Lipids (2008) 43:1–17
DOI 10.1007/s11745-007-3111-z

REVIEW

Role of Fatty Acid Binding Proteins and Long Chain Fatty Acids in Modulating Nuclear Receptors and Gene Transcription

Friedhelm Schroeder · Anca D. Petrescu · Huan Huang · Barbara P. Atshaves · Avery L. McIntosh · Gregory G. Martin · Heather A. Hostetler · Aude Vespa · Danilo Landrock · Kerstin K. Landrock · H. Ross Payne · Ann B. Kier

Received: 10 April 2007 / Accepted: 26 July 2007 / Published online: 19 September 2007
© AOCS 2007

Abstract Abnormal energy regulation may significantly contribute to the pathogenesis of obesity, diabetes mellitus, cardiovascular disease, and cancer. For rapid control of energy homeostasis, allosteric and posttranslational events activate or alter activity of key metabolic enzymes. For longer impact, transcriptional regulation is more effective, especially in response to nutrients such as long chain fatty acids (LCFA). Recent advances provide insights into how poorly water-soluble lipid nutrients [LCFA; retinoic acid (RA)] and their metabolites (long chain fatty acyl Coenzyme A, LCFA-CoA) reach nuclei, bind their cognate ligand-activated receptors, and regulate transcription for signaling lipid and glucose catabolism or storage: (i) while serum and cytoplasmic LCFA levels are in the 200 μM–mM range, real-time imaging recently revealed that LCFA and LCFA-CoA are also located within nuclei (nM range); (ii) sensitive fluorescence binding assays show that LCFA-activated nuclear receptors [peroxisome proliferator-activated receptor-α (PPARα) and hepatocyte nuclear factor 4α (HNF4α)] exhibit high affinity (low nM K_ds) for LCFA (PPARα) and/or LCFA-CoA (PPARα, HNF4α)—in the same range as nuclear levels of these ligands; (iii) live and fixed cell immunolabeling and imaging revealed that some cytoplasmic lipid binding proteins [liver fatty acid binding protein (L-FABP), acyl CoA binding protein (ACBP), cellular retinoic acid binding protein-2 (CRABP-2)] enter nuclei, bind nuclear receptors (PPARα, HNF4α, CRABP-2), and activate transcription of genes in fatty acid and glucose metabolism; and (iv) studies with gene ablated mice provided physiological relevance of LCFA and LCFA-CoA binding proteins in nuclear signaling. This led to the hypothesis that cytoplasmic lipid binding proteins transfer and channel lipidic ligands into nuclei for initiating nuclear receptor transcriptional activity to provide new lipid nutrient signaling pathways that affect lipid and glucose catabolism and storage.

Keywords L-FABP · ACBP · PPARα · HNF4α · CRABP · Fatty acid · Transgenic mice

Abbreviations

LCFA	Long chain fatty acids
L-FCFA-CoA	Long chain fatty acyl Coenzyme A
L-FABP	Liver fatty acid binding protein
A-FABP	Adipocyte FABP
H-FABP	Heart FABP
K-FABP	Keratinocyte FABP
I-FABP	Intestinal FABP
B-FABP	Brain FABP
ACBP	Acyl CoA binding protein
CRABP	Cellular retinoic acid binding protein
PPAR	Peroxisome proliferator-activated receptor
HNF4α	Hepatocyte nuclear factor-4α
RA	Retinoic acid
RXR	Retinoic acid X receptor
SCP-2	Sterol carrier protein-2
WT	Wild-type

F. Schroeder (✉) · A. D. Petrescu · H. Huang ·
B. P. Atshaves · A. L. McIntosh · G. G. Martin ·
H. A. Hostetler · A. Vespa
Department of Physiology and Pharmacology,
Texas A&M University, TVMC, College Station,
TX 77843-4466, USA
e-mail: fschroeder@cvm.tamu.edu

D. Landrock · K. K. Landrock · H. R. Payne · A. B. Kier
Department of Pathobiology, Texas A&M University, TVMC,
College Station, TX 77843-4467, USA

Introduction

Long chain fatty acids (LCFA) have been known for some time to serve as components of biological membranes and are also used for metabolic fuel. LCFA are not only precursors of signaling molecules; they are also endogenous ligands [1–3] for nuclear receptors that initiate transcription of multiple genes involved in LCFA (β-oxidation, lipoprotein) and glucose metabolism. Concomitantly, LCFA down-regulate genes involved in insulin signaling (e.g. protein tyrosine phosphatase) (rev. in [4–6]). Abnormal activation of the nuclear peroxisome proliferator-activated receptors (PPARs) contributes to lipotoxicity associated with obesity, insulin resistance, type 2 diabetes, and hyperlipidemia (rev. in [5, 7]).

Mammals have evolved both short/rapid acting and long/slower mechanisms to control metabolism. Rapid allosteric control and posttranslational modification activate/deactivate enzymes or alter protein stability within seconds to minutes [5]. Most effective for longer-lasting control (hours to days) is transcriptional regulation of at least two types of receptors [8]: (i) hydrophilic ligands (e.g. diazapines) bind with cell surface membrane receptors, activating cascades of second messengers, which transmit signals to transcription factors that control expression of target genes; and (ii) in contrast, hydrophobic ligands (fatty acids, retinoic acid, vitamins, hormones) must actually enter the cell and be transported to the nucleus, interacting with intracellular and nuclear receptors that serve as nutrient sensors [8, 9]. These hydrophobic ligands act as modulators of transcription factors, exerting regulatory functions directly at the gene level [8]. Because nuclear receptors such as PPAR isoforms (α, β, γ), HNF4α, thyroid receptor (T_3R), glucocorticoid receptor (GR), liver X receptor (LXR), retinoic acid X receptor (RXR), and others regulate transcription of genes involved in lipid and glucose metabolism [5, 9–13], there is great interest in discovery of pharmaceutical antagonists of these receptors to reduce/prevent the deleterious effects of LCFA and LCFA-CoA in obesity, diabetes mellitus, and cardiovascular disease. This focus has led to important discoveries that certain hydrophobic xenobiotics and metabolites/analogues of LCFA including LCFA-CoA are high-affinity ligands that inhibit transcriptional activity of their respective nuclear receptor.

However, the identity of endogenous ligands for PPARα and HNF4α has been elusive. Clearly, dietary LCFA regulate activity of PPARα and HNF4α to induce transcription of genes encoding enzymes and proteins of LCFA and carbohydrate metabolism in cells [14–20] and animals [21], but until recently it was not clear whether LCFA themselves versus their metabolites LCFA-CoA exhibit the requisite characteristics generally acknowledged as hallmarks of physiologically significant ligands: (i) presence in the nucleus, but at levels sufficiently low not to saturate the nuclear receptors, (ii) high affinity binding, with K_ds in the range of physiological concentrations of the ligands in nuclei; (iii) ligand-induced conformational change in the nuclear receptor; and (iv) ligand-induced alterations in coregulator recruitment to the nuclear receptor [7, 22–25]. Further, until recently little was known regarding how hydrophobic ligands [e.g. LCFA, LCFA-CoA, retinoic acid (RA)] could be transported to the nucleus.

Since elevated levels of LCFA and LCFA-CoA are characteristic of several chronic metabolic disorders, including obesity, diabetes mellitus, hyperlipidemia, and cardiovascular disease [26], it is important to resolve mechanism(s) that regulate intracellular and nuclear LCFA/LCFA-CoA concentrations for optimal LCFA and glucose metabolic homeostasis [27]. This review focuses on recent evidence supporting one hypothesis, "exemplified for liver, that transfer and channeling of LCFA to PPARα in the nucleus can be mediated by L-FABP" (Fig. 1).

Dietary LCFA Activate Nuclear Receptors PPARα and HNF4α: Functional Data

Early studies of PPARα and HNF4α ligand specificity illustrate the difficulty in determining the nature of the endogenous ligands of these ligand-activated nuclear receptors. High-fat diets increase PPARα-activated gene expression, especially of L-FABP and β-oxidative enzymes, stimulating LCFA β-oxidation, regardless of whether dietary LCFA are polyunsaturated,

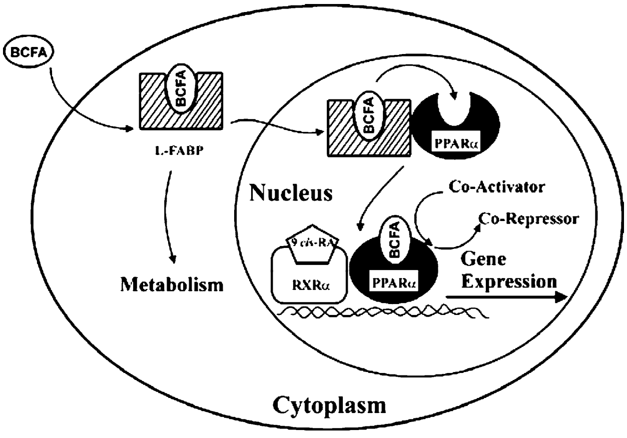

Fig. 1 Selective cooperation between L-FABP and PPARα in branched-chain fatty acid signaling to the nucleus. BCFA, branched-chain fatty acid; L-FABP, liver fatty acid binding protein; RXRα, retinoic acid X receptor α; 9 *cis*-RA, 9 *cis*-retinoic acid

monounsaturated, or saturated [13, 16, 21]. While straight-chain LCFA (unsaturated > saturated) stimulate PPARα transactivation [14, 16, 18, 23, 28], they are relatively non-selective and effective on all three PPAR isoforms (α, β, γ) [29]. In contrast, branched-chain LCFA (pristanic acid, phytanic acid) selectively activate only PPARα [29], particularly in liver [30], and more effectively than any other dietary LCFA or synthetic peroxisome proliferator drugs [29, 31]. Plasma of healthy individuals contains <10 μM phytanic and <3 μM pristanic acid, levels that activate PPARα in cultured cells [29]. In patients with peroxisomal disorders (Refsum, Zellweger, and other peroxisomal abnormalities), plasma phytanic and pristanic acid levels rise to 8,000 and 80 μM, respectively [29, 32].

While together these data suggest that the LCFA activate PPARα, nutritional studies and activation assays do not discriminate whether dietary LCFA are themselves PPARα ligands, induce endogenous PPARα ligands, or are metabolized to active PPARα ligands [16]. Early studies with radioligand binding assays indicated that saturated LCFA and VLCFA (except for arachidonic acid) were very poorly or not bound by PPARα (see below). However, this apparent contradiction of dietary saturated LCFA and very long chain fatty acids (VLCFA) directly activating PPARα [21] was recently resolved by showing that metabolites of saturated LCFA and VLCFA (LCFA-CoA and VLCFA-CoA) are the actual high-affinity PPARα ligands [2, 3]. Mouse studies lend further support for the potential importance of LCFA-CoA in regulating PPARα: (i) peroxisome proliferators induce expression of acyl-CoA oxidase (AOX) and bifunctional protein (BPE), the first two enzymes of the β-oxidation pathway [33], and increase the level of CoA thioesters of peroxisome proliferators [34, 35]; (ii) 2-bromopalmitate, a general inhibitor of fatty acid thioesterification, inhibits bezafibrate induction of peroxisomal proliferation [36]; (iii) AOX gene ablation increases serum VLCFA, and since VLCFA-CoA are not β-oxidized in AOX-null mice, they accumulate and hyperactivate PPARα [37]. Conversely, ablation of the adrenoleukodystrophy gene (prevents VLCFA and/or VLCFA-CoA from being transported to peroxisomes) increases VLCFA (but not VLCFA-CoA) levels and does not alter PPARα activity [38]. These data show that gene alterations resulting in high acyl-CoA elicit PPARα activation, while gene alterations leading to reduced acyl-CoA result in PPARα inactivation.

With HNF4α activation, dietary saturated fatty acids increase plasma levels of lipid rich lipoproteins (VLDL, LDL, HDL) and their constituent apolipoproteins, while dietary unsaturated fatty acids decrease plasma levels of these lipoproteins and their apolipoproteins [39]. This fatty acid nutrient regulation of serum lipids and lipoproteins has been ascribed to transcriptional modulation of HNF4α activated genes encoding apolipoproteins (AI, AII, B, CIII) [40, 41]. Dietary fatty acids modulate HNF4α transactivation in a highly selective manner, consistent with LCFA-CoA representing the activating ligand rather than LCFA (rev. in [42–45]). Mutations in HNF4α form the basis of mature onset diabetes of the young (MODY-1), while agonist LCFA-CoA ligands rescue MODY-1 mutants of HNF4α in transactivation assays [45].

In summary, the above data show that dietary LCFA regulate the PPARα- and HNF4α-mediated transcription of genes involved in LCFA and glucose metabolism. However, it was not clear from earlier studies whether LCFA and their acyl CoA represented the endogenous ligands of these nuclear receptors. For LCFA and LCFA-CoA to represent physiologically significant endogenous ligands they must meet the classical criteria of ligand-activated nuclear receptors (summarized in Table 1). These criteria provide a mechanistic framework accounting for current observations, and establish LCFA and LCFA-CoA as physiologically relevant ligands for these nuclear receptors.

LCFAs and LCFA-CoAs must be Present Within the Nucleus

Serum LCFA levels exceed the solubility of LCFA (1–100 μM) by several orders of magnitude: 200–600 μM under normal conditions, 1 mM under fasting, and up to 8 mM in Refsum's disease, diabetes, cancer, and sepsis (rev. in [29, 32, 46]). Because LCFA are potent detergents and thus toxic at higher concentrations, serum LCFA are almost completely bound by albumin such that the concentration of free unbound LCFA available for uptake into cells is quite low, 2–67 nM, depending on the assay (rev. in [46]). Still, cultured cells can generally take up unbound LCFA from media very rapidly ($t_{1/2}$ of minutes) into the cytoplasm (rev. in [46]). Because of their potent detergent action at high concentration, once taken up the LCFA are rapidly (sec to min) converted to LCFA-CoA by fatty acyl

Table 1 Essential criteria for LCFA or LCFA-CoA activated nuclear receptors: PPARs and HNF4α

	Criterion
1	LCFA or LCFA-CoA levels in nuclear envelope and nucleoplasm are low (nM range)
2	Nuclear receptors have high affinity (nM K_ds) for LCFAs or LCFA-CoAs
3	LCFA or LCFA-CoA binding alters nuclear receptor conformation
4	LCFA or LCFA-CoA binding alters cofactor recruitment

CoA synthase activity at the plasma membrane—a process that can be facilitated by certain fatty acid binding proteins in the cytoplasm (rev. in [46, 47]). While LCFA-CoA are less potent detergents than LCFA, cellular LCFA-CoA levels are generally 10–100 fold lower than LCFA levels because the LCFA-CoA are more rapidly utilized for metabolism (esterification, oxidation), regulation of receptor/enzyme activity, and/or transport to nuclei to potentially regulate transcriptional activity of LCFA-CoA dependent nuclear receptors (rev. in [27, 48, 49]).

However, to be physiologically significant ligands and regulators of nuclear receptors, these LCFA and/or their LCFA-CoA metabolites must: (i) be able to enter nuclei and (ii) nucleoplasmic concentrations of these ligands must be in the same affinity range as the nuclear receptors for these ligands. Whether these ligands enter nuclei was originally addressed by purifying nuclei through subcellular fractionation, in which it was determined that LCFA and LCFA-CoA were detectable [50–54]. However, such experiments could not discriminate contributions from contaminating adherent endoplasmic reticulum (ER) fragments and ligand binding to nuclear membranes, versus actual distribution into nucleoplasm. These potential problems were resolved by real-time confocal and/or multiphoton imaging of a naturally-occurring fluorescent, slowly metabolizable LCFA (*cis*-parinaric acid) as well as non- and poorly-metabolizable synthetic fluorescent LCFA (NBD-stearic acid, BODIPY-C16, BODIPY-C12) and a non-hydrolyzable fluorescent synthetic LCFA-CoA (BODIPY-C16-S-S-CoA) in intact living cells [55–57]. While much of the fluorescent LCFA and LCFA-CoA was present outside the nucleus, significant amounts also colocalized with a nucleic acid dye such that the intracellular distribution was of the order: outside the nucleus $\gg$ nuclear membrane $>$ more dense structures within the nucleoplasm $>$ diffuse nucleoplasm [56]. Thus LCFA and LCFA-CoA are indeed present in nuclei and, more importantly, distributed throughout the nucleoplasm of both fixed and live cells.

Secondly, measurement of LCFA and LCFA-CoA concentrations within the nucleus was initially also addressed by chemical analysis of nuclei isolated by subcellular fractionation, in which nuclear LCFA and LCFA-CoA concentrations were measured in the high µM range (rev. in [55, 56]). Such experiments could not discriminate contributions due to esterase activity on LCFA-CoA and more complex lipids to release LCFA, redistribution of LCFA and LCFA-CoA from other intracellular sites, or differences in the proportion of LCFA and LCFA-CoA in the nuclear envelope versus nucleoplasm. In later experiments, real-time confocal and multiphoton imaging of naturally-occurring and synthetic fluorescent LCFA and LCFA-CoA in living cells measured nucleoplasmic LCFA levels at 39–69 nM [55, 56] and nucleoplasmic LCFA-CoA levels at <10 nM [56], levels consistent with earlier calculations [48, 49].

PPARα and HNF4α must Exhibit Specific, High Affinity (nM K_d*s) for LCFA and/or LCFA-CoA*

While LCFA are currently considered putative, physiologically significant endogenous ligands of PPARα, earlier data did not support this hypothesis. As initially measured by radioligand competition and indirect binding assays, PPARα had a low affinity for unsaturated LCFA (10–50 µM $K_d s$), and did not bind saturated LCFA or LCFA-CoA [15, 17]. These µM $K_d s$ would be several orders of magnitude higher than nuclear LCFA and LCFA-CoA concentrations. Unanswered was whether LCFA or LCFA-CoA alter conformation of PPARα and/or alter coactivator binding, both hallmarks of ligand-activated nuclear receptors (rev. in [1, 2]). More recent data utilizing new assays not requiring separation of bound from free lipidic ligands (LCFA, LCFA-CoA) showed that radioligand binding assays produce significant levels of non-specific binding [15] and underestimate PPARα affinities for LCFA [46] and LCFA-CoA [58, 59]. The newer fluorescence-based assays showed that PPARα has high affinity (1–20 nM $K_d s$) for unsaturated LCFA, saturated LCFA-CoA, unsaturated LCFA-CoA, unsaturated and saturated VLCFA-CoA, and branched-chain BCFA-CoA, as well as similar or somewhat weaker affinity for fibrates and branched-chain fatty acids (both PPARα agonists) [1–3, 60]. In contrast, saturated LCFA, saturated VLCFA, and unsaturated VLCFA (PPARα agonists) as well glitazones (PPARγ agonists) do not or only weakly bind to PPARα [2, 3, 61, 62]. LCFA-CoA binding to PPARα did not require hydrolysis of LCFA-CoA to the free acid form (LCFA), since PPARα bound non-hydrolyzable *S*-hexadecyl-CoA (S-C16-CoA) with high affinity (K_d = 10 nM) [2, 3].

In the case of HNF4α, earlier studies on the HNF4α ligand binding domain (LBD) suggested that HNF4α did not contain a ligand binding site for either LCFA or LCFA-CoA [63]. Indeed, initial studies using radioligand competition and indirect binding assays showed that the full-length HNF4α had low affinity for unsaturated LCFA-CoA (1–4 mM $K_d s$) and did not bind saturated LCFA [24, 42, 64]. Further, LCFA, but not LCFA-CoA, was bound by truncated HNF4α ligand binding domain (LBD) constructs that were missing both the N-terminal domains and more importantly the C-terminal F domain (52.5% of the protein) [64]. This reversal of ligand specificity was primarily due to deletion of the C-terminal F domain since deletion of the N-terminal domains had little effect on ligand affinity or specificity [64]. Confirming the effect of C-terminal F-domain truncation on ligand specificity, X-ray crystallography of truncated HNF4α constructs detected only bound LCFA [64]. Since LCFA-CoA are very unstable under conditions necessary for crystallization of HNF4α (i.e. several weeks at room temperature) [65], lack of the terminal F domain, instability of LCFA-CoA under crystallization conditions, and the fact that HNF4α exhibits thioesterase activity [65, 66] could account for LCFA-CoA not being observed by x-ray crystallography [24, 65, 67, 68]. Interestingly, the LCFA binding site identified by X-ray crystallography is located within a classic LBD [66–68], has weak affinity for LCFA [24, 45, 64] and does not alter its conformation in response to LCFA binding [24, 66–68]. More recent fluorescence data have shown that both unsaturated and saturated LCFA-CoA are bound in a second site with high affinity (i.e. low nM K_ds) by full-length HNF4α [24, 45, 64, 66]. LCFA-CoA binding was subsequently confirmed by mass spectrometry of full-length HNF4α [66]. Mass spectrometry also detected a second ligand binding site which was discrete from the LCFA-CoA binding site, bound only LCFA, and bound LCFA in this site were not displaced by adding exogenous LCFA [66]. While X-ray crystallography studies also showed that the bound LCFA could not be displaced by exogenous LCFA, it is not known if the LCFA binding site determined by mass spectrometry is identical to that determined by X-ray crystallography. Since LCFA bound to HNF4α did not alter structure, and LCFA that are poorly metabolized to LCFA-CoA do not affect HNF4α transactivation [42, 45], the physiological function if any of the LCFA bound within the HNF4α second ligand site remains to be shown.

In summary, PPARα (exhibits high affinity for unsaturated LCFA and nearly all LCFA-CoA and VLCFA-CoA, but not saturated LCFA or VLCFA. Thus select LCFA and all LCFA-CoA/VLCFA-CoA satisfy the high affinity and location requirements for physiologically significant ligands that activate PPARα [1]. These data help to explain why dietary or exogenous saturated LCFA and both saturated and unsaturated VLCFA alter transcriptional activity of PPARα even though they are weak ligands. In contrast, select LCFA-CoA (but not unsaturated or saturated LCFA) satisfy the high affinity requirements for ligands that enhance or inhibit full-length HNF4α transactivation [45, 66]. What remains to be shown, however, is whether LCFA or LCFA-CoA directly bind with PPARα or HNF4α in nuclei of living cells.

LCFA and LCFA-CoA Binding must Alter PPARα and HNF4α Conformation

Recent studies by circular dichroism, quenching of intrinsic aromatic amino acid fluorescence, and protease susceptibility have all demonstrated that LCFA and/or LCFA-CoA alter the conformation of PPARα and HNF4α (rev. in [2, 3, 66]). All high affinity (but not low/no affinity) endogenous or synthetic ligands alter PPARα conformation [2, 3]. Likewise, high affinity (but not low/no affinity) endogenous or synthetic ligands alter conformation of full-length HNF4α [24, 64] as well as HNF4α constructs retaining the C-terminal F-domain, which is the largest F domain (near 80aa) of any nuclear receptor examined to date [64]. Finally, circular dichroism studies of HNF-4α in the absence and presence of various acyl-CoA ligands demonstrated that saturated versus polyunsaturated acyl-CoA differentially altered HNF-4α secondary structure conformation [64], suggesting that different lipid ligands could modulate HNF-4α activity by inducing conformational changes in the structure of HNF-4α [64].

LCFA and LCFA-CoA Alter Cofactor Recruitment to PPARα and HNF4α

It has been shown that high affinity (but not low/no affinity) endogenous or synthetic LCFA and LCFA-CoA alter PPARα coactivator binding [2, 3]. Conversely, select LCFA-CoA but not LCFA alter DNA binding and/or coactivator recruitment to HNF4α (rev. in [42, 43, 45]).

Potential Roles of LCFA and LCFA-CoA Binding Proteins in Regulating Nuclear Receptors

Fatty acid binding proteins represent a large family of soluble proteins that bind LCFA and, in most cases LCFA-CoA, with high affinity (rev. in [46]). Although these proteins were generally named after the tissue in which they were first discovered, most occur in multiple tissues. For example, liver fatty acid binding protein (L-FABP) is expressed at highest amounts in liver and intestine, as well as in lower quantities in kidney and several other tissues (rev. in [4, 46, 69–75]). All tissues examined to date express one or more FABP (L-FABP, adipose A-FABP, intestine I-FABP, heart H-FABP, brain B-FABP), often at a relatively high level, representing as much as 2–5% of cytosolic protein and concentrations of 200–1,000 μM depending on genetic status [76], sex (rev. in [46, 69]), physiological status (rev. in [46]), and induction by peroxisome proliferators (rev. in [46]). In addition, all tissues examined contain the ubiquitous acyl CoA binding protein (ACBP), usually present at several fold-lower levels than the FABPs in the same tissue (rev. in [27, 48, 49, 77, 78]). ACBP and various FABPs are generally expressed at highest levels in tissues that exhibit the highest LCFA metabolic activity, such as liver and heart (rev. in [27, 48, 49, 77, 78]). ACBP in combination with select FABPs may regulate the nuclear concentration of LCFA and LCFA-CoA by one or more of the following mechanisms.

ACBP and FABPs have Ligand Affinities in the Same Range as those of Nuclear Receptors

To effectively transport and donate bound LCFA and/or LCFA-CoA, ACBP and FABPs must have affinities in the same range or slightly weaker than those exhibited by nuclear receptors, such as PPARα and HNF4α described previously, and indeed this parallel affinity is the case. For example, native liver L-FABP exists in two isoforms which exhibit high affinity for LCFA (K_ds of 8–60 nM, depending on the isoform) and LCFA-CoA (K_ds of 14–110 nM, depending on the isoform) [59]. L-FABP binds unsaturated LCFA with 2–3 fold higher affinity than saturated LCFA, while affinities for both types of LCFA-CoA are more similar (rev. in [59, 79]). ACBP exhibits a higher affinity, but only for LCFA-CoA (K_ds of 0.6–7 nM) [48, 49, 80]. ACBP binds LCFA-CoA with the following order of affinities: saturated > unsaturated > polyunsaturated [80, 81]. However, it must be noted that some studies based on titration microcalorimetry, a method that uses relatively high concentrations of proteins and ligands (e.g. 130,000 nM), yields K_ds of 1–10 nM for ACBP (rev. in [48, 49, 82]) while K_ds for L-FABP are 1,000 nM [83]. The reasons for the discrepancy are not clear but may be related to the fact that fluorescence binding assays use very low concentrations of proteins and ligands (e.g. 180 nM) below the critical micellar concentration of the LCFA-CoA ligand [59, 80], while titration microcalorimetry uses relatively high concentrations of proteins and ligands (e.g. 130,000 nM) above the critical micellar concentration of LCFA-CoA ligand (rev. in [48, 49, 82]). While LCFA-CoA levels above the critical micelle concentration apparently do not affect calculation of binding affinities for proteins with very high affinities such as with ACBP for LCFA-CoA, titration microcalorimetry with lower LCFA-CoA binding affinity proteins such as L-FABP results in underestimation of the binding affinity by one to two orders of magnitude. These data indicate that while ACBP is a higher LCFA-CoA affinity protein than L-FABP, the difference is not 1,000-fold, but rather in the range of 10–50 fold depending on the ligand. Further, the physiological significance of both proteins in LCFA-CoA metabolism was confirmed by a variety of studies indicating that not only ACBP, but also L-FABP [27, 79, 84] enhance acyl transferase enzymes (GPAT, ACBP) in vitro (rev. in [85]). Additionally, studies with livers of gene targeted mice indicate that, while ACBP alters both fatty acyl CoA pool size and acyl chain distribution [81], L-FABP alters cytosolic fatty acyl CoA binding capacity, albeit not fatty acyl CoA pool size [86]. Thus, both L-FABP and ACBP exhibit physiologically significant LCFA-CoA affinities, slightly weaker or in the same range as PPARα and HNF4α-consistent with these proteins being able to effectively donate bound LCFA and LCFA-CoA to the nuclear receptors.

FABPs Enhance LCFA Uptake into the Cell: Role in LCFA-CoA Pool Size

Studies with transfected cells overexpressing FABPs (L-FABP, I-FABP, A-FABP, H-FABP) and with cultured primary hepatocytes from L-FABP null mice show that FABP enhance LCFA uptake 1.5–5 fold (rev. in [46, 79, 87–92]). FABPs may enhance LCFA uptake either by acting as acceptors from plasma membrane LCFA transport/translocase proteins and/or by enhancing intracellular metabolism of LCFA (rev. in [46, 79, 87–92]).

Since FABPs enhance LCFA uptake, they may thereby increase intracellular LCFA pool size and thus increase intracellular availability of LCFA for targeting to the nucleus. Consistent with this possibility are: (i) FABPs can extract LCFA from membranes and increase their solubility in aqueous buffer (rev. in [46, 79, 87–89]). (ii) The LCFA binding sites of native L-FABP isolated from liver are 76% occupied by LCFA (rev. in [79]). (iii) Studies with L-FABP gene-ablated mice indicate that L-FABPs accounts for 90% of the cytosolic LCFA binding capacity in liver (rev. in [46, 93]). Despite these findings, however, studies with gene-targeted mice indicate that L-FABP gene ablation does not decrease liver LCFA pool size [93] or LCFA-CoA pool size [86]. L-FABP gene ablation did alter LCFA-CoA acyl chain distribution [86]. The lack of effect on LCFA and LCFA-CoA pool sizes may be explained by the fact that L-FABP enhances the activities of both catabolic (oxidative) and anabolic (esterification) pathways of LCFA metabolism—thereby maintaining the respective pool sizes. For example, tissue levels of FABPs correlate with LCFA oxidative activity [94–97] and L-FABP expression enhances LCFA (via LCFA-CoA) oxidation with isolated liver mitochondria [98, 99], in transfected cells overexpressing L-FABP [92], and in wild-type as compared to L-FABP null mice [86, 91, 93, 100–102]. Furthermore, L-FABP stimulates LCFA esterification (via LCFA-CoA) with isolated liver microsomes [79, 85, 89, 103], in transfected cells overexpressing L-FABP (rev. in [46, 104]), and in wild-type as compared to L-FABP null mice [86, 91, 93, 102]. In contrast to L-FABP, ACBP increases LCFA-CoA pool size by extracting LCFA-CoA from membranes (rev. in [81]), in yeast overexpressing ACBP [105], and in transgenic mice overexpressing ACBP [81]. Interestingly, ACBP also enhances LCFA catabolic (oxidation) and anabolic (esterification) pathways of LCFA metabolism in vitro [58, 81, 87, 106, 107] and in vivo [81].

In summary, since tissue total (cytosol plus membranes) LCFA-CoA concentrations are generally 10–100 fold lower than LCFA concentrations, these studies indicate that hepatic L-FABP and ACBP levels are sufficient to extract almost all available LCFA and LCFA-CoA from membranes and from cytosol (rev. in [46, 48, 49, 79]). Furthermore, ACBP expression increases LCFA-CoA pool size, while L-FABP expression does not alter either LCFA or LCFA-CoA pool size, likely due to its higher affinity for LCFA-CoA as compared to L-FABP.

FABPs Enhance LCFA Intracellular Trafficking

Studies with a variety of cultured cell lines overexpressing L-FABP [46, 108–112] and with hepatocytes from wild-type and L-FABP gene-ablated mice [91] indicate that several members of the FABP family (L-FABP, I-FABP) enhance LCFA intracellular diffusion/trafficking. There have been no published reports, to our knowledge, examining the effect of FABPs or ACBP on LCFA-CoA diffusion/transport through the cytoplasm. Thus, based on the finding that FABPs facilitate intracellular transport and trafficking of bound LCFA, the possibility that FABPs may facilitate LCFA trafficking to/into nuclei for interaction with nuclear receptors must be considered. By analogy it may be predicted that the LCFA-CoA binding proteins (e.g. L-FABP, ACBP) may likewise facilitate trafficking of this ligand into nuclei.

FABPs Enhance LCFA and LCFA-CoA Distribution into Nuclei, both Nuclear Membrane and Nucleoplasm

LCFA binds to purified nuclei only in the presence of L-FABP [113]. However, such in vitro studies do not discriminate whether L-FABP only transfers bound LCFA to the cytoplasmic face of the nuclear envelope or actually facilitates LCFA transport into nuclei. This issue was recently addressed by use of confocal and multiphoton microscopy of naturally-occurring, slowly-metabolizable fluorescent LCFA (*cis*-parinaric acid) and non- or very poorly-metabolizable synthetic fluorescent LCFA (NBD-stearic acid, BODIPY-C16, BODIPY-C12) and LCFA-CoA (BODIPY-C16-S-S-CoA) [55–57]. Real-time imaging of these probes in live L-cell fibroblasts overexpressing L-FABP and in cultured primary hepatocytes from L-FABP null mice demonstrated that L-FABP enhances distribution of: (i) LCFA into nuclei, both into nucleoplasm and within the nuclear envelope, and (ii) LCFA-CoA into nuclei, primarily diffuse in nucleoplasm with less within the nuclear membrane. Thus, L-FABP distributes LCFA and LCFA-CoA to and into nuclei, but unknown is whether L-FABP cotransfers bound LCFA/LCFA-CoA through the nuclear envelope into the nucleoplasm (Fig. 2, Pathway 1), or just to the nuclear envelope for subsequent release and diffusion of LCFA/LCFA-CoA into the nucleoplasm (Fig. 2, Pathway 2). Nuclear pores are sufficiently large to accommodate diffusion not only of the LCFA and LCFA-CoA ligands (<1 kDa) but also of 14 kDa L-FABP complexes with these ligands (rev. in [56]).

FABPs, ACBP, and CRABP-2 Enter Nuclei (Fig. 2, Pathway 1): Role of Ligands

Several members of the FABP family have been detected in nuclei and nucleoplasm, as shown by confocal imaging of living cells expressing GFP-tagged FABPs, indirect immunofluorescence confocal imaging of fixed cells, and immunogold electron microscopy of fixed cells: L-FABP in nuclei of hepatocytes as well as transfected cells (L-cells, ES cells) [56, 85, 114], H-FABP in cardiac myocytes as well as in transfected CV1 and 3T3-L1 cells [115, 116] K-FABP in transfected CV1, 3T3–L1, and COS1 cells [116, 117], and CRABP-2 in MCF7 cells [118, 119]. In L-cell fibroblasts overexpressing L-FABP (0.4% of cytosolic protein, 10 fold lower than in liver), L-FABP exhibited punctate and clustered distribution in the nucleoplasm [56]. However, when transfected into adipocytes, L-FABP is not detected in nuclei—suggesting that nuclear localization of some members of the FABP family may be cell type specific (rev. in [4]). Furthermore, the localization of FABPs in nuclei as well as cytoplasm is specific for select members of the FABP family, since another member of the FABP family, CRABP-1, is not detected in nuclei [118].

Similarly, a member of a separate LCFA-CoA binding protein family, i.e. ACBP, has also been detected in nuclei. Immunofluorescence microscopy, confocal microscopy and immunogold electron microscopy detect significant amounts of ACBP in nuclei of fixed transfected cells (CV1, 3T3-L1, COS7) overexpressing ACBP [117, 120, 121], rat and mouse hepatoma cells that normally express high amounts of ACBP [120, 121], as well as normal rat and mouse liver hepatocytes [120, 121]. This pattern of distribution was also detected by immunofluorescence confocal microscopy of endogenous ACBP in mouse hepatoma cells (Fig. 3e–h). To assure that this distribution was not due to a fixation or immunolabeling artifacts, a recently developed approach was used for real-time imaging of ACBP in living cells [122]. Purified recombinant ACBP was chemically labeled with small (<1 kDa) fluorescent tags such as Cy5, incorporated into living cells, and intracellular distribution was examined by confocal microscopy (Fig. 3e–h) [123]. ACBP (Fig. 3e) and the nuclear marker Hoechst 33342 (Fig. 3f) were then simultaneously imaged through

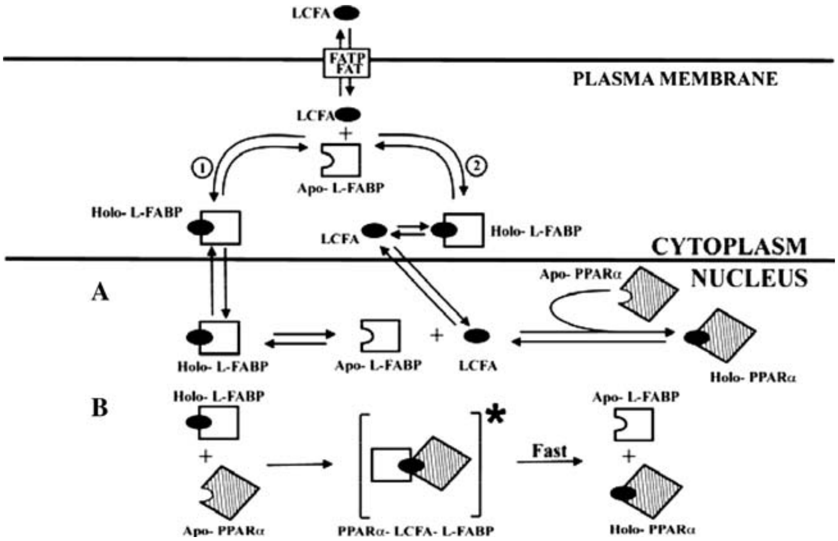

Fig. 2 Mechanisms of LCFA transfer from L-FABP to PPARα within the nucleus. Suggested pathways by which L-FABP may deliver LCFAs to PPARα: (*A*) diffusional and (*B*) collisional/complex

separate photomultipliers. When only colocalized pixels were shown (Fig. 3g), it was apparent that ACBP was significantly colocalized with the DNA binding dye in nuclei of living cells. A pixel fluorogram indicated that 22% of ACBP was colocalized with nuclei (Fig. 3f). These results in living cells confirm the findings of immunofluorescence and immunogold labeling of fixed cells and indicate that significant amounts of ACBP are distributed to nuclei.

While these data clearly show that many members of the FABP family can enter nuclei, it is less clear whether ligands enhance FABPs targeting/transport into the nucleoplasm (Fig. 2, Pathway 1). Some fluorescence imaging studies have shown that ligands enhanced distribution of GFP-A-FABP, GFP-K-FABP, and GFP-CRABP-2 (but not GFP-CRABP-1) into nuclei of living COS1 cells [116, 118]. In contrast, another study using immunolabeling fluorescence microscopy and confocal microscopy showed that ligands did not alter the distribution of ACBP, A-FABP, and K-FABP into nuclei of fixed transfected CV1 or 3T3–L1 cells [117]. The reasons for the discrepancy are not known, but may relate to the cell type, FABP expression level, use of live versus fixed cells, use of GFP vs antibodies to decorate the FABPs, or other as yet unresolved factors.

In summary, several members of the FABP family as well as ACBP are present at significant levels in nuclei and nucleoplasm—consistent with these small sized proteins being able to enter nuclei through the nuclear pores. A cluster of basic amino acids in some FABPs (e.g. C-terminal region of A-FABP and K-FABP) and a cluster of lysine residues (far C-terminal region) of ACBP, both apparent only in the respective three-dimensional folded protein structures, have been suggested to resemble a nuclear localization signal [117]. However, the fact that yeast ACBP does not contain such a region, but nevertheless is significantly localized to nuclei suggests that additional as yet unresolved factors are involved [117]. Finally, several, but not all, studies indicate that ligands can enhance the distribution of the FABPs into nuclei under at least some conditions—suggesting cotransport of FABP-ligand complexes through the nuclear pores into the nucleoplasm.

FABPs Directly Bind Nuclear Receptors

Growing evidence indicates that multiple members of the FABP family interact directly with nuclear receptors, especially PPARs and RAR (Table 2). For example, co-immunoprecipitation, immunofluorescence colocalization, and transactivation assays (despite some disagreement regarding enhancement or inhibition of transactivation [116, 117]) suggest that several members of the FABP family interact with nuclear receptors to transfer bound ligands: CRABP-2 with RAR [116, 118, 119, 124]; A-FABP and K-FABP with PPARγ and β isoforms, respectively, but not PPARα [116, 117]; H-FABP with PPARα [116]; ILBP with farnesoid X receptor (FXR), an interaction augmented by bound bile acid [125]. Likewise, transactivation, coimmunoprecipitation, two-hybrid assay, and immunofluorescence colocalization indicate that L-FABP binds with both PPARα (Fig. 2, L-FABP/PPARα complex) and PPARγ [18, 56, 126]. However, such indirect assays do not provide direct proof of physical association between the FABP family of proteins with their respective nuclear receptors. The finding that L-FABP does not contain an LXXLL domain characteristic of proteins bound by PPARα [18] suggests that L-FABP either interacts with PPARα through an unidentified domain, or that these

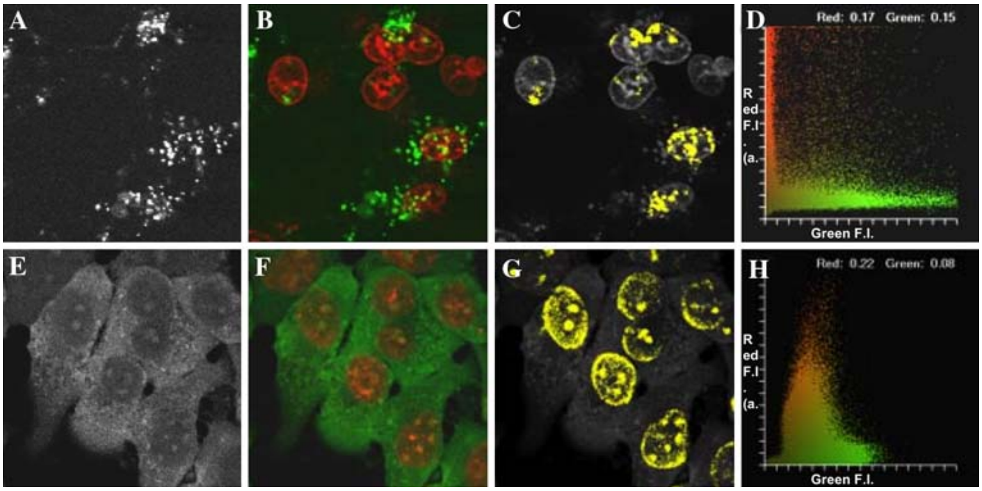

Fig. 3 Intracellular localization of exogenous ACBP in living COS-7 cells, and endogenous ACBP in fixed mouse hepatoma cells. **a–d** Live COS-7 cells were incubated with Cy5-ACBP/Pep-1 and counterstained with nuclear marker Hoechst 33342 before LSCM imaging. **a** Fluorescence image of Cy5-labeled ACBP. **b** Fluorescence image overlay of Cy5-ACBP (*red*) and nuclear marker (*green*). **c** Colocalized pixels are shown in *yellow*. **d** Fluorograph of colocalization analysis of image in panel **b**. **e–h** Mouse hepatoma cells were preincubated with nuclear marker Hoechst 33342, then fixed and labeled with primary antibody against ACBP and Texas-Red-labeled secondary antibody. **e** Indirect immunofluorescence image of ACBP. **f** Overlay of fluorescence images from ACBP (*green*) and nuclear marker (*red*). **g** Colocalized pixels from panel **f** are shown in *yellow*. **h** Fluorograph of colocalization analysis of image in panel **f**

Table 2 Cytoplasmic LCFA and LCFA-CoA binding proteins and nuclear receptors

Cytoplasmic protein	Acronym	Nuclear receptor
FABP family		
Liver FABP	L-FABP	PPARα, PPARγ
Heart FABP	H-FABP	PPARα
Adipocyte FABP	A-FABP	PPARγ
Keratinocyte FABP	K-FABP	PPARβ
Cellular retinoic acid binding protein-2	CRABP-2	RAR
Ileal lipid binding protein[a]	ILBP	FXR
ACBP family		
Acyl CoA binding protein	ACBP	HNF4α

Cytoplasmic LCFA and LCFA-CoA binding proteins enter nuclei, bind with nuclear receptors with high affinity for LCFA/LCFA-CoA, and thereby regulate transcriptional activity of nuclear receptors

[a] Interaction augmented by bound bile acid

assays do not demonstrate direct molecular interaction. With the latter possibility, positive results with the above assays could arise from L-FABP interacting with intermediary protein(s) that in turn bind to PPARα, L-FABP enhancing release of endogenous PPARα ligands [16], and/or L-FABP enhancing formation of additional LCFA metabolite(s) which binds PPARα as exemplified by LCFA-CoAs [2, 3, 47, 127–129].

Despite these reservations, several recent studies have provided molecular details of FABP/nuclear receptor interaction, including intermolecular distance between the proteins, affinity of the proteins for each other, conformational changes upon interaction, and the mechanism(s) whereby ligand cargo is transferred between these proteins. Physical interaction between purified CRABP-2 and RAR proteins was indicated by coimmunoprecipitation [118]. Likewise, physical interaction between purified A-FABP and PPARγ as well as between K-FABP and PPARβ has been shown by coimmunoprecipitation [116]. Circular dichroism has shown that interaction of purified L-FABP and PPARα alters protein conformation [57]. Likewise, a fluorescence resonance energy transfer (FRET) demonstrated that purified L-FABP binds PPARα with high affinity [57]. Finally, FRET between purified L-FABP and PPARα showed these proteins interacting with very close intermolecular distance, i.e. a few angstroms [57]. This was confirmed by immunofluorescence and immunogold electron microscopy. Although L-FABP overexpressed in transfected L-cell fibroblasts has been detected in nuclei, most of this distribution appeared distinct from that of PPARα [56]. However, subsequent double immunogold electron microscopic observations in cultured primary hepatocytes indicate that significant amounts of L-FABP and PPARα in the punctuately distributed regions of the nucleoplasm are in close proximity [57].

In summary, both indirect (coimmunoprecipation, two hybrid, transactivation) and direct (circular dichroism, FRET-based K_ds, FRET-based intermolecular distance in fixed cells, immunogold EM) binding assays show that FABPs interact with select nuclear receptors (PPAR isoforms, RAR, and HNF4α). The ligand-dependence of these interactions remains to be elucidated. Taken together, these studies indicate that the FABPs may selectively cooperate with the respective nuclear receptors in providing a signaling pathway for LCFA metabolism. However, molecular mechanisms and physiological impact of these interactions remain to be resolved.

ACBP Directly Binds Nuclear Receptors: HNF4α

ACBP, a member of a separate LCFA-CoA binding protein family, interacts directly with the nuclear receptor HNF4α (Table 2). A model similar to that for the L-FABP/PPARα interaction (Figs. 1, 2) is illustrated in Fig. 4. In this model, ACBP interacts with the ligand binding domain of HNF4α to elicit a conformational change and/or transfer bound LCFA-CoA ligand to elicit a conformational change which in turn alters coregulator recruitment and transactivation. Whether other LCFA-CoA binding proteins compete with ACBP for binding and differentially modulating transcriptional activity of this nuclear receptor is not known (Fig. 4). This model is supported by both indirect and direct interaction assays.

Indirect assays such as coimmunoprecipitation, mammalian two hybrid, and transactivation indicate that ACBP directly interacts with HNF4α [120]. It has been reported that HNF4α transactivation is stimulated by saturated acyl-CoAs like C14:0- and C16:0-CoA, and inhibited by polyunsaturated C18:2-, C18:3-, C20:5-CoA thioesters [130]. Thus, depending on the LCFA-CoA species bound to ACBP, the type of ACBP/LCFA-CoA complex may regulate the type of interaction/activation observed.

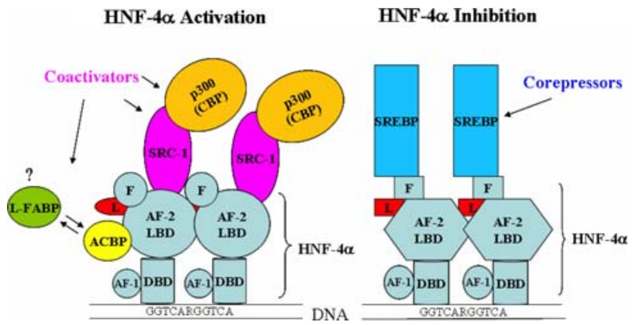

Fig. 4 Suggested modulation of HNF-4α transactivation by specific acyl-CoA ligands, and acyl-CoA-binding proteins ACBP and L-FABP. The DNA sequence shown in the diagram is a specific response element in promoters of HNF-4α target genes. AF-1, DBD, AF2, LBD, F are HNF-4α activation function 1 (ligand-independent), DNA-binding domain, activation function-2 (ligand-dependent), ligand binding domain, and F-regulatory domain at the C-terminus of HNF-4α molecule, respectively. L, ACBP, L-FABP are denotations for ligands (saturated-round shape, or polyunsaturated-square shape), acyl-CoA binding protein and liver fatty acid binding protein, respectively. SRC-1/p300 are complexes of coactivators which contribute to increasing the transcription when recruited by HNF-4α to the target gene promoter. SREBP-1 is a transcription factor reported to negatively regulate HNF-4α transcription activity. In this model, it is assumed that depending on the structure of HNF-4α ligand or on the interaction of HNF-4α with ligand binding proteins like ACBP and L-FABP, the conformation of HNF-4α is significantly altered—thereby resulting in recruiting of either coactivator complexes (such as SRC-1/p300) or corepressor transcriptional factors like (SREBP-1)

While such indirect assays do not provide direct proof of physical association between ACBP with this nuclear receptor, perhaps the strongest direct evidence to date that these lipid binding proteins may physically interact with nuclear receptors has been obtained for the ACBP/HNF4α complex [120, 122]: (i) interaction of pure ACBP and HNF4α proteins significantly altered the protein secondary structure; (ii) HNF4α bound ACBP with high affinity (K_d ∼60–110 nM); (iii) the intermolecular distance between HNF4α and bound ACBP determined by FRET was 73 Å; (iv) double immunofluorescence labeling confocal microscopy FRET demonstrated an intermolecular distance of 53Å between HNF4α and bound ACBP in fixed cells; (v) double immunogold electron microscopy showed an intermolecular distance of 43 Å between HNF4α and bound ACBP [120]. These molecular interactions were specific, since ACBP did not interact with/bind β-galactosidase (a cytosolic enzyme), Sp1 (a coregulator of nuclear receptors) and GR (glucocorticoid receptor in the nucleus). However, recent evidence from our laboratory indicates that HNF-4α interacts with multiple LCFA-CoA binding proteins, not just ACBP, as demonstrated by in vitro FRET between fluorescent tagged L-FABP and HNF4α as well as between ACBP and HNF4α (not shown).

In summary, both indirect (coimmunoprecipation, yeast two hybrid, mammalian two hybrid, transactivation) and direct (circular dichroism, FRET-based K_ds, FRET-based intermolecular distance in fixed cells, immunogold EM) binding assays show that ACBP interacts with select nuclear receptors (HNF4α). Again, the ligand-dependence of these interactions remains to be elucidated. Taken together, these studies indicate that ACBP may also selectively cooperate with a nuclear receptor (HNF4α), analogous to FABPs cooperating with nuclear receptors (PPARs), in providing a signaling pathway for LCFA metabolism.

Interaction Between Nuclear Receptors (HNF4α, PPARα) and ACBP/FABP in Liver

If FABP/ACBP directly channel ligands to nuclear receptors, this could represent a significant mechanism of gene regulation. This direct association of ACBP with HNF-4α would ensure HNF-4α binding to LCFA-CoA while precluding the availability of LCFA-CoA for interaction with

PPARα. Since LCFA-CoA are endogenous, high-affinity ligands of both HNF-4α [24] and PPARα [2, 3], this would shift the balance of transcriptional regulation to HNF-4α. The binding of saturated LCFA-CoA to HNF-4α would result in increased HNF-4α activity [24] and decreased PPARα activity (due to lack of availability for binding and activation) [2], while unsaturated LCFA-CoA would decrease HNF-4α activity and possibly increase or decrease PPARα activity. Similarly, L-FABP binding to either PPARα or HNF-4α could provide a direct route of transport for both LCFA and LCFA-CoA, while ensuring that these ligands interacted exclusively with one nuclear receptor and preventing their interaction with the other.

Moreover, interaction of ACBP with HNF-4α, both in the presence and absence of ligands, directly stimulates HNF-4α transactivation [120], while ACBP inhibits PPARα transactivation [62, 117]. Since HNF-4α and PPARα both regulate downstream transcription through the binding of similar DR1 sequences [43, 131], ACBP may again shift the transcriptional control to HNF-4α, rather than PPARα, by allowing preferential DNA binding by HNF-4α. Given that HNF-4α and PPARα compete for the same co-activators and co-repressors (rev in [132]), cross-talk between these nuclear receptors could represent a pertinent tool for maintaining energy homeostasis in the liver, and FABP/ACBP may function to regulate this cross-talk.

Interaction of Proteins within Nuclear Receptor/Coregulator Complexes: HNF4α, Coactivators, and Corepressors

The interaction of HNF-4α with ACBP (Fig. 4) and PPARα with L-FABP (not shown) is thought to elicit downstream alterations in coactivator and corepressor protein association (Fig. 4). To date, however, there are very few if any data directly demonstrating the individual interactions between specific proteins in such complexes. A first approach to study multi-protein nuclear receptor complexes by triple immunolabeling confocal fluorescence microscopy and FRET (fluorescence resonance energy transfer) was applied to HNF4α. Rat hepatoma cells in culture were demonstrated to express detectable amounts of HNF-4α, coactivators of HNF4α (SRC-1, p300) and corepressors of HNF4α (SREBP-1) by Western blotting (not shown). Rat hepatoma cells were fixed and labeled with primary antibodies (rabbit anti-HNF-4α, mouse anti-p300, mouse SBEBP-1, goat anti-SRC-1) and with fluorescent dye-labeled secondary antibodies (i.e. FITC-anti-mouse IgG, Cy3-anti-rabbit IgG, Cy5-anti-goat IgG). If three proteins are closely bound into a complex, by this technique it would be possible to detect Cy5 sensitized emission at 680 nm by excitation of FITC at 488 nm, as excitation of FITC at 488 nm could result in FRET from FITC to Cy3, which in turn would be followed by FRET from Cy3 to Cy5. Two examples demonstrate the feasibility of this approach.

First, triple immunolabeling confocal FRET imaging of fixed cells demonstrated specific physical complex formation between HNF4α and coactivators (SRC-1 and p300) in fixed cells (Fig. 5). Excitation of FITC/p300 at 488 nm, resulted in: (i) a fluorescence image with emission at 530 nm from p300 molecules inside hepatoma cells (Fig. 5a); (ii) a FITC → Cy3 FRET image with emission at 600 nm, from HNF-4α molecules (Fig. 5b) due to close interaction of HNF-4α with p300; (iii) a Cy3 → Cy5 FRET image with emission at 680 nm from SRC-1 molecules closely associated to HNF-4α molecules (Fig. 5c). Images obtained with excitation of Cy3 at 568 nm and Cy5 at 647 nm are shown in Fig. 5d–i; by direct excitation of Cy3/HNF-4α both HNF-(α and SRC-1 molecules were detected, being associated within a FRET distance of less than 100 Å.

Second, triple immunolabeling confocal FRET imaging of fixed cells demonstrated that, in contrast to the coactivator p300, the corepressor SREBP-1 was not detected within a complex of HNF4α with SRC-1 (Fig. 6). Thus, excitation of FITC/SREBP-1 resulted in a fluorescence emission image of SREBP-1 (Fig. 6a), a FRET image of Cy3/HNF-4α (Fig. 6b) but not a further FRET image of Cy5/SRC-1 (Fig. 6c) suggesting that the cells contained HNF-4α molecules that were complexed with SREBP-1, but these complexes did not contain SRC-1. Excitation of Cy3/HNF-4α resulted in emission fluorescence image of HNF-4α (Fig. 6e) and FRET image of SRC-1, indicating that a subpopulation of HNF-4α molecules were associated with SRC-1; the fact that no FITC → Cy3 → Cy5 FRET image from SREBP-1 → HNF-4α → SRC-1 (Fig. 6a–c) was detected in panel C even though there were HNF-4α/SRC-1 complexes, strongly indicates that SREBP-1 was not associated with HNF-4α that was complexed with SRC-1. This was in agreement with previous publications reporting SREBP-1 as a negative coregulator of HNF-4α, by reporter gene assays [133].

These triple-immunolabeling confocal imaging FRET studies illustrate for the first time the direct physical proximities of coactivators and corepressors with a nuclear receptor (HNF4α) involved in fatty acid and glucose metabolism. What remains to be done is to apply these approaches to resolve the effects of the LCFA-CoA binding proteins (ACBP, FABPs) on these intermolecular interactions.

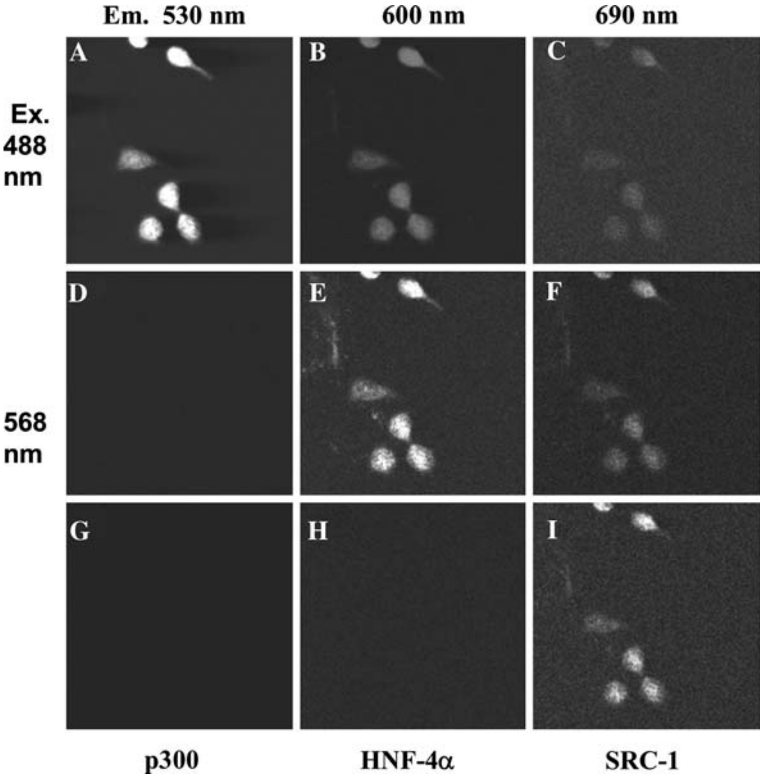

Fig. 5 Interaction of HNF-4α with coactivators p300 and SRC-1. T-7 cells were labeled with primary antibodies against p300, HNF-4α and SRC-1 and secondary antibodies conjugated to FITC, Cy3 and Cy5, respectively. **a** FITC/p300 detected with excitation at 488 nm; **b** Cy3/HNF-4α detected with excitation of FITC at 488 nm, due to FRET; **c** Cy5/SRC-1 detected with excitation of FITC at 488 nm, due to double FRET. **d**–**f** show images in *green*, *red* and *blue* channels, respectively, when excited at 568 nm (for Cy3); fluorescence Cy5 in F is due to FRET; **g**–**i** show fluorescence images in channels *green*, *red* and *blue* channels, when excited at 647 nm (for Cy5)

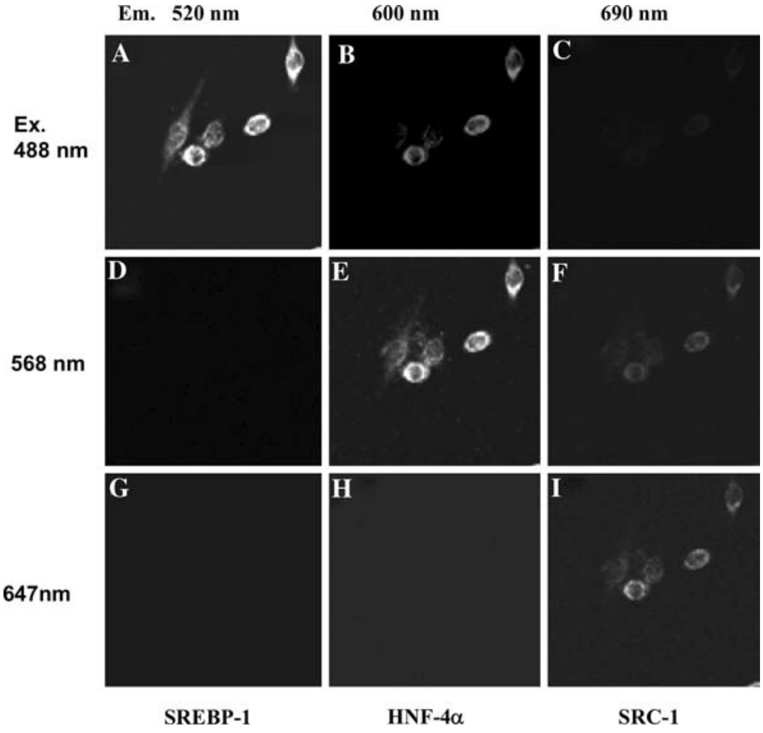

Fig. 6 Interaction of HNF-4α with coactivator SRC-1 and corepressor SREBP-1. T-7 cells were labeled with primary antibodies against SREBP-1, HNF-4α and SRC-1 and secondary antibodies conjugated to FITC, Cy3 and Cy5, respectively. **a** FITC/SREBP-1 detected with excitation at 488 nm; **b** Cy3/HNF-4α detected with excitation of FITC at 488 nm, due to FRET; **c** Cy5/SRC-1 detected with excitation of FITC at 488 nm, due to double FRET. **d**–**f** show images in *green*, *red* and *blue* channels, respectively, when excited at 568 nm (for Cy3); fluorescence of Cy5 in F is due to FRET; **g**–**i** show fluorescence images in channels *green*, *red* and *blue* channels, when excited at 647 nm (for Cy5)

Direct Channeling of Ligands between FABPs and Nuclear Receptors

Several studies with purified proteins indicate that by binding to nuclear receptors, different FABPs may directly channel bound ligands to the receptors. For example, CRABP-2 transfers bound retinoic acid (a poorly soluble nuclear regulatory ligand) to the nuclear receptor RAR in vitro [116] via transient collisional interactions (rev. in [4, 118, 119, 124]). Likewise, A-FABP directly channels bound ligands to PPARγ, but K-FABP does not [116]. However, complexes of these proteins all appeared to be transient collisional interactions. Whether this is the case for interactions between other FABPs or ACBP with nuclear receptors remains to be shown.

Summary/Conclusions

The past few years have seen great advances in our understanding of potential contributions of FABPs and ACBP to nuclear signaling mediated through PPARs, RAR, and HNF4α. The overall picture that is emerging is illustrated by Fig. 2, Pathway 1. In this proposed scheme, FABPs and ACBP enhance uptake of lipidic ligands (LCFA, RA, and/or LCFA-CoA), bind these ligands with high affinity in the cytoplasm, cotransport this cargo to nuclei and through the nuclear pores into the nucleoplasm, form complexes with nuclear receptors exhibiting even higher affinity for the respective ligands, and directly channel this cargo to the respective nuclear receptors to regulate receptor activation. Thus, the FABPs and ACBP may act as nutrient sensors [1, 4, 5]. For example, LCFA-mediated PPARα activation enhances L-FABP transcription (rev. in [23]) while PPARα gene ablation reduces L-FABP expression, especially during fasting [13, 134, 135]. These data suggest that by transporting LCFA (or LCFA-CoA) to PPARα in the nucleus, L-FABP may in part regulate its own expression (rev. in [5, 18]). These data suggest that other FABPs and ACBP may also in part regulate their own expression.

Acknowledgments This work was supported in part by the USPHS, National Institutes of Health grants DK41402 (FS and ABK), NIH P20 GM72041 (Project 2, ABK and FS) and DK70965 (BPA).

References

1. Lin Q, Ruuska SE, Shaw NS, Dong D, Noy N (1999) Ligand selectivity of the peroxisome proliferator-activated receptor α. Biochem 38:185–190
2. Hostetler HA, Petrescu AD, Kier AB, Schroeder F (2005) Peroxisome proliferator-activated receptor α interacts with high affinity and is conformationally responsive to endogenous ligands. J Biol Chem 280:18667–18682
3. Hostetler HA, Kier AB, Schroeder F (2006) Very-long-chain and branched-chain fatty acyl-CoAs are high affinity ligands for the peroxisome proliferator-activated receptor α (PPARα). Biochemistry 45:7669–7681
4. Adida A, Spener F (2002) Intracellular lipid binding proteins and nuclear receptors inolved in branched-chain fatty acid signaling. Prost Leukot Essen Fatty Acids 67:91–98
5. Desvergne B, Michalik L, Wahli W (2004) Be fit or be sick: peroxisome proliferator-activated receptors are down the road. Mol Endocrinol 18:1321–1332
6. Frederiksen KS, Wulf EM, Wassermann K, Sauerberg P, Fleckner J (2003) Identification of hepatic transcriptional changes in insulin-resistant rats treated with peroxisome proliferator activated receptor-α agonists. J Mol Endocrinol 30:317–329
7. Francis GA, Fayard E, Picard F, Auwerx J (2003) Nuclear receptors and the control of metabolism. Annu Rev Physiol 65:261–311
8. Schoonjans K, Staels B, Auwerx J (1996) Role of the peroxisome proliferator-activated receptor (PPAR) in mediating the effects of fibrates and fatty acids on gene expression. J Lipid Res 37:907–925
9. Jump DB (2004) Fatty acid regulation of gene transcription. Crit Rev Clin Lab Sci 41:41–78
10. Pawar A, Jump DB (2003) Unsaturated fatty acid regulation of peroxisome proliferatoractivated receptor α activity in primary rat hepatocytes. J Biol Chem 278:35931–35939
11. Jump DB, Clarke SD (1999) Regulation of gene expression by dietary fat. Annu Rev Nutr 19:63–90
12. Kersten S, Desvergne B, Wahli W (2000) Roles of PPARs in health and disease. Nature 405:421–424
13. Kersten S, Seydoux J, Peters JM, Gonzalex FJ, Desvergne B, Wahli W (1999) Peroxisome proliferator-activated receptor α mediates the adaptive response to fasting. J Clin Inv 103:1489–1498
14. Gottlicher M, Widmark E, Li Q, Gustafsson JA (1992) Fatty acids activate a chimera of the clofibric acid-activated receptor and the glucocorticoid receptor. Proc Natl Acad Sci 89:4653–4657
15. Forman BM, Chen J, Evans RM (1999) Hypolipidemic drugs, polyunsaturated fatty acids, and eicosanoids are ligands for peroxisome proliferator-activated receptors alpha and delta. Proc Natl Acad Sci 94:4312–4317
16. Keller H, Dreyer C, Medin J, Mahfoudi A, Ozato K, Wahli W (1993) Fatty acids and retinoids control lipid metabolism through activation of peroxisome proliferator activated receptorretinoid X receptor heterodimers. Proc Natl Acad Sci 90:2160–2164
17. Kliewer SA, Sundseth SS, Jones SA, Brown PJ, Wisely GB, Koble CS, Devchand P, Wahli W, Willson TM, Lenhard JM, Lehmann JM (1997) Fatty acids and eicosanoids regulate gene expression through direct interactions with peroxisome proliferator-activated receptors α and γ. Proc Natl Acad Sci 94:4318–4323
18. Wolfrum C, Borrmann CM, Borchers T, Spener F (2001) Fatty acids and hypolipidemic drugs regulate PPARα and PPARγ gene expression via L-FABP: a signaling path to the nucleus. Proc Natl Acad Sci 98:2323–2328
19. Krey G, Braissant O, L'Horset F, Kalkhoven E, Perroud M, Parker MG, Wahli W (1997) Fatty acids, eicosanoids, and hypolipidemic agents identified as ligands of peroxisome proliferator-activated receptors by coactivator-dependent receptor ligand assay. Mol Endocrinol 11:779–791
20. Banner CD, Gottlicher M, Widmark E, Sjovall J, Rafter JJ, Gustafsson J (1993) A systematic analytical chemistry/cell assay approach to isolate activators of orphan nuclear receptors from biological extracts: characterization of peroxisome proliferator-activated receptor activators in plasma. J Lipid Res 34:1583–1591
21. Bonilla S, Redonnet A, Noel-Suberville C, Pallet V, Garcin H, Higueret P (2000) High-fat diets affect the expression of nuclear retinoic acid receptor in rat liver. Br J Nutr 83:665–671
22. Xu J, Nawaz Z, Tsai SY, Tsai MJ, O'Malley BW (1996) The extreme C terminus of the progesterone receptor contains a transcriptional repressor domain that functions through a putative corepressor. Proc Natl Acad Sci USA 93:12195–12199
23. Escher P, Wahli W (2000) Peroxisome proliferator activated receptors: insights into multiple cellular functions. Mutat Res 448:121–138

24. Petrescu AD, Hertz R, Bar-Tana J, Schroeder F, Kier AB (2002) Ligand specificity and conformational dependence of the hepatic nuclear factor-4α (HNF-4α). J Biol Chem 277:23988–23999
25. Svensson S, Osteberg T, Jacobsson M, Norstrom C, Stefansson K, Hallen D, Johansson IC, Zachrisson K, Ogg D, Jendeberg L (2003) Crystal structure of the heterodimeric complex of LXRα and RXRβ ligand binding domains in a fully agonistic form. EMBO J 22:4625–4633
26. McGarry JD, Dobbins RL (1999) Fatty acids, lipotoxicity, and insulin secretion. Diabetologia 42:128–138
27. Gossett RE, Frolov AA, Roths JB, Behnke WD, Kier AB, Schroeder F (1996) Acyl-CoA binding proteins: multiplicity and function. Lipids 31:895–918
28. Lemberger T, Desvergne B, Wahli W (1996) Peroxisome proliferator-activated receptors. Annu Rev Cell Dev Biol 12:335–363
29. Zomer AWM, van der Burg B, Jansen GA, Wanders RJA, Poll-The BT, van der Saag PT (2000) Pristanic acid and phytanic acid: naturally occurring ligands for the nuclear receptor peroxisome proliferator-activated receptor α. J Lipid Res 41:1801–1807
30. Wolfrum C, Spener F (2000) Fatty acids as regulators in lipid metabolism. Eur J Lip Sci Technol 102:746–762
31. Hanhoff T, Wolfrum C, Ellinghaus P, Seedorf U, Spener F (2001) Pristanic acid is activator of peroxisome proliferator activated receptor alpha. Eur J Lipid Sci 103:75–80
32. Steinberg D (1995) Refsums disease. In: Scriver CR, Beaudet AL, Sly WS, Vallee D (eds) The metabolic and molecular basis of inherited disease. McGraw-Hill, New York
33. Reddy JK, Goel SK, Nemali MR, Crrino JJ, Laffler TG, Reddy MK, Sperbeck SJ, Osumi T, Hashimoto T, Lalwani ND, Rao MS (1986) Transcriptional regulation of peroxisomal fatty acyl-CoA oxidase and enoyl-CoA hydratase/3-hydroxyacyl-CoA dehydrogenase in rat liver by peroxisome proliferators. Proc Natl Acad Sci 83:1747–1751
34. Berge R, Stensland E, Aarsland A, Tsegai G, Osmundsen H, Aarsaether N, Gjellesvik DR (1987) Induction of cytosolic clofibroyl-CoA hydrolase activity in liver of rats treated with clofibrate. Biochim Biophys Acta 918:60–66
35. Aarsland A, Berge RK (1991) Peroxisome proliferating sulphur and oxy-substituted fatty acid analogues are activated to acyl coenzyme A thioesters. Biochem Pharmacol 41:53–61
36. Hertz R, Bar-Tana J (1987) Prevention of peroxisomal proliferation by carnitine palmitoyltransferase inhibitors in cultured rat hepatocytes and in vivo. Biochem J 245:387–392
37. Fan CY, Pan J, Usuda N, Yeldandi AV, Rao MS, Reddy JK (1998) Steatohepatitis,spontaneous peroxisome proliferation and liver tumors in mice lacking peroxisomal fattyacyl-CoA oxidase. J Biol Chem 273:15639–15645
38. Reddy JK, Hashimoto T (2001) Peroxisomal β-oxidation and peroxisome proliferatoractivatedreceptor α: an adaptive metabolic system. Annu Rev Nutr 21:193–230
39. Grundy SM, Denke MA (1990) Dietary influence on serum lipids and lipoproteins. J Lipid Res 31:1149–1172
40. Hayhurst GP, Lee YH, Lambert G, Ward JM, Gonzalez FJ (2001) Hepatocyte nuclear factor 4α (nuclear receptor 2A1) is essential for maintenance of hepatic gene expression and lipid homeostasis. Mol Cell Biol 21:1393–1403
41. Sladek FM (1994) In: Tronche F, Yaniv M (eds) Liver gene expression, VRG Landes, Austin
42. Hertz R, Magenheim J, Berman I, Bar-Tana J (1998) Fatty acyl-CoA thioesters are ligands of hepatic nuclear factor-4α. Nature 392:512–516
43. Rajas F, Gautier A, Bady I, Montano S, Mithieux G (2002) Polyunsaturated fatty acyl CoA suppress the glucose-6-phosphate promoter activity by modulating the DNA binding of hepatocyte nuclear factor 4α. J Biol Chem 277:15736–15744
44. Hertz R, Sheena V, Kalderon B, Berman I, Bar-Tana J (2001) Suppression of hepatocyte nuclear factor-4α by acyl-CoA thioesters of hypolipidemic peroxisome proliferators. Biochem Pharmacol 61:1057–1062
45. Hertz R, Ben-Haim M, Petrescu A, Kalderon B, Berman I, Eldad N, Schroeder F, Bar-Tana J (2003) Rescue of MODY-1 by agonist ligands of hepatocyte nuclear factor-4α. J Biol Chem 278:22578–22585
46. McArthur MJ, Atshaves BP, Frolov A, Foxworth WD, Kier AB, Schroeder F (1999) Cellular uptake and intracellular trafficking of long chain fatty acids. J Lipid Res 40:1371–1383
47. Burrier RE, Manson CR, Brecher P (1987) Binding of acyl-CoA to liver fatty acid binding protein: effect on acyl-CoA synthesis. Biochim Biophys Acta 919:221–230
48. Faergeman NJ, Knudsen J (1997) Role of long-chain fatty acyl-CoA esters in the regulation of metabolism and in cell signaling. Biochem J 323:1–12
49. Knudsen J, Jensen MV, Hansen JK, Faergeman NJ, Neergard T, Gaigg B (1999) Role of acyl CoA binding protein in acyl CoA transport, metabolism, and cell signaling. Mol Cell Biochem 192:95–103
50. Song M, Rebel G (1987) Rat liver nuclear lipids. Composition and biosynthesis. Bas Appl Histochem 31:377–387
51. Bucki R, Zendzian-Piotrowska M, Nawrocki A, Gorski J (1997) Effect of increased uptake of plasma fatty acids by the liver on lipid metabolism in the hepatocellular nuclei. Prost Leukot Essen Fatty Acids 57:27–31
52. Ves-Losada A, Mate SM, Brenner RR (2001) Incorporation and distribution of saturated and unsaturated fatty acids into nuclear lipids of hepatic cells. Lipids 36:273–282
53. Ves-Losada A, Brenner RR (1996) Long-chain fatty acyl-CoA synthetase enzymatic activity in rat liver cell nuclei. Mol Cell Biochem 159:1–6
54. Losada AV, Brenner RR (1998) Incorporation of delta-5 desaturase substrate (dihomogammalnolenic acid, 20:3 n-6) and product (arachidonic acid 20:4 n-6) into rat liver cell nuclei. Prost Leukot Essen Fatty Acids 59:39–47
55. Huang H, Starodub O, McIntosh A, Kier AB, Schroeder F (2002) Liver fatty acid binding protein targets fatty acids to the nucleus: real-time confocal and multiphoton fluorescence imaging in living cells. J Biol Chem 277:29139–29151
56. Huang H, Starodub O, McIntosh A, Atshaves BP, Woldegiorgis G, Kier AB, Schroeder F (2004) Liver fatty acid binding protein colocalizes with peroxisome proliferator receptor alpha and enhances ligand distribution to nuclei of living cells. Biochemistry 43:2484–2500
57. McIntosh A, Atshaves BP, Huang H, Payne HR, Hostetler HA, Davis J, Kier AB, Schroeder F (2007) Liver fatty acid binding protein gene ablation reduces nuclear targeting of fatty acid and fatty acyl-CoA in cultured mouse primary hepatocytes. Biochem J (submitted)
58. Gossett RE, Edmondson RD, Jolly CA, Cho TH, Russell DH, Knudsen J, Kier AB, Schroeder F (1998) Structure and function of normal and transformed murine acyl-CoA binding proteins. Arch Biochem Biophys 350:201–213
59. Frolov A, Cho TH, Murphy EJ, Schroeder F (1997) Isoforms of rat liver fatty acid binding protein differ in structure and affinity for fatty acids and fatty acyl-CoAs. Biochemistry 36:6545–6555
60. Wolfrum C, Borchers T, Sacchettini JC, Spener F (2000) Binding of fatty acids and peroxisome proliferators to orthologous fatty acid binding proteins from human, murine, and bovine liver. Biochemistry 39:1469–1474
61. Murakami K, Ide T, Nakazawa T, Okazaki T, Mochizuki T, Kadowaki T (2001) Fatty-acyl-CoA thioesters inhibit recruitment of steroid receptor co-activator 1 to α and γ isoforms of

peroxisome-proliferator-activated receptors by competing with agonists. Biochem J 353:231–238
62. Elholm M, Dam I, Jorgenesen C, Krogsdam AM, Holst D, Kratchamarova I, Gottlicher M, Gustafsson JA, Berge RK, Flatmark T, Knudsen J, Mandrup S, Kristiansen K (2001) Acyl-CoA esters antagonize the effects of ligands on peroxisome proliferator-activated receptor α conformation, DNA binding, and interaction with cofactors. J Biol Chem 276:21410–21416
63. Bogan AA, Dallas-Yang Q, Ruse MD, Maeda Y, Jiang G, Nepomuceno L, Scanlan TS, Cohen FE, Sladek FM (2000) Analysis of protein dimerization and ligand binding of orphan receptor HNF4α. J Mol Biol 302:831–851
64. Petrescu A, Huang H, Hertz R, Bar-Tana J, Schroeder F, Kier AB (2005) Role of regulatory F-domain in hepatocyte nuclear factor-4α ligand specificity. J Biol Chem 280:16714–16727
65. Schroeder F, Huang H, Hostetler HA, Petrescu AD, Hertz R, Bar-Tana J, Kier AB (2005) Stability of fatty acyl CoA thioester ligands of hepatocyte nuclear factor-4α and peroxisome proliferator-activated receptor-α. Lipids 40:559–568
66. Hertz R, Kalderon B, Byk T, Berman I, Zátara G, Mayer R, Bar-Tana J (2005) Thioesterase activity and acyl-CoA/fatty acid cross talk of hepatocyte nuclear factor-4α. J Biol Chem 280:24451–24461
67. Dhe-Paganon S, Duda K, Iwamoto M, Chi YI, Shoelson SE (2002) Crystal structure of the HNF4α ligand binding domain in complex with endogenous fatty acid ligand. J Biol Chem 277:37973–37976
68. Wisely GB, Miller AB, Davis RG, Thornquest AD, Johnson R, Spitzer T, Sefler A, Shearer B, Moore JT, Miller AB, Willson TM, Williams SP (2002) Hepatocyte nuclear factor 4 is a transcription factor that constitutively binds fatty acids. Structure 10:1225–1234
69. Paulussen RJA, Veerkamp JH (1990) Intracellular fatty acid-binding proteins characteristics and function. In: Hilderson HJ (ed) Subcellular biochemistry. Plenum Press, New York
70. Veerkamp JH, Maatman RG, Prinsen CF (1992) Fatty acid-binding proteins: structural and functional diversity. Biochem Soc Trans 20:801–805
71. Bass NM (1988) The cellular fatty acid binding proteins: aspects of structure, regulation, and function. Int Rev Cytol 111:143–184
72. Banaszak L, Winter N, Xu Z, Bernlohr DA, Cowan S, Jones TA (1994) Lipid-binding proteins: a family of fatty acid and retinoid transport proteins. Adv Protein Chem 45:89–151
73. Matarese V, Stone RL, Waggoner DW, Bernlohr DA (1989) Intracellular fatty acid trafficking and the role of cytosolic lipid binding proteins. Prog Lipid Res 28:245–272
74. Borchers T, Spener F (1994) Fatty acid binding proteins. In: Hoekstra D (ed) Current topics in membranes, Academic, Orlando
75. Haunerland NH, Spener F (2004) Fatty acid binding proteins—insights from genetic manipulations. Prog Lipid Res 43:328–349
76. Seedorf U, Raabe M, Ellinghaus P, Kannenberg F, Fobker M, Engel T, Denis S, Wouters F, Wirtz KWA, Wanders RJA, Maeda N, Assmann G (1998) Defective peroxisomal catabolism of branched fatty acyl coenzyme A in mice lacking the sterol carrier protein-2/sterol carrier protein-x gene function. Genes Dev 12:1189–1201
77. Knudsen J, Faergeman NJ, Skott H, Hummel R, Borsting C, Rose TM, Andersen JS, Hojrup P, Roepstorff P, Kristiansen K (1994) Yeast acyl-CoA-binding protein: acyl-CoA-binding affinity and effect on intracellular acyl-CoA pool size. Biochem J 302:479–485
78. Faergeman NJ, Wadum MCT, Feddersen S, Burton BB, Knudsen J (2007) Acyl-CoA binding proteins: structural and functional conservation over 2000 MYA. Mol Cell Biochem (in press)
79. Schroeder F, Jolly CA, Cho TH, Frolov AA (1998) Fatty acid binding protein isoforms: structure and function. Chem Phys Lipids 92:1–25
80. Frolov AA, Schroeder F (1998) Acyl coenzyme A binding protein: conformational sensitivity to long chain fatty acyl-CoA. J Biol Chem 273:11049–11055
81. Huang H, Atshaves BP, Frolov A, Kier AB, Schroeder F (2005) Acyl-coenzyme A binding protein expression alters liver fatty acyl coenzyme A metabolism. Biochemistry 44:10282–10297
82. Faergeman NJ, Sigurskjold BW, Kragelund BB, Andersen KV, Knudsen J (1996) Thermodynamics of ligand binding to acyl-coenzyme A binding protein studied by titration calorimetry. Biochemistry 35:14118–14126
83. Rolf B, Oudenampsen-Kruger E, Borchers T, Faergeman NJ, Knudsen J, Lezius A, Spener F (1995) Analysis of the ligand binding properties of recombinant bovine liver-type fatty acid binding protein. Biochim Biophys Acta 1259:245–253
84. Chao H, Zhou M, McIntosh A, Schroeder F, Kier AB (2003) Acyl-CoA binding protein and cholesterol differentially alter fatty acyl CoA utilization by microsomal acyl CoA: cholesterol transferase. J Lipid Res 44:72–83
85. Bordewick U, Heese M, Borchers T, Robenek H, Spener F (1989) Compartmentation of hepatic fatty-acid-binding protein in liver cells and its effect on microsomal phosphatidic acid biosynthesis. Biol Chem Hoppe-Seyler 370:229–238
86. Martin GG, Huang H, Atshaves BP, Binas B, Schroeder F (2003) Ablation of the liver fatty acid binding protein gene decreases fatty acyl-CoA binding capacity and alters fatty acyl-CoA pool distribution in mouse liver. Biochemistry 42:11520–11532
87. Jolly CA, Wilton DA, Schroeder F (2000) Microsomal fatty acyl-CoA transacylation and hydrolysis: fatty acyl-CoA species dependent modulation by liver fatty acyl-CoA binding proteins. Biochim Biophys Acta 1483:185–197
88. Jolly CA, Hubbell T, Behnke WD, Schroeder F (1997) Fatty acid binding protein: stimulation of microsomal phosphatidic acid formation. Arch Biochem Biophys 341:112–121
89. Jolly CA, Murphy EJ, Schroeder F (1998) Differential influence of rat liver fatty acid binding protein isoforms on phospholipid fatty acid composition: phosphatidic acid biosynthesis and phospholipid fatty acid remodeling. Biochim Biophys Acta 1390:258–268
90. Wolfrum C, Buhlman C, Rolf B, Borchers T, Spener F (1999) Variation of liver fatty acid binding protein content in the human hepatoma cell line HepG2 by peroxisome proliferators and antisense RNA affects the rate of fatty acid uptake. Biochim Biophys Acta 1437:194–201
91. Atshaves BP, McIntosh AL, Lyuksyutova OI, Zipfel WR, Webb WW, Schroeder F (2004) Liver fatty acid binding protein gene ablation inhibits branched-chain fatty acid metabolism in cultured primary hepatocytes. J Biol Chem 279:30954–30965
92. Atshaves BP, Storey S, Huang H, Schroeder F (2004) Liver fatty acid binding protein expression enhances branched-chain fatty acid metabolism. Mol Cell Biochem 259:115–129
93. Martin GG, Danneberg H, Kumar LS, Atshaves BP, Erol E, Bader M, Schroeder F, Binas B (2003) Decreased liver fatty acid binding capacity and altered liver lipid distribution in mice lacking the liver fatty acid-binding protein gene. J Biol Chem 278:21429–21438
94. Glatz JF, Baerwaldt CC, Veerkamp JH, Kempen HJ (1984) Diurnal variation of cytosolic fatty acid-binding protein content and of palmitate oxidation in rat liver and heart. J Biol Chem 259:4295–4300

95. Veerkamp JH, van Moerkerk HT (1986) Peroxisomal fatty acid oxidation in rat and human tissues. Effect of nutritional state, clofibrate treatment and postnatal development in the rat. Biochim Biophys Acta 875:301–310
96. Veerkamp JH (1995) Fatty acid transport and fatty acid-binding proteins. Proc Nutr Soc 54:23–37
97. Veerkamp JH, van Moerkerk HT (1993) Fatty acid-binding protein and its relation to fatty acid oxidation. Mol Cell Biochem 123:101–106
98. Pande SV (1973) Reversal by CoA of palmityl-CoA inhibition of long chain acyl-CoA synthetase activity. Biochim Biophys Acta 306:15–20
99. Woldegiorgis G, Bremer J, Shrago E (1985) Substrate inhibition of carnitine palmitoyltransferase by palmitoyl-CoA and activation by phospholipids and proteins. Biochim Biophys Acta 837:135–140
100. Martin GG, Atshaves BP, McIntosh AL, Kier AB, Schroeder F (2007) Effect of gender and age-dependent obesity on lipid metabolism in liver fatty acid binding protein (L-FABP) gene ablated mice. J Nutr (submitted)
101. Erol E, Kumar LS, Cline GW, Shulman GI, Kelly DP, Binas B (2004) Liver fatty acid-binding protein is required for high rates of hepatic fatty acid oxidation but not for the action of PPAR-α in fasting mice. FASEB J 18:347–349
102. Newberry EP, Xie Y, Kennedy S, Buhman KK, Luo J, Gross RW, Davidson NO (2003) Decreased hepatic triglyceride accumulation and altered fatty acid uptake in mice with deletion of the liver fatty acid binding protein gene. J Biol Chem 278:51664–51672
103. Jolly CA, Hubbell T, Behnke WD, Schroeder F (1997) Fatty acid binding protein: stimulation of microsomal phosphatidic acid formation. Arch Biochem Biophys 341:112–121
104. Murphy EJ, Schroeder F (1997) Sterol carrier protein-2 mediated cholesterol esterification in transfected L-cell fibroblasts. Biochim Biophys Acta 1345:283–292
105. Mandrup S, Jepsen R, Skott H, Rosendal J, Hojrup P, Kristiansen K, Knudsen J (1993) Effect of heterologous expression of acyl-CoA-binding protein on acyl-CoA level and composition in yeast. Biochem J 290:369–374
106. Bhuiyan AKMJ, Pande SV (1994) Carnitine palmitoyltransferase activities: effects of serum albumin, acyl-CoA binding protein and fatty acid binding protein. Mol Cell Biochem 139:109–116
107. Bhuiyan AKMJ, Pande SV (1994) Carnitine palmitoyltransferase activies: effects of serum albumin, ACBP, and FABP. Mol Cell Biochem 139:109–116
108. Luxon BA, Weisiger RA (1993) Sex differences in intracellular fatty acid transport: role of cytoplasmic binding proteins. Am J Physiol 265:G831–G841
109. Weisiger RA (1996) Cytoplasmic transport of lipids: role of binding proteins. Comp Biochem Physiol 115B:319–331
110. Phelps-Luby K, Weisiger RA (1996) Role of cytoarchitecture in cytoplasmic transport. Comp Biochem Physiol 115B:295–306
111. Weisiger RA (2005) Cytosolic fatty acid binding proteins catalyze two distinct steps in intracellular transport of their ligands. Mol Cell Biochem 239:35–42
112. Murphy EJ (1998) L-FABP and I-FABP expression increase NBD-stearate uptake and cytoplasmic diffusion in L-cells. Am J Physiol 275:G244–G249
113. Lawrence JW, Kroll DJ, Eacho PI (2000) Ligand dependent interaction of hepatic fatty acid binding protein with the nucleus. J Lipid Res 41:1390–1401
114. Schroeder F, Atshaves BP, Starodub O, Boedeker AL, Smith R, Roths JB, Foxworth WB, Kier AB (2001) Expression of liver fatty acid binding protein alters growth and differentiation of embryonic stem cells. Mol Cell Biochem 219:127–138
115. Borchers T, Unterberg C, Rudel H, Robenek H, Spener F (1989) Subcellular distribution of cardiac fatty acid-binding protein in bovine heart muscle and quantitation with an enzyme-linked immunosorbent assay. Biochim Biophys Acta 1002:54–61
116. Tan NS, Shaw NS, Vinckenbosch N, Liu P, Yasmin R, Desvergne B, Wahli W, Noy N (2002) Selective cooperation between fatty acid binding proteins and peroxisome proliferatoractivated receptors in regulating transcription. Mol Cell Biol 22:5114–5127
117. Hellendie T, Antonius M, Sorensen RV, Hertzel AV, Bernlohr DA, Kolvraa S, Kristiansen K, Mandrup S (2000) Lipid binding proteins modulate ligand-dependent trans-activation by peroxisome proliferator-activated receptors and localize to the nucleus as well as the cytoplasm. J Lipid Res 41:1740–1751
118. Budhu AS, Noy N (2002) Direct channeling of retinoic acid between cellular retinoic acid binding protein II and retinoic acid receptor sensitizes mammary carcinoma cells to retinoic acid induced growth arrest. Mol Cell Biol 22:2632–2641
119. Delva L, Bastie JN, Rochette-Egly C, Kraiba R, Balitrand N, Despouy G, Chambon P, Chomienne C (1999) Physical and functional interactions between cellular retinoic acid binding protein II and the retinoic acid-dependent nuclear complex. Mol Cell Biol 19:7158–7167
120. Petrescu AD, Payne HR, Boedeker AL, Chao H, Hertz R, Bar-Tana J, Schroeder F, Kier AB (2003) Physical and functional interaction of acyl-CoA-binding protein with hepatocyte nuclear factor-4α. J Biol Chem 278:51813–51824
121. Elholm M, Garras A, Neve S, Tarnehave D, Lund TB, Skorve J, Flatmark T, Kristiansen K, Berge RK (2000) Long chain acyl-CoA esters and acyl-CoA binding protein are present in the nucleus of rat liver cells. J Lipid Res 41:538–545
122. Petrescu AD, Vespa A, McIntosh AL, Schroeder F, Kier AB (2007) Structural and functional characterization of a new recombinant histidine-tagged acyl-CoA binding protein (ACBP) from mouse. Biochemistry (submitted)
123. Bandichhor R, Petrescu AD, Vespa A, Kier AB, Schroeder F, Burgess K (2006) Synthesis of a new water soluble rhodamine derivative and application to intracellular imaging. J Am Chem Soc 128:10688–10689
124. Dong D, Ruuska SE, Levinthal DJ, Noy N (1999) Distinct roles for cellular retinoic acid binding proteins I and II in regulating signaling by retinoic acid. J Biol Chem 274:23695–23698
125. Nakahara M, Furuya N, Takagaki K, Sugaya T, Hirota K, Fukamizu A, Kanda T, Fujii H, Sato R (2005) Ileal bile acid binding protein, functionally associated with the farnesoid X receptor or the ileal bile acid transporter, regulates bile acid activity in the small intestine. J Biol Chem 280:42283–42289
126. Wolfrum C, Ellinghaus P, Fobker M, Seedorf U, Assmann G, Borchers T, Spener F (1999) Phytanic acid is ligand and transcriptional activator of murine liver fatty acid binding protein. J Lipid Res 40:708–714
127. Ockner RK, Manning JA (1976) Fatty acid binding protein. Role in esterification of absorbed long chain fatty acid in rat intestine. J Clin Inv 58:632–641
128. ul-Haq R, Shrago E, Christodoulides L, Ketterer B (1985) Purification and characterization of fatty acid binding protein in mammalian lung. Exp Lung Res 9:43–55
129. McCormack M, Brecher P (1987) Effect of liver fatty acid binding protein on fatty acid movement between liposomes and rat liver microsomes. Biochem J 244:717–723
130. Li Q, Yamamoto N, Morisawa S, Inoue A (1993) Fatty acyl-CoA binding activity of the nuclear thyroid hormone receptor. J Cell Biochem 51:458–464
131. Kliewer SA, Umesono K, Noon DJ, Heyman RA, Evans RM (1992) Convergence of 9-cisretinoic acid and peroxisome

proliferator signaling pathways through heterodimer formation of their receptors. Nature 358:771–774

132. Perissi V, Rosenfeld MG (2005) Controlling nuclear receptors: the circular logic of cofactor cycles. Mol Cell Biol 6:542–554

133. Yamamoto T, Shimano H, Nakagawa Y, Ide T, Yahagi N, Matsuzuka T, Nakakuki M, Takahashi A, Suzuki H, Sone H, Toyoshima H, Sato R, Yamada N (2004) SREBP-1 interacts with hepatocyte nuclear factor-4α and interferes with PGC-1 recruitment to suppress hepatic gluconeogenic genes. J Bio Chem 279:12027–12035

134. Hashimoto T, Fujita T, Usuda N, Cook W, Qi C, Peters JM, Gonzalez FJ, Yeldandi AV, Rao MS, Reddy JK (1999) Peroxisomal and mitochondrial fatty acid β-oxidation in mice nullizygous for both PPARα and peroxisomal fatty acyl-CoA oxidase. J Biol Chem 274:19228–19236

135. Lee SST, Pineau T, Drago J, Lee EJ, Owens JW, Kroetz DL, Fernandez-Salguero PM, Wesphal H, Gonzalez FJ (1995) Targeted disruption of the alpha isoform of the peroxisome proliferator-activated receptor gene in mice results in abolishment of the pleiotrophic effects of peroxisome proliferators. Mol Cell Biol 15:3012–3022

Lipids (2008) 43:19–28
DOI 10.1007/s11745-007-3117-6

ORIGINAL ARTICLE

Estradiol Favors the Formation of Eicosapentaenoic Acid (20:5n-3) and n-3 Docosapentaenoic Acid (22:5n-3) from Alpha-Linolenic Acid (18:3n-3) in SH-SY5Y Neuroblastoma Cells

Jean-Marc Alessandri · Audrey Extier · Bénédicte Langelier · Marie-Hélène Perruchot · Christine Heberden · Philippe Guesnet · Monique Lavialle

Received: 27 June 2007 / Accepted: 27 August 2007 / Published online: 3 October 2007
© AOCS 2007

Abstract Whether neurosteroids regulate the synthesis of long chain polyunsaturated fatty acids in brain cells is unknown. We examined the influence of 17-β-estradiol (E2) on the capacity of SH-SY5Y cells supplemented with α-linolenic acid (ALA), to produce eicosapentaenoic acid (EPA), docosapentaenoic acid (DPA) and docosahexaenoic acid (DHA). Cells were incubated for 24 or 72 h with ALA added alone or in combination with E2 (ALA + E2). Fatty acids were analyzed by gas chromatography of ethanolamine glycerophospholipids (EtnGpl) and phosphatidylcholine (PtdCho). Incubation for 24 h with ALA alone increased EPA and DPA in EtnGpl, by 330 and 430% compared to controls ($P < 0.001$) and DHA by only 10% ($P < 0.05$). Although DHA increased by 30% ($P < 0.001$) in ALA + E2-treated cells, the difference between the ALA and ALA + E2 treatments were not significant after 24 h (Anova-1, Fisher's test). After 72 h, EPA, DPA and DHA further increased in EtnGpl and PtdCho of cells supplemented with ALA or ALA + E2. Incubation for 72 h with ALA + E2 specifically increased EPA (+34% in EtnGpl, $P < 0.001$) and DPA (+15%, $P < 0.001$) compared to ALA alone. Thus, SH-SY5Y cells produced membrane EPA, DPA and DHA from supplemental ALA. The formation of DHA was limited, even in the presence of E2. E2 significantly favored EPA and DPA production in cells grown for 72 h. Enhanced synthesis of ALA-elongation products in neuroblastoma cells treated with E2 supports the hypothesis that neurosteroids could modulate the metabolism of PUFA.

Keywords Docosahexaenoic acid · Eicosapentaenoic acid · Docosapentaenoic acid · Estradiol · Long-chain PUFA synthesis · Ethanolamine-glycerophospholipids · Phosphatidylcholine · Neuroblastoma cells

Abbreviations

DHA	Docosahexaenoic acid (22:6n-3)
DPA	n-3 Docosapentaenoic acid (22:5n-3)
E2	17-β estradiol
EPA	Eicosapentaenoic acid (20:5n-3)
ER	Estrogen receptors
EtnGpl	ethanolamine glycerophospholipids
ALA	α-Linolenic acid
MUFA	Monounsaturated fatty acids
PPAR	Peroxisome proliferator-activated receptors
PtdCho	Phosphatidylcholine
PtdSer	Phosphatidylserine
PUFA	Polyunsaturated fatty acids
SFA	Saturated fatty acids
TEFA	Trienoic fatty acids
THA	Tetracosahexaenoic acid (24:6n-3)

Introduction

Clinical and epidemiological studies suggest that both n-3 polyunsaturated fatty acids (PUFA) [1] and estrogens [2] influence memory and cognition and protect neurons from degenerative or inflammatory processes. Neonatal neuronal cells synthesize neurosteroids, in which they promote the dendritic growth, spinogenesis and synaptogenesis [3]. Steroid hormones also act as trophic factors in the brain

J.-M. Alessandri (✉) · A. Extier · B. Langelier · M.-H. Perruchot · C. Heberden · P. Guesnet · M. Lavialle
Unit of Lipid Nutrition and Regulation of Brain Functions, Nu.Re.Li.Ce, INRA, Jouy-en-Josas, France
e-mail: Jean-Marc.Alessandri@jouy.inra.fr

under a variety of normal and pathological conditions [4]. On the other hand, studies using stable isotope tracer methods in men and women (reviewed in Ref. [5]) and clinical studies in steroid-treated subjects [6, 7] have suggested that estrogens regulate the metabolic fate of the essential PUFA, 18:3n-3 (α-linolenic acid, ALA) and 18:2n-6 (linoleic acid, LA), i.e., their β-oxidation to acetylCoA or their conversion into long-chain derivatives. The end product of ALA metabolic conversion, docosahexaenoic acid (DHA, 22:6n-3) is the major structural and functional n-3 PUFA in the membranes of brain and retinal cells (reviewed in Ref. [8, 9]). One notable effect of DHA at the cellular level, comparable to that of neurosteroids, is to activate the expression of neuronal differentiation genes and to stimulate the neurite outgrowth [10, 11].

DHA is supplied directly by dietary fats rich in long-chain n-3 PUFA (fat fishes and marine oils), or by hepatic synthesis [12] through successive desaturations and elongations of ALA. Upstream of DHA, the conversion of ALA produces two major membrane long-chain derivatives, eicosapentaenoic acid (EPA, 20:5n-3) and n-3 docosapentaenoic acid (n-3 DPA or DPA, 22:5n-3). In normal physiological conditions, EPA and DPA do not accumulate in the brain, contrary to DHA. It has been demonstrated in rodents that the extent to which the liver produces and delivers ALA-derived DHA to the brain (and other tissues) depends on the concentration of DHA in the diet [13, 14]. Brain endothelial cells and glial cells may also provide neurons with newly formed DHA, suggesting that synthesis of long-chain n-3 PUFAs is a constitutive process in the brain [15–17]. Whether estrogens and neurosteroids regulate the brain lipid metabolism and the balance of long-chain PUFA in neural membranes is unknown.

The extent to which dietary ALA contributes to the n-3 long-chain PUFA status in brain tissue throughout a human's life remains to be clarified. Stable isotope tracer studies in human adults suggest that only a small percentage of the ingested ALA that is not stored or oxidised is available for conversion to DHA [18–20]. In this respect, gender-related differences may be particularly informative since less ALA appeared to be converted to DHA in men than in women [21–23]. This is supported by the observation that there are compositional differences in the blood lipids of men and women that are not due to dietary habits; women have higher DHA concentrations in plasma phosphatidylcholine, triacylglycerol and non-esterified fatty acids than do men [24]. Actually, EPA and DPA are the principal metabolic products of orally-administered ALA in the blood of young men [21]. Moreover, differences in DHA status of pregnant women at varying gestational ages suggest that changes in the hormonal status may produce variations in metabolic capacity for long-chain PUFA synthesis [25, 26]. Changes in the blood lipid fatty acid compositions of human adults after steroid treatment also suggest that estrogens promote the metabolic conversion of PUFA [6, 7]. In summary, it is suggested that steroid hormones like estrogen regulate the metabolic fate of ALA through its partitioning between anabolic and catabolic pathways (reviewed in Ref. [5]).

We have shown that n-3 PUFA metabolism in human neuroblastoma SH-SY5Y cells reflects the physiological limitation of DHA synthesis [27]. This study uses the same model to determine whether 17-β-estradiol (E2), the most potent biological form of estrogen, promotes ALA conversion into membrane long-chain derivatives. We examined the effect of E2 on the incorporation of ALA-elongation products in phospholipids of growing cells. Neuroblastoma cells in culture are spontaneously depleted in DHA, and they respond to graded concentrations of non-esterified DHA by increasing their membrane DHA to physiological values [28]. These cells also increase their membrane EPA, DPA and DHA in response to supplemental ALA, though the maximum incorporation of ALA-derived DHA into phospholipids is 70% lower than that of supplemental DHA dosed at matched concentrations [27]. Since the SH-SY5Y cells can produce membrane EPA, DPA and DHA from supplemental ALA, this model is convenient for studying the regulation of long-chain n-3 synthesis. In this study, we examined the capacity of E2 to modulate the restoration of long-chain n-3 PUFAs in the membrane phospholipids of growing cells supplemented with ALA.

Experimental Procedure

Culture

SH-SY5Y cells were obtained from the European Collection of Animal Cell Culture (Porton Down, Salisbury, UK). Cells were plated out on 75-cm^2 flasks, grown for 3 days in DMEM with 10% FCS, and incubated for 24 or 72 h with 10 ml of this medium containing the E2-vehicle (CTRL), 10 nM E2 alone (E2), 30 µM ALA alone (ALA), or E2 plus 30 µM ALA (ALA + E2). In the group ALA + E2, E2 was dosed at two concentrations, 0.5 or 10 nM. The sodium salts of ALA (Nu-Chek Prep, Elysian, MN, USA) were directly dissolved in the medium at 37 °C [28, 29]. E2 in the parent solution was dissolved in ethanol (vehicle); the final concentration of ethanol in all batches was equal to 0.1% (preliminary trials with control cultures in 10% FCS showed that ethanol had no effect at this concentration on cell growth and phospholipid fatty acid composition).

Lipid Analysis

Membrane fatty acid compositions were analyzed on triplicate flasks. The composition of each flask was determined by capillary gas chromatography of the ethanolamine-glycerophospholipids (EtnGpl) and the phosphatidylcholine (PtdCho). The phosphatidylserine (PtdSer) was also analyzed in control cells. The cells were trypsinized, harvested by centrifugation and washed with phosphate buffer saline (PBS) containing 50 µM fatty acid-free albumin (Sigma Chimie, Saint Quentin Fallavier, France) to remove free fatty acids. The total lipids were extracted from one volume of cell homogenate with four volumes of chloroform/methanol (2:1, by vol) in the presence of 0.005 % (by weight) butyl-hydroxytoluene (BHT). The lipid bottom phase was washed, dried, solubilized in chloroform and stored at –80 °C until separation of phospholipid classes by solid-phase extraction on 500 mg-prepacked aminopropyl cartridges (J.T. Baker, Deventer, The Netherlands) [28, 29]. The cartridges were equilibrated beforehand with eluent I (isopropanol/chloroform, 1:2, by vol). Each sample of total lipids was dried under nitrogen, resolubilized in 250 µl of eluent I and deposited onto a single-use cartridge, which was immediately eluted successively with 3 ml of eluent I, 3 ml of diethylether/acetic acid (98:2, by vol), 1 ml of acetonitrile, 8 ml of acetonitrile/*n*-propanol (3:1, by vol) to recover the phosphatidylcholine (ChoGpl) fraction, and then with 2 ml of acetonitrile/*n*-propanol (1:1, by vol) and 3 ml of methanol to recover the EtnGpl fraction (the latter consisted in a mixture of phosphatidylethanolamine and 1-*O*-alkylenyl-2-acyl glycerophosphoethanolamine). The PtdSer fraction was recovered by eluting with isopropanol/methanolic HCl (4:1, vol/vol). The three phospholipid fractions were dried under a nitrogen flux and transmethylated by methanol at 90°C in the presence of BF_3. The fatty acid methyl esters were extracted, washed and injected through the on-column injector of a gas chromatograph equipped with a retention gap and a CP-WAX 52 CB bonded fused-silica capillary column of a 0.25 mm i.d. and 60-m length (Varian, Les Ullis, France). The oven temperature was programmed for 79–212 °C, at a heating rate of 4 °C/min. The instrument responses attributable to fatty acid methyl esters (excluding dimethylacetals) were automatically integrated in proportion to their masses, and their factor response and Kovats's equivalent chain length (ECL) were compared with standard compounds. The fatty acid methyl ester of 20:3n-9 (ECL = 20.6 ± 0.05) was identified by reference to the peak specifically found in liver phospholipids of n-3 deficient rats (routinely reared in our laboratory). The corresponding elongation product, 22:3n-9, was identified in the cell phospholipids by comparing the ECL value of this peak to the ECL of 20:3n-9 incremented by two points (ECL of 22:3n-9 = 22.6 ± 0.05).

Statistical Analysis

We used "Statview + Graphics" software (Abacus Concepts Inc., Berkeley, CA, USA). Means were compared by one way-analysis of variance followed by post hoc analysis. Fisher multiple comparison test was used to compare differences in fatty acid contents among the eight treatments, each of the different group defining one item of one category, the treatment category (anova-1), i.e., CTRL, E2, ALA and ALA + E2 at 24 and 72 h, respectively.

Results

Distribution of n-3 Long-chain PUFA in Cell Phospholipids

The concentrations of EPA, DPA and DHA in the EtnGpl, PtdSer and PtdCho fractions of cells grown for 72 h in standard conditions are reported in Fig. 1. The sum EPA + DPA + DHA accounted for 140 ± 8 mmol/mol of EtnGpl, 75.5 ± 8.6 mmol/mol of PtdSer and 15.3 ± 1.6 mmol/mol of PtdCho. Thus, the EtnGpl fraction from control cells contained 1.8- and 9.1-times more n-3 long chain PUFAs than PtdSer and PtdCho. DHA was the major n-3 long-chain PUFA in EtnGpl (95 ± 8.7 mmol DHA/mol of EtnGpl, or 4.75 ± 0.4 mol DHA %). In the PtdSer fraction, EPA (25 mmol/mol PtdSer or 1.25 mol %), DPA (21 mmol/mol PtdSer or 1.05 mol %) and DHA (29 mmol/mol PtdSer or 1.45 mol %) were distributed almost equally (Fig. 1). Thus, the EtnGpl fraction of SH-SY5Y cells contained 1.8-time more n-3 long-chain PUFAs and three times more DHA than PtdSer. Owing to this specific composition, we focused on the impact of E2 and ALA supplementation within the EtnGpl fraction.

Effect of Culture Stage on the Standard Phospholipid Fatty Acid Composition

The duration of culture changed the fatty acid composition in non-supplemented cells cultured for 24 or 72 h with 10% FCS. In the EtnGpl fraction (Table 1, CTRL-72 h vs. CTRL-24h), there was a significant increase of 18:1n-9 (+29%), 18:1n-7 (+18%) and of the n-9 long-chain trienoic fatty acids (TEFA), 20:3n-9 (+115%) and 22:3n-9 (+20%). The total n-6 fatty acids decreased by 24%, mainly 22:4n-6 (–39%) and 22:5n-6 (–33%). The n-3 fatty acids also tended to decrease with the duration of culture (not significant at $P < 0.001$). In the PtdCho fraction (Table 2, CTRL-72 h vs. CTRL-24 h), the 18:1n-9 content also increased by 29%, and that of 16:1n-9 by 12%, while the n-6 fatty acids decreased by 39%. The increase of MUFA in PtdCho was

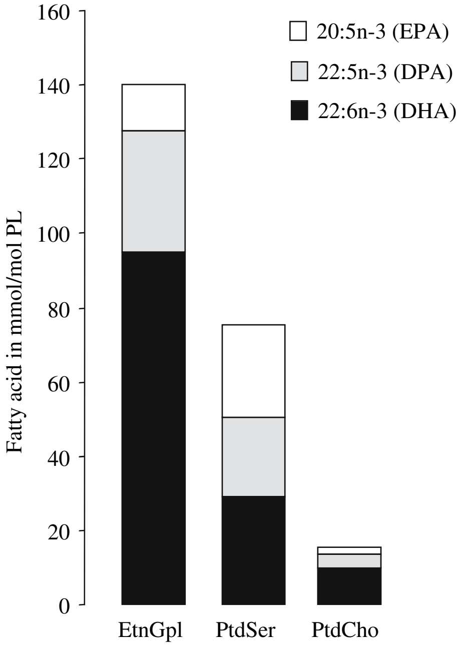

Fig. 1 Distribution of the n-3 long-chain PUFAs in the EtnGpl, PtdSer and PtdCho fractions of SH-SY5Y cells grown for 72 h in a medium containing 10% FCS. Values are expressed in mmol of fatty acid/mol of phospholipid

mainly compensated by a decrease of the major saturated fatty acids, 16:0 (–15%) and 18:0 (–7%). These data show that, in the absence of ALA supplementation, the status in EPA, DPA and DHA did not "spontaneously" improved with the duration of culture. However, it is noteworthy that the n-9 TEFA increased, indicating that the SH-SY5Ycells have the constitutive capacity to produce Δ6- and Δ5-desaturated long-chain fatty acids.

Response of Cells to ALA Alone

Cells responded to 24 h incubation with 30 μM ALA by increasing EtnGpl the two main elongation-products of ALA, EPA (+330%, $P < 0.001$) and DPA (+430%, $P < 0.001$) (Table 1, ALA-24 h vs. CTRL-24h). The DHA content also increased by 10% (significant only at $P < 0.05$, not reported in Table 1). After 72 h of incubation with 30 μM ALA alone, EPA had increased by 780% ($P < 0.001$), DPA by 850% ($P < 0.001$) and DHA by 65% ($P < 0.001$) (Table 1, ALA-72 h vs. CTRL-24 h). Thus, the growing cells had markedly increased their production of membrane EPA, DPA and DHA throughout the 72 h incubation with supplemental ALA. The increase of EPA, DPA and DHA mainly occurred at the expense of the n-9 TEFA (–38 and –51% at 24 and 72 h, respectively, compared with CTRL-24 h) and of n-6 PUFA (–20 and –55%). The same significant changes were observed in the PtdCho fraction (Table 2); in comparison with control cells cultured for 24 h, EPA increased in the PtdCho of ALA-supplemented cells by 900 and 1,000% at 24 and 72 h, respectively, DPA by 567 and 1,130%, and DHA by 22 and 67%. These data clearly indicate that SH-SY5Y cells are able to synthesize all the long-chain n-3 fatty acids from the precursor ALA and strongly suggest that the production of neoformed DHA is limited in comparison with that of EPA and DPA.

Effect of E2 on the Response of Cells to ALA

The incubation of cells for 24 or 72 h with 0.5 nM E2 (data not shown) or 10 nM E2 alone had no effect on EPA, DPA and DHA (Table 1, E2-24 h vs. CTRL-24 h, and E2-72 h vs. CTRL-72 h). By itself, E2 had no significant impact on the fatty acid profile in non-supplemented cells.

The incubation with 30 μM ALA and 10 nM E2 during 24 h led to a significant increase (+30%, $P < 0.001$) of DHA in EtnGpl (Table 1, ALA + E2-24 h vs. E2-24 h). As stated in the above paragraph, DHA increased by only 10% ($P < 0.05$) upon incubation with ALA alone (Table 1, ALA-24 h vs. CTRL-24 h, not significant at $P < 0.001$). Thus, E2 produced a small gain of neoformed DHA upon the 24 h treatment with ALA + E2, though the difference in DHA between the two groups (ALA + E2 vs. ALA alone) was not significant at $P < 0.001$ (Table 1). In brief, the sole effect of E2 after 24 h was to improve the statistical level of significance of the DHA increase observed in cells supplemented with ALA compared to non-supplemented cells.

The incubation with ALA + E2 resulted after 72 h in a further increase of EPA (+34%) and DPA (+15%) compared to cells incubated with ALA alone (Table 1, ALA + E2-72 h vs. ALA-72 h). However, there was no additional effect on DHA upon incubation with ALA + E2 compared to incubation with ALA alone (Table 1, ALA + E2-72 h vs. ALA-72 h). Therefore, E2 differentially promoted the production of the different ALA-derived long-chain fatty acids. E2 mainly increased EPA and DPA after 72 h.

The individual data of EPA, DPA and DHA are presented under a piled form in Fig. 2. The upper panel of Fig. 2 shows that incubation of cells for 72 h with 30 μM ALA and 10 nM E2 induced the sum EPA + DPA + DHA to increase ($P < 0.001$) in comparison with incubation with ALA alone. This gain in n-3 long-chain PUFAs affected EPA and DPA, not DHA. The same trend was observed at 72 h with the dose of 0.5 nM E2, although it did not reach a significant level. The lower panel of Fig. 2 shows that the TEFAs decreased with ALA supplementation and further decreased in the presence of 0.5 or 10 nM E2 ($P < 0.04$),

Table 1 Fatty acid composition (mol%) in EtnGpl of cells incubated for 24 or 72 h with vehicle, 30 μM ALA, 10 nM E2, or 30 μM ALA plus 10 nM E2 (mean ± SD; *n* = 3 flasks per treatment)

	24 h				72 h			
	CTRL	E2	ALA	ALA + E2	CTRL	E2	ALA	ALA + E2
14:0	0.9 ± 0.1	0.9 ± 0.05	0.9 ± 0.2	0.7 ± 0.3	1.5 ± 0.5	1.0 ± 0.1	0.8 ± 0.05	0.7 ± 0.04
16:0	8.3 ± 0.4	7.9 ± 0.3	8.1 ± 0.8	7.8 ± 0.6	9.6 ± 0.8	7.8 ± 0.9	7.6 ± 0.2	7.5 ± 1.1
18:0	18.9 ± 0.2 bc	18.6 ± 0.2 bc	19.8 ± 0.9 c	19.3 ± 0.2 bc	16.8 ± 1.4 ab	15.9 ± 0.5 a	18.4 ± 0.6 bc	18.7 ± 0.9 bc
∑SFA	28.8 ± 0.8 b	27.9 ± 0.2 ab	29.3 ± 0.4 b	28.3 ± 0.5 ab	28.2 ± 2.5 ab	24.9 ± 1.2 a	26.7 ± 0.8 ab	26.7 ± 0.7 ab
16:1n-9	2.1 ± 0.1	2.1 ± 0.1	1.8 ± 0.1	1.8 ± 0.1	2.5 ± 0.6	3.6 ± 0.5 a	1.7 ± 0.1	1.6 ± 0.2
16:1n-7	1.3 ± 0.1	1.4 ± 0.1	1.3 ± 0.1	1.4 ± 0.2	1.4 ± 0.2	1.7 ± 0.1	1.3 ± 0.1	1.3 ± 0.1
18:1n-9	16.0 ± 0.1 ab	16.6 ± 0.1 b	15.2 ± 0.5 a	15.9 ± 0.1 ab	20.6 ± 0.3 c	21.4 ± 0.4 c	16.4 ± 0.7 ab	15.1 ± 0.6 a
18:1n-7	3.3 ± 0.1 b	3.3 ± 0.1 b	3.1 ± 0.1 b	3.1 ± 0.1 b	3.9 ± 0.1 c	3.9 ± 0.1 c	2.6 ± 0.1 a	2.4 ± 0.1 a
∑MUFA	24.7 ± 0.4 bc	25.3 ± 0.2 c	22.7 ± 0.6 ab	23.5 ± 0.4 bc	28.9 ± 0.5 d	31.0 ± 1.0 d	23.1 ± 0.9 ab	21.1 ± 0.9 a
20:3n-9	2.6 ± 0.05 bc	2.9 ± 0.06 c	2.0 ± 0.1 ab	2.1 ± 0.04 ab	5.6 ± 0.4 d	5.9 ± 0.3 d	1.9 ± 0.2 a	1.5 ± 0.1 a
22:3n-9	5.5 ± 0.04 c	5.6 ± 0.1 c	3.0 ± 0.1 b	3.1 ± 0.1 b	6.6 ± 0.9 cd	6.9 ± 0.3 d	2.1 ± 0.3 ab	1.6 ± 0.2 a
∑TEFA	8.1 ± 0.05 c	8.5 ± 0.2 c	5.0 ± 0.2 b	5.2 ± 0.1 b	12.2 ± 1.3 d	12.8 ± 0.4 d	4.0 ± 0.5 ab	3.1 ± 0.3 a
18:2n-6	1.3 ± 0.1 b	1.3 ± 0.1 b	1.3 ± 0.1 b	1.3 ± 0.1 b	0.6 ± 0.1 a	0.5 ± 0.1 a	0.4 ± 0.1 a	0.3 ± 0.1 a
18:3n-6	1.5 ± 0.3	1.4 ± 0.1	1.5 ± 0.3	1.1 ± 0.5	0.7 ± 0.2	0.6 ± 0.2	0.5 ± 0.1	0.5 ± 0.1
20:2n-6	1.2 ± 0.3 c	1.2 ± 0.2 c	0.9 ± 0.03 c	0.9 ± 0.1 c	0.5 ± 0.1 b	0.5 ± 0.05 b	0.1 ± 0.03 a	0.1 ± 0.05 a
20:4n-6	14.5 ± 0.2 cd	15.4 ± 0.3 d	12.0 ± 0.3 b	13.4 ± 0.1 bc	13.7 ± 1.0 c	14.0 ± 0.5 cd	8.0 ± 0.5 a	7.2 ± 0.5 a
22:4n-6	8.4 ± 0.1 e	7.6 ± 0.2 de	6.1 ± 0.2 c	5.8 ± 0.1 bc	5.1 ± 0.5 b	5.2 ± 0.4 b	3.3 ± 0.3 a	2.9 ± 0.1 a
22:5n-6	2.7 ± 0.02 c	2.6 ± 0.07 c	1.7 ± 0.04 b	1.7 ± 0.01 b	1.8 ± 0.1 b	1.8 ± 0.2 b	1.0 ± 0.1 a	0.9 ± 0.1 a
∑n-6	29.6 ± 0.7 c	29.6 ± 0.4 c	23.8 ± 0.6 b	24.3 ± 0.6 b	22.4 ± 1.4 b	22.6 ± 0.8 b	13.2 ± 0.9 a	11.9 ± 0.7 a
18:3n-3	0.4 ± 0.1	0.4 ± 0.2	0.6 ± 0.3	0.3 ± 0.1	0.6 ± 0.1	0.6 ± 0.1	0.8 ± 0.2	1.0 ± 0.3
20:5n-3	0.6 ± 0.1 a	0.7 ± 0.02 a	2.6 ± 0.5 b	2.4 ± 0.2 b	0.6 ± 0.06 a	0.7 ± 0.02 a	5.3 ± 0.7 c	7.1 ± 0.9 d
22:5n-3	1.8 ± 0.03 a	1.9 ± 0.01 a	9.6 ± 0.6 b	8.7 ± 0.2 b	1.6 ± 0.01 a	1.5 ± 0.1 a	17.1 ± 1.3 c	19.6 ± 1.2 d
22:6n-3	5.8 ± 0.1 ab	5.7 ± 0.2 ab	6.4 ± 0.6 bc	7.4 ± 0.1 c	4.7 ± 0.4 a	4.5 ± 0.5 a	9.6 ± 0.3 d	9.5 ± 0.9 d
∑n-3	8.7 ± 0.1 a	8.7 ± 0.1 a	19.2 ± 0.7 b	18.8 ± 0.3 b	7.6 ± 0.2 a	7.3 ± 0.7 a	32.9 ± 2.1 c	37.2 ± 1.5 d

Values with different superscripts are significantly different (Anova-1 and Fisher's test, $P < 0.001$)

SFA saturated fatty acids, *MUFA* monounsaturated fatty acids, *TEFA* trienoic fatty acids

which indicated that cells responded to ALA + E2 treatment by decreasing the production of n-9 TEFAs and by increasing that of ALA-elongation products. Since ALA + E2 modified in an opposite manner the production of long-chain n-3 PUFAs and that of n-9 TEFAs, we used the ratio of the sum [EPA + DPA + DHA] to the sum [20:3n-9 + 22:3n-9] as a biochemical marker of the propensity of ALA-supplemented cells to produce membrane long-chain n-3 PUFAs. The values of the Σn-3/ΣTEFA ratio are reported in Fig. 3. The figure shows that combining ALA supplementation, incubation with E2 and prolongation of treatment produced the greatest increase ($P < 0.005$) of this ratio, both in EtnGpl and PtdCho.

Discussion

We studied the effect of estradiol on the conversion of ALA to long-chain products by neuroblastoma cells. The results on ALA supplementation in growing SH-SY5Y cells support our previous data that ALA is efficiently converted into EPA, DPA and DHA [27]. We had previously shown that the formation of membrane DHA occurs only within a very restricted range of concentration of its upstream precursors (either ALA, EPA or DPA), whereas that of DPA from ALA or EPA follows a saturating dose-response pattern [27]. Moreover, it has been shown in primary culture that rat astrocytes dosed with ALA incorporate DPA into their membranes, not DHA [30]. The response of SH-SY5Y cells to ALA is thus particularly efficient, although their membrane incorporation of neoformed DHA is readily limited in comparison with that of DPA. We suggested that the formation of DHA in these cells is constitutively limited, or possibly submitted to down-regulation [27].

In physiological conditions, endogenous DPA is produced in the endoplasmic reticulum by successive desaturations and elongations of ALA. DPA is further

Table 2 Fatty acid composition (mol%) in PtdCho of cells incubated for 24 or 72 h with vehicle, 30 µM ALA, 10 nM E2, or 30 µM ALA plus 10 nM E2 (mean ± SD; $n = 3$ flasks per treatment)

	24 h				72 h			
	CTRL	E2	ALA	ALA + E2	CTRL	E2	ALA	ALA + E2
14:0	4.2 ± 0.2	4.0 ± 0.1	4.0 ± 0.1	4.1 ± 0.03	4.0 ± 0.3	4.0 ± 0.1	3.8 ± 0.1	3.8 ± 0.2
16:0	36.7 ± 0.5 cd	35.2 ± 0.3 b	36.9 ± 0.6 d	36.7 ± 0.1 cd	31.2 ± 0.2 a	31.2 ± 0.1 a	35.1 ± 0.5 b	35.5 ± 0.3 bc
18:0	7.1 ± 0.7 bc	5.6 ± 0.1 a	6.5 ± 0.6 ab	5.9 ± 0.1 a	6.6 ± 0.1 ab	6.6 ± 0.1 ab	8.0 ± 0.2 cd	8.5 ± 0.4 d
∑SFA	48.4 ± 1.3 c	45.1 ± 0.2 b	47.9 ± 1.1 c	47.0 ± 0.2 bc	42.2 ± 0.5 a	42.1 ± 0.2 a	47.3 ± 0.7 bc	48.2 ± 0.7 c
16:1n-9	6.5 ± 0.1 c	6.8 ± 0.1 cd	5.3 ± 0.1 b	5.4 ± 0.1 b	7.3 ± 0.2 d	7.0 ± 0.1 cd	4.3 ± 0.1 a	4.3 ± 0.5 a
16:1n-7	2.3 ± 0.1 a	2.4 ± 0.1 a	2.9 ± 0.1 b	2.9 ± 0.1 b	2.2 ± 0.1 a	2.2 ± 0.1 a	2.2 ± 0.1 a	2.3 ± 0.1 a
16:1n-5	1.2 ± 0.05 b	1.2 ± 0.05 b	1.2 ± 0.05 b	1.3 ± 0.05 b	0.8 ± 0.1 a	0.7 ± 0.1 a	0.8 ± 0.1 a	0.9 ± 0.1 a
18:1n-9	25.3 ± 0.7 ab	27.3 ± 0.1 bc	24.5 ± 0.6 a	25.3 ± 0.3 ab	32.7 ± 0.5 d	33.3 ± 0.2 d	27.8 ± 1.1 c	26.1 ± 1.0 abc
18:1n-7	7.0 ± 0.2 bc	7.5 ± 0.05 c	6.4 ± 0.2 ab	6.7 ± 0.1 b	7.9 ± 0.1 c	7.9 ± 0.1 c	6.5 ± 0.3 ab	6.0 ± 0.3 a
other	0.5 ± 0.3	0.8 ± 0.1	0.6 ± 0.03	0.7 ± 0.1	0.8 ± 0.02	0.7 ± 0.01	0.5 ± 0.1	0.4 ± 0.1
∑MUFA	42.9 ± 1.1 ab	46.0 ± 0.05 b	40.9 ± 0.9 a	42.4 ± 0.4 a	51.7 ± 0.3 c	51.9 ± 0.2 c	42.2 ± 1.4 a	40.1 ± 1.7 a
20:3n-9	0.9 ± 0.1 b	1.0 ± 0.1 b	0.5 ± 0.05 a	0.6 ± 0.05 a	1.1 ± 0.1 b	1.1 ± 0.1 b	0.5 ± 0.05 a	0.4 ± 0.05 a
22:3n-9	0.9 ± 0.1 b	0.9 ± 0.03 b	0.5 ± 0.03 a	0.5 ± 0.01 a	0.9 ± 0.01 b	0.9 ± 0.02 b	0.4 ± 0.06 a	0.3 ± 0.01 a
∑TEFA	1.8 ± 0.2 b	1.9 ± 0.1 b	1.0 ± 0.06 a	1.1 ± 0.02 a	2.0 ± 0.02 b	2.0 ± 0.02 b	0.9 ± 0.1 a	0.8 ± 0.1 a
18:2n-6	0.4 ± 0.04	0.4 ± 0.03	0.6 ± 0.1	0.6 ± 0.03	0.4 ± 0.03	0.4 ± 0.03	0.5 ± 0.04	0.6 ± 0.04
20:4n-6	2.8 ± 0.1 c	2.9 ± 0.01 c	2.5 ± 0.1 b	2.7 ± 0.02 c	1.3 ± 0.05 a	1.3 ± 0.03 a	1.4 ± 0.04 a	1.3 ± 0.01 a
22:4n-6	1.1 ± 0.1 b	1.1 ± 0.1 b	0.9 ± 0.1 b	1.0 ± 0.1 b	0.7 ± 0.01 a	0.7 ± 0.01 a	0.6 ± 0.02 a	0.5 ± 0.01 a
22:5n-6	0.4 ± 0.02 c	0.4 ± 0.01 c	0.3 ± 0.01 b	0.3 ± 0.01 b	0.2 ± 0.01 a	0.2 ± 0.01 a	0.2 ± 0.01 a	0.2 ± 0.01 a
∑n-6	5.4 ± 0.1 b	5.5 ± 0.4 b	5.5 ± 0.6 b	5.5 ± 0.04 b	3.3 ± 0.2 a	3.2 ± 0.2 a	3.2 ± 0.1 a	3.1 ± 0.1 a
18:3n-3	0.2 ± 0.05	0.1 ± 0.05	0.5 ± 0.2	0.2 ± 0.05	0.1 ± 0.05	0.1 ± 0.05	0.2 ± 0.05	0.3 ± 0.06
20:5n-3	0.1 ± 0.05 a	0.1 ± 0.03 a	1.0 ± 0.3 b	0.9 ± 0.1 b	0.1 ± 0.01 a	0.1 ± 0.01 a	1.1 ± 0.2 b	1.4 ± 0.4 b
22:5n-3	0.3 ± 0.1 a	0.3 ± 0.01 a	2.0 ± 0.2 b	1.8 ± 0.07 b	0.2 ± 0.02 a	0.2 ± 0.02 a	3.7 ± 0.5 c	4.5 ± 0.6 c
22:6n-3	0.9 ± 0.03 b	0.9 ± 0.04 b	1.1 ± 0.07 c	1.3 ± 0.04 c	0.5 ± 0.1 a	0.4 ± 0.06 a	1.5 ± 0.1 d	1.7 ± 0.03 d
∑n-3	1.5 ± 0.1 a	1.4 ± 0.1 a	4.7 ± 0.6 b	4.1 ± 0.2 b	0.9 ± 0.1 a	0.8 ± 0.01 a	6.5 ± 0.8 c	8.0 ± 1.0 c

Values with different superscripts are significantly different (Anova-1 and Fisher's test, $P < 0.001$)

SFA saturated fatty acids, *MUFA* monounsaturated fatty acids, *TEFA* trienoic fatty acids

elongated and desaturated into tetracosahexaenoic acid (THA, 24:6n-3) that moves to peroxisomes and is shortened into DHA by one cycle of β-oxidation (Sprecher's pathway) [31, 32]. We have suggested that limitation of the peroxisomal step of DHA synthesis could account for the membrane accretion of its upstream metabolites, EPA and DPA [27]. In contrast, the incorporation of supplemental DHA into SH-SY5Y cell phospholipids follows a dose-response saturation curve that is comparable to the curve of DHA repletion in the brain of newborn rats deprived of n-3 fatty acids and fed after weaning a diet enriched in microalgal DHA [28]. Therefore, the uptake and phospholipid acylation of preformed DHA is fully operational in SH-SY5Y cells, whereas the terminal synthesis of DHA is limited, possibly at the peroxisomal step. The present study addressed the question of the estrogen action on the conversion pathway.

In cells incubated with ALA alone compared to non-supplemented cells, DHA increased in EtnGpl by 10% ($P < 0.05$) after 24 h and by 104% ($P < 0.001$) after 72 h. In the presence of 10 nM E2, the neoformed DHA increased in comparison with matched control cells by 30 and 110%, at 24 and 72 h, respectively ($P < 0.001$, Table 1). In the PtdCho fraction, DHA increased after 24 h by 22 and 44%, in the absence and in the presence of E2, respectively, and by 200 and 325% after 72 h. Thus, E2 slightly enhanced the formation of ALA-derived DHA in cells cultured for 24 h, though the combination of ALA with E2 did not produce a greater content in membrane DHA compared to supplementation with ALA alone. Moreover, the impact on DHA was weak and transient, since E2 did not favor higher DHA content after 72 h. It clearly appeared that prolongation of incubation (from 24 to 72 h) with ALA resulted by itself in a more marked increase of membrane DHA. However, the prolongation of incubation also resulted in the membrane accretion of EPA and DPA, and E2 at 10 nM augmented this time-dependent effect. In parallel, the n-9 TEFAs decreased with the

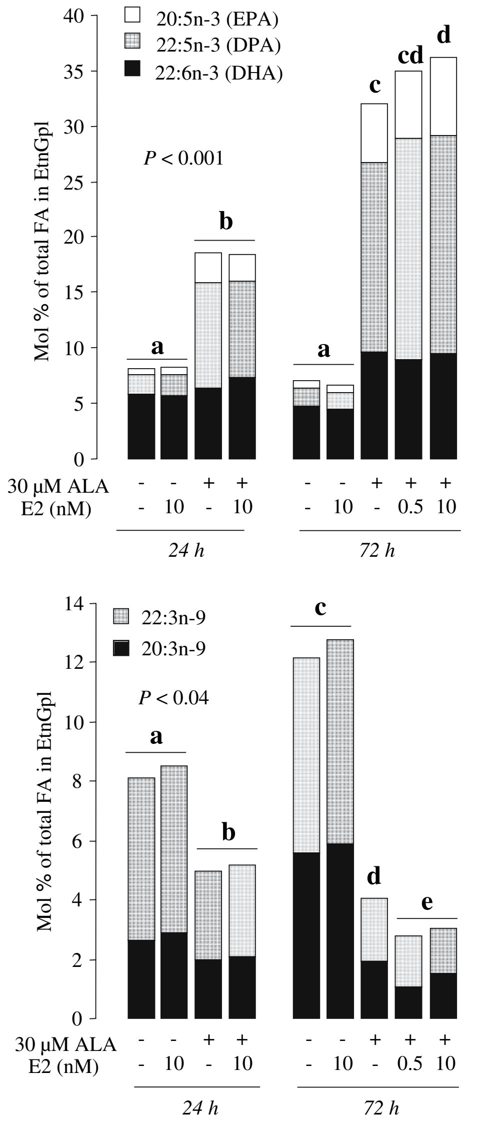

Fig. 2 Distribution of n-3 long-chain PUFAs (*upper panel*) and n-9 TEFA (*lower panel*) in EtnGpl of SH-SY5Y cells cultured for 24 or 72 h in a medium containing 10% FCS and 30 μM ALA used alone or in combination with 0.5 or 10 nM E2. Values are expressed in mol% of total fatty acids in EtnGpl (see Table 1 for individual mean values and SD). Different superscripts correspond to significant differences in the sum of n-3 PUFAs (*upper panel*, $P < 0.001$) or in the sum of n-9 TEFA (*lower panel*, $P < 0.04$)

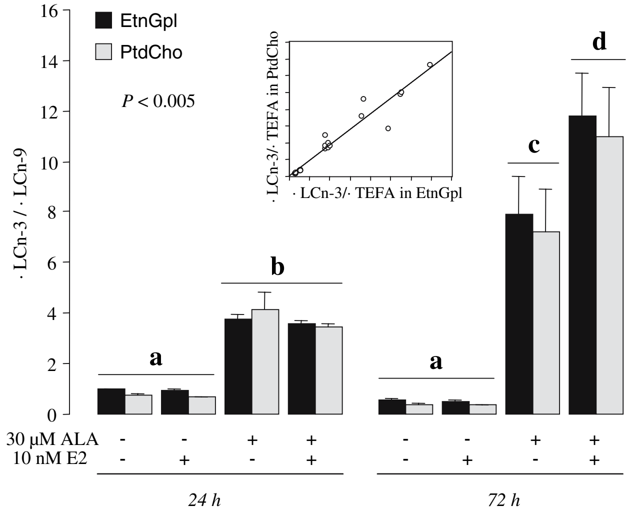

Fig. 3 Values of the sum of n-3 long-chain PUFAs to the sum of n-9 TEFA ratio in EtnGpl of cells cultured for 24 or 72 h in a medium containing 10% FCS and 30 μM ALA used alone or in combination with 10 nM E2. Different superscripts correspond to different ratio values ($P < 0.005$). The insert illustrates the correlation between the ratio values in PtdCho and EtnGpl

prolongation of incubation with ALA, and E2 accentuated this decrease. We propose to use the ratio of the sum of n-3 long-chain products to the sum of n-9 TEFAs as a biochemical marker of the restoration of the n-3 status in cultured cells. The ratio values were almost identical in EtnGpl and PtdCho (insert of Fig. 3); therefore it may be supposed that changes of this ratio in membranes reflect sizeable metabolic changes in cells. The data reported in Fig. 3 clearly show that incubation with ALA restored the n-3 PUFAs status in a time-dependent manner and that the combination of ALA with E2 produced the highest “ratio of restoration”. With a ratio value of 1, the non-supplemented cells must be considered as being deficient in n-3 long-chain PUFAs; the ratio increased four times after 24 h of incubation with ALA, eight times after 72 h (time effect) or 12-times when cells were exposed to ALA + E2 during 72 h. In summary, the increase of EPA and DPA was the major change induced by E2 after 72 h incubation of cells with ALA and E2. Although E2 favored the production of membrane EPA and DPA, its effect was not sufficient to complete that of DHA. Mitochondrial oxidation of ALA could not account for the limited production of neoformed DHA since supplemental ALA was efficiently converted into EPA and DPA (ALA was not more degraded in the presence of E2 than in its absence). The whole data suggest that E2 mainly produced the progressive membrane accumulation of the major upstream metabolic precursors of DHA, EPA and DPA.

The growing SH-SY5Y cells are able to incorporate preformed (non-esterified) DHA in their phospholipids. We previously showed that the maximum incorporation of preformed DHA into neuroblastoma cell phospholipids matches that of rat brain membranes [28]. Therefore, the limitation in membrane DHA production does not seem to be due to alteration of acylCoA synthesis or to impairment of esterification into phospholipids. We assume that production of membrane DHA is limited at the stage of DHA terminal synthesis, possibly at the peroxisomal step. The peroxisomal shortening of THA to DHA involves complex trafficking of the very long-chain acylCoA between the endoplasmic reticulum and the peroxisomes [32], which could be impaired in SH-SY5Y cells. We have previously shown that the SH-SY5Y cells express the mRNAs encoding for the main enzymes of peroxisomal β-oxidation, though the mRNA abundances of the L- and D-bifunctional peroxisomal proteins were particularly low in standard conditions of culture [27]. We suggested that the low expression of proteins or enzymes related to the peroxisomal function could form a "metabolic bottleneck". In this respect, hormonal, coactivators or other environmental signals including stimulants of peroxisomal activities would be necessary for completing the DHA synthesis in these cells.

Putative Mode of Action of E2

Estrogens exert their action on cell functions through genomic and non-genomic pathways. E2 binds to specific nuclear receptors (estrogen receptors, ER) which dimerize and directly bind to response elements of DNA; E2 may also interact with membrane receptors coupled to the activation of protein G-dependent kinases, producing changes in gene expression through the recruitment of other transcription factors (reviewed in [33]). A broad range of E2-responsive genes can be regulated by these mechanisms, including those involved in brain functions (reviewed in [34]). Our hypothesis is that changes in the transcription of lipid metabolism genes could account for the effect of E2 on the production of membrane n-3 long-chain PUFAs in ALA-supplemented cells. The transcription of most of these genes, notably those encoding desaturases [35, 36] and peroxisomal enzymes [37–39], are regulated by nuclear receptors which are recruited to the target promoters upon the binding of exogenous compounds (peroxisome proliferators) or of endogenous ligands (PUFA and PUFA-derived signaling molecules). We have shown that the mRNAs of the three peroxisome proliferator-activated receptors (PPAR) isotypes (α, β/δ and γ) are expressed in SH-SY5Y cells [27], and unpublished results from our laboratory indicated to us that the ERβ isotype (*ESR2* human gene) is also expressed in these cells. Numerous studies have shown that complex cross-stalks exist between the PPAR and ER signaling pathways, depending on the gender [40–42] and on tissue or cell specificity [43–45]. There is also evidence that transcription of PPARα itself can be triggered by E2 [46]. On the other hand, chemical agonists of PPARα have been shown to alter the expression of estrogen-metabolizing enzymes, notably the 17-β-hydroxysteroid dehydrogenase type IV (*17BHSD-4* human gene) [47]. It must be emphasized that the 17BHSD-4 gene product, also known as D-bifunctional protein or multifunctional protein-2, is that involved in the peroxisomal β-oxidation of both estradiol and very long-chain fatty acids [48, 49], and precisely in the β-oxidation of THA to DHA [50–52]. It is tempting to speculate that an E2-dependent stimulation of the PPAR-signaling pathway may modulate the membrane fatty acid composition through changes in the expression of PUFA metabolizing genes. In conclusion, our data suggest that estradiol is able to modulate the upstream production of membrane n-3 long-chain PUFA by neural cells in culture.

Acknowledgments This work was supported by grants from the Institut National de la Recherche Agronomique (INRA) and from the Organisation Nationale Interprofessionnelle des Graines et Fruits Oléagineux (ONIDOL).

References

1. Young G, Conquer J (2005) Omega-3 fatty acids and neuropsychiatric disorders. Reprod Nutr Dev 45:1–28
2. Wise PM, Dubal DB, Rau SW, Brown CM, Suzuki S (2005) Are estrogens protective or risk factors in brain injury and neurodegeneration? Reevaluation after the women's health initiative. Endocr Rev 26:308–312
3. Tsutsui K, Sakamoto H, Shikimi H, Ukena K (2004) Organizing actions of neurosteroids in the Purkinje neuron. Neurosci Res 49:273–279
4. Garcia-Segura LM, Azcoitia I, DonCarlos LL (2001) Neuroprotection by estradiol. Prog Neurobiolol 63:29–60
5. Burdge GC, Calder PC (2005) Conversion of α-linolenic acid to longer-chain polyunsaturated fatty acids in human adults. Reprod Nutr Dev 45:581–597
6. Giltay EJ, Gooren LJG, Toorians AWFT, Katan MB, Zock PL (2004) Docosahexaenoic acid concentrations are higher in women than in men because of estrogenic effects. Am J Clin Nutr 80:1167–1174
7. Giltay EJ, Duschek EJ, Katan MB, Zock PL, Neele SJ, Netelenbos JC (2004) Raloxifene and hormone replacement therapy increase arachidonic acid and docosahexaenoic acid levels in postmenopausal women. J Endocrinol 182:399–408
8. Alessandri JM, Guesnet P, Vancassel S, Astorg P, Denis I, Langelier B, Aïd S, Poumès-Ballihaut C, Champeil-Potokar G, Lavialle M (2004) Polyunsaturated fatty acids in the nervous system, evolution of concepts and nutritional implications throughout life. Reprod Nutr Dev 44:509–538
9. McCann JC, Ames BN (2005) Is docosahexaenoic acid, an n-3 long-chain polyunsaturated fatty acid, required for development of normal brain function ? An overview of evidence from cognitive and behavioral tests in humans and animals. Am J Clin Nutr 82:281–295
10. Rojas CV, Martinez JI, Flores I, Hoffman DR, Uauy R (2003) Gene expression analysis in human fetal retinal explants treated with docosahexaenoic acid. Invest Ophthalmol Vis Sci 44:3170–3177
11. Kawakita E, Hashimoto M, Shido O (2006) Docosahexaenoic acid promotes neurogenesis in vitro and in vivo. Neuroscience 139:991–997
12. Igarashi M, DeMar JC Jr, Ma K, Chang L, Bell JM, Rapoport SI (2007) Upregulated liver conversion of alpha-linolenic acid to docosahexaenoic acid in rats on a 15 week n-3 PUFA-deficient diet. J Lipid Res 48:152–164
13. DeMar JC, Ma K, Chang L, Bell JM, Rapoport SI (2005) Alpha-linolenic acid does not contribute appreciably to docosahexaenoic acid within brain phospholipids of adult rats fed a diet enriched in docosahexaenoic acid. J Neurochem 94:1063–1076

14. Igarashi M, Ma K, Chang L, Bell JM, Rapoport SI, DeMar JC Jr (2006) Low liver conversion rate of alpha-linolenic to docosahexaenoic acid in awake rats on a high-docosahexaenoate-containing diet. J Lipid Res 47:1812–1822
15. Moore SA (2001) Polyunsaturated fatty acid synthesis and release by brain-derived cells in vitro. J Mol Neurosci 16:195–200
16. Williard DE, Harmon SD, Kaduce TL, Preuss M, Moore SA, Robbins MEC, Spector AA (2001) Docosahexaenoic acid synthesis from n-3 polyunsaturated fatty acids in differentiated rat brain astrocytes. J Lipid Res 42:1368–1376
17. Williard DE, Harmon SD, Kaduce TL, Spector AA (2002) Comparison of 20-, 22-, and 24-carbon n-3 and n-6 polyunsaturated fatty acid utilization in differentiated rat brain astrocytes. Prostaglandins Leukot Essent Fatty Acids 67:99–104
18. Pawlosky RJ, Hibbeln JR, Novotny JA, Salem N Jr (2001) Physiological compartmental analysis of alpha-linolenic acid metabolism in adult humans. J Lipid Res 42:1257–1265
19. Pawlosky RJ, Hibbeln JR, Lin Y, Goodson S, Riggs P, Sebring N, Brown GL, Salem N Jr (2003) Effects of beef- and fish-based diets on the kinetics of n-3 fatty acid metabolism in human subjects. Am J Clin Nutr 77:565–572
20. Burdge GC, Finnegan YE, Minihane AM, Williams CM, Wootton SA (2003) Effect of altered dietary n-3 fatty acid intake upon plasma lipid fatty acid composition, conversion of [13C]alpha-linolenic acid to longer-chain fatty acids and partitioning towards beta-oxidation in older men. Br J Nutr 90:311–321
21. Burdge GC, Jones AE, Wootton SA (2002) Eicosapentaenoic and docosapentaenoic acids are the principal products of alpha-linolenic acid metabolism in young men. Br J Nutr 88:355–363
22. Burdge GC, Wootton SA (2002) Conversion of alpha-linolenic acid to eicosapentaenoic, docosapentaenoic and docosahexaenoic acids in young women. Br J Nutr 88:411–420
23. Burdge GC, Wootton SA (2003) Conversion of alpha-linolenic acid to palmitic, palmitoleic, stearic and oleic acids in men and women. Prostaglandins Leukot Essent Fatty Acids 69:283–290
24. Bakewell L, Burdge GC, Calder PC (2006) Polyunsaturated fatty acid concentrations in young men and women consuming their habitual diets. Br J Nutr 96:93–99
25. Postle AD, Al MD, Burdge GC, Hornstra G (1995) The composition of individual molecular species of plasma phosphatidylcholine in human pregnancy. Early Hum Dev 43:47–58
26. Cunnane SC, Francescutti V, Brenna JT, Crawford MA (2000) Breast-fed infants achieve a higher rate of brain and whole body docosahexaenoate accumulation than formula-fed infants not consuming dietary docosahexaenoate. Lipids 35:105–111
27. Langelier B, Alessandri JM, Perruchot MH, Guesnet P, Lavialle M (2005) Changes of the transcriptional and fatty acid profiles in response to n-3 fatty acids in SH-SY5Y neuroblastoma cells. Lipids 40:719–728
28. Alessandri JM, Poumès-Ballihaut C, Langelier B, Perruchot MH, Raguénez G, Lavialle M, Guesnet P (2003) Incorporation of docosahexaenoic acid into nerve membrane phospholipids, bridging the gap between animals and cultured cells. Am J Clin Nutr 78:702–710
29. Goustard-Langelier B, Alessandri JM, Raguenez G, Durand G, Courtois Y (2000) Phospholipid Incorporation and metabolic conversion of n-3 polyunsaturated fatty acids in the Y79 retinoblastoma cell line. J Neurosci Res 60:678–685
30. Innis SM, Dyer RA (2002) Brain astrocyte synthesis of docosahexaenoic acid from n-3 fatty acids is limited at the elongation of docosapentaenoic acid. J Lipid Res 43:1529–1536
31. Voss A, Reinhart M, Sankarappa S, Sprecher H (1991) The metabolism of 7, 10, 13, 16, 19-docosapentaenoic acid to 4, 7, 10, 13, 16, 19-docosahexaenoic acid in rat liver is independent of a Δ4-desaturase. J Biol Chem 266:19995–20000
32. Luthria DL, Mohammed BS, Sprecher H (1996) Regulation of the biosynthesis of 4, 7, 10, 13, 16, 19-docosahexaenoic acid. J Biol Chem 271:16020–16025
33. Bjornstrom L, Sjoberg M (2005) Mechanisms of estrogen receptor signaling, convergence of genomic and nongenomic actions on target genes. Mol Endocrinol 19:833–842
34. Balthazart J, Ball GF (2006) Is brain estradiol a hormone or a neurotransmitter ? Trends Neurosci 29:241–249
35. Tang C, Cho HP, Nakamura MT, Clarke SD (2003) Regulation of human delta-6 desaturase gene transcription, identification of a functional direct repeat-1 element. J Lipid Res 44:686–695
36. Nakamura MT, Cheon Y, Li Y, Nara TY (2004) Mechanisms of regulation of gene expression by fatty acids. Lipids 39:1077–1083
37. Reddy JK, Goel SK, Nemali MR, Carrino JJ, Laffler TG, Reddy MK, Sperbeck SJ, Osumi T, Hashimoto T, Lalwani ND, Rao MS (1986) Transcription regulation of peroxisomal fatty acyl-CoA oxidase and enoyl-CoA hydratase/3-hydroxyacyl-CoA dehydrogenase in rat liver by peroxisome proliferators. Proc Natl Acad Sci USA 83:1747–1751
38. Jia Y, Qi C, Zhang Z, Hashimoto T, Rao MS, Huyghe S, Suzuki Y, Van Veldhoven PP, Baes M, Reddy JK (2003) Overexpression of peroxisome proliferator-activated receptor-α (PPAR(α)-regulated genes in liver in the absence of peroxisome proliferation in mice deficient in both L- and D-forms of enoyl-CoA hydratase/dehydrogenase enzymes of peroxisomal β-oxidation system. J Biol Chem 278:47232–47239
39. Tugwood JD, Issemann I, Anderson RG, Bundell KR, McPheat WL, Green S (1992) The mouse peroxisome proliferator activated receptor recognizes a response element in the 5′ flanking sequence of the rat acyl CoA oxidase gene. EMBO J 11:433–439
40. Djouadi F, Weinheimer CJ, Saffitz JE, Pitchford C, Bastin J, Gonzalez FJ, Kelly DP (1998) A gender-related defect in lipid metabolism and glucose homeostasis in peroxisome proliferator-activated receptor alpha-deficient mice. J Clin Invest 102:1083–1091
41. Jalouli M, Carlsson L, Améen C, Lindén D, Ljungberg A, Michalik L, Edén S, Wahli W, Oscarsson J (2003) Sex difference in hepatic peroxisome proliferator-activated receptor expression: influence of pituitary and gonadal hormones. Endocrinology 144:101–109
42. Ciana P, Biserni A, Tatangelo L, Tiveron C, Sciarroni AF, Ottobrini L, Maggi A (2007) A novel peroxisome proliferator-activated receptor responsive element-luciferase reporter mouse reveals gender specificity of peroxisome proliferator-activated receptor activity in liver. Mol Endocrinol 21:388–400
43. Jacobs MN, Dickins M, Lewis DF (2003) Homology modelling of the nuclear receptors, human oestrogen receptor beta (hERβ), the human pregnane-X-receptor (PXR), the Ah receptor (AhR) and the constitutive androstane receptor (CAR) ligand binding domains from the human oestrogen receptor alpha (hERα) crystal structure, and the human peroxisome proliferator activated receptor alpha (PPARα) ligand binding domain from the human PPARγ crystal structure. J Steroid Biochem Mol Biol 84:117–132
44. Bonofiglio D, Gabriele S, Aquila S, Catalano S, Gentile M, Middea E, Giordano F, Ando S (2005) Estrogen receptor alpha binds to peroxisome proliferator-activated receptor response element and negatively interferes with peroxisome proliferator-activated receptor gamma signaling in breast cancer cells. Clin Cancer Res 11:6139–6147
45. Min G (2006) Different modulation of ER-mediated transactivation by xenobiotic nuclear receptors depending on the estrogen response elements and estrogen target cell types. Ann NY Acad Sci 1091:244–257
46. Campbell SE, Mehan KA, Tunstall RJ, Febbraio MA, Cameron-Smith D (2003) 17β-Estradiol upregulates the expression of

peroxisome proliferator-activated receptor alpha and lipid oxidative genes in skeletal muscle. J Mol Endocrinol 31:37–45

47. Corton JC, Bocos C, Moreno ES, Merritt A, Cattley RC, Gustafsson JA (1997) Peroxisome proliferators alter the expression of estrogen-metabolizing enzymes. Biochimie 79:151–162
48. Adamski J, Leenders F, Carstensen JF, Kaufmann M, Markus MM, Husen B, Tesdorpf JG, Seedorf U, de Launoit Y, Jakob F (1997) Steroids, fatty acyl-CoA, and sterols are substrates of 80-kDa multifunctional protein. Steroids 62:159–163
49. Baes M, Huyghe S, Carmeliet P, Declercq PE, Collen D, Mannaerts GP, Van Veldhoven PP (2000) Inactivation of the peroxisomal multifunctional protein-2 in mice impedes the degradation of not only 2-methyl-branched fatty acids and bile acid intermediates but also of very long chain fatty acids. J Biol Chem 275:16329–16336
50. Su HM, Moser AB, Moser HW, Watkins PA (2001) Peroxisomal straight-chain acyl-CoA oxidase and D-bifunctional protein are essential for the retroconversion step in docosahexaenoic acid synthesis. J Biol Chem 276:38115–38120
51. Ferdinandusse S, Denis S, Mooijer PAW, Zhang Z, Reddy JK, Spector AA, Wanders RJA (2001) Identification of the peroxisomal β-oxidation enzymes involved in the biosynthesis of docosahexaenoic acid. J Lipid Res 42:1987–1995
52. Ferdinandusse S, van Grunsven EG, Oostheim W, Denis S, Hogenhout EM, Ijlst L, van Roermund CWT, Waterham HR, Goldfischer S, Wanders RJ (2002) Reinvestigation of peroxisomal 3-ketoacyl-CoA thiolase deficiency, identification of the true defect at the level of D-bifunctional protein. Am J Hum Genet 70:1589–1593

Lipids (2008) 43:29–35
DOI 10.1007/s11745-007-3116-7

ORIGINAL ARTICLE

Soy-Based Infant Formula Supplemented with DHA and ARA Supports Growth and Increases Circulating Levels of these Fatty Acids in Infants

Dennis Hoffman · Ekhard Ziegler · Susan H. Mitmesser · Cheryl L. Harris · Deborah A. Diersen-Schade

Received: 31 May 2007 / Accepted: 21 August 2007 / Published online: 3 October 2007
© AOCS 2007

Abstract Healthy term infants ($n = 244$) were randomized to receive: (1) control, soy-based formula without supplementation or (2) docosahexaenoic acid–arachidonic acid (DHA + ARA), soy-based formula supplemented with at least 17 mg DHA/100 kcal (from algal oil) and 34 mg ARA/100 kcal (from fungal oil) in a double-blind, parallel group trial to evaluate safety, benefits, and growth from 14 to 120 days of age. Anthropometric measurements were taken at 14, 30, 60, 90, and 120 days of age and 24-h dietary and tolerance recall were recorded at 30, 60, 90, and 120 days of age. Adverse events were recorded throughout the study. Blood samples were drawn from subsets of 25 infants in each group. Capillary column gas chromatography was used to analyze the percentages of fatty acids in red blood cell (RBC) lipids and plasma phospholipids. Compared with the control group, percentages of fatty acids such as DHA and ARA in total RBC and plasma phospholipids were significantly higher in infants in the DHA + ARA group at 120 days of age ($P < 0.001$). Growth rates did not differ significantly between feeding groups at any assessed time point. Supplementation did not affect the tolerance of formula or the incidence of adverse events. Feeding healthy term infants soy-based formula supplemented with DHA and ARA from single cell oil sources at concentrations similar to human milk significantly increased circulating levels of DHA and ARA when compared with the control group. Both formulas supported normal growth and were well tolerated.

Keywords Soy-based formula · Term infants · Infant formula · Docosahexaenoic acid · Arachidonic acid · LCPUFA · Infant growth

Introduction

Docosahexaenoic acid (22:6ω3; DHA) and arachidonic acid (20:4ω6; ARA) are long-chain polyunsaturated fatty acids (LCPUFAs) that accumulate rapidly in the brain from the last trimester of fetal gestation until at least 2 years of age [1, 2]. Human breast milk provides DHA and ARA for growth as well as retinal and central nervous system development and function [3–7]. Infants unable to breastfeed or weaned from breastfeeding now benefit from supplementation of DHA and ARA in many commercial infant formulas. Supplementation of DHA and ARA from single cell algal and fungal sources at median worldwide human milk levels [8–10] in both premature and term infants has resulted in red blood cell (RBC) concentrations of the LCPUFAs comparable to those of breast-fed infants [11–13]. Clinical evidence of improved visual acuity and cognitive development in term infants up to 18 months of age [12, 14–18] and enhanced growth in premature infants [19, 20] has resulted from inclusion of DHA and ARA at worldwide human milk levels in milk-based formulas. In addition, a follow-up study of 4-year-olds who received formula supplemented with DHA and ARA at those levels as infants, demonstrated visual and IQ maturation similar to that of breast-fed subjects [7].

D. Hoffman
Retina Foundation of the Southwest, Dallas, TX, USA

E. Ziegler
Department of Pediatrics,
University of Iowa Hospital and Clinic,
Iowa City, IA, USA

S. H. Mitmesser (✉) · C. L. Harris · D. A. Diersen-Schade
Mead Johnson Nutritionals, 2400 W. Lloyd Expressway,
Evansville, IN 47721, USA
e-mail: susan.mitmesser@bms.com

Not all infants can tolerate a cow's milk-based formula, and some parents prefer a vegetarian product. Primary clinical indications for discontinued use of cow's milk-based formula include immunoglobulin E-mediated milk allergy (commonly associated with eczema), documented lactose intolerance following infectious diarrhea, lactase deficiency, and galactosemia [21, 22]. In such instances, soy-based formulas have been endorsed by The American Academy of Pediatrics as a safe and effective alternative [21]. An estimated 25–36% of formula-fed infants in the United States receive a soy-based infant formula at some time in the first year of life [21, 22].

To date, no published data are available for supplementation of soy-based infant formula with DHA and ARA. Given the extensive use of soy-based formulas and the developmental advantages afforded by routine supply of exogenous DHA and ARA in cow's milk-based formulas, we felt it prudent to examine the growth, tolerance, and possible benefits of supplementation in a soy-based matrix. In this study we examined the effects of a soy-based formula supplemented with single cell oil sources of DHA and ARA at worldwide human milk levels on growth, tolerance, and the percentage of DHA and ARA (i.e., vegetarian sources) in RBCs and plasma phospholipids when fed to term infants from 14 to 120 days of age.

Experimental Procedure

Subjects

Healthy term infants were recruited at 13 pediatric centers in the United States for a double-blind, randomized, controlled parallel group study. Eligible participants were 12–16 days of age, had a minimum birth weight of 2,500 g, and solely received formula at least 24 h prior to randomization. Exclusion criteria included: history of underlying disease or malformation that could interfere with growth and development; large-for-gestational-age infants whose mothers were diabetic; breastfeeding within 24 h prior to randomization; evidence of formula intolerance or poor intake at time of randomization; weight at randomization less than 98% of birth weight; enlarged liver or spleen; or plans to move outside of the study area within the study time frame (120 days).

Parents or guardians provided written informed consent prior to enrollment. The research protocol and informed consent forms adhered to the Declaration of Helsinki (including the October 1996 amendment) and were approved by the institutional review board/ethics committee of each participating institution. The study was conducted in compliance with good clinical practices.

Study Protocol

Two hundred and forty-four infants (control, $n = 120$; DHA + ARA, $n = 124$) enrolled in the study were stratified by gender and randomized to receive one of two formulas: (1) control, soy formula without supplementation (Enfamil ProSobee®, Mead Johnson & Company, Evansville, IN) or (2) DHA + ARA, soy formula supplemented with a minimum of 17 mg DHA/100 kcal from algal oil and 34 mg ARA/100 kcal from fungal oil (Enfamil ProSobee® LIPIL®, Mead Johnson & Company, Evansville, IN). Aside from the addition of DHA and ARA, the formulas were identical in all other respects. The supplemented levels of DHA and ARA were similar to reported median amounts of DHA (~0.3% by weight of fatty acids) and ARA (~0.6%) found in human milk worldwide [8–10].

Infants received study formulas from 14 to 120 days of age. Body weight and length, head circumference, and atopic dermatitis scores were recorded at 14, 30, 60, 90, and 120 days of age. Evidence of atopic dermatitis was determined using the SCORAD index [23] which quantifies the extent, distribution, and severity of rashes and the presence and severity of associated itching and sleep loss. Parents or guardians completed a family history of allergy and a survey of possible factors in the home and child care environments that might affect the infant's risk of atopy, such as cigarette smoke, pets, dust, and mold. At each study visit following initial enrollment at 14 days of age, parents or care givers completed a questionnaire on dietary intake and tolerance from the previous 24 h. Adverse events were monitored throughout the study period.

Blood Sample Analysis

At five investigative sites, blood samples from a subset of infants (25 per group) were collected by venipuncture into EDTA Vacutainer tubes at 14 and 120 days of age. Only sites with experience handling clinical blood samples and appropriate sample storage facilities provided blood samples. For fatty acid analysis, plasma and RBC were separated by centrifugation and frozen. Samples were shipped on dry ice to the Retina Foundation of the Southwest (Dallas, TX) where lipids were isolated, fractionated, and analyzed by capillary column gas chromatography as previously described [12]. Fatty acid methyl esters from RBC lipids and plasma phospholipid fractions were expressed as a percentage of total fatty acids by weight. Outcomes were expressed as percentages of DHA, ARA, and other fatty acids in RBC phosphatidylethanolamine (PE) and phosphatidylcholine (PC) fractions, total RBC lipids, and plasma phospholipids. A portion of the blood sample was also used for comprehensive metabolic panel of blood chemistry analyses including glucose, cholesterol, triglycerides, electrolytes, and kidney, liver, and pancreas function markers.

Statistical Analysis

Statistical comparisons were made between control and DHA + ARA formula groups. Analyses were performed using SAS version 8 (Cary, NC). Weight gain from 14 to 120 days was the primary outcome used to establish that formulas supported adequate growth. The sample size was chosen to be able to detect a 3 g/day difference in weight gain with 80% power ($\alpha = 0.05$; one-tailed). For all subsequent comparisons, *P* values are based on two-tailed tests. Analysis of variance was used to analyze formula intake, stool frequency and characteristics, anthropometrics (achieved growth, length, and head circumference), SCORAD grade, and blood lipid and chemistry data. Analysis of covariance was used to analyze growth rate. Race, gender, family history of allergy, home and child care environments, study discontinuation rate, and adverse events were analyzed by Fisher's Exact test. The van Elteren test, stratified by study site, was used to analyze metabolic blood panel results.

Results

Infants

Of the original 244 infants enrolled, three infants (control, $n = 2$; DHA + ARA, $n = 1$) did not receive study formula and were excluded from subsequent analyses. At study entry (14 days of age) infants in the control group were significantly heavier and longer than those in the DHA + ARA group (Table 1), although head circumference did not differ significantly between groups. Groups were similar for race and gender distribution, family history of allergy, and home and child care environments (data not shown). A total of 182 infants (control, $n = 86$; DHA + ARA, $n = 96$) completed the study.

Table 1 Infant characteristics at study entry

	Control	DHA + ARA
Total number of subjects	118	123
Number of male/female	66/52	67/56
Weight (g)[a]	3,677.8 ± 45	3,575.4 ± 44*
Length (cm)[a]	52.3 ± 0.2	51.8 ± 0.2*
Head circumference (cm)[a]	36.1 ± 0.1	35.8 ± 0.1

[a] Mean ± standard error

* Significant difference between groups, $P < 0.05$

Growth and Tolerance

Growth rate, as assessed by mean daily gains of weight, length, and head circumference, did not differ statistically between groups from 14 to 120 days of age (Table 2). The mean achieved weight was significantly higher for infants in the control versus the DHA + ARA group at 30 and 90 days of age ($P < 0.05$; data not shown). The mean achieved weight for males (Fig. 1, upper panel) and females (lower panel) in both formula groups, however, fell between the 25th and 75th percentile of normal infant weight-for-age when plotted on the US Centers for Disease Control (CDC) standard growth chart [24]. Mean achieved length was higher for infants in the control group at all time points ($P < 0.05$; data not shown) and mean achieved head circumference did not differ significantly between groups at any assessed time point (data not shown).

Formula intake, stool frequency, and stool characteristics were similar for infants in both groups (data not shown). Both formulas were well tolerated as reported by parental assessment of fussiness, diarrhea, and constipation, with the only difference between groups being a higher incidence of excessive gas in the control group than the DHA + ARA group at 60 days of age (15% vs. 5%; $P = 0.026$). Minimal incidence of atopic dermatitis, as assessed by mean SCORAD indices, was noted for infants in each study group at all time points. For example, at 120 days of age mean SCORAD values were 2.9 ± 0.76 for the control group ($n = 85$) versus 2.3 ± 0.72 for the DHA + ARA group ($n = 93$, $P = 0.374$). Given the SCORAD index range of 0–103 with disease severity indicated by a higher score, mean values from this study signified a very low occurrence of atopic dermatitis.

There were no significant differences between groups for total discontinuation rates (control, $n = 32$ [27%] vs. DHA + ARA, $n = 27$ [22%]; $P = 0.37$) or for discontinuation due to feeding-related issues (control, $n = 23$ [19%] vs. DHA + ARA, $n = 19$ [15%]; $P = 0.615$). The most common reasons for discontinuation were diarrhea (control, DHA + ARA: $n = 8$, $n = 5$), vomiting ($n = 8$, $n = 4$), and fussiness ($n = 6$, $n = 6$). Significant differences between groups in adverse events included gastroesophageal reflux

Table 2 Mean weight, length, and head circumference growth rates from 14 to 120 days of age

	Control	DHA + ARA
Total number of subjects	86	93
Weight (g/day)[a]	27.8 ± 0.8	27.3 ± 0.7
Length (cm/day)[a]	0.10 ± 0.002	0.10 ± 0.002
Head circumference (cm/day)[a]	0.05 ± 0.001	0.05 ± 0.001

[a] Mean ± standard error

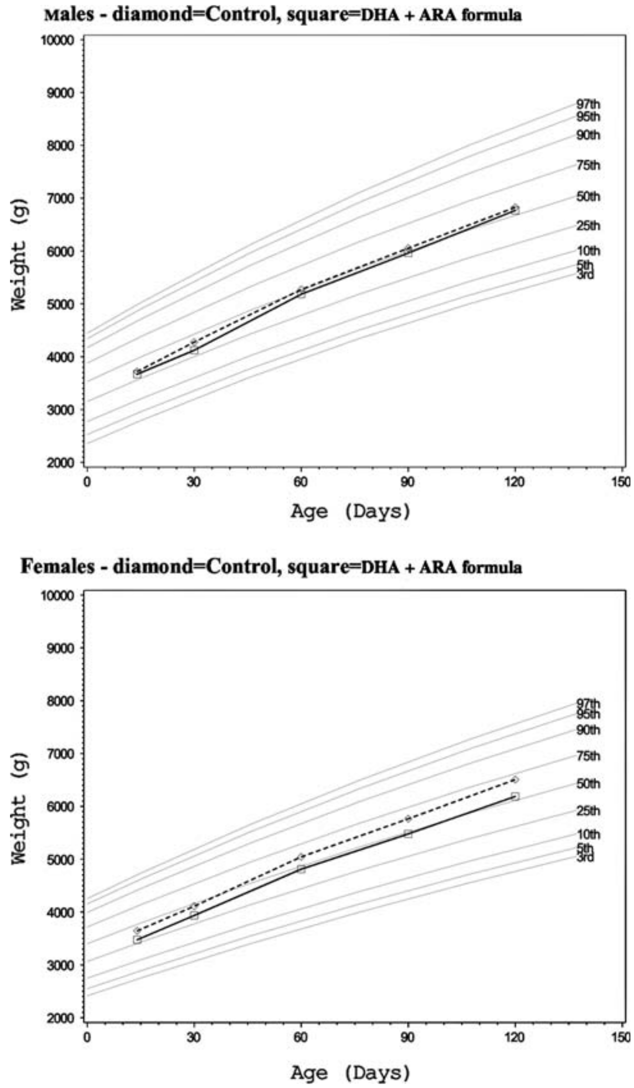

Fig. 1 Mean achieved weights of male participants (*upper panel*) and female participants (*lower panel*) with CDC reference percentiles (3–97) from 14 to 120 days of age. Control formula group, *diamonds*; DHA + ARA formula group, *squares*

(control, $n = 13$ vs. DHA + ARA, $n = 3$; $P = 0.009$) and incidence of metabolic or nutritional difficulties (control: weight loss, $n = 3$; poor weight gain, $n = 2$; Type 1 Glutaric Acidemia, $n = 1$ vs. DHA + ARA: $n = 0$ for any category; $P = 0.013$). Serious adverse events were reported for 12 infants (control, $n = 6$; DHA + ARA, $n = 6$). In each of these cases, the investigator stated that the serious adverse event was unrelated to the study product.

Blood Lipids and Blood Chemistry

No significant differences in mean fatty acid percentages were detected between groups for total RBC lipids or plasma phospholipids at 14 days of age in a subset of infants (control, $n = 25$; DHA + ARA, $n = 22$; data not shown). Results from infants at 120 days of age are reported in Table 3. In the $\omega3$ fatty acid family, the percentage of DHA in total fatty acids was significantly higher in total RBC lipids from infants in the DHA + ARA group versus the control (6.23 vs. 2.47%, $P < 0.001$; Table 3). DHA was also significantly higher in plasma phospholipids in infants from the DHA + ARA group (5.04 vs. 1.67%, $P < 0.001$). Percentages of α-linolenic acid (18:3ω3; ALA) and docosapentaenoic acid (22:5ω3) in total RBC lipids ($P = 0.019$ and $P < 0.001$, respectively) and plasma phospholipids ($P < 0.001$ for both fatty acids) were significantly lower in the DHA + ARA group.

In the $\omega6$ fatty acid family, ARA as a percentage of total fatty acids was significantly higher in total RBC lipids from infants in the DHA + ARA group versus the control (16.27 vs. 13.97%, $P < 0.001$). ARA was also significantly higher in plasma phospholipids in infants in the DHA + ARA group (13.46 vs.7.33%, $P < 0.001$). Mean percentages of linoleic acid (18:2ω6), γ-linolenic acid (18:3ω6), eicosadienoic acid (20:2ω6), dihomo-γ-linolenic acid (20:3ω6), and docosapentaenoic acid (22:5ω6) were significantly lower in total RBC lipids and plasma phospholipids from infants in the DHA + ARA group as compared with the control (see individual P values in Table 3). Fatty acid profiles of RBC PE and PC fractions were not reportable due to technical problems during analysis. There were no statistical differences in blood chemistry profiles between groups at 14 or 120 days of age (data not shown).

Discussion

The present study showed that a soy-based infant formula supplemented with DHA and ARA supported growth rates and tolerance of term infants as well as commercially available soy-based formula without these fatty acids, and increased DHA and ARA status similar to milk-based formulas with similar levels of added DHA and ARA. The American Academy of Pediatrics Task Force on Clinical Testing of Infant Formulas [25] stated that rate of weight gain (g/day) is the most beneficial component of the clinical evaluation of infant formula and recommended that a difference in weight gain of more than 3 g/day over 3–4 months be considered nutritionally significant. Our study found no differences in rate of weight gain over the 4-month study. Daily gains in length and head circumference (cm/day) also did not differ between the formula groups. In addition, weights in both groups, when compared with CDC infant reference data [24], fell between the 25th and 75th percentiles of both male and female weight-for-age growth curves. Although achieved weight means were significantly higher at 30 and 90 days of age and achieved

Table 3 Fatty acid levels (percent of total fatty acids) in infant blood lipid fractions at 120 days of age

Fatty acid	Total RBC		Plasma phospholipids	
	Control	DHA + ARA	Control	DHA + ARA
n-3 Fatty acids				
18:3n-3	0.23 ± 0.02	0.18 ± 0.01***	0.19 ± 0.01	0.15 ± 0.01*
18:4n-3	0.10 ± 0.01	0.10 ± 0.01	0.03 ± 0.01	0.04 ± 0.01
20:3n-3	0.01 ± 0.00	0.00 ± 0.00	0.02 ± 0.00	0.02 ± 0.00
20:5n-3	0.79 ± 0.04	0.75 ± 0.04	0.40 ± 0.14	0.68 ± 0.13
22:5n-3	1.12 ± 0.05	0.66 ± 0.04*	0.44 ± 0.02	0.21 ± 0.02*
22:6n-3	2.47 ± 0.18	6.23 ± 0.16*	1.67 ± 0.14	5.04 ± 0.13*
n-6 Fatty acids				
18:2n-6	15.28 ± 0.42	12.58 ± 0.39*	27.48 ± 0.52	21.49 ± 0.48*
18:3n-6	0.10 ± 0.01	0.07 ± 0.01**	0.12 ± 0.01	0.08 ± 0.01*
20:2n-6	0.45 ± 0.01	0.39 ± 0.01*	0.40 ± 0.01	0.36 ± 0.01***
20:3n-6	1.97 ± 0.08	1.26 ± 0.07*	2.50 ± 0.10	1.62 ± 0.10*
20:4n-6	13.97 ± 0.33	16.27 ± 0.30*	7.33 ± 0.32	13.46 ± 0.29*
22:2n-6	0.14 ± 0.02	0.11 ± 0.02	0.04 ± 0.00	0.04 ± 0.00
22:4n-6	3.88 ± 0.12	3.61 ± 0.11	0.45 ± 0.01	0.43 ± 0.01
22:5n-6	1.23 ± 0.5	0.75 ± 0.05*	1.14 ± 0.06	0.66 ± 0.06*

Least square mean ± SE Control group, $n = 15$; DHA + ARA group, $n = 16$

* Significant difference between groups, $P \leq 0.001$

** Significant difference between groups, $P = 0.01$

*** Significant difference between groups, $P = 0.019$

length means were higher in the control group at all time points, these differences were consistent with those upon study entry, when the control group was significantly heavier and longer on average than the DHA + ARA group.

Questions have been raised as to how some other components of soy formulas (e.g., phytoestrogens) affect growth and long-term health [21, 22]. Previous clinical reports, however, have demonstrated that soy-based formulas promoted normal growth in term infants [21, 22, 26–28]. In addition, a study of adults found that long-term growth, health, and reproductive outcomes are comparable between individuals who received soy- or cow's milk-based formula as infants [29]. The American Academy of Pediatrics has concluded that soy based formulas are safe and effective feedings for infants whose nutritional needs are not met by human milk or cow's milk formula [21]. Our study adds further support to this conclusion and demonstrates that the addition of DHA and ARA at levels similar to those found in worldwide breast milk does not negatively influence growth [29].

Both the marketed control and the DHA + ARA supplemented soy-based formulas were well tolerated by infants in this study as evidenced by similarities in parental assessment of tolerance, formula intake, stool frequency and characteristics, and low occurrence of atopic dermatitis throughout the study. Serum chemistry values for a wide variety of metabolic parameters were similar for infants in both groups at 14 and 120 days of age. Rates of study discontinuation and adverse events were similar between formula groups and incidence of serious adverse events was low and deemed unrelated to the study products by participating physicians. Previous clinical evidence also indicates infant tolerance of soy-based formulas, with favorable comparison to cow's milk-based formula [22, 30, 31]. Our study demonstrated that the soy-based control formula and soy-based formula supplemented with DHA and ARA were equally well tolerated by infants, with very low incidence of allergic manifestations.

Concentrations of DHA and ARA in RBC and plasma phospholipids have been widely evaluated as outcomes in studies of milk-based formula-fed and breast-fed infants [3, 6, 11–17, 32–34]. In the current study, mean fatty acid percentages were similar between control and DHA + ARA groups at 14 days of age. Similar to trials with term infants fed milk-based formulas [12, 32–34], infants fed a soy-based formula supplemented with DHA and ARA had significantly higher percentages of fatty acids as DHA and ARA in RBC lipids and plasma phospholipids at 120 days of age than infants fed an unsupplemented soy-based formula. Previously published levels of RBC and plasma phospholipid DHA and ARA from a clinical trial of term infants fed a control milk-based formula without DHA or ARA [12] were similar to those of infants fed the control soy-based formula in this study. For example, mean total RBC DHA and ARA percentages for infants fed control soy-based formula in the current study were 2.47 and 13.97%, respectively, compared with 2.52 and 13.9%, respectively, for control milk-based formula in the earlier study [12]. Likewise, the RBC and plasma phospholipid DHA and ARA values for infants fed milk-based formulas supplemented with 0.32–0.36% of fatty acids as DHA and 0.64–0.72% as ARA [12, 13] were similar to concentrations measured in those blood fractions in the DHA + ARA group in the current study. Blood levels of DHA and ARA measured in infants in the DHA + ARA group at 120 days of age also were similar to those demonstrated in breast-fed infants where representative breast milk contained 0.29% DHA and 0.56% ARA [12]. For example, total RBC DHA and ARA were 6.23% and 16.27%, respectively, for the DHA + ARA group in the current study, compared with 4.97% and 15.9%, respectively, for the breast-fed group and 6.77% and 17.1%, respectively, for the supplemented milk-based formula in the earlier study [12]. Thus, the addition of DHA and ARA to soy-based formula produces similar responses in blood DHA and ARA as addition of similar levels to milk-based formula, as well as similar responses as comparable levels of breast milk DHA and ARA. The significant increase at 120 days of age in the DHA + ARA group further suggests that feeding term infants a soy-based formula supplemented with preformed DHA and ARA increases the levels of circulating DHA and ARA available for brain and retinal development and functions similarly to breast-fed infants [12, 18].

Significant differences in percentages of other PUFA in RBC lipids and plasma phospholipids seen in the DHA + ARA group compared with control also parallel, for the most part, changes seen in previous studies of milk-based formulas [12, 13, 16, 17, 32–34]. Lower blood levels of DHA precursors ALA (18:3ω3) and docosapentaenoic (22:5ω3), and ARA precursors linoleic (18:2ω6), γ-linolenic (18:3ω6), and dihomo-γ-linolenic (20:3ω6), as well as eicosadienoic (20:2ω6) and docosapentaenoic (22:5ω6) acids in the DHA + ARA group were consistent with supplemental feeding or feeding higher levels of DHA and ARA, as previously noted [13, 16, 17, 34]. Breast-fed infants have also been shown to have lower percentages of linoleic acid and ALA in total RBC and plasma phospholipids [12] and lower linoleic acid in RBC PC and PE [32] than infants fed control milk-based formula without added DHA and ARA. Blood levels of linoleic acid and ALA were comparable among infants fed human milk with 0.29% DHA and 0.56% ARA and infants fed milk-based formula with 0.36% DHA and 0.72% ARA in the earlier study [12], and infants fed soy-based formula with 0.32% DHA and 0.64% ARA in the current study; mean total RBC and plasma phospholipid linoleic acid across the three groups ranged from 10.9% to 12.58% and 20.2% to 21.49%, respectively, and mean ALA values for both blood fractions across all three groups were less than 0.2%. Our data demonstrate that the addition of DHA and ARA to soy-based formula results in similar responses in blood PUFA levels at similar levels of DHA and ARA in milk-based formulas and in breast milk [12], and provide further evidence that the conversion of ALA and linoleic acid to DHA and ARA, respectively, does not compensate for lack of dietary DHA and ARA [13].

Supplementation of formulas with DHA and ARA is now a widely accepted method of attempting to reproduce concentrations typical of human breast milk and to parallel developmental benefits. The current study is unique in comparing growth, tolerance, and blood chemistry outcomes between infants who received commercially available soy-based formulas with or without DHA and ARA supplementation. Both formulas supported normal growth of infants, and tolerance for each formula was similar between groups. Supplementation of soy-based formula with preformed DHA and ARA from single cell oil sources also resulted in circulating levels of DHA and ARA comparable to previous clinical data from breast-fed infants and infants who received cow's milk-based formula supplemented with median worldwide levels of DHA and ARA. These results demonstrate that feeding soy-based formulas supplemented with DHA and ARA supports infant growth and achieves increased levels of circulating DHA and ARA.

Acknowledgments This study was supported by a grant from Mead Johnson & Company. The authors wish to thank study investigators and their staff for their cooperation, including Barbara Alexander, M.D. (Pediatric Associates, Hollywood, FL), Dean Antonson, M.D. (The Center for Human Nutrition, Omaha, NE), Janet Barnes, M.D. (New Orleans, LA), Azzam Baker, M.D. (Riverside Pediatric Group, Secaucus, NJ), Wesley Burks, M.D. (Arkansas Children's Hospital, Little Rock, AR), William M. Crecelius, M.D. (Welborn Clinic, Evansville, IN); James Hubbard, M.D. (Medical Associates Clinic, Dubuque, IA); William H. Johnson, Jr., M.D. (Birmingham, AL), Barry Kroll, M.D. (Margiotti & Kroll Pediatrics, Newtown, PA); Matthew Sadof, M.D. (Baystate Pediatric Group, Springfield, MA); Charles Sheaffer, M.D. (Chapel Hill, NC); and Eric Slosberg, M.D. (ProMed Pediatrics, Kalamazoo, MI). The participation of parents and infants in this study is gratefully acknowledged. We also acknowledge valuable contributions from Julia Boettcher, R.D., M.S. and Suzanne I. Stolz in the execution and completion of this study. We are grateful to Dianna K.H. Wheaton, K.J. James, and L.E. Wiedemann for fatty acid analysis conducted at the Retina Foundation. Additionally, we would like to acknowledge Jennifer Wampler, Ph.D. for her contributions to the manuscript development.

References

1. Martinez M (1992) Tissue levels of polyunsaturated fatty acids during early human development. J Pediatr 120:S129–S138
2. Innis SM (2003) Perinatal biochemistry and physiology of long-chain polyunsaturated fatty acids. J Pediatr 143:S1–S8

3. Carlson SE, Werkman SH, Peeples JM, Cooke RJ, Tolley EA (1993) Arachidonic acid status correlates with first year growth in preterm infants. Proc Natl Acad Sci USA 90:1073–1077
4. Makrides M, Neumann MA, Byard RW, Simmer K, Gibson RA (1994) Fatty acid composition of brain, retina, and erythrocytes in breast- and formula-fed infants. Am J Clin Nutr 60:189–194
5. Lauritzen L, Hansen HS, Jorgensen MH, Michaelsen KF (2001) The essentiality of long chain n-3 fatty acids in relation to development and function of the brain and retina. Prog Lipid Res 40:1–94
6. Innis SM, Gilley J, Werker J (2001) Are human milk long-chain polyunsaturated fatty acids related to visual and neural development in breast-fed term infants? J Pediatr 139:532–538
7. Birch EE, Garfield S, Castaneda Y, Hughbanks-Wheaton D, Uauy R, Hoffman D (2007) Visual acuity and cognitive outcomes at 4 years of age in a double-blind, randomized trial of long-chain polyunsaturated fatty acid-supplemented infant formula. Early Hum Dev 83:279–284
8. Innis SM (1992) Human milk and formula fatty acids. J Pediatr 120:S56–S61
9. Koletzko B, Thiel I, Abiodun PO (1992) The fatty acid composition of human milk in Europe and Africa. J Pediatr 120:S62–S70
10. Brenna JT, Varamini B, Jensen RG, Diersen-Schade DA, Boettcher JA, Arterburn LM (2007) Docosahexaenoic and arachidonic acid concentrations in human breast milks worldwide. Am J Clin Nutr 85:1457–1464
11. Clandinin MT, Van Aerde JE, Parrott A, Field CJ, Euler AR, Lien EL (1997) Assessment of the efficacious dose of arachidonic and docosahexaenoic acids in preterm infant formulas: fatty acid composition of erythrocyte membrane lipids. Pediatr Res 42:819–825
12. Hoffman DR, Birch EE, Birch DG, Uauy R, Castaneda YS, Lapus MG, et al. (2000) Impact of early dietary intake and blood lipid composition of long-chain polyunsaturated fatty acids on later visual development. J Pediatr Gastroenterol Nutr 31:540–553
13. Hoffman DR, Wheaton DK, James KJ, Tuazon M, Diersen-Schade DA, Harris CL, et al. (2006) Docosahexaenoic acid in red blood cells of term infants receiving two levels of long-chain polyunsaturated fatty acids. J Pediatr Gastroenterol Nutr 42:287–292
14. Birch EE, Hoffman DR, Uauy R, Birch DG, Prestidge C (1998) Visual acuity and the essentiality of docosahexaenoic acid and arachidonic acid in the diet of term infants. Pediatr Res 44:201–209
15. Birch EE, Garfield S, Hoffman DR, Uauy R, Birch DG (2000) A randomized controlled trial of early dietary supply of long-chain polyunsaturated fatty acids and mental development in term infants. Dev Med Child Neurol 42:174–181
16. Birch EE, Hoffman DR, Castaneda YS, Fawcett SL, Birch DG, Uauy RD (2002) A randomized controlled trial of long-chain polyunsaturated fatty acid supplementation of formula in term infants after weaning at 6 wk of age. Am J Clin Nutr 75:570–580
17. Hoffman DR, Birch EE, Castaneda YS, Fawcett SL, Wheaton DH, Birch DG, et al. (2003) Visual function in breast-fed term infants weaned to formula with or without long-chain polyunsaturates at 4 to 6 months: a randomized clinical trial. J Pediatr 142:669–677
18. Morale SE, Hoffman DR, Castaneda YS, Wheaton DH, Burns RA, Birch EE (2005) Duration of long-chain polyunsaturated fatty acids availability in the diet and visual acuity. Early Hum Dev 81:197–203
19. Innis SM, Adamkin DH, Hall RT, Kalhan SC, Lair C, Lim M, et al. (2002) Docosahexaenoic acid and arachidonic acid enhance growth with no adverse effects in preterm infants fed formula. J Pediatr 140:547–554
20. Clandinin MT, Van Aerde JE, Merkel KL, Harris CL, Springer MA, Hansen JW, et al. (2005) Growth and development of preterm infants fed infant formulas containing docosahexaenoic acid and arachidonic acid. J Pediatr 146:461–8
21. AAP (1998) Soy protein-based formulas: recommendations for use in infant feeding. Pediatr 101:148–153
22. Merritt R, Jenks B (2004) Safety of soy-based infant formulas containing isoflavones: the clinical evidence. J Nutr 134:1220S–1224S
23. Severity scoring of atopic dermatitis: the SCORAD index (1993) Consensus report of the European task force on atopic dermatitis. Dermatology 186:23–31
24. Ogden CL, Kuczmarski RJ, Flegal KM, Mei Z, Guo S, Wei R, et al. (2002) Centers for disease control and prevention 2000 growth charts for the United States: improvements to the 1977 national center for health statistics version. Pediatrics 109:45–60
25. American Academy of Pediatrics (1988) Clinical testing of infant formulas with respect to nutritional suitability for term infants. Report to the FDA. Committee on Nutrition. AAP Elk Grove Village, IL
26. Fomon S, Ziegler E (1992) Isolated soy protein in infant feeding. In: Steinke F, Waggle D, Volgarev M (eds) New protein foods in human health: nutrition, prevention, and therapy. CRC, Boca Raton
27. Churella HR, Borschel MW, Thomas MR, Breen M, Jacobs J (1994) Growth and protein status of term infants fed soy protein formulas differing in protein content. J Am Coll Nutr 13:262–267
28. Lasekan JB, Ostrom KM, Jacobs JR, Blatter MM, Ndife LI, Gooch WM 3rd, et al. (1999) Growth of newborn, term infants fed soy formulas for 1 year. Clin Pediatr (Phila) 38:563–571
29. Strom BL, Schinnar R, Ziegler EE, Barnhart KT, Sammel MD, Macones GA, et al. (2001) Exposure to soy-based formula in infancy and endocrinological and reproductive outcomes in young adulthood. JAMA 286:807–814
30. Seppo L, Korpela R, Lonnerdal B, Metsaniitty L, Juntunen-Backman K, Klemola T, et al. (2005) A follow-up study of nutrient intake, nutritional status, and growth in infants with cow milk allergy fed either a soy formula or an extensively hydrolyzed whey formula. Am J Clin Nutr 82:140–145
31. Osborn DA, Sinn J (2006) Soy formula for prevention of allergy and food intolerance in infants. Cochrane Database Syst Rev 4:CD003741
32. Auestad N, Montalto MB, Hall RT, Fitzgerald KM, Wheeler RE, Connor WE, et al. (1997) Visual acuity, erythrocyte fatty acid composition, and growth in term infants fed formulas with long chain polyunsaturated fatty acids for one year. Ross pediatric lipid study. Pediatr Res 41:1–10
33. Auestad N, Halter R, Hall RT, Blatter M, Bogle ML, Burks W, et al. (2001) Growth and development in term infants fed long-chain polyunsaturated fatty acids: a double-masked, randomized, parallel, prospective, multivariate study. Pediatrics 108:372–381
34. Birch EE, Castaneda YS, Wheaton DH, Birch DG, Uauy RD, Hoffman DR (2005) Visual maturation of term infants fed long-chain polyunsaturated fatty acid-supplemented or control formula for 12 mo. Am J Clin Nutr 81:871–879

Lipids (2008) 43:37–43
DOI 10.1007/s11745-007-3129-2

ORIGINAL ARTICLE

Oral Administration of Dihomo-γ-Linolenic Acid Prevents Development of Atopic Dermatitis in NC/Nga Mice

**H. Kawashima · N. Tateishi · A. Shiraishi ·
N. Teraoka · T. Tanaka · A. Tanaka ·
H. Matsuda · Y. Kiso**

Received: 24 August 2007 / Accepted: 17 October 2007 / Published online: 6 November 2007
© AOCS 2007

Abstract Disorders of the metabolism of essential fatty acids (EFAs) are related to atopic dermatitis (AD). Concentrations of dihomo-γ-linolenic acid (DGLA), an EFA, in the serum of AD patients are lower than those in healthy volunteers. Recently we developed a fermented DGLA oil, and examined whether oral administration of DGLA prevents development of dermatitis in NC/Nga mice, which spontaneously develop human AD-like skin lesions. NC/Nga mice were fed a diet either containing or not containing DGLA for 8 weeks under in air-uncontrolled conventional circumstances. Clinical skin severity scores were significantly lower in mice fed DGLA than in mice not fed it. Scratching behavior and plasma total IgE levels were also reduced in the DGLA group, in association with histological improvement. DGLA suppressed clinical severity of skin lesions dose-dependently, with an increase in DGLA contents in phospholipids of skin, spleen, and plasma. Discontinuation of DGLA administration resulted in the onset of dermatitis and a decrease in DGLA contents in skin, spleen, and plasma. These findings indicate that oral administration of DGLA effectively prevents the development of AD in NC/Nga mice, and that DGLA in phospholipids is a compound of key importance in the development and prevention of dermatitis.

Keywords Atopic dermatitis · NC/Nga · Dihomo-γ-linolenic acid · DGLA · Arachidonic acid · Essential fatty acid

Introduction

Atopic dermatitis (AD) is a chronic and relapsing skin disorder associated with allergic inflammation, and is related to disorders of polyunsaturated fatty acid metabolism. Among these fatty acids, dihomo-γ-linolenic acid (DGLA, 8,11,14-eicosatrienoic acid) may be a compound of key importance, since DGLA concentration in the serum of AD patients was significantly lower than in that of healthy volunteers [1], and DGLA is metabolized to anti-inflammatory eicosanoids such as those of the prostaglandin (PG) 1-series and 15-hydroxyeicosatrienoic [2–4]. With the goal of increasing the DGLA level in AD patients, clinical trials have been performed using oil containing γ-linolenic acid (GLA, 6,9,12-octadecatrienoic acid), the precursor of DGLA, and some have found that GLA was effective for AD [5, 6]. However, GLA was sometimes not effectively converted to DGLA in AD patients, resulting in insufficient increases in DGLA concentration and an insufficient therapeutic effect [7, 8].

Although DGLA exists widely in the human body and daily animal-source foods, it had not been available previously. Therefore, there were only a few pioneering studies in which DGLA ethyl ester were fed to rats and rabbits [9, 10]. Recently, a new fermentation technique using an oleaginous fungus *Mortierella alpina* has recently been established, enabling industrial production of DGLA-containing oil [11].

H. Kawashima (✉) · N. Tateishi · A. Shiraishi ·
N. Teraoka · T. Tanaka · Y. Kiso
Institute for Health Care Science, Suntory Ltd,
1-1-1, Wakayamadai, Shimamoto-cho,
Mishima-gun, Osaka 618-8503, Japan
e-mail: hiroshi_kawashima@suntory.co.jp

A. Tanaka · H. Matsuda
Graduate School,
Institute of Symbiotic Science and Technology,
Tokyo University of Agriculture and Technology,
Tokyo, Japan

DGLA oil consists almost entirely of triglycerides, in which the proportion of DGLA is approximately 40%. As expected, DGLA contents of liver and serum were increased much more effectively in rats fed DGLA oil than in those fed GLA oil [12]. These findings suggest the possibility that oral intake of DGLA may increase DGLA contents in skin and prevent AD. In the present study, the effects of oral administration of DGLA on AD were examined using NC/Nga mice, which spontaneously develop AD-like skin lesions that are pathologically and immunologically quite similar to those found in human AD [13–15]. We also determined the DGLA content in skin, and examined whether it is related to the severity of AD in NC/Nga mice.

Experimental Procedures

Mice

We used male and female NC/Nga mice maintained in air-uncontrolled conventional circumstances. These mice manifested severe skin lesions very similar to those of human AD [13]. The mice were fed a defined diet with or without DGLA from 5 to 12 weeks of age. The care and handling of the animals were in accordance with the 'Tokyo University of Agriculture and Technology Animal Experiment Guidelines, April 2001'.

Diet and Reagents

The mice were given a pellet diet and water ad libitum. The diet was a modified AIN-76A containing 5% (w/w) lipids, which consisted of a mixture of DGLA oil, corn oil, lard, or olive oil. DGLA oil is a triglyceride oil extracted from the fungus *Mortierella alpina*. In brief, the oil was extracted from the biomass of *M. alpina* obtained by fermentation [11], and purified by traditional edible oil refining procedures to obtain an oil containing approximately 40% DGLA. The fatty acid composition of each diet administered is shown in Table 1. Fatty acid compositions of diets were adjusted to be similar to each other, for the amounts of total $n-6$ fatty acids (LA + GLA + DGLA) to be approximately 40%. The DGLA content in DGLA diet was 0.6 g/kg diet, while DGLA contents in the high-, medium-, low-, and very-low-DGLA diets were 0.5, 0.24, 0.13, and 0.06 g/kg diet, respectively. Mice ($n = 7$) were fed diet for 8 weeks, from 5 to 12 weeks of age. In the discontinuation experiment, mice were fed high-DGLA diet from 5 to 10 weeks of age, and the control or high-DGLA diet for the final 2 weeks, i.e., from 66 to 79 days of age. All chemicals used were purchased from Sigma-Aldrich, unless otherwise indicated. The experimental designs of the diets and the digestion period are summarized in Fig. 1.

Table 1 Fatty acid composition of lipids in each experimental diet

Diet	Fatty acid composition (%)[a]						
	16:0	18:0	18:1	18:2	18:3	20:3	Others
Control	15.1	6.4	34.5	39.5	nd	nd	4.5
DGLA	14.9	6.3	32.8	26.9	1.0	12.5	5.6
High-DGLA	15.8	6.2	32.3	28.4	0.7	10.5	6.1
Medium-DGLA	16.0	6.3	33.0	34.6	0.4	4.8	4.9
Low-DGLA	15.8	6.3	31.3	39.7	0.6	2.5	3.8
Very-low-DGLA	15.9	6.4	32.7	39.8	0.5	1.2	3.5

nd not detected

[a] Fatty acids are indicated by number of carbons:number of double bond(s): *16:0* palmitic acid, *18:0* stearic acid, *18:1* oleic acid, *18:2* linoleic acid, *18:3* γ-linolenic acid, *20:3* dihomo-γ-linolenic acid. Others include α-linolenic acid and small amounts of saturated fatty acids

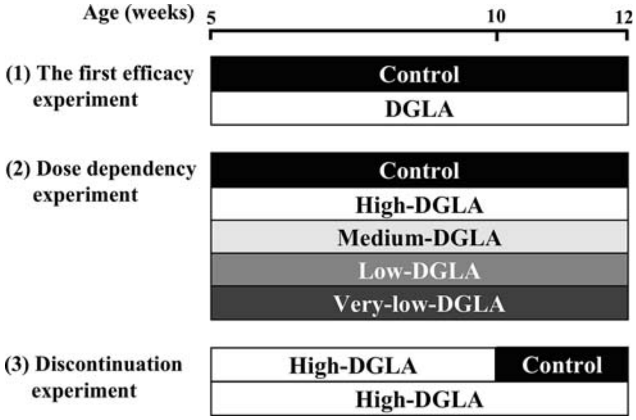

Fig. 1 Experimental designs of the diets and the digestion period. The fatty acid composition of each diet is indicated in Table 1

Clinical Skin Severity Score and Scratching Analysis

Clinical features of dermatitis were scored two to four times a week, from 10 to 12 weeks of age, according to criteria described previously [13], which consisted of five major clinical signs and symptoms of AD: itching, erythema/hemorrhage, edema, excoriation/erosion, and scaling/dryness. The scratching behavior of the mice was recorded and analyzed at 10 and 12 weeks of age using a SCLABA system (Noveltec Inc., Kobe, Japan), a novel analyzer that quantifies the scratching behavior of mice for a fixed period of time [16]. Scratching behavior was quantified as the frequency and duration of scratching per 20 min in the double-blind evaluation.

Histological Examination and Plasma IgE Determination

Dorsal skin specimens were fixed in 10% formalin. The fixed specimens were embedded in paraffin, and sliced sections were stained with hematoxylin and eosin. Total plasma IgE was measured by a sandwich ELISA (Yamasa Co., Chiba, Japan).

Fatty Acid Analysis

Dorsal skin, spleen, and plasma were stored in a freezer (−80 °C), and analyzed as soon as possible. Lipids in these specimens were extracted by chloroform/methanol according to the Folch methods [17], and separated into neutral lipids and phospholipids by thin-layer chromatography with silica gel 60 (Merck, Darmstadt). The solvent system consisted of hexane/diethyl ether (7:3, by vol). Fatty acid residues in the phospholipid fractions were analyzed as described previously [18]. In brief, each fraction with an additional internal standard (pentadecanoic acid) was incubated in methanolic HCl at 50 °C for 3 h for transmethylation of fatty acid residues. Fatty acid methyl esters were extracted with *n*-hexane and analyzed by capillary gas-liquid chromatography.

Statistical Analyses

The clinical skin severity scores were analyzed by two-way analyses of variance (ANOVA), and followed by Dunnett multiple comparison test. The other data were analyzed by Dunnett multiple comparison test or two-tailed unpaired Student's *t*-test.

Results

Clinical Severity of Skin Lesions of NC/Nga Mice Fed DGLA

Neither body weight nor weight gain differed between the two groups (data not shown). Clinical signs of dermatitis were effectively prevented by oral intake of DGLA (Fig. 2a, b). Although the score gradually increased, and reached 9.14 ± 1.03 (mean ± SEM) at day 84 in control mice fed no DGLA, it seldom increased and was in fact

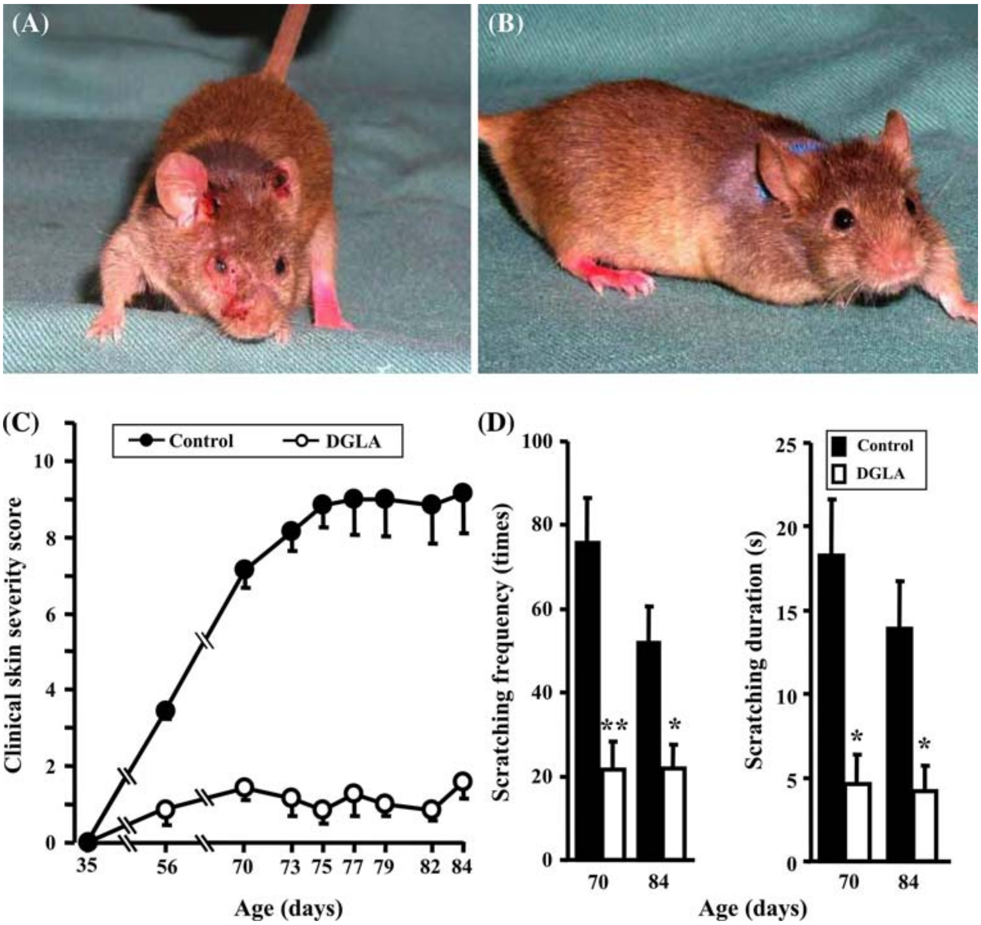

Fig. 2 Prevention of dermatitis by DGLA in NC/Nga mice. Typical overall status of control (**a**) and DGLA-fed (**b**) mice at 84 days of age (Blue pigment was applied to quantify scratching.) (**c**) Clinical skin severity scores for control (*closed circles*) and DGLA-fed (*open circles*) mice. (**d**) Frequency of scratching per 20 min of control (*closed bars*) and DGLA-fed (*open bars*) mice. Each value represents the mean ± SEM of seven mice. $^*P < 0.05$, $^{**}P < 0.01$ versus control

significantly lower in mice fed DGLA (1.57 ± 0.43 at day 84) (Fig. 2c) ($P < 0.01$ by ANOVA). Since itching is one of the most important unpleasant symptoms of AD, we attempted to quantify itching by analyzing the scratching behavior using an SCLABA system. Scratching behaviors were recorded as frequency and duration of scratching per 20 min, and were significantly reduced at 70 and 84 days of age in mice fed DGLA (Fig. 2d). Histological examination at 84 days of age revealed that oral intake of DGLA prevented epidermal hyperplasia, dermal edema, and infiltration of inflammatory cells in dorsal skin (Fig. 3a, b). At 84 days of age, total plasma IgE levels were very high in control mice (64.2 ± 15.1 µg/ml) and significantly lower in mice fed DGLA (15.6 ± 1.4 µg/ml).

Dose-dependency of Effects of DGLA and Incorporation of DGLA in Skin

Neither body weight nor weight gain differed among groups (data not shown). The decrease in clinical severity of skin lesions caused by DGLA was dose-dependent (Fig. 4), and the clinical skin severity was significantly reduced only in the high-DGLA group ($P < 0.05$ by ANOVA). Scores were relatively low in the medium- and low-DGLA groups, though they were not significantly reduced. The score in the very-low-DGLA group was almost the same as that in the control group.

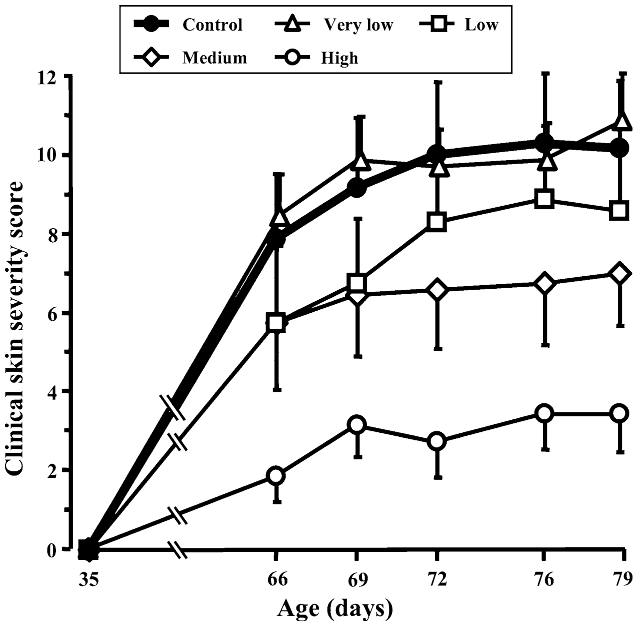

Fig. 4 Clinical skin severity scores of mice in the control (*closed circles*) and high- (*open circles*), medium- (*open rhombuses*), low- (*open squares*) and very-low-DGLA (*open triangles*) groups. Each value represents the mean ± SEM of seven mice

We quantified fatty acids in phospholipids of the dorsal skin to determine whether the DGLA content in skin was increased by oral intake of DGLA (Fig. 5). The DGLA content in phospholipids was 0.75 ± 0.10% (mean ± SEM)

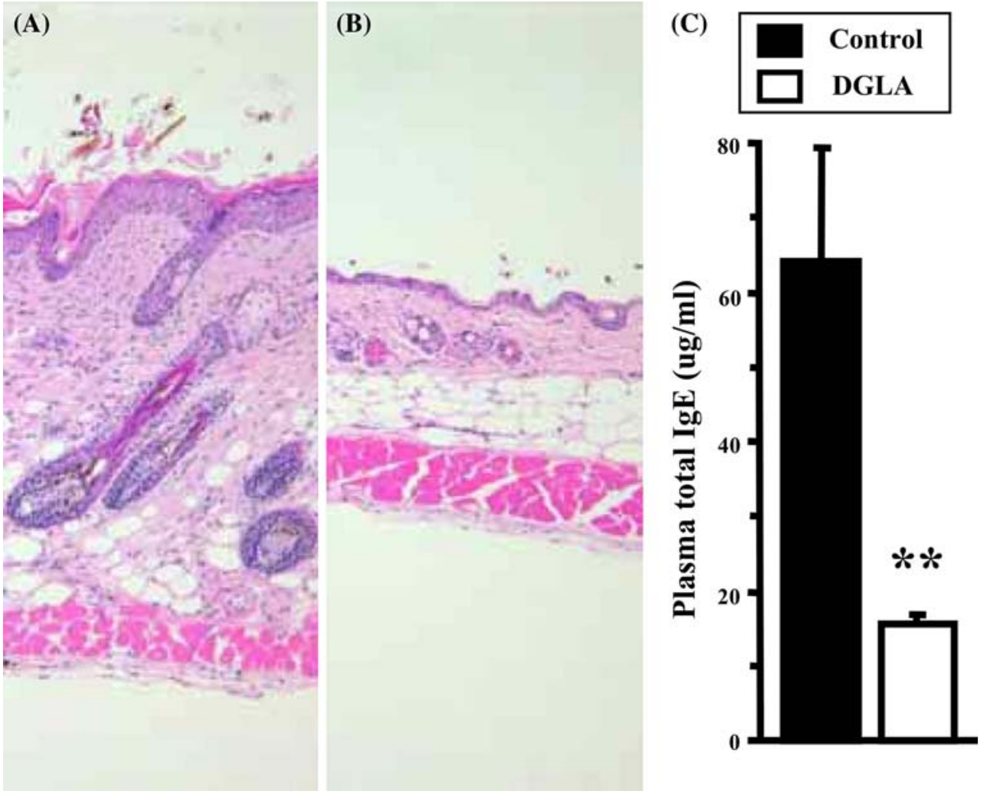

Fig. 3 Prevention by DGLA of histological skin lesions and elevation of total plasma IgE levels in NC/Nga mice. Hematoxylin and eosin-stained sections of dorsal skin specimens of control (**a**) and DGLA-fed (**b**) mice (×100). **c** Total plasma IgE levels of control (*closed bars*) and DGLA-fed (*open bars*) mice. Each value represents the mean ± SEM of seven mice. **$P < 0.01$ versus control

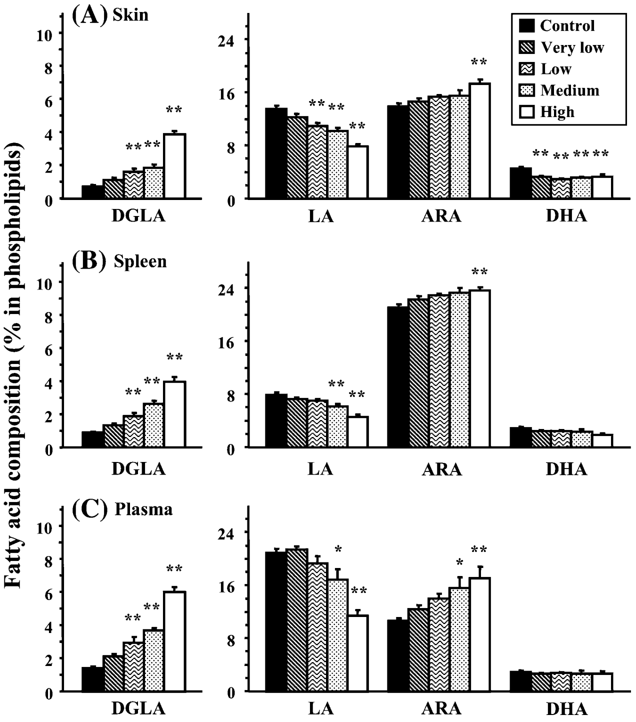

Fig. 5 Fatty acid composition of phospholipids of dorsal skin (**a**), spleen (**b**), and plasma (**c**) in control (*closed bars*) and very-low- (*hatched bars*), low- (*wavy-lined bars*), medium- (*gray bars*), and high-DGLA (*open bars*) groups. Each value represents the mean ± SEM of seven mice. *$P < 0.05$, **$P < 0.01$ versus control

of total fatty acids in the control group, and increased dose-dependently to reach 3.89 ± 0.20% in the high-DGLA group. The ARA content was 13.95 ± 0.48% in the control group, and also increased gradually to reach 17.45 ± 0.58% in the high-DGLA group. The content of LA, which was decreased in diets with DGLA supplementation, decreased dose-dependently with the dose of DGLA. The proportions of other fatty acids in skin were unchanged by DGLA ingestion (data not shown). In the spleen, fatty acid composition differed from that in skin, e.g., the proportion of ARA was relatively high. However, the effects of DGLA ingestion were similar to those in skin; the DGLA content increased drastically, the ARA content increased slightly, the LA content decreased, and the DHA content remained unchanged with DGLA ingestion. The effects of DGLA on fatty acids in plasma were also similar, though the ARA level was rather low in the control group and increased drastically with an increase in the DGLA content in the diet.

Effects of Discontinuation of DGLA Ingestion

Neither body weight nor weight gain differed among the groups (data not shown). The clinical skin severity score in the discontinuation group was low at first, but increased soon after and was significantly higher than that in the continuation group after day 72 (Fig. 6) ($P < 0.05$ by ANOVA). DGLA contents in skin, spleen, and plasma were significantly decreased in the discontinuation group, to almost the same level as in control mice fed no DGLA throughout the experiment. The LA content increased significantly, while changes in ARA and DHA levels were rather small (Fig. 7).

Discussion

Oral administration of DGLA markedly suppressed the development of dermatitis in NC/Nga mice under air-uncontrolled conventional circumstances. DGLA reduced not only the clinical skin severity of dermatitis, but also scratching behavior and plasma total IgE levels. DGLA decreased the clinical severity of skin lesions in dose-dependent fashion, with an increase in DGLA contents in phospholipids of skin, spleen, and plasma. Furthermore, discontinuation of DGLA administration resulted in the onset of dermatitis and the decrease in DGLA contents in skin, spleen, and plasma. These findings show that oral administration of DGLA is very effective in preventing the development of dermatitis in NC/Nga mice, and that DGLA in phospholipids is a compound of key importance in both the development and prevention of dermatitis.

Although the efficacy of DGLA in preventing dermatitis was strong, the mechanism by which it does so is unclear.

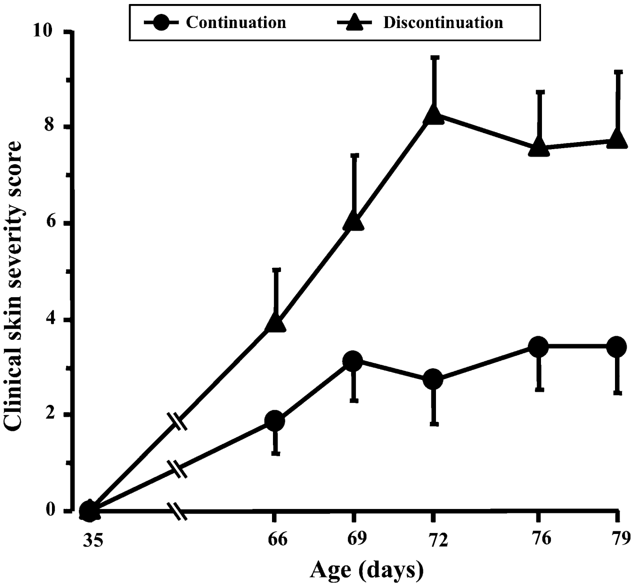

Fig. 6 Clinical skin severity scores of mice fed DGLA until day 79 (continuation group, *closed circles*), or fed DGLA until day 66 and no DGLA from days 66 to 79 (discontinuation group, *closed triangles*). Each value represents the mean ± SEM of seven mice

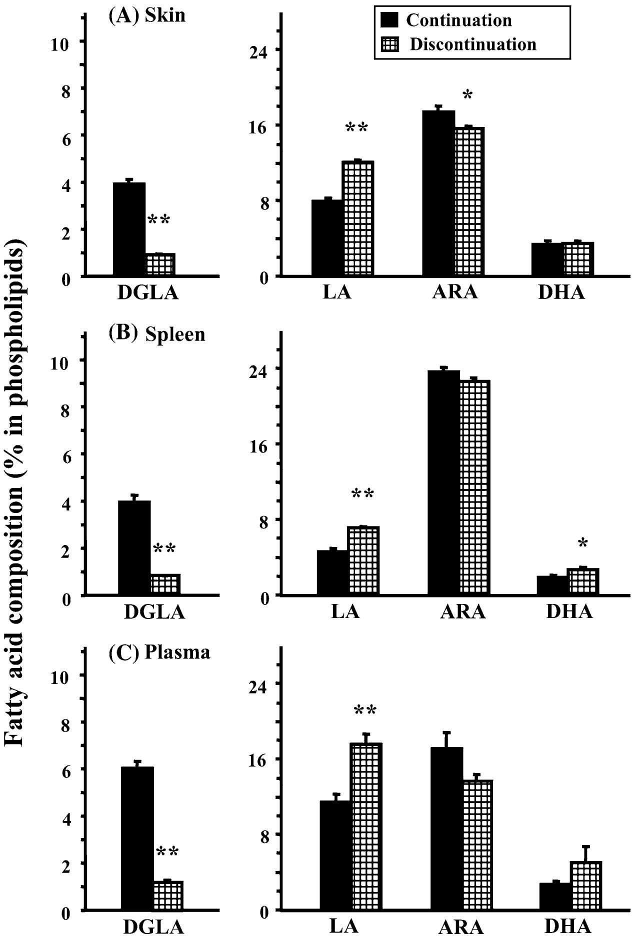

Fig. 7 Fatty acid composition of phospholipids of dorsal skin (**a**), spleen (**b**), and plasma (**c**) in the continuation (*closed bars*) and discontinuation (*lined bars*) groups. Each value represents the mean ± SEM of seven mice. $*P < 0.05$, $**P < 0.01$ versus control

One of mediators related to the effects of DGLA may be the unique eicosanoids derived from DGLA, since various eicosanoids have been found to affect the immune system. PGE1 and 15-hydroxyeicosatrienoic acid, which have unique functions, including anti-inflammatory effects [3] and inhibition of leukotriene B_4 production [5], are candidate mediators of the effects of DGLA. Indeed, both were detected in the skin in guinea pigs fed GLA [19]. It will be of great interest to determine whether these eicosanoids are involved in mediating the prevention of dermatitis in NC/Nga mice. The existence and involvement of the candidate mediators in various tissues were examined at the next stage.

DGLA was incorporated and increased in contents not only in skin and plasma, but also in the spleen. In a previous study, DGLA levels were increased in liver and serum in rats fed DGLA [12]. These findings suggest that oral administration of DGLA increases systemic concentrations of DGLA. Although the increase in DGLA in skin is clearly of greatest importance, systemic increases in DGLA concentration may have systemic effects as well, such as the suppression of the plasma total IgE level. Determination of fatty acid profiles showed that ARA contents in skin, spleen, and plasma were also increased dose-dependently by DGLA, and were higher in the high-DGLA group, in which AD was prevented the most effectively. This indicates that a portion of DGLA must be metabolized to ARA in mice, which is thought to be reasonable because DGLA is the direct precursor of ARA in the biosynthetic pathway of essential fatty acids. However, the increase in ARA did not trigger allergy or inflammation here, although $n - 6$ fatty acids are reported to trigger inflammation [20]. This is interesting evidence that the increase in omega-6 fatty acids does not always induce inflammation.

Since NC/Nga mice are widely considered to be a suitable model for human AD, oral administration of DGLA may be useful for preventing human AD. If this DGLA oil is useful, it must be ingested because its DGLA content is high, i.e., approximately 40% of this oil consists of DGLA. Another important finding of the present study is that both the DGLA content in skin and efficacy in prevention of dermatitis were related to the DGLA content in plasma. This suggests that the DGLA content in skin and expected efficacy in preventing dermatitis can be estimated by monitoring the DGLA content in plasma. The kinetics of absorption of DGLA in humans needs to be determined.

In this study, we have demonstrated the marked efficacy of DGLA in preventing dermatitis in NC/Nga mice. Human studies and examination of the mechanisms by which DGLA exerts these effects are needed.

Acknowledgments This research was supported in part by the New Energy and Industrial Technology Development Organization, Japan.

References

1. Manku MS, Horrobin DF, Morse N, Kyte V, Jenkins K (1982) Reduced levels of prostaglandin precursors in the blood of atopic patients. Prostaglandins Leukot Med 9:615–628
2. Dooper MM, Wassink L, M'Rabet L, Graus YM (2002) The modulatory effects of prostaglandin-E on cytokine production by human peripheral blood mononuclear cells are independent of the prostaglandin subtype. Immunology 107:152–159
3. Zurier RB, Quagliate F (1971) Effect of prostaglandin E1 on adjuvant arthritis. Nature 234:304–305
4. Iversen L, Fogh K, Kragballe K (1992) Effect of dihomogammalinolenic acid and its 15-lipoxygenase metabolite on eicosanoid metabolism by human mononuclear leukocytes in vitro: selective inhibition of the 5-lipoxygenase pathway. Arch Dermatol Res 284:222–226
5. Wright S, Burton JL (1982) Oral evening-primrose-seed oil improves atopic eczema. Lancet 2:1120–1122
6. Morse PF, Horrobin DF, Manku MS, Stewart JC, Allen R, Littlewood S, Wright S, Burton J, Gould DJ, Holt PJ (1989) Meta-analysis of placebo-controlled studies of the efficacy of Epogam

in the treatment of atopic eczema. Relationship between plasma essential fatty acid changes and clinical response. Br J Dermatol 121:75–90

7. Henz BM, Jablonska S, van de Kerkhof PC, Stingl G, Blaszczyk M, Vandervalk PG, Veenhuizen R, Muggli R, Raederstorff D (1999) Double-blind, multicentre analysis of the efficacy of borage oil in patients with atopic eczema. Br J Dermatol 140:685–688
8. Takwale A, Tan E, Agarwal S, Barclay G, Ahmed I, Hotchkiss K, Thompson JR, Chapman T, Berth-Jones J (2003) Efficacy and tolerability of borage oil in adults and children with atopic eczema: randomised, double blind, placebo controlled, parallel group trial. BMJ 327:1385
9. Danon A, Heimberg M, Oates JA (1975) Enrichment of rat tissue lipids with fatty acids that are prostaglandin precursors. Biochim Biophys Acta 388:318–330
10. Knapp HR, Oelz O, Whorton AR, Oates JA (1978) Effects of feeding ethyl-dihomo-gamma-linolenate on rabbit renomedullary lipid composition and prostaglandin production in vitro. Lipids 13:804–808
11. Kawashima H, Akimoto K, Higashiyama K, Fujikawa S, Shimizu S (2000) Industrial production of dihomo-γ-linolenic acid by a $\Delta5$ desaturase-defective mutant of *Mortierella alpina* 1S-4 fungus. J Am Oil Chem Soc 77:1135–1138
12. Umeda-Sawada R, Fujiwara Y, Ushiyama I, Sagawa S, Morimitsu Y, Kawashima H, Ono Y, Kiso Y, Matsumoto A, Seyama Y (2006) Distribution and metabolism of dihomo-gamma-linolenic acid (DGLA, 20:3*n*-6) by oral supplementation in rats. Biosci Biotechnol Biochem 70:2121–2130
13. Matsuda H, Watanabe N, Geba GP, Sperl J, Tsudzuki M, Hiroi J, Matsumoto M, Ushio H, Saito S, Askenase PW, Ra C (1997) Development of atopic dermatitis-like skin lesion with IgE hyperproduction in NC/Nga mice. Int Immunol 9:461–466
14. Tanaka A, Muto S, Jung K, Itai A, Matsuda H (2007) Topical application with a new NF-κB inhibitor improves atopic dermatitis in NC/NgaTnd Mice. J Invest Dermatol 127:855–863
15. Sawada J, Morita H, Tanaka A, Salminen S, He F, Matsuda H (2007) Ingestion of heat-treated Lactobacillus rhamnosus GG prevents development of atopic dermatitis in NC/Nga mice. Clin Exp Allergy 37:296–303
16. Orito K, Chida Y, Fujisawa C, Arkwright PD, Matsuda H (2004) A new analytical system for quantifying scratching behaviour in mice. Br J Dermatol 150:33–38
17. Folch J, Lees M, G.H.S. Stanley GHS (1957) A simple method for the isolation and purification of total lipids from animal tissues. J Biol Chem 226:497–509
18. Sakuradani E, Kobayashi M, Shimizu S (1999) $\Delta9$-Fatty acid desaturase from arachidonic acid-producing fungus: unique gene sequence and its heterologous expression in a fungus. Eur J Biochem 260:208–216
19. Miller CC, McCreedy CA, Jones AD, Ziboh VA (1988) Oxidative metabolism of dihomogammalinolenic acid by guinea pig epidermis: evidence of generation of anti-inflammatory products. Prostaglandins 35:917–938
20. Calder PC (2006) Polyunsaturated fatty acids and inflammation. Prostaglandins Leukot Essent Fatty Acids 75:197–202

Lipids (2008) 43:45–53
DOI 10.1007/s11745-007-3128-3

ORIGINAL ARTICLE

The Percentage of n-3 Highly Unsaturated Fatty Acids in Total HUFA as a Biomarker for Omega-3 Fatty Acid Status in Tissues

Ken D. Stark

Received: 24 August 2007 / Accepted: 16 October 2007 / Published online: 6 November 2007
© AOCS 2007

Abstract A blood biomarker of omega-3 fatty acid intake and tissue status could serve as a modifiable risk factor for cardiovascular disease. The percentage of omega-3 highly unsaturated fatty acid (HUFA $\geq$ 20 carbons and $\geq$3 double bonds) in the total HUFA pool (the n-3 HUFA score) was examined as a potential blood biomarker of omega-3 fatty acids in tissues. The fatty acid composition of total lipid extracts (TLE) and phospholipid (PL) fractions were determined for plasma and erythrocytes samples of human subjects (n = 20) and the n-3 HUFA score and the sum of eicosapentaenoic acid (EPA) and docosahexaenoic acid (DHA) were compared. Omega-3 fatty acids in blood and tissues of rats (n = 31) and pigs (n = 48) were also determined and the associations were compared. The n-3 HUFA score is more consistent across plasma and erythrocytes, with strong correlations between TLE and PL in plasma (r = 0.93) and erythrocytes (r = 0.94). The n-3 HUFA score was less variable and blood levels correlated strongly with various animal tissues. The n-3 HUFA score is a useful blood biomarker that does not require the isolation of the PL class thereby supporting high throughput analyses. The strength of association between the n-3 HUFA score and disease risk needs to be examined.

Keywords Omega-3 fatty acids · Docosahexaenoic acid · Eicosapentaenoic acid · Biomarker · Plasma · Erythrocyte

Introduction

Dietary supplementation with omega-3 fatty acids from fish oil has been demonstrated to significantly reduce the risk of death from coronary heart disease (CHD) and sudden cardiac death in secondary prevention trials [1]. Higher dietary intake and higher blood levels of omega -3 fatty acids, specifically eicosapentaenoic acid (20:5n-3, EPA) and docosahexaenoic acid (22:6n-3, DHA), are associated with decreased risk of sudden cardiac death in western populations [2–4]. The mechanism of the prevention of sudden cardiac death has not been fully elucidated but is likely related to anti-arrhythmic [5] and lowered resting heart rates [6]. EPA and DHA mediated triacylglycerol-lowering, anti-hypertensive, and anti-inflammatory effects may also reduce CHD risk [7, 8]. This mounting evidence has led to several recommendations for the intake of omega-3 fatty acids for optimal heart health [9].

The fatty acid composition of adipose tissue is considered to be the best choice for the assessment of long-term dietary intake of fatty acids due to a slow turnover rate, with blood fractions reflecting shorter-term intakes [10]. Given the invasiveness of adipose tissue biopsies, a blood based biomarkers would be preferred for large observational and clinical trials. Recently it has been proposed that the level of EPA + DHA in erythrocyte membranes (the Omega-3 Index) could be used as a new risk factor for CHD mortality [11]. The selection of the Omega-3 Index over other blood based biomarkers is based largely on a single study demonstrating a significant correlation between erythrocytes and cardiac tissue [12] as compared with plasma but other measures of assessing these omega-3 long-chain polyunsaturated fatty acids (LCPUFA) or highly unsaturated fatty acids (HUFA, $\geq$20 carbons and $\geq$3 carbon-carbon, double bonds) in blood do exist and are

---

K. D. Stark (✉)
The Laboratory of Nutritional and Nutraceutical Research,
Department of Kinesiology, University of Waterloo, Waterloo,
ON, Canada N2L 3G1
e-mail: kstark@uwaterloo.ca

untested. In particular, the use of the percentage of omega-3 HUFA in the total HUFA pool as a biomarker of omega-3 fatty acid status has been defined previously [13] and has been demonstrated to have the potential to have smaller coefficient of variation and better correlate with plasma and erythrocytes [14]. This is based on the competition between these fatty acids for the sn-2 position of phospholipids (PL) and the use of the term HUFA over LCPUFA tends to emphasize the important physiological difference from other PUFA in addition to the longer chemical carbon chain length. The HUFA pool is largely dominated by arachidonic acid (AA, 20:4n-6) in Western diets. Increased omega-3 fatty acid intake increases tissue levels of EPA and DHA and decreases other HUFA, an antagonistic effect that was observed originally by Mohrhauer and Holman [15].

In the present study, the use of EPA + DHA as a marker for omega-3 fatty acid status is compared to the use of the percentage of omega-3 HUFA in total HUFA (n-3 HUFA score) in human blood samples. As these biomarkers have the potential to be developed into a risk factor for chronic disease, total lipid extracts (TLE) and PL fractions were examined. A fatty acid risk factor derived from TLE would be advantageous as it would facilitate high throughput analyses to a much greater extent than a specific lipid fraction such as PL. The ability of omega-3 fatty acid blood biomarkers to correlate with omega-3 fatty acid levels in various tissues was also examined in rat and in pig tissues.

Methods

Human Blood Samples

Blood samples were obtained at Wayne State University in Detroit, MI as previously described [16]. The study was approved by the Wayne State University Human Investigations Committee and informed consent was obtained from all participants. Briefly, fasting blood samples (15 ml) were collected by venipuncture into heparinized tubes. Samples were kept cold (4 °C) until centrifuged (5 min × 2,000*g*) to separate plasma from erythrocytes and each fraction was frozen and stored at −75 °C until analysis. Women with known fatty acid metabolism disorders and diabetics were excluded from the study. Twenty-five samples from non-pregnant women were analyzed. TLE were prepared from plasma [17] and erythrocyte [18] with an internal standard (23:0, or 22:3n-3; Nu-Check Prep, Elysian, MN, USA). An aliquot of TLE from each sample was taken and PL fractions were isolated by thin layer chromatography using a mixture of heptane/diethyl ether glacial acetic acid (60:40:2 by volume) as described previously [19]. Both the TLE and PL preparations were then methylated with boron trifluoride in methanol (14% wt./vol.; Alltech Assoc., Deerfield, IL, USA) [20]. The fatty acid methyl esters were analyzed by capillary gas chromatography according to Salem et al. [21] on an Agilent 6890N gas chromatograph (Agilent, Palo Alto, CA, USA) with a 0.25 mm × 30 m DB-FFAP column (J&W Scientific, La Palma, CA, USA).

Rat Tissue Samples

Animal tissues were obtained from male Long-Evans rats raised on diets either adequate or deficient in omega-3 fatty acids as described previously [22–24]. Experimental procedures were approved by the Animal Care and Use Committee of the National Institute on Alcohol Abuse and Alcoholism, NIH. Briefly, pregnant (3-day gestation) Long Evans rats were purchased from Charles River (Portage, MI, USA) and placed on an essential fatty acid adequate diet and raised in an animal facility under conventional conditions. At 2-day post-natal males pups from 10 litters were randomly allocated to one of five groups containing ten pups each. The control group was allowed to be dam-reared while the other four groups were hand-reared on artificial milk. The fat content of the artificial milk consisted of hydrogenated coconut oil/medium chain triglyceride fat supplemented with ethyl esters of specific fatty acids (Nu-Check Prep) including 18:1n-9 ethyl ester, 18:2n-6 ethyl ester, 22:6n-3 ethyl ester, and 22:5n-6 ethyl ester. All four of the milks contained 18:2n-6 while the others were supplemented with 1% DHA, 1% docosapentaenoic acid (DPA, 22:5n-6), 1% DHA : DPA (2:1). Therefore, three of the diets (including dam-reared) were adequate in omega-3 fatty acid content, while two were omega-3 fatty acid deficient. Rats were raised and eventually transferred to a pelleted diet containing the same fat profile. The adult male rats were then sacrificed at approximately 20 weeks of age. Plasma, erythrocytes, liver, heart, brain, and adipose tissues were collected following decapitation and frozen at −80 °C until fatty acids from TLE were analyzed as described above. Detailed fatty acid compositions will be presented elsewhere. Samples for each and every tissue were successfully collected and analyzed for 31 rats. Seven of these rats were dam-reared with another 14 of these rats consuming adequate amounts of omega-3 fatty acids as DHA. Ten rats were on omega-3 fatty acid deficient diets.

Pig Tissue Samples

Tissues from pigs fed varying levels of fatty acids as described elsewhere [25, 26] were examined according to omega-3 fatty acid biomarkers. The study methods and procedures were approved by the Shur-Gain Agresearch Animal Care Committee. Pregnant Yorkshire-Landrace sows (Maple Leaf Foods Agresearch, Burford, ON, Canada) were randomly fed either a control diet or a diet high in α-linolenic acid (18:3n-3) from ∼1 week prior to parturition until weaning. The diets consisted of base commercial pig feed (Shur-Gain Feed # 694, Guelph, ON, Canada) containing 477 g/kg of corn, 270 g/kg of soy bean meal, 75 g/kg of wheat middlings, 74 g/kg of whey powder, 36.2 g/kg of fish meal, 10 g/kg of limestone, 7 g/kg of dicalcium phosphate, 3.3 g/kg of salt, and 17.6 g/kg of a vitamin/mineral supplement. The control diet consisted of the base pig feed supplemented with 50 g/kg of sunflower oil, while the high-α-linolenic acid diet consisted of the same base pig feed supplemented with 15 g/kg of sunflower oil and 35 g/kg of flaxseed oil. The feeds were similar in levels of saturates and monounsaturates and varied with respect to linoleic and α-linolenic acid (1.9% vs. 17.8% and 61.9% vs. 45.4% of total fatty acids for α-linolenic acid in the low- and high-α-linolenic acid and linoleic acid (18:2n-6) in the low- and high-α-linolenic acid feeds, respectively). The piglets in the present study suckled from their respective sows consuming either the control or high-α-linolenic acid. At 14 days old, suckling pigs per dietary treatment were randomly allocated to several different nurseries. After weaning, pigs consumed diets with the same α-linolenic acid content as their respective sows until the end of the study. Pigs were anesthetized and killed at 14, 35, or 49 days old for tissue fatty acid analysis. Blood samples were anti-coagulated with citrate. Liver, brain, and carcass from which the viscera were removed were completely homogenized four times using a Hobart Grinder with 0.12 cm dye. Total lipids of plasma and portion of homogenized liver, carcass, and brain were extracted into chloroform–methanol (2:1, v/v). Non-esterified heptadecanoic acid (Sigma, St. Louis, MO, USA) was added as an internal standard to an aliquot of the total fatty acid extract to quantitate total lipids. Total lipids were then recovered and saponified in methanolic potassium hydroxide (60 g potassium hydroxide/L-methanol) for 1 h at 100 °C and the fatty acids were converted to fatty acid methyl esters using 14% boron trifluoride-methanol at 100 °C for 30 min (Sigma) under nitrogen. Fatty acid methyl esters were analyzed by gas liquid chromatography using a capillary column (J&W Scientific DB-23, 30 m × 0.25 mm, ID), in a Hewlett-Packard 5890A gas liquid chromatograph (Palo Alto, CA, USA) with automated sample delivery and injection (Hewlett-Packard 7671A) and peak integration (Hewlett-Packard 3393 integrator). Total lipid fatty acids were quantified on the basis of the proportion in each chromatogram of the corresponding internal standard added to each sample.

Data Analysis and Statistics

Individual fatty acids were determined and ratios and sums of interest were calculated. These included the sum of 20:5n-3 + 22:6n-3, the ratio of total n-3 PUFA divided by total n-6 PUFA, and the percentage of n-3 HUFA in total HUFA. The impact of including 22:5n-3 (DPAn-3) in the summation of 20:5n-3 + 22:6n-3 was also examined. HUFAs were considered to be fatty acids with ≥20 carbons in length and ≥3 carbon-carbon, double bonds. The equation for calculation was: (20:3n-3 + 20:5n-3 + 22:5n-3 + 22:6n-3)/(20:3n-3 + 20:5n-3 + 22:5n-3 + 22:6n-3 + 20:3n-6 + 20:4n-6 + 22:4n-6 + 22:5n-6 + 20:3n-9) × 100. A comparison of TLE and PL fractions in plasma and erythrocytes were compared by two-way ANOVA. Mean comparisons for the rat and pig tissues were made by ANOVA. Tukey's Honestly Significantly Different (HSD) test was used for individual mean comparisons when significant *F*-values were determined. Pearson's correlations were also determined to examine the association of the n-3 HUFA score in blood fractions with other blood measures of omega-3 fatty acid status, and the associations between blood fractions and various tissues in rats and pigs. The corresponding n-3 HUFA score and EPA + DHA correlations between blood and animal tissues were compared by Fisher's Exact *Z*-test. All statistics were completed with SPSS for Windows statistical software (release 11.5.1; SPSS Inc., Chicago, IL, USA).

Results

Comparison of the Omega-3 Status of Different Blood Fractions in Humans

The percentage of EPA and DHA in blood of the present study participants was low with a relatively low level of variance in each fraction and as determined by various indices (Table 1). The percentages of EPA and DHA were compared according to plasma versus erythrocytes and TLE versus PLs by two-way ANOVA. The percentage of EPA in plasma was significantly higher ($P < 0.001$) as compared with erythrocytes with no significant effect of the TLE versus the PL isolate. A significant interactive effect ($P < 0.001$) was determined for the percentage of DHA with all four individual means significantly different by Tukey's HSD ($P < 0.05$) testing. Plasma TLE contained the lowest percentage of DHA followed by plasma PL, erythrocyte PL, and erythrocyte TLE containing the highest. The interactive effect observed for DHA persisted for the EPA + DHA values, EPA + DPAn-3 + DHA, the n-3 HUFA score and the ratio of total n-3 PUFA to total n-6 PUFA ($P < 0.001$ for all except $P = 0.016$ for the n-3

Table 1 Biomarkers for omega-3 fatty acid status in human blood

Biomarker	Mean ± SD (n = 25)	CV%	n-3 HUFA score	
			Plasma TLE	Erythrocyte TLE
			Pearson's r	
20:5n-3[1]				
Plasma TLE[2]	0.45 ± 0.16^{a}	35.6	0.66**	0.46*
Erythrocyte TLE	0.36 ± 0.16^{ab}	44.4	0.48*	0.51**
Plasma PL[3]	0.45 ± 0.19^{a}	42.2	0.63**	0.47*
Erythrocyte PL	0.29 ± 0.06^{b}	20.7	0.27	0.40
22:6n-3[1]				
Plasma TLE	1.27 ± 0.46^{a}	36.2	0.72**	0.70**
Erythrocyte TLE	3.07 ± 0.60^{b}	19.5	0.69**	0.86**
Plasma PL	2.03 ± 0.63^{c}	31.0	0.70**	0.71**
Erythrocyte PL	2.57 ± 0.52^{d}	20.2	0.61**	0.83**
EPA + DHA[4]				
Plasma TLE	1.72 ± 0.57^{a}	33.1	0.77**	0.70**
Erythrocyte TLE	3.43 ± 0.67^{c}	19.5	0.73**	0.89**
Plasma PL	2.49 ± 0.74^{b}	29.7	0.76**	0.72**
Erythrocyte PL	2.87 ± 0.55^{b}	19.2	0.61**	0.83**
n-3 HUFA Score[5]				
Plasma TLE	16.63 ± 2.72^{a}	16.4	–	0.76**
Erythrocyte TLE	20.17 ± 2.26^{b}	11.2	0.76**	–
Plasma PL	17.35 ± 2.85^{a}	16.4	0.93**	0.79**
Erythrocyte PL	18.44 ± 2.08^{ab}	11.3	0.67**	0.94**
Totals n-3/n-6				
Plasma TLE	0.07 ± 0.02^{a}	23.4	0.84**	0.62**
Erythrocyte TLE	0.17 ± 0.03^{d}	14.1	0.75**	0.89**
Plasma PL	0.10 ± 0.03^{b}	25.8	0.77**	0.65**
Erythrocyte PL	0.15 ± 0.02^{c}	14.0	0.65**	0.96**

Means within a biomarker with different alphabetical superscripts were significantly different by Tukey's HSD after significant F-tests were determined by two-way ANOVA, $P < 0.05$

HUFA highly unsaturated fatty acid (≥20 carbons, ≥3 carbon-carbon double-bonds), *TLE* total lipid extract, *PL* phospholipid fraction

* $P < 0.05$

** $P < 0.01$

[1] Expressed as % by weight of total fatty acids

[2] Total lipids from Folch extraction were methylated and analyzed by gas chromatography

[3] Phospholipid fraction was methylated and analyzed by gas chromatography after isolation from total lipid extraction by thin layer chromatography

[4] EPA + DHA = 20:5n-3 + 22:6n-3

[5] n-3 HUFA Score = % of omega-3 HUFA in total HUFA

HUFA score). The EPA + DHA values were significantly lower in plasma TLE and the highest in erythrocyte TLE with plasma PL and erythrocyte PL demonstrating no difference. Including DPAn-3 in the sum of EPA + DHA resulted in each mean being significantly different by Tukey's HSD as the mean values all increased (approximately 20% in plasma to 2.14 ± 0.63 in TLE and 3.16 ± 0.80 in PL, and approximately 33% in erythrocytes to 5.08 ± 0.73 in TLE and 4.30 ± 0.6 in PL). The individual means were also significantly different for each ratio of n-3/n-6. The individual mean differences for the n-3 HUFA scores were restricted to erythrocyte TLE being significantly higher than plasma TLE and PL ($P < 0.001$) but not erythrocyte PL ($P = 0.075$).

The n-3 HUFA scores from plasma and erythrocyte TLE were significantly correlated with other measured markers of omega-3 status except the % EPA in erythrocyte PL (Table 1). Correlations between TLE and PL fractions within a blood fraction were particularly strong with $r = 0.93$ for plasma TLE and PL n-3 HUFA scores and $r = 0.94$ for erythrocyte TLE and PL n-3 HUFA scores. Corresponding correlation coefficients within a biomarker were: $r = 0.94$ for plasma TLE EPA + DHA and PL EPA + DHA and $r = 0.92$ for erythrocyte TLE EPA + DHA and PL EPA + DHA; $r = 0.93$ for plasma TLE EPA + DPAn-3 + DHA and PL EPA + DPAn-3 + DHA and $r = 0.92$ for erythrocyte TLE EPA + DPAn-3 + DHA and PL EPA + DPAn-3 + DHA; and $r = 0.92$ for plasma TLE n-3/n-6 and PL n-3/n-6 and $r = 0.92$ for erythrocyte TLE n-3/n-6 and PL n-3/n-6.

Associations of Blood n-3 HUFA Scores to Tissue Levels of Omega-3 Fatty Acids in Animals

The n-3 HUFA score and the EPA + DHA sum both vary in magnitude across various tissue and organs in the control animals (Figs. 1, 2). In the TLE of tissues analyzed from dam reared rats, the n-3 HUFA score and the EPA + DHA values were the highest in brain at 51.3 ± 1.3 and 12.18 ± 0.62%, respectively. Liver, heart, and adipose TLE had similar n-3 HUFA scores, but different omega-3 indices. Plasma and erythrocytes were statistically similar by both the n-3 HUFA score and EPA + DHA, but a larger sample size would likely elicit a difference between plasma and erythrocytes by EPA + DHA values as a post hoc paired t-test between plasma and erythrocyte EPA + DHA values indicate a significant difference ($P < 0.05$). These observations were reflected in the tissues of the pigs on the control diet; however there were smaller differences between the various tissues particularly when the omega-3 status was expressed as the n-3 HUFA score (Fig. 2). The pig brain tissue had the highest n-3 HUFA score and EPA + DHA-value (27.4 ± 2.9 and 6.7 ± 1.3%, respectively). In the pig, the n-3 HUFA scores for plasma, liver, and carcass were all significantly lower than the brain score, but did not differ from each other, while the EPA + DHA-values were all significantly different from

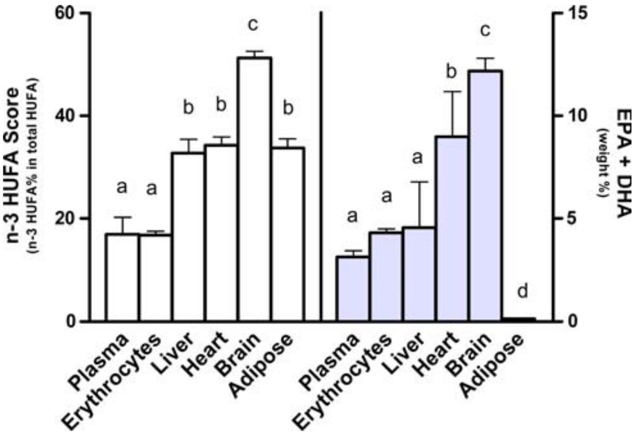

Fig. 1 The n-3 HUFA scores and EPA + DHA values of total lipid extracts from tissues of dam-reared rats. Mean ± SD, $n = 7$. *Different alpha* superscripts indicate significantly different values ($P < 0.05$) by Tukey's Honestly Significant Difference Test following significance by one-way ANOVA ($P < 0.05$). *EPA* eicosapentaenoic acid (20:5n-3), *DHA* docosahexaenoic acid (22:6n-3), *HUFA* highly unsaturated fatty acid (≥20 carbons, ≥3 carbon-carbon double-bonds)

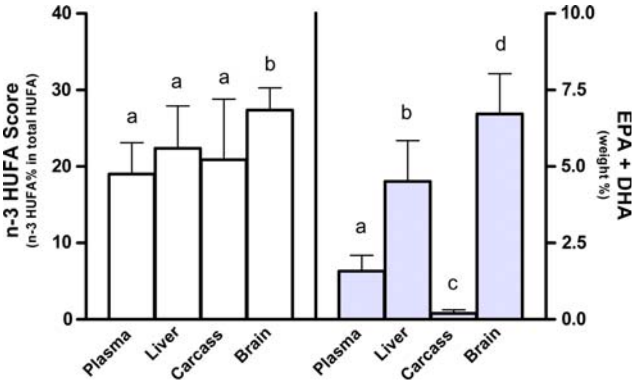

Fig. 2 The n-3 HUFA scores and EPA + DHA-values of total lipid extracts from tissues of pig raised on a control diet. Mean ± SD, $n = 25$. *Different alpha* superscripts indicate significantly *different values* ($P < 0.05$) by Tukey's Honestly Significant Difference Test following significance by one-way ANOVA ($P < 0.05$). *EPA* eicosapentaenoic acid (20:5n-3), *DHA* docosahexaenoic acid (22:6n-3), *HUFA* highly unsaturated fatty acid (≥20 carbons, ≥3 carbon-carbon double-bonds)

each other with carcass EPA + DHA having the lowest value (0.19 ± 0.12%). The sum of EPA + DPAn-3 + DHA reflected the sum of EPA + DHA statistically for tissues from both rats and pigs (data not shown). The ratio of n-3/n-6 for individual tissues tended to resemble the pattern of n-3 HUFA score, except adipose n-3/n-6 was significantly less than n-3/n-6 in liver and heart and similar to n-3/n-6 in plasma and erythrocytes in the rat and liver n-3/n-6 was significantly higher than plasma and carcass (data not shown).

The amount of omega-3 fatty acids in plasma and erythrocyte can correlate well with various organ tissues by the n-3 HUFA score, the EPA + DHA sum and the ratio of total n-3 to n-6 PUFA (Tables 2, 3). Correlations between n-3 HUFA score blood markers with the various tissues tended to be more robust than those determined by EPA + DHA and to a lesser extent the ratio of n-3/n-6. In a sample of rats that included both omega-3 deficient and omega-3 adequate rats, both plasma, and erythrocytes were significantly correlated with liver, heart, brain, and adipose tissue. The correlations between blood n-3 HUFA scores and liver were significantly greater than the corresponding EPA + DHA values by Fisher's exact *Z*-test ($P < 0.001$). The correlations between n-3 HUFA scores in blood and adipose were also significantly greater than corresponding n-3/n-6 correlations.

Removing the omega-3 deficient animals from the analysis results in increased error in correlation determination as evidenced by increased SD for slope and *Y*-intercepts (Fig. 3) and resulted in generally lower correlations between omega-3 status in blood markers and tissues. In the omega-3 adequate rats, all of these n-3 HUFA score correlations remained significant ($P < 0.05$) except for plasma n-3 HUFA score and heart n-3 HUFA score ($r = 0.42$, $P = 0.06$). For the EPA + DHA-values, heart and adipose indices correlated to neither plasma nor erythrocytes, and plasma and liver EPA + DHA did not correlate. Correlations based on the sum of EPA + DPAn-3 + DHA (not shown) resulted in slight but not significant increases in selected correlations as compared to EPA + DHA. However, the significant differences between correlations for EPA + DHA and the n-3 HUFA score for plasma-heart and erythrocyte–adipose in the omega-3 adequate rats disappeared when DPAn-3 was added to EPA and DHA. There was no increase in the correlation between plasma and liver EPA + DHA when DPAn-3 was added. Also in the omega-3 adequate rats, the n-3/n-6 ratio correlations were slightly more robust than the sum of EPA + DHA. The n-3/n-6 correlation between erythrocyte and heart was lower than the corresponding n-3 HUFA score correlation ($P < 0.05$ by Fisher's exact *Z*-test). The n-3/n-6 correlations for blood and adipose tended to be stronger than the n-3 HUFA score correlations, but did not reach significance (plasma–adipose, $P = 0.052$, and erythrocyte–adipose, $P = 0.070$ by Fisher's exact *Z*-test).

Correlations for the omega-3 biomarkers between plasma TLE and liver, carcass, and brain TLE from pigs feed varying amounts of omega-3 fatty acids were also determined and compared. The n-3 HUFA score and n-3/n-6 ratio correlations were similar and tended to be higher than the correlations based on the sum of EPA + DHA (Table 3) with the inclusion of DPAn-3 in the sum making no difference (not shown). Plasma correlated with all

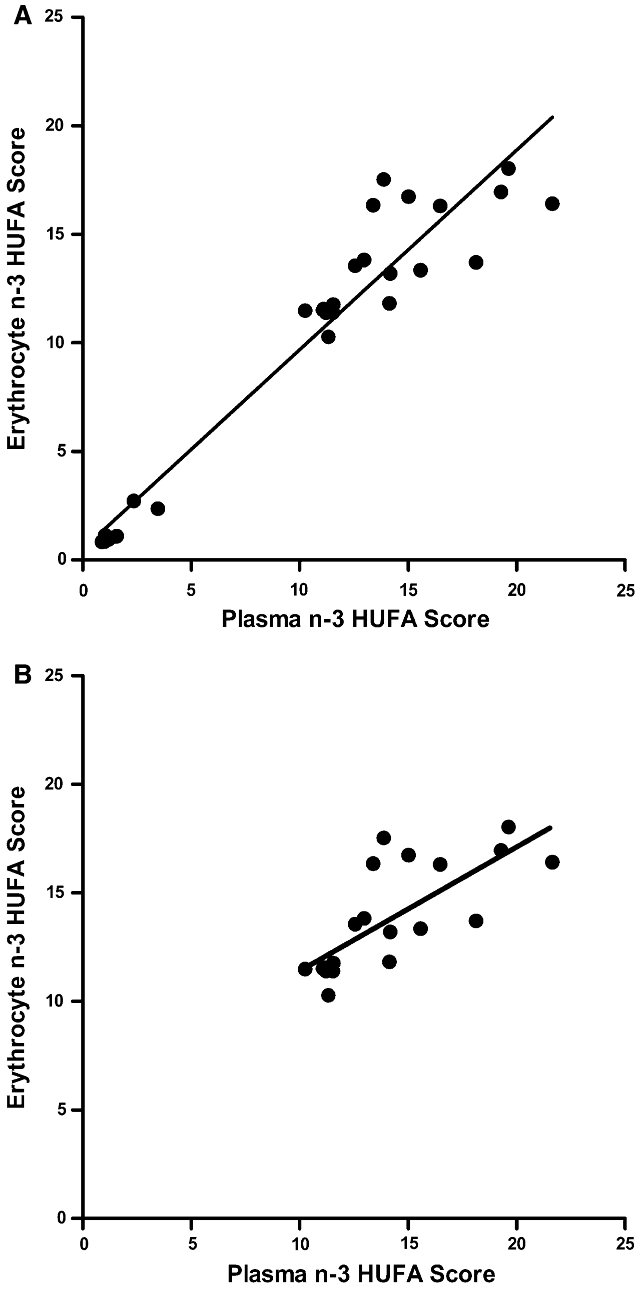

Fig. 3 The n-3 HUFA score of total lipid extract of erythrocytes versus plasma. **a** Omega-3 deficient and adequate rats ($n = 31$). Slope = 0.9197 ± 0.04807, *Y*-intercept = 0.4874 ± 0.5743. **b** Omega-3 adequate rats only ($n = 21$). Slope = 0.5716 ± 0.1157, *Y*-intercept = 5.685 ± 1.673. *HUFA* highly unsaturated fatty acid (≥20 carbons, ≥3 carbon-carbon double-bonds)

values except brain by EPA + DHA ($r = 0.10$, $P = 0.50$) and EPA + DPAn-3 + DHA ($r = 0.13$, $P = 0.37$). Although the n-3 HUFA score and n-3/n-6 correlations tended to be stronger than the EPA + DHA correlations (with and without DPAn-3), the differences did not reach significance by Fisher's Exact *Z*-test.

Discussion

The n-3 HUFA score is a suitable biomarker for omega-3 status in human blood and appears to offer several advantages over the sum of EPA + DHA. The present study demonstrates that (1) the differences between TLE and PL lipid classes of blood fractions are minimal when omega-3 fatty acid status is expressed as the n-3 HUFA score as compared with EPA + DHA and n-3/n-6; (2) the association between omega-3 fatty acid status in blood with various tissues was more robust when predicted by the n-3 HUFA score for liver, heart and brain as compared to EPA + DHA and for heart when compared to n-3/n-6.

Plasma and erythrocytes tend to be the blood fractions analyzed most often, although whole blood, platelets and leukocytes have been analyzed as well. Platelets and leukocytes require extra isolation steps that limit their utility as potential biomarkers. Erythrocytes, due to a longer half-life, have been considered to reflect diet intakes over a longer period as compared with plasma. However, this assumption fails to account for the short half-lives of fatty acids in erythrocyte membranes (7–9 h) [27]. Consistent with the short half-lives of erythrocyte fatty acid membranes, recent evidence suggests that erythrocytes respond to dietary interventions in a similar time course as do plasma pools, possibly through active fatty acid exchange [28]. Differences in fatty acid composition between blood fractions as observed in the EPA + DHA values in plasma TLE (1.72 ± 0.57%) and erythrocyte TLE (3.43 ± 0.67%) in the present study are reflective of the lipid class characteristics of the blood fraction. The lipid classes of tissues have been presented previously [29]. Erythrocytes contain ~32% phosphatidyl choline, 21% phosphatidyl ethanolamine, and have a large cholesterol component (30%), while plasma tends to be dominated by triacylglycerols (49%) with 24% phosphatidyl choline, 16% cholesteryl esters, and minor contributions from phosphatidyl ethanolamine.

Expressing the plasma and erythrocyte omega-3 status in TLE as the n-3 HUFA score reduces the differences between the different blood fractions by focusing on the HUFA pool. Glycerolipid synthesis typically results in a saturated fatty acid (14:0, 16:0, 18:0) in the *sn*-1 position and a 16 or 18 carbon unsaturated fatty acid (16:1n-7, 18:1n-7, 18:1n-9, 18:2n-6, and 18:3n-3) in the *sn*-2 position of the molecule. HUFA such as EPA, DHA, and AA are not extensively incorporated in triacylglycerols. HUFA tend to be *trans*-esterified into the *sn*-2 position of PLs, reflecting their structural and cell-signaling roles in membranes. In addition, phosphatidyl ethanolamine has a tendency to have greater amounts of DHA *trans*-esterified into the *sn*-2 position as compared with phosphatidyl choline [30]. While the isolation of the PL class of plasma

Table 2 Biomarkers for Omega-3 fatty acid status in rat tissues

Tissue	Omega-3 deficient and omega-3 adequate rats ($n = 31$)				Omega-3 adequate rats ($n = 21$)			
	Pearson's *r* Plasma	*P*-value	Erythrocytes		Plasma		Erythrocytes	
n-3 HUFA score								
Plasma	–		0.96	<0.001	–		0.75	<0.001
Liver	0.98	<0.001	0.99	<0.001	0.89	<0.001	0.85	<0.001
Heart	0.93	<0.001	0.97	<0.001	0.42	0.06	0.68	0.001
Brain	0.93	<0.001	0.96	<0.001	0.55	0.01	0.79	<0.001
Adipose	0.93	<0.001	0.97	<0.001	0.47	0.03	0.70	<0.001
EPA + DHA								
Plasma	–		0.96	<0.001	–		0.64	0.002
Liver	0.76***	<0.001	0.76***	<0.001	0.43**	0.06	0.58	0.006
Heart	0.87	<0.001	0.94	<0.001	−0.22*	0.34	−0.11**	0.96
Brain	0.95	<0.001	0.99*	<0.001	0.46	0.04	0.62	0.003
Adipose	0.88	<0.001	0.93	<0.001	−0.08	0.74	−0.05**	0.84
Totals n-3/n-6								
Plasma	–		0.97	<0.001	–		0.82	<0.001
Liver	0.96	<0.001	0.97	<0.001	0.72	<0.001	0.72	<0.001
Heart	0.88	<0.001	0.93	<0.001	−0.12	0.61	0.04*	0.85
Brain	0.93	<0.001	0.97	<0.001	0.52	0.02	0.73	<0.001
Adipose	0.77*	<0.001	0.74***	<0.001	0.82	<0.001	0.90	<0.001

Significantly different than corresponding n-3 HUFA score correlation by Fisher's Exact *Z*-test, *$P < 0.05$

** $P < 0.01$

*** $P < 0.001$

and various tissues is preferred for examining cell membrane composition, this requires an extra analytical step that would prove difficult to automate for high-throughput analyses. Examining the amount of omega-3 HUFA in the total HUFA pool in TLE is a good reflection of the status of the *sn*-2 position of PLs. The correlations between the n-3 HUFA score in plasma TLE and PL was 0.93 and in erythrocyte TLE and PL was 0.94 in the present study.

Table 3 Biomarkers for omega-3 fatty acid status in pig tissues

Tissue	Pigs ($n = 48$)	
	Pearson's *r* Plasma	*P*-value
n-3 HUFA score		
Liver	0.83	<0.001
Carcass	0.76	<0.001
Brain	0.44	0.002
EPA + DHA		
Liver	0.71	<0.001
Carcass	0.54	<0.001
Brain	0.10	0.50
Totals n-3/n-6		
Liver	0.83	<0.001
Carcass	0.79	<0.001
Brain	0.48	0.001

There is significant evidence to conclude that omega-3 HUFAs are important for supporting optimal brain and heart function, likely at the level of cellular membrane structure [6, 11, 31]. The ability to predict omega-3 HUFA levels in these tissues is highly relevant for determining the utility of a biomarker. In the present study, the associations between various tissues and blood fractions tended to be stronger when expressed as n-3 HUFA score as compared with EPA + DHA. This was particularly evident when omega-3 deficient animals were excluded from the analyses (Table 2) as predicting the linear relationship is more variable with the smaller range in the data (Fig. 3). Associations as determined by n-3 HUFA scores tend to be more robust and are well-suited for examinations in humans given that the minimum n-3 HUFA score in plasma TLE in the present human sample was 12.99%.

As presently described, the n-3 HUFA score is more inclusive than EPA + DHA as DPAn-3 is part of the equation. Evidence for DPAn-3 specific health benefits is very limited and impossible to isolate from EPA and DHA [32, 33]. However the content of DPAn-3 can be equivalent and often higher than EPA with the notable exception being plasma [24] and increased DPAn-3 can decrease the production of AA-derived eicosanoids [33]. The inclusion of DPAn-3 in the sum of EPA + DHA resulted in minor but non-significant increases in the correlations between blood and tissues. The stronger correlations between tissues with the n-3 HUFA score appears to be attributed less to the inclusion of DPAn-3 and more to the use of a relative expression as the ratio of n-3 to n-6 PUFA also appeared more robust than the summation of EPA + DHA.

The EPA + DHA blood levels in the present human sample are at the low end of the range observed in humans [34]. This is a reflection of the low and homogeneous intake of omega-3 fatty acids in the present population [14] even as compared with other North Americans [35, 36]. Although the present findings are limited to a small and tightly defined human sample, the observations are supported by similar observations in rat and pig studies. While the present evidence for the use of the n-3 HUFA score is far from conclusive, it is substantial enough to provoke further comparisons in larger studies; in particular, associations with disease risk are required. However, determining the n-3 HUFA score is easily completed on new and existing fatty acid composition data, and as demonstrated by the present study, is not dependent on a specific blood fraction.

Acknowledgments I would like to acknowledge Norman Salem Jr. and Sun-Young Lim for providing the rat tissue data and Stephen Cunnane for providing pig tissue data. I would like to acknowledge William Lands for inspiring the analysis and concepts presented herein. Ken Stark received salary support and was supported by a Gender and Sex Determinants of Cardiovascular Disease: from Bench to Beyond (GENESIS) Young Investigator salary award.

References

1. GISSI-Prevenzione Investigators (1999) Dietary supplementation with n-3 polyunsaturated fatty acids and vitamin E after myocardial infarction: results of the GISSI-Prevenzione trial. Gruppo Italiano per lo Studio della Sopravvivenza nell'Infarto miocardico. Lancet 354:447–455
2. Albert CM, Hennekens CH, O'Donnell CJ, Ajani UA, Carey VJ, Willett WC, Ruskin JN, Manson JE (1998) Fish consumption and risk of sudden cardiac death. JAMA 279:23–28
3. Albert CM, Campos H, Stampfer MJ, Ridker PM, Manson JE, Willett WC, Ma J (2002) Blood levels of long-chain n-3 fatty acids and the risk of sudden death. N Engl J Med 346:1113–1118
4. Lemaitre RN, King IB, Mozaffarian D, Kuller LH, Tracy RP, Siscovick DS (2003) n-3 Polyunsaturated fatty acids, fatal ischemic heart disease, and nonfatal myocardial infarction in older adults: the Cardiovascular Health Study. Am J Clin Nutr 77:319–325
5. Leaf A, Albert CM, Josephson M, Steinhaus D, Kluger J, Kang JX, Cox B, Zhang H, Schoenfeld D (2005) Prevention of fatal arrhythmias in high-risk subjects by fish oil n-3 fatty acid intake. Circulation 112:2762–2768
6. Mozaffarian D, Geelen A, Brouwer IA, Geleijnse JM, Zock PL, Katan MB (2005) Effect of fish oil on heart rate in humans: a meta-analysis of randomized controlled trials. Circulation 112:1945–1952
7. Mozaffarian D (2007) JELIS, fish oil, and cardiac events. Lancet 369:1062–1063
8. Yokoyama M, Origasa H, Matsuzaki M, Matsuzawa Y, Saito Y, Ishikawa Y, Oikawa S, Sasaki J, Hishida H, Itakura H, Kita T, Kitabatake A, Nakaya N, Sakata T, Shimada K, Shirato K (2007) Effects of eicosapentaenoic acid on major coronary events in hypercholesterolaemic patients (JELIS): a randomised open-label, blinded endpoint analysis. Lancet 369:1090–1098
9. Kris-Etherton PM, Harris WS, Appel LJ (2002) Fish consumption, fish oil, omega-3 fatty acids, and cardiovascular disease. Circulation 106:2747–2757
10. Baylin A, Campos H (2006) The use of fatty acid biomarkers to reflect dietary intake. Curr Opin Lipidol 17:22–27
11. Harris WS, Von Schacky C (2004) The Omega-3 Index: a new risk factor for death from coronary heart disease? Prev Med 39:212–220
12. Harris WS, Sands SA, Windsor SL, Ali HA, Stevens TL, Magalski A, Porter CB, Borkon AM (2004) Omega-3 fatty acids in cardiac biopsies from heart transplantation patients: correlation with erythrocytes and response to supplementation. Circulation 110:1645–1649
13. Lands WE (1995) Long-term fat intake and biomarkers. Am J Clin Nutr 61:721S–725S
14. Stark KD, Beblo S, Murthy M, Buda-Abela M, Janisse J, Rockett H, Whitty JE, Martier SS, Sokol RJ, Hannigan JH, Salem N Jr (2005) Comparison of bloodstream fatty acid composition from African-American women at gestation, delivery, and postpartum. J Lipid Res 46:516–525
15. Mohrhauer H, Holman RT (1963) The effect of dose level of essential fatty acids upon fatty acid composition of the rat liver. J Lipid Res 58:151–159
16. Stark KD, Beblo S, Murthy M, Whitty JE, Buda-Abela M, Janisse J, Rockett H, Martier SS, Sokol RJ, Hannigan JH, Salem N Jr (2005) Alcohol consumption in pregnant, black women is associated with decreased plasma and erythrocyte docosahexaenoic acid. Alcohol Clin Exp Res 29:130–140
17. Folch J, Lees M, Stanley GHS (1957) A simple method for the isolation and purification of total lipids from animal tissues. J Biol Chem 226:497–509
18. Reed CF, Swisher SN, Marinetti GV, Eden EG (1960) Studies of the lipids of the erythrocyte. I. Quantitative analysis of the lipids of normal human red blood cells. J Lab Clin Med 56:281–289
19. Rapoport SI, Chang MC, Spector AA (2001) Delivery and turnover of plasma-derived essential PUFAs in mammalian brain. J Lipid Res 42:678–685
20. Morrison WR, Smith LM (1964) Preparation of fatty acid methyl esters and dimethylacetals from lipids with boron fluoride-methanol. J Lipid Res 5:600–608
21. Salem N Jr, Reyzer M, Karanian J (1996) Losses of arachidonic acid in rat liver after alcohol inhalation. Lipids 31(Suppl 1):S153–S156
22. Lim SY, Hoshiba J, Salem N Jr (2005) An extraordinary degree of structural specificity is required in neural phospholipids for optimal brain function: n-6 docosapentaenoic acid substitution for docosahexaenoic acid leads to a loss in spatial task performance. J Neurochem 95:848–857
23. Stark KD, Lim SY, Salem N Jr (2007) Docosahexaenoic acid and n-6 docosapentaenoic acid supplementation alter rat skeletal muscle fatty acid composition. Lipids Health Dis 6:13
24. Stark KD, Lim SY, Salem N Jr (2007) Artificial rearing with docosahexaenoic acid and n-6 docosapentaenoic acid alters rat tissue fatty acid composition. J Lipid Res 48:2471–2477
25. Bazinet RP, McMillan EG, Cunnane SC (2003) Dietary alpha-linolenic acid increases the n-3 PUFA content of sow's milk and the tissues of the suckling piglet. Lipids 38:1045–1049
26. Bazinet RP, McMillan EG, Seebaransingh R, Hayes AM, Cunnane SC (2003) Whole-body beta-oxidation of 18:2omega6 and 18:3omega3 in the pig varies markedly with weaning strategy and dietary 18:3omega3. J Lipid Res 44:314–319

27. Staufenbiel M (1988) Fatty acids covalently bound to erythrocyte proteins undergo a differential turnover in vivo. J Biol Chem 263:13615–13622
28. Skeaff CM, Hodson L, McKenzie JE (2006) Dietary-induced changes in fatty acid composition of human plasma, platelet, and erythrocyte lipids follow a similar time course. J Nutr 136:565–569
29. Christie WW (1985) Rapid separation and quantification of lipid classes by high performance liquid chromatography and mass (light-scattering) detection. J Lipid Res 26:507–512
30. Lemaitre-Delaunay D, Pachiaudi C, Laville M, Pousin J, Armstrong M, Lagarde M (1999) Blood compartmental metabolism of docosahexaenoic acid (DHA) in humans after ingestion of a single dose of [(13)C]DHA in phosphatidylcholine. J Lipid Res 40:1867–1874
31. Salem N Jr, Litman B, Kim HY, Gawrisch K (2001) Mechanisms of action of docosahexaenoic acid in the nervous system. Lipids 36:945–959
32. Conquer JA, Cheryk LA, Chan E, Gentry PA, Holub BJ (1999) Effect of supplementation with dietary seal oil on selected cardiovascular risk factors and hemostatic variables in healthy male subjects. Thromb Res 96:239–250
33. Murphy MG, Wright V, Scott J, Timmins A, Ackman RG (1999) Dietary menhaden, seal, and corn oils differentially affect lipid and ex vivo eicosanoid and thiobarbituric acid-reactive substances generation in the guinea pig. Lipids 34:115–124
34. Dewailly E, Blanchet C, Gingras S, Lemieux S, Holub BJ (2003) Fish consumption and blood lipids in three ethnic groups of Quebec (Canada). Lipids 38:359–365
35. Denomme J, Stark KD, Holub BJ (2005) Directly quantitated dietary (n-3) fatty acid intakes of pregnant Canadian women are lower than current dietary recommendations. J Nutr 135:206–211
36. Innis SM, Elias SL (2003) Intakes of essential n-6 and n-3 polyunsaturated fatty acids among pregnant Canadian women. Am J Clin Nutr 77:473–478

Lipids (2008) 43:55–64
DOI 10.1007/s11745-007-3124-7

ORIGINAL ARTICLE

Dietary Structured Lipids and Phytosteryl Esters: Blood Lipids and Cardiovascular Status in Spontaneously Hypertensive Rats

**Byung Hee Kim · Kevin D. Sandock ·
Tom P. Robertson · Stephen J. Lewis ·
Casimir C. Akoh**

Received: 2 August 2007 / Accepted: 1 October 2007 / Published online: 6 November 2007
© AOCS 2007

Abstract This study examined the dietary effects of enzymatically modified sesame oil with caprylic acid (structured lipids, SL) and phytosteryl esters (PE) on blood lipid profiles and cardiovascular parameters of spontaneously hypertensive rats (SHR) fed high-fat and high-cholesterol (HFHC) diets. The dietary groups were: normal diet (control), sesame oil (SO), SL, SO fortified with PE (SOP), and SL fortified with PE (SLP). After 9 weeks of feeding, the body weights, liver weights, and liver weight/body weight ratios in all HFHC-fed groups were higher than controls. Plasma total and LDL cholesterol levels in all HFHC-fed groups were similar to one another but higher than those in controls. Plasma HDL cholesterol levels in rats fed SOP and SLP were higher than those in controls or rats fed SO and SL. Plasma HDL/total cholesterol ratios in rats fed SOP and SLP were similar to those in controls and were higher than those in rats fed SO and SL. There was no difference in plasma lipid profiles between rats fed SO and SL. Arterial blood pressures (BP) in conscious HFHC-fed rats were similar to those in controls whereas heart rates (HR) in all HFHC-fed groups were similar to one another but were higher than that in controls. These findings demonstrate that (1) the dietary effects of SL on plasma lipid profiles and resting BP and HR are similar to those of SO, (2) PE had positive effects on plasma lipid profiles, and (3) 9-week intake of SL and PE did not have pronounced effects on resting BP but induced tachycardia in SHR.

B. H. Kim · C. C. Akoh (✉)
Department of Food Science and Technology,
The University of Georgia,
Athens, GA 30602-7610, USA
e-mail: cakoh@uga.edu

K. D. Sandock · T. P. Robertson · S. J. Lewis
Department of Physiology and Pharmacology,
The University of Georgia, Athens, GA, USA

Keywords Sesame oil · Structured lipids · Phytosteryl esters · Plasma lipid profiles · Spontaneously hypertensive rats · Cardiovascular parameters

Abbreviations

BP	Arterial blood pressures
DBP	Diastolic arterial blood pressures
HDL	High density lipoprotein
HFHC	High-fat and high-cholesterol
HR	Heart rates
LCT	Long chain triacylglycerol
LDL	Low density lipoprotein
MAP	Mean arterial blood pressures
MLM-type	Type of triacylglycerols containing medium chain fatty acids esterified at *sn*-1,3 positions and long chain fatty acids at *sn*-2 position
PE	Phytosteryl esters
PP	Arterial pulse pressures
SBP	Systolic arterial blood pressures
SHR	Spontaneously hypertensive rats
SL	Structured lipids
SLP	Structured lipids fortified with phytosteryl esters
SO	Sesame oil
SOP	Sesame oil fortified with phytosteryl esters

Introduction

Structured lipids are triacylglycerols that have been restructured by incorporation of new fatty acids to change the composition and positional distribution of fatty acids from the native state by chemical or enzymatic methods [1]. Among several types of structured lipids, MLM-type structured lipids are triacylglycerols comprising medium chain fatty acids esterified at *sn*-1,3 positions and long chain fatty acids at *sn*-2 position of the glycerol backbone. MLM-type structured lipids can be synthesized by attaching medium chain fatty acids into long chain triacylglycerols (LCT) with the help of *sn*-1,3 regiospecific lipases. These MLM-type structured lipids are expected to have different physiological attributes from LCT, the typical triacylglycerol forms of many edible fats and oils, because of the presence of both medium chain and long chain fatty acids in the same triacylglycerol molecules. For example, when compared to LCT, they are expected to deliver the energy more rapidly via oxidation of the more hydrophilic medium chain fatty acids and less likely to be deposited in the adipose tissue due to the predominant transportation of medium chain fatty acids via the portal vein to the liver rather than through the lymphatic system [1–5]. Therefore, MLM-type structured lipids with proper balance of medium chain fatty acids and long chain fatty acids, such as essential fatty acids (e.g., linoleic acid) and hypocholesterolemic fatty acids (e.g., oleic acid [6]), might have positive effects on blood lipid profiles and cardiovascular status of humans as well as meeting essential fatty acid requirements while providing the benefits of medium chain fatty acids described above. Although MLM-type structured lipids are expected to have different physiological attributes from LCT, there are few studies evaluating the dietary effects of MLM-type structured lipids, especially their effects on cardiovascular status of animals and humans.

On the other hand, phytosterols are known to have hypocholesterolemic effects by lowering plasma total and low density lipoprotein (LDL) cholesterol levels without affecting plasma high density lipoprotein (HDL) cholesterol levels in humans and some animals, such as rabbits [7–10]. The cholesterol-lowering mechanisms of phytosterols in humans are still not known in detail. Recently, the inhibited absorption of cholesterol in intestine arising from chemical structure similarities between phytosterols and cholesterol is believed to be the main mechanism of their hypocholesterolemic effects [11]. Besides, other mechanisms such as competition with cholesterol for solubilization in dietary mixed micelles, co-crystallization with cholesterol to form insoluble mixed crystals, and interference with the hydrolysis process by lipases and cholesterol esterases are suggested to be responsible for their hypocholesterolemic effects [11]. However, phytosterols have limitations as dietary supplements because they have very poor solubilities in edible oil and have very high melting points. To overcome such physical problems of free phytosterols, phytosteryl esters (fatty acid ester forms of phytosterols) are preferred in food formulation. Because phytosteryl esters have much enhanced solubility in oils and much lower melting point compared to their corresponding phytosterols, they can be easily incorporated into a wide variety of diets and fat/oil-based diets and food products. Moreover, many recent studies have shown that phytosteryl esters can also effectively reduce plasma total and LDL cholesterol levels similar to phytosterols in humans [12–15].

The aim of our study was to investigate the dietary effects of sesame oil-based MLM-type structured lipids and phytosteryl esters on the blood lipid profiles and cardiovascular parameters of spontaneously hypertensive rats (SHR), a widely studied animal model of cardiovascular disorders (e.g., essential hypertension) of humans [16, 17]. The principal hypotheses of our study were: (1) the dietary effects of the structured lipids (MLM-type triacylglycerols) on the blood lipid profiles and cardiovascular status of SHR would be different from those of original sesame oil (LCT; i.e., LLL-type); and (2) dietary phytosteryl esters would have positive effects on the blood lipid profiles in SHR.

Materials and Methods

Materials

Sesame oil was purchased from Spectrum Organic Product, Inc. (Petaluma, CA, USA). Caprylic acid (C8:0, purity >98%) was obtained from Aldrich Chemical Company (Milwaukee, WI, USA). Phytosteryl esters (from vegetable oil deodorizates) were donated by Cargill Inc. (Minneapolis, MN, USA). Lipozyme RM IM, an *sn*-1,3 regiospecific immobilized lipase from *Rhizomucor miehei* was provided by Novozymes North America, Inc. (Franklinton, NC, USA).

Structured Lipids Synthesis

The sesame oil-based structured lipids (MLM-type) were synthesized by Lipozyme RM IM-catalyzed acidolysis reaction of sesame oil with caprylic acid as described previously [18].

Fatty Acid Profiles of Fat Source

Total and positional fatty acid profiles of fat sources of experimental diets were analyzed according to the procedures described previously [18].

Rats

All animal studies were performed according to the National Institutes of Health Guide for the Care and Use of Laboratory Animals (NIH Publications No. 80–23) revised in 1996. All protocols were approved by the Animal Care and Use Committee of the University of Georgia. Four-week-old male SHR ($n = 30$) were obtained from Harlan (Madison, WI, USA). They were randomly assigned to one of five different dietary groups described below ($n = 6$ per group). The rats were individually housed in cages under controlled temperature (21 ± 1 °C) and lighting (12 h light/dark cycle). The rats were fed diets and water ad libitum for 9 weeks. Diet intakes were recorded daily and body weights were measured weekly. After the cardiovascular measurements described below, the rats were killed by decapitation and then their organs (liver, heart, and kidney) were removed and weighed.

Diets

Normal diet for the control rats was purchased from Labdiet (Brentwood, MO, USA). The fat and cholesterol contents of the normal diet were 4.5 and 0.02% of total diet weight, respectively. The high-fat and high-cholesterol (HFHC) diets were prepared and pelleted by Research Diets (New Brunswick, NJ, USA). Four different kinds of HFHC diets were made for four different dietary groups: *sesame oil (SO), structured lipids (SL), sesame oil fortified with phytosteryl esters (SOP), and structured lipids fortified with phytosteryl esters (SLP)* (Table 1). The four formulations for HFHC dietary groups were identical in composition, except for the type of fat. The HFHC diets contained SO, SL, SOP, or SLP as a fat source (20% of total diet weight), respectively. Dietary cholesterol was adjusted to 0.56% of total diet weight in all HFHC diets. The amount of phytosteryl esters added in the HFHC diets for the groups SOP and SLP was adjusted to 0.54% of total diet weight (2.4 g/2,000 kcal) approximately corresponding to a therapeutic level (1.5–3.0 g/day) for hypocholesterolemic effects in humans [14, 15, 19–25]. All HFHC diets were almost isoenergetic (diets for groups SO and SL, 4.54 kcal/g; diets for groups SOP and SLP 4.50 kcal/g).

Surgeries, Blood Collection and Cardiovascular Measurements

Twelve hours before the surgeries were performed, all rats were deprived of food. Water was freely available. All rats were anesthetized with pentobarbital sodium (50 mg/kg, i.p.) and a catheter (PE-50) was placed in a femoral artery to record systolic arterial blood pressure (SBP), diastolic arterial blood pressure (DBP), pulse pressure (PP), and mean arterial blood pressure (MAP) [26, 27]. The catheters were exteriorized to the back of the neck and all wounds were liberally coated with triple antibiotic (neomycin, polymixin B, and bacitracin) ointment (Fougera, NY, USA) and then sutured. The arterial catheter was connected to a pressure transducer that was coupled to a computerized data acquisition system (PowerLab Chart, version 4.0.4, ADI Instruments, Colorado Springs, CO, USA) to record resting arterial blood pressures and heart rate (HR), which was derived from PP by way of an internal cardiotachometer in the data acquisition system [26, 27]. Once the resting cardiovascular parameters were recorded, 2 mL of blood was taken via the arterial catheter for subsequent determination of plasma lipid profiles described below. The rats were returned to their home cages in a room maintained on a 12 h light/dark cycle. Food and water were freely available. The rats were given 2 days to recover from the above surgeries. On the day of data recording, the arterial catheter of each conscious rat was connected to the pressure transducer and recording equipment as described above.

Plasma Lipid Profiles

Blood plasma samples were analyzed to determine total, HDL, and LDL cholesterols, and triacylglycerol levels. Total and HDL cholesterol levels were determined by the cholesterol oxidase method with Equal reagents (Equal Diagnostics, Exton, PA, USA), respectively. Plasma triacylglycerols levels were determined by the glycerol phosphate oxidase method with Amresco reagents (Amresco Inc., Solon, OH, USA). The measurements were conducted using a Roche/Hitachi 717 analyzer (Roche Diagnostics, Indianapolis, IN, USA). Plasma LDL cholesterol level was calculated using the Friedwald calculation, LDL cholesterol = total cholesterol − (triacylglycerol/5 + HDL cholesterol).

Statistical Analysis

The data are presented as mean ± SEM and were analyzed by one-way or repeated-measures analysis of variance (ANOVA) [28] followed by Student's modified t test with the Bonferroni correction for multiple comparisons between means using the error mean square (EMS) terms from the ANOVA [29]. A value of $P < 0.05$ denoted statistical significance.

Table 1 Composition of experimental diets

Ingredient			High-fat and high-cholesterol (HFHC) diet							
	Control		SO		SL		SOP		SLP	
	Weight (g/kg)	Calorie (%)	Weight (g/kg)	Calorie (%)	Weight (g/kg)	Calorie (%)	Weight (g/kg)	Calorie (%)	Weight (g/kg)	Calorie (%)
Protein	234	28	227	20	227	20	227	20	227	20
Carbohydrate	499	60	459	40	459	40	459	41	459	41
Fat	45	12	200	40	200	40	194.6	39	194.6	39
(kcal/g)	(3.34)		(4.54)		(4.54)		(4.50)		(4.50)	
Casein			224		224		224		224	
L-Cystine			3		3		3		3	
Corn starch	Laboratory Rodent Diet 5001 (Labdiet, Brentwood, MO, USA)[a]		112		112		112		112	
Maltodextrin			112		112		112		112	
Sucrose			224		224		224		224	
Cellulose			56		56		56		56	
Sesame oil			200				194.6			
Structured lipids					200				194.6	
Phytosteryl esters							5.4		5.4	
Cholesterol	0.2		5.6		5.6		5.6		5.6	
Minerals[b]			50		50		50		50	
Vitamins[c]			13		13		13		13	

SO sesame oil, *SL* structured lipids, *SOP* sesame oil fortified with phytosteryl esters, *SLP* structured lipids fortified with phytosteryl esters

[a] Ingredients: ground corn, dehulled soybean meal, dried beet pulp, fish meal, ground oats, brewers dried yeast, cane molasses, dehydrated alfalfa meal, dried whey, wheat germ, porcine meat meal, wheat middlings, animal fat preserved with BHA, salt, calcium carbonate, choline chloride, cholecalciferol, vitamin A acetate, folic acid, pyridoxine hydrochloride, DL-methionine, thiamin mononitrate, calcium pantothenate, nicotinic acid, DL-alpha tocopheryl acetate, cyanocobalamin, riboflavin, ferrous sulfate, manganous oxide, zinc oxide, ferrous carbonate, copper sulfate, zinc sulfate, calcium iodate, cobalt carbonate

[b] Composed of RD-96 Salt Mix without calcium, phosphorus, and potassium, 11 g/kg; dicalcium phosphate, 14 g/kg; calcium carbonate, 6 g/kg; potassium citrate monohydrate, 19 g/kg. RD-96 Salt Mix without calcium, phosphorus, and potassium contains the following (g/kg): sodium chloride, 259.0; magnesium oxide, 41.9; magnesium sulfate, 257.6; chromium potassium sulfate, 1.925; cupric carbonate, 1.05; sodium fluoride, 0.2; potassium iodate, 0.035; ferric citrate, 21.0; manganous carbonate, 12.25; ammonium molybdate, 0.3; sodium selenite, 0.035; zinc carbonate, 5.6; sucrose, 399.105

[c] Composed of Vitamin Mix for AIN-76A Rodent Diet, 11 g/kg; choline bitartrate 2 g/kg. Vitamin Mix for AIN-76A Rodent Diet contains the following (g/kg): vitamin A palmitate (500,000 IU/g), 0.8; vitamin D_3 (100,000 IU/g), 1.0; vitamin E acetate (500 IU/g), 10.0; menadione sodium bisulfite, 0.08; biotin (1%), 2.0; cyancocobalamin (0.1%), 1.0; folic acid, 0.2; nicotinic acid, 3.0; calcium pantothenate, 1.6; pyridoxine HCl, 0.7; riboflavin, 0.6; thiamin HCl, 0.6; sucrose, 978.42

Results

Fatty Acid Compositions of Fat Sources

Total and positional fatty acid compositions of fat sources of experimental diets are given in Table 2. Major fatty acids of control diet were oleic acid (27.2 mol%), linoleic acid (26.5 mol%), palmitic acid (20.2 mol%), and linolenic acid (17.6 mol%). Accordingly, the fat in the control diet originated from a mixture of animal fat and vegetable oil (see Table 1 legend). Two major fatty acids of sesame oil were oleic acid (37.0 mol%) and linoleic acid (48.4 mol%). The total content of palmitic acid in sesame oil was 10.0 mol%. Whereas, structured lipids presented reduced total contents of palmitic acid (3.1 mol%), oleic acid (19.4 mol%), and linoleic acid (30.0 mol%), respectively, compared to the original sesame oil. Total caprylic acid content of structured lipids was 45.8 mol%. The content of caprylic acid found at *sn*-2 position of the structured lipids was 3.7 mol%. Major fatty acids present at the *sn*-2 position of original sesame oil (oleic acid, 40.2 mol%; linoleic acid, 57.3 mol%) remained almost intact at that position in the structured lipids (oleic acid, 36.4 mol%; linoleic acid, 57.2 mol%). The incorporation of caprylic acid into *sn*-1,3 positions, as we intended by using Lipozyme RM IM (an *sn*-1,3 regiospecific lipase) in the synthesis of structured lipids, reached 66.8 mol%. These results demonstrate that MLM-type structured lipids were successfully produced from sesame oil and caprylic acid.

Table 2 Total and positional fatty acid compositions of sesame oil and structured lipids (mol%)

Fatty acid	Total			*sn*-2			*sn*-1,3[a]		
	Control	SO	SL	Control	SO	SL	Control	SO	SL
C8:0	ND[b]	ND	45.8 ± 0.2	ND	ND	3.7 ± 0.1	ND	ND	66.8 ± 0.2
C10:0	ND	ND	ND	ND	ND	ND	ND	ND	ND
C12:0	ND	Trace[b]	ND	ND	ND	ND	ND	Trace	ND
C14:0	1.8 ± 0.1	Trace	ND	ND	ND	ND	2.7 ± 0.1	Trace	ND
C14:1	ND	ND	ND	ND	ND	ND	ND	ND	ND
C16:0	20.2 ± 0.4	10.0 ± 0.0	3.1 ± 0.1	34.7 ± 1.1	1.1 ± 0.0	1.5 ± 0.0	12.9 ± 0.1	14.4 ± 0.0	4.0 ± 0.1
C16:1	3.0 ± 0.0	0.1 ± 0.0	0.1 ± 0.0	ND	0.1 ± 0.0	Trace	4.4 ± 0.0	0.1 ± 0.0	0.1 ± 0.0
C18:0	3.7 ± 0.1	3.6 ± 0.0	1.1 ± 0.0	3.7 ± 0.3	0.3 ± 0.0	0.4 ± 0.1	3.6 ± 0.3	5.3 ± 0.0	1.5 ± 0.0
C18:1*n-9*	27.2 ± 0.4	37.0 ± 0.0	19.4 ± 0.1	19.2 ± 1.2	40.2 ± 0.4	36.4 ± 0.0	31.3 ± 0.0	35.4 ± 0.2	11.0 ± 0.1
C18:2*n-6*	26.5 ± 0.6	48.4 ± 0.0	30.0 ± 0.0	34.5 ± 0.3	57.3 ± 0.5	57.2 ± 0.1	22.5 ± 0.8	44.0 ± 0.2	16.3 ± 0.0
C18:3*n-3*	17.6 ± 1.6	0.9 ± 0.0	0.5 ± 0.0	7.9 ± 2.2	1.0 ± 0.0	0.8 ± 0.0	22.5 ± 1.2	0.8 ± 0.0	0.3 ± 0.0
SFA[d]	25.6 ± 0.6	13.6 ± 0.0	50.1 ± 0.1	38.4 ± 0.8	1.5 ± 0.1	5.6 ± 0.1	19.2 ± 0.5	19.7 ± 0.0	72.3 ± 0.1
USFA[e]	74.4 ± 0.6	86.4 ± 0.0	49.9 ± 0.1	61.6 ± 0.8	98.5 ± 0.1	94.4 ± 0.1	80.8 ± 0.5	80.3 ± 0.0	27.7 ± 0.1

Data are presented as mean ± SEM, $n = 2$

See Table 1 legend for description of abbreviations

SFA saturated fatty acid, *USFA* unsaturated fatty acid, *ND* not detected

[a] *sn*-1,3 (mol%) = [3 × Total (mol%)−*sn*-2 (mol%)]/2

[b] <0.05 mol%

Diet Intake, Weight Gain and Food Efficiency Ratio

The total diet intakes, weight gains and food efficiency ratios (FER, weight gain for 9 weeks/diet intake for 9 weeks) in the five dietary groups are summarized in Table 3. The diets began when the rats were 4 weeks old and continued until they were 13 weeks old. Although the rats in each group ate similar ($P > 0.05$, for all comparisons) amounts of food, the HFHC dietary groups, i.e., the rats fed SO, SL, SOP, and SLP put on more ($P < 0.05$, for all comparisons) weight, and accordingly had higher ($P < 0.05$, for all comparisons) FER values than the control group.

Table 3 Total diet intake, weight gain and food efficiency ratio

	Dietary group				
	Control	SO	SL	SOP	SLP
Diet intake (g/day)	16 ± 1	15 ± 1†	15 ± 1†	15 ± 1	16 ± 1
Weight gain (g/9 weeks)	263 ± 4	303 ± 8*,†	296 ± 9*,†	284 ± 7*	296 ± 7*
FER[a]	16 ± 1	36 ± 1*,†	35 ± 1*,†	35 ± 1*	34 ± 1*

Data are presented as mean ± SEM, $n = 6$

See Table 1 legend for description of abbreviations

[a] Food efficiency ratio; FER = (weight gain for 9 weeks/diet intake for 9 weeks) × 100

* $P < 0.05$, versus control

† $P > 0.05$, SO versus SL

Body and Organ Weights

After 9 weeks of feeding, the body weights, organ (liver, heart, and kidney) weights, and organ weights to body weight ratios of HFHC dietary groups were compared to those of control rats fed normal diet. The body weights (BW) of the groups SO (333 ± 7 g), SL (339 ± 12 g), SOP (319 ± 7 g), and SLP (338 ± 7 g) were substantially greater than that of control group (304 ± 4 g), respectively ($P < 0.05$, for all comparisons). The liver weights (LW) and liver weight to body weight ratios (LW/BW × 1,000) of the rats fed SO (LW = 17.1 ± 0.6 g; LW/BW × 1,000 = 51.3 ± 1.1), SL (LW = 16.6 ± 0.7 g; LW/BW × 1,000 = 48.9 ± 0.6), SOP (LW = 16.5 ± 0.7 g; LW/BW × 1,000 = 51.5 ± 1.3), and SLP (LW = 17.3 ± 0.7 g; LW/BW × 1,000 = 51.2 ± 1.9) were substantially greater than those of control rats (LW = 9.6 ± 0.5 g; LW/BW × 1,000 = 31.6 ± 3.1), respectively ($P < 0.05$, for all comparisons). Whereas, the heart weights, heart weight to body weight ratios, kidney weights, and kidney weight to body weight ratios of the rats fed SO, SL, SOP, and SLP were similar to those of control rats (data are not shown; $P > 0.05$, for all comparisons).

Plasma Lipid Profiles

Plasma lipid profiles in the five dietary groups are shown in Fig. 1. The plasma total and LDL cholesterol levels and LDL to total cholesterol ratios were similar ($P > 0.05$, for all comparisons) in all HFHC dietary groups but were higher ($P < 0.05$, for all comparisons) than those in the control group. However, the plasma HDL cholesterol levels in the rats fed phytosteryl esters, i.e., the groups SOP and SLP were higher than those in the control group and the other HFHC dietary groups such as SO and SL ($P < 0.05$, for all comparisons). Furthermore, the plasma HDL to total cholesterol ratios in the groups SOP and SLP were also higher ($P < 0.05$, for all comparisons) than those in the groups SO and SL and were similar ($P > 0.05$, for all comparisons) to that in the control group. The plasma triacylglycerol levels were similar ($P > 0.05$, for all comparisons) in all HFHC dietary groups but were lower ($P < 0.05$, for all comparisons) than that in the control group. On the other hand, no distinct differences were found in the overall plasma lipid profiles between groups SO and SL ($P > 0.05$, for both comparisons).

Resting Cardiovascular Parameters in Anesthetized Rats

Resting values for the cardiovascular parameters in the five dietary groups recorded under pentobarbital anesthesia are summarized in Fig. 2. Resting parameters in the control group were similar to those reported previously [30–32]. As can be seen, resting SBP values in the HFHC dietary groups were lower than those in the control group ($P < 0.05$, for all comparisons). Resting DBP value in the rats fed SL was lower than that in the control group ($P < 0.05$, for both comparisons). The PP values in the rats fed SOP or SLP were lower than that in the control group ($P < 0.05$, for both comparisons). Resting HR value of the rats fed SO was higher than that of the control rats ($P < 0.05$, for both comparisons). On the other hand, all resting arterial blood pressures, i.e., SBP, DBP, PP, and MAP and resting HR in the rats fed SL tended to be slightly lower than those in the rats fed SO but the differences were not significant ($P > 0.05$, for both comparisons).

Resting Cardiovascular Parameters in Conscious Rats

Resting values for the cardiovascular parameters in the five dietary groups of conscious rats are summarized in Fig. 3. Resting parameters in the control rats were similar to those reported previously [33–35]. As can be seen, resting HR values in all HFHC dietary groups were substantially higher than that in the control rats ($P < 0.05$, for all comparisons). However, resting arterial blood pressures, i.e., SBP, DBP, PP, and MAP in all HFHC dietary groups were similar to those in the control group ($P > 0.05$, for all comparisons), with one exception. Specifically, the PP value for the rats fed SLP was lower than that of the control rats ($P < 0.05$, for both comparisons). On the other hand, all resting arterial blood pressures tended to be slightly lower in the group SL than in the group SO; whereas, resting HR tended to be slightly higher in the group SL than in the group SO. However, the differences were not significant ($P > 0.05$, for both comparisons).

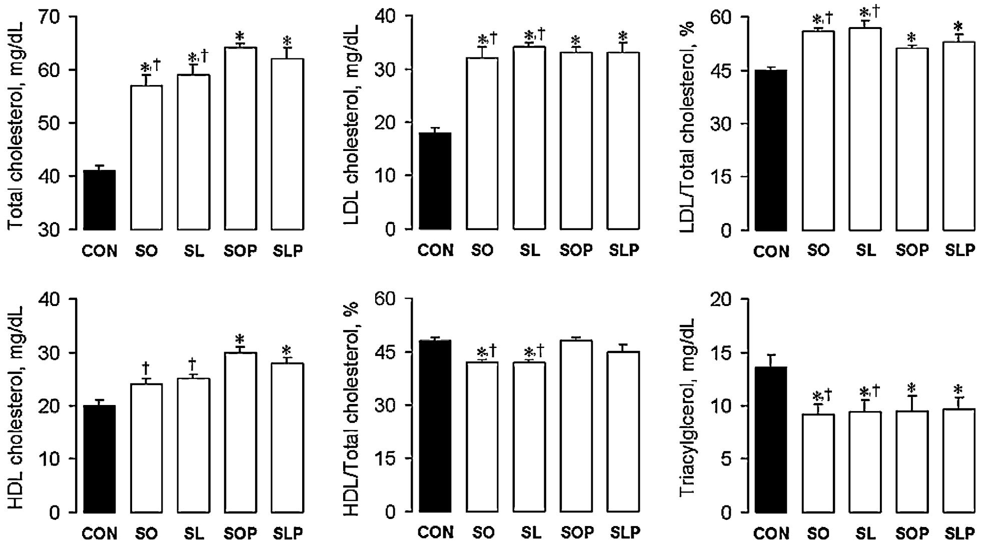

Fig. 1 Dietary effects on plasma lipid profiles: total cholesterol; LDL cholesterol: LDL/total cholesterol ratio; HDL cholesterol; HDL/total cholesterol ratio; triacylglycerol. Treatment groups: *CON*, control; *SO*, sesame oil; *SL*, structured lipids; *SOP*, sesame oil fortified with phytosteryl esters; *SLP*, structured lipids fortified with phytosteryl esters. The data are presented as mean ± SEM. $^*P < 0.05$, versus control. $^\dagger P > 0.05$, SO versus SL

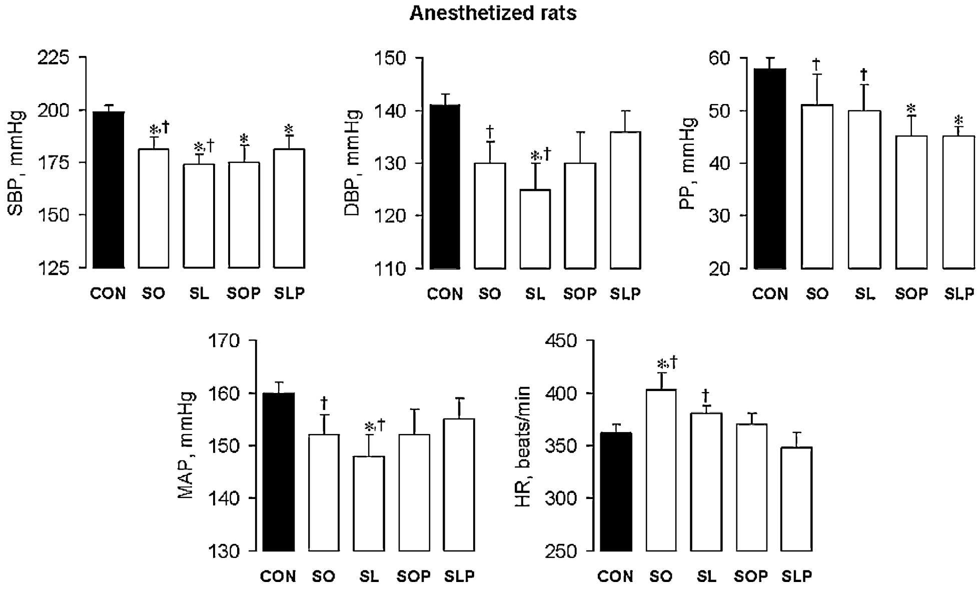

Fig. 2 Dietary effects on resting cardiovascular parameters in *anesthetized rats*: systolic arterial blood pressure (*SBP*); diastolic arterial blood pressure (*DBP*); pulse pressure (*PP*); mean arterial blood pressure (*MAP*); heart rate (*HR*). Treatment groups: *CON*, control; *SO*, sesame oil; *SL*, structured lipids; *SOP*, sesame oil fortified with phytosteryl esters; *SLP*, structured lipids fortified with phytosteryl esters. The data are presented as mean ± SEM. *$P < 0.05$, versus control. $^{\dagger}P > 0.05$, SO versus SL

Discussion

Effects of Dietary MLM-Type Structured Lipids

The present study showed that the dietary effects of MLM-type structured lipids produced from sesame oil and caprylic acid on the plasma lipid profiles in SHR were not different from those of original sesame oil. The major rationale for MLM-type structured lipids development is based on (1) the difference in the metabolic aspects of long chain fatty acids by their positional distribution in triacylglycerol and (2) the rapid metabolism of medium chain fatty acids in triacylglycerol. The long chain fatty acids at the *sn*-2 position of the triacylglycerol are preferentially absorbed and stored in humans compared to the long chain fatty acids located at the *sn*-1,3 positions since triacylglycerols are hydrolyzed into free fatty acids and *sn*-2 monoacylglycerols by lipoprotein lipase, and *sn*-2 monoacylglycerols readily form mixed micelles with bile salts [36, 37]. The medium chain fatty acids are poorly transported through the lymphatic system [38]. Instead, they are readily absorbed and transported through the portal system especially when they are at the *sn*-1,3 positions in triacylglycerol and this leads to more rapid absorption of MLM-type structured lipids compared to LCT [4, 37–39]. The total contents of the principal long chain fatty acids (e.g., palmitic, oleic, and linoleic acids) of original sesame oil were reduced in the structured lipids due to their replacement with caprylic acid. However, their *sn*-2 positional contents were similar in both sesame oil and

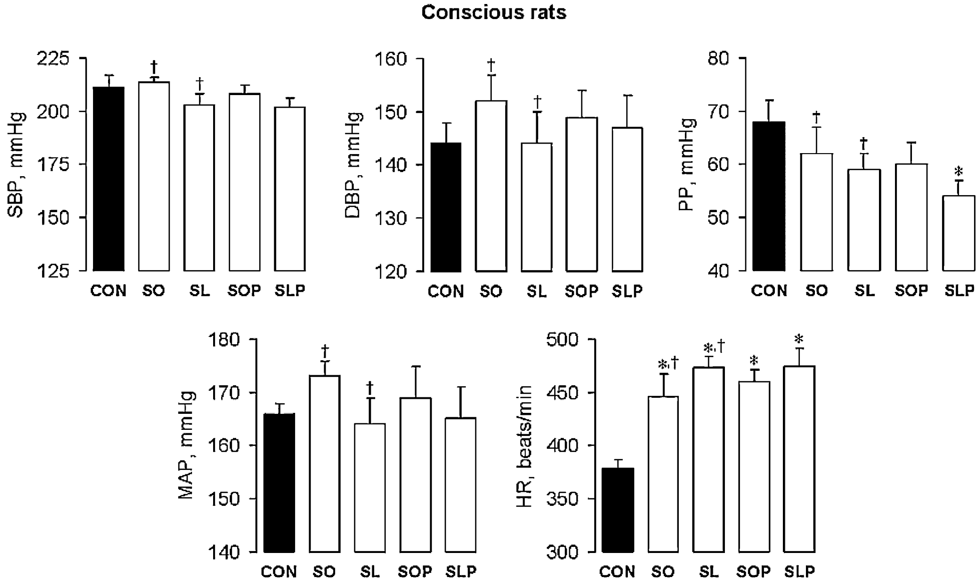

Fig. 3 Dietary effects on resting cardiovascular parameters in *conscious rats*: systolic arterial blood pressure (*SBP*); diastolic arterial blood pressure (*DBP*); pulse pressure (*PP*); mean arterial blood pressure (*MAP*); heart rate (*HR*). Treatment groups: *CON*, control; *SO*, sesame oil; *SL*, structured lipids; *SOP*, sesame oil fortified with phytosteryl esters; *SLP*, structured lipids fortified with phytosteryl esters. The data are presented as mean ± SEM. *$P < 0.05$, versus control. $^{\dagger}P > 0.05$, SO versus SL

structured lipids because most caprylic acids were incorporated at *sn*-1,3 positions in the structured lipids. Therefore, the similarity in *sn*-2 positional fatty acid profiles between sesame oil and structured lipids as well as more efficient absorption of structured lipids compared to sesame oil might be the reasons for the lack of difference in their dietary effects on plasma lipid profiles.

On the other hand, the effects of *sn*-1,3 positional fatty acid profiles of both oils on plasma lipid profiles were also shown to be comparable to each other. Cater et al. [40] suggested that medium chain fatty acids including caprylic acid might be hypercholesterolemic and hypertriglyceridemic. They found that a medium chain triacylglycerol diet, where 43% of total dietary calories were provided as caprylic acid and capric acid tended to increase plasma LDL cholesterol and triacylglycerol levels in humans compared to a high oleic acid oil diet even though the medium chain triacylglycerol diet slightly lowered plasma LDL cholesterol level compared to a high palmitic acid oil diet [40]. Accordingly, the structured lipids should have been more hypercholesterolemic and more hypertriglyceridemic than original sesame oil because of their reduced content of oleic acid and considerable high content of caprylic acid. However, the present study showed that both SHR fed sesame oil and those fed structured lipids presented similar plasma total and LDL cholesterol levels as well as similar plasma triacylglycerol levels. It is very complicated to distinguish between the dietary effects of total and individual fatty acids. Nevertheless, the possible explanations are: first, the caprylic acid contents of our experimental diets containing structured lipids (i.e., diets for structured lipids dietary group and structured lipids fortified with phytosteryl esters dietary group) were approximately 18% of total dietary calories, which was considerably lower than the caprylic acid levels in their diets [40]; and second, the effects of caprylic acid, which are mostly located at *sn*-1,3 positions in the structured lipids were counterbalanced by the reduced contents of major long chain fatty acids, such as palmitic, oleic, and linoleic acids present at the same positions even though the individual fatty acids would have different effects.

Effects of Dietary Phytosteryl Esters

The present study showed that the plasma HDL cholesterol levels were distinctly increased in the rats fed phytosteryl esters (i.e., the rats fed sesame oil fortified with phytosteryl esters and those fed structured lipids fortified with phytosteryl esters) compared to control rats or those fed sesame oil or structured lipids alone. Moreover, the plasma HDL/total cholesterol ratios in the rats fed phytosteryl esters were similar to that in control rats. These results indicate that dietary phytosteryl esters have positive effects on blood cholesterol profiles in SHR, as reported in humans and rabbits by others [8–10]. However, the phytosteryl esters-fed rats presented higher plasma total and LDL cholesterol levels as well as higher plasma LDL to total cholesterol ratios than control rats. These results are probably related to the fact that the diets containing phytosteryl esters have higher dietary fat and/or dietary cholesterol levels than control diets. In the case that the phytosteryl esters-fed rats are administered with the same levels of dietary fat and/or dietary cholesterol to those of the control diets, they are expected to present reduced plasma total and LDL cholesterol levels compared to the levels reported in the present study. The effects of high dietary fat levels in SHR are additionally discussed below.

Effects of High Dietary Fat Levels

The body weights, liver weights and liver weight to body weight ratios were higher in all HFHC dietary groups compared to the controls. In addition, the HFHC diets increased plasma total and LDL cholesterol levels compared to normal diets. As such, it appears that high dietary fat and/or cholesterol levels induce obesity and fatty liver in SHR. In contrast, heart and kidney weights and their weights to body weight ratios in the HFHC dietary groups were similar to those of the controls. The heart weights of SHR are higher than in normotensive control rats and this hypertrophy is a direct result of the higher blood pressures in SHR [16, 41]. Accordingly, the lack of effect of the HFHC diets on heart weights in the SHR is in line with the lack of major effects of the diets on resting arterial blood pressures in conscious SHR (see below).

The finding that resting systolic blood pressures of the HFHC dietary groups were lower than in controls under pentobarbital anesthesia suggests that arterial compliance was increased by these diets. This is a provocative finding and suggests that the timing and duration of high-fat feeding as well as the state of consciousness of the animal plays a major role in the expression of the changes in cardiovascular status. The finding that resting arterial pressures of the conscious HFHC dietary groups were not different to the control group is also provocative since there is evidence that high-fat diets increase arterial pressures in normotensive rats [42, 43]. The finding that the resting heart rates of the HFHC dietary groups were higher than in the controls suggests that these diets affect cardiac pacemaker activity. Whether this is due to direct effects on pacemaker cells (i.e., effects on intrinsic pacemaker activity) or changes in the release of sympathetic and parasympathetic neurotransmitters and/or their signaling mechanisms remains to be determined.

Summary

The present study demonstrates that the dietary effects of sesame oil-based MLM-type structured lipids on the plasma lipid profiles and cardiovascular parameters (resting arterial blood pressures and heart rates) of SHR are not different from those of original sesame oil (LCT). Dietary phytosteryl esters have positive effects on the plasma cholesterol profiles in SHR. However, our findings have the limitation of applicability to humans because the rat models have traditionally not been as ideal as other rodent models (e.g., hamsters and guinea pigs) for testing the effects of dietary lipids on blood lipid and lipoprotein lipid profiles [44]. Despite the lack of obvious effects of 9-week intake of structured lipids and phytosteryl esters on resting arterial blood pressures, lower or higher dietary intakes of these compounds may have positive effects on cardiovascular status of SHR. However, these different diets elicit tachycardia in SHR. Moreover, it is important to recognize the distinct possibility that the effect of high fat diets on blood pressure, heart rate and other cardiovascular parameters may differ in SHR compared with normotensive rats.

References

1. Akoh CC (2002) Structured lipids, In: Akoh CC, Min DB (eds) Food lipids–chemistry, nutrition, and biotechnology. 2nd edn, Marcel Dekker, New York
2. Iwasaki Y, Yamane T (2000) Enzymatic synthesis of structured lipids. J Mol Catal B Enzym 10:29–140
3. Xu X, Balchen S, Høy CE, Alder-Nissen J (1998) Pilot batch production of specific-structured lipids by lipase-catalyzed interesterification: preliminary study on incorporation and acyl migration. J Am Oil Chem Soc 75:301–308
4. Bach AC, Babayan VK (1982) Medium-chain triglycerides: an update. Am J Clin Nutr 36:50–962
5. Bray GA, Lee M, Bray TL (1980) Weight gain of rats fed medium-chain triglycerides is less than rats fed long-chain triglycerides. Int J Obes 4:7–32
6. Hayes DG, Gulari E (1992) Formation of polyol-fatty acid esters by lipases in reverse micellar media. Biotechnol Bioeng 40:110–118
7. Wester I (2000) Cholesterol-lowering effect of plant sterols. Eur J Lipid Sci Technol 102:37–44
8. Lees AM, Mok HY, Lees RS, McCluskey MA, Grundy SM (1977) Plant sterols as cholesterol-lowering agents: clinical trials in patients with hypercholesterolemia and studies of sterol balance. Atherosclerosis 28:325–338
9. Beveridge JM, Haust HL, Connel WF (1964) Magnitude of the hypocholesterolemic effect of dietary sitosterol in man. J Nutr 83:119–122
10. Pollak OJ (1953) Successive prevention of experimental hypercholesterolemia and cholesterol atherosclerosis in the rabbit. Circulation 7:696–701
11. Trautwein EA, Duchateau GSMJE, Lin YG, Mel'nikov SM, Molhuizen HOF, Ntanios FY (2003) Proposed mechanisms of cholesterol-lowering action of plant sterols. Eur J Lipid Sci Technol 105:171–185
12. Neil HA, Meijer GW, Roe LS (2001) Randomised controlled trial of use by hypercholesterolaemic patients of a vegetable oil sterol-enriched fat spread. Atherosclerosis 156:329–337
13. Law M (2000) Plant sterol and stanol margarines and health. Br Med J 320:861–864
14. Weststrate JA, Meijer GW (1998) Plant sterol-enriched margarines and reduction of plasma total- and LDL-cholesterol concentrations in normocholesterolaemic and mildly hypercholesterolaemic subjects. Eur J Clin Nutr 52:334–343
15. Jones PJH, MacDougall DE, Ntanios F, Vanstone CA (1997) Dietary phytosterols as cholesterol-lowering agents in humans. Can J Physiol Pharmacol 75:217–227
16. Lerman LO, Chade AR, Sica V, Napoli C (2005) Animal models of hypertension: an overview. J Lab Clin Med 146:160–173
17. Shimamoto K, Ura N (2006) Mechanisms of insulin resistance in hypertensive rats. Clin Exp Hypertens 28:543–552
18. Kim BH, Akoh CC (2006) Characteristics of structured lipid prepared by lipase-catalyzed acidolysis of roasted sesame oil and caprylic acid in a bench-scale continuous packed bed reactor. J Agric Food Chem 54:5132–5141
19. Miettinen TA, Gylling H (2004) Plant stanol and sterol esters in prevention of cardiovascular diseases. Ann Med 36:126–134
20. Katan MB, Grundy SM, Jones P, Law M, Miettinen T, Paoletti R (2003) Efficacy and safety of plant stanols and sterols in the management of blood cholesterol levels. Mayo Clin Proc 78:965–978
21. Noakes M, Clifton P, Ntanios F, Shrapnel W, Record I, McInerney J (2002) An increase in dietary carotenoids when consuming plant sterols or stanols is effective in maintaining plasma carotenoid concentrations. Am J Clin Nutr 75:79–86
22. Nestel P, Cehun M, Pomeroy S, Abbey M, Weldon G (2001) Cholesterol-lowering effects of plant sterol esters and non-esterified stanols in margarine, butter and low-fat foods. Eur J Clin Nutr 55:1084–1090
23. Hendriks HFJ, Weststrate JA, van Vliet T, Meijer GW (1999) Spreads enriched with three different levels of vegetable oil sterols and the degree of cholesterol lowering in normocholesterolaemic and mildly hypercholesterolaemic subjects. Eur J Clin Nutr 53:319–327
24. Ling WH, Jones PJH (1995) Dietary phytosterols: a review of metabolism, benefits and side effects. Life Sci 57:195–206
25. Miettinen TA, Puska P, Gylling H, Vanhanen H, Vartiainen E (1995) Reduction of serum cholesterol with sitostanol-ester margarine in a mildly hypercholesterolemic population. N Engl J Med 333:1308–1312
26. Lewis SJ, Hashmi-Hill MP, Owen JR, Sandock K, Robertson TP, Bates JN (2006) The vasodilator potency of the endothelium-derived relaxing factor, L-S-nitrosocysteine, is impaired in conscious spontaneously hypertensive rats. Vascul Pharmacol 44:476–490
27. Lewis SJ, Hashmi-Hill MP, Owen JR, Sandock K, Robertson TP, Bates JN (2006) ACE inhibition restores the vasodilator potency of the endothelium-derived relaxing factor, L-S-nitrosocysteine, in conscious spontaneously hypertensive rats. Vascul Pharmacol 44:491–507
28. Winer BJ (1971) Statistical principles of experimental design. 2nd edn, McGraw-Hill, New York
29. Wallenstein S, Zucker CL, Fleiss JC (1980) Some statistical methods useful in circulation research. Circ Res 47:1–9
30. Possas O, Johnson AK, Lewis SJ (2006) Role of nitrosyl factors in the hindlimb vasodilation produced by baroreceptor afferent nerve stimulation. Am J Physiol 290: R741–R748
31. Graves JE, Kooy NW, Lewis SJ (2006) L-β,β-Dimethylcysteine attenuates the hemodynamic responses elicited by systemic injections of peroxynitrite in anesthetized rats. Br J Pharmacol 148:7–15

32. Whalen EJ, Bates JN, Johnson AK, Lewis SJ (2006) Down-regulation of propranolol-sensitive β-adrenoceptor signaling after inhibition of nitric oxide synthesis. Br J Pharmacol 147:755–764
33. Whalen EJ, Schoorlemmer GHM, Beltz TG, Johnson AK, Lewis SJ (2001) Effects of chronic lesions of the anteroventral region of the third ventricle on cardiac β-adrenoceptor function in conscious rats. Brain Res 913:82–85
34. Lewis SJ, Hoque A, Bates JN (2005) Differentiation of L- and D-S-nitrosothiol recognition sites. J Cardiovasc Pharmacol 46:660–671
35. Lewis SJ, Graves JE, Bates JN, Kooy NW (2005) Peroxynitrite elicits dysfunction of stereoselective S-nitrosocysteine recognition sites. J Cardiovasc Pharmacol 46:637–645
36. Kubow S (1996) The influence of positional distribution of fatty acids in native, interesterified and structure-specific lipids on lipoprotein metabolism and atherogenesis. J Nutr Biochem 7:530–541
37. Jandacek RJ, Whiteside JA, Holcombe BN, Volpenhein RA, Taulbee JD (1987) The rapid hydrolysis and efficient absorption of triglycerides with octanoic acid in the 1 and 3-positions and long chain fatty acid in the 2-position. Am J Clin Nutr 45:940–945
38. Tso P, Karlstad MD, Bistrian BR, DeMichele SJ (1995) Intestinal digestion, absorption, and transport of structured triglycerides and cholesterol in rats. Am J Physiol 268:G568–G577
39. Straarup EM, Høy CE (2000) Structured lipids improve fat absorption in normal and malabsorbing rats. J Nutr 130:2802–2808
40. Cater NB, Heller HJ, Denke MA (1997) Comparison of the effects of medium-chain triacylglycerols, palm oil, and high oleic sunflower oil on plasma triacylglycerol fatty acid and lipid and lipoprotein concentrations in humans. Am J Clin Nutr 65:41–45
41. Touyz RM (2004) Reactive oxygen species, vascular oxidative stress, and redox signaling in hypertension: what is the clinical significance? Hypertension 44:248–252
42. Uemura K, Mori N (2006) Influence of age and sex on high-fat diet-induced increase in blood pressure. Nagoya J Med Sci 68:109–114
43. Song GY, Gao Y, Di YW, Pan LL, Zhou Y, Ye JM (2006) High-fat feeding reduces endothelium-dependent vasodilation in rats: differential mechanisms for saturated and unsaturated fatty acids? Clin Exp Pharmacol Physiol 33:708–713
44. Beher WT, Baker GD, Penney DG (1963) A comparative study of the effects of bile acids and cholesterol on cholesterol metabolism in the mouse, rat, hamster and guinea pig. J Nutr 79:523–530

Lipids (2008) 43:65–77
DOI 10.1007/s11745-007-3132-7

ARTICLE

Comparison of Low Fat and Low Carbohydrate Diets on Circulating Fatty Acid Composition and Markers of Inflammation

Cassandra E. Forsythe · Stephen D. Phinney · Maria Luz Fernandez · Erin E. Quann · Richard J. Wood · Doug M. Bibus · William J. Kraemer · Richard D. Feinman · Jeff S. Volek

Received: 5 July 2007 / Revised: 24 October 2007 / Accepted: 25 October 2007 / Published online: 29 November 2007
© AOCS 2007

Abstract Abnormal distribution of plasma fatty acids and increased inflammation are prominent features of metabolic syndrome. We tested whether these components of metabolic syndrome, like dyslipidemia and glycemia, are responsive to carbohydrate restriction. Overweight men and women with atherogenic dyslipidemia consumed ad libitum diets very low in carbohydrate (VLCKD) (1504 kcal:%CHO:fat:protein = 12:59:28) or low in fat (LFD) (1478 kcal:%CHO:fat:protein = 56:24:20) for 12 weeks. In comparison to the LFD, the VLCKD resulted in an increased proportion of serum total n-6 PUFA, mainly attributed to a marked increase in arachidonate (20:4n-6), while its biosynthetic metabolic intermediates were decreased. The n-6/n-3 and arachidonic/eicosapentaenoic acid ratio also increased sharply. Total saturated fatty acids and 16:1n-7 were consistently decreased following the VLCKD. Both diets significantly decreased the concentration of several serum inflammatory markers, but there was an overall greater anti-inflammatory effect associated with the VLCKD, as evidenced by greater decreases in TNF-α, IL-6, IL-8, MCP-1, E-selectin, I-CAM, and PAI-1. Increased 20:4n-6 and the ratios of 20:4n-6/20:5n-3 and n-6/n-3 are commonly viewed as pro-inflammatory, but unexpectedly were consistently inversely associated with responses in inflammatory proteins. In summary, a very low carbohydrate diet resulted in profound alterations in fatty acid composition and reduced inflammation compared to a low fat diet.

Keywords Arachidonic acid · Palmitoleic acid · Ketogenic diet · Saturated fat · Metabolic syndrome

Abbreviations

VLCKD	Very low carbohydrate ketogenic diet
LFD	Low fat diet
PL	Phospholipid
CE	Cholesteryl ester
CVD	Cardiovascular disease
RDA	Recommended daily allowance
BMI	Body mass index
IL	Interleukin
TNF-α	Tumor necrosis factor-α
VEGF	Vascular endothelial growth factor
IFN-γ	Interferon-γ
EGF	Epidermal growth factor
MCP-1	Monocyte chemotactic protein-1
ICAM-1	Intracellular cellular adhesion molecule-1
VCAM-I	Vascular cellular adhesion molecule-I
NF-κB	Nuclear factor-kappa B

C. E. Forsythe · E. E. Quann · W. J. Kraemer · J. S. Volek (✉)
Department of Kinesiology, University of Connecticut,
2095 Hillside Road, Unit 1110, Storrs, CT 06269-1110, USA
e-mail: jeff.volek@uconn.edu

S. D. Phinney
School of Medicine, University of California, Davis, CA, USA

M. L. Fernandez · R. J. Wood · J. S. Volek
Department of Nutritional Science, University of Connecticut,
Storrs, CT, USA

D. M. Bibus
University of Minnesota and Lipid Technologies, LLC,
Austin, MN, USA

R. D. Feinman
Department of Biochemistry, SUNY Downstate Medical Center,
Brooklyn, NY, USA

CRP	C-reactive protein
TAG	Triglycerides

Introduction

Development of metabolic syndrome (insulin resistance syndrome) is associated with altered composition of circulating fatty acids characterized by higher saturated fatty acids (14:0, 16:0), higher palmitoleic acid (16:1n-7, the MUFA product derived from palmitic acid), higher dihomo-γ-linolenic acid (20:3n-6, the precursor of arachidonic acid), and lower levels of linoleic acid (18:2n-6) [1]. The effect of dietary fatty acid composition on circulating fatty acids [2] is not well understood. Two recent studies demonstrated that consumption of a diet higher in saturated fat resulted in lower circulating palmitic acid (16:0) in cholesteryl ester compared to a diet low in saturated fat [3, 4], a paradox likely explained by the level of carbohydrate [5] whose increase is known to be associated with de novo fatty acid synthesis [6] and decreased fatty acid oxidation. We have previously described a comparison between a very low carbohydrate diet (VLCKD) and a low fat diet (LFD) in subjects with features of metabolic syndrome. A notable finding was an inverse relationship between dietary and plasma saturated fatty acids (SFA). The VLCKD, with three-fold greater dietary SFA than the LFD, showed a consistently greater reduction in plasma SFA compared to the LFD [7].

Metabolic syndrome is generally defined by high fasting glucose, triglycerides (TG), blood pressure and waist circumference, and low HDL cholesterol. Resistance to the effects of insulin provides a metabolic basis for changes in these disparate physiologic markers as well an increasing number of associations that extend beyond the original description of the syndrome almost 20 years ago [8]. New features that appear to be associated with metabolic syndrome include disturbed circulating fatty acid composition, perturbed lipid metabolism and increased oxidative stress and inflammation [9]. Fatty acids contribute to overall inflammatory balance by several mechanisms. In macrophages, SFA activate toll-like receptor signaling leading to activation of nuclear factor-kappa B (NF-κB) and expression of cyclooxygenase-2 [10, 11]. NF-κB is a transcription factor that regulates over 100 genes, many with an established role in inflammatory responses and atherosclerosis, and may therefore represent a crucial link between fatty acids, metabolic syndrome and atherogenesis [12]. Arachidonic acid (20:4n-6) in membranes is commonly assumed to have a deleterious effect on overall inflammatory balance because of its enzymatic conversion to proinflammatory, proaggregative, and vasoconstrictive eicosanoids (e.g., prostaglandin E_2, thromboxane A_2, leukotrienes B_4). Arachidonic acid is also capable of non-enzymatic conversion to other proinflammatory bioactive products (F2-isoprostanes) via interaction with molecular oxygen. In contrast, eicosanoids derived from the 20-carbon n-3 PUFA, eicosapentaenoic acid (20:5n-3), have less potent inflammatory effects [13]. A recent report showed a marked increase in the plasma 20:4n-6/20:5n-3 ratio in subjects consuming a VLCKD, while CRP, a marker of constitutive inflammation, decreased slightly [14]. The relations between inflammatory markers and arachidonic acid metabolism are complex [15], and may be further modified by the level of dietary carbohydrate.

Carbohydrate restriction is generally effective at ameliorating those physiologic markers associated with metabolic syndrome: high fasting glucose and insulin, and particularly the atherogenic dyslipidemia characterized by high TG and low HDL [16–19]. The effects are presumed to be attributed to better regulation of plasma glucose and insulin levels and improvement in the hyperinsulinemia/insulin resistance that are fundamental features of metabolic syndrome. Here we evaluated circulating fatty acid composition in three lipid fractions as well as a large number of inflammatory makers and show that a VLCKD results in profound alterations in fatty acid composition and reduced inflammatory markers to a greater extent than a low fat diet.

Materials and Methods

Study Design and Subjects

Details of this investigation have been described previously [7]. In brief, 40 overweight men and women aged 18–55 year with a BMI >25 kg/m^2 participated in this 12 week randomized, controlled, dietary intervention trial comparing a VLCKD to a LFD. All participants were required to have atherogenic dyslipidemia defined by moderately elevated TG (150 to 500 mg/dl) and low HDL [<40 (men) or <50 (women) mg/dl]. The two dietary groups were balanced for gender, age and BMI. Exclusion criteria were any metabolic and endocrine disorders, use of glucose-lowering, lipid-lowering or vasoactive prescriptions or supplements, consumption of a VLCKD, or weight loss >5.0 kg in the past 3 months. Habitual physical activity was maintained throughout the study intervention and was documented daily. Blood was drawn at baseline and after 12 week of diet intervention in the morning after a 12 h overnight fast and a 24 h abstinence from alcohol and strenuous exercise. All procedures were approved by the Institutional Review Board of the University of Connecticut, and all participants provided written informed consent.

Dietary Intervention

Subjects received individual and personalized dietary counseling from Registered Dietitians during the dietary intervention. No explicit instructions were provided regarding caloric intake for either diet to allow expression of any non-cognitive aspects on food intake. Subjects received weekly follow-up counseling during which body mass was measured, compliance was assessed, and further dietetic education was provided. Dietary intake and compliance was assessed with detailed and weighed 7-day food records at baseline, during weeks one, 6, and 12, and was analyzed for energy and macro/micronutrient content using NUTRITIONIST PRO™ (Version 1.5, First Databank Inc, The Hearst Corporation, San Bruno, CA, USA). The nutrient analysis program had no missing values for the nutrients reported and the database was extensively updated with new foods and individualized recipes. All subjects were given a multi-vitamin/mineral complex that provided micronutrients at levels $\leq$100% of the RDA.

The main goal of the VLCKD was to restrict carbohydrate to a level that induced a low level of ketosis. Subjects monitored their level of ketosis daily using urine reagent strips. In this diet there were no restrictions on the intake of fat from saturated and unsaturated sources or the intake of cholesterol. Examples of foods consumed by the subjects included unlimited amounts of beef, poultry, fish, eggs, oils and heavy cream; moderate amounts of hard cheeses, low carbohydrate vegetables and salad dressings; and small amounts of nuts, nut butters and seeds. Subjects restricted fruit and fruit juices, dairy products (with the exception of heavy cream and hard cheese), breads, grains, pasta, cereal, high carbohydrate vegetables, and desserts. Subjects were instructed to avoid all low carbohydrate breads and cereal products, and were limited to a maximum of one sugar alcohol-containing, low carbohydrate snack per day.

The LFD was designed to provide <10% of total calories from saturated fat and <300 mg cholesterol. Foods encouraged included whole grains (breads, cereals, and pastas), fruit/fruit juices, vegetables, vegetable oils, low-fat dairy and lean meat products. Standard diabetic exchange lists were used to ensure a macronutrient balance of protein (~20% energy), fat (~25% energy), and carbohydrate (~55% of energy).

Blood Analyses

Whole blood was collected into tubes with no preservative or EDTA and centrifuged at 1500×*g* for 15 min and 4°C, and promptly aliquoted into separate storage tubes which were stored at 75 °C until analyzed for serum fatty acid composition and plasma inflammatory markers. An aliquot of anti-coagulated whole blood (~3 ml) was sent to a certified medical laboratory (Quest Diagnostics, Wallingford, CT, USA) for a white blood cell differential count.

Inflammatory Biomarkers

The Evidence Investigator™ Biochip Array technology (Randox Laboratories Ltd, UK) that uses sandwich chemiluminescent immunoassays to simultaneously detect multiple analytes from a single sample was used to determine the following serum cytokines and adhesion molecules: IL-6, IL-8, vascular endothelial growth factor (VEGF), TNF-α, IFN-γ, epidermal growth factor (EGF), monocyte chemotactic protein-1 (MCP-1), intracellular cellular adhesion molecule-1 (ICAM-1), vascular cellular adhesion molecule-I (VCAM-I), E-selectin, P-selectin and L-selectin. In addition, serum C-reactive protein (CRP) was determined on an IMMULITE Automated Analyzer using the commercially available immulite chemiluminescent enzyme immunometric assay (Immulite®, Diagnostic Products Corp, Los Angeles, CA, USA) and plasma plasminogen-activator inhibitor-1 (PAI-1) was determined utilizing the Luminex 200 analyzer (Luminex Corp, Austin, TX, USA) using an immunoassay kit from LINCO Research.

Fatty Acid Composition

Serum lipids were extracted according to the method of Bligh–Dyer whereby mixtures of plasma, methanol, chloroform and water were prepared such that lipid is recovered in a chloroform layer. The resulting lipid extracts were maintained under an atmosphere of nitrogen following extraction and kept frozen prior to additional processing. Immediately prior to lipid class separation, lipid samples were dried under a gentle stream of nitrogen, rediluted in 50 μl of chloroform and prepared for lipid class separation. Lipid classes including total TAG, PL and CE were separated on commercial silica gel G plates (AnalTech, Newark, DE, USA). The chromatographic plates were developed in a solvent system consisting of distilled petroleum ether (bp 30–60 °C):diethyl ether:acetic acid (80:20:1, by vol). Following development, the silica gel plates were sprayed with a methanolic solution containing 0.5% 2,7-dichlorofluorescein which was then used to visualize lipid classes under ultraviolet light. Desired corresponding lipid bands were then scraped into Teflon line screw cap tubes. The samples were then transesterified with boron trifluoride (10%) in excess methanol (Supelco, Bellefonte, PA, USA) in an 80 °C water bath for 90 min. Resulting fatty acid methyl esters were extracted with water and petroleum ether and stored frozen until gas chromatographic analysis was performed.

Lipid class fatty acid methyl ester composition was determined by capillary gas chromatography. Methyl ester samples were blown to dryness under nitrogen and resuspended in hexane. Resulting fatty acid methyl esters were separated and quantified with a Shimadzu capillary gas chromatograph (GC17) utilizing a 30 m Restek free fatty acid phase (FFAP) coating and EZChrom software. The instrument temperature was programmed from 190 to 240 °C at 7°C/min with a final hold of 10 min, separating and measuring fatty acid methyl esters ranging from 12:0 to 24:1. The detector temperature was 250 °C. Helium carrier gas was used at a flow rate of 1.4 ml/min. and a split ratio of 1:25. Chromatographic data was collected and processed with EZChrom software (Scientific Products, CA, USA). Fatty acids were identified by comparison to authentic fatty acid standards and quantitated with peak area and internal standard. Resulting data are expressed in percent composition. Individual peaks, representing as little as 0.05% of the fatty acid methyl esters, were distinguished.

Statistical Analyses

All statistical analyses were done with Statistica software (StatSoft Inc, Tulsa, OK, USA). A 2 × 2 ANOVA with one between effect (VLCKD vs. LFD) and one within effect (Week 0 vs. Week 12) was used to compare biochemical responses over time in both groups. Significant main or interaction effects were further analyzed using a Fishers LSD post hoc test. Relationships among selected variables were examined using Pearson's product-moment correlation coefficient. The alpha level for significance was set at 0.05.

Results

Dietary Intake and MetS Responses

Dietary nutrient intake and responses of MetS biomarkers will be presented elsewhere [7]. In brief, subjects in both groups reduced energy intake to approximately 1500 kcal/day, but the diets had markedly different macronutrient distributions based upon the analysis of individual diet records (VLCKD, %CHO:fat:protein = 12:59:28) and (LFD, %CHO:fat:protein = 56:24:20) (Table 1). Dietary saturated fat and cholesterol intake were significantly higher during the VLCKD than the LFD. The LFD led to improvements in some metabolic markers, but subjects following the VLCKD had consistently greater weight loss,

Table 1 Daily nutrient intake and serum cholesterol responses of men and women who consumed low carbohydrate and low fat diets

Variables	VLCKD (*n* = 20)		LFD (*n* = 20)		2 × 2 ANOVA	
	Baseline	Intervention	Baseline	Intervention	Time	T × G
Energy (kcal)	2351 ± 617	1504 ± 494	2082 ± 445	1478 ± 435	0.000	0.154
Protein (g)	94.6 ± 28.5	104.8 ± 33.6	82.3 ± 17.6	71.5 ± 21.3	0.756	0.009
Protein (%)	16.2 ± 3.1	28.1 ± 4.4	15.8 ± 2.6	19.6 ± 4.4	0.000	0.000
Carbohydrate (g)	270.3 ± 67.2	44.8 ± 18.9	266.8 ± 74.7	208.3 ± 69.6	0.000	0.000
Carbohydrate (%)	46.6 ± 7.7	12.4 ± 5.2	50.9 ± 10.1	55.8 ± 7.9	0.000	0.000
Total Fat (g)	97.0 ± 35.2	100.2 ± 37.9	78.5 ± 29.5	40.0 ± 17.5	0.004	0.001
Total Fat (%)	36.2 ± 6.7	58.9 ± 5.4	33.0 ± 9.8	23.8 ± 6.8	0.000	0.000
Saturated Fat (g)	34.2 ± 14.3	36.4 ± 12.9	26.0 ± 11.1	11.7 ± 5.9	0.012	0.002
Monounsaturated Fat (g)	19.2 ± 6.5	26.4 ± 11.1	18.0 ± 9.6	8.9 ± 4.7	0.830	0.000
Polyunsaturated Fat (g)	12.4 ± 7.4	12.4 ± 7.8	10.6 ± 7.4	5.1 ± 3.1	0.064	0.019
18:1n-9 (g)	14.0 ± 5.0	20.9 ± 9.5	11.6 ± 6.9	6.5 ± 3.8	0.289	0.000
18:2n-6 (g)	7.4 ± 6.0	7.7 ± 5.1	5.8 ± 4.7	2.9 ± 2.0	0.215	0.042
18:3n-3 (mg)	989 ± 1199	879 ± 746	575 ± 398	325 ± 198	0.139	0.439
20:5n-3 (mg)	8 ± 10	46 ± 81	32 ± 50	32 ± 58	0.047	0.050
22:6n-3 (mg)	24 ± 24	117 ± 184	83 ± 116	82 ± 154	0.049	0.052
Alcohol (%)	0.9 ± 1.8	0.7 ± 1.4	0.3 ± 0.5	0.9 ± 2.0	0.232	0.056
Cholesterol (mg)	354 ± 120	605 ± 262	267 ± 111	144 ± 80	0.044	0.000
Dietary Fiber (g)	13.1 ± 3.5	9.4 ± 4.9	15.8 ± 6.6	17.3 ± 9.6	0.083	0.021
Serum total cholesterol (mg/dl)	208.0 ± 26.0	196.5 ± 34.9	204.0 ± 31.5	194.5 ± 34.0	0.016	0.816
Serum LDL-C (mg/dL)	130.4 ± 21.8	135.4 ± 31.4	127.9 ± 31.3	125.9 ± 32.1	0.357	0.357
Serum HDL-C (mg/dl)	35.8 ± 6.9	40.4 ± 9.6	38.7 ± 6.2	38.4 ± 5.5	0.001	0.000

Values are mean ± SD calculated from 7 days of weight food records at baseline (week 0) and 7 days during weeks 1, 6, and 12 (Intervention) decreased adiposity, improved glycemic control and insulin sensitivity and more favorable TAG, HDL-C and total cholesterol/HDL-C ratio responses. In addition to these markers for MetS, the VLCKD subjects showed more favorable responses in alternative indicators of atherogenic dyslipidemia and cardiovascular risk: postprandial lipemia, apo B, apo A-1, the apo B/Apo A-1 ratio, LDL particle distribution and postabsorptive and postprandial vascular function. Most striking, we reported that despite a threefold higher intake of dietary saturated fat during the VLCKD compared to the LFD, circulating saturated fatty acids in TAG and CE were significantly decreased, as was 16:1n-7, an endogenous marker of lipogenesis. There were profound changes, as well, in other fatty acids in circulating TG, PL, and CE fractions (Tables 2–4).

Circulating Triglyceride Fatty Acids

Compared to the LFD, consumption of the VLCKD resulted in a significantly greater increase in TG n-6 PUFA, mainly attributed to a marked increase in arachidonic acid: 17 of 20 subjects in VLCKD showed marked increases while only 7 of 20 subjects on LFD showed increases in 20:4n-6 and these were more modest in amplitude (Table 2). In both groups, n-3 PUFA was decreased due largely to lower α-linolenic acid (18:3n-3) and 20:5n-3. The n-6/n-3 and arachidonic/eicosapentaenoic acid ratios were, on average, nearly doubled in response to the VLCKD and virtually unchanged by the LFD: 15 of 20 subjects on VLCKD showed increases in the n-6/n-3 ratios, while only 8 of 20 of the LFD showed increases. In contrast to the response in 20:4n-6, the metabolic intermediates in the biosynthetic pathway, especially 20:3n-6, were decreased after the VLCKD. As previously reported, total MUFA was unchanged but 16:1n-7 and total SFA was significantly decreased in response to the VLCKD.

Circulating Phospholipid Fatty Acids

The pattern of fatty acid changes seen in the TAG fraction was also found in circulating phospholipids: consumption of the VLCKD was associated with an increase in n-6 PUFA, again primarily due to a distinct increase in 20:4n-6 (Fig 1a), whereas 18:3n-6 and 20:3n-6 were markedly decreased (Table 3). The VLCKD was associated with a significant reduction in 18:3n-3, 18:4n-3, 20:4n-3, and 20:5n-3. However docosahexaenoic acid (22:6n-3) was increased so that total n-3 PUFA was not significantly changed. Compared to the LFD, ingestion of the VLCKD resulted in a significant increase in total PUFA and the ratio of n-6/n-3 (Fig. 1b) and arachidonic/eicosapentaenoic acid (Fig. 1c). In comparison to the LFD, total MUFA was significantly decreased in response to the VLCKD due to significant decreases in the most abundant MUFA, 18:1n-9, and a consistent reduction in 16:1n-7.

Circulating Cholesteryl Ester Fatty Acids

The patterns of CE fatty acid responses to diet resembled that in TG and PL, and in general were more dramatic in this lipid fraction (Table 4). Total n-6 PUFA was significantly increased in response to the VLCKD due to a large increase in 18:2n-6 and a smaller increase in 20:4n-6: most of the VLCKD group showed a significant increase in 20:4n-6 while only five of the LFD group showed an increase. On the other hand total n-3 PUFA was significantly decreased due to a reduced proportion of 18:3n-3 and 20:5n-3 in response to the VLCKD but, similar to other fractions, there was an increase in 22:6n-3. The n-6/n-3 and arachidonic/eicosapentaenoic acid ratios were unchanged in response to the LFD but increased sharply after consumption of the VLCKD. Total MUFA decreased in response to the VLCKD, again due to a reduced proportion of 18:1n-9 and a striking decrease in 16:1n-7.

Inflammatory Markers

Both diets led to a similar significant reduction in the acute phase reactant C-reactive protein (−23%), VEGF (−21%), P-selectin (−11%), and a trend for EGF (−38%), and V-CAM (−6%); however, there was an overall greater anti-inflammatory effect associated with the VLCKD as evidenced by significantly greater decreases in the proinflammatory cytokine TNF-α (−32 vs. −12%), the chemokines IL-8 (−33 vs. 4%) and MCP-1 (−24 vs. −5%), and the adhesion molecules E-selectin (−34 vs. −14%) and I-CAM (−17 vs. −3%) (Table 5). There was also a trend for a greater reduction in IL-6 (−35%) in response to the VLCKD ($P = 0.07$). Plasminogen-activator inhibitor-1 (PAI-1) has antifibrinolytic functions, and was also reduced more in subjects consuming the VLCKD compared to LFD (−34 vs. −8%). There was no effect of the interventions on leukocyte subpopulations.

Correlations

The results described above are surprising in that consumption of the VLCKD showed substantially greater increases in arachidonic acid and the arachidonic/eicosapentaenoic acid and n-6/n-3 ratios that are commonly viewed as contributing to an overall proinflammatory state,

Table 2 Serum triglyceride fatty acid responses of men and women who consumed low carbohydrate and low fat diets

Variables	VLCKD ($n = 20$)		Low Fat ($n = 20$)		2 × 2 ANOVA	
	Week 0	Week 12	Week 0	Week 12	Time	T × G
Total TG (mg/dl)	210.9 ± 57.9	103.7 ± 44.1	187.1 ± 57.6	151.2 ± 38.0	0.000	0.000
SFA						
12:0	0.09 ± 0.09	0.04 ± 0.06	0.06 ± 0.10	0.06 ± 0.13	0.271	0.108
14:0	1.94 ± 0.61	1.02 ± 0.40	1.86 ± 0.88	1.71 ± 0.61	0.000	0.001
15:0	0.27 ± 0.07	0.25 ± 0.05	0.28 ± 0.10	0.28 ± 0.08	0.478	0.527
16:0	27.07 ± 4.14	24.26 ± 1.65	24.86 ± 2.31	23.99 ± 1.86	0.002	0.092
18:0	3.66 ± 1.06	3.45 ± 0.66	3.32 ± 1.09	2.86 ± 0.48	0.051	0.466
20:0	0.06 ± 0.03	0.05 ± 0.04	0.04 ± 0.03	0.04 ± 0.03	0.354	0.901
22:0	0.03 ± 0.03	0.05 ± 0.03	0.03 ± 0.03	0.04 ± 0.03	0.079	0.584
24:0	0.01 ± 0.02	0.02 ± 0.04	0.00 ± 0.01	0.00 ± 0.00	0.514	0.155
Total SFA	33.13 ± 5.03	29.15 ± 1.39	30.45 ± 3.98	28.98 ± 2.45	0.000	0.086
MUFA						
14:1	0.22 ± 0.15	0.06 ± 0.09	0.18 ± 0.17	0.17 ± 0.13	0.000	0.004
15:1	0.04 ± 0.03	0.04 ± 0.05	0.03 ± 0.02	0.04 ± 0.04	0.627	0.659
16:1n-7	4.53 ± 1.07	3.10 ± 0.69	4.54 ± 0.98	4.53 ± 1.10	0.000	0.000
17:1	0.29 ± 0.06	0.26 ± 0.08	0.29 ± 0.10	0.29 ± 0.07	0.248	0.264
18:1n-9	36.31 ± 3.18	38.67 ± 2.73	38.91 ± 2.75	39.50 ± 2.90	0.015	0.132
20:1n-7	0.07 ± 0.03	0.05 ± 0.02	0.07 ± 0.02	0.07 ± 0.03	0.015	0.100
20:1n-9	0.27 ± 0.07	0.27 ± 0.08	0.31 ± 0.07	0.31 ± 0.07	0.912	0.672
22:1n-9	0.05 ± 0.03	0.05 ± 0.03	0.04 ± 0.03	0.03 ± 0.03	0.454	0.352
Total MUFA	41.78 ± 3.51	42.50 ± 2.99	44.37 ± 2.92	44.93 ± 3.25	0.292	0.900
n-6 PUFA						
18:2n-6	19.04 ± 3.58	22.19 ± 3.09	19.36 ± 4.36	19.99 ± 3.09	0.010	0.078
18:3n-6	0.45 ± 0.19	0.38 ± 0.17	0.38 ± 0.18	0.41 ± 0.23	0.517	0.102
20:2n-6	0.20 ± 0.07	0.18 ± 0.07	0.21 ± 0.08	0.21 ± 0.09	0.616	0.259
20:3n-6	0.34 ± 0.10	0.26 ± 0.06	0.33 ± 0.07	0.33 ± 0.08	0.001	0.003
20:4n-6	1.17 ± 0.35	1.70 ± 0.55	1.04 ± 0.27	1.16 ± 0.35	0.000	0.002
22:4n-6	0.18 ± 0.04	0.21 ± 0.06	0.17 ± 0.04	0.17 ± 0.04	0.040	0.049
22:5n-6	0.14 ± 0.07	0.27 ± 0.18	0.15 ± 0.10	0.13 ± 0.07	0.033	0.004
Total n-6	21.51 ± 3.59	25.18 ± 2.86	21.64 ± 4.24	22.39 ± 3.13	0.004	0.048
n-3 PUFA						
18:3n-3	1.10 ± 0.44	0.90 ± 0.51	1.04 ± 0.35	1.13 ± 0.60	0.494	0.080
18:4n-3	0.39 ± 0.21	0.27 ± 0.17	0.46 ± 0.20	0.44 ± 0.18	0.009	0.042
20:3n-3	0.04 ± 0.03	0.02 ± 0.02	0.03 ± 0.02	0.03 ± 0.04	0.054	0.051
20:4n-3	0.06 ± 0.04	0.02 ± 0.03	0.04 ± 0.03	0.04 ± 0.04	0.019	0.005
20:5n-3	0.15 ± 0.05	0.12 ± 0.04	0.13 ± 0.06	0.16 ± 0.11	0.696	0.025
22:5n-3	0.24 ± 0.06	0.29 ± 0.09	0.25 ± 0.08	0.28 ± 0.10	0.011	0.497
22:6n-3	0.31 ± 0.16	0.42 ± 0.16	0.27 ± 0.11	0.33 ± 0.23	0.019	0.486
Total n-3	2.30 ± 0.57	2.05 ± 0.63	2.22 ± 0.44	2.41 ± 0.72	0.790	0.039
n-9 PUFA						
20:3n-9	0.09 ± 0.04	0.12 ± 0.05	0.12 ± 0.06	0.13 ± 0.09	0.012	0.455
Total PUFA	23.90 ± 3.91	27.35 ± 3.11	23.97 ± 4.34	24.94 ± 3.56	0.006	0.106
Total HUFA	4.66 ± 0.73	4.98 ± 0.75	4.41 ± 0.64	4.74 ± 0.97	0.034	0.986
Total n-9	36.85 ± 3.24	39.05 ± 2.77	39.44 ± 2.68	40.02 ± 2.84	0.023	0.170
n-6/n-3	9.74 ± 2.20	13.16 ± 3.49	10.04 ± 2.47	9.74 ± 2.26	0.002	0.000
20:4n-6/20:5n-3	7.69 ± 1.82	14.76 ± 6.21	8.73 ± 3.44	9.33 ± 6.05	0.000	0.002

Values are weight percent (mean ± SD)

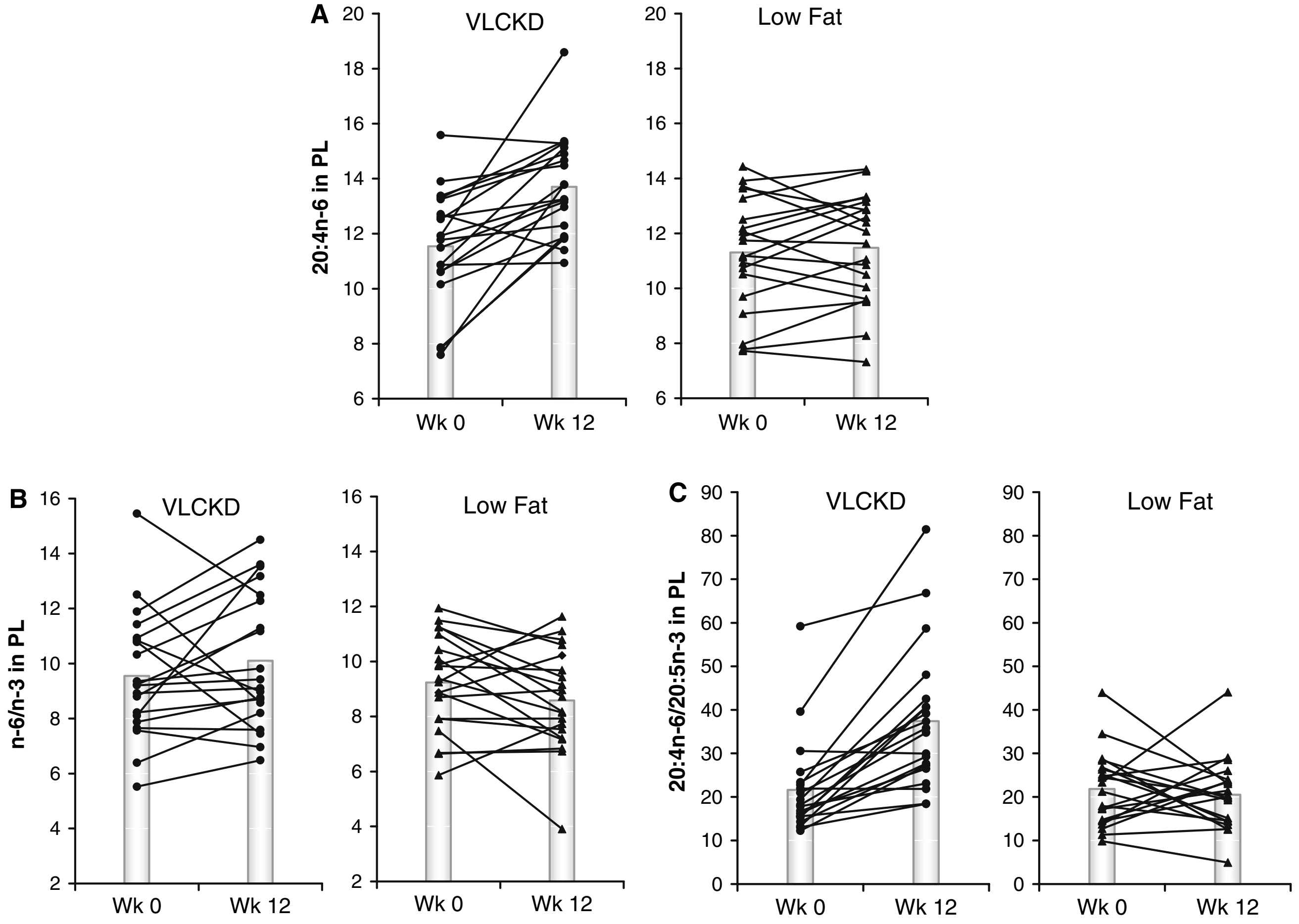

Fig. 1 Individual responses in serum phospholipid arachidonic acid (20:4n-6) (**a**), the n-6/n-3 ratio (**b**) and the arachidonic/eicosapentaenoic acid ratio (20:4n-6/20:5n-3) (**c**) in subjects who consumed a very low carbohydrate ketogenic diet (VLCKD) or a low fat diet for 12 weeks. *Shaded bars* indicate mean responses

while simultaneously there was a significant decrease in many inflammatory markers. An analysis of these data bears out the idea that changes in the fatty acid proxies were consistently inversely associated with responses in most of the inflammatory markers we measured (Fig. 2). The fatty acid with the most consistent positive association with changes in inflammatory markers was palmitoleic acid (16:1n-7). The correlations between weight loss and changes in inflammatory markers were generally small and not significant. As shown in Fig. 3 for two of the more important markers TNF-α and IL-8, there is essentially no correlation.

Discussion

Because of the continued emphasis on dietary recommendations for cardiovascular disease and general health, the relation between dietary fat intake and plasma fatty acids and inflammatory markers is of great importance. The findings presented here support our hypothesis that the components of metabolic syndrome are distinctly those that respond favorably to reduction in dietary carbohydrate [19]. Responses in fatty acid composition to the VLCKD in this study were exactly opposite to the fatty acid profile recently shown to be associated with development of metabolic syndrome over a 20 year period in previously healthy men (i.e., higher circulating 14:0, 16:0, 16:1n-7, 18:1n-9, 18:3n-6, and 20:3n-6, and lower levels of 18:2n-6) [1]. Abnormal fatty acid composition and inflammatory status are now recognized as prominent features of metabolic syndrome, and are reliably improved in subjects consuming a low carbohydrate diet compared to a low fat diet.

Acute ingestion of carbohydrate clearly induces an increase in reactive oxygen species and activation of proinflammatory pathways [9], and isocaloric high carbohydrate [20] and high glycemic [21] diets are associated with increased biomarkers of inflammation. In the context of hypocaloric diets, we showed that reducing dietary total

Table 3 Serum phospholipid fatty acid responses of men and women who consumed low carbohydrate and low fat diets

Variables	VLCKD (*n* = 20)		Low fat (*n* = 20)		2 × 2 ANOVA	
	Week 0	Week 12	Week 0	Week 12	Time	T × G
Total phospholipids (mg/dl)	196 ± 25	170 ± 33	183 ± 28	173 ± 30	0.001	0.135
SFA						
14:0	0.34 ± 0.12	0.28 ± 0.12	0.35 ± 0.13	0.36 ± 0.15	0.186	0.094
15:0	0.16 ± 0.03	0.17 ± 0.03	0.18 ± 0.06	0.18 ± 0.05	0.224	0.681
16:0	26.62 ± 1.64	26.87 ± 1.52	26.46 ± 1.59	27.02 ± 1.49	0.107	0.512
18:0	13.83 ± 1.25	12.76 ± 0.97	14.20 ± 1.58	13.56 ± 1.22	0.000	0.217
20:0	0.13 ± 0.04	0.18 ± 0.04	0.13 ± 0.03	0.13 ± 0.03	0.000	0.001
22:0	0.41 ± 0.11	0.57 ± 0.21	0.36 ± 0.11	0.35 ± 0.07	0.000	0.000
24:0	0.35 ± 0.11	0.48 ± 0.21	0.27 ± 0.12	0.26 ± 0.10	0.006	0.001
Total SFA	41.84 ± 1.30	41.31 ± 1.45	41.94 ± 1.17	41.88 ± 1.00	0.127	0.231
MUFA						
14:1	0.03 ± 0.06	0.07 ± 0.09	0.09 ± 0.09	0.10 ± 0.09	0.134	0.331
15:1	0.35 ± 0.11	0.54 ± 0.21	0.25 ± 0.16	0.29 ± 0.14	0.001	0.035
16:1n-7	0.92 ± 0.23	0.60 ± 0.17	0.86 ± 0.18	0.86 ± 0.23	0.000	0.000
17:1	0.28 ± 0.10	0.41 ± 0.17	0.26 ± 0.10	0.27 ± 0.08	0.002	0.007
18:1n-9	10.95 ± 1.60	9.88 ± 1.17	11.38 ± 0.94	11.67 ± 1.26	0.122	0.009
20:1n-7	0.05 ± 0.03	0.03 ± 0.01	0.04 ± 0.02	0.04 ± 0.02	0.011	0.020
20:1n-9	0.10 ± 0.02	0.12 ± 0.03	0.12 ± 0.05	0.13 ± 0.03	0.000	0.244
22:1n-9	0.05 ± 0.06	0.06 ± 0.04	0.06 ± 0.06	0.06 ± 0.05	0.754	0.654
24:1	0.42 ± 0.13	0.58 ± 0.22	0.37 ± 0.11	0.42 ± 0.11	0.000	0.041
Total MUFA	13.14 ± 1.68	12.29 ± 1.14	13.43 ± 1.09	13.84 ± 1.37	0.392	0.015
n-6 PUFA						
18:2n-6	22.99 ± 3.09	23.74 ± 2.69	22.66 ± 3.09	22.13 ± 2.74	0.807	0.162
18:3n-6	0.17 ± 0.06	0.10 ± 0.02	0.14 ± 0.04	0.14 ± 0.03	0.000	0.002
20:2n-6	0.29 ± 0.05	0.25 ± 0.07	0.34 ± 0.09	0.32 ± 0.08	0.008	0.234
20:3n-6	3.67 ± 0.82	2.29 ± 0.55	3.78 ± 0.76	3.50 ± 0.72	0.000	0.000
20:4n-6	11.54 ± 2.05	13.70 ± 1.82	11.31 ± 2.05	11.48 ± 1.97	0.000	0.001
22:4n-6	0.44 ± 0.08	0.40 ± 0.09	0.43 ± 0.10	0.42 ± 0.09	0.023	0.222
22:5n-6	0.41 ± 0.13	0.39 ± 0.11	0.38 ± 0.10	0.36 ± 0.13	0.379	0.883
Total n-6	39.50 ± 2.17	40.86 ± 2.04	39.04 ± 1.53	38.34 ± 1.53	0.246	0.001
n-3 PUFA						
18:3n-3	0.20 ± 0.08	0.15 ± 0.06	0.15 ± 0.07	0.19 ± 0.13	0.684	0.015
18:4n-3	0.13 ± 0.04	0.08 ± 0.04	0.13 ± 0.05	0.13 ± 0.07	0.000	0.003
20:3n-3	0.03 ± 0.02	0.03 ± 0.02	0.04 ± 0.03	0.04 ± 0.04	0.752	0.999
20:4n-3	0.12 ± 0.06	0.03 ± 0.02	0.10 ± 0.02	0.09 ± 0.05	0.000	0.000
20:5n-3	0.61 ± 0.20	0.42 ± 0.15	0.60 ± 0.27	0.68 ± 0.48	0.264	0.009
22:5n-3	0.81 ± 0.15	0.74 ± 0.16	0.87 ± 0.22	0.86 ± 0.20	0.044	0.104
22:6n-3	2.43 ± 0.84	2.80 ± 0.81	2.48 ± 0.62	2.71 ± 0.83	0.023	0.592
Total n-3	4.33 ± 0.90	4.24 ± 0.89	4.37 ± 0.80	4.69 ± 1.19	0.419	0.164
n-9 PUFA						
20:3n-9	0.09 ± 0.03	0.06 ± 0.03	0.10 ± 0.06	0.10 ± 0.05	0.048	0.092
Total PUFA	43.92 ± 1.89	45.17 ± 1.76	43.51 ± 1.11	43.14 ± 1.16	0.073	0.001
Total HUFA	20.64 ± 2.58	21.19 ± 1.90	20.51 ± 2.50	20.68 ± 2.32	0.323	0.599
Total n-9	11.55 ± 1.59	10.71 ± 1.16	12.02 ± 0.98	12.38 ± 1.29	0.341	0.021
n-6/n-3	9.55 ± 2.29	10.11 ± 2.46	9.24 ± 1.75	8.58 ± 1.84	0.879	0.062
20:4n-6/20:5n-3	21.59 ± 11.05	37.41 ± 16.28	21.86 ± 8.52	20.52 ± 8.20	0.000	0.000

Values are weight percent (mean ± SD)

Table 4 Serum cholesteryl ester fatty acid responses of men and women who consumed low carbohydrate and low fat diets

Variables	VLCKD (*n* = 20)		Low fat (*n* = 20)		2 × 2 ANOVA	
	Week 0	Week 12	Week 0	Week 12	Time	T × G
Total cholesteryl ester (mg/dl)	224 ± 35	224 ± 47	215 ± 42	199 ± 31	0.337	0.308
SFA						
14:0	0.79 ± 0.18	0.51 ± 0.13	0.69 ± 0.23	0.59 ± 0.24	0.000	0.010
15:0	0.17 ± 0.07	0.15 ± 0.05	0.14 ± 0.07	0.13 ± 0.09	0.274	0.475
16:0	11.23 ± 1.13	10.40 ± 0.84	10.79 ± 1.03	10.67 ± 0.88	0.011	0.052
18:0	1.15 ± 0.28	1.00 ± 0.22	1.29 ± 0.64	1.24 ± 0.69	0.268	0.596
20:0	0.05 ± 0.05	0.06 ± 0.03	0.05 ± 0.04	0.09 ± 0.09	0.009	0.035
22:0	0.01 ± 0.03	0.01 ± 0.01	0.01 ± 0.01	0.00 ± 0.01	0.222	0.501
24:0	0.01 ± 0.01	0.00 ± 0.01	0.02 ± 0.09	0.01 ± 0.05	0.737	0.863
Total SFA	13.41 ± 1.48	12.13 ± 0.91	12.98 ± 1.29	12.74 ± 1.21	0.002	0.028
MUFA						
14:1	0.79 ± 0.59	0.71 ± 0.56	0.94 ± 0.66	0.94 ± 0.63	0.785	0.779
15:1	0.05 ± 0.03	0.04 ± 0.05	0.02 ± 0.02	0.04 ± 0.09	0.606	0.218
16:1n-7	3.28 ± 0.90	1.84 ± 0.46	3.02 ± 1.01	2.98 ± 1.20	0.000	0.000
17:1	0.17 ± 0.09	0.14 ± 0.08	0.18 ± 0.08	0.16 ± 0.08	0.154	0.829
18:1n-9	17.77 ± 2.89	16.47 ± 1.69	17.52 ± 1.77	17.97 ± 1.44	0.290	0.034
20:1n-9	0.06 ± 0.06	0.04 ± 0.03	0.10 ± 0.10	0.11 ± 0.12	0.653	0.499
22:1n-9	0.02 ± 0.05	0.01 ± 0.03	0.04 ± 0.16	0.01 ± 0.03	0.260	0.583
24:1	0.00 ± 0.00	0.00 ± 0.02	0.03 ± 0.12	0.00 ± 0.00	0.444	0.263
Total MUFA	21.95 ± 2.47	22.22 ± 1.71	22.14 ± 3.65	19.26 ± 2.06	0.015	0.004
n-6 PUFA						
18:2n-6	52.41 ± 4.90	56.44 ± 4.08	53.23 ± 4.52	53.05 ± 3.60	0.014	0.008
18:3n-6	1.05 ± 0.40	0.50 ± 0.16	0.95 ± 0.33	0.92 ± 0.28	0.000	0.000
20:2n-6	0.07 ± 0.10	0.04 ± 0.03	0.05 ± 0.06	0.04 ± 0.05	0.093	0.483
20:3n-6	0.90 ± 0.23	0.59 ± 0.13	0.89 ± 0.17	0.85 ± 0.17	0.000	0.000
20:4n-6	7.39 ± 1.73	7.78 ± 1.73	7.57 ± 1.73	7.74 ± 1.75	0.001	0.008
22:4n-6	0.00 ± 0.00	0.00 ± 0.01	0.00 ± 0.01	0.00 ± 0.00	0.672	0.173
22:5n-6	0.05 ± 0.03	0.04 ± 0.04	0.09 ± 0.18	0.08 ± 0.16	0.855	0.997
Total n-6	61.87 ± 5.22	66.57 ± 2.89	62.79 ± 3.23	62.69 ± 2.47	0.003	0.002
n-3 PUFA						
18:3n-3	0.60 ± 0.15	0.45 ± 0.14	0.51 ± 0.11	0.53 ± 0.21	0.056	0.009
18:4n-3	0.14 ± 0.05	0.08 ± 0.04	0.14 ± 0.04	0.10 ± 0.09	0.001	0.363
20:3n-3	0.03 ± 0.03	0.03 ± 0.05	0.04 ± 0.07	0.02 ± 0.03	0.169	0.320
20:4n-3	0.05 ± 0.07	0.01 ± 0.03	0.03 ± 0.04	0.02 ± 0.03	0.002	0.128
20:5n-3	0.50 ± 0.16	0.37 ± 0.10	0.57 ± 0.26	0.61 ± 0.37	0.154	0.017
22:5n-3	0.03 ± 0.08	0.01 ± 0.01	0.02 ± 0.02	0.03 ± 0.06	0.759	0.165
22:6n-3	0.40 ± 0.12	0.45 ± 0.14	0.37 ± 0.12	0.44 ± 0.18	0.012	0.520
Total n-3	1.74 ± 0.27	1.39 ± 0.23	1.67 ± 0.33	1.75 ± 0.52	0.015	0.000
Total PUFA	63.61 ± 5.15	67.96 ± 2.85	64.46 ± 3.15	64.44 ± 2.37	0.004	0.004
Total HUFA	1.13 ± 1.58	11.48 ± 1.88	11.17 ± 1.98	11.35 ± 1.84	0.308	0.743
Total n-9	18.64 ± 3.18	17.25 ± 1.78	18.63 ± 1.83	19.02 ± 1.37	0.280	0.057
n-6/n-3	36.69 ± 8.46	49.59 ± 10.34	39.24 ± 9.32	38.26 ± 9.35	0.000	0.000
20:4n-6/20:5n-3	16.24 ± 6.80	26.56 ± 11.83	15.63 ± 7.87	14.59 ± 4.94	0.001	0.000

Values are weight percent (mean ± SD)

Table 5 Inflammatory responses of men and women who consumed low carbohydrate and low fat diets

Variables	VLCKD ($n = 20$)		Low fat ($n = 20$)		2 × 2 ANOVA	
	Week 0	Week 12	Week 0	Week 12	Time	T × G
WBC ($\times 10^9$/l)	6.2 ± 1.4	5.9 ± 1.4	5.9 ± 1.8	5.9 ± 2.2	0.471	0.427
Neutrophils ($\times 10^9$/μl)	3507 ± 877	3460 ± 1172	3368 ± 1500	3428 ± 1460	0.971	0.783
Lymphocytes ($\times 10^9$/μl)	2039 ± 648	1741 ± 439	1899 ± 509	1892 ± 668	0.076	0.090
Monocytes ($\times 10^9$/μl)	402 ± 135	451 ± 215	506 ± 274	422 ± 153	0.659	0.106
Eosinophils ($\times 10^9$/μl)	210 ± 169	176 ± 130	184 ± 105	164 ± 81	0.297	0.785
Basophils ($\times 10^9$/μl)	26 ± 21	21 ± 17	24 ± 13	27 ± 17	0.752	0.310
CRP (mg/dl)	0.6 ± 0.6	0.5 ± 0.5	0.4 ± 0.5	0.3 ± 0.4	0.028	0.858
IL-6 (pg/ml)	8.4 ± 9.3	5.5 ± 7.6	6.3 ± 8.7	6.3 ± 9.0	0.064	0.073
IL-8 (pg/ml)	8.5 ± 4.4	5.7 ± 2.8	9.4 ± 9.7	9.8 ± 11.0	0.033	0.007
VEGF (pg/ml)	162 ± 130	122 ± 96	129 ± 130	109 ± 113	0.004	0.293
TNF-α (pg/ml)	2.8 ± 1.6	1.9 ± 2.0	2.6 ± 1.8	2.3 ± 1.7	0.000	0.017
IFN-γ (pg/ml)	2.2 ± 1.5	1.7 ± 1.9	2.0 ± 1.4	2.2 ± 1.5	0.543	0.261
EGF (pg/ml)	12.6 ± 11.6	6.9 ± 8.1	20.7 ± 22.4	13.7 ± 22.9	0.060	0.841
MCP-1 (pg/ml)	380 ± 134	288 ± 120	323 ± 102	307 ± 123	0.002	0.023
I-CAM (ng/ml)	360 ± 84	299 ± 64	338 ± 69	328 ± 57	0.001	0.008
V-CAM (ng/ml)	549 ± 101	512 ± 113	567 ± 139	536 ± 135	0.060	0.874
E-selectin (ng/ml)	18.9 ± 9.2	12.4 ± 5.0	16.7 ± 5.3	14.4 ± 4.1	0.000	0.014
P-selectin (ng/ml)	125 ± 27	107 ± 27	122 ± 28	112 ± 28	0.002	0.301
L-selectin (ng/ml)	1148 ± 210	1091 ± 197	1081 ± 167	1098 ± 126	0.398	0.128
PAI-1 (ng/ml)	45.0 ± 20.7	29.5 ± 10.1	38.3 ± 11.5	35.2 ± 12.6	0.001	0.026

Values are mean ± SD

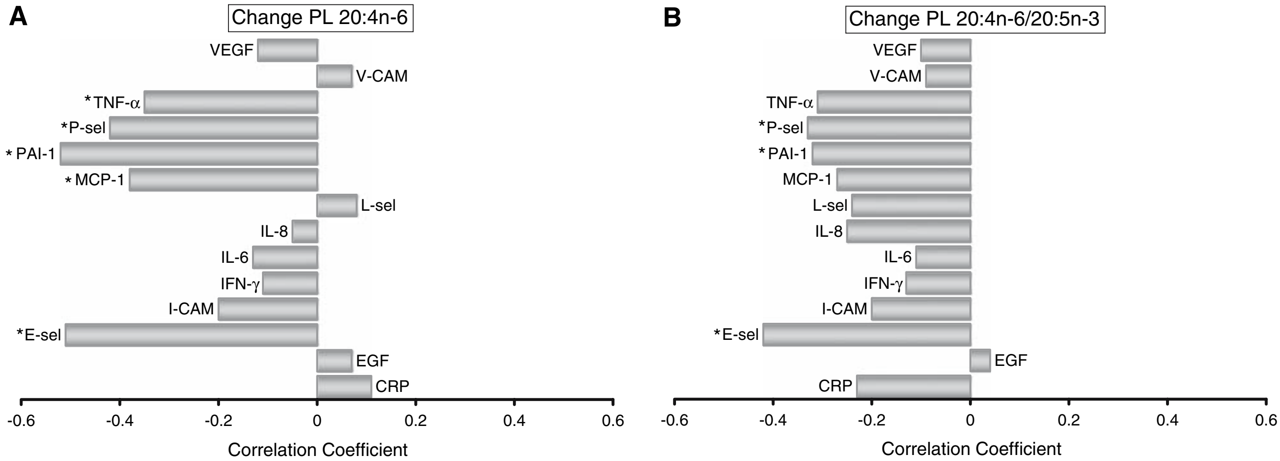

Fig. 2 Associations between changes in markers of inflammation and changes in PL arachidonic acid (**a**), and the 20:4n-6/20/5n-3 ratio (**b**). *Individual bars* represent Pearson correlation coefficients *($P < 0.05$)

and saturated fat only had a small effect on circulating inflammatory markers whereas reducing carbohydrate led to considerably greater reductions in a number of proinflammatory cytokines, chemokines, and adhesion molecules. These data implicate dietary carbohydrate rather than dietary fat as a more significant nutritional factor contributing to inflammatory processes; although increased fat in the presence of high carbohydrate may be particularly deleterious. Dietary carbohydrate also has a fundamental role in determining fatty acid composition of lipids and membranes, and it is the endogenous fatty acids (as opposed to the exogenous dietary fatty acids) that influence inflammation by acting as ligands for receptors or transcription factors that regulate inflammatory signaling cascades or serving as substrates for proinflammatory bioactive products.

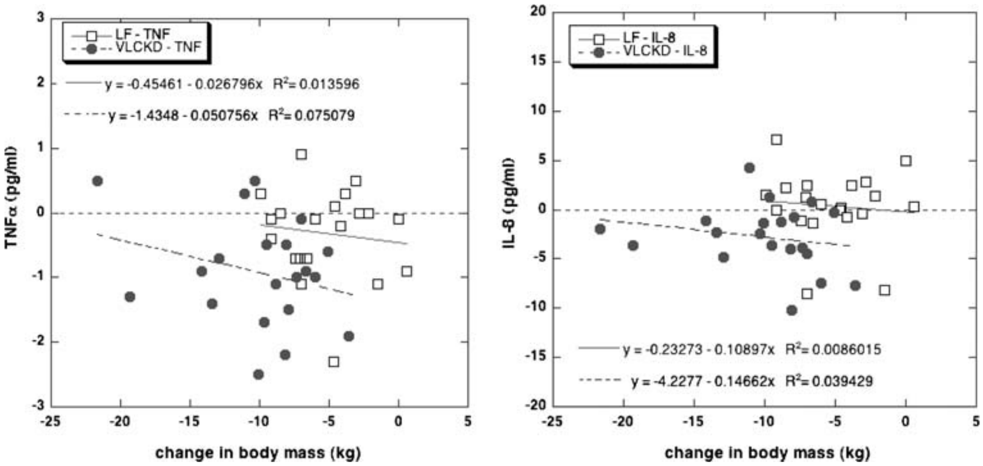

Fig. 3 Associations between weight loss and changes in TNF-α and IL-8

Despite the two diet groups consuming roughly the same caloric intake and all losing at least some weight, there were larger reductions in the VLCKD group in TNF-α, IL-8, MCP-1, PAI-1, E-selectin and I-CAM, while these markers showed little change on low fat suggesting that it is the macronutrient composition not weight loss or caloric reduction that is key. Most of the inflammatory markers did not correlate with weight loss. A correlation would not have proved that weight loss caused change in inflammatory markers but the lack of correlation makes it extremely unlikely. As shown in Fig. 3, there is essentially no correlation and if anything the associations tend to go in the opposite direction of what is expected if weight loss caused change in markers. In both cases, individuals with the largest reductions in inflammatory markers tended to be in the middle of the weight-loss range. The question of weight loss as a stimulus versus a response has been raised before with regard to other effects of carbohydrate restriction. Our group [22] and others [16, 18, 23] have consistently shown that there is a benefit to atherogenic dyslipidemia, glycemic control, and insulin from reduction in carbohydrate independent of weight loss. We therefore suggest that reduction in carbohydrate is primary, and weight loss (more precisely caloric restriction) is not the controlling variable.

One of the most striking responses in fatty acid composition was the increase in arachidonic acid and total n-6 PUFA in subjects consuming a VLCKD. Rather than being a negative factor within lipid membranes, increased arachidonic acid appears to be a beneficial outcome of weight-reducing diets associated with greater lipolysis [24]. The increase in plasma arachidonic acid only in response to the low carbohydrate diet is best explained by decreased degradation presumably due to less interaction with reactive oxygen species [25]. Increased production from 18:2n-6 was unlikely since the metabolic intermediates 18:3n-6 and 20:3n-6 were reduced in all three circulating fractions and there was no increase in 20:3n-9, which typically occurs in cases where PUFA anabolism is increased [13, 25]. Since arachidonic acid was elevated in all circulating fractions, a shift from other pools is unlikely. This is supported by the fact that fat loss was only moderately greater on the VLCKD compared to the LFD (−5.6 vs. −3.7 kg), and by week 12, the rate of weight loss on both diets was low. Given that daily dietary contribution of arachidonic acid is on the order of 0.5% of the total body pool [26] also suggests reduced degradation as the major explanation. Thus, an increase in the proportion of arachidonic acid resulting from a diet that restricts carbohydrate may be due to lower catabolism (i.e. better preservation) and therefore reduced formation of proinflammatory products. The consistent inverse associations between changes in arachidonic acid and responses in inflammatory markers indicate that the adverse effects of arachidonic acid are due to metabolites produced subsequent to its release from membranes rather than the proportion of the intact fatty acid.

The 19% rise in PL arachidonic acid in the low carbohydrate group (from 11.54 to 13.70 wt%) is consistent with the change seen after 12 weeks of a very low calorie diet in a more obese population (e.g,, from 9.16 to 11.77 wt%) [24]. Given the regulatory role of arachidonic acid as a ligand for PPAR and in gene expression (e.g., fatty acid synthase) [27], this degree of rise in 20:4n-6 has the potential to influence fuel partitioning. In the obese Zucker rat, the increase in liver PL arachidonic acid from 22.68 to 25.23 wt% (an 11% change) induced by feeding 18:3n-6 was associated with significant reductions in food intake and body fat content [28].

Scenarios associated with less oxidative stress should result in better preservation of the substrate arachidonic acid, due to the interaction of free radicals with several steps in its metabolism. Inflammatory cytokines are known to increase production of hydroxyl radicals which in turn initiate arachidonic acid release and breakdown. The VLCKD in this study resulted in significantly greater reductions in several proinflammatory markers including TNF-α, E-selectin, ICAM-1, and IL-8, that were related to the increase in arachidonic acid. The significantly greater reduction in TNF-α in subjects following the VLCKD is of interest in that it is one of the agents known to activate NF-κB a major transcription factor regulating cytokines, chemokines and adhesion molecules (TNF-α, MCP-1, IL-8, E-selectin, and ICAM-1) [12, 29]. The reduction in all of these agents by the VLCKD suggests that the antiinflammatory effects of carbohydrate restriction may be mediated via down regulation of NF-κB expression [30]. We have previously found that guinea pigs fed high-cholesterol atherogenic diets demonstrated significant increases in aortic TNF-α, an effect that was attenuated by reduction in dietary carbohydrate [31].

Hypercaloric high carbohydrate feeding stimulates the production of several fatty acids including 16:0, the major lipogenic product, and palmitoleic acid (16:1n-7), the product of Δ9 desaturase. Palmitoleic acid is a minor constituent in dietary fat and its increase is a marker of lipogenesis [32] and its presence has been linked to higher levels of adiposity [33, 34]. In this study, the VLCKD resulted in concurrent reductions in both 16:0 and 16:1n-7 in both TG and CE lipid fractions despite an increase in dietary saturated fat load. The significant reduction in dietary saturated fat in the LFD led to little decrease in total saturates and essentially no change in 16:1n-7, with one subject actually showing a drastic increase. The greater decrease in circulating SFA in response to carbohydrate restriction may have contributed to the larger decline in several inflammatory markers that are regulated by NF-κB [10, 11]. The decrease in circulating saturated fatty acids on the VLCKD is likely due to greater oxidation of the saturated fat from both diet and endogenous lipolysis, and a reduction in de novo lipogenesis.

In summary, carbohydrate restricted diets that are proportionately high in saturated fatty acids show very different results from what might be expected [7, 18]. A VLCKD significantly increases arachidonic acid levels, presumably due to a better preservation as a result of reduced oxidative stress and decreased inflammation. Sparing of arachidonic acid (by reducing its degradation to oxy-lipids) may provide a signaling mechanism by which dietary carbohydrate restriction favorably alters lipid metabolism and inflammatory processes [27].

Acknowledgments This work was supported by the Dr. Robert C. Atkins Foundation.

References

1. Warensjo E, Riserus U, Vessby B (2005) Fatty acid composition of serum lipids predicts the development of the metabolic syndrome in men. Diabetologia 48:1999–2005
2. Dougherty RM, Galli C, Ferro-Luzzi A, Iacono JM (1987) Lipid and phospholipid fatty acid composition of plasma, red blood cells, and platelets and how they are affected by dietary lipids: a study of normal subjects from Italy, Finland, and the USA. Am J Clin Nutr 45:443–455
3. King IB, Lemaitre RN, Kestin M (2006) Effect of a low-fat diet on fatty acid composition in red cells, plasma phospholipids, and cholesterol esters: investigation of a biomarker of total fat intake. Am J Clin Nutr 83:227–236
4. Raatz SK, Bibus D, Thomas W, Kris-Etherton P (2001) Total fat intake modifies plasma fatty acid composition in humans. J Nutr 131:231–234
5. Phinney SD (2006) The low fat paradox—do dietary carbohydrates increase circulating saturated fatty acids? Am J Clin Nutr 84:461–462
6. Parks EJ (2002) Changes in fat synthesis influenced by dietary macronutrient content. Proc Nutr Soc 61:281–286
7. Volek JS, Feinman RD, Phinney SD, Forsythe CE, Silvestre R, Judelson D, Quann EE, Wood RJ, Puglisi MJ, LaBonte CC, Kraemer WJ, Bibus DM, Contois JH, Fernandez ML (2007) Comparative effects of dietary restriction of carbohydrate or fat on circulating saturated fatty acids and atherogenic dyslipidemia. (Submitted)
8. Reaven GM (1988) Banting lecture 1988. Role of insulin resistance in human disease. Diabetes 37:1595–1607
9. Dandona P, Aljada A, Chaudhuri A, Mohanty P, Garg R (2005) Metabolic syndrome: a comprehensive perspective based on interactions between obesity, diabetes, and inflammation. Circulation 111:1448–1454
10. Lee JY, Hwang DH (2006) The modulation of inflammatory gene expression by lipids: mediation through Toll-like receptors. Mol Cells 21:174–185
11. Lee JY, Zhao L, Youn HS, Weatherill AR, Tapping R, Feng L, Lee WH, Fitzgerald KA, Hwang DH (2004) Saturated fatty acid activates but polyunsaturated fatty acid inhibits Toll-like receptor 2 dimerized with Toll-like receptor 6 or 1. J Biol Chem 279:16971–16979
12. de Winther MP, Kanters E, Kraal G, Hofker MH (2005) Nuclear factor kappaB signaling in atherogenesis. Arterioscler Thromb Vasc Biol 25:904–914
13. Calder PC (2006) Polyunsaturated fatty acids and inflammation. Prostaglandins Leukot Essent Fatty Acids 75(3):197–202
14. Johnston CS, Tjonn SL, Swan PD, White A, Hutchins H, Sears B (2006) Ketogenic low-carbohydrate diets have no metabolic advantage over nonketogenic low-carbohydrate diets. Am J Clin Nutr 83:1055–1061
15. Peplow PV (1996) Actions of cytokines in relation to arachidonic acid metabolism and eicosanoid production. Prostaglandins Leukot Essent Fatty Acids 54:303–317
16. Feinman RD, Volek JS (2006) Low carbohydrate diets improve atherogenic dyslipidemia even in the absence of weight loss. Nutr Metab (Lond) 3:24
17. Feinman RD, Westman EC, Volek JS (2006) Low carbohydrate and low fat diets in diabetes, cardiovascular disease and metabolic syndrome. Cellscience Reviews 3, no. 1 (http://www.cellscience.com/reviews9/Low_carbohydrate_low_fat_diets_in_disease. html)
18. Krauss RM, Blanche PJ, Rawlings RS, Fernstrom HS, Williams PT (2006) Separate effects of reduced carbohydrate intake and weight loss on atherogenic dyslipidemia. Am J Clin Nutr 83:1025–1031
19. Volek JS, Feinman RD (2005) Carbohydrate restriction improves the features of metabolic syndrome. Metabolic syndrome may be defined by the response to carbohydrate restriction. Nutr Metab (Lond) 2:31
20. Kasim-Karakas SE, Tsodikov A, Singh U, Jialal I (2006) Responses of inflammatory markers to a low-fat, high-carbohydrate diet: effects of energy intake. Am J Clin Nutr 83:774–779

21. Liu S, Manson JE, Buring JE, Stampfer MJ, Willett WC, Ridker PM (2002) Relation between a diet with a high glycemic load and plasma concentrations of high-sensitivity C-reactive protein in middle-aged women. Am J Clin Nutr 75:492–498
22. Volek JS, Sharman MJ, Gomez AL, Scheett TP, Kraemer WJ (2003) An isoenergetic very low carbohydrate diet improves serum HDL cholesterol and triacylglycerol concentrations, the total cholesterol to HDL cholesterol ratio and postprandial pipemic responses compared with a low fat diet in normal weight, normolipidemic women. J Nutr 133:2756–2761
23. Gannon MC, Nuttall FQ (2006) Control of blood glucose in type 2 diabetes without weight loss by modification of diet composition. Nutr Metab (Lond) 3:16
24. Phinney SD, Davis PG, Johnson SB, Holman RT (1991) Obesity and weight loss alter serum polyunsaturated lipids in humans. Am J Clin Nutr 53:831–838
25. Sullivan PG, Rippy NA, Dorenbos K, Concepcion RC, Agarwal AK, Rho JM (2004) The ketogenic diet increases mitochondrial uncoupling protein levels and activity. Ann Neurol 55:576–580
26. Zhou L, Nilsson A (2001) Sources of eicosanoid precursor fatty acid pools in tissues. J Lipid Res 42:1521–1542
27. Brash AR (2001) Arachidonic acid as a bioactive molecule. J Clin Invest 107:1339–1345
28. Phinney SD, Tang AB, Thurmond DC, Nakamura MT, Stern JS (1993) Abnormal polyunsaturated lipid metabolism in the obese Zucker rat, with partial metabolic correction by gamma-linolenic acid administration. Metabolism 42:1127–1140
29. Monaco C, Paleolog E (2004) Nuclear factor kappaB: a potential therapeutic target in atherosclerosis and thrombosis. Cardiovasc Res 61:671–682
30. Shin WS, Szuba A, Rockson SG (2002) The role of chemokines in human cardiovascular pathology: enhanced biological insights. Atherosclerosis 160:91–102
31. Fernandez ML, Volek JS (2006) Guinea pigs: a suitable animal model to study lipoprotein metabolism, atherosclerosis and inflammation. Nutr Metab (Lond) 3:17
32. Aarsland A, Wolfe RR (1998) Hepatic secretion of VLDL fatty acids during stimulated lipogenesis in men. J Lipid Res 39:1280–1286
33. Okada T, Furuhashi N, Kuromori Y, Miyashita M, Iwata F, Harada K (2005) Plasma palmitoleic acid content and obesity in children. Am J Clin Nutr 82:747–750
34. Kunesova M, Hainer V, Tvrzicka E, Phinney SD, Stich V, Parizkova J, Zak A, Stunkard AJ (2002) Assessment of dietary and genetic factors influencing serum and adipose fatty acid composition in obese female identical twins. Lipids 37:27–32

Lipids (2008) 43:79–89
DOI 10.1007/s11745-007-3133-6

ARTICLE

A Reliable Biomarker Derived from Plasmalogens to Evaluate Malignancy and Metastatic Capacity of Human Cancers

**Rosina E. Smith · Pablo Lespi · María Di Luca ·
Claudia Bustos · Fernando A. Marra ·
María J. T. de Alaniz · Carlos A. Marra**

Received: 12 June 2007 / Revised: 25 October 2007 / Accepted: 30 October 2007 / Published online: 29 November 2007
© AOCS 2007

Abstract Antigen tumor markers employed in monitoring therapeutical approaches are limited by their specificity (Sp) and sensitivity (Se). The aim of this study was to investigate the suitability of a lipid tumor marker derived from ether-linked phospholipids and to compare it with others usually assayed in clinical practice. Complex lipids from normal and pathological breast, lung, and prostate tissue were isolated and analyzed by TLC and c-GLC methods. Results were compared as pooled samples, or by means of the averaged percent changes with respect to the composition observed in the normal tissue of the same patient. Sp, Se, negative-predictive (NPV) and positive-predictive values (PPV) were established for conventional markers and for the proposed lipid-derived marker. Results demonstrated that the content of monoenoic fatty acyl chains was significantly increased in total lipids, phosphatidylethanolamine, and especially in ethanolamine-containing ether lipids of neoplastic tissues with respect to their corresponding normal ones. Major changes were observed in the plasmalogen sub-fraction where the ratio monoenoic/saturated fatty acids can distinguish with high Se normal tissues from either benign or neoplastic tissues from breast, lung, or prostate lesions. Analyses of fatty acyl chains from ethanolamine-containing plasmalogens provided a reliable tumor marker that correlated with high Se and linearity with metastases spreading. This fact may be useful in prognosis of the most frequently observed human cancers.

Keywords Ether-lipids · Breast · Lung · Prostate · Tumor markers · Human

List of abbreviations

ADAG	Alkyldiacylglycerols
BL	Benign (lesions or tissues)
C	Normal
CEA	Carcinoembryonic antigen
ChoGpl	Choline glycerophospholipids
EtnGpl	Ethanolamine glycerophospholipids
FAs	Fatty acids
FAMEs	Fatty acid methyl esters
GEDE-A	1-*O*-alkyl-2,3-diacyl-*sn*-glycerol
GEDE-E	1-*O*-alkenyl-2,3-diacyl-*sn*-glycerol
NEO	Neoplastic (lesions or tissues)
NPV	Negative-predictive value

R. E. Smith · P. Lespi
Hospital Penna, Bahía Blanca, Pcia. de Buenos Aires, Argentina

P. Lespi · F. A. Marra
Hospital San Martín, La Plata, Argentina

M. Di Luca
Hospital Rossi, Cátedra de Patología. Facultad de Ciencias Médcias de la UNLP, La Plata, Argentina

M. Di Luca · F. A. Marra
Hospital Meléndez, Adrogué, Pcia. de Buenos Aires,
La Plata, Argentina

C. Bustos
Hospital Rossi, Servicio de Histopatología, La Plata, Argentina

F. A. Marra
Clínica Vaccarini, Servivio de Medicina General,
La Plata, Argentina

M. J. T. de Alaniz · C. A. Marra (✉)
INIBIOLP (Instituto de Investigaciones Bioquímicas de
La Plata), CONICET-UNLP, Cátedra de Bioquímica.
Facultad de Ciencias Médicas de la Universidad Nacional de
La Plata, Calles 60 y 120, 1900 La Plata, Argentina
e-mail: camarra@atlas.med.unlp.edu.ar

PakCho	Plasmanylcholine (1-*O*-alkyl-2-acyl-*sn*-glycero-3-phosphocholine)
PakEtn	1-*O*-alkyl-2-acyl-*sn*-glycero-3-phosphoethanolamine (plasmanylethanolamine)
PlsCho	Plasmenylcholine (1-*O*-alk-1′-enyl-2-acyl-*sn*-glycero-3-phosphocholine)
PlsEtn	1-*O*-alk-1′-enyl-2-acyl-*sn*-glycero-3-phosphoethanolamine (plasmenylethanolamine)
PtdEtn	Diacyl-*sn*-glycero-3-phosphoethanolamine
PtdCho	Diacyl-*sn*-glycero-3-phosphocholine
PPV	Positive-predictive value
PSA	Prostatic specific antigen
PUFAs	Polyunsaturated fatty acids
Se	Sensitivity
Sp	Specificity

Introduction

Plasmalogens make up approximately 18% of the total phospholipid mass in humans; however, their content varies widely among tissues. The bulk of the 1-*O*-alk-1′-enyl-2-acyl-*sn*-glycero-3-phosphoethanolamine (plasmenylethanolamine or PlsEtn) pool may represent up to 70% of the ethanolamine phospholipids depending on the tissue analyzed [1]. 1-*O*-alkyl-2-acyl-*sn*-glycero-3-phosphoethanolamine (plasmanylethanolamine or PakEtn) and diacyl-*sn*-glycero-3-phosphoethanolamine (PtdEtn) represent the other species present in the ethanolamine glycerophospholipids (EtnGpl) [1]. Concerning neutral lipids, several authors proposed alkyldiacylglycerols (ADAG) as a lipid class marker for malignant tissues. Important contributions in this field were made by Snyder et al. [2, 3], Mangold and Paltauf [4], and Nagan and Zoeller [1] among others. Traditionally, an excess of 1% ADAG in neutral lipids may indicate malignant degeneration, and values observed may be as high as 6% [4]. As a general rule, amounts of PakEtn + PlsEtn over 4% of total phospholipids correlated with neoplastic transformation [4]. However, this reference parameter was obtained comparing lipid compositions from neoplastic and normal tissue samples (of the same type) obtained from donors or normal subjects free from cancer lesions. A meaningful comparison should only be plausible between tumorous and healthy tissue samples of the same patient [4]. Lin et al. [5] performed a study in which hepatocellular carcinomas were compared with the residual hepatic tissue free from tumor cells. They found that ADAG in the neutral lipid fraction exhibited an increased concentration of hexadecyl-glycerol and lower proportions of C18-glyceryl ethers in hepatocellular carcinomas with respect to non-malignant liver tissue. In spite of the fact that higher concentrations of neutral ADAG and cholesterol were found in this kind of tumor, no differences between levels of ether-linked phosphoglycerides, triacylglycerides, and lipid phosphorous were observed [3, 5]. So far, no similar studies have been carried out. Thus, no information concerning PakEtn and PlsEtn content and their fatty acid composition has been reported for normal and pathological samples from the same patient. This may be due to problems with surgical protocols, since the collection of cancer and normal tissues from the same patient is not easy. We explored in detail if there was a compositional marker derived from the fatty acyl pattern of polar and/or neutral lipids and if it correlated with the metastatic dissemination of the most prevalent cancers in our country (and probably in most industrialized nations). Several samples of lung, breast, and prostate cancer tissues were taken and studied in comparison with normal tissues obtained from the same patient in order to investigate which lipid profile (if any) correlated better with histopathological characteristics of cancer tissues and/or predicted metastatic spreading of the primary tumor. Tumor markers usually employed in clinical practice were also determined and compared with the results obtained from lipid analyses.

Experimental Procedure

Chemicals

All solvents used were HPLC grade from Carlo Erba, Milan, Italy. Standards for thin-layer chromatography (TLC) and capillary gas-liquid chromatography (c-GLC) were purchased from Nu-Check-Prep., Elysian, MN. 2′,7′-Dichlorofluorescein, boron trifluoride in methanol (14%), phospholipase C from *Bacillus cereus* (type IV, 1,500 U/mg protein), β-mercaptoethanol, sphingomyelin, PtdCho, PtdEth, inorganic salts and other chemicals used in sample preparation and processing were from Sigma Chem. Co., St. Louis, MO.

Patients and Tissue Samples

Lung, breast, and prostate tissues were obtained by surgical procedures and analyzed with the written consent of the patients. This study followed the Helsinki protocol for handling human specimens. Patients were recruited from five public and private health institutions and the survey involved a total of 677 paired samples (C: normal, BL: hyperplastic-displastic, and NEO: malignant tissues from the same patient) collected for 6 years. In most cases samples were obtained surgically. Other samples were obtained by performing a 3-mm needle disposable punch biopsy using a ultrasound guide. This procedure provides approx. 9 mg of tissue, enough for performing all the analyses. Two portions of tissue from each patient were analyzed, one from a pathological lesion and the other from (assumed) normal tissue. Each portion was divided into two sub-portions. One of them was processed for histopathological examination (PBS with 10% formalin) and the other for lipid analyses. Normal tissue surrounding the lesion was checked for any infiltration of abnormal cells. Suspicious normal samples were excluded from the study together with the corresponding paired (pathological) sample. Each sample was identified with an encrypted code which did not include any information concerning the origin and/or characteristics of the tissues examined. Thus, pathologists, biochemists, and laboratory technicians processed the samples under a blind protocol. At the end of the study, histopathological classification, biochemical determinations, and clinical stage of the samples were revealed and correlated with lipid analyses. For each type of pathological tissue the clinical state of patients and also the criteria for classification of samples (benign or neoplastic) were evaluated following international scores such as those recommended by the American Joint Committee on Cancer Staging, World Health Organization, or Gleason scale [6–8]. Presence and localization of metastases were explored by specific medical studies such as magnetic resonance, X-ray computed tomography, and radioisotopic densitography. Table 1 shows a summary of the main characteristics of patients and samples.

Blood Samples and Biochemical Markers

Morning fasting blood samples were obtained from the antecubital vein on the day of tissue collection. Plasma was separated by centrifugation in the cold at 600 × g (15 min), aliquoted, frozen at −20 °C (no more than one week), and

Table 1 Main characteristics of subjects and samples analyzed

	Tissue		
	Breast	Lung	Prostate
Mean age (years)[a]	61 (53–76)	64 (49–81)	74 (55–86)
n	222	226	229
Sex (n_F; $\%_F$) (n_M; $\%_M$)[b]	(222; 100)	(78; 32.9) (148; 67.1)	(229; 100)
Body weight (kg)[c]	68.4 ± 3.1	75.1 ± 2.0	78.0 ± 4.2
Body mass index (kg/m^2)[c]	26.0 ± 1.5	24.3 ± 1.1	25.8 ± 2.3
Weight loss (kg; %)[d]	(3.1 ± 0.2; 4.5 ± 0.1)	(6.7 ± 0.8; 8.9 ± 0.4)	(4.9 ± 0.5; 6.6 ± 0.3)
Tumor histopathology[b,e]			
Squamous cell carcinoma		(26; 11.5) (54; 23.9)	
Undifferentiated large-cell carcinoma		(3; 1.3) (11; 4.9)	
Adenocarcinoma (ADC)	(148; 66.6)	(14; 6.2) (31; 13.7)	(173; 75.5)
Small cell ADC		(21; 9.3) (26; 11.5)	
Intraductal ADC	(41;18.5)		
Ductal ADC	(90; 40.5)		
Lobulillar ADC	(13; 5.9)		
Medullary ADC	(4; 1.7)		
Extracapsular ADC (C1,C2)			(27; 11.8)
Metastasized ADC (D1,D2)			(146; 63.7)
Fibrous degeneration	(33; 14.9)		
Localized adenoma	(41; 18.5)		(56; 24.5)
Mesenchymal tumor		(6; 2.7) (11; 4.9)	
Hamartoma		(8; 3.5) (15; 6.6)	

At the time of recruitment most patients (71%) were hospitalized for medical tests and/or antitumor treatment (chemotherapy, surgery, radiation, or a combination of these procedures). The meanings of the superscript letters is as follows:

[a] Mean age (range)

[b] ($n_{F:\text{female}}$; % female with respect to total sample) ($n_{M:\text{males};}$ % males with respect to total sample)

[c] At the time of sampling, expressed as the mean ± 1SD (standard deviation)

[d] Weight loss (cancer patients) within the preceding 6 months expressed as (mean ± 1SD; percentage with respect to initial weight)

[e] Classification based on the American Joint Committee on Cancer Staging, World Health Organization, or Gleason Score

used for tumor marker determinations. Marker antigens assayed were (cut-off in parenthesis): total PSA (<5 ng/ml), CA-125 (<35 UI/ml), CA-15.3 (<30 UI/ml), CA-19.9 (<25 UI/ml), and CA-27.29 (<38 UI/ml). Determinations were performed according to the procedures recommended by manufacturers of the commercial kits (streptavidin technology of ELISA from Boehringer-Mannheim Immunodiagnostics, Germany, ES-300 BM auto-analyzer), or Abbott Lab., Buenos Aires, Argentina (AXSYM auto-analyzer). CEA (<5 ng/ml) was also determined by enzyme immunoassay (SRL, Fukuoka, Japan). Sensitivity (Se), specificity (Sp), positive predictive value (PPV), and negative-predictive values (NPV) were defined and calculated as described in detail by Kuralay et al. [9]. Briefly, for all samples correctly or incorrectly identified by the histological, laboratory, or other complementary studies as being malignant or benign (nonmalignant) were defined as true positive (TP), false positive (FP), true negative (TN), and false negative (FN). The term "positive" was referred to histological by proven malignant sample while benign tissues were referred as "negative" histological findings. Se was defined as TP/(TP + FN), Sp as TN/(TN + FP), PPV as TP/(TP + FP), and NPV as TN/(FN + TN).

Lipid Analyses

Samples were homogenized on ice with PBS (pH: 7.4, 100 µl per mg wet tissue) using a Potter-Elvejehm glass-Teflon homogenizer. An aliquot of 20 µl was taken for protein measurement [10] and the remainder was treated with Folch reactive [11]. After processing the samples according to Folch methodology, an aliquot of the final extract was taken to determine total lipid content gravimetrically [12] on a XP56-Delta Range Mettler Toledo balance. The evaporated residue was used for quantitative phosphorus determination according to Chen et al. [13]. Another aliquot was analyzed as described by Park et al. [14] in order to separate neutral ether lipids (ADAG) into their components, 1-*O*-alkyl-2,3-diacyl-*sn*-glycerol (GEDE-A), 1-*O*-alkenyl-2,3-diacyl-*sn*-glycerol (GEDE-E), and triacylglycerides (TAG). The remainder of the total lipid extract was separated into various phospholipid subclasses using thin-layer chromatography (TLC) with a biphasic solvent system [15]. TLC was performed in hermetic pre-equilibrated cubes (Sigma Chem. Co., St. Louis, MO) on pre-coated silica gel 60 plates from Merck (Darmstadt, Germany). Phospholipid bands were visualized under ultraviolet light after spraying with 2′,7′-dichlorofluorescein solution and exposure to ammonia vapor. Lipids were identified comparing them with pure standards run in the same plate. In order to separate plasmalogens and DAG components from the PtdCho and PtdEth fractions the spots were scrapped-off and quantitatively eluted with chloroform/methanol (1:2, by vol). Isolated PtdCho and PtdEth were incubated with phospholipase C following the method of Mangold and Totani [16]. The resulting diacylglycerides were then acetylated with acetic anhydride/pyridine (10:5, by vol), and the products were separated by TLC using hexane/diethyl

Table 2 Marker antigens in plasma samples from patients with breast, lung, and prostate tumors

Tissue	Breast		Lung		Prostate	
Histopathology	BL	NEO	BL	NEO	BL	NEO
n	74	148	40	186	56	73
CA-125[a]	160 ± 34	873 ± 202[*]	83 ± 14	1037 ± 244[*]	ND	ND
CA-15.3[b]	96 ± 21	919 ± 195[*]	ND	ND	38 ± 6	318 ± 64[*]
CA-19.9[c]	ND	ND	31 ± 8	505 ± 191[*]	ND	ND
CA-27.29[d]	111 ± 29	1006 ± 197[*]	ND	ND	ND	ND
CEA[e]	40 ± 17	477 ± 165[*]	46 ± 7	355 ± 106[*]	13 ± 5	425 ± 113[*]
PSA[e]	ND	ND	ND	ND	37 ± 9	306 ± 170[*]

Data correspond to date of tissue collection and they were expressed as the mean of the number of samples indicated as *n* ± 1 SD. Patients were studied periodically after diagnose to correlate results with tumor progression and/or spreading

ND Non determined

[*] Significantly different ($P < 0.01$) compared with BL samples

Cut-off values and units for each marker are indicated with a superscript letter as follows:

[a] <35 UI/ml

[b] <30 UI/ml

[c] <25 UI/ml

[d] <38 UI/ml

[e] <5 ng/ml

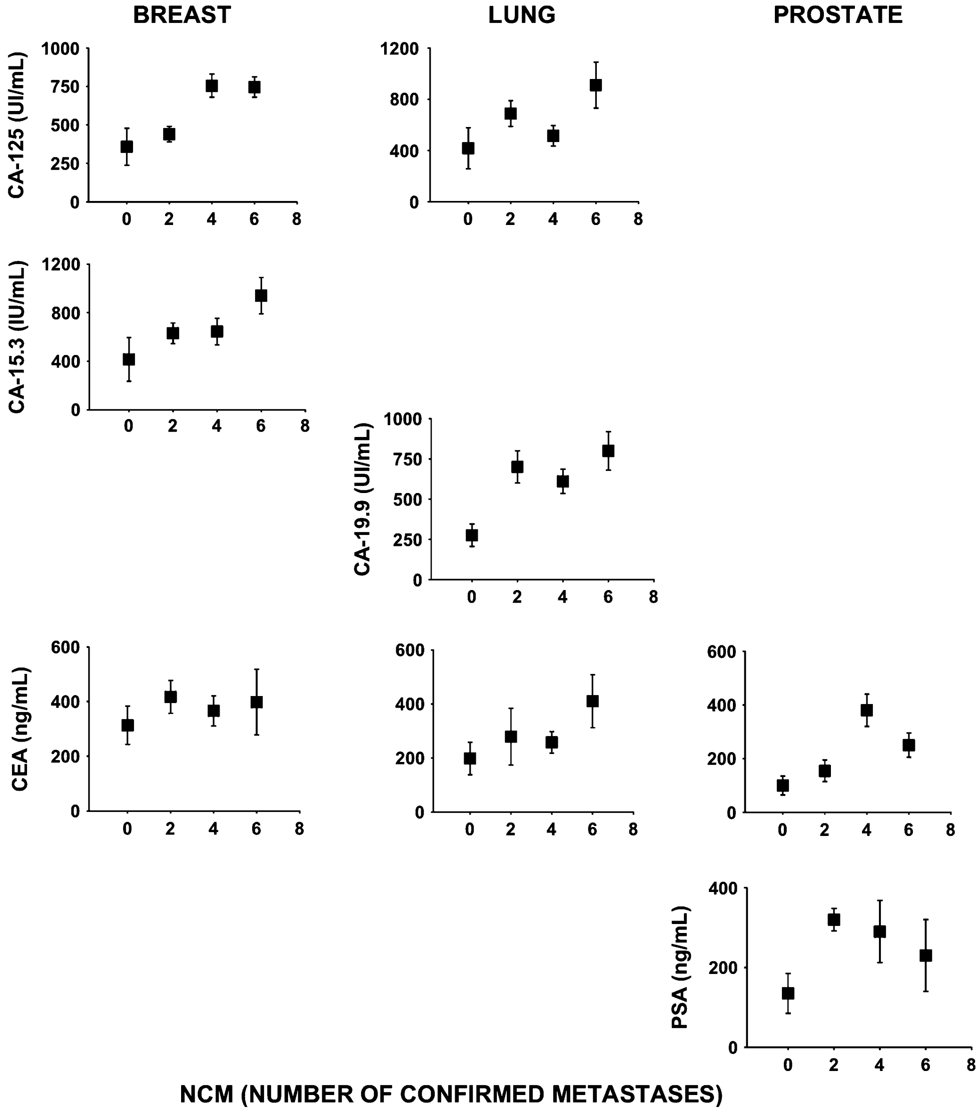

Fig. 1 Correlation between number of confirmed metastases (NCM) and various antigen markers for breast, lung and prostate. Number of neoplastic samples processed was smaller than the total number of patients studied since only those cases with confirmed number of metastases were included (101, 129, and 73 for breast, lung, and prostate, respectively)

ether/acetic acid (90:10:1, by vol) as first solvent system and toluene as second developing solvent [17]. Bands were scrapped-off the plate and transmethylated using F_3B (14% in methanol) under nitrogen atmosphere for 45 min at 80 °C. Monopentadecanoin was added to all the tubes as an internal standard. Fatty acid methyl esters (FAMEs) from the ether lipid species were separated from the aldehyde derivatives by TLC using toluene as a solvent and quantitatively analyzed using a Hewlett Packard HP 6890 Series GC System Plus (Avondale, PA) equipped with a terminal computer integrator [18].

Graphic Software and Statistical Treatment of Data

Data were reported as the mean ± 1 standard deviation (SD). Statistical significance was tested by student *t*-test or by ANOVA (analysis of variance) plus Bonferroni test. Correlation and regression analyses and data plotting were performed with the aid of Systat (version 12.0 for Windows) from SPSS Science (Chicago, IL), Sigma Scientific Graphing Software (version 8.0) from Sigma Chem. Co. (St. Louis, MO), and/or GB-STAT Professional Statistics Program (version 4.0) from Dynamic Microsystems Inc. (Silver Springs). Multivariable regression analyses were performed as described by Kleinbaum and Kupper [19].

Results and Discussion

Patients and Tumor Markers

Our study was carried out with a representative (characteristic) population of neoplastic samples, composed of a typical distribution of cancer types (Table 1). Histopathological data were in agreement with previous studies performed in Western countries [20]. Tumor marker levels (Table 2) were also in accordance with data previously reported for each kind of tumor [21–24]. These values of tumor markers are often useful for monitoring the evolution of patients; however, some of them may not be helpful in detecting recurrence. For example, we found that CA-125, CA-19.9, CA-27.29, CEA, and total PSA remained unaltered in a significant proportion of cases in which large spreading of primary tumors was detected by other tests such as radioisotopic and/or X-ray scanning (data not shown). Total PSA was the antigen that showed the best correlation with clinical status. Notwithstanding, it was within normal values in 12% patients with prostate cancer detected by digital rectal and scanner exams, and then corroborated by histological studies after needle punch biopsy. Moreover, spreading of primary prostatic or breast tumors with bone metastases was not correlated with a significant raise in any of the antigen markers tested in 22 and 31% of the samples analyzed, respectively. In addition, approximately 25% of patients with metastatic dissemination of primary lung cancer (especially in central nervous system and liver) showed no significant changes with respect to the starting level of the antigenic markers.

Sp and Se of tumor markers are topics under continuous evaluation. The ideal marker would be a molecule which only appears in patients with a specific malignancy, and it would correlate directly with stage and response to treatment. Up till now, no tumor marker has met this requirement. Thus, establishment of a biochemical index for either diagnosis of cancer, or management of patients with neoplastic diseases remains as one of the important goals to be achieved in cancer research. It is accepted that measurement of one antigen concentration in plasma is not recommended as a useful diagnostic tool in malignancy.

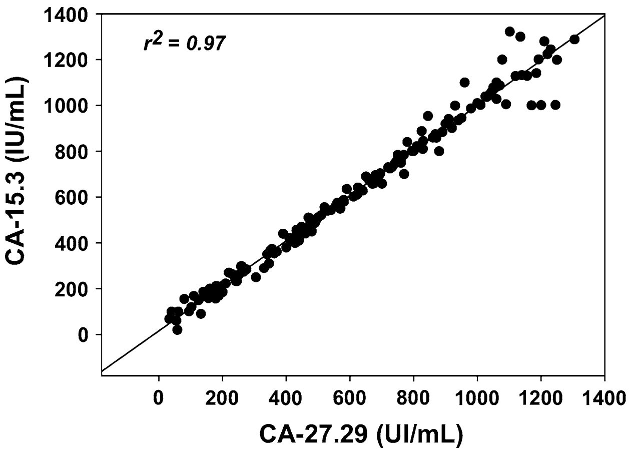

Fig. 2 Linear correlation between plasma levels of antigens CA-15.3 and CA-27.29 was determined as described in "Experimental Procedure" for 148 patients with breast cancer

In this regard, multivariable regression analyses of data in relation to tumor marker concentrations and clinical status of patients (summarized in Figs. 1 and 2, and in Tables 2 and 3) led us to these conclusions: (1) high levels of conventional markers did not directly correlate ($r^2 < 0.80$) with both stage and /or spreading of the primary tumor. (2) simultaneous determinations of two or more antigenic tumor markers did not improve PPV and NPV values ($0.58 < r^2 < 0.73$), and (iii) specifically, tumor markers CA-15.3 and CA-27.29 were directly proportional between them ($r^2 = 0.97$). Thus, simultaneous determinations of these two antigens do not offer advantages over the measurement of each marker alone. These statements confirm previous suggestions and findings made by other researchers [25–30] and answered the question raised by Klee et al [31]. It is important to remark that even the association of two or three of these markers (CA-125 + CA-15.3 + CEA; CA-125 + CA-19.9 + CEA; or PSA + CEA for breast, lung, and prostate cancers, respectively) could not significantly improve PPV and NPV values compared with prognosis or spreading predictions based on determinations of the primary marker alone (Table 3).

The optimal interpretation of tumor markers requires knowledge about both methodological limitations and the course of the disease in a particular patient. Even in those cases where these conditions were met, the correlation with clinical status was poor. For that reason we explored the usefulness of other tumor markers derived from ether lipid

Table 3 Sensitivity (Se), specificity (Sp), and negative- and positive-predictive values (NPV; PPV) of marker antigen levels tumors from human breast, Lung, and Prostate

	Tissue	Parameters			
		Se	Sp	NPV	PPV
CA-125	Breast	84	90	90	95
	Lung	89	92	96	89
CA-15.3	Breast	66	91	88	93
CA-19.9	Lung	87	96	94	95
CA-27.29	Breast	64	91	89	93
CEA	Breast	46	80	68	76
	Lung	53	75	77	72
	Prostate	38	89	65	70
PSA	Prostate	93	92	100	94
CA-125 + CA-15.3 + CEA	Breast	91	90	92	95
CA-125 + CA-19.9 + CEA	Lung	99	97	98	97
PSA + CEA	Prostate	100	93	100	96

Values were calculated as indicated in the experimental part. For simplicity only three types of associations between markers were shown. Data were calculated on the day of tissue collection. Patients were studied periodically after diagnosis to correlate results with tumor progression and/or spreading

Table 4 Absolute amounts of lipids of normal (C), benign (BL), and neoplastic (NEO) samples from human breast, lung, and prostate tissues

Tissues	Breast			Lung			Prostate		
Histopathology	C	BL	NEO	C	BL	NEO	C	BL	NEO
n	222	74	148	226	40	186	229	56	173
GEDE-A	0.5 ± 0.1	1.9 ± 0.3*	4.6 ± 0.5*,**	1.3 ± 0.2	1.8 ± 0.5	2.8 ± 0.3*	0.6 ± 0.1	0.9 ± 0.2	1.7 ± 0.3*,**
GEDE-E	0.7 ± 0.1	1.6 ± 0.4	3.3 ± 0.8*	0.7 ± 0.1	0.9 ± 0.2	1.3 ± 0.3*	0.5 ± 0.1	0.8 ± 0.2	2.2 ± 0.7*
PakEtn	0.7 ± 0.1	1.6 ± 0.2*	3.9 ± 0.4*,**	4.6 ± 0.3	6.6 ± 0.6	8.9 ± 0.5*	0.8 ± 0.2	0.8 ± 0.3	1.5 ± 0.4*,**
PlsEtn	1.1 ± 0.2	2.4 ± 0.3	5.8 ± 0.4*,**	11.5 ± 2.4	19.8 ± 3.0	24.1 ± 2.9*	3.3 ± 0.4	6.0 ± 1.8*	12.5 ± 3.0*
PakCho	0.5 ± 0.1	0.6 ± 0.1	2.1 ± 0.3*,**	1.0 ± 0.2	1.5 ± 0.4	2.9 ± 0.3*	0.6 ± 0.1	0.5 ± 0.3	1.6 ± 0.2*,**
PlsCho	0.8 ± 0.2	1.2 ± 0.3	3.5 ± 0.7*	2.3 ± 0.3	3.3 ± 0.7	4.4 ± 0.4*	0.8 ± 0.2	1.1 ± 0.3	3.6 ± 0.3*,**

Results were expressed as μg of each lipid subclass per mg protein, and they correspond to the mean ± SD of the number of samples indicated as *n*

Statistically different ($P < 0.01$) *compared with C, **compared with BL

compositional analysis of biopsy samples to perform histopathological studies.

Lipids and Fatty Acyl Composition of Ether Lipids as Tumor Markers

As a first approach in searching for a new lipid marker for human tumor tissues, we followed the strategy employed in this kind of investigation, that is, to compare pooled results between normal and malignant tissues classified according to their histopathological criteria and obtained from different patients. Table 4 shows data obtained from the analyses of neutral and polar ether lipid subclasses among normal, BL and NEO samples from breast, lung, and prostate human tissues. Results corresponded to absolute amounts of lipids (μg per mg tissue protein). They were pooled and averaged as a function of their histopathological classification on the day of collection. In agreement with previous studies from other researchers we found that tumor tissues were significantly enriched in GEDE-A and GEDE-E [4, 32–34]. Interestingly, concerning lung, no differences were found between normal and BL samples. Similar conclusions can be obtained examining the data obtained from PakEtn, PlsEtn, PakCho and PlsCho. Notwithstanding, the EtnGpl sub-fraction exhibited higher Se than ChoGpl since changes observed in ethanolamine-containing plasmalogens were more pronounced than those of choline. Drastic modification of data interpretation occurred when the results were separately compared. We calculated the amount of each lipid subclass with respect to the content of the same lipid in normal sample from the same patient. Table 5 shows the mean values obtained after these calculations. Data were expressed as ratios of the absolute amount of lipids (μg/mg protein). In the tumors studied, we found significant differences between normal, BL, and NEO samples. Moreover, differences observed among groups were even more evident than those observed

Table 5 Mean values of ratios between the content of ether lipids in benign (BL) or neoplastic (NEO) and normal (C) samples in human breast, lung, and prostate tissues

Tissues	Breast		Lung		Prostate	
Histopathology	BL	NEO	BL	NEO	BL	NEO
n	74	148	40	186	56	173
GEDE-A	4.2 ± 0.2*	10.1 ± 0.3*,**	1.9 ± 0.1*	3.9 ± 0.2*,**	1.5 ± 0.1*	4.7 ± 0.1*,**
GEDE-E	3.5 ± 0.4*	5.8 ± 0.2*,**	1.8 ± 0.2*	3.2 ± 0.1$^{*, **}$	2.4 ± 0.2*	4.8 ± 0.2*,**
PakEtn	4.1 ± 0.1*	7.0 ± 0.2*,**	2.0 ± 0.2*	4.5 ± 0.2*,**	1.9 ± 0.1*	5.6 ± 0.1$^{*, **}$
PlsEtn	2.7 ± 0.1*	6.9 ± 0.1*,**	3.1 ± 0.2*	6.3 ± 0.3*,**	3.5 ± 0.2*	7.8 ± 0.1*,**
PakCho	1.8 ± 0.1*	4.7 ± 0.2*,**	1.5 ± 0.1*	3.9 ± 0.1*,**	2.1 ± 0.1*	3.9 ± 0.2*,**
PlsCho	2.0 ± 0.2*	5.4 ± 0.1*,**	2.0 ± 0.2*	4.2 ± 0.2*,**	3.0 ± 0.2*	5.1 ± 0.2*,**

Results were expressed as the mean of ratios between the absolute amount (μg/mg protein) of each lipid subclass in BL or NEO samples and the content measured in normal tissues from the same patient ± 1SD of the number of analyses indicated as *n*. SD of normal samples was between 8 and 19% of the mean value depending on the group of samples analyzed

Statistically significant ($P < 0.01$) *compared with control, **compared with BL in the previous analyses (Table 4). Thus, using this type of analysis all the groups were statistically different from each other.

As reported by other authors [4, 32–34], pooled samples had a lower proportion of PakEtn or PakCho than PlsEtn or PlsCho. We calculated the relative proportion of GEDE-A to GEDE-E, and the PakEtn/PlsEtn and PakCho/PlsCho ratios. The content of GEDE-A compared to GEDE-E decreased in NEO samples from the three tissues studied, while the proportion between plasmanyl- and plasmenyl-derived compounds (in both PE and PC) increased in BL and in NEO sample tissues with respect to the normal ones. An important conclusion was that changes in EtnGpl were more pronounced than those in ChoGpl. Analytical ratios shown in Table 6 would be useful for the classification of samples according to their histopathological characteristics. However, there were two major problems with these calculations: (a) except in the case of plasmalogen ratios, no differences were found between BL and normal samples, and (b) they did not reflect the fact that individual samples may not differ from the mean values obtained for the corresponding histopathological group and, consequently, they would be misclassified. Considering PakEtn/PlsEtn and PakCho/PlsCho ratios as the most discriminating biomarkers, 31.4, 26.2 and 12.5% of NEO samples from breast, lung and prostate (respectively) were classified as normal samples when compared with the means shown in Table 4. However, they became malignant when comparisons were made against those values obtained from normal tissue from the same patient. Using the same strategy of comparison, BL samples from breast, lung and prostate were 25.0, 20.1 and 11.3% misclassified. These records were similar to those obtained using the conventional primary antigenic tumor markers as discriminators.

As a second approach to find a more reliable lipid tumor marker, analyses of fatty acyl composition of each ether lipid subclass isolated from normal and pathological samples were carried out. Significant changes in fatty acyl composition were easily observed directly on the chromatograms even without ulterior calculations of peak areas (data not shown). This pattern represented a “finger print” and it was a constant finding in the samples analyzed. The main changes observed involved the proportion of monoenoic to saturated fatty acids and also the relative amount of PUFAs to saturated fatty acids. For these reasons, the absolute amount (nmoles per mg protein) of fatty acyl chains in each lipid subclass from normal, BL and NEO samples was calculated and used to obtain several analytical ratios. A few selected (statistically significant) ratios were presented in Table 7. They were expressed as the percent change calculated by comparing the absolute content of fatty acyl chains of BL or NEO samples with the

Table 6 Ratio between ether-lipid subclasses in normal (C), benign (BL), and neoplastic (NEO) human tissues

Tissue	Breast			Lung			Prostate		
Histopathology	C	BL	NEO	C	BL	NEO	C	BL	NEO
n	222	74	148	226	40	186	229	56	173
GEDE-A ± GEDE-E/ Total plasmalogens	0.24 ± 0.05^a	0.39 ± 0.06^a	0.47 ± 0.08^b	0.08 ± 0.01^a	0.11 ± 0.01^a	0.18 ± 0.03^b	0.20 ± 0.04^a	0.19 ± 0.02^a	0.21 ± 0.03^a
GEDE-A/ GEDE-E	5.01 ± 0.42^a	6.33 ± 0.22^a	2.70 ± 0.22^b	1.91 ± 0.21^a	2.02 ± 0.16^a	1.30 ± 0.11^b	1.22 ± 0.11^a	0.91 ± 0.19^a	0.78 ± 0.03^a
PakEtn/ PlsEtn	0.58 ± 0.07^a	0.92 ± 0.10^b	1.64 ± 0.06^c	0.33 ± 0.03^a	0.57 ± 0.04^b	0.91 ± 0.06^c	0.21 ± 0.04^a	0.45 ± 0.02^b	0.74 ± 0.01^c
PakCho/ PlsCho	0.23 ± 0.01^a	0.44 ± 0.03^b	0.67 ± 0.05^c	0.40 ± 0.03^a	0.82 ± 0.06^b	1.11 ± 0.08^c	0.63 ± 0.08^a	0.87 ± 0.05^b	1.15 ± 0.04^c

Ratios were calculated from the absolute amounts (μg/mg protein) of each lipid subclass. They were expressed as the mean of the number of samples indicated as n ± 1SD

Lipids were determined chromatographically using internal standards or phosphorous measurements

Different superscript letters within each row -of the same kind of tissue- are significantly different at $P < 0.01$ or lesser

Table 7 Analytical markers of fatty acyl composition of lipids from benign (BL) and neoplastic (NEO) samples of human breast, lung and prostate

Histopathology	Breast		Lung		Prostate	
	BL	NEO	BL	NEO	BL	NEO
n	74	148	40	186	56	173
Total lipids						
Σ Monoethylenic/Σ Saturated	66 ± 7*	144 ± 17*,**	39 ± 6*	127 ± 15*,**	51 ± 4*	185 ± 19*,**
18:2n − 6 + 18:3n − 3/20:4 (n − 6)	54 ± 8*	196 ± 21*,**	27 ± 5*	222 ± 17*,**	36 ± 5*	193 ± 12*,**
18:2n − 6/Σ PUFAs	43 ± 5*	232 ± 25*,**	31 ± 7*	204 ± 21*,**	49 ± 4*	209 ± 15*,**
Σ (n − 3)/Σ (n − 6)	−21 ± 2*	−39 ± 4*,**	11 ± 3	−40 ± 5*,**	−8 ± 2	−53 ± 4*,**
EtnGpl						
Σ Monoethylenic/Σ Saturated	58 ± 3*	195 ± 13*,**	30 ± 3*	193 ± 13*,**	65 ± 7*	303 ± 25*,**
18:2n − 6 + 18:3n − 3/20:4 (n − 6)	49 ± 4*	107 ± 14*,**	36 ± 4*	131 ± 19*,**	57 ± 6*	148 ± 17*,**
18:2n − 6/Σ PUFAs	33 ± 5*	121 ± 27*,**	27 ± 2*	97 ± 6*,**	38 ± 4*	106 ± 12*,**
Σ (n − 3)/Σ (n − 6)	−7 ± 2	−11 ± 3	4 ± 1	−13 ± 2	−5 ± 1	−16 ± 4
PlsEtn						
Σ Monoethylenic/Σ Saturated	74 ± 5*	303 ± 18*,**	28 ± 2*	298 ± 21*,**	76 ± 8*	355 ± 20*,**
18:2n − 6 + 18:3n − 3/20:4 (n − 6)	31 ± 3*	90 ± 6*,**	19 ± 2	49 ± 3*,**	27 ± 3*	67 ± 5*,**
18:2n − 6/Σ PUFAs	35 ± 4*	76 ± 7*,**	15 ± 3	34 ± 5*,**	19 ± 3	46 ± 6*,**
Σ (n − 3)/Σ (n − 6)	−6 ± 1	−5 ± 1	11 ± 2	10 ± 3	−7 ± 1	−12 ± 3

Data were calculated as percent change with respect to normal tissue of each individual sample

total lipids unfractionates (neutral plus polar) lipids, *EtnGpl* ethanolamine glycerophospholipids (PtdEtn + PakEtn + PlsEtn), *PlsEtn* plasmalogen fraction of ethanolamine phospholipids

Calculations were averaged and expressed as the mean ± 1SM. *n* Indicates the number of samples within each category

Statistical differences ($P < 0.01$) were noted as * for BL or NEO vs. control, and ** for NEO vs. BL

amount measured in the normal tissue of the same patient. Similar calculations were made concerning the fatty acyl composition of GEDE-A, GEDE-E, and DAG. However, in those cases the statistical differences, though significant, were of lesser extension. Thus, we focused our attention in fatty acyl composition of PakEtn and PlsEtn sub-fractions. Ratios allowed the differentiation not only of NEO samples from normal tissue, but also of BL from NEO samples with high Se and Sp. These statistical differences almost disappeared when ratios were calculated in pooled samples since values of SD were notoriously increased. This fact can be attributed to a marked variability observed in the baseline contents of fatty acyl chains among patients under different nutritional conditions, concomitant pathologies, therapeutical approaches, hormonal status, gender, age, and other factors which are not easily controlled. In agreement with this, reports from other laboratories have attempted to characterize plasma fatty acyl profile in patients undergoing benign and/or neoplastic illness with a variable success [35–37].

From the data reported in Table 7 we calculated Se, Sp, NPV, and PPV for the different lipid markers studied. The best results were obtained for Σ monoenoic/Σ saturated fatty acids in PlsEtn showing major changes with minor dispersion together with an excellent correlation with clinical status of patients. Se and Sp were between 96 and 100%, and NPV and PPV values were both over 97%. Figure 3 shows correlation studies between the lipid marker and the spreading capacity of primary tumors. Interestingly, in all of the tumors studied we found a linear correlation, ($0.96 < r^2 < 0.98$) that agreed with the clinical prognosis of each kind of damage. It seems that this lipid marker does not depend on the nature of the tumor, but it clearly reflects the mestastatic potential of the primary cancer even when an accurate quantification of this condition is so difficult to obtain. Extrapolation of the regression lines to zero metastases yielded values of percent change (Σ monoenoic/Σsaturated) PlsEtn FAs which would correspond to a tumor with a hypothetically null spreading capacity. These values were similar to those obtained for BL samples (Table 7). Thus, the proposed marker has an excellent correlation with clinical status of the patient, especially number of metastases. Probably, it may be limited to the follow-up of the patient and to distinguish between BL and NEO samples in conflicting histopathological examinations in which complementary studies would be required. A population study at large scale may confirm the utility of the marker in prognosis, but our results are promising. We demonstrated that this highly sensitive marker is, at least, equally or even better than the existing clinical chemistry tumor markers.

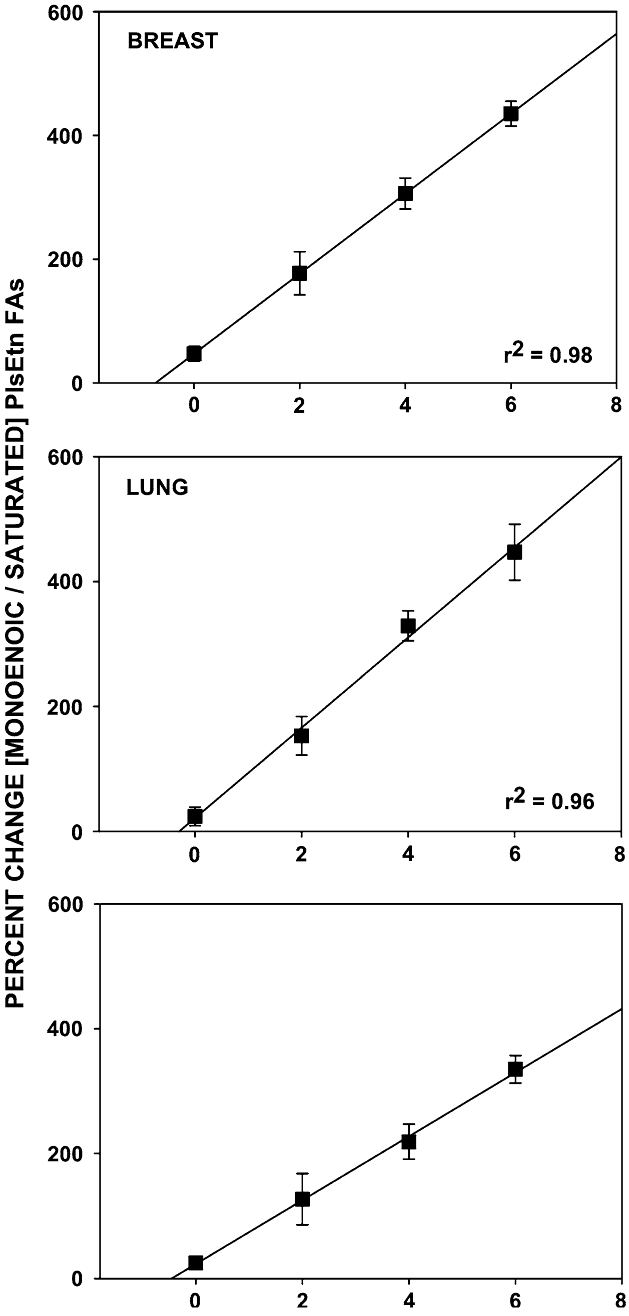

Fig. 3 Correlations between the relative content of monoenoic fatty acyl chains in PlsEtn and number of confirmed metastases (NCM) in 101 breast, 129 lung, and 73 prostate neoplastic samples. Calculations were done upon the percent change of the amount of monoenoic fatty acyl chains in PlsEtn of neoplastic samples with respect to normal tissue of the same patient. We included only those patients in which complementary studies confirmed the presence and number of metastases. Linear regression coefficients were calculated electronically using the software mentioned in "Experimental Procedure"

Surprisingly, the early findings reported in this field on lipid biochemistry have not been further developed for decades. So, we expect that our contribution may stimulate future research in this area.

Conclusions

To the best of our knowledge, this is the first time that a biochemical marker derived from composition studies of ethanolamine-containing plasmalogens provides a reliable index capable of distinguishing between BL and NEO tissues, and it correlates linearly with metastases spreading in vivo. Lipid analyses were performed with minor amounts of tissue and may be carried out with a relatively low number of complex instruments. Samples could be obtained during punch needle biopsy for histopathological examination. Results displayed high Se and excellent clinical correlation, and they would have interesting applications in prognosis of the most frequently observed human cancers.

Acknowledgments We are very grateful to the surgeons who contributed to this study. The authors also thank Elsa Claverie and Norma Cristalli for excellent technical assistance. Partially supported by grants from CIC, CONICET and UNLP, Argentina.

References

1. Nagan N, Zoeller RA (2001) Plasmalogens: biosynthesis and functions. Prog Lipid Res 40:199–229
2. Snyder F (1999) The ether lipid trail: a historical perspective. Biochim Biophys Acta 1436:265–278
3. Snyder F, Lee TC, Wykle RL (2002) Ether-linked lipids and their bioactive species. In: Vance DE, Vance JE (eds) Biochemistry of lipids, lipoproteins and membranes. Elsevier Science BV, Amsterdam, pp 233–262
4. Mangold HK, Paltauf F (1983) Ether lipids as chemical indicators in neoplasms. In: Mangold HK, Paltauf F (eds) Ether lipids. Biochemical and biomedical aspects. Academic, London, pp 248–251
5. Lin HJ, Ho FCS, Lee CLH (1978) Abnormal distribution of O-alkyl groups in the neutral glycerolipids from human hepatocellular carcinomas. Cancer Res 38:946–949
6. Mostofi FK, Davis CJ Jr, Sesterhenn IA (1992) Pathology of carcinoma of the prostate. Cancer 70:235–253
7. Mostofi FK, Murphy GP, Mettlin C (1995) Pathology review in an early prostate cancer detection program: results from the American Cancer Society-National Prostate Cancer Detection Project. Prostate 27:7–12
8. Travis WD, Colby TV, Corrin B (1999) Histological typing of lung and pleural tumors. World Health Organization International Histological Classification of Tumors, 3rd edn. Springer, Berlin
9. Kuralay F, Tokgöz Z, Cömlekci A (2000) Diagnostic usefulness of tumor marker levels in pleural effusions of malignant and benign origin. Clin Chim Acta 300:43–55
10. Bradford MM (1976) A rapid and sensitive method for the quantitation of microgram quantities of protein utilizing the principle of protein-dye binding. Anal Biochem 72:248–254
11. Folch J, Lees M, Sloane Stanley GH (1957) A simple method for the isolation and purification of total lipids from animal tissues. J Biol Chem 226:497–509
12. Marra CA, Alaniz MJT de (2000) Calcium deficiency modifies polyunsaturated fatty acid metabolism in growing rats. Lipids 35:983–990

13. Chen PS, Toribara TY, Warner H (1956) Microdetermination of phosphorus. Anal Chem 28:1756–1758
14. Park JH, Park EJ, Kim KS, Yeo YK (1995) Changes in ether-linked phospholipids in rat kidney by dietary α-Linolenic acid in Vivo. Lipids 30:541–546
15. Neskovic NM, Kostic DM (1968) Quantitative analysis of rat liver phospholipids by a two-step thin-layer chromatographic procedure. J Chromatogr 35:297–300
16. Mangold HK, Totani N (1983) Procedures for the analysis of ether lipids. In: Mangold HK, Paltauf F (eds) Ether Lipids. Biochemical and biomedical aspects. Academic, London, pp 377–387
17. Yeo YK, Philbrick DJ, Holub BJ (1989) Altered acyl chain compositions of alkylacyl, alkenylacyl, and diacyl subclasses of choline and ethanolamine glycerophospholipids in rat heart by dietary fish oil. Biochim Biophys Acta 1001:25–30
18. Marra CA, Alaniz MJT de (1989) Influence of testosterone administration on the biosynthesis of unsaturated fatty acids in male and female rats. Lipids 24:1014–1019
19. Kleinbaum DG, Kupper LL (1997) Applied regression analysis and other multivariable methods, (3rd edn.) Duxbury Press, MA
20. Boring CC, Squires TS, Tong T, Montgomery S (1994) Cancer statistics. Cancer J Clin 44:7–26
21. Giai M, Roagna R, Ponzone R, Biglia N (1996) TPS and CA 15.3 serum values as a guide for treating and monitoring breast cancer patients. Anticancer Res 16:875–881
22. De La Lande B, Hacene K, Florias JL, Alatrakchi N, Pichon MF (2002) Prognostic value of CA 15.3 kinetics for metastatic breast cancer. Int J Biol Markers 17:231–238
23. Sawabata N, Okada M, Higashiyama K (2006) Diagnostic strategy based on preoperative serum CEA levels in clinical stage IA NSCLC. J Clin Oncol 24:17011
24. D́Nistrian AM, Schwartz MK, Greenberg EJ, Smith CA, Schwartz DC (1991) Evaluation of CAM26, CAM29, CA 15–3 and CEA as circulating tumor markers in breast cancer patients. Tumor Biol 12:82–90
25. Daoud E, Bodor G (1991) CA-125 concentrations in malignant and nonmalignant disease. Clin Chem 37:1968–1974
26. Correale M, Abbate I, Gargano G (1992) Analytical and clinical evaluation of a new tumor marker in breast cancer: CA 27.29. Int J Biol Markers 7:43–46
27. Devine PL, Walsh MD, McGuckin MA (1995) Prostate-specific antigen (PSA) and cancer-associated serum antigen (CASA) in distinguishing benign and malignant prostate disease. Int J Biol Markers 10:221–225
28. Rodríguez de Paterna L, Arnaiz F, Esternoz J, Ortuno B, Lanzos E (1995) Study of serum tumor markers CEA, CA 15.3 and CA 27.29 as diagnostic parameters in patients with breast carcinoma. Int J Biol Markers 10:24–29
29. Pamies RJ, Crawford DR (1996) Tumor markers: an update. Med Clin North Am 80:185–199
30. Roulston JE (2002) Screening with tumor markers: critical issues. Mol Biotechnol 20:153–62
31. Klee GG, Schreiber WE (2004) MUC1 gene-derived glycoprotein assays for monitoring breast cancer (CA 15–3, CA 27.29, BR): are they measuring the same antigen? Arch Pathol Lab Med 128:1131–1135
32. Snyder F, Blank ML, Morris HP (1969) Occurrence and nature of O-alkyl and O-alk-1-enyl moieties of glycerol in lipids of Morris transplanted hepatomas and normal rat liver. Biochim Biophys Acta 176:502–510
33. Snyder F, Wood R (1969) Alkyl and alk-1-enyl ethers of glycerol in lipids from normal and neoplastic human tissues. Cancer Res 29:251–257
34. Howard BV, Morris HP, Bailey JM (1972) Ether-lipids, α-glycerol phosphate dehydrogenase, and growth rate in tumors and cultured cells. Cancer Res 32:533–1538
35. Yang YJ, Lee SH, Hong SJ, Chung BC (1999) Comparison of fatty acid profiles in the serum of patients with prostate cancer and benign prostatic hyperplasia. Clin Biochem 32:405–409
36. Aronson WJ, Glaspy JA, Reddy ST, Reese D, Heber D, Bagga D (2001) Modulation of Omega-3/Omega-6 polyunsaturated ratios with dietary fish oils in men with prostate cancer. Urology 58:283–288
37. Zuijdgeest-Van Leeuwen SD, Van Der Heijden MS, Rietveld T (2002) fatty acid composition of plasma lipids in patients with pancreatic, lung and oesophageal cancer in comparison with healthy subjects. Clin Nutr 21:225–230

Lipids (2008) 43:91–95
DOI 10.1007/s11745-007-3122-9

SHORT COMMUNICATION

Δ6 Desaturase mRNA Abundance in HepG2 Cells Is Suppressed by Unsaturated Fatty Acids

**Roxanne Portolesi · Barry C. Powell ·
Robert A. Gibson**

Received: 16 April 2007 / Accepted: 26 September 2007 / Published online: 25 October 2007
© AOCS 2007

Abstract The effect of unsaturated fatty acids on the abundance of Δ6 desaturase (D6D) mRNA and the fatty acid composition of HepG2 cell membranes was examined. Supplementation of HepG2 cells with oleic acid (18:1n-9, OA), linoleic acid (18:2n-6, LA), α-linolenic acid (18:3n-3, ALA), arachidonic acid (20:4n-6, AA) or eicosapentaenoic acid (20:5n-3, EPA) reduced D6D mRNA abundance by 39 ± 6.6, 40 ± 2.2, 31 ± 5.2, 55 ± 4.8, and 52 ± 5.0%, respectively, compared with control cells. Despite the reduction in D6D mRNA abundance, the level of D6D conversion products (20:3n-9, EPA and AA) in OA, ALA and LA supplemented cells, respectively, was elevated above that in control cells. Our results suggest that although unsaturated fatty acids decrease the abundance of D6D mRNA by as much as 50%, the conversion of polyunsaturated fatty acids and accumulation of long chain polyunsaturated fatty acids (LCPUFA) in HepG2 cell phospholipids continues to occur.

Keywords Fatty acid synthesis ·
Long chain polyunsaturated fatty acids ·
Peroxisome proliferators-activated receptor (PPAR)

Abbreviations

AA	Arachidonic acid
ALA	α-Linolenic acid
DHA	Docosahexaenoic acid
DPA	Docosapentaenoic acid
EPA	Eicosapentaenoic acid
LA	Linoleic acid
OA	Oleic acid
D6D	Δ6 Desaturase
cDNA	Complementary DNA
SE	Standard error

Introduction

Δ6 desaturase (D6D) is the first and rate-limiting enzyme involved in the desaturation and elongation of 18 carbon polyunsaturated fatty acids (PUFA) to long chain PUFA (LCPUFA). Dietary studies indicate that hepatic D6D mRNA expression is induced by diets low in linoleic acid (18:2n-6, LA) and α-linolenic acid (18:3n-3, ALA) and suppressed by diets rich in vegetable or marine oils [1–3]. D6D mRNA expression may be used as a surrogate marker for the activity of the enzyme as some studies in rodent have shown that the suppression of D6D mRNA expression by dietary PUFA is

---

R. Portolesi
Department of Paediatrics and Child Health, Flinders University,
Adelaide, Australia

B. C. Powell
Child Health Research Institute,
Children, Youth and Women's Health Service,
Adelaide, Australia

B. C. Powell
Discipline of Paediatrics, University of Adelaide, Adelaide,
Australia

B. C. Powell
School of Biological Sciences, Flinders University, Adelaide,
Australia

R. A. Gibson (✉)
Nutrition and Functional Food Science,
Discipline of Plant and Food Science, School of Agriculture,
Food and Wine, University of Adelaide, Waite Road,
Glen Osmond, SA 5064, Australia
e-mail: robert.gibson@adelaide.edu.au

associated with reduced D6D activity [3, 4]. Nuclear run-on analysis suggests that the suppression of D6D mRNA expression by PUFA is due to regulation at the transcriptional level [3], supposedly via peroxisome proliferators-activated receptors (PPARs), which bind to peroxisome proliferator-activated receptor response elements (PPRE) on the D6D gene [5–7]. There appears to be species differences in response to PPAR agonists. PPAR agonists cause hepatic peroxisome proliferation, hepatomegaly and, with prolonged administration, hepatocarcinogenesis, in rodents [8] yet human hepatocytes and HepG2 cells do not exhibit peroxisome proliferators-dependent peroxisome proliferation or induction of peroxisome proliferator-associated genes [9]. While D6D appears to be the rate-limiting step in the desaturation–elongation pathway, the overall regulation of the pathway and the correlation between D6D mRNA expression and the fatty acid composition of cell lipids is unclear and may involve several points of metabolic control. This study aimed to examine the effect of fatty acid supplementation on the mRNA abundance of D6D and fatty acid composition of HepG2 cells, a human cell line commonly used to study LCPUFA metabolism.

Materials and Methods

Materials

DMEM, FBS, penicillin, streptomycin and trypsin were purchased from JRH Biosciences (Victoria, Australia). FFA and authentic lipid standards were obtained from Nu-Check-Prep Inc (Elysian, MN, USA). BSA was from Sigma (St Louis, MO, USA). All other chemicals and reagents were of analytical grade.

Cell Culture

HepG2 cells (human hepatoma cell line) were obtained from American Type Culture Collection (Rockville, MD, USA) and cultured in DMEM supplemented with 10% FBS, 2 mM L-glutamine, 50 U/ml penicillin and 37.5 U/ml streptomycin. A series of experiments were performed to determine the cell culture conditions that produced the greatest accumulation of DHA in HepG2 cell phospholipids following supplementation with ALA, without a significant reduction in cell number or viability (data not shown). These conditions are described herein. Cells were grown and seeded into 6-well plates and supplemented with fatty acids bound to BSA as described previously [10]. Stock solutions of FFA were prepared in ethanol at a concentration of 10 mg/ml and diluted in serum free medium to achieve final concentrations of 71 µM OA, 71 µM LA, 72 µM ALA, 66 µM AA or 66 µM EPA. These concentrations effectively elevated the accumulation of the supplemented fatty acid above that observed in control cells whilst maintaining cell viability. The final concentration of ethanol in the media was 0.2%. Control cells were cultured in serum-free medium supplemented with an equivalent concentration of ethanol and BSA. After 48 h incubation with fatty acid-supplemented media, the cells were harvested for fatty acid or RNA extraction. Cells were used between passage 15 and 20. Cell viability was assessed by trypan blue exclusion.

Fatty Acid Analysis

Lipids were extracted from cells with chloroform/methanol (2:1, by vol) according to the method of Folch et al. [11]. Phospholipids were separated from other lipid classes by TLC (Silica Gel 60 H Merck Darmstadt, Germany) and transesterified by methanolysis to form fatty acid methyl esters (FAME). The resulting FAME were separated and quantified by gas chromatography as described previously [10].

RNA Extraction

Total RNA was isolated using a commercially available kit (Qiagen, CA, USA). Real-time quantitative PCR analysis (Corbett Rotorgene, Sydney, Australia) using SYBR® green fluorescence was used to determine the abundance of D6D mRNA relative to the house keeping gene, cyclophilin A using the comparative C_T (Threshold cycle) method. Two µg of total RNA was reverse transcribed with random hexamers according to the manufacturers instructions (Ambion, Austin, TX, USA). Each amplification mixture (20 µl) contained 0.5 µl of cDNA, 90 nM forward D6D primer (5′-CTG CCAACTGGTGGAATCATC), 90 nM reverse D6D primer (5′-ACAAACACGTGCAGCATGTTC) and PCR master mix (Stratagene, La Jolla, CA, USA). Published primer sequences were used for the forward and reverse D6D primers [12]. The forward and reverse cyclophilin A primers were 5′-GGTTGGATGGCAAGCATGTG and 5′-TGCTGG TCTTGCCATTCCTG, respectively. DNA sequences of the amplification products were determined by direct sequencing to confirm their identities with reported cDNA sequences of corresponding proteins [13] (GenBank Accession Number AF084559).

Statistical Analysis

Fatty acid analyses were performed on means of at least three separate replicates. Mean D6D mRNA abundance was compared from at least five separate replicates. ANOVA and Bonferroni post hoc statistical tests (SPSS Inc. Chicago, IL, USA) were used to compare means following fatty acid supplementation. Statistical significance was defined as ($P < 0.05$). Data are expressed as mean ± standard error (SE).

Results

Δ6 Desaturase mRNA Abundance

In cells supplemented with OA, LA, ALA, AA or EPA, the abundance of D6D mRNA was significantly ($P < 0.05$) reduced by 39 ± 6.6, 40 ± 2.2, 31 ± 5.2, 55 ± 4.8 and 52 ± 5.0%, respectively (Fig. 1) compared with control cells maintained in serum-free media with BSA. Analysis of D6D mRNA abundance before fatty acid supplementation and then at 1, 2, 6, 12, 24 and 48 h following supplementation with 72 μM ALA showed a significant reduction in D6D mRNA abundance at 24 h (data not shown). However, following 48 h supplementation, the time after which the medium was refreshed, the D6D mRNA abundance was equivalent to that observed in cells harvested immediately prior to supplementation. The suppression of D6D mRNA was not specific to any particular class of fatty acid as all fatty acids tested suppressed D6D mRNA abundance. Western blot analysis of HepG2 whole cell protein lysates using polyclonal rat antibodies [14] did not adequately identify the D6D protein in HepG2 cells (data not shown).

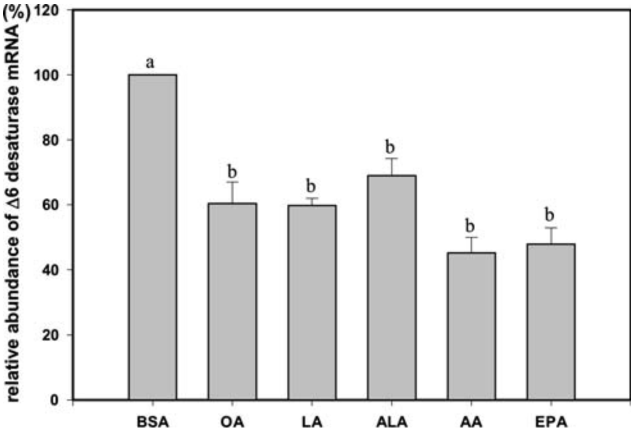

Fig. 1 Relative abundance of Δ6 desaturase mRNA compared with the housekeeping gene, cyclophilin A, in HepG2 cells following 48 h supplementation with oleic acid (18:1n-9, *OA*), linoleic acid (18:2n-6, *LA*), α-linolenic acid (18:3n-3, *ALA*), arachidonic acid (20:4n-6, *AA*) and eicosapentaenoic acid (20:5n-3, *EPA*) compared with control cells (BSA). Values are means ± SE of at least five replicates. Values with different symbols are significantly different ($P < 0.05$) from each other by one-way ANOVA with Bonferroni post-hoc analysis

Fatty Acid Analysis

The fatty acid composition of HepG2 cell phospholipids following supplementation with fatty acids is shown in Table 1. Despite the reduction in D6D mRNA abundance by all fatty acids examined, the concentration of D6D conversion products (20:3n-9, AA and EPA), in respective OA, LA and ALA supplemented cells were elevated above that observed in control cells. There was a significant increase in the level of OA and its product, 20:3n-9, in cells supplemented with 71 μM OA. In HepG2 cells supplemented with 71 μM LA, the level of LA and AA in cell phospholipids increased significantly ($P < 0.05$) compared with control cells. In ALA-supplemented cells, the level of ALA, EPA, DPA and DHA in cell phospholipids was increased. Following supplementation with 66 μM AA, the level of AA in HepG2 cell phospholipids increased dramatically, as did the level of 22:5n-6, which increased tenfold from 0.17 ± 0.01% total fatty acids in control cells to 1.73 ± 0.10% total fatty acids. In HepG2 cells supplemented with 66 μM EPA, the level of EPA in cell phospholipids increased from 0.14 ± 0.02% total fatty acids in control cells to 14.95 ± 0.51% total fatty acids. The level of DPA and DHA also increased significantly ($P < 0.05$) (Table 1).

Discussion

The mRNA abundance of D6D in HepG2 cells was significantly reduced following supplementation with OA, LA, ALA, AA or EPA compared with control. Dietary PUFA is reportedly a major regulator of D6D mRNA expression [15] which may influence the accumulation of LCPUFA in cell membranes. The suppression of D6D mRNA abundance by PUFA has been described previously in human neuroblastoma cells [16] and HepG2 cells [3]. However, these studies did not correlate D6D mRNA expression with the fatty acid composition of cell lipids. Nara et al. [12] showed that the abundance of D6D mRNA was reduced by approximately 50% in HepG2 cells supplemented with AA, EPA and DHA for 24 h whereas OA had no effect. The difference in the effect of OA between our study and that of Nara et al. [12] may be due to their inclusion of insulin and dexamethasone, two hormones that influence the expression of PPAR [17] and indeed, D6D [18].

In vivo studies also demonstrate that dietary OA does not affect D6D mRNA expression [1–3, 19], which may be attributed to mechanisms in vivo that are not apparent in vitro. One study suggests that D6D mRNA expression may be modulated indirectly by the metabolic state of the animal. In rats supplemented with the PPARα agonist

Table 1 Fatty acid composition of HepG2 cell phospholipids of cells supplemented with oleic acid (18:1n-9, OA), linoleic acid (18:2n-6, LA), α-linolenic acid (18:3n-3, ALA), arachidonic acid (20:4n-6, AA) or eicosapentaenoic acid (20:5n-3, EPA). Values are means ± SE of at least three replicates

Fatty acid	BSA control % total fatty acids	71 μM OA	71 μM LA	72 μM ALA	66 μM AA	66 μM EPA
Total saturates	29.63 ± 0.18^{a}	28.05 ± 0.32^{a}	34.55 ± 0.30^{b}	$35.29 \pm 1.44^{b,c}$	$36.31 \pm 0.62^{b,d}$	$38.57 \pm 0.60^{c,d}$
18:1n-9 OA	20.69 ± 0.52^{a}	30.74 ± 0.66^{b}	9.86 ± 0.87^{c}	11.23 ± 0.75^{c}	9.94 ± 0.68^{c}	10.16 ± 0.66^{c}
Total monounsaturates	51.99 ± 0.27^{a}	48.42 ± 0.29^{a}	26.92 ± 1.67^{b}	32.34 ± 1.60^{c}	$29.57 \pm 0.19^{b,c}$	$29.26 \pm 0.26^{b,c}$
20:3n-9	5.36 ± 0.36^{a}	7.37 ± 0.19^{b}	2.12 ± 0.19^{c}	2.24 ± 0.21^{c}	1.92 ± 0.03^{c}	1.85 ± 0.00^{c}
Total n-9	33.19 ± 0.31^{a}	44.96 ± 0.57^{b}	15.02 ± 1.22^{c}	17.56 ± 1.20^{c}	15.71 ± 0.72^{c}	15.28 ± 0.72^{c}
18:2n-6 LA	0.73 ± 0.06^{a}	0.59 ± 0.03^{a}	15.92 ± 0.24^{b}	0.86 ± 0.01^{a}	0.63 ± 0.03^{a}	0.61 ± 0.02^{a}
18:3n-6	0.11 ± 0.03^{a}	0.08 ± 0.00^{a}	0.43 ± 0.01^{b}	0.09 ± 0.02^{a}	0.10 ± 0.05^{a}	0.06 ± 0.03^{a}
20:3n-6	0.48 ± 0.02^{a}	0.36 ± 0.01^{a}	2.83 ± 0.20^{b}	0.43 ± 0.01^{a}	0.47 ± 0.08^{a}	0.34 ± 0.03^{a}
20:4n-6 AA	2.94 ± 0.14^{a}	2.56 ± 0.07^{a}	10.60 ± 0.83^{b}	2.64 ± 0.08^{a}	22.53 ± 0.65^{c}	2.39 ± 0.03^{a}
22:5n-6	0.17 ± 0.01^{a}	0.16 ± 0.01^{a}	1.19 ± 0.17^{b}	0.14 ± 0.03^{a}	1.73 ± 0.10^{c}	0.07 ± 0.00^{a}
Total n-6	4.78 ± 0.28^{a}	3.80 ± 0.12^{a}	32.22 ± 1.70^{b}	4.40 ± 0.13^{a}	27.83 ± 0.73^{c}	3.51 ± 0.11^{a}
18:3n-3 ALA	0.11 ± 0.13^{a}	0.01 ± 0.01^{a}	0.05 ± 0.00^{a}	7.05 ± 0.53^{b}	0.02 ± 0.02^{a}	0.03 ± 0.00^{a}
20:5n-3 EPA	0.14 ± 0.02^{a}	0.08 ± 0.00^{a}	0.07 ± 0.01^{a}	7.07 ± 0.74^{b}	0.04 ± 0.01^{a}	14.95 ± 0.51^{c}
22:5n-3 DPA	0.24 ± 0.06^{a}	0.30 ± 0.01^{a}	0.17 ± 0.01^{a}	1.91 ± 0.31^{b}	0.23 ± 0.02^{a}	5.38 ± 0.21^{c}
22:6n-3 DHA	2.61 ± 0.08^{a}	$2.14 \pm 0.06^{a,c}$	2.11 ± 0.06^{a}	3.93 ± 0.22^{b}	1.48 ± 0.14^{c}	4.48 ± 0.13^{b}
Total n-3	3.95 ± 0.29^{a}	2.53 ± 0.07^{a}	2.75 ± 0.07^{a}	22.69 ± 1.44^{b}	2.35 ± 0.07^{a}	25.35 ± 0.39^{b}

Values with different superscripts are significantly different from each other ($P < 0.05$) within each fatty acid group by one-way ANOVA with Bonferroni post-hoc test

WY14643, the fatty acid oxidation enzymes, acyl CoA oxidase, L-bifunctional protein and cytochrome P450 4A1 were all significantly induced within 4 h of treatment, with maximum induction occurring at 28 h [20]. D6D mRNA abundance was not significantly elevated at 4 h and it was only after 28 h that significance was reached [20]. The increased expression of D6D mRNA after 28 h suggests that its induction was secondary to the induction of the oxidation enzymes by WY1463 and may be compensatory. Interestingly, the level of OA in liver phospholipids was elevated [20] following treatment with WY14643 and may indicate an increased synthesis of OA de novo, as occurs in essential fatty acid deficient states. Moreover, PPAR agonists induce peroxisome proliferation in rodents [21]. Therefore, changes in fatty acid metabolism may also be attributable to the increased demand for fatty acids as constituents of phospholipids in the expanding peroxisome population [9]. It is questionable whether the changes in the fatty acid composition of cell lipids is directly attributable to the increased mRNA expression of D6D by WY14643 but rather the increased demand for fatty acid oxidation as a result of PPAR activation. The effect of D6D mRNA expression on the fatty acid composition of cell lipids is still unclear.

Despite a reduction in D6D mRNA abundance by up to 50%, the accumulation of fatty acid conversion products was increased compared with control cells. The fatty acid composition of cell lipids may be influenced by various parameters and highlights the need to examine D6D mRNA expression concurrent with the expression of oxidation enzymes and enzyme activity. Further studies that examine the effect of D6D overexpression by transfection of a D6D expression vector or the effect of knockdown of D6D mRNA by short interfering RNA, on the fatty acid composition of cell lipids, may help in describing a relationship between the two.

Acknowledgments Roxanne Portolesi is a Dairy Australia postgraduate student and RAG is a Senior NHMRC Research Fellow. The authors are grateful to Professor Philippe LeGrand, Laboratoire de Biochimie, INRA-ENSA, 35590 Saint-Gilles, France, who donated the polyclonal anti-rat Δ6 desaturase antibodies.

References

1. Cho HP, Nakamura MT, Clarke SD (1999) Cloning, expression, and nutritional regulation of the mammalian delta-6 desaturase. J Biol Chem 274:471–477
2. Nakamura MT, Cho HP, Clarke SD (2000) Regulation of hepatic delta-6 desaturase expression and its role in the polyunsaturated fatty acid inhibition of fatty acid synthase gene expression in mice. J Nutr 130:1561–1565
3. Tang C, Cho HP, Nakamura MT, Clarke SD (2003) Regulation of human {Delta}-6 desaturase gene transcription: identification of a functional direct repeat-1 element. J Lipid Res 44:686–695
4. Gasperikova D, Demcakova E, Ukropec J, Klimes I, Sebokova E (2002) Insulin resistance in the hereditary hypertriglyceridemic rat is associated with an impairment of delta-6 desaturase expression in liver. Ann N Y Acad Sci 967:446–453

5. Clarke SD, Jump DB (1994) Dietary polyunsaturated fatty acid regulation of gene transcription. Annu Rev Nutr 14:83–98
6. Kliewer SA, Sundseth SS, Jones SA, Brown PJ, Wisely GB, Koble CS, Devchand P, Wahli W, Willson TM, Lenhard JM, Lehmann JM (1997) Fatty acids and eicosanoids regulate gene expression through direct interactions with peroxisome proliferator-activated receptors alpha and gamma. Proc Natl Acad Sci USA 94:4318–4323
7. Smith SA (2002) Peroxisome proliferator-activated receptors and the regulation of mammalian lipid metabolism. Biochem Soc Trans 30:1086–1090
8. Lawrence JW, Li Y, Chen S, DeLuca JG, Berger JP, Umbenhauer DR, Moller DE, Zhou G (2001) Differential gene regulation in human versus rodent hepatocytes by peroxisome proliferator-activated receptor (PPAR) alpha. PPAR alpha fails to induce peroxisome proliferation-associated genes in human cells independently of the level of receptor expression. J Biol Chem 276:31521–31527
9. Kawashima Y, Musoh K, Kozuka H (1990) Peroxisome proliferators enhance linoleic acid metabolism in rat liver. Increased biosynthesis of omega 6 polyunsaturated fatty acids. J Biol Chem 265:9170–9175
10. Portolesi R, Powell BC, Gibson RA (2007) Competition between 24:5n-3 and ALA for u6 desaturase may limit the accumulation of DHA in HepG2 cell membranes. J Lipid Res (in press)
11. Folch J, Lees M, Sloane-Stanley GH (1957) A simple method for the isolation and purification of total lipids from animal tissues. J Biol Chem 226:497–509
12. Nara TY, He WS, Tang C, Clarke SD, Nakamura MT (2002) The E-box like sterol regulatory element mediates the suppression of human delta-6 desaturase gene by highly unsaturated fatty acids. Biochem Biophys Res Commun 296:111–117
13. Marquardt A, Stohr H, White K, Weber BH (2000) cDNA cloning, genomic structure, and chromosomal localization of three members of the human fatty acid desaturase family. Genomics 66:175–183
14. D'andrea S, Guillou H, Jan S, Catheline D, Thibault JN, Bouriel M, Rioux V, Legrand P (2002) The same rat Delta6-desaturase not only acts on 18- but also on 24-carbon fatty acids in very-long-chain polyunsaturated fatty acid biosynthesis. Biochem J 364:49–55
15. Nakamura MT, Nara TY (2004) Structure, function, and dietary regulation of delta6, delta5, and delta9 desaturases. Annu Rev Nutr 24:345–376
16. Langelier B, Alessandri JM, Perruchot MH, Guesnet P, Lavialle M (2005) Changes of the transcriptional and fatty acid profiles in response to n-3 fatty acids in SH-SY5Y neuroblastoma cells. Lipids 40:719–728
17. Steineger HH, Sorensen HN, Tugwood JD, Skrede S, Spydevold O, Gautvik KM (1994) Dexamethasone and insulin demonstrate marked and opposite regulation of the steady-state mRNA level of the peroxisomal proliferator-activated receptor (PPAR) in hepatic cells. Hormonal modulation of fatty-acid-induced transcription. Eur J Biochem 225:967–974
18. Saether T, Tran TN, Rootwelt H, Christophersen BO, Haugen TB (2003) Expression and regulation of delta5-desaturase, delta6-desaturase, stearoyl-coenzyme A (CoA) desaturase 1, and stearoyl-CoA desaturase 2 in rat testis. Biol Reprod 69:117–124
19. Matsuzaka T, Shimano H, Yahagi N, Amemiya-Kudo M, Yoshikawa T, Hasty AH, Tamura Y, Osuga J, Okazaki H, Iizuka Y, Takahashi A, Sone H, Gotoda T, Ishibashi S, Yamada N (2002) Dual regulation of mouse delta(5)- and delta(6)-desaturase gene expression by SREBP-1 and PPARalpha. J Lipid Res 43:107–114
20. Song HW, Nara TY, Nakamura MT (2002) Delayed induction of delta-6 and delta-5 desaturases by a peroxisome proliferator. Biochem Biophys Res Commun 299:832–838
21. Hsu MH, Savas U, Griffin KJ, Johnson EF (2001) Identification of peroxisome proliferator-responsive human genes by elevated expression of the peroxisome proliferator-activated receptor alpha in HepG2 cells. J Biol Chem 276:27950–27958

Lipids (2008) 43:97–103
DOI 10.1007/s11745-007-3121-x

METHODS

Fourier Transform Near Infrared Spectroscopy: A Newly Developed, Non-Invasive Method To Measure Body Fat

Non-invasive body fat content measurement using FT-NIR

H. Azizian · J. K. G. Kramer · S. B. Heymsfield ·
S. Winsborough

Received: 25 July 2007 / Accepted: 7 September 2007 / Published online: 6 November 2007
© AOCS 2007

Abstract An FT-NIR technique is reported to provide a fast, accurate and low cost method of determining in-vivo human body fat content. The body fat content of 353 healthy subjects (154 males and 199 females) of various height, weight, and age were measured by FT-NIR and compared to 420 subjects investigated by magnetic resonance imaging (MRI). The procedure involved scanning each subject's upper ear that provided a necessary reflectance surface and proved representative of the subject's subcutaneous fat content. The average FT-NIR spectrum was compared to a reference mixture with known and similar fat content and composition to that of humans. The FT-NIR response was incorporated into an empirical equation using the ratio of subcutaneous to total body fat from MRI data, taking into account the subject's gender, height, weight and age. The results on the two data sets were similar and demonstrated that the FT-NIR technique can be used to obtain a measure of the body fat content of individuals, similar to that using MRI. In addition, the FT-NIR was used to more accurately monitor the fat content of sleep apnea patients.

Keywords Body fat · Fourier transform near infrared spectroscopy · Obstructive sleep apnea · Human · Magnetic resonance imaging · Obesity

Introduction

According to a recent Statistics Canada Report 57% of men and 40% of women in Canada are considered overweight or obese[1] [1]. Overweight is defined by a body mass index (BMI) of >25, and obesity >30, and it is linked to several diseases, including hypertension, diabetes mellitus, hyperlipidemia, coronary artery disease, obstructive sleep apnea, and cancers of the breast, uterus, prostate and colon [1, 2]. The BMI guidelines assume that body mass is closely associated with body fatness [3]. However, some overweight individuals are not necessarily overfat (e.g., bodybuilders), while others having a normal BMI have a high percentage of their body weight as fat [3]. This suggests that we need a more reliable indicator of obesity for actual body fat measurement.

BMI is one of several ways to determine body fat or monitor obesity. Other techniques include skinfold thickness, circumference, bioelectrical impedance, dual energy X-ray absorptiometry, underwater weighing, computed tomography, and near-infrared interactance. The vast majority of these measurements are indirect and based on

H. Azizian (✉) · S. Winsborough
NIR Technologies Inc., 1312 Fairmeadow Trail,
Oakville, ON, Canada L6M 2M2
e-mail: hazizian@nirtechnologies.com

J. K. G. Kramer
Food Research Program, Agriculture and Agri-Food Canada,
Guelph, ON, Canada

S. B. Heymsfield
Body Composition Laboratory and Weight Control Unit,
St. Luke's-Roosevelt Hospital Center,
New York, NY 10025, USA

Present Address:
S. B. Heymsfield
Merck and Co., Inc., Clinical Research, Metabolism,
Whitehouse Station, NJ, USA

---

[1] Body mass index (BMI), by sex, household population aged 18 and over excluding pregnant women, Canada, provinces, territories, health regions and peer groups, 2003. http://www.statcan.ca/english/freepub/82–221-XIE/00604/tables/html/1228_03.htm.

assumptions and models. Magnetic resonance imaging (MRI) has been used as a more reliable technique, but it is expensive and inaccessible. As a result, we have developed a new technique to directly scan and evaluate subcutaneous body fat content in humans using Fourier Transform near infrared (FT-NIR) spectroscopy. The FT-NIR response can be compared to reference materials with known fat content and composition or used in an empirical equation with height, weight, gender and age as covariates.

The use of near infrared spectroscopy to determine fat content in humans was first reported in 1984 [4]. Ruchti et al. [5] reported the use of bovine fat as a reference material in their NIR determinations of the human fat content. We have shown that there are significant differences between bovine and human fat in composition, and since the FT-NIR signal is based on the fatty acid profile of the fat, a more appropriate reference material was developed that more closely resembled the human fatty acid composition [6]. Recent improvements in the resolution of FT-NIR spectroscopy coupled with chemometric analysis has allowed for the complete fatty acid profiling of fats and oils including *trans* fatty acids [7–9].

Methods

Subjects

Data were obtained from five different locations in Ontario: Mississauga City Hall, Mississauga South Common Mall, Mississauga River Grove Community Centre, Mississauga Meadowvale Community Centre, and Fitness Corner, Port Elgin. A total of 353 subjects (199 females and 154 males) were scanned, and their height, weight, and age recorded (as provided by the subjects). All subjects were required to read the information sheet describing the procedure and then sign a consent form.

FT-NIR Methods and Procedures

A Matrix-F FT-NIR Spectrometer equipped with a standard fibre optic probe from Bruker Optics in combination with OPUS (Optics Users Software) software was used to obtain the spectra. Several body parts were examined to obtain reliable and intense spectra. Most abdominal and arm measurements proved unusable because of high dispersion and low signal to noise ratio. It was found that the upper ear yielded the best spectral characteristics for this study with the least amount of background noise and water interference, and strong reflectance signal. The resulting absorption spectra were a composite of different components in the sample. The fibre optic probe carrying the near infrared light was held against the back of the subjects' upper ear to avoid eye contact; see demonstration of technique in [10]. On average five measurements of five scans each per subject were taken (for a total scan time of 25 s) and the resulting absorption spectra were averaged. The averaged spectrum was then integrated focusing on the frequencies associated with the fat peaks to obtain the FT-NIR response. This response proved to be related to subcutaneous fat of the subjects, and was matched against the FT-NIR response of the reference material with a known fat content [6].

FT-NIR Reference Material

Preliminary results indicated that bovine fat used by Ruchti et al. [5] did not resemble human body fat composition and hence could not be used as a FT-NIR reference. Figure 1 shows the second derivative spectra of human, reference material and bovine fat; the latter showed a more pronounced peak for saturated fatty acids and less unsaturated fatty acids compared to human fat. In addition, a clear chemical shift of about 8 cm^{-1} wavenumbers was evident in the bovine fat at 5,777 cm^{-1} compared to human fat spectrum at 5,785 cm^{-1}. This chemical shift and the profile differences have a significant effect on the quantitative determination in near infrared spectroscopy. A more suitable reference material was prepared consisting of water, fat, and protein, which more closely resembled human body fat profile (Fig. 1). To generate a calibration curve, the FT-NIR response of increasing amounts of fat in the reference material was measured (Fig. 2). These results were used to obtain the calibration curve (Fig. 3). The underlying protein signal from the cartilage was established by purchasing pig's ears and measuring the FT-NIR

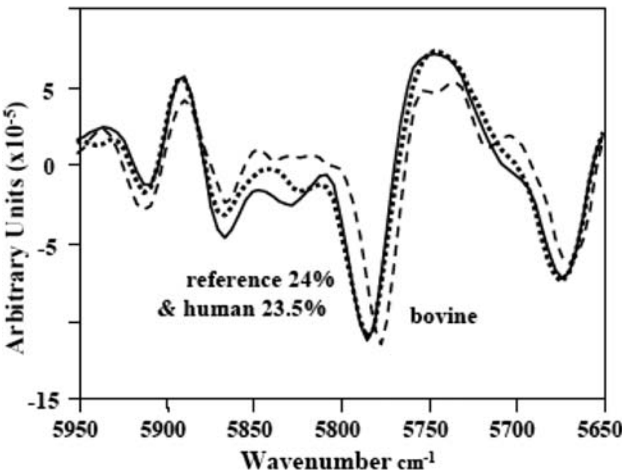

Fig. 1 Second derivative spectra for bovine, human, and the reference material: *dashed line*, bovine; *dotted line*, reference 24%; *solid line*, human 23.5%

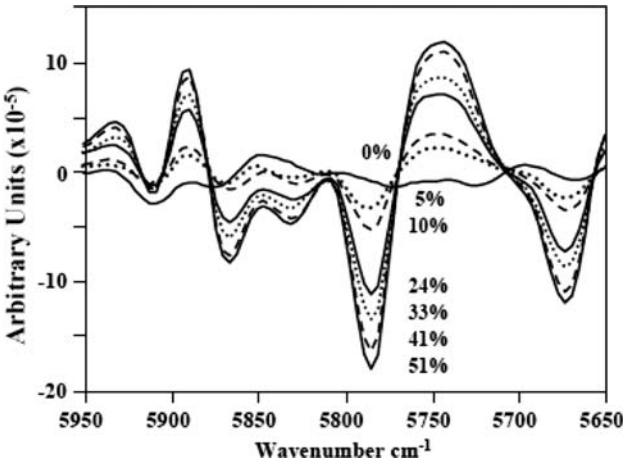

Fig. 2 FT-NIR response in the fat region of the reference materials containing 0–51% fat: *solid line* 0%; *dotted line* 5%; *dashed line* 10%; *solid line* 24%; *dotted line* 33%; *dashed line* 41%; *solid line* 51%

spectra with the skin plus fat layer, and after removal of the outer layers, recording the signal of the cartilage.

FT-NIR Empirical Equation

The fat content measurement results using the reference material with known fat content were verified by developing an empirical equation. This equation was based on the existing body surface area equations [11, 12] and the ratio of subcutaneous to total fat content from MRI studies taking gender and age into consideration, which were combined with the FT-NIR response. It was assumed that the total body fat volume could be determined by measuring the body surface area multiplied by the thickness of subcutaneous fat layer. The values of the FT-NIR response were substituted for the thickness of subcutaneous fat layer in these equations.

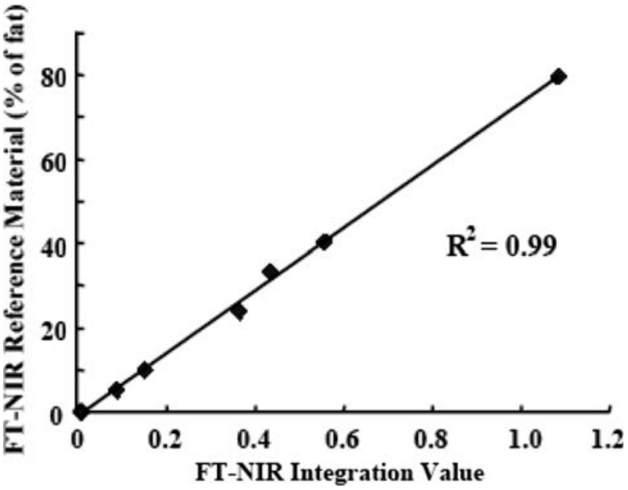

Fig. 3 Calibration curve for fat content determination

Magnetic Resonance Imaging Methods and Procedures

Methods and procedures for the collection of MRI data were published [13].

Results

Representative values for both female and male subjects are shown in Table 1. Their body fat content was measured by FT-NIR spectroscopy and determined using the calibration curve (Fig. 3).

A number of subjects were compared according to height, weight, age, BMI and fitness level to observe differences in their fat content (Table 2). One pair is shown in Fig. 4, which shows the second derivative spectrum for male subjects 1007 and 1010. Subject 1007 was involved in bodybuilding activities, while subject 1010 is an average male. Both subjects were of a similar weight and height with a similar BMI. The FT-NIR spectrum for subject 1010 in Fig. 4 shows more intense fat peaks than that for subject 1007, indicating a higher body fat content. The data in Table 2 demonstrate that BMI is an unreliable measure of body fat content, and confirms the findings by other that fat percentage measurements are more informative than BMI [3].

An empirical equation was developed based on the assumption that subcutaneous fat thickness, substituted by FT-NIR response and multiplied by body surface area generates subcutaneous fat volume. The surface area was determined using existing body surface area equations [11, 12]. The ratio of subcutaneous to total adipose tissue was obtained from MRI data that was necessary to convert the FT-NIR response (subcutaneous) to total body fat content. Figure 5 shows the MRI data for subcutaneous/total adipose tissue ratio with respect to age and gender. As can be seen, at a younger age, almost 95% of the adipose tissue for males and 97% for females is stored subcutaneously. A separate empirical equation for males and females was developed using the body surface area equations and MRI ratio of subcutaneous to total adipose tissue, and incorporating a factor for the FT-NIR response. These equations are shown below:

$$\text{Female}\quad \mathrm{TBF} = \frac{64.719\mathrm{N} \times \mathrm{W}^{0.51456} \times \mathrm{H}^{0.42246}}{(-0.001\mathrm{A} + 0.989)\mathrm{W}}$$

$$\text{Male}\quad \mathrm{TBF} = \frac{64.719\mathrm{N} \times \mathrm{W}^{0.51456} \times \mathrm{H}^{0.42246}}{(-0.003\mathrm{A} + 0.997)\mathrm{W}}$$

TBF total body fat; N NIR response; W weight in kg; H height in cm; A age in years.

The scanned data for 353 subjects were re-analyzed for body fat content using the FT-NIR empirical equations, and

Table 1 Body fat content of representative female or male subjects using FT-NIR spectroscopy

ID No.	Gender	Age	Height (cm)	Weight (kg)	FT-NIR response	BMI	FT-NIR Fat % equation	FT-NIR Fat % reference
1002	F	24	165	61.4	0.46	23	36	33
1006	F	21	163	67.3	0.38	25	28	27
1009	F	27	163	72.0	0.26	27	19	18
1011	F	47	156	60.5	0.35	25	28	25
1020	F	43	165	68.0	0.71	25	54	52
1022	F	56	168	85.9	0.45	30	31	33
1025	F	48	173	68.2	0.50	23	39	36
1027	F	39	165	72.7	0.38	27	28	27
1033	F	46	163	62.0	0.64	23	51	47
1036	F	44	155	59.1	0.24	25	19	17
1038	F	37	170	61.4	0.50	21	40	36
1039	F	51	155	72.7	0.41	30	30	30
1001	M	49	174	79.1	0.26	26	19	19
1005	M	21	183	79.5	0.14	24	10	9
1007	M	25	188	93.0	0.07	26	5	4
1010	M	23	191	95.0	0.28	26	19	20
1014	M	22	185	90.0	0.23	26	16	16
1018	M	24	170	63.6	0.20	22	16	14
1019	M	24	178	95.4	0.31	30	20	22
1023	M	40	178	75.0	0.29	24	22	21
1029	M	42	198	78.8	0.31	20	24	22
1031	M	31	175	77.3	0.23	25	17	16
1034	M	21	185	88.6	0.29	26	20	21
1042	M	60	173	78.0	0.20	26	15	14

Mean and standard deviations for all females were: age 43 ± 14 years; height 163 ± 7 cm; weight 64 ± 10 kg; FT-NIR response 0.39 ± 0.11; BMI 24 ± 4; body fat content by FT-NIR 29 ± 8%. Mean and standard deviations for all males were: age 39 ± 16 years; height 178 ± 7 cm; weight 82 ± 13 kg; FT-NIR response 0.22 ± 0.09; BMI 26 ± 3; body fat content by FT-NIR 16 ± 7%. The percent (%) body fat content for each of the subjects was calculated using the equations and the reference material

comparing the results to those using the FT-NIR reference material. Setting the intercept at 0, a significant linear correlation was found ($R^2 = 0.94$) tested using a two-tailed paired t test ($P < 0.0001$), as shown in Fig. 6 (all data). Table 1 includes the determination of percent (%) body fat using the reference material and the empirical equation for each of the representative male and female subjects (the last two columns). The results using the empirical equation were dependent upon subjects accurately reporting their height and weight, which may explain some minor discrepancies between the two data sets. These equations are very sensitive to age, weight and the NIR response. For example a change of 0.02 in the NIR response would result in 1% drop in body fat %, and in some minor cases up to 2% drop in both female and male subjects. The same is true for the age coefficient. Switching the empirical equation for males and females

Table 2 Effect of physical activity on subject's body fat content

ID No.	Gender	Age	Height (cm)	Weight (kg)	Activity level	FT-NIR fat response	BMI	FT-NIR Fat %
1007	M	25	188	93	High—body building	0.07	26	4
1010	M	23	191	95	Average	0.28	26	20
1005	M	21	183	80	High—body building	0.14	24	10
1131	M	18	183	80	Active	0.24	24	17
1156	M	22	175	82	High—fitness training	0.12	27	8
1132	M	23	173	80	Active	0.23	27	16
1201	F	26	165	61	Active	0.29	22	21
1002	F	24	165	61	Average	0.46	22	34
1211	F	25	157	55	Active	0.26	22	19
1015	F	24	158	55	Average	0.43	22	32

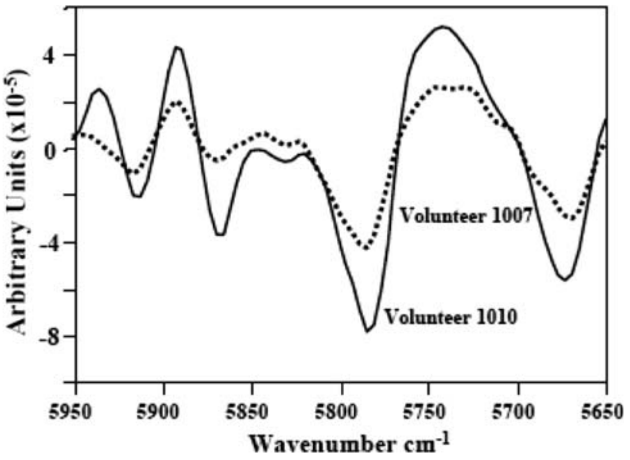

Fig. 4 Second derivative comparisons for two subjects with the same BMI but different body fat content: *dotted line*, volunteer 1007; *Solid line*, volunteer 1010

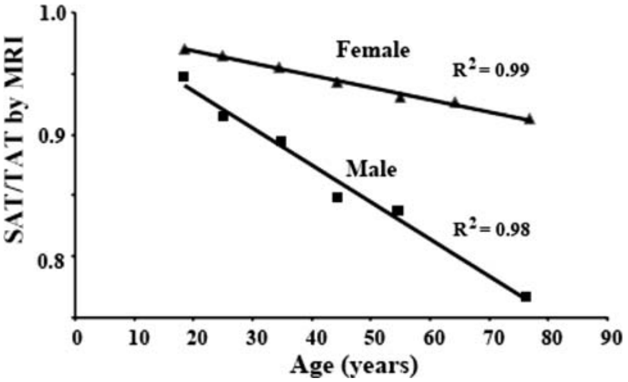

Fig. 5 Subcutaneous to total fat ratio with respect to age for males and females as determined by MIR: SAT, Subcutaneous Adipose Tissue; TAT, Total Adipose Tissue; MRI, magnetic resonance imaging

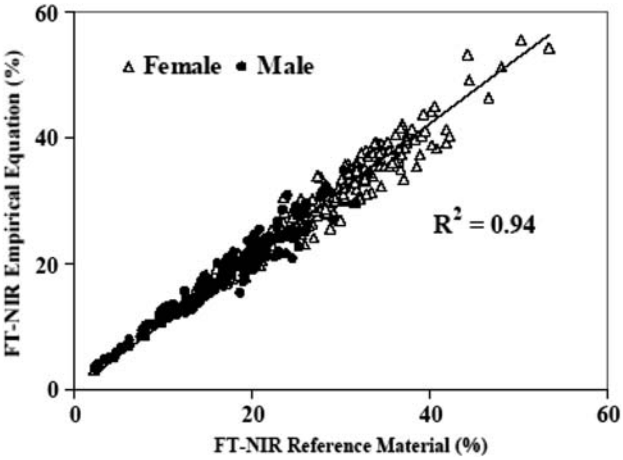

Fig. 6 Comparison of two FT-NIR methods for determining fat content for males and females

result in a fat % difference of up to 2%. This is due to the difference in the slope of subcutaneous to total ratio in males and females (see Fig. 5). Figure 6 also shows that the majority of male subjects are located at the lower end of the scale, whereas female subjects are located at the higher end of the scale confirming that, on average, females have more body fat than males [3].

A comparison between the FT-NIR data for 353 subjects in Ontario and MRI data for 420 subjects from the St. Luke's-Roosevelt Hospital in New York was subsequently performed. The FT-NIR and MRI data for 39 pairs of subjects were matched according to gender, age, height and weight. Table 3 shows representative comparisons for 10 female pairs and 10 male pairs. The R^2 value for all 39 pairs was 0.96 with a two-tailed P value of $P = 0.0468$. The last two columns in Table 3 show the % fat content measured by the FT-NIR and MRI for the paired subjects. The only discrepancies would be similar to the example provided in which a body builder is compared to an average person with similar weight and height (Table 2). Although the two subject groups were measured using two different techniques (FT-NIR and MRI) the results show a remarkable resemblance in body fat content. The comparison of these two groups was to some extent justified since both groups were from North America with similar life styles and diets.

The FT-NIR technique was recently applied to also monitor body fat content of sleep apnea patients. The patient was diagnosed with obstructive sleep apnea having an Apnea Hypopnea Index (AHI) of 15.2 (event/h); below 10 is considered normal. The person's weight was 81.8 kg and height 1.74 m for a BMI of 27.0. The patient then underwent a weight loss program losing 6.8 kg, which corresponded to a 9% drop in body fat content as measured by FT-NIR (25–16%), or a decrease in BMI from 27.0–24.8. A subsequent obstructive sleep apnea test showed a marked improvement in the AHI down from 15.2 to 2.5 (event/h).

Discussion

The body fat content of 353 subjects was measured by FT-NIR spectroscopy and determined using the calibration curve. The results were confirmed by calculating the fat volume using an empirical equation that was developed based on substituting the FT-NIR response for the subcutaneous fat thickness and the body surface area. A comparison between FT-NIR and MRI data for 39 pairs of subjects were matched according to gender, age, height and weight ($R^2 = 0.96$, $P = 0.0468$). Both groups were from North America with similar life styles and diets.

Table 3 Comparison of FT-NIR and MRI results for selected female or male subjects

Gender	ID No.	Age	Height (cm)	Weight (kg)	BMI	Fat % by FT-NIR	Fat % by MRI
F1	NIR 1141	17	157	56	23	35	–
	MRI 153	20	158	58	23	–	35
F2	NIR 1202	18	165	58	21	20	–
	MRI 190	23	162	51	19	–	20
F3	NIR 1285	25	168	57	20	25	–
	MRI 146	24	163	59	22	–	23
F4	NIR 1149	22	170	64	22	27	–
	MRI 166	24	170	65	22	–	28
F5	NIR 1370	27	170	55	19	28	–
	MRI 105	27	170	55	19	–	28
F6	NIR 1060	27	160	68	27	30	–
	MRI 1184	29	158	65	26	–	29
F7	NIR 1191	30	156	59	24	30	–
	MRI 233	30	157	56	23	–	31
F8	NIR 1204	36	163	61	23	28	–
	MRI 313	36	160	58	23	–	29
F9	NIR 1078	42	168	74	26	37	–
	MRI 0329	42	167	73	26	–	37
F10	NIR 1253	66	168	61	22	31	–
	MRI 267	70	164	61	23	–	32
M1	NIR 1323	20	180	68	21	17	–
	MRI 202	20	183	73	22	–	17
M2	NIR 1375	20	180	70	22	8	–
	MRI 336	22	181	72	22	–	8
M3	NIR 1010	23	191	95	26	21	–
	MRI 17816	25	185	96	28	–	22
M4	NIR 1018	24	170	64	22	14	–
	MRI 0011	25	173	65	22	–	13
M5	NIR 1017	25	183	68	20	10	–
	MRI 17486	25	187	70	20	–	11
M6	NIR 1195	25	180	80	25	11	–
	MRI 32	26	178	78	25	–	12
M7	NIR 1031	31	175	77	25	17	–
	MRI 129	31	176	74	24	–	18
M8	NIR 1059	37	180	86	27	18	–
	MRI 0111	38	181	88	27	–	19
M9	NIR 1123	40	178	86	27	19	–
	MRI 2	38	181	88	27	–	19
M10	NIR 1001	49	174	79	26	19	–
	MRI 415	49	174	78	26	–	20

The newly developed method based on FT-NIR shows the potential for a quick, accurate and relatively inexpensive determination of human body fat content. Previous NIR studies were not successful since dispersive NIR technology and inappropriate reference materials were used [4, 5]. The discovery of using the back of the upper ear providing a suitable reflectance surface for the NIR light, as well as, the finding that the fat layer was representative of the subcutaneous fat in the human subjects proved to be important steps in this research. The reflectance of NIR light could not be obtained by measuring other body parts due to dispersion of the NIR light. The MRI data established that a high percentage of body fat was stored subcutaneously (Fig. 5), which was used to correlate the subcutaneous fat layer on the back of the upper ear to the whole body fat content. The significant correlation of the FT-NIR to the MRI data suggests that the upper ear was representative of the whole body fat content when measured using FT-NIR spectroscopy.

Although, the FT-NIR and MRI tests were performed on different subjects at different locations and times, the correlation between the results of the two techniques is notable and the similarities are gender neutral with no obvious differences for scanning male or female subjects. The similarity of life styles and diets between the two study groups allowed for a comparison of the two techniques. The ultimate test of acceptance for the FT-NIR technique would be a direct validation using both techniques and several groups of male and female subjects, old and young, normal and obese.

These results demonstrate the potential of using FT-NIR to measure the body fat content of human subjects rapidly and accurately providing data comparable to the more costly and less accessible MRI technique. The FT-NIR technique is a low cost, portable and safe method that could prove valuable to determine the fat content of individuals being treated for obesity and sleep apnea and to more accurately monitor weight loss. The FT-NIR method has already been used for fatty acid profiling of fats and oils and there is the potential of doing the same for humans.

Acknowledgments The authors acknowledge partial financial contributions by the Industrial Research Assistance Program of National Research Council in Canada, and David Hawks a technology advisor from that center. The authors also acknowledge the technical assistance of Anthony Kamalian, Michael Younikian, and Carolyn Winsborough in the scanning sessions.

References

1. Douketis JD, Paradis G, Keller H, Martinea C (2005) Canadian guidelines for body weight classification in adults: application in clinical practice to screen for overweight and obesity and to assess disease risk. Can Med Assoc J 172:995–998
2. Douketis JD, Feightner JW, Attia J, Feldman WF (1999) Examination Canadian task force on the periodic health. Periodic health examination, 1999 update: 1. Detection, prevention and treatment of obesity. Can Med Assoc J 160:513–525

3. Gallagher D, Heymsfield SB, Heo M, Jebb SA, Murgatroyd PR, Yakamoto Y (2000) Healthy percentage body fat ranges: an approach for developing guidelines based on body mass index. Am J Clin Nutr 72:694–701
4. Conway JM, Norris KH, Boldwell CE (1984) A new approach for the estimation of body composition: infrared interactance. Am J Clin Nutr 40:1123–1130
5. Ruchti TL, Malin SF, Hazen KH, Makarewicz MR, Acosta GM (2002) Classification and characterization of tissue through features related to adipose tissue. Canadian Patent Application 2 397 611 (Jul 26, 2001)
6. Azizian H, Winsborough S, Younikian M, Winsborough C (2003) Method of in-vivo measurement of fat content of a body and apparatus thereof. Canadian Patent No. 2,404,891 (Issued November 18, 2003)
7. Azizian H, Kramer JKG (2005) A rapid method for the quantification of fatty acids in fats and oils with emphasis on *trans* fatty acids using Fourier transform near infrared spectroscopy (FT-NIR). Lipids 40:855–867
8. Azizian H, Kramer JKG, Winsborough SL (2007) Factors influencing the FA determination in fats and oils using Fourier transform near infrared spectroscopy. Eur J Lipid Sci Technol 109:960–968
9. Azizian H, Kramer JKG, Kamalian AR, Hernandez M, Mossoba MM, Winsborough SL (2004) Quantification of *trans* fatty acids in food products by GC, ATR-FTIR, and FT-NIR methods. Lipid Technol 16:229–231
10. Azizian H, Kramer JKG (2005) A non-invasive analytical tool for many applications. Inform 16:656–658
11. Du Bois D, Du Bois EF (1916) A formula to estimate the approximate surface area if height and weight be known. Arch Intern Med 17:863–871
12. Gehan EA, George SL (1970) Estimation of human body surface area from height and weight. Cancer Chemother Rep (Part 1) 54:225–235
13. Engelson ES, Kofler DP, Tan YX, Agin D, Wang J, Pierson RN Jr, Heymsfield SB (1999) Fat distribution in HIV-infected patients reporting truncal enlargement quantified by whole-body magnetic resonance imaging. Am J Clin Nutr 69:1162–1169

Lipids (2008) 43:105–106
DOI 10.1007/s11745-008-3156-7

EDITORIAL

Editorial

Eric J. Murphy

Published online: 31 January 2008
© AOCS 2008

Dear Readers:

In their Letter to the Editor in this issue of *Lipids*, Drs. Bosetti and Toscano highlight an important issue: the need for the persons involved as reviewers in the peer-review system to disclose potential conflicts of interest regarding the manuscript or the authors.

Certainly someone who has a financial stake in the area of research presented in a submitted manuscript should declare potential conflicts of interest without regard to which side of the peer-review system that individual belongs. For instance, if someone from a competing company is asked to review a manuscript that could impact the reviewer's own projects and downstream drug revenue, the reviewer should declare that conflict to the assigned Associate Editor. The Associate Editor will consult with either the assigning Senior Associate Editor or me to determine whether that person should continue in the review of the said manuscript. Although this is a clear-cut issue, what about those of us who reside primarily in the academic arena? Here, people can be ruthless if they perceive that another person's work intrudes into their domain. In short, I have just been scooped! Under this circumstance, the best way to prevent the scoop by a reviewer is to delay the other individual's manuscript, through such means as tardy reviews and a request for a large number of unnecessary experiments or by rejecting the manuscript altogether. Hence, how do we police this behavior, which is clearly not well defined and is highly variable? Whereas we try on the editorial side to weed out the "unfair" reviews, we first must catch them. We strive to do our best in this area and overall I think our efforts are commendable.

Overall, I think that our own collective maliciousness is often more damaging than all of the big-time financial conflicts of interest. When I was interviewed for the Editor-in-Chief position, I repeated a statement that I learned from my mentor, Professor Lloyd Horrocks. That is, be fair in the review process, and combine this fairness with a great deal of rigor. I train my postdoctoral fellows to review manuscripts with fairness and rigor. I teach my students and post-doctoral fellows the mantra, "Likes and dislikes have no place in science." Whether I like or dislike a person does not affect my decision during a review or in making a decision at the level of Editor-in-Chief. Fairness with rigor is the absolute key to the process.

So what about disclosures? At *Lipids*, we formally ask all authors to disclose any potential conflicts of interest regarding the submitted manuscript. For most of us, this is a minor issue. For my lab, every manuscript submitted to *Lipids* has an inherent conflict in that I am Editor-in-Chief. I make such a disclosure and, like all other authors, suggest potential reviewers and editorial staff; but from there on I am blinded to the process just like everyone else. But these types of disclosures are the easy ones.

The issue raised by Bosetti and Toscano is with the review side. At *Lipids*, we ask reviewers to note any scientific misconduct issues in manuscripts, but should we also ask them to note any potential conflicts? I for one have always expected reviewers to know when to recuse themselves, and over the years I have seen numerous people do this, running the gamut from big names in the field to emerging stars to graduate students reviewing their first manuscript. So these

E. J. Murphy (✉)
Department of Pharmacology,
Physiology and Therapeutics,
School of Medicine and Health Sciences,
University of North Dakota,
501 North Columbia Road,
Grand Forks, ND 58203, USA
e-mail: emurphy@medicine.nodak.edu

types of people once again fall into the category that Lloyd spoke about all those many years ago.

I think the cause for concern is those individuals who are quite ambitious but lack ambition. This is something Stephen R. Lorenz, a three-star US Air Force general noted to a group of young, newly commissioned officers. He told them to surround themselves with people with ambition, not with ambitious people. The key element is that scientists who recuse themselves voluntarily are people perhaps with ambition, but who certainly are not ambitious. They are team players who recognize the fact that, despite their best efforts, they just cannot be fair to the authors during the review process, and to be fair, they recuse themselves. The ambitious scientists are those individuals who recognize that they can help themselves by harming others through the review process.

How do we ultimately police these individuals? At this point, it is impossible, as we are all subject to the frailties that come from being human. I, like French philosopher Jean-Jacques Rousseau (1712–1778), feel that most of us are good and will strive to do the right thing. For those reviewers who do not fit into this model, we need to be vigilant at the editorial level to limit the impact that these types of people have on the peer-review process.

My best wishes to everyone for a prosperous and healthy New Year.

Sincerely,

Eric J. Murphy
Editor-in-Chief, *Lipids*

Lipids (2008) 43:107–108
DOI 10.1007/s11745-007-3134-5

LETTER TO THE EDITOR

Is It Time to Standardize Ethics Guiding the Peer Review Process?

Francesca Bosetti · Christopher D. Toscano

Received: 11 October 2007 / Revised: 30 October 2007 / Accepted: 30 October 2007 / Published online: 29 November 2007
© AOCS 2008

Abstract While most scientific journals have well defined ethics requirements for authors, very few journals explicitly specify the ethics standards that govern the actions of editors, editorial board members, and reviewers. We believe it is time to create a standardized policy for all medical and scientific journals that guides the ethical conduct of all stakeholders in the peer review process.

Keywords Ethics · Conflict of interest · Peer review

In their recent article, James et al. [1] comment on the role of medical journals and the peer review process in the assessment of the cardiovascular risk of rofecoxib (Vioxx®), a selective cyclooxygenase-2 (COX-2) inhibitor. The authors conclude that the commercial success of rofecoxib, despite the existence of convincing data regarding its severe cardiovascular risks, provides a case-study of the failure of the medical journals and peer review process in directing appropriate drug usage. While it is an important review of the COX-2 inhibitor controversy in its own right, we believe that the article by James et al. indirectly raises a more general issue on the need for more stringent standards of ethical conduct for all participants in the peer review process. With the current movement to formalize the ethical regulations and guidelines for activities in science [2], we propose that it is time for universal adoption of standardized and written guidelines by peer-reviewed scientific journals regarding the ethical conduct of all stakeholders in the peer review process.

While most scientific journals have well defined ethics requirements for authors, very few journals explicitly specify, in writing, the ethics standards that govern the actions of editors, editorial board members, and reviewers. In fact, it has been determined that of journals that require conflict of interest disclosures by authors, more than 50% do not currently require editors or reviewers to disclose financial or other conflicts of interest [3]. With two of the major publishers of scientific journals, Elsevier and Blackwell Publishing, and the HHS Office of Research of Integrity having offered suggested guidelines for ethical conduct in the peer review process [4–6], it is staggering that this number of peer-reviewed journals has been slow to adopt a standardized, written policy of ethics governing editors, reviewers and authors alike.

We submit that it is time for all scientific journals to adopt a standardized and written code of ethics which governs all stakeholders in the peer review process and not just the authors of manuscripts. This endeavor should be undertaken via the guidance of the Editors-in-Chief and should include at the minimum:

(1) An explicitly stated policy in the Journal and its website regarding the ethical standards expected of authors, editors and reviewers.
(2) A mandated disclosure of real or perceived conflicts of interest of authors, editors, members of the editorial board and reviewers during the submission process.
(3) A detailed mechanism for editors or reviewers with real or perceived potential conflict of interests to recuse themselves from assignments that represent a conflict of interest.

F. Bosetti (✉) · C. D. Toscano
Brain Physiology and Metabolism Section,
National Institute on Aging, National Institutes of Health,
Bethesda, MD 20892, USA
e-mail: frances@mail.nih.gov

We by no means suggest that the above measures be accepted as the sole measures for standardizing ethics in the peer review process. Other entities, as stated above, have provided more comprehensive guidelines for ethical conduct for all participants in the peer review process [4–6]. Our objective in writing this letter, however, is to begin the long overdue dialog regarding the adoption of written ethical guidelines by scientific journals for all stakeholders in the peer review process. We feel that creating standardized guidelines for all medical and scientific journals will prevent conflict of interest controversies involving the peer-review process. Further and most important, these ethical guidelines will act to increase the trust of both authors and readers in a fair and ethical peer review process, with the ultimate goal of improving the quality and credibility of science.

References

1. James MJ, Cook-Johnson RJ, Cleland LG (2007) Selective COX-2 inhibitors, eicosanoid synthesis and clinical outcomes: a case study of system failure. Lipids 42:779–785
2. National Institutes of Health Ethics Program, Principles of Ethical Conduct for Government Officers and Employees http://ethics.od.nih.gov/principl.htm (Accessed: 5 October, 2007)
3. Cooper RJ, Gupta M, Wilkes MS, Hoffman JR (2005) Conflict of interest disclosure policies and practices of peer-reviewed biomedical journals. J Gen Intern Med 21:1248–1252
4. Ethics of Peer Review: a guide for manuscript reviewers http://ori.hhs.gov/education/products/yale/prethics.pdf (Accessed: 5 October, 2007)
5. Publication Ethics http://www.blackwellpublishing.com/Publicationethics/#ethical_policy_template (Accessed: 5 October, 2007)
6. Ethical Guidelines for Journal Publication http://www.elsevier.com/wps/find/intro.cws_home/ethical_guidelines#Duties%20of%20Editors (Accessed: 5 October, 2007)

Lipids (2008) 43:109–115
DOI 10.1007/s11745-007-3127-4

ORIGINAL ARTICLE

Octacosanol Administration to Humans Decreases Neutral Sterol and Bile Acid Concentration in Feces

Sylvia Keller · Franziska Gimmler · Gerhard Jahreis

Received: 8 June 2007 / Accepted: 18 October 2007 / Published online: 15 November 2007
© AOCS 2007

Abstract To investigate octacosanol (OC) metabolism in humans and its influence on cholesterol metabolism, two studies were conducted. In the first study ten healthy women received daily 30 mg OC for a period of 4 weeks. Blood and feces samples were collected at baseline and after the intervention. Serum concentrations of total cholesterol, LDL cholesterol, and HDL cholesterol were not altered following OC administration. Concentrations of excreted cholesterol end products decreased with the intervention (neutral sterols: 24.6 ± 9.7 mg/g vs. 20.3 ± 7.5 mg/g dry matter, $P < 0.05$; bile acids: 6.47 ± 3.89 mg/g vs. 4.03 ± 2.26 mg/g dry matter, $P < 0.05$). OC was not detected in serum samples, but the fecal OC concentration increased after the intervention period (11 ± 7 µg/g vs. 817 ± 179 µg/g dry matter, $P < 0.05$). In the second kinetic study on three participants, OC was identified in serums after oral application of 50 mg OC within 8 h. The decrease in the concentration of fecal cholesterol end products may underline a systemic effect of OC on cholesterol metabolism, even though the serum cholesterol levels were not influenced.

Keywords Bile acid · Cholesterol · LDL cholesterol · Neutral sterol · Octacosanoic acid · Octacosanol · Policosanol

Abbreviations

BA	Bile acid
FA	Fatty acid
FAME	Fatty acid methyl ester
NS	Neutral sterol
OC	Octacosanol
TC	Total cholesterol

Introduction

Octacosanol (OC) is a main component of the fatty alcohol mixture policosanol, which is found in plant waxes. There is evidence suggesting that fatty alcohols modulate the serum cholesterol concentration in human subjects [1]. In various human studies, a daily supplement of 5–20 mg policosanol decreased the LDL cholesterol concentration between 19 and 31% and the total cholesterol (TC) concentration between 13 and 23%. Long-term studies have shown that HDL cholesterol levels increased in the range of 8–29% [2]. A daily dose of 40 mg policosanol seems to be effective in reducing the serum triacylglycerol concentration [3]. Comparative studies have demonstrated that policosanol used for the treatment of hypercholesterolemia is equally or even more effective, than the use of statins [4–6]. In contrast, Cubeddu et al. [7] found no additional effect of a policosanol-statin combination in comparison to statin alone. Apart from the study by Cubeddu et al. [7], none of two other placebo-controlled studies have revealed an influence of a daily 20 mg policosanol supplement on cholesterol levels [8, 9]. Moreover, in a randomized, double blind, placebo-controlled study, the intake of up to 80 mg/day of policosanol did not affect the serum LDL cholesterol concentration in patients with hypercholesterolemia or

---

Dual first authorship. S. Keller and F. Gimmler having contributed equally to the basic science presented.

S. Keller · F. Gimmler · G. Jahreis (✉)
Department of Nutritional Physiology, Institute of Nutrition,
Friedrich Schiller University, Dornburger Street 24,
07743 Jena, Germany
e-mail: b6jage@uni-jena.de

combined hyperlipidemia [10]. In view of these findings, current policosanol doses seem to be ineffective for improving serum cholesterol profiles.

The conversion of fatty alcohols to fatty acids (FAs) was discovered by Rizzo et al. in 1987 [11]. Octacosanoic acid was produced when human fibroblasts were incubated with OC. This conversion of fatty alcohol into FAs via oxidation has been corroborated in vivo. Following oral administration of OC, the corresponding octacosanoic acid was identified in animal plasma [12]. Hence, octacosanoic acid was postulated as the active metabolite of OC [13]. Moreover, the effects of fatty alcohols are often equated to their respective FAs. Thus, these FAs were used as test substances in several studies [14–17].

However, fatty alcohols may themselves have an influence on the physiological processes. Being the main component of policosanol, OC was often employed as a test substance, but triacontanol was also shown to exert an influence on cholesterol synthesis in vitro [18, 19]. To date, the mechanisms through which policosanol lowers cholesterol levels have not yet been elucidated. Studies indicate that fatty alcohols inhibit synthesis of endogenous cholesterol, without a direct inhibition of the activity of HMG-CoA reductase, a key enzyme involved in the biosynthesis of cholesterol. Policosanol may reduce HMG-CoA reductase activity by depressing de novo synthesis and/or stimulating degradation of HMG-CoA reductase [20–22]. In addition, it was found that policosanol-related suppression of HMG-CoA reductase activity is mediated indirectly through AMP-kinase activation [19].

Most of the studies related to pharmacokinetics and metabolism of OC in human and animal subjects were performed using radioactively labeled OC [23–26]. A study examining the absorption and metabolism of unlabeled fatty alcohol in humans has not yet been found in the current literature. In animals fed unlabeled fatty alcohol mixtures, policosanol was not detected in the small intestine, liver, adipose, and plasma [27]. In contrast, OC was measured in plasma samples of rats and monkeys, which had been orally administered 60 mg policosanol/kg and 10 mg policosanol/kg, respectively [12]. These findings point to a direct absorption of the fatty alcohols in the mucosa cells without complete conversion to FA metabolites.

The aim of the two studies was to investigate OC metabolism in humans and its influence on cholesterol metabolism. Therefore, methods for determining OC and octacosanoic acid in human serum and feces were established. The effect on the total body cholesterol pool was examined with reference to the concentrations of serum cholesterol, and the fecal cholesterol end products [neutral sterols (NSs) and bile acids (BAs)].

Materials and Methods

Study Conditions

Ten healthy women (age: 25.5 ± 2.7 years; BMI: 21.5 ± 2.8 kg/m^2) with normal to mildly elevated TC concentrations (TC: 5.39 ± 0.87 mmol/l) participated in the first study. Pregnant subjects or those with diabetes mellitus, and subjects on medication for lowering lipid levels were excluded. All participants were informed about the study conditions in both verbal and written form. Written consent was given by participating subjects. The local Ethics Committee of the Friedrich Schiller University of Jena approved the study protocol.

The participants received a daily dose of 30 mg OC for 4 weeks. They were instructed to maintain their usual eating habits and to ingest one 10 mg OC capsule at each principal meal. The last capsule was administered 1 h before blood samples were drawn. Preparation of the OC capsules involved homogenizing and dosing 10 mg OC (Lesstanol®/Natural OC > 90%, Garuda inc., Exeter, CA, USA) and 200 mg glucose into gelatin capsules.

Blood samples were obtained from fasting subjects at the beginning and at the end of the study, in addition to collecting 24-h feces samples. Serum was separated from blood cells by centrifugation at 1,700*g* for 10 min at room temperature and stored at −80 °C until analysis. Aliquots of feces samples were lyophilized, milled, and stored at −20 °C. The participants completed two 3-day dietary records prior to the sample collection days in order to itemize the food intake, especially the fat and cholesterol consumption.

In a separate second study, three volunteers consumed a total of 50 mg OC within 8 h. The dose was divided into five 10 mg applications and was administered 8, 6, 4, 2, and 1 h before drawing blood samples. Serum samples were pooled before analysis.

Parameter for Cholesterol Metabolism

Cholesterol concentrations in serum (TC, LDL cholesterol, and HDL cholesterol) were determined after enzymatic preparation as previously described [28]. Concentrations of fecal NSs (cholesterol, coprostanol, coprostanone, cholestanol, cholestanone) and fecal BAs (primary BAs: cholic acid, chenodeoxycholic acid; secondary BAs: deoxycholic acid, iso-deoxycholic acid, 12-keto deoxycholic acid, lithocholic acid, iso-lithocholic acid) were determined using gas chromatography according to a method established by Keller and Jahreis [29].

Octacosanol Analysis

For OC analysis, either 6 ml serum or 200 mg of lyophilized feces were added to vessels containing the internal standard (20 µg tricosanol for serum samples, 200 µg tricosanol for feces samples). Hydrolysis of esterified fatty alcohols was established by applying freshly prepared ethanolic sodium hydroxide. Proteins were precipitated with methanol and OC extraction was carried out by using of trichloromethane. *N*,*O*-bis(trimethylsilyl)-trifluoro acetamide was employed to silylate the fatty alcohols.

The OC trimethylsilyl ethers from serum samples were measured using GC-MS (GCMS-QP5000, Shimadzu, Kyoto, Japan). The procedure for serum OC analysis followed an optimized temperature program (200 °C for 2 min, 10 °C/min to 240 °C, 1 °C/min to 255 °C, 255 °C for 1 min, 4 °C/min to 270 °C, 1 °C/min to 274 °C) using a capillary column (ZB5, 30 m, 0.25 mm, 0.25 µm; Phenomenex, Torrance, CA, USA). The sample (5 µl) was injected in split mode (1:10) at 280 °C. Helium served as the carrier gas at a constant linear velocity of 35 cm/s. The interface temperature was adjusted to 300 °C. The mass spectrometric detection was realized in multi ion current mode with $m/z = 397.45$ amu for tricosanol as an internal standard and $m/z = 467.6$ amu for OC. Analysis of fecal OC was performed using a gas chromatograph Shimadzu GC 17A (Kyoto, Japan, capillary column: Optima δ3, 30 m, 0.25 mm, 0.25 µm, Macherey Nagel, Dueren, Germany). The injection of 1 µl sample solution was carried out in split mode (1:50) at 280 °C. Hydrogen was used as the mobile phase at a constant velocity of 45 cm/s. The temperature of the flame ionization detector was kept at 300 °C. The oven temperature was raised from 70 °C to 220 °C (70 °C for 2 min, 10 °C/min to 180 °C, 2 °C/min to 220 °C, 220 °C for 5 min).

Octacosanoic Acid Analysis

To determine octacosanoic acid in human feces and serum samples, an aliquot of 100 mg fecal fat or 15 mg serum lipid extract was prepared to form FA methyl esters (FAMEs) as described previously [30]. Analytical measurement of the saturated FAs (C4:0, C10:0, C12:0, C13:0, C14:0, C15:0, C16:0, C17:0, C18:0, C20:0, C21:0, C22:0, C23:0, C24:0, C25:0, C28:0) was carried out using the GC-FID (GC 17A, Shimadzu Kyoto, Japan) equipped with a capillary column (DB 225 MS, 60 m, 0.25 mm, 0.25 µm, Agilent, Palo Alto, CA, USA).

Data Handling and Statistical Methods

Evaluation of the dietary records was carried out using the software PRODI® (5.0 expert, Nutri-Science, Freiburg, Germany). Chromatogram analysis was conducted employing LabSolutions Software Class 5000® and GCMSsolution® (Shimadzu, Kyoto, Japan). Statistical analyses of the experimental results were accomplished utilizing SPSS® for Windows® (version 11.5.1, SPSS Inc., Chicago, IL, USA) with the paired *t*-test. The statistical test criteria for a probability level (*P*) less than 0.05 was necessary for a sample concentration difference to be considered as significant when performing baseline intervention comparisons. The results were stated as mean ± standard deviation.

Results

Dietary Records

Evaluation of the 3-day dietary records revealed no differences in daily fat and cholesterol intake between baseline and intervention (Table 1).

Parameter of Cholesterol Metabolism

Intervention with OC did not influence cholesterol concentrations in the serum samples (Table 2). The concentrations of TC, LDL cholesterol, and LDL/HDL were reduced in their means, but no significance could be verified. The concentration of the cardio-protective HDL cholesterol did not rise after intervention with OC.

Table 1 Fat and cholesterol intake at baseline and after octacosanol intervention, $n = 10$

	Baseline	Intervention	*P*-value[d]
Fat intake (g/day)[a,c]	72.3 ± 21.6	68.0 ± 18.2	0.673
Cholesterol intake (mg/day)[b,c]	202 ± 111	197 ± 117	0.937

[a] Mean of fat intake (g/day) ± SD

[b] Mean of cholesterol intake (mg/day) ± SD

[c] Data were evaluated using 3-day dietary records

[d] Data were generated using paired *t*-test

Table 2 Serum cholesterol concentrations at baseline and after octacosanol intervention (mmol/l), $n = 10$

	Baseline	Intervention	*P*-value[b]
TC[a]	5.39 ± 0.87	5.19 ± 0.96	0.337
LDL cholesterol[a]	3.43 ± 1.14	3.32 ± 1.05	0.438
HDL cholesterol[a]	1.62 ± 0.32	1.61 ± 0.29	0.889
LDL/HDL	2.27 ± 1.10	2.16 ± 0.93	0.210

TC total cholesterol

[a] Mean of cholesterol concentrations (mmol/l) ± SD

[b] Data were generated using paired *t*-test

The fecal concentration of total NSs was significantly reduced after intervention with OC. The concentration of excreted cholesterol itself did not differ between baseline and intervention samples (Table 3). The total fecal concentration of BAs decreased after intervention with OC due to a significant reduction of secondary BAs.

Parameter of Octacosanol Metabolism

Octacosanol trimethyl silyl ethers could not be identified in the serum samples collected in the first study. In the pooled serum of the second study, we succeeded in determining silylated OC qualitatively. On measuring the fragment *m*/*z* = 467.6 amu, two different peaks were visible (Fig. 1a). After adding the OC standard to this serum sample, the peak at 29.8 min could be identified as OC (Fig. 1b), though it could not be quantified.

Table 3 Fecal concentrations of neutral sterols and bile acids at baseline and after octacosanol intervention (mg/g dry matter), *n* = 10

	Baseline	Intervention	*P*-value[d]
Total NSs[a,b]	24.6 ± 9.7	20.3 ± 7.5	0.048
Cholesterol[b]	4.21 ± 5.26	3.63 ± 4.61	0.559
Metabolites[a,b]	20.4 ± 13.1	16.6 ± 10.2	0.061
Total BAs[bc]	6.47 ± 3.89	4.03 ± 2.26	0.007
Primary BAs[b,c]	0.42 ± 0.23	0.38 ± 0.20	0.212
Secondary BAs[b,c]	6.05 ± 3.94	3.65 ± 2.25	0.009

NS neutral sterol, *BA* bile acid

[a] Metabolites: sum of coprostanol, coprostanone, cholestanol, and cholestanone concentration

[b] Mean of NSs and BAs concentrations (mg/g dry matter) ± SD

[c] Primary BAs: sum of cholic acid and chenodeoxycholic acid concentration; secondary BAs: sum of deoxycholic acid, iso-deoxycholic acid, 12-keto deoxycholic acid, lithocholic acid, and iso-lithocholic acid concentration

[d] Data were generated using paired *t*-test

The fecal concentration of OC was significantly elevated after intervention in comparison to the baseline concentration (Fig. 2, Table 4). However, it was also found that two study participants were low-converters of cholesterol. There are indeed different patterns of colonic neutral steroid conversion in the human population [31]. In the high-converters accounting for the majority of the human population, more than 50% of cholesterol is transformed into coprostanol by the microflora. In contrast, low-converters have a conversion rate below 50% and are identifiable by high fecal cholesterol and low coprostanol concentrations [29]. In this study, results of the OC concentration in the feces samples of the two low-converters were excluded from statistical analysis, because chromatographic co-elution of OC and cholesterol occurred, when the excretion of cholesterol was exceptionally high.

The octacosanoic acid metabolite of OC could not be identified in any of the serum samples after the intervention. Independent of the OC intervention, octacosanoic acid was excreted to a small extent with feces (Table 4). The fecal saturated FA pattern after the intervention was unchanged in comparison to the baseline FA pattern.

Discussion

In the current study involving ten healthy women receiving a daily dose of 30 mg OC for a period of 4 weeks, two major effects were observed. Firstly, the concentration of circulating cholesterol in blood remained unaltered after OC supplementation, and secondly, fecal concentration of cholesterol in the form of NSs and BAs was decreased, due possibly to a reduction of the total body cholesterol pool.

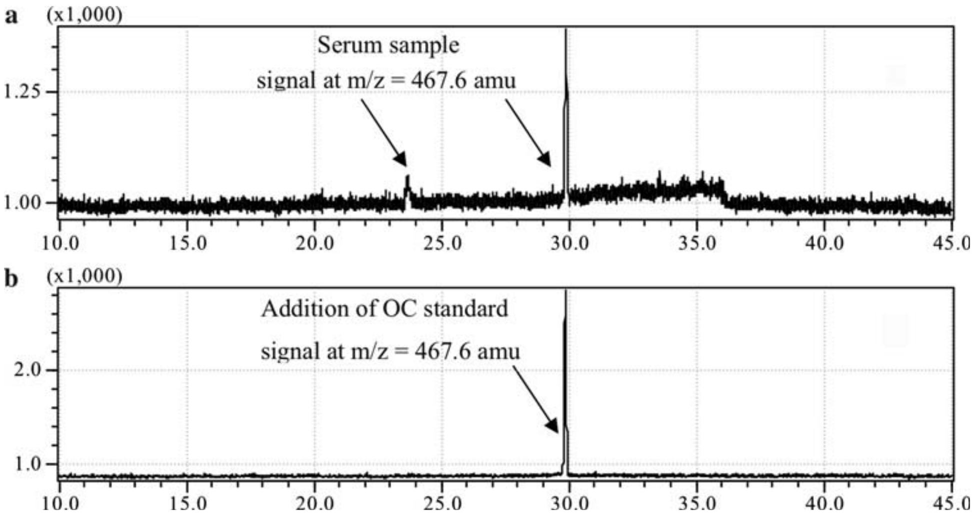

Fig. 1 Chromatogram (*m*/*z* = 467.6 amu) of a serum sample (**a**) and of the same serum sample after addition of the octacosanol standard (**b**)

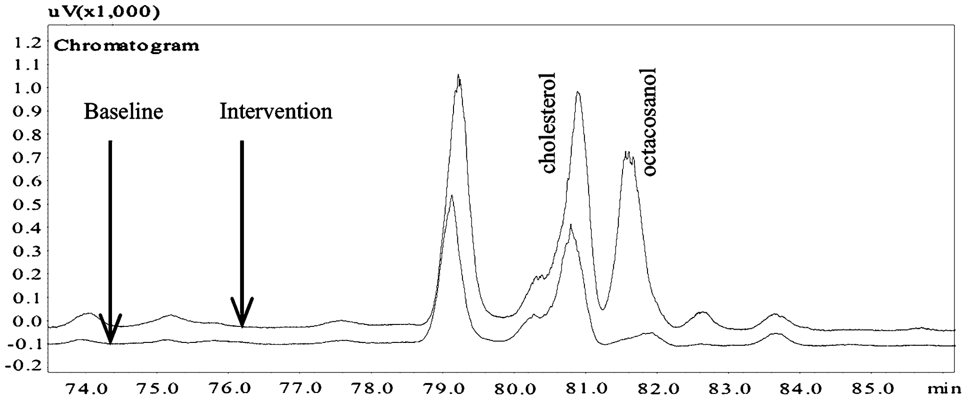

Fig. 2 Chromatogram comparison of fecal octacosanol at baseline and after octacosanol intervention

Table 4 Fecal concentrations of octacosanol and octacosanoic acid at baseline and after octacosanol intervention

	Baseline	Intervention	*P*-value[c]
Octacosanol, (n = 8)[a] (μg/g dry matter)	11.2 ± 7.4	816 ± 179	<0.001
Octacosanoic acid, (n = 10)[b] [% of saturated FAMEs]	0.12 ± 0.07	0.11 ± 0.14	0.880

[a] Mean of octacosanol concentration (μg/g dry matter) ± SD

[b] Mean of octacosanoic acid concentration (% of saturated FAMEs) ± SD

[c] Data were generated using paired *t*-test

In addition to efficient cholesterol homeostasis in healthy subjects, the sustained TC and LDL cholesterol concentrations may be explained by the small study population or the short period of supplementation. In addition, a daily dose of 30 mg OC may have been ineffective. In other studies, a reduction in the TC and LDL cholesterol concentrations occurred after six or more weeks [32]. However, Hernández et al. [33] found decreased LDL cholesterol concentrations after 4 weeks of a daily 20 mg-policosanol supplementation in a double blind, placebo-controlled study. The results of our study are consistent with the study of Lin et al. [9], which also revealed no changes in lipid parameters during a 4-week intervention with a daily dose of 20 mg policosanol.

Although the circulating cholesterol concentration remained unchanged after OC supplementation, there was a significant decrease in the concentration of the excreted cholesterol products NSs and BAs. The excretion of NSs and BAs strongly depends, in addition to other factors, on the consumed dietary fat. However, the evaluation of the 3-day dietary records revealed neither a difference in the fat, nor in the cholesterol intake between the baseline and the intervention period.

The reduction in the total body cholesterol pool may have several explanations, e.g., a down-regulated cholesterol absorption in the small bowel, a diminished hepatic cholesterol synthesis, an up-regulated hepatic BA synthesis, and finally, an elevated cholesterol and/or BA excretion. It has in fact been shown that fatty alcohols are capable of suppressing cholesterol synthesis by indirectly inhibiting the key enzyme HMG-CoA reductase in hepatoma cells in vitro [19]. Moreover, the total body cholesterol pool may decrease as a result of a reduced hepatic cholesterol synthesis. Additionally, Shefer et al. [34] have emphasized that a change in the rate of hepatic cholesterol synthesis may influence the production of BAs. Thus, HMG-CoA reductase may function as a secondary regulatory mechanism for BA production [34]. A reduced cholesterol synthesis in the liver would result in a diminished BA production and subsequently in decreased cholesterol and BA excretion. Contrary to this hypothesis, results obtained from an in vivo study supplementing policosanol in hamsters did not substantiate a reduced cholesterol synthesis after policosanol treatment [35].

To date, no one has succeeded in detecting the unlabeled fatty alcohols and their corresponding FAs in the serum following oral administration of unlabeled fatty alcohols in human subjects. Further, it could not be demonstrated in humans that fatty alcohols are themselves absorbed and are capable of inducing a systemic effect [18]. We were not able to detect OC in the serum samples in our first study. The applied dose of 20 mg/day and an absorption rate of approximately 10% [18] may have been too low to allow verification of OC in serum samples. Assuming absorption of 5 mg of OC at a rate of 10% in an average serum volume of 2.5 l in healthy adults, then an absolute amount of 0.01 mg OC should be detectable in the 5 ml serum samples. In the serum samples from the second kinetic study in which three participants consumed 50 mg OC within 8 h the identification of OC was confirmed. Therefore, the presence of OC in the serum samples provided the evidence for a direct absorption of the non-metabolized fatty alcohols. In fact, a direct absorption of OC in plasma after oral administration has been documented in studies in rats and monkeys [12]. However, this finding is inconsistent with earlier assumptions from Hargrove et al. [36], who postulated that fatty alcohols are already converted to FAs in the mucosa cell.

Experiments with [^{3}H]-OC indicated that fatty alcohols are excreted mainly via the feces [23]. The results of our study corroborate this excretion pathway as seen by the significant increase in the concentration of fecal OC after supplementation. Furthermore, we noted a baseline excretion of OC in all study participants. However, a bacterial synthesis of fatty alcohols in the colon or even a dietary intake could explain this baseline excretion of OC. Contrary to our findings, no excretion of fatty alcohols was observed in the control group feces in the study with hamsters by Ng et al. [37].

Although results of studies with human fibroblasts indicate a conversion of OC to octacosanoic acid [12], to date, this metabolism has not been verified in humans. Our results from analysis of fecal and serum samples could not confirm the formation of octacosanoic acid from OC, though a serum concentration of octacosanoic acid below the limit of detection cannot be excluded.

Thus, study data suggest the absorption of non-metabolized OC, which is detectable in serum after oral consumption of OC. In addition, although the serum cholesterol concentration was not influenced, the decrease in the concentration of the fecal cholesterol end products may underline a systemic effect of OC on cholesterol metabolism.

References

1. Nies LK, Cymbala AA, Kasten SL, Lamprecht DG, Olson KL (2006) Complementary and alternative therapies for the management of dyslipidemia. Ann Pharmacother 40:1984–1992
2. Varady KA, Wang Y, Jones P (2003) Role of policosanols in the prevention and treatment of cardiovascular disease. Nutr Rev 61:376–383
3. Janikula M (2002) Policosanol: a new treatment for cardiovascular disease? Altern Med Rev 7:203–217
4. Crespo N, Illnait J, Más R, Fernández L, Fernández J, Castaño G (1999) Comparative study of the efficacy and tolerability of policosanol and lovastatin in patients with hypercholesterolemia and noninsulin dependent diabetes mellitus. Int J Clin Pharmacol Res 19:117–127
5. Fernández JC, Más R, Castaño G, Menéndez R, Amor A, González RM, Alvarez E (2001) Comparison of the efficacy, safety and tolerability of policosanol versus fluvastatin in elderly hypercholesterolaemic women. Clin Drug Investig 21:103–113
6. Castaño G, Menéndez R, Más R, Amor A, Fernández JL, González RL, Lezcay M, Alvarez E (2002) Effects of policosanol and lovastatin on lipid profile and lipid peroxidation in patients with dyslipidemia associated with type 2 diabetes mellitus. Int J Clin Pharmacol Res 22:89–100
7. Cubeddu LX, Cubeddu RJ, Heimowitz T, Restrepo B, Lamas G, Weinberg GB (2006) Comparative lipid-lowering effects of policosanol and atorvastatin: a randomized, parallel, double-blind, placebo-controlled trial. Am Heart J 152:982.e1–982.e5
8. Greyling A, De Witt C, Oosthuizen W, Jerling JC (2006) Effects of a policosanol supplement on serum lipid concentrations in hypercholesterolemic subjects. Br J Nutr 95:968–975
9. Lin Y, Rudrum M, Van der Wielen RPJ, Trautwein EA, McNeill G, Sierksma A, Meijer GW (2004) Wheat germ policosanol failed to lower plasma cholesterol in subjects with normal to mildly elevated cholesterol concentrations. Metabolism 53:1309–1314
10. Berthold HK, Unverdorben S, Degenhardt R, Bulitta M, Gouni-Berthold I (2006) Effect of policosanol on lipid levels among patients with hypercholesterolemia or combined hyperlipidemia. A randomized controlled trial. J Am Med Assoc 295:2262–2269
11. Rizzo WB, Craft DA, Dammann AL, Phillips MW (1987) Fatty alcohol metabolism in cultured human fibroblasts. Evidence for a fatty alcohol cycle. J Biol Chem 262:17412–17419
12. Menéndez R, Marrero D, Más R, Fernández I, González L, González RM (2005) In vitro and in vivo study of octacosanol metabolism. Arch Med Res 36:113–119
13. Más R (2000) Policosanol. Hypolipidemic antioxidant treatment of atherosclerosis. Drugs Future 25:569–586
14. Menéndez R, Más R, Amor AM, Rodeiro I, González RM, Alfonso JL (2001) Inhibition of cholesterol biosynthesis in cultured fibroblasts by D003, a mixture of very long chain saturated fatty acids. Pharmacol Res 44:299–304
15. Castaño G, Más R, Fernández L, López E, Gutiérrez JA, Illnait J, Fernández JC, Gámez R, Alvarez E (2002) Assessment of the effects of D-003, a new antiplatelet and lipid-lowering compound, in healthy volunteers. A phase I clinical study. Drugs R D 3:337–348
16. Castaño G, Más R, Fernández L, Illnait J, López E, Gámez R, Mendoza S, Fernández J, Mesa M (2003) Effects of D-003 on the lipid profile of patients with type II hypercholesterolaemia. A phase II clinical study. Clin Drug Investig 23:789–802
17. Menéndez R, Más R, Pérez J, González RM, Jiménez S (2004) Oral administration of D-003, a mixture of very long chain fatty acids prevents casein-induced endogenous hypercholesterolemia in rabbits. Can J Physiol Pharmacol 82:22–29
18. Gouni-Berthold I, Berthold HK (2002) Policosanol: clinical pharmacology and therapeutic significance of a new lipid-lowering agent. Am Heart J 143:356–365
19. Singh DK, Li L, Porter TD (2006) Policosanol inhibits cholesterol synthesis in hepatoma cells by activation of AMP-kinase. J Pharmacol Exp Ther 318:1020–1026
20. Menéndez R, Fernández SI, Del Rio A, González RM, Fraga V, Amor AM, Más RM (1994) Policosanol inhibits cholesterol biosynthesis and enhances low density lipoprotein processing in cultured human fibroblasts. Biol Res 27:199–203
21. Menéndez R, Arruzazabala L, Más R, Del Rio A, Amor AM, González RM, Carbajal D, Fraga V, Molina V, Illnait J (1997) Cholesterol-lowering effect of policosanol on rabbits with hypercholesterolemia induced by a wheat starch-casein diet. Br J Nutr 77:923–932
22. Menéndez R, Amor AM, Rodeiro I, González RM, González PC, Alfonso JL, Más R (2001) Policosanol modulates HMG-CoA reductase activity in cultured fibroblasts. Arch Med Res 32:8–12
23. Menéndez R, Sotolongo V, Fraga V, Amor AM, González R, Del Rio A, Jiménez S, Pérez N, Más R (1996) Plasma levels and total radioactivity excretion in healthy volunteers after oral 3H-octacosanol administration. Rev CENIC Cien Biol 27:32–35
24. Kabir Y, Kimura S (1993) Biodistribution and metabolism of orally administered octacosanol in rats. Ann Nutr Metab 37:33–38
25. Kabir Y, Kimura S (1994) Distribution of radioactive octacosanol in response to exercise in rats. Nahrung 38:373–377
26. Kabir Y, Kimura S (1995) Tissue distribution of (8-^{14}C)-octacosanol in liver and muscle of rats after serial administration. Ann Nutr Metab 39:279–284

27. Marinangeli CPF, Kassis AN, Jain D, Ebine N, Cunnane SC, Jones PJH (2007) Comparison of composition and absorption of sugarcane policosanol. Br J Nutr 97:381–388
28. Ditscheid B, Keller S, Jahreis G (2005) Cholesterol metabolism is affected by calcium phosphate supplementation in humans. J Nutr 135:1678–1682
29. Keller S, Jahreis G (2004) Determination of underivatised sterols and bile acid trimethyl silyl ether methyl esters by gas chromatography-mass spectrometry-single ion monitoring in faeces. J Chromatogr B Analyt Technol Biomed Life Sci 813:199–207
30. Kraft J, Hanske L, Möckel P, Zimmermann S, Härtl A, Kramer JKG, Jahreis G (2006) The conversion efficiency of trans-11 and trans-12 18:1 by Δ9-desaturation differs in rats. J Nutr 136:1209–1214
31. Wilkins TD, Hackman AS (1974) Two patterns of neutral steroid conversion in the feces of normal north Americans. Cancer Res 34:2250–2254
32. Pepping J (2003) Policosanol. Am J Health Syst Pharm 60:1112–1115
33. Hernández F, Illnait J, Más R, Castaño G, Fernádez L, González M, Cordovi N, Fernandez JC (1992) Effect of policosanol on serum lipids and lipoproteins in healthy volunteers. Curr Ther Res Clin Exp 51:568–575
34. Shefer S, Hauser S, Lapar V, Mosbach EH (1973) Regulatory effects of sterols and bile acids on hepatic 3-hydroxy-3-methyl-glutaryl CoA reductase and cholesterol 7α-hydroxylase in the rat. J Lipid Res 14:573–580
35. Wang YW, Jones PJH, Pischel I, Fairow C (2003) Effects of policosanols and phytosterols on lipid levels and cholesterol biosynthesis in hamsters. Lipids 38:165–170
36. Hargrove JL, Greenspan P, Hartle DK (2004) Nutritional significance and metabolism of very long chain fatty alcohols and acids from dietary waxes. Exp Biol Med 229:215–226
37. Ng CH, Leung KY, Huang Y, Chen ZY (2005) Policosanol has no antioxidant activity in human low-density lipoprotein but increases excretion of bile acids in hamsters. J Agric Food Chem 53:6289–6293

Lipids (2008) 43:117–124
DOI 10.1007/s11745-007-3138-1

ORIGINAL ARTICLE

Primary Hypercholesterolemia, Carotid Atherosclerosis and Insulin Resistance Among Chinese

Kuo-Liong Chien · Chiau-Suong Liau · Ming-Fong Chen · Yuan-Teh Lee · Jiann-Shing Jeng · Bao-Show Hwang · Ta-Chen Su

Received: 5 June 2007 / Accepted: 30 October 2007 / Published online: 15 December 2007
© AOCS 2007

Abstract We investigated the genetic contributions to carotid atherosclerosis and insulin resistance in Chinese patients with primary hypercholesterolemia. A family study of probands from the outpatient clinics in patients with high low-density-lipoprotein cholesterol levels was conducted. A total of 62 families (360 subjects) underwent carotid ultrasonography and insulin resistance measurement. The correlation coefficients of carotid intima-media thickness (IMT) were high among spouse, parent–offspring, and sibling pairs (0.39, 0.38 and 0.35, respectively). All insulin indices and IMT had significant estimates of heritability, of which fasting insulin had the highest heritability (0.410 ± 0.104, $P = 0.0001$), followed by homeostasis model assessment (HOMA) (0.395 ± 0.108, $P = 0.0001$). The estimated heritability of IMT was significant (0.185 ± 0.103, $P = 0.025$) but not of plaque score. Bivariate genetic coefficient between IMT and HOMA was 0.569 ± 0.292, while the environmental coefficient was 0.028 ± 0.103. The study confirms a relationship between insulin resistance and atherosclerosis and, in particular, between insulin resistance and the thickening of the arterial wall. Moreover, it shows that genetics influence both insulin resistance and atherosclerosis, implying that the management of insulin resistance may benefit the prevention of atherosclerotic disease in familial hypercholesterolemia.

Keywords Hypercholesterolemia · Insulin resistance · Carotid atherosclerosis · Family study

Abbreviations

CA	Carotid atherosclerosis
CCA	Common carotid artery
ECCA	Extracranial carotid artery
FRSPH	Familial-related severe primary hypercholesterolemia
HDL-C	High-density lipoprotein density
HOMA	Homeostasis model assessment
hs-CRP	High-sensitivity C-reactive protein
IMT	Intima-media thickness
LDL-C	Low-density lipoprotein cholesterol

Introduction

Carotid atherosclerosis (CA) is a subclinical disease associated with cardiovascular disease and risk factors among ethnic Chinese [1, 2]. Although hypertension and related

---

K.-L. Chien
Institute of Preventive Medicine, School of Public Health,
National Taiwan University, Taipei, Taiwan
e-mail: klchien@ntu.edu.tw

K.-L. Chien · C.-S. Liau · M.-F. Chen · Y.-T. Lee · T.-C. Su
Division of Cardiology, Department of Internal Medicine,
National Taiwan University Hospital, National Taiwan
University College of Medicine, Taipei, Taiwan

C.-S. Liau
Cardiovascular Center, Tzu-Chi Hospital, Hsin-Dian, Taipei,
Taiwan

J.-S. Jeng · B.-S. Hwang
Department of Neurology, National Taiwan University Hospital,
National Taiwan University College of Medicine, Taipei,
Taiwan

T.-C. Su (✉)
Department of Environmental and Occupational Medicine,
National Taiwan University Hospital, Taipei, Taiwan
e-mail: tachensu@ntu.edu.tw

atherosclerotic risk factors are associated with the progression of CA, genetic factors also play an important role [3–5]. Previous familial aggregation studies showed significant heritability on the carotid artery intima-medial thickness (IMT) and plaque scores [4, 6, 7]. Moreover, genome-wide linkage results showed several genomic loci for determining carotid IMT trait [7–10].

Although there is evidence of genetic components for CA traits, there are several issues yet to be answered. First, the inconsistent genomic loci from genome-wide linkage results have implied genetic heterogeneity over genetic components controlling trait. Second, geographic and racial/ethnic variations of CA has been reported [5–7, 11–15], however, little information is available in ethnic Chinese. Moreover, previous studies have shown that age, gender, insulin resistance, diabetes, metabolic syndrome, and family history were related to CA [9, 16–22]; however, association of these factors with CA have not been simultaneously examined in a family-based genetic study. In addition, hereditary factors have not been studied in ethnic Chinese. We designed a family-based genetic study that focused on ethnic Chinese, where the probands were recruited from hyperlipidemic clinics, in order to explore the genetic correlation and heritability of various CA traits. We also collected information on confounding factors, especially on metabolic syndrome and insulin resistance, to investigate the association with CA.

Materials and Methods

Study Subjects

This family study was conducted in hyperlipidemic outpatient clinics after developing standard procedures for recruiting probands and their family members in the university hospital [23]. Familial hypercholesterolemia screening was conducted in 2002 at the lipid clinic of the National Taiwan University Hospital and consecutive patients were recruited as proband. These probands were diagnosed as having familial-related severe primary hypercholesterolemia (FRSPH) on the basis of having low density lipoprotein-cholesterol (LDL-C) levels in themselves and in two or more first-degree relatives that were above 190 mg/dL and/or the presence of tendinous xanthomas within the kindred [24]. The spouses and first-degree relatives were invited to participate in the study.

Individuals with some types of secondary hyperlipidemia, including nephrotic syndrome, obstructive liver disease, or hypothyroidism, and those who refused to provide informed consents, were excluded. The response rate was 90%. The genetic basis of FRSPH is heterogeneous. The most common autosomal dominant form of FH is caused by mutation in the LDL receptor gene (LDLR) on chromosome 19 in band 19p13.2. There are a number of other less frequent forms of this disorder. They include type B hypercholesterolemia which is caused by ligand-defective apolipoprotein B-100 (APOB), and autosomal dominant hypercholesterolemia 3 (HCHOLA3) which is caused by mutation in the PCSK9 gene. In addition, the differences in frequencies of specific mutations between populations should be considered. Instead of absence of genetic confirmation, we defined our study subjects as FRSPH [24]. All of the subjects received a detailed medical history review and physical examination.

The design was family study, based on the hypercholesterolemic patient as a proband and the first-degree relatives were recruited [25]. The study was approved by the Institutional Review Board of the National Taiwan University Hospital, and all of the subjects gave their informed consent. The procedure of collecting data was standardized, and was followed by the physicians and assistants in measuring the variables. We recruited a total of 360 members in the 62 families, which included three to six patients of hypercholesterolemia in each family, into our study. The subjects underwent examinations for anthropometric measurements, blood pressure, lipid profile, and carotid ultrasound measurements. Information on family history and medical diseases was obtained from each participant by trained assistants, using a structured questionnaire. Patient's socio-demographic characteristics, lifestyle, personal and family history of diseases, and history of hospitalization were also collected. Regular exercise habit was defined as the participants undertaking sports and leisure physical activity daily. Blood pressure was measured after resting for 10 min, with the subjects in the sitting position, while body weight was measured using a calibrated balance. Body mass index was calculated as weight (kilogram) divided by height (meter) squared. The circumference of the smallest part of waist and the thickest part of the hip in the standing position were also measured.

Blood Chemistry and Lipid Measurement

Overnight fasting (>12 h) blood samples were collected for measurements of glucose, total cholesterol, high-density lipoprotein cholesterol (HDL-C), and triglyceride by standard enzymatic methods with an automatic multi-channel chemical analyzer (Hitachi 7450, Hitachi Corp., Tokyo, Japan) in the central laboratory of the National Taiwan University Hospital. LDL-C value was calculated by the Friedewald's formula [26]. Blood samples for glucose analysis were drawn into glass test tubes, each containing 80 mol/L fluoride/oxalate reagents. After centrifugation at 4 °C, 1,500*g* for 10 min, glucose levels were measured on the supernatant by enzymatic assay (Merck 3389 commercial kit, Germany) in an Eppendorf 5060 autoanalyzer.

For the following assays, blood samples were first centrifuged at 3,000 rpm for 15 min within 30 min of collection, and then stored at −70 °C until assayed. Serum insulin level was measured using a Microparticle Enzyme immunoassay (AxSYM Insulin, Abbott Diagnostic, Tokyo, Japan). Serum high-sensitivity C-reactive protein (hs-CRP) was measured using a chemi-luminescent enzyme-labeled immunometric assay (Immulite C-Reactive Protein, Diagnostic Products Co., Los Angeles).

Insulin Resistance Indices

Several measurements and parameters were used for insulin resistance indices. First, fasting insulin and glucose levels were used because fasting hyperinsulinemia was considered an important indicator of insulin resistance [27]. Second, homeostasis model assessment (HOMA) using the formula: [fasting insulin (mU/L) × fasting glucose (mg/dL) × 0.05551]/22.5 was also used [28]. The numbers of metabolic syndrome components, defined by high blood pressure, high waist circumference, high fasting glucose, high triglyceride and low HDL-C status, were also utilized. Finally, we defined the metabolic syndrome status according to the criteria of the number of components more than or equal to three [29].

Extracranial Carotid Artery Ultrasound Measurements

The protocol and methods of CA measurements have been reported previously [1, 2, 30]. A Hewlett-Packard SONO 4500 ultrasound system (Andover, MA, USA) with a 3–11 MHz real-time B-mode scanner was used for evaluation, which included observation of the longitudinal and transverse views of the extracranial carotid artery (ECCA) bilaterally. An experienced ultrasonographer performed carotid ultrasonography while the patient was supine with the neck extended in a mild lateral rotation. Carotid end-organ disease was assessed by maximal IMT at the common carotid artery (CCA) and by ECCA plaque score. Two measurements of maximal IMT at CCA 0–20 mm proximal to the carotid bifurcation were obtained bilaterally. For future and subsequent off-line analysis, all scans were recorded on super-VHS videotape. Observers were blinded to the subjects' health status and risk factors. Intra-class correlation coefficients of intra-observer were about 0.70–0.87 for both sides of CCA IMT measurements, as reported previously [31]

Method for quantifying plaque score has been described previously [1, 31]. Briefly, a focal thickening of IMT with >50% of thickness than the adjacent IMT was considered as an atherosclerotic plaque. A grade was assigned for each chosen segment: grade 0 for normal or no observable plaque; grade 1 for a small plaque with diameter stenosis <30%; grade 2 for a medium plaque with 30–49% diameter stenosis or multiple small plaques; grade 3 for one large plaque with 50–99% diameter stenosis or multiple plaques with at least one medium plaque; and grade 4 for 100% occlusion.

Extracranial carotid artery segments, including the proximal and distal CCA (>20 and 0–20 mm distal to the bulb bifurcation, respectively), bulb, internal carotid artery, and external carotid artery, were examined bilaterally. The plaque score was calculated by adding up the plaque grades of ten segments of the ECCA. Reproducibility of the plaque grade scoring expressed good agreement with a kappa value of 0.70 [1, 31].

Statistical Analysis

Carotid atherosclerosis and insulin resistance indices, including fasting insulin, glucose and HOMA values, were presented in mean and standard deviation. We specified the above values by gender. Skewness and kurtosis of triglyceride, fasting glucose, insulin, and HOMA values were large due to a non-normal distribution. Logarithm-transformed variables were used for further genetic analysis but due to familial correlation, the statistical difference between genders was not tested. We have four IMT measurements at CCA for each participant, so mixed effect models can be applied in the analysis to increase the detection power in limited study samples. The mixed models were used to test the significance of contributions of IR indices to IMT of CCA and plaque score values in all family members [32].

The intra-familial correlation coefficients of carotid atherosclerosis traits were measured in different pairs, including spouse, parent–offspring, and siblings, by the FCOR program in SAGE [33]. Heritability estimates of carotid indices in the families were estimated by the variance component model, which was incorporated in the SOLAR software [34].

Results

Description of Study Participants

Compared with men, women tended to be older and to have higher total cholesterol, HDL, and LDL cholesterol levels, as well as lower waist circumference, uric acid, fasting insulin, HOMA values (Table 1). BMI and blood pressure

Table 1 Demographic and insulin resistance index risk profiles in the family study (by gender)

Characteristics	Men ($N = 166$)		Women ($N = 194$)	
	Mean	SD	Mean	SD
Age (years)	39.2	17.5	45.5	17.1
Body mass index (kg/m^2)	23.8	4.1	22.7	3.7
Systolic blood pressure (mmHg)	113.4	14.9	114.4	18.8
Diastolic blood pressure (mmHg)	73.9	10.3	72.4	10.7
Waist circumference (cm)	83.3	11.8	77	10.3
Total cholesterol (mg/dL)	239.9	66.8	264	73.5
Triglyceride (mg/dL)	138	103.1	113.9	72.3
HDL cholesterol (mg/dL)	51.3	14.8	62.4	13.5
LDL cholesterol (mg/dL)	149.6	59.5	164.6	64.7
Serum creatinine (mg/dL)	0.96	0.17	0.73	0.13
Uric acid (mg/dL)	7.58	1.67	5.83	1.63
Fasting glucose (mg/dL)	91.9	13	92.1	14.1
Fasting insulin (mU/L)	9.31	7.78	7.81	6.18
HOMA	2.17	1.88	1.83	1.54
Intima media thickness (mm)	0.06	0.01	0.06	0.02
Plaque score	0.12	0.29	0.14	0.27
Characteristics	*N*	%	*N*	%
Diabetes mellitus—yes	2	1.2	5	2.6
Hyperlipidemia—yes	88	53	117	60.3
Education group				
≤9 years	25	15.3	43	23.2
>9 years	138	84.7	142	76.8
Job type				
Labor work	31	18.9	45	23.4
House work	1	0.6	64	33.3
Nil	25	15.2	19	9.9
Business and office	107	65.2	64	33.3
Marital status				
Couple	93	56.4	123	64.4
Single	72	43.6	68	35.6
Smoking				
Current	40	24.1	9	4.7
Nil	113	68.1	183	94.8
Quit	13	7.8	1	0.5
Alcohol drinking				
Current	43	27	4	2.1
Nil	114	71.7	181	95.8
Quit	2	1.3	4	2.1
Exercise				
Non-regular	63	38.2	81	42.4
Regular	102	61.8	110	57.6
Metabolic syndrome				
No	127	84.1	140	82.8
Yes	24	15.9	29	17.2

in women were comparable with those in men. Carotid atherosclerosis indices, including IMT and plaque scores, were similar between genders. Most patients had hyperlipidemic status, educational level ≥9 years, and regular exercise habits. Their jobs were business and official work. Men had higher proportions of smoking and alcohol drinking habits. The prevalence rates of metabolic syndrome, defined by AHA/NHLBI criteria, were 15.9% in men and 17.2% in women.

Predictor of Carotid Atherosclerosis by Insulin Resistance Indices

We estimated the effects of association between carotid atherosclerosis and various insulin resistance indices (Table 2) using the mixed models. In the univariate model, all insulin resistance indices were associated well with IMT. The magnitude of effects was reduced somewhat after age and gender adjustment. In the multivariate models that incorporated age, gender, obesity, married status, smoking, drinking, education and sport habits, the insulin resistance indices of fasting insulin, glucose, HOMA were still significant predictors for IMT values ($P = 0.030$, 0.003, and 0.019, respectively). Metabolic syndrome component numbers and status were non-significant predictors for IMT in multivariate models. For plaque scores, most of the estimated parameters were not statistically significant in the multivariate models, and only fasting glucose was a significant predictor for plaque score (0.00325 ± 0.00107, $P = 0.003$). Insulin resistance indices were associated with IMT values, not with plaque scores.

Familial Correlation and Heritability

In all of the family members, there were 45 spouse pairs, 266 parent–offspring pairs, and 236 sibling pairs. Familial correlation coefficients and heritability estimates were shown in Table 3. The coefficients of parent–offspring and sibling pairs were higher than those of spouses in insulin resistance and carotid atherosclerosis indices. Among these, the IMT coefficients were higher among spouse, parent–offspring, and sibling pairs (0.389, 0.376, and 0.354, respectively). Gender specific parent–offspring correlation coefficients varied much: mothers had higher coefficients than fathers in insulin resistance indices (0.426 in mother–daughter, 0.322 in mother–son, 0.043 in father–daughter, and −0.083 in father–son for HOMA, respectively).

For IMT values, the coefficients were equal in mother–daughter and father–son pairs (0.454 and 0.489, respectively). The coefficients of plaque scores varied much and

Table 2 Estimated parameters and standard errors of various insulin resistance indices for the intima media thickness and plaque scores in the study population, after adjusted for familial correlation by mixed models

	Intima media thickness, mm			Plaque score		
	Estimated parameter	Standard error	*P* value	Estimated parameter	Standard error	*P* value
1. Univariate						
Fasting insulin, mU/L	0.00018	0.00013	0.157	0.00154	0.00228	0.499
Fasting glucose, mg/dL	0.00033	0.00006	<0.0001	0.00602	0.00108	<0.0001
HOMA	0.00113	0.00051	0.029	0.01366	0.00937	0.146
Metabolic syndrome	0.00748	0.00105	<0.0001	0.09434	0.02052	<0.0001
2. Age, sex adjusted						
Fasting insulin, mU/L	0.00018	0.00009	0.059	0.00175	0.00194	0.367
Fasting glucose, mg/dL	0.00011	0.00005	0.022	0.00285	0.00099	0.004
HOMA	0.00081	0.00038	0.036	0.00988	0.00795	0.216
Metabolic syndrome	0.00215	0.00089	0.016	0.01406	0.01982	0.479
3. Multivariate adjusted[a]						
Fasting insulin, mU/L	0.00021	0.00010	0.030	0.00240	0.00194	0.217
Fasting glucose, mg/dL	0.00016	0.00005	0.003	0.00325	0.00107	0.003
HOMA	0.00092	0.00039	0.019	0.01203	0.00802	0.135
Metabolic syndrome	0.00154	0.00091	0.094	−0.00632	0.02037	0.757

[a] Adjusted covariates in multivariate models included age, gender, obesity, married, smoking, drinking, education, and sport habits

high in sibling and spouse pairs. All insulin resistance indices and IMT had significant heritability estimates, and the highest heritability values were fasting insulin (0.410 ± 0.104, *P* = 0.0001), then HOMA (0.395 ± 0.108, *P* = 0.0001). The estimated heritability of IMT was significant (0.185 ± 0.103, *P* = 0.025) but the plaque score heritability was not statistically different.

Genetic and environmental correlation between CA and insulin resistance in bivariate models showed that genetic correlation coefficients were higher (0.999 in HOMA vs. insulin and 1.00 in IMT vs. plaque score). Genetic coefficients between IMT and HOMA were 0.569 ± 0.292 and environmental coefficients were 0.028 ± 0.103.

Discussion

The study confirms a relationship between insulin resistance and atherosclerosis and, in particular, between insulin resistance and the thickening of the arterial wall. Moreover,

Table 3 Familial correlation coefficients, heritability and standard error estimates for insulin resistance indices and carotid atherosclerosis in the study population

Familial pair type	Number of pairs	Correlation coefficients				
		Fasting insulin	Fasting glucose	HOMA	Intima media thickness	Plaque score
Spouse	45	0.140	0.013	0.155	0.389	0.451
Parent–offspring	266	0.219	0.056	0.222	0.376	0.135
Sibling	236	0.255	0.188	0.201	0.354	0.301
Mother–daughter	84	0.410	0.015	0.426	0.454	0.016
Mother–son	89	0.316	0.307	0.322	0.349	0.256
Father–daughter	44	0.010	0.307	0.043	0.172	0.167
Father–son	49	−0.079	−0.282	−0.083	0.489	0.080
Sister–sister	71	−0.032	0.082	−0.075	0.362	0.363
Sister–brother	118	0.319	0.297	0.278	0.371	0.392
Brother–brother	47	0.259	0.414	0.262	0.293	−0.048
Heritability		0.410	0.370	0.395	0.185	0.062
Standard error		0.104	0.181	0.108	0.103	0.085
P value		0.0001	0.018	0.0001	0.025	0.212

it shows that genetics influence both insulin resistance and atherosclerosis. This family-based study on ethnic Chinese clearly demonstrated the association between insulin resistance indices and CA, which showed significant heritability values among the study subjects. The more novel component of this study is the effort to consider joint genetic determinants of IMT and insulin resistance.

The relationship between insulin resistance indices and IMT had been previously demonstrated among young Italian women [16]. Although some studies did not show an association of insulin resistance and carotid IMT [35, 36], most studies have shown a positive relation between insulin resistance and carotid IMT [16, 37, 38]. The implications of the study involve several aspects. First, as ascertained from hyperlipidemic patients, family members showed significant familial aggregation of insulin resistance indices and CA. These findings also echoed results in other population-based studies [18, 22, 39, 40]. Our study differentiated two traits of CA, i.e., IMT and plaque score. IMT had higher heritability and familial correlation than plaque score in the study population, while advanced plaque score did not have significant heritability, which were different from those of Mexican American families [10]. Moreover, heritability for IMT was higher for the spouse than for the parent–offspring and sibling, which implied that common environmental factors were as important as genetic factors. Insulin resistance coefficients were ten times higher in the mother–daughter than in the father–daughter, indicating that maternal transmission of glucose metabolism and insulin resistance was much more important than paternal transmission. The hypothesis of excess maternal transmission in diabetes and related traits has been postulated [41]. The mechanisms of female predominance in terms of transmission were proposed as the unique maternal genetic and environmental effects [42], with gestational diabetes having a strong effect on offspring diabetic risk [43]. Our data showed a higher heritability from maternal lineage than paternal one.

We emphasized the relationship between insulin resistance indices and CA, which were taken into consideration together. For predicting CA, various insulin resistance indices, such as fasting insulin, glucose, HOMA, and metabolic syndrome components, had positive effects on IMT, but not plaque scores. High plaque scores were an indicator of more advanced CA, which was evident in men over 40 years of age and in post-menopausal women. With regards to plaque scores, this study did not show a significant heritability between family members whom only IMT values were affected by markers of insulin resistance. The relative young age in these families, with a mean age of 39 and 45 years in men and women, respectively, might be the reason of lack of heritability. As age increases, the association of plaque severity with insulin resistance might be more apparent [10, 22, 39, 40, 44]. Our participants were in a higher education and official job and tended to maintain a healthy lifestyle, which may blunt the progress of carotid atherosclerosis. Social class disparities in atherosclerosis were observed among general population: adults in US with higher social class keeping a healthier lifestyle, such as exercise and smoking cessation [45].

The strength of our study includes the complete measurements of insulin resistance indices and CA, and the focus on hypercholesterolemic proband populations. The study limitation is that we cannot separate the pure genetic factors from shared common household factors in the estimates of heritability. The high genetic correlation observed seems counterintuitive since this parameter requires that there is a significant heritability to both traits separately. Relatively small sample size in this study may limit the power, especially after being stratified by different relative pairs.

In conclusion, our finding confirms significant heritability for IMT and HOMA, in line with many previous studies, and demonstrates a moderately high genetic correlation between these two traits, implying that common genes contribute to variation in both traits. The association and heritability of insulin resistance and CA were evident among hypercholesterolemic proband families. The results imply that potential pleiotropy exists among these traits. As knowledge of clinical phenotypes and the technical improvement in post-human genome era, the genetic locus of complex traits, such as insulin resistance and CA will be revealed in the near future.

Acknowledgments This study was partially funded by NSC 94-2314-B-002-300 grant from the National Science Council, Taiwan, and the National Taiwan University Hospital.

References

1. Su TC, Jeng JS, Chien KL, Sung FC, Hsu HC, Lee YT (2001) Hypertension status is the major determinant of carotid atherosclerosis: a community-based study in Taiwan. Stroke 32:2265–2271
2. Su TC, Lee YT, Chou S, Hwang WT, Chen CF, Wang JD (2006) Twenty-four-hour ambulatory blood pressure and duration of hypertension as major determinants for intima-media thickness and atherosclerosis of carotid arteries. Atherosclerosis 184:151–156
3. Lange LA, Bowden DW, Langefeld CD et al (2002) Heritability of carotid artery intima-medial thickness in type 2 diabetes. Stroke 33:1876–1881
4. Moskau S, Golla A, Grothe C, Boes M, Pohl C, Klockgether T (2005) Heritability of carotid artery atherosclerotic lesions: an ultrasound study in 154 families. Stroke 36:5–8
5. Xiang AH, Azen SP, Buchanan TA et al (2002) Heritability of subclinical atherosclerosis in Latino families ascertained through a hypertensive parent. Arterioscler Thromb Vasc Biol 22:843–848

6. Sayed-Tabatabaei FA, van Rijn MJ, Schut AF et al (2005) Heritability of the function and structure of the arterial wall: findings of the Erasmus Rucphen family (ERF) study. Stroke 36:2351–2356
7. Pankow JS, Heiss G, Evans GW et al (2004) Familial aggregation and genome-wide linkage analysis of carotid artery plaque: the NHLBI family heart study. Hum Hered 57:80–89
8. Fox CS, Cupples LA, Chazaro I et al (2004) Genome-wide linkage analysis for internal carotid artery intimal medial thickness: evidence for linkage to chromosome 12. Am J Hum Genet 74:253–261
9. Wang TJ, Nam BH, D'Agostino RB et al (2003) Carotid intima-media thickness is associated with premature parental coronary heart disease: the Framingham heart study. Circulation 108:572–576
10. Hunt KJ, Duggirala R, Goring HH et al (2002) Genetic basis of variation in carotid artery plaque in the San Antonio family heart study. Stroke 33:2775–2780
11. Juonala M, Viikari JS, Kahonen M et al (2005) Geographic origin as a determinant of carotid artery intima-media thickness and brachial artery flow-mediated dilation: the cardiovascular risk in Young Finns study. Arterioscler Thromb Vasc Biol 25:392–398
12. Tatsukawa M, Sawayama Y, Maeda N et al (2004) Carotid atherosclerosis and cardiovascular risk factors: a comparison of residents of a rural area of Okinawa with residents of a typical suburban area of Fukuoka, Japan. Atherosclerosis 172:337–343
13. Fox CS, Polak JF, Chazaro I et al (2003) Genetic and environmental contributions to atherosclerosis phenotypes in men and women: heritability of carotid intima-media thickness in the Framingham heart study. Stroke 34:397–401
14. Juo SH, Lin HF, Rundek T et al (2004) Genetic and environmental contributions to carotid intima-media thickness and obesity phenotypes in the Northern Manhattan family study. Stroke 35:2243–2247
15. North KE, MacCluer JW, Devereux RB et al (2002) Heritability of carotid artery structure and function: the Strong heart family study. Arterioscler Thromb Vasc Biol 22:1698–1703
16. De PG, Ciccone M, Pannacciulli N et al (2000) Lower insulin sensitivity as an independent risk factor for carotid wall thickening in normotensive, non-diabetic, non-smoking normal weight and obese premenopausal women. Int J Obes Relat Metab Disord 24:825–829
17. Hunt KJ, Williams K, Rivera D et al (2003) Elevated carotid artery intima-media thickness levels in individuals who subsequently develop type 2 diabetes. Arterioscler Thromb Vasc Biol 23:1845–1850
18. Kitamura A, Iso H, Imano H et al (2004) Carotid intima-media thickness and plaque characteristics as a risk factor for stroke in Japanese elderly men. Stroke 35:2788–2794
19. Larsen JR, Brekke M, Bergengen L et al (2005) Mean HbA1c over 18 years predicts carotid intima media thickness in women with type 1 diabetes. Diabetologia 48:776–779
20. Pannacciulli N, De PG, Ciccone M, Rizzon P, Giorgino F, Giorgino R (2003) Effect of family history of type 2 diabetes on the intima-media thickness of the common carotid artery in normal-weight, overweight, and obese glucose-tolerant young adults. Diabetes Care 26:1230–1234
21. Sigurdardottir V, Fagerberg B, Hulthe J (2004) Preclinical atherosclerosis and inflammation in 61-year-old men with newly diagnosed diabetes and established diabetes. Diabetes Care 27:880–884
22. Tzou WS, Douglas PS, Srinivasan SR et al (2005) Increased subclinical atherosclerosis in young adults with metabolic syndrome: the Bogalusa heart study. J Am Coll Cardiol 46:457–463
23. Chien KL, Chen WJ, Hsu HC, Su TC, Chen MF, Lee YT (2006) Major gene effects on apolipoprotein B concentrations in families of adolescents—Results from a community-based study in Taiwan. Clin Chim Acta 365:194–199
24. Lin LY, Liau CS, Yang WS, Su TC (2005) Decreased serum adiponectin in adolescents and young adults with familial primary hypercholesterolemia. Lipids 40:163–167
25. Chien KL, Hsu HC, Su TC, Chen MF, Lee YT (2006) Heritability and major gene effects on left ventricular mass in the Chinese population: a family study. BMC Cardiovasc Disord 6:37
26. Friedewald WT, Levy RI, Fredrickson DS (1972) Estimation of the concentration of low-density lipoprotein cholesterol in plasma, without use of the preparative ultracentrifuge. Clin Chem 18:499–502
27. Chien KL, Lee YT, Sung FC, Hsu HC, Su TC, Lin RS (1999) Hyperinsulinemia and related atherosclerotic risk factors in the population at cardiovascular risk: a community-based study. Clin Chem 45:838–846
28. Matthews DR, Hosker JP, Rudenski AS, Naylor BA, Treacher DF, Turner RC (1985) Homeostasis model assessment: insulin resistance and beta-cell function from fasting plasma glucose and insulin concentrations in man. Diabetologia 28:412–419
29. NCEP (2002) Third Report of the National Cholesterol Education Program (NCEP) Expert Panel on Detection, Evaluation, and Treatment of High Blood Cholesterol in Adults (Adult Treatment Panel III) final report. Circulation 106:3143–3421
30. Su TC, Jeng JS, Wang JD et al (2006) Homocysteine, circulating vascular cell adhesion molecule and carotid atherosclerosis in postmenopausal vegetarian women and omnivores. Atherosclerosis 184:356–362
31. Su TC, Jeng JS, Chien KL, Torng PL, Sung FC, Lee YT (1999) Measurement reliability of common carotid artery intima-media thickness by ultrasonographic assessment. J Med Ultrasound 7:73–79
32. Liang KY, Zeger SL (1993) Regression analysis for correlated data. Annu Rev Public Health 14:43–68
33. SAGE (1997) Statistical analysis for genetic epidemiology, Release 3.1. Computer program package available from the Department of Epidemiology and Biostatistics, Rammelkamp Center for Education and Research, Metro Health Campus, Case Western Reserve University, Cleveland. In.
34. Almasy L, Blangero J (1998) Multipoint quantitative-trait linkage analysis in general pedigrees. Am J Hum Genet 62:1198–1211
35. Larsson H, Berglund G, Ahren B (2003) Insulin sensitivity, insulin secretion, and glucose tolerance versus intima-media thickness in nondiabetic postmenopausal women. J Clin Endocrinol Metab 88:4791–4797
36. Snehalatha C, Vijay V, Suresh MR et al (2001) Lack of association of insulin resistance and carotid intimal medial thickness in non-diabetic Asian Indian subjects. Diabetes Metab Res Rev 17:444–447
37. Golden SH, Folsom AR, Coresh J, Sharrett AR, Szklo M, Brancati F (2002) Risk factor groupings related to insulin resistance and their synergistic effects on subclinical atherosclerosis: the atherosclerosis risk in communities study. Diabetes 51:3069–3076
38. Yang B, Li TD, Wang JS, Zhi G, Jin WS, Xu Y (2005) Insulin resistance and carotid atherosclerosis in 221 patients with potential hyperglycemia. Chin Med Sci J 20:108–111
39. Joakimsen O, Bonaa KH, Stensland-Bugge E, Jacobsen BK (1999) Age and sex differences in the distribution and ultrasound morphology of carotid atherosclerosis: the Tromsö Study. Arterioscler Thromb Vasc Biol 19:3007–3013
40. Mathiesen EB, Joakimsen O, Bonaa KH (2001) Prevalence of and risk factors associated with carotid artery stenosis: the Tromsö study. Cerebrovasc Dis 12:44–51
41. Lin RS, Lee WC, Chou P, Fu CC (1994) Maternal role in type 2 diabetes mellitus: indirect evidence for a mitochondrial inheritance. Int J Epidemiol 23:886–890

42. Mahtani MM, Widen E, Lehto M et al (1996) Mapping of a gene for type 2 diabetes associated with an insulin secretion defect by a genome scan in Finnish families. Nat Genet 14:90–94
43. McLean M, Chipps D, Cheung NW (2006) Mother to child transmission of diabetes mellitus: does gestational diabetes program Type 2 diabetes in the next generation? Diabet Med 23:1213–1215
44. De MM, Panico S, Iannuzzi A et al (2002) Association of obesity and central fat distribution with carotid artery wall thickening in middle-aged women. Stroke 33:2923–2928
45. Kanjilal S, Gregg EW, Cheng YJ et al (2006) Socioeconomic status and trends in disparities in 4 major risk factors for cardiovascular disease among US adults, 1971–2002. Arch Intern Med 166:2348–2355

Lipids (2008) 43:125–131
DOI 10.1007/s11745-007-3131-8

ORIGINAL ARTICLE

LXR Agonist Increases the Lymph HDL Transport in Rats by Promoting Reciprocally Intestinal ABCA1 and apo A-I mRNA Levels

**Masao Sato · Yayoi Kawata · Kazuo Erami ·
Ikuo Ikeda · Katsumi Imaizumi**

Received: 20 August 2007 / Accepted: 23 October 2007 / Published online: 15 November 2007
© AOCS 2007

Abstract Liver and intestine are major sites of apo A-I synthesis in mammals. ABCAI is reported to be involved in the secretion of nascent HDL from cultured intestinal cells. However, whether ABCA1 participates in the secretion of nascent HDL from the intestine has not been assessed directly in vivo. This study examined the effect of a synthetic LXR-agonist "TO" on the lymphatic transport of HDL in thoracic duct-cannulated rats. The feeding of a TO-containing diet resulted in an increased transport of cholesterol and apo A-I in the lymph $d > 1.063$ g/ml lipoprotein fraction than did the feeding of a control diet without TO. The transport of cholesterol in whole lymph was lower, whereas the transport of apo A-I was higher, in the TO group. The abundance of mRNAs for ABCAI and apo A-I in the intestine was increased in the TO group. Furthermore, although the TO-containing diet reportedly increased the serum HDL concentration in intact mice and rats, no such effect was observed in the cannulated rats. The LXR agonist stimulated in vivo the synthesis of nascent HDL by increasing reciprocally the mRNA for ABCAI and apo A-I in the intestine, thereby contributing to an increase in the circulating HDL.

Keywords ABCA1 · Apo A-I · Intestine · Lymph · LXR/RXR · Nascent HDL

Abbreviations

ABC	ATP-binding cassette transporter
LXR	Liver X receptor
RXR	Retinoid X receptor
SREBP-1	Sterol regulatory element binding protein-1
TO	TO-901317

Introduction

Clinical studies have established a negative correlation between the level of high density lipoprotein (HDL) cholesterol in serum and frequency of ischemic heart disease [1]. HDL particles play a role in a reverse transport process by which excessive cholesterol is pulled out from the peripheral tissues and transferred to the liver.

The serum HDL is believed to be synthesized from precursor HDL, which is secreted by the liver and intestine, or during the catabolism of triacylglycerol-rich lipoproteins [1]. ATP-binding cassette transporter A1 (ABCA1) is a lipid pump that effluxes cholesterol and phospholipids from the cells to apolipoprotein (apo) A-I [2]. ABCA1-deficient mice had low HDL cholesterol levels [3] and human ABCA1 transgenic mice had increased plasma HDL cholesterol levels [4], demonstrating the importance of ABCA1 in the formation of HDL. Liver X receptor (LXR) forms a hetero dimer with the retinoid X receptor (RXR)

M. Sato · Y. Kawata · K. Erami · K. Imaizumi (✉)
Laboratory of Nutrition Chemistry,
Department of Bioscience and Biotechnology,
Faculty of Agriculture, Graduate School,
Kyushu University, Fukuoka 812-8581, Japan
e-mail: imaizumi@agr.kyushu-u.ac.jp

M. Sato
e-mail: masaos@agr.kyushu-u.ac.jp

I. Ikeda
Laboratory of Food and Biomolecular Science,
Department of Food Function and Health,
Division of Bioscience and Biotechnology for Future
Bioindustries, Graduate School of Agricultural Science,
Tohoku University, Sendai 981-8555, Japan

and this dimer binds to the LXR response element in the promoter sequence of ABCA1 [5]. As ligands of LXR, several oxidized cholesterols, such as 22(R)-hydroxycholesterol have been identified [6]. Furthermore, Repa et al. reports that when LXRα/β double knock-out mice and C57BL/65/129SV mice as the wild type were fed a diet containing 0.2% cholesterol and TO-901317 (TO) as an LXR agonist, the abundance of the intestinal ABCA1 mRNA increased only in the wild type mice [7].

ABCA1 is abundant in not only macrophages but also the liver and small intestine [8]. Recent studies suggest that significant numbers of HDL particles are assembled at the hepatocyte surface [9, 10]. In addition, it has been reported that the expression of ABCA1 in macrophages has a minimal contribution to plasma HDL levels [11]. Timmis et al. [12] demonstrated that hepatic ABCA1 is essential for the lipidation of nascent apo A-I and the maintenance of the majority of the plasma HDL pool.

Although the physiological role of ABCA1 in the small intestine has yet to be clarified, Ohama et al. [13] showed that ABCA1 protein is expressed at the basolateral site of CaCo-2 cells, the expression is enhanced by incubating the cells with LXR/RXR agonists, and the efflux of cholesterol is induced by apo A-I at the basolateral but not apical site. The study therefore suggests that ABCA1 may be involved in vivo in the formation and secretion of intestinal HDL, but this hypothesis has not been demonstrated in vivo. In this study, we evaluated the role of intestinal ABCA1 expression in the lymphatic transport of HDL in rats with permanent cannulation of the thoracic duct. Our results demonstrate that a LXR agonist increases the lymphatic HDL transport from the intestine by promoting reciprocally ABCA1 and apo A-I expression.

Materials and Methods

Animals and Diet

Male SD rats, 8-weeks old, obtained from Seiwa Experimental Animals (Fukuoka, Japan) and maintained in a temperature-controlled room (23 °C), were trained to consume a control diet twice a day from 10:00–11:00 and 16:00–17:00, respectively, for 5 days. The control diet was based on the AIN-93G [14] formulation as described previously [15] and supplemented with soybean oil (100 g/kg diet) and cholesterol (10 g/kg diet). To the control diet was added TO-901317 (TO: Cayman, MI, USA) at 0.056 g/kg diet (TO diet). The amount was based on the report showing that the effective level of TO is 3 mg/kg body weight in a meal [7]. On day 6, all the rats were anesthetized with Nembutal prior to permanent cannulation of the thoracic duct lymph as described previously [15]. Briefly, a cannula (SH silicon tube, 0.5 mm i.d. and 1.0 mm o.d., Kaneka Medics, Osaka, Japan) filled with heparinized saline was inserted into the thoracic duct and secured within the abdominal cavity. The rats were returned to their cages and provided with the control diet or the TO diet twice a day as just described. On day 9, the rats were attached to a long PE cannula (0.58 mm i.d. and 0.97 mm o.d., Becton Dickinson and Company, MD, USA) to collect the lymph. The end of the cannula was 5–10 cm below the bottom of the cage in order to allow the lymph to drain into the cannula. The lymph was collected for 20 min, and the rats were then given free access to the control diet or TO diets for 30 min. At this time, the lymph was collected every hour for 7 h. The lymph was collected in a tube containing an inhibitor for lecithin-cholesterol acyltransferase, 1 mM 5,5′-dithionitrobenzoic acid in 0.75 M phosphate buffer solution. After fibrin was removed, ethylenediaminetetraacetic acid at a final concentration of 0.01% was added to the lymph solutions. The lymph was subjected to ultracentrifugation to isolate the lymph $d > 1.063$ g/ml fraction as described below. The rats were anesthetized with diethylether and sacrificed by collecting aortic blood. The intestine was immediately excised and then divided into proximal and distal sites to strip the mucosa for the total RNA preparation. The liver was also excised and used for RNA preparation and lipid determination.

The rats had free access to deionized water throughout the feeding periods and during lymph collection. Experiments were carried out following the Guidelines for Animal Experiments at the Faculty of Agriculture and the Graduate Course, Kyushu University, Fukuoka, Japan, and Law No.105 and Notification (No. 6) of the Government of Japan

Measurement of mRNA Levels for Specific cDNA in the Intestinal Mucosa and the Liver

Total cellular RNA was isolated from the small intestine and liver using guanidium thiocyanate/cesium chloride ultracentrifugation as described by Sato et al. [16] and used for Northern blotting as described by Thomas [17]. Hybridization was performed in hybridization solution containing cDNA labeled with [α-^{32}P] deoxycytidine triphosphate (dCTP) (3,000 Ci/mmol, ICN Co., CA, USA) using a multiprime DNA labeling system (Amersham Pharmacia Biotech, Tokyo, Japan) according to the manufacturers instruction, as described elsewhere [16]. Rat cDNAs for ABCA1 (GenBank No.: NM178095, GeneID: 313210), G5 (GenBank No.: NM053754, GeneID: 114628) and G8 (GenBank No. NM130414, GeneID: 155192), and apo A-I [18] were cloned from rat liver cDNA by the reverse transcription PCR method. Rat ABC G5 and G8 and sterol regulatory element binding protein (SREBP)-1 cDNAs were cloned full length. Rat ABC A1 cDNA was partly cloned: 392 bp from bp 2,616 to 3,007. The primer sequences were 5′-CAAGGTATCGGGGTCCAATG (5′-primer) and 5′-CATTATGCTGGGGACAGACT (3′-primer) for ABCA1, 5′-GCTGGCCATGGGTGAGCTGCCC TTTCTG and 5′-TCTTACCTATCTGCTAATCAGGTAG TCC for ABCG5, 5′-ATGGCTCAGACGACCAAAGAGG AGA and 3′-TGAACATCACCAATCTTGAATTGAC for ABCG8 and 5′-ATGAAAGCTGCAGTGTTGGCTGCC and 5′-CGGTCACTAAGCGTTCAGCTTCTTCTTTTT for apo A-I. All cDNA sequences were ensured by a DNA autosequencer (Gene Rapid, Amersham Pharmacia Biotech, Tokyo, Japan) to match the reported sequences. The apo A-IV cDNA clone as a plasmid was provided by Gordon [19]. Human ribosomal 18s RNA cDNA clones as a plasmid were obtained from American Type Culture Collection (Rockville, MD, USA). Quantification of the hybridization signals was carried out with a bio-imaging analyzer (BAS-1000, Fuji Photo Film Co., Tokyo, Japan). The results were expressed as a relative value after normalization to ribosomal 18s RNA.

Preparation of Lymph HDL Fraction

The lymph was adjusted to a density of 1.063 by addition of KBr, and ultracentrifuged at 100,000×*g* (Beckman TLA100.2 rotor, Beckman Instruments, USA) for 20 h at 15 °C. Lipoprotein fractions of density >1.063 g/ml and density <1.063 g/ml were designated as the HDL fraction and non-HDL fraction, respectively.

Measurement of Serum and Liver Lipid Concentrations

Serum triacylglycerol, total cholesterol and phospholipid levels were measured using enzyme assay kits (Triglyceride *G* Test, Cholesterol *C* Test and Phospholipid *B* Test, respectively). The kits were purchased from Wako Pure Chemical Industries, Osaka, Japan. Serum HDL-cholesterol levels were measured using a precipitate and enzymatic assay kit (HDL-C 2: Daiichi Chemical Industry, Tokyo, Japan). Liver lipids were extracted by the method of Folch et al. [20] and cholesterol [15], triacylglycerol [21] and phospholipid [8] levels were measured as described elsewhere. The lipids of the lymph HDL and non-HDL fractions were extracted by the method of Folch et al. [20] and cholesterol levels were measured by gas liquid chromatography as described elsewhere [15]. The apo A-I level was determined by immuno electrophoresis using anti rat apo A-I rabbit serum and expressed as arbitrary units against a reference serum from rats [16].

Statistical Analysis

The data were expressed as the mean ± SEM. The significance of differences was determined with Student's *t* test. The statistical analysis was carried out with Statcel (OMS, Saitama, Japan) and Microsoft Excel 2000 (Microsoft, Redmond, WA, USA). Differences were considered to be statistically significant at $P < 0.05$.

Results

During the training period (day 1–5), all the rats consumed a control diet twice a day (16.2 ± 0.4 and 15.0 ± 1.1 g/day for the control and TO groups, respectively, $n = 6$). After the operation (day 7–8), rats consumed the control diet and TO diet, respectively, twice a day (11.1 ± 0.9 and 10.1 ± 1.6 g/day for control and TO group, respectively). As expected, food consumption was lower at day 7–8 than day 1–5. At day 9, both groups of rats consumed the diet for 30 min (5.2 ± 0.4 and 5.2 ± 0.9 g for the control and TO groups, respectively). The type of diet had no significant effect on food consumption.

Although there was no difference in the lymph flow prior to the feeding of the control and TO diets, consumption of the TO diet resulted in a remarkable reduction in lymph flow (8.52 ± 0.99 ml/7 h and 4.80 ± 1.13 ml/7 h for the control and TO groups, respectively, $P < 0.05$). The TO diet also resulted in a reduction in lymph flow (13.7 ± 1.62 ml/7 h and 8.21 ± 0.780 ml/7 h for the control and TO groups, respectively, $P < 0.05$) and the rate of transport of cholesterol (14.0 ± 1.37 mg/7 h and 9.02 ± 0.70 mg/7 h for the control and TO groups, respectively, $P < 0.05$), triacylglycerols (341.7 ± 31.2 mg/7 h and 220.9 ± 25.9 mg/7 h for the control and TO groups, respectively, $P < 0.05$), and phospholipids (32.4 ± 3.5 mg/7 h and 25.2 ± 2.1 mg/7 h for the control and TO groups, respectively) in our preliminary study.

As shown in Fig. 2a, the TO diet resulted in a decrease in the transport of cholesterol for 7 h in the total lymph and $d < 1.063$ g/ml fraction. However, the transport for 7 h in the $d > 1.063$ g/ml fraction was greater in the TO group than the control group. As shown in Fig. 2b, the lymphatic output of apo A-I was higher in the TO group. Such a difference was attributed to an increased output of apo A-I in the $d > 1.063$ g/ml fraction in the TO group (Fig. 2).

Table 1 and Fig. 1 shows the relative abundances of the mRNAs for ABC proteins, apoproteins, and SREBP-1 in intestinal mucosa and liver isolated from rats after the of

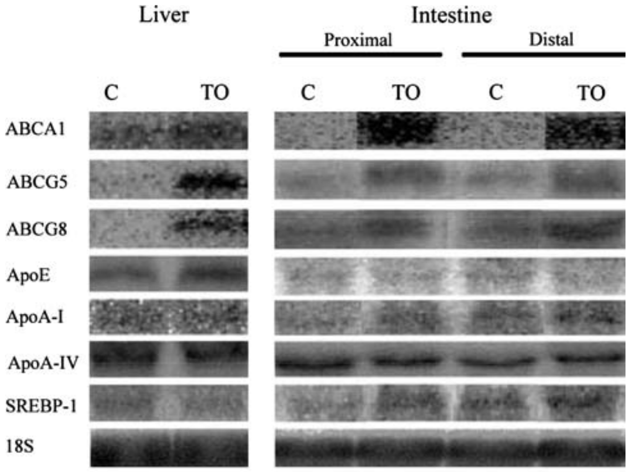

Fig. 1 The mRNA expression of ABCA1, ABCG5, ABCG8, ApoE, SREBP-1, ApoA-I and ApoA-IV were analyzed by Northern blot analysis. Signals were quantitated by image analysis. Each value was normalized for the ribosomal RNA 18S signal

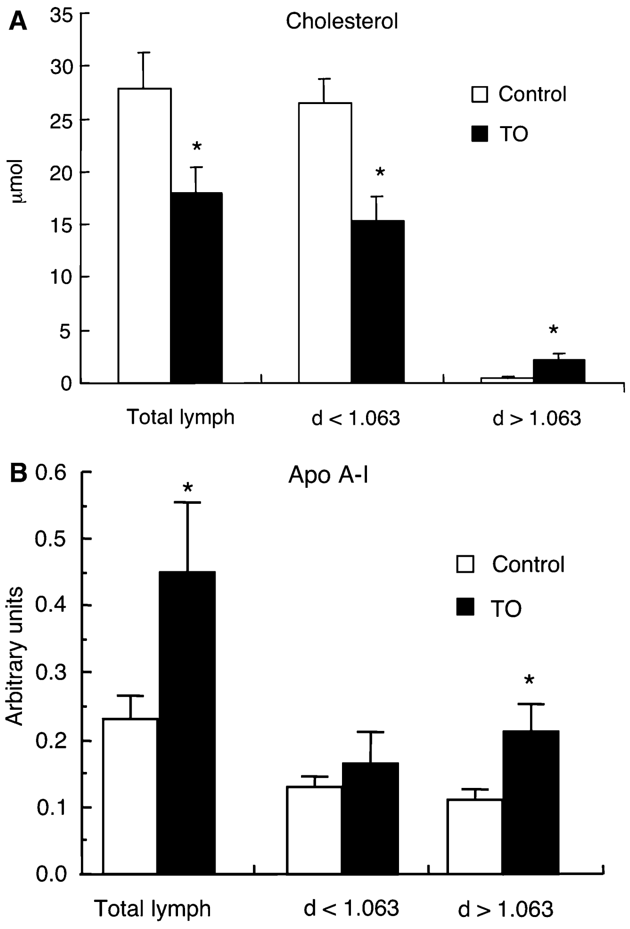

Fig. 2 The effect of dietary TO on cholesterol contents (**a**) and apo A-I contents of total lymph and non-HDL and HDL fractions (**b**) collected for 7 h. Values for six rats per group are means ± SEM. Values for apo A-I are represented as the area of the immunoprecipitation by immuno electrophoresis. *Asterisk*, significantly different from the control group, $P < 0.05$

lymph was collected. The abundance of mRNAs for ABCA1, G5 and G8, apo A-I, and SREBP-1 in the proximal intestine was higher in the TO group than the control group. The extent of the increase was most prominent for the ABCA1 mRNA. The TO diet also resulted in an increase in mRNA abundance for ABC proteins, apo A-I and SREBP-1, in the distal intestine. In the liver, the TO diet resulted in an increased abundance of mRNAs for ABC proteins and SREBP-1. However, there was no significant difference in apo A-I mRNA abundance between the dietary groups. The extent of the increase for ABCG5/8 mRNA abundance in the liver appeared to be greater than that for the corresponding ABCA1. The consumption of TO had no significant effect on the mRNA abundance for apo A-IV and apo E in the intestine and liver.

The TO diet resulted in an increased concentration of triacylglycerol in serum (257 ± 33 for the TO diet and 100 ± 33 mg/dl for the control diet, $n = 6$, $P < 0.05$). The concentration of triacylglycerols in the liver was also higher in the TO than control group (79.9 ± 10.9 versus 12.0 ± 1.9 mg/g liver, respectively, $n = 6$, $P < 0.05$). There was no significant difference in the concentration of HDL-cholesterol in serum between the groups (17.9 ± 3.0 and 18.9 ± 2.5 mg/dl for the TO and control group, respectively, $n = 6$, $P > 0.1$).

Discussion

The present study showed that consumption of TO, an artificially made LXR agonist, resulted in an elevation of cholesterol and apo A-I levels in the lymph $d > 1.063$ g/ml fraction. Although it remains to be determined if cholesterol and apo A-I exist simultaneously as a lipoprotein particle such as a nascent HDL, Green et al. reported that rat intestine secretes discoidal HDL in the lymph $d > 1.063$ g/ml fraction [23]. Furthermore, Wu et al. [24] and Imaizumi et al. [25] showed that rat intestine actively produces apo A-I, which is used as a constituent of chylomicrons and nascent HDL in the lymph. Accordingly, the present study suggests that the LXR agonist increases the secretion of nascent HDL particles from the intestine.

Recent studies have established that the lipidation of HDL apoproteins occurs primarily after their secretion and that ABCA1 is a crucial participant in the early lipidation of newly secreted apo A-I [26]. The present study showed that the TO diet resulted in increased mRNA levels of ABCA1 and apo A-I suggesting increased levels of these proteins in the intestinal mucosa. That the apo A-I levels in the lymph and the HDL fraction were higher in the TO group than in the control group indicates indirectly the active synthesis of apo A-I in the intestinal mucosa.

Table 1 Relative mRNA levels for ABC proteins, apoproteins and SREBP1 in the proximal intestine and liver in rats fed the control and TO diet

	Liver		Proximal intestine		Distal intestine	
	Control	TO	Control	TO	Control	TO
ABCA1	100 ± 13.6	188 ± 10.8*	100 ± 36.0	1127 ± 99.0*	100 ± 15.7	1557 ± 273*
ABCG5	100 ± 28.4	629 ± 96.5*	100 ± 16.6	284.0 ± 10.1*	100 ± 6.3	194 ± 10.6*
ABCG8	100 ± 15.9	996 ± 272*	100 ± 20.4	324.0 ± 6.7*	100 ± 6.9	262 ± 28.6*
Apo A-I	100 ± 13.9	110 ± 7.2	100 ± 9.0	180.0 ± 10.0*	100 ± 14.9	118 ± 7.8*
Apo A-IV	100 ± 12.6	141 ± 32.8	100 ± 19.1	109.0 ± 5.6	100 ± 9.1	148 ± 5.0
Apo E	100 ± 9.7	147 ± 20.2	100 ± 15.6	94.4 ± 3.7	100 ± 24.2	91 ± 9.6
SREBP-1	100 ± 16.4	158 ± 15.6*	100 ± 13.9	171.0 ± 15.1*	100 ± 7.6	109 ± 9.4

Values are means ± SEM; $n = 6$ per group. The significance of difference between the two diet groups of liver and proximal and distal intestines was analyzed by Student's *t* test

* Significantly different from rats fed the control diet ($P < 0.05$)

Although ABCA1 protein levels were not determined in the present study, the increased HDL-cholesterol level in the lymph in the TO group suggests an increased level of ABCA1 protein at the basolateral site of the intestine, because it is reported that LXR/RXR ligands enhance the expression of ABCA1 on the basolateral surface of CaCo-2 cells [13, 27, 28] and efficient basolateral cholesterol efflux occurs during the absorption of dietary cholesterol in chickens [29]. It is also reported that apo A-I is secreted independent of lipids and that the lipid-poor apo A-I can accept cholesterol from ABCA1 which plays a role in the TG-rich lipoprotein-independent transport of cholesterol across the intestinal epithelial cells [13, 27, 28]. Accordingly, it is likely that the TO-diet -dependent increase in the transport of HDL-cholesterol is attributable to the increased expression of ABCA1 and apo A-I.

Feeding mice a TO-containing diet has been reported to result in an increased level of HDL cholesterol [7]. In our preliminary study, in rats whose thoracic lymph duct was not cannulated, the TO diet resulted in an increased serum HDL cholesterol concentration compared with the control diet (36.4 ± 1.2 and 26.4 ± 1.7 mg/dl for the TO and control groups, respectively, $n = 5$, $P < 0.05$). As shown in the present study, however, there was no significant difference in the serum HDL-cholesterol level in the cannulated rats indicating that the increase in intestinal HDL synthesis caused by the TO contributes to the elevation in the serum HDL level. Brunham et al. [30] treated mice with the synthetic LXR agonist GW3965. GW3965 significantly increased plasma HDL cholesterol levels in wild-type mice and mice lacking hepatic ABCA1, and this effect was completely abrogated in mice lacking intestinal ABCA1. They have insisted that activation of intestinal ABCA1 can lead to an increase in HDL level. Therefore, in this study, serum HDL level in cannulated rats did not arise because of lacking HDL derived from lymph secreted from intestine.

The ABCA1 gene has a responsive site for the complex LXR/RXR ligand [6]. No such responsive element has been reported for the apo A-I gene in the mouse or rat. In fact, apo A-I gene in the liver and intestine of mice remained unaffected by a LXR agonist [31]. Alternatively, a rise in the apo A-I mRNA level caused by a LXR agonist has been reported in chondrocytes from chick embryo tibiae [32] and epithelial cells from canine gallbladder [33]. Therefore, it remains possible that an increased efflux of cholesterol from the basolateral site through an ABCA1-mediated pathway triggered a change in the apo A-I mRNA abundance. Therefore, there may be an indirect regulatory mechanism by which LXR agonists act on apo A-I expression in rat intestine.

In the present study, the extent of the change in the abundance of mRNAs for the ABCA1 and ABCG5/8 genes, which have the responsive element for the LXR/RXR gene differed between the intestine and liver. Namely, the effect of TO was prominent in the intestine for ABCA1 and in the liver for ABCG5/8. These results indicate that there exists a mechanism regulating tissue-dependent expression of ABCA1 and ABCG5/8 due to the TO-diet. According to Tamehiro et al. [34], there are two types of ABCA1 transcripts: a LXR-responsive element-dependent transcript which is found in the intestine and the peripheral tissues including macrophages and a novel liver-type promoter which is activated by sterol regulatory element-binding protein-2. Expression of the latter is suppressed by dietary cholesterol in experimental animals. The intestine contains only the peripheral-type transcript, whereas the liver has both types. In the present study, the diet contained cholesterol, hence resulting in a less prominent increase in abundance for the liver type ABCA1 mRNA than for the intestine type ABCA1 mRNA. It remains unclear why the TO-diet exerted a more pronounced change in the abundance of ABCG5/8 mRNA in the liver than intestine.

In the present study, the TO diet resulted in an elevation of SREBP-1 mRNA abundance 1.7-fold higher than the control diet. In contrast, Brunham et al. [30] reported that administration of GW3965 as an agonist of LXR to wild-type mice elevated the level of SREBP1c mRNA to 30-fold compared to the vehicle administration without cholesterol input. The different response to LXR agonist appears to the amount of cholesterol in the diet, feeding period of the agonist and the amount of the agonist injected.

Dietary fat has been reported to increase lymph flow [35]. In the present study, it was found that the TO-diet resulted in a decreased lymph flow compared to the control. The suppression appears to be relevant to a decrease in the transport of lymphatic cholesterol, triacylglycerols, and phospholipids. The suppression of lymph flow may be partly due to the decrease in intestinal nitric oxide (NO), the expression of which was suppressed by a LXR agonist [36]. In fact, NO production in the gut has been reported to increase gastrointestinal peristaltic motion [37]. Thus, the inhibition of NO production by the agonist may lower lymph flow, thereby delaying lipid absorption. Alternatively, the TO-diet may have increased intestinal fluid flow from the mucosal site to the luminal site thereby resulting in an increase in sterol transport from the mucosal site to the luminal site in mice fed an LXR/RXR agonist [38]. Furthermore, it remains the possibility that TO-diet might influence the bile acid synthesis thereby influence the absorption of cholesterol [39].

In summary, the present study demonstrated for the first time that treatment with a LXR agonist promotes the transport of lymph HDL possibly by enhancing reciprocally the expression of the ABCA1 and apo A-I genes.

References

1. Eisenberg S (1984) High density lipoprotein metabolism. J Lipid Res 25:1017–1058
2. Brooks-Wilson A, Marcil M, Clee SM, Zhang LH, Roomp K, van Dam M, Yu L, Brewer C, Collins JA, Molhuizen HO, Loubser O, Ouelette BF, Fichter K, Ashbourne-Excoffon KJ, Sensen CW, Scherer S, Mott S, Denis M, Martindale D, Frohlich J, Morgan K, Koop B, Pimstone S, Kastelein JJ, Hayden MR (1999) Mutations in ABC1 in Tangier disease and familial high-density lipoprotein deficiency. Nat Genet 22:336–345
3. McNeish J, Aiello RJ, Guyot D, Turi T, Gabel C, Aldinger C, Hoppe KL, Roach ML, Royer LJ, de Wet J, Broccardo C, Chimini G, Francone OL (2000) High density lipoprotein deficiency and foam cell accumulation in mice with target with targeted disruption of ATP-binding cassette transporter-1. PNAS 97:4245–4250
4. Singaraja RR, Bocher V, James ER, Clee SM, Zhang LH, Leavitt BR, Tan B, Brooks-Wilson A, Kwok A, Bissada N, Yang YZ, Liu GQ, Tafuri SR, Fievet C, Wellington CL, Staels B, Hayden MR (2001) Human ABCA1 BAC transgenic mice show increased high density lipoprotein cholesterol and apoAI-dependent efflux stimulated by an internal promoter containing liver X receptor response elements in intron 1. J Biol Chem 276:33969–33979
5. Costet P, Luo Y, Wang N, Tall AR (2000) Sterol-dependent transactivation of the ABC1 promoter by the liver X receptor/retinoid X receptor. J Biol Chem 275:28240–28245
6. Janowski BA, Willy PJ, Devi TR, Falck JR, Mangelsdorf DJ (1996) An oxysterol signalling pathway mediated by the nuclear receptor LXR α. Nature 383:728–731
7. Repa JJ, Turley SD, Lobaccaro JMA, Medina J, Li L, Lustig K, Shan B, Heyman RA, Dietschy JM, Mangelsdorf DJ (2000) Regulation of absorption and ABC1-mediated efflux of cholesterol by RXR heterodimers. Science 289:1524–1529
8. Drobnik W, Lindenthal B, Lieser B, Ritter M, Weber TC, Liebisch G, Giesa U, Igel M, Borsukova H, Buchler C, Fung-Leung WP, Von Bergmann K, Schmitz G (2001) ATP-binding cassette transporter A1 (ABCA1) affects total body sterol metabolism. Gastroenterology 120:1203–1211
9. Vaisman BL, Lambert G, Amar M, Joyce C, Ito T, Shamburek RD, Cain WJ, Fruchart-Najib J, Neufeld ED, Remaley AT, Brewer HB Jr, Santamarina-Fojo S (2001) ABCA1 overexpression leads to hyperalphalipoproteinemia and increased biliary cholesterol excretion in transgenic mice. J Clin Invest 108:303–309
10. Wellington CL, Brunham LR, Zhou S, Singaraja RR, Visscher H, Allison Gelfer A, Ross C, James E, Liu G, Huber MT, Yang YZ, Parks RJ, Groen A, Fruchart-Najib J, Hayden MR (2003) Alterations of plasma lipids in mice via adenoviral-mediated hepatic overexpression of human ABCA1. J Lipid Res 44:1470–1480
11. Haghpassand M, Bourassa PA, Francone OL, Aiello RL (2001) Monocyte/macrophage expression has minimal contribution to plasma HDL levels. J Clin Invest 108:1315–1320
12. Timmins JM, Lee JY, Boudyguina EB, Kluckman KD, Brunham LR, Mulya A, Gebre AK, Coutinho JM, Colvin PL, Smith TL, Hayden MR, Maeda N, Parks JS (2005) Targeted inactivation of hepatic Abca1 causes profound hypoalphalipoproteinemia and kidney hypercatabolism of apo A-I. J Clin Invest 115:1333–1342
13. Ohama T, Hirano K, Zhang ZY, Aoki R, Tsujii K, Nakagawa-Toyama Y, Tsukamoto K, Ikegami C, Matsuyama A, Ishigami M, Sakai N, Hiraoka H, Ueda K, Yamashita S, Matsuzawa Y (2002) Dominant expression of ATP-binding cassette transporter-1 on basolateral surface of Caco-2 cells stimulated by LXR/RXR ligands. Biochem Biophys Res Commun 296:625–630
14. Reeves PG, Nielsen FH, Fahey GC Jr (1993) AIN-93 purified diets for laboratory rodents: final report of the American Institute of Nutrition ad hoc Writing Committee on the reformulation of the AIN-76A rodent diet. J Nutr 123:1939–1951
15. Tomoyori H, Kawata Y, Higuchi T, Ichi I, Sato H, Sato M, Ikeda I, Imaizumi K (2004) Phytosterol oxidation products are absorbed in the intestinal lymphatics in rats but do not accelerate atherosclerosis in apolipoprotein E–deficient mice. J Nutr 134:1690–1696
16. Sato M, Imaizumi K, Mori H, Sugano M (1992) Regulation of intestinal apo A-IV mRNA abundance in rat pups during fasting and refeeding. Biochem Biophys Acta 1165:93–101
17. Thomas PS (1983) Hybridization of denatured RNA transferred or dotted nitrocellulose paper. Method Enzymol 100:255–266
18. Poncin JE, Martial JA, Gielen JE (1984) Cloning and structure analysis of the rat apolipoprotein A-I cDNA. Eur J Biochem 140:493–498
19. Boguski MS, Elshourbagy N, Taylor JM, Gordon JI (1984) Rat apolipoprotein A-IV contains 13 tandem repetitions of a 22-amino acid segment with amphipathic helical potential. PNAS 81:5021–5025
20. Folch J, Lees M, Sloane Stanley GH (1957) A simple method for the isolation and purification of total lipids from animal tissue. J Biol Chem 226:497–509
21. Fletcher MJ (1968) A colorimetric method for estimating serum triglycerides. Clin Chim Acta 22:393–399

22. Rouser G, Siakotos AN, Fleischer S (1966) Quantitative analysis of phospholipids by thin-layer chromatography and phosphorus analysis of spots. Lipids 1:85–86
23. Green PH, Tall AR, Glickman RM (1979) Rat intestine secretes discoid high density lipoprotein. J Clin Invest 61:528–534
24. Wu AL, Windmueller HG (1979) Relative contributions by liver and intestine to individual plasma apolipoproteins in the rat. J Biol Chem 254:7316–7322
25. Imaizumi K, Havel RJ, Fainaru M, Vigne JL (1978) Origin and transport of the A-I and arginine-rich apolipoproteins in mesenteric lymph of rats. J Lipid Res 19:1038–1046
26. Rader DJ (2006) Molecular regulation of HDL metabolism and function: implications for novel therapies. J Clin Invest 116:3090–3100
27. Iqbal J, Anwar K, Hussain MM (2003) Multiple, independently regulated pathways of cholesterol transport across the intestinal epithelial cells. J Biol Chem 278:31610–31620
28. Murthy S, Born E, Mathur SN, Field FJ (2002) LXR/RXR activation enhances basolateral efflux of cholesterol in CaCo-2 cells. J Lipid Res 43:1054–1064
29. Mulligan JD, Flowers MT, Tebon A, Bitgood JJ, Wellington C, Hayden MR, Attie AD (2003) ABCA1 is essential for efficient basolateral cholesterol efflux during the absorption of dietary cholesterol in chickens. J Biol Chem 278:13356–13366
30. Brunham LR, Kruit JK, Pape TD, Parks JS, Kuipers F, Hayden MR, (2006) Tissue-specific induction of intestinal ABCA1 expression with a liver X receptor agonist raises plasma HDL cholesterol levels. Circ Res 99:672–674
31. Jiang XC, Beyer TP, Li Z, Liu J, Quan W, Schmidt RJ, Zhang Y, Bensch WR, Eacho PI, Cao G (2003) Enlargement of high density lipoprotein in mice via liver X receptor activation requires apolipoprotein E and is abolished by cholesteryl ester transfer protein expression. J Biol Chem 278:49072–49078
32. Gentili C, Tutolo G, Pianezzi A, Cancedda R, Cancedda FD (2005) Cholesterol secretion and homeostasis in chondrocytes: a liver X receptor and retinoid X receptor heterodimer mediates apolipoprotein A-I expression. Matrix Biol 24:35–44
33. Lee J, Tauscher A, Seo DW, Oram JF, Kuver R (2003) Cultured gallbladder epithelial cells synthesize apolipoproteins A-I and E. Am J Physiol Gastrointest Liver Physiol 285:G630–G641
34. Tamehiro N, Shigemoto-Mogami Y, Kakeya T, Okuhira K, Suzuki K, Sato R, Nagao T, Nishimaki-Mogami T (2007) SREBP-2- and LXR-driven dual promoter regulation of hepatic ABCA1 gene expression:mechanism underlying the unique response to cellular cholesterol status. J Biol Chem 10.1074/jbc.M701228200
35. Sylvén C, Borgström B (1968) Absorption and lymphatic transport of cholesterol in the rat. J Lipid Res 9:596–601
36. Joseph SB, Castrillo A, Laffitte BA, Mangelsdorf DJ, Tontonoz P (2003) Reciprocal regulation of inflammation and lipid metabolism by liver X receptors. Nat Med 9:213–219
37. Calignano A, Whittle BJ, Rosa MD, Moncada S (1992) Involvement of endogenous nitric oxide in the regulation of rat intestinal motility in vivo. Eur J Pharmacol 229:273–276
38. Igel M, Giesa U, Lütjohann D, Klaus von Bergmann K (2003) Comparison of the intestinal uptake of cholesterol, plant sterols, and stanols in mice. J Lipid Res 44:533–538
39. Sehayek E, Ono JG, Shefer S, Nguyen LB, Wang N, Batta AK, Salen G, Smith JD, Tall AR, Breslow JL, (1998) Biliary cholesterol excretion: a novel mechanism that regulates dietary cholesterol absorption. PNAS 95:10194–10199

Lipids (2008) 43:133–141
DOI 10.1007/s11745-007-3125-6

ORIGINAL ARTICLE

Brachial Artery Intima-Media Thickness and Echogenicity in Relation to Lipids and Markers of Oxidative Stress in Elderly Subjects:-The Prospective Investigation of the Vasculature in Uppsala Seniors (PIVUS) Study

Lars Lind · Jessika Andersson · Monika Rönn · Thomas Gustavsson · Peter Holdfelt · Johannes Hulthe · Anders Elmgren · Kersti Zilmer · Mihkel Zilmer

Received: 21 June 2007 / Accepted: 3 September 2007 / Published online: 15 November 2007
© AOCS 2007

Abstract The aim of the present study was to relate brachial artery intima-media thickness (IMT) and the grey scale median of the intima-media complex (IM-GSM) to traditional cardiovascular risk factors and markers of inflammation and oxidative stress. In the Prospective Study of the Vasculature in Uppsala Seniors (PIVUS) study, a population-based study of 1016 subjects aged 70, brachial artery IMT and IM-GSM, who were evaluated by ultrasound. Lipids, thirteen markers of inflammation and nine markers of oxidative stress were measured. The Framingham risk score was related to IMT ($p < 0.0001$), but not to the IM-GSM. In univariate analysis, HDL-cholesterol, serum triglycerides, fasting glucose, smoking, HOMA insulin resistance index and oxidized LDL levels were related to IMT. HDL and LDL-cholesterol, triglycerides, VCAM-1, e-selectin, leukocyte count, conjugated diens, baseline conjugated diens (BCD)-LDL, antibodies to ox-LDL, the GSSG/GSH glutathione ratio and homocysteine were related to IM-GSM. In multiple regression models, HDL-cholesterol, fasting glucose and oxLDL levels were the independently related to IMT ($p = 0.01$–0.04), while serum triglycerides, BCD-LDL and the GSSG/GSH ratio were independently related to IM-GSM ($p = 0.0001$–0.004). In conclusion, in addition to traditional lipid variables, markers of oxidative stress were associated with both thickness and echogenicity of the brachial artery intima-media complex. Thus, both thickness and echogenicity of the brachial artery intima-media complex might be useful biomarkers in the future.

Keywords Lipids · Ultra sound · Artery · Oxidation · Intima-media

Introduction

The IMT of the carotid artery is a commonly used measure of atherosclerosis. IMT of the carotid artery has been shown to be reduced by intensive statin treatment [1] and to predict cardiovascular events in epidemiological cohort studies [2]. It has recently been shown that brachial artery IMT is correlated to common carotid artery IMT [3]. Thus, also brachial artery IMT might serve as a marker of cardiovascular risk.

Although several studies have evaluated the echogenicity of carotid artery plaque as the GSM by image analysis [4, 5], few attempts have been made to characterize the intima-media complex with a similar grey scale analysis. It is evident from the visual inspection of the intima-media complex in both the carotid and brachial artery that a great variation in echogenicity does exist.

L. Lind (✉) · J. Andersson · M. Rönn
Department of Medicine, Uppsala University Hospital,
751 85 Uppsala, Sweden
e-mail: lars.lind@medsci.uu.se

T. Gustavsson · P. Holdfelt
Department of Signals and Systems,
Chalmers University of Technology,
Gothenburg, Sweden

J. Hulthe
Wallenberg laboratory, Sahlgrenska University Hospital,
Gothenburg, Sweden

A. Elmgren
AstraZeneca R&D, Mölndal, Sweden

K. Zilmer · M. Zilmer
Department of Biochemistry, University of Tartu,
Estonia, Sweden

However, the usefulness of this information has however not yet been studied.

In order to validate the usefulness of the evaluation of the brachial artery IMT and GSM of the intima-media complex (IM-GSM), these two brachial artery characteristics were related to traditional cardiovascular risk factors included in Framingham risk score and the metabolic syndrome (MetS). Furthermore, since both inflammation and oxidative stress have been advocated to play an important role in the development of atherosclerosis, we used data from the PIVUS study, a population-based cohort study initiated in more than 1000 subjects aged 70 living in the community of Uppsala, Sweden [6], to study the relationships between brachial artery IMT and GSM of the intima-media complex and traditional risk factors as well as markers of inflammation and oxidative stress. The hypothesis tested was that both the brachial artery IMT and GSM of the intima-media complex would be related to traditional risk factors. This hypothesis is biologically plausible, since carotid artery IMT [2], as well as echolucent plaques predict future cardiovascular events [7].

Material and Methods

Subjects

The eligible subjects were all aged 70 living in the community of Uppsala, Sweden. The subjects were chosen from the register of community inhabitants and were invited in a randomized order. The subjects received an invitation by letter within 2 months of their 70th birthday. Of the 2025 subjects invited, 1016 subjects participated giving a participation rate of 50.1%.

The study was approved by the Ethics Committee of the University of Uppsala and the participants gave informed consent.

Basic Investigation

The participants were asked to answer a questionnaire about their medical history, smoking habits, and regular medication.

All subjects were investigated in the morning after an over-night fast. No medication or smoking was allowed after midnight. After recording their height, weight, abdominal and hip circumference, an arterial cannula was inserted in the brachial artery for blood sampling (and later regional infusions of vasodilators, see Ref. 6]. Thereafter, the ultrasonographic evaluation took place in the contralateral arm.

Blood pressure was measured by a calibrated mercury sphygmomanometer in the non-cannulated arm to the nearest mmHg after at least 30 min of rest and the average of three recordings was used. Traditional lipid variables and fasting blood glucose were measured by standard laboratory techniques. From these data, the Framingham risk score was calculated [8].

Approximately 10% of the cohort reported a history of coronary heart disease, 4% reported stroke and 9% diabetes mellitus. Almost half the cohort reported some cardiovascular medication (45%), with antihypertensive medication being the most prevalent (32%). Fifteen percent reported use of statins, while insulin and oral antiglycemic drugs were reported in 2 and 6%, respectively (see Ref. 6 for details).

As the participation rate in this cohort was only 50%, we carried out an evaluation of cardiovascular disorders and medications in 100 consecutive non-participants. The prevalences of cardiovascular drug intake, history of myocardial infarction, coronary revascularization, antihypertensive medication, statin use and insulin treatment were similar to those in the investigated sample, while the prevalences of diabetes, congestive heart failure and stroke tended to be higher among the non-participants (see Ref. 6 for details).

Brachial Artery IMT and GSM

The brachial artery was assessed by external B-mode ultrasound imaging 2–3 cm above the elbow (Acuson XP128 with a 10-MHz linear transducer, Acuson Mountain View, California, USA). The image was digitized and imported into the AMS (Artery Measurement Software) automated software [9, 10] for dedicated analysis of IMT and GSM. A maximal 10-mm segment with good image quality was chosen for analysis.

The program automatically identifies the borders of the IMT of the far wall and the inner diameter of the vessel and calculates IMT and the diameter from around 100 discrete measurements through the 10-mm long segment. This automated analysis was capable of being manually corrected if not found appropriate on visual inspection.

A Region Of Interest (ROI) was placed manually around the intima-media segment that was evaluated for IMT and the program calculates the intima-media GSM (IM-GSM) from analysis of the individual pixels within the ROI on a scale from 0 (black) to 256 (white). The blood was used as the reference for black and the adventitia was the reference for white. See Fig. 1 for an illustration of the measurements.

The mean length of the evaluated segment was 6.9 (SD 1.9) mm when subjects with a segment recording less

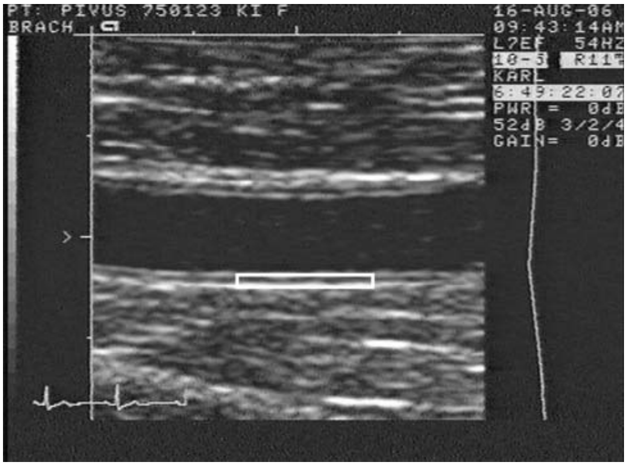

Fig. 1 Measurement of intima-media thickness (IMT) and echogenicity (grey scale median) of the intima-media complex (IM-GSM) of the brachial artery far wall. A region of interest (ROI) is created by the computer software used and manually adjusted if necessary. The length of this ROI is 5–10 mm. In this figure, a strict rectangular ROI has been indicated for graphical reasons, but in practice the ROI is very tightly adjusted by use of about 200 measurement points to closely fit the blood-intima interface and the media-adventitia interface. IMT is measured by the mean of about 100 thickness measurements and IM-GSM by the median of the grey scale of all pixels included in the ROI

than 3 mm were excluded, leaving 945 subjects with valid recordings.

The digitized measurements were repeated in 30 random subjects giving coefficients of variations for IMT and IM-GSM of 7.8 and 5.0%, respectively.

Insulin Resistance and the Metabolic Syndrome

Serum insulin was measured by an enzymatic-immunological assay (Boehringer Mannheim). HOMA insulin resistance index was defined as: fasting blood glucose × serum insulin/22.5 [11].

The metabolic syndrome was defined according to the NECP/ATP III criteria [12]. Three of the following five criteria should be fulfilled: Blood pressure >130/85 mmHg or antihypertensive treatment, fasting blood glucose > 5.6 mmol/l, serum triglycerides >1.7 mmol/l, waist circumference >102 cm in men and >88 cm in women, HDL-cholesterol <1.0 mmol/l in men and <1.3 in women.

Markers of Inflammation

High sensitive CRP was measured in human serum by an ultra sensitive particle enhanced immunoturbidimetric assay (Orion Diagnostica, Espoo, Finland) on a Konelab 20 autoanalyser (Thermo Clinical Labsystems, Espoo, Finland). The inter assay coefficient of variation was 3.2%.

Cytokines, chemokines and adhesion molecules were analysed on the Evidence® array biochip analyser (Randox Laboratories, Ltd, Crumlin, UK) [13].

The functional sensitivity for the different inflammatory markers were as follows: IL-1 alpha: 0.5 pg/ml, IL-1 beta: 0.8: IL-2: 4.1, IL-4: 2.8: IL-6: 0.3, IL-8: 1.5, IL-10: 1.0: INF-gamma: 1.8, TNF-alpha 1.8, MCP-1 19.4, ICAM-1: 18.6, VCAM-1:3.1, e-selectin 3.1, p-selectin 11.2, l-selectin 32.8, CRP: 0.1, Leukocyte count 0.2.

Due to a poor sensitivity for IL-1 alpha and beta, IL-4 and IL-10 with a large number of subjects with undetectable levels, these four cytokines were excluded from the analysis.

Markers of Oxidative Stress

Baseline conjugated dienes of LDL (BCD-LDL) were measured by using a method validated and reported in detail before [14]. For BCD-LDL, the coefficients of variance for within-assay and between-assay precision were 4.4 and 4.5%, respectively. Enzyme-linked immunoabsorbent assay (ELISA) kits (Mercodia, AB) were used to determine serum oxidized LDL, within-assay variation coefficient was 6.3% and between-assay CV was 4.7%, respectively [15]. ELISA kit (BioMedica) was applied to assay autoantibodies to Ox LDL (oLAB), with intra assay and inter assay values 4.3 and 6.0%, respectively. All glutathione indices, CD and TAOC values were measured and calculated as described previously [16]. Homocysteine was measured by using an Enzyme Immunoassay method (Axis-Shield Diagnostics Ltd) with an intra assay coefficient of 6.8%.

Markers of inflammation and oxidative stress were not evaluated in the young healthy reference sample

Statistics

Non-normally distributed variables were log-transformed in order to achieve a normal distribution. This was, however, not achieved for some of the variables. ANOVA or Mann–Witney *U* test was therefore used to evaluate differences between groups. Relationships between continuous variables were evaluated by Pearson's and Spearman's correlation coefficients and multiple regression analysis. Two-tailed significance values were given with $p < 0.05$ regarded as significant. StatView (SAS inc, NC; USA) was used for calculations.

Results

Basic Statistics of Risk Factors, Brachial Artery IMT and IM-GSM

Basic risk factor statistics and data on brachial artery IMT and IM-GSM in the PIVUS sample are given in Table 1.

Relationship between Brachial Artery IMT and IM-GSM

Brachial artery IMT and IM-GSM were inversely correlated ($r = -0.07$, $p = 0.025$).

Relation to Framingham Risk Score

Of the evaluated brachial artery characteristics, IMT, but not IM-GSM, was related to Framingham risk score (see Table 2 for details).

Of the variables in the Framingham risk score, HDL-cholesterol, smoking and fasting glucose were significantly related to brachial artery IMT. Both LDL and HDL-cholesterol were related to IM-GSM (see Table 2 for details).

Table 1 Basic characteristics and major cardiovascular risk factors in the sample

n	1016
Females (%)	50.2
Height (cm)	169 (9.1)
Weight (kg)	77 (14)
Waist circumference (cm)	91 (12)
BMI (kg/m^2)	27.0 (4.3)
Waist/hip ratio	0.90 (0.075)
SBP (mmHg)	150 (23)
DBP (mmHg)	79 (10)
Heart rate (beats/min)	62 (8.7)
Serum cholesterol (mmol/l)	5.4 (1.0)
LDL-cholesterol (mmol/l)	3.3 (0.88)
HDL-cholesterol (mmol/l)	1.5 (0.42)
Serum triglycerides (mmol/l)	1.3 (0.60)
Fasting blood glucose (mmol/l)	5.3 (1.6)
Currently smoking (%)	11
IMT (mm)	0.41 (0.08)
IM-GSM (units)	104 (39)

Means are given with SD in parenthesis. *SBP* Systolic blood pressure, *DBP* Diastolic blood pressure, *BMI* Body mass index, *IMT* brachial artery intima-media thickness, *IM-GSM* the grey scale median of the intima-media complex (IM-GSM)

Table 2 Univariate relationships between brachial artery intima-media thickness (IMT), the grey scale median of the intima-media complex (IM-GSM) and Framingham risk score and individual cardiovascular risk factors included in the score, as well as serum triglycerides, body mass index (BMI), waist circumference and the HOMA index

	IMT	IM-GSM
Framingham risk score	0.14 (0.0001)	−0.04 (0.18)
SBP	0.05	−0.01
DBP	0.02	−0.06
LDL-cholesterol	<0.01	0.10 (0.003)
HDL-cholesterol	−0.18 (0.0001)	0.14 (0.0001)
Triglycerides	0.09 (0.009)	−0.07 (0.037)
Smoking (pack-years)	0.10 (0.003)	0.03
Fasting glucose	0.11 (0.001)	−0.03
BMI	0.05	−0.05
Waist circumference	0.05	−0.03
HOMA index	0.08 (0.033)	−0.05

Pearson's correlation coefficients are given with *p*-values in parenthesis if <0.05

See Table 1 for abbreviations. *HOMA* Homeostatic model assessment

Relations to the Metabolic Syndrome

None of evaluated brachial artery characteristics were significantly different when subjects with the metabolic syndrome were compared with those without.

However, when related to the five different components included in the MetS definition, IMT was related to HDL-cholesterol, serum triglycerides and fasting glucose, but not to blood pressure or waist circumference. IM-GSM was related to HDL-cholesterol and serum triglycerides, but not to the other three components of the MetS (see Table 2 for details).

The HOMA insulin resistance index was significantly related to IMT, but not significantly to IM-GSM. BMI was not related to any of the brachial artery indices (see Table 2 for details).

Inflammatory Markers

Brachial artery IMT was not significantly related to any of the inflammatory makers (see Table 3), while IM-GSM was inversely correlated with VCAM-1, e-selectin and leukocyte count.

Oxidative Stress Markers

Of the oxidative stress markers, only the level of oxidized LDL was related to brachial artery IMT. IM-GSM, on the

Table 3 Univariate relationships between brachial artery characteristics and markers of inflammation and oxidative stress

	IMT	IM-GSM	Median	10th to 90th percentile
TNF-alpha (pg/ml)	−0.04	<0.01	3.7	2.3–7.1
IL-2 (pg/ml)	−0.05	0.03	3.6	2.6–14.3
IL-6 (pg/ml)	0.03	0.02	4.1	1.2–66.1
IL-8 (pg/ml)	−0.05	<0.01	6.4	3.1–13.6
MCP-1 (pg/ml)	−0.04	<0.01	386	250–569
Interferon-gamma(pg/ml)	−0.04	<0.01	1.6	0–3.8
ICAM-1 (mg/L)	−0.03	<0.01	344	265–470
VCAM-1 (mg/L)	0.06	−0.08 (0.020)	518	394–695
e-selectin (mg/L)	<0.01	−0.07 (0.037)	14.7	8.5–23.0
p-selectin (mg/L)	<0.01	−0.05	101	70–134
l-selectin (mg/L)	−0.06	−0.02	706	570–890
CRP (mg/L)	−0.02	0.02	1.2	0.4–3.9
Leukocyte count	0.05	−0.07 (0.033)	5.5	4.0–7.8
OxLDL (U/l)	0.08 (0.020)	−0.02	126	77–197
OLAB (mU/l)	0.01	−0.09 (0.009)	317	107–1400
BCD-LDL (umol/l)	0.02	0.14 (0.0001)	21	13–31
CD (umol/l)	<0.01	−0.10 (0.003)	39	29–54
Homocysteine (umol/l)	0.01	−0.07 (0.037)	9.9	6.7–15.3
TAOC (%)	−0.04	−0.02	37	33–43
TGSH (ug/ml)	−0.04	0.02	877	684–1157
GSSG (ug/ml)	−0.01	0.23 (0.0001)	68	44–113
GSH (ug/ml)	−0.04	−0.02	812	612–1072
GSSG/GSH ratio	0.02	0.26 (0.0001)	0.082	0.057–0.127

Spearmańs correlation coefficients are given with *p*-values in parenthesis if <0.05. Median and the 10th to 90th percentile are given to the right. *IM* intima-media, *IMT* Intima-media thickness, *TNF* Tumor necrosis factor, *IL* Interleukin, *MCP* Monocyte chemoattractive protein, *ICAM* Intracellular adhesion molecule, *VCAM* Vascular cell adhesion molecule, *CRP* C-reactive protein, *Ox LDL* Oxidized LDL, *oLAB* antibodies against oxLDL, *CD* Conjugated diens, *BCD* Baseline CD, *TAOC* Total antioxidant capacity, *TGSH* Total glutathion level, *GSSG* oxidized glutathione, *GSH* reduced glutation

other hand, was related to oxidized LDL antibody, CD and homocysteine in a negative way and to BCD-LDL, GSSG and the GSSG/GSH ratio in a positive way.

Multiple Regression Models

In the first multiple regression model, brachial artery IMT was the dependent variable. The independent variables were the traditionally risk factors, inflammatory markers and markers of oxidative stress that in the univariate analysis showed a *p*-value less than 0.05 when related to IMT (see Tables 2, 3 for details). Also gender was included as an independent variable.

As could be seen in Table 4, HDL-cholesterol (inversely), oxLDL and fasting glucose were the variables being independently related to brachial artery IMT in the regression model. The R2 for this model with only significant variables included was 0.07.

In the second multiple regression model, brachial artery IM-GSM was the dependent variable. Like in the first model above, the independent variables were the traditionally risk factors, inflammatory markers and markers of oxidative stress that in the univariate analysis showed a *p*-value less than 0.05 when related to IM-GSM (see Tables 2, 3 for details). Gender was also included as an independent variable.

Table 4 Multiple regression analysis with brachial artery intima-media thickness (IMT) as the dependent variable and the traditional risk factors, markers of inflammation and oxidative stress being related in univariate analysis (see Tables 3, 4, 5 for details) as independent variables together with gender (coded 0 for males and 1 for females)

	Partial correlation coefficient	*p*-value
Gender	−0.14	0.0001
HDL-cholesterol	−0.09	0.019
Smoking (pack-years)	0.03	0.34
OxLDL	0.09	0.016
Fasting glucose	0.08	0.024
Serum triglycerides	0.02	0.66

OxLDL Oxidized LDL

Table 5 Multiple regression analysis with brachial artery intima-media grey scale median (IM-GSM) as the dependent variable and the traditional risk factors, markers of inflammation and oxidative stress being related in univariate analysis (see Tables 3, 4, 5 for details) as independent variables together with gender (coded 0 for males and 1 for females)

	Partial correlation coefficient	*p*-value
Gender	0.07	0.045
HDL-cholesterol	0.06	0.10
Serum triglycerides	−0.12	0.004
LDL-cholesterol	0.01	0.75
VCAM-1	0.01	0.85
e-selectin	−0.02	0.48
Leukocyte count	−0.01	0.80
GSSG/GSH ratio	0.23	0.0001
BCD-LDL	0.18	0.0001
Homocysteine	−0.06	0.064

See Table 3 for abbreviations

In this second multiple model, serum triglycerides (inversely), the GSSG/GSH ratio and BCD-LDL were independently related to IM-GSM (see Table 5 for details). The R2 for this model with only significant variables included was 0.13.

Discussion

The present study showed that the Framingham score was related to brachial artery IMT, but not to IM-GSM. However, when the individual risk factors were analyzed, risk factors related to lipid metabolism included in the Framingham risk score or the metabolic syndrome were related to IM-GSM. Furthermore, when oxidative stress and inflammatory markers were also analysed in multiple regression models, both traditional lipid variables and markers of oxidative stress were independently associated with both IMT and IM-GSM, while markers of inflammation were not.

Strength of the Association and the Issue of Multiple Testing

In the present study most of the significant associations (except for the glutathione ratio) showed correlation coefficients that were rather modest (0.10–0.15), despite being highly significant, and the biological relevance might be questioned. It should, however, be emphasized that most such relationships are attenuated with age and higher values are usually seen in younger subjects with fewer disorders and medications. Furthermore, the multiple regression models show several factors to determine IMT and IM-GSM so that no single factor would be of uttermost importance limiting the correlation coefficients.

Although the primary aim of the present study was to investigate the relationships between brachial artery IMT and IM-GSM vs. established risk factors in order to see if these measurements were related to the risk factors in a plausible way, and thereby justify the future measurement of these vascular wall characteristics in the brachial artery, we also had information on multiple markers of inflammation and oxidative stress and added those to the study in order to obtain a more complete picture, since both inflammation and oxidative stress have been suggested as being involved in atherosclerosis.

By doing so, many correlation tests were performed. Since this was a study of exploratory character, we did not adjust for multiple testing (which by applying the Bonferroni correction would result in a critical *p*-value of 0.00075) and report unadjusted *p*-values to give a more broad view. Using this approach, it is evident that some of the relationships reported might be false positive, but it must be emphasized that all significant relationships are directed in the hypothesized direction and all are biologically highly plausible. However, it is obvious with this approach that all findings must be considered with great caution until reproduced by others.

Measurements of Brachial Artery IMT and IM-GSM

In the present cohort of elderly subjects it was possible to evaluate brachial artery far-wall IMT and IM-GSM is the vast majority of patients (94%), when the criteria of at least 3 mm length of evaluable intima-media complex was applied. A proper measurement in the near wall was much harder to obtain and was therefore not included in the present study. The reproducibility (CV) of the IMT and IM-GSM were in the range of 5–8%, being satisfactory.

While IMT is an established measure of the vascular wall [1, 2], the IM-GSM is less commonly used. GSM analysis has previously mainly been performed on plaques and then found to be related to histological features of the plaque, such as the elastin and calcium content, as well as to the size of the lipid-rich necrotic core [17]. However, the histological correlate to variations in the IM-GSM has not been evaluated. The finding the IM-GSM was related to some of the common risk factors, as well as to markers of inflammation and oxidative stress, does, however, suggest that the IM-GSM is a measure that is of biological relevance.

The intimal reflection line is included in the measurement of IM-GSM. Our experience is that the echogenicity of this reflection line is most often related to the echogenicity of the more darker space below. Furthermore, since the intimal reflection line only consists of 10–20% of all pixels in the ROI, it is not believed that the inclusion of this part would distort the measurement of IM-GSM.

Relationships to the Framingham Risk Score

The Framingham score was only related to brachial artery IMT, but not to IM-GSM. The reason for this is not clear since when analyzing the different components in the Framingham risk score, LDL-cholesterol and HDL-cholesterol were both related to IM-GSM.

Of the different components in the Framingham score, HDL was most closely related to both IMT and IM-GSM in an independent way. Thus, low levels of HDL were associated with both a thick and echolucent intima-media complex. This relationship seems biologically plausible, since low levels of HDL, as well as a thick intima-media complex and echolucent plaques are predictive of future cardiovascular events [2, 7].

Relationships to the Metabolic Syndrome

Despite the fact that brachial artery IMT was related to three of the five components of the MetS and IM-GSM was related to two of them, no alterations in IMT or IM-GSM were seen in subjects with the MetS. This was clearly contrary to the original hypothesis and emphasizes that the metabolic syndrome is composed of different clinical entities, rather than a uniform pathogenetic mechanism.

One of the proposed uniting mechanisms in the syndrome is abdominal obesity, but no relationship was seen between waist circumference and IMT or IM-GSM. On the other hand, another proposed unifying mechanism of the syndrome, insulin resistance, was found to be related to IMT. This relation was, however, weak and of borderline significance.

Relationships to Inflammatory Markers

Different inflammatory markers, such as CRP, a number of cytokines, adhesion molecules and leukocyte count have all been found to be related to carotid artery IMT in previous studies [18–26].

In the present study, no markers of inflammation, including CRP, were related to brachial artery IMT. Although several investigators have reported a relationship between CRP and carotid artery IMT [19, 21, 23, 25, 27], a number of studies were not able to find such a relationship [20, 22, 28–31]. Thus, the role of CRP as a determinant of IMT in the carotid and brachial arteries is still far from being clear.

In contrast to IMT, several of the inflammatory markers measured in the present study were related to the grey scale of the intima-media complex. In the past, grey scale analysis has only been applied to overt atherosclerotic plaque and a relationship between echolucent plaque in the carotid artery and CRP levels have been reported [32, 33]. The present study expands that knowledge of a relationship between inflammation and the grey scale of the intima-media complex in the brachial artery. It should, however, be pointed out that these relationships were rather weak and did not persist in the multiple regression models.

Relationships to Oxidative Stress Markers

Previous studies have shown both markers of intracellular oxidative stress, such as glutathione [27], and markers of lipid peroxidation, such as oxLDL and oxLDL antibodies [34–39] to be related to carotid artery IMT, although not every study has been able to reproduce these results [40, 41]. In the present study, oxLDL was the major oxidative marker measured being related to brachial artery IMT. This was valid also after adjustment for traditional risk factors and was of the same magnitude as the relationships between IMT and HDL-cholesterol or fasting glucose.

Both markers of the intracellular oxidative stress defense (the GSSG/GSH ratio) and the defense against LDL oxidation (BCD-LDL) were independently related to brachial artery IM-GSM after adjustment of traditional risk factors and inflammatory markers.

Glutathione, an intracellular antioxidant widely distributed in human tissues, acts as a cofactor for glutathione peroxidase. This enzyme reduces H_2O_2, a reactive oxidant species produced during the course of metabolism, to oxidized glutathione (GSSG) and water [42]. The low levels of the GSSG/GSH ratio that characterized subjects with an echolucent intima-media complex could be a result of a low glutathione peroxidase activity, indicating a reduced antioxidant activity.

Thus, although the exact histological correlates of the IM-GSM are not known, these data suggest that oxidative mechanisms, together with circulating lipids, might play a part in the determination of brachial artery IM-GSM.

Clinical Usefulness

Since clinical atherosclerosis is uncommon in the brachial artery, it is not likely that measurements of IMT and IM-GSM in the brachial artery would be a useful tool for atherosclerosis detection. However, since we detected an association between IM-GSM and lipids, as well as markers of oxidative stress, IM-GSM might be used for risk prediction in the future, but first it has to be shown in prospective studies that IM-GSM is a predictor for future cardiovascular events with an additive value to conventional risk factors.

Limitation of the Study

The present sample was limited to Caucasians aged 70. Caution should therefore be made in drawing conclusions with regard to other ethnic- and age groups.

The present study had a moderate participation rate. Therefore, we carried out an evaluation of cardiovascular disorders and medications in 100 consecutive subjects who did not wish to participate [6]. The prevalences of cardiovascular drug intake, history of myocardial infarction, coronary revascularization, antihypertensive medication, statin use and insulin treatment were similar to those in the investigated sample, while the prevalences of diabetes, congestive heart failure and stroke tended to be higher among the non-participants.

In conclusion, the present study showed that in addition to traditional lipid variables, markers of oxidative stress were independently related to both thickness and echogenicity of the brachial artery intima-media complex, suggesting that an evaluation of both the thickness and echolucency of the brachial artery intima-media complex to be of value to study the atherosclerotic process and cardiovascular risk.

Acknowledgments The outstanding work performed at the endothelium laboratory by Nilla Fors, Jan Hall, Kerstin Marttala and Anna Stenborg in the collection and processing of the data is gratefully acknowledged. We also wish to thank the staff at Analytical Biochemistry at AstraZeneca for performing the analyses of cytokines, chemokines, and adhesion molecules. The financial support from Uppsala University, the Thureus foundation and AstraZeneca R&D is highly valued.

References

1. Taylor AJ, Kent SM, Flaherty PJ, Coyle LC, Markwood TT, Vernalis MN (2002) ARBITER: Arterial Biology for the Investigation of the Treatment Effects of Reducing Cholesterol: a randomized trial comparing the effects of atorvastatin and pravastatin on carotid intima medial thickness. Circulation 106:2055–2060
2. O'Leary DH, Polak JF, Kronmal RA, Manolio TA, Burke GL, Wolfson SK Jr (1999) Carotid-artery intima and media thickness as a risk factor for myocardial infarction and stroke in older adults. Cardiovascular Health Study Collaborative Research Group. N Engl J Med 340:14–22
3. Agewall S, Henareh L, Jogestrand T (2005) Intima-media complex of both the brachial artery and the common carotid artery are associated with left ventricular hypertrophy in patients with previous myocardial infarction. J Hypertens 23:119–125
4. El-Barghouty NM, Levine T, Ladva S, Flanagan A, Nicolaides A (1996) Histological verification of computerised carotid plaque characterisation. Eur J Vasc Endovasc Surg 11:414–416
5. Fosse E, Johnsen SH, Stensland-Bugge E, Joakimsen O, Mathiesen EB, Arnesen E, Njolstad I (2006) Repeated visual and computer-assisted carotid plaque characterization in a longitudinal population-based ultrasound study: the Tromso study. Ultrasound Med Biol 32:3–11
6. Lind L, Fors N, Hall J, Marttala K, Stenborg A (2005) A comparison of three different methods to evaluate endothelium-dependent vasodilation in the elderly: the Prospective Investigation of the Vasculature in Uppsala Seniors (PIVUS) study. Arterioscler Thromb Vasc Biol 25:2368–2375
7. Schmidt C, Fagerberg B, Hulthe J (2005) Non-stenotic echolucent ultrasound-assessed femoral artery plaques are predictive for future cardiovascular events in middle-aged men. Atherosclerosis 181:125–130
8. Wilson PW, D'Agostino RB, Levy D, Belanger AM, Silbershatz H, Kannel WB (1998) Prediction of coronary heart disease using risk factor categories. Circulation 97:1837–1847
9. Liangu Q, Wendelhag I, Wikstrand J, Gustavsson T (2000) A multiscale dynamic programming procedure for boundary detection in ultrasonic artery images. IEEE Trans Med Imaging 19:127–142
10. Wendelhag I, Liang Q, Gustavsson T, Wikstrand J (1997) A new automated computerized analyzing system simplifies readings and reduces the variability in ultrasound measurement of intima-media thickness. Stroke 28:2195–2200
11. Matthews DR, Hosker JP, Rudenski AS, Naylor BA, Treacher DF, Turner RC (1985) Homeostasis model assessment: insulin resistance and beta-cell function from fasting plasma glucose and insulin concentrations in man. Diabetologia 28:412–419
12. Executive summary of the third report of the national cholesterol education program (NECP) expert panel on detection, education, treatment of high blood cholesterol in adults (ATP III). (2001) JAMA 285:2486–2497
13. FritzGerald SP, Lamont JV, McConnell RI, Benchikh O (2005) Development of a high-throughput automated analyser using biochip array technology. Clin Chem 51:1165–1176
14. Ahotupa M, Marniemi J, Lehtimäki T, Talvinen K, Raitakari O, Vasankari T, Viikari J, Luoma J, Ylä-Herttuala S (1998) Baseline diene conjugation in LDL lipids as a direct measure of in vivo LDL oxidation. Clin Biochem 31:257–261
15. Annuk M, Fellstrom B, Akerblom O, Zilmer K, Vihalemm T, Zilmer M (2001) Oxidative stress markers in pre-uremic patients. Clin Nephrol 56:308–314
16. Annuk M, Zilmer M, Lind L, Linde T, Fellström B (2001) Oxidative stress and endothelial function in chronic renal failure. J. Am Soc Nephrology 12:2747–2754
17. Goncalves I, Lindholm MW, Pedro LM, Dias N, Fernandes e Fernandes J, Fredrikson GN, Nilsson J, Moses J, Ares MP (2004) Elastin and calcium rather than collagen or lipid content are associated with echogenicity of human carotid plaques. Stroke 35:2795–2800
18. Ambrosius W, Kazmierski R, Michalak S, Kozubski W (2006) Anti-inflammatory cytokines in subclinical carotid atherosclerosis. Neurology 66:1946–1948
19. Reinehr T, Kiess W de Sousa G, Stoffel-Wagner B, Wunsch R (2006) Intima media thickness in childhood obesity: relations to inflammatory marker, glucose metabolism, and blood pressure. Metabolism 55:113–118
20. Larsson PT, Hallerstam S, Rosfors S, Wallen NH (2005) Circulating markers of inflammation are related to carotid artery atherosclerosis. Int Angiol 24:43–51
21. Schillinger M, Exner M, Mlekusch W, Sabeti S, Amighi J, Nikowitsch R, Timmel E, Kickinger B, Minar C, Pones M,

Lalouschek W, Rumpold H, Maurer G, Wagner O, Minar E (2005) Inflammation and Carotid Artery-Risk for Atherosclerosis Study (ICARAS). Circulation 111:2203–2209

22. Elkind MS, Rundek T, Sciacca RR, Ramas R, Chen HJ, Boden-Albala B, Rabbani L, Sacco RL (2005) Interleukin-2 levels are associated with carotid artery intima-media thickness. Atherosclerosis 180:181–187
23. Magyar MT, Szikszai Z, Balla J, Valikovics A, Kappelmayer J, Imre S, Balla G, Jeney V, Csiba L, Bereczki D (2003) Early-onset carotid atherosclerosis is associated with increased intima-media thickness and elevated serum levels of inflammatory markers. Stroke 34:58–63
24. Temelkova-Kurktschiev T, Koehler C, Henkel E, Hanefeld M (2002) Leukocyte count and fibrinogen are associated with carotid and femoral intima-media thickness in a risk population for diabetes. Cardiovasc Res 56:277–283
25. Sitzer M, Markus HS, Mendall MA, Liehr R, Knorr U, Steinmetz H (2002) C-reactive protein and carotid intimal medial thickness in a community population. J Cardiovasc Risk 9:97–103
26. Rohde LE, Lee RT, Rivero J, Jamacochian M, Arroyo LH, Briggs W, Rifai N, Libby P, Creager MA, Ridker PM. (1998) Circulating cell adhesion molecules are correlated with ultrasound-based assessment of carotid atherosclerosis. Arterioscler Thromb Vasc Biol 18:1765–1770
27. Ashfaq S, Abramson JL, Jones DP, Rhodes SD, Weintraub WS, Hooper WC, Vaccarino V, Harrison DG, Quyyumi AA (2006) The relationship between plasma levels of oxidized and reduced thiols and early atherosclerosis in healthy adults. J Am Coll Cardiol 47:1005–1011
28. Hee Choi S, Chang Kim H, Woo Ahn C, Keun Cho H, Soo Cha B, Chung YS, Woo Lee K, Chul Lee H, Bum Huh K, Kim DJ (2005) Is high-sensitivity C-reactive protein associated with carotid atherosclerosis in healthy Koreans? Eur J Cardiovasc Prev Rehabil 12:548–554
29. Leinonen ES, Hiukka A, Hurt-Camejo E, Wiklund O, Sarna SS, Mattson Hulten L, Westerbacka J, Salonen RM, Salonen JT, Taskinen MR (2004) Low-grade inflammation, endothelial activation and carotid intima-media thickness in type 2 diabetes. J Intern Med 256:119–127
30. Sigurdardottir V, Fagerberg B, Hulthe J (2004) Preclinical atherosclerosis and inflammation in 61-year-old men with newly diagnosed diabetes and established diabetes. Diabetes Care 27:880–884
31. Folsom AR, Pankow JS, Tracy RP, Arnett DK, Peacock JM, Hong Y, Djousse L, Eckfeldt JH (2001) Investigators of the NHBLI Family Heart Study Association of C-reactive protein with markers of prevalent atherosclerotic disease. Am J Cardiol 88:112–117
32. With Noto AT, Bogeberg Mathiesen E, Amiral J, Vissac AM, Hansen JB (2006) Endothelial dysfunction and systemic inflammation in persons with echolucent carotid plaques. Thromb Haemost 96:53–59
33. Yamagami H, Kitagawa K, Nagai Y, Hougaku H, Sakaguchi M, Kuwabara K, Kondo K, Masuyama T, Matsumoto M, Hori M (2004) Higher levels of interleukin-6 are associated with lower echogenicity of carotid artery plaques. Stroke 35:677–681
34. Magyar MT, Szikszai Z, Balla J, Valikovics A, Kappelmayer J, Imre S, Balla G, Jeney V, Csiba L, Bereczki D (2003) Early-onset carotid atherosclerosis is associated with increased intima-media thickness and elevated serum levels of inflammatory markers. Stroke 34:58–63
35. Wallenfeldt K, Fagerberg B, Wikstrand J, Hulthe J (2004) Oxidized low-density lipoprotein in plasma is a prognostic marker of subclinical atherosclerosis development in clinically healthy men. J Intern Med 256:413–420
36. Karvonen J, Paivansalo M, Kesaniemi YA, Horkko S (2003) Immunoglobulin M type of autoantibodies to oxidized low-density lipoprotein has an inverse relation to carotid artery atherosclerosis. Circulation 108:2107–2112
37. Hulthe J, Fagerberg B (2002) Circulating oxidized LDL is associated with subclinical atherosclerosis development and inflammatory cytokines (AIR Study). Arterioscler Thromb Vasc Biol 22:1162–1167
38. Hulthe J, Wiklund O, Hurt-Camejo E, Bondjers G (2001) Antibodies to oxidized LDL in relation to carotid atherosclerosis, cell adhesion molecules, and phospholipase A(2). Arterioscler Thromb Vasc Biol 21:269–274
39. Fukumoto M, Shoji T, Emoto M, Kawagishi T, Okuno Y, Nishizawa Y (2000) Antibodies against oxidized LDL and carotid artery intima-media thickness in a healthy population. Arterioscler Thromb Vasc Biol 20:703–707
40. Demuth K, Drunat S, Girerd X, Moatti N, Paul JL, Safar M, Boutouyrie P (2002) Homocysteine is the only plasma thiol associated with carotid artery remodeling. Atherosclerosis 165:167–174
41. Jedryka-Goral A, Pasierski T, Zabek J, Widerszal-Bazyl M, Radkiewicz P, Szulczyk GA, Wojciechowska B, Bugajska J (2006) Risk factors for atherosclerosis in healthy employees-a multidisciplinary approach. Eur J Intern Med 17:247–253
42. Stocker R, Keaney JF Jr (2004) Role of oxidative modifications in atherosclerosis. Physiol Rev 84:1381–1478

Lipids (2008) 43:143–149
DOI 10.1007/s11745-007-3148-z

ORIGINAL ARTICLE

Apoptotic Effects of Dietary and Synthetic Sphingolipids in Androgen-Independent (PC-3) Prostate Cancer Cells

Kyle D. Kent · Elizabeth A. Clubbs ·
W. James Harper · Joshua A. Bomser

Received: 8 November 2007 / Accepted: 11 December 2007 / Published online: 10 January 2008
© AOCS 2008

Abstract Stress-induced activation and metabolism of plasma membrane sphingolipids results in intracellular ceramide accumulation and has been shown to induce apoptosis in human prostate cancer cells. This effect has been observed using synthetic ceramide analogs, such as C6-ceramide; however, the effects of naturally-occurring sphingolipids, such as C18-ceramide and sphingomyelin (CerPCho), on apoptosis and prostate cancer cell proliferation have not been examined. The results of the present study demonstrate that natural (CerPCho, C18-ceramide) and synthetic (C6-ceramide) sphingolipids reduced PC-3 cell proliferation by 15 ± 1.8, 17 ± 2.5, and 46 ± 2.1%, respectively ($P < 0.05$). These reductions in proliferation were due, in part, to increased cellular apoptosis. Treatment of PC-3 cells with CerPCho and C18-ceramide significantly increased apoptosis by 3.0 ± 0.8 and 3.6 ± 0.6%, respectively, compared to the untreated control, while the synthetic C6-ceramide significantly increased apoptosis by 55.7 ± 0.4%. C6-ceramide-induced apoptosis was associated with cell cycle arrest in the G_2/M phase, decreased extracellular signal-regulated kinase (ERK1/2) signaling and activation of the cell cycle regulatory protein, retinoblastoma (pRb). Treatment of PC-3 cells with C18-ceramide and CerPCho did not alter cell cycle distribution, pRb or ERK1/2 activation. Taken together, these results suggest that natural and synthetic sphingolipids induce apoptosis in PC-3 cells via distinct signaling mechanisms and potencies.

Keywords Apoptosis · Cancer · Ceramide · Prostate · Sphingomyelin

Introduction

Prostate cancer is the second leading cause of cancer related death in the United States [1]. Although the 5-year survival rate of prostate cancer is nearly 100% when detected during early stages of the disease, the survival rate plunges to only 33% in those patients with metastatic, androgen-independent prostate cancer [1]. Androgen-independent prostate cancer is very resilient and largely chemoresistant, primarily due to defects in apoptotic signaling. Strategies to circumvent defective apoptotic signaling may sensitize these chemoresistant cells to undergo apoptosis.

The membrane sphingolipid sphingomyelin (CerPCho) plays an important role in regulation of cell signaling and apoptosis. In response to cellular stress, the phosphatidylcholine (PtdCho) headgroup of CerPCho is cleaved by sphingomyelinase (SMase), resulting in accumulation of ceramide. Accumulation of ceramide can alter membrane fluidity and modulate signal transduction cascades leading to cell cycle arrest and/or apoptosis [2–7]. Ceramide-induced apoptosis is an important mechanism by which damaged cells are efficiently destroyed and removed. However, alterations in CerPCho metabolism during

K. D. Kent · W. J. Harper
Department of Food Science and Technology,
The Ohio State University, 2015 Fyffe Rd,
Columbus 43210-1097, OH, USA

E. A. Clubbs · J. A. Bomser
OSU Interdisciplinary PhD Program in Nutrition,
The Ohio State University, Columbus 43210, OH, USA

J. A. Bomser (✉)
Department of Human Nutrition, The Ohio State University,
1787 Neil Ave, 325 Campbell Hall, Columbus 43210, OH, USA
e-mail: bomser.1@osu.edu

carcinogenesis results in decreased ceramide accumulation and resistance to apoptosis [8].

Mammalian cells have several enzymes which limit accumulation of ceramide, so that undamaged cells do not unnecessarily undergo apoptosis. Ceramide can be converted back to CerPCho via CerPCho synthase, while glucosylceramide synthase reduces the toxicity of ceramide via glycosylation [2, 6, 9]. Ceramidase converts ceramide to sphingosine which is ultimately converted to sphingosine-1-phosphate, an anti-apoptotic compound [6]. Many cancer cell types overexpress these enzymes, leading to lower basal levels of ceramide and increased resistance to chemotherapeutic agents that induce ceramide accumulation [9–13]. Androgen-independent prostate cancer cells (designated PC-3 cells) also appear to have defects in accumulation of ceramide resulting in resistance to apoptosis. Although the exact mechanism is currently unknown, it appears that the inability of these cells to accumulate ceramide is independent of de novo ceramide synthesis [14].

Sphingolipids are of particular interest in anticancer therapy due to the apoptotic effects of their metabolites, particularly ceramide. One possible strategy to accumulate ceramide in tumors cells is via delivery of dietary sources of CerPCho. Dietary CerPCho has previously been shown to inhibit the progression of colon cancer in mice and the formation of preneoplastic hepatic lesions in rats due to altered sphingolipid metabolism and reduced intracellular ceramide concentrations [15, 16]. Synthetic ceramides (short acyl group, $<C_8$) have previously been shown to induce apoptosis in an androgen-independent, multi-drug resistant prostate cancer cell line [14]; however, there are concerns that synthetic ceramide accumulation may result in different cellular effects than their natural sphingolipid derived ceramide counterparts (long acyl group, $>C_{16}$). Naturally-occurring sphingolipids, such as CerPCho, are found in a variety of food products and are efficiently absorbed postprandially. However, the apoptotic effects of such naturally-occurring dietary sphingolipids in the prostate are largely unknown. Therefore, the present study examines the ability of exogenous CerPCho to induce apoptosis in the chemoresistant PC-3 cell line.

Materials and Methods

Reagents

CerPCho, C6-ceramide, PtdCho, 3-[4,5- dimethylthiazol-2-yl]-2-,5-diphenyltetrazolium bromide (MTT), ribonuclease A, and propidium iodide were obtained from Sigma-Aldrich Co (St. Louis, MO, USA). C18-ceramide was obtained from Fisher Scientific (Fairlawn, NJ, USA). The Annexin V-FITC apoptosis detection kit was purchased from Oncogene Research Products (San Diego, CA, USA). The ECL Plus Western Blotting Detection Reagents kit was purchased from Amersham Biosciences (Piscataway, NJ, USA). Phospho-p44/42 mitogen activated protein kinase (MAPK) [Thr202/Tyr204] (p-ERK 1/2), p44/42 MAPK (total ERK 1/2), phospho-pRb [Ser807/811] (pRb), pRb (4H1) monoclonal (total pRb), phospho-cdc2 (p-cdc2), total cdc2, anti-rabbit horseradish peroxidase (HRP)-linked IgG, and anti-mouse HRP-linked IgG were purchased from Cell Signaling Technology, Inc. (Beverly, MA, USA). Media and tissue culture supplies were obtained from Invitrogen Corporation (Carlsbad, CA, USA).

Cell Culture and Lipid Preparation

Human prostate cancer cells (PC-3, ATCC #CRL-1435) were maintained in RPMI 1640 supplemented with 10% fetal bovine serum at 37 °C, 5% CO_2, and 90% relative humidity. Upon reaching 90% confluency, cells were trypsinized and seeded into the appropriate tissue culture vessels for each experiment. C6-ceramide was solubilized in DMSO and added to growth medium at a solvent concentration at 0.5%. CerPCho was solubilized in methanol and added to growth medium at a solvent concentration of 0.25%. C18-ceramide and PtdCho were solubilized in a chloroform:methanol (1:1) solution and added to growth medium at a solvent concentration of 0.25%. Growth medium containing the lipids was sonicated for 30 min at 37 °C followed by passage of the medium through a 0.2-μm sterile filter.

Cell Proliferation

To determine the effects of CerPCho, C6-ceramide, C18-ceramide, and PtdCho on PC-3 cell proliferation, cells were seeded in 96-well tissue culture plates at an initial concentration of 2.5×10^4 cells/well. Following an overnight incubation, cells were treated with CerPCho, C18-ceramide, C6-ceramide, and PtdCho at the indicated concentrations and time intervals. After incubation, cell proliferation was determined by the MTT assay as described previously [17]. Changes in cellular proliferation are expressed as a percent of control (given as 100%).

Annexin V-FITC Binding

PC-3 cells were seeded in 60-mm dishes at an initial concentration of 10^6 cells/dish and treated with CerPCho (244 μM), C18-ceramide (353 μM), C6-ceramide

(63 µM), or vehicle alone for 24 h. Following the indicated treatments, cells were collected and analyzed according to the directions provided by the Annexin V-FITC apoptosis detection kit (Oncogene Research Products). In brief, media was collected from each dish and cells were trypsinized from the dishes and washed using PBS. Annexin V-FITC was added to each sample followed by 15 min incubation at room temperature in the dark. Medium containing Annexin V-FITC was removed and cells were resuspended in a propidium iodide solution and stored on ice away from light until analyzed. For each sample, a digital micrograph was taken (200× magnification) under bright field conditions, as well as under green and blue fluorescent filters. Cells expressing only green fluorescence under the blue filter were considered early apoptotic. Cells expressing green/red or red fluorescence were considered late apoptotic. The percentage of apoptotic cells was determined by dividing the total number of early and late apoptotic cells by the total number of cells as counted under bright field. Significant difference from the untreated control is designated by *($P < 0.05$).

Flow Cytometry

PC-3 cells were seeded in 60-mm dishes at an initial concentration of 10^6 cells/dish. Following the indicated treatments with CerPCho, C18-ceramide, C6-ceramide for 24 h, or vehicle alone cells were collected and analyzed according to the procedure of Darzynkiewicz et al. [18]. In brief, media was collected from each dish and cells were trypsinized from the dishes and washed using PBS containing 0.1% bovine serum albumin. The cells were fixed in 70% ethanol and stored at 4 °C until analysis. For analysis, cells were washed using PBS, centrifuged at $1250\times g$, resuspended in a propidium iodide staining solution containing ribonuclease A, and incubated for 30 min at room temperature away from light. A minimum of 20,000 events per sample was measured for DNA content by propidium iodine staining using the BD FACS Calibur flow cytometer and cell cycle distribution was determined using the software program Modfit®.

Cell Harvesting and Immunoblotting

PC-3 cells were seeded in 60-mm dishes at an initial concentration of 10^6 cells/dish. Following the indicated treatments cells were harvested and protein concentrations for each sample were determined using the bicinchoninic acid assay. Crude proteins isolated and separated on a 10% SDS-polyacrylamide gel and transferred to a nitrocellulose membrane. Immunoblot was performed using primary antibodies (phospho-ERK1/2, total-ERK1/2, phospho-pRb, total-Rb, phospho-cdc2, total-cdc2) at recommended dilutions in TTBS (1 × tris buffered saline (TBS) with 0.1% Tween-20) overnight at 4 °C. Following incubation with secondary antibodies, protein signals were visualized on autoradiography film, and quantified by densitometry using Scion imaging software (Frederick, Maryland).

Statistical Analysis

Statistical significance was determined using two-way analysis of variance with Tukey's post hoc comparisons ($n = 3$). Differences were considered significant at $P < 0.05$.

Results

Sphingolipids Reduce PC-3 Cell Proliferation

The concentration dependent effects of PtdCho, CerPCho, C18-ceramide, and C6-ceramide on PC-3 cell proliferation (24 h) are given in Fig. 1a. Proliferation of PC-3 cells was significantly decreased by 13.4 ± 2.3%, and 15.1 ± 1.8% following treatment with 122 and 244 µM CerPCho, respectively ($P < 0.05$), compared to untreated controls. C18-ceramide reduced cell proliferation by 15–17% at all concentrations tested while the negative control PtdCho did not affect proliferation. Cell proliferation was significantly decreased by 21 ± 3.6, 35 ± 3.4, and 46 ± 2.1% following treatment with 6, 16, and 63 µM C6-ceramide, respectively ($P < 0.05$), compared to untreated controls.

PC-3 cells treated with CerPCho and C18-ceramide exhibited only modest reductions in proliferation over time (Fig. 1b). CerPCho (244 µM) reduced PC-3 cell proliferation by 17 ± 1.8, 13 ± 1.8, and 18 ± 1.8% at 24, 48, and 72 h post-treatment, respectively ($P < 0.05$), compared to untreated controls. C18-ceramide (353 µM) reduced proliferation by 17 ± 2.5, 19 ± 1.7, and 22 ± 3.3%, respectively ($P < 0.05$), compared to untreated controls. C6-ceramide (63 µM) reduced proliferation by 46 ± 2.1, 68 ± 2.6, and 72 ± 3.6% at 24, 48, and 72 h post-treatment, respectively ($P < 0.05$), compared to untreated controls. PtdCho (253 µM) did not reduce cell proliferation.

Sphingolipid-Induced Apoptosis

CerPCho (244 µM) and C-18 ceramide (353 µM) significantly increased the amount of apoptotic cells by nearly

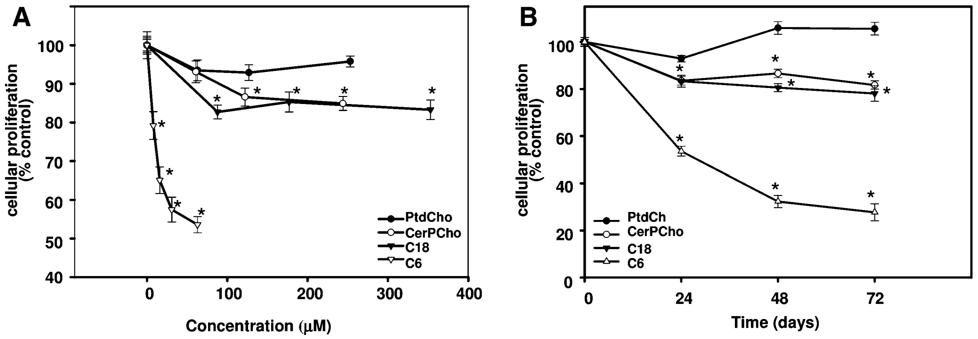

Fig. 1 Concentration and time dependent effects of PtdCho, CerPCho, C18-ceramide, and C6-ceramide on PC-3 cell proliferation. Cell proliferation was measured using the MTT assay. **a** PC-3 cells were treated 24 h with increasing concentrations of PtdCho (*closed circles*), CerPCho (*open circles*), C18-ceramide (*closed triangles*), C6-ceramide (*open triangles*) (**b**) PC-3 cells were treated for increasing time intervals with PtdCho (253 μM, *closed circles*), CerPCho (244 μM, *open circles*), C18-ceramide (353 μM, *closed triangles*, and C6-ceramide (63 μM, *open triangles*). Significant difference from the untreated control is designated by *($P < 0.05$).

twofold as compared to the untreated control ($P < 0.05$) (Table 1). The increase in total apoptosis induced by CerPCho and C18-ceramide was represented by an increase in the population of early apoptotic cells. C6-ceramide significantly induced a 16-fold increase in the population of apoptotic cells as compared to the untreated control, and significantly increased the population of late apoptotic cells ($P < 0.05$).

Exogenous Sphingolipids Do Not Alter PC-3 Cell Cycle Distribution

The effects of ceramides on cell cycle distribution are given in Table 2. CerPCho significantly increased the population of apoptotic cells sevenfold as compared to the untreated control ($P < 0.05$) without affecting the proportions of cells in the G_1, S, and G_2 phases. C18-ceramide increased apoptosis was nearly sixfold that of the untreated cells; however, this was not statistically different from the untreated control ($P = 0.1$). C18-ceramide did not alter the ratios of cells in the G_1, S, and G_2 phases compared to the control. C6-ceramide alone significantly increased the population of apoptotic cells to 41 ± 1.0% as compared to 1.8 ± 1.0% apoptosis of the untreated control ($P < 0.05$) and induced a twofold increase in the population of cells in the G_2 phase of the cell cycle while reducing the populations of G_1 and S phase cells five and twofold, respectively, compared to the untreated control ($P < 0.05$).

Table 1 Apoptosis of PC-3 cells treated with CerPCho (244 μM), C18-ceramide (353 μM), C6-ceramide (63 μM), or vehicle treated control was measured by Annexin V-FITC staining following 24 h treatment

	Total apoptosis (%)	Early apoptosis (%)	Late apoptosis (%)
Control	3.6 ± 0.3	1.5 ± 0.3	2.1 ± 0.3
CerPCho	6.6 ± 0.8*	3.6 ± 0.8*	3.0 ± 0.7
C18-ceramide	7.2 ± 0.6*	4.4 ± 0.6*	2.7 ± 0.3
C6-ceramide	59.3 ± 0.4*	3.5 ± 1.0	55.8 ± 0.7*

* Significant difference from the untreated control ($P < 0.05$)

Inhibition of ERK1/2 by C6-ceramide but not CerPCho and C18-ceramide

The concentration and time dependent effects of the sphingolipids on ERK1/2 are given in Fig. 2. Treatment with CerPCho (Fig. 2a, b) and C18-ceramide (data not shown) did not reduce ERK1/2 at any concentration tested. ERK1/2 activation decreased in a concentration and time dependent manner following treatment with C6-ceramide (Fig. 2c, d). The decrease in ERK1/2 activation was greatest at 12 h post-treatment, with a small rebound in activity observed 24 h post-treatment.

Table 2 Cell cycle analysis of PC-3 cells treated with CerPCho (244 μM), C18-ceramide (353 μM), C6-ceramide (63 μM), or vehicle treated control was measured by flow cytometric techniques following 24 h treatment

	Apoptosis (%)	G1 (%)	G2 (%)	*S* (%)
Control	1.8 ± 1.8	36.2 ± 0.9	34.0 ± 1.2	30.0 ± 1.6
CerPCho	13.3 ± 2.5*	31.0 ± 1.4	36.2 ± 1.3	32.8 ± 2.5
C18-ceramide	10.4 ± 5.6	29.7 ± 3.7	33.3 ± 0.9	37.0 ± 3.4
C6-ceramide	40.7 ± 1.0*	7.0 ± 2.0*	77.6 ± 1.9*	15.4 ± 0.1*

* Significant difference from the untreated control ($P < 0.05$)

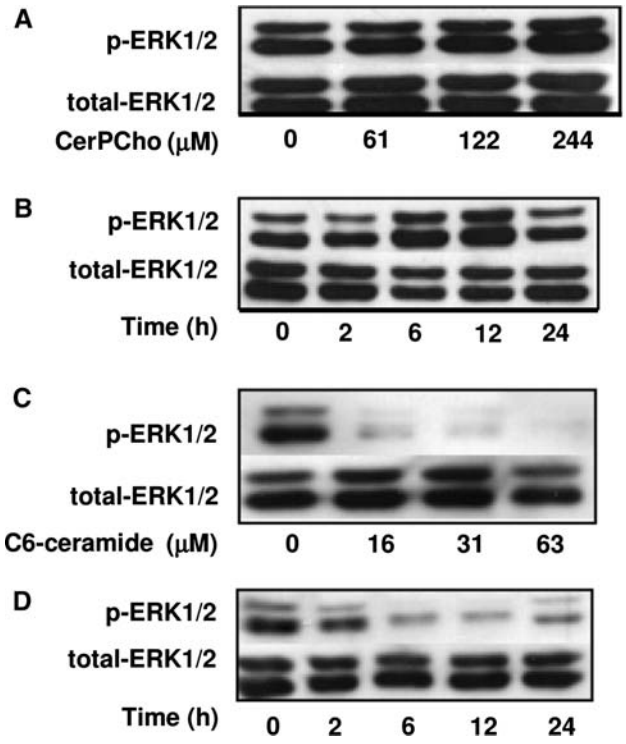
A
p-ERK1/2
total-ERK1/2
CerPCho (μM) 0 61 122 244
B
p-ERK1/2
total-ERK1/2
Time (h) 0 2 6 12 24
C
p-ERK1/2
total-ERK1/2
C6-ceramide (μM) 0 16 31 63
D
p-ERK1/2
total-ERK1/2
Time (h) 0 2 6 12 24

Fig. 2 Concentration and time dependent effects of CerPCho and C6-ceramide on ERK1/2 activation. **a** Active ERK1/2 (p-ERK1/2) was measured by immunoblot in PC-3 cells following 24 h treatment with CerPCho (0–244 μM). **b** Time dependent (0–24 h) activation of ERK1/2 following treatment of cells with 244 μM CerPCho. **c** Active ERK1/2 (p-ERK1/2) was measured by immunoblot in PC-3 cells following 24 h treatment with C6-ceramide (0–63 μM). **d** Time dependent (0–24 h) activation of ERK1/2 following treatment of cells with 63 μM C6-ceramide. All experiments were performed independently at least three times with an $n = 3$. Total ERK1/2 (t-ERK1/2) was used as the loading control

Sphingolipid-Induced Activation of Cell Cycle Regulatory Proteins

The concentration and time dependent effects of CerPCho and C6 ceramide on pRb and cdc2 activation are given in Fig. 3. Treatment with CerPCho (Fig. 3a) and C18-ceramide (data not shown) did not affect activation of pRb or cdc2 at any concentration tested. pRb activation (dephosphorylation) increased in a concentration and time dependent manner following treatment with C6-ceramide (Fig. 3b). The increase in pRb activation was greatest at 6 h post-treatment. However, C6 ceramide did not alter the activity of cdc2 at any concentration tested.

Discussion

Humans consume 115–140 g of sphingolipids per year from sources such as meat, dairy, fruits, legumes, and vegetable products [19–21]. Plasma lipoproteins contain significant amounts of sphingolipids such as CerPCho and ceramide [22], suggesting that dietary sphingolipids reach peripheral tissues and may influence a variety of cellular processes including proliferation and apoptosis [21]. Dietary sphingolipids, such as CerPCho, localize in the plasma membrane of cells and release ceramide intracellularly in response to cellular stress, resulting in ceramide accumulation and apoptosis [2–7]. Many cancer cell types overexpress enzymes which limit ceramide accumulation, thereby increasing resistance to chemotherapeutic agents that induce apoptosis [12, 13, 23]. Several studies suggest that overwhelming the cancer cell with short acyl synthetic

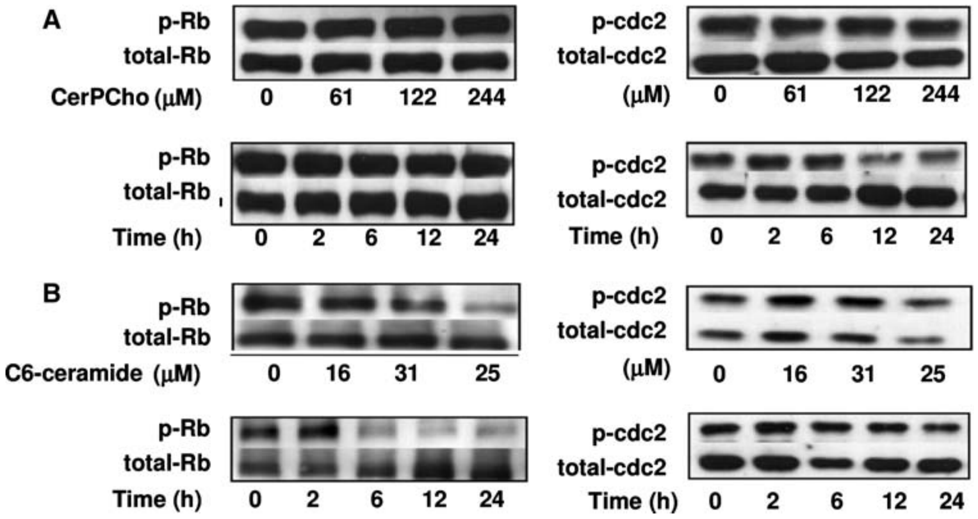
A
p-Rb
total-Rb
CerPCho (μM) 0 61 122 244
p-cdc2
total-cdc2
(μM) 0 61 122 244
p-Rb
total-Rb
Time (h) 0 2 6 12 24
p-cdc2
total-cdc2
Time (h) 0 2 6 12 24
B
p-Rb
total-Rb
C6-ceramide (μM) 0 16 31 25
p-cdc2
total-cdc2
(μM) 0 16 31 25
p-Rb
total-Rb
Time (h) 0 2 6 12 24
p-cdc2
total-cdc2
Time (h) 0 2 6 12 24

Fig. 3 Concentration and time dependent effects of CerPCho and C6-ceramide on pRb and cdc2 phosphorylation. **a** pRb and cdc2 phosphorylation was measured by immunoblot in PC-3 cells following 24 h treatment with CerPCho (0–244 μM) or following treatment with 244 μM CerPCho for 0–24 h. **b** pRb and cdc2 phosphorylation was measured by immunoblot in PC-3 cells following 24 h treatment with C6-ceramide (0–63 μM) or following treatment with 63 μM C6-ceramide for 0–24 h. All experiments were performed independently at least three times with an $n = 3$. Total pRb and total cdc2 was used as the loading control

ceramides may mitigate the effects of these enzymes and result in increased apoptosis [14, 24]. However, to date, the antiproliferative effects of naturally-occurring ceramides have not been explored.

The results of the present study show that naturally-occurring ceramides, CerPCho and C18-ceramide, and the synthetic C6-ceramide can reduce PC-3 cell proliferation via apoptosis. The apoptotic effects of C6-ceramide were more robust than those of the CerPCho and C18-ceramide. This is most likely due to differences in the uptake, metabolism, and/or cellular localization of long versus short chain acyl ceramides. Long acyl chain ceramides and CerPCho (containing long acyl chain ceramide) are unable to penetrate the plasma membrane without metabolic stimulation, [3, 7, 16, 25], whereas, short acyl chain ceramides, such as C6-ceramide, are able to penetrate the plasma membrane thereby significantly increasing intracellular ceramide concentrations.

Several studies have demonstrated that cellular ceramide accumulation inhibits the proliferation of monoblastic leukemia, glomerular mesangial, and vascular smooth muscle cells via reduced ERK1/2 activity and increased apoptosis [26–28]. In agreement with these previous reports, the present study shows that C6-ceramide inhibited ERK1/2 activity and increased apoptosis in the PC-3 cell line. Short acyl ceramides have been shown to induce G_0/G_1 cell cycle arrest [29]. However, in the present study, G_2/M arrest was observed following treatment of PC-3 cells with C6-ceramide, despite activation of pRb, the major G_0/G_1 cell cycle check point protein. We hypothesize that G_0/G_1 cell cycle arrest was not observed because of the significant amount of cellular apoptosis induced by C6-ceramide 24 h following treatment [30, 31]. Surprisingly, changes in cdc2 activity, a cell cycle check point protein in the G_2/M phase, were not observed upon treatment of PC-3 cells with C6-ceramide. A possible explanation for this observation is that a majority of those cells arrested in the G_2/M phase following C6-ceramide treatment may already be undergoing apoptosis [32]. In contrast to C6-ceramide, naturally-occurring long acyl chain ceramides did not alter cell signaling or cell cycle distribution, yet a modest increase in PC-3 apoptosis was observed. The mechanism by which long acyl chain ceramides induce apoptosis in the PC-3 cell line remains to be elucidated.

The results of the present study suggest that naturally-occurring and synthetic sphingolipids reduce proliferation of androgen-independent prostate cancer cells via increased apoptosis. Increased dietary consumption of naturally-occurring long acyl chain sphingolipids may represent a novel chemopreventive strategy to increase prostate cancer cell apoptosis via intracellular ceramide accumulation. Dietary feeding studies are necessary to further support this hypothesis.

Acknowledgments This project was supported in part by grant P30 CA16058, National Cancer Institute, Bethesda, MD and by state and federal funds appropriated to The Ohio State University, Ohio Agriculture Research and Development Center.

References

1. American Cancer Society (2007) Facts and figures. http://www.cancer.org
2. Kolesnick R (2002) The therapeutic potential of modulating the ceramide/sphingomyelin pathway. J Clin Invest 110:3–8
3. Mimeault M (2002) New advances on structural and biological functions of ceramide in apoptotic/necrotic cell death and cancer. FEBS Lett 530:9–16
4. Molkentin J (1999) Bioactive lipids naturally occurring in bovine milk. Nahrung 431:185–189
5. Parodi PW (1999) Conjugated linoleic acid and other anticarcinogenic agents of bovine milk fat. J Dairy Sci 82:1339–1349
6. Tepper AD, Diks SH, van Blitterswijk WJ, Borst J (2000) Glucosylceramide synthase does not attenuate the ceramide pool accumulating during apoptosis induced by CD95 or anti-cancer regimens. J Biol Chem 275:34810–34817
7. van Blitterswijk WJ, van der Luit A, Veldman RJ, Verheij M, Borst J (2003) Ceramide: second messenger or modulator of membrane structure and dynamics? J Biochem 369:199–211
8. Padron JM (2006) Sphingolipids in anticancer therapy. Curr Med Chem 13:755–770
9. Itoh M, Kitano T, Watanabe M, Kondo T, Yabu T, Taguchi Y, Iwai K, Tashima M, Uchiyama T, Okazaki T (2003) Possible role of ceramide as an indicator of chemoresistance: decrease of the ceramide content via activation of glucosylceramide synthase and sphingomyelin synthase in chemoresistant leukemia. Clin Cancer Res 8:415–423
10. Kester M, Kolesnick R (2003) Sphingolipids as therapeutics. Pharmacol Res 47:365–371
11. Reynolds CP, Maurer BJ, Kolesnick RN (2004) Ceramide synthesis and metabolism as a target for cancer therapy. Cancer Lett 206:169–180
12. Selzner M, Bielawska A, Morse MA, Rüdiger HA, Sindram D, Hannum YA, Clavien PA (2001) Induction of apoptotic cell death and prevention of tumor growth by ceramide analogues in metastatic human colon cancer. Cancer Res 61:1233–1240
13. Senchekov A, Litvak DA, Cabot MC (2001) Targeting ceramide metabolism—a strategy for overcoming drug resistance. J Natl Canc Inst 93:347–357
14. Wang XZ, Beebe JR, Pwiti L, Bielawska A, Smyth MJ (1999) Aberrant sphingolipid signaling is involved in the resistance of prostate cancer cell lines to chemotherapy. Cancer Res 59:5842–5848
15. Lemonnier LA, Dillehay DL, Vespremi MJ, Abrams J, Brody E, Schmelz EM (2003) Sphingomyelin in the suppression of colon tumors: prevention versus intervention. Arch Biochem Biophys 419:129–138
16. Silins I, Nordstrand M, Högberg J, Stenius U (2003) Sphingolipids suppress preneoplastic rat hepatocytes in vitro and in vivo. Carcinogenesis 24:1077–1083
17. Wang X, Clubbs EA, Bomser JA (2006) Genistein modulates prostate epithelial cell proliferation via estrogen- and extracellular signal-regulated kinase-dependent pathways. J Nutr Biochem 17:204–210
18. Darzynkiewicz Z, Bruno S, Del Bino G, Gorczyca W, Hotz MA, Lassota P, Traganos F (1992) Features of apoptotic cells measured by flow cytometry. Cytometry 13:795–808

19. Ahn EH, Schroeder JJ (2002a) Bioactive sphingolipids are constituents of soy and dairy products. J Food Sci 67:522–524
20. Merrill AH Jr, Schmelz EM, Dillehay DL, Spiegel S, Shayman JA, Schroeder JJ, Riley RT, Voss KA, Wang E (1997) Sphingolipids–the enigmatic lipid class: biochemistry, physiology, and pathophysiology. Toxicol Appl Pharmacol 142:208–225
21. Vesper H, Schmelz EM, Nikolova-Karakashian MN, Dillehay DL, Lynch DV, Merrill AH Jr (1999) Sphingolipids in food and the emerging importance of sphingolipids to nutrition. J Nutr 129:1239–1250
22. Schiller J, Zschörnig O, Petković M, Müller M, Arnhold J, Arnold K (2001) Lipid analysis of human HDL and LDL by MALDI-TOF mass spectrometry and 31P-NMR. J Lipid Res 42:1501–1508
23. Seelan RS, Qian C, Yokomizo A, Bostwick DG, Smith DI, Liu W (2000) Human acid ceramidase is overexpressed but not mutated in prostate cancer. Genes Chromosomes Cancer 29:137–146
24. Oh JE, So KS, Lim SJ, Kim Y (2006) Induction of apoptotic cell death by a ceramide analog in PC-3 prostate cancer cells. Arch Pharm Res 29:1140–1146
25. Shabbits JA, Mayer LD (2003) Intracellular delivery of ceramide lipids via liposomes enhances apoptosis in vitro. Biochim Biophys Acta 1612:98–106
26. Bourbon NA, Yun J, Berkey D, Wang Y, Kester M (2001) Inhibitory actions of ceramide upon PKC-ε/ERK interactions. Am J Physiol Cell Physiol 280:C1403-C1411
27. Coroneos E, Wang Y, Panuska JR, Templeton DJ, Kester M (1996) Sphingolipid metabolites differentially regulate extracellular signal-regulated kinase and stress-activated protein kinase cascades. J Biochem 316:13–17
28. Jarvis WD, Fornari FA Jr, Auer KL, Freemerman AJ, Szabo E, Birrer MJ, Johnson CR, Barbour SE, Dent P, Grant S (1997) Coordinate regulation of stress- and mitogen-activated protein kinases in the apoptotic actions of ceramide and sphingosine. Mol Pharmacol 52:935–947
29. Ragg SJ, Kaga S, Berg KA, Ochi A (1998) The mitogen-activated protein kinase pathway inhibits ceramide-induced terminal differentiation of a human monoblastic leukemia cell line, U937. J Immunol 161:1390–1398
30. Jayadev S, Liu B, Bielawska AE, Lee JY, Nazaire F, Pushkareva MY, Obeid LM, Hannun YA (1995) Role for ceramide in cell cycle arrest. J Biol Chem 270:2047–2052
31. Ogretmen B, Pettus BJ, Rossi MJ, Wood R, Usta J, Szulc Z, Bielawska A, Obeid LM, Hannun YA (2002) Biochemical mechanisms of the generation of endogenous long chain ceramide in response to exogenous short chain ceramide in the A549 human lung adenocarcinoma cell line. J Biol Chem 277:12960–12969
32. Oberhammer FA, Hochegger K, Froschl G, Tiefenbacher R, Pavelka M (1994) Chromatin condensation during apoptosis is accompanied by degradation of lamin A + B, without enhanced activation of cdc2 kinase. J Cell Biol 126:827–837

Lipids (2008) 43:151–159
DOI 10.1007/s11745-007-3145-2

ORIGINAL ARTICLE

Chemical Properties of Epidermal Lipids, Especially Sphingolipids, of the Antarctic Minke Whale

Keita Yunoki · Hajime Ishikawa · Yutaka Fukui · Masao Ohnishi

Received: 12 November 2007 / Accepted: 6 December 2007 / Published online: 10 January 2008
© AOCS 2007

Abstract It is well known that sphingolipids specifically exist in the terrestrial mammal epidermis and correlate with skin barrier functions. However, the lipid properties of the marine mammal epidermis have not been examined in detail. We thus investigated the chemical composition of lipid components, especially sphingolipids, in the black epidermis (outer skin) of Antarctic minke whales (six mature and six immature specimens). Complex lipid fractions mainly contained cerebroside (CE), cholesteryl sulfate and sphingomyelin (SM), as well as two glycerophospholipids. Moreover, in the superficial layer of the black epidermis, CE was richly abundant but phospholipids were scarce. As component fatty acids, the non-hydroxy monounsaturated very long chain fatty acids (VLFA) within 34 carbons were generally present in CE and SM in the black epidermis. CE also consisted of α-hydroxy fatty acids with monounsaturation within C34 (17%) and a slight proportion of ω-hydroxy ones (32:1 and 34:1), the latter being probably derived from acyl-CE. Component sphingoid bases of both sphingolipids were predominantly 4-sphingenine (64%), followed by a C16 analogue (21%). When comparing these by different maturities, mature whales showed sphingolipid profiles with higher levels of unsaturated fatty acids and with shorter sphingoid base chains than those of immature ones. Component analysis revealed that CE sugars were 67% glucose and 33% galactose, and α-hydroxy fatty acids only bound to galactose.

Keywords Cerebroside · Sphingomyelin · Complex lipids · Sphingolipid · Ceramide · Marine mammal · Whale · Cetacean · Epidermis · Galactose

Introduction

The skin is the largest biological organ, and it is in constant contact with the outside world. It functions as a barrier to maintain homeostasis in the body. In particular, the superficial epidermis of terrestrial mammals, such as humans, forms the stratum corneum consisting of an intercellular lipid matrix [1]. The intercellular space of the stratum corneum contains 40–50% ceramide, 20–33% cholesterol, 7–13% free fatty acid, 0–7% cholesteryl sulfate, and 0–20% cholesteryl ester [2, 3]. Ceramides, the most predominant intercellular lipid, are enzymatically derived from cerebroside and sphingomyelin synthesized in epidermal cells [4, 5]. The ceramide is localized in the stratum corneum and has a role in its barrier properties. It has been reported that sphingolipids and their hydrolyzing enzymes are also present in the epidermis of some terrestrial mammals, including pigs and mice [6–10]. Moreover, it was found that enzyme suppression could impair epidermal barrier properties [5, 11]. Therefore, epidermal lipids are generally regarded as playing an important role in the maintenance of the barrier against

K. Yunoki · Y. Fukui · M. Ohnishi (✉)
Department of Agricultural and Life Science,
Obihiro University of Agriculture and Veterinary Medicine,
Obihiro, Hokkaido 080-8555, Japan
e-mail: mohnishi@obihiro.ac.jp

K. Yunoki
e-mail: yunoki@obihiro.ac.jp

H. Ishikawa
The Institute of Cetacean Research, Toyomi-cho,
Tokyo 104-0055, Japan

excessive transcutaneous water loss in terrestrial mammals. Additionally, in terrestrial mammals, the chemical composition of epidermal sphingolipids has been investigated in detail [7, 12, 13].

In contrast, the properties of epidermal barrier functions in marine mammals, which are not exposed to dry stress, have not been examined in detail, although they may have greatly differing barrier requirements to terrestrial mammals.

Since the whale, a marine mammal, has been utilized as an oil source in the past, intensive research has been carried out into the chemical composition of their fat [14–19]. It was found that the pilot whale epidermis contains cerebroside and sphingomyelin by TLC analysis [20]; however, chemical research on lipids in the whale epidermis, which hardly contains any fat, is very limited. Thus, we used the outer black epidermis of minke whales of different ages and investigated the chemical compositions of the lipid components, especially sphingolipids.

Materials and Methods

Materials

The present study was approved by the Animal Experimental Committee of Obihiro University of Agricultural and Veterinary Medicine in accordance with the Guiding Principles for the Care and Use of Research Animals. Antarctic minke whales *Balaenoptera bonaerensis* were obtained from the Japanese Whale Research Program under Special Permit in the Antarctic (JARPA) in the 2004/2005 seasons. All the whales used in the present study were killed by explosive harpoons which have been recognized as the best humane killing method of whales by the International Whaling Commission and provided by the Schedule III (Capture) in the International Convention for the Regulations of Whaling. Twelve male whales were divided into two groups, with each six mature and immature whales, according to body length and body weight. Average body length and weight (± standard deviation) were 8.4 (±0.4) m and 6.5 (±0.5) t for mature whales, respectively, and 6.3 (±0.9) m and 2.9 (±1.1) t for immature ones, respectively. Whale skins with black and fatty epidermis were cut from the back of each whale on the ship and were immediately frozen. Then, the fatty and black (approximately 0.4 mm thick) epidermis specimens were carefully separated with a knife. As for one black epidermis specimen from the mature whale, a superficial layer (24 wt%) and inner layer (76 wt%) were respectively separated.

Extraction and Detection of Total Lipids

Black and fatty epidermis samples (5 g) were extracted twice with chloroform–methanol (2:1, *v*/*v*) and once with chloroform–methanol (1:2, *v*/*v*) for 1 h, respectively, after homogenization (Polytron, Kinematica, Switzerland). After filtration using filter paper (Advantec No. 2, Toyo Roshi Kaisha, Japan), the extracts were combined and washed once with water in a ratio of chloroform–methanol–water (8:4:3, *v*/*v*/*v*) [21]. After partition, the lower phase was concentrated to dryness using a rotary evaporator, and the lipids were weighed to yield the total lipids (175–220 mg from black epidermis). Total lipids were analyzed by silicic acid TLC (Silica gel 60, 0.25 mm, Merck, Germany) with hexane–diethylether–acetic acid (80:20:1, *v*/*v*/*v*) and chloroform–methanol–water (65:25:4, *v*/*v*/*v*) to detect neutral and complex lipids, respectively. CE species were visualized after spraying with anthrone/sulfuric acid, followed by heating. Free ceramide was detected with chloroform–methanol–water (90:10:1, *v*/*v*/*v*).

Separation of Complex Lipids and Sphingolipids from the Epidermis

A part (150 mg) of total lipids obtained from the black epidermis were subjected to silicic acid column chromatography. Neutral and complex lipid (47–59 mg) fractions were eluted from the column with chloroform and methanol, respectively [22]. Additionally, a part (30 mg) of the complex lipid fraction from three whales was hydrolyzed with 0.4 M KOH/methanol at 37 °C for 2 h [23], then placed in Sep-Pak Plus Silica Cartridges (Waters, Milford, USA). After removing the neutral lipids from the cartridge with chloroform and chloroform/acetic acid (99:1, *v*/*v*), CE was eluted with chloroform–methanol (2:1, *v*/*v*), and SM was eluted with chloroform–methanol (1:4, *v*/*v*) [24]. The CE fraction also contained cholesteryl sulfate and lactosylceramide. Also, a part of each complex lipid fraction was separated by preparative silicic acid TLC (Silica gel 60, 0.25 mm, Merck, Germany) with chloroform–methanol–water (65:25:4, *v*/*v*/*v*), and CE with two main bands, made visible by spraying the plate with 0.001% primuline solution followed by UV irradiation, was respectively recovered from the silica gel.

Methanolysis and TMS-Derivatization of Lipids

The lipid samples (1 mg) were reacted with 5% HCl/methanol at 100 °C for 3 h. After cooling, the fatty acid methyl esters were extracted three times with *n*-hexane after the addition of water. Sphingolipid fractions (1 mg) were reacted with 1 M HCl/methanol at 70 °C for 18 h to analyze sphingoid base [25]. After removing the fatty acid methyl esters three times with *n*-hexane, the lower phase was adjusted to pH 10 by the addition of 4 M NaOH. The sphingoid base released was then extracted three times with diethylether after the addition of water. Sphingoid bases were converted to TMS-ether derivatives. Fatty acid methyl ester fractions of CE were also converted to TMS-ether derivatives to determine *ω*-hydroxy fatty acid. In the CE fractions, the residue (water phase) was dried by evaporation under a nitrogen gas, in which methylglycosides were converted to TMS-ethers [26]. Standard D-mannose, D-glucose and lactose monohydrate (Wako, Osaka, Japan) were also prepared in the same way.

HPLC Analysis

The alkaline stable lipid fractions after alkaline hydrolysis of total lipids were analyzed by normal-phase HPLC according to the method of Sugawara and Miyazawa with slight modification under the following conditions [27]. Instrument: Shimadzu LC-10AD (Kyoto, Japan); mobile phase—solvent A: chloroform and solvent B: methanol–water (95:5 *v*/*v*); gradient (solvent B%): 0–15 (1–25%), 15–25 (25–90%), 25–30 min (90–95%), hold for 10 min, 40–45 min (95–1%); column: LiChrospher Si 60 (column size, 250 mm × 4 mm i.d.; particle size: 5 µm, Merck, Germany); flow rate: 1 ml/min; injection volume: 20 µl; column temperature: 40 °C; detector: Shimadzu ELSD-LT (70 °C, 350 kPa). The amounts of CE and SM were calculated from the calibration curves of standard CE (lower spot from the bovine brain, Doosan Serdary Research Laboratories, Toronto, Canada) and SM (from the bovine brain, Sigma, St Louis, USA). All data are averages ± SD of independent experiments from three whales.

GC and GC–MS Analyses

Fatty acid methyl esters and sphingoid base-TMS-ether derivatives were analyzed using a Shimadzu GCMS-QP2010 (Kyoto, Japan) under the following conditions. Column: ULBON HR-1 (50 m × 0.25 mm i.d., 0.25 µm, Shinwa Chemical Industries, Japan); temperature program for fatty acid analysis: 80–180 (15 °C/min), 180–320 °C (2 °C/min), held at 320 °C for 35 min; temperature program for sphingoid base analysis: 150–260 (8 °C/min), 260–320 °C (2 °C/min), held at 320 °C for 2 min; carrier gas: helium; detect: EI 70 eV. Fatty acid methyl esters (same conditions with GC–MS as above-mentioned) and methylglycoside–TMS ethers were analyzed using a Shimadzu GC-2010 (Kyoto, Japan) equipped with FID under the following conditions. Column ULBON HR-1 (50 m × 0.25 mm i.d., 0.25 µm, Shinwa Chemical Industries, Japan); temperature program: 80–180 (15 °C/min), 180–250 (2 °C/min), 250–300 °C (4 °C/min); carrier gas: nitrogen. The double bonds were estimated just by comparing GC retention times. Analytical data of lipid analyses for total and complex lipids and sphingolipid fractions are averages from six independent experiments, and means ± SD are presented. Analytical data for sugars are averages from two independent experiments.

Statistical Analysis

Statistical significance for lipid profiles between mature and immature whales was evaluated by analysis of variance (ANOVA). The *P* value <0.05 was regarded as statistically significant.

Results and Discussion

Fatty Acid Compositions of Total Lipids in Black and Fatty Epidermis

Yields of total lipids obtained from the fatty and black epidermis of six mature whales and their fatty acid compositions are shown in Table 1. The average total lipid content of six whale fatty epidermis was 72.3%. At least 23 fatty acids from C14 to C22, including unsaturated fatty acids, were detected, with oleic acid (18:1) and palmitoleic acid (16:1) the major components. Also, a significant amount (13.3%) of n-3 highly unsaturated fatty acids (HUFA), including icosapentaenoic acid (20:5), docosapentaenoic acid (22:5) and docosahexaenoic acid (22:6), were present. In contrast, the average total lipid content of six whale black epidermis was 4.0%, which was considerably lower than that of the fatty epidermis. Thirty-four fatty acids from C14 to C34 were detected as component fatty acids (Table 1). Major fatty acids of the black epidermis were 18:1 and 16:1, in common with the fatty epidermis; however, the former was high and the latter was low compared to the fatty epidermis. Also, arachidonic acid (20:4) was much higher than the fatty epidermis. The composition of 20:5 was close to that of the fatty epidermis, whereas 22:5 and 22:6 were low. As a noteworthy difference, the black epidermis contained very long chain (~C34) monounsaturated fatty acids, which could not be detected in the fatty epidermis.

Although it was reported that icosenoic acid (20:1) was characteristically high in the blubber and muktuk of marine mammals [28], it was a minor constituent (0.8–1.6%) in whale skins. The proportion of HUFA in the whale fatty epidermis was lower than that of seals (approximately 20% 20:5 and 22:6) and higher than that of narwhals (5%).

Table 1 Fatty acid compositions (mol%) of total lipids between fatty and black epidermis

Fatty acids	Fatty epidermis	Black epidermis
14:0	8.0 ± 0.4	2.3 ± 0.3
14:1n-5	4.5 ± 0.9	0.7 ± 0.2
15:0	0.3 ± 0.1	0.1 ± 0.1
16:0	6.7 ± 1.6	10.0 ± 0.9
16:1n-9	0.4 ± 0.1	–
16:1n-7	22.7 ± 2.4	10.2 ± 0.9
17:0	0.1 ± 0.1	–
17:1n-8	0.3 ± 0.0	–
18:0	1.1 ± 0.4	7.4 ± 0.3
18:1n-11	0.3 ± 0.0	–
18:1n-9	25.0 ± 1.5	34.5 ± 1.0
18:1n-7	8.8 ± 0.3	6.5 ± 0.7
18:2n-6	3.1 ± 0.1	3.8 ± 0.3
18:3n-3	1.8 ± 1.6	–
20:0	0.1 ± 0.1	0.4 ± 0.0
20:1n-9	0.8 ± 0.2	1.3 ± 1.1
20:1n-7	–	0.3 ± 0.1
20:2n-6	0.5 ± 0.1	–
20:3n-6	0.4 ± 0.2	0.7 ± 0.1
20:4n-6	0.6 ± 0.1	5.6 ± 0.6
20:4n-3	1.2 ± 0.2	–
20:5n-3	6.3 ± 1.2	7.2 ± 0.5
22:0	–	0.4 ± 0.1
22:1n-9	–	0.3 ± 0.2
22:1n-7	–	0.1 ± 0.0
22:5n-3	2.9 ± 0.4	0.7 ± 0.1
22:6n-3	4.1 ± 0.9	1.3 ± 0.3
23:0	–	0.1 ± 0.1
24:0	–	1.3 ± 0.2
24:1n-9	–	1.7 ± 0.3
24:1n-7	–	0.3 ± 0.1
25:0	–	0.2 ± 0.1
26:0	–	0.2 ± 0.0
26:1n-9	–	0.4 ± 0.1
26:1n-7	–	0.3 ± 0.1
28:1n-9	–	0.3 ± 0.0
28:1n-7	–	0.3 ± 0.1
30:1n-9	–	0.1 ± 0.1
30:1n-7	–	0.1 ± 0.1
32:1n-9	–	0.6 ± 0.2
34:1n-9	–	0.3 ± 0.1
Total lipid yields (%)	72.3 ± 17.7	4.0 ± 0.4

Values represent means of six whales ± SD

Lipid Components in the Black Epidermis

Silicic acid TLC of total lipids from the black epidermis of mature whales is shown in Fig. 1. As neutral lipid classes, five components including acylsterol (AS), triacylglycerol (TAG), free fatty acids (FFA), free cholesterol (FS) and diacylglycerol (DAG) were detected (Fig. 1A). As complex lipid classes, five components including cerebroside (CE), lactosylceramide (LC), phosphatidylethanolamine (PE), cholesteryl sulfate (CS), phosphatidylcholine (PC) and sphingomyelin (SM) were found (Fig. 1b). CE and SM were largely found with two upper and lower spots on TLC. When complex lipids obtained from superficial (24 wt%) and inner (76 wt%) layers were analyzed by TLC (Fig. 1c), the former contained a high amount of CE and the latter contained a high amount of phospholipids such as PC and SM. LC was only detected in the superficial layer. A small spot with a positive reaction to the anthrone reagent above the CE spot was found (Fig. 1c), although it was hardly detected from total lipids of the whole black epidermis (Fig. 1b). It was considered to be an acyl-CE, since it disappeared after alkaline hydrolysis (data not shown). Free ceramide was found in extremely small amounts (data not shown).

It was thus shown that CE and SM were present in complex lipid fractions from the black epidermis of Antarctic minke whales as major sphingolipids, as in other

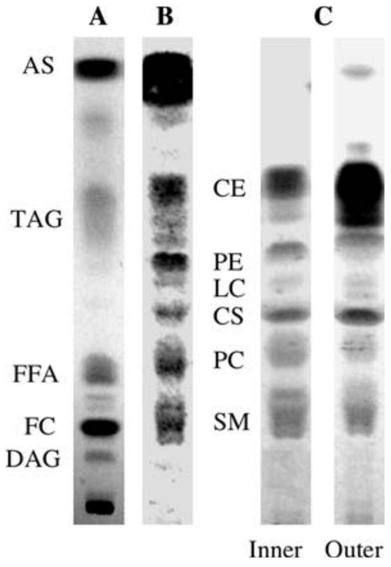

Fig. 1 Lipid components in the mature whale black epidermis. **a** Hexane–diethyl ether–acetic acid (80:20:1, *v*/*v*/*v*); **b**, **c** chloroform–methanol–water (65:25:4, *v*/*v*/*v*). Inner and outer indicate the complex lipid fractions of inner (76 wt%) and superficial (24 wt%) layers of the black epidermis, respectively. *AS* Acylsterol, *TAG* triacylglycerol, *FFA* free fatty acid, *FC* free cholesterol, *DAG* diacylglycerol, *CE* cerebroside, *PE* phosphatidylethanolamine, *LC* lactosylceramide, *CS* cholesteryl sulfate, *PC* phosphatidylcholine, *SM* sphingomyelin

whales [20]. Moreover, CE increased in the superficial layer, accompanied by a decreased level of phospholipids, as previously described in other cetaceans (*Phocena phocena*) [29]. Epidermal lipids, except for sphingolipids, contained relatively higher levels of FFA and sterol lipids including CS, FC and AS. It can be said that lipid composition of the whale black epidermis is similar to that of the human stratum corneum [2, 3].

Fatty Acid Compositions of Complex Lipid Fractions in the Black Epidermis

Fatty acid compositions of complex lipid fractions from the black epidermis from six mature whales are shown in Table 2. The proportion of complex lipid fraction of total lipids was 34.8%. Thirty-two non-hydroxy fatty acids from C14 to C34, 14 α-hydroxy fatty acids from C22 to C34 and four dimethylacetals with C18 and C20 were detected. As the proportions of three components, non-hydroxy fatty acids were predominant at 88% followed by 10% dimethylacetals and 2% hydroxy fatty acids. Major non-hydroxy fatty acids were 18:1, 16:0 and stearic acid (18:0). The compositions of saturated fatty acids, including 16:0 and 18:0 as well as VLFA within C34 (18%), were higher than those of total lipids. Major α-hydroxy fatty acids were hydroxy lignoceric acid (24h:0), hydroxy nervonic acid (24h:1) and hydroxydocosenoic acid (22h:1). Very long chain hydroxymonoenoic acids within C34 were also significantly present.

Since dimethylacetals are released from acidic hydrolysis of the alkenylether bond, the existence of this compound indicates that the complex lipid fractions contained plasmalogen. It was assumed that the proportion of plasmalogen in complex lipid fractions was approximately 20%, since plasmalogen has one alkenylether and one acyl moiety. As for terrestrial animals, our previous research showed that chicken skin contained a significant amount of plasmalogen (in submission). Further study is needed to clarify the physiological function of skin plasmalogen.

Contents and Fatty Acid Compositions of Cerebroside and Sphingomyelin in the Black Epidermis

The contents of CE and SM in the black epidermis were 5.7 and 4.2% of the total lipids, respectively. The total sphingolipid content (9.9%) was lower than the porpoise epidermis [29], indicating that epidermal sphingolipid contents significantly differ among species, although it is necessary to take the different analytical method into consideration.

Table 2 Constituents of complex lipid fractions in the mature black epidermis

Non-hydroxy acid		α-Hydroxy acid		Dimethylacetal	
Species	mol%	Species	mol%	Species	mol%
14:0	1.6 ± 0.4	22αh:0	3.8 ± 1.0	18:0	31.9 ± 4.6
14:1n-5	0.4 ± 0.2	22αh:1n-9	7.2 ± 1.2	20:0	15.6 ± 4.7
15:0	0.2 ± 0.0	24αh:0	22.7 ± 3.4	20:1n-9	29.8 ± 2.1
16:0	15.1 ± 2.4	24αh:1n-9	21.8 ± 1.5	20:1n-7	22.8 ± 2.4
16:1n-7	4.3 ± 1.1	26αh:0	7.9 ± 1.3		
18:0	12.1 ± 1.6	26αh:1n-9	6.8 ± 0.9		
18:1n-9	23.3 ± 2.2	26αh:1n-7	4.2 ± 1.1		
18:1n-7	3.4 ± 0.5	28αh:0	0.4 ± 0.1		
18:2n-6	4.3 ± 0.8	28αh:1n-9	3.2 ± 0.7		
20:0	1.0 ± 0.1	28αh:1n-7	3.5 ± 0.5		
20:1n-9	0.6 ± 0.5	30αh:1n-9	4.2 ± 0.3		
20:1n-7	0.3 ± 0.1	30αh:1n-7	4.4 ± 0.6		
20:3n-6	0.9 ± 0.1	32αh:1n-9	7.4 ± 0.9		
20:4n-6	6.2 ± 1.3	34αh:1n-9	2.5 ± 0.4		
20:5n-3	5.6 ± 1.6				
22:0	1.3 ± 0.5				
22:1n-9	0.4 ± 0.2				
22:1n-7	0.3 ± 0.1				
22:5n-3	0.3 ± 0.1				
22:6n-3	0.8 ± 0.2				
24:0	4.0 ± 1.8				
24:1n-9	5.4 ± 1.6				
24:1n-7	0.8 ± 0.3				
26:0	0.9 ± 0.3				
26:1n-9	1.6 ± 0.4				
26:1n-7	0.9 ± 0.1				
28:1n-9	0.2 ± 0.1				
28:1n-7	0.2 ± 0.1				
30:1n-9	0.5 ± 0.2				
30:1n-7	0.4 ± 0.1				
32:1n-9	1.8 ± 0.5				
34:1n-9	0.9 ± 0.4				

Values represent means of six whales ± SD

Fatty acid compositions of CE and SM fractions of three mature whales are shown in Table 3. CE consisted of 23 non-hydroxy fatty acids and 16 hydroxy fatty acids, the former being predominant (82%). Major non-hydroxy fatty acids were 24:0, 24:1 and 16:0. Hydroxy fatty acids consisted of not only α-hydroxy types ranging from C22 to C34, but also two ω-hydroxy types (32h:1 and 34h:1), the latter in a slight amounts (4.5%). Major α-hydroxy fatty acids were 24h:0, 24h:1 and 22h:1. SM consisted of 21 non-hydroxy fatty acids and 2 α-hydroxy acids (22h:1 and 24h:1), the former accounting for almost all the total (96.7%). Major non-hydroxy fatty

Table 3 Fatty acid compositions (mol%) of sphingolipid fractions in the black epidermis

Non-hydroxy acid			Hydroxy acid		
Species	CE	SM	Species	CE	SM
14:0	0.5 ± 0.2	1.0 ± 0.2	22αh:0	3.3 ± 1.0	–
16:0	10.9 ± 1.4	13.9 ± 1.7	22αh:1n-9	5.0 ± 0.7	66.0 ± 3.1
18:0	9.7 ± 1.1	9.0 ± 1.2	24αh:0	27.4 ± 2.8	–
18:1n-9	3.9 ± 0.4	–	24αh:1n-9	16.3 ± 1.6	34.0 ± 2.6
18:1n-7	2.5 ± 0.3	–	26αh:0	9.2 ± 1.5	–
20:0	1.1 ± 0.1	7.1 ± 0.7	26αh:1n-9	6.0 ± 0.8	–
22:0	2.3 ± 0.6	6.1 ± 1.9	26αh:1n-7	4.0 ± 1.1	–
22:1n-9	0.2 ± 0.1	0.3 ± 0.1	28αh:0	0.5 ± 0.2	–
22:1n-7	0.3 ± 0.1	0.9 ± 0.3	28αh:1n-9	3.1 ± 0.6	–
24:0	13.6 ± 2.3	15.4 ± 2.8	28αh:1n-7	4.6 ± 0.8	–
24:1n-9	13.2 ± 1.9	29.5 ± 3.5	30αh:1n-9	3.7 ± 0.2	–
24:1n-7	2.3 ± 0.5	4.0 ± 1.6	30αh:1n-7	4.0 ± 0.5	–
26:0	4.8 ± 1.3	2.1 ± 0.6	32αh:1n-9	6.2 ± 0.8	–
26:1n-9	5.0 ± 0.8	3.0 ± 0.7	34αh:1n-9	2.2 ± 0.3	–
26:1n-7	4.3 ± 0.6	1.0 ± 0.1	32ωh:1n-9	3.4 ± 0.4	–
28:0	0.2 ± 0.1	0.1 ± 0.1	34ωh:1n-9	1.1 ± 0.3	–
28:1n-9	2.9 ± 1.3	0.5 ± 0.1			
28:1n-7	1.8 ± 1.1	0.7 ± 0.2			
30:1n-9	3.3 ± 0.8	0.8 ± 0.3			
30:1n-7	3.2 ± 0.4	0.8 ± 0.2			
32:1n-9	8.8 ± 2.1	2.4 ± 0.5			
32:1n-7	0.8 ± 0.3	0.2 ± 0.1			
34:1n-9	4.4 ± 1.4	1.2 ± 0.3			

Values represent the means of six whales ± SD

CE Cerebroside, *SM* sphingomyelin

acids were 24:1, 24:0 and 16:0. The proportion of major VLFA, including 32:1 and 34:1, of SM was lower than CE.

It was considered that ω-hydroxy fatty acids detected from CE fractions after alkaline hydrolysis were derived from acyl-CE, which is present in small amounts in the epidermal superficial layer as shown in Fig. 1c. The proportion of ω-hydroxy fatty acids was only 0.8% of the total acids of CE, which was considerably lower than the 3% in the pig [7]. Additionally, human and pig epidermal CE generally consist of almost all saturated fatty acids of both non-hydroxy and hydroxy types [4, 7], whereas whale epidermal CE consist of abundant monounsaturated fatty acids. Moreover, human and hairless mouse epidermal SM contained a significant amount of hydroxy fatty acids (11 and 45%, respectively) [10], whereas whale epidermal SM predominantly consisted of non-hydroxy fatty acids.

Table 4 Sphingoid base compositions (mol%) of sphingolipids in the black epidermis

Sphingoid bases	CE	SM
d14:1^{4trans}	2.1 ± 0.1	3.1 ± 0.2
d16:0	2.3 ± 0.3	3.0 ± 0.3
d16:1^{4trans}	21.2 ± 1.3	21.7 ± 0.8
d16:2	0.6 ± 0.2	0.7 ± 0.2
d17:1	0.7 ± 0.2	1.3 ± 0.4
d18:0	2.8 ± 0.9	3.1 ± 0.8
d18:1^{4trans}	63.9 ± 1.8	64.5 ± 1.3
d18:2	1.3 ± 0.4	1.4 ± 0.2
d19:1	0.7 ± 0.2	0.7 ± 0.1
d20:0	0.2 ± 0.1	0.1 ± 0.1
d20:1	0.7 ± 0.1	0.4 ± 0.1
t16:0	0.8 ± 0.2	–
t18:0	2.4 ± 0.6	–
t20:0	0.3 ± 0.1	–
d16:1/d18:1	0.33 ± 0.02	0.34 ± 0.02

Values represent means of six whales ± SD

CE Cerebroside, *SM* sphingomyelin, *d* dihydroxy, *t* trihydroxy

Sphingoid Base Composition of Cerebroside and Sphingomyelin in the Black Epidermis

Compositions of sphingoid bases from CE and SM fractions are shown in Table 4. CE consisted of 11 dihydroxy bases and 3 trihydroxy bases, the latter being only minimal (4%). The component sphingoid base predominantly consisted of 4-sphingenine (d18:1), followed by a C16 analogue of 4-sphingenine (d16:1). Sphingoid base compositions of SM almost corresponded with those of CE, except for having no trihydroxy base.

The major component sphingoid base of whale epidermal sphingolipids was d18:1, corresponding to that of other terrestrial mammals, including humans, pigs and murine [4, 7, 10, 12, 30]; however, the proportion of trihydroxy base was considerably lower than human [4] and pig epidermis [7, 12]. As minor components, human and murine epidermis contained d20:1 [4] and d17:1 [10], respectively, whereas the whale black epidermis characteristically contained sphingoid bases with shorter chain lengths ($<$C16).

Comparison of Lipid Profiles Between Mature and Immature Whales

Lipid profiles of mature and immature whale epidermis are shown in Table 5. In the fatty epidermis, only non-hydroxy fatty acids were detected, and consisted of more than 80% unsaturated fatty acids (UFA). Particularly, the HUFA (20:5, 22:5 and 22:6) of immature whales showed a significantly higher proportion than mature ones. In the black epidermis, the differences between mature and immature whales were slight in terms of lipid yield and proportion of complex lipid fraction. Moreover, the proportions of complex lipid constituents such as non-hydroxy fatty acids (87–88%), α-hydroxy acids (2%) and dimethylacetals (10–11%) hardly showed any difference between the two whale groups. However, the proportion of UFA of mature whales was significantly higher than immature ones. In CE and SM fractions from three whales, mature whales epidermis generally contained more UFA than immature ones. As for the component sphingoid base, the d16:1/d18:1 ratio generally showed higher values in mature whales than immature ones. As for sphingolipid contents, mature and immature whales contained high levels of CE and SM, respectively, although they were not statistically significant due to great individual differences.

Taken together, it was shown that the sphingolipids in the whale black epidermis were sugar- and phosphorylcholine-binding types, having characteristic chemical properties of fatty acids with monounsaturation and sphingosine base with shorter carbon lengths, compared to terrestrial mammals, which became marked with maturity.

Table 5 Comparison of lipid profiles between mature and immature whales

	Mature	Immature
Fatty epidermis		
Total lipid fraction		
Lipid yields (wt%)	72.3 ± 17.7	78.0 ± 8.2
Non-hydroxy UFA	83.6 ± 2.5	81.4 ± 1.3
HUFA n-3	13.3 ± 2.4	17.3 ± 1.2*
Black epidermis		
Total lipid fraction		
Lipid yields (wt%)	4.0 ± 0.4	4.3 ± 0.3
Non-hydroxy UFA	77.0 ± 1.1	75.8 ± 1.1
Complex lipid fraction		
Lipid yield (wt%)	34.8 ± 2.3	33.1 ± 3.7
Non-hydroxy acid	87.6 ± 1.7	86.8 ± 1.1
Non-hydroxy UFA	63.8 ± 1.4	57.6 ± 3.4*
α-Hydroxy acid	2.4 ± 1.7	2.1 ± 0.6
α-Hydroxy UFA	65.2 ± 3.1	56.8 ± 6.5*
Dimethylacetal	10.0 ± 1.6	11.1 ± 1.3
Cerebroside fraction		
Non-hydroxy UFA	56.9 ± 1.9	52.0 ± 1.8*
Hydroxy UFA	59.6 ± 2.1	53.4 ± 3.0*
d16:1/d18:1	0.33 ± 0.02	0.21 ± 0.02*
Sphingomyelin fraction		
Non-hydroxy UFA	45.3 ± 2.8	41.3 ± 1.9
d16:1/d18:1	0.34 ± 0.02	0.25 ± 0.01*
Sphingolipid contents (wt%)		
Per total lipids		
Cerebroside	5.7 ± 2.0	4.1 ± 0.85
Sphingomyelin	4.2 ± 0.47	4.6 ± 0.33
Per black epidermis		
Cerebroside	0.22 ± 0.05	0.17 ± 0.03
Sphingomyelin	0.16 ± 0.01	0.19 ± <0.01

Values represent the means of six whales ± SD, except for sphingolipid contents ($n = 3$)

HUFA highly unsaturated fatty acids, UFA unsaturated fatty acids

* Significantly different ($P < 0.05$) between mature and immature whales

Composition Data of Cerebroside in the Black Epidermis

Composition data of cerebroside from the black epidermis are summarized in Table 6. CE consisted of glucose and galactose in a ratio of 67:33. Moreover, glucose and galactose at more than 85% were detected in the upper and lower spots of CE on TLC, respectively. The upper spot contained almost only non-hydroxy fatty acids (>95%), while the lower spot contained non- and α-hydroxy acids by 46 and 54%, respectively. Sphingoid base hardly showed any differences in either CE spot.

In animal epidermis, it was reported that galactocerebroside was present in pig epidermal cells, accounting for 13% of total CE [12]. The pig galactocerebroside mainly consisted of fatty acids with shorter chains, such as C16 non-hydroxy fatty acid and C14–C16 α-hydroxy acids, than glucocerebroside (C16–C30 as non-hydroxy fatty acids and C18–C30 as α-hydroxy acids). On the other hand, whale

Table 6 Compositions data of cerebroside in the whale black epidermis

Cerebroside[a]	Carbohydrate[b]	Fatty acid (mol%)[c]		Sphingoid base[d]	Yield (mol%)[e]
Upper	Glucose	Non-hydroxy (C14–C34)	(>95)	d18:1, d16:1	67
Lower	Galactose	Non-hydroxy (C14–C28)	(46)	d18:1, d16:1	33
		α-Hydroxy (C22–C34)	(54)		

d Dihydroxy

[a] Separated from TLC with chloroform–methanol–water (65:25:4, *v*/*v*/*v*)

[b] Determined from an alkali stable lipid fraction

[c] Chain length of major components are indicated in parentheses

[d] Only those comprising more than 10% are listed

[e] Calculated from carbohydrate contents by GC analysis (mol%)

epidermal galactocerebroside (33% of total CE) was higher than in pigs and consisted of fatty acids with very long chains, although non-hydroxy fatty acids consisted of a slightly shorter chain (~C28) than glucocerebroside. Since the galactocerebroside was probably derived from epidermal melanocytes [12], it was assumed that galactocerebroside was abundantly present in the whale black epidermis with a high amount of melanin pigment. Menon et al. assumed that glycoconjugate, namely cerebroside, in the lamellar body of the cetacean epidermis may be important for cell-to-cell adhesion and be consistent in part with their water barrier requirements, or may contribute to streamlining due to a reduction in frictional resistance [29]. This study also revealed that whales accumulate cerebroside, but not free ceramide, in the superficial layer of the epidermis. Moreover, in general, the aliphatic chains in the ceramides of the terrestrial mammals are mainly long-chain saturated fatty acids with a high melting point and are mostly in a solid crystalline or gel state, exhibiting low lateral diffusion properties with low permeability at physiological temperatures [31]. These lipids have an obvious role in the barrier properties of the skin, limiting loss of water even in a dry environment on land. In contrast, whale epidermal lipids not only serve a similar role to the terrestrial mammal epidermis such as the prevention of efflux of body components, but also increase the proportion of unsaturated fatty acids to adapt to the colder skin surface temperatures in their habitats. An increased level of unsaturated sphingolipids would offer certain advantages such as protection from thermal crystallization of lipids at low seawater temperatures, and greater flexibility on a molecular level to provide superior streamlining [29]. Additionally, sphingoid bases with a relatively shorter chain may be important to maintain cellular membrane fluidity. These features probably become prominent in grown whales.

References

1. Norlén L (2001) Skin barrier structure and function: the single gel phase model. J Invest Dermatol 117:830–836
2. Wertz PW, Swartzendruber DC, Madison KC, Downing DT (1987) Composition and morphology of epidermal cyst lipids. J Invest Dermatol 89:419–425
3. Norlén L, Nicander I, Lundsjö A, Cronholm T, Forslind B (1998) A new HPLC-based method for the quantitative analysis of inner stratum corneum lipids with special reference to the free fatty acid fraction. Arch Dermatol Res 290:508–516
4. Hamanaka S, Hara M, Nishio H, Otsuka F, Suzuki A, Uchida Y (2002) Human epidermal glucosylceramides are major precursors of stratum corneum ceramides. J Invest Dermatol 119:416–423
5. Schmuth M, Man MQ, Weber F, Gao W, Feingold KR, Fritsch P, Elias PM, Holleran WM (2000) Permeability barrier disorder in Niemann–Pick disease: sphingomyelin–ceramide processing required for normal barrier homeostasis. J Invest Dermatol 115:459–466
6. Gray GM, Yardley HJ (1975) Lipid compositions of cell isolated from pig, human, and rat epidermis. J Lipid Res 16:434–440
7. Wertz PW, Downing DT (1983) Glucosylceramides of pig epidermis: structure determination. J Lipid Res 24:1135–1139
8. Bowser PA, Gray GM (1978) Sphingomyelinase in pig and human epidermis. J Invest Dermatol 70:331–335
9. Takagi Y, Kriehuber E, Imokawa G, Elias PM, Holleran WM (1999) Beta-glucocerebrosidase activity in mammalian stratum corneum. J Lipid Res 40:861–869
10. Uchida Y, Hara M, Nishio H, Sidransky E, Inoue S, Otsuka F, Suzuki A, Elias PM, Holleran WM, Hamanaka S (2000) Epidermal sphingomyelins are precursors for selected stratum corneum ceramides. J Lipid Res 41:2071–2082
11. Takagi Y, Nakagawa H, Yaginuma T, Takema Y, Imokawa G (2005) An accumulation of glucosylceramide in the stratum corneum due to attenuated activity of beta-glucocerebrosidase is associated with the early phase of UVB-induced alteration in cutaneous barrier function. Arch Dermatol Res 297:18–25
12. Hamanaka S, Yamaguchi Y, Yamamoto T, Asagami C (1988) Occurrence of galactosylceramide in pig epidermal cells. Biochim Biophys Acta 961:374–377
13. Wertz PW, Downing DT (1989) omega-Hydroxyacid derivatives in the epidermis of several mammalian species. Comp Biochem Physiol B 93:265–269

14. Brockerhoff H, Hoyle RJ, Hwang PC, Litchfield C (1967) Positional distribution of fatty acids in depot triglycerides of aquatic animals. Lipids 3:24–29
15. Hansen IA, Cheah CC (1969) Related dietary and tissue lipids of the sperm whale. Comp Biochem Physiol 31:757–761
16. Hamilton RJ, Long M, Raine MY (1972) Sperm whale oils. 3. Alkanes and alcohols. J Am Oil Chem Soc 49:307–310
17. Spencer GF, Tallent WH (1973) Sperm whale oil analysis by gas chromatography and mass spectrometry. J Am Oil Chem Soc 50:202–206
18. Litchfield C, Greenberg AJ, Ackman RG, Eaton CA (1978) Distinctive medium chain wax esters, triglycerides and diacylglyceryl esters in the head fats of the Pacific beaked whales, *Berardius bairdi*. Lipids 13:860–866
19. Lok CM, Folkersma B (1979) Composition of wax esters and triacylglycerols in the melon and blubber fats of young sowerby's whale, *Mesopladon bidens*. Lipids 14:872–875
20. Birkby CS, Wertz PW, Downing DT (1982) The polar lipids from keratinized tissues of some vertebrates. Comp Biochem Physiol 73:239–242
21. Folch J, Lees M, Sloane SGH (1957) A simple method for the isolation and purification of total lipids from animal tissues. J Biol Chem 226:497–509
22. Rouser G, Kritchevsky G, Yamamoto A (1967) Column chromatographic and associated procedures for separation and determination of phosphatides and glycolipids. In: Marinetti GV (eds) Lipid chromatographic analysis. Marcel Dekker, New York, pp 99–161
23. Fujino Y, Ohnishi M (1983) Sphingolipids in wheat grain. J Cereal Sci 1:159–168
24. Hanahan DJ, Dittmer JC, Warashima E (1957) A column chromatographic separation of classes of phospholipids. J Biol Chem 228:685–700
25. Gaver RC, Sweeley CC (1965) Methods for methanolysis of sphingolipids and direct determination of long-chain bases by gas chromatography. J Am Oil Chem Soc 42:294–298
26. Fujino Y, Ohnishi M (1976) Structure of cerebroside in *Aspergillus oryzae*. Biochim Biophys Acta 486:161–171
27. Sugawara T, Miyazawa T (1999) Separation and detection of glycolipids from edible plant sources by high-performance liquid chromatography and evaporative light-scattering detector. Lipids 34:1231–1237
28. Innis SM, Kuhnlein HV (1987) The fatty acid composition of northern-Canadian marine and terrestrial mammals. Acta Med Scand 222:105–109
29. Menon GK, Grayson S, Brown BE, Elias PM (1986) Lipokeratinocytes of the epidermis of a cetacean (*Phocena phocena*). Histochemistry, ultrastructure, and lipid composition. Cell Tissue Res 244:385–394
30. Hamanaka S, Nakazawa S, Yamanaka M, Uchida Y, Otsuka F (2005) Glucosylceramide accumulates preferentially in lamellar bodies in differentiated keratinocytes. Br J Dermatol 152:426–434
31. Rawlings AV (1995) Skin waxes: their composition, properties, structures and biological significance. In: Hamilton RJ (eds) Waxes: chemistry, molecular biology and functions. Oily, Dundee, pp 223–256

Lipids (2008) 43:161–169
DOI 10.1007/s11745-007-3136-3

METHODS

Capturing Proteins that Bind Polyunsaturated Fatty Acids: Demonstration Using Arachidonic Acid and Eicosanoids

Thomas G. Brock

Received: 25 August 2007 / Accepted: 6 November 2007 / Published online: 15 December 2007
© AOCS 2007

Abstract Polyunsaturated fatty acids (PUFA) and their biological derivatives, including the eicosanoids, have numerous roles in physiology and pathology. Although some eicosanoids are known to act through receptors, the molecular actions of many PUFA remain obscure. As the three-dimensional structure of eicosanoids allows them to specifically bind and activate their receptors, we hypothesized that the same structure would allow other proteins to associate with PUFA and eicosanoids. Here, we demonstrate that biotinylation of arachidonic acid and its oxygenated derivatives 5-hydroxyeicosatetraenoic acid (5-HETE) and leukotriene (LT) B_4 can be used to pull down associated proteins. Separation of proteins by two-dimensional gel electrophoresis indicated that a large number of proteins bound each lipid and that proteins could distinguish between two enantiomers of 5-HETE. Individual proteins, identified by matrix assisted laser desorption/ionization-time of flight mass spectrometry, included proteins that are known to bind lipids, including albumin and phosphatidylethanolamine-binding protein, as well as several novel proteins. These include cytoskeletal proteins, such as actin, moesin, stathmin and coactosin-like protein, and G protein signaling proteins, such as Rho GDP dissociation inhibitor 1 and nucleoside diphosphate kinase B. This method, then, represents a relatively simple and straightforward way to screen for proteins that directly associate with, and are potentially modulated by, PUFA and their derivatives.

Keywords Leukotrienes · 5-Hydroxyeicosatetraenoic acid · Moesin · Stathmin · Coactosin-like protein · Rho GDP dissociation inhibitor 1 · Nucleoside diphosphate kinase B

Abbreviations

ARA	Arachidonic acid
ACH	Arachidic acid
HETE	Hydroxyeicosatetraenoic acid
HpETE	Hydroperoxyeicosatetraenoic acid
LT	Leukotriene
MALDI-TOF	Matrix assisted laser desorption/ionization-time of flight
PUFA	Polyunsaturated fatty acid
RBL	Rat basophilic leukemia

Introduction

Polyunsaturated fatty acids (PUFA) play important roles in health and disease. For example, increasing the consumption of ω-3 PUFA reduces the risk of coronary heart disease [1–3] and decreases ischemic heart disease [4, 5]. On the other hand, the ω-6 PUFA arachidonic acid (ARA) can form ω-6 eicosanoids that exacerbate arrhythmogenic events [6, 7] and decreasing excessive ω-6 eicosanoid action can reduce the risk of ischemic heart disease [8–10]. Although these PUFA have profound effects on physiology, the specific actions of PUFA at the molecular and cellular levels are diverse and poorly understood.

Chemically, PUFA include long chain hydrocarbon molecules with numerous carbon–carbon double bonds. The double bonds represent sites of chemical reactivity

---

T. G. Brock (✉)
Department of Internal Medicine, University of Michigan,
Ann Arbor, MI 48109, USA
e-mail: brocko@umich.edu

with potential for enzymatic modification. For example, ARA is a twenty carbon PUFA with four double bonds (20:4). It can be modified by the enzyme 5-lipoxygenase, which inserts molecular oxygen at the fifth carbon to produce 5(*S*)-hydroperoxyeicosatetraenoic acid (5(*S*)-HpETE; reviewed in [11]). This PUFA can be modified by peroxidases to produce 5(*S*)-hydroxyeicosatetraenoic acid (5(*S*)-HETE), a biologically active monohydroxylated PUFA. Alternatively, 5(*S*)-HpETE can be further metabolized along the 5-lipoxygenase pathway to produce the dihydroxylated PUFA leukotriene (LT) B_4 or the glutathione-containing LTC_4. Whereas ARA induces apoptosis in neurons [12] and in leukemic cells [13, 14] or activates a variety of cell types [15, 16], LTB_4 and 5(*S*)-HETE are best known as chemoattractants and activators of leukocytes, and LTC_4 is recognized to promote contraction of smooth muscle and secretion of mucus from goblet cells (reviewed in [17]). Thus, enzymes recognize specific PUFA and alter them to produce a variety of novel constructs that have unique functions. The multitude of products that can be produced from ARA are called eicosanoids, whereas the smaller group produced solely by the 5-lipoxygenase pathway are the LT.

Structurally, the carbon–carbon double bonds in PUFA provide a degree of rigidity that is not found in saturated FA. As a result, each of the PUFA and their derivatives has a unique three-dimensional structure. This structure allows these lipids to interact with specific receptors. For example, LTB_4 binds to and activates two G-protein coupled receptors, the high affinity BLT_1 [18] and the lower affinity BLT_2 [19]. Similarly, LTC_4 activates two other receptors, $CysLT_1$ and $CysLT_2$. Consistent with the high specificity of lipid for protein, LTB_4 does not activate $CysLT_1$ or $CysLT_2$ at physiological concentrations, and LTC_4 does not activate BLT_1 or BLT_2. Relevant to this study, the interaction of these eicosanoids with their receptors results in conformational changes of the receptors with their consequential activation. This suggests that, if PUFA associate with non-receptor proteins, they may alter protein shape, resulting in modification of protein function.

We hypothesized that the distinctive structure of PUFA and eicosanoids should allow them to interact with specific soluble proteins other than traditional receptors. For example, it is known that ARA can bind directly to protein phosphatase 5 [20], binds to [21] and activates [22] S100A8/A9, and directly activates a GTP-binding protein in neutrophils [23]. Here, we describe a method for objectively capturing proteins that associate with PUFA and eicosanoids. We use proteins from the rat basophilic leukemia (RBL-1) cell line because it is mast cell like, in that it releases ARA, makes LT and responds to LT.

Materials and Methods

Cells and Cell Lysates

RBL cells (RBL-1, American Type Culture Collection, Manassas, VA) were grown under 5% CO_2 in Minimal Essential Medium alpha (Invitrogen) with 10% fetal bovine serum, 182 units/mL penicillin G sodium, 182 µg/mL streptomycin sulfate, 455 µg/mL amphotericin B. 2×10^7 cells were suspended in lysis buffer (137 mM NaCl, 10 mM phosphate buffer, pH 7.4, 2.7 mM KCl, 1 mM EGTA, protease inhibitor cocktail (Roche Applied Science, Indianapolis, IN), sonicated, centrifuged at 14,000×*g* (5 min, 4 °C) and supernatant collected as total soluble proteins from RBL cells.

Isolation of PUFA-Binding Proteins

PUFA (ARA, ACH, 5(*S*)-HETE, 5(*R*)-HETE, or LTB_4) were biotinylated using the EZ-Link Biotin PEO-Amine kit (Pierce, Rockford IL), according to manufacturer's directions. Briefly, PUFA were diluted to 10 mg/mL in 2-(*N*-morpholino)ethane sulfonic acid (MES) buffer, pH 4.5, mixed with biotin (21 mg/mL) and 1-ethyl-3-[3-dimethyl aminopropyl] carbodiimide hydrochloride crosslinker (20 mg/mL), with mixing on rotator for 2 h at RT. Total soluble proteins from RBL cells were mixed with FA-biotin solution, without purification of the FA-biotin preparation, at an approx 1:1 molar ratio, on rotator for 1 h at RT. Samples of the cell protein/FA-biotin preparation were mixed with avidin immobilized on beaded agarose (Pierce) for 1 h at RT and centrifuged 1 min at 3,000×*g*. The resulting pellet was washed three times with TBS and FA-binding proteins recovered by elution with 400 mM NaCl in PBS. In some experiments, the supernatant, partially depleted of FA-binding proteins, was mixed with additional immobilized avidin and centrifuged to remove remaining FA-binding proteins, producing a protein fraction that was highly depleted of FA-binding proteins.

Gel Electrophoresis and Protein Identification

Protein samples were dialyzed overnight in PBS with stirring at 4 °C, mixed with SDS-PAGE sample buffer, boiled, separated by SDS-PAGE using a 12% Tris-HCl gel and stained with Coomassie. For two-dimensional gel electrophoresis, samples were mixed with isoelectric focusing buffer and separated using ReadyStrip IPG strips, pH 3–10, in the Protean IEF Cell (Bio-Rad Laboratories, Hercules CA). After focusing, strips were equilibrated using iodoacetamide, separated by SDS-PAGE using a 12% Tris-HCl gel and stained with Coomassie. Isolated proteins were subjected to matrix assisted laser desorption/ionization-time of flight (MALDI-TOF) ms and tandem ms, with fragments sequenced by the Michigan Proteome Consortium at the University of Michigan. Initial analysis involved searching the NCBInr database; subsequent analysis included BLAST searching the SwissProt database for proteins matching all peptide sequences from tandem mass spectrometry. Calculated kDa and p*I* values for proteins were obtained through SwissProt.

Densitometric Analysis

Regions of images from SDS-PAGE results were analyzed using ImageJ 1.33, with quantitation of grayscale values of pixels measured by ImageJ and plotted using GraphPad Prism 3.00.

Results

Isolation of Fatty Acid-Associated Proteins

Soluble proteins were used in this study, excluding membrane-associated proteins, which have extensive hydrophobic regions that would interact non-specifically with various FA (although many soluble proteins will also have accessible hydrophobic regions). As a first evaluation, proteins from these total soluble protein preparations were separated into those proteins that could be pulled down using different FA and those that were resistant to capture. Here, the polyunsaturated ARA (20 carbon, 4 double bonds) was compared with the saturated arachidic acid (ACH, 20:0). An initial evaluation of the proteins captured by fatty acids indicated that a surprisingly large number of proteins associated with both ARA and ACH (Fig. 1a). Prominent bands could be readily identified in the fatty acid-associated samples, which were largely absent from the fatty acid-depleted samples. Densitometric analysis of a region of the ARA-depleted sample (lane 2) and the ARA-associated samples (lane 3) indicated two major peaks that were unique to the latter sample (Fig. 1b). In addition, while many bands were associated with both ARA (lane 3) and ACH (lane 5), some bands appeared to be more abundant in one than the other (Fig. 1c), suggesting some degree of specificity. In control experiments, essentially no protein bound to beads alone or to beads after incubation with biotin alone without fatty acid, as determined by SDS-PAGE analysis of fractions eluted from washed beads processed in parallel (not shown).

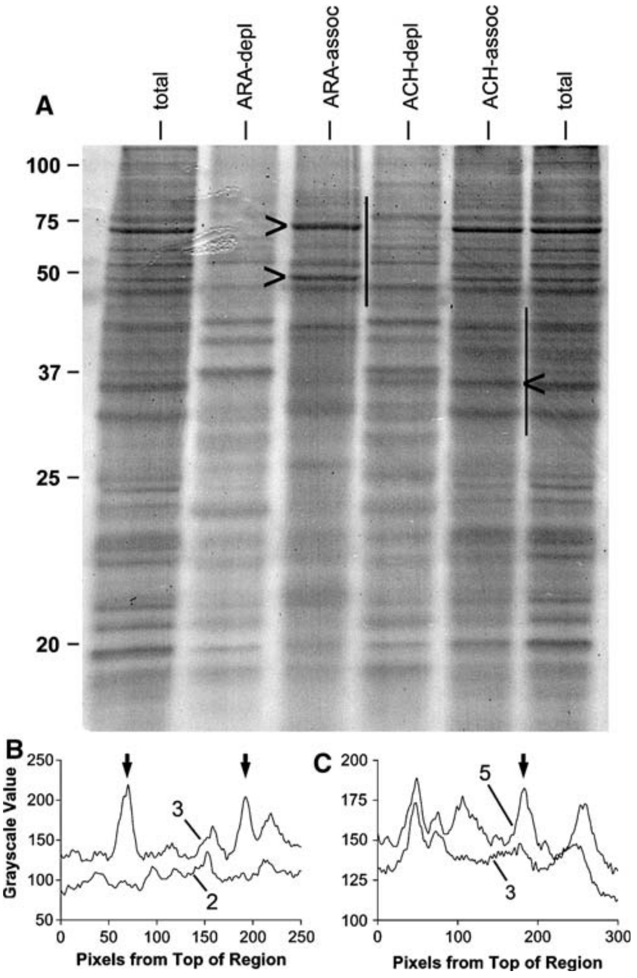

Fig. 1 Separation of ARA-associated proteins from proteins that do not associate with ARA from total soluble proteins of RBL1 cells. **a** SDS-PAGE analysis. Total soluble proteins of RBL1 cells ("total") were incubated with either ARA-biotin or ACH-biotin and the proteins that associated ("assoc") with the fatty acids were captured using avidin agarose. The remaining proteins, depleted of fatty acid-associated proteins, are also presented ("depl"). >, more abundant in ARA-assoc than ARA-depleted; <, more abundant in ACH-assoc than ARA-assoc. **b** Densitometric analysis of regions of ARA-depleted (*2*) and ARA-associated (*3*) lanes; region denoted by bar adjacent to *lane 3*. **c** Densitometric analysis of regions of ARA-associated (*3*) and ACH-associated (*5*) lanes; region corresponds to bar at *lane 5*

Identification of Some ARA-Associating Proteins

The large number of proteins that were pulled down by FA in this protocol indicated that additional separation steps would be required to identify individual FA-associating proteins. Parallel separation of total proteins and ARA-associated proteins by 2-dimensional gel electrophoresis again supported the conclusion that this protocol was capturing a subset of total proteins that bound ARA (Fig. 2).

Some of the most abundant (heavily staining) proteins that associated with ARA were identified by MALDI-TOF

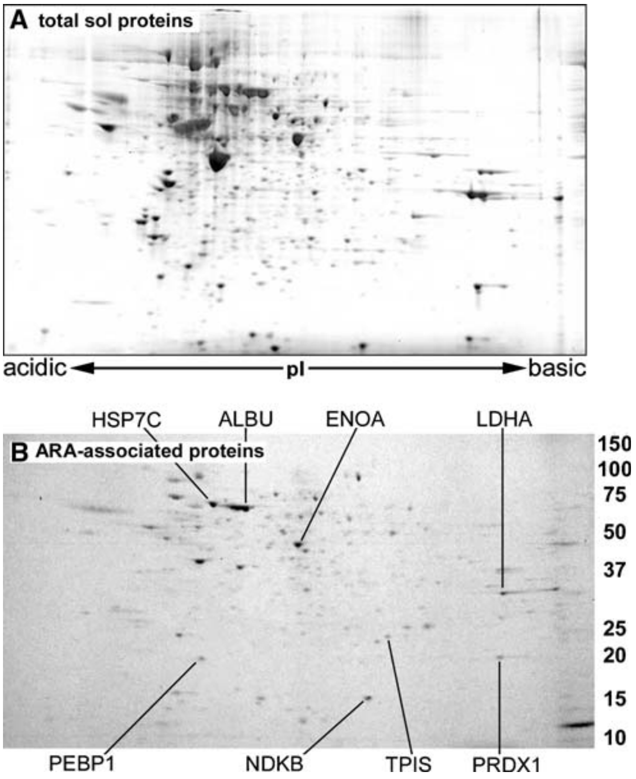

Fig. 2 Two-dimensional separation of total soluble proteins compared with ARA-associating proteins from RBL1 cells. **a** Total soluble proteins. **b** ARA-associating proteins. Coomassie-stained spots were analyzed by MALDI-TOF ms/ms and sequenced peptides used to identify proteins. Abbreviations refer to proteins detailed in Table 1. Migration of molecular weight markers indicated at right of (**b**)

mass spectrometric analysis followed by database searches. In each case, individual peptide sequences were further queried by BLAST search for unique identities. For example, one protein provided the peptides FEELNADLFR, TTPSYVAFTDTER, IINEPTAAAIAYGLDK and TFTNAVVTVPAYFNDSQR; the first three peptides are shared by various heat shock proteins, including heat shock-related 70 kDa protein 2 (HSP72), but the fourth peptide is unique to heat shock cognate 71 kDa protein (HSP7C). The position of this protein on the two-dimensional gel, and some others that were positively identified, is indicated in Fig. 2b. Additional proteins that were identified as ARA-associating proteins are provided in Table 1, grouped according to function, with predicted kDa and p*I* values. Supporting their identification were correlations between the kDa and calculated p*I* values of the proteins and the position of the spots on the gels. Also, when peptide sequences were species specific, the identified isoform was from rat (or from mouse, if a rat protein sequence was not in SwissProt), consistent with these proteins being produced in a rat cell line.

Identification of Proteins Associating with 5-HETE and LTB_4

As noted above, 5(*S*)-HETE can be a significant product of 5-LO metabolism of ARA. Several studies have examined the importance of the stereochemistry on function by comparing the effects of 5(*S*)- versus 5(*R*)-HETE. In short, some effects can be induced by both [24], whereas others are stereospecific [25, 26]. We compared 5(*S*)- vs. 5(*R*)-HETE in their capacity to bind proteins. Remarkably, both enantiomers retained many proteins (Fig. 3). Also, the similarity between the two sets of proteins was very high. Importantly, the major differences between the proteins were seen in horizontal groups of proteins (boxed in Fig. 3), which commonly represent proteins with different degrees of post-translational modification. Indeed, identification of selected pairs of spots using MALDI-TOF mass spectrometry verified that they were identical, recognized as Rho GDP-dissociation inhibitor 1 (GDIR), eukaryotic translation initiation factor 5A-2 (IF5A2), coactosin-like protein (COTL1) and SH3 domain-binding glutamic acid-rich-like protein 3 (SH3L3). Typically, 5(*S*)-HETE selectively captured the more acidic version and 5(*R*)-HETE bound the more basic protein. Additional proteins identified from the 5(*S*)-HETE gel are listed in Table 2.

Finally, two-dimensional gel separation of proteins that associated with LTB_4 revealed at least 20 proteins (not shown). A partial list of the most abundant proteins is given in Table 2. These are grouped according to known roles.

Discussion

This study presents a relatively simple and straightforward approach for capturing proteins that associate with PUFA and their derivatives. An asset of the approach is that it allows novel interactions to be discovered objectively. Through this approach, we have identified groups of proteins involved in protein synthesis, cytoskeletal function, Rho functioning and glycolysis that can associate with ARA. Some of these same proteins and roles are also shared with 5-HETE, suggesting that it can act like a second messenger akin to ARA. Perhaps most surprisingly, several proteins were found to associate with LTB_4, a lipid mediator whose actions are thought to be solely receptor-mediated. This suggests that at least some of the effects of LTB_4, as well as 5-HETE and ARA, may be through direct lipid-protein interactions.

Lipids, due to their hydrophobic nature, are first thought to associate with membranes. However, PUFA may have higher affinities for certain proteins than for membranes. For example, PUFA will partition into liposomal membranes in an aqueous solution, but will leave those

Table 1 Identification of some of the proteins that associate with ARA

Enzyme	Abbrev.	Accession	kDa	p*I*	Role(s)
Elongation factor 1-gamma	EF1G	Q68FR6	50	6.31	Protein synthesis; probably anchors the complex to other cellular components
Elongation factor 2	EF2	P05197	95.3	6.41	Protein synthesis; promotes the GTP-dependent translocation of the nascent protein chain
Eukaryotic translation initiation factor 5A-2	IF5A2	Q9GZV4	16.8	5.38	Protein synthesis; promotes the formation of the first peptide bond
Actin, cytoplasmic 1	ACTB	P60711	41.7	5.29	Motility
Moesin	MOES	O35763	67.7	6.16	Probably involved in connections of major cytoskeletal structures to the plasma membrane
Stathmin	STMN1	P13668	17.3	5.76	Prevents assembly and promotes disassembly of microtubules; Binds to two alpha/beta-tubulin heterodimers
Rho GDP-dissociation inhibitor 1	GDIR	Q99PT1	23.4	5.12	Inhibits dissociation of GDP from and the subsequent binding of GTP to Rho proteins
Nucleoside diphosphate kinase B	NDKB	P19804	17.3	6.91	Synthesis of nucleoside triphosphates other than ATP; negatively regulates Rho activity
Triosephosphate isomerase	TPIS	P48500	26.8	6.89	D-glyceraldehyde 3-phosphate = glycerone phosphate
Alpha-enolase	ENOA	P04764	47.1	6.16	Glycolysis, growth control, hypoxia tolerance, allergic responses, fibrinolysis
L-lactate dehydrogenase A chain	LDHA	P04642	36.5	8.45	Anaerobic glycolysis; (*S*)-lactate + NAD+ = pyruvate + NADH
Peroxiredoxin-1	PRDX1	Q63716	22.1	8.27	Redox regulation; eliminating peroxides; regulating H2O2
Heat shock cognate 71 kDa protein	HSP7C	P63018	70.9	5.37	Chaperone
Phosphatidylethanolamine-binding protein 1	PEBP1	P31044	20.8	5.47	Binds ATP, opioids and PE; Serine protease inhibitor
Serum albumin [Precursor]	ALBU	P02770	68.7	6.09	Regulates colloidal osmotic pressure of blood: binds water, Ca(2+), Na(+), K(+), fatty acids, hormones, bilirubin and drugs

Proteins were identified by BLAST search of SwissProt using at least two peptide sequences obtained by MALDI-TOF ms/ms analysis of two-dimensional gel samples. Abbreviation and SwissProt accession numbers, as well as predicted kDa and p*I* obtained using sequence analysis tools at SwissProt, are included

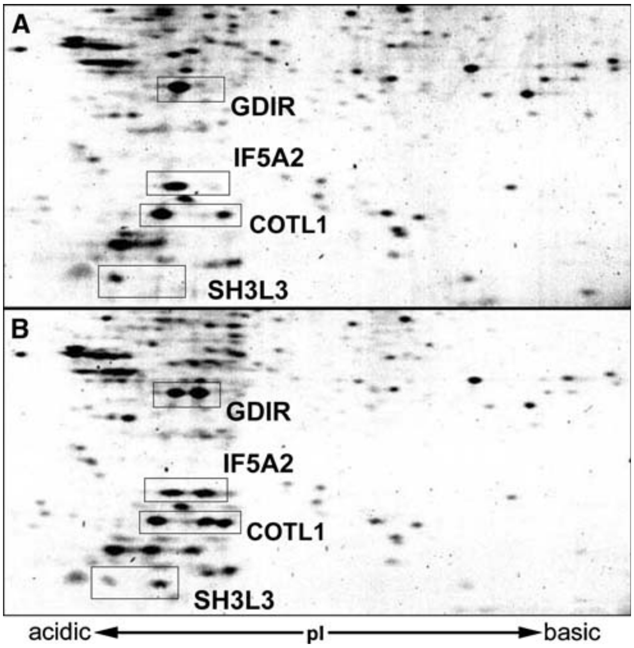

Fig. 3 Selected region of 2-D PAGE analysis of proteins that associate with 5(*S*)-HETE versus 5(*R*)-HETE. **a** 5(*S*)-HETE-associated proteins. **b** 5(*R*)-HETE-associated proteins. Region corresponds to approx. 10–37 kDa and p*I* 4.5–8. Abbreviations refer to proteins detailed in Table 2

membranes to associate with added albumin [27]. Furthermore, ARA will leave albumin to associate with classical fatty acid-binding proteins (FABP), again due to differences in affinity. This indicates that soluble proteins, like albumin and FABP, can have higher affinities for PUFA than do liposomal membranes.

An important question may be whether previous studies support any of the PUFA-protein interactions here. That is, are any of these interactions biologically important, or do they just reflect the interaction of a lipid with a hydrophobic portion of a protein? First, the unique profile of proteins observed for each of the PUFA/eicosanoids argues against all of the interactions being non-specific interactions. Second, the capture of albumin, while not surprising, serves as a positive control. Albumin is recognized to serve the physiologically important function of regulating the colloidal osmotic pressure of blood through its binding of fatty acids, cations, hormones, bilirubin and drugs. Perhaps most intriguing is the case of the Rho GDP-dissociation inhibitor 1 (GDIR). It is well established that PUFA, including ARA, activate the production of reactive oxygen species in leukocytes [28, 29]. The GTP-bound (activated) form of Rac is required for activation of NADPH oxidase [30]. In resting leukocytes, GDIR inhibits the activation of Rac by directly binding to the GDP-bound (inactive) form of Rac, preventing guanine–nucleotide exchange and activation. In a comparison of the ability of different lipids to alter GDIR binding, ARA and other PUFA, but not saturated fatty acids, caused almost complete dissociation of GDIR from Rac, leading to activation of Rac [31]. The identification of the same protein binding to 5(*S*)-HETE suggests that this derivative of ARA may also modulate Rac activation through GDIR. Finally, similar approaches using biotinylation of 15-deoxy-$\Delta^{12,14}$-prostaglandin J_2 have been used to show that this PGD_2 metabolite interacts with cytoskeletal [32, 33] and mitochondrial [34] proteins. These results underscore the versatility of this approach and strengthen the assertion that ARA metabolites may directly interact with proteins.

The role of PUFA to alter protein–protein interactions, demonstrated for GDIR [31], may also apply to other results from this study. Heat shock cognate 71 kDa protein (HSP7C) was found to bind ARA. ARA has been shown to cause the dissociation of two HSP proteins, approx. 70 and 90 kDa, from protein phosphatase 5, leading to inactivation and degradation of the phosphatase [35], suggesting, at least that the interaction of ARA with HSP7C may serve to dissociate it from target proteins. In contrast with this, ARA has been shown to promote a physical interaction between phospholipase C-γ and a multimeric activating protein, AHNAK [36]. Similarly, ARA promotes translocation of p47-phox [37] and assembly of the NADPH oxidase complex [38]. Thus, PUFA may alter protein functions by facilitating the assembly or disassembly of protein complexes.

Many of the oxidized lipids that are produced from PUFA are relatively unstable and reactive. For example, the 5-LO product LTA_4 has been shown to form stable adducts with nucleotides through covalent binding [39, 40]. Also, lipid hydroperoxides may be decomposed by antioxidants to produce DNA-reactive electrophiles [41]. Relevant to this study, biotinylated derivatives of 15-HETE have been shown to form complexes with proteins that are stable enough to withstand SDS-PAGE and electrophoretic transfer [42]. This suggests that some lipid-protein associations may be very stable.

Another interesting finding relates to L-lactate dehydrogenase A chain (LDHA), which is known to mediate the conversion of lactate to pyruvate, with concomitant generation of NADH from NAD^+. Either transient hypoxia [43] or ischemia [44] produces a rapid release of arachidonic acid associated with a marked increase in lactate and decreases in pyruvate and ATP. It seems possible that arachidonic acid might directly associate with LDHA and inhibit lactate dehydrogenase activity.

Proteins also show specificity for specific PUFA. For example, the different FABP clearly favor certain PUFA over others [45]. Similarly, 5-lipoxygenase, which initiates the synthesis of LTs from ARA, prefers ARA over other PUFA [46] and was detected in ARA-associated proteins

Table 2 Identification of some of the proteins that associate with 5(S)-HETE and LTB$_4$

Enzyme	Abbrev.	Accession	kDa	pI	Role(s)
5s-HETE binding prots					
Elongation factor 2	EF2	P05197	95.3	6.41	Protein synthesis; promotes the GTP-dependent translocation of the nascent protein chain
Eukaryotic translation initiation factor 5A-2	IF5A2	Q9GZV4	16.8	5.38	Protein synthesis; promotes the formation of the first peptide bond
Coactosin-like protein	COTL1	Q9CQI6	15.9	5.28	Binds to F-actin in a calcium-independent manner; has no direct effect on actin depolymerization
Tropomyosin alpha-4 chain	TPM4	P09495	28.5	4.66	Binds to actin filaments in muscle and non-muscle cells; in non-muscle cells, implicated in stabilizing cytoskeleton actin filaments
Stathmin	STMN1	P13668	17.3	5.76	Destabilizes microtubules; binds to two alpha/beta-tubulin heterodimers
Rho GDP-dissociation inhibitor 1	GDIR	Q99PT1	23.4	5.12	Inhibits dissociation of GDP from and the subsequent binding of GTP to Rho proteins
SH3 domain-binding glutamic acid-rich-like protein 3	SH3L3	Q91VW3	10.5	5.02	Could act as a modulator of glutaredoxin biological activity
LTB4 binding prots					
Actin, cytoplasmic 2	ACTG	P63259	41.8	5.31	Motility
Profilin-1	PROF1	P62963	15	8.46	Complexes with actin
Nucleoside diphosphate kinase B	NDKB	P19804	17.3	6.91	Synthesis of nucleoside triphosphates other than ATP; negatively regulates Rho activity
Fructose-bisphosphate aldolase A	ALDOA	P05064	39.4	8.3	Glycolysis: D-fructose 1,6-bisphosphate = glycerone phosphate + D-glyceraldehyde 3-phosphate
Peroxiredoxin-1	PRDX1	Q63716	22.1	8.27	Redox regulation; eliminating peroxides; regulating H2O2
Serum albumin (Precursor)	ALBU	P02770	68.7	6.09	Regulates colloidal osmotic pressure of blood: binds water, Ca(2+), Na(+), K(+), fatty acids, hormones, bilirubin and drugs

Proteins were identified by BLAST search of SwissProt using at least two peptide sequences obtained by MALDI-TOF ms/ms analysis of two-dimensional gel samples. Abbreviation and SwissProt accession numbers, as well as predicted kDa and pI obtained using sequence analysis tools at SwissProt, are included but not in the ACH-associated proteins (not shown). Also, certain proteins were more abundant in the ACH-associated fraction than in the ARA-associated fractions (Fig. 1), suggesting specificity. This specificity must, at least in part, be due to the shape and structure of the PUFA. This specificity of protein for PUFA may be so exquisite that it may distinguish between stereochemistry of a hydroxyl group, as seen in the difference between the proteins that bind 5(*S*)- and 5(*R*)-HETE (Fig. 3).

The specificity of protein for PUFA points to a drawback of the approach used in this study. Since the biotin moiety is at the carboxyl terminus, proteins that specifically target that site will be missed. For example, FA associate with classical FABP, like the human epidermal-FABP, with the carboxyl group of the FA directly interacting with side chains of key amino acids within the FABP [47]. As a result, this approach did not capture these well-known FABP, and perhaps many other proteins.

Another drawback of this approach is that it will not reveal which proteins interact directly with lipids, as opposed to those that associate indirectly by binding to a true PUFA-associating protein. For example, it is possible that the different cytoskeletal proteins (e.g., actin, moesin, stathmin, coactosin-like protein, profilin) may have been pulled down together, with only one of these proteins truly associating with ARA.

In summary, we present a relatively simple stepwise approach for the discovery of proteins that associate with PUFA and their derivatives. This approach can be used with any lipid with a free carboxyl terminus. Given the large number of proteins that were observed on the two-dimensional gels presented here, it appears that PUFA interact with many proteins. The diversity of PUFA and PUFA derivatives suggests that numerous interactions can be discovered with this approach.

Acknowledgments This research was supported by generous funding from the Undergraduate Research Opportunities Program at the University of Michigan, as well as by National Institutes of Health grant R01 AI43574. The technical expertise of Lindsay Nixon and Rebecca Oas is also acknowledged.

References

1. Simopoulos AP, Leaf A, Salem NJ (1999) Workshop on the essentiality of and recommended dietary intakes for omega-6 and omega-3 fatty acids. J Am Coll Nutr 18:487–489
2. de Deckere EAM, Korver O, Verschuren PM, Katan MB (1998) Health aspects of fish and n-3 polyunsaturated fatty acids from plant and marine origin. Eur J Clin Nutr 52:749–753
3. Hirafuji M, Machida T, Hamaue N, Minami M (2003) Cardiovascular protective effects of n-3 polyunsaturated fatty acids with special emphasis on docosahexaenoic acid. J Pharmacol Sci 92:308–316
4. Burr ML, Fehily AM, Rogers S, Welsby E, King S, Sandham S (1989) Diet and reinfarction trial (DART): design, recruitment, and compliance. Eur Heart J 10:558–567
5. Marchioli R, Barzi F, Bomba E, Chieffo C, Di Gregorio D, Di Mascio R, Franzosi MG, Geraci E, Levantesi G, Maggioni AP, Mantini L, Marfisi R, Mastrogiuseppe G, Mininni N, Nicolosi GL, Santini M, Schweiger C, Tavazzi L, Tognoni G, Tucci C, Valagussa F, Investigators G-P (2002) Early protection against sudden death by n-3 polyunsaturated fatty acids after myocardial infarction: time-course analysis of the results of the Gruppo Italiano per lo Studio della Sopravvivenza nell'Infarto Miocardico (GISSI)-Prevenzione. Circulation 105:1897–1903
6. Kang JX, Leaf A (1994) Effects of long-chain polyunsaturated fatty acids on the contraction of neonatal rat cardiac myocyte. Proc Natl Acad Sci USA 91:9886–9890
7. Xiao Y-F, Gomez AM, Morgan JP, Lederer WJ, Leaf A (1997) Suppression of voltage-gated L-type Ca^{2+} currents by polyunsaturated fatty acids in adult and neonatal rat ventricular myocytes. Proc Natl Acad Sci USA 94:4182–4187
8. Framework MGPR (1998) Thrombosis prevention trial: randomised trial of low-intensity oral anticoagulation with warfarin and low-dose aspirin in the primary prevention of ischemic heart disease in men at increased risk. Lancet 351:233–241
9. Ridker PM, Manson JE, Buring JE, Goldhaber SZ, Hennekens CH (1991) The effect of chronic platelet inhibition with low-dose aspirin on atherosclerotic progression and acute thrombosis: clinical evidence from the Physicians' Health Study. Am Heart J 122:1588–1592
10. Steering Committee PHSRG (1989) Final report on the aspirin component of the ongoing Physicians' Health Study. N Engl J Med 321:129–135
11. Murphy RC, Gijón MA (2007) Biosynthesis and metabolism of leukotrienes. Biochem J 405:379–395
12. Baskin DS, Ngo H, Didenko V (2003) Thimerosal induces DNA breaks, caspase-3 activation, membrane damage, and cell death in cultured human neurons and fibroblasts. Toxicol Sci 74:361–368
13. Woo KJ, Lee TJ, Bae JH, Jang BC, Song DK, Cho JW, Suh SI, Park JW, Kwon TK (2006) Thimerosal induces apoptosis and G2/M phase arrest in human leukemia cells. Mol Carcinog 45:657–666
14. Cao Y, Pearman AT, Zimmerman GA, McIntyre TM, Prescott SM (2000) Intracellular unesterified arachidonic acid signals apoptosis. Proc Natl Acad Sci USA 97:11280–11285
15. Tinel H, Wehner F, Kinne RK (1997) Arachidonic acid as a second messenger for hypotonicity-induced calcium transients in rat IMCD cells. Pflugers Arch 433:245–253
16. van der Zee L, Nelemans A, den Hertog A (1995) Arachidonic acid is functioning as a second messenger in activating the Ca^{2+} entry process on H1-histaminoceptor stimulation in DDT1 MF-2 cells. Biochem J 305:859–864
17. Flamand N, Mancuso P, Serezani CHC, Brock TG (2007) Leukotrienes: mediators that have been typecast as villains. Cell Mol Life Sci 64:2657–2670
18. Yokomizo T, Izumi T, Chang K, Takuwa Y, Shimizu T (1997) A G-protein-coupled receptor for leukotriene B_4 that mediates chemotaxis. Nature 387:620–624
19. Yokomizo T, Kato K, Terawaki K, Izumi T, Shimizu T (2000) A second leukotriene B(4) receptor, BLT2. A new therapeutic target in inflammation and immunological disorders. J Exp Med 192:421–432
20. Skinner J, Sinclair C, Romeo C, Armstrong D, Charbonneau H, Rossie S (1997) Purification of a fatty acid-stimulated protein-serine/threonine phosphatase from bovine brain and its identification as a homolog of protein phosphatase 5. J Biol Chem 272:22464–22471

21. Siegenthaler G, Roulin K, Chatellard-Gruaz D, Holtz R, Saurat JH, Hellman U, Hagens G (1997) A heterocomplex formed by the calcium-binding proteins MRP8 (S100-A8) and MRP-14 (S100A9) binds unsaturated fatty acids with high affinity. J Biol Chem 272:9371–9377
22. Bouzidi F, Doussiere J (2004) Binding of arachidonic acid to myeloid-related proteins (S100A8/A9) enhances phagocytic NADPH oxidase activation. Biochem Biophys Res Commun 325:1060–1065
23. Abramson SB, Leszczynska-Piziak J, Weissmann G (1991) Arachidonic acid as a second messenger. Interactions with a GTP-binding protein of human neutrophils. J Immunol 147:231–236
24. Bittleman DB, Casale TB (1995) 5-Hydroxyeicosatetraenoic acid (HETE)-induced neutrophil transcellular migration is dependent upon enantiomeric structure. Am J Respir Cell Mol Biol 12:260–267
25. Rossi AG, Thomas MJ, O'Flaherty JT (1988) Stereospecific bioactions of 5-hydroxyeicosatetraenoate. FEBS Lett 240:163–166
26. O'Flaherty J, Rossi A (1993) 5-Hydroxyicosatetraenoate stimulates neutrophils by a stereospecific, G protein-linked mechanism. J Biol Chem 268:14708–14714
27. Ek-Von Mentzer BA, Zhang F, Hamilton JA (2001) Binding of 13-HODE and 15-HETE to phospholipid bilayers, albumin, and intracellular fatty acid binding proteins. Implications for transmembrane and intracellular transport and for protection from lipid peroxidation. J Biol Chem 276:15575–15580
28. Kakinuma K (1974) Effects of fatty acids on the oxidative metabolism of leukocytes. Biochim Biophys Acta 348:76–85
29. Badwey J, Curnutte J, Karnovsky M (1981) *cis*-polyunsaturated fatty acids induce high levels of superoxide production by human neutrophils. J Biol Chem 256:12640–12643
30. Heyworth PG, Knaus UG, Xu X, Uhlinger DJ, Conroy L, Bokoch GM, Curnutte JT (1993) Requirement for posttranslational processing of Rac GTP-binding proteins for activation of human neutrophil NADPH oxidase. Mol Biol Cell 4:261–269
31. Chuang TH, Bohl BP, Bokoch GM (1993) Biologically active lipids are regulators of Rac.GDI complexation. J Biol Chem 268:26206–26211
32. Stamatakis K, Sánchez-Gómez FJ, Pérez-Sala D (2006) Identification of novel protein targets for modification by 15-deoxy-Delta12,14-prostaglandin J_2 in mesangial cells reveals multiple interactions with the cytoskeleton. J Am Soc Nephrol 17:89–98
33. Aldini G, Carini M, Vistoli G, Shibata T, Kusano Y, Gamberoni L, Dalle-Donne I, Milzani A, Uchida K (2007) Identification of actin as a 15-deoxy-Delta12,14-prostaglandin J_2 target in neuroblastoma cells: mass spectrometric, computational, and functional approaches to investigate the effect on cytoskeletal derangement. Biochemistry 46:2707–2718
34. Landar A, Shiva S, Levonen AL, Oh J-Y, Zaragoza C, Johnson MS, Darley-Usmar VM (2006) Induction of the permeability transition and cytochrome c release by 15-deoxy-Delta12,14-prostaglandin J_2 in mitochondria. Biochem J 394:185–195
35. Zeke T, Morrice N, Vázquez-Martin C, Cohen PT (2005) Human protein phosphatase 5 dissociates from heat-shock proteins and is proteolytically activated in response to arachidonic acid and the microtubule-depolymerizing drug nocodazole. Biochem J 385:45–56
36. Sekiya F, Bae YS, Jhon DY, Hwang SC, Rhee SG (1999) AHNAK, a protein that binds and activates phospholipase C-γ1 in the presence of arachidonic acid. J Biol Chem 274:13900–13907
37. Sellmayer A, Obermeier H, Danesch U, Aepfelbacher M, Weber PC (1996) Arachidonic acid increases activation of NADPH oxidase in monocytic U937 cells by accelerated translocation of p47-phox and co-stimulation of protein kinase C. Cell Signal 8:397–402
38. Uhlinger DJ, Tyagi SR, Inge KL, Lambeth JD (1993) The respiratory burst oxidase of human neutrophils. Guanine nucleotides and arachidonate regulate the assembly of a multicomponent complex in a semirecombinant cell-free system. J Biol Chem 268:8624–8631
39. Reiber DC, Murphy RC (2000) Covalent binding of LTA_4 to nucleosides and nucleotides. Arch Biochem Biophys 379:119–26
40. Hankin JA, Jones DN, Murphy RC (2003) Covalent binding of leukotriene A_4 to DNA and RNA. Chem Res Toxicol 16:551–561
41. Lee SH, Oe T, Blair IA (2001) Vitamin C-induced decomposition of lipid hydroperoxides to endogenous genotoxins. Science 292:2083–2086
42. Kang LT, Vanderhoek JY (1997) Synthesis and use of a novel biotinylated probe for the chemiluminescent detection of proteins that bind 15-hydroxyeicosatetraenoic acid. Anal Biochem 250:119–122
43. Ikeda M, Busto R, Yoshida S, Santiso M, Martinez E, Ginsberg MD (1988) Cerebral phosphoinositide, triacylglycerol and energy metabolism during severe hypoxia and recovery. Brain Res 459:344–350
44. Katayama Y, Shimizu J, Suzuki S, Perrier H, Prasit P, Wang Z, Vickers PJ (1990) Role of arachidonic acid metabolism on ischemic brain edema and metabolism. Adv Neurol 52:105–108
45. Zimmerman AW, van Moerkerk HT, Veerkamp JH (2001) Ligand specificity and conformational stability of human fatty acid-binding proteins. Int J Biochem Cell Biol 33:865–876
46. Charleson S, Evans JF, Léger S, Perrier H, Prasit P, Wang Z, Vickers PJ (1994) Structural requirements for the binding of fatty acids to 5-lipoxygenase-activating protein. Eur J Pharmacol 267:275–280
47. Hohoff C, Börchers T, Rüstow B, Spener F, van Tilbeurgh H (1999) Expression, purification, and crystal structure determination of recombinant human epidermal-type fatty acid binding protein. Biochemistry 38:12229–12239

Lipids (2008) 43:171–180
DOI 10.1007/s11745-007-3130-9

METHODS

High-Throughput Analysis of Plasma Fatty Acid Methyl Esters Employing Robotic Transesterification and Fast Gas Chromatography

M. Athar Masood · Norman Salem Jr

Received: 10 August 2007 / Accepted: 22 October 2007 / Published online: 15 December 2007
© AOCS 2007

Abstract Fatty acid analysis is an important research tool, and indices derived from essential fatty acid contents serve as useful biomarkers related to cardiovascular and other chronic disease risk. Both clinical and basic studies of essential fatty acid composition are becoming ever larger in magnitude leading to delays while the rather laborious lipid analyses are performed. A robotic transesterification procedure has been developed for high-throughput analysis of plasma fatty acid methyl esters. In this approach, robots perform most steps including plasma and reagent transfer, transesterification reaction via heating at 80 °C in open tubes with multiple reagent additions, followed by two-phase extraction and transfer of lipid extracts to GC vials. The vials are then placed directly onto a GC autosampler carousel for robotic sample injection. An improved fast GC method is presented in which the peaks of interest are eluted within 6 min. This method is readily scalable to prepare and analyze 200 samples per day (1,000 samples per week) so that large clinical trials can be accommodated.

Keywords Robotic transesterification ·
Plasma fatty acid methyl esters ·
Fast gas chromatographic ·
High throughput sample preparation ·
High throughput gas chromatography · Essential fatty acids

Introduction

Fatty acids are important components of biological membranes and their measurement is useful from a variety of biological perspectives. The chain length, degree of unsaturation and other structural features of fatty acids are one determinant of the physico-chemical properties of biological membranes [1, 2]. Essential fatty acids are the focus of many compositional [3–5], physiological [6–8], behavioral [9–14] and metabolic experiments [15–19]. The n-3 polyunsaturates eicosapentaenoic acid (20:5n-3, EPA) and docosahexaenoic acid (22:6n-3, DHA) have been inversely associated with several disease states in epidemiological studies [20–23]. They antagonize the n-6 polyunsaturated arachidonic acid (20:4n-6, AA) and the eicosanoids that are produced from it [24, 25]. Moreover, the blood stream contents of these n-3 and n-6 polyunsaturates provide an important biomarker of cardiovascular disease risk [21, 22, 24]. EPA and DHA intake and tissue content have been related to sudden cardiac death and arrhythmias [26–29]. These observations have led to many clinical experiments and more recently large clinical trials (e.g., GISSI study [30], primary prevention CVD [31],

---

Electronic supplementary material The online version of this article (doi:10.1007/s11745-007-3130-9) contains supplementary material, which is available to authorized users.

M. A. Masood · N. Salem Jr
Laboratory of Membrane Biochemistry and Biophysics,
National Institutes on Alcohol Abuse and Alcoholism,
National Institutes of Health, Rockville, MD, USA

N. Salem Jr (✉)
5625 Fishers Lane, Room 3N-07, MSC 9410, Bethesda,
MD 20892-9410, USA
e-mail: nsalem@niaaa.nih.gov

Present Address:
M. A. Masood
Laboratory of Proteomics and Analytical Technologies,
Advanced Technology Program, SAIC-Frederick, Inc.,
National Cancer Institute at Frederick, P. O. Box B, Frederick,
MD 21702, USA
e-mail: masoodaa@mail.nih.gov

AREDS2 [32], DINO infant [33], NINDS Alzheimer's [34]), where the effects of increased EPA and/or DHA intake are examined in various pathological states.

Thus the analysis of fatty acid profiles in tissues, particularly blood components, has become increasingly important as endpoints in clinical trials, as biomarkers in cross-sectional studies and as measures of compliance. Such trials may generate very large numbers of samples for analysis necessitating quick, efficient and inexpensive analytical methods for fatty acid analysis. The standard methods for such analysis typically involve total lipid extraction followed by a laborious transmethylation procedure, methyl ester extraction, concentration and gas chromatographic analysis. It is typical for this labor-intensive methodology to consume 2 days of a skilled chemist's efforts for 10–20 samples. As a result, it has not been generally feasible to study thousands of subjects where each subject in a clinical trial can generate many samples. Clearly, a high throughput method for fatty acid analysis is needed.

In previous work from our laboratory, a simplified chemical procedure was developed for lipid transmethylation [35] that was based upon the Lepage and Roy procedure [36]. A method for fast gas chromatography of the typical profile of fatty acid methyl esters found in biological samples was also introduced [35, 37]. This paper presents a complete method for robotic transmethylation and analysis of plasma lipids. Plasma is directly reacted without prior lipid extraction, as in the Lepage and Roy method, and a robot carries out the reaction, methyl ester extraction and sample concentration, leaving the sample in a GC autosampler vial ready for injection. A faster method for GC analysis is also presented here. Together, these methods are efficient and cost effective. They may potentially increase laboratory productivity by an order of magnitude. These procedures may be used as the basis for a high-throughput method suitable for analysis of large populations such as are found in clinical trials.

Materials and Methods

Reagents and Plasma Samples

Acetyl chloride, 2[6]-di-*tert*-butyl-*p*-cresol (butylated hydroxytoluene, BHT), analytical grades methanol, hexane and toluene, and K_2CO_3 were purchased from Sigma-Aldrich Chemical Co. (St Louis, MO, USA). BHT was added to methanol (50 μg BHT/sample) to prevent fatty acid oxidation. The internal fatty acid standards (23:0 methyl ester, and 22:3n-3) and external (GLC-462) were purchased from Nu-Chek Prep (Elysian, MN, USA). Internal standard solutions were prepared by dissolving them, respectively, in the methanol BHT solution at a concentration of 250 μg/ml. Blood was collected by venipuncture into a heparinized tube and was immediately centrifuged for 5 min at 2,000×*g*. The resulting plasma was then aliquoted in batches of 5 ml, frozen and stored at −80 °C. The 13 mm × 100 mm Pyrex disposable culture tubes for transesterification reactions were purchased from PGC Scientific (Frederick, MD, USA).

For the robotic transesterification procedure, Stock A and Stock B reagents were prepared in bulk. The 2.4 ml of Stock Solution A required initially for the reaction of 100–200 μl aliquots of plasma included 1.9 ml of methanol, 100 μl of acetyl chloride, 0.3 ml of toluene, and 100 μl each of the two internal standard solutions (containing 25 μg of 23:0 and 20 μg of 22:3n-3 as ethyl esters). Each 900 μl volume of Stock B solution was comprised of 740 μl of methanol, 40 μl of acetyl chloride solution, and 120 μl of toluene.

Robotic Apparatus

A 1.5-m long Freedom EVO robot equipped with a liquid handling arm (LH-arm), a multi-channel 1-ml syringe pipetting system with an integrated liquid detection system and liquid detection disposable tips, a robotic manipulator arm, a fast wash pump and a syringe wash station, low disposable tips ejector option, and a nitrogen manipulation station was purchased from Tecan US Inc. (Research Triangle Park, NC, USA). The working space on the Tecan deck also includes other peripherals such as tip rack with a waste tip disposal station, twelve 13-mm test tube carrier racks each with a capacity to hold up to 16 plasma vials along the *y*-axis, three troughs for holding reagents, a reaction block, and a heated GC vial sample block. The layout of the robotic deck is illustrated in Fig. 1. The Tecan EVOware™ scripting programming language is used to control the robotic arm and other modules. The temperature regulated GC vial sample block and the heating-cooling reaction block were custom made by J-Kem Scientific Inc. (St Louis, MO, USA) and are under computer control. The reaction block is composed of a hot plate connected to a chiller through a cryogenic solenoid valve which regulates the flow of cooling liquid. The GC vial sample plate and reaction block hot plate are an array containing 16 × 12 holes to hold a maximum of 192 GC vials (13-mm diameter) and 192 reaction tubes of 13 × 100 mm dimension, respectively. Both the reaction block and GC vial block are controlled by a digital temperature controller either via a local module or by a program driver that was incorporated into the software of the Tecan programming command set running under Windows. The robot was encased in a hood fabricated by

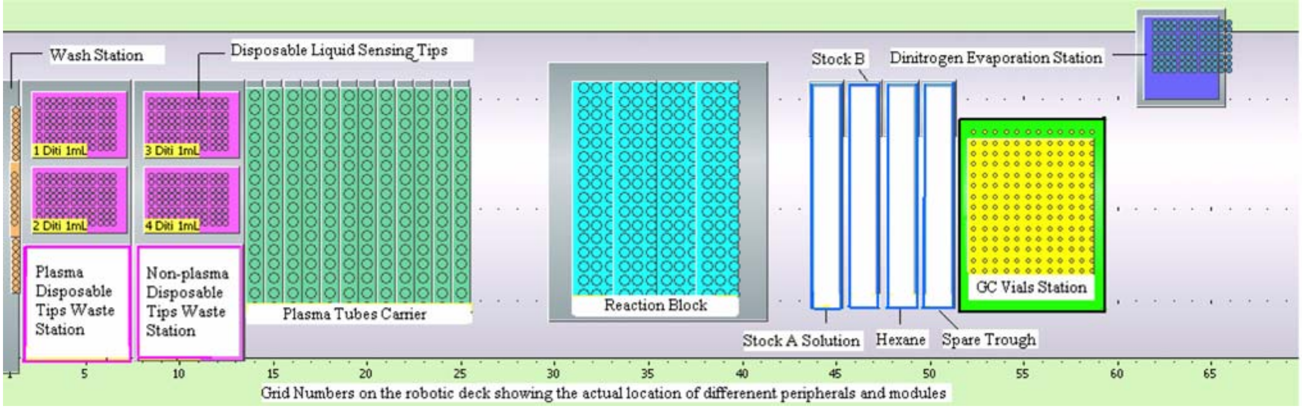
Wash Station
Disposable Liquid Sensing Tips
1 Diti 1mL
2 Diti 1mL
3 Diti 1mL
4 Diti 1mL
Plasma Disposable Tips Waste Station
Non-plasma Disposable Tips Waste Station
Plasma Tubes Carrier
Reaction Block
Stock B
Dinitrogen Evaporation Station
GC Vials Station
Stock A Solution
Hexane
Spare Trough
5
10
15
20
25
30
35
40
45
50
55
60
65
Grid Numbers on the robotic deck showing the actual location of differenent peripherals and modules

Fig. 1 Diagrammatic representation of the layout of the robotic deck

Airline Hydraulics (Bensalem, PA, USA) and is connected at the top to an exhaust outlet and is well ventilated.

Instrumentation

Fast GC Analyses

Analyses were performed on an Agilent 6890N Network Gas Chromatograph (Agilent Technologies, Palo Alto, CA, USA) equipped with a split/splitless injector, a 7683 automatic liquid sampler and flame ionization detector. The GC was also equipped with a 208-V power supply to enable fast temperature ramping. The column used was a DB-FFAP of 15 m × 0.1 mm i.d. × 0.1 μm film thickness (J&W Scientific from Agilent Technologies, Palo Alto, CA, USA). Instrument control and data collection was performed by a GC Chemstation, Rev. B.01.01 (Agilent Technologies, Palo Alto, CA, USA). Temperature program was as follows: initial conditions, 150 °C with 0.25 min hold; ramp 35 °C/min to 200 °C, 7 °C/min to 225 °C with a 3.2 min hold and then 80 °C/min to 245 °C with 2.75 min hold. Instrumental conditions were as follows: carrier gas was H_2 at a flow rate of 56 cm/s and a constant head pressure of 344.7 kPa; FID detector set at 250 °C; air and N_2 make-up gas flow rates of 450 and 10 ml/min; respectively, with a split ratio of 100:1; sampling frequency of 50 Hz; autosampler injections of 2 μl volume. Run time for a single sample was 11 min with all the fatty acid peaks of interest eluting within 8 min of the injection time. The sample injection-to-injection time was 16 min including a re-equilibration time of 1.50 min. The liner used was split with a cup containing no glass wool.

For the development of a faster GC method, a constant flow mode of 0.6 ml/min was used using the same column as above. Temperature program was as follows: initial conditions, 160 °C with 0.10 min hold; ramp 60 °C/min to 220 °C with a 0.5 min hold, 80 °C/min to 175 °C, 70 °C/min to 230 °C with 1.82 min hold, 70 °C/min to 220 °C with 0.96 min hold, and final ramping at 60 °C/min to 245 °C with 2.40 min hold. Instrumental conditions were as follows: carrier gas was H_2 at a starting flow rate of 58 cm/s and a starting head pressure of 344.7 kPa; FID detector set at 250 °C; air and N_2 make-up gas flow rates of 450 and 10 ml/min, respectively; split ratio of 100:1; sampling frequency of 50 Hz; autosampler injections of 2 μl volume. Run time for a single sample was 8.69 min with all the fatty acid peaks of interest eluting within 5.8 min of the injection time. The sample injection-to-injection time was 12 min, including a re-equilibration time of 1.50 min. The data was quantified according to a method previously described [35].

Transesterification Methods

The standard Lepage and Roy transesterification method [36] was used as the reference point for comparisons to samples generated by the robotic method. All manipulations were performed under a nitrogen atmosphere. Briefly, 200 μl of plasma and 100 μl each of the two internal standard solutions (providing 25 μg of 23:0 and 20 μg of 22:3n-3 methyl ester) were added to 13 mm × 100 mm borosilicate or Pyrex screw-capped glass tubes, followed by an addition of 2 ml of a methanol:hexane (4:1 v/v) mixture. Samples were vortexed and the tubes were placed on ice, and then acetyl chloride (200 μl) was added dropwise while swirling the tubes. The tubes were tightly capped under nitrogen, and heated at 100 °C for 60 min. Afterwards, the samples were placed on ice, uncapped, and neutralized by the addition of 5 ml of a 6% solution of K_2CO_3. The tubes were recapped and vortexed for 1 min followed by centrifugation for 2 min at 3,000 rpm on a refrigerated tabletop centrifuge at 9 °C to separate the mixture into two phases and the upper (organic) phase was collected. The extraction procedure was repeated on the lower phase by adding 0.5 ml of hexane, vortexing and centrifuging. The organic phases were combined and evaporated under nitrogen to a volume of 75–100 µl. This solution was transferred to a GC vial, and the vial was crimped under nitrogen for FAME analysis by GC. All reactions were performed in sextet in a well ventilated fume hood.

Automated Robotic Transesterification Procedure

For robotic transesterification procedure Stock A and Stock B reagents were freshly prepared in bulk as stated above. The hexane solution and the bulk stock solutions A and B were placed in three different Teflon troughs. Plasma sample vials were placed on the carrier racks and clean uncapped pyrex tubes were labeled and placed in the reaction block (Fig. 1). The robot was initialized and the prompt for the number of samples to be processed is answered. Then the liquid handling arm (LH-arm) picks up disposable tips, aspirates 100–200 µl of plasma per tip, and then dispenses the plasma into the reaction tubes on the reaction block. Tips are ejected into a waste tip dispenser for biohazardous waste (labeled as "plasma disposable tips waste station" in Fig. 1) between plasma samples to avoid cross-contamination. The process is repeated until all plasma samples have been pipetted into reaction tubes. The LH-arm then obtains a fresh set of eight disposable tips and adds 800 µl of stock solution A to each reaction tube three times (2.4 ml total). The tips are then ejected into a general purpose waste tip dispenser. The program then issues a command to the reaction block to heat to 80 °C for 2.5 h. During the course of the 2.5 h reaction time, five additions of 0.9 ml each of stock B solution (every 20 m) are performed by the robot to prevent complete drying of the reaction tubes as well as to compensate for evaporation of the solution and to complete the transesterification reaction. This multiple addition helps to wash down the sides of the tubes and thus yield a complete reaction. Also after each round of addition of the stock B solution, the LH-arm was stationed away from the reaction block in order to minimize exposure of the robot arm pneumatics to corrosive vapors arising from the heated reaction tubes. However, corrosion is still a possibility and so the instrument accuracy is validated every day by weighing a certain volume of liquid that is dispensed by the LH-arm. After the last addition, the reaction block was allowed to cool to 25 °C via a command issued by the program. This sets the solenoid sensor to open to allow chilled fluid (10 °C) to circulate around the reaction block to bring the temperature down to 20 °C within approximately 30 min. The LH-arm picks up a fresh set of disposable tips, aspirates 700 µl of hexane from the third trough and dispenses this into each of the reaction tubes. After this task is performed, the tips are ejected. The LH-arm obtains fresh tips, aspirates 400 µl of the upper hexane phase and dispenses it at the bottom of the reaction tube, forcing the hexane to mix with the aqueous phase as it passes thru. This mixing step is repeated 20 times followed by the ejection of the tips. It was observed that 15–20 hexane aspirations for extraction of FAMEs was sufficient since fewer than 15 aspiration cycles resulted in incomplete extraction and more than 20 aspiration cycles did not produce any benefit. The LH-arm then obtains a fresh set of disposable tips and aspirates from the reaction tubes 250 µl of the upper phase hexane solution. The system is able to detect the position at which it becomes immersed in the hexane solution as it is lowered into the tube through detection of a change in pressure (or by capacitance for detection of the interface between the two liquids). The hexane is transferred into GC vials positioned in the GC vial block. Tips must be changed prior to mixing or sampling a new set of tubes. Since only the tips come in contact with sample tube contents and a new tip is used for each step, there is no possibility of sample cross-contamination. The GC vials can be heated in order to concentrate the sample through hexane evaporation.

Results and Discussion

Validation of Robotic Transmethylation Procedure

In a previous publication from this laboratory, we demonstrated that a simplification of the Lepage and Roy procedure could produce valid results [35]. In that work an "open tube" method was implemented that was amenable to robotic application. This chemical procedure was transferred to a robotic procedure as described above. A bulk plasma sample was transmethylated by the fully automated robotic method and the results compared to the standard Lepage and Roy procedure ($n = 6$). A second set of samples were similarly treated with the robotic procedure, and the hexane extracts were subjected to heating in the GC vial station in order to concentrate the extract further (Table 1). The mean values for each fatty acid concentration are similar in the three methods. The coefficients of variation are as good or better in the robotic method as the standard method. The fatty acid percentages in the three methods are very similar. The robotic method was in this way validated for plasma analysis. We have run the robotic method with an n of up to 40 samples and obtained similar results. The fatty acids measured here are

Table 1 Comparison of human plasma fatty acid concentrations in standardized and robotic methods using fast gas chromatography ($n = 6$)

Fatty acids	Standardized method			Robotic method				Robotic method (concentrated)			
	Mean (μg/ml)	CV (%)	Percentage of total fatty acids	Mean (μg/ml)	CV (%)	Percentage of total fatty acids	Difference (%)	Mean (μg/ml)	CV (%)	Percentage of total fatty acids	Difference[a] (%)
14:0	26.4	7.3	1.1	25.7	1.7	1.1	−2.5	27.1	1.9	1.2	2.5
16:0	538.2	6.5	22.5	568.3	2.6	24.1	5.6	538.8	1.6	23.1	0.1
18:0	198.0	6.6	8.3	214.1	3.1	9.1	8.1	206.0	1.1	8.8	4.0
20:0	6.4	4.9	0.3	6.8	1.8	0.3	5.7	7.2	3.4	0.3	12.7
22:0	19.7	2.2	0.8	21.5	5.1	0.9	9.1	21.4	5.0	0.9	8.6
24:0	16.0	1.4	0.7	17.2	4.7	0.7	7.0	17.3	6.3	0.7	8.0
Total saturates	804.8	6.1	33.6	853.6	1.5	36.2	6.1	817.8	1.1	35.0	1.6
16:1n-7	45.7	9.9	1.9	44.5	4.7	1.9	−2.6	42.5	8.7	1.8	−7.0
18:1n-7	43.9	5.7	1.8	42.7	4.4	1.8	−2.8	41.3	4.4	1.8	−5.9
18:1n-9	416.9	8.7	17.4	379.0	4.0	16.1	−9.1	390.4	0.8	16.7	−6.4
20:1n-9	2.7	5.7	0.1	2.8	3.6	0.1	1.8	2.6	7.4	0.1	−5.3
24:1n-9	19.8	2.3	0.8	18.7	3.0	0.8	−5.5	21.6	8.0	0.9	9.5
Monounsaturates	529.0	7.6	22.1	487.6	3.8	20.7	−7.8	498.4	1.1	21.3	−5.8
18:2n-6	663.1	8.1	27.7	636.1	3.6	26.9	−4.1	641.6	0.5	27.5	−3.2
18:3n-6	12.4	8.2	0.5	11.8	2.2	0.5	−4.9	10.6	0.7	0.5	−14.2
20:2n-6	4.9	7.2	0.2	5.0	2.2	0.2	0.7	5.1	3.4	0.2	2.2
20:3n-6	38.0	3.9	1.6	35.8	4.0	1.5	−5.8	36.2	3.3	1.5	−4.8
20:4n-6	192.5	3.0	8.0	188.5	2.6	8.0	−2.1	184.0	1.8	7.9	−4.4
22:4n-6	7.0	8.5	0.3	6.6	7.4	0.3	−4.8	6.6	5.9	0.3	−5.7
22:5n-6	5.4	8.4	0.2	5.0	2.6	0.2	−7.1	5.1	6.8	0.2	−7.0
Total n-6 PUFA	923.3	6.5	38.6	888.8	3.3	37.6	−3.7	889.1	0.7	38.1	−3.7
18:3n-3	15.5	6.5	0.6	14.3	7.6	0.6	−7.9	14.7	6.2	0.6	−5.4
20:5n-3	38.8	2.3	1.6	40.3	3.8	1.7	4.0	41.5	7.7	1.8	7.2
22:5n-3	17.8	2.6	0.7	16.3	6.3	0.7	−8.2	17.0	7.4	0.7	−4.2
22:6n-3	63.4	3.1	2.7	60.0	2.3	2.5	−5.5	57.5	4.0	2.5	−9.3
Total n-3 PUFA	135.5	2.6	5.7	130.8	3.2	5.5	−3.4	130.8	4.0	5.6	−3.5
Total PUFA	1,058.8	6.0	44.3	1,019.7	3.1	43.2	−3.7	1,019.9	1.1	43.7	−3.7
Total fatty acid	2,392.6	5.8	100.0	2,360.9	2.1	100.0	−1.3	2,336.1	0.8	100.0	−2.4

[a] Percentage difference of the concentration values

the common ones reported for many other mammalian tissue analyses as well.

Fatty acid extraction using 10% decane in pentane has also been used as an alternative extraction solvent. During heating in the GC vial block, the pentane is easily evaporated leaving mainly the decane volume containing the methyl esters. It is also possible to leave an open GC vial on the GC autosampler and allow it to evaporate prior to analysis. We encountered some difficulties with dripping during the LH-arm transfer of pentane to the GC vials. However, this problem was overcome by first aspirating and dispensing pentane prior to sample transfer.

Another difficulty is the leaching of organic compounds from the disposable tips. The black tips used for capacitance based detection are worse in this respect, in our experience. These impurities elute primarily in the first 1.5 min of the GC run. They create difficulties for automated peak integration of minor peaks of 10–14 carbons with zero or one double bonds. Tips from a variety of vendors have given similar results, however, the clear tips used in pressure-based sensing exhibit a lower level of leaching.

Improvements in the Fast GC Method

We earlier developed a Fast GC method utilizing a DB-FFAP column of dimensions 15 m × 0.1 mm i.d. × 0.1 μm film thickness. A high temperature program was used in which all the fatty acid peaks of interest eluted within 8 min of injection, with a sample to sample injection time of 16 min (Fig. 2a). An attempt was made to further

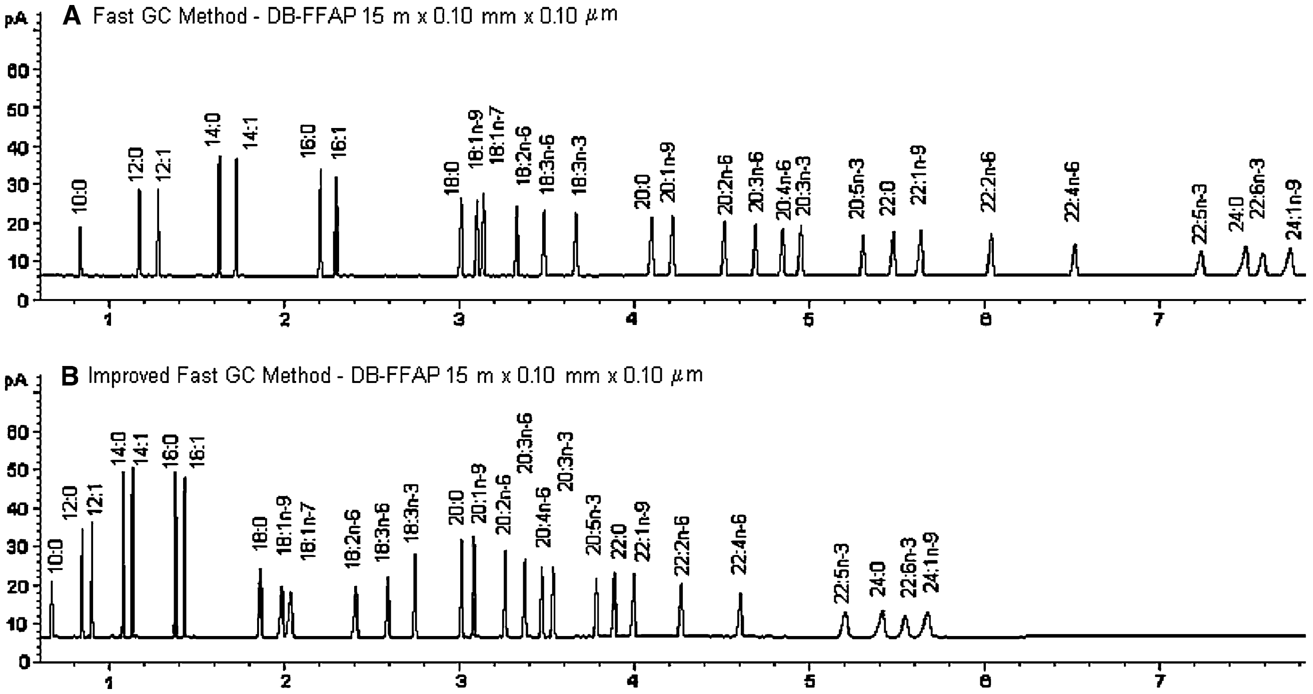

Fig. 2 Improvements in Fast GC methods for separation of a mixed FAME external reference standard

shorten the GC run times using an aggressive, single ramp method of 40 °C or 50 °C/min and starting from 135 to 150 °C up to 240 °C. However, this approach resulted in overlaps of critical peaks found in a 28 component quantitative standard (Nu Chek Prep 462); 18:1n-9, 18:1n-7 and 24:1n-9, 22:6n-3 were the overlapping peak pairs in this case. A method was then developed based on the constant flow mode of operation in which the oven temperature was ramped up and down to effect critical pair separation. With this method, peaks of interest eluted in less than 6 min and sample-to-sample injection time was under 13 min allowing for the elution of cholesterol (Fig. 2b). An initial hold time of 0.10 min and starting temp of 160 °C was used. We observed that even a small decrease in the hold time or a slight increase in the initial oven temperature results in coelution of the 10:0 and 12:0 peaks with the solvent peak. Similarly, small changes (e.g., 0.10 m) in the hold times after the temperature ramps resulted in a loss of peak separation. Use of the constant pressure mode instead of the constant volume mode using an identical temperature program led to an increase of 1 min in analysis time but maintained good separation of peaks. GC Methods have been published where the fatty acid components elute within 2 min [38], however these methods are not feasible for the analysis of FAMEs from plasma samples due to the coelution of several critical pairs (18:1n-9, 18:1n-7 and 24:1n-9, 22:6n-3) which then prevent correct quantitation.

The improved fast GC method that we have developed has been applied to the separation of plasma fatty acid methyl esters. In both the former method and the faster method, all of the peaks of interest are well separated, even with the shorter analysis time with the improved method (Fig. 3). The concentrations of human plasma fatty acids obtained by the robotic method and determined by both fast GC and by the improved GC method are presented in Table 2. Very similar results were obtained for each fatty acid concentration and its percentage of total fatty acids, and the CV values were similar between the two. Thus the faster GC method is suitable for fatty acid analyses of human plasma and can significantly reduce analytical run times.

Detecting the liquid interface is one of the most critical steps in developing a high throughput transesterification automation application. The Tecan robot integrated liquid detection system employs two different physical principles: detection of changes in capacitance (c-LLD) or pressure (p-LLD). Both types of detection have been used in our studies. The capacitance-based system is useful for detecting an alkane–aqueous interface. This was used in collecting the upper phase as interface detection is followed by a 1-mm retraction into the organic layer. Pressure detection detects an air–liquid interface. This is useful when aspiration of only the upper organic phase is desired, such as when transferring the methyl ester extracts into GC vials or during the mixing phase when upper phase is squirted thru the lower phase.

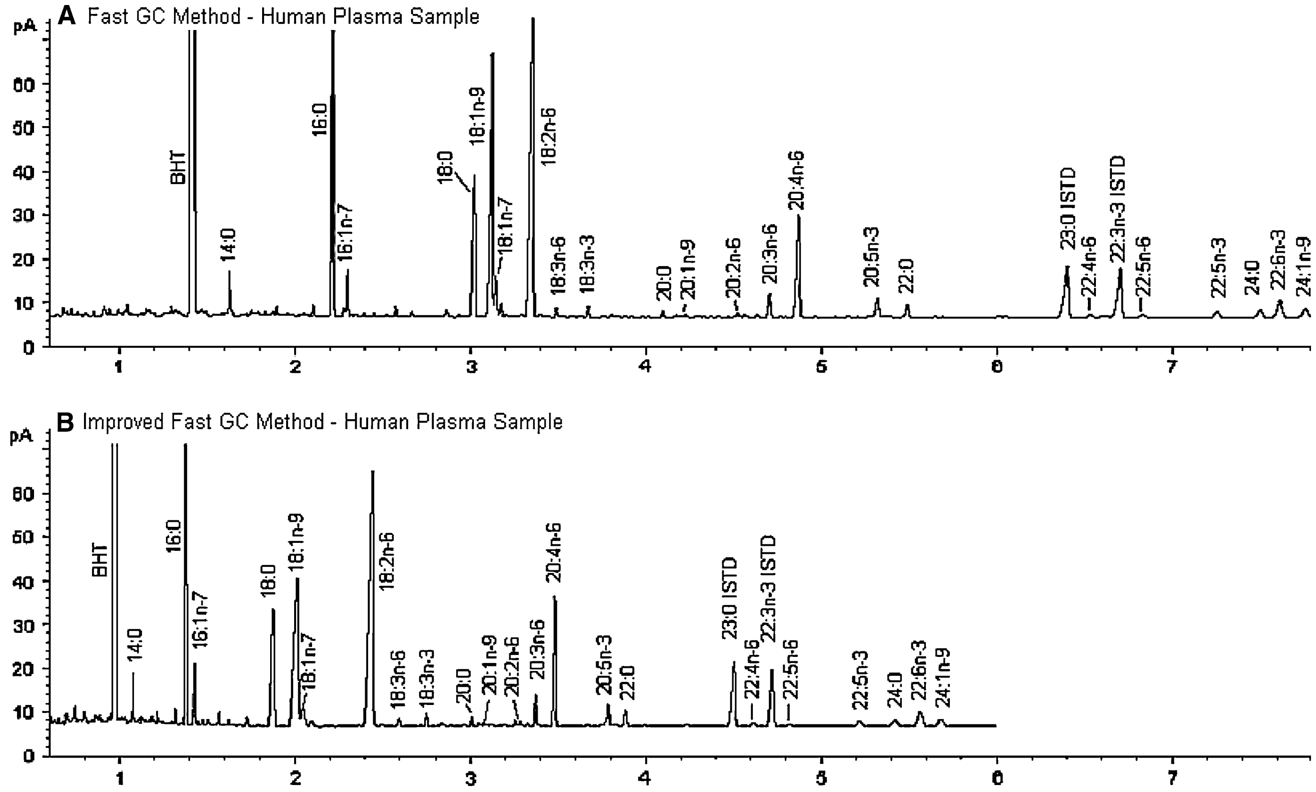

Fig. 3 Comparison of fast and improved GC method gas chromatograms of human plasma FAME, including 23:0 and 22:3n-3 internal standards. Sample was prepared robotically. *BHT* butylated hydroxytoluene

The simplified transmethylation procedure used here dispensed with several steps once considered to be necessary. These steps include addition of cold acetyl chloride drop-wise, working under a nitrogen atmosphere, base addition for reaction mixture neutralization, vortexing, centrifugation and multiple extractions. Results in Table 1 and also our previous analysis [35] demonstrate that these steps are unnecessary or can be replaced by simple pipetting procedures that the robotic arm can perform. Such procedures were devised to overcome difficulties in implementing robotic processes that mimic the traditional chemical procedure. For example, vortexing can be performed by a robot using specialized apparatus, but it is a slow process whereby one sample at a time is mixed. Similarly, some robots are capable of centrifuging samples with integrated centrifuges, but this is a laborious, technically challenging and time-consuming process. What is required is for the organic and aqueous phases to be well mixed and then separated to effect methyl ester extraction. This has been achieved here by repeated mixing by aspirating the upper phase, moving the tip to the bottom of the tube and rapidly dispensing the organic solvent thru the aqueous phase. The organic phase can then be transferred into GC vials after the phases have settled and concentrated further for fast GC analysis, if necessary. Use of an internal standard has obviated the need for complete upper phase transfer and multiple extractions. The use of fast GC also makes possible the analysis of a lower concentration of solutes and, if an appropriate amount of plasma is used, no organic phase concentration may be required. Alternatively, if a microanalysis is required where sample is limited, the organic phase can be concentrated by heating the GC vial rack, and multiple extractions may be performed to increase solute concentrations.

The robotic method described here has been applied to the simultaneous analysis of larger numbers of samples. For example, preliminary experiments transmethylated and analyzed the same bulk plasma sample 40 times. When multiple sets of eight samples are to be analyzed, the program may perform the mixing steps, change tips, wait for a prescribed length of time, and then perform the transfer of the upper phase extract into the GC vials. Another alternative that may improve overall efficiency with a larger number of samples is to perform the mixing step on two sets of eight samples, and then return to the first set for upper phase transfer to GC vials. This creates a delay time that will allow adequate phase separation and also maintain a controlled and constant interval for mixing and sampling for each set of tubes to be processed. This method is then amenable to the analysis of 192 samples in one batch. In

Table 2 Comparison of human plasma fatty acid concentrations in the robotic methods using improved methods for fast gas chromatography ($n = 6$)

Fatty acids	Fast GC method			Improved fast GC method			Difference[a] (%)
	Mean (µg/ml)	CV (%)	Percentage of total fatty acids	Mean (µg/ml)	CV (%)	Percentage of total fatty acids	
14:0	25.7	1.7	1.1	27.2	5.5	1.1	5.7
16:0	568.3	2.6	24.1	573.3	4.1	23.8	0.9
18:0	214.1	3.1	9.1	220.2	4.4	9.1	2.9
20:0	6.8	1.8	0.3	6.6	4.6	0.3	−3.1
22:0	21.5	5.1	0.9	21.3	6.1	0.9	−1.0
24:0	17.2	4.7	0.7	17.6	9.8	0.7	2.5
Total saturates	853.6	1.5	36.2	866.2	3.8	35.9	1.5
16:1n-7	44.5	4.7	1.9	41.1	7.6	1.7	−7.6
18:1n-7	42.7	4.4	1.8	41.3	7.9	1.7	−3.2
18:1n-9	379.0	4.0	16.1	392.5	3.1	16.3	3.6
20:1n-9	2.8	3.6	0.1	2.7	7.6	0.1	−2.0
24:1n-9	18.7	3.0	0.8	20.3	5.0	0.8	8.5
Monounsaturates	487.6	3.8	20.7	497.9	2.7	20.6	2.1
18:2n-6	636.1	3.6	26.9	650.2	5.6	27.0	2.2
18:3n-6	11.8	2.2	0.5	11.3	4.6	0.5	−4.3
20:2n-6	5.0	2.2	0.2	5.1	6.3	0.2	2.4
20:3n-6	35.8	4.0	1.5	38.8	8.4	1.6	8.3
20:4n-6	188.5	2.6	8.0	196.4	2.8	8.1	4.2
22:4n-6	6.6	7.4	0.3	6.6	5.8	0.3	−1.2
22:5n-6	5.0	2.6	0.2	5.2	6.7	0.2	3.0
Total n-6 PUFA	888.8	3.3	37.6	913.4	4.1	37.9	2.8
18:3n-3	14.3	7.6	0.6	15.4	5.4	0.6	7.5
20:5n-3	40.3	3.8	1.7	37.7	3.0	1.6	−6.5
22:5n-3	16.3	6.3	0.7	16.9	8.8	0.7	3.4
22:6n-3	60.0	2.3	2.5	63.8	4.8	2.6	6.4
Total n-3 PUFA	130.8	3.2	5.5	133.7	3.2	5.5	2.2
Total PUFA	1,019.7	3.1	43.2	1,047.1	3.4	43.4	2.7
Total fatty acid	2,360.9	2.1	100.0	2,411.2	3.2	100.0	2.1

[a] Percentage difference of the concentration values

combination with the rapid GC methodology presented, two GCs can process the 192 samples within 1 day. This method then results in an order of magnitude increase in productivity and makes possible large clinical studies.

This method may then be used for both cross-sectional studies of populations and for monitoring compliance in interventional trials with fatty acid supplements and for the use of essential fatty acid related parameters as biomarkers for disease or disease risk. It should also be noted that where more detailed information is required concerning lipid class and molecular species content, that mass spectrometric techniques may be used for highly efficient analyses [39–41].

Analysis of about 200 samples per day would generate over 5,000 peaks per day that must be correctly assigned and entered into spreadsheets. This is a non-trivial task that requires automation. It will be the next step in development of a high throughput system for analysis of large sets of clinical samples.

Acknowledgments This research was supported by the Intramural Research Program of the National Institutes of Health, NIAAA. The authors wish to thank Dr. William E. M. Lands for his help and encouragement during the course of these studies.

References

1. Grossfield A, Feller SE, Pitman MC (2006) Contribution of omega-3 fatty acids to the thermodynamics of membrane protein solvation. J Phys Chem B Condens Matter Mater Surf Interfaces Biophys 110:8907–8909
2. Eldho NV, Feller SE, Nagle ST, Polozov IV, Gawrisch K (2003) Polyunsaturated docosahexaenoic vs docosapentaenoic acid-

differences in lipid matrix properties from the loss of one double bond. J Am Chem Soc 125:6409–6421

3. Harris JL, Hibbeln JR, Mackey RH, Muldoon MF (2003) Statin treatment alters fatty acid composition in hypercholesterolemic patients. Circulation 107:119
4. Salem N Jr, Hullin F, Yoffe AM, Karanian JW, Kim HY (1989) Fatty acid and phospholipid species composition of rat tissues after a fish oil diet. Adv Prostaglandin Thromboxane Leukot Res 19:618–622
5. Salem N Jr (1989) Omega-3 fatty acids: molecular and biochemical aspects. In: Spiller G, Scala J (eds) New protective roles of selective nutrients in human nutrition. Liss AR, New York, pp 263–317
6. Makrides M, Neumann MA, Simmer K, Pater J, Gibson RA (2000) A critical appraisal of the role of dietary long chain polyunsaturated fatty acids on neural indices of term infants: a randomized, controlled trail. Pediatrics 105:32–38
7. Weisenger HS, Armitage JA, Sinclair AJ, Vingrys AJ, Burns P, Weisinger RS (2001) Perinatal omega-3 fatty acid deficiency affects blood pressure later in life. Nat Med 7:258–259
8. Neuringer M, Connor WE, Lin DS, Barstad L, Luck S (1986) Biochemical and functional effects of prenatal and postnatal omega 3 fatty acid deficiency on retina and brain in rhesus monkeys. Proc Natl Acad Sci 83:4021–4025
9. Bourre JM, Francois M, Youyou A, Dumont O, Piciotti M, Pascal G, Durand G (1989) The effects of dietary alpha-linolenic acid on the composition of nerve membranes, enzymatic activity, amplitude of electrophysiological parameters, resistance to poisons and performance of learning tasks in rats. J Nutr 119:1880–1892
10. Yamamoto N, Saitoh M, Moriuchi A, Nomura M, Okuyama H (1987) Effects of dietary alpha-linolenate/linoleate balance on brain lipid compositions and learning ability of rats. J Lipid Res 28:144–151
11. Moriguchi T, Salem N Jr (2003) Recovery of brain docosahexaenoate leads to recovery of spatial task performance. J Neurochem 87:297–309
12. Carlson SE, Werkman SH, Peeples JM, Wilson WM (1994) Growth and development of premature infants in relation to omega 3 and omega 6 fatty acid status. World Rev Nutr Diet 75:63–69
13. Willats P, Forsyth JS, DiModugno MK, Varma S, Colvin M (1998) Effects of long-chain polyunsaturated fatty acids in infant formula on problem solving at 10 months of age. Lancet 352:688–691
14. Birch EE, Garfield S, Hoffman DR, Uauy R, Birch DG (2000) A randomized controlled trial of early dietary supply of long-chain polyunsaturated fatty acids and mental development of in term infants. Dev Med Child Neurol 42:174–181
15. Contreras MA, Greiner RS, Chang MC, Myers CS, Salem N Jr, Rapoport SI (2000) Nutritional deprivation of alpha-linolenic acid decreases but does not abolish turnover and availability of unacylated docosahexaenoic acid and docosahexaenoyl-CoA in rat brain. J Neurochem 75:2392–2400
16. Su HM, Bernardo L, Mirmiran M, Hong MX, Thomas CN, Nathanielsz PW, Thomas BR (1999) Bioequivalence of dietary alpha-linolenic and docosahexaenoic acids as sources of docosahexanenoate accretion in brain and associated organs of neonatal baboons. Pediatr Res 45:87–93
17. Lefkowitz W, Lim SY, Lin Y, Salem N Jr (2005) Where does the developing brain obtain its docosahexaenoic acid? Relative contribution of dietary [alpha]-linolenic acid, docosahexaenoic acid, and body stores in the developing rat. Pediatr Res 57:157–165
18. Pawlosky RJ, Hibbeln JR, Lin Y, Goodson S, Riggs P, Sebring N, Brown GL, Salem N Jr (2003) Effects of beef- and fish-based diets of the kinetics of n-3 fatty acid metabolism in human subjects. Am J Clin Nutr 77:565–572
19. Lin YH, Pawlosky RJ, Salem N Jr (2005) Simultaneous quantitative determination of deuterium- and carbon-13-labeled essential fatty acids in rat plasma. J Lipid Res 46:1974–1982
20. Simopoulos AP (2004) The traditional diet of Greece and cancer. Eur J Cancer Prev 13:219–230
21. Harris WE (2007) Omega-3 fatty acids and cardiovascular disease: a case for omega-3 index as a new risk factor. Pharmacol Res 55:217–223
22. Lands WEM (1995) Long-term fat intake and biomarkers. Am J Clin Nutr 61:721S-725S
23. von Schacky C (2007) Omega-3 fatty acids and cardiovascular disease. Curr Opin Clin Nutr Metab Care 10:129–135
24. Lands WEM, Libelt B, Morris A, Kramer NC, Prewitt TE, Bowen P, Schmeisser D, Davidson M, Burns JH (1992) Maintenance of lower proportions of (n-6) eicosanoid precursors in phospholipids of human plasma in response to added dietary (n-3) fatty acids. Biochim Biophys Acta 1180:147–162
25. Lands WEM (1993) Eicosanoids and health. Ann N Y Acad Sci 676:40–59
26. Albert CM, Campos H, Stampfer MJ, Ridker PM, Manson JE, Willett WC, Ma J (2002) Blood levels of long-chain n-3 fatty acids and the risk of sudden death. N Engl J Med 346:1113–1118
27. Lemaitre RN, King IB, Mozaffarian D, Kuller LH, Tracy RP, Siscovick DS (2003) n-3 Polyunsaturated fatty acids, fatal ischemic heart disease, and nonfatal myocardial infarction in older adults: the cardiovascular health study. Am J Clin Nutr 77:319–325
28. Simon JA, Hodgkins ML, Browner WS, Neuhaus JM, Bernert JT Jr, Hulley SB (1995) Serum fatty acids and the risk of coronary heart disease. Am J Epidemiol 142:469–476
29. Kang JX, Leaf A (1996) The cardiac antiarrhythmic affects of polyunsaturated fatty acids. Lipids 31:S41–S44
30. Marchiolli R, Barzi F, Bomba E, Chieffo C, Di Gregorio D, Di Mascio R, Franzosi MG, Geraci E, Levantesi G, Maggioni AP, Mantini L, Marfisi RM, Mastrogiuseppe G, Mininni N, Nicolosi GL, Santini M, Schweiger C, Tavazzi L, Tognoni G, Tucci C, Valagussa F (2002) Early protection against sudden death by n-3 polyunsaturated fatty acids after myocardial infarction: time course analysis of the results of the gruppo italiano per lo studio della sopravvivenza nell'infarto miocardico (GISSI)-Prevenzione. Circulation 105:1897–1903
31. Mihrshahi S, Peat JK, Webb K, Tovey ER, Marks GB, Mellis CM, Leeder SR (2001) The childhood asthma prevention study (CAPS): design and research protocol of a randomized trial for the primary prevention of asthma. Control Clin Trials 22:333–354
32. Coleman H, Chew E, AREDS2 (2007) Nutritional supplementation in age-related macular degeneration. Curr Opin Ophthalmol 3:220–223
33. Smithers LG, McPhee AJ, Gibson RA, Makrides M (2004) Visual development of preterm infants fed high dose docosahexaenoic acid. Asia Pac J Clin Nutr 13:S50
34. New Alzheimer's clinical trials to be undertaken by NIA nationwide consortium. http://www.nia.nih.gov/Alzheimers/ResearchInformation/NewsReleases/PR20061017ADC
35. Masood MA, Stark KD, Salem N Jr (2005) A simplified and efficient method for the analysis of fatty acid methyl esters suitable for large clinical studies. J Lipid Res 46:2299–2305
36. Lepage G, Roy CC (1986) Direct transesterification of all classes of lipids in a one-step reaction. J Lipid Res 27:114–120
37. Stark KD, Salem N Jr (2005) Fast gas chromatography methods and column selection for the identification of fatty acid methyl esters from mammalian samples. Lipid Technol 17:181–185

38. Thermo Application Note 10058, http://www.thermo.com/com/cda/products/product_application_details/1,12075,00.html
39. Kuksis A (2007) Lipidomics in triacylglycerol and cholesteryl and cholesterol ester oxidation. Front Biosci 12:3203–3246
40. Merrill AH Jr, Sullards MC, Allegood JC, Kelly S, Wang E (2005) Sphingolipidomics: high-throughput, structure-specific, and quantitative analysis of sphingolipids by liquid chromatography tandem mass spectrometry. Methods 36:207–224
41. Han X, Gross RW (2005) Shotgun lipidomics: electrospray ionization mass spectrometric analysis and quantitation of cellular lipidomes directly from crude extracts of biological samples. Mass Spectrom Rev 24:367–412

Lipids (2008) 43:181–186
DOI 10.1007/s11745-007-3140-7

METHODS

Validation of a Rapid Measure of Blood PUFA Levels in Humans

Eileen Bailey-Hall · Edward B. Nelson ·
Alan S. Ryan

Received: 27 September 2007 / Accepted: 15 November 2007 / Published online: 15 December 2007
© AOCS 2007

Abstract An assay involving a finger stick and filter paper blood spotting was developed to determine polyunsaturated fatty acid (PUFA) levels in blood. Capillary whole blood from a finger stick was blotted on antioxidant impregnated filter paper, air dried, saponified and methylated using sodium hydroxide and boron trifluoride in methanol. The method differed from those described previously because separation of plasma and red blood cells (RBCs) was not needed, thin-layer chromatography (TLC) was not required to separate phospholipids, initial extraction of lipids before transesterification was not necessary, and the fatty acid methyl ester (FAME) method was able to methylate steryl esters, free fatty acids, and sphingomyelins. Twenty-six subjects provided blood samples by finger stick and venipuncture. Levels of long-chain polyunsaturated fatty acids (LC-PUFA) from capillary whole blood were correlated with those from RBCs and PLs in venous blood ($P < 0.001$, R^2 ranged from 0.64 to 0.86). Although highly significant ($P < 0.002$), the R^2 values for the correlation between arachidonic acid (ARA) levels in capillary whole blood with ARA levels in RBCs and plasma phospholipids (PLs) were relatively lower ($R^2 = 0.31$–0.41, respectively). Results indicate that the described finger stick assay represents a fast, reliable method to measure specific LC-PUFA levels.

Keywords Polyunsaturated fatty acid levels · Phospholipid levels · Finger stick · Blood assay

---

E. Bailey-Hall (✉) · E. B. Nelson · A. S. Ryan
Martek Biosciences Corporation, 6480 Dobbin Road,
Columbia, MD 21045, USA
e-mail: ebailey@martek.com

Abbreviations

AOCS	American Oil Chemists' Society
ARA	Arachidonic acid
DHA	Docosahexaenoic acid
DPAn-6	Docosapentaenoic acid
EPA	Eicosapentaenoic acid
FAME	Fatty acid methyl esters
LC-PUFA	Long-chain polyunsaturated fatty acids
PLs	Plasma phospholipids
PUFA	Polyunsaturated fatty acids
RBCs	Red blood cells
TLC	Thin-layer chromatography

Introduction

The fatty acid composition of red blood cells (RBCs) and plasma phospholipids (PLs) is commonly used to evaluate certain medical conditions, estimate nutritional status, and measure compliance of investigational drug use in clinical trials. Only a few investigators have developed and described methods to measure quickly the levels of fatty acids in blood using techniques other than venipuncture. Ohta et al. [1] described a method for analyzing the fatty acids in plasma lipids from a 50 µL finger-tip blood sample. The method involved initial separation of whole blood into plasma and red blood cells (RBCs) and needed thin-layer chromatography (TLC) prior to fatty acid methyl ester (FAME) analysis to isolate the phospholipid fraction [1]. Inoue et al. [2] described a method of fatty acid analysis using a dried blood spot on filter paper to screen for adrenoleukodystrophy, an x-linked recessive disorder characterized by progressive demyelination of cerebral white matter and adrenal insufficiency. This method involved initial extraction of the blood lipids from the filter paper matrix prior to methanolyis with MeOH/HCL [2]. Ichihara et al. [3] described a finger stick and FAME technique to analyze the fatty acid composition of glycerolipids in blood or breast milk. These authors developed a method to prepare BHT impregnated filter paper to collect blood. However, free fatty acids, steryl esters, and sphingomyelins were not methylated using the reported alkaline methanolyis FAME procedure [3]. Finally, Marangoni et al. [4] described a finger stick assay to analyze the fatty acid composition of circulating lipids. In their analysis, percentage levels of fatty acids in blood total lipids from a finger stick were analyzed in volunteers who consumed differing amounts of fish and meat. The samples obtained had high levels of triglycerides and not only phospholipids since total blood lipids were analyzed. Correlations between fatty acids in venous blood and capillary whole blood were not provided. These authors used MeOH/HCL as a methylating agent and not BF_3/MeOH as recommended by the American Oil Chemists' Society (AOCS) [5]. In some studies, it appears that acid-catalyzed procedures using MeOH/HCL result in incomplete transesterification of triglycerides [6].

Presently, the most common method of measuring PUFA levels in blood involves venipuncture. However, this method is often time consuming, involves an invasive technique for blood collection, and is costly. Standard analysis using venipuncture to determine PUFA levels in RBCs and PLs involves several steps, including: (1) the collection of whole blood, (2) the separation of whole blood into RBCs and plasma by centrifugation, (3) the washing of the RBCs with isotonic saline to remove white cell and plasma contamination, (4) the organic extraction of the total lipids from the RBCs and plasma, (5) the separation of PLs by TLC, and (6) the saponification and methylation of the RBC total lipids and PLs for analysis by gas chromatography.

The purpose of this paper is to describe an accurate, inexpensive, and minimally invasive finger stick assay to measure LC-PUFA levels in capillary whole blood. The method described here differs from those used previously because separation of plasma and RBCs is not needed, TLC is not required to separate phospholipids, initial extraction of lipids before transesterification is not necessary, and the FAME method is able to methylate steryl esters, free fatty acids, and sphingomyelins. Further, the method described herein uses BF_3/MeOH as a methylating agent as recommended by the AOCS [5]. Mean mole percent LC-PUFA levels in capillary whole blood are compared with those from RBCs and PLs in venous blood. Correlations based on the type of assay used (finger stick or venipuncture) are reported for several important LC-PUFA [docosahexaenoic acid (DHA), docosapentaenoic acid (DPAn-6), eicosapentaenoic acid (EPA), and arachidonic acid (ARA)]. These correlations are particularly useful because LC-PUFA levels in RBCs and PLs are most often used as indicators of dietary intake of these fatty acids.

Materials and Methods

Twenty-six healthy subjects between the ages of 25 and 66 volunteered to participate. The study was approved by the New England Institutional Review Board, Wellesley, MA, and written informed consent was obtained prior to enrollment. Volunteers were recruited at Martek Biosciences Corporation where the study was conducted. The sample may have included individuals who routinely consume omega-3 dietary supplements.

Venipuncture Assay

Samples were taken from both fasting and non-fasting subjects. Using standard phlebotomy techniques, approximately 4 ml of whole blood was collected from each subject by venipuncture and placed into an EDTA vacutainer tube. The tubes were centrifuged to separate the plasma from the RBCs. The RBCs were washed two times with isotonic saline to remove plasma and white blood cell contamination. The plasma and RBCs were purged with nitrogen and stored at −80 °C until analysis. Plasma and erythrocyte lipids were extracted using the methods described by Folch [7] and Bligh and Dyer [8], respectively. Plasma (400 μl) and RBCs (500 μl) were used for extraction. The phospholipid fraction was isolated from the plasma total lipids by TLC on silica gel plates developed in a 60:40:3 ratio solution (v/v/v) of hexane:ether:acetic acid. Internal standard (23:0 fatty acid) was added to the plasma phospholipid subfraction and RBC total lipids. We used 23:0 fatty acid as an internal standard because it is not typically detected in the analyses described here. The lipids were saponified with 0.5 N NaOH in methanol, and the resulting fatty acids were methylated using 14% BF_3 in methanol at 100 °C for 30 min and then extracted with hexane. The FAMEs were separated by capillary column gas chromatography on an Agilent Series 6890 System equipped with a 30 m FAMEWAX^{TM} (Restek, State College, PA) column. A 48:1 split flow ratio with helium as a carrier gas and a programmed temperature gradient (130–250 °C) was used. FAMEs were identified by flame ionization detection. Retention times were compared to a mixed fatty acid methyl ester standard from NuChek Prep (Elysian, MN). Fatty acids were quantified by comparison to the 23:0 internal standard (NuChek Prep Elysian, MN). Concentrations of fatty acids were not reported in the present study because blood volumes from the finger stick assay were not determined.

Finger Stick Assay

BHT impregnated filter paper squares (Whatman 3MM chromatography paper, Whatman Inc.) were prepared according to the methods described by Ichihara et al. [3]. These authors demonstrated that BHT minimized fatty acid oxidation. A drop of capillary blood was obtained from each subject by piercing the fingertip with a lancet device (BD Genie^{TM} Lancet, Emergency Medical Products). A piece of filter paper was applied to the finger. The blood sample was dried overnight at room temperature and then stored for 1 day at −80 °C, the standard storage temperature for RBCs and plasma. The filter paper samples were transferred to test tubes with 23:0 fatty acid internal standard, directly saponified with NaOH, and methylated with 14% BF_3 in methanol with no prior extraction step. The resultant FAMEs were analyzed by gas chromatography using the aforementioned method except that a split flow of 20:1 was used. The finger stick assay involved direct transesterification and methylation of the fatty acids without prior lipid extraction.

Statistical Analyses

All statistics were conducted using Minitab^{TM}. Means, standard deviations, and ranges were calculated for levels of PUFA in capillary whole blood and for PUFA in RBCs and PLs from venous blood. One-way ANOVA with the post hoc Tukey's test was used to determine significant difference between levels of PUFA from the assays. Spearman's rank correlation was used to determine the strength of the association between each assay and levels of LC-PUFA. An $\alpha = 0.05$ was used to determine statistical significance.

Results

Table 1 shows the mean mole percent levels, their standard deviations and ranges for the fatty acids obtained from each assay. Not surprisingly, values for most mean mole percent

Table 1 Mean mole percent levels of fatty acids from the finger stick and venipuncture assays

Fatty acid	RBCs from venipuncture Mean ± SD (range) mol%	PLs from venipuncture Mean ± SD (range) mol%	Capillary whole blood from finger stick Mean ± SD (range) mol%
14:0	0.53 ± 0.23 (0.20–1.12)^{a}	0.36 ± 0.10 (0.18–0.67)^{b}	0.81 ± 0.22 (0.55–1.53)^{c}
16:0	26.83 ± 1.29 (22.94–29.37)^{a}	28.89 ± 1.67 (25.77–31.71)^{b}	24.58 ± 1.57 (22.46–28.00)^{c}
18:0	10.00 ± 0.85 (8.35–12.79)^{b}	14.61 ± 1.18 (11.07–16.37)^{a}	13.77 ± 1.96 (9.68–17.55)^{a}
20:0	0.11 ± 0.03 (0.07–0.16)^{a}	0.13 ± 0.03 (0.06–0.19)^{b}	0.16 ± 0.03 (0.09–0.22)^{c}
22:0	0.20 ± 0.07 (0.08–0.34)^{a}	0.15 ± 0.05 (0.08–0.28)^{b}	0.18 ± 0.03 (0.10–0.23)^{ab}
24:0	0.48 ± 0.18 (0.18–0.81)^{b}	0.13 ± 0.04 (0.06–0.22)^{a}	0.19 ± 0.10 (0.00–0.32)^{a}
16:1	0.43 ± 0.17 (0.21–1.04)^{a}	0.55 ± 0.20 (0.33–1.16)^{a}	1.27 ± 0.51 (0.67–2.72)^{b}
18:1n-9	14.78 ± 1.17 (11.19–16.57)^{a}	8.49 ± 1.25 (6.49–11.95)^{b}	15.99 ± 1.95 (11.80–19.85)^{c}
18:1n-7	1.80 ± 0.21 (1.40–2.16)	1.99 ± 0.33 (1.38–2.67)	1.86 ± 0.32 (1.40–2.84)
20:1n-9	0.29 ± 0.10 (0.16–0.55)^{a}	0.15 ± 0.04 (0.08–0.30)^{b}	0.23 ± 0.13 (0.10–0.63)^{a}
24:1	0.42 ± 0.16 (0.09–0.72)^{b}	0.14 ± 0.07 (0.00–0.25)^{a}	0.09 ± 0.09 (0.00–0.23)^{a}
18:2n-6	14.59 ± 2.71 (9.08–25.27)^{b}	22.52 ± 2.60 (14.51–26.03)^{a}	23.66 ± 2.99 (14.78–29.09)^{a}
18:3n-6	0.07 ± 0.08 (0.00–0.40)^{a}	0.08 ± 0.04 (0.03–0.21)^{a}	0.25 ± 0.12 (0.06–0.63)^{b}
20:2n-6	0.39 ± 0.10 (0.21–0.61)^{a}	0.37 ± 0.02 (0.21–0.54)^{a}	0.29 ± 0.13 (0.16–0.80)^{b}
20:3n-6	1.44 ± 0.26 (1.11–2.01)^{a}	2.56 ± 0.66 (1.52–3.95)^{b}	1.18 ± 0.24 (0.77–1.73)^{a}
20:4n-6	12.24 ± 1.19 (10.03–14.94)^{a}	10.62 ± 1.27 (8.14–13.43)^{b}	8.06 ± 1.03 (5.69–10.05)^{c}
22:4n-6	2.49 ± 0.55 (1.28–3.46)^{a}	0.33 ± 0.10 (0.18–0.61)^{b}	0.84 ± 0.20 (0.44–1.29)^{c}
22:5n-6	0.50 ± 0.17 (0.19–0.88)^{b}	0.31 ± 0.16 (0.12–0.73)^{a}	0.27 ± 0.12 (0.00–0.51)^{a}
18:3n-3	0.32 ± 0.11 (0.18–0.67)^{a}	0.27 ± 0.08 (0.19–0.51)^{a}	0.55 ± 0.18 (0.36–1.19)^{b}
20:5n-3	0.76 ± 0.42 (0.27–2.06)	0.78 ± 0.52 (0.21–2.41)	0.55 ± 0.33 (0.18–1.59)
22:5n-3	1.40 ± 0.33 (0.55–1.89)^{b}	0.58 ± 0.15 (0.35–0.86)^{a}	0.64 ± 0.19 (0.38–1.06)^{a}
22:6n-3	4.89 ± 1.18 (2.24–7.25)^{a}	4.36 ± 1.24 (1.65–7.03)^{a}	2.76 ± 0.77 (1.14–4.34)^{b}

Different superscripts indicate significant differences between groups, $P < 0.05$

levels of fatty acids from RBC, PLs, and capillary whole blood differed significantly ($P < 0.05$) from each other because each sample type contained differing amounts of triglyceride, phospholipid, free fatty acids, and steryl esters. There was substantial inter-individual variation in levels of LC-PUFA as demonstrated by the wide range of values.

For only two fatty acids (18:1n-7 and 20:5n-3) from capillary whole blood, RBCs, and PLs, the values for mean mole percent levels were not significantly different ($P > 0.05$). Of the 22 fatty acids considered, the values for mean mole percent fatty acid levels from capillary whole blood and PLs were not significantly different for 9 fatty acids. Values for capillary whole blood and RBCs mean mole percent fatty acid levels were not significantly different for five fatty acids. For PLs and RBCs, mean mole percent fatty acid levels were not significantly different for seven fatty acids.

No assay had consistently higher or lower mole percent values compared with the other assays. However, the mean mole percent value for DHA was about 150% lower in capillary whole blood than in RBCs and PLs.

Table 2 shows the correlations between levels of certain LC-PUFA in capillary whole blood with those from RBCs and PL in venous blood. The association between LC-PUFA levels in RBC and PLs is also provided. Capillary whole blood DHA, EPA, and DPAn-6 mole percent levels were highly correlated to those in RBCs and PLs (see Figs. 1, 2 for DHA). Although highly significant ($P < 0.002$), the R^2 values for the correlation of ARA levels in capillary whole blood with ARA levels in RBCs and PLs were relatively low ($R^2 = 0.31$ and 0.41, respectively). Notably, the R^2 values for the correlation of ARA between capillary whole blood and RBCs and PLs were higher than those for the correlation of ARA between RBCs and PLs ($R^2 = 0.24$).

Table 2 Correlations for LC-PUFA from the finger stick and venipuncture assays

Fatty acid	P value	R^2 value
DHA C22:6n-3		
Finger stick versus RBCs	<0.001	0.74
Finger stick versus PLs	<0.001	0.86
RBC versus PLs	<0.001	0.84
EPA C20:5n-3		
Finger stick versus RBCs	<0.001	0.68
Finger stick versus PLs	<0.001	0.64
RBC versus PLs	<0.001	0.71
DPA C22:5n-6		
Finger stick versus RBCs	<0.001	0.74
Finger stick versus PLs	<0.001	0.77
RBC versus PLs	<0.001	0.49
ARA C20:4n-6		
Finger stick versus RBCs	0.002	0.31
Finger stick versus PLs	<0.001	0.41
RBC versus PLs	<0.012	0.24

Discussion

The present study describes an accurate, inexpensive, and minimally invasive finger stick assay to measure LC-PUFA levels in capillary whole blood. Measures of DHA and ARA are particularly important because these LC-PUFA are present in the brain, retina, and other neural tissues [9]. LC-PUFA have well established benefits for infant cognitive and visual function [10–14], cardiovascular health [15–21], and may play an important role in neural and visual health during the aging process [22–25].

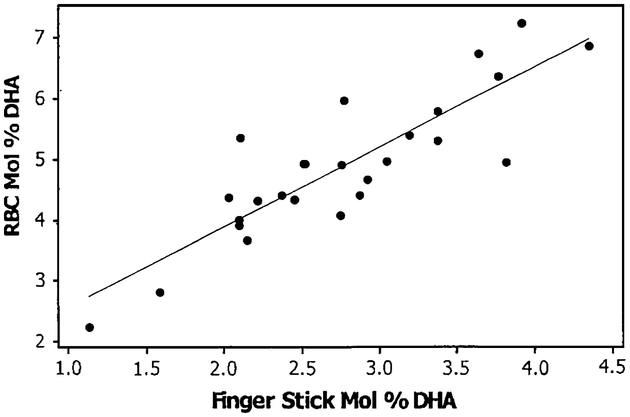

Fig. 1 Relationship between mole percent DHA levels from capillary whole blood and RBC DHA levels from venous blood in subjects with variable LC-PUFA intakes

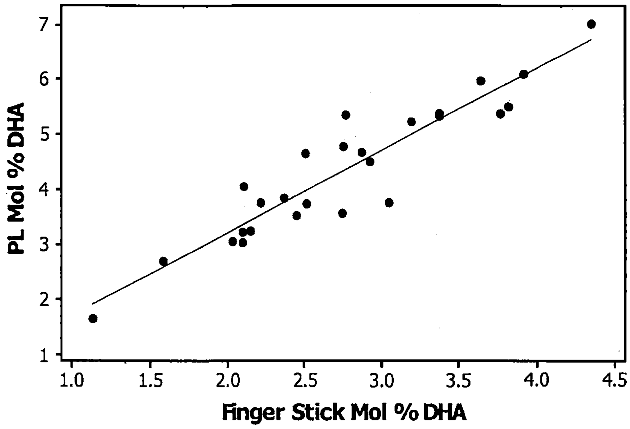

Fig. 2 Relationship between mole percent DHA levels from capillary whole blood and PL DHA from venous blood in subjects with variable LC-PUFA intakes

Due to differing dietary intakes of PUFA, there was substantial inter-individual variation in levels found in RBCs, PLs, and capillary whole blood as demonstrated by the wide ranges of values. It is evident that the majority of mean mole percent levels of fatty acids from RBCs, PLs, and capillary whole blood were significantly different from each other. These differences probably reflected differing amounts of triglyceride, phospholipid, free fatty acids, and steryl esters in each sample type.

For DHA, the mean mole percent value was much lower in capillary whole blood than in RBCs or PLs. Since phospholipid is the predominant lipid class in RBCs it is reasonable to expect a higher level of DHA in RBCs and PLs compared with that found in capillary whole blood. One of the limitations of the finger stick assay is that is uses whole blood total lipids rather than RBCs and plasma phospholipids. This may produce results that show artificially lower levels of DHA due to the presence of less DHA-containing lipid components such as triglycerides. This is particularly relevant in individuals with hyperlipidemia. This problem may be ameliorated by asking subjects to fast before the blood draw.

Levels for DHA, DPAn-6 and EPA from both assays were highly correlated ($P < 0.001$, R^2 ranged from 0.64 to 0.86). However, the correlation between ARA from capillary whole blood and ARA from RBCs and PLs was not as strong as compared to the other LC-PUFA. As suggested by Ichihara et al. [3], correlation with ARA may be improved when the ARA level is expressed as a proportion of fatty acids, using the ratio ARA/(EPA + DHA) as an indicator of n-6/n-3 status. The ratios calculated from both assays were highly correlated for RBCs ($R^2 = 0.91$, $P < 0.001$) and for PLs ($R^2 = 0.93$, $P < 0.001$). Although the ratio ARA/(EPA + DHA) improves the correlation with ARA and provides information about n-6/n-3 status, it does not provide specific information about the level of ARA. The narrow range of levels for ARA also may account for the low R^2 values for the resulting correlations. For DHA, EPA, and DPAn-6, the range of levels is much greater than that found for ARA. The narrow range of levels for ARA is found in diets that contain differing amounts of ARA and other PUFA.

DHA has been shown to incorporate into the steryl ester fraction and to be circulating as a free fatty acid [26]. We used the AOCS recommended BF_3/MeOH methylating agent because free fatty acids, steryl esters, and sphingomyelins are not methylated using the alkaline methanolyis FAME procedure. The BF_3/MeOH FAME method will methylate these lipid classes and therefore give a more accurate assessment of blood PUFA status [26]. Notably, the BF_3/MeOH FAME method is appropriate for measuring fatty acid levels in whole blood because the triglycerides are transesterified.

Although Ohta et al. [1] described a method for the rapid analysis of plasma phospholipids, the method involved initial separation of the whole blood into plasma and RBCs and included a TLC step prior to FAME analysis to isolate the phospholipid fraction. Both procedures are eliminated in our method as the whole blood is directly methylated without prior whole blood or TLC separation.

The finger stick assay described here represents a rapid, minimally invasive, and cost effective method to determine LC-PUFA levels, notably DHA and EPA, in capillary whole blood. The assay may be useful for the determination of subject compliance in clinical trials, particularly when LC-PUFA are administered.

References

1. Ohta A, Mayo MC, Kramer N, Lands WEM (1990) Rapid analysis of fatty acids in plasma lipids. Lipids 25:742–747
2. Inoue K, Suzuki Y, Yajima S, Shimozawa N, Orii T, Kondo N (1997) Very long chain fatty acid analysis of dried blood spots on filter paper to screen for adrenoleukodystrophy. Clin Chem 43:2197–2198
3. Ichihara K, Waku K, Yamaguchi C, Saito K, Shibahara A, Miyatani S, Yamamoto K (2002) A convenient method for determination of the C 20–22 PUFA composition of glycerolipids in blood and breast milk. Lipids 37:523–526
4. Marangoni F, Colombo C, Galli C (2004) A method for the direct evaluation of the fatty acid status in a drop of blood from a fingertip in humans: applicability to nutritional and epidemiological studies. Anal Biochem 326:267–272
5. Morrison WR, Smith LM (1964) Preparation of fatty acid methyl esters and dimethylacetals from lipids with boron fluoride-methanol. J Lipid Res 5:600–608
6. Kohn G, van der Ploeg P, Mobius M, Sawatzki G (1996) Influence of the derivatization procedure on the results of the gas chromatographic fatty acid analysis of human milk and infant formula. Z Ernahrungswiss 35:226–234
7. Folch J, Lees M, Sloane Stanley GH (1957) A simple method for the isolation and purification of total lipids from animal tissue. J Biol Chem 226:497–509
8. Bligh EG, Dyer WJ (1959) A rapid method of total lipid extraction and purification. Can J Biochem Physiol 37:911
9. Innis SM (2007) Dietary (n-3) fatty acids and brain development. J Nutr 137:855–859
10. Agostini C, Trojan S, Bellu R, Riva E, Giovannini M (1995) Neurodevelopmental quotient of healthy term infants at 4 months and feeding practice: the role of long-chain polyunsaturated fatty acids. Pediatr Res 38:262–266
11. Hoffman DR, Birch EE, Castaneda YS, Fawcett SL, Wheaton DH, Birch DG, Uauy R (2003) Visual function in breast-fed term infants weaned to formula with or without long-chain polyunsaturates at 4 to 6 months: a randomized clinical trial. J Pediatr 142:668–677
12. Uauy R, Hoffman DR, Mena P, Llanos A, Birch EE (2003) Term infant studies of DHA and ARA supplementation on neurodevelopment: results of randomized controlled trials. J Pediatr 143:S17–S25
13. Morale SE, Hoffman DR, Castaneda YS, Wheaton DH, Burns RA, Birch EE (2005) Duration of long-chain polyunsaturated fatty acids availability in the diet and visual acuity. Early Hum Dev 81:197–203

14. SanGiovanni JP, Berkey CS, Dwyer JT, Colditz GA (2000) Dietary essential fatty acids, long-chain polyunsaturated fatty acids, and visual resolution acuity in healthy full-term infants: a systematic review. Early Hum Dev 57:165–188
15. GISSI-Prevenzione Investigators (1999) Dietary supplementation with n-3 polyunsaturated fatty acids and vitamin E after myocardial infarction: results from the GISSI Prevenzione trial. Lancet 354:447–455
16. von Schacky C (2003) The role of omega-3 fatty acids in cardiovascular disease. Curr Atheroscler Rep 5:139–145
17. Harris WS (2005) Extending the cardiovascular benefits of omega-3 fatty acids. Curr Atheroscler Rep 7:375–380
18. Moore C, Bryant S, Mishra G, Krebs J, Browning L, Miller G, Jebb S (2006) Oily fish reduces plasma triacylglycerols: a primary prevention study in overweight men and women. Nutrition 22:1012–1024
19. Mori TA, Bao DQ, Burke V, Puddey IB, Beilin LJ (1999) Docosahexaenoic acid but not eicosapentaenoic acid lowers ambulatory blood pressure and heart rate in humans. Hypertension 34:253–260
20. Leaf A, Kang JX, Xiao YF, Billman GE, Voskuyl RA (1999) The antiarrhythmic and anticonvulsant effects of dietary n-3 fatty acids. J Membr Biol 172:1–11
21. Pischon T, Hankinson SE, Hotamisligil GS, Rifai N, Willett WC, Rimm EB (2003) Habitual dietary intake of n-3 and n-6 fatty acids in relation to inflammatory markers among US men and women. Circulation 108:155–160
22. Green KN, Martinez-Coria H, Khashwji H, Hall EB, Yurko-Mauro K, Ellis L, LaFerla FM (2007) Dietary docosahexaenoic acid and docosapentaenoic acid ameliorate amyloid-β and tau pathology via a mechanism involving presenilin 1 levels. J Neurosci 16:4385–4395
23. Lim GP, Calon F, Morihara T, Yang F, Teter B, Ubeda O, Salem Jr N, Frautschy SA, Cole GM (2005) A diet enriched with omega-3 fatty acid docosahexaenoic acid reduces amyloid burden in an aged Alzheimer mouse model. J Neurosci 25:3032–3040
24. Morris M, Evans D, Bienias J, Tangney CC, Bennett DA, Wilson RS, Aggarwal N, Schneider J (2003) Consumption of fish and n-3 fatty acids and risk of incident Alzheimer disease. Arch Neurol 60:940–946
25. SanGiovanni JP, Chew EY (2005) The role of omega-3 long-chain polyunsaturated fatty acids in health and disease of the retina. Prog Retin Eye Res 24:87–138
26. Arterburn LM, Oken HA, Hoffman JP, Bailey-Hall EB, Chung G, Rom D, Hamersley J, McCarthy D (2007) Bioequivalence of docosahexaenoic acid from different algal oils in capsules and in DHA-fortified food. Lipids (in press)

Lipids (2008) 43:187–196
DOI 10.1007/s11745-007-3141-6

METHODS

Direct Microwave Transesterification of Fingertip Prick Blood Samples for Fatty Acid Determinations

Jeff M. Armstrong · Adam H. Metherel ·
Ken D. Stark

Received: 6 November 2007 / Accepted: 16 November 2007 / Published online: 15 December 2007
© AOCS 2007

Abstract Omega-3 polyunsaturated fatty acid (PUFA) dietary intakes and tissue levels are positively associated with various health benefits. The development of cost efficient, high throughput methodologies would enable research in large clinical and population studies, and clinical fatty acid profiling. Microwave heating for the transesterification of blood fatty acids was examined. Samples were collected by venous puncture and fingertip prick onto chromatography paper. Aliquots of serum, plasma, erythrocytes and whole blood were prepared from venous blood. Boron trifluoride in methanol was used for transesterification but sample preparation and heating varied. Fatty acid determinations and markers of omega-3 fatty acid status including the sum of eicosapentaenoic acid and docosahexaenoic acid, the ratio of total n-3 PUFA to n-6 PUFA, and the percentage of n-3 highly unsaturated fatty acids (HUFA, $\geq$20 carbons and $\geq$3 carbon–carbon double bonds) in total HUFA were compared. Quantitative determinations indicate that microwave transesterification results in significantly lower estimates of monounsaturates and polyunsaturates, possibly through incomplete transesterification of triacylglycerols. However, qualitative estimates of omega-3 fatty acid status were relatively similar. Fingertip prick blood collection combined with direct transesterification by microwave may be a very rapid method to estimate omega-3 fatty acid status for selected applications.

Keywords Plasma · Erythrocytes · Whole blood · Fingertip · Omega-3 fatty acid · EPA · DHA · HUFA

Abbreviations

BF_3/MeOH	Boron trifluoride in methanol
BHT	Butylated hydroxytoluene
DHA	Docosahexaenoic acid (22:6n-3)
DMA	Dimethyl acetal
EDTA	Ethylene diaminetetraacetic acid
EPA	Eicosapentaenoic acid (20:5n-3)
FAME	Fatty acid methyl ester
HUFA	Highly unsaturated fatty acids
PUFA	Polyunsaturated fatty acid
TLC	Thin layer chromatography
17:0 PC	1,2-Diheptadecanoyl-*sn*–glycero-3-phosphocholine
17:0 TG	Triheptadecanoin

Introduction

Epidemiological and interventional trials have shown that n-3 polyunsaturated fatty acids (PUFA), specifically docosahexaenoic acid (22:6n-3, DHA) and eicosapentaenoic acid (20:5n-3, EPA) have significant cardio-protective effects [1–5]. These cardio-protective effects are mediated through various mechanisms including anti-arrhythmia [5, 6], anti-thrombosis [7], triacylglycerol-lowering [8],

---

Electronic supplementary material The online version of this article (doi:10.1007/s11745-007-3141-6) contains supplementary material, which is available to authorized users.

J. M. Armstrong · A. H. Metherel · K. D. Stark (✉)
Department of Kinesiology, Laboratory of Nutritional and Nutraceutical Research, University of Waterloo, N2L 3G1 Waterloo, ON, Canada
e-mail: kstark@uwaterloo.ca

and heart rate-lowering [9]. An intake of 750 mg/d has been proposed as a target intake to provide significant anti-arrhythmic benefits, as well as additional cardiovascular benefits [10]. Blood measures of n-3 PUFA have been demonstrated to be a biomarker of dietary n-3 PUFA intake [11]. It has been proposed that n-3 fatty acid measures in blood could be developed into an independent risk factor for coronary heart disease mortality [12]. Large-scale clinical, intervention and population-based studies are needed to support the use of blood measures of n-3 PUFA as a risk factor for cardiovascular disease.

The conventional determination of fatty acids in blood is a multi-step process that requires highly trained manual labor. High throughput and cost efficient determinations of fatty acids would enable large research initiatives and support routine fatty acid profiling during clinical screening. Fast gas chromatography for the determination of fatty acids in human blood has been demonstrated previously [13, 14]. It has also been demonstrated that fatty acid methyl esters (FAMEs) can be prepared by direct transesterification without prior lipid extraction [15–17] and that these steps can be made amenable to robotics [14]. Fingertip prick blood sampling techniques can also eliminate the requirement for a trained phlebotomist for sample collection [18–20] and the samples absorbed on chromatography paper can be directly transesterified to yield for FAMEs for gas chromatography analysis [20]. FAME preparation remains time-consuming with conventional methylation often requiring 1 hour with convectional heat to catalyze the reaction [20,21], although reaction times as short as 10 min have been utilized when the transesterification of sphingolipids is not of interest [21,22]. Microwave irradiation has been substituted for convectional heating during the production of FAMEs from phospholipids isolated from brain lipids [23], but this technique has neither been adapted widely nor tested exhaustively.

In the present study, the use of direct microwave transesterification was compared to the traditional use of convectional heat for the preparation of FAMEs. A primary interest was the determination of n-3 PUFA status by rapid methods from venipuncture and fingertip prick blood samples. Biomarkers of n-3 PUFA status compared include EPA + DHA with and without the addition of docosapentaenoic acid (22:5n-3, DPAn-3), the ratio of total n-3 PUFA to total n-6 PUFA, and the percentage of n-3 highly unsaturated fatty acids ($\geq$20 carbons, $\geq$3 carbon–carbon, double bonds, HUFA) in total HUFA [24]. Analyses of fingertip blood samples were compared to analyses performed on erythrocyte and plasma total lipid extracts, plasma phospholipids, and whole blood total lipids with and without prior lipid extraction.

Methods

Blood Samples

Blood was collected on one occasion by venous puncture and by fingertip prick (see below for details) from a fasted male subject, 21 years of age for initial qualitative comparisons. The samples were prepared under a series of conditions (see Table 1 for a summary). A quantitative and qualitative comparison between convectional block heating and microwave heating for transesterification was completed on blood collected on a single occasion from a fasted male subject, 25 years of age. The study and methods were reviewed and received clearance from the Office of Research Ethics at the University of Waterloo.

Table 1 Blood collection and sample preparation conditions

Sample	Abbreviation	Collection	Extraction	Methanolysis
Serum total lipids	Serum	Venous	Yes	Convectional heat 60 min
Plasma total lipids	Plasma	Venous	Yes	Convectional heat 60 min
Plasma phospholipid	Plasma PL	Venous	Yes	Convectional heat 60 min
Erythrocyte total lipids	Erythrocyte	Venous	Yes	Convectional heat 60 min
Whole blood total lipids	WB Ext Con60	Venous	Yes	Convectional heat 60 min
	WB Con15	Venous	Yes	Convectional heat 15 min
	WB Ext Micro	Venous	Yes	Microwave (45 s)
	WB Drop Micro	Venous	No	Microwave (45 s)
	WB Paper Micro	Venous onto paper	No	Microwave (45 s)
	FTP Dir Con60	FTP onto paper	No	Convectional heat 60 min
	FTP Dir Con15	FTP onto paper	No	Convectional heat 15 min
	FTP Dir Micro	FTP onto paper	No	Microwave (45 s)

PL phospholipid; *WB* whole blood; *Ext* lipid extraction prior to transesterification; *Con60* convectional heating for 60 min; *Con15* convectional heating for 15 min; *Micro* microwave heating; *Drop* blood dropped into solvent without absorbent; *Paper* blood absorbed onto chromatography paper; *FTP* fingertip prick blood; *Dir* direct transesterification

Finger Prick Samples

Finger prick blood samples were obtained by puncturing the fingertip with a sterile, disposable, lancing device (A.R. Medicom Inc., Montreal, QC, Canada). Blood was absorbed on a thin strip (3.0 cm × 0.5 cm) of chromatography paper (Analtech, Newark, DE) as the processing of chromatography paper for fatty acid analysis produced no peaks during gas chromatography in agreement with previous findings [20]. The incorporation of 2,6-di-*tert*-butyl-4-methylphenol (butylated hydroxytoluene, BHT) into the absorbent was not necessary as samples in the present study were not stored, but prepared immediately after collection [20]. Each fingertip prick blood sample consisted of enough blood to saturate approximately 0.5 cm × 1.0 cm of chromatography paper. This section of chromatography paper with absorbed blood was cut into and completely submerged in the transesterification solvents to prevent combustion during heating, particularly with microwave heating. Conventional extraction of lipids was bypassed for the fingertip prick samples and they were prepared by direct transesterification with boron trifluoride in methanol (BF_3/MeOH, 14% w/v; Alltech Associates, Deerfield, IL) with the addition of hexane.

Venous Blood Samples

Venous blood was collected from the antecubital vein by a trained technician into 10 ml evacuated tubes (Vacutainer; Becton Dickinson, Franklin Lakes, NJ) with ethylene diaminetetraacetic acid (EDTA) as an anticoagulant for plasma, erythrocyte and whole blood preparations and without EDTA for serum preparations. Whole blood from the EDTA blood collection was aliquoted (100 µl each) into borosilicate glass tubes (13 mm × 10 mm, Fisher Scientific). Strips of chromatography paper were dipped into collected whole blood to compare blood collected from the antecubital vein to fingertip prick collected blood. Plasma and erythrocytes, and serum were prepared from EDTA blood and clotted blood, respectively, by centrifugation at 3,000 rpm for 15 min. The erythrocytes were washed twice with 3 ml of sodium chloride solution (0.9% in water, B. Braun Medical, Irvine, CA) to remove plasma and leukocytes. Washed erythrocytes were aliquoted by weight (0.16–0.18 g) for preparation of FAMEs.

Conventional Sample Preparation

Total lipids from plasma, serum and whole blood samples were extracted according to the method described by Folch et al. [25]. Briefly, 3 ml chloroform:methanol (2:1 v/v) containing an 3.33 µg/ml of an internal standard (22:3n-3 ethyl ester; Nu-Chek Prep, Elysian, MN) and 50 µg/ml BHT (Sigma–Aldrich Inc., St. Louis, MO) was added to each 100 µl sample and vortexed for 1 min. Sodium phosphate solution (500 µl of 0.5 M) was added, and samples were mixed by inversion and centrifuged at 3,000 rpm for 5 min. The organic phase was collected, evaporated to dryness under nitrogen gas and lipids were redissolved in 300 µl of hexane for direct transesterification or 100 µl of chloroform for phospholipid isolation (plasma only). Erythrocytes were prepared according to Reed et al. [26]. Briefly, 1 ml of cold methanol (containing 50 µg BHT and 20 µg 22:3n-3 ethyl ester internal standard) was added to erythrocytes (0.16–0.18 g) and vortexed for 1 ml to lyse cells. Chloroform (1 ml) was then added, followed by vortexing and storage overnight at −80 °C. The following day, samples were thawed, vortexed, and then centrifuged at 3,000 rpm for 10 min. The supernatant was collected, and the remaining pellet was reextracted using 2 ml chloroform:methanol (1:1 v/v). The extracted supernatants were combined and 1.8 ml of water was added to separate the aqueous and organic phases [27]. The organic phase was collected and lipids isolated as described for plasma, serum and whole blood.

Plasma phospholipids were also isolated by thin layer chromatography (TLC) [28]. Briefly, total lipid extracts of plasma were applied to silica gel plates (Whatman, Clifton, NJ) and lipids were separated using a mixture of heptane: diethylether: methylene chloride (60:40:2 by volume; J.T. Baker, Phillipsburg, NJ). Samples were run alongside a TLC reference standard (TLC 18–5 A, Nu-Chek Prep, Elysian, MN), visualized with 2′,7′-dichlorofluorescein (Sigma, St. Louis, MO) under ultraviolet light and the phospholipid band collected for transesterification.

Total lipid extracts of serum, plasma, erythrocytes, and whole blood and plasma phospholipids in 300 µl of hexane were transesterified using 1 ml of BF_3/MeOH (14% w/v) without prior saponification as described previously [21] with convectional heat by a block heater for 60 min at 90°C. The use of convectional heat by block heater for 60 min was also used on a set of fingertip blood samples. The use of convectional heat for only 15 min was also examined on whole blood and fingertip prick blood samples.

Direct Microwave Transesterification

Fingertip blood on chromatography paper, whole blood on chromatography paper, and whole blood dropped directly into the solvents were prepared by direct microwave transesterification using 1 ml BF_3/MeOH (14% w/v) with the addition of 300 µl of hexane with BHT added.

A commercial microwave oven (model MW8107WAC, 1,000 W; Emerson, Toronto, ON) was used at power level 4 for 45 s for the transesterification of fatty acids to FAMEs. Lower power settings or less time proved to be insufficient to carry out the reaction, and more aggressive reaction conditions did not improve results and increased the risk of explosion (data not shown). Although the settings were optimal for our commercial microwave oven, it is important to note that these settings differed from those presented previously [23]. This is likely due to high variation in household microwave ovens. After heating by microwave, samples were allowed to cool to room temperature and the FAMEs collected in the hexane after the addition of additional hexane and deionized water. The hexane layer containing the FAMEs was collected, dried to a volume of 100 µl and capped under nitrogen, and stored at −80°C until analysis by gas chromatography.

Quantitative Comparisons

Initial qualitative results warranted further investigation between the use of direct transesterification for FAME generation by convectional and microwave heating. Whole blood samples (50 µl each) were aliquoted directly into 1 ml BF_3/MeOH (14% w/v) with the addition of hexane (300 µl). BHT and an internal standard (22:3n-3 methyl ester, Nu-Chek Prep) were added to the hexane previously. Samples were then heated by either block heating (60 min at 90°C) or microwave heating (power level 4 for 45 s) as described above. Note that 22:3n-3 ethyl ester, an internal standard we use to indicate complete transesterification for convectional techniques was not completely transesterified by microwave transesterification as both methyl and ethyl esters of 22:3n-3 were detected when only 22:3n-3 ethyl ester was included. Concentrations of individual fatty acids were determined based on the peak area of a calibrated internal standard (22:3n-3 methyl ester) after peaks areas were adjusted by individual peak response factors as determined by a 28 component qualitative standard mixture GLC-462, Nu-Chek Prep).

The transesterification of fatty acids bound specifically to triacylglycerols or phospholipids was examined. Triheptadecanoin (17:0 TG, Nu-Chek) and 1,2-diheptadecanoyl-*sn*-glycero-3-phosphocholine (17:0 PC, Avanti Polar Lipids Inc., Alabaster, AL) were purchased and FAMES prepared by direct transesterification methods with convectional and microwave heat.

Gas Chromatography Analysis

Analyses were performed on a Shimadzu 17-A gas chromatograph (Shimadzu, Columbia, MD) with a fused silica capillary column (DB-FFAP), 30 m × 0.25 mm inner diameter × 0.25 µm film thickness (J&W Scientific, Agilent Technologies, Palo Alto, CA). A Shimadzu AOC-17 automatic injector was used, and 2 µl of each sample were injected, at a split ratio of 8:1 and injector temperature of 250 °C. Samples were detected with a flame ionization detector at 250 °C. The temperature program consisted of an initial temperature of 130 °C with 1 min hold, ramp 4 °C/min to 178 °C, 1 °C/min to 195 °C with 17 min hold, and 40 °C/min to 245 °C with 12 min hold. Pressure was held constant at 106 kPa, and the carrier gas was H_2. Shimadzu Class-VP software was used for integration. Peaks with retention times and fatty acids were detected as compared to an external standard (GLC-462).

Gas Chromatography Mass Spectrometry (GC-MS) Analysis

Individual peaks, particularly dimethyl acetal (DMA) peaks were confirmed with GC-MS analysis on a 3800 gas chromatograph equipped with a Varian 4000 ion trap mass spectrometer in external EI mode (Varian Canada Inc., Mississauga, ON). DMAs were identified with target ion mass to charge ratios (*m/z*) of 255, 281 and 283 for 16:0 DMA, 18:1 DMA and 18:0 DMA, respectively[29,30]. The fatty acid methyl esters in hexane were injected onto a DB-FFAP 30 m × 0.25 mm i.d. × 25 µm film thickness, capillary column (J&W Scientific from Agilent Technologies, Mississauga, ON) interfaced directly onto the ion source with helium as the carrier gas. Initial column temperature was 50 °C with a 1 min hold followed by a 30 °C/min ramp to 130 °C, an 8 °C/min ramp to 175 °C, a 1 °C/min ramp to 210 °C, and a 30 °C/min ramp to 245 °C with a 30 min hold at the end. The injector and transfer line were maintained at 260 °C and 250 °C, respectively. The source temperature and manifold temperatures were 180 and 50 °C, respectively. The low mass range was selected as 50 *m/z* to exclude air and water contaminants, and the high mass range was 400 *m/z* to include the full range of fatty acid methyl esters. A target total ion count of 20,000 was selected with a maximum ionization time of 65,000 µs, and an emission current of 25 µA for the ion trap. In addition, a 3 µScan average for each data point resulting in a 0.55 s maximum scan time was utilized.

Data Analyses and Statistics

The fatty acid composition of blood samples and common biomarkers for expressing omega-3 PUFA status were determined. These included EPA + DHA, EPA + DPAn-

Table 2 Fatty acid composition of various blood samples by conventional techniques

Fatty acids	Serum Total lipid	Plasma Total lipid	Plasma Phospholipid	Erythrocytes Total lipid	Whole blood Total lipid
mol% of total fatty acids					
14:0	1.34 ± 0.01^{d}	1.37 ± 0.03^{d}	0.77 ± 0.09^{b}	0.45 ± 0.01^{a}	1.01 ± 0.01^{c}
16:0	23.01 ± 0.10^{a}	23.01 ± 0.35^{a}	30.40 ± 0.58^{c}	24.59 ± 0.38^{b}	23.07 ± 0.12^{a}
18:0	5.45 ± 0.03^{a}	5.52 ± 0.21^{a}	12.09 ± 0.61^{c}	13.06 ± 0.52^{c}	8.87 ± 0.09^{b}
20:0	0.13 ± 0.01^{a}	0.13 ± 0.01^{a}	0.33 ± 0.06^{b}	0.31 ± 0.02^{b}	0.19 ± 0.01^{a}
22:0	0.34 ± 0.02^{a}	0.32 ± 0.04^{a}	0.86 ± 0.04^{c}	1.18 ± 0.05^{d}	0.59 ± 0.02^{b}
23:0	0.15 ± 0.01^{a}	0.13 ± 0.02^{a}	0.33 ± 0.01^{c}	0.20 ± 0.01^{b}	0.14 ± 0.01^{a}
24:0	0.28 ± 0.02^{a}	0.26 ± 0.03^{a}	0.71 ± 0.05^{b}	3.00 ± 0.16^{d}	1.07 ± 0.03^{c}
SFA	30.81 ± 0.15^{a}	30.89 ± 0.65^{a}	46.30 ± 0.83^{d}	41.92 ± 0.55^{c}	35.09 ± 0.23^{b}
16:0 DMA	0.21 ± 0.03^{a}	0.21 ± 0.02^{a}	0.30 ± 0.02^{a}	1.64 ± 0.13^{c}	0.68 ± 0.04^{b}
18:0 DMA	0.05 ± 0.03^{ab}	0.08 ± 0.01^{b}	n.d.^{a}	0.45 ± 0.02^{d}	0.18 ± 0.03^{c}
18:1 DMA	n.d.^{a}	n.d.^{a}	n.d.^{a}	0.37 ± 0.02^{c}	0.14 ± 0.02^{b}
Total DMA	0.25 ± 0.05^{a}	0.29 ± 0.02^{a}	0.30 ± 0.02^{a}	2.45 ± 0.16^{c}	1.01 ± 0.09^{b}
14:1	0.12 ± 0.01	0.13 ± 0.01	0.05 ± 0.10	0.02 ± 0.05	0.09 ± 0.06
16:1n-7	3.57 ± 0.13^{c}	3.57 ± 0.07^{c}	0.84 ± 0.07^{a}	0.89 ± 0.13^{a}	2.54 ± 0.10^{b}
18:1n-7	1.86 ± 0.04^{c}	1.83 ± 0.04^{bc}	1.51 ± 0.05^{a}	1.53 ± 0.03^{a}	1.72 ± 0.03^{b}
18:1n-9	19.38 ± 0.10^{d}	19.26 ± 0.45^{d}	8.26 ± 0.07^{a}	12.40 ± 0.17^{b}	17.02 ± 0.13^{c}
20:1n-9	0.35 ± 0.05	0.33 ± 0.02	0.39 ± 0.12	0.36 ± 0.04	0.29 ± 0.05
24:1n-9	0.44 ± 0.02^{a}	0.44 ± 0.05^{a}	1.18 ± 0.03^{b}	3.14 ± 0.16^{c}	1.22 ± 0.04^{b}
MUFA	25.79 ± 0.12^{d}	25.65 ± 0.40^{d}	12.37 ± 0.48^{a}	18.54 ± 0.50^{b}	22.95 ± 0.07^{c}
18:2n-6	29.61 ± 0.05^{d}	29.51 ± 0.41^{d}	22.17 ± 0.38^{b}	11.35 ± 0.18^{a}	23.14 ± 0.10^{c}
18:3n-6	0.37 ± 0.01^{b}	0.37 ± 0.01^{b}	0.07 ± 0.14^{a}	0.08 ± 0.06^{a}	0.29 ± 0.01^{b}
20:2n-6	0.26 ± 0.01^{b}	0.28 ± 0.01^{bc}	0.33 ± 0.08^{b}	0.30 ± 0.01^{b}	0.10 ± 0.01^{a}
20:3n-6	0.70 ± 0.01^{a}	0.71 ± 0.02^{a}	1.57 ± 0.04^{b}	0.75 ± 0.01^{a}	0.73 ± 0.01^{a}
20:4n-6	5.50 ± 0.04^{a}	5.56 ± 0.12^{a}	9.40 ± 0.11^{c}	13.23 ± 0.15^{d}	8.75 ± 0.04^{b}
22:4n-6	0.20 ± 0.01^{a}	0.20 ± 0.01^{a}	0.41 ± 0.07^{b}	3.06 ± 0.02^{d}	1.22 ± 0.01^{c}
22:5n-6	0.11 ± 0.01^{a}	0.11 ± 0.01^{a}	0.25 ± 0.02^{b}	0.45 ± 0.02^{c}	0.14 ± 0.07^{a}
n-6 PUFA	36.74 ± 0.09^{c}	36.73 ± 0.33^{c}	34.28 ± 0.22^{b}	29.22 ± 0.26^{a}	34.37 ± 0.16^{b}
18:3n-3	0.91 ± 0.01^{c}	0.91 ± 0.01^{c}	0.28 ± 0.08^{a}	0.18 ± 0.01^{a}	0.65 ± 0.01^{b}
20:5n-3	0.56 ± 0.01^{a}	0.55 ± 0.02^{a}	0.81 ± 0.06^{b}	0.53 ± 0.01^{a}	0.53 ± 0.01^{a}
22:5n-3	0.48 ± 0.01^{a}	0.49 ± 0.03^{a}	0.94 ± 0.07^{b}	2.22 ± 0.02^{d}	1.11 ± 0.01^{c}
22:6n-3	0.72 ± 0.02^{a}	0.75 ± 0.02^{a}	1.52 ± 0.05^{c}	1.99 ± 0.06^{d}	1.17 ± 0.02^{b}
n-3 PUFA	2.67 ± 0.03^{a}	2.70 ± 0.07^{a}	3.59 ± 0.33^{b}	4.92 ± 0.06^{c}	3.45 ± 0.02^{b}
PUFA	39.41 ± 0.12^{c}	39.43 ± 0.31^{c}	37.87 ± 0.43^{b}	34.14 ± 0.25^{a}	37.82 ± 0.17^{b}

Values are means ± SD, $n = 4$. *SFA* saturated fatty acids; *DMA* dimethyl acetal; *MUFA* monounsaturated fatty acids; *PUFA* polyunsaturated fatty acids. Fatty acids with different alphabetical superscripts are statistically different by Tukey's HSD after significant F value by one-way ANOVA, $P < 0.01$

3 + DHA, the ratio of n-3 to n-6 PUFA and the % of n-3 HUFA in total HUFA. The equation for calculation of the % of n-3 HUFA in total HUFA was: (20:3n-3 + 20:5n-3 + 22:5n-3 + 22:6n-3)/(20:3n-3 + 20:5n-3 + 22:5n-3 + 22:6n-3 + 20:3n-6 +20:4n-6 + 22:4n-6 + 22:5n-6 + 20:3n-9) × 100. The qualitative determinations of various blood fractions were compared by one-way ANOVA with comparisons of individual means by Tukey's Honestly Significantly Difference (HSD) tests as were whole blood samples including fingertip prick samples that varied by preparation techniques. Due to the number of statistical comparisons made, significance was inferred when $P < 0.01$. The comparisons of quantitative determinations in human blood and with standards were made by paired t-tests with significance inferred at $P < 0.05$. All values are expressed as means ± SD.

Results

Blood Fractions

The fatty acid composition of human blood is dependent on the blood fraction collected (Table 2). Fatty acid compositions of serum and plasma total lipid extracts were similar, while plasma phospholipid and erythrocyte total lipid had significantly higher percentages of saturated fatty acids and lower percentages of monounsaturated fatty

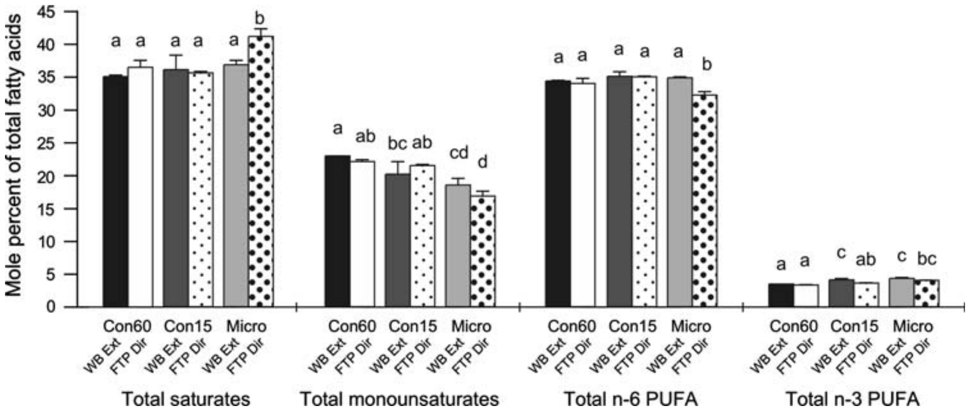

Fig. 1 The effects of transesterification by convectional heat for 60 min and 15 min or by microwave on lipid extracts from whole blood and blood absorbed on chromatography paper from a fingertip prick. Values are means ± SD, $n = 4$. Bars with different alphabetical superscripts within a grouping are statistically different by Tukey's HSD after significant F value by one-way ANOVA, $P < 0.01$

acids, and slightly lower polyunsaturated fatty acids. A closer examination of the polyunsaturated fatty acids indicate that in plasma and serum total lipid, the significantly higher amounts linoleic acid (18:2n-6) are responsible for this difference, as the HUFAs such as arachidonic acid (20:4n-6, AA) and DHA are higher in the erythrocytes and plasma phospholipid. Theses differences are to be expected and are largely dictated by differences in the lipid classes, with plasma and serum total lipids containing lipoproteins with significant amounts of triacylglycerols and cholesterol esters [31] that contain a higher proportion of oleic (18:1n-9) and linoleic acid, and lower proportions of HUFAs.

In the present blood samples, there were higher proportions of HUFAs, except EPA and 20:3n-6 in erythrocytes. Erythrocytes also had much lower levels of 18:2n-6 and 16:0, but higher levels of 18:1n-9, 24:1n-9 (found mainly in sphingolipids) and dimethyl acetals (DMAs, derived from the methylation of plasmologens). Differences in plasma phospholipids and erythrocytes is largely determined by the higher proportion of inner leaflet membranes with significantly higher amounts of phosphatidylethanolamine in erythrocytes as compared to phosphatidylcholine dominated monolayers of lipoproteins [31]. Whole blood total lipid fatty acid compositions reflect the mixture of erythrocyte and plasma total lipids with fatty acid percentages falling intermediary of the two extremes.

Convectional Versus Microwave Heat

The use of convectional heat at 90 °C for 60 min, convectional heat at 90 °C for 15 min and microwave heat at power level 4 for 45 s for the transesterification of lipid extracts from whole blood and fingertip prick blood on chromatography paper demonstrated significant differences in fatty acid composition (Fig. 1). Direct transesterification of fingertip blood by microwave methylation differed from the other methods to the greatest degree. Specifically, the percentage of saturates was significantly higher and the percentage of monounsaturates were lower with direct microwave transesterification. Interestingly, prior lipid extraction of whole blood followed by microwave methylation resulted in values more similar to those obtained by transesterification mediated by convectional heat, suggesting that sample matrix was affecting microwave transesterification. In regards to PUFA, the differences were less pronounced. An additional experiment comparing microwave transesterification on whole blood lipid extract, whole blood dipped in chromatography paper, whole blood added directly to the solvent mixture, and fingertip prick blood on chromatography paper was completed (Fig. 2). Direct transesterification of fingertip prick blood on chromatography paper and whole blood without prior lipid extraction (on chromatography paper or directly

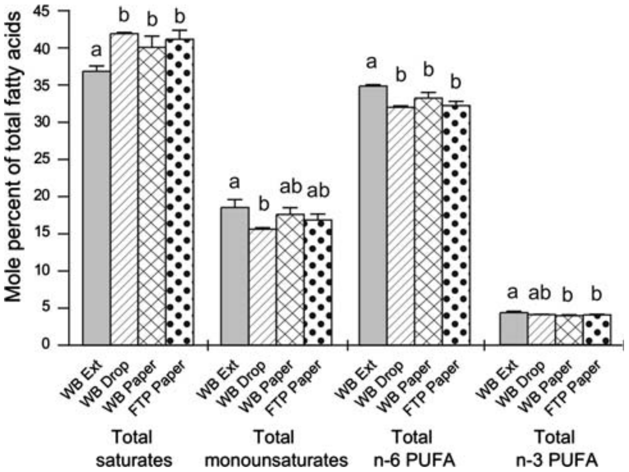

Fig. 2 The effects of transesterification by microwave on whole blood with and without prior extraction, and blood absorbed on chromatography paper from venous sampling and from a fingertip prick. Values are means ± SD, $n = 4$. Bars with different alphabetical superscripts within a grouping are statistically different by Tukey's HSD after significant F value by one-way ANOVA, $P < 0.01$

Table 3 Qualitative and quantitative determinations after direct transesterification of whole blood using convectional heat and microwave heat

Fatty acids	Qualitative		Quantitative	
	Convectional (mol% of total fatty acids)	Microwave (mol% of total fatty acids)	Convectional (μg/ml)	Microwave (μg/ml)
14:0	0.76 ± 0.05	0.83 ± 0.05	14.0 ± 0.6	12.1 ± 1.5
16:0	20.65 ± 0.56	22.82 ± 1.03	426 ± 9	375 ± 39
18:0	9.88 ± 0.23	17.19 ± 1.03**	226 ± 4	314 ± 38
20:0	0.24 ± 0.02	0.26 ± 0.03	5.95 ± 0.32	5.14 ± 0.69
22:0	0.64 ± 0.05	0.25 ± 0.09*	17.5 ± 0.5	5.31 ± 1.45*
23:0	0.17 ± 0.01	0.06 ± 0.03*	4.83 ± 0.22	1.40 ± 0.52*
24:0	1.45 ± 0.19	0.38 ± 0.27	43.0 ± 3.2	8.89 ± 5.35*
SFA	34.03 ± 1.02	42.32 ± 1.88*	767 ± 21	790 ± 94
16:0 DMA	0.56 ± 0.34	1.46 ± 0.54	11.7 ± 6.0	24.3 ± 8.5
18:0 DMA	0.61 ± 0.33	1.99 ± 0.64	14.1 ± 6.4	36.6 ± 11.3
18:1 DMA	0.18 ± 0.09	0.55 ± 0.20	4.25 ± 1.85	10.1 ± 3.5
Total DMA	1.35 ± 0.75	4.01 ± 1.38	30.0 ± 14.1	71.0 ± 23.3
14:1	0.01 ± 0.02	0.05 ± 0.01	0.24 ± 0.34	0.72 ± 0.18
16:1n-7	1.34 ± 0.12	0.70 ± 0.15*	27.5 ± 2.6	11.3 ± 1.9**
18:1n-7	1.43 ± 0.02	1.25 ± 0.03*	32.6 ± 0.8	22.6 ± 1.5*
18:1n-9	15.35 ± 0.24	12.14 ± 1.34	349 ± 9	219 ± 18**
20:1n-9	0.76 ± 0.12	0.38 ± 0.01*	19.0 ± 1.8	7.53 ± 0.48**
22:1n-9	0.11 ± 0.03	0.06 ± 0.01	2.93 ± 0.66	1.32 ± 0.17
24:1n-9	1.99 ± 0.18	0.56 ± 0.39*	58.4 ± 2.5	12.7 ± 6.2*
MUFA	21.00 ± 0.39	15.15 ± 1.83	494 ± 9	285 ± 20**
18:2n-6	19.24 ± 0.64	14.96 ± 2.12	434 ± 12	267 ± 27*
18:3n-6	0.30 ± 0.03	0.21 ± 0.05	6.79 ± 0.36	3.66 ± 0.72*
20:2n-6	0.23 ± 0.01	0.19 ± 0.02*	5.75 ± 0.10	3.80 ± 0.20*
20:3n-6	1.12 ± 0.04	1.04 ± 0.02*	27.7 ± 0.4	20.4 ± 1.3*
20:4n-6	6.70 ± 0.21	6.40 ± 0.13*	164 ± 2	125 ± 9*
22:4n-6	0.53 ± 0.02	0.59 ± 0.06*	14.3 ± 0.1	12.5 ± 1.8
22:5n-6	0.16 ± 0.01	0.12 ± 0.02	4.17 ± 0.39	2.56 ± 0.44
n-6 PUFA	28.29 ± 0.91	23.60 ± 2.02	657 ± 15	437 ± 28*
18:3n-3	0.54 ± 0.02	0.43 ± 0.07	12.0 ± 0.4	7.56 ± 0.99*
20:5n-3	2.47 ± 0.10	2.21 ± 0.05	60.1 ± 1.4	42.8 ± 2.6*
22:5n-3	1.46 ± 0.06	1.54 ± 0.09	38.7 ± 0.3	32.5 ± 3.2
22:6n-3	5.77 ± 0.33	5.23 ± 0.06	152 ± 4	110 ± 8*
n-3 PUFA	10.23 ± 0.51	9.41 ± 0.09	263 ± 6	193 ± 14*
PUFA	38.52 ± 1.42	33.01 ± 2.01	920 ± 20	629 ± 37*
Total fatty acids			2,180 ± 46	1,704 ± 126

Values are means ± SD, $n = 4$. *SFA* saturated fatty acids; *DMA* dimethyl acetal; *MUFA* monounsaturated fatty acids; *PUFA* polyunsaturated fatty acids. Significantly different than convectional by paired *t*-test

* $P < 0.05$; ** $P < 0.001$

dropped in solvents) resulted in similar determinations which were different than when lipids were previously extracted. Individual fatty acid results are presented in detail in Supplementary Table I.

Quantitative Determinations

Quantitative determinations of fatty acids (μg/ml) in whole blood using convectional heating and microwave indicated a greater number of significant differences as compared to when the data was expressed as a relative percentage of total fatty acids (Table 3). The total fatty acid concentration tended to be lower with microwave methylation (2180 ± 46 vs. 1704 ± 46, $P = 0.052$). There was no difference in the concentration of total saturates, although there were significantly lower determinations of 22:0, 23:0 and 24:0, possibly reflecting lower rates of transesterification of sphingolipids. Total monounsaturated fatty acids as determined by microwave transesterification were significantly lower and only 58% of the total monounsaturates as determined by convectional heat. The determinations of

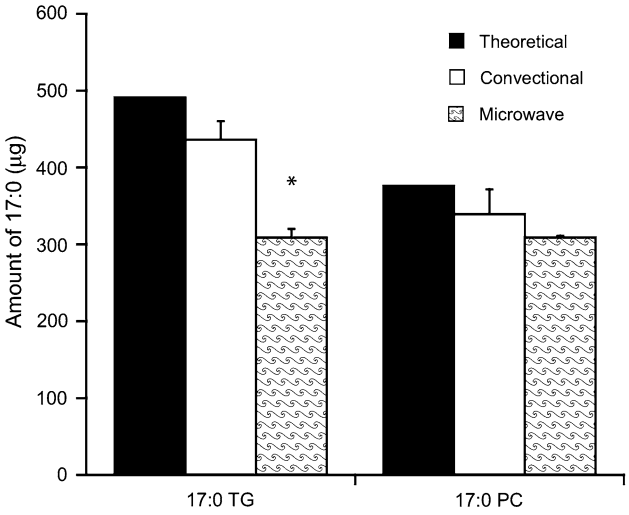

Fig. 3 The amount of heptadecanoic acid (17:0) determined from triheptadecanoin (17:0 TG) and diheptadecanoyl phosphatidylcholine (17:0 PC) by transesterification with convectional and microwave heat. Values are means ± SD, *n* = 4. *Significantly different from convectional heat by paired *t*-test, $P < 0.05$

PUFAs were also significantly lower with microwave with microwave determinations being only 68% of the convectional heat. Within the PUFAs, the 18 carbon PUFAs tended to reflect the determinations in monounsaturates with microwave determinations being only 60% of convectional heat while HUFA determinations by microwave were 75% of convectional determinations with no difference in the n-6 versus n-3 HUFAs. Interestingly, DMA estimates were slightly, but not significantly higher when prepared by microwave transesterification.

Direct transesterification of 17:0 TG and 17:0 PC standards by convectional and microwave heating indicated that convectional heating resulted in estimates relative similar to theoretical yields. Determinations by microwave heating tended to be lower than convectional heating for phospholipids ($P = 0.06$), but were significantly lower for triacylglycerols ($P = 0.01$) (Fig. 3).

Biomarkers of n-3 Status

Biomarkers of n-3 PUFA status were determined for all qualitative analyses including different blood fractions and different methodologies (Fig. 4). The range of values were: 1.28 ± 0.02 to 2.52 ± 0.04 for EPA + DHA; 1.76 ± 0.03 to 4.74 ± 0.06 for EPA + DPAn-3 + DHA; 20.10 ± 0.15 to 22.14 ± 1.26 for the % of n-3 HUFA in total HUFA; and 0.073 ± 0.001 to 0.168 ± 0.003 for n-3/n-6. The lowest value for each biomarker came from serum or plasma and the highest value came from erythrocytes, except for the % on n-3 HUFA in total HUFA. Expressing values as the % of n-3 HUFA in total HUFA resulted in a much tighter range across methodologies. As a result, the lowest value (fingertip prick blood transesterified with convectional heat) was different only from the highest value (plasma phospholipid). The highest value (plasma phospholipid) was statistically similar to serum, plasma, erythrocyte and 15 min convectional transesterified whole blood lipid extract determinations.

Overall, microwave heating tended to result in slightly higher estimates in biomarkers of n-3 PUFA status as compared with convectional heating for 60 min, but differences were not consistent when compared to convectional heating for 15 min. When expressed as the % of n-3 HUFA in total HUFA, the increases with microwave heating were not present.

Discussion

The conventional methods for fatty acid determinations compared in the present study are by no means exhaustive, but were focused on incorporating several common methods used to estimate n-3 PUFA levels in human blood samples. Although a major focus was on examining the utility of microwave transesterification, the analysis of various blood fractions including fingertip blood were compared to promote are more comprehensive understanding of measures of n-3 PUFA. The use of microwave heating for transesterification of fatty acids for analysis by gas chromatography has potential, but it appears utility may be limited to rapid, qualitative estimates of n-3 PUFA status with some loss of precision and accuracy. Fingertip prick blood sample collection however, proved to be an effective and inexpensive method for whole blood sample collection when only total lipid fatty acid composition is of interest as demonstrated previously [20].

There is very limited literature examining the use of microwave energy for driving fatty acid transesterification reactions [23,32]. The present study is the first to document significant limitations in the use of microwave transesterification in place of convectional transesterification. The present study indicates that direct microwave transesterification of whole blood can result in significantly higher qualitative estimates of saturated fatty acids and lower estimates of monounsaturated fatty acids. Quantitative analyses indicate that the determination of saturated fatty acids by microwave transesterification is in fact similar to convectional heat, but that polyunsaturates and monounsaturates in particular are significantly underestimated. Very low determinations of monounsaturates (mainly 18:1n-9) and 18:2n-6 specifically among PUFAs suggested that transesterification rates may differ by lipid class. The use of 17:0 TG and 17:0 PC confirmed that microwave

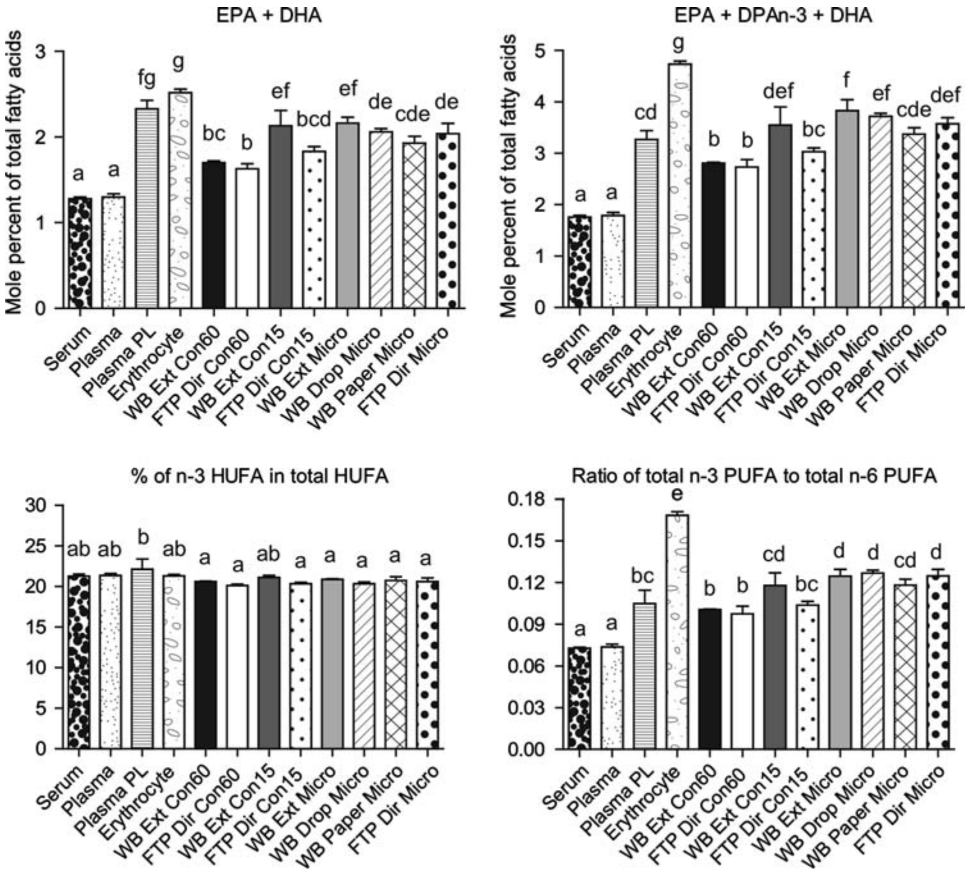

Fig. 4 Values of n-3 fatty acids biomarkers as determined from various blood fractions and by various analytical methods. Values are means ± SD, $n = 4$. Bars with different alphabetical superscripts within a grouping are statistically different by Tukey's HSD after significant F value by one-way ANOVA, $P < 0.01$

transesterification had significant discrepancies with the transesterification of triacylglycerols as compared with convectional heat. These differences may partly explain differences observed in quantitative and qualitative estimates of fatty acid composition. Microwave transesterification also resulted in lower determinations of fatty acids associated with sphingolipids such as 24:1n-9, a phenomenon previously observed and duplicated in the present study when BF_3/MeOH direct transesterification by convectional heating is <60 min [21].

The use of microwave heating for the preparation of FAMEs requires further research. In the present study, we were biased towards one-step direct transesterification methods that are more suitable for robotic automation. Whole blood is a challenging matrix to analyze given that it is a mixture of lipid classes with mono- and bi-layer membranes and various proteins. Limitations with the use of microwave heating may be reduced if other approaches are examined rather than just direct transesterification. Sample preparation techniques such as the isolation of individual lipid classes and the saponification of lipids prior to derivatisation may be more amenable to microwave based methylation. Increasing the percentage of BF_3 in methanol, or the use of catalysts other than BF_3/MeOH may improve quantitative fatty acid determinations with microwave transesterification. Using research scale microwave synthesizers appears relevant, although these instruments are considerable more expensive than household microwave ovens. These alternative approaches may however introduce other limitations such as an increase in sample handling time and the loss of free or esterified fatty acids in multi-step techniques, and the increased risk of generating methoxy-substituted fatty acids with higher BF_3 concentrations [33].

Despite the limitations of microwave driven transesterifications of blood samples, we have found that it has utility. Although the quantitative estimates by microwave transesterification were lower than by convection transesterification, the decrease in accuracy was consistent for n-3 and n-6 HUFAs. Therefore, when the data is expressed as the % of n-3 HUFA in total HUFA, the absolute values determined with microwave transesterification are very close to values determined by convectional heating. Therefore when direct microwave transesterification is combined with fingertip prick blood collection and fast gas chromatography [13,14] n-3 PUFA status for a single individual can be determined in under 30 min. This is quicker than dietary assessment tools, and is particularly useful when screening research participants for n-3 PUFA intervention studies and other blood biochemical parameters are not of interest.

The present findings also support further consideration of the % of n-3 HUFA in total HUFA as a universal blood biomarker for n-3 HUFA status [24]. The tight range of this biomarker across various blood fractions and methods in the present study as compared to other markers provides a significant advantage in knowledge translation and public health targets. Adding 750 mg of EPA + DHA to the typical North American diet as proposed for significant cardioprotection [10] without changing in other fatty acid intakes should result in a % of n-3 HUFA in total HUFA of 44% using equations developed by Lands et al. [34]. A target of 40% of n-3 HUFA in total HUFA corresponds to a lower risk of mortality from myocardial infarction [35,36] and roughly corresponds to an EPA + DHA value of 8% of total fatty acids in erythrocytes [12].

The use of the % of n-3 HUFA in total HUFA as an n-3 biomarker, and microwave heating require further assessment. For the % of n-3 HUFA in total HUFA, determinations across individuals consuming a range of n-3 PUFA, and an assessment of the ability of this biomarker to predict disease risk are required. In addition, the % of n-3 HUFA in total HUFA largely characterizes the *sn*-2 position of membrane phospholipids [24] and therefore health/disease associations may be limited to *sn*-2 related physiological mechanisms. Fatty acid biological effects mediated by 18:2n-6 and 18:3n-3 for example, may not be represented by this biomarker. The use of direct microwave transesterification for preparation of FAMEs also requires testing across a wider range of fatty acid compositions. Additional modifications and testing of microwave transesterification/methylation is definitely required, however it can serve as a rapid, qualitative assessment of n-3 fatty acid status. The potential application of cheap, rapid qualitative methods for clinical screening is dependent not only on further developments of such methods, but also continued efforts to associate n-3 biomarkers to disease risk so that healthy recommendations and targets can be made that will allow specificity and sensitivity evaluations of these high throughput, novel methods.

Acknowledgements Operating funds were provided by a start-up award from the University of Waterloo and infrastructure was purchased through a Canada Foundation of Innovation and the Ontario Research Fund matching grants. K.D.S. received partial salary support through a GENESIS Young Investigator Award and J.M.A held a NSERC Undergraduate Student Research Award for a portion of the study.

References

1. Schmidt EB, Skou HA, Christensen JH, Dyerberg J (2000) Public Health Nutr 3:91–98
2. Albert CM, Hennekens CH, O'Donnell CJ, Ajani UA, Carey VJ, Willett WC, Ruskin JN, Manson JE (1998) JAMA 279:23–28
3. Albert CM, Campos H, Stampfer MJ, Ridker PM, Manson JE, Willett WC, Ma J (2002) N Engl J Med 346:1113–1118
4. Connor WE (2000) Am J Clin Nutr 71:171S–175S
5. GISSI-Prevenzione Investigators (1999) Lancet 354:447–455
6. Kang JX, Leaf A (1996) Circulation 94:1774–1780
7. Von Schacky C, Fischer S, Weber PC (1985) J Clin Invest 76:1626–1631
8. Harris WS, Rothrock DW, Fanning A, Inkeles SB, Goodnight SH Jr, Illingworth DR, Connor WE (1990) Am J Clin Nutr 51:399–406
9. Mozaffarian D, Geelen A, Brouwer IA, Geleijnse JM, Zock PL, Katan MB (2005) Circulation 112:1945–1952
10. Mozaffarian D, Rimm EB (2006) JAMA 296:1885–1899
11. Kobayashi M, Sasaki S, Kawabata T, Hasegawa K, Akabane M, Tsugane S (2001) Eur J Clin Nutr 55:643–650
12. Harris WS, Von Schacky C (2004) Prev Med 39:212–220
13. Stark KD, Salem N Jr (2005) Lipid Tech 17:181–185
14. Masood A, Stark KD, Salem N Jr (2005) J Lipid Res 46:2299–2305
15. Lepage G, Roy CC (1984) J Lipid Res 25:1391–1396
16. Kang JX, Wang J (2005) BMC Biochem 6:5
17. Lepage G, Roy CC (1986) J Lipid Res 27:114–120
18. Ohta A, Mayo MC, Kramer N, Lands WE (1990) Lipids 25:742–747
19. Inoue K, Suzuki Y, Yajima S, Shimozawa N, Orii T, Kondo N (1997) Clin Chem 43:2197–2198
20. Marangoni F, Colombo C, Galli C (2004) Anal Biochem 326:267–272
21. Morrison WR, Smith LM (1964) J Lipid Res 4:600–608
22. Harris WS, Sands SA, Windsor SL, Ali HA, Stevens TL, Magalski A, Porter CB, Borkon AM (2004) Circulation 110:1645–1649
23. Banerjee P, Dawson G, Dasgupta A (1992) Biochim Biophys Acta 1110:65–74
24. Stark KD (2007) Lipids. doi:10.1007/s11745-007-3128-3
25. Folch J, Lees M, Sloane Stanley GHS (1957) J Biol Chem 226:497–509
26. Reed CF, Swisher SN, Marinetti GV, Eden EG (1960) J Lab Clin Med 56:281–289
27. Bligh EG, Dyer WJ (1959) Can J Biochem Physiol 37:911–917
28. Skipski VP, Good JJ, Barclay M, Reggio RB (1968) Biochim Biophys Acta 152:10–19
29. Hara A, Taketomi T (1988) J Biochem (Tokyo) 104:1011–1015
30. Takemoto Y, Suzuki Y, Horibe R, Shimozawa N, Wanders RJ, Kondo N (2003) Brain Dev 25:481–487
31. Christie WW (1985) J Lipid Res 26:507–512
32. Itonori S, Takahashi M, Kitamura T, Aoki K, Dulaney JT, Sugita M (2004) J Lipid Res 45:574–581
33. Lough AK (1964) Nature 202:795
34. Lands WE, Libelt B, Morris A, Kramer NC, Prewitt TE, Bowen P, Schmeisser D, Davidson MH, Burns JH (1992) Biochim Biophys Acta 1180:147–162
35. Lands WE (2005) Ann N Y Acad Sci 1055:179–192
36. Dolecek TA (1992) Proc Soc Exp Biol Med 200:177–182

Lipids (2008) 43:197–205
DOI 10.1007/s11745-007-3139-0

ORIGINAL ARTICLE

Identification and Characterization of Hamster Stearoyl-CoA Desaturase Isoforms

Jian Wang · Lan Yu · He Wang · Yunling Gao · James P. Schrementi · Regina K. Porter · David A. Yurek · Mingshang Kuo · Chen-Shian Suen · Guoqing Cao · James S. Bean · Raymond F. Kauffman · Yuewei Qian

Received: 29 June 2007 / Accepted: 8 November 2007 / Published online: 15 December 2007
© AOCS 2007

Abstract Stearoyl-CoA desaturase (SCD) catalyzes the formation of monounsaturated fatty acids from saturated fatty acids. It plays a key role in lipid metabolism and energy expenditure in mammals. In mice, four SCD isoforms (SCD1–4) have been identified. Here we report the identification of cDNA sequences corresponding to SCD1, SCD2 and SCD3 of golden hamster. The deduced amino acid sequences of these hamster SCD (hmSCD) isoforms display a high degree of homologies to their mouse counterparts (mouse SCD). Polyclonal antibodies specific to rodent SCDs detected proteins of predicted size in the human embryonic kidney 293 cells transfected with hmSCD cDNAs. Microsome fractions prepared from these cells also displayed increased SCD activity versus cells transfected with vector alone. Real-time reverse transcription-polymerase chain reaction analysis revealed the highest expression of hmSCD1 in liver and adipose tissue, while the highest hmSCD2 expression was detected in the brain. Very low levels of hmSCD3 mRNA can be detected in the tissues tested. This report is the first description of three SCD isoforms in the hamster and will provide useful tools in the further study of fatty acids metabolism in this species.

Keywords Stearoyl-CoA desaturase · Hamster

Abbreviations

Bp	Base pair(s)
cDNA	DNA complementary to RNA
GAPDH	Glyceraldehyde-3-phosphate dehydrogenase
HDL	High density lipoprotein
kb	Kilobase(s) or 1,000 bp
PCR	Polymerase chain reaction
RT	Reverse transcription
SCD	Stearoyl-CoA desaturase
TLC	Thin-layer chromatography
VLDL	Very low density lipoprotein
CDS	Coding sequence

Introduction

Stearoyl-CoA desaturase (SCD) catalyzes the formation of monounsaturated fatty acids from long-chain saturated fatty acids [1]. In mammalian systems, this is the first committed step in the formation of unsaturated fatty acids. The mammalian SCD enzyme is an integrated endoplasmic reticulum (ER) membrane-protein. Its function requires two additional polypeptides: NADH-cytochrome b5 reductase and cytochrome b5. The SCD protein is comprised of over 62% non-polar amino acid residues and is largely embedded in the ER membrane, with active sites exposed to the cytosol. A site-directed mutagenesis study confirmed that clusters of histidine-rich motifs are required

J. Wang (✉) · L. Yu · Y. Gao · J. P. Schrementi ·
R. K. Porter · C.-S. Suen · G. Cao · J. S. Bean · R. F. Kauffman
Cardiovascular and Diabetes Drug Discovery,
Lilly Research Labs, Lilly Corporate Center, DC 0434,
Indianapolis, IN 46285, USA
e-mail: jyw@lilly.com

H. Wang · Y. Qian
Integrative Biology, Lilly Research Labs, DC 0343,
Indianapolis, IN 46285, USA

D. A. Yurek · M. Kuo
Discovery Chemistry, Lilly Research Labs, DC 0343,
Indianapolis, IN 46285, USA

for catalytic activity [2]. The preferred substrates for SCD are palmitoyl-CoA and stearoyl-CoA, which are converted into palmitoleoyl-CoA and oleoyl-CoA, respectively.

Recent studies suggest that mammalian SCD plays an important role in lipid metabolism and energy balance [3]. The naturally occurring SCD1-deficient mouse strains (asebia mouse) displayed impaired hepatic triglyceride and cholesterol ester biosynthesis, as well as a deficiency in wax ester and alkyl diacylglycerol. The SCD1-/- mice also have low plasma triglyceride levels in the very low density lipoprotein (VLDL) particle and reduced VLDL secretion from the liver. Dietary supplementation of triolein or tripalmitolein cannot normalize hepatic and plasma triglyceride levels [4]. SCD1-/- mice are also resistant to diet-induced weight gain and diabetes and display an attenuated obesity phenotype in a leptin-deficient background [5]. Human epidemiology studies have demonstrated a reverse correlation between hepatic SCD activity and plasma levels of high density lipoprotein (HDL) [6]. In cultured macrophage cells, SCD expression inhibited ABCA1-mediated cholesterol efflux [7]. It has been proposed that monounsaturated fatty acids phosphorylate and destabilized ABCA1 through a phospholipase D2 pathway [8]. Macrophages isolated from type 2 diabetic patients displayed increased SCD activity compared to non-diabetic controls, correlating with increased atherosclerosis risk in diabetes patients [9]. Taken together, these data suggest that SCD1 has potential implications in metabolic syndromes associated with dyslipidemia, obesity and type 2 diabetes.

Four SCD (SCD1–4) isoforms have been characterized in the mouse [10, 11]. All four mouse SCD (mSCD) genes are located in a 200 kb stretch on chromosome 19. It has been suggested that all the four mSCD genes are derived from tandem gene duplication events [10]. Two SCD isoforms have been identified in humans. Human SCD1 is the human ortholog of mSCD1 and displays similar tissue distribution [12]. Human SCD5 does not have a mouse ortholog, but displays a tissue distribution pattern similar to mSCD2 [13, 14].

The golden Syrian hamsters have been used as a valuable animal model for studying lipoprotein cholesterol metabolism and atherosclerosis. Compared to other rodent models, the hamster has the advantage of a lipoprotein profile similar to that of humans, largely due to the presence of the endogenous cholesterol ester transfer protein (CETP) activity [15]. Similar to humans, plasma non-HDL cholesterol and triglycerides levels increase in response to a diet rich in cholesterol and fatty acids in hamsters. Hamsters also develop early atherosclerosis lesions similar to those found in the early stages of human disease [16, 17]. Therefore, hamsters appear to be a good model to study the effect of SCD on lipoprotein cholesterol metabolism and the early stages of atherosclerosis. However, the hamster SCD (hmSCD) isoforms and their expression patterns have not been reported.

Here we report the identification and characterization of hmSCD1, hmSCD2 and hmSCD3. We show that all three cDNAs encode polypeptides with SCD activity. Real-time reverse transcription (RT)-polymerase chain reaction (PCR) analysis shows that the tissue distribution of hmSCD isoforms is similar to that of mSCD's, with the highest expression of SCD1 detected in adipose tissue and liver, and highest SCD2 expression detected in brain. To our knowledge, this is the first report on the three hmSCD isoforms. The identification and characterization of the hmSCD isoforms should facilitates our study of lipoprotein metabolism in relation to fatty acid desaturation in this animal model.

Materials and Methods

Animals

Male golden Syrian hamsters were obtained from Harlan (Indianapolis, IN, USA) and housed individually in stainless steel suspended rodent cages with free access to normal rodent diet (Purina 5001) and water. For tissue collection, hamsters were sacrificed by CO_2 euthanasia. White adipose tissue, heart, brain, liver, kidney, intestine, lung and skeletal muscle samples were collected, rinsed in phosphate-buffered saline, quick frozen in liquid nitrogen and stored at −80 °C. Use of hamster was approved by the Institutional Animal Care and Use Committees of the American Association for Accreditation of Laboratory Animal Care and Lilly Research Laboratories in accordance with the National Institutes of Health Guide for the Care and Use of Laboratory Animals.

Cloning of Hamster SCD cDNAs

Gene-specific primers corresponding to regions of the translation start and termination codons of hmSCD1 and hmSCD2 were designed using the cDNA sequences of mouse and rat SCD isoforms. The forward primer for hmSCD1 is 5′-ATGCCGGCCCACATGCTCCAAGAGAT, and the reverse primer for hmSCD1 is 5′-TCAGCTACTCTTGTGACTCCCGTCTCCA; the forward primer for hmSCD2 is 5′-ATGCCGGCCCACATACTGCAAGAG ATG and the reverse primer for hmSCD2 is 5′-GAACA GGAACTGCAAGACCCCACACTC. Gene-specific primers corresponding to regions of the translation starting and termination codons of hmSCD3 were designed according to the cDNA sequence of published hmSCD3 (FAR-17c). The forward primer for hmSCD3 is 5′-GCCACCATGCCAGG

ACACTTGCTAC and reverse primer for hmSCD3 is 5′-TC AGCCACTCTTGCAGCTCCCATCTCC.

The PCR was performed using the high-fidelity pfx DNA polymerase (Invitrogen, Carlsbad, CA, USA) and the gene-specific primers with cDNA prepared from hamster liver or brain as template. PCR reaction products were directly cloned into the pCRII-TOPO vector (Invitrogen, Carlsbad, CA, USA). Three clones for each gene were amplified and sequenced. In all genes, 100% consensus was reached among different clones for each gene.

For subcloning into mammalian expression vectors, each hmSCD cDNA was cut from the pCRII-TOPO vector with appropriate restriction endonucleases, separated on a 1.2% agarose gel and purified with the Qiaquick gel purification kit from Qiagen (Valencia, CA, USA). The purified cDNA fragments were ligated into the similarly restriction-digested mammalian expression vector pcDNA3.1 and transformed into H101B competent cells (Invitrogen, Carlsbad, CA, USA). The resulting subcloned products, pcDNA3.1-hmSCD1, pcDNA3.1-hmSCD2 and pcDNA3.1-hmSCD3, were confirmed by restriction digestion.

Real-time Polymerase Chain Reaction

Total RNA from hamster tissue samples was isolated using the Trizol reagent following protocols recommended by the manufacturer (Invitrogen, Carlsbad, CA, USA). RNA samples were treated with DNase I and extracted with phenol/chloroform to remove any contaminating genomic DNA. The first strand cDNA was prepared by RT with 2 μg of RNA in a 20 μl reaction volume using the Superscript II kit (Invitrogen). Quantitative sequence detection was carried out on an ABI PRISM 7700 instrument (Applied Biosystems, Foster City, CA, USA) using the Universal Master Mix from Applied Biosystems following recommended conditions (Applied Biosystems Foster City, CA, USA). The nucleotide probes and primers for hmSCD1, hmSCD2, hmSCD3 and glyceraldehyde-3-phosphate dehydrogenase (GAPDH) were designed using Primer Express version 2.0 (Applied Biosystems), and were synthesized by Operon Biotechnologies, Inc. (Huntsville, Al, USA). Primer and probe sequences are listed in Table 1. The PCR cycle number at which each assay target reached the threshold detection line (C_t value) for each gene was determined. The difference in C_t value (ΔC_t) between each SCD isoform (unkn-C_t) and GAPDH (GAPDH-C_t) was calculated as ΔC_t = unkn-C_t − GAPDH-C_t. The relative abundance of mRNA normalized against that of GAPDH for each SCD isoform in each sample was calculated using the following equation: relative mRNA level = $2^{\Delta C_t}$. The difference in ΔC_t value ($\Delta\Delta C_t$) between SCD isoforms was used to compare mRNA abundance between different SCD isoforms in the same tissue using the formula $\Delta\Delta C_t$ = unkn1 ΔC_t − unkn2 ΔC_t.

Statistical Methods

For the analysis of hmSCD mRNA levels in hamster tissues, same tissue samples from two different animals were collected and RNA isolated separately. RT-PCR reaction was run as quadruplicate for each RNA sample. C_t values and relative mRNA abundance were calculated for each PCR reaction. Mean values and standard deviations were calculated from the eight ΔC_t values using the $\Delta\Delta C_t C_t$ as described [18].

Cell Transfection, Immunoblotting and Stearoyl-CoA Desaturase Activity

Human embryonic kidney (HEK) 293 cells grown on 10 cm culture dishes were transiently transfected with plasmid DNA using Lipofectamine reagent (Invitrogen) following the recommended protocol. Cells were collected 48 h after transfection and microsome fractions were prepared using the differential centrifugation method as described earlier [13]. Microsome fractions were re-suspended in buffer A (50 mM Tris pH. 7.5, 250 mM sucrose, 1 mM EDTA and 0.1 mM DTT) and stored at −80 °C until use.

Microsome membranes (40 μg) were separated on a precast 10% SDS polyacrylamide gel (Invitrogen) and transferred to nylon membranes. Immunoblotting analysis was performed with goat polyclonal antibodies SC-14720 and SC-14722 from Santa Cruz Biotechnology (Santa Cruz, CA, USA) followed by Alexa Fluor 680-conjugated goat anti-rabbit IgG (Invitrogen). Immunoblots were developed

Table 1 Primer and probe sequences used in real-time RT-PCR reaction

	Forward primer	Reverse primer	Probe
HmSCD1	ctccggaagcctgcagaat	gggcggatgtcttcttcca	cgggagaagcagaagaccgttccc
HmSCD2	gcagatgttcgccctgaaat	tttctccagacgtactccagctt	tatatgaccccagctaccaggatgaggagg
HmSCD3	ccttgcagagaccctttactatgc	cacgactctgatgagggtgtga	atgaagggtgctgggaccgacg
GAPDH	cggatttggccgtattgg	tggcaacaacttccactttgc	cctggttaccagggctgccttcactt

and visualized with the Odysse Infrared Imaging System (Li-Cor Inc, Lincoln, NE, USA).

The thin-layer chromatography (TLC) method was employed for the measurement of desaturase activity using ^{14}C-labeled stearoyl-CoA as substrate (55 µCi/umol, ARC, St Louis, MO, USA) as described earlier [13]. Each reaction mixture contained 0.2 µCi of ^{14}C-labeled stearoyl-CoA and 50 µg of microsome fraction from transfected cells. Saturated and monounsaturated fatty acid methyl esters were separated by 10% $AgNO_3$-impregnated TLC using hexane/diethyl ether (9:1) as developing solution. Following chromatography, the plate was air dried and exposed to a phosphor image screen. A Molecular Imager FX equipment (Bio-RAD, Hercules, CA, USA) was used to visualize and quantify the ^{14}C-labeled fatty acids. Band intensities corresponding to saturated and monounsaturated fatty acids were used to calculate the percentage of conversion and enzyme activity.

Results

Cloning and Identification of Hamster Stearoyl-CoA Desaturase Isoforms

We first attempted to see if hmSCD sequences are available in the National Center for Biotechnology Information database. In the database, one cDNA sequence (FAR-17c, L26956) is described as golden hmSCD. FAR-17c was initially identified as an mRNA induced by androgen in male golden hamster's flanking tissue [19] but displayed high homology to mSCD1. Therefore, it was listed as hmSCD. However, a more detailed sequence alignment of the amino acid sequence of FAR-17c with that of mSCD isoforms revealed that it is more closely homologous to mSCD3 than to mSCD1 and mSCD2. The sequence of the first 10 amino acids in the N-terminal of FAR-17c is MPGHLLQEEM, which is 100% identical to that of mSCD3. In contrast, the sequence of first 10 amino acids of mSCD1 and mSCD2 are MPAHMLQEIS and MPAHILQEIS, respectively. The predicted amino acid sequence of FAR-17c is 91.2% identical to that of mSCD3, but only 86.2% identical to mSCD1 and 82.5% to mSCD2. These data suggest that FAR-17c is the golden hamster ortholog of mSCD3.

Alignment of the nucleotide sequences showed more than 90% homology between the mouse and rat SCD1 and also between mouse and rat SCD2. The first 25 nucleotides of mSCD1 coding sequence (CDS) are 100% identical to those of rat SCD1. The last 25 nucleotides of mSCD1 CDS differ from those of rat SCD1 by only one nucleotide. Similarly, there is only one nucleotide difference found in the first 25 nucleotides of mouse and rat SCD2 CDS. Since golden hamster DNA sequences are also very homologous to that of mouse and rat, we speculated that the first and last 25 nucleotides of hmSCD1 and hmSCD2 would be also highly homologous to those of mouse and rat SCD1 and SCD2. To clone the hmSCD1 and hmSCD2 cDNA, we designed primers according to the first and last 25 nucleotides of rat SCD1 and SCD2 CDS. PCR was performed using the pfx DNA polymerase and cDNA libraries prepared from mRNA of hamster liver and brain tissues, respectively. PCR products were directly cloned into the PCR cloning vector pCRII-TOPO. Plasmid DNA was isolated from several clones of each PCR reaction and sequenced. In all three SCD isoforms, 100% consensus was reached among different clones for each gene.

Figure 1 shows the predicted amino acid sequences of hmSCD1, hmSCD2 and hmSCD3. The hmSCD1 cDNA has an open reading frame (ORF) with a predicted peptide of 358 amino acids. The predicted hmSCD1 peptide is 94.1% identical to the amino acid sequence of mSCD1 and 92.5% identical to that of rat SCD1. The hmSCD2 cDNA has an ORF with a predicted peptide of 359 amino acids. The predicted hmSCD2 peptide is 94.7 and 96.1% identical to the amino acid sequences of mouse and rat SCD2, respectively. The hmSCD3 cDNA has an ORF with a predicted peptide of 354 amino acids and is 91.2% identical to that of mSCD3. Table 2 shows the identity and similarity among the predicted amino acid sequences of the various rodent SCD isoforms. The nucleotide sequences of hmSCD1 and hmSCD2 cDNA have been submitted to Genbank under the accession number EU003989 and EU003990, respectively.

Expression and Enzymatic Activities of Hamster SCD Isoforms

To determine if the hmSCD cDNA's we cloned code for active SCDs, these cDNA's were subcloned into mammalian expression vector pcDNA3.1. HEK 293 cells were transiently transfected with either vector DNA or plasmid DNA encoding the three hmSCD isoforms. Microsome fractions were prepared from these transfected cells and immunoblotting analysis was performed. Figure 2a shows the immunoblotting data using a goat polyclonal antibody specific for SCD1 and SCD3 of mouse and rat (SC-14720). A polypeptide about 40 kDa was detected in 293 cells transfected with either hmSCD1 or hmSCD3. These bands likely represent the hmSCD1 and hmSCD3, respectively, because the same antibody detected bands of similar size in cells transfected with rat SCD1 and SCD3 (data not shown). SC-14720 also detected a faint band at the same size in both vector and pcDNA-hmSCD2 transfected cells. These bands likely represent the endogenous human SCD1

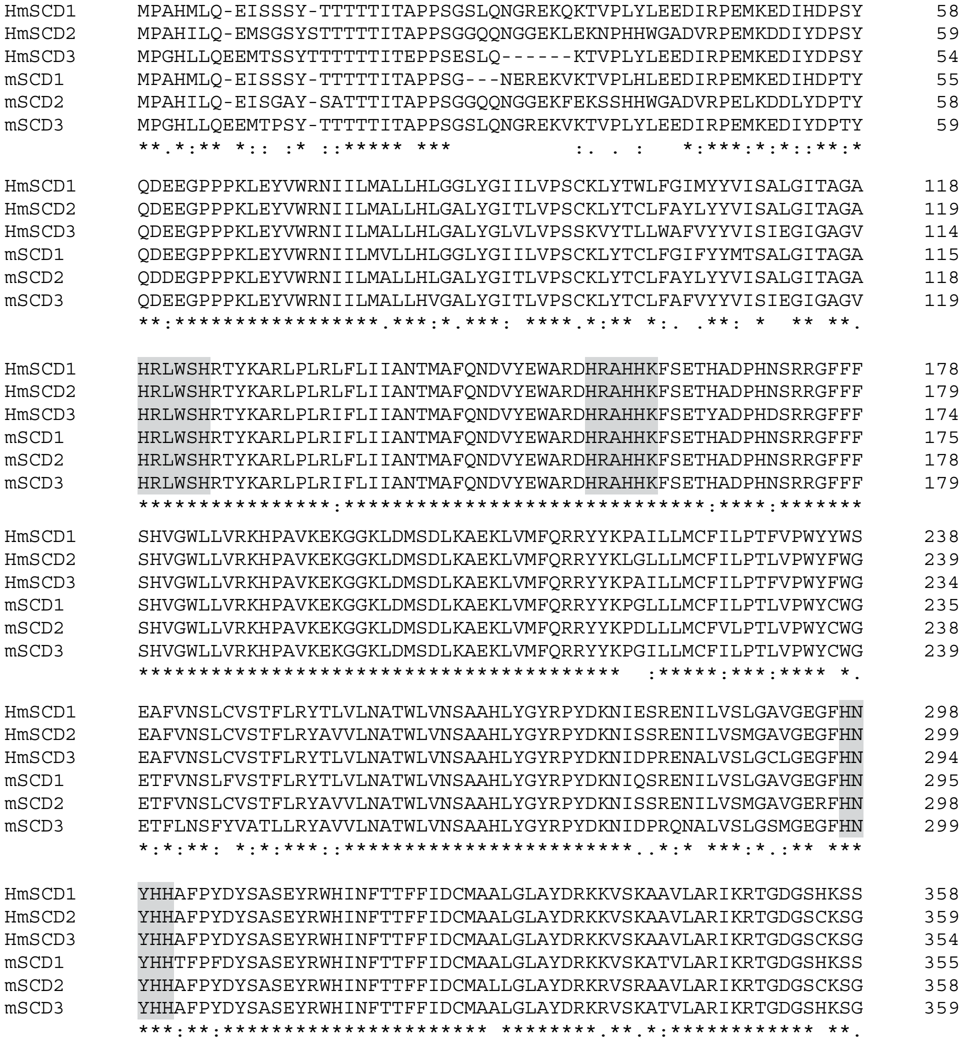

```
HmSCD1    MPAHMLQ-EISSSY-TTTTTITAPPSGSLQNGREKQKTVPLYLEEDIRPEMKEDIHDPSY    58
HmSCD2    MPAHILQ-EMSGSYSTTTTTITAPPSGGQQNGGEKLEKNPHHWGADVRPEMKDDIYDPSY    59
HmSCD3    MPGHLLQEEMTSSYTTTTTTITEPPSESLQ------KTVPLYLEEDIRPEMKEDIYDPSY    54
mSCD1     MPAHMLQ-EISSSY-TTTTTITAPPSG---NEREKVKTVPLHLEEDIRPEMKEDIHDPTY    55
mSCD2     MPAHILQ-EISGAY-SATTTITAPPSGGQQNGGEKFEKSSHHWGADVRPELKDDLYDPTY    58
mSCD3     MPGHLLQEEMTPSY-TTTTTITAPPSGSLQNGREKVKTVPLYLEEDIRPEMKEDIYDPTY    59
          **.*:** *:: :* ::***** ***          :. . :   *:***:*:*::**:*

HmSCD1    QDEEGPPPKLEYVWRNIILMALLHLGGLYGIILVPSCKLYTWLFGIMYYVISALGITAGA    118
HmSCD2    QDEEGPPPKLEYVWRNIILMALLHLGALYGITLVPSCKLYTCLFAYLYYVISALGITAGA    119
HmSCD3    QDEEGPPPKLEYVWRNIILMALLHLGALYGLVLVPSSKVYTLLWAFVYYVISIEGIGAGV    114
mSCD1     QDEEGPPPKLEYVWRNIILMVLLHLGGLYGIILVPSCKLYTCLFGIFYYMTSALGITAGA    115
mSCD2     QDDEGPPPKLEYVWRNIILMALLHLGALYGITLVPSCKLYTCLFAYLYYVISALGITAGA    118
mSCD3     QDEEGPPPKLEYVWRNIILMALLHVGALYGITLVPSCKLYTCLFAFVYYVISIEGIGAGV    119
          **:*****************.***:*.***: ****.*:** *:. .**: *  ** **.

HmSCD1    HRLWSHRTYKARLPLRLFLIIANTMAFQNDVYEWARDHRAHHKFSETHADPHNSRRGFFF    178
HmSCD2    HRLWSHRTYKARLPLRLFLIIANTMAFQNDVYEWARDHRAHHKFSETHADPHNSRRGFFF    179
HmSCD3    HRLWSHRTYKARLPLRIFLIIANTMAFQNDVYEWARDHRAHHKFSETYADPHDSRRGFFF    174
mSCD1     HRLWSHRTYKARLPLRIFLIIANTMAFQNDVYEWARDHRAHHKFSETHADPHNSRRGFFF    175
mSCD2     HRLWSHRTYKARLPLRLFLIIANTMAFQNDVYEWARDHRAHHKFSETHADPHNSRRGFFF    178
mSCD3     HRLWSHRTYKARLPLRIFLIIANTMAFQNDVYEWARDHRAHHKFSETHADPHNSRRGFFF    179
          ****************:******************************:****:*******

HmSCD1    SHVGWLLVRKHPAVKEKGGKLDMSDLKAEKLVMFQRRYYKPAILLMCFILPTFVPWYYWS    238
HmSCD2    SHVGWLLVRKHPAVKEKGGKLDMSDLKAEKLVMFQRRYYKLGLLLMCFILPTLVPWYFWG    239
HmSCD3    SHVGWLLVRKHPAVKEKGGKLDMSDLKAEKLVMFQRRYYKPAILLMCFILPTFVPWYFWG    234
mSCD1     SHVGWLLVRKHPAVKEKGGKLDMSDLKAEKLVMFQRRYYKPGLLLMCFILPTLVPWYCWG    235
mSCD2     SHVGWLLVRKHPAVKEKGGKLDMSDLKAEKLVMFQRRYYKPDLLLMCFVLPTLVPWYCWG    238
mSCD3     SHVGWLLVRKHPAVKEKGGKLDMSDLKAEKLVMFQRRYYKPGILLMCFILPTLVPWYCWG    239
          ****************************************  :*****:***:**** *.

HmSCD1    EAFVNSLCVSTFLRYTLVLNATWLVNSAAHLYGYRPYDKNIESRENILVSLGAVGEGFHN    298
HmSCD2    EAFVNSLCVSTFLRYAVVLNATWLVNSAAHLYGYRPYDKNISSRENILVSMGAVGEGFHN    299
HmSCD3    EAFVNSLCVSTFLRYTLVLNATWLVNSAAHLYGYRPYDKNIDPRENALVSLGCLGEGFHN    294
mSCD1     ETFVNSLFVSTFLRYTLVLNATWLVNSAAHLYGYRPYDKNIQSRENILVSLGAVGEGFHN    295
mSCD2     ETFVNSLCVSTFLRYAVVLNATWLVNSAAHLYGYRPYDKNISSRENILVSMGAVGERFHN    298
mSCD3     ETFLNSFYVATLLRYAVVLNATWLVNSAAHLYGYRPYDKNIDPRQNALVSLGSMGEGFHN    299
          *:*:**: *:*:***::************************..*:* ***:*.:** ***

HmSCD1    YHHAFPYDYSASEYRWHINFTTFFIDCMAALGLAYDRKKVSKAAVLARIKRTGDGSHKSS    358
HmSCD2    YHHAFPYDYSASEYRWHINFTTFFIDCMAALGLAYDRKKVSKAAVLARIKRTGDGSCKSG    359
HmSCD3    YHHAFPYDYSASEYRWHINFTTFFIDCMAALGLAYDRKKVSKAAVLARIKRTGDGSCKSG    354
mSCD1     YHHTFPFDYSASEYRWHINFTTFFIDCMAALGLAYDRKKVSKATVLARIKRTGDGSHKSS    355
mSCD2     YHHAFPYDYSASEYRWHINFTTFFIDCMALLGLAYDRKRVSRAAVLARIKRTGDGSCKSG    358
mSCD3     YHHAFPYDYSASEYRWHINFTTFFIDCMAALGLAYDRKRVSKATVLARIKRTGDGSHKSG    359
          ***:**:********************** ********.**.*:************ **.
```

Fig. 1 Alignment of the predicted amino acid sequences of hamster SCD1 (*hmSCD1*), hamster SCD2 (*hmSCD2*), hamster SCD3 (*hmSCD3*), mouse SCD1 (*mSCD1*), mouse SCD2 (*mSCD2*) and mouse SCD3 (*mSCD3*). The one letter amino acid code is used. *Spaced endash* indicates a gap and *asterisk* indicates identical amino acids. The three histidine motifs that are 100% conserved are *shaded*

Table 2 Comparison of % identity and % similarity between SCD isoforms from different mouse, rat and the hamster (hmSCD)

% Identity	% Similarity								
	Mouse SCD2	Rat SCD2	HmSCD2	HmSCD1	Mouse SCD1	Rat SCD1	HmSCD3	Mouse SCD3	Mouse SCD4
Mouse SCD2		98.9	97.5	91.6	91.5	92.5	90.4	91.6	86.1
Rat SCD2	96.1		98.0	91.9	92.1	93.0	90.7	92.2	86.4
HmSCD2	94.7	96.1		93.3	92.7	93.6	92.1	92.5	87.0
HmSCD1	86.3	87.2	89.7		96.1	96.1	94.4	93.0	87.5
Mouse SCD1	86.5	87.0	88.7	94.1		96.9	90.7	93.8	87.0
Rat SCD1	84.9	86.9	87.7	92.5	93.2		93.2	94.1	88.7
HmSCD3	82.5	83.9	86.7	90.1	86.2	88.7		94.9	84.4
Mouse SCD3	84.6	85.5	86.6	88.5	89.0	88.5	91.2		85.3
Mouse SCD4	79.9	81.6	81.6	80.5	79.6	82.2	78.5	78.8	

protein in 293 cells because the band in vector (pcDNA3) transfected cells has a similar intensity to that appearing in cells transfected with pcDNA-hmSCD2. A different antibody, SCD-14722 was used to detect the hmSCD2 in 293 cells. This antibody was raised against mSCD2 and it detected a 40 kDa band present only in 293 cells transfected with pcDNA3.1-hmSCD2 (Fig. 2b).

The TLC method was employed for the measurement of desaturase activity using ^{14}C-labeled stearoyl-CoA as substrate. As shown in Fig. 2c, the microsome fraction

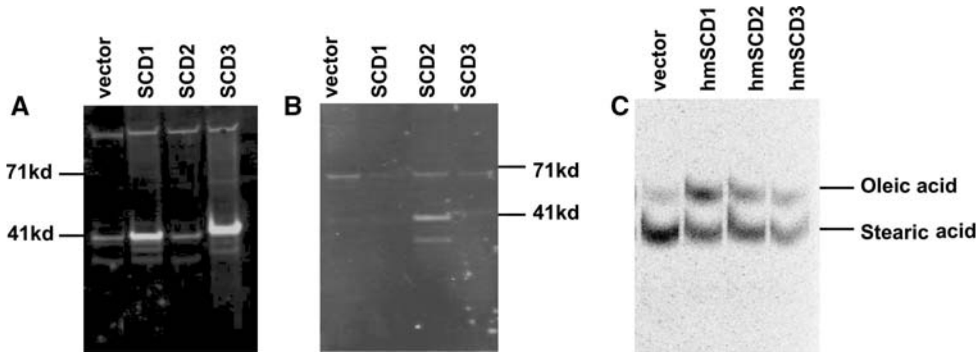

Fig. 2 Expression and enzymatic activity of hamster SCD isoforms. **a** Microsome fractions (40 µg) from HEK 293 cells transiently transfected with pcDNA3.1 (*vector*), pcDNA3.1-hmSCD1 (*SCD1*), pcDNA3.1-hmSCD2 (*SCD2*) or pcDNA3.1-hmSCD3 (*SCD3*) were separated on a SDS-PAGE gel and probed with an antibody recognizing the N-terminal peptide of mouse SCD1. The molecular weight markers indicated are alcohol dehydrogenase (41 kD) and BSA (71 kD). **b** Immunoblotting analysis of the same microsome fractions with a SCD2-specific antibody. **c** Representative images of TLC plates showing the substrate and product of the SCD reaction using microsome fraction of 293 cells transfected with pcDNA3.1 (*vector*), pcDNA3.1-hmSCD1 (*hmSCD1*), pcDNA3.1-hmSCD2 (*hmSCD2*) and pcDNA3.1-hmSCD3 (*hmSCD3*). Positions of the methyl esters of ^{14}C-labeled stearic acid and oleic acid are marked

prepared from 293 cells transfected with the various hmSCD cDNA isoforms displayed increased SCD activity compared to microsomes from vector-transfected cells. Each reaction mixture contained same amount of microsome fraction as judged by total protein concentration. Due to the potential different reactivity of SCD antibodies used toward different hmSCD isoforms, as well as different transfection efficiency, we could not accurately assess if similar amount of SCD proteins are present in each reaction. Thus, a quantitative comparison of enzyme activity between the different hmSCD isoforms was not possible. Nevertheless, our data suggest that all three hmSCD isoforms encode proteins with functional SCD activity.

Tissue Distribution of Hamster SCD mRNAs

To determine the tissue distribution of the three hmSCD isoforms, specific real-time PCR primers and probes for the three hmSCD isoforms were designed in regions that differ among the three cDNA sequences. Total RNA was isolated from white adipose tissue, brain, heart, liver, lung, kidney, intestine and skeletal muscle of hamsters. First strand cDNA was synthesized with the Superscript cDNA synthesis kit (Invitrogen). Real-time PCR reactions were carried out using the isoform-specific primers and probes and cDNA prepared from different hamster tissues. Quadruplicates PCR reaction was run for each cDNA samples.

The relative mRNA levels of different SCD isoforms in different tissues were calculated from C_t values of each PCR reaction normalized using the C_t value of GAPDH from the same cDNA prep. As shown in Fig. 3a, the highest hmSCD1 mRNA level was detected in white adipose tissue and liver. The highest SCD2 mRNA levels were detected in the brain, white adipose tissue and liver (Fig. 3b). In general, SCD3 mRNA was detectable in several hamster tissues including liver, lung and white adipose tissue (Fig. 3c). However, the overall level of SCD3 mRNA was very low with the C_t values nearing the lower limit of detection (40 cycles). Therefore, the comparison of SCD3 mRNA level between different tissues might not be accurate.

We also tried to determine the relative abundance of each hmSCD isoforms in the same tissue by comparing delta C_t values in each tissue. Figure 4 shows the comparative mRNA levels of each SCD isoform in white adipose tissue, brain and liver. While SCD1 was the predominant isoform expressed in hamster white adipose tissue and liver (Fig. 4a, c), SCD2 mRNA seemed to be the predominant isoform in the brain (Fig. 4b). On the other hand, mRNA levels of hmSCD3 were very low compared to either hmSCD1 or hmSCD2 in all the tissues tested.

Discussions

Among the rodent species, the hamster is the species with lipid metabolism most similar to humans. It has been a widely used as animal model for the study of dyslipidemia and atherosclerosis [15]. Unlike the mouse or rat, the hamster has lower plasma HDL levels due to the presence of endogenous CETP activity [20]. It has been used to study the effects of bile acid sequestrants, a-1 adrenergic inhibitor and doxazin on lipid levels and aortic fatty streak formation. The HMG-CoA reductase inhibitor lovastatin has been shown to inhibit the formation of atherosclerotic lesions in hamsters fed a high-fat diet [16].

The SCD is a key enzyme in lipid metabolism in mammals. Four SCD isoforms have been identified from the mouse and rat. Only one SCD isoform has been

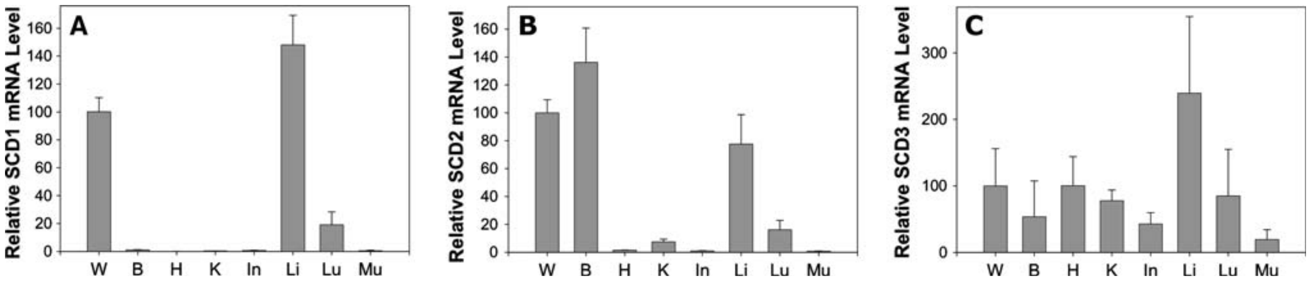

Fig. 3 Tissue distribution of hamster SCD mRNA's determined by real-time quantitative PCR analysis. **a** Histogram shows the relative mRNA levels of hmSCD1 in adult hamster white adipose tissue (*W*), brain (*B*), heart (*H*), kidney (*K*), intestine (*In*), liver (*Li*), lung (*Lu*) and skeletal muscle (*Mu*). The relative mRNA abundance was calculated by the delta C_t (ΔC_t) method using mRNA of GAPDH as internal standard. For each tissue, two samples from two different animals were analyzed and quadruplicate PCR reactions were run for each sample. Mean values and standard deviations were calculated from the eight ΔC_t values representing the two tissue samples. The mRNA level of hmSCD1 in white adipose tissue was set at 100. **b** Relative mRNA levels of hmSCD2 in adult hamster tissues. The mRNA level of hmSCD2 in white adipose tissue was set at 100. **c** Relative mRNA level of hmSCD3 in adult hamster tissues. The mRNA level of hamster SCD3 in white adipose tissue was set at 100

described in the hamsters (FAR-17c). In this report, we describe for the first time the identification and characterization of hmSCD1, hmSCD2 and hmSCD3. The predicted amino acid sequences of hmSCD1, hmSCD2 and hmSCD3 displayed high degree of homology to their mouse or rat orthologs. Using a real-time RT-PCR method, we showed that the expression pattern of hmSCD1, hmSCD2 and hmSCD3 is similar to their mouse counter parts. Finally, we presented data showing that all three hmSCD isoforms encode proteins with functional SCD activity.

Sequence analysis revealed that the previously cloned FAR-17c is the hmSCD3. FAR-17c was originally cloned as an androgen-dependent gene in the flank organs of hamster [19]. Northern blot analysis detected a band that migrated similarly to 18S RNA in the sebaceous glands and liver, and weakly in the lungs. There was also a strong band at the 28S position in the brain tissue of female hamster. However, the Northern blot analysis for FAR-17c was performed using the full length hmSCD3 cDNA as probe. Due to the high level of homology at the nucleotide sequence level in the CDS region of hmSCD isoforms, it is possible that the full length SCD3 cDNA probe could also detect SCD1 and SCD2 mRNA. Zheng et al. [11] reported tissue distribution data of mSCD1, mSCD2 and mSCD3 using cDNA's corresponding to the respective 5′ UTR region as probes. They show that SCD3 expression is limited to mouse skin, whereas the highest SCD1 mRNA level was detected in liver and the highest SCD2 mRNA level was detected in brain. To accurately measure the relative mRNA level of the hmSCD isoforms, we designed our real-time PCR primers and probes in regions that displayed the least homology among the three cDNA sequences. The tissue distribution pattern of hmSCD isoforms measured through our real-time PCR method is very similar to the reported expression pattern of SCD isoforms in the mice [10, 11].

Mouse SCD4 has been shown to be expressed exclusively in the heart and its expression is induced by a high-carbohydrate fat-free diet and by a liver-X-receptor agonist in mice [10]. The rat ortholog of mSCD4 has not been published. However, one cDNA sequence in Genbank (XM_574671) shows the highest homology to mSCD4 and

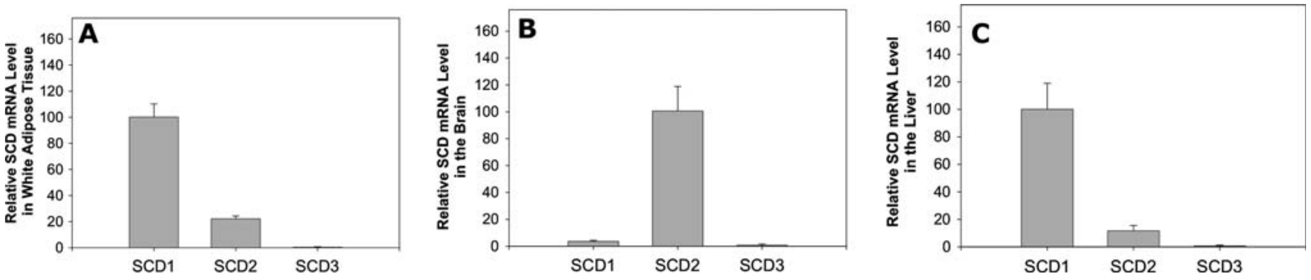

Fig. 4 Relative mRNA level of different SCD isoforms in adult hamster white adipose tissue, brain and liver. **a** Histogram shows the relative mRNA levels of hmSCD1, hmSCD2 and hmSCD3 in adult hamster white adipose tissues. The mRNA level of hmSCD1 in white adipose tissue was set at 100. **b** Histogram shows the relative mRNA levels of hmSCD1, hmSCD2 and hmSCD3 in adult hamster brain. The mRNA level of hmSCD2 in brain tissue was set at 100. **c** Histogram shows the relative mRNA levels of hmSCD1, hmSCD2 and hmSCD3 in adult hamster liver. The mRNA level of hmSCD1 in liver was set at 100

is probably the rat ortholog of SCD4. We attempted several PCR reactions using primers corresponding to regions of translation start and termination codes of XM_574671. However, this effort did not yield any successful cDNA clones. Thus, we have not been able to clone the hamster ortholog of mSCD4 at the present time.

Ideta et al. [19] reported no desaturase activity from the African green monkey kidney cells (COS7) transfected with a expression vector encoding FAR-17c cDNA under the control of SV40 promoter. Using the TLC method and ^{14}C-labeled stearoyl-CoA as substrate, we investigated the desaturase of the three hmSCD cDNAs. The microsome fraction from HEK 293 cells transfected with the hmSCD1, hmSCD2 and hmSCD3 displayed increased SCD activities compared to microsome fraction from HEK 293 cells transfected with the vector alone. Additionally, antibody specific to rodent SCD protein detected polypeptides with predicted size from the transfected cells. These data suggest that all three hmSCD isoforms reported here encode polypeptides with functional SCD activities. Using the microsome fraction from Hela cells transfected with cDNA of different mSCD isoforms, Miyazaki et al. [21] reported that mSCD1, mSCD2 and mSCD4 can use both palmitoyl-coenzyme A (16:0) and stearoyl-coenzyme A (18:0) as substrate whereas mSCD3 can only use palmitoyl-coenzyme A as substrate [21]. Our data suggest that hmSCD3 can also use stearoyl-coenzyme A as substrate under our experimental conditions. The discrepancy between these two studies is not clear at this time. The difference in the cell-type used between the two reports might contribute to the different results. It is also possible that hmSCD3 prefer palmitoyl-coenzyme A (16:0) as substrate but can also use stearoyl-coenzyme A (18:0) in the absence of palmitoyl-coenzyme A. Further studies are needed to determine the substrate selectivity of hmSCD isoforms.

Two SCD isoforms, SCD1 and SCD5 have been identified in humans. Human SCD1 showed the highest level of homology to mouse and rat SCD1 and displayed a similar expression pattern as mSCD1. The expression pattern of hmSCD1 shown here is also similar to that of human and mSCD1 with the highest expression detected in adipose tissue and liver. SCD1 null mice [5] are resistant to high fat diet-induced adiposity and insulin resistance. They also displayed greatly reduced plasma VLDL and triglyceride levels, but no significant changes in LDL and HDL cholesterol level. Since cholesterol metabolism in hamster displayed more similarity to that of humans, it would be interesting to investigate the effect of SCD1 inhibition on cholesterol metabolism and the development of atherosclerosis in hamster under hypercholesterolemic conditions.

The highest mRNA level of hmSCD2 was detected in the brain of adult hamster (Fig. 4b). This expression pattern is similar to that of mSCD2 in adult mice and SCD5 in adult human and bovine [22]. In the mice, SCD2-deficient resulted in a skin permeability barrier defect in the neonates. Compared to wild type mice, plasma triglycerides levels decreased in the neonatal mSCD2-/- mice but not adult mSCD2-/- mice [23]. These data suggest that mSCD2 is required for the liver and skin development during embryonic and neonatal stages. Adult mSCD2-/- mice displayed twisted tail suggesting SCD2 is also required for normal tail development. However, neuronal defect was not described in the SCD2-/- mice. Thus the function of rodent SCD2 or human and bovine SCD5 in central nervous system of adult animals remains to be delineated.

The mRNA levels of hmSCD3 was very low or barely detectable in the tissue we tested that include adipose tissue, brain, heart, liver, kidney, lung, intestine and skeletal muscle. In the mice, it was reported that SCD3 expression was limited to the skin [11]. We did not test the skin tissues of hamster for SCD3 expression at the current study. Future studies are needed to understand the expression and function of hmSCD3.

In summary, here we report for the first time the identification of hmSCD1 and hmSCD2. We also show that the previously identified hmSCD (FAR-17c) is the hmSCD3. The identification and characterization of hmSCD isoforms will provide useful tools in our study of lipoprotein metabolism and atherosclerosis in this animal model.

Acknowledgments We would like to thank Liyun Ding and Julia Cao for technical assistance and Dr Marian Mosior for helpful discussions.

References

1. Enoch HG, Catala A, Strittmatter P (1976) Mechanism of rat liver microsomal stearyl-CoA desaturase. Studies of the substrate specificity, enzyme-substrate interactions, and the function of lipid. J Biol Chem 251:5095–5103
2. Heinemann FS, Korza G, Ozols J (2003) A plasminogen-like protein selectively degrades stearoyl-CoA desaturase in liver microsomes. J Biol Chem 278:42966–42975
3. Ntambi JM, Miyazaki M (2004) Regulation of stearoyl-CoA desaturases and role in metabolism. Prog Lipid Res 43:91–104
4. Miyazaki M, Kim Y, Gray-Keller MP, Attie AD, Ntambi JM (2000) The biosynthesis of hepatic cholesterol esters and triglycerides is impaired in mice with a disruption of the gene for stearoyl-CoA desaturase 1. J Biol Chem 275:30132–30138
5. Cohen P, Miyazaki M, Socci ND, Hagge-Greenberg A, Liedtke W, Soukas AA, Sharma R, Hudgins LC, Ntambi JM, Friedman JM (2002) Role for stearoyl-CoA desaturase-1 in leptin-mediated weight loss. Science 297:240–243
6. Attie AD, Krauss RM, Gray-Keller MP, Brownlie A, Miyazaki M, Kastelein JJ, Lusis AJ, Stalenhoef AF, Stoehr JP, Hayden MR, Ntambi JM (2002) Relationship between stearoyl-CoA desaturase activity and plasma triglycerides in human and mouse hypertriglyceridemia. J Lipid Res 43:1899–1907
7. Sun Y, Hao M, Luo Y, Liang CP, Silver DL, Cheng C, Maxfield FR, Tall AR (2003) Stearoyl-CoA desaturase inhibits ATP-

binding cassette transporter A1-mediated cholesterol efflux and modulates membrane domain structure. J Biol Chem 278:5813–5820

8. Wang Y, Oram J (2005) Unsaturated fatty acids phosphorylate and destabilize ABCA1 through a phospholipase D2 pathway. J Biol Chem 280:35896–35903
9. Senanayake S, Brownrigg LM, Panicker V, Croft KD, Joyce DA, Steer JH, Puddey IB, Yeap BB (2007) Monocyte-derived macrophages from men and women with type 2 diabetes mellitus differ in fatty acid composition compared with non-diabetic controls. Diabetes Res Clin Pract 75:292
10. Miyazaki M, Jacobson MJ, Man W, Cohen P, Asilmaz E, Friedman JM, Ntambi JM (2003) Identification and characterization of murine SCD4, a novel heart-specific stearoyl-CoA desaturase isoform regulated by leptin and dietary factors. J Biol Chem 278:33904–33911
11. Zheng Y, Prouty SM, Harmon A, Sundberg JP, Stenn KS, Parimoo S (2001) Scd3—a novel gene of the stearoyl-CoA desaturase family with restricted expression in skin. Genomics 71:182–191
12. Zhang L, Ge L, Parimoo S, Stenn K, Prouty SM (1999) Human stearoyl-CoA desaturase: alternative transcripts generated from a single gene by usage of tandem polyadenylation sites. Biochem J 340:255–264
13. Wang J, Yu L, Schmidt RE, Su C, Huang X, Gould K, Cao G (2005) Characterization of HSCD5, a novel human stearoyl-CoA desaturase unique to primates. Biochem Biophy Res Commun 332:735–742
14. Beiraghi S, Zhou M, Talmadge CB, Went-Sumegi N, Davis JR, Huang D, Saal H, Seemayer TA, Sumegi J (2003) Identification and characterization of a novel gene disrupted by a pericentric inversion inv(4)(p13.1q21.1) in a family with cleft lip. Gene 309:11–21
15. Spady DK, Dietschy JM (1983) Sterol synthesis in vivo in 18 tissues of the squirrel monkey, guinea pig, rabbit, hamster, and rat. J Lipid Res 24:303–315
16. Otto J, Ordovas JM, Smith D, van Dongen D, Nicolosi RJ, Schaefer EJ (1995) Lovastatin inhibits diet induced atherosclerosis in F1B golden Syrian hamsters. Atherosclerosis 114:19–31
17. Nistor A, Bulla A, Fillip DA, Radu A (1987) The hyperlipidemic hamsters as a model of experimental atherosclerosis. Atherosclerosis 68:159–173
18. Livak KA, Schmittgen TD (2001) Analysis of relative gene expression data using real-time quantitative PCR and the 2-$\Delta\Delta C_t$ method. Methods 25:402–408
19. Ideta R, Seki T, Adachi K (1995) Sequence analysis and characterization of FAR-17c, an androgen-dependent gene in the flank organs of hamsters. J Dermatol Sci 9:94–106
20. Trautwein EA, Liang J, Hayes KC (1993) Cholesterol gallstone induction in hamsters reflects strain differences in plasma lipoproteins and bile acid profiles. Lipids 28:305–312
21. Miyazaki M, Bruggink SM, Ntambi JM (2006) Identification of mouse palmitoyl-coenzyme A {Delta}9-desaturase. J Lipid Res 47:700–704
22. Lengi AJ, Corl BA (2007) Identification and characterization of a novel bovine stearoyl-CoA desaturase isoform with homology to human SCD5. Lipids 42:499–508
23. Miyazaki M, Dobrzyn A, Elias PM, Ntambi JM (2005) Stearoyl-CoA desaturase-2 gene expression is required for lipid synthesis during early skin and liver development. Proc Natl Acad Sci USA 102:12501–12506

Lipids (2008) 43:207–213
DOI 10.1007/s11745-007-3150-5

ORIGINAL ARTICLE

Identification and Functional Expression of a Δ9-Fatty Acid Desaturase from *Psychrobacter urativorans* in *Escherichia coli*

Yan Li · Matthias Dietrich · Rolf D. Schmid · Bingfang He · Pingkai Ouyang · Vlada B. Urlacher

Received: 2 October 2007 / Accepted: 18 December 2007 / Published online: 7 February 2008
© AOCS 2008

Abstract The Δ9-fatty acid desaturase is a key enzyme in the synthesis of unsaturated fatty acids. The fatty acid composition of membrane phospholipids in *Psychrobacter urativorans* is characterized by a high degree of desaturation at Δ9 position. Based on CODEHOP-mediated PCR strategy, a novel gene designated as *PuFAD9*, putatively encoding a Δ9-fatty acid desaturase (*Pu*FAD9), was isolated from *P. urativorans*. The gene consists of 1,455 bp and codes for 484 amino acids. Analysis of the amino acid sequence reveals three histidine clusters and a hydropathy profile, typical for membrane-bound desaturases. Activity of the *Pu*FAD9 protein, recombinantly expressed in *Escherichia coli* was confirmed by GC-MS analysis of the cellular fatty acid composition. It was found that the ratio between palmitoleic and palmitic acid in *E. coli* cells heterologously expressing the *PuFAD9* gene was significantly affected by IPTG induction and the growth temperature.

Keywords Δ9-Fatty acid desaturase · Degenerate primer · Gene expression · Fatty acid composition

Abbreviations

IPTG	Isopropyl-*β*-D-thiogalacto-pyranoside
MOPS	3-Morpholinopropanesulfonic acid
PMSF	Phenylmethylsulfonyl fluoride

Y. Li · M. Dietrich · R. D. Schmid · V. B. Urlacher (✉)
Institute of Technical Biochemistry, University of Stuttgart,
Stuttgart 70569, Germany
e-mail: Vlada.Urlacher@itb.uni-stuttgart.de

Y. Li · B. He · P. Ouyang
College of Life Science and Pharmacy,
Nanjing University of Technology, Nanjing 210009, China

Introduction

Fatty acid desaturases belong to a family of enzymes that catalyze O_2-dependent dehydrogenation [1]. They have been found in prokaryotes, lower and higher eukaryotes [2]. There are three classes of fatty acid desaturases: soluble acyl carrier protein desaturases, membrane-bound acyl-CoA desaturases and acyl-lipid desaturases. Despite the differences in cellular localization and substrate spectra, three classes of desaturases share several common characteristics regarding their reaction mechanism, including the requirement of molecular oxygen, NAD(P)H, an electron transport system (ferredoxin-NADP$^+$ oxidoreductase and ferredoxin, or cytochrome b_5 reductase and cytochrome b_5) [3]. Each fatty acid desaturase creates an unsaturated bond at a fixed position by "counting" from the carboxyl end of the fatty acids. Incorporation of the first *cis*-double bond at the central (C9–C10) position catalyzed by Δ9-desaturases has an essential effect on membrane physical properties [4], because the balance between saturated and unsaturated fatty acids (UFAs) is, probably, of higher importance than the type of UFA in membrane phospholipids [5]. This event is also a crucial step in polyunsaturated fatty acid (PUFA) synthesis pathways, since all other desaturases require the existence of a previous double bond at the Δ9 position of the fatty acid [6]. Although a number of integral membrane or membrane-bound Δ9-desaturase genes have been isolated [7] and the related information was submitted to the public databases, these enzymes are less well understood than the soluble Δ9-ACP desaturases. One of the reasons for that is the difficulties in obtaining sufficient quantities of these purified enzymes [8]. Heterologous expression of membrane proteins in appropriate hosts would provide enough material for biochemical analysis and the analysis of their structure–function relationships [9–12].

Psychrobacter urativorans DSM 14009 (formerly named as *Micrococcus cryophilus* ATCC 15174) has an unusual fatty acid composition of its membrane phospholipids, containing at least 95% monounsaturated fatty acids (C16:1Δ9 and C18:1Δ9) [13]. The desaturase activity and regiospecificity of *P. urativorans* were studied in in vivo experiments, revealing the presence of a highly active and membrane-bound Δ9-fatty acid desaturase [14–16]. In this study, we report identification and cloning of a gene from *P. urativorans* encoding for Δ9-fatty acid desaturase and its functional characterization by heterologous expression in *Escherichia coli*.

Experimental Procedures

Chemicals and Enzymes

All chemicals were purchased from Fluka (Buchs, Switzerland). Restriction endonucleases, T4 DNA ligase, Taq DNA polymerase and Pfu DNA polymerase were obtained from Fermentas (St Leon-Rot, Germany).

Bacterial Strains

P. urativorans DSM 14009 was purchased from the German Resource Center for Biological Material (DSMZ, Braunschweig, Germany). *E. coli* DH5α (Clontech, Staint-Germain-en-Laye, France) strain was routinely used for gene cloning and plasmid propagation. *E. coli* Rosetta (DE3) (Novagen, Merck Chemicals Ltd., Nottingham, UK) supports translation of rare codons and therefore was used as host for heterologous expression of the desaturase from *P. urativorans*. All strains were stored and cultivated as recommended by the suppliers.

PCR-Based Cloning

Genomic DNA of *P. urativorans* was isolated using the standard phenol/chloroform precipitation protocol [17]. Degenerate primers were designed using CODEHOP strategy (http://bioinformatics.weizmann.ac.il/blocks/codehop.html) as follows: DE1 (CGGATCCACCACA GGCANGTNGAYRA) and DE2 (CGAAGATGTGGTGG AAGTTGTGRTANCCYTC). They were used for the CODEHOP PCR and demonstrate high identity to certain regions of putative *Psychrobacter arcticus* 273-4 (GenBank accession no. YP_264647) and *Psychrobacter cryohalolentis* K5 desaturases (GenBank accession no. YP_580264).

Subsequently, the primers EX1 (CACCTACTATAA TCCATACAAGTTATTGTTAT) and EX2 (GATAGAGG GAAGGAGAARCGT) were derived from the flanking regions of those two genes. MD1 (GTTCTATCTTTAGT-CAAGTCTGGAATGT) and MD2 (CGCTTAGTATTGA CTCACCATTTCACT) are the gene-specific primers derived from the DNA fragment obtained by the CODEHOP PCR. Another two PCR reactions were carried out using the primers EX1 and MD1, and EX2 and MD2, respectively, to get the information of the whole gene sequence. Gene fragments, obtained after each PCR were purified by gel-extraction (QIAGEN, Hilden, Germany) and sequenced directly or after ligation into the vector of pGEM®-T Easy (Promega, Mannheim, Germany).

Sequence Analysis

Sequence analysis was carried out using a BLAST search program (http://www.ncbi.nlm.nih.gov/blast/). Multiple sequence alignment of putative Δ9-desaturases was performed with Clustalx1.81 [18]. The distribution of the hydrophobic amino acids was analyzed using Kyte–Doolittle hydropathy scale with a window size of 19 (http://www.expasy.ch/cgi-bin/protscale.pl) [19]. Transmembrane (TM) regions of the protein were predicted with TMHMM (transmembrane Hidden Markov Model) (http://www.cbs.dtu.dk/services/TMHMM/) [20]. The signal sequence analysis was done using a signal peptide prediction server (http://www.cbs.dtu.dk/services/SignalP-3.0/) [21].

Construction of Plasmid for Gene Expression in *E. coli*

The full-length gene encoding a desaturase-like protein from *P. urativorans* was amplified by PCR using primers McB (CGGGATCCATGATTGCAAAAACAGCAAT) and McX (CCGCTCGAG TTACTAAGCGGCTTTGCT). The *BamH*I and *Xho*I restriction endonuclease sites in the primer sequences are underlined. The PCR product was isolated and digested with *BamH*I and *Xho*I restriction endonucleases and then ligated into the pET21a(+) expression vector (Novagen, Darmstadt, Germany). Positive transformants were screened on LB agar plates with ampicillin and chloromycetin resistance. The resultant positive plasmid, named as pEPUD9, was validated by control PCR, restriction enzyme digestion and subsequent sequencing.

Expression of Desaturase from *P. urativorans* in *E. coli*

Individual colonies of *E. coli* Rosetta (DE3) cells transformed with the plasmid pEPUD9 were grown in 5 mL LB medium containing 100 μg/mL ampicillin and 34 μg/mL chloromycetin at 37 °C until OD_{600} reached approximately 1. Then aliquots of the cultures were taken to inoculate 400 mL of fresh LB medium supplemented with corresponding antibiotics. Cells were cultivated until the OD_{600} value reached 0.6–0.8, then IPTG was added at a final concentration of 0.4 mM and the incubation was shifted to different temperatures (15, 25 and 37 °C). At various intervals after addition of IPTG, the cells were harvested from 50 mL culture. Centrifugation was done at 5,000*g* for 15 min at 4 °C. The pellets were washed once with MOPS–NaOH buffer (pH 7.5, 50 mM) that contained 10 mM $MgCl_2$, and stored at −80 °C until use. Control experiments were performed under the same experimental conditions using *E. coli* transformants containing empty plasmid pET21a(+).

Preparation of Membranes

The frozen cells were thawed at room temperature and resuspended in appropriate volume of lysis buffer (MOPS–NaOH buffer (pH 7.5, 50 mM) containing 10 mmol/L $MgCl_2$, 1 mmol/L PMSF, 0.1 U/mL DNase) and lysed by sonication. The lysate containing soluble proteins and solubilized membranes was clarified by centrifugation at 16,100*g* for 15 min at 4 °C. The supernatant was subjected to ultracentrifugation at 100,000*g* for 40 min at 4 °C to separate membrane and soluble protein fractions.

Gel-Electrophoresis and Western Blotting Analysis

Aliquots of soluble, insoluble, and membrane fractions were analyzed for protein expression by SDS-polyacrylamide gel electrophoresis (SDS-PAGE) [22] on a 12% polyacrylamide gel followed by either Coomassie staining or Western blotting. For the latter detection method, the bands were transferred onto a nitrocellulose membrane using a Trans-Blot SD Semi-Dry Electrophoretic Transfer Cell (Bio-Rad, Munich, Germany) at a constant voltage of 15 V for 30 min at room temperature. The blotting and detection were done using T7 tag antibody HRP conjugate (Novagen, Merck Chemicals Ltd., Nottingham, UK) according to the manufacturer's instructions.

Analysis of Total Cellular Fatty Acid Composition

About 40 mg of *E. coli* cells (wet weight) were resuspended in 1 mL of 15% (w/v) NaOH in methanol/water (1:1, by vol) and saponified according to the MIDI protocol (Microbial Identification System, Microbial ID Inc., Newark, DE, USA). After saponification, the pH of reaction solution was adjusted to 2.0 with HCl (aq). Then, the fatty acids were extracted with diethyl ether. The extract was subsequently dried over anhydrous magnesium sulfate and trimethylsilyl (TMS)-derivatized. TMS derivatives were separated and analyzed by Gas chromatography-mass spectrometry (GC-MS) (GCMS QP2010, Shimadzu, Japan). The GC was equipped with a 30-m FS-supreme column (internal diameter 0.25 mm, film thickness 0.25 μM) using helium as carrier gas with a linear velocity of 30 cm/s. The column temperature program was composed of an initial hold at 140 °C for 1 min, ramping at 2 °C per min to 240 °C, followed by heating until 300 °C with 30 °C per min, and a final hold at 300 °C for 6 min. The injector temperature was 250 °C.

Results

Cloning of the *PuFAD9* Gene

A DNA fragment of about 400 bp was amplified from *P. urativorans* using CODEHOP primers DE1 and DE2 [23], which were derived from two sequences, RIHHKHVDD and EGYHNFHHIF corresponding to the highly conserved histidine motifs of putative Δ9-desaturases in *P. cryohalolentis* K5, *Pseudoalteromonas haloplanktis* TAC125 and other strains shown in Fig. 1. The amplified DNA-fragment showed a high identity to putative desaturase genes in *P. cryohalolentis* K5 (84%) and *P. arcticus* 273-4 (83%). For identification of the unknown parts of the gene, two subsequent PCR reactions were carried out using primers EX1 and MD1, EX2 and MD2 (see "Experimental Procedures"). After the full gene sequence was deduced from the sequences of the three PCR products, the resulting sequence information was confirmed by sequencing both strands of the target gene and submitted to GenBank (accession no. EF617339). The nucleotide sequence had an open reading frame of 1,455 bp, designated as *PuFAD9*, encoding a 484 amino acid polypeptide with a calculated molecular weight of 55 kDa and a theoretical isoelectric point of 8.88.

Comparison of Amino Acid Sequences

A Blast search revealed that the primary structure of the putative desaturase from *P. urativorans* was quite similar to those of other known Δ9-fatty acid desaturases, with a 79% identity to *P. arcticus* 273-4, a 78% identity to *P. cryohalolentis* K5, a 67% identity to *Psychrobacter* sp.

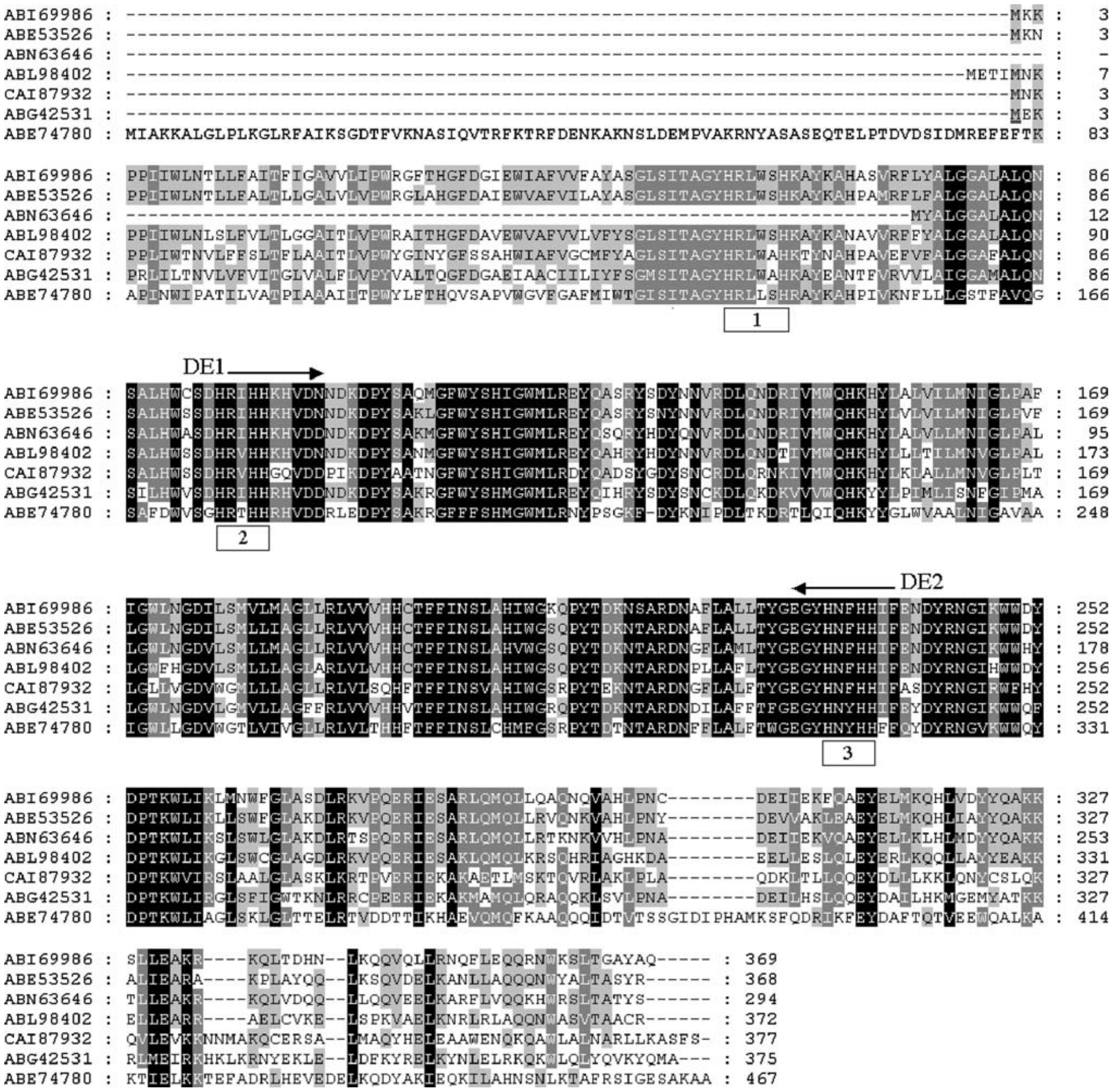

```
ABI69986 : --------------------------------------------------------------------------------MKK :   3
ABE53526 : --------------------------------------------------------------------------------MKN :   3
ABN63646 : ----------------------------------------------------------------------------------- :   -
ABL98402 : ----------------------------------------------------------------------------METIMNK :   7
CAI87932 : --------------------------------------------------------------------------------MNK :   3
ABG42531 : --------------------------------------------------------------------------------MEK :   3
ABE74780 : MIAKKALGLPLKGLRFAIKSGDTFVKNASIQVTRFKTRFDENKAKNSLDEMPVAKRNYASASEQTELPTDVDSIDMREFEFTK :  83

ABI69986 : PPIIWLNTLLFAITFIGAVVLIPWRGFTHGFDGIEWIAFVVFAYASGLSITAGYHRLWSHKAYKAHASVRFLYALGGALALQN :  86
ABE53526 : PPIIWLNTLLFALTLLGALVLVPWRGLAHGFDAIEWVAFVILAYASGLSITAGYHRLWSHKAYKAHPAMRFLFALGGALALQN :  86
ABN63646 : -----------------------------------------------------------------------MYALGGALALQN :  12
ABL98402 : PPIIWLNLSLFVLTLGGAITLVPWRAITHGFDAVEWVAFVVLVFYSGLSITAGYHRLWSHKAYKANAVVRFFYALGGALALQN :  90
CAI87932 : PPLIWTNVLFFSLTFLAAITLVPWYGINYGFSSAHWIAFVGCMFYAGLSITAGYHRLWAHKTYNAHPAVEFVFALGGAFALQN :  86
ABG42531 : PRLILTNVLVFVITGLVALFLVPYVALTQGFDGAEIAACIILIYFSGMSITAGYHRLWAHKAYEANTFVRVVLAIGGAMALQN :  86
ABE74780 : APINWIPATILVATPIAAAIITPWYLFTHQVSAPVWGVFGAFMIWTGISITAGYHRLLSHRAYKAHPIVKNFLLLGSTFAVQG : 166

ABI69986 : SALHWCSDHRIHHKHVDNNDKDPYSAQMGFWYSHIGWMLREYQASRYSDYNNVRDLQNDRIVMWQHKHYLALVILMNIGLPAF : 169
ABE53526 : SALHWSSDHRIHHKHVDNNDKDPYSAKLGFWYSHIGWMLREYQASRYSNYNNVRDLQNDRIVMWQHKHYLVLVILMNIGLPVF : 169
ABN63646 : SALHWASDHRIHHKHVDDNDKDPYSAKMGFWYSHIGWMLREYQSQRYHDYQNVRDLQNDRIVMWQHKHYLALVLLMNIGLPAL :  95
ABL98402 : SALHWSSDHRVHHKHVDNNDKDPYSANMGFWYSHIGWMLREYQAHRYHDYNNVRDLQNDTIVMWQHKHYLLLTILMNVGLPAL : 173
CAI87932 : SALHWSSDHRVHHGQVDDPIKDPYAATNGFWYSHIGWMLRDYQADSYGDYSNCRDLQRNKIVMWQHKHYLKLALLMNVGLPLT : 169
ABG42531 : SILHWVSDHRIHHRHVDDNDKDPYSAKRGFWYSHMGWMLREYQIHRYSDYSNCKDLQKDKVVVWQHKYYLPIMLISNFGIPMA : 169
ABE74780 : SAFDWVSGHRTHHRHVDDRLEDPYSAKRGFFSHMGWMLRNYPSGKF-DYKNIPDLTKDRTLQIQHKYYGLWVAALNIGAVAA : 248

ABI69986 : IGWLNGDILSMVLMAGLLRLVVVHHCTFFINSLAHIWGKQPYTDKNSARDNAFLALLTYGEGYHNFHHIFENDYRNGIKWWDY : 252
ABE53526 : LGWLNGDILSMLLIAGLLRLVVVHHCTFFINSLAHIWGSQPYTDKNTARDNAFLALLTYGEGYHNFHHIFENDYRNGIKWWDY : 252
ABN63646 : LGWLNGDVLSMLLMAGLLRLVVVHHCTFFINSLAHVWGSQPYTDKNTARDNGFLAMLTYGEGYHNFHHIFENDYRNGIKWWHY : 178
ABL98402 : LGWFHGDVLSMLLLAGLARLVLVHHCTFFINSLAHIWGSQPYTDKNTARDNPLLAFLTYGEGYHNFHHIFENDYRNGIHWWDY : 256
CAI87932 : LGLLVGDVWGMLLLAGLLRLVLSQHFTFFINSVAHIWGSRPYTEKNTARDNGFLALFTYGEGYHNFHHIFASDYRNGIRWFHY : 252
ABG42531 : LGWLNGDVLGMVLLAGFFRLVVVHHVTFFINSLAHIWGRQPYTDKNTARDNDILAFFTFGEGYHNYHHIFEYDYRNGIKWWQF : 252
ABE74780 : IGWLLGDVWGTLVIVGLLRLVLTHHFTFFINSLCHMFGSRPYTDTNTARDNFFLALFTWGEGYHNYHHFFQYDYRNGVKWWQY : 331

ABI69986 : DPTKWLIKLMNWFGLASDLRKVPQERIESARLQMQLLQACNQVAHLPNC--------DEIIEKFQAEYELMKQHLVDYYQAKK : 327
ABE53526 : DPTKWLIKLLSWFGLAKDLRKVPQERIESARLQMQLLRVQNKVAHLPNY--------DEVVAKLEAEYELMKQHLIAYYQAKK : 327
ABN63646 : DPTKWLIKSLSWLGLAKDLRTSPQERIESARLQMQLLRTKNKVVHLPNA--------DEIIEKVQAEYELLKLHLMDYYQAKK : 253
ABL98402 : DPTKWLIKGLSWCGLAGDLRKVPQERIESAKLQMQLKRSQHRIAGHKDA--------EELLESLQLEYERLKQQLLAYYEAKK : 331
CAI87932 : DPTKWVIRSLAALGLASKLKRTPVERIEKAKAETLMSKTQVRLAKLPLA--------QDKLTLLQQEYDLLLKKLQNYCSLQK : 327
ABG42531 : DPTKWLIRGLSFIGWTKNLRRCPEERIEKAKMAMQLQRAQQKLSVLPNA--------DEILHSLQQEYDAILHKMGEMYATKK : 327
ABE74780 : DPTKWLIAGLSKLGLTTELRTVDDTTIKHAEVQMQFKAAQQQIDTVTSSGIDIPHAMKSFQDRIKFEYDAFTQTVEEWQALKA : 414

ABI69986 : SLLEAKR----KQLTDHN--LKQQVQLLRNQFLEQQRNWKSLTGAYAQ----- : 369
ABE53526 : ALIEARA----KPLAYQQ--LKSQVDELKANLLAQQQNWYALTASYR------ : 368
ABN63646 : TLLEAKR----KQLVDQQ--LLQQVEELKARFLVQQKHWRSLTATYS------ : 294
ABL98402 : ELLEARR----AELCVKE--LSPKVAELKNRLRLAQQNWASVTAACR------ : 372
CAI87932 : QVLEVKKNNMAKQCERSA--LMAQYHELEAAWENQKQAWLALNARLLKASFS- : 377
ABG42531 : RLMEIRKHKLKRNYEKLE--LDFKYRELKYNLELRKQKWLQLYQVKYQMA--- : 375
ABE74780 : KTIELKKTEFADRLHEVEDELKQDYAKIEQKILAHNSNLKTAFRSIGESAKAA : 467
```

Fig. 1 Multiple alignments of amino acid sequences of putative Δ9-desaturase of *Psychrobacter cryohalolentis* K5 (GenBank accession no. ABE74780), *Pseudoalteromonas haloplanktis* TAC125 (GenBank accession no. CAI87932), *Pseudoalteromonas atlantica* T6c (GenBank accession no. ABG42531), *Shewanella amazonensis* SB2B (GenBank accession no. ABL98402), *Shewanella baltica* OS155 (GenBank accession no. ABN63646), *Shewanella frigidimarina* NCIMB 400 (GenBank accession no. ABI69986), and *Shewanella denitrificans* OS-217 (GenBank accession no. ABE53526) using Clustalx1.81 [18]. Three conserved histidine clusters (one of HXXXXH and two of HXXHH) are indicated by the *boxes* numbered 1, 2, and 3. The overlines with an *arrow* indicate the sequences used for designing the primers DE1 and DE2

PRwf-1 and a 50% identity to *Acinetobacter* sp. ADP1. Figure 2 shows the distribution of the hydrophobic amino acids of *P. urativorans* desaturase, typical for a membrane protein, as identified using the Kyte–Doolittle hydropathy scale [19]. The histidine-rich motifs, HXXXXH (155–160), HXXHH (192–196) and HXXHH (329–333), which are highly conserved among membrane-bound acyl-CoA and acyl-lipid desaturases and proposed to form the potential diiron active site [24], are shown as the bold “H” in Fig. 2. The prediction of TM helices by TMHMM [20] indicated that the deduced protein contained four hydrophobic domains between amino acids 104–126, 136–158, 250–269 and 273–295, which would be long enough to span the membrane bilayer twice, with both the N- and C-termini

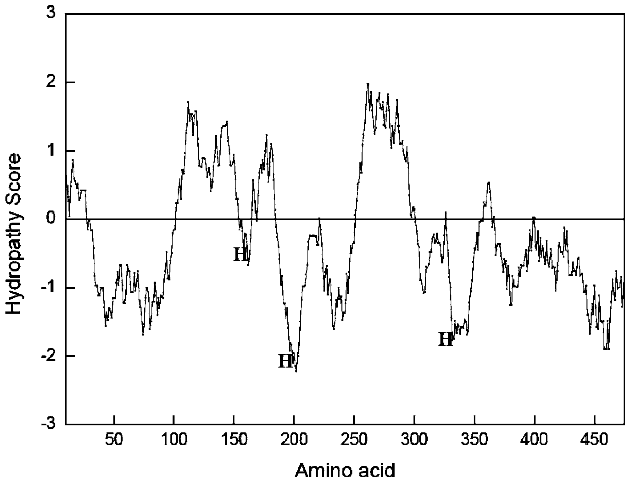

Fig. 2 Kyte–Doolittle Hydropathy plot derived from the amino acid sequence of *P. urativorans* desaturase. A window size of 19 amino acids was used to search for a transmembrane region in this protein. The hydrophobic residues are shown above zero, whereas the hydrophilic residues are below zero

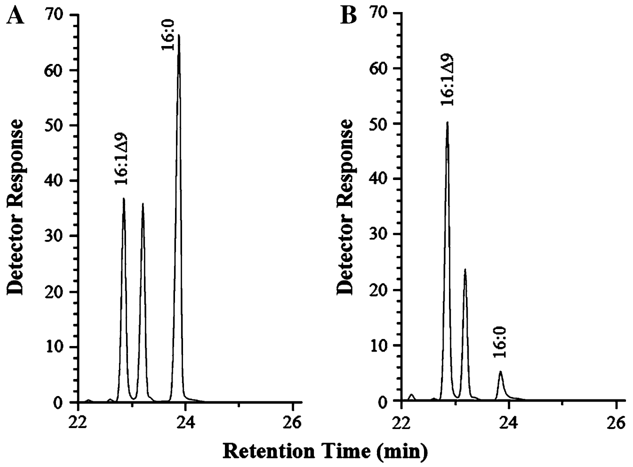

Fig. 3 Gas chromatograms of TMS derivatives of C16 fatty acids isolated from *E. coli* Rosetta (DE3) cells transformed with the control vector pET21a (+) (**a**); or cells expressing the recombinant plasmid pEPUD9 (**b**). The peak at the retention time of 23.2 min was identified as 3-trimethylsilyloxymyristic acid according to MS data. 3-Hydroxymyristic acid is a component of the hydrophilic outer membrane polysaccharides [28]

facing the cytosol. This prediction is consistent with the topology model of Δ9-stearoyl-CoA desaturase from other species [25, 26]. A possible N-terminal signal (MIAKTAMGLPLKGLRLA) sequence was also predicted by SignalP-NN [21, 27].

Heterologous Expression of *PuFAD9* in *E. coli*

The *PuFAD9* gene was cloned into pET21a(+) *E. coli* expression vector, resulting in the target protein, fused with a T7 tag at N-terminus. Protein expression has been performed as described in "Experimental Procedures". *E. coli* cells transformed with empty pET21a(+) vector cultivated under the same conditions were used as negative control. Since the target protein expressed in *E. coli* contained a T7 tag at the N-terminus, its detection has been achieved by Western blot, using the T7 tag antibody. Results showed that protein bands corresponding to an approximate molecular weight of 60 kDa, were present in lysate and membrane fractions of the recombinant *E. coli* cells (data not shown). However, the predominant portion of the protein was incorporated into cellular membrane. The reason why the molecular weight was a bit larger than the predicted value has not been clarified, besides the fact that some additional amino acids came from the fused T7 tag.

E. coli itself contains type II fatty acid synthase rather than fatty acid desaturases. Four major fatty acids, C14:0 (myristic acid), C16:0 (palmitic acid), C16:1Δ9 (palmitoleic acid), and C18:1Δ11 (*cis*-vaccenic acid), among which palmitate, palmitoleate, and *cis*-vaccenate are components of the membrane phospholipids, are found in *E. coli* cells. Two minor components, C12:0 (lauric acid) and 3-hydroxymyristic acid are found exclusively in the hydrophilic outer membrane polysaccharides [28]. GC-MS analysis of trimethylsilylated derivatives of cellular fatty acids indicated changes in the pattern of palmitate and palmitoleate in *E. coli* cells upon expression of *PuFAD9* (Fig. 3). The amount of palmitoleate increased from 34 to 88%, while the amount of palmitate decreased from 66 to 11% during expression at 15 °C. This result demonstrates that *PuFAD9* from *P. urativorans* indeed encodes a Δ9-fatty acid desaturase that can be actively expressed in *E. coli.*

In Vivo Study of *P. urativorans* Δ9-Fatty Acid Desaturase Expressed in *E. coli.*

The optimal growth temperature for *P. urativorans* in the psychrophilic habitat is 18–22 °C [29]. To investigate the temperature effect on functional expression of the desaturase in *E. coli*, cells transformed with pEPUD9 plasmid were harvested 6 h after expression at 15, 25 and 37 °C (Fig. 4). The ratio of palmitoleic to palmitic acid in the recombinant cells at 15 °C was 2.4 times smaller than at 25 °C, which fitted well with the levels of the expressed enzyme detected by western blotting at both temperatures. Although Western blot shows that the protein is expressed (Fig. 4b), no accumulation of palmitoleic acid was observed at 37 °C, probably due to the loss of enzyme activity at this temperature which is compatible with the maximum growth temperature limit of *P. urativorans* at 25 °C. The Δ9-desaturase in recombinant cells was not

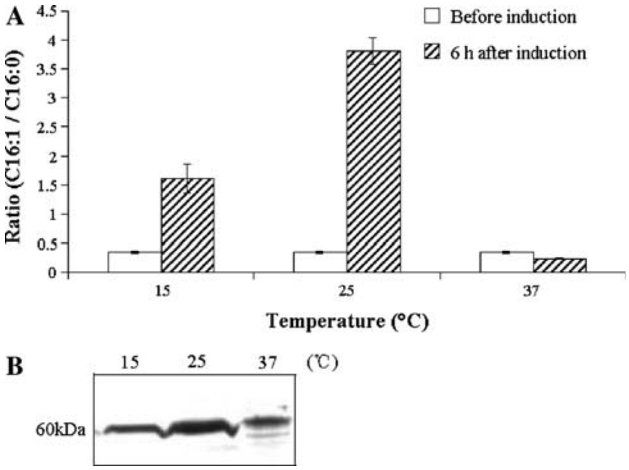

Fig. 4 The ratio of palmitoleic acid to palmitic acid (**a**) and western blotting analysis (**b**) of the cells transformed with pEPUD9 after the expression for 6 h at 15, 25 and 37 °C. For western blot, *E. coli* cultures (equal to 1 mL of cell suspension with $OD_{600} = 0.2$) were pelleted by centrifugation and heated with SDS loading buffer at 95 °C for 10 min

detectable before the addition of IPTG to the culture, indicating that the *PuFAD9* gene was strictly regulated. The desaturation level of C16 fatty acids was 79% at 25 °C whereas only 61% at 15 °C when measured 6 h after induction. These results suggest that the conversion of palmitic acid into palmitoleic acid catalyzed by this desaturase can be controlled by expression time and temperature.

Discussion

Cloning and expression of the genes coding for the desaturases and elongases which are critical enzymes involved in the biogenesis of most of the PUFAs, have important biotechnological potential [7]. Introduction of the Δ9-desaturase gene into cells capable of producing an UFA can enhance the conversion to palmitoleic acid and oleic acid as starting compounds of UFAs. Particularly when a putative electron transport partner or a gene coding for another desaturase is combined with the Δ9-desaturase by a recombinant DNA technology, the improved productivity of some desired PUFAs could be expected [30]. In this sense, besides the soluble Δ9-ACP desaturases, the other two classes of membrane-bound Δ9-desaturases in different species could be regarded as alternative desaturase resource for more efficient production of PUFAs. However, although most research has been done on the Δ9 acyl-lipid desaturase isolated from cyanobacteria [31–34], the number of prokaryotic Δ9-desaturase enzymes that have been investigated in detail is much smaller than those from fungi [35, 36], higher plants [10, 37], fish [38] and mammals [39] so far. In the present study, a novel gene that encodes a membrane-bound Δ9-fatty acid desaturase from *P. urativorans* has been cloned and, to our knowledge, for the first time, successfully expressed in *E. coli*. The product of this gene fused with T7 tag has an approximate molecular mass of 60 kDa. Enzymatic activity of the target protein was confirmed by GC-MS analysis of the cellular fatty acid composition, to demonstrate that this enzyme was expressed in the heterologous host in active form and the desaturation reaction can be carried out in an *E. coli* host cell effectively. Growth temperature has an effect not only on the synthesis, but also on the activity of the desaturase, which was reflected by desaturation of palmitic acid. It is very likely that the *P. urativorans* desaturase expressed in *E. coli* accepted electrons from the host's ferredoxin [40]. However, further work is needed to clarify the electron transport system and substrate specificity of the enzyme.

Acknowledgments This work is part of the joint project between Nanjing University of Technology and the University of Stuttgart on Biosystems Engineering of Desaturation, which is in the framework of a Baden-Wuerttemberg—Shanghai/Jiangsu Exchange Program on Systems Biology and Biosystems Engineering.

References

1. Buist PH (2004) Fatty acid desaturases: selecting the dehydrogenation channel. Nat Prod Rep 21:249–262
2. Los DA, Murata N (1998) Structure and expression of fatty acid desaturases. Biochim Biophys Acta 1394:3–15
3. Shanklin J, Cahoon EB (1998) Desaturation and related modifications of fatty acids. Annu Rev Plant Physiol Plant Mol Biol 49:611–641
4. Macartney AI, Maresca B, Cossins AR (1994) Acyl-CoA desaturases and the adaptive regulation of membrane lipid composition. In: Cossins AR (ed) Temperature adaptation of biological membranes. Portland Press, London
5. Guschina IA, Harwood JL (2006) Mechanisms of temperature adaptation in poikilotherms. FEBS Lett 580:5477–5483
6. Lopez Alonso D, Garcia-Maroto F, Rodriguez-Ruiz J, Garrido JA, Vilches MA (2003) Evolution of the membrane-bound fatty acid desaturase. Biochem Syst Ecol 31:1111–1124
7. Warude D, Joshi K, Harsulkar A (2006) Polyunsaturated fatty acids: biotechnology. Crit Rev Biotechnol 26:83–93
8. Schmidt H, Dresselhaus T, Buck F, Heinz E (1994) Purification and PCR-based cDNA cloning of a plastidial n-6 desaturase. Plant Mol Biol 26:631–642
9. Li MC, Li H, Wei DS, Xing LJ (2006) Cloning and molecular characterization of Delta12-fatty acid desaturase gene from *Mortierella isabellina*. World J Gastroenterol 12:3373–3379
10. Marillia EF, Giblin EM, Covello PS, Taylor DC (2002) A desaturase-like protein from white spruce is a Delta9 desaturase. FEBS Lett 526:49–52
11. Hongsthong A, Subudhi S, Sirijuntarat M, Cheevadhanarak S (2004) Mutation study of conserved amino acid residues of *Spirulina* Delta6 acyl-lipid desaturase showing involvement of histidine 313 in the regioselectivity of the enzyme. Appl Microbiol Biotechnol 66:74–84
12. Na-Ranong S, Laoteng K, Kittakoop P, Tanticharoen M, Cheevadhanarak S (2006) Targeted mutagenesis of a fatty acid

Delta6 desaturase from *Mucor rouxii*: role of amino acid residues adjacent to histidine-rich motif II. Biochem Biophys Res Commun 339:1029–1034

13. Russell NJ (1971) Alteration in fatty acid chain length in *Micrococcus cryophilus* grown at different temperatures. Biochim Biophys Acta 231:254–256
14. Russell NJ (1977) Desaturation of fatty acids by the psychrophilic bacterium *Micrococcus cryophilus*. Biochem Soc Trans 5:1492–1494
15. Russell NJ (1978) The positional specificity of a desaturase in the psychrophilic bacterium *Micrococcus cryophilus* (ATCC 15174). Biochim Biophys Acta 531:179–186
16. Foot M, Jeffcoat R, Russell NJ (1983) Some properties, including the substrate in vivo, of the Delta9-desaturase in *Micrococcus cryophilus*. Biochem J 209:345–353
17. Sambrook J, Russell DW (2000) Molecular cloning, 3rd edn. Cold Spring Harbor Laboratory, New York
18. Thompson JD, Gibson TJ, Plewniak F, Jeanmougin F, Higgins DG (1997) The CLUSTAL_X windows interface: flexible strategies for multiple sequence alignment aided by quality analysis tools. Nucleic Acids Res 25:4876–4882
19. Kyte J, Doolittle RF (1982) A simple method for displaying the hydropathic character of a protein. J Mol Biol 157:105–132
20. Moller S, Croning MD, Apweiler R (2001) Evaluation of methods for the prediction of membrane spanning regions. Bioinformatics 17:646–653
21. Bendtsen JD, Nielsen H, von Heijne G, Brunak S (2004) Improved prediction of signal peptides: SignalP 3.0. J Mol Biol 340:783–795
22. Schagger H, von Jagow G (1987) Tricine-sodium dodecyl sulfate-polyacrylamide gel electrophoresis for the separation of proteins in the range from 1 to 100 kDa. Anal Biochem 166:368–379
23. Rose TM (2005) CODEHOP-mediated PCR—a powerful technique for the identification and characterization of viral genomes. Virol J 2:20
24. Shanklin J, Whittle E, Fox BG (1994) Eight histidine residues are catalytically essential in a membrane-associated iron enzyme, stearoyl-CoA desaturase, and are conserved in alkane hydroxylase and xylene monooxygenase. Biochemistry 33:12787–12794
25. Stukey JE, McDonough VM, Martin CE (1990) The OLE1 gene of *Saccharomyces cerevisiae* encodes the Delta9 fatty acid desaturase and can be functionally replaced by the rat stearoyl-CoA desaturase gene. J Biol Chem 265:20144–20149
26. Man WC, Miyazaki M, Chu K, Ntambi JM (2006) Membrane topology of mouse stearoyl-CoA desaturase 1. J Biol Chem 281:1251–1260
27. Nielsen H, Engelbrecht J, Brunak S, von Heijne G (1997) Identification of prokaryotic and eukaryotic signal peptides and prediction of their cleavage sites. Protein Eng 10:1–6
28. Subrahmanyam S, Cronan JE Jr (1998) Overproduction of a functional fatty acid biosynthetic enzyme blocks fatty acid synthesis in *Escherichia coli*. J Bacteriol 180:4596–4602
29. McLean LR, Sulzbacher WL, Mudd S (1951) *Micrococcus cryophilus*, spec. nov.; a large coccus especially suitable for cytologic study. J Bacteriol 62:723–728
30. Shimizu S, Kobayashi M (2002) Delta9 desaturase gene. US Patent 6,448,055
31. Sakamoto T, Wada H, Nishida I, Ohmori M, Murata N (1994) Delta9 Acyl-lipid desaturases of cyanobacteria. Molecular cloning and substrate specificities in terms of fatty acids, sn-positions, and polar head groups. J Biol Chem 269:25576–25580
32. Kiseleva LL, Serebriiskaya TS, Horvath I, Vigh L, Lyukevich AA, Los DA (2000) Expression of the gene for the Delta9 acyl-lipid desaturase in the thermophilic cyanobacterium. J Mol Microbiol Biotechnol 2:331–338
33. Chintalapati S, Prakash JS, Gupta P, Ohtani S, Suzuki I, Sakamoto T, Murata N, Shivaji S (2006) A novel Delta9 acyl-lipid desaturase, DesC2, from cyanobacteria acts on fatty acids esterified to the sn-2 position of glycerolipids. Biochem J 398:207–214
34. Maali R, Shimshilashvili KhR, Pchelkin VP, Tsydendambaev VD, Nosov AM, Los DA, Goldenkova-Pavlova IV (2007) Comparative expression in *Escherichia coli* of the native and hybrid genes for acyl-lipid Delta9 desaturase. Genetika 43:176–182
35. Stukey JE, McDonough VM, Martin CE (1989) Isolation and characterization of OLE1, a gene affecting fatty acid desaturation from *Saccharomyces cerevisiae*. J Biol Chem 264:16537–16544
36. MacKenzie DA, Carter AT, Wongwathanarat P, Eagles J, Salt J, Archer DB (2002) A third fatty acid Delta9 desaturase from *Mortierella alpina* with a different substrate specificity to ole1p and ole2p. Microbiology 148:1725–1735
37. Lindqvist Y, Huang W, Schneider G, Shanklin J (1996) Crystal structure of Delta9 stearoyl-acyl carrier protein desaturase from castor seed and its relationship to other di-iron proteins. Embo J 15:4081–4092
38. Chang BE, Hsieh SL, Kuo CM (2001) Molecular cloning of full-length cDNA encoding Delta9 desaturase through PCR strategies and its genomic organization and expression in grass carp (Ctenopharyngodon idella). Mol Reprod Dev 58:245–254
39. Miyazaki M, Bruggink SM, Ntambi JM (2006) Identification of mouse palmitoyl-coenzyme a Delta9-desaturase. J Lipid Res 47:700–704
40. Knoell HE, Knappe J (1974) *Escherichia coli* ferredoxin, an iron-sulfur protein of the adrenodoxin type. Eur J Biochem 50:245–252

Lipids (2008) 43:215–225
DOI 10.1007/s11745-007-3146-1

ORIGINAL PAPER

Developmental, Hormonal, and Nutritional Regulation of Porcine Adipose Triglyceride Lipase (ATGL)

Jeffrey A. Deiuliis · Jonghyun Shin · Dongryeoul Bae · Michael J. Azain · Richard Barb · Kichoon Lee

Received: 24 July 2007 / Accepted: 6 December 2007 / Published online: 10 January 2008
© AOCS 2008

Abstract Adipose triglyceride lipase (ATGL) is a newly identified lipase. We report for the first time the porcine ATGL sequence and characterize ATGL gene and protein expression in vitro and in vivo. Adult pig tissue expresses ATGL at high levels in the white adipose and muscle tissue relative to other tested tissues. We show that within the white adipose tissue ATGL is expressed at higher levels in the adipocyte than in the stromal-vascular fraction. Additionally, ATGL expression increases dramatically in the subcutaneous adipose during adipose development and maturation, as well as during in vitro adipogenesis. Peroxisome proliferator-activated receptor gamma transcript levels increased concomitant with ATGL gene expression, suggesting a possible role in the regulation of ATGL by adipogenic regulators. In vitro treatment of differentiated primary pig preadipocytes with insulin and forskolin decreased ATGL gene expression in a dose-dependent manner, suggesting ATGL transcript levels are hormone sensitive. In vivo experimentation showed that calorie-restriction in gilts resulted in increased ATGL mRNA and protein levels in subcutaneous and peri-renal fat tissues. Our data demonstrate that ATGL expression reacts to hormonal stimuli and plays a role in catecholamine-induced lipolysis in porcine adipose tissue.

Keywords Adipose triglyceride lipase (ATGL) · Lipolysis · Delta like homolog 1 (DLK1) · Peroxisome proliferator-activated receptors gamma (PPARγ) · Adipose tissue · Pig

Introduction

Due to a variety of similar physiological and anatomical characteristics, including a tendency to overeat, pigs are used as models for human diseases including obesity and cardiovascular disease [1, 2]. Understanding the lipolytic pathway in pigs has an application to researchers of human diseases. Lipase enzymes catalyze the breakdown of stored triglycerides, a process known as lipolysis, to fatty acids and glycerol. Adipose triglyceride lipase (ATGL), a newly discovered lipase, hydrolyzes the first ester bond of stored triglycerides, releasing nonesterified free fatty acids [3]. ATGL protein is associated with lipid droplets and is found at high levels in adipose tissue, but is also present in other tissues that have lipid stores [4]. ATGL activity has been shown to be required for all PKA-stimulated fatty acid and glycerol release in murine embryonic fibroblast adipocytes [5] and is the rate-limiting step in hormone-induced lipolysis [3, 6]. The product, diacylglycerol, is hydrolyzed by activated hormone sensitive lipase (HSL), which has a higher substrate affinity for diacylglycerol than triglyceride [6]. Thus, ATGL and HSL work in concert to mobilize free fatty acid stores from lipid storing tissues.

J. A. Deiuliis · J. Shin · D. Bae · K. Lee (✉)
Department of Animal Sciences, The Ohio State University,
2029 Fyffe Rd, Columbus, OH 43210, USA
e-mail: lee.2626@osu.edu

J. A. Deiuliis · J. Shin · K. Lee
The Ohio State University Interdisciplinary Human Nutrition
Program, The Ohio State University, Columbus, OH 43210,
USA
e-mail: deiuliis.1@osu.edu

M. J. Azain
Animal and Dairy Science Department, University of Georgia,
Athens, GA 30602, Greece

R. Barb
Russell Agricultural Research Center, USDA-ARS,
Athens, GA 30604, Greece

Fasting has been shown to increase ATGL transcript levels in mice [7]. Human obesity is associated with decreased catecholamine-induced lipolysis and decreased HSL expression in adipocytes [8]. A study of the level of HSL and ATGL gene expression showed that the abundance of the two transcripts in human adipose tissue was highly correlated to habitual dietary conditions during a low calorie diet [8]. This suggests a common regulatory mechanism(s) for the two genes [8]. Studies in mice suggest that dexamethasone induces ATGL gene expression, whereas tumor necrosis factor alpha, isoproterenol, and insulin downregulate ATGL gene expression in 3T3-L1 preadipocytes [7, 9]. However, regulation of ATGL at the molecular level remains unclear. The role ATGL plays in tissues during adipogenesis and times of calorie restriction as well as the transcriptional response to metabolic stimuli in most mammals is unknown. Our experiments are the first to characterize ATGL gene expression in pigs. We investigated pATGL gene expression in various tissues, in the subfractions of the adipose, during development, during in vitro preadipocyte differentiation, and after food restriction.

Materials and Methods

Animals

All in vitro work was performed using adipose tissue collected from Landrace pigs: primary preadipocyte culture (7–12 day old pigs, 6 piglets total), tissue fractionation and tissue distribution (120 days), ontogeny (embryo, 105 days of gestation; adult, 120 days; 3 pigs per group). The adipose is a rapidly developing tissue with rapid histological changes occurring during late gestational and early post-natal development, thus samples from 105 days fetal and 6 days post-natal were included in the ontogeny study [10, 11]. The calorie restriction study used 12 adult (164 days of age) commercially crossbred ovariectomized gilts weighing between 80–100 kg with a mean weight of 79 kg. Six were fed a calorie restricted (1 kg/days) diet while control pigs were fed ad libitum ~3 kg/days for two weeks before tissue collection. At the conclusion of the experiment, the control group gained an average of 8.2 kg and the calorie restricted group lost an average of 2.5 kg. Samples were collected from the subcutaneous adipose (inner and outer) and the peri-renal adipose (pad proximate the kidneys). Protein and total RNA were isolated for use in immunoblotting and quantitative real-time RT-PCR, respectively. All animal procedures were approved by the institutional animal care and use committee.

RNA Isolation and Preparation of cDNA for Cloning

RNA was isolated from pig adipose samples using Trizol™ (Invitrogen) according to the manufacturer's instructions. RNA quality was assessed by agarose gel electrophoresis. Approximately 1 µg of total RNA was reverse transcribed according to the manufacturer's instructions (Invitrogen Life Technologies—M-MLV reverse transcriptase) [12].

ATGL Cloning and Design of Primers

cDNA from pig adipose was used as a template for PCR. Two sets of primers were designed according to two porcine sequences: The Institute for Genome Research (TIGR) database sequences TC276632 and TC277702. The TIGR sequences showed homology to human (Genbank accession numbers: AY894804, NM_020376), mouse (AJ278476, AK031609), and cow (XM_864571) ATGL cDNA. A MJ Research PTC-200 thermal cycler and DNA Taq polymerase (Invitrogen) were used for all PCR reactions. The PCR products were separated by electrophoresis on a 1% agarose gel and the appropriate band(s) excised and gel extracted using the Qiagen Gel Extraction Kit. The product was then ligated to the pCR 2.1-TOPO vector using the TOPO TA Cloning Kit (Invitrogen). Positive clones were sequenced by The Ohio State University sequencing core facility using an Applied Biosystems 3730 DNA Analyzer. The resulting sequences confirmed sequence identity by homology to the mouse and human by identification of characteristic enzyme domains. Real-time primers were then designed to measure ATGL gene expression ("F2" 5′-GCACCTTCATTCCCGTGTAC-3′, "R2" 5′-CGAGAGATGTGCAAGCAGGG-3′). Primers were designed to span genomic introns, thus avoiding amplification of genomic DNA possibly present in RNA samples. PCR reactions using F2/R2 primers were optimized for use in real-time PCR.

Real-Time PCR Detection of Total Gene Expression

Real-time PCR was performed using SYBR green I nucleic acid dye (Molecular Probes Invitrogen detection technologies) on an ABI 7300. AmpliTaq Gold™ (Applied Biosystems, Roche New Jersey) was used in all real-time reactions as was the following thermal profile: 95 °C 10 m, 40 cycles of 94 °C 30 s, 60 °C 60 s, and 82 °C 30 s. The C_T values for the internal control (cyclophilin) and target genes, as determined by the ABI software, were used to calculate gene expression using the $2^{-\Delta\Delta Ct}$ method [13]. All target genes were normalized to cyclophilin and displayed as a relative fold-change. Randomly selected samples from all real-time runs were resolved by agarose gel electrophoresis to ensure the production of one product. In addition, dissociation/melting curves yielded single peaks, indicating a single product with lack of primer dimers. “No template” negative controls were included in all PCR reactions to detect possible contamination.

Protein Isolation and Immunoblotting

Approximately 80 mg of tissue was homogenized in 800 µl of lysis buffer (1% Triton X-100, 150 mM NaCl, 20 mM HEPES pH 7.5, 10% glycerol, 1 mM EDTA, 100 mM NaF, 100 µM sodium orthovanadate, 1 mM PMSF, and 10 µl/ml commercial protease inhibitor cocktail). The protein content of cell lysate was determined using the bicinchoninic acid (BCA) Protein Assay Kit (Pierce Chemical). Samples were separated by SDS-PAGE using the mini-Protean system (Bio-RadHer). The protein was wet-transferred to a PVDF membrane (Amersham Biosciences Hybond-P^{TM}), blocked in 5% nonfat dry milk (NFDM) in 1x-TBST (0.1% Tween 20) and incubated overnight at 4 °C with primary antibody specific to ATGL (Cayman Chemical, 1:1000) in 5% NFDM. After washing in 1x-TBST, blots were incubated with the appropriated HRP-conjugated secondary antibody for 1 h at room temperature. Blots were washed before addition of ECL plus^{TM} (Amersham Biosciences) and bands were detected with Hyperfilm^{TM} (Amersham Biosciences).

Porcine Stromal-Vascular and Adipocyte Cell Fractionation

Adipose tissue (5 g) was removed from 120 day old pigs, minced, and incubated with 3.2 mg/ml collagenase II (Sigma-Aldrich) for 1 h in a shaking waterbath (180 rpm, 37 °C) to separate adipose tissue into adipocyte and stromal-vascular fractions (SVF). After treatment, the suspension was passed through a 100 µm nylon cell strainer to remove undigested tissue. The filtrate was centrifuged at $200\times g$ for 5 min and the top layer (adipocyte fraction) and the pellet (SVF) were collected for RNA isolation [14]. Separation of fractions was verified by marker genes delta like homolog 1 (DLK1) (preadipocyte) [12, 15] and peroxisome proliferator-activated receptor (PPARγ) (adipocyte) [12, 16].

Primary Pig Preadipocyte Culture and Differentiation

The separated stromal-vascular portion of the tissue fractionation was plated in DMEM supplemented with 10% fetal bovine serum (FBS) and antibiotics. The media was refreshed every 24 h until confluence (~5 days) and during the differentiation protocol. The cells were differentiated similar to our previous publication [17]. Briefly, 1 day after confluence cells were treated with 80 nM dexamethasone for 2 days followed by 5 µg/ml insulin, 5 µg/ml transferrin, 0.5 mM isobutyl-1-methylxanthine, and 5 ng/ml selenium for 4 days. Cells were maintained in growth media until 10 days post-differentiation before use in experiments resulting in approximately 60% differentiation. This method is based on those published by Hausman and colleagues [18–20]. The cells were serum starved for 6 h before treatment with insulin, epinephrine, or forskolin for 12 h. Samples were immediately frozen at −80 °C after collection.

Bioinformatics and Statistical Analyses

ClustalX was used for multiple amino acid sequence alignment [21]. Genedoc^{TM} was used for creation of cDNA and amino acid alignment figures. Gene expression data were subjected to a one-way ANOVA procedure of SAS^{TM} (SAS Inst., Inc.) followed by Fisher’s Protected LSD. Comparison of two means was accomplished by a Student’s *t*-test [22]. The minimum level of significance was set at $P < 0.05$.

Results

ATGL cDNA and Amino Acid Sequences

We identified several partial pig ATGL sequences in The Institute for Genomic Research (TIGR) database that were homologous to human (Genbank accession #AY894804) and murine ATGL (#AK031609). Porcine ATGL cDNA (Genbank accession #EU047807) was cloned using primers designed based on these sequences (Fig. 1). Analysis of amino acid homology shows that porcine ATGL protein is more homologous to the mouse (83%) than the human (78%). The first 180 amino acids of the ATGL protein represent the patatin domain (PFAM accession PF01734) which is responsible for the lipolytic activity of ATGL (Fig. 2) [23, 24]. Porcine ATGL has a hydrophobic domain (Leu309-Ser396) which may be necessary for association with the lipid-droplet [23, 24]. The consensus sequence within the patatin domain for the serine lipase motif (GXGXXG) was GCGFLG and the serine hydrolase motif (GXSXG) was GASAG in all three species compared.

ATGL Gene Expression Levels Differ between Adipose Tissue Fractions

Among the tissues analyzed, pig white adipose, skeletal muscle, and cardiac muscle tissues showed the highest

Fig. 1 Porcine ATGL cDNA sequence. The full length pig ATGL cDNA (Genbank accession #EU047807) is shown with start and stop codons (*underlined*) at +4 and +1462, respectively

```
           *        20         *        40         *        60         *        80         *
: GCGATGTTCCCCAAAGAGACGACGTGGAACATCTCGTTCGCGGGTTGCGGCTTCCTCGGCGTCTACCACGTCGGCGTGGCCTCCTGTCTC :   90

         100         *       120         *       140         *       160         *       180
: CGCGAGCACGCGCCCTTCCTAGTGGCCAACGCCAAGCACATCTACGGCGCCTCGGCTGGGGCGCTCGTGGCCACGGCCCTGGTTACCGGG :  180

           *       200         *       220         *       240         *       260         *
: GTCTGCCTGGGTGATACTGGCGCCAGCATCATCGAGGTGTCGAAGGAGGCCCGGAAGCGGTTCTTGGGCCCACTGCACCCCTCCTTCAAC :  270

         280         *       300         *       320         *       340         *       360
: CTGGTGAAGACCATCCGTGGCTGCCTGGTGAAAATCCTGCCCGCCGACAGCCACGAGCGGGCCAGCGGCCGCCTGGGCATCTCCCTGACC :  360

           *       380         *       400         *       420         *       440         *
: CGCGTCTCCGACGGCGAAAATGTCATCATAACCCACTTCGCCGCCAGGGAGGAGCTCATCCAGGCCAACGTCTGCAGCACCTTCATTCCC :  450

         460         *       480         *       500         *       520         *       540
: GTGTACTGCGGCCTCATTCCACCTGCTCTCCAGGGCGAGCGCTACGTGGACGGTGGCATCTCAGACAACCTGCCTCTCTACGAACTCAAG :  540

           *       560         *       580         *       600         *       620         *
: AGCACCATCACCGTGTCCCCCTTCTCGGGCGAGAGCGACATCTGCCCGCAGGACAGCTCCACCAACATCCACGAGCTCCGCGTCACCAAC :  630

         640         *       660         *       680         *       700         *       720
: ACCAGCATCCAGTTCAGCCTGCGCAACCTCTACCGCCTCTCCAAGGCCCTGTTCCCGCCCGAGCCCCTGGTGCTTCGAGAGATGTGCAAG :  720

           *       740         *       760         *       780         *       800         *
: CAGGGTTACAGGGACGGCCTGCGCTTCCTGCGGCGGAACGGCCTCCTGAACCGGCCCAACCCCTTGCTGGCGCTGCCTCCCGCCTGCCCC :  810

         820         *       840         *       860         *       880         *       900
: CGTGCCCCCGAGGAGGAAGATGCCCCGAAGGCCGAGGTGGCCGAGGAGAGGGCCGGAGCCAAGGAGCCCTTGCAGCTGCCCACAAGTGAT :  900

           *       920         *       940         *       960         *       980         *
: AGCATCCTGGAGCACCTGCCCTCGAGGCTCAATGACGCCCTGCTGGAGGCCTGCATGGAGCCCACGGACCTGCTGAGCACCCTGTCCAAC :  990

        1000         *      1020         *      1040         *      1060         *      1080
: CTGCTGCCCGTGCGTCTGGCCACAGCCATGATGGTGCCCTACACGCTGCCGCTGGAGAGCGCCGTGTCCTTCACCGTCCGCTTGCTGGAG : 1080

           *      1100         *      1120         *      1140         *      1160         *
: TGGCTGCCCGACGTCCCGGAGGACATCCGGTGGATAAAGGAGCAGACAGGCAGTATCTGCCAGTACCTGGTGATGCGCGCCAAGAGGAAG : 1170

        1180         *      1200         *      1220         *      1240         *      1260
: CTGGGCAGGCACCTGCCCTCCAGGCTGACGGAGCAGGTGGAGCTGCGGCGCTCGCAGTCGCTGCCCTCTGTGCCCCTGTCCTGCGCCGCC : 1260

           *      1280         *      1300         *      1320         *      1340         *
: TACGGCGGGGTGCTGCCCAGCTGGATGCGCAACAGCCTCTCGCTGGGGGACGTGCTGGCCAAGTGGGAGGAGCGCCAGCGCCAGCTGCTG : 1350

        1360         *      1380         *      1400         *      1420         *      1440
: CTGGGTCTCTTCTGCACCAACACTGCCTTCCCGCCCGACGCCCTGCGCATGCTCGCCCCAGCGGGTCCTGCCCCCGCACCCTCGCAGCAC : 1440

           *      1460         *      1480         *      1500         *
: CCGCCCGGCTCCCCCCCCTGCTGAGCGCCCCTGCTCCGGCCTTCTCCAGGGCCCTGGGGTCCCAGTGCTGA : 1511
```

relative gene expression of ATGL (Fig. 3a). Skeletal muscle expression of ATGL is of comparable magnitude to that of the subcutaneous white adipose. Cardiac muscle showed higher expression on average than the intestine, kidney, liver, lung, and spleen. Western blot data show that ATGL protein levels in white adipose are much higher than other tissues (Fig. 3b).

The adipose tissue is composed of two general fractions, the SVF and the adipocyte fraction. The SVF accounts for at least one half of the cells of the adipose and includes fibroblasts, macrophages, and preadipocytes (mesenchymal stem cells) [25]. It is important to determine which adipose tissue subfraction is expressing ATGL because it lends insight into the role of the gene product in the whole tissue. While collagenase digestion and the subsequent separation are not absolute, we show (Fig. 3c) that delta like homolog 1 (DLK1), a preadipocyte marker gene, is significantly higher in the SVF and that PPARγ, an adipocyte marker gene, is significantly higher in the adipocyte fraction, indicating effective separation. Our data showed (Fig. 3c) that ATGL expression was, on average, 14-fold higher in the adipocyte fraction compared to the SVF, suggesting that adipocytes dominantly express ATGL in adipose tissue and that ATGL expression may be induced during adipogenesis.

Ontogeny of ATGL Gene Expression in the Adipose and During Differentiation of Primary Pig Preadipoctyes

To confirm the induction of ATGL during in vivo adipose development, we collected subcutaneous fat tissue from embryonic day E105, 6 day, and 120 day old pigs (*n* of

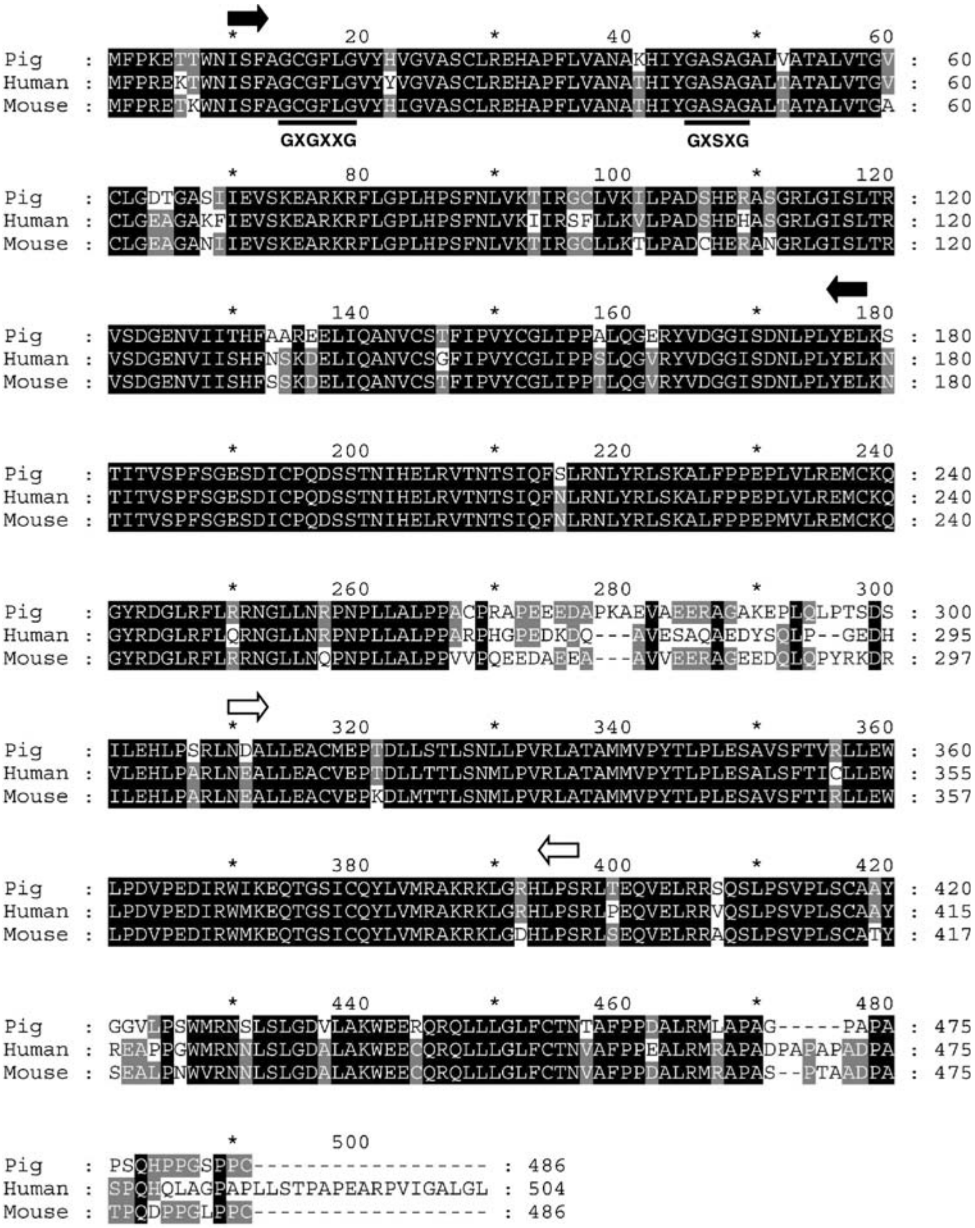
* 20 * 40 * 60
Pig : MFPKETTWNISFAGCGFLGVYHVGVASCLREHAPFLVANAKHIYGASAGALVATALVTGV : 60
Human : MFPREKTWNISFAGCGFLGVYYVGVASCLREHAPFLVANATHIYGASAGALTATALVTGV : 60
Mouse : MFPRETKWNISFAGCGFLGVYHIGVASCLREHAPFLVANATHIYGASAGALTATALVTGA : 60
GXGXXG
GXSXG
* 80 * 100 * 120
Pig : CLGDTGASIIEVSKEARKRFLGPLHPSFNLVKTIRGCLVKILPADSHERASGRLGISLTR : 120
Human : CLGEAGAKFIEVSKEARKRFLGPLHPSFNLVKIIRSFLLKVLPADSHEHASGRLGISLTR : 120
Mouse : CLGEAGANIIEVSKEARKRFLGPLHPSFNLVKTIRGCLLKTLPADCHERANGRLGISLTR : 120
* 140 * 160 * 180
Pig : VSDGENVIITHFAAREELIQANVCSTFIPVYCGLIPPALQGERYVDGGISDNLPLYELKS : 180
Human : VSDGENVIISHFNSKDELIQANVCSGFIPVYCGLIPPSLQGVRYVDGGISDNLPLYELKN : 180
Mouse : VSDGENVIISHFSSKDELIQANVCSTFIPVYCGLIPPTLQGVRYVDGGISDNLPLYELKN : 180
* 200 * 220 * 240
Pig : TITVSPFSGESDICPQDSSTNIHELRVTNTSIQFSLRNLYRLSKALFPPEPLVLREMCKQ : 240
Human : TITVSPFSGESDICPQDSSTNIHELRVTNTSIQFNLRNLYRLSKALFPPEPLVLREMCKQ : 240
Mouse : TITVSPFSGESDICPQDSSTNIHELRVTNTSIQFNLRNLYRLSKALFPPEPMVLREMCKQ : 240
* 260 * 280 * 300
Pig : GYRDGLRFLRRNGLLNRPNPLLALPPACPRAPEEEDAPKAEVAEERAGAKEPLQLPTSDS : 300
Human : GYRDGLRFLQRNGLLNRPNPLLALPPARPHGPEDKDQ---AVESAQAEDYSQLP--GEDH : 295
Mouse : GYRDGLRFLRRNGLLNQPNPLLALPPVVPQEEDAEEA---AVVEERAGEEDQLQPYRKDR : 297
* 320 * 340 * 360
Pig : ILEHLPSRLNDALLEACMEPTDLLSTLSNLLPVRLATAMMVPYTLPLESAVSFTVRLLEW : 360
Human : VLEHLPARLNEALLEACVEPTDLLTTLSNMLPVRLATAMMVPYTLPLESALSFTICLLEW : 355
Mouse : ILEHLPARLNEALLEACVEPKDLMTTLSNMLPVRLATAMMVPYTLPLESAVSFTIRLLEW : 357
* 380 * 400 * 420
Pig : LPDVPEDIRWIKEQTGSICQYLVMRAKRKLGRHLPSRLTEQVELRRSQSLPSVPLSCAAY : 420
Human : LPDVPEDIRWMKEQTGSICQYLVMRAKRKLGRHLPSRLPEQVELRRVQSLPSVPLSCAAY : 415
Mouse : LPDVPEDIRWMKEQTGSICQYLVMRAKRKLGDHLPSRLSEQVELRRAQSLPSVPLSCATY : 417
* 440 * 460 * 480
Pig : GGVLPSWMRNSLSLGDVLAKWEERQRQLLLGLFCTNTAFPPDALRMLAPAG-----PAPA : 475
Human : REAPPGWMRNNLSLGDALAKWEECQRQLLLGLFCTNVAFPPEALRMRAPADPAPAPADPA : 475
Mouse : SEALPNWVRNNLSLGDALAKWEECQRQLLLGLFCTNVAFPPDALRMRAPAS--PTAADPA : 475
* 500
Pig : PSQHPPGSPPC------------------ : 486
Human : SPQHQLAGPAPLLSTPAPEARPVIGALGL : 504
Mouse : TPQDPPGLPPC------------------ : 486

Fig. 2 Amino acid sequence alignment of pig, human, and mouse ATGL. *Black shading* indicates identical amino acids and *gray shading* indicates amino acids in the same R groups. The patatin domain is located between the *filled arrows* (I10-L178) and the hydrophobic domain between the *unfilled arrows* (L309-S396). Within the patatin domain, the glycine-rich, serine lipase motif (GXGXXG) is *underlined* as well as the serine hydrolase motif (GXSXG). *Dashes* represent gaps in the amino acid sequence that are necessary for alignment according to the default parameters of ClustalX

pigs = 3 for each time point) and expression of ATGL at mRNA and protein levels was quantified by real-time RT-PCR and Western blot analyses, respectively. Embryonically, porcine subcutaneous fat tissue expresses very low levels of ATGL when compared to the levels detected in adults (Fig. 4a). Even at 6 days after birth, pigs have relatively low levels of ATGL. The dramatic increase in ATGL during development was further confirmed at the protein level by immunoblotting (Fig. 4b). This suggested that adipogenesis or tissue maturation resulted in increased ATGL expression. In order to study if preadipocyte differentiation resulted in an increase in ATGL transcript, primary pig preadipocytes were grown in culture and differentiated. During differentiation, we found that levels of ATGL increased concomitantly with differentiation. We showed (Fig. 4) that increases in PPARγ in the pig during maturation occurred simultaneously with ATGL gene expression and that PPARγ and ATGL gene expression increased during adipogenesis (Fig. 5).

Hormonal Effects on ATGL Gene Expression in Differentiated Primary Pig Adipocytes

In order to determine if ATGL transcript levels were sensitive to hormonal signals, we cultured, differentiated, and treated primary pig pre-adipocytes with an anabolic and catabolic compound. Fully differentiated pig adipocytes treated with insulin for six hours showed a statistically significant decrease in ATGL gene expression (Fig. 6a). As

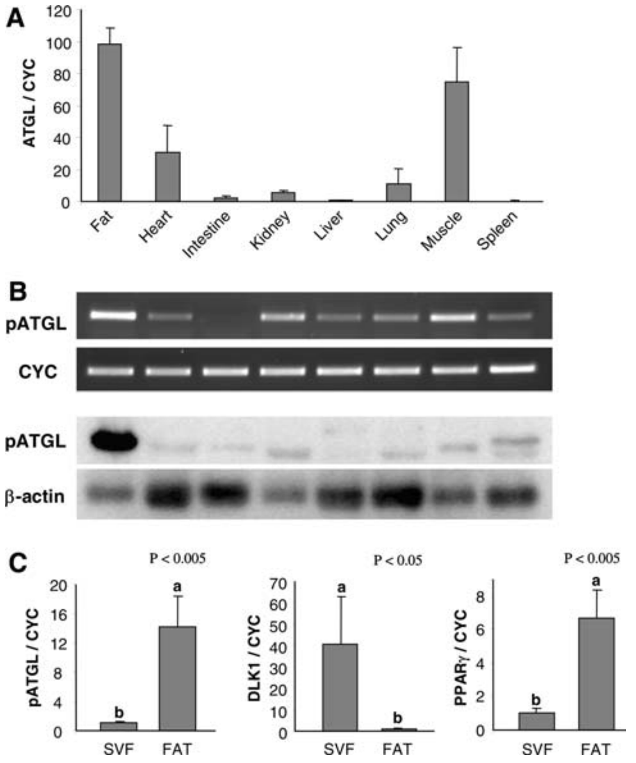

Fig. 3 ATGL gene expression in pig tissues and adipose tissue fractions. (**a**) Total RNA was isolated from various pig tissues. The mRNA expression of porcine ATGL was determined by quantitative real-time RT-PCR and expressed as a ratio to cyclophilin mRNA. The tissue distribution of the porcine ATGL gene expression was also assessed by RT-PCR, followed by agarose gel electrophoresis and ethidium bromide staining Cyclophilin was used as a housekeeping gene control. (**b**) Equal amounts of protein from whole tissue lysates were separated by SDS-PAGE and protein expression levels were determined by immunoblotting using an antibody specific to ATGL. Beta-actin is provided as an internal control. (**c**) Relative ATGL gene expression in the adipocyte and stromal-vascular (SV) fraction of digested tissues from two 12 day old piglets. Total DLK1 expression, a preadipocyte marker, is shown in addition to PPARγ expression, an adipocyte marker, both of which are normalized to cyclophilin

previously discussed, isoproterenol decreases ATGL transcript levels in mice. Isoproterenol binds the beta-adrenergic receptors, leading to activation of protein kinase A (PKA) signaling. In order to show a role for PKA signaling in ATGL gene expression, we used the specific PKA activator, forskolin. We found that forskolin decreased ATGL gene expression in a dose-dependent manner (Fig. 6b), providing a role for PKA signaling in the regulation of ATGL transcript levels.

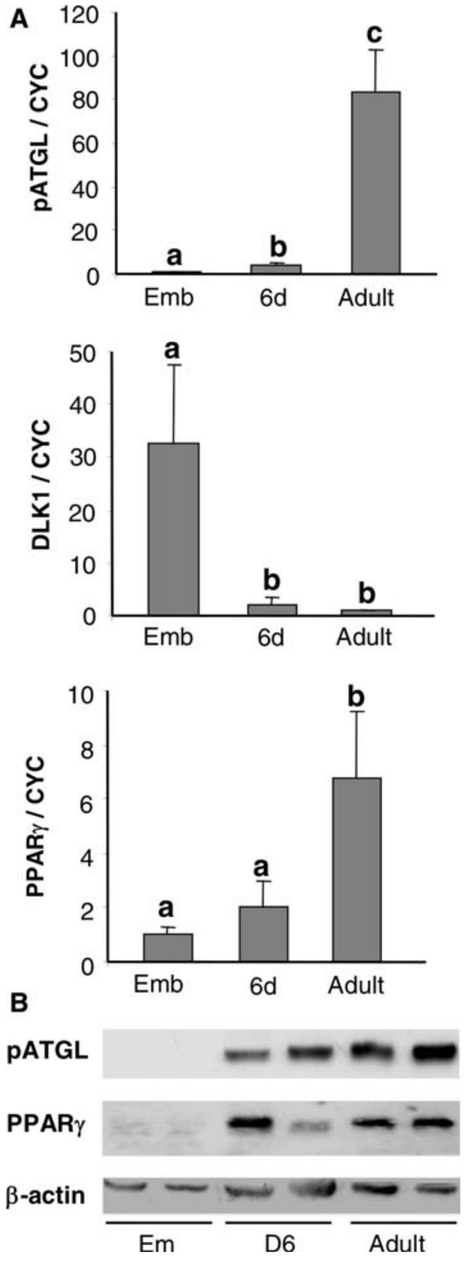

Fig. 4 ATGL expression during development of the pig. (**a**) Total RNA was isolated from 70-day old fetal, 6-day old and 120-day old pig adipose tissues. Porcine ATGL, DLK1 and PPARγ expressions in pig adipose tissue at three different ages were analyzed by quantitative real-time RT-PCR. Bar charts represent data from at least three animals per group performed in duplicate and are corrected for cyclophilin. Data reported as means ± SEM. The level of ATGL expression at day 140 was significantly higher than those of the fetus and 6-day old pigs (ANOVA, $P < 001$). The levels of DLK1 expression in fetal adipose tissue were significantly lower than those at day 6 and 140 (ANOVA, $P < 0001$). PPARγ expression increased with increasing age (**b**) ATGL and PPARγ protein was measured by Western blot analysis; β-actin was used as an internal control

Sensitivity of ATGL Expression to Calorie Restriction in the Peri-renal and Subcutaneous Fat Depots

The regulation of ATGL expression is unknown, although it has been shown that ATGL gene expression is decreased by insulin and epinephrine in vitro. The decreases in ATGL gene expression due to individual hormones in vitro, both catabolic and anabolic, suggest that ATGL expression in

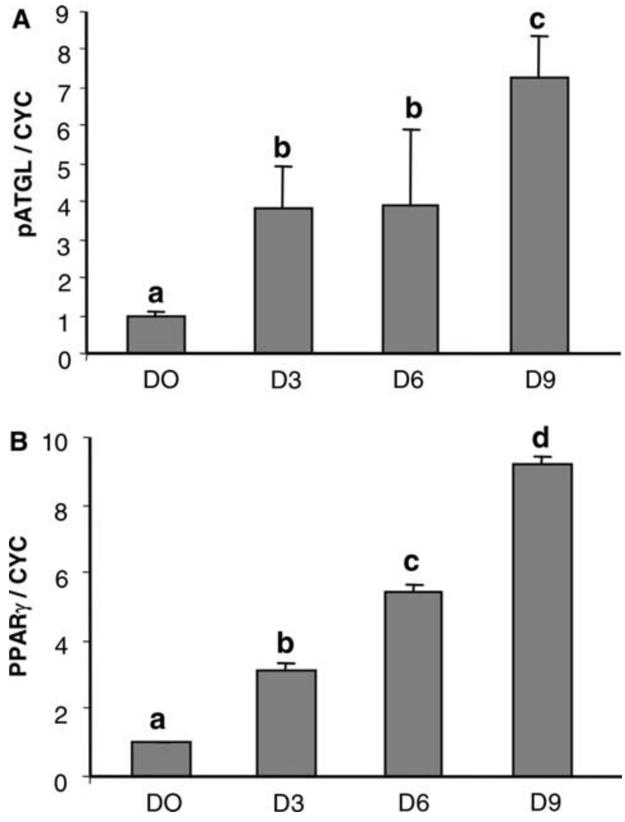

Fig. 5 ATGL gene expression during differentiation. Total RNA was isolated from d0 to d9 during adipogenic differentiation of adipose stromal-vascular cells. The mRNA expression of ATGL and PPARγ genes was determined by quantitative real-time RT–PCR and expressed as a ratio to cyclophilin mRNA. The bars indicate means ± SEM (the number of pigs = 3)

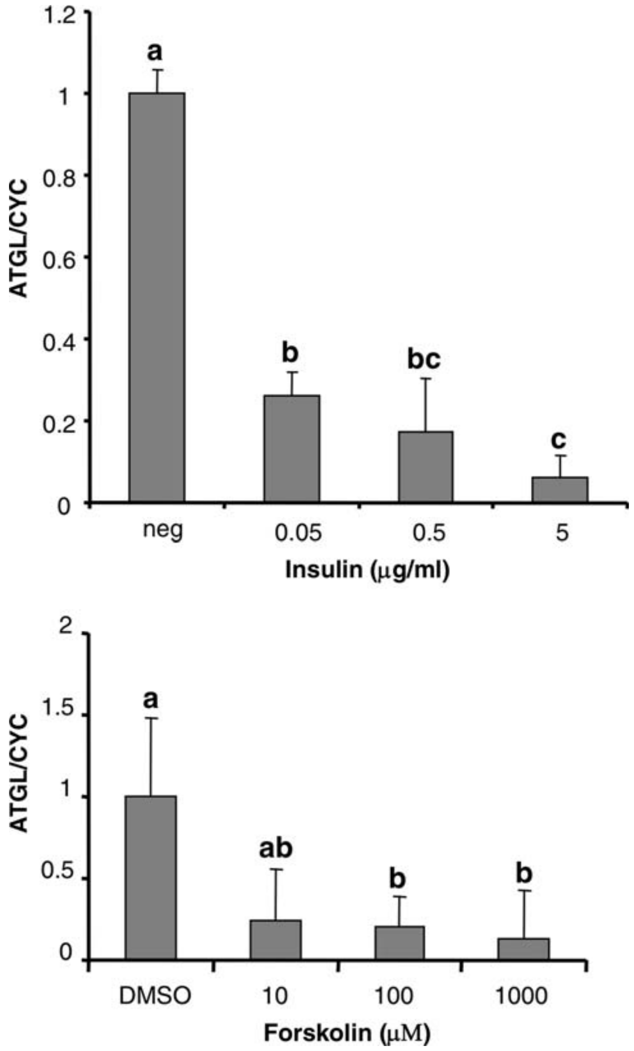

Fig. 6 Sensitivity of ATGL gene expression to hormonal signals in vitro. The differentiated porcine adipocytes in culture were treated with insulin and forskolin at indicated doses for 12 h. The mRNA expression of ATGL gene was determined by quantitative real time RT–PCR and expressed as a ratio to cyclophilin mRNA. The bars indicate means ± SEM (the number of pigs = 3)

vivo may be sensitive to metabolic hormones. Our data show that ATGL expression is increased by calorie restriction in the peri-renal and subcutaneous fat depots of pigs (Fig. 7). Hormone sensitive lipase (HSL) gene expression does not significantly change during calorie restriction. The lipolytic activity of HSL serves as an internal control because it is regulated at the protein level by PKA-mediated phosphorylation. Interestingly, DLK1 increased dramatically in the adipose of calorie-restricted pigs. We used immunoblotting to confirm the increased expression of ATGL at the protein level in the peri-renal and subcutaneous fat of the pig (Fig. 8a, b).

Discussion

Triglycerides stored in white adipose tissue (WAT) represent the primary energy storage form in animals. When caloric intake does not meet caloric expenditures, the body relies on the process of lipolysis in WAT to provide non-esterified fatty acids to tissues as an energy substrate. The regulation of lipolysis is an incompletely understood process which can vary greatly between species. This variability is largely due to species-specific differences in sensitivity to hormonal stimuli caused by variations in hormone receptor abundance and sequence [26]. In addition, the existence of lipases that have not been characterized adds a new dimension of complexity. Do inter-species variations in lipase enzyme sequence and/or function determine a species' or individual's unique lipolytic system? ATGL is a newly identified lipase that has only been described in a few mammalian species.

The 180 amino acids at the N-terminal were identified as a patatin-like domain in the Pfam protein family database. The patatin-like domain overlaps with the α/β hydrolase domain located at amino acids 25–240. These domains contain a glycine-rich motif (G*X*G*XX*G) and the active

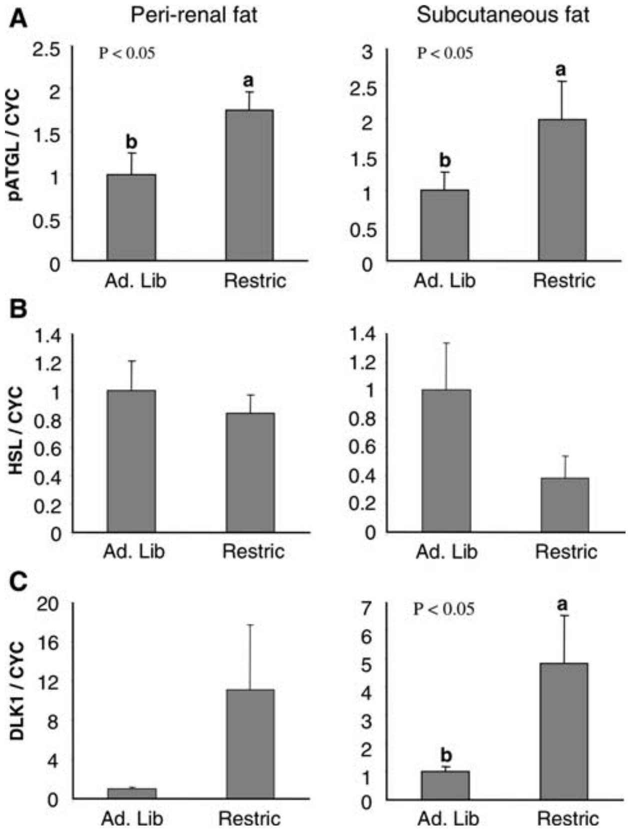

Fig. 7 ATGL gene expression in ad libitum versus calorie-restricted pigs. The ad libitum group was fed 3 kg/days and the calorie restricted group was fed 1 kg/days of a grower diet for 9 days. Total RNA isolated from peri-renal and subcutaneous adipose tissues was analyzed by quantitative real-time RT–PCR for ATGL, HSL and DLK1. Cyclophilin expression was used as a housekeeping gene control

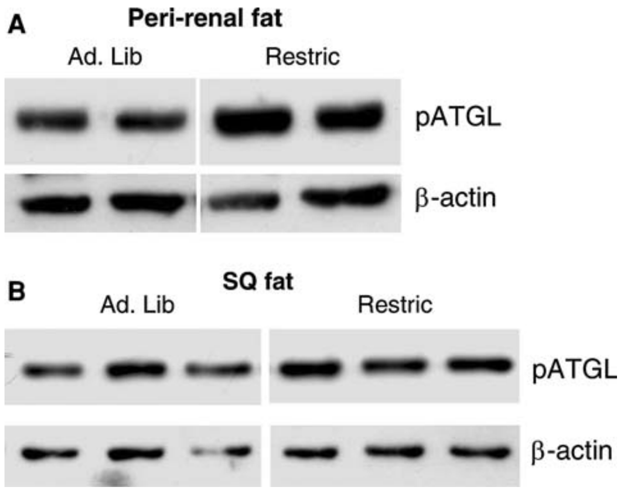

Fig. 8 ATGL protein levels in ad libitum versus calorie-restricted pigs. Total protein isolated from two groups was subjected to Western blot analysis for ATGL protein ATGL protein levels in (**a**) perirenal and (**b**) subcutaneous fat *β*-actin was used to indicate equal sample loading

serine hydrolase motif (G*X*S*X*G). The patatin-like domain also contains a brummer box (BB) that is conserved across patatin-like domain-containing proteins belonging to the nutrin family of proteins [24]. We show a high level of sequence conservation across species. In addition, the hydrophobic area of the protein from Leu309-Ser396 shows conserved homology. The hydrophobic domain has been shown to be associated with ATGL localization to the lipid-droplet [23]. Mutations within the hydrophobic domain of ATGL do not affect whole-cell lipase activity; however, ATGL cannot effectively localize to the adiposome. Localization of ATGL to the lipid droplet is essential for hydrolysis of stored triglyceride, explaining the phenotype presented by patients suffering from neutral lipid storage disorders (NLSDs) [23]. In addition, of the 12 identified single nucleotide polymorphisms in humans with three SNPs changing amino acids sequences, some have been correlated with free fatty acid, serum glucose levels, and the risk for type II diabetes [27]. However, the pig amino acid sequences at these SNP sites are identical to the sequences of normal human ATGL. Amino acids 267–300 are variable between species and no significant conservation is seen near the carboxyl terminus of the ATGL after amino acid 470. The pig sequence data supports the biological and evolutionary advantage to maintaining the patatin-like domain and the hydrophobic domain of ATGL across species.

ATGL has been shown to be associated with the lipid droplet [4]. Therefore, it is logical to assume that tissues with a greater abundance of accumulated triglyceride, and thus a larger lipid droplet, will have increased levels of ATGL. High relative expression of ATGL in WAT is consistent with expression in mice; however, ATGL gene expression in pig muscle seems to be high relative to most tissues tested [28]. Pig muscle ATGL expression is probably due to the presence of adiposomes (lipid droplets in the cells) within the muscle fibers themselves as well as the presence of intramuscular fat. Both skeletal and cardiac muscle use fatty acids as a preferred fuel substrate under certain conditions. ATGL gene expression in muscle was shown to be high while protein levels were not. The reason for this is unclear; however, one might explain this by differences in translation efficiencies or degradation rates between the tissues. NLSDs in humans are the result of mutations in both alleles of the ATGL gene and are characterized by ectopic fat droplet presence in leukocytes, bone marrow, skin, and muscle [23]. In addition, ATGL knockout mice accumulate large amounts of lipid in the heart causing premature death [29]. ATGL (+/−) mice presented cardiac triglyceride content at twice the level of wild-type mice [29]. Thus, the presence of ATGL may allow for enhanced catecholamine-induced hydrolysis of stored lipid in the mature porcine.

This indicates that embryonic and post-natal pigs have immature adipose tissues that are not effective at high levels of lipolysis and beta-oxidation, suggesting a reliance on a consistent supply of nutrients from the mother. Also, newborn piglets increase body fat mass from 3% to 15% by weaning at 21 days of age [30] with dramatic increases in fat cell size and expression of adipocyte marker genes [31]. High ATGL expression in the adult is probably due to a large population of mature adipocytes in adipose tissue, which was supported by the increased expression of adipogenic marker gene, PPARγ, and reduction in expression of preadipocyte marker gene, DLK1. Downregulation of DLK1 expression would theoretically allow for maximal adipocyte differentiation in rapidly growing piglets. It is important to note that DLK1 gene expression levels were very high in the embryo and dramatically decreased in the 6 d and adult pig, resulting in reduction of anti-adipogenic activities of DLK1 during in vivo differentiation of adipose tissue. PPARγ showed an inverse relationship to DLK1 and a direct relationship to ATGL as we stated previously concerning tissue fractionation. It is important to note that ATGL expression levels have been shown to be altered in states of obesity. For instance, genetically obese (ob/ob) mice have been shown to have decreased ATGL transcript levels in white adipose compared to normal weight controls suggesting a role for ATGL transcript regulation in body fat mass control [7]. Interestingly, ATGL-deficient mice exhibit fat cell hypertrophy and mild obesity [29]. These states suggest that ATGL function plays a role in whole body lipid content. Although the possible association of ATGL with whole body lipid content in pigs has not been studied, ATGL transcription levels may influence carcass adipose and meat quality.

The in vitro and in vivo data suggests that ATGL gene expression is controlled directly or indirectly by adipogenesis. Adipogenesis is a complex process regulated in large part by PPARγ. Transfection of 3T3-L1 cells with ATGL promoter-luciferase constructs followed by treatment with a PPARγ ligand resulted in transactivation, indicating that ATGL gene expression may be controlled by PPARγ mediated signals [28]. PPARγ may directly regulate ATGL gene transactivation by binding to the promoter of the ATGL gene or indirectly increase ATGL gene expression levels by upregulating an adipogenic factor that regulates ATGL expression. This suggests that ATGL transactivation may be controlled by an adipogenic transcription factor such as PPARγ [22]. However, further studies to elucidate this relationship are needed.

Decreased ATGL transcript levels due to insulin treatment are likely caused by phosphoinositide-3 kinase (PI3K) signaling events. Binding of insulin to the insulin receptor leads to PI3K and Akt activation. In a mouse adipocyte cell line, 3T3-L1, insulin-mediated ATGL decrease was rescued by a PI3K inhibitor [28]. We showed that forskolin treatment also decreased ATGL transcript levels. Forskolin activates adenyl-cyclase, resulting in increased intracellular cyclic AMP levels and the activation of PKA signaling. PKA signaling affects many cellular processes and activation of this pathway may directly or indirectly regulate ATGL transcription. Calorie-restriction increases ATGL, catecholamine, and glucocorticoid levels, as well as decreases levels of insulin. Translating the data between the two systems is complex. Calorie restriction in the pig most likely decreased serum insulin levels compared to the ad libitum group. This may reduce the potent inhibition of PI3K signaling via insulin stimulation as seen in vitro. Also, calorie restriction-induced glucocorticoid release may also increase ATGL expression as did dexamethasone in vitro. The inconsistency resides in the response to catecholamine-induced PKA signaling with ATGL decreasing in vitro but increasing in vivo when catecholamine levels should be higher than the ad libitum group. This incompatibility may be due to interactions between the hormonal signaling pathways in vivo which cannot be, or are difficult to, recapitulate in culture.

The calorie-restriction experiment yielded a novel finding; restriction increased DLK1 gene expression. This may be explained by a proportional increase in the number of SV cells per gram of tissue as adipocytes lose lipid mass during restriction. Alternatively, DLK1 may play, as of yet, an undefined role in the adipose during times of calorie restriction [32]. The upregulation of DLK1 may function to prevent cells within the adipose from undergoing differentiation, thus maintaining preadipocytes in times of a negative energy balance and possibly leading to an increased population of preadipocytes. This is supported by transgenic overexpression of DLK1 in mouse adipose tissue, resulting in decreased fat mass and increased endogenous DLK1 gene expression [15]. Alternatively, food restriction results in decreased adipose tissue mass by inhibition of adipogenesis and catabolic events such as lipolysis, which may have led to the indirect upregulation of the DLK1 gene expression. In adipose tissue, expression of the DLK1 antisense decreased amounts of endogenous DLK1 and promoted adipocyte differentiation, whereas overexpression of the DLK1 gene inhibited adipocyte development in vitro [33]. In addition, our previous studies clearly indicate that overexpression of the DLK1 gene in adipose tissue of transgenic mice inhibited adipocyte development and knockout of the DLK1 gene induced the obesity phenotype in mice [15, 34]. In pigs, DLK1 served as a reliable preadipocyte marker as shown by greater expression of DLK1 in the subcutaneous adipose of embryonic pigs and the stromal-vascular tissue fraction of adult pigs [12].

The sensitivity of the pig ATGL gene to hormonal stimuli both in vitro and in vivo suggests a role for ATGL in hormone-induced lipolysis. Before the identification of ATGL, HSL was regarded as the hormonally-controlled master regulator of lipolysis. The mechanisms that control ATGL-mediated initiation of lipolysis are not understood. While some researchers report that ATGL is affected by hormonal stimuli, others speculate that ATGL is only involved in basal lipolysis. Though our study does not directly measure lipolysis we do show that ATGL gene and protein expression are altered by hormonal stimuli in vitro and in vivo, respectively, suggesting that hormonally sensitive signaling pathways converge on factors that effect ATGL gene expression. Both anti- and pro-lipolytic hormones downregulated ATGL in the pig, similar to that reported in mice. It has been shown that PKA activating compounds, such as epinephrine and forskolin, induce lipolysis while decreasing ATGL gene expression levels, suggesting that ATGL may not be regulated at a transcriptional level. It has been shown that ATGL is not a direct substrate of PKA and there are no data showing evidence of regulation at a protein level [3]. It is also important to note that ATGL gene and protein expression levels increase during calorie restriction. Previous studies showed that feed restriction in pigs results in decreased transcript levels in some genes (fatty acid synthase, lipoprotein lipase, leptin) involved with energy partitioning [35–37]. During food restriction in our study, pig insulin levels should be lower than during ad libitum feeding which would allow for ATGL levels to increase. However, epinephrine levels in restricted pigs would also be elevated on average in comparison to ad libitum fed pigs. This suggests that individual hormones tested in vitro do not accurately recapitulate the complex metabolic signals that undoubtedly intersect on ATGL. Further elucidation of the biochemical regulation of ATGL enzyme activity may clarify the intricacy between whole body metabolism and the convergence of hormonal signaling effects on ATGL.

Acknowledgments This work was supported by an Ohio Agriculture Research and Development Center (K. Lee) seed grant and HK Biotech (K. Lee). This work was partially supported by the Korean Science and Engineering Foundation Grant (J. Shin, No.C00137).

References

1. Guillerm-Regost C, Louveau I, Sebert SP, Damon M, Champ MM, Gondret F (2006) Cellular and biochemical features of skeletal muscle in obese Yucatan minipigs. Obesity (Silver Spring) 14:1700–1707
2. Turk JR, Henderson KK, Vanvickle GD, Watkins J, Laughlin MH (2005) Arterial endothelial function in a porcine model of early stage atherosclerotic vascular disease. Int J Exp Pathol 86:335–345
3. Zimmermann R, Strauss JG, Haemmerle G, Schoiswohl G, Birner-Gruenberger R, Riederer M, Lass A, Neuberger G, Eisenhaber F, Hermetter A, Zechner R (2004) Fat mobilization in adipose tissue is promoted by adipose triglyceride lipase. Science 306:1383–1386
4. Smirnova E, Goldberg EB, Makarova KS, Lin L, Brown WJ, Jackson CL (2006) ATGL has a key role in lipid droplet/adiposome degradation in mammalian cells. EMBO Rep 7:106–113
5. Miyosh H, Perfield JW, Souza SC, Shen WJ, Zhang HH, Stancheva ZS, Kraemer FB, Obin MS, Greenberg AS (2007) Control of adipose triglyceride lipase action by serine 517 of perilipin A globally regulates protein kinase A-stimulated lipolysis in adipocytes. J Biol Chem 282:996–1002
6. Haemmerle G, Zimmermann R, Strauss JG, Kratky D, Riederer M, Knipping G, Zechner R (2002) Hormone-sensitive lipase deficiency in mice changes the plasma lipid profile by affecting the tissue-specific expression pattern of lipoprotein lipase in adipose tissue and muscle. J Biol Chem 277:12946–12952
7. Villena JA, Roy S, Sarkadi-Nagy E, Kim KH, Sul HS (2004) Desnutrin, an adipocyte gene encoding a novel patatin domain-containing protein, is induced by fasting and glucocorticoids: ectopic expression of desnutrin increases triglyceride hydrolysis. J Biol Chem 279:47066–47075
8. Langin D, Dicker A, Tavernier G, Hoffstedt J, Mairal A, Ryden M, Arner E, Sicard A, Jenkins CM, Viguerie N, Van HV, Gross RW, Holm C, Arner P (2005) Adipocyte lipases and defect of lipolysis in human obesity. Diabetes 54:3190–3197
9. Kralisch S, Klein J, Lossner U, Bluher M, Paschke R, Stumvoll M, Fasshauer M (2005) Isoproterenol, TNFalpha, and insulin downregulate adipose triglyceride lipase in 3T3-L1 adipocytes. Mol Cell Endocrinol 240:43–49
10. Bilak SR, Bremner EM, Robson RM (1987) Composition of intermediate filament subunit proteins in embryonic, neonatal and postnatal porcine skeletal muscle. J Anim Sci 64:601–606
11. Hausman GJ, Kauffman RG (1986) The histology of developing porcine adipose tissue. J Anim Sci 63:642–658
12. Deiuliis JA, Li B, Lyvers-Peffer PA, Moeller SJ, Lee K (2006) Alternative splicing of delta-like 1 homolog (DLK1) in the pig and human. Comp Biochem Physiol B Biochem Mol Biol 145:50–59
13. Livak KJ, Schmittgen TD (2001) Analysis of relative gene expression data using real-time quantitative PCR and the 2(-Delta Delta C(T)) method. Methods 25:402–408
14. Fernyhough ME, Vierck JL, Hausman GJ, Mir PS, Okine EK, Dodson MV (2007) Primary adipocyte culture: adipocyte purification methods may lead to a new understanding of adipose tissue growth and development. Cytotechnology 46:163–172
15. Lee K, Villena JA, Moon YS, Kim KH, LeeS, Kang C, Sul HS (2003) Inhibition of adipogenesis and development of glucose intolerance by soluble preadipocyte factor-1 (Pref-1). J Clin Invest 111:453–461
16. Tontonoz P, Hu E, Spiegelman BM (1994) Stimulation of adipogenesis in fibroblasts by PPAR gamma 2, a lipid-activated transcription factor. Cell 79:1147–1156
17. Li B, Zerby HN, Lee K (2007) Heart fatty acid binding protein is upregulated during porcine adipocyte development. J Anim Sci 85:1651–1659
18. Hausman GJ, Poulos S (2004) Recruitment and differentiation of intramuscular preadipocytes in stromal-vascular cell cultures derived from neonatal pig semitendinosus muscles. J Anim Sci 82:429–437
19. Hausman GJ, Poulos SP (2005) A method to establish co-cultures of myotubes and preadipocytes from collagenase digested neonatal pig semitendinosus muscles. J Anim Sci 83:1010–1016
20. Hentges EJ, Hausman GJ (1989) Primary cultures of stromal-vascular cells from pig adipose tissue: the influence of

glucocorticoids and insulin as inducers of adipocyte differentiation. Domest Anim Endocrinol 6:275–285

21. Thompson JD, Gibson TJ, Plewniak F, Jeanmougin F, Higgins DG (1997) The CLUSTAL_X windows interface: flexible strategies for multiple sequence alignment aided by quality analysis tools. Nucleic Acids Res 25:4876–4882
22. Kershaw EE, Schupp M, Guan HP, Gardner NP, Lazar MA, Flier JS (2007) PPARg regulates adipose triglyceride lipase in adipocytes in vitro and in vivo. Am J Physiol Endocrinol Metab, Sep 11
23. Fischer J, Lefevre C, Morava E, Mussini JM, Laforet P, Negre-Salvayre A, Lathrop M, Salvayre R (2007) The gene encoding adipose triglyceride lipase (PNPLA2) is mutated in neutral lipid storage disease with myopathy. Nat Genet 39:28–30
24. Gronke S, Mildner A, Fellert S, Tennagels N, Petry S, Muller G, Jackle H, Kuhnlein RP (2005) Brummer lipase is an evolutionary conserved fat storage regulator in Drosophila. Cell Metab 1:323–330
25. Hausman GJ (1985) The comparative anatomy of adipose tissue. In: Cryer A, Van, RL (eds) New perspectives in adipose tissue: structure, function and development. Butterworths, London, pp 1–21
26. Bergen WG, Mersmann HJ (2005) Comparative aspects of lipid metabolism: impact on contemporary research and use of animal models. J Nutr 135:2499–2502
27. Schoenborn V, Heid IM, Vollmert C, Lingenhel A, Adams TD, Hopkins PN, Illig T, Zimmermann R, Zechner R, Hunt SC, Kronenberg F (2006) The ATGL gene is associated with free fatty acids, triglycerides, and type 2 diabetes. Diabetes 55:1270–1275
28. Kim JY, Tillison K, Lee JH, Rearick DA, Smas CM (2006) The adipose tissue triglyceride lipase ATGL/PNPLA2 is downregulated by insulin and TNF-alpha in 3T3-L1 adipocytes and is a target for transactivation by PPARgamma. Am J Physiol Endocrinol Metab 291:E115–E127
29. Haemmerle G, Lass A, Zimmermann R, Gorkiewicz G, Meyer C, Rozman J, Heldmaier G, Maier R, Theussl C, Eder S, Kratky D, Wagner EF, Klingenspor M, Hoefler G, Zechner R (2006) Defective lipolysis and altered energy metabolism in mice lacking adipose triglyceride lipase. Science 312:734–737
30. Manners MJ, McCrea MR (1963) Changes in the chemical composition of sow-reared piglets during the 1st month of life. Br J Nutr 17:495–513
31. McNeel RL, Ding ST, Smith EO, Mersmann HJ (2000) Expression of porcine adipocyte transcripts during differentiation in vitro and in vivo. Comp Biochem Physiol B Biochem Mol Biol 126:291–302
32. Abdallah BM, Jensen CH, Gutierrez G, Leslie RG, Jensen TG, Kassem M (2004) Regulation of human skeletal stem cells differentiation by Dlk1/Pref-1. J Bone Miner Res 19:841–852
33. Smas CM, Chen L, Sul HS (1997) Cleavage of membrane-associated pref-1 generates a soluble inhibitor of adipocyte differentiation. Mol Cell Biol 17:977–988
34. Moon YS, Smas CM, Lee K, Villena JA, Kim KH, Yun EJ, Sul HS (2002) Mice lacking paternally expressed Pref-1/Dlk1 display growth retardation and accelerated adiposity. Mol Cell Biol 22:5585–5592
35. Hart HA, Azain MJ, Hausman GJ, Reeves DE, Barb CR (2007) Failure of short-term feed restriction to affect luteinizing hormone and leptin secretion or subcutaneous adipose tissue expression of leptin in the prepuberal gilt. Can J Anim Sci 87:191–197
36. McNeel RL, Ding ST, Smith EO, Mersmann HJ (2000) Effect of feed restriction on adipose tissue transcript concentrations in genetically lean and obese pigs. J Anim Sci 78:934–942
37. McNeel RL, Mersmann HJ (2000) Nutritional deprivation reduces the transcripts for transcription factors and adipocyte-characteristic proteins in porcine adipocytes. J Nutr Biochem 11:139–146

Lipids (2008) 43:227–230
DOI 10.1007/s11745-007-3144-3

COMMUNICATION

Docking of Fatty Acids into the WIF Domain of the Human Wnt Inhibitory Factor-1

Tomas Malinauskas

Received: 10 September 2007 / Accepted: 4 December 2007 / Published online: 7 February 2008
© AOCS 2008

Abstract Palmitoylated Wnt proteins comprise a conserved family of secreted signaling molecules associated with variety of human cancers. WIF domain of the human WIF (Wnt inhibitory factor)-1 is sufficient for Wnt binding and signaling inhibition. Detailed interactions between Wnt and WIF-1 are not known. Computational docking was employed to identify a possible fatty acid binding site in the WIF domain. A putative binding site was identified inside the domain. WIF domain exhibited the highest affinity for C16:0–C18:0 (−22 kJ/mol free energy of binding) fatty acids. The results suggest a role of the WIF domain as a palmitoyl binding domain required for WIF-1 binding to palmitoylated Wnt and signaling inhibition.

Keywords Wnt inhibitory factor-1 · WIF domain · Wnt · Lipoprotein · Signaling · Palmitoylation · Docking · Fatty acids · Cancer

Electronic supplementary material The online version of this article (doi:10.1007/s11745-007-3144-3) contains supplementary material, which is available to authorized users.

T. Malinauskas
Faculty of Chemistry, Vilnius University,
Naugarduko 24, LT-03225 Vilnius, Lithuania

T. Malinauskas (✉)
Division of Structural Biology, University of Oxford,
The Henry Wellcome Building for Genomic Medicine,
Roosevelt Drive, Oxford OX3 7BN, UK
e-mail: tomas.malinauskas@gmail.com; tomas@strubi.ox.ac.uk

Introduction

Palmitoylated wingless-type (Wnt) proteins comprise a conserved family of secreted signaling molecules [1]. They play key roles during embryogenesis and adult tissue homeostasis. Canonical Wnt proteins bind to the Frizzled (Fz)/low-density-lipoprotein-receptor-related protein (LRP) complex at the target cell surface (Fig. 1). These cell surface receptors can transduce a signal through several cytoplasmic proteins eventually leading to the transcription of target genes. Aberrant regulation of the Wnt pathway is associated with variety of human cancers and degenerative diseases [2].

Wnt antagonists interrupt binding of Wnts to their receptors [3]. Antagonists form two functional classes. Members of the sFRP class (which includes secreted Frizzled-related proteins (sFRP) [4], WIF (Wnt inhibitory factor)-1 [5–10] and Cerberus [11]) bind to the Wnt proteins and inhibit their ability to interact with the receptor complex. Members of the Dickkopf class [12] inhibit Wnt signaling by binding to the LRP component of the Wnt receptor complex. Interactions between Wnts and their antagonists remain elusive due to the lack of tertiary structures.

The Wnt inhibitory factor-1 is a secreted protein of 379 amino acid residues that binds to palmitoylated Wnt protein and inhibits its activity [5]. WIF domain (about 140 residues) of WIF-1 is sufficient for Wnt binding and signaling inhibition. The tertiary structure of the WIF domain was solved using NMR spectroscopy [6]. The unexpected association between detergent Brij-35 [dodecylpoly(ethyleneglycolether)$_{23}$] and the WIF domain suggests its affinity for alkyl chains and palmitoylated Wnts. Removal of the palmitate leads to the loss of Wnt activity. Wnt proteins are difficult to purify due to inefficient secretion [13], high degree of insolubility [1]; the WIF domain tends to precipitate [6]. Thus detailed interactions between

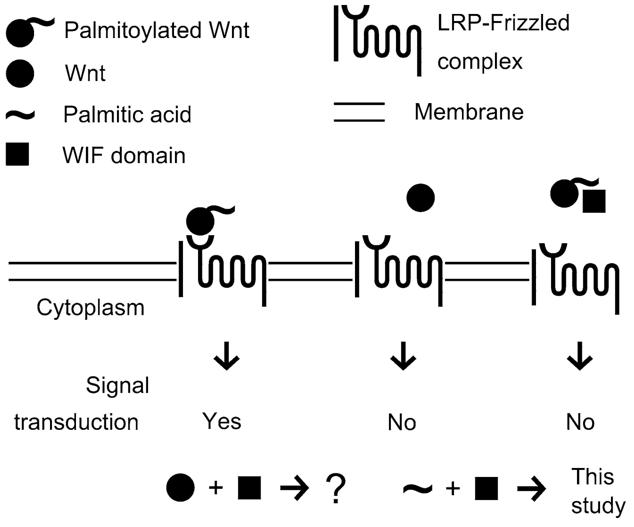

Fig. 1 Role of palmitoylation in Wnt signaling. Canonical Wnt signaling pathway is initiated when palmitoylated Wnt binds to the Frizzled and LRP5/6 receptor complex at the cell surface. Loss of palmitoyl or presence of WIF domain leads, by unknown mechanism, to inactivation of signal transduction. This study aims to propose thermodynamically favorable interactions between palmitoylated Wnt and WIF domain

palmitoylated Wnt and WIF-1 remain hardly approachable by traditional biochemical methods. Computational studies presented here aim to determine a possible fatty acid binding site in the WIF domain and propose thermodynamically favorable interactions in the Wnt signaling pathway associated with variety of cancers and intercellular communication.

Experimental Procedures

Twenty conformers representing the NMR structure of the WIF domain of the human WIF-1 were downloaded from the Protein Data Bank (PDB ID code 2D3J). The average structure of 20 conformers was calculated and each conformer was aligned with it individually. The RMSD (root mean square deviation) between the average structure and individual conformers was calculated. The best fitting (lowest all-atom RMSD value, 0.57 Å) conformer (MODEL 1 from 2D3J file) was selected for docking studies. As a control experiment, palmitic acid (C16:0) was docked with all of the 20 WIF domain conformers. The same fatty acid binding site with similar C16:0 conformations and free energy of binding ($\Delta G_{\text{binding}}$) was identified in all of the 20 WIF domain conformers (Supplementary Fig. 1).

Structures of fatty acids were constructed manually using program ACD/ChemSketch 10.02. Energy minimization of the three-dimensional structures was performed using CHARMM force field [14] as implemented in the ChemSketch prior to docking.

Molecular docking was carried out using program AutoDock 4.0 [15] in order to identify possible binding sites and conformations of fatty acids, estimate $\Delta G_{\text{binding}}$. The estimation function of $\Delta G_{\text{binding}}$ is based on an empirical function derived by linear regression analysis of a set of diverse protein-ligand complexes with known inhibition constants in the AutoDock 4.0. All torsions of fatty acids except double bonds were unconstrained during the docking. The protein was treated as a rigid body. Docking was accomplished using the Lamarckian genetic algorithm (LGA) with the following modifications of the default parameters leading to higher accuracy of calculations. Atomic interaction energy grid maps were calculated with 0.3 Å (the default is 0.375 Å) grid spacing. The WIF domain was placed in a 39 × 90 × 39 Å box. The space of the box covered the whole WIF domain and the space beyond. Thus identification of the fatty acid binding site both on the surface and inside the domain was possible. A hundred conformers of each fatty acid were generated during the docking experiment (Suppl. Fig. 2). The maximum number of energy evaluations was set to 1×10^6.

Results and Discussion

To aid the experimental analysis of interactions between the palmitoylated protein Wnt and its antagonist WIF-1, binding of fatty acids to the available tertiary structure of the WIF domain was investigated. The surface of the WIF domain was probed to identify sites that are energetically most favorable for interaction with the flexible ligand.

Fatty acid docking revealed no binding sites at the outer surface of the WIF domain. A hydrophobic binding site was observed between hydrophobic residues of strand 4 (Phe65, Trp67) and 8 (Val128/130/132) surrounded by Leu12, Leu14 and Val110 inside the domain (Fig. 2). Residues Phe65 and Trp67 are highly conserved within the WIF domains (also identified in the extracellular domains of Ryk (receptor-like tyrosine kinase) [16], Wnt binding protein) although their function remains unknown. Leu12 is not associated with any secondary structure element and may serve as a flexible boundary of the entry point for alkyl chain into the hydrophobic site.

Free energies of fatty acid binding to the WIF domain were estimated. $\Delta G_{\text{binding}}$ decreased gradually from approx. −14 to −22 kJ/mol for saturated fatty acids C8:0–C16:0 (Fig. 3). A steady increase of $\Delta G_{\text{binding}}$ was observed for fatty acids with a longer alkyl chain. Unfavorable $\Delta G_{\text{binding}}$ for longer acids might be explained by steric hindrances between limited-size binding site and fatty acids. It is noteworthy that the lowest $\Delta G_{\text{binding}}$ of approx. −22 kJ/mol was observed for C16:0–C18:0 in case

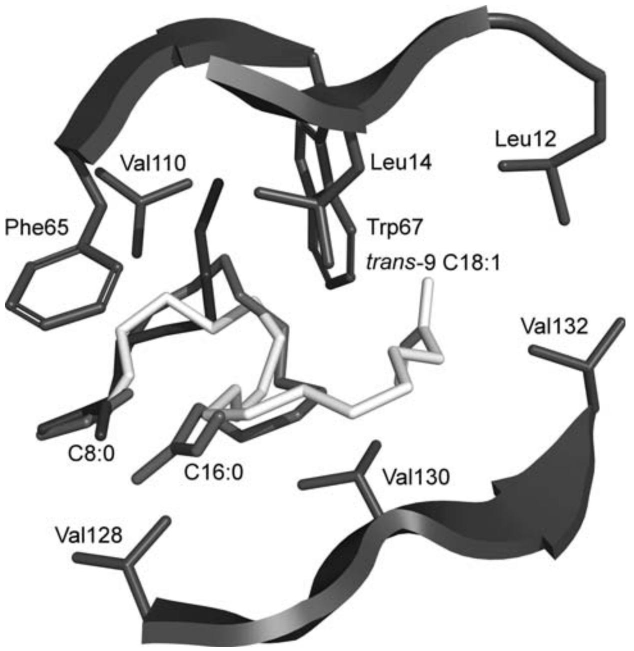

Fig. 2 Docking of fatty acids inside the hydrophobic site of the WIF domain. *Light grey arrows* represent fragments of the β-strands 1 (Leu14), 4 (Phe65, Trp67), and 8 (Val128/130/132) [6]. Carbon backbone and carboxyl group of the C8:0 (−14.6 kJ/mol), C16:0 (palmitic acid, −24.9 kJ/mol), and *trans*-9 C18:1 (−24.5 kJ/mol) lowest $\Delta G_{\text{binding}}$ solutions are shown as *black*, *grey* and *light grey stick* models, respectively. Coordinates of the complex are provided as the electronic supplementary material (PDB file)

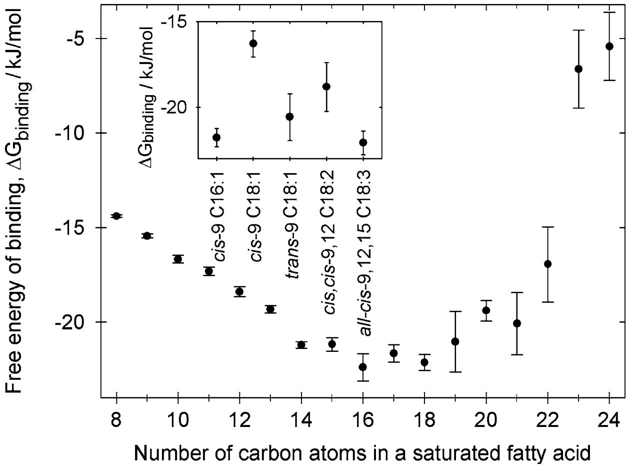

Fig. 3 Free energy of binding between the WIF domain and various fatty acids. The *inset* shows $\Delta G_{\text{binding}}$ for unsaturated fatty acids. Average values were derived from five fatty acid conformers exhibiting the lowest $\Delta G_{\text{binding}}$. RMSD between five lowest energy conformers increased from 0.75 to 2.9 Å with increasing length of fatty acid chain (C8–C24) (Suppl. Fig. 3). The height of the *error bar* is equal to the standard deviation in all of the figures

of saturated fatty acids. This suggests that the WIF domain might serve as the palmitoyl binding domain during the binding between palmitoylated Wnt and WIF-1.

No significant differences in the $\Delta G_{\text{binding}}$ between even and odd chain fatty acids were observed. The influence of double C-C bonds on $\Delta G_{\text{binding}}$ remained negligible in the case of C16:0 versus *cis*-9 C16:1 (Fig. 3, an inset). Interestingly, the *trans*-9 C18:1 lowest energy conformer exhibited the $\Delta G_{\text{binding}}$ of −24.5 kJ/mol (Fig. 2) while the corresponding *cis*-9 C18:1 conformer docked with the $\Delta G_{\text{binding}}$ of −18.2 kJ/mol. The identified differences between C18 fatty acid isomers probably could be explained by limitations of the program as no specific interactions between double C-C bond and WIF domain were observed (Fig. 2). However, it is tempting to speculate that Wnt signaling might be regulated using alternative saturated or unsaturated alkyl chains on the Wnt proteins.

To summarize, the putative fatty acid binding site was identified inside the WIF domain of the Wnt antagonist human WIF-1 using the computational docking method. The WIF domain exhibited the highest affinity for C16:0–C18:0 (−22 kJ/mol free energy of binding). The results suggest a possible role of the WIF domain as a palmitoyl binding domain required for WIF-1 binding to palmitoylated Wnt. Although molecular docking and NMR studies indicate high affinity of the WIF domain for alkyl chains, determination of the tertiary structure of palmitoylated Wnt in complex with its antagonist WIF-1 are highly desirable for the understanding of Wnt signaling pathway.

References

1. Willert K, Brown JD, Danenberg E, Duncan AW, Weissman IL, Reya T, Yates JR 3rd, Nusse R (2003) Wnt proteins are lipid-modified and can act as stem cell growth factors. Nature 423:448–452. doi:10.1038/nature01611
2. Logan CY, Nusse R (2004) The Wnt signaling pathway in development and disease. Annu Rev Cell Dev Biol 20:781–810. doi:10.1146/annurev.cellbio.20.010403.113126
3. Kawano Y, Kypta R (2003) Secreted antagonists of the Wnt signalling pathway. J Cell Sci 116:2627–2634. doi:10.1242/jcs.00623
4. Jones SE, Jomary C (2002) Secreted frizzled-related proteins: searching for relationships and patterns. Bioessays 24:811–820. doi:10.1002/bies.10136
5. Hsieh JC, Kodjabachian L, Rebbert ML, Rattner A, Smallwood PM, Samos CH, Nusse R, Dawid IB, Nathans J (1999) A new secreted protein that binds to Wnt proteins and inhibits their activities. Nature 398:431–436. doi:10.1038/18899
6. Liepinsh E, Banyai L, Patthy L, Otting G (2006) NMR structure of the WIF domain of the human Wnt-inhibitory factor-1. J Mol Biol 357:942–950. doi:10.1016/j.jmb.2006.01.047
7. Hunter DD, Zhang ML, Ferguson JW, Koch M, Brunken WJ (2004) The extracellular matrix component WIF-1 is expressed during, and can modulate, retinal development. Mol Cell Neurosci 27:477–488. doi:10.1016/j.mcn.2004.08.003
8. Lin YC, You L, Xu Z, He B, Yang CT, Chen JK, Mikami I, Clement G, Shi Y, Kuchenbecker K, Okamoto J, Kashani-Sabet M, Jablons DM (2007) Wnt inhibitory factor-1 gene transfer inhibits melanoma cell growth. Hum Gene Ther 18:379–386. doi:10.1089/hum.2006.005

9. Chan SL, Cui Y, van Hasselt A, Li H, Srivastava G, Jin H, Ng KM, Wang Y, Lee KY, Tsao GS, Zhong S, Robertson KD, Rha SY, Chan AT, Tao Q (2007) The tumor suppressor Wnt inhibitory factor 1 is frequently methylated in nasopharyngeal and esophageal carcinomas. Lab Invest 87:644–650. doi:10.1038/labinvest.3700547
10. Queimado L, Lopes CS, Reis AM (2007) WIF-1, an inhibitor of the Wnt pathway, is rearranged in salivary gland tumors. Genes Chromosomes Cancer 46:215–225. doi:10.1002/gcc.20402
11. Piccolo S, Agius E, Leyns L, Bhattacharyya S, Grunz H, Bouwmeester T, De Robertis EM (1999) The head inducer Cerberus is a multifunctional antagonist of Nodal, BMP and Wnt signals. Nature 397:707–710. doi:10.1038/17820
12. Glinka A, Wu W, Delius H, Monaghan AP, Blumenstock C, Niehrs C (1998) Dickkopf-1 is a member of a new family of secreted proteins and functions in head induction. Nature 391:357–362. doi:10.1038/34848
13. Bradley RS, Brown AM (1995) A soluble form of Wnt-1 protein with mitogenic activity on mammary epithelial cells. Mol Cell Biol 15:4616–4622
14. Brooks BR, Bruccoleri RE, Olafson BD, States DJ, Swaminathan S, Karplus M (1983) CHARMM: A program for macromolecular energy, minimization, and dynamics calculations. J Comput Chem 4:187–217. doi:10.1002/jcc.540040211
15. Morris GM, Goodsell DS, Halliday RS, Huey R, Hart WE, Belew RK, Olson AJ (1998) Automated docking using a Lamarckian genetic algorithm and an empirical binding free energy function. J Comput Chem 19:1639–1662. doi:10.1002/(SICI)1096-987X(19981115)19:14<1639::AID-JCC10>3.0.CO;2-B
16. Patthy L (2000) The WIF module. Trends Biochem Sci 25:12–13. doi:10.1016/S0968-0004(99)01504-2

Lipids (2008) 43:231–241
DOI 10.1007/s11745-007-3142-5

ORIGINAL ARTICLE

Oral Nanoparticulate Atorvastatin Calcium is More Efficient and Safe in Comparison to Lipicure® in Treating Hyperlipidemia

A. K. Meena · D. Venkat Ratnam · G. Chandraiah · D. D. Ankola · P. Rama Rao · M. N. V. Ravi Kumar

Received: 8 October 2007 / Accepted: 23 November 2007 / Published online: 10 January 2008
© AOCS 2007

Abstract Atorvastatin calcium (AC) is a second-generation 3-hydroxy-3-methylglutaryl-CoA reductase inhibitor approved for clinical use as a lipid lowering agent. AC, the world's best selling drug is associated with poor oral bioavailability and serious adverse effects like rhabdomyolysis on chronic administration. A biodegradable nanoparticulate approach was introduced here with a view to improving the efficacy and safety of AC. Poly lactide-*co*-glycolic acid (PLGA) nanoparticles containing atorvastatin calcium were prepared using two stabilizers i.e. didodecyl dimethyl ammonium bromide (DMAB) and Vitamin E tocopheryl polyethylene glycol 1000 succinate (Vit E-TPGS) using a co-solvent approach by emulsion–diffusion–evaporation method. AC loaded PLGA nanoparticles prepared using DMAB and Vit E-TPGS were found to be 120.0 ± 4.2 nm and 140.0 ± 1.5 nm (z-average) in size respectively. In vitro release studies at pH 7.4 revealed a zero order release profile for nanoparticles. Efficacy and safety parameters of the prepared nanoparticles against marketed formulation were evaluated in high fat diet fed (hyperlipidemic) rats. It was found that atorvastatin calcium nanoparticles were equally effective in comparison to Lipicure®, at a 66%-reduced dose in treating the hyperlipidemia characterized by alterations in PTC, LDL-C, VLDL-C, HDL-C, PTG and PGL in the high fat diet fed rats. On the other hand, when evaluated for safety, nanoparticulate formulation showed no/negligible myotoxicity characterized by lower PC, BUN, CK, LDH and AST levels in comparison to the marketed formulation.

Keywords Bioavailability · Hyperlipidemia · Nanoparticles · Oral delivery · Rhabdomyolysis

Abbreviations

AC	Atorvastatin calcium
AST	Aspartate amino transferase
BUN	Blood urea nitrogen
PTC	Plasma total cholesterol
PTG	Plasma triglyceride
LDL-C	Low-density lipoprotein cholesterol
HDL-C	High-density lipoprotein cholesterol
VLDL-C	Very low-density lipoprotein cholesterol
CK	Creatinine kinase
LDH	Lactate dehydrogenase
PC	Plasma creatinine
NPD	Normal pellet diet
HFD	High fat diet

Introduction

Statins are the treatment of choice for the management of hyperlipidemia because of their proven efficacy.

A. K. Meena · D. V. Ratnam · D. D. Ankola ·
M. N. V. R. Kumar (✉)
Department of Pharmaceutics,
National Institute of Pharmaceutical Education
and Research (NIPER), Phase-X, S. A. S. Nagar,
Punjab 160062, India
e-mail: mnvrkumar@niper.ac.in; mnvrkumar@yahoo.com

G. Chandraiah · P. R. Rao
Department of Pharmacology and Toxicology,
National Institute of Pharmaceutical Education
and Research (NIPER), Phase-X, S. A. S. Nagar,
Punjab 160062, India

G. Chandraiah · D. D. Ankola · P. R. Rao · M. N. V. R. Kumar
Center for Pharmaceutical Nanotechnology,
National Institute of Pharmaceutical Education
and Research (NIPER), Phase-X, S. A. S. Nagar,
Punjab 160062, India

Atorvastatin, the leading drug among statins, inhibits the enzyme 3-hydroxy-3-methyl-glutaryl coenzyme A (HMG CoA) reductase resulting in reduced cholesterol synthesis. The salt form of the drug, atorvastatin calcium is most widely used for the treatment of hyperlipidemia. The statin market is increasing globally because of the associated risk of cardiovascular disorders with elevated lipid profiles.

All the drug candidates of statin group exhibit varied absorption rates upon oral administration. The oral absorption of atorvastatin is 30% and bioavailability is only 12% [1]. Atorvastatin is absorbed primarily from the intestine and to a lesser extent from the stomach and presystemic metabolism is the major cause for the poor bioavailability. Lau et al. [2] showed that saturable transport system involves in the hepatic uptake of atorvastatin in rats in vivo. Metabolic studies in animals revealed that more than 98% of the dose of atorvastatin was recovered in the feces within 48 h [3]. It was also reported that atorvastatin is metabolized extensively by cytochrome P-450 3A4 which was found extensively in the gut wall and liver [4].

Patients under statin treatment sometimes suffer from a number of serious adverse effects such as myopathy and rhabdomyolysis. The incidence of statin-induced rhabdomyolysis is low in clinical trials in which high risk patients were excluded. However, increased scrutiny shows that the incidence is higher when applied outside of these trials [5, 6]. The detailed mechanism is unknown but it was suggested that inhibition of HMG-CoA reductase may directly cause this myotoxicity [7]. It was thought that the exposure of statins to extrahepatic tissues leads to adverse effects, with diminutive pharmacological effect [8]. The most common explanations include the deficiency of one of three main end products: cholesterol deficiency with secondary abnormal membrane behavior, coenzyme Q_{10} deficiency causing abnormal mitochondrial respiratory function, or prenylated protein abnormalities causing imbalances in intracellular protein messaging [9]. The root cause is related to increased distribution or accumulation of atorvastatin calcium in the muscles.

We hypothesize that oral nanoparticulate formulations by virtue of their unique uptake mechanism and sustained release of the loaded drug would improve the efficacy of atorvastatin and at the same time reduce the associated side effects. Therefore, the present work deals with the development of atorvastatin calcium nanoparticles using a biodegradable polymer, poly(lactide-*co*-glycolate) (PLGA) and their evaluation in hyperlipidemic rats for efficiency as well as safety.

Experimental Procedure

Nanoparticle Preparation and Characterization

Nanoparticles of AC were prepared by an emulsion–diffusion–evaporation technique with modifications [10]. AC has poor solubility in routinely used organic solvents, thus a co-solvent approach was adopted to formulate nanoparticles using poly(ethylene glycol) 400 (PEG 400) (S.d. fine-chem, India). 0.5 ml PEG 400 was used to dissolve required amount of AC (2.5–25 mg) while 50 mg PLGA (50:50) molecular weight 38,400 Da (Boehringer Ingelheim, Germany) was dissolved in 2.5 ml ethyl acetate followed by mixing both the solutions (organic phase) at room temperature. The organic phase was then added to the 5 ml aqueous phase containing either DMAB (Aldrich, USA) or Vit E-TPGS (Peboc, UK) as stabilizer at 1% *w*/*v* strength. This is homogenized at 15,000 rpm for 5 min using a high-speed homogenizer (Polytron PT4000, Switzerland) to form emulsion. The organic solvent was allowed to diffuse overnight at room temperature, which was facilitated by adding 20 ml water. The prepared nanoparticles were characterized using a zeta sizer (Nano ZS, Malvern Instruments, Malvern, UK) for size (average of 5 measurements for one batch) and zeta potential (average of 20 measurements for a batch). Three batches with each stabilizer were prepared in the same manner. The surface morphology of nanoparticles was analyzed by AFM (Veeco Bioscope II) that was attached with a Nikon eclipse TE 2000-S microscope. The system was run by Nanoscope software. The nanoparticles suspension was placed on the silicon wafer with the help of a micropipette and allowed to dry in air. The microscope was vibration damped and measurements were made using commercial pyramidal Si_3N_4 tip (Veeco's CA, USA). The cantilever used for scanning had a length of 325 μm and a width of 26 μm with a nominal force constant 0.1 N/m.

The drug-loading was optimized by preparing the particles at different initial loadings (5–50% *w*/*w* of polymer). Entrapment efficiency is the percentage of drug incorporated in the nanoparticles. It was determined by centrifuging (25,000*g* and 10,000*g* for 5 min, respectively, for DMAB and Vit E-TPGS stabilized nanoparticles) the drug-loaded nanoparticles and separating the supernatant and pellet. The pellet was washed and dissolved in ethyl acetate followed by extraction of the drug. The drug content in the pellet and supernatant were analyzed using a validated HPLC method [11].

In Vitro Drug Release Studies

The release of atorvastatin calcium from the nanoparticles was determined by a dialysis membrane method. Freshly made PLGA nanoparticles of DMAB or Vit E-TPGS (single batch is approximately 20 ml), were centrifuged (at 25,000*g* for DMAB and 10,000*g*, for 5 min, for Vit E-TPGS stabilized particles) and redispersed in 2 ml of phosphate buffer and put in the dialysis bags (Sigma) with a molecular mass cut-off of 12,000 Da. The bags were suspended in vials containing 5 ml phosphate buffer (pH 7.4). All the vials were kept in a shaking water bath maintained at 37 °C and 100 rpm. The release medium was completely replaced with 10 mM phosphate buffer at predetermined intervals of 2, 4, 6, 8, 12 and 24 h on first day followed by sampling at 24 h interval every day till the release was observed. The amount of atorvastatin calcium released in the medium was estimated using HPLC method.

Animals

Male Sprague-Dawley (SD) rats (180–200 g) were procured from the central animal facility of the Institute. The animals were housed in standard polypropylene cages (three rats/cage) and maintained under controlled room temperature (22 ± 2 °C) and humidity (55 ± 5%) with 12 h light and 12 h dark cycle. All the rats were fed with commercially available rat normal pellet diet (NPD) (Amrut Diet, New Delhi) and water ad libitum, prior to the dietary manipulation. The guidelines of committee for the purpose of control and supervision of experiments on animals (CPCSEA), Government of India were followed and prior permission was sought from the institutional animal ethics committee for conducting the study.

Development of Hyperlipidemic Rats

Except for the control group, which was fed NPD all the other group animals were fed high fat diet (HFD). The HFD comprises 58% fat, 25% protein and 17% carbohydrate, as a percentage of total kcal. The composition is described in Table 1 and preparation of HFD is described elsewhere [12].

Experimental Design

The rats were divided into seven groups of *n* = 6. One group received NPD and all other groups received HFD. Groups receiving HFD were again divided into no treatment, and treatment groups. After 4 weeks, the animals were treated with Lipicure® (HLI), AC loaded nanoparticles of DMAB (HAD) & Vit E-TPGS (HAE), and blank nanoparticles of DMAB (HBD) & Vit E-TPGS (HBE). Treatment was carried out for 2 weeks till the end of the sixth week. Drug treatment groups (HLI, HAD & HAE) received a dose of atorvastatin calcium equivalent to 3 mg/kg atorvastatin, through the oral route using an oral gavage needle. The blank nanoparticle groups (HBD & HBE) received the blank nanoparticles containing an equivalent polymer amount, which was associated with the AC nanoparticle dose. Dosing frequency was once every 3 days in the case of nanoparticles and daily for the commercial formulation (Table 2). Blood sampling was done after two, four, six, seven, and eight weeks and various biochemical parameters related to hyperlipidemia and atorvastatin toxicity were studied.

Table 1 Composition of high fat diet

Ingredients	Diet (g/kg)
Powdered NPD	365
Lard	310
Casein	250
Cholesterol	10
Vitamin and mineral mix	60
DL-Methionine	03
Sodium chloride	01
Yeast powder	01

Estimation of Biochemical Parameters

Plasma total cholesterol levels (PTC), plasma triglyceride levels (PTG), high-density lipoprotein cholesterol (HDL-C), plasma glucose levels (PGL), plasma creatinine levels (PC), blood urea nitrogen levels (BUN) were estimated using commercially available diagnostic kits (Accurex® kits,). Plasma enzyme activities of creatinine kinase (CK), lactate dehydrogenase (LDH) and aspartate transaminase

Table 2 Treatment regimen applied for hyperlipidemic rat model

Group	Frequency of dosing	AC dose (mg/kg)	Total AC Dose[a] (mg)
NPD	–	–	–
HFD	–	–	–
HLI	Daily	3	11.25
HAD	Once every 3 days	3	3.75
HAE	Once every days	3	3.75
HBD	Once every 3 days	–	–
HBE	Once every 3 days	–	–

[a] Dose for a 250 g body weight rat for 15 days

(AST) were estimated using commercially available diagnostic kits (Pointe Scientific Inc., USA and Crest Biosystems, India, respectively). Low-density lipoprotein cholesterol (LDL-C) levels were calculated using the Friedewald formula [13].

Results and Discussion

Nanoparticle Preparation and Characterization

Previous reports from our laboratory clearly indicate that water insoluble drugs can be efficiently loaded onto PLGA nanoparticles using various surfactants [10, 14–17]. However, considering the poor solubility of AC in common organic solvents used to make nanoparticles, a co-solvent approach [10] was adopted with suitable modifications. The particle preparation process was optimized for varied drug loading using DMAB and Vit E-TPGS as surfactants. The previous findings from our laboratory indicate that DMAB can lead to particles of about 80–200 nm in size irrespective of the polymer molecular weight, copolymer composition and the drug used [15–17] depending upon the process conditions. Furthermore, the studies indicate that the in vivo fate of these carrier systems is strongly influenced by their size, where the circulation times were thought to be dictated by their size and the release profiles by molecular weight and copolymer composition [16]. On the other hand, literature reports indicate that Vit E-TPGS is a surfactant with the natural ability to increase the absorption across the GIT [18–20], therefore, Vit E-TPGS was used as a second surfactant to make the AC loaded particles and compared with the particles made of DMAB for their efficacy. The blank particles (without the drug) made of DMAB and Vit E-TPGS as surfactants were found to be in the size range of 95 and 201 nm, respectively, whereas a slight increase in the size was observed for the drug loaded particles with DMAB as surfactant, which corroborates our previous findings as well as the literature reports that drug loading would add on to the size [10, 15, 16, 20–22]. However, such effect was not seen with Vit E-TPGS, rather a drastic decrease in the particle size was observed, which remains to be understood (Table 3). The zeta potential values of the particles are indicative of the surfactant nature, where, DMAB lead to cationic particles on contrary Vit E-TPGS resulted in negatively charged particles. The polydispersity index for both the formulations indicates the preparations have a very narrow polydispersity, the characteristic highly desirable in drug delivery applications (Table 3). Furthermore, these particles were characterized by Atomic Force Microscope for shape and size and the results obtained clearly indicate that the particles are spherical in shape with smooth surfaces (Fig. 1) and the size of the particles was comparable with that of the size obtained by zeta sizer measurements.

In Vitro Release Studies

Nanoparticles were prepared using a biocompatible and biodegradable copolymer PLGA. The release of drug from the biodegradable particles occurs through several mechanisms of which the release mediated through (1) diffusion (2) surface erosion (3) bulk degradation and (4) a combined degradation/diffusion process are of importance [22]. No initial burst effect was observed with either of the formulations prepared using DMAB and Vit E-TPGS as the surfactant. A constant release rate for a period of 30 days was observed at an average release rate of 85.01 and 87.55 μg/day for DMAB and Vit E-TPGS particles, with 50% of the drug being released in 15 days (Fig. 2a, b). The cumulative release was fitted into different release models: zero order, first order, Higuchi's square root plot, and Hixon–Crowell cube root plot. The model giving a correlation coefficient close to unity was taken as the order of release. A zero order release pattern was observed with DMAB and Vit E-TPGS stabilized nanoparticles with r^2 of 0.990 and 0.987. We have also fitted the data for the first part of the release curve ($M_t/M_\infty < 0.6$) into the Korsmeyer-Peppas equation ($M_t/M_\infty = Kt^n$) and we got n values of 0.367 and

Table 3 Characteristics of the nanoparticles used in the present study

Parameters	Blank nanoparticles		AC loaded nanoparticles[b]	
	DMAB	TPGS	DMAB	TPGS
Size (nm)	95.6 ± 4.8	201.0 ± 2.6	120.0 ± 4.2	140.0 ± 1.5
Polydispersity index	0.310 ± 0.005	0.170 ± 0.004	0.126 ± 0.007	0.150 ± 0.020
Zeta potential[a] (mV)	119.0 ± 2.6	−17.3 ± 5.5	70.0 ± 2.3	−16.6 ± 1.2
Entrapment efficiency (%)	–	–	37.82 ± 6.40	34.54 ± 1.96

Values are depicted as mean ± SD (*n* = 6)

[a] pH of the nanoparticles was in the range of 4.5–6.0

[b] Initial drug loading is 20% *w*/*w* of polymer

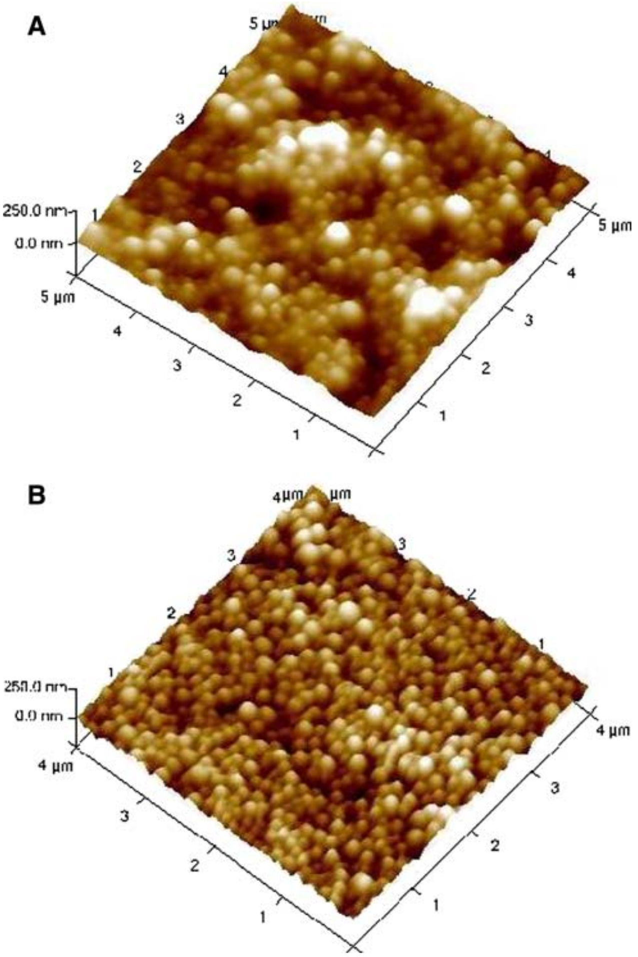

Fig. 1 Atomic force micrographs of atorvastatin calcium loaded nanoparticles prepared using DMAB (**a**) and Vit E-TPGS (**b**) as the stabilizer

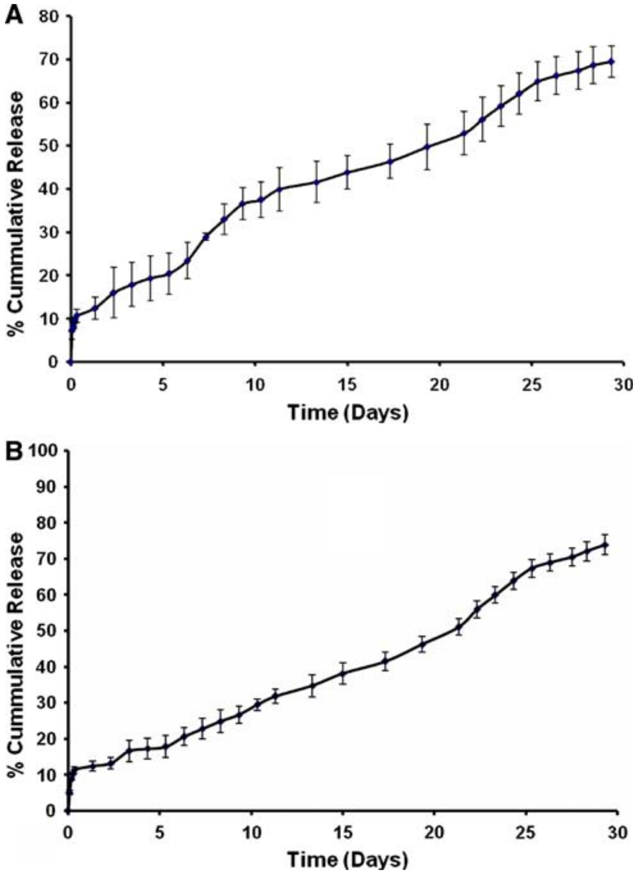

Fig. 2 In vitro release of atorvastatin calcium from DMAB (**a**) and vit E-TPGS (**b**) particles in phosphate buffer at pH 7.4 and values are depicted as mean ± SD ($n = 3$)

0.366 for DMAB and Vit E-TPGS particles, however the regression was very poor with r^2 0.928 and 0.892, respectively, making it difficult to comment on the mechanism of the drug release. M_t/M_∞ is the fraction of drug released up to time t, K is the kinetic constant and n is the release exponent indicative of the release mechanism. From the values, it can only be understood that the mechanism by which the drug was released is non-Fickian. The chances are more towards a non-fickian case II release because of the good r^2 value obtained with the zero order profile.

Traditionally, polymers that undergo surface erosion (polyanhydrides) are expected to release the entrapped drug at zero-order rate, where degradation and release show a strong correlation, in contrast, polymers that undergo bulk erosion (PLGA) are expected to release the entrapped drug primarily by diffusion followed by degradation showing a weak correlation between the degradation and release profile [22, 23]. However, no study has been reported in the literature, to see if the final manipulation of those surface-eroding and bulk-eroding polymers into implants, microparticles, nanoparticles would change the fate of release kinetics. A series of studies conducted in our laboratory as well as by other workers with many water insoluble drugs using PLGA in the form of nanoparticles did show zero-order release profiles [14, 16, 17]. On the other hand, we did observe a Higuchi release pattern for molecules like ellagic acid, where the particles were made by a co-solvent approach leading us to conclude that the incorporation of PEG-400 would have made the difference [10, 21]. However, the present study with AC nanoparticles demonstrating the zero-order release profile does not support the foregoing statement. Taking together all the possibilities, it appears that the drug release kinetics is not only influenced by the polymer, but also by the final form of the product (implant, nano-microparticle), the drug, preparation process, sink conditions, sample withdrawal (aliquot or complete replacement of the medium) etc. On a different note, in vitro release studies with polymeric particulate systems might not be of real significance, considering the difficulties involved in establishing IVIVC,

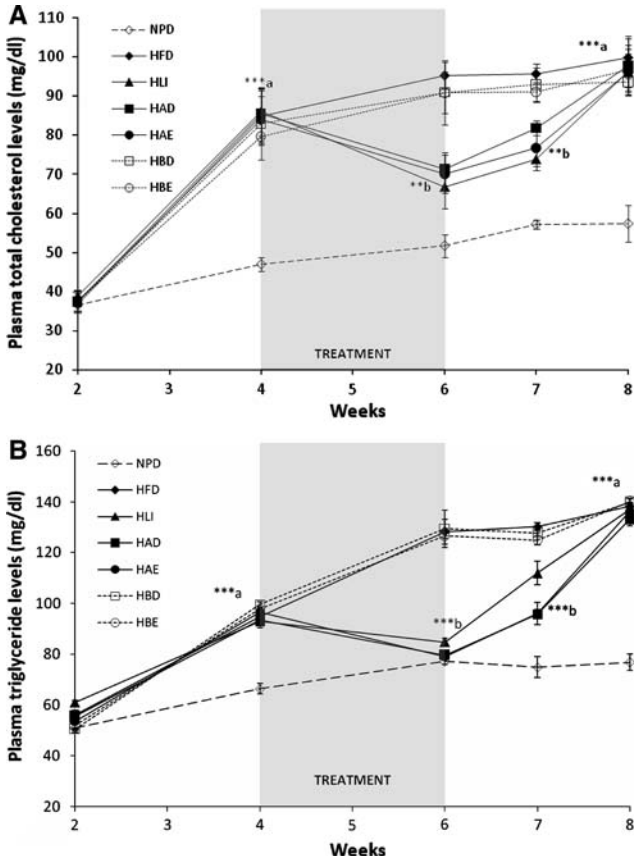

Fig. 3 Plasma total cholesterol levels (**a**) and plasma triglyceride levels (**b**). NPD- normal pellet diet, HFD- high fat diet only, HLI- hyperlipidemic rats treated with commercial formulation (Lipicure®), HAD- hyperlipidemic rats treated with DMAB stabilized nanoparticles of AC, HAE- hyperlipidemic rats treated with Vit E-TPGS stabilized nanoparticles, HBD- hyperlipidemic rats treated with blank DMAB stabilized nanoparticles, HBE- hyperlipidemic rats treated with blank TPGS stabilized nanoparticles. Values are depicted as mean ± SEM ($n = 6$). ***$P < 0.001$, **$P < 0.01$; **a** NPD versus all other groups; **b** HFD versus HLI, HAD and HAE at same week

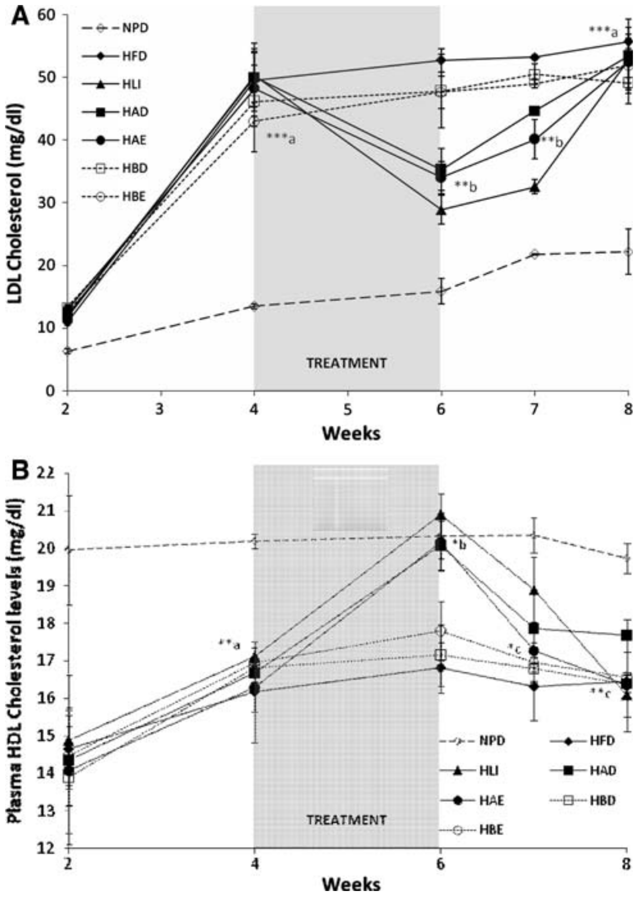

Fig. 4 Plasma LDL-cholesterol levels (**a**) and HDL-cholesterol levels (**b**). NPD- normal pellet diet, HFD- high fat diet only, HLI- hyperlipidemic rats treated with commercial formulation (Lipicure®), HAD- hyperlipidemic rats treated with DMAB stabilized nanoparticles of AC, HAE- hyperlipidemic rats treated with Vit E-TPGS stabilized nanoparticles, HBD- hyperlipidemic rats treated with blank DMAB stabilized nanoparticles, HBE- hyperlipidemic rats treated with blank TPGS stabilized nanoparticles. Values are depicted as mean ± SEM ($n = 6$). ***$P < 0.001$, **$P < 0.01$, *$P < 0.05$; **a** NPD versus all other groups; **b** HFD versus HLI, HAD, HAE and NPD; **c** NPD versus HFD, HLI, HAE, HBD and HBE at same week

nevertheless, such studies would certainly give an insight for new polymers that are synthesized.

In Vivo Efficacy Parameters

The study revealed that after 4 weeks of HFD treatment the biochemical parameters PTC, PTG (Fig. 3a, b), and LDL-C levels were elevated, where as HDL-C levels decreased significantly (Fig. 4a, b). The plasma glucose levels were also elevated with this treatment (Fig. 5). During the forth and sixth weeks different groups were treated as described in Table 2. Competitive inhibition of HMG CoA reductase by the AC decreases intracellular cholesterol synthesis. The associated reduction in concentration induces LDL-receptor expression leading to an increase in LDL-C clearance from plasma. Two direct mechanisms have been suggested for the reduction of triglycerides by atorvastatin calcium. Firstly, marked inhibition of cholesterol synthesis would impair the assembly and secretion of VLDL particles, of which cholesterol is an essential component, therefore causing a reduction in triglyceride levels. Secondly, reduction in hepatic cholesterol levels would lead to an increase in LDL-receptor expression and hence increased binding of VLDL and LDL particles reduction in both cholesterol and triglyceride levels [24]. There have been a number of clinical trials reporting the HDL-C increasing beneficial effect of atorvastatin [25], however, there is no established mechanism explaining this phenomenon. Another pleiotropic effect of atorvastatin includes insulin sensitization through which it reduces the glucose levels to some extent. Post hoc analysis of the West of Scotland

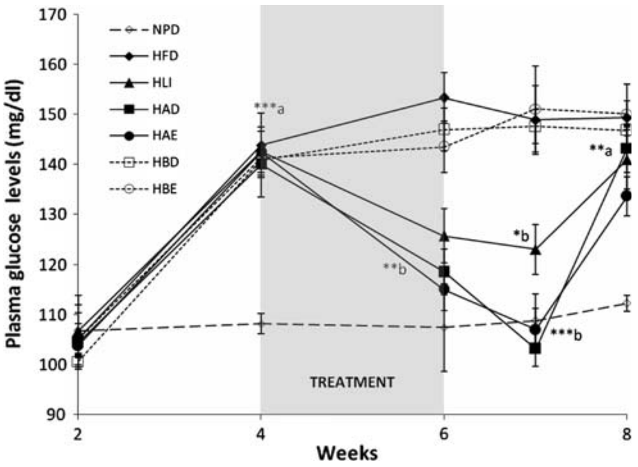

Fig. 5 Plasma glucose levels. NPD- normal pellet diet, HFD- high fat diet only, HLI- hyperlipidemic rats treated with commercial formulation (Lipicure®), HAD- hyperlipidemic rats treated with DMAB stabilized nanoparticles of AC, HAE- hyperlipidemic rats treated with Vit E-TPGS stabilized nanoparticles, HBD- hyperlipidemic rats treated with blank DMAB stabilized nanoparticles, HBE- hyperlipidemic rats treated with blank TPGS stabilized nanoparticles. Values are depicted as mean ± SEM ($n = 6$). $^{*}P < 0.05$, **a** HLI versus all other groups at that week

Coronary Prevention Study (WOSCOPS) observed an intriguing and unexpected significant reduction in the development of diabetes with statin therapy, suggesting a potential for regulating multiple complications associated with type II diabetes [26]. Recently atorvastatin treatment of insulin-resistant, fructose-fed hamsters appeared to ameliorate hepatic insulin resistance based on an increase in the tyrosine phosphorylation status of insulin receptors [27].

At the end of treatment (after six weeks) both the types of drug nanoparticles and commercial formulation of atorvastatin calcium had shown almost equal effects in assuaging the elevated levels of PTC, PTG, VLDL, LDL-C and reducing HDL-C levels. The exciting outcome of this study is that nanoparticles are as efficient as the commercial formulation although the nanoparticles were used at one-third the dose of the commercial formulation. Nanoparticles have been reported to increase the absorption of the encapsulated drugs when compared to the suspension form or any simple formulation type of the drug [28, 29]. By the virtue of enhanced absorption and the sustained release of drug these nanoparticles might have shown equal effects as the commercial formulation, which was given once daily. From this we can say that a once-in-3-days regimen of nanoparticles matched the once-daily regimen of the commercial formulation and showed a similar trend in the assuaging of different efficacy parameters during the treatment and elevation of the same parameters during the follow up after stoppage of treatment.

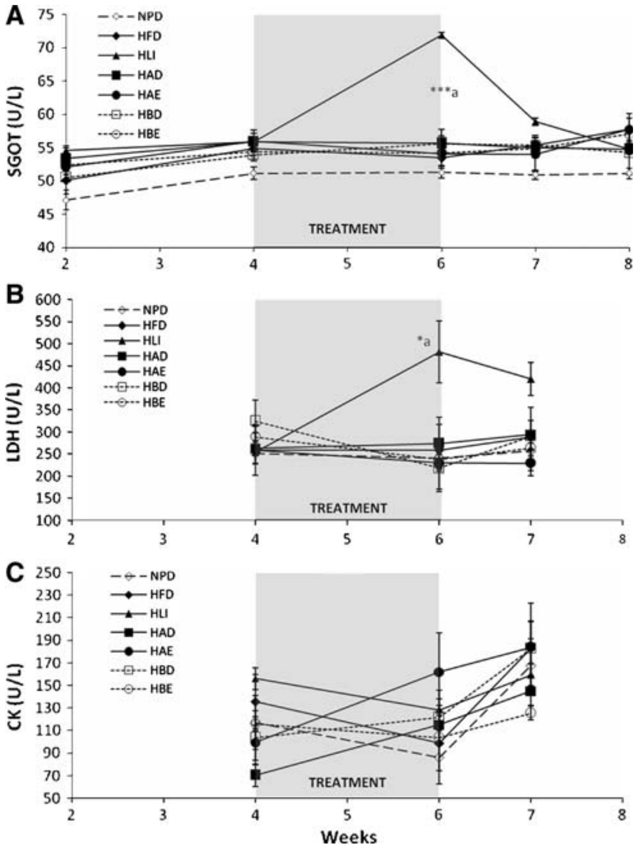

Fig. 6 Activities of different enzymes, SGOT (**a**), LDH (**b**) and CK (**c**). NPD- normal pellet diet, HFD- high fat diet only, HLI- hyperlipidemic rats treated with commercial formulation (Lipicure®), HAD- hyperlipidemic rats treated with DMAB stabilized nanoparticles of AC, HAE- hyperlipidemic rats treated with Vit E-TPGS stabilized nanoparticles, HBD- hyperlipidemic rats treated with blank DMAB stabilized nanoparticles, HBE- hyperlipidemic rats treated with blank TPGS stabilized nanoparticles. Values are depicted as mean ± SEM ($n = 6$). $^{***}P < 0.001$, $^{*}P < 0.05$; **a** HLI versus all other groups at that week

The literature has reported improved particle uptake in vivo and in vitro cell culture models when nanoparticles were coated with mucoadhesive polymers such as chitosan or surfactants like Vit E-TPGS as well as the size dependent uptake, where smaller particles are absorbed better than larger ones [10, 14–16, 18]. Therefore, the present investigation aimed at screening two different formulations made of distinctly different surfactants DMAB and Vit E-TPGS, where DMAB leads to particles of smallest size as discussed in the foregoing sections, on the other hand, Vit E-TPGS with ability to enhance the absorption across the GIT. In our previous studies we have seen distinct differences in the bioavailability with different sized particles, where smaller particles showed better circulations times [16]. In the present study, we have not seen any difference in the efficacy of the two formulations though there is a significant difference in the particle size (Table 3) further supporting the hypothesis described above, that the size and nature of the surfactant can

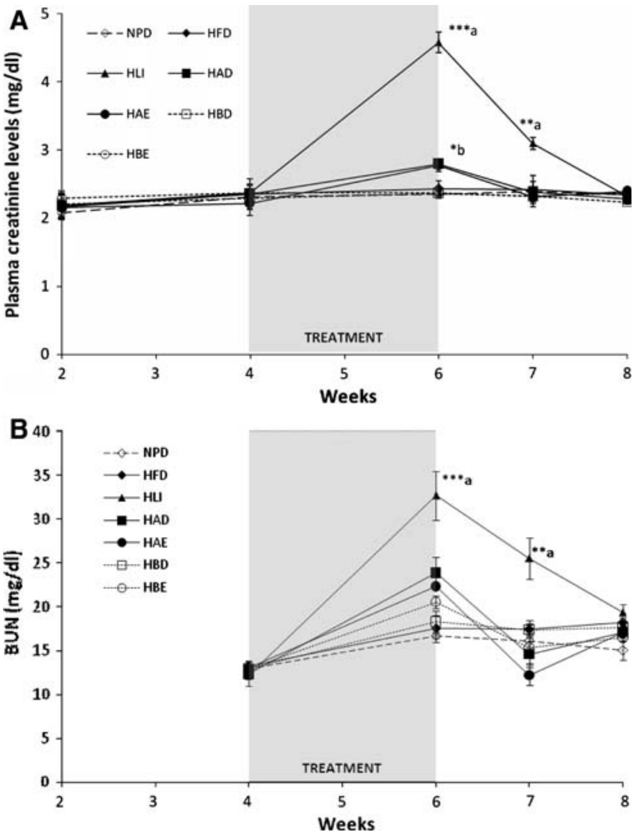

Fig. 7 Plasma creatinine levels (**a**) and blood urea nitrogen levels (**b**). NPD- normal pellet diet, HFD- high fat diet only, HLI- hyperlipidemic rats treated with commercial formulation (Lipicure®), HAD- hyperlipidemic rats treated with DMAB stabilized nanoparticles of AC, HAE- hyperlipidemic rats treated with Vit E-TPGS stabilized nanoparticles, HBD- hyperlipidemic rats treated with blank DMAB stabilized nanoparticles, HBE- hyperlipidemic rats treated with blank TPGS stabilized nanoparticles. Values are depicted as mean ± SEM ($n = 6$). $^{***}P < 0.001$, $^{**}P < 0.01$, $^{*}P < 0.05$, **a** HLI versus all other groups; **b** HAD and HAE versus all other groups at that week

influence the overall performance of the formulations. After six weeks, the treatment was stopped and the same parameters were followed until the biochemical parameters matched the HFD control animals. The levels elevated gradually with time and reached the HFD control levels at the end of the 8th week. Though the nanoparticulate AC showed similar/better effects in comparison to Lipicure®, at a 66%-reduced dose, the formulations did not show any activity beyond sixth week, which was comparable to Lipicure® treated groups and this could be due to particle elimination or limited dose administered in comparison to the Lipicure® (3.75 vs. 11.25 mg total dose) (Table 2). The elevation trend of efficacy parameters of both types of nanoparticles from sixth to eighth week is completely overlapped with the trend followed by the commercial formulation. On the other hand the blank nanoparticles were equivalent to the HFD group indicating least possible effect of nanoparticles as such without the drug.

During the treatment period (four to six weeks) the treatment groups (Lipicure® and both the nanoparticles formulations) effectively reduced the PTC, PTG, VLDL-C, LDL-C levels and elevated the HDL-C, however, the same was found to increase and decrease in the case of HDL-C by the seventh week and further matched the HFD group by the eighth week. The intriguing finding in the study is the effectiveness of the nanoparticulate groups at a 66%-reduced dose in comparison to Lipicure®.

Safety Parameters

Concern over the safety of the HMG-CoA reductase inhibitors, or statins, followed the worldwide withdrawal of cerivastatin in 2001, a drug that had been thought to be relatively free of serious adverse effects over the 4 years it was marketed [29]. Further concern followed documentation of the hazards of rosuvastatin after regulatory approval by the US Food and Drug Administration (FDA) and marketing [30]. Nowadays, there are increasing numbers of reports on the atorvastatin associated complications. The elimination half-life of atorvastatin is longer when compared with some other statins. There are more chances of tissue accumulation of AC on repeated administration. Due to its long elimination half-life and the presence of detectable plasma levels of active metabolites for a prolonged period of time (>24 h), AC can accumulate in the plasma, achieving a steady state drug concentration after multiple doses. After a single atorvastatin dose on day 1, drug concentrations increased more than proportionally with a 5–80 mg dose range. Atorvastatin equivalent concentrations achieved a steady state by the third day of multiple dosing [31]. $C_{\max}$ and AUC increased more than proportionally with dose during multiple administrations. Atorvastatin accumulation was 1.6-fold and 3.3-fold on the 22nd day after once- and twice-daily administration, respectively. From the efficacy parameters, it is evident that the nanoparticulate formulations are equally effective to Lipicure® at a 66%-lower dose, on the other hand, nanoparticulate formulations showed no/negligible toxicity, which could be due the following two reasons, (1) nanoparticles can protect the drug from being degraded, instant metabolism and can release the entrapped drug at a sustained rate all contributing to improved efficacy and reduced toxicity, (2) nanoparticles can modify the tissue distribution and could be quite different from the native drug distribution profiles.

There were no significant changes in CK levels with the commercial formulation and nanoparticulate formulation (Fig. 6). AST levels and LDH levels were increased with HLI treatment (Fig. 6). Commercial AC formulation

Table 4 Safety and efficacy parameters with different treatments in hyperlipidemic rats at sixth week

Biochemical parameters	NPD	HFD	HLI	HAD	HAE	HBD	HBE
PTC (mg/dl)	51.68 ± 2.88	95.21 ± 3.45^{***a}	66.77 ± 5.60^{**b}	71.33 ± 4.25^{**b}	70.04 ± 4.88^{**b}	90.87 ± 8.17	90.79 ± 5.36
LDL-C (mg/dl)	15.89 ± 2.01	52.73 ± 1.82^{***a}	28.92 ± 2.32^{**b}	35.32 ± 3.36^{**b}	34.06 ± 2.58^{**b}	47.81 ± 5.88	47.65 ± 2.55
VLDL-C (mg/dl)	15.45 ± 1.53	25.66 ± 0.79^{***a}	16.95 ± 1.46^{***b}	15.93 ± 0.58^{***b}	15.82 ± 1.77^{***b}	25.90 ± 1.01	25.34 ± 1.29
HDL-C (mg/dl)	20.34 ± 0.62	16.82 ± 1.35^{***a}	20.90 ± 0.56^{*b}	20.08 ± 0.65^{*b}	20.16 ± 0.75^{*b}	17.16 ± 0.82	17.80 ± 0.78
PTG (mg/dl)	77.26 ± 1.23	128.28 ± 4.79^{***a}	84.75 ± 1.60^{***b}	79.66 ± 1.20^{***b}	79.10 ± 0.74^{***b}	129.50 ± 7.37	126.69 ± 1.01
PGL (mg/dl)	107.42 ± 8.80	153.33 ± 5.03^{***a}	125.75 ± 5.40^{**b}	118.54 ± 4.56^{**b}	115.03 ± 4.28^{**b}	147.03 ± 4.30	143.55 ± 5.10
PC (mg/dl)	2.36 ± 0.06	2.43 ± 0.11	4.58 ± 0.15^{***c}	2.80 ± 0.07^{*c}	2.78 ± 0.09^{*c}	2.37 ± 0.03	2.37 ± 0.04
BUN (mg/dl)	16.71 ± 0.25	17.54 ± 1.55	32.71 ± 2.81^{***c}	23.88 ± 1.76	22.32 ± 0.33	18.34 ± 1.24	20.57 ± 0.71
CK (U/L)	86.14 ± 14.58	98.88 ± 10.37	128.32 ± 10.93	115.09 ± 17.08	162.05 ± 34.31	121.82 ± 11.62	103.69 ± 39.46
LDH (U/L)	241.18 ± 76.52	259.09 ± 25.13	481.25 ± 70.03^{*c}	274.64 ± 59.03	230.35 ± 19.22	218.57 ± 47.13	237.36 ± 18.01
AST (U/L)	51.31 ± 0.91	53.45 ± 1.53	71.87 ± 0.45^{***c}	55.68 ± 2.05	54.11 ± 1.86	55.57 ± 1.15	54.22 ± 0.97

PTC, Plasma total cholesterol; LDL-C, Low density lipoprotein cholesterol; VLDL-C, very low density lipoprotein cholesterol; HDL-C, High density lipoprotein cholesterol; PTG, plasma triglyceride levels; PGL, Plasma glucose levels; PC, Plasma creatinine; BUN, Blood urea nitrogen; CK, Creatinine kinase; LDH, Lactate dehydrogenase; AST, Aspartate aminotransferase; NPD, normal pellet diet; HFD, High fat diet; HLI, hyperlipidemic rats treated with commercial formulation (Lipicure®); HAD, hyperlipidemic rats treated with DMAB stabilized nanoparticles of AC; HAE, hyperlipidemic rats treated with TPGS stabilized nanoparticles; HBD, hyperlipidemic rats treated with blank DMAB stabilized nanoparticles; HBE, hyperlipidemic rats treated with blank TPGS stabilized nanoparticles

All values are at the sixth week and are depicted as mean ± SEM ($n = 6$)

*** $P < 0.001$, ** $P < 0.01$, ** $P < 0.05$

[a] Versus NPD

[b] Versus HFD, HBD and HBE

[c] Versus NPD and HFD

increased the levels of PC, which are indicative of muscle as well as kidney toxicity, which was not observed with nanoparticles (Fig. 7a). A similar case is with the other marker measured for renal failure, BUN (Fig. 7b). All these toxicity parameters if raised were only with the commercial formulation and not with the nanoparticles. Overall, the nanoparticles at reduced dose and frequency showed no adverse effects without compromising the efficacy.

The Clinical Advisory on Statins made a significant step towards standardization of the terms in myotoxicity [32]. Rhabdomyolysis required muscle symptoms with marked creatine kinase elevation typically substantially greater than ten times the upper limit of the normal, with a creatinine elevation consistent with pigment nephropathy and usually with brown urine with myoglobinuria. Although this is an improvement over prior classifications, the requirement that creatine kinase exceed ten times the upper limit of normal is arbitrary and excludes some cases of serious muscle toxicity. It is also unclear why the diagnosis of rhabdomyolysis, a muscle disorder, should require evidence of renal impairment. There is no specific biomarker available to date for the statin induced myotoxicity. Elevation of PC with or without elevation of CK is generally used to establish the myotoxicity of statins with elevation of other parameters like LDH, AST, and BUN [33, 34]. The remarkable observation of this study was that the adverse effects of atorvastatin calcium were suppressed when nanoparticles were used. The reason could be the reduced total dose and frequency with sustained release of the nanoparticles resulting in reduced accumulation of the drug upon chronic treatment. It is well established that the adverse effects of atorvastatin calcium are dose dependent. From the literature it is evident that chronic treatment with atorvastatin calcium results in accumulation and exposure of statins to extra hepatic tissues leading to adverse effects [35]. Lipid lowering drugs may induce necrotizing myopathy of the direct type. The fundamental change may be a disturbance of the integrity of the plasma membrane of the muscle fiber, allowing an efflux of calcium ions into the fiber which leads to over contraction and breakdown of the contractile apparatus and to a disturbance of protein synthesis and mitochondrial metabolism, culminating in death of the fiber. This reaction is dose-dependent [35].

Conclusion

The possible approaches in managing hyperlipidemia include life style management and drug therapy. However, drug therapy was adopted very rapidly by physicians as well as patients. After the introduction of atorvastatin onto the market, it has become the best selling drug in this category. However, there have been certain reports recently reporting the toxicity of atorvastatin. The feasibility of nanoparticulate delivery of AC, capable of releasing the entrapped drug in a sustained fashion over a period of time has been evaluated in hyperlipidemic rats. The study clearly demonstrates the proof of the concept that drug delivery systems can improve the performance of the drugs and minimize the side effects (Table 4), in this case AC nanoparticulate formulations.

Acknowledgments AKM acknowledges a NIPER MS fellowship. Financial support in the form of a research grant (IR/SO/LF-03/2006) from the Department of Science and Technology (DST), Government of India, is gratefully acknowledged. Authors acknowledge Mr. Vijender Singh Beniwal for the AFM studies.

References

1. Shitara Y, Sugiyama Y (2006) Pharmacokinetic and pharmacodynamic alterations of 3-hydroxy-3-methylglutaryl coenzyme A (HMG-CoA) reductase inhibitors: drug–drug interactions and interindividual differences in transporter and metabolic enzyme functions. Pharmacol Ther 112:71–105
2. Lau YY, Okochi H, Huang Y, Benet LZ (2006) Multiple transporters affect the disposition of atorvastatin and its two active hydroxy metabolites: application of in vitro and ex situ systems. J Pharmacol Exp Ther 316:762–771
3. Black AE, Sinz MW, Hayes RN, Woolf TF (1998) Metabolism and excretion studies in mouse after single and multiple oral doses of the 3-hydroxy-3-methylglutaryl-CoA reductase inhibitor atorvastatin. Drug Metab Dispos 26:755–763
4. Bottorff MB (2006) Statin safety and drug interactions: clinical implications. Am J Cardiol 97:S27
5. Cannon CP, Braunwald E, McCade CH, Rader DJ, Rouleau JL, Belder R, Joyal SV, Hill KA, Pfeffer MA, Skene AM (2004) Intensive versus moderate lipid lowering with statins after acute coronary syndromes. N Engl J Med 350:1495–1504
6. Graham DJ, Staffa JA, Shatin D, Andrade SE, Schech SD, Grenade LL, Gurwitz JH, Chan KA, Goodman MJ, Platt R (2004) Incidence of hospitalized rhabdomyolysis in patients treated with lipid-lowering drugs. J Am Med Assoc 292:2585–2590
7. Thompson PD, Clarkson P, Karas RH (2003) Statin associated myopathy. J Am Med Assoc 289:1681–1690
8. Sirtori CR (1993) Tissue selectivity of hydroxymethylglutaryl coenzyme A (HMG CoA) reductase inhibitors. Pharmacol Ther 60:431–459
9. Antons KA, Williams CD, Baker SK, Phillips PS (2006) Clinical perspectives of statin-induced rhabdomyolysis. Am J Med 119:400–409
10. Bala I, Bhardwaj V, Hariharan S, Sitterberg J, Bakowsky U, Kumar MNVR (2005) Design of biodegradable nanoparticles: a novel approach to encapsulating poorly soluble phytochemical ellagic acid. Nanotechnology 16:2819–2822
11. Shen HR, Li ZD, Zhong MK (2006) HPLC assay and pharmacokinetic study of atorvastatin in beagle dogs after oral administration of atorvastatin self-microemulsifying drug delivery system. Pharmazie 61:18–20
12. Srinivasan K, Viswanad B, Asrat L, Kaul CL, Ramarao P (2005) Combination of high-fat diet-fed and low-dose streptozotocin-treated rat: a model for type 2 diabetes and pharmacological screening. Pharmacol Res 52:313–320
13. Friedewald WT, Levy RI, Fredrickson DS (1972) Estimation of the concentration of low-density lipoprotein cholesterol in plasma, without use of the preparative ultracentrifuge. Clin Chem 18:499–502
14. Hariharan S, Bhardwaj V, Bala I, Sitterberg J, Bakowsky U, Kumar MNVR (2006) Design of estradiol loaded PLGA nanoparticulate formulations: a potential oral delivery system for hormone therapy. Pharm Res 23:184–195
15. Ankola DD, Viswanad B, Bhardwaj V, Ramarao P, Kumar MNVR (2007) Development of potent oral nanoparticulate formulation of coenzyme Q10 for treatment of hypertension: can the simple nutritional supplements be used as first line therapeutic agents for prophylaxis/therapy? Eur J Pharm Biopharm 67:361–369
16. Mittal G, Sahana DK, Bhardwaj V, Kumar MNVR (2007) Estradiol loaded PLGA nanoparticles for oral administration: effect of polymer molecular weight and copolymer composition on release behavior in vitro and in vivo. J Control Release 119:77–85
17. Italia JL, Bhatt DK, Bhardwaj V, Tikoo K, Kumar MNVR (2007) PLGA nanoparticles for oral delivery of cyclosporine: nephrotoxicity and pharmacokinetic studies in comparison to Sandimmune Neoral. J Control Release 119–206:197–206
18. Zhang Z, Feng SS (2006) Self-assembled nanoparticles of poly(lactide)-Vitamin ETPGS copolymers for oral chemotherapy. Int J Pharm 324:191–198
19. Mu L, Feng SS (2003) PLGA/TPGS nanoparticles for controlled release of paclitaxel: effects of the emulsifier and drug loading ratio. J Control Release 86:33–48
20. Song KC, Lee HS, Choung IY, Cho KI, Ahn Y, Choi EJ (2006) The effect of type of organic phase solvents on the particle size of poly(D,L-lactide-*co*-glycolide) nanoparticles. Colloids Surf A Physicochem Eng Aspects 276:162–167
21. Sonaje K, Italia JL, Sharma G, Bhardwaj V, Tikoo K, Kumar MNVR (2007) Development of biodegradable nanoparticles for oral delivery of ellagic acid and evaluation of their antioxidant efficacy against cyclosporine A-induced nephrotoxicity in rats. Pharm Res 24:899–908
22. Mogi T, Ohtake N, Yoshida M, Chimura R, Kamaga Y, Ando S, Tsukamoto T, Nakajima T, Uenodan H, Otsuka M, Matsuda Y, Ohshima H, Makino K (2000) Sustained release of 17β-estradiol from poly (lactide-*co*-glycolide) microspheres in vitro and in vivo. Colloids Surf B Biointerfaces 17:153–165
23. Panyam J, Dali MM, Sahoo SK, Ma W, Chakravarthi SS, Amidon GL, Levy RJ, Labhasetwar V (2003) Polymer degradation and in vitro release of a model protein from poly(D,L-lactide-co-glycolide) nano-and microparticles. J Control Release 92:173–187
24. Lea AP, McTavish D (1997) Atorvastatin. A review of its pharmacology and therapeutic potential in the management of hyperlipidemias. Drugs 53:828–847
25. Rogers SL, Magliano DJ, Levison DB, Webb K, Clarke PJ, Grobler MP, Liew D (2007) A dose-specific meta-analysis of lipid changes in randomized controlled trials of atorvastatin and simvastatin. Clin Ther 29:242–252
26. Freeman DJ, Norrie J, Sattar N, Neely RDG, Cobbe SM, Ford I, Isles C, Lorimer AR, Macfarlane PW, McKillop JH, Packard CJ, Shepherd J, Gaw A (2001) Pravastatin and the development of diabetes mellitus. Circulation 103:357–362
27. Mangaloglu L, Iderstine SV, Chen B, Taghibiglou C, Cheung R, Adeli K (2000) Effect of atorvastatin (Lipitor^{TM}) on VLDL-apoB and VLDL-triglyceride overproduction in vivo in an insulin resistant hamster model. Atherosclerosis 151:45

28. Sakuma S, Suzuki N, Kikuchi H, Hiwatari K, Arikawa K, Kishida A, Akashi M (1997) Absorption enhancement of orally administered salmon calcitonin by polystyrene nanoparticles having poly (*N*-isopropylacrylamide) branches on their surfaces. Int J Pharm 158:69–78
29. Omar MA, Wilson J, Cox TS (2001) Rhabdomyolysis and HMG-CoA reductase inhibitors. Ann Pharmacother 35:1096–1107
30. Wolfe SM (2004) Dangers of rosuvastatin identified before and after FDA approval. Lancet 363:2189–2190
31. Cilla D, whitfield LR, Gibson DM, Sedman AJ, Posvar EL (1996) Multiple-dose pharmacokinetics, pharmacodynamics, and safety of atorvastatin, an inhibitor of HMG-CoA reductase, in healthy subjects. Clin Pharmacol Ther 60:687–695
32. Pasternak RC, Smith SC, Bairey-Merz CN, Grundy SM, Cleeman JI, Lenfant C (2002) ACC/AHA/NHLBI Clinical advisory on the use and safety of statins. Stroke 33:2337–2341
33. Hodel C (2002) Myopathy and rhabdomyolysis with lipid-lowering drug. Toxicol Lett 128:159–168
34. Rimon D, Ludatscher R, Cohen L (1984) Clofibrate-induced muscular syndrome. Case report with ultrastructural findings and review of the literature. Isr J Med Sci 20:1082–1086
35. Ghirlanda G, Oradei A, Manto A, Lippa S, Uccioli L, Caputo S, Greco AV, Littarru GP (1993) Evidence of plasma CoQ10-lowering effect by HMG-CoA reductase inhibitors: a double-blind, placebo-controlled study. J Clin Pharmacol 33:226–229

Lipids (2008) 43:243–249
DOI 10.1007/s11745-008-3151-z

COMMUNICATION

Identification of Lysophosphatidylcholine–Chlorohydrin in Human Atherosclerotic Lesions

**M. C. Messner · C. J. Albert ·
J. McHowat · D. A. Ford**

Received: 13 November 2007 / Accepted: 24 December 2007 / Published online: 7 February 2008
© AOCS 2008

Abstract Lysophosphatidylcholine (LysoPtdCho) levels are elevated in sera in patients with atherosclerosis and in atherosclerotic tissue. Previous studies have shown that reactive chlorinating species attack plasmalogens in human coronary artery endothelial cells (HCAEC), forming lysoPtdCho and lysoPtdCho–chlorohydrin (lysoPtdCho–ClOH). The results herein demonstrate for the first time that lysoPtdCho–ClOH is elevated over 60-fold in human atherosclerotic lesions. In cultured HCAEC, 18:0 lysoPtdCho–ClOH led to a statistically significant increase in P-selectin cell-surface expression, but unlike 18:1 lysoPtdCho did not lead to cyclooxygenase-2 protein expression. These data show that 18:0 lysoPtdCho–ClOH is elevated in atherosclerotic tissue and may have unique pro-atherogenic properties compared to lysoPtdCho.

Keywords Myeloperoxidase · Reactive chlorinating species (RCS) · Plasmalogen · P-selectin

Abbreviations

RCS	Reactive chlorinating species
LysoPtdCho	Lysophosphatidylcholine
ClOH	Chlorohydrin
lysoPtdCho–ClOH	Lysophosphatidylcholine–chlorohydrin
PtdCho–ClOH	Phosphatidylcholine–chlorohydrin
FFA–ClOH	Free fatty acid chlorohydrin
HCAEC	Human coronary artery endothelial cells
MPO	Myeloperoxidase
GC–MS	Gas chromatography–mass spectrometry
ESI–MS	Electrospray ionization–mass spectrometry
HOCl	Hypochlorous acid
LDL	Low-density lipoprotein
2-ClHDA	2-chlorohexadecanal

Introduction

Lysophosphatidylcholine (LysoPtdCho) is elevated in atherosclerotic lesions from monkey [1], rat [2], and human [3] and may be an important pro-atherogenic mediator. LysoPtdCho comes from a variety of sources including the enzymatic action of a variety of phospholipase A_2s (PLA_2) on low-density lipoprotein (LDL) and membrane phosphatidylcholine (PtdCho) [4]. Numerous studies have shown that serum levels of lysoPtdCho are elevated from patients that have chronic inflammatory conditions such as renal failure on hemodialysis [5], diabetes [6], cancer [7], asthma [8], and atherosclerosis [9].

Activated monocytes and a subpopulation of macrophages release myeloperoxidase (MPO), which is an enzyme that catalyzes the production of reactive chlorinating species (RCS) such as hypochlorous acid (HOCl) [10]. Levels of MPO are elevated in atherosclerotic plaques

---

M. C. Messner · C. J. Albert · J. McHowat · D. A. Ford (✉)
Department of Biochemistry and Molecular Biology,
St Louis University School of Medicine,
1402 South Grand Boulevard,
St Louis, MO 63104, USA
e-mail: fordda@slu.edu

J. McHowat
Department of Pathology,
St Louis University School of Medicine,
1402 South Grand Boulevard, St Louis, MO 63104, USA

[11], as well as MPO-derived oxidation products such as 3-chlorotyrosine [12] and 2-chlorohexadecanal (2-ClHDA) [3]. It has been shown that phosphatidylcholine-chlorohydrins (PtdCho–ClOHs) are produced from isolated LDL treated with physiologically-relevant concentrations of HOCl [13]. PtdCho–ClOHs have been shown to elicit ATP depletion and necrosis in HL60, U937, Jurkat, and THP-1 cells [14, 15]. Additionally, Dever et al. [15] demonstrated that 25–50 μM PtdCho–ClOHs increased leukocyte adhesion to mouse artery segments by P-selectin expression [16] and increased caspase-3 activity [15]. There are several classes of phospholipase A_2 (PLA_2) that function to release the *sn*-2 fatty acid chains from the glycerol backbone of PtdCho, thereby potentially releasing free fatty acid-chlorohydrins (FFA–ClOHs). FFA–ClOHs cause ATP depletion [15] and cell death of erythrocytes [17] and endothelial cells [18]. In particular, administration of linoleic acid monochlorohydrin elicited decreased muscle tension using an isolated guinea-pig heart papillary muscle preparation [6].

Plasmalogens are a subclass of glycerophospholipids enriched in the cells of the cardiovascular system, and is thought to play an important role in normal heart function, as well as serve as an endogenous lipoprotein antioxidant [19]. Recently, our lab and others have shown that RCS attack of plasmenylcholine in liposomes and in human coronary artery endothelial cells (HCAEC) yields lysoPtdCho [20, 21] and lysoPtdCho-chlorohydrin (lysoPtdCho–ClOH) [21–23]. Additionally, we have shown that HOCl preferentially targets lysoPtdCho in comparison to PtdCho [22]. Since lysoPtdCho is elevated in atherosclerotic lesions and is preferentially targeted by RCS in vitro, the present study was designed to determine that lysoPtdCho–ClOH levels increase in atherosclerotic lesions. We show here, for the first time, that lysoPtdCho–ClOH is elevated in atherosclerotic lesions, and that lysoPtdCho–ClOH induces P-selectin cell-surface expression on HCAEC.

Materials and Methods

Lipids

Lysoplasmenylcholine (1-*O*-hexadec-1′-enyl-GPC) was prepared from bovine heart lecithin and purified as described previously [24]. 1-*O*-Hexadec-1′-enyl-2-heptadec-10′-enoyl-GPC (16:0–17:1 plasmenylcholine), 1-*O*-hexadec-1′-enyl-2-octadec-9′-enoyl-GPC (16:0–18:1 plasmenylcholine), and 1-*O*-hexadec-1′-enyl-2-nonadec-10′-enoyl-GPC (16:0–19:1 plasmenylcholine) were synthesized by an anhydrous reaction utilizing 1-*O*-hexadec-1′-enyl-GPC and heptadec-10′-enoyl chloride, octadec-9′-enoyl chloride, and nonadec-10′-enoyl chloride, respectively, as precursors and dimethylaminopyridine as a catalyst. The reactions were purified sequentially by normal phase HPLC and then by reversed phase HPLC. Purity of the plasmalogen fraction was confirmed by ESI–MS and quantified by GC following acid methanolysis using arachidic acid as an internal standard. 16:0–17:1 and 16:0–19:1 plasmenylcholine were treated with tenfold molar excess HOCl [25, 26], which simultaneously cleaved the vinyl ether bond and formed 17:0 and 19:0 lysoPtdCho–ClOH, respectively. The desired reaction product, lysoPtdCho–ClOH, was purified by HPLC, quantified by Bartlett [27], extracted in chloroform and stored at −20 °C under N_2. All other materials were of the highest grade available and were purchased from Sigma–Aldrich or Fisher.

Cell Culture

HCAEC (Cell Applications) were seeded onto 60 or 35-mm^2 6-well tissue culture dishes and cultured in EGM-2-MV (Lonza) at 37 °C in a 5% CO_2 and 95% air atmosphere. Experiments were performed on ~80% confluent monolayers (~1×10^6 cells/60-mm^2 dish) between passages 5 and 9. HCAEC growth medium was replaced with growth medium containing 2% FBS for 4–6 h prior to experiments. Lipids were dried under a stream of nitrogen and reconstituted in ethanol at a concentration of 0.1% (v/v) per well. Lipids were mixed with EGM-2MV and added by pipette to each dish dropwise for a final concentration of 1–50 μM, while control dishes received 0.1% ethanol vehicle mixed into EGM-2MV.

Human Tissue

Atherosclerotic and normal aortic tissue was collected from human postmortem autopsy specimens as authorized by Saint Louis University Institutional Review Board Protocol #10014. In general, tissues were harvested 6–12 h postmortem and then were sequentially rinsed, and submerged in PBS supplemented with 100 μM diethylenetriamine-pentaacetic acid and 100 μM butylhydroxytoluene, frozen in liquid N_2, and stored at −80 °C until analysis. Normal tissue was collected from subjects showing no overt indications of atherosclerotic vascular disease. Frozen tissue was weighed and then crushed in a liquid nitrogen-chilled mortar and pestle. Lipids and internal standards 17:0 and 19:0 lysoPtdCho–ClOH were added to the crushed tissue in methanol/chloroform/saline (2.5:1.5:1 v/v/v). After 5 min, chloroform was added resulting in a 1:1:0.8 methanol/chloroform/saline ratio [28]. The extracted organic phase was stored in chloroform at −20 °C under N_2 until analysis.

Electrospray Ionization–Tandem Mass Spectrometry

Lipid extracts were reconstituted in methanol containing 10 μM NaOH and analyzed by ESI–MS in the direct infusion mode at a flow rate of 1–3 μL/min using Thermo Electron TSQ Quantum Ultra instrumentation. The choline glycerophospholipids yield intense $[M + Na]^+$ adduct ions by electrospray ionization in the positive ion mode. Tandem mass spectrometry was performed on selected ions (collision energies were ∼32–38 eV). To detect lysoPtdCho and lysoPtdCho– molecular species, survey scan and neutral loss scanning of 95 amu (NL 95) was employed. Spectra were averaged at 3–5 min and processed utilizing Xcalibur software (Thermo), and molecular species were quantified by comparing the ion intensity of individual molecular species to that of the internal standards. The differences in ^{13}C isotope effects (Z_1) between the endogenous 16:0 and 18:0 lysoPtdCho–ClOH and the internal standards 17:0 and 19:0 lysoPtdCho–ClOH were corrected [29].

P-selectin Surface Expression

P-selectin expression on the surface of HCAEC was measured by a modified ELISA with nonpermeabilized monolayers using a modified version of the method described by Willam et al. [30]. HCAEC, grown to confluence in 24-well plates, were incubated with indicated lipids in Hanks' buffer for 5 min at 37 °C in 95% O_2/5% CO_2. At the end of incubations, buffer was quickly removed and cells were immediately fixed with 1% paraformaldehyde overnight at 4 °C. Cells were then washed 3 times with PBS and then blocked with Tris-buffered saline containing 0.1% Tween 20 (v/v) supplemented with 0.8% BSA (w/v) and 0.5% fish gelatin (w/v) for 1 h at 24 °C. Primary goat polyclonal antibody (1:500) for P-selectin (Santa Cruz) was used before treatments with horseradish peroxidase-conjugated rabbit-anti-goat secondary antibody (1:5,000). Subsequently, each well was incubated in the dark with the 3,3′,5,5′-tetramethylbenzidine liquid substrate system. Reactions were stopped by the addition of sulfuric acid, and color development was measured with a microtiter plate spectrophotometer (Wallac) at 450 nm [3].

Western Blotting

HCAEC monolayers in 60-mm^2 dishes were exposed to various experimental conditions in the presence of 2% FBS-supplemented EGM-2-MV. At the end of the treatment, the medium was aspirated from the dishes and monolayers were rinsed with PBS. Cells were scraped in SDS sample buffer containing DTT, boiled, and subjected to SDS-PAGE utilizing 10% polyacrylamide gels followed by transfer of proteins to polyvinylidene difluoride (PVDF)-plus membranes (GE Waters) for Western blot analysis. Blots were probed with an antibody to COX-2 (1:1,000) (Zymed) and an HRP-conjugated secondary antibody (1:7,000) (Sigma). Blots were stripped (0.1 M glycine, pH 2.5) and, following extensive washing, reprobed with an antibody to *β*-actin (1:5,000) (Abcam) and probed with an HRP-conjugated goat-anti-rabbit (1:7,000) (Sigma). Immunoreactive bands were visualized by exposure to autoradiographic film following incubation with enhanced chemiluminescence reagent (GE Healthcare).

Data Analysis

Data were normalized to the respective control mean values and are expressed as means ± SEM. Statistical analyses of data were performed by *t*-test and $P \leq 0.05$ was considered statistically significant.

Results

Lipid extracts from both atherosclerotic and normal human aorta samples were analyzed by ESI–MS. Previous studies have shown that unsaturated lysoPtdCho is present in higher levels of atherosclerotic lesions [3] and that MPO-derived oxidation products such as 3-chlorotyrosine [12] and the α-chlorofatty aldehyde, 2-ClHDA [3], have been detected in lesions. Since MPO-derived RCS have been shown to attack lysoPtdCho to produce lysoPtdCho–ClOH [21–23], ESI–MS was used to assess lysoPtdCho–ClOH accumulation in atherosclerotic lesions. Initial inspection of the spectra from normal and atherosclerotic tissue in the positive ion mode show noticeable differences, qualitatively revealing an increase in lysoPtdCho molecular species, which include *m/z* 518, 542, 544, 546, and 566, corresponding to 16:0, 18:2, 18:1, 18:0, and 20:4 lysoPtdCho, respectively (Fig 1a). Neutral loss scanning of 95 amu, which corresponds to the combined neutral loss of the trimethylamine and HCl [22], was utilized to detect chlorinated choline glycerophospholipid species. Figure 1b (traces 1 and 2) shows molecular ions with NL 95 scanning of lipid extracts from normal tissue extracted in the presence of synthetic internal standards 17:0 and 19:0 lysoPtdCho–ClOH at *m/z* 582 and 610, respectively. Figure 1b (traces 3 and 4) shows molecular ions with NL 95 scanning from atherosclerotic tissue extracted in the presence of synthetic internal standards (e.g., *m/z* 582 and 610) and demonstrate the appearance of 18:0 lysoPtdCho–ClOH at *m/z* 596. Atherosclerotic tissue also contains 16:0 lysoPtdCho–ClOH (*m/z* 568).

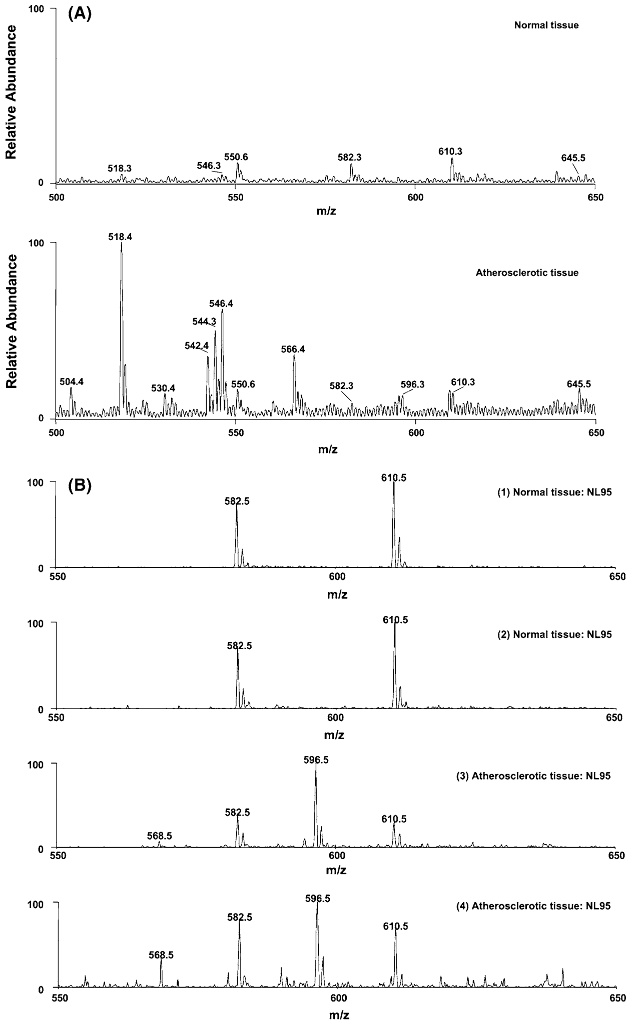

Fig. 1 18:0 LysoPtdCho–ClOH is detected in atherosclerotic tissue. Lipids from normal and atherosclerotic aorta were analyzed by ESI–MS in positive ion mode with spectra from a survey scan shown in **a** and neutral loss scanning of 95 amu (**b**). The spectra of molecular ions from normal tissue (spectra 1 and 2) show the synthetic internal standards 17:0 and 19:0 lysoPtdCho–ClOH at *m/z* 582 and 610, respectively. The spectra of molecular ions atherosclerotic tissue contain 16:0 lysoPtdCho–ClOH at *m/z* 568, 18:0 lysoPtdCho–ClOH at *m/z* 596, and the synthetic internal standards (spectra 3 and 4)

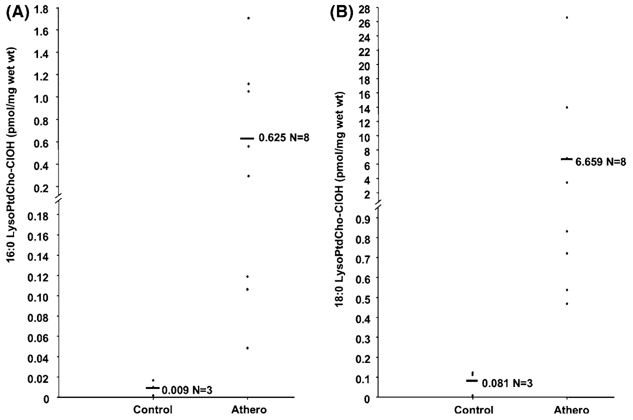

Fig. 2 16:0 and 18:0 LysoPtdCho–ClOH molecular species are elevated in atherosclerotic tissue. Lipids from normal and atherosclerotic aorta tissue were extracted and analyzed by direct infusion ESI–MS using neutral loss scanning of 95 amu in positive ion mode. Quantification of 16:0 and 18:0 lysoPtdCho–ClOH was performed by comparison to the relative intensities of the internal standards 17:0 and 19:0 lysoPtdCho–ClOH, respectively, as described in "Materials and Methods"

Utilizing neutral loss scanning of 95 amu, the relative abundance of 18:0 and 16:0 lysoPtdCho–ClOH were compared to the relative intensities of the internal standards for quantification. Atherosclerotic tissue contains approximately 69-fold more 16:0 lysoPtdCho–ClOH and 82-fold more 18:0 lysoPtdCho–ClOH than normal tissue (Fig. 2). However, 18:0 lysoPtdCho–ClOH is about 10.7-fold more abundant than 16:0 lysoPtdCho–ClOH. This likely reflects the abundance of 18:1 lysoPtdCho compared to 16:1 lysoPtdCho in atherosclerotic tissue (see Fig. 1a, spectra 2). Other unsaturated lysoPtdCho molecular species, such as 18:2 and 20:4 lysoPtdCho (e.g., *m/z* 544 and 566, respectively), are elevated in atherosclerotic tissue compared to control tissue (Fig. 1a). The accumulation of these unsaturated lysoPtdCho molecular species in atherosclerotic vascular tissue has previously been shown [3], which likely reflect phospholipase A_1 or lipase activity directed at phosphatidylcholine or alternatively RCS attack of unsaturated plasmenylcholine molecular species [3]. It should be appreciated that lysoPtdCho molecular species containing multiple chlorohydrin residues were not observed in atherosclerotic tissue as well as in our previous in vitro studies [22]. These findings are similar to those of Panasenko et al. [31] who showed that multi-chlorohydrin species are unstable and degrade to short-chained lysoPtdCho molecular species.

Endothelial activation, and subsequent dysfunction, is recognized as a major hallmark in the development and progression of atherosclerosis [32]. LysoPtdCho induces a wide range of pro-atherogenic effects [33], however the effects of lysoPtdCho–ClOHs are unknown. Two critical events in the development of atherosclerosis are cell-surface expression of proteins that tether blood monocytes to inflamed endothelium and release of chemotactic molecules [34]. Figure 3 shows that 10 μM 18:0 lysoPtdCho–ClOH elicits HCAEC surface expression of P-selectin at levels similar to that elicited by platelet activating factor [3]. The results suggest that lysoPtdCho–ClOH may function to recruit leukocytes to the endothelium by inducing an increase in coronary artery endothelial cell surface expression of P-selectin, an adhesion factor implicated in the development of vascular inflammation [35].

Cyclooxygenase-2 (COX-2) is an inducible enzyme that catalyzes the production of prostaglandin H_2 (PGH_2) from phospholipid-derived arachidonic acid [36, 37]. COX-2 is

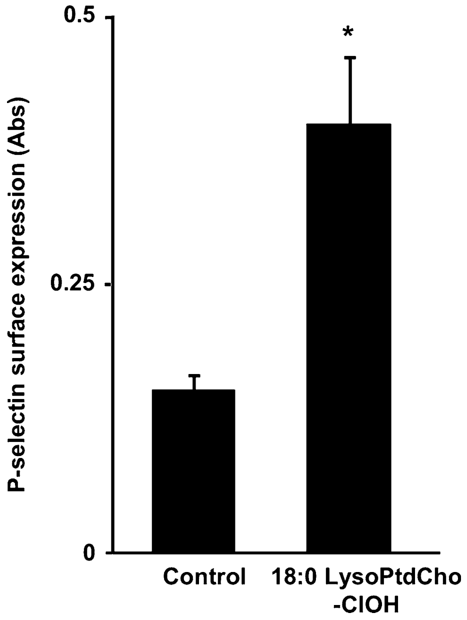

Fig. 3 P-selectin is expressed on the surface of HCAEC following 18:0 lysoPtdCho–ClOH treatment. HCAEC were treated with Hank's buffer alone (control) or buffer containing 10 µM 18:0 lysoPtdCho–ClOH for 5 min. A modified ELISA was utilized to assay P-selectin cell surface expression and is expressed as increased absorbance, $P < 0.01$

highly expressed in atherosclerotic plaques [38] and increased COX-2 expression in endothelial cells has been shown to increase prostacyclin production [39]. Under normal conditions, prostacyclin has a variety of effects in the vasculature, including inhibiting platelet aggregation and adhesion, relaxing smooth muscle cells, and inhibiting leukocyte activation and adhesion [40]. Palmitoyl lysoPtdCho has been shown to induce COX-2 protein expression in vascular endothelial cells [41–43]. Our previous studies showed that unsaturated lysoPtdCho is elevated in human atherosclerotic plaques [3]. Robust COX-2 protein expression was elicited in HCAEC by 50 µM 18:1 lysoPtdCho, whereas only slight induction of COX-2 was seen following 50 µM 18:0 lysoPtdCho, and no COX-2 expression was observed after treatment with 18:0 lysoPtdCho–ClOH (Fig. 4).

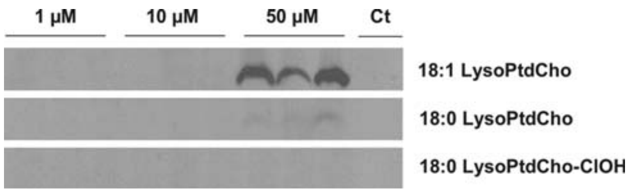

Fig. 4 18:1 LysoPtdCho induces COX-2 protein expression. HCAEC were treated with vehicle or were treated with 1, 10, or 50 µM (in triplicate) of various lysoPtdCho for 8 h. Western blotting was performed for COX-2 and β-actin

Discussion

Myeloperoxidase is found in human atherosclerotic lesions [11] and is localized in the shoulder regions of the plaque [44]. Products from MPO-derived RCS attack of tissue targets include, 3-chlorotyrosine, which is elevated sixfold in human atherosclerotic vascular tissue compared to normal vascular tissue [45]. Previous studies have shown that RCS attack of plasmenylcholine leads to the formation of unsaturated lysoPtdCho [20, 21] and α-chlorofatty aldehyde [46] (Scheme 1). Furthermore unsaturated lysoPtdCho is targeted by RCS leading to the production of lysoPtdCho–ClOH [21, 22] (Scheme 1). α-Chlorofatty aldehydes [3], were the first chlorinated lipids found in atherosclerotic lesions and are elevated ~1400-fold in atherosclerotic aorta. In this study, we utilized a soft ionization technique, ESI–MS/MS, and determined that human atherosclerotic tissue contains 69-fold more 16:0 and 82-fold more 18:0 lysoPtdCho–ClOH than normal tissue. Similar to our previous in vitro studies, only chlorohydrins derived from monoenoic lysoPtdCho molecular species were detected which likely reflects the instability of the lysoPtdCho chlorohydrins produced from polyunsaturated molecular species of lysoPtdCho [31].

LysoPtdCho is elevated in atherosclerotic lesions [3] and in sera of people with atherosclerosis [9]. Interestingly the mechanism leading to the production of unsaturated molecular species of lysoPtdCho (e.g. 20:4 lysoPtdCho as observed as *m/z* 566 in Fig. 1a) reflects a combination of activation of phospholipase A_1 lipase activities and RCS attack of plasmenylcholine molecular species. The results from this study demonstrate that 18:1 lysoPtdCho induces increased COX-2 protein expression in HCAEC. There are contradictory reports on the role of COX-2 in the development of atherosclerosis. Recent studies show that prostanoid synthases, such as those responsible for the synthesis of PGE_2, PGD_2, $PGF_2\alpha$, PGI_2, and TXA, differentially couple with upstream COX-1 and COX-2 and that colocalization is essential for terminal prostanoid production. Prostanoid synthases preferentially localize to either COX isozyme, and some localize to both COX-1 and COX-2 depending on the stimulus [47]. It appears that the addition of a chlorohydrin moiety across the alkene bond led to the ablation of the robust increase in COX-2 protein induced by 18:1 lysoPtdCho in HCAEC. The elevation of 18:1 lysoPtdCho in atherosclerotic tissue may confer anti-atherogenic properties in endothelial cells by increasing COX-2 protein expression and prostacyclin production. If this is the case, chlorohydrin formation of 18:1 lysoPtdCho due to RCS attack, leads to a molecular species that is unable to elicit COX-2 expression. If, however, 18:1 lysoPtdCho induces preferential coupling of pro-atherogenic PGE_2 or TXA to COX-2, further oxidation to 18:0

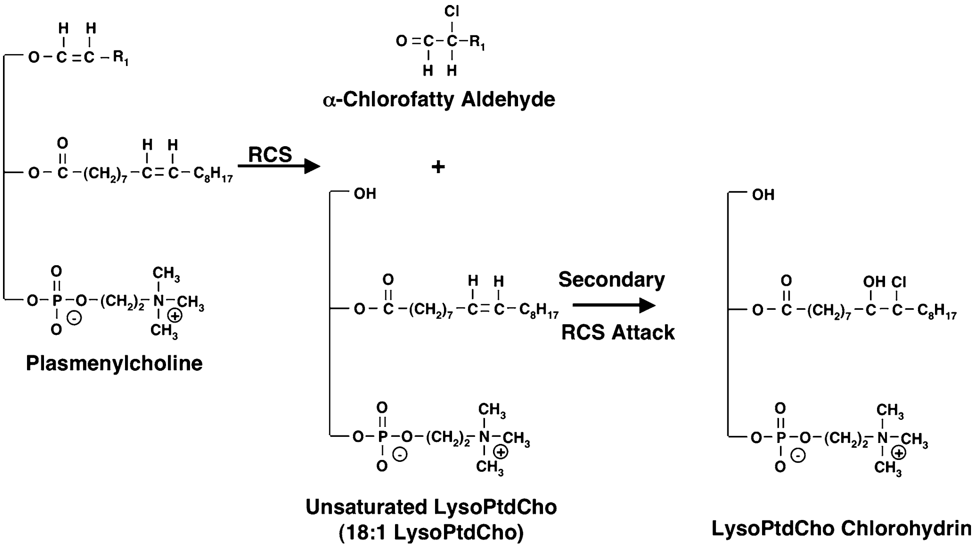

Scheme 1 Scheme of RCS attack of plasmenylcholine to yield 18:1 lysoPtdCho and 18:0 lysoPtdCho–ClOH. RCS attacks plasmenylcholine resulting in the release of an α-chlorofatty aldehyde and unsaturated molecular species of lysoPtdCho. LysoPtdCho undergoes further oxidation by RCS to yield lysoPtdCho–ClOH

lysoPtdCho–ClOH would prevent further pro-atherogenic prostaglandin production.

Previous studies have demonstrated that 2-ClHDA is a potent neutrophil chemoattractant, while unsaturated lysoPtdCho increases P-selectin surface expression on HCAEC [3, 20]. The results from this study show that 18:0 lysoPtdCho–ClOH also leads to increased P-selectin surface expression on HCAEC, which may function to recruit more MPO-containing leukocytes to sites of inflammation. RCS attack of plasmenylcholine may lead to the production of molecular species that lead to both leukocyte attraction and adhesion. Collectively these data suggest that lysoPtdCho–ClOH in injured blood vessels may propagate inflammation by facilitating leukocyte recruitment through a mechanism leading to P-selectin surface expression on endothelial cells.

Collectively the data presented herein show that lysoPtdCho–ClOH accumulate in human atherosclerotic tissue and have a potential role in the inflammatory state of the atherosclerotic lesion. It will be important in future studies to determine the accumulation and role of these lipids in early stages of atherosclerotic tissue as well as determine the tissue distribution of lysoPtdCho–ClOH at lesion sites as well as adjacent tissue. It will also be of great importance to determine that lysoPtdCho–ClOH are associated with oxidized LDL in the subintima. It would then follow that levels of 16:0 and 18:0 molecular species of lysoPtdCho–ClOH in blood LDL could potentially serve as a marker of coronary artery disease risk. It would be of interest as well to determine the choline glycerophospholipid, lysoPtdCho and lysoPtdCho–ClOH molecular species profile in diet-controlled studies comparing diets enriched in either monoenoic, saturated or cardioprotective ω-3 fatty acids. Further studies on these novel chlorinated lipids as well as other blood-borne chlorinated lipids derived from MPO activity may prove to be important in the development of biomarkers for cardiovascular disease.

References

1. Portman OW, Alexander M (1969) Lysophosphatidylcholine concentrations and metabolism in aortic intima plus inner media: effect of nutritionally induced atherosclerosis. J Lipid Res 10:158–165
2. Hara A, Taketomi T (1990) Characterization and change of phospholipids in the aorta of Watanabe hereditable hyperlipidemic rabbit. Jpn J Exp Med 60:311–318
3. Thukkani AK, McHowat J, Hsu FF, Brennan ML, Hazen SL, Ford DA (2003) Identification of alphachloro fatty aldehydes and unsaturated lysophosphatidylcholine molecular species in human atherosclerotic lesions. Circulation 108:3128–3133
4. Chakraborti S (2003) Phospholipase A(2) isoforms: a perspective. Cell Signal 15:637–665
5. Sasagawa T, Suzuki K, Shiota T, Kondo T, Okita M (1998) The significance of plasma lysophospholipids in patients with renal failure on hemodialysis. J Nutr Sci Vitaminol (Tokyo) 44:809–818
6. Iwase M, Yamada Y, Uemura H, Nakaya H, Takatori T, Nagao M, Iwadate K (1997) Effect of monochlorohydrins of linoleic acid on guinea pig cardiac papillary muscles. Biochem Biophys Res Comm 231:295–298
7. Okita M, Gaudette DC, Mills GB, Holub BJ (1997) Elevated levels and altered fatty acid composition of plasma lysophosphatidylcholine(lysoPC) in ovarian cancer patients. Int J Cancer 71:31–34
8. Mehta D, Gupta S, Gaur SN, Gangal SV, Agrawal KP (1990) Increased leukocyte phospholipase A2 activity and plasma lysophosphatidylcholine levels in asthma and rhinitis and their relationship to airway sensitivity to histamine. Am Rev Respir Dis 142:157–161
9. Lavi S, McConnell JP, Rihal CS, Prasad A, Mathew V, Lerman LO, Lerman A (2007) Local production of lipoprotein-associated phospholipase A2 and lysophosphatidylcholine in the coronary circulation: association with early coronary atherosclerosis and endothelial dysfunction in humans. Circulation 115:2715–2721

10. Harrison JE, Schultz J (1976) Studies on the chlorinating activity of myeloperoxidase. J Biol Chem 251:1371–1374
11. Daugherty A, Dunn JL, Rateri DL, Heinecke JW (1994) Myeloperoxidase, a catalyst for lipoprotein oxidation, is expressed in human atherosclerotic lesions. J Clin Invest 94:437–444
12. Hazen SL, Heinecke JW (1997) 3-Chlorotyrosine, a specific marker of myeloperoxidase-catalyzed oxidation, is markedly elevated in low density lipoprotein isolated from human atherosclerotic intima. J Clin Invest 99:2075–2081
13. Jerlich A, Pitt AR, Schaur RJ, Spickett CM (2000) Pathways of phospholipid oxidation by HOCl in human LDL detected by LC-MS. Free Radic Biol Med 28:673–682
14. Dever G, Stewart LJ, Pitt AR, Spickett CM (2003) Phospholipid chlorohydrins cause ATP depletion and toxicity in human myeloid cells. FEBS Lett 540:245–250
15. Dever G, Wainwright CL, Kennedy S, Spickett CM (2006) Fatty acid and phospholipid chlorohydrins cause cell stress and endothelial adhesion. Acta Biochim Pol 53:761–768
16. Dever GJ, Benson R, Wainwright CL, Kennedy S, Spickett CM (2007) Phospholipid chlorohydrin induces leukocyte adhesion to ApoE−/− mouse arteries via upregulation of P-selectin. Free Radic Biol Med. doi:10.1016/j.freeradbiomed.2007.10.038
17. Carr AC, Vissers MC, Domigan NM, Winterbourn CC (1997) Modification of red cell membrane lipids by hypochlorous acid and haemolysis by preformed lipid chlorohydrins. Redox Rep 3:263–271
18. Vissers MC, Carr AC, Winterbour CC (2001) Fatty acid chlorohydrins and bromohydrins are cytotoxic to human endothelial cells. Redox Rep 6:49–55
19. Vance JE (1990) Lipoproteins secreted by cultured rat hepatocytes contain the antioxidant 1-alk-1-enyl-2-acylglycerophosphoethanolamine. Biochim Biophys Acta 1045:128–134
20. Thukkani AK, Hsu FF, Crowley JR, Wysolmerski RB, Albert CJ, Ford DA (2002) Reactive chlorinating species produced during neutrophil activation target tissue plasmalogens: production of the chemoattractant, 2-chlorohexadecanal. J Biol Chem 277:3842–3849
21. Lessig J, Schiller J, Arnhold J, Fuchs B (2007) Hypochlorous acid-mediated generation of glycerophosphocholine from unsaturated plasmalogen glycerophosphocholine lipids. J Lipid Res 48:1316–1324
22. Messner MC, Albert CJ, Hsu FF, Ford DA (2006) Selective plasmenylcholine oxidation by hypochlorous acid: formation of lysophosphatidylcholine chlorohydrins. Chem Phys Lipids 144:34–44
23. Panasenko OM, Vakhrusheva T, Tretyakov V, Spalteholz H, Arnhold J (2007) Influence of chloride on modification of unsaturated phosphatidylcholines by the myeloperoxidase/hydrogen peroxide/bromide system. Chem Phys Lipids 149:40–51
24. Han XL, Zupan LA, Hazen SL, Gross RW (1992) Semisynthesis and purification of homogeneous plasmenylcholine molecular species. Anal Biochem 200:119–124
25. Hazen SL, Hsu FF, Duffin K, Heinecke JW (1996) Molecular chlorine generated by the myeloperoxidasehydrogen peroxide-chloride system of phagocytes converts low density lipoprotein cholesterol into a family of chlorinated sterols. J Biol Chem 271:23080–23088
26. Thomas EL, Fishman M (1986) Oxidation of chloride and thiocyanate by isolated leukocytes. J Biol Chem 261:9694–9702
27. Dittmer JC, Douglas MG (1969) Quantitative determination of phosphoinositides. Ann NY Acad Sci 165:515–525
28. Bligh EG, Dyer WJ (1959) A rapid method of total lipid extraction and purification. Can J Biochem Physiol 37:911–917
29. Han X, Gross RW (2005) Shotgun lipidomics: electrospray ionization mass spectrometric analysis and quantitation of cellular lipidomes directly from crude extracts of biological samples. Mass Spectrom Rev 24:367–412
30. Willam C, Schindler R, Frei U, Eckardt KU (1999) Increases in oxygen tension stimulate expression of ICAM-1 and VCAM-1 on human endothelial cells. Am J Physiol 276:H2044–H2052
31. Panasenko OM, Spalteholz H, Schiller J, Arnhold J (2003) Myeloperoxidase-induced formation of chlorohydrins and lysophospholipids from unsaturated phosphatidylcholines. Free Radic Biol Med 34:553–562
32. Deanfield JE, Halcox JP, Rabelink TJ (2007) Endothelial function and dysfunction: testing and clinical relevance. Circulation 115:1285–1295
33. Kougias P, Chai H, Lin PH, Lumsden AB, Yao Q, Chen C (2006) Lysophosphatidylcholine and secretory phospholipase A2 in vascular disease: mediators of endothelial dysfunction and atherosclerosis. Med Sci Monit 12:RA5–RA16
34. Ley K, Reutershan J (2006) Leucocyte-endothelial interactions in health and disease. Handb Exp Pharmacol 97–133
35. Blann AD, Nadar SK, Lip GY (2003) The adhesion molecule P-selectin and cardiovascular disease. Eur Heart J 24:2166–2179
36. Masferrer JL, Seibert K, Zweifel B, Needleman P (1992) Endogenous glucocorticoids regulate an inducible cyclooxygenase enzyme. Proc Natl Acad Sci USA 89:3917–3921
37. Kraemer SA, Meade EA, DeWitt DL (1992) Prostaglandin endoperoxide synthase gene structure: identification of the transcriptional start site and 5′-flanking regulatory sequences. Arch Biochem Biophys 293:391–400
38. Schonbeck U, Sukhova GK, Graber P, Coulter S, Libby P (1999) Augmented expression of cyclooxygenase-2 in human atherosclerotic lesions. Am J Pathol 155:1281–1291
39. Jones DA, Carlton DP, McIntyre TM, Zimmerman GA, Prescott SM (1993) Molecular cloning of human prostaglandin endoperoxide synthase type II and demonstration of expression in response to cytokines. J Biol Chem 268:9049–9054
40. Vane JR, Botting RM (1995) Pharmacodynamic profile of prostacyclin. Am J Cardiol 75:3A–10A
41. Kirtikara K, Raghow R, Laulederkind SJ, Goorha S, Kanekura T, Ballou LR (2000) Transcriptional regulation of cyclooxygenase-2 in the human microvascular endothelial cell line, HMEC-1: control by the combinatorial actions of AP2, NF-IL-6 and CRE elements. Mol Cell Biochem 203:41–51
42. Zembowicz A, Jones SL, Wu KK (1995) Induction of cyclooxygenase-2 in human umbilical vein endothelial cells by lysophosphatidylcholine. J Clin Invest 96:1688–1692
43. Rikitake Y, Hirata K, Kawashima S, Takeuchi S, Shimokawa Y, Kojima Y, Inoue N, Yokoyama M (2001) Signaling mechanism underlying COX-2 induction by lysophosphatidylcholine. Biochem Biophys Res Commun 281:1291–1297
44. Sugiyama S, Okada Y, Sukhova GK, Virmani R, Heinecke JW, Libby P (2001) Macrophage myeloperoxidase regulation by granulocyte macrophage colony-stimulating factor in human atherosclerosis and implications in acute coronary syndromes. Am J Pathol 158:879–891
45. Hazen SL, Heinecke JW (1997) 3-Chlorotyrosine, a specific marker of myeloperoxidase-catalyzed oxidation, is markedly elevated in low density lipoprotein isolated from human atherosclerotic intima. J Clin Inv 99:2075–2081
46. Albert CJ, Crowley JR, Hsu FF, Thukkani AK, Ford DA (2001) Reactive chlorinating species produced by myeloperoxidase target the vinyl ether bond of plasmalogens: identification of 2-chlorohexadecanal. J Biol Chem 276:23733–23741
47. Ueno N, Takegoshi Y, Kamei D, Kudo I, Murakami M (2005) Coupling between cyclooxygenases and terminal prostanoid synthases. Biochem Biophys Res Commun 338:70–76

Lipids (2008) 43:251–258
DOI 10.1007/s11745-007-3137-2

ORIGINAL ARTICLE

Altered Lipid Response in Hamsters Fed *cis*-9, *trans*-11+*trans*-8,*cis*-10 Conjugated Linoleic Acid Mixture

Vishnee Bissonauth · P. Yvan Chouinard · Johanne Marin · Nadine Leblanc · Denis Richard · Hélène Jacques

Received: 16 August 2007 / Accepted: 6 November 2007 / Published online: 15 December 2007
© AOCS 2007

Abstract The objective of the present study was to compare the effects of *cis*-9,*trans*-11 + *trans*-8,*cis*-10 conjugated linoleic acid (CLA) mixture to those of *cis*-9,*trans*-11 + *trans*-10,*cis*-12 CLA mixture and linoleic acid (LA) on lipoprotein profile, hepatic lipids, body composition and digestibility of dietary fat in hamsters ($n = 17$) fed diets containing 2% of experimental fat (w/w) for 28 days. The *cis*-9,*trans*-11 + *trans*-10,*cis*-12 CLA mixture showed higher LDL cholesterol concentrations than LA and the *cis*-9,*trans*-11 + *trans*-8,*cis*-10 CLA mixture. The *cis*-9,*trans*-11 + *trans*-8,*cis*-10 CLA mixture induced similar plasma LDL cholesterol and hepatic lipid concentrations, and coefficient of digestibility as LA, indicating no effect of the *trans*-8,*cis*-10 CLA isomer on these lipid parameters. On the other hand, the *cis*-9, *trans*-11 + *trans*-8,*cis*-10 CLA mixture induced higher plasma VLDL cholesterol and triglycerides than LA and the *cis*-9,*trans*-11 + *trans*-10,*cis*-12 CLA mixture. The *cis*-9,*trans*-11 + *trans*-8,*cis*-10 CLA mixture also induced the highest plasma glucose concentrations compared with the two other groups, indicating an impairment of glycemic control. No differences in body composition were noted between the three groups. The present results thus show that the *cis*-9,*trans*-11 + *trans*-8,*cis*-10 CLA mixture can deteriorate plasma VLDL cholesterol and triglycerides in hamsters, possibly due to an increased flux of glucose.

Keywords Conjugated linoleic acid · Isomers · Lipoproteins · Lipid metabolism · Body composition · Hamsters

Abbreviations

CLA	Conjugated linoleic acid
DM	Dry matter
LA	Linoleic acid
LDL	Low density lipoproteins
VLDL	Very low-density lipoproteins
HDL	High-density lipoproteins
ED	Experimental diets
NPD	Nonpurified diet

Introduction

Conjugated linoleic acid (CLA) represents a series of heterogeneous polyunsaturated fatty acids that exist as positional and geometric isomers of conjugated octadecadienoic acid (18:2) varying in double bonding pattern. Unlike linoleic acid (LA), which is a single unique molecule, several different CLA isomers are possible depending on which carbon atom the double bonds are relocated and the resulting isomeric reconfigurations [1]. CLA is found in foods such as beef and lamb, as well as dairy foods derived

---

V. Bissonauth · J. Marin · N. Leblanc · H. Jacques (✉)
Department of Food Science and Nutrition and Institute of Nutraceuticals and Functional Foods, Laval University,
2425 Agriculture St, Paul-Comtois Building,
G1V 0A6 Quebec, QC, Canada
e-mail: helene.jacques@aln.ulaval.ca

P. Y. Chouinard
Department of Animal Sciences and Institute of Nutraceuticals and Functional Foods, Laval University, 2425 Agriculture St, Paul-Comtois Building, G1V 0A6 Quebec, QC, Canada

D. Richard
Department of Anatomy and Physiology, Laval University,
1050 Medicine Ave, Ferdinand-Vandry Building,
G1V 0A6 Quebec, QC, Canada

from these ruminant sources, formed largely as a result of rumen microbial isomerisation of dietary linoleic acid as well as desaturation of octadecanoic acid derivatives. Of these, the predominant geometric isomer of CLA in foods is the *cis*-9,*trans*-11 C18:2, followed by *trans*-7,*cis*-9 C18:2, *cis*-11,*trans*-13 C18:2, *trans*-8,*cis*-10 C18:2 and the *trans*-10,*cis*-12 C18:2 [2]. CLA produced chemically is available as dietary supplement, usually containing equal amounts of *cis*-9,*trans*-11 CLA, and *trans*-10,*cis*-12 CLA as well as a proportion of other fatty acids [3]. The most dominant CLA isomer in milk fat is *cis*-9,*trans*-11 C18:2. Recent work has shown that this isomer can be transformed into *trans*-8,*cis*-10 C18:2 by heating butterfat under specific conditions [4].

A number of animal studies, primarily in rodents, showed that the consumption of CLA results in beneficial effects on plasma lipids and lipoproteins [5–9], atherogenic risk [8, 10] and body fat accumulation [5, 9, 11, 12]. In the majority of the animal studies, the CLA preparations used have been either individual *cis*-9,*trans*-11 CLA isomer (90%), *trans*-10,*cis*-12 CLA isomer (90%) or mixtures of CLA isomers, i.e. usually mixtures of 30–40% of each of the *cis*-9,*trans*-11 and *trans*-10,*cis*-12 isomers, the residue consisting of various less common isomers [13]. The effects of CLA on plasma lipids and body composition have been first attributed specifically to the *trans*-10,*cis*-12 CLA isomer [14–16]. However, CLA does not appear to produce identical results in all studies due to variations in experimental conditions such as age, dose, duration of the study, animal species, food consumption, body weight and initial metabolic status. A recent study conducted in our laboratory [17] showed that *trans*-10,*cis*-12 CLA isomer fed to hamsters had an undesirable effect on plasma lipids by increasing LDL cholesterol concentrations but had no impact on body composition.

Until now, most investigations have studied the effects of the individual or mixed *cis*-9,*trans*-11 + *trans*-10,*cis*-12 CLA isomers, and few have addressed the effects of *trans*-8,*cis*-10 CLA isomer on plasma lipoproteins. In the present study, we thus compared, under isoenergetic conditions, the effects of a mixture of *cis*-9,*trans*-11 + *trans*-8,*cis*-10 CLA isomers to those of a mixture of *cis*-9,*trans*-11 + *trans*-10,*cis*-12 CLA isomers and LA on plasma and hepatic lipids, body composition and other related metabolic parameters in hamsters. The highest concentration of *trans*-8,*cis*-10 CLA isomer that could be obtained was 35% in the *cis*-9,*trans*-11 + *trans*-8,*cis*-10 CLA mixture, since individual purified *trans*-8,*cis*-10 CLA isomer was not available on the market. Although it was highly speculative due to lack of scientific data, we hypothesized that the *cis*-9,*trans*-11 + *trans*-8,*cis*-10 CLA mixture would induce different effects on plasma and hepatic lipids as well as on body composition than the *cis*-9,*trans*-11 and *trans*-10,*cis*-12 CLA mixture in hamsters.

Experimental Procedures

Experimental Diets

All animals were assigned to one of the three experimental diets varying in CLA isomers, namely a 50:50 *cis*-9,*trans*-11 + *trans*-10,*cis*-12 CLA mixture, a CLA mixture consisting of *cis*-9,*trans*-11 + *trans*-8,*cis*-10 (as approximately 40% *cis*-9,*trans*-11 CLA and 35% *trans*-8,*cis*-10 CLA), and LA. The latter fatty acid was used as the reference fatty acid. The CLA mixtures were supplied by Natural ASA (Hovdebygda, Norway). The fatty acid composition of the three experimental groups is shown in Table 1.

Table 2 shows the composition of the experimental diets (ED). Except for lard, which was purchased from a local supermarket, all dietary ingredients were provided by MP Biomedical Inc (Aurora, OH). To minimize the oxidation of the fatty acids, BHT was added to the diets [18]. As confirmed by bomb calorimetry using an automatic adiabatic calorimeter (Model 1241, Parr Instruments, Moline, IL), the three purified diets were isoenergetic, providing 4,7 kcal/g each. Diets were also found to be isonitrogenous and isolipidic. The protein content of each diet (N × 6.25) (20–22% w/w) was assayed by Leco FP-528 (ISO 34/SC 5, Principle of Dumas). The lipid content of each diet measured by Manual Soxtec System HT6 (Tecator AB, Box70.S-2601, HOGANAS, Sweden) was approximately 12.0–12.6% (w/w). The dry matter of each diet was also measured by Fisher Econo Temp Laboratory Oven Model 30G. The percentage of water obtained from the samples was between 6 and 6.5% (w/w).

Table 1 Fatty acid composition of the three experimental fats (Provided by Natural ASA)

Fatty acid	LA	*cis*-9,*trans*-11 + *trans*-10,*cis*-12 CLA	*cis*-9,*trans*-11 + *trans* 8,*cis*-10 CLA
16:0	0.1	0.1	<0.1
18:0	0.4	<0.1	<0.1
cis-9 18:1	5.3	5.0	3.6
cis-9,*cis*-12 18:2	93.0	0.7	0.7
cis-9,*trans*-11 18:2	–	44	42
trans-10,*cis*-12 18:2	–	44	0.8
trans-8,*cis*-10 18:2	–	–	35
Other conjugated 18:2[a,b]	<0.1	5.1	18

LA linoleic acid, *CLA* conjugated linoleic acid

[a] Principally *cis*-*cis*-9,11 & 10,12 + *trans*-*trans*-9,11 & 10,12

[b] For *cis*-9,*trans*-11 + *trans*-8,*cis*-10 CLA mixture, 5.6% are *trans*-8,*trans*-10, *trans*-9,*trans*-11 and *trans*-10,*trans*-12

Table 2 Composition (w/w) of the five experimental purified diets

Ingredient	(%)
Casein	23
DL-methionine	0.3
Cornstarch	38.2
Sucrose	15
Lard	10
CLA or LA[a]	2
Cellulose	5
Minerals AIN-93	3.5
Vitamins AIN-93VX	1
CaHPO4	1.5
Choline Bitartrate	0.2
Cholesterol	0.3
BHT[b]	0.002

[a] Conjugated linoleic acid or linoleic acid

[b] Butylated Hydroxytoluene

Experimental Animals

Fifty-one growing golden Syrian hamsters (Charles River laboratories, St-Constant, QC, Canada) weighing 50–60 g on arrival were housed individually in plastic cages. The temperature (20 ± 2°C) and relative humidity (45–55%) of the animal room were constant, and the hamsters were kept under a daily light–dark cycle (0900 to 2100). Upon arrival, hamsters were maintained on a ground non purified (NPD) commercial diet (Purina, St Louis, MO) for 6 days to adapt them to their new environment. Following this adaptation period, they were then randomly assigned to one of the three dietary groups on the basis of their body weight and feed intake during the 6-day adaptation period ($n = 17$ per group). They were then gradually transferred to their respective purified diet differing in lipid source by feeding a mixture of ground NPD and experimental diet over a 5-day period (25%ED/75%NPD for 3 days, 50%ED/50%NPD for 1 day and 75%ED/25%NPD for 1 day).

Experimental diets and tap water were provided once daily on an ad libitum basis for a 28-day period. Records of food intake and body weight were taken every morning. This protocol was approved by the Animal Care Committee of Laval University according to the guidelines of the Canadian Council on Animal Care.

At day zero, prior to the 28-day feeding 100%ED period, measurements of body composition were taken when the hamsters were on front in the Piximus apparatus (Lunar, Madison, WI). After a 12-h fast, animals were weighed and anaesthetized with isoflurane in order to proceed to the measurement of body fat and lean mass with the help of X-ray from the sternum to the tail of the hamster. At the end of the 28-day feeding 100%ED period, similar body composition measurements were taken before sacrifice.

On day 18–20, hamsters were transferred to individual stainless-steel wire bottom mesh cages, for a 3-day feces collection. Feces were weighed and stored at −80 °C until further analysis.

Laboratory Analyses

After 28 days on experimental diets and after a 12-h overnight fast, immediately after body composition measurements, blood samples were collected by cardiac puncture in tubes containing disodium EDTA (0.05%). After blood collection, hamsters were quickly sacrificed by asphyxia with CO_2. Epididymal tissue and liver were rapidly removed, weighed, and frozen in liquid nitrogen and stored at −80 °C until subsequent analysis. Plasma was separated by centrifugation at 2,500 rpm for 10 min. An aliquot of plasma was frozen at −80 °C for further total lipid, glucose and insulin determinations. Another aliquot was stored at 4 °C until the next day.

The day following blood sampling, lipoproteins were separated from fresh plasma by ultracentrifugation (TL-100 Tabletop Ultracentrifuge, Beckman, Palo Alto, CA) at 100,000 rpm and 15 °C for 120 min using a TLA-100.4 rotor. The density of plasma samples was adjusted to 1.063 g/ml by adding a solution of NaBr–NaCl 1.478 g/ml [19]. A two-step density gradient was formed by layering the density-adjusted plasma underneath NaCl solution ($d = 1.006$ g/ml). Triglyceride-rich lipoproteins, chylomicrons and very low-density lipoproteins (VLDL) ($d <$ 1.006 g ml), low-density lipoproteins (LDL) ($1.006 < d < 1.063$ g/ml) and high-density lipoproteins (HDL) ($1.06 < d < 1.21$ g/ml) were then fractionated. Coomassie blue (5% w/w) was used as a dye to locate the lipoprotein fractions. Plasma cholesterol and triglycerides were measured in these lipoproteins as well as in the total fresh plasma using the Triglycerides/GB and CHOD-PAP enzymatic kits (Roche Diagnostics, Laval, Quebec). Phospholipids in plasma were determined using Phospholipids B Enzymatic colorimetric Method (Wako Chemicals USA).

According to the method of Folch et al. [20], hepatic lipids were extracted with chloroform/methanol (2:1, v/v). Hepatic triglycerides and cholesterol were then measured using the Triglycerides/GB and CHOD-PAP enzymatic kits (Roche Diagnostics, Laval, Quebec), as described above.

Plasma glucose was measured with a glucose oxidase method [21] using a glucose analyzer (Technicon RA-TX), and the plasma insulin level was measured by radioimmunoassay using rat insulin standards and polyethylene glycol for separation [22].

In order to determine fecal fat content, extraction with anhydrous diethyl ether (Soxtec System HT 1043 Extraction Unit; Tecator Inc., Höganäs, Sweden) after acid hydrolysis (4M HCL) for 30 min (Soxtec System 1047 Hydrolysing Unit; Tecator Inc.) was performed on lyophilized and ground feces [23].

Statistical Analysis

Results were analyzed using the general linear model (GLM) procedure of the Statistical Analysis System (SAS Institute, Cary, NC, USA). When statistically significant diet effects were detected by ANOVA (at a probability level inferior to 0.05), Tukey's studentized range (HSD) test was performed to identify differences among diet groups. However data on fecal fat content were log-transformed in order to normalize their distribution prior to statistical analysis. All data, including those on fecal fat content, are presented in tables as non-transformed means ± SEM. Pearson correlation coefficients were used to quantify the univariate associations among variables.

Results

Food Intake and Body Weight and Composition

At the end of the 28-day experimental period, hamsters displayed similar daily food intake and body weight gain regardless to the lipid source (Table 3).

Table 3 Mean food intake and body weight of male hamsters fed the five purified diets for 28 days

	LA	*cis*-9,*trans*-11 + *trans*-10,*cis*-12 CLA	*cis*-9,*trans*-11 + *trans*-8,*cis*-10 CLA
Mean food intake (g/day)	6.7 ± 0.2	7.0 ± 0.2	6.5 ± 0.1
Initial body weight (g)	69 ± 1	70 ± 1	67 ± 1
Final body weight (g)	99 ± 2	102 ± 2	97 ± 2
Body weight gain (g)	30 ± 2	31 ± 1	30 ± 2

Values are mean ± SEM. For abbreviations see Table 1

Number of animals: $n = 17$, except for *cis*-9,*trans*-11 + *trans*-10,*cis*-12 CLA, $n = 16$

Diets were similar in content, except for the source of fat: *LA* linoleic acid, *CLA* conjugated linoleic acid having different isomerisation

Plasma Lipids

The CLA mixtures used in this study differently affected LDL cholesterol as well as VLDL cholesterol and triglyceride concentrations (Table 4). The *cis*-9,*trans*-11 + *trans*-10,*cis*-12 CLA mixture induced higher LDL cholesterol concentrations than the *cis*-9,*trans*-11 + *trans*-8,*cis*-10 CLA mixture and LA. On the other hand, feeding the *cis*-9,*trans*-11 + *trans*-8,*cis*-10 CLA mixture increased VLDL cholesterol and triglyceride concentrations compared to LA and the *cis*-9,*trans*-11 + *trans*-10,*cis*-12 CLA mixture.

Plasma Glucose and Insulin

The *cis*-9,*trans*-11 + *trans*-8,*cis*-10 CLA mixture showed the highest plasma glucose concentration compared to the other two groups. However, no significant differences were observed for plasma insulin among the three experimental diets (Table 5).

Hepatic Lipids

Hepatic cholesterol concentrations of the animals fed the *cis*-9,*trans*-11 + *trans*-10,*cis*-12 CLA mixture were

Table 4 Plasma lipids of male hamsters fed the five purified diets for 28 days

	LA	*cis*-9,*trans*-11 + *trans*-10,*cis*-12 CLA	*cis*-9,*trans*-11 + *trans*-8,*cis*-10 CLA
Total cholesterol (mmol/L)	5.3 ± 0.3	6.0 ± 0.3	6.2 ± 0.2
VLDL cholesterol (mmol/L)	2.0 ± 0.3^b	1.8 ± 0.1^b	2.7 ± 0.2^a
LDL cholesterol (mmol/L)	0.7 ± 0.1^b	1.0 ± 0.1^a	0.7 ± 0.1^b
HDL cholesterol (mmol/L)	3.0 ± 0.2	3.0 ± 0.2	2.9 ± 0.1
Total triglycerides (mmol/L)	2.5 ± 0.2	3.0 ± 0.3	3.3 ± 0.3
VLDL triglycerides (mmol/L)	2.4 ± 0.3^b	2.7 ± 0.4^b	3.7 ± 0.3^a
LDL triglycerides (mmol/L)	0.06 ± 0.02	0.06 ± 0.01	0.05 ± 0.01
HDL triglycerides (mmol/L)	0.1 ± 0.01	0.1 ± 0.01	0.1 ± 0.01
Total phospholipids (mmol/L)	3.9 ± 0.2	4.5 ± 0.3	4.0 ± 0.1

Values are mean ± SEM. Number of animals: $n = 17$, except for *cis*-9,*trans*-11 + *trans*-10,*cis*-12 CLA, $n = 16$

Diets were similar in content, except for the source of fat: *LA* linoleic acid; *CLA* conjugated linoleic acid having different isomerisation

[a,b] Mean values within a row not sharing a common letter were significantly different ($P < 0.05$)

Table 5 Glycemia and insulinemia of male hamsters fed the five purified diets for 28 days

	LA	*cis*-9,*trans*-11 + *trans*-10,*cis*-12 CLA	*cis*-9,*trans*-11 + *trans*-8,*cis*-10 CLA
Glycemia (mmol/L)	14 ± 1^{a}	15 ± 1^{a}	18 ± 1^{b}
Insulinemia (pmol/L)	444 ± 144	381 ± 92	507 ± 186

Values are mean ± SEM. Number of animals: $n = 17$, except for *cis*-9,*trans*-11 + *trans*-10,*cis*-12 CLA, $n = 16$

Diets were similar in content, except for the source of fat: *LA* linoleic acid; *CLA* conjugated linoleic acid having different isomerisation

[a,b] Mean values within a row not sharing a common letter were significantly different ($P < 0.05$)

significantly lower to those of animals fed either LA and the *cis*-9,*trans*-11 + *trans*-8,*cis*-10 CLA mixture. No difference was observed neither on hepatic triglyceride concentrations nor on liver weight between the three dietary groups (Table 6).

Body Composition

The hamsters from the three diet groups had a similar weight gain (30–31 g/day on the average) (Table 3). In accordance with this result, no difference was observed neither in body composition (lean mass, fat mass, total (fat + lean) mass, percentage fat, bone mass content and bone mass density) nor in the weight of epididymal fat pads between our three experimental groups (Table 7).

Fat Digestibility

The *cis*-9,*trans*-11 + *trans*-8,*cis*-10 CLA mixture and LA feeding led to lower fecal fat content than the *cis*-9,*trans*-11 + *trans*-10,*cis*-12 CLA mixture (Table 8). We also calculated a coefficient of digestibility of dietary fat [(fat intake − fat excreted)/fat intake] in order to take into account fat intake in addition to fecal fat. Based on those calculations, the *cis*-9,*trans*-11 + *trans*-8,*cis*-10 CLA mixture and LA had thus similar and higher coefficient of digestibility than the *cis*-9,*trans*-11 + *trans*-10,*cis*-12 CLA mixture (Table 8).

Discussion

Previous and current researches have focused their attention on the *cis*-9,*trans*-11 isomer and *trans*-10,*cis*-12 isomer and the CLA mixture composed of these two forms usually at a ratio of approximately 50:50 because they are produced in high quantities successfully by various methodologies. There is however, an increasing awareness that the other isomers may be responsible for certain metabolic changes [24]. Recently, a CLA mixture composed of *cis*-9,*trans*-11 + *trans*-8,*cis*-10 isomers has been produced. The results of the present study demonstrate that feeding a CLA mixture composed of *cis*-9,*trans*-11 + *trans*-8,*cis*-10 isomers induced higher plasma concentrations of VLDL cholesterol and triglycerides concomitant with higher plasma glucose compared with LA and the *cis*-9,*trans*-11 + *trans*-10,*cis*-12 CLA mixture in hamsters.

The *cis*-9,*trans*-11 + *trans*-8,*cis*-10 CLA mixture induced similar plasma LDL cholesterol and hepatic lipid concentrations, and coefficient of digestibility than LA, indicating no effect of the *trans*-8,*cis*-10 CLA isomer on these parameters. The *trans*-10,*cis*-12 isomer has been previously identified, rather than the *cis*-9,*trans*-11, as the ingredient being responsible for the biological effects on plasma lipids [5, 6, 14, 17]. In the present study, our data show that the *cis*-9,*trans*-11 + *trans*-10,*cis*-12 CLA mixture can increase LDL cholesterol and decrease hepatic cholesterol as previously did the *trans*-10,*cis*-12 isomer in

Table 6 Liver weight and hepatic lipids of male hamsters fed the five purified diets for 28 days

	LA	*cis*-9,*trans*-11 + *trans*-10,*cis*-12 CLA	*cis*-9,*trans*-11 + *trans*-8,*cis*-10 CLA
Liver weight (g)	4.9 ± 0.2	5.3 ± 0.2	5.1 ± 0.1
Hepatic triglycerides (μmoL/g)	7.1 ± 0.8	6.1 ± 1.1	5.9 ± 0.7
Total hepatic triglycerides (μmoL)^{c}	32 ± 4	32 ± 3	30 ± 3
Hepatic cholesterol (μmoL/g)	83 ± 4^{a}	62 ± 6^{b}	83 ± 4^{a}
Total hepatic cholesterol (μmoL)^{d}	392 ± 30^{a}	338 ± 32^{b}	420 ± 33^{a}

Values are mean ± SEM. Number of animals: $n = 17$, except for *cis*-9,*trans*-11 + *trans*-10,*cis*-12 CLA, $n = 16$

Diets were similar in content, except for the source of fat: *LA* linoleic acid; *CLA* conjugated linoleic acid having different isomerisation

[a,b] Mean values within a row not sharing a common letter were significantly different ($P < 0.05$)

[c] Total hepatic triglycerides = hepatic triglyceride concentrations × liver weight

[d] Total hepatic cholesterol = hepatic cholesterol concentrations × liver weight

Table 7 Body composition of male hamsters on day 0 and after 28 days of purified diets

	Day	LA	*cis*-9,*trans*-11 + *trans*-10,*cis*-12 CLA	*Cis*-9,*trans*-11 + *trans*-8,*cis*-10 CLA
Lean body mass (g)	0	52 ± 0.9	53 ± 1	50 ± 1
	28	73 ± 2	75 ± 2	72 ± 1
Body fat mass (g)	0	12 ± 0.5	11 ± 0.4	11 ± 0.4
	28	21 ± 1.0	22 ± 0.7	20 ± 0.6
Total (fat + lean) (g)	0	70 ± 1	64 ± 2	62 ± 2
	28	94 ± 2	97 ± 2	92 ± 2
Percentage body fat (%)	0	18 ± 0.5	18 ± 0.4	18 ± 0.4
	28	22 ± 0.5	22 ± 0.4	22 ± 0.5
Bone mass content (g)	0	0.8 ± 0.02	0.8 ± 0.02	0.8 ± 0.02
	28	1.5 ± 0.03	1.5 ± 0.04	1.4 ± 0.03
Bone mass density (g/cm^2)	0	0.05 ± 0.001	0.05 ± 0.001	0.05 ± 0.001
	28	0.1 ± 0.001	0.1 ± 0.001	0.1 ± 0.001
Epididymal fat tissue (g)	0	ND	ND	ND
	28	2.1 ± 0.2	2.4 ± 0.1	2.2 ± 0.1

Values are mean ± SEM. Number of animals: $n = 17$, except for *cis*-9,*trans*-11 + *trans*-10,*cis*-12 CLA, $n = 16$

Diets were similar in content, except for the source of fat: *LA* linoleic acid; *CLA* conjugated linoleic acid having different isomerisation

ND not determined

hamsters under physiological isoenergetic conditions [17]. These results suggest that the *cis*-9,*trans*-11 + *trans*-10,*cis*-12 CLA mixture may cause redistribution of cholesterol between serum and tissues leading to a lower level of hepatic cholesterol but a higher level of LDL cholesterol. Because this redistribution can result in part from variations in VLDL secretion and hydrolysis into the circulation and less affinity of LDL particles with LDL receptors following *trans*-10,*cis*-12 CLA feeding in hamsters, further studies on VLDL and LDL metabolism are thus necessary to gain more insight into this controversial result.

In the present work, reductions in hepatic cholesterol observed following *cis*-9,*trans*-11 + *trans*-10,*cis*-12 CLA mixture may also be attributed to decreased intestinal absorption of dietary fats. The *cis*-9,*trans*-11 + *trans*-10,*cis*-12 CLA mixture indeed lowered the coefficient of digestibility of dietary lipids and enhanced fecal fat content compared with LA. These results agree well with those of Terpstra et al. [25] observing increased energy lost in feces of mice fed *cis*-9,*trans*-11 + *trans*-10,*cis*-12 CLA mixture. Yeung et al. [26] have also shown a greater fecal neutral lipid (cholesterol and coprostanol) output in *cis*-9,*trans*-11 + *trans*-10,*cis*-12 CLA mixture fed hamsters and noted a downregulation of intestinal acyl CoA: cholesterol acyltransferase (ACAT) activity, an enzyme involved in the esterification and storage of intestinal cholesterol, associated with increased fecal sterols in hamsters following CLA mixture supplementation. According to Wrenn et al. [27], intestinal cholesterol is esterified before it is assembled in the chylomicrons and secreted into the lymphatic system. We thus hypothesized that the *cis*-9,*trans*-11 + *trans*-10,*cis*-12 CLA mixture may interfere with the absorption of dietary fats and cholesterol either by interfering with the action of intestinal fatty acid-binding proteins or by inhibiting ACAT activity in intestinal cells or both.

The most novel result of the present study is the demonstration that the *cis*-9,*trans*-11 + *trans*-8,*cis*-10 CLA

Table 8 Mean fecal fat content and coefficient of digestibility of dietary fat in male hamsters fed the three purified diets

	LA	*cis*-9,*trans*-11 + *trans*-10,*cis*-12 CLA	*cis*-9,*trans*-11 + *trans*-8,*cis*-10 CLA
Fecal fat content (% DM basis)[c]	3.44 ± 0.1[b]	4.89 ± 0.27[a]	4.03 ± 0.16[b]
Coefficient of digestibility[d]	0.964 ± 0.008[a]	0.943 ± 0.004[b]	0.957 ± 0.003[a]

Values are mean ± SEM. Number of animals: $n = 15$

Diets were similar in content, except for the source of fat: *LA* linoleic acid; *CLA* conjugated linoleic acid having different isomerisation

[a,b] Mean values within a row not sharing a common letter were significantly different ($P < 0.05$)

[c] Mean fecal fat content from pooled fecal samples, which were collected from day 18 to 20

[d] Coefficient of digestibility = (fat intake − fat excreted)/fat intake

mixture increased plasma VLDL cholesterol and triglyceride concentrations. It is unlikely that this effect can be attributed to the *cis*-9,*trans*-11 CLA isomer contained in the mixture since in a previous study using similar experimental conditions than this one [17], feeding hamsters with the *cis*-9,*trans*-11 isomer only did not modify VLDL composition as compared to LA. There is thus a high possibility that the *trans*-8,*cis*-10 CLA found at 35% in this mixture might be the physiologically active CLA isomer regarding VLDL cholesterol and triglyceride concentrations in the present study. However, because there were 18% of other minor isomers such as *cis*-*cis*-9,11 & 10,12 + *trans*-*trans* 8,10 & 9,11 & 10,12 in this CLA mixture (Table 1), we cannot completely exclude a contribution of those minor isomers in the deterioration of VLDL composition.

Based on normal fasting glucose concentrations of 3.6–9.5 mmol/L in hamsters [28], it appears that the lard-based diet in golden Syrian hamsters induced hyperglycemia under our control conditions (LA group). In the present study, the *cis*-9,*trans*-11 + *trans*-8,*cis*-10 CLA mixture compared with LA and the *cis*-9,*trans*-11 + *trans*-10,*cis*-12 CLA mixture worsened the existing hyperglycemia of our hamsters from 14 to 18 mmol/L, although plasma insulin levels were not different among the three experimental groups. There is a possibility that an increased hepatic lipogenesis stimulated by an increased flux of glucose could explain, at least in part, some of the increase of VLDL triglycerides in the animals fed the *cis*-9,*trans*-11 + *trans*-8,*cis*-10 CLA mixture. We also observed a slight positive correlation between VLDL triglycerides and percentage body fat ($r = 0.31, P = 0.007, n = 50$), suggesting a slightly greater transport of free fatty acids from adipose tissue to the liver that can also be used for de novo hepatic VLDL triglyceride synthesis. However, plasma free fatty acid concentrations have not been measured to support this explanation. The impact of the *cis*-9,*trans*-11 + *trans*-8,*cis*-10 CLA mixture on glucose tolerance, however, remains to be studied further.

In conclusion, we confirmed part of our hypothesis that the effects of *cis*-9,*trans*-11 + *trans*-8,*cis*-10 CLA mixture on plasma lipids differed from those of *cis*-9,*trans*-11 + *trans*-10,*cis*-12 CLA mixture by causing a deterioration of VLDL cholesterol and triglycerides associated with increased plasma glucose. Future studies are thus required to study the impact of the *cis*-9,*trans*-11 + *trans*-8,*cis*-10 CLA mixture on hepatic VLDL secretion into the circulation, on postheparin lipoprotein lipase and hepatic triglyceride lipase activities in plasma as well as on insulin sensitivity.

Acknowledgments The assistance of Pierre Samson and Roxanne Papineau, for their dedicated technical help which was greatly appreciated. This research was supported by research funding from the Dairy Farmers of Canada.

References

1. Kelly GS (2001) Conjugated linoleic acid: a review. Altern Med Rev 6:367–382
2. Eulitz K, Yurawecz MP, Sehat N, Fritsche J, Roach JA, Mossoba MM, Kramer JK, Adlof RO, Ku Y (1999) Preparation, separation, and confirmation of the eight geometrical *cis*/*trans* conjugated linoleic acid isomers 8, 10- through 11, 13 18:2. Lipids 34:873–877
3. McLeod RS, LeBlanc AM, Langille MA, Mitchell PL, Currie DL (2004) Conjugated linoleic acids, atherosclerosis, and hepatic very-low-density lipoprotein metabolism. Am J Clin Nutr 79:1169S–1174S
4. Destaillats F, Japiot C, Chouinard PY, Arul J, Angers P (2005) Rearrangement of rumenic acid in ruminant fats: a marker of thermal treatment. J Dairy Sci 88:1631–1635
5. Wang YM, Nagao K, Inoue N, Ujino Y, Shimada Y, Nagao T, Iwata T, Kamegai T, Yamauchi-Sato Y, Yanagita T (2006) Isomer-specific anti-obese and hypolipidemic properties of conjugated linoleic acid in obese OLETF rats. Biosci Biotechnol Biochem 70:355–362
6. Navarro V, Zabala A, Macarulla MT, Fernandez-Quintela A, Rodriguez VM, Simon E, Portillo MP (2003) Effects of conjugated linoleic acid on body fat accumulation and serum lipids in hamsters fed an atherogenic diet. J Physiol Biochem 59:193–199
7. Faulconnier Y, Arnal MA, Patureau Mirand P, Chardigny JM, Chilliard Y (2004) Isomers of conjugated linoleic acid decrease plasma lipids and stimulate adipose tissue lipogenesis without changing adipose weight in post-prandial adult sedentary or trained wistar rats. J Nutr Biochem 15:741–748
8. Nicolosi RJ, Rogers EJ, Kritchevsky D, Scimeca JA, Huth PJ (1997) Dietary conjugated linoleic acid reduces plasma lipoproteins and early aortic atherogenesis in hypercholesterolemic hamsters. Artery 22:266–277
9. Gavino VC, Gavino G, Leblanc MJ, Tuchweber B (2000) An isomeric mixture of conjugated linoleic acids but not pure *cis*-9, *trans*-11-octadecadienoic acid affects body weight gain and plasma lipids in hamsters. J Nutr 130:27–29
10. Kritchevsky D, Tepper SA, Wright S, Tso P, Czarnecki SK (2000) Influence of conjugated linoleic acid (CLA) on establishment and progression of atherosclerosis in rabbits. J Am Coll Nutr 19:472S–477S
11. DeLany JP, Blohm F, Truett AA, Scimeca JA, West DB (1999) Conjugated linoleic acid rapidly reduces body fat content in mice without affecting energy intake. Am J Physiol 276:R1172–R1179
12. Park Y, Albright KJ, Liu W, Storkson JM, Cook ME, Pariza MW (1997) Effect of conjugated linoleic acid on body composition in mice. Lipids 32:853–858
13. Larsen TM, Toubro S, Astrup A (2003) Efficacy and safety of dietary supplements containing CLA for the treatment of obesity: evidence from animal and human studies. J Lipid Res 44:2234–2241
14. De Deckere EA, van Amelsvoort JM, McNeil GP, Jones P (1999) Effects of conjugated linoleic acid (CLA) isomers on lipid levels and peroxisome proliferation in the hamster. Br J Nutr 82:309–317
15. Park Y, Storkson JM, Albright KJ, Liu W, Pariza MW (1999) Evidence that the *trans*-10, *cis*-12 isomer of conjugated linoleic acid induces body composition changes in mice. Lipids 34:235–241
16. Nagao K, Wang YM, Inoue N, Han SY, Buang Y, Noda T, Kouda N, Okamatsu H, Yanagita T (2003) The 10*trans*, 12*cis* isomer of conjugated linoleic acid promotes energy metabolism in OLETF rats. Nutrition 19:652–656
17. Bissonauth V, Chouinard Y, Marin J, Leblanc N, Richard D, Jacques H (2006) The effects of t10, c12 CLA isomer compared

with c9, t11 CLA isomer on lipid metabolism and body composition in hamsters. J Nutr Biochem 17:597–603
18. Reeves PG, Nielsen FH, Fahey GC Jr (1993) AIN-93 purified diets for laboratory rodents: final report of the American Institute of Nutrition ad hoc writing committee on the reformulation of the AIN-76A rodent diet. J Nutr 123:1939–1951
19. Hatch FT, Lees RS (1968) Practical methods for plasma lipoprotein analysis. Adv Lipid Res 6:1–68
20. Folch JM, Lees M, Sloane Stanley GH (1957) A simple method for the isolation and purification of total lipids from animal tissues. J Biol Chem 226:497–509
21. Richterich R, Dauwalder H (1971) Zur Bertimmung der Plasmaglucokonzentration mit der Hexokinase-Glucose-6-Phosphat-Dehydrogenase Methode. Schweiz Med Wochenschr 101:615–618
22. Desbuquois B, Aurbach GD (1971) Use of polyethylene glycol to separate free and antibody-bound peptide hormones in radioimmunoassays. J Clin Endocr Metab 37:732–738
23. Association of Official Analytical Chemists (1984) Official methods of analysis. 14th edn. AOAC, Washington
24. Banni S (2002) Conjugated linoleic acid metabolism. Curr Opin Lipidol 13:261–266
25. Terpstra AH, Beynen AC, Everts H, Kocsis S, Katan MB, Zock PL (2002) The decrease in body fat in mice fed conjugated linoleic acid is due to increases in energy expenditure and energy loss in the excreta. J Nutr 132:940–945
26. Yeung CHT, Yang L, Wang J, Chen ZY (2000) Dietary conjugated linoleic acid mixture affects the activity of intestinal acyl coenzyme A: cholesterol acyltransferase in hamsters. Br J Nutr 84:935–941
27. Wrenn SM Jr, Parks JS, Immermann FW, Rudel L (1995) ACAT inhibitors CL 283,546 and CL 283,796 reduce LDL cholesterol without affecting cholesterol absorption in African green monkeys. J Lipid Res 36:1199–1210
28. Field KJ, Sibold AL (1999) The laboratory hamster and gerbil. CRC, Boca Raton

Lipids (2008) 43:259–273
DOI 10.1007/s11745-007-3143-4

METHODS

Combining Results of Two GC Separations Partly Achieves Determination of All *cis* and *trans* 16:1, 18:1, 18:2 and 18:3 Except CLA Isomers of Milk Fat as Demonstrated Using Ag-Ion SPE Fractionation

John K. G. Kramer · Marta Hernandez · Cristina Cruz-Hernandez · Jana Kraft · Michael E. R. Dugan

Received: 24 October 2007 / Accepted: 2 December 2007 / Published online: 24 January 2008
© AOCS 2008

Abstract Milk fat is a complex mixture of geometric and positional isomers of monounsaturated and polyunsaturated, including short-, long- and branch-chain fatty acids (FAs). There has been partial success to resolve this mixture of FAs using different GC temperature programs, or a combination of GC isothermal and temperature programs. To overcome the problem associated with overlapping isomers prior silver-ion separation was recommended. However, this procedure is time consuming and not practical for routine analysis. In addition, previous methods focused mainly on the *trans* and *cis* isomers of 18:1. The present method takes advantage of differences in the relative elution times between different types of FAs. The method involved analyzing each milk fat using the same highly polar 100-m capillary column and GC instrument, and conducting two separations using temperature programs that plateau at 175 and 150 °C. The relative shift among the geometric and positional isomers at these two temperature settings was enough to permit identification of most of the *trans* and *cis* 16:1, 18:1 and 20:1, the *c*/*t*-18:2 and the *c*/*c*/*t*-18:3 isomers found in milk fat. The identity of these FAs was confirmed by prior separation of the total fatty acid methyl esters (FAMEs) of milk fat using Ag$^+$-SPE columns, and comparing the fractions to the total milk fat. The Ag$^+$-SPE technique was modified to obtain pure saturated, *trans*- and *cis*-monounsaturated and diunsaturated FAMEs. By combining the results from these two separate GC analyses, knowing the elution order, it was possible to determine most of the geometric and positional isomers of 16:1, 18:1, 20:1, 18:2 and 18:3 without a prior silver-ion separation. Only few minor FAs could not be resolved, notable the conjugated linoleic acid isomers that still required the complimentary Ag$^+$-HPLC separation. The two GC temperature programs have been successfully used to routinely analyze most FA isomers in total milk and beef fats in about 200 min without the use of prior silver-ion separations.

Keywords Gas chromatography · Ag-ion SPE · Milk fat · *cis* and *trans* isomers

Abbreviations

Ag$^+$-HPLC	Silver ion-high performance liquid chromatography
Ag$^+$-TLC	Silver ion-thin layer chromatography
CLA	Conjugated linoleic acid
FA	Fatty acid
FAME	Fatty acid methyl ester
GC	Gas chromatography
HPLC	High-performance liquid chromatography
MUFA	Monounsaturated fatty acid
PHVO	Partially hydrogenated vegetable oil
PUFA	Polyunsaturated fatty acid
SPE	Solid phase extraction
SFA	Saturated fatty acid

J. K. G. Kramer (✉) · M. Hernandez · C. Cruz-Hernandez
Guelph Food Research Center, Agriculture and Agri-Food
Canada, 93 Stone Road West, N1G5C9 Guelph, ON, Canada
e-mail: kramerj@agr.gc.ca

J. Kraft
Department of Animal Science, University of Vermont,
Burlington, VT 05405-0148, USA

M. E. R. Dugan
Lacombe Research Center, Agriculture and Agri-Food Canada,
Lacombe, AB, Canada

Introduction

Considerable efforts have been made in the past few years to modify the profile of milk fats by increasing such fatty acids (FAs) as rumenic (9*c*11*t*-18:2) and vaccenic acids (11*t*-18:1), as well as essential FAs and the long-chain polyunsaturated fatty acids (PUFAs), but their comprehensive analysis has proven challenging. Milk fat is already a complex mixture of up to 400 different FAs [1]. These can be short or long (4–26 carbons), branched or not, saturated, unsaturated (0–6 double bonds) or conjugated, and there are all possible geometric and positional isomers of mono-, di-, highly unsaturated poly- and conjugated FAs. Some FAs also contain hydroxyl, keto, or cyclic functional groups. By far the most common and convenient method to analyze such a complex mixture of FAs is by gas chromatography (GC) as their fatty acid methyl esters (FAMEs). There is general agreement that 100 m highly polar flexible fused-silica capillary columns are absolutely mandatory to help resolve this isomeric mixture [2–7]. Most researchers have used the 100% cyanopropylpolysiloxane coated phases (CP-Sil 88 by Varian Inc.; SP 2560 by Supelco Inc.; HP88 by Agilent Technol.) [2–13], while others have chosen slightly less polar phases equivalent to 70% cyanopropylpolysiloxane (BPX-70 by SGE Co. [14, 15] or CP Select by Varian Inc. [16]) that are slightly longer (BPX-70 at 120 m, and CP Select at 200 m) but more stable because these stationary phases are bonded.

The ideal method would be a single GC analysis but this is currently not possible. Therefore, several different approaches have been used to analyze the complete FA composition of milk fat. We developed a GC temperature program starting at 45 °C to resolve the short-chain FAs followed by a plateau temperature at 175 °C during the elution of the 18:1 isomers to resolve as many of the 16:1, 18:1 and 18:2 isomers as possible [3, 5, 9]. Decreasing the plateau temperature to 170 [11] or 165 °C [7], or introducing two plateau stages at 100 and 175 °C [13], did not improve the separation. To provide a definitive composition of many of these FA isomers, a prior separation of geometric isomers was introduced using silver ion-thin layer chromatography (Ag^+-TLC) followed by a GC analysis of the fractions at a low isothermal temperature of 120 °C that resolved all the 18:1 isomers except 6*t*-8*t*-18:1 and 6*c*-8*c*-18:1 [2, 3, 5–8, 14]. Prior fractionation using Ag^+-TLC has also been used to identify overlapping isomers in the 16:1 [17], 18:2 [18], and 18:3/20:1 [19] regions.

An alternative approach was to resolve the total milk fat FAMEs using one GC column to resolve the total milk lipids, followed by second GC operation at isothermal temperatures between 160 and 180 °C with a 100-m highly polar column to resolve the 18:1 isomers. The isothermal GC separations were performed using either the same [13, 20], or a different GC column [2, 17–19]. Some isothermal separations gave a partial resolution of 15*t*-18:1 from 9*c*-18:1, but with little improvement in the separation of the remaining 18:1 isomers. This approach requires two separate GC analyses and addressed only the resolution of 18:1 isomers, while ignoring overlapping in the 16:1, 18:2 and 18:3/20:1 regions.

Another technique was recently reported in which the FAMEs from milk fat were analyzed by GC using the 100-m highly polar columns, and the *cis*- and *trans*-18:1 isomers were isolated using reversed-phase HPLC followed by GC analyses [14]. This method is complicated involving two different instruments, at least three GC separations, and again only addressing the overlapping 18:1 isomers.

The analyses of the different conjugated linoleic acid (CLA) isomers is particularly challenging since many of the isomers do not separate under any of the isothermal or temperature program GC conditions [5, 6, 9, 12], even at isothermal conditions at 120 °C [3]. Therefore, regardless of the GC method used, a complimentary Ag^+-HPLC separation will be necessary to resolve most of the CLA isomers [21]. The final CLA isomer composition can then be determined by combining the GC and Ag^+-HPLC results [5, 6].

It is interesting to note that operating the GC under different isothermal temperature conditions has been shown to resolve overlapping peaks by taking advantage of differences in the relative elution times of different FA families. For example, the 20:1 and 18:3 isomers were resolved by decreasing the temperature from 180 to 155 °C that partly reversed the elution order of the 20:1 and 18:3 isomers relative to each other [22]. Several overlapping saturated FAMEs were also identified amongst the 18:1 and 18:2 isomers in milk fat by conducting isothermal separations between 130 and 190 °C [18].

In the present communication a GC method is described in which total milk lipids were analyzed using the same 100-m polar capillary column and two complementary GC temperature programs that resolved most of the 16:1, 18:1, 18:2, 18:3 and 20:1 isomers without the need for a prior argentation or reversed-phase chromatographic separation. Employing the two complementary GC temperature programs took advantage of changes in the elution order at different temperatures, the high efficiency of the 100-m polar capillary column to resolve FA isomers, and consistent column characteristics and detector responses when using the same GC column for both temperature programs. Partial support for the identity of the FAME isomers in milk fat was obtained by comparing the results with separations prepared using silver ion-solid phase extraction (Ag^+-SPE) columns recently available from Supelco Inc. (Bellefonte, PA). The separation of saturated, *trans*, *cis*, dienes, and trienes FAME fractions was achieved by modifying the solvent system reported recently for the Ag^+-SPE columns [23]. In this study, four milk lipids were selected that differed greatly in their total *trans*-18:1 content and isomer profile to demonstrate the effectiveness of resolving FAME pairs in the 16:1, 18:1/18:2, and 18:3/20:1 regions, particularly when adjacent isomers had large asymmetric distributions.

Materials and Methods

Selected milk fats were obtained from a previous study [24]. They were transesterified using $NaOCH_3$ as previously described [5, 25]. Details of the Ag^+-HPLC methodology for the complimentary separation and analysis of the CLA isomers were previously published [3, 5, 26]. All chemicals and solvents were of analytical grade.

Ag^+-SPE Cartridges

Ag^+-SPE cartridges (750 mg/6 mL) were purchased from Supelco Inc. (Bellafonte, PA). Before use, the cartridges were conditioned with 4 mL of acetone to remove any moisture followed by 4 mL of hexane. Total methylated lipids (about 1 mg total FAMEs in 1 mL hexane) were applied onto the column and eluted with 6 mL volumes of hexane containing increasing amounts of acetone: 99:1 (v/v) eluted saturated FAMEs, 96:4 (v/v) eluted mono-*trans* FAMEs plus the *t*/*t* FAME isomers of CLA; 90:10 (v/v) eluted mono-*cis* FAMEs plus the *c*/*t* FAME isomers of CLA; 0:100 (v/v) eluted dienoic FAMEs. This was followed by 3% acetonitrile in acetone to elute trienoic FAMEs, and 6% acetonitrile in acetone to elute tetraenoic FAMEs. All fractions were taken to dryness in a stream of N_2, reconstituted in an appropriate volume of hexane for analysis by GC.

Gas Chromatography (GC)

A Hewlett Packard Model 5890 Series II GC was used and equipped with a flame ionization detector operated in splitless mode and flushed 0.3 min after injection, an autosampler (HP Model 7673), a 100-m CP-Sil 88 fused capillary column (Varian Inc., Mississauga, ON) and a software program (Agilent ChemStation, Version A.10). Injector and detector temperatures were kept at 250 °C. Hydrogen was used as carrier gas at a flow rate of 1 mL/min and for the flame ionization detector at 40 mL/min. The other gases were purified air at 250 mL/min and N_2 makeup gas at 25 mL/min. The injection volume was 1 µL of FAME mixtures containing about 1–2 µg/µL. The three temperature programs evaluated are summarized in Table 1. Each milk fat was routinely analyzed using the three GC programs in series in this study but only the results of the 175 and 150 °C programs were used in determining the final analysis.

FAME Standards

The FAMEs were compared to a GC reference standard (#463) and spiked with a mixture of four positional CLA isomers (#UC-59M) and long-chain saturated FAMEs 21:0, 23:0 and 26:0; all FAMEs were obtained from Nu-Chek Prep Inc. (Elysian, MN). A branch-chain FAs standard was available from Matreya Inc. (Pleasant Gap, PA). Identification of the *trans*-18:1, 16:1 and 20:1 isomers are based on principles of silver-ion separation, selected isomers in the GC reference standard #463, and on comparison with previously published reports [2, 3, 5, 19, 27]. A few *t*/*t*- and *c*/*t*-18:2 and *c*/*c*/*t*-18:3 standards were available, i.e., 9*t*12*t*-18:2 in GC standard #463, and previously synthesized 9*c*12*t*- and 9*t*12*c*-18:2, and 9*c*12*c*15*t*-, 9*c*12*t*15*c*- and 9*t*12*c*15*c*-18:3 [4]. The assignment of the remaining *c*/*t*-18:2 isomers was based on GC chromatographic principles, known diet related metabolites, and on comparison with previously published reports [18, 28]. It is important to evaluate each GC column with the standards given there are slight differences between columns even from the same supplier [5, 29].

Combining Selective Sections from the Two GC Programs

It was found that comprehensive FA analysis could be achieved by combining the results of the 175 and 150 °C temperature programs. The 175 °C results were used as the quantitative reference, while the results at 150 °C were used to complement or correct these data. When selecting

Table 1 Details of the three GC temperature programs evaluated

Descriptions	175 °C	163 °C	150 °C
Initial temperature (°C)	45	45	45
Time (min)	4	4	4
First rate of increase (°C/min)	13	13	13
Plateau temperature (°C)	175	163	150
Time (min)	27	37	47
Second rate of increase (°C/min)	4	4	4
Final temperature (°C)	215	215	215
Time (min)	35	40	35
Total time (min)	86	103.8	110.33

groups of FAs to be corrected, the beginning and end position of the FA cluster should be baseline resolved and each cluster should contain the same FAs from both GC separations. In the case of the 18:1 isomers the region from 4*t*-18:1 to 19:0/15*c*-18:1 was selected, for the 16:1 isomers the 4*t*-16:1 to 17:0/13*c*-16:1 region was selected, and for the 20:1/18:3 isomers the 18:3n-6 to 18:3n-3/13*c*-20:1 region was used. The 175 °C results were calculated as relative percent of total FAMEs, while only the integrated values were used from the 150 °C results to calculate the corrected composition. If a specific FA was resolved in both chromatographic separations, the 175 °C value was chosen. Sample calculations are provided in the Results and discussion and in the tables. It should be noted that in attempting to calculate FAs present in trace amounts by difference, these can at times result in negative values. The short-chain FAs from 4:0 to 11:0 were corrected for mass discrepancy using the correction factors published by Wolff et al. [30].

Results and Discussions

To evaluate this method, four milk fats were selected from a recent study in which cows were fed a barley-corn based concentrate containing a mixture of 4.5% sunflower oil and 0.5% fish oil in which the concentrate to forage ratio was 50:50 [24]. These milk fats showed great differences in the total *trans*-18:1 content and isomer distribution. One milk fat contained 3% total *trans*-18:1 and showed a pattern of 18:1 isomers general seen in commercial milk fats in Canada [5, 6] (Fig. 1, milk fat A), while the other three milk fats selected contained much higher levels of total *trans*-18:1 (13–21%) that is often observed when diets with a high concentrate (consisting of corn, barley or wheat, etc.) to forage ratio, and/or PUFAs are fed. In these samples the predominant *trans*-18:1 isomer was either 11*t* (Fig. 1, milk fat B), 10*t* (Fig. 1, milk fat D) or both (Fig. 1, milk fat C). The separations shown in Fig. 1 were those obtained using the temperature program with a plateau at 175 °C. Except for the milk fat low in total *trans* (Fig. 1, milk fat A), most of the *trans*-18:1 isomers from 6*t*-8*t*- to 11*t*-18:1 were not well resolved that often leads to misidentification of the isomers.

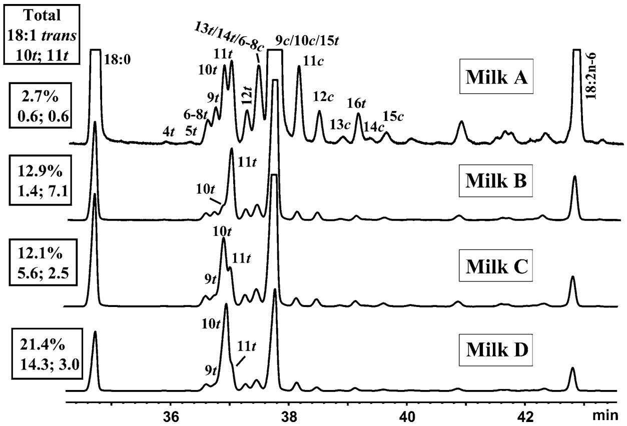

Fig. 1 Partial GC chromatogram of the four milk fats selected (*A*–*D*) are shown from 18:0 to 18:2n-6. The total *trans*-, 10*t*- and 11*t*-18:1 content of each of the milk fats is listed on the *left* hand side. The *trans*- and *cis*-18:1 isomers are identified. The 175 °C GC temperature program was used for the analysis of these milk fats; see specifics of GC program in Table 1

Three separate GC temperature programs were evaluated in this study (Table 1). Decreasing the temperature at the plateau from 175 to 163 and 150 °C resulted in a marked improvement in the separation of the isomers 6*t*-8*t*- to 11*t*-18:1 (Fig. 2). The resolution of these isomers is crucial when evaluating milk fats with increased levels of total *trans*-18:1 to determine whether 11*t*- (Fig. 2, milk fat B) or 10*t*-18:1 (Fig. 2, milk fats C and D) was predominantly produced. At 175 °C the isomers adjacent to the major *trans*-18:1 isomers were barely recognizable, while at 150 °C all isomers were clearly resolved. The decrease in temperature from 175 to 150 °C resulted in an increase in the elution times of the *trans*-18:1 isomers relative to the saturated FAs (carbon number increased by about 0.2), which improved the resolution of the *trans* isomers, while the elution times of the *cis*-18:1 isomers relative to the saturated FAs remained virtually the same. This relative shift among the geometric 18:1 isomer with temperature resulted in 15*t*-18:1 eluting between 9*c*- and 11*c*-18:1 at 163 °C, and coeluting with 11*c*-18:1 at 150 °C (Fig. 2). There was also a reversal in the elution sequence of 16*t*- and 14*c*-18:1; at 175 °C 16*t*-18:1 eluted slightly before, at 163 °C coeluted with, and at 150 °C slightly after 14*c*-18:1. Confirmation of identification will be provided based on silver ion separation, see below.

Confirmation of 18:1 Isomers Using Ag^+-SPE Separated Fractions

To establish identification of all the geometric and positional 18:1 isomers in total milk FAMEs, fractions were prepared using Ag^+-SPE cartridges to separate the total milk fat FAMEs based on the number and geometric configuration of double bonds. The procedure using Ag^+-SPE columns was modified to yield highly purified fractions of saturated, mono *trans* plus *t*,*t*-CLA, mono *cis* plus *c*/*t*-CLA, and diene FAMEs; the more polyunsaturated fractions are not presented. The Ag^+-SPE fractions obtained from each of the milk fats were compared to the total FAME mixture from each milk fat at 175 °C (Fig. 3), 163 °C (Fig. 4) and 150 °C (Fig. 5). In each of these

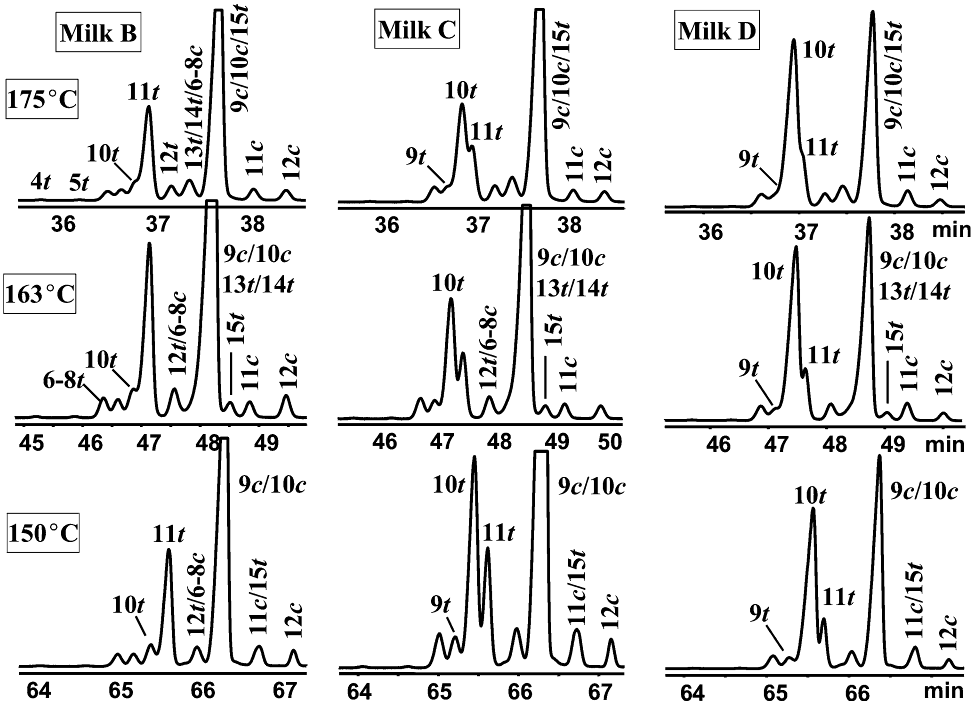

Fig. 2 Partial GC chromatogram of three milk fats (*B–D*) are shown from 4*t*- to 12*c*-18:1 that contained a high total *trans*-18:1 content. Separations were performed using the 175 °C (*top row*), 163 °C (*middle row*) and 150 °C (*bottom row*) GC programs. Selected *trans*- and *cis*-18:1 isomers are identified to indicate the changes in the elution order of these 18:1 isomers with temperature

figures the region between 9*c*-18:1 and 18:2n-6 was enlarged and inserted for clarity in the partial GC chromatogram of total milk fat.

Each of the temperature programs provided a slightly different separation that made possible the identification of all the *trans*-18:1 isomers either directly or indirectly by difference (Figs. 3, 4, 5). The isomers 4*t*- to 11*t*-18:1 were best resolved at 150 °C (Fig. 5). The 12*t*-18:1 isomer was only free of interfering *cis*-18:1 isomers at 175 °C (Fig. 3); at both 163 and 150 °C it coeluted with 6*c*-8*c*-18:1 (Figs. 4, 5). On the other hand, 13*t*-/14*t*-18:1 coeluted with 6*c*-8*c*-18:1 at 175 °C (Fig. 3) and with 9*c*-18:1 at 163 and 150 °C (Figs. 4, 5). The 15*t*-18:1 isomer coeluted with 9*c*-18:1 at 175 °C and with 11*c*-18:1 at 150 °C, but was resolved at 163 °C (Fig. 4). Generally, either the GC separations at 175 °C (Fig. 3) or 150 °C (Fig. 5) provided an adequate separation of 16*t*- and 14*c*-18:1.

The 6*c*-8*c*-18:1 isomers are generally minor components in milk fat but they can be determined by difference from

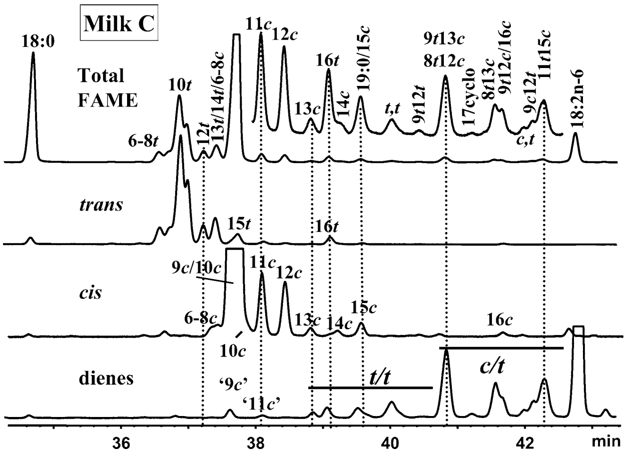

Fig. 3 Partial GC chromatogram of milk fat C separated using GC program 175 °C and showing the 18:0 to 18:2n-6 region. An enlargement of the 11*c*-18:1 to 11*t*15*c*-18:2 is inserted for clarity. The *trans*, *cis* and diene fractions isolated from total milk fat FAMEs using Ag^{+}-SPE columns and are compared to the total milk fat FAMEs. The structure of all the *t*/*t*-18:2 isomers, except 9*t*12*t*-18:2 is unknown. The assignments of most *c*/*t*-18:2 isomers and methyl 11-cyclohexylundecanoate (17cyclo) is tentative, and based on comparison with some standards (9*c*12*t*-18:2 and 9*t*12*c*-18:2) and on previously published reports [4,18,19]

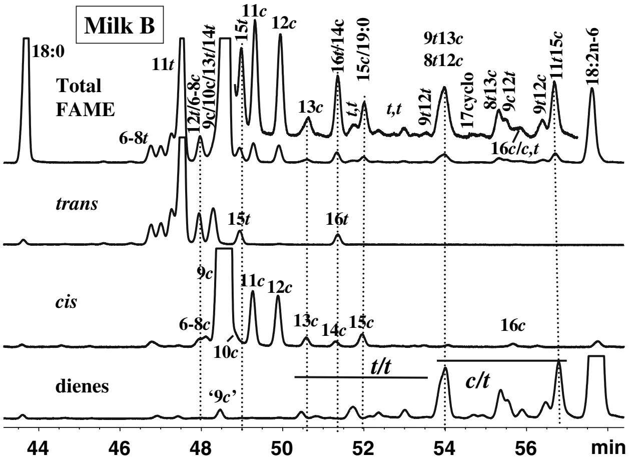

Fig. 4 Partial GC chromatogram of milk fat B separated using GC program 163 °C and showing the 18:0 to 18:2n-6 region. An enlargement of the 11*c*-18:1 to 11*t*15*c*-18:2 is inserted for clarity. For remaining description see caption Fig. 3

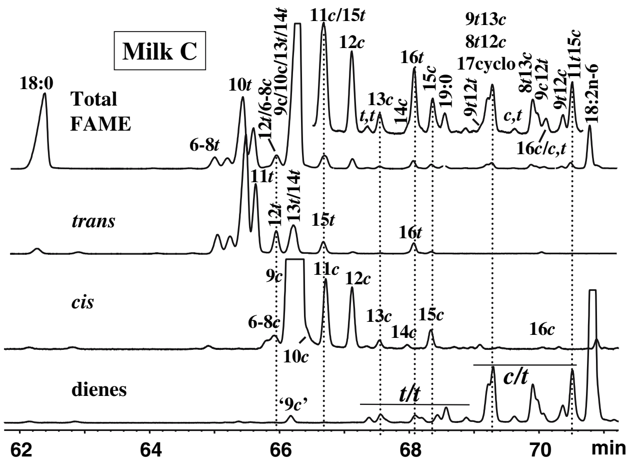

Fig. 5 Partial GC chromatogram of milk fat C separated using GC program 150 °C and showing the 18:0–18:2n-6 region. An enlargement of the 11*c*-18:1–11*t*15*c*-18:2 is inserted for clarity. For remaining description see caption Fig. 3

the 13*t*-/14*t*-18:1 peak at 175 °C (Fig. 3), or from the 12*t*-18:1 peak at 163 and 150 °C (Figs. 4, 5). The predominant 9*c*-18:1 isomer contained 10*c*- and 15*t*-18:1 at 175 °C (Fig. 3), and 10*c*- plus 13*t*-/14*t*-18:1 at 163 and 150 °C (Figs. 4, 5). Unfortunately, the minor 10*c*-18:1 isomer cannot be resolved from the 9*c*-18:1 peak under any of these temperature conditions; and even at an isothermal conditions at 120 °C a separation was not often always possible because of the predominance of the 9*c*-18:1 isomer [5, 6, 31]. The 11*c*- and 12*c*-18:1 isomers are free of interferences at 175 °C (Fig. 3) and 163 °C (Fig. 4), however, at 150 °C 15*t*- coeluted with 11*c*-18:1 (Fig. 5). The isomers 13*c*-, 15*c*- and 16*c*-18:1 all coeluted with *t*,*t*- or *c*/*t*-18:2 isomers using all GC programs (Figs. 3, 4, 5). In the case of 13*c*-18:1, the coeluting *t*,*t*-18:2 isomer was similar in abundance, while 16*c*-18:1 was a minor component compared to the coeluting *c*/*t*-18:2 isomers (Fig. 5).

Representative Calculations of the 18:1 Isomers

The region from 4*t*-18:1 to 15*c*-18:1/19:0 in the 175 and 150 °C GC separations was chosen to calculate all the 18:1 isomers except 16*c*-18:1, since it encompasses all the same FAs in both chromatograms, and the terminal FAMEs were base line resolved. Table 2 lists each of the peaks identified in both chromatograms. Also included in Table 2 is the best GC program, or combination of programs to calculate the correct composition for each of the 18:1 isomers. To determine the concentration of any FA isomer from the 150 °C results, simply multiply the ratio of area counts of that FA over the total area count of 4*t*-18:1 to 15*c*-18:1/19:0 at 150 °C by the total relative percent of all FAMEs from 4*t*-18:1 to 15c-18:1/19:0 at 175 °C. Examples of several FAs are included in Table 2. Several 18:1 isomers could not be resolved using this method, i.e., 6*t*-8*t*-, 6*c*-8*c*-, 13*t*/14*t*-, and 9*c*/10*c*-18:1. The first two groups of isomers have never been resolved by GC, while the last two pairs can be resolved, but only at low isothermal conditions after prior argentation separation. Unequivocal identification of all the *trans*- and *cis*-18:1 can be obtained by analyzing the *trans* and *cis* fraction from Ag$^+$-SPE at a low isothermal temperature condition of 120 °C that resolved the isomers except 6*t*-8*t*-18:1 (Fig. 6) and 6*c*-8*c*-18:1 (results not presented). These results have been previously reported [3, 5, 6, 8, 17, 19], and therefore will not be discussed further.

Resolution of the 18:2 Isomers

Seldom discussed is the presence of *t*,*t*- and *c*/*t*-18:2 isomers in the region between 13*c*-18:1 and 18:2n-6, with few exceptions [4, 18, 19]. The peaks in this region were enlarged and appropriately inserted in Figs. 3, 4, 5, and the isolated diene fraction from each of the milk fats was included in each of these figures. In general, the *t*,*t*-18:2 isomers eluted ahead of the *c*/*t*-18:2 isomers on these GC columns in the region between 13*c*-18:1 and 9*t*13*c*/8*t*12*c*-18:2. The magnitude of the interferences of these *t*,*t*-18:2 isomers in total milk fat was not previously recognize; see diene fraction in Figs. 3, 4, 5. Selectively using the 175 and 150 °C program provides a more accurate estimate of the *cis*-18:1 isomers among these 18:2 dienes. The structure of most of the *t*,*t*-18:2 isomers remain to be identified, other than 9*t*12*t*-18:2, for which a standard is available. However, this isomer is only present as a trace component in milk fat.

The major *c*/*t*-18:2 peak in milk fat was 9*t*13*c*- plus 8*t*12*c*-18:2 that was partially resolved at 150 °C (Fig. 5). The 8*t*13*c*- plus 9*c*12*t*-18:2 isomers coelute with 16*c*-18:1 and they were partially resolved at all the temperatures. The third group of *c*/*t*-18:2 isomers include 9*t*12*c*-, 11*t*15*c*- plus an unknown *c*/*t*-18:2 isomer evident from the separations. The identification and resolution of the *c*/*t*-18:2 isomers in milk fat are of particular interest since they arise as intermediates of PUFA metabolism by rumen bacteria, for instance, 11*t*15*c*-18:2 is a metabolite of 18:3n-3. Therefore, many of the *t*,*t*- and *c*/*t*-18:2 isomers in milk fat might be different from those found in partially hydrogenated vegetable oils (PHVOs) that arise by random processes. Canola and soybean oils that contain both 18:2n-6 and 18:3n-3 were shown to give rise to four major (9*t*13*c*-, 9*c*12*t*-, 9*t*12*c*-, 9*c*15*c*-18:2) and seven minor isomers (9*t*12*t*-, 8*t*12*c*-, 8*t*13*c*-, 8*c*13*c*-, 9*t*15*c*-, 10*t*15*c*- and 9*c*13*c*-18:2) during partial hydrogenation [32]. If the *trans* containing dienoic FA isomers are confirmed as contributing to the development of coronary heart disease [33],

Table 2 Resolution of the geometric and positional 18:1, 16:1 and 20:1/18:3 isomers using the two GC programs

Fatty acids	175 °C	150 °C	Best GC program
Determination of the 18:1 isomers			
4*t*-18:1	4*t*-18:1	4*t*-18:1	175 °C
5*t*-18:1	5*t*-18:1	5*t*-18:1	175 °C
6*t*-8*t*-18:1	6*t*-8*t*-18:1	6*t*-8*t*-18:1	150 °C
9*t*-18:1	9*t*-18:1	9*t*-18:1	150 °C
10*t*-18:1	10*t*-18:1	10*t*-18:1	150 °C
11*t*-18:1	11*t*-18:1	11*t*-18:1	150 °C
12*t*-18:1	12*t*-18:1	**12t**/6*c*-8*c*-18:1	175 °C
6*c*-8*c*-18:1	13*t*/14*t*/**6c-8c**-18:1	12*t*/**6c-8c**-18:1	150 °C-(12*t*) 175 °C
13*t*/14*t*-18:1	**13t/14t**/6*c*-8*c*-18:1	9*c*/10*c*/**13t/14t**-18:1	175 °C-(6*c*-8*c*) calc
9*c*/10*c*-18:1	**9c/10c**/15*t*-18:1	**9c/10c**/13*t*/14*t*-18:1	175 °C-(15*t*) calc
15*t*-18:1	9*c*/10*c*/**15t**-18:1	11*c*/**15t**-18:1	150 °C-(11*c*) 175 °C
11*c*-18:1	11*c*-18:1	**11c**/15*t*-18:1	175 °C
12*c*-18:1	12*c*-18:1	12*c*-18:1	175 °C
13*c*-18:1	**13c-18:1**/*tt*-18:2	13*c*-18:1	150 °C
14*c*-18:1	14*c*-18:1	14*c*-18:1	175 °C
16*t*-18:1	16*t*-18:1	16*t*-18:1	175 °C
15*c*-18:1	**15c**-18:1/19:0	15*c*-18:1	150 °C
19:0	15*c*-18:1/**19:0**	19:0	150 °C
	X = % total FAME[a]	Y = Total area count[b]	
Determination of the 16:1 isomers			
4*t*-16:1	4*t*-16:1	4*t*-16:1	175 °C
5*t*-16:1	5*t*-16:1	5*t*-16:1	175 °C
17:0 iso	**17:0 iso**/6*t*/7*t*/8*t*-16:1	9*t*-16:1/**17:0 iso**	150 °C-(9*t*) 175 °C
6*t*-7*t*-16:1	17:0 iso/**6t/7t**/8*t*-16:1	6*t*-7*t*-16:1	150 °C
8*t*-16:1	17:0 iso/6*t*/7*t*/**8t**-16:1	8*t*-16:1	150 °C
9*t*-16:1	9*t*-16:1	**9t-16:1**/17:0 iso	175 °C
10*t*-16:1	10*t*-16:1	10*t*-16:1	175 °C
11*t*/12*t*-16:1	11*t*/12*t*-16:1	7*c*/**11t/12t**-16:1	175 °C
13*t*-16:1	7*c*/**13t**-16:1/17:0 ai	13*t*-16:1	150 °C
17:0 ai	7*c*/13*t*-16:1/**17:0 ai**	9*c*-16:1/**17:0 ai**	150 °C-(9*c*) 175 °C
7*c*-16:1	**7c**/13*t*-16:1/17:0 ai	**7c**/11*t*/12*t*-16:1	150 °C-(11*t*/12*t*) 175 °C
9*c*-16:1	9*c*-16:1	**9c-16:1**/17:0 ai	175 °C
10*c*-16:1	10*c*-16:1	10*c*-16:1	175 °C
11*c*-16:1	11*c*-16:1	**11c**/14*t*-16:1	175 °C
12*c*-16:1	**12c**/14*t*-16:1/17:0	12*c*-16:1	150 °C
13*c*-16:1	13*c*-16:1	13*c*-16:1	175 °C
14*c*-16:1	Not in partial GC graph	14*c*-16:1	150 °C
17:0	12*c*/14*t*-16:1/**17:0**	17:0	150 °C
14*t*-16:1	12*c*/**14t**-16:1/17:0	11*c*/**14t**-16:1	150 °C-(11*c*) 175 °C
	M = % total FAME[c]	N = Total area count[d]	
Determination of the 20:1/18:3 isomers			
18:3n-6	18:3n-6	18:3n-6	175 °C
9*c*12*c*15*t*-18:3	**cct-18:3**/6*t*-11*t*-20:1	9*c*12*c*15*t*-18:3	150 °C
6*t*-11*t*-20:1	**6t-11t-20:1**/*cct*-18:3	6*t*-11*t*-20:1	150 °C
12*t*-20:1	12*t*-20:1	12*t*-20:1	175 °C
13*t*-20:1	13*t*-20:1	13*t*-20:1	175 °C
14*t*-20:1	**14t**/9*c*-20:1	**14t**/9*c*-20:1	Cannot be resolved

Table 2 continued

Fatty acids	175 °C	150 °C	Best GC program
15*t*/16*t*-20:1	15*t*/16*t*-20:1	**15*t*/16*t***/11*c*-20:1/*tcc*-18:3	175 °C
9*c*-20:1	9*c*-20:1	14*t*/**9*c***-20:1	175 °C
9*t*/12*c*/15*c*-18:3	11*c*-20:1/***tcc*-18:3**	15*t*/16*t*/11*c*-20:1/***tcc*-18:3**	175 °C-(11*c*) calc
11*c*-20:1	**11*c*-20:1**/*tcc*-18:3	15*t*/16*t*/**11*c***-20:1	150 °C-(15*t*/16*t*) 175 °C
13*c*-20:1	**13*c*-20:1**/18:3n-3	13*c*-20:1	150 °C
18:3n-3	13*c*-20:1/**18:3n-3**	18:3n-3	150 °C
	P = % total FAME[e]	*Q* = Total area count[f]	

Included is the suggested GC program to give the best results and the footnote has sample calculations

ai Anteiso, *calc* calculated, *cct* or *tcc* isomers of 18:3n-3; *FAMEs* fatty acid methyl esters

[a] *X* Total % FAMEs of 4*t*-18:1 to 15*c*-18:1/19:0 from GC results at 175 °C

[b] *Y* Total area response of FAMEs 4*t*-18:1 to 15*c*-18:1/19:0 from GC results at 150 °C

[c] *M* Total % FAMEs of 4*t*-16:1 to 13*c*-16:1/17:0 from GC results at 175 °C

[d] *N* Total area response of FAMEs 4*t*-16:1 to 13*c*-16:1/17:0 from GC results at 150 °C

[e] *P* Total % FAMEs of 18:3n-6 to 18:3n-3/13*c*-20:1 from GC results at 175 °C

[f] *Q* Total area response of FAMEs 18:3n-6 to 18:3n-3/13*c*-20:1 from GC results at 150 °C

Calculating the concentration of 9*t*-18:1 taken from the 150 °C results:

% [9*t*-18:1] = (area count of 9*t*-18:1 at 150 °C) (*X* % total FAMEs of 18:1 region)/(*Y* total area count of 18:1 region at 150 °C)

Calculating the concentration of 6*c*-8*c*-18:1 using values from both GC programs:

% [6*c*-8*c*-18:1] = [(area count of 12*t*/6*c*-8*c*-18:1 at 150 °C) (*X* % total FAMEs of 18:1 region)/(*Y* total area count of 18:1 region at 150 °C)] – [% 12*t*-18:1 taken from 175 °C results]

Calculating the concentration of 15*t*-18:1 using values from both GC programs:

% [15*t*-18:1] = [(area count of 11*c*/15*t*-18:1 at 150 °C) (*X* % total FAMEs of 18:1 region)/(*Y* total area count of 18:1 region at 150 °C)]–[% 11*c*-18:1 taken from 175 °C results]

Calculating the concentration of 9*c*/10*c*-18:1 using values from both GC programs:

% [9*c*/10*c*-18:1] = [% 9*c*/10*c*/15*t*-18:1 taken from 175 °C results] – [% 15*t*-18:1, calculation shown above]

then the differences in the *c*/*t*-18:2 isomer composition between milk fat and PHVOs will need to be examined closer to differentiate these two *trans*-containing fats. The combination of these two GC programs will be helpful to provide this information.

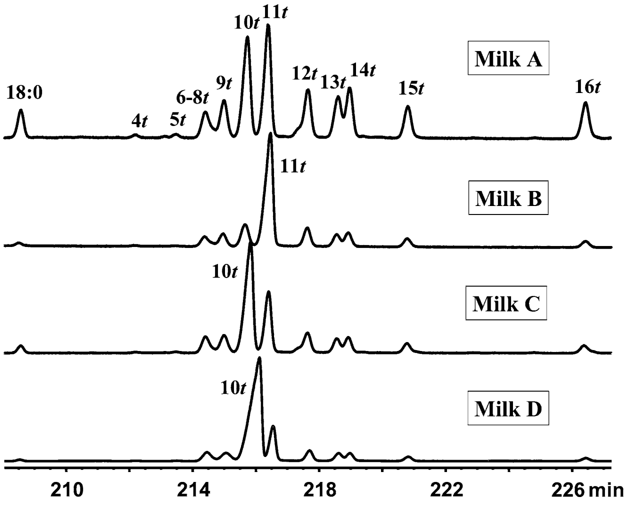

Fig. 6 Partial GC chromatogram of the 18:1 region of the *trans* fraction isolated from all four milk fats selected (*A*–*D*) using Ag$^+$-SPE chromatography and analyzed by GC operated isothermally at 120 °C. Details regarding the Ag$^+$-SPE separation are provided in Materials and methods section

Resolution of FA Isomers in the 16:1 Region

The 16:1 region is as complex as the 18:1 region, consisting of overlapping C17 branch-chain FAs, and *cis*- and *trans*-16:1 isomers. Precht and Molkentin [17] demonstrated with human milk fat that an inaccurate identification of these FAs leads to wrong conclusions as to a potential cause of coronary heart disease. These authors confirmed the identity of each of these FAs after prior separation using Ag$^+$-TLC and subsequent GC analysis of the fractions. In this study, we evaluated the results of the three GC temperature programs to see whether the FA composition of milk fat can be determined without prior argentation fractionation.

The separation of two milk fats is presented because the high content of total *trans* FAs markedly affected the 16:1 profile. The GC separation of a milk fat with a low content of total *trans* fat and analyzed using the 175 °C program is shown in Fig. 7, and the milk fat with a higher total *trans* content is shown in Fig. 8. In each figure the total milk fat separation was compared with the *trans*, *cis* and saturated fractions obtained using the Ag$^+$-SPE columns. At 175 °C both of the 17:0 branch-chain FAs coeluted, 17:0 iso with 6*t*- to 8*t*-16:1, and 17:0 anteiso with 7*c*- and 13*t*-16:1 (Figs. 7, 8). The *trans*-16:1 isomers were present as small peaks in the milk fat with a low total *trans* content; only small peaks corresponding to 9*t*- and 11*t*-/12*t*-16:1 were evident in the total milk fat (Fig. 7). On the other hand, when the total *trans* content was high, it was difficult to differentiate 17:0 iso among the *trans*-16:1 isomers, and the contribution of 13*t*- and 7*c*-16:1 to 17:0 anteiso were not negligible (Fig. 8). Several of the *trans*- and *cis*-16:1 isomers were well resolved using the 175 °C program, such as 9*t*-, 10*t*-, 11*t*-/12*t*-, 9*c*-, 10*c*-, 11*c*- and 13*c*-16:1 (Figs. 7, 8), while the minor isomers 12*c*- and 14*t*-16:1 coeluted with 17:0 at 175 °C. The assignment of the geometric 16:1 isomers was based on argentation chromatographic principles (number and geometric configuration of double bonds), on several authentic FAME standards, and on agreement with published reports in which the isomers were confirmed by GC/MS [17].

Lowering the plateau from 175 to 150 °C caused a similar relative shift among the *trans*- and *cis*-16:1 isomers as was observed among the 18:1 isomers, resulting in an altered pattern of elution of these FA isomers (Fig. 9). For example, at 150 °C there was a near baseline resolution of 8*t*- and 9*t*-16:1, but now 11*t*-/12*t*-16:1 and 7*c*-16:1, 13*t*-16:1 and 17:0, and 11*c*- and 14*t*-16:1 coeluted. There was also a shift of the branch-chain FAs relative to both the *trans*- and *cis*-16:1 isomers, such that 17:0 iso now coeluted with 9*t*-16:1, and 17:0 anteiso with 9*c*-16:1. At 150 °C several *trans*- and *cis*-16:1 isomers were well resolved, such as 4*t*- to 8*t*-, 10*t*-, 10*c*-, 12*c*-, 13*c*- and 14*c*-16:1 (Fig. 9). A section is included in Table 2 that summarizes the *trans*- and *cis*-16:1 isomers, and how best to determine the concentration of each of these isomers. For the 16:1 isomers the region from 6*t*-8*t*- to 17:0/13*c*-18:1 was selected.

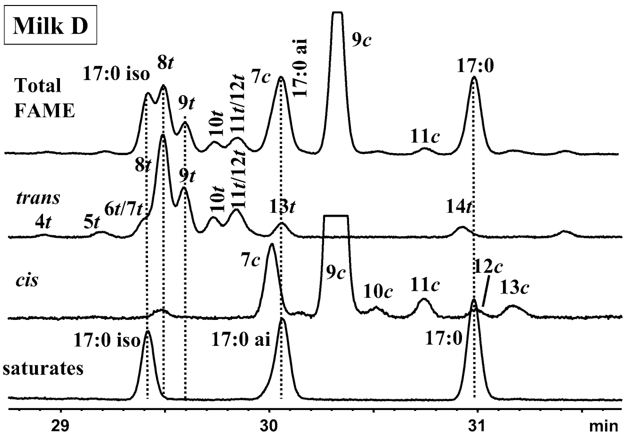

Fig. 8 Partial GC chromatogram of milk fat D separated using GC program 175 °C and showing the 16:1 region. The total milk FAMEs were compared to the *trans*, *cis* and saturated FA fractions isolated from total milk fat FAMEs using Ag$^+$-SPE columns. For remaining description see caption Fig. 7

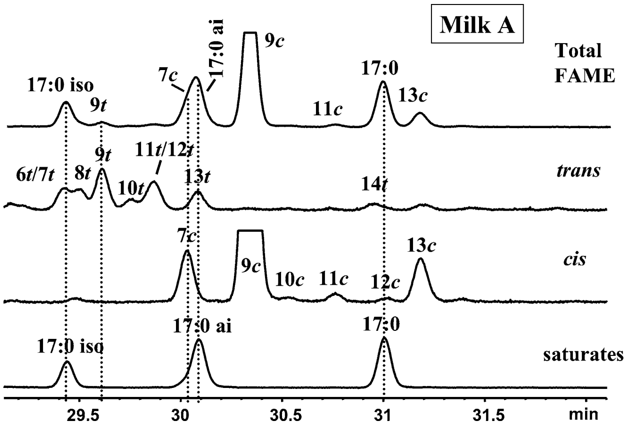

Fig. 7 Partial GC chromatogram of milk fat A separated using GC program 175 °C and showing the 16:1 region. The total milk FAMEs were compared to the *trans*, *cis* and saturated FA fractions isolated from total milk fat FAMEs using Ag$^+$-SPE columns. Details regarding the Ag$^+$-SPE separation are provided in Materials and methods. The assignments of several FAs were based on available standards (17:0, branch-chain FAs, and 9*t*- and 9*c*-16:1), while the others are based on silver-ion chromatographic principles and on a previously published report [17]

The individual *trans*-16:1 isomers isolated from the four milk fats by Ag$^+$-SPE are compared at the two GC temperature programs (Fig. 10). The separations were improved for each of the milk fats by decreasing the temperature from 175 to 150 °C, and there was a partial resolution of the 11*t*-/12*t*-16:1 pair at 150 °C. It is of

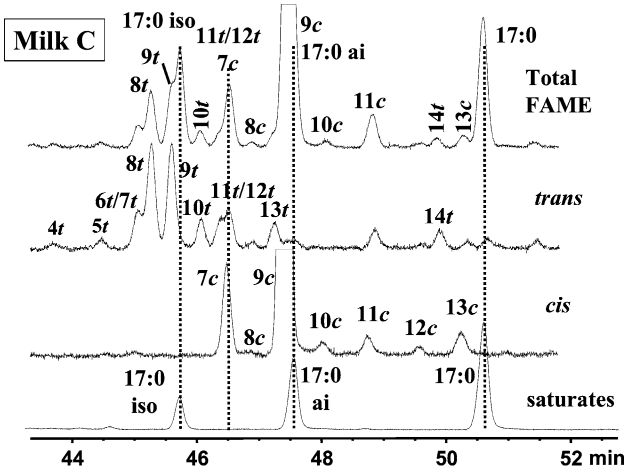

Fig. 9 Partial GC chromatogram of milk fat C separated using GC program 150 °C and showing the 16:1 region. The total milk FAMEs were compared to the *trans*, *cis* and saturated FA fractions isolated from total milk fat FAMEs using Ag$^+$-SPE columns. For remaining description see caption Fig. 7

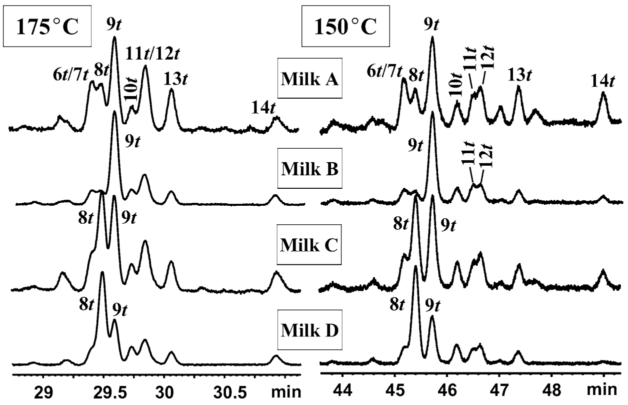

Fig. 10 Comparison of the *trans*-16:1 isomers from the *trans* fraction isolated using Ag$^+$-SPE columns of all four milk fats (*A*–*D*) that were separated by GC using the 175 and 150 °C temperature program. The assignments were based on silver-ion chromatographic principles and on a previously published report [17]. A partial separation of the 11*t*- and 12*t*-16:1 isomers was observed at 150 °C

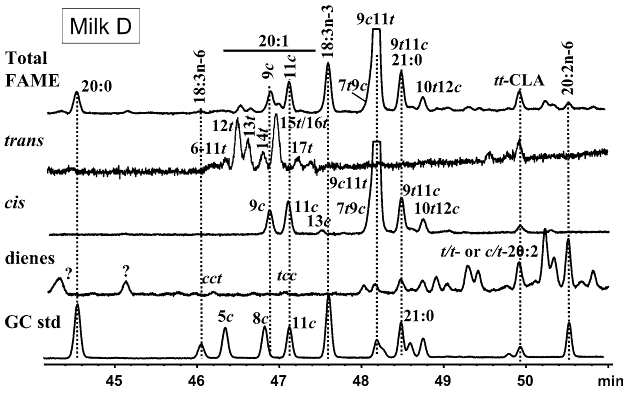

Fig. 11 Partial GC chromatogram of milk fat A separated using GC program 175 °C and showing the 20:0 to 20:2 region. The total milk FAMEs were compared to the *trans*, *cis* and diene fractions isolated from total milk fat FAMEs using Ag$^+$-SPE columns, and the GC standard #463 spiked with the CLA isomers and 21:0. The assignments of several FAs were based on available standards, on silver-ion chromatographic principles, and on previously published reports [4, 17, 27, 39]. The peaks in the diene fraction isolated using Ag$^+$-SPE and eluting before 20:2n-6 are *t*/*t*- or *c*/*t*-20:2 isomers that were confirmed by high-resolution selected-ion mass spectrometry [39] but their structure remains unknown

interest to note that the *trans*-16:1 isomers have a similar pattern as the *trans*-18:1 isomers, except being two carbons shorter. The milk fat with the predominant 11*t*-18:1 isomers (Fig. 2, milk fat B) had 9*t*-16:1 as the major *trans*-16:1 isomers (Fig. 10, milk fat B), and the milk fat with the predominant 10*t*-18:1 isomers (Fig. 2, milk fat D) had 8*t*-16:1 as the major *trans*-16:1 isomers (Fig. 10, milk fat D). On the other hand, the milk fat enriched with both 10*t*- and 11*t*-18:1 (Fig. 2, milk fat C) contained high amounts of both 8*t*- and 9*t*-16:1 (Fig. 10, milk fat C). Peroxisomal oxidation is a well-recognized process of FAs metabolism in cells in which FAs are chain-shortening [34]. The CLA isomers were also observed to convert to 16:2 products in rats [35, 36]. This is the first report demonstrating that altering the *trans*-18:1 profile affected the *trans*-16:1 isomer composition consistent with the expected peroxisomal oxidation products from the *trans*-18:1 isomers. It is unlikely that the *trans*-16:1 isomers were formed by biohydrogenation from C16 PUFA (16:2 or 16:3) precursors, analogous to 18:2n-6 and 18:3n-3 giving rise to *trans*-18:1 in ruminants [10–13, 20, 28], since C16 PUFAs were not present in the cow's diet. Furthermore, the presence of the peroxisomal oxidation products in milk fat does not exclude the possibility of their formation in other tissues and then being transferred into milk. It should be noted that the remaining milk fats from this feeding study [24] from which these four examples were selected also showed the same pattern in of the *trans*-18:1 and *trans*-16:1 isomers (data not shown).

Resolution of FA Isomers in the 20:1/18:3 Region

The 20:1/18:3 region in milk fat consists mainly of a mixture of overlapping *cis* and *trans*-20:1 and geometric and positional 18:3 isomers. The predominant FAs in this region are 9*c*- and 11*c*-20:1 and 18:3n-3, with minor amounts of 13*c*-20:1 and 18:3n-6 (Figs. 11, 12). However, depending on the diet fed to dairy cows, substantial amounts of either *trans*-20:1, *c*/*c*/*t*-18:3, or both can be present. The dairy cows in this study were fed a 50:50 forage to concentrate mixture containing sunflower oil that was high in 18:2n-6 [24], and therefore the milk fat had significantly elevated levels of *trans*-20:1 isomers (*trans* fraction), and only trace amounts of the 18:3 isomers (diene fraction) (Figs. 11, 12). Dairy cows fed diets supplemented with either soybean or canola oil would be

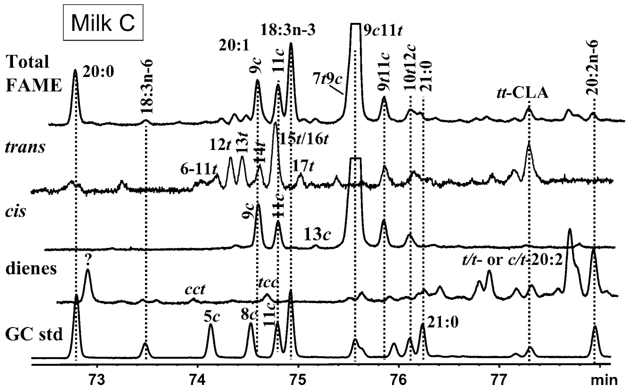

Fig. 12 Partial GC chromatogram of milk fat C separated using GC program 150 °C and showing the 20:0–20:2 region. The total milk FAMEs were compared to the *trans*, *cis* and diene fractions isolated from total milk fat FAMEs using Ag$^+$-SPE columns, and the GC standard #463 spiked with the CLA isomers and 21:0. For remaining description see caption Fig. 11

expected to have a more complex pattern of *trans*-20:1 and *c*/*c*/*t*-18:3 isomers in the milk fat, since these oils contain substantial amounts of 18:3n-3 compared to sunflower oil used in the feeding study from which these milk fats were taken [24]. There were two unknown peaks in the diene fraction near 20:0 (labeled unknown, '?') that appear to elute in the *c*,*t*,*t*- and *t*,*t*,*t*-18:3 region, but their identification will need to be confirmed by GC/MS.

The major *trans*-20:1 isomers were resolved from the *cis*-20:1 isomers at both 175 and 150 °C, i.e., the isomers 6*t*- to 13*t*-20:1 eluted well ahead of 9*c*-20:1 in both 175 and 150 °C (Figs. 11, 12). The unresolved 15*t*-/16*t*-20:1 pair was resolved from the *cis*-20:1 isomers only at 175 °C (Fig. 11), while 13*c*-20:1 was well separated at 150 °C (Fig. 12). However, the minor 14*t*-20:1 isomer could not be separated using either temperature program. The major *c*/*c*/*t*-18:3 isomers in the milk fat are 9*c*12*c*15*t*- and 9*t*12*c*15*c*-18:3 with trace amounts of 9*c*12*t*15*c*-18:3. The 9*c*12*c*15*t*-18:3 isomer eluting shortly after 18:3n-6, the 9*t*12*c*15*c*-18:3 isomers was best resolved from the 20:1 isomers at 150 °C (Fig. 12). A similar shift in the 20:1 and 18:3 isomers with temperature was previously reported by Wolf [22]. A summary of the FAs in the 20:1/18:3 region ranging from 18:2n-6 to 18:3n-3 is included in Table 2 and the GC program that is best used for their analysis.

Only the *trans*-20:1 isomers profile of the high *trans* containing milk fats are compared in Fig. 13. The low total *trans* milk fat (milk fat A) was not included since the *trans*-20:1 isomers in this sample were present only in trace amounts. The unresolved pair of 15*t*-/16*t*-20:1 was the predominant peak among the *trans*-20:1. This is the first report showing evidence that the pattern of the *trans*-18:1 isomers in milk fat were similar to the *trans*-20:1 isomers, except for being two carbons longer. The milk fat with the predominant 11*t*-18:1 isomer (Fig. 2, milk fat B) gave rise to increased levels of 13*t*-20:1 (Fig. 13, milk fat B), while the milk fat with the predominant 10*t*-18:1 isomer (Fig. 2, milk fat D) gave rise to 12*t*-20:1 (Fig. 13, milk fat D). The milk fat contained similar amounts of 10*t*- and 11*t*-18:1 (Fig. 2, milk fat C) gave rise to both 12*t*- and 13*t*-20:1 (Fig. 13, milk fat C). This suggests that the *trans*-18:1 isomers were chain-elongated to the *trans*-20:1 isomers. Analogous to the argument above for the *trans*-16:1 isomers, the origin of *trans*-20:1 isomers could not have been C20 PUFAs, but the site of chain-elongation is not clear.

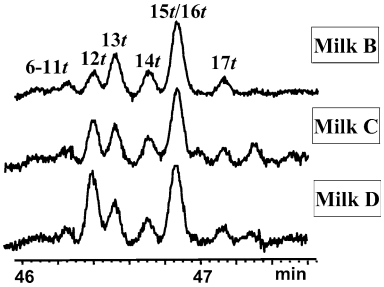

Fig. 13 Comparison of the *trans*-20:1 isomers from the *trans* fraction isolated using Ag$^+$-SPE columns of milk fats B to D that were separated by GC using the 175 °C temperature program. The assignments were based on silver-ion chromatographic principles and on a previously published report [27]

Resolution of CLA Isomers

There was no difference in the separation of the CLA isomers using either of the two temperature programs; 9*c*11*t*-, 7*t*9*c*- and 8*t*10*c*-18:2 coeluted, as well as 9*c*11*c*- and 11*t*13*c*-18:2 and most of the *t*,*t*-18:2 isomers (10*t*12*t*- to 7*t*9*t*-18:2) (Figs. 11, 12). However, some of the isomers were resolved at both temperatures, such as 9*t*11*c*-, 10*t*12*c*-, 11*c*13*t*- and 11*t*13*t*-18:2. Lowering the GC temperature to 120 °C was successful in resolving the *trans*-18:1 isomers, but it did not further resolve the CLA isomers [3]. Therefore, a complete resolution of all the CLA isomers still requires the use of a complimentary Ag$^+$-HPLC technique, since the separation of the CLA isomers is not possible by any GC program [5, 21, 26, 37]. The argument has often been made that the isomers coeluting with the major CLA isomer 9*c*11*t*-18:2 can be estimated as constant percentage of total CLA [13]. However, such an assumption may not be valid when analyzing milk and meat fats from ruminants fed different diets that greatly impact the rumen bacterial population [5, 6, 38]. Preliminary results from a survey of North American milk and meat samples show substantial amounts of 7*t*9*c*-18:2 that occasionally are present at similar levels as 9*c*11*t*-18:2 in these fats [6]. Not separating these isomers will leads to inaccuracies and misinterpretations of FA metabolism in these animals.

There are two major interferences in the CLA region with GC analysis, 21:0 [3, 5, 29, 39] and several isomers of 20:2 [39]. The elution of 21:0 depends on the polarity of the GC column, and slight differences in polarity caused 21:0 to elute anywhere between 9*t*11*c*- and 9*c*11*c*/11*t*13*c*-18:2 [3, 5, 6, 29, 39] using the 175 °C GC program. Therefore, inclusion of 21:0 is necessary for all GC standards for analyzing CLA [5, 6]. Using the same GC column and decreasing the temperature from 175 to 150 °C increased the elution time of 21:0 relative to the CLA isomers. In the present separation 21:0 eluted with 9*t*11*c*-18:2 at 175 °C (Fig. 11), and between 10*t*12*c*- and 9*c*11*c*/11*t*13*c*-18:2 at 150 °C (Fig. 12). Several 20:2 isomers were identified in the diene fraction that eluted in the CLA region and may result in misidentification of minor *c*,*c*- and *t*,*t*-CLA isomers at both temperatures (Figs. 11, 12). The presence of 20:2 isomers in the CLA region was previously confirmed by GC/MS using high-resolution select-ion recording at m/z 322.2872 [39].

The FA Composition of the Milk Fats

The complete FA composition of all four milk fats as determined by combining the results of the two GC temperature programs are presented in Table 3; and the individual *trans* and *cis* isomer of 16:1, 18:1 and 20:1/18:3 are listed separately in Table 4. Most of the geometric and positional isomers of the MUFAs in milk fat were analyzed without prior separation of the total milk FAMEs. The isomers were confirmed by comparison to milk fat fractions isolated using Ag$^+$-SPE columns. There are some isomers that could not resolved apart from those that cannot be resolved even at 120 °C (6*t*/7*t*-16:1, 6*t*-8*t*-18:1, 6*c*-8*c*-18:1, 4*t*-11*t*-20:1), and they included 11*t*/12*t*-16:1, 13*t*/14*t*-18:1, 9*c*/10*c*-18:1, 15*t*/16*t*-20:1, 9*c*/14*t*-20:1 and 11*c*-20:1/*tcc*-18:3 (Table 4). In some cases one of the two FAs is present in milk fat in trace amounts (10*c*-18:1, 14*t*-20:1, *ctc*-18:3). Identification of some isomers (11*t*- and 12*t*-16:1, 13*t*- and 14*t*-18:1, 15*t*- and 16*t*-20:1) if required, will require the more elaborate prior argentation chromatographic separation followed by GC analyses at low isothermal conditions [3, 5, 17, 19]. The individual *t*/*t*- and *c*/*t*-18:2 are not separately listed in the Table 4 because the identity of most of these isomers will need to be confirmed by GC/MS, while the *c*/*c*/*t*-18:3 were only present in trace amounts. The proposed current GC method in this communication was successfully applied for the analysis of beef and muskox lipids [40], and the method is now fully described.

Table 3 Total fatty acid composition of the four selected milk fats as determined using the two GC programs

Fatty acids	Milk fat A	Milk fat B	Milk fat C	Milk fat D
4:0	3.86	2.26	3.21	1.74
6:0	2.32	1.17	1.85	0.81
7:0	0.04	0.01	0.01	0.02
8:0	1.36	0.63	1.10	0.40
9:0	0.06	0.02	0.02	0.02
10:0	2.93	1.43	2.31	0.85
9*c*-10:1	0.01	0.01	0.01	0.01
11:0	0.41	0.12	0.25	0.08
11:1/12:0	3.49	1.92	2.67	1.31
13iso	0.02	0.02	0.03	0.02
13ai	0.10	0.05	0.07	0.04
13:0	0.12	0.08	0.06	0.07
9*c*-12:1	0.10	0.05	0.07	0.03
14iso	0.07	0.07	0.08	0.04
13:1	0.01	0.00	0.01	0.00
14:0	11.39	8.59	8.72	6.98
15iso	0.16	0.14	0.19	0.10
15ai	0.43	0.40	0.40	0.28
9*c*-14:1	1.03	0.77	0.79	0.81
15:0	1.17	1.05	0.84	1.05
16 iso	0.21	0.19	0.27	0.15
16:0	33.82	21.16	21.91	22.54
$\sum$ *trans*-16:1	0.14	0.58	0.89	0.96
$\sum$ *cis*-16:1	1.87	2.08	1.56	1.58
17:0iso	0.21	0.53	0.13	0.30
17:0ai	0.47	0.10	0.69	0.31
17:0	0.51	0.57	0.48	0.47
18:0 iso	0.05	0.05	0.07	0.05
5*c*-17:1	0.04	0.01	0.01	0.01
7*c*-17:1	0.03	0.71	0.04	0.03
9*c*-17:1	0.21	1.72	0.23	0.18
11*c*-17:1	0.00	0.04	0.02	0.01
18:0	6.54	9.35	7.44	8.06
$\sum$ *trans*-18:1	2.71	12.53	12.11	21.40
$\sum$ *cis*-18:1	18.84	22.65	20.72	19.60
19:0	0.05	0.07	0.13	0.15
$\sum$ *tt*-18:2	0.07	0.20	0.11	0.18
9*t*12*t*-18:2	0.02	0.05	0.03	0.09
9*c*13*t*/8*t*12*c*-18:2	0.25	0.57	0.52	0.44
17cyclo	0.01	0.02	0.02	0.02
8*t*13*c*-18:2	0.10	0.26	0.19	0.18
9*c*12*t*-18:2/16*c*-18:1	0.10	0.18	0.18	0.19
9*t*12*c*-18:2	0.03	0.10	0.11	0.13
11*t*15*c*-18:2	0.13	0.38	0.45	0.41
18:2n-6	1.85	2.56	3.51	3.20
9*c*15*c*-18:2	0.02	0.04	0.06	0.04
20:0	0.12	0.19	0.19	0.14

Reason for Choosing the Two GC Temperature Programs for Milk Fat Analysis

It is well known that the analysis of milk and beef fat requires the use of GC temperature programs rather than isothermal GC conditions. On the other hand, isothermal GC conditions were proven to be sufficient to resolve the FA isomers of PHVO mainly because plant oils and fats are devoid of short-chain and branch-chain FAs, and do not contain significant amounts of C16 and C20 PUFAs that would give rise to complex mixtures of 16:1 and 20:1 geometric and positional isomers during partial hydrogenation or deodorization. For this reason, an official method was successfully established to analyze the FA isomers of PHVOs using an isothermal GC program, since these oils/fats contain only 18:1, 18:2 and 18:3 isomers [41–43]. However, it is becoming increasingly evident that the analysis of milk fat requires more than one GC temperature program as previously recommended [5]. There are too many unresolved FAs that necessitated a prior separation of the total milk fat FAMEs using argentation chromatographic techniques. However, the latter procedures are

Table 3 continued

Fatty acids	Milk fat A	Milk fat B	Milk fat C	Milk fat D
18:3n-6	0.04	0.02	0.03	0.02
cct-18:3	0.00	0.03	0.02	0.02
∑ *trans*-20:1	0.04	0.12	0.13	0.15
∑ *cis*-20:1	0.23	0.30	0.38	0.36
18:3n-3	0.32	0.33	0.39	0.29
9*c*11*t*-18:2	0.45	1.58	3.25	1.32
9*t*11*c*-18:2/21:0	0.04	0.13	0.07	0.23
10*t*12*c*-18:2	0.02	0.06	0.03	0.08
9*c*11*c*/11*t*13*c*-18:2	0.01	0.01	0.02	0.01
11*t*13*t*-18:1	0.02	0.01	0.01	0.01
9*t*11*t*/10*t*12*t*-18:2	0.04	0.06	0.08	0.11
∑ *c*/*t*-20:2	0.04	0.11	0.16	0.14
20:2n-6	0.03	0.03	0.05	0.03
22:0	0.03	0.07	0.06	0.06
20:3n-6	0.09	0.07	0.10	0.04
20:3n-3	0.01	0.02	0.04	0.03
20:4n-6	0.14	0.05	0.12	0.05
23:0	0.01	0.01	0.01	0.02
20:5n-3	0.01	0.02	0.01	0.02
24:0	0.05	0.04	0.07	0.04
26:0	0.04	0.01	0.03	0.01
22:5n-3	0.06	0.05	0.08	0.05
22:6n-3	0.02	0.03	0.05	0.02
∑ SFA	70.51	51.27	54.12	47.03
∑ *cis*-MUFA	22.77	26.09	24.01	21.91
∑ *trans* MUFA	2.84	15.17	11.49	23.16
∑ *trans*-18:1	2.68	12.61	12.03	21.33
∑ n-6 PUFA	2.11	2.71	3.78	3.33
∑ n-3 PUFA	0.41	0.47	0.69	0.48
∑ *c*/*t*-18:2	0.77	1.90	1.86	1.88

Some FA pairs cannot be resolved using either GC programs

lengthy, require a certain amount of expertise, and are not practical for routine analyses. The present method of analyzing total milk fat using the 175 and the 150 °C temperature programs takes advantage of differences in the elution times of different types of FAs with temperature to resolve most of the FAs in milk fat. We considered selecting the 163 °C GC temperature program either by itself or in combination of other GC programs because it was possible to resolve 15*t*-18:1. However, this single advantage was outweighed by an insufficient separation of the 6-8*t*- to 11*t*-18:1 isomers, and many other unresolved overlaps in the remaining chromatogram. Choosing the 175 and the 150 °C temperature programs maximized the differences between the FA families sufficiently to determine most of the different FA isomers, some by differences.

Table 4 The *trans*- and *cis*-isomer composition of the four selected milk fats as determined using the two GC programs

Fatty acids	Milk fat A	Milk fat B	Milk fat C	Milk fat D
trans-16:1				
6*t*/7*t*-16:1	0.04	0.09	0.07	0.09
8*t*-16:1	0.03	0.05	0.20	0.39
9*t*-16:1	0.04	0.20	0.36	0.19
10*t*-16:1	0.00	0.06	0.06	0.08
11*t*/12*t*-16:1	0.03	0.13	0.14	0.13
13*t*-16:1	0.00	0.04	0.04	0.04
14*t*-16:1	-0.02	0.01	0.00	0.01
cis-16:1				
7*c*-16:1	0.18	0.18	0.12	0.16
8*c*-16:1	0.02	0.03	0.02	0.03
9*c*16:1	1.63	1.72	1.29	1.21
10*c*-16:1	0.02	0.03	0.03	0.03
11*c*-16:1	0.02	0.04	0.03	0.04
12*c*-16:1	0.00	0.03	0.03	0.04
13*c*-16:1	0.00	0.05	0.04	0.06
trans-18:1				
6*t*-8*t*-18:1	0.25	0.76	0.91	1.15
9*t*-18:1	0.21	0.75	0.82	0.83
10*t*-18:1	0.58	1.36	5.58	14.26
11*t*-18:1	0.60	6.95	2.47	2.97
12t-18:1	0.25	0.69	0.63	0.53
13*t*/14*t*-18:1	0.46	1.09	1.00	0.82
15*t*-18:1	0.08	0.39	0.23	0.31
16*t*-18:1	0.24	0.54	0.38	0.47
cis-18:1				
6*c*-8*c*-18:1	0.26	0.70	0.50	1.08
9*c*/10*c*-18:1	17.48	19.96	18.39	16.23
11*c*-18:1	0.62	0.80	0.72	1.21
12*c*-18:1	0.25	0.69	0.63	0.53
13*c*-16:1	0.06	0.12	0.14	0.23
14*c*-18:1	0.05	0.11	0.09	0.07
15*c*-18:1	0.12	0.26	0.26	0.24
trans-20:1				
6*t*-11*t*-20:1	0.00	0.01	0.02	0.02
12*t*-20:1	0.00	0.03	0.02	0.05
13*t*-20:1	0.04	0.03	0.03	0.03
15*t*/16*t*-20:1	0.00	0.05	0.07	0.05
cis-20:1				
9*c*-20:1(14*t*-20:1)	0.16	0.18	0.20	0.15
11*c*-20:1(*tcc*-18:3)	0.05	0.08	0.14	0.17
13*c*-20:1	0.02	0.04	0.04	0.03

Values in brackets are minor coeluting FA isomers that cannot be resolved using either GC program

Identification of the geometric and positional isomers of 16:1, 18:1, 18:2, 18:3 and 20:1 was accomplished by comparing the total milk lipids with fractions isolated by argentation chromatographic techniques. In this case, the silver-ion separation was accomplished using Ag$^+$-SPE columns. The solvent mixtures were modified to provide pure fractions of saturated, *trans*- and *cis*-monounsaturated and diunsaturated FAMEs. The Ag$^+$-SPE method proved to be easier and in general gave improved separations compared to those obtained using Ag$^+$-TLC [5, 6]. Combining the results from these two separate GC analyses, and establishing the elution order of most FA isomers, made it possible to determine many of the geometric and positional isomers of 16:1, 18:1, 20:1, 18:2 and 18:3 without a prior silver ion chromatographic separation. Only few minor FAs remained unresolved notably the CLA isomers that still require Ag$^+$-HPLC separation. The total time required for the two GC temperature program was about 200 min per sample.

References

1. Jensen RG (2002) The composition of bovine milk lipids: January 1996 to December 2000. J Dairy Sci 85:295–350
2. Precht D, Molkentin J (1996) Rapid analysis of the isomers of *trans*-octadecenoic acid in milk fat. Int Dairy J 6:791–809
3. Kramer JKG, Cruz-Hernandez C, Zhou J (2001) Conjugated linoleic acid and octadecenoic acids: analysis by GC. Eur J Lipid Sci Technol 103:600–609
4. Kramer JKG, Blackadar CB, Zhou J (2002) Evaluation of two GC columns (60-m SUPELCOWAX 10 and 100-m CP Sil 88) for analysis of milkfat with emphasis on CLA, 18:1, 18:2 and 18:3 isomers, and short- and long-chain FA. Lipids 37:823–835
5. Cruz-Hernandez C, Deng Z, Zhou J, Hill AR, Yurawecz MP, Delmonte P, Mossoba MM, Dugan MER, Kramer JKG (2004) Methods for analysis of conjugated linoleic acid and trans-18:1 isomers in dairy fats by using a combination of gas chromatography, silver-ion thin-layer chromatography/gas chromatography, and silver-ion liquid chromatography. J AOAC Int 87:545–562
6. Cruz-Hernandez C, Kramer JKG, Kraft J, Santercole V, Or-Rashid M, Deng Z, Dugan MER, Delmonte P, Yurawecz MP (2006) Systematic analysis of *trans* and conjugated linoleic acids in the milk and meat of ruminants. In: Yurawecz MP, Kramer JKG, Gudmundsen O, Pariza MW, Banni S (eds) Advances in conjugated linoleic acid research, vol 3. AOCS, Champaign, pp 45–93
7. Destaillats F, Golay P-A, Joffre F, de Wispelaere M, Hug B, Giuffrida F, Fauconnot L, Dionisi F (2007) Comparison of available analytical methods to measure *trans*-octadecenoic acid isomeric profile and content by gas–liquid chromatography in milk fat. J Chromatography A 1145:222–228
8. Precht D, Molkentin J (1997) *Trans*-geometrical and positional isomers of linoleic acid including conjugated linoleic acid (CLA) in German milk and vegetable fats. Fett/Lipid 99:319–326
9. Kramer JKG, Fellner V, Dugan MER, Sauer FD, Mossoba MM, Yurawecz MP (1997) Evaluating acid and base catalysts in the methylation of milk and rumen fatty acids with special emphasis on conjugated dienes and total *trans* fatty acids. Lipids 32:1219–1228
10. Piperova LS, Teter BB, Bruckental I, Sampugna J, Mills SE, Yurawecz MP, Fritsche J, Ku K, Erdman RA (2000) Mammary lipogenic enzyme activity, *trans* fatty acids and conjugated linoleic acids are altered in lactating dairy cows fed a milk fat-depressing diet. J Nutr 130:2568–2574
11. Shingfield KJ, Ahvenjrvi S, Toivonen V, Ärölä A, Nurmela KVV, Huhtanen P, Griinari JM (2003) Effect of fish oil on biohydrogenation of fatty acids and milk fatty acid content in cows. Anim Sci 77:165–179
12. Shingfield KJ, Reynolds CK, Lupoli B, Toivonen V, Yurawecz MP, Delmonte P, Griinari JM, Grandison AS, Beever DE (2005) Effects of forage type and proportion of concentrate in the diet on milk fatty acid composition in cows given sunflower oil and fish oil. Anim Sci 80:225–238
13. Shingfield KJ, Reynolds CK, Hervás G, Griinari JM, Grandison AS, Beever DE (2006) Examination of the persistency of milk fatty acid composition responses to fish oil and sunflower oil in the diet of dairy cows. J Dairy Sci 89:714–732
14. Juanéda P (2002) Utilisation of reversed-phase high-performance liquid chromatography as an alternative to silver-ion chromatography for the separation of *cis*- and *trans*-C18:1 fatty acid isomers. J Chromatography A 954:285–289
15. Destaillats F, Trottier J P,.Galvez JMG, Angers P (2005) Analysis of α-linolenic acid biohydrogenation intermediates in milk fat with emphasis on conjugated linolenic acids. J Dairy Sci 88:3231–3239
16. Flachowsky G, Erdmann K, Huether L, Jahreis G, Moeckel P, Lebzien P (2006) Influence of roughage/concentrate ratio and linseed oil on the concentration of *trans*-fatty acids and conjugated linoleic acid in duodenal chyme and milk fat of late lactating cows. Arch Anim Nutr 60:501–511
17. Precht D, Molketin J (2000) Identification and quantitation of *cis*/*trans* C16:1 and C17:1 fatty acid positional isomers in German human milk lipids by thin-layer chromatography and gas chromatography/mass spectrometry. Eur J Lipid Sci Technol 102:102–113
18. Precht D., Molkentin J (2003) Overestimation of linoleic acid and *trans*-C18:2 isomers in milk fats with emphasis on *trans* Δ9, *trans* Δ12-octadecadienoic acid. Milchwissenschaft 58:30–34
19. Precht D, Molketin J (1999) C18:1,C18:2 and C18:3 *Trans* and *cis* fatty acid isomers including conjugated *cis* Δ9, *trans* Δ11 linoleic acid (CLA) as well as total fat composition of German human milk lipids. Nahrung 43:233–244
20. Griinari JM, Dwyer DA, McGuire MA, Bauman DE, Palmquist DL, Nurmela KVV (1998) *Trans*-octadecenoic acids and milk fat depression in lactating dairy cows. J Dairy Sci 81:1251–1261
21. Sehat N, Rickert R, Mossoba MM, Kramer JKG, Yurawecz MP, Roach JAG, Adlof RO, Morehouse KM, Fritsche J, Eulitz KD, Steinhart H, Ku Y (1999) Improved separation of conjugated fatty acid methyl esters by silver ion-high-performance liquid chromatography. Lipids 34:407–413
22. Wolff RL (1994) Analysis of alpha-linolenic acid geometrical isomers in deodorized oils by capillary gas–liquid chromatography on cyanoalkyl polysiloxane phases: a note of caution. J Am Oil Chem Soc 71:907–909
23. Supelco Technical Report (2006) Discovery® Ag-Ion SPE for FAME fractionation and *cis*/*trans* separation. Sigma-Aldrich.-Com/Supelco, email: supelco@sial.com, Bellefonte, PA
24. Cruz-Hernandez C, Kramer JKG, Kennelly JJ, Glimm DR, Sorensen BM, Okine EK, Goonewardene LA, Weselake RJ (2007) Evaluating the conjugated linoleic acid and *trans* 18:1 isomers in milk fat of dairy cows fed increasing amounts of sunflower oil and a constant level of fish oil. J Dairy Sci 90:3786–3801
25. Chouinard PY, Corneau L, Barbano DM, Metzger LE, Bauman DE (1999) Conjugated linoleic acids alter milk fatty acid composition and inhibit milk fat secretion in dairy cows. J Nutr, 129:1579–1584
26. Sehat N, Yurawecz MP, Roach JAG, Mossoba MM, Kramer JKG, Ku Y (1998) Silver ion high-performance liquid

chromatographic separation and identification of conjugated linoleic acid isomers. Lipids 33:217–221

27. Precht D, Molkentin J (2000) Recent trends in the fatty acid composition of German sunflower margarines, shortenings and cooking fats with emphasis on individual C16:1, C18:1, C18:2, C18:3 and 20:1 *trans* isomers. Nahrung 44:222–228
28. Precht D, Hagemeister H, Kanitz W, Voigt J (2002) *Trans* fatty acids and conjugated linoleic acids in milk fat from dairy cows fed a rumen-protected linoleic acid rich diet. Kieler Milchwirtschaftliche Forschungsberichte 54:225–242
29. Kramer JKG, Cruz-Hernandez C, Deng Z, Zhou J, Jahreis G, Dugan MER (2004) Analysis of conjugated linoleic acid and *trans*-18:1 isomers in synthetic and animal products. Am J Clin Nutr 79(Suppl.):1137S–1145S
30. Wolff RL, Bayard CC, Fabien RJ (1995) Evaluation of sequential methods for the determination of butterfat fatty acid composition with emphasis on *trans*-18:1 acids. Application to the study of seasonal variations in French butters. J Am Oil Chem Soc 72:1471–1483
31. Precht D, Molkentin J, Destaillats F, Wolff RL (2001) Comparative studies on individual isomeric 18:1 acids in cow, goat, and ewe milk fats by low-temperature high-resolution capillary gas–liquid chromatography. Lipids 36:827–832
32. Ratnayake WMN, Pelletier G (1992) Positional and geometrical isomers of linoleic acid in partially hydrogenated oils. J Am Oil Chem Soc 69:95–105
33. Lemaitre RN, King IB, Mozaffarian D, Sotoodehnia N, Rea TD, Kuller LH, Tracy RP, Siscovick DS (2006) Plasma phospholipids trans fatty acids, fatal ischemic heart disease, and sudden cardiac death in older adults. The cardiovascular health study. Circulation 114:209–215
34. Osmunsen H, Brenner J, Pedersen JI (1991) Review. metabolic aspects of peroxisomal β-oxidation. Biochim Biophys Acta 1085:141–158
35. Sébédio J-L, Angioni E, Chardigny JM, Grégoire S, Juanéda P, Berdeaux O (2001) The effect of conjugated linoleic acid isomers on fatty acid profiles of liver and adipose tissues and their conversion to isomers of 16:2 and 18:3 conjugated fatty acids in rats. Lipids 36:575–582
36. Demizieus L, Degrace P, Gresti J, Loreau O, Noël J-P, Chardigny J-M, Sébédio J-L, Clouet P (2002) Conjugated linoleic acid isomers in mitochondria: evidence for an alteration of fatty acid oxidation. J Lipid Res 43:2112–2122
37. Yurawecz MP, Roach JAG, Sehat N, Mossoba MM, Kramer JKG, Frische J, Steinhart H, Ku Y (1998) A new conjugated linoleic acid isomer, 7 *trans*, 9 *cis*-octadecadienoic acid, in cow milk, cheese, beef and human milk and adipose tissue. Lipids 33:803–809
38. Klieve AV, Hennessy D, Ouwerkerk D, Forster RJ, Mackie RI, Attwood GT (2003) Establishing populations of *Megasphaera elsdenii* YE 34 and *Butyrivibrio fibrisolvens* YE 44 in the rumen of cattle fed high grain diets. J Appl Microbiol 95:621–630
39. Roach JAG, Yurawecz MP, Kramer JKG, Mossoba MM, Eulitz K, Ku Y (2000) Gas chromatography–high resolution selected-ion mass spectrometric identification of trace 21:0 and 20:2 fatty acids eluting with conjugated linoleic acid isomers. Lipids 35:797–802
40. Dugan MER, Kramer JKG, Robertson WM, Meadus WJ, Aldai N, Rolland DC (2007) Comparing subcutaneous adipose tissue in beef and muskox with emphasis on *trans* 18:1 and conjugated linoleic acids. Lipids 42:509–518
41. AOCS Official Method Ce 1h-05, Determination of *cis*-, *trans*-, saturated, monounsaturated and polyunsaturated fatty acids in vegetable or non-ruminant animal oils and fats by capillary GLC, AOCS, Champaign
42. Ratnayake WMN, Plouffe LJ, Pasquier E, Gagnon C (2002) Temperature-sensitive resolution of *cis*- and *trans*-fatty acid isomers of partially hydrogenated vegetable oils on SP-2560 and CP-Sil 88 capillary columns. J AOAC 85:1112–1118
43. Ratnayake WMN, Hansen SL, Kennedy MP (2006) Evaluation of the CP-Sil 88 and SP-2560 GC columns used in the recently approved AOCS Official Method Ce 1h-05: Determination of *cis*-, *trans*-, saturated, monounsaturated, and polyunsaturated fatty acids in vegetable or non-ruminant animal oils and fats by capillary GLC method. J Am Oil Chem Soc 83:475–488

Lipids (2008) 43:275–280
DOI 10.1007/s11745-008-3153-x

METHODS

Quantification of Pentafluorobenzyl Oxime Derivatives of Long Chain Aldehydes by GC–MS Analysis

**Viral V. Brahmbhatt · Christopher Nold ·
Carolyn J. Albert · David A. Ford**

Received: 4 December 2007 / Accepted: 8 January 2008 / Published online: 7 February 2008
© AOCS 2008

Abstract Negative ion mass spectrometric techniques, for compounds having good ionization properties, such as pentafluorobenzyl derivatives, are believed to be more sensitive than positive ion methods. Preparation of PFB oximes of fatty aldehydes from crude lipid extracts is problematic due to the release of free aldehydes from plasmalogens during derivatization. Accordingly, in these studies plasmalogens were removed by silicic acid column chromatography prior to pentafluorobenzyl derivatization. This simple purification step to remove plasmalogens is shown to facilitate the quantification of long-chain aldehydes by analysis of their pentafluorobenzyl oxime derivatives utilizing gas chromatography–mass spectrometry in the negative ion chemical ionization mode. The limit of detection for long chain fatty aldehydes using this method is 0.5 pmol and it is linear over two orders of magnitude. Silicic acid column chromatography followed by electrospray ionization mass spectrometry demonstrated that plasmalogens were removed (the detection limit for this analyses was ≤0.3 pmol). Furthermore, we have exploited the utility and sensitivity of this method to identify increases in hexadecanal and octadecanal in 3-amino-1,2,4-triazole treated human neutrophils.

Keywords Gas chromatography · Mass spectrometry · Aldehydes · Pentafluorobenzyl · Hexadecanal · Octadecanal · Aminotriazole · Negative ion chemical ionization

Abbreviations

AAG	1-*O*-alk-1′-enyl-2-acyl-*sn*-glycerol
di-16:0 GPC	1,2-Dihexadecanoyl-*sn*-glycero-3-phosphocholine
di-20:0 GPC	1,2-Diicosanoyl-*sn*-glycero-3-phosphocholine
16:0-18:1 pPC	1-*O*-hexadec-1′-enyl-2-octadec-9′-enoyl-*sn*-glycero-3-phosphocholine
2-ClHDA	2-Chlorohexadecanal
ATZ	3-Amino-1,2,4-triazole
DAG	Diacylglycerol
DI-ESI-MS/MS	Direct-infusion electrospray ionization tandem mass spectrometry
GC–MS	Gas chromatography–mass spectrometry
HCAEC	Human coronary artery endothelial cells
HNE	4-Hydroxynonenal
MDA	Malondialdehyde
NICI	Negative ion chemical ionization
18:0 SM	*N*-octadecanoyl sphingosylphosphorylcholine
PFB	Pentafluorobenzyl
PC	Phosphatidylcholine
SIM	Selected ion monitoring
TLC	Thin layer chromatography

Introduction

Lipid oxidation through a variety of enzymatic and non-enzymatic mechanisms can lead to the formation of

---

Electronic supplementary material The online version of this article (doi:10.1007/s11745-008-3153-x) contains supplementary material, which is available to authorized users.

V. V. Brahmbhatt · C. Nold · C. J. Albert · D. A. Ford (✉)
Department of Biochemistry and Molecular Biology,
St Louis University School of Medicine,
1100 South Grand Blvd, St Louis, MO 63104, USA
e-mail: fordda@slu.edu

aldehydes [1, 2]. The generation of aldehydes from polyunsaturated fatty acids through the attack of reactive oxidizing species is considered particularly facile and leads to the formation of aldehydes such as 4-hydroxynonenal (HNE) and malondialdehyde (MDA) [3–5]. Both, HNE and MDA have been extensively studied and are involved in numerous signaling pathways [1, 2, 6]. Besides short-chain aldehydes, the formation of long-chain aldehydes such as 2-chlorohexadecanal (2-ClHDA) and 2-hexadecenal is also known [7, 8]. 2-ClHDA is a neutrophil chemoattractant and can also inhibit endothelial nitric oxide synthase [9, 10]. Thus, knowledge of the overall load of aldehydes can provide an insight into the pathogenesis of diseases related to oxidative stress.

Aldehydes have been measured by a variety of techniques including spectrophotometry [11, 12] and mass spectrometry. Derivatization techniques that introduce electron-withdrawing groups enhance the sensitivity of analyte signal using negative ion mode detection [13]. Hence, pentafluorobenzyl (PFB) oxime derivatization of aldehydes followed by gas chromatography-mass spectrometry (GC–MS) analysis has been a commonly employed technique for aldehyde quantification. Mass spectrometric determination of PFB oximes has been performed by electron impact [14] and negative ion chemical ionization (NICI) [15]. While most of these studies were performed for short-chain aldehydes, detection of long-chain aldehydes in biological tissue has not been studied in depth. We have previously quantified α-chlorinated fatty aldehydes and 2-hexadecenal as their PFB oximes utilizing GC–MS in NICI mode [7, 8]. However, for measurement of long-chain saturated aldehydes in biological tissue, thin layer chromatography (TLC) separated aldehydes were oxidized to the corresponding acids, followed by their quantification as bromophenacyl esters [16].

Plasmalogens are a major phospholipid subclass in many mammalian tissues [17]. Plasmalogens contain a masked fatty aldehyde in the *sn*-1 position and in presence of acidic conditions this aldehyde is released [17, 18]. This property of plasmalogens may impede the utilization of some derivatization techniques that can be applied for lipid analyses. It is likely that the conversion of free fatty aldehydes to PFB oximes in crude lipid extracts will lead to the release of fatty aldehydes from plasmalogen pools potentially rendering this technique ineffective. In this report, we separate plasmalogens from aldehydes prior to their derivatization utilizing silicic acid column chromatography. After removal of plasmalogens from crude lipid extracts long-chain aldehydes can then be quantified following conversion to their PFB oximes with subsequent analysis in the NICI mode. We use the method to detect changes in the aldehyde content of 3-amino-1,2,4-triazole (ATZ) treated human neutrophils.

Experimental Procedures

Materials

Hexadecanal and octadecanal were synthesized using Dess-Martin oxidation as described [19]. [d_4]-Hexadecanal was synthesized utilizing Mancuso oxidation of [d_4]-hexadecanol, which was prepared by reduction of the corresponding acid. A similar procedure has been described earlier [9]. Bovine heart phosphatidylcholine (PC), 1,2-dihexadecanoyl-*sn*-glycero-3-phosphocholine (di-16:0 GPC) and1,2-diicosanoyl-*sn*-glycero-3-phosphocholine (di-20:0 GPC) were purchased from Avanti Polar Lipids. 1-*O*-hexadec-1′-enyl-2-octadec-9′-enoyl-*sn*-glycero-3-phosphocholine (16:0–18:1 pPC) was synthesized as described previously [20] and *N*-octadecanoyl sphingosylphosphorylcholine (18:0 SM) was purchased from Matreya, Inc. Human coronary artery endothelial cells (HCAEC) were purchased from Cambrex and maintained according to manufacturer's protocol. Silicic acid columns (1 ml) were purchased from Sigma. All other reagents were obtained either from Sigma or Fisher.

Silicic Acid Column Separation

Organic extracts of either HCAEC or neutrophils were obtained after a modified Bligh and Dyer extraction [21]. [d_4]-hexadecanal was added in methanol as the internal standard during extraction. Organic extracts were dried and resuspended in 500 μl chloroform. Each extract was loaded onto a pre-equilibrated Silicic acid column (pre-equilibration was performed with 10 ml chloroform) and eluted with 5 ml of chloroform. The void and elute fractions were collected in 15 ml screw-top tubes, and these fractions were sequentially dried under nitrogen and aldehydes were derivatized to their PFB oximes for GC–MS analysis. In parallel studies bovine heart PC (150 μg) was suspended in 500 μl chloroform and subjected to silicic acid column chromatography. The void and elute fractions were sequentially dried under nitrogen, resuspended in a 4:1 mixture of methanol/chloroform and subjected to direct-infusion electrospray ionization tandem mass spectrometry (DI-ESI-MS/MS). Following silicic acid column chromatography, organic extracts were dried and resuspended in a 4:1 mixture of methanol/chloroform (1 ml). These were injected onto the electrospray ionization interface (TSQ Quantum Ultra, Thermo-Fisher Corporation) at a flow rate of 3 μl/min (after addition of the internal standard di-20:0 PC at 1.3 pmol/μl). Spectra were averaged over 3–5 min and processed utilizing Xcalibur software. Ions were monitored in the positive ion mass scan mode. The limit of detection for this specific assay for plasmalogens at dilutions similar to those used for analyses is ≤0.3 pmol (in 1 ml).

PFB Oxime Derivatization and GC–MS Analysis

Silicic acid column chromatography column-purified extracts or known amounts of aldehydes or lipids (100 µg) were taken, dried and derivatized to their respective PFB oximes utilizing PFB hydroxylamine as the reagent. The PFB oximes were resuspended in 50–100 µl of petroleum ether and analyzed by GC–MS as described earlier [8]. The analyses were performed either by mass scan analysis from *m/z* 100 to 800 or by selected ion monitoring (SIM) of the $[\mathrm{M\text{-}HF}]^-$ ion of the PFB oximes of respective aldehydes. The ions monitored for the PFB oximes of hexadecanal, octadecanal and [d_4]-hexadecanal were *m/z* 415, *m/z* 443 and *m/z* 419, respectively.

Limit of Detection

HCAEC were incubated on 60 mm plates to confluency. The media was discarded and the cells were scraped with 1:1 mixture of methanol/saline (1 ml × 2). Varying amounts of [d_4]-hexadecanal were added in methanol (0–50 pmol). Organic extracts collected using a Bligh and Dyer extraction were subjected to silicic acid column chromatography. The chloroform extracts were derivatized by PFB hydroxylamine and analyzed by GC–MS for [d_4]-hexadecanal. The area under the curve was integrated using the Chemstation software and plotted against the amount of [d_4]-hexadecanal added.

Neutrophil ATZ Treatment

Human neutrophils were isolated from whole blood as described earlier [9]. A total of 0.5×10^6 neutrophils/ml were incubated in the presence or absence of 10 mM ATZ at 37 °C for 10 min. The reactions were terminated with the addition of methanol containing 20 pmol of [d_4]-hexadecanal as the internal standard. Following an extraction, samples were subjected to silicic acid column chromatography. Column eluates were derivatized and analyzed by GC–MS. The calculations were based on linear response curves generated for hexadecanal and octadecanal against [d_4]-hexadecanal.

Results

Plasmalogens are a subclass of lipids with a vinyl ether bond at the *sn*-1 position. The vinyl ether bond is readily susceptible to breakdown under acidic [17, 18] and oxidative conditions [7, 16, 22]. Since PFB hydroxylamine derivatization requires acidic conditions we tested the stability of the vinyl ether bond, the acyl ester and the amide bond under derivatization conditions. Derivatization was performed in the presence of 16:0–18:1 pPC, di-16:0 GPC and 18:0 SM and the derivatives were analyzed by GC–MS. As shown in Fig. 1, the vinyl ether bond in plasmalogens degrades to generate the PFB oxime of hexadecanal (Fig. 1a). For reference, the chromatogram, mass spectrum and fragment ions of the PFB oxime of hexadecanal are provided as supplementary data (supplementary data Fig. 1). However, the acyl ester bonds and the amide bond are stable (Fig. 1b, c). Thus to quantify aldehydes, which would be of similar structure to the alkenyl chains of plasmalogens, prior separation is necessary.

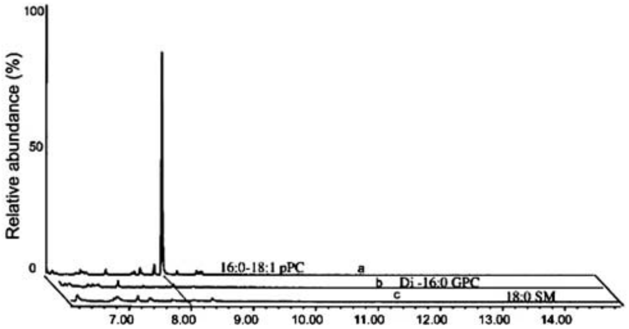

Fig. 1 Vinyl ether susceptibility of PFB hydroxylamine derivatization. 16:0–18:1 pPC (**a**), di-16:0 GPC (**b**) and 18:0 SM (**c**) were derivatized by PFB hydroxylamine and analyzed by GC–MS in the NICI utilizing the mass scan mode. Representative chromatograms obtained are shown. Each condition was repeated three times

To separate plasmalogens from aldehydes, we used silicic acid column chromatography. Pre-equilibrated silicic acid columns were loaded with bovine heart PC in chloroform. Bovine heart PC was chosen because it contains ∼33% plasmalogens. The void and the chloroform elute were collected and analyzed by DI-ESI-MS/MS. As seen in Fig. 2, the sodiated adduct of plasmalogens present at *m/z* 764.7 and 790.7 in bovine heart PC (Fig. 2a) are absent in the chloroform elute after silicic acid column chromatography (Fig. 2b). The major PC species are outlined in supplementary data (Table 1). The internal standard seen at *m/z* 868.8 (sodiated adduct of di-20:0 GPC) was added for comparison after silicic acid column chromatography. Thus, it was concluded that silicic acid column chromatography would successfully be able to separate the plasmalogens and since aldehydes are neutral lipids they should readily elute in chloroform. Following this, the aldehydes could be derivatized to their PFB oximes and analyzed by GC–MS.

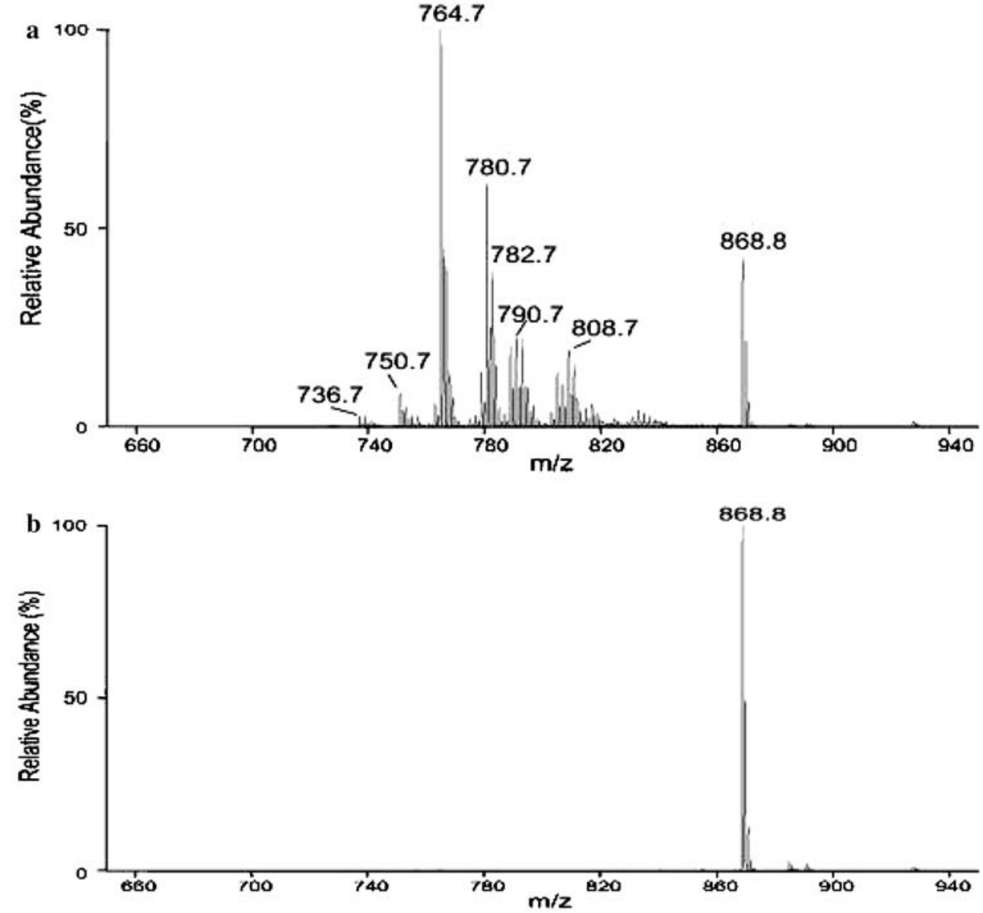

Fig. 2 Silicic acid column chromatography: 150 μg of bovine heart PC was analyzed either directly (**a**) or after silicic acid column separation (**b**) by DI-ESI-MS/MS. The internal standard di-20:0 GPC was added just prior to analysis

Table 1 Major phosphatidylcholine (PC) species in bovine heart by DI-ESI-MS/MS

m/z of $[M+Na]^+$	Molecular species
750.7	32:3 GPC
764.7	34:2 pPC
766.7	34:1 pPC
780.7	34:2 GPC
782.7	34:1 GPC
790.7	36:4 pPC
792.7	36:3 pPC
794.7	36:2 pPC
804.7	36:4 GPC
806.7	36:3 GPC
808.7	36:2 GPC
810.7	36:1 GPC
868.8	40:0 GPC (internal standard)

Column 1: The *m/z* of sodiated adducts ($[M+Na]^+$

Column 2: The numbers denote the total carbons and double bonds present at the *sn*-1 and the *sn*-2 position of the PC species

GPC glycerophosphatidylcholine species with acyl chains at the *sn*-1 and the *sn*-2 position; *pPC* denotes plasmenylcholine species

To test limit of detection of our method we synthesized [d_4]-hexadecanal and added it to HCAEC prior to Bligh and Dyer extraction. The cellular extracts were separated on a silicic acid column, derivatized and analyzed for [d_4]-hexadecanal. Figure 3 shows the plot of the amount of [d_4]-hexadecanal added against the area under the chromatographic peak for $[M-HF]^-$ ion of its PFB oxime at *m/z* 419. The lowest amount we were able to easily detect was 0.5 pmol (inset). The dashed line represents 95% confidence limits of the linear detection curve.

Further, we treated human neutrophils with ATZ, an inhibitor of hydrogen peroxide scavenging enzymes such as catalase (EC 1.11.1.6) [23] and myeloperoxidase (EC 1.11.1.7) [24]. It was anticipated that ATZ would increase fatty aldehyde levels since it reduces the removal of reactive oxygen species by catalase. Indeed, as shown in Fig. 4, ATZ causes an increase in hexadecanal and octadecanal. The calculations were based on linear response curves generated for hexadecanal and octadecanal against the internal standard, [d_4]-hexadecanal (supplementary data Fig. 2). Collectively, these data suggest the sensitivity and utility of the method for quantification of long-chain aldehydes under biologically relevant conditions.

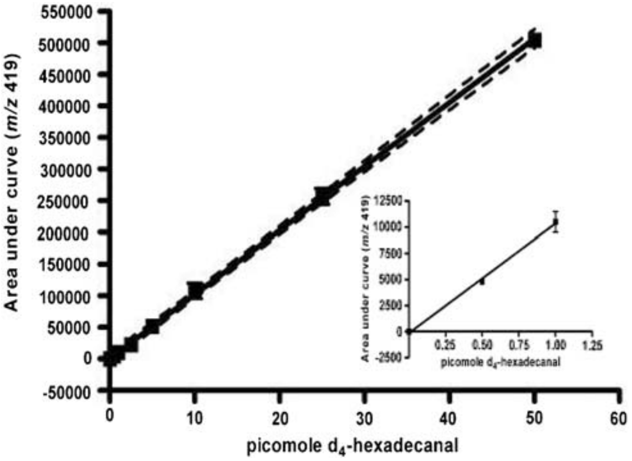

Fig. 3 Limit of detection: varying amounts of [d_4]-hexadecanal (0–50 pmol) was added to HCAEC prior to extraction. The cell extracts were then separated over a Si column and analyzed by GC–MS after derivatization. The figure shows the linear plot of the integrated area under the curve for chromatographic peak of *m/z* 419 against the known initial amount of [d_4]-hexadecanal. The individual points represent the mean with standard deviation of the measured area for that amount. The *dashed lines* represent the 95% confidence limits of the linear curve. The inset shows magnification of the lower end of the plot. GraphPad Prism (GraphPad Software, Inc, CA) was used for curve plotting and statistical analyses

Discussion

Quantification of long-chain aldehydes as PFB derivatives from crude lipid extracts of biological tissue poses a special problem due to the presence of masked aldehydes in plasmalogens. Earlier, TLC separation has been used to separate polar lipids such as plasmalogens from long-chain aldehydes prior to their detection after oxidation to the acid followed by bromophenacyl esterification and liquid chromatography. Results from this study demonstrated that plasmalogens are targeted by free radicals but this method was not quantitative and employed radioactivity [16]. Additionally, others have employed HPLC with UV detection yielding a sensitivity for detection of ~6 pmol [12, 25]. These methods are time-consuming, employ acidic conditions used for TLC separation, and the sensitivity of these assays for aldehyde measurement is less than that described in the method herein. In the present method we have separated plasmalogen phospholipids from fatty aldehydes by a simple silicic acid column step. Conversion of the partially purified fatty aldehydes to their pentafluorobenzyl oximes followed by GC–MS analyses using negative ion chemical ionization allows very sensitive (limit of detection of 0.5 pmol and a linear range of two orders of magnitude), rapid and accurate measurements of fatty aldehydes from biological tissues. Furthermore, we have used this new methodology to demonstrate increases in hexadecanal in ATZ-treated human neutrophils.

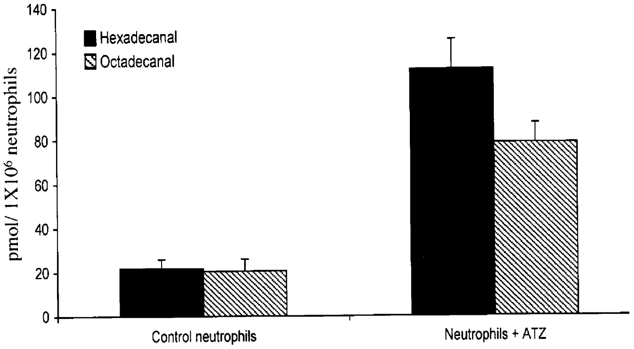

Fig. 4 Long-chain aldehydes increase in ATZ treated neutrophils. Isolated human neutrophils were treated with 10 mM ATZ for 10 min. The amount of hexadecanal and octadecanal in untreated and treated neutrophils was measured utilizing [d_4]-hexadecanal as the internal standard as outlined in "Experimental Procedures"

Several groups including ours have shown that vinyl ether linked diglycerides (e.g., AAG) are present in cells. This method for the measurement of long chain fatty aldehydes could have some aldehydes generated from AAG since this diglyceride co-elutes with the neutral lipids present in the void and chloroform elute of the silicic acid column. In the present study we have shown that fatty aldehydes range between ~20 and 120 pmol/10^6 neutrophils. Others have shown that cytochalasin B primed human neutrophils have AAG levels up to 1.2 pmol/10^6 neutrophils while basal AAG levels are two orders of magnitude less [26]. Thus, it is unlikely that AAG in neutrophils would significantly effect the fatty aldehyde determinations in these studies. Additionally TLC of crude lipid extracts has been used to separate plasmalogens and AAG from long-chain aldehydes prior to their measurement [16]. Our studies comparing TLC separation with silicic acid column chromatography indicate a modest increase in fatty aldehyde measurement using TLC purification over silicic acid column chromatography (data not shown). This likely reflects the masked aldehyde release from alkenyl bond containing lipids due to the presence of acetic acid in conventionally used TLC solvent systems [27].

Taken together these studies demonstrate the utility of a novel method to quantitate long chain fatty aldehydes that couples the ease of silicic acid column chromatography to remove plasmalogens with the sensitivity of quantifying their PFB oxime derivatives. It is likely that this technique will be extremely useful in measuring these lipids in tissues that are susceptible to oxidative stress.

Acknowledgments This research was supported by National Institutes of Health grants HL 74214 (DAF) and RR19232 (DAF) as well as Grant-in-Aid 0650044Z (DAF) and Pre-doctoral fellowship grant 0710121Z (VVB) from the American Heart Association.

References

1. O'Brien PJ, Siraki AG, Shangari N (2005) Aldehyde sources, metabolism, molecular toxicity mechanisms, and possible effects on human health. Crit Rev Toxicol 35:609–662
2. Uchida K (2000) Role of reactive aldehyde in cardiovascular diseases. Free Radic Biol Med 28:1685–1696
3. Esterbauer H, Jurgens G, Quehenberger O, Koller E (1987) Autoxidation of human low density lipoprotein: loss of polyunsaturated fatty acids and vitamin E and generation of aldehydes. J Lipid Res 28:495–509
4. Porter NA, Caldwell SE, Mills KA (1995) Mechanisms of free radical oxidation of unsaturated lipids. Lipids 30:277–290
5. Yin H, Porter NA (2005) New insights regarding the autoxidation of polyunsaturated fatty acids. Antioxid Redox Signal 7:170–184
6. Esterbauer H, Schaur RJ, Zollner H (1991) Chemistry and biochemistry of 4-hydroxynonenal, malonaldehyde and related aldehydes. Free Radic Biol Med 11:81–128
7. Albert CJ, Crowley JR, Hsu FF, Thukkani AK, Ford DA (2001) Reactive chlorinating species produced by myeloperoxidase target the vinyl ether bond of plasmalogens: identification of 2-chlorohexadecanal. J Biol Chem 276:23733–23741
8. Brahmbhatt VV, Hsu FF, Kao JL, Frank EC, Ford DA (2007) Novel carbonyl and nitrile products from reactive chlorinating species attack of lysosphingolipid. Chem Phys Lipids 145:72–84
9. Thukkani AK, Hsu FF, Crowley JR, Wysolmerski RB, Albert CJ, Ford DA (2002) Reactive chlorinating species produced during neutrophil activation target tissue plasmalogens: production of the chemoattractant, 2-chlorohexadecanal. J Biol Chem 277:3842–3849
10. Marsche G, Heller R, Fauler G, Kovacevic A, Nuszkowski A, Graier W, Sattler W, Malle E (2004) 2-chlorohexadecanal derived from hypochlorite-modified high-density lipoprotein-associated plasmalogen is a natural inhibitor of endothelial nitric oxide biosynthesis. Arterioscler Thromb Vasc Biol 24:2302–2306
11. Kim SS, Gallaher DD, Csallany AS (1999) Lipophilic aldehydes and related carbonyl compounds in rat and human urine. Lipids 34:489–496
12. Csallany AS, Kim SS, Gallaher DD (2000) Response of urinary lipophilic aldehydes and related carbonyl compounds to factors that stimulate lipid peroxidation in vivo. Lipids 35:855–862
13. Hunt DF, Stafford GC, Crow FW, Russell JW (1976) Pulsed positive negative ion chemical ionization mass spectrometry. Anal Chem 48:2098–2104
14. Kawai Y, Takeda S, Terao J (2007) Lipidomic analysis for lipid peroxidation-derived aldehydes using gas chromatography-mass spectrometry. Chem Res Toxicol 20:99–107
15. Hsu FF, Hazen SL, Giblin D, Turk J, Heinecke JW, Gross ML (1999) Mass spectrometric analysis of pentafluorobenzyl oxime derivative of reactive biological aldehydes. Int J Mass Spectr 187:795–812
16. Morand OH, Zoeller RA, Raetz CR (1988) Disappearance of plasmalogens from membranes of animal cells subjected to photosensitized oxidation. J Biol Chem 263:11597–11606
17. Nagan N, Zoeller RA (2001) Plasmalogens: biosynthesis and functions. Prog Lipid Res 40:199–229
18. Hayashi H, Hara M (1997) 1-Alkenyl group of ethanolamine plasmalogen derives mainly from de novo-synthesized fatty alcohol within peroxisomes, but not extraperoxisomal fatty alcohol or fatty acid. J Biochem (Tokyo) 121:978–983
19. Dess DB, Martin JC (1983) Readily accessible 12-I-5 oxidant for the conversion of primary and secondary alcohols to aldehydes and ketones. J Org Chem 48:4155–4156
20. Han XL, Zupan LA, Hazen SL, Gross RW (1992) Semisynthesis and purification of homogeneous plasmenylcholine molecular species. Anal Biochem 200:119–124
21. Bligh EG, Dyer WJ (1959) A rapid method of total lipid extraction and purification. Can J Biochem Physiol 37:911–917
22. Zoeller RA, Lake AC, Nagan N, Gaposchkin DP, Legner MA, Lieberthal W (1999) Plasmalogens as endogenous antioxidants: somatic cell mutants reveal the importance of the vinyl ether. Biochem J 338(Pt 3):769–776
23. Margoliash E, Novogrodsky A, Schejter A (1960) Irreversible reaction of 3-amino-1:2:4-triazole and related inhibitors with the protein of catalase. Biochem J 74:339–348
24. Nauseef WM, Metcalf JA, Root RK (1983) Role of myeloperoxidase in the respiratory burst of human neutrophils. Blood 61:483–492
25. Seppanen CM, Csallany AS (2001) Simultaneous determination of lipophilic aldehydes by high-performance liquid chromatography in vegetable oil. J Am Oil Chem Soc 78:1253–1260
26. Tyagi SR, Burnham DN, Lambeth JD (1989) On the biological occurrence and regulation of 1-acyl and 1-O-alkyl-diradylglycerols in human neutrophils. Selective destruction of diacyl species using *Rhizopus* lipase. J Biol Chem 264:12977–12982
27. Kates M (1986) in Laboratory techniques in biochemistry and molecular biology. In: Burdon RH, Knippenberg PHV (eds) vol. 3, part 2, 2nd revised edn. Elsevier, New York

Lipids (2008) 43:281–288
DOI 10.1007/s11745-007-3135-4

METHODS

Determination of Tertiary-butylhydroquinone and Its Metabolites in Rat Serum by Liquid Chromatography–Ion Trap Mass Spectrometry

Wen Huang · Yinchun Gu · Hai Niu

Received: 14 September 2007 / Accepted: 30 October 2007 / Published online: 10 January 2008
© AOCS 2007

Abstract A new method applying sensitive and selective liquid chromatography coupled with mass spectrometry (LC/MS/MS) for analyzing tertiary-butylhydroquinone (TBHQ) and its metabolites in rat serum was validated. Using an extracted ion chromatogram (EIC) of *m/z* 149, free TBHQ was observed in rat serum after dosing TBHQ at 350 mg/kg to male and female Sprague–Dawley (SD) rats. Four major metabolites of TBHQ were identified—a TBHQ-sulfate, two TBHQ-sulfate-derived substances and a TBHQ-glucuronide through MS^n spectra. Besides its simplicity, the sample treatment allows one to obtain a very good recovery of analysts, namely around 95%. This result suggests that the method described here is useful for the analysis of TBHQ and its metabolites in rat serum. Moreover, the metabolism of TBHQ was investigated using the method. After oral administration, TBHQ appear to be more completely absorbed and bio-transformed by males than females, which may result in higher acute oral toxicity of TBHQ for males than females.

Keywords Tertiary-butylhydroquinone (TBHQ) · Metabolites · Liquid chromatography–ion trap mass spectrometry (LC/ITMS)

Introduction

Tertiary-butylhydroquinone (TBHQ) is one of the most commonly used antioxidants for preventing lipid peroxidation because of its chemical stability, availability and low cost [1, 2]. The toxicological effects of TBHQ, however, have been the subject of controversy in recent years [3–6]. Because of its possible toxicity, most countries of the world have regulations for controlling the use of TBHQ in food applications. For example, TBHQ is permitted in fatty foods up to a maximum limit of 200 mg/kg in China and USA, whereas it has not been approved as a food antioxidant yet in Japan and the European Union.

To evaluate the safety of TBHQ, several methods have been carried out for the analysis of TBHQ in body fluids as well as foods including Fourier transform infrared (FTIR) spectroscopy, colorimetry, UV–visible photometry, electroanalytical–voltammetry, paper and thin-layer chromatography, gas and liquid chromatography [7–11]. Most of these methods require long analysis times and laborious sample treatment techniques in addition to low resolution. Meanwhile, it has been found that they are limited in studying biological samples, such as analysis of metabolites, which is a very important study in the pharmacokinetics and toxicology of TBHQ. These reasons have prompted the need to establish an effective and convenient method for evaluating safety by analytical monitoring of TBHQ and its metabolites.

W. Huang (✉)
Institute for Nanobiomedical Technology and Membrane Biology, State Key Lab of Biotherapy of Human Diseases, Cancer Center, West China Hospital, West China Medical School, Sichuan University, No 1, Keyuan 4 Lu, Gaopeng Avenue, Hi-Tech Zone, Chengdu 610041, China
e-mail: hwpharm@tom.com

Y. Gu
School of Light Industry and Food, Sichuan University, Chengdu 610065, China

H. Niu
Mathematical College, Sichuan University, Chengdu 610064, China

HPLC coupled with mass spectrometry (MS) is currently unique technique being developed for monitoring antioxidant content and studying compound structure. In particular, MS/MS triple quadrupole mass spectrometry in the multiple reaction monitoring modes (MRM) provides excellent speed, sensitivity and selectivity. In our previous study, we established a rapid, sensitive, precise and accurate quantitative method for the measurement of TBHQ in commercial edible oil by liquid chromatography/tandem mass spectrometry (LC/MS/MS) [12].

For this paper, we developed a fast and precise HPLC/MS/MS method capable of quantifying TBHQ and its metabolites in rat serum (biological sample) after oral administration.

Experimental Procedure

Reagents

The purity of TBHQ (J & K Chemica, Augsburg, Germany) was better than 98%. Methanol and acetonitrile (Fisher Scientific, Pittsburgh, PA) were of HPLC grade. Water was purified using a Milli-Q gradient system (Millipore Corporation, Genay Cedex, France).

Animal Handling and Sample Collection

Adult Sprague–Dawley (SD) rats, weighing 160 ± 10 g, were obtained from Department of Laboratory Animal Science of Peking University (Beijing, China). Both male and female rats were used in each experiment. The rats were maintained on the basal diet and tap water throughout the study and were not fasted before dosing, as dosing after an overnight fast resulted in mortality [13].

To identify the metabolites of TBHQ, the rats were divided into two groups (four rats/group). Rats in group 1, as control group, were assigned to receive corn oil at a gavage dose of 1 ml, respectively. Rats in group 2 were to receive TBHQ dissolved in corn oil at a gavage dose of 350 mg/kg, respectively. All rats at 1.2 h after oral administration were killed by cutting behind their heads using scissors. And then, the blood samples from the rats' necks were immediately collected into EP (Epoxy epoxide) tubes (0.5 ml of blood sample/rat).

To study distributions of TBHQ and its metabolites in rat serum, the rats were divided into four groups (six rats/group). Group 1–4 were to receive corn oil at a gavage dose of 1 ml, and TBHQ dissolved in corn oil at gavage doses of 7, 350 and 700 mg/kg, respectively After oral administration, serial blood samples (0.25 ml sample/rat) were collected from tail using clip at 0.08, 0.25, 0.5, 1, 2, 3, 5, 7, 9, 12, 24 and 48 h. Following centrifugation of the blood samples at 12,000 rpm/min for 20 min, each serum sample was collected and stored at −20°C until analyzed.

Metabolite Identification

During metabolite identification, serum samples were analyzed only after a simple pretreatment procedure to avoid losing any possible metabolite. Three times the volume of methanol was added to deposit proteins. After centrifugation at 12,000 rpm/min for 20 min, the upper liquid was transferred to a filter with a 0.22 μm membrane.

The serum samples were analyzed using liquid chromatography–ion trap mass spectrometry (LC/ITMS) on an Agilent 1100 Series LC/MSD Trap system (Wilmington, PA) consisting of a G1312A binary pump, a G1306 A diode array detector, a G1313A automatic sample injector, a G1316A column oven, an G1379A on-line vacuum degasser, and electrospray ionization (ESI) source. The injection volume was 1 μl. The mobile phase was a mixture of methanol and water (60:40 v/v) pumped at 0.15 ml/min. For ESI, the nebulizer flow was at 35 psi and the drying gas flow was at 8 l/min and 350 °C. Free TBHQ in serum was analyzed by extracted ion chromatograms (EICs) of its MS^2 characteristic product ion. Major metabolites of TBHQ were distinguished from complex serum matrix by MS^1 analysis, and then they were identified by their characteristic product ion mass spectra of MS^n analysis.

Quantitative Analysis of TBHQ and its Metabolites in Rat Serum

Each rat serum sample (100 μl) was diluted with water (100 μl), and then ethyl acetate (1 ml) was added for lipid–lipid extraction. The mixture was vortexed for 3 min on a roller shaker and centrifuged at 12,000 r/min for 20 min. The organic phase (ethyl acetate) was then separated from the aqueous phase. The ethyl acetate extracts were collected and evaporated to dryness at 25 °C under a gentle stream of nitrogen gas, and the residue was finally dissolved in 100 μl methanol for TBHQ quantitative analysis. As for the aqueous phase, 200 μl of methanol was added to deposit proteins, and after centrifugation100 μl of the final supernatant was transferred to a sample bottle for quantitative analyses of the metabolites.

TBHQ was quantified using an external standard prepared in a blank serum matrix with a concentration range of 49–5,030 μg/l. Due to lack of standards, the metabolites were semi-quantified using TBHQ as standard. The stock standard solution containing about 1 mg/ml of TBHQ in methanol was prepared and shielded from light and stored at 4 °C for a maximum of one month for analysis. The matrix-assisted standards were prepared in the same way as the samples. To evaluate accuracy and precision, we prepared and analyzed six serum samples, each containing three different concentrations of TBHQ (328, 998, 1,969 µg/l). The precision was obtained as the inter-day and intra-day coefficient of variation [relative standard deviation (RSD %)]. The limit of detection (LOD) was considered as the concentration that produced a signal-to-noise (S/N) ratio of 3. The recovery was determined by comparing the peak areas of TBHQ obtained for the samples (328, 998, 1,969 µg/l, $n = 6$) that were subjected to the extraction procedure with those obtained from blank serum that were spiked post-extraction at the corresponding concentrations.

TBHQ and its metabolites contents in non-pretreatment and post-pretreatment serum samples were determined for evaluating the stability after samples were stored at −20 °C for 1, 2, 3 and 7 days and at room temperature for 12 and 24 h.

Statistical Analysis

Data are presented as mean ± SD. The results were statistically analyzed by analysis of variance (ANOVA) followed by Fisher's test. Differences were considered significant at $P < 0.01$.

Results and Discussion

Metabolite Identification by LC/ITMS

Analysis of standard solution of TBHQ showed that TBHQ was well ionized to parent ion *m/z* 165 with the retention time of 5.3 min in negative ionization mode, while TBHQ had no response in positive ionization mode. In the MS^2 spectrum (Fig. 1), the product ions of *m/z* 165 were *m/z* 149 and *m/z* 108. The main product ion *m/z* 149 was due to the methyl cleavage from tertiary butyl of TBHQ and the other product ion *m/z* 108 came from the cleavage of tertiary butyl of TBHQ. In order to avoid the serum interference, extracted ion chromatograms (EICs) of the main product ion *m/z* 149 were used to identify free TBHQ in rat serum. In Fig. 2, an apparent peak of the main product ion *m/z* 149 was observed at the retention time of 5.3 min in rat serum after 350 mg/kg of oral administration. This indicates the presence of free TBHQ in rat serum following oral administration.

Total ion chromatograms (TICs) obtained in positive and negative ionization modes in Fig. 3 showed that possible metabolites were found in the region with retention time of 3–4 min in the negative ionization mode, while no metabolites were observed in the positive ionization mode. Mass spectral analysis of the peak of metabolites revealed four major ionic parent masses $[M-H]^-$ at *m/z* 245 (M1), *m/z* 305 (M2), *m/z* 327 (M3) and *m/z* 341 (M4) (Fig. 4).

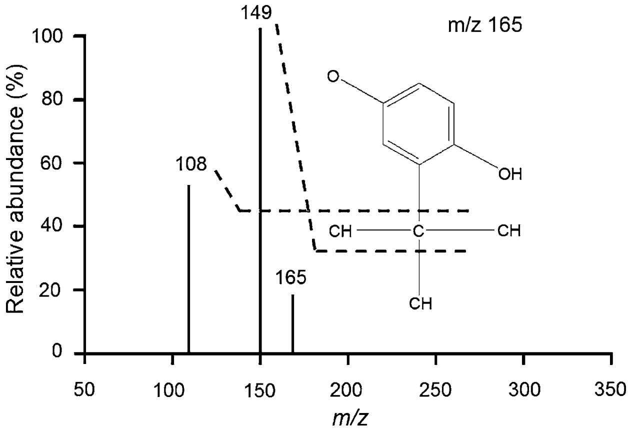

Fig. 1 MS–MS product ion spectrum and the predominant fragmentation patterns of TBHQ

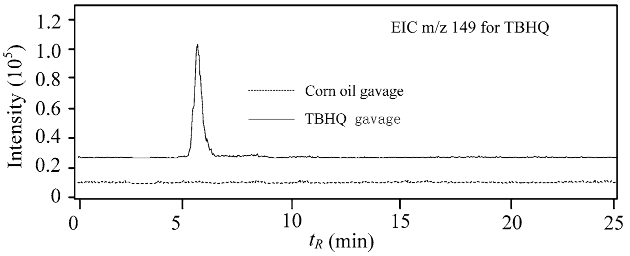

Fig. 2 EICs of *m/z* 149 (MS^2) observed in rat serum following oral administration of corn oil and TBHQ, respectively

MS^2 and MS^3 mass spectra of the major metabolites of TBHQ are given in Fig. 5. For M1 ($[M-H]^-$ at *m/z* 245), a major product ion was *m/z* 165 (loss of SO_3) using LC/MS^2 (Fig. 5a1). MS^3 spectral analysis showed that the product ions of *m/z* 165 were *m/z* 149 (loss of the methyl of tertiary butyl of TBHQ) and *m/z* 108 (loss of the tertiary butyl of TBHQ), as evident in Fig. 5a2, consistent with the fragmentation pathway of TBHQ (Fig. 1). The characteristic fragmentation pathway of *m/z* 245 (M1) can be noted in Fig.6 [14]. The metabolite M1 was identified as a direct sulfate conjugate of TBHQ.

MS^2 and MS^3 spectra of M2 ($[M-H]^-$ at *m/z* 305) and M3 ($[M-H]^-$ at *m/z* 327) were shown in Fig. 5b, c, respectively. Using LC/MS^2, a major product ion was *m/z* 245, for both M2 and M3 (Fig. 5b1, c1). MS^3 spectral analysis indicated that product ions of *m/z* 245 were *m/z* 165 and *m/z* 81, as evident in Fig. 5b2 and c2, consistent

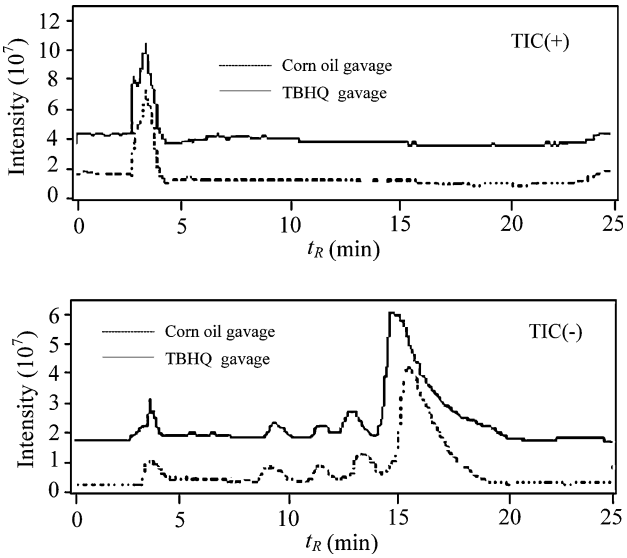

Fig. 3 Total ion chromatograms (MS^1) observed in rat serum following oral administration of corn oil and TBHQ, respectively

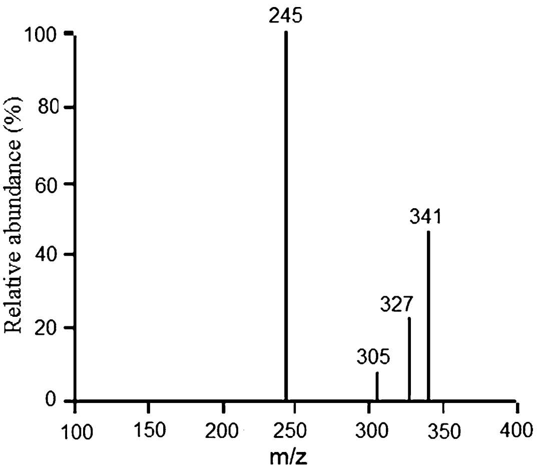

Fig. 4 Average spectrum of the peak with retention time of 3–4 min following oral administration of TBHQ, obtained by subtracting the average spectrum in the region of 3–4 min following oral administration of corn oil

with the fragmentation pathway of M1. So both M2 and M3 were derived from M1 (a sulfate conjugate of TBHQ). However, the structures of M2 and M3 have not yet been completely identified in the present studies.

For M4 ($[M-H]^-$ at *m/z* 341), MS^2 spectral analysis (Fig. 5d1) showed that a major product ion was *m/z* 165 (from loss of $C_6H_6O_6$), the other product ion were *m/z* 175, a characteristic product ion of glucuronide conjugates [15], and *m/z* 113 (the loss of CO_2 and H_2O from *m/z* 175). MS^3 spectral analysis from Fig. 5 d2 indicated that product ions of *m/z* 165 were *m/z* 149 and *m/z* 108, which are MS–MS product ions of TBHQ. The characteristic fragmentation

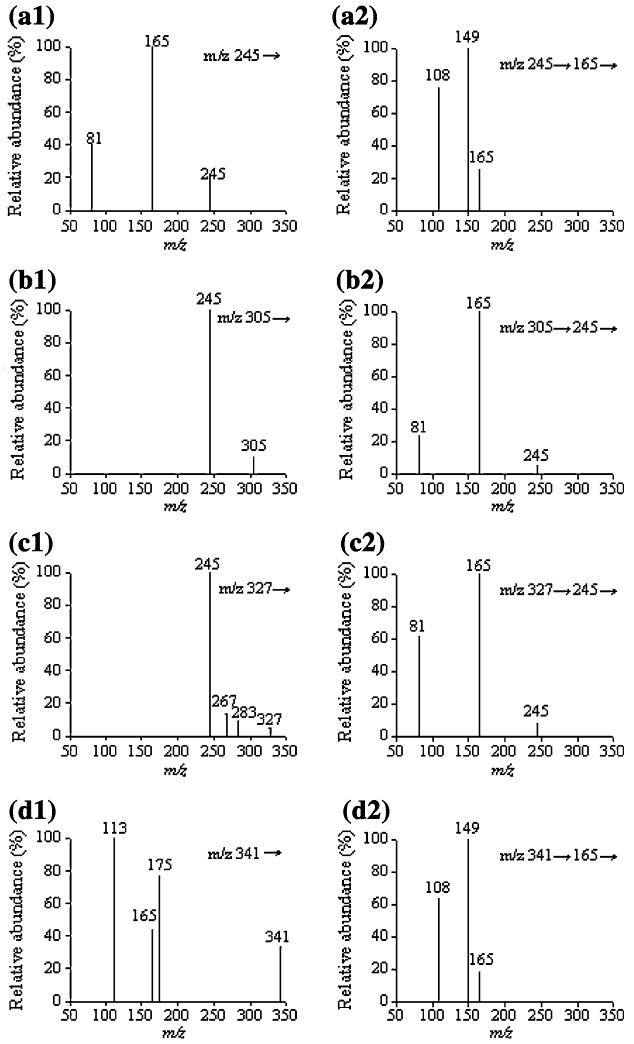

Fig. 5 Mass spectra of the major metabolites of TBHQ in rat serum following oral administration of TBHQ dissolved in corn oil at a dosage of 350 mg/kg. a1 and a2: MS^2 and MS^3 mass spectra of M1 (*m/z* 245 → 165); b1 and b2: MS^2 and MS^3 mass spectra of M2 (*m/z* 305 → 245); c1 and c2: MS^2 and MS^3 mass spectra of M3 (*m/z* 327 → 245); d1 and d2: MS^2 and MS^3 mass spectra of M4 (*m/z* 341 → 165)

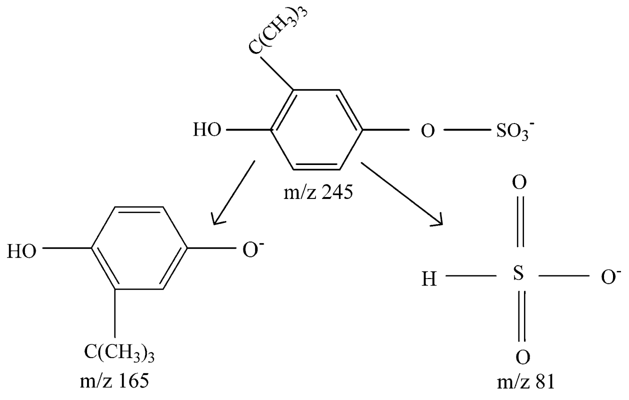

Fig. 6 Fragmentation pathway of *m/z* 245 (M1)

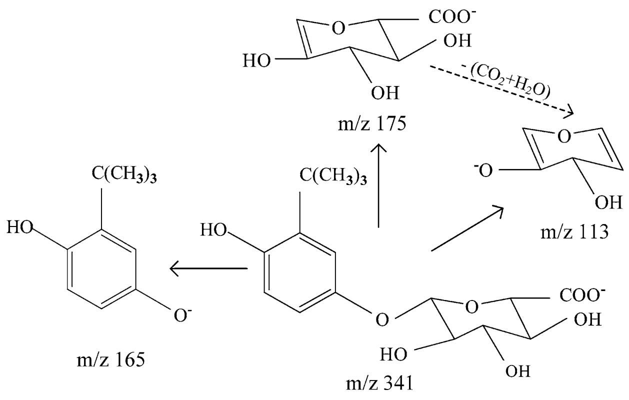

Fig. 7 Fragmentation pathway of *m/z* 341 (M4)

pathway of *m/z* 341 (M4) can be seen in Fig. 7. M4 was identified as a glucuronide conjugate of TBHQ.

The results indicate that besides free TBHQ, TBHQ is mainly metabolized to a TBHQ-sulfate, a TBHQ-glucuronide and two derivatives from TBHQ-sulfate in rat serum after oral administration. These findings are consistent with those results reported in the literature [13, 16]. Astill et al. reported that 57–74% of the administered TBHQ was eliminated in the urine as the sulfate conjugate. Ikeda et al. observed metabolites consisted of TBHQ-glucuronide, TBHQ-sulfate and unidentified polar substances in rat urine by thin-layer radiochromatography following sample treatment with β-glucuronidase and sulfatase.

Serum Distribution of TBHQ and its Metabolites

As evident in Fig. 8, TBHQ and its metabolites were able to be separated very well and the separations did not suffer from interference of rat serum substrate using LC/ITMS. Therefore, TBHQ's MS^2 characteristic product ion and its MS^1 product ions based on extracted ion chromatograms (EICs) were employed for quantitation of free TBHQ and semi-quantitation of its metabolites in rat serum.

The concentration of TBHQ in rat serum was quantified using an external standard prepared in a blank matrix. The calibration curve was obtained by plotting the peak area of EIC *m/z* 149 (MS^2) against the concentration of TBHQ. The calibration curve ($Y = 401.2X + 39{,}958.9$) showed good linearity over the concentration range of 49–5,030 μg/l with the coefficient (r^2) of 0.9985. The detection limit of TBHQ for serum samples was 14 μg/l ($S/N = 3$). The recoveries of TBHQ in serum ($n = 6$) were 96.1 ± 11.9, 93.4 ± 6.7 and 95.5 ± 9.4%. The intra-day relative standard deviations (RSDs) ($n = 6$) were 14.8, 10.3 and 7.7% and the inter-day RSDs over three consecutive days were 20.6, 14.4 and 8.3%. The results show that the method could be used for quantifying TBHQ in rat serum.

Under the adopted LC/ITMS conditions, peaks of TBHQ and its metabolites appear with retention times of 5.3 and 3–4 min, respectively. The nearness of their chromatographic retention times suggests that the polarities

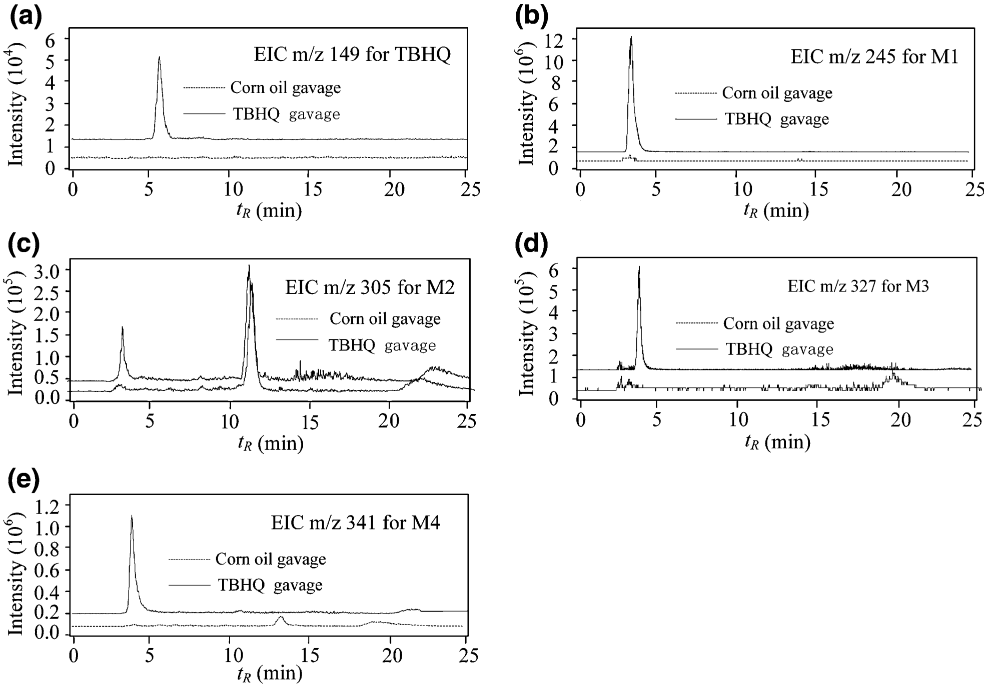

Fig. 8 Extracted ion chromatograms for quantitation of free TBHQ and its metabolites in rat serums following oral administration of corn oil at a dosage of 1 ml and TBHQ dissolved in corn oil at a dosage of 350 mg/kg. **a** Product ion *m/z* 149 from MS^2 spectrum for free TBHQ; **b** *m/z* 245 from MS^1 spectrum for M1; **c** *m/z* 305 from MS^1 spectrum for M2; **d** *m/z* 327 from MS^1 spectrum for M3; **e** *m/z* 341 from MS^1 spectrum for M4

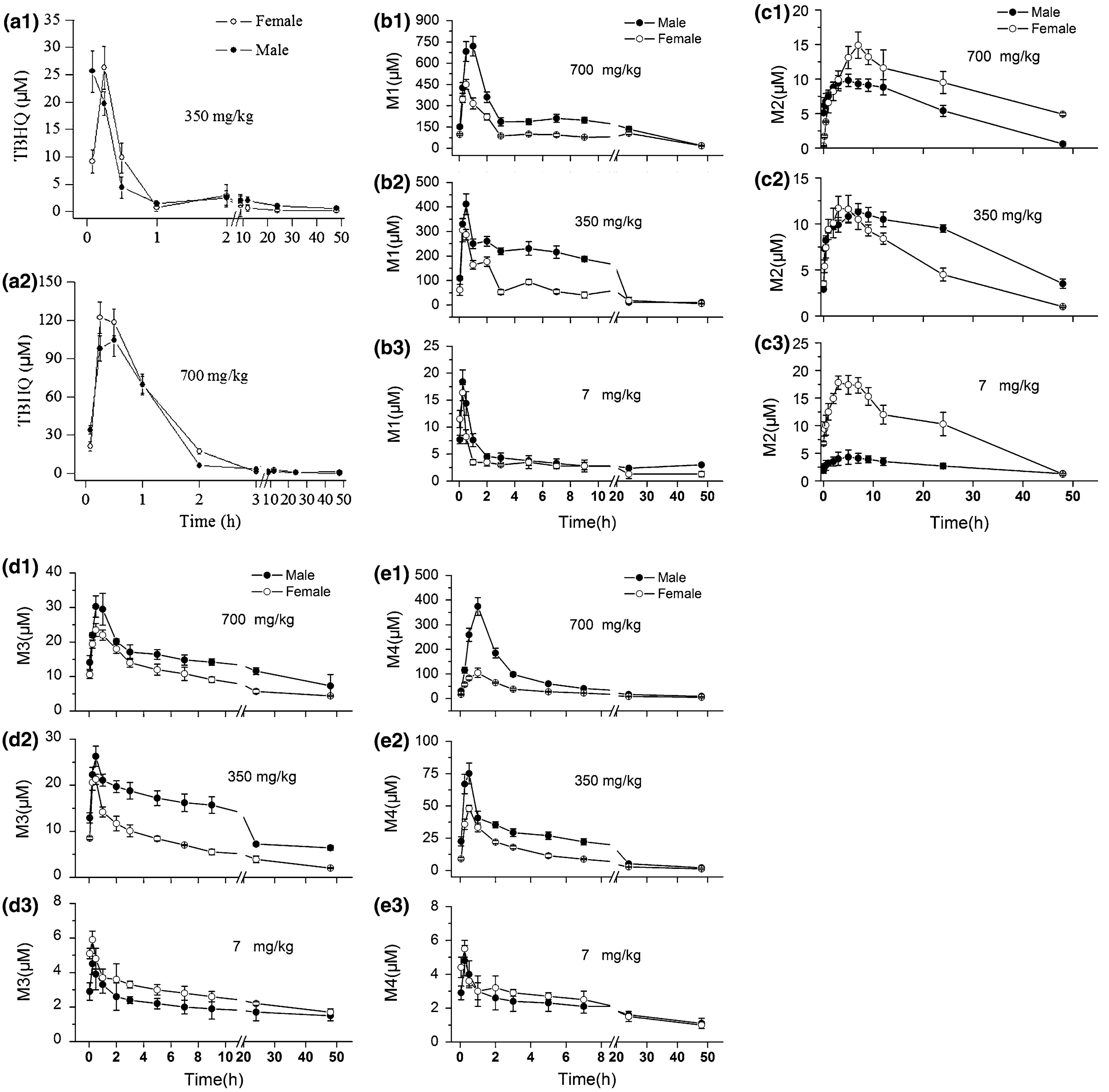

Fig. 9 Serum concentration–time profiles for TBHQ and its metabolites in both male and female rats after oral administration of TBHQ at a single dose of 7, 350 or 700 mg/kg. **a1** and **a2** for TBHQ; **b1**, **b2** and **b3** for M1; **c1**, **c2** and **c3** for M2; **d1**, **d2** and **d3** for M3; **e1**, **e2** and **e3** for M4. *Error bars* represent SD

of TBHQ and its metabolites are quite similar. The MS^1 response of a compound is decided by its polarity to some extent. So, using TBHQ standards, the semi-quantification of its metabolites is acceptable for metabolic kinetics study. In the research, the MS^1 responses of per unit concentration were defined to be equivalent for TBHQ and its metabolites; the calibration curve was obtained by plotting the peak area of EIC *m/z* 165 against the concentration of TBHQ. The coefficient (r^2) of the calibration curve ($Y = 817.2X - 74268.5$) was 0.9893, suggesting that the curve could work well for semi-quantifying the metabolites of TBHQ in rat serum.

The stabilities of TBHQ and its metabolites in post-pretreated and non-pretreated serum samples were evaluated by putting the samples at −20 °C for 24, 48 h, 3 and 7 days and at room temperature for 12 and 24 h. The results indicate that TBHQ and its metabolites in post-pretreated serum samples were stable at −20 °C within

7 days and RSDs were less than 6.3%; post-pretreated samples were stable at room temperature within 24 h and with RSDs of less than 7.1%; in non-pretreated samples they were stable at −20 °C for 7 days with RSDs of less than 8.3%. Afterwards samples were stored at −20 °C for 24, 48 h, 3 and 7 days and at room temperature for 12 and 24 h. In the experiment, the samples used for quantitation of TBHQ and its metabolites were stored at −20 °C for 7 days.

The acceptable daily intake (ADI) was 0–0.7 mg/kg body weight allocated by the Joint FAO/WHO Expert Committee on Food Additives (JECFA). Generally, rats could tolerate poisons approximately ten times higher than humans. The LD_{50} for TBHQ was found to be between 700 and 1,000 mg/kg for rats [15]. On the basis of this information, rats were administered TBHQ with a single dose of 7, 350 or 700 mg/kg. After a single dose of 700 mg/kg TBHQ, two male rats died within 2 h, whereas no female rats died.

The serum concentrations of TBHQ and its metabolites M1–M4 of both male and female rats after oral administration of TBHQ at doses of 7, 350 and 700 mg/kg were determined (Fig. 9). The serum levels of TBHQ reached peaks at 0.08–0.50 h after oral administration of 350 and 700 mg/kg TBHQ, and then the concentrations decreased rapidly and TBHQ disappeared from the serum after 5 h, as shown in Fig. 9a1 and a2, while the concentration of free TBHQ in the serum samples at the dose of 7 mg/kg was not detected because it was lower than the limit of detection. Following oral administration of 7, 350 and 700 mg/kg TBHQ, the maximum levels of M1 (Fig. 9b1, b2, b3), M3 (Fig. 9d1, d2 and d3) and M4 (Fig. 9e1, e2, e3) were observed at 0.25–1.00 h in rat serum, while the maximum levels of M2 (Fig. 9c1, c2, c3) were observed at 3.00–7.00 h. The concentrations of M1–M4 decreased slowly and most metabolites had been eliminated from the serum after 24–48 h. Meanwhile, it was observed in the experiment that after oral administration of 350 and 700 mg/kg (except 7 mg/kg), the total concentrations of TBHQ in serum were much higher for males than for females during the metabolic process ($P < 0.01$). It seems that TBHQ could be more completely absorbed by males than by females after oral administration, which may result in higher acute oral toxicity of TBHQ for males than females. This may explain why two males ($n = 6$) died, but no females ($n = 6$) died at the high dose of 700 mg/kg. Meanwhile, it was also found that the serum concentrations of M1, M3 and M4 appeared to be much higher for males than females ($P < 0.01$) during the metabolic process, while that TBHQ and M2 appeared no significant differences between male and female ($P > 0.05$). These results suggest that one or two of the metabolites M1, M3 and M4 are likely to be poisonous, but further toxicological studies on these metabolites are required to elucidate it.

Conclusions

A rapid and sensitive LC/ITMS method with simple treatment of samples was established for accurate quantitation of TBHQ and semi-quantitation of its metabolites in rat serum. Moreover, apparent sex difference in the metabolism of TBHQ were found. After oral administration, TBHQ appears to be more completely absorbed and bio-transformed by males than females, which may result in higher acute oral toxicity of TBHQ for males than females.

Acknowledgments Financial support of this research was from the National Key Technologies R&D Program of China with grant no. 2001BA804A21. Sincere thanks are to Dr Pengpenhao at Peking University for providing technical assistance in the experimental studies.

References

1. Rojas M, Brewer M (2007) Effect of natural antioxidants on oxidative stability of cooked, refrigerated beef and pork. J Food Sci 72:282–288
2. Gámez-Mezaa B, Noriega-Rodrígueza J, Medina-Juáreza LA, Ortega-Garcíaa J, Cázarez-Casanovaa R, Angulo-Guerrerob O (1999) Antioxidant activity in soybean oil of extracts from Thompson grape bagasse. J Am Oil Chem Soc 76:1445–1447
3. Min DB, Schweizer D (1983) Gas chromatographic determination of butylated hydroxyanisole, butylated hydroxytoluene and tertiary butyl hydroquinone in soybean oil. J Food Sci 48:73–74
4. Okubo T, Yokoyama Y, Kano K, Kano I (2003) Cell death induced by the phenolic antioxidant tert-butylhydroquinone and its metabolite tert-butylquinone in human monocytic leukemia U937 cells. Food Chem Toxicol 41:679–688
5. Hirokazu H, Mitsuhiro O, Kiyoe O, Sadako K, Tetsuo A (2003) Increase of antioxidative potential by tert-butylhydroquinone protects against cell death associated with 6-hydroxydopamine-induced oxidative stress in neuroblastoma SH-SY5Y cells. Mol Brain Res 119:125–131
6. Mohamed H (2003) Testicular toxicity of dibromoacetonitrile and possible protection by tertiary butylhydroquinone. Pharmacol Res 47:509–515
7. Ammawath W, Che MY, Baharin B, Abdul-Rahman R (2004) A new method for determination of tert-butylhydroquinone (TBHQ) in RBD palm olein with FTIR spectroscopy. J Food Lipids 11:266–277
8. Min-hua Y, Hsiu-jung L, Youk-meng C (2002) A rapid gas chromatographic method for direct determination of BHA, BHT and TBHQ in edible oils and fats. Food Res Int 35:627–633
9. Christian P, Liliane M (2002) Quantification of synthetic phenolic antioxidants in dry foods by reversed-phase HPLC with photodiode array detection. Food Chem 77:93–100
10. Warner K, Dunlap C (2006) Effects of expeller-pressed/physically refined soybean oil on frying oil stability and flavor of french-fried potatoes. J Am Oil Chem Soc 83:435–441
11. Yueqing G, Qingcui C, Liang F, Ting W, Jiannong Y (2006) Determination of phenolic antioxidants by micellar electrokinetic

capillary chromatography with electrochemical detection. Food Chem Toxicol 94:157–162

12. Wen H, Hai N, Bi S, Minli Y, Jixin J (2007) HPLC coupled to ion trap-ms/ms for analysis of tertiary-butylhydroquinone in edible oil samples. J Food Lipids (in press)
13. Ikeda G, Sapienza P, Ross I (1998) Distribution and excretion of radiolabelled tert-butylhydroquinone in Fischer 344 rats. Food Chem Toxicol 36:907–914
14. Chen HX, Chen Y, Du P, Han FM, Wang H, Zhang HS (2006) Sensitive and specific liquid chromatographic–tandem mass spectrometric assay for atropine and its eleven metabolites in rat urine. J Pharm Biomed Anal 40:142–150
15. Aresta A, Carbonara T, Palmisano F, Zambonin C (2006) Profiling urinary metabolites of naproxen by liquid chromatography–electrospray mass spectrometry. J Pharm Biomed Anal 41:1312–1316
16. Astill B, Terhaar C, Krasavage W, Wolf G, Roudabush R, Fassett D (1975) Safety evaluation and biochemical behavior of monotertiarybutylhydroquinone. J Am Oil Chem Soc 52:53–58

Lipids (2008) 43:289–299
DOI 10.1007/s11745-008-3158-5

ORIGINAL ARTICLE

SNPs of the *FADS* Gene Cluster are Associated with Polyunsaturated Fatty Acids in a Cohort of Patients with Cardiovascular Disease

Giovanni Malerba · Linda Schaeffer · Luciano Xumerle · Norman Klopp · Elisabetta Trabetti · Michele Biscuola · Ugo Cavallari · Roberta Galavotti · Nicola Martinelli · Patrizia Guarini · Domenico Girelli · Oliviero Olivieri · Roberto Corrocher · Joachim Heinrich · Pier Franco Pignatti · Thomas Illig

Received: 23 April 2007 / Accepted: 23 January 2008 / Published online: 5 March 2008
© AOCS 2008

Abstract Polymorphisms of the human Δ-5 (*FADS1*) and Δ-6 (*FADS2*) desaturase genes have been recently described to be associated with the level of several long-chain n-3 and n-6 polyunsaturated fatty acids (PUFAs) in serum phospholipids. We have genotyped 13 single nucleotide polymorphisms (SNPs) located on the *FADS1–FADS2–FADS3* gene cluster (chromosome 11q12–13.1) in 658 Italian adults (78% males; mean age 59.7 ± 11.1 years) participating in the Verona Heart Project. Polymorphisms and statistically inferred haplotypes showed a strong association with arachidonic acid (C20:4n-6) levels in serum phospholipids and in erythrocyte cell membranes (rs174545 adjusted *P* value for multiple tests, $P < 0.0001$ and $P < 0.0001$, respectively). Other significant associations were observed for linoleic (C18:2n-6), alpha-linolenic (C18:3n-3) and eicosadienoic (C20:2n-6) acids. Minor allele homozygotes and heterozygotes were associated to higher levels of linoleic, alpha-linolenic, eicosadienoic and lower levels of arachidonic acid. No significant association was observed for stearidonic (C18:4n-3), eicosapentaenoic (C20:5n-3) and docosahexaenoic (C22:6n-3) acids levels. The observed strong association of *FADS* gene polymorphisms with the levels of arachidonic acid, which is a precursor of molecules involved in inflammation and immunity processes, suggests that SNPs of the *FADS*1 and *FADS*2 gene region are worth studying in diseases related to inflammatory conditions or alterations in the concentration of PUFAs.

Keywords Fatty acid metabolism · Fatty acids · Genetics · Metabolism · Miscellaneous desaturases · n-6/n-3 fatty acids · Specific lipids

Introduction

Polyunsaturated fatty acids (PUFAs) are known to play crucial roles in various cellular functions—for example, as components of the cell membrane and precursors of important mediators of inflammation, such as eicosanoids [1]. They can affect membrane fluidity and cholesterol content and influence the generation of signaling molecules. Several studies have reported an association between PUFAs and the development and outcomes of several complex diseases [2–7].

The levels of PUFAs greatly depend on diet and metabolic pathways. The key enzymes in PUFA metabolism are the Δ-5 and Δ-6 desaturases, which are encoded by the *FADS1* and *FADS2* gene, respectively [8–10]. These two genes are located on the desaturase gene cluster on chromosome 11 (11q12–13.1). This cluster also includes a *FADS*3 gene that shares 52 and 62% sequence identity with

---

Electronic supplementary material The online version of this article (doi:10.1007/s11745-008-3158-5) contains supplementary material, which is available to authorized users.

G. Malerba (✉) · L. Xumerle · E. Trabetti · M. Biscuola ·
U. Cavallari · R. Galavotti · P. F. Pignatti
Department of Mother and Child, and Biology–Genetics,
Section of Biology and Genetics,
University of Verona, Verona, Italy
e-mail: giovanni.malerba@univr.it

L. Schaeffer · N. Klopp · J. Heinrich · T. Illig
Helmholtz Zentrum Muenchen, German Research Center
for Environmental Health, Institute of Epidemiology,
Neuherberg, Germany

N. Martinelli · P. Guarini · D. Girelli · O. Olivieri ·
R. Corrocher
Department of Clinical and Experimental Medicine,
University of Verona, Verona, Italy

the above-mentioned genes, respectively, as well as a cytochrome b5-like domain and a multiple membrane-spanning desaturase region. Consequently, it is surmised that *FADS3* encodes for another desaturase of as-yet unknown activity [8].

Schaeffer et al. [11] recently reported the association of single nucleotide polymorphisms (SNPs) in the *FADS1–FADS2* gene cluster with the levels of n-6 and n-3 fatty acids in serum phospholipids. However, they did not test this association in erythrocyte cell membranes. Erythrocytes provide a simple, highly suitable model for the study of fatty acid metabolism, because these cells lack desaturase and elongase enzymes and their membrane fatty acid composition closely resembles that of circulating lipoproteins, which in turn are assembled in the liver. Moreover, erythrocyte fatty acids are less influenced than serum phospholipids by short-term variations in dietary intake and can, therefore, be considered as suitable biological markers of relatively long time periods (weeks or a few months) [13]. *FADS* gene polymorphisms may contribute to the regulation of the levels of several PUFAs in various tissues; as such, they may be involved in disorders related to different arrangements of PUFA composition.

The aim of this study was to test—in a Northern Italian population of cardiovascular patients—the hypothesis that *FADS*1, *FADS*2, and *FADS3* gene polymorphisms correlate with the levels of fatty acids in serum phospholipids and erythrocyte membranes.

Methods

Study Population

Northern Italian subjects were recruited as a part of a cardiovascular survey study, the Verona Heart Project (VRHP). Details on the enrolment criteria have been described elsewhere [13].

In the present study we genotyped a total of 658 subjects who had been referred for coronography due to cardiovascular disease. These patients were not on lipid-lowering treatment, and data on their PUFA levels were available.

Each patient was characterized for possible confounders of PUFA levels, such as age (mean 59.7 ± 11.1 years), gender (78% males), body mass index (BMI; mean 26.03 ± 3.38 kg/m^2), hypertension (50%), smoking status (58% smokers), plasma triglycerides (TGs; 3.80 ± 0.97 m*M*), high-density lipoprotein (HDL) cholesterol (1.30 ± 0.38 m*M*), low-density lipoprotein (LDL) cholesterol (3.80 ± 0.97 m*M*), total cholesterol (5.72 ± 1.08 m*M*), diabetes (12%) and status of cardiovascular disease [414 individuals had coronary atherosclerotic disease (CAD), as established by angiography, and 244 individuals had angiographically documented normal coronary arteries].

The study was approved by our Institutional Review Board. Written informed consent was obtained from all patients.

Measurement of Fatty Acid Levels

Fatty acids levels were measured as previously described [14]. Blood samples were collected after an overnight fast, transported to the laboratory within 1 h and processed immediately. Analyses of the serum phospholipids (100 μl) and erythrocyte membranes (250 μl packed erythrocytes hemolyzed in an equal volume of double distilled water) fatty acids were performed on total lipids extracted using 4.5 ml isopropanol:chloroform (11:7, v:v) containing 0.45 m*M* 2,6-di-ter-*p*-cresol/l as antioxidant. A gas-chromatographic method [Hewlett Packard 5980 chromatograph equipped with an HP-FFAP phase column (length 25 m, internal diameter 0.2 mm, phase column 0.3 μm); Hewlett Packard, Palo Alto, CA] based on a direct fatty acid transesterification technique was used, as previously described [12]. The peaks were identified and quantified by comparison with commercially available reference fatty acids (Sigma, St. Louis, MO). Fatty acid C17:0 was used as the internal standard. The areas of the peaks were measured and subsequently quantified using a PC Vectra QS/16S equipped with HP-3365 Chem Station software (Hewlett Packard) working with the operative system Microsoft Windows 3.0. The level of each fatty acid was expressed as grams per 100 g total fatty acid methyl esters (% by wt). Fatty acids from C12:0 to C26:0 were measured, and unidentified peaks accounted for <0.5% of the total. Each sample was analyzed in duplicate, and all coefficients of variation were <5%.

Some descriptive statistics on fatty acid values are given in Table 1.

SNPs and Genotyping

Thirteen SNPs tagging the most common haplotypes of the *FADS* gene region from the reported European Community Respiratory Health Survey (ECHRS) study [11] and six additional SNPs from the HapMap project (http://www.hapmap.org) were selected. Table 2 presents a description of the SNPs used. Figure 1 shows the position of the SNP relative to *FADS* gene cluster region.

Genotyping was performed using the same methods and in the same laboratory as previously described [11]. Briefly, genotyping was performed using matrix-assisted laser desorption/ionization time-of-flight mass spectrometry (MALDI-TOF MS) to detect allele-specific primer extension products (Mass Array, Sequenom, San Diego,

Table 1 Fatty acid content in serum phospholipids and erythrocyte membrane

PUFA	Acid name	Serum PUFA ($n = 658$)		Erythrocyte PUFA ($n = 656$)		Correlation
		Mean (%)	SD	Mean (%)	SD	r
C18:2n-6	Linoleic	24.40	6.00	9.40	0.75	0.70
C18:3n-3	Alpha-linolenic	0.44	0.2	0.10	0.17	0.38
C18:4n-3	Stearidonic	0.36	0.2	0.38	0.31	0.31
C20:2n-6	Eicosadienoic	0.23	0.22	0.27	0.26	0.64
C20:4n-6	Arachidonic	9.82	1.97	19.03	1.43	0.60
C20:5n-3	Eicosapentaenoic	0.78	0.42	0.68	0.26	0.78
C22:6n-3	Docosahexaenoic	2.45	0.74	6.30	1.3	0.75

PUFA Polyunsaturated fatty acids, *SD* standard deviation, *r* correlation coefficient

Fatty acid content is expressed as mean percentage of the total fatty acid level of either serum phospholipids or erythrocyte membranes. PUFAs were measured in 658 individuals. Information on erythrocyte PUFAs is missing for two individuals ($n = 656$). Correlation: Pearson's correlation between serum and erythrocyte PUFA. All correlations were statistically significant ($P < 0.05$)

Table 2 Characteristics of the 13 genotyped SNPs in the *FADS* gene region for the VRHP study population

SNP	Gene	Position	Major allele	Minor allele	Minor allele frequency
rs174545	*FADS*1	61325882	G	C	0.29
rs174556	*FADS*1	61337211	C	T	0.24
rs174561	*FADS*1	61339284	T	C	0.25
rs3834458	Intergenic *FADS*1/*FADS*2	61351497	T	Del	0.30
rs174570	*FADS*2	61353788	C	T	0.11
rs2524299	*FADS*2	61361358	A	T	0.09
rs174583	*FADS*2	61366326	C	T	0.32
rs174589	*FADS*2	61372379	C	G	0.20
rs498793	*FADS*2	61381281	G	A	0.41
rs174611	*FADS*2	61384457	T	C	0.25
rs17831757	Intergenic *FADS*2/*FADS*3	61391776	T	C	0.10
rs174627	Intergenic *FADS*2/*FADS*3	61394042	C	T	0.13
rs1000778	*FADS*3	61411881	G	A	0.24

VRHP Verona Heart Project, *SNP* single nucleotide polymorphism

Position in basepairs was derived from dbSNP Build 126, based on NCBI Human Genome Build 36.1 (March 2006) of chromosome 11. Allele frequency was calculated in the VRHP study population ($n = 658$)

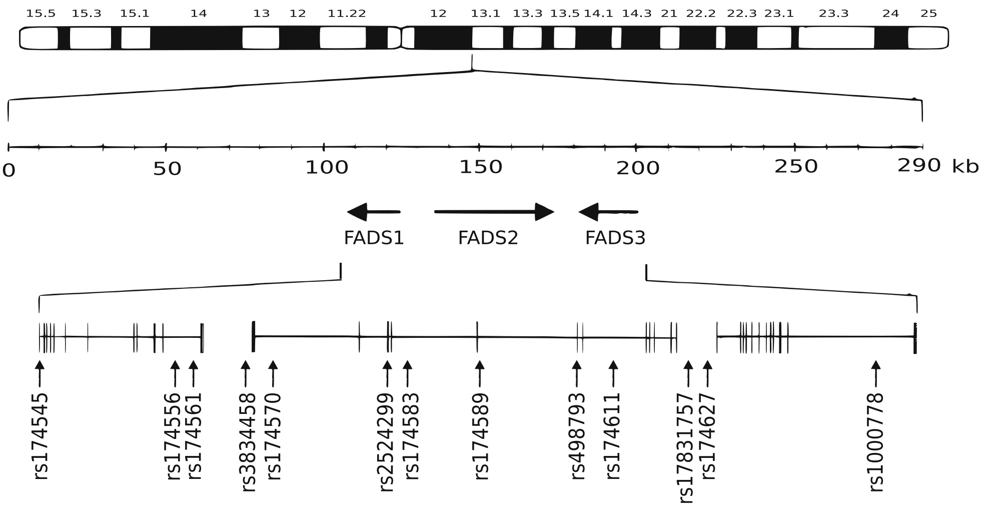
15.5
15.3
15.1
14
13
12
11.22
12
13.1
13.3
13.5
14.1
14.3
21
22.2
22.3
23.1
23.3
24
25
0
50
100
150
200
250
290 kb
FADS1
FADS2
FADS3
rs174545
rs174556
rs174561
rs3834458
rs174570
rs2524299
rs174583
rs174589
rs498793
rs174611
rs17831757
rs174627
rs1000778

Fig. 1 Location on chromosome 11, gene position and structure of the *FADS*1–*FADS*2–*FADS*3 gene cluster. *Horizontal arrows* indicate the direction of gene transcription. *Vertical bars* indicate exons. The position of markers used is shown at the *bottom*

CA). The primers for the PCR analyses were designed using Sequenom's MassArrayAssayDesign program.

The SNP association analysis was performed using R, a free software environment for statistical computing and graphics [15]. Haplotypes were reconstructed and analyzed using the haplo.glm function of the R library Haplo.Stats (http://mayoresearch.mayo.edu/mayo/research/biostat/splusfunctions.cfm) [16].

Statistical Analysis

a. Fatty acids

Fatty acid levels were treated as quantitative traits. The distribution of each PUFA is summarized by mean and standard deviation values. All potential confounders, such as age, gender, BMI, smoking status and CAD status, were included as covariates in the statistical models.

b. SNP Analysis

Hardy–Weinberg equilibrium was tested for each SNP locus, and significance was ascertained by the permutation tests implemented in the JenoHWE program, which is part of the Jenoware project (http://medgen.univr.it/jenoware by Dr. Luciano Xumerle). Lewontin's disequilibrium coefficient D' and the squared correlation coefficient (R^2) were estimated. Pairwise linkage disequilibrium was calculated for each pair of SNPs. Linear regression models including covariates were used for testing the association of SNPs with quantitative traits.

c. Haplotypes Analysis

Generalized linear regression models were used analyzing haplotype association with quantitative traits, assuming an additive inheritance model. Haplotype frequency was inferred from the investigated SNPs by an EM algorithm calculating maximum likelihood estimates given the genotypes on unknown phase (http://www-gene.cimr.cam.ac.uk/clayton/software/). Haplotype analysis was performed either by using haplotypes from all the 13 SNPs (from rs174544 up to rs1000778; 612 fully genotyped subjects) or by focusing on the windows of consecutive SNPs within linkage disequilibrium (LD) blocks. The windows of LD blocks were determined according to the method proposed by Kamatani [17]. All haplotypes with an estimated frequency higher than 2% were modeled. Each possible haplotype combination per individual entered the model as a weighted observation according to the approach 'EM by the method of weights' [18]. Rare haplotypes (frequency <2%) were pooled and included in the model as a group called 'haplo.rare'.

d. Estimation of Significance Values

The significance value of each association was estimated by permuting the phenotype and performing that statistical analysis in at least 1000 replicates and counting the number of replicates that presented a value greater than the value obtained from the statistical analysis of the original data set. This procedure was performed for single SNPs (10,000 replicates for each phenotype), 13-SNP haplotypes (1000 replicates for each phenotype and 10,000 replicates for phenotypes showing stronger association) and haplotype block-based association analysis (10,000 replicates for each LD block and phenotype).

e. Multiple Testing

Adjustment for multiple tests was achieved by estimating the significance level of the single test taking into account the number of statistical tests computed for either single SNP or haplotype analyses.

- SNPs. Due to a possible high LD between some of the SNPs, the estimated number of effective loci of the 13 SNPs was calculated according to the spectral decomposition method by Nyholt [19]. The nominal significance level of a single test was conservatively adjusted by a correction factor calculated as the number of effective loci × the 14 analyzed fatty acids (seven fatty acids in serum phospholipids + seven fatty acids in erythrocyte membrane, respectively). The *P* values of single tests were multiplied by the correction factor, and adjusted *P* values of greater than 1 were set to 1. All *P* values of single SNP analyses reported in the paper are the adjusted *P* values.
- Haplotypes. The significance level of the statistical tests was set to the significance level of a single test (i.e. 0.05) divided by the sum of 1 (analysis of the 13 SNPs haplotype) plus the number of LD blocks identified in the cluster region × the number of phenotypes investigated. The *P* values for the haplotype analyses reported here are not corrected for multiple tests.

Results

PUFAs in Serum and Erythrocyte Membranes

The content of fatty acids in serum and the erythrocyte membrane for seven n-6 and seven n-3 PUFAs was determined in 658 individuals from Northern Italy, as shown in Table 1. All coefficients of variations of PUFA measurements were less than 5%.

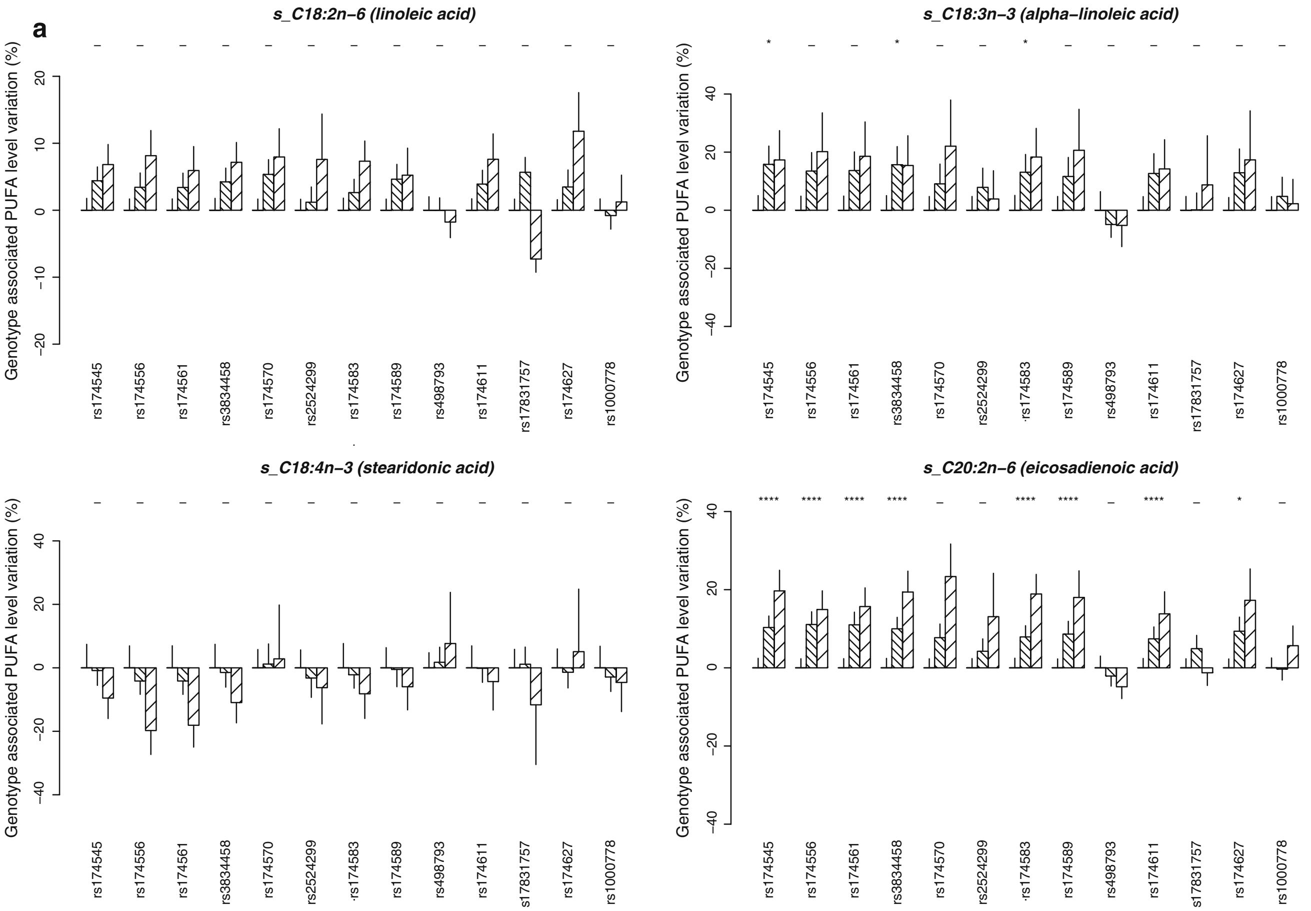

Fig. 2 Association analysis of 13 single nucleotide polymorphisms (SNPs) in the *FADS* gene cluster with the levels of polyunsaturated fatty acids in serum phospholipids and the erythrocyte membrane of 658 individuals. In each graph and for each SNP, the *first bar* represents the reference, which is the mean level of the PUFA for major allele homozygotes. The *height of the second and third bars* indicates the percentage change in the PUFA level in heterozygotes and minor allele homozygotes, respectively, calculated as the difference between the value for that PUFA and the reference value, divided by the reference value. The *vertical lines* indicate standard errors. *Asterisks* indicate significances after correction for multiple testing from general linear regression analyses: *$P < 0.05$, **$P < 0.001$, ***$P < 0.0001$. Table 1 in the Electronic Supplementary Material reports the PUFA mean levels for each SNP stratified by genotype as well as the significance (P value) of the statistical test comparing the PUFA mean levels among the genotypes

A significant correlation ($P < 0.0001$) between serum and erythrocyte membrane was observed for each of the PUFAs (Table 1).

Genetic Structure of the Region

Genotyping was performed with 13 SNPs in the *FADS* gene cluster. All genotyped SNPs were found to be polymorphic in the VRHP study. The minor allele frequency (MAF) ranged from 9 to 41%, as shown in Table 2. The frequency of most SNPs ranged between 20 and 30%, with only one SNP (rs2524299) showing a MAF <10% (9.1%). The mean genotyping success rate (GSR) was 99.0%, with the lowest GSR being 97.4%. The genotype distribution for each SNP was consistent with Hardy–Weinberg equilibrium. Three LD blocks were observed in the gene cluster [17]: block-1 from rs174545 to rs3834458; block-2 from rs2524299 to rs174589; block-3 from rs174611 to rs174627. Markers rs174545 and rs3834458 located in a highly preserved LD block (block-1) and markers rs174556 and rs174561 located in the same LD block showed a particularly high correlation ($R^2 > 0.98$). As haplotype analysis was performed on each of the three LD blocks and on the entire 13-SNP window, the significance at the nominal level of 5% for a single test was set to $P = 0.00089$ {i.e. $0.05/[(1 + 3) \times 14]$; see Methods}. Therefore, a haplotype association was considered to be significant after multiple test adjustment when $P < 0.00089$.

Association of PUFAs with Single SNPs

The results of the single SNP association analysis with fatty acids (658 individuals) are summarized for serum phospholipids or the erythrocyte membrane by graphical

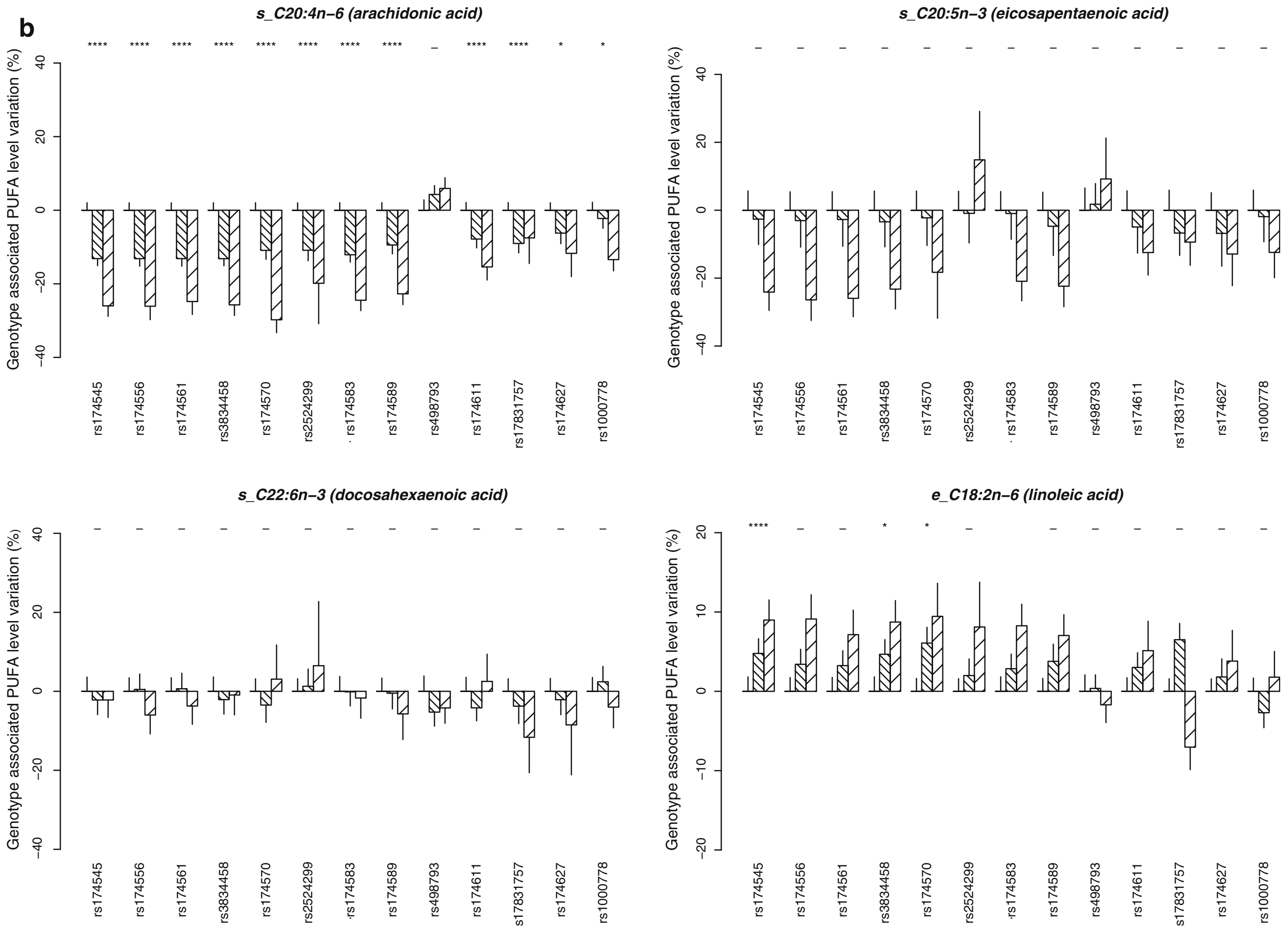

Fig. 2 continued

representation in Fig. 2; for more detailed results, see Table 1 in the Electronic Supplementary Material.

The association study was performed by adjusting the PUFA level for potential confounders (i.e. age, gender, BMI, smoking status and CAD status). In order to adjust for multiple testing the *P* values of the single tests were multiplied by 112 (eight effective loci × the 14 analyzed fatty acids). After this correction, highly significant results were observed for the majority of the SNPs and serum phospholipids or erythrocyte membrane for arachidonic acid in the region from rs174545 up to rs174570 (adjusted-*P* values <0.0001 for serum and for erythrocyte membranes). Carriers of the minor variants showed significantly lower levels of arachidonic acid. Carriers of the minor alleles of rs174545, rs3834458, and rs174583 also showed significant associations with an increase in the serum phospholipid n-3 fatty acid alpha-linolenic acid, while carriers of the minor alleles of SNPs rs174545 up to rs3834458, and rs174583, rs174589, rs174611 and rs174627 showed a significant association with an increased level of eicosadienoic acid (C20:2n-6) in serum phospholipids. In erythrocyte membranes, the rare variants of rs174545, rs3834458, rs174570, and rs174583 showed significant associations with an increase in linoleic acid, and rs174545 up to rs3834458, and rs174583 showed significant associations with an increase in eicosadienoic acid (C20:2n-6).

Similar significant results were also observed in the subgroup of individuals without coronary heart disease (244/658 individuals; data not shown).

Association of PUFAs with the Genetic Region

Haplotypes were reconstructed with all 13 SNPs. Table 3 shows the estimated 13-SNP haplotype frequency for haplotypes showing a frequency of more than 2%. Six common haplotypes can be seen to account for 74% of the estimated haplotypes and rare haplotypes to account for the remaining 26%. The two most common haplotypes (haplo.base and haplo.4; Table 3) carry major alleles at each

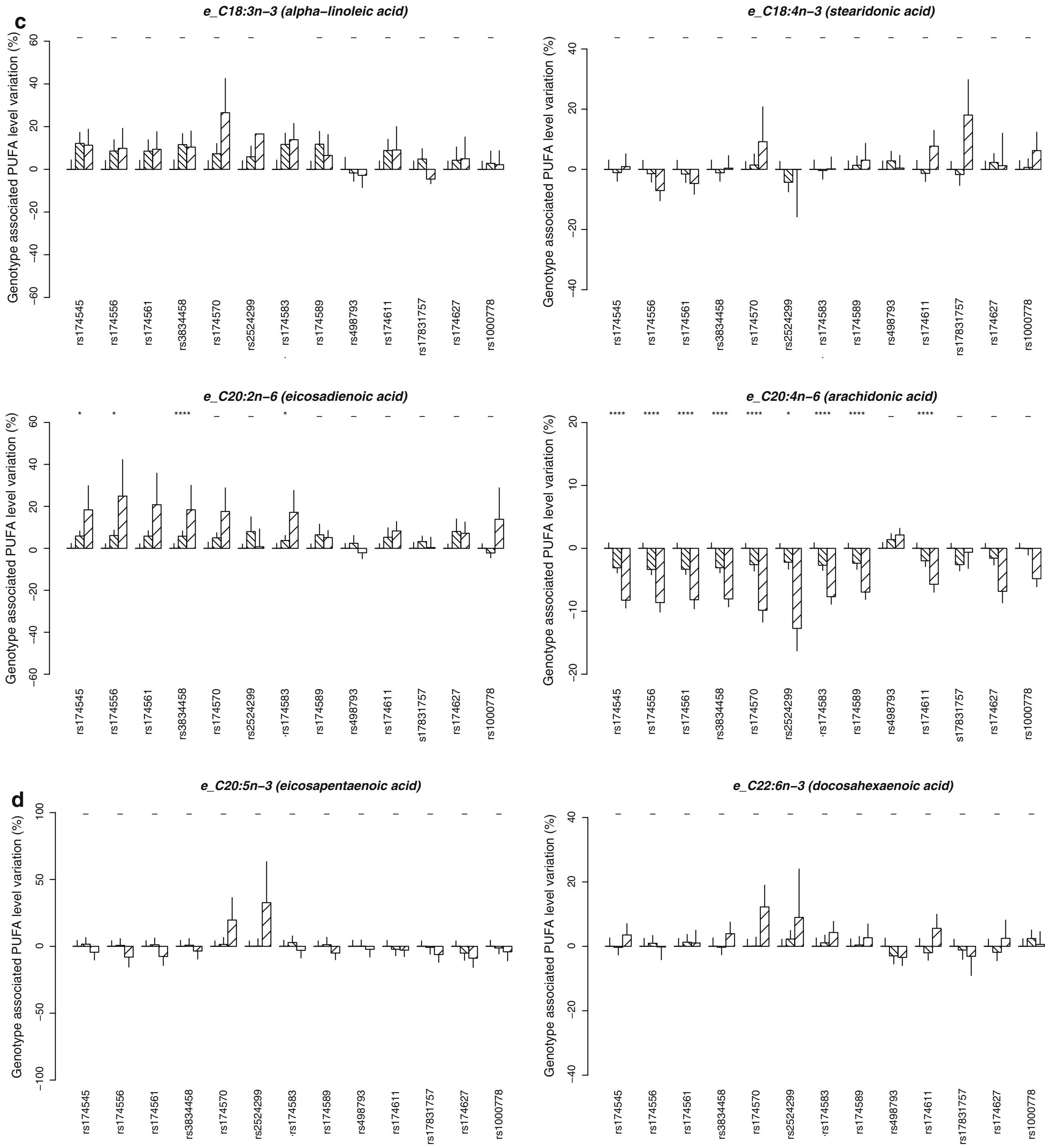

Fig. 2 continued

SNP locus, with the exception of rs498793, which shows the minor allele in haplo.base. The association study was performed with each one of the seven PUFAs investigated in both serum phosholipids and in erythrocyte membranes, as shown in Table 4. The results reveal a significant association (threshold after multiple test adjustment: $P < 0.00089$) between the *FADS* cluster haplotypes and the level of arachidonic acid in serum phospholipids and in the membrane of red blood cells (RBCs) (Table 4). No other significant association was observed.

Table 3 *FADS* gene cluster haplotype frequencies

Haplotype	rs174545	rs174556	rs174561	rs3834458	rs174570	rs2524299	rs174583	rs174589	rs498793	rs174611	rs17831757	rs174627	rs1000778	Haplotype frequency
haplo.base	G	C	T	T	C	A	C	C	A	T	T	C	G	0.3229
haplo.1	C	T	C	Del	C	A	T	G	G	C	T	T	A	0.0583
haplo.2	C	T	C	Del	T	T	T	C	G	T	T	C	G	0.0212
haplo.3	C	C	T	Del	T	A	T	G	G	C	C	C	G	0.0388
haplo.4	G	C	T	T	C	A	C	C	G	T	T	C	G	0.2664
haplo.5	G	C	T	T	C	A	C	C	G	T	T	C	A	0.0327
haplo.rare	*	*	*	*	*	*	*	*	*	*	*	*	*	0.2597

Haplo.rare all of the haplotypes showing an individual frequency below 2%, *haplo.base* the more frequent haplotype; it is used as a reference in generalized linear models in the association analyses with PUFA

Association of PUFAs with three LD Blocks in the *FADS* Gene Cluster

For further refining of the genetic data, we carried out an association analysis between the *FADS* gene cluster LD block and PUFA levels. The LD block structure and frequency of haplotypes within the three LD blocks are shown in Table 5.

Table 6 shows the results of the LD block-based haplotype association analysis performed for the seven PUFAs in the serum and RBC, respectively. This table shows non-corrected P values. After correction for multiple tests the haplotype associations with the PUFA levels remained statistically significant (nominal level of 5% for a single test) only for arachidonic acid (serum: blocks 1, 2, 3; RBC: blocks 1, 2). No significant association was observed for linoleic, alpha-linolenic, stearidonic, eicosadienoic, eicosapentaenoic and docosahexaenoic acids.

Discussion

We report here the association of 13 *FADS* gene cluster polymorphisms and the level of several PUFAs in serum phospholipids (SP) and the membrane of red blood cells (RBC), as measured in 658 Italian individuals. We observed a very strong association between arachidonic acid levels in SP, as has been reported previously [11], and, for the first time, in RBCs. Weaker but still significant associations were observed between single SNPs and linoleic (SP), alpha-linolenic (SP, RBC) and eicosadienoic

Table 4 Thirteen-SNP haplotype association analysis

PUFA	Acid name	Haplotype analysis P value[a]	
		Serum	Red blood cells
C18:2n-6	Linoleic	0.49	0.0122
C18:3n-3	Alpha-linolenic	0.25	0.0541
C18:4n-3	Stearidonic	0.57	0.35
C20:2n-6	Eicosadienoic	0.0081	0.15
C20:4n-6	Arachidonic	<0.0001***	0.0002***
C20:5n-3	Eicosapentaenoic	0.70	0.44
C22:6n-3	Docosahexaenoic	0.68	0.30

[a] P value: Significance level of the model containing the genetic factor (haplotypes) versus the model without the genetic factors. P values were not adjusted for multiple tests. Arachidonic acid showed a significant association in serum phospholipids and in erythrocyte membrane (=significant association after correction for multiple tests; *** $P < 0.00089$; see Methods). Eicosadienoic showed an association in serum phospholipids, and linoleic acid showed an association in erythrocyte membranes, but both these associations were not significant after correction for multiple tests

Table 5 Linkage disequilibrium (LD) blocks and haplotype frequency

FADS gene cluster LD blocks								
Block 1			Block 2			Block 3		
(rs174545–rs3834458)			(rs2524299–rs174589)			(rs174611–rs174627)		
Hap. id	Haplotype	%	Hap id	Haplotype	%	Hap id	Haplotype	%
1a	C T C Del	23.7	2a	A T C	2.6	3a	C T C	2.8
1b	C C T Del	4.9	2b	A T G	19.8	3b	C T T	12.8
			2c	T T C	8.8	3c	C C C	9.2
1Bl	G C T T	70.6	2Bl	A C C	68	3Bl	T T C	74.3

SNPs between parentheses define left and right bounds for each LD block. Blocks 1, 2, and 3 contain three, four and four common haplotypes, respectively. Three LD blocks were identified. Haplotypes with an estimated frequency below 2% are not reported

Hap id identifier of the haplotype, *haplotype* alleles at consecutive SNPs, *1Bl, 2Bl, 3Bl* most common haplotype in blocks 1, 2 and 3, respectively

Table 6 Linkage disequilibrium (LD) block-based haplotype association analysis

PUFA[a]	Block-1		Block 2		Block-3	
	P value[b]	Effect and haplotype id[c]	*P* value	Effect and haplotype id	*P* value	Effect and haplotype id
s_C18:2n-6	1.84×10^{-1}	ns	2.31×10^{-1}	ns	7.06×10^{-2}	ns
e_C18:2n-6	8.9×10^{-3}	+1a,1b	3.99×10^{-2}	+2b,2c	1.64×10^{-2}	+3c
s_C18:3n-3	1.20×10^{-1}	ns	1.25×10^{-1}	ns	8.87×10^{-2}	ns
e_C18:3n-3	3.54×10^{-1}	ns	2.31×10^{-1}	ns	2.81×10^{-2}	ns
s_C18:4n-3	1.95×10^{-1}	ns	2.57×10^{-1}	ns	3.65×10^{-1}	ns
e_C18:4n-3	2.17×10^{-1}	ns	1.452×10^{-1}	ns	2.88×10^{-1}	ns
s_C20:2n-6	3.2×10^{-3}	+1a,1b	1.01×10^{-2}	+2b,2c	1.00×10^{-2}	+3b,3c
e_C20:2n-6	6.40×10^{-2}	ns	4.51×10^{-2}	+2b,2c	9.16×10^{-2}	ns
s_C20:4n-6	<0.0001***	−1a, 1b	<0.0001***	−2a, 2b, 2c	<0.0001***	−3a, 3b, 3c
e_C20:4n-6	<0.0001***	−1a, 1b	<0.0001***	−2a, 2b, 2c	4.3×10^{-3}	−3a, 3b, 3c
s_C20:5n-3	4.74×10^{-1}	ns	3.59×10^{-1}	ns	4.79×10^{-1}	ns
e_C20:5n-3	5.69×10^{-1}	ns	8.64×10^{-1}	ns	1.10×10^{-1}	ns
s_C22:6n-3	1.45×10^{-1}	ns	6.85×10^{-1}	ns	8.72×10^{-2}	+3a
e_C22:6n-3	2.14×10^{-1}	ns	4.03×10^{-1}	ns	5.88×10^{-2}	+3a

[a] *PUFA* names preceded with a 's_' or a 'e_' are referred to serum or erythrocyte membrane, respectively

[b] *P* value: Significance level of the model containing the genetic factor versus the model without the genetic factor. *P* values are not corrected for multiple testing. Covariates are included in the models. *** Significant *P* values after adjustment for multiple tests ($P < 0.00089$)

[c] Effect and haplotypes: The sign (+/−) indicates the effect of the reported haplotypes, that is the increase or decrease of PUFA level with respect to the reference haplotype of each LD block. Only the haplotypes with a significant ($P < 0.05$) σ-value in the Generalized Linear Model are reported. Haplotypes are indicated by the Hap id reported in Table 5. ns, No statistically significant effect

(SP, RBC) acids. In particular, SNP rs174583 was associated with all the three acids. Significant associations were also confirmed in the subgroup of individuals without coronary heart disease.

The *FADS* gene cluster was studied using 13 SNPs tagging the most common haplotypes. These 13 SNPs span a region that contains three *FADS* genes, including the *FADS*3 gene. *FADS*3 is a gene with an unknown function, although it is presumed to have a desaturase activity on the basis of its sequence homology with the other *FADS* genes.

The LD block structure of the whole region was studied in order to detect sub-regions of highly correlated SNPs that ideally represent the smallest and non-redundant source of variability that can be used independently in the association analyses of the region. Three LD blocks were identified (see Table 5). Block 1 (four SNPs, from rs174545 to rs3834458) contains three SNPs in the *FADS*1 gene and one SNP between the *FADS1* and *FADS2* genes; block 2 (three SNPs, from rs2524299 to rs174589) contains three SNPs in the *FADS2* gene; block 3 (three SNPs, rs174611 to rs174627) contains one SNP in the *FADS2* gene and two SNPs between the *FADS2* and *FADS3* genes. A similar LD structure was also observed in the ECHRS study by Schaeffer et al. [11]. It is noteworthy that the strongest association was observed with arachidonic acid levels, confirming the results of the previous study [11] (see Table 7). Furthermore, in accordance with the results of Schaeffer et al., the most frequent haplotype shows an opposite effect with respect to all the other haplotypes, indicating that the most common haplotype exerts a different effect from all other haplotypes (see Table 7). Therefore, the *FADS* gene cluster polymorphisms are likely to contribute to the variability of PUFA levels in the short-term the serum component (as initially indicated by Schaeffer et al. [11]) and in medium-term compartments, such as erythrocytes (as indicated in this study). Although detailed information on their mode of action remains elusive, PUFAs appear to affect many different biological systems (hormone production, lipid peroxidation products, transcription events, membrane structure and function), and it can be argued that they act at a fundamental level that is common to most cells [20]. At the present time, we cannot know whether the association described here could be extended to long-term compartments, such as adipose tissue, or generalized to other tissues. However, Baylin et al. recently described an association of the rs3834458 marker, mapping in the LD block-1 of the present paper, with serum and adipose tissue PUFA levels [21]. This result suggests that *FADS* gene cluster polymorphisms may affect the PUFA levels of long-term compartments as well as short- and medium-term compartments. To the best of the authors' knowledge, no study has actually reported whether the studied polymorphisms are functionally related to desaturase activity or whether they simply tag the true and still unknown causal genetic variant.

Since arachidonic acid is the precursor of prostaglandins, leukotrienes and related compounds, all of which have important roles in inflammation and in the regulation of immunity, *FADS* gene polymorphisms now represent novel candidates to be studied in eicosanoid-related disorders. However, PUFA levels are expressed as a percentage of total lipids and not as an absolute value (e.g. concentration). Therefore, we were able to detect relative differences in the PUFA levels due to the genetic component but we were unable to study mechanisms as these depend on the absolute value of PUFA levels (i.e. concentration).

Desaturase activity represents only a part of the mechanisms involved in the regulation of PUFAs, and several other components, such as sex, diet, age, BMI and hypertension, are factors known to be associated with variations in the levels of PUFAs [22–25].

The association of single SNPs with the levels of linoleic, alpha-linolenic and eicosadienoic acids indicates that *FADS* gene polymorphisms are likely to influence the levels of several PUFAs. Linoleic and alpha-linolenic acids are a substrate of Δ-6 desaturase (*FADS2* gene), and eicosadienoic acid is the product of the elongation process of linoleic acid. Therefore, these associations may reflect a

Table 7 Haplotype frequency of block 1 and association with arachidonic acid levels in the VRHP and ECRHS [12] studies

Block 1—haplotypes			Frequency %	Study[a]	β-coef[b]	P value[c]
rs174556	rs174561	rs3834458				
C	T	T	68.6	ECRHS	Base-line	
			70.6	VRHP serum	Base-line	
				VRHP RBC	Base-line	
T	C	Del	25.7	ECRHS	−1.17	<0.0001
			23.7	VRHP serum	−1.41	<0.0001
				VRHP RBC	−0.768	<0.0001
C	T	Del	3.5	ECRHS	−1.12	<0.0001
			4.9	VRHP serum	−1.19	<0.0001
				VRHP RBC	−0.55	2.2×10^{-3}
<1%			2.3	ECRHS	−0.40	0.7
			0.8	VRHP serum	n.d	
				VRHP RBC	n.d	

[a] ECRHS (European Community Respiratory Health Survey) analysis was determined in serum phospholipids only; VRHP serum arachidonic acid in serum phospholipids; VRHP RBC, arachidonic acid in the red blood cell membranes

[b] *β-coef* estimated coefficient for the haplotype in the generalized linear model with respect to the baseline-haplotype values, *n.d.* not determined

[c] *P* value significance of the hypothesis that the β-coef value is different from 0

The haplotype with highest frequency (CTT) is associated to higher levels of arachidonic acid (all the other haplotypes are associated to lower levels) relationship with Δ-6 desaturation activity. The lack of association with the other PUFAs may be due to a true absence of any association with causative genetic factors or to the effect of other factors, such as diet, or other processes involved in the regulation of the proportion of different types of PUFAs. For example, studies reporting that docosahexaenoic acid level does not strongly correlate with dietary intake indicate an independent regulation of docosahexaenoic acid [22].

Overall, the results of this study suggest that *FADS1* and *FADS2* gene polymorphisms are likely to be important factors contributing to the variability in PUFA levels in several tissues, such as serum phospholipids, tightly regulated tissues as the phospholipid membrane and in tissues with low turnover [21].

In conclusion, the association of the *FADS1* and *FADS2* gene region—but not the *FADS3* gene region—indicates that polymorphisms of these two genes contribute to the variability of several PUFAs, such as linoleic, alpha-linolenic, eicosadienoic acids and, most of all, arachidonic acid. As modifications in PUFA levels have been observed in several diseases, these genes may therefore represent a susceptibility factor worth investigating.

Acknowledgments We thank Patrizia Pattini (Department of Internal Medicine, University of Verona) for her excellent help in measuring serum and erythrocyte fatty acids. This work was supported by grants from Italian Ministry of University and Research, Veneto region, and by the German National Genome Research Network (NGFN).

References

1. Jump DB (2002) Dietary polyunsaturated fatty acids and regulation of gene transcription. Curr Opin Lipidol 13:155–164
2. Serhan CN (2005) Novel omega-3-derived local mediators in anti-inflammation and resolution. Pharmacol Ther 105:7–21
3. Simopoulos AP (2002) Omega-3 fatty acids in inflammation and autoimmune diseases. J Am Coll Nutr 21:495–505
4. Thies F, Miles EA, Nebe-von-Caron G, Powell JR, Hurst TL, Newsholme EA, Calder PC (2001) Influence of dietary supplementation with long-chain n-3 or n-6 polyunsaturated fatty acids on blood inflammatory cell populations and functions and on plasma soluble adhesion molecules in healthy adults. Lipids 36:1183–1193
5. Harbige LS (1998) Dietary n-6 and n-3 fatty acids in immunity and autoimmune disease. Proc Nutr Soc 57:555–562
6. Bazinet RP, Douglas H, McMillan EG, Wilkie BN, Cunnane SC (2004) Dietary 18:3 omega3 influences immune function and the tissue fatty acid response to antigens and adjuvant. Immunol Lett 95:85–90
7. Palmer LJ, Daniels SE, Rye PJ, Gibson NA, Tay GK, Cookson WO, Goldblatt J, Burton PR, LeSöuef PN (1998) Linkage of chromosome 5q and 11q gene markers to asthma-associated quantitative traits in australian children. Am J Respir Crit Care Med 158:1825–1830
8. Marquardt A, Stöhr H, White K, Weber BH (2000) Cdna cloning, genomic structure, and chromosomal localization of three members of the human fatty acid desaturase family. Genomics 66:175–183
9. Cho HP, Nakamura MT, Clarke SD (1999) Cloning, expression, and nutritional regulation of the mammalian delta-6 desaturase. J Biol Chem 274:471–477
10. Cho HP, Nakamura M, Clarke SD (1999) Cloning, expression, and fatty acid regulation of the human delta-5 desaturase. J Biol Chem 274:37335–37339
11. Schaeffer L, Gohlke H, Muller M, Heid IM, Palmer LJ, Kompauer I, Demmelmair H, Illig T, Koletzko B, Heinrich J (2006) Common genetic variants of the *FADS1 FADS2* gene cluster and their reconstructed haplotypes are associated with the fatty acid composition in phospholipids. Hum Mol Genet 15:1745–1756
12. Olivieri O, Stanzial AM, Girelli D, Trevisan MT, Guarini P, Terzi M, Caffi S, Fontana F, Casaril M, Ferrari S (1994) Selenium status, fatty acids, vitamins a and e, and aging: the nove study. Am J Clin Nutr 60:510–517
13. Trabetti E, Biscuola M, Cavallari U, Malerba G, Girelli D, Olivieri O, Martinelli N, Corrocher R, Pignatti PF (2006) On the association of the oxidised ldl receptor 1 (*olr1*) gene in patients with acute myocardial infarction or coronary artery disease. Eur J Hum Genet 14:127–130
14. Olivieri O, Martinelli N, Sandri M, Bassi A, Guarini P, Trabetti E, Pizzolo F, Girelli D, Friso S, Pignatti PF, Corrocher R (2005) Apolipoprotein c-iii, n-3 polyunsaturated fatty acids, and "insulin-resistant" t-455c apoc3 gene polymorphism in heart disease patients: example of gene–diet interaction. Clin Chem 51:360–367
15. R Development Core Team (2006) R. A language and environment for statistical computing. R Foundation for Statistical Computing. R Development Core Team,Vienna
16. Lake SL, Lyon H, Tantisira K, Silverman EK, Weiss ST, Laird NM, Schaid DJ (2003) Estimation and tests of haplotype–environment interaction when linkage phase is ambiguous. Hum Hered 55:56–65
17. Kamatani N, Sekine A, Kitamoto T, Iida A, Saito S, Kogame A, Inoue E, Kawamoto M, Harigai M, Nakamura Y (2004) Large-scale single-nucleotide polymorphism (snp) and haplotype analyses, using dense snp maps, of 199 drug-related genes in 752 subjects: the analysis of the association between uncommon snps within haplotype blocks and the haplotypes constructed with haplotype-tagging SNPs. Am J Hum Genet 75:190–203
18. Ibrahim JG (1990) Incomplete data in generalized linear models. J Am Stat Assoc 85:765–769
19. Nyholt DR (2004) A simple correction for multiple testing for single-nucleotide polymorphisms in linkage disequilibrium with each other. Am J Hum Genet 74:765–769
20. Stillwell W, Shaikh SR, Zerouga M, Siddiqui R, Wassall SR (2005) Docosahexaenoic acid affects cell signaling by altering lipid rafts. Reprod Nutr Dev 45:559–579
21. Baylin A, Ruiz-Narvaez E, Kraft P, Campos H (2007) Alpha-linolenic acid, delta6-desaturase gene polymorphism, and the risk of nonfatal myocardial infarction. Am J Clin Nutr 85:554–560
22. James MJ, Ursin VM, Cleland LG (2003) Metabolism of stearidonic acid in human subjects: comparison with the metabolism of other n-3 fatty acids. Am J Clin Nutr 77:1140–1145
23. Sands SA, Reid KJ, Windsor SL, Harris WS (2005) The impact of age, body mass index, and fish intake on the EPA and DHA content of human erythrocytes. Lipids 40:343–347
24. Cao J, Schwichtenberg KA, Hanson NQ, Tsai MY (2006) Incorporation and clearance of omega-3 fatty acids in erythrocyte membranes and plasma phospholipids. Clin Chem 52:2265–2272
25. Jump DB (2002) Dietary polyunsaturated fatty acids and regulation of gene transcription. Curr Opin Lipidol 13:155–164

Lipids (2008) 43:301–312
DOI 10.1007/s11745-008-3161-x

ORIGINAL ARTICLE

Molecular Mechanism of Age-Specific Hepatic Lipid Accumulation in PPARα (+/−):LDLR (+/−) Mice, an Obese Mouse Model

Yufeng Li · Eiko Sugiyama · Shin Yokoyama · Lingling Jiang · Naoki Tanaka · Toshifumi Aoyama

Received: 4 October 2007 / Accepted: 12 February 2008 / Published online: 12 March 2008
© AOCS 2008

Abstract This study aimed to clarify the molecular mechanisms of age-specific hepatic lipid accumulation accompanying hyperinsulinemia in a peroxisome proliferator-activated receptor α (PPARα) (+/−):low-density lipoprotein receptor (LDLR) (+/−) mouse line. The hepatic fat content, protein amounts, and mRNA levels of genes involved in hepatic lipid metabolism were analyzed in 25-, 50-, 75- and 100-week-old mice. Severe fatty liver was confirmed only in 50- and 75-week-old mice. The hepatic expression of proteins that function in lipid transport and catabolism did not differ among the groups. In contrast, the mRNA levels and protein amounts of lipogenic enzymes, including acetyl-coenzyme A carboxylase-1, fatty acid synthase, and glycerol-3-phosphate acyltransferase, enhanced in the mice with fatty liver. Elevated mRNA and protein levels of lipoprotein lipase and fatty acid translocase, which are involved in hepatic lipid uptake, were also detected in mice with fatty liver. Moreover, both protein and mRNA levels of sterol regulatory element-binding protein-1 (SREBP-1), a transcription factor regulating lipid synthesis, had age-specific patterns similar to those of the proteins described above. Therefore, the age-specific fatty liver found in the PPARα (+/−):LDLR (+/−) mouse line is probably caused by age-specific expression of SREBP-1 and its downstream lipogenic genes, coordinated by the increased uptake of lipids. All of these factors might be affected by age-specific changes in serum insulin concentration.

Keywords Lipid biosynthesis · Lipid uptake · Lipid catabolism · Peroxisome proliferator-activated receptor α · Low-density lipoprotein receptor · Sterol regulatory element-binding protein-1 · Insulin

Abbreviations

ACC-1	Acetyl-CoA carboxylase-1
ACO	Acyl-CoA oxidase
CoA	Coenzyme A
C_T	Cycle threshold
DBF	Peroxisomal D-type bifunctional protein
FAS	Fatty acid synthase
FAT	Fatty acid translocase
FATP	Fatty acid transport protein
GAPDH	Glyceraldehyde-3-phosphate dehydrogenase
GPAT	Glycerol-3-phosphate acyltransferase
HTGL	Hepatic triglyceride lipase
LACS	Long chain acyl-CoA synthase
LDLR	Low-density lipoprotein receptor
L-FABP	Liver fatty acid-binding protein
LPL	Lipoprotein lipase

Y. Li · E. Sugiyama · N. Tanaka · T. Aoyama
Department of Metabolic Regulation,
Institute on Aging and Adaptation,
Shinshu University Graduate School of Medicine,
Matsumoto 390-8621, Japan
e-mail: fengfly@sch.md.shinshu-u.ac.jp

E. Sugiyama (✉)
Department of Nutritional Science,
Nagano Prefectural College, Nagano 380-8525, Japan
e-mail: eikoyoko@nagano-kentan.ac.jp

S. Yokoyama
Department of Psychiatry,
Shinshu University School of Medicine,
Matsumoto 390-8621, Japan

L. Jiang
Department of Biochemistry,
Hebei Medical University,
050017 Shijiazhuang, Hebei, China

MCAD	Medium chain acyl-CoA dehydrogenase
MTP	Microsomal triglyceride transfer protein
PAGE	Polyacrylamide gel electrophoresis
PCR	Polymerase chain reaction
PPAR	Peroxisome proliferator-activated receptor
PT	Peroxisomal thiolase
SD	Standard deviation
SDS	Sodium dodecyl sulfate
SREBP-1	Sterol regulatory element-binding protein-1
T1	Short chain-specific 3-ketoacyl-CoA thiolase

Introduction

Fatty liver disease is divided into two broad categories: alcoholic fatty liver disease and nonalcoholic fatty liver disease. The etiologic factors of the two entities are quite different, but the pathologic changes of the liver are nearly the same. Simple fatty liver, as the basic process of fatty liver disease, is the most common cause of abnormal liver function and can progress to steatohepatitis, cirrhosis, and even hepatocellular carcinoma through a metabolic pathway [1]. Fatty liver is also found frequently among persons infected with hepatitis C virus [2, 3]. Furthermore, nonalcoholic fatty liver disease is strongly associated with obesity, visceral fat accumulation, insulin resistance, and so on [4–8]. It is also recognized as a risk factor of cardiovascular diseases [9].

Insulin resistance and hyperinsulinemia are known to be central to the development of fatty liver [10]. Insulin is an anabolic hormone that promotes the synthesis and storage of carbohydrates, lipids, and proteins, as well as inhibiting their degradation and release into the circulation [11]. A high level of insulin may be one of the factors leading to the development of fatty liver, although the underlying mechanisms remain elusive. The insulin-responsive transcription factor participating in hepatic lipid metabolism has been identified as sterol regulatory element-binding protein-1 (SREBP-1) [12]. SREBP-1 is one of the SREBPs that belong to the basic helix-loop-helix-leucine zipper family of transcription factors; it plays an essential role in the regulation of lipogenesis [13–15]. Studies have shown that elevated SREBP-1 levels were associated with fatty liver in *ob/ob* mice and transgenic mice [14], whereas the disruption of SREBP-1 reduced the expression of lipogenic enzymes as well as the triglyceride content in liver of Lep^{ob}/Lep^{ob} mice [15].

It is also known that peroxisome proliferator-activated receptors (PPARs), the ligand-activated nuclear receptors, mediate the critical transcriptional regulation of genes associated with lipid homeostasis [16]. There are three PPAR isoforms, designated PPARα, PPARβ (also called δ), and PPARγ, which exhibit distinct tissue distribution [17]. PPARα is expressed at high levels in the liver, kidney, and heart [17]. PPARα-null [PPARα (−/−)] mice chronically fed a high fat diet or fasted for a short-term often develop severe fatty liver, because of their considerably diminished hepatic β-oxidation capacity [18]. We have reported that PPARα regulates mitochondrial fatty acid catabolism under constitutive conditions in the liver [19], heart [20], and kidney [21], although many publications have presented that PPARα mainly regulates peroxisomal β-oxidation through the experiments by activating its ligands [22, 23]. Our recent studies using PPARα (−/−) mice indicated that it also plays a protective role in different pathological conditions such as alcoholic liver disease [24] and proximal tubular cell injury induced by acute fatty acid toxicity [25]. In contrast, PPARβ is ubiquitously expressed [17]. The role of PPARβ in liver is still controversial, although a recent paper proposed that PPARβ might regulate hepatic expression of genes modulating glucose homeostasis [26]. PPARγ is the well-known major PPAR form in white adipose tissue, however, is poorly expressed in liver [17]. Liver-specific PPARγ disruption contributes in protecting mouse liver from the development of steatosis in leptin-deficient mice [27], which suggests that PPARγ may play an important role in hepatic triglyceride accumulation.

In addition, low-density lipoprotein receptor (LDLR) also plays an important role in hepatic lipid uptake [28]. LDLR-null [LDLR (−/−)] mice often develop atherosclerosis [29], obesity and severe hyperlipidemia [30] on a high-fat diet.

We have recently developed a novel mouse line, PPARα (+/−):LDLR (+/−) mice by mating PPARα (−/−) and LDLR (−/−) mice [31]. The average body weight increased around the age of 50 and 75 weeks compared with that at the age of 25 weeks, and then rapidly dropped nearly to the level of 25-week-old mice until at the age of 100 weeks. Serum insulin concentrations were also changed in the age-specific manner (25-week-old mice, 368 ± 119 pg/ml; 50-week-old mice, 1,021 ± 205 pg/ml; 75-week-old mice, 652 ± 198 pg/ml; 100-week-old mice, 356 ± 91 pg/ml), which was coincident with the changes of body weight [31].

This mouse line represents obesity, visceral fat accumulation, hypertriglyceridemia, severe fatty liver, and hyperinsulinemia (after 25–30 weeks of age) [31]. Therefore, the PPARα (+/−):LDLR (+/−) mice may be useful for the long-term study of these metabolic diseases. To clarify the molecular mechanism of age-specific fatty liver in the PPARα (+/−):LDLR (+/−) mice may be important for the prevention and treatment of liver diseases and metabolic disorders and their complications in human. However, the precise mechanism of pathogenesis of these symptoms remains unclear.

As such, we aimed to clarify the molecular mechanism of age-specific lipid accumulation in the PPARα (+/−):LDLR (+/−) mice.

Materials and Methods

Animals

PPARα (−/−) mice (hybrids of Sv/129 cross C57BL/6N genetic background) were produced as described previously [32], and LDLR (−/−) mice (hybrids of Sv/129 cross C57BL/6J genetic background) were obtained from Jackson Laboratories (Bar Harbor, ME, USA). LDLR (−/−) mice were crossbred with PPARα (−/−) mice to obtain the PPARα (+/−):LDLR (+/−) mice, as described previously [31]. All mice were genotyped by polymerase chain reaction (PCR) analysis from tail genomic DNA. Since age-specific abnormalities were not seen in female PPARα (+/−):LDLR (+/−) mice, male mice were adopted. All mice were housed in a specific pathogen-free barrier facility with a 12/12-h dark–light cycle, and fed a standard chow and water ad libitum. Male 4-week-old mice ($n = 20$) were randomly divided into four groups. The mice of each group ($n = 5$) were killed by cervical dislocation after 6-h food deprivation at the age of 25, 50, 75 and 100 weeks, respectively, according to the symptoms of the age-specific obesity. Liver tissues were removed and cut in some pieces, and some were subjected to histological analysis. The others were quick-frozen on dry ice, and stored at −80 °C until used. Experimental procedures were performed in accordance with protocols approved by the Institutional Animal Care and Research Advisory Committee.

Histological Analysis

The removed liver tissue of the four experimental groups (25-, 50-, 75- and 100-week-old mice, $n = 5$ in each group) was fixed in 4% paraformaldehyde in phosphate-buffered saline at 4 °C overnight and equilibrated in 30% sucrose overnight. The tissue was embedded at the optimal cutting temperature. Ten-micrometer frozen sections were prepared (three sections were selected every five sections from the serial section of each mouse for each experimental group). Then the sections were incubated with oil red O solution for 10 min, followed by washing with 60% isopropanol and counter staining with hematoxylin. Five microscopic fields in the pericentral area of liver lobuli were randomly selected in each section and photomicrographed at a magnification of 200×. The proportion of areas of lipid droplets stained with oil red O to those of hepatocytes was assessed by morphometric analysis using MetaView software (Universal Imaging Corp, Downington, PA, USA).

Biochemical Analysis

Total lipids were extracted from the liver samples from the mice in the four experimental groups according to Folch's method with minor modifications [33]. Briefly, frozen liver pieces (50 mg) were homogenized in 2.1 ml of chloroform/methanol (2:1, v/v) to extract lipids and incubated at 37 °C for 40 min. After the incubation and removing insoluble substances, 0.2 ml of water was added to the extract in order to make two phases. The lower phase was carefully collected, and 0.83 volume of chloroform/methanol/water (3:48:47, v/v/v) so called "theoretical upper phase" was added and vigorously mixed to re-extract. Then the lower phase was carefully collected again and combined to dry under nitrogen gas. The dried samples were dissolved into 125 µl of 2-propanol and centrifuged at $10{,}000\times g$ for 3 min to remove insoluble substances. The supernatant was subjected to the determination of triglycerides and free fatty acids using the Triglyceride E-WAKO kit (Wako Pure Chemical Industries Ltd., Osaka, Japan) and the NEFA C-WAKO kit (Wako Pure Chemical Industries Ltd.), respectively.

Microsomal triglyceride transfer protein (MTP) activity was measured with the MTP assay kit (Roar Biomedical, New York, NY, USA). The MTP source was prepared with liver homogenate according to the manufacturer's protocol. Donor vesicles (10 µl) containing fluorescent neutral lipid (triglyceride) and acceptor vesicles (10 µl) were incubated with 20 µl of liver homogenate (containing 15 µg protein) in the total volume of 400 µl of assay buffer at 37 °C for 4 h. MTP activity was then measured as an increase in fluorescence intensity at an excitation wavelength of 465 nm and an emission wavelength of 535 nm.

Messenger RNA Determination

Total RNA from frozen liver samples of mice in the four experimental groups was isolated using the RNeasy mini kit according to the manufacture's protocol (Qiagen GmbH., Hilden, Germany). RNA was treated with DNase (Qiagen GmbH., Hilden, Germany) to remove residual contaminating genomic DNA. The amount and quality of RNA was determined by spectrophotometry. To confirm the purity of the RNA samples, the total RNA (3 µg) was subjected to 1% formaldehyde agarose gel-electrophoresis, and then visualized under UV light. The RNA samples were transferred to cDNA by SuperScript$^{\mathrm{TM}}$ First-Strand Synthesis System with the oligo-dT primer (Invitrogen Life Technologies, Carlsbad, CA, USA). Final concentration of each sample was adjusted at 20 ng/µl. We designed gene-specific primers using Primer Express Software (Applied Biosystems, Foster City, CA, USA). The sequences and GenBank accession numbers of the primer sets are listed in Table 1. Most of the standard plasmid DNAs for real-time quantitative PCR were constructed by the pT7Blue T-Vector System and the Wizard Plus SV Minipreps DNA Purification System (Promega Co., Madison, WI, USA). The standard plasmid DNAs of acyl-coenzyme A (CoA) oxidase (ACO), lipoprotein lipase (LPL), and SREBP-1 were constructed with the pGEM-T Easy Vector System I (Promega Co.). Real-time quantitative PCR was performed using the SYBR$^{®}$ Premix Ex Taq$^{\text{TM}}$ (Applied Biosystems) on the ABI Prism 7700 Sequence Detection System (Applied Biosystems). We ran each sample (25 ng of cDNA) in triplicate final concentration of 0.4 µM of each primer set. The PCR condition was set to 95 °C for 10 s, followed by 40 cycles of 95 °C for 5 s and 60 °C for 34 s.

Fold change in target mRNA relative to glyceraldehyde-3-phosphate dehydrogenase (GAPDH) was calculated according to the method reported by Livak and Schmittgen [34]. After completion of the real-time quantitative PCR, baseline limits were set according to the manufacturer (i.e., at least three cycles before the rise of the earliest amplification). The threshold was set to lie in the middle of the exponential phase of the amplification plot, so that efficiency values truly reflect the reaction dynamic at the cycle threshold (C_T). Relative quantification of gene expression was evaluated by utilizing the comparative C_T. The C_T value for each mRNA reaction was subtracted from the respective C_T value of the GAPDH as an internal control, resulting in the ΔC_T value. The ΔC_T value of the 25-week-old mice group was arbitrarily used as a constant that was subtracted from all other ΔC_T values to determine the $\Delta\Delta C_T$ value. The fold change was then generated for each mRNA by calculating $2^{-\Delta\Delta CT}$.

Preparation of Whole Liver Lysate and Nuclear Fraction for Western Blotting

The frozen liver tissue of mice in the four experimental groups (50 mg) was lysed with 200 µl of 20 mM sodium phosphate buffer (pH 7.4) containing 250 mM sucrose, 10 mM EDTA, and protease inhibitors, using a high-speed mixer homogenizer. The homogenate was centrifuged at 8,000×*g* for 5 min at 4 °C, and the supernatant was used as whole liver lysate. Meanwhile, nuclear extract was isolated using a nuclear extraction kit (Sigma, St. Louis, MO, USA) to analyze transcription factors. Briefly, 100 mg of liver tissue was added to 1 ml of lysis buffer containing 10 mM HEPES, pH 7.9, 1.5 mM $MgCl_2$, 10 mM KCl, 1 mM dithiothreitol, and protease inhibitors. The tissue was homogenized and centrifuged at 11,000×*g* for 20 min at 4 °C. The pellet was resuspended in 140 µl of extraction buffer containing 20 mM HEPES, pH 7.9, 1.5 mM $MgCl_2$, 0.42 M NaCl, 0.2 mM EDTA, 25% glycerol, 1 mM dithiothreitol, and protease inhibitors. After centrifugation at 20,000×*g* for 5 min at 4 °C, the pellet was collected, suspended with 100 µl of 20 mM sodium phosphate buffer (pH 7.4), and used as the nuclear fraction. Whole liver lysate or nuclear fraction (100 µl each) was added with 100 µl of

Table 1 Sequences and GenBank accession numbers of primers

Genes	Acc. no.	Forward primer (5′–3′)	Reverse primer (5′–3′)
ACC-1	XM_193604	GGGCACAGACCGTGGTAGTT	CAGGATCAGCTGGGATACTGAGT
ACO	NM_015729	TGGTATGGTGTCGTACTTGAATGAC	AATTTCTACCAATCTGGCTGCAC
FAS	XM_126624	ATCCTGGAACGAGAACACGATCT	AGAGACGTGTCACTCCTGGACTT
FAT	NM_007643	CCAAATGAAGATGAGCATAGGACAT	GTTGACCTGCAGTCGTTTTGC
FATP	NM_011977	ACCACCGGGCTTCCTAAGG	CTGTAGGAATGGTGGCCAAAG
GAPDH	M32599	TGCACCACCAACTGCTTAG	GGATGCAGGGATGATGTTCTG
GPAT	NM_008149	GGCTACGTCCGAGTGGATTTT	AACATCATTCGGTCTTGAAGGAA
HTGL	NM_008280	ACGGGAAGAACAAGATTGGAAG	CGTTCCCTCAAACATAGGGC
LACS	NM_007981	TCCTACGGCAGTGATCTGGTG	GGTTGCCTGTAGTTCCACTTGTG
LDLR	NM_010700	GATGGACCAGGCCCCTAACT	GGTGTCAGCCACAGATACGCT
L-FABP	NM_017399	GCAGAGCCAGGAGAACTTTGAG	TTTGATTTTCTTCCCTTCATGCA
LPL	M63335	CGCTCCATTCATCTCTTCATT	GGCAGAGCCCTTTCTCAAAGG
MCAD	NM_007382	TGCTTTTGATAGAACCAGACCTACAGT	CTTGGTGCTCCACTAGCAGCTT
MTP	NM_008642	GAGCGGTCTGGATTTACAACG	GTAGGTAGTGACAGATGTGGCTTTTG
PPARα	NM_011144	CCTCAGGGTACCACTACGGAGT	GCCGAATAGTTCGCCGAA
PPARβ	XM_128500	TCAACATGGAATGTCGGGTG	ATACTCGAGCTTCATGCGGATT
PPARγ	NM_011146	TTCCACTATGGAGTTCATGCTTGT	TCCGGCAGTTAAGATCACACCTA
SREBP-1	AB017337	GCCCACAATGCCATTGAGA	GCAAGAAGCGGATGTAGTCGAT

20 mM sodium phosphate buffer (pH 7.4) containing 2% (w/w) sodium dodecyl sulfate (SDS), sonicated twice, and subjected to Western blotting.

Western Blotting

The protein concentration of the whole liver lysate and nuclear fraction was determined using the BCA protein assay kit (Applied Biosystems). Whole liver lysate or nuclear fraction (60 μg protein) was loaded in each well, and subjected to 10% SDS-polyacrylamide gel electrophoresis (PAGE), except for acetyl-CoA carboxylase-1 (ACC-1) and fatty acid synthase (FAS) which were subjected to 6% SDS-PAGE. Proteins were then transferred to a nitrocellulose membrane at 10 V, 2 mA/cm^2 for 1.5 h, except ACC-1 and FAS which were transferred under 10 V, 2 mA/cm^2 for 5 h. The membrane was incubated with the primary antibody followed by the secondary alkaline phosphatase–conjugated goat anti-rabbit IgG antibody (Stratech Scientific Ltd., Newmarket, UK) (1:2,000 dilution). Primary antibodies were used as follows: anti-long chain acyl-CoA synthase (LACS), anti-medium chain acyl-CoA dehydrogenase (MCAD), anti-ACO, anti-short chain-specific 3-ketoacyl-CoA thiolase (T1), anti-peroxisomal D-type bifunctional protein (DBF), anti-peroxisomal thiolase (PT), and anti-liver fatty acid-binding protein (L-FABP) antibodies were prepared as described previously [19, 35, 36]. The following antibodies were purchased from Santa Cruz Biotechnology, Inc. (Santa Cruz, CA, USA): anti-ACC-1 (FL-114), anti-FAS (C-20), anti-LDLR (C-20), anti-LPL (H-53), anti-fatty acid translocase (FAT) (H-300), anti-SREBP-1 (H-160), anti-PPARα (H-98), anti-PPARβ (H-74), anti-PPARγ (H-100), anti-β-actin (H-196), and anti-histone H3 (FL-136). Anti-glycerol-3-phosphate acyltransferase (GPAT) was purchased from ABNOVA (Abnova Co., Taibei, Taiwan). Dilution was performed 200-fold for most of the antibodies commercially available, except for anti-β-actin and anti-histone H3 (250-fold), anti-GPAT (750-fold). The band intensity was quantified by densitometric scanning with the software Image Quant Version 5.2 (Molecular Dynamics, Sunnyvale, CA, USA). The band intensity for the proteins involved in β-oxidation and L-FABP was normalized to that of β-actin, and those for the nuclear proteins were normalized to that of histone H3. The result was subsequently expressed as the fold changes relative to that of 25-week-old PPARα (+/−):LDLR (+/−) mice.

Statistical Analysis

Statistical analysis was performed using SPSS program (SPSS 10.0, SPSS Science, Chicago, Illinois, USA). One-way ANOVA with repeated measure of the age factor was used to analyze group differences. Total freedom value was shown as *F*, and freedom values between groups and within groups are expressed in parentheses. If a significant interaction was observed, Scheffe' post hoc testing was used to determine pairwise differences between mean. A *P* value of less than 0.05 was considered to be statistically significant. Data were expressed as mean ± standard deviation (SD).

Results

Histological and Biochemical Analysis in Liver Samples

To examine hepatic morphological conditions in the mice, the liver sections were stained with oil red O, which specifically detects neutral lipids such as triglycerides. The area stained with oil red O increased by 2- to 2.5-fold in 50- and 75-week-old mice compared with 25-week-old mice, then decreased in 100-week-old mice similar to the level of 25-week-old mice [F (3, 16) = 17.771, $P = 0.000$; 25- vs. 50-week-old mice, $P < 0.01$; 50- vs. 100-week-old mice, $P < 0.01$; and 75- vs. 100-week-old mice, $P < 0.05$, respectively] (Fig. 1a, b). In addition, the hepatic triglycerides and free fatty acids increased by approximately threefold until the age of 50 weeks and later decreased with aging, which are consistent with the previous report [31] [triglycerides: F (3, 16) = 17.773, $P = 0.000$; 25- vs. 50-week-old mice, $P < 0.01$; 50- vs. 100-week-old mice, $P < 0.01$; and 75- vs. 100-week-old mice, $P < 0.01$; free fatty acids: F (3, 16) = 8.187, $P = 0.003$; 25- vs. 50-week-old mice, $P < 0.01$; 50- vs. 100-week-old mice, $P < 0.01$] (Fig. 1c, d).

Analysis of Genes Related to the Synthesis of Fatty Acids and Triglycerides

Figure 2 shows the expression levels of the enzymes involved in lipid synthesis such as ACC-1, FAS, and GPAT at the age of 25, 50, 75 and 100 weeks. Both the mRNA and protein levels of ACC-1 increased by approximately twofold in 50- and 75-week-old mice compared with 25-week-old mice, and then decreased in 100-week-old mice to the level of 25-week-old mice [mRNA levels: F (3, 16) = 17.167, $P = 0.000$, 25- vs. 50-week-old mice, $P < 0.01$; 50- vs. 100-week-old mice, $P < 0.01$; and 75- vs. 100-week-old mice, $P < 0.01$; protein levels: F (3, 16) = 9.850, $P = 0.001$, 25- vs. 50-week-old mice, $P < 0.01$; 50- vs. 100-week-old mice, $P < 0.01$; and 75- vs. 100-week-old mice, $P < 0.05$]. FAS exhibited similar age-specific changes in both the mRNA and protein levels [mRNA: F (3, 16) =16.864, $P = 0.000$; protein: F (3, 16) = 10.225, $P = 0.001$], as well as GPAT

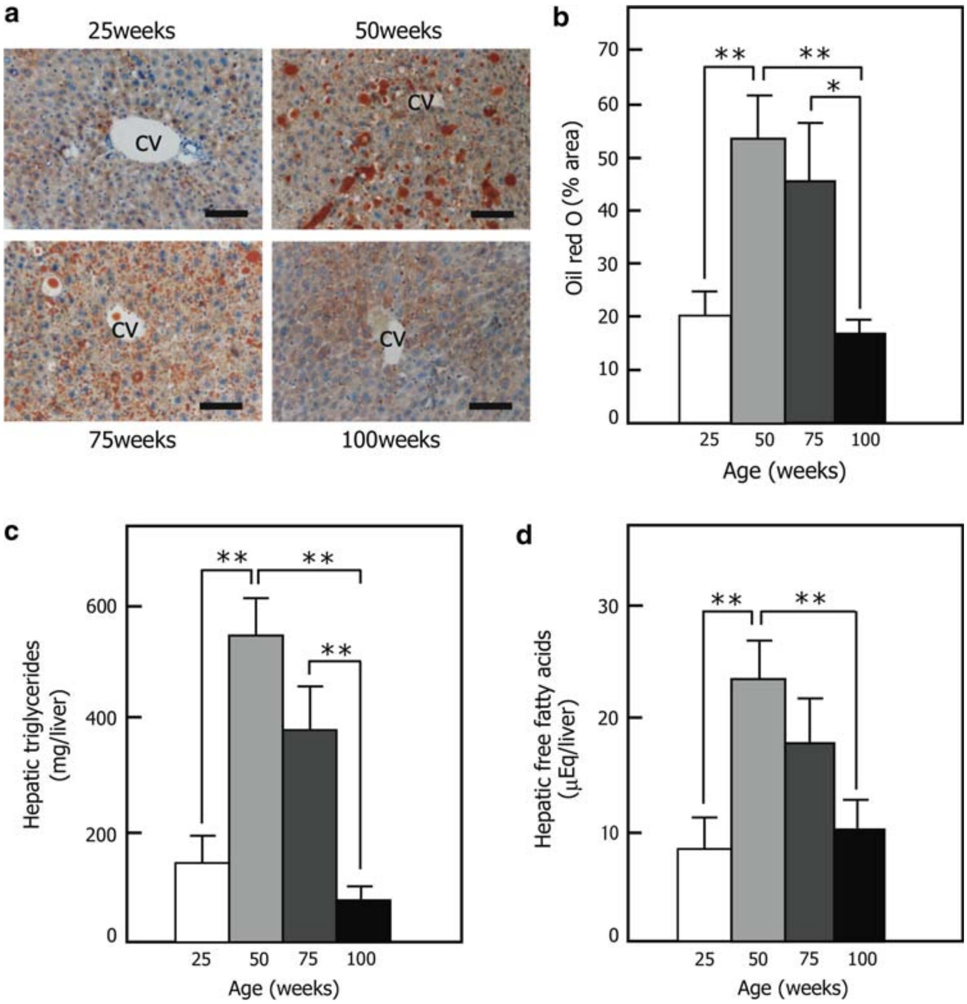

Fig. 1 Hepatic oil red O staining and the amounts of hepatic triglycerides and free fatty acids in PPARα (+/−):LDLR (+/−) mice at the age of 25, 50, 75, and 100 weeks. **a** Representative images of oil red O-stained liver sections. CV denotes central vein, and each *bar* indicates 50 μm. **b** Morphometric analysis of oil red O-stained liver sections. Fifteen pericentral areas of liver lobuli were photomicrographed in each mouse, and the areas of lipid droplets were quantified as described in "Materials and Methods". Results are expressed as mean ± SD ($n = 5$). * $P < 0.05$, and ** $P < 0.01$ between the indicated groups. The contents of hepatic triglycerides (**c**) and free fatty acids (**d**). All of the manipulations were as described in "Materials and Methods". Results are expressed as mean ± SD ($n = 5$). * $P < 0.05$, and ** $P < 0.01$ between the indicated groups

[mRNA: F (3, 16) = 16.520, $P = 0.000$; protein: F (3, 16) = 13.052, $P = 0.000$].

Analysis of Genes Related to the Uptake of Fatty Acids and Triglycerides

The hepatic levels of the proteins that function in hepatic lipid uptake are displayed in Fig. 3. The expression of LDLR decreased in 50-week-old mice compared with 25-week-old mice, and then increased in 100-week-old mice approximately to the level of 25-week-old mice [mRNA: F (3, 16) = 5.982, $P = 0.010$; protein: F (3, 16) = 5.058, $P = 0.017$; 50- vs. 25-week-old mice, $P < 0.05$]. In contrast, the expression of LPL increased in 50- and 75-week-old mice than that in 100-week-old mice [mRNA: F (3, 16) = 6.717, $P = 0.007$; protein: F (3, 16) = 8.796, $P = 0.002$; 50- vs. 100-week-old mice, $P < 0.05$; 75- vs. 100-week-old mice, $P < 0.05$]. The expression of FAT increased by approximately 1.5- to 2-fold in 50- and 75-week-old mice compared with 25-week-old mice, and then decreased in 100-week-old mice approximately to the level of 25-week-old mice [mRNA: F (3, 16) = 16.548, $P = 0.000$; protein: F (3, 16) = 13.802, $P = 0.000$; 25- vs. 50-week-old mice, $P < 0.01$; 50- vs. 100-week-old mice, $P < 0.01$; and 75- vs. 100-week-old mice, $P < 0.05$]. Whereas, the hepatic mRNA levels of fatty acid transport protein (FATP) and hepatic TG lipase (HTGL) were similar among all the groups [FATP: F (3, 16) = 0.680, $P = 0.581$; HTGL: F (3, 16) = 0.399, $P = 0.757$].

Analysis of Genes Participating in Fatty Acid Catabolism and Triglyceride Secretion

Next, we determined both the mRNA and protein levels of enzymes involved in both mitochondrial and peroxisomal fatty acid β-oxidation. Figure 4 shows the results for LACS, MCAD, and ACO, which are representative enzymes of fatty acid β-oxidation. There were no significant changes in mRNA expression among the different age groups for all the enzymes [LACS: F (3, 16) = 1.112, $P = 0.382$; MCAD: F

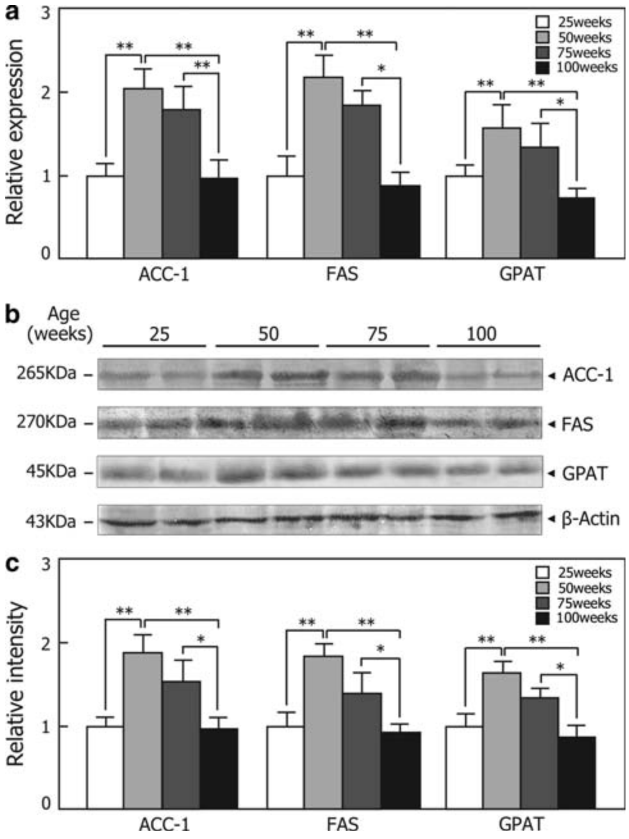

Fig. 2 Hepatic expression of lipogenic enzymes in PPARα (+/−):LDLR (+/−) mice at the age of 25, 50, 75, and 100 weeks. **a** Changes in the expression of ACC-1, FAS, and GPAT at the presented ages. The expression was determined by real-time PCR method, normalized to that of GAPDH, and subsequently expressed as the fold changes relative to that of 25-week-old PPARα (+/−):LDLR (+/−) mice. Results are expressed as mean ± SD ($n = 5$). * $P < 0.05$, and ** $P < 0.01$ between the indicated groups. **b** Western blot analysis of ACC-1, FAS, and GPAT. Whole liver lysate (60 μg of protein) was loaded in each lane. The band of β-actin was used as a loading control. Results are representative of three independent experiments. The apparent molecular weight is indicated on the *left*. **c** Quantification of the protein amounts of ACC-1, FAS, and GPAT. The band intensity was quantified densitometrically, normalized to that of β-actin, and subsequently expressed as the fold changes relative to that of 25-week-old PPARα (+/−):LDLR (+/−) mice. Results are expressed as mean ± SD ($n = 5$). * $P < 0.05$, and ** $P < 0.01$ between the indicated groups

(3, 16) = 1.033, $P = 0.413$; ACO: F (3, 16) = 0.660, $P = 0.592$] (Fig. 4a). These protein amounts were also constant among the groups (Fig. 4b, c). Furthermore, no differences were found in the expression and protein amounts of other genes such as T1, DBF, and PT, which are also involved in β-oxidation (data not shown).

We also investigated the expression of L-FABP and MTP, which are representative proteins participating in intracellular lipid trafficking in hepatocytes and secretion of triglycerides from hepatocytes, respectively. No differences of the gene expression and protein amounts of L-FABP were detected [mRNA: F (3, 16) = 1.984, $P = 0.170$; protein: F (3, 16) = 2.157, $P = 0.146$] (Fig. 5a, b). The gene expression and activities of MTP were also unchanged among the groups [mRNA: F (3, 16) = 3.429, $P = 0.052$; activity: F (3, 16) = 2.387, $P = 0.120$] (Fig. 5c, d).

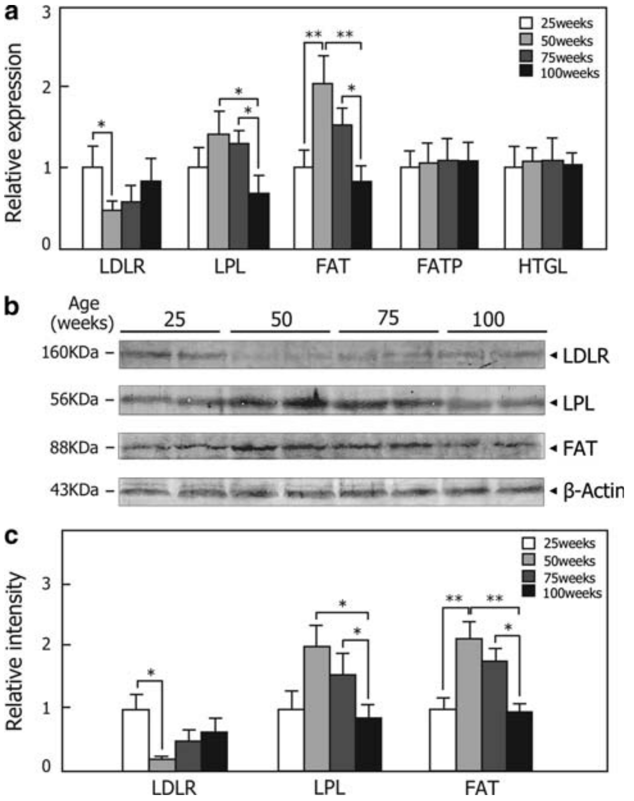

Fig. 3 Hepatic expression of the genes involved in lipid uptake in PPARα (+/−):LDLR (+/−) mice at the age of 25, 50, 75 and 100 weeks. **a** Changes in mRNA levels of LDLR, LPL, FAT, FATP, and HTGL at the presented ages. The expression was determined by real-time PCR method, normalized to that of GAPDH, and subsequently expressed as the fold changes relative to that of 25-week-old PPARα (+/−):LDLR (+/−) mice. Results are expressed as mean ± SD ($n = 5$). * $P < 0.05$, and ** $P < 0.01$ between the indicated groups. **b** Western blot analysis of LDLR, LPL, and FAT. Whole liver lysate (60 μg of protein) was loaded in each lane. The band of β-actin was used as a loading control. Results are representative of three independent experiments. The apparent molecular weight is indicated on the *left*. **c** Quantification of the protein amounts of LDLR, LPL, and FAT. The band intensity was quantified densitometrically, normalized to that of β-actin, and subsequently expressed as the fold changes relative to that of 25-week-old PPARα (+/−):LDLR (+/−) mice. Results are expressed as mean ± SD ($n = 5$). * $P < 0.05$, and ** $P < 0.01$ between the indicated groups

Determination of the Expression of Transcription Factors

We further evaluated the expression of transcription factors regulating hepatic lipid homeostasis. As comparison, we also presented the results of 50-week-old PPARα (+/+):LDLR (−/−) mice, which exhibit no

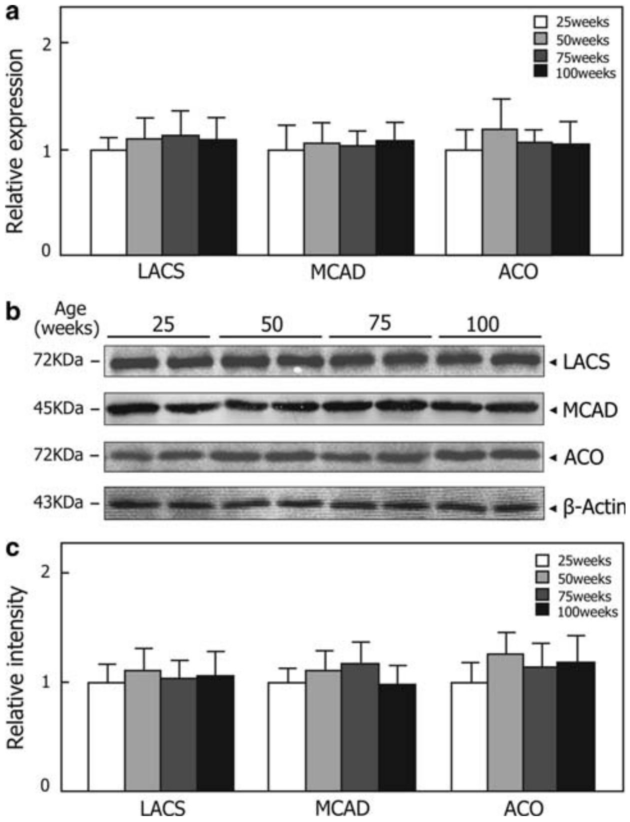

Fig. 4 Hepatic expression of fatty acid β-oxidation enzymes in PPARα (+/−):LDLR (+/−) mice at the age of 25, 50, 75 and 100 weeks. **a** Changes in mRNA levels of LACS, MCAD, and ACO at the presented ages. The expression was determined by real-time PCR method, normalized to that of GAPDH, and subsequently expressed as the fold changes relative to that of 25-week-old PPARα (+/−):LDLR (+/−) mice. Results are expressed as mean ± SD ($n = 5$). **b** Western blot analysis of LACS, MCAD, and ACO. Whole liver lysate (60 µg of protein) was loaded in each lane. The band of β-actin was used as a loading control. Results are representative of three independent experiments. The apparent molecular weight is indicated on the *left*. **c** Quantification of the protein amounts of LACS, MCAD, and ACO. The band intensity was quantified densitometrically, normalized to that of β-actin, and subsequently expressed as the fold changes relative to that of 25-week-old PPARα (+/−):LDLR (+/−) mice. Results are expressed as mean ± SD ($n = 5$)

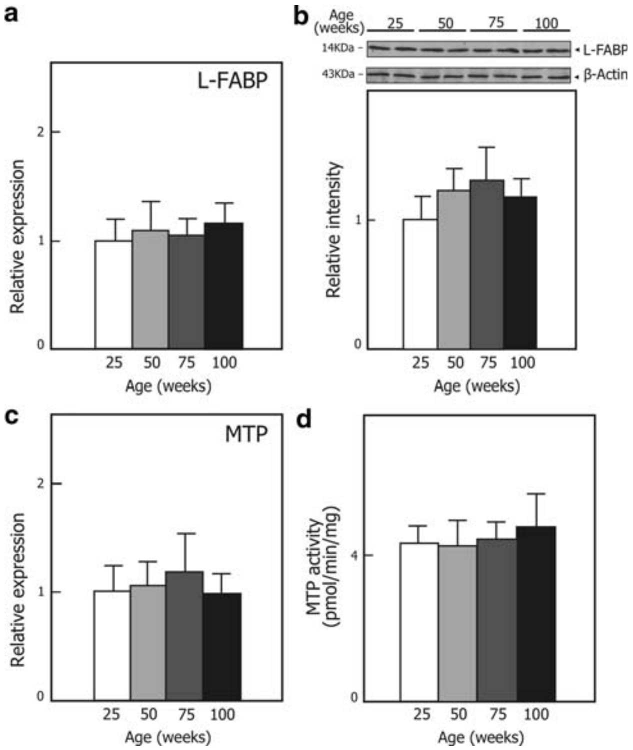

Fig. 5 Analysis of L-FABP and MTP in PPARα (+/−):LDLR (+/−) mice at the age of 25, 50, 75 and 100 weeks. **a** The mRNA levels of L-FABP. The levels were determined by real-time PCR method, normalized to that of GAPDH, and subsequently expressed as the fold changes relative to that of 25-week-old PPARα (+/−):LDLR (+/−) mice. Results are expressed as mean ± SD ($n = 5$). **b** Western blot analysis of L-FABP (*upper panel*) and quantification of the protein amounts (*lower panel*). Whole liver lysate (60 µg of protein) was loaded in each lane. The band intensity was quantified densitometrically, normalized to that of β-actin, and subsequently expressed as the fold changes relative to that of 25-week-old PPARα (+/−):LDLR (+/−) mice. Results are expressed as mean ± SD ($n = 5$). **c** The mRNA levels of MTP. The levels were determined by real-time PCR method, normalized to that of GAPDH, and subsequently expressed as the fold changes relative to that of 25-week-old PPARα (+/−):LDLR (+/−) mice. Results are expressed as mean ± SD ($n = 5$). **d** The activity of MTP. All of the procedures were as described in "Materials and Methods". Results are mean ± SD ($n = 5$)

hepatic steatosis and obesity [31]. Both the mRNA and protein levels of PPARα tended to increase until the age of 75 weeks, but markedly dropped in 100-week-old PPARα (+/−):LDLR (+/−) mice [mRNA: F (3, 16) = 9.608, $P = 0.002$; protein: F (3, 16) = 8.747, $P = 0.002$; 50- vs. 100-week-old mice, $P < 0.01$; 75- vs. 100-week-old mice, $P < 0.01$] (Fig. 6). The expression levels of PPARα in 50- and 75-week-old PPARα (+/−):LDLR (+/−) mice were higher than expected, but those in 100-week-old PPARα (+/−):LDLR (+/−) mice were much lower compared with 50-week-old PPARα (+/+):LDLR (−/−) mice.

On the other hand, no differences were found at the mRNA and protein levels of PPARβ [mRNA: F (3, 16) = 1.164, $P = 0.327$; protein: F (3, 16) = 1.150, $P = 0.331$] and PPARγ [mRNA: F (3, 16) = 3.472, $P = 0.059$; protein: F (3, 16) = 3.350, $P = 0.064$] (Fig. 6).

The hepatic mRNA and protein levels of SREBP-1 increased by 1.5- to 2-fold in 50- and 75-week-old mice compared with 25-week-old mice, then decreased in 100-week-old mice approximately to the level of 25-week-old mice [mRNA: F (3, 16) = 12.319, $P = 0.001$; protein: F (3, 16) = 12.965, $P = 0.000$; 25- vs. 50-week-old mice, $P < 0.01$; 50- vs. 100-week-old mice, $P < 0.01$; and 75- vs. 100-week-old mice, $P < 0.05$] (Fig. 6).

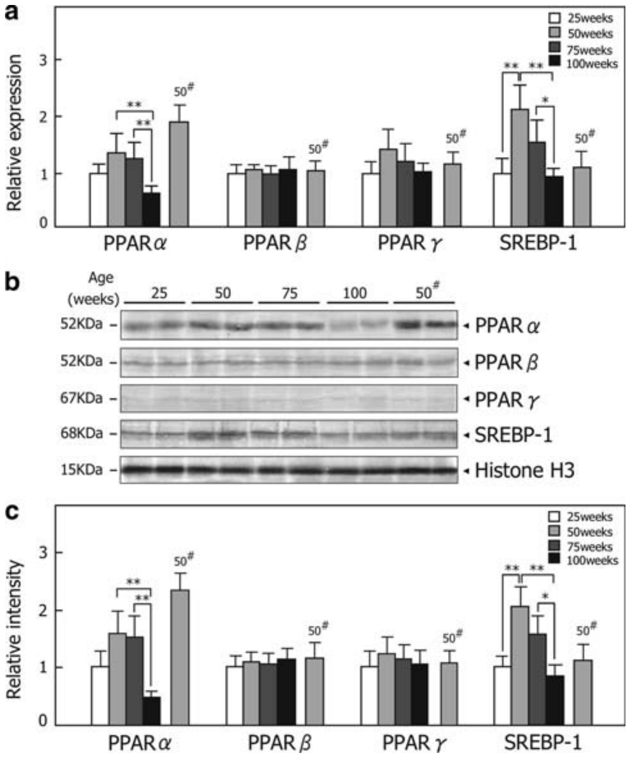

Fig. 6 Hepatic expression of transcription factors in PPARα (+/−):LDLR (+/−) mice at the age of 25, 50, 75 and 100 weeks. **a** Changes in mRNA levels of PPARα, PPARβ, PPARγ, and SREBP-1. The expression was determined by real-time PCR method, normalized to that of GAPDH, and subsequently expressed as the fold changes relative to that of 25-week-old PPARα (+/−):LDLR (+/−) mice. As comparison, data obtained from 50-week-old PPARα (+/+):LDLR (−/−) mice are shown as $^{\#}$ 50. Results are expressed as means ± SD ($n = 5$). * $P < 0.05$, and ** $P < 0.01$ between the indicated groups. **b** Western blot analysis of PPARs and SREBP-1. Hepatocyte nuclear fraction (60 μg of protein) was loaded in each lane. The band of histone H3 was used as a loading control. Results are representative of three independent experiments. The apparent molecular weight is indicated on the *left*. $^{\#}$50, 50-week-old PPARα (+/+):LDLR (−/−) mice. **c** Quantification of the nuclear amounts of PPARs and SREBP-1. The band intensity was quantified densitometrically, normalized to that of histone H3, and subsequently expressed as the fold changes relative to that of 25-week-old PPARα (+/−):LDLR (+/−) mice. Results are expressed as mean ± SD ($n = 5$). $^{\#}$50, 50-week-old PPARα (+/+): LDLR (−/−) mice; * $P < 0.05$, and ** $P < 0.01$ between the indicated groups

Discussion

Fatty liver presents an excessive accumulation of lipids in hepatocytes. The cause of lipid accumulation in liver may possibly be due to enhanced de novo lipogenesis, activating lipid uptake, lowering lipid catabolism, and reducing lipoprotein secretion rates. Development of studies in this field has contributed to a better understanding of the cause of fatty liver in spite of remaining unknown problems [37].

In the present study, we confirmed the finding described in our previous paper that severe fatty liver was found in 50- and 75-week-old PPARα (+/−):LDLR (+/−) mice [31]. The gene expression and the amounts of proteins participating in lipogenesis and lipid uptake were increased in 50- and 75-week-old mice compared with 25- and 100-week-old mice. Notably, enhanced gene expression and protein amounts of transcription factor SREBP-1 were also detected only in the 50- and 75-week-old mice, which presented severe fatty liver. Several studies using different animal models demonstrated that the development of fatty liver was not necessarily associated with the changes in the molecules involved in lipogenesis and/or lipid uptake [38–41]. To date, there has not been enough evidence to conclude that enhanced lipogenesis and/or lipid uptake is the consequence of hepatic steatosis. Therefore, increased expression of these genes is considered to be the cause of the hepatic lipid accumulation in our mouse model.

FAS, ACC-1, and GPAT are key enzymes in de novo fatty acid and triglyceride synthesis in mammals. SREBP-1 is well-known as the dominant transcription factor regulating gene expression of these lipogenic enzymes in the liver [13]. FAS [42], ACC-1 [42] and GPAT [43] are also known to be regulated by SREBP-1. In our study, gene expression of FAS, ACC-1, GPAT, and SREBP-1 was changed simultaneously in accordance with the extent of lipid accumulation (Figs. 1, 2, 6). These results indicate that severe fatty liver in PPARα (+/−):LDLR (+/−) mice is associated with increased expression of SREBP-1 and its downstream lipogenic genes.

Insulin is known to stimulate hepatic lipid synthesis by selectively up-regulating the expression of SREBP-1 [12, 44–46]. Various studies have indicated that insulin regulates the expression of SREBP-1 principally at the transcriptional level in vivo [44, 45] as well as in vitro [46]. The regulation by insulin is considered to be a result of activating several SREBP-1 responding motifs in its promoter region [47]. In our study, both the mRNA and protein levels of the mature form of SREBP-1 changed in the age-specific manner (Fig. 6b, e), and the changes were consistent with those in serum insulin concentration on the basis of the result from the previous study [31]. Therefore, we propose that insulin probably up-regulates the age-specific expression of SREBP-1 in PPARα (+/−): LDLR (+/−) mice. It is conceivable that this up-regulation also occurs at both the transcriptional and post-translational levels. Of interest, Okamoto et al. [48] reported that the SREBP-1 expression in brain was affected by age, the mRNA levels of which increased between 4 and 80 weeks of age and did not decrease in aged rats (over 80 weeks of age). Neither hormones nor metabolic changes affect those of SREBP-1. This difference in liver and brain indicates that the age-specific SREBP-1 expression in liver in our PPARα (+/−):LDLR (+/−) mice is quite unique.

Other important molecules in this study, LPL and FAT increased in 50- and 75-week-old mice and decreased in 100-week-old mice (Fig. 3). The expression of LPL and FAT is known to be regulated by PPARα, because ligand-activating experiments showed induction of the expression of LPL [49] or FAT [50]. In our study, the mRNA and protein amounts of PPARα presented age-specific changes in PPARα (+/−):LDLR (+/−) mice, all of which were lower than those in PPARα (+/+):LDLR (−/−) mice (Fig. 6). In our experimental conditions (constitutive conditions), the expression of PPARα is probably much lower than that of PPARα in the conditions activated by PPARα ligands. Meanwhile, PPARα target genes such as LACS, MCAD, ACO, and L-FABP were unchanged among all the groups [14, 17] (Figs. 4, 5). Therefore, we consider that other factors except PPARα activation probably contribute to the age-specific expression of LPL and FAT in the PPARα (+/−):LDLR (+/−) mice. To date, several pieces of evidence have supported the stimulatory functions of insulin on fatty acid uptake, through regulating FAT and LPL in cardiac myocytes [51], skeletal muscle [52], and adipose tissue [53], although little is known about the effect of insulin on the expression of them in liver. Considering the close association between changes in expression of FAT and LPL and those in serum insulin concentration described in the previous paper [31], our findings suggest that insulin probably plays some roles in the regulation of lipid uptake in the liver by inducing the expression of LPL and FAT (Fig. 3).

The mechanism of the age-specific changes in serum insulin concentration found in PPARα (+/−):LDLR (+/−) mice is still obscure. Experimental disruption of PPARα improves insulin resistance in LDLR (−/−) mice [54] and apolipoprotein E-null mice [55]. In our PPARα (+/−):LDLR (+/−) mice, higher expression of PPARα than expected might contribute to the induction of insulin resistance in 50- and 75-week-old mice, while lower expression of PPARα after 75 weeks of age might lead to the improvement of insulin resistance [31]. Furthermore, insufficient gene expression of LDLR might contribute to the development of hyperlipidemia, which is also considered an important factor in the development of fatty liver and insulin resistance.

Decreases in hepatic lipid accumulation in 100-week-old mice may be caused by spontaneous improvement of hyperinsulinemia and the resultant down-regulation of lipogenic enzymes. On the basis of the concept that PPARα deficiency can ameliorate insulin sensitivity in the insulin-resistant status [3, 54, 55], it is postulated that these phenomena found in 100-week-old mice might be related to spontaneous reduction in PPARα expression. However, its precise mechanism remains unclear. Since several studies have indicated that aging leads to a decrease in the activity and the expression of PPARα in rat liver [56, 57], heart [58] and spleen [59], we speculate that aging seems to be one of the contributors of PPARα reduction in 100-week-old PPARα (+/−):LDLR (+/−) mice. Further study is needed to address this issue.

In conclusion, the development of the fatty liver found in PPARα (+/−):LDLR (+/−) mice is linked with the elevated hepatic expression of SREBP-1 and its downstream genes involved in lipogenesis, accompanied by increased lipid uptake. Insulin appeared to play a predominant role in age-specific hepatic lipid accumulation in this mouse line. Our observations will be helpful to increase understanding of hepatic lipid homeostasis and may contribute to the overall knowledge of the onset of fatty liver diseases accompanying the metabolic syndrome.

References

1. Reddy JK, Rao MS (2006) Lipid metabolism and liver inflammation II. Fatty liver disease and fatty acid oxidation. Am J Physiol Gastrointest Liver Physiol 290:852–858
2. Asselah T, Rubbia-Brandt L, Marcellin P, Negro F (2006) Steatosis in chronic hepatitis C: why does it really matter? Gut 55:123–130
3. Tanaka N, Moriya K, Kiyosawa K, Koike K, Gonzalez FJ, Aoyama T (2008) PPARα activation is essential for HCV core protein-induced hepatic steatosis and hepatocellular carcinoma in mice. J Clin Invest 118: 683–694
4. Jakobsen MU, Berentzen T, Sørensen TI, Overvad K (2007) Abdominal obesity and fatty liver. Epidemiol Rev 29:77–87
5. Utzschneider KM, Kahn SE (2006) Review: The role of insulin resistance in nonalcoholic fatty liver disease. J Clin Endocrinol Metab 91:4753–4761
6. Tanaka N, Tanaka E, Sheena Y, Komatsu M, Okiyama W, Misawa N, Muto H, Umemura T, Ichijo T, Matsumoto A, Yoshizawa K, Horiuchi A, Kiyosawa K (2006) Useful parameters for distinguishing nonalcoholic steatohepatitis with mild steatosis from cryptogenic chronic hepatitis in the Japanese population. Liver Int 26:956–963
7. Tanaka N, Ichijo T, Okiyama W, Mutou H, Misawa N, Matsumoto A, Yoshizawa K, Tanaka E, Kiyosawa K (2006) Laparoscopic findings in patients with nonalcoholic steatohepatitis. Liver Int 26:32–38
8. Tanaka N, Sano K, Horiuchi A, Tanaka E, Kiyosawa K, Aoyama T (2008) Highly-purified eicosapentaenoic acid treatment improves nonalcoholic steatohepatitis. J Clin Gastroenterol (in press)
9. Targher G, Arcaro G (2007) Non-alcoholic fatty liver disease and increased risk of cardiovascular disease. Atherosclerosis 191:235–240
10. Abdelmalek MF, Diehl AM (2007) Nonalcoholic fatty liver disease as a complication of insulin resistance. Med Clin North Am 91:1125–1149
11. Saltiel AR, Kahn CR (2001) Insulin signalling and the regulation of glucose and lipid metabolism. Nature 414:799–806
12. Ferré P, Foretz M, Azzout-Marniche D, Bécard D, Foufelle F (2001) Sterol-regulatory-element-binding protein 1c mediates insulin action on hepatic gene expression. Biochem Soc Trans 29:547–552

13. Shimano H (2000) Sterol regulatory element-binding protein-1 as a dominant transcription factor for gene regulation of lipogenic enzymes in the liver. Trends Cardiovasc Med 10:275–278
14. Shimomura I, Bashmakov Y, Horton JD (1999) Increased levels of nuclear SREBP-1c associated with fatty livers in two mouse models of diabetes mellitus. J Biol Chem 274:30028–30032
15. Yahagi N, Shimano H, Hasty AH, Matsuzaka T, Ide T, Yoshikawa T, Amemiya-Kudo M, Tomita S, Okazaki H, Tamura Y, Iizuka Y, Ohashi K, Osuga J, Harada K, Gotoda T, Nagai R, Ishibashi S, Yamada N (2002) Absence of sterol regulatory element-binding protein-1 (SREBP-1) ameliorates fatty livers, but not obesity of insulin resistance in *Lep*^{ob}/*Lep*^{ob} mice. J Biol Chem 277:19353–19357
16. Lee CH, Olson P, Evans RM (2003) Minireview: lipid metabolism, metabolic diseases, and peroxisome proliferator-activated receptors. Endocrinology 144:2201–2207
17. Braissant O, Foufelle F, Scotto C, Dauça M, Wahli W (1996) Differential expression of peroxisome proliferator-activated receptors (PPARs): tissue distribution of PPAR-α, -β, and -γ in the adult rat. Endocrinology 137:354–366
18. Kersten S, Seydoux J, Peters JM, Gonzalez FJ, Desvergne B, Wahli W (1999) Peroxisome proliferator-activated receptor α mediates the adaptive response to fasting. J Clin Invest 103:1489–1498
19. Aoyama T, Peters JM, Iritani N, Nakajima T, Furihata K, Hashimoto T, Gonzalez FJ (1998) Altered constitutive expression of fatty acid-metabolizing enzymes in mice lacking the peroxisome proliferator- activated receptor α (PPARα). J Biol Chem 273:5678–5684
20. Watanabe K, Fujii H, Takahashi T, Kodama M, Aizawa Y, Ohta Y, Ono T, Hasegawa G, Naito M, Nakajima T, Kamijo Y, Gonzalez FJ, Aoyama T (2000) Constitutive regulation of cardiac fatty acid metabolism through peroxisome proliferator-activated receptor α associated with age-dependent cardiac toxicity. J Biol Chem 275:22293–22299
21. Kamijo Y, Hora K, Tanaka N, Usuda N, Kiyosawa K, Nakajima T, Gonzalez FJ, Aoyama T (2002) Identification of functions of peroxisome proliferator-activated receptor α in proximal tubules. J Am Soc Nephrol 13:1691–1702
22. Schoonjans K, Martin G, Staels B, Auwerx J (1997) Peroxisome proliferator-activated receptors, orphans with ligands and functions. Curr Opin Lipidol 8:159–166
23. Tanaka N, Moriya K, Kiyosawa K, Koike K, Aoyama T (2008) Hepatitis C virus core protein induces spontaneous and persistent activation of peroxisome proliferator-activated receptor α in transgenic mice: implications for HCV-associated hepatocarcinogenesis. Int J Cancer 122:124–131
24. Nakajima T, Kamijo Y, Tanaka N, Sugiyama E, Tanaka E, Kiyosawa K, Fukushima Y, Peters JM, Gonzalez FJ, Aoyama T (2004) Peroxisome proliferator-activated receptor α protects against alcohol-induced liver damage. Hepatology 40:972–980
25. Kamijo Y, Hora K, Kono K, Takahashi K, Higuchi M, Ehara T, Kiyosawa K, Shigematsu H, Gonzalez FJ, Aoyama T (2007) PPARα protects proximal tubular cells from acute fatty acid toxicity. J Am Soc Nephrol 18:3089–3100
26. Lee CH, Olson P, Hevener A, Mehl I, Chong LW, Olefsky JM, Gonzalez FJ, Ham J, Kang H, Peters JM, Evans RM (2006) PPARδ regulates glucose metabolism and insulin sensitivity. Proc Natl Acad Sci USA 103:3444–3449
27. Matsusue K, Haluzik M, Lambert G, Yim SH, Gavrilova O, Ward JM, Brewer B Jr, Reitman ML, Gonzalez FJ (2003) Liver-specific disruption of PPARγ in leptin-deficient mice improves fatty liver but aggravates diabetic phenotypes. J Clin Invest 111:737–747
28. Dietschy JM (1997) Theoretical considerations of what regulates low-density-lipoprotein and high-density-lipoprotein cholesterol. Am J Clin Nutr 65:1581–1589
29. Ishibashi S, Goldstein JL, Brown MS, Herz J, Burns DK (1994) Massive xanthomatosis and atherosclerosis in cholesterol-fed low density lipoprotein receptor-negative mice. J Clin Invest 93:1885–1893
30. Towler DA, Bidder M, Latifi T, Coleman T, Semenkovich CF (1998) Diet-induced diabetes activates an osteogenic gene regulatory program in the aortas of low density lipoprotein receptor-deficient mice. J Biol Chem 273:30427–30434
31. Sugiyama E, Tanaka N, Nakajima T, Kamijo Y, Yokoyama S, Li Y, Gonzalez FJ, Aoyama T (2006) Haploinsufficiency in the PPARα and LDL receptor genes leads to gender- and age-specific obesity and hyperinsulinemia. Biochem Biophys Res Commun 350:370–376
32. Lee SS, Pineau T, Drago J, Lee EJ, Owens JW, Kroetz DL, Fernandez-Salguero PM, Westphal H, Gonzalez FJ (1995) Targeted disruption of the α isoform of the peroxisome proliferator-activated receptor gene in mice results in abolishment of the pleiotropic effects of peroxisome proliferators. Mol Cell Biol 15:3012–3022
33. Folch J, Lees M, Sloane Stanley GH (1957) A simple method for the isolation and purification of total lipids from animal tissues. J Biol Chem 226:497–509
34. Livak KJ, Schmittgen TD (2001) Analysis of relative gene expression data using real-time quantitative PCR and the $2^{-\Delta\Delta CT}$ method. Methods 25:402–408
35. Aoyama T, Uchida Y, Kelley RI, Marble M, Hofman K, Tonsgard JH, Rhead WJ, Hashimoto T (1993) A novel disease with deficiency of mitochondrial very-long-chain acyl-CoA dehydrogenase. Biochem Biophys Res Commun 191:1369–1372
36. Aoyama T, Souri M, Ushikubo S, Kamijo T, Yamaguchi S, Kelley RI, Rhead WJ, Uetake K, Tanaka K, Hashimoto T (1995) Purification of human very-long-chain acyl-coenzyme A dehydrogenase and characterization of its deficiency in seven patients. J Clin Invest 95:2465–2473
37. Goldberg IJ, Ginsberg HN (2006) Ins and outs modulating hepatic triglyceride and development of nonalcoholic fatty liver disease. Gastroenterology 130:1343–1346
38. Albarado DC, McClaine J, Stephens JM, Mynatt RL, Ye J, Bannon AW, Richards WG, Butler AA (2004) Impaired coordination of nutrient intake and substrate oxidation in melanocortin-4 receptor knockout mice. Endocrinology 145:243–252
39. Goetzman ES, Tian L, Wood PA (2005) Differential induction of genes in liver and brown adipose tissue regulated by peroxisome proliferator-activated receptor-α during fasting and cold exposure in acyl-CoA dehydrogenase-deficient mice. Mol Genet Metab 84:39–47
40. Gudbrandsen OA, Rost TH, Berge RK (2006) Causes and prevention of tamoxifen-induced accumulation of triacylglycerol in rat liver. J Lipid Res 47:2223–2232
41. Zhang YL, Hernandez-Ono A, Siri P, Weisberg S, Conlon D, Graham MJ, Crooke RM, Huang LS, Ginsberg HN (2006) Aberrant hepatic expression of PPARγ2 stimulates hepatic lipogenesis in a mouse model of obesity, insulin resistance, dyslipidemia, and hepatic steatosis. J Biol Chem 281:37603–37615
42. Shimano H, Horton JD, Hammer RE, Shimonura I, Brown MS, Goldstein JL (1996) Overproduction of cholesterol and fatty acids causes massive liver enlargement in transgenic mice expressing truncated SREBP-1a. J Clin Invest 98:1575–1584
43. Ericsson J, Jackson SM, Kim JB, Spiegelman BM, Edwards PA (1997) Identification of glycerol-3-phosphate acyltransferase as an adipocyte determination and differentiation factor 1- and sterol regulatory element-binding protein-responsive gene. J Biol Chem 272:7298–7305
44. Foretz M, Guichard C, Ferre P, Foufelle F (1999) Sterol regulatory element binding protein-1c is a major mediator of insulin

action on the hepatic expression of glucokinase and lipogenesis-related genes. Proc Natl Acad Sci USA 96:12737–12742
45. Azzout-Marniche D, Becard D, Guichard C, Foretz M, Ferre P, Foufelle F (2000) Insulin effects on sterol regulatory-element-binding protein-1c (SREBP-1c) transcriptional activity in rat hepatocytes. Biochem J 2:389–393
46. Deng X, Cagen LM, Wilcox HG, Park EA, Raghow R, Elam MB (2002) Regulation of the rat SREBP-1c promoter in primary rat hepatocytes. Biochem Biophys Res Commun 290:256–262
47. Cagen LM, Deng X, Wilcox HG, Park EA, Raghow R, Elam MB (2005) Insulin activates the rat sterol-regulatory-element-binding protein 1c (SREBP-1c) promoter through the combinatorial actions of SREBP, LXR, Sp-1 and NF-Y *cis*-acting elements. Biochem J 385:207–216
48. Okamoto K, Kakuma T, Fukuchi S, Masaki T, Sakata T, Yoshimatsu H (2006) Sterol regulatory element binding protein (SREBP)-1 expression in brain is affected by age but not by hormones or metabolic changes. Brain Res 1081:19–27
49. Schoonjans K, Peinado-Onsurbe J, Lefebvre AM, Heyman RA, Briggs M, Deeb S, Staels B, Auwerx J (1996) PPARα and PPARγ activators direct a distinct tissue-specific transcriptional response via a PPRE in the lipoprotein lipase gene. EMBO J 15:5336–5348
50. Motojima K, Passilly P, Peters JM, Gonzalez FJ, Latruffe N (1998) Expression of putative fatty acid transporter genes are regulated by peroxisome proliferator-activated receptor α and γ activators in a tissue- and inducer-specific manner. J Biol Chem 273:16710–16714
51. Dyck DJ, Steinberg G, Bonen A (2001) Insulin increases FA uptake and esterification but reduces lipid utilization in isolated contracting muscle. Am J Physiol Endocrinol Metab 281:600–607
52. Luiken JJ, Dyck DJ, Han XX, Tandon NN, Arumugam Y, Glatz JF, Bonen A (2002) Insulin induces the translocation of the fatty acid transporter FAT/CD36 to the serum membrane. Am J Physiol Endocrinol Metab 282:491–495
53. Wu G, Brouckaert P, Olivecrona T (2004) Rapid downregulation of adipose tissue lipoprotein lipase activity on food deprivation: evidence that TNF-α is involved. Am J Physiol Endocrinol Metab 286:711–717
54. Bernal-Mizrachi C, Weng S, Feng C, Finck BN, Knutsen RH, Leone TC, Coleman T, Mecham RP, Kelly DP, Semenkovich CF (2003) Dexamethasone induction of hypertension and diabetes is PPAR-α dependent in LDL receptor-null mice. Nat Med 9:1069–1075
55. Tordjman K, Bernal-Mizrachi C, Zemany L, Weng S, Feng C, Zhang F, Leone TC, Coleman T, Kelly DP, Semenkovich CF (2001) PPARα deficiency reduces insulin resistance and atherosclerosis in apoE-null mice. J Clin Invest 107:1025–1034
56. Sanguino E, Ramón M, Michalik L, Wahli W, Alegret M, Sánchez RM, Vázquez-Carrera M, Laguna JC (2004) Lack of hypotriglyceridemic effect of gemfibrozil as a consequence of age-related changes in rat liver PPARα. Biochem Pharmacol 67:157–166
57. Ye P, Wang ZJ, Zhang XJ, Zhao YL (2005) Age-related decrease in expression of peroxisome proliferator-activated receptor α(and its effects on development of dyslipidemia. Chin Med J (Engl) 118:1093–1098
58. Iemitsu M, Miyauchi T, Maeda S, Tanabe T, Takanashi M, Irukayama-Tomobe Y, Sakai S, Ohmori H, Matsuda M, Yamaguchi I (2002) Aging-induced decrease in the PPAR-α level in hearts is improved by exercise training. Am J Physiol Heart Circ Physiol 283:1750–1760
59. Gelinas DS, McLaurin J (2005) PPAR-α expression inversely correlates with inflammatory cytokines IL-1β and TNF-α in aging rats. Neurochem Res 30:1369–1375

Lipids (2008) 43:313–324
DOI 10.1007/s11745-008-3164-7

ORIGINAL ARTICLE

Hepatic and Adipose Tissue Depot-Specific Changes in Lipid Metabolism in Late-Onset Obese (LOB) Rats

Fredrik Frick · Randip Hume · Iain C. Robinson · Staffan Edén · Jan Oscarsson

Received: 30 October 2007 / Accepted: 19 February 2008 / Published online: 12 March 2008
© AOCS 2008

Abstract Transgenic Late-onset OBesity (LOB) rats slowly develop a male-specific, autosomal dominant, obesity phenotype with a specific increase in peri-renal white adipose tissue (WAT) depot and preserved insulin sensitivity (Bains et al. in Endocrinology 145:2666–2679, 2004). To better understand the remarkable phenotype of these rats, the lipid metabolism was investigated in male LOB and non-transgenic (NT) littermates. Total plasma cholesterol (C) levels were normal but total plasma triacylglycerol (TAG) (2.8-fold) and hepatic TAG content (25%) was elevated in LOB males. Plasma VLDL-C and VLDL-TAG levels were higher while plasma apoB levels were 60% lower in LOB males. Increased hepatic TAG secretion explained the increased VLDL levels in LOB males. The hepatic gene expression of FAS, SCD-1, mitochondrial (mt)GPAT, and DGAT2 was up-regulated in both old obese and young non-obese LOB rats. Lipoprotein lipase (LPL) activity in heart and epididymal white adipose tissue (WAT) was unchanged, while LPL activity was increased in peri-renal WAT (30%) and decreased in soleus muscle (40%). Moreover, FAS, SCD-1 and DGAT2 gene expression was increased in peri-renal, but not in epididymal WAT. Basal lipolysis was reduced or unchanged and β-adrenergic stimulated lipolysis was reduced in WAT from both old obese and young non-obese LOB rats. To summarize, the obese phenotype of LOB male rats is associated with increased hepatic TAG production and secretion, a shift in LPL activity from skeletal muscle to WAT, reduced lipolytic response in WAT depots and a specific increase in expression of genes responsible for fatty acid and TAG synthesis in the peri-renal depot.

Keywords Lipoproteins · Apolipoprotein B · Lipoprotein lipase · SCD-1 · FAS · DGAT1 · DGAT2 · Mitochondrial GPAT · Adiponectin · Lipoprotein lipase · Lipolysis

Introduction

Obesity is associated with insulin resistance and ectopic TAG storage in skeletal muscle and liver [1–4]. An increased free fatty acid (FFA) release from adipocytes and changed adipocytokine production in adipose tissue is probably of major importance for the development of ectopic lipid storage and insulin resistance [1, 3–5]. The dyslipidemia associated with insulin resistance is characterised by high plasma levels of TAG and apolipoprotein (apo) B, and low levels of HDL-cholesterol (C) in humans

---

F. Frick and R. Hume contributed equally to this work.

F. Frick (✉) · J. Oscarsson
Department of Bioscience, AstraZeneca R&D,
Pepparedsleden 1, 431 83 Mölndal, Sweden
e-mail: Fredrik.Frick@astrazeneca.com

R. Hume · I. C. Robinson
Division of Molecular Neuroendocrinology,
National Institute for Medical Research, Mill Hill,
London NW7 1AA, UK

R. Hume · I. C. Robinson
Anacrine Ltd, 1-3 Burtonhole Lane,
London NW7 1AD, UK

F. Frick · J. Oscarsson
Department of Physiology/Endocrinology,
The Sahlgrenska Academy at Göteborg University,
Göteborg, Sweden

S. Edén
Department of Medicine, The Sahlgrenska Academy
at Göteborg University, Göteborg, Sweden

[3, 6]. In insulin-resistant rodent models, such as ob/ob mice and Zucker rats, plasma levels of TAG, apoB and total C are increased, while HDL-C levels are largely unchanged [7–9].

The LOB rat (Late-onset OBesity) model, first described by Bains et al. [10], develops a male-specific, late-onset, central obesity despite a normal intake of low fat diet. These rats were originally generated to study the regulation of the vasopressin/oxytocin (VP/OT) locus targeting human GH to the posterior pituitary [11]. However, as previously reported [1] one of the lines differed from the other lines since it slowly developed an obesity phenotype with unusual characteristics. The most pronounced change in the LOB rats was an approximately threefold increase in the peri-renal fat depots in LOB males compared to NT littermates. This increase was almost entirely attributed to an increase in adipocyte number [10]. Remarkably, despite severe central obesity, transgenic rats were able to retain a normal glucose metabolism with a heightened insulin sensitivity compared to non-transgenic (NT) littermates. It is likely that the preserved adipocyte size in the context of obesity and the increased plasma adiponectin levels [5] observed in the LOB rats [10] to a large extent contributed to the normal glucose metabolism in this obese phenotype.

Obesity associated with normal adipocyte size and preserved insulin sensitivity is a unique feature compared to other existing rodent models of obesity with insulin resistance. This phenotype therefore clearly differentiates the LOB rats from obese insulin resistant rodents like the obese (ob/ob) mouse [4, 12] and the Zucker (fa/fa) rat [13].

The underlying genetic cause of the phenotype seen in LOB rats has yet to be determined. Here we sought to analyse the changes in lipid and lipoprotein metabolism in both old obese and young non-obese LOB rats in an attempt to identify potential mechanisms that favor central fat deposition in these rats.

Materials and Methods

Animals

Experiments were performed following Institutional and National guidelines. All rats were bred and housed under controlled conditions (22 °C, 12 h light, 12 h dark cycle), with access to food and water ad libitum. The diet was standard rat chow (3.4% fat, 18.8% protein, 3.7% fibre, 3.8% ash, 60.3% carbohydrate, 15.6 MJ/kg (Special Diet Services, Witham, UK). The male rats were 10–12 months of age at sacrifice if not otherwise stated. At this age the LOB rats are severely obese and weighed ~30% more than their controls as previously described [10]. For all studies, control animals referred to as NT are non-transgenic littermates from the same strain colonies.

Plasma Analyses

TAG and total cholesterol concentrations (cholesterol + cholesteryl esters) were determined by enzymatic colorimetric assays (MPR2: TG/GPO-PAP and Chl/CHOD-PAP, Boehringer Mannheim, Germany). The intra-assay coefficient of variation (CV) was 3% for the TAG assay and 4% for the cholesterol assay. Plasma apolipoprotein B (apo B) and apolipoprotein E (apo E) concentrations were determined by an electroimmunoassay (EIA) as previously described [14, 15]. The intra- and inter-assay CV for the apo B assay was 5.3 and 8.6% respectively. Plasma glucose concentrations were measured by the MPR3 Glucose/GOD-PAP method (Boehringer Mannheim). Serum FFA concentrations were measured with a NEFA kit (Wako Chemicals, Neuss, Germany).

Lipoprotein profiles were obtained by gel filtration using fast protein liquid chromatography (FPLC) equipment (Pharmacia Upjohn, Uppsala, Sweden) as previously described [16]. TAG and total cholesterol concentrations were determined with enzymatic colorimetric assays as described above. VLDL ($d < 1.006$ g/ml), IDL/LDL (d 1.006–1.063 g/ml) and HDL (d 1.063–1.21 g/ml) are indicated based on the elution profile of density fractions after sequential ultracentrifugation.

ApoB in the FPLC fractions was determined by western blotting as previously described [17] using enhanced chemiluminescence (ECL) protocol (Amersham Pharmacia Biotech, Buckinghamshire, UK).

In Vivo Hepatic Triacylglycerol Secretion and Clearance

TAG secretion rate in vivo was measured by intravenous administration of Triton WR1339 [16, 18]. Plasma TAG levels were analysed as described above, and hepatic TAG secretion rate was calculated from the slope of the curve and expressed as micromoles per hour per gram liver. The plasma TAG clearance rate was calculated as the ratio between hepatic TAG secretion rate and the basal plasma TAG levels before Triton WR1339 administration (μmol/min:μmol/ml).

Total Amount of Lipids in the Liver

Frozen liver was homogenized in ice-cold double distilled water (6 ml/g tissue). Total lipid content was then extracted from the homogenate according to Bligh and Dyer [19]. After evaporation of the chloroform phase under a stream of N_2 the extracted lipids were dissolved in isopropanol.

TAG and total cholesterol concentrations were determined as described above.

Lipoprotein Lipase Activity

Lipoprotein lipase activity in heart, skeletal muscle and white adipose tissue (WAT) depots was determined according to the method of Peterson et al. [20]. The substrate emulsion used was Intralipid®, labelled with [^{3}H]-triolein (Dr Krabisch, Lund University, Lund, Sweden). Samples were incubated in triplicates at 25 °C. Liberated fatty acids were extracted [21] and quantified in a liquid scintillation counter. Activity was expressed as mU/g tissue (1 mU = 1 nmol FFA released per minute).

β-Adrenergic Stimulated Lipolysis

Isolated fat cells were obtained using a method similar to that previously described by Rodbell [22] with the modifications made by Gause et al. [23]. For each incubation, 100 µl of the 50/50 cell-suspension was added to plastic vials containing 2 ml incubation medium, supplemented with 4% BSA (fraction V, Sigma Chem.), in the absence (basal lipolysis) or presence of 10^{-5} M isoproterenol (Isoproterenol, Noradrenaline, Sigma Chem.). In parallel, 100 µl 50/50 cell-suspension was added to Dole's solution, for subsequent extraction of lipids [24]. After incubation for 2 h at 37 °C, cells and medium were separated by centrifugation (2,400 rpm, 3 min) through silicon oil (Kebo Lab, Spånga, Sweden). The glycerol content in the medium was determined using an enzymatic colorimetric assay (GY105, Randox, Randox Laboratories, United Kingdom) and taken as an index of lipolysis. The rate of lipolysis was expressed as nmol glycerol released per mg TAG.

cDNA Synthesis and Quantitative Real-Time PCR

Total RNA was isolated with TRIZOL® Reagent (Invitrogen). To remove contaminating DNA, total RNA was treated with DNA-free™ (Ambion, Austin, TX, USA). First-strand cDNA was synthesized with SuperScript™ First-Strand Synthesis System (Invitrogen). Quantitative real time PCR analyses were performed with Applied Biosystems 7500 Real-Time PCR System (96 wells). All samples were analysed in triplicates. The expression data were normalized against the endogenous control acid ribosomal phosphoprotein P0 (36B4). The expression of 36B4 was not influenced by the introduced transgene. The relative expression levels were calculated according to the formula $2^{-\Delta Ct}$, where ΔCt is the difference in threshold cycles (Ct) values between the target gene and the 36B4 endogenous control. Each gene, except for PPARγ2 (see below), was analysed using FAM™ labelled probes obtained from TaqMan® Gene Expression Assays (Applied Biosystems): FAS (fatty acid synthase, Rn00569117_m1), SCD-1 (stearoyl-CoA desaturase-1, Rn00594894_g1), DGAT1 (acyl-CoA:diacylglycerol O-acyltransferase 1, Rn00584870_m1), DGAT2 (acyl-CoA:diacylglycerol O-acyltransferase 2, Rn01506781_m1), mtGPAT (mitochondrial glycerol-3-phosphate acyltransferase, Rn00568620_m1), Adiponectin (adipocyte complement related protein of 30 kDa, Rn00595250_m1) and FABP4 (fatty acid binding protein 4, Rn00670361_m1). For PPARγ2 (peroxisome proliferator activated receptor γ2), specific primers (forward: 5′-TT TTATGCTGTTATGGGTGAAACTCT-3′, reverse: 5′-AG TGCTCATAGGCAGTGCATCA-3′) was used to amplify a 86 bp long fragment of rat PPARγ2 cDNA (Acc No. NM_013124).

Statistical Analysis

Values are expressed as means ± SEM. Comparisons between groups were made by one-way Analysis of Variance (ANOVA) followed by Bonferroni test for pairwise differences in multiple groups or using Student's *t*-test. When appropriate, values were normalized by transformation to logarithms. A difference of $P < 0.05$ was considered significant: NS = non-significant.

Results

Plasma Lipids and Lipoprotein Profiles

As has been shown previously [10], total plasma cholesterol (C) levels were normal (Fig. 1a) but total plasma TAG levels were elevated ~2.8-fold in 10- to 12-month-old LOB males (Fig. 1b). Size-exclusion chromatography analysis showed a marked increase in both VLDL-C and TAG levels (Fig. 2a, b) while LDL-C and HDL-C levels were slightly lower in LOB rats. This analysis was performed on three separate occasions with each analysis giving similar results. Surprisingly, in spite of the elevated levels of VLDL, apo B levels were ~60% lower in LOB males compared to NT males (Fig. 2c). No significant changes were detected in plasma levels of apo E (NT 100.0 ± 6.4 vs. LOB 105.8 ± 6.7 expressed as percent of NT, $n = 10$) or free fatty acid (FFA) levels (NT 0.31 ± 0.04 vs. LOB 0.38 ± 0.08 mM, $n = 6$).

Hepatic Triacylglycerol Secretion Rate

It was subsequently investigated whether the increase in plasma VLDL levels was due to an increased hepatic TAG secretion. Hepatic TAG secretion in vivo was measured by

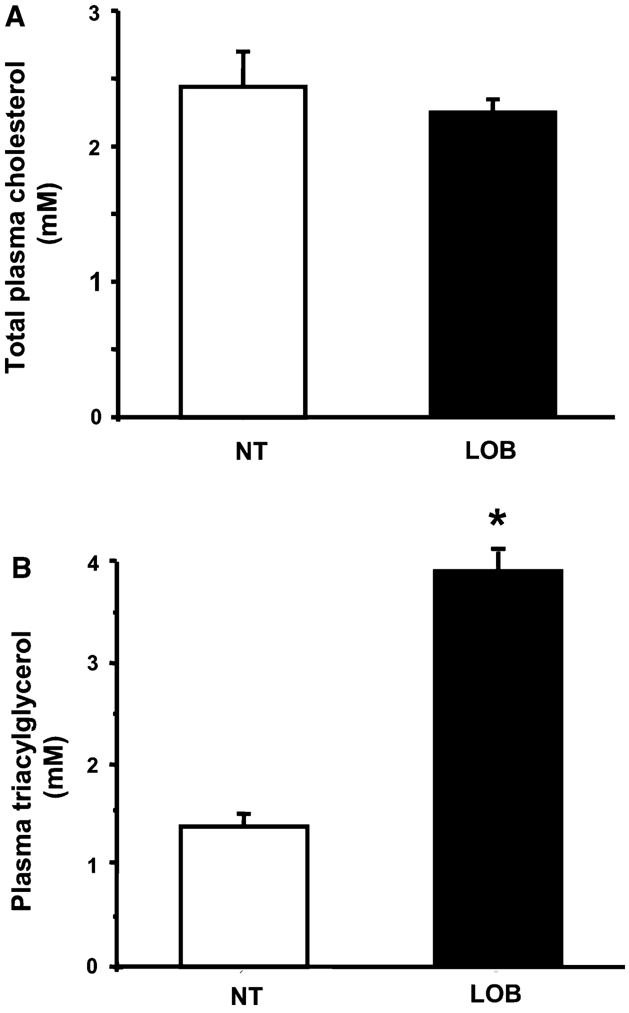

Fig. 1 Plasma total cholesterol and TAG levels. Total cholesterol (**a**) and TAG (**b**) concentrations were determined in LOB rats (LOB) and non-transgenic littermates (NT) by enzymatic colorimetric assays as described in "Materials and Methods". The animals were sacrificed between 0900 and 1100 hours without prior fasting. Results are presented as means ± SEM, $n = 6$. *$P < 0.05$ LOB versus NT rat (unpaired Student's *t*-test)

administering Triton WR1339 via the tail vein. LOB rats showed a significant increase in hepatic TAG secretion compared with NT male rats (Fig. 3a, b). To estimate the peripheral tissues ability to remove TAG from the circulation, the plasma TAG clearance rate was calculated. LOB males had significantly higher plasma TAG clearance rate when compared to NT rats (Fig. 3c).

Lipid Content in the Liver

To investigate whether hepatic lipid content changed in parallel with hepatic TAG secretion, hepatic TAG and C content were measured (Table 1). Hepatic TAG content was significantly higher in LOB rats compared to non-transgenic rats. However, there was no significant difference in hepatic total cholesterol content.

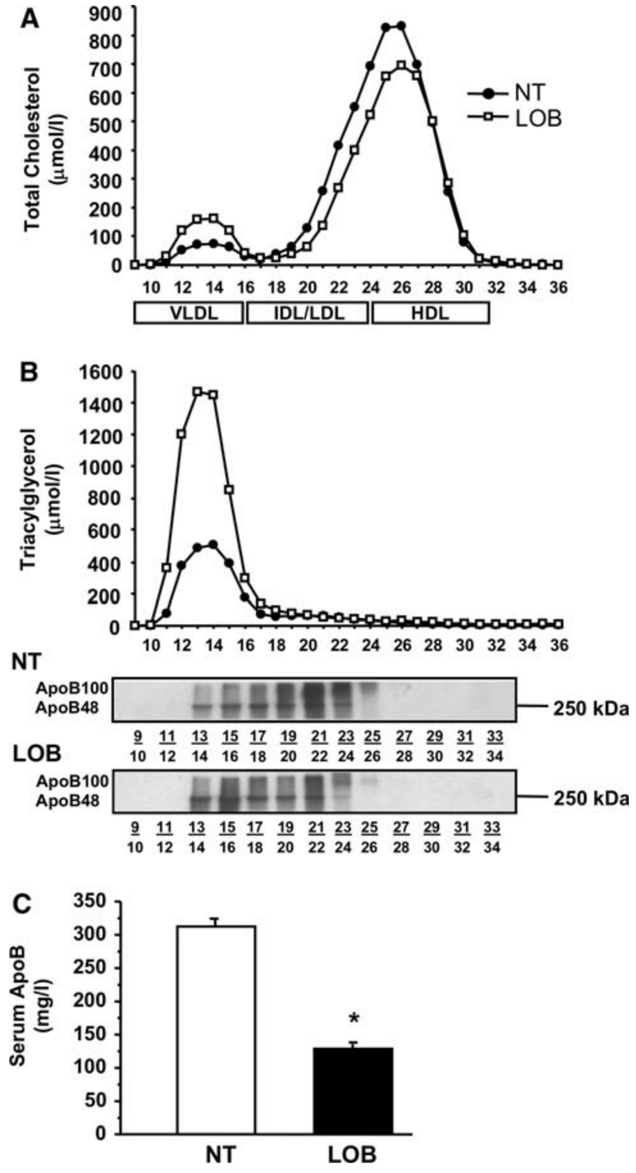

Fig. 2 Size distribution of serum lipoproteins and serum levels of apoB. Size distribution of serum lipoproteins in LOB rats (LOB) and non-transgenic littermates (NT) rats is shown for total cholesterol (**a**) and TAG (**b**) concentrations. The density classes of lipoproteins obtained by sequential ultracentrifugation, VLDL ($d < 1.006$ g/ml), IDL/LDL (d 1.006–1.063 g/ml) and HDL (d 1.063–1.21 g/ml) are indicated. Data was obtained from pooled serum from six rats in each group. Similar results were obtained in three separate experiments. Below the lipoprotein profiles are Western blot data showing apoB in the fractions; assayed as described in "Materials and Methods". Briefly, in each lane adjacent FPLC fractions were pooled in pairs (9 µl each). Serum apo B concentrations (**c**) were determined by an electroimmunoassay as described in "Materials and Methods". Results are presented as means ± SEM, $n = 5$. The animals were killed between 0900 and 1100 hours without prior fasting. *$P < 0.05$ LOB versus NT rats (unpaired Student's *t*-test)

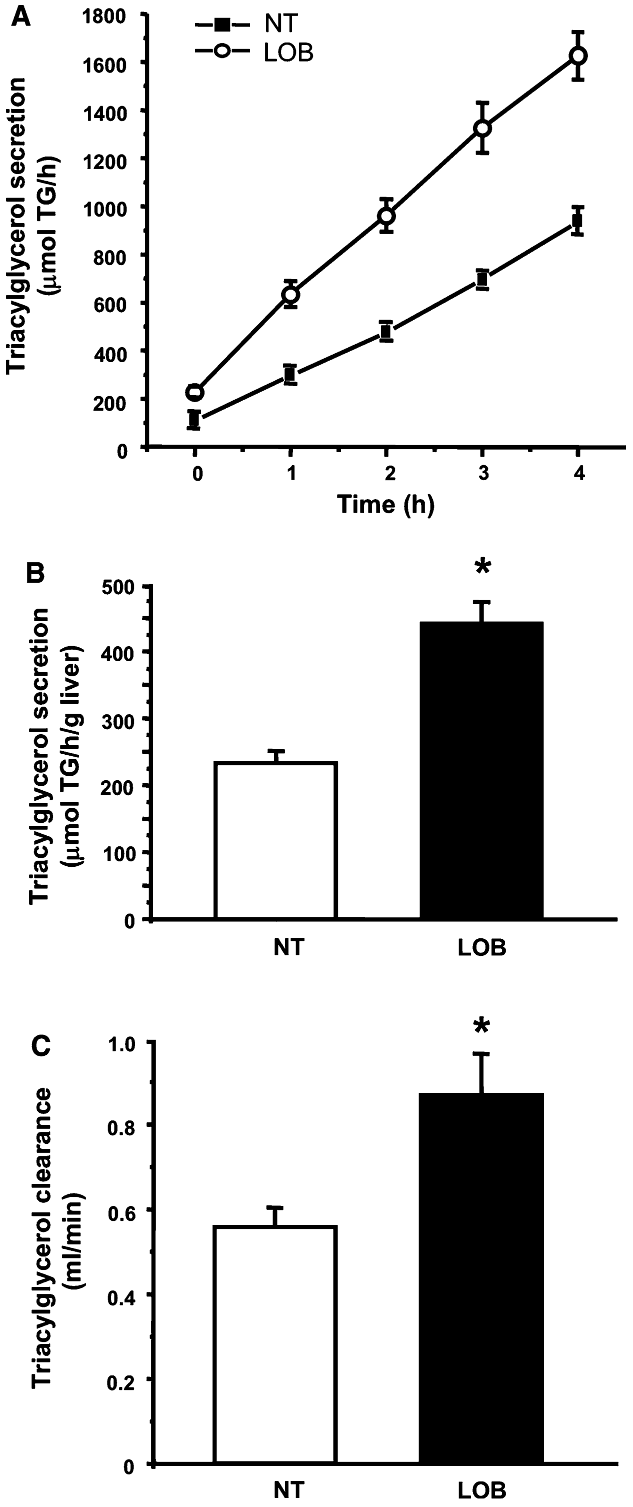

Fig. 3 Hepatic TAG secretion and plasma TAG clearance rate in ▶ vivo. TAG secretion rate in vivo from LOB rats (LOB) and non-transgenic littermates (NT) rats was measured after i.v. administration of Triton WR1339 (500 mg/kg). Serum TAG were determined before (0 min) and 60, 120, 180 and 240 min after Triton administration (**a**). TAG secretion rate was calculated from the slope of the curves (**b**). TAG clearance rate (ml/min) was calculated as the ratio between hepatic TAG secretion rate and the basal plasma TAG levels before Triton WR1339 administration (µmol TAG/min:µmol/ml) (**c**). Results are presented as means ± SEM, $n = 7$. $^{*}P < 0.05$ LOB versus NT rats (unpaired Student's *t*-test)

Hepatic Gene Expression

The marked increase in hepatic TAG secretion and the parallel increase in hepatic TAG content lead us to investigate the gene expression of five different hepatic enzymes involved in de novo lipogenesis or TAG synthesis. Figure 4 shows that the mRNA expression of FAS, SCD1, mtGPAT and DGAT2 was up-regulated in both old (10–12 months) and young (1.5–2 months) LOB rats compared to NT rats. However, the expression of DGAT1 was significantly higher only in old LOB rats.

Lipoprotein Lipase Activity

The importance of lipoprotein lipase (LPL) for the turnover of TAG-rich lipoproteins is well documented [25]. The activity of lipoprotein lipase (LPL) is an important first step in plasma TAG clearance and FFA delivery to adipose and muscle tissues. Lipoprotein lipase activity was therefore measured in heart, soleus muscle and the peri-renal and epididymal white adipose tissue (WAT) depots. There were no significant differences in heart or epididymal WAT LPL activity between LOB rats and NT rats (Fig. 5a, c). However, LPL activity was higher in peri-renal WAT (~30%) and lower in soleus muscle (~40%) in LOB rats (Fig. 5b, d). This shift in LPL activity ratio between adipose and muscle tissues would favour an increased TAG deposition into the peri-renal adipose depot that would contribute to the increased central obesity observed in LOB rats [10].

Adipose Tissue Gene Expression

Fatty acids liberated by LPL are re-esterified in adipocytes to TAG. An alternative source of fatty acids for TAG synthesis is de novo lipogenesis. Gene expression of some enzymes important for lipogenesis and TAG synthesis were therefore determined in epididymal and peri-renal WAT. As shown in Fig. 6, the gene expression of SCD-1 and DGAT1 was not different between LOB rats and their controls in epididymal WAT. Unexpectedly, FAS and DGAT2 mRNA levels were lower in LOB rats in this WAT depot. In contrast to the findings in epididymal WAT, the expression of all these genes except DGAT1, was significantly higher in peri-renal WAT of LOB rats than in lean littermates (Fig. 6). These results indicate a marked difference in regulation of genes involved in fatty acid and TAG synthesis between the WAT depots.

Table 1 Lipid content in liver

Groups	Liver triacylglycerol (µmol/g liver)	Liver total cholesterol (µmol/g liver)
NT	7.8 ± 0.2	4.6 ± 0.1
LOB	9.1 ± 0.2*	4.9 ± 0.2

The content of triacylglycerol and total cholesterol in liver of LOB and non-transgenic littermate controls (NT) rats was determined as described in "Materials and Methods". Animals were sacrificed at 12 months of age. Results are presented as means ± SEM, $n = 5$–6. * $P < 0.05$ LOB versus NT rat (unpaired Student's *t*-test)

Our previous study [10] has shown that LOB rats are more sensitive to a PPARγ agonist, and moreover, treatment with PPARγ agonists have shown to reduce adipocyte size [13] and increase adiponectin mRNA levels in adipocytes [26]. Hence, mRNA expression of PPARγ2 was also measured in epididymal and peri-renal WAT from LOB and NT rats. There was a trend towards higher expression of PPARγ2 in both epididymal and peri-renal WAT from LOB as compared to NT littermates (epididymal WAT ($2^{-\Delta Ct}$): LOB, 0.033 ± 0.009, NT, 0.022 ± 0.016, $n = 5$–6, peri-renal WAT ($2^{-\Delta Ct}$): LOB, 0.095 ± 0.023, NT, 0.069 ± 0.030, $n = 4$–5). In our previous study, it was shown that LOB males had markedly higher plasma levels of adiponectin [10]. To determine if the increased plasma levels of adiponectin were associated with changed gene expression, adiponectin mRNA was measured in both WAT depots. Interestingly, adiponectin mRNA levels were not significantly different between LOB males and littermate NT controls (epididymal WAT ($2^{-\Delta Ct}$): LOB, 3.42 ± 0.19, NT, 3.22 ± 0.04, $n = 4$–5, peri-renal WAT ($2^{-\Delta Ct}$): LOB, 2.57 ± 0.10, NT, 2.46 ± 0.12, $n = 4$).

Another unique model of obesity associated with preserved insulin sensitivity is the FABP4 (aP2) null mouse [27] on a ob/ob background [28]. We therefore measured FABP4 mRNA expression in WAT depots. There was no significant difference in FABP4 mRNA levels between LOB males and littermate controls (epididymal WAT ($2^{-\Delta Ct}$): LOB, 1.77 ± 0.08, NT, 1.48 ± 0.08, $n = 4$, peri-renal WAT ($2^{-\Delta Ct}$): LOB, 2.30 ± 0.20, NT, 1.83 ± 0.16, $n = 4$).

β-Adrenergic Stimulated Lipolysis

We next investigated the lipolytic response in peri-renal and epididymal WAT using glycerol release from isolated adipocytes as an index of lipolysis during non-stimulated conditions (basal lipolysis) and during β-adrenergic stimulation. β-adrenergic stimulated lipolysis was lower in both peri-renal and epididymal WAT from LOB rats compared to non-transgenic rats (Fig. 7a, b). Basal lipolysis was significantly lower in epididymal WAT, but unchanged in peri-renal WAT, from LOB versus NT rats (Fig. 7b). Lipolysis was also investigated in 2-month-old non-obese LOB rats. The basal lipolysis in epididymal and peri-renal WAT was similar in young NT and LOB rats (data not shown). The isoproterenol (10^{-5} M) stimulated lipolysis in epididymal WAT was 33.3 ± 0.8 and 18.0 ± 0.7 µM/mg TAG (mean ± SD, $n = 2$) in young NT and LOB rats, respectively. The isoproterenol (10^{-5} M) stimulated lipolysis in peri-renal WAT was 33.3 ± 1.6 and 16.5 ± 0.7 µM/mg TAG (mean ± SD, $n = 2$) in young NT and LOB rats, respectively. The similar findings in the young non-obese LOB rats and old obese LOB rats indicate that the obesity did not cause the decreased lipolysis of LOB rats.

Discussion

In contrast to most other obese rodent models [4, 13, 29, 30], the LOB rats have unchanged plasma levels of insulin and glucose as well as normal or improved insulin sensitivity and glucose tolerance [10]. Possible clues to the well preserved glucose homeostasis in the context of marked obesity were the previous findings of high plasma levels of adiponectin and unchanged adipocyte size [10]. The obese phenotype was not explained by GH deficiency, since GH treatment of LOB rats, increased body weight gain and the size of the peri-renal fat depot [10]. In addition, other GH deficient lines did not show this obese phenotype [1]. Moreover, LOB rats did not show increased food intake or decreased body temperature [10]. The genetic basis of this phenotype is currently under investigation and is unclear. It may result from a combinational effect of transgene insertion and transgene expression, since the phenotype only manifests in a single line. The intriguing obesity of these rats prompted us to further investigate lipid and lipoprotein metabolism in more detail to gain further understanding of the phenotype of LOB rats. We report here that the specific growth of the peri-renal WAT depot was associated with a unique regulation of LPL activity and genes involved in fatty acid and TAG synthesis in that depot.

An increased hepatic TAG secretion and not a decreased turnover of circulating TAG resulted in increased plasma VLDL-TAG levels. Interestingly, increased hepatic TAG secretion is also observed in ob/ob mice and Zucker rats [7, 9, 29]. In contrast to the obese Zucker rat [29], the LOB rats showed enhanced calculated TAG clearance indicating a fundamental difference in TAG metabolism. Opposite to the findings in LOB rats, insulin resistant rodent models also have increased total plasma cholesterol [7, 9] and apo B levels [8]. The increase in hepatic TAG content was

Fig. 4 Hepatic mRNA expression. Hepatic mRNA expression of FAS (**a**), SCD-1 (**b**), DGAT1 (**c**), DGAT2 (**d**) and mtGPAT (**e**) in young non-obese (1.5–2 months) and old-obese (10–12 months) LOB rats compared with non-transgenic littermates (NT). The animals were sacrificed between 0900 and 1100 hours without prior fasting. The mRNA levels were measured with Applied Biosystems 7500 Real-Time PCR System (96 wells). All samples were analysed in triplicates and expression data normalized against the endogenous control 36B4. Results are presented as means ± SEM, $n = 5$–7. *$P < 0.05$ LOB versus NT rats (unpaired Student's *t*-test)

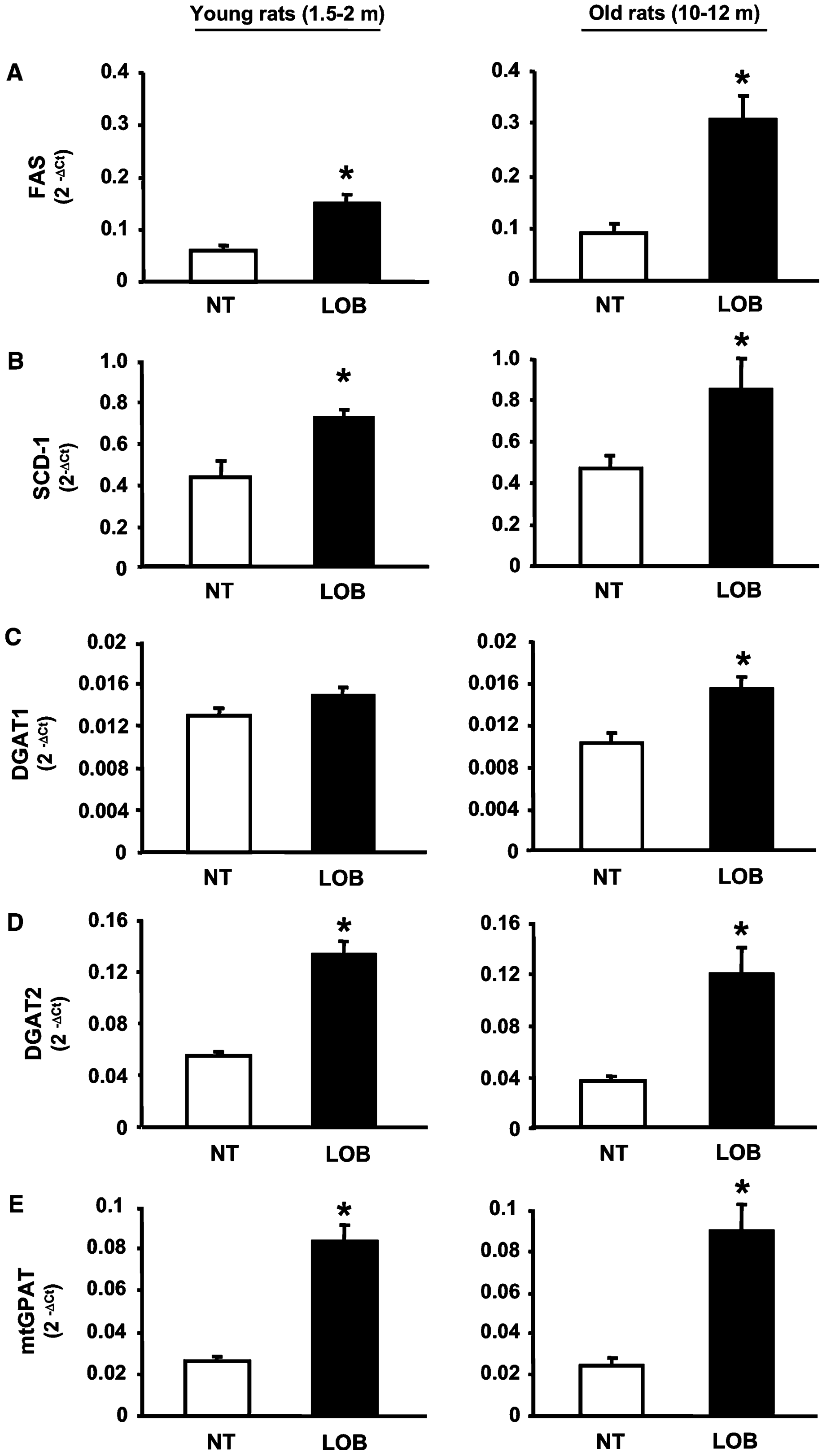

much less pronounced in the LOB rats than observed in ob/ob mice [9] and Zucker rats [7]. We conclude that de novo lipogenesis in the liver was likely enhanced in LOB rats since the lipolysis in WAT was reduced in the context of increased hepatic TAG content and secretion. Expression of the lipogenic genes, like FAS and SCD-1 was increased

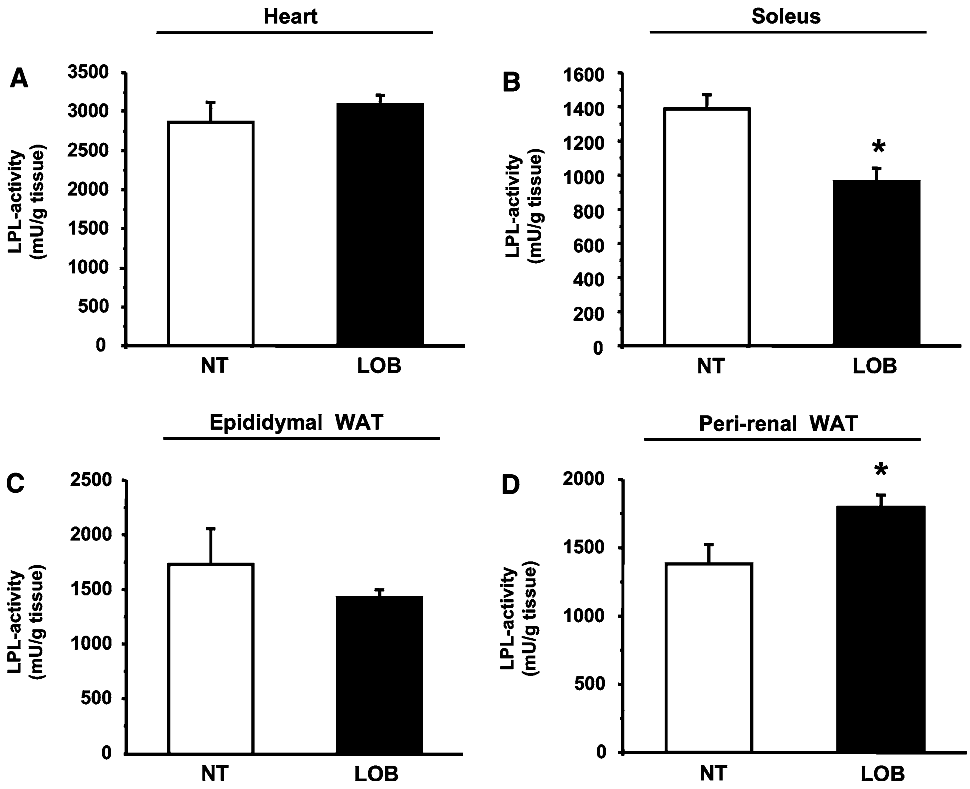

Fig. 5 Lipoprotein lipase activity. Lipoprotein lipase (LPL) activity in heart (**a**), soleus muscle (**b**), epididymal white adipose tissue (WAT) (**c**) and peri-renal WAT (**d**) from 12-month-old LOB rats and non-transgenic littermates (NT). Animals were sacrificed between 0900 and 1200 hours. Lipoprotein lipase activity was analysed as described in "Materials and Methods". Results are presented as means ± SEM, $n = 6$. *$P < 0.05$ LOB versus NT rats (unpaired Student's *t*-test)

in both young and old LOB males. Mitochondrial (mt)GPAT and DGAT2 mRNA, genes important in TAG synthesis were also up-regulated. Increased hepatic expression of mtGPAT results in increased hepatic TAG secretion and mild hypertriglyceridemia [31]. Over-expression of DGAT2 in the liver results in liver steatosis without changed hepatic TAG secretion [32]. The exact role of DGAT2 in VLDL assembly is not clear, since silencing DGAT2 in fat fed mice decreases both hepatic steatosis and TAG secretion [33]. On the other hand, hepatic over-expression of DGAT1 is specifically related to increased hepatic TAG secretion and also results in increased adipose tissue mass [32]. Therefore, the higher DGAT1 expression in old LOB rats probably contributes to the increased hepatic TAG secretion.

Interestingly, the increase in VLDL in LOB rats was accompanied by a ~60% reduction in apoB. The mechanisms behind the low plasma apoB levels remain to be explored. However, hepatic insulin resistance and hyperinsulinemia is accompanied with increased hepatic secretion of apoB [6] and insulin prevents apoB secretion [34]. Therefore, the preserved insulin sensitivity of LOB rats [10] might contribute to low plasma apoB levels.

LPL activity was increased specifically in the peri-renal WAT. With the lower LPL activity in skeletal muscle of LOB rats, these changes contribute to a shift in fatty acid flux towards the peri-renal depot [25]. A similar shift in LPL activity from muscle to adipose tissue has been described for the insulin-resistant obese Zucker rat [35, 36], indicating that this shift in LPL activity might be a general phenomena of obesity. Thus, the changed balance in LPL activity towards the peri-renal WAT would result in an increased availability of TAG-derived fatty acids in that tissue.

The increased LPL activity would not lead to increased TAG synthesis in the peri-renal WAT depot if balanced by decreased capacity for TAG synthesis. The increased expression of mtGPAT and DGAT2 in peri-renal WAT of LOB rats indicated increased capacity for TAG synthesis. The expression of DGAT2 is higher than DGAT1 in adipose as indicated in this study and by others [37]. Ob/ob mice, high fat fed mice and IRS2-/-mice showed increased DGAT2 and decreased DGAT1 expression in WAT [38]. In contrast, LOB rats showed unchanged DGAT1 expression. The mechanisms behind the changed expression of DGAT1 and DGAT2 in LOB rats remain unclear.

Interestingly, hepatic lipogenesis is increased, but expression of lipogenic genes are unchanged in WAT in overt human obesity [39]. Therefore, it was of interest that FAS and SCD-1 expression was up-regulated in LOB peri-renal fat but not in epididymal fat. Increased SCD-1 expression may be of importance in obesity since SCD-1 knock-out in ob/ob mice resulted in a dramatic decrease in their body weight [40]. The increased SCD-1 expression in

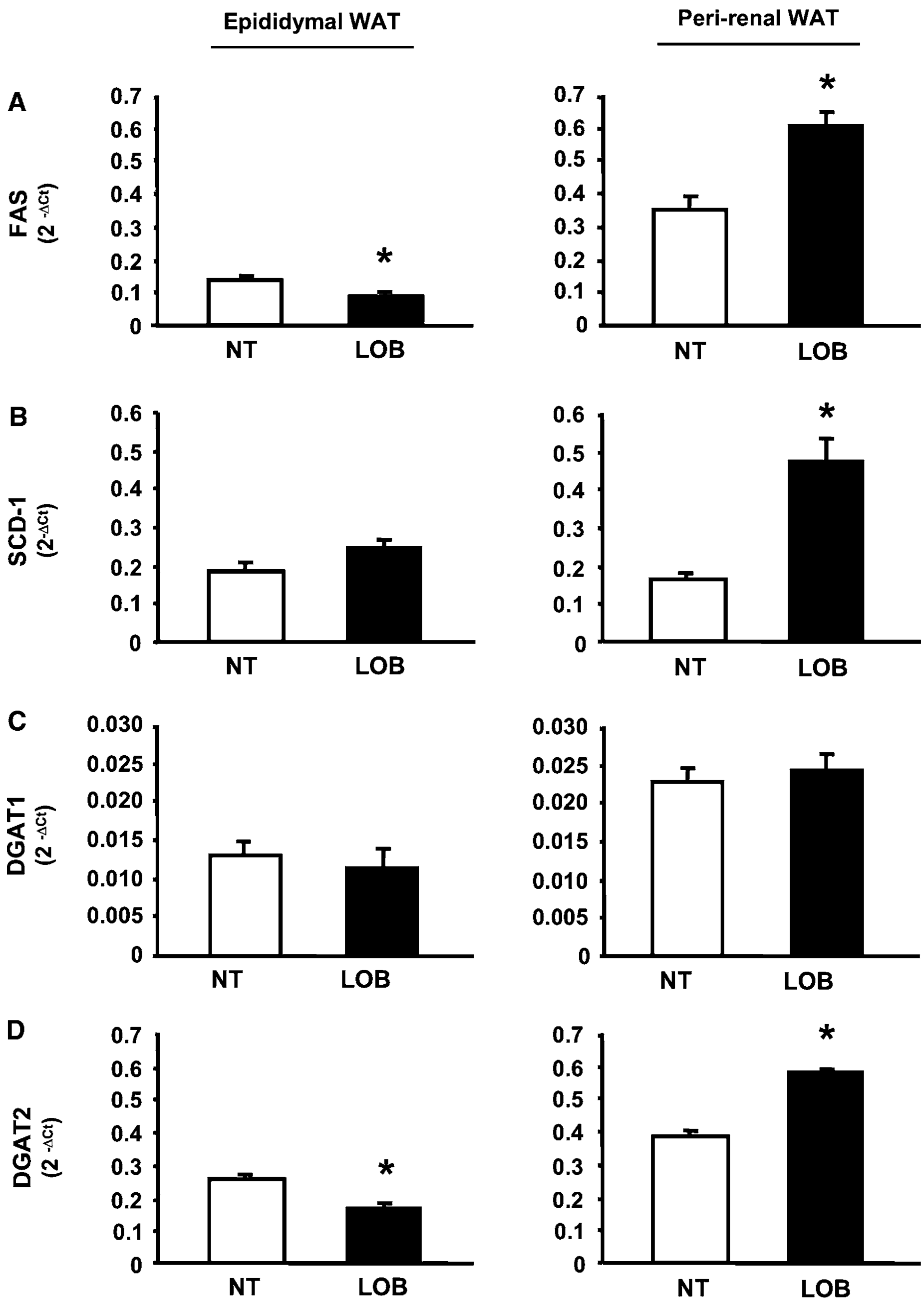

Fig. 6 Adipose tissue mRNA expression. Epididymal and peri-renal white adipose tissue (WAT) mRNA expression of FAS (**a**), SCD-1 (**b**), DGAT1 (**c**), DGAT2 (**d**) in 10- to 12-month LOB rats compared with non-transgenic littermates (NT). The animals were sacrificed between 0900 and 1100 hours without prior fasting. The mRNA levels were measured with Applied Biosystems 7500 Real-Time PCR System (96 wells). All samples were analysed in triplicates and expression data normalized against the endogenous control 36B4. Results are presented as means ± SEM, $n = 4$–6. *$P < 0.05$ LOB versus NT rats (unpaired Student's *t*-test)

liver and peri-renal WAT in LOB males may thus contribute to their specific increase in peri-renal WAT.

In the LOB rat, β-adrenergic stimulated lipolysis was lower in peri-renal and epididymal WAT compared with NT rats. Non-stimulated or basal lipolysis was significantly lower in the epididymal depot and tended to be lower also in peri-renal WAT. Since the peri-renal depot is preferentially enlarged in LOB rats, differences in lipolysis cannot fully explain the growth of that WAT. Interestingly, corresponding results were obtained with young males before their obese phenotype is evident. This finding suggests that both peri-renal and epididymal WAT depots in young non-obese LOB male rats are predisposed to a reduced lipolytic response. Recently, it was reported that isolated adipocytes derived from the subcutaneous depot of obese subjects were larger and showed unchanged catecholamine-induced lipolysis but markedly enhanced basal lipolysis [41]. Insulin resistant ob/ob mice and Zucker rats also display increased adipocyte size and increased basal lipolysis per cell [13, 42, 43]. Therefore, the lower basal lipolysis observed in LOB rats is in sharp contrast to the findings in obese humans and obese insulin resistant rodents [10] and again could contribute to a preserved insulin sensitivity [1].

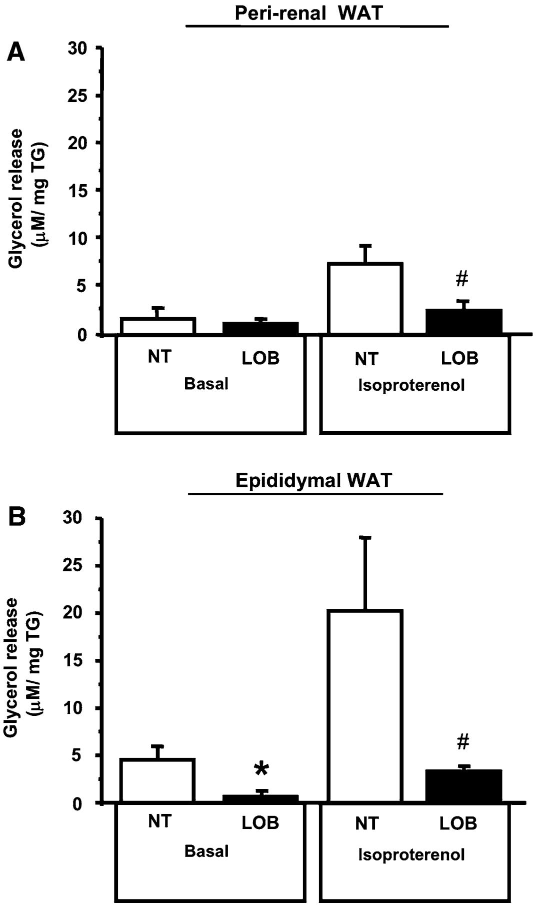

Fig. 7 Basal and β-adrenergic stimulated lipolysis in white adipose tissue (WAT). Peri-renal and epididymal WAT depots were freshly dissected and adipocytes acutely isolated by collagenase incubation. Incubation was then performed in absence (basal lipolysis) or presence of isoproterenol (10^{-5} M). Glycerol release from isolated adipocytes was used as an index of lipolysis. Basal and β-adrenergic stimulated lipolysis in peri-renal WAT (**a**) and epididymal WAT (**b**) from 12-month-old LOB and NT rats were investigated. Results are presented as means ± SEM. Peri-renal lipolysis was investigated in five LOB and three NT rats, while epididymal WAT lipolysis was investigated in five NT and five LOB rats. Comparisons between groups were made by one-way analysis of variance (ANOVA), followed by Bonferroni test between individual groups. $^{*}P < 0.05$ basal lipolysis LOB versus NT rats, $\#P < 0.05$ β-adrenergic stimulated lipolysis LOB versus NT rats

Another important factor for insulin sensitivity is the adipocyte-derived hormone adiponectin [5]. Obese humans and obese insulin resistant rodent models show decreased adipose expression of adiponectin mRNA and plasma adiponectin levels [30, 44, 45]. In contrast, LOB rats have elevated plasma adiponectin levels [10]. We report here that adiponectin mRNA expression is unchanged suggesting the increased plasma levels of adiponectin in LOB rats is primarily due to expanded visceral WAT mass. Recently, ob/ob mice over-expressing adiponectin were shown to become even more obese but with improved insulin sensitivity [46]. Similar to LOB rats, the adiponectin transgenic ob/ob mice showed smaller adipocytes and increased DGAT1 expression and LPL activity in WAT [46]. Thus, the LOB rat resembles this adiponectin transgenic ob/ob mouse.

In summary, LOB male rats show increased hepatic TAG production, a shift in LPL activity from skeletal muscle to WAT, reduced TAG lipolysis in WAT depots and a specific increase in genes responsible for fatty acid and TAG synthesis in the peri-renal depot.

Several findings in the old obese LOB rat were also observed in the young lean animals, including reduced lipolysis and altered expression of genes involved in lipogenesis and TAG synthesis, indicating that the obesity per se was not the cause of these hepatic and adipose tissue-specific changes in lipid metabolism in the LOB rat.

In view of the most surprising feature of the LOB phenotype, that obese LOB male rats exhibit enhanced insulin sensitivity [10], it seems likely that the quality of the adipose tissue is most important for the metabolic consequences of obesity. Thus, enhanced capacity of TAG production, decreased or unchanged basal lipolysis and preserved adiponectin expression of adipocytes would be part of a response that hinders fatty acids from ectopic storage and the subsequent development of insulin resistance.

Acknowledgments We are grateful to Birgitta Odén for technical assistance. This work was supported by grants 8269 (SE) and 14291 (JO) from the Swedish Medical Research Council and the Swedish Heart and Lung Foundation.

References

1. Heilbronn L, Smith SR, Ravussin E (2004) Failure of fat cell proliferation, mitochondrial function and fat oxidation results in ectopic fat storage, insulin resistance and type II diabetes mellitus. Int J Obes Relat Metab Disord 28(Suppl 4):S12–S21
2. Unger RH (2003) Lipid overload and overflow: metabolic trauma and the metabolic syndrome. Trends Endocrinol Metab 14:398–403
3. Lewis GF, Carpentier A, Adeli K, Giacca A (2002) Disordered fat storage and mobilization in the pathogenesis of insulin resistance and type 2 diabetes. Endocr Rev 23:201–229
4. Kahn BB, Flier JS (2000) Obesity and insulin resistance. J Clin Invest 106:473–481
5. Kadowaki T, Yamauchi T (2005) Adiponectin and adiponectin receptors. Endocr Rev 26:439–451
6. Taskinen MR (2005) Type 2 diabetes as a lipid disorder. Curr Mol Med 5:297–308
7. Fukuda N, Azain MJ, Ontko JA (1982) Altered hepatic metabolism of free fatty acids underlying hypersecretion of very low density lipoproteins in the genetically obese Zucker rats. J Biol Chem 257:14066–14072
8. Elam MB, von Wronski MA, Cagen L, Thorngate F, Kumar P, Heimberg M, Wilcox HG (1999) Apolipoprotein B mRNA editing and apolipoprotein gene expression in the liver of

hyperinsulinemic fatty Zucker rats: relationship to very low density lipoprotein composition. Lipids 34:809–816

9. Bartels ED, Lauritsen M, Nielsen LB (2002) Hepatic expression of microsomal triglyceride transfer protein and in vivo secretion of triglyceride-rich lipoproteins are increased in obese diabetic mice. Diabetes 51:1233–1239
10. Bains RK, Wells SE, Flavell DM, Fairhall KM, Strom M, Le Tissier P, Robinson IC (2004) Visceral obesity without insulin resistance in late-onset obesity rats. Endocrinology 145:2666–2679
11. Wells SE, Flavell DM, Bisset GW, Houston PA, Christian H, Fairhall KM, Robinson IC (2003) Transgenesis and neuroendocrine physiology: a transgenic rat model expressing growth hormone in vasopressin neurones. J Physiol 551:323–336
12. Kaplan ML, Trout JR, Leveille GA (1976) Adipocyte size distribution in ob/ob mice during preobese and obese phases of development. Proc Soc Exp Biol Med 153:476–482
13. Okuno A, Tamemoto H, Tobe K, Ueki K, Mori Y, Iwamoto K, Umesono K, Akanuma Y, Fujiwara T, Horikoshi H, Yazaki Y, Kadowaki T (1998) Troglitazone increases the number of small adipocytes without the change of white adipose tissue mass in obese Zucker rats. J Clin Invest 101:1354–1361
14. Oscarsson J, Olofsson SO, Bondjers G, Eden S (1989) Differential effects of continuous versus intermittent administration of growth hormone to hypophysectomized female rats on serum lipoproteins and their apoproteins. Endocrinology 125:1638–1649
15. Sjoberg A, Oscarsson J, Olofsson SO, Eden S (1994) Insulin-like growth factor-I and growth hormone have different effects on serum lipoproteins and secretion of lipoproteins from cultured rat hepatocytes. Endocrinology 135:1415–1421
16. Frick F, Linden D, Ameen C, Eden S, Mode A, Oscarsson J (2002) Interaction between growth hormone and insulin in the regulation of lipoprotein metabolism in the rat. Am J Physiol Endocrinol Metab 283:E1023–E1031
17. Frick F, Bohlooly YM, Linden D, Olsson B, Tornell J, Eden S, Oscarsson J (2001) Long-term growth hormone excess induces marked alterations in lipoprotein metabolism in mice. Am J Physiol Endocrinol Metab 281:E1230–E1239
18. Li X, Catalina F, Grundy SM, Patel S (1996) Method to measure apolipoprotein B-48 and B-100 secretion rates in an individual mouse: evidence for a very rapid turnover of VLDL and preferential removal of B-48- relative to B-100-containing lipoproteins. J Lipid Res 37:210–220
19. Bligh EG, Dyer WJ (1959) A rapid method of total lipid extraction and purification. Can J Biochem Physiol 37:911–917
20. Peterson J, Olivecrona T, Bengtsson-Olivecrona G (1985) Distribution of lipoprotein lipase and hepatic lipase between plasma and tissues: effect of hypertriglyceridemia. Biochim Biophys Acta 837:262–270
21. Spooner PM, Garrison MM, Scow RO (1977) Regulation of mammary and adipose tissue lipoprotein lipase and blood triacylglycerol in rats during late pregnancy. Effect of prostaglandins. J Clin Invest 60:702–708
22. Rodbell M, Krishna G (1974) Preparation of isolated fat cells and fat cell "ghosts"; methods for assaying adenylate cyclase activity and levels of cyclic AMP. Methods Enzymol 31:103–114
23. Gause I, Eden S, Isaksson O, DiGirolamo M, Smith U (1985) Changes in growth hormone binding and metabolic effects of growth hormone in rat adipocytes following hypophysectomy. Acta Physiol Scand 124:229–238
24. Dole VP, Meinerz H (1960) Microdetermination of long-chain fatty acids in plasma and tissues. J Biol Chem 235:2595–2599
25. Preiss-Landl K, Zimmermann R, Hammerle G, Zechner R (2002) Lipoprotein lipase: the regulation of tissue specific expression and its role in lipid and energy metabolism. Curr Opin Lipidol 13:471–481
26. Maeda N, Takahashi M, Funahashi T, Kihara S, Nishizawa H, Kishida K, Nagaretani H, Matsuda M, Komuro R, Ouchi N, Kuriyama H, Hotta K, Nakamura T, Shimomura I, Matsuzawa Y (2001) PPARgamma ligands increase expression and plasma concentrations of adiponectin, an adipose-derived protein. Diabetes 50:2094–2099
27. Hotamisligil GS, Johnson RS, Distel RJ, Ellis R, Papaioannou VE, Spiegelman BM (1996) Uncoupling of obesity from insulin resistance through a targeted mutation in aP2, the adipocyte fatty acid binding protein. Science 274:1377–1379
28. Uysal KT, Scheja L, Wiesbrock SM, Bonner-Weir S, Hotamisligil GS (2000) Improved glucose and lipid metabolism in genetically obese mice lacking aP2. Endocrinology 141:3388–3396
29. Oakes ND, Thalen PG, Jacinto SM, Ljung B (2001) Thiazolidinediones increase plasma-adipose tissue FFA exchange capacity and enhance insulin-mediated control of systemic FFA availability. Diabetes 50:1158–1165
30. Altomonte J, Harbaran S, Richter A, Dong H (2003) Fat depot-specific expression of adiponectin is impaired in Zucker fatty rats. Metabolism 52:958–963
31. Linden D, William-Olsson L, Ahnmark A, Ekroos K, Hallberg C, Sjogren HP, Becker B, Svensson L, Clapham JC, Oscarsson J, Schreyer S (2006) Liver-directed overexpression of mitochondrial glycerol-3-phosphate acyltransferase results in hepatic steatosis, increased triacylglycerol secretion and reduced fatty acid oxidation. Faseb J 20:434–443
32. Yamazaki T, Sasaki E, Kakinuma C, Yano T, Miura S, Ezaki O (2005) Increased very low density lipoprotein secretion and gonadal fat mass in mice overexpressing liver DGAT1. J Biol Chem 280:21506–21514
33. Yu XX, Murray SF, Pandey SK, Booten SL, Bao D, Song XZ, Kelly S, Chen S, McKay R, Monia BP, Bhanot S (2005) Antisense oligonucleotide reduction of DGAT2 expression improves hepatic steatosis and hyperlipidemia in obese mice. Hepatology 42:362–371
34. Phung TL, Roncone A, Jensen KL, Sparks CE, Sparks JD (1997) Phosphoinositide 3-kinase activity is necessary for insulin-dependent inhibition of apolipoprotein B secretion by rat hepatocytes and localizes to the endoplasmic reticulum. J Biol Chem 272:30693–30702
35. Bessesen DH, Robertson AD, Eckel RH (1991) Weight reduction increases adipose but decreases cardiac LPL in reduced-obese Zucker rats. Am J Physiol 261:E246–251
36. Hartman AD (1981) Lipoprotein lipase activities in adipose tissues and muscle in the obese Zucker rat. Am J Physiol 241:E108–E115
37. Cases S, Stone SJ, Zhou P, Yen E, Tow B, Lardizabal KD, Voelker T, Farese RV Jr (2001) Cloning of DGAT2, a second mammalian diacylglycerol acyltransferase, and related family members. J Biol Chem 276:38870–38876
38. Suzuki R, Tobe K, Aoyama M, Sakamoto K, Ohsugi M, Kamei N, Nemoto S, Inoue A, Ito Y, Uchida S, Hara K, Yamauchi T, Kubota N, Terauchi Y, Kadowaki T (2005) Expression of DGAT2 in white adipose tissue is regulated by central leptin action. J Biol Chem 280:3331–3337
39. Diraison F, Dusserre E, Vidal H, Sothier M, Beylot M (2002) Increased hepatic lipogenesis but decreased expression of lipogenic gene in adipose tissue in human obesity. Am J Physiol Endocrinol Metab 282:E46–51
40. Ntambi JM, Miyazaki M (2004) Regulation of stearoyl-CoA desaturases and role in metabolism. Prog Lipid Res 43:91–104
41. Langin D, Dicker A, Tavernier G, Hoffstedt J, Mairal A, Ryden M, Arner E, Sicard A, Jenkins CM, Viguerie N, van Harmelen V, Gross RW, Holm C, Arner P (2005) Adipocyte lipases and defect of lipolysis in human obesity. Diabetes 54:3190–3197

42. Jolly SR, Lech JJ, Menahan LA (1978) Influence of genetic obesity in mice on the lipolytic response of isolated adipocytes to isoproterenol and ACTH-(1–24). Horm Metab Res 10:223–227
43. Lebrazi H, Chomard P, Dumas P, Autissier N (1990) Lipolysis in isolated epididymal adipocytes from genetically obese Zucker rat treated with 3,5,3′-L-triiodothyronine. Acta Endocrinol (Copenh) 122:379–384
44. Hu E, Liang P, Spiegelman BM (1996) AdipoQ is a novel adipose-specific gene dysregulated in obesity. J Biol Chem 271:10697–10703
45. Milan G, Granzotto M, Scarda A, Calcagno A, Pagano C, Federspil G, Vettor R (2002) Resistin and adiponectin expression in visceral fat of obese rats: effect of weight loss. Obes Res 10:1095–1103
46. Kim JY, van de Wall E, Laplante M, Azzara A, Trujillo ME, Hofmann SM, Schraw T, Durand JL, Li H, Li G, Jelicks LA, Mehler MF, Hui DY, Deshaies Y, Shulman GI, Schwartz GJ, Scherer PE (2007) Obesity-associated improvements in metabolic profile through expansion of adipose tissue. J Clin Invest 117:2621–2637

Lipids (2008) 43:325–333
DOI 10.1007/s11745-008-3157-6

ORIGINAL ARTICLE

Eicosapentaenoic Acid Supplementation for Chronic Hepatitis C Patients During Combination Therapy of Pegylated Interferon α-2b and Ribavirin

Aiko Kawashima · Ikuyo Tsukamoto · Tomoko Koyabu · Yasuko Murakami · Takayo Kawakami · Naoko Kakibuchi · Kouichi Takaguchi · Keiji Kita · Misako Okita

Received: 30 July 2007 / Accepted: 25 January 2008 / Published online: 5 March 2008
© AOCS 2008

Abstract Eicosapentaenoic acid (EPA) (1.8 g/day) was administered to 12 chronic hepatitis C patients receiving combination therapy of pegylated interferon (PEG-IFN) α-2b and ribavirin for 48 weeks (EPA group). Twelve patients were not administered EPA (control group). All patients also received vitamin E and C (300, 600 mg/day, respectively) during the therapy. Serum alanine aminotransferase improved to a normal level in 8 of 12 patients from the EPA group and 6 of 12 patients from the control group after 12 weeks. Lymphocyte counts decreased significantly after 8 weeks in the control group, but not the EPA group. T-helper (Th) 1 decreased after 4 weeks in the control group, but not in the EPA group (two-way ANOVA; $P < 0.05$). Th1/Th2 ratios were elevated in 9 of 12 patients in the EPA group, and 3 out of 12 in the control group ($P < 0.05$) after 8 weeks. After 12 weeks, the arachidonic acid/EPA molar ratio of erythrocyte membrane phospholipid correlated negatively with the leukocyte count ($n = 24$, $r = -0.439$, $P < 0.05$) and the neutrophil count ($n = 24$, $r = -0.671$, $P < 0.02$). The hemoglobin level improved after 48 weeks compared with 24 weeks in only the EPA group. These findings suggest that EPA supplementation may be useful in therapy for chronic hepatitis C.

Keywords Eicosapentaenoic acid · Chronic hepatitis C patients · Pegylated interferon α-2b · Erythrocyte membrane · Leukocyte

A. Kawashima (✉) · I. Tsukamoto · M. Okita
Department of Natural Science and Ecological Awareness,
Graduate School of Humanities and Sciences,
Nara Women's University, Kitauoyanishimachi,
Nara 630-8506, Japan
e-mail: faa_kawashima@cc.nara-wu.ac.jp

T. Koyabu · Y. Murakami · T. Kawakami
Department of Nutritional Science,
Faculty of Health and Welfare Science,
Okayama Prefectural University,
Soja 719-1197, Japan

N. Kakibuchi
Department of Food and Nutrition, Setouchi Junior College,
Mitoyo 767-8511, Japan

K. Takaguchi
Department of Internal Medicine,
Kagawa Prefectural Central Hospital,
Takamatsu 760-8557, Japan

K. Kita
Kita Clinic, Takamatsu 761-0104, Japan

Introduction

Hepatitis C virus (HCV) infection is one of the main causes of chronic liver disease and the most common cause of hepatocellular carcinoma [1, 2]. Increased oxidative stress caused by mitochondrial injury [3], hepatocellular iron accumulation [4], and the direct effect of the HCV core protein [5], in addition to reactive oxygen species production related to the immune response [6], are reported in HCV-infected patients, and enhanced oxidative stress has been shown to be involved in the progression to hepatic fibrosis and hepatocellular carcinoma [7–10]. In a previous study, we observed decreased polyunsaturated fatty acids (PUFA) in phospholipids of mononuclear cells and plasma α-tocopherol, and increased thiobarbituric acid reactive substances (TBARS) in HCV-infected patients, and suggested that these findings may accompany enhanced oxidative stress [11]. Improvement in fatty acid composition and the serum alanine aminotransferase (ALT) level was observed in HCV-infected patients who were administered vitamin E [12], and a significant decrease in eicosapentaenoic acid (EPA) in phospholipids of mononuclear cells during combination therapy of interferon (IFN) α-2b and ribavirin and a significant correlation between the arachidonic acid (ARA)/EPA molar ratio and the serum ALT level were seen in chronic hepatitis C patients [13].

A major therapeutic goal in HCV-infected patients is to achieve early eradication of the virus, and combination therapy using pegylated (PEG)-IFN α-2b and ribavirin induces a higher sustained virological response than interferon monotherapy [14, 15]. However, hematological abnormalities, mainly hemolytic anemia resulting from the oxidative damage to membranes, are a known side effect of combination therapy [15, 16].

The deformability and vulnerability of erythrocyte membranes to oxidative stress is affected by the fatty acid composition of membrane phospholipids [17]. Dietary n-3 PUFA has been shown to influence signaling complexes and to suppress T-cell cytokines in vivo by altering T-cell raft composition [18]. EPA has a wide variety of physiological actions such as regulating the T-helper (Th) 1-type response associated with chronic inflammatory disease and antagonizing the production of inflammatory eicosanoids from ARA [19]. EPA supplementation in patients with chronic hepatitis C is reported to improve ribavirin-related anemia [20], and it was suggested that the increased EPA level in erythrocyte membranes may be associated with increased membrane fluidity and viscoelastic properties of erythrocyte membranes [21]. We also reported that EPA supplementation improved the serum ALT level and prevented a decrease in lymphocyte counts, which were significantly decreased from the baseline during the treatment in non-EPA supplemented patients receiving combination therapy of IFN α-2b and ribavirin, and suggested the usefulness of EPA supplementation for the treatment of HCV-infected patients [22]. However, longer and more detailed research is required to confirm its efficacy.

The aim of the present study was to confirm the effectiveness of EPA supplementation combined with vitamin E and C for the prevention of hematological abnormalities and improve the immune cell response in chronic hepatitis C patients receiving PEG-IFN α-2b and ribavirin combination therapy. Therefore, we administered EPA with vitamin E and C for 48 weeks, and examined the effects on hematological and immunological parameters.

Experimental Procedures

Subjects

Twenty-four chronic hepatitis C patients with genotype 1b and high viral load ($\geq 10^5$ IU/ml) (13 males and 11 females) treated at Kagawa Prefectural Central Hospital were enrolled in the present study. Patients with detectable hepatitis B virus surface antigen, other potential causes of chronic liver disease, human immunodeficiency virus infection, poorly controlled diabetes mellitus, or cardiovascular disease were excluded.

Study Design

We obtained written informed consent from all patients and randomized them into an EPA supplementation group (EPA group: seven males and five females, 62.5 ± 2.5 year) and a no supplementation group (control group: six males and six females, 56.7 ± 2.4 year). Patients in the EPA group received 1,800 mg/day of EPA ethyl ester (EPADEL S600, Mochida Pharmaceutical Co. Ltd., Tokyo, Japan). Six capsules (300 mg EPA ethyl ester/capsule) were administered per day orally after three meals (two capsules after each meal) for 48 weeks. All patients in both groups received 300 mg/day of vitamin E (Juvela, one tablet contains 50 mg of tocopherol acetate, Eisai, Tokyo, Japan) and 600 mg/day of vitamin C (Cinal, one packet contains 200 mg of ascorbic acid, SHIONOGI & CO., LTD., Osaka, Japan) orally, in addition to injections of PEG-IFN α-2b (PegIntron, Schering-Plough K. K., Osaka, Japan) once a week for 48 weeks, and daily oral ribavirin (Revetol, Schering-Plough K. K., Osaka, Japan) for 48 weeks. At the baseline no significant differences were observed in the distribution of the histological diagnosis for grading inflammation or staging fibrosis. Patients graded as inflammation 1, 2, 3 and unknown included 7, 1, 2 and 2 in the EPA group and 7, 4, 1 and 0 in the control group, respectively, and the number of patients staged as 1, 2, 3, 4 and unknown included 2, 3, 3, 2 and 2 in the EPA group and 4, 5, 1, 2 and 0 in the control group. The patients were required to avoid iron or other antioxidant supplements during the treatment period.

Blood samples were obtained from each patient immediately before the initiation of therapy (0 week) and 4, 8, 12, 24 and 48 weeks after the start of therapy.

The experiment was designed in accordance with the principles of the Declaration of Helsinki of the World Medical Association and was approved by the Ethics Committee of Kagawa Prefectural Central Hospital.

Analytical Methods

We determined routine clinical laboratory parameters, such as erythrocyte, leukocyte and platelet counts, hemoglobin level, and serum ALT and aspartate aminotransferase (AST) activities. Flow cytometry was used to characterize and distinguish CD^{4+} T cells as Th1 or Th2, as defined by their cytokine production (IFN-γ and IL-4, respectively). To determine the rate of blastogenesis of lymphocytes by phytohemagglutinin (PHA), lymphocytes isolated from heparinized peripheral blood were used. After adding PHA (10 μg/ml), lymphocytes (1×10^5 counts) were incubated for 64 h at 37 °C under 5% CO_2. Then, ^{3}H-thymidine was added and they were incubated for 8 more hours. After harvesting the cells, ^{3}H-thymidine incorporated into cells was determined using a liquid scintillation counter. The ratio of ^{3}H-thymidine incorporation into PHA-treated cells to the control without PHA was calculated [stimulation index (SI)].

Plasma was separated by centrifugation of blood samples containing EDTA-2Na at 1,600×g for 15 min at 4 °C. The erythrocyte layer was drawn off into another tube and washed three times with saline (4 °C) to determine the fatty acid composition in erythrocyte membrane phospholipids. All samples were stored at −80 °C until assayed.

The α-tocopherol concentration in plasma was determined according to a modification of the method of Milne et al. [23], as described previously.

Total lipids were extracted from erythrocyte membranes suspended in saline by the method of Bligh and Dyer [24]. Phospholipids were separated by one-dimensional thin-layer chromatography using a silica gel plate (Silica Gel 60; Merck, Darmstadt, Germany) and a solvent system of petroleum ether/ethyl ether/acetic acid (80:20:1, v/v). The spots corresponding to phospholipids were scraped from the plate and transmethylated for 2 h at 90 °C using acetylchloride:methanol (5:50, v/v). A known amount of heptadecanoic acid (17:0) was used as an internal standard. Fatty acid methyl esters were analyzed by gas-chromatography (Model GC-14A; Shimazu, Kyoto, Japan) as described previously [12].

Statistical Analysis

Values are expressed as the means ± standard errors (SE). Statistical analyses were done using SPSS v. 13.0 (SPSS Inc., Chicago, IL, USA). Two-way ANOVA was performed to assess the presence or absence of an EPA × time interaction. Significance of difference during the treatment was examined using Friedman's test followed by Wilcoxon *t* test with Bonferroni correction post hoc analysis. Group differences were tested for significance using the Mann–Whitney *U* test. Differences between observed and expected frequency were tested using Fisher's test. Correlation coefficients were calculated using Spearman's rank-correlation analysis. All *P* values are two-tailed and values of $P < 0.05$ were taken as indicating significance.

Results

Completion of the Assigned Therapy

Four patients in the control group changed hospitals after 24 weeks and discontinued the treatment. Two patients in each group discontinued the treatment between 24 weeks and 37 weeks under the direction of a physician, because they had no virologic response. One patient in the EPA group changed therapeutic measures because of neuropsychiatric symptoms after 30 weeks under the advice of a doctor. Consequently, in this study, all patients were analyzed until 12 weeks for the early response, and the long-term observation results of 15 patients (6 patients in the control group and 9 patients in the EPA group) were analyzed until the end of therapy (48 weeks).

Clinical Data up to 12 weeks

BMI and clinical data up to 12 weeks of therapy are shown in Table 1. No significant differences were observed in the dose of PEG-IFN α-2b or ribavirin during treatment between the two groups. The serum ALT level decreased significantly in the EPA group ($P < 0.01$), but not in the control group. The blood cells were significantly decreased during the therapy in both groups (Friedman's test). However several differences were observed between the groups. In the control group, the lymphocyte count decreased significantly after 8 weeks, whereas no significant decrease was observed in the EPA group. The neutrophil count decreased significantly after 8 weeks of therapy in both groups; however, the counts in the EPA group were significantly higher than those in the control group at 8 weeks and 12 weeks. The platelet count in the EPA group was significantly decreased only at 4 weeks and was maintained the basal level thereafter, whereas a significant decrease was observed throughout the observation period in the control group. The hemoglobin level decreased significantly following 4 weeks of therapy in both groups. Serum albumin did not change throughout therapy in either group. The plasma α-tocopherol level increased significantly at 4 weeks and was maintained at a high level throughout therapy in both groups.

T Cell Subsets and Lymphocyte Blastogenesis up to 8 weeks

The Th1 in the control group decreased significantly ($P < 0.05$), but the Th1 in the EPA group was maintained at the basal level during the observation periods (two-way ANOVA; $P < 0.05$, Table 2). As a result, the Th1/Th2 balance improved in the EPA group compared with the

Table 1 BMI and clinical data during therapy

	Group	PEG-IFN α-2b and ribavirin combination therapy				Friedman's test *P*
		0 week	4 weeks	8 weeks	12 weeks	
BMI (kg/m^2)	Control	24.7 ± 1.0	24.3 ± 1.0	24.0 ± 1.0*	23.7 ± 0.9*	<0.001
	EPA	23.4 ± 0.8	22.8 ± 0.8*	22.7 ± 0.8*	22.6 ± 0.7*	<0.001
Albumin (g/dL)	Control	3.8 ± 0.1	3.8 ± 0.1	3.8 ± 0.1	3.8 ± 0.1	NS
	EPA	3.8 ± 0.1	3.8 ± 0.1	3.8 ± 0.1	3.8 ± 0.1	NS
ALT (U/L)	Control	61 ± 7	40 ± 8	39 ± 8	44 ± 8	NS
	EPA	102 ± 20	54 ± 10	48 ± 10*	50 ± 11*	<0.01
Erythrocytes (×10^4/μL)	Control	446 ± 14	408 ± 16*	378 ± 16**	360 ± 18**	<0.0001
	EPA	443 ± 9	402 ± 9*	376 ± 9*	373 ± 11**	<0.0001
Hemoglobin (g/dL)	Control	13.9 ± 0.3	12.7 ± 0.4*	11.8 ± 0.4**	11.3 ± 0.4**	<0.0001
	EPA	14.0 ± 0.3	12.6 ± 0.2*	11.9 ± 0.2*	11.9 ± 0.3**	<0.0001
Leukocytes (/μL)	Control	5,033 ± 267	3,617 ± 328*	3,300 ± 273**	3,108 ± 233**	<0.001
	EPA	5,492 ± 418	4,150 ± 247*	3,858 ± 202*	3,758 ± 243*	<0.001
Lymphocytes (/μL)	Control	2,183 ± 222	1,926 ± 242	1,692 ± 221*	1,488 ± 194*	<0.001
	EPA	2,152 ± 216	1,968 ± 148	1,711 ± 134	1,583 ± 163	<0.05
Neutrophils (/μL)	Control	2,178 ± 154	1,233 ± 172	1,162 ± 106*	1,135 ± 66*	<0.01
	EPA	2,676 ± 248	1,658 ± 157	1,624 ± 138*,***	1,692 ± 107*,****	<0.01
Platelets (×10^4/μL)	Control	18.0 ± 1.5	13.6 ± 1.3**	13.4 ± 1.0**	13.9 ± 1.2**	<0.0001
	EPA	15.8 ± 1.5	12.4 ± 1.2*	13.3 ± 1.6	13.3 ± 1.5	<0.05
Plasma α-tocopherol (μg/mL)	Control	7.6 ± 0.5	15.1 ± 0.7*	17.4 ± 1.6*	15.8 ± 1.4*	<0.001
	EPA	8.6 ± 0.8	18.3 ± 1.3**	19.6 ± 1.3**	18.1 ± 1.2**	<0.001

Mean ± SE

BMI body mass index, *ALT* alanine aminotransferase

* $P < 0.05$; ** $P < 0.01$, compared with 0 week (Friedman's test followed by Wilcoxon's test with Bonferroni correction); *** $P < 0.05$; **** $P < 0.001$; compared with control group (Mann–Whitney *U*-test), control group; $n = 12$, EPA group; $n = 12$

Table 2 T cell subsets and lymphocyte blastogenesis during therapy

	Group	PEG-IFN α-2b and ribavirin combination therapy			Friedman's test *P*
		0 week	4 weeks	8 weeks	
T helper 1 (%)	Control	36.3 ± 2.8	33.9 ± 2.8*	32.5 ± 2.7**	<0.05
	EPA	34.0 ± 3.9	35.8 ± 4.0	35.7 ± 1.7	NS
T helper 2 (%)	Control	2.0 ± 0.2	1.8 ± 0.2	2.0 ± 0.2	NS
	EPA	1.7 ± 0.2	1.8 ± 0.2	1.7 ± 0.2	NS
PHA$^+$ (CPM)	Control	35,321 ± 3,050	33,133 ± 2,612	33,919 ± 2902	NS
	EPA	34,042 ± 2,437	36,376 ± 2,251	35,955 ± 3,249	NS
PHA$^-$ (CPM)	Control	285 ± 50	293 ± 54	237 ± 32	NS
	EPA	255 ± 45	184 ± 14	210 ± 38	NS
SI (PHA$^+$/PHA$^-$)	Control	169.2 ± 30.2	149.5 ± 26.7	172.0 ± 27.7	NS
	EPA	183.4 ± 35.0	211.2 ± 20.5***	214.5 ± 38.2	NS

Mean ± SE

PHA phytohemagglutinin, *SI* stimulation index, % percentage of lymphocytes

** $P < 0.01$, * $P < 0.05$; compared with 0 week (Friedman's test followed by Wilcoxon's test with Bonferroni correction). *** $P < 0.05$ compared with control group (Mann–Whitney *U* test), control group; $n = 12$, EPA group; $n = 12$

control group, as shown in Fig. 1. The SI of the PHA-induced lymphocyte blast formation test in the EPA group was significantly higher compared with that of the control group at 4 weeks of therapy, but the SI did not increase significantly during therapy in either group. HCV RNA disappeared in 3 of 12 (25.0%) in the EPA group and 5 of

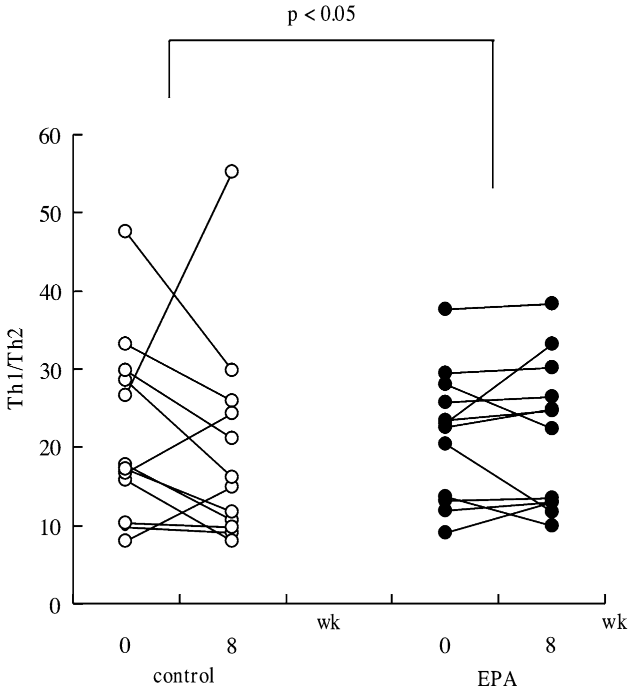

Fig. 1 Th1/Th2 ratio in the EPA group (*filled circles*), and the control group (*open circles*), before and after 8 weeks of treatment. A significant increase was observed in the EPA group compared with the control group (Fisher's test)

12 (41.7%) in the control group at 12 weeks ($P > 0.50$, Fisher's test).

Fatty Acid Composition of Erythrocyte Membrane Phospholipids up to 12 weeks

In the EPA group, EPA and docosapentaenoic acid (DPA) increased significantly ($P < 0.01$, respectively) after EPA supplementation and the EPA level was elevated to two times the basal level after 12 weeks, but in the control group, EPA did not change during therapy (Table 3). Conversely, the ARA/EPA ratio decreased markedly only in the EPA group (two-way ANOVA; $P < 0.05$).

Correlation between Clinical Data and ARA/EPA Ratio in Phospholipids of the Erythrocyte Membrane after 12 weeks

Considering all individuals as a group, negative correlations between ARA/EPA ratio in erythrocyte membrane phospholipids and leukocyte count ($n = 24$, $r = -0.439$, $P < 0.05$) and neutrophil count ($n = 24$, $r = -0.671$, $P < 0.05$) were observed. Also, the ARA/EPA ratio in erythrocyte membrane phospholipids correlated negatively with lymphocyte count in the control group ($n = 12$, $r = -0.671$, $P < 0.05$), but there was no such correlation in all patients.

Clinical Data at the End of Therapy

Nine subjects in the EPA group (six males and three females, 61.1 ± 3.3 year) and six subjects in the control group (four males and two females, 58.7 ± 2.8 year) were able to continue the treatment for 48 weeks. Erythrocyte count, hemoglobin level and platelet count for 48 weeks are shown in Fig. 2. Erythrocyte count, hemoglobin level and platelet count decreased significantly up to 24 weeks in both groups. In the EPA group, the erythrocyte count tended to improve at 48 weeks of therapy compared with 24 weeks (Fig. 2a). Hemoglobin level and platelet count in the EPA group increased significantly at 48 weeks compared with 24 weeks, but no significant improvement was observed in the control group (Fig. 2b, c). Accordingly, significant increases in hemoglobin level and platelet count were observed in the EPA group compared with the control group at 48 weeks (hemoglobin level; $P < 0.05$, platelet count; $P < 0.05$, Fisher's test). Mean levels of leukocyte count, neutrophil count and lymphocyte count decreased in both groups up to 48 weeks. However, leukocyte and lymphocyte counts increased in five of nine patients in the EPA group and one of six patients in the control group, respectively, although the difference was not significant ($P > 0.10$, Fisher's test). Serum ALT level improved in four of six subjects in the control group and seven of nine subjects in the EPA group by the end of therapy ($P = 1.0$ Fisher's test). At the end of therapy, HCV RNA had disappeared in five of six (83.3%) subjects in the control group and six of nine (66.7%) subjects in the EPA group ($P > 0.5$, Fisher's test).

Discussion

In the present study, we evaluated the effects of EPA supplementation combined with vitamin E and C in chronic hepatitis C patients receiving PEG-IFN α-2b and ribavirin combination therapy for 48 weeks. As shown in Table 3, EPA in erythrocyte membrane phospholipids increased significantly in the patients who received daily oral EPA ethyl ester capsules. Plasma α-tocopherol levels also increased in all patients at 4 weeks after the beginning of therapy. These results reflected good compliance with orally administered EPA and vitamin E.

In IFN α-2b and ribavirin combination therapy, hematologic abnormalities have been observed as a common side effect [25, 26]. Although the mechanism remains uncertain, it may be due to both hemolytic anemia caused by ribavirin [27] and bone marrow suppression caused by IFN [28, 29]. Ribavirin-induced hemolytic anemia is thought to be caused by accumulation of ribavirin in

Table 3 Fatty acid composition (mol%) of phospholipids in erythrocyte membrane during therapy

	Group	PEG-IFN α-2b and ribavirin combination therapy				Friedman's test *P*
		0 week	4 weeks	8 weeks	12 weeks	
18:2n-6	Control	8.64 ± 1.50	7.04 ± 1.37	7.88 ± 1.21	6.94 ± 0.57	NS
	EPA	7.90 ± 1.52	6.55 ± 0.59	7.96 ± 0.83	8.59 ± 0.86	NS
20:4n-6	Control	8.11 ± 0.97	5.65 ± 0.88*	6.82 ± 1.28	8.38 ± 0.77	NS
	EPA	7.15 ± 0.86	5.37 ± 0.59*	5.85 ± 0.72	6.30 ± 0.57****	NS
20:5n-3	Control	1.04 ± 0.15	0.89 ± 0.14	0.78 ± 0.14	1.02 ± 0.15	NS
	EPA	1.02 ± 0.13	1.69 ± 0.16**,***	1.96 ± 0.43**,****	2.14 ± 0.19**,***	<0.01
22:5n-3	Control	1.55 ± 0.65	0.62 ± 0.12*	0.83 ± 0.14	1.18 ± 0.11	NS
	EPA	1.29 ± 0.34	1.12 ± 0.35	1.63 ± 0.37	2.34 ± 0.31**,***	<0.01
22:6n-3	Control	4.81 ± 0.92	3.03 ± 0.68*	4.44 ± 0.67	5.45 ± 0.58	NS
	EPA	3.93 ± 0.52	3.05 ± 0.45	4.92 ± 1.02	4.25 ± 0.62	NS
ARA/EPA	Control	8.67 ± 0.78	7.60 ± 1.13	10.45 ± 1.98	10.56 ± 1.90	NS
	EPA	7.15 ± 0.45	3.22 ± 0.29**,***	4.27 ± 0.83**,***	3.01 ± 0.20**,***	<0.0001

Mean ± SE

ARA arachidonic acid, *EPA* eicosapentaenoic acid

* $P < 0.05$; ** $P < 0.01$, compared with 0 week (Friedman's test followed by Wilcoxon's test with Bonferroni correction); *** $P < 0.01$, **** $P < 0.05$; compared with control group (Mann–Whitney *U* test), Control group; $n = 12$, EPA group; $n = 12$

erythrocytes and oxidative stress in the erythrocyte membrane [30]. In the present study, erythrocyte counts and hemoglobin levels markedly decreased in both groups after 4 weeks of the therapy. However, over long-term (48 weeks) observation, the erythrocyte count tended to increase and the hemoglobin level improved significantly in the EPA group. Although the exact mechanism of these effects was unclear, it is thought that the increased level of EPA may be associated with the increased membrane fluidity and viscoelastic properties of erythrocyte membranes [31, 32], allowing erythrocytes to avoid erythrophagocytic extravascular destruction during IFN and ribavirin combination therapy, as suggested by Ide et al. [20]. The long-term outcome is not yet known, but it is thought that EPA administration over the long-term may improve stability and prevent destruction of erythrocytes.

Poynard et al. [33] reported decreases in leukocyte and lymphocyte counts during IFN therapy either in combination with ribavirin or as monotherapy. In the present study, the lymphocyte count in the EPA group did not decrease compared with the basal level, but the leukocyte count decreased significantly in both groups after 4 weeks of therapy. These results are similar to those in our previous study [22], in which EPA supplementation for 24 weeks in chronic hepatitis C patients receiving combination therapy of IFN α-2b and ribavirin prevented decreases in leukocyte and lymphocyte counts. It was reported that the side effects caused by PEG-IFN α-2b/ribavirin combination therapy were more serious compared with those caused by IFN α-2b because PEG-IFN α-2b is a conjugated protein and its metabolism and excretion are prolonged [15, 25, 26]. This may explain some of the differences between the observations in these past studies and the present study. The neutrophil count was higher in the EPA group compared with the control group at 8 and 12 weeks. The neutrophil count was reported to decline rapidly within the first 2 weeks of therapy [28]. A decrease in the neutrophil count is one of the main causes of therapy discontinuation. The phagocytosis of neutrophils is thought to play a role in virus eradication. Therefore, the prevention of a decrease in neutrophil count by EPA supplementation can be expected to contribute to HCV elimination, but this was unclear in the present study. In addition, the leukocyte count and neutrophil count in all subjects, and lymphocyte count in the control group, correlated negatively with the ARA/EPA ratio in erythrocyte membrane phospholipids. The significantly lower ARA/EPA level observed in the erythrocyte membrane suggests the same effect of EPA supplementation in other cell membranes. EPA supplementation induced significant increases in EPA and DPA, but not docosahexaenoic acid (DHA). Cell membrane phospholipids are characterized by having high PUFAs, such as ARA, EPA and DHA. Changing the fatty acid composition of immune cells affects phagocytosis, T-cell signaling and antigen presentation capability [34], and lipid composition in rafts, especially n-3 PUFAs, modulates immunological cell functions [18].

A high level of T-helper 2 cytokines is observed in chronic hepatitis C patients [30]. Combination therapy aims to increase type 1 cytokine expression in order to

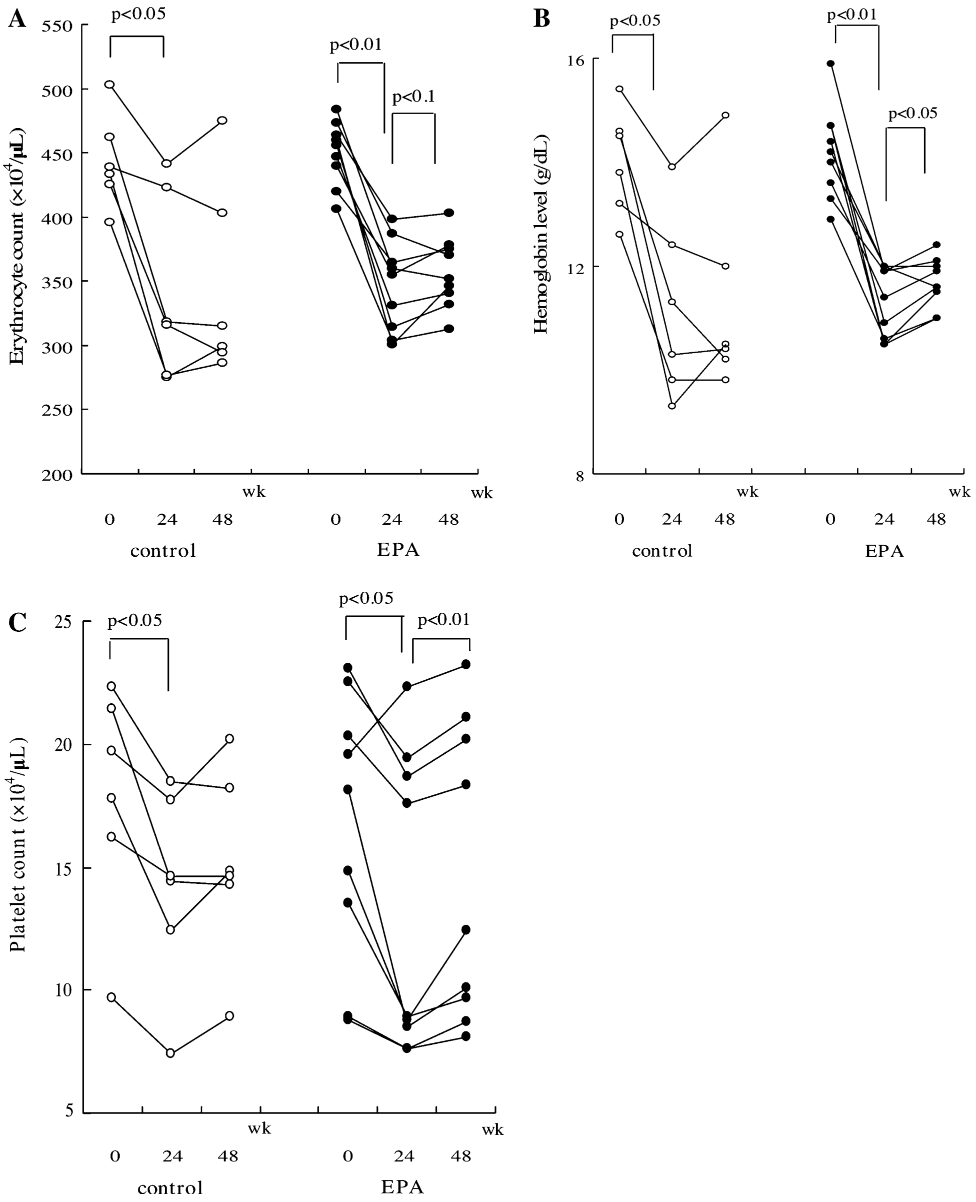

Fig. 2 **a** Erythrocyte count in the patients observed over 48 weeks. EPA group (*filled circles*, $n = 9$) and control group (*open circles*, $n = 6$), Wilcoxon's *t* test. **b** Hemoglobin concentration in the patients observed over 48 weeks. EPA group (*filled circle*, $n = 9$) and control group (*open circle*, $n = 6$), Wilcoxon's *t* test. **c** Platelet count in the patients observed over 48 weeks. EPA group (*filled circle*, $n = 9$) and control group (*open circle*, $n = 6$), Wilcoxon's *t* test

switch the T-cell phenotype from type 2 to type 1, as well as to inhibit the early phase of viral infection [30]. Type 1 cytokines, IL-2, IFN-γ and tumor necrosis factor (TNF)-α induce activation of cytotoxic lymphocytes and recruitment of natural killer cells and macrophages, which induce destruction of HCV-infected cells. It was reported that EPA supplementation had no effect on the proportions of T lymphocytes, T-helper cells, cytotoxic T cells, natural killer cells, or B lymphocytes in healthy subjects [35–37]. In the present study, however, the Th1/Th2 balance was elevated in 75% of subjects in the EPA group at 4 weeks, during the early stage of treatment, and it was higher than in the control group, in which it was elevated in 25% of subjects. Therefore, it is suggested that EPA administration may have beneficial immunomodulatory effects, although no virological effects were observed.

In conclusion, EPA supplementation with vitamins E and C prevented a decrease in the lymphocyte count and elevated the Th1/Th2 balance in the early stage of therapy, and in the long-term, it induced an improvement in the erythrocyte count and hemoglobin level in chronic hepatitis C patients during combination therapy with PEG-IFN α-2b and ribavirin. These observations suggested that EPA supplementation with antioxidative vitamins may be useful when administered with combination therapy for HCV-related chronic hepatitis. More long-term prognosis research should be performed to confirm this treatment.

Acknowledgments This study was supported by Grants-in-Aid for Scientific Research from the Ministry of Education, Culture, Sports, Science and Technology of Japan.

References

1. Tong MJ, EL-Farra NS, Reikes AR, Co RL (1995) Clinical outcomes after transfusion-associated hepatitis C. N Engl J Med 332:1463–1466
2. Saito I, Miyamura T, Ohbayashi A, Harada H, Katayama T, Kikuchi S, Watanabe Y, Koi S, Onji M, Ohta Y, Choo Q-L, Houghton M, Kuo G (1990) Hepatitis C virus infection is associated with the development of hepatocellular carcinoma. Proc Natl Acad Sci USA 87:6547–6549
3. Okuda M, Li K, Beard MR, Showalter LA, Scholle F, Lemon SM, Weinman SA (2002) Mitochondrial injury, oxidative stress, and antioxidant gene expression are induced by hepatitis C virus core protein. Gastroenterology 122:366–375
4. Bonkovsky HL, Banner BF, Rothman AL (1997) Iron and chronic viral hepatitis. Hepatology 25:759–768
5. Moriya K, Nakagawa K, Santa T, Shintani Y, Fujie H, Miyoshi H, Tsutsumi T, Miyazawa T, Ishibashi K, Horie T, Imai K, Todoroki T, Kimura S, Koike K (2001) Oxidative stress in the absence of inflammation in a mouse model for hepatitis C virus-associated hepatocarcinogenesis. Cancer Res 61:4365–4370
6. Bureau C, Bernad J, Chaouche N, Orfila C, Beraud M, Gonindard C, Alric L, Vinel J-P, Pipy B (2001) Nonstructural 3 protein of hepatitis C virus triggers an oxidative burst in human monocytes via activation of NADPH oxidase. J Biol Chem 276:23077–23083
7. Yadav D, Hertan HI, Schweitzer P, Norkus EP, Pitchumoni CS (2002) Serum and liver micronutrient antioxidants and serum oxidative stress in patients with chronic hepatitis C. Am J Gastroenterol 97:2634–2639
8. Parola M, Robino G (2001) Oxidative stress-related molecules and liver fibrosis. J Hepatol 35:297–306
9. Pratico D, Iuliano L, Basili S, Ferro D, Camastra C, Cordova C, FitzGerald GA, Violi. F (1998) Enhanced lipid peroxidation in hepatic cirrhosis. J Investig Med 46:51–57
10. Loguercio C, Federico A (2003) Oxidative stress in viral and alcoholic hepatitis. Free Radic Biol Med 34:1–10
11. Okita M, Tomioka K, Ota Y, Sasagawa T, Osawa T, Sakai N, Kawaguchi M, Itoshima T (2003) Arachidonic acid in mononuclear cells and its clinical significance in HCV cirrhotic patients. Nutrition 19:727–732
12. Ota Y, Sasagawa T, Suzuki K, Tomioka K, Nagai A, Niiyama G, Kawanaka M, Yamada G, Okita M (2004) Vitamin E supplementation increases polyunsaturated fatty acids of RBC membrane in HCV-infected patients. Nutrition 20:358–363
13. Murakami Y, Nagai A, Kawakami T, Hino K, Kitase A, Hara Y, Okuda M, Okita K, Okita M (2006) Vitamin E and C supplementation presents decrease of eicosapentaenoic acid in mononuclear cells in chronic hepatitis C patients during combination therapy of interferon α-2b and ribavirin. Nutrition 22:114–122
14. Manns MP, McHutchison JG, Gordon SC, Rustgi VK, Shiffman M, Reindollar R, Goodman ZD, Koury K, Ling M, Albrecht JK (2001) Peginterferon Alfa-2b plus ribavirin compared with interferon Alfa-2b plus ribavirin for initial treatment of chronic hepatitis C: a randomised trial. Lancet 358:958–965
15. Lindsay KL, Trepo C, Heintges T, Shiffman ML, Gordon SC, Hoefs JC, Schiff ER, Goodman ZD, Laughlin M, Yao R, Albrecht JK, the Hepatitis Interventional Therapy Group (2001) A randomized, double-blind trial comparing pegylated interferon Alfa-2b to interferon Alfa-2b as initial treatment for chronic hepatitis C. Hepatology 34:395–403
16. Levent G, Ali A, Ahmet A, Polat EC, Aytac C, Ayse E, Ahmet S (2006) Oxidative stress and antioxidant defense in patients with chronic hepatitis C patients before and after pegylated interferon Alfa-2b plus ribavirin therapy. J Transl Med 4:25
17. Kumar VV (1993) Lipid molecular shapes and membrane architecture. Indian J Biochem Biophys 30:135–138
18. Switzer KC, McMurray DN, Chapkin RS (2004) Effects of dietary n-3 polyunsaturated fatty acids on T-cell membrane composition and function. Lipids 39:1163–1170
19. Calder PC, Yaqoob P, Thies F, Wallace FA, Miles EA (2002) Fatty acids and lymphocyte functions. Br J Nutr 87:S31–S48
20. Ide T, Okamura T, Kumashiro R, Koga Y, Hino T, Hisamochi A, Ogata K, Tanaka K, Kuwahara R, Seki R, Sata M (2003) A pilot study of eicosapentaenoic acid therapy for ribavirin-related anemia in patients with chronic hepatitis C. Int J Mol Med 11:729–732
21. Mabile L, Piolot A, Boulet L, Fortin LJ, Doyle N, Rodriguez C, Davignon J, Blache D, Lussier-Cacan S (2001) Moderate intake of n-3 fatty acids is associated with stable erythrocyte resistance to oxidative stress in hypertriglyceridemic subjects. Am J Clin Nutr 74:449–456
22. Tomioka K, Kakibuchi N, Murakami Y, Kawakami T, Takaguchi K, Kita K, Okita M (2005) Effects of eicosapentaenoic acid supplementation in the treatment of chronic hepatitis C patients. J Nutr Sci Vitaminol 51:419–425
23. Milne DB, Botnen J (1986) Retinol, α-tocopherol, lycopene, and α- β-carotene simultaneously determined in plasma by isocratic liquid chromatography. Clin Chem 32:874–876
24. Bligh EG, Dyer WJ (1959) A rapid method of total lipid extraction and purification. Can J Biochem Physiol 37:911–917
25. Fried MW (2002) Side effects of therapy of hepatitis C and their management. Hepatology 36:S237–S244
26. Ong JP, Younossi ZM (2004) Managing the hematologic side effects of antiviral therapy for chronic hepatitis C: anemia, neutropenia, and thrombocytopenia. Cleve Clin J Med 71:S17–S21
27. Franceschi LD, Fattovich G, Turrini F, Ayi K, Brugnara C, Manzato F, Noventa F, Stanzial AM, Solero P, Corrocher R (2000) Hemolytic anemia induced by ribavirin therapy in patients with chronic hepatitis C virus infection: role of membrane oxidative damage. Hepatology 31:997–1004
28. Balan V, Schwartz D, Wu GY, Muir AJ, Ghalib R, Jackson J, Keeffe EB, Rossaro L, Burnett A, Goon BL, Bowers PJ, Leitz GJ, for the HCV Natural History Study Group (2005) Erythropoietic response to anemia in chronic hepatitis C patients receiving combination pegylated interferon/ribavirin. Am J Gastroenterol 100:299–307
29. De Franceschi L, Fattovich G, Turrini F, Ayi K, Brugnara C, Manzato F, Noventa F, Stanzial AM, Solero P, Corrocher R (2000) Hemolytic anemia induced by ribavirin therapy in patients with chronic hepatitis C virus infection: role of membrane oxidative damage. Hepatology 31:997–1004
30. Lau JYN, Tam RC, Liang TJ, Hong Z (2002) Mechanism of action of ribavirin in the combination treatment of chronic HCV infection. Hepatology 35:1002–1009
31. Terano T, Hirai A, Hamazaki T, Kobayashi S, Fujita T, Tamura Y, Kumagai A (1983) Effect of oral administration of highly purified eicosapentaenoic acid on platelet function, blood viscosity and red cell deformability in healthy human subjects. Atherosclerosis 46:321–331
32. Hino K, Murakami Y, Nagai A, Kitase A, Hara Y, Furutani T, Ren F, Yamaguchi Y, Yutoku K, Yamashita S, Okuda M, Okita M, Okita K (2006) α-Tocopherol and ascorbic acid attenuates the ribavirin-induced decrease of eicosapentaenoic acid in erythrocyte membrane in chronic hepatitis C patients. J Gastroenterol Hepatol 21:1269–1275

33. Poynard T, Marcellin P, Lee SS, Niederau C, Minuk GS, Ideo G, Bain V, Heathcote J, Zeuzem S, Trepo C, Albrecht J, for the International Hepatitis Interventional Therapy Group (1998) Randomised trial of interferon α2b plus ribavirin for 48 weeks or for 24 weeks versus interferon α2b plus placebo for 48 weeks for treatment of chronic infection with hepatitis C virus. Lancet 352:1426–1432
34. Calder PC (2007) Immunomodulation by omega-3 fatty acids. Prostaglandins Leukot Essent Fatty Acids 77:327–335
35. Yaqoob P, Pala HS, Cortina-Borja M, Newsholme EA, Calder PC (2000) Encapsulated fish oil enriched in α-tocopherol alters plasma phospholipid and mononuclear cell fatty acid compositions but not mononuclear cell functions. Eur J Clin Invest 30:260–274
36. Wallace FA, Miles EA, Calder PC (2003) Comparison of the effects of linseed oil and different doses of fish oil on mononuclear cell function in healthy human subjects. Br J Nutr 89:679–689
37. Miles EA, Banerjee T, Wells SJ, Calder PC (2006) Limited effect of eicosapentaenoic acid on T-lymphocyte and natural killer cell numbers and functions in healthy young males. Nutrition 22:512–519

Lipids (2008) 43:335–342
DOI 10.1007/s11745-008-3160-y

ORIGINAL ARTICLE

Conjugated Linoleic Acids and CLA-Containing Phospholipids Inhibit NO Formation in Aortic Endothelial Cells

Kimberly J. Jenko · Jack Y. Vanderhoek

Received: 11 December 2007 / Accepted: 12 February 2008 / Published online: 12 March 2008
© AOCS 2008

Abstract This study examined the effects of five CLA isomers and the non-conjugated LA on nitric oxide (NO) production, an important modulator of vasodilation, inflammation, and cytotoxicity. Bovine aortic endothelial cells (BAECs) were pretreated with pure CLAs (c9, c11-, c9, t11-, t9, t11-, t10, c12-, c11, c13-CLA) and the non-conjugated c9, c12-analog, then stimulated by the ionophore A23187 followed by fluorescence monitoring of NO production. CLAs (5 μM) decreased NO formation in the range of 20–40% relative to non-fatty acid-treated controls with the t9, t11- and t10, c12-CLAs being the most effective. The inhibitory effect of either of these CLAs was not time dependent over a 120 min time interval. Phosphatidylcholine (PC) and phosphatidylethanolamine (PE) play crucial roles in membrane structure and cell signaling. Since CLAs are usually esterified in these phospholipids (PLs), the effects of three CLA-containing PLs and 2-linoleoyl-PC on NO production by A23187-stimulated BAECs were also examined. c9, t11-CLA-PC and 2-linoleoyl-PC dose-dependently inhibited NO production over a 60–1,000 μM concentration range whereas c9, c11-CLA-PC and c9, t11-CLA-PE were ineffective. Both c9, t11-CLA-PC and linoleoyl-PC exhibited a time-dependent decrease in NO production from 5 to 120 min. The results of the present study suggest that the influence of several C18 polyunsaturated fatty acids incorporated into cellular phospholipids on the A23187-induced formation of NO by BAECs is strongly dependent on the positional and geometric nature of the double bonds.

Keywords CLA isomers · NO · Endothelial cells · Phospholipids · Linoleic acid

Abbreviations

BAEC	Bovine aortic endothelial cells
CLA	Conjugated linoleic acid
DAN	2, 3-Diaminonaphthalene
ECGS	Endothelial cell growth supplement
FBS	Fetal bovine serum
FU	Fluorescence units
L-Gln	L-Glutamine
HBSS	Hank's balanced salt solution
NO	Nitric oxide
NOS	Nitric oxide synthase
c9, c11-CLA-PC	1-Stearoyl-2-(c9, c11-octadecadienoyl)-*sn*-glycerol-3-phosphocholine
linoleoyl-PC	1-Stearoyl-2-linoleoyl-*sn*-glycerol-3-phosphocholine
c9, t11-CLA-PC	1-Stearoyl-2-(c9, t11-octadecadienoyl)-*sn*-glycerol-3-phosphocholine
c9, t11-CLA-PE	1-Stearoyl-2-(c9, t11-octadecadienoyl)-*sn*-glycerol-3-phosphoethanolamine
PL	Phospholipid

Introduction

Nitric oxide has emerged as an important signaling molecule that is involved in the regulation of a number of physiological and pathophysiological situations. For example, NO is a major mediator of endothelial function

---

K. J. Jenko · J. Y. Vanderhoek (✉)
Department of Biochemistry and Molecular Biology,
The George Washington University School of Medicine,
2300 Eye Street, N.W., Washington, DC 20037, USA
e-mail: bcmjyv@gwumc.edu

and depending on the cell type and concentrations, it has been shown to have both vasoconstrictor and vasodilator effects [1]. In certain inflammatory and neurodegenerative diseases, NO appears to have both cytoprotective and cytotoxic effects [2, 3]. Nitric oxide can be produced by either the constitutive (c) or inducible (i) isoforms of NOS. A number of posttranslational control mechanisms, including acylation, phosphorylation and translocation, regulate the cNOS, including the NOS present in endothelial cells (eNOS) [4]. Among its many effects, calcium also plays an important role in stimulating eNOS but not iNOS [5]. Several reports have shown that the ionophore A23187, commonly used to increase intracellular calcium concentrations, stimulated NO production by eNOS in endothelial cells and macrophages [4–8] but was ineffective in increasing NO formation cells containing iNOS [9, 10].

Conjugated linoleic acid is a family of conjugated di-unsaturated fatty acids consisting of a number of positional and *cis*/*trans* isomers of linoleic acid. These CLAs were found to be present in foods such as beef and dairy products obtained from ruminant animals. Although we, as well as others, have shown that CLA is incorporated into the phospholipid fraction of cellular membranes [11, 12], it appears that nearly all studies examining the biological effects of CLA have used the free fatty acid form of this lipid.

Several studies have reported varying effects of CLA isomers on NO formation. Coen et al. [13] determined that treatment of bradykinin-stimulated BAECs with a mixture of CLA isomers increased nitrite (a product of NO) production up to 50% relative to bradykinin-treated cells. On the other hand, Eder and coworkers [14] reported that incubation of HAECs with either c9, t11- or t10, c12-CLA decreased NO production relative to untreated cells. Treatment of interferon γ-stimulated mouse macrophages, lipopolysaccharide-enhanced murine macrophages and lipopolysaccharide/interferon γ-stimulated mouse mesangial cells with a CLA isomeric mixture all resulted in decreased NO formation relative to control cells [15, 16].

As none of these studies addressed the effects of all, currently commercially available, individual CLA isomers on NO production, we decided to determine how these isomers affected NO formation by BAECs stimulated by the ionophore A23187. Since Ohashi et al. [17] reported that several phospholipids stimulated NO production in BAECs, we hypothesized that CLA-containing PLs could directly affect NO formation. Consequently, we also examined whether (and if so, how) certain CLA containing PLs influenced NO release from both non-stimulated and A23187-stimulated BAECs.

Materials and Methods

The c9, c11-, c9, t11-, t9, t11-, t10, c12-, and c11, t13-CLA isomers were purchased from Matreya Inc. (Pleasant Gap, PA, USA). 1-stearoyl-2-(c9, t11-octadecadienoyl)-*sn*-glycerol-3-phosphocholine (18:0–18:2 (c9, t11) PC), 1-stearoyl-2-(c9, c11-octadecadienoyl)-*sn*-glycerol-3-phosphocholine (18:0–18:2 (c9, c11) PC), 1-stearoyl-2-(c9, t11-octadecadienoyl)-*sn*-glycerol-3-phosphoethanolamine (18:0–18:2 (c9, t11) PE), and 1-stearoyl-2-linoleoyl-*sn*-glycerol-3-phosphocholine (18:0–18:2 PC) were synthesized by Avanti Polar Lipids, Inc. (Alabaster, AL, USA). BAECs were obtained from the Coriell Institute for Medical Research (Camden, NJ, USA), and the DMEM/F12 50/50 mix, penicillin–streptomycin, HBSS (without phenol red), trypsin-EDTA, and FBS solution were purchased from Mediatech, Inc. Heparin, ECGS from bovine pituitary, HEPES, EDTA, fatty acid-free BSA, NAD, L(+) lactic acid, sodium nitrite, 2,3-diaminonaphthalene, A23187 and L-glutamine were purchased from Sigma-Aldrich, Corp. (St Louis, MO, USA).

Cell Culture of BAECs

BAECs were grown in Corning T-150 flasks with 20 ml DMEM/F12 medium supplemented with 15% FBS, ECGS (0.02 mg/ml), heparin (0.05 mg/ml), penicillin–streptomycin (1,000 I.U., 1,000 μg/ml), and incubated at 37 °C in 5% CO_2 for 3–4 days as previously described [18]. After reaching approximately 90% confluence, the cells were subcultured by removing the growth media, washed twice with 5 ml EDTA solution [1× HBSS supplemented with HEPES (12 mg/ml) and EDTA (4 mg/ml), pH 7.4], and detached from the flask with 2 ml 1× trypsin-EDTA solution for 1 min. After addition of 6 ml growth media to the flask, an aliquot of cells was counted in a hemocytometer. To each Corning T-25 flask containing 3 ml of growth media, 130,000 cells were added. Only BAECs from passage numbers 8–10 were used.

Preparation of CLA-BSA Solutions and Phospholipid Solutions

CLA-BSA complexes were prepared by mixing the appropriate amounts of CLA and 2% BSA-DMEM/F12 solution as previously described [18] and added to the cells for 18 h. Phospholipid solutions were prepared by first evaporating the chloroform under nitrogen from the appropriate amount of PL solution followed by the addition of 2% complete media in DMEM/F12. The solution was sonicated using a sonifier cell disruptor (Heat Systems-ultrasonics, Inc. Plainview, NY, USA) twice at 0 °C for 10 s at a setting of 30 and further diluted with 2% complete media. Four milliliters of the phospholipids mixtures (60, 250 μM, 1 mM final concentration) were added to the flasks containing 130,000 cells/flask for 18 h at 37 °C.

NO Assay

The nitric oxide protocol was modified from procedures reported by Rathel et al. [19] and Misko et al. [20]. After 18 h, control cells or cells pretreated with CLA-BSA or PL solutions were rinsed twice with 2.5 ml HBSS. Four milliliters HBSS (without phenol red) pH 7.4, were added followed by addition of 2 μM DAN (final concentration) and 2 μM A23187 (final concentration). After incubating at 37 °C for 5 or 20 min with the DAN reagent, triplicate samples of 200 μl each of the cell media were removed by pipette and transferred directly into a 96 well plate and the reaction was terminated with the addition of 5 μl of 2.8 N NaOH. Fluorescence measurements were immediately taken using a Synergy^{TM} HT multi-detection microplate reader (BioTek Instruments, Inc. Winooski, VT, USA) with excitation at 360 nm and emission read at 460 nm.

To confirm that the formation of NO could be inhibited (using this protocol), cells were treated with either 0.5 or 5 mM L-glutamine/HBSS (final concentration) for 30 min followed by the addition of 2 μM each of A23187 and DAN. After an additional 5 and 20 min, triplicate samples were removed and measured for fluorescence with the microplate reader.

All data expressed in fluorescent units (FUs) were generated by subtracting fluorescence values measured in unstimulated cells from fluorescence values generated from A23187-stimulated cells treated with or without various agents.

LDH Activity Assay and Statistical Analysis

Cell viability was assessed by determining lactate dehydrogenase release into the medium as previously described [18]. Viability measurements of BAECs treated with either CLA isomers (or CLA-containing PLs) and A23187 were not significantly different from either resting cells or cells stimulated with A23187 alone (results not shown). Data were analyzed by Student's *t* test and one-way ANOVA.

Results

In order to determine the effect of CLA isomers and CLA-containing PL on NO production in resting cells, BAECs were treated with t10, c12-CLA (concentration range 0.3–100 μM) but failed to produce any significant change in NO production compared to cells not treated with CLA. Similar results were obtained with c9, c11-, c9, t11-, t9, t11-, and c11, t13-CLA (not shown). Likewise, NO production was not significantly affected when resting BAECs treated with 60–1,000 μM c9, c11-CLA-PC were compared to untreated control cells. In view of these results, it was decided to examine the effects of CLAs and CLA-PLs on stimulated BAECs.

Treatment of cells with ionophore A23187 stimulated NO formation in a dose-dependent manner as shown in Fig. 1. Although 0.1 μM A23187 had no effect, 0.5, 1 and 2 μM increased NO production from 1,456 ± 412 FU to 9,940 ± 324 FU ($n = 4$) relative to non-stimulated cells (after 5 min, non-stimulated cells generated 9,222 ± 1,083 FU, $n = 5$). Cells incubated with A23187 for 5 or 20 min produced similar quantities of NO but a 17% decrease was observed over a 120 min incubation period (Fig. 1 insert). To confirm that NO production in this system could be inhibited by a known NO inhibitor, the effect of glutamine was tested [21]. Pre-incubation of BAECs with 5 mM glutamine for 30 min followed by treatment with 1 μM A23187 for 5 or 20 min decreased NO formation by 33 ± 16 and 46 ± 22%, respectively ($P < 0.05$, $n = 4$, Fig. 2).

The effects of various CLA isomers on NO production by A23187-stimulated BAECs are shown in Fig. 3. Cells were first incubated for 18 h with either 2% BSA or 2% BSA complexed with 5 μM pure CLA isomer. After washing the cells to remove the BSA or CLA-BSA, the cells were treated with 2 μM A23187 and 2 μM DAN for

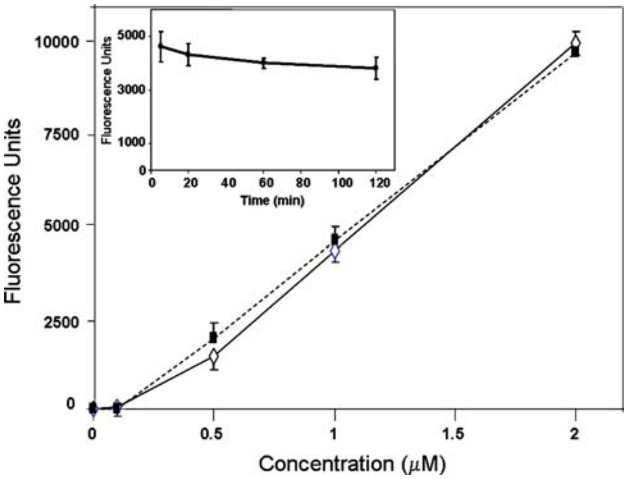

Fig. 1 The effect of A23187 on NO production in BAECs. BAECs (130,000 per flask) were treated for 18 h with 4 ml of 2% complete medium. Next, the cells were rinsed with HBSS and incubated at 37 °C with different concentrations of A23187 followed by 2 μM DAN (final concentration). Samples were collected after either 5 (*ldiamonds*) or 20 (*filled squares*) min and measured for fluorescence. The results are expressed as fluorescence units. The values are mean ± SD from four experiments. *Insert*: with incubation times greater than 5 min, the DAN was added 10 min prior to the collection of samples and then analyzed for fluorescence

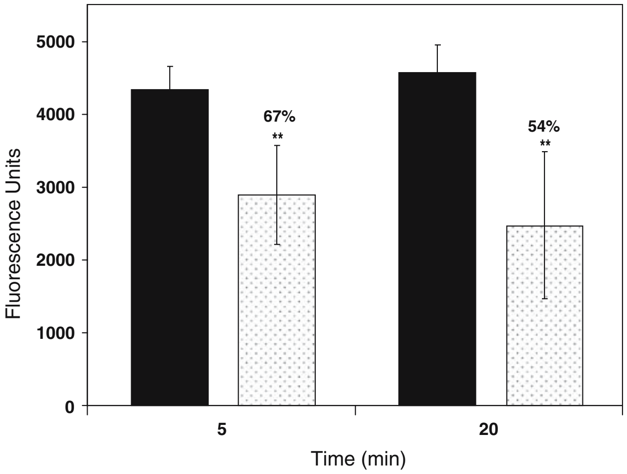

Fig. 2 The effect of L-glutamine on NO formation by A23187-stimulated BAECs. BAECs (130,000 per flask) were placed in T-25 flasks containing 3 ml growth media/flask and grown for 24 h. The cells were rinsed and treated for 18 h with 4 ml of 2% complete media. After washing with HBSS, the cells were incubated at 37 °C for 30 min with 4 ml 5 mM L-Gln/HBSS (final concentration). Next, 1 μM A23187 and 2 μM DAN (final concentrations) were added and after either 5 or 20 min, samples were collected and assayed for fluorescence. The results of single samples from four experiments are expressed as fluorescence units. The *numbers* above the columns indicate % control values. The values are mean ± SD. ** $P < 0.05$ when compared to A23187 control

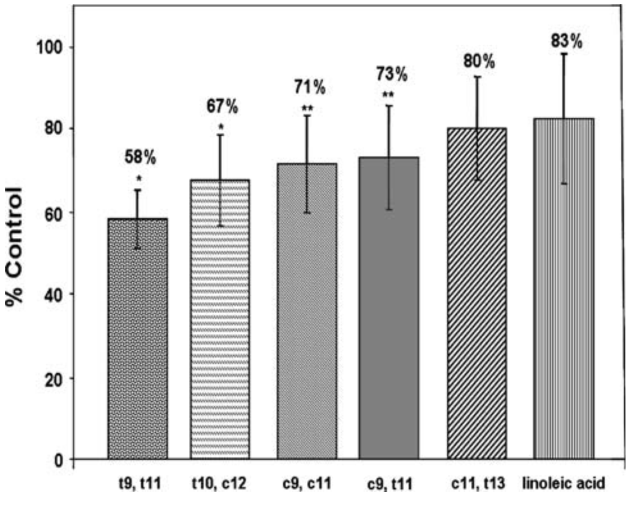

Fig. 3 The effect of 5 μM CLA isomers and linoleic acid on NO production by A23187-stimulated BAECs. BAECs (130,000 per flask) were treated for 18 h at 37 °C with either 4 ml of 2% BSA or 4 ml 2% BSA complexed with 5 μM (final concentration) of c9, t11-, c9, c11-, t10, c12-, t9, t11-, 11, 13-CLA, and linoleic acid. After washing the cells, 2 μM A23187 (final concentration) and 2 μM DAN were added and samples were collected after 5 min and analyzed for fluorescence. Values are expressed as % control compared to BSA/A23187 (100%) and are generated from four experiments. The *numbers* above each column indicate % control values. The values are mean ± SD. * $P \le 0.01$, ** $P \le 0.05$ when compared to A23187 control

5 min followed by fluorescence measurements to determine NO formation. Treatment of BAECs with t9, t11-CLA resulted in a decrease of 42 ± 7.1% ($P \le 0.01$, $n = 4$) in NO formation which was somewhat greater than that observed with t10, c12-CLA (33 ± 11, $P \le 0.01$, $n = 4$). The c9, c11-, c9, t11-, and the c11, t13-CLA isomers were somewhat less effective (29 ± 12, 27 ± 13 and 20 ± 13%, respectively, $P \le 0.05$, $n = 4$). Linoleic acid, the corresponding non-conjugated c9, c12-isomer, decreased NO production by 17 ± 16% ($n = 4$). Similar results were observed with 60 and 120 μM CLA concentrations (results not shown).

We next examined whether CLA-containing PLs could influence NO formation in A23187-stimulated BAECs. The structures of these PLs as well as the non-conjugated linoleoyl-PC are shown in Fig. 4. BAECs were treated for 18 h with either 2% complete medium or 2% medium containing 60, 250 or 1,000 μM PLs. After rinsing, the cells were treated with 2 μM A23187 and 2 μM DAN for 20 min followed by NO determinations. As shown in Fig. 5 (top), 1,000 μM c9, t11-CLA-PC decreased NO formation 31 ± 5.3% ($P \le 0.01$, $n = 5$) with smaller decreases observed at 60 and 250 μM. Changing the head group to PE (c9, t11-CLA-PE) did not result in any inhibitory potency which was also observed with c9, c11-CLA-PC (Fig. 5 bottom). On the other hand, 1,000 μM of the non-conjugated linoleoyl-PC analog resulted in a 37 ± 13% ($P \le 0.01$, $n = 9$) inhibition of NO formation (Fig. 5 bottom).

To determine whether the inhibitory effects of certain CLA-pretreated BAECs on NO production were dependent on the incubation time of these cells with A23187, time

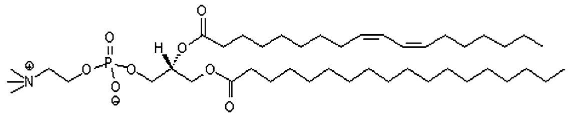

1-stearoyl-2-(c9, c11- octadecadienoyl)-*sn*-glycero-3-phosphocholine
(c9, c11-CLA-PC)

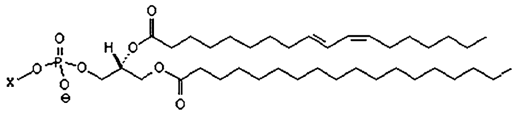

1-stearoyl-2-(c9, t11- octadecadienoyl)-*sn*-glycero-3-phosphate
X = $CH_2CH_2N^+(CH_3)_3$, c9, t11-CLA-PC
X = $CH_2CH_2NH_3^+$, c9, t11-CLA-PE

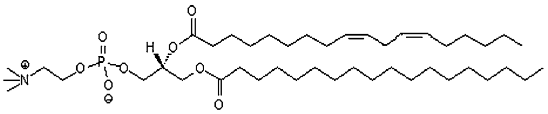

1-stearoyl-2-(c9, c12- linoleoyl)-*sn*-glycero-3-phosphocholine
(linoleoyl- PC)

Fig. 4 Structures of phospholipids. Structures of c9, c11-CLA-PC, c9, t11-CLA-PC, c9, t11-CLA-PE, and 2-linoleoyl-PC

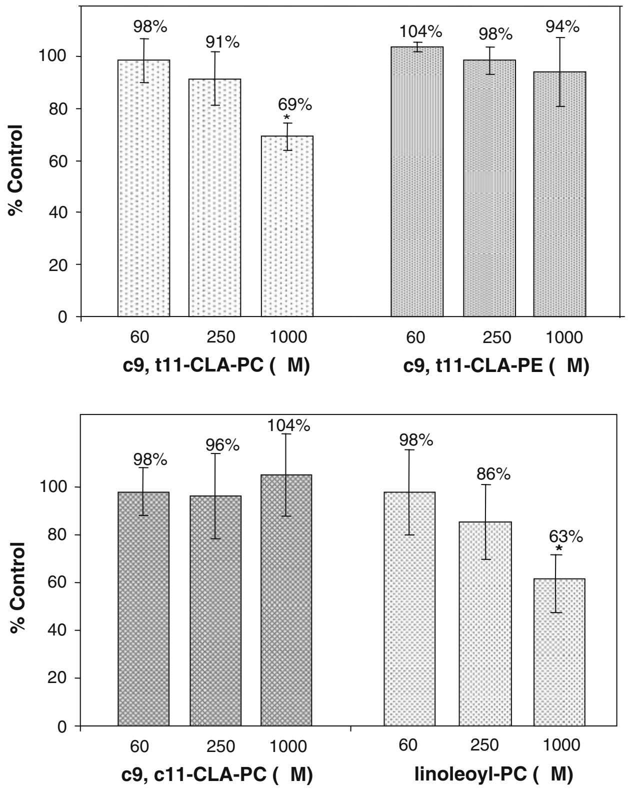

Fig. 5 The effect of conjugated and non-conjugated octadienoic acid-containing PLs on NO production in A23187-stimulated BAECs. The protocol is the same as described in the legend of Fig. 3 except BAECs were treated at 37 °C with either 4 ml 2% complete media or 4 ml 2% complete media containing 60, 250, or 1,000 μM c9, t11-CLA-PC, linoleoyl-PC (Fig. 5 *top*) and c9, c11-CLA-PC, c9, t11-CLA-PE (Fig. 5 *bottom*). Samples were collected 20 min after A23187 addition and analyzed for fluorescence. Values are expressed as % control compared to 2% complete media/A23187 (100%) and are generated from four experiments. The *numbers* above each column indicate % control values. The values are means ± SD. * $P \leq 0.01$, ** $P \leq 0.05$ when compared to the A23187 control (=100%)

course experiments were carried out. BAECs were first pretreated with 5 μM t9, t11-CLA for 18 h, then exposed to A23187 for 5 min which resulted in a 42 ± 7% ($n = 4$) reduction in NO formation relative to A23187-stimulated cells (Fig. 6, top). Increasing the incubation time after A23187 stimulation to 120 min, adding the DAN 10 min prior to collection of samples, and taking fluorescence readings did not result in a statistically significant change in decreased NO production (28 ± 14%, $n = 6$). Similar results were obtained with t10, c12-CLA (results not shown). Using the same approach with BAECs pretreated with 1,000 μM c9, t11-CLA-PC followed by a 5 min incubation with A23187 resulted in a 20 ± 15% ($n = 5$) decrease in NO formation whereas 120 min after stimulation with A23187 produced a 45 ± 11% ($n = 6$) reduction in NO generation (Fig. 6, bottom). This figure also showed that the c9, c11-CLA-PC isomer was about half as effective 120 min after A23187 stimulation since NO production had decreased by 24 ± 12% ($n = 5$) compared to control values. Finally, the non-conjugated linoleoyl-PC analog exhibited the largest time dependent effect. Pretreatment of BAECs with 1,000 μM linoleoyl-PC followed by stimulation with A23187 decreased NO formation 21 ± 13% ($n = 5$) after 5 min and by 76 ± 15% ($n = 6$) after 120 min compared to control cells after these incubation periods (Fig. 6, top).

Discussion

Coen et al. [13] showed that bradykinin stimulation of BAECs pretreated with a CLA isomeric mix, consisting primarily of the c9, t11- and t10-c12-isomers, potentiated

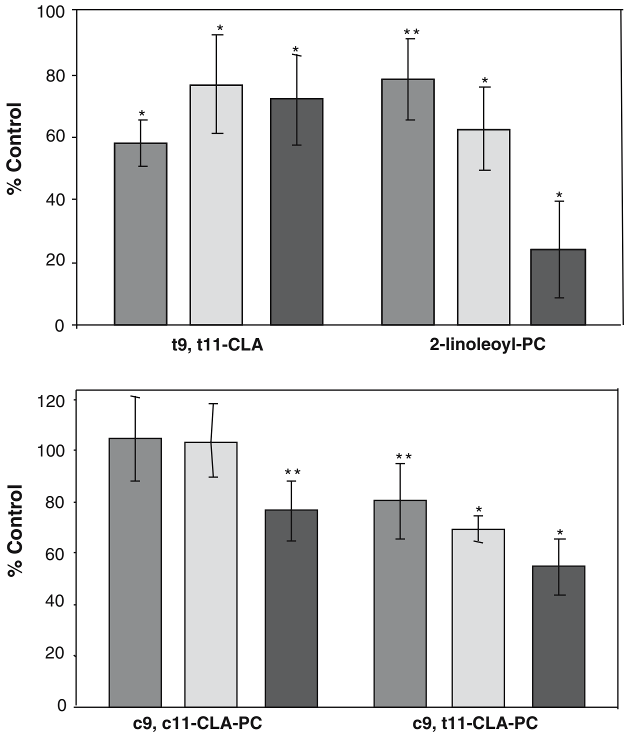

Fig. 6 The effect of incubation time on NO production by A23187-stimulated BAECs. BAECs (130,000 per flask) were treated for 18 h at 37 °C with either 5 μM (final concentrations) of t9, t11-CLA complexed with 2% BSA in DMEM/F12 as described in the legend of Fig. 3, or with 1,000 μM 2-linoleoyl-PC, c9, t11-CLA-PC, or c9, c11-CLA-PC in 2% complete media as indicated in the legend of Fig. 5. After washing the cells, 2 μM A23187 (final concentration) was added at time 0 followed by addition of 2 μM DAN (final concentration) either right after A23187 for the 5 min (*light shaded bar*) time point or at 10 min prior to collection of samples at 20 (*checkered bar*) and 120 (*dark shaded bar*) min and analyzed for fluorescence. Values are expressed as % control compared to A23187 stimulation after these incubation times, and are the average of triplicate samples from two or three experiments. The values are mean ± SD. * $P \leq 0.01$, ** $P \leq 0.05$ when compared to A23187 control (=100%)

NO formation up to 40%. Others reported that these two CLA isomers or a mixture of CLA isomers decreased NO production by various cells stimulated by lipopolysaccharide and/or interferon-γ [14–16, 22]. In contrast to other investigators, we used A23187 as the cellular stimulus in this study of the effects of pure CLA isomers on NO generation by BAECs. We observed that pretreatment of BAECs with 5 μM of either t9, t11-, t10, c12-, c9, c11-, c9, t11- or c11, t13-CLA followed by A23187 stimulation for 5 min decreased NO production in the range of 20–42% compared to untreated cells stimulated with A23187. The non-conjugated linoleic acid was the least effective of the unsaturated fatty acids tested. As a number of reports have determined that the CLA concentration in human serum was between 7 and 70 μM [23, 24], our finding that 5 μM CLA is an effective concentration suggests that this is within the physiological concentration range of this fatty acid. Interestingly, neither we nor the other groups (using different cells, stimuli, experimental conditions and higher concentrations of CLA) found more than 40% inhibition of NO formation [13–15, 22]. These results suggest that there is little structural selectivity of the octadecadienoic acids for the NOS since the location and *cis*/*trans* isomerism of the double bonds do not appear to be major determinants for decreasing NO formation. This contrasts with our findings of much greater selectivity of CLA isomers for inhibiting the cyclooxygenase–prostanoid complex in platelets and endothelial cells [12, 25]. Furthermore, we as well as others [14] have observed that higher concentrations (up to 120 μM) of different CLA isomers did not produce stronger inhibitory effects on NO production. A possible explanation for this apparent non-concentration effect is that pretreatment of BAECs with various CLA isomers could generate an intermediate metabolite whose formation is already at maximal capacity at 5 μM CLA and whose inhibitory effect is maximized at about 40%. Although no significant differences in NO production between most of the CLA isomers was observed, there was a statistically significant difference ($P \leq 0.05$) between cells pretreated with t9, t11-CLA and c11, t13-CLA. Possible explanations for the different results obtained by Coen et al. [13] using bradykinin and our results with A23187 include the use of different experimental conditions (e.g. incubation times with stimulus, CLA composition and concentrations used) and that receptor-mediated events involve different pathways and mechanisms than ionophore-modulated reactions.

It has been well established that pretreatment of cells with unsaturated fatty acids leads to their incorporation into the cellular lipids, especially the PL fraction. We and others have shown that supplementation of the growth media with CLA isomers resulted into their esterification into membrane PLs [11, 12]. Since Ohashi et al. [17] had reported that 1-palmitoyl-2-oleoyl-PC and its PE and PS analogs enhanced endothelial nitric oxide synthase, we examined whether treating BAECS with various CLA-containing PLs could affect NO production. Pretreatment of BAECs with 1,000 μM, c9, t11-CLA-PC decreased A23187-activated NO formation by 31% after 20 min whereas both c9, t11-CLA-PE and c9, c11-CLA-PC were ineffective. However, the inhibitory effectiveness of linoleoyl-PC (37%) was comparable to that of c9, t11-CLA-PC. These results suggest that efficacy of PL on A23187-stimulated NO production are dependent both on the nature of the fatty acid esterified in the two position of the PL as well as the identity of the PL head group. It is interesting to note that while pretreatment of BAECs with c9, t11- and c9, c11-CLA resulted in comparable decreases in NO formation after A23187 stimulation, only the c9, t11-CLA-PC was effective when added in the PL form. One possible explanation is that when BAECs are pretreated with CLA isomers, they become incorporated into a variety of PLs, some (or all) of which may inhibit NO production. Hence it is feasible that the inhibitory PL of the c9, t11-CLA is the PC form whereas the inhibitory PL of the c9, c11-CLA isomer is not the PC analog but may be another PL class.

A number of mechanistic possibilities can be envisaged to explain the inhibitory effects of the CLA isomers on A23187-induced NO formation. In view of Li's reports that eicosapentaenoic acid and docosahexaenoic acids modified the lipid composition in caveolae of endothelial cells and modulated the cellular eNOS activity as well as a number of studies that have documented incorporation of CLA into cellular lipids [11, 12, 26, 27], it is possible that this CLA-induced modification of lipid milieu (or the addition of certain CLA-containing phospholipids) could have a negative effect on the eNOS activity in BAECs. Another possible mechanism could involve a cyclooxygenase metabolite. It is well known that A23187 stimulates cytosolic phospholipases to release arachidonic acid which can then be metabolized to cyclooxygenase products such as prostacyclin [28]. Furthermore, a number of studies have documented a relationship between NO production and prostanoid formation including a recent one by Niwano who reported that beraprost, a stable analog of prostacyclin, stimulated eNOS activity in BAECs [3, 29]. Since c9, t11- and t10, c12-CLA isomers were reported to inhibit macrophage phospholipase A_2 activity and we, as well as others, have shown that CLA isomers decreased the formation of cyclooxygenase products in endothelial cells, it is possible that CLA pretreatment of BAECs decreased production of endogenously generated prostacyclin (or other cyclooxygenase metabolites) which could explain the decrease in NO formation observed in our study [13, 14, 25, 30].

The 2-linoleoyl-PC, c9, t11-CLA-PC and the c9, c11-CLA-PC all exhibited a time-dependent inhibitory effect on A23187-stimulated NO formation by BAECs over a 2-h period, with the 2-linoleoyl-PC being the most effective (76% decrease), followed by c9, t11-CLA-PC (45% decrease) with the c9, c11-CLA-PC (24% decrease) and t9, t11-CLA (28% decrease) being the least potent. These results suggest that certain octadecadienoic acid-containing PLs may have both short and long term effects on the NO synthase system. Although the mechanism of this time-dependent effect is unknown, one can speculate that these PLs may be slowly converted to other, more effective, inhibitors of the NO synthase system.

In conclusion, the results of this report indicate that pretreatment of BAECs with five different CLA isomers decreased A23187-stimulated NO production between 20 and 40% relative to non-CLA treated controls. Furthermore, our study is the first to demonstrate that when testing certain CLA-containing PLs, e.g. the c9, t11-CLA-PC and the 2-linoleoyl-PC analog, on this system, NO production was inhibited (whereas two other CLA-containing PLs were ineffective) and that this inhibition was time dependent. These results support the hypothesis that CLA-containing PLs may directly influence specific enzymatic systems, e.g. nitric oxide synthases, in the cellular milieu.

References

1. Rastaldo R, Paglioro P, Cappello S, Penna C, Mancardi D, Westerhof N, Losano G (2007) Nitric oxide and cardiac function. Life Sci 81:779–793
2. Wiley JW (2007) The many faces of nitric oxide: cytotoxic, cytoprotective or both. Neurogastroenterol Motil 19:541–544
3. Mariotto S, Suzuki Y, Persichini T, Colasanti M, Suzuki H, Cantoni O (2007) Cross-talk between NO and arachidonic acid in inflammation. Curr Med Chem 14:1940–1944
4. Fleming I, Busse R (2003) Molecular mechanisms involved in the regulation of the endothelial nitric oxide synthase. Am J Physiol Regul Integr Comp Physiol 284:R1–R12
5. Nathan C, Xie Q-W (1994) Nitric oxide synthases: roles, tolls and controls. Cell 78:915–918
6. Fulton D, Gratton J-P, Sessa WC (2001) Post-translational control of endothelial nitric oxide synthase: why isn't calcium/calmodulin enough? J Pharm Exp Therap 299:818–824
7. Kimura C, Oike M, Ohnaka K, Nose Y, Ito Y (2003) Constitutive nitric oxide production in bovine aortic and brain microvascular endothelial cells: a comparative study. J Physiol 554:721–730
8. Miles PR, bowman L, Rengasamy A, Huffman L (1998) Constitutive nitric oxide production by rat alveolar macrophages. Am J Physiol 274:L360–L368
9. Shen L-J, Lin W-C, Beloussow K, Hosoya K-I, Terasaki T, Ann DK, Shen W-C (2003) Recombinant arginine deiminase as a differential modulator of inducible (iNOS) and endothelial (eNOS) nitric oxide synthetase activity in cultured endothelial cells. Biochem Pharmacol 66:1945–1952
10. Korhone R, Kankaanranta H, Lahti A, Lahde M, Knowles RG, Moilanen E (2001) Bi-directional effects of the elevation of intracellular calcium on the expression of inducible nitric oxide synthase in J774 macrophages exposed to low and to high concentrations of endotoxin. Biochem J 354:351–358
11. Ha YL, Storkson J, Pariza MW (1990) Inhibition of benzo(a)-pyrene-induced mouse forestomach neoplasia by conjugated dienoic derivatives of linoleic acid. Cancer Res 50:1097–1101
12. Al-Madaney MM, Kramer JKG, Deng Z, Vanderhoek JY (2003) Effects of lipid-esterified isomers on platelet function: evidence for stimulation of platelet phospholipase activity. Biochim Biophys Acta 1635:75–82
13. Coen PM, Cummins PM, Birney YA, Devery R, Cahill PA (2004) Modulation of nitric oxide and 6-keto-prostaglandin $F_{1\alpha}$ production in bovine aortic endothelial cells by conjugated linoleic acid. Endothelium 11:211–220
14. Eder K, Schleser S, Becker K, Körting R (2003) Conjugated linoleic acids lower the release of eicosanoids and nitric oxide from human aortic endothelial cells. J Nutr 133:4083–4089
15. Iwakiri Y, Sampson DA, Allen KGD (2002) Suppression of cyclooxygenase-2 and inducible nitric oxide synthase expression by conjugated linoleic acid in murine macrophages. Prostaglandins, Leukot Essent Fatty Acids 67:435–443
16. Sheu JN, Lin TH, Lii CK, Chen CC, Chen HW, Liu KL (2006) Contribution of conjugated linoleic acid to the suppression of inducible nitric oxide synthase expression and transcription factor activation in stimulated mouse mesangial cells. Food Chem Toxicol 44:409–416
17. Ohashi Y, Katayama M, Hirata K, Suematsu M, Kawashima S, Yokoyama M (1993) Activation of nitric oxide synthase from cultured aortic endothelial cells by phospholipids. Biochem Biophys Res Commun 195(3):1314–1320
18. Lai KL, Torres-Duarte AP, Vanderhoek JY (2005) 9-Trans, 11-trans: antiproliferative and proapoptotic effects on bovine endothelial cells. Lipids 40:1107–1116
19. Rathel T, Leikert JF, Vollmar AM, Dirsch VM (2003) Application of 4,5-diaminofluorescein to reliably measure nitric oxide released from endothelial cells in vitro. Biol Proced Online 5:136–142
20. Misko TP, Schilling RJ, Salvemini D, Moore WM, Currie MG (1993) A fluorometric assay for the measurement of nitrite in biological samples. Anal Biochem 214:11–16
21. Meininger C, Wu G (1997) L-glutamine inhibits nitric oxide synthesis in bovine venular endothelial cells. J Pharmacol and Exp Ther 281:448–453
22. Shen CL, Dunn DM, Henry JH, Yong L, Watkins BA (2004) Decreased production of inflammatory mediators in human osteoarthritic chondrocytes by conjugated linoleic acids. Lipids 39:161–166
23. Fogerty AC, Ford GL, Svoronos D (1988) Octa-9, 11-dienoic acid in foodstuffs and in the lipids of human blood and breast milk. Nutr Rep Intl 38:937–944
24. Huang Y-C, Luedecke LO, Shultz TD (1994) Effect of cheddar cheese consumption on plasma conjugated linoleic acid concentrations in men. Nutr Res 14:373–386
25. Torres-Duarte AP, Vanderhoek JY (2003) Conjugated linoleic acid exhibits stimulatory and inhibitory effects on prostanoid production in human endothelial cells and platelets. Biochim Biophys Acta 1640:69–76
26. Li Q, Zhang Q, Wang M, Zhao S, Ma J, Luo N, Li N, Li Y, Xu G, Li J (2007) Eicosapentaenoic acid modifies lipid composition in caveolae and induces translocation of endothelial nitric oxide synthase. Biochimie 89:169–177
27. Li Q, Zhang Q, Wang M, Liu F, Zhao S, Ma J, Luo N, Li N, Li Y, Xu G, Li J (2007) Docosahexaenoic acid affects endothelial nitric oxide synthase in caveolae. Arch Biochem Biophys 466:250–259
28. Hong SL, McLaughlin NJ, Tzeng CY, Patton G (1985) Prostacyclin synthesis and deacylation of phospholipids in human

endothelial cells: comparison of thrombin, histamine and ionophore A23187. Thromb Res 38:1–10

29. Niwano K, Arai M, Tomaru K, Uchiyama T, Ohyama Y, Kurabayashi M (2003) Transcriptional stimulation of the eNOS gene by the stable prostacyclin analogue breaprots is mediated through cAMP-responsive element in vascular endothelial cells. Close link between PGI2 signal and NO pathways. Circ Res 93:523–530
30. Stachowska E, Dziedziejko V, Safranow K, Gutowska I, Adler G, Ciechanowicz A, Machalinski B, Chlubek D (2007) Inhibition of phospholipase A2 activity by conjugated linoleic acids in human macrophages. Eur J Nutr 46:28–33

Lipids (2008) 43:343–352
DOI 10.1007/s11745-008-3152-y

ORIGINAL ARTICLE

Membrane Lipid Composition Plays a Central Role in the Maintenance of Epithelial Cell Adhesion to the Extracellular Matrix

María Gabriela Márquez · Francisco Leocata Nieto · María C. Fernández-Tome · Nicolás Octavio Favale · Norma Sterin-Speziale

Received: 29 October 2007 / Accepted: 30 December 2007 / Published online: 21 February 2008
© AOCS 2008

Abstract Focal contacts (FC) are membrane-associated multi-protein complexes that mediate cell-extracellular matrix (ECM) adhesion. FC complexes are inserted in detergent-resistant membrane microdomains enriched in phosphatidylinositol-4,5-bisphosphate (PtdIns(4,5)P_2); however, the influence of membrane lipid composition in the preservation of FC structures has not been extensively addressed. In the present work, we studied the contribution of membrane lipids to the preservation of renal epithelial cell adhesion structures. We biochemically characterized the lipid composition of membrane-containing FC complexes. By using cholesterol and PtdIns(4,5)P_2 affecting agents, we demonstrated that such agents did not affect any particular type of lipid but induced the formation of new FC-containing domains of completely different lipid composition. By using both biochemical approaches and fluorescence microscopy we demonstrated that phospholipid composition plays an essential role in the in vivo maintenance of FC structures involved in cell-ECM adhesion.

Keywords Membrane lipids · Focal contacts · Collecting duct cells · Cell-extracellular matrix adhesion

Abbreviations

DRM	Detergent-resistant membrane domains
ECM	Extracellular matrix
FC	Focal contacts
IB	Immunoblotting
IP	Immunoprecipitation
CD	Methyl-β-cyclodextrin

Introduction

Tissue organization depends on structures that enable cells to attach to the extracellular matrix (ECM). Focal contacts (FC), the most stable points of cell tethering to the ECM, are multi-protein complexes that reach the outside of the cell from the cytoplasm through the cell membrane and contact the actin-cytoskeleton inside the cell with ECM proteins [1, 2]. FC assembly occurs by the binding of the integrin-extracellular domain to the ECM proteins followed by the interaction of the β-integrin cytoplasmic domain with talin, which, in turn, binds vinculin [3–5]. The acidic phospholipid, phosphatidylinositol-4,5-bisphosphate (PtdIns(4,5)P_2), acts as a regulator of both actin dynamics and FC turnover [6], and many cytoskeleton proteins involved in cell adhesion bind PtdIns(4,5)P_2 in order to be

---

This work was supported by the National Council for Scientific and Technologic Research-CONICET, (PIP-05557 grant) and by the University of Buenos Aires, (UBACYT -B064 grant), by ANPCYT (PME 2003, RES. No 123) and by the National University of La Rioja (Exp. 5623/05).

M. G. Márquez
Instituto de Investigaciones en Ciencias de la Salud Humana (IICSHUM), Universidad Nacional de La Rioja, 5300 la Rioja, Argentina

M. G. Márquez · M. C. Fernández-Tome · N. O. Favale · N. Sterin-Speziale (✉)
IQUIFIB-CONICET, C1113AAD Buenos Aires, Argentina
e-mail: speziale@ffyb.uba.ar

F. Leocata Nieto · M. C. Fernández-Tome · N. O. Favale · N. Sterin-Speziale
Departamento de Ciencias Biológicas,
Facultad de Farmacia y Bioquímica,
Universidad de Buenos Aires, C1113AAD Buenos Aires,
Argentina

either activated or inactivated [7]. It is accepted that both vinculin activation and integrin binding to talin are dependent on plasma membrane local availability of PtdIns(4,5)P_2 [8].

Both talin and vinculin need to be inserted into the phospholipid bilayer to form FC plaques. Earlier in vitro studies have demonstrated that the insertion of either vinculin or talin into the lipid bilayer depends on the bilayer phospholipid composition [9]. On the other hand, it has been reported that many of the molecular components that regulate cell-ECM adhesion are associated with cholesterol-enriched detergent-resistant membrane microdomains (DRM), which are also enriched in PtdIns(4,5)P_2 [10]. It is considered that the specific interactions with phosphoinositides could serve to recruit cytoskeletal proteins to particular membrane domains, in which specific lipids are thought to be accumulated [10].

In spite of the relevance that membrane lipids appear to have for FC assembly, there are no previous reports on the membrane lipid composition where FC are located in vivo or on how changes in local membrane composition contribute to FC maintenance.

In the present study, we first performed the biochemical characterization of the membrane domains where FC complexes are located in renal papillary collecting duct cells. Thereafter, by combining biochemical and immunofluorescence studies, we obtained experimental evidence showing how specific changes in the membrane lipid composition in vivo are a sufficient condition to affect the maintenance of FC, thus demonstrating that membrane lipid composition plays a central role in the maintenance of cell-ECM adhesion.

Materials and Methods

Silicagel plates for thin layer chromatography (TLC) were from Merck. X-ray film was obtained from the Eastman Kodak Co. Neomycin, LiCl, methyl-β-cyclodextrin, Collagenase Type II, Fast 3,3′diaminobenzidine tablets and monoclonal antibodies against vinculin and talin and phalloidin-FITC were from the Sigma Chemical Co (St. Louis, MO, USA). Biotinylated anti PtdIns(4,5)P_2 was from Echelon Biosciences Inc. (Lake City, UT), FITC-conjugated goat F(ab)$_2$ to mouse IgG was from Jackson ImmunoResearch Inc. (West Grove, PA) and ABC complex/HRP Kit was from Dako Lab (Glostrup, Denmark). Protein A/G PLUS Agarose was obtained from Santa Cruz Biotechnology Inc (Burlingame, CA). All culture reagents were from Gibco (Gibco, Invitrogen, USA). All other reagents and chemicals were of analytical grade (Sigma, Merck or Mallinckrodt) and purchased from local commercial suppliers.

Animals and Tissue Preparation

Adult male Wistar rats were sacrificed by cervical dislocation and both kidneys removed. Renal papillae were isolated by scalpel and scissors dissection and sliced (0.5 mm thick) by using a Stadie-Riggs microtome. Papillary slices were collected in ice-cold 10 mM Tris–HCl, pH 7.4, containing 140 mM NaCl, 5 mM KCl, 2 mM $MgSO_4$, 1 mM $CaCl_2$ and 5.5 mM glucose (TBS) and incubated at 37 °C in a metabolic shaking bath either in the absence or in the presence of membrane-affecting agents: 5 mM methyl-β-cyclodextrin or 1 mM neomycin or 10 mM LiCl for 30, 10 or 120 min, respectively. Incubations were stopped on ice and immediately homogenized in 10 vol of a solution 0.25 M sucrose containing 25 mM Tris–HCl, pH 7.4, 3 mM $MgCl_2$, 2 mM EGTA, 1 mM PMSF, 10 μg/mL aprotinin and 1 mM Na_3VO_4 and, successively centrifuged at 860 g for 10 min, 8,000 g for 20 min, and 105,000 g for 60 min; the resultant pellet corresponding to microsomal fraction was used for further studies.

Detergent-Resistant Membrane Isolation

Triton X-100 insoluble membrane fractions were performed by the two-step centrifugation process described by Ito el al. [11]. Briefly, microsomes were resuspended in one vol of ice-cold PBS containing 1 mM PMSF, 10 μg/mL aprotinin and 1 mM Na_3VO_4. Then, one volume of 0.2% (v/v) Triton X-100 in PBS was added, mixed and incubated at 4 °C for 20 min. Samples were layered on 30% (w/v) sucrose and centrifuged at 225,000*g* at 4 °C for 2.5 h. Pellets were discarded and supernatants diluted with 0.1% Triton X-100 in PBS up to 10% (w/v) sucrose and centrifuged at 225,000*g* at 4 °C for 2.5 h. The resultant pellet contained the Triton X-100 insoluble membrane fraction while supernatants were considered as the soluble membrane fraction (S fraction). Throughout this paper we termed DRM as the 0.1% Triton X-100 insoluble membranes that sediment in 10% sucrose after centrifuging for 2.5 h at 225,000 g. For the biochemical studies we used DRM isolated from microsomal fractions instead of the plasmatic membrane because in our experimental conditions no detergent resistant pellet was obtained from the isolated endoplasmatic reticulum. Thus, our microsomal DRM only represented resistant domains from the plasmatic membrane.

Lipid Analysis

Total lipids were obtained in the lower chloroformic phase of the Bligh and Dyer extraction procedure [12]. From total lipid extracts, individual phospholipids and phosphoinositides were separated and quantified as previously reported [13, 14], and the cholesterol content determined by the method based on the cholesterol-oxidase enzyme reaction [15]. Phospholipid biosynthesis was studied by incubating papillary slices in TBS containing 0.1 μCi/mL of [^{32}P]-sodium orthophosphate ([^{32}P]-Pi) at 37 °C in a metabolic shaking bath. After 60 min incubation, samples were homogenized, DRM and S fractions obtained, and phospholipids and polyphosphoinositides separated. Radioactive lipids were visualized by autoradiography and iodine vapors and quantified by liquid scintillation counting.

Fatty Acid Determination

Following phospholipid separation by TLC, spots were scraped off and stored under nitrogen atmosphere at −20 °C. The lipids were *trans*-esterified with acetyl chloride in methanol at 100 °C for 1 h. After cooling, K_2CO_3 was added, and the methyl esters were extracted with benzene. Thereafter, the extracts were evaporated under stream of nitrogen and stored at −20 °C. Methyl esters were analyzed by gas chromatography using a Gas Chromatograph (Series GC-8A) equipped with a flame ionization detector and 30 m × 0.25 mm DR-23 capillary column. The temperature was programmed from 175 to 240 °C at a rate of 3 °C/min. Nitrogen was used as the carrier gas. The chromatographic peaks were identified by comparison of the retention time with those of standards and the percentage composition of each fatty acid was calculated from the proportionality of peak areas by an automatic integrator.

Phospholipid Determination

For the quantification of phospholipids, specific areas of the TLC plates were scraped off and digested with 70% perchloric acid in the presence of ammonium molybdate (0.5%), for 2 h in a heating block at 180 °C. The resulting inorganic phosphate was assayed with a Fiske–Subbarow reagent [16].

Immunoprecipitation and Western Blot Analysis

Aliquots containing 100 μg of protein of DRM or S fractions were pre-cleared by incubation at 4 °C with protein A/G Plus-Agarose and, after centrifugation, supernatants were incubated at 4 °C for 1 h with 2 μg of monoclonal antibody against PtdIn(4,5)P2 (plus 2.5 μg of rabbit anti-mouse IgM) or monoclonal antibody against vinculin. Thereafter, protein A/G Plus- Agarose was added and incubated overnight at 4 °C with gentle shaking. The immunoprecipitates were washed three times with HNTG buffer (20 mM Hepes pH 7.5, 150 mM NaCl, 0.1 % (v/v) Triton X-100 and 10 % w/v glycerol), resuspended in Laemmli buffer and boiled for 5 min prior to Western blot analysis. Proteins were resolved in 8 % SDS-PAGE, electrotransferred to PVDF membranes and detected with the antibody of interest. Primary interaction was evidenced by using ECL Kit (GE Healthcare Life Sciences). When necessary, membranes were stripped and reprobed with the antibody of interest and evidenced with the ABC/HRP complex and 3, 3′diaminobenzidine. The intensity of each band was estimated by optical densitometry with a Gel-Pro Analyzer version 3.1 (Media Cybernetics, USA).

Cell Culture and Fluorescence Microscopy

Primary culture of papillary collecting duct cells was performed by means of Stokes et al.'s procedure [17]. Briefly, renal papillae were minced to 1–2 mm^3 pieces and incubated at 37 °C in sterile TBS containing 0.1% (w/v) collagenase under 95% O_2/5% CO_2 for 40 min. From collagenase digestion, a "crude-pellet", containing most papillary cell types and tubular elements, was obtained by centrifugation at 175 g for 10 min. The pellet was washed twice and resuspended in Dulbecco's modified Eagle's medium (DMEM) with F-12 (1:1), 10% (v/v) fetal bovine serum, 100 U/mL penicillin and 100 μg/mL streptomycin, and an "enriched-papillary collecting duct pellet" was obtained by centrifuging at 60 g for 1 min. Pellets were resuspended in DMEM-F12 and aliquots placed on sterile dry-glass coverslips. After 96 h, the cells grown on coverslips were incubated at 37 °C in TBS containing 1 mM neomycin, 5 mM CD or 10 mM LiCl for 10, 30 min, or 24 h, respectively, and then the cover slips were transferred to cold PBS. For immunofluorescence labeling cells were washed with PBS and fixed with methanol (at −20 °C for 10 min) and acetone (at −20 °C for 4 min), blocked with 3% (v/v) goat normal serum in PBS. After fixation, cells were stained with mouse anti vinculin or mouse anti talin overnight at 4 °C in goat serum containing PBS. Detection of primary antibodies was performed with FITC conjugated F $(a\acute{b})_2$ fragment goat anti-mouse IgG (Jackson Immuno Research) secondary antibody. Finally, cells were washed in PBS and mounted using Vectashield Mounting Media (Vector Lab) and stored at 4 °C until analysis. Specimens were examined with an Olympus FV300 Confocal Microscopy (Model BX61), with an acquisition software FluoView version 3.3 provided by the manufacturer. The confocal images were analyzed using the Image-Pro Plus version 5.1.2 software (Media Cybernetics, USA). All adhesion sites (focal contacts) in 10–15 randomly selected cells were analyzed for generation of quantitative data sets for each treatment, and three independent experiments were performed. Cells were examined with a 100X Plan Apo oil objective (NA 1.4), resulting in a pixel length of 0.1388 μm after performing the spatial calibration. To even out background variations in our immunofluorescence images, we applied a "flatten filter". To select the intensity range of the objects (focal contacts) to be counted, we applied the software command to perform the "segmentation" of the image. The total number of vinculin- and talin- immunostained FC per cell was counted. To do so, the contour of each cell in the confocal image (area of interest) was manually drawn by using the mouse pointer of the program.

Statistics

Results were expressed as mean ± SE. We used the unpaired *t*-test for comparison between DRM and S fractions. Data from control and different treatments were analyzed by ANOVA and significant differences were assessed by "a posteriori" Dunnett Multiple Comparisons test ($P < 0.05$).

Results

Renal Papillary Focal Contact (FC) Complexes are Localized in Specific Detergent-Resistant Membranes

We first evaluated the presence of FC proteins vinculin and talin in 0.1% Triton X-100 resistant (DRM) and soluble (S) fractions. As seen in Fig. 1a, anti-vinculin recognized a 116-kDa band in both fractions. By contrast, anti-talin recognized a 225-kDa band only in the DRM fraction (Fig. 1b). It is considered that PtdIns(4,5)P_2 is an essential lipid for FC stabilization [1, 2]; therefore, we next determined whether vinculin and talin were associated with PtdIns(4,5)P_2 in both DRM and S fractions. Thus, PVDF membranes were stripped and retested with anti PtdIns(4,5)P_2 antibody. Two bands were clearly detected in DRM but not in the S fraction (Fig. 1 C). The highest molecular mass band (~225 kDa) was compatible with PtdIns(4,5)P_2 association with talin, while the second band (molecular mass ~116 kDa) was consistent with PtdIns(4,5)P_2 bound to vinculin. In order to confirm whether vinculin and talin were, in fact, bound to PtdIns(4,5)P_2, we immunoprecipitated DRM and S fractions with anti-PtdIns(4,5)P_2 and then, vinculin and talin were detected by Western blot. In DRM, both vinculin and talin were pulled down by PtdIns(4,5)P_2 antibody, while no bands were evident in immunoprecipitates from the S fraction (Fig. 1d, e). To verify the presence of assembled FC complexes in DRM, talin–vinculin interaction was addressed by performing an immunoprecipitation with anti-vinculin and then, talin was detected by Western blot in the precipitate. As seen in Fig. 1f, a positive band (molecular mass ~225 kDa) was obtained with anti talin, thus reflecting vinculin–talin association. The presence of vinculin bound to PtdIns(4,5)P_2, together with talin–vinculin association in DRM, constitute the biochemical expression of the existence of FC complexes in DRM isolated from rat renal papillae.

Biochemical Characterization of FC-Containing DRMs

Once established that FC complexes were located in DRM, we characterized the DRM lipid composition in

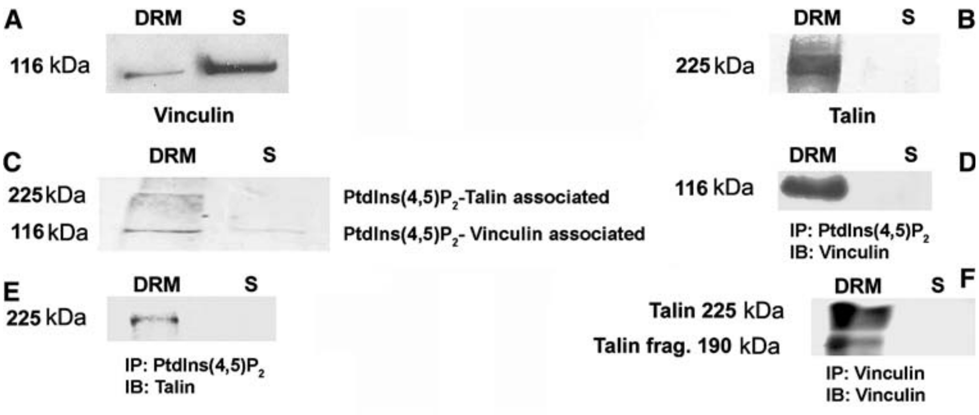

Fig. 1 Biochemical protein-characterization of DRMs from renal papillary cells. DRM and S fractions were obtained from renal papillae as described in "Materials and Methods", and equivalent amounts of protein were resolved by electrophoresis and immunoblotted for vinculin (**a**) and talin (**b**). Representative membranes were stripped and evaluated for PtdIns(4,5)P_2 (**c**). DRM and S were immunoprecipitated (IP) for PtdIns(4,5)P_2 (**d**, **e**), and for vinculin (**f**) and then immunoblotted (IB) with the indicated antibody. Results correspond to a representative experiment of five individual assays

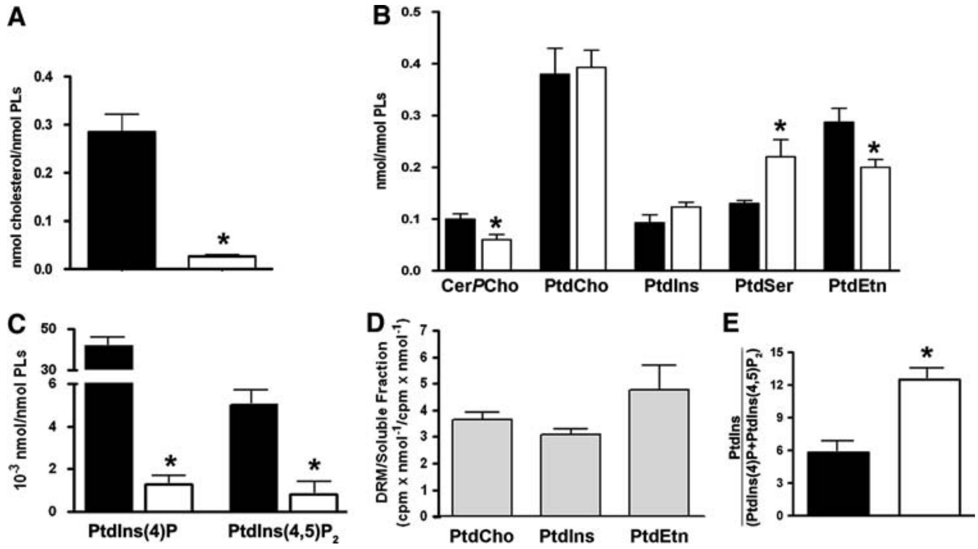

Fig. 2 Lipid characterization of DRM (*black*) and S fractions (*white*). Endogenous content of cholesterol (**a**), individual phospholipids (**b**), and polyphosphoinositides (**c**) was determined on DRM and S aliquots, according to the methodology described for each kind of molecule. **d** [^{32}P]-phospholipids ratio and **e** [^{32}P]-PtdIns and [^{32}P]-PtdIns(4)P$_2$ plus [^{32}P]-PtdIns(4,5)P$_2$ ratio. (Mean ± SE, $n = 5$). *Significantly different from the S fraction, $P < 0.05$. *PLs* phospholipids

comparison with the S fractions. As seen in Fig. 2a, cholesterol concentration was ten times higher in DRM than in S fractions (Fig. 2a). With respect to the phospholipid profile (Fig. 2b), DRM showed a 70% increase in sphingomyelin (CerPCho), accompanied by a 30% increase in phosphatidylethanolamine (PtdEtn) and a 40% decrease in phosphatidylserine (PtdSer) but no differences were found in phosphatidylcholine (PtdCho) and phosphatidylinositol (PtdIns) concentrations. The study of individual phospholipid fatty acid composition revealed that DRM are enriched in arachidonic acid mainly due to PtdEtn, which doubled its content with respect to PtdEtn in S fractions (Table 1). The amount of DRM-polyphosphoinositides, PtdIns(4)P and PtdIns(4,5)P$_2$, was several times higher than in the S fraction, denoting the massive accumulation of these acidic phospholipids in our papillary DRM (Fig. 2c). In order to determine whether or not DRM-associated phospholipids were metabolically active, we evaluated [^{32}P]-Pi incorporation into phospholipids. [^{32}P]-Pi specific activity, expressed as [^{32}P]-Pi per nmol of each phospholipid, was obtained and the DRM/S ratio calculated for each individual phospholipid. As seen in Fig. 2d, [^{32}P]-Pi incorporation was more than three times higher in DRM than in S fraction. It is known that PtdIns(4)P and PtdIns(4,5)P$_2$ are formed by PtdIns phosphorylation by specific kinases. As a reflection of such a dynamic process, we analyzed the ratio between [^{32}P]-PtdIns and [^{32}P]-PtdIns(4)P plus [^{32}P]-PtdIns(4,5)P$_2$ in DRM and S

Table 1 Fatty acid profile of DRM and soluble fraction phospholipids

	CerPCho		PtdCho		PtdIns		PtdSer		PtdEtn	
	DRM (%)	S (%)	DRM (%)	S (%)	DRM (%)	S (%)	DRM (%)	S (%)	DRM (%)	S (%)
14:0	4.6	4.0	1.2	2.0	4.5	5.0	4.2	4.5	1.7	2.8
16:0	37.7	37.4	27.5	33.0	32.9	35.3	28.8	33.4	17.7	21.0
16:1	1.6	1.7		1.3	1.3	1.9	1.4	1.3		2.4
17:0	1.7	1.8	1.5	1.4	1.7	1.6	1.5	1.5	1.1	2.7
18:0	33.8	34.8	21.8	26.0	40.8	38.8	40.3	40.5	30.5	25.8
18:1		1.4	16.6	12.5		2.1	6.1	3.4	5.6	6.4
18:2			10.9	8.1			1.9	1.1	3.6	1.9
18:3										2.6
20:0	1.7	1.8	0.9	0.9			1.0			2.9
20:2		0.8	0.4							
20:4			14.7	11.3		0.7	6.2	4.1	33.1	16.0
22:0	4.5	4.1	0.7	0.9	7.9	4.9	1.6	2.3	1.0	2.2
22:1		0.5			2.1	2.3				
23:0	1.0	0.8								
24:0	4.6	3.4							2.1	
26:0										3.5

Phospholipids present in both DRM and soluble fraction were isolated and specific fatty acid profile was determined for each phospholipid as described in "Materials and Methods". The table shows the results of one representative experiment ($n = 3$)

fractions. As seen in Fig. 2e, the DRM ratio was around half of the S fraction ratio, reflecting that polyphosphoinositide synthesis in DRM is twice higher than in the S fraction.

Altogether, these results demonstrate that FC complexes are located in cholesterol-CerPCho-polyphosphoinositide-enriched membrane domains, which show an exceptionally high phospholipid biosynthesis with respect to the S fraction (Fig. 2d). The high polyunsaturated PtdEtn content, plus the enrichment in polyphosphoinositides, suggests that such DRM correspond to the inner leaflet of the plasma membrane, which is consistent with the fact that FC are the cytoplasmic face of the cell contact site [18].

Effect of Membrane-Affecting Agents in DRM Compositions

Methyl-β-cyclodextrin (CD), a known cholesterol-depleting agent, decreased cholesterol content by 35%, and also induced an overall change in phospholipid profile (Fig. 3a). The most significant change was the great augmentation in CerPCho and PtdIns, counterbalanced by the decrease in PtdCho and PtdEtn content, while PtdIns(4)P and PtdIns(4,5)P_2 did not significantly change.

Neomycin, a known PtdIns(4,5)P_2 sequestering agent [19, 20], provoked an unexpected 60% loss in cholesterol concentration, which was accompanied by a slight decrease in CerPCho and PtdSer, and an increase in PtdEtn content. Neomycin also increased PtdIns(4,5)P_2 by 65% while PtdIns(4)P concentration fell about 10% (Fig. 3b).

The treatment with LiCl, which blocks phosphoinositides synthesis [21], evoked an increase in cholesterol and CerPCho content by 35 and 25%, respectively, accompanied by a decrease in PtdCho, an important PtdIns and PtdSer enrichment. No changes in PtdEtn content were observed. Both PtdIns(4)P and PtdIns(4,5)P_2 contents were diminished, accounting for a 50 and 25% decrease, respectively (Fig. 3c).

These results show that instead of evoking an effect on a single membrane lipid, each membrane-affecting agent appears to induce an unexpected overall change in the DRM-lipid profile, thus bringing about a DRM of different lipid composition.

Influence of Changes in DRM Lipid Composition on FC Maintenance

In order to obtain a morphological correlation of the biochemical findings, we performed primary cultures of collecting duct cells and studied the FC by immunofluorescence microscopy. As shown in Fig. 4a, vinculin-stained FC appeared as bright and elongated structures (arrowheads). Vinculin immunoreactivity was also observed diffusively distributed in the cytoplasm. By contrast, talin immmunoreactivity was exclusively found in

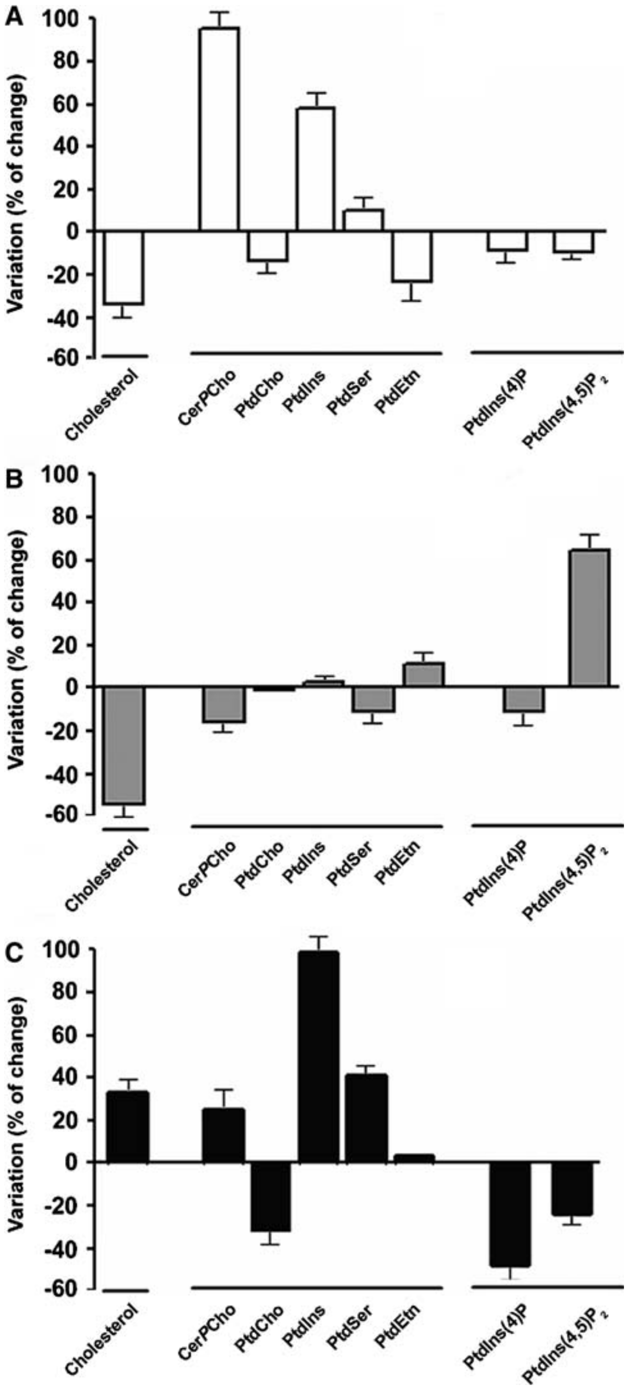

Fig. 3 Changes in lipid composition of DRMs after treatment with membrane-affecting agents. Renal papillary slices were treated with **a** 5 mM CD, **b** 1 mM Neomycin, or **c** 10 mM LiCl, and DRMs were isolated. Variation of cholesterol, individual phospholipids, and polyphosphoinositides is expressed as percentage of control (Mean ± SE, $n = 5$)

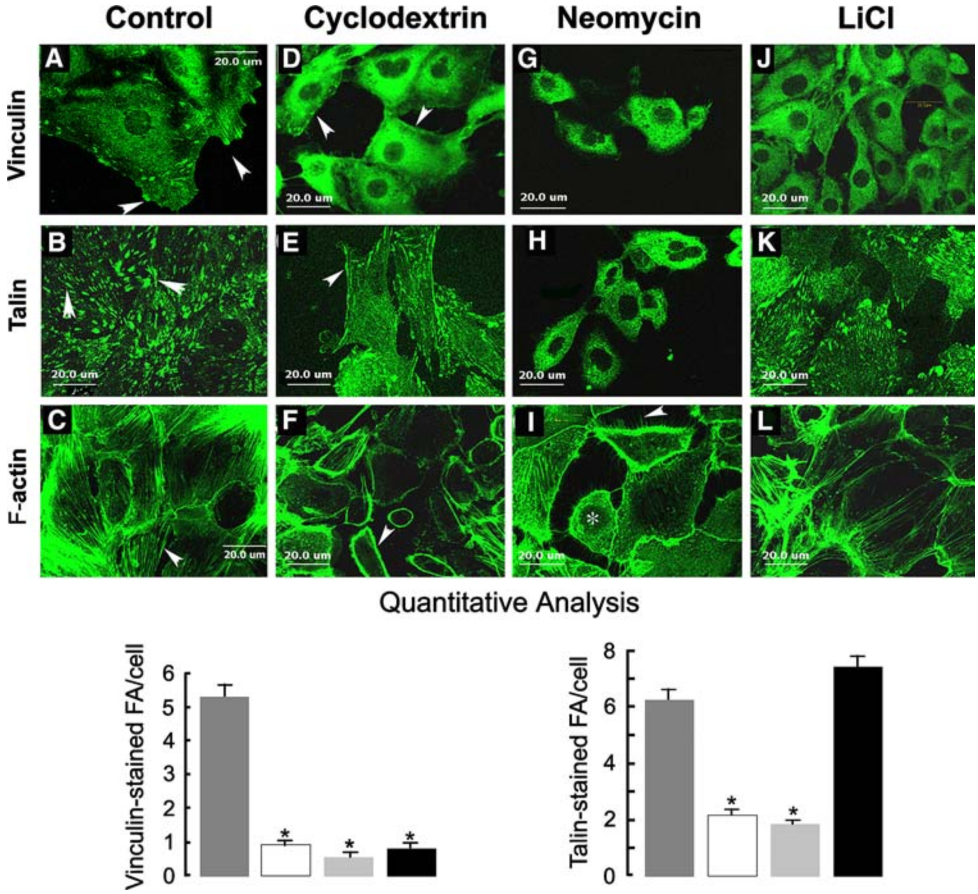

Fig. 4 Effect of changes in DRM lipid composition on FC plaques. Cultured collecting duct cells were treated with 5 mM CD, 1 mM Neo, or 10 mM LiCl. After fixation, cells were immunostained with antibodies against vinculin (**a**, **d**, **g**, **j**) and talin (**b**, **e**, **b**, **k**), and with FITC-phalloidin (**c**, **f**, **i**, **l**). Primary monoclonal interactions were evidenced by using goat anti-mouse IgG–FITC secondary antibody and analyzed with confocal microscopy. Representative images of three independent experiments are shown. *Scale bar* 20 μm. Quantization of the number of vinculin-stained, and talin-stained FC per cell were calculated by the image analysis program, and performed as described in "Materials and Methods". *Bar graphs* results are expressed as mean ± SE. *Significantly different from control, $P < 0.01$

FC, appearing as abundant bright plaques morphologically heterogeneous (Fig. 4b, arrowheads).

Treatment of cultured cells with CD caused dissipation of vinculin-stained FC (Fig. 4 and quantitative analysis). Immunoreactivity increased in discrete zones of the plasma membrane (arrowhead) and was also accumulated in the perinuclear zone (Fig. 4d). Talin-stained FC were also affected by CD and an unusual accumulation in specific zones of the plasma membrane was also observed (Fig. 4e, arrowhead and quantitative analysis). Taken together, these results demonstrate that although a fraction of vinculin and talin remained in the plasma membrane, the assembly of these proteins in FC was almost completely impaired by CD. Consistent with the dissipation of FC, CD induced almost complete disappearance of stress fibers. F-actin appeared as a cortical network in rounded cells (Fig. 4f, arrowhead), typical of isolated–detached cells but not of cells that constitute organized epithelial tissues.

As seen in Fig. 4g and quantitative analysis, the specific PtdIns(4,5)P_2 sequestering agent neomycin induced almost complete loss of both vinculin- and talin-stained FC. Both proteins appeared densely accumulated in the cytosol with a punctuate appearance neighboring the nucleus (Fig. 4g, h). Consistent with the dissipation of FC, stress fibers almost disappeared and arrangements of peripherical actin-based structures were evident (Fig. 4i, arrowhead). Phalloidin-stained images also allowed us to visualize cells that were in the process of retraction (Fig. 4i, asterisk).

The treatment of culture cells with LiCl induced a decrease in the number of vinculin-stained FC per cell (Fig. 4j and quantitative analysis). By contrast, neither the quantity of talin-stained FC nor F-actin distribution in cultured cells was affected (Fig. 4k, l, and quantitative analysis). The preservation of actin organization in stress fibers explains the maintenance of cellular morphology observed after LiCl treatment (Fig. 4l).

Discussion

In the present report, we biochemically studied FC complexes obtained from rat renal papillae and then defined their morphological correlation in papillary collecting duct cells primary cultures. By using a two-step centrifugation procedure and changing sucrose concentration, we were able to demonstrate that FC complexes are part of a detergent resistant membrane fraction, highly enriched in cholesterol and phosphoinositides and whose phospholipid constituents are subjected to a very high turn-over.

FC has been previously associated with detergent resistant domains and also with local membrane accumulation of PtdIns(4,5)P_2 [22] and it has been recently shown that they can regulate membrane order [23], thus supporting the notion that actin-containing cytoskeleton can promote lateral segregation of cholesterol–sphingomyelin enriched detergent resistant domains [24]. However, a direct demonstration of the existence of such resistant domains and their biochemical characterization has not been reported before. Here, we were able to detect the FC complex in a Triton X-100 resistant lipid domain and we propose that the lipid composition of such DRM corresponds to the physiological environment where FC are inserted.

For the isolation of DRM we used a low Triton X-100 concentration (0.1%). It has been demonstrated in stomach smooth muscle that at such a detergent and similar sucrose concentration most of vinculin was efficiently solubilized while sphingomyelin remained insoluble [24]. Consistent with this observation, we also found the bulk of vinculin in the soluble fraction, but this fraction of vinculin did not correspond to the FC-vinculin since it did not interact with PtdIns(4,5)P_2 nor with talin. Moreover, talin, which is immediately degraded by calpain if it is not assembled into FC, was only found in the detergent resistant domain. Since vinculin, besides being part of FC, can also form adherent junctions, it is possible that the bulk of the solubilized vinculin corresponds to vinculin present in adherent junctions, as suggested previously [23].

FC cannot be detected in histological preparations from intact tissue, but they can be observed in cultured cells. Therefore, we took advantage of the fact that cultured papillary collecting duct cells preserve their tendency to interact with their self-formed ECM, mimicking their behavior in intact tissue. Therefore, we established a parallelism between the biochemical data obtained from papillary microsomes and the morphological observations from immunofluorescence microscopy performed in primary cultures of collecting duct cells. By using such experimental strategy, we demonstrated that membrane lipid composition affects the in vivo preservation of FC as clearly shown by the immunofluorescence images. At first, we showed that the various membrane-affecting agents differently affect FC, depending on their capacity to change the membrane lipid composition. Consistent with previous observations in smooth muscle cells [24], the treatment with CD did not lead to DRM elimination. Instead, CD induced cholesterol decrease but also membrane lipid redistribution, which resulted in a net increase of the CerPCho content in DRM. It has been reported that DRM serves as a platform for PtdIns(4,5)P_2 accumulation induced by FC proteins [22], and that such PtdIns(4,5)P_2 accumulation serves to stabilize the assembled FC [6]. However, here we show that, although polyphosphoinositides were still accumulated in CD-treated DRMs, FC did not persist assembled as seen in the immunofluorescence images. Based on these observations, we can suggest that polyphosphoinositide accumulation in DRM is not sufficient to stabilize FC; but polyphosphoinositides must be included in a DRM with a specific lipid composition in order to guarantee an efficient FC stabilization.

The effect of neomycin on cytoskeleton organization has currently been attributed to a failure in the PtdIns(4,5)P_2 availability to bind cytoskeletal proteins but the membrane lipid composition was not studied [22]. The present results clearly show that apart from its well known action as PtdIns(4,5)P_2 sequestering-agent, neomycin simultaneously evokes a dramatic decrease in the DRM cholesterol content. Therefore, we suggest that the deleterious effect of neomycin on FC can be due not only to the loss of PtdIns(4,5)P_2 availability but also to a decrease in cholesterol content, which with no doubt changes the physico-chemical properties of the new formed DRM.

It has been previously shown that LiCl dissipates FC in neural cells [22]. However, here we show that the inhibition of polyphosphoinositide synthesis by LiCl induces a restructuration rather than a dissipation of FC. It is known that FC are hierarchical structures where additional FC proteins assemble as they mature. Talin is the first protein that forms FC, while vinculin is added thereafter [25]. Thus, even without vinculin, talin-containing FC can still be present, thus conforming the minimal FC assembling. Thus, the apparent controversy with the previous observations [22] resides in the fact that the authors studied only vinculin-stained but not talin-stained FC. It is known that vinculin has to be bound to PtdIns(4,5)P_2 to stay in FC plaques [26]. The selective dissipation of vinculin from assembled FC can be explained considering their different affinities for membrane lipids. Thus, vinculin binding to PtdIns(4,5)P_2 is of low affinity, while binding to PtdIns is of high affinity but does not serve to assemble vinculin into FC [27]. Thus, the lowering in PtdIns(4,5)P_2 content, together with the high increase in PtdIns produced by LiCl, may account for the dissipation of vinculin from FC. By contrast, talin has high affinity to bind PtdIns(4)P [27], thus the decreased concentration of DRM–PtdIns(4)P, could be still enough to bind talin. On the other hand, it appears that the new DRM conformation, where cholesterol and CerPCho increased their concentration, could result favorable to stabilize talin-containing FC. Moreover, it has been reported that LiCl affects 20:4n-6 turnover by altering the expression of $cPLA_2$ [28]; however, whether or not such effect is also involved in the dissipation of vinculin-containing FC needs further demonstration.

Investigations on the interaction of the cytoskeleton components with artificial membranes, and in more detail with membrane lipids were started in the 1980s [29]. However, no direct evidence on the effect of changes in the membrane lipid composition in biological membranes on FC structures exists. It is currently considered that PtdIns(4,5)P_2 is the membrane phospholipid that plays the crucial role in the maintenance of assembled FC. However, our results demonstrated that such pool of polyphosphoinositides has to be part of a domain of specific lipid composition to serve as a membrane lipid stabilizing FC plaques. Among membrane lipids, and taking in consideration that the decrease in cholesterol was a common feature in the deleterious effect of CD and Neo, we suggest that the enrichment in cholesterol is in fact the crucial lipid for evoking the lipid environment to maintain the FC plaques assembled.

We used the various membrane affecting agents only as a tool to study the influence of membrane lipid composition on FC maintenance. However, it is of interest to point out that both neomycin and LiCl are pharmacological agents of known nephrotoxic effects. In this context, our results could be also pharmacologically relevant. Indeed, neomycin is an aminoglycoside antibiotic known to cause tubular necrosis [30, 31]. Thus, the disruption of the cell-extracellular matrix adhesion demonstrated by the present data could be an explanation for the deleterious effect caused by neomycin treatments since it is known that epithelial cells have to be bound to the extracellular matrix in order to survive and not die by anoikis. On the other hand, LiCl is used for the treatment of some human mental diseases [32, 33] and it is known that long-term treatment with this agent provokes alterations in the renal capacity for concentrating urine [34]. Although the pharmacological dose is lower (0.8–1 mM) than the concentration that we used, chronic low doses could also affect FC. The impairment of vinculin-contained FC reported here could be a primary cause that progressively affects cell-ECM adhesion, thus affecting renal function. Moreover, the alteration in membrane lipid composition, mostly cholesterol enrichment, could disturb the location or the function of membrane transporter systems involved in normal renal tubular physiology, thus affecting the urine concentration process.

In conclusion, in this work we show evidence about the importance of the lipid composition of the specific membrane lipid domain, where FC are included, and suggest that it could be relevant for the maintenance of the structures that tether the collecting duct epithelial cells to the extracellular matrix.

Acknowledgments We thank Mr. Roberto Fernández for confocal microscope technical assistance.

References

1. Zamir E, Geiger B (2001) Molecular complexity and dynamics of cell-matrix adhesions. J Cell Sci 114:3583–3590
2. Critchley DR (2000) Focal adhesions: the cytoskeletal connection. Curr Opin Cell Biol 12:133–139
3. Jockusch BM, Bubeck P, Giehl K, Kroemker M, Moschner J, Rothkegel M, Rüdiger M, Schlüter K, Stanke G, Winkler J (1995) The molecular architecture of focal adhesions. Annu Rev Cell Dev Biol 11:379–416
4. Petit V, Thiery J-P (2000) Focal adhesion structure and dynamics. Biol Cell 92:477–494
5. Wozniak MA, Modzelewska L, Kwong L, Kelly PJ (2004) Focal adhesion regulation of cell behavior. Biochim Biophys Acta 1692:103–119
6. Chandrasekar I, Stradal T, Holt MR, Entschladen F, Jockusch BM, Ziegler WH (2005) Vinculin acts as a sensor in lipid regulation of adhesion-site turnover. J Cell Sci 118:1461–1472
7. Sechi AS, Wehland J, Horwitz AF (2000) The actin cytoskeleton and plasma membrane connection: PtdIns(4,5)P_2 influences cytoskeletal protein activity at the plasma membrane. J Cell Sci 113:3685–3695
8. Martel V, Racaud-Sultan C, Dupe S, Marie C, Paulhe F, Galmiche A, Block MR, Albiges-Rizo C (2001) Conformation, localization, and integrin binding of talin depend on its interaction with phosphoinositides. J Biol Chem 276:21217–21227
9. Isenberg G, Niggli V (1998) Interaction of cytoskeletal proteins with membrane lipids. Int Rev Cytol 178:73–122
10. Simons K, Ikonen E (1997) Functional rafts in cell membranes. Nature 387:569–572
11. Ito J, Nagayasu Y, Yokoyama S (2000) Cholesterol-sphingomyelin interaction in membrane and apolipoprotein-mediated cellular cholesterol efflux. J Lipid Res 41:894–904
12. Bligh EG, Dyer WJ (1959) A rapid method of total lipid extraction and purification. Can J Biochem Phys 37:911–917
13. Sterin-Speziale NB, Kahane VL, Setton CP, Fernández MC, Speziale EH (1992) Compartmental study of rat renal phospholipid metabolism. Lipids 27:10–14
14. Catz SD, Sterin-Speziale NB (1996) Bradykinin stimulates phosphoinositide turnover and phospholipase C but do not phospholipase D and NADPH oxidase in human neutrophils. J Leukoc Biol 59:591–597
15. Richmond W (1973) Preparation and properties of a cholesterol oxidase from *Nocardia* sp. and its application to the enzymatic assay of total cholesterol in serum. Clin Chem 19:1350–1356
16. Barlett GR (1959) Phosphorus assay in column chromatography. J Biol Chem 234:466–468
17. Stokes JB, Grupp C, Kinne RKH (1987) Purification of rat papillary collecting duct cells: functional and metabolic assessment. Am J Physiol 253:F251–F262
18. Pokutta S, Weis WI (2002) The cytoplasmic face of cell contact sites. Curr Opin Struct Biol 12:255–262
19. Gabev E, Kasianowicz J, Abbott T, McLaughlin S (1989) Binding of neomycin to phosphatidylinositol 4,5-bisphosphate (PIP2). Biochim Biophys Acta 979:105–112
20. Rebecchi M, Peterson A, McLaughlin S (1992) Phosphoinositide-specific phospholipase C-delta 1 binds with high affinity to phospholipid vesicles containing phosphatidylinositol 4,5-bisphosphate. Biochem 31:12742–12747
21. Batty IH, Downes CP (1994) The inhibition of phosphoinositide synthesis and muscarinic-receptor-mediated phospholipase C activity by Li^+ as secondary, selective, consequences of inositol depletion in 1321N1 cells. Biochem J 297:529–537
22. Laux T, Fukami K, Thelen M, Golub T, Frey D, Caroni P (2000) GAP43, MARCKS, and CAP23 modulates PI(4,5)2 at

plasmalemmal rafts, and regulate cell cortex actin dynamics through a common mechanism. J Cell Biol 149:1455–1471

23. Gaus K, Lay SL, Balasubramanian N, Schwatz MA (2006) Integrin-mediated adhesion regulates membrane order. J Cell Biol 174:728–734
24. Babiychuk EB, Draeger A (2006) Biochemical characterization of detergent-resistant membranes: a systematic approach. Biochem J 397:407–416
25. Zaidel-Bar R, Cohen M, Addadi L, Geiger B (2004) Hierarchical assembly of cell-matrix adhesion complexes. Biochem Soc Trans 32:416–420
26. Gilmore AP, Burridge K (1996) Regulation of vinculin binding to talin and actin by phosphatidyl-inositol-4–5-bisphosphate. Nature 381:531–535
27. Di Paolo G, Pellegrini L, Letinic K, Cestra G, Zoncu R, Voronov S, Chang S, Guo J, Wenk MR, De Camilli P (2002) Recruitment and regulation of phosphatidylinositol phosphate kinase type 1γ by the FERM domain of talin. Nature 420:85–93
28. Rosenberger TA, Villacreses NE, Contreras MA, Bonventre JV, Rapoport SI (2003) Brain lipid metabolism in the cPLA2 knockout mouse. J Lipid Res 44:109–117
29. Niggli V, Burner MM (1987) Interaction of the cytoskeleton with the plasma membrane. J Membr Biol 100:97–121
30. Clark CH (1977) Toxicity of aminoglycoside antibiotics. Mod Vet Pract 58:594–598
31. Nagai J, Takano M (2004) Molecular aspects of renal handling of aminoglycosides and strategies for preventing the nephrotoxicity. Drug Metab Pharmacokinet 19(3):159–170
32. Atack JR (2000) Lithium, phosphatidylinositol signaling and bipolar disorder: the role of inositol monophosphatase. In: Manji HK, Bowden CL, Belmaker RH (eds) Bipolar medications mechanisms of action. American Psychiatric Press, Washington, pp 1–30
33. Kim H, McGrath BM, Silverstone PH (2005) A review of the possible relevance of inositol and the phosphatidylinositol second messenger system (PI-cycle) to psychiatric disorders-focus on magnetic resonance spectroscopy studies. Human Psychopharmacol 20(5):309–326
34. Markowitz GS, Radhakrishnan J, Kambham N, Valeri AM, Hines WH, D'Agati VD (2000) Lithium nephrotoxicity: a progressive combined glomerular and tubulo-interstitial nephropathy. J Am Soc Nephrol 11(8):1439–1448

Lipids (2008) 43:353–360
DOI 10.1007/s11745-008-3159-4

ORIGINAL ARTICLE

Delayed Metabolism of Postprandial Triglyceride-Rich Lipoproteins in Subjects with Echolucent Carotid Plaques

Ann-Trude With Notø · Ellisiv Bøgeberg Mathiesen · Jan Brox · Johan Björkegren · John-Bjarne Hansen

Received: 17 October 2007 / Accepted: 28 January 2008 / Published online: 5 March 2008
© AOCS 2008

Abstract Subjects with echolucent carotid plaques have an increased risk of ischemic cerebrovascular events independent of degree of stenosis. Low plasma lipoprotein lipase (LPL) activity promotes a proatherogenic lipid profile, and delayed chylomicron clearance is a risk factor for atherosclerosis. This study was conducted to determine plasma LPL activity and postprandial metabolism of triglycerides in relation to carotid plaque morphology. Plaque echogenicity was assessed by B-mode ultrasound and analysis of the grey scale median (GSM). Echolucent plaques were defined as GSM ≤ 63 (the median) and echogenic plaques as GSM > 63, and 57 subjects with carotid plaques and 38 subjects without carotid plaques were recruited. Blood samples were collected before and at 2-h interval for 8 h after a standard high fat meal. LPL activity and mass was determined before and after heparin administration. Postheparin LPL activity was decreased in subjects with echolucent plaques compared to subjects with echogenic plaques ($P = 0.06$) and to controls ($P = 0.04$). Plaque echogenicity increased linearly with increasing levels of postheparin LPL activity ($P = 0.02$) and mass ($P = 0.03$). Subjects with echolucent plaques had delayed postprandial clearance of chylomicron triglycerides compared to controls ($P = 0.04$). Low postheparin LPL activity due to attenuated mobilization of LPL from capillary endothelium may play an important role in the formation of echolucent plaques by modulation of postprandial lipids and subsequent fat accumulation in the arterial wall.

Keywords Lipoprotein lipase · Chylomicrons · Lipoprotein metabolism · Triglyceride metabolism · Atherosclerosis

Introduction

Postprandial lipemia is a physiological phenomenon occurring several times a day. Elevated postprandial levels of triglyceride-rich lipoproteins (TRLs) have been associated with both coronary [1] and carotid [2] artery atherosclerosis. Zilversmit [3] proposed that atherosclerosis, at least in part, is a postprandial disease, and hypothesized that accumulation of triglyceride-rich dietary lipoproteins promoted formation of atherosclerosis, due to reduced clearance and thereby prolonged exposure of the vascular wall to TRL. More recent studies provide new perspective to this hypothesis by reporting a particular efficient penetration and selective retention of chylomicron remnants in sites of lesion formation [4]. The "response to retention" hypothesis of atherosclerosis suggests that intimal deposition is proportional to the concentration of circulating plasma lipoproteins [5].

A.-T. W. Notø · J.-B. Hansen (✉)
Center for Atherothrombotic Research in Tromsø (CART),
Institute of Clinical Medicine, University of Tromsø,
9037 Tromsø, Norway
e-mail: john.bjarne.hansen@unn.no

A.-T. W. Notø
e-mail: anntrude@fagmed.uit.no

E. B. Mathiesen
Department of Neurology, Institute of Clinical Medicine,
Tromsø, Norway

J. Brox
Department of Clinical Chemistry, University of Tromsø,
Tromsø, Norway

J. Björkegren
The Atherosclerosis Research Unit,
King Gustaf V Research Institute, Karolinska Institutet,
Stockholm, Sweden

Triglycerides in the core of TRL in circulating blood are hydrolyzed by the action of endothelial cell-bound lipoprotein lipase (LPL) representing the principal enzyme that removes triglycerides from the bloodstream [6]. The functional pool of LPL is anchored to heparin sulphate proteoglycans (HSPGs) at the surface of vascular endothelium, and only low levels are found in the circulation [6]. Unfractionated heparin has higher affinity for LPL than heparin sulphate, and heparin infusion will therefore displace LPL from the endothelial surface into circulating blood [7]. The amount of LPL released after a bolus dose of heparin is used as a measure of functional LPL and assumed to reflect the LPL availability at the endothelial surface [8]. A deficiency of LPL is associated with increased plasma levels of chylomicrons, suggesting that triglyceride hydrolysis is important for the clearance of these particles [9]. Furthermore, LPL has also been shown to enhance the uptake of remnant lipoproteins by the liver [10].

The carotid arteries are readily accessible to ultrasound imaging and evaluation of atherosclerotic plaque morphology. Plaques that appear echolucent are lipid-rich, covered by a thinner fibrous cap, whereas echogenic plaques have higher content of fibrous tissue and calcification [11]. Studies have shown that echolucent carotid plaques are associated with high risk for ischemic cerebrovascular events (CVE) independent of the degree of stenosis [12]. The purpose of the present study was to investigate whether plaque echolucency was associated with lowered plasma LPL activity, elevated postprandial triglycerides, and delayed clearance of postprandial TRL in subclinical carotid stenosis.

Materials and Methods

Study Participants

The study was performed at the Clinical Research Centre at the University Hospital of North Norway in Tromsø.

The participants were recruited from a population health study (the fifth survey of The Tromsø Study in 2001), which included ultrasound examination of the carotid arteries. Subjects were eligible for the plaque group if they were aged 56–80 years and had one plaque or more in the carotid bifurcation or internal carotid artery at the screening with a plaque thickness of $\geq$2.5 mm and plaque morphology classified as echolucent (grade 1) or echogenic (grade 4) according to the Gray–Weale criteria [13]. Subjects in the same age groups without plaques in their carotid arteries were used as controls. Exclusion criteria included the following conditions: regular use of lipid-lowering drugs or oral anticoagulants, cancer or other serious life-threatening medical conditions, hypothyroidism, renal, hepatic, or psychiatric disease, and current abuse of alcohol or drugs. Coronary artery disease (CAD) was defined as prior or present angina pectoris, myocardial infarction and peripheral vascular disease. Cerebrovascular event (CVE) was defined as transient ischemic attacks, stroke and amaurosis fugax. The study included 57 subjects with and 38 subjects without carotid plaques. Informed written consent was obtained from the participants, and the regional ethical committee approved the study.

Ultrasound Examination

The ultrasound examination was performed as described previously [14, 15]. Plaque morphology in terms of echogenicity was assessed by analysis of grey scale content of the plaques and calculation of grey scale median (GSM). Assessment of plaque morphology was made in all plaques present in the near and far walls of the common carotid, the bifurcation, and the internal carotid arteries on both sides (12 locations). All examinations and measurements of all plaques were recorded on videotapes. Stored B-mode images were subsequently transferred to a personal computer and digitized into frames of 768 × 576 pixels of 256 grey levels each (0 = black and 256 = white) with the use of a commercially available video grabber card (meteor II/Matrox Intellicam). Measurements of plaque area were made with the use of the Adobe Photoshop image-processing program (version 7.0.1), by tracing around the perimeter of each plaque with a cursor. The grey-level distribution and grey-scale median (GSM) of each plaque was calculated. Normalization of GSM was performed according to the method by El-Barghouty [16]. A fixed area of the lumen of the carotid artery (300 pixels), the brightest area of the innermost adventitia adjacent to the plaque (150 pixels), and the plaque were marked. The plaque image was normalized by adjusting linearly their grey tonal range so that the lumen were assigned a GSM of 1 and the adventitia 200 [17]. After standardization, the GSM of the plaques were re-calculated. In subjects with more than one plaque, the standardized GSM of the total plaque area was estimated as a weighted mean of the GSM value of each single plaque.

The area of each plaque was divided by the total area of plaques in each subject, and this fraction was multiplied with each plaques normalized GSM value. All scores were added to calculate the total normalized GSM score for each subject. Echolucent plaques were defined as GSM at or below the median ($\leq$63) and echogenic plaques as plaques with a GSM above the median (>63).

Fat Tolerance Test

A fat-tolerance test was conducted using a test meal prepared from standard porridge cream containing 70% of calories from fat of which 66% saturated fat, 32% monounsaturated fat and 2% polyunsaturated fat. A weight-adjusted meal (1 g fat/kg body weight) was served at 8:00 a.m. and consumed within 15 min. Blood samples for isolation of chylomicrons (CM), and serum- and plasma preparations were collected before the meal and every second hour during the next 8 h.

Isolation of Chylomicrons and Measurements of Serum Lipids and Apolipoproteins

Chylomicrons were isolated by over-layering 8 ml EDTA plasma with 5 ml of NaCl solution (density 1.006 kg/l NaCl solution with 0.02% sodium azide and 0.01% EDTA) in a cellulose nitrate tube (Beckman Instruments Inc, CA, USA) and centrifuged in a Beckman SW40 Ti swinging bucket rotor at 20.000 rpm for 1 h at 4 °C. The CM, with Svedberg flotation (Sf) rates > 400, were carefully removed by aspiration from the top of the tube, divided into three aliquots in cryovials, flushed with nitrogen, and frozen at −70 °C until further analysis.

Serum lipids were analysed on a Cobas Mira S (Roche Diagnostics, F. Hoffmann-La Roche Ltd, Basel, Switzerland) with reagents from ABX Diagnostics (Montpellier, France). Total cholesterol (CHOD-PAP) and triglycerides (GPO-PAP) were measured with enzymatic colorimetric methods. Low-density lipoprotein (LDL) and high-density lipoprotein cholesterol were measured by selective inhibition colorimetric assays (LDL cholesterol direct and HDL cholesterol direct, respectively, ABX Diagnostics). Serum apolipoprotein AI (apo-AI) and apolipoprotein B (apo-B) were analysed by turbidimetry on Cobas Mira S with reagents from ABX Diagnostics, whereas apolipoproteins CII and CIII were analysed by turbidimetry with reagents from Kamyia Biomed Comp (Seattle, WA, USA). Serum apolipoprotein E (apoE) was measured by an enzyme-linked immunosorbent assay, Apo-Tek ApoE^{TM} (PerImmune Inc., Rockville, MD, USA) and genotyping of apoE was performed according to Hixson and Vernier [18] with slight modifications.

Lipoprotein Lipase Measurements

Eight hours after ingestion of the test meal, blood was drawn into vacutainers (Becton Dickinson) containing heparin as anticoagulant and the heparinized blood was immediately placed on ice. Unfractionated heparin was given as a bolus injection (100 IU/kg body weight) on the contra-lateral arm to mobilize LPL from the endothelial surface into the circulation. A second blood sample was obtained exactly 15 min after heparin administration and immediately placed on ice. Heparinized plasma was recovered within 30 min by centrifugation ($2{,}000 \times g$ for 10 min) at 4 °C, divided into aliquots of 1.0 ml in cryovials, flushed with nitrogen, and frozen at −70 °C until further analysis. LPL activity was determined as described by Olivecrona et al. [7]. In short, sonicated emulsion of ^{3}H-oleic acid-labelled triolein in 20% Intralipid (Fresenius Kabi) was used as substrate. Samples were preincubated for 2 h on ice with 0.5 vol goat antibodies to hepatic lipase (HL) to suppress HL activity. LPL activity is expressed in mU/ml corresponding to nanomole of fatty acids released per millilitre per minute. The samples were quantitated in triplicate, and postheparin plasma from pooled normal control persons were used to correct for inter-assay variation. LPL mass was measured in heparin plasma with a commercial ELISA kit (MARKIT-M LPL ELISA, Dainippon Sumitomo Pharma Co., Ltd., Osaka, Japan) according to the instructions made by the manufacturer.

Statistics

Subjects with carotid plaques were divided in two groups, the echogenic group, defined as GSM > 63 ($n = 28$) and the echolucent group, defined as GSM ≤ 63 ($n = 29$). The extent of postprandial triglyceridemia was assessed by the total area under the curve (AUC) and incremental area under the curve (AUCi) for plasma triglycerides and plasma chylomicron triglycerides, and by the triglyceride response (TGR), defined as the average of the two highest postprandial triglyceride concentrations minus baseline concentrations. Continuous variables are presented as mean [95% confidence interval (CI)], and categorical data as proportions (n). Serum triglycerides, LPL activity, apolipoprotein CII and CIII were not normally distributed and therefore logarithmically transformed. Differences in continuous and categorical variables between groups were analyzed by ANOVA and the χ^2 test, respectively. When indicated by a F value below 0.05, a post hoc test using the Bonferroni method was performed to identify significant group differences. Linear trends were tested by multiple regression analysis. Differences between groups in total and chylomicron triglycerides over time were analyzed by general linear models (GLM). All analyses were performed using SPSS (SPSS Inc. Chicago, Illinois, USA) for windows software, version 14.0.

Results

Characteristics of the study participants, including carotid plaque characteristic, are shown in Table 1. There were no

Table 1 Baseline characteristics of the study participants with echolucent and echogenic carotid plaques and subjects without carotid plaques (controls)

	Echolucent (n = 29)	Echogenic (n = 28)	Controls (n = 38)	P values
Male (%)	55 (16)	54 (15)	50 (19)	0.9
Age (years)	68.7 (66.2–71.2)	70.2 (68.0–72.5)	68.0 (66.0–70.0)	0.3
Currently smoking (%)	18 (5)	29 (8)	24 (9)	0.6
Body mass index (kg/m^2)	25.5 (24.1–26.9)	26.4 (24.8–28.0)	27.4 (25.8–27.3)	0.1
Systolic blood pressure (mmHg)	127 (120–135)	131 (123–139)	129 (124–135)	0.7
Diastolic blood pressure (mmHg)	74 (68–78)	75 (71–78)	75 (72–78)	0.9
CVE (%)	0	4 (1)	5 (2)	0.5
CAD (%)	14 (4)	18 (5)	13 (5)	0.9
Diabetes (%)	3 (1)	7 (2)	0	0.3
Hypertension (%)	21 (6)	32 (9)	29 (11)	0.6
β-blockers (%)	17 (5)	11 (3)	13 (5)	0.8
Platelet inhibitors (%)	10 (3)	25 (7)	13 (5)	0.3
Degree of stenosis (%)	39(33–45)	37(32–42)		0.6
Number of plaques	2.1(1.5–2.6)	2.3(1.7–2.9)		0.6
Total plaque area (mm^2)	6.3 (3.1–9.1)	5.1 (3.3–6.8)		0.4
Grey scale median (pixels)	40.4 (36.2–44.7)	88.6 (81.7–95.6)		<0.001

Values are means (95% CI) or percentages (n)

significant differences between groups with regard to traditional risk factors. None of the participants had experienced TIA, one had experienced amaurosis fugax and two had experienced stroke. There were no differences in regular use of drugs or presence of CAD between groups. The median GSM value was 63.0 pixels (range 19.0–137.0) (Table 1). Except for GSM, no differences in plaque characteristics were observed between the echolucent and echogenic plaque groups.

Fasting lipid and apolipoprotein levels are shown in Table 2. Subjects with echolucent plaques had lower HDL cholesterol levels than subjects with echogenic plaques and controls. To further investigate the relation between plaque echogenicity and HDL cholesterol linear regression analysis was performed. HDL cholesterol increased linearly across tertiles (T) of GSM (HDL T1 = 1.28 mmol/l (0.92–1.79), HDL T2 = 1.59 mmol/l (1.35–1.87), HDL T3 = 1.79 mmol/l (1.53–2.03), P for trend = 0.04). The ratio between total and HDL cholesterol was significantly higher in subjects with echolucent plaques compared to controls. In addition, subjects with echolucent plaques had lower apo-AI levels, and the ratio between apo-B and apo-AI was significantly higher in subjects with carotid plaques than the control group (Table 2). The apo-CII/apo-CIII

Table 2 Fasting lipid and apolipoprotein levels in subjects with echolucent and echogenic carotid plaques, and in subjects without carotid plaques (controls)

	Carotid plaques		Controls (n = 38)	P values
	Echolucent (n = 29)	Echogenic (n = 28)		
Total cholesterol (mmol/l)	6.45 (5.91–7.00)	6.43 (5.98–6.88)	6.07 (5.69–6.46)	0.4
LDL cholesterol (mmol/l)	4.14 (3.76–4.51)	4.17 (3.80–4.54)	3.76 (3.46–4.06)	0.1
HDL cholesterol (mmol/l)	1.59 (1.36–1.82)	1.74 (1.52–1.95)	1.77 (1.63–1.91)	0.4
Total triglycerides (mmol/l)	1.27 (0.99–1.56)	1.08 (0.83–1.33)	1.13 (0.96–1.30)	0.5
Total cholesterol/HDL cholesterol (ratio)	4.31(3.73–4.90)	3.98 (3.53–4.42)	3.56 (3.28–3.84)	0.04
Apolipoprotein AI (g/l)	1.13 (1.24–1.43)	1.40 (1.30–1.51)	1.44 (1.36–1.51)	0.3
Apolipoprotein B (g/l)	1.13 (1.06–1.21)	1.14 (1.07–1.21)	1.04 (0.98–1.11)	0.09
Apolipoprotein CII (mg/l)	41.8 (34.1–49.5)	38.8 (32.6–45.0)	38.7 (34.8–42.6)	0.7
Apolipoprotein CIII (mg/ml)	102.3 (85.8–118.8)	97.7 (81.3–114.1)	98.1 (87.2–109.2)	0.9
Apolipoprotein E (mg/l)	42.1 (36.7–47.5)	40.7 (35.5–45.8)	45.7 (40.5–50.9)	0.3
Apo-B/Apo-AI (ratio)	0.87 (0.79–0.94)	0.85 (0.76–0.94)	0.74 (0.68–0.80)	0.03
Apo-CII/Apo-CIII (ratio)	0.41 (0.38–0.44)	0.41 (0.37–0.46)	0.41 (0.38–0.44)	0.9

Values are means (95% CI)

ratio was equal in all groups. The apoE genotype did not differ between groups, where 57% of the participants had the E3/3 isoform, 30% E3/4, 1% E4/4, 0% E2/2, 9% E2/3 and 2% had the E2/4 isoform.

Plasma levels of pre- and postheparin LPL activity, LPL mass and LPL specific activity are shown in Table 3. Postheparin LPL activity was decreased in subjects with echolucent plaques (112.2 mU/ml, 96.6–130.3 mU/ml) (mean, 95% CI) compared to subjects with echogenic plaques (137.3 mU/ml, 118.9–158.5 mU/ml, $P = 0.06$) and to controls (137.5 mU/ml, 121.6–155.5 mU/ml, $P = 0.04$). The differences between groups remained unchanged after adjustments for age, BMI, use of β-blockers, apoE polymorphism, and serum concentrations of apo-CII and apo-CIII. Similar differences between groups were found in postheparin LPL mass, whereas the specific activity for postheparin LPL was equal between groups. To further investigate the relationship between LPL and plaque echogenicity (GSM), trend analysis revealed a significant increase in GSM across tertiles of postheparin LPL activity ($P = 0.02$) and LPL mass, whereas no linear trend was found for GSM across tertiles of LPL specific activity (Fig. 1). The relations between GSM and postheparin LPL activity and LPL mass remained significant after adjustment for age, BMI, use of β-blockers, apoE polymorphism, and serum concentrations of apo-CII and apo-CIII ($P = 0.03$ and 0.046, respectively). Univariate analyses were conducted to determine predictors of GSM. Different fasting and postprandial lipid parameters, age, sex, BMI, apolipoproteins, and LPL activity were tested. Postheparin LPL activity was the only variable that correlated significant with GSM ($r = 0.32$, $P = 0.02$).

Plasma concentrations of CM-triglycerides (upper panel) and total triglycerides (lower panel) after ingestion of the test meal are shown in Fig. 2. Subjects with echolucent plaques had significantly higher levels of CM-triglycerides 6 and 8 h after ingestion of the meal compared to controls even after adjusting for age, sex, smoking status, use of β-blockers, and fasting CM-triglyceride levels (Fig. 2, upper panel). Six hours after the meal the CM-triglyceride level tended to be higher in subjects with echolucent plaques compared to echogenic plaques ($P = 0.06$). Repeated measurement analysis was performed to identify differences between groups over time. The postprandial CM-triglyceride-curve (time × group) was significantly different ($P = 0.004$) between echolucent plaques and controls, and not significantly different between the plaque groups ($P = 0.3$) (Fig. 2, upper panel). The postprandial triglyceride-curve (time × group) tended to be different ($P = 0.08$) between echolucent plaques and controls, and not significantly different between the plaque groups ($P = 0.2$) (Fig. 2, lower panel). No differences between groups were observed with regard to TGR, AUC and AUCi for triglycerides and CM-triglycerides (Table 3).

Table 3 Lipoprotein lipase mass and activity, and characteristics of triglyceride-rich lipoproteins after a fat tolerance test in subjects with echolucent and echogenic carotid plaques, and in subjects without carotid plaques (controls)

	Carotid plaques		Controls ($n = 38$)	P values
	Echolucent ($n = 29$)	Echogenic ($n = 28$)		
Prehep LPL				
Activity (mU/ml)	0.87 (0.68–1.07)	1.01 (0.66–1.36)	1.32 (0.83–1.81)	0.3
Protein (ng/ml)	72.6 (57.5–87.7)	108.5 (31.8–185.2)	76.6 (64.6–88.7)	0.4
Specific act (mU/ng)	0.02 (0.01– 0.02)	0.02 (0.01– 0.03)	0.02 (0.01–0.03)	0.9
Posthep LPL				
Activity (mU/ml)	112.2 (96.6–130.3)	137.3 (118.9–158.5)	137.5 (121.6–155.5)	0.07
Protein (ng/ml)	613.5 (523.5–703.6)	786.5 (627.8–945.2)	744.9 (666.0–823.7)	0.07
Specific act (mU/ng)	0.20 (0.18–0.22)	0.20 (0.18 –0.23)	0.20 (0.19–0.22)	0.9
Triglycerides				
AUC (mmol/h/l)	14.1 (11.1–17.0)	12.1 (9.8–14.4)	13.0 (11.0–14.9)	0.6
AUCi (mmol/h/l)	3.87 (2.77–4.97)	3.46 (2.76–4.16)	3.95 (2.87–5.03)	0.8
TGR (mmol/l)	0.79 (0.60–0.98)	0.74 (0.60–0.88)	0.89 (0.68–1.09)	0.5
Chylomicrons				
AUC (mmol/h/l)	1458.0 (1110.7–1805.3)	1400.1 (1110.5–1689.8)	1365.6 (1087.4–1643.8)	0.9
AUCi (mmol/h/l)	1154.3 (837.3–1471.3)	1074.3 (857.3–1291.3)	1098.3 (849.8–1346.8)	0.9
TGR (mmol/l)	229.2 (168.1–290.2)	221.6 (174.0–269.1)	240.5 (187.0–294.0)	0.9

Values are means (95% CI)

AUC area under the curve, *AUCi* incremental area under the curve, *TGR* triglyceride response

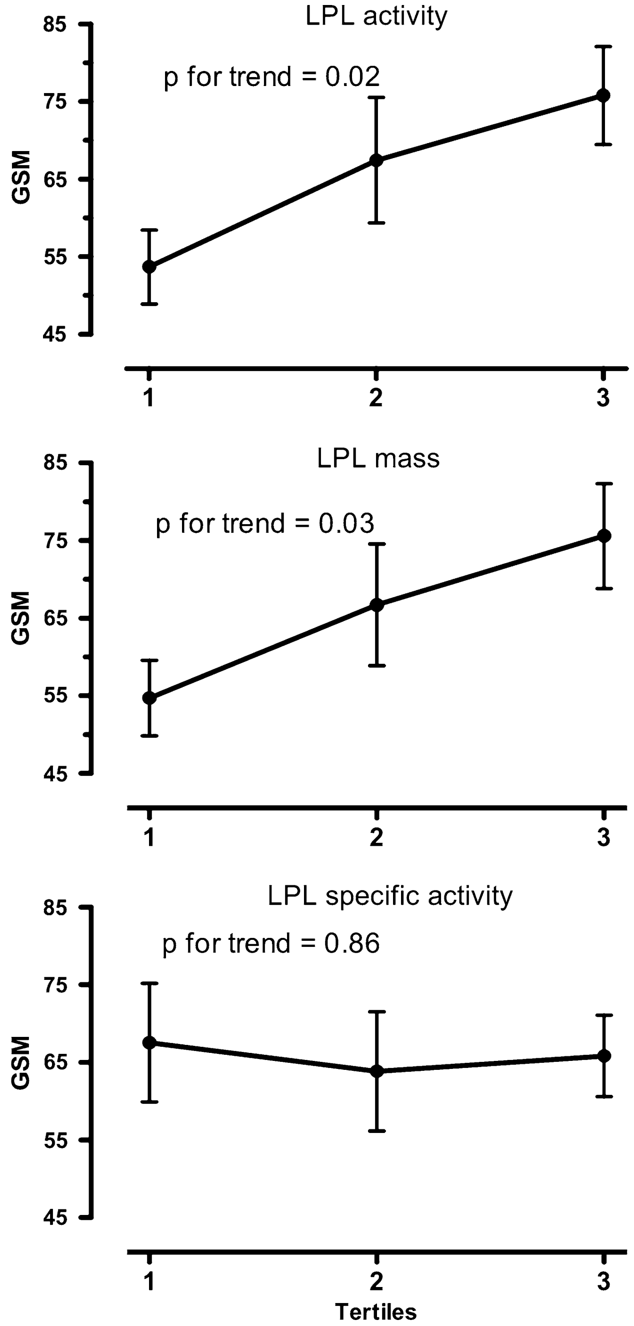

Fig. 1 Line graph showing relation between tertiles of postheparin lipoprotein lipase (LPL) activity (*upper panel*; T1: <110 mU/ml, T2: 110–154 mU/ml, T3:>154 mU/ml), LPL mass (*middle panel*; T1: <535 ng/ml, T2: 535–795 ng/ml, T3: >795 ng/ml), specific LPL activity (*lower panel*; T1: <0.18 mU/ng, T2: 0.18–0.22 mU/ml, T3: >0.22 mU/ml) and grey scale median (GSM). Values are means ± SEM

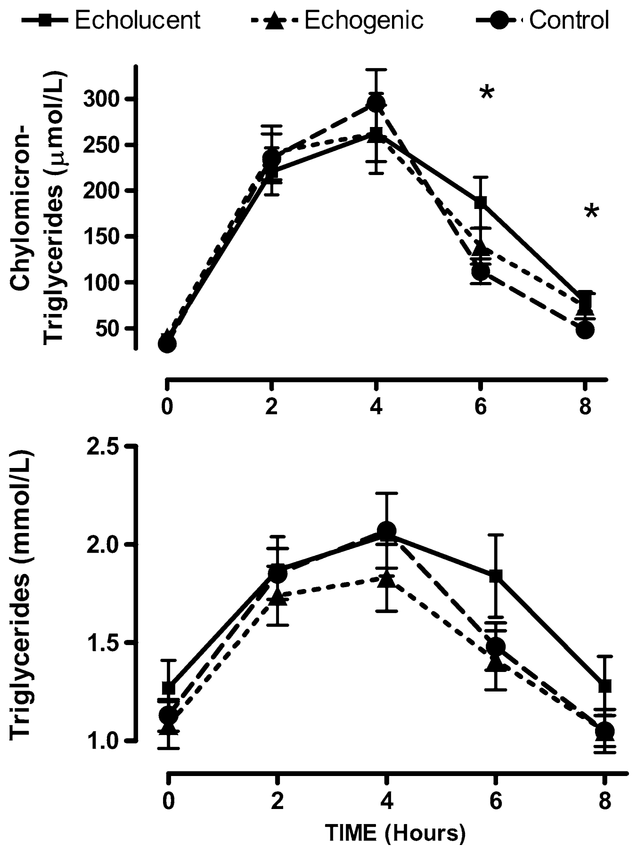

Fig. 2 Line graphs showing time-course concentrations of chylomicron triglycerides (*upper panel*) and total triglycerides (*lower panel*) after a fat tolerance test in subjects with echolucent ($n = 29$) and echogenic ($n = 28$) carotid plaques, and in subjects without carotid plaques (controls, $n = 38$). Values are means ± SEM. $^*P < 0.05$ for difference between echolucent and control groups

Discussion

In the present study we investigated postheparin LPL activity and postprandial levels of TRL in plasma from subjects with subclinical carotid plaques and healthy controls. To the best of our knowledge, the present study is the first to report a distinct decrease in LPL activity associated with echolucent carotid plaques and a linear increase in plaque echogenicity with increasing postheparin LPL activity. The decreased postheparin LPL activity was accompanied by delayed clearance of TRL in subjects with echolucent plaques.

Several studies support the concept that postprandial TRL are predictors for the presence, severity, and progression of atherosclerotic diseases [1, 2]. Despite the fact that plaque morphology is established as an independent risk factor for CVE, only few studies have focused on the relation between postprandial TRL and qualitative aspects of the carotid plaques. In patients with neurological symptoms and significant stenosis (≥50%) of the relevant carotid artery, plaque echogenicity, assess by GSM, was in univariate analysis negatively associated with BMI, fasting triglycerides, triglyceride response, and VLDL/chylomicron remnant in blood collected 4 h after a fat-rich meal. However, multiple regression analysis revealed only fasting triglycerides and IDL cholesterol as independent predictors for GSM, and concluded that increased plasma levels of TRL predicted echolucency of carotid plaques [19]. In a case-control study including patients with neurological symptoms and ≥50% carotid stenosis, Kofoed et al. [20] confirmed increased levels of fasting and postprandial TRL in patients with echolucent plaques with the most pronounced findings in women.

Neither the triglyceride response nor the AUC for TRL were higher in subjects with echolucent carotid plaques in our study. The reason(s) for the apparent differences between our and previous findings is not known, but many potential explanations exist. First, we recruited participants with subclinical carotid plaques from a population-based survey in contrast to patients attending an outpatient clinic with neurological symptoms [19, 20]. Patients are expected to have more pronounced lipid disturbances with increased fasting triglycerides and severe disease, and both fasting triglycerides [19] and severity of disease (1) are established predictors for postprandial triglyceridemia. Second, both age [21] and BMI [19] are determinants for both postprandial triglyceridemia and GSM. In our study, no age or BMI differences appeared between groups. In contrast, both age and BMI were predictors for GSM in patients with carotid plaques and neurological symptoms [19]. Altogether, our study supports previous findings that neither the triglyceride response nor AUC for TRL are independent predictors for carotid plaque echolucency.

Previous studies on the relation between plaque morphology and postprandial triglycerides did not assess clearance of TRL from the circulation since TRL in plasma was not measured more than 4 h after the meal [19, 20]. Thus, for the first time, we report a delayed clearance of TRL in subjects with echolucent carotid plaques. A delayed clearance would imply a prolonged postprandial triglyceridemia and lead to an unfavourable translocation of cholesteryl-esters from HDL to CM [22]. Experimental studies also suggest that plasma accumulation of remnant lipoproteins is not just an associated feature of an atherogenic lipoprotein profile, but that TRL remnants themselves contribute to the pathogenesis of atherosclerosis. Chylomicron remnants in the intima of the vascular wall are derived from postprandial lipoproteins [23], and TRL can be taken up directly by macrophages without prior modification and form foam cells [24]. Chylomicron remnants contain 40 times more cholesterol per particle than do LDL particles, and consequently, exposure and retention of apo-B48 lipoproteins in the arterial wall may pose a significant atherogenic risk [25]. Our finding of a delayed clearance of TRL in subjects with echolucent carotid plaques support the concept that prolonged exposure of the vessel wall to TRL remnants may promote the formation of echolucent carotid plaques.

In our study, delayed clearance of postprandial TRL in subjects with echolucent carotid plaques was associated with decreased postheparin LPL activity. The decreased LPL activity may be due to lowered specific enzyme activity or attenuated mobilization of LPL from the capillary endothelium. In our study, the specific activity of postheparin LPL was similar in all groups, but lowered LPL activity in subjects with echolucent plaques was associated with attenuated mobilization of LPL mass, and linear relations were established between plaque echogenicity (GSM) and LPL activity and mass. These findings do suggest that attenuated mobilization of LPL from capillary endothelium was the main reason for decreased postheparin LPL activity in subjects with echolucent plaque. However, it remained to be settled whether attenuated mobilization of LPL is due to actual lowered concentration of LPL at the endothelial surface or incomplete release of LPL by heparin from the endothelial surface. CM clearance, both lipolysis and hepatic uptake, is sensitive to LPL activity [26, 27]. Thus, decreased LPL activity may slow CM clearance in both stages. Both environmental and genetic factors are known to affect LPL activity [26]. In the present study, neither age, use of β-blockers, nor apoE polymorphisms and serum concentrations of apo-CII and apo-CIII could explain decreased LPL activity in subjects with echolucent carotid plaques.

LPL activity contributes to the regulation of HDL cholesterol and partly explains the inverse relation between postprandial TRL and HDL cholesterol [26]. Even though HDL cholesterol was not significantly decreased among subjects with echolucent carotid plaques, HDL cholesterol increased significantly with plaque echogenicity providing further support for the hypothesis that HDL cholesterol is a predictor for plaque morphology in carotid stenosis [28].

In conclusion, subjects with echolucent carotid plaques had decreased postheparin LPL activity accompanied by a delayed clearance of postprandial TRL. Thus, our findings support a novel property of LPL in determining plaque morphology most probably by subsequent modulation of postprandial TRL.

Acknowledgments CART is supported by an independent grant from Pfizer AS. ATW Notø was financed by a grant from Norwegian Health Association. EB Mathiesen was financed by a grant from the Norwegian Research Council. The study has received a grant from the Center for Research in Elderly in Tromsø. We thank Birgit Svensson, Kristin Sørensen and Hege Appelbom Iversen at CART for their excellent technical assistance.

Conflict of interest disclosure The authors of this manuscript have nothing to disclose.

References

1. Patsch JR, Miesenbock G, Hopferwieser T, Muhlberger V, Knapp E, Dunn JK, Gotto AM Jr, Patsch W (1992) Relation of triglyceride metabolism and coronary artery disease. Studies in the postprandial state. Arterioscler Thromb 12:1336–1345

2. Boquist S, Ruotolo G, Tang R, Bjorkegren J, Bond MG, de Faire U, Karpe F, Hamsten A (1999) Alimentary lipemia, postprandial triglyceride-rich lipoproteins, and common carotid intima-media thickness in healthy, middle-aged men. Circulation 100:723–728
3. Zilversmit DB (1979) Atherogenesis: a postprandial phenomenon. Circulation 60:473–485
4. Proctor SD, Vine DF, Mamo JC (2004) Arterial permeability and efflux of apolipoprotein B-containing lipoproteins assessed by in situ perfusion and three-dimensional quantitative confocal microscopy. Arterioscler Thromb Vasc Biol 24:2162–2167
5. Williams KJ, Tabas I (1998) The response-to-retention hypothesis of atherogenesis reinforced. Curr Opin Lipidol 9:471–474
6. Eckel RH (1989) Lipoprotein lipase. A multifunctional enzyme relevant to common metabolic diseases. N Engl J Med 320:1060–1068
7. Olivecrona T, Olivecrona G (1999) Lipoprotein and hepatic lipases in lipoprotein metabolism. In: Betteridge DJ, Illingworth DR, Shepard J (eds) Lipoproteins in health and disease. Arnold, London, pp 223–246. Ref Type: Generic
8. Olivecrona T, Olivecrona G (2000) Determination and clinical significance of lipoprotein lipase and hepatic lipase In: Rifai N, Warnick G, Dominiczak M (eds) Handbook of lipoprotein testing. AACC Press, Washington DC, pp 479–497. Ref Type: Generic
9. Brunzell JD, Miller NE, Alaupovic P, St Hilaire RJ, Wang CS, Sarson DL, Bloom SR, Lewis B (1983) Familial chylomicronemia due to a circulating inhibitor of lipoprotein lipase activity. J Lipid Res 24:12–19
10. Beisiegel U, Weber W, Bengtsson-Olivecrona G (1991) Lipoprotein lipase enhances the binding of chylomicrons to low density lipoprotein receptor-related protein. Proc Natl Acad Sci USA 88:8342–8346
11. Gronholdt ML (1999) Ultrasound and lipoproteins as predictors of lipid-rich, rupture-prone plaques in the carotid artery. Arterioscler Thromb Vasc Biol 19:2–13
12. Mathiesen EB, Bonaa KH, Joakimsen O (2001) Echolucent plaques are associated with high risk of ischemic cerebrovascular events in carotid stenosis: the Tromsø study. Circulation 103:2171–2175
13. Gray-Weale AC, Graham JC, Burnett JR, Byrne K, Lusby RJ (1988) Carotid artery atheroma: comparison of preoperative B-mode ultrasound appearance with carotid endarterectomy specimen pathology. J Cardiovasc Surg (Torino) 29:676–681
14. Joakimsen O, Bonaa KH, Stensland-Bugge E (1997) Reproducibility of ultrasound assessment of carotid plaque occurrence, thickness, and morphology. The Tromsø study. Stroke 28:2201–2207
15. Vik A, Mathiesen EB, Noto AT, Sveinbjornsson B, Brox J, Hansen JB (2007) Serum osteoprotegerin is inversely associated with carotid plaque echogenicity in humans. Atherosclerosis 191:128–134
16. El-Barghouty N, Geroulakos G, Nicolaides A, Androulakis A, Bahal V (1995) Computer-assisted carotid plaque characterization. Eur J Vasc Endovasc Surg 9:389–393
17. Elatrozy T, Nicolaides A, Tegos T, Griffin M (1998) The objective characterisation of ultrasonic carotid plaque features. Eur J Vasc Endovasc Surg 16:223–230
18. Hixson JE, Vernier DT (1990) Restriction isotyping of human apolipoprotein E by gene amplification and cleavage with HhaI. J Lipid Res 31:545–548
19. Gronholdt ML, Nordestgaard BG, Wiebe BM, Wilhjelm JE, Sillesen H (1998) Echo-lucency of computerized ultrasound images of carotid atherosclerotic plaques are associated with increased levels of triglyceride-rich lipoproteins as well as increased plaque lipid content. Circulation 97:34–40
20. Kofoed SC, Gronholdt ML, Bismuth J, Wilhjelm JE, Sillesen H, Nordestgaard BG (2002) Echolucent, rupture-prone carotid plaques associated with elevated triglyceride-rich lipoproteins, particularly in women. J Vasc Surg 36:783–792
21. Cohn JS, McNamara JR, Cohn SD, Ordovas JM, Schaefer EJ (1988) Postprandial plasma lipoprotein changes in human subjects of different ages. J Lipid Res 29:469–479
22. Tall AR (1993) Plasma cholesteryl ester transfer protein. J Lipid Res 34:1255–1274
23. Proctor SD, Mamo JC (1998) Retention of fluorescent-labelled chylomicron remnants within the intima of the arterial wall–evidence that plaque cholesterol may be derived from postprandial lipoproteins. Eur J Clin Invest 28:497–503
24. Bradley WA, Gianturco SH (1994) Triglyceride-rich lipoproteins and atherosclerosis: pathophysiological considerations. J Intern Med Suppl 736:33–39
25. Proctor SD, Mamo JC (1996) Arterial fatty lesions have increased uptake of chylomicron remnants but not low-density lipoproteins. Coron Artery Dis 7:239–245
26. Otarod JK, Goldberg IJ (2004) Lipoprotein lipase and its role in regulation of plasma lipoproteins and cardiac risk. Curr Atheroscler Rep 6:335–342
27. Hussain MM, Goldberg IJ, Weisgraber KH, Mahley RW, Innerarity TL (1997) Uptake of chylomicrons by the liver, but not by the bone marrow, is modulated by lipoprotein lipase activity. Arterioscler Thromb Vasc Biol 17:1407–1413
28. Mathiesen EB, Bonaa KH, Joakimsen O (2001) Low levels of high-density lipoprotein cholesterol are associated with echolucent carotid artery plaques: the Tromsø study. Stroke 32:1960–1965

Lipids (2008) 43:361–372
DOI 10.1007/s11745-007-3147-0

ORIGINAL ARTICLE

Analysis of Human Oral Mucosa Ex Vivo for Fatty Acid Compositions Using Fourier-transform Infrared Spectroscopy

Satoshi Yoshida · Yuhki Okazaki · Takumi Yamashita · Hiroshi Ueda · Reza Ghadimi · Akihiro Hosono · Tsutomu Tanaka · Kiyonori Kuriki · Sadao Suzuki · Shinkan Tokudome

Received: 6 August 2007 / Accepted: 11 December 2007 / Published online: 10 January 2008
© AOCS 2008

Abstract The purpose of this research was to develop an infrared spectroscopic technique (Fourier transform infrared spectroscopy with attenuated total reflectance system; FTIR-ATR) for non-invasive measurement of saturated and unsaturated fatty acid compositions in human oral mucosa obtained from three nationalities; Iranian, Vietnamese, and Indonesian. The histogram patterns of fatty acid compositions for three nationalities suggest that the pattern of unsaturated fatty acids were quite different, although the distribution profiles of fatty acid to lipid ratios in FTIR-ATR has a similar normal pattern with small difference in skewness and mode. The second derivative infrared spectra of the mucosal tissues in the wavenumber regions from 1,600 to 1,760 cm^{-1} and 2,800 to 3,050 cm^{-1} were analyzed with partial least squares (PLS) multivariate regression analysis method. With this analysis method we compared predicted values with the measured values of ten categorized fatty acid compositions, i.e., **a**(saturated C17 or lower), **b**(C16:1 + C17:1), **c**(C18:0), **d**(C18:1), **e**(C18:2), **f**(saturated C20 or longer), **g**(C20:3 + C20:4), **h**(C22:1 + C24:1), **i**(C22:6), **j**(γC18:3). Almost all fatty acid compositions of oral mucosa were well predicted with differences between predicted and measured values within ±5% of total, however, errors were relatively larger in minor components such as C22:6 than major components.

S. Yoshida (✉) · Y. Okazaki · T. Yamashita · H. Ueda
Department of Biomolecular Science,
Faculty of Engineering, Gifu University,
Gifu 501-1193, Japan
e-mail: xyosida@gifu-u.ac.jp

R. Ghadimi · A. Hosono · T. Tanaka · K. Kuriki · S. Suzuki · S. Tokudome
Department of Health Promotion and Preventive Medicine,
Nagoya City University School of Medicine,
Nagoya 467-8601, Japan

Keywords Fatty acids · Composition · FTIR · Human oral mucosa · Multivariate analysis

Abbreviations

FTIR	Fourier-transform infrared
ATR	Attenuated total reflectance
PLS	Partial least squares
PBS	Phosphate buffered saline
PUFA	Polyunsaturated fatty acids

Introduction

Dietary fatty acids including saturated, monounsaturated and polyunsaturated fatty acids play important physiological roles for human health [1]. Epidemiological research using fatty acid compositional analyses of human body fluids or tissues may be important for assessment of the effectiveness of dietary fatty acids on the physiology of the human body. However, the measurement of fatty acid compositions in tissues involves tedious and time-consuming procedures for extraction and derivatization of fatty acids from tissues for subsequent analyses with gas-chromatography or high-performance liquid chromatography. This standard method may not be practically suitable for large scale (more than several thousands of subjects) epidemiological research, because it would take a long time to measure fatty acid compositions of a large sample size even with high-throughput gas- or liquid-chromatographic techniques.

On the other hand, vibrational spectroscopy such as Raman, near-infrared and mid-infrared spectroscopy may provide useful techniques to measure lipid compositions in food and human body-derived samples such as blood, saliva, lipoproteins and oral mucosa [2–7]. Especially, Whittaker et al. [3] reported that Fourier-transform infrared spectroscopy with attenuated total reflectance (FTIR-ATR) could be used for rapid discrimination of food-borne bacteria with their extracted fatty acid methyl esters and multivariate statistical analysis. We reported [4] that polyunsaturated fatty acid species in dietary oils could be predicted using FTIR-ATR system. We also reported [5] that non-destructive FTIR-ATR measurement of human oral mucosa could monitor diurnal changes of polyunsaturated fatty acids in the mucosa. With these spectroscopic and statistical methods, we may complete fatty acid compositional analysis for epidemiological studies on a large scale in a much shorter time. Lam et al. [6] also reported that FTIR and chemometrics revealed low density lipoprotein oxidation with protein conformational changes and provided a simple rapid technique for measuring primary and secondary oxidation products.

The purpose of this research was to determine whether FTIR-ATR technique used for measurement of the infrared spectrum of oral mucosa ex vivo may predict fatty acid compositions in the mucosa and to explore at what level of identification of fatty acid species could be achieved by multivariate analysis. If this analysis technique provided reasonably reliable results for the assay of fatty acid compositions, this would greatly shorten time from sampling to getting results and lower the costs because only a minimum amount of reagent would be necessary for fatty acid analysis with the use of the multivariate statistical analysis. This would then become a suitable method for epidemiological and clinical researches.

Materials and Methods

Preparation of Oral Mucosa

A total of 425 oral mucosal samples from Iranian (100 samples), Indonesian (175 samples), and Vietnamese (150 samples) subjects were collected for epidemiologic research by the team of Nagoya City University (Dr. S. Tokudome as the leader). Those oral mucosal tissues after collecting with cotton-wiping were suspended in 0.25 M sucrose with phosphate buffered saline (PBS; 50 mM Na_2-K-phosphate buffer and 0.7% NaCl, pH 7.3) and frozen with dry-ice to ship to Japan. The samples were then stored at −80 °C until use. After thawing, the oral mucosal samples were washed in sucrose-free phosphate buffered saline two times with centrifugation at 5,000*g* for 5 min. The mucosal pellet (soft solid) thus obtained was directly subjected, after separation with a spatula, in part to Fourier transform infrared spectral analysis with an attenuated total reflectance (ATR) probe (diamond ATR), and the other part to methyl-esterification for fatty acid analysis with gas chromatography-mass spectrometry.

Fatty Acid Determination by Gas Chromatography–Mass Spectrometry

The washed mucosal pellet was suspended in 50 µl of PBS buffer, and dried with flushing with N_2 gas. To the dried sample was added 0.15 ml of methanolic HCl (5%; GL-Science, Japan) and 0.35 ml of dehydrated methanol, and heated at 100°C in dry-bath unit for 4 h in Teflon-coated screw-capped glass tubes. The resulting fatty acid methyl esters, after cooling, were extracted in 1 ml of hexane (Nakarai Tesque Co., Japan), and stored until use at − 20 °C. Before measurement, the hexane phase was dried by flushing with N_2 gas, and dissolved in 10 µl of hexane. 0.8 µL of the sample solution in hexane was injected into a gas chromatography-mass spectrometry system (GC; Agilent technologies: MS, GC-Mate II, JEOL, Japan) with a capillary column (BPX-70, SGE Co., Japan; 30 m in length, 0.32 mm in internal diameter, and 0.25 µm in film thickness). The temperature program in gas-chromatography was set at 100 °C for 2 min, and raised linearly from 100 to 250 °C at a 10 °C/min rate, and kept at 250 °C for 8 min. Identification of fatty acids was carried out using standard fatty acid methyl esters (Funakoshi, Japan) and mass spectrum of each fatty acid methyl ester. In some cases, fatty acid methyl esters thus obtained from oral mucosa were filtered and purified through Florisil-column (Florisil-SepPak Plus cartridges, Waters, MA, USA) to remove some sterols and hydroxyl fatty acids if occurred. Initially the column was washed with hexane-diethylether (85:15) extensively and then 100% hexane, and fatty acid methyl esters obtained in hexane were applied to the column, and washed with hexane-diethylether (95:5), and then eluted by hexane-diethylether (85:15), and concentrated by N_2 gas flushing. This Florisil-column treatment of fatty acid methyl esters could not change principally the gas chromatographic pattern of oral mucosa-derived fatty acid methyl esters appeared in the region from C14 to C24 fatty acids.

Fatty Acid Analysis by Fourier-Transform Infrared Spectroscopy with Partial Least Squares (PLS) Regression Analysis

For measurement of the mucosal pellet, we used Fourier-transform infrared spectroscopy with a diamond attenuated total reflectance system (FTIR-ATR system; TravelIR, SensIR (Smiths Detection Co. at present), Columbus, OH, USA). Nearly 0.5 µl of the mucosal pellet was placed on the surface of the ATR probe and dried by air-blowing for 1 min, and measured at 4 cm^{-1} resolution with 48 accumulations. The duplicate data for one sample were averaged and used for calculation. The spectral data were transformed to the second derivative form and normalized adjusting the intensity at 1,650 cm^{-1} to a constant value.

We reported previously [8] that the ratio [2850]/[1650] in the second derivative form of infrared spectrum had a good linear correlation with the lipid (triacylglycerol) to protein ratio (mg/mg). This relationship is also true for the ratio [2850]/[1540], and in this paper we have adopted this [2850]/[1540] ratio for a large number of human mucosal tissues. The reason is that the accidental contamination of water or water vapor influences the absorption spectrum at around 1,650 cm^{-1} more than that at 1,540 cm^{-1}, and thus the ratio [2850]/[1540] may be more robust to this contamination than the ratio [2850]/[1650].

For predicting the fatty acid composition from the infrared spectrum of tissues, it may be necessary to obtain information of fatty acids from the spectrum including the profile of unsaturated bonds (*cis*-alkene, HC=CH; peak position and intensity at around 3,010 cm^{-1}), profile of methyl ($–CH_3$; peak position and intensity at around 2,875 cm^{-1}), profile of methylene ($–CH_2–$; peak position and intensity at around 2,850 cm^{-1}), profile of fatty ester (–C(=O)–O–R) or free fatty acid carboxylate ($–C(=O)O^-$); peak position and intensity at around 1,740 or 1,710 cm^{-1}, respectively). The infrared spectral intensity itself is also dependent on the sample handling such as change of contact area of the samples on the ATR probe, and this artifactual variation of intensity may be corrected by normalization of the spectrum by adjusting the protein infrared absorbance at 1,650 (amide I) or 1,540 cm^{-1} (amide II) to a constant value.

To adopt a wide variety of fatty acid compositions, it may be reasonable to select samples randomly with various ratios [2850]/[1540] or [2850]/[1650], for building Partial Least Squares (PLS) models, as the change of ratio [2850]/[1540] did not practically reflect any specific fatty acid change, but reflected the integrated changes of all fatty acids. The information of the infrared spectrum including absorption intensity of methylene may be used for PLS model building, and a wider range of spectral intensities should be adopted for ameliorating the fitness of unknown sample data to the PLS model.

Partial least squares (PLS) regression analysis for the FTIR-ATR spectrum of oral mucosa was done using Sirius software (PRS; Bergen, Norway). As a model learning process, 6–8 samples with known fatty acid compositions were used, and the IR absorption data between 3,050 and 2,800 cm^{-1}, and between 1,750 and 1,600 cm^{-1} were extracted into spread sheet software (as Excel files, Microsoft), and transferred to the PLS software. Increasing the number of samples for the model learning process to 10 could not improve results. The PLS model was constructed up by setting the cross validation to 2 as a stop criterion and the maximum number of components to 6. After a suitable PLS model was constructed for subsets such as **a**(saturated C17 or lower), **b**(C16:1 + C17:1), **c**(C18:0), **d**(C18:1), **e**(C18:2), **f**(saturated C20 or longer), **g**(C20:3 + C20:4), **h**(C22:1 + C24:1), **i**(C22:6), and **j**(γC18:3), those components were predicted for the unknown mucosal samples. Oral mucosa contained a certain amount of odd-numbered fatty acids and very-long-saturated fatty acids (longer than C22), and these components were summarized with other fatty acids. The number of classified species of fatty acids for prediction by PLS analysis was controlled to less than 10 in order to shorten the working time of the PLS software.

Results

Figure 1a shows typical second derivative and absolute (insert) infrared (IR) spectra of human oral mucosal pellet, and the fatty methylene IR absorption originated from CH symmetric stretching mode was observed at around 2,850 cm^{-1} and protein amide II at around 1,540 cm^{-1}. The intensity ratio ([2850]/[1540]) between 2,850 cm^{-1} and 1,540 cm^{-1} in the second derivative spectrum was calculated and the distribution of the ratio values is shown in Fig. 1b as histograms for three nationalities: Iranian, 100 samples; Indonesian, 170 samples; Vietnamese, 150 samples. The intensity ratio at around 0.16 was the mode, and from 0.12 to 0.2 the distribution of the intensity ratio showed nearly normal distribution, but a little distorted shape.

Five groupings were temporarily made using the distribution of ratio [2850]/[1540] for mucosal samples according to classes as shown in Fig. 1b, and four samples were randomly picked up from each group. Then fatty acid composition of each sample was determined with gas chromatography-mass spectrometry as shown in Fig. 2a. In oral mucosa, fatty acids from C14:0 to C26:0 were mainly observed and it was noticed that long saturated even- and odd-numbered fatty acids were abundant in oral mucosa. Among polyunsaturated fatty acids (PUFA), C18:2n-6 was also abundant, while small amount of C18:3n-6 (γ-linolenic acid), C20:3n-6, C20:4n-6 (arachidonic acid; AA) and C22:6n-3 (docosahexaenoic acid; DHA) were also detected. In Fig. 2a′ shown was an example of a little contaminated pattern. The pattern of fatty acid methyl esters from oral mucosa (an example shown in Fig. 2a) was not basically changed by florisil-column treatment, suggesting no hydroxyl fatty acids content. In minor components there were many atypical fatty acid peaks and

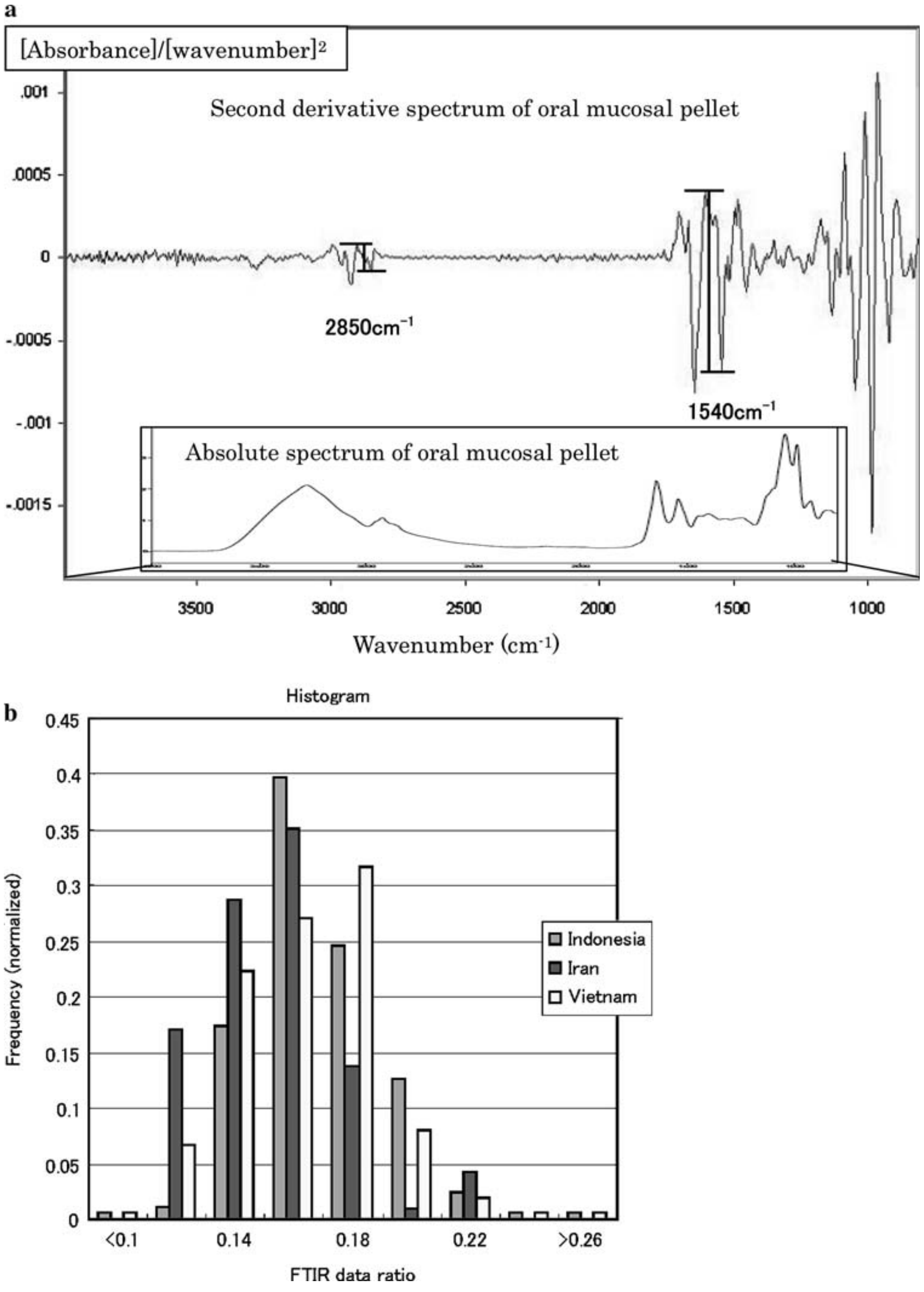

Fig. 1 Infrared spectrum of oral mucosa measured by FTIR-ATR system in the second derivative and absolute spectrum (insert) forms (**a**), and the normalized distribution of methylene/amide II ratios ([2850]/[1540]) for three nationalities (**b**). The distributions of the ratio as histograms show distinct features among three nationalities (100–170 samples). Those mucosal samples were collected in a city in Iran or Vietnam (Ho Chi Mihn City) or Indonesia (Semarang)

those showed typical fatty methyl ester mass fragment patterns (containing ex., m/z = 74 and 87). At present those minor peaks were not identified in this paper.

In Fig. 2b, the relationships between fatty acid contents (percentage in all fatty acids) and infrared absorption intensity ratios ([2850]/[1540]) was shown for each sample. In the case of saturated fatty acids (C14 to C26) and monounsaturated fatty acids (MUFA) no correlations were observed for Iranian samples with infrared absorption ratio ([2850]/[1540]). No correlation was observed for other nationalities either. On the other hand, the amount of PUFA may have a weak but significant negative correlation ($R = -0.56$; $P < 0.05$, $n = 20$) with the ratio of the infrared absorption bands. However, this correlation could not be observed in other nationalities (Indonesia and Vietnam) samples (data not shown).

The intensity of methylene 2,850 cm^{-1} band may be affected by both the amount of total fatty acids and the balance between saturated and unsaturated fatty acids, and even the species of unsaturated fatty acids such as linoleic

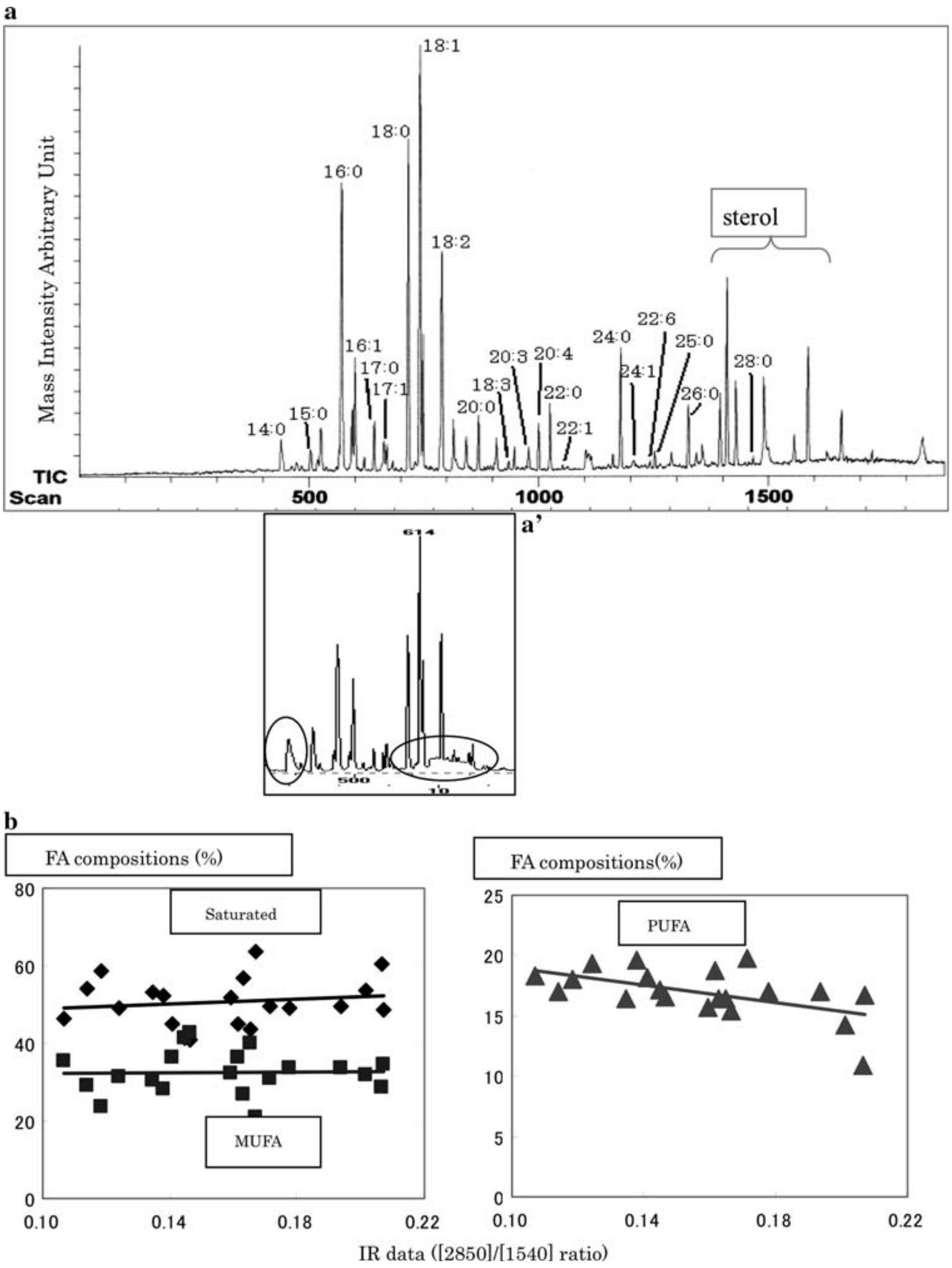

Fig. 2 A gas chromatographic pattern of fatty acids of oral mucosa, a typical case in (**a**) and a low contaminated form in (**a′**), and the correlations between fatty acid composition and the [2850]/[1540] ratio (**b**). The fatty acid methyl esters and some sterol compounds formed after 5% methanolic HCl treatment of oral mucosa were extracted in hexane and injected into gas chromatography-mass spectrometry. Total ion chromatogram was shown in (**a**). In (**a′**) inserted pattern, contaminated broad bands were shown in circles. The correlations between saturated or mono-unsaturated or polyunsaturated fatty acid compositions and the infrared methylene to amide II absorbance ratio showed almost no correlations for saturated and mono-unsaturated fatty acids. Exceptionally polyunsaturated fatty acid (PUFA) compositions, mainly linoleic acid, in Iranian samples showed good correlation with the infrared absorbance ratios [2850]/[1540]

and eicosatetraenoic acids, may affect the methylene infrared absorption intensity differently. The increase in polyunsaturated fatty acid may contribute to the intensity of 2,850 cm^{-1} less than that of saturated or monounsaturated fatty acids. The intensity of band at 2,850 cm^{-1} may result from integration of all fatty acids in the mucosa.

In Table 1, the present fatty acid compositional data are compared with the published human oral mucosal fatty acid compositions [9, 10]. Although the origin of oral mucosal tissues were very different, the compositions of saturated (S) C14–17, C18:0, C18:1, and C18:2 were comparable for these three cases. The composition of monounsaturated (M) C16–17 of the present case was much larger than the other two reports (12.5 vs. 4–5), and this may be caused by including the composition of C17:1 in the present case. The other two reports did not show the chromatographic patterns and the content of C17:1. Fatty acid composition of oral mucosa shows very different profile from that of other organs, and C22:4, C22:5, C20:5, and C22:5 which are frequently observed in internal organ cells such as liver, brain and blood cells could be hardly detected in oral mucosa. However, C20:3 and C20:4 (n-6 fatty acids) and C22:6 (n-3 fatty acid) were detected in oral mucosa, and those may be used as markers of those polyunsaturated fatty acid contents in the body.

Table 1 Comparison of reported human oral mucosal fatty acid compositions

Fatty acids (% of total)	S14–17^{a}	M16–17^{a}	18:0	18:1	18:2	20:3 + 20:4	22:6	18:3
Connor et al. [9] (PL)^{b}	15.5 (C14, C16)	5.7 (C16)	11.5	25.2	14.7	2.9 (C20:4)	0.9	0.3 (α)^{c}
Terashi et al. [10] (US, whole lipids)^{d}	24.2 (C14, C16)	4.3	16.9	20.3	14.5	12.6	1.9	0.0 (γ)^{c}
Present (5 averaged ; Iran, whole lipids)	24.0	12.5	13.4	20.4	11.1	3.2	0.45	1.0 (γ)^{c}

[a] S and M represent saturated and monounsaturated fatty acids, respectively, with numbered carbon chain lengths

[b] Infant cheek phospholipids (PL); [9]

[c] α and γ represent α-linolenate and γ-linolenate, respectively

[d] Adult oral mucosal tissues; [10]

Partial Least Square Regression Analysis of Mucosal Fatty Acids

Figure 3 shows the second derivative infrared spectra of several samples after normalizing the amide I band intensity. The spectral regions (windows) used were 1,600–1,750 cm^{-1} and 2,800–3,050 cm^{-1}. These regions were used for evaluation of the relative amount of fatty acids against the amount of proteins in the mucosa and of the balance between saturated and unsaturated fatty acids with different chain length and extent of unsaturation. Especially the extent of unsaturation could be detected by the infrared absorption peak position and shape originated from *cis*-alkene (HC=CH) CH stretching mode usually observed at around 3,010 cm^{-1} [5, 7].

Next these spectroscopic data were analyzed using PLS software (Sirius), and the data of fatty acid compositions for the corresponding samples were also analyzed. Both the

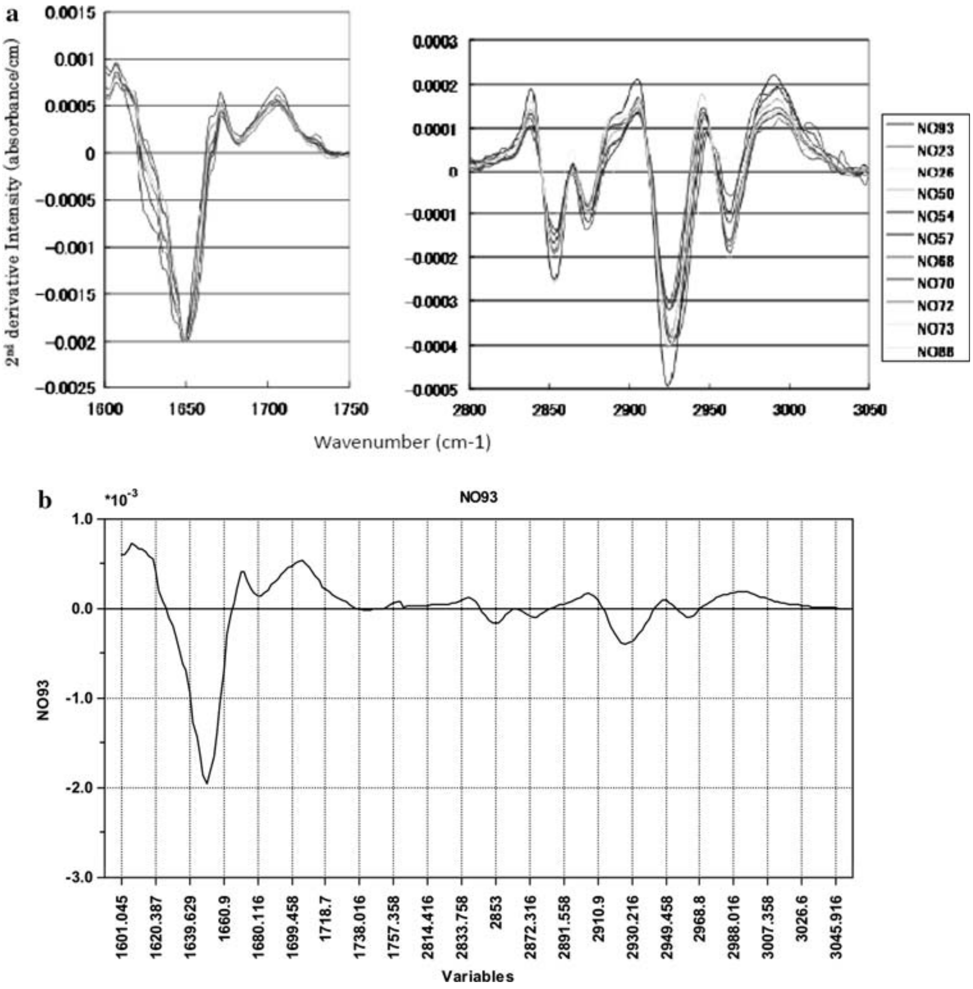

Fig. 3 Examples (from the Iranian samples) of infrared spectra in the second derivative form of oral mucosa with normalizing the absorbance at 1,649 cm^{-1} (amide I) to a constant value (−0.002). (**a**) Second derivative spectra for 11 examples (overlaid) in two wavenumber windows. (**b**) An example spectrum used for the PLS analysis after combining the two wavenumber regions. For PLS model construction, these two wavenumber regions (protein region at around 1,650 cm^{-1} and fatty acid region at around 2,850 cm^{-1}) were used, because these regions contain enough information to obtain relative contents of saturated and unsaturated fatty acids

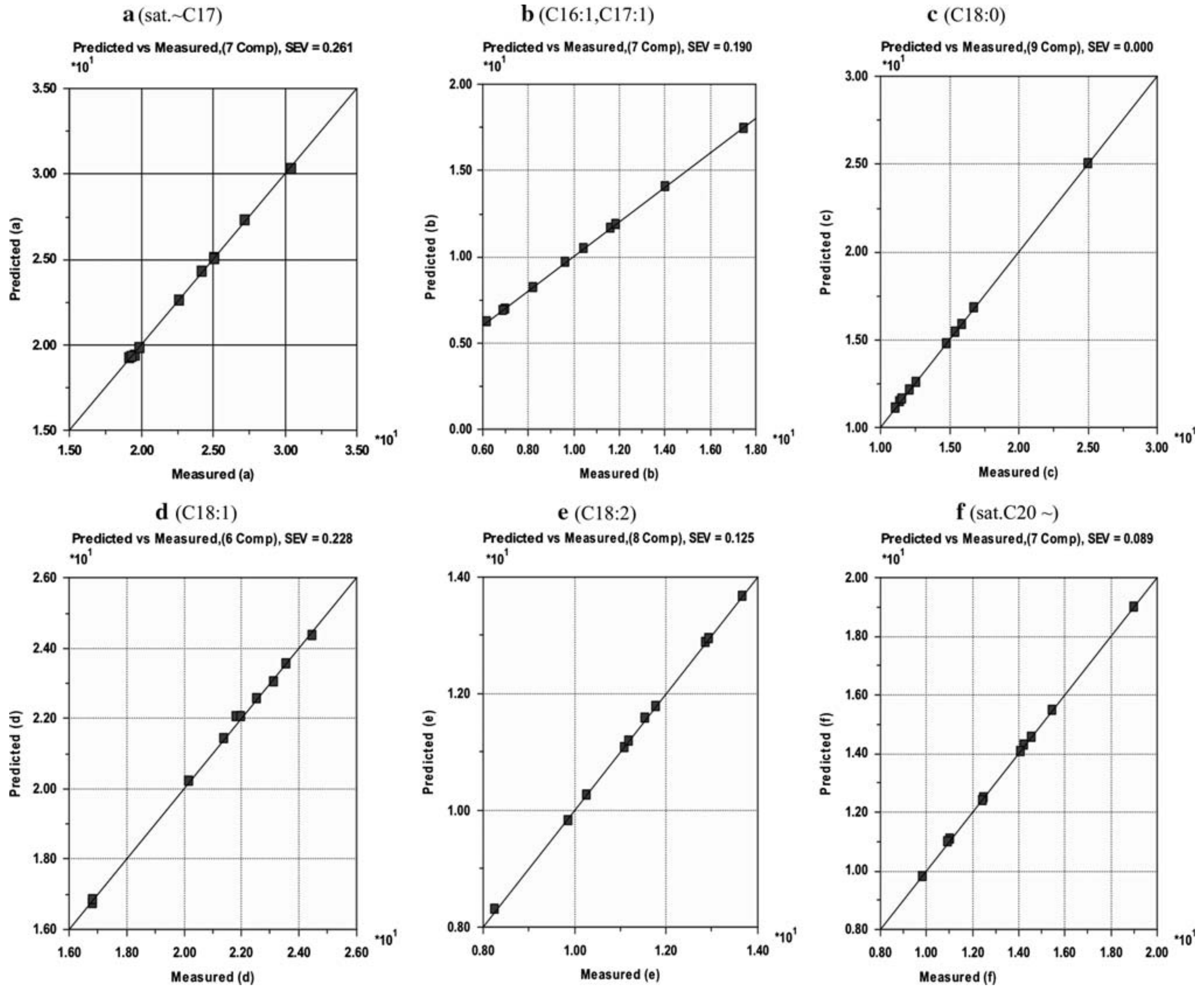

Fig. 4 Correlation plots between predicted and measured values of the fatty acid groups (**a** to **f**). In these cases the correlation coefficient (R^2) was almost 0.98–1.00 after a suitable PLS model was constructed for ten subjects. SEV(standard error of validation) for each regression analysis was noted from 0.000 to 0.261, and the component numbers used for the regression were from 6 to 9

spectroscopic and fatty acid compositional data were used to construct the suitable PLS models and to determine some PLS parameters including the number of groups in cross validation and stop criteria for cross validation, and the maximum number of components with a significant level of 0.05. Here we represented data for Iranian samples, however, the data for the other two countries showed similar results as long as we used the learning data of their own countries for construction of PLS model.

Figure 4 shows the results of plots for [measured] (m) vs. [predicted](p) values after construction of PLS model for the composition (%) of fatty acid(s) or fatty acid groups of Iranian samples. All plots showed good correlations with the coefficient of almost 1.00. In this case, the fatty acids or fatty acid groups are (**a**) saturated fatty acids including C14, C15, C16, C17 acids, (**b**) monounsaturated C16 and C17 acids, (**c**) stearic acid (C18:0), (**d**) oleic acid (C18:1), (**e**) linoleic acid (C18:2), (**f**) very-long-chain saturated fatty acids including C20, C22, C24, C25, C26, C28 acids. Other fatty acids and fatty acid groups were also evaluated (not shown here), for (**g**) C20:3 + C20:4, (**h**) C22:1 + C24:1, (**i**) C22:6, and (**j**) γC18:3, and similar results were obtained. The minor fatty acid, γC18:3, could be hardly detected clearly for Indonesian and Vietnamese samples. The discrimination of the gas chromatographic peak whether alpha- or gamma-linolenic acid was done by a mass spectrometric technique comparing with the mass spectrum of the standard fatty acid methyl esters as shown in Fig. 5.

Under this condition of PLS regression analysis we tried to predict fatty acid compositions of mucosal samples

a Oral mucosa C18:3 methyl ester (M^+=m/z 292), *mainly C18:3n-6 (γ-linolenate)

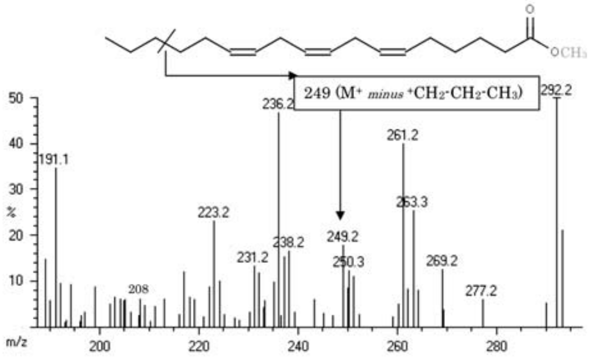

b Standard α-linolenic acid (C18:3n-3) methyl ester

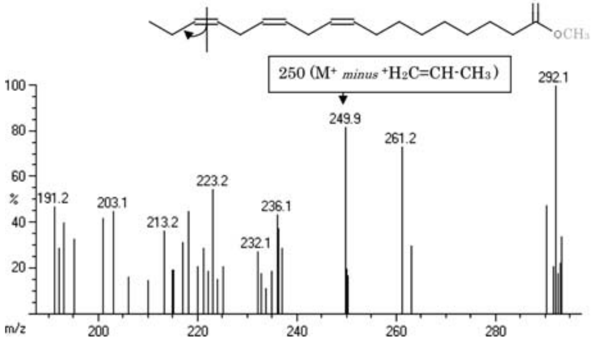

Fig. 5 Comparison of mass spectra of C18:3 methyl ester isomers. In (**a**), mass spectrum of oral mucosal C18:3 methyl ester with molecular ion (M^+) at m/z = 292. In (**b**), the mass spectrum of authentic alpha-linolenic acid (C18:3n-3) methyl ester was shown. The presence of fragment ions at 249.2 in (**a**) and 249.9 in (**b**) show mucosal C18:3 is not alpha-linolenic acid, but gamma-linolenic acid (C18:3n-6) mainly

which were not used in the learning process for constructing PLS parameters. A part of results is shown in Table 2. In this table, the predicted and the measured values of fatty acid compositions were shown in percent. The difference between the predicted and observed values were within ±5% of total fatty acids, depending on the species of fatty acids. Some samples showed a little worse prediction, and these samples contained unusual contaminants as detected in the gas chromatographic patterns (Fig. 2a′), which might be caused in part through the sampling of oral mucosa. When the relative deviation from the measured value was denoted as DM (%; deviation from the measured value), the averaged DM for compositional groups (**a** to **f**) with relatively higher contents over 10% of all fatty acids was 10.8 DM (%; ±8.4 SD). For minor components (group **g** to **j**) with relatively lower contents below 5% of all fatty acids, the averaged DM was 35 DM(%;±20 SD), and this large DM value for minor components may be resulted partly from background noise and some contamination in the gas chromatography and FTIR.

Figure 6 shows the distributions for fatty acid groups (**c, d, e, i**) in 34 samples of Iranian subjects after predicting the compositions. The distribution profile of long saturated fatty acid (C18:0) represented the mode was at 13–17 (%) with long lobe up to 37(%), while unsaturated C18 fatty acids (C18:1 and C18:2) showed a little distorted bell-shaped distributions, and these data showed similar mean values to the measured samples. The distribution of C18:0 (**c**) was similar to that of saturated C14 to C17 fatty acids (**a**), and also the distribution of C18:1 (**d**) is similar to that of monounsaturated C16 to C17 (**b**) (data not shown). A minor component (C22:6 (**i**)) showed wide range of distribution, and fractions with very low content of C22:6 was remarkable. The distribution of C20:3 + C20:4 (**g**) was similar to that of C22:6 (data not shown).

Figure 7 shows the distributions of measured fatty acids of oral mucosa obtained from Vietnamese (Vn) and Indonesian (Id). The distribution of C18:0 was similar in both nationalities, whereas that of C18:1 or C18:2 was different in both. The distribution of C22:6 shows the content of C22:6 in the Vietnamese samples was a little higher on average than that of Indonesian.

When comparing Fig. 6 with Fig. 7, the contents of C18:0 and C18:1 were higher in Fig. 6 (Iranian) than in Fig.7 (Vn and Id), whereas those of C18:2 and C22:6 were lower in Fig. 6 than in Fig. 7. These differences in fatty acid contents, such as lower contents of polyunsaturated fatty acids in the Iranian group than in the Vietnamese and Indonesian groups, may be easily recognizable in these histograms, and thus the compositional analysis of fatty acids by FTIR-ATR and PLS methods may become possible and suitable for rough screening of oral mucosal samples when noise and contamination levels in the measurement of mucosal samples with FTIR and GCMS are adequately suppressed.

Discussion

This paper has described infrared spectroscopic and multivariate analysis methods to quantitate the relative amounts of various fatty acids in human oral mucosa. This technique may provide ideally a great advantage to fatty acid analysis in the fields of food science, preventive medicine and epidemiology.

We have demonstrated that the fat to protein ratios ([2850]/[1540] ratios) showed a nearly Gaussian distribution for each nationality. However, the distribution profile of [2850]/[1540] ratio for each nationality had a slightly different feature (in skewness and mode). For example, for Iranian samples the profile showed a larger contribution from the lower ratios, and for Indonesian samples a larger contribution from higher ratios. For Vietnamese samples the mode value (0.18) was larger

Table 2 Predicted and measured values of fatty acid compositions of oral mucosa based on learning of six subjects using PLS analysis

		s14–17[a]	m16–17[b]	18:0[c]	18:1[d]	18:2[e]	s20–28[f]	20:3 + 20:4[g]	m22–24[h]	22:6[i]	γ18:3[j]
#72	Pred	20.6	13.4	11.1	23.4	10.1	12.5	4.9	1.47	0.56	1.0
	Meas	19.9	14.0	12.6	21.4	13.7	12.5	4.0	0.99	0.34	0.65
	Δ	0.7	−0.6	−1.5	2.0	−3.6	0.0	0.9	0.48	0.22	0.35
#73	Pred	26	11.1	13.2	18.5	9.5	15.2	3.5	1.31	0.46	0.56
	Meas	25	11.9	11.6	20.2	11.8	12.4	3.2	1.79	0.62	1.44
	Δ	1	−0.8	1.6	−1.7	−2.3	2.8	0.3	−0.48	−0.16	−0.88
#88	Pred	19.6	12.9	10.9	22.0	11.2	14.6	5.4	1.5	0.7	0.95
	Meas	19.7	16.5	12.0	21.6	10.5	11.9	3.8	1.9	0.68	1.6
	Δ	−0.1	−3.6	−1.1	0.4	0.7	2.7	1.6	−0.4	0.02	−0.65

Pred Predicted values in % of total, *Meas* measured values with GCMS in % of total, Δ difference ([Pred] − [Meas]) values in % of total

[a] s14–17, saturated fatty acids with chain length from C14 to C17

[b] m16–17, monounsaturated fatty acids with chain length from C16 to C17

[c] 18:0, stearic acid

[d] 18:1, oleic acid

[e] 18:2, linoleic acid

[f] saturated fatty acids with chain length from C22 to C28

[g] 20:3 + 20:4, eicosatrienoic acid plus eicosatetraenoic acid (arachidonic acid)

[h] m22–24, monounsaturated fatty acids with chain length from C22 to C24

[i] 22:6, docosahexaenoic acid

j γ18:3, gamma-linolenic acid

than that (0.16) of other samples (Iranian and Indonesian). The intensity at 1,650 or 1,540 cm^{-1} may correspond to the amount and density of oral mucosal proteins on the surface of ATR probe, and this intensity may not be changed practically when normal test subjects were used and contact area of the sample on the ATR probe was constant. This infrared absorption peak ratio ([2850]/[1540] or [2850]/[1650]) may, practically, correspond to the relative amount of fatty acids in the oral mucosal sample comparing with the amount of protein, and actually the ratio, [2850]/[1650], has a linear correlation with the triglyceride/protein ratio as we have reported previously [8], and it is also true for the ratio [2850]/[1540]. As the contact area of the dried pellet sample on the ATR probe is hard to control experimentally and exactly, it was necessary to use this ratio [2850]/[1540] for assaying the relative changes of lipids or fatty acids in mucosal samples. This ratio in the oral mucosa may be related to the extent of dietary intake and accumulation of lipids in body tissues, and thus to the life style of the nation on average.

The ratio of infrared absorptions, [2850]/[1540], is not directly related to the content of specific fatty acid, but related to a complex integration of each saturated and unsaturated fatty acids or roughly to the amount of total fatty acids as described in the method section. It might be exceptional that the [2850]/[1540] ratio for Iranian samples had a weak inversed relationship with the amount of polyunsaturated fatty acids (mainly C18:2) as shown in Fig. 2b (right). For other nationalities there was no relationship between the [2850]/[1540] ratio and the amount of polyunsaturated fatty acids.

Thus, the ratio of infrared absorptions, [2850]/[1540], may be mainly referred to the relative amount of total fatty acids compared to the amount of proteins, and 20 samples were picked out for fatty acid determination using gas chromatography-mass spectrometry. These samples were selected impartially from the group with wide range of distribution of the [2850]/[1540] ratio. After obtaining the information for the fatty acid compositions and normalized infrared spectra of the mucosal samples, we proceeded to the multivariate analysis to construct suitable PLS regression parameters. It was important to obtain the normalized spectra (second derivative form), which were adjusted to the same value for the amide I infrared absorption intensities of the selected mucosal samples.

Many papers have been published recently concerning multivariate analysis methods for fatty acid compositional analyses [11–14] using vibrational spectroscopy. These papers have proved that vibrational spectroscopies such as Raman, near-infrared, and mid-infrared spectroscopy are useful in combination with multivariate analyses such as the PLS (partial least squares) regression analysis method

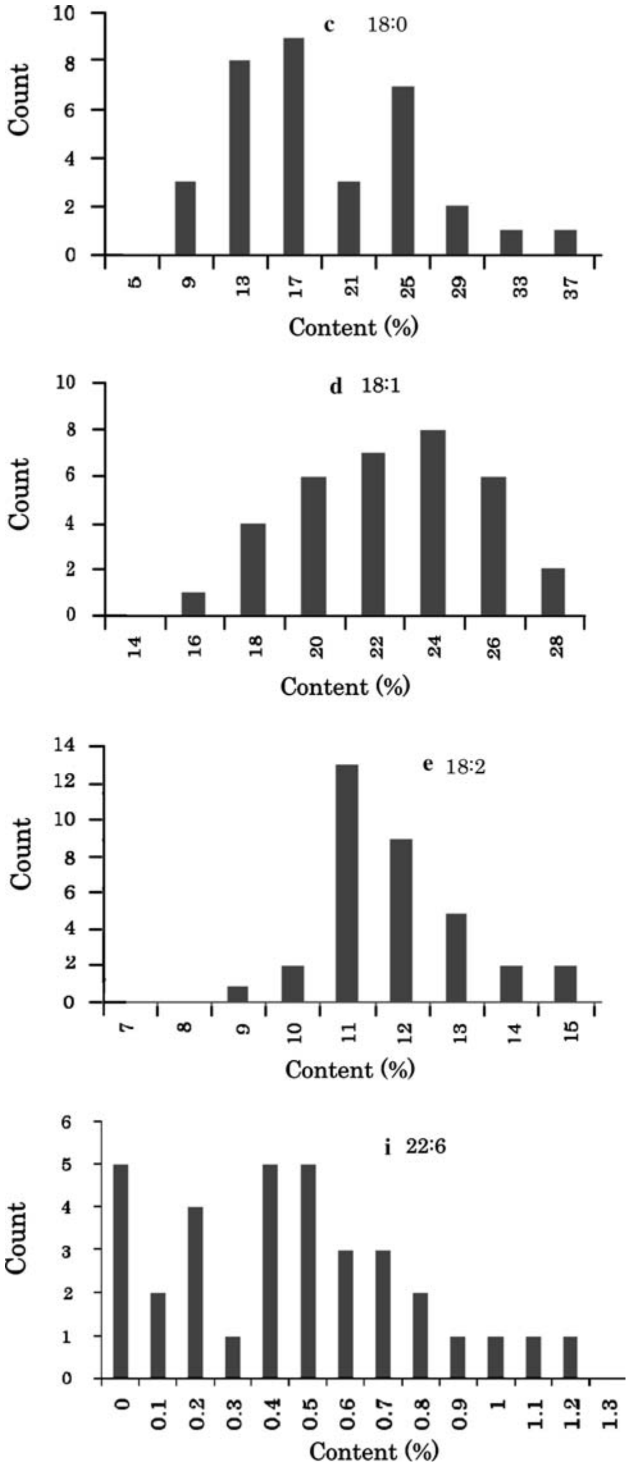

Fig. 6 Histograms for four predicted fatty acid compositions of 34 oral mucosal samples (Iranian). In these histograms, the x-axes represent the contents in % of the fatty acids

for the prediction of fatty acid compositions in biological materials, for example in adipose tissues. These methods may have a great advantage in the analysis of fatty acids and other biomolecular compositions as these analyses can be done very rapidly for a large number of samples compared to normal chromatographic methods.

Beattie et al. [12] reported that the bulk unsaturation parameters and abundance of polyunsaturated fatty acids of several adipose tissues could be predicted by Raman spectroscopy using multivariate analysis. In that report, the Raman spectra of adipose tissues from several species in the range between 800 and 1,800 cm^{-1} were used for analysis, and the correlation coefficients of the contents of several major fatty acids were reported to be from 0.8 to 0.97. They reported that Raman analysis has the advantage of giving good correlation coefficients without the need for prior solvent extraction steps in the analysis. On the other hand, Ripoche and Guillard [13] reported when using FTIR that the prediction of fatty acid composition of unextracted adipose tissue gave poor correlation coefficient (R^2 = 0.69–0.79). Improvement of the coefficient in our case (Fig. 4) may result mainly from using less noisy second derivative infrared spectra in the selected wavenumber regions. Afseth et al. [14] reported using Raman and near-IR spectroscopic methods and that Raman spectroscopy was suitable for predicting the total level of unsaturation, and both Raman and near-IR spectroscopy were feasible for rapid quantification of fat composition in complex food model systems.

It may be important to apply vibrational spectroscopy including mid-IR spectroscopy to the estimation of fatty acid compositions in biological tissues and model mixtures with selecting the normalized absorption—wavenumber sets. These sets of the spectra contain information regarding the quality and quantity of both methylene (CH_2) stretching mode and *cis*-alkene (originated from unsaturated fatty acids; HC=CH) CH stretching mode with comparing relative intensities of those bands with protein amide I or II band intensity. Basically the fatty acid compositions (% of total fatty acids) may be determined with information regarding to the length of fatty chains and the degree of unsaturation in fatty acids, and the length of fatty chains may affect principally the intensity and peak position of infrared absorption of the methylene stretching mode and the degree of unsaturation may affect the intensity and peak position of alkene infrared absorption. The methylene infrared absorption could be measured at around 2,850 ~2,920 cm$^{-1,}$ and the intensity and shape of the absorption peaks may contain necessary information regarding the length of the fatty chains and a part of the methylene absorption shape may be affected by the extent of unsaturation and position of unsaturated bonds through changing the packing mode of lipid membranes or micelles.

On the other hand, the infrared absorption of *cis*-double bond(alkene) could be measured at around 3,010 cm^{-1}, and the intensity and shape of the alkene peak may contain

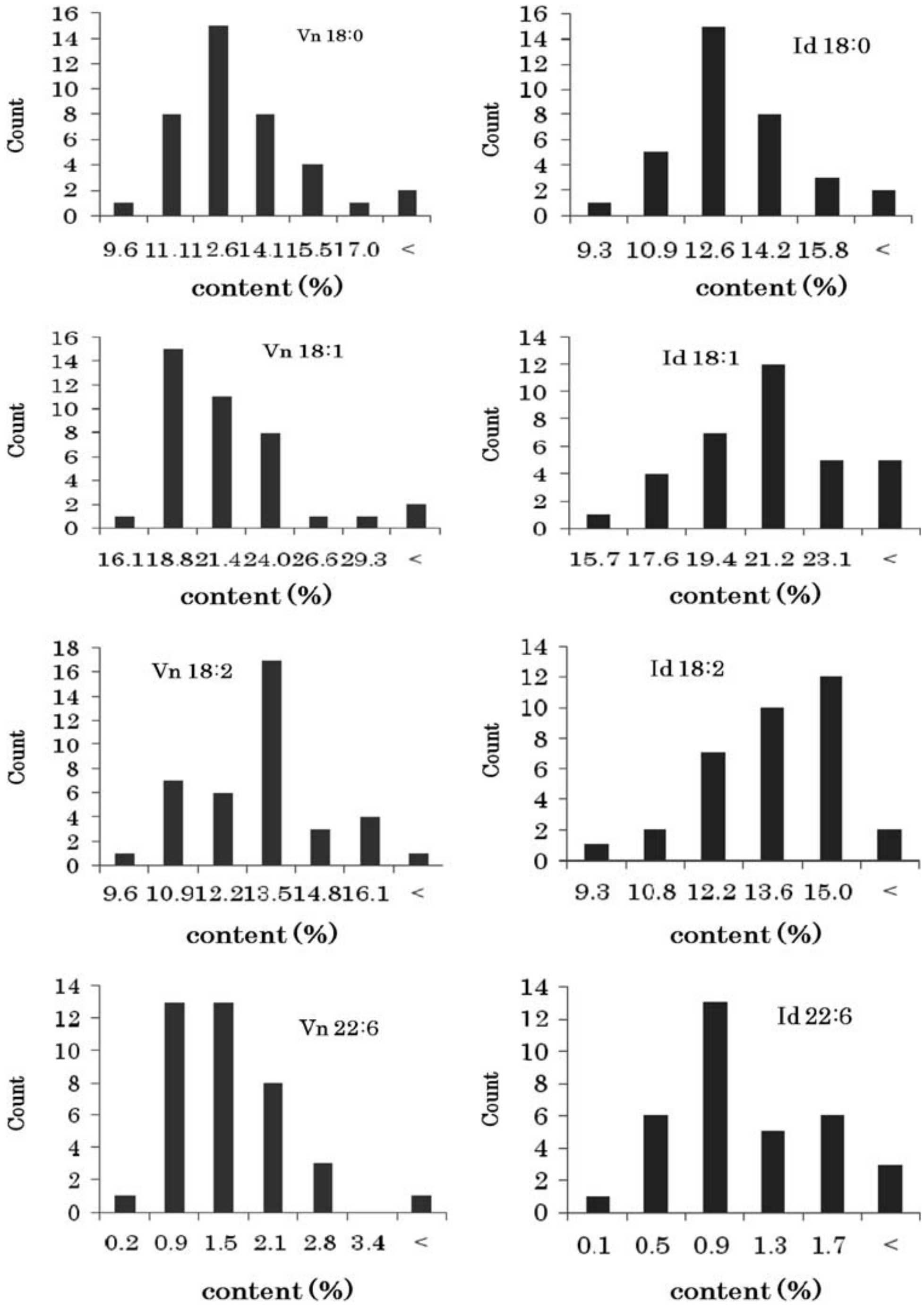

Fig. 7 Histograms for four measured fatty acids compositions of oral samples from Vietnamese and Indonesian subjects. In these histograms, the x-axes represent contents in % of the fatty acids. Vt, Vietnamese; Id, Indonesian

the information about the extent of unsaturation and the position of the double bonds [4]. The infrared absorption for *trans*-double bond could be measured [15] at 966 cm^{-1}, however, in the normal human tissue the content of *trans*-unsaturated fatty acids may be negligible. Furthermore we employed the second derivative form of the infrared spectra, which enhanced the quality of the absorption peak position and shape as shown in Fig. 3.

Based on these considerations, it may be reasonable for the prediction of fatty acid compositions by PLS regression analysis to use the normalized infrared spectrum between 2,800 and 3,050 cm^{-1}. Actually the correlation coefficient for each fatty acid, as shown in Fig. 4, was high enough for prediction of fatty acid compositions of oral mucosa. However, it should be noted that the PLS models presented are not universal.

References

1. Lands WEM (2005) Fish, Omega-3, and human health. 2nd edn. AOCS Press, Champaign, ISBN 1-893997-81-2
2. Azizian H, Kramer JK (2005) A rapid method for the quantification of fatty acids in fats and oils with emphasis on trans fatty acids using Fourier Transform near infrared spectroscopy (FT-NIR). Lipids 40:855–867
3. Whittaker P, Mossoba MM, Al-Khaldi S, Fry S, Dunkel VC, Tall BD, Yurawecz MP (2003) Identification of food borne bacteria by infrared spectroscopy using cellular fatty acid methyl esters. J Microbiol Methods 55:709–716
4. Yoshida S, Yoshida H (2003) Nondestructive analyses of unsaturated fatty acid species in dietary oils by attenuated total reflectance with Fourier transform infrared spectroscopy. Biopolymers 70:604–613
5. Yoshida S, Yoshida H (2004) Noninvasive analyses of polyunsaturated fatty acids in human oral mucosa in vivo by Fourier-transform infrared spectroscopy. Biopolymers 74:403–412
6. Lam HS, Proctor A, Nyalala J, Morris MD, Smith WG (2004) Quantitative determination of low density lipoprotein oxidation by FTIR and chemometric analysis. Lipids 39:687–692
7. Kinder R, Ziegler C, Wessels JM (1997) Gamma-irradiation and UV-C light-induced lipid peroxidation: a Fourier transform-infrared absorption spectroscopic study. Int J Radiat Biol 71:561–571
8. Nagase Y, Yoshida S, Kamiyama K (2005) Analysis of human tear fluid by Fourier transform infrared spectroscopy. Biopolymers 79:18–27
9. Connor SL, Zhu N, Anderson GJ, Hamill D, Jaffe E, Carlson J, Connor WE (2000) Cheek cell phospholipids in human infants: a marker of docosahexaenoic and arachidonic acids in the diet, plasma, and red blood cells. Am J Clin Nutr 71:21–27
10. Terashi H, Izumi K, Rhodes LM, Marcelo CL (2000) Human stratified squamous epithelia differ in cellular fatty acid composition. J Dermatol Sci 24:14–24
11. Kansiz M, Billman-Jacobe H, McNaughton D (2000) Quantitative determination of the biodegradable polymer Poly(beta-hydroxybutyrate) in a recombinant *Escherichia coli* strain by use of mid-infrared spectroscopy and multivariate statistics. Appl Environ Microbiol 66:3415–3420
12. Beattie JR, Bell SE, Borgaard C, Fearon A, Moss BW (2006) Prediction of adipose tissue composition using Raman spectroscopy: average properties and individual fatty acids. Lipids 41:287–294
13. Ripoche A, Guillard AS (2001) Determination of fatty acid composition of pork fat by Fourier transform infrared spectroscopy. Meat Sci 58:299–304
14. Afseth NK, SegtnanVH, Marquardt BJ, Wold JP (2005) Raman and near-infrared spectroscopy for quantification of fat composition in a complex food model system. Appl Spectrosc 59:1324–1332
15. Mossoba MM, Yurawecz MP, Delmonte P, Kramer JK (2004) Overview of infrared methodologies for trans fat determination. J AOAC Int 87:540–544

Lipids (2008) 43:373–382
DOI 10.1007/s11745-007-3149-y

ORIGINAL ARTICLE

Inhibitory Effects of Cholesterol Derivatives on DNA Polymerase and Topoisomerase Activities, and Human Cancer Cell Growth

Chisato Ishimaru · Yuko Yonezawa · Isoko Kuriyama · Masayuki Nishida · Hiromi Yoshida · Yoshiyuki Mizushina

Received: 10 September 2007 / Accepted: 7 December 2007 / Published online: 24 January 2008
© AOCS 2008

Abstract This paper describes the inhibitory activities of cholesterol derivatives such as cholesterol, sodium cholesteryl sulfate, cholesteryl-5α, 6α-epoxide, cholesteryl chloride, cholesteryl bromide, and cholesteryl hemisuccinate (compounds **1**–**6**, respectively) against DNA polymerase (pol), DNA topoisomerase (topo), and human cancer cell growth. Among the compounds tested, compounds **2** and **6** revealed themselves to be potent inhibitors of animal pols, and the IC_{50} values for pols were 0.84–11.6 and 2.9–148 μM, respectively. Compounds **2**, **3** and **6** inhibited the activity of human topo II, with IC_{50} values of 5.0, 12.5 and 120 μM, respectively. Compounds **2**, **3** and **6** also suppressed human cancer cell (promyelocytic leukemia cell line, HL-60) growth, and LD_{50} values were 8.8, 20.2 and 72.3 μM, respectively, suggesting that cell growth inhibition had the same tendency as the inhibition of topos rather than pols. Compounds **2** and **6** arrested the cells in S and G2/M phases, compound **3** arrested the cells in the G2/M phase, and these compounds also increased sub-G1 phase in the cell cycle. These results suggested that the effect of cell cycle arrest might be effective on both pols and topos activities. From these findings, the action mode of cholesterol derivatives as anti-cancer compounds is discussed.

Keywords Cholesterol derivatives · Sodium cholesteryl sulfate · Cholesteryl-5α, 6α-epoxide · Cholesteryl hemisuccinate · Enzyme inhibitor · DNA polymerase · DNA topoisomerase · Cell growth inhibition · Cell cycle arrest

Abbreviations

Clog P	Calculated log P
DMSO	Dimethyl sulfoxide
HPBMC	Normal peripheral blood mononuclear cells
dTTP	2′-Deoxythymidine 5′-triphosphate
dNTP	2′-Deoxyribonucleotide 5′-triphosphate
dsDNA	Double-stranded DNA
IC_{50}	50% Inhibitory concentration
LD_{50}	50% Lethal dose
pol	DNA-directed DNA polymerase (E.C. 2.7.7.7)
topo	DNA topoisomerase

Introduction

DNA polymerase (pol) catalyzes the addition of deoxyribonucleotides to the 3′-hydroxyl terminus of primed double-stranded DNA (dsDNA) molecules [1]. The human genome encodes 14 pols which conduct cellular DNA synthesis [2]. Eukaryotic cells reportedly contain three replicative types: pols α, δ, and ε, mitochondrial pol γ, and at least twelve repair types: pols β, δ, ε, ζ, η, θ, ι, κ, λ, μ, and σ and REV1 [3].

DNA topoisomerases (topos) are key enzymes that control the topological state of DNA. There are two classes of topos: type I enzymes, which act by transiently nicking one of the two DNA strands, and type II enzymes, which nick both DNA strands are dependent on ATP, are involved

C. Ishimaru · Y. Yonezawa · I. Kuriyama · M. Nishida ·
H. Yoshida · Y. Mizushina (✉)
Laboratory of Food & Nutritional Sciences,
Department of Nutritional Science, Kobe-Gakuin University,
Nishi-ku, Kobe, Hyogo 651-2180, Japan
e-mail: mizushin@nutr.kobegakuin.ac.jp

H. Yoshida · Y. Mizushina
Cooperative Research Center of Life Sciences,
Kobe-Gakuin University, Nishi-ku,
Kobe, Hyogo 651-2180, Japan

in many vital cellular processes that influence DNA replication, transcription, recombination, integration and chromosomal segregation [4].

DNA metabolic enzymes such as pols and topos are not only essential for DNA replication, repair and recombination, but are also involved in cell division. Selective inhibitors of these enzymes are considered as a group of potentially useful anti-cancer and anti-parasitic agents, because some inhibitors suppress human cancer cell proliferation and have cytotoxicity [5–8].

Cholesterol is a steroid alcohol that is essentially insoluble in aqueous solutions. In mammals, it is normally solubilized by its association with other lipids, such as phospholipids or bile acids; thus, most cholesterol is found in cell membranes, plasma lipoproteins, and bile [9]. Cholesterol can be esterified with a fatty acid to form cholesteryl esters [10]. The latter form discrete lipid droplets in cells, especially in cells of steroidogenic tissues, and in the lipid core of low-density lipoproteins in blood [11]. Most cholesterols are synthesized by the liver and other tissues, including the adrenal glands and reproductive organs. Some cholesterol is absorbed from dietary sources. The most common sterol of eukaryotes is a key constituent of cell membranes and works as the precursor of bile acids, cholecalciferol (vitamin D) and steroid hormones including cortisol, cortisone, aldosterone and sex hormone progesterone in vertebrates [12].

The purpose of this study was to find the novel bioactivity of cholesterol and its related compounds. Herein, we describe the inhibitory activities of various cholesterol derivatives against DNA metabolic enzymes such as pols and topos, and cellular proliferation processes such as DNA replication of human cancer cells (HL-60). It was discussed that cholesterol derivatives could have anti-cancer activity.

Materials and Methods

Materials

Six cholesterol-related compounds—cholesterol (compound **1**), sodium cholesteryl sulfate (compound **2**), cholesteryl-5α, 6α-epoxide (compound **3**), cholesteryl chloride (compound **4**), cholesteryl bromide (compound **5**) and cholesteryl hemisuccinate (compound **6**), aphidicolin, camptothecin, and etoposide were purchased from Sigma-Aldrich (St Louis, MO, USA). The chemical structures of the compounds are shown in Fig. 1. Nucleotides and chemically synthesized DNA template-primers, such as poly(dA) and oligo$(dT)_{12-18}$, and radioisotope reagents such as $[^3H]$-dTTP (2′-deoxythymidine 5′-triphosphate) (43 Ci/mmol) were purchased from GE Healthcare Bio-Science Corp. (Buckinghamshire, UK). Supercoiled pBR322 plasmid dsDNA was obtained from Takara Bio Inc. (Kyoto, Japan). All other reagents were of analytical grade and were purchased from Nacalai Tesque, Ltd (Kyoto, Japan).

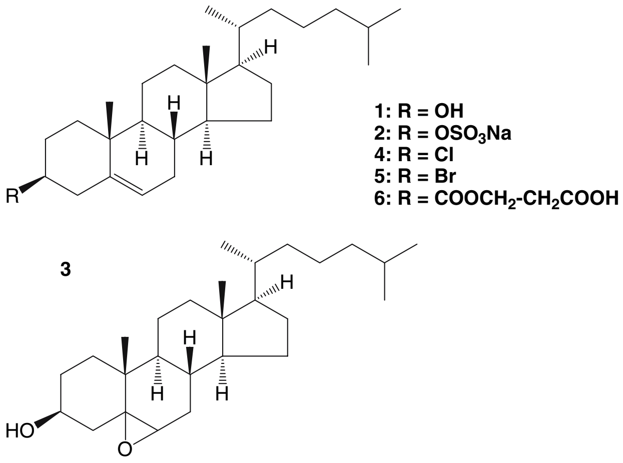

Fig. 1 Structures of cholesterol derivatives. Compound **1**: cholesterol, compound **2**: sodium cholesteryl sulfate, compound **3**: cholesteryl-5α, 6α-epoxide, compound **4**: cholesteryl chloride, compound **5**: cholesteryl bromide, and compound **6**: cholesteryl hemisuccinate

Enzymes

Pol α was purified from the calf thymus by immuno-affinity column chromatography, as described by Tamai et al. [13]. Recombinant rat pol β was purified from *E. coli* JMpβ5, as described by Date et al. [14]. The human pol γ catalytic gene was cloned into pFastBac, and histidine-tagged enzyme was expressed using the BAC-TO-BAC HT Baculovirus Expression System according to the supplier's manual (Life Technologies, MD, USA) and purified using ProBoundresin (Invitrogen Japan, Tokyo, Japan) [15]. Human pols δ and ε were purified by the nuclear fractionation of human peripheral blood cancer cells (Molt-4) using the second subunit of pols δ and ε-conjugated affinity column chromatography, respectively [16]. Recombinant human His-pol λ was overexpressed and purified according to a method described by Shimazaki et al. [17]. Fish pol δ was purified from the testis of cherry salmon (*Oncorhynchus masou*) [18]. Fruit fly pols α, δ and ε were purified from early embryos of *Drosophila melanogaster*, as described by Aoyagi et al. [19, 20]. Pols I (α-like) and II (β-like) from a higher plant, cauliflower inflorescence, were purified according to the methods outlined by Sakaguchi et al. [21]. The Klenow fragment of pol I from *E. coli* was purchased from Worthington Biochemical Corp. (Freehold, NJ, USA). *Taq* pol, T4 pol, T7 RNA polymerase and T4 polynucleotide kinase were purchased from Takara (Kyoto, Japan). Bovine pancreas deoxyribonuclease I was obtained from Stratagene Cloning Systems (La Jolla, CA, USA). Purified human placenta topos I and II were purchased from TopoGen, Inc. (Columbus, OH).

DNA Polymerase Assays

The reaction mixtures for pol α, pol β, plant pols and prokaryotic pols have been described previously [22, 23], and those for pol γ, and pols δ and ε were as described by Umeda et al. [15] and Ogawa et al. [24], respectively. The reaction mixture for pol λ was the same as that for pol β. For pols, poly(dA)/oligo(dT)$_{12–18}$ (A/T = 2/1) and dTTP were used as the DNA template-primer and nucleotide (i.e., 2′-deoxyribonucleotide 5′-triphosphates, dNTP) substrate, respectively.

The cholesterol derivatives (i.e., compounds **1**–**6**) were dissolved in dimethyl sulfoxide (DMSO) at various concentrations and sonicated for 30 s. Aliquots of 4 μl of sonicated samples were mixed with 16 μl of each enzyme (final amount 0.05 units) in 50 mM Tris–HCl (pH7.5) containing 1 mM dithiothreitol, 50% glycerol and 0.1 mM EDTA, and kept at 0 °C for 10 min. These inhibitor-enzyme mixtures (8 μl) were added to 16 μl of each of the enzyme standard reaction mixtures, and incubation was carried out at 37 °C for 60 min, except for *Taq* pol, which was incubated at 74 °C for 60 min. Activity without the inhibitor was considered 100%, and the remaining activity at each concentration of the inhibitor was determined relative to this value. One unit of pol activity was defined as the amount of enzyme that catalyzed the incorporation of 1 nmol of dNTP (i.e., dTTP) into synthetic DNA template-primers within 60 min at 37 °C under the normal reaction conditions for each enzyme [22, 23].

Measurement of DNA Topoisomerase Activity

The catalytic activity of topo I was determined by detecting supercoiled plasmid DNA (i.e., form I) in its nicked form (i.e., form II) [25]. The topo I reaction was performed in 20 μl of reaction mixture containing 10 mM Tris-HCl (pH 7.9), pBR322 DNA (250 ng), 1 mM EDTA, 150 mM NaCl, 0.1% bovine serum albumin (BSA), 0.1 mM spermidine, 5% glycerol, 2 μl of DMSO dissolved cholesterol-related compounds (i.e., compounds **1**–**6**), and 2 units of topo I. The catalytic activity of topo II was analyzed in the same manner except that the reaction mixture contained 50 mM Tris–HCl (pH 8.0), 120 mM KCl, 10 mM $MgCl_2$, 0.5 mM ATP, 0.5 mM DTT, supercoiled pBR322 DNA (250 ng) and 2 units of topo II [25]. The reaction mixtures were incubated at 37 °C for 30 min, followed by 1% SDS and 1 mg/ml proteinase K digestion, and then 2 μl of loading buffer was added, consisting of 5% sarkosyl, 0.0025% bromophenol blue and 25% glycerol. To study the binding of enzyme and DNA based on mobility shifts, SDS denaturation and proteinase K digestion were omitted. The mixtures were subjected to 1% agarose gel electrophoresis in TBE buffer. Agarose gel was stained with ethidium bromide (EtBr) and the DNA was visualized under UV light.

Other Enzyme Assays

The primase activity of pol α, the activities of T7 RNA polymerase, T4 polynucleotide kinase and bovine deoxyribonuclease I were measured by standard assays according to the manufacturer's specifications, as described by Tamiya-Koizumi et al. [26], Nakayama et al. [27], Soltis et al. [28], and Lu and Sakaguchi [29], respectively.

Investigation of Cytotoxicity on Cultured Cells

To investigate the effects of cholesterol derivatives (i.e., compounds **1**–**6**) on cultured cells, human blood corpuscle cells, derived from a cancer patient, such as promyelocytic leukemia cell line HL-60 and acute T lymphoblastic leukemia cell line Molt-4, and normal peripheral blood mononuclear cells (HPBMC) were used. HL-60 cells (IFO 50022) and Molt-4 cells (IFO 50362) were supplied by the Health Science Research Resources Bank (Osaka, Japan). HPBMC was obtained from Dainippon Sumiotomo Pharma Co. Ltd (Osaka, Japan). The cells were routinely cultured in RPMI 1640 medium supplemented with 10% fetal bovine serum, 100 μg/ml streptomycin, 100 unit/ml penicillin, and 1.6 μg/ml $NaHCO_3$. They were cultured at 37 °C in standard medium in a humidified atmosphere of 5% CO_2-95% air. The cytotoxicity of the compounds was investigated as follows. High concentrations (10 mM) of the compounds were dissolved in DMSO and stocked. Approximately 1×10^4 cells per well were inoculated in 96-well micro plates, and then the compound stock solution was diluted to various concentrations and applied to each well. After incubation for 24 h, the survival rate was determined by MTT (3-(4,5-dimethylthiazol-2-yl)-2,5-diphenyl tetrazolium bromide) assay [30] and trypan blue stain method [31].

Cell Cycle Analysis

The cellular DNA content for cell cycle analysis was determined as follows: Aliquots of 3×10^5 HL-60 cells were harvested into a 35-mm dish, and incubated with medium containing compounds **2**, **3** and **6** for various times. The cells were then washed with ice-cold PBS three times by centrifugation, fixed with 70% (v/v) ethanol, and stored at −20 °C. DNA was stained with PI (3,8-diamino-5-[3-(diethylmethylammonio)propyl]-6-phenylphenanthridinium diiodide) staining solution for at least 10 min at room temperature in the dark. Fluorescence intensity was measured by FACSCanto flow cytometer in combination with FACSDiVa software (BD (Becton, Dickinson and Company), NJ, USA).

Results

Effects of Cholesterol Derivatives on Mammalian DNA Polymerases α, β and λ

The chemical structures of cholesterol (compound **1**) and its related compounds (i.e., compounds **2**–**6**), which were commercially available, are shown in Fig. 1. First, the inhibitory activity of calf pol α, rat pol β and human pol λ against 100 μM of each compound was investigated (Fig. 2). In mammalian pols, pol α and pols β and λ were used as representative replicative pols and repair/recombination-related pols, respectively [2, 3]. Compounds **2** and **6** significantly inhibited the activities of these pols, and the other compounds had no influence on the activities of mammalian pols, although compounds **4** and **5**, which consist of one halogen atom, slightly inhibited pol λ activity. As a positive control, we measured the inhibition of these pol activities using the same concentration (i.e., 100 μM) of aphidicolin, which is a known inhibitor of replicative pols α, δ and ε, and the inhibitory effect on pol α of compounds **2** and **6** was stronger than that of aphidicolin. Compound **2** showed the strongest inhibition of pols α, β and λ activities in the tested compounds, and 50% inhibition was observed at doses of 2.8, 1.7 and 0.84 μM, respectively (Table 1). When activated DNA (i.e., DNA digested by bovine deoxynuclease I) was used as the DNA template-primer instead of poly(dA)/oligo(dT)$_{12–18}$ (A/T = 2/1), the mode of inhibition by these compounds did not change (data not shown).

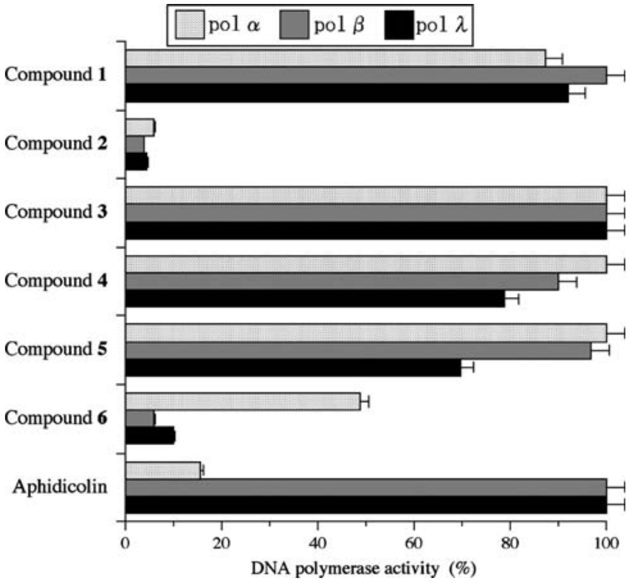

Fig. 2 Effect of cholesterol derivatives on the activities of mammalian pols. One hundred μM of each compound and aphidicolin was incubated with calf pol α, rat pol β and human pol λ (0.05 units each). Pol activities were measured as described in the "Materials and Methods" section. Enzymatic activity in the absence of the compound was taken as 100%. Data are the mean ± SEM of three independent experiments

Effects of Cholesterol Derivatives on Human DNA Topoisomerases I and II

We next, as the secondary screening for DNA metabolic enzyme inhibition, investigated the inhibitory effects of compounds **1** to **6** against human topos I and II, which have single-stranded and dsDNA nicking activity, respectively [4]. As shown in Fig. 3a, 100 μM of compounds **2** and **6** significantly inhibited the activity of topo I, and IC$_{50}$ values were 7.5 and 25.0 μM, respectively (Table 1). These results suggested that the inhibitory activity of these cholesterol-related compounds between mammalian pols and human topo I had the same tendency (Fig. 2). On the other hand, topo II inhibition was shown by 100 μM of compounds **2**, **3** and **6**, and the other compounds, **1**, **4** and **5** were not affected (Fig. 3b). Camptothecin and etoposide, which are known topo I and topo II inhibitors, respectively, also inhibited the nicking activities of topos I and II with IC$_{50}$ values of 85 and 70 μM, respectively (Fig. 3). These findings showed that compounds **2** and **6** were stronger inhibitors of topo I than camptothecin, and compounds **2** and **3** were stronger inhibitors of topo II than etoposide.

The Effects of Cholesterol Derivatives on Various DNA Polymerases and other DNA Metabolic Enzymes

Compound **2** inhibited the activities of mammalian pols tested (i.e., pols α, β, γ, δ, ε and λ), with an IC$_{50}$ value of 0.84–9.1 μM (Table 1). The pol λ inhibitory effect of compound **2** was the strongest in mammalian pols. Compound **6** also had inhibitory effects against the mammalian pols tested, and selectively inhibited pols β and λ, which are family X pols [32, 33], with IC$_{50}$ values of 2.9 and 6.3 μM, respectively (Table 1). This compound moderately suppressed the activities of the pol A family (i.e., pol γ)

Table 1 IC$_{50}$ values of cholesterol derivatives for the activities of various DNA polymerases and other DNA metabolic enzymes

Enzyme	IC$_{50}$ values of compounds (μM)					
	1	2	3	4	5	6
Mammalian DNA polymerases						
Calf DNA polymerase *α*	>200	2.8	>200	>200	>200	96.8
Rat DNA polymerase *β*	>200	1.7	>200	>200	>200	2.9
Human DNA polymerase *γ*	>200	9.1	>200	>200	>200	131
Human DNA polymerase *δ*	>200	7.7	>200	>200	>200	89.2
Human DNA polymerase *ε*	>200	8.5	>200	>200	>200	148
Human DNA polymerase *λ*	>200	0.84	>200	>200	>200	6.3
Fish DNA polymerase						
Cherry salmon DNA polymerase *δ*	>200	9.6	>200	>200	>200	94.6
Insect DNA polymerases						
Fruit fly DNA polymerase *α*	>200	3.0	>200	>200	>200	97.6
Fruit fly DNA polymerase *δ*	>200	11.6	>200	>200	>200	92.5
Fruit fly DNA polymerase *ε*	>200	10.0	>200	>200	>200	99.1
Plant DNA polymerases						
Cauliflower DNA polymerase *α*	>200	>200	>200	>200	>200	>200
Cauliflower DNA polymerase *β*	>200	>200	>200	>200	>200	>200
Prokaryotic DNA polymerases						
E. coli DNA polymerase I	>200	>200	>200	>200	>200	>200
Taq DNA polymerase	>200	>200	>200	>200	>200	>200
T4 DNA polymerase	>200	>200	>200	>200	>200	>200
Other DNA metabolic enzymes						
Calf Primase of DNA polymerase *α*	>200	>200	>200	>200	>200	>200
T7 RNA polymerase	>200	>200	>200	>200	>200	>200
T4 Polynucleotide kinase	>200	>200	>200	>200	>200	>200
Bovine Deoxyribonuclease I	>200	>200	>200	>200	>200	>200
Human DNA topoisomerase I	>200	7.5	>200	>200	>200	25.0
Human DNA topoisomerase II	>200	5.0	12.5	>200	>200	120

Compound **1**: cholesterol, Compound **2**: sodium cholesteryl sulfate, Compound **3**: cholesteryl-5*α*, 6*α*-epoxide, Compound **4**: cholesteryl chloride, Compound **5**: cholesteryl bromide, Compound **6**: cholesteryl hemisuccinate

These compounds were incubated with each enzyme. Enzymatic activity was measured as described in "Materials and Methods". Enzyme activity in the absence of the compounds was taken as 100%

and pol B family (i.e., pols *α*, *δ* and *ε*) [32], and 50% inhibition was observed at concentrations of 131 and 89.2–148 μM, respectively. The inhibitory effect of compound **2** on mammalian pols was stronger than that of compound **6**.

Furthermore, compounds **2** and **6** inhibited animal pols from fish (cherry salmon) pol *δ*, and insects (fruit fly) pols *α*, *δ* and *ε* at almost the same concentration as the inhibition of mammalian pols (Table 1). On the other hand, these compounds had no significant influence on the activities of pols I (*α*-like pol) and II (*β*-like pol) from plants (cauliflower) and prokaryotes such as the Klenow fragment of *E. coli* pol I, *Taq* pol and T4 pol.

In the DNA metabolic enzymes tested, the activities of human topos II were inhibited by not only compounds **2** and **6**, but also compound **3**, and the order of the inhibitory effect was as follows: compound **2** > compound **3** > compound **6** (Table 1). These compounds did not influence the activities of the other DNA metabolic enzymes tested, including calf primase of pol *α*, T7 RNA polymerase, T4 polynucleotide kinase and bovine deoxyribonuclease I.

To determine whether the inhibitor resulted in binding to DNA or the enzyme, the interaction of compounds **2**, **3** and **6** with dsDNA was investigated based on the thermal transition of dsDNA with or without the compound. The Tm of dsDNA with an excess amount of each compound (100 μM) was measured using a spectrophotometer equipped with a thermoelectric cell holder. In the concentration range used, no thermal transition of Tm was observed, whereas ethidium bromide used as a positive control, a typical intercalating compound, produced clear thermal transition. These observations indicated that these compounds did not intercalate to DNA as a template-primer, and the compound might directly bind to the enzyme and inhibit its activity.

Furthermore, we studied the mechanism of the inhibitory effect of cholesterol derivatives on human cancer cells.

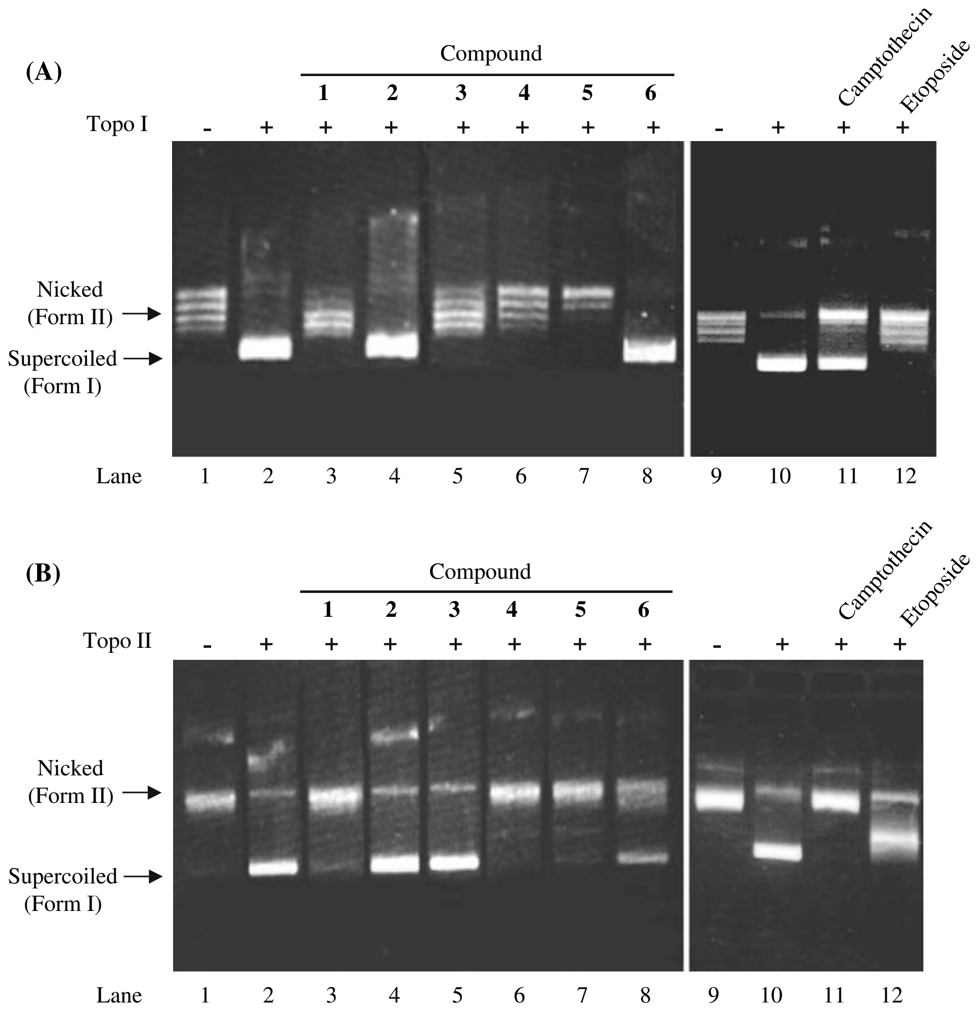

Fig. 3 Effect of cholesterol derivatives on human topos I and II. **a** topo I and **b** topo II. Supercoiled plasmid DNA was mixed with the enzyme and 100 µM of compounds **1**–**6**, and camptothecin and etoposide dissolved in DMSO (*lanes* 3–8, and 11 and 12, respectively). *Lanes* 1–2 and 9–10, no compounds. *Lanes* 2–8 and 10–12, 2 units of topo enzyme; *lanes* 1 and 9, no enzyme. Plasmid DNA of 0.25 µg was added to each of the *lanes*. Photographs of ethidium bromide-stained gels are shown

Effects of Cholesterol Derivatives on Cultured Human Cancer Cells

Pols and topos have recently emerged as important cellular targets for chemical intervention in the development of anti-cancer agents. Cholesterol and its related compounds (i.e., compounds **1**–**6**) could, therefore, be useful in chemotherapy and we investigated the cytotoxic effect of six compounds against three cultured cells of human blood corpuscles, two human leukemia cell lines, HL-60 and Molt-4, and HPBMC. HL-60 is a mutant cell line, which has a p53 gene deletion, and Molt-4 is a normal cell line, which has a p53 gene. As shown in Fig. 4a, 50 and 100 µM of compound **2** had the strongest growth inhibitory effect on HL-60 cancer cell line in the tested compounds, and compounds **3** and **6** were the second strongest, and cell proliferation was not influenced by the other compounds. The suppression of cell growth had the same tendency as the inhibition of topo II among the compounds (Fig. 3b), suggesting that the cause of cancer cell influence might be the activity of topo II. On the other hand, the same concentrations of aphidicolin, camptothecin and etoposide, which are inhibitors of replicative pols, topo I and topo II, respectively, completely suppressed the growth of HL-60 cells (Fig. 4a).

The influence of compounds **1**–**6** on Molt-4 cell growth showed the same tendency as that on HL-60 cells, and the cell growth effect on the HL-60 cell line had almost the same cytotoxicity as that on the Molt-4 cell line (Fig. 4b), suggesting that p53 protein expression had no relation to cell growth inhibition by cholesterol derivatives, which are selective inhibitors of pols and topos. The normal blood corpuscle cell line, HPBMC, was not influenced the growth by these compounds (Fig. 4c). As a result, compounds **2**, **3** and **6** could selectively inhibit the growth of human cancer cells, and could be come anti-cancer drugs.

Therefore, we concentrated our efforts on compounds **2**, **3** and **6**, and aphidicolin (a representative pol inhibitor) and etoposide (a representative topo inhibitor) against HL-60 cells in the latter part of this study. Compounds **2**, **3** and **6**, aphidicolin and etoposide suppressed HL-60 cell growth in a dose-dependent manner, and 50% cytotoxicity of these compounds was observed at doses of 8.8, 20.2, 72.3, 7.0

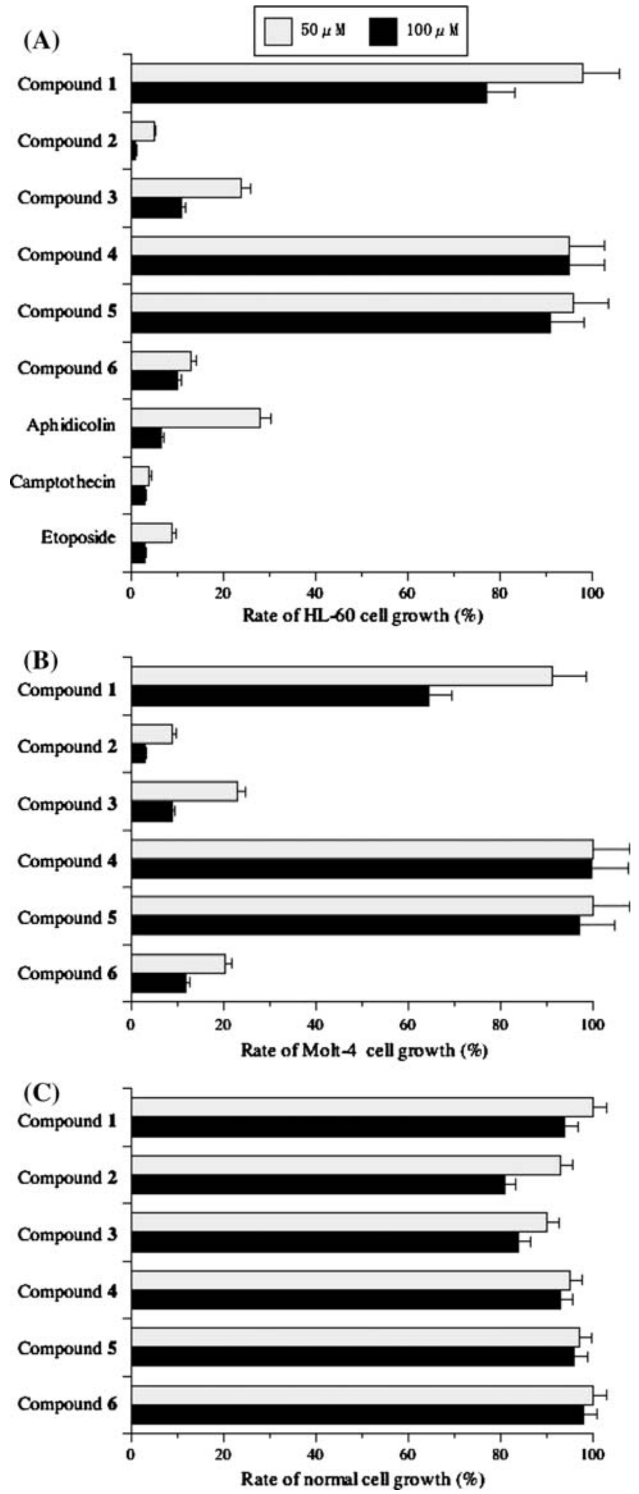

◀ **Fig. 4** Effect of cholesterol derivatives on the proliferation of human cultured blood corpuscle cell growth. Each compound (50 and 100 μM) was added to the culture of a leukemia cell line HL-60 (**a**) and Molt-4 (**b**), and normal peripheral blood mononuclear cells (HPBMC) (**c**). The cells were incubated for 24 h, and the rate of cultured cell growth inhibition was determined by MTT assay [30] for cancer cells (i.e., HL-60 and Molt-4) and by trypan blue stain method [31] for HPBMC. Cell growth inhibition of the cancer cells in the absence of the compound was taken as 100%. Data are the mean ± SEM of five independent experiments

and 1.5 μM, respectively, after 24 h of treatment. These results showed that the LD_{50} value in vivo of compounds **2**, **3** and **6** on HL-60 cells was almost the same as IC_{50} values in vitro on pols and/or topos.

We investigated in more detail which inhibition by these compounds is effective for cancer cell proliferation, that of pols or topos.

Effects on the Cell Cycle Progression of Compounds **2**, **3** and **6**

Next, we analyzed whether compounds **2**, **3** and **6** affected the cell cycle distribution of each compound-treated cell. The cell cycle fraction was recorded after 6, 12 and 24 h of treatment with the LD_{50} value of each compound, and the ratio of the four phases (i.e., sub-G1, G0/G1, S and G2/M) in the cell cycle is shown in Fig. 5. Consequently, among cells treated with compound **2** for time-dependent incubation, the population of cells in the S and G2/M phases increased (1.3- and 2.8-fold increase of S and G2/M phases for 24 h incubation, respectively), and the percentage of cells in the G1 phase significantly, 2.0-fold, decreased for 24 h (Fig. 5a). The cell cycle effect of compound **6** had the same tendency as that of compound **2** (Fig. 5b). Aphidicolin, which is a replicative pols (i.e., pols α, δ and ε) inhibitor, moderately arrested the cell cycle in the S phase (Fig. 5d), and etoposide, which is a classical topo II inhibitor, 4.6-fold strongly arrested the cell cycle in the G2/M phase (Fig. 5e). Compounds **2** and **6**, therefore, might be effective in the inhibition of both pols and topos for the incubation of cells, because these compounds inhibited the activities of mammalian pols and human topos, and the inhibitory effect on pols was the almost same as that on topos in vitro (Table 1). On the other hand, compound **3** led to an increase in the population of HL-60 cells in the G2/M phase (6.4–24.2%), to decrease the population of cells in the G1 phases (65.0–32.8%), and the S phase was hardly affected (25.9–29.4%) for 24 h (Fig. 5b), suggesting that this compound arrested the G2/M phase in the cells by inhibition of topo II. These results indicated that the cell cycle arrest of cancer cells by cholesterol derivatives might be affected by the inhibitory activities of both pols and topos.

As shown in Fig. 5, all compound tested, which inhibited the activities of pols and/or topos, also time-dependently increased the sub-G1 phase (i.e., the rate of DNA fragmentation in HL-60 cells) in the cell cycle. The findings suggested that these compounds induced DNA fragmentation in the cells, and the effect of the compounds must involve a combination of growth arrest and cell death. These cholesterol derivatives, therefore, should be

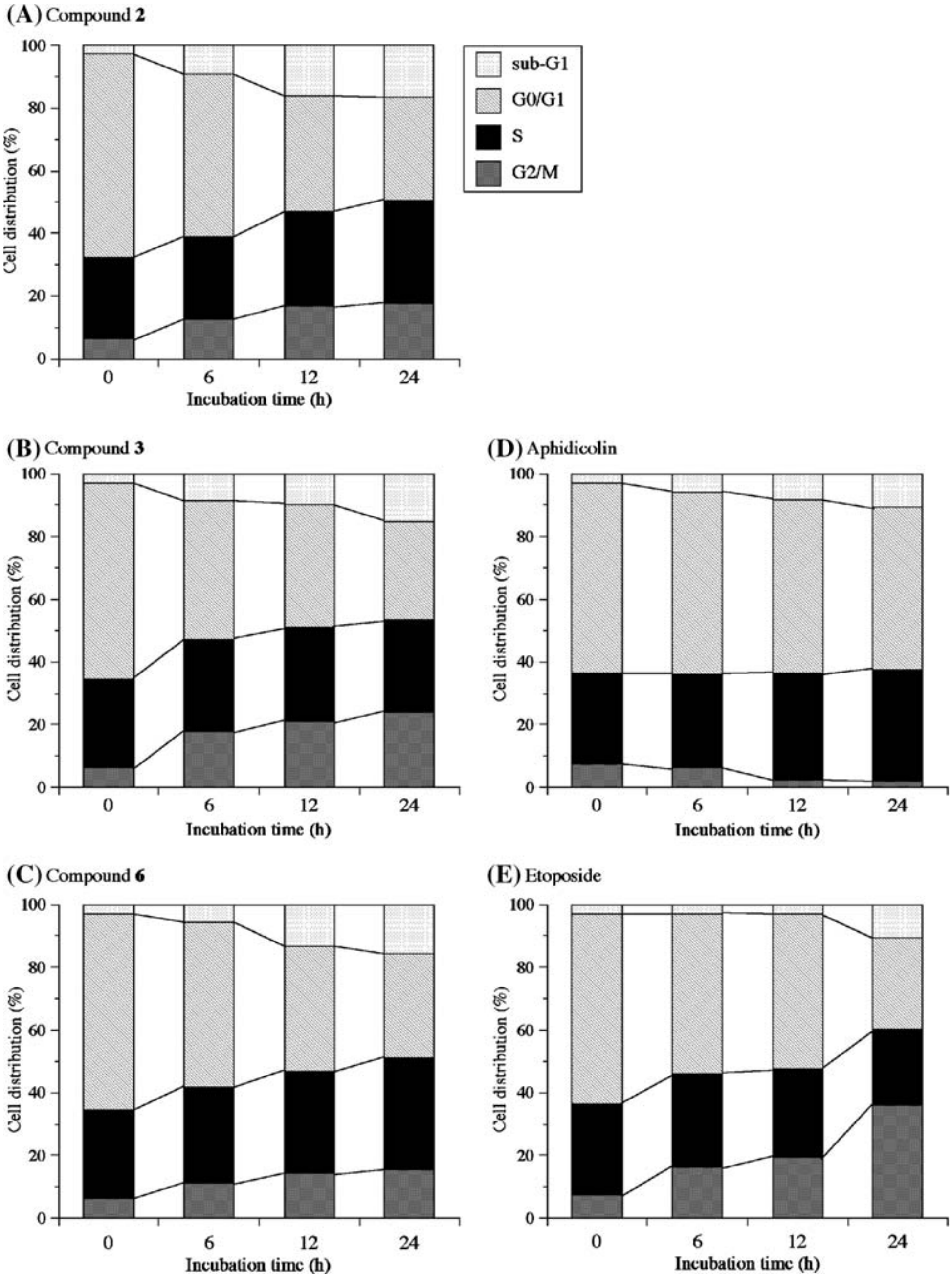

Fig. 5 The effect of compounds **2**, **3** and **6** on the cell cycle. HL-60 cells were incubated with 8.8 µM of compound **2** (**a**), 20.2 µM of compound **3** (**b**), 72.3 µM of compound **6** (**c**), 7 µM of aphidicolin (**d**) and 1.5 µM of etoposide (**e**) for 0, 6, 12 and 24 h. Cell cycle distribution was calculated as the percentage of cells in sub-G1, G0/G1, S and G2/M phases. All experiments were performed three times

considered the lead compound in potentially useful cancer chemotherapy agents.

Discussion

As described in this report, we found that some cholesterol derivatives, such as sodium cholesteryl sulfate (compound **2**), cholesteryl-5α, 6α-epoxide (compound **3**), and cholesteryl hemisuccinate (compound **6**), inhibited the activities of DNA metabolic enzymes, such as pols and/or topos, and also suppressed human cancer cell growth (Figs. 2–4, Table 1). In particular, compounds **2** and **6** might be potent and selective inhibitors of animal pols and topos, and compound **3** could be a specific inhibitor of human topo II. The suppression of cell growth had the same tendency as the inhibition of topo II rather than pols and topo I among the cholesterol derivatives, suggesting that the cause of cancer cell influence might be the activity of topo II. To analyze the cell proliferation and growth of topo II in cancer cells, studies on the effects of small interfering RNAs (siRNA) of topo II-treated cells are now underway in our laboratory.

Table 2 Clog *P* values and calculated p*K*a values of cholesterol derivatives

Compound	Clog *P*	p*K*a
1	9.85 ± 0.28	15.0 ± 0.7
2	10.14 ± 0.64	−3.5 ± 0.2
3	8.07 ± 0.42	15.2 ± 0.7
4	11.48 ± 0.30	ND
5	11.71 ± 0.29	ND
6	10.32 ± 0.46	4.4 ± 0.2

Compound **1**: cholesterol, Compound **2**: sodium cholesteryl sulfate, Compound **3**: cholesteryl-5α, 6α-epoxide, Compound **4**: cholesteryl chloride, Compound **5**: cholesteryl bromide, Compound **6**: cholesteryl hemisuccinate

Unless otherwise noted, both the Clog *P* values and p*K*a values of compounds **1**–**6** were obtained from the calculated properties in SciFinder Scholar, which were originally calculated using Advanced Chemistry Development (ACD/Lab) Software V8.14 for Solaris (ACD/Labs)

ND: not detected

We focused on the calculated log *P* (Clog *P*) value (partition coefficients for octanol/water) and p*K*a of the cholesterol derivatives as chemical properties (Table 2). The values of Clog *P*, which indicate hydrophobicity, in compounds **1**–**6** were almost in the same range (8.07–11.71). Since compounds **2** and **6** inhibited the activities of mammalian and fish pols and human topo I in the cholesterol derivatives tested (Table 1, Figs. 2, 3a), the low p*K*a value of the compounds must be important for inhibition. These findings suggested that acidic moieties, such as sulfate and hemisuccinate groups, could be essential, and did not influence the hydrophobicity of the compound in inhibition. In particular, compound **2** showed the strongest inhibition in the tested compounds, and it was revealed that the inhibition of pols and topos activities by compound **2** influenced not only cell proliferation but also the cell cycle. These observations indicated that the sulfate group of compound **2** might be important for inhibition. Djuric et al. [34] reported that compound **2** had little effect on the proliferation of both MCF-7 and MCF-10 cells, which are human breast tumor cell line and human normal-like human breast cell line, respectively, and the different data between their report and our results may be the different species of human cancer cell lines. The more detailed mechanism by which compound **2** inhibits cell growth will be addressed in further studies.

Cholesterol is a lipid partly provided by the diet, although only about 20–25% of human body cholesterol comes from food, the rest being made by the body itself [11]. A person of average weight will have rather more than 100 g of cholesterol in their body and the body makes about 700 mg of cholesterol each day. The actual amount varies with the individual and also with the amount received from food. If the amount supplied in the diet is reduced, the body compensates by making more for itself. The body normally has more cholesterol than it needs and some of the excess is made into bile salts, which help with the digestion of fat. It is this excess cholesterol in the body which some consider harmful in relation to coronary heart disease, gallstones, and cancer.

In the human body, cholesterol derivatives such as cholesteryl sulfate (compound **2**) and cholesteryl-5α, 6α-epoxide (compound **3**) were produced by cholesterol sulfotransferase [35] and autoxidation [12], respectively. Compound **2** is a second messenger of the η isoform of protein kinase C mediating squamous differentiation, and inhibits the tumor promotional phase in mouse skin carcinogenesis [35]. Detailed studies on the action mechanism of the inhibition between tumor promotion and pols/topos activities are currently being undertaken. Compound **2** is present at approximately 300 μg/100 ml (i.e., 6.1 μM) in human body [36], and this concentration is almost the same inhibitory dose in pols/topos activities and cancer cell growth. This finding suggests that the results in this in vitro report may directly influence anti-cancer effects in the in vivo human body. Since synthesized derivatives from cholesterol in the body may possible work in anti-cancer activity, a diet containing cholesterol prevents cancer disease.

Acknowledgments We are grateful for the donations of calf pol α by Dr. M. Takemura of Tokyo University of Science (Tokyo, Japan), rat pol β by Dr. A. Matsukage of Japan Women's University (Tokyo, Japan), human pol γ by Dr. M. Suzuki of Nagoya University School of Medicine (Nagoya, Japan), human pols δ and ε by Dr. K. Sakaguchi of Tokyo University of Science (Chiba, Japan), and human pol λ by Dr. O. Koiwai of Tokyo University of Science (Chiba, Japan). This work was supported in part by a Grant-In-Aid for Kobe-Gakuin University Joint Research (A), and "Academic Frontier" Project for Private Universities: matching fund subsidy from the Ministry of Education, Science, Sports, and Culture of Japan (MEXT), 2006–2010, (Y. M. and H. Y.). Y. M. acknowledges a Grant-in-Aid for Young Scientists (A) (No. 19680031) from MEXT, and a Grant-In-Aid from the Nakashima Foundation (Japan).

References

1. Kornberg A, Baker TA (1992) DNA replication. Chapter 6, 2nd edn. Freeman, New York, pp 197–225
2. Bebenek K, Kunkel TA (2004) DNA repair and replication. In: Yang W (ed) Advances in protein chemistry, vol 69. Elsevier, San Diego, pp 137–165
3. Friedberg EC, Feaver WJ, Gerlach VL (2000) The many faces of DNA polymerases: strategies for mutagenesis and for mutational avoidance. Proc Natl Acad Sci USA 97:5681–5683
4. Wang JC (1996) DNA topoisomerases. Annu Rev Biochem 65:635–692
5. Chakraborty AK, Majumder HK (1988) Mode of action of pentavalent antimonials: specific inhibition of type I DNA topoisomerase of *Leishmania donovani*. Biochem Biophys Res Commun 152:605–611

6. Liu LF (1989) DNA topoisomerase poisons as antitumor drugs. Annu Rev Biochem 58:351–375
7. Ray S, Hazra B, Mittra B, Das A, Majumder HK (1998) Diospyrin, a bisnaphthoquinone: a novel inhibitor of type I DNA topoisomerase of *Leishmania donovani*. Mol Pharmacol 54:994–999
8. Sakaguchi K, Sugawara F, Mizushina Y (2002) Inhibitors of eukaryotic DNA polymerases. Seikagaku 74:244–251
9. Mouritsen OG, Zuckermann MJ (2004) What's so special about cholesterol? Lipids 39:1101–1113
10. Wilke MS, Clandinin MT (2005) Influence of dietary saturated fatty acids on the regulation of plasma cholesterol concentration. Lipids 40:1207–1213
11. Ostlund RE Jr (2007) Phytosterols, cholesterol absorption and healthy diets. Lipids 42:41–45
12. Smith LL (1981) Cholesterol autoxidation. Plenum Press, New York
13. Tamai K, Kojima K, Hanaichi T, Masaki S, Suzuki M, Umekawa H, Yoshida S (1988) Structural study of immunoaffinity-purified DNA polymerase α-DNA primase complex from calf thymus. Biochim Biophys Acta 950:263–273
14. Date T, Yamaguchi M, Hirose F, Nishimoto Y, Tanihara K, Matsukage A (1988) Expression of active rat DNA polymerase β in *Escherichia coli*. Biochemistry 27:2983–2990
15. Umeda S, Muta T, Ohsato T, Takamatsu C, Hamasaki N, Kang D (2000) The D-loop structure of human mtDNA is destabilized directly by 1-methyl-4-phenylpyridinium ion (MPP+), a parkinsonism-causing toxin. Eur J Biochem 267:200–206
16. Oshige M, Takeuchi R, Ruike R, Kuroda K, Sakaguchi K (2004) Subunit protein-affinity isolation of Drosophila DNA polymerase catalytic subunit. Protein Expr Purif 35:248–256
17. Shimazaki N, Yoshida K, Kobayashi T, Toji S, Tamai T, Koiwai O (2002) Over-expression of human DNA polymerase λ in *E. coli* and characterization of the recombinant enzyme. Genes Cells 7:639–651
18. Yamaguchi T, Saneyoshi M, Takahashi H, Hirokawa S, Amano R, Liu X, Inomata M, Maruyama T (2006) Synthetic Nucleoside and Nucleotides. 43. Inhibition of vertebrate telomerases by carbocyclic oxetanocin G (C.OXT-G) triphosphate analogues and influence of C.OXT-G treatment on telomere length in human HL60 cells. Nucleosides Nucleotides Nucleic Acids 25:539–551
19. Aoyagi N, Matsuoka S, Furunobu A, Matsukage A, Sakaguchi K (1994) *Drosophila* DNA polymerase δ: Purification and characterization. J Biol Chem 269:6045–6050
20. Aoyagi N, Oshige M, Hirose F, Kuroda K, Matsukage A, Sakaguchi K (1997) DNA polymerase ε from *Drosophila melanogaster*. Biochem Biophys Res Commun 230:297–301
21. Sakaguchi K, Hotta Y, Stern H (1980) Chromatin-associated DNA polymerase activity in meiotic cells of lily and mouse. Cell Struct Funct 5:323–334
22. Mizushina Y, Tanaka N, Yagi H, Kurosawa T, Onoue M, Seto H, Horie T, Aoyagi N, Yamaoka M, Matsukage A, Yoshida S, Sakaguchi K (1996) Fatty acids selectively inhibit eukaryotic DNA polymerase activities in vitro. Biochim Biophys Acta 1308:256–262
23. Mizushina Y, Yoshida S, Matsukage A, Sakaguchi K (1997) The inhibitory action of fatty acids on DNA polymerase β. Biochim Biophys Acta 1336:509–521
24. Ogawa A, Murate T, Suzuki M, Nimura Y, Yoshida S (1998) Lithocholic acid, a putative tumor promoter, inhibits mammalian DNA polymerase β. Jpn J Cancer Res 89:1154–1159
25. Yonezawa Y, Tsuzuki T, Eitsuka T, Miyazawa T, Hada T, Uryu K, Murakami-Nakai C, Ikawa H, Kuriyama I, Takemura M, Oshige M, Yoshida H, Sakaguchi K, Mizushina Y (2005) Inhibitory effect of conjugated eicosapentaenoic acid on human DNA topoisomerases I and II. Arch Biochem Biophys 435:197–206
26. Tamiya-Koizumi K, Murate T, Suzuki M, Simbulan CG, Nakagawa M, Takamura M, Furuta K, Izuta S, Yoshida S (1997) Inhibition of DNA primase by sphingosine and its analogues parallels with their growth suppression of cultured human leukemic cells. Biochem Mol Biol Int 41:1179–1189
27. Nakayama C, Saneyoshi M (1985) Inhibitory effects of 9-β-D-xylofuranosyladenine 5′-triphosphate on DNA-dependent RNA polymerase I and II from cherry salmon (*Oncorhynchus masou*). J Biochem (Tokyo) 97:1385–1389
28. Soltis DA, Uhlenbeck OC (1982) Isolation and characterization of two mutant forms of T4 polynucleotide kinase. J Biol Chem 257:11332–11339
29. Lu BC, Sakaguchi K (1991) An endo-exonuclease from meiotic tissues of the basidiomycete *Coprinus cinereus*: Its purification and characterization. J Biol Chem 266:21060–21066
30. Mosmann T (1983) Rapid colorimetric assay for cellular growth and survival: application to proliferation and cytotoxicity assays. J Immunol Methods 65:55–63
31. Ramanchandra S, Studzinski GP (1995) Cell growth and apoptosis, a practical approach. In: Stuzinskin GP (ed) IRL Press, Oxford, pp 119–142
32. Burgers PM, Koonin EV, Bruford E, Blanco L, Burtis KC, Christman MF, Copeland WC, Friedberg EC, Hanaoka F, Hinkle DC, Lawrence CW, Nakanishi M, Ohmori H, Prakash L, Prakash S, Reynaud CA, Sugino A, Todo T, Wang Z, Weill JC, Woodgate R (2001) Eukaryotic DNA polymerases: proposal for a revised nomenclature. J Biol Chem 276:43487–43490
33. Aravind L, Koonin EV (1999) DNA polymerase β-like nucleotidyltransferase superfamily: identification of three new families, classification and evolutionary history. Nucleic Acids Res 27:1609–1618
34. Djuric Z, Heilbrun LK, Lababidi S, Everett-Bauer CK, Fariss MW (1997) Growth inhibition of MCF-7 and MCF-10A human breast cells by alpha-tocopheryl hemisuccinate, cholesteryl hemisuccinate and their ether analogs. Cancer Lett 111:133–139
35. Chida K, Murakami A, Tagawa T, Ikuta T, Kuroki T (1995) Cholesterol sulfate, a second messenger for the η isoform of protein kinase C, inhibits promotional phase in mouse skin carcinogenesis. Cancer Res 55:4865–4869
36. Strott CA, Higashi Y (2003) Cholesterol sulfate in human physiology: what's it all about? J Lipid Res 44:1268–1278

Lipids (2008) 43:383–390
DOI 10.1007/s11745-008-3163-8

ORIGINAL ARTICLE

Inhibition of Serum Cholesterol Oxidation by Dietary Vitamin C and Selenium Intake in High Fat Fed Rats

M. Menéndez-Carreño · D. Ansorena · F. I. Milagro · J. Campión · J. A. Martínez · I. Astiasarán

Received: 28 November 2007 / Accepted: 17 February 2008 / Published online: 12 March 2008
© AOCS 2008

Abstract Cholesterol oxidation products (COPs) have been considered as specific in vivo markers of oxidative stress. In this study, an increased oxidative status was induced in Wistar rats by feeding them a high-fat diet (cafeteria diet). Another group of animals received the same diet supplemented with a combination of two different antioxidants, ascorbic acid (100 mg/kg rat/day) and sodium selenite (200 µg/kg rat/day) and a third group fed on a control diet. Total and individual COPs analysis of the different diets showed no differences among them. At the end of the experimental trial, rats were sacrificed and serum cholesterol, triglycerides and COPs were measured. None of the diets induced changes in rats body weight, total cholesterol and triglycerides levels. Serum total COPs in rats fed on the high-fat diet were 1.01 µg/ml, two times the amount of the control rats (0.47 µg/ml). When dietary antioxidant supplementation was given, serum total COPs concentration (0.44 µg/ml) showed the same levels than those of the rats on control diet. 7*β*-hydroxycholesterol, formed non-enzymatically via cholesterol peroxidation in the presence of reactive oxygen species, showed slightly lower values in the antioxidant-supplemented animals compared to the control ones. This study confirms the importance of dietary antioxidants as protective factors against the formation of oxysterols.

Keywords Antioxidants · Ascorbic acid · Cafeteria diet · COPs · Lipid oxidation

---

M. Menéndez-Carreño · D. Ansorena (✉) ·
F. I. Milagro · J. Campión · J. A. Martínez · I. Astiasarán
Department of Nutrition, Food Science,
Physiology and Toxicology, University of Navarra,
C/ Irunlarrea s/n, 31008 Pamplona, Spain
e-mail: dansorena@unav.es

Introduction

Cholesterol is an unsaponifiable lipid prone to oxidation by reactive oxygen species (ROS), light, UV light, ionizing radiation, chemical catalysts, enzymatic reactions and other oxidizing conditions, leading to the formation of cholesterol oxidation products (COPs) [1–2]. Some studies have pointed out that COPs can be absorbed from the diet in rats [3–6].

It has been demonstrated that COPs may produce a wide range of adverse biological outcomes including cytotoxicity, apoptosis, mutagenesis, carcinogenesis, diabetes and metabolic disorders, their main negative effect being the development of atherosclerosis [7–13]. Also, it has been shown that the presence of COPs in diet promotes fatty streak lesion formation in several different animal models of atherosclerosis [6].

In this context, certain oxysterols, 7*β*-hydroxycholesterol and 7-ketocholesterol, have been suspected not only as oxidative stress inducers, which are associated with an increase in the risk of atherosclerosis [14–16] but also as specific markers of oxidative stress [17]. There is evidence that oxidized lipoproteins play a key role in the pathogenesis of atherosclerosis and especially both oxysterols are found at significantly increased levels in atherosclerotic lesions [14, 18–20].

The endogenous formation of oxysterols in relation to the influence of the type of diet and the consumption of antioxidants has hardly been studied so far [21–22]. Some data suggest that a greater intake of antioxidative vitamins such as vitamin E, vitamin C and *β*-carotene are associated with a reduced risk of atherosclerotic vascular disease [23], which may happen through different mechanisms such as inhibition of LDL oxidation, cell lipid peroxidation and cell-mediated oxidation of LDL and reduction in blood cholesterol levels [24]. In this sense, ascorbic acid could limit lipid peroxidation, protecting partially oxidized LDL against further oxidative modification [25]. On the other hand, selenium is known to play an important role in cytoprotection against cholesterol oxide-induced vascular damage in the vascular wall of rats [26]. Combinations of selenium and vitamin E have been shown to contribute to protection of the vascular endothelium and to control the oxidative status and altered lipid metabolism in the liver [27–28]. No data have been found about the combination of selenium and vitamin C.

In this article, we hypothesized that the dietary intake of a combination of two different antioxidants (ascorbic acid and selenium) could prevent cholesterol oxide formation in rats fed on a high-fat diet.

Materials and Methods

Animals, Diets and Experimental Design

Male Wistar rats, supplied by the Applied Pharmacobiology Center (CIFA, Pamplona, Spain), were housed at 21–23 °C with a 12 h light cycle (8:00 a.m. to 8:00 p.m.) and assigned into three different dietary groups. One group of animals (Control group, C) were fed a standard pelleted diet (Harlan Iberica, Barcelona, Spain) containing 16.62% of the energy as protein, 73.16% of the energy as carbohydrate and 10.22% of the energy as lipids by dry weight. The second group of animals (Cafeteria, Caf) was fed on a high-fat diet in order to generate a diet-induced obesity model as previously reported [29]. High-fat diet components were paté, bacon, chips, cookies, chocolate and chow with proportions 2:1:1:1:1:1 and the diet was given to each rat daily. The composition of this Cafeteria diet was 9.26% of the energy as protein, 31.58% of the energy as carbohydrates and 59.15% of the energy as lipids by dry weight (430 kcal/100 g in the Cafeteria diet vs. 350 kcal/100 g in the pelleted diet). Cafeteria diet was supplemented in a third group of animals (Caf + Aox) with a daily dose of vitamin C (100 mg/kg rat) + sodium selenite (200 μg/kg rat) both mixed into the food. Animals had ad libitum access to water and food during the experimental trial. Body weight was recorded daily. At the end of the experimental period (72 days), animals were sacrificed by decapitation and blood and tissue samples were immediately collected and weighed. All the procedures were performed according to national and institutional guidelines of the Animal Care and Use Committee at the University of Navarra.

Diet Composition

Moisture was determined according to the Association of Official Analytical Chemists (AOAC) method [30]. Total fat was determined by an extraction with petroleum ether according to the AOAC [31]. Protein was analyzed using the Kjeldahl method for the determination of nitrogen [32], using 6.25 as the factor to transform nitrogen into protein. Ash was determined by incineration using the method of the AOAC [33]. Quantitative fat extraction was made with a chloroform–methanol mixture using the method of Folch et al. [34]. Cholesterol content was analyzed by gas chromatography according to Kovacs et al. [35]. Derivatization to obtain the trimethyl silyl ethers of cholesterol was performed. A Perkin-Elmer Autosystem XL gas chromatograph equipped with an HP1 column (30 m × 0.25 mm × 0.1 μm) was used. The oven temperature was 265°C. The temperature of both the injection port and detector was 285 °C. Cholesterol identification and quantitation was done by using pure 5α-cholestane (Sigma, St Louis, MO, USA) as an internal standard, where 1 ml was added to the sample as a solution (2 mg/ml), previously to the extraction procedure. A Perkin-Elmer Turbochrom programme was used for quantitation. COPs determination in diets was performed using 0.5 g of the Folch extract of the correspondent diet adding 1 ml of 19-hydroxycholesterol (20 μg/ml) as internal standard. Ten milliliters of 1 N KOH solution in methanol were then added to perform a cold saponification at room temperature for 20 h, in darkness and under continuous agitation in an orbital shaker (Rotaterm P; Selecta, Barcelona) at 100 rpm. The unsaponifiable material was extracted with diethyl ether and purified by silica SPE according to Guardiola et al. [36]. COPs were finally eluted from the cartridge with acetone. Samples solutions of COPs were derivatized to trimethylsilyl (TMS) ethers according to a modified version of the method described by Dutta et al. [38]. After drying the solvent, 400 μl of Tri-Sil reagent were added and the tubes were kept at 60 °C for 45 min. The solvent was evaporated under a stream of nitrogen and the TMS-ether derivates were dissolved in 400 μl of hexane. Dissolved samples were filtrated prior to GC-MS analysis in order to avoid damage to the capillary column. Gas chromatography-Mass spectrometry analysis was performed on a CG 6890N Hewlett Packard device coupled to a 5975 Mass Selective Detector (Agilent Technologies, Inc., CA, USA). The TMS-ether derivates of COPs were separated on a capillary column Varian VF-5ms CP8947 (50 m × 250 μm × 0.25 μm film thickness) (Varian, France). Oven temperature conditions were optimized in order to achieve a proper separation of the individual compounds. The oven was programmed with an initial temperature of 75 °C, heated to 250 °C at a rate of 30 °C/min, raised to 290 °C at rate of 8 °C/min, and finally, it was raised to 292 °C at a rate of 0.05 °C/min. High purity helium was used as the carrier gas at a flow rate of 1 ml/min. The inlet pressure used was 13.40 psi. The injector temperature was 250 °C and the transfer line to detector at 280 °C. The samples were injected in a splitless mode with an injection volume of 1 μl. The mass spectrometer was operated in electron impact ionization (70 eV). Identification of the peaks was made by the characteristic ion fragmentation of the standard substances and the quantification was made using select ion monitoring program using the internal standard method.

Serum Measurements

Serum triacylglycerides were determined with the RANDOX kit (Randox Laboratories LTD, UK) and cholesterol level with the Cholesterol-CP kit (Haribo, ABX diagnostic, Montpellier, France). All these measurements were adapted for COBAS MIRA equipment (Roche, Switzerland). COPs in serum were analyzed following the method described in Menéndez-Carreño et al. (in press) [37]. Lipids from serum were extracted from serum according to a modified version of the method described by Folch et al. [34] using chloroform–methanol (2:1; v/v). One milliliter of serum was introduced into a centrifuge tube, and 6 ml of chloroform and 3 ml of methanol were added. After shaking on vortex for 1 min, samples were then centrifuged at 4,000 rpm for 15 min to facilitate phase separation using a Hermle Z320 centrifuge (Apeldoorn, The Netherlands). The chloroform (lower) layer was transferred to a test tube taking care of not transferring any solid material which remains at the interface between the upper and lower phases. Ten milliliters of 1 N KOH solution in methanol and 1 ml of stock solution of the internal standard, 19-hydroxycholesterol (20 μg/ml), were then added to perform a cold saponification at room temperature for 20 h, in darkness and under continuous agitation in an orbital shaker (Rotaterm P; Selecta, Barcelona) at 100 rpm. A total of 100 mg/kg of butylhydroxytoluene was added as an antioxidant in order to avoid COPs artifact formation during the saponification. The extraction of the unsaponifiable material, the purification and further analysis of COPs was exactly the same as explained above for the determination of COPs in diets.

Statistical Analysis

All results are expressed as means ± standard deviations of the mean. The differences between the groups were evaluated by one-way ANOVA, and Tukey post hoc test was applied when suitable (SPSS 15.0 packages for Windows, Chicago, IL, USA). A level of probability of $p < 0.05$ was set as being statistically significant. A Pearson correlation test was performed between COPs content in the diets and in the serum samples.

Results

Control (C) and cafeteria diets (Caf and Caf + Aox diets) presented different macronutrient profiles, as shown in Table 1, especially in relation to the fat content, seven times higher in cafeteria diets. This diverse macronutrient distribution of the diets led to 20% more energy in both high-fat diets in comparison to the standard one. Regarding the cholesterol content, it was significantly lower in chow diet than in the two cafeteria ones, and a similar trend was detected for the COPs content, being 7.5 times higher in the cafeteria diets. Analyzing specifically oxysterols, 7-ketocholesterol was the main oxysterol in all the three diets (Table 2), being less abundant in the control one and more abundant in the cafeteria diets.

These results led to percentages of cholesterol oxidation significantly higher in C (0.68%) than in Caf and Caf + Aox diets, which did not show significant differences between them (0.25 and 0.24%, respectively). However, the total oxysterol content of the diet was much higher in both cafeteria diets with no differences between them, suggesting that the antioxidant supplementation of the diet does not affect the amount of oxysterols ingested.

Whereas the body weight of the animals at the beginning of the experimental trial was similar within the three groups, the two groups fed on cafeteria diets gained significantly more weight than rats fed chow pellets (Table 3).

Table 1 General composition (g/100 g) and energy value (kcal/100 g) for the three tested diets

	Control diet (C)	Cafeteria diet (Caf)	Cafeteria selenium vitamin C diet (Caf + Aox)
Moisture (g/100 g)	12.13 ± 0.10 a	25.55 ± 0.10 b	25.33 ± 0.04 b
Total fat (g/100 g)	4.03 ± 0.4 a	28.32 ± 0.14 b	28.33 ± 0.08 b
Protein (g/100 g)	14.75 ± 0.08 c	9.97 ± 0.10 a	9.98 ± 0.07 a
Carbohydrates (g/100 g)	64.93 ± 0.11 c	33.90 ± 0.17 a	34.02 ± 0.13 a
Ash (g/100 g)	4.16 ± 0.07 b	2.25 ± 0.08 a	2.35 ± 0.04 a
Energy (kcal/100 g product)	354.99 ± 0.37 a	430.45 ± 1.87 b	430.38 ± 0.84 b

Results are expressed as means ± standard deviations, $n = 10$. Values in the same row bearing different letters are significantly different ($p < 0.05$)

Table 2 Cholesterol content and cholesterol oxidation products of the three tested diets

	Control diet (C)	Cafeteria diet (Caf)	Cafeteria selenium vitamin C diet (Caf + Aox)
7α-Hydroxycholesterol (μg/g fat)	0.11 ± 0.01 a	0.57 ± 0.01 b	0.55 ± 0.02 b
7β-Hydroxycholesterol (μg/g fat)	0.07 ± 0.00 a	0.44 ± 0.01 b	0.44 ± 0.03 b
5,6β-Epoxycholesterol (μg/g fat)	n.d.	1.44 ± 0.08 a	1.47 ± 0.10 a
5,6α-Epoxycholesterol (μg/g fat)	n.d.	0.33 ± 0.02 a	0.36 ± 0.04 a
Cholestanetriol (μg/g fat)	0.04 ± 0.00 a	0.18 ± 0.01 b	0.21 ± 0.0 b
25-Hydroxycholesterol (μg/g fat)	n.d.	n.d.	n.d.
7-Ketocholesterol (μg/g fat)	0.47 ± 0.0 a	2.42 ± 0.11 b	2.31 ± 0.09 b
Cholesterol (mg/100g)	2.75 ± 0.15 a	58.02 ± 4.07 b	57.95 ± 5.13 b
Total COPs (μg/g fat)	0.70 ± 0.02 a	5.39 ± 0.11 b	5.34 ± 0.38 b
Percentage of cholesterol oxidation (%)	0.68 ± 0.02 b	0.25 ± 0.03 a	0.24 ± 0.03 a

Cholesterol and individual COPs were analyzed in quadruplicate in the three different diets. Total COPs is the sum of all individual COPs detected. Percentage of cholesterol oxidation (%) = (total COPs diet/cholesterol diet) × 100. Results are expressed as means ± standard deviations, $n = 10$. Values in the same row bearing different letters are significantly different ($p < 0.05$)

n. d. Non-determined compound

Table 3 Body weight changes of rats fed on three different diets

	Control diet (C)	Cafeteria diet (Caf)	Cafeteria selenium vitamin C diet (Caf + Aox)
Initial weight (g)	260.6 ± 16.4 a	263.9 ± 21.87 a	268.1 ± 21.82 a
Final weight (g)	427.6 ± 32.4 a	533.5 ± 79.78 b	512.1 ± 62.26 b
Weight gain (g)	167.0 ± 18.9 a	269.6 ± 62.65 b	244.0 ± 45.01 b

Results are expressed as means ± standard deviations, $n = 10$. Values in the same row bearing different letters are significantly different ($p < 0.05$)

As no significant differences were found for weight gain between the two cafeteria diets and the weights of their white adipose tissue depots were similar (data not shown), we can conclude that antioxidant addition did not affect animals weight, adiposity and growth.

Regarding the analysis of serum lipid metabolites, neither total cholesterol nor triglyceride levels differed among the three groups of rats (Table 4). Although HDL-cholesterol was not measured in the C group, no differences were found between the two cafeteria-fed groups.

In this study, seven different COPs were analyzed in serum rats from the three experimental groups; 7α-hydroxycholesterol, 7β-hydroxycholesterol, 5,6β-epoxycholesterol, 5,6α-epoxycholesterol, cholestanetriol, 25-hydroxycholesterol and 7-ketocholesterol, but only 7α-hydroxycholesterol, 7β-hydroxycholesterol, cholestanetriol and 7-ketocholesterol could be quantified in all the serum samples (Table 4). Cholestanetriol was detected in all the cafeteria-fed animals, but only in seven and six out of ten samples in Caf + Aox and C groups, respectively.

As a result of this dietary treatment over 72 days, the most abundant serum oxysterol in all the three groups was 7-ketocholesterol. Its levels reached 38.3% of total COPs in the case of the control group and 52.2 and 47.7% for the Caf and Caf + Aox animals. The total amount of serum oxysterols was significantly increased in rats fed on the cafeteria diet compared to the C group, with significant increments in all the oxysterols quantified (Table 4). However, the Caf + Aox diet decreased the different serum oxysterol concentrations to the levels of the control rats, which in the case of 7β-hydroxycholesterol, was even significantly lower than that of the control animals.

In summary, as shown in Fig. 1, animals fed on the cafeteria diet showed a higher percentage of serum oxysterols than the control rats, indicating a pro-oxidant effect of the diet. However, the supplementation of this diet with antioxidants resulted in a normalization of the circulating oxysterol levels, demonstrating a protective effect of the supplementation that could have beneficial effects on different metabolic features related to glycemia control and atherogenesis.

Discussion

High-fat diets have been traditionally used for generating overweight in rats, the cafeteria diet being a variation of them [29]. As a result, animals might develop obesity,

Table 4 Lipid metabolites and cholesterol oxidation products in serum of rats fed on three different diets

	Control diet (C)	Cafeteria diet (Caf)	Cafeteria selenium vitamin C diet (Caf + Aox)
Cholesterol (mg/dl)	78.36 ± 10.15 a	79.69 ± 12.59 a	79.46 ± 12.93 a
HDL (mg/dl)	n.a.	27.59 ± 3.80 a	27.31 ± 4.35 a
TG (mg/dl)	115.89 ± 4.25 a	110 ± 33.73 a	99.33 ± 20.71 a
7α-Hydroxycholesterol (µg/ml)	0.14 ± 0.04 a	0.20 ± 0.06 b	0.14 ± 0.04 a
7β-Hydroxycholesterol (µg/ml)	0.09 ± 0.03 b	0.14 ± 0.03 c	0.06 ± 0.03 a
5,6β-Epoxycholesterol (µg/ml)	n.d.	n.d.	n.d.
5,6α-Epoxycholesterol (µg/ml)	n.d.	n.d.	n.d.
Cholestanetriol (µg/ml)	0.05 ($n = 6$) ± 0.03 a	0.14 ± 0.04 b	0.03 ($n = 7$) ± 0.03 a
25-Hydroxycholesterol (µg/ml)	n.d.	n.d.	n.d.
7-Ketocholesterol (µg/ml)	0.18 ± 0.04 a	0.53 ± 0.15 b	0.21 ± 0.07 a
Total COPs (µg/ml)	0.47 ± 0.10 a	1.01 ± 0.17 b	0.44 ± 0.11 a

Total COPs is the sum of all individual COPs detected. Results are expressed as means ± standard deviations, $n = 10$. Values in the same row bearing different letters are significantly different ($p < 0.05$)

n.a. Non-analyzed compound, *n.d.* non-detected compound

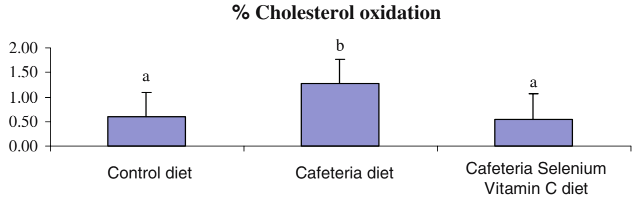

Fig. 1 Percentage of cholesterol oxidation products in serum samples of rats fed on three different diets. Percentage of cholesterol oxidation (%) = (serum total COPs/serum cholesterol) × 100. Groups bearing different letters are significantly different ($p < 0.05$)

insulin resistance, hyperglycemia, fatty liver, oxidative stress, and, in some cases, lipid metabolism disturbances. Our model of obesity in rats, in agreement with previous results of our own group, achieves adiposity and weight gain but does not induce fasting hypertriglyceridemia or hypercholesterolemia [29, 38].

In this study, it was found that oxidative stress was effectively induced by the high-fat diet, as the levels of total COPs were significantly higher than those of the control group. This pro-oxidant effect of the cafeteria diet has been associated with an impairment of some obesity-related features such as non-alcoholic fatty liver, diabetes and atherogenesis [39], and the supplementation of this diet with a high dose of ascorbic acid has recently been reported to protect against body weight gain and adiposity [40]. However, in this study, the diet supplementation with a lower dose of vitamin C induced no changes in body weight and adiposity during the assayed period. The use by other authors of similar or higher doses of vitamin C during long periods has shown no toxic or deleterious effects in similar animal models [41–44].

Rats fed on very high cholesterol diets usually present increased serum oxysterol levels [22]. Other studies have shown that, although a cholesterol-rich diet supplemented with vitamins E and C induces hypercholesterolemia in rabbits, it was able to reduce lipid peroxidation and lipoprotein modification [45]. Ringseis and Eder [21] pointed out that, as a consequence of antioxidant-induced inhibition of lipid peroxidation, it is reasonable to assume that the formation of COPs in animal tissues would be inhibited by these compounds, although this effect requires more studies. On the other hand, in vitro trials have demonstrated that cholesterol is susceptible to oxidation under selenium deficiency-induced oxidative stress [46]. In that study, a significant increase in the amounts of 7-hydroxycholesterol was detected due to the selenium deficiency. In fact, selenium has been widely used as an antioxidant, with doses of up to 2 µg/g body weight in rats [47–48], and has been reported to protect from vascular damage induced by COPs [32]. The effect of dietary selenium on the reduction of COPs formation in the serum could be mediated by GSH-dependent selenoperoxidases, such as GPx, which have been implicated in the defence against oxidized low density lipoproteins [49]. In this sense, different papers showed a significant correlation between dietary selenium concentration and GPx levels [50–53].

This study also showed that the control group, which had a standard feeding, led to COPs concentrations in the serum being significantly lower than those animals fed on a high-fat diet (cafeteria group). The values for total COPs both for control and modified groups were similar to those found by Mahfouz and Kummerov [22] in rats fed on high cholesterol diets for 4 months. The cafeteria diet did not affect the total serum cholesterol and triglyceride levels as expected, but increased the serum COPs levels. Increasing dietary vitamin C and selenium in a high-fat diet prevented the oxidation of circulating cholesterol.

Thus, the intake of the antioxidants mixture included in the cafeteria diet can efficiently decrease the oxidation process affecting cholesterol. As total cholesterol levels were not modified by the different dietary treatments, the percentage of cholesterol oxidation also showed significant differences between the cafeteria diet and the others.

One remarkable finding is the fact that serum 7β-hydroxycholesterol levels in the Caf + Aox diet group were even slightly lower than those obtained for the control group. Ringseis and Eder [21] demonstrated that insufficient vitamin E in the diet increased the formation of 7β-hydroxycholesterol in rats fed on salmon oil. Most of the 7β-hydroxycholesterol is formed non-enzymatically via cholesterol peroxidation in the presence of ROS [54]. As 7β-hydroxycholesterol is formed in the presence of ROS, it is likely influenced by the antioxidative status [21]. Yoshida et al. [55] measured 7α-hydroperoxycholesterol, 7β-hydroperoxycholesterol and 7-ketocholesterol as well as 7α-hydroxycholesterol and 7β-hydroxycholesterol were measured as total 7-hydroxycholesterol in samples of human plasma because their usefulness for the assessment of oxidative stress in animal and in vivo experiments. They concluded that 7β-hydroxycholesterol may be a better biomarker for oxidative stress than 7α-hydroxycholesterol. As the consumption of selenium and antioxidants suppresses ROS formation by different mechanisms [56], it is reasonable to suppose that endogenous formation of 7β-hydroxycholesterol could have been suppressed by the high intake of vitamin C and selenium. In fact, no correlation was found between the level of 7β-hydroxycholesterol in the diet and in its content in the serum samples ($r = 0.26$, $p < 0.05$) pointing to an endogenous formation of this compound.

Arca et al. [57] found that familial combined hyperlipidemia patients are prone to a condition of oxidative stress, as shown by the presence of increased levels of COPs. Thus, oxidative stress should be taken into account to explain the increased cardiovascular risk in these patients. Moreover, 7β-hydroxycholesterol and 7-ketocholesterol are biomarkers for oxidative stress in patients with atherosclerosis [17], and it has been demonstrated the interconversion of these compounds in humans [58]. 7-Ketocholesterol was the most abundant oxysterol in the three groups of rats, showing a positive correlation [$r = 0.66$, ($p < 0.01$)] with the data obtained from the diet.

In conclusion, the concentrations of oxysterols were influenced by the dietary fat, but also by the vitamin C and selenium intake. The fact that the concentration of COPs was reduced by increasing dietary vitamin C and selenium supply confirms the importance of antioxidants as a protective factor against the formation of oxysterols from a high-fat dietary pattern.

Acknowledgments We thank Plan Investigador de la Universidad de Navarra (PIUNA), Linea Especial (LE/97), Asociación de Amigos de la Universidad de Navarra (ADA), Gobierno de Navarra (Departamento de Educación y Departamento de Industria) and Ministerio de Educación y Ciencia (Programa Ramón y Cajal, 2002) for their contribution to the financial support of this research work.

References

1. Russel D (2000) Oxysterol biosynthetic enzymes (review). Biochim Bhophys Acta 1529:126–135
2. Savage GP, Dutta P, Rodriguez-Estrada MT (2002) Cholesterol oxides: their occurrence and methods to prevent their generation in foods. Asia Pac J Clin Nutr 11(1):72–78
3. Osada K, Sasaki E, Sugano M (1994) Lymphatic absorption of oxidized cholesterol in rats. Lipids 29:555–559
4. Vine DF, Mamo J, Beilin L, Mori T, Croft K (1998) Dietary oxysterols are incorporated in plasma triglyceride-rich proteins, increase their susceptibility to oxidation and increase aortic cholesterol concentration of rabbits. J Lipid Res 39(10):1995–2004
5. Staprans I, Pan XM, Rapp JH, Grunfeld C, Feingold KR (2000) Oxidized cholesterol in the diet accelerates the development of atherosclerosis in LDL receptor—and apoliprotein E-deficient mice. Arterioscler Thromb Vasc Biol 20(3):708–714
6. Staprans I, Pan XM, Rapp JH, Feingold KR (2005) The role of dietary oxidized cholesterol and oxidized fatty acids in the development of atherosclerosis. Mol Nutr Food Res 49:1075–1082
7. Schroepfer GJ Jr (2000) Oxysterols: modulators of cholesterol metabolism and others processes. Physiol Rev 80:361–554
8. Zhou Q, Wasowicz E, Handler B, Fleisher L, Kummerov FA (2000) An excess concentration of oxysterols in the plasma is cytotoxic to cultured endothelial cells. Atherosclerosis 149:191–197
9. Leonarduzzi G, Sottero B, Poli G (2002) Oxidized products of cholesterol: Dietary and metabolic origin and proatherosclerotic effects (review). J Nutr Biochem 13:700–710
10. Dobarganes C, Márquez-Ruiz G (2003) Oxidized fats in foods. Curr Opin Clin Nutr Metab Care 6:157–163
11. Rimner A, Al Makdessi S, Sweidan H, Wischhusen J, Rabenstein B, Shatat K, Mayer P, Spyridopoulos I (2005) Relevance and mechanism of oxysterol stereospecificity in coronary artery disease. Free Radic Biol Med 38:535–544
12. Ryan E, Chopra J, McCarthy F, Maguire AR, O'Brien N (2005) Qualitative and quantitative comparison of the cytotoxic and apoptotic potential of phytosterol oxidation products with their corresponding cholesterol oxidation products. Br J Nutr 94(3): 443–451
13. Ferderbar S, Pereira EC, Apolinário ME, Bertolami MC, Faludi A, Monte O, Calliari LE, Sales JE, Gagliardi AR, Xavier HT, Abdalla DSP (2007) Cholesterol oxides as biomarkers of oxidative stress in type 1 and type 2 diabetes mellitus. Diabetes Metab Res Rev 23:35–42
14. Brown AJ, Jessup W (1999) Oxysterols and atherosclerosis. Atherosclerosis 142:1–28
15. Bjorkhem I, Diczfalusy U (2002) Oxysterols. Friends, foes or just fellow passengers. Arterioscler Thromb Vasc Biol 22:734–742
16. Arca M, Natoli S, Micheletta F, Riggi S, Di Angelantonio E, Montali A, Antonini MT, Antonini R, Diczfalusy U, Iuliano L (2007) Increased plasma levels of oxysterols, in vivo markers of oxidative stress, in patients with familial combined

hyperlipidemia: reduction during atorvastatin and fenofibrate therapy. Free Radic Biol Med 42:698–705
17. Yoshida Y, Niki E (2004) Detection of lipid peroxidation in vivo: total hydroxyoctadecadienoic acid and 7-hydroxycholesterol as oxidative stress marker. Free Radic Res 38(8):787–794
18. Hultén LM, Lindmark H, Diczfalusy U, Björkhem I, Ottosson M, Liu Y, Bondjers G, Wicklund O (1996) Oxysterols present in atherosclerotic tissue decrease the expression of lipoprotein lipase messenger RNA in human monocyte-derived macrophages. J Clin Invest 97(29):461–468
19. Colles SM, Irwin KC, Chisolm GM (1996) Roles of multiple oxidized LDL lipids in cellular injury: dominance of 7β-hydroperoxycholesterol. J Lipid Res 37(9):2018–2028
20. García-Cruset S, Carpenter KL, Guardiola F, Stein BK, Mitchinson MJ (2001) Oxysterols profiles of normal human arteries, fatty streaks and advanced lesions. Free Radic Res 53(1):31–41
21. Ringseis R, Eder K (2002) Insufficient dietary vitamin E increases the concentration of 7β-hydroxycholesterol in tissues of rats fed salmon oil. J Nutr 132(12):3732–3735
22. Mahfouz MM, Kummerov FA (2000) Cholesterol-rich diets have different effects on lipid peroxidation, cholesterol oxides, and antioxidant enzymes in rats and rabbits. J Nutr Biochem 11:293–302
23. Rimm EB, Stampfer MJ (2000) Antioxidants for vascular disease. Med Clin North Am 84(1):239–249
24. Fuhrman B, Aviram M (2001) Anti-atherogenicity of nutritional antioxidants. IDrugs 4(1):82–92
25. Retsky KL, Frei B (1995) Vitamin C prevents metal ion-dependent initiation and propagation of lipid peroxidation in human low-density lipoprotein. Biochim Biophys Acta 1257(3):279–287
26. Huang K, Liu H, Chen Z, Xu H (2002) Role of selenium in cytoprotection against cholesterol oxide-induced vascular damage in rats. Atherosclerosis 162(1):137–144
27. Douillet C, Bost M, Accominotti M, Borson-Chazot F, Ciavatti M (1998) Effect of selenium and vitamin E supplements on tissue lipids, peroxides, and fatty acid distribution in experimental diabetes. Lipids 33(4):393–399
28. Douillet C, Bost M, Accominotti M, Borson-Chazot F, Ciavatti M (1998) Effect of selenium and vitamin E supplementation on lipid abnormalities in plasma, aorta, and adipose tissue of Zucker rats. Biol Trace Elem Res 65(3):221–236
29. Milagro FI, Campión J, Martinez JA (2006) Weight gain induced by high-fat feeding involves increased liver oxidative stress. Obesity 14(7):1118–1123
30. AOAC (2002) Determination of moisture content. 950.46. In: Official methods of analysis, 17th edn. Association of Official Analytical Chemists, Gaithersburg
31. AOAC (2002) Determination of fat (crude) o ether extract in meat. 960.39. In: Official methods of analysis 17th edn. Association of Official Analytical Chemists, Gaithersburg
32. AOAC (2002) Determination of protein content in meat. 928.08. In: Official method of analysis, 17th edn. Association of Official Analytical Chemists, Gaithersburg
33. AOAC (2002) Ash of meat. 920.153. In: Official methods of analysis, 17th edn. Association of Official Analytical Chemists, Gaithersburg
34. Folch J, Lees M, Sloane Stanley GH (1957) A simple method for the isolation and purification of total lipids from animal tissues. J Biol Chem 226:497–509
35. Kovacs MIP, Anderson WE, Ackman RG (1979) A simple method for the determination of cholesterol and some plant sterols in fishery-based food products. J Food Sci 44:1299–1301, 1305
36. Guardiola F, Codony R, Rafecas M, Boatella J (1995) Comparison of three methods for the determination of oxysterols in spray-dried egg. J Chromatogr A 705:289–304
37. Menéndez-Carreño M, García-Herreros C, Astiasarán I, Ansorena D (2008) Validation of a gas chromatography-mass spectrometry method for the analysis of sterol oxidation products in serum. J Chromatogr B. doi:10.1016/j.jchromb.2008.01.036
38. Dutta PC (1997) Studies on phytosterol oxides. II: effect of storage on the content in potato chips prepared in different vegetable oils. J Am Oil Chem Soc 74(6):659–666
39. Campión J, Martinez JA (2004) Ketoconazole, an antifungal agent, protects against adiposity induced by a cafeteria diet. Horm Metab Res 36(7):485–491
40. Neri S, Signorelli SS, Torrisi B, Pulvirenti D, Mauceri B, Abate G, Ignaccolo L, Bordonaro F, Cilio D, Calvagno S, Leotta C (2005) Effects of antioxidant supplementation on postprandial oxidative stress and endothelial dysfunction: a single-blind, 15-day clinical trial in patients with untreated type 2 diabetes, subjects with impaired glucose tolerance, and healthy controls. Clin Ther 27(11):1764–1773
41. Campión J, Milagro FI, Fernández D, Martínez JA (2006) Differential gene expression and adiposity reduction induced by ascorbic acid supplementation in a cafeteria model of obesity. J Physiol Biochem 62(2):71–80
42. Cartier R, Bouchard D (1998) The beneficial effect of natural antioxidants on the endothelial function of regenerated endothelium. Ann Chim 52(8):827–833
43. Cederberg J, Eriksson UJ (2005) Antioxidative treatment of pregnant diabetic rats diminishes embryonic dysmorphogenesis. Birth Defects Res A Clin Mol Teratol 73(7):498–505
44. García-Díaz D, Campión J, Milagro FI, Martínez JA (2007) Adiposity dependent apelin gene expression: relationships with oxidative and inflammation markers. Mol Cell Biochem 305(1–2):87–94
45. Mahfouz MM, Kawano H, Kummerow FA (1997) Effect of cholesterol-rich diets with and without added vitamins E and C on the severity of atherosclerosis in rabbits. Am J Clin Nutr 66(5):1240–1249
46. Saito Y, Yoshida Y, Niki E (2007) Cholesterol is more susceptible to oxidation than linoleates in cultured cells under oxidative stress induced by selenium deficiency and free radicals. FEBS Lett 581(22):4349–4354
47. Erbayraktar Z, Yilmaz O, Artmann AT, Cehreli R, Coker C (2007) Effects of selenium supplementation on antioxidant defense and glucose homeostasis in experimental diabetes mellitus. Biol Trace Elem Res 118(3):217–226
48. Tirosh O, Levy E, Reifen R (2007) High selenium diet protects against TNBS-induced acute inflammation, mitochondrial dysfunction, and secondary necrosis in rat colon. Nutrition 23(11–12):878–886
49. Thomas JP, Geiger PG, Girotti AW (1993) Lethal damage to endothelial cells by oxidized low density lipoprotein: role of selenoperoxidases in cytoprotection against lipid hydroperoxide and iron-mediated reactions. J Lipid Res 34:479–490
50. Hafeman DG, Sunde RA, Hoekstra WG (1974) Effect of dietary selenium or erythrocyte and liver glutathione peroxidase in the rat. J Nutr 104(5):580–587
51. Contempre B, Denef JF, Dumont JE Many MC (1993) Selenium deficiency aggravates the necrotizing effects of a high iodide dose in iodine deficient rats. Endocrinology 132(4):1866–1868
52. Lei XG, Evenson JK, Thompson KM, Sunde RA (1995) Glutathione peroxidase and phospholipid hydroperoxide glutathione peroxidase are differentially regulated in rats by dietary selenium. J Nutr 125(6):1438–1446
53. Zhang Z, Miyatake S, Saiki M, Asahi M, Yakawa H, Toda H, Kikuchi H, Yoshimura SI, Hashimoto N (2000) Selenium and glutathione peroxidase mRNA in rat glioma. Biol Trace Elem Res 73(1):67–76

54. Emanuel A, Hassel CA, Addis PB, Bergmann SD, Zavoral JH (1991) Plasma cholesterol oxidation products (oxysterols) in human subjects fed a meal rich in oxysterols. J Food Sci 56(3):843–847
55. Yoshida Y, Saito Y, Hayakawa M, Habuchi Y, Imai Y, Sawai Y (2007) Levels of peroxidation in human plasma and erythrocytes: comparison between fatty acids and cholesterol. Lipids 42(5):439–449
56. Saito Y, Yoshida Y, Akazawa T, Takahashi K, Niki E (2003) Cell death caused by selenium deficiency and protective effect of antioxidants. J Biol Chem 278(41):39428–39434
57. Arca M, Natoli S, Micheletta F, Riggi S, Di Angelantonio E, Montali A, Antonini MT, Antonini R, Diczfalusy U, Iuliano L (2007) Increased plasma levels of oxysterols, in vivo markers of oxidative stress, in patients with familial combined hyperlipidemia: Reduction during atorvastatin and fenofibrate therapy. Free Radic Biol Med 42:698–705
58. Larsson H, Böttiger Y, Iuliano L, Diczfalusy U (2006) Oxysterol mixtures, in atheroma-relevant proportions, display synergistic and proapoptotic effects. Free Radic Biol Med 43:695–761

Lipids (2008) 43:391–400
DOI 10.1007/s11745-008-3168-3

ORIGINAL ARTICLE

Erucic Acid is Differentially Taken up and Metabolized in Rat Liver and Heart

**Cameron C. Murphy · Eric J. Murphy ·
Mikhail Y. Golovko**

Received: 24 November 2007 / Accepted: 26 February 2008 / Published online: 19 March 2008
© AOCS 2008

Abstract Because X-linked adrenoleukodystrophy is treated using erucic acid (22:1n-9), we assessed its metabolism in rat liver and heart following infusion of [14-^{14}C]22:1n-9 (170 Ci/kg) under steady-state-like conditions. In liver, 2.3-fold more tracer was taken up as compared to heart, accounted entirely by increased incorporation into the organic fraction (4.2-fold). The amount of tracer entering the aqueous fraction, which represents β-oxidation, was not different between groups; however a significantly elevated proportion of tracer was in the heart aqueous fraction. In both tissues, 76% of the radioactivity found in the organic fraction was esterified in neutral lipids, while only about 10% was found esterified into phospholipids. In liver, 56% of lipid radioactivity was found in cholesteryl esters, whereas in heart 64% was found in triacylglycerols. Because 22:1n-9 can be chain shortened, we assessed tracer metabolism using phenacyl fatty acid derivatives esterified from saponified esterified neutral lipid (triacylglycerol/cholesteryl ester) and phospholipid fractions. In heart esterified neutral lipids, 75% of tracer was recovered as 22:1n-9 and only 10% as oleic acid (18:1n-9), while in liver only 25% of the tracer was recovered as 22:1n-9, while 50% was found as stearic acid (18:0) and 10% as 18:1n-9. In liver and heart phospholipids, the tracer was distributed amongst the n-9 fatty acid family. Thus, 22:1n-9 under went tissue selective metabolism, with conversion to 18:0 the dominant pathway in the liver presumably for export in the neutral lipids, while in heart it was found primarily as 22:1n-9 in neutral lipids and used for β-oxidation.

Keywords Erucic acid · Fatty acid uptake · Lipid · Phospholipid · Cholesteryl ester · Triacylglycerol · Fatty acid metabolism

Abbreviations

BBB	Blood brain barrier
CE	Cholesteryl esters
Cer*P*Cho	Sphingomyelin
ChoGpl	Choline glycerophospholipids
CNS	Central nervous system
EtnGpl	Ethanolamine glycerophospholipids
FFA	Free fatty acids
PL	Phospholipids
PtdIns	Phosphatidylinositol
PtdSer	Phosphatidylserine
SFA	Saturated fatty acids
TAG	Triacylglycerols
VLCFA	Very-long-chain saturated fatty acids
X-ALD	X-linked adrenoleukodystrophy
16:0	Palmitic acid
18:0	Stearic acid
18:1n-9	Oleic acid
20:4n-6	Arachidonic acid
22:1n-9	Erucic acid

C. C. Murphy · E. J. Murphy (✉) · M. Y. Golovko
Department of Pharmacology,
Physiology, and Therapeutics,
School of Medicine and Health Sciences,
University of North Dakota,
501 N. Columbia Rd, Grand Forks,
ND 58202-9037, USA
e-mail: emurphy@medicine.nodak.edu

E. J. Murphy
Department of Chemistry, University of North Dakota,
Grand Forks, ND 58202-9037, USA

Introduction

X-linked adrenoleukodystrophy (X-ALD) is characterized by elevated very long chain saturated fatty acids (VLCFA) in plasma [1, 2] and in tissue [2, 3]. The clinical manifestations of X-ALD include adrenal insufficiency and rapid demyelination in the central nervous system (CNS) [4]. Accompanying this demyelination is a rise in brain cholesteryl ester mass [5, 6], which is extensively esterified with 26:0 [2]. Lorenzo's oil (LO) is a dietary therapy with restricted saturated fatty acid ingestion in combination with ingestion of a triacylglycerol (TAG) form of erucic acid (22:1n-9), which effectively reduces plasma levels of VLCFA found in X-ALD patients [7–9]. Although the use of LO is controversial because early studies demonstrated the absence of 22:1n-9 from the brain of treated patients [7, 10, 11] and because of its limited effectiveness in ameliorating the progression of CNS demyelination in patients with advanced X-ALD [7–9]. Recent evidence indicates that it has a strong potential in limiting the onset of CNS demyelination following early intervention in X-ALD patients [12–14]. The lack of elevated 22:1n-9 in brains from treated X-ALD patients suggests limited uptake into the CNS, perhaps as a result of poor movement of 22:1n-9 across the blood brain barrier (BBB). Recent work from our laboratory demonstrates that 22:1n-9 crosses the BBB and is found esterified into brain esterified neutral lipid (NL) and phospholipid (PL) pools as primarily 18:1n-9 due to the rapid chain shortening of 22:1n-9 [15]. The entry and metabolism of 22:1n-9 in the brain supports the results of recent clinical trials demonstrating that LO reduces clinical symptoms of X-ALD when administered early in life [12–14].

Although we have studied the metabolism of 22:1n-9 in the brain [15], previous studies have focused on its metabolism in the heart due to its reported impact on heart physiology [16, 17]. In cultured cells, 22:1n-9 is rapidly esterified into TAG and to a lesser extent into PL pools [18–21]. Similar results are reported in isolated organs [22–25], and in intact animals [26–28]. Although 22:1n-9 is poorly oxidized to CO_2 [29, 30], it is quickly converted into oleic acid (18:1n-9) in vivo and in isolated tissues and cultured cells [15, 18, 19, 24, 26–28, 31–35]. This conversion is presumably through peroxisome localized β-oxidation [19, 33, 36], although a possible mitochondrial pathway for 22:1n-9 oxidation can not be excluded [26, 27]. Whole liver and liver cells are capable of converting 22:1n-9 into 18:1n-9 more efficiently than other organs and cell types [18, 28–32], leading to the conclusion that liver plays a central role in 22:1n-9 utilization with other organs utilizing 18:1n-9 exported from liver after 22:1n-9 chain shortening [33].

However, in most of these previous studies examining 22:1n-9 metabolism in vivo, the animals were fed high oil diets rich in 22:1n-9. Under these experimental conditions, peroxisomal β-oxidation is increased, thus increasing the conversion of 22:1n-9 to 18:1n-9 in cultured heart and liver cells [19, 33, 36, 37]. In contrast, constant exposure of the brain to 22:1n-9 alters the pools in which it is found esterified, with minimal impact on 22:1n-9 chain shortening to 18:1n-9 [15]. Pulse infusion studies using labeled 22:1n-9 in vivo also demonstrate an increase in chain shortening even in animals fed with regular diets [26–28]. In these studies, the initial concentration of 22:1n-9 is much higher than its normal physiological levels found in plasma. These conditions would distort 22:1n-9 metabolism because 22:1n-9 esterification into PL or TAG pools is concentration dependent [22]. Similar concentration dependence is observed for 20:4n-9 targeting to heart lipid pools, where under non-physiologically high concentrations it is incorporated into TAG pools [38–40], whereas under conditions using a steady-state tracer infusion, 20:4n-6 is predominantly targeted to PL pools [41]. This demonstrates the utility of the method used herein to study fatty acid metabolism under conditions in which there is minimal alteration of the plasma unesterified fatty acid concentration during infusion of the radiotracer. Thus, high superphysiological concentrations (mM range) of labeled 22:1n-9 used in experiments with perfused organs and cultured cells would significantly alter 22:1n-9 metabolism. Until now, no studies have been done to study 22:1n-9 metabolism in heart and liver under steady-state conditions using low 22:1n-9 concentrations that do not perturb plasma concentrations found in intact animals fed with a regular diet.

Previously, we have demonstrated that under steady-state-like conditions 7% of infused [14-^{14}C]22:1n-9 is recovered as [^{14}C]18:0 from plasma [15], suggesting possible contamination of the tracer. Although the chemical purity of the tracer was >92% pure by GLC, no 18:0 was observed [15]. This observation led us to propose that 22:1n-9 may be rapidly converted into saturated fatty acids (SFA) in liver and then exported into plasma. Despite the fact the 22:1n-9 conversion into monounsaturated fatty acids has been extensively studied, only one study addressed the question of 22:1n-9 conversion into SFA, but this study was done using cultured heart cells [21], demonstrating a need to more fully understand the dynamics of 22:1n-9 metabolism in liver and heart of intact animals.

In the present study, we extend our previous work using samples from our previous study [15] to examine the uptake and incorporation of [14-^{14}C]22:1n-9 into liver and heart lipids as well as its metabolism under steady-state-like conditions using a well established infusion protocol where normal plasma fatty acid concentrations are unaltered by tracer infusion [42–48]. We demonstrate that 2.3-

fold more [14-^{14}C]22:1n-9 was taken up into liver as compared to heart and that the bulk of [14-^{14}C]22:1n-9 radioactivity was incorporated into the NL, mainly into heart TAG and into liver cholesteryl esters (CE) pools, while significantly lesser amounts were esterified into liver and heart PL (<10%). In NL fraction, the bulk of the radioactivity in heart was recovered as 22:1n-9, while in liver NL the bulk of the radioactivity was recovered as 18:0. These data indicate that under steady-state-like conditions, the predominant pathway for 22:1n-9 metabolism in liver is conversion into 18:0 and subsequent incorporation into NL pool, mainly into CE, whereas in the heart, the bulk of 22:1n-9 is incorporated into the NL pool as 22:1n-9 and then presumably used for β-oxidation.

Materials and Methods

Animals

Male Sprague-Dawley rats (150–200 g) were obtained from Charles River Laboratories (St. Louis, MO) and maintained on standard laboratory rat chow diet (Purina rodent chow) and water ad libitum. This study was conducted in accordance with the National Institutes of Health Guidelines for the Care and Use of Laboratory Animals (NIH Publication 80-23) under an animal protocol approved by the IACUC at the University of North Dakota (Protocol 0110-1).

Tracer Preparation

Tracer preparation was performed as previously described [15]. Briefly, the custom synthesized [14-^{14}C] 22:1n-9 (specific activity 53 mCi/mmol, Moravek Biochemical, Brea, CA) was solubilized in 5 mM Hepes (pH 7.4) buffer containing “essentially fatty acid free” bovine serum albumin (50 mg/mL; Sigma Chemical Co, St. Louis, MO). Solubilization was facilitated using a bath sonicator for 45 min at 45 °C. Tracer was infused at a dose of 170 µCi/kg [15, 49]. Previously we determined tracer purity to be >92% by GLC, based upon total peak area [15]. Because we reported 6.5% of the tracer in plasma was found as [^{14}C]18:0, we assessed radiochemical purity of the [14-^{14}C]22:1n-9 using HPLC analysis and found that it the radiochemical purity of the tracer was >99%.

Rat Surgery and Tracer Infusion

Rat surgery and tracer infusion was performed as previously described [15]. Briefly, rats were anesthetized with halothane (1–3%) and PE-50 catheters inserted into the femoral artery and vein. Using an infusion pump (BS-8000, Braintree Scientific, Inc., Braintree, MA), awake rats were infused 3–4 h following recovery from anesthesia with 170 µCi/kg of [14-^{14}C]22:1n-9 via the femoral vein over 10 min at a constant rate of 0.4 mL/min to achieve steady-state-like plasma radioactivity. Prior to and during the infusion, arterial blood samples (200 µL) were taken to determine plasma radioactivity (see Golovko et al. [15]). Following infusion, the rats were killed using pentobarbital (100 mg/kg, intravenous). Liver and heart were rapidly removed and frozen in liquid nitrogen. The tissue was stored at −80 °C until used.

Blood Extraction

To account for the contribution of residual blood to tissue radioactivity, whole blood was extracted using a two-phase extraction [50]. Residual blood in heart and liver was estimated to be 24 and 17%, respectively based upon literature values [51, 52]. Previously using this infusion protocol, we demonstrated that 95% radioactivity in blood is found as free fatty acid, whereas 2.5% is found in phospholipids, and 2.5% is found in triacylglycerols [41, 53].

Tissue Lipid Extraction

To determine tracer incorporation into liver and heart individual lipid compartments, lipids were extracted using a two-phase extraction procedure [50]. Briefly, frozen tissues were pulverized under liquid nitrogen temperatures into a fine homogeneous powder and lipids from the tissue powders were extracted using chloroform/methanol (2:1 by vol) in a Tenbroeck tissue homogenizer. The tissue mass in grams was multiplied by a correction factor of 1.28 to convert it to an equivalent value in mL [54], which represents one volume. The tissue was homogenized in 17 volumes of chloroform-methanol (2:1 by vol), the solvent removed and the homogenizer rinsed with 3 volumes of chloroform/methanol (2:1 by vol). This rinse was added to the original sample and 4 volumes of 0.9% KCl solution were added to the combined lipid extract. The extract was mixed by vortexing and the phases separated by centrifugation. The upper aqueous phase and proteinaceous interphase were transferred to a 20 mL scintillation vial for counting. The lower organic phase was washed twice with 2 mL of theoretical upper phase (chloroform/methanol/water, 3:48:47 by vol) and the phases again separated by centrifugation. Each wash was removed and added to the previously removed upper phase. The lower organic phase was then dried under nitrogen and then dissolved in hexane-2-propanol (3:2 by vol) containing 5.5% water.

To analyze tracer metabolism to other fatty acids and its subsequent distribution within esterified fatty acids found in NL and PL fractions, lipids from liver and heart tissue (200 mg, wet weight) were extracted using single phase extraction procedure [55, 56]. Briefly, tissue powder was homogenized in 1.8 mL hexane/2-propanol (3:2 by vol) per 0.1 g tissue and quantitatively transferred to a test tube. The homogenizer was rinsed with an additional 3 mL of hexane/2-propanol (3:2 by vol) and added to the original extract. The protein-containing residue was pelleted by centrifugation and the lipid bearing organic fraction was removed and stored under a N_2 atmosphere at −80 °C until it was used to assess tracer elongation and chain shortening.

Thin Layer Chromatography

Tissue PL were separated by thin layer chromatography (TLC) on heat-activated Whatman silica gel-60 plates (20 cm × 20 cm, 250 μm) using two different solvent systems. The first system used a chloroform/methanol/acetic acid/water (60:30:3:1 by vol) solvent system that resolves cardiolipin (Ptd_2Gro), phosphatidic acid (PtdOH), and ethanolamine glycerophospholipids (EtnGpl) [53]. Because this first system does not separate phosphatidylserine (PtdSer) and phosphatidylinositol (PtdIns), these two phospholipids were separated using a chloroform/methanol/acetic acid/water (50:37.5:3.5:2 by vol) solvent system [57]. Phospholipids were visualized using iodine vapor.

Heart and liver NL were separated by TLC on heat-activated Whatman silica gel-60 plates (20 cm × 20 cm, 250 μm) and developed in petroleum ether/diethyl ether/acetic acid (70:30:1.3 by vol) solvent system that resolves cholesterol, cholesteryl esters, diacylglycerols, nonesterified fatty acids, and triacylglycerols [58].

All lipid fractions were identified using authentic standards (Doosan–Serdary, Englewood Cliffs, NJ, and NuChek Prep, Elysian, MN). Bands corresponding to the appropriate lipid fractions were removed from the TLC plate by scrapping and transferred into 20 mL liquid scintillation vials and 0.5 mL of water was added followed by 10 mL of Scintiverse BD (Fisher Scientific, Pittsburgh, PA). Radioactivity was quantified by liquid scintillation counting using a Beckman LS 5000 CE liquid scintillation counter.

Analysis of Tracer Conversion in Esterified NL and PL Fractions

To determine the elongation and chain shortening of the infused tracer by heart and liver, extracted heart and liver lipids were separated into PL and NL fractions using silicic acid column chromatography (Clarkson Chemical Co., Inc., Williamsport, PA) [59]. To remove nonesterified fatty acids from the NL fraction, it was then separated by TLC as described above using the petroleum ether/diethyl ether/acetic acid (70:30:1.3 by vol) solvent system, except that lipid fractions were visualized using 6-*p*-toluidino-2-naphthalenesulfonic acid [60]. TAG and CE were collected by scraping the bands off the TLC plate, and were then extracted off the silica by adding 1.5 mL of water followed by three successive washes of the aqueous phase with 3 mL of hexane/2-propanol (3:2 by vol). For each wash, the elution mixture was vigorously mixed for 1 min by vortexing and the two phases were separated by centrifugation. The upper lipid-containing phase was aspirated and saved for fatty acid analysis and subsequent washes were added to this original wash.

Fatty acids from PL fraction and from the combined TAG and CE fractions were separated and quantified after conversion to their corresponding phenacyl esters [61, 62]. Briefly, solvent containing the PL and TAG/CE lipid fractions was removed under a stream of nitrogen and the lipids subjected to saponification at 100 °C for 30 min in 2% KOH in ethanol, which was then acidified with HCl. The released fatty acids were extracted with hexane, the hexane evaporated using nitrogen, and phenacyl esters were then prepared by the addition of acetone containing 2-bromoacetophenone (10 mg/mL) (Sigma) and triethylamine (10 mg/mL) (Sigma) followed by heating at 100 °C for 5 min followed by addition of acetic acid (2 mg/mL) and then the samples were heated for an additional 5 min.

Individual fatty acid phenacyl esters were separated by high performance liquid chromatography (HPLC) on a C-18(2) Luna column (Phenomenex, Torrance, CA) as previously described [15] with a modified elution program that allows resolution of VLCFA. Fatty acids were identified using fatty acid standards (NuChek Prep, Elysian, MN) converted to phenacyl esters. The HPLC system was controlled by a Beckman 127 solvent module (Fullerton, CA). The eluent was monitored at 242 nm using a Beckman 166 ultraviolet/visible light detector. The gradient system used was composed of water (solvent A) and acetonitrile (solvent B). Column temperature was maintained at 37 °C. The flow rate was 1 mL/min, and the initial percentage of B was 80%. The percentage of B was increased to 90% over 1 min at 350 min, increased to 96% over 1 min. at 490 min, and returned to 80% over 1 min at 550 min. Eluent from HPLC containing individual fatty acid phenacyl esters was concentrated by reducing the volume to 1 mL under a stream of nitrogen and 15 mL of Scintiverse BD was added and the samples were mixed by vortexing. After mixing, all samples were allowed to stabilize for at least 1 h before the radioactivity was quantified by liquid scintillation counting using a Beckman LS 6500 liquid scintillation counter.

Statistical Analysis

Statistical analysis was done using InStat (GraphPad, San Diego, CA) and a two-tailed, unpaired Student's *t* test. Values were considered statistically significant when $p < 0.05$.

Results

Plasma Curve

The plasma curve for these awake, male rats infused with [14-^{14}C]22:1n-9 (i.v.) was previously published [15] and indicates that the radiotracer was near steady-state-like conditions and that the plasma concentration of unesterified (free) 22:1n-9 is 6 µM.

Uptake and Distribution of 22:1n-9 in Liver and Heart

In liver and heart, the amount of tracer, expressed as nCi/g ww, found in the total extract, in the organic fraction (lipid containing), and in the aqueous fraction, which represents products of β-oxidation [41, 63, 64] was determined (Fig. 1). Under steady-state-like conditions, significantly more tracer was taken up by the liver (2.3-fold) as compared to the heart. When the unilateral incorporation coefficient for liver and heart uptake was calculated [41–45], which normalizes the amount of tracer taken up into a given tissue by the amount of tracer infused into the rat, the liver had taken up significantly more tracer (2.3-fold) as compared to heart (data not shown). The percentage of the infused tracer removed by the heart was 0.82 ± 0.33%, while that removed by the liver was 1.63 ± 0.45%. Again, using this calculation, the liver removed 2.0-fold more tracer than did heart. The increase in liver total uptake was accounted for by a significantly higher incorporation of tracer (4.2-fold) into the liver organic fraction as compared with heart. However, no differences were found between liver and heart in amount of tracer found in the aqueous fraction. However, in heart a significantly greater proportion of radioactivity was found in the aqueous fraction (63.2 ± 5.8%) as compared to liver (22.9 ± 2.9%), indicating that in the heart 2.8-fold more tracer underwent β-oxidation relative to the liver.

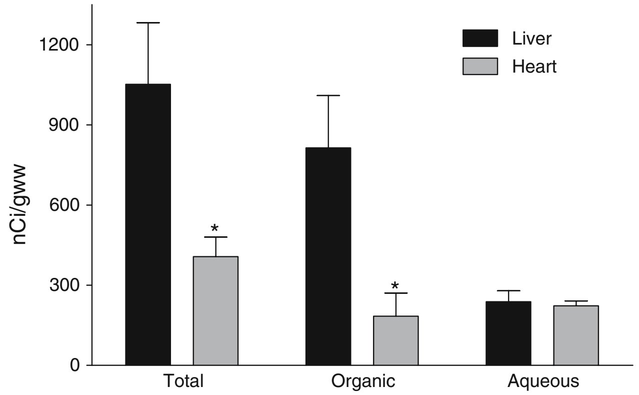

Fig. 1 Uptake of [14-^{14}C]22:1n-9 by heart and liver values are expressed as mean ± SD, where $n = 5$ heart and $n = 6$ for liver. The * indicates statistical significance from liver, $p < 0.05$

Distribution of Tracer in Liver and Heart Lipid Pools

To determine into which lipid compartments the tracer entered in liver and heart, the incorporation of the tracer into individual lipid fractions was determined (Fig. 2). Significantly more tracer (nCi/g ww) went into liver total PL, unesterified (free) fatty acids, and CE as compared to heart (Fig. 2, *top panel*). However, the amount of tracer entering into the TAG pool was not different between groups. These values illustrate two important points. First, that very little tracer entered into the phospholipid pools.

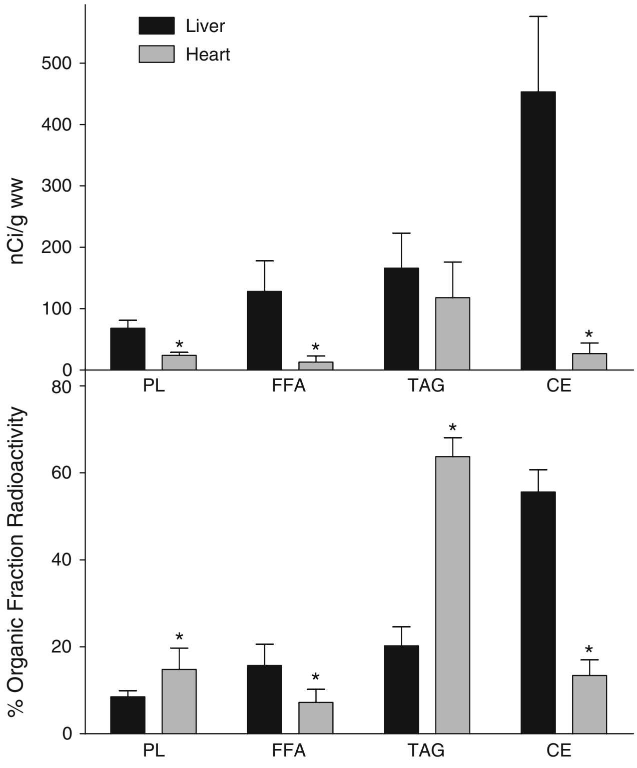

Fig. 2 Distribution of infused [14-^{14}C]22: 1n-9 amongst different heart and liver lipid fractions values are expressed as mean ± SD, where $n = 5$ heart and $n = 6$ for liver. The * indicates statistical significance from liver, $p < 0.05$. In the *top panel*, values are expressed as nCi/g ww, while in the *bottom panel*; these values are expressed as percent of total organic fraction radioactivity. PL: phospholipids; FFA: free fatty acids; TAG: triacylglycerols; CE: cholesteryl esters

Second, that the amount of tracer entering the CE pool was tremendously different between groups.

However, it is also important to determine the proportion of tracer targeted to each of the respective lipid pools (Fig. 2, *lower panel*). Under steady-state-like conditions, the bulk of the infused tracer in heart was found in TAG pool (63.7 ± 4.4%), while the remainder was distributed between the total PL, unesterified (free) fatty acids, and CE. In stark contrast, in liver the bulk of the infused tracer was found in CE (55.6 ± 5.1%), with the remaining tracer distributed between the other lipid fractions. These data indicate that under steady-state-like conditions the intact liver targets 22:1n-9 for esterification into different lipid metabolic pools than in the heart.

Distribution of Tracer in Individual Phospholipid Classes

The distribution of the infused tracer in liver and heart individual PL classes was also determined and values are expressed as % of total phospholipid radioactivity (Fig. 3). In both liver and heart, the bulk of the infused tracer was incorporated into CholGpl, Cer*P*Cho, and EtnGpl. The rest of the tracer was found distributed amongst the other phospholipids.

Metabolism of [14-^{14}C]22:1n-9 to Other Fatty Acids in Liver and Heart

To determine whether the infused [14-^{14}C]22:1n-9 was chain elongated or shortened, we determined the distribution of radioactivity found in other monounsaturated and saturated fatty acids in the total phospholipid fraction from liver and heart (Fig. 4). We observed minimal of elongation of [14-^{14}C]22:1n-9 to [16-^{14}C]24:1n-9 in liver and heart, however we did find that in liver and heart PL fractions, 64.2 ± 10.9% and 41.1 ± 8.2% of radioactivity, respectively, was found in products derived from chain shortening of [14-^{14}C]22:1n-9. The terminal pool was found to be 18:1n-9, in which form 41.8 ± 5.4% and 30.8 ± 6.6% of the tracer was found in liver and heart PL, respectively. Limited carbon recycling into SFA was found in liver and heart, as only 6.9 ± 2.3% of the tracer was found in liver PL SFA (mainly as 18:0, 3.0 ± 1.3%) and only 7.0 ± 3.3% of the tracer was found in the heart PL SFA fraction (mainly as 16:0, 4.2 ± 3.2%).

Similar to the PL pool in liver and heart, the combined TAG/CE pool contained products of chain shortening, mainly in the form of 18:1n-9 form. However, the distribution into this pool was much lower (12.9 ± 3.1% and 10.0 ± 1.7% in liver and heart, respectively) than what was observed in the PL pool. These data support previous observations showing that 22:1n-9 is readily chain shortened and that it accumulates as 18:1n-9 as the terminal pool. Limited carbon recycling into SFA was found in the heart TAG/CE fraction (Fig. 5). In stark contrast, in the liver TAG/CE fraction, 54.2 ± 9.0% of the tracer was recovered in SFA form, mainly as 18:0 (48.4 ± 4.5%). These data support our assumption that 22:1n-9 was rapidly converted into 18:0 in liver, which can then be exported into plasma, thereby accounting for our observation of 6.5% of the tracer in the plasma being in the form of [^{14}C]18:0.

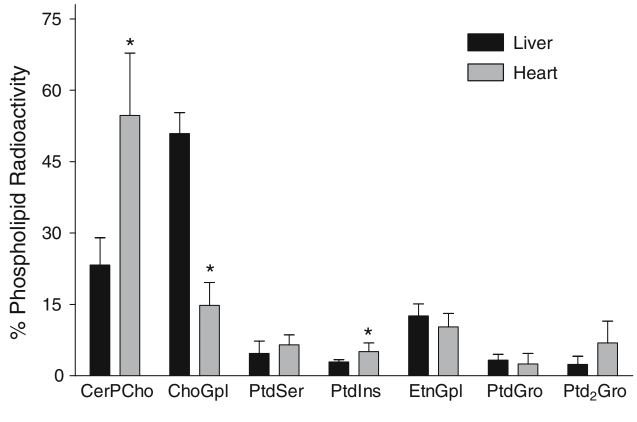

Fig. 3 Distribution of infused [14-^{14}C]22:1n-9 amongst individual heart and liver phospholipid classes values are expressed as mean ± SD, where $n = 5$ heart and $n = 6$ for liver. The * indicates statistical significance from liver, $p < 0.05$. *CerPCho* sphingomyelin, *ChoGpl* choline glycerophospholipids, *PtdSer* phosphatidylserine, *PtdIns* phosphatidylinositol, *EtnGpl* ethanolamine glycerophospholipids, *PtdOH* phosphatidic acid, *Ptd$_2$Gro* cardiolipin

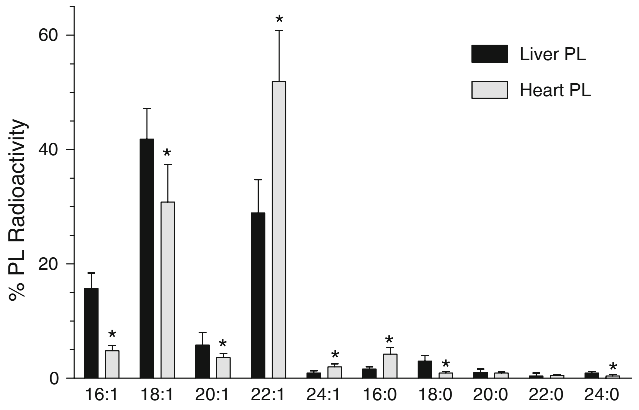

Fig. 4 Distribution of radioactivity amongst different fatty acids derived from the total tissue phospholipid fraction Values are expressed as mean ± SD, where $n = 5$ heart and $n = 6$ for liver. The * indicates statistical significance from liver, $p < 0.05$. These values are expressed as *percent* of total phospholipid fraction radioactivity. The abbreviations are: 16:1: palmitoleic acid; 18:1: oleic acid; 20:1: gondoic acid; 22:1: erucic acid; 24:1: nervonic acid; 16:0: palmitic acid; 18:0: stearic acid; 20:0: arachidic acid; 22:0: behenic acid; 24:0: lignoceric acid

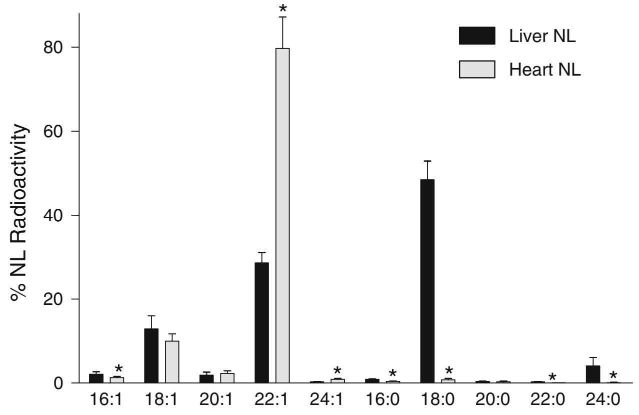

Fig. 5 Distribution of radioactivity amongst different fatty acids in the combined tissue TAG/CE fraction Values are expressed as mean ± SD, where $n = 5$ heart and $n = 6$ for liver. The * indicates statistical significance from liver, $p < 0.05$. These values are expressed as percent of total phospholipid fraction radioactivity. The abbreviations are: 16:1: palmitoleic acid; 18:1: oleic acid; 20:1: gondoic acid; 22:1: erucic acid; 24:1: nervonic acid; 16:0: palmitic acid; 18:0: stearic acid; 20:0: arachidic acid; 22:0: behenic acid; 24:0: lignoceric acid

Discussion

Although 22:1n-9 metabolism has been extensively studied in different model systems, it is important to note that in these other studies, the experimental conditions used may dramatically impact normal 22:1n-9 metabolism, potentially impacting interpretation. For example, feeding animals high oil diets or diets rich in 22:1n-9 increases the ability of the liver and heart to oxidize 22:1n-9 [19, 33, 36, 37], thus providing metabolic results that are difficult to interpret and perhaps erroneous relative to more steady-state conditions. Because the metabolism of 22:1n-9 is concentration dependent [22], it is important to use studies that avoid perturbing the normal plasma concentration of the fatty acid of interest [41]. Recently, we demonstrated the uptake into and metabolism of [14-^{14}C]22:1n-9 in rat brain [15]. Herein, we present data from hearts and livers isolated from the rats used in our previous study [15]. Unlike the many other studies examining 22:1n-9 metabolism, this is the first study to examine liver and heart 22:1n-9 metabolism under steady-state-like conditions.

Under these steady-state-like conditions, 2.3-fold more tracer was incorporated into liver as compared with heart (Fig. 1). These data are consistent with results showing increased liver uptake relative to that by heart under a number of experimental conditions. Following pulse infusion (i.v.) with [14-^{14}C]22:1n-9, liver radioactivity is 10–15 fold higher than that found in heart, kidneys, or spleen radioactivity after pulse i.v. infusion of [28]. Similar results are observed following pulse infusion of tritiated 22:1n-9 [26, 27]. We did not see such a large difference between heart and liver uptake, this is more than likely because the concentration of labeled 22:1n-9 used in pulse infusion experiments was about 10-fold higher than that used in our experimental paradigm, certainly high enough to alter the normal plasma concentration of 22:1n-9. This is critical because liver fatty acid uptake is directly related to fatty acid plasma concentration [65], which is consistent with our lower difference between liver and heart uptake at steady-state conditions.

Furthermore, targeting of tracer to lipid pools is also highly dependent upon tracer concentration. We observed that 7 and 16% of the tracer was in the unesterified free fatty acid (FFA) fraction, in heart and liver, respectively (Fig. 2), which is substantially lower than those obtained under other experimental conditions when concentrations of [^{14}C]22:1n-9 are in the mM range. Under these supra-physiological conditions, 80% of the tracer is recovered in the unesterified FFA fraction in perfused liver [24], 36–90% of the tracer in this fraction in hepatocytes [18, 34], and 20–62% of the tracer in this fraction in perfused heart [23, 25, 26, 66]. While we find only 23% of the infused [14-^{14}C]22:1n-9 was found in the aqueous fraction of the liver, this value was two times higher than that observed in vitro [24, 34, 35]. These data indicate that under steady-state-like conditions, more 22:1n-9 that entered the liver was subjected to β-oxidation rather than esterified into lipids. Thus, the concentration of infused tracer is critical for not only tissue uptake, but metabolism of the tracer by the tissue as well as distribution of tracer into specific metabolic pools.

In liver and heart, the bulk of the infused [14-^{14}C]22:1n-9 found in the organic fraction was incorporated into the NL fractions, but the targeting to individual NL (TAG and CE) was radically different between liver and heart (Fig. 2). However, the distribution of radioactivity between the total PL and NL fractions was similar for liver and heart, which is consistent with tracer distribution between these fractions following pulse-infusion [26, 27], in perfused heart [22, 23, 25, 66], in perfused liver [24, 35], and in hepatocytes incubated with 22:1n-9 [34]. Interestingly, 22:1n-9 distribution between PL and NL fractions is independent of fatty acid concentration used for heart perfusion [22]. We also found that the tracer was mainly found in ChoGpl, Cer$\underline{P}$Cho, and EtnGpl in liver and heart phospholipids (Fig. 3), which appears to be independent of experimental conditions, since a similar distribution was shown in heart cell cultures [20], in liver cell cultures [67], and in perfused heart [22].

We [15] and others have shown that 22:1n-9 is readily converted into 18:1n-9 through chain shortening pathway in various organs and cell types [18, 19, 24, 26–28, 31–35], however none of these studies have addressed conversion of 22:1n-9 to other fatty acids under steady-state-like conditions or its conversion into saturated fatty acids (SFA). Previously we found that >91% of the infused tracer was recovered as plasma 22:1n-9, with 6.5% of the tracer found in plasma found as 18:0 under steady-state-like conditions [15]. Because the radiochemical purity of the custom-synthesized tracer was >99% for [14-^{14}C]22:1n-9 (as shown by radiochemical HPLC analysis), it is unlikely that the 18:0 was derived from the tracer, but rather via conversion of 22:1n-9 to 18:0 in liver through carbon recycling followed by export into plasma. This is consistent with our observation reported herein that the liver took up significantly more tracer and that by others demonstrating that the liver has a central role in 22:1n-9 metabolism [33].

In brain, we demonstrated that [14-^{14}C]22:1n-9 is chain shortened predominantly to [10-^{14}C]18:1n-9 [15]. In livers and hearts isolated from these same rats, we demonstrate that 31 and 42% of PL radioactivity was found as 18:1n-9, respectively (Fig. 4). These results confirm previous reports showing that 22:1n-9 is quickly converted into 18:1n-9 in all models studied [15, 18, 19, 24, 26, 27, 31–35]. Presumably, this conversion is through peroxisome localized β-oxidation [33, 36, 68]. In contrast, 80% of heart NL radioactivity was recovered as 22:1n-9 in which TAG radioactivity represents 70% of total lipid radioactivity. This is consistent with the observation that up to 80% of heart TAG radioactivity remains in 22:1n-9 form after pulse infusion of [^{14}C]22:1n-9 [26, 28]. These data indicate that the heart TAG pool may serve as a transient pool for 22:1n-9 before its β-oxidation, similar to the proposed role for TAG pools comprised of other fatty acids in heart [41, 53] and this role may be independent of the 22:1n-9 concentrations used in the experiment.

Although 22:1n-9 conversion into monounsaturated FA has been extensively studied, no studies have demonstrated the conversion of 22:1n-9 into SFA in liver and only one study addressed this conversion in cultured heart cells [21]. In the present study, we demonstrate that half of the tracer conversion was limited in the heart as it was found in [14-^{14}C]22:1n-9 (Figs. 4 and 5), which is consistent with results from cultured heart cells [21]. The high amount of radioactive 18:0 in the liver esterified NL fraction explains our previous observation that 7% of infused [14-^{14}C]22: 1n-9 is found as radioactive 18:0 in plasma [15].

There are two possible explanations for the high rate of conversion of the tracer into SFA. First, the tracer could be chain shortened to 18:1n-9 that is then saturated via the reversal of the Δ-9 desaturase. However, there is no evidence for a reversal of Δ-9 desaturase activity. Second, the complete β-oxidation of 22:1n-9 and recycling of the radioactive carbons for 18:0 biosynthesis. This is not without precedence, as in brain a significant portion (>30%) of infused fatty acid radiotracer is found as radioactive amino acids made via Krebs cycle intermediates within a 10 min time frame [63, 64]. Hence, the rapidity of these processes has been observed in the past and is an important indicator of how fast these processes work in vivo.

In summary, under steady-state-like physiological conditions more of the infused [14-^{14}C]22:1n-9 (2.3-fold) was taken up by the liver as compared to heart. It is important to note that significantly more tracer was targeted for β-oxidation in the heart as compared to liver, consistent with the high distribution of radioactivity into heart TAG pools. This is significant because these pools have a high rate of incorporation in vivo [53], consistent with a high degree of turnover to provide fatty acids for β-oxidation. In both tissues, the bulk of tracer radioactivity was incorporated into the esterified NL fraction, found mainly in TAG in heart and CE in liver. In the heart NL fraction, the radioactivity was found predominantly as 22:1n-9, whereas it was mainly found as 18:0 in liver NL fraction, demonstrating a rapid conversion of 22:1n-9 into saturated fatty acids. The underlying importance of this finding is that during the treatment of X-ALD using LO, which contains a high level of 22:1n-9, its ingestion may lead to an increase in saturated fatty acid burden. Because patients on LO have a restricted saturated fatty acid diet our finding may have clinical ramifications. The high levels of [^{14}C]18:0 found in liver TAG/CE is consistent with the presence of this fatty acid (6.5%) in the plasma of rats, indicating that the liver rapidly (<10 min) metabolized the [14-^{14}C]22:1n-9 and exported the TAG/CE containing the [^{14}C]18:0 into the plasma. Collectively, these data indicate that under steady state-like conditions, the liver has a greater capacity to take up 22:1n-9 as compared with heart, where significant amounts of this fatty acid is metabolized to form saturated fatty acids, while in the heart this fatty acid remains more intact and it is targeted for pools destined for use in heart for β-oxidation.

Acknowledgments The authors thank Dr. Carole Haselton for her excellent surgical and technical assistance and editorial suggestions and Mrs. Cindy Murphy for typing and preparation of the manuscript. This work was supported by grant from The Myelin Project to EJM and in part by a project (EJM) on a COBRE Grant from the National Institute of Health P20 RR17699.

References

1. Moser HW, Moser AB, Frayer KK, Chen W, Schulman JD, O'Neill BP, Kishimoto Y (1981) Adrenoleukodystrophy: increased plasma content of saturated very long chain fatty acids. Neurology 31:1241–1249
2. Igarashi M, Schaumburg HH, Powers J, Kishimoto Y, Kolodny E, Suzuki K (1976) Fatty acid abnormality in adrenoleukodystrophy. J Neurochem 26:851–860

3. Theda C, Moser AB, Powers JM, Moser HW (1992) Phospholipids in X-linked adrenoleukodystrophy white matter-fatty acid abnormalities before the onset of demyelination. J Neurol Sci 110:195–204
4. Dubois-Dalcq M, Feigenbaum V, Aubourg P (1999) The neurobiology of X-linked adrenoleukodystrophy, a demyelinating peroxisomal disorder. Trends Neurosci 22:4–12
5. Wilson R, Sargent JR (1993) Lipid and fatty acid composition of brain tissue from adrenoleukodystrophy patients. J Neurochem 61:290–297
6. Paintlia AS, Gilg AG, Khan M, Signh AK, Barbosa E, Singh I (2003) Correlation of very long chain fatty acid accumulation and inflammatory disease progression in childhood X-ALD implications for potential therapies. Neurobiol Dis 14:425–439
7. Rizzo WB, Leshner RT, Odone A, Dammann AL, Craft DA, Jensen ME, Jennings SS, Davis S, Jaitly R, Sgro JA (1989) Dietary erucic acid therapy for X-linked adrenoleukodystrophy. Neurology 39:1415–1422
8. Kaplan PW, Tusa RJ, Shankroff J, Heller J, Moser HW (1993) Visual evoked potentials in adrenoleukodystrophy: a trial with glycerol trioleate and Lorenzo oil. Ann Neurol 34:169–174
9. Odone A, Odone M (1989) Lorenzo's oil a new treatment for adrenoleukodystrophy. J Pediatr Neurosci 5:55–61
10. Rasmussen M, Moser AB, Borel J, Khangoora S, Moser HW (1994) Brain, liver, and adipose tissue erucic and very long chain fatty acid levels in adrenoleukodystrophy patients treater with glyceryl trierucate and trioleate oils (Lorenzo's oil). Neurochem Res 19:1073–1082
11. Poulos A, Gibson R, Sharp P, Beckman K, Grattan-Smith P (1994) Very long chain fatty acids in X-linked adrenoleukodystrophy brain after treatment with Lorenzo's oil. Ann Neurol 36:741–746
12. Moser HW, Raymond GV, Koehler W, Sokolowski P, Hanefeld F, Korenke GC, Green A, Loes DJ, Hunneman DH, Jones RO, Lu S-E, Uziel G, Blasco MLG, Roels F (2003) Evaluation of the preventive effect of glyceryl trioleate-trierucate ("Lorenzo's oil") therapy in X-linked adrenoleukodystrophy: results of two concurrent trials. Adv Exp Med Biol 544:369–387
13. Moser HW, Raymond GV, Lu S-E, Muenz LR, Moser AB, Xu J, Jones RO, Loew DJ, Melhem ER, Dubey P, Bezman L, Brereton NH, Odone A (2005) Follow-up of 89 asymptomatic patients with adrenoleukodystrophy treated with Lorenzo's oil. Arch Neurol 62:1073–1080
14. Ferri R, Chance PF (2005) Lorenzo's oil: advances in the treatment of neurometabolic disorders. Arch Neurol 62:1045–1046
15. Golovko MY, Murphy EJ (2006) Uptake and metabolism of plasma derived euricic acid by rat brain. J Lipid Res 47:1289–1297
16. Kramer JKG, Farnworth ER, Johnston KM, Wolynetz MS, Modler HW, Sauer FD (1990) Myocardial changes in newborn piglets fed sow milk or milk replacer diets containing different levels of erucic acid. Lipids 25:729–737
17. Kramer JKG, Sauer FD, Wolynetz MS, Farnworth ER, Johnston KM (1992) Effects of dietary saturated fat on erucic acid induced myocardial lipidosis in rats. Lipids 27:619–623
18. Norseth J, Christophersen BO (1978) Chain shortening of erucic acid in isolated liver cells. FEBS Lett 88:353–357
19. Christiansen RZ, Christiansen EN, Bremer J (1979) The stimulation of erucate metabolism in isolated rat hepatocytes by rapeseed oil and hydrogenated marine oil-containing diets. Biochim Biophys Acta 573:417–429
20. Rogers CG (1977) Lipid composition and erucic acid in rat liver cells in culture. Lipids 12:1043–1049
21. Pinson A, Padieu P (1974) Erucic acid oxidation by beating heart cells in culture. FEBS Lett 39:88–90
22. Sauer FD, Kramer JKG, Forester GV, Butler KW (1989) Palmitic and erucic acid metabolism in isolated perfused hearts from weanling pigs. Biochim Biophys Acta 1004:205–214
23. Vasdev SC, Kako KJ (1976) Metabolism of erucic acid in the isolated perfused rat heart. Biochim Biophys Acta 431:22–32
24. Rønneberg R, Hølmer G, Lambertsen G (1986) Effects of feeding high-fat diets to rats: metabolism of erucic acid (C 22:1 n-9) in the perfused liver and secretion of metabolites to the perfusate. Ann Nutr Metab 30:345–356
25. Ward B, Harris P (1984) A comparison of the short-term incorporation of erucic acid and oleic acid in the perfused guinea-pig heart. J Mol Cell Cardiol. 16:897–903
26. Caselli C, Carlier H, Bezard J (1990) Erucic acid metabolism in rat heart. A combined biochemical and radioautographical study. Arch Int Physiol Biochim 98:377–395
27. Caselli C, Bernard A, Bezard J, Carlier H (1992) Erucic acid metabolism in rat liver: a combined biochemical and radioautographical study. Arch Int Physiol Biochim Biophys 100:309–320
28. Ong N, Bezard J, Lecerf J (1977) Incorporation and metabolic conversion of erucic acid in various tissues of the rat in short term experiments. Lipids 12:563–569
29. Carroll KK (1962) Levels of radioactivity in tissues and in expired carbon dioxide after administration of 1-C^{14}-labeled palmitic acid, 2-C^{14}-labelled erucic acid, or 2-C^{14}-labelled nervonic acid to rats. Can J Biochem Physiol 40:1229–1238
30. Reubsaet FAG, Veerkamp JMF, Monnens LAH (1989) Total and peroxisomal oxidation of various saturated and unsaturated fatty acids in rat liver, heart and M quadriceps. Lipids 24:945–950
31. Clouet P, Bezard J (1978) Chain shortening of erucic acid by subcellular particles isolated from liver and heart of rat. FEBS Lett 93:165–168
32. Clouet P, Bezard J (1979) In vitro conversion of erucic acid by microsomes and mitochondria from liver, kidneys and heart of rats. Lipids 14:268–273
33. Christiansen EN, Thomassen MS, Christiansen RZ, Osmundsen H, Norum KR (1979) Metabolism of erucic acid in perfused rat liver: increased chain shortening after feeding partially hydrogenated marine oil and rapeseed oil. Lipids 14:829–835
34. Rønneberg R, Hølmer G, Lambertsen G (1987) Comparative metabolism of erucic and oleic acid in hepatocytes from rats fed partially hydrogenated marine oil or palm oil. Ann Nutr Metab 31:160–169
35. Hølmer G, Rønneberg R (1986) Influence of dietary fat on metabolism of (14-^{14}C)erucic acid in the perfused rat liver. Distribution of metabolites in lipid classes. Lipids 21:395–400
36. Neat CE, Thomassen MS, Osmundsen H (1980) Induction of peroxisomal β-oxidation in rat liver by high-fat diets. Biochem J 186:369–371
37. Norseth J (1979) The effect of feed rats with partially hydrogenated marine oil or rapeseed oil on the chain shortening of erucic acid in perfused heart. Biochim Biophys Acta 575:1–9
38. Hohl CM, Rosen P (1987) The role of arachidonic acid in rat heart cell metabolism. Biochim Biophys Acta 921:356–363
39. Hagve T-A, Sprecher H (1989) Metabolism of long-chain polyunsaturated fatty acids in isolated cardiac myocytes. Biochim Biophys Acta 1001:338–344
40. Saddik M, Lopaschuk GD (1991) The fate of arachidonic acid and linoleic acid in isolated working rat hearts containing normal or elevated levels of coenzyme A. Biochim Biophys Acta 1086:217–224
41. Murphy EJ, Rosenberger TA, Patrick CB, Rapoport SI (2000) Intravenously injected [1-^{14}C]arachidonic acid targets phospholipids, and [1-^{14}C]palmitic acid targets neutral lipids in hearts of awake rats. Lipids 35:891–898

42. Robinson PJ, Noronha J, DeGeorge JJ, Freed LM, Nariai T, Rapoport SI (1992) A quantitative method for measuring regional in vivo fatty acid incorporation into and turnover within brain phospholipids: review and critical analysis. Brain Res Rev 17:187–214
43. Rapoport SI (1996) In vivo labeling of brain phospholipids by long-chain fatty acids: relation to turnover and function. Lipids 31:S97–S101
44. Rapoport SI, Chang MCJ, Spector AA (2001) Delivery and turnover of plasma-derived essential PUFAs in mammalian brain. J Lipid Res 42:678–685
45. Rapoport SI (2005) In vivo approaches and rationale for quantifying kinetics and imaging brain lipid metabolic pathways. Prostaglandins Other Lipid Mediat 77:185–196
46. Golovko MY, Færgeman NJ, Cole NB, Castagnet PI, Nussbaum RL, Murphy EJ (2005) α-Synuclein gene-deletion decreases brain palmitate uptake and alters the palmitate metabolism in the absence of α-synuclein palmitate binding. Biochemistry 44:8251–8259
47. Golovko MY, Rosenberger TA, Færgeman NJ, Feddersen S, Cole NB, Pribill I, Berger J, Nussbaum RL, Murphy EJ (2006) Acyl-CoA synthetase activity links wild-type but not mutant α-synuclein to brain arachidonate metabolism. Biochemistry 45:6956–6966
48. Golovko MY, Rosenberger TA, Feddersen S, Færgeman NJ, Murphy EJ (2007) α-Synuclein gene ablation increases docosahexaenoic acid incorporation and turnover in brain phospholipids. J Neurochem 101:201–211
49. Freed LM, Wakabayashi S, Bell JM, Rapoport SI (1994) Effect of inhibition of β-oxidation on incorporation of [U-^{14}C]palmitate and [1-^{14}C]arachidonate into brain lipids. Brain Res 645:41–48
50. Folch J, Lees M, Sloan Stanley GH (1957) A simple method for the isolation and purification of total lipides from animal tissues. J Biol Chem 226:497–509
51. Smith BSW (1970) A comparison of ^{125}I and ^{51}Cr for measurement of total blood volume and residual blood content of tissues in the rat; evidence for accumulation of ^{51}Cr by tissues. Clinica Chimica Acta 27:105–108
52. Regoeczi E, Taylor P (1978) The net weight of the rat liver. Growth 42:451–456
53. Patrick CB, Rosenberger TA, McHowat J, Rapoport SI, Murphy EJ (2005) Arachidonic acid incorporation and turnover is decreased in sympathetically denervated rat heart. Am J Physiol 288:2611–2619
54. Radin NS (1988) Lipid extraction. In: Boulton AA, Baker GB, Horrocks LA (eds) Neuromethods 7 lipids and related compounds. Humana Press, Clifton, pp 1–62
55. Hara A, Radin NS (1978) Lipid extraction of tissues with a low-toxicity solvent. Anal Biochem 90:420–426
56. Saunders RD, Horrocks LA (1984) Simultaneous extraction and preparation for high-performance liquid chromatography of prostaglandins and phospholipids. Anal Biochem 143:71–75
57. Jolly CA, Hubbell T, Behnke WD, Schroeder F (1997) Fatty acid binding protein: stimulation of microsomal phosphatidic acid formation. Arch Biochem Biophys 341:112–121
58. Marcheselli VL, Scott BL, Reddy TS, Bazan NG (1988) Quantitative analysis of acyl group composition of brain phospholipids, neutral lipids, and free fatty acids. In: Boulton AA, Baker GB, Horrocks LA (eds) Neuromethods 7 lipids and related compounds. Humana Press, Clifton, pp 83–110
59. Murphy EJ, Schroeder F (1997) Sterol carrier protein-2 mediated cholesterol esterification in transfected L-cell fibroblasts. Biochim Biophys Acta 1345:283–292
60. Jones M, Keenan RW, Horowitz P (1982) Use of 6-p-toluidino-2-naphthalenesulfonic acid to quantitate lipids after thin-layer chromatography. J Chromatogr 237:522–524
61. Wood R, Lee T (1983) High-performance liquid chromatography of fatty acids: quantitative analysis of saturated, monoenoic, polyenoic and geometrical isomers. J Chromatogr 254:237–246
62. Chen H, Anderson RE (1992) Quantitation of phenyl esters or retinal fatty acids by high-performance liquid chromatography. J Chromatogr 578:124–129
63. Miller JC, Gnaedinger JM, Rapoport SI (1987) Utilization of plasma fatty acid in rat brain: distribution of [^{14}C]palmitate between oxidative and synthetic pathways. J Neurochem 49:1507–1514
64. Gnaedinger JM, Miller JC, Latker CH, Rapoport SI (1988) Cerebral metabolism of plasma ^{14}Cpalmitate in awake adult rat: subcellular localization. Neurochem Res. 13:21–29
65. Berk PD, Stump DD (1999) Mechanisms of cellular uptake of long chain free fatty acids. Mol Cell Biochem 192:17–31
66. Norseth J, Christiansen EN, Christophersen BO (1979) Increased chain shortening of erucic acid in perfused heart from rats fed rapeseed oil. FEBS Lett 97:163–165
67. Rogers CG (1977) Erucic acid and phospholipids of newborn rat heart cells in culture. Lipids 12:375–381
68. Christiansen RZ, Christopherson BO, Bremer J (1977) Monoethylenic C_{20} and C_{22} fatty acids in marine oil and rapeseed oil. Studies on their oxidation and on their relative ability to inhibit palmitate oxidation in heart and liver mitochondria. Biochim Biophys Acta 487:28–36

Lipids (2008) 43:401–408
DOI 10.1007/s11745-008-3172-7

ORIGINAL ARTICLE

NPC1L1 and SR-BI are Involved in Intestinal Cholesterol Absorption from Small-Size Lipid Donors

Ziad Haikal · Barbara Play · Jean-François Landrier · Annie Giraud · Odette Ghiringhelli · Denis Lairon · Dominique Jourdheuil-Rahmani

Received: 12 November 2007 / Accepted: 3 March 2008 / Published online: 29 March 2008
© AOCS 2008

Abstract In the human intestinal content after a meal, cholesterol is dispersed in a complex mixture of emulsified droplets, vesicles, mixed micelles and precipitated material. The aim of this study was to determine the contribution of the main intestinal cholesterol transporters (NPC1L1, SR-BI) to the absorption processes, using different cholesterol-solubilizing donors. Cholesterol donors prepared with different taurocholate concentrations were added to an apical medium of differentiated TC7/Caco-2 cells. As the taurocholate concentrations increased, cholesterol donor size decreased (from 712 to 7 nm in diameter), which enhanced cholesterol absorption in a dose-dependent manner (38-fold). Two transport processes were observed: (1) absorption from large donors exhibited low-capacity transport with no noticeable transporter contribution; (2) efficient cholesterol absorption occurs from small lipid donors ($\leq$23 nm diameter), mainly due to NPC1L1 and SR-BI involvement. In addition, bile acids significantly increased mRNA and protein expression of NPC1L1, but not of SR-BI. In conclusion, bile acids present in the intestinal lumen and the micelles enhance intestinal cholesterol transport into the cell by two different regulatory processes: by reducing the lipid donor size, so that small-size mixed micelles can more easily access brush-border membrane transporters, and by increasing the expression level of the enterocyte NPC1L1. These mechanisms could account for the important inter-individual variations observed in cholesterol intestinal absorption.

Keywords Cholesterol absorption · NPC1L1 · SR-BI · Bile acids · Vesicle · Mixed micelles

Abbreviations

BA	Bile acids
CL	Cholesterol
DCA	Deoxycholic acid
DMEM	Dulbecco's modified Eagle's medium
NPC1L1	Niemann–Pick C1-like 1
SR-BI	Scavenger receptor class B type I
TCA	Taurocholic acid

Introduction

Dietary and biliary cholesterol (CL) absorption contributes, along with regulation of CL biosynthesis, to maintaining a tight control of CL homeostasis. However, the mechanisms of intestinal CL absorption are not yet fully understood. They involve a multistep process which is regulated by multiple genes and different protein-facilitated processes at the enterocyte level. The scavenger receptor class B type I (SR-BI) is a membrane glycoprotein. When localized at the brush-border membrane, it facilitates intestinal absorption of CL and other lipid nutrients [1–4]. Recently, the Niemann–Pick C1-like 1 (NPC1L1) transporter was identified as being critical to CL absorption [5–7]. However, its involvement in intestinal CL absorption is not fully

---

This work was supported by grants from the Nouvelle Société Française d'Athérosclérose and from the Comité Nutrition et Santé, Institut Appert, France.

Z. Haikal · B. Play · J.-F. Landrier · A. Giraud ·
O. Ghiringhelli · D. Lairon · D. Jourdheuil-Rahmani (✉)
INRA, UMR1260 «Nutriments Lipidiques et Prévention des Maladies Métaboliques», INSERM, U476,
Univ Aix-Marseille 1, Univ Aix-Marseille 2,
Faculté de Médecine, IPHM-IFR 125, 27 bld Jean Moulin,
13385 Marseille, France
e-mail: Dominique.Jourdheuil-Rahmani@pharmacie.univ-mrs.fr

understood and its cell surface and/or intracellular localization is still debated. While some reports indicate that NPC1L1 is located at the cell surface in animal enterocytes [7–9] and Caco-2 cells [1, 10, 11], others describe NPC1L1 as being an intracellular [12], endosomal protein [5]. Moreover, very recent studies have confirmed the presence of NPC1L1 in both regions [1, 13, 14]. Some authors have proposed that the observed differences in the cellular location of NPC1L1 might depend on the differentiated state of the cultured cells [10]. NPC1L1 possibly cooperates with SR-BI to mediate intestinal CL absorption in humans [1, 8]. Members of the ATP-binding cassette (ABC) family are involved in efflux processes. ABCG5 and ABCG8 constitute apical sterol export pumps that promote active efflux of CL from enterocytes back into the intestinal lumen for excretion [15, 16], thus limiting intestinal CL absorption. ABCA1 located at the basolateral membrane of the enterocyte is involved in the efflux process of CL towards circulating HDL lipoproteins [17–19]. The respective roles of these transporters are still under investigation.

Within the gut lumen, dietary CL is emulsified with triglycerides and other lipids into oily droplets (1–100 μm) [20]. As intraluminal fat digestion occurs, vesicles are generated at the surface of emulsions which are then partly dispersed in mixed micelles [21]. Vesicles are large unilamelar aggregates (40–100 nm), and mixed micelles have a much smaller size ($\sim$10 nm). Little is known about intestinal absorption of CL from vesicles, while micelle CL absorption is thought to be essential. Bile acids (BAs) are mainly present in mixed micelles and even in vesicles, but also exist in monomer form [20]. BAs are required for efficient CL absorption; in the absence of BAs, CL absorption is markedly reduced [22, 23]. They are recognized as being important lipid-solubilizing molecules. However, several investigators have reported that the best BA for lipid solubilization is not the best for intestinal CL absorption [24–26]. The role that BA plays in facilitating CL absorption by the enterocytes may thus extend beyond their CL solubilization properties.

Very little information is available about the possible interactions between the various kinds of dispersed lipid aggregates present in the intestinal lumen and the different intestinal CL transporters. Thus, we hypothesized that BAs incorporated into lipid-donors are involved in the CL absorption regulation processes through direct or indirect interactions with intestinal cholesterol transporters (NPC1L1 and SR-BI). The data obtained with differentiated human intestinal TC7/Caco-2 cells show, for the first time, that donor size and/or BA per se play a key role in the regulation of intestinal CL absorption through several interactions with CL transporters.

Materials and Methods

Materials

Trypsin–EDTA, nonessential amino acids, antibiotics and cell culture media were obtained from Gibco BRL (Cergy Pontoise, France). Cell culture materials were obtained through Becton Dickinson (Le Pont de Claix, France). Mouse monoclonal IgG raised against the external domain (amino acids 104–294) of human SR-BI, also known as CLA-1, was purchased from BD Transduction Laboratories (Lexington, KY, USA). Polyclonal antibodies to NPC1L1 raised in rabbit against an external domain (amino acids 596–610) were purchased from Abcam (Cambridge, UK). The specificity of NPC1L1 antibodies was checked using blocking peptide (Cayman Chemical, Ann Arbor, MI, USA). [^{3}H]-CL (1.44/TBq/mmol) was purchased from Amersham International (Little Chalfont, UK). Radioactivity was measured by liquid scintillation counting (TRi-Carb 1600 Packard, Meriden, CT, USA) in the presence of Emulsifier Safe for aqueous media or Insta-Fluor Plus for all organic samples obtained through Perkin-Elmer (Waltham, MA, USA).

Measurement of Lipid Donor Size

As an estimate of the size of the lipid particles, the intensity-weighted mean diameter (z-average diameter) and the polydispersity index were determined by photon correlation spectroscopy (Zetasizer Nano ZS, Malvern Instruments, Malvern, UK; 633-nm He–Ne laser) at 25 °C. All measurements were performed with 10-min runs, and results are expressed as mean values of at least three measurements [27].

Cell Culture Conditions

The TC7 cells, a clone of human intestinal cell-line Caco-2, were used between passages 30 and 50 as previously described [28, 29]. Stocks of cells were cultured in Dulbecco's Modified Eagle Medium (DMEM) containing 25 mM glucose, supplemented with 1% nonessential amino acids and 20% heat-inactivated (30 min, 56 °C) fetal calf serum in a 10% CO_2 humidified incubator at 37 °C. When the cells reached 70–80% confluence, monolayers were subcultured at 2.5×10^5 cells in 0.25% trypsin–EDTA (1 mM) on 23.1-mm-diameter PET culture inserts (1 μm pore size). The inserts were fitted into six-well culture plates with 1 ml apical and 2 ml basolateral culture medium. The experiments were performed on day 21 after plating; i.e., after cells had reached confluence and made a tight monolayer as checked by transepithelial electrical resistance.

Absorption Measurement

CL donors at a final concentration of 2 mM phosphatidylcholine, 0.03 mM monoacylglycerol, 0.5 mM oleic acid sodium salt, 0.1 mM CL and traces of [^{3}H]-CL were obtained with 2, 3, 4, 5, 6 and 8 mM taurocholic acid (TCA). TCA-free CL donors were also prepared; one part was used without treatment (0) and the other part was sonicated for 10 min at 4 dB (0s) (Sonifier 250, Branson, Danbury, CT, USA). CL donors were added to the apical side and cells were incubated for 3 h at 37 °C, as previously published [28]. At the end of the experiment, the radioactivities of the basolateral and apical media were measured. Cell CL was extracted using hexane/isopropanol (3/2 V/V). Cell proteins were extracted using a membrane protein extraction kit (Pierce, Rockford, IL, USA) and quantified (BCA kit from Pierce). When necessary, before CL donor addition, cells were incubated for 2 min with antibodies diluted in DMEM (8 µg/ml anti-SR-BI, 5 µg/ml anti-NPC1L1).

Western Blot Analysis

Cell proteins were denatured in sample buffer containing SDS and *β*-mercaptoethanol, separated by 10% SDS-PAGE (10% acrylamide gels), and electroblotted onto nitrocellulose membranes (Pierce). Nonspecific binding sites were blocked using 5% non-fat dried milk followed by overnight incubation at 4 °C with primary antibodies directed against NPC1L1 (1/200) or SR-BI (1/2,000). After washing, the membranes were incubated with peroxidase-labeled antibody raised against rabbit IgG (NPC1L1 detection) or mouse IgG (SR-BI). Blots were developed by chemiluminescence detection for NPC1L1 and SR-BI (Pierce). Loading controls were performed on the same membrane with GAPDH or *β*-actin. Apparent molecular mass was determined using standards (Fermentas, Vilnius, Lithuania). Protein expression levels were quantified using a Bio-1D++ gel image analysis system (Vilber-Lourmat, Marne la Vallée, France).

RNA Isolation, Reverse Transcription, and Real-Time PCR

Total RNA was isolated from incubated cells using TRIzol reagent (Invitrogen, Carlsbad, CA, USA). One microgram of each RNA was reverse-transcribed by random priming, using MMLV enzyme (Invitrogen, Carlsbad, CA, USA). Five microliters of each cDNA, from a final reaction volume of 100 µl, were used for real-time PCR, which was performed on Mx3005P (Stratagene, La Jolla, CA, USA) using qPCR Mastermix Plus SYBR green I (Eurogentec, Liege Science Park, Belgium). The primers used are listed in Table 1. Constitutively expressed 18S rRNA was measured as an internal standard for sample normalization. Relative mRNA levels were calculated using the comparative threshold cycle ($2^{-\Delta\Delta C_t}$) method [30]. Each PCR was performed in triplicate.

Data Analysis

Results are expressed as mean (±SD) values of nmol CL accumulated into the cell per cellular protein milligram ($n = 3$). Differences between data were explored using one-way analysis of variance (ANOVA) for factorial, nonrepeated values, and using Fischer test, with P values ≤ 0.05 considered significant. SPSS 11.0 software (SPSS Inc., Chicago, IL, USA) was used for statistical analysis.

Results

CL Donor-size and TCA Concentration

Cholesterol donors were prepared in the presence or not of TCA, and their diameter was measured (Table 2). Without TCA, very large particles (1,025 ± 24 nm) were obtained which decreased in size after sonication (46 ± 3 nm). In the presence of increasing TCA concentrations (2–8 mM), chosen within physiological range [20, 31], the CL donor diameter varied from 712 ± 25 to 7 ± 1 nm. At 4 mM TCA, small donors with diameters of <50 nm (vesicles) were found in the medium. Mixed micelles were observed for TCA concentrations ≥ 5 mM. The smallest CL donor (7 ± 1 nm) was obtained with 8 mM TCA. Higher TCA concentrations were not used because of their cellular toxicity.

Regulation of CL Cell Absorption by TCA Concentration and Lipid Donor Size

Because of the heterogeneity of the parental population of Caco-2 cells, the selected experimental model was the TC7 clone of the human intestinal cell-line, which had previously been characterized for cholesterol absorption studies

Table 1 Sequences of oligonucleotides used for real-time PCR

Oligonucleotides	Sequence (5′-3′)
NPC1L1 for	GGCAGACCTCCCAAGTCGA
NPC1L1 rev	ATCCTTGAAGGTGAGCGGG
SR-BI for	CGGCTCGGAGAGCGACTAC
SR-BI rev	GGGCTTATTCTCCATCATCACC
18S for	CGCCGCTAGAGGTGAAATTCT
18S rev	CATTCTTGGCAAATGCTTTCG

Table 2 CL cell uptake from different CL donors

TCA (mM)	Size (nm)	Cell uptake (nmol/mg protein)		
		Control	+anti NPC1L1	+anti SR-BI
0	1,025 ± 24	0.19 ± 0.02	0.17 ± 0.07 (87%)	0.17 ± 0.04 (90%)
0s	46 ± 3	0.81 ± 0.06	0.42 ± 0.01** (51%)	0.59 ± 0.09 (73%)
2	712 ± 25	0.66 ± 0.07	0.45 ± 0.02* (71%)	0.63 ± 0.04 (96%)
3	350 ± 15	1.11 ± 0.04	0.76 ± 0.02* (68%)	0.78 ± 0.02* (70%)
4	47 ± 5	1.74 ± 0.06	0.99 ± 0.13* (57%)	0.93 ± 0.08* (54%)
5	18 ± 2	2.73 ± 0.63	1.22 ± 0.23** (45%)	1.48 ± 0.24** (54%)
6	12 ± 3	3.81 ± 0.35	1.62 ± 0.35** (44%)	2.00 ± 0.16** (53%)
8	7 ± 1	7.37 ± 1.64	4.49 ± 0.74* (61%)	5.28 ± 0.47* (72%)

CL cell uptake was measured after 3 h of incubation of TC7 cells with several CL donors added to the apical medium. The donors were prepared either without TCA (0 and 0s mM) or with TCA. Antibodies directed at SR-BI or NPC1L1 were added or not (control) before incubation with lipid donors. Percentages were determined as compared to the respective control values, $*P < 0.05$, $** P < 0.01$

[29]. When the TCA concentration was increased (from 2 to 8 mM; Fig. 1a; Table 2), CL cell absorption was markedly enhanced (×11). The intercept on the x-axis of the extrapolated line obtained for high absorption values gave a TCA concentration of 3.9 mM.

Cholesterol cell absorption increased as the lipid donor size decreased (Fig. 1b), and exhibited two different processes. The first one ($R^2 = 0.998$), observed with large donors and vesicles (1,025−47 nm), was particularly slow and exhibited a low transport capacity. CL cell absorption was increased ninefold when vesicles (47 ± 5 nm) were compared to large particles (1,025 ± 24 nm). The second one ($R^2 = 0.882$), only observed with micelle donors (18−7 nm), was much more efficient. Indeed, CL cell absorption was increased 38-fold using mixed micelles (7 ± 1 nm) as compared to large particles (1,025 ± 24 nm). The calculated maximal donor diameter promoting efficient cell absorption was 23.49 ± 0.27 nm, which fitted with the mixed micelle size [5]. To test the role of BA in these processes, TCA-free donors were prepared. Using the small TCA-free donors, the CL cell absorption was increased (×4) compared to when the large ones were used (Table 2). Thus, the donor size is an important factor per se in the regulation of CL absorption by BA, but other regulations can take place.

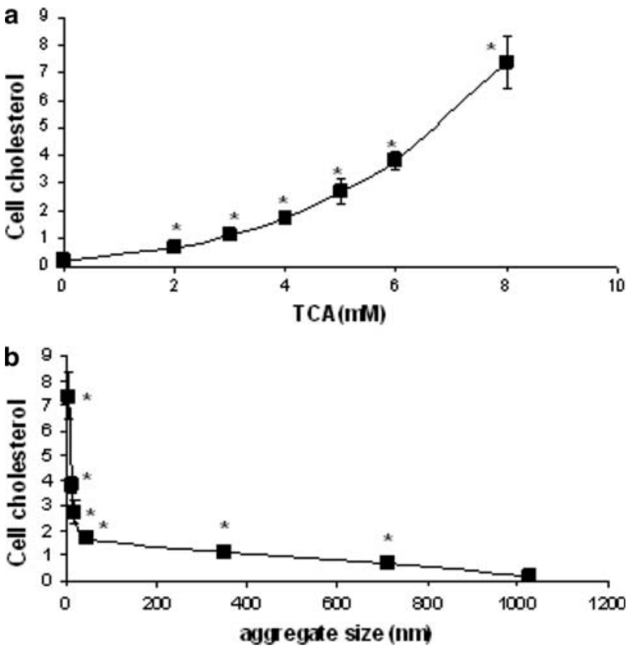

Fig. 1 Effects of TCA concentration (**a**) and CL donor size (**b**) on CL cell absorption (nmol/mg). Results are expressed as mean ± SD ($n = 3$), $*P < 0.05$

Contribution of NPC1L1 and SR-BI to CL Absorption Processes

To quantify the involvement of the main intestinal CL transporters in the absorption processes from each lipid donor, cell absorption was measured in the presence or not (control) of specific antibodies directed at NPC1L1 and SR-BI, added to the apical medium (Table 2). These antibodies were inefficient at modulating the CL cell absorption from large donors (1,025 ± 24 nm), but they significantly reduced CL cell absorption from small donors. The inhibitory effect of anti-NPC1L1 and anti-SR-BI abruptly increased in the presence of very small donors (≤45 nm), i.e., from 4mM TCA. The most important effect was observed in the presence of mixed micelles (56% NPC1L1 inhibition, 47% SR-BI inhibition) at 6 mM TCA. For the smallest CL donor used (7 ± 1 nm), the inhibitory effects of antibodies were reduced, so a saturation process was observed. Using lipid donors of comparable sizes obtained with or without TCA (47 and 46 nm, respectively), similar reductions (43–49 for NPC1L1 and 46–27% for SR-BI, respectively) were observed in both cases. Thus, the presence of BA is not essential for the interactions between lipid donors and intestinal transporters. These data confirm that BA regulation takes place at the brush-border membrane, where intestinal cholesterol transporters are mainly localized.

NPC1L1 and SR-BI Protein Expression Levels

NPC1L1 and SR-BI protein levels were quantified in TC7 cells after incubation with different CL donors. NPC1L1 protein level increased in a dose-dependent manner with TCA concentrations (Fig. 2a). A fivefold increase in NPC1L1 protein level (7.03 ± 0.76 vs. 1.49 ± 0.13 relative levels) was observed after cell incubation in the presence of donors prepared with (8 mM) or without (0 mM) TCA, respectively. Comparable protein expression level was obtained using TCA-free particles with either very large or small diameters. Thus, the mixed micelle size is not involved in this regulation path; TCA is efficient per se. Conversely, the SR-BI protein level was unchanged, whatever the experimental conditions (Fig. 2b). TCA was not able to modulate its expression level, but post-transcriptional regulations which regulate the transporter activity and/or its turnover may take place.

Regulation of SR-BI and NPC1L1 Gene Expression by Bile Salts

To confirm the ability of BA to up-regulate the NPC1L1 expression at mRNA level, we treated TC7 cells with TCA or deoxycholic acid (DCA) for 3 h. Both treatments induced a significant increase in the NPC1L1 mRNA level (Fig. 3a), but were inefficient at modulating SR-B1 transcription levels (Fig. 3b). It is worth noting that the well-known FXR target gene small heterodimer partner (SHP) was also up-regulated by this BA treatment (data not shown).

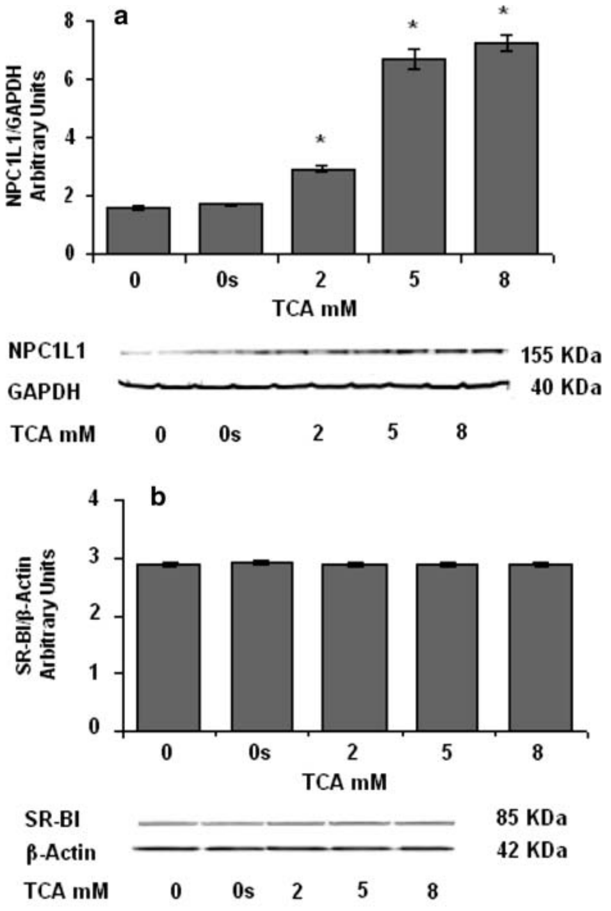

Fig. 2 Effects of TCA concentration on NPC1L1 (**a**) and SR-BI (**b**) protein expression levels in TC7 cells. Two different TCA-free lipid donors were used, one with large (0) and one with small diameters obtained after sonication (0s). Expression levels were corrected to GAPDH for NPC1L1 and to β-actin for SR-BI. Results are expressed as the mean ± SD ($n = 3$), *$P < 0.05$

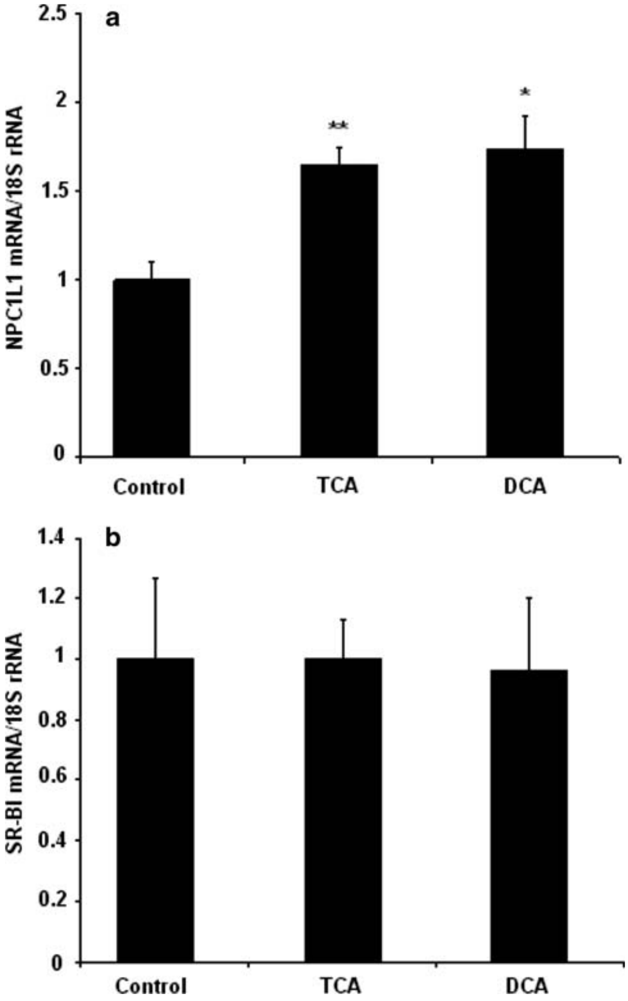

Fig. 3 Effect of BA on NPC1L1 (**a**) and SR-BI (**b**) mRNA expression levels in TC7 cells. Differentiated cells were incubated in the presence of 100 μM TCA or 100 μM DCA added to the apical medium. NPC1L1 and SR-BI expression were evaluated by quantitative RT-PCR and corrected with 18S rRNA gene expression. Results are expressed as mean ± SD ($n = 3$), *$P < 0.05$,**$P < 0.01$

Discussion

After a meal, dietary and biliary CL are present in the human intestinal content in the form of a complex mixture of emulsified droplets, vesicles, mixed micelles as well as precipitated material [20, 21]. Different CL transporters located at the enterocyte brush-border have recently been identified [10, 32], which has raised the key issue of possible interactions between components of CL donors and intestinal transporters with regard to CL absorption.

First, we observed that CL donor size is one determinant of CL cell transport. Indeed, the CL cell transport was increased fourfold after a marked size reduction (from 1,025 to 46 nm) of BA-free lipid donors (Table 2). Moreover, when lipid donors with increased TCA concentrations were dispersed, the CL donor size decreased and CL transport increased in a dose-dependent manner up to 38-fold (Table 2), exhibiting a negative relationship (Fig. 1b). Such a correlation is in agreement with a recent in vivo study showing that cholic acid supplementation enhances CL absorption in humans [33], and this has already been suggested by an in vitro study indicating that CL transfer from TCA micelles is faster than from other donor particles not containing bile salts [34]. Two different absorption processes were observed (Fig. 1b). With very large donors, a poorly efficient absorption process independent of NPC1L1 or SR-BI transporters takes place. It is likely a passive process [35]. In contrast, with small donors (mixed micelles), NPC1L1 and SR-BI contribute to a very efficient CL cell uptake. The minimum TCA concentration enabling efficient CL absorption (i.e., 3.9 mM) was comparable to the critical micellar concentration of TCA (around 4 mM) in such conditions. Indeed, when the BA concentration exceeds the critical micellar concentration, as occurs in vivo [20, 31], mixed micelles formed from vesicles made of amphipathic lipids and CL, leading to small-size donors (7–12 nm). This clearly means that efficient intestinal CL absorption requires both mixed micelles and intestinal CL transporters. The main reason for this is that enterocytes have an apical brush-border membrane made of many microvilli where the CL transporters (NPC1L1 and SR-BI) are present in Caco-2 cells [1, 10, 11]. The space between the microvilli ranges from 5 to 20 nm. To optimally access this space, CL donors should likely not be larger than it; indeed, we found in this work that the maximum donor size for efficient CL absorption is about 23 nm.

However, for a lipid donor size of the same order of magnitude (46 or 47 nm), the addition of TCA enhanced CL cell absorption twofold (Table 2). In addition, BA (TCA or DCA) up-regulated the NPC1L1 mRNA and protein levels (Figs. 2, 3). Thus, for the first time, we demonstrated that BAs also regulate intestinal CL absorption by activating an intracellular pathway, leading to an increase in the NPC1L1 protein level. Such a regulation of NPC1L1 by BA has already been suggested, with five days of dietary cholic acid supplementation increasing CL absorption in NPC1L1 (+/+) mice, but not in NPC1L1 (−/−) mice [7]. The presence of such an intracellular regulation explains why CL absorption was enhanced by increasing the BA level in mixed micelles [10]. It also indicates that the effects of BA on CL absorption are not solely due to their detergent capacity, in line with some previous experiments [24–26]. The molecular regulations induced by BA are unknown, but BAs are activating ligands of the farnesoid X receptor, a nuclear receptor with established roles in BA and lipid metabolisms [36]. After stimulating this nuclear receptor expression, intestinal CL transport was altered as well as the expression level of ABC family transporters [37]. The hypothesis that farnesoid X receptor is involved in the intracellular path induced by BA to up-regulate the NPC1L1 expression levels is currently under investigation. Surprisingly, SR-BI expression levels were not regulated by BA in this study. However, BAs were unable to regulate SR-BI expression levels in the rat model [38], whereas a reduction of the SR-BI protein levels was observed in mice with altered bile delivery and impaired CL absorption [39]. Experimental conditions may explain these differences, since only acute regulations could be observed in the present study (cells were incubated for just 3 h for sustained viability).

In conclusion, CL solubilized in mixed micelles can access the brush-border membrane transporters more easily, and is thus efficiently absorbed. In addition, BA absorbed by the enterocyte can elicit per se an intracellular signaling pathway which increases the expression of the main intestinal CL transporter, NPC1L1. Thus intestinal CL absorption is regulated by both the size and the components of the mixed micelles. In this context, these data confirm that the physicochemical environment of the lumen plays a major role in CL absorption efficiency. This can account, at least in a large part, for the important inter-individual variations observed in the rate of CL intestinal absorption.

Acknowledgments We thank G. Diraison and Malvern Instruments (Vénissieux, France) for technical assistance. We thank L. Cara for his helpful comments about the preparation of the experiment.

References

1. Sane AT, Sinnett D, Delvin E, Bendayan M, Marcil V, Menard D, Beaulieu JF, Levy E (2006) Localization and role of NPC1L1 in cholesterol absorption in human intestine. J Lipid Res 47:2112–2120
2. Bietrix F, Yan D, Nauze M, Rolland C, Bertrand-Michel J, Comera C, Schaak S, Barbaras R, Groen AK, Perret B, Terce F, Collet X (2006) Accelerated lipid absorption in mice overexpressing intestinal SR-BI. J Biol Chem 281:7214–7219

3. Reboul E, Abou L, Mikail C, Ghiringhelli O, Andre M, Portugal H, Jourdheuil-Rahmani D, Amiot MJ, Lairon D, Borel P (2005) Lutein transport by Caco-2 TC-7 cells occurs partly by a facilitated process involving the scavenger receptor class B type I (SR-BI). Biochem J 387:455–461
4. Hauser H, Dyer JH, Nandy A, Vega MA, Werder M, Bieliauskaite E, Weber FE, Compassi S, Gemperli A, Boffelli D, Wehrli E, Schulthess G, Phillips MC (1998) Identification of a receptor mediating absorption of dietary cholesterol in the intestine. Biochemistry 37:17843–17850
5. Davies JP, Scott C, Oishi K, Liapis A, Ioannou YA (2005) Inactivation of NPC1L1 causes multiple lipid transport defects and protects against diet-induced hypercholesterolemia. J Biol Chem 280:12710–12720
6. Davis HR Jr, Zhu LJ, Hoos LM, Tetzloff G, Maguire M, Liu J, Yao X, Iyer SP, Lam MH, Lund EG, Detmers PA, Graziano MP, Altmann SW (2004) Niemann-Pick C1 Like 1 (NPC1L1) is the intestinal phytosterol and cholesterol transporter and a key modulator of whole-body cholesterol homeostasis. J Biol Chem 279:33586–33592
7. Altmann SW, Davis HR Jr, Zhu LJ, Yao X, Hoos LM, Tetzloff G, Iyer SP, Maguire M, Golovko A, Zeng M, Wang L, Murgolo N, Graziano MP (2004) Niemann-Pick C1 Like 1 protein is critical for intestinal cholesterol absorption. Science 303:1201–1204
8. Labonte ED, Howles PN, Granholm NA, Rojas JC, Davies JP, Ioannou YA, Hui DY (2007) Class B type I scavenger receptor is responsible for the high affinity cholesterol binding activity of intestinal brush border membrane vesicles. Biochim Biophys Acta 1771:1132–1139
9. Iyer SP, Yao X, Crona JH, Hoos LM, Tetzloff G, Davis HR Jr, Graziano MP, Altmann SW (2005) Characterization of the putative native and recombinant rat sterol transporter Niemann-Pick C1 Like 1 (NPC1L1) protein. Biochim Biophys Acta 1722:282–292
10. Yamanashi Y, Takada T, Suzuki H (2007) Niemann-Pick C1-like 1 overexpression facilitates ezetimibe-sensitive cholesterol and beta-sitosterol uptake in CaCo-2 cells. J Pharmacol Exp Ther 320:559–564
11. Mathur SN, Watt KR, Field FJ (2007) Regulation of intestinal NPC1L1 expression by dietary fish oil and docosahexaenoic acid. J Lipid Res 48:395–404
12. Knopfel M, Davies JP, Duong PT, Kvaerno L, Carreira EM, Phillips MC, Ioannou YA, Hauser H (2007) Multiple plasma membrane receptors but not NPC1L1 mediate high-affinity, ezetimibe-sensitive cholesterol uptake into the intestinal brush border membrane. Biochim Biophys Acta 1771:1140–1147
13. Field FJ, Watt K, Mathur SN (2007) Ezetimibe interferes with cholesterol trafficking from the plasma membrane to the endoplasmic reticulum in CaCo-2 cells. J Lipid Res 48:1735–1745
14. Yu L, Bharadwaj S, Brown JM, Ma Y, Du W, Davis MA, Michaely P, Liu P, Willingham MC, Rudel LL (2006) Cholesterol-regulated translocation of NPC1L1 to the cell surface facilitates free cholesterol uptake. J Biol Chem 281:6616–6624
15. Duan LP, Wang HH, Wang DQ (2004) Cholesterol absorption is mainly regulated by the jejunal and ileal ATP-binding cassette sterol efflux transporters Abcg5 and Abcg8 in mice. J Lipid Res 45:1312–1323
16. Lee MH, Lu K, Hazard S, Yu H, Shulenin S, Hidaka H, Kojima H, Allikmets R, Sakuma N, Pegoraro R, Srivastava AK, Salen G, Dean M, Patel SB (2001) Identification of a gene, ABCG5, important in the regulation of dietary cholesterol absorption. Nat Genet 27:79–83
17. Calpe-Berdiel L, Rotllan N, Palomer X, Ribas V, Blanco-Vaca F, Escola-Gil JC (2005) Direct evidence in vivo of impaired macrophage-specific reverse cholesterol transport in ATP-binding cassette transporter A1-deficient mice. Biochim Biophys Acta 1738:6–9
18. Albrecht C, Simon-Vermot I, Elliott JI, Higgins CF, Johnston DG, Valabhji J (2004) Leukocyte ABCA1 gene expression is associated with fasting glucose concentration in normoglycemic men. Metabolism 53:17–21
19. Mulligan JD, Flowers MT, Tebon A, Bitgood JJ, Wellington C, Hayden MR, Attie AD (2003) ABCA1 is essential for efficient basolateral cholesterol efflux during the absorption of dietary cholesterol in chickens. J Biol Chem 278:13356–13366
20. Armand M, Borel P, Pasquier B, Dubois C, Senft M, Andre M, Peyrot J, Salducci J, Lairon D (1996) Physicochemical characteristics of emulsions during fat digestion in human stomach and duodenum. Am J Physiol 271:G172–G183
21. Hernell O, Staggers JE, Carey MC (1990) Physical-chemical behavior of dietary and biliary lipids during intestinal digestion and absorption. 2. Phase analysis and aggregation states of luminal lipids during duodenal fat digestion in healthy adult human beings. Biochemistry 29:2041–2056
22. Woollett LA, Wang Y, Buckley DD, Yao L, Chin S, Granholm N, Jones PJ, Setchell KD, Tso P, Heubi JE (2006) Micellar solubilisation of cholesterol is essential for absorption in humans. Gut 55:197–204
23. Siperstein MD, Chaikoff IL, Reinhardt WO (1952) C14-Cholesterol. V. Obligatory function of bile in intestinal absorption of cholesterol. J Biol Chem 198:111–114
24. Watt SM, Simmonds WJ (1984) Effects of four taurine-conjugated bile acids on mucosal uptake and lymphatic absorption of cholesterol in the rat. J Lipid Res 25:448–455
25. Reynier MO, Montet JC, Crotte C, Marteau C, Gerolami A (1981) Intestinal cholesterol uptake from mixed micelles. In vitro effects of taurocholate, taurochenodeoxycholate and tauroursodeoxycholate. Biochim Biophys Acta 664:616–619
26. Cohen BI, Raicht RF, Mosbach EH (1977) Sterol metabolism studies in the rat. Effects of primary bile acids (sodium taurochenodeoxycholate and sodium taurocholate) on sterol metabolism. J Lipid Res 18:223–231
27. Kaszuba M, Jones MN (1999) Hydrogen peroxide production from reactive liposomes encapsulating enzymes. Biochim Biophys Acta 1419:221–228
28. Play B, Salvini S, Haikal Z, Charbonnier M, Harbis A, Roussel M, Lairon D, Jourdheuil-Rahmani D (2003) Glucose and galactose regulate intestinal absorption of cholesterol. Biochem Biophys Res Commun 310:446–451
29. Salvini S, Charbonnier M, Defoort C, Alquier C, Lairon D (2002) Functional characterization of three clones of the human intestinal Caco-2 cell line for dietary lipid processing. Br J Nutr 87:211–217
30. Livak KJ, Schmittgen TD (2001) Analysis of relative gene expression data using real-time quantitative PCR and the 2(-Delta Delta C(T)) Method. Methods 25:402–408
31. Horter D, Dressman JB (2001) Influence of physicochemical properties on dissolution of drugs in the gastrointestinal tract. Adv Drug Deliv Rev 46:75–87
32. Levy E, Spahis S, Sinnett D, Peretti N, Maupas-Schwalm F, Delvin E, Lambert M, Lavoie MA (2007) Intestinal cholesterol transport proteins: an update and beyond. Curr Opin Lipidol 18:310–318
33. Woollett LA, Buckley DD, Yao L, Jones PJ, Granholm NA, Tolley EA, Tso P, Heubi JE (2004) Cholic acid supplementation enhances cholesterol absorption in humans. Gastroenterology 126:724–731
34. Thurnhofer H, Schnabel J, Betz M, Lipka G, Pidgeon C, Hauser H (1991) Cholesterol-transfer protein located in the intestinal brush-border membrane. Partial purification and characterization. Biochim Biophys Acta 1064:275–286

35. Thurnhofer H, Hauser H (1990) Uptake of cholesterol by small intestinal brush border membrane is protein-mediated. Biochemistry 29:2142–2148
36. Kuipers F, Stroeve JH, Caron S, Staels B (2007) Bile acids, farnesoid X receptor, atherosclerosis and metabolic control. Curr Opin Lipidol 18:289–297
37. Cantafora A, Blotta I, Rivabene R, Pisciotta L, Bertolini S (2003) Evaluation of RNA messengers involved in lipid trafficking of human intestinal cells by reverse-transcription polymerase chain reaction with competimer technology and microchip electrophoresis. Electrophoresis 24:3748–3754
38. Kamisako T, Ogawa H, Yamamoto K (2007) Effect of cholesterol, cholic acid and cholestyramine administration on the intestinal mRNA expressions related to cholesterol and bile acid metabolism in the rat. J Gastroenterol Hepatol 22:1832–1837
39. Voshol PJ, Schwarz M, Rigotti A, Krieger M, Groen AK, Kuipers F (2001) Down-regulation of intestinal scavenger receptor class B, type I (SR-BI) expression in rodents under conditions of deficient bile delivery to the intestine. Biochem J 356:317–325

Lipids (2008) 43:409–417
DOI 10.1007/s11745-008-3155-8

ORIGINAL ARTICLE

Effects of a Single and Short-Term Ingestion of Diacylglycerol on Fat Oxidation in Rats

**Noriko Osaki · Shinichi Meguro · Kouji Onizawa ·
Tomohito Mizuno · Akira Shimotoyodome ·
Tadashi Hase · Ichiro Tokimitsu**

Received: 28 October 2007 / Accepted: 9 January 2008 / Published online: 21 February 2008
© AOCS 2008

Abstract This study examines the effect of diacylglycerol (DAG) oil consisting mainly of 1,3-species on fat oxidation as a possible mechanism for anti-obesity. We examined the following: (1) the long-term (23-week) effects of a DAG oil diet on the development of obesity; (2) the effect of a single ingestion of DAG oil on fat oxidation; and, (3) the short-term (2-week) effect of a DAG oil diet on fat metabolism in rats. Rats fed a DAG oil diet accumulated significantly less body fat compared to rats fed a triacylglycerol (TAG) oil diet, each oil possesses a similar fatty acid composition. More ^{14}C-CO$_2$ was expired and less ^{14}C-radioactivity was incorporated into visceral fat after administration of a tracer emulsion containing 1,3-[oleoyl-1-^{14}C] diolein compared to [carboxyl-^{14}C] triolein. Indirect calorimetry showed respiratory quotients were significantly lower in the DAG oil diet group than in the TAG oil diet group. More ^{14}C-CO$_2$ was expired and less ^{14}C-radioactivity was incorporated into visceral fat in the DAG oil diet group than in the TAG oil diet group after a single intragastric administration of [carboxyl-^{14}C] triolein. These results suggest the following. (1) DAG oil has an inhibitory effect on diet-induced fat accumulation. (2) 1,3-DAG, a major component of DAG oil, is more susceptible to oxidation. (3) A short-term ingestion of DAG oil increases fat utilization at the whole body level and results in increased oxidation of dietary fat. The stimulated fat oxidation might be one explanation for the anti-obesity effect of long-term DAG oil ingestion.

Keywords Anti-obesity · ^{14}C-labeled · Diacylglycerol · 1,3-Diolein · 1(3),2-Diolein · Fat oxidation · Oxygen consumption · Rat · Respiratory quotients · Triolein

Introduction

The metabolic syndrome can be defined as a state of metabolic dysregulation characterized by insulin resistance, obesity, and a predisposition to type 2 diabetes, dyslipidemia, premature atherosclerosis, and other diseases [1–3]. Especially in individuals with abdominal obesity, metabolic syndrome is the result of an imbalance between energy intake and energy expenditure. Therefore, food ingredients affecting energy expenditure may help people manage their weight.

Diacylglycerol (DAG) as a natural component of various edible oils, contains only two esterified fatty acyl chains in contrast to triacylglycerol (TAG). DAG oil is an edible oil containing 80–90% of DAG, approximately 70% of DAG exists as 1,3-DAG, and its energy value is practically the same as ordinary oil containing TAG [4–6]. Results from studies in animals and humans demonstrate that DAG oil has metabolic characteristics distinct from those of TAG oil, although the two have a similar fatty acid composition, and that these characteristics can be beneficial in preventing and managing the accumulation of visceral fat and the postprandial elevations of triacylglycerol in serum and chylomicron [4, 5, 7–15]. Kimura et al. [16] reported that DAG oil infusion in rats led to higher fat oxidation compared with TAG oil, although the two have a similar fatty acid composition. Saito et al. [17] reported that compared with a TAG oil-containing meal, a DAG oil-containing meal tended to produce significantly lower

---

N. Osaki (✉) · S. Meguro · K. Onizawa · T. Mizuno ·
A. Shimotoyodome · T. Hase · I. Tokimitsu
Biological Science Laboratories, Kao Corporation,
2606 Akabane, Ichikaimachi, Haga, Tochigi 321-3497, Japan
e-mail: osaki.noriko@kao.co.jp

postprandial respiratory quotient (RQ) in healthy humans. Kamphuis et al. [18] also reported that consumption of DAG oil in place of TAG oil increased fat oxidation in healthy humans. These previous results indicated that a single ingestion of DAG oil increases fat oxidation, and also indicated that DAG oil might be more easily oxidized than TAG oil. In addition, a short-term ingestion of DAG oil, instead of TAG oil, increased β-oxidation and its related gene expression in either liver or intestine of rodents [9–11, 19]. These results also indicated that a short-term ingestion of DAG oil might increase fat oxidation in the whole body and that might induce the oxidation of dietary fat and/or body fat. Therefore, the aim of this study was to examine the effect of DAG oil ingestion on fat oxidation as a possible mechanism for anti-obesity. This study was composed of three experiments:

1. In Experiment 1, we examined the long-term effects of DAG- and TAG-oil (having similar fatty acid compositions) on the development of obesity in rats.
2. In Experiment 2, we investigated the effect of a single ingestion of DAG oil on fat oxidation using 1(3), 2-[oleoyl-1-^{14}C] diolein (^{14}C-1(3),2-diolein), 1,3-[oleoyl-1-^{14}C] diolein (^{14}C-1,3-diolein) in comparison with [carboxyl-^{14}C] triolein (^{14}C-triolein).
3. In Experiment 3, we studied the effect of short-term (2-week) DAG oil ingestion on fat metabolism in comparison with TAG oil.

Experimental Procedure

Test Oils

DAG oil was prepared by esterifying glycerol with fatty acids from soybean oil and rapeseed oil using the method of Huge-Jensen et al. [20]. TAG oil was prepared by mixing rapeseed oil, safflower oil, and perilla oil. The fatty acid compositions of the TAG and DAG oils, analyzed by gas chromatography, are shown in Table 1. The fatty acid composition of the DAG oil was very similar to that of the TAG oil. The DAG concentration of the DAG oil was 85.8 g/100 g and the ratio of 1(3),2- to 1,3-DAG was 32.5:67.5.

Table 1 Fatty acid compositions of TAG and DAG oils[a]

Fatty acid	TAG	DAG
C16	5.7	3.1
C16:1	0.2	–
C18	2.1	1.2
C18:1	37.9	38.9
C18:2	45.2	47.8
C18:3	7.4	8.0
C20	0.4	0.2
C20:1	0.6	0.5
C22	0.2	0.2
C22:1	0.1	0.1
C24	0.1	–
C24:1	0.1	–

[a] Percentage by weight

Materials

[Carboxyl-^{14}C] Triolein (^{14}C-triolein; Purity: >97%, Specific activity: 3.0–4.4 GBq/mM) was purchased from Perkin Elmer Life Science, Inc (Boston, MA, USA). 1(3),2- [oleoyl-1-^{14}C] Diolein (^{14}C-1(3),2-diolein; Purity: >95%, Specific activity: 629 MBq/mM) and 1,3- [oleoyl-1-^{14}C] diolein (^{14}C-1,3-diolein; Purity: >95%, Specific activity: 492 MBq/mM) were obtained from Daiichi Chemical Co., Ltd. (Tokyo, Japan). Casein, cellulose powder, mineral mixture AIN-76, vitamin mixture AIN-76 (containing choline bitartrate), and α-potato starch were obtained from Oriental Yeast (Tokyo, Japan). Casein sodium, sucrose, lecithin (from egg), and 1 N sodium hydroxide solution were purchased from Wako Pure Chemical Industries, Ltd (Osaka, Japan). Bovine serum albumin, xanthan-gum, and ethanolamine were purchased from Sigma Chemical Co. (St. Louis, MO, USA).

Tracer Emulsion with ^{14}C-Labeled Fat

The tracer emulsion with ^{14}C-labeled fat was prepared in the same manner as in a previous report, with minor modification [21]. The "[^{14}C] TAG emulsion" (w/w) contained ^{14}C-triolein (1.74 kBq/g) in TAG oil (4.61%); the "[^{14}C] 1(3),2-DAG emulsion" (w/w) contained ^{14}C-1(3),2-diolein (1.74 kBq/g) in DAG oil (4.61%), and the "[^{14}C] 1,3-DAG emulsion" (w/w) contained ^{14}C-1,3-diolein (1.74 kBq/g) in DAG oil (4.61%). Each tracer emulsion contained casein sodium (4.61%), sucrose (11.88%), cellulose powder (0.92%), mineral mixture AIN-76 (0.81%), vitamin mixture AIN-76 (0.23%), bovine serum albumin (1.92%), xanthan-gum (0.23%), lecithin (from egg) (0.19%) and distilled water (74.56%), and was prepared through emulsification by sonicater.

Animals and Experimental Design

The animal experiments were performed with the approval of the Ethics Committee for Experimental Animals of the

Kao Corporation. The animals were housed in a temperature- and humidity-controlled environment (22 ± 2°C, 55 ± 10%) under a 12-h light/dark cycle. Male SD rats (7 weeks old) used in Experiments 1 and 3 or 2 were purchased from CLEA Japan (Tokyo, Japan) or Charles River Japan (Kanagawa, Japan), respectively. During the acclimatization periods (7-days), they had free access to a commercial rodent diet CE-2 (CLEA Japan) and to drinking water.

In Experiment 1, we investigated the long-term effects of DAG oil on development of obesity. After acclimatization periods, the rats were divided into three groups ($n = 7$/group). The body weight of each group was approximately equal. Each rat ingested either the low-TAG, TAG, or DAG oil diet for a 23-week period (Table 2). The energy values for each diet were calculated from the macronutrient composition, using values of 16.7, 16.7, 38.9, and 39.6 kJ/g for carbohydrate, protein, DAG and TAG oil, respectively. All rats were allowed access to water and food ad libitum. Food intake was recorded every 3 or 4 days. A week before the final day of Experiment 1, the amounts of food consumed and of feces in a 48-h period were measured and fat contents of the diets and of the feces were extracted according to the method used by Jeejeebhoy et al. [22]. Calculation of fat digestibility was based on the fat contents of diets and of feces. On the final day of Experiment 1, a blood sample was collected via the abdominal aorta from the anaesthetized rats under non-fasting conditions between 9 and 11 am. The fat pads were then dissected from each rat, and the weight of visceral fat (retroperitoneal, epididymal, mesenteric, and perirenal fats), and inguinal fat were determined. Serum triacylglycerol, total cholesterol, and glucose concentrations were determined using the following enzyme assay kits, respectively: L-type Wako TG-H; L-type Wako CHO-H; and L-type Glu2 (all from Wako, Osaka, Japan). Serum insulin and leptin were measured using rat insulin and leptin enzyme immunoassay (EIA) kits (both from Morinaga, Yokohama, Japan) according to the manufacturer's instructions.

Table 2 Composition of the diets

Ingredient	Dietary group(g/100 g diet)		
	Low-TAG	TAG	DAG
TAG oil	5.0	20.0	–
DAG oil	–	–	20.0
α-Potato starch	66.5	41.5	41.5
Sucrose	–	10.0	10.0
Casein	20.0	20.0	20.0
Cellulose	4.0	4.0	4.0
Mineral mix[a]	3.5	3.5	3.5
Vitamin mix[b]	1.0	1.0	1.0

[a] AIN-76 prescription

[b] AIN-76 prescription + choline bitartrate (20 g/100 g)

In Experiment 2, we compared ^{14}C-1,3-diolein (Exp.2–1) and ^{14}C-1(3),2-diolein (Exp.2–2) with ^{14}C-triolein in fat oxidation. After acclimatization periods on the commercial rodent diet (CE-2), the rats were divided into two groups: Exp.2–1 ([^{14}C] 1,3-DAG group versus [^{14}C] TAG group, ($n = 12$/group)), and Exp.2–2 ([^{14}C] 1(3),2-DAG group versus [^{14}C] TAG group, ($n = 12$/group)). The body weight of each group was approximately equal (Exp.2–1: [^{14}C] 1,3-DAG group and [^{14}C] TAG group = 293.4 ± 2.5 g and 294.7 ± 2.6 g, Exp.2–2: [^{14}C] 1(3),2-DAG group and [^{14}C] TAG group = 303.6 ± 4.0 g and 306.0 ± 3.5 g). After intragastric administration of each tracer emulsion (7.23 g; 12.33 kBq/kg rat body weight of "[^{14}C] TAG emulsion", "[^{14}C] 1(3),2-DAG emulsion", or "[^{14}C] 1,3-DAG emulsion"), rats were placed in individual, airtight metabolic cages (Sugiyama-gen, Tokyo, Japan) and maintained for 22 h at 22 ± 2°C. Air was drawn through the cages at 300 mL/min. The air entering the cage was first passed through 1 N sodium hydroxide solution to remove atmospheric carbon dioxide and then passed through silica gel blue (Wako Pure Chemical Industries, Ltd) to remove water vapor. The gas expired by the rats was trapped in a trough gas collection chamber containing 50% ethanolamine solution (300 mL). A 1-mL aliquot of the expired ^{14}C-CO$_2$ was collected at 2, 4, 6, 8, 10, and 22 h after administration of each tracer emulsion. At 22 h after administration of each tracer emulsion, the rats were euthanized and blood, liver, and white adipose tissues as visceral fat (mesenteric, epididymal, perirenal and retroperitoneal) were collected for radioactivity measurement.

In Experiment 3, we investigated the effects of short-term ingestion of DAG oil on fat oxidation in the whole body (Exp.3–1) and on ^{14}C-triolein oxidation as dietary fat (Exp.3–2), in comparison with TAG oil.

In Exp.3–1, after acclimatization periods, the rats were divided into two groups ($n = 7$/group). The body weight of each group was approximately equal. Each rat ingested either a TAG or a DAG oil diet for 2 weeks (Table 2). All rats were allowed access to water and food ad libitum. After the 2-week ingestion of each diet, the respiratory metabolic performance of each rat was measured using an indirect calorimetric system. (Oxymax Respirometer system v5.61, Columbus Instruments, Columbus, OH, USA). In the respiration chamber, each rat was allowed access to water and each diet ad libitum. Each metabolic chamber had a 5 L. Air flow through the chambers, and expired airflow from the chambers was adjusted to 2.0 L/min and 1.0 L/min, respectively. Oxygen consumption (VO$_2$), carbon dioxide exhaustion, and spontaneous motor activity were measured and recorded, from 5 pm on the first day until 4 pm of the second day, every 10 min for the 23-h period, and then the average values of each hour-period were determined. The RQ value was calculated using an Oxymax respirometer system and the following formula: RQ = carbon dioxide exhaustion/oxygen consumption. The spontaneous motor activity of each rat was examined with SCANET SV-10 (Toyo Sangyo Co., Ltd., Toyama, Japan). The fat oxidation value was calculated using the method of Ishihara et al. [23]. The motor activity was assessed as a single count when the animal moved from one region of the measurement area, which was optically divided by multiple lenses, to a neighboring region.

In Exp.3–2, after acclimatization periods, the rats were divided into two groups ($n = 8$/group). The body weight of each group was approximately equal. Each rat ingested either a TAG or a DAG oil diet for 2 weeks (Table 2). All rats were allowed access to water and food ad libitum. After a 2-week ingestion of each diet, each rat was intragastrically given a "[^{14}C] TAG emulsion", then was placed in an individual airtight metabolic cage and maintained for 22-hour with collection of aliquots for trapping of (^{14}C-CO_2) in the same manner as Experiment 2. At 22-hour after administration of the [^{14}C] TAG emulsion, the rats were euthanized and blood, liver, and white adipose tissues as visceral fat were collected for radioactivity measurement, as in Experiment 2.

Radioactivity Measurements

Liver and white adipose tissue samples were weighed and then homogenized in a Polytron homogenizer (Glen Mills Inc., Clifton, NJ, USA). A 250-mg aliquot of homogenate was treated with 1 mL Solvable (Perkin Elmer Life Science, Inc) for 2 h at 50°C and with 200 µL of 30% hydrogen peroxide for 30 min at 50 °C. A 100-µL aliquot of blood sample was treated with 0.5 mL Solvable and 300 µL of 30% hydrogen peroxide. Radioactivity in each aliquot was quantitated by liquid scintillation analyzer (Tri-Carb 2550 TR/LL, Packard Instrument Company, Meriden, CT, USA).

Statistical Analyses

The data are presented as the mean ± SEM. Statistical differences were determined using a student *t*-test or Fisher's protected least significant difference test. A repeated measures ANOVA was used to investigate changes in energy expenditure and expired ^{14}C-CO_2 levels. A statistical model was constructed using the effects of treatment, time and interaction of treatment × time. In all analysis, significance was defined as $P < 0.05$. These statistical calculations were performed with Stat View for Windows, version 5.0 (SAS Institute, Cary, NC, USA).

Results

Experiment 1: Effect of Long-Term Ingestion of DAG Oil on Development of Obesity

Consistent with earlier reports [7–11], ingestion of a DAG oil diet significantly reduced body fat accumulation compared with a TAG oil diet in rats.

The TAG oil diet (a high-TAG oil diet) significantly increased body weight and fat pads weight compared with a low-TAG oil diet. On the other hand, rats fed a DAG oil diet accumulated less total visceral, retroperitoneal and inguinal fat weight by 21, 32, and 27%, respectively, as compared with a TAG oil diet (Table 3). No significant difference was observed in the average energy intake and fat digestibility between the TAG and the DAG oil diet groups (Table 3), suggesting that reduced body fat

Table 3 Body weight, energy intake, body fat weight, and digestibility

	Dietary group		
	Low-TAG	TAG	DAG
Initial body weight (g)	250.9 ± 4.5	252.8 ± 3.5	252.7 ± 2.8
Final body weight (g)	642.7 ± 17.4^{a}	725.5 ± 31.1^{b}	663.8 ± 20.3^{ab}
Energy intake (kJ/rat/day)	366.3 ± 2.9^{a}	381.6 ± 3.7^{b}	370.9 ± 3.4^{ab}
Visceral fat weight			
Total visceral fat (g)	58.4 ± 5.0^{a}	84.2 ± 7.0^{b}	66.8 ± 4.3^{a}
Retroperitoneal fat (g)	20.6 ± 2.5^{a}	30.7 ± 3.5^{b}	20.8 ± 0.7^{a}
Epididymal fat (g)	16.3 ± 1.2^{a}	22.7 ± 1.6^{b}	20.6 ± 1.9^{ab}
Mesenteric fat (g)	15.0 ± 1.4^{a}	23.6 ± 2.0^{b}	19.1 ± 1.6^{ab}
Perirenal fat (g)	6.5 ± 0.9^{a}	7.2 ± 0.4^{b}	6.4 ± 0.5^{ab}
Inguinal fat (g)	14.2 ± 1.2^{a}	22.2 ± 2.3^{b}	16.3 ± 1.2^{a}
Fat digestibility (%)	82.9 ± 0.9^{a}	94.9 ± 0.1^{b}	95.4 ± 0.2^{b}

Exp.1: Rats were euthanized after a 23-week ingestion of the respective diets, and the body fat weight was determined. Food intake was measured throughout the study. Values are mean ± SEM ($n = 7$); those with different letters are significantly different by Fisher's PLSD, $P < 0.05$

accumulation in the DAG oil diet group was not related to reduced energy intake. No significant difference was observed in non-fasting serum parameters between the TAG and the DAG oil diet groups, whereas non-fasting leptin level was significantly higher in the TAG oil diet group than the low-TAG oil diet group (Table 4).

Experiment 2: Comparison of Oxidation in ^{14}C-1,3-Diolein (Exp.2–1) and ^{14}C-1(3),2-Diolein (Exp.2–2) with ^{14}C-Triolein

We investigated the effects of DAG isomers, 1,3-DAG and 1(3),2-DAG, in comparison with TAG, on fat oxidation and incorporation of dietary fat into visceral fat, liver, and blood using ^{14}C-1,3-diolein, ^{14}C-1(3),2-diolein, and ^{14}C-triolein. The expired ^{14}C-CO_2 is shown in Fig. 1. The expired ^{14}C-CO_2 in the rats administered the [^{14}C] 1,3-DAG emulsion (^{14}C-1,3-diolein) was increased compared with the [^{14}C] TAG emulsion (^{14}C-triolein) (Exp.2–1; Fig. 1a). In contrast, the expired ^{14}C-CO_2 in the rats administered the [^{14}C] 1(3),2-DAG emulsion (^{14}C-1(3),2-diolein) was equal to the [^{14}C] TAG emulsion (^{14}C-triolein) (Exp.2–2; Fig. 1b). Table 5 shows the ^{14}C contents in visceral fat, liver and blood at 22 h after administration of each tracer emulsion. The ^{14}C content in visceral fat after [^{14}C] 1,3-DAG emulsion administration was significantly less compared to [^{14}C] TAG emulsion (Exp.2–1). In contrast, incorporation of ^{14}C radioactivity into visceral fat was similar between [^{14}C] 1(3),2-DAG and [^{14}C] TAG emulsion (Exp.2–2). The ^{14}C contents in liver and blood did not differ between the groups (Exp.2–1 and Exp.2–2).

Table 4 Serum analysis

	Dietary group		
	Low-TAG	TAG	DAG
Triacylglycerol (mg/dl)	212.2 ± 39.2	159.0 ± 21.9	139.5 ± 21.7
Total cholesterol (mg/dl)	104.8 ± 7.4	93.1 ± 6.7	93.4 ± 4.6
Glucose (mg/dl)	193.5 ± 7.8	188.7 ± 4.1	190.3 ± 7.9
Insulin (ng/ml)	4.1 ± 0.9	3.9 ± 0.4	3.7 ± 0.3
Leptin (ng/ml)	18.4 ± 1.7^a	24.1 ± 1.9^b	20.1 ± 1.5^{ab}

Exp.1: Blood was collected from anesthetized rats under non-fasting conditions. Values are mean ± SEM ($n = 7$); those with different letters are significantly different by Fisher's PLSD, $P < 0.05$

Experiment 3: Effect of Short-Term Ingestion of DAG Oil on Fat Oxidation

Exp.3–1: Fat Oxidation at a Whole Body Level

Body weight at 2 weeks after ingestion of TAG and DAG oil diets were 360.7 ± 5.3 and 361.8 ± 3.9 g, and energy intakes at 2 weeks were 407.2 ± 9.4 and 405.9 ± 4.0 kJ/rat/day, respectively, with no significant differences between the groups. VO_2, RQ, fat oxidation, and spontaneous motor activity for the 23-h feeding period in the respiration chamber (with access to water and each diet ad libitum) are shown in Fig. 2. Energy intake for 23 h of the TAG and the DAG oil diets were 267.0 ± 15.3 and 231.7 ± 25.7 kJ/rat, respectively, with no significant

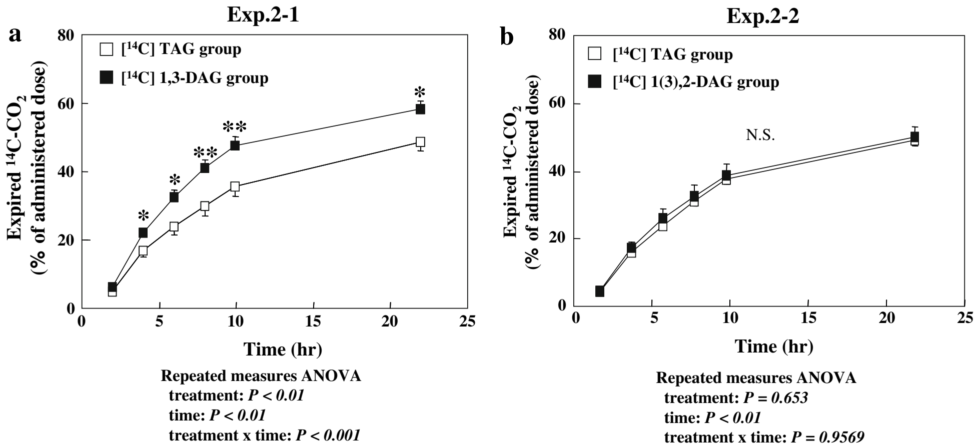

Fig. 1 a The expired ^{14}C-CO_2 in the rats that ingested the commercial rodent diet (CE-2) and received a [^{14}C] 1,3-DAG emulsion compared with a [^{14}C] TAG emulsion in Exp.2–1. *Open squares* represent the [^{14}C] TAG group and *closed squares* represent the [^{14}C] 1,3-DAG group. **b** The expired ^{14}C-CO_2 in the rats that received a [^{14}C] 1(3),2-DAG emulsion compared with a [^{14}C] TAG emulsion in Exp.2–2. *Open squares* represent the [^{14}C] TAG group and *closed squares* represent the [^{14}C] 1(3),2-DAG group. Values are expressed as mean ± SEM ($n = 12$). A symbol at each time point indicates a significant difference between the groups by Student's *t*-test: $^*P < 0.05$, $^{**}P < 0.01$. Significant differences by repeated measures ANOVA are shown under the graphs

Table 5 [^{14}C] contents (% of administered dose) in visceral fat, liver, blood and expired CO_2

	Exp.2–1		Exp.2–2	
	[^{14}C] 1,3-DAG group	[^{14}C] TAG group	[^{14}C] 1(3),2-DAG group	[^{14}C] TAG group
Visceral fat				
Epididymal	2.81 ± 0.38*	4.05 ± 0.42	3.72 ± 0.50	3.63 ± 0.41
Mesenteric	1.34 ± 0.23*	2.33 ± 0.34	1.90 ± 0.30	1.78 ± 0.18
Perirenal	0.44 ± 0.07*	0.70 ± 0.07	0.65 ± 0.10	0.58 ± 0.05
Retroperitoneal	1.32 ± 0.26*	2.20 ± 0.30	1.93 ± 0.33	2.11 ± 0.20
Total	5.91 ± 0.90*	9.28 ± 1.07	8.19 ± 1.18	8.10 ± 0.74
Liver	1.46 ± 0.08	1.53 ± 0.10	1.43 ± 0.09	1.71 ± 0.16
Blood	0.49 ± 0.02	0.48 ± 0.02	0.39 ± 0.03	0.37 ± 0.03
Expired CO_2	58.31 ± 2.40*	48.60 ± 2.62	50.18 ± 3.09	49.31 ± 1.50

Exp.2–1: Rats that ingested the commercial rodent diet (CE-2) were administered either the [^{14}C] 1,3-DAG emulsion or the [^{14}C] TAG emulsion. Exp.2–2: Rats that ingested the commercial rodent diet (CE-2) were administered either the [^{14}C] 1(3),2-DAG emulsion or the [^{14}C] TAG emulsion. At 22-h after administration of each tracer emulsion, the rats were euthanized and blood, liver, and white adipose tissues were collected for radioactivity measurement. The expired $^{14}C-CO_2$ was collected at 2, 4, 6, 8, 10, and 22 h after administration of each tracer emulsion. Values are mean ± SEM ($n = 12$).

* Significantly different from the [^{14}C] TAG group, $P < 0.05$

difference between the groups. VO_2 and spontaneous motor activity values were equal between the groups. RQ values in the DAG oil diet group were lower than in the TAG oil diet group. Fat oxidation measurements in the DAG oil diet group at 2, 3, and 9 am were higher than in the TAG oil diet group.

Exp.3–2: ^{14}C-Labeled Dietary Fat Oxidation

Body weight at 2 weeks after ingestion of the TAG and the DAG oil diets were 377.1 ± 9.7 and 370.3 ± 7.2 g, and energy intakes at 2 weeks were 362.9 ± 15.9 and 362.9 ± 15.7 kJ/rat/day, respectively, with no significant differences between the groups. The expired $^{14}C-CO_2$ after intragastric administration of [^{14}C] TAG emulsion was significantly higher in the DAG oil diet group compared to the TAG oil diet group following a 2-week ingestion of each diet (Fig. 3). The ^{14}C contents in mesenteric, epididymal, and perirenal fat were significantly less in the DAG oil diet group than in the TAG oil diet group (Table 6). In addition, the ^{14}C contents in total visceral fat were less in the DAG oil diet group than in the TAG oil diet group. The ^{14}C contents in liver and blood did not differ between the groups.

Discussion

Consistent with previous reports [7–11], a long-term ingestion of DAG oil significantly reduced body fat accumulation compared with TAG oil, which has a similar fatty acid composition. Also consistent with previous reports, neither energy intake nor fat excretion in feces differed significantly between TAG and DAG oil diets [6, 9], suggesting that reduced body fat accumulation in the DAG oil diet group was not related to reduced energy intake.

Fat balance, calculated as the difference between dietary fat intake and fat oxidation and excretion, has been suggested as a key factor of fat mass regulation [24]. Fat oxidation at the whole-body level must be assessed by indirect calorimetry, whereas dietary fat oxidation is assessed using expired labeled-CO_2 after administration of stable isotope- or isotope-labeled fat. Piers et al. [25] demonstrated using indirect calorimetry that fat oxidation was higher after a single ingestion of a high monounsaturated fat meal compared to a high saturated fat meal. Bessesen et al. [26] reported that the expired $^{14}C-CO_2$ was lower after a single administration of ^{14}C-stearic acid compared to ^{14}C-oleic and linolenic acid. Shimomura et al. [27] reported that the diets high in saturated fat were associated with an increase in body weight. The above studies together suggest that increased fat oxidation may contribute to improvement of obesity.

^{14}C-1,3-DAG-derived ^{14}C-radioactivity was expired more as $^{14}C-CO_2$ and incorporated less into visceral fat compared to ^{14}C-TAG. In contrast, ^{14}C-1(3),2-DAG was metabolized similarly as ^{14}C-TAG. These results suggest that 1,3-DAG, a major component of DAG oil, is more susceptible to oxidation and less accumulated in visceral fat compared to TAG after a single administration.

Several studies demonstrated that a single ingestion of DAG oil affected fat metabolism differentially from TAG oil. Kimura et al. [16] reported that a single administration of DAG oil emulsion decreased RQ values compared with TAG oil emulsion in rats. Kamphuis et al. [18] reported

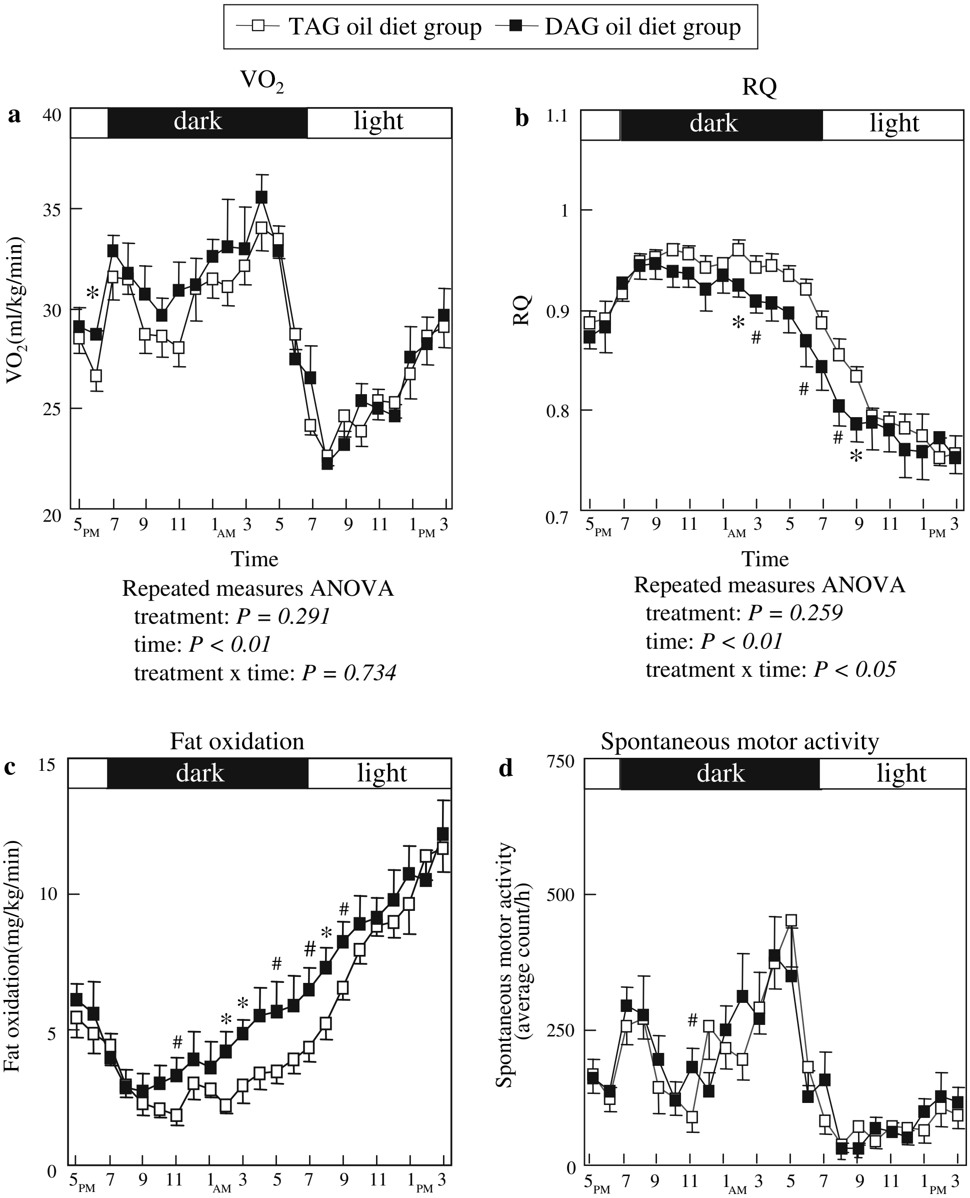

(a) Repeated measures ANOVA
treatment: $P = 0.291$
time: $P < 0.01$
treatment x time: $P = 0.734$

(b) Repeated measures ANOVA
treatment: $P = 0.259$
time: $P < 0.01$
treatment x time: $P < 0.05$

(c) Repeated measures ANOVA
treatment: $P = 0.215$
time: $P < 0.01$
treatment x time: $P = 0.129$

(d) Repeated measures ANOVA
treatment: $P = 0.789$
time: $P < 0.01$
treatment x time: $P = 0.604$

Fig. 2 Changes in VO$_2$ (**a**), RQ (**b**), fat oxidation (**c**), and spontaneous motor activity (**d**) for the 23-h feeding period in a respiration chamber after a 2-week ingestion of either the TAG or DAG oil diet in Exp.3–1. *Open circles* represent the TAG oil diet group and *closed circles* represent the DAG oil diet group. Values are expressed as mean ± SEM ($n = 7$). Differences in values between the groups by Student's *t*-test: #$P < 0.1$, *$P < 0.05$. Significant differences by repeated measures ANOVA are shown under the graphs

that the ingestion of a DAG oil-containing meal increased fat oxidation in humans. Saito et al. [17] also reported that the ingestion of a DAG oil-containing meal decreased RQ values. The higher susceptibility of 1,3-DAG to oxidation found in this study is consistent with the above previous studies.

The present study also demonstrated that the fat oxidation is higher in 1,3-DAG compared with TAG. In contrast, 1(3),2-DAG is oxidized in a similar manner as TAG. The reason 1,3-DAG and TAG are differentially susceptible to oxidation is still unclear. The differential metabolic pathway of each acylglycerol may offer an explanation. Kondo et al. [12] demonstrated that 1,3-diolein was hydrolyzed to 1(3)-monoolein and fatty acids, and triolein was hydrolyzed to 1(3),2-diolein, 2-monoolein and fatty acids through digestion by pancreatic lipase in the small intestine in mice. In addition, 1,3-diolein was less susceptible to enzymatic TAG re-synthesis compared with 1(3),2-diolein. Murase et al. [10] reported that the amount of fatty acid, as digestion products, was higher with DAG oil than with

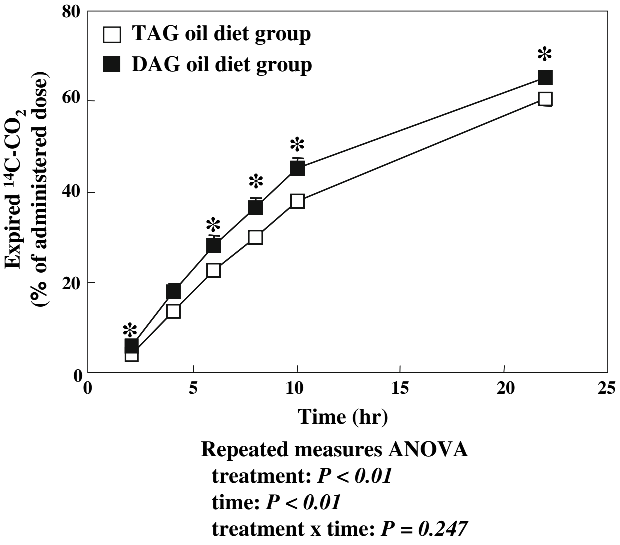

Fig. 3 The expired ^{14}C-CO$_2$ in the rats that received the [^{14}C] TAG emulsion after a 2-week ingestion of the TAG or DAG oil diet in Exp.3–2. *Open squares* represent the TAG oil diet group and *closed squares* represent the DAG oil diet group. Values are expressed as mean ± SEM ($n = 8$). A symbol at each time point indicates a significant difference between the groups by Student's *t*-test. Significant differences by repeated measures ANOVA are shown under the graph

Table 6 [^{14}C] contents (% of administered dose) in visceral fat, liver, blood and expired CO$_2$

	Dietary group	
	TAG	DAG
Visceral fat		
Epididymal	1.05 ± 0.11	0.65 ± 0.08*
Mesenteric	0.78 ± 0.07	0.55 ± 0.05*
Perirenal	0.44 ± 0.04	0.28 ± 0.04*
Retroperitoneal	0.86 ± 0.13	0.53 ± 0.08
Total	3.14 ± 0.30	2.00 ± 0.24*
Liver	3.17 ± 0.13	3.05 ± 0.24
Blood	0.47 ± 0.03	0.47 ± 0.02
Expired CO$_2$	60.73 ± 1.51	65.43 ± 0.94*

Exp.3–2: Rats that ingested TAG oil diet or DAG oil diet for 2 weeks were administered the [^{14}C] TAG emulsion. At 22-hour after administration of [^{14}C] TAG emulsion, the rats were euthanized and blood, liver, and white adipose tissues were collected for radioactivity measurement. The expired ^{14}C-CO$_2$ was collected at 2, 4, 6, 8, 10, and 22 h after administration of [^{14}C] TAG emulsion. Values are mean ± SEM ($n = 8$)

* Significantly different from the TAG diet group, $P < 0.05$

TAG oil in the small intestine of mice. While Nemali et al. [28] reported that the liver, kidney, small intestine, and heart were active organs on β-oxidation. According to these previous reports, decreased TAG re-synthesis and increased fatty acid production in the small intestine may contribute to the increased oxidation of 1,3-DAG. On the other hand, we hypothesized that the oxidation of 1(3),2-DAG was similar to that of TAG because 1(3),2-DAG is a main digestive product of TAG. However, further detailed experiments are required to clarify these speculations.

In Experiment 3, we demonstrated that a short-term ingestion of DAG oil led to increased fat utilization at a whole-body level, increased dietary fat oxidation, and decreased dietary fat incorporation into visceral fat compared with TAG oil. Murata et al. [19] reported that a 2-week ingestion of DAG oil increased β-oxidation activity, its related enzymes activities, and reduced fat synthesis-related enzyme activities in the liver. Murase et al. [10] also observed that a 10-day ingestion of DAG oil increased β-oxidation in the small intestine in mice. These results suggest that a short-term ingestion of DAG oil may activate hepatic and intestinal β-oxidation at the tissue level. In this study, we revealed for the first time that a short-term ingestion of DAG oil stimulates fat metabolism at a whole-body level. In addition, we demonstrated for the first time that a short-term ingestion of DAG oil resulted in a stimulation of dietary fat oxidation.

In conclusion, this study shows the following: (1) DAG oil has an inhibitory effect on diet-induced fat accumulation compared to TAG oil; (2) 1,3-DAG, a major component of DAG oil, is more susceptible to oxidation compared to TAG or 1(3),2-DAG; and, (3) a short-term ingestion of DAG oil increases fat utilization at a whole-body level, and results in increased oxidation of dietary fat compared to TAG oil. The stimulated fat oxidation might be one explanation for the anti-obesity effect of long-term DAG oil ingestion.

References

1. Eckel RH, Grundy SM, Zimmet PZ (2005) The metabolic syndrome. Lancet 365:1415–1428
2. Weiss R, Dziura J, Burgert TS, Tamborlane WV, Taksali SE, Yeckel CW, Allen K, Lopes M, Savoye M, Morrison J, Sherwin RS, Caprio S (2004) Obesity and the metabolic syndrome in children and adolescents. N Engl J Med 350:2362–2374
3. Chew GT, Gan SK, Watts GF (2006) Revisiting the metabolic syndrome. Med J Aust 185:445–449
4. Tada N, Yoshida H (2003) Diacylglycerol on lipid metabolism. Curr Opin Lipidol 14:29–33
5. Tada N (2004) Physiological actions of diacylglycerol outcome. Curr Opin Clin Nutr Metab Care 7:145–149
6. Taguchi H, Nagao T, Watanabe H, Onizawa K, Matsuo N, Tokimitsu I, Itakura H (2001) Energy value and digestibility of dietary oil containing mainly 1,3-diacylglycerol are similar to those of triacylglycerol. Lipids 36:379–382
7. Nagao T, Watanabe H, Goto N, Onizawa K, Taguchi H, Matsuo N, Yasukawa T, Tsushima R, Shimasaki H, Itakura H (2000) Dietary diacylglycerol suppresses accumulation of body fat compared to triacylglycerol in men in a double-blind controlled trial. J Nutr 130:792–797

8. Maki KC, Davidson MH, Tsushima R, Matsuo N, Tokimitsu I, Umporowicz DM, Dicklin MR, Foster GS, Ingram KA, Anderson BD, Frost SD, Bell M (2002) Consumption of diacylglycerol oil as part of a reduced-energy diet enhances loss of body weight and fat in comparison with consumption of a triacylglycerol control oil. Am J Clin Nutr 76:1230–1236
9. Murase T, Mizuno T, Omachi T, Onizawa K, Komine Y, Kondo H, Hase T, Tokimitsu I (2001) Dietary diacylglycerol suppresses high fat and high sucrose diet-induced body fat accumulation in C57BL/6J mice. J Lipid Res 42:372–378
10. Murase T, Aoki M, Wakisaka T, Hase T, Tokimitsu I (2002) Anti-obesity effect of dietary diacylglycerol in C57BL/6J mice: dietary diacylglycerol stimulates intestinal lipid metabolism. J Lipid Res 43:1312–1319
11. Meng X, Zou D, Shi Z, Duan Z, Mao Z (2004) Dietary diacylglycerol prevents high-fat diet-induced lipid accumulation in rat liver and abdominal adipose tissue. Lipids 39:37–41
12. Kondo H, Hase T, Murase T, Tokimitsu I (2003) Digestion and assimilation features of dietary DAG in the rat small intestine. Lipids 38:25–30
13. Murata M, Ide T, Hara K (1994) Alteration by diacylglycerol of the transport and fatty acid composition of lymph chylomicron in rats. Biosci Biotech Biochem 58:1416–1419
14. Taguchi H, Watanabe H, Onizawa K, Nagao T, Gotoh N, Yasukawa T, Tsushima R, Shimasaki H, Itakura H (2000) Double-blind controlled study on the effects of diacylglycerol on postprandial serum and chylomicron triacylglycerol responses in healthy humans. J Am Coll Nutr 19:789–796
15. Tada N, Watanabe H, Matsuo N, Tokimitsu I, Okazaki M (2001) Dynamics of postprandial remnant-lipoprotein particles in serum after loading of diacylglycerols. Clin Chem Acta 311:109–117
16. Kimura S, Tsuchiya H, Inage H, Meguro S, Matsuo N, Tokimitsu I (2006) Effects of dietary diacylglycerol on the energy metabolism. Int J Vitam Nutr Res 76:75–79
17. Saito S, Tomonobu K, Hase T, Tokimitsu I (2006) Effects of diacylglycerol on postprandial energy expenditure and respiratory quotient in healthy subjects. Nutrition 22:30–35
18. Kamphuis MM, Mela DJ, Westerterp-Plantenga MS (2003) Diacylglycerols affect substrate oxidation and appetite in humans. Am J Clin Nutr 77:1133–1139
19. Murata M, Ide T, Hara K (1997) Reciprocal responses to dietary diacylglycerol of hepatic enzymes of fatty acid synthesis and oxidation in the rat. Br J Nutr 77:107–121
20. Huge-Jensen B, Galluzzo DR, Jensen RG (1988) Studies on free and immobilized lipases from mucor miehei. J Am Oil Chem Soc 65:905–910
21. Ramirez I (1987) Diet texture, moisture and starch type in dietary obesity. Physiol Behav 41:149–154
22. Jeejeebhoy KN, Ahmad S, Kozak G (1970) Determination of fecal fats containing both medium and long chain triglycerides and fatty acids. Clin Biochem 3:157–163
23. Ishihara K, Oyaizu S, Fukuchi Y, Mizunoya W, Segawa K, Takahashi M, Mita Y, Fukuya Y, Fushiki T, Yasumoto K (2003) A soybean peptide isolate diet promotes postprandial carbohydrate oxidation and energy expenditure in type II diabetic mice. J Nutr 133:752–757
24. Flatt JP (1995) Use and storage of carbohydrate and fat. Am J Clin Nutr 61:952S–959S
25. Piers LS, Walker KZ, Stoney RM, Soares MJ, O'Dea K (2002) The influence of the type of dietary fat on postprandial fat oxidation rates: monounsaturated (olive oil) vs saturated fat (cream). Int J Obes Relat Metab Disord 26:814–821
26. Bessesen DH, Vensor SH, Jackman MR (2000) Trafficking of dietary oleic, linolenic, and stearic acids in fasted or fed lean rats. Am J Physiol Endocrinol Metab 278:E1124–E1132
27. Shimomura Y, Tamura T, Suzuki M (1990) Less body fat accumulation in rats fed a sunflower oil diet than in rats fed a beef tallow diet. J Nutr 120:1291–1296
28. Nemali MR, Usuda N, Reddy MK, Oyasu K, Hashimoto T, Osumi T, Rao MS, Reddy JK (1988) Comparison of constitutive and inducible levels of expression of peroxisomal beta-oxidation and catalase genes in liver and extrahepatic tissues of rat. Cancer Res 48:5316–5324

Lipids (2008) 43:419–429
DOI 10.1007/s11745-008-3167-4

ORIGINAL ARTICLE

GCG-Rich Tea Catechins are Effective in Lowering Cholesterol and Triglyceride Concentrations in Hyperlipidemic Rats

**Sang Min Lee · Chae Wook Kim · Jung Kee Kim ·
Hyun Jung Shin · Joo Hyun Baik**

Received: 12 November 2007 / Accepted: 21 February 2008 / Published online: 26 March 2008
© AOCS 2008

Abstract The (−)-gallocatechin gallate (GCG) concentration in some tea beverages can account for as much as 50% of the total catechins, as a result of sterilization. The present study aims to examine the effects of GCG-rich tea catechins on hyperlipidemic rats and the mechanisms associated with regulating cholesterol metabolism in the liver. By performing heat epimerization of (−)-epigallocatechin gallate (EGCG), we manufactured a mixture of catechins that had a GCG content of approximately 50% (w/w). In sucrose-rich diet-induced hyperlipidemic rats, the GCG-rich tea catechins exhibited strong activity in reducing plasma cholesterol and triglyceride concentrations. Furthermore, the hepatic cholesterol and triglyceride concentrations that had increased as a result of the sucrose-rich diet were reduced due to GCG-rich tea catechins consumption. In order to investigate the hyperlipidemic mechanism of GCG-rich tea catechins, we examined the hepatic expressions of LDL receptor and HMG-CoA reductase in hyperlipidemic rats. We further evaluated the action of purified GCG on LDL receptor activity, which is a key contributor to the regulation of cholesterol concentrations. We found that purified GCG increased LDL receptor protein level and activity to a greater extent than EGCG. In conclusion, our study indicates that GCG-rich tea catechins in tea beverages may be effective in preventing hyperlipidemia by lowering plasma and hepatic cholesterol concentrations.

Keywords GCG-rich catechins · Hyperlipidemia · LDL receptor activity

Abbreviations

EGCG	(−)-Epigallocatechin gallate
GCG	(−)-Gallocatechin gallate
HDL	High density lipoprotein
LDL	Low density lipoprotein
VLDL	Very low density lipoprotein
LDLR	Low density lipoprotein receptor
HMG-CoA	3-Hydroxy-3-methylglutaryl coenzyme A

Introduction

Hypercholesterolemia is one of the major risk factors for the development of atherosclerosis. Epidemiological studies have been reported which show a significant inverse relationship between the consumption of tea beverages and plasma cholesterol concentration [1, 2]. The health benefits of green tea have been attributed mainly to catechins, particularly (−)-epigallocatechin gallate (EGCG), which is the most abundant catechin in green tea [3, 4]. Animal studies have shown that EGCG inhibited cholesterol absorption and lowered plasma cholesterol concentration [5, 6]. It was found that EGCG enhanced the removal of intravenously injected ^{14}C-cholesterol from plasma in rats

S. M. Lee · H. J. Shin · J. H. Baik (✉)
Green Tea Research Team, Food Research Institute,
R&D Center, Amorepacific Corporation, 314-1 Bora-dong,
Giheung-gu, Yongin-si, Gyeonggi-do, South Korea
e-mail: jhbaik@amorepacific.com

C. W. Kim
Pre-clinic Research Team, Pharmaceutical Research Institute,
R&D Center, Amorepacific Corporation, 314-1 Bora-dong,
Giheung-gu, Yongin-si, Gyeonggi-do, South Korea

J. K. Kim
Healthfood Research Team, Food Research Institute,
R&D Center, Amorepacific Corporation, 314-1 Bora-dong,
Giheung-gu, Yongin-si, Gyeonggi-do, South Korea

[7]. This increased clearance rate of cholesterol might have been due to an increased LDL receptor expression, as this is the main mechanism by which cholesterol is removed from the circulation [8]. Kuhn et al. [9] found that EGCG was able to increase LDL receptor protein expression with subsequent up-regulation of LDL receptor gene transcription. Moreover, Bursill and Roach [10] found that EGCG significantly increased LDL receptor binding activity. These studies might explain the effect of EGCG on regulating cholesterol concentration by increasing LDL receptor activity.

Canned and bottled tea beverages are widely consumed in Asian countries and are gaining popularity worldwide. During pasteurization, these products are generally autoclaved at 120 °C for several minutes. It has been known that during pasteurization, considerable amounts (approximately 50%) of catechins undergo epimerization at the two-position to form (−)-catechin, (−)-gallocatechin, (−)-catechin gallate, and (−)-gallocatechin gallate (GCG) [11]. It has been reported that the GCG concentration of total catechins could increase from approximately 1.5% to as much as 50% in some tea beverages [11]. The relatively high GCG concentration in tea beverages is due to the thermal conversion of a major tea catechin, EGCG.

Although the consumption of bottled green tea beverages is increasing, several physiological functions involving the regulation of plasma lipid concentrations have been reported for EGCG; however, studies on GCG-rich tea catechins are limited. Recently, Ikeda et al. [12] found that tea catechins rich in GCG were more effective in inhibiting cholesterol absorption than tea catechins rich in EGCG. In addition, Kobayashi et al. [13] reported that heat-epimerized catechins had identical cholesterol-lowering activity as green tea catechins in cholesterol-fed rats. Except for its inhibitory effect on cholesterol absorption, other mechanisms by which GCG-rich tea catechins reduce plasma lipid concentrations are not known. In the present study, we manufactured a mixture of catechins that contained approximately 50% (w/w) GCG by the heat epimerization of EGCG. By using GCG-rich tea catechins, we evaluated the effect on lipid concentrations in hyperlipidemic rats induced by a sucrose-rich diet. Furthermore, we analyzed the cholesterol and triglyceride concentrations in the liver which is the main tissue that regulates lipid metabolism.

Human and animal cells possess at least two mechanisms for obtaining the cholesterol necessary for the formation of membranes, steroid hormones, and bile acids. They can either obtain this cholesterol by means of receptor-mediated endocytosis of LDL, an event that involves the LDL receptor, or synthesize cholesterol de novo using 3-hydroxy-3-methylglutaryl coenzyme A reductase (HMG-CoA reductase) as a rate-limiting enzyme [14]. Under certain conditions, the LDL level in plasma is determined by a balance between the activities of LDL receptor and HMG-CoA reductase in the liver. The LDL receptor has been found to regulate and lower plasma cholesterol concentration, while HMG-CoA reductase, a rate-limiting enzyme that catalyzes the conversion of HMG-CoA to mevalonic acid, is known as the critical enzyme for cholesterol de novo synthesis in our body [15]. In order to study the mechanism of the hypercholesterolemic effect of GCG-rich tea catechins, hepatic LDL receptor activity and HMG-CoA reductase levels were measured. In addition, based on previous studies that evaluated the effect of EGCG on increasing LDL receptor activity, we further analyzed the effect of purified GCG on LDL receptor expression and activity in HepG2 cells.

Materials and Methods

Chemical Reagents

(−)-Epigallocatechin gallate (EGCG, E4143) and (−)-gallocatechin gallate (GCG, G6782) were purchased from Sigma (St. Louis, MO, USA) for in vitro experiments. Penicillin–streptomycin, Dulbecco's modified Eagle's medium (DMEM), and fetal bovine serum (FBS) were purchased from GIBCO-BRL of Life Technologies (New York, NY, USA). Specific antibodies for LDL receptor and HMG-CoA reductase were purchased from Abcam (ab14056) and SantaCruz (sc-27578), respectively. For measurements of LDL receptor activity, fluorescence probe (BODIPY) labeled LDL was purchased from Molecular probe, Inc (Eugene, OR, USA). For the manufacture of GCG-rich tea catechins, pure EGCG powder was obtained from TEAVIGO$^{\mathrm{TM}}$ (94% purity), which was a registered trademark of DSM Nutritional Products (Parsippany, NJ, USA). GCG-rich tea catechins were manufactured by autoclaving the pure EGCG powder at 120 °C for 30 min. The EGCG and GCG concentrations as a result of heat epimerization are shown in Table 1. Initially, we intended to compare the effects of absolute GCG and EGCG in vivo. However, we realized that purchasing GCG powder from Sigma-Aldrich in order to include a group of rats administrated with only GCG (90 ~ 100%) would involve prohibitive costs. Moreover, the EGCG provided by Sigma-Aldrich is too expensive for animal experiments.

Table 1 EGCG and GCG contents (%) of the GCG-rich tea catechins

	EGCG	GCG	EGCG + GCG
Raw EGCG material	94	0	94
GCG-rich tea catechins	46.6	46.1	92.7

Therefore, due to high material costs, we used pure EGCG powder from TEAVIGO™ and manufactured GCG-rich tea catechins by autoclaving the TEAVIGO™ samples for our in vivo experiments. The purity of EGCG for the in vitro and in vivo experiments was 95 and 94%, respectively. Although we obtained EGCG powder from TEAVIGO™ instead of Sigma-Aldrich, we believe this did not show any different metabolism results between in vitro and in vivo experiments, since the EGCG for each experiment was the same compound and the content of EGCG was similar.

Sucrose-Rich Diet-Induced Hyperlipidemic Rats

Studies were carried out using male Sprague-Dawley rats (Orient Bio Company, Korea); each weighing approximately 200 g. The experiments were conducted under the Korea Association for Laboratory Animal Science's guidelines for the care and use of experimental animals. The amorepacific institutional animal care and use committee had approved the use of animals in the experiments. Seven-week-old rats were randomly divided into the following groups: control diet (CD), sucrose-rich diet (SRD), EGCG (E), and GCG-rich tea catechins (G), with six animals per group. All rats were provided free access to experimental diet and fluid for 30 days. The composition of the diets is shown in Table 2 [16]. The CD and SRD groups consumed distilled water. EGCG and the GCG-rich tea catechins were prepared in distilled water (0.2% w/v) and the rats in E and G groups consumed each of the designated fluids ad libitum. The fluids containing EGCG and the GCG-rich tea catechins were freshly prepared, and the intakes were measured on every other day. Body weight and food intakes were measured three times a week.

Table 2 Composition of the experimental diets

Ingredient	Control diet (CD) (g/kg diet)	Sucrose-rich diet (SRD) (g/kg diet)
Casein	200	200
Corn starch	397.5	0
Sucrose	100	600
Dextrose	130	30
Soybean oil	70	70
Cellulose	50	50
AIN-93G mineral mix	35	35
AIN-93G vitamin mix	10	10
L-Cystine	3	3
Choline bitartrate	2.5	2.5
t-Butylhydroquinone	0.014	0.014

Modified from the AIN-93 purified rodent diet

Analysis of Plasma Total Triglyceride, Total Cholesterol, HDL Cholesterol, LDL Cholesterol, and VLDL Cholesterol Concentrations

Venous blood for measuring lipid concentrations was collected from the retro-orbital sinus of the animals on day 30. Plasma samples were separated from the whole blood by centrifugation at 3,000*g* for 10 min. Plasma total triglyceride, total cholesterol, HDL cholesterol, and LDL cholesterol concentrations were determined according to the protocol provided by DiaSys Diagnostic Systems (Holzheim, Germany). Based on the total cholesterol and HDL cholesterol that were measured, we calculated the VLDL + LDL cholesterol concentration by using modified Friedewald formula [17]. The VLDL + LDL cholesterol level for each sample was obtained using the following formula:

$$\text{VLDL} + \text{LDL cholesterol} = \text{total cholesterol} - \text{HDL cholesterol}.$$

Analysis of the Total Hepatic Triglyceride and Cholesterol Concentrations

Liver tissue was extracted using the standard Folch [18] extraction technique as described below. Homogenized liver (100 mg, wet weigh) was first mixed with 5 mL methanol containing 0.2% butylated hydroxytoluene, followed immediately by the addition of 10 mL chloroform, and vortexed vigorously for 30 s. The homogenate was centrifuged at 3,000*g* for 10 min and we separated the homogenate to obtain a crude extract solution. The crude extract was mixed thoroughly with 0.2 times its volume of water, and the mixture was separated into two phases by centrifugation. The upper phase was aspirated; it was completely removed by rinsing the inter-phase three times with small amounts of pure upper phase solvents. The lower organic layer was transferred to a tube and stored at −20 °C. The total hepatic cholesterol and triglyceride concentrations were measured using EnzyChrom Cholesterol Assay Kit (BioAssay Systems, Hayward, CA, USA) and L-Type Triglyceride H reagents (Wako, Osaka, Japan), respectively.

Detection of LDL Receptor Activity and HMG-CoA Reductase in the Rat Liver

Low-density lipoprotein receptor and HMG-CoA reductase were detected by using western blotting with specific antibodies [10, 19]. Liver samples and HepG2 cells were lysed using cell lysis buffer (Cell Signaling Technology, Beverly, MA, USA). The protein concentration was determined using a BCA assay kit (Pierce, Rockford, IL, USA). Proteins (30 μg) were resolved on 10% NuPAGE gels run in an MES buffer system (Invitrogen, Carlsbad, CA, USA) and transferred to nitrocellulose membranes according to the manufacturer's protocol. Immunoreactive proteins were revealed by enhanced chemiluminescence with ECL+ (Amersham Biosciences, Piscataway, NJ, USA). Anti-actin antibody (Sigma, A2066) was used to assess equal loading of the protein. Quantification of each protein was carried out by using the Image J software program.

HepG2 Cell Culture and Catechins Treatment

Human hepatoblastoma cells, HepG2, obtained from American type Culture Collection (Rockville, MD, USA) were used to quantify LDL receptor activity. Cells were seeded into 6-well or 96-well plates (Nunc, Rochester, NY, USA), and were cultured in DMEM supplemented with 10% fetal bovine serum (FBS) and 100 U/mL penicillin–streptomycin (Gibco, grand Island, NY, USA). Cells were grown for 48 h at 37 °C in an atmosphere of 5% CO_2. After an additional 24 h of incubation with FBS-free DMEM, cells were incubated for 24 h with DMEM containing different concentrations (0, 10, 50 μM) of the purified tea catechins.

Measurement of LDL Receptor Activity with a Fluorescence Detector

After a 48-h period of culture in DMEM supplemented with FBS, cells were switched to DMEM containing 0.5% human serum albumin for an additional 24 h. BODIPY-LDL (20 μg protein/mL) was incubated with HepG2 cells for 2 h at 37 °C. At the end of the incubation period, cells were extensively washed with phosphate-buffered saline, 200 μl (for 96 well) isopropanol was added to each well, and plates were gently shaken using an orbital shaker for 20 min. BODIPY-LDL fluorescence in each of isopropanol extracts was determined using a Victor^2 1420 multi-label counter (Wallac, Boston, MA, USA) with excitation and emission wavelengths set at 485 and 535 nm, respectively. By representing the total amount of BODIPY-LDL versus time, the specific activity of each sample was expressed as microgram of LDL protein per minute per milligram cellular protein, as described elsewhere [20].

Measurement of LDL Receptor Activity with a Flow Cytometer

Fluorescence was measured with a FACScalibur flow cytometer (BD bioscience, San Jose, CA, USA) equipped with 15 mW, 488 nm, air-cooled argon laser and linked to a Macintosh Quadra 650 computer with CellQuest software (BD bioscience). Forward scatter and side scatter were adjusted to exclude debris and dead cells. The emission of BODIPY LDL was measured at 530 ± 15 nm (FL1-H). Fluorescence signals of FL1-H were recorded on logarithmically transformed intensity scale in a histogram. The LDL receptor activity of each sample was expressed as the mean of FL1-H intensity.

Statistical Analysis

Data were presented as mean ± standard deviation (SD). Statistical analyses were performed using one-way ANOVA with post-hoc Tukey–Kramer's tests for comparisons between two groups or multiple groups, respectively. Differences were considered significant at $P < 0.05$ or $P < 0.01$.

Results

Effects of EGCG and the GCG-Rich Tea Catechins on the Food Intake, Fluid Intake, and Body Weight Gain of Rats on the Sucrose-Rich Diet

To evaluate the possibility that GCG-rich tea catechins play an effective role in buffering increases in plasma cholesterol and triglyceride levels, we investigated their effects in sucrose-rich diet-induced hyperlipidemic rats. We first examined the food intake, fluid intake, and body weight gain of rats on the sucrose-rich diet (Table 3). The daily food intakes were almost similar between the groups,

Table 3 Food intake, fluid intake, and body weight gain of rats fed indicated diet and beverage

Group	Diet and beverage	Food intake (g/day)	Fluid intake	Body weight gain (g/30day)
CD	CD + distilled water	22.1 ± 1.9	39.2 ± 7.0	247.1 ± 9.3
SRD	SRD + distilled water	21.0 ± 1.8	37.5 ± 4.6	246.8 ± 8.3
E	SRD + 0.2% EGCG	18.7 ± 1.5*	28.9 ± 4.6*	221.0 ± 9.9*
G	SRD + 0.2% GCG-rich tea catechins	19.0 ± 1.5*	26.1 ± 3.0*	225.0 ± 7.0*

Data are expressed as mean ± SD, *N* = 6. Significant differences from the SRD group is shown with an asterisk

CD Control diet, *SRD* sucrose-rich diet, *E* EGCG, *G* GCG-rich tea catechins

* $P < 0.05$

whereas fluid intakes were significantly suppressed in the E and G groups. The average food intakes (mean ± SD) for the CD, SRD, E, and G groups were 22.1 ± 1.9, 21.0 ± 1.8, 18.7 ± 1.5 and 19.0 ± 1.5 g/day. The food intakes of E and G groups were significantly decreased about 2 g per day, compared to CD and SRD groups. The average fluid intakes (mean ± SD) were 39.2 ± 7.0, 37.5 ± 4.6, 28.9 ± 4.6, and 26.1 ± 3.0 g/day for the CD, SRD, E, and G groups, respectively. Although the fluid intakes were decreased significantly in the E and G groups as compared to the CD and SRD groups, the amount of GCG-rich tea catechins consumed by the G group was not significantly different from that of EGCG consumed by the E group. No difference in body weight gain was observed between the SRD and CD groups. However, body weight gain significantly decreased after the consumption of EGCG and the GCG-rich tea catechins. This result is consistent with a previous study that showed that dietary supplementation with EGCG for 1 month attenuated diet-induced obesity and decreased body weight of mice [21]. The reduced food intakes in E and G groups may influence the reduced body weight gain.

GCG-Rich Tea Catechins Decreased Plasma Cholesterol and Triglyceride Concentrations Significantly in Sucrose-Rich Diet-Induced Hyperlipidemic Rats

In sucrose-rich diet-induced hyperlipidemic rats, the total plasma cholesterol concentration in the SRD group was elevated to 123.8%, as compared to the CD group. The consumption of GCG-rich tea catechins significantly normalized the plasma cholesterol concentration, which was augmented by the sucrose-rich diet (Fig. 1a). Although EGCG seemed to decrease plasma cholesterol concentration, significant difference was not observed between E and SRD groups with one-way ANOVA statistical test. The sucrose-rich diet caused an increase in the total plasma triglyceride concentration to 155.5% of the CD group on day 30. Fluids containing EGCG and the GCG-rich tea catechins reduced the total plasma triglyceride concentration to 126 and 120%, respectively. The difference between EGCG and the GCG-rich tea catechins was not clear on the effects of decreasing cholesterol and triglyceride concentrations (Fig. 1b).

The plasma lipoprotein cholesterol concentrations are depicted in Table 4. None of the groups showed a significant alteration in their plasma LDL cholesterol concentrations. The sucrose-rich diet increased HDL cholesterol to 136%, as compared to the level found in the control diet group. The increased HDL cholesterol concentration was almost normalized in the GCG-rich tea catechins-supplemented group. Significant reduction in HDL cholesterol concentration was observed in G group. Instead of direct measurement of VLDL cholesterol, we could calculate VLDL + LDL cholesterol level by using the Friedewald formula. Although the VLDL + LDL cholesterol concentration between SRD and G groups was not significantly different, GCG-rich tea catechins tended to lower the plasma VLDL + LDL cholesterol level. Therefore, the normalized plasma total cholesterol concentration in G group might be attributed to the reduced HDL and VLDL + LDL cholesterol concentrations.

Consuming the GCG-Rich Tea Catechins was Effective in Decreasing the Hepatic Cholesterol and Triglyceride Concentrations

The liver is well known as the main tissue that regulates plasma cholesterol and triglyceride concentrations [22].

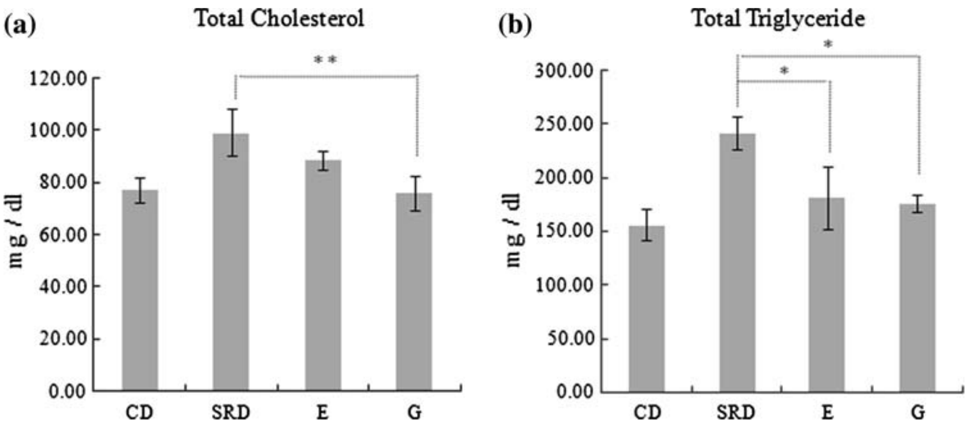

Fig. 1 Effects of GCG-rich tea catechins on the plasma **a** cholesterol and **b** triglyceride concentrations of sucrose-rich diet-induced hyperlipidemic rats. GCG-rich tea catechins significantly reduced plasma cholesterol and triglyceride concentrations in sucrose-rich diet-induced hyperlipidemic rats. Significant differences from the SRD group are presented with *asterisks*. $*P < 0.05$, $**P < 0.01$, *CD* control diet, *SRD* sucrose-rich diet, *E*: EGCG, *G*: GCG-rich tea catechins

Table 4 Effects of EGCG and the GCG-rich tea catechins on lipoprotein cholesterol concentrations (mg/dl)

Group	HDL-C	LDL-C	(VLDL + LDL)-C[a]
CD	55.57 ± 5.60*	13.67 ± 2.89	19.70 ± 5.37
SRD	75.63 ± 6.15	11.13 ± 2.08	23.67 ± 5.29
E	64.57 ± 5.56	13.33 ± 1.53	24.30 ± 2.26
G	57.23 ± 9.26*	12.33 ± 0.58	18.97 ± 3.02

Data are expressed as means ± SD, $N = 6$. An asterisk indicates significant difference from the SRD group

* $P < 0.05$

[a] (VLDL + LDL)-C is calculated by using a modified Friedewald formula

Table 5 Effects of EGCG and the GCG-rich tea catechins on the total hepatic cholesterol and triglyceride concentrations (mg/g)

Group	Cholesterol	Triglyceride
CD	3.56 ± 0.30**	9.08 ± 0.77*
SRD	8.53 ± 1.17	14.38 ± 1.37
E	3.66 ± 0.32**	11.83 ± 2.50
G	3.56 ± 0.60**	8.55 ± 0.32*

Data are expressed as mean ± SD for each group, $N = 3$. Asterisk indicates significant difference from SRD group

CD Control diet, *SRD* sucrose-rich diet, *E* EGCG, *G* GCG-rich tea catechins

* $P < 0.05$

** $P < 0.01$

A sucrose-rich diet has been proven to be lipogenic and elevates the hepatic triglyceride concentration [23]. In this study, it increased hepatic cholesterol concentration to nearly 2.4-fold that of control. Although the increase in cholesterol concentration was significantly attenuated by EGCG and the GCG-rich tea catechins in the fluids, the effects of the E and G groups were similar (Table 5). The hepatic triglyceride concentration was significantly elevated by approximately 160% in the SRD group as compared to the CD group. However, the GCG-rich tea catechins almost normalized the hepatic triglyceride content, whereas EGCG tended to decrease the triglyceride concentration to some degree which was augmented by the sucrose-rich diet (Table 5).

Expressions of Hepatic LDL Receptor and HMG-CoA Reductase Remained Unchanged Despite the Administration of EGCG and the GCG-Rich Tea Catechins in Sucrose-Rich Diet-Induced Hyperlipidemic Rats

An increase in the LDL receptor expression is the main mechanism by which cholesterol is removed from circulation [16]. Further, the LDL receptor is reported to be the main factor that regulates hepatic lipid concentrations [18]. To confirm the involvement of the LDL receptor in lowering plasma and hepatic lipid concentrations, we examined the hepatic expression of the LDL receptor in the sucrose-rich diet-induced hyperlipidemic rats. The hepatic LDL receptor was elevated by the sucrose-rich diet. Although EGCG was known to increase LDL receptor expression [10], the consumption of EGCG and the GCG-rich tea catechins did not additionally increase LDL receptor expression (Fig. 2a). Figure 2b shows the expression of hepatic HMG-CoA reductase for each group after 30 days of treatment. The sucrose-rich diet did not affect hepatic HMG-CoA reductase expression, and no significant differences were found between the rats supplemented with EGCG and the GCG-rich tea catechins and those in the SRD group.

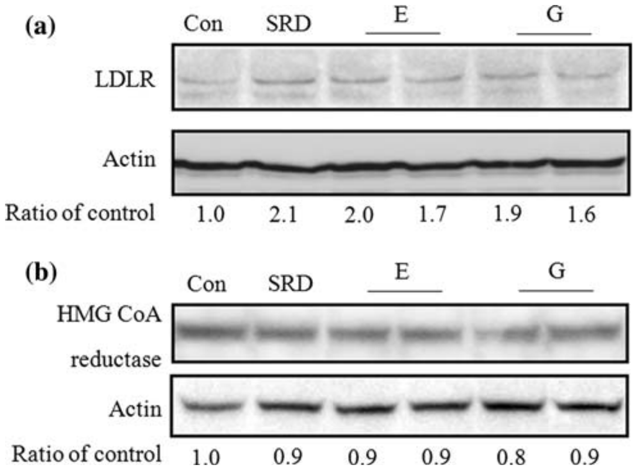

Fig. 2 Effects of GCG-rich tea catechins on the hepatic LDL receptor and HMG-CoA reductase expressions in hyperlipidemic rats. **a** Hepatic LDL receptor and **b** HMG-CoA reductase expressions remained unchanged among the SRD, E, and G groups. *CD* control diet, *SRD* sucrose-rich diet, *E* EGCG, *G* GCG-rich tea catechins, *LDLR* LDL receptor

GCG Was More Effective in Increasing the Expression of the LDL Receptor than EGCG

The GCG-rich tea catechins were effective in reducing cholesterol and triglyceride concentrations. Although the expression of the LDL receptor was not changed apparently in the E and G groups, we considered that purified EGCG and GCG could have different effects on LDL receptor expression. Therefore, we further investigated the effect of purified EGCG and GCG on the expression of LDL receptor by using HepG2 cells. Recently, EGCG was reported to increase LDL receptor expression in HepG2 cells [10]. In this study, we revealed for the first time that incubation with GCG (50 μM) significantly increased LDL receptor protein expression (∼450% of control, **$P < 0.01$) over the effect of EGCG (Fig. 3a, b). This result indicates that the effect of

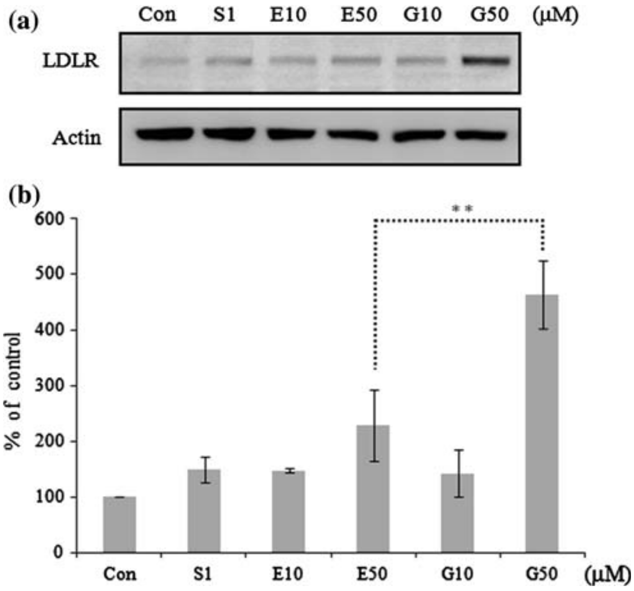

Fig. 3 LDL receptor expression in HepG2 cells treated with either EGCG or GCG GCG was more effective in increasing the LDL receptor expression than EGCG. **a** LDL receptor protein was determined by using western blotting with a polyclonal anti-LDL receptor antibody. **b** Quantitative results of the LDL receptor expression, $**P < 0.01$. *Con* control, *S* simvastatin, *E* EGCG, *G* GCG

GCG on up-regulating of the LDL receptor is significantly greater than that of EGCG, while both EGCG and GCG increase the expression of the LDL receptor.

GCG Increased the LDL Receptor Activity to a Greater Extent than EGCG

To confirm the effectiveness of GCG in up-regulating LDL receptor, we measured the LDL receptor activity with a fluorometer by using fluorescence probe, BODIPY labeled LDL. GCG treatment increased LDL receptor activity significantly ($*P < 0.05$), compared to EGCG treatment. LDL receptor activity increased in a concentration-dependent manner by GCG treatment, showing ~2-fold induction over the control at 50 μM (Fig. 4a). Further, to validate the effect of GCG on LDL receptor activity, the association of LDL–LDL receptor was assessed by flow cytometer. Like as evaluated by the flourometer, GCG treatment increased LDL–LDL receptor association more than EGCG (Fig. 4b). During 24 h treatment of the simvastatin, EGCG, and GCG, mean of FL1-H intensity that represents the LDL–LDL receptor association was 135.2, 138.2, and 150.5% of the control, respectively. Simvastatin, a drug for hyperlipidemia, was used for a positive control. When we measured LDL receptor activity with a flow cytometer, however, it could not detect each cell's fluorescence properly with 50 μM of EGCG and GCG, respectively. Maybe this undetectable result was caused by strong cell–cell adhesion. Although the effect of GCG was apparent in 50 μM with the fluorometer, observing the fluorescence of each cell with flow cytometer was limited in that concentration due to the strong cell–cell adhesion. This could be related with a previous report that EGCG increased mRNA expressions of cell adhesion proteins in the 25 μM and above concentrations [24]. To sum up, this result strongly suggests that GCG increases the LDL receptor activity effectively, compared to EGCG.

Discussion

The aim of this study is to elucidate the effectiveness of GCG-rich tea catechins in modulating cholesterol and triglyceride concentrations in vivo and to investigate the effective mechanisms. We manufactured GCG-rich tea catechins, in which GCG concentration was as high as 50% of the total catechins from the process of heat epimerization. For hyperlipidemic animal experiments, sucrose-rich diet was used to induce hyperlipidemia in rats. This diet-induced hyperlipidemia is relatively similar to the physiological condition that arises as a result of dietary habits such as the consumption of daily food.

Table 3 shows the diet and fluid consumption of each animal group. The daily diet and fluid intakes of the E and G groups were significantly lesser than those of the SRD group. Moreover, the total body weight gains in the E and G groups were greatly decreased, as compared to those in the SRD group. This difference in body weight gain could be attributed to the dietary reduction implemented in the above mentioned groups. Green tea catechins are known to activate many cellular mechanisms for reducing body weight. Studies in adipocyte cell lines and animal models have demonstrated that EGCG inhibits extracellular signal-related kinases (ERK), activates AMP-activated protein kinases (AMPK), modulates adipocyte marker proteins, and down-regulates lipogenic enzymes [25].

A sucrose-rich diet induces hypertriglyceridemia and elevates the triglyceride concentration in the plasma and liver as early as within 3 weeks in rats [16, 23]. Long-term feeding on a sucrose-rich diet results in a steady state of hyperlipidemia and hyperglycemia. Consistent with previous studies, the sucrose-rich diet exerted its lipogenic effect on day 30. The consumption of GCG-rich tea catechins inhibited the hypertriglyceridemia as well as hypercholesterolemia induced by the sucrose-rich diet (Fig. 1). There was no significant difference between EGCG and the GCG-rich tea catechins with regard to reducing the plasma cholesterol and triglyceride concentrations in sucrose-rich diet-induced hyperlipidemic rats.

(−)-Epigallocatechin gallate and the GCG-rich tea catechins decrease plasma lipid concentrations without

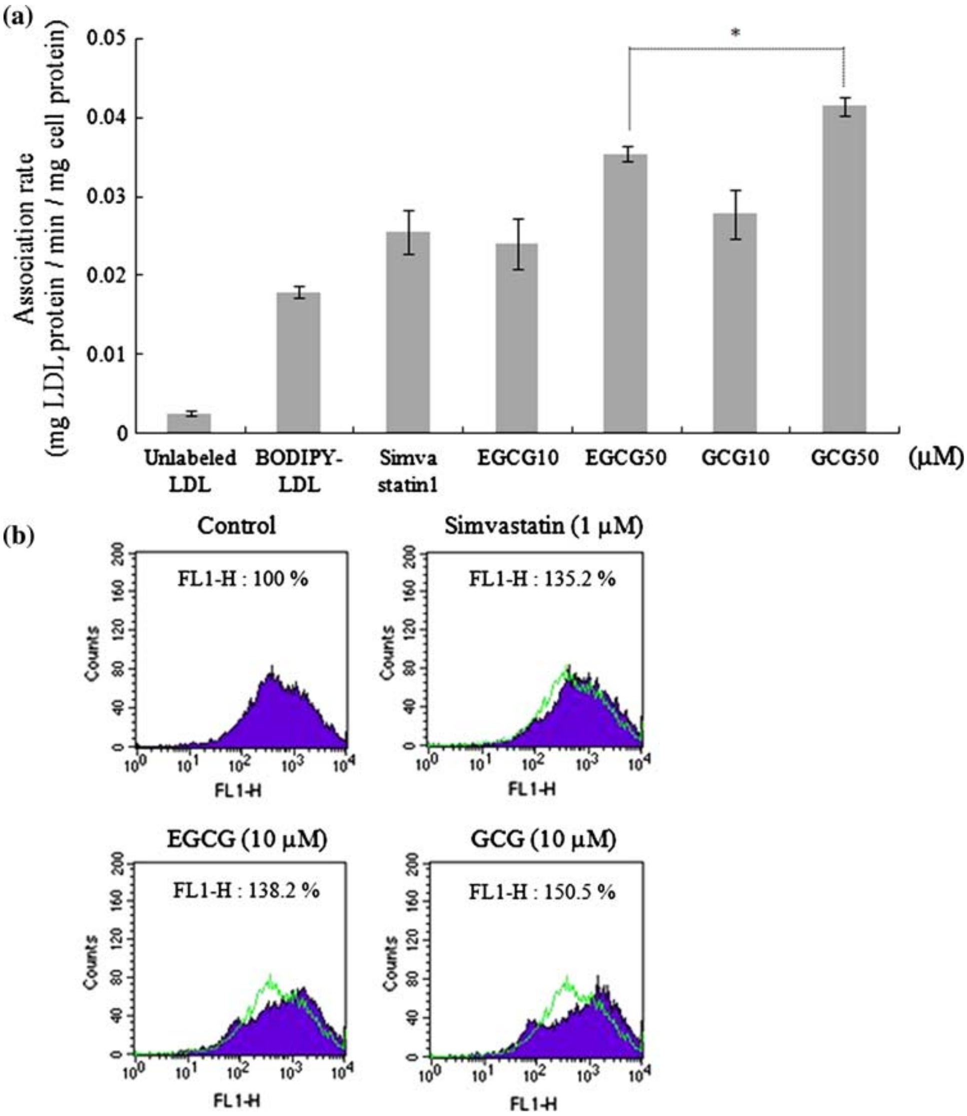

Fig. 4 GCG is more effective in increasing LDL receptor activity than EGCG. **a** LDL receptor activity by using a fluorescence detector The specific activity of each sample was expressed in micrograms of LDL protein per minute per milligram of cellular protein $*P < 0.05$. **b** LDL receptor activity using a flow cytometer The emission of fluorescent LDL was measured at 530 ± 15 nm (FL1-H). The LDL receptor activity in each sample was expressed as the mean of FL1-H intensity. *Con* control, *S* simvastatin, *E* EGCG, *G* GCG

affecting the LDL cholesterol level. According to a recent study, LDL cholesterol is not altered significantly by the consumption of green tea catechins in vivo. Bursill and Roach [26] proposed that administration of green tea catechins had no effect on plasma LDL cholesterol concentration in rats. However, other human studies have reported the effect of green tea extracts in decreasing plasma LDL cholesterol concentration. Additional studies of green tea in regulating LDL cholesterol concentration should be carried out including in vivo experiments.

In this study, as compared to the SRD group, the G group showed a significant reduction in HDL cholesterol concentration. Yang et al. [16] reported that all green and black tea extracts, with the exception of those obtained from oolong tea, failed to increase plasma HDL cholesterol concentration in rats; on the contrary, green tea extracts were found to lower HDL cholesterol concentration after 25 days of treatment. Weber et al. [6] also showed that dietary treatment involving 1% EGCG tended to decrease HDL cholesterol concentration, although there were no significant changes in the HDL level. Therefore, it is necessary to conduct further investigation into the effect of green tea catechins on HDL cholesterol regulation. As regards VLDL + LDL cholesterol concentration, the consumption of GCG-rich tea catechins seemed to decrease VLDL + LDL cholesterol, as calculated using a modified Friedewald formula. The normalization of the sucrose-rich diet-induced total cholesterol induction could be caused by the reduction in VLDL + LDL cholesterol. The decrease in HDL and VLDL + LDL cholesterol levels—effected by the GCG-rich tea catechins—shows that GCG-containing tea drinks can regulate plasma cholesterol concentration. The way in which GCG-containing tea drinks are able to influence these lipoprotein cholesterol concentrations also needs further, more specific investigation.

A sucrose-rich diet elevated the hepatic cholesterol and triglyceride concentrations (Table 5). EGCG and the GCG-rich tea catechins had a similar effect on decreasing hepatic cholesterol concentration. However, the GCG-rich tea catechins almost normalized hepatic triglyceride concentration induced by the sucrose-rich diet. Although green tea extracts were known for reducing hepatic triglyceride content [16], we revealed for the first time that GCG-rich tea catechins were effective on reducing hepatic cholesterol and triglyceride concentrations. Both EGCG and the GCG-rich tea catechins may modulate lipid metabolism in the liver.

A high expression of the LDL receptor is related to plasma cholesterol absorption by the liver, and LDL uptake by the receptor is a compensatory mechanism in terms of cholesterol homeostasis [27]. We investigated the hepatic LDL receptor expression, regarded as the chief mechanism in plasma cholesterol transport [10], in sucrose-rich diet-induced rats. The sucrose-rich diet elevated the hepatic expression of the LDL receptor. It is known that a sucrose-rich diet stimulates the biosynthesis of very low-density lipoproteins in the rat liver [28]. In cultures from rats fed on a sucrose-rich diet, the production of apolipoprotein E was found to be twice the amount produced by the control diet [28]. Moreover, Patsch et al. [29] reported that in the livers of sucrose-fed rats, the abundance of cellular apo A-IV mRNA increased to 185% of the control values. Although a sucrose-rich diet is found to increase lipoprotein-related components, the effect of such a diet on LDL receptor expression is not reported thus far. The consumption of EGCG and the GCG-rich tea catechins did not affect LDL receptor expression in the sucrose-rich diet-induced hyperlipidemic rats (Fig. 2). These catechins seemed to reduce the LDL receptor expression, to some extent, as compared to that found in the SRD group. The increased LDL receptor expression of the SRD group may be regarded as an adaptive response aimed at buffering the higher plasma lipid concentrations induced by the sucrose-rich diet.

Mammalian cells receive cholesterol by the uptake of lipoproteins; they also produce their own cholesterol. Cholesterol synthesis regulation keeps cellular and plasma cholesterol concentrations at a precisely controlled level; moreover, cholesterol synthesis is regulated by the activity of the microsomal enzyme HMG-CoA reductase and is determined by both the amount of protein present and the degree of activation of the enzyme [14]. In our study, we investigated hepatic HMG-CoA reductase expression in sucrose-rich diet-induced hyperlipidemic rats. There was no difference in the HMG-CoA reductase expressions for all animal groups. This result is consistent with a previous report indicating that the activity of HMG-CoA reductase is not affected by Lung Chen tea, a Chinese green tea [30]. Therefore, EGCG and the GCG-rich tea catechins are not involved in regulating the levels of the rate-limiting cholesterol synthesis enzyme HMG-CoA reductase.

It is evident from in vitro and in vivo studies that green tea catechins inhibit the intestinal absorption of dietary lipids. Studies in vitro indicated that green tea catechin, particularly EGCG, interfered with the digestion and micellar solubilization of lipids, which are critical steps in the intestinal absorption of dietary fat, cholesterol, and other lipids. Based on these results, blocking lipid absorption using tea catechins is likely to be an important way of reducing plasma cholesterol and triglyceride concentrations. In this study, we used hyperlipidemic rats induced by a sucrose-rich diet that contained the same quantity of lipids as the diet of rats in the other groups. Therefore, the effect of the sucrose-rich diet on increasing lipid concentrations could not be attributed to a high dietary fat supply—it was the result of an abnormality in lipid metabolism with respect to lipoproteins. Therefore, we suggest that the inhibition of intestinal lipid absorption is not the main reason for the lipid-lowering effect of tea catechins in the sucrose-rich diet-induced hyperlipidemic rat model. Regarding carbohydrates absorption, it was revealed that black and green tea extracts caused malabsorption of carbohydrates in healthy men [31]. Moreover, in vitro experiments have shown that some constituents of green tea inhibited the activity of α-amylase [32] and α-glucosidase [33]. However, inhibition of sucrose absorption by green tea catechins has not been reported so far.

Elevated plasma concentrations of LDL and LDL oxidation are recognized as playing an important role in atherogenesis [34] and increasing the efficiency of lipid clearance by raising LDL receptor activity is an efficient way to lower plasma cholesterol concentration [35]. Several in vitro and in vivo studies have shown that EGCG enhanced LDL receptor activity and decreased lipid concentrations [6, 10]. Bursill and Roach [10] demonstrated that green tea polyphenol, EGCG, increased LDL receptor activity and LDL receptor expression in human cells in vitro. In the present work, we reported that GCG had a stronger effect on increasing LDL receptor activity than EGCG in hepG2 cells (Fig. 4). This effect was accompanied by an increase in LDL receptor protein expression (Fig. 3). This mechanism may be pivotal for GCG-rich tea catechins to decrease lipid concentrations.

In our results, there is a discrepancy between the determination of LDL receptor activity by blotting and by a fluorescent method. According to previous reports, LDL receptor mRNA level, amount of LDL receptor protein and functional cellular LDL binding activity were consistent across the three measurements [36]. In that study, human LDL was conjugated to colloidal gold (LDL–gold) and the cell-bound LDL–gold was quantified using silver enhancement solution. However, another study reported that incubation of liver cells with citrus flavonoids caused a fivefold increase in LDL receptor mRNA level and a twofold increase in LDL binding activity [37]. LDL was radiolabeled with ^{125}I using the iodine monochloride technique for the measurement of LDL receptor binding activity. Given this, the difference between LDL receptor activity and LDL receptor expression seemed to be dependent on which methods were used to detect the LDL receptor activity. By measuring the fluorescent probe 3,3′-dioctadecylindocarbocyanine (Dil), which is a similar fluorescent material to that used in our study, Munoz et al. [20] revealed that LDL obtained during the walnut diet showed a 50% increase in the association rate to the LDL receptor in human hepatoma HepG2 cells. Therefore, an almost twofold increase of LDL receptor activity in our study can be significantly effective.

The LDL receptor is regulated at the transcriptional level by a family of membrane-bound transcription factors, the sterol response element binding proteins (SREBPs). In response to a decrease in cellular cholesterol availability, SREBP is processed proteolytically, and the active fragment migrates to the nucleus where it interacts with sterol response elements present in the promoter of LDL gene and activates LDL transcription [38]. Kuhn et al. [9] proposed that the up-regulation of LDL receptor expression induced by green tea polyphenols was caused by the inhibition of ubiquitin/-mediated degradation of active SREBP-2. He reported that green tea catechin, EGCG, potently inhibited proteasomal activity in HepG2 cells. Significantly, in connection with proteasome inhibition, the cleavage and active SREBP-2/p68 protein expression was enhanced after EGCG treatment. Subsequently, EGCG also increased LDL receptor proteasome expression by inhibiting proteasomal activity and increasing active SREBP-2 expression. With respect to this effect on proteasomal activity, a comparison experiment between EGCG and GCG is needed for elucidating apparent mechanism for regulating LDL receptor expression. Moreover, further studies should analyze the role played by GCG in LDL receptor regulation in the SREBP-2 related transcriptional level.

The results of our study show that GCG-rich tea catechins are effective in reducing cholesterol and triglyceride concentrations in hyperlipidemic rats. This may be consistent with a recent report that GCG-rich tea catechins are more effective in inhibiting cholesterol absorption than EGCG-rich tea catechins [12]. High GCG contents of the GCG-rich tea catechins may cause this effect. Moreover, our experiments support that GCG, a major catechin produced by the heat epimerization from EGCG, has a stronger effect to increase the LDL receptor activity than EGCG. Several structure–activity relationship studies revealed that the difference between the stereoscopic structures of EGCG and GCG contributed to their different effects [39–41]. An epitome of this is the binding of GCG to the active site of tyrosinase with a greater affinity than EGCG [42]. Furthermore, an electron spin resonance study indicated that the antioxidant activity of GCG was stronger than that of EGCG [43]. This effect of GCG is thought to be a result of the difference in the conformational structure of the epimer, EGCG. Furthermore, in vivo investigations are necessary to clarify the absorption, distribution, and metabolism of GCG, in comparison with EGCG.

Although various physiological functions of EGCG have been reported in many papers, for the first time, this study shows that GCG-rich tea catechins have strong effects on lowering cholesterol and triglyceride concentrations in hyperlipidemic rats. In the process of manufacturing bottled green tea beverages, relatively high amounts of GCG are produced due to the epimerization from EGCG during sterilization. Because some bottled green tea beverages have a GCG content of more than 50%, we may be able to decrease plasma and hepatic lipid concentrations by drinking green tea beverages abundant in GCG-rich tea catechins.

References

1. Imai K, Nakachi K (1995) Cross sectional study of effects of drinking green tea on cardiovascular and liver diseases. Br Med J 310(6981):693–696 (PubMed: 7711535)
2. Kono S, Shinchi K, Wakabayashi K, Honjo S, Todoroki I, Sakurai Y, Imanishi K, Nishikawa H, Ogawa S, Katsurada M (1996) Relation of green tea consumption to serum lipids and lipoproteins in Japanese men. J Epidemiol 6(3):128–133 (PubMed: 8952216)
3. Yang CS, Landau JM (2000) Effects of tea consumption on nutrition and health. J Nutr 130(10):2409–2412 (PubMed: 11015465)
4. Zaveri NT (2006) Green tea and its polyphenolic catechins: medicinal uses in cancer and noncancer applications. Life Sci 78(18):2073–2080 (PubMed: 16445946)
5. Wang S, Noh SK, Koo SI (2006) Epigallocatechin gallate and caffeine differentially inhibit the intestinal absorption of cholesterol and fat in ovariectomized rats. J Nutr 136(11):2791–2796 (PubMed: 11015465)
6. Raederstorff DG, Schlachter MF, Elste V, Weber P (2003) Effect of EGCG on lipid absorption and plasma lipid levels in rats. J Nutr Biochem 14(6):326–332 (PubMed: 12873714)
7. Chisaka T, Matsuda H, Kubomura Y, Mochizuki M, Yamahara J, Fujimura H (1988) The effect of crude drugs on experimental hypercholesteremia: mode of action of (−)-epigallocatechin gallate in tea leaves. Chem Pharm Bull 36(1):227–233 (PubMed: 3378286)
8. Brown MS, Goldstein JL (1986) A receptor-mediated pathway for cholesterol homeostasis. Science 232(4746):34–47 (PubMed: 3513311)
9. Kuhn DJ, Burns AC, Kazi A, Dou QP (2004) Direct inhibition of the ubiquitin-proteasome pathway by ester bond-containing green tea polyphenols is associated with increased expression of sterol regulatory element-binding protein 2 and LDL receptor. Biochim Biophys Acta 1682(1–3):1–10 (PubMed: 15158750)
10. Bursill CA, Roach PD (2006) Modulation of cholesterol metabolism by the green tea polyphenol (−)-epigallocatechin gallate in

cultured human liver (HepG2) cells. J Agric Food Chem 54(5):1621–1626 (PubMed: 16506810)

11. Chen Z, Zhu QY, Tsang D, Huang Y (2001) Degradation of green tea catechins in tea drinks. J Agric Food Chem 49(1):477–482 (PubMed: 11170614)
12. Ikeda I, Kobayashi M, Hamada T, Tsuda K, Goto H, Imaizumi K, Nozawa A, Sugimoto A, Kakuda T (2003) Heat-epimerized tea catechins rich in gallocatechin gallate and catechin gallate are more effective to inhibit cholesterol absorption than tea catechins rich in epigallocatechin gallate and epicatechin gallate. J Agric Food Chem 51(25):7303–7307 (PubMed: 14640575)
13. Kobayashi M, Unno T, Suzuki Y, Nozawa A, Sagesaka Y, Kakuda T, Ikeda I (2005) Heat-epimerized tea catechins have the same cholesterol-lowering activity as green tea catechins in cholesterol-fed rats. Biosci Biotechnol Biochem 69(12):2455–2458 (PubMed: 16377909)
14. Goldstein JL, Brown MS (1984) Progress in understanding the LDL receptor and HMG-CoA reductase, two membrane proteins that regulate the plasma cholesterol. J Lipid Res 25(13):1450–1461 (PubMed: 6397553)
15. Bisgaier CL, Essenburg AD, Auerbach BJ, Pape ME, Sekerke CS, Gee A, Wolle S, Newton RS (1997) Attenuation of plasma low density lipoprotein cholesterol by select 3-hydroxy-3-methylglutaryl coenzyme A reductase inhibitors in mice devoid of low density lipoprotein receptors. J Lipid Res 38(12):2502–2515 (PubMed: 9458274)
16. Yang M, Wang C, Chen H (2001) Green, oolong and black tea extracts modulate lipid metabolism in hyperlipidemia rats fed high-sucrose diet. J Nutr Biochem 12(1):14–20 (PubMed: 11179857)
17. Friedewald WT, Levy RI, Fredrickson DS (1972) Estimation of the concentration of low-density lipoprotein cholesterol in plasma, without use of the preparative ultracentrifuge. Clin Chem 18(6):499–502 (PubMed: 4337382)
18. Folch J, Lees M, Slovan Stanley GH (1957) A simple method for the isolation and purification of total lipides from animal tissues. J Biol Chem 226(1):497–509 (PubMed: 13428781)
19. Wassmann S, Faul A, Hennen B, Scheller B, Bohm M, Nickenig G (2003) Rapid effect of 3-hydroxy-3-methylglutaryl coenzyme a reductase inhibition on coronary endothelial function. Circ Res 93(9):e98–e103 (PubMed: 14551237)
20. Munoz S, Merlos M, Zambon D, Rodriguez C, Sabate J, Ros E, Laguna JC (2001) Walnut-enriched diet increases the association of LDL from hypercholesterolemic men with human HepG2 cells. J Lipid Res 42(12):2069–2076 (PubMed: 11734580)
21. Klaus S, Pultz S, Thone-Reineke C, Wolfram S (2005) Epigallocatechin gallate attenuates diet-induced obesity in mice by decreasing energy absorption and increasing fat oxidation. Int J Obes (Lond) 29(6):615–623 (PubMed: 15738931)
22. Jiang J, Nilsson-Ehle P, Xu N (2006) Influence of liver cancer on lipid and lipoprotein metabolism. Lipids Health Dis 5:4 (PubMed: 16515689)
23. Lombardo YB, Drago S, Chicco A, Fainstein-Day P, Gutman R, Gagliardino JJ, Gomez Dumm CL (1996) Long-term administration of a sucrose-rich diet to normal rats: relationship between metabolic and hormonal profiles and morphological changes in the endocrine pancreas. Metabolism 45(12):1527–1532 (PubMed: 8969287)
24. Park HJ, Shin DH, Chung WJ, Leem K, Yoon SH, Hong MS, Chung JH, Bae JH, Hwang JS (2006) Epigallocatechin gallate reduces hypoxia-induced apoptosis in human hepatoma cells. Life Sci 78(24):2826–2832 (PubMed: 16445947)
25. Moon HS, Lee HG, Choi YJ, Kim TG, Cho CS (2007) Proposed mechanisms of (-)-epigallocatechin-3-gallate for anti-obesity. Chem Biol Interact 167(2):85–98 (PubMed: 17368440)
26. Bursill CA, Roach PD (2007) A green tea catechin extract upregulates the hepatic low-density lipoprotein receptor in rats. Lipids 42(7):621–627 (PubMed: 17582541)
27. Spady DK, Turley SD, Dietschy JM (1985) Rates of low density lipoprotein uptake and cholesterol synthesis are regulated independently in the liver. J Lipid Res 26(4):465–472. (PubMed: 4009063)
28. Strobl W, Gorder NL, Fienup GA, Lin-Lee YC, Gotto AM Jr, Patsch W (1989) Effect of sucrose diet on apolipoprotein biosynthesis in rat liver. Increase in apolipoprotein E gene transcription. J Biol Chem 264(2):1190–1194 (PubMed: 2463248)
29. Radosavljevic M, Lin-Lee YC, Soyal SM, Strobl W, Seelos C, Gotto AM Jr, Patsch W (1992) Effect of sucrose diet on expression of apolipoprotein genes A-I, C-III and A-IV in rat liver. Atherosclerosis 95(2–3):147–156 (PubMed: 1418089)
30. Yang TT, Koo MW (2000) Chinese green tea lowers cholesterol level through an increase in fecal lipid excretion. Life Sci 66(5):411–423 (PubMed: 10670829)
31. Zhong L, Furne JK, Levitt MD (2006) An extract of black, green, and mulberry teas causes malabsorption of carbohydrate but not of triacylglycerol in healthy volunteers. Am J Clin Nutr 84(3):551–555 (PubMed: 16960168)
32. Zhang J, Kashket S (1998) Inhibition of salivary amylase by black and green teas and their effects on the intraoral hydrolysis of starch. Caries Res 32(3):233–238 (PubMed: 9577990)
33. Oki T, Matsui T, Matsumoto K (2000) Evaluation of alpha-glucosidase inhibition by using an immobilized assay system. Biol Pharm Bull 23(9):1084–1087 (PubMed: 10993209)
34. Witztum JL, Steinberg D (1991) Role of oxidized low density lipoprotein in atherogenesis. J Clin Invest 88(6):1785–1792 (PubMed: 1752940)
35. Brown MS, Goldstein JL (2004) Lowering plasma cholesterol by raising LDL receptors. Atheroscler Suppl 5(3):57–59 (PubMed: 15531276)
36. Pal S, Thomson AM, Bottema CD, Roach PD (2002) Polyunsaturated fatty acids downregulate the low density lipoprotein receptor of human HepG2 cells. J Nutr Biochem 13(1):55–63 (PubMed: 11834220)
37. Wilcox LJ, Borradaile NM, de Dreu LE, Huff MW (2001) Secretion of hepatocyte apoB is inhibited by the flavonoids, naringenin and hesperetin, via reduced activity and expression of ACAT2 and MTP. J Lipid Res 42(5):725–734 (PubMed: 11352979)
38. Brown MS, Goldstein JL (1997) The SREBP pathway: regulation of cholesterol metabolism by proteolysis of a membrane-bound transcription factor. Cell 89(3):331–340 (PubMed: 9150132)
39. Sanae F, Miyaichi Y, Kizu H, Hayashi H (2002) Effects of catechins on vascular tone in rat thoracic aorta with endothelium. Life Sci 71(21):2553–2562 (PubMed: 12270760)
40. Satoh K, Sakamoto Y, Ogata A, Nagai F, Mikuriya H, Numazawa M, Yamada K, Aoki N (2002) Inhibition of aromatase activity by green tea extract catechins and their endocrinological effects of oral administration in rats. Food Chem Toxicol 40(7):925–933 (PubMed: 12065214)
41. Kajiya K, Kumazawa S, Nakayama T (2001) Steric effects on interaction of tea catechins with lipid bilayers. Biosci Biotechnol Biochem 65(12):2638–2643 (PubMed: 11826958)
42. No JK, Soung DY, Kim YJ, Shim KH, Jun YS, Rhee SH, Yokozawa T, Chung HY (1999) Inhibition of tyrosinase by green tea components. Life Sci 65(21):PL241–PL246 (PubMed: 10576599)
43. Guo Q, Zhao B, Shen S, Hou J, Hu J, Xin W (1999) ESR study on the structure-antioxidant activity relationship of tea catechins and their epimers. Biochim Biophys Acta 1427(1):13–23 (PubMed: 10082983)

Lipids (2008) 43:431–439
DOI 10.1007/s11745-008-3162-9

ORIGINAL ARTICLE

Structural Importance of the Acyl Group in Substrate Specificity of Purified Bovine Lysophospholipase D

Xi-Wen Liu · Dai-Eun Sok · Hong-Sun Yook · Cheon-Bae Sohn · Sun Yung Ly · Mee Ree Kim

Received: 1 October 2007 / Accepted: 15 February 2008 / Published online: 12 March 2008
© AOCS 2008

Abstract The structural importance of the acyl group in lysophosphatidylcholine (LPC) as substrate of purified bovine lysophospholipase D (lysoPLD) was investigated. Among LPCs with saturated acyl chains, the K_m value decreased according to the length of the acyl chain (C12–C16) up to the palmitoyl group, while the V_m value showed no remarkable change. But, the extension of the acyl size to C18, as observed with 1-stearoyl LPC (K_m, 8.5 mM), rather resulted in a remarkable increase in the K_m value. Meanwhile, the introduction of one double bond in the C18 saturated acyl chain led to a remarkable reduction in the K_m value, as observed with 1-oleoyl LPC (K_m, 0.48 mM). Furthermore, 1-linoleoyl LPC (K_m, 56 μM) with two double bonds exhibited a smaller K_m value than 1-oleoyl LPC, suggesting that the unsaturation degree might be important in augmenting the binding affinity of LPCs. A similar phenomenon was also observed with 1-arachidonoly LPC (K_m, 79 μM) or 1-docosahexaenoyl LPC (K_m, 36 μM). Overall, the order of catalytic efficiency (V_m/K_m value) of those LPCs seemed to be affected by the K_m value rather than the V_m value, which differed by at most threefold among LPC derivatives. Next, the introduction of a hydroperoxide group into 1-linoleoyl-LPC or 1-arachidonoyl LPC led to a further reduction in K_m values (1-hydroperoxylinoleoyl LPC, 26 μM; 1-hydroperoxyarachidonoyl LPC, 33 μM), accompanied by a further increase in the V_m/K_m values. Additionally, phosphatidylcholines (PCs) with an oxidized acyl chain at *sn*-2 position were found to be efficient as 1-palmitoyl LPC as substrates of lysoPLD. Taken together, the catalytic efficiency of LPCs or oxidized PCs as substrates of lysoPLD seems to be determined by the property of the acyl chain, length of the acyl chain, unsaturation degree and oxidation status.

Keywords Substrate specificity · Lysophospholipase D · LPC · Oxidized PC · Acyl chain · Unsaturation · Oxidation

Abbreviations

LysoPLD	Lysophospholipase D
LPC	Lysophosphatidylcholine
LPA	Lysophosphatidic acid
PC	Phosphatidylcholine
AzPC	1-Palmitoyl-2-azelaoyl-*sn*-glycero-3-phosphocholine
PGPC	1-Palmitoyl-2-glutaroyl-*sn*-glycero-3-phosphocholine

Introduction

Lysophospholipase D (lysoPLD) activity is known to catalyze the conversion of lysophosphatidylcholine (LPC) to lysoPA (lysophosphatidic acid), a potent lipid signaling molecule in numerous cellular responses [1]. LysoPLD was first reported to be present in the microsomal fraction [2], and later, extracellular lysoPLD was found to be present in plasma [3], various tissues and body fluids [4–6]. Recently,

X.-W. Liu · H.-S. Yook · C.-B. Sohn · S. Y. Ly ·
M. R. Kim (✉)
Department of Food and Nutrition,
Chungnam National University, Gung-Dong 220,
Yuseong-Gu, Taejon 305-764, South Korea
e-mail: mrkim@cnu.ac.kr

D.-E. Sok
College of Pharmacy, Chungnam National University,
Gung-Dong 220, Yuseong-Gu, Taejon 305-764, South Korea

extracellular lysoPLD, belonging to the ecto-nucleotide pyrophosphatase/phosphodiesterase family, was shown to correspond to autotoxin, a tumor cell motility-stimulating factor [7]. Thereafter, endeavors to regulate the extracellular lysoPLD activity have been attempted [8].

Concerning the substrates of lysoPLD, only LPC had been considered to be a substrate for serum lysoPLD, but subsequent studies demonstrated that lysoPLD could act on other lysophospholipids [9] and sphingosylphosphorylcholine [10]. Nonetheless, only LPC has been used as a lysoPLD substrate in a routine assay, since LPC, abundantly present in plasma, corresponds to an endogenous substrate. Although the level of LPC in plasma [9–16] amounts up to 200 μM, the concentration of LPA, generated from the hydrolysis of LPC, is limited to the micromolar level [11–13] in human plasma, where lysoPLD is constitutively active [9, 17]. Therefore, it has been suggested that lysoPLD-catalyzed hydrolysis of LPC may be regulated by endogenous factors in vivo. One explanation is that lysoPLD activity in blood may be inhibited by endogenous LPAs, cyclic LPAs and sphingosine 1-phosphate, corresponding to strong inhibitors of lysoPLD [18, 19]. Our recent study indicated that LPAs with unsaturated acyl chains expressed more potent inhibition of lysoPLD than those with saturated acyl chains [19]. It may also be that the amount of free form LPC available for the interaction with lysoPLD can limit the formation of LPA in plasma. In support of this, blood lysoPLD was observed to express affinity for free form LPCs, equilibrated with albumin- and lipoprotein-bound forms in plasma [20]. In addition, the conversion of LPC to LPA in plasma was higher for free forms of unsaturated acyl type LPCs than free forms of saturated acyl type LPCs. Thus, it was assumed that lysoPLD activity in rat plasma might show a preference for unsaturated LPCs over saturated LPCs. However, there has been no extensive study to clarify the structural requirement of acyl group in the hydrolysis of LPCs by purified lysoPLD.

Separately, lysoPLD was reported to convert the bioactive platelet activating factor (1-alky-2-acetyl PAF) to 1-alkyl-2-acetyl phosphatidic acid [20, 21]. In addition, lysoPAF was also hydrolyzed by lysoPLD to produce alkyl type LPC, which is physiologically active [21, 22]. From these, lysoPLD was supposed to be implicated in the metabolism of choline glycerophospholipids with an alkyl group at *sn* 1 and a short acyl chain at *sn* 2. In this regard, it was assumed that oxidized phosphatidylcholines (PCs), which accumulate during oxidative damage of membranes, might be substrates for lysoPLD. Nevertheless, there has been no study on the lysoPLD-catalyzed hydrolysis of oxidized PCs.

In this study, the structural requirement of the acyl chain in lysoPLD-catalyzed hydrolysis of LPCs was examined, and additionally the role of oxidized PCs as substrates for lysoPLD was investigated.

Experimental Procedures

Materials

DEAE sephacel, concanavalin A-sepharose, heparin-agarose, phenyl-agarose, choline oxidase, peroxidase (horse radish), soybean lipoxygenase (lipoxidase Type I-B), phospholipase A_2 (honey bee venom), 2,2′-azino-bis(3-ethylbenzthiazoline-6-sulfonic acid) were purchased from Sigma Chemical Co. (St Louis, MO, USA), and 1-linoleoyl LPA and 1-arachidonoyl LPA were from Echelon Co. (Salt Lake City, UT, USA). LPCs, phosphatidylcholines, 1-palmitoyl-2-azeuroyl phosphatidylcholine, 1-palmitoyl-2-glutaryl phosphatidylcholine and 1-alkyl-2-acetoyl-*sn*-glycero-3-phosphocholine (PAF) were procured from Avanti Polar Lipids, Inc. (Alabaster, AL, USA). 1-Linoleoyl LPC, 1-arachidonoyl LPC and 1-docosahexaenoyl LPC were prepared from PLA_2-catalyzed hydrolysis of the corresponding PC as described previously [23, 24]. 1-Hydroperoxylinoleoyl LPC, 1-hydroperoxyarachidonoyl LPC and 1-hydroperoxydocosahexaenoyl LPC were prepared from soybean lipoxygenase-1-catalyzed oxygenation of the corresponding LPC as reported before [24, 25].

Purification of LysoPLD from Fetal Bovine Serum

LysoPLD was purified from fetal bovine serum (JRH Biosciences, Inc, Lenexa, KS, USA) according to a slight modification of the previously reported methods [19, 26, 27] employing ammonium sulfate fractionation (30–60%), DEAE sephacel chromatography, concanavalin A sepharose affinity chromatography, heparin agarose affinity chromatography, phenyl agarose hydrophobic interaction chromatography, second DEAE sephacel chromatography and finally FPLC employing a Superpose 12 column. The protein amount was determined by the Bradford method [28]. The purified enzyme possessed a specific activity of approximately 3,700 nmol/h/mg protein in the hydrolysis of 1-palmitoyl LPC.

Spectrophotometric Assay of LysoPLD Activity

The determination of lysoPLD activity was carried out by measuring the amount of choline released from exogenously added LPC; briefly, lysoPLD (1.6 U) was incubated with 1 mM 1-palmitoyl LPC (MW, 495.6) in 100 mM Tris buffer, pH 9.0 (0.2 ml) containing 500 mM NaCl, 5 mM $MgCl_2$ and 0.05% Triton X-100 for 30 min at 37 °C. To avoid the interference by artifacts, a short-time (30 min) incubation was chosen. Then, to the assay mixture was added choline oxidase (3 U/ml) and horseradish peroxidase (1 U/ml) and finally, 2,2′-azino-bis(3-ethylbenzthiazoline-6-sulfonic acid) was included to 1 mM. After a 2-min incubation at room temperature, the change of absorbance at 415 nm was determined [26, 27]. One unit is expressed as the capability of lysoPLD to release 1 nmol of choline from 1-palmitoyl LPC per hour at 37 °C.

Determination of V_{max} and K_m Values of LPCs, PAF or Oxidized PCs

LysoPLD (1.6 U) was incubated with various concentrations (0.01–30 mM) of each LPC or oxidized PC in 100 mM Tris buffer, pH 9.0 (0.2 ml) containing 500 mM NaCl, 5 mM $MgCl_2$ and 0.05% Triton X-100 for 30 min at 37 °C. The amount of choline was determined as described above. The kinetic values were obtained according to Lineweaver–Burk plot analyses as described before [19, 26]. The catalytic efficiency of the substrate is defined as the value of V_m/K_m.

Oxygenation of 1-Linoleoyl LPA and 1-Arachidonoyl LPA

Oxygenation of 1-linoleoyl LPA or 1-arachidonoyl LPA was carried out as described in the previous publication [24, 25]. Briefly describing, each LPA (400 μM) was incubated with soybean lipoxygenase-1 (10 U/ml) in 150 μl of 50 mM borax buffer pH 9.0. After 10 min, the oxygenation products were loaded into a C_{18} Sep-pack column (3 cm × 1 cm), which was washed out with distilled water, and then the products were eluted with methanol. Finally, the methanol elute was concentrated, and used for the inhibition of lysoPLD activity.

Inhibition of LysoPLD activity by 1-Hydroperoxylinoleoyl LPA or 1-Hydroperoxyarachidonoyl LPA

LysoPLD (1.6 U) was incubated with 1-palmitoyl LPC (0.2–1.0 mM) in the presence of 1-hydroperoxylinoleoyl LPA or 1-hydroperoxyarachidonoyl LPA of different concentrations in 100 mM Tris buffer, pH 9.0 containing 500 mM NaCl, 5 mM $MgCl_2$ and 0.05% Triton X-100 for 30 min at 37 °C. The remaining lysoPLD activity was determined spectrophotometrically as described above. The K_i values were obtained according to Lineweaver–Burk plot analyses as described before [19, 29]. Separately, the K_i value was determined using a fluorogenic substrate (FS-3) as described previously [19, 30]; lysoPLD was incubated with FS-3 (0.5–4 μM) in the presence of each hydroperoxylated LPA in 100 μl of 50 mM Tris buffer pH 8.0 containing 140 mM NaCl, 5 mM KCl, 1 mM CaCl, 1 mM $MgCl_2$ and bovine serum albumin (1 mg/ml) for 30 min at room temperature. The change of fluorescent intensity was measured at 520 nm with the excitation at 480 nm.

Statistical Analysis

All statistical analyses were performed using a SPSS program for Windows. Statistical assessments were performed using ANOVA for the initial demonstration of significance at $P < 0.05$, followed by post hoc Duncan's multiple-range test [31].

Results

Determination of Kinetic Values of Various Lysophosphatidylcholines as LysoPLD Substrates

Previously [8, 18, 26], it had been reported that lysoPLD activity in rat plasma catalyzed the hydrolysis of LPCs with various acyl groups, and PCs with short acyl chains. However, the study of the role of LPCs as substrates was limited to LPCs with palmitoyl, myristoyl or oleoyl group, despite the availability of LPCs with various acyl groups, saturated or unsaturated. Thus, the structural requirement of the acyl chain for LPCs as substrate of lysoPLD remains to be clarified. Here, lysoPLD activity was determined by measuring the amount of choline released from lysoPLD-catalyzed hydrolysis of LPCs in the assay buffer (Tris buffer, pH 9.0) containing 500 mM NaCl, 5 mM $MgCl_2$, and 0.05% Triton X-100. First, when the K_m value and V_m value of 1-palmitoyl LPC, displaying a typical pattern of saturation kinetics, were determined by double-reciprocal plot analysis (Fig. 1a), it was found to possess K_m and V_m values of 147 μM and 2,011 nmol/h/mg, respectively. Similarly, the kinetic values of the other LPCs were also determined (Table 1). Among LPCs with saturated fatty acyl chains, the catalytic efficiency, reflected by the V_m/K_m value, was observed to be the highest for 1-palmitoyl LPC, followed by 1-myristoyl LPC (K_m, 273 μM; V_m, 2,622 nmol/h/mg), 1-lauroyl LPC (K_m, 2,291 μM; V_m, 2,717 nmol/h/mg) and 1-stearoyl LPC (K_m, 8,512 μM; V_m, 2,244 nmol/h/mg). Thus, the catalytic efficiency appeared to be proportional to the size of the acyl chain (C12–C16) up to the palmitoyl group, but the extension of the acyl size to C18, as observed with 1-stearoyl LPC, resulted in a remarkable decrease. Noteworthy, a similar relationship was also found between the size of the acyl group and the K_m values, which differed by 320 -fold among saturated acyl type LPCs. Therefore, the order of catalytic efficiency of LPCs seemed to be affected by the K_m value rather than the V_m value, which differed by at most threefold among

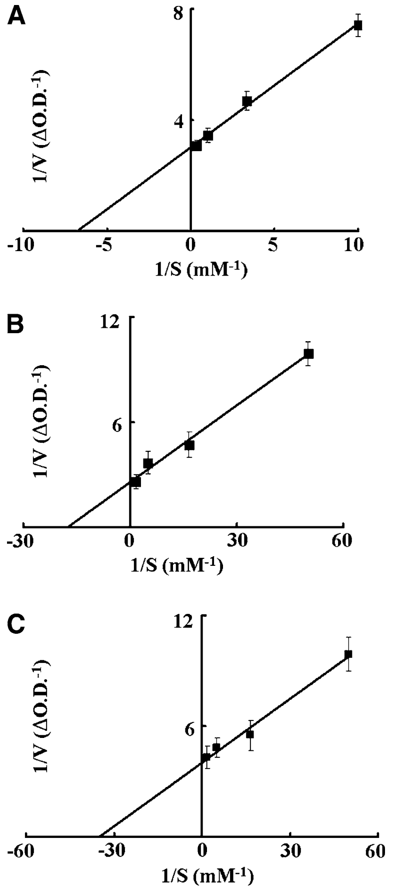

Fig. 1 Lineweaver–Burk double reciprocal plot for lysoPLD-catalyzed hydrolysis of LPCs LysoPLD (1.6 U) was incubated with each LPC in 100 mM Tris buffer (pH 9.0) containing 500 mM NaCl, 5 mM $MgCl_2$ and 0.05% Triton X-100 for 30 min at 37 °C. **a** 1-Palmitoyl LPC; **b** 1-linoleoyl LPC; **c** 1-hydroperoxylinoleoyl LPC. Data were expressed as means ± S.D. of three experimental sets

LPC derivatives. Meanwhile, the introduction of one double bond in the C18 saturated acyl chain led to a remarkable decrease in the K_m value; 1-stearoyl LPC (K_m, 8,512 μM) vs. 1-oleoyl LPC (K_m, 477 μM). From these, it was supposed that the catalytic efficiency of LPCs might be also governed by the unsaturation degree of the acyl chain. In this regard, LPCs with polyunsaturated fatty acyl chains were tested for their efficiency as a substrate of lysoPLD. As demonstrated in Fig. 1b, the hydrolysis of 1-linoleoyl LPC by lysoPLD followed classical Michaelis–Menten kinetics as observed with 1-palmitoyl LPC (Fig. 1a); the K_m and V_m values of 1-linoleoyl LPC were estimated to be 56 μM and 2,077 nmol/h/mg, respectively. Thus, the catalytic efficiency of 1-linoleoyl LPC was much greater than that of 1-stearoyl LPC or 1-oleoyl LPC, which contains the same carbon number. In addition, the K_m value and the V_m value of 1-arachidonoyl LPC were estimated to be 79 μM and 2,100 nmol/h/mg, respectively, and the K_m value and the V_m value of 1-docosahexaenoyl LPC were estimated to be 36 μM and 1,116 nmol/h/mg, respectively. In comparison, 1-linoleoyl LPC appeared to express a higher V_m/K_m value than 1-arachidonoyl LPC or 1-docosahexaenoyl LPC. However, the smallest K_m value was expressed by 1-docosahexaenoyl LPC, followed by 1-linoleoyl LPC and 1-arachidonoyl LPC. This led to the notion that the property of the acyl chain might affect the catalytic efficiency of polyunsaturated acyl type LPCs. In this regard, we examined the kinetic values of LPCs with oxidized acyl chains.

Effect of Oxidation on the Catalytic Efficiency of LPC with Polyunsaturated Fatty Acyl Chains

It is well known that polyunsaturated fatty acids are susceptible to oxidation [32, 33]. Likewise, LPCs with polyunsaturated fatty acyl chains were found to be readily subjected to enzymatic oxygenation [24, 25]. In the attempt to see whether the oxidation could alter the catalytic efficiency of LPCs as substrate, 1-linoleoyl LPC was subjected to enzymatic or non-enzymatic oxidation, and then kinetic values of oxidized LPC were determined. First, when 1-linoleoyl LPC was exposed to non-enzymatic oxidation such as HOCl oxidation or copper ion-catalyzed oxidation, and the kinetic values of oxidized LPC were determined, there was no great change (<10%) of V_{max} value or K_m value. Next, 1-linoleoyl LPC was subjected to oxygenation by soybean lipoxygenase-1 to produce 1-hydroperoxylinoleoyl LPC. When the kinetic values of 1-hydroperoxylinoleoyl LPC were determined (Fig. 1c), the K_m value and the V_{max} value were estimated to be 26 μM and 1,450 nmol/h/mg, respectively (Table 1). Thus, the K_m value of 1-hydroperoxylinoleoyl LPC was reduced by 2.2-fold, compared to that of 1-linoleoyl LPC (K_m, 56 μM). Additionally, the K_m value (33 μM) of 1-hydroperoxyarachidonoyl LPC decreased by 2.4-fold, compared to that of 1-arachidonoyl LPC. However, the K_m value of 1-docosahexanoyl LPC was not altered remarkably after the exposure to soybean lipoxygenase-1. When the V_m values were compared, there was a modest decrease in the V_m value after the exposure of each polyunsaturated fatty acyl type LPC to soybean lipoxygenase-1 (Table 1). Taken together, the oxygenation of 1-linoleoyl-LPC or 1-arachidonoyl LPC with soybean lipoxygenase-1 led to some reduction in the K_m value, thereby leading to a further increase in the V_m/K_m value; 1-linoleoyl-LPC (V_m/K_m, 37.5 nmol/h/mg/μM) vs. 1-hydroperoxylinoleoyl-LPC (V_m/K_m, 56.1 nmol/h/mg/μM) and 1-arachidonoyl-LPC (V_m/K_m, 27.5 nmol/h/mg/μM) vs. 1-hydroperoxyarachidonoyl LPC (V_m/K_m, 39.6 nmol/h/mg/μM). However, such an oxygenation failed to affect the V_m/K_m values of 1-docosahexaenpoyl LPC remarkably, suggesting that the beneficial effect of lipoxygenation was not pronounced positively in the case of 1-docosahexaenoyl LPC with six double bonds. In a separate experiment, there

Table 1 K_m and V_m values of LPCs

Acyl moiety	K_m (μM)	V_{max} (nmol/h/mg)	V_{max}/K_m (nmol/h/mg/μM)
1-Lauroyl	2,291 ± 539	2,717 ± 401	1.3 ± 0.5
1-Myristoyl	273 ± 79	2,622 ± 305	9.7 ± 3.0
1-Palmitoyl	147 ± 12	2,011 ± 152	13.4 ± 1.8
1-Stearoyl	8,512 ± 1,828	2,244 ± 433	0.3 ± 0.1
1-Oleoyl	477 ± 44	1,967 ± 207	4.1 ± 0.5
1-Linoleoyl	56 ± 6^{a}	2,077 ± 258	37.5 ± 4.5^{a}
1-Hydroperoxylinoleoyl	26 ± 4^{b}	1,450 ± 234	56.1 ± 9.8^{b}
1-Hydroxylinoleoyl	35 ± 4^{c}	1,444 ± 255	40.9 ± 4.1^{a}
1-Arachidonoyl	79 ± 12^{d}	2,100 ± 233	27.5 ± 5.0^{c}
1-Hydroperoxyarachidonoyl	33 ± 6^{c}	1,294 ± 256	39.6 ± 5.5^{a}
1-Hydroxyarachidonoyl	46 ± 7^{ac}	1,883 ± 304	42.3 ± 3.2^{a}
1-docosahexaenoyl	36 ± 4^{c}	1,116 ± 156	31.0 ± 2.3^{c}
1-Hydroperoxydocosahexaenoyl	34 ± 3^{c}	994 ± 120	29.5 ± 3.2^{c}
1-Hydroxydocosahexaenoyl	35 ± 7^{c}	1,066 ± 202	29.7 ± 5.2^{c}

LysoPLD (1.6 U) was incubated with each LPC in 100 mM Tris buffer (pH 9.0) containing 500 mM NaCl, 5 mM $MgCl_2$ and 0.05% Triton X-100 for 30 min at 37 °C. The kinetic values were obtained according to Lineweaver–Burk plot analysis. Data were expressed as mean ± S.D. of three experimental sets. Values were expressed as mean ± S.E. of at least three independent experiments. Mean values with the same letter are not significantly different ($P < 0.05$, $n = 3$)

was approximately twofold increase of K_m values after reduction of hydroperoxy group to hydroxyl group; 1-hydroperoxylinoleoyl-LPC (K_m, 26 μM) vs. 1-hydroxylinoleoyl-LPC (K_m, 35 μM) and 1-hydroperoxyarachidonoyl-LPC (K_m, 33 μM) vs. 1-hydroxyarachidonoyl-LPC (K_m, 46 μM).

Inhibition of LysoPLD by 1-Hydroperoxylinoleoyl LPA or 1-Hydroperoxyarachidonoyl LPA

Since the introduction of a peroxide group into linoleoyl or arachidonoyl chain caused a remarkable increase of binding affinity of LPC toward to lysoPLD, it was supposed that the hydro(pero)xide group might be responsible for the increased affinity of acyl chain to lysoPLD. In an attempt to support this idea, 1-linoleoyl-LPA and 1-arachidonoyl-LPA were oxygenated to produce 1-hydroperoxylinoleoyl-LPA or 1-hydroperoxyarachidonoyl-LPA [24, 25], and the effect of oxygenation on the inhibitory potency of those LPAs was examined. As shown in Fig. 2, it was found that lysoPLD-catalyzed hydrolysis of 1-palmitoyl LPA was inhibited competitively by 1-hydroperoxylinoleoyl LPA in a dose-dependent manner. According to the double-reciprocal plot analysis (Fig. 2a), the K_i value of 1-hydroperoxylinoleoyl LPA was estimated to be 1.14 μM (Table 2), which was found to be lower than K_i value (1.8 μM) of 1-linoleoyl LPA reported previously [19]. Likewise, the K_i value (2.68 μM) of 1-hydroperoxyarachidonoyl LPA was smaller than that (3.4 μM) of 1-arachidonoyl LPA reported previously [19]. Thus, the incorporation of peroxide group markedly enhanced the binding of polyunsaturated acyl type LPAs toward lysoPLD. Separately, it was found that lysoPLD-catalyzed hydrolysis of FS-3, fluorescent substrate [30], was inhibited by 1-hydroperoxylinoleoyl LPA in a dose-dependent manner at relatively low concentrations. According to the double-reciprocal plot analysis (Fig. 2b), the K_i value of 1-hydroperoxylinoleoyl LPA was estimated to be 0.14 μM (Table 2), which was found to be lower than the K_i value (0.21 μM) of 1-linoleoyl LPA reported previously [19]. Likewise, the K_i value (0.25 μM) of 1-hydroperoxyarachidonoyl LPA was smaller than that (0.55 μM) of 1-arachidonoyl LPA reported previously [19]. Thus, the incorporation of peroxide group markedly enhanced the binding affinity of LPAs with polyunsaturated fatty acyl chain toward lysoPLD.

Hydrolysis of Oxidized PCs by LysoPLD

Previous studies [20, 21] indicated that PAF, containing an acetyl group at the *sn*-2 position, could be utilized as a substrate for lysoPLD. Therefore, PCs with short acyl derivatives at *sn*-2 were supposed to be used as lysoPLD substrates. In this respect, the oxidized PCs such as 1-palmitoyl-2-azelaoyl-*sn*-glycero-3-phosphocholine (AzPC) and 1-palmitoyl-2-glutaroyl-*sn*-glycero-3-phosphocholine (PGPC) were tested for their efficacy as substrates of lysoPLD. The hydrolysis of AzPC or PGPC by lysoPLD followed classic Michaelis–Menten kinetics as observed with 1-palmitoyl LPC. In a Lineweaver–Burk plot analysis (Fig. 3a), the K_m and V_m values of AzPC were estimated to be 203 μM and 1,533 nmol/h/mg, respectively (Table 3). In

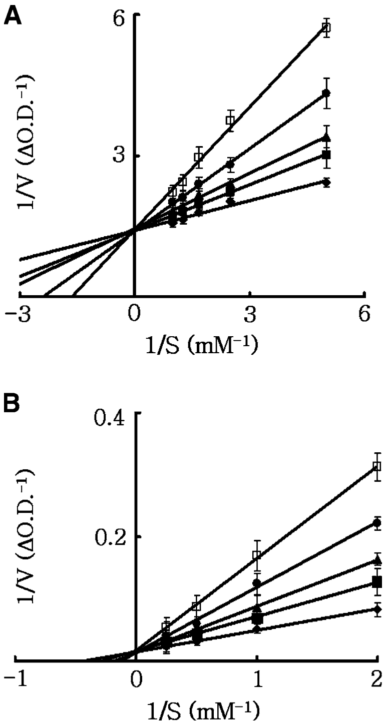

Fig. 2 Inhibitory effect of LPAs on lysoPLD-catalyzed hydrolysis of 1-palmitoyl LPC or FS-3. **a** LysoPLD (1.6 U) was incubated with 1-palmitoyl LPC (0.2–1.0 mM) in the presence of 1-hydroperoxylinoleoyl LPA in 100 mM Tris buffer (pH 9.0) containing 500 mM NaCl, 5 mM $MgCl_2$ and 0.05% Triton X-100 for 30 min at 37 °C. *Filled diamonds* indicate the control, *filled squares* indicate 0.5 µM, *filled triangles* indicate 1 µM, *filled circles* indicate 2 µM, *open squares* indicate 4 µM. Data were expressed as means ± S.D. of three experimental sets. **b** LysoPLD (1.6 U) was incubated with FS-3 (0.5–4 µM) in the presence of 1-hydroperoxylinoleoyl LPA in 100 µl of 50 mM Tris buffer pH 8.0 containing 140 mM NaCl, 5 mM KCl, 1 mM CaCl, 1 mM $MgCl_2$ and BSA (1 mg/ml) for 30 min at 25 °C. *Filled diamonds* indicate control, *filled squares* indicate 0.03 µM, *filled triangles* indicate 0.1 µM, *filled circles* indicate 0.3 µM, *open squares* indicate 1 µM. Data were expressed as means ± S.D. of three experimental sets

addition (Fig. 3b), PGPC showed the K_m value of 146 µM and the V_m value of 2,172 nmol/h/mg. Although the K_m value of AzPC or PGPC was greater than that of PAF (K_m, 71 µM), the V_m value of those oxidized PCs was greater than that of PAF. Overall, the catalytic efficiency (V_m/K_m) of AzPC or PGPC was close to that of PAF or 1-palmitoyl LPC.

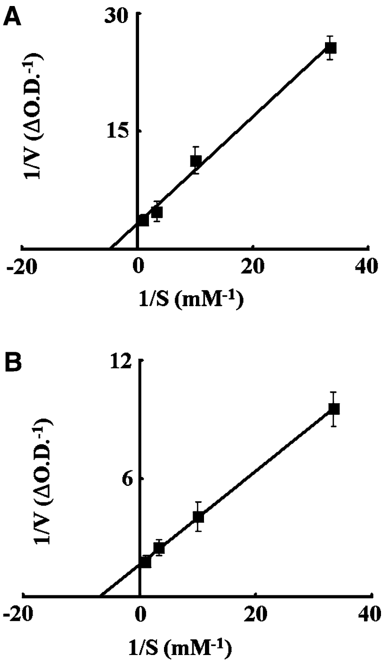

Fig. 3 Lineweaver–Burk double reciprocal plot for lysoPLD-catalyzed hydrolysis of oxidized phosphatidylcholines. **a** LysoPLD (1.6 U) was incubated with AzPC in 100 mM Tris buffer (pH 9.0) containing 500 mM NaCl, 5 mM $MgCl_2$ and 0.05% Triton X-100 for 30 min at 37 °C. **b** LysoPLD (1.6 U) was incubated with PGPC as described in **a**. Data were expressed as mean ± S.D. of three experimental sets

Thus, it is suggested that AzPC and PGPC may be utilized efficiently as a substrates for lysoPLD.

Discussion

Our present study shows that the K_m value of LPCs with saturated acyl chains varies greatly (up to 320-folds) according to the length of the acyl chain. It is worth noting that the introduction of one double bond in stearoyl LPC led to a remarkable enhancement of binding affinity as illustrated with 1-oleoyl LPC. Furthermore, 1-linoleoyl LPC with two double bonds expressed a much smaller K_m value than 1-oleoyl LPC, reaffirming that the unsaturation degree might be one of the factors in determining the K_m

Table 2 K_i values of 1-hydroperoxylinoleoyl LPA or 1-hydroperoxyarachidonoyl LPA in the inhibition of LysoPLD activity

Acyl group	Spectrophotometric assay, K_i (µM)	Fluorometric assay, K_i (µM)
1-Hydroperoxylinoleoyl	1.14 ± 0.13	0.14 ± 0.01
1-Hydroperoxyarachidonoyl	2.68 ± 0.61	0.25 ± 0.02

LysoPLD (1.6 U) was incubated with 1-palmitoyl LPC (0.2–1.0 mM) in the presence of each LPA as described in Fig. 2. Separately, lysoPLD (1.6 U) was incubated with FS-3 (0.5–4 µM) in the presence of each LPA. The K_i values were determined as described in Fig. 2, and the values were expressed as mean ± S.D. of three experimental sets

Table 3 K_m and V_{max} values of oxidized phosphatidylcholines

	K_m (μM)	V_{max} (nmol/h/mg)	V_{max}/K_m (nmol/h/mg/μM)
AzPC	203 ± 11	1,533 ± 134	7.6 ± 1.0
PGPC	146 ± 20	2,172 ± 288	14.9 ± 1.2
PAF (1-Alkyl-2-acetoyl)	71 ± 5	1,228 ± 122	17.3 ± 2.5

LysoPLD (1.6 U) was incubated with each oxidized PC in 100 mM Tris buffer (pH 9.0) containing 500 mM NaCl, 5 mM $MgCl_2$ and 0.05% Triton X-100 for 30 min at 37 °C. The K_m and V_{max} values were obtained as described in Table 1. Data were expressed as mean ± S.D. of three experimental sets

value of LPCs. Furthermore, such a beneficial effect of unsaturation was more remarkable for 1-docosahexaenoyl LPC. In contrast, the V_m value of LPCs was less dependent on the type of acyl chain; the differences of V_m values, among LPCs with saturated acyl chains (C12–C16), were limited to at most threefold. Taken together, the order of catalytic efficiency of LPCs with saturated acyl chains seems to be more intimately related to the K_m value than the V_m value of LPCs, suggesting that the catalytic efficiency of LPCs may be determined largely by the binding affinity of the acyl chain. Such a difference in the K_m values of LPCs might be due to the difference in the micellar concentrations of LPCs, since the K_m value decreased with increasing length of the acyl chains (C12–C16), inversely proportional to the critical micellar concentration (CMC) values [34, 35]. However, this is not supported by the finding that 1-stearoyl LPC, possessing a smaller CMC value, possessed a higher K_m value than 1-palmitoyl LPC. Furthermore, the K_m values of LPCs with saturated fatty acyl chain, possessing smaller CMC values, were greater than those of LPCs with unsaturated acyl chains. Alternatively, it is conceivable that the smaller K_m values of LPCs may be related to the greater product inhibition of lysoPLD by LPAs [8, 19], produced during the incubation of LPCs with lysoPLD. However, this is not supported by the previous finding that the inhibitory potency of LPAs with saturated acyl chains increases with decreasing length of the acyl chain (C14–C20) [19]. From these, it is supposed that the direct binding of the LPC monomer to the lysoPLD active site is important for lysoPLD-catalyzed hydrolysis of LPCs. It is interesting to find that the structural requirement of the acyl chain in the hydrolysis of LPCs by lysoPLD is somewhat similar to that in the inhibition of lysoPLD by LPAs [19]; the unsaturated fatty acyl type is preferred to the saturated fatty acyl type for the interaction of lysoPLD with either LPCs or LPAs. Moreover, the contributory role of the oxygenated acyl chain was commonly observed in the hydrolysis of LPCs by lysoPLD as well as the inhibition of lysoPLD by LPAs. Taken together, the interaction of lysoPLD with LPCs seems to be governed strictly by the property of the acyl chain, depending on the length of the acyl chain, the unsaturation degree and the oxygenation of the acyl chain.

A previous report [20, 26] indicated that PCs with short acyl chains as well as PAF could be utilized as a substrate of lysoPLD. The present study with oxidized PCs may add to the list of substrates for lysoPLD. AzPC and PGPC, corresponding to oxidized PCs with oxidized acyl chains at the *sn*-2 position, were also found to be good substrates of lysoPLD. From the similarity of catalytic efficiency between of oxidized PCs and 1-palmitoyl LPC, it is suggested that oxidized PCs can go through the metabolic pathway, which is mediated by lysoPLD in vivo [3–5].

Previously, it was reported that the lysoPLD-induced conversion of endogenous unsaturated LPCs was more favorable than saturated LPCs in rat plasma [20]. A possible explanation is that lysoPLD shows a higher affinity for free forms of unsaturated acyl type LPCs than free forms of saturated acyl type LPCs. Therefore, the substrate specificity of lysoPLD for LPCs is supposed to be a primary factor responsible for the conversion of LPCs into LPAs in plasma. In support of this, the order (1-linoleoyl LPC > 1-arachidonoyl LPC ~ 1-palmitoyl LPC > 1-oleoyl LPC > 1-stearoyl LPC) for the yield in the conversion of LPCs to LPAs in plasma [20] seems to agree well with that for catalytic efficiency (V_m/K_m) of those LPCs in this present study. However, the substrate specificity of purified bovine lysoPLD toward LPCs seemed to somewhat differ from that reported previously [26]. The discrepancy might be explained by the difference of kinetic analysis used and/or the assay conditions [19, 26, 27]; the previous study employed a prolonged incubation (up to 24 h), where LPAs, produced from the incubation of lysoPLD with LPCs, might have interfered with lysoPLD-catalyzed hydrolysis of LPC through the product inhibition [8].

Here, the structure activity relationship of LPCs as substrates of lysoPLD was established, based on the catalytic efficiency (K_m/V_m). Bovine lysoPLD expressed higher substrate specificity for LPCs with unsaturated acyl chains than those with saturated acyl chains. Noteworthy, the oxygenation of the unsaturated fatty acyl chain remarkably reduced the K_m values of unsaturated fatty acyl type LPCs, resulting in a further increase in catalytic efficiency. In addition, PCs with an oxidized acyl chain were as efficient as 1-palmitoyl LPC or PAF as substrates for lysoPLD. Thus, lysoPLD may be implicated in the metabolism of choline phospholipids such as LPCs, oxidized PCs and PAF. In other words, these choline phospholipids may compete with each other as substrates of lysoPLD in the in vivo system. In this regard, it is conceivable that polyunsaturated acyl type LPCs, showing smaller K_m values, may suppress the lysoPLD-catalyzed hydrolysis of alkyl type LPCs, saturated acyl type LPCs, oxidized PCs or PAF, expressing higher K_m values. Furthermore, this may lead to the notion that the level of physiologically active LPAs may be regulated by the level of polyunsaturated acyl type LPCs in the blood, which remains to be clarified in the near future.

Acknowledgments This study was supported by the Korea Research Foundation Grant funded by the Korean Government (MOEHRD, Basic Research Promotion Fund) (KRF-2007-531-C00067).

References

1. van Meeteren LA, Moolenaar WH (2007) Regulation and biological activities of the autotaxin-LPA axis. Prog Lipid Res 46:145–160
2. Wykle RL, Schremmer JM (1974) A lysophospholipase D pathway in the metabolism of ether-linked lipids in brain microsomes. J Biol Chem 249:1742–1746
3. Yamashita M, Homma H, Inoue K, Nojima S (1983) The metabolism of platelet activating factor in platelets and plasma of various animals. J Toxicol Sci 8:177–188
4. Tokumura A, Miyake M, Nishioka Y, Yamano S, Aono T, Fukuzawa K (1999) Production of lysophosphatidic acids by lysophospholipase D in human follicular fluids of in vitro fertilization patients. Biol Reprod 61:195–199
5. Tokumura A, Fujimoto H, Yoshimoto O, Nishioka Y, Miyake M, Fukuzawa K (1999) Production of lysophosphatidic acid by lysophospholipase D in incubated plasma of spontaneously hypertensive rats and Wistar Kyoto rats. Life Sci 65:245–253
6. Gesta S, Simon M, Rey A, Sibrac D, Girard A, Lafontan M, Valet P, Saulnier-Blache J (2002) Secretion of a lysophospholipase D activity by adipocytes, involvement in lysophosphatidic acid synthesis. J Lipid Res 43:904–910
7. Clair T, Lee HY, Liotta LA, Stracke ML (1997) Autotaxin is an exoenzyme possessing 5′-nucleotide phosphodiesterase/ATP pyrophosphatase and ATPase activities. J Biol Chem 272:996–1001
8. van Meeteren LA, Ruurs P, Christodoulou E, Goding JW, Takakusa H, Kikuchi K, Perrakis A, Nagano T, Moolenaar WH (2005) Inhibition of autotaxin by lysophosphatidic acid and sphingosine 1-phosphate. J Biol Chem 280:21155–21161
9. Aoki J, Taira A, Takanezawa Y, Kishi Y, Hama K, Kishimoto T, Mizuno K, Saku K, Taguchi R, Arai H (2002) Serum lysophosphatidic acid is produced through diverse phospholipase pathways. J Biol Chem 277:39696–39702
10. Clair T, Aoki J, Koh E, Bandle RW, Nam SW, Ptaszynska MM, Mills GB, Schiffmann E, Liotta LA, Stracke ML (2003) Autotaxin hydrolyzes sphingosylphosphorylcholine to produce the regulator of migration, sphingosine-1-phosphate. Cancer Res 63:5446–5453
11. Sano T, Baker D, Virag T, Wada A, Yatomi Y, Kobayashi T, Igarashi Y, Tigyi G (2002) Multiple mechanisms linked to platelet activation result in lysophosphatidic acid and sphingosine 1-phosphate generation in blood. J Biol Chem 277:21197–21206
12. Eichholtz T, Jalink K, Fahrenfort I, Moolenaar WH (1993) The bioactive phospholipid lysophosphatidic acid is released from activated platelets. Biochem J 291:677–680
13. Baker DL, Morrison P, Miller B, Riely CA, Tolley B, Westermann AM, Bonfrer JM, Bais E, Moolenaar WH, Tigyi G (2002) Plasma lysophosphatidic acid concentration and ovarian cancer. J Am Med Assoc 287:3081–3082
14. Okita M, Gaudette DC, Mills GB, Holub BJ (1997) Elevated levels and altered fatty acid composition of plasma lysophosphatidylcholine (lysoPC) in ovarian cancer patients. Int J Cancer 71:31–34
15. Croset M, Brossard N, Polette A, Lagarde M (2000) Characterization of plasma unsaturated lysophosphatidylcholines in human and rat. Biochem J 345:61–67
16. Ojala PJ, Hirvonen TE, Hermansson M, Somerharju P, Parkkinen J (2007) Acyl chain-dependent effect of lysophosphatidylcholine on human neutrophils. J Leukoc Biol 82:1501–1509
17. Aoki J (2004) Mechanisms of lysophosphatidic acid production. Semin Cell Dev Biol 15:477–489
18. Baker DL, Fujiwara Y, Pigg KR, Tsukahara R, Kobayashi S, Murofushi H, Uchiyama A, Murakami-Murofush K, Koh E, Bandle RW, Byun HS, Bittman R, Fan D, Murph M, Mills GB, Tigyi G (2006) Carba analogs of cyclic phosphatidic acid are selective inhibitors of autotaxin and cancer cell invasion and metastasis. J Biol Chem 281:22786–22793
19. Liu XW, Sok DE, Yook HS, Sohn CB, Chung YJ, Kim MR (2007) Inhibition of lysophospholipase D activity by unsaturated lysophosphatidic acids or seed extracts containing 1-linoleoyl and 1-oleoyl lysophosphatidic acid. J Agric Food Chem 55:8717–8722
20. Tokumura A, Nishioka Y, Yoshimoto O, Shinomiya J, Fukuzawa K (1999) Substrate specificity of lysophospholipase D which produces bioactive lysophosphatidic acids in rat plasma. Biochim Biophys Acta 1437:235–245
21. Sugimoto S, Sugimoto H, Aoyama C, Aso C, Mori M, Izumi T (2006) Purification and characterization of lysophospholipase D from rat brain. Biochim Biophys Acta 1761:1410–1418
22. Tokumura A, Sinomiya J, Kishimoto S, Tanaka T, Kogure K, Sugiura T, Satouchi K, Waku K, Fukuzawa K (2002) Human platelets respond differentially to lysophosphatidic acids having a highly unsaturated fatty acyl group and alkyl ether-linked lysophosphatidic acids. Biochem J 365:617–628
23. Roberts MF, Deems RA, Dennis EA (1977) Dual role of interfacial phospholipid in phospholipase A2 catalysis. Proc Natl Acad Sci USA 74:1950–1954
24. Huang LS, Kim MR, Jeong TS, Sok DE (2007) Linoleoyl lysophosphatidic acid and linoleoyl lysophosphatidylcholine are efficient substrates for mammalian lipoxygenases. Biochim Biophys Acta 1770:1062–1070
25. Huang LS, Kim MR, Sok DE (2007) Oxygenation of 1-docosahexaenoyl lysophosphatidylcholine by lipoxygenases; conjugated hydroperoxydiene and dihydroxytriene derivatives. Lipids 42:981–990
26. Tokumura A, Majima E, Kariya Y, Tominaga K, Kogure K, Yasuda K, Fukuzawa K (2002) Identification of human plasma lysophospholipase D, a lysophosphatidic acid-producing enzyme, as autotaxin, a multifunctional phosphodiesterase. J Biol Chem 277:39436–39442
27. Umezu-Goto M, Kishi Y, Taira A, Hama K, Dohmae N, Takio K, Yamori T, Mills GB, Inoue K, Aoki J, Arai H (2002) Autotaxin has lysophospholipase D activity leading to tumor cell growth and motility by lysophosphatidic acid production. J Cell Biol 158:227–233
28. Bradford M (1976) A rapid and sensitive method for quantitation of microgram quantities of protein utilizing the principle of protein-dye binding. Anal Biochem 72:248–254
29. Egmond MR, Brunori M, Fasella PM (1976) The steady-state kinetics of the oxygenation of linoleic acid catalysed by soybean lipoxygenase. Eur J Biochem 61:93–100
30. Ferguson CG, Bigman CS, Richardson RD, van Meeteren LA, Moolenaar WH, Prestwich GD (2006) Fluorogenic phospholipid substrate to detect lysophospholipase D/autotaxin activity. Org Lett 8:2023–2026

31. Steel RGD, Torrie JH (1960) Analysis of variance I: the one-way classification, principles and procedures of statistics. McGraw-Hill, New York, pp 99–132
32. Arlt S, Beisiegel U, Kontush A (2002) Lipid peroxidation in neurodegeneration: new insights into Alzheimer's disease. Curr Opin Lipidol 13:289–294
33. Christopher J, Axelrod B (1971) On the different positional specificities of peroxidation of linoleate shown by two isozymes of soybean lipoxygenase. Biochem Biophys Res Commun 44:731–736
34. Li Z, Mintzer E, Bittman R (2004) The critical micelle concentrations of lysophosphatidic acid and sphingosylphosphorylcholine. Chem Phys Lipids 130:197–201
35. Kumar VV, Baumann WJ (1991) Lanthanide-induced phosphorus-31 NMR downfield chemical shifts of lysophosphatidylcholines are sensitive to lysophospholipid critical micelle concentration. Biophys J 59:103–107

Lipids (2008) 43:441–450
DOI 10.1007/s11745-008-3174-5

ORIGINAL ARTICLE

Unusual Fatty Acids in the Fat Body of the Early Nesting Bumblebee, *Bombus pratorum*

Josef Cvačka · Edita Kofroňová · Soňa Vašíčková ·
Karel Stránský · Pavel Jiroš · Oldřich Hovorka ·
Jiří Kindl · Irena Valterová

Received: 6 December 2007 / Accepted: 6 March 2008 / Published online: 26 March 2008
© AOCS 2008

Abstract Unusual fatty acids with 24, 26, and 28 carbon atoms were found in triacylglycerols (TAGs) isolated from fat body tissue of bumblebee *Bombus pratorum*. The most abundant one was (*Z*,*Z*)-9,19-hexacosadienoic acid. Its structure was determined by mass spectrometry after derivatization with dimethyl disulfide and by infrared spectroscopy. ECL (equivalent chain length) values of its methyl ester were determined on both DB-1 and DB-WAX capillary columns. (*Z*,*Z*)-9,19-Hexacosadienoic acid is quite rare in nature. So far it has been identified only in marine sponges, and this work is the first evidence of its occurrence in a terrestrial organism. HPLC/MS analysis of the bumblebee TAGs showed that (*Z*,*Z*)-9,19-hexacosadienoic acid is present in one third of all TAG molecular species. As it was found in all sn-TAG positions, it is likely that (*Z*,*Z*)-9,19-hexacosadienoic acid is transported to tissues. Interestingly, labial gland secretion of *B. pratorum* was found to contain (*Z*,*Z*)-7,17-pentacosadiene, a hydrocarbon with markedly similar double bond positions and geometry. Possible biosynthetic relationships between these two compounds are discussed.

Keywords Bumblebees · *Bombus pratorum* · Fat body lipids · Fatty acids · Marking pheromone biosynthesis · Triacylglycerol analysis

Introduction

In insects, fat body is the major storage site for nutrients. Most lipid stores are triacylglycerols (TAGs). It is assumed that the fat body TAGs originate mainly from dietary fats absorbed by midgut epithelium during times of feeding. In addition, lipid reserves can be biosynthesized de novo from carbohydrates [1]. The fat body is also a key center of metabolism, which responds to the physiological and biochemical needs of insects. Lipids are mobilized in the form of 1,2-diacylglycerols and transported to tissues. Fatty acids (FAs) are known to be essential precursors in the biosynthesis of many important compounds, including eicosanoids, pheromones, cuticular hydrocarbons, and other semiochemicals [2]. It is hypothesized that FAs released from fat body of bumblebee males might serve as precursors of their marking pheromones [3]. The most common FAs found in insect fat bodies are palmitic, palmitoleic, stearic, oleic and linoleic acids [4–6]. The same FAs also prevail in bumblebees, and we have shown that the FA composition as well as the composition of TAGs in this genus are clearly species-specific [7]. Large differences exist among species, whereas variations within the species are substantially less significant. In our effort to prove connections between fat body TAGs and bumblebee male marking pheromones, several species were investigated, including the early nesting bumblebee *Bombus pratorum*. This is a relatively small bee with a bright yellow thorax and strikingly orange tail that is common all over Europe. The fat body of this species was found to

---

J. Cvačka · E. Kofroňová · S. Vašíčková · K. Stránský ·
P. Jiroš · O. Hovorka · J. Kindl · I. Valterová (✉)
Institute of Organic Chemistry and Biochemistry,
Academy of Sciences of the Czech Republic,
Flemingovo nám. 2, 166 10 Prague, Czech Republic
e-mail: irena@uochb.cas.cz

E. Kofroňová · P. Jiroš
Institute of Chemical Technology, Technická 5,
166 28 Prague, Czech Republic

contain rare FAs which have not been detected in any other insect species so far.

In this work we report on long-chain FAs with 24, 26 and 28 carbon atoms found in the fat body of the male bumblebee *B. pratorum*. Possible connections between the most abundant long-chain (*Z*,*Z*)-9,19-hexacosadienoic acid and labial gland secretion (marking pheromone) components are discussed.

Materials and Methods

Insect Material and Sample Preparation

The bumblebee males of *Bombus (Pyrobombus) pratorum* (Linnaeus, 1761) were collected during the summer season 2006 in the north region of the Czech Republic and transported to the laboratory. After immobilization of males in cold (−18°C), their peripheral fat bodies were carefully dissected. The fat body tissue from each individual was transferred into a glass vial with 100 µL of $CHCl_3/CH_3OH$ (1:1, *v*/*v*) containing di-*tert*-butyl-4-methylphenol (Fluka, Buchs, Switzerland) at a concentration of 25 mg/mL. Samples were sonicated for 15 min and stored at −18 °C.

Isolation of Triacylglycerols

The tissue was thoroughly crushed using a glass stick and extracted three times with 100 µL of $CHCl_3/CH_3OH$ (1:1, *v*/*v*). The combined crude extract was separated on a pre-cleaned glass TLC plate (76 mm × 36 mm) coated with 0.2 mm of Adsorbosil Plus silica gel [Applied Science Laboratories, Alltech Associates, Inc., Deerfield, IL, USA; with gypsum (12%)] using a hexane/diethyl ether/formic acid (80:20:1) mobile phase. TLC zones were visualized by spraying Rhodamine 6G solution (0.05% in ethanol). The band containing TAGs ($R_F = 0.6$) was scraped off the plate and extracted with 7 mL of freshly distilled diethyl ether. The solvent was evaporated to dryness under argon stream. The samples were reconstituted in chloroform to a concentration of 1% and stored in sealed glass ampoules under argon at −18 °C until analyzed. The absolute amounts of TAGs isolated from samples 1–5 were 0.2, 0.4, 0.8, 0.9, and 0.1 mg, respectively.

Transesterification and DMDS Derivatization

TAG samples were transesterified using a method described earlier [8]. Briefly, TAGs were dissolved in $CHCl_3/CH_3OH$ (2:3, *v*/*v*) in a small glass ampoule. After adding acetyl chloride (Fluka), the ampoule was sealed and placed in a water bath at 70 °C. This procedure prevents the loss of volatile FAMEs during transesterification. After 90 min the ampoule was opened and the reaction mixture was neutralized with silver carbonate (Lachema, Brno, Czech Republic). To determine double bond position(s), FAMEs were derivatized with dimethyl disulfide (DMDS). The transesterified mixture was filtered through a column with a small amount of silica gel and evaporated to dryness under a stream of argon. The residues were dissolved in 50 µL of DMDS (Merck, Darmstadt, Germany), which was precleaned by filtration through silica gel. A diethyl ether solution of iodine (Lachema, 12.5 µL, 60 µg/µL) was added and the reaction mixture was shaken for 24 h at laboratory temperature. Finally, hexane (60 µL) was added, the excess of iodine was removed by 5% solution of sodium thiosulfate, and the hexane layer was separated and directly injected onto the GC column.

Gas Chromatography/Mass Spectrometry

FAMEs and their DMDS derivatives were analyzed using a 6890N gas chromatograph (Agilent, Santa Clara, CA, USA) coupled to a 5975B quadrupole mass spectrometer and equipped with a fused silica capillary column HP-5 ms (30 m × 0.25 mm, 0.25 µm, Agilent). The carrier gas was helium at 1 mL/min. The injector was operated in splitless mode at 230 °C. The temperature program for FAMEs: 40 °C (1 min), then 50 °C/min to 140 °C, then 3 °C/min to 320 °C (20 min). The temperature program for DMDS derivatives: 70 °C (1 min), then 10 °C/min to 320 °C (20 min). Standard 70 eV mass spectra were recorded in the mass range (m/z) of 25–600; a 4-min solvent delay was used. The temperatures of the transfer line, ion source and quadrupole were 250, 230 and 150 °C, respectively.

Gas Chromatography/Flame Ionization Detection

FAMEs were quantified and their ECL (equivalent chain length) values were determined using an HP 5890A gas chromatograph (Hewlett-Packard, Palo Alto, CA, USA) equipped with a flame ionization detector (FID). Two fused silica capillary columns were used: (a) DB-WAX (30 m × 0.25 mm, 0.25 µm, J&W Scientific, USA) and (b) DB-1 (30 m × 0.25 mm, 0.25 µm, J&W Scientific, Folsom, CA, USA). The injector and detector temperatures were 230 and 250 °C, respectively. The injector was operated in split mode with a split ratio of 20:1. The carrier gas was hydrogen (87 kPa, $\bar{u} = 40$ cm/s for DB-WAX and 95 kPa, $\bar{u} = 41$ cm/s for DB-1); nitrogen was used as make-up gas (25 mL/min). Temperature program: (a) 45 °C (2 min), then 15 °C/min to 150 °C, then 4 °C/min to 320 °C (5 min) (FAME quantification on DB-WAX column); (b) isothermally at 220 °C (60 min) (both columns, for determining ECL values). Data were collected with an HP 3393A integrator (Hewlett-Packard). ECL values were calculated from the retention times of FAMEs and co-injected FAME standards (22:0–28:0, both odd and even) using a program written in GW-BASIC [9].

Gas Chromatography/Infrared Spectroscopy

Double-bond positions were determined using an Agilent 6850 gas chromatograph connected to an Equinox 55 FT-IR spectrometer (Bruker Optics Inc., Ettlingen, Germany). A DB-5 column (30 m × 0.32 mm, 0.25 µm, J&W Scientific) was used for the separations; the injector temperature was 220 °C (splitless mode), while the carrier gas was He at a flow rate of 2.5 mL/min. The temperature program: 50 °C (0 min), then 50 °C/min to 150 °C (0 min), then 1 °C/min to 240 °C (5 min). A liquid nitrogen-cooled photoconductive mercury-cadmium-telluride (MCT) detector was used with an FT-IR resolution of 8 cm^{-1}; the light pipe temperature was 200 °C. Methyl (*E*)-hexadec-9-enoate and methyl (*Z*)-hexadec-9-enoate (Applied Science Laboratories; 20 mg/mL in cyclohexane) were used as standards for infrared (IR) spectra of unsaturated methyl esters.

High-Performance Liquid Chromatography/Mass Spectrometry

HPLC was performed on a TSP liquid chromatograph (Thermo Separation Products, Piscataway, NJ, USA) with an ion-trap mass spectrometric detector (LCQ classic) controlled by Xcalibur software (Thermo Finnigan Corp., San Jose, CA, USA). TAGs were separated on two Nova-Pak C18 stainless steel columns (300 × 3.9 and 150 × 3.9 mm, 4 µm, Waters Corp., Milford, MA, USA) connected in series. The mobile phase was mixed from acetonitrile (A) and 2-propanol (B) [10]. A linear gradient from 0 to 70% of B in 108 min (1.0 mL/min) was followed by a linear gradient to 100% B (150 min, 0.7 mL/min). The columns were kept at 30 °C during analyses. The mobile phase was mixed post-column in a low dead volume T-piece with 100 mM ammonium acetate prepared in 2-propanol/water 1:1 (v/v), at a flow rate of 10 µL/min. The full scan mass spectra were recorded in the mass range (m/z) of 75–1,300, the temperatures of the vaporizer and heated capillary were set to 400 and 200 °C, respectively; the corona discharge current was 4.5 µA. TAGs were identified using the TriglyAPCI software [11] and quantified from reconstructed chromatograms calculated for $[M+H]^+$ and $[M+NH_4]^+$ molecular adducts [7].

Results and Discussions

Identification of Fatty Acids

TAGs from fat body of bumblebee males were transesterified and analyzed by GC/MS. Methyl esters of both saturated and unsaturated FAs were found. To determine the position(s) of double bond(s) in FA chains, DMDS derivatives were prepared [12]. DMDS derivatives of monoenic FAs provided molecular ions $M^{+\bullet}$ accompanied by less intense ions formed by the loss of methoxy ($M^{+\bullet}$-31) and methylthio ($M^{+\bullet}$-47) radicals from the molecular ions. The most abundant peaks resulted from α-cleavage between the two carbon atoms originally constituting the double bond, and these ions were denominated A^+ ($[CH_3(CH_2)_nCH = S–CH_3]^+$) and B^+ ($[CH_3–S = CH(CH_2)_mCOOCH_3]^+$) in this work. Neutral losses of methanethiol from A^+ and methanol and methanethiol from B^+ were also observed ($[A-48]^+$, $[B-32]^+$ and $[B-32-48]^+$, respectively). In the low-mass region, fragment ions of the C_nH_{2n-1} series, $[CH_2=S–CH_3]^+$ (*m/z* 61), and methyl ester-related ions at *m/z* 74 and 87 were found.

The most abundant dienoic acid found in *B. pratorum* contained 26 carbons, and the mass spectrum of its methyl ester (M = 406) is shown in Fig. 1a. The corresponding DMDS derivative provided a mass spectrum (Fig. 1b) with a molecular ion at *m/z* 594, which indicated the formation of a tetrasubstituted acyclic derivative. Therefore, at least

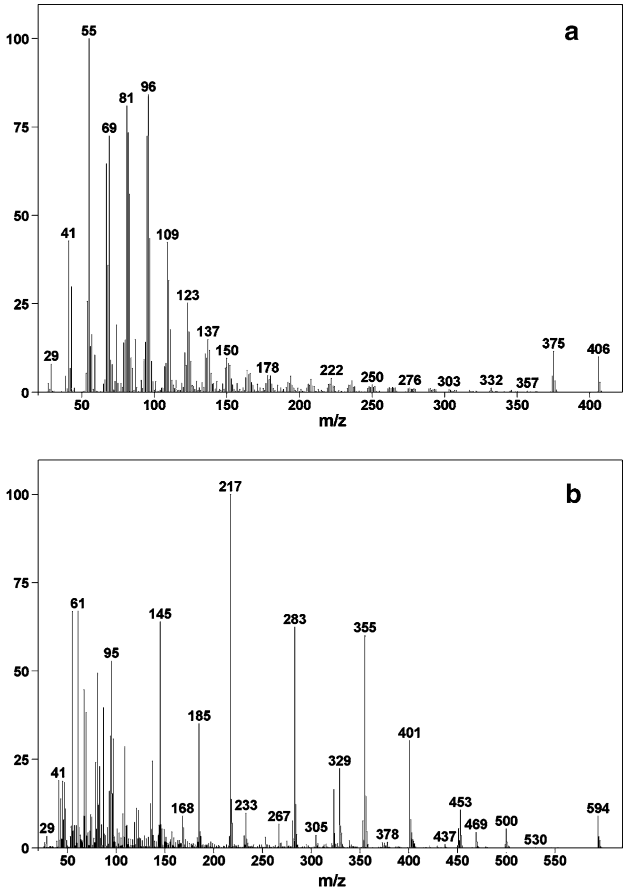

Fig. 1 Mass spectra of (*Z*,*Z*)-9,19-hexacosadienoic acid methyl ester (**a**) and its DMDS derivative (**b**)

four methylene groups separating the two double bonds were expected [13]. An ion at *m/z* 500 corresponded to the elimination of both methanethiol and thioformaldehyde. Further losses of methoxy or methylthio radicals resulted in ions at *m/z* 469 and 453, respectively. As two double bonds existed in the molecule, two pairs of diagnostic ions were expected. However, only two ions were found; the other two diagnostic ions lost neutral molecules giving the secondary fragments. Based on the fragmentation, the spectrum was interpreted as 9,19-hexacosadienoic acid methyl ester. Figure 2 indicates the expected fragments after α-cleavage between the carbons originally constituting the double bonds, which were labeled A^+, B^+, C^+, and D^+ here. The diagnostic ions A^+ and D^+ were found at *m/z* 145 and 217, respectively; D^+ was the spectrum base peak. The B^+ and C^+ eliminated neutral molecules, either methanethiol, giving *m/z* 401 ($[B\text{-}48]^+$) and *m/z* 329 ($[C\text{-}48]^+$), or both methanethiol and thioformaldehyde, providing *m/z* 355 ($[B\text{-}48\text{-}46]^+$) and 283 ($[C\text{-}48\text{-}46]^+$), respectively. In addition, B^+ eliminated methanol from the methyl ester moiety ($[B\text{-}48\text{-}46\text{-}32]^+$; *m/z* 323). Ions A^+ and D^+ also provided additional fragments after the elimination of neutral molecules, giving *m/z* 97 ($[A\text{-}48]^+$), *m/z* 185 ($[D\text{-}32]^+$) and *m/z* 137 ($[D\text{-}32\text{-}48]^+$). The low-mass region contained ions of the C_nH_{2n-1} series, the *m/z* 67, 81, 95, 109 series, $[CH_2 = S\text{–}CH_3]^+$ (*m/z* 61), and methyl ester-related ions at *m/z* 74 and *m/z* 87. The identities of all common FAMEs were also confirmed by determining ECL values and comparing them with published data [14].

The geometric configuration of double bonds in 9,19-hexacosadienoic acid methyl ester was determined by IR spectroscopy. Unsaturated dienoic compounds with at least one (*E*)-double bond provide a characteristic strong band at 990–965 cm^{-1} assigned to the =C–H out-of-plane deformation vibration [15]. Compounds with a (*Z*)-double bond do not provide a signal in this area, but show a typical band from =C–H stretch absorption at 3,028–3,011 cm^{-1} [16]. The IR spectrum of 9,19-hexacosadienoic acid methyl ester (Fig. 3) did not show any signal that could be attributed to (*E*)-double bond(s). By contrast, a well-resolved band at 3,012 cm^{-1} was found, which indicated the presence of double bond(s) with a (*Z*)-configuration. Other bands were those expected for methyl esters (1,758 cm^{-1} (C=O stretching), 1,176 cm^{-1} (C–O stretching), 1,651 cm^{-1} (C=C stretching), and 718 cm^{-1} ($\text{–}(CH_2)_n$-skeletal overlapping with =CH deformation).

Based on the MS and IR data, we have concluded that structure of the most abundant dienoic acid is (*Z*,*Z*)-9,19-hexacosadienoic acid [(*Z*,*Z*)-9,19-26:2].

ECL values of (*Z*,*Z*)-9,19-Hexacosadienoic Acid Methyl Ester

To characterize the retention behavior of the (*Z*,*Z*)-9,19-26:2 methyl ester for future reference, ECL values at 220 °C were determined. The measurements were done in quadruplicate on both nonpolar (DB-1) and polar (DB-WAX) stationary phases, and the values obtained are listed in Table 1.

Quantification of Fatty Acids

The compositions of the FAs were determined by GC/FID, because this technique provides almost identical response factors for FAMEs [17]. FAs identified in the fat body of *B. pratorum* and their relative abundances are summarized in

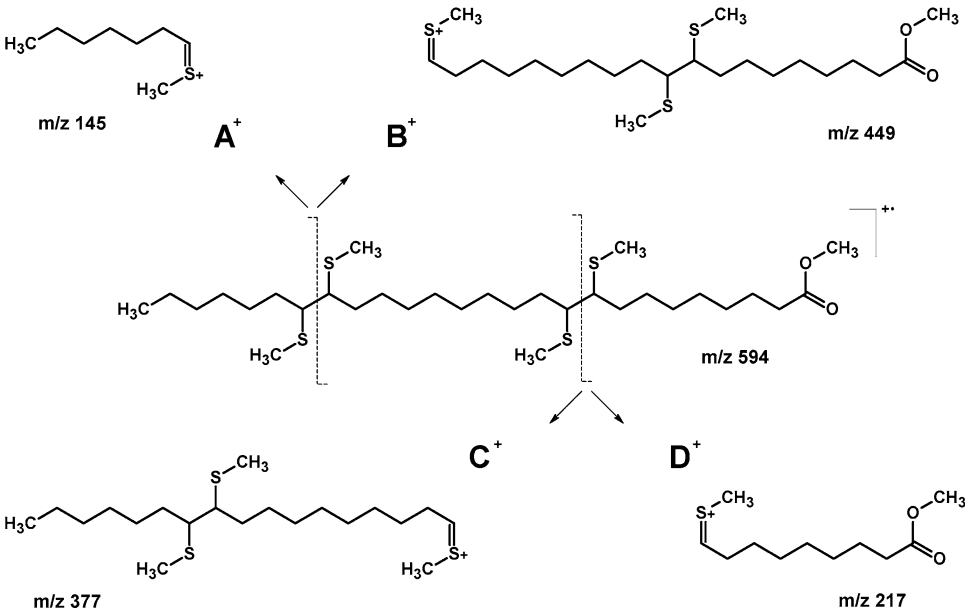

Fig. 2 Labels of the main fragments expected in the EI mass spectrum of the DMDS derivative of (*Z*,*Z*)-9,19-hexacosadienoic acid methyl ester

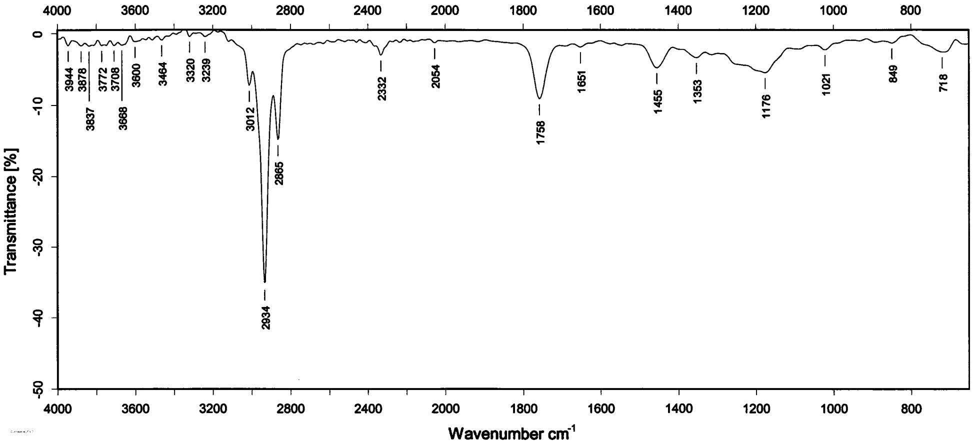

Fig. 3 Infrared spectrum of (*Z*,*Z*)-9,19-hexacosadienoic acid methyl ester

Table 1 ECL values of (*Z*,*Z*)-9,19-hexacosadienoic acid methyl ester

Column	ECL ± SD
DB-WAX	26.461 ± 0.002
DB-1	25.393 ± 0.003

Table 2. To compare variations between individuals, results for five bumblebees collected in different localities and at different times during the season are given.

The fat body was found to contain only even FAs, with the exception of pentadecanoic acid, which was present at trace levels. Palmitic acid was the most abundant saturated acid; stearic, myristic, and lauric acids were also detected, but at lower concentrations. FAs with one double bond prevailed in the samples. Oleic acid itself formed about one-third and together with *cis*-vaccenic acid more than half of all acids. The typical position of the double bond in the monoenoic FAs was 9, but FAs with other double bond positions (11 or 13) also occurred. Among polyenoic acids, (*Z*,*Z*)-9,19-26:2, linoleic and α-linolenic acid were detected.

Whereas most of the FAs found in *B. pratorum* are common in bumblebees [7], those with 24 and 26 carbon atoms have not been detected in this genus and they are quite rare in nature. Males of six bumblebee species (*Bombus lucorum*, *B. terrestris*, *B. lapidarius*, *B. hypnorum*, *B. hortorum*, and *B. confusus*) underwent analyses of TAGs in their pool lipids, but none of the species contained fatty acids longer than 22 carbon atoms [7]. 9,19-26:2 has so far been identified only in marine sponges [18–22]. Even there, its concentrations are substantially lower than those of the more common isomer 5,9-26:2. Morales and Lichtfield [18] showed in labeling experiments with *Microciona prolifera* that 9,19-26:2 is biosynthesized from 9-16:1 by chain elongation followed by Δ^9 desaturation. The reaction intermediate 19-26:1 was found in high quantities in the sponge. By contrast, *B. pratorum* produces 9-26:1 as the only monoenic FA with 26 carbons, which might be indicative of a different biosynthetic pathway (e.g., Δ^9 desaturation of 26:0 followed by Δ^{19} desaturation). However, no data on the biosynthesis of 9,19-26:2 in bumblebees are available at the moment. 9,19-26:2 has also been found in the marine sponges *Dysidea fragilis* [19], *Halichondria panicea* [20], and *Hymeniacidon sanguinea* [21, 22].

Monounsaturated 9-26:1 and 9-24:1 were detected in *B. pratorum* at trace levels, but they are more common in nature than 9,19-26:2. Several papers reported their presence in both marine [19–26] and freshwater [27, 28] sponges. Their abundances are also low, at percent or subpercent levels. Marine fish have been shown to contain 9-24:1 in substantially lower quantities than isomeric 15-24:1 [29]. Higher levels of monoenic 9-24:1 and 9-26:1 were only found in the bacteria *Mycobacterium tuberculosis* [30] and *Francisella tularensis* [31]. So far there has been no evidence of 9,19-26:2, 9-26:1 or 9-24:1 in insects or any other higher organism.

Composition of Triacylglycerols

HPLC/MS was employed to elucidate the structures of intact TAGs and thus to reveal how the rare long-chain FAs are bonded to the glycerol backbone [32]. Fat body of *B. pratorum* was found to contain more than 80 different TAG molecular species (Table 3). The most abundant TAGs were those which are common in bumblebees ([16:0, 18:1, 18:1] and [18:1, 18:1, 18:1]). Note that 18:1 might represent oleic and/or *cis*-vaccenic acid, as both of them were detected by GC/MS. Equivalent carbon number (ECN) values of TAGs from *B. pratorum* ranged from 38 to 66, i.e., up to unusually high values for bumblebees [7]. In accordance with GC data, rare long-chain FAs with 24 and 26 carbons were detected. In addition, FAs with 28 carbons and two or one double bonds were found, although at sub-percent levels. 9,19-26:2 occupied at least one position in one-third of all TAG molecular species. Not surprisingly, the most abundant TAGs with this acid also

Table 2 Fatty acids identified in triacylglycerols from the fat body of male *B. pratorum*

Fatty acid	Relative peak area (%)					
	Sample 1	Sample 2	Sample 3	Sample 4	Sample 5	Mean ± SD
12:0	1.3	3.7	4.3	13.1	2.2	3.7 ± 4.2
14:0	3.1	5.4	6.0	8.5	2.8	5.4 ± 2.1
9-14:1	0.2	0.2	0.2	1.0	0.2	0.2 ± 0.3
15:0	<0.1	0.1	<0.1	<0.1	0.2	<0.1
16:0	21.9	18.5	19.1	14.5	17.7	18.5 ± 2.4
9-16:1	9.0	6.2	7.7	11.7	7.2	7.7 ± 1.9
11-16:1	0.4	1.4	1.4	0.7	0.8	0.8 ± 0.4
18:0	1.2	0.7	0.7	0.4	1.1	0.7 ± 0.3
9-18:1	40.5	35.1	32.9	32.5	38.6	35.1 ± 3.2
11-18:1	9.9	19.5	17.3	12.6	17.5	17.3 ± 3.6
9,12-18:2	0.6	1.3	2.2	0.8	0.7	0.8 ± 0.6
9,12,15-18:3	2.8	2.6	3.4	2.5	2.7	2.7 ± 0.3
20:0	0.2	0.1	0.2	0.2	0.3	0.2 ± 0.1
9-20:1	<0.1	<0.1	<0.1	<0.1	<0.1	<0.1
13-20:1	<0.1	<0.1	<0.1	<0.1	<0.1	<0.1
22:0	0.1	0.1	0.3	0.3	0.5	0.3 ± 0.1
24:0	0.2	<0.1	<0.1	<0.1	0.2	<0.1
9-24:1	0.2	<0.1	<0.1	<0.1	0.1	<0.1
9-26:1	0.2	0.2	0.3	<0.1	0.4	0.2 ± 0.1
9,19-26:2	8.1	5.0	4.0	1.1	6.7	5.0 ± 2.4

contained 18:1, 16:1 or 16:0, i.e., the main FAs occurring in this bumblebee. 9,19-26:2 occupied one (e.g., [18:1, 26:2, 18:1], [16:0, 18:1, 26:2]), two (e.g., [26:2, 18:1, 26:2], [26:2, 16:1, 26:2]), or even all three positions ([26:2, 26:2, 26:2]), which is unusual. Other long-chain FAs, 24:1, 24:2, 26:1, 28:1 and 28:2, were found in a small number of TAGs, mostly at very low concentrations. It is important to note that the assignment of FAs to a particular sn position (distinguishing sn-2 from sn-1/3) is based on the intensities of diacylglycerol fragments observed in the mass spectra. Besides the position, the fragment intensities are to some extent also affected by the structures of FAs. Also, unlike GC/FID, TAG response factors in HPLC/APCI-MS are generally not equal. Therefore, the FA positions and quantities of individual TAGs shown in Table 3 are burdened with some uncertainty, which cannot be avoided without using authentic TAG standards. Despite these limitations, HPLC/APCI-MS provided valuable information on TAGs. An example chromatogram showing the separation of TAGs from *B. pratorum* is given in Fig. 4.

9,19-Hexacosadienoic Acid and Labial Gland Composition

FAs identified in the fat body were compared with the composition of the cephalic labial gland secretion of *B. pratorum* males. Bumblebees use the secretions as scent marks for denoting prominent objects along the patrolling routes. The scent—which contains marking pheromone—attracts females for mating [33]. The composition of labial gland secretions is strictly species-specific. The biosynthesis of the marking pheromone components has not been completely clarified yet [34]. We attempt to explore the idea that FAs stored in the fat body might serve as the precursors of non-terpenic components of the labial gland secretions. The marking pheromone blend of *B. pratorum* contains isoprenoids (farnesol, geranylgeranyl acetate, farnesyl acetate), alcohols (11-octadecenol, hexadecanol [35]), and both saturated and unsaturated hydrocarbons [36, 37]. The hydrocarbon (*Z*,*Z*)-7,17-pentacosadiene is a medium-abundance component; it forms 9% of the labial gland secretion, which represents about 80% of all hydrocarbons. This rare diene has not been detected in the marking pheromone of any other bumblebee species. One can speculate about its biosynthesis from 9,19-26:2 by decarboxylation [38], as shown in Fig. 5. 9,19-26:2 is bonded in several relatively abundant TAGs in two or even all three positions, which ensures the presence of this acid in the transport of 1,2-diacylglycerols. Thus, the acid might be available to the labial gland for pheromone synthesis. Similar biosynthetic transformations to that proposed for 9,19-26:2 might also apply for 9-24:1 and 9-26:1. The

Table 3 Triacylglycerols identified in the fat body of male *B. pratorum*

ECN	CN:DB	t_R (min)	Triacylglycerol(s)[a]	Peak area [rel. (%)]					
				Sample 1	Sample 2	Sample 3	Sample 4	Sample 5	Mean ± SD
38	46:4	52.6	[12:0, 16:1, 18:3]	–	0.1	0.1	0.3	–	0.1 ± 0.1
	44:3	53.7	[12:0, 14:0, 18:3]	–	–	0.1	0.3	–	<0.1 ± 0.1
40	54:7	58.6	[18:3, 18:1, 18:3], [18:3, 18:2, 18:2]	–	0.1	0.3	0.1	0.1	0.1 ± 0.1
	52:6	60.0	[16:0, 18:3, 18:3]	0.2	0.1	0.2	0.1	0.1	0.1 ± 0.1
	48:4	59.4	[12:0, 18:1, 18:3]	0.3	0.5	0.8	1.4	0.2	0.5 ± 0.4
	46:3	60.7	[12:0, 18:3, 16:0], [14:0, 14:0, 18:3]	0.2	0.3	0.4	0.7	0.1	0.3 ± 0.2
	42:1	60.5	[12:0, 18:1, 12:0], [12:0, 16:1, 14:0]	–	0.2	0.2	1.7	0.1	0.2 ± 0.6
42	54:6	64.3	[18:2, 18:2, 18:2]	–	0.2	0.4	0.2	0.2	0.2 ± 0.1
	52:5	64.6	[16:1, 18:1, 18:3]	1.1	1.0	1.4	1.3	1.0	1.1 ± 0.2
	50:4	66.0	[16:0, 16:1, 18:3], [14:0, 18:1, 18:3], [14:0, 18:2, 18:2]	1.4	1.1	1.9	1.7	0.8	1.4 ± 0.4
	48:3	67.3	[14:0, 14:0, 20:3]	–	0.3	0.5	0.5	0.1	0.3 ± 0.2
	48:3	65.4	[12:0, 18:1, 18:2]	0.3	0.4	0.4	0.9	0.1	0.4 ± 0.3
	46:2	65.7	[12:0, 16:1, 18:1]	0.4	1.0	0.9	4.0	0.5	0.9 ± 1.3
	44:1	67.1	[12:0, 18:1, 14:0], [12:0, 16:1, 16:0],	0.2	1.1	0.9	3.9	0.3	0.9 ± 1.3
	42:0	68.5	[12:0, 14:0, 16:0]	–	0.1	0.1	0.3	–	0.1 ± 0.1
44	54:5	70.3	**[18:1, 18:3, 18:1]**	2.3	3.5	4.3	2.7	3.2	**3.2 ± 0.7**
	52:4	71.9	**[16:0, 18:3, 18:1], [16:0, 18:2, 18:2]**	5.0	4.0	6.1	3.3	4.3	**4.3 ± 1.0**
	50:3	73.3	[16:0, 16:0, 18:3]	0.7	0.4	0.7	0.3	0.3	0.4 ± 0.2
	50:3	70.6	[16:1, 16:1, 18:1], [18:1, 14:1, 18:1]	1.1	1.3	1.5	2.5	1.1	1.3 ± 0.5
	48:2	71.7	**[12:0, 18:1, 18:1]**	1.9	4.3	3.4	9.7	2.5	**3.4 ± 2.8**
	46:1	73.3	**[12:0, 18:1, 16:0], [14:0, 14:0, 18:1]**	1.0	3.4	2.5	6.2	1.3	**2.5 ± 1.9**
	44:0	75.0	[14:0, 14:0, 16:0], [12:0, 16:0, 16:0]	–	0.2	0.2	0.2	–	0.2 ± 0.1
46	54:4	75.8	[18:2, 18:1, 18:1]	0.8	1.7	1.8	1.3	1.2	1.3 ± 0.3
	52:3	76.1	**[18:1, 16:1, 18:1]**	4.8	6.3	6.6	8.4	7.9	**6.6 ± 1.2**
	50:2	77.6	**[18:1, 14:0, 18:1], [16:0.16:1, 18:1]**	6.9	8.0	7.2	10.3	7.6	**7.6 ± 1.2**
	48:1	79.2	**[14:0, 18:1, 16:0], [16:0, 16:1, 16:0]**	1.8	3.0	2.4	3.0	1.3	**2.4 ± 0.7**
	46:0	81.0	[14:0, 16:0, 16:0]	–	0.1	0.1	0.1	–	0.1 ± 0.1
48	54:3	81.6	**[18:1, 18:1, 18:1]**	7.4	11.9	8.8	9.4	15.2	**9.4 ± 2.8**
	52:2	83.2	**[16:0, 18:1, 18:1]**	12.3	14.6	11.6	10.4	17.8	**12.3 ± 2.6**
	50:1	85.0	**[16:0, 18:1, 16:0]**	2.5	2.3	2.1	1.3	1.9	**2.1 ± 0.4**
	48:0	87.1	[16:0, 16:0, 16:0]	–	0.1	0.1	–	–	<0.1 ± 0.1
50	62:6	85.2	[18:2, 18:2, 26:2]	–	–	0.6	0.2	0.3	0.2 ± 0.2
	60:5	86.7	[16:1, 18:2, 26:2]	0.3	0.2	0.4	0.1	0.2	0.2 ± 0.1
	58:4	86.1	[16:1, 16:1, 26:2]	0.3	0.2	0.2	0.2	0.2	0.2 ± 0.1
	56:3	86.9	[18:1, 18:1, 20:1], [12:0, 26:2, 18:1]	1.0	1.1	1.0	1.0	1.5	1.0 ± 0.2
	54:2	88.9	[18:1, 16:0, 20:1], [18:1, 18:1, 18:0]	0.8	0.8	0.9	0.8	1.3	0.8 ± 0.2
	52:1	90.6	[16:0, 18:1, 18:0]	0.3	0.2	0.2	0.1	0.3	0.2 ± 0.1
52	62:5	90.4	[18:2, 26:2, 18:1], [18:1, 16:1, 26:2]	0.5	0.4	0.5	0.2	0.3	0.4 ± 0.1
	60:4	90.7	[16:1, 26:2, 18:1]	2.1	1.3	1.5	0.8	1.4	1.4 ± 0.4
	58:3	92.2	[16:0, 16:1, 26:2], [18:1, 14:0, 26:2]	1.3	0.6	1.1	0.6	1.0	1.0 ± 0.3
	56:2	94.2	[18:1, 18:1, 20:0]	0.4	0.2	0.4	0.2	0.3	0.3 ± 0.1
54	62:4	95.7	**[18:1, 26:2, 18:1]**	8.3	4.3	4.1	1.9	5.3	**4.3 ± 2.1**
	60:3	97.1	**[16:0, 18:1, 26:2]**	3.7	2.2	3.2	1.4	3.4	**3.2 ± 0.9**
	58:2	98.7	[16:0, 26:2, 16:0]	0.4	0.2	0.5	0.2	0.3	0.3 ± 0.1

Table 3 continued

ECN	CN:DB	t_R (min)	Triacylglycerol(s)[a]	Peak area [rel. (%)]					
				Sample 1	Sample 2	Sample 3	Sample 4	Sample 5	Mean ± SD
56	70:7	98.2	[18:3, 26:2, 26:2]	0.9	0.7	0.7	0.1	0.2	0.7 ± 0.3
	66:5	99.1	[16:1, 26:2, 24:2]	0.6	0.2	0.5	0.1	0.1	0.2 ± 0.2
	64:4	99.9	[18:1, 18:1, 28:2], [18:1, 26:2, 20:1]	1.8	0.7	0.8	0.4	0.9	0.8 ± 0.5
	62:3	101.9	[18:1, 18:1, 26:1], [18:1, 26:2, 18:0]	1.3	0.6	0.8	0.4	1.1	0.8 ± 0.3
	60:2	103.9	[16:0, 18:1, 26:1]	0.3	0.1	0.3	0.2	0.4	0.3 ± 0.1
58	68:5	103.0	**[26:2, 16:1, 26:1]**	4.3	2.5	2.4	0.8	1.6	**2.4 ± 1.2**
	66:4	104.3	[14:0, 26;2, 26:2], [22:1, 18:1, 26:2]	1.3	0.5	0.9	0.3	0.5	0.5 ± 0.4
	64:3	106.2	[18:1, 18:1, 28:1]	0.4	0.1	0.4	0.1	0.3	0.3 ± 0.1
	62:2	107.8	[18:0, 18:0, 26:2], [18:1, 18:1, 26:0]	0.1	–	0.1	0.1	0.1	0.1 ± 0.1
60	70:5	107.2	**[26:2, 18:1, 26:2]**	9.2	6.5	4.8	1.5	4.7	**4.8 ± 2.5**
	68:4	108.4	[16:0, 26:2, 26:2]	2.5	1.7	2.0	0.5	1.5	1.7 ± 0.6
	66:3	110.5	[16:0, 24:1, 26:2], [18:1, 22:0, 26:2]	0.2	0.1	0.2	0.1	0.2	0.2 ± 0.1
62	72:5	111.0	[26:2, 18:1, 28:2]	1.3	0.7	0.6	0.2	0.5	0.6 ± 0.4
	70:4	113.3	[26:2, 18:1, 26:1]	1.8	1.0	1.6	0.4	1.3	1.3 ± 0.5
	68:3	114.9	[16:0, 26:1, 26:2], [18:2, 26:1, 24:0]	0.3	0.2	0.4	0.1	0.3	0.3 ± 0.1
64	72:4	117.6	[20:0, 26:2, 26:2], [16:0, 28:2, 28:2]	0.4	0.2	0.2	0.1	0.3	0.2 ± 0.1
	70:3	119.1	[18:1, 26:1, 26:1]	0.1	0.1	–	0.1	0.1	0.1 ± 0.1
66	78:6	118.3	[26:2, 26:2, 26:2]	0.9	0.5	0.3	–	0.2	0.3 ± 0.3

The most abundant TAGs are shown in bold

CN number of carbon atoms in fatty acids in TAG; *DB* number of double bonds in the carbon chains of fatty acids

[a] TAG abbreviations reflect the assumed positions of FAs on the glycerol backbone. As APCI MS cannot distinguish between acyls in the sn-1 and sn-3 positions, the TAG abbreviations in the table do not differentiate between these two positions; FA residues in sn-1/3 were ordered by increasing molecular weight

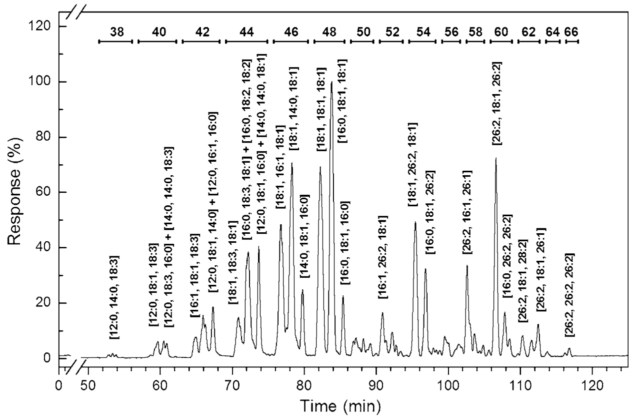

Fig. 4 HPLC/APCI-MS chromatogram of triacylglycerols isolated from the fat body of male bumblebee *B. pratorum*. The numbers in the upper part of the figure are ECN values

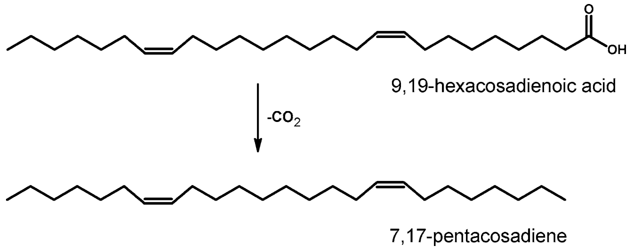

Fig. 5 Proposed biosynthesis of (*Z*,*Z*)-7,17-pentacosadiene in male marking pheromone of *B. pratorum* from (*Z*,*Z*)-9,19-hexacosadienoic acid

expected products, 8-tricosene and 8-pentacosene, were detected in the labial gland, though only at trace levels. Furthermore, tricosadiene and heptacosadiene are present in minor quantities in the pheromonal gland, which corresponds well with the presence of 24:2 and 28:2 acids in TAGs. Clearly, our findings support the hypothesis about a connection between pheromone biosynthesis and FAs in the fat body, but more research is needed.

Concluding Remarks

In conclusion, unique FAs with 24, 26 and 28 carbon atoms were identified in the fat body of *B. pratorum*. Among them, (*Z*,*Z*)-9,19-hexadecadienoic acid was the most abundant, comprising up to 8% of all FAs. In this work we have also shown remarkable similarities between the structure of this acid and the main hydrocarbon component of the male marking pheromone. Due to the uncommon structure of its acid and labial gland secretion component(s), *B. pratorum* represents a convenient model for studying marking pheromone biosynthesis.

Acknowledgments The financial support from the Grant Agency of the Academy of Sciences of the Czech Republic (A4055403), by the Ministry of Education of the Czech Republic (2B06007), and by the Academy of Sciences of the Czech Republic (research project No. Z40550506) is acknowledged with appreciation.

References

1. Canavoso LE, Jouni ZE, Karnas KJ, Pennington JE, Wells MA (2001) Fat metabolism in insects. Annu Rev Nutr 21:23–46. doi:10.1146/annurev.nutr.21.1.23
2. Stanley-Samuelson DW, Nelson DR (ed) (1993) Insect lipids: chemistry, biochemistry and biology. University of Nebraska Press, Lincoln, NE
3. Luxová A, Valterová I, Stránský K, Hovorka O, Svatoš A (2003) Biosynthetic studies on marking pheromones of bumblebee males. Chemoecology 13:81–87. doi:10.1007/s00049-003-0230-8
4. Bashan M, Cakmak O (2005) Changes in composition of phospholipid and triacylglycerol fatty acids prepared from prediapausing and diapausing individuals of *Dolycoris baccarum* and *Piezodorus lituratus* (Heteroptera: Pentatomidae). Ann Entomol Soc Am 98:575–579. doi:10.1603/0013-8746(2005)098[0575:CICOPA]2.0.CO;2
5. Hoback WW, Rana RL, Stanley DW (1999) Fatty acid compositions of phospholipids and triacylglycerols of selected tissues, and fatty acid biosynthesis in adult periodical cicadas, *Magicicada septendecim*. Comp Biochem Physiol A Mol Integr Physiol 122:355–362. doi:10.1016/S1095-6433(99)00018-5
6. Canavoso LE, Bertello LE, de Lederkremer RM, Rubiolo ER (1998) Effect of fasting on the composition of the fat body lipid of *Dipetalogaster maximus*, *Triatoma infestans* and *Panstrongylus megistus* (Hemiptera: Reduviidae). J Comp Physiol B 168:549–554. doi:10.1007/s003600050176
7. Cvačka J, Hovorka O, Jiroš P, Kindl J, Stránský K, Valterová I (2006) Analysis of triacylglycerols in fat body of bumblebees by chromatographic methods. J Chromatogr A 1101:226–237. doi:10.1016/j.chroma.2005.10.001
8. Stránský K, Jursík T (1996) Simple quantitative transesterification of lipids. 1. Introduction. Fett/Lipid 98:65–71. doi:10.1002/lipi.19960980206
9. Stránský K, Jursík T, Vítek A, Skořepa J (1992) An improved method of characterizing fatty-acids by equivalent chain-length values. J High Res Chromatogr 15:730–740. doi:10.1002/jhrc.1240151107
10. Holčapek M, Lísa M, Jandera P, Kabátová N (2005) Quantitation of triacylglycerols in plant oils using HPLC with APCI-MS, evaporative light-scattering, and UV detection. J Sep Sci 28:1315–1333. doi:10.1002/jssc.200500088
11. Cvačka J, Krafková E, Jiroš P, Valterová I (2006) Computer-assisted interpretation of atmospheric pressure chemical ionization mass spectra of triacylglycerols. Rapid Commun Mass Spectrom 20:3586–3594. doi:10.1002/rcm.2770
12. Dunkelblum E, Tan SH, Sikl PJ (1985) Double-bond location in monounsaturated fatty acids by dimethyl disulfide derivatization and mass spectrometry: application to analysis of fatty acids in pheromone glands of four Lepidoptera. J Chem Ecol 11:265–277. doi:10.1007/BF01411414
13. Vincenti M, Guglielmetti G, Cassani G, Tonini C (1987) Determination of double bond position in diunsaturated compounds by mass spectrometry of dimethyl disulfide derivatives. Anal Chem 59:694–699. doi:10.1021/ac00132a003
14. Stránský K, Jursík T, Vítek A (1997) Standard equivalent chain length values of monoenic and polyenic (methylene interrupted) fatty acids. J High Res Chromatogr 20:143–158. doi:10.1002/jhrc.1240200305
15. Hamilton RJ, Cast J (1999) Spectral properties of lipids (the chemistry and technology of oils and fats). Sheffield Academic Press Ltd., Sheffield, UK
16. Attygalle AB, Svatoš A, Wilcox C, Voerman S (1994) Gas-phase infrared spectroscopy for determination of double bond configuration of monounsaturated compounds. Anal Chem 66:1696–1703. doi:10.1021/ac00082a016
17. Christie WW (2003) Lipid analysis: isolation, separation, identification and structural analysis of lipids. The Oily Press, Bridgwater, UK
18. Morales RW, Litchfield C (1977) Incorporation of 1–14C-acetate into C26 fatty acids of the marine sponge *Microciona prolifera*. Lipids 12:570–576. doi:10.1007/BF02533383
19. Christie WW, Brechany EY, Stefanov K, Popov S (1992) The fatty acids of the sponge *Dysidea fragilis* from the Black Sea. Lipids 27:640–644. doi:10.1007/BF02536125
20. Rod'kina SA, Latyshev NA, Imbs AB (2003) Fatty acids from the Sea of Japan sponge *Halichondria panicea*. Russ J Bioorg Chem (Translation of Bioorganicheskaya Khimiya) 29:382–386. doi:10.1023/A:1024957403078
21. Christie WW, Brechany EY, Marekov IN, Stefanov KL, Andreev SN (1994) The fatty acids of the sponge *Hymeniacidon sanguinea* from the Black Sea. Comp Biochem Physiol B Biochem Mol Biol 109B:245–252. doi:10.1016/0305-0491(94)90008-6
22. Nechev J, Christie WW, Robaina R, de Diego F, Popov S, Stefanov K (2004) Chemical composition of the sponge *Hymeniacidon sanguinea* from the Canary Islands. Comp Biochem Physiol A Mol Integr Physiol 137:365–374. doi:10.1016/j.cbpb.2003.10.016
23. Lam WK, Hahn S, Ayanoglu E, Djerassi C (1989) Phospholipid studies of marine organisms. 22. Structure and biosynthesis of a novel brominated fatty acid from a hymeniacidonid sponge. J Org Chem 54:3428–3432. doi:10.1021/jo00275a032
24. Carballeira NM, Reyes ED, Shalabi F (1993) Identification of novel iso/anteiso nonacosadienoic acids from the phospholipids of the sponges *Chondrosia remiformis* and *Myrmekioderma styx*. J Nat Prod 56:1850–1855. doi:10.1021/np50100a032
25. Carballeira NM, Pagan M, Rodriguez AD (1998) Identification and total synthesis of novel fatty acids from the caribbean sponge *Calyx podatypa*. J Nat Prod 61:1049–1052. doi:10.1021/np9801413
26. Rod'kina SA (2005) Fatty acids from the sponge *Tedania dirhaphis*. Chem Nat Comp 41:289–292. doi:10.1007/s10600-005-0131-x
27. Dembitsky VM, Řezanka T, Kashin AG (1993) Comparative study of the endemic freshwater fauna of Lake Baikal-II. Unusual lipid composition of two sponge species *Baicalospongia bacillifera* and *Baicalospongia intermedia* (family Lubomirskiidae, class Demospongiae). Comp Biochem Physiol B Biochem Mol Biol 106B:825–831. doi:10.1016/0305-0491(93)90037-6
28. Dembitsky VM, Řezanka T, Kashin AG (1994) Comparative study of the endemic freshwater fauna of Lake Baikal. VI. Unusual fatty acid and lipid composition of the endemic sponge *Lubomirskia baicalensis* and its amphipod crustacean parasite *Brandtia* (*Spinacanthus*) *parasitica*. Comp Biochem Physiol B

Biochem Mol Biol 109B:415–426. doi:10.1016/0305-0491(94)90024-8

29. Shantha NC, Ackman RG (1991) Fish oil tetracosenoic acid isomers and GLC analyses of polyunsaturated fatty acids. Lipids 26:237–239. doi:10.1007/BF02543978
30. Takayama K, Qureshi N, Schnoes HK (1978) Isolation and characterization of the monounsaturated long chain fatty acids of *Mycobacterium tuberculosis*. Lipids 13:575–579. doi:10.1007/BF02535818
31. Nichols PD, Mayberry WR, Antworth CP, White DC (1985) Determination of monounsaturated double-bond position and geometry in the cellular fatty acids of the pathogenic bacterium *Francisella tularensis*. J Clin Microbiol 21:738–740
32. Mottram HR, Evershed RP (1996) Structure analysis of triacylglycerol positional isomers using atmospheric pressure chemical ionisation mass spectrometry. Tetrahedron Lett 37:8593–8596. doi:10.1016/0040-4039(96)01964-8
33. Kullenberg B, Bergström G, Ställberg-Stenhagen S (1970) Volatile components of the cephalic marking secretion of male bumblebees. Acta Chem Scand 24:1481–1483
34. Lanne BS, Bergström G, Wassgren A-B, Törnbäck B (1987) Biogenetic pattern of straight chain marking compounds in male bumble bees. Comp Biochem Physiol 88B:631–636. doi:10.1016/0305-0491(87)90355-5
35. Svenson BG, Bergström G (1977) Volatile marking secretions from the labial gland of North European *Pyrobombus* D. T. males (Hymenoptera, Apidae). Insectes Soc 24:213–224. doi:10.1007/BF02227172
36. Ponchau O, Terzo M, Aytekin M, Valterová I, Iserbyt S, Michez D, Rasmont P (2006) The geographical variability of the secretions of the cephalic labial glands of *Bombus pratorum* L. males. In: XVth IUSSI Congr, Washington, DC, 30 July–5 Aug 2006, p 526
37. Cahlíková L (2008) Isolation and identification of compounds influencing the behavior of Hymenoptera. PhD Thesis, Institute of Chemical Technology, Prague, Czech Republic
38. Tillman JA, Seybold SJ, Jurenka RA, Blomquist GJ (1999) Insect pheromones—an overview of biosynthesis and endocrine regulation. Insect Biochem Mol Biol 29:481–514. doi:10.1016/S0965-1748(99)00016-8

Lipids (2008) 43:451–456
DOI 10.1007/s11745-008-3173-6

ORIGINAL ARTICLE

Effect of Substitution of High Stearic Low Linolenic Acid Soybean Oil for Hydrogenated Soybean Oil on Fatty Acid Intake

Maureen A. DiRienzo · Shawna L. Lemke · Barbara J. Petersen · Kim M. Smith

Received: 19 November 2007 / Accepted: 6 March 2008 / Published online: 26 March 2008
© AOCS 2008

Abstract High stearic, low α-linolenic acid soybean oil (HSLL) has been developed via traditional breeding to serve as a substitute for partially hydrogenated soybean oils used in food manufacturing. The purpose of this study was to estimate the impact on fatty acid intake in the United States if HSLL were substituted for partially hydrogenated soybean oils used in several food categories, including baked goods, shortenings, fried foods, and margarines. Using National Health and Nutrition Examination Survey (NHANES) data (1999–2002), baseline intakes of five fatty acids and trans fatty acids (TFA) were determined at the mean and 90th percentile of fat consumption. Then intakes of these fatty acids were determined after HSLL was substituted for 100% of the partially hydrogenated soybean oils used in these four food categories. The results show that baseline intake of stearic acid is 3.0% energy at the mean and 3.3% energy at the 90th percentile. Use of HSLL could increase stearic acid intake to about 4–5% energy. Mean intakes of TFA could decrease from 2.5 to 0.9% energy, and intake of palmitic acid would remain unchanged. Use of HSLL as a substitute for partially hydrogenated soybean oils would result in changes in the fatty acid composition of the US diet consistent with current dietary recommendations.

Keywords Dietary fat · Edible oils · Atherosclerosis · Saturated fatty acids · Trans fatty acids · Hydrogenation

Abbreviations

HSLL	High stearic acid, low α-linolenic acid soybean oil
NHANES	National Health and Nutrition Examination Survey
TFA	Trans fatty acids

Introduction

The recent United States Food and Drug Administration regulation [1] to require trans fatty acid (TFA) labeling on packaged food products has prompted food manufacturers to find alternatives to partially hydrogenated soybean oils used in formulating bakery products and margarines and in fried foods. Partially hydrogenated soybean oils provided about 9 billion lbs of oil to the diet in the United States [2], and so it is not a small undertaking to find functional alternatives for this amount of oil. For frying applications, alternatives, such as low α-linolenic acid soybean oil, have been made available to the food industry. Low α-linolenic acid soybean oil reduces or eliminates the need to hydrogenate prior to use in food processing; thus, the TFA content of foods fried in this oil is also reduced or eliminated.

Bakery products and margarines require the use of solid fats to provide the desired functionality. The choices of solid fats have included animal fats, such as lard, tallow and butter, and tropical oils, such as palm, palm kernel and coconut, but these have nutritional disadvantages in that they contain high amounts of hypercholesterolemic lauric (12:0), myristic (14:0), and palmitic (16:0) saturated fatty acids. In fact, it was the recognition in the 1980s that these saturated fatty acids raise serum cholesterol and thus the

---

M. A. DiRienzo · S. L. Lemke (✉)
Monsanto Company, 800 N Lindbergh Blvd,
St. Louis, MO 63167, USA
e-mail: Shawna.lin.lemke@monsanto.com

B. J. Petersen · K. M. Smith
Exponent Inc., 1150 Connecticut Ave NW Suite 1100,
Washington, DC 20036, USA

risk of coronary heart disease that prompted population-based dietary advice to reduce their intake. Partially hydrogenated oils were then used by food manufacturers to replace animal fats and tropical oils because it was not known at that time that the TFAs they contain also have adverse effects on blood lipids. Food manufacturers now face the challenge of replacing partially hydrogenated vegetable oils while not reverting to the use of animal fats and tropical oils.

Soybean oils high in stearic acid and low in α-linolenic acid (HSLL) are being developed using conventional breeding methods to provide a new solid fat alternative for food manufacturers. The stearic acid molecules are positioned at the sn 1,3 positions on the triacylglycerols. The oil provides the functionality of solid fats and can be used in a variety of food applications, such as shortening for baked goods and in margarines. In addition, the high stearic acid coupled with the low α-linolenic acid composition make this oil suitable for deep fat frying as well.

Although stearic acid is a saturated fatty acid, its consumption does not significantly alter serum total and HDL cholesterol the way other saturated fatty acids, such as lauric, myristic and palmitic acids, do [3]. Numerous clinical studies have shown that the consumption of stearic acid does not raise serum cholesterol levels, even when added to the diet in amounts far in excess of typical intake [4]. Furthermore, clinical studies have shown that stearic acid does not adversely affect other markers of heart health when present in the diet at about twice current intake levels [5, 6]. Thus, HSLL could provide an ideal alternative for food manufacturers needing solid fat functionality and stability while avoiding the negative health consequences associated with certain saturated fatty acids.

If HSLL is to be used instead of partially hydrogenated soybean oil in food formulations, it is important to first determine the impact this use could have on fatty acid intakes. Ideally this substitution would cause TFA intake to decrease, but not at the expense of undesirable changes in intakes of other fatty acids.

The purpose of this study was to estimate the potential dietary impact of substituting HSLL for 100% of the partially hydrogenated soybean oils used in four major food categories: baked goods, margarines, shortenings and frying oils. The impact on mean and 90th percentile intakes of palmitic, stearic, oleic, linoleic, and α-linolenic acids and TFA was determined for the total US population.

Materials and Methods

Food and soybean oil consumption data were derived from the National Health and Examination Survey (NHANES 1999–2002) [7], which were the most recent data available at the time of the study. The NHANES (1999–2002) is a complex, multistage, probability sample designed to be representative of the civilian US population. The survey collects one-day food intake data, in addition to nutrition, demographic, and health information. The NHANES survey over-samples minorities, low-income groups, and children, and statistical weights are provided by the National Center for Health Statistics to adjust for the differential probabilities of selection. Participants included 9,965 subjects in 1999–2000 and 11,039 subjects in 2001–2002. The NHANES is a large survey specifically designed to allow the estimation of food and nutrient intakes by the US population. The NHANES and its predecessor surveys have been used by the US Department of Agriculture for more than 70 years to estimate food and nutrient intake and to evaluate the impact of proposed policy changes.

The NHANES database does not have fatty acid compositions for the hydrogenated soybean oil component of foods; therefore, we extrapolated from the USDA's database of the fatty acid profiles, including trans fatty acids, of 214 foods [8]. When this database did not provide the fatty acid profiles for specific versions of hydrogenated soybean oils used to prepare certain foods, these fatty acids were estimated, using information from the fats/oils industry [Banks D (2003) Approximate composition of hydrogenated soy oils used in nine broad food categories, personal communication]. The methods used to assign these fatty acid profiles to hydrogenated soybean oils in foods have been described previously [9]. Exponent's proprietary software program FARE version 7.95™ was used to conduct the intake and substitution analyses. Other publicly available statistical software programs such as SAS or STATA can be used to evaluate data from NHANES and the USDA. The FARE™ software is currently used by the Center for Food Safety and Applied Nutrition (CFSAN) within the US Food and Drug Administration.

Two versions of HSLL, HSLL1 and HSLL2, were evaluated. These two versions differ primarily in their stearic and linoleic acid contents. The lower stearic acid content of HSLL1 is associated with a higher content of linoleic acid. Conversely, the higher content of stearic acid in HSLL2 is accompanied by a lower content of linoleic acid. The fatty acid compositions of HSLL1 and HSLL2 compared to regular soybean oil and partially hydrogenated soybean oil are shown in Table 1. The analyses substituted these two versions of HSLL for the partially hydrogenated soybean oils in the following food categories:

- All baked goods: including yeast breads and rolls, quick breads, cakes, cookies, pies, pastries, crackers, salty snacks, pancakes, and waffles
- Home use shortenings

Table 1 Fatty acid compositions of two versions of HSLL, regular soybean oil, and hydrogenated soybean oil

Fatty acid	Regular soybean oil [8] % Fatty acids	Hydrogenated soybean oil [19]	HSLL1	HSLL2
Palmitic	10.1	10.8	9.3	8.0
Stearic	3.6	12.1	18.7	30.0
Oleic	21.2	30.2	19.8	23.2
Linoleic	51.3	4.4	44.5	37.1
Linolenic	6.8	0.2	3.1	3.0
TFA	0.7	32.8	0.39	0.5

HSLL1 High stearic low linolenic acid soybean oil version 1, *HSLL2* high stearic low linolenic acid soybean oil version 2, *TFA* trans fatty acids

- French fries, and all fried meat, poultry, and fish (commercially and home-prepared)
- Margarines (stick, tub, and light varieties)

The three forms of margarines were assigned the following formulations: stick margarine, 80% fat, of which 50% was HSLL, 10% was partially hydrogenated soybean oil, and 20% was regular soybean oil; tub margarine, 70% fat, of which 33% was HSLL, 2% was partially hydrogenated soybean oil and 35% was regular soybean oil; and light spreads, 40% fat, of which 19% was HSLL, 1% partially hydrogenated soybean oil and 20% regular soybean oil. The fatty acid compositions of these oils are provided in Table 1.

Data on fatty acid intakes were generated on the total population mean and 90th percentile. Intakes of palmitic, stearic, oleic, linoleic, and α-linolenic acids, and TFA were evaluated. The data are expressed as percent of total energy intake (% energy), which was calculated by multiplying grams of fatty acid/day at the mean (or 90th percentile) by 9 cal/g and dividing by the total energy at the mean (or 90th percentile).

Results

This analysis used food consumption data from NHANES (1999–2002) to determine baseline fatty acid intakes from the diet, and then fatty acid intakes were determined after replacement with either HSLL1 or HSLL2 for partially hydrogenated soybean oil in foods in the four categories of interest. Figures 1 and 2 provide the results of these analyses.

The results show that the US diet provided on average 3.0% energy from stearic acid. At the 90th percentile of total fat intake, stearic acid provided 3.3% energy. Use of HSLL1 or HSLL2 resulted in an increase in mean intake of stearic acid from a baseline of 3.0–3.7 or 4.5% energy, respectively. For 90th percentile consumers of fat, use of HSLL1 or HSLL2 resulted in an increase in intake of stearic acid from 3.3% energy to 4.3% or 5.4% energy, respectively.

Use of either HSLL resulted in decreases in TFA intake from a baseline mean of 2.5% (3.0% at the 90th percentile) to 0.9% energy. This reduction was accompanied by no increase in palmitic acid intake. Substitution of either HSLL for partially hydrogenated soybean oil also produced increases in mean and 90th percentile intakes of linoleic acid of about 1.5–2% energy, decreases in mean and 90th percentile intakes of oleic acid of about 1% energy, and slight increases in the intake of α-linolenic acid.

Discussion

This study demonstrates the overall positive dietary impact of using HSLL to replace partially hydrogenated soybean oil in four food categories: baked goods; home-use shortenings; French fries and fried meat, poultry and fish; and margarines and spreads. Mean intake of TFA could decrease to 0.9% energy from 2.5–3.0% energy with no concomitant increase in palmitic acid. Intake of stearic acid could increase from a baseline mean of 3.0% energy (3.3% at the 90th percentile) to about 4% energy for average consumers of fat and to about 5% energy for 90th-percentile consumers of fat. Intakes of linoleic and α-linolenic acids could increase, and intakes of oleic acid decrease; these changes maintain or improve the fatty acid intake of the diet to be more in line with current dietary recommendations [3]. The categories chosen for substitution were ones for which HSLL has appropriate functionality and so the potential to be selected by food manufacturers. One limitation of the study is that the actual impact of HSLL on the diet will depend on how and to what degree food manufacturers select HSLL to replace partially hydrogenated oils, and cannot be fully characterized until reformulation is complete.

The effects of stearic acid on cardiovascular health endpoints have been extensively studied and recently reviewed [4–6, 10–17], and will not be reviewed in detail here. It has long been recognized that stearic acid does not share the hypercholesterolemic effects of shorter chain saturated fatty acids, such as lauric, myristic and palmitic acids [11]. In a recent well-designed and controlled study, Judd et al. [12] compared the effects of diets containing an additional 8% energy from stearic acid (STE) versus lauric + myristic + palmitic acid (LMP) versus TFA versus a blend of stearic acid + TFA (STE/TFA) versus oleic acid (OL) versus carbohydrate (CHO) on blood lipids. The STE diet produced the lowest total cholesterol and low-density

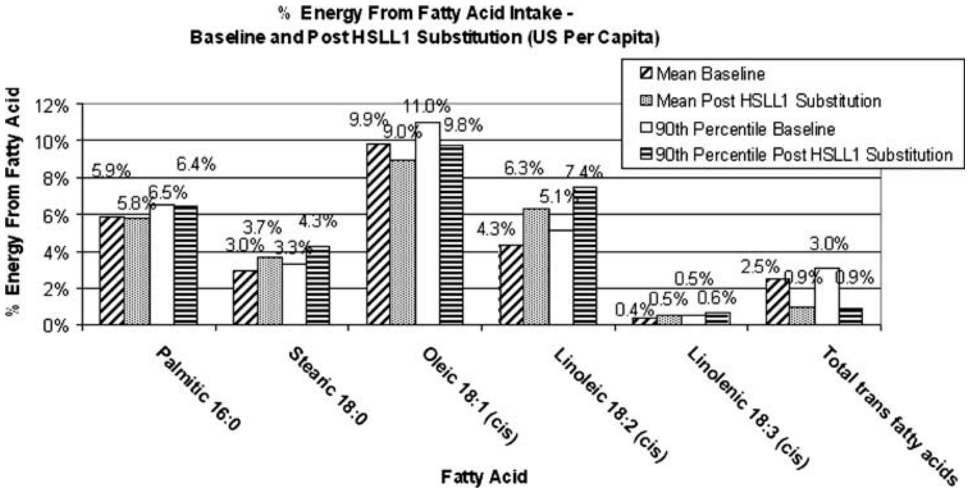

Fig. 1 US per capita fatty acid intake (% energy) after substitution of HSLL1 in four food categories, mean and 90th percentile

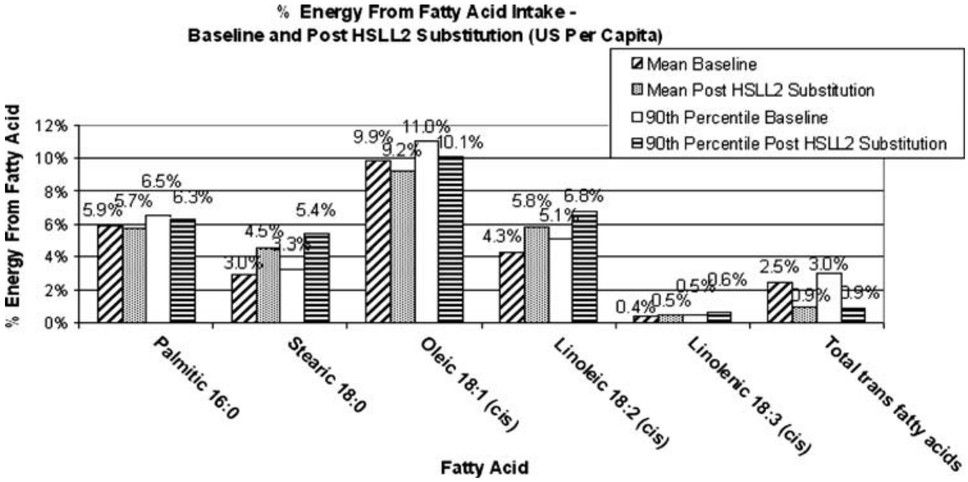

Fig. 2 US per capita fatty acid intake (% energy) after substitution of HSLL2 in four food categories, mean and 90th percentile

lipoprotein–cholesterol concentrations among the STE, LMP, TFA and STE/TFA diets, and the effects of the STE diet on these endpoints were not different from those observed for the CHO diet. These results are particularly relevant because they demonstrate the effects on plasma lipids of different types of dietary fats that could substitute for each other in food applications. The work of Judd et al. [12] indicates that using a high stearic acid fat to replace partially hydrogenated oil or oils high in lauric, myristic and palmitic acids would result in lower total and LDL cholesterol.

More recent research has sought to determine whether there are any potentially undesirable effects of stearic acid on other cardiovascular health indicators, such as inflammatory markers and hemostatic risk factors. For example, as part of the study by Judd et al. [12] described above, Baer et al. [13] determined the effects of six different diets on a variety of inflammatory markers in healthy men. They found that the STE diet did not result in levels of E-selectin, C-reactive protein, or IL-6 that were different from those found in the CHO group. The STE diet did raise levels of fibrinogen significantly versus the CHO diet, raising concern that dietary stearic acid could be pro-inflammatory. However, stearic acid did not consistently lead to increased fibrinogen levels in this study, since there were no significant effects on fibrinogen levels by the STE/TFA diet. The fibrinogen concentration on the CHO diet was 2.74 g/L, and on the STE/TFA diet, 2.75 g/L. The amount of stearic acid in the STE/TFA diet, 6.9% energy, in the study by Baer et al. [13] is higher than the 5.0% energy estimated to be the 90th percentile intake of stearic acid in the present study.

Thijssen et al. [5] compared the thrombogenic effects of diets containing comparable fat compositions except for 7% energy as either stearic, oleic or linoleic acids. Healthy male and female subjects consumed each diet for five weeks in a randomized, cross-over design. At the end of each period, ex vivo and in vitro platelet aggregation and variables of coagulation, fibrinolysis and hematology were assessed. There were no differences among the three dietary fatty acids in effects on indices of coagulation and fibrinolytic activity, i.e., Factor VII amidolytic activity, fibrinogen, prothrombin fragment 1 and 2, plasminogen activator inhibitor, and tissue plasminogen activator (tPA/PAI-1) complexes. There also were no significant effects of diet on ex vivo and in vitro platelet aggregation. When data from male subjects were considered separately from those of female subjects, the ex vivo platelet aggregation time following the linoleic acid diet was prolonged when compared to the stearic acid diet, but there was no difference ($P < 0.05$) between the stearic and oleic acid diets. Mean platelet volume for both male and female subjects was significantly lower following the high stearic acid diet versus the high oleic and high linoleic acid diets. Thijssen and coworkers concluded that their data refute the suggestion that stearic acid is thrombogenic.

In the review by Kris-Etherton et al. [4], it was shown that most clinical trials of the effects of stearic acid on health-related endpoints have used dietary concentrations of stearic acid of about 7–13% energy. Compared to the results shown in this study, these levels are well in excess of what is likely achievable in the US diet. In their review, Kris-Etherton et al. [4] concluded that even if stearic acid intake increased to 9% energy, "…it is unlikely that any adverse effects of this level of stearic acid would be observed". The increase in stearic acid intake from 3.0 energy to about 4–5% energy, as estimated in this study, represents the outer limit of possibility, since it assumed that 100% of the partially hydrogenated soybean oil used in four categories of foods would be replaced by HSLL1 or HSLL2. Thus, the expected intake of stearic acid is likely to be less than 5% energy as the result of using HSLL1 or HSLL2.

Note that the use of either HSLL1 or HSLL2 could result in decreases in TFA intake from a mean of 2.5–0.9% energy. The ability of these oils to replace partially hydrogenated soybean oils used in baked goods accounts for much of their significant potential to reduce intake of TFA while not increasing intake of palmitic acid. A recent clinical study [18] has shown that the use of palm oil to replace partially hydrogenated soybean oil would result in undesirable effects on lipoprotein profiles when compared to soy and canola oils. The authors concluded that palm oil would not be a good substitute for partially hydrogenated fats.

As food manufacturers seek alternatives to partially hydrogenated oils, they must weigh their formulation needs against the need to deliver optimal nutrition. High stearic, low α-linolenic acid soybean oils provide the opportunity to deliver stability and functionality to a variety of foods while also avoiding the negative health consequences associated with other saturated fatty acids. This study has shown that the use of HSLL1 or HSLL2 to replace partially hydrogenated soybean oil in four food categories could increase the intake of stearic acid from a mean of 3.0% energy to about 4% energy (at the 90th percentile, 3.3% energy baseline to about 5% energy). This increased level of stearic acid intake is well below the levels studied in numerous clinical trials that have shown no adverse effects on markers of cardiovascular health. Moreover, such a substitution could achieve a significant reduction in the intake of TFA while not increasing the intake of palmitic acid.

References

1. Department of Health and Human Services, Food and Drug Administration (2003) Food labeling: trans fatty acids in nutrition labeling, nutrient content claims, and health claims. Fed Regist 68(133):41434–41506
2. Golbitz P, Hayes K, Hartford G, Jordon J, Jost A (2006) Soya and oilseeds bluebook. Soyatech, Bar Harbor, ME
3. Department of Health and Human Services (HHS) and the Department of Agriculture (USDA) (2005) Dietary guidelines for Americans (Health and Human Services Publication; Home and Garden Bulletin No. 232). http://www.healthierus.gov/dietaryguidelines. Accessed Aug 2007
4. Kris-Etherton PM, Griel AE, Psota TL, Gebauer SK, Zhang J, Etherton TD (2005) Dietary stearic acid and risk of cardiovascular disease: intake, sources, digestion, and absorption. Lipids 40:1193–2001
5. Thijssen MAMA, Hornstra G, Mensink R (2005) Stearic, oleic and linoleic acids have comparable effects on markers of thrombotic tendency in healthy human subjects. J Nutr 135:2805–2811
6. Tholstrup T (2005) Influence of stearic acid on hemostatic risk factors in humans. Lipids 40:1229–1235
7. National Center for Health Statistics (NCHS)(2007) The National Health and Nutrition Examination Survey (NHANES) 1999–2002. Public Data Release 1999–2002. http://www.cdc.gov/nchs/about/major/nhanes/nhanes99_00.htm. Accessed Aug 2007
8. US Department of Agriculture, Agriculture Research Service (2007) Fat and fatty acid content of selected foods containing *trans*-fatty acids. http://www.nal.usda.gov/fnic/foodcomp/Data/Other/trans_fa.pdf. Accessed Aug 2007
9. DiRienzo M, Astwood J, Petersen B, Smith K (2006) Effect of substitution of low linolenic acid soybean oil for hydrogenated soybean oil on fatty acid intake. Lipids 41:149–157
10. Sanders TAB, Berry SEE (2005) Influence of stearic acid on postprandial lipemia and hemostatic function. Lipids 40:1221–1227
11. Mensink RP (2005) Effects of stearic acid on plasma lipid and lipoproteins in humans. Lipids 40:1201–1205
12. Judd JT, Baer DJ, Clevidence BA, Kris-Etherton P, Muesing RA, Iwane M (2002) Dietary *cis* and *trans* monounsaturated and saturated FA and plasma lipids and lipoproteins in men. Lipids 37:123–131
13. Baer DJ, Judd JT, Clevidence BA, Tracy RP (2004) Dietary fatty acids affect plasma markers of inflammation in healthy men fed controlled diets: a randomized crossover study. Am J Clin Nutr 79:969–973
14. Berry SEE, Miller GJ, Sanders TAB (2007) The solid fat content of stearic-acid rich fats determines their postprandial effects. Am J Clin Nutr 85:1486–1494
15. Mensink RP, Zock PL, Kester ADM, Katan MB (2003) Effects of dietary fatty acids and carbohydrates on the ratio of serum total to hdl cholesterol and on serum lipids and apolipoproteins:

a meta-analysis of 60 controlled trials. Am J Clin Nutr 77:1146–1155

16. Thijssen MA, Mensink RP (2005) Small differences in the effects of stearic acid, oleic acid, and linoleic acid on the serum lipoprotein profile of humans. Am J Clin Nutr 82:510–516
17. Tholstrup T, Marckmann P, Jespersen J, Sandstrom B (1994) Fat high in stearic acid favorably affects blood lipids and Factor VII coagulant activity in comparison with fats high in palmitic acid or high in myristic and lauric acids. Am J Clin Nutr 59:371–377
18. Vega-Lopez S, Ausman LM, Jalbert SM, Erkkila AT, Lichtenstein AH (2006) Palm and partially hydrogenated soybean oils adversely alter lipoprotein profiles compared with soybean and canola oils in moderately hyperlipidemic subjects. Am J Clin Nutr 84:54–62
19. US Department of Agriculture, Agriculture Research Service (2007) Search the Nutrient Database Laboratory for standard reference. http://www.nal.usda.gov/fnic/foodcomp/search. Accessed Aug 2007

Lipids (2008) 43:457–460
DOI 10.1007/s11745-008-3154-9

COMMUNICATION

Ricinoleic Acid in Common Vegetable Oils and Oil Seeds

Kouhei Yamamoto · Akemi Kinoshita ·
Akira Shibahara

Received: 20 July 2007 / Accepted: 9 January 2008 / Published online: 21 February 2008
© AOCS 2008

Abstract An original gas chromatography/mass spectrometry method for quantifying trace amounts of ricinoleic acid (12-hydroxy-*cis*-9-octadecenoic acid) is detailed. Data are presented on trace amounts of ricinoleic acid found in several common vegetable oils and oils extracted from common oil seeds: e.g., ca. 30 ppm in commercial olive oil was the lowest amount; and ca. 2,690 ppm in oil extracted from cottonseeds was the highest amount.

Keywords Ricinoleic acid · 12-hydroxy-*cis*-9-octadecenoic acid · Common vegetable oils · Common oil seeds · Gas chromatography/mass spectrometry

Abbreviations

GC/MS	Gas chromatography/mass spectrometry
IS	Internal standard
OTMS	*O*-trimethylsilylated

Introduction

With current testing methods, ricinoleic acid (12-hydroxy-*cis*-9-octadecenoic acid), the characteristic acyl component of castor bean oil [1–3] can only be quantified at the percent level. For quantifying trace amounts of ricinoleic acid, our research group developed a method using gas chromatography/mass spectrometry (GC/MS). While we were developing this method, we unexpectedly found that ricinoleic acid is in many common vegetable oils.

In this communication, we introduce this method and present the data confirming the presence of ricinoleic acid.

Materials and Methods

Materials and Chemicals

Rapeseeds were supplied by an oil manufacturer; other oil seeds and vegetable oils were purchased from local markets. Standard castor oil, authentic ricinoleic acid (purity 87%) and 3-hydroxyhexadecanoic acid (purity 98%) were from Wako Pure Chemical Industries (Osaka, Japan). Triolein (purity 99%) was from Nu-Chek Prep (Elysian, MN). Other chemicals were of the highest reagent grade available.

Preparation of Derivatives from Oil Samples

Samples were ten kinds of vegetable oils and the oils (extracted by the method of Folch et al. [4]) of four kinds of oil seeds. The internal standard (IS), 3-hydroxyhexadecanoic acid (50 µg), was added to each 50 mg sample, and then these samples were methanolyzed with 0.5 M KOH/methanol (1 mL) and successively methylated with 14% BF_3/methanol (1.5 mL), under the same conditions as those described in our previous research [5]. After adding a saturated NaCl aqueous solution (5 mL), the resultant fatty acid methyl esters were extracted three times with hexane (3 mL each time). The hexane layers were combined, dehydrated and evaporated to dryness. The residue

---

K. Yamamoto · A. Kinoshita · A. Shibahara (✉)
Department of Clinical Nutrition, Osaka Prefecture University,
7-30 Habikino 3-chome, Habikino 583-8555, Japan
e-mail: shibahar@rehab.osakafu-u.ac.jp

containing fatty acid methyl esters was dissolved in hexane (1 mL). This was poured into a glass column (30 cm × 15 mm i.d.) packed with 8 g of Wakogel C-300 (Wako Pure Chemical Industries) and 3 g of anhydrous Na_2SO_4. The esters with straight carbon chains were removed from the column by passing through a solution of ether/hexane (10:90, by vol.) (50 mL). The remaining esters with hydroxyl groups on their carbon chains were recovered from the column by passing acetone (50 mL) through. This recovered fraction was evaporated to dryness, dissolved in dehydrated pyridine (0.3 mL), and then trimethylsilylated with 0.2 mL of a reagent mixture [trimethylchlorosilane/*N*-trimethylsilylimidazole/*N*,*O*-bis(trimethylsilyl)trifluoroacetamide] (1:1:1, by vol.) under the usual conditions. After standing for 10 min at room temperature, the *O*-trimethylsilylated (-OTMS) methyl ester derivatives of each sample were analyzed by GC/MS.

Preparation of the Standard Mixtures for the Calibration Curve

Eight different standard mixtures were prepared—each contained different amounts (0, 0.5, 1, 2, 5, 10, 20 and 50 μg) of authentic ricinoleic acid with the same amount (50 μg) of 3-hydroxyhexadecanoic acid (IS). These standard mixtures were methylated, trimethylsilylated, and analyzed by GC/MS. The conditions for methylating and trimethylsilylating were the same as those described above.

GC/MS Conditions

The derivatives of fatty acid methyl ester-OTMS were analyzed on an SPB-50 capillary column (30 m × 0.25 mm i.d., 0.25 μm film, chemically bonded type, Supelco, Bellefonte, PA) connected to a Shimadzu QP-2010 mass spectrometer (Kyoto, Japan) with a computer on-line system. The column temperature was programmed at 180 °C isothermally for 2 min, increased to 240 °C at a rate of 3 °C/min, to 290 °C at a rate of 60 °C/min, and held at 290 °C isothermally for 8 min. The other operating conditions were as follows: injector temperature, 280 °C; interface temperature, 280 °C; ion source temperature, 200 °C; carrier gas, helium (linear gas velocity of 35 cm/s); split ratio, 1/25; ionizing energy, 70 eV; and scanning range, 70–400 *m/z* (0.5 s/cycle).

Results and Discussion

Calibration Curve for Determining the Amounts of Ricinoleic Acid

The eight different standard mixtures were analyzed by GC/MS to get the calibration curve used for determining the trace amounts of ricinoleic acid in the oil samples. Figure 1a shows the mass chromatogram of one of the standard mixtures; methyl 3-hydroxyhexadecanoate-OTMS (derived from the IS) elutes at 11.9 min and methyl ricinoleate-OTMS elutes at 16.9 min.

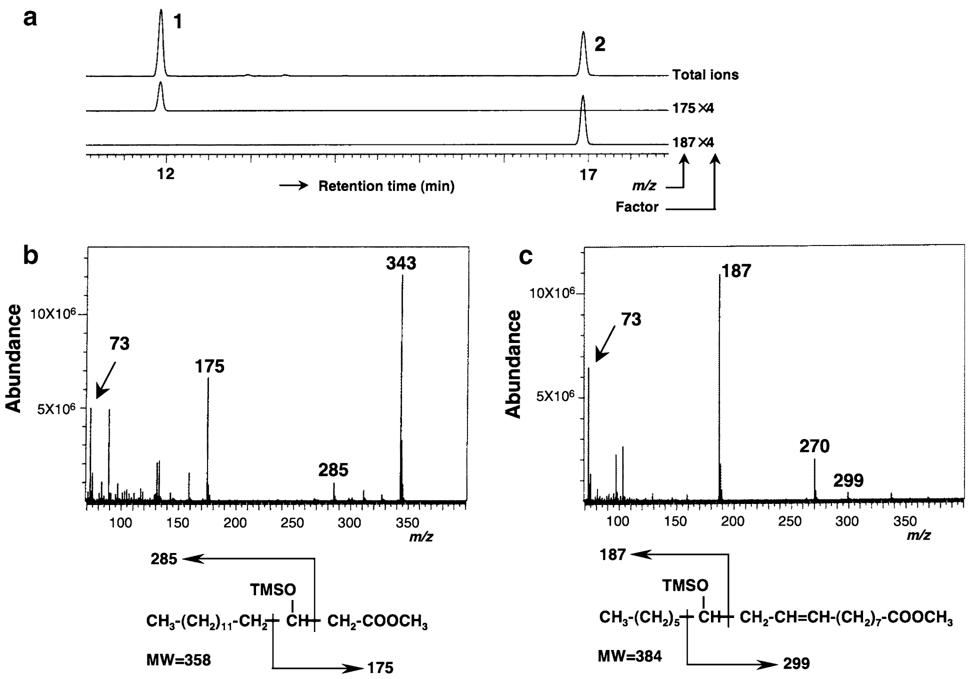

Fig. 1 Mass chromatogram of one of the standard mixtures of methyl 3-hydroxyhexadecanoate and methyl ricinoleate after trimethylsilylation (**a**), and mass spectra of trimethylsilylated derivatives of methyl 3-hydroxyhexadecanoate (**b**) and of methyl ricinoleate (**c**). In mass chromatogram A, peak 1 (retention time, 11.9 min) is the trimethylsilylated derivative of methyl 3-hydroxyhexadecanoate (internal standard) and peak 2 (retention time, 16.9 min) is the trimethylsilylated derivative of methyl ricinoleate. Mass spectra (**b**) and (**c**) are taken from the tops of peak 1 and peak 2 in mass chromatogram A. Mass spectral elucidations and the GC/MS conditions are given in the text

Figure 1b shows the electron impact mass spectrum of methyl 3-hydroxyhexadecanoate-OTMS. The α-cleavage at the silyl ether group gives the fragment ions at *m/z* 175 and at *m/z* 285. The ion at *m/z* 343 (M^+-15) is due to the loss of the methyl group (one of three methyl groups of the silyl group) from the molecular ion at *m/z* 358. The major ion at *m/z* 73, $(CH_3)_3Si^+$, is a typical ion originating from the trimethylsilylated compound.

In the mass spectrum of methyl ricinoleate-OTMS (Fig. 1c), the α-cleavage at the silyl ether group gives the fragment ions at *m/z* 187 and at *m/z* 299. The migration ion (TMS rearrangement ion) at *m/z* 270, CH_2–CH = CH–$(CH_2)_7$–C^+(=OTMS)–OCH_3, is present, indicating the locations of the hydroxyl group at the C-12 carbon and the double bond at the C-9 and C-10 carbons. These mass spectral elucidations agree with those in other research [6, 7].

With mass chromatography, we traced the fragment ions at *m/z* 175 (from methyl 3-hydroxyhexadecanoate-OTMS) and at *m/z* 187 (from methyl ricinoleate-OTMS) from the eight different standard mixtures to get the calibration curve.

The value *V*, indicating the peak area ratio of these two fragment ions, is calculated with the following formula: *V* = peak area of the ion at *m/z* 187/peak area of the ion at *m/z* 175. Plotting the value *V* for the eight different standard mixtures (on the *y*-axis) against the known amounts of ricinoleic acid (on the *x*-axis) gives the calibration curve in Fig. 2. Value *V* increases in direct proportion to the increasing amounts of ricinoleic acid (from 0 to 50 µg). This GC/MS method is suitable for quantifying ricinoleic acid at the ppm level.

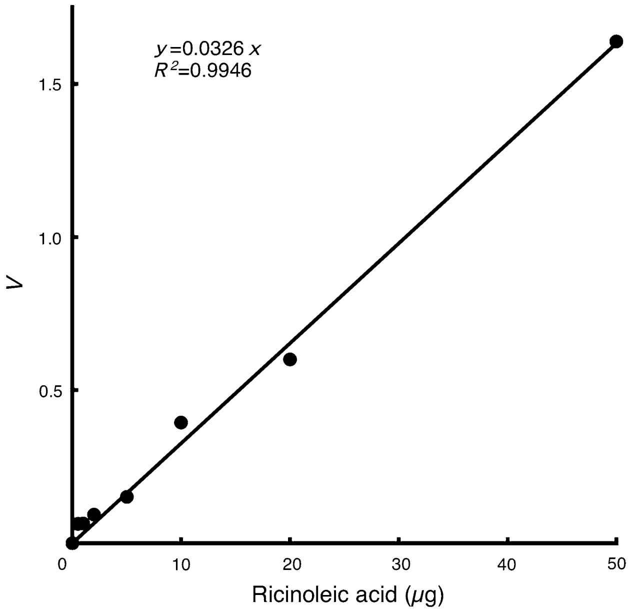

Fig. 2 Calibration curve for determining the amounts of ricinoleic acid. Known amounts of ricinoleic acid in the eight different standard mixtures are plotted on the *x*-axis. The values *V*, indicating the peak area ratio of the two fragment ions, are plotted on the *y*-axis. The value *V* is calculated with the following formula: *V* = peak area of the ion at *m/z* 187/peak area of the ion at *m/z* 175, where the ion at *m/z* 187 is from the trimethylsilylated derivative of methyl ricinoleate and the ion at *m/z* 175 is from the trimethylsilylated derivative of methyl 3-hydroxyhexadecanoate. Each value *V* is an average of triplicate determinations

Recovery Test

As the model experiment, 32 µg of standard castor oil was added to 50 mg of triolein. This was analyzed (five times, independently), and there was an average of 95% recovery for ricinoleic acid (6.2% CV).

Ricinoleic Acid in Common Vegetable Oils and Oil Seeds

Using this method, we analyzed ten kinds of vegetable oils, and all the oils contain ricinoleic acid (Table 1). Figure 3 illustrates the mass spectrum of methyl ricinoleate-OTMS taken from the soybean oil analysis, and it agrees with the spectrum of authentic methyl ricinoleate-OTMS (Fig. 1c).

We considered the possibility that these vegetable oils were contaminated, with castor oil or another contaminant containing ricinoleic acid, in the refining process during

Table 1 Amounts of ricinoleic acid in common vegetable oils and oils from seeds

Type of oil	Ricinoleic acid (ppm)[a]
Coconut	33 ± 1
Corn	209 ± 6
Cottonseed	1,695 ± 80
Extracted from seed[b]	2,688 ± 397
Olive	31 ± 1
Rapeseed	208 ± 40
Extracted from seed[b]	171 ± 37
Rice bran[c]	243 ± 8
Safflower	54 ± 19
Sesame	212 ± 17
Extracted from seed[b]	138 ± 23
Soybean	542 ± 27
Extracted from seed[b]	344 ± 51
Sunflower	181 ± 3

[a] Mean value and standard deviation from triplicate determinations

[b] Extracted in our laboratory according to the method of Folch et al. [4]

[c] We found an isomer of ricinoleic acid in rice bran oil. The details will be reported elsewhere

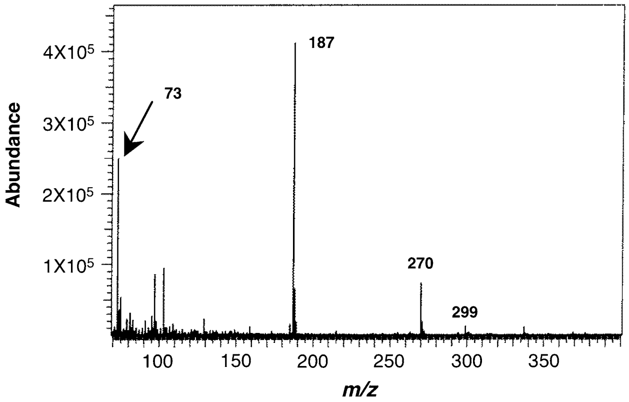

Fig. 3 Mass spectrum of trimethylsilylated derivative of methyl ricinoleate, taken from the soybean oil analysis

production. To check this, we directly extracted oil from four kinds of oil seeds (according to the method of Folch et al. [4], routinely used in lipid laboratories). In these cases, as well, ricinoleic acid is quantified (Table 1).

From our data, we may conclude that many common vegetable oils and oil seeds contain ricinoleic acid.

This easy and sensitive GC/MS method can be a strong tool for those who need to determine trace amounts of ricinoleic acid in the food, cosmetic or pharmaceutical industries and also in research laboratories.

Possible Mechanism for Ricinoleic Acid Biosynthesis

The oil-producing plants (reported here) must have enzyme systems involving ricinoleic acid bioformation. Plant lipid researchers fully understand the biosynthetic pathway for ricinoleic acid in castor bean [3, 8–11]; an enzyme system catalyzes the production of ricinoleate by direct hydroxylation of oleate (*cis*-9-octadecenoate) attaching to phosphatidylcholine (the immediate substrate: oleoyl-phosphatidylcholine). We do not know, however, if this enzyme system exists in the plants we analyzed.

In addition, fatty acyl hydroxylases and desaturases have similar amino acid sequences and similar reaction mechanisms [7, 9–11]. Our findings may help researchers studying the ricinoleate-synthesizing enzyme and the linoleate-synthesizing enzyme in higher plants.

References

1. Smith CR Jr (1970) Occurrence of unusual fatty acids in plants. Prog Chem Fats Other Lipids 11:137–177
2. Badami RC, Patil KB (1981) Structure and occurrence of unusual fatty acids in minor seed oils. Prog Lipid Res 19:119–153
3. Gunstone FD, Harwood JL, Dijkstra AJ (eds) (2007) The lipid handbook, 3rd edn. Taylor & Francis, Boca Raton
4. Folch J, Lees M, Sloane Stanley GH (1957) A simple method for the isolation and purification of total lipides from animal tissues. J Biol Chem 226:497–509
5. Shibahara A, Yamamoto K, Nakayama T, Kajimoto G (1986) *cis*-Vaccenic acid in mango pulp lipids. Lipids 21:388–394
6. Kleiman R, Spencer GF (1973) Gas chromatography–mass spectrometry of methyl esters of unsaturated oxygenated fatty acids. J Am Oil Chem Soc 50:31–38
7. van de Loo FJ, Broun P, Turner S, Somerville C (1995) An oleate 12-hydroxylase from *Ricinus communis* L. is a fatty acyl desaturase homolog. Proc Natl Acad Sci USA 92:6743–6747
8. Stymne S (1993) Biosynthesis of 'uncommon' fatty acids and their incorporation into triacylglycerols. In: Murata N, Somerville CR (eds) Biochemistry and molecular biology of membrane and storage lipids of plants. American Society of Plant Physiologists, Rockville, pp 150–158
9. Harwood JL (1996) Recent advances in the biosynthesis of plant fatty acids. Biochim Biophys Acta 1301:7–56
10. Shanklin J, Cahoon EB (1998) Desaturation and related modifications of fatty acids. Annu Rev Plant Physiol Plant Mol Biol 49:611–641
11. Voelker T, Kinney AJ (2001) Variations in the biosynthesis of seed-storage lipids. Annu Rev Plant Physiol Plant Mol Biol 52:335–361

Lipids (2008) 43:461–466
DOI 10.1007/s11745-008-3166-5

COMMUNICATION

From Aquatic to Terrestrial Food Webs: Decrease of the Docosahexaenoic Acid/Linoleic Acid Ratio

Apostolos-Manuel Koussoroplis · Charles Lemarchand · Alexandre Bec · Christian Desvilettes · Christian Amblard · Christine Fournier · Philippe Berny · Gilles Bourdier

Received: 26 November 2007 / Accepted: 22 February 2008 / Published online: 12 March 2008
© AOCS 2008

Abstract Fatty acid composition of the adipose tissue of six carnivorous mammalian species (European otter *Lutra lutra*, American mink *Mustela vison*, European Mink *Mustela lutreola*, European polecat *Mustela putorius*, stone marten *Martes foina* and European wild cat *Felis silvestris*) was studied. These species forage to differing degrees in aquatic and terrestrial food webs. Fatty acid analysis revealed significant differences in polyunsaturated fatty acid composition between species. More specifically, our results underline a gradual significant decrease in the docosahexaenoic acid (DHA)/linoleic acid (LNA) ratio of carnivore species as their dependence on aquatic food webs decreases. In conclusion, the use of the DHA/LNA ratio in long-term studies is proposed as a potential proxy of changes in foraging behaviour of semi-aquatic mammals.

Keywords Biomarkers · Carnivorous mammals · Conservation · Diet · Docosahexaenoic acid · Fatty acids · Food webs · Linoleic acid · Peritoneal fat

Abbreviations

ARA	Arachidonic acid
ALA	α-Linolenic acid
DHA	Docosahexaenoic acid
EPA	Eicosapentaenoic acid
LNA	Linoleic acid
MUFA	Monounsaturated fatty acid
PUFA	Polyunsaturated fatty acid
SAFA	Saturated fatty acid
TFAW	Total fatty acid weight

Introduction

Recent legal protection and conservation programs allowed many endangered species to re-colonise their habitats. Nevertheless, these species have to cope now with disturbed biotopes and prey populations. The re-colonising success of these species in their disturbed niches suggests a change in their foraging strategies [1, 2]. However, these diet modifications are very difficult to evaluate in a low density context [3]. Indeed, direct observation of faeces analysis give only a snapshot of the animals' diet.

On the other hand, fatty acid storage tissue composition has been successfully used in many cases as an accurate and time-integrating proxy of carnivorous mammals' diets [4–7]. The latter is based on the fact that some dietary fatty acids are stored in the adipose tissues without important modifications and thus can be used as biomarkers [4].

Lipids from aquatic and terrestrial primary producers exhibit differences in fatty acid signatures [8]. Phytoplanktonic microalgae can produce n-3 polyunsaturated fatty acids (PUFAs) in large quantities [8–11]. In contrast, few terrestrial plants (e.g. Berries, Olives) contain significant amounts of α-linolenic acid (18:3n-3, ALA), whereas many

A.-M. Koussoroplis (✉) · C. Lemarchand · A. Bec · C. Desvilettes · C. Amblard · G. Bourdier
Laboratoire LMGE, UMR CNRS 6023,
Equipe Réseaux Trophiques Aquatiques,
Université Blaise Pascal, 24, Avenue des Landais,
63177 Aubière, France
e-mail: a-manuel.KOUSSOROPLIS@univ-bpclermont.fr

C. Fournier
GREGE, Route de Préchac, 33730 Villandraut, France

P. Berny
Laboratoire de Biologie et Toxicologie, ENVL, BP83,
69280 Marcy l'Etoile, France

more synthesize and store large amounts of linoleic acid (18:2n-6, LA) [12]. Highly unsaturated PUFAs (e.g. 20:4n-6; ARA, 20:5n-3; EPA, 22:6n-3; DHA) are involved in a wide range of physiological processes. As most animals lack the specific fatty acid desaturases required to insert double bonds in the n-3 and the n-6 position, these compounds have to be obtained by the animals from their diet [13, 14]. This results in a high conservation of these molecules along food webs, from primary producers to final consumers [15, 16]. Consequently, each type of food web shows a "typical" fatty acid profile [17, 18]. In aquatic food webs n-3 PUFAs dominate over n-6 PUFAs by a factor of 5–20 [17, 19]. The opposite is true for terrestrial food webs where n-6 PUFAs are more abundant than n-3 PUFAs [20]. Thus, we expect that gradual transitions from one food web to another are followed by a gradual evolution of fatty acid proportions The major aim of this study is to investigate the evolution of PUFA patterns along a gradual transition from aquatic to terrestrial food webs.

In this context, fatty acid composition of the peritoneal fat of six carnivore species (*Mammalia*, *Carnivora*) was analysed. The analysed species (European otter *Lutra lutra*, Linnaeus 1758 American mink *Mustela vison*, Schreber 1777, European mink *Mustela lutreola*, Linnaeus 1761, European polecat *Mustela putorius*, Linnaeus 1758, Stone marten *Martes foina*, Erxleben 1777 and European wild cat *Felis sylvestris*, Schreber 1777) were chosen in order to illustrate a continuous decreasing gradient of aquatic food web exploitation (Fig. 1).

Materials and Methods

Carnivore Sampling

Six species of two families of carnivores were chosen in order to illustrate a continuous decreasing gradient of aquatic food web exploitation (Fig. 1), and sampled in France between 2002 and 2006. Species were mainly chosen in the Mustelidae family: (American mink, $n = 13$; European otter, $n = 17$; European mink, $n = 17$; European polecat, $n = 13$; stone marten, $n = 13$) and one species was chosen in the Felidae family (European wild cat, $n = 14$). For ethical, legal and technical reasons, only freshly conserved (maximum 24 h) wild animals killed by road traffic were collected, using existent French networks in animal studies. Peritoneal adipose tissues were sampled and deep-frozen (−80 °C) before the lipid analysis.

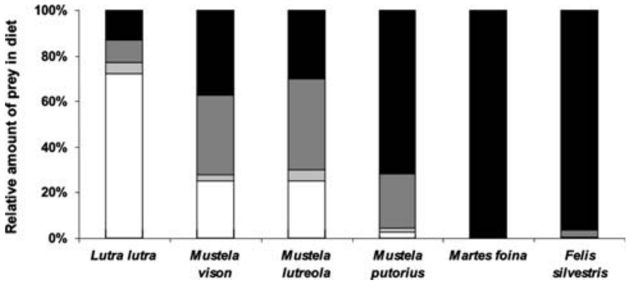

Fig. 1 Schematic representation of food source origin of the studied carnivorous mammals. *White*: fish; *clear grey*: crayfish; *dark grey*: amphibians; *black*: terrestrial food (birds, mammals, fruits, terrestrial invertebrates); Data synthesised from previous studies [35–39]

Lipid and Statistical Analysis

Total lipids were extracted from tissue samples with a chloroform/methanol (2:1, *v*/*v*) mixture [21]. Fatty acid methyl esters were obtained by hydrolysis in methanolic NaOH and esterification in methanolic H_2SO_4 [10]. Fatty acid analyses were carried out on a Chrompack CP 9001 gas chromatograph equipped with a Supelco® Omegacoax™ column and a FID detector (260 °C) (split injection; injector temperature: 260 °C; carrier gas: helium; oven rise from 140 to 245 °C at 3 °C min^{-1}). Individual fatty acid methyl esters are identified by comparing retention times with those obtained from Supelco® standards and laboratory standards. Fatty acid methyl esters were quantified using 13:0 as an internal standard that is added before the derivation of fatty acids.

Statistical differences in DHA, LNA and DHA/LNA compositions among sampled species were analysed with the Kruskal–Wallis test and when significant, two-by-two species comparisons were made with the Mann–Whitney *U* test. Correlation was calculated with Spearman's correlation coefficient (r_s). *P* values less than 0.05 where considered significant.

Results and Discussion

SAFA and MUFA Patterns

A total of 87 individuals were analysed for fatty acid composition (Table 1). Saturated fatty acids (SAFA) varied from 29.3 (European otter) to 55.3% (stone marten) of the total fatty acids weight (TFAW). As already observed [4, 22] for other mammals, SAFA are dominated by 16:0 (17.2% of the TFAW for otter, 31.4% for stone marten) and to a lesser extent by 18:0 (4.9% of the TFAW for otter to 22.8% of the TFAW for stone marten).

The monounsaturated fatty acids (MUFA) ranged from 21.4 (stone marten) to 45.0% (European mink) of TFAW. As observed for other carnivorous mammals [4, 22, 23] 18:1n-9 was the dominant fatty acid in MUFA, varying from 20.0 (stone marten) to 40.6% (European mink) of TFAW. Substantial or high levels of 16:1n-7 were also observed, ranging from 1.4 (stone marten) to 8.3% (European otter).

Table 1 Fatty acid composition of peritoneal adipose tissue of the six carnivorous mammal species studied

	Lutra lutra (n = 17)	*Mustela vison* (n = 13)	*Mustela lutreola* (n = 17)	*Mustela putorius* (n = 13)	*Martes foina* (n = 13)	*Felis silvestris* (n = 14)
14:0	4.0 ± 1.8	3.8 ± 1.8	2.5 ± 0.8	2.9 ± 0.8	1.1 ± 1.2	1.5 ± 1.2
15:0	1.0 ± 0.5	3.5 ± 3.0	Tr	0.6 ± 0.3	Tr	2.1 ± 1.9
16:0	17.2 ± 3.6	18.4 ± 8.6	20.5 ± 3.5	18.8 ± 3.4	31.4 ± 10.5	19.3 ± 4.7
17:0	0.8 ± 0.3	0.6 ± 0.3	0.5 ± 0.3	0.8 ± 0.5	Tr	1.1 ± 1.4
18:0	4.9 ± 1.9	8.5 ± 1.2	8.9 ± 2.9	16.3 ± 16.1	22.8 ± 7.3	10.6 ± 4.4
20:0	Tr	Tr	Tr	Tr	–	Tr
Br. SAFA	1.4 ± 1.1	Tr	Tr	Tr	–	Tr
SAFA	29.3 ± 5.3	34.8 ± 4.9	32.4 ± 5.0	39.4 ± 14.5	55.3 ± 9.3	34.6 ± 8.7
16:1n-7	8.3 ± 3.2	3.7 ± 1.5	3.4 ± 1.8	2.1 ± 1.1	1.4 ± 1.1	2.0 ± 0.6
18:1n-7	1.6 ± 2.2	–	Tr	Tr	Tr	Tr
18:1n-9	28.4 ± 2.7	37.6 ± 7.2	40.6 ± 10.1	27.0 ± 9.7	20.0 ± 7.1	38.5 ± 14.0
20:1n-11 + 1n-9	1.7 ± 1.0	1.1 ± 0.7	1.0 ± 0.7	Tr	Tr	0.6 ± 0.5
MUFA	40.0 ± 4.9	42.4 ± 7.4	45.0 ± 9.2	29.1 ± 10.9	21.4 ± 7.3	41.1 ± 14.3
16:2n-4	Tr	–	–	–	–	–
16:3n-4	0.9 ± 0.6	Tr	Tr	Tr	–	Tr
18:2n-6*	10.6 ± 2.8	15.2 ± 5.5	14.8 ± 4.4	18.2 ± 4.4	11.1 ± 3.3	15.9 ± 5.1
18:3n-6	Tr	Tr	Tr	Tr	Tr	Tr
18:3n-3	4.0 ± 2.2	1.8 ± 1.2	1.7 ± 1.1	7.3 ± 7.9	Tr	2.6 ± 2.8
18:4n-3	Tr	–	–	–	–	–
20:2n-6	0.8 ± 0.4	Tr	Tr	0.6 ± 0.5	Tr	Tr
20:3n-6	0.6 ± 0.4	Tr	Tr	Tr	1.0 ± 0.9	Tr
20:4n-6	2.2 ± 1.0	1.0 ± 0.6	1.1 ± 0.6	1.2 ± 1.0	5.5 ± 4.3	2.3 ± 3.8
20:3n-3	Tr	Tr	Tr	Tr	–	Tr
20:4n-3	Tr	Tr	–	–	–	–
20:5n-3	1.2 ± 0.9	Tr	Tr	Tr	Tr	Tr
22:4n-6	0.9 ± 0.5	Tr	0.6 ± 0.4	0.5 ± 0.3	1.3 ± 1.3	Tr
22:5n-6	Tr	Tr	0.6 ± 0.4	Tr	Tr	Tr
22:5n-3	2.7 ± 0.7	0.9 ± 0.5	0.8 ± 0.6	1.3 ± 0.8	2.5 ± 1.9	1.6 ± 1.5
22:6n-3*	4.4 ± 1.2	1.2 ± 0.8	1.1 ± 0.7	0.6 ± 0.3	Tr	Tr
PUFA	28.3 ± 4.6	20.1 ± 6.8	20.7 ± 6.4	29.7 ± 9.3	21.4 ± 7.3	22.4 ± 9.2
NI	0.9 ± 0.8	Tr	Tr	Tr	Tr	Tr
Sum n-3	12.3 ± 2.4	3.9 ± 2.2	3.6 ± 2.3	9.2 ± 8.4	2.5 ± 2.1	4.2 ± 4.3
Sum n-6	15.1 ± 3.9	16.2 ± 6.1	17.1 ± 5.2	20.3 ± 5.2	18.9 ± 6.3	18.2 ± 6.6
22:6/18:2*	0.46 ± 0.22	0.09 ± 0.07	0.08 ± 0.06	0.04 ± 0.02	0.01 ± 0.02	0.02 ± 0.04

Values are the mean percentages of total fatty acid weight (TFAW) ± standard deviations

Tr trace amounts (<0.5% TFAW), *Br. SAFA* sum of branched saturated fatty acids, *MUFA* sum of mono unsaturated fatty acids, *PUFA* sum of poly unsaturated fatty acids, – not detected, *NI* not identified

* Significant difference amongst six studied species Kruskall–Wallis $P < 0.001$ (only for 18:2n-6, 22:6n-3 and 22:6/18:2)

Variations in PUFA Patterns

The polyunsaturated fatty acids (PUFA) make up 20.1% (American mink) to 29.7% (European polecat) of TFAW, and are dominated by the n-6 FAs (52.4–89.1% of the total weight of PUFA, data not shown). For all sampled species, 18:2n-6 (linoleic acid, LA) counts for more than half of the weight of n-6 PUFAs (data not shown). High concentrations of LNA (from 10.6 to 18.2% of TFAW for otter and polecat, respectively) were also observed in terrestrial mammalian carnivores in previous studies [4, 24] and certainly reflect the abundance of this FA in terrestrial food webs [12, 18].

In contrast, n-3 FAs show stronger variations ranging from 10.9% (stone marten) to 42.5% (European otter) of total PUFA weight (data not shown) and are dominated by 18:3n-3 (α-linolenic acid, ALA) as well as by 22:6n-3 (docosahexaenoic acid, DHA) and to a lesser extent by

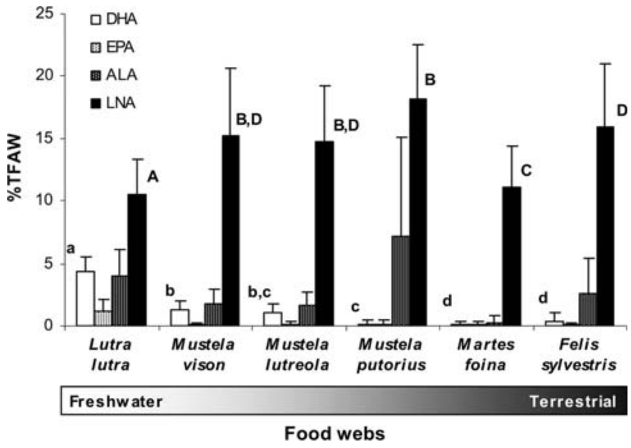

Fig. 2 Mean values of four major PUFAs in the peritoneal adipose tissue of the sampled carnivorous mammals, according to their degree of aquatic food web exploitation. For simplification reasons only the DHA and LNA statistical differences are presented. Data labelled with the *same letter* are not significantly different (Mann–Whitney, $P < 0.05$)

22:5n-3 (Table 1). Species with aquatic prey-based diet (Fig. 1) show up to tenfold higher concentrations of DHA than species that predate exclusively on terrestrial prey (Fig. 2). A dietary-influence of DHA and EPA concentrations linked to fish consumption has already been documented for American minks kits fed on a fish-oil supplemented diet [4]. Indeed, DHA is abundant in both marine and freshwater fishes [14, 19]. Although freshwater fishes can also be a source of ALA [8, 25, 26] the high concentration of this FA observed for the European polecat (7.3% of TFAW) is probably not completely due to fish consumption. Indeed, the results suggest that important ALA amounts of aquatic origin are associated with high DHA amounts, as observed for the European otter and both mink species (Fig. 2). Moreover, European polecats rarely consume fish (Fig. 1) and ALA could come from berries consumption, since berries are known to contain significant amounts of ALA [12]. Furthermore, the European polecat is known to complete its diet with fruits and berries (Fig. 1). In contrast with DHA, the LNA concentration tends to be increased in carnivorous mammals with more "terrestrial" diets (Fig. 2).

The DHA/LNA Ratio

The decrease in DHA as well as the increasing tendency of LNA in carnivorous mammals from aquatic to terrestrial food webs seems to be confirmed when comparing our results to those from other studies (Fig. 3). Indeed, animals foraging strictly in aquatic food webs, such as dolphins or marine seals, are characterized by the highest DHA/LNA ratios whereas freshwater seals exhibit lower DHA/LNA ratios when compared to marine mammals. A previous study successfully used the n-3/n-6 fatty acid ratio to distinguish marine from freshwater populations of genetically related seals [23]. The great abundance of n-6 PUFAs in freshwater food webs has been suggested to be due to a greater terrestrial input of organic matter [18]. Indeed, river food webs are often based on the use of terrestrial plant detrital material by macroinvertebrates [27]. Moreover, in lakes, a recent study has suggested that 22–55% of assimilated carbon by the major freshwater "herbivore" *Daphnia* sp. is derived from terrestrial organic matter [28]

Fig. 3 Mean values of DHA/LNA ratio in adipose tissue of carnivorous mammals belonging to different food webs. *Dagger*: data estimated from Samuel and Worthy [33]; *double dagger* data estimated from Käkelä and Hyvärinen [23]; *asterisks* data estimated from Grahl-Nielsen et al. [22]. *No symbol*: data from present study. *Above*: DHA/LNA ratio in peritoneal adipose tissue of carnivorous mammals from this study. Data labelled with the *same letter* are not significantly different (Mann–Whitney, $P < 0.05$)

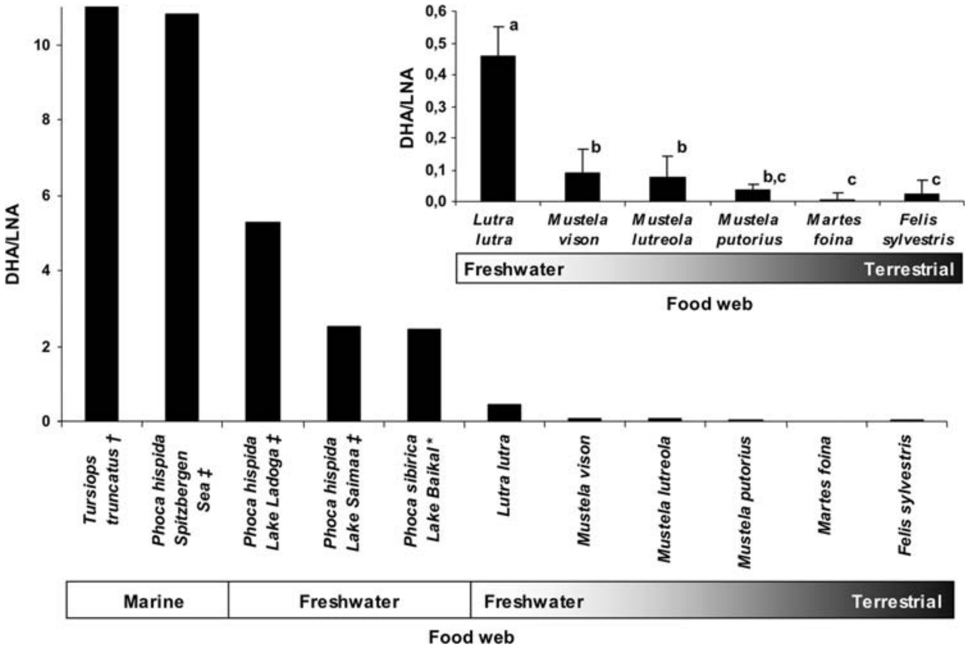

which could be rich in LNA [29]. Thus, inputs of terrestrial organic matter could partially explain the abundance of n-6 PUFAs and more particularly LNA in freshwater food webs. However, terrestrial influence may also occur under the form of phosphorus loading. It has recently been shown that sestonic concentrations of n-3 highly unsaturated fatty acids (such as DHA or EPA) decreased along a trophic state gradient from oligotrophic to eutrophic lakes [30]. For evident reasons the authors established the decrease of DHA with increasing total phosphorus by sampling different lakes. It is tempting to speculate that the decrease of DHA could occur in a given lake over a long-term temporal scale corresponding to its natural eutrophication. This could imply that the DHA/LNA ratios that are observed in a given aquatic food web gradually evolve towards more terrestrial values. However, Müller-Navarra et al. [30] did not mention any increase of LNA with increasing total phosphorus. Nevertheless, phytoplankton composition in eutrophic lakes is often dominated by Cyanobacteria or Chlorophyceae, which do not produce DHA but can contain relatively high amounts of LNA [9, 31].

DHA/LNA Ratio Gradient from Aquatic to Terrestrial Food Webs

Because of the terrestrial influence and specific processes occurring in freshwater food webs, the DHA/LNA ratio can distinguish marine from freshwater mammals. For example, dolphins and seals foraging in marine food webs exhibit high DHA/LNA ratios ranging from 11 (Bottlenose dolphin *Tursiops truncatus*) to 11.82 (Ringed seal *Phoca hispida*), whereas freshwater seals exhibit ratios ranging from 2.5 to 5.29 (Fig. 3). Continental carnivorous mammals foraging partially or totally in terrestrial food webs exhibit much lower DHA/LNA ratios, ranging from 0.46 (European otter) to 0.01 (stone marten). More interestingly, the gradual decrease of the ratio is correlated with decreasing aquatic food web exploitation ($r_s = 0.957$, $P < 0.05$) (Fig. 3).

The decrease in the DHA/LNA ratio from aquatic to terrestrial food webs led us to consider DHA/LNA ratio of carnivorous mammals as a proxy evaluating their connection strength to these two types of food webs. Nevertheless, the mean values of the DHA/LNA ratio of the animals sampled in this study exhibit an important individual variability (Fig. 3). As these animals were collected in different geographic areas and at different seasons, this variability could reflect geographical and temporal differences in foraging behaviour [32]. Furthermore, other parameters such as age, sex or physiological state should also be taken into account when considering this variability [22, 33].

Thus, further studies are required to better understand the dietary FA accumulation patterns and their variations among and within species. Moreover, more attention should be paid on adipose tissue turnover rates in order to establish more precisely the links between DHA/LNA ratio and dietary shifts. Once these parameters are known, it should be possible to determine whether the striking difference in the DHA/LNA ratios between otters and freshwater seals (Fig. 3) is relevant. If so, our results could suggest that the re-colonising otters sampled for this study are more strongly connected to terrestrial food webs than expected. This phenomenon has already been observed for American minks sharing the same biotope with otters. These two species are niche competitors, and their competition in a disturbed biotope can result in a switch of the mink's diet from aquatic to terrestrial prey [1, 34].

In conclusion, we suggest that the DHA/LNA ratio is a useful tool for the assessment of the dietary plasticity of carnivorous mammals. The use of the DHA/LNA ratio in long-term studies could allow to evaluate in which manner changes in foraging behaviour are linked to population dynamics of semi-aquatic species in different geographical areas.

References

1. Bonesi L, Chanin P, Macdonald DW (2004) Competition between Eurasian otter *Lutra lutra* and American mink *Mustela vison* probed by niche shift. Oikos 106:19–26
2. Bonesi L, Macdonald DW (2004) Differential habitat use promotes sustainable coexistence between the specialist otter and the generalist mink. Oikos 106:509–519
3. Kruuk H (2002) Hunters and hunted, relationships between carnivores and people. Cambridge University Press, Cambridge
4. Iverson SJ, Field C, Don Bowen W, Blanchard W (2004) Quantitative fatty acids signature analysis: a new method of estimating predator diets. Ecol Monogr 74:211–235
5. Rouvinen K, Kiiskinen T (1989) Influence of dietary fat source on the body fat composition of mink (*Mustela vison*) and blue fox (*Alopex lagopus*). Acta Agric Scand 39:279–288
6. Wamberg S, Olesen CR, Hansen HO (1992) Influence of dietary sources of fat on lipid synthesis in mink (*Mustela lutreola*) mammary tissue. Comp Chem Physiol A 103:199–204
7. Colby RH, Mattacks CA, Pond CM (1993) The gross anatomy, cellular structure, and fatty acid composition of adipose tissue in captive polar bears (*Ursus maritimus*). Zoo Biol 12:267–275
8. Napolitano GE (1998) Fatty acids as trophic and chemical markers in freshwater ecosystems. In: Arts MT, Wainman BC (eds) Lipids in freshwater ecosystems, pp 21–44
9. Ahlgren G, Gustavsson IB, Boberg M (1992) Fatty acid content and chemical composition of freshwater algae. J Phycol 28:37–50
10. Desvilettes C, Bourdier G, Breton JC (1997) Use of fatty acids for the assessment of zooplankton grazing on bacteria, protozoan and microalgae. Freshw Biol 38:629–637
11. Volkman JK, Barrett SM, Blackburn SI, Mansour MP, Sikes EL, Gelin F (1998) Microalgal biomarkers: a review of recent research developments. Org Geochem 29:1163–1179
12. Malainey ME, Przybylski RS, Sherriff BL (1999) Fatty acid composition of native food plants and animals of Western Canada. J Archaeol Sci 26:83–94

13. Arts MT (1998) Lipids in freshwater zooplankton: selected ecological and physiological aspects. In: Arts MT, Wainman BC (eds) Lipids in freshwater ecosystems, pp 71–86
14. Sargent JR, Bell JG, Bell MV, Henderson RJ, Tocher DR (1993) The metabolism of phospholipids and polyunsaturated fatty acids in fish. Aquaculture: fundamental and applied research. In: Lahlou B, Vitiello P (eds) Coastal and estuarine studies, vol 43. American Geophysical Union, Washington DC, pp 103–124
15. Brett MT, Müller-Navarra DC (1997) The role of highly unsaturated fatty acids in aquatic foodweb processes. Freshw Biol 38:483–499
16. Arts MT, Ackman RG, Holub BG (2001) "Essential fatty acids" in aquatic ecosystems: a crucial link between diet and human health and evolution. Can J Fish Aquat Sci 58:122–137
17. Henderson RJ, Tocher DR (1987) The lipid composition and biochemistry of freshwater fish. Prog Lipid Res 26:28–347
18. Olsen Y (1998) Lipids and essential fatty acids in aquatic food webs: what can freshwater ecologists learn from mariculture? In: Arts MT, Wainman BC (eds) Lipids in freshwater ecosystems, pp 161–202
19. Ahlgren G, Blomqvist P, Boberg M, Gustavsson IB (1994) Fatty acid content of the dorsal muscle—an indicator of fat quality in freshwater fish. J Fish Biol 45:131–157
20. Skjervold H (1992) Lifestyle diseases and the human diet. How should the new discoveries influence the food production? Collection of articles printed in The Journal of Dairy Industry of Norway. Ås-Trykk, Norway, p 48
21. Folch J, Lees M, Sloane-Stanley GH (1957) A simple method for the isolation and purification of total lipids from animal tissues. J Biol Chem 226:497–509
22. Grahl-Nielsen O, Halvorsen A-K, Bodoev N, Averina L, Radnaeva L, Pronin N, Käkelä R, Petrov E (2005) Fatty acid composition of blubber of the Baikal seal *Phoca sibirica* and its marine relative, the ringed seal *P. hispida*. Mar Ecol Prog Ser 305:261–274
23. Käkelä R, Hyvärinen H (1998) Composition of polyunsaturated fatty acids in the liver of freshwater and marine ringed seals (*Phoca hispida* ssp.) differs largely due to the diet of seals. Comp Biochem Physiol B 120:231–237
24. Mustonen AM, Nieminen P (2006) Fatty acid composition in the central and peripheral adipose tissues of the sable (*Martes zibellina*). J Therm Biol 31:617–625
25. Käkelä R, Ackman RG, Hyvärinen H (1995) Very long chain polyunsaturated fatty acids in the blubber of ringed seals (*Phoca hispida* sp.) from Saimaa, Lake Ladoga, the Baltic Sea and Spitbergen. Lipids 30:725–731
26. Smith RJ, Hobson KA, Koopman HN, Lavigne DM (1996) Distinguishing between populations of fresh- and salt-water harbour seals (*Phoca vitulina*) using stable-isotopes ratios and fatty acid profiles. Can J Fish Aquat Sci 53:272–279
27. Wallace JB, Webster JR (1996) The role of macroinvertebrates in stream ecosystem function. Annu Rev Entomol 41:115–139
28. Pace ML, Cole JJ, Carpenter SR, Kitchell JF, Hodgson JR, Van de Bogert MC, Bade DL, Kritzberg ES, Bastviken D (2004) Whole-lake carbon-13 additions reveal terrestrial support of aquatic food webs. Nature 427:240–243
29. Bec A, Desvilettes C, Véra A, Lemarchand C, Fontvielle D, Boudier G (2003) Nutritional quality of a freshwater heterotrophic flagellate: trophic upgrading of its microalgal diet for *Daphnia hyalina*. Aquat Microb Ecol 32:203–207
30. Müller-Navarra DC, Brett MT, Park S, Chandra S, Ballantyne AP, Zorita E, Goldman CR (2004) Unsaturated fatty acid content in seston and tropho-dynamic coupling in lakes. Nature 427: 69–71
31. Bec A, Martin-Creuzburg D, von Elert E (2006) Trophic upgrading of autotrophic picoplankton by the heterotrophic nonaflagellate *Paraphysomonas* sp. Limnol Oceanogr 51:1699–1707
32. Ben-David M, Flynn FW, Schell DM (1997) Annual and Seasonal changes in diets of martens: evidence from stable isotope analysis. Oecologia 111:280–291
33. Samuel AM, Worthy GAJ (2004) Variability in fatty acid composition of bottlenose dolphin (*Tursiops truncatus*) blubber as a function of body site, season, and reproductive state. Can J Zool 82:1933–1942
34. Clode D, Macdonald DW (1995) Evidence for food competition between mink (*Mustela vison*) and otter (*Lutra lutra*) on Scottish islands. J Zool 237:435–444
35. Goszczynski J (1976) Composition of the food of martens. Acta Theriol 21:527–534
36. Libois R, Waechter A (1991) La fouine (*Martes foina*). In: Artois M, Delattre P (eds) Encyclopédie des Carnivores de France. Société Française d'Etude et de Protection des Mammifères, Nort/Erdre, n°10
37. Libois R, Fellous A, Rosoux R, Fournier P, Siberchicot O (1998) The diet of the European Mink, *Mustela lutreola*, in south-western France: preliminary results. In: Reg S (ed) Euro-Americano mammal congress. Santiago de Compostela, 19–24th July 1998
38. Sidorovich V, Kruuk H, Macdonald DW, Maran T (1998) Diets of semi-aquatic carnivores in northern Belarus, with implications for population changes. Symp Zool Soc Lond 71:177–190
39. Clavero M, Prenda J, Delibes M (2003) Trophic diversity of the otter (*Lutra lutra* L.) in temperate and Mediterranean freshwater habitats. J Biogeogr 30:761–769

Lipids (2008) 43:467–470
DOI 10.1007/s11745-008-3169-2

COMMUNICATION

A Pivotal Role of the Human Kidney in Catabolism of HDL Protein Components Apolipoprotein A-I and A-IV but not of A-II

Jonas Heilskov Graversen · Graciela Castro · Abdelmejid Kandoussi · Henning Nielsen · Erik Ilsø Christensen · Anthony Norden · Søren Kragh Moestrup

Received: 14 November 2007 / Accepted: 27 February 2008 / Published online: 19 March 2008
© AOCS 2008

Abstract Renal handling of major HDL components was studied by analyzing urine from patients with Fanconi syndrome, a rare renal proximal tubular reabsorption failure, including dysfunction of the kidney HDL receptor, cubilin. A high urinary excretion of apolipoprotein A-I and A-IV corresponding to a major part of the metabolism of these proteins was measured. In contrast, no urinary excretion of apolipoprotein A-II which is more hydrophobic and tighter bound to HDL was found. Control urines displayed absence of the three apolipoproteins. Urinary excretion of phospholipids, triglycerides, cholesterol and cholesterol esters in patients was as low as in controls. In conclusion, these data indicate that the human kidney is a major site for filtered nascent apolipoprotein A-I and A-IV but not for HDL particles.

Keywords Lipid biochemistry · Apolipoproteins · Lipoproteins · HDL · Lipoproteins · Renal function · Physiology

Abbreviations

apoA-I	Apolipoprotein A-I
apoA-II	Apolipoprotein A-II
apoA-IV	Apolipoprotein A-IV
HDL	High-density lipoprotein

Introduction

The high density lipoprotein (HDL) plasma level, including its major protein component apolipoprotein A-I (apoA-I), is inversely correlated to the incidence of cardiovascular diseases [1]. ApoA-I's anti-atherosclerotic properties, have led to a focus on apoA-I metabolism and apoA-I based therapies [2–6]. The plasma level of HDL/apoA-I is correlated to the catabolic rate rather than production rate of apoA-I [7]. Whereas the liver and steroid organs are major site for uptake of HDL lipids, there are diverging data on the catabolism of the HDL particles and protein components.

In studies of elimination of human and murine apoA-I in mice models and hamster apoA-I in hamster, the liver was found to be the major organ for clearance of apoA-I [8–10], whereas in rats the kidney was found to be the major site [11]. These different observations may be due to species differences as well as the apoA-I labeling procedures used. The latter is indicated by a study in rabbits showing that 70% of injected human apoA-I was cleared by the kidneys, whereas ^{125}I- labeled apoA-I was cleared substantially faster, and predominantly by liver [12]. Furthermore, the

---

Abdelmejid Kandoussi: Deceased.

J. H. Graversen (✉) · H. Nielsen · S. K. Moestrup
Department of Medical Biochemistry,
University of Aarhus, 8000 Aarhus C, Denmark
e-mail: jhg@biokemi.au.dk

E. I. Christensen
Department of Cell biology, University of Aarhus,
8000 Aarhus C, Denmark

G. Castro · A. Kandoussi
Institut Pasteur, INSERM U545, Lille, France

A. Norden
Department of Clinical Biochemistry,
Addenbrooke's Hospital, Cambridge, UK

S. K. Moestrup
Department of Clinical Biochemistry,
Aarhus University Hospital, Aarhus, Denmark

catabolic site of apoA-I may depend on its degree of lipidation and binding strength to the entire HDL particle. Studies of the apoA-I clearance in mice transgenic for human apoA-I indicate that the liver preferentially takes up apoA-I associated to particles [13, 14].

In rodent kidney, apoA-I uptake is accounted for by glomerular filtration and subsequent recognition by cubilin in the proximal tubules leading to endocytosis and degradation [15].

To define the role of the human kidney in HDL clearance we compared the renal handling of HDL apoA-I, apoA-II and apoA-IV and HDL lipid components in human Fanconi syndrome patients with failure in megalin and cubilin-mediated protein re-absorption in the proximal tubules [16].

Materials and Methods

Fanconi Syndrome Patients and Specimen Collection

Patients with the rare Fanconi syndrome had the following diagnoses: Dent's disease caused by mutations in the ClC-5 chloride channel (Patients 3–5 and 8); Lowe syndrome (Patients 6 and 7) and autosomal dominant idiopathic Fanconi syndrome (Patients 1 and 2). All patients had well-preserved renal glomerular function estimated by creatinine clearance and had been described previously [16]. Sample collection and calculation of 24 h excretion based on creatinine values was conducted as described [16].

Urine Analysis

Western blot analysis was conducted using rabbit polyclonal antibodies against apoA-I, apoA-II and apoA-IV. Urine concentrations of apoA-I were measured by an enzyme-linked immunosorbent assay (ELISA) as described [2]. Two-dimensional gel-electrophoresis analysis of urinary apoA-I and A-IV was carried out as described [17]. Lipids were extracted from 60 ml urine samples and phospholipids and cholesterol concentrations determined as described [18–20]. Creatinine, α_1-microglobulin and albumin were determined as described [16].

Immunocytochemistry Studies of Human Proximal Tubules

Normal, uninvolved human renal tissue was obtained from resected renal carcinoma kidneys and 0.8 µm cryosections prepared [21]. The sections were incubated with rabbit anti-human apoA-I antibody. As negative control, sections were incubated with secondary antibodies alone or non-specific rabbit IgG.

Results

Analysis of Urine from Fanconi Patients

Substantial reabsorption of apoA-I in the human proximal tubules was indicated by apoA-I immunoreactivity in lysosomal-like vesicles proximal tubule cells of normal human kidney cortex (Fig. 1). An estimate of the clearance of apoA-I in the kidneys was obtained by analyzing urine of Fanconi patients having failure in tubular reabsorption with high urinary protein excretion.

Western blotting showed a substantial secretion of full-length apoA-I (Fig. 1) and ELISA of patients urine showed apoA-I levels ranging from 7.8 to 178 µg/ml (mean 73 ± 55 µg/ml, Table 1) corresponding to an excretion of

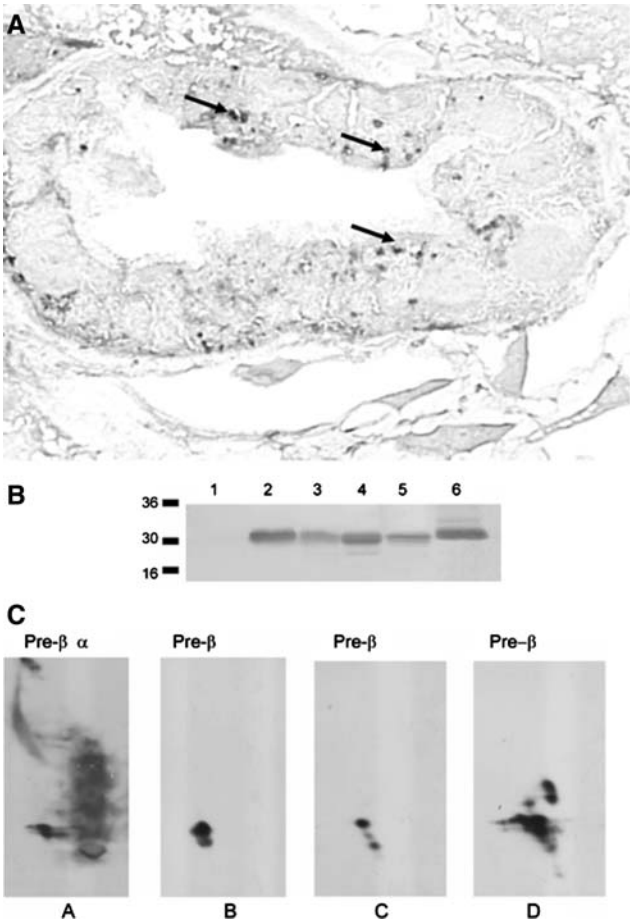

Fig. 1 Immunochemical detection of apoA-I in normal human renal cortex and urine of Fanconi patients. **a** Immunohistochemical detection of apoA-I in normal human proximal tubules, seen as a vesicular staining (*arrows*) in agreement with uptake into endosomes and lysosomes. **b** SDS-PAGE and Western blotting of apoA-I in urine samples. *Lane 1* control urine, *lane 2* patient 1, *lane 3* patient 4, *lane 4* patient 6, *lane 5* patient 8, *lane 6* human plasma HDL. **c** Two-dimensional gel-electrophoresis and Western blotting of apoA-I in normal plasma and in urine of three Fanconi patients, with indications of areas with apoA-I exhibiting pre-β and α migration

Table 1 Excretion of apoA-I, α_1-microglobulin, albumin and creatinine in urine from Fanconi patients

Patient no.	ApoA-I		α_1-microglobulin		Albumin		Creatinine	
	µg/ml	mg/24 h	µg/ml	mg/24 h	µg/ml	mg/24 h	mM	mmol/24 h
1	108	328	242	734	73	222	4.3	13
2	39	31	513	411	193	154	15.4	12
3	60	192	215	697	148	478	5.2	17
4	39	104	232	621	187	501	4.7	13
5	8	28	66	235	266	956	7.2	26
6	178	580	297	969	974	3173	4.9	16
7	47	173	240	885	187	687	4.3	16
8	108	209	354	685	175	339	5.1	10

205 ± 181 mg apoA-I/24 h with 0.5 g/24 h being the maximum value. No apoA-I was detected in urine from control individuals (sensitivity limit 0.01 µg/ml). Measurement of urinary creatinine, albumin and α_1-microglobulin (Table 1) suggested normal filtration rates in the patients.

Western blotting detected also a high apoA-IV content but no apoA-II in the urines. The level of apoA-IV in urine was by semiquantitative immunoblotting of 2-D gels measured to 8–86 µg/ml, (mean 42 ± 30 µg/ml), corresponding to a total daily urinary excretion of 6–172 mg apoA-IV (mean 120 ± 89 mg/day). This is in the range of what is previously reported [22, 23]. No apo-A-II or apoA-IV was detected by western blotting of control urine.

ApoA-I from urine exhibited pre-β_1 migration in 2-D gel-electrophoresis (Fig. 1) indicating that apoA-I was represented by pre-β_1 particles or less lipidated including the nascent apoA-I form (which also exhibits pre-β_1 migration). Low apoA-I lipidation was further indicated by the very low contents of phospholipids, cholesterol, cholesterol esters and triglyceride determined by thin layer chromatography of lipids extracted from urine of patients and controls. In the urine of the two patients (3 and 4) the phospholipid concentrations were 0.82 and 2.87 mg/l, respectively, whereas cholesterol concentrations were 1.59 and 1.92 mg/l, respectively. In two healthy individuals similar phospholipid (0.86 and 0.62 mg/l) and cholesterol (1.21 and 1.45 mg/l) concentrations were measured.

Discussion

By taking advantage of the fact that Fanconi patients in the urine excretes filtered proteins that otherwise would be reabsorbed in the proximal tubules [16], we measured the urinary content of the major HDL apoA proteins to get further insight into the role of the kidney in HDL clearance. Using proteomic methods apoA-I and apoA-IV have previously been identified in the urine of Fanconi syndrome patients [24], but a comparative quantitative approach has to our knowledge not been done. Although this approach for estimating normal renal filtration of a protein has its limitations and may underestimate the true values we find it justified because the Fanconi disease has no observed effect on lipoprotein levels [25], glomerular filtration rates and glomerular sieving coefficients [16]. The data showed a high urinary excretion of apoA-I amounting to at least 0.2–0.5 g/day, that is about 50% of the daily synthesis of apoA-I previously estimated to 9–14 mg apoA-I/kg in humans [7, 26].

Consistent with previous data on HDL catabolism in animal models showing a high apoA-I clearance in kidney but a very low HDL cholesteryl ester uptake [10, 11], the data indicate that apoA-I is catabolized in a lipid-poor form. Lipidation of apoA-I and rearrangement into the lipid loaded helix-belt formation [27, 28] may therefore protect apoA-I from catabolism. The absence of this protection may therefore contribute to hypercatabolism of HDL and very low apoA-I and plasma HDL levels in Tangier disease patients with failure in ABCA-1-mediated phospholipid and cholesterol efflux to apoA-I [29–31].

Renal failure surprisingly also causes a decrease in HDL cholesterol [32] but an increase in the fraction of free apoA-I [33] thus indicating that increased extrarenal metabolism of HDL counteracts a failed renal filtration of nascent apoA-I. Hemodialysis of renal failure patients is also reported to further increase the plasma pre-β fraction of HDL and free apoA-I [32, 33], indicating that this treatment does not compensate for the absent apoA-I filtration in the kidney

ApoA-II is not excreted in the urine of Fanconi patients, presumably due to the strong hydrophobicity of apoA-II protecting it from dissociation from the HDL particle and subsequent glomerular filtration. Concordant with a stronger association of apoA-II to HDL, transgenic mice overexpressing apoA-II have an increased renal catabolism of apoA-I, presumably displaced from HDL by apoA-II [34].

In conclusion, these data indicate that the human kidney is a major site for filtering nascent apoA-I and A-IV, whereas there is no evidence for filtration of HDL holoparticles.

Acknowledgment This work was supported by The Danish Medical Research Council.

References

1. Srivastava RA, Srivastava N (2000) High density lipoprotein, apolipoprotein A-I, and coronary artery disease. Mol Cell Biochem 209(1–2):131–144
2. Graversen JH, Laurberg JM, Andersen MH, Falk E, Nieland J, Christensen J, Etzerodt M, Thogersen HC, Moestrup SK (2008) Trimerization of apolipoprotein A-I retards plasma clearance and preserves antiatherosclerotic properties. J Cardiovasc Pharmacol 51(2):170–177
3. Newton RS, Krause BR (2002) HDL therapy for the acute treatment of atherosclerosis. Atheroscler Suppl 3(4):31–38
4. Nicholls SJ, Tuzcu EM, Sipahi I, Schoenhagen P, Crowe T, Kapadia S, Nissen SE (2006) Relationship between atheroma regression and change in lumen size after infusion of apolipoprotein A-I Milano. J Am Coll Cardiol 47(5):992–997
5. Singh IM, Shishehbor MH, Ansell BJ (2007) High-density lipoprotein as a therapeutic target: a systematic review. JAMA 298(7):786–798
6. von Eckardstein A, Nofer JR, Assmann G (2001) High density lipoproteins and arteriosclerosis. Role of cholesterol efflux and reverse cholesterol transport. Arterioscler Thromb Vasc Biol 21(1):13–27
7. Marsh JB, Welty FK, Schaefer EJ (2000) Stable isotope turnover of apolipoproteins of high-density lipoproteins in humans. Curr Opin Lipidol 11(3):261–266
8. Spady DK, Woollett LA, Meidell RS, Hobbs HH (1998) Kinetic characteristics and regulation of HDL cholesteryl ester and apolipoprotein transport in the apoA-I-/- mouse. J Lipid Res 39(7):1483–1492
9. Wang N, Arai T, Ji Y, Rinninger F, Tall AR (1998) Liver-specific overexpression of scavenger receptor BI decreases levels of very low density lipoprotein ApoB, low density lipoprotein ApoB, and high density lipoprotein in transgenic mice. J Biol Chem 273(49):32920–32926
10. Woollett LA, Spady DK (1997) Kinetic parameters for high density lipoprotein apoprotein AI and cholesteryl ester transport in the hamster. J Clin Invest 99(7):1704–1713
11. Glass CK, Pittman RC, Keller GA, Steinberg D (1983) Tissue sites of degradation of apoprotein A-I in the rat. J Biol Chem 258(11):7161–7167
12. Braschi S, Neville TA, Maugeais C, Ramsamy TA, Seymour R, Sparks DL (2000) Role of the kidney in regulating the metabolism of HDL in rabbits: evidence that iodination alters the catabolism of apolipoprotein A-I by the kidney. Biochemistry 39(18):5441–5449
13. Lee JY, Lanningham-Foster L, Boudyguina EY, Smith TL, Young ER, Colvin PL, Thomas MJ, Parks JS (2004) Prebeta high density lipoprotein has two metabolic fates in human apolipoprotein A-I transgenic mice. J Lipid Res 45(4):716–728
14. Lee JY, Parks JS (2005) ATP-binding cassette transporter AI and its role in HDL formation. Curr Opin Lipidol 16(1):19–25
15. Kozyraki R, Fyfe J, Kristiansen M, Gerdes C, Jacobsen C, Cui S, Christensen EI, Aminoff M, de la Chapelle A, Krahe R et al (1999) The intrinsic factor-vitamin B12 receptor, cubilin, is a high-affinity apolipoprotein A-I receptor facilitating endocytosis of high-density lipoprotein. Nat Med 5(6):656–661
16. Norden AG, Lapsley M, Lee PJ, Pusey CD, Scheinman SJ, Tam FW, Thakker RV, Unwin RJ, Wrong O (2001) Glomerular protein sieving and implications for renal failure in Fanconi syndrome. Kidney Int 60(5):1885–1892
17. Castro GR, Fielding CJ (1988) Early incorporation of cell-derived cholesterol into pre-beta-migrating high-density lipoprotein. Biochemistry 27(1):25–29
18. Bartlett GR (1959) Phosphorus assay in column chromatography. J Biol Chem 234(3):466–468
19. Bhandaru RR, Srinivasan SR, Pargaonkar PS, Berenson GS (1977) A simplified colorimetric micromethod for determination of serum cholesterol. Lipids 12(12):1078–1080
20. Bligh EG, Dyer WJ (1959) A rapid method of total lipid extraction and purification. Can J Biochem Physiol 37(8):911–917
21. Christensen EI, Nielsen S, Moestrup SK, Borre C, Maunsbach AB, de Heer E, Ronco P, Hammond TG, Verroust P (1995) Segmental distribution of the endocytosis receptor gp330 in renal proximal tubules. Eur J Cell Biol 66(4):349–364
22. Lingenhel A, Lhotta K, Neyer U, Heid IM, Rantner B, Kronenberg MF, Konig P, von Eckardstein A, Schober M, Dieplinger H et al (2006) Role of the kidney in the metabolism of apolipoprotein A-IV: influence of the type of proteinuria. J Lipid Res 47(9):2071–2079
23. Seishima M, Muto Y (1987) An increased apo A-IV serum concentration of patients with chronic renal failure on hemodialysis. Clin Chim Acta 167(3):303–311
24. Cutillas PR, Chalkley RJ, Hansen KC, Cramer R, Norden AG, Waterfield MD, Burlingame AL, Unwin RJ (2004) The urinary proteome in Fanconi syndrome implies specificity in the reabsorption of proteins by renal proximal tubule cells. Am J Physiol Renal Physiol 287(3):F353–F364
25. van't Hoff WG (1996) Biology and genetics of inherited renal tubular disorders. Exp Nephrol 4(5):253–262
26. Ooi EM, Watts GF, Farvid MS, Chan DC, Allen MC, Zilko SR, Barrett PH (2005) High-density lipoprotein apolipoprotein A-I kinetics in obesity. Obes Res 13(6):1008–1016
27. Li L, Chen J, Mishra VK, Kurtz JA, Cao D, Klon AE, Harvey SC, Anantharamaiah GM, Segrest JP (2004) Double belt structure of discoidal high density lipoproteins: molecular basis for size heterogeneity. J Mol Biol 343(5):1293–1311
28. Martin DD, Budamagunta MS, Ryan RO, Voss JC, Oda MN (2006) Apolipoprotein A-I assumes a "looped belt" conformation on reconstituted high density lipoprotein. J Biol Chem 281(29):20418–20426
29. Lee JY, Timmins JM, Mulya A, Smith TL, Zhu Y, Rubin EM, Chisholm JW, Colvin PL, Parks JS (2005) HDLs in apoA-I transgenic Abca1 knockout mice are remodeled normally in plasma but are hypercatabolized by the kidney. J Lipid Res 46(10):2233–2245
30. Oram JF (2000) Tangier disease and ABCA1. Biochim Biophys Acta 1529(1–3):321–330
31. Timmins JM, Lee JY, Boudyguina E, Kluckman KD, Brunham LR, Mulya A, Gebre AK, Coutinho JM, Colvin PL, Smith TL et al (2005) Targeted inactivation of hepatic Abca1 causes profound hypoalphalipoproteinemia and kidney hypercatabolism of apoA-I. J Clin Invest 115(5):1333–1342
32. Mekki K, Bouchenak M, Remaoun M, Belleville JL (2004) Effect of long-term hemodialysis on plasma lecithin: cholesterol acyltransferase activity and the amounts and compositions of HDL2 and HDL3 in hemodialysis-treated patients with chronic renal failure: a 9-year longitudinal study. Med Sci Monit 10(8):CR439–CR446
33. Duval F, Frommherz K, Atger V, Drueke T, Lacour B (1989) Influence of end-stage renal failure on concentrations of free apolipoprotein A-1 in serum. Clin Chem 35(6):963–966
34. Julve J, Escola-Gil JC, Ribas V, Gonzalez-Sastre F, Ordonez-Llanos J, Sanchez-Quesada JL, Blanco-Vaca F (2002) Mechanisms of HDL deficiency in mice overexpressing human apoA-II. J Lipid Res 43(10):1734–1742

Lipids (2008) 43:471–483
DOI 10.1007/s11745-008-3182-5

ORIGINAL ARTICLE

Monoacylglycerols Activate Capsaicin Receptor, TRPV1

Yusaku Iwasaki · Orine Saito · Manabu Tanabe · Kimiko Inayoshi · Kenji Kobata · Shuichi Uno · Akihito Morita · Tatsuo Watanabe

Received: 3 January 2008 / Accepted: 17 April 2008 / Published online: 15 May 2008
© AOCS 2008

Abstract Transient receptor potential vanilloid subtype 1 (TRPV1) is known as capsaicin (CAP) receptor and activated by CAP. Activation of TRPV1 by CAP increases energy expenditure and thermogenesis in rodents or human. Therefore, TRPV1 may be target for energy expenditure enhancement and thermogenesis. To search for novel TRPV1 agonist, we screened 19 types of foods by using TRPV1-expressing HEK293 cells. TRPV1 was activated by hexane extract of wheat flour, and its functional compounds were 1-monoacylglycerols containing oleic, linoleic, and α-linolenic acids. Their potencies (EC_{50}) were about 50 times larger than that of CAP and their efficacies (maximal response) were about half of that of CAP. TRPV1 was activated by 1-monoacylglycerols (MGs) having C18 and C20 unsaturated and C8–C12 saturated fatty acid (FA). Moreover, 2-MGs having C18 and C20 unsaturated FA acted on TRPV1 with the same potency. On the other hand, no activation of TRPV1 was induced by MGs having C16 and C18 saturated FA, di- or triacylglycerols of C18:1 FA. Pain-relating aversive responses were induced when TRPV1-activating 1-monoacylglycerols (50 mM) was administered subcutaneously into rat hind paw. These effects were inhibited by the co-injection of capsazepine (10 mM) which is a TRPV1 competitive antagonist. These results suggested that these 1-monoacylglycerols activate TRPV1 in vitro and in vivo.

Keywords Monoacylglycerol · TRPV1 · Pungency · Capsaicin

Abbreviations

AEA	Arachidonoylethanolamide (Anandamide)
2-AGE	2-Arachidonyl glycerol ether
CAP	Capsaicin
CPZ	Capsazepine
DG	Diacylglycerol
DRG	Dorsal root ganglion
EtOAc	Ethyl acetate
FA	Fatty acid
MG	Monoacylglycerol
OEA	Oleoylethanolamide
TG	Triacylglycerol
TRPV1	Transient receptor potential vanilloid 1

Introduction

Transient receptor potential vanilloid subtype 1 (TRPV1) is a non-selective cation channel activated by noxious heat (>43 °C), protons, and capsaicin (CAP), a pungent ingredient of red pepper (Fig. 1). TRPV1 is mainly expressed in sensory neurons [1, 2]. TRPV1 functions as nociceptor, and is involved in pungent taste by red pepper intake and pain by inflammation or other stimuli [3]. A variety of natural products and endogenous compounds other than CAP have been identified as the TRPV1 agonists. For example, gingerols and shogaols (pungent compounds of ginger), piperine (pungent compound of black or white pepper), and sanshools (pungent compounds of Japanese pepper) have been identified as natural compounds, and anandamide (arachidonoylethanolamide, AEA; Fig. 1) and *N*-arachidonyl dopamine as endogenous TRPV1 agonists [4–6].

Y. Iwasaki · O. Saito · M. Tanabe · K. Inayoshi · K. Kobata · S. Uno · A. Morita · T. Watanabe (✉)
Graduate School of Nutritional and Environmental Sciences and Global COE Program, University of Shizuoka, 52-1 Yada, Suruga-ku, Shizuoka 422-8526, Japan
e-mail: watanbt@u-shizuoka-ken.ac.jp

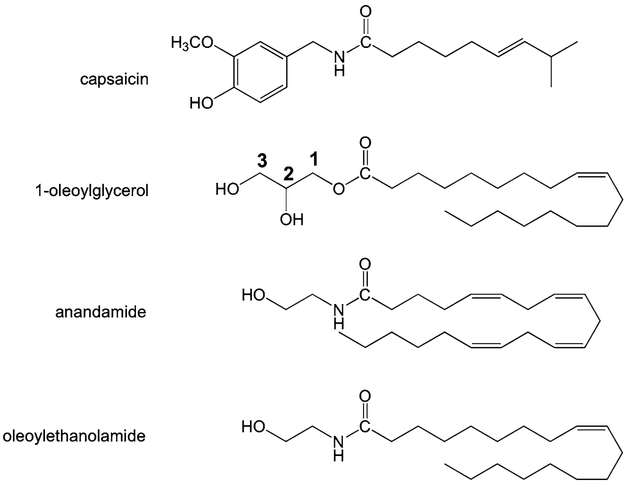

Fig. 1 Chemical structures of capsaicin, 1-oleoylglycerol, anandamide and oleoylethanolamide

Activation of TRPV1 plays a role not only in transmission of pungent or pain sensations but also in CAP-induced energy expenditure enhancement and thermogenesis [3, 7, 8]. CAP increases energy expenditure (oxygen consumption) and body temperature by first stimulating the sympathetic nerves and then stimulating adrenaline secretion from the adrenal gland [9–14]. Adrenaline secretion via the activation of sympathetic nervous system plays a key role in energy consumption [15], and it is very important for CAP-induced energy expenditure enhancement. CAP-induced adrenaline secretion and core temperature increment were blocked by pretreatment with capsazepine (CPZ), a TRPV1 competitive antagonist [13, 16]. Recently, it has been reported that CAP intake could not prevent obesity in TRPV1-knockout mice [17] although CAP prevented body fat accumulation in normal rats and mice [18, 19]. These results indicate that TRPV1 activity is very important for CAP-induced anti-obesity. Therefore, TRPV1-activating food ingredients may exert for CAP-like action on energy expenditure enhancement and prevention of obesity that is a serious risk factor for life style-related diseases including impaired glucose and lipid metabolism [20].

In the present study, we screened 19 types of foods by using intracellular Ca^{2+} imaging of TRPV1-expressing HEK293 cells. We found that hexane extract of wheat flour increased intracellular calcium concentration ($[Ca^{2+}]_i$) in TRPV1-expressing HEK293 cells. This extract was fractionated by repeated chromatography, and 1-monoacylglycerols (MGs) having oleic, linoleic, and α-linolenic acid as acyl components were determined as TRPV1 agonists. These MGs not only activated TRPV1 both in vitro [recombinant TRPV1-expressing HEK293 cells and endogenous TRPV1 expressing mouse dorsal root ganglion (DRG)] and in vivo (hind paw irritancy test). TRPV1 was activated by not only 1-MGs binding C18 and C20 unsaturated and C8–C12 saturated fatty acids (FAs) but also 2-MGs binding C18 and C20 unsaturated FAs. Therefore, TRPV1-activating MGs may be useful for increasing energy expenditure.

Materials and Methods

Reagents

Capsaicin and CPZ were purchased from Sigma. Fura-2 AM and fluo-4 AM were obtained from Molecular Probes Inc. (Eugene, OR, USA). All other lipid chemicals such as MGs, diacylglycerol (DGs), triacylglycerols (TGs), FAs and glycerol were of guaranteed reagent grade or higher. These compounds were dissolved in dimethyl sulfoxide (DMSO) and stored at −20 °C. All food materials were purchased from a local market. Wheat flour was obtained from Nisshin Flour Milling Inc. (Tokyo, Japan).

Extraction and Purification of Wheat Flour

Wheat flour (1,029 g) was extracted with hexane (10 L), and this extract was purified as shown in Fig. 3. Each fraction was examined for TRPV1 activity by using TRPV1-expressing HEK293 cells. The fraction positive for TRPV1 activity was further purified. Briefly, the hexane extract from wheat flour (7,900 mg) was partitioned with hexane/methanol (MeOH)/H_2O (200/97/3, by vol.). The MeOH layer (3,278 mg) that activated TRPV1 was chromatographed on silica gel (36 mm × 90 mm) with a stepwise elution of hexane/ethyl acetate (EtOAc) and MeOH. The fraction eluted with EtOAc (Fr. 4, 205 mg) was rechromatographed on silica gel (15 mm× 120 mm) with hexane/EtOAc (1/1), and Fr. 4–2 (127.6 mg) was obtained as the active fraction. Fr. 4-2 was further purified by solid-phase extraction (MEGA BE-C18, 1 g, 6 mL, BOND ELUT) with MeOH as an eluent, and Fr. 4-2-M (63.2 mg) was obtained as a single spot by thin-layer chromatography (TLC) along with the development of sulfuric acid.

Identification and Quantification of Monoacylglycerols in Wheat Flour

^{1}H-NMR spectra (TMS as the internal standard) were recorded on a JEOL α-400 instrument (Tokyo, Japan) at 399.65 MHz. The ^{1}H-NMR spectra of Fr. 4-2-M ($CDCl_3$) were δ 5.35 (2.9H, m), δ 4.21 (1.0H, dd, $J = 4.6$, 11.2 Hz, H-1a), δ 4.15 (1.0H, dd, $J = 6.0$, 11.6 Hz, H-1b), δ 3.93 (0.83H, quint, $J = 5.0$ Hz, H-2), δ 3.83 (0.19H, d, $J = 4.8$), δ 3.70 (1.0H, dd, $J = 4.0$, 11.2 Hz, H-3a), δ 3.60 (1.0H, dd, $J = 6.0$, 11.2 Hz, H-3b), δ 2.77 (2.3H, t,

$J = 6.0$ Hz), δ 2.35 (3.1H, t, $J = 7.6$ Hz), δ 2.05 (3.6H, m), δ 1.63 (2.4H, m), δ 1.29 (18.8H, m), δ 0.89 (3.2H, m).

Quantitative and qualitative analyses of lipids were carried out using TLC with flame ionization detection (TLC-FID) on Iatroscan MK-5 (Mitsubishi Kagaku Iatron Inc., Tokyo, Japan). The analysis conditions were as follows: flow rate of hydrogen, 160 mL/min; flow rate of air, 2.0 L/min; scanning speed, 30 s/scan. The purified sample of wheat flour (Fr. 4-2-M) spotted on the rod-silica gel treated with 3% borate and a 2-stage development system was used to separate the compound classes. The first stage was developed with chloroform, and the second separation comprised the development in chloroform/MeOH/25% ammonia water (700/4/1, by vol.). The total crude MG content in wheat flour was determined with the calibration curve for 1-oleoylglycerol [1-MG (18:1)] as the standard. The samples spotted with the TLC rods were developed twice with hexane/diethyl ether/acetic acid (5/5/0.1, by vol.).

In order to analyze the acyl components in MGs, gas chromatography/mass spectrometry (GC/MS) was performed with HP 6890 Series (Hewlett Packard, CA, USA). WCOT fused silica CP-Sil 88 column (0.25 mm × 50 m; Varian, Inc., Palo Alto, CA, USA) was used with helium at a flow rate of 1 mL/min for the separation of the sample. The injector temperature was set at 260 °C. The column oven temperature was changed from 160 to 240 °C (3 °C/min). FAs methyl esters from Fr. 4-2-M were obtained by reaction with 0.5 N NaOH/MeOH and 14% BF_3/MeOH. The GC/MS spectrum of Fr. 4-2-M showed five peaks at 7.37 min (hexadecanoic acid methyl ester; concordance rate, 97%), 9.71 min (octadecanoic acid methyl ester, 97%), 10.47 min (9*Z*-octadecenoic acid methyl ester, 99%), 11.66 min (9*Z*, 12*Z*-octadecadienoic acid methyl ester, 99%), and 13.13 min (9*Z*, 12*Z*, 15*Z*-octadecatrienoic acid methyl ester, 95%).

Direct determination of the MG structure with liquid chromatography/mass spectrometry (LC/MS) was performed using a NANOSPACE 51-1 HPLC system (Shiseido, Tokyo, Japan) connected to an LCQ MS (Thermo Fisher Sci., Watham, MA, USA). Unison UK-C18 150 × 2 mm (3 μm) column (Imtakt, Kyoto, Japan) with a flow rate of 0.2 mL/min was used for the separation of the sample. The linear gradient was used as follows: first condition, acetic acid (0.1%)/acetonitrile (30/70, by vol.); from 0 to 10 min, 1/99 (by vol.); then held up to 20 min. The MS condition used was as follows: ionization, APCI; ion polarity, positive; vaporizer temperature, 250 °C; sheath gas flow rate, 80 arb; aux gas flow rate, 0 arb; discharge current, 5 mA; capillary temperature, 200 °C; and capillary voltage, 10 V. Standard MGs were measured using the selected ion monitoring mode. 1-MGs (16:0 and 18:0) were detected as $[M + H]^+$-H_2O, while others were detected as $[M + H]^+$. The retention times of standard lipids [1-MGs having palmitic (1-MG16:0), stearic (1-MG18:0), oleic (1-MG18:1), linoleic (1-MG18:2), and α-linolenic acids (1-MG18:3)] were detected at 11.48, 14.92, 12.08, 9.85, and 8.28 min, respectively.

Animals

Male 6-week-old Sprague-Dawley rats and male 5-week-old C57BL/6 Cr mice (Japan SLC, Shizuoka, Japan) were housed at least for 1 week under conditions of controlled temperature (23 ± 1 °C), humidity (55 ± 5%), and lighting (light on, 7:00–19:00 hours). Food and water were available ad libitum. Animal experiment procedures conformed to the Guidelines for the Care and Use of Laboratory Animals of the University of Shizuoka.

Rats were handled for 1 week to get them habituated to humans for the behavior experiment. On the day of the behavior experiment, the rats were placed individually in transparent cages (21 cm × 31 cm × 13 cm) and maintained for at least 10 min in order to stabilize their behavior.

Measurement of Intracellular Calcium Concentration in TRPV1-Expressing HEK293 Cells and DRG Cells of Mice

HEK293 cells that stably expressed rat-TRPV1 (named as HEK293VR11 cells [21]) were generated according to the methods reported by Caterina et al. with minor modifications [1]. The HEK293VR11 cells were maintained in Dulbecco's modified Eagle's medium containing 10% fetal bovine serum, 100 units/mL of penicillin, 100 μg/mL of streptomycin, and 250 ng/mL of amphotericin B at 37 °C under 5% CO_2/air. The cells were sub-cultured every week, and the highest passage number used was 35. We confirmed that HEK293VR11 cells up to passage 35 showed almost equal responses to CAP.

Measurement of the intracellular calcium concentration ($[Ca^{2+}]_i$) of HEK293VR11 cells was performed using a previously reported method [21]. Briefly, the HEK293VR11 cells were loaded with cytoplasmic calcium indicator fura-2 AM (5 μM) or fluo-4 AM (2.5 μM) in a loading buffer (5.37 mM KCl, 0.441 mM KH_2PO_4, 137 mM NaCl, 0.336 mM $Na_2HPO_4 \cdot 7H_2O$, 5.56 mM glucose, 20 mM HEPES, 1 mM $CaCl_2$, and 0.1% bovine serum albumin at pH 7.4) at 37 °C for 30 min. The time-dependent changes in fluorescence (fura-2: excitation wavelength of 340 and 380 nm and emission wavelength of 500 nm; fluo-4: excitation wavelength of 485 nm and emission wavelength of 540 nm) were recorded using a CAF-110 fluorospectrophotometer (Jasco, Tokyo, Japan) and analyzed using PowerLab (AD Instruments, NSW, Australia). The test compounds and extracted fractions of foods were dissolved in DMSO and applied at 0.1 or 0.3% concentration to the cells. In some experiments, CPZ (100 μM, dissolved in DMSO) was added at least 1 min prior to the addition of the test compound. Each data value was expressed as a percent response to 10 μM CAP in each experiment. Curve fitting and parameter estimation were carried out using Prism 4 software (GraphPad Software, San Diego, CA, USA).

Dorsal root ganglia from all spinal levels of male C57BL/6 mice (5∼6 weeks old) were rapidly dissected and dissociated by incubation for 20 min in a solution of culture medium [Earl's balanced salt solution with 10% fetal bovine serum, 100 units/mL of penicillin, 100 μg/mL of streptomycin, 250 ng/mL of amphotericin B, 2 mM L-alanyl-L-glutamine, and 1× MEM vitamin solution (Sigma)] containing 1.25 mg/mL collagenase P (Roche, Basel, Swiss). Cells were gently triturated using fire-polished Pasteur pipettes and centrifugated in culture medium to separate cells from debris. Cells were resuspended and plated onto coverslips coated with poly-L-lysin. Cells were cultured in medium with 50 ng/mL nerve growth factor (Sigma). Calcium imaging experiments were performed 18∼36 h after plating using fluorescence microscopy. DRG neurons were loaded with fluo-4 AM (5 μM) for 30 min at 37 °C.

Hind Paw Irritancy Test

Pain behaviors such as licking or biting produced by the local injection of chemicals into the hind paw have been used as a model of chemogenic nociception in rats [22, 23]. Experimental methods were similar to those reported previously [5]. Briefly, 15 μL of the test reagent solution (0.5 or 50 mM) in saline containing 5% DMSO and 10% Tween 80 was subcutaneously injected into the hind paw by using a 27-G needle on a 1-mL syringe. The total time spent on licking and biting in the injected paw was measured for 3 min after the injection. In some experiments, CPZ (10 mM) was coadministered with the test solution. Only 1 hind paw was examined per test. The other hind paw was examined at least 24 h after the first experiment.

Eye-Wiping Test

The eye-wiping test [24] was used for evaluating the pungency of compounds. Experimental methods were the same as those reported previously [5]. Briefly, using a micropipette, 15 μL of the test solution (0.5 or 5 mM) in saline containing 5% DMSO and 10% Tween 80 was instilled into an eye of the animal. The tip of the micropipette was cut at approximately 10 mm from the top to increase the size of the instillation drop. The number of wiping movements per minute after the administration was counted. Only 1 eye was examined per test. The other eye was examined at least 24 h after the first experiment.

Statistical Analysis

All data were indicated as mean ± SEM. These statistical analyses were carried out by using the Prism 4 software. In the aversive behavior tests, the treatment effects were analyzed by one-way ANOVA (nonparametric), and the differences between the mean values were evaluated by using Tukey's multiple comparison test. In other tests, the differences between the compounds and vehicle treatments on different days were evaluated by using the unpaired *t*-test. Similarly, the differences between CPZ treatment and non-treatment on different days were also evaluated by using the unpaired *t*-test. Differences with $P < 0.05$ were considered to be significant.

Results

1-Monoacylglycerols in Wheat Flour Activate TRPV1

A total of 19 types of food extracts (onion, Chinese chive, garlic, welsh onions (white and green types), shallot, Japanese pepper, myoga (*Zingiber mioga*), perilla, peach, American cherry, Konbu (*Laminaria japonica*), cucumber, tomato, bitter melon, egg plant, apple, kiwi fruit, and wheat flour) were examined for TRPV1 activation by calcium imaging of TRPV1-expressing HEK293 cells. Of all extracts, we found that the hexane extract of wheat flour (300 μg/mL) increased the intracellular calcium concentration ($[Ca^{2+}]_i$) in TRPV1-expressing HEK293 cells, and this activity was half the maximum response to 10 μM CAP (Fig. 2a, e). On the other hand, this extract induced only a small response in native HEK293 cells (Fig. 2b, e). Accordingly, this extract certainly contained specific TRPV1-activating compounds. TRPV1 activation in sensory neurons induces pain or pungent sensation. However, unlike red pepper, wheat flour is not pungent. Therefore, wheat flour may contain a weak-pungent or a non-pungent TRPV1 agonist.

Wheat flour extract was purified by silica gel and octadecyl silica (ODS) column chromatography (Fig. 3). Purified fraction (Fr.) 4-2-M (5 μg/mL) increased the $[Ca^{2+}]_i$ in the TRPV1-expressing HEK293 cells but not in the native HEK293 cells (Fig. 2c–e). Furthermore, the preadministration of 100 μM CPZ, a TRPV1-specific antagonist, completely inhibited the response in the TRPV1-expressing HEK293 cells to Fr. 4-2-M (15 μg/mL) (non-treatment, 333.4 ± 26.2 nM ($n = 3$); CPZ treatment, 2.50 ± 0.379 nM ($n = 3$), values are $\Delta[Ca^{2+}]_i$). These

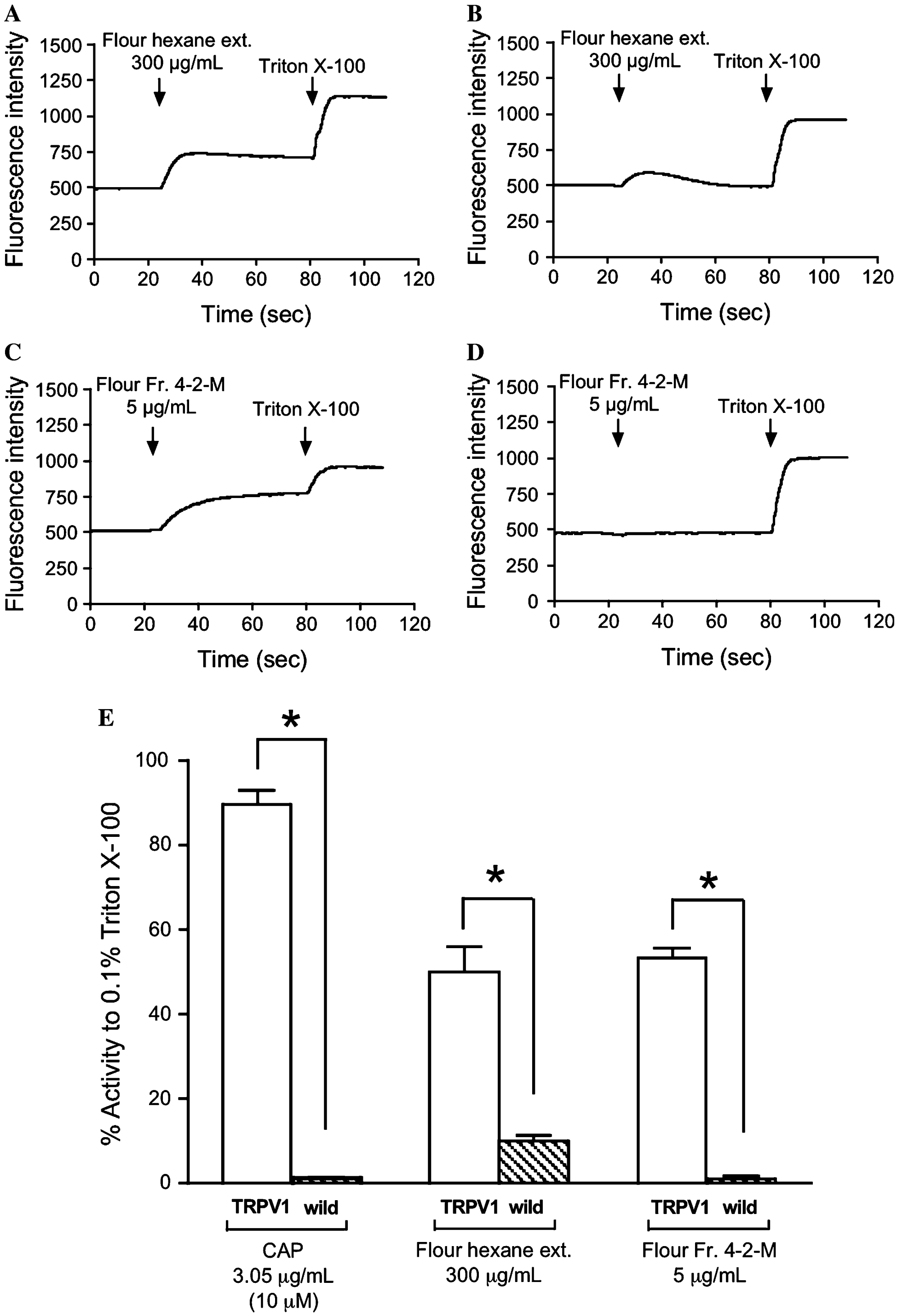

Fig. 2 Transient receptor potential vanilloid subtype 1 is activated by wheat flour extract. Time course of fluorescence changes by fluo-4 AM in TRPV1-expressing HEK293 cells (**a**, **c**) and parent HEK293 cells (**b**, **d**) are shown. Triton X-100 (0.1%) was added to obtain maximum fluorescence. (**e**) Calcium responses of the parent (wild-type, open bar) and TRPV1-expressing HEK293 cells (TRPV1, hatched bar) by capsaicin (CAP) and wheat flour extract. These values are mean ± SEM ($n = 3$). *Asterisk* indicates a significant difference between each cell type ($P < 0.01$)

results clearly show that the purified fraction has a specific TRPV1 activity.

A part of the ^{1}H-NMR spectrum of Fr. 4-2-M was fitted with a glycerol portion of 1-palmitoylglycerol: δ 4.21 (1.0H, dd, $J = 4.6$, 11.2 Hz, H-1a), δ 4.15 (1.0H, dd, $J = 6.0$, 11.6 Hz, H-1b), δ 3.93 (0.83H, quint, $J = 5.0$ Hz, H-2), δ 3.70 (1.0H, dd, $J = 4.0$, 11.2 Hz, H-3a), δ 3.60 (1.0H, dd, $J = 6.0$, 11.2 Hz, H-3b). According to this, Fr. 4-2-M was estimated to be a 1-MG analogue. In agreement with this speculation, 1-MG peak ($R_f = 0.586$) was mainly detected in the TLC with FID analysis of Fr. 4-2-M (Fig. 4a). A small peak of R_f 0.480 was consistent with the 2-oleoylglycerol [2-MG (18:1)] standard (Fig. 4a). TLC/FID analysis showed that Fr. 4-2-M was composed of mainly 1-MG and small part of 2-MG, but the exact ratio of MGs could not be got because the sensitivity of FTD differed significantly depending on the degree of unsaturation for acyl moiety in MGs.

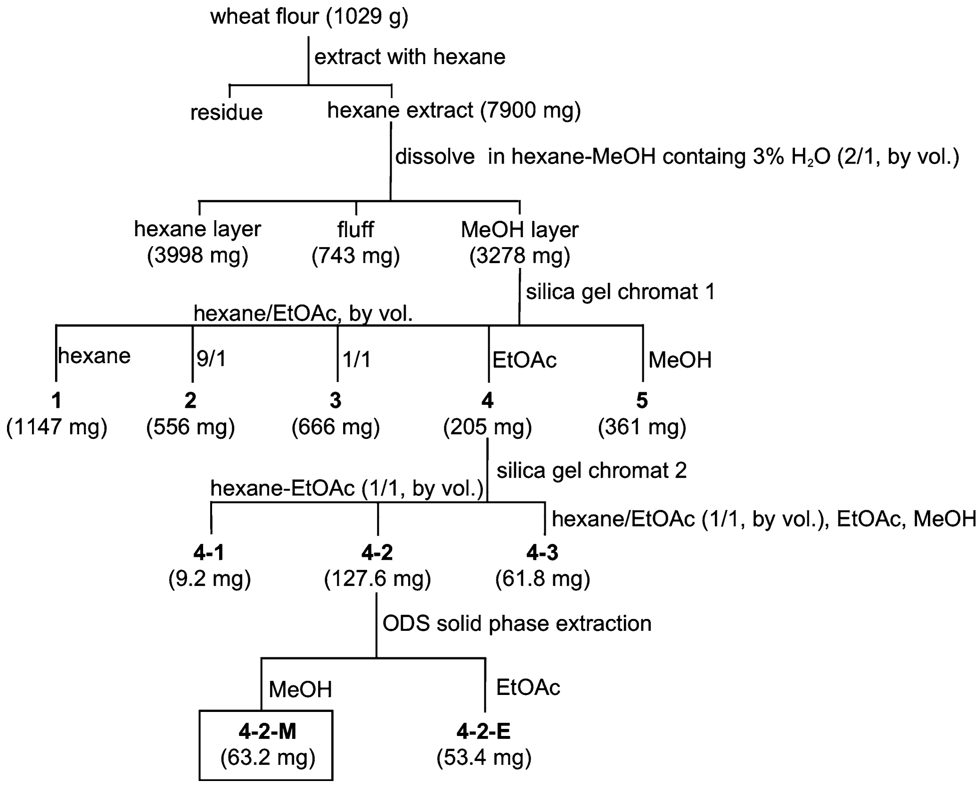
wheat flour (1029 g)
extract with hexane
residue
hexane extract (7900 mg)
dissolve in hexane-MeOH containg 3% H₂O (2/1, by vol.)
hexane layer (3998 mg)
fluff (743 mg)
MeOH layer (3278 mg)
silica gel chromat 1
hexane/EtOAc, by vol.
hexane
9/1
1/1
EtOAc
MeOH
1 (1147 mg)
2 (556 mg)
3 (666 mg)
4 (205 mg)
5 (361 mg)
silica gel chromat 2
hexane-EtOAc (1/1, by vol.)
hexane/EtOAc (1/1, by vol.), EtOAc, MeOH
4-1 (9.2 mg)
4-2 (127.6 mg)
4-3 (61.8 mg)
ODS solid phase extraction
MeOH
EtOAc
4-2-M (63.2 mg)
4-2-E (53.4 mg)

Fig. 3 Purification of TRPV1-activating compounds in wheat flour EtOAc, ethyl acetate; MeOH, methanol; ODS, octadecyl silica

The chemical structure of the acyl portion of 1-MG in Fr. 4-2-M could not be identified from the ^{1}H-NMR spectra. Therefore, the FA was analyzed by GC/MS after the BF_3/MeOH methanolysis of Fr. 4-2-M to identify the acyl portion of 1-MG. The GC/MS analysis revealed palmitic (16:0), stearic (18:0), oleic (18:1), linoleic, (18:2) and α-linolenic acids (18:3) as the constituted FAs of 1-MG.

The chemical structures of 1-MGs in Fr. 4-2-M were directly analyzed by LC/MS. 1-MGs of 16:0, 18:0, 18:1, 18:2, and 18:3 FAs were detected in Fr. 4-2-M, and the weight ratios of these 1-MGs were calculated to be 31.2, 0.302, 55.7, 12.5, and 0.302%, respectively (Fig. 4b).

The TRPV1 activities of the five types of 1-MGs were measured using standards in 100 μM concentration. 1-MGs (18:1, 18:2, and 18:3) increased the $[Ca^{2+}]_i$ in the TRPV1-expressing HEK293 cells; however, 1-MGs of 16:0 and 18:0 did not (Fig. 5a). These responses were inhibited by 100 μM CPZ (Fig. 5a) and were not observed in the parent HEK293 cells [414 ± 29.3, 411 ± 35.8, 433 ± 35.1 nM for HEK293VR11 cells (100 μM, $n = 3$), 44.7 ± 8.31, 45.9 ± 7.40, 44.3 ± 9.83 nM for HEK29 cells (100 μM, $n = 3$), respectively]. Values are $\Delta[Ca^{2+}]_i$), showing a TRPV1-specific action of 1-MGs of 18:1, 18:2, and 18:3. The dose–response curves for TRPV1 activation by 1-MGs containing oleic, linoleic, and α-linolenic acids were comparable, and their potency (EC_{50}) was 50 to 100 times higher than that of CAP, and their efficacy (% activity in response to 10 μM CAP) was approximately 50% (Fig. 5b; Table 1). Moreover, the dose–response curve of Fr. 4-2-M [total content of TRPV1-activating MGs (18:1, 18:2, and 18:3) was 68.5% by LC/MS] was roughly consistent with that of 1-MGs of 18:1, 18:1, and 18:3 (Fig. 5c). Consequently, it was concluded that 1-MGs of 18:1, 18:2, and 18:3 were the TRPV1-activating compounds in wheat flour.

The total crude MG content in wheat flour was 197 μg/g by quantitative TLC/FID analysis.

Other Foods Containing TRPV1-Activating MGs

Active compounds in wheat flour were identified to be 1-MGs containing oleic, linoleic, and α-linolenic acids. The hexane extracts of onion (*Allium cepa*) (onion powder; GABAN, Tokyo, Japan) and myoga (*Z. mioga*) also activated TRPV1 in the above described screening. The main active compounds in onion extract were also 1-MGs of 18:1, 18:2, and 18:3 FAs. Myoga extract contained the same 1-MGs (18:2 and 18:3) and additional 2-MGs of 18:2 and 18:3 FAs. The contents of these MGs were as small as the level of wheat flour.

TRPV1 Activity of Other Lipid Compounds

Transient receptor potential vanilloid subtype 1 was activated by 1-MGs binding oleic, linoleic, and α-linolenoic acids but not 1-MGs binding stearic and palmitic acids

Fig. 4 Chromatograms of TLC/FID (**a**) and LC/MS (**b**) analysis of purified flour extract (Fr. 4-2-M)

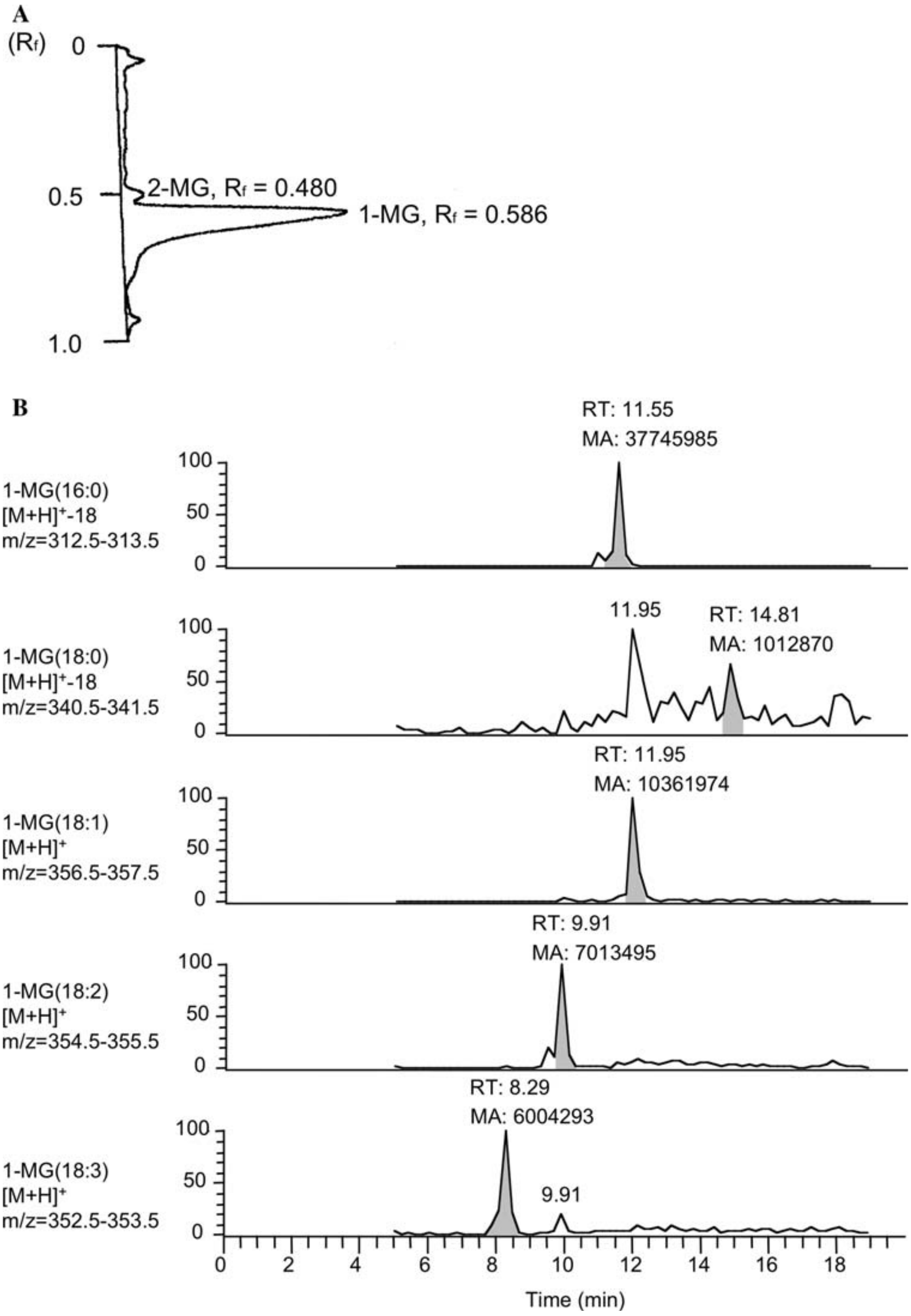

(Fig. 5a). This result suggested that acyl moiety of MG is very important for TRPV1 activity. To decide important acyl moiety of MG, we examined TRPV1 activities for 1-MGs having FAs of varied length. In saturated FAs, 1-MGs (8:0, 10:0, and 12:0) increased $[Ca^{2+}]_i$ of HEK293VR11 cells. However, by increasing carbon chain length of acyl moiety the effect was reduced (Fig. 6a). Although 1-MG of C18 saturated FA [1-MG(18:0)] could not act on HEK293VR11 cells, 1-MGs of C18 unsaturated FA [1-MG(18:1, 18:1*trans*, 18:2, 18:3 and 20:4] increased $[Ca^{2+}]_i$ of HEK293VR11 cells (Fig. 6a). Moreover, 2-MG of C18:1, C18:2 and C20:4 increased $[Ca^{2+}]_i$ of HEK293VR11 cells (Fig. 6a). These responses of 1-MGs and 2-MGs on HEK293VR11 cells were inhibited by CPZ, suggesting that these 1-MGs and 2-MG specifically acted on TRPV1 (Fig. 6b). All TRPV1-activated MGs except 1-MG(8:0) had the equivalent TRPV1 potencies (EC_{50}) and efficacies (maximum response) respectively (Table 1).

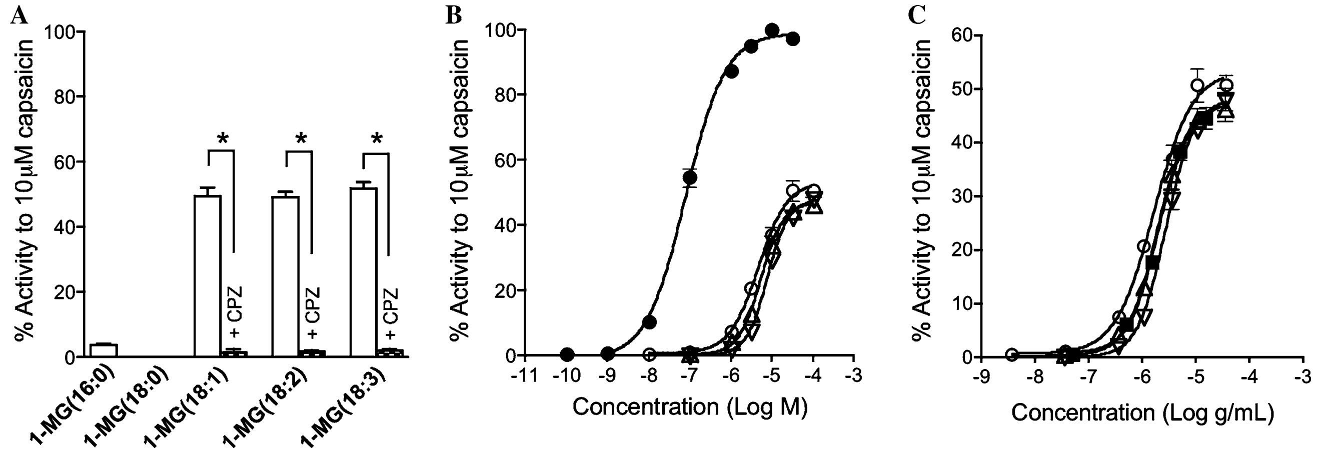

Fig. 5 Transient receptor potential vanilloid subtype 1 (TRPV1) activities by monoacylglycerols (MGs) as measured by intracellular Ca^{2+} concentration in TRPV1-expressing HEK293 cells. **a** *White bars* indicate TRPV1 activities by 100 μM MGs having 16:0, 18:0, 18:1, 18:2, and 18:3 fatty acids, respectively. *Checked bars* indicate TRPV1 activities by these MGs after pretreatment with 100 μM capsazepine (CPZ). These values are mean ± SEM ($n = 3$). *Asterisk* indicates a significant difference between each cell type ($P < 0.01$). **b**, **c** Dose–response curves of capsaicin (CAP, *closed circle*), 1-MGs of 18:1, 18:2, and 18:3 (*open circle*, *open triangle*, and *open inverted triangle*, respectively), and Fr. 4-2-M of wheat flour extract (*filled square*). These values are mean ± SEM ($n = 3$–10)

These potency values were 20 to 150 times higher than that of CAP, and these efficacies were half to that of CAP. The potency of 1-MG(8:0) was only large in comparison with MGs, and its EC_{50} was 195.9 μM (Table 1). These results suggest that middle-chain and long-chain unsaturated acyl moiety of MGs are very important structure for activating TRPV1.

There are other glycerol-based compounds than MGs, i.e., 1,2-DGs, 1,3-DGs, and TGs. Therefore, we investigated whether or not 1,2-DGs, 1,3-DGs, and TGs binding long acyl chain could activate TRPV1. No responses were induced by the DGs and TGs used [1,2-DG(16:0); 100 μM, others; 100 μM, Fig. 6a]. Moreover, some FAs (FA, 300 μM) and glycerol (300 μM) increased little or no $[Ca^{2+}]_i$ of HEK293VR11 cells (Fig. 6c). These results were consistent with previous reports [25, 26].

Anandamide (AEA) and oleoylethanolamide (OEA) were identified as endovanilloids (Fig. 1) [25, 27]. Structure of 1-MGs is similar to that of AEA and OEA. Moreover, It was reported that 2-arachidonyl glycerol ether (2-AGE, noladin ether), which was known as endocannabinoid [28], increased $[Ca^{2+}]_i$ of TRPV1-expressing

Table 1 TRPV1 activation potencies of capsaicin, monoacylglycerols (MGs), anandamide (AEA), oleoylethanolamide (OEA), and 2-arachidonyl glycerol ether (2-AGE)

Compounds	pEC_{50} (−log M)	EC_{50} (μM)	Maximum response (%)	Number of experiments
Capsaicin	7.09 ± 0.0310	0.0819	99.0 ± 1.15	4–10
1-MG(8:0)	3.71 ± 0.0710	195.9	54.6 ± 2.84	3–5
1-MG(10:0)	4.90 ± 0.0565	12.6	50.6 ± 1.70	3–10
1-MG(12:0)	5.10 ± 0.0639	8.01	44.9 ± 1.59	3–10
1-MG(18:1)	5.32 ± 0.0518	4.78	53.3 ± 1.96	3
1-MG(18:1 *trans*)	5.41 ± 0.140	3.88	46.8 ± 3.40	3–6
1-MG(18:2)	5.21 ± 0.0524	6.19	50.1 ± 1.79	3–5
1-MG(18:3)	5.07 ± 0.0380	5.60	50.3 ± 1.41	3–6
1-MG(20:4)	5.81 ± 0.0895	1.55	58.6 ± 2.67	3–4
2-MG(18:1)	5.37 ± 0.0844	4.27	50.4 ± 2.33	3–6
2-MG(18:2)	5.48 ± 0.0496	3.34	59.0 ± 19.4	3
2-MG(20:4)	5.60 ± 0.0869	2.54	59.8 ± 2.64	3–7
AEA	5.69 ± 0.0126	2.02	63.6 ± 0.546	3
OEA	5.60 ± 0.0554	2.53	60.9 ± 2.42	3
2-AGE	5.71 ± 0.0917	1.97	48.3 ± 2.23	3

Maximum responses were normalized to the 10 μM CAP-induced response. pEC_{50} values and maximum responses are indicated as mean ± SEM, and EC_{50} is expressed as the mean value

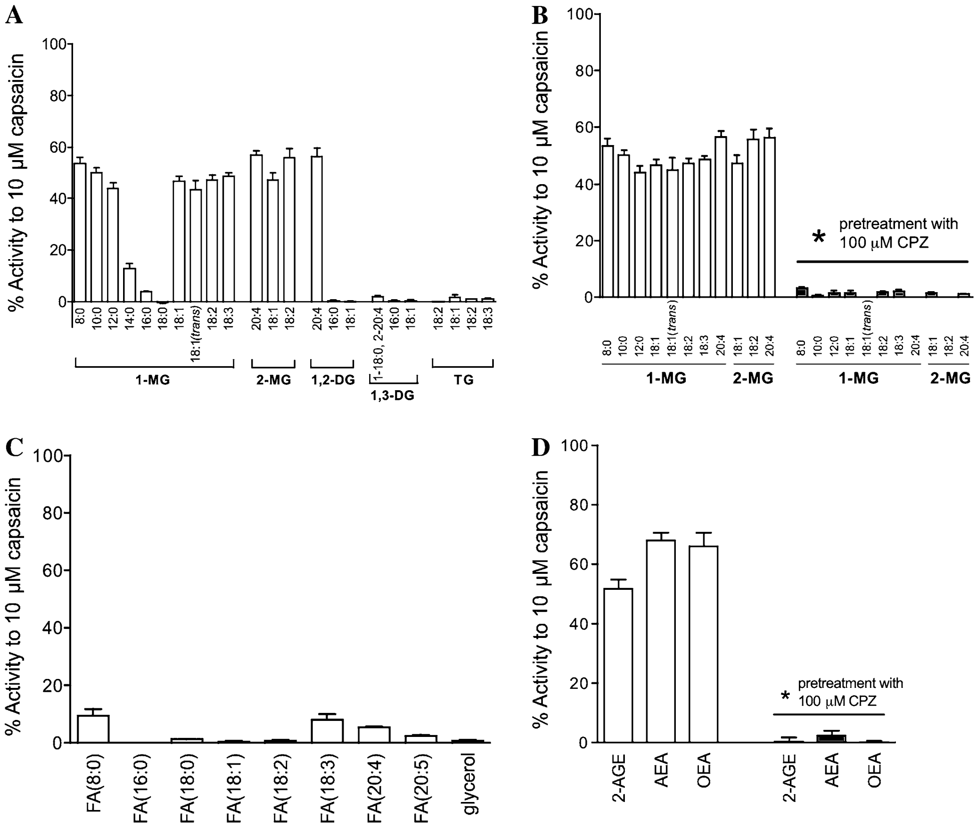

Fig. 6 Transient receptor potential vanilloid subtype 1 (TRPV1) activities of lipid-related compounds as measured by intracellular Ca^{2+} concentration in TRPV1-expressing HEK293 cells. **a** Calcium responses by 1-monoacylglycerols (1-MGs), 2-MGs, diacylglycerols (DGs) and triacylglycerols (TGs). Concentrations of 1-MG(8:0) and 1,2-DG(16:0) were 1,000 and 10 μM, respectively. Other's concentrations were 100 μM. **b** Suppressive effect of capsazepine (CPZ, 100 μM) on the MGs-induced responses. CPZ was treated 1 min before samples injection. **c** Calcium responses by fatty acids (FA) and glycerol (300 μM). **d** TRPV1 activities of 2-arachidonyl glycerol ether (2-AGE), anandamide (AEA), and oleoylethanolamide (OEA) (100 μM). *White bars* indicate calcium responses by sample only. *Gray bars* indicate calcium responses by CPZ treatment 1 min before sample addition. These values are mean ± SEM (**a** and **b**: $n = 3$–13, **c**: $n = 3$–4, **d**: $n = 3$–7). *Asterisk* indicates a significant difference between each groups with or without CPZ, $P < 0.05$

HEK293 cells [29]. TRPV1 activities of effective MGs in this study were compared with those of AEA, OEA, and 2-AGE. These compounds increased $[Ca^{2+}]_i$ in TRPV1-expressing HEK293 cells in concentration-dependent manner as shown in Table 1. These effects were TRPV1 specific because they were inhibited by CPZ (Fig. 6d). TRPV1 activities of AEA and OEA were in agreement with those of previous reports [29–31]. Additionally, TRPV1 activities of MGs were almost identical to those of AEA, OEA, and 2-AGE (Table 1).

Effect of 1-MG(18:1) to Mouse DRG Neurons

Transient receptor potential vanilloid subtype 1 is mainly expressed in sensory neuron of such as DRG and trigeminal nerve [1, 2]. We examined the effect of 1-MG (18:1) to endogenous TRPV1 expressed in mouse DRG neurons. $[Ca^{2+}]_i$ of DRG neurons were increased by 100 μM 1-MG(18:1), and all these neurons were responded to 10 μM CAP (67 cells, Fig. 7a). On the other hand, small number of neurons were activated by only 10 μM CAP (10 cells, Fig. 7a). The percentage of MG positive neurons/CAP positive neurons was 87%. Moreover, all cells that were activated by 100 μM 1-MG (18:1) were significantly inhibited by 100 μM CPZ ($n = 10$, Fig. 7b). These results suggested that 1-MG (18:1) also activates endogenous TRPV1 of mouse DRG.

Irritant Response after Subcutaneous Injection of Monoacylglycerols into Hind Paw

Activation of TRPV1 in the somatic sensory neurons carries pain signals to the brain. In fact, subcutaneous administration of CAP into mouse or rat hind paws induced licking and biting behaviors, which are the characteristic actions in response to a painful sensation [5, 22, 23, 32].

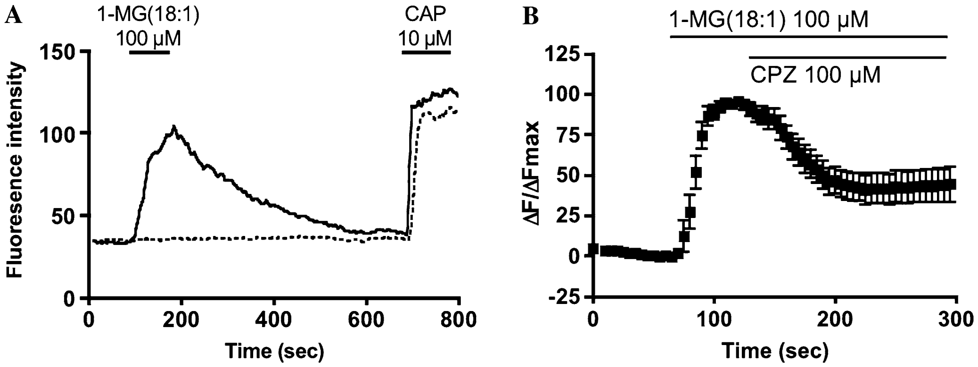

Fig. 7 1-MG (18:1) increases cytosolic Ca^{2+} concentration ($[Ca^{2+}]_i$) in mouse sensory neurons. **a** Two types of representative charts are shown. One is both 100 µM 1-MG(18:1)- and 10 µM CAP-positive neuron (*unbroken line*, $n = 67$), the other is 10 µM CAP-positive and 100 µM 1-MG(18:1)-negative neuron (*broken line*, $n = 10$). **b** 1-MG (18:1)-induced increases in $[Ca^{2+}]_i$ were inhibited by capsazepine (CPZ) in mouse DRG neurons ($n = 10$)

Thus, we investigated whether the subcutaneous injection of TRPV1-activating 1-MGs into rat hind paw induced an irritant behavior.

From the results obtained, the concentration of TRPV1-activating 1-MGs to produce TRPV1 activation was 100-fold the concentration of CAP; thus, 50 mM 1-MG solution was administrated subcutaneously into the rat hind paw. First, we confirmed that vehicle injection elicited no licking and biting behaviors (Fig. 8a). 1-MGs of 18:1, 18:2, and 18:3 induced these behaviors to the same extent or even greater than that induced by 0.5 mM CAP (Fig. 8a). The coadministration of CPZ (10 mM) significantly diminished these irritant responses (Fig. 8b). These data indicated that 1-MGs (18:1, 18:2, and 18:3) activated TRPV1 in vivo. As predicted, 1-MG (18:0) and 1, 3-dilinoleoylglycerol (50 mM), which could not activate TRPV1, did not elicit aversive responses (Fig. 8a).

TRPV1-Activating MGs have no Pungency

As functional food compounds, pungency is an important factor. Many TRPV1 activators induce a pungent taste. On the other hand, capsiate (a red pepper compound), olvanil (CAP's synthetic analogue), and [10]-shogaol (a ginger compound) were identified to be less or non-pungent TRPV1 agonists [5, 32]. Therefore, we examined the pungencies of the TRPV1-activating MGs by a rat eye-wiping assay. This assay has often been used for evaluating the pungency of plant ingredients and chemical compounds [24]. The number of eye-wiping movements observed during 1 min after 0.5 mM CAP application was approximately 27 times/min (Fig. 8c). On the other hand, 1-MGs of 18:1, 18:2, and 18:3 did not induce eye-wiping movements as well as vehicle (Fig. 8c) although they activated TRPV1 in vitro and in vivo (Figs. 5, 8a, c). Thus, these MGs were thought to have no pungent taste.

Discussion

Since CAP induces energy expenditure enhancement and thermogenesis via the activation of TRPV1 [8], other TRPV1 activators in foods may play a role in energy expenditure. In this study, we searched for food ingredients activating TRPV1. We found that TRPV1 was activated by hexane extract of wheat flour which do not have pungency although most of foods contained TRPV1 activators have pungency such as hot pepper, ginger, and pepper. Active compounds in wheat flour were identified to be 1-MG having oleic, linoleic, and α-linolenic acids. Lipid-related TRPV1 agonists reported thus far are 12-(*S*)-hydroperoxyeicosatetraenoic acid, AEA, OEA, and 2-AGE [26, 29]. Omega-3 polyunsaturated FAs activated TRPV1 only when TRPV1 sensitivity was high by phorobol 12, 13-dibutyrate (PDBu)-induced phosphorylation [33]. In the present study, we first report that 1-MG or 2-MG containing C18 and C20 unsaturated- or a C8–C12 FAs activated TRPV1, and excited sensory neurons expressing TRPV1. In addition, the TRPV1 activities of such MGs were almost identical to those of AEA, OEA, or 2-AGE (Table 1) [30, 31].

Transient receptor potential vanilloid subtype 1 potencies (EC_{50}) for these MGs were near to those of [6]-gingerol (4.55 µM) or piperine (2.69 µM) that are the pungent compounds of ginger or pepper, respectively [5, 34] (Table 1). However, these efficacies (maximum response) for MGs were half for that of CAP (Table 1). On the other hand, TRPV1 activities of such MGs were almost the same levels as that of AEA or OEA, known as endovanilloid (Table 1). Movahed et al. examined TRPV1 activity of endogenous C18 *N*-acylethanolamines having stearic, oleic, linoleic, and α-linolenic acids [31]. *N*-Acylethanolamine of saturated C18 (stearic acid) did not activate TRPV1, while other *N*-acylethanolamines binding unsaturated C18 FAs activated TRPV1 at the same EC_{50}s.

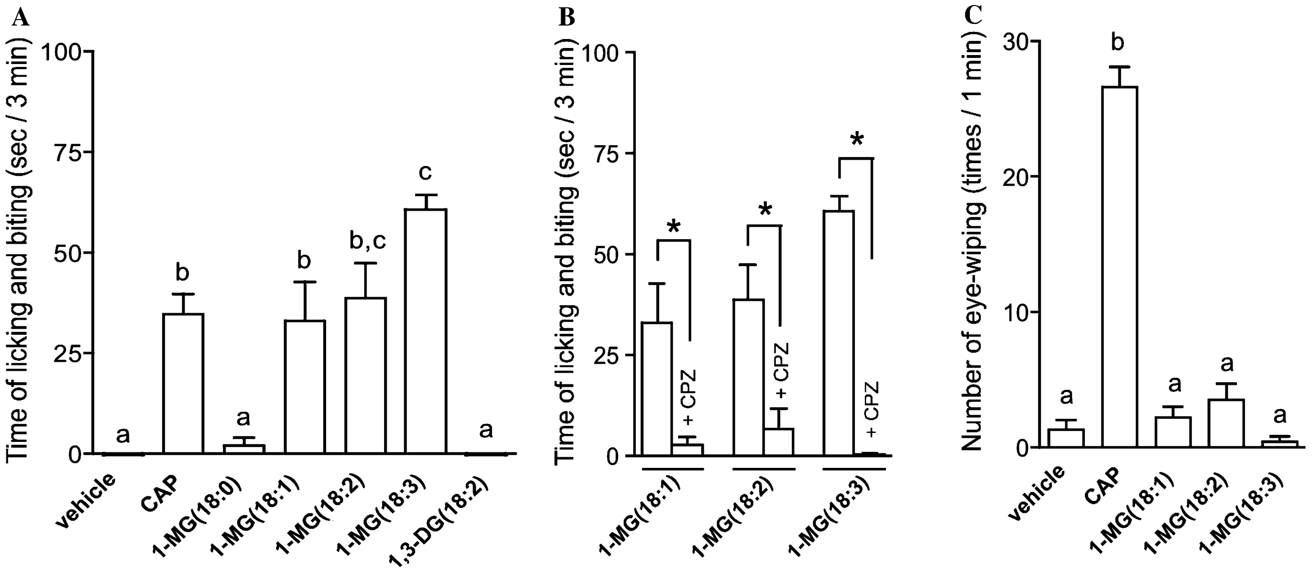

Fig. 8 Aversive responses of rats induced by TPRV1-activating monoacylglycerols (MGs) after the subcutaneous hind paw injection or eye instillation. (**a**) The total time spent on licking and biting the injected hind paw was measured for 3 min after the injection of the vehicle, capsaicin (CAP, 0.5 mM), MGs (50 mM), and 1,3-dilinoleoylglycerol [1,3-DG (18:2), 50 mM]. **b** The total time spent on licking and biting was measured for 3 min after the injection of the TRPV1-activating MGs (50 mM) with or without capsazepine (CPZ, 10 mM) administration. **c** The number of eye-wiping movements was counted for 1 min after the administration of vehicle, CAP (0.5 mM), or TRPV1-activating MGs (50 mM). The values are mean ± SEM (**a**: $n = 5$, **b**: $n = 4$–6, **c**: $n = 6$–12). *Different letters* indicate significant differences, $P < 0.05$. *Asterisk* indicates a significant difference between the groups with or without CPZ, $P < 0.05$

These results are consistent with structure activity relationships for TRPV1 activity of MGs in this study. Moreover, we confirmed that TRPV1 was activated by both 1-MG(18:1) having oleic acid and 1-MG(18:1*trans*) having elaidic acid at the same potencies. Geometric configuration (*cis* or *trans*) of acyl moiety in 1-MG affects molecular size, and 1-MG(18:1*cis*) is smaller than 1-MG(18:1*trans*). This result suggested that important thing for TRPV1 activation might be not a molecular size but the existence of double bounds in acyl moiety of MG.

The potency of TRPV1 activation generally correlates with pungency. But some compounds having high lipophilicity, such as capsiate, olvanil and [10]-shogaol, are strong TRPV1 agonists with low or no pungency [5, 32]. The probable reason why capsiate, olvanil, and [10]-shogaol are not pungent is that these substances cannot reach the epithelium-covered TRPV1-expressing trigeminal nerve endings in the mouth or eye due to their high lipophilicity [5, 32]. The TRPV1-activating MGs may have a high lipophilicity because they are lipids with long-chain FAs. In fact, the lipophilicity of 1-MGs of 18:1, 18:2, and 18:3 was higher than that of CAP and roughly equal to that of olvanil, as revealed by ODS-TLC analysis performed with MeOH/water [ratio, 9/1; the R_f value: CAP, 0.73; olvanil, 0.36; 1-MG (18:1), 0.30; 1-MG (18:2), 0.38; and 1-MG (18:3), 0.43]. Therefore, these MGs are believed to have no pungency and activate TRPV1 via the same mechanism as capsiate, olvanil, and [10]-shogaol.

Capsiate is very low pungent CAP analogue isolated from non-pungent red pepper ‘CH-19 Sweet’ [35]. Capsiate activates TRPV1 with the same potency [32], and increases energy expenditure via TRPV1 activation as well as CAP [13, 36, 37]. For some people who dislike CAP, CAP is too pungent to intake for increasing energy expenditure. From this point of view, capsiate is very useful as it is very low pungent. MGs which activated TRPV1 also may be useful food ingredients to increase energy expenditure like capsiate.

These MGs are minor constituents in foods. In fact, the total crude MG content of wheat flour was 197 μg/g. However, when vegetable oils are ingested, 2-MGs containing oleic or linoleic acids are produced by the lipase digestion of dietary TGs in the small intestine. TRPV1 is expressed at several locations such as myenteric ganglia and mucosa in the lower gastrointestinal tract, and its activation may be related to provide a sensory integration of chemical, physical, or inflammatory stimuli [38]. Therefore, TRPV1 activation by MGs might participate in the control of digestion or absorption of fat.

In the present study, we identified 1- or 2-MGs containing oleic, linoleic, or α-linolenic acids as TRPV1 activators in wheat flower, onion, and myoga. MGs binding to not only C18 and C20 unsaturated FAs but also C8–C12 saturated FAs activated recombinant and endogenous TRPV1 in vitro. Moreover, 1-MGs of 18:1, 18:2, or 18:3 acted on the sensory neurons via TRPV1 in vivo. However, the physiological function through the activation of TRPV1 is not clear now. Study on the effect of 1-MG intake for fat accumulation in rodents is now in progress.

Acknowledgments This work was supported in part by Daikin Air-Conditioning R & D Lab., Osaka, Japan, The Nisshin Seifun Foundation, Tokyo, Japan, and a Grant-in-Aid for Scientific Research from the Japan Society for Promotion of Science.

References

1. Caterina MJ, Schumacher MA, Tominaga M, Rosen TA, Levine JD, Julius D (1997) The capsaicin receptor: a heat-activated ion channel in the pain pathway. Nature 389:816–824
2. Tominaga M, Caterina MJ, Malmberg AB, Rosen TA, Gilbert H, Skinner K, Raumann BE, Basbaum AI, Julius D (1998) The cloned capsaicin receptor integrates multiple pain-producing stimuli. Neuron 21:531–543
3. Immke DC, Gavva NR (2006) The TRPV1 receptor and nociception. Semin Cell Dev Biol 17:582–591
4. Calixto JB, Kassuya CA, Andre E, Ferreira J (2005) Contribution of natural products to the discovery of the transient receptor potential (TRP) channels family and their functions. Pharmacol Ther 106:179–208
5. Iwasaki Y, Morita A, Iwasawa T, Kobata K, Sekiwa Y, Morimitsu Y, Kubota K, Watanabe T (2006) A nonpungent component of steamed ginger-[10]-shogaol-increases adrenaline secretion via the activation of TRPV1. Nutr Neurosci 9:169–178
6. Sugai E, Morimitsu Y, Iwasaki Y, Morita A, Watanabe T, Kubota K (2005) Pungent qualities of sanshool-related compounds evaluated by a sensory test and activation of rat TRPV1. Biosci Biotechnol Biochem 69:1951–1957
7. Caterina MJ (2007) Transient receptor potential ion channels as participants in thermosensation and thermoregulation. Am J Physiol 292:R64–R76
8. Iwai K, Yazawa A, Watanabe T (2003) Roles as metabolic regulators of the non-nutrients, capsaicin and capsiate, supplemented to diets. Proc Jpn Acad Ser B 79B:207–212
9. Kawada T, Watanabe T, Takaishi T, Tanaka T, Iwai K (1986) Capsaicin-induced beta-adrenergic action on energy metabolism in rats: influence of capsaicin on oxygen consumption, the respiratory quotient, and substrate utilization. Proc Soc Exp Biol Med 183:250–256
10. Watanabe T, Kawada T, Yamamoto M, Iwai K (1987) Capsaicin, a pungent principle of hot red pepper, evokes catecholamine secretion from the adrenal medulla of anesthetized rats. Biochem Biophys Res Commun 142:259–264
11. Watanabe T, Kawada T, Kurosawa M, Sato A, Iwai K (1988) Adrenal sympathetic efferent nerve and catecholamine secretion excitation caused by capsaicin in rats. Am J Physiol 255:E23–E27
12. Ohnuki K, Moritani T, Ishihara K, Fushiki T (2001) Capsaicin increases modulation of sympathetic nerve activity in rats: measurement using power spectral analysis of heart rate fluctuations. Biosci Biotechnol Biochem 65:638–643
13. Ohnuki K, Haramizu S, Watanabe T, Yazawa S, Fushiki T (2001) CH-19 sweet, nonpungent cultivar of red pepper, increased body temperature in mice with vanilloid receptors stimulation by capsiate. J Nutr Sci Vitaminol (Tokyo) 47:295–298
14. Kobayashi A, Osaka T, Namba Y, Inoue S, Lee TH, Kimura S (1998) Capsaicin activates heat loss and heat production simultaneously and independently in rats. Am J Physiol 275:R92–R98
15. Blaak EE, Van Baak MA, Kemerink GJ, Pakbiers MT, Heidendal GA, Saris WH (1994) Beta-adrenergic stimulation of energy expenditure and forearm skeletal muscle metabolism in lean and obese men. Am J Physiol 267:E306–E315
16. Watanabe T, Sakurada N, Kobata K (2001) Capsaicin-, resiniferatoxin-, and olvanil-induced adrenaline secretions in rats via the vanilloid receptor. Biosci Biotechnol Biochem 65:2443–2447
17. Zhang LL, Yan Liu D, Ma LQ, Luo ZD, Cao TB, Zhong J, Yan ZC, Wang LJ, Zhao ZG, Zhu SJ, Schrader M, Thilo F, Zhu ZM, Tepel M (2007) Activation of transient receptor potential vanilloid type-1 channel prevents adipogenesis and obesity. Circ Res 100:1063–1070
18. Kawada T, Hagihara K, Iwai K (1986) Effects of capsaicin on lipid metabolism in rats fed a high fat diet. J Nutr 116:1272–1278
19. Ohnuki K, Haramizu S, Oki K, Watanabe T, Yazawa S, Fushiki T (2001) Administration of capsiate, a non-pungent capsaicin analog, promotes energy metabolism and suppresses body fat accumulation in mice. Biosci Biotechnol Biochem 65:2735–2740
20. Fujioka S, Matsuzawa Y, Tokunaga K, Tarui S (1987) Contribution of intra-abdominal fat accumulation to the impairment of glucose and lipid metabolism in human obesity. Metabolism 36:54–59
21. Morita A, Iwasaki Y, Kobata K, Iida T, Higashi T, Oda K, Suzuki A, Narukawa M, Sasakuma S, Yokogoshi H, Yazawa S, Tominaga M, Watanabe T (2006) Lipophilicity of capsaicinoids and capsinoids influences the multiple activation process of rat TRPV1. Life Sci 79:2303–2310
22. Carlton SM, Zhou S, Du J, Hargett GL, Ji G, Coggeshall RE (2004) Somatostatin modulates the transient receptor potential vanilloid 1 (TRPV1) ion channel. Pain 110:616–627
23. Jimenez-Andrade JM, Zhou S, Du J, Yamani A, Grady JJ, Castaneda-Hernandez G, Carlton SM (2004) Pro-nociceptive role of peripheral galanin in inflammatory pain. Pain 110:10–21
24. Szolcsanyi J, Jancso-Gabor A (1975) Sensory effects of capsaicin congeners I. Relationship between chemical structure and pain-producing potency of pungent agents. Arzneimittelforschung 25:1877–1881
25. Zygmunt PM, Petersson J, Andersson DA, Chuang H, Sorgard M, Di Marzo V, Julius D, Hogestatt ED (1999) Vanilloid receptors on sensory nerves mediate the vasodilator action of anandamide. Nature 400:452–457
26. Hwang SW, Cho H, Kwak J, Lee SY, Kang CJ, Jung J, Cho S, Min KH, Suh YG, Kim D, Oh U (2000) Direct activation of capsaicin receptors by products of lipoxygenases: endogenous capsaicin-like substances. Proc Natl Acad Sci USA 97:6155–6160
27. Ahern GP (2003) Activation of TRPV1 by the satiety factor oleoylethanolamide. J Biol Chem 278:30429–30434
28. Hanus L, Abu-Lafi S, Fride E, Breuer A, Vogel Z, Shalev DE, Kustanovich I, Mechoulam R (2001) 2-Arachidonyl glyceryl ether, an endogenous agonist of the cannabinoid CB1 receptor. Proc Natl Acad Sci USA 98:3662–3665
29. Duncan M, Millns P, Smart D, Wright JE, Kendall DA, Ralevic V (2004) Noladin ether, a putative endocannabinoid, attenuates sensory neurotransmission in the rat isolated mesenteric arterial bed via a non-CB1/CB2 G(i/o) linked receptor. Br J Pharmacol 142:509–518
30. Sprague J, Harrison C, Rowbotham DJ, Smart D, Lambert DG (2001) Temperature-dependent activation of recombinant rat vanilloid VR1 receptors expressed in HEK293 cells by capsaicin and anandamide. Eur J Pharmacol 423:121–125
31. Movahed P, Jonsson BA, Birnir B, Wingstrand JA, Jorgensen TD, Ermund A, Sterner O, Zygmunt PM, Hogestatt ED (2005) Endogenous unsaturated C18 *N*-acylethanolamines are vanilloid receptor (TRPV1) agonists. J Biol Chem 280:38496–38504
32. Iida T, Moriyama T, Kobata K, Morita A, Murayama N, Hashizume S, Fushiki T, Yazawa S, Watanabe T, Tominaga M (2003) TRPV1 activation and induction of nociceptive response by a

non-pungent capsaicin-like compound, capsiate. Neuropharmacology 44:958–967
33. Matta JA, Miyares RL, Ahern GP (2007) TRPV1 is a novel target for omega-3 polyunsaturated fatty acids. J Physiol 578:397–411
34. Witte DG, Cassar SC, Masters JN, Esbenshade T, Hancock AA (2002) Use of a fluorescent imaging plate reader–based calcium assay to assess pharmacological differences between the human and rat vanilloid receptor. J Biomol Screen 7:466–475
35. Kobata K, Todo T, Yazawa S, Iwai K, Watanabe T (1998) Novel capsaicinoid-like substances, capsiate and dihydrocapsiate, from the fruits of a nonpungent cultivar, CH-19 Sweet, of pepper (*Capsicum annuum* L.). J Agric Food Chem 46:1695–1697
36. Kawabata F, Inoue N, Yazawa S, Kawada T, Inoue K, Fushiki T (2006) Effects of CH-19 sweet, a non-pungent cultivar of red pepper, in decreasing the body weight and suppressing body fat accumulation by sympathetic nerve activation in humans. Biosci Biotechnol Biochem 70:2824–2835
37. Hachiya S, Kawabata F, Ohnuki K, Inoue N, Yoneda H, Yazawa S, Fushiki T (2007) Effects of CH-19 Sweet, a non-pungent cultivar of red pepper, on sympathetic nervous activity, body temperature, heart rate, and blood pressure in humans. Biosci Biotechnol Biochem 71:671–676
38. Ward SM, Bayguinov J, Won KJ, Grundy D, Berthoud HR (2003) Distribution of the vanilloid receptor (VR1) in the gastrointestinal tract. J Comp Neurol 465:121–135

Lipids (2008) 43:485–497
DOI 10.1007/s11745-008-3176-3

ORIGINAL ARTICLE

N-3 Polyunsaturated Fatty Acids Modulate In-Vitro T Cell Function in Type I Diabetic Patients

Sid Ahmed Merzouk · Meriem Saker · Karima Briksi Reguig · Nassima Soulimane · Hafida Merzouk · Baya Guermouche · Abdelsslam Yahia Berrouiguet · Aziz Hichami · Michel Narce · Naim Akhtar Khan

Received: 19 February 2008 / Accepted: 23 March 2008 / Published online: 8 April 2008
© AOCS 2008

Abstract In this work, we assessed the in-vitro effects of eicosapentaenoic acid (EPA; C20:5n-3) and docosahexaenoic acid (DHA; C22:6n-3) (final concentration, 15 μM) on T cell blastogenesis, interleukin-2 and -4 (IL-2, IL-4) secretion, fatty acid composition and intracellular oxidative status in type I diabetic patients with or without complications. Con A stimulated lymphocyte proliferation, glucose uptake, intracellular reduced glutathione levels and catalase activity were lower in diabetics as compared to controls, regardless to the presence of complications. EPA and DHA diminished T-lymphocyte proliferation and IL-2 production but enhanced IL-4 secretion in both diabetic and control groups. No changes in the levels of reduced glutathione and in the activities of catalase and SOD were observed in control T cells cultured in the presence of EPA and DHA. However, in diabetic patients, addition of n-3 PUFA to culture induced an increase in T cell levels of reduced glutathione and hydroperoxide, and in activities of catalase and SOD. Low levels of arachidonic acid (C20:4n-6) were found in plasma membrane phospholipids of lymphocytes from diabetic patients compared to controls. Incubation of lymphocytes with EPA and DHA was associated with an incorporation of these fatty acids in membrane phospholipids. In conclusion, the beneficial effects of n-3 PUFA on T cell functions in type I diabetes could be attributed to their suppressive action and modulation of cytokine secretion, and to the improvement of intracellular oxidative status.

Keywords Diabetes · Docosahexaenoic acid · Eicosapentaenoic acid · Interleukins · Lymphocytes · Oxidant status · Polyunsaturated fatty acids

Abbreviations

AA	Arachidonic acid
CAT	Catalase
Con A	Concanavalin A
DHA	Docosahexaenoic acid
EPA	Eicosapentaenoic acid
GSH	Reduced glutathione
HDL-C	High density lipoprotein-cholesterol
IDDM	Insulin dependent diabetes mellitus
IL-2	Interleukin-2
IL-4	Interleukin-4
PBL	Peripheral blood lymphocytes
PUFA	Polyunsaturated fatty acids
PL	Phospholipids

S. A. Merzouk
Département de Physique, Faculté des Sciences,
Université de Tlemcen, Tlemcen, Algeria

M. Saker · N. Soulimane · H. Merzouk (✉) · B. Guermouche
Département de Biologie Moléculaire et Cellulaire,
Faculté des Sciences, Université de Tlemcen, Tlemcen, Algeria
e-mail: hafidamerzouk_2@hotmail.com

K. B. Reguig
Laboratoire d'Ecobiotoxicologie,
Université de Sidi Belabbess, Tlemcen, Algeria

A. Y. Berrouiguet
Service de Diabétologie,
Centre Hospitalo-Universitaire de Tlemcen, Tlemcen, Algeria

A. Hichami · N. A. Khan
UPRES EA 4183 "Lipides and Signalisation Cellulaire",
Faculté des Sciences de la Vie, 6 Boulevard Gabriel,
21000 Dijon, France

M. Narce
UMR 866 "Lipides, Nutrition, Cancer",
Faculté des Sciences de la Vie, 6 Boulevard Gabriel,
21000 Dijon, France

ROS	Reactive oxygen species
SOD	Superoxide dismutase
TCR	T cell receptor
TG	Triglycerides

Introduction

The pathogenesis of diabetes mellitus is multifactorial and hence, abnormalities in the immune system have been well established in type 1 and type 2 diabetic subjects [1–4]. A high susceptibility to infection has been described in diabetes mellitus patients, which may be caused by several defects of the immunological defense mechanism [2]. Impairment of polymorphonuclear leukocyte phagocytosis and reduction in granulocyte phagocytic capacity have been reported with increased plasma glucose concentration in diabetic patients [5]. The most dramatic defect that occurs in diabetes mellitus is related to abnormalities of T cell function. Abnormal lymphocyte subpopulations, decreased numbers and activity of T-cytotoxic cells, the presence of activated T cells, and increased number and activity of natural killer (NK) cells have been reported in diabetes [1, 6, 7].

Type 1 diabetes is an autoimmune disease resulting from the selective destruction of insulin-producing β cells by autoreactive T cells [1, 8]. An in-vivo activation of T cells in diabetes is typically reflected by increased serum levels of their products, namely interleukin-2 (IL-2) and the soluble interleukin-2 receptor (sIL-2R). In fact, the CD4+ T cells involved in the mechanisms underlying type 1 diabetes exhibit predominantly a Th1 phenotype, characterized by the secretion of high amounts of IL-2 and IFN-δ [9]. Conversely, CD4+ T cells of the Th2 subset may exhibit regulatory functions that control the development of type 1 diabetes [10, 11].

Paradoxically, a reduced in-vitro production of IL-2 upon mitogen stimulation is found in these patients, associated with an impaired proliferation response in mitogen-activated peripheral blood mononuclear cells [1, 12]. In fact, most of the studies have indicated that T cell growth is triggered exclusively by the production of IL-2 and the consequent expression of its surface receptor [13].

Moreover, the impaired immune function in diabetes could be partly associated with insulin deficiency [1], since insulin modulates cell growth and differentiation [14] and mitogen-activated lymphocyte proliferation [15]. In addition, insulin has an anti-inflammatory effect [16]. Glucose is essential for lymphocyte function, and diabetes causes marked changes in lymphocyte metabolism [4].

There is overwhelming evidence for the effects of n-3 polyunsaturated fatty acids (PUFA) on inflammatory diseases, and they exert beneficial effects in various inflammatory disorders [17]. Dietary n-3 PUFA induce changes in membrane fatty acid composition specially alterations in lipid raft composition, membrane fluidity, receptor distribution; prostaglandin biosynthesis which may influence T cell mediated immune responses [18, 19]. Besides, PUFA have been shown to modulate lymphocyte proliferation, IL-2 production, IL-2 receptor (IL-2R) expression, antigen presentation and natural killer cell activity [19–22]. In addition, the effects of n-3 PUFAS especially EPA (eicosapentaenoic) and DHA (docosahexaenoic acid), on ex vivo lymphocyte functions as judged by mitogen stimulation, have been consistent in both human and animal studies showing suppressed responses [19–22].

Previous studies have demonstrated that n-3 PUFA decrease T cell proliferation [21, 23], cytokine secretion [23], intracellular enzyme activity [24] and gene transcription [25] and modulate antigen presentation through the HLA class I pathway [26]. Additionally, n-3 PUFA suppress T cell proliferative capacity attributed to a reduction in IL-2 production and/or function, and to enhancement of counter regulatory IL-4-driven Th2 cells [27]. Previous studies on the effects of n-3 PUFA on apoptosis in purified T cells indicated that dietary n-3 PUFA preferentially promote apoptosis in a T cell subset exhibiting a Th1 cytokine profile [28]. This exciting observation provides yet another unique mechanism by which n-3 PUFA exert a significant and selective effect on T cell proinflammatory function.

Other factors implicated in different forms of apoptosis are reactive oxygen species (ROS). Several studies have provided evidence for the involvement of ROS in apoptosis of T cell blasts [29]. Apoptosis in these cells is the consequence of changes in mitochondrial permeability and the subsequent release of ROS. Studies performed with primary T cells, however, indicate that the formation of intracellular ROS is necessary for T cell activation and IL-2 secretion but also regulates activation induced T cell apoptosis, therefore suggesting that intracellular ROS could play a role in peripheral T cell homeostasis [30].

The steady-state formation of ROS produced during cell metabolism is normally balanced by a similar rate of consumption by antioxidants. Under normal conditions, protective intracellular enzymes mainly catalase and superoxide dismutase, and cellular non-enzymatic antioxidants such as glutathione prevent ROS accumulation. Oxidative stress may result from imbalance in this pro-oxidant-antioxidant equilibrium. Oxidative stress was found to influence functional characteristics of T lymphocytes with critical implications on proximal and distal T cell receptor (TCR) signaling events [31].

T lymphocyte oxidative stress could originate from environmental free radicals or intracellular enzyme activity.

Diabetes mellitus is associated with increased oxidative stress. Increased production of reactive oxygen species as well as reduced antioxidant defense mechanisms have been suggested to play a role in type 1 diabetic patients [32]. Oxidative stress plays an important role in the etiology of diabetic complications such as atherosclerosis, a major cause of morbidity and mortality in these patients. The following mechanisms are thought to be involved in the increased oxidative stress in diabetes mellitus: hyperglycemia, oxygen free radical generation due to nonenzymatic protein glycosylation, autoxidation of glucose and glycation products, and changes in antioxidant defense systems [32–34].

Despite the various markers of oxidative stress in diabetes mellitus and its implications in the development of diabetes complications, it is not well known whether T lymphocytes affected by this oxidative stress had suppressive proliferative responses to n-3 PUFA supplementation in vitro. In addition, it is still unclear whether impaired lymphocyte proliferation responses occur in diabetic patients with or without complications, and whether EPA and DHA have modulatory effects on cell mediated immune responses in diabetes mellitus regardless to complications.

Therefore, the present study was undertaken to assess in-vitro effects of n-3 PUFA (EPA and DHA) on mitogen-stimulated proliferation, cytokine production, fatty acid composition and oxidant/antioxidant status of T lymphocytes in type 1 diabetic patients with or without complications.

Materials and Methods

Subjects

A total of 38 type I diabetic patients were recruited from the Department of Diabetics, University Hospital of Tlemcen (Algeria). Medical records were screened by specialist physicians. The diabetic type I patients were divided into two groups: group I consisted of type I diabetic patients without complications (20 patients); group II consisted of patients with complications. Complications in the diabetic patients included coronary artery disease in ten type I diabetics, diagnosed by clinical symptoms of angina pectoris, electrocardiogram examination or documented myocardial infarction and renal failure (RF) in eight patients, evaluated by significant renal impairment such as abnormal creatinine or macroalbuminuria. All diabetic patients received insulin. In addition, diabetic patients with RF were treated by angiotensin converting enzyme inhibitors. Diabetic patients with coronary artery disease were treated by calcium antagonists.

Twenty-six control subjects were selected. Controls and diabetic subjects were matched with respect to age and body mass index (BMI) as determined by the weight and height of patients. The characteristics of patients are given in Table 1. The study was approved by the ethical committee of the Tlemcen University Hospital and informed written consent was obtained from all the subjects.

Blood Samples

Samples were collected at approximately the same time each day (between 7 and 8 o'clock in the morning) to

Table 1 Characteristics of the study groups

	Controls	Type I diabetics	
		Without complications	With complications
Number	26	20	18
M/F ratio	15/11	11/9	10/8
Age (years)	28.50 ± 1.37	29.05 ± 1.82	30.50 ± 2.21
BMI (Kg/m^2)	22.83 ± 2.42	21.86 ± 1.53	22.17 ± 2.31
Duration of disease (years)	–	5.00 ± 0.52	9.00 ± 1.44
Fasting glucose (mmol/l)	4.72 ± 0.45	8.87 ± 0.52*	12.24 ± 1.51*
Hb A1C (%)	4.50 ± 0.40	7.56 ± 0.81*	9.89 ± 0.50*
Total cholesterol (mmol/l)	5.63 ± 0.51	5.53 ± 0.53	5.87 ± 0.81
Triglycerides (mmol/l)	1.50 ± 0.42	1.65 ± 0.61	2.59 ± 0.23*
HDL-C (mmol/l)	1.82 ± 0.20	1.64 ± 0.43	1.00 ± 0.20*

Values are means ± SD. The significance of the differences between two groups was determined by Student's *t* test. *$P < 0.05$, diabetic subjects versus controls

BM body mass index, *HDL-C* high density lipoprotein-cholesterol minimize diurnal variations, and before morning insulin injection or any drugs used for diabetic patients. Fasting venous blood samples were collected in two heparinized tubes from each patient. From the first blood sample, plasma was collected for analysis of glucose, glycosylated hemoglobin (Hb A1C) and lipids. The second blood sample was used for immediate lymphocyte isolation.

Laboratory Methods

Plasma Determination

Glycosylated hemoglobin levels (Hb A1C) were determined using a Stambio laboratory kit (P350-050, USA). Plasma glucose was determined by the glucose oxidase method using a glucose analyzer (Beckman Instruments, Fullerton, CA, USA). Plasma triglyceride, total cholesterol and HDL-cholesterol contents were determined by using enzymatic methods, according to the instructions furnished with the kit (Boehringer, Mannheim, Germany).

Lymphocyte Proliferation Assay

Peripheral blood lymphocytes were isolated from heparinized venous blood using differential centrifugation (400*g* for 40 min) on a density gradient of Ficoll-Paque (pharmacia biotech, UK). The peripheral blood lymphocytes (PBL) at the interface of plasma and Ficoll-Paque were collected and washed twice with RPMI 1640 culture medium (Gibco, USA). After washing and counting, the cells were resuspended in a tissue culture medium at 2×10^6 cells/ml. For proliferation assay, 1.5×10^5 cells were cultured in triplicate in 200 µl of medium RPMI 1640 containing 25 mM HEPES buffer supplemented with 10% heat-inactivated fetal calf serum, L-glutamine (2 mM), 2-mercaptoethanol (5×10^{-5} M), penicillin (100 UI/ml) and streptomycin (100 µg/ml) with or without concanavalin A (Sigma St Louis, MO) at a final concentration of 5 µg/ml. This concentration of Con A was found optimal to activate T cells (results not shown). Cultures were performed in 96-well flat-bottomed microtiter plates (Nunc, Paris, France) and maintained at 37 °C in humidified 5% CO_2 atmosphere for 48 h. This culture time was optimal for cytokine secretion. To determine the effects of n-3 PUFA, lymphocytes were also incubated with EPA and DHA (Sigma St Louis, MO) as described by Purasiri et al. [35]. The fatty acids were initially dissolved in ethanol. The stock solution of EPA and DHA in ethanol was diluted in RPMI 1640 culture medium immediately before use (to minimize oxidation) and was added to the cultures at a final concentration of 15 µM (final concentration of ethanol 0.1%). Control cells were mixed with equivalent amounts of ethanol to reach a final concentration of 0.1% ethanol. In preliminary experiments, we have found that this fatty acid concentration (15 µM) induced maximal inhibition of lymphocyte proliferation while cell viability was unaffected. After incubation, cells were harvested by washing with RPMI 1640 medium. Cell viability was controlled by trypan blue exclusion test. Proliferation was monitored by direct cell counts, and confirmed by [3-(4,5-dimethylthiazol-2-yl)-2,5-diphenyl tetrazolium bromide] (MTT; Sigma) assay as described by Mosmann [36].

Interleukin-2 and -4 Quantification

Aliquots of culture supernatants were used to quantitate IL-2 and IL-4 by using commercially available ELISA kits (R&D System, Oxford, UK), as per instructions furnished by the manufacturer. The results are expressed as pg/ml.

Analysis of Lymphocyte Phospholipid Fatty Acids

Lipids from T lymphocytes were extracted according to the method of Bligh and Dyer [37]. Phospholipids were separated on silica gel by thin layer chromatography. Fatty acid composition was analysed by gas–liquid chromatography as previously reported [34].

Glucose Uptake by Lymphocytes

After incubation period, the supernatant of the culture was collected and used for the measurement of glucose as described above. Glucose uptake by lymphocytes after in vitro incubation with Con A for 48 h was calculated by comparing the glucose concentration in the supernatant of cultured cells from controls or diabetics with that of glucose in the supernatant without lymphocytes.

Lymphocyte Oxidant/Antioxidant Markers

GSH Measurement

Glutathione (GSH) levels were measured using a Bioxytech GSH-400 kit (OXIS International, Inc., Portland, OR, USA). Briefly, cells were resuspended in 500 µl of 5% (w/v) metaphosphoric acid and were homogenized. After centrifugation of the homogenate at 3,000*g* for 10 min, 100 µl of the supernatant was transferred to 800 µl of 200 mM potassium phosphate containing 0.2 mM diethylenetriamine pentacetic acid and 0.025% (w/v) lubrol. Then 50 µl of 12 mM chromogenic reagent and 50 µl of 30% NaOH were added, and the mixture was incubated at 25°C for 10 min in the dark. The absorbance at 400 nm was measured, and the GSH concentration was then determined with the GSH standard curve obtained at 400 nm.

Determinations of Lymphocyte Antioxidant Enzyme Activities

After different incubations and cell collection, lymphocytes were washed once, resuspended in chilled 10 mM phosphate buffer (pH 7.0) containing 0.15 M NaCl, sonicated for 30 s and then centrifuged at 15,000*g* for 20 min. Aliquots of the supernatant fractions were used to determine the activities of catalase and the total activity of Superoxide dismutase (Cu, Zn-SOD and Mn-SOD) according to established methods. Briefly, catalase (CAT, EC 1.11.1.6) activity was measured by spectrophotometric analysis of the rate of hydrogen peroxide decomposition at 240 nm [38]. Enzyme activity was expressed as U/mg of protein. The activity of the total SOD was measured by the NADPH oxidation procedure [39] and expressed as units of SOD per mg of protein. Protein content was determined using a Lowry protein kit.

Determination of Lymphocyte Hydroperoxides

To determine markers of lipid peroxidation, hydroperoxides were measured, in sonicated lymphocyte supernatant, by the ferrous ion oxidation-xylenol orange assay (Fox2) in conjunction with a specific ROOH reductant, triphenylphosphine (TPP), according to the method of Nourooz-Zadeh et al. [40]. This method is based on the principle of the rapid peroxide-mediated oxidation of Fe2+ to Fe3+ under acidic conditions. The latter, in the presence of xylenol orange, forms a Fe3+—xylenol orange complex which can be measured spectrophotometrically at 560 nm. Hydroperoxide content in the samples was determined as a function of the mean absorbance difference of samples with and without elimination of ROOH by TPP. Calibration was done with standard peroxides such as hydrogen peroxide.

Statistical Analysis

Data are expressed as mean ± SEM. Statistical analysis were carried out using STATISTICA (version 4.1, Statsoft, Paris, France). The significance of the differences between two groups was determined by Student's *t* test. Multiple comparisons were performed using ANOVA followed by the least significant difference (LSD) test. $P < 0.05$ was considered to represent statistical significant differences.

Results

Hb A1C, Plasma Glucose, Cholesterol, Triglyceride and HDL-Cholesterol Levels

Significant differences were found between diabetic and control subjects for plasma glucose and HbA1C levels which were high in all diabetic patients regardless to complications (Table 1). However, the highest values were apparent in type I diabetes mellitus associated to complications. HDL-cholesterol amounts were lower only in type I diabetes mellitus with complications compared to control and diabetic patients without complications. Plasma triglyceride (TG) levels were significantly increased in type I diabetic patients with complications as compared to these patients without complications and to controls.

Effects of n-3 Fatty Acids on T cell Blastogenesis

Figure 1 shows that mitogen induced cell proliferation, as expressed by cell number, was significantly diminished in both type I diabetic patients with or without complications, as compared to controls. Con A, a T cell-specific mitogen, significantly stimulated lymphocyte proliferation in both diabetic and control subjects. Addition of insulin to culture medium potentiated Con A-stimulated T cell proliferation in all groups. Addition of EPA and DHA to the culture medium resulted in inhibition of Con A-stimulated lymphocyte proliferation, whether the cells were treated with insulin or not, in both diabetic and control groups (Fig. 2), as shown by the reduction in cell number. Inhibition of lymphocyte proliferation was more pronounced with EPA than DHA. Nonetheless, lymphocyte proliferation was always significantly diminished in diabetic patients, regardless of complications. However, the lowest values

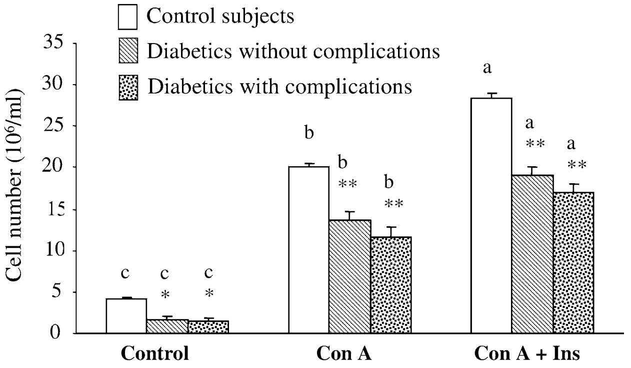

Fig. 1 Resting and mitogen-stimulated T cell proliferation in diabetic and control subjects. 1.5×10^5 cells per well were incubated in 96 well microplates in the presence or absence of concanavalin A (Con A, 5 µg/ml) and insulin (Ins, 5 µg/ml). Cultures were performed in triplicate for 48 h. Proliferation was monitored by direct cell counts, and confirmed by MTT method. The values are mean ± SEM of triplicate assays of subjects composed of following numbers: controls, 26; type I diabetics without complications, 20; type I diabetics with complications, 18. The significance of the differences between two groups was determined by Student's *t* test. Multiple comparisons were performed using ANOVA followed by the least significant difference (LSD) test. The values in diabetic subjects are significantly different (*$P < 0.05$; **$P < 0.01$) as compared to respective control subjects in each incubation. *a*, *b*, *c*, *d* denote significant differences between different incubations within a group ($P < 0.05$)

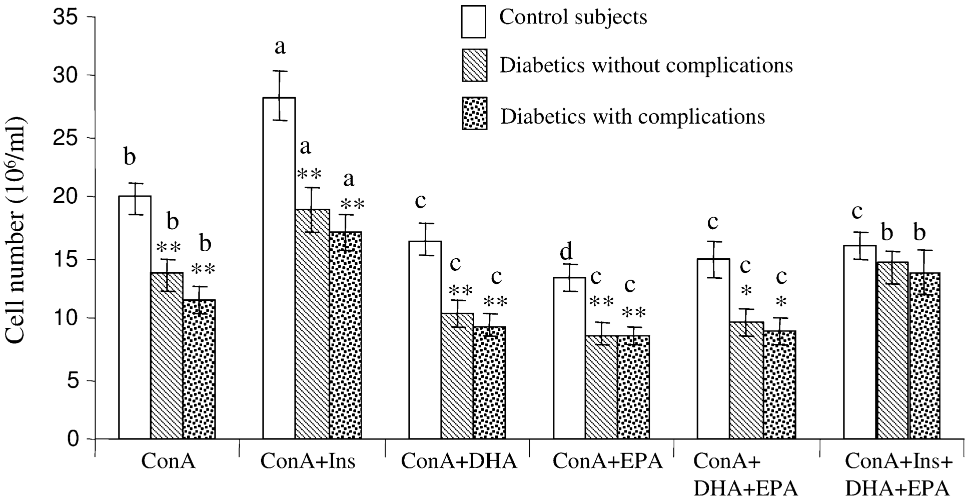

Fig. 2 Effects of EPA and DHA on mitogen-stimulated T cell proliferation in diabetic and control subjects. 1.5×10^5 cells per well were incubated in 96 well microplates in the presence or absence of the following agents: concanavalin A (Con A, 5 µg/ml), eicosapentaenoic acid (EPA, 15 µM), docosahexaenoic acid (DHA, 15 µM), insulin (Ins, 5 µg/ml). The values are mean ± SEM of triplicate assays. The values in diabetic subjects are significantly different ($*P < 0.05$; $**P < 0.01$) as compared to respective control subjects in each incubation. *a*, *b*, *c*, *d* denote significant differences between different incubations within a group ($P < 0.05$)

were observed in diabetic patients with complications. As far as insulin is concerned, its addition to the culture medium did not affect the suppressive effects of EPA and DHA, and the results showed similar patterns as to those obtained with Con A-activated lymphocytes in both control and diabetic subjects (Fig. 2).

Effects of n-3 Fatty Acids on Interleukin-2 and Interleukin-4 (IL-2 and IL-4) Production

IL-2 and IL-4 production was increased by Con A in both diabetic and control groups (Table 2). The data showed that T cells in control and diabetic patients stimulated with Con A for 48 h secreted significantly more IL-2 than IL-4. Because Th1 cells secrete high levels of IL-2, Con A appears to have generated a Th1-like phenotype. Insulin exerted no significant effect on IL-2 secretion induced by Con A. However, it induced a significant increase in IL-4 production by Con A stimulated lymphocytes in both diabetic and control groups.

The effects of EPA and DHA on IL-2 production are parallel to those seen on the proliferation responses. IL-2 levels showed a significant diminution following exposure to EPA and DHA. The addition of insulin in these culture mediums did not affect IL-2 production (data not shown). Production of IL-2 by lymphocytes from type I diabetic patients was significantly diminished compared to controls, the lowest values being in diabetics with complications. However, in the presence of insulin and the combination of the two fatty acids, DHA and EPA, IL-2 amounts secreted by Con A stimulated lymphocytes from diabetics were not significantly different from those of controls (Table 2).

Incubation of T lymphocytes with EPA or DHA was associated with significantly higher production of IL-4 in all groups. The greatest production was observed with the combined n-3 PUFA. Adding insulin to culture mediums containing either EPA or DHA did not affect IL-4 production (data not shown). However, addition of insulin to culture medium with the combined n-3 PUFA potentiated the effects of the combined EPA and DHA on Con A-stimulated T cell production of IL-4 in all groups (Table 2). On the other hand, in the presence of n-3 PUFA, IL-4 production by T cells was significantly increased in diabetic patients than in controls.

Fatty Acid Composition of Lymphocyte Phospholipids

The basal fatty acid composition of phospholipid of lymphocytes from diabetic patients was significantly different from that of controls (Table 3). In fact, type I diabetic patients showed a significant increase in the proportion of C18:2n-6 and a significant decrease in the proportion of C20:4n-6 in their lymphocyte phospholipids as compared to controls, regardless to the presence of complications.

Lymphocytes stimulated with Con A showed a significant increase in the proportion of C18:1 and a decrease in the proportion of C18:0, C18:2n-6 and C20:4n-6 compared to basal fatty acid composition, in both diabetic and control groups. As expected, the proportion of DHA in phospholipids in lymphocytes incubated with DHA was significantly higher than in cells cultured without DHA. Similarly, the EPA content of phospholipids from lymphocytes incubated with EPA contained significant high proportion of EPA. The

Table 2 Production of IL-2 and IL-4 by stimulated lymphocytes from diabetic and control subjects

	Control 1	Type I diabetics	
		Uncomplicated	Complicated
IL-2(Pg/ml)			
Basal	890.55 ± 46.22^{a}	856.18 ± 47.25a	810.50 ± 70.16a
Con A	6,900.25 ± 432.15^{b}	5,600.32 ± 330.54*, ^{b}	4,270.58 ± 250.35**, $^{b,\ \dagger}$
Con A + Ins	6,547.85 ± 345.50^{b}	5,508.56 ± 328.64*, ^{b}	4,846.42 ± 300.33*,$^{\dagger,\ b}$
Con A + DHA	3,450.32 ± 167.31^{c}	2,565.30 ± 108.50*, ^{c}	2,051.50 ± 230.45*,$^{\dagger,\ c}$
Con A + EPA	3,009.45 ± 231.7^{d}	1,980.52 ± 306.65*, ^{d}	1,765.75 ± 100.53*,$^{\dagger,\ d}$
Con A + DHA + EPA	2,599 ± 311.65^{e}	2,164 ± 200.35 ^{d}	1,645 ± 187.64*, $^{\dagger,\ d}$
Con A + Ins + DHA + EPA	2,278 ± 442^{e}	2,005.50 ± 306^{d}	1,809 ± 323.52^{d}
IL-4 (Pg/ml)			
Basal	15 ± 3.87^{a}	18 ± 2.54^{a}	17.50 ± 3.65^{a}
Con A	47.89 ± 4.78^{b}	52.43 ± 5.32^{b}	56.86 ± 6.33^{b}
Con A + Ins	165.76 ± 12.54^{c}	387 ± 23*, ^{c}	399.45 ± 28.75*, ^{c}
Con A + DHA	1,500 ± 48.95^{d}	1,875 ± 67*, ^{d}	1,796.57 ± 75.98*, ^{d}
Con A + EPA	1,234 ± 42.58^{e}	1,654 ± 56.40*, ^{e}	1,561.62 ± 67.90*, ^{e}
Con A + DHA + EPA	1,854.87 ± 83.75^{f}	2,506.06 ± 118*, ^{f}	2,478.50 ± 99.35*, ^{f}
Con A + Ins + DHA + EPA	2,279.56 ± 25.68^{g}	2,808.57 ± 105.33*, ^{g}	2,711.04 ± 79.55*, ^{g}

Values are means ± SD. Total of 1.5×10^5 cells per well (or 10^6 cells/ml) were incubated in 96 well microplates in the presence or absence of the following agents: concanavalin A (Con A, 5 µg/ml), eicosapentaenoic acid (EPA, 15 µM), docosahexaenoic acid (DHA, 15 µM), insulin (Ins, 5 µg/ml) in triplicate assays. Different letters (a, b, c, d, e, f, g) denote significant differences between different incubations within a group ($P < 0.05$). Values with the same letter are not significantly different

* Comparison between diabetic and control groups *$P < 0.05$; **$P < 0.01$

† Denote significant differences between uncomplicated and complicated diabetics $P < 0.05$

concentration of C20:4n-6 (AA) was lower in phospholipids of lymphocytes following exposure to DHA and EPA. These modifications were observed in both control and diabetic groups, regardless to complications. However, lower incorporation of n-3 PUFA and lower loss of AA was observed on diabetic membranes than in controls. The addition of insulin in culture mediums did not affect membrane fatty acid composition (data not shown).

Glucose Uptake by Lymphocytes

Glucose uptake by T cells was measured after in vitro incubation for 48 h. As shown in Table 4, glucose uptake by resting lymphocytes from diabetic patients was significantly lower than that from control subjects, the lowest values being in diabetics with complications. The addition of Con A and insulin increased significantly glucose uptake, but the values remained still lower in diabetics than in controls.

Glucose uptake was not affected by the addition of EPA or DHA in the medium. Adding insulin to these mediums did not change glucose uptake in the presence of either EPA or DHA (data not shown). However, in the presence of insulin and the combined n-3 PUFA, glucose uptake by lymphocytes from diabetics patients was not significantly different from that of control cells (Table 4).

Cellular GSH and Hydroperoxide Contents of Stimulated Lymphocytes

Analyses of glutathione levels in T lymphocytes from diabetic patients showed several significant differences from normal controls. First, as shown in Table 5, T lymphocytes from diabetic patients had significantly decreased reduced glutathione levels, the lowest values being in diabetics with complications. Second, in the presence of Con A, lymphocytes exhibited increased intracellular levels of reduced glutathione, and addition of insulin to culture medium potentiated Con A effects in all groups. Third, glutathione levels of control lymphocytes were not sensitive to n-3 PUFA adding in the medium. Adding insulin to these mediums did not change cellular GSH in the presence of either EPA or DHA (data not shown). However, EPA and DHA produced a significant increase in reduced glutathione levels in lymphocytes from diabetic patients, the highest values being in the presence of insulin and combined n-3 PUFA.

Table 3 Fatty acid composition of lymphocyte phospholipids in diabetic patients and control subjects

	Controls	Type I diabetics	
		Uncomplicated	Complicated
14:0			
Basal	5.18 ± 1.04^{a}	6.63 ± 1.01^{a}	5.66 ± 1.43^{a}
Con A	5.15 ± 1.11^{a}	5.63 ± 0.99^{a}	4.77 ± 1.33^{a}
DHA	5.04 ± 0.89^{a}	5.37 ± 1.07^{a}	5.89 ± 0.97^{a}
EPA	5.84 ± 1.01^{a}	5.66 ± 1.23^{a}	5.99 ± 1.21^{a}
16:0			
Basal	25.18 ± 2.03^{a}	24.33 ± 2.45^{a}	24.82 ± 1.63^{a}
Con A	25.55 ± 2.31^{a}	24.15 ± 2.01^{a}	24.16 ± 2.08^{a}
DHA	25.91 ± 2.39^{a}	24.82 ± 2.09^{a}	24.34 ± 1.94^{a}
EPA	25.89 ± 2.41^{a}	24.62 ± 1.87^{a}	24.93 ± 1.64^{a}
16:1			
Basal	6.14 ± 1.14^{a}	7.16 ± 0.88^{a}	7.55 ± 1.03^{a}
Con A	7.13 ± 1.01^{a}	7.22 ± 1.47^{a}	7.14 ± 0.99^{a}
DHA	6.19 ± 1.23^{a}	7.07 ± 1.25^{a}	6.44 ± 0.95^{a}
EPA	6.83 ± 0.87^{a}	7.37 ± 1.32^{a}	7.45 ± 1.01^{a}
18:0			
Basal	20.06 ± 1.44^{a}	22.15 ± 1.52^{a}	23.04 ± 2.12^{a}
Con A	18.15 ± 1.06^{b}	20.36 ± 1.08^{b}	20.67 ± 1.22^{b}
DHA	18.73 ± 1.45^{b}	19.88 ± 1.39^{b}	20.04 ± 1.11^{b}
EPA	18.06 ± 1.53^{b}	19.89 ± 1.63^{b}	19.55 ± 1.04^{b}
18:1			
Basal	13.89 ± 1.06^{b}	12.33 ± 0.93^{b}	11.69 ± 1.08^{b}
Con A	19.98 ± 1.13^{a}	19.58 ± 1.12^{a}	20.08 ± 1.08^{a}
DHA	19.57 ± 1.30^{a}	19.67 ± 1.28^{a}	19.75 ± 1.45^{a}
EPA	20.03 ± 1.82^{a}	19.57 ± 1.77^{a}	19.11 ± 1.33^{a}
18:2n-6			
Basal	9.66 ± 0.87^{a}	14.04 ± 0.45*, ^{a}	14.69 ± 1.08*, ^{a}
Con A	8.09 ± 0.75^{b}	11.88 ± 0.71*, ^{b}	12.03 ± 1.10*, ^{b}
DHA	8.68 ± 0.65^{b}	11.06 ± 0.92*, ^{b}	11.54 ± 1.06*, ^{b}
EPA	8.12 ± 0.67^{b}	10.67 ± 0.82*, ^{b}	10.98 ± 1.24*, ^{b}
18:3n-3			
Basal	1.38 ± 0.49^{a}	1.58 ± 0.37^{a}	1.56 ± 0.29^{a}
Con A	1.39 ± 0.25^{a}	1.27 ± 0.35^{a}	1.29 ± 0.24^{a}
DHA	1.28 ± 0.54^{a}	1.36 ± 0.24^{a}	1.38 ± 0.28^{a}
EPA	1.42 ± 0.33^{a}	1.39 ± 0.30^{a}	1.54 ± 0.23^{a}
20:4n-6			
Basal	13.85 ± 1.01^{a}	8.72 ± 1.11*, ^{a}	7.89 ± 1.03*, ^{a}
Con A	10.64 ± 1.12^{b}	6.83 ± 0.90*, ^{b}	6.58 ± 0.70*, ^{b}
DHA	7.06 ± 1.04^{c}	6.18 ± 0.89^{b}	6.09 ± 0.64^{b}
EPA	7.02 ± 0.66^{c}	6.68 ± 0.72^{b}	6.44 ± 0.57^{b}
20:5n-3			
Basal	1.99 ± 0.58^{b}	1.08 ± 0.69^{b}	1.33 ± 0.50^{b}
Con A	1.87 ± 0.43^{b}	1.19 ± 0.55^{b}	1.56 ± 0.60^{b}
DHA	1.68 ± 0.51^{b}	1.38 ± 0.56^{b}	1.44 ± 0.51^{b}
EPA	4.64 ± 0.42^{a}	2.42 ± 0.36*, ^{a}	2.38 ± 0.53*, ^{a}
22:6n-3			
Basal	2.47 ± 0.64^{b}	1.98 ± 0.77^{b}	1.77 ± 0.80^{b}
Con A	2.04 ± 0.71^{b}	1.89 ± 0.65^{b}	1.70 ± 0.53^{b}
DHA	5.86 ± 0.89^{a}	3.21 ± 0.38*, ^{a}	3.09 ± 0.62*, ^{a}
EPA	2.15 ± 0.52^{b}	1.73 ± 0.62^{b}	1.63 ± 0.48^{b}

Values are means ± SEM. Values are expressed as a percentage of total fatty acids. Total of 1.5×10^5 cells per well (or 10^6 cells/ml) were incubated in 96 well microplates in the presence or absence of the following agents: concanavalin A (ConA, 5 μg/ml), eicosapentaenoic acid (EPA, 15 μM), docosahexaenoic acid (DHA, 15 μM), insulin (Ins, 5 μg/ml) in triplicate assays. Fatty acid composition was determined in resting lymphocytes before any addition (basal), after mitogen addition (Con A), and after n-3 PUFA addition (DHA or EPA). Comparison between diabetic and control groups $^{*}P < 0.05$

Different letters denote significant differences between different incubations within a group ($P < 0.05$). Values with the same letter are not significantly different

Hydroperoxides, markers of lipid peroxidation, were significantly increased in T lymphocytes from diabetics compared to control values (Table 5). In the presence of Con A, hydroperoxide levels were higher than basal values and the addition of insulin did not affect these levels. Addition of EPA or/and DHA in the culture medium produced significant increases in hydroperoxide levels in all groups. Adding insulin to these mediums did not change hydroperoxide levels in the presence of either EPA or DHA (data not shown). However, in the presence of insulin and combined n-3 PUFA, no significant difference was noted between diabetic and control groups.

Lymphocyte Cellular Antioxidant Enzyme Activities

Resting lymphocyte catalase activity was significantly lower in the two groups of type I diabetes mellitus when compared with controls (Table 6). However, no significant difference in basal SOD activity was observed between type I diabetic groups and controls.

In the presence of Con A, catalase and SOD activities were enhanced in lymphocytes from diabetic and control subjects. This effect was amplified when insulin was added to culture medium. Catalase activity was reduced while SOD activity was enhanced in stimulated lymphocytes from diabetics compared to controls. The treatment with n-3 PUFA had no effect on catalase and SOD activities in all groups. Adding insulin to mediums did not change catalase and SOD activities in the presence of either EPA or DHA (data not shown).

Table 4 Glucose uptake by lymphocytes from diabetic and control subjects

μg/48 h/10^5 cells	Controls	Type I diabetics	
		Uncomplicated	Complicated
Basal	11.72 ± 3.76^{a}	4.85 ± 1.05*, ^{a}	3.67 ± 1.03*, ^{a}
Con A	95.43 ± 10.18^{a}	57.32 ± 9.27*, ^{a}	39.54 ± 8.32*, $^{\dagger, a}$
Con A + Ins	129.67 ± 12.35^{b}	98.56 ± 10.75*, ^{b}	87.38 ± 11.04*, ^{b}
Con A + DHA	98.45 ± 11.56^{a}	60.32 ± 7.36*, ^{a}	49.83 ± 8.02*, ^{a}
Con A + EPA	104 ± 23.05^{a}	63.32 ± 8.11*, ^{a}	53.48 ± 7.70*, ^{a}
Con A + DHA + EPA	100.36 ± 21.50 ^{a}	65.98 ± 8.45*, ^{a}	55.77 ± 8.59*, ^{a}
Con A + Ins + DHA + EPA	133.04 ± 20.13^{b}	103 ± 18.04^{b}	101.50 ± 20.08^{b}

Values are mean ± SEM. Total of 1.5 × 10^5 cells per well (or 10^6 cells/ml) were incubated in 96 well microplates in the presence or absence of the following agents: concanavalin A (Con A, 5 μg/ml), eicosapentaenoic acid (EPA, 15 μM), docosahexaenoic acid (DHA, 15 μM), insulin (Ins, 5 μg/ml) in triplicate assays. Glucose uptake was calculated by subtracting the glucose content in the medium after in vitro incubations for 48 h from the glucose content in preculture medium

* Comparison between diabetic and control groups $P < 0.05$

† Denote significant differences between uncomplicated and complicated diabetics $P < 0.05$

Different letters (a, b) denote significant differences between different incubations within a group ($P < 0.05$). Values with the same letter are not significantly different

Table 5 Cellular GSH and hydroperoxide contents of stimulated lymphocytes from diabetic and control subjects

	Controls	Type I diabetics	
		Uncomplicated	Complicated
GSH (nM/10^6 cells)			
Basal	8.45 ± 1.67^{a}	4.09 ± 0.98*, ^{a}	2.34 ± 0.67*, $^{\dagger, a}$
Con A	15.68 ± 2.76^{b}	9.05 ± 3.23*, ^{b}	6.76 ± 2.14*, $^{\dagger, b}$
Con A + Ins	30.04 ± 3.11^{c}	18.16 ± 2.88*, ^{d}	10.32 ± 2.21*, $^{\dagger, c}$
Con A + DHA	14.25 ± 1.33^{b}	14.32 ± 1.17^{c}	11.75 ± 1.64*, ^{c}
Con A + EPA	13.06 ± 2.05^{b}	14.66 ± 3.05^{c}	10.34 ± 1.86*, ^{c}
Con A + DHA + EPA	15.87 ± 2.11^{b}	14.98 ± 1.14^{c}	12.63 ± 1.17*, ^{c}
Con A + Ins + DHA + EPA	28.86 ± 3.53^{c}	24.99 ± 3.27^{e}	19.65 ± 1.33*, ^{d}
Hydroperoxides (nM/10^6 cells)			
Basal	1.35 ± 0.19^{a}	1.87 ± 0.28*, ^{a}	1.90 ± 0.37*, ^{a}
Con A	2.85 ± 0.15^{b}	3.56 ± 0.10*, ^{b}	3.76 ± 0.22*, ^{b}
Con A + Ins	2.97 ± 0.26^{b}	3.76 ± 0.14*, ^{b}	3.83 ± 0.11*, ^{b}
Con A + DHA	8.50 ± 1.23^{c}	15 ± 1.13*, ^{d}	17.34 ± 1.08*, ^{d}
Con A + EPA	7.35 ± 1.34^{c}	13.27 ± 1.32*, ^{d}	15.89 ± 1.52*, ^{d}
Con A + DHA + EPA	8.94 ± 1.41^{c}	15.37 ± 1.45*, ^{d}	17.68 ± 2.44*, ^{d}
Con A + Ins + DHA + EPA	7.08 ± 1.53^{c}	8.32 ± 1.81^{c}	8.56 ± 1.78^{c}

Values are means ± SEM. Total of 1.5 × 10^5 cells per well (or 10^6 cells/ml) were incubated in 96 well microplates in the presence or absence of the following agents: concanavalin A (Con A, 5 μg/ml), eicosapentaenoic acid (EPA, 15 μM), docosahexaenoic acid (DHA, 15 μM), insulin (Ins, 5 μg/ml) in triplicate assays. Different letters (a, b, c, d) denote significant differences between different incubations within a group ($P < 0.05$). Values with the same letter are not significantly different

* Comparison between diabetic and control groups $P < 0.05$

† Denote significant differences between uncomplicated and complicated diabetics $P < 0.05$

Discussion

To gain further insight into the immunomodulatory effects of n-3 PUFA, the present study was conducted to examine in-vitro proliferation of T lymphocytes from diabetic patients with or without complications and from healthy subjects, cultured with n-3 PUFA, eicosapentaenoic acid (EPA) and docosahexaenoic acid (DHA). Behaviour of oxidative stress biomarkers in T lymphocytes was also analyzed. To our knowledge, this is the first study to

Table 6 Cellular antioxidant enzyme activities of stimulated lymphocytes from diabetic and control subjects

Catalase (U/mg protein)	Controls	Type I diabetics	
		Uncomplicated	Complicated
Basal	8.56 ± 1.24^{a}	4.23 ± 0.98*,^{a}	3.57 ± 0.65*,$^{\dagger, a}$
Con A	16.85 ± 1.05^{b}	10.07 ± 1.13*,^{b}	8.36 ± 0.85*,$^{\dagger, b}$
Con A + Ins	25.28 ± 3.54^{c}	17.25 ± 1.08*,^{c}	15.63 ± 1.17*,^{c}
Con A + DHA	18.45 ± 1.76^{b}	16.78 ± 1.97^{c}	16.50 ± 1.23^{c}
Con A + EPA	15.35 ± 2.87^{b}	15.47 ± 2.56^{c}	14.32 ± 3.01^{c}
Con A + DHA + EPA	18.38 ± 49^{b}	18.28 ± 2.69^{c}	17.37 ± 2.44^{c}
Con A + Ins + DHA + EPA	28.63 ± 2.58^{c}	26.67 ± 3.33^{d}	25.93 ± 3.77^{d}
SOD (U/mg protein)			
Basal	80.32 ± 4.76^{a}	74.23 ± 8.93^{a}	78.50 ± 6.77^{a}
Con A	141.19 ± 12.34^{b}	189.45 ± 22.54*,^{b}	178.05 ± 20.24*,^{b}
Con A + Ins	169.78 ± 18.90^{c}	235.32 ± 21.05*,^{c}	229.28 ± 28.93*,^{c}
Con A + DHA	148.35 ± 23.89^{b}	209 ± 26.86*,^{b}	199.73 ± 22.02*,^{b}
Con A + EPA	138.07 ± 31.22^{b}	185.35 ± 30.21*,^{b}	187.38 ± 25.30*,^{b}
Con A + DHA + EPA	155.06 ± 28.93^{b}	203.57 ± 39.44*,^{b}	200.57 ± 31.06*,^{b}
Con A + Ins + DHA + EPA	182.39 ± 37.84^{c}	217.99 ± 32.10$^{b, c}$	208.09 ± 27.43$^{b, c}$

Values are means ± SEM. Total of 1.5×10^5 cells per well (or 10^6 cells/ml) were incubated in 96 well microplates in the presence or absence of the following agents: concanavalin A (Con A, 5 μg/ml), eicosapentaenoic acid (EPA, 15 μM), docosahexaenoic acid (DHA, 15 μM), insulin (Ins, 5 μg/ml) in triplicate assays. Different letters (a, b, c, d) denote significant differences between different incubations within a group ($P < 0.05$). Values with the same letter are not significantly different

* Comparison between diabetic and control groups $P < 0.05$

† Denote significant differences between uncomplicated and complicated diabetics $P < 0.05$

investigate the in vitro effects of n-3 PUFA (EPA, DHA) on T lymphocyte proliferation, cytokine production combined to lymphocyte antioxidant/oxidant status in diabetes regarding the influence of metabolic control. In the population studied, abnormalities in lipids (high TG, low HDL-C) were seen only in diabetic patients with complications. However, high fasting glucose and HbA1C levels were observed in all type I diabetics.

In this study, we determined cell proliferation by counting the number of viable cells and by the MTT method. Con A, a T cell specific mitogen, significantly stimulated lymphocyte proliferation in both diabetic and control subjects. T cells in control and diabetic patients stimulated with Con A for 48 h secreted significantly more IL-2 than IL-4. Because Th1 cells secrete high levels of IL-2, Con A appears to have generated a Th1-like phenotype.

We also observed that mitogen-activated lymphocyte proliferation was lower in diabetic patients than that in healthy subjects. Basal and Con A stimulated IL-4 production was not affected by diabetes.

However, IL-2 production was diminished in type I diabetic patients, the lowest values were seen in diabetic patients with complications. Other investigators have also reported that IDDM patients not only showed a depressed response of lymphocytes to T cell mitogen but also lower IL-2 production when compared with matched controls [1, 5, 6, 9]. The explanation of decreased in vitro proliferative response may be that lymphocyte in diabetic patients are subjected to in-vivo activation of the immune system. In this case, their further in-vitro proliferation will be reduced compared to those from control subjects. It is well known that Con A acts, mainly, on resting (quiescent) T cells. In fact, several studies have reported a significant increase in the percent of in-vivo activated T-lymphocytes in diabetic patients [6, 7, 41], which play a role in the progression of chronic complications [1, 6–9]. Since impaired immune function in diabetes is partly associated with insulin deficiency and activated lymphocytes possess insulin receptors, we were tempted to investigate the effects of insulin on T cell activation. Hence, we have observed that insulin potentiated Con A-stimulated T cell proliferation, indicating that insulin deficiency in diabetes mellitus might be partly responsible for immunosuppression. In addition, insulin has no effect on IL-2 production while it increased IL-4 secretion by lymphocytes, due probably to its anti inflammatory effect [16]. Insulin effect on IL-4 secretion was more pronounced in diabetic patients. This observation is in accordance with previous publications reporting IL-4 secretion in response to insulin in individuals with type 1 diabetes [11] and increased mitogen induced secretion of IL-4 by insulin from PBMCs [42].

We further observed that in vitro EPA and DHA significantly reduced lymphocyte proliferation in both diabetic and control groups. The immuno-suppressive action was more pronounced with EPA. The suppressed T-lymphocyte proliferative response of EPA and DHA is supported with the observations of other investigators who have also reported that n-3 PUFA significantly diminished mitogen activated lymphocyte proliferation [19–23]. There are several possible mechanisms as to how n-3 PUFA may exert their inhibitory effects. Firstly, both EPA and DHA reduced IL-2 secretion by Con A-stimulated lymphocytes, suggesting that the suppressed lymphoproliferation is due in part to a reduction in IL-2 production [21, 22]. However, IL-4 production was enhanced by n-3 PUFA. These data are consistent with previous observations showing an increase in IL-4-dependent Th2 proliferation after n-3 PUFA feeding [28], and indicate that n-3 PUFA act differently on distinct T cell subsets. It has been shown that dietary n-3 PUFA shift the Th1/Th2 balance toward the Th2 pole by suppression of Th1 development rather than enhancement of Th2 development [43].

In the presence of combined n-3 PUFA and insulin, lymphocytes from diabetic patients secreted similar amounts of IL-2 but higher levels of IL-4 compared to that from controls, which probably reflected a regulatory effect of n-3 PUFA on Th cell phenotypes in diabetes, in favor of an anti-inflammatory phenotype.

Incubation of lymphocytes with fatty acids in vitro resulted in marked alterations in fatty acid composition [18, 19, 44]. Dietary DHA alter T cell plasma membrane microdomain lipid composition and influence the plasma membrane partitioning of signaling proteins that regulate T cell activation in vivo [45]. In our study, the addition of DHA or EPA to culture media was accompanied with a predominant composition of DHA or EPA in phospholipids of T cell membrane from control and diabetic patients. These effects appeared to result from alterations in lipid raft composition of T cells, as indicated by several previous investigations [18, 44, 45].

In our study, suppressed proliferation response may be also due to arachidonic acid (AA) substitution by EPA and DHA in lymphocyte membrane phospholipids as observed in our study. We should recall that turnover of membrane phospholipids is an early event in T cell activation which implies arachidonic acid liberation and its metabolism [44]. Similarly, low levels of this n-6 fatty acid, observed in diabetic subjects, may contribute to depressed T cell proliferation in type I diabetes, regardless to complications. Stimulation with Con A also brings about changes in lymphocyte fatty acid composition. Mitogenic activation of lymphocyte is associated with a decrease in the proportions of stearic, linoleic and arachidonic acids and an increase in the proportion of oleic acid, in accordance with other studies [46]. It is interesting to note that lymphocytes from type I diabetic patients responded to EPA and DHA in a manner similar to those from healthy subjects despite the altered initial fatty acid composition.

Glucose is essential for lymphocyte function, and it is the main energy source for mature lymphocytes, especially at the stage of proliferation after in vitro stimulation with mitogens. Diabetes causes marked changes in lymphocyte metabolism [4]. We found that glucose uptake by T lymphocytes was significantly lower in diabetic than in control subjects, the lowest value being in diabetes with complications. In addition, insulin enhanced Con A stimulated glucose uptake by T cells from controls and diabetics. Lymphocyte proliferation in type I diabetes might be also due to the impairment of glucose uptake by lymphocytes. Indeed, EPA and DHA had no effect on in vitro glucose uptake by lymphocytes from both control and diabetic subjects. However, in the presence of combined n-3 PUFA and insulin, T cell glucose uptake in diabetic patients was not significantly different from that in controls.

Our results on oxidative stress biomarkers in T lymphocytes showed that these cells are submitted to an oxidative stress in type I diabetes. In fact, abnormalities in glutathione levels were observed in T lymphocytes from diabetic patients compared with cells from healthy controls, with significantly decreased intracellular levels of reduced glutathione (GSH), the lowest values being in diabetes with complications. We have previously reported that oxidative stress is induced by both the increases in free radicals and disturbance of the free radical scavenging system in type I diabetes mellitus [33, 34]. We also observed that Con A involved an increased glutathione level in T lymphocytes in both diabetic and control subjects, and insulin potentiated this effect. It has been demonstrated that enhancement of intracellular GSH concentration results in an increased lymphocyte response to mitogen stimulation [47].

Our findings indicated that catalase activity was reduced while SOD activity was normal in basal T lymphocytes from diabetics. Stimulation with Con A and insulin enhanced catalase and SOD activities in T cells from diabetic and control subjects. Thus, the increase in GSH levels and in catalase and SOD activities could be adaptative responses to oxidative stress following T cell receptor activation.

Hydroperoxides were measured as a marker of lipid peroxidation. We have previously assessed elevated levels of hydroperoxides in plasma from type 1 diabetic patients [34]. High hydroperoxide levels in our diabetic patients could result from their hyperglycemia. Lipid peroxidation is initiated when membrane PUFA interact with ROS which include hydrogen peroxide (H_2O_2). Our results showed that basal T cell hydroperoxide levels were increased in diabetic versus controls. Addition of Con A enhanced hydroperoxide levels following T cell activation in all groups.

As far as the effects of n-3 PUFA are concerned, we found that the hydroperoxide content was increased in T cells from control and diabetic patients. N-3 PUFA are highly susceptible to lipid peroxidation. No changes in the levels of GSH and in the activities of catalase and SOD were observed in control T cells cultured in the presence of EPA and DHA. However, in diabetic patients, addition of n-3 PUFA to culture induced an increase in T cell levels of GSH and hydroperoxide, and activities of catalase and SOD. These findings suggested a defect in the utilization of GSH or an upregulation of the enzymes responsible for GSH production and recuperation of extracellular GSH with a resultant increase in intracellular levels of GSH in diabetic lymphocytes exposed to n-3 PUFA. It was clear that the oxidant/antioxidant status of T lymphocyte from diabetic patients was more sensitive to the presence of n-3 PUFA than those from controls. Interestingly, we noted that in the presence of combined EPA and DHA and insulin, the oxidant/antioxidant status of T lymphocyte from diabetic patients became similar to that found in control subjects, with only minor perturbations in diabetes with complications. We suggested that the diabetic T cells, in the presence of n-3 PUFA, regulate their intracellular oxidative status; this could be considered as one mechanism that resulted in the benefits of n-3 PUFA.

In conclusion, the present study demonstrates that type I diabetes mellitus is associated to in vitro reduced T lymphocyte proliferation, IL-2 secretion and glucose uptake, altered fatty acid composition of T lymphocyte membrane phospholipids and oxidant/antioxidant status, regardless to the presence of complications. EPA and DHA possessed immunosuppressive properties and have similar effects on T cell functions of diabetic patients as in healthy subjects. EPA and DHA inhibit in vitro T cell proliferation, IL-2 secretion and enhance IL-4 production with a shift away from Th1 response to Th2 phenotype. Although EPA and/or DHA alone had no effects on behaviour of oxidative stress biomarkers, combined n-3 PUFA in the presence of insulin improved T cell intracellular oxidative status in type I diabetes mellitus. The beneficial effects of n-3 PUFA on T cell functions in type I diabetes could be attributed to their suppressive action and modulation of cytokine secretion, and to the improvement of intracellular antioxidant status.

Acknowledgments This work was supported by the French Foreign office (International Research Extension Grants 01 MDU 531) and by financial support from the Algerian Health investigation office (ANDRS, no.02/15/02/00 001). Thanks are due to J. Gresti for his technical assistance. A contingent grant from the Burgundy region is also acknowledged.

References

1. Itoh M (1989) Immunological aspects of diabetes mellitus: prospects for pharmacological modification. Pharmacol Ther 44:351–406
2. Shah BR, Hux JE (2003) Quantifying the risk of infectious diseases for people with diabetes. Diabetes Care 26:510–513
3. Balasubramanyam M, Premanand C, Mohan V (2002) The lymphocyte as a cellular model to study insights into the pathophysiology of diabetes and its complications. Ann NY Acad Sci 958:399–402
4. Otton R, Mendonca JR, Curi R (2002) Diabetes causes marked changes in lymphocyte metabolism. J Endocrinol 174:55–61
5. Delamaire M, Maugendre D, Moreno M, Le Goff MC, Allannic H, Genetet B (1997) Impaired leucocyte functions in diabetic patients. Diabet Med 14:29–34
6. Lindley S, Dayan CM, Bishop A, Roep BO, Peakman M, Tree TIM (2005) Defective suppressor function in CD4_CD25_ T-Cells from patients with type 1 diabetes. Diabetes 54:92–99
7. Hoffman WH, Helman SW, Passmore G (2001) Acute activation of peripheral lymphocytes during treatment of diabetic ketoacidosis. J Diabet Complicat 15:144–149
8. Seyfert-Margolis V, Gisler TD, Asare AL, Wang RS, Dosch HM, Brooks-Worrell B, Eisenbarth GS, Palmer JP, Greenbaum CJ, Gitelman S, Nepom G, Bluestone JA, Herold KC (2006) Analysis of T-Cell assays to measure autoimmune responses in subjects with type 1 diabetes. Diabetes 55:2588–2594
9. Arif S, Tree TI, Astill TP, Tremble JM, Bishop AJ, Dayan CM, Roep BO, Peakman M (2004) Autoreactive T cell responses show proinflammatory polarization in diabetes but a regulatory phenotype in health. J Clin Invest 113:451–463
10. Hill N, Sarvetnick N (1996) Cytokines: promoters and dampeners of autoimmunity. Curr Opin Immunol 14:791–792
11. Tiittanen M, Huupponen JT, Knip M, Vaarala O (2006) Insulin treatment in patients with Type 1 diabetes induces upregulation of regulatory T-cell markers in peripheral blood mononuclear cells stimulated with insulin in vitro. Diabetes 55:3446–3454
12. Giordano C, Panto F, Caruso C (1989) Interleukin-2 and soluble interleukin-2 receptor secretion defect in vitro in newly diagnosed type 1 diabetic patients. Diabetes 38:310–315
13. Cantrell DA, Smith KA (1984) The interleukin-2 T cell system: a new cell growth model. Science 224:1312–1316
14. Saltiel AR (1990) Second messengers of insulin action. Diabetes Care 13:244–256
15. Hunt P, Eardley DD (1986) Suppressive effects of insulin and insulin-like growth factor–1 (IGF1) on immune responses. J Immunol 136:3994–3999
16. Dandona P, Aljada A, Mohanty P (2002) The anti-inflammatory and potential anti-atherogenic effect of insulin: a new paradigm. Diabetologia 45:924–930
17. Jump DB (2002) The biochemistry of n-3 polyunsaturated fatty acids. J Biol Chem 277:8755–8758
18. Li Q, Wang M, Tan L, Wang C, Ma J, Li N, Xu G, Li J (2005) Docosahexaenoic acid changes lipid composition and interleukin-2 receptor signaling in membrane rafts. J Lipid Res 46:1904–1913
19. Harbige LS (1998) Dietary n-6 and n-3 fatty acids in immunity and autoimmune disease. Proc Nutr Soc 57:555–562
20. Kelly DS (2001) Modulation of human immune and inflammatory responses by dietary fatty acids. Nutrition 17:669–673
21. Jolly CA, Jiang YH, Chapkin RS, Mc Murray DN (1997) Dietary n-3 polyunsaturated fatty acids suppress murine lymphoproliferation, interleukin-2 secretion, and the formation of diacylglycerol and ceramide. J Nutr 127:37–43

22. Calder PC, Newsholme EA (1992) Polyunsaturated fatty acids suppress human peripheral blood lymphocyte proliferation and interleukin-2 production. Clin Sci 82:695–700
23. Stulnig TM (2003) Immunomodulation by polyunsaturated fatty acids: mechanisms and effects. Int Arch Allergy Immunol 132:310–321
24. Zeyda M, Szekeres AB, Saemann R, Geyeregger H, Stockinger H, Zlabinger GJ, Waldhausl W, Stulnig TM (2003) Suppression of T cell signaling by polyunsaturated fatty acids: selectivity in inhibition of mitogen-activated protein kinase and nuclear factor activation. J Immunol 170:6033–6039
25. Clarke SD (2001) Polyunsaturated fatty acid regulation of gene transcription: a molecular mechanism to improve the metabolic syndrome. J Nutr 131:1129–1132
26. Raza Shaikh S, Edidin M (2007) Immunosuppressive effects of polyunsaturated fatty acids on antigen presentation by human leukocyte antigen class I molecules. J Lipid Res 48:127–138
27. Arrington JL, Chapkin RS, Switzer KC, Morris JS, McMurray DN (2001) Dietary n-3 polyunsaturated fatty acids modulate purified murine T-cell subset activation. Clin Exp Immunol 123:1–10
28. Switzer KC, McMurray DN, Morris JS, Chapkin RS (2003) N-3 polyunsaturated fatty acids promote activation-induced cell death in murine T lymphocytes. J Nutr 133:496–503
29. Williams MS, Henkart PA (1996) Role of reactive oxygen intermediates in TCR-induced death of T cell blasts and hybridomas. J Immunol 157:2395–2402
30. Hildeman DA, Mitchell T, Teague TK (1999) Reactive oxygen species regulate activation-induced T cell apoptosis. Immunity 10:735–744
31. Cope AP (2002) Studies of T-cell activation in chronic inflammation. Arthritis Res 4:197–211
32. Aronson D (2008) Hyperglycemia and the pathobiology of diabetic complications. Adv Cardiol 45:1–16
33. Merzouk S, Hichami A, Madani S, Merzouk H, Yahia Berrouiguet A, Prost J, Moutairou K, Chabane-Sari N, Khan NA (2003) Antioxidant status and levels of different vitamins determined by HPLC in diabetic subjects with multiple complications. Gen Physiol Biophys 22:15–27
34. Merzouk S, Hichami A, Sari A, Madani S, Merzouk H, Yahia Berrouiguet A, Lenoir-Rousseaux JJ, Chabane-Sari N, Khan NA (2004) Impaired oxidant/antioxidant status and LDL-fatty acid composition are associated with increased susceptibility to peroxidation of LDL in diabetic patients. Gen Physiol Biophys 23:387–399
35. Purasiri P, Mckechnie A, Heys SD, Eremin O (1997) Modulation in vitro of human natural cytotoxicity, lymphocyte proliferative response to mitogens and cytokine production by essential fatty acids. Immunology 92:166–172
36. Mosmann T (1983) Rapid colorimetric assay for cellular growth and survival: application to proliferation and cytotoxicity assays. J Immunol Methods 65:55–63
37. Bligh EG, Dyer WJ (1959) A rapid method of total lipid extraction and purification. Can J Physiol Pharmacol 37:911–917
38. Aebi H (1974) Catalase. In: H U Bergmeyer (ed) Methods of enzymatic analysis, 2nd edn. Verlag Chemie GmbH, Weinheim, pp 673–684
39. Elstner EF, Youngman RJ, Obwald W (1983) Superoxide dismutase. In: H U Bergmeyer (ed) Methods of enzymatic analysis, 3rd edn. Verlag Chemie GmbH, Weinheim, vol 3 pp 293–302
40. Nourooz-Zadeh J, Tajaddini-Sarmadi J, Ling KLE, Wolff PS (1996) Low-density lipoprotein is the major carrier of lipid hydroperoxides in plasma. Relevance to determination of total plasma lipid hydroperoxide concentrations. Biochem J 313:781–786
41. Chen C, Lee WH, Yun P, Snow P, Liu CP (2003) Induction of autoantigen-specific Th2 and Tr1 regulatory T cells and modulation of autoimmune diabetes. J Immunol 171:733–744
42. Kretowski A, Mysliwiec J, Szelachowska M, Kinalski M, Kinalska I (1999) Insulin increases in vitro production of Th2 profile cytokines in peripheral blood cultures in subjects at high risk of diabetes type 1 and patients with newly diagnosed IDDM. Horm Metab Res 31:289 –292
43. Zhang P, Smith R, Chapkin RS, McMurray DN (2005) Dietary n-3 Polyunsaturated fatty acids modulate the Th1/Th2 balance towards the Th2 pole by suppression of Th1 development. J Nutr 135:1745–1751
44. Raza Shaikh S, Edidin M (2006) Polyunsaturated fatty acids, membrane organization, T cells, and antigen presentation. Am J Clin Nutr 84:1277–1289
45. Fan YY, Ly LH, Barhoumi R, McMurray DN, Chapkin RS (2004) Dietary docosahexaenoic acid suppresses T-cell protein kinase C-theta lipid raft recruitment and interleukin-2 production. J Immunol 173:6151–6160
46. Yaqoob P, Newsholme EA, Calder PC (1995) Influence of cell culture conditions on diet-induced changes in lymphocyte fatty acid composition. Biochim Biophys Acta 1255:333–340
47. Fidelus RK, Tsan MF (1986) Enhancement of intracellular glutathione promotes lymphocyte activation by mitogen. Cell Immunol 97:155–163

Lipids (2008) 43:499–506
DOI 10.1007/s11745-008-3171-8

ORIGINAL ARTICLE

Dietary Perilla Oil Inhibits Proinflammatory Cytokine Production in the Bronchoalveolar Lavage Fluid of Ovalbumin-Challenged Mice

**Hui-Hsiang Chang · Chin-Shun Chen ·
Jin-Yuarn Lin**

Received: 7 December 2007 / Accepted: 2 March 2008 / Published online: 2 April 2008
© AOCS 2008

Abstract To evaluate the anti-inflammatory effects of different dietary oils on ovalbumin-sensitized and -challenged mice. Experimental BALB/c mice were fed with different diets containing 5% corn oil [rich in linoleic acid, 18:2n-6 polyunsaturated fatty acids (PUFA), as a control diet], 5% perilla oil (rich in α-linolenic acid, 18:3n-3 PUFA) or 5% compound oil containing 50% corn oil and 50% perilla oil, for 5 consecutive weeks. The leukocyte count, inflammatory mediators, and cytokine levels, including proinflammatory and Th1/Th2 cytokines in the bronchoalveolar lavage fluid (BALF) from the mice were determined. The results showed that 5% compound oil administration significantly ($P < 0.05$) decreased eosinophilic infiltration. Dietary perilla oil could not significantly ($P > 0.05$) decrease the eosinophil accumulation or the secretions of inflammatory mediators such as prostaglandin E_2 (PGE_2), histamine, nitric oxide and eotaxin. However, dietary perilla oil significantly ($P < 0.05$) reduced proinflammatory cytokine (TNF-α, IL-1β and IL-6) and Th1 cytokine (IFN-γ and IL-2) production. The production of Th2 cytokine IL-10, but not IL-4 and IL-5, was also significantly inhibited by perilla oil administration. The results suggest that dietary perilla oil might alleviate inflammation via decreasing the secretion of pro-inflammatory cytokines in BALF, but failed to regulate the Th1/Th2 balance toward Th1 pole during the Th2-skewed allergic airway inflammation.

Keywords Perilla oil · n-3 Polyunsaturated fatty acids (PUFA) · Proinflammatory cytokines · Th1/Th2 balance · Ovalbumin-sensitized and -challenged mice

Introduction

In the modern Western dietary pattern there is an increase in the consumption of total fat and n-6 polyunsaturated fatty acids (PUFAs), but a decrease in n-3 PUFAs and antioxidants. The changes in dietary lipid patterns are potent promoters of many chronic diseases [1]. Asthma, one of the chronic inflammatory airway disorders may be related to dietary lipids [2]. Reasonably, daily modification of the dietary lipid pattern may alleviate asthmatic damage.

Asthma is recognized as a T-helper type 2 (Th2)-skewed allergic disease [3]. Th2-type cells are important in humoral immunity and defense against extracellular pathogens [4] via eosinophilic infiltration, as well as IgE and IgG1 production in vivo [5]. Th2-type cytokines include interleukin (IL)-4, IL-5, IL-6, IL-9, IL-10, and IL-13. IL-4 and IL-13 are implicated in isotype switching of B-cells to produce IgE. IL-5 promotes the differentiation, recruitment, and survival of eosinophils [6]. In contrast to the Th2 cells, Th1 cells are characterized by the production of IL-2, interferon (IFN)-γ and tumor necrosis factor (TNF)-α. Th1 cells promote cell-mediated immunity to destroy intracellular pathogens [4], inhibit eosinophilic infiltration, IgE and IgG1 production, and strengthen IgG2a production in vivo [5]. Th1-skewed immune responses are generally pro-inflammatory and may result in autoimmune

H.-H. Chang · C.-S. Chen · J.-Y. Lin (✉)
Department of Food Science and Biotechnology,
National Chung Hsing University, 250 Kuokuang Road,
Taichung 40227, Taiwan, ROC
e-mail: jinlin@nchu.edu.tw

H.-H. Chang
Department of Food Technology, Tajen University,
20 Weishin Road, Yanpu Shiang, Pingtung, Taiwan, ROC

and chronic inflammatory diseases. However, Th2-skewed immune responses may cause asthma and allergy [7]. Whether it is possible to maintain the Th1/Th2 balance through dietary modification, especially the dietary lipid pattern, is an important issue in immunology.

Many animal experiments and clinical intervention studies indicate that long-chain n-3 polyunsaturated fatty acids (PUFAs) such as eicosapentaenoic acid (EPA, 20:5n-3) and docosahexaenoic acid (DHA, 22:6n-3) from fish oil have anti-inflammation effects [8]. However, arachidonic acid (ARA, 20:4n-6), which is a component of phospholipids in the cell membrane, may produce ARA-derived eicosanoid inflammatory mediators, e.g. leukotriene (LT) B_4 and prostaglandin (PG) E_2 [9]. It has been found that EPA (n-3 PUFA) supplementation can replace ARA as an eicosanoid substrate to inhibit ARA metabolism and decrease inflammation status resulting from inflammatory eicosanoids [10].

In contrast to linoleic acid (18:2n-6), which is abundant in vegetable oils such as corn oil, and converted to ARA in animal cells [11], α-linolenic acid (ALNA, 18:3n-3), which exists in green leafy vegetables, as well as some seed and vegetable oils such as flaxseed oil and perilla oil, is a possible precursor of EPA and DHA. However, ALNA use to replicate the effects of EPA or DHA is still not properly justified in vivo. Perilla oil is obtained from the seeds of *Perilla frutescenes*, and exhibits high n-3 fatty acid ALNA bioavailability [12]. Perilla oil consists of about 50–60% ALNA in the form of triglycerides. ALNA has been recognized as an essential fatty acid in nutrition [13]. Increase uptakes of ALNA have similar effects as EPA and DHA on health and chronic disease control [14]. Weanling NIN wistar rats that consumed 10% perilla seed oil in their diet for 18 weeks suffered no toxicological effects [15]. Generally, perilla oil is valuable more for its medicinal benefit than its flavor, such as uses for chemopreventive effects on tumors [16] and plasma triacylglycerol level [17]. Recently, Kim and Choi [18] indicated that dietary perilla oil showed effects similar to that of fish oil on EPA and DHA accumulation in the hepatic membrane fraction of male Sprague Dawley rats. Perilla seeds are widely used to treat asthma in traditional Chinese medicine. However, the medicinal effects of dietary perilla oil administration on asthmatic airway inflammation have been scarcely discussed. As perilla oil is rich in ALNA, we hypothesized that it has physiological effects, especially in immunomodulation, like EPA and DHA. Thus, perilla oil was selected for study.

This study evaluated the anti-inflammatory and immuno-modulatory potential of perilla oil (rich in n-3 PUFA) using ovalbumin (OVA)-sensitized and -challenged allergic inflammatory murine models. The diet consisted of 5% corn oil (rich in linoleic acid, 18:2n-6) as the control diet. The immune responses in the bronchoalveolar lavage fluid (BALF) from the experimental mice were determined to evaluate the effects of perilla oil administration on airway inflammation and allergic characteristics.

Methods

Materials, Experimental Animals and Feeds

The experimental feed was prepared according to the recommendation of the American Institute of Nutrition AIN-76 [19] and varied only in lipid composition. The basic composition of each feed, expressed in g/100 g, contained 40 g sucrose, 25 g corn starch, 20 g casein, 5 g fiber, 3.5 g mineral mixture, 1 g vitamin mixture, 0.3 g DL-methionine, 0.2 g choline bitartrate and 5 g lipid. The components of each feed were thoroughly mixed and stored at −20°C. There were three kinds of lipid used in the experiment. Perilla oil (PER) rich in α-linolenic acid (>60.5%) was purchased from MasterAsia Marketing Co. (Taipei, Taiwan, ROC) as the source of n-3 fatty acid. Corn oil (COR) rich in linoleic acid but poor in α-linolenic acid (<2%) was purchased from Chang Chi Foodstuff Factory Co. (Taichung, Taiwan, ROC) as a control and the source of n-6 fatty acids. Compound oil (COR-PER) was a mixture containing 50% corn oil and 50% perilla oil.

Female BALB/c ByJNarl mice (6 weeks old) were obtained from the National Laboratory Animal Center, National Applied Research Laboratories, National Science Council in Taipei, ROC and maintained at the Department of Food Science and Biotechnology at National Chung Hsing University College of Agriculture and Natural Resources in Taichung, Taiwan, ROC. The animal room was kept on a 12-h light and 12-h dark cycle. Constant temperature (25 ± 2°C) and humidity were maintained. The mice were housed and kept on a chow diet (laboratory standard diet) to acclimatize for 2 weeks before feeding the experimental diet. After this equilibrium period, the mice were divided into four groups varied by oil source and sensitized treatments: non-sensitized control (PBS/COR, $n = 12$), dietary control (OVA/COR, $n = 8$), OVA/COR-PER ($n = 8$) and OVA/PER ($n = 9$). Each group was fed with the specified experimental diets for 5 consecutive weeks. Mice food intake and body weight were measured twice a week during the study period. There were no differences in food intake, feed efficiency and body weight gain between the four groups.

OVA-Sensitized and -Challenged Allergic Inflammation Murine Model

To test the effects of n-3 and/or n-6 fatty acids on airway inflammation, the mice (8 weeks old) were sensitized and challenged to induce allergic airway inflammation. The mouse allergic airway inflammation model was manipulated as described by Lin et al. [20] and Ye et al. [21]. In brief, the mice were sensitized using an intraperitoneal injection (i.p.) of 0.2 ml alum-precipitated antigen containing 8 μg of ovalbumin (OVA, albumin chicken egg grade III, Sigma A-5378, MO, USA) and 2 mg $Al(OH)_3$ to induce primary immunity after supplementation of the specified experimental diets for 1 week. Two booster injections of this alum-OVA mixture were given 7 and 14 days later, respectively. Non-sensitized control mice received alum–phosphate-buffered saline (PBS, 137 mM NaCl, 2.7 mM KCl, 8.1 mM Na_2HPO_4, 1.5 mM KH_2PO_4, pH 7.2–7.4, 0.2 μm filtered) only. One week later, the mice were then challenged by aerosolized OVA at a concentration of 5 mg OVA per milliliter PBS for 60 min, twice at 3 day intervals and repeated twice in 24 h. The aerosolized OVA were produced using an ultrasonic nebulizer (sw918, Shinmed). Non-sensitized control mice received PBS only. Two days later, the animals were anesthetized with diethyl ether, exsanguinated using retro-orbital venous plexus puncture and immediately euthanized using CO_2 inhalation. The bronchoalvelor lavage fluid (BALF) was collected and assayed for cytokines and other inflammatory mediators. The experimental design is given in Fig. 1.

Collection of BALF and Cellular Differential Counts

The BALF collection and differential cell counts were modified from the methods described by Ye et al. [21]. The mice were anesthetized with diethyl ether, exsanguinated using retro-orbital venous plexus puncture and immediately euthanized using CO_2 inhalation. Using a cannula, their lungs were immediately lavaged through the trachea with 5 aliquots of 0.6 ml Hank's balanced salts solution (HBSS) which was free of ionized calcium and magnesium (HyClone). The bronchoalveolar lavage fluid (BALF) was centrifuged at 400*g* for 10 min at 4°C. The supernatant (BALF) volume was determined and stored at −70°C for future assay. The cell pellet was resuspended in minimum essential medium (MEM, HyClone) containing 10% bovine serum albumin (HyClone) and the final cell density was 1×10^6 cells/ml. Total cells counts were determined with a hemocytometer using the trypan blue dye exclusion method. Cytocentrifuged preparations were stained with Liu's stain for differential cell counts. Based on standard morphologic criteria, a minimum of 200 cells were counted and classified as macrophages, lymphocytes, or eosinophils.

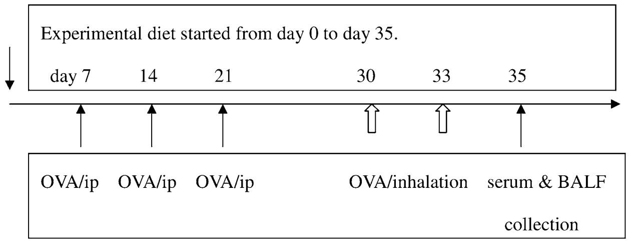

Fig. 1 Sensitization and challenge protocols for inducing allergic airway inflammation. Mice were sensitized with OVA/alum at days 7, 14, 21. The sensitized mice were then challenged twice with aerosolized OVA for 60 min at days 30, 33. The challenge was administered twice a day. All experimental mice were sacrificed at day 35 and their bronchoalveolar lavage fluids (BALF) were collected and analyzed

Assay Inflammatory Mediators in BALF

Histamine

The BALF histamine level was determined using the Histamine-ELISA kit (Cat. No. A05890, SPI-BIO). The procedure was carried out according to the manufacturer's instructions for use.

Prostaglandin E_2 (PGE_2)

The BALF PGE_2 level was determined using the competitive enzyme immunoassay method (Prostaglandin E_2 Express EIA Kit, Cat. No.500141, Cayman).

Nitric Oxide (NO)

Aliquots of 80 μl BALF samples and standards (0–100 μM sodium nitrite (Sigma S-2252) dissolved in double distilled water) were pipetted into the 96-microplate wells (Nunc). Aliquots of 160 μl Griess reagent were then added into each well to develop the color. The Griess reagent was freshly prepared from Reagent A and B at a ratio of 1:1 (Reagent A: 2% (w/v) sulfanilamide (Sigma S-9251) dissolved in 2.5% (v/v) phosphoric acid; Reagent B: 0.2% (w/v) *N*-1-naphthylethylene diamide dihydrochloride (Sigma N-9125) dissolved in 2.5% (v/v) phosphoric acid). After incubation for 10 min, the plate was read on a plate reader (ELISA reader, ASYS/HITECH Jupiter) at 540 nm. Using the standard curve, the NO concentration for each unknown sample was determined.

Protein

The BALF protein content was analyzed using the Bio-Rad protein assay dye reagent concentrate (Cat. no. 500-0006), according to the accompanying instructions, using a 96-well micro-titre plate.

Measurement of Cytokine and Chemokine Levels in BALF by an ELISA

IL-1β, IL-2, IL-4, IL-5, IL-6, IL-10, IFN-γ and TNF-α

Cytokine (IL-1β, IL-2, IL-4, IL-5, IL-6, IL-10, IFN-γ, TNF-α) levels in BALF were determined using sandwich ELISA kits, respectively. The IL-1β, IL-2, IL-4, IL-5, IL-6, IL-10, IFN-γ and TNF-α concentrations were assayed according to the cytokine ELISA protocol of manufacturer's instructions (mouse DuoSet ELISA Development system, R&D Systems). The sensitivity of these cytokine assays was <15.6 pg/ml.

Eotaxin

The BALF eotaxin concentration was determined using the mouse eotaxin sandwich ELISA kit (Quantikine M murine, R&D Systems). The eotaxin concentration was assayed according to the manufacturer's instructions. The sensitivity of this assay was <15.6 pg/ml.

Statistical analysis

Data were expressed as means ± SD. Data within OVA-sensitized treatment are analyzed using analysis of variance (ANOVA) followed by Duncan's test. Data between the dietary control and non-sensitized control are analyzed using unpaired Student's *t*-test. Differences between the dietary control and non-sensitized control or among OVA-sensitized groups were considered statistically significant if $P < 0.05$.

Table 1 Effects of OVA-sensitization and -challenge on differential indicators in bronchoalveolar lavage fluid (BALF) from BALB/c experimental mice

Indicators in BALF	Treatments	
	PBS/COR	OVA/COR
Cellularity		
Total cells ($\times 10^5$/mouse)	5.7 ± 3.4	21.5 ± 14.4*
Monocytes/macrophages (%)	86.3 ± 11.7	32.2 ± 11.5*
Lymphocytes (%)	11.7 ± 11.3	1.87 ± 1.69
Eosinophils (%)	1.9 ± 1.1	65.9 ± 12.4*
Inflammatory mediators		
Protein (μg/mouse)	266 ± 96	368 ± 139
Eotaxin (pg/mouse)	270 ± 108	356 ± 107
PGE_2 (ng/mouse)	1.18 ± 0.80	6.75 ± 3.95*
Histamine (pmol/mouse)	10.40 ± 3.94	9.79 ± 3.55
Nitric oxide (nmol/mouse)	5.10 ± 1.57	5.68 ± 2.83
Pro-inflammatory cytokines		
IL-1β (pg/mouse)	34.3 ± 26.5	29.6 ± 19.6
TNF-α (pg/mouse)	280 ± 223	216 ± 128
IL-6 (pg/mouse)	289 ± 204	257 ± 134
Th1-type cytokines		
IFN-γ (pg/mouse)	118.6 ± 104.8	77.6 ± 56.5
IL-2 (pg/mouse)	155 ± 92	167 ± 46
Th2-type cytokines		
IL-4 (pg/mouse)	161 ± 90	161 ± 84
IL-5 (pg/mouse)	265 ± 196	222 ± 110
IL-10 (pg/mouse)	548 ± 315	418 ± 190

Data are presented as means ± SD (n = 6–9). Asterisk (*) means significantly ($P < 0.05$) different from the PBS/COR group within the same row analyzed using unpaired Student's *t*-test

Results

The OVA-Sensitization and -Challenge Effects on Differential Indicators in Bronchoalveolar Lavage Fluid (BALF) from BALB/c Experimental Mice

The OVA-sensitization and -challenge effects on differential indicators in BALF from BALB/c experimental mice are shown in Table 1. The results showed that sensitization and challenge with OVA significantly ($P < 0.05$) increased an influx of total leukocytes (increase from 5.7 ± 3.4 × 10^5 to 21.5 ± 14.4 × 10^5 cells/mouse) into the lungs and airways. Challenge with OVA significantly increased an infiltration of eosinophils (increase from 1.9 ± 1.1 to 65.9 ± 12.4%) but decreased the monocytes/macrophages (decrease from 86.3 ± 11.7 to 32.2 ± 11.5%) infiltration into the lungs and airways. Challenge with OVA also significantly increased PGE_2 (increase from 1.18 ± 0.80 to 6.75 ± 3.95 ng/mouse) secretion into the lungs and airways. However, the other measured BALF indicators did not significantly change after OVA sensitization and challenge (OVA/COR group) compared to the sensitization control (PBS/COR) group.

Effects of Different Dietary Oil on Cellularity of BALF from OVA-Sensitized and -Challenged Mice

Effects of different dietary oils on cellularity of BALF from OVA-sensitized and -challenged mice are shown in Table 2. Total leukocyte count in BALF from experimental mice that consumed the diet containing perilla oil (OVA/COR-PER, OVA/PER) did not significantly change compared to the dietary control (OVA/COR). Among the OVA-sensitized and -challenged groups, dietary compound oil (COR-PER) significantly increased the percentage of monocytes/macrophages (increase from 32.2 ± 11.5 to 52.7 ± 18.8%), whereas decreased that of eosinophils

Table 2 Effects of different dietary oil on total leukocytes and cell distributions in bronchoalveolar lavage fluid (BALF) from OVA-sensitized and -challenged BALB/c mice

Groups	Total cells ($\times 10^5$/mouse)	Monocytes/macrophages (%)	Lymphocytes (%)	Eosinophils (%)
OVA/COR	21.5 ± 14.4	32.2 ± 11.5^a	1.87 ± 1.69	65.9 ± 12.4^b
OVA/COR-PER	17.0 ± 9.7	52.7 ± 18.8^b	0.71 ± 0.82	46.6 ± 18.1^a
OVA/PER	34.1 ± 16.6	29.1 ± 14.8^a	2.69 ± 2.90	68.3 ± 16.8^b

Data are presented as means ± SD ($n = 6$–9). Data within the same column not sharing the same superscript letters are significantly different ($P < 0.05$) from each other analyzed using analysis of variance (ANOVA) followed by Duncan's test

Table 3 Effects of different dietary oil on protein and eotaxin levels in bronchoalveolar lavage fluid (BALF) from OVA-sensitized and -challenged BALB/c mice

Groups	Protein (μg/mouse)	Eotaxin (pg/mouse)
OVA/COR	368 ± 139	356 ± 107
OVA/COR-PER	412 ± 142	371 ± 124
OVA/PER	478 ± 63	442 ± 174

Data are presented as means ± SD ($n = 6$–10). Data within the same column are analyzed by analysis of variance (ANOVA) followed by Duncan's test. There is no significant difference among groups. The sensitivity of eotaxin kit was about <7.8 pg/ml

(decrease from 65.9 ± 12.4 to 46.6 ± 18.1%) in BALF. The percentages of lymphocytes in BALF did not significantly differ among groups.

Effects of Different Dietary Oil on Inflammatory Mediator Levels in BALF from OVA-Sensitized and -Challenged Mice

Effects of different dietary oil on eotaxin and protein levels in BALF are shown in Table 3. Effects of different dietary oil on inflammatory mediator levels in BALF are shown in Table 4. The results showed that perilla oil administration did not significantly affect protein, eotaxin, and inflammatory mediator levels in BALF.

Table 4 Effects of different dietary oil on inflammatory mediators of bronchoalveolar lavage fluid (BALF) from OVA-sensitized and -challenged BALB/c mice

Groups	PGE_2 (ng/mouse)	Histamine (pmol/mouse)	Nitric oxide (nmol/mouse)
OVA/COR	6.75 ± 3.95	9.79 ± 3.55	5.68 ± 2.83
OVA/COR-PER	8.21 ± 6.65	10.15 ± 6.95	5.41 ± 1.47
OVA/PER	10.91 ± 5.04	12.28 ± 3.80	5.87 ± 1.70

Data are presented as means ± SD ($n = 6$–11). Data within the same column are analyzed by analysis of variance (ANOVA) followed by Duncan's test. There is no significant difference among groups. The detection limit of the kits used in this study: PGE_2 36 pg/ml; Histamine 0.5 nM

Table 5 Effects of different dietary oils on the levels of pro-inflammatory cytokines IL-1β, TNF-α and IL-6 in bronchoalveolar lavage fluid (BALF) from OVA-sensitized and -challenged BALB/c mice

Groups	IL-1β (pg/mouse)	TNF-α (pg/mouse)	IL-6 (pg/mouse)
OVA/COR	29.6 ± 19.6^b	216 ± 128^b	257 ± 134^b
OVA/COR-PER	24.7 ± 6.3^{ab}	178 ± 52^{ab}	227 ± 45^{ab}
OVA/PER	12.5 ± 7.1^a	108 ± 60^a	141 ± 53^a

Data are presented as means ± SD ($n = 6$–11). Data within the same column not sharing the same superscript letters are significantly different ($P < 0.05$) from each other analyzed using analysis of variance (ANOVA) followed by Duncan's test

Effects of Different Dietary Oil on the Levels of Pro-inflammatory Cytokines in BALF from OVA-Sensitized and -Challenged Mice

Table 5 shows the effects of different dietary oil on the levels of pro-inflammatory cytokines IL-1β, TNF-α and IL-6 in BALF from OVA-sensitized and -challenged mice through 5 weeks feeding. Sensitization and challenge with OVA did not significantly influence the secretion of pro-inflammatory cytokines, but dietary perilla oil significantly decreased these pro-inflammatory cytokines levels in BALF of OVA-sensitized and -challenged mice.

Effects of Different Dietary Oils on the Levels of Th1/Th2 Cytokines in BALF from OVA-Sensitized and -Challenged Mice

To evaluate the effects of different dietary oils on the secretion of Th1/Th2 cytokines in the local tissues of lungs and airways, the amounts of Th1 cytokines (IFN-γ and IL-2) and Th2 cytokines (IL-4, IL-5 and IL-10) in BALF were measured (Tables 6, 7). Dietary perilla oil significantly decreased the levels of Th1 cytokines in BALF; IFN-γ level decreased from 77.6 ± 56.5 to 21.9 ± 27.5 pg/mouse and IL-2 level decreased from 153 ± 42 to 110 ± 28 pg/mouse (Table 6). The levels of Th2 cytokines IL-4, IL-5, and IL-10 in BALF from experimental mice

Table 6 Effects of different dietary oils on the levels of Th1-type cytokines in bronchoalveolar lavage fluid (BALF) from OVA-sensitized and -challenged BALB/c mice

Group	IFN-γ (pg/mouse)	IL-2 (pg/mouse)
OVA/COR	77.6 ± 56.5^{b}	153 ± 42^{ab}
OVA/COR-PER	67.7 ± 19.7^{b}	175 ± 64^{b}
OVA/PER	21.9 ± 27.5^{a}	110 ± 28^{a}

Data are presented as mean ± SD ($n = 6$–11). Data within the same column not sharing the same superscript letters are significantly different ($P < 0.05$) from each other analyzed using analysis of variance (ANOVA) followed by Duncan's test

Table 7 Effects of different dietary oil on the levels of Th2-type cytokines in bronchoalveolar lavage fluid (BALF) from OVA-sensitized and -challenged BALB/c mice

Group	IL-4 (pg/mouse)	IL-5 (pg/mouse)	IL-10 (pg/mouse)
OVA/COR	161 ± 84	222 ± 110	418 ± 190^{b}
OVA/COR-PER	174 ± 34	206 ± 43	378 ± 84^{ab}
OVA/PER	121‘± 31	137 ± 55	242 ± 92^{a}

Data are presented as means ± SD ($n = 6$–11). Data within the same column not sharing the same superscript letters are significantly different ($P < 0.05$) from each other analyzed using analysis of variance (ANOVA) followed by Duncan's test

were decreased by dietary perilla oil administration (Table 7). Especially, IL-10 levels significantly decreased (decrease from 418 ± 190 to 242 ± 92 pg/mouse).

Effects of Different Dietary Oils on the Secretion Ratios of Th1/Th2 Cytokines in BALF from OVA-Sensitized and -Challenged Mice

To compare the secretion ratios between Th1and Th2 cytokine levels in BALF, the secretion ratios of Th1/Th2 cytokine displayed as IFN-γ/IL-4, IFN-γ/IL-5 and IFN-γ/(IL-4 + IL-5) are shown in Fig. 2. The results showed that sensitization and challenge with OVA slightly decreased the secretion ratio of Th1/Th2 cytokine in BALF. However, dietary perilla oil administration significantly decreased the secretion ratios of Th1/Th2 cytokines in BALF (IFN-γ/IL-4, decrease from 0.49 ± 0.32 to 0.15 ± 0.17; IFN-γ/IL-5, decrease from 0.36 ± 0.06 to 0.12 ± 0.13; IFN-γ/(IL-4 + IL-5), decrease from 0.18 ± 0.10 to 0.07 ± 0.08).

Discussion

The purpose of this study was to evaluate the effects of perilla oil administration on airway inflammation using an allergic asthma animal model. The established animal model significantly increased the flux of total leukocytes, especially eosinophils, as well as PGE_2 release into the bronchoalveolar tissues (Table 1), and slightly increased the Th2-skewed inclination in BALF (Fig. 2) compared to OVA/COR with the PBS/COR group. The levels of non-specific and anti-OVA specific IgE were significantly increased in the sera after OVA-sensitization and -challenge treatments (data not shown). Mice sensitized and challenged with OVA exhibited asthma-like symptoms [20], e.g. allergic airway inflammation, infiltration of differential cells, such as eosinophils, into the lungs and airways, and chemical mediator releases including inflammatory eicosanoids, histamine, Th1/Th2 cytokines, nitric oxide (NO), or eotaxin [3]. This study suggests that an intermediate airway inflammation mouse model was achieved. This airway inflammation mouse model (Fig. 1) might be suitable for evaluating the effects of different dietary lipids on the airway inflammation in vivo. Unfortunately, no significant up-regulation of cytokines occurred as expected in BALF in the established experimental animal model (Table 1). Undoubtedly, this might limit the results interpretation and relevance. Therefore, cytokine levels secreted by lymphocytes from the spleen or other lymphoid organs remain to be further clarified to compensate for the lack in the model.

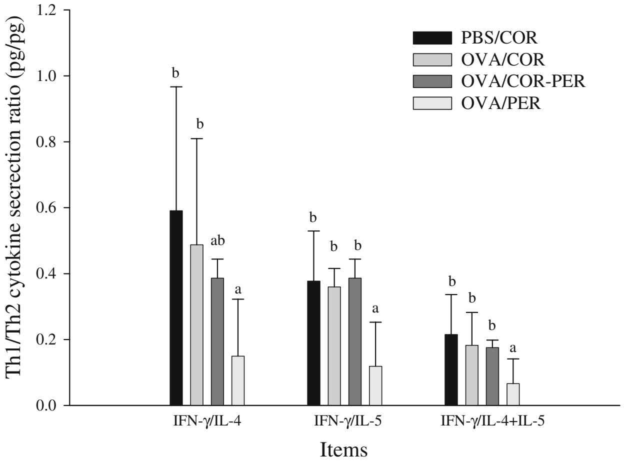

Fig. 2 Effects of different dietary oils on Th1/Th2 cytokine secretion ratios in bronchoalveolar lavage fluid (BALF) from BALB/c mice in an OVA-sensitized and -challenged asthmatic murine model. Data are presented as mean ± SD ($n = 6$–11). Within the same Th1/Th2 cytokine item not sharing the same letters are significantly different ($P < 0.05$) from each other analyzed using analysis of variance (ANOVA) followed by Duncan's test

In this study perilla oil rich in ALNA (18:3n-3) and corn oil rich in linoleic acid (18:2n-6) were selected and subjected to the allergic airway inflammation animal study. The compound oil consisted of n-3/n-6 fatty acid (PER/COR) exhibited the best anti-allergic effects via significantly decreasing eosinophils, but increasing monocytes/macrophages infiltration into the airways (Table 2). Although lymphocytes in BALF did not significantly change, the decrease in eosinophilic infiltration suggested that compound oil (COR-PER) administration might remodel the inflammatory condition of the airways via decreasing vasodilation, mucus hypersecretion and bronchoconstriction [22, 23]. However, perilla oil administration alone could not significantly change the eosinophilic infiltration status in the airways. The anti-eosinophilic infiltration effect mechanism using a mixture of perilla and corn oils remains to be further clarified. To further clarify the effects of n-3 or n-6 PUFA, this study suggests that an ovalbumin sensitized group fed a diet supplemented with 5% of oil not rich in n-3 or n-6 fatty acids should be added. The added group will be helpful to further decipher the anti-inflammatory effects due to the anti-inflammatory effects of n-3 fatty acids or the lack of inflammatory effects of n-6 fatty acids.

The suppressive effects of n-3 PUFAs, such as EPA and DHA, on the production of arachidonic acid-derived eicosanoids have been reported [2, 24, 25]. Perilla oil was proposed to have anti-inflammatory potential for its high bioavailability of the n-3 fatty acid ALNA (18:3n-3) [12]. Contrary to our hypothesis, dietary perilla oil did not significantly affect the levels of inflammatory mediators in BALF such as protein, eotaxin, PGE_2, histamine, and nitric oxide (Tables 3, 4). Although the n-3 PUFAs such as EPA and DHA inhibit the production of inflammatory eicosanoids [24, 25], the synthesis of EPA and DHA from their precursor ALNA (18:3n-3) is low efficiency in cells [26, 27]. This study further hypothesized that ALNA (n-3, PUFA) from perilla oil having lower anti-eicosanoid effects than those of EPA and DHA (n-3, PUFA) from fish oil might result from its low conversion efficiency from ALNA to EPA and DHA in vivo. The low conversion efficiency from ALNA to EPA and DHA in vivo might decrease the anti-eicosanoid effect of perilla oil. To further clarify whether or not the ALNA in the perilla oil is converted to EPA or DHA and speculate the mechanisms by which EPA and DHA may cause immuno-modulation, the tissue fatty acid composition of experimental mice should be analyzed. Unfortunately, this study did not analyzed the fatty acid composition in relevant cells or tissues. However, Kim and Choi (2005) have analyzed fatty acid composition in tissues and have demonstrated that both dietary corn oil (rich in C18:2n-6, 57.29%) and dietary perilla oil (rich in C18:3n-3, 61.49%) indeed reflected their fatty acid composition upon hepatic microsomal phospholipids of male Sprague–Dawley rats either through 4-day feeding or 4-week feeding [18]. They reported that total n-6 and n-3 fatty acid composition in hepatic microsomal phospholipids of the experimental rats, fed with 10% corn oil and 10% perilla oil diet through 4-day feeding, were 46.85% (Σn-6), and 4.47% (Σn-3), as well as 32.57% (Σn-6), and 22.58% (Σn-3, including considerable EPA and DHA), respectively [18]. Comparatively the fatty acid composition of C20:4 in the analyzed tissue were 30.10 and 17.73%, respectively [18]. Although only 5% perilla oil diet was used in this study, this study suggests that the anti-inflammatory activity of dietary perilla oil might be partially via increasing n-3 fatty acid composition, but decreasing C20:4 (arachidonic acid) composition in vivo.

To further elucidate the effects of dietary perilla oil administration on cytokine secretions in BALF, pro-inflammatory cytokines including IL-1β, IL-6 and TNF-α, and Th1/Th2 cytokines were determined. The results revealed that dietary perilla oil administration significantly inhibits the production of pro-inflammatory cytokines, IL-1β, IL-6 and TNF-α, in BALF (Table 5). Undoubtedly, perilla oil administration exhibited anti-inflammatory potential via inhibiting the production of pro-inflammatory cytokines. Since the fatty acid composition (purity) in perilla oil was >99.9%, this study suggests that the effective components in perilla oil are fatty acids but not other components. However, the effective components in perilla oil and their immuno-regulatory mechanism should be further clarified.

Furthermore, this study showed that both Th1 (IFN-γ and IL-2) and Th2 (IL-10), especially Th1 cytokine secretions were significantly inhibited by dietary perilla oil, suggesting that perilla oil administration might also have immunosuppressive effects on Th1 cells from OVA-sensitization and -challenge mice (Tables 6, 7). IL-10 is generally synthesized in a lower level at the late stage of inflammation [28, 29] to inhibit Th1 cell and delayed-type hypersensitivity responses [6]. Thus, the decrease in Th1 cytokine production might also result in a significant decrease of IL-10 production in vivo. Recent evidences have indicated that lipid micro domains in the T-cell plasma membrane are remodeled using a dietary lipid consisting of n-3 PUFA, EPA and DHA [30–33]. Long-chain n-3 PUFAs suppress Th1-cell, but not Th2-cell, development [34, 35], and modulate the Th1/Th2 balance toward the Th2 pole [36–38]. The results from this study also exhibited that perilla oil, which is rich in ALNA (n-3 PUFA), regulated the Th1/Th2 balance toward to Th2-skewed inclination in the asthmatic model as compared to corn oil (rich in n-6 PUFA) administration (Fig. 2). The Th2-skewed immune response is disadvantage to allergic diseases.

In conclusion, the results from this study showed that perilla oil administration might alleviate bronchoalveolar inflammation by decreasing the secretion of pro-inflammatory cytokines (TNF-α, IL-1β and IL-6) and Th1 cytokines (IFN-γ and IL-2) into the local lung and airway tissues, but failed to regulate the Th1/Th2 balance toward the Th1 pole during the Th2-skewed allergic airway inflammation.

References

1. Simopoulos AP (2002) The importance of the ratio of omega-6/omega-3 essential fatty acids. Biomed Pharmacother 56:365–379
2. Spector SL, Surette ME (2003) Diet and asthma: has the role of dietary lipids been overlooked in the management of asthma? Ann Allergy Asthma Immunol 90:371–377
3. Kay AB (2003) Immunomodulation in asthma: mechanisms and possible pitfalls. Curr Opin Pharmacol 3:220–226
4. Opal SM, DePalo VA (2000) Anti-inflammatory cytokines. Chest 117:1162–1172
5. Morokata T, Ishikawa J, Yamada T (1999) Differential susceptibility of C57BL/6 and DBA/2 mice to ovalbumin-induced pulmonary eosinophilia regulated by Th1/Th2-type cytokines. Immunol Lett 70:127–134
6. Riffo-Vasquez Y, Spina D (2002) Role of cytokines and chemokines in bronchial hyperresponsiveness and airway inflammation. Pharmacol Ther 94:185–211
7. Kidd P (2003) Th1/Th2 balance: the hypothesis, its limitations, and implications for health and disease. Altern Med Rev 8:223–246
8. Calder PC, Yaqoob P, Thies F, Wallace FA, Miles EA (2002) Fatty acids and lymphocyte functions. Br J Nutr 87:S31–48
9. Wong KW (2005) Clinical efficacy of n-3 fatty acid supplementation in patients with asthma. J Am Diet Assoc 105:98–105
10. Calder PC (2005) Polyunsaturated fatty acids and inflammation. Biochem Soc Trans 33:423–427
11. Burdge GC, Calder PC (2005) Conversion of alpha-linolenic acid to longer-chain polyunsaturated fatty acids in human adults. Reprod Nutr Dev 45:581–597
12. Kurowska EM, Dresser GK, Deutsch L, Vachon D, Khalil W (2003) Bioavailability of omega-3 essential fatty acids from perilla seed oil. Prostaglandins Leukot Essent Fatty Acids 68:207–212
13. Burdge GC (2006) Metabolism of α-linolenic acid in humans. Prostaglandins Leukot Essent Fatty Acids 75:161–168
14. Simopoulos AP (1991) Omega-3 fatty acids in health and disease and in growth and development. Am J Clin Nutr 54:438–463
15. Longvah T, Deosthale YG, Kumar PU (2000) Nutritional and short term toxicological evaluation of perilla seed oil. Food Chem 70:13–16
16. Futakuchi M, Cheng JL, Hirose M, Kimoto N, Cho YM, Iwata T, Kasai M, Tokudome S, Shirai T (2002) Inhibition of conjugated fatty acids derived from safflower or perilla oil of induction and development of mammary tumors in rats induced by 2-amino-1-methyl-6-phenylimidazo[4,5-b]pyridine (PhIP). Cancer Lett 178:131–139
17. Kim HK, Choi S, Choi H (2004) Suppression of hepatic fatty acid synthase by feeding α-linolenic acid rich perilla oil lowers plasma triacylglycerol level in rats. J Nutr Biochem 15:485–492
18. Kim HK, Choi H (2005) Stimulation of acyl-CoA oxidase by α-linolenic acid-rich perilla oil lowers plasma triacylglycerol level in rats. Life Sci 77:1293–1306
19. AIN (1977) Report of the American Institute of Nutrition ad hoc Committee on Standards for Nutritional Studies. J Nutr 107:1340–1348
20. Lin JY, Chen ML, Lin BF (2006) *Ganoderma tsugae* in vivo modulates Th1/Th2 and macrophage responses in an allergic murine model. Food Chem Toxicol 44:2025–2032
21. Ye YL, Huang WC, Lee YL, Chiang BL (2002) Interleukin-12 inhibits eotaxin secretion of cultured primary lung cells and alleviates airway inflammation in vivo. Cytokine 19:76–84
22. Kay AB, Phipps S, Robinson DS (2004) A role for eosinophils in airway remodelling in asthma. Trends Immunol 25:477–482
23. Wills-Karp M, Karp CL (2004) Eosinophils in asthma: remodeling a tangled tale. Science 305:1726–1729
24. Calder PC (2006) n-3 Polyunsaturated fatty acids, inflammation, and inflammatory diseases. Am J Clin Nutr 83:S1505–1519
25. Mickleborough TD, Murray RL, Ionescu AA, Lindley MR (2003) Fish oil supplementation reduces severity of exercise-induced bronchoconstriction in elite athletes. Am J Respir Crit Care Med 168:1181–1189
26. Deckelbaum RJ, Worgall TS, Seo T (2006) n-3 Fatty acids and gene expression. Am J Clin Nutr 83:S1520–1525
27. Cunnane SC (2003) Problems with essential fatty acids: time for a new paradigm? Prog Lipid Res 42:544–568
28. Lin JY, Tang CY (2007) Interleukin-10 administration inhibits TNF-α and IL-1β, but not IL-6 secretion of LPS-stimulated peritoneal macrophages. J Food Drug Anal 15:48–54
29. Lin JY, Lai YS, Liu CJ, Wu AR (2007) Effects of lotus plumule supplementation before and following systemic administration of lipopolysaccharide on the splenocyte responses of BALB/c mice. Food Chem Toxicol 45:486–493
30. Fan YY, McMurray DN, Ly LH, Chapkin RS (2003) Dietary (n-3) polyunsaturated fatty acids remodel mouse T-cell lipid rafts. J Nutr 133:1913–1920
31. Diaz O, Berquand A, Dubois M, Di Agostino S, Sette C, Bourgoin S, Lagarde M, Nemoz G, Prigent AF (2002) The mechanism of docosahexaenoic acid-induced phospholipase D activation in human lymphocytes involves exclusion of the enzyme from lipid rafts. J Biol Chem 277:39368–39378
32. Jolly CA, Jiang YH, Chapkin RS, McMurray DN (1997) Dietary (n-3) polyunsaturated fatty acids suppress murine lymphoproliferation, interleukin-2 secretion, and the formation of diacylglycerol and ceramide. J Nutr 127:37–43
33. Stulnig TM, Huber J, Leitinger N, Imre EM, Angelisova P, Nowotny P, Waldhausl W (2001) Polyunsaturated eicosapentaenoic acid displaces proteins from membrane rafts by altering raft lipid composition. J Biol Chem 276:37335–37340
34. Switzer KC, McMurray DN, Morris JS, Chapkin RS (2003) (n-3) Polyunsaturated fatty acids promote activation-induced cell death in murine T lymphocytes. J Nutr 133:496–503
35. Switzer KC, Fan YY, Wang N, McMurray DN, Chapkin RS (2004) Dietary n-3 polyunsaturated fatty acids promote activation-induced cell death in Th1-polarized murine CD4+ T-cells. J Lipid Res 45:1482–1492
36. Zhang P, Smith R, Chapkin RS, McMurray DN (2005) Dietary (n-3) polyunsaturated fatty acids modulate murine Th1/Th2 balance toward the Th2 pole by suppression of Th1 development. J Nutr 135:1745–1751
37. Ly LH, Smith R, Switzer KC, Chapkin RS, McMurray DN (2006) Dietary eicosapentaenoic acid modulates CTLA-4 expression in murine CD4+ T-cells. Prostaglandins Leukot Essent Fatty Acids 74:29–37
38. Zhang P, Kim W, Zhou L, Wang N, Ly LH, McMurray DN, Chapkin RS (2006) Dietary fish oil inhibits antigen-specific murine Th1 cell development by suppression of clonal expansion. J Nutr 136:2391–2398

Lipids (2008) 43:507–515
DOI 10.1007/s11745-008-3165-6

ORIGINAL ARTICLE

Increased Postprandial Triglyceride-Rich Lipoprotein Levels in Elderly Survivors of Myocardial Infarction

Samira Lekhal · Trond Børvik · Arne Nordøy · John-Bjarne Hansen

Received: 25 January 2008 / Accepted: 18 February 2008 / Published online: 4 April 2008
© AOCS 2008

Abstract Postprandial triglyceride-rich lipoproteins (TRL) levels are a predictor for coronary atherosclerosis. The aim of the study was to compare fasting high density lipoprotein (HDL) cholesterol, plasma lipoprotein lipase (LPL) activity, and postprandial TRL between elderly survivors of myocardial infarction (MI) and healthy controls. A case-control study was performed in 44 elderly patients 65–85 years of age with a previous history of MI and 43 age- and sex-matched healthy controls. Each participant underwent physical examination and was given a standard oral fat load with subsequent blood sampling over the next 8 h. Total and chylomicron triglycerides were assessed by area under the curve (AUC), incremental are under the curve (AUCi) and triglyceride response (TGR). Elderly MI patients had significantly lower postheparin LPL activity (87.4 ± 36.9 mU/ml) (mean ± 1 SD) than healthy controls (106.0 ± 29.0 mU/ml) ($P = 0.014$). Decreased postheparin LPL activity was accompanied by significant increased and delayed clearance of postprandial TRL. Fasting HDL cholesterol was significantly lower in elderly MI patients than controls (1.45 ± 0.32 and 1.66 ± 0.47 mmol/l, respectively, $P = 0.048$). Multiple regression analysis revealed postheparin LPL activity as an independent predictor for postprandial TRL and fasting HDL cholesterol. Logistic regressions analysis revealed HDL cholesterol, triglycerides measured 2 h after the oral fat load, and postheparin LPL activity as independent predictors for MI. Our findings indicate that decreased fasting HDL cholesterol is associated with increased postprandial triglyceridemia which could be a target for life-style and therapeutic interventions in patients at risk for cardiovascular disease.

Keywords Lipoproteins · Triglyceride metabolism · Lipoprotein · Lipase · Hyperlipidemia · HDL · LDL metabolism · Plasma lipids

Introduction

More than 20 years ago, Zilversmit [1] proposed that atherosclerosis is, at least in part, a postprandial disease, and hypothesised that accumulation of TRL promoted formation of atherosclerosis, due to reduced clearance and thereby prolonged exposure of the vascular wall to TRL. More recent studies provide new perspective to this hypothesis by reporting a particular efficient penetration and selective retention of chylomicron remnants in sites of lesion formation [2, 3]. Patients with coronary artery disease (CAD) have delayed elimination of postprandial TRL [4, 5], and plasma concentrations of postprandial remnants have been related to the progression of coronary lesions [6]. Furthermore, increased and delayed postprandial hyperlipidemia has been reported to be a strong predictor for CAD verified by angiography in middle-aged men with severe disease [4].

Lipoprotein lipase (LPL) is the major lipase in lipoprotein metabolism [7]. The enzyme is synthesized by and released from parenchymal cells in many tissues, and becomes anchored to heparan sulphate proteoglycans (HSPGs) at the endothelial surface [7]. LPL hydrolyzes triglycerides in chylomicrons (CM) and very low-density lipoproteins (VLDL), providing fatty acids to the underlying tissues [8]. A delay in chylomicron clearance would

---

S. Lekhal (✉) · T. Børvik · A. Nordøy · J.-B. Hansen
Center for Atherothrombotic Research in Tromsø,
Department of Medicine, Institute of Clinical Medicine,
University of Tromsø, 9037 Tromsø, Norway
e-mail: samira.lekhal@fagmed.uit.no

imply prolonged postprandial hyperlipidemia, which supposedly leads to increased deposition of chylomicron contents in the arterial wall and to an unfavourable translocation of cholesteryl-esters from high density lipoprotein (HDL) to CM [1, 4]. Deficiency of LPL or its cofactor apo-CII is known to induce accumulation of CM in plasma, suggesting that triglyceride hydrolysis is important for clearance of these particles [9]. Furthermore, low levels of LPL activity, as encountered in patients with partial LPL deficiency, are associated with premature atherosclerosis and accelerated progression of atherogenesis [10], and low postheparin LPL activity is related to severe angina pectoris in men with angiographically documented CAD [11].

Low HDL cholesterol is known to be a strong and independent risk factor for CAD [12], which remains significant even at old age [13, 14]. In humans, LPL activity contributes to the regulation of HDL cholesterol and may partly explain the inverse relation between postprandial TRL and HDL cholesterol [5, 15, 16]. In addition, postheparin LPL activity is associated with HDL cholesterol [17, 18] and inversely correlated to the magnitude of postprandial hyperlipidemia in normolipidemic patients [19].

The purpose of the present study was to compare fasting HDL cholesterol, plasma LPL activity, and postprandial TRL in elderly patients with a previous history of myocardial infarction (MI) with apparently healthy controls. To address these questions we performed a case-control study among elderly, normotriglyceridemic survivors of acute MI more than a year prior to the investigation and in healthy age- and sex-matched controls. Our hypothesis was that low fasting HDL cholesterol may be a marker of decreased LPL activity accompanied by increased and delayed clearance of postprandial TRL.

Materials and Methods

Patients and Study Design

Medical records of consecutive patients between 65 and 85 years of age with the diagnosis acute MI were obtained from the archives at the University Hospital of North Norway in Tromsø. The diagnosis acute MI was verified by diagnostic criteria such as chest pain, pathological ECG and increase in serum concentration of cardiac markers. The inclusion criteria were; suffering of acute MI 1–4 years before the present investigation without any major coronary events (i.e. hospitalization for angina pectoris, reinfarction, coronary angioplasty or ACB surgery) afterwards, both genders, and age between 65 and 85 years at diagnosis. The exclusion criteria were; regular use of drugs interfering with the coagulation system, chronic inflammatory diseases, renal or liver disease, cancer, hypothyroidism, serious hypertension, abuse of alcohol or drugs, and psychiatric diseases. One age- and sex-matched healthy person for each case was recruited from the general population and invited to a screening visit. At the screening visit, a complete medical history, physical examination and blood samples were taken with special emphasis on exclusion criteria were conducted on both cases and controls. Absence of diseases, and cardiovascular diseases in particular, for the healthy controls were confirmed by searching into their medical records. Height and weight were measured with the patients in light clothing without shoes and body mass index (BMI) was calculated. Blood pressure was recorded in seated position by the use of an automatic device (Dinamap Vital Signs Monitor). Three recordings were made at 1 min intervals, and the mean of the two last values was used in this report. A 75-g oral glucose tolerance test was performed on the first visit. Impaired fasting glucose (fasting plasma glucose 6.1–6.9 mmol/l), impaired glucose tolerance (fasting glucose < 7.0 mmol/l and 2 h plasma glucose from 7.8 to 11.0 mmol/l) and diabetes (fasting glucose ≥ 7.0 mmol/l or 2 h plasma glucose ≥ 11.1 mmol/l or on antidiabetic treatment) were defined according to WHO criteria. Eligible persons (44 cases and 43 controls) were invited to a second visit during which the participants were subjected to a fat tolerance test. Informed written consent was obtained from the participants, and the Regional Board of Research Ethics approved the study. The study was performed at the Clinical Research Centre at the University Hospital of North Norway in Tromsø.

Fat Tolerance Test

A fat tolerance test was conducted using a test meal prepared as a standard cream porridge containing 70% of calories from fat of which 66% saturated fat, 32% monounsaturated fat and 2% polyunsaturated fat. A weight-adjusted meal (1 g fat per kg body weight) was served at 8:00 a.m. and consumed over a 15 min period. The participants were allowed to drink 350 ml calorie-free beverages (diet soda) and eat an apple during the following 8 h. Blood samples for isolation of CM, and serum and plasma preparations were collected after 12 h fasting, before the meal and every second hour during the next 8 h.

Measurement of Plasma Glucose, Serum lipids, Apolipoproteins and Isolation of Chylomicrons

Serum was prepared by clotting whole blood in a glass tube at room temperature for 1 h and then centrifuged at 2,000*g* for 15 min at 22 °C. Blood for plasma preparation was collected into vacutainers (Becton Dickinson, Meylan

Cedex, France) containing 0.129 M sodium citrate (1 vol anticoagulant and 9 vol whole blood) as anticoagulant. Plasma glucose was measured (Gluco-quant Glucose/HK, Roche Diagnostics GmbH, Mannheim, Germany) in fasting plasma and 2 h after a 75 g oral glucose tolerance test according to the manufacturers instructions. Serum lipids were analyzed on a Hitachi 737 Automatic Analyzer (Boehringer Mannheim, Germany) with reagents from the manufacturer. Total cholesterol was measured with an enzymatic colorimetric method (CHOD-PAP) and HDL cholesterol was assayed by the same procedure after precipitation of lower density lipoproteins with heparin and manganese chloride as described by Burstein et al. [20]. Total triglycerides and chylomicron triglycerides concentration was determined with an enzymatic colorimetric test (GPO-PAP). Low-density lipoprotein (LDL) cholesterol was calculated by the formula of Friedewald et al. [21]. Apo-AI and apo-B100 were measured immunochemically by rate nephelometry, using the Array Protein System from Beckman Instruments Inc. (Brea, CA, USA). CM were isolated by over layering 8 ml EDTA plasma with 5 ml of NaCl solution (a density 1.006 kg/l NaCl solution with 0.02% sodium azide and 0.01% EDTA) in a cellulose nitrate tube (Beckman Instruments Inc., CA, USA) and centrifuged in a Beckman SW40 Ti swinging bucket rotor at 20,000 rpm for 1 h at 4 °C. The CM, with Svedberg flotation (Sf) rates >400, were carefully removed by aspiration from the top of the tube divided into three aliquots in cryovials, flushed with nitrogen, and frozen at −70 °C until further analysis.

Lipoprotein Lipase Activity

Eight hours after ingestion of the test meal, blood was drawn into vacutainers (Becton Dickinson) containing heparin as anticoagulant and the heparinised blood was immediately placed on ice. Unfractionated heparin was given as a bolus injection (100 IU/kg body weight) on the contra lateral arm to mobilize LPL from the endothelial surface into the circulation, and a second blood sample was obtained 15 min after heparin administration and immediately placed on ice. Heparinised plasma was recovered within 30 min by centrifugation (2,000×*g* for 10 min) at 4 °C, divided into aliquots of 1.0 ml in cryovials, flushed with nitrogen, and frozen at −70 °C until further analysis. LPL activity was determined as described by Olivecrona et al. [22]. In short, sonicated emulsion of ^{3}H-oleic acid-labelled triolein in 20% Intralipid (Fresenius Kabi, Halden, Norway) was used as substrate. Samples were preincubated for 2 h on ice with 0.5 vol goat antibodies to hepatic lipase (HL) to suppress HL activity. LPL activity is expressed in mU/ml corresponding to nanomole of fatty acids released per millilitre per minute. The samples were quantitated in duplicate, and postheparin plasma from pooled normal control persons was used to correct for interassay variation.

Statistics

All variables were checked for frequency distribution. The extent of postprandial hypertriglyceridemia was assessed by the total area under the curve (AUC) and incremental area under the curve (AUCi) for triglycerides and chylomicron triglycerides, and by the triglyceride response (TGR), defined as the average of the two highest postprandial triglyceride concentrations minus baseline concentration. Unpaired t test was used to compare differences between groups. χ^2 (Chi-square) test was used to compare groups on categorical variables. General linear models for univariate analysis of variance were used for adjustments. Pearson's correlation coefficients were used to examine correlations between continuous variables. Linear regression models were used to test linear trends. Multiple linear regression models were used to assess independent predictors of AUCi for serum triglycerides, AUCi for CM and HDL cholesterol. Multiple logistic regression models were performed with case-control status for MI with triglycerides measured 2 h after the fat load, postheparin LPL activity and HDL cholesterol. All analyses were performed using SPSS (SPSS Inc. Chicago, Illinois, USA) for windows software, version 14.0. Two-sided P values (<0.05) were considered statistically significant. Values are mean ± SD if not otherwise stated.

Results

Characteristics of elderly survivors of MI and age- and sex-matched healthy controls are shown in Table 1. Patients had significantly higher frequency of hypertension and lower measured blood pressure and heart rate than healthy controls. The apparent discrepancy between higher frequency of hypertension and actual lowered blood pressure and heart rate among MI patients is most probably explained by their frequent use of β-blockers (Table 1). Elderly MI patients tended to have a higher frequency of diabetes mellitus, but impaired fasting glucose and impaired glucose tolerance were equally distributed between groups.

Serum lipids and apolipoproteins in elderly survivors of MI and their age- and sex-matched controls are shown in Table 2. Elderly MI patients had significantly lower total cholesterol, LDL cholesterol and HDL cholesterol than control persons in crude analysis and after adjustment for BMI, diabetes mellitus and regular use of statins. Apo-AI was lower in MI patients in crude analysis, but the difference between groups disappeared after adjustment for

Table 1 Characteristics of elderly survivors of myocardial infarction and age- and sex-matched healthy controls

Variables	MI patients (n = 44)	Healthy controls (n = 43)	P values
Age (years)	73.4 ± 5.4	73.7 ± 5.4	0.76
Gender (% men)	77 (34)	77 (33)	0.95
Smoking (%)	5 (2)	9 (4)	0.43
BMI (kg/m^2)	27.4 ± 3.8	26.0 ± 3.9	0.10
Diabetes mellitus (%)	11 (5)	0 (0)	0.06
Hypertension (%)	66 (29)	5 (2)	<0.001
Systolic BP (mmHg)	137 ± 21	148 ± 22	0.02
Diastolic BP (mmHg)	71 ± 10	84 ± 11	<0.001
Heart rate (beats/min)	60 ± 8	68 ± 12	<0.001
Glucose (mmol/l)	5.5 ± 0.8	5.2 ± 0.5	0.10
Impaired fasting glucose	5 (2)	7 (3)	0.68
Impaired glucose tolerance	5 (2)	7 (3)	0.68
Statins (%)	48 (21)	0 (0)	<0.001
Ca-antagonists (%)	9 (4)	14 (6)	0.48
β-blockers (%)	68 (30)	5 (2)	<0.001
Diuretics (%)	32 (14)	2 (1)	<0.001
ACE-inhibitors (%)	18 (8)	5 (2)	0.09
Nitrates (%)	48 (21)	0 (0)	<0.001
Aspirin (%)	95 (42)	7 (3)	<0.001

Values are mean ± SD or percentage with absolute numbers in brackets

Table 2 Serum concentrations of fasting lipids and apolipoproteins in elderly survivors of myocardial infarction and age- and sex-matched healthy controls

Variables	MI patients (n = 44)	Healthy controls (n = 43)	P values	
			P1	P2
Total cholesterol (mmol/l)	5.24 ± 1.16	6.40 ± 1.12	<0.001	0.002
LDL cholesterol (mmol/l)	3.23 ± 0.97	4.28 ± 0.92	<0.001	<0.001
HDL cholesterol (mmol/l)	1.45 ± 0.32	1.66 ± 0.47	0.02	0.05
Triglycerides (mmol/l)	1.12 ± 0.44	1.11 ± 0.45	0.91	0.38
Apolipoprotein-AI (g/l)	1.46 ± 0.26	1.61 ± 0.30	0.01	0.28
Apolipoprotein-B (g/l)	1.08 ± 0.26	1.09 ± 0.23	0.78	0.69

Values are mean ± SD

P1, crude analyses; P2, adjusted for BMI, presence of diabetes mellitus, and regular use of statins

BMI, diabetes and use of statins. No difference between groups was observed with regard to fasting serum triglycerides.

To investigate the time-course of postprandial triglyceride-rich lipoproteins (TRL) in elderly patients with and without a previous history of MI, the participants were subjected to a standard fat meal, and total serum triglycerides and chylomicron triglycerides were measured over time (Fig. 1 and Table 3). The MI patients had increased peak concentrations of total triglycerides, increased total and incremental AUC, which reached significance after adjustment for BMI, diabetes and use of statins. Even more pronounced differences between groups with regard to peak concentrations and both total and incremental AUC were observed for chylomicron triglycerides. Statistical adjustments for use of cardiovascular drugs (statins, β-blockers, Ca-antagonists, diuretics) and concurrent diseases (diabetes mellitus and hypertension) among MI patients did not influence differences between groups. The MI patients had significantly higher levels of chylomicron triglycerides 8 h after the fat load (P = 0.018). Furthermore, we found a significant correlation between fasting TG and AUCi for total triglycerides in patients (r = 0.51, P = 0.001), but not in controls (r = 0.21, P = 0.193).

Preheparin LPL activity was similar in the two groups, whereas elderly MI patients had significantly lower

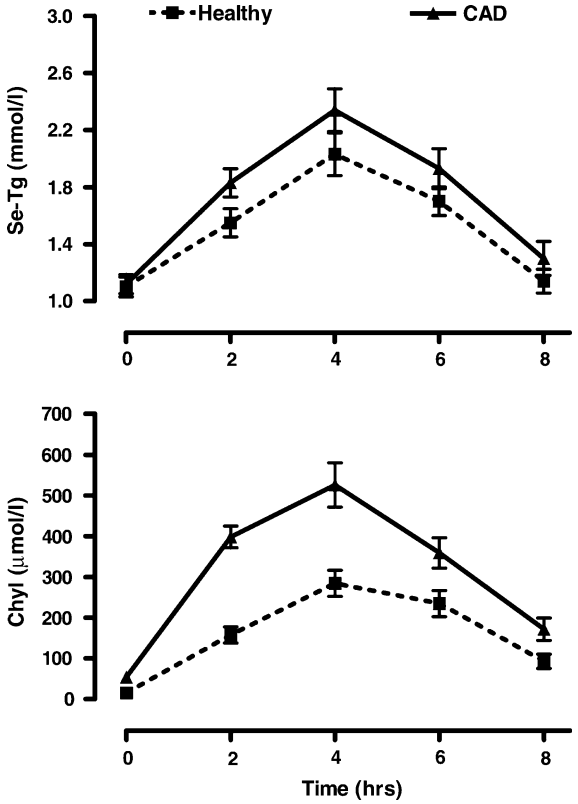

Fig. 1 Line graph showing postprandial concentrations of total triglycerides (*upper panel*) and chylomicron triglycerides (*lower panel*) over time after a standard fat meal in elderly patients with a previous history of myocardial infarction ($n = 44$) and healthy age- and sex-matched controls ($n = 43$). Values are mean ± SEM

postheparin LPL activity than age- and sex-matched controls in crude analysis ($P = 0.014$) (Table 3). Statistical adjustments for smoking, BMI, use of cardiovascular drugs (statins, β-blockers, Ca-antagonists, diuretics) and concurrent diseases (Diabetes Mellitus and hypertension) among MI patients did not influence the differences between groups. In the total study population ($n = 87$), postheparin LPL activity was inversely correlated with fasting TG levels ($r = -0.29$, $P = 0.008$), incremental AUC for total triglycerides ($r = -0.39$, $P < 0.001$) and chylomicron triglycerides ($r = -0.41$, $P < 0.001$). Furthermore, a significant positive correlation was found between postheparin LPL activity and fasting HDL cholesterol for both patients ($r = 0.40$, $P = 0.013$) and healthy controls ($r = 0.34$, $P = 0.037$). Multiple linear regression analyses were performed to determine independent predictors for incremental AUC for triglycerides (TG-AUCi), incremental AUC for chylomicron triglycerides (CM-AUCi) and HDL cholesterol (Table 4). Triglycerides measured 2 h after the oral fat load was independent predictors for TG-AUCi, whereas triglycerides measured 2 h after fat load and postheparin LPL activity were significant independent predictors for CM-AUCi. Postheparin LPL activity was the only significant predictor for HDL cholesterol in the model. The included variables in the model explained 51% of the variation in TG-AUCi, 43% of the variation in CM-AUCi, and 19% of the variation in HDL cholesterol.

To study the predictive role of triglycerides measured 2 h after the fat load, postheparin LPL activity and HDL cholesterol for MI in elderly, multiple logistic regression analysis were performed (Table 5). Postheparin LPL activity ($P = 0.02$), triglycerides measured 2 h after the fat load ($P = 0.05$) and HDL cholesterol ($P = 0.02$) were independent predictors for MI in elderly. After adjusting for BMI and statin prescription, postheparin LPL activity ($P = 0.02$) and triglycerides measured 2 h after the fat load

Table 3 Serum concentrations of postprandial total triglycerides and chylomicron triglycerides measured as total area under the curve (AUC), incremental area under the curve (AUCi) and triglyceride response (TGR), and lipoprotein lipase activity during 8 h after intake of a standard fat meal in elderly survivors of myocardial infarction and age- and sex-matched healthy controls

Variables	MI patients ($n = 44$)	Healthy controls ($n = 43$)	*P* values	
			*P*1	*P*2
Triglycerides				
AUC (mmol/h/l)	14.65 ± 6.00	12.94 ± 4.81	0.16	0.04
AUCi (mmol/h/l)	3.94 ± 2.53	5.64 ± 3.38	0.01	0.03
TGR (mmol/l)	1.12 ± 0.66	0.82 ± 0.50	0.02	0.03
Chylomicrons				
AUC (μmol/h/l)	2683.9 ± 1387.3	1437.8 ± 956.1	<0.001	<0.001
AUCi (μmol/h/l)	2358.4 ± 1334.2	1346.8 ± 951.6	<0.001	<0.001
TGR (μmol/l)	451.6 ± 252.0	270.5 ± 188.8	<0.001	0.003
LPL activity				
Preheparin (mU/ml)	1.5 ± 2.3	1.2 ± 0.9	0.39	0.71
Postheparin (mU/ml)	87.4 ± 36.9	106.0 ± 29.0	0.01	0.01

Values are mean ± SD

*P*1 crude analyses, *P*2 adjusted for BMI, presence of diabetes mellitus, and regular use of statins

Table 4 Predictors for incremental area under the curve for total triglycerides (TG-AUCi), chylomicrons (CM-AUCi) and HDL cholesterol in elderly survivors of myocardial infarction and controls (n = 87) using a multiple linear regression model

Independent variables	Dependent variables					
	TG-AUCi		CM-AUCi		HDL-Chol	
	β	t	β	t	β	t
Triglycerides 2 h (mmol/l)	2.97	6.34**	1045.7	5.08**	−0.06	−0.81
HDL (mmol/l)	−1.35	−1.83	−236.7	−0.74		
Postheparin LPL (mU/ml)	−0.01	−1.11	−7.68	−1.92*	0.004	2.52*
BMI (kg/m^2)	−0.09	−1.32	21.10	0.65	−0.02	−1.87
R^2	0.51		0.43		0.19	

Values are standardized beta coefficients (β) and t values

* $P < 0.05$; ** $P < 0.001$

Table 5 Logistic regression models with case-control status for triglycerides measured 2 h after the fat load, postheparin LPL activity and HDL cholesterol

Variables	OR (95% CI)	OR*
HDL-cholesterol (mmol/l)	0.26 (0.08–0.81)	0.32 (0.07–1.44)
Triglycerides, 2 h (mmol/l)	1.99 (1.00–4.03)	2.54 (1.00–6.44)
LPL activity (mU/ml)	0.89 (0.84–0.97)	0.89 (0.68–0.99)

Values are crude and adjusted odds ratios (OR) with 95% confidence intervals

OR* adjusted for BMI and prescription of statins. Units are 1 mmol/l for serum lipids and 10 mU/ml for postheparin LPL activity

(P = 0.05) remained as independent predictors in the model.

Discussion

The present study showed that decreased fasting HDL cholesterol in elderly survivors of MI was associated with lowered postheparin LPL activity accompanied by increased postprandial TRL. To the best of our knowledge, our study is the first to show these metabolic changes in elderly MI patients.

In our study, elderly survivors of MI had increased peak concentrations, elevated AUC and delayed clearance of both total triglycerides and chylomicron triglycerides. Similar findings have previously been reported in middle-aged male subjects with severe CAD [4]. Although other studies have reported delayed clearance of TRL in CAD patients [5, 23], they were not able to demonstrate increased postprandial levels of TRL [5, 23, 24]. Previous studies have shown a significant association between fasting triglycerides and postprandial TRL [5, 24]. A significant correlation between fasting triglycerides and postprandial TRL in elderly MI patients was confirmed in our study, and multiple regression analysis revealed triglycerides measured 2 h after the fat load as a strong and independent predictor for the magnitude of postprandial increase in TRL and the presence of CAD.

Postprandial lipoprotein changes in healthy persons aged 22–79 years showed that elderly people had significantly increased [25] and prolonged postprandial hypertriglyceridemia compared to healthy young persons [26]. Thus, both age and the presence of CAD are known predictors for increased and delayed clearance of postprandial TRL. Our findings of a pronounced increase in peak concentrations and delayed clearance of postprandial TRL in elderly MI patients may indicate that age contributes to reinforcing the effect on postprandial handling of TRL.

Obesity, insulin resistance, and dyslipidemia including low levels of HDL cholesterol are important elements of the metabolic syndrome [27] associated with increased risk for cardiovascular disease [28, 29] and type 2 diabetes [30]. Insulin resistance is associated with endothelial dysfunction [31] with subsequent impaired metabolism of TRLs by LPLs [32]. Persons with obesity [33] and diabetes mellitus type 2 [34] are reported to have increased levels of postprandial TRLs. In our study, elderly MI patients tended to have higher BMI and to have a higher frequency of diabetes mellitus type 2 than the healthy controls. However, the increased levels of postprandial TRL in elderly MI patients remained significant even after adjusting for BMI and diabetes mellitus.

Statin treatment is known to reduce the postprandial triglyceridemia [35–38] in a Dose-Dependent manner by 5–30% [39]. In the present study, almost 50% of the MI patients regularly used statins. Thus, it is likely correct to assume that the actual difference in postprandial levels of TRL between groups was underestimated in our study. Both non-selective and β1-selective β-blockers increase fasting plasma triglycerides [40]. In our study, all patients were using β1-selective β-blockers which are reported not to affect postprandial TRL [41] and postheparin LPL activity [42]. However, adjustments for use of cardiovascular drugs (statins, β-blockers, Ca-antagonists, diuretics) among MI patients did not influence the differences between groups.

The "response to retention" hypothesis of atherosclerosis suggests that intimal deposition is proportional to the concentration of circulating proatherogenic lipoproteins [43, 44]. Experimental studies suggest that plasma accumulation of remnant lipoproteins is not just an associated feature of an atherogenic lipoprotein profile, but that TRL remnants themselves contribute to the pathogenesis of atherosclerosis. Chylomicron remnants in the intima are derived from postprandial lipoproteins [2, 45], and TRL can be taken up directly by macrophages without prior modification and form foam cells [46]. Apo-B48 containing chylomicron remnants may contain up to 40 times more cholesterol per particle than do LDL particles, and consequently, exposure and retention of apo-B48 containing postprandial lipoproteins in the arterial wall may pose a significant atherogenic risk [2]. The present study supports the hypothesis that both increased and delayed postprandial hyperlipidemia are associated with CAD, and suggests that increased postprandial hypertriglyceridemia is a stronger predictor for CAD in old age. Thus, it may be speculated that increased and delayed postprandial levels of TRL among elderly may contribute to increased risk for CAD in older men and women [47].

The amount of LPL released after a bolus dose of heparin is used as a measure of functional LPL and assumed to reflect the LPL availability at the endothelial surface [22]. Inconsistent data has been reported on postheparin LPL activity in CAD. In two independent studies in young normotriglyceridemic CAD patients, both no change [5] and decreased [17] postheparin LPL activity has been reported. In the latter study, hypertriglyceridemic patients did not have decreased LPL activity [17]. However, a large cohort study among dyslipidemic CAD patients less than 70 years of age showed a significant decrease in postheparin LPL activity [48]. In the present study, normotriglyceridemic elderly survivors of MI had significantly lower postheparin LPL activity than healthy controls. Both environmental and genetic factors are known to affect LPL activity [7]. Postheparin LPL activity decreases with advancing age [25]. Use of β-blockers was earlier reported to inhibit LPL activity [49], whereas more recent studies have shown no influence of regular use of β-blockers [11, 48]. In the present study, the differences in postheparin LPL activity remained significant even after adjustments for use of cardiovascular drugs and concurrent diseases among the MI patients.

Chylomicron clearance, both lipolysis and hepatic uptake, is sensitive to LPL activity [7]. Thus, decreased LPL activity may slow chylomicron clearance in both stages. In our study, multiple regression analysis revealed that postheparin LPL activity was an independent predictor for both fasting HDL and postprandial TRL. Decreased postheparin LPL activity was associated with low HDL cholesterol and increased postprandial TRL, a lipid profile that is associated with increased risk for atherosclerosis [4, 5, 50]. Genetic studies have reported that individuals, who are heterozygous for LPL mutations that reduce enzymatic activity, are predisposed to premature atherosclerosis [51, 52]. Conversely, a variant of LPL that is associated with increased activity has been shown to protect against coronary heart disease [53]. Thus, our findings support a novel property of LPL in CAD either directly or indirectly by subsequent modulation of HDL cholesterol and postprandial TRL.

In conclusion, elderly MI patients had decreased fasting HDL cholesterol associated with metabolic disturbances such as decreased postheparin LPL activity and increased postprandial triglyceridemia. Increased postprandial triglyceridemia could be a target for life-style changes, i.e. weight loss [54], physical exercise [55] and dietary supplementation of polyunsaturated n-3 fatty acids [38, 56], and therapeutic interventions, i.e. statin treatment [35–37].

Acknowledgments CART is supported by an independent grant from Pfizer Norway AS. The study has received a grant from the Center for Research in the Elderly.

Conflict of interest statement There are no conflicts of interest.

References

1. Zilversmit DB (1979) Atherogenesis: a postprandial phenomenon. Circulation 60:473–485
2. Proctor SD, Mamo JC (1996) Arterial fatty lesions have increased uptake of chylomicron remnants but not low-density lipoproteins. Coron Artery Dis 7:239–245
3. Proctor SD, Vine DF, Mamo JC (2004) Arterial permeability and efflux of apolipoprotein B-containing lipoproteins assessed by in situ perfusion and three-dimensional quantitative confocal microscopy. Arterioscler Thromb Vasc Biol 24:2162–2167
4. Patsch JR, Miesenbock G, Hopferwieser T, Muhlberger V, Knapp E, Dunn JK, Gotto AM Jr, Patsch W (1992) Relation of triglyceride metabolism and coronary artery disease. Studies in the postprandial state. Arterioscler Thromb 12:1336–1345
5. Groot PH, van Stiphout WA, Krauss XH, Jansen H, van Tol A, van Ramshorst E, Chin-On S, Hofman A, Cresswell SR, Havekes L (1991) Postprandial lipoprotein metabolism in normolipidemic men with and without coronary artery disease. Arterioscler Thromb 11:653–662
6. Karpe F, Steiner G, Uffelman K, Olivecrona T, Hamsten A (1994) Postprandial lipoproteins and progression of coronary atherosclerosis. Atherosclerosis 106:83–97
7. Otarod JK, Goldberg IJ (2004) Lipoprotein lipase and its role in regulation of plasma lipoproteins and cardiac risk. Curr Atheroscler Rep 6:335–342

8. Olivecrona T, Olivecrona G (1999) Lipoprotein and hepatic lipases in lipoprotein metabolism. In: Betterbridge DJ, Illingworth DR, Shepard J (eds) Lipoproteins in health and disease. Arnold, London, pp 223–246
9. Brunzell JD, Miller NE, Alaupovic P, St Hilaire RJ, Wang CS, Sarson DL, Bloom SR, Lewis B (1983) Familial chylomicronemia due to a circulating inhibitor of lipoprotein lipase activity. J Lipid Res 24:12–19
10. Jukema JW, van Boven AJ, Groenemeijer B, Zwinderman AH, Reiber JH, Bruschke AV, Henneman JA, Molhoek GP, Bruin T, Jansen H, Gagne E, Hayden MR, Kastelein JJ (1996) The Asp9 Asn mutation in the lipoprotein lipase gene is associated with increased progression of coronary atherosclerosis. REGRESS Study Group, Interuniversity Cardiology Institute, Utrecht, The Netherlands. Regression Growth Evaluation Statin Study. Circulation 94:1913–1918
11. Kastelein JJ, Jukema JW, Zwinderman AH, Clee S, van Boven AJ, Jansen H, Rabelink TJ, Peters RJ, Lie KI, Liu G, Bruschke AV, Hayden MR (2000) Lipoprotein lipase activity is associated with severity of angina pectoris. REGRESS Study Group. Circulation 102:1629–1633
12. Miller NE, Thelle DS, Forde OH, Mjos OD (1977) The Tromsø heart-study. High-density lipoprotein and coronary heart-disease: a prospective case-control study. Lancet 1:965–968
13. Zimetbaum P, Frishman WH, Ooi WL, Derman MP, Aronson M, Gidez LI, Eder HA (1992) Plasma lipids and lipoproteins and the incidence of cardiovascular disease in the very elderly. The Bronx Aging Study. Arterioscler Thromb 12:416–423
14. Weverling-Rijnsburger AW, Jonkers IJ, van Exel E, Gussekloo J, Westendorp RG (2003) High-density vs low-density lipoprotein cholesterol as the risk factor for coronary artery disease and stroke in old age. Arch Intern Med 163:1549–1554
15. Kolovou GD, Anagnostopoulou KK, Pilatis N, Kafaltis N, Sorodila K, Psarros E, Cokkinos DV (2004) Low fasting low high-density lipoprotein and postprandial lipemia. Lipids Health Dis 3:18–26
16. Karpe F, Bard JM, Steiner G, Carlson LA, Fruchart JC, Hamsten A (1993) HDLs and alimentary lipemia. Studies in men with previous myocardial infarction at a young age. Arterioscler Thromb 13:11–22
17. Tornvall P, Olivecrona G, Karpe F, Hamsten A, Olivecrona T (1995) Lipoprotein lipase mass and activity in plasma and their increase after heparin are separate parameters with different relations to plasma lipoproteins. Arterioscler Thromb Vasc Biol 15:1086–1093
18. Jackson RL, Yates MT, McNerney CA, Kashyap ML (1990) Relationship between post-heparin plasma lipases, triglycerides and high density lipoproteins in normal subjects. Horm Metab Res 22:289–294
19. Patsch JR, Prasad S, Gotto AM Jr, Patsch W (1987) High density lipoprotein2. Relationship of the plasma levels of this lipoprotein species to its composition, to the magnitude of postprandial lipemia, and to the activities of lipoprotein lipase and hepatic lipase. J Clin Invest 80:341–347
20. Burstein M, Scholnick HR, Morfin R (1970) Rapid method for the isolation of lipoproteins from human serum by precipitation with polyanions. J Lipid Res 11:583–595
21. Friedewald WT, Levy RI, Fredrickson DS (1972) Estimation of the concentration of low-density lipoprotein cholesterol in plasma, without use of the preparative ultracentrifuge. Clin Chem 18:499–502
22. Olivecrona T (2000) Determination and clinical significance of lipoprotein lipase and hepatic lipase In: Rifai N, Warnwick G, Dominiczak M (eds) Handbook of lipoprotein testing. AACC Press, Whasington, pp 429–497
23. Przybycien K, Kornacewicz-Jach Z, Torbus-Lisiecka B, Naruszewicz M (2000) Is abnormal postprandial lipemia a familial risk factor for coronary artery disease in individuals with normal fasting concentrations of triglycerides and cholesterol? Coron Artery Dis 11:377–381
24. Schaefer EJ, Audelin MC, McNamara JR, Shah PK, Tayler T, Daly JA, Augustin JL, Seman LJ, Rubenstein JJ (2001) Comparison of fasting and postprandial plasma lipoproteins in subjects with and without coronary heart disease. Am J Cardiol 88:1129–1133
25. Cohn JS, McNamara JR, Cohn SD, Ordovas JM, Schaefer EJ (1988) Postprandial plasma lipoprotein changes in human subjects of different ages. J Lipid Res 29:469–479
26. Cassader M, Gambino R, Ruiu G, Marena S, Bodoni P, Pagano G (1996) Postprandial triglyceride-rich lipoprotein changes in elderly and young subjects. Aging (Milano) 8:421–428
27. Grundy SM, Cleeman JI, Daniels SR, Donato KA, Eckel RH, Franklin BA, Gordon DJ, Krauss RM, Savage PJ, Smith SC Jr, Spertus JA, Spertus JA, Costa F (2005) Diagnosis and management of the metabolic syndrome. An American Heart Association/National Heart, Lung, and Blood Institute Scientific Statement. Circulation 112:2735–52
28. Isomaa B, Almgren P, Tuomi T, Forsen B, Lahti K, Nissen M, Taskinen MR, Groop L (2001) Cardiovascular morbidity and mortality associated with the metabolic syndrome. Diabetes Care 24:683–689
29. Malik S, Wong ND, Franklin SS, Kamath TV, L'Italien. GJ, Pio JR, Williams GR (2004) Impact of the metabolic syndrome on mortality from coronary heart disease, cardiovascular disease, and all causes in united states adults. Circulation 110:1245–1250
30. Maggio CA, Pi-Sunyer FX (2003) Obesity and type 2 diabetes. Metab Clin North Am 32:805–22
31. Kim JA, Montagnani M, Kon Koh K, Quon MJ (2006) Reciprocal relationships between insulin resistance and endothelial dysfunction: molecular and phatophysiological mechanisms. Circulation 113:1888–1904
32. Inoue T, Saniabadi AR, Matsunaga R, Hoshi K, Yaguchi I, Morooka S (1998) Impaired endothelium-dependent acetylcholine-induced coronary artery relaxation in patients with high serum remnant lipoprotein particles. Atherosclerosis 139:363–367
33. Lewis GF, O'Meara NM, Soltys PA, Blackman JD, Iverius PH, Druetzler AF, Getz GS, Polonsky KS (1990) Postprandial lipoprotein metabolism in normal and obese subjects: comparison after the vitamin A fat-loading test. J Clin Endocrinol Metab 33:1041–1050
34. Hirano T, Yoshino G, Kashiwazaki K, Adachi M (2001) Doxazosin reduces prevalence of small dense low density lipoprotein and remnant-like particle cholesterol levels in nondiabetic and diabetic hypertensive patients. Am J Hypertens 14:908–913
35. Schaefer EJ, McNamara JR, Tayler T, Daly JA, Gleason JA, Seman LJ, Ferrari A, Rubenstein JJ (2002) Effects of atorvastatin on fasting and postprandial lipoprotein subclasses in coronary heart disease patients versus control subjects. Am J Cardiol 90:689–696
36. Boquist S, Karpe F, Danell-Toverud K, Hamsten A (2002) Effects of atorvastatin on postprandial plasma lipoproteins in postinfarction patients with combined hyperlipidaemia. Atherosclerosis 162:163–170
37. van Wijk JP, Halkes CJ, De Jaegere PP, Plokker HW, Erkelens DW, Cabezas MC (2003) Normalization of daytime triglyceridemia by simvastatin in fasting normotriglyceridemic patients with premature coronary sclerosis. Atherosclerosis 171:109–116
38. Nordoy A, Bonaa KH, Sandset PM, Hansen JB, Nilsen H (2000) Effect of omega-3 fatty acids and simvastatin on hemostatic risk

factors and postprandial hyperlipemia in patients with combined hyperlipemia. Arterioscler Thromb Vasc Biol 20:259–265

39. Karpe F (2002) Postprandial lipemia–effect of lipid-lowering drugs. Atheroscler Suppl 3:41–46
40. Vyssoulis GP, Karpanou EA, Pitsavos CE (1992) Differentiation of β-blocker effects on serum lipids and apolipoproteins in hypertensive patients with normolipidemic profiles. Eur Heart J 13:1506–1513
41. Boquist S, Ruotolo G, Hellenius M-L, Danell-Toverud K, Karpe F, Hamsten A (1998) Effects of cardioselective β-blocker on postprandial triglyceride-rich lipoproteins, low density lipoprotein particle size and glucose-insulin homeostasis in middle-aged men with modestly increased cardiovascular risk. Atherosclerosis 2:391–400
42. Rubba P, De Simone B, Marotta TA (1989) Adrenergic blocking agents and lipoprotein lipase activity. J Endocrinol Invest 12:119–122
43. Williams KJ, Tabas I (1995) The response-to-retention hypothesis of early atherogenesis. Arterioscler Thromb Vasc Biol 15:551–561
44. Cohn JS (1998) Postprandial lipemia: emerging evidence for atherogenicity of remnant lipoproteins. Can J Cardiol 14(Suppl B):18B–27B
45. Proctor SD, Mamo JC (1998) Retention of fluorescent-labelled chylomicron remnants within the intima of the arterial wall–evidence that plaque cholesterol may be derived from postprandial lipoproteins. Eur J Clin Invest 28:497–503
46. Bradley WA, Gianturco SH (1994) Triglyceride-rich lipoproteins and atherosclerosis: pathophysiological considerations. J Intern Med Suppl 736:33–39
47. Kannel WB (1997) Cardiovascular risk factors in the elderly. Coron Artery Dis 8:565–575
48. Henderson HE, Kastelein JJP, Zwinderman AH, Gagne E, Jukema JW, Reymer PWA, Groenemeyer BE, Lie KI, Bruschke AVG, Hayden MR, Jansen H (1999) Lipoprotein lipase activity is decreased in a large cohort of patients with coronary artery disease and is associated with changes in lipids and lipoproteins. J Lipid Res 40:735–743
49. Day JL, Metcalfe J, Simpson N, Lowenthal L (1984) Adrenergic mechanisms in the control of plasma lipids in man. Am J Med 76:94–96
50. Miller GJ, Miller NE (1975) Plasma-high-density-lipoprotein concentration and development of ischaemic heart-disease. Lancet 1:16–19
51. Reymer PW, Gagne E, Groenemeyer BE, Zhang H, Forsyth I, Jansen H, Seidell JC, Kromhout D, Lie KE, Kastelein J (1995) A lipoprotein lipase mutation (Asn291Ser) is associated with reduced HDL cholesterol levels in premature atherosclerosis. Nat Genet 10:28–34
52. Nordestgaard BG, Abildgaard S, Wittrup HH, Steffensen R, Jensen G, Tybjaerg-Hansen A (1997) Heterozygous lipoprotein lipase deficiency: frequency in the general population, effect on plasma lipid levels, and risk of ischemic heart disease. Circulation 96:1737–1744
53. Gagne SE, Larson MG, Pimstone SN, Schaefer EJ, Kastelein JJ, Wilson PW, Ordovas JM, Hayden MR (1999) A common truncation variant of lipoprotein lipase (Ser447X) confers protection against coronary heart disease: the Framingham Offspring Study. Clin Genet 55:450–454
54. James AP, Watts GF, Barrett PH, Smith D, Pal S, Chan DC, Mamo JC (2003) Effect of weight loss on postprandial lipemia and low-density lipoprotein receptor binding in overweight men. Metabolism 52:136–141
55. Gill JM, Mees GP, Frayn KN, Hardman AE (2001) Moderate exercise, postprandial lipaemia and triacylglycerol clearance. Eur J Clin Invest 31:201–207
56. Williams CM, Moore F, Morgan L, Wright J (1992) Effects of n-3 fatty acids on postprandial triacylglycerol and hormone concentrations in normal subjects. Br J Nutr 68:655–666

Lipids (2008) 43:517–524
DOI 10.1007/s11745-008-3177-2

ORIGINAL ARTICLE

Fat Utilization in Healthy Subjects Consuming Diacylglycerol Oil Diet: Dietary and Whole Body Fat Oxidation

**Masanobu Hibi · Hideto Takase · Koichi Yasunaga ·
Tohru Yamaguchi · Ushio Harada ·
Yoshihisa Katsuragi · Ichiro Tokimitsu**

Received: 22 August 2007 / Accepted: 25 March 2008 / Published online: 12 April 2008
© AOCS 2008

Abstract Several studies in animals and humans have reported beneficial effects of diacylglycerol (DAG) on lipid and energy metabolism. We assessed the effect of DAG versus triacylglycerol (TAG) treatment on total energy expenditure (TEE), total fat oxidation (Fox) and respiratory quotient (RQ), and measured the oxidation rate of each oil using a respiratory chamber and the ^{13}C-stable isotope. Eleven healthy subjects participated in a double-blind, randomized crossover study. Subjects consumed an energy maintenance diet consisting of 55% of total calories from carbohydrate, 15% from protein and 30% from fat during both the 3-day pre-chamber and 36-h chamber period. Fifty percent of the fat was test oil, containing either DAG oil or TAG oil. The oxidation rate of ingested test oils was determined by monitoring $^{13}CO_2$ excretion in the breath from ^{13}C-labeled diolein or ^{13}C-labeled triolein. There were no significant differences in TEE, RQ and total Fox between the DAG and TAG treatment in the overall analysis. In the subgroup analysis, DAG treatment decreased RQ significantly in subjects with a high fat ratio (HFR) compared to TAG treatment. In addition, ingested diolein oxidation in DAG treatment was significantly faster than triolein oxidation in TAG treatment in the HFR group. Enhanced fat utilization with DAG treatment and rapid oxidation of ingested DAG may, at least in part, explain the greater loss of body weight and body fat related to DAG consumption found in the weight-loss studies.

M. Hibi (✉) · H. Takase · K. Yasunaga · T. Yamaguchi ·
U. Harada · Y. Katsuragi · I. Tokimitsu
Health Care Food Research Laboratories, Kao Corporation,
2-1-3, Bunka, Sumida-ku, Tokyo 131-8501, Japan
e-mail: hibi.masanobu@kao.co.jp

Keywords Diacylglycerol · Obesity · Total energy expenditure · Respiratory quotient · Total fat oxidation · Ingested fat oxidation · Respiratory chamber · ^{13}C-stable isotope

Introduction

The prevalence of obesity has increased worldwide. Obesity is an important risk factor for chronic diseases such as coronary heart disease, hypertension and diabetes. Genetic predisposition, physical inactivity, and composition of habitual diets are some of the factors identified as causes of obesity [1]. Among these, the amount of dietary fat in a usual diet is considered to be important in the development of obesity [2]. Therefore, it would be beneficial to have a dietary fat with properties of enhanced fat oxidation.

Diacylglycerol (DAG) oil reportedly has nutritional properties distinct from triacylglycerol (TAG) oil due to its different chemical structure [3–5]. Human studies in the US and Japan have demonstrated that long-term ingestion of DAG oil enhanced loss of body weight and body fat, in comparison with TAG oil [6–9]. Animal studies have also shown lower fat accumulation after DAG oil feeding compared to TAG oil feeding [10]. Although the mechanisms are still speculative, these effects are most likely attributable to enhanced β-oxidation in the liver and small intestine [11–13].

Recently, a few studies in humans examined the effect of DAG on fat utilization. Kamphuis et al. [14] showed significantly increased total fat oxidation (Fox) and reduced respiratory quotient (RQ) with DAG consumption compared to TAG consumption, with no difference in total energy expenditure (TEE). Saito et al. [15] reported significantly lower postprandial RQ and a trend toward higher postprandial energy expenditure after DAG ingestion. Although significantly increased total fat utilization after DAG consumption was found in these studies, whether the oxidation rate of ingested DAG itself contributes to the enhanced total fat utilization is yet to be examined.

The combination technique of the respiratory chamber and fatty acid labeled with ^{13}C stable isotope enables the accurate determination of ingested fat oxidation during practical daily life activities over a long period of time. The primary objective of this study was to determine the effects of short-term DAG consumption on energy metabolism, with special attention paid to the rate of ingested DAG oxidation.

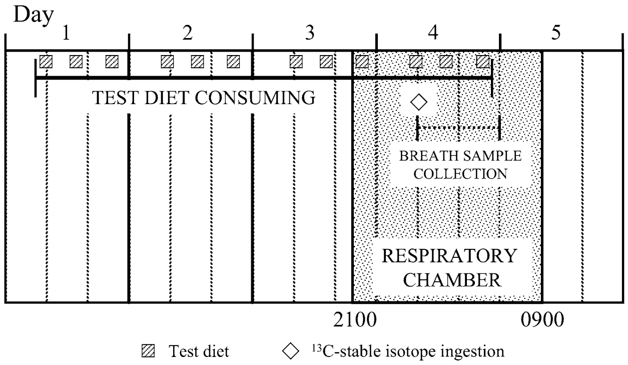

Fig. 1 Schematic representation of test diet consuming periods and measurement of energy metabolism and substrate utilization in respiratory chamber

Table 1 Fatty acid and glyceride compositions of test oils

	TAG	DAG
Glyceride composition (wt.%)		
Monoglyceride	ND	0.4
Diglyceride	1.0	84.1
Triglyceride	99.0	15.5
Fatty acid composition (wt.%)		
C14:0	0.1	0.9
C16:0	6.4	4.0
C18:0	2.4	1.5
C18:1	33.7	36.4
C18:2	48.8	47.1
C18:3	7.5	9.3
C20:0	0.4	0.2

ND not detectable

Methods

Subjects

Eight males and six females [age: 38.5 ± 5.5 years; body mass index (BMI): 24.2 ± 2.7 kg/m^2] were recruited from the local population. After receiving a full explanation of the study, all subjects gave their informed consent to participate in the study, which was approved by the Clinical Research Ethical Committee of Shibuya Core Clinic (Tokyo, Japan). All subjects were healthy according to their medical histories. All were non-smokers, and had no metabolic disorders. The study was performed in accordance with the principles of the Helsinki Declaration.

Study Design

The study was a randomized, double-blind, placebo-controlled crossover design with three stays in a respiratory chamber. After the first chamber stay, which acclimated the subjects to the process, they were randomized into either the DAG or TAG diet group for the second chamber stay. Then, they had a 4-week rest period before crossing over and receiving the opposite test diet for the third chamber stay. Each test diet was consumed for a 4-day period, including the period of the chamber stay from the night of day 3 until the morning of day 5 (Fig. 1).

Test Oils

The DAG oil used in the present study was prepared from soybean oil and rapeseed oil in the presence of immobilized lipase [16]. The prepared DAG oil contained more than 80% diacylglycerol and the ratio of 1(3),2-diacylglycerol to 1,3-diacylglycerol was approximately 3:7. TAG oil was prepared by mixing rapeseed, safflower and perilla oils so the fatty acid composition was similar to that of DAG oil. Fatty acid and glyceride compositions are shown in Table 1. The test oil was served as a mayonnaise-type food that contained 66.3 wt.% of the test oil.

Test Diet and Chamber Protocol

Total energy intake of the test diet was calculated for each subject by multiplying the subject's estimated basal metabolic rate (BMR) by a physical activity level of 1.4. BMR was estimated using the Harris–Benedict equation [17]. The macronutrient composition of the test diet was made up of 55% of total calories from carbohydrate, 15% from protein and 30% from fat. Fifty percent of the total fat was taken from the test oil served as a mayonnaise-type food. The test diet was allocated as 30% for breakfast, 30% for lunch and 40% for dinner.

Subjects were required to consume the test diet provided by the study investigator for a 4-day period, including the chamber stay. Subjects entered the respiratory chamber at

2100 hours on day 3 and left at 0900 hours on day 5. During the 36-h stay in the respiratory chamber, subjects were served dinner at 2100 hours on day 3, breakfast at 0900 hours, lunch at 1500 hours and dinner at 2100 hours on day 4. In the respiratory chamber, subjects were required to perform two sessions of a 20-min bicycle exercise at a rate of 120 heartbeats/min at 1430 and 2030 hours. The metabolic data in the respiratory chamber were analyzed at 36-h and at 24-h after from entering the respiratory chamber at 2100 hours on day 3 to 2100 hours on day 4.

Anthropometrics and Body-Composition Measurement

Body weight, height and whole-body dual-energy X-ray absorptiometry (DEXA, Hologic Inc., QRD 4500 W, Waltham, MA) measurement were performed during the washout period. Measurements of fat mass (FM), fat-free mass (FFM) and body fat ratio (BFR) were made with the use of Hologic Systems Software according to procedures outlined in the Hologic QRD 4500 User's Guide. Body fat ratio (BFR) was calculated using the following equation: BFR (%) = FM/(FM + FFM) × 100.

Respiratory Chamber

The whole-room respiratory chamber was a 16-m^3 room with a bed, chair, desk, sink, toilet, exercise bike (Combi Wellness Co. Ltd., Tokyo, Japan), telephone, personal computer, radio and CD player. The room temperature was set at 25 °C, the humidity was set at 50% and the fresh air rate was set at 100 L/min. A fan drew mixed air (sample air) out of the chamber, while fresh air was forced into the chamber by the resulting negative pressure. The air samples were dried using a gas sampling unit (Shimadzu Corp., CPF-8000, Kyoto, Japan) and analyzed using a mass spectrometer (Thermo Fisher Scientific, VG PRIMA δB, Cheshire, UK), which was calibrated biweekly using standard gas (N_2 78.08%, CO_2 0.033%, O_2 20.95% and Ar 0.934%). The flow rate exhausted from the chamber was measured by a mass flow meter (Yamatake Corp., CMQ0200J-K, Tokyo, Japan). The oxygen consumption (VO_2) and carbon dioxide production (VCO_2) were calculated using the method reported by Brown et al. [18]. Gas concentration was analyzed every 14 s and data were calculated every 5 min to obtain stable and accurate gas concentration. The gas concentration for 5 min was determined from the mid-point of the least square linear regression lines in this time period. The fresh air was analyzed every hour. TEE was calculated by VO_2 and VCO_2 according to the method of Weir [19]. Total Fox were calculated using the following formula [20]:

$$\text{Total Fox (g/d)} = 1.718 \times VO_2 - 1.718 \times VCO_2 - 0.315 \times P$$

The sleeping metabolic rate (SMR) was defined as the lowest mean energy expenditure over three consecutive hours between 0000 and 0800 hours [21]. P is protein oxidation (g/d) calculated from protein intake.

Oxidation Rate of Ingested Test Oil

^{13}C-labeled diolein and triolein, used as probes for measurement of ingested test oil oxidation, were synthesized from ^{13}C-labeled oleic acid (purity of oleic acid >99%, ^{13}C >99%, Isotec Inc., OH) and free glycerol using the method described by Watanabe et al. [16] and purified with silica gel liquid chromatography. The glyceride composition of each probe was determined by gas–liquid chromatography (Table 2). The ratio of ^{13}C-labelled 1(3),2-diolein and 1,3-diolein was approximately 3:7. ^{13}C-labeled diolein or triolein at a dose of 900 mg was added to the DAG and TAG diets as a portion of breakfast at 0900 hours on day 4. Breath samples were collected into aluminum bags (GL Science Inc., Japan) before breakfast (baseline) and then hourly for a period of 8-h, and again at 10 and 15-h. Enrichment of $^{13}CO_2$ in the breath was analyzed by isotope ratio mass spectrometry (Sercon, ANCA-GSL, UK). The oxidation rates of the ^{13}C-labeled diolein and triolein were calculated as the dose recovery rate in the breath, described by Murphy et al. [22], with some modification as follows:

$$\begin{aligned}\text{Atom\%} &= {}^{13}CO_2/({}^{12}CO_2 + {}^{13}CO_2)\\ &\quad \times 100\,{}^{13}\text{C excretion to } {}^{13}\text{C administered ratio}\\ &= (\text{Atom\%}^{T} - \text{Atom\%}^{B})/100 \times VCO_2^{T}/(M \times 22.4)\end{aligned}$$

where Atom%^{B} denotes the Atom% at baseline, Atom%^{T} denotes Atom% at each time, VCO_2^T denotes the VCO_2 measured by the respiratory chamber for 1 h prior to the time point of breath sample collection, and M denotes the molar of ^{13}C-labeled oleic acid administered in diolein or triolein. The ^{13}C dose recovery in breath (%) was measured for 15 h at each time point after the test meal ingestion. The cumulative dietary triolein or diolein oxidation was

Table 2 Glyceride compositions of ^{13}C tri- or diolein

	TAG	DAG
Glyceride composition (wt.%)		
Monoglyceride	0.26	1.71
Diglyceride	3.94	96.14
Triglyceride	95.80	2.15
Free fatty acid	1.12	0.33

determined from the cumulative values of ^{13}C dose recovery in breath.

Statistical Analysis

Data are presented as means ± SD. Possible differences in TEE, RQ and total Fox between TAG treatment and DAG treatment were analyzed using a paired *t* test. At first, relationships between the differences in metabolic parameters in TAG versus DAG treatment and the subjects' body compositions were assessed by a Spearman rank correlation coefficient. The subgroup analysis was performed when significant correlation was found. Analysis of variance (ANOVA) models were generated using a PROC MIXED procedure. Repeated measures ANOVA was used to assess the effects of treatment-by-time interactions on delta from the baseline in ^{13}C doses recovered in breath. Statistical analyses were performed with the SAS systems for Windows (release 8.2, SAS Institute Inc., Cary, NC).

Results

Subjects and Baseline Characteristics

Of the 14 subjects enrolled, 2 did not complete the study. One subject discontinued for private reasons and the other subject withdrew for medical reasons unrelated to the study treatment. Of 12 subjects who completed the study, 1 was excluded from the analysis because of menstruation in the respiratory chamber. As a result, the data of 11 subjects (6 men and 5 women) were used for the analysis. The baseline characteristics of subjects are shown in Table 3.

Table 3 Baseline characteristics of subjects

	All	HFR	LFR
Sex (M/F)	M = 6/F = 5	M = 2/F = 4	M = 4/F = 1
Age (year)	38.5 ± 5.5	37.2 ± 5.6	40.0 ± 5.7
Weight (kg)	67.1 ± 8.6	67.3 ± 8.4	66.9 ± 9.7
Height (cm)	166.4 ± 6.4	164.3 ± 6.8	168.9 ± 5.5
BMI (kg/m^2)	24.2 ± 2.7	24.9 ± 2.9	23.4 ± 2.5
FFM (kg)	48.6 ± 8.1	45.6 ± 7.4	52.1 ± 8.1
FM (kg)	17.3 ± 4.6	19.8 ± 4.6	14.3 ± 2.3[a]
Body fat ratio (%)	26.3 ± 6.2	30.2 ± 5.6	21.6 ± 2.6[a]

Values are means ± SD

[a] Significant difference from HFR group at baseline by unpaired *t* test ($p < 0.05$)

Energy Expenditure and Substrate Utilization

TEE, RQ and total Fox for 36 h are shown in Table 4. The data from all subjects showed no significant differences in TEE, RQ and total Fox for 36 h between TAG and DAG treatment. TEE in TAG and DAG treatment were 11.52 ± 1.62 and 11.41 ± 1.68 MJ, respectively. The energy intake for all subjects was 8.88 ± 1.01 MJ during the test period per day. This value agreed with the appropriate intake as defined by the guidelines of the Ministry of Health and Welfare in Japan. The energy intake in respiratory chamber stays for 36 h was 12.43 ± 1.42 MJ. Energy balance for 36 h was slightly positive in both groups and did not differ between TAG and DAG treatment (0.91 ± 0.93 and 1.02 ± 1.11 MJ, respectively). During the 24 h inside the respiratory chamber, TEE was 8.18 ± 1.17 MJ in TAG treatment and 8.11 ± 1.18 MJ in DAG treatment. TEE for 24 h did not differ between treatments. Both 36-h TEE and SMR (mean values of two nights in the chamber) positively correlated with FFM in the TAG treatment (FFM vs. 36-h TEE; $r = 0.745$, $p = 0.009$, FFM vs. SMR; $r = 0.718$, $p = 0.013$). Mean RQ and total Fox for the 36-h analyses showed no significant differences between the TAG and DAG treatments (RQ; 0.867 ± 0.020 and 0.870 ± 0.020, total Fox; 94.4 ± 29.8 and 90.3 ± 29.8 g, for TAG and DAG, respectively). For 24 h, mean RQ and total Fox also showed no significant differences between TAG and DAG treatments (RQ; 0.867 ± 0.020 and 0.869 ± 0.023, total Fox; 66.9 ± 20.8 and 64.8 ± 22.3 g, for TAG and DAG, respectively).

In order to further examine the metabolic effect of DAG on fat utilization, we conducted a post-hoc subgroup analysis. ΔRQ for each subject was calculated by subtracting the 36-h RQ in the DAG treatment from that in the TAG treatment and their correlation with various anthropometric parameters were examined. Among various parameters, a strong positive correlation of ΔRQ in body fat ratio was found, suggesting enhanced fat utilization in the subjects with higher body fat ratio ($r = 0.855$, $p < 0.001$, Fig. 2).

After observing this significant correlation, subgroup analyses were performed with the two subgroups divided by median of body fat ratio (24.4%): the high fat ratio (HFR) group and the low fat ratio group (LFR). The HFR group consisted of six subjects (two men and four women), and the LFR group consisted of five subjects (four men and one woman). At baseline, there were no significant differences in fat-free mass and BMI between the two subgroups (Table 3). In each subgroup, the parameters for energy metabolism were compared between TAG and DAG treatments. Mean RQ for 36 h in the HRF group was significantly lower with DAG treatment than with TAG

Table 4 Energy expenditure and substrate utilization during 36 hours of treatment with diacylglycerol or triacylglycerol consumption

	TAG			DAG		
	All	HFR	LFR	All	HFR	LFR
TEE (MJ/36 h)	11.52 ± 1.62	11.30 ± 1.52	11.77 ± 1.87	11.41 ± 1.68	11.35 ± 1.86	11.47 ± 1.65
36-h RQ	0.867 ± 0.020	0.875 ± 0.021	0.857 ± 0.016	0.870 ± 0.020	0.869 ± 0.023[a]	0.871 ± 0.019
Total Fox (g/36 h)	94.4 ± 29.8	84.7 ± 30.3	106.1 ± 27.7	90.3 ± 29.8	91.9 ± 36.3	88.3 ± 23.7

Values are means ± SD

[a] Significantly lower than TAG on HFR group (paired *t* test): $p = 0.003$

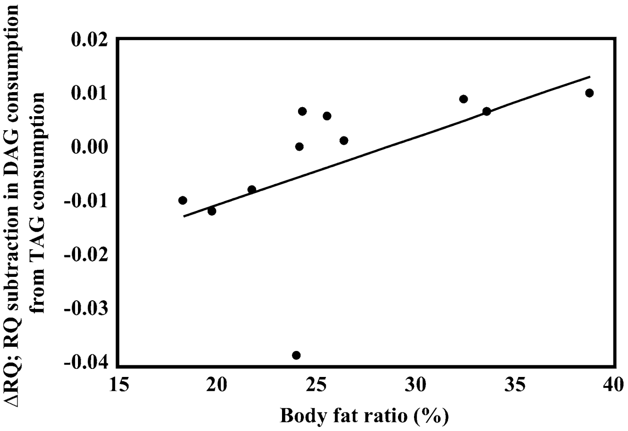

Fig. 2 Correlation of body fat rate with difference in RQ between DAG and TAG treatment. ΔRQ for each subject was calculated by subtracting 36-h RQ in DAG treatment from that in TAG treatment. The relationships between the ΔRQ and the subjects' body compositions were assessed by a Spearman rank correlation coefficient ($r = 0.855$, $p < 0.001$)

treatment ($p = 0.003$), but the LFR group did not show a difference between the TAG and DAG treatments (Table 4). TEE and total Fox for 36 h did not differ significantly between treatments in each subgroup.

Oxidation of Ingested Test Fat

Oxidation of ingested test fat was assessed for 15 h by measuring ^{13}C-labeled CO_2 after ingestion of ^{13}C diolein or ^{13}C triolein on day 4. The recovery rates of $^{13}CO_2$ in the breath peaked at 6 h and had almost returned to baseline at 15 h (0.78 ± 0.22 and 0.70 ± 0.12%, TAG and DAG, respectively). The cumulative recovery of $^{13}CO_2$ in the breath of all subjects during the 15-h period is not significantly different between treatment groups (29.0 ± 5.7 and 29.4 ± 4.7%, for TAG and DAG, respectively). Subgroup analyses were performed with the two subgroups. The cumulative values of $^{13}CO_2$ in breath over 15 h did not differ significantly between the TAG and DAG treatments (LFR; 32.0 ± 4.8 and 29.8 ± 3.8%, HFR; 26.6 ± 5.5 and 29.1 ± 5.8%, for TAG and DAG, respectively). The time course of the cumulative recovery rate for $^{13}CO_2$ in the HFR group is shown in Fig. 3. The repeated measures ANOVA showed significant ($p = 0.008$) treatment-by-time interaction in the time course for cumulative recovery of $^{13}CO_2$ in the HFR group.

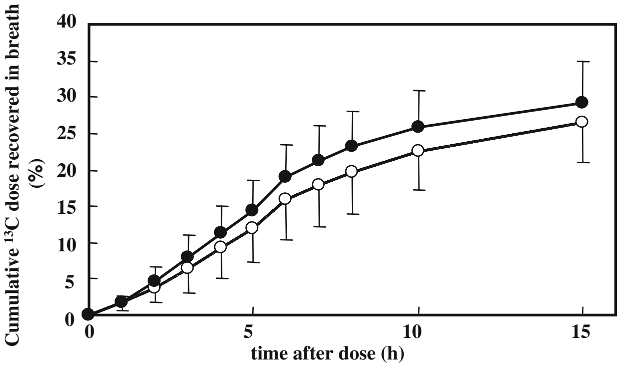

Fig. 3 Cumulative $^{13}CO_2$ recovery in breath over 15 h in the HFR group. Time zero corresponds to the time of [^{13}C] enriched meal ingestion. The cumulative dietary triolein or diolein oxidation determined from cumulative values of ^{13}C dose recovery in breath. *Closed circles*, diolein; *open circles*, triolein. Data are shown as means ± SD. The repeated measures ANOVA showed significant ($p = 0.008$) treatment-by-time interaction in the time course for cumulative recovery of $^{13}CO_2$ in the HFR group

Discussion

In the present study, the effect of short-term DAG treatment on energy metabolism was investigated with emphasis on the rate of ingested DAG oxidation using the combination technique of a respiratory chamber and fatty acid labeled with ^{13}C-stable isotope. In the analysis of all subjects, TEE, RQ and total Fox during 36-h showed no difference between TAG and DAG treatments. Because the subjects in our study had various backgrounds, their BMI varied from 19.8 to 29.3 kg/m^2, and body fat ratio varied from 18.3 to 38.7%, so the metabolic parameters were greatly influenced by the physical parameters. However, we found that the extent of reduction of RQ caused by DAG treatment had a positive correlation with the body fat ratio of each subject (Fig. 2). In the post-hoc subgroup analysis, significantly lower RQ was observed in DAG treatment compared to TAG treatment, suggesting that DAG treatment increased fat utilization. Though the results from the post-hoc subgroup analysis provide limited evaluation, it is noteworthy that DAG oil showed an enhanced fat utilization in subjects with higher body fat ratios.

Kamphuis et al. [14] investigated the effect of DAG treatment over 36 h, determined by use of a respiratory chamber. In 12 female subjects (average body fat ratio; 32.5 ± 5.3%), they observed significantly lower RQ but no change in TEE in DAG treatment compared to TAG treatment. These results are consistent with those obtained from the present study with the HFR subgroup with respect to the body fat ratio of the subjects and the extent of the reduction in RQ. Indeed the reductions in RQ level in the study conducted by Kamphuis and in the present study were 0.006 and 0.005, respectively. Although the RQ measured in the respiratory chamber was affected by energy balance, by PFC balance of intake and by the subjects' own background, it is an appropriate predictor of weight loss [23, 24]. The subjects who rely less on fat oxidation have a tendency to gain weight, possibly because they are more prone to store excess energy as fat [25]. The enhanced fat utilization that occurs with DAG oil consumption changes fat balance (fat intake minus fat oxidation). Fat balance over the short-term (days), which is measured by a respiratory chamber, is possibly more closely related to energy balance over the long term (weeks or months) [26]. In the present study, we observed only the difference between DAG treatment and TAG treatment on fat utilization to explain the differences in the effect that DAG oil and TAG oil appears to have on body fat stores. Based on these results, it can be assumed that over the long term DAG oil consumption has a different effect on energy expenditure and energy intake.

Several long-term clinical trials have indicated that DAG consumption results in a loss of body weight and body fat in healthy, non-obese men and women, as well as with obese men and women. In the study with 38 male subjects conducted by Nagao et al. [7], subjects who consumed DAG over 4 months experienced 1.5 kg more reduction in body weight compared to subjects who consumed TAG. Whereas, in the present study, in the HFR subgroup, experienced a total Fox increased of 4 g/d (NS) with DAG consumption compared to TAG consumption, which estimates 0.48 kg of weight loss for 4 months based on the simple extrapolation. In addition, subjects in the present study consumed DAG approximately three-fold more than subjects in the study of Nagao et al. Taking these discrepant levels in total Fox and dosages of DAG into consideration, the increased total Fox on short-term DAG treatment observed from the present study cannot completely explain the full-extent of weight loss reported in the study of long-term DAG consumption, suggesting that other factors may contribute to the weight loss with a long-term DAG consumption. In C57BL/6J mice, which are a model for diet-induced obesity, the small intestinal β-oxidation activity and mRNA expression of lipid metabolism-related molecules were markedly increased after long-term intake of DAG oil [12]. Further studies are needed to examine the relationship precisely between alteration in energy metabolism and body weight loss associated with long-term DAG consumption.

Ingested fat oxidation was investigated next, to gain further insight into the mechanism responsible for enhanced fat utilization after short-term DAG treatment. The oxidation of ingested fat was assessed using the combination technique of a respiratory chamber and ^{13}C-labeled diolein or triolein. The mean ^{13}C-labeled triolein oxidation over 15-h after oral administration was 29.0 ± 5.7% in the present study. This level is similar to data reported previously [27, 28]. The rates of ingested ^{13}C-labeled diolein and triolein oxidation were compared (Fig. 3). The repeated measures ANOVA showed significant ($p = 0.008$) treatment-by-time interaction in the time course for cumulative recovery of $^{13}CO_2$ in the HFR group. We found small, but significant, differences in oxidation kinetics between DAG and TAG. This rapid oxidation of ingested DAG may partly explain increased total fat utilization in DAG treatment compared to TAG treatment.

Insulin is the most potent regulator in postprandial fat metabolism through the mediation of lipoprotein lipase (LPL) and hormone-sensitive lipase (HSL) [29]. Saito et al. [15] reported lower postprandial insulin and RQ after loading with a DAG meal compared to a TAG meal. The lower postprandial insulin levels after DAG consumption compared to TAG consumption indicated a smaller stimulus in the direction of fat storage and increased postprandial fat utilization through the regulation of LPL and HSL, which may be associated with the present findings of increased total fat utilization in DAG treatment. The mechanism of pronounced fat utilization of DAG, observed only in the HFR group, is yet to be clarified, and further investigation is needed. Nagao et al. [7] reported that weight loss by long-term DAG consumption was pronounced in the subjects with higher intra-abdominal fat areas, which is partially explained by the present results in the HFR group. 1,3-DAG, a major component of DAG oil, is more susceptible to the beneficial effect against obesity compared to TAG or 1(3),2-DAG; Previous and present results suggest that 1,3-DAG might up-regulate fat utilization leading to greater β-oxidation in the intestine and liver, and/or via insulin action (Fig. 4).

In conclusion, TEE, RQ and total Fox for 36 h in the respiratory chamber showed no differences between DAG

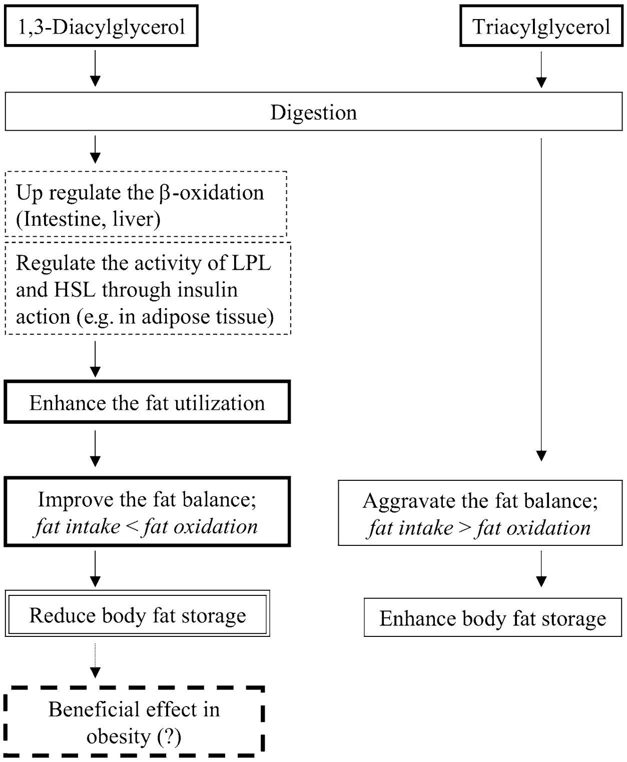
1,3-Diacylglycerol
Triacylglycerol
Digestion
Up regulate the β-oxidation (Intestine, liver)
Regulate the activity of LPL and HSL through insulin action (e.g. in adipose tissue)
Enhance the fat utilization
Improve the fat balance; fat intake < fat oxidation
Aggravate the fat balance; fat intake > fat oxidation
Reduce body fat storage
Enhance body fat storage
Beneficial effect in obesity (?)

Fig. 4 Diagrammatic representation of the effects of 1,3-DAG on fat metabolism. The differential metabolic pathway of 1,3-DAG is speculated to up-regulate the fat utilization leading to the greater β-oxidation in intestine and liver, and/or via the insulin action. In the present study, it was shown that oxidation of ingested DAG was more rapid than that of TAG in subjects with a high body fat ratio (HFR). Simultaneously, fat utilization after a DAG meal was greater than that after a TAG meal in HFR subjects. These changes of fat utilization may reduce a body fat storage through the improvement of fat balance under free-living conditions

treatment and TAG treatment in all subjects. However, post-hoc analysis showed that oxidation of ingested DAG was more rapid than that of TAG, and that fat utilization after a DAG meal was greater than that after a TAG meal in HFR subjects. Although further analyses are needed to examine these increases in fat utilization, these changes experienced by HFR subjects may in part explain the greater loss of body weight and body fat found in weight-loss studies after DAG oil consumption.

Acknowledgments This work was supported by the Kao Corporation. None of the authors of this manuscript have any conflicts of interest. We deeply appreciate the instruction and advice given Dr. Shigeru Kobayashi, Chief Surgeon, Tokyo Rinkai Hospital, during this study.

References

1. Prentice AM, Poppitt SD (1996) Importance of energy density and macronutrients in the regulation of energy intake. Int J Obes Relat Metab Disord 20:S18–23
2. Bray GA, Popkin BM (1998) Dietary fat intake does affect obesity! Am J Clin Nutr 68:1157–1173
3. Abdel-Nabey AA, Shehata AAY, Ragab MH, Rossell JB (1992) Glycerides of cottonseed oils from Egyptian and other varieties. Riv Ital Stostanze Grasse 69:443–447
4. D' Alonzo RP, Kozarek WJ, Wade RL (1982) Glyceride composition of processed fats and oils as determined by glass capillary gas chromatography. J Am Oil Chem Soc 58:1416–1419
5. Rudkowska I, Roynette CE, Demonty I, Vanstone CA, Jew S, Jones PJ (2005) Diacylglycerol: efficacy and mechanism of action of an anti-obesity agent. Obes Res 13:1864–1876
6. Maki KC, Davidson MH, Tsushima R, Matsuo N, Tokimitsu I, Umporowicz DM, Dicklin MR, Foster GS, Ingram KA, Anderson BD, Frost SD, Bell M (2002) Consumption of diacylglycerol oil as part of a reduced-energy diet enhances loss of body weight and fat in comparison with consumption of a triacylglycerol control oil. Am J Clin Nutr 76:1230–1236
7. Nagao T, Watanabe H, Goto N, Onizawa K, Taguchi H, Matsuo N, Yasukawa T, Tsushima R, Shimasaki H, Itakura H (2000) Dietary diacylglycerol suppresses accumulation of body fat compared to triacylglycerol in men in a double-blind controlled trial. J Nutr 130:792–797
8. Teramoto T, Watanabe H, Ito K, Omata Y, Furukawa T, Shimoda K, Hoshino M, Nagao T, Naito S (2004) Significant effects of diacylglycerol on body fat and lipid metabolism in patients on hemodialysis. Clin Nutr 23:1122–1126
9. Matsuyama T, Shoji K, Watanabe H, Shimizu M, Saotome Y, Nagao T, Matsuo N, Hase T, Tokimitsu I, Nakaya N (2006) Effects of diacylglycerol oil on adiposity in obese children: initial communication. J Pediatr Endocrinol Metab 19:795–804
10. Murase T, Mizuno T, Omachi T, Onizawa K, Komine Y, Kondo H, Hase T, Tokimitsu I (2001) Dietary diacylglycerol suppresses high fat and high sucrose diet-induced body fat accumulation in C57BL/6J mice. J Lipid Res 42:372–378
11. Murata M, Ide T, Hara K (1997) Reciprocal responses to dietary diacylglycerol of hepatic enzymes of fatty acid synthesis and oxidation in the rat. Br J Nutr 77:107–121
12. Murase T, Aoki M, Wakisaka T, Hase T, Tokimitsu I (2002) Anti-obesity effect of dietary diacylglycerol in C57BL/6J mice: dietary diacylglycerol stimulates intestinal lipid metabolism. J Lipid Res 43:1312–1319
13. Kondo H, Hase T, Murase T, Tokimitsu I (2003) Digestion and assimilation features of dietary DAG in the rat small intestine. Lipids 38:25–30
14. Kamphuis MM, Mela DJ, Westerterp-Plantenga MS (2003) Diacylglycerols affect substrate oxidation and appetite in humans. Am J Clin Nutr 77:1133–1139
15. Saito S, Tomonobu K, Hase T, Tokimitsu I (2005) Effects of diacylglycerol on postprandial energy expenditure and respiratory quotient in healthy subjects. Nutrition 22:30–35
16. Watanabe T, Shimizu M, Sugiura M, Sato M, Kohori J, Yamada N, Nakanishi K (2003) Optimization of reaction conditions for the production of DAG using immobilized 1,3-regiospecific lipase lipozyme RM IM. J Am Oil Chem Soc 80:1201–1207
17. Harris JA, Benedict FG (1919) A biometric study of basal metabolism in man. Carngie Institution, Washington
18. Brown D, Cole TJ, Dauncey MJ, Marrs RW, Murgatroyd PR (1984) Analysis of gaseous exchange in open-circuit in-direct calorimetry. Med Biol Eng Comput 22:333–338
19. Weir JB (1949) New methods for calculating metabolic rate with special reference to protein metabolism. Nutrition 6:213–221
20. Brouwer E (1957) On simple formulae for calculating the heat expenditure and the quantities of carbohydrate and fat oxidized in metabolism of men and animals, from gaseous exchange (oxygen intake and carbonic acid output) and urine-N. Acta Physiol Pharmacol Neerl 6:795–802

21. Schrauwen P, van Marken Lichtenbelt WD, Westerterp KR (1997) Energy balance in a respiration chamber: individual adjustment of energy intake to energy expenditure. Int J Obes Relat Metab Disord 21:769–774
22. Murphy JL, Jones A, Brookes S, Wootton SA (1995) The gastrointestinal handling and metabolism of [1–13C] palmitic acid in healthy women. Lipids 30:291–298
23. Zurlo F, Lillioja S, Esposito-Del Puente A, Nyomba BL, Raz I, Saad MF, Swinburn BA, Knowler WC, Bogardus C, Ravussin E (1990) Low ratio of fat to carbohydrate oxidation as predictor of weight gain: study of 24-h RQ. Am J Physiol 259:E650–E657
24. Schutz Y (1995) Abnormalities of fuel utilization as predisposing to the development of obesity in humans. Obes Res 3:173S–178S
25. Seidell JC, Muller DC, Sorkin JD, Andres R (1992) Fasting respiratory exchange ratio and resting metabolic rate as predictors of weight gain: the Baltimore Longitudinal Study on Aging. Int J Obes Relat Metab Disord 16:667–674
26. Schutz Y (2004) Concept of fat balance in human obesity revisited with particular reference to de novo lipogenesis. Int J Obes Relat Metab Disord 28(Suppl 4):S3–S11
27. DeLany JP, Windhauser MM Champagne CM, Bray GA (2000) Differential oxidation of individual dietary fatty acids in humans. Am J Clin Nutr 72:905–911
28. Jones PJ, Pencharz PB, Clandinin MT (1985) Whole body oxidation of dietary fatty acids: implications for energy utilization. Am J Clin Nutr 42:769–777
29. Fielding BA, Frayn KN (1998) Lipoprotein lipase and the disposition of dietary fatty acids. Br J Nutr 80:495–502

Lipids (2008) 43:525–531
DOI 10.1007/s11745-008-3186-1

ORIGINAL ARTICLE

The Influence of Maternal Early to Mid-Gestation Nutrient Restriction on Long Chain Polyunsaturated Fatty Acids in Fetal Sheep

Yunhua Zhou · Mark Nijland · Myrna Miller ·
Stephen Ford · Peter W. Nathanielsz · J. Thomas Brenna

Received: 7 June 2007 / Accepted: 17 April 2008 / Published online: 15 May 2008
© AOCS 2008

Abstract The early to mid-gestational period (days 28–78) in sheep is the period of most rapid placental development. Maternal nutrient restriction (MNR) in this phase has negative consequences on fetal growth and development, predisposing the fetus to disease in adult life. The influence of MNR on fetal tissue fatty acids has not been reported. Ewes were fed to 50% (MNR) or 100% (control fed) of total digestible nutrients from days 28 to 78 of gestation. At 78 days, fetuses were sacrificed and the fatty acids in fetal liver, lung and muscle as well as maternal and fetal plasma were analyzed. Most fatty acids were not influenced by MNR. The n-3 long chain PUFA eicosapentaenoic acid (20:5n-3, EPA) concentration (μg/mg) was low and more than doubled in the MNR sheep. Similarly, docosapentaenoic acid (22:5n-3, DPA) increased by 60, 19, and 38% in liver, lung, and muscle, respectively. Neither docosahexaenoic acid (22:6n-3, DHA) nor any of n-6 PUFA changed. Arachidonic acid (20:4n-6; ARA) increased in MNR maternal plasma as a percent of total fatty acids only, while in MNR fetal plasma only EPA increased. These results provide the first indication that MNR in early to mid-gestation influences the profiles of LCPUFA in fetal tissues, and suggest that metabolic processes involving LCPUFA should be considered in evaluations of the impact of maternal nutriture on perinatal health.

Keywords Lipid metabolism · Metabolism · n-3 Fatty acids · Nutrition · Fatty acids · Maternal nutrient restriction

Introduction

The concept of developmental programming during fetal and neonatal life is well established. Extensive epidemiological evidence indicates that the nutritional and hormonal environment encountered by the fetus is a strong determinant of not only fetal growth but also disease risk in later life [1, 2]. These epidemiological findings are strongly supported by an increasing number of animal studies [3] indicating that fetal physiological development and organ sensitivity, including that of the lung, heart, and skeletal muscle, are significantly altered by maternal nutrient restriction (MNR). These adaptations may lead to predisposition of offspring to cardiovascular disease, type II diabetes and obesity in adult life [4–9].

Long chain polyunsaturated fatty acids (LCPUFA) have diverse roles in tissue function. Docosahexaenoic acid (DHA, 22:6n-3) and arachidonic acid (ARA, 20:4n-6) play critical roles in neurodevelopment during the perinatal period [10, 11]. LCPUFA are structural components of cell membranes and DHA is highly concentrated in brain grey matter and retina rod photoreceptors [11, 12]. Evidence from various studies suggests that retinal function and learning

Y. Zhou · J. T. Brenna (✉)
Division of Nutritional Sciences, Cornell University, Ithaca,
NY 14853, USA
e-mail: jtb4@cornell.edu

M. Nijland
Center for Pregnancy and Newborn Research,
Department of Obstetrics and Gynecology,
University of Texas Health Science Center,
San Antonio, TX, USA

M. Miller · S. Ford · P. W. Nathanielsz
Department of Animal Science, University of Wyoming,
Laramie, WY, USA

Present Address:
Y. Zhou
Institute of Nutrition, Shanghai, China

ability may be permanently impaired if there is a reduction in the accumulation of sufficient DHA during intrauterine life [13, 14]. ARA is associated with normal intrauterine growth, including weight and head circumference [15]. The precursors, linoleic acid (LA, 18:2n-6) and α-linolenic acid (ALA, 18:3n-3), are converted into LCPUFA by alternating desaturation (Δ6 and Δ5 desaturases) and chain elongation, however most studies indicate that the process is inefficient in humans and primates [16]. In addition to the well-studied ARA and eicosapentaenoic acid (EPA, 20:5n-3)-derived eicosanoids, recent studies indicate that DHA and EPA are substrates for potent bioactive compounds involved in the resolution phase of inflammation [17] and in neuroprotection [18]. Studies in rats demonstrate that n-3 LCPUFA, notably EPA and DHA, modulate the expression and repression in brain of a number of genes that are involved in structure, energy metabolism, neurotransmission, signal transduction and regulation [19–21].

The fatty acid pattern found in the walls of umbilical blood vessels suggests that the essential fatty acid status of a developing fetus is marginally sufficient [22, 23]. Supplementation of pregnant mothers with LCPUFA has been shown to improve offspring LCPUFA status [24]. However, the availability of the PUFA/LCPUFA to the fetus depends not only on the maternal dietary intake but also on the function of the placenta and the many physiological and biochemical adaptations that occur during pregnancy.

The pregnant sheep has been studied extensively to determine the effects of nutrient restriction during various periods of gestation [25]. Apart from these studies, there is a great deal of information on the influence of maternal dietary fatty acids on tissue fatty acids, particularly of the fetus. Tissue fatty acids differ in their sensitivity to diet: ARA is generally much less sensitive to diet than DHA, for instance [12]. The impact of other maternal dietary factors on fetal tissue PUFA is much less studied. Nothing is known about the influence of pure calorie restriction on fetal PUFA, and there are scant data on gene expression or related factors to guide formulation of a rational and grounded hypothesis. We therefore undertook an exploratory study to evaluate the impact of MNR on fetal fatty acids in sheep tissues. The present study was designed to determine the impact of MNR from early- to mid-gestation on profiles of fatty acids in maternal and fetal sheep to better understand the metabolism of LCPUFA in situations of maternal restriction.

Materials and Methods

Animals and Tissue Collection

All protocols were approved by the University of Wyoming Institutional Animal Care and Use Committee. Details of the diet and procedures used have been published elsewhere [7] and will be summarized here. The diet is based on beet pulp solids with fatty acid composition shown in Table 1. 18:2n-6 and 18:3n-3 are the only sources of the respective essential fatty acids, and their ratio of about 9–1 is similar to that of the human western diet. The fatty acids 16:0 and 18:1n-9 make up almost 50% of the balance of the fatty acids.

On day 28 of gestation, ewes were randomly assigned to a control-fed group ($n = 6$; 100% NRC requirements) and a nutrient-restricted group ($n = 6$; fed 50% NRC requirements). On day 78 of gestation ewes were given an overdose of sodium pentobarbital (Abbott Laboratories, Abbott Park, IL) and exsanguinated, and fetuses were removed. Fetal organs including liver, lung and muscle and maternal and fetal plasma were stored in a −80 °C freezer until analyzed.

Lipid Extraction and Analysis

Organ samples were processed by one step homogenization/extraction/methylation method of Garces and Mancha [26]. About 0.1 g sample was weighted and placed into a Pyrex tube. Two ml heptane, 1.4 ml of freshly made aqueous reagent (methanol: 2,2-dimethyl-3-pentanol:H_2SO_4 = 85:11:4 by volume) and 1.6 ml of organic reagent (heptane:toluene = 63:37 by volume) were added. Freshly prepared di-heptadecanoyl-phosphatidylcholine (Matreya, Inc Pleasant Gap, PA, USA) was also added as internal standard before extraction. After mixing the contents the tubes were stoppered and placed in a shaking water bath at 80 °C for 2 h. Upon cooling, tubes are thoroughly vortexed to yield a homogeneous solution similar in appearance to tissue homogenized by a rotary blade homogenizer. Two ml of saturated NaCl are then added, and after vortexing, phase separation was accomplished by centrifugation at 3,500 rpm for 10 min. The organic layer was removed by nitrogen evaporation.

All the purified FAME was dissolved in 200 μl heptane and stored in a −20 °C freezer until analysis.

Table 1 Composition of selected fatty acids in maternal feed

	Mean ± SD (%, w/w)
16:0	35.4 ± 3.8
Other SFA	6.5 ± 0.6
18:1n-9	12.7 ± 1.5
Other MUFA	7.1 ± 0.9
18:2n-6	30.7 ± 4.3
18:3n-3	3.4 ± 0.2
18:3 isomers	4.1 ± 0.1
n-6/n-3	9

Total FAME were analyzed by gas chromatography (GC) (Hewlett Packard 5890 series II GC with flame ionization detector; BPX-70 capillary column: 60 m × 0.32 mm I.D. × 0.25 µm film; SGE, Austin, TX, using H_2 as carrier gas). Each fatty acid was identified by GC-Covalent Adduct Chemical Ionization tandem mass spectrometry [27]. Quantitative profiles were calibrated using methyl-17:0 as an internal standard and an equal weight FAME mixture (68A; Nuchek Prep, Elysian, MN) to derive response factors for each FAME. Chromatography conditions and calibration details have been reported previously [28]. The concentration of each fatty acid from 14 to 24 carbons is expressed as µg fatty acid per mg wet tissue weight or mg fatty acid per ml plasma.

Statistics

Data are expressed as means ± SD. Concentrations of fatty acids in differently fed groups were tested for significant differences. A *t*-test was performed on a pairwise basis with significance declared at $P < 0.05$. Statistics were calculated using functions provided in Excel 2000 for WinXP (Microsoft, Redmond, WA). No correction for multiple comparisons was applied.

Table 2 Fetal and fetal organ weights from conceptuses on day 78 of gestation from control–fed and nutrient-restricted ewes

	Control fed ($n = 6$)	Nutrient restricted ($n = 6$)
Fetal weight (g)	268 ± 28	211 ± 21*
Liver (g)	15.9 ± 2.4	13.4 ± 1.5*
Lung (g)	13.7 ± 1.8	10.8 ± 2.0*
Ld[a] muscle (g)	2.5 ± 0.4	2.1 ± 0.3*

* Means ± SD within a row and measurement differ ($P < 0.05$)

[a] Longissimus dorsi muscle

Results

Table 2 presents weights of the fetuses and several organs. MNR reduced fetal body weight about 21%, with reductions of 16, 21, and 17% in liver, lung, and longissimus dorsi muscle weights, respectively.

Table 3 presents the maternal and fetal plasma fatty acid concentrations, expressed as mg/ml plasma; in cases in which the proportion of fatty acids as a weight percent of total (%, w/w) was significant, these data are presented as well. As expected, fetal plasma had enhanced 20:4n-6 and 22:6n-3 compared to maternal plasma, as well as 20:3n-9 (Mead acid). Significant differences in plasma fatty acid concentrations were not found for any fatty acid in either compartment. A 13% decrease in 16:0 as %, w/w was found in fetal plasma due to MNR, while in maternal plasma MNR induced a 24% increase in 18:1 and a 14% decrease in 20:4n-6.

Table 4 presents the effects of MNR fetal liver, lung and skeletal muscle fatty acid composition. MNR did not induce changes in the overwhelming majority of saturated and monounsaturated fatty acid concentrations compared with control group. There was an increase of 24% in

Table 3 Fetal and maternal plasma fatty acids concentrations

Fatty acid	Fetal plasma		Maternal plasma	
	C	MNR	*C*	MNR
16:0	0.30 ± 0.03, 25.3 ± 1.2	0.25 ± 0.04, 22.1 ± 1.7**	0.38 ± 0.05	0.39 ± 0.02
18:0	0.18 ± 0.03	0.18 ± 0.03	0.25 ± 0.08	0.23 ± 0.04
16:1n-9/n-7	0.088 ± 0.02	0.081 ± 0.010	0.058 ± 0.006	0.058 ± 0.005
18:1n-9/n-7	0.31 ± 0.04	0.31 ± 0.04	0.24 ± 0.04 (18.7 ± 1.1)	0.31 ± 0.04 (23.1 ± 1.6**)
20:3n-9	0.040 ± 0.013	0.035 ± 0.006	0.022 ± 0.006	0.020 ± 0.007
18:2n-6	0.054 ± 0.013	0.046 ± 0.023	0.18 ± 0.03	0.17 ± 0.01
20:4n-6	0.098 ± 0.016	0.097 ± 0.016	0.063 ± 0.009 (4.89 ± 0.31)	0.057 ± 0.011 (4.28 ± 0.51**)
18:3n-3	–[a]	–[a]	–[a]	–[a]
20:5n-3	0.024 ± 0.007	0.031 ± 0.005	0.023 ± 0.026	0.027 ± 0.011
22:5n-3	0.027 ± 0.007	0.031 ± 0.005	0.032 ± 0.009	0.039 ± 0.007
22:6n-3	0.063 ± 0.003	0.054 ± 0.012	0.037 ± 0.007	0.037 ± 0.008
Σfatty acid	1.16 ± 0.11	1.11 ± 0.12	1.29 ± 0.17	1.33 ± 0.12

All fatty acids are presented as mean ± SD, in units of mg/ml. In cases of significant differences ($P < 0.05$) for %, w/w, these units are entered in the same cell immediately below

ND not detected

* Different from control ($P < 0.05$). ** Different from control only when expressed as relative weight percent of fatty acids (%, w/w)

[a] Trace, below quantifiable levels

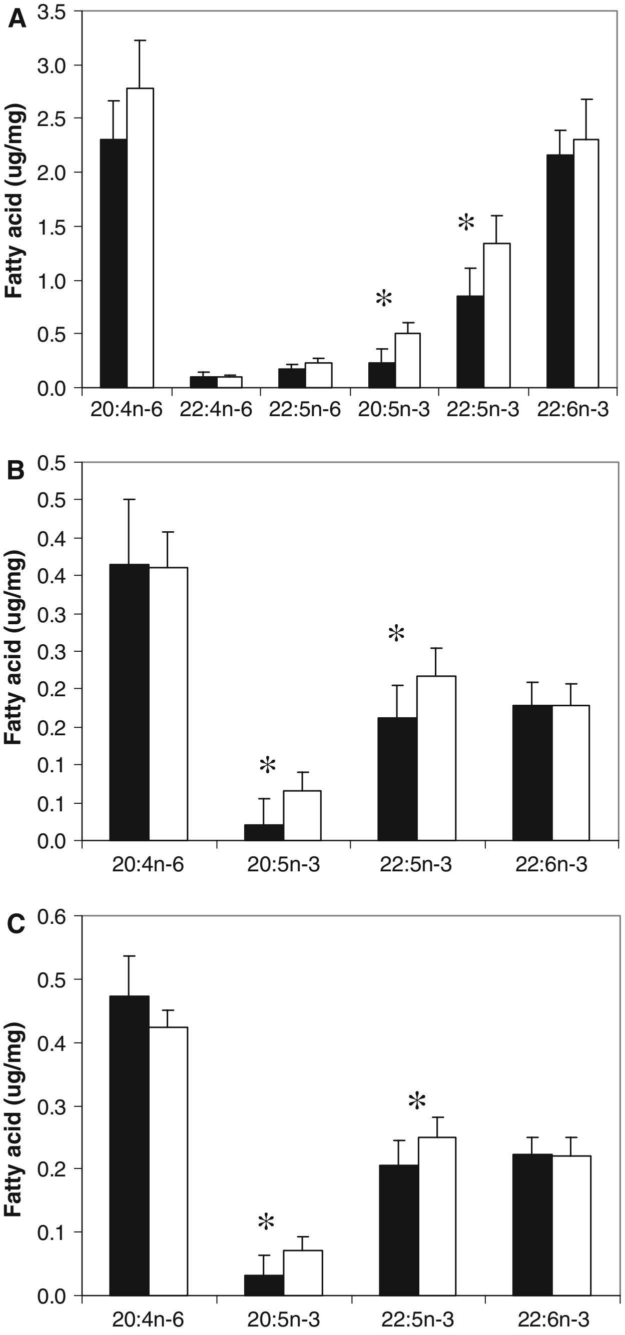

Fig. 1 LCPUFA composition in Control (*filled square*) and MNR (*open square*) fetal sheep tissue. **a** Liver, **b** lung, **c** muscle. $^{*}P < 0.05$

nervonic acid (24:1n-9) in liver and a 17% increase in the %, w/w of nervonic acid in muscle. Similar to saturates and monounsaturates, there were no changes in n-6 PUFA due to MNR in the three tissues studied.

MNR Did Induce Changes in n-3 PUFA

Figure 1 presents selected results for fetal tissue LCPUFA. In liver, 20:5n-3 increased more than twofold, from 0.23 to 0.51 µg/mg, while 22:5n-3 increased 60%, from 0.84 to 1.34 µg/mg. 20:5n-3 increased 2–3 fold in lung and muscle, from lower base levels, and the increases in lung and muscle 22:5n-3 concentrations were similarly attenuated, with only the lung concentration value reaching significance. The muscle 22:5n-3 %, w/w was significant. In stark contrast, 22:6n-3 was not affected by MNR and no trend in means was apparent.

Discussion

The literature is replete with studies showing that the fatty acid composition of various diets influence tissue fatty acid composition. In contrast, these are the first results to show that MNR of a single diet alters fatty acid composition of tissues, in this case fetal tissue. Some but not all-long chain n-3 PUFA were selectively altered but not in plasma, with no other major changes in concentrations.

Augmentation of 20:5n-3 and 22:5n-3 but not in 22:6n-3 is reminiscent of a large body of work in humans in which 18:3n-3 intake is increased through the use of supplements [16]. For supplementation of many grams of 18:3n-3 for several weeks, adult human plasma and platelet 18:3n-3, 20:5n-3, and 22:5n-3 are increased, in decreasing order of enhancement, while 22:6n-3 concentrations do not change. This pattern is also seen for breast milk of 18:3n-3 supplemented women [29]. These changes are generally regarded as health-promoting. In the present study, 18:3n-3 concentrations were too low for reliable quantitative analysis due, presumably, to rumen organism saturation of much of the incoming 18:3n-3. However, the pattern of increases in 20:5n-3 and 22:5n-3 in MNR group may be indicative of entry of 18:3n-3 into a similar desaturation/elongation pathway within the fetus. It is widely believed that the final steps in the synthesis of 22:6n-3 (and 22:5n-6) involve the translocation of 24:6n-3 and 24:5n-6 from endoplasmic reticulum to peroxisomes, where partial oxidation by acyl-CoA oxidase generates 22:6n-3 and 22:5n-6 [30]. The regulatory mechanism of these final steps is not established, but could perhaps explain why 22:6n-3 is unaffected by MNR though the upstream intermediates are increased.

Recent studies report that 50% of NRC caloric intake produced ewes with 7.4% of body weight loss during early to mid gestation [7], with fetuses markedly smaller in the restricted group than in the control group. Restricted fetuses exhibited greater right- and left-ventricular and liver weights per unit fetal weight. In addition, maternal and fetal blood glucose concentrations were reduced in MNR groups. Kwon et al. [31] demonstrated that 50% global nutrient restriction markedly reduced concentrations of total α-amino acids and polyamines in the ovine

Table 4 Fetal tissue fatty acids concentrations (mean ± SD, μg/mg wet weight)

Fatty acid	Liver		Lung		Muscle	
	C	MNR	*C*	MNR	*C*	MNR
14:0	0.34 ± 0.03	0.37 ± 0.08	0.2 ± 0.06	0.17 ± 0.04	0.23 ± 0.02	0.22 ± 0.04
15:0	0.12 ± 0.03	0.13 ± 0.03	0.09 ± 0.01	0.09 ± 0.01	0.07 ± 0.03	0.08 ± 0.01
16:0	4.20 ± 0.43	4.83 ± 0.73	1.63 ± 0.14	1.61 ± 0.18	1.62 ± 0.16	1.72 ± 0.14
18:0	3.88 ± 0.41	4.22 ± 0.31	0.84 ± 0.1	0.82 ± 0.11	1.28 ± 0.11	1.29 ± 0.09
20:0	0.1 ± 0.03	0.1 ± 0.01	0.1 ± 0.03	0.08 ± 0.04	0.09 ± 0.02	0.09 ± 0.02
22:0	0.18 ± 0.03	0.22 ± 0.05	0.09 ± 0.02	0.08 ± 0.02	0.08 ± 0.01	0.09 ± 0.02
24:0	ND[a]	ND	0.13 ± 0.02	0.12 ± 0.04	0.09 ± 0.02	0.08 ± 0.02
16:1n-5	ND	ND	0.06 ± 0.01	0.06 ± 0.02	0.1 ± 0.02	0.1 ± 0.02
16:1n-7	0.36 ± 0.07	0.395 ± 0.042	0.18 ± 0.02	0.16 ± 0.03	0.18 ± 0.01	0.17 ± 0.02
18:1n-7	0.91 ± 0.11	0.95 ± 0.14	0.29 ± 0.03	0.28 ± 0.03	0.45 ± 0.03	0.42 ± 0.04
20:1n-7	0.05 ± 0.01	0.055 ± 0.009	ND	ND	ND	ND
20:3n-7	0.09 ± 0.03	0.08 ± 0.03	0.04 ± 0.01	0.03 ± 0.01	0.04 ± 0.01	0.04 ± 0.02
17:1**	ND	ND	0.05 ± 0.02 (0.71 ± 0.24)	0.03 ± 0.01 (0.48 ± 0.07**)	0.07 ± 0.02	0.06 ± 0.02
18:1	ND	ND	0.09 ± 0.03	0.07 ± 0.04	0.11 ± 0.02	0.13 ± 0.03
19:1	0.06 ± 0.01 (0.28 ± 0.05)	0.05 ± 0.02 (0.22 ± 0.05**)	ND	ND	ND	ND
22:3	0.07 ± 0.03	0.07 ± 0.03	0.09 ± 0.01	0.08 ± 0.02	0.12 ± 0.02	0.11 ± 0.03
16:1n-9	0.29 ± 0.04	0.33 ± 0.06	0.17 ± 0.01	0.17 ± 0.02	0.17 ± 0.01	0.17 ± 0.02
18:1n-9	3.07 ± 0.39	3.26 ± 0.53	1.58 ± 0.16	1.59 ± 0.18	2.33 ± 0.12	2.32 ± 0.13
trans 18:1n-9	0.06 ± 0.01	0.06 ± 0.01	ND	ND	ND	ND
20:1n-9	0.1 ± 0.01	0.12 ± 0.03	0.06 ± 0.01	0.05 ± 0.01	0.07 ± 0.01	0.08 ± 0.02
22:1n-9	0.1 ± 0.04	0.09 ± 0.03	0.06 ± 0.03	0.05 ± 0.01	0.06 ± 0.01	0.05 ± 0.03
24:1n-9	0.42 ± 0.07	0.52 ± 0.07*	0.13 ± 0.03	0.12 ± 0.02	0.16 ± 0.01 (1.8 ± 0.1)	0.18 ± 0.03 (2.1 ± 0.2**)
20:2n-9	0.08 ± 0.01	0.1 ± 0.03	ND	ND	ND	ND
20:3n-9	0.63 ± 0.17	0.62 ± 0.23	0.26 ± 0.03	0.25 ± 0.06	0.38 ± 0.04	0.32 ± 0.07
18:2n-6	0.26 ± 0.02	0.28 ± 0.04	0.06 ± 0.02	0.07 ± 0.02	0.08 ± 0.01	0.08 ± 0.02
20:3n-6	0.18 ± 0.05	0.23 ± 0.04	0.03 ± 0.01	0.03 ± 0.02	0.04 ± 0.01	0.05 ± 0.03
20:4n-6	2.31 ± 0.36	2.78 ± 0.44	0.37 ± 0.09	0.36 ± 0.05	0.47 ± 0.06	0.42 ± 0.03
22:4n-6	0.1 ± 0.04	0.1 ± 0.02	ND	ND	ND	ND
22:5n-6	0.17 ± 0.05	0.22 ± 0.05	ND	ND	ND	ND
18:3n-3	[b]	[b]	[b]	[b]	[b]	[b]
20:5n-3	0.23 ± 0.14	0.51 ± 0.09*	0.02 ± 0.04	0.07 ± 0.02*	0.03 ± 0.03	0.07 ± 0.02*
22:5n-3	0.84 ± 0.27	1.34 ± 0.26*	0.16 ± 0.04	0.22 ± 0.04*	0.21 ± 0.04 (2.4 ± 0.4)	0.25 ± 0.03 (2.9 ± 0.4**)
22:6n-3	2.16 ± 0.24	2.30 ± 0.38	0.18 ± 0.03	0.18 ± 0.03	0.22 ± 0.03	0.22 ± 0.03
Σfatty acid	21.4 ± 2.06	24.4 ± 2.9	6.94 ± 0.73	6.84 ± 0.77	8.74 ± 0.48	8.81 ± 0.61

Fatty acids without "n-" designations are of unspecified double bond position. Differences as %, w/w presented below

* Different from control ($P < 0.05$). ** Different from control only when expressed as relative weight percent of fatty acids (%, w/w)

[a] *ND* not detected

[b] Trace, below quantifiable levels

maternal and fetal plasma and in fetal allantoic and amniotic fluids at both mid and late gestation. Our data indicate that n-3 LCPUFA are also affected by MNR. The changes observed here due to nutrient restriction operated specifically on long chain n-3 PUFA in the fetal tissues investigated and did not influence n-6 PUFA in the fetus.

The rate-limiting step in long chain PUFA synthesis is usually considered to be the initial conversion of 18:2n-6 and 18:3n-3 to 18:3n-6 and 18:4n-3 by the action of Δ6-desaturase [32], the product of FADS2 gene, and further synthesis of 20:3(n-6) and 20:4(n-3) requires Δ5 desaturase [33], coded by FADS1. Δ6 and Δ5 desaturase activities have been shown in human fetal liver microsomes from as early as 17 weeks of gestation [34, 35].

Both Δ6 and Δ5 desaturases are activated by insulin and depressed by glucagon, adrenaline, and glucocorticoids [36]. A considerable body of work has explored the underlying regulatory mechanisms of desaturases and elongases [37–42]. They can be upregulated by peroxisomal proliferator-activated receptor-α (PPARα) and sterol-regulatory element binding protein-1 (SREBP-1). PPARα was required for WY14643-mediated induction of elongase-5 (Elovl-5), Elovl-6, and Δ5, Δ6 and Δ9 desaturases. Increased nuclear SREBP-1 is correlated with enhanced expression of Elovl-6, Δ5, Δ6 and Δ9 desaturases. Δ6 desaturase activity can be downregulated by glucocorticoids and by an increased abundance of LCPUFA products [32, 43, 44]. The promoter region of FADS2 (Δ6-desaturase) contains the response element for the ligand-activated transcription factor PPARα [40]. Binding of 22:6n-3 to PPARα suppresses transcription of Δ6-desaturase and so would be expected to down-regulate conversion of LNA to longer-chain PUFA. Nutrient restriction in sheep over the same early period of gestation that we have studied, leads to increased mRNA for PPARα in fetal adipose tissue [45].

A plausible hypothesis to explain our results is that MNR-induced fetal hypoglycemia induced higher insulin secretion, which may in turn increase desaturase and elongase activities in fetal liver. These may be involved in the regulation of transcription factors, particularly PPARα and SREBP-1. Decreased amino acids and inadequate energy may also participate in the activation.

20:4n-6 is the most important substrate for synthesis of highly bioactive eicosanoids that regulate many aspects of cellular and tissue metabolism. 20:4n-6 tissue concentrations are much less subject to dietary influence than the n-3 fatty acids in primates [46], and this tighter control may in part explain why the maternal and fetal plasma 20:4n-6 remained stable in MNR, and decreased as a percentage of fatty acids in maternal plasma to do so. The activated desaturases and elongases preferentially impact the n-3 PUFA production pathway leading to the increase of concentrations of 20:5n-3 and 22:5n-3 while not affecting n-6 LCPUFA concentrations. Common use of enzymes for n-3 and n-6 desaturation and elongation, as is also widely believed, does not explain why 20:5n-3 concentrations were more than doubled while 20:4n-6 was unaffected. Either the presence of family-specific (n-3 or n-6) isozymes or differential affinities of the acylation pathways could explain this result.

In conclusion, these data provide the first examination of fatty acid levels in fetal tissues and plasma of MNR ewes. The PUFA data reveal that during early- to mid-gestation, fetal n-3 PUFA are most influenced among fatty acids by nutrient restriction, and these changes do not parallel that of the ewe. Alterations PUFA metabolism in fetal development are known to induce lasting deficiencies in the CNS [47] and thus fetal programming for abnormal conditions in later life is warranted based on these results. Moreover, changes in LCPUFA profiles may provide a marker for identifying those at risk of developing adulthood disease. Knowledge obtained from the effects of restricted fetal nutrition will be useful in developing guidelines for consumption of essential fatty acids by mothers in a manner that is specific to each pregnancy (Fig. 1).

Acknowledgments Yunhua Zhou acknowledges a fellowship from International Nutrition Foundation for career development support.

References

1. Barker DJP (1999) Fetal programming and public health. RCOG Press, London, pp 3–11
2. Barker DJP (1998) Mothers, babies and disease in later life, 2nd edn. Churchill Livingstone, Edinburgh
3. Armitage JA, Khan IY, Taylor PD, Nathanielsz PW, Poston L (2004) Developmental programming of the metabolic syndrome by maternal nutritional imbalance: how strong is the evidence from experimental models in mammals? J Physiol 561:355–377
4. Zhu MJ, Ford SP, Means WJ, Hess BW, Nathanielsz PW, Du M (2006) Maternal nutrient restriction affects properties of skeletal muscle in offspring. J Physiol 575:241–250
5. Gnanalingham MG, Mostyn A, Gardner DS, Stephenson T, Symonds ME (2006) Developmental regulation of the lung in preparation for life after birth: hormonal and nutritional manipulation of local glucocorticoid action and uncoupling protein-2. J Endocrinol 188:375–386
6. Ozanne SE, Nicholas Hales C (2005) Poor fetal growth followed by rapid postnatal catch-up growth leads to premature death. Mech Ageing Dev 126:852–854
7. Vonnahme KA, Hess BW, Hansen TR, McCormick RJ, Rule DC, Moss GE, Murdoch WJ, Nijland MJ, Skinner DC, Nathanielsz PW, Ford SP (2003) Maternal undernutrition from early- to mid-gestation leads to growth retardation, cardiac ventricular hypertrophy, and increased liver weight in the fetal sheep. Biol Reprod 69:133–140
8. Selak MA, Storey BT, Peterside I, Simmons RA (2003) Impaired oxidative phosphorylation in skeletal muscle of intrauterine growth-retarded rats. Am J Physiol Endocrinol Metab 285:E130–E137
9. Symonds ME, Bird JA, Clarke L, Gate JJ, Lomax MA (1995) Nutrition, temperature and homeostasis during perinatal development. Exp Physiol 80:907–940
10. Heird WC, Lapillonne A (2005) The role of essential fatty acids in development. Annu Rev Nutr 25:549–571
11. Lauritzen L, Hansen HS, Jorgensen MH, Michaelsen KF (2001) The essentiality of long chain n-3 fatty acids in relation to development and function of the brain and retina. Prog Lipid Res 40:1–94

12. Diau GY, Hsieh AT, Sarkadi-Nagy EA, Wijendran V, Nathanielsz PW, Brenna JT (2005) The influence of long chain polyunsaturate supplementation on docosahexaenoic acid and arachidonic acid in baboon neonate central nervous system. BMC Med 3:11
13. Innis SM (1991) Essential fatty acids in growth and development. Prog Lipid Res 30:39–103
14. Uauy R, Treen M, Hoffman DR (1989) Essential fatty acid metabolism and requirements during development. Semin Perinatol 13:118–130
15. Leaf AA, Leighfield MJ, Costeloe KL, Crawford MA (1992) Long chain polyunsaturated fatty acids and fetal growth. Early Hum Dev 30:183–191
16. Brenna JT (2002) Efficiency of conversion of alpha-linolenic acid to long chain n-3 fatty acids in man. Curr Opin Clin Nutr Metab Care 5:127–132
17. Serhan CN (2006) Novel chemical mediators in the resolution of inflammation: resolvins and protectins. Anesthesiol Clin 24:341–364
18. Bazan NG (2006) Cell survival matters: docosahexaenoic acid signaling, neuroprotection and photoreceptors. Trends Neurosci 29:263–271
19. Kitajka K, Sinclair AJ, Weisinger RS, Weisinger HS, Mathai M, Jayasooriya AP, Halver JE, Puskas LG (2004) Effects of dietary omega-3 polyunsaturated fatty acids on brain gene expression. Proc Natl Acad Sci USA 101:10931–10936
20. Kitajka K, Puskas LG, Zvara A, Hackler L Jr, Barcelo-Coblijn G, Yeo YK, Farkas T (2002) The role of n-3 polyunsaturated fatty acids in brain: modulation of rat brain gene expression by dietary n-3 fatty acids. Proc Natl Acad Sci USA 99:2619–2624
21. Muskiet FA, van Goor SA, Kuipers RS, Velzing-Aarts FV, Smit EN, Bouwstra H, Dijck-Brouwer DA, Boersma ER, Hadders-Algra M (2006) Long-chain polyunsaturated fatty acids in maternal and infant nutrition. Prostaglandins Leukot Essent Fatty Acids 75:135–144
22. Hornstra G, van Houwelingen AC, Simonis M, Gerrard JM (1989) Fatty acid composition of umbilical arteries and veins: possible implications for the fetal EFA-status. Lipids 24:511–517
23. Al MD, Hornstra G, van der Schouw YT, Bulstra-Ramakers MT, Huisjes HJ (1990) Biochemical EFA status of mothers and their neonates after normal pregnancy. Early Hum Dev 24:239–248
24. Connor WE, Lowensohn R, Hatcher L (1996) Increased docosahexaenoic acid levels in human newborn infants by administration of sardines and fish oil during pregnancy. Lipids 31(Suppl):S183–S187
25. McMillen IC, Robinson JS (2005) Developmental origins of the metabolic syndrome: prediction, plasticity, and programming. Physiol Rev 85:571–633
26. Garces R, Mancha M (1993) One-step lipid extraction and fatty acid methyl esters preparation from fresh plant tissues. Anal Biochem 211:139–143
27. Michaud AL, Diau GY, Abril R, Brenna JT (2002) Double bond localization in minor homoallylic fatty acid methyl esters using acetonitrile chemical ionization tandem mass spectrometry. Anal Biochem 307:348–360
28. Su HM, Bernardo L, Mirmiran M, Ma XH, Corso TN, Nathanielsz PW, Brenna JT (1999) Bioequivalence of dietary alpha-linolenic and docosahexaenoic acids as sources of docosahexaenoate accretion in brain and associated organs of neonatal baboons. Pediatr Res 45:87–93
29. Francois CA, Connor SL, Bolewicz LC, Connor WE (2003) Supplementing lactating women with flaxseed oil does not increase docosahexaenoic acid in their milk. Am J Clin Nutr 77:226–233
30. Ferdinandusse S, Denis S, Mooijer PA, Zhang Z, Reddy JK, Spector AA, Wanders RJ (2001) Identification of the peroxisomal beta-oxidation enzymes involved in the biosynthesis of docosahexaenoic acid. J Lipid Res 42:1987–1995
31. Kwon H, Ford SP, Bazer FW, Spencer TE, Nathanielsz PW, Nijland MJ, Hess BW, Wu G (2004) Maternal nutrient restriction reduces concentrations of amino acids and polyamines in ovine maternal and fetal plasma and fetal fluids. Biol Reprod 71:901–908
32. Cho HP, Nakamura MT, Clarke SD (1999) Cloning, expression, and nutritional regulation of the mammalian delta-6 desaturase. J Biol Chem 274:471–477
33. Sprecher H (1981) Biochemistry of essential fatty acids. Prog Lipid Res 20:13–22
34. Poisson JP, Dupuy RP, Sarda P, Descomps B, Narce M, Rieu D, Crastes de Paulet A (1993) Evidence that liver microsomes of human neonates desaturate essential fatty acids. Biochim Biophys Acta 1167:109–113
35. Rodriguez A, Sarda P, Nessmann C, Boulot P, Leger CL, Descomps B (1998) Delta6- and delta5-desaturase activities in the human fetal liver: kinetic aspects. J Lipid Res 39:1825–1832
36. Brenner RR (2003) Hormonal modulation of delta6 and delta5 desaturases: case of diabetes. Prostaglandins Leukot Essent Fatty Acids 68:151–162
37. Jakobsson A, Westerberg R, Jacobsson A (2006) Fatty acid elongases in mammals: their regulation and roles in metabolism. Prog Lipid Res 45:237–249
38. Matsuzaka T, Shimano H, Yahagi N, Amemiya-Kudo M, Yoshikawa T, Hasty AH, Tamura Y, Osuga J, Okazaki H, Iizuka Y, Takahashi A, Sone H, Gotoda T, Ishibashi S, Yamada N (2002) Dual regulation of mouse delta(5)- and delta(6)-desaturase gene expression by SREBP-1 and PPARalpha. J Lipid Res 43:107–114
39. Nakamura MT, Nara TY (2003) Essential fatty acid synthesis and its regulation in mammals. Prostaglandins Leukot Essent Fatty Acids 68:145–150
40. Tang C, Cho HP, Nakamura MT, Clarke SD (2003) Regulation of human delta-6 desaturase gene transcription: identification of a functional direct repeat-1 element. J Lipid Res 44:686–695
41. Wang Y, Botolin D, Christian B, Busik J, Xu J, Jump DB (2005) Tissue-specific, nutritional, and developmental regulation of rat fatty acid elongases. J Lipid Res 46:706–715
42. Wang Y, Botolin D, Xu J, Christian B, Mitchell E, Jayaprakasam B, Nair MG, Peters JM, Busik JV, Olson LK, Jump DB (2006) Regulation of hepatic fatty acid elongase and desaturase expression in diabetes and obesity. J Lipid Res 47:2028–2041
43. Cho HP, Nakamura M, Clarke SD (1999) Cloning, expression, and fatty acid regulation of the human delta-5 desaturase. J Biol Chem 274:37335–37339
44. Marra CA, de Alaniz MJ, Brenner RR (1986) Modulation of delta 6 and delta 5 rat liver microsomal desaturase activities by dexamethasone-induced factor. Biochim Biophys Acta 879:388–393
45. Bispham J, Gardner DS, Gnanalingham MG, Stephenson T, Symonds ME, Budge H (2005) Maternal nutritional programming of fetal adipose tissue development: differential effects on messenger ribonucleic acid abundance for uncoupling proteins and peroxisome proliferator-activated and prolactin receptors. Endocrinology 146:3943–3949
46. Hsieh AT, Anthony JC, Diersen-Schade DA, Rumsey SC, Lawrence P, Li C, Nathanielsz PW, Brenna JT (2007) The influence of moderate and high dietary long chain polyunsaturated fatty acids (LCPUFA) on baboon neonate tissue fatty acids. Pediatr Res 61:537–545
47. Li D, Weisinger HS, Weisinger RS, Mathai M, Armitage JA, Vingrys AJ, Sinclair AJ (2006) Omega 6 to omega 3 fatty acid imbalance early in life leads to persistent reductions in DHA levels in glycerophospholipids in rat hypothalamus even after long-term omega 3 fatty acid repletion. Prostaglandins Leukot Essent Fatty Acids 74:391–399

Lipids (2008) 43:533–548
DOI 10.1007/s11745-008-3181-6

ORIGINAL ARTICLE

The Identification of Mono-, Di-, Tri-, and Tetragalactosyldiacylglycerols and their Natural Estolides in Oat Kernels

**Robert A. Moreau · Douglas C. Doehlert ·
Ruth Welti · Giorgis Isaac · Mary Roth ·
Pamela Tamura · Alberto Nuñez**

Received: 27 November 2007 / Accepted: 8 April 2008 / Published online: 15 May 2008
© AOCS 2008

Abstract Oat kernels were extracted with methanol, and glycolipid-enriched fractions were prepared using silica solid phase extraction. Using direct infusion electrospray ionization (ESI) tandem mass spectrometry (MS), high performance liquid chromatography (HPLC)-ESI-MS, and HPLC-atmospheric pressure chemical ionization (APCI)-MS, we confirmed previous reports that digalactosyldiacylglycerol (DGDG) was the most abundant glycolipid in oat kernels and confirmed a previous report of the presence of a DGDG mono-estolide in oat kernels. In the current study we also identified several additional natural galactolipid estolides: two new DGDG estolides (di- and tri-estolides), two trigalactosyldiacylglycerol (TriGDG) estolides (mono- and di-estolides), and one tetragalactosyldiacylglycerol (TetraGDG) estolide (mono-estolide). The levels of total galactolipid estolides in oat kernels were estimated to be about 29% of the total glycolipid fraction. To our knowledge, this report is the first evidence of natural di- and tri-estolides of polar lipids.

Keywords Oat kernels · Estolides · Digalactosyldiacylglycerol · Trigalactosyldiacylglycerol · Tetragalactosyldiacylglycerol · Galactolipid · Mass spectrometry

Abbreviations

APCI	Atmospheric pressure chemical ionization
CID	Collision-induced dissociation
DAG	Diacylglycerol
DGDG	Digalactosyldiacylglycerol
DGMG	Digalactosylmonoacylglycerol
ESI	Electrospray ionization
ELSD	Evaporative light scattering detector
EIC	Extracted ion chromatogram
HPLC	High-performance liquid chromatography
MS	Mass spectrometry
MGDG	Monogalactosyldiacylglycerol
NL	Neutral loss
NP	Normal-phase
RP	Reverse-phase
SPE	Solid phase extraction
MS/MS	Tandem mass spectrometry
TetraGDG	Tetragalactosyldiacylglycerol
TIC	Total ion chromatogram
TriGDG	Trigalactosyldiacylglycerol
TriGMG	Trigalactosylmonoacylglycerol

Mention of trade names or commercial products in this publication is solely for the purpose of providing specific information and does not imply recommendation or endorsement by the US Department of Agriculture.

R. A. Moreau · A. Nuñez
US Department of Agriculture, Agricultural Research Service,
Eastern Regional Research Center, Wyndmoor, PA 19038, USA

D. C. Doehlert
US Department of Agriculture, Agricultural Research Service,
Cereal Crops Research Unit, Fargo, ND 58105, USA

R. Welti · G. Isaac · M. Roth · P. Tamura
Kansas Lipidomics Research Center, Division of Biology,
Kansas State University, Manhattan, KS 66506, USA

R. A. Moreau (✉)
Crop Conversion Science and Engineering Research Unit,
ERRC, ARS, USDA, 600 East Mermaid Lane, Wyndmoor,
PA 19038, USA
e-mail: Robert.Moreau@ars.usda.gov

Introduction

Although the major lipid components of most biological membranes are phospholipids, the most abundant lipids of plant chloroplasts are the galactolipids, MGDG and DGDG [1]. In addition to their occurrence in chloroplasts, MGDG and DGDG have been observed in significant levels in oat kernels and other seeds [2]. Smaller amounts of two other galactolipids have also been detected in some plant tissues; TriGDG has been reported in wheat [3], potatoes [4], rice [5], Adzuki beans [6], and pumpkin [5, 7, 9]; TetraGDG has been reported in rice [5].

Hamberg et al. [9] previously reported that oat kernels contain significant amounts of an unusual hydroxy fatty acid, 15(*R*)–hydroxylinoleic acid (avenoleic acid), and later [10] described an unusual galactolipid containing this fatty acid in oat kernels (Fig. 1), containing this fatty acid. The galactolipid was a DGDG with 15(*R*)–hydroxylinoleic acid esterified to the sn-2 position of the glycerol and a third fatty acid esterified to the free OH on the hydroxy fatty acid (Fig. 1). This "acyl-DGDG" is a natural estolide. An estolide is formed when a hydroxy fatty acid is esterified to another fatty acid [11]. Natural estolides are rare, but natural triacylglycerol estolides have been described in the seed oils of three species of *Sebastiana* [11–13], in ergot oil [14], in *Lesquerella oil* [15], and more recently, in castor oil [16]. Synthetic estolides have been prepared from common vegetable oils [17] and from oils that contain hydroxy fatty acids such as those in *Lesquerella* and castor oil [18]. The current study employs HPLC-MS and direct infusion ESI-MS/MS to characterize additional unusual glycolipids in oat kernels and oat oil.

Materials and Methods

Materials

Oats (*Avena sativa* L., cv Morton) were grown in the field in Fargo, North Dakota. DGDG for HPLC standardization was purchased from Matreya, Inc., Pleasant Gap, PA.

Extraction of Lipids

Oat grain was dehulled with a Codema (Codema, Inc., Eden Prairie, MN) compressed air oat dehuller. Oat groats (caryopses) were steamed with a vegetable steamer for 20 min to inactivate hydrolytic enzymes. Enzyme-inactivated groats were ground with a Retsch (Haan, Germany) Z-200 centrifugal mill with a 0.5 mm collar screen. For polar lipid extraction, a sample of 10 g of flour was extracted in 50 ml of methanol in a 150 ml Corex (Corning, New York) centrifuge bottle. Solvent and flour were mixed thoroughly by vortexing and shaking the sealed bottle by hand. The bottle was centrifuged at 1,500*g* for 15 min to pellet particulates, and the supernatant was removed. The pellet was suspended in 20 ml methanol and shaken vigorously by hand to extract a second time. The bottle was centrifuged as before and the supernatant pooled with the first supernatant. About 15 g of sodium sulfate were added to the extract to remove traces of water, and the extract was filtered through Whatman (Middlesex, UK) #1 filter paper. Solvent was reduced to about 15 ml with a rotary evaporator, using an aspirator to draw a vacuum, with a water bath temperature of 42 °C. The remaining extract was divided into three tubes and evaporated to dryness under nitrogen, on a block evaporator at 48 °C. Samples were stored under nitrogen at −80 °C until further fractionation.

Glycolipid Fractionation Via Solid Phase Extraction

Crude oat oil extracts (80–200 mg) were dissolved in chloroform/methanol (9:1, by vol). A silica SPE column (10 g silica in a 75 ml column) was equilibrated with chloroform, and the crude extract was applied to the column. Neutral lipids were eluted with 100 ml chloroform/acetone (4:1, by vol). Glycolipids were eluted with 100 ml acetone/methanol (9:1, by vol), and phospholipids were eluted with 100 ml methanol [19]. Solvent was removed by a rotary evaporator under the conditions described above. Several ml of acetone/methanol (9:1, by vol) were added to

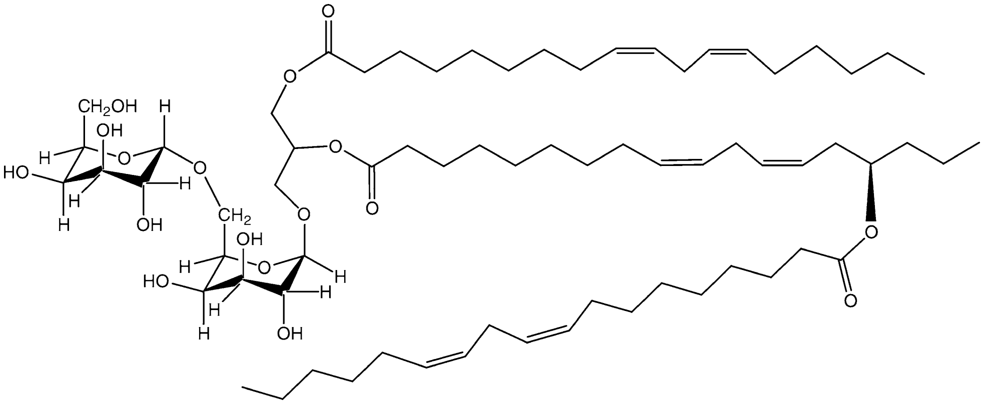

Fig. 1 The structure of the DGDG mono-estolide (DGDG 54:6) reported by Hamberg et al. [10]. Exact mass ($C_{69}H_{118}O_{17}$), 1,218.8369 Da; average mass, 1,219.69 Da; *m/z* of $[M + NH_4]^+$ ($C_{69}H_{122}O_{17}N$), 1,236.8707

each flask, and several grams of sodium sulfate were added to remove moisture. Solvent was removed by pipette and several more ml of solvent added to the flask and mixed before the solvent was removed and pooled with the first aliquot of solvent. The combined aliquots were filtered with Whatman #541 filter paper and evaporated to dryness under nitrogen, on a block evaporator at 48 °C.

Subfractions enriched in the putative Tri- and TetraGDG were generated. Thirty to one-hundred milligrams of the total glycolipid fraction (eluted with acetone/methanol (9:1, by vol) as described above) were loaded onto a silica SPE column equilibrated with chloroform. Subfraction 1 was eluted with 100 ml of chloroform/acetone (1:1, by vol). Subfraction 2, which contained primarily DGDG and its estolides, was eluted with 100 ml chloroform/acetone (1:4, by vol). Subfraction 3, which was enriched in TriGDG and TetraGDG, was eluted with acetone/methanol (9:1, by vol). Solvents were evaporated with a rotary evaporator, and samples were stored dry under nitrogen at −80 °C.

ESI-MS/MS

An aliquot of the oat total glycolipid SPE fraction in chloroform was combined with solvents, such that the ratio of chloroform/methanol/300 mM ammonium acetate in water was 300:665:35 (by vol) and the final volume was 1 ml. This solution was introduced by continuous infusion into the ESI source on a triple quadrupole MS/MS (API 4000, Applied Biosystems, Foster City, CA), using an autosampler (LC Mini PAL, CTC Analytics AG, Zwingen, Switzerland) fitted with the required injection loop for the acquisition time, and presented to the ESI needle at 30 μl/min. The collision gas pressure was set at 1 (arbitrary units). The collision energy, with nitrogen in the collision cell, was 84 V. The declustering potential was 215 V, the entrance potential was 15 V, and the exit potential was 17 V. The mass analyzers were adjusted to a resolution of 0.7 Da full width at half height. For each spectrum, 9–150 continuum scans were averaged in multiple channel analyzer (MCA) mode. The source temperature (heated nebulizer) was 100 °C, the interface heater was on, +5.5 kV or −4.5 kV was applied to the electrospray capillary, the curtain gas was set at 20 (arbitrary units), and the two ion source gases were set at 45 (arbitrary units). DGDG species were detected by neutral loss (NL) of “341” (digalactose minus H minus $H_2O + NH_4^+$; NL setting, 341.13 Da) to identify the $[M + NH_4]^+$ ions of DGDG and DGMG, neutral loss of “503” (trigalactose minus H minus $H_2O + NH_4^+$; NL setting, 503.18 Da) to identify the $[M + NH_4]^+$ ions of TriGDG and TriGMG, and neutral loss of “665” (tetragalactose minus H minus $H_2O + NH_4^+$; NL setting, 665.24 Da) to identify the $[M + NH_4]^+$ ions of TetraGDG. Sequential neutral loss scans of the extracts produced a series of spectra with each spectrum revealing a class of lipid species containing a common head group fragment.

Multiple acyl precursor scanning in negative ion mode was combined with head group neutral loss ion scanning to identify and quantify DGDG species with specified individual acyl chains [20]. Briefly, scans of the head group (NL 341 in positive ion mode) and acyl anions (precursors of *m/z* 255.23, 277.22, 279.23, 281.25, 283.28, 295.23, 305.25, 307.26, and 309.28 in negative ion mode) were performed in the DGDG mass range (*m/z* 900–1,050). The neutral loss of 341 scan (to identify the $[M + NH_4]^+$ ions of DGDG) was used to quantify the total amount of each galactolipid at each nominal mass in comparison to internal standards (DGDG 16:0/18:0 (0.49 nmol) and DGDG 18:0/18:0 (0.71 nmol)). By integrating data from the acyl precursor scans with those from the neutral loss head group scan, individual molecular species (i.e., with both acyl chains identified) were quantified.

ESI-MS/MS Product Ion Analysis

The structures of the galactolipid species were discerned by product ion analysis in the positive mode as $[M + NH_4]^+$ ions. The solvent was chloroform/methanol/300 mM ammonium acetate in water (300:665:35, by vol). The collision energy was 45 V.

Normal-Phase HPLC, HPLC-APCI-MS, and HPLC-ESI-MS Methods for Lipid Class Analysis

Normal-phase (NP) polar lipid HPLC analyses were performed on a Hewlett Packard Model 1100 HPLC, with autosampler, and detected by both an HP Model 1100 diode-array UV-visible detector (Agilent Technologies, Avondale, PA) and a Sedex Model 55 ELSD (Richard Scientific, Novato, CA), operated at 40 °C and a nitrogen gas pressure of 2 bars. The column was a LiChrosorb, 3 mm diameter and 100 mm length, 7 micron DIOL (Chrompack, Raritan, NJ). The ternary gradient had a constant flow rate of 0.5 ml/min, with solvent A = hexane/acetic acid (1000:1, by vol), solvent B = isopropanol, and solvent C = aqueous 50 mM ammonium formate. Gradient timetable: at 0 min, 90:10:0, by vol (%A/%B/%C); at 30 min, 58:38:2, by vol; at 40 min, 12:80:8, by vol; at 50 min, 12:80:8, by vol; at 51 min, 50:50:0, by vol; at 52 min, 90:10:0, by vol; and at 60 min, 90:10:0, by vol. Using this method, the retention times of the polar lipid standards were: MGDG, 10.5 min and DGDG, 20.5 min. For HPLC-APCI-MS, the column effluent was routed into an Agilent 1100 MSD mass spectrometer operated with APCI in the positive mode in the range of *m/z* 200–2,000, with drying gas at 6.0 l/min, nebulizer pressure at 60 psi, drying gas temperature at 350 °C, vaporizer gas temperature at 325 °C, capillary voltage of 4,000 V, corona current of 4.0 μA, and fragmentor at 80 V. For HPLC-ESI-MS, the column effluent was routed into an Agilent 1100 MSD mass spectrometer operated with ESI in the positive mode in the range of *m/z* 200–2,000, with the fragmentor at 5 V, drying gas at 6 l/min, nebulizing pressure at 50 psi, drying gas temperature at 300 °C, and a capillary voltage of 5,500 V.

Reverse-Phase HPLC and HPLC-ESI-MS Method for Lipid Class Analysis

For the reverse-phase (RP) analyses the HPLC, ELSD, and MS parameters were as described above. The column was a Prevail C18, 3 micron particle size (2.1 × 150 mm), from Alltech Associates, Northfield, IL. The binary gradient had a flow rate of 0.2 ml/min, with solvent A = methanol/water/ammonium formate (95:5:0.126, vol/vol/w), and solvent B = isopropanol. Gradient timetable: at 0 min, 100:0, by vol (%A/%B); at 5 min, 100:0, by vol; at 40 min, 60:40, by vol; at 45 min, 60:40, by vol; at 46 min, 100:0, by vol; and at 60 min, 100:0, by vol.

Lipid Nomenclature and Mass Description

Lipid molecular species are described as "X y:z", where X indicates the class of galactolipid, y indicates the total number of carbon atoms in the fatty acyl moieties, and z indicates the total number of carbon-carbon double bonds in the fatty acyl groups. For example, the DGDG mono-estolide previously reported [10] is abbreviated DGDG 54:6 because it is a DGDG with three 18–carbon fatty acids and a total of 6 double bonds. For clarification, nominal masses are provided in parentheses.

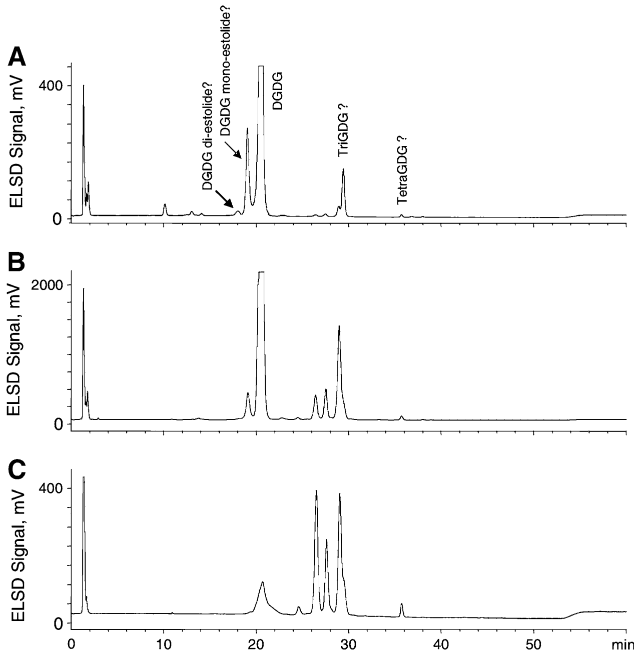

Fig. 2 NP-HPLC-ELSD chromatogram of the classes of lipids in: **a** the oat total glycolipid fraction, **b** oat glycolipid subfraction 2, and **c** oat glycolipid subfraction 3

Results and Discussion

Normal-Phase HPLC-ELSD Separation of the Oat Kernel Glycolipids Indicated the Presence of Multiple Lipid Classes

In our previous report on oat kernel lipids, the levels of DGDG and phospholipids were quantified using normal-phase HPLC with evaporative light scattering detection [2]. For the current study this HPLC method was modified by increasing the proportions of both isopropanol and water in the hexane/acetic acid/isopropanol/water system to

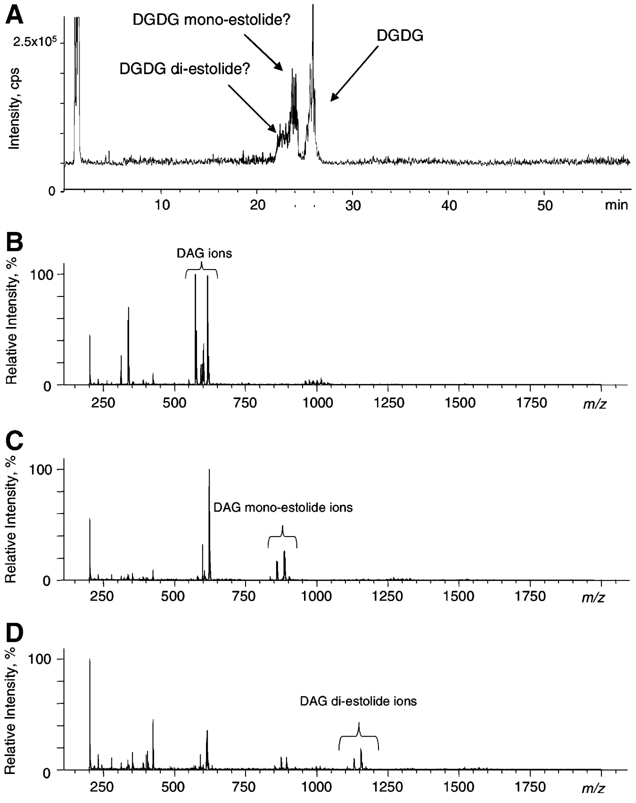

Fig. 3 NP-HPLC-APCI-MS to identify classes of glycolipids in the oat total glycolipid fraction. **a** Total ion chromatogram (TIC) of the oat glycolipid fraction when separated in NP-HPLC-APCI-MS in the positive ion mode, **b** spectrum of the peak at 24.7 to 26.9 min in **a**, which has the same retention time as commercial DGDG, **c** spectrum of the peak at 23.3 to 24.7 min in **a**, which is tentatively identified as DGDG mono-estolide (Fig. 1), and **d** spectrum of the peak at 21.8 to 23.3 min in **a**, which is tentatively identified as DGDG di-estolide

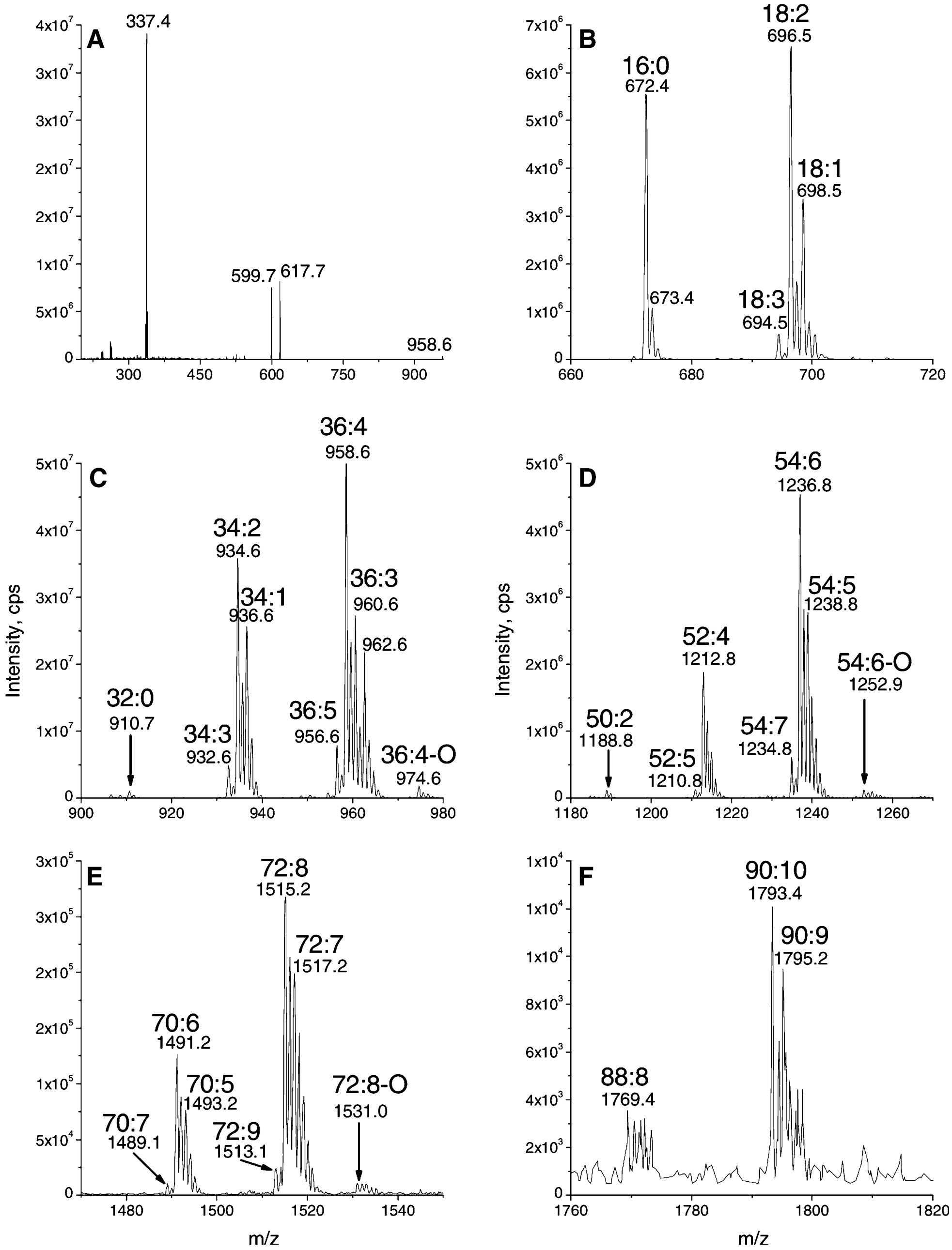

Fig. 4 Fragmentation of DGDG and neutral loss scans identifying digalactosyl acylglycerol species in the oat glycolipid SPE fraction. **a** Product ion spectrum of DGDG 36:4 $[M + NH_4]^+$ ion at *m/z* 958 (nominal mass). **b–f** Scans of neutral loss of 341, showing **b** DGMG species, **c** DGDG species, **d** DGDG mono-estolide species, **e** DGDG di-estolide species, and **f** DGDG tri-estolide species

potentially permit the separation of very polar glycolipids (Fig. 2). As expected, DGDG (identified by co-chromatography with commercial DGDG standard) eluted at 20 min and was the major class of lipid detected in the total glycolipid fraction obtained by SPE (Fig. 2a). A smaller peak eluting at 19 min was proposed to be the DGDG mono-estolide previously reported [10]. A very small peak eluted at 18 min; its retention time suggested that it may be a DGDG di-estolide. Two other groups of peaks also appeared in the regions of 26–30 min and 35–39 min, and based on their retention times as compared with those determined in previous analyses of more polar glycolipids in other plants [3–8], their structures were postulated to be TriGDG and TetraGDG, respectively. NP-HPLC-ELSD analyses of two glycolipid subfractions, also prepared by SPE, indicated that subfraction 2 contained higher levels of the 26–30 min series of peaks (Fig. 2b), and in subfraction 3, these unknown peaks in the region of 26–30 min were the major components (Fig. 2c). The small putative TetraGDG peaks in the region of 35–39 min in the total glycolipid fraction (Fig. 2a) were also present in glycolipid subfraction 2 (Fig. 2b) and subfraction 3 (Fig. 2c).

Table 1 The fatty acyl combinations that make up the DGDG species were identified by multiple acyl precursor scanning in negative ion mode, in combination with neutral loss head group scanning in positive ion mode

DGDG species	% of total DGDG	Acyl species
DGDG 32:0	0.7	16:0/16:0
DGDG 34:3	3.2	16:0/18:3 (79%) > 16:1/18:2
DGDG 34:2	26.3	16:0/18:2 (99+%) > 16:1/18:1
DGDG 34:1	10.3	16:0/18:1 (99+%) > 16:1/18:0
DGDG 36:6	0.6	18:3/18:3
DGDG 36:5	4.8	18:3/18:2
DGDG 36:4	31.7	18:2/18:2 (94%) > 18:3/18:1 > 16:1/20:3
DGDG 36:3	9.6	18:2/18:1 (97%) > 16:0/20:3 > 18:3/18:0 > 16:1/20:2
DGDG 36:2	8.8	18:1/18:1 (79%) > 18:2/18:0 (21%) > 16:0/20:2
DGDG 36:1	0.8	18:1/18:0 (96%) > 16:0/20:1
DGDG 36:5-OH	0.1	18:3/18:2-OH (51%)
DGDG 36:4-OH	1.0	18:2/18:2-OH (97%)
DGDG 36:3-OH	0.2	18:1/18:2-OH (91%)

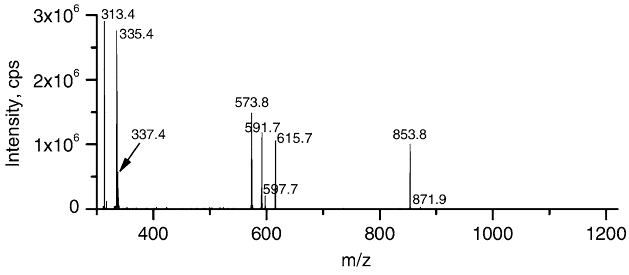

Fig. 5 Product ion spectrum of DGDG 52:4, *m/z* 1212 (nominal mass), a DGDG mono-estolide species containing the fatty acids 18:2, 16:0 and 18:2-OH

Identification of DGDG, DGDG Mono-Estolide and DGDG Di-Estolide Using Normal-Phase HPLC-APCI-MS

APCI-MS was employed previously for the structural characterization of DGDG and other glycolipids in red bell pepper [21]. In that study, the major ions observed were fragments attributed to loss of digalactose (i.e., protonated diacylglycerol (DAG)) and loss of digalactose and one fatty acid (i.e., protonated monoacylglycerol); the precursor DGDG ions were observed to be of low intensity. Using an NP-HPLC system similar to the one in the previous experiment, APCI-MS in the positive mode was used to obtain structural information about the three DGDG peaks identified in Fig. 2a. In this experiment (Fig. 3a), the HPLC conditions described in our previous report were used [2], and DGDG eluted at about 26 min, whereas it eluted at about 20 min under the conditions used in the analyses depicted in Fig. 2. The major peaks in the APCI-MS spectrum of the putative DGDG peak (Fig. 3b) were in the mass range consistent with DAG ions. The APCI-MS spectra of the putative mono-estolide (Fig. 3c) and di-estolide DGDG (Fig. 3d) species contained ions consistent with loss of digalactose from each species, leaving fragments consistent with protonated DAG mono- and di-estolides, respectively. Thus, the APCI data (Fig. 3) support the tentative identifications of the three peaks (Fig. 2a), but stronger evidence was sought to confirm the identifications.

ESI-MS/MS Neutral Loss Scanning Reveals Digalactosyl Acylglycerol Molecular Species

Precursor or neutral loss scanning by ESI-MS/MS can be utilized to identify the lipid species within a lipid class [22]. ESI-MS/MS is the main tool employed in the new field of “lipidomics” and has been employed to characterize the “lipidome” of humans, other animals, and plants [20, 23–26]. Figure 4a shows that, in the positive mode, in solvent containing ammonium acetate, DGDG species underwent neutral loss of ammoniated digalactose minus H_2O (NL 341; the neutral fragment is $C_{12}H_{23}O_{10}N$) or ammoniated digalactose (NL 359; the neutral fragment is $C_{12}H_{25}O_{11}N$). Specifically, the ammoniated precursor ion of DGDG 36:4 at *m/z* 958.6 (958) underwent neutral loss of 341 or 359 to produce the fragments observed at *m/z* 617.7 (617) and *m/z* 599.7 (599). (Loss of an “ammoniated digalactose minus H_2O” is equivalent to the loss of the ammoniated digalactose with the bridging oxygen left behind as a glycerol hydroxyl group.) In this product ion spectrum, the peak at *m/z* 337.4 (337) was a protonated 18:2 esterified to glycerol minus H_2O ($C_{21}H_{37}O_3$), indicating that the major molecular species of DGDG 36:4 was DGDG 18:2/18:2. Small peaks at *m/z* 335 (nominal) and *m/z* 339 (nominal) correspond to analogous acylglycerol fragments, indicating that DGDG 36:4 contained a smaller amount of DGDG 18:3/18:1.

To elucidate the varied digalactosyl acylglycerol species in the glycolipid SPE extract, NL 341 scans were utilized

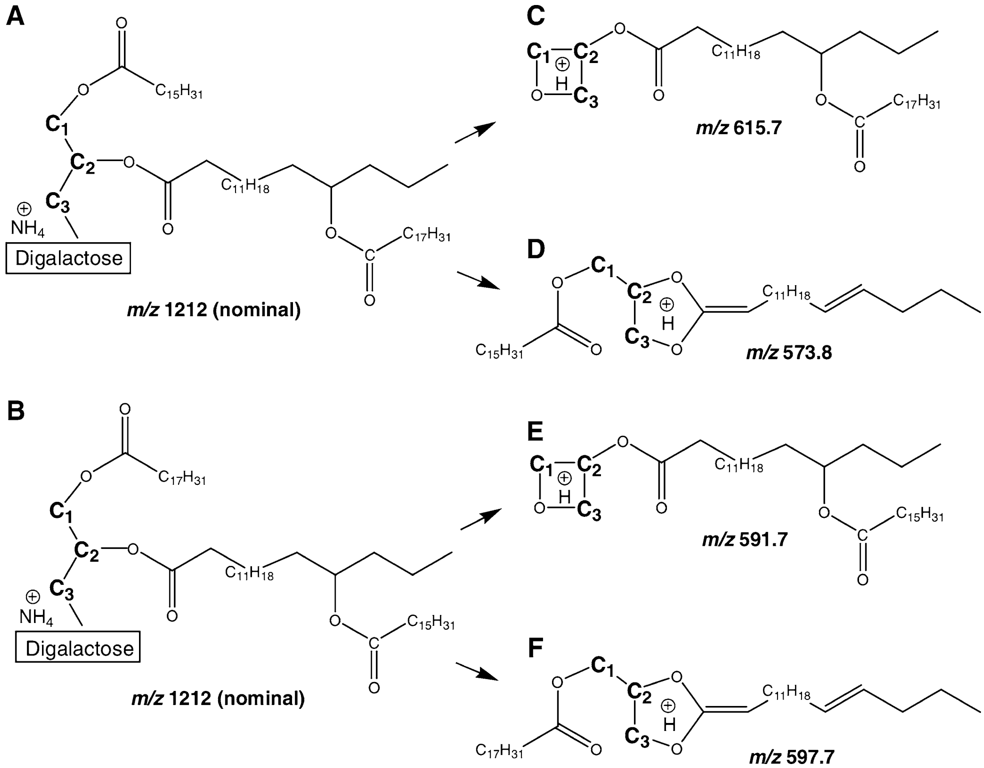

Fig. 6 Proposed structures of ammoniated DGDG 52:4 mono-estolide, *m/z* 1212 (nominal mass), and CID fragments at *m/z* 615, 573, 591, and 597 (nominal mass), based on structures demonstrated for triacylglycerol and phosphatidylethanolamine [27, 28]. Please note that, although we have indicated the glycerol carbons by C_1, C_2, and C_3, we have no information to indicate esterification to specific glycerol positions. We also do not know the position of carbon-carbon double bonds. **a** DGDG 52:4, with 16:0 and 18:2-OH/18:2 esterified to glycerol. **b** DGDG 52:4, with 18:2 and 18:2-OH/16:0 esterified to glycerol. **c** Fragment resulting from loss of ammoniated digalactose and 16:0 from structure in **a**. **d** Fragment resulting from loss of ammoniated digalactose and 18:2 from structure in **a**. **e** Fragment resulting from loss of ammoniated digalactose and 18:2 from structure in **b**. **f** Fragment resulting from loss of ammoniated digalactose and 16:0 from structure in **b**

(Fig. 4b–f). These spectra depict the molecular species of DGDG and provide the total number of acyl carbons: total number of carbon-carbon double bonds. Figure 4b shows the NL 341 scan in the mass range corresponding to DGMG species; these peaks represent species with only one acyl moiety per molecule. To identify the individual acyl chains associated with the non-estolide DGDG class, as depicted in Fig. 4c, multiple acyl precursor scanning in the negative ion mode [20], in combination with quantitative analysis of the DGDG class via the NL 341 scan in the positive mode, was carried out (Table 1). Hydrogenated DGDG species were used as internal standards. The data indicate that two DGDG species, 16:0/18:2 and 18:2/18:2 accounted for over half of the DGDG. A little over 1% of the DGDG (non-estolide) species contained 18:2–OH, consistent with the presence of 15(*R*)-hydroxylinoleic acid (avenoleic acid) [9, 10].

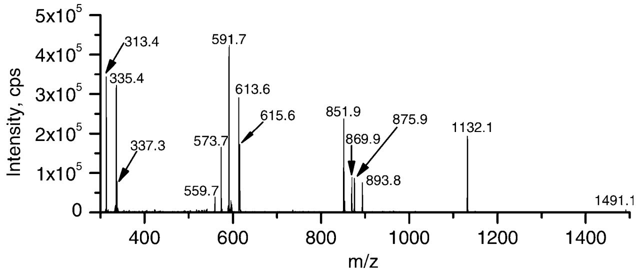

Fig. 7 Product ion spectrum of DGDG 70:6, *m/z* 1,490 (nominal mass), a DGDG di-estolide species containing the fatty acids 18:2, 16:0 and 2 18:2-OH species

Figure 4d–f shows that NL 341 scanning of the glycolipid SPE extract produced mass spectral peaks consistent with the identification of mono-, di-, and tri-estolides, respectively. Product ion spectra of specific mono-, di-, and tri-estolides of DGDG also were consistent with these identifications. The spectra suggest that some estolides are made up of multiple isomeric species. Figure 5 shows the product ion spectrum of the compound tentatively identified as DGDG 52:4, a DGDG mono-estolide species containing the fatty acids 18:2, 16:0 and 18:2-OH. The ammoniated DGDG 52:4 $[M + NH_4]^+$ ion at *m/z* 1212 (nominal, not visible in figure) underwent neutral loss to

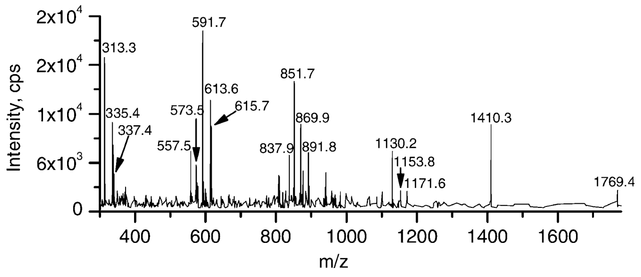

Fig. 8 Product ion spectrum of DGDG 88:8, *m/z* 1,768 (nominal mass), a DGDG tri-estolide species containing the fatty acids 18:2, 16:0 and 3 18:2-OH species

m/z 871.9 (871) or 853.8 (853). These species are likely to be due to loss of an ammoniated digalactose minus H_2O ($C_{12}H_{23}O_{10}N$; 341 Da) or an ammoniated digalactose ($C_{12}H_{25}O_{11}N$; 359 Da). The low abundance peak observed at *m/z* 871.9 (871) is likely to represent a protonated diacylglycerol mono-estolide containing the fatty acids 18:2, 16:0, and 18:2-OH. The more abundant fragment at *m/z* 853.8 (853) is likely to depict a conventional diacylglycerol-like fragment that lost the bridging oxygen during collision-induced dissociation (CID) [27, 28]. The peaks observed at *m/z* 615.7 (615) and 597.7 (597) contain

Fig. 9 Fragmentation of TriGDG and neutral loss scans identifying trigalactosyl acylglycerol species. **a** Product ion spectrum of TriGDG 36:4 $[M + NH_4]^+$ ion at *m/z* 1,120 (nominal mass). **b–e** Scans of neutral loss of 503, showing **b** TriGMG species, **c** TriGDG species, **d** TriGDG mono-estolide species, and **e** TriGDG di-estolide species

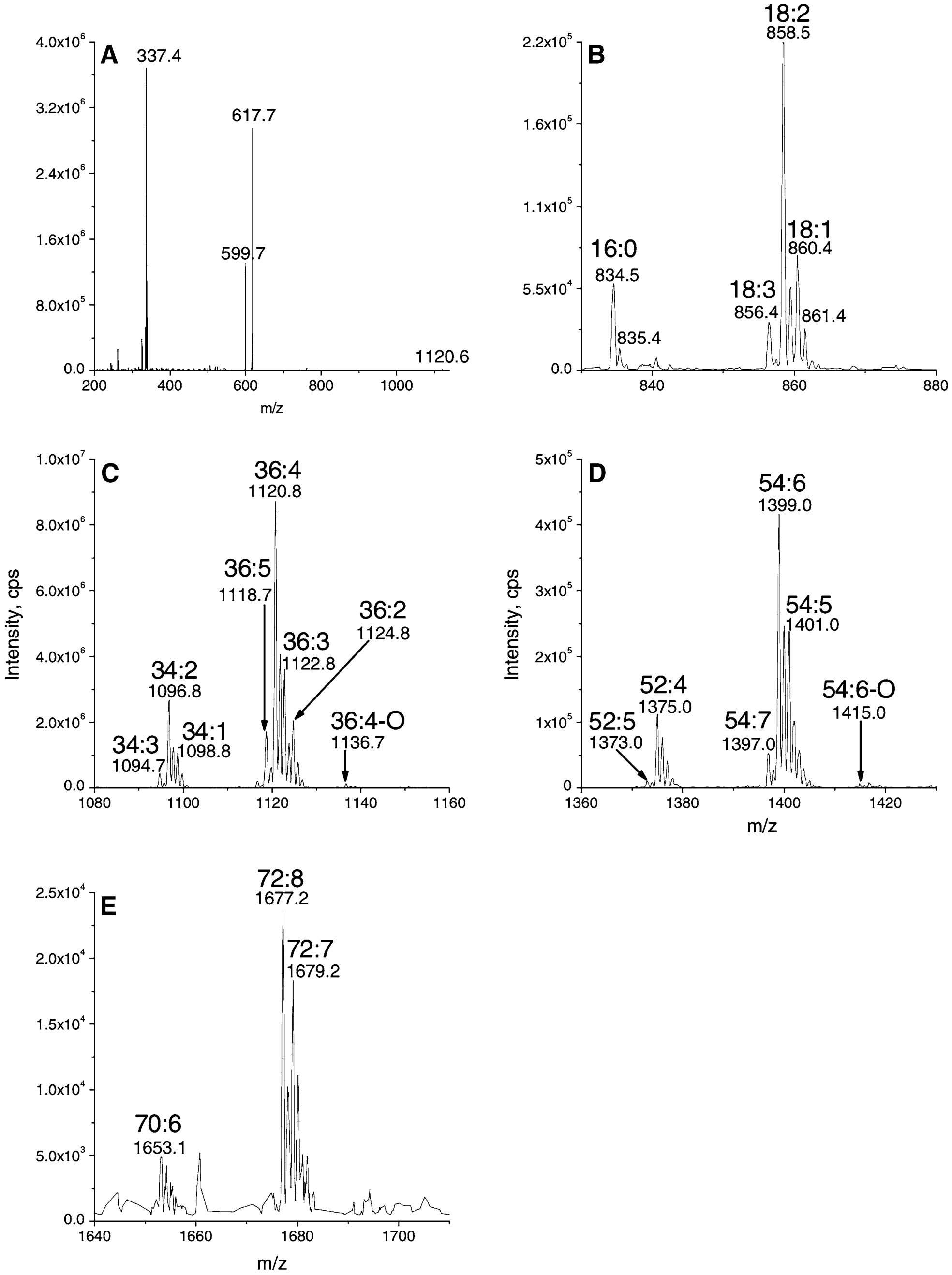

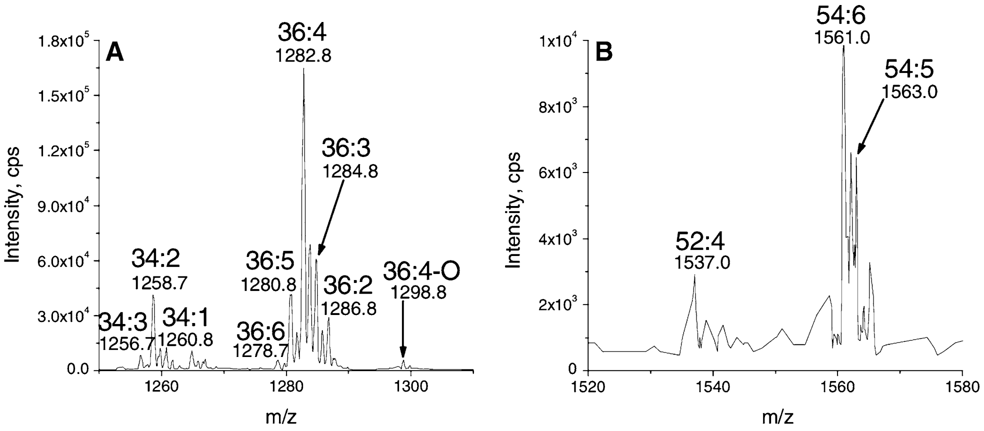

Fig. 10 Neutral loss scans identifying tetragalactosyldiacylglycerol species. TetraGDGs are identified in scans for neutral loss of an ammoniated tetragalactose minus H_2O ($C_{24}H_{43}O_{20}N$; 665 Da). Scans of neutral loss of 665, showing **a** TetraGDG species and **b** TetraGDG mono-estolide species

glycerol, one 18:2-OH, and one 18:2 fatty acid; the 16:0 fatty acid has been lost. These two peaks differ only in the amount of dehydration (1 dehydration for 615; 2 for 597). The peaks at *m/z* 591.7 (591) and 573.8 (573) likely represent fragments with glycerol, one 18:2-OH, and one 16:0 fatty acid; the 18:2 fatty acid has been lost. Again, these two peaks differ only in the amount of dehydration (1 dehydration for 591; 2 for 573). These four peaks may depict fragments originating from two different isomers of the DGDG 52:4 mono-estolide species. Figure 6 shows two possible structures for DGDG 52:4, one with 16:0 and an 18:2-OH/18:2 linked moiety each esterified to the glycerol (Fig. 6a). Another possible structure has 18:2 and an 18:2-OH/16:0 linked moiety each esterified to the glycerol (Fig. 6b). When the ammoniated digalactose head group and one fatty acid are lost during CID, the resulting structures can be stabilized by cyclization, by analogy to the structures produced during CID of triacylglycerols and phosphatidylethanolamines [27, 28], resulting in different apparent amounts of dehydration (Fig. 6c–f). Loss of the 16:0 esterified to glycerol, along with the head group, from the structure in Fig. 6a, can produce the ion seen at *m/z* 615.7 (615; Figs. 5, 6c). Loss of the 18:2 esterified to 18:2-OH, along with the head group, from the same structure (Fig. 6a) can produce the ion seen at *m/z* 573.8 (573; Figs. 5, 6d). The DGDG 52:4 isomer shown in Fig. 6b can fragment during CID in the same manner. Loss of the glycerol-esterified fatty acid, 18:2, along with the head group, can produce the ion seen at *m/z* 591.7 (591; Figs. 5, 6e). Loss of the 18:2-OH-esterified fatty acid, 16:0, along with the head group, can produce the ion seen at m/z 597.7 (597; Figs. 5, 6f). In comparing Fig. 6c with 6f or 6e with 6d, loss of ammoniated digalactose + loss of a fatty acid from the glycerol backbone results in one apparent dehydration, whereas loss of ammoniated digalactose + loss of the same fatty acid from the 18:2-OH-esterified position results in two apparent dehydrations. The peak observed in Fig. 5 at *m/z* 337.4 (337) is tentatively identified as protonated 18:2 esterified to glycerol minus H_2O ($C_{21}H_{37}O_3$). The peak observed at *m/z* 335.4 (335) appears to correspond to protonated 18:2-OH esterified to glycerol minus 2 H_2O ($C_{21}H_{35}O_3$), while the peak at *m/z* 313.4 (313) most likely represents protonated 16:0 esterified to glycerol minus H_2O ($C_{19}H_{37}O_3$). Again, these products are likely to have been cyclized, by analogy to structures formed in phosphatidylethanolamine fragmentation [28]. The presence in the spectrum of peaks representing each of the three fatty acids esterified to the glycerol is also consistent with DGDG 52:4 being a mixture of DGDG 16:0/18:2-O-18:2 (Fig. 6a) and DGDG 18:2/18:2-O-16:0 (Fig. 6b). The larger size of the peak at *m/z* 313.4 (313; acylglycerol 16:0 minus H_2O) as compared to the peak at *m/z* 337.4 (337; acylglycerol 18:2 minus H_2O) suggests that DGDG 16:0/18:2-O-18:2 was likely the more abundant species.

Figure 7 shows the product ion spectrum of putative DGDG 70:6, a DGDG di-estolide species containing the fatty acids 18:2, 16:0 and two 18:2-OH species. The ammoniated 70:6 DGDG $[M + NH_4]^+$ ion observed at *m/z* 1,491.1 (1,490) underwent neutral loss of 341 or 359 Da, like the mono-estolide, to yield the small peak at *m/z* 1,149 (nominal) and the larger peak observed at *m/z* 1,132.1 (1,131). The *m/z* 1,149 (nominal) peak represents loss of an ammoniated digalactose minus H_2O ($C_{12}H_{23}O_{10}N$; 341 Da), leaving a protonated diacylglycerol di-estolide. Loss of the intact digalactosyl moiety (NL 359) formed a conventional diacylglycerol-like fragment ion at *m/z* 1,132.1 (1,131) [27, 28]. The peak observed at *m/z* 893.8 (893), by analogy to the proposed structures for DGDG 52:4 detailed above in Fig. 6, most likely represents a protonated monoacylglycerol di-estolide, with two 18:2-OH groups and one 18:2 minus 1 H_2O; 16:0, along with the head group, was lost from the glycerol backbone. The peak at *m/z* 875.9 (875) probably represents its isomer, a protonated diacylglycerol mono-estolide. The 16:0 fatty acid was most likely lost from an 18:2-OH linkage, resulting in an additional

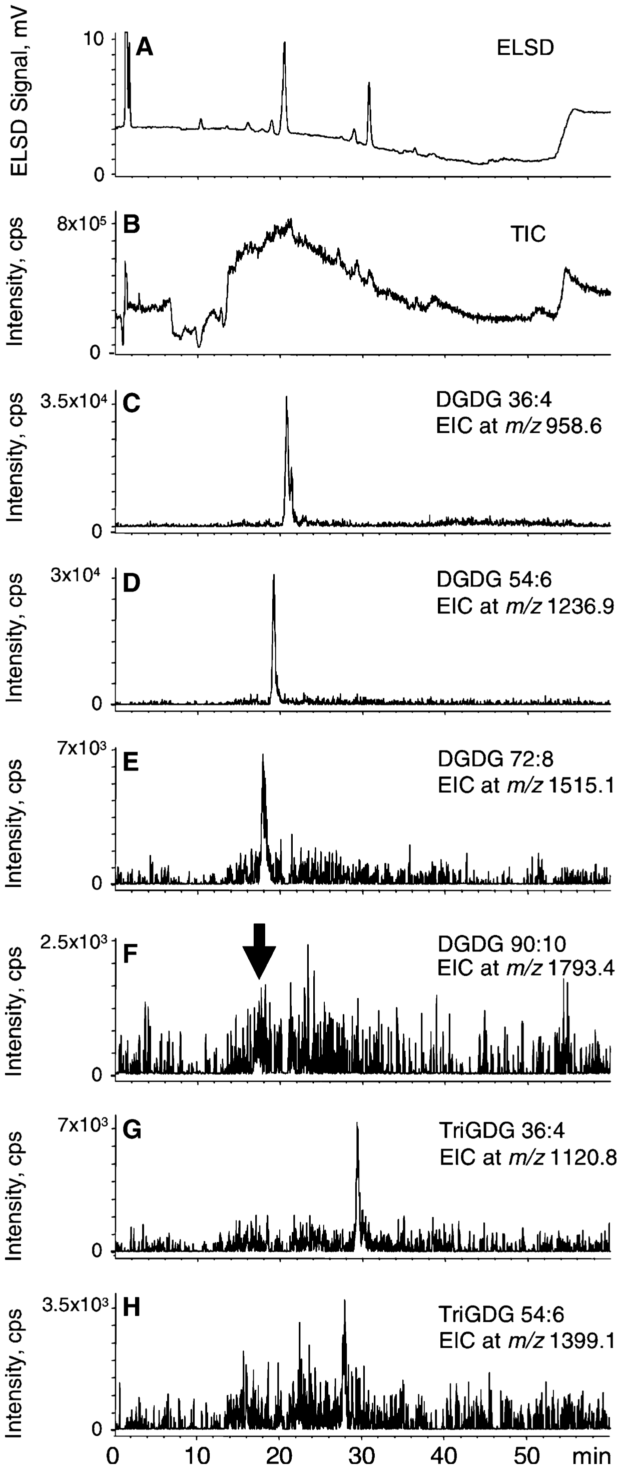

Fig. 11 NP-HPLC chromatograms of the oat total glycolipid SPE fraction. **a** NP-HPLC-ELSD chromatogram, **b** positive ESI TIC, *m/z* 200–2,000, **c** EIC of *m/z* 958.6, a major DGDG non-estolide, DGDG 36:4, **d** EIC of *m/z* 1,236.9, a major DGDG mono-estolide, DGDG 54:6, **e** EIC of *m/z* 1515.1, a major DGDG di-estolide, DGDG 72:8, **f** EIC of *m/z* 1,793.4, a major DGDG tri-estolide, DGDG 90:10 (The *arrow* indicates the possible location of this very small peak), **g** EIC of *m/z* 1,120.8, a major TriGDG non-estolide, TriGDG 36:4, and **h** EIC of *m/z* 1,399.1, a major TriGDG mono-estolide, TriGDG 54:6

dehydration. Likewise, the peaks at *m/z* 869.9 (869) and 851.9 (851) are likely to represent separate isomers of protonated glycerol esterified with two 18:2-OH and one 16:0, with one or two dehydrations, respectively. The peaks in the range *m/z* 573 to 615 represent additional acyl losses. The peaks at *m/z* 615.6 (615) and 597 (nominal) are consistent with protonated 18:2 and 18:2-OH esterified to glycerol, with the higher mass ion representing a protonated monoacylglycerol mono-estolide minus 1 H_2O and the lower mass ion representing a protonated diacylglycerol minus 2 H_2O. The peaks at *m/z* 613.6 (613) and 595 (nominal) are likely to represent protonated fragments with two 18:2-OH fatty acids esterified to glycerol with 2 or 3 dehydrations. The peaks at *m/z* 591.7 (591) and 573.7 (573) are tentatively identified as protonated 16:0 and 18:2-OH esterified to glycerol minus 1 and 2 H_2O, respectively. On the other hand, the peak at *m/z* 559.7 (559) may represent a free fatty acid protonated mono-estolide made up of 18:2-OH and 18:2. The peak at *m/z* 337 is likely to correspond to protonated 18:2 esterified to glycerol minus H_2O ($C_{21}H_{37}O_3$). The peak at *m/z* 335 may represent protonated 18:2-OH esterified to glycerol minus 2 H_2O ($C_{21}H_{35}O_3$), while the peak at *m/z* 313 is probably protonated 16:0 esterified to glycerol minus H_2O ($C_{19}H_{37}O_3$). These data indicate that DGDG 70:6 most likely was a mixture of

Table 2 Identification of the major galactolipids and estolides in oats and their abbreviations and ammoniated ion masses

Galactolipid molecular species	Abbreviation	*m/z* of $[M + NH_4]^+$
DGDG	DGDG 34:2	934.6
	DGDG 36:4	958.6
DGDG-with 1 hydroxy FA	DGDG 36:4-OH	974.6
DGDG mono-estolide	DGDG 52:4	1,212.9
	DGDG 54:6	1,236.9
	DGDG 54:7	1,234.9
DGDG mono-estolide with free OH	DGDG 54:6-OH	1,252.9
DGDG di-estolide	DGDG 70:6	1,491.1
	DGDG 72:8	1,515.1
DGDG tri-estolide	DGDG 88:8	1,769.4
	DGDG 90:10	1,793.4
TriGDG	TriGDG 34:2	1,096.7
	TriGDG 36:4	1,120.8
TriGDG-with 1 hydroxy FA	TriGDG 36:4-OH	1,136.7
TriGDG mono-estolide	TriGDG 54:6	1,399.1
TriGDG di-estolide	TriGDG 72:8	1,677.4
TetraGDG	TetraGDG 34:2	1,258.9
	TetraGDG 36:4	1,282.9
TetraGDG mono-estolide	TetraGDG 54:6	1,561.2

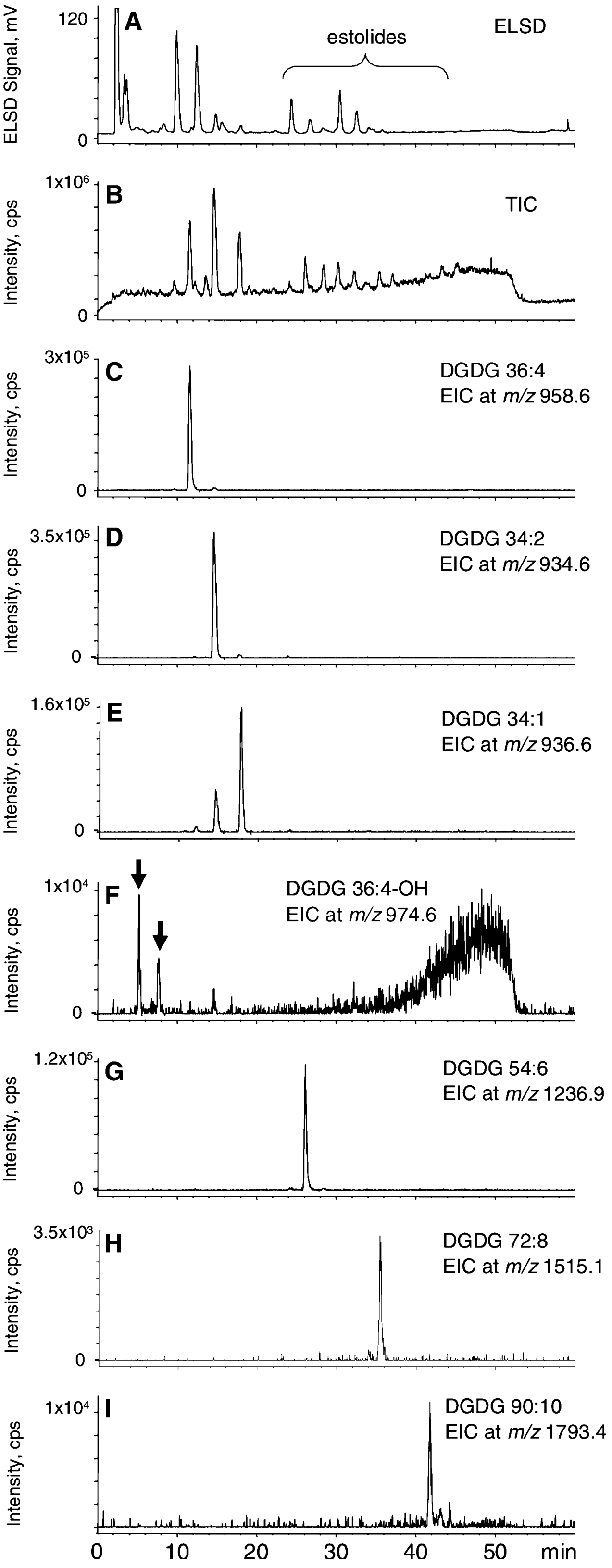

Fig. 12 RP-HPLC chromatograms of the oat total glycolipid SPE▶ fraction. **a** RP-HPLC-ELSD chromatogram, **b** positive ESI TIC, *m/z* 200–2,000, **c** EIC of *m/z* 958.6, a major DGDG non-estolide, DGDG 36:4, **d** EIC of *m/z* 934.6, a major DGDG non-estolide, DGDG 34:2, **e** EIC of *m/z* 936.6, a major DGDG non-estolide, DGDG 34:1, **f** EIC of *m/z* 974.6, a major DGDG non-estolide with a free hydroxyl group, DGDG 36:4-OH (The *peaks* marked by the *arrows* are both candidates for authentic DGDG 36:4-OH; the identity of the lipids in the large broad peak at 40–55 min is unknown.), **g** EIC of *m/z* 1,236.9, a major DGDG mono-estolide, DGDG 54:6, **h** EIC of *m/z* 1,515.1, a major DGDG di-estolide, DGDG 72:8, and **i** EIC of *m/z* 1,793.4, a major DGDG tri-estolide, DGDG 90:10

isomers, including DGDG 16:0/18:2-O-18:2-O-18:2 and DGDG 18:2/18:2-O-18:2-O-16:0. The presence of additional arrangements of the fatty acids, such as 18:2-O-18:2/18:2-O-16:0, cannot be ruled out by these data.

Similarly, Fig. 8 shows the product ion spectrum of the peak tentatively assigned as DGDG 88:8, a DGDG tri-estolide species containing the fatty acids 18:2, 16:0 and three 18:2-OH species. The ammoniated DGDG 88:8 $[M + NH_4]^+$ ion at *m/z* 1,769.4 (1,768) underwent neutral loss to the peaks observed at *m/z* 1,410. 3 (1,409) and 1,427 (nominal). These probably represent loss of an ammoniated digalactose (NL 359) and an ammoniated digalactose minus H_2O (NL 341). Thus, the peak at 1,410.3 (1,409) lost the bridging glycerol-galactose oxygen and is probably a conventional diacylglycerol-like fragment [27, 28]. The peaks at *m/z* 1,171.6 (1,171) and 1,153.8 (1,153) are likely to represent a protonated monoacylglycerol tri-estolide with one dehydration and a protonated diacylglycerol di-estolide with two dehydrations, respectively, with three 18:2-OH groups and one 18:2 each, by analogy to the proposed structures for DGDG 52:4 in Fig. 6. The peaks observed at *m/z* 1,147 (nominal) and 1,130.2 (1,129) probably reflect protonated glycerol esterified with three 18:2-OH and one 16:0 minus 1 or 2 H_2O. The peaks in the range *m/z* 851.7 (851) to 893 (nominal) represent additional acyl losses. The small peak at *m/z* 893 (nominal) represents a protonated fragment with two 18:2-OH and one 18:2 esterified to glycerol minus H_2O. The peaks at *m/z* 891.8 (891) and 873 (nominal) are likely to represent a protonated fragment with three 18:2-OH esterified to glycerol with either 2 or 3 dehydrations. The peaks observed at *m/z* 869.9 (869) and 851.7 (851) probably are protonated 16:0 and two 18:2-OH esterified to glycerol minus 1 or 2 H_2O. On the other hand, the peak at *m/z* 837.9 (837) may represent a free fatty acid protonated di-estolide species made up of two 18:2-OH and 18:2. The peaks in the range *m/z* 573.5 (573) to 615.7 (615) represent further acyl losses leading to species with two acyl chains. The peaks at *m/z* 615.7 (615) and 597 (nominal) probably represent protonated 18:2 and 18:2-OH esterified to glycerol, either a protonated monoacylglycerol mono-estolide with one dehydration or a protonated diacylglycerol with two dehydrations, respectively. The peaks at *m/z* 613.6 (613) and 595 (nominal) are consistent with a protonated fragment with two 18:2-OH esterified to glycerol with 2 or 3

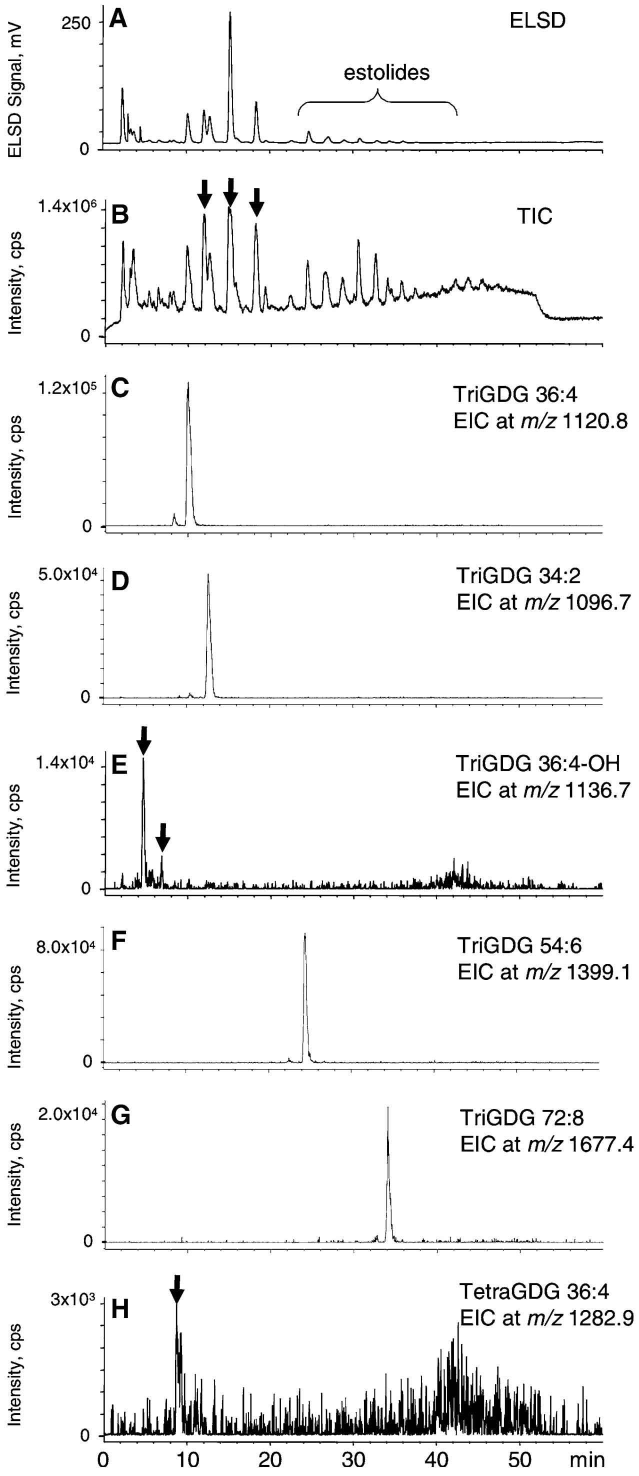

◀**Fig. 13** RP-HPLC chromatograms of the oat total glycolipid SPE subfraction 2, enriched in DGDG and TriGDG. **a** RP-HPLC-ELSD chromatogram, **b** positive ESI TIC, *m/z* 200–2,000 (The retention times of the three major non-estolide DGDG peaks previously identified in Fig. 12c–e were labeled with *arrows*), **c** EIC of *m/z* 1,120.8, a major TriGDG non-estolide, TriGDG 36:4, **d** EIC of *m/z* 1,096.7, a major TriGDG non-estolide, TriGDG 34:2, **e** EIC of *m/z* 1,136.7, a major TriGDG non-estolide with a free hydroxyl group, TriGDG 36:4-OH, **f** EIC of *m/z* 1,399.1, a major TriGDG mono-estolide, TriGDG 54:6, **g** EIC of *m/z* 1,677.4, a major TriGDG di-estolide, TriGDG 72:8, and **h** EIC of *m/z* 1,282.9, a major TetraGDG non-estolide, TetraGDG 36:4

dehydrations. The peak at *m/z* 591.7 (591) and that observed at *m/z* 573.5 (573) are likely to show protonated 16:0 and 18:2-OH esterified to glycerol minus 1 or 2 H_2O. The peak at *m/z* 557.5 (557) may represent a free fatty acid protonated mono-estolide species made up of two 18:2-OH minus H_2O. The peak at *m/z* 337 is likely to be protonated 18:2 esterified to glycerol minus H_2O ($C_{21}H_{37}O_3$). The peak at *m/z* 335 is protonated 18:2-OH esterified to glycerol minus 2 H_2O ($C_{21}H_{35}O_3$), while the peak at *m/z* 313 is probably protonated 16:0 esterified to glycerol minus H_2O ($C_{19}H_{37}O_3$). These data imply that the tentatively assigned DGDG 88:8 was a mixture of isomers, including DGDG 16:0/18:2-O-18:2-O-18:2-O-18:2 and DGDG 18:2/18:2-O-18:2-O-18:2-O-16:0. Again, the presence of additional arrangements of the fatty acids, such as 18:2-O-18:2/18:2-O-18:2-O-16:0, cannot be ruled out by these data.

ESI-MS/MS of Trigalactosyldiacylglycerol and Tetragalactosyldiacylglycerol Species

The product ion spectrum shown in Fig. 9a indicates that, in the positive mode, in solvent containing ammonium acetate, putative TriGDG species underwent a neutral loss of ammoniated trigalactose minus H_2O (NL 503). Specifically, the ammoniated precursor ion of TriGDG 36:4 at *m/z* 1,120.6 (1,120) underwent neutral loss to *m/z* 617.7 (617). The observed fragment is consistent with loss of an ammoniated trigalactose minus H_2O ($C_{18}H_{33}O_{15}N$; 503 Da). The peak observed at *m/z* 337.4 (337) is a protonated 18:2 esterified to glycerol minus H_2O ($C_{21}H_{37}O_3$), indicating that the major molecular species of TriGDG 36:4 was TriGDG 18:2/18:2. Peaks at *m/z* 335 (nominal) and 339 (nominal) correspond to analogous acylglycerol fragments indicating that TriGDG 36:4 contains a smaller amount of TriGDG 18:3/18:1. Scanning for NL 503 (Fig. 9b–e) can be used to identify TriGMGs, TriGDGs, TriGDG mono-estolides, and TriGDG di-estolides, respectively. Similarly, in the positive mode, in solvent containing ammonium acetate, TetraGDGs underwent a neutral loss of ammoniated tetragalactose minus H_2O (NL 665), and scanning for NL 665 displays species of TetraGDG and TetraGDG mono-estolide (Fig. 10a, b).

Normal-phase HPLC-ESI-MS Evidence for the Structural Identification of Glycolipids and their Estolides in the Oat Total Glycolipid Fraction

Based on the numerous glycolipids and estolides that were identified by ESI-MS/MS (Figs. 4, 5, 7, 8, 9, 10), we used

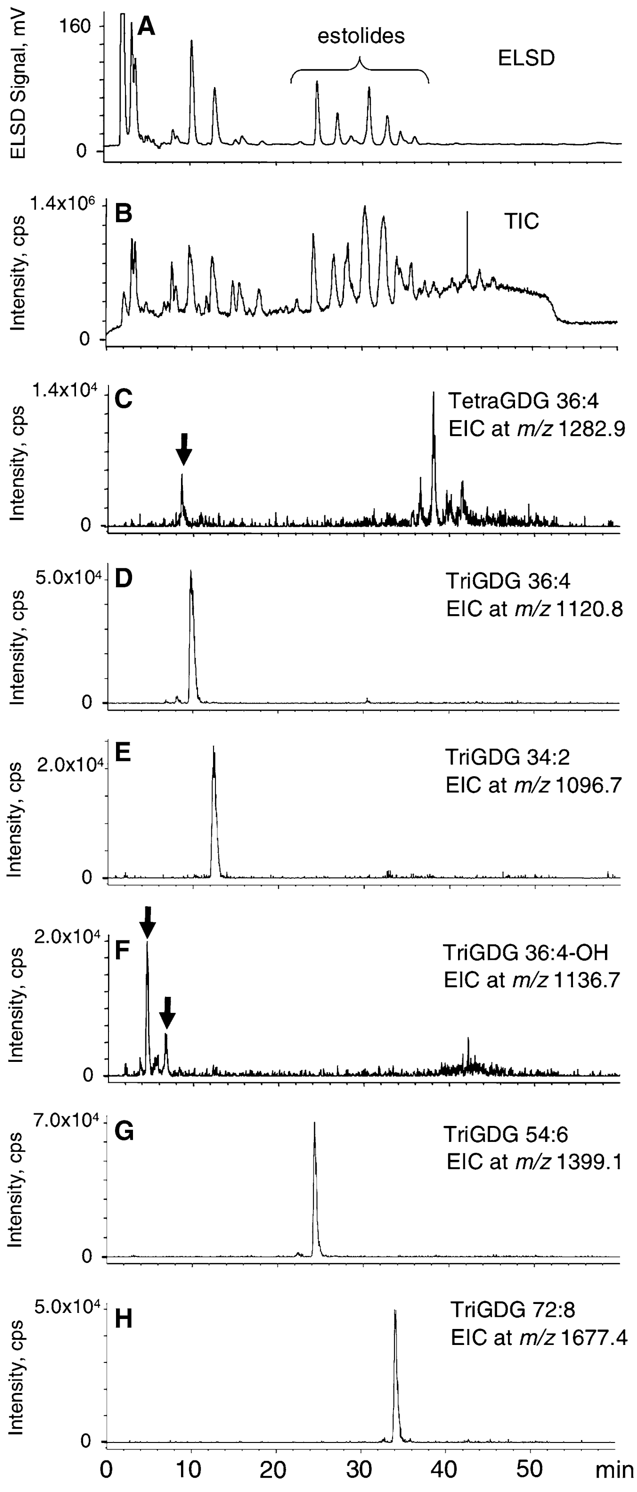

◀ **Fig. 14** RP-HPLC chromatograms of the oat total glycolipid SPE subfraction 3, enriched in TriGDG and TetraGDG. **a** RP-HPLC-ELSD chromatogram, **b** positive ESI TIC, *m/z* 200–2,000, **c** EIC of *m/z* 1,282.9, a major TetraGDG non-estolide, TetraGDG 36:4 (The probable retention time of authentic TetraGDG 36:4 was identified with an *arrow*; the identity of the lipids in the multiple peaks at 35–45 min is unknown.), **d** EIC of *m/z* 1,120.8, a major TriGDG non-estolide, TriGDG 36:4, **e** EIC of *m/z* 1,096.7, a major TriGDG non-estolide, TriGDG 34:2, **f** EIC of *m/z* 1,136.7, a major TriGDG non-estolide with a free hydroxyl group, TriGDG 36:4-OH, **g** EIC of *m/z* 1,399.1, a major TriGDG mono-estolide, TriGDG 54:6, and **h** EIC of *m/z* 1,677.4, a major TriGDG di-estolide, TriGDG 72:8

NP-HPLC-ESI-MS to try to identify some of the same lipids. The HPLC-ELSD chromatogram is shown in Fig. 11a. To assist in this evaluation, the major [M + NH$_4$]$^+$ ions identified in Figs. 4, 9, and 10 are listed in Table 2, and we searched for these "extracted ions" in the NP-HPLC-ESI-MS total ion chromatogram (TIC) (Fig. 11b); the results are plotted as "extracted ion chromatograms" (EIC) (Fig. 11c–h). Early attempts to employ ESI produced very few ions, and it was only after we added ammonium formate to the mobile phase that we started to obtain good ESI spectra. After we began routinely including ammonium formate in our mobile phase, the [M + NH$_4$]$^+$ ions were present in the greatest abundance (we saw very little of the [M + H]$^+$ and [M + Na]$^+$ ions), so we focused our attention on [M + NH$_4$]$^+$. Even with ammonium formate, the TIC for the normal-phase separation contained a very high background (Fig. 11b). However, by examining the EICs, we were able to identify peaks that corresponded to the major [M + NH$_4$]$^+$ ions of: non-estolide DGDG (DGDG 36:4) (Fig. 11c), DGDG mono-estolide (DGDG 54:6) (Fig. 11d), DGDG di-estolide (DGDG 72:8) (Fig. 11e), DGDG tri-estolide (DGDG 90:10) (Figure 11f, with an arrow indicating the possible location of this very small peak, which is consistent with the expected retention time for this hydrophobic DGDG estolide), non-estolide TriGDG (TriGDG 36:4) (Fig. 11g), and TriGDG mono-estolide (TriGDG 54:6) (Fig. 11h).

Reverse-Phase HPLC-ESI-MS Evidence for the Structural Identification of Glycolipids and their Estolides in the Oat Total Glycolipid Fraction

RP-HPLC-ESI-MS was also employed to identify the glycolipids and their estolides determined above by ESI-MS/MS. The HPLC-ELSD chromatogram is shown in Fig. 12a. The major difference that was observed when switching to the reverse phase HPLC method was that the reverse phase TIC (Fig. 12b) contained much less background noise than the comparable normal phase TIC (Fig. 11b). Examination of the EICs revealed several large sharp peaks that corresponded to the major [M + NH$_4$]$^+$ ions of: four non-estolide DGDGs (DGDG 36:4, 34:2, 34:1, and 36:4-OH) (Fig. 12c–f), DGDG mono-estolide (DGDG 54:6) (Fig. 12g), DGDG di-estolide (DGDG 72:8) (Fig. 12h), and DGDG tri-estolide (DGDG 90:10) (Fig. 12i). The putative DGDG 34:1 EIC (Fig. 12e) likely shows both an A + 2 isotope peak of the more abundant DGDG 34:2 (coeluting with DGDG 34:2, Fig. 12d) and

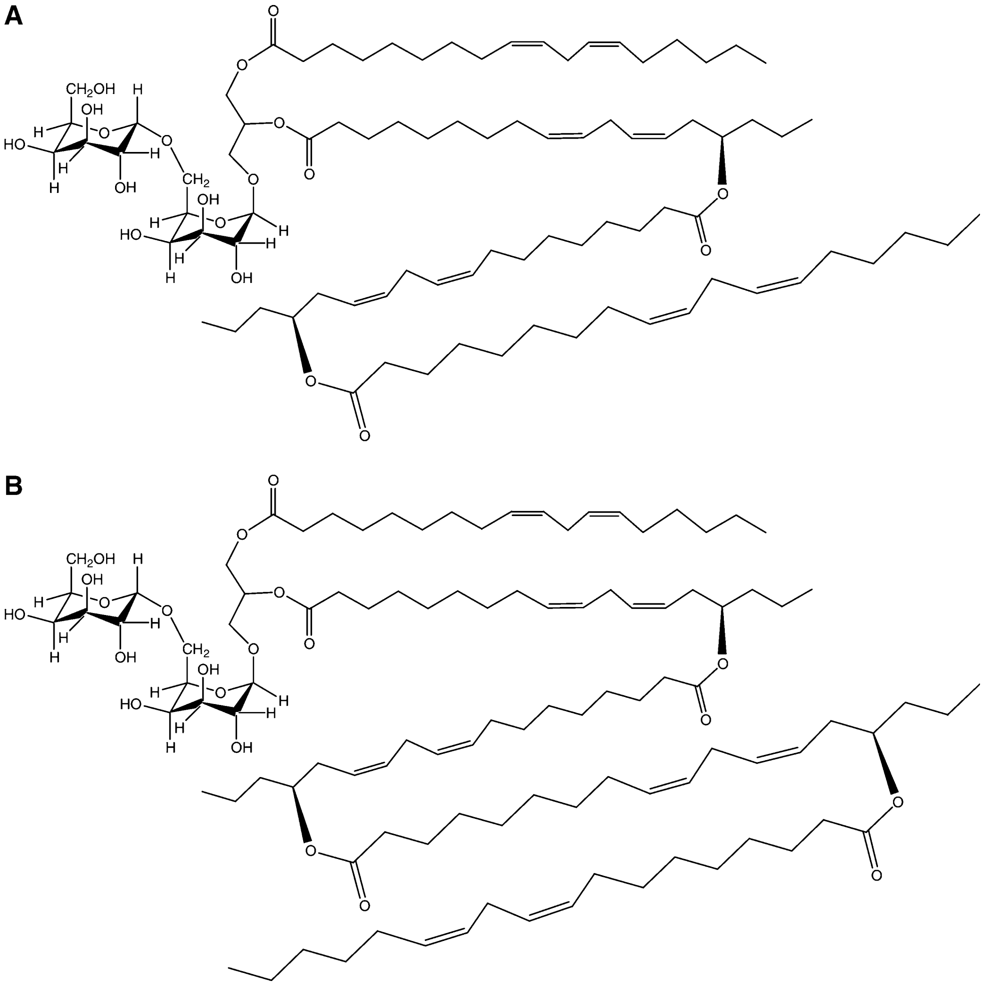

Fig. 15 Proposed structures of: **a** a DGDG di-estolide (DGDG 72:8) identified in this study by HPLC-MS and MS/MS. Exact mass ($C_{87}H_{148}O_{19}$), 1,497.0615 Da; *m/z* of $[M + NH_4]^+$ ($C_{87}H_{152}O_{19}N$), 1,515.0953. **b** A DGDG tri-estolide (DGDG 90:10) identified in this study by HPLC-MS and MS/MS. Exact mass ($C_{105}H_{178}O_{21}$), 1,775.2861 Da; *m/z* of $[M + NH_4]^+$ ($C_{105}H_{182}O_{21}N$), 1,793.3199. In these figures the estolide is shown esterified to the sn-2 position of glycerol, as suggested by Hamberg [10], but our data do not preclude the possibility that some or all of the estolides may be esterified at sn-1

DGDG 34:1, eluting slightly later. The EIC for DGDG 36:4-OH shows two sharp peaks (Fig. 12f). The location of the peaks is consistent with the notion that the presence of an extra OH would cause DGDG 36:4-OH to elute early in RP-HPLC, but it is not clear which peak is DGDG 36:4-OH, nor is the identity of the lipids in the large broad peak at 40–55 min in Fig. 12f known.

Reverse-Phase HPLC-ESI-MS Evidence for the Structural Identification of Glycolipids and their Estolides in the Oat Glycolipid Subfraction 2

As noted previously, oat glycolipid subfraction 2 contained high levels of DGDG and moderate levels of the putative TriGDG peaks (eluting at 26–30 min in Fig. 2). The RP-HPLC-ELSD chromatogram (Fig. 13a) and RP-HPLC-ESI-MS-TIC (Fig. 13b) revealed peaks at 10–20 min that appeared to correspond to non-estolides and peaks at about 20–40 min that corresponded to estolides. The retention times of the three major non-estolide DGDG peaks previously identified in Fig. 12c–e were labeled with arrows in Fig. 13b. The EICs revealed peaks that were tentatively identified as the major $[M + NH_4]^+$ ions of: non-estolide TriGDGs 36:4, 34:2, and 36:4-OH (Fig. 13c–e), TriGDG mono-estolide (TriGDG 54:6) (Fig. 13f), and TriGDG di-estolide (TriGDG 72:8) (Fig. 13g). It is unknown which early-eluting peak corresponds to TriGDG 36:4-OH in Fig. 13e. The EIC for *m/z* 1,282.9, corresponding to TetraGDG 36:4 (Fig. 13h), revealed weak peaks at about 9 (marked) and 40–42 min; the peak at 9 min exhibits a slightly shorter elution time than TriGDG 36:4 (Fig. 13c), consistent with expected behavior for TetraGDG 36:4 on a reverse-phase column.

Reverse Phase HPLC-ESI-MS Evidence for the Structural Identification of Glycolipids and their Estolides in the Oat Glycolipid Subfraction 3

As noted previously, oat glycolipid subfraction 3 was enriched in the putative TriGDG peaks (eluting at 26–30 min in Fig. 2) and contained a small putative TetraGDG peak (eluting at about 36 min). When analyzed via reverse-phase HPLC-ESI-MS (Fig. 14), the EICs revealed peaks that corresponded to the major $[M + NH_4]^+$ ions of TriGDG non-estolide and estolide peaks as identified in Fig. 13. The EIC of TetraGDG 36:4 revealed weak peaks at about 9 and 35–45 min (Fig. 14c) that were slightly stronger than those observed above (Fig. 13h). Based on its early elution time and the polar structure of TetraGDG, we speculate that the peak at 9 min is probably authentic TetraGDG and the peaks of less polar compounds at 35–45 min probably correspond to estolides with the same mass.

Estimation of the Total Amount of Estolides in Oat Lipids

The main objective of the current study was to provide structural evidence for the occurrence of several galactolipids and their estolides in oat kernels. In a future study we plan to report a comprehensive quantitative analysis of the levels of galactolipids and their estolides in several cultivars of oat kernels. However, we believe that it is important to estimate their approximate levels in this report to demonstrate that they are present in more than trace amounts. Using direct infusion electrospray ionization mass spectrometry we estimate that the oat glycolipid fraction contains: 58 mol% DGDG non-estolides, 25 mol% DGDG estolides, 8 mol% TriGDG non-estolides, 4 mol% TriGDG estolides, 0.3 mol% TetraGDG non-estolides, and 0.1 mol% TetraGDG estolides. Estolides therefore comprise about 29% of the total glycolipid fraction and 10% of the total methanol-extractable lipid fraction (based on the SPE fractionation yields).

Conclusion

We have confirmed the presence of DGDG mono-estolide (Fig. 1) in oat kernels, as previously reported by Hamberg et al. [10], and we have demonstrated that it is the most abundant estolide in oat kernels, but it is not the only estolide. Two larger DGDG estolides (di- and tri-estolides) (Fig. 15), two TriGDG estolides (mono- and di-estolides), and one TetraGDG estolide (mono-estolide) were also tentatively identified. The amounts of various estolide species did not vary, regardless of whether the oats were steamed to inactivate lipases before extraction, as in this study, or whether the oats were extracted directly (data not shown). To our knowledge, this report is the first evidence of natural di- and tri-estolides of polar lipids.

Acknowledgments We thank the reviewers for their detailed comments, which helped us to improve the manuscript. Kansas Lipidomics Research Center was supported by National Science Foundation (EPS 0236913, MCB 0455318, DBI 0521587), Kansas Technology Enterprise Corporation, Kansas IDeA Network of Biomedical Research Excellence (INBRE) of National Institute of Health (P20RR16475), and Kansas State University. This is contribution 08–122-J from the Kansas Agricultural Experiment Station.

References

1. Dörmann P, Benning C (2002) Galactolipids rule in seed plants. Trends Plant Sci 7:112–118
2. Moreau RA, Powell MJ, Singh V (2003) Pressurized liquid extraction of polar and nonpolar lipids in corn and oats with hexane, methylene chloride, isopropanol, and ethanol. J Am Oil Chem Soc 80:1063–1067
3. Morrison WR (1978) Wheat lipid composition. Cereal Chem 55:548–558
4. Galliard T (1969) The isolation and characterization of trigalactosyl diglyceride from potato tubers. Biochem J 115:335–339
5. Fujino Y, Miyazawa T (1979) Chemical structures of mono-, di-, tri-, and tetraglycosylglycerides in rice bran. Biochim Biophys Acta 572:442–451
6. Kojima M, Seki K, Ohnishi M, Ito S, Fujino Y (1990) Structure of novel glyceroglycolipids in Adzuki bean (*Vigna angularis*) seeds. Biochem Cell Biol 68:59–64
7. Ito S, Fujino Y (1975) Trigalactosyl diglyceride of pumpkin. Phytochemistry 14:1445–1447
8. Sugawara T, Miyazawa T (1999) Separation and determination of glycolipids from edible plant sources by high-performance liquid chromatography and evaporative-light scattering detection. Lipids 34:1231–1237
9. Hamberg M, Hamberg G (1996) 15(*R*)-Hydroxylinoleic acid, an oxylipin from oat seeds. Phytochemistry 42:729–732
10. Hamberg M, Liepinsh E, Otting G, Griffiths W (1998) Isolation and structure of a new galactolipid in oat seeds. Lipids 33:355–363
11. Spitzer V, Tomberg W, Pohlentz G (1997) Structure analysis of an allene-containing estolide tetraester triglyceride in the seed oil of *Sebastiana commersonionia* (Euphorbiaceae). Lipids 32:549–557
12. Sprecher HW, Maier R, Barber M, Holman RT (1965) Structure of an optically active allene-containing tetraester triglyceride isolate from the seed oil of *Sapium sebiferum*. Biochemistry 4:1856–1863
13. Heimermann WH, Holman RT (1972) Highly optically active triglycerides from *Sebastiana ligustrina* and related species. Phytochemistry 11:799–802
14. Morris LJ, Hall SW (1966) The structures of glycerides in ergot oil. Lipids 1:188–196
15. Hayes DG, Kleiman R, Bliss SP (1955) The triglyceride composition, structure, and presence of estolides in the oils of *Lesquerella* and related species. J Am Oil Chem Soc 72:559–569
16. Lin J-T, Arcinas A, Harden LR, Fagerquist CK (2006) Identification of (12-ricinoleolylricinoleoyl) diricinoleoylglycerol, and acylglycerol containing four acyl chains, in castor (*Ricinus communis* L.) oil by LC-ESI-MS. J Agric Food Chem 54:3498–3504
17. Isbell TA, Kleiman R (1994) Characterization of estolides from acid-catalyzed condensation of oleic acid. J Am Oil Chem Soc 71:379–383
18. Isbell TA, Cermak SC (2002) Synthesis of triglyceride estolides from *Lesquerella* and castor oils. J Am Oil Chem Soc 79:1227–1233
19. Ohm JB, Chung OK (1999) Estimation of free glycolipids in wheat flour by HPLC. Cereal Chem 76:873–876

20. Buseman CM, Tamura P, Sparks AA, Baughman EJ, Maatta S, Zhao J, Roth MR, Esch SW, Shah J, Williams TD, Welti R (2006) Wounding stimulates the accumulation of glycerolipids containing oxophytodienoic acid and dinor-oxophytodienoic acid in *Arabidopsis* leaves. Plant Physiol 142:28–39
21. Yamauchi R, Aizawa K, Inakuma T, Kato K (2001) Analysis of molecular species of glycolipids in fruit pastes of red bell pepper (*Capsicum annuum* L.) by high-performance liquid chromatography-mass spectrometry. J Agric Food Chem 49:622–627
22. Welti R, Wang X (2004) Lipid species profiling: A high-throughput approach to identify lipid compositional changes and determine the function of genes involved in lipid metabolism and signaling. Curr Opin Plant Biol 7:337–344
23. Brügger B, Erben G, Sandhoff R, Wieland FT, Lehmann WD (1997) Quantitative analysis of biological membrane lipids at the low picomole level by nano-electrospray ionization tandem mass spectrometry. Proc Natl Acad Sci USA 94:2339–2344
24. Devaiah SP, Roth MR, Baughman E, Li M, Tamura P, Jeannotte R, Welti R, Wang X (2006) Quantitative profiling of polar glycerolipid species and the role of phospholipase Dα1 in defining the lipid species in *Arabidopsis* tissues. Phytochemistry 67:1907–1924
25. Welti R, Li W, Li M, Sang Y, Biesiada H, Zhou H-E, Rajashekar CB, Williams TD, Wang X (2002) Profiling membrane lipids in plant stress responses: role of phospholipase Dα in freezing-induced lipid changes in Arabidopsis. J Biol Chem 277:31994–32002
26. Welti R, Wang X, Williams TD (2003) Electrospray ionization tandem mass spectrometry scan modes for plant chloroplast lipids. Anal Biochem 314:149–152
27. Hsu F-F, Turk J (1999) Structural characterization of triacylglycerols as lithiated adducts by electrospray ionization mass spectrometry using low-energy collisionally activated dissociation on a triple stage quadrupole instrument. J Am Soc Mass Spec 10:587–599
28. Hsu F-F, Turk J (2000) Characterization of phosphatidylethanolamine as a lithiated adduct by triple quadrupole tandem mass spectrometry with electrospray ionization. J Mass Spectrom 35:596–606

Lipids (2008) 43:549–557
DOI 10.1007/s11745-008-3175-4

ORIGINAL ARTICLE

The Digestibility and Accumulation of Dietary Phytosterols in Atlantic Salmon (*Salmo salar* L.) Smolt Fed Diets with Replacement Plant Oils

Matthew R. Miller · Peter D. Nichols ·
Chris G. Carter

Received: 21 November 2007 / Accepted: 12 March 2008 / Published online: 12 April 2008
© AOCS 2008

Abstract Phytosterols occur in high concentration in canola (*Brassica napus* L.) and other vegetable oils such as from the borage plant Echium (*Echium plantagineum* L.). We investigated if Atlantic salmon (*Salmo salar*) digest and accumulate dietary phytosterols in significant amounts in muscle and liver. Phytosterols are lipid soluble, lower cholesterol and reduce the risk of coronary heart disease in humans. We aimed to determine if fatty fish, such as salmon, can be used as a delivery source of this functional food component. Three diets containing canola oil (CO), Echium oil (EO) and fish oil (FO) were fed to Atlantic salmon smolt over 9 weeks. The digestibility of natural abundances of phytosterols by Atlantic salmon was poor compared to cholesterol. However, phytosterols accumulated in liver and muscle of fish. Significantly increased concentrations of 24-methylenecholesterol, campesterol, β-sitosterol and total phytosterol occurred in livers of EO fed fish compared to FO fed fish. Campesterol concentrations increased in CO fed fish compared to the FO fed fish. We demonstrated that natural abundances of dietary phytosterols are digested by and accumulated in liver and white muscle of Atlantic salmon smolt. However, phytosterol levels in salmon muscle will not be a major source of phytosterols in human diets and would not be expected to significantly effect human cardiovascular health.

Keywords Replacement oil · Fatty acids · Phytosterols · Canola oil · Echium oil · Sitosterol · Vegetable oil · Fish oil

Abbreviations

ADC	Apparent digestibility coefficients
ALA	α-Linolenic acid
ANOVA	One-way analysis of variance
BSFTA	*N*,*O*-Bis(trimethylsilyl)-trifluoroacetamide
CHD	Coronary heart disease
CMC	Carboxymethyl cellulose
DM	Dry matter
FA	Fatty acid(s)
GC	Gas chromatography
GC–MS	Gas chromatography–mass spectroscopy
LC	Long chain ($\geq C_{20}$)
LDL	Low-density lipoprotein
PCB	Polychlorinated biphenyls
PUFA	Polyunsaturated fatty acid(s)
SDA	Stearidonic acid
SE	Standard error
ST	Sterol(s)
TLC–FID	Thin layer chromatography–flame ionised detection
TLE	Total lipid extract
tr	Trace amounts
$\omega 3$	Omega 3
$\omega 3$ LC-PUFA	Omega 3 long chain ($\geq C_{20}$)-polyunsaturated fatty acid(s)

M. Miller was supported by an Australian Postgraduate Award (APA) and a CSIRO Food Futures Flagship postgraduate award.

M. R. Miller · C. G. Carter
School of Aquaculture,
Tasmanian Aquaculture and Fisheries Institute,
University of Tasmania, Locked Bag 1370,
Launceston, TAS 7250, Australia

M. R. Miller (✉) · P. D. Nichols
School of Aquaculture, CSIRO Food Futures Flagship
and CSIRO Marine and Atmospheric Research,
GPO Box 1538, Hobart, TAS 7001, Australia
e-mail: matthew.miller@utas.edu.au

$\omega 6$ Omega 6
WW Wet weight

Introduction

Phytosterols, a general term applied to a large number of plant-derived sterols, are found in all tissues of higher plants and are often enriched in seeds and seed oils [1, 2]. Phytosterols are natural, organic compounds with a molecular nucleus of 17 carbon atoms and a characteristic three-dimensional arrangement of four rings. Phytosterols can act as a structural component in the plant cell membrane, a role played in mammalian cells by cholesterol [2]. Unlike cholesterol, which has an alkyl side chain of 8 carbon atoms, the side chain of phytosterols generally contains 9 or 10 carbon atoms with alkyl substitution at C_{24}. Phytosterols have wide bioactivity in humans, and in particular are considered an efficacious cholesterol-lowering agent and consequently may have a preventive role against cardiovascular disease [2, 3]. Phytosterols may also have a role in cancer prevention [2, 4]. Consequently, some margarines, butters, spreads and breakfast cereals are enriched with phytosterols and promoted as "functional foods" [5, 6].

Due to increasing demand and prices, reduced availability, the possibility of organic contaminants (such as dioxins and polychlorinated biphenyls (PCB)), and increased knowledge about fishing impacts, fish oil is being replaced in part with plant oils such as canola and soy in formulated/commercial feeds for aquaculture species [7]. Replacement oil diets have become an industry priority and over the last 20 years there has been increased scientific activity focused on the effects of substituting fish oil with plant oils, including effects on fish growth and health and on flesh quality. Limited research has been performed examining phytosterols in farmed Atlantic salmon (*Salmo salar*). The replacement of fish oil with plant oils in aquafeeds will increase dietary amounts of phytosterols. However, it has yet to be evaluated to what extent Atlantic salmon digest and accumulate phytosterols from dietary plant oils.

Pulp and paper mill effluent has been shown to affect reproductive and endocrine function in fish and this is thought to be due to the large amount of phytosterols, in particular β-sitosterol. In vivo and in vitro studies suggest that large amounts of β-sitosterol can affect fish endocrine activity and reproduction via many mechanisms/actions on numerous pathways [8].

The digestibility of phytosterols is poor in humans, and to our knowledge has yet to be evaluated in Atlantic salmon or in any other fish species. With the increased use of plant oils and meal in aquafeeds, minor components such as phytosterols will be increasingly introduced into aquaculture diets and it is necessary to examine how they are digested by salmon. Phytosterols have been shown to have potential health benefits to the human consumer, in particular as a cholesterol-lowering agent. Therefore farmed Atlantic salmon fed a replacement plant oil diet may be a novel and further delivery source of phytosterols to humans. Assessment of how they are accumulated and concentrated in tissues such as liver and muscle of Atlantic salmon fed on replacement oil diets is needed to gauge any possible advantageous affect to the consumer. This study aims to assess digestibility and accumulation in white muscle and liver of phytosterols from two experimental plant oil diets (canola and Echium) compared with a traditional fish oil diet fed to Atlantic salmon smolt.

Material and Methods

Experimental Diets

Three diets were formulated to compare canola oil (CO), Echium oil (EO) and fish oil (FO) (Table 1). Fish meal was defatted three times using a 2:1 mixture of hexane and ethanol (400 ml/100g fish meal). Full fat soybean meal (Hamlet Protein A/S, Horsens, Denmark), casein (MP Biomedicals Australasia Pty Ltd, Seven Hills, NSW, Australia), wheat gluten (Starch Australasia, Lane Cove,

Table 1 Ingredient, lipid and sterol composition (g/kg dry matter) of experimental diets

	Diet		
	CO	EO	FO
Ingredient composition (g/kg)			
Fish meal (defatted)	150	150	150
Casein	150	150	150
Wheat gluten	100	100	100
Soybean meal	180	180	180
Fish oil	0	0	200
Canola oil	200	0	0
Echium oil	0	200	0
Pre gel starch	127	127	127
Vitamin mix[a]	3	3	3
Mineral mix[b]	5	5	5
Stay C[c]	3	3	3
Chlorine chloride	2	2	2
Supernat	40	40	40
CMC	10	10	10
Sodium mono phosphate	20	20	20
Yttrium oxide	10	10	10
Chemical composition (g/kg WW)			

Table 1 continued

	Diet		
	CO	EO	FO
Dry matter	919.4	925.2	904.3
Crude protein	344.0	333.5	331.7
Crude fat	242.4	250.4	241.8
Energy (MJ/kg WW)	18.9	18.6	18.4
FAME (g/kg WW)			
Total SFA	20.4	23.9	62.9
Total MUFA	105.7	38.5	49.5
Total ω3	12.4	67.6	46.0
Total ω6	45.2	56.2	18.7
Total PUFA	58.3	123.9	71.0
Sterols and stanols (g/kg WW)			
Cholesterol[d]	1.6	2.6	6.7
Cholestanol[e]	ND	ND	0.1
24-Methylenecholesterol[f]	0.3	0.6	0.3
Phytosterols (g/kg WW)			
Brassicasterol[g]	0.6	ND	0.0
Campesterol[h]	2.1	1.8	0.4
Stigmasterol[i]	0.1	ND	ND
β-sitosterol[j]	3.4	2.4	1.2
Isofucosterol[k]	0.4	1.3	0.2
Other minor sterols[l]	0.3	0.2	0.2
Total phystosterols	6.8	5.6	1.9

EO Echium oil Crossential SA14 from Croda chemicals, *CO* canola oil, *FO* fish oil, *SFA* saturated fatty acids, *MUFA* monounsaturated fatty acids, *PUFA* polyunsaturated fatty acids, *CMC* carboxymethyl cellulose, *ND* not determined

[a] Vitamin mix (ASV4) supplied per kilogram of feed: 2.81 mg thiamine HCL, 1.0 mg riboflavin, 9.15 mg pyridoxine HCL, 25 mg nicotinic acid, 54.35 mg calcium D-pantothenate, 750 mg myo-inositol, 0.38 mg D-biotin, 2.5 mg folic acid, 0.03 mg cyanocobalamin, 6,350 IU retinol acetate, 2,800 IU cholecalciferol, 100 IU DL α-tocopherol acetate, 5 g menadione sodium bisulphate, 100 mg Roche rovimix E50

[b] Mineral mix (TMV4) supplied per kilogram of feed: 117 mg $CuSO_4 \cdot 5H_2O$, 7.19 mg KI, 1,815 mg $FeSO_4 \cdot 7H_2O$, 307 mg $MnSO_4 \cdot H_2O$, 659 mg $ZnSO_4 \cdot 7H_2O$, 3.29 mg Na_2SeO_3, 47.7 mg $CoSO_4 \cdot 7H_2O$

[c] L-Ascorbyl-2-polyphosphate (Stay-C, Roche Vitamins Australia, Frenchs Forest, NSW, Australia)

[d] Cholest-5-en-3β-ol

[e] 5α-Cholestan-3β-ol

[f] 24-Methylcholesta-5,24(28)-dien-3β-ol

[g] 24-Methylcholesta-5,22E-dien-3β-ol

[h] 24-Methylcholest-5-en-3β-ol

[i] 24-Ethylcholesta-5,22E-dien-3β-ol

[j] 24-Ethylcholest-5-en-3β-ol

[k] 24-Ethylcholesta-5,24(28)Z-dien-3β-ol

[l] Other minor sterols included 24-ethyl-5α-cholest-7-en-3β-ol, 4,4,14-trimethyl-5α-cholesta-8,24-dien-3β-ol (lanosterol), and other undetermined sterols

NSW, Australia) and BOIIC pre-gelatinised maize starch (Penford Australia Limited, Lane Cove, NSW, Australia) were used as ingredients. Echium oil was supplied as Crossential SA14 (Croda Chemicals, East Yorkshire, UK). Fish oil was from jack mackerel, *Trachurus symmetricus* L., (Skretting Australia, Cambridge, TAS, Australia) and a domestic refined source of pure canola oil was used (Steric Trading Pty Ltd, Villawood, NSW, Australia). Stay-C and Rovimix E50 were purchased from Roche Vitamins Australia (Frenchs Forest, NSW, Australia), and the remaining ingredients were purchased from Sigma-Aldrich (Castle Hill, NSW, Australia). Yttrium oxide was used as a digestibility marker. The diets were manufactured into 3 mm diameter pellets using a California Pellet Mill (CL-2), dried and stored at 5 °C [9].

Growth Experiment

The experiment was conducted at the School of Aquaculture, University of Tasmania (Launceston, TAS, Australia). Atlantic salmon (*S. salar* L.) parr (≈87.9 g) were obtained from Springfield Fisheries hatchery (Scottsdale, TAS, Australia), acclimated for 14 days in 300 l tanks and fed a commercial feed (Skretting). Prior to the experiment the fish were slowly adapted to seawater over a 21 day period. The tanks were held at a constant temperature of 12.0 °C under a natural photoperiod. Water was treated through physical, UV and biofilters. Dissolved oxygen, pH, ammonia, nitrate, nitrite, and salinity were monitored daily to ensure water quality remained within parameters recommended for Atlantic salmon [10]. The fish were held in an average of 27.4 ± 0.2 ppm saltwater. The experiment was conducted in accordance with the University of Tasmania Animal Ethics guidelines (Investigation A0008392).

At the start of the experiment fish (average weight 106.9 g) were anaesthetized (50 mg/1, benzocaine), their weight and length measured, and three fish were killed to measure initial lipid content and composition. Twenty-five fish were randomly re-allocated into each of twelve 300 l tanks, and 4 tanks were randomly allocated to each dietary treatment. The four diets were fed in triplicate at a ration of 1.8% body weight per day (% BW/d) in two equal feeds at 0900 and 1700 hours by automatic belt feeders. Every 7 days the total feed consumption (kg DM) was estimated from the amount of uneaten feed in Guelph-type sediment collectors [11, 12]. Every 3 weeks all fish were anaesthetized (50 mg/1, benzocaine) and batch-weighed. Fish were starved the day prior to weighing.

At the end of the experiment (day 84), fish were starved for 1 day prior to being anaesthetized (50 mg/1, benzocaine) and their weight and length measured. Three fish, which had doubled their initial weight, per tank were killed by a blow to the head after immersion in anaesthetic.

Samples of white muscle (approx 0.7 g), dissected from below the dorsal fin, and liver (average 2.7 g) were taken and frozen at −80 °C until analysis [7].

On days 86–90, faecal samples were collected from sediment collectors between 1100–1700 and 1900–0900 hours, freeze–dried and used in the analysis of digestibility [12]. The apparent digestibility coefficients (ADC) were calculated using the standard formula $\text{ADC} (\%) = 100 - [100((Y_{\text{diet}}/Y_{\text{faeces}}) \times ((ST_{\text{faeces}}/ST_{\text{diet}}))]$, where Y is percentage of yttrium oxide and ST is the % of particular sterols [13]. This calculation does not take into account possible dealkylation of phytosterols to cholesterol.

Sterol Extraction and Isolation

All samples (tissue, faeces and diets) were freeze–dried and extracted overnight using a modified Bligh and Dyer protocol [14]. This involved a single phase extraction, $CHCl_3$/MeOH/H_2O (1:1:0.9, by vol), followed by phase separation to yield a total lipid extract (TLE).

Lipid classes were analysed using an Iatroscan MK V thin-layer chromatography-flame ionization detector (TLC-FID) analyser (Iatron Laboratories, Japan). Samples of the TLE were spotted onto silica gel SIII Chromarods (5 µm particle size) and developed in a glass tank lined with pre-extracted filter paper. The solvent system used for the lipid separation was hexane:diethyl ether:acetic acid (60:17:0.1 v/v/v) [15]. After development for 25 min, the chromarods were oven-dried and analysed immediately to minimise adsorption of atmospheric contaminants. Lipid classes were quantified by DAPA software (Kalamunda, WA, Australia). The FID was calibrated for each compound class: phosphatidylcholine (retention factor 0.00), cholesterol (0.30), oleic acid (0.46); wax ester (derived from fish oil, 0.89) and triacylglycerol (derived from fish oil, 0.74).

An aliquot of the TLE was treated with 2 ml of 5% w/v KOH in 80:20 MeOH:H_2O (60 °C, 3h, milli-Q water). Following the addition of water, sterols were extracted into hexane/chloroform (4:1 v/v, 3 × 1.5 ml), transferred to vials, reduced under a stream of nitrogen and stored in chloroform. Samples were treated with *N*,*O*-bis(trimethylsilyl)-trifluoroacetamide (BSTFA) to form trimethylsilyl (TMS) ether derivatives (of free sterols) prior to instrument analysis.

Concentrations of plant sterols were determined by gas chromatography. Samples were made up to a known volume with a internal injection standard containing methyl nonadecanate and analysed by gas chromatography (GC) using an Agilent Technologies 6890N GC (Palo Alto, CA, USA) equipped with an Equity^{TM}-1 fused silica capillary column (15 m × 0.1 mm i.d., 0.1 µm film thickness), an FID, a split/splitless injector and an Agilent Technologies 7683 Series autosampler. Helium was the carrier gas. Samples were injected in splitless mode at an oven temperature of 120 °C. After 3 min, the oven temperature was raised to 270 °C at 10 °C per min and finally to 290 °C at 5 °C/min^{-1} holding at 290 °C for 5 min. Peaks were quantified with Agilent Technologies GC ChemStation software (Palo Alto, CA, USA).

Individual components were identified from mass spectral data and by comparing retention time data with those obtained for authentic and laboratory standards. GC–mass spectrometric (GC–MS) analyses were performed on a Finnigan Thermoquest GCQ GC–mass spectrometer fitted with an on-column injector and using Thermoquest Xcalibur software (Austin, TX, USA). The GC was equipped with an HP-5 cross-linked methyl silicone fused silica capillary column (50 m × 0.32 mm i.d.). Helium was used as the carrier gas, with operating conditions previously described [16]. Sterols were identified from comparison to known spectra and major ion fragments [17]. The stereochemistry was not determined for the C_{24} position. The retention times for the major sterols were cholesterol 20.33 min, cholestanol 20.73 min, 24-methylenecholesterol 21.51 min, brassicasterol 20.85 min, campesterol 21.63 min, stigmasterol 22.17 min, *β*-sitosterol 22.77 min and isofucosterol 22.92 min.

Statistical Analysis

Mean values are reported as plus or minus the standard error of the mean. Normality and homogeneity of variance were confirmed and percentage data were arcsin transformed prior to analysis. Comparison between means was by one-way analysis of variance (ANOVA) followed by multiple comparisons using Tukey–Kramer HSD. Significance was accepted at probabilities of 0.05 or less. Statistical analysis was performed using SPSS for Windows version 11.

Results

Growth Results

There was no significant difference in the final weight, final length or growth between fish fed the three experimental diets. Fish of an average weight (106.8 g) were grown on the three experimental diets for 12 weeks to an average sampled weight of 236.5 g.

Sterol (ST) Composition

There was no significant difference in the sterol content in the white muscle between dietary treatments as determined by TLC–FID analysis (Table 2). There was significantly

Table 2 Sterol and lipid content (wet weight) of white muscle and livers of Atlantic salmon smolt fed canola oil (CO), Echium oil (EO) and fish oil (FO) diets

Sterol content (mg/100g)	Initial (±SE)	CO (±SE)	EO (±SE)	FO (±SE)	*f*
White muscle	21.6 ± 4.8	15.0 ± 6.0	12.4 ± 6.5	13.9 ± 3.1	
Liver	139.9 ± 18.4^{a}	263.8 ± 34.3^{b}	144.7 ± 18.0^{a}	139.7 ± 11.8^{a}	7.9
Lipid content (mg/g)					
White muscle	17.9 ± 2.9	28.0 ± 3.4	30.1 ± 6.2	26.8 ± 4.9	
Liver	29.0 ± 2.2^{a}	49.1 ± 3.5^{b}	38.3 ± 2.4^{a,b}	35.8 ± 2.7^{a}	7.3

[a, b] Mean values across the row not sharing a common superscript were significantly different as determined by Tukey–Kramer HSD; $df = 3{,}40$, $P < 0.01$

higher total sterol content in the liver (263.8 mg/100 g) of the fish fed the CO diet. Cholesterol was the major sterol in all tissues, irrespective of diet, but the amounts of minor sterols varied. There were significantly ($P < 0.01$) higher concentrations of total phytosterols in the liver and white muscle in both the CO and EO fed fish compared to the FO or initial fish (Tables 3, 4). This equated to a fourfold increase in the white muscle and a twofold increase in the liver in total phytosterol concentrations in EO and CO fish compared to the FO fish. There were significant differences in the sterol composition of the liver (Table 4). There was a sevenfold significant ($P < 0.01$) increase in concentrations of campesterol (full chemical names for all sterols are contained in the footnote for Table 1) in the liver of both the CO and EO fish compared to the FO or initial fish. There were significant ($P < 0.01$) increases in concentrations of β-sitosterol and 24-methylenecholesterol in the liver of EO fish compared to that of the FO or initial fish. This equated to a sevenfold increase in β-sitosterol in the EO fish compared with the FO fish. There was a significantly ($P < 0.01$) higher concentration of cholestanol in the initial fish compared to the CO and EO fish. There was a significant ($P < 0.01$) five to ninefold increase in the concentrations of other minor sterols including 24-ethyl-5α-cholest-7-en-3β-ol, lanosterol, and other undetermined sterols in the liver of CO and EO fish.

There was no significant difference in the sterol composition (%) between the white muscle for fish fed the three diet treatments (Table 3). However, although not significant, the same trends in increased concentration of individual phytosterols that occurred in the liver were observed in the white muscle. There was a three to fivefold increase in the amount of β-sitosterol and a twofold increase in campesterol in the white muscle of fish fed EO and CO diets compared with the FO fish.

Digestibility of Phytosterols

There was no significant difference between the ADC of cholesterol between the three diet treatments (Table 5).

Table 3 Sterol composition (mg/100g wet weight) of white muscle of Atlantic salmon smolt fed canola oil (CO), Echium oil (EO) and fish oil (FO) diets

Sterol	Initial (±SE)	CO (±SE)	EO (±SE)	FO (±SE)	*f*
Cholesterol	25.7 ± 2.2	15.4 ± 2.0	15.2 ± 2.0	13.6 ± 2.8	
Cholestanol	0.2 ± 0.2	0.0 ± 0.0	0.0 ± 0.0	0.0 ± 0.0	
Brassicasterol	0.0 ± 0.0	0.2 ± 0.1	0.1 ± 0.1	0.1 ± 0.0	
24-Methylenecholesterol	0.2 ± 0.1	0.1 ± 0.1	0.4 ± 0.1	0.1 ± 0.0	
Campesterol	0.1 ± 0.1	0.2 ± 0.0	0.2 ± 0.1	0.0 ± 0.0	
Stigmasterol	0.0 ± 0.0	0.0 ± 0.0	0.0 ± 0.0	0.0 ± 0.0	
β-sitosterol	0.0 ± 0.0	0.3 ± 0.2	0.5 ± 0.3	0.0 ± 0.0	
Isofucosterol	0.0 ± 0.0	0.1 ± 0.0	0.0 ± 0.0	0.0 ± 0.0	
Other minor sterols[c]	0.1 ± 0.0	0.1 ± 0.0	0.0 ± 0.0	0.0 ± 0.0	
Total phytosterols[d]	0.2 ± 0.1^{a}	0.9 ± 0.2^{b}	0.8 ± 0.3^{b}	0.2 ± 0.1^{a}	8.5

Systematic names for all sterols are contained in the footnote for Table 1

[a, b] Mean values across the row not sharing a common superscript were significantly different as determined by Tukey–Kramer HSD; $df = 3{,}36$, $P < 0.01$

[c] Other minor sterols including 24-ethyl-5α-cholest-7-en-3β-ol, lanosterol, and other undetermined sterols

[d] Includes all C_{28} and C_{29} sterols excluding 24-methylenecholesterol

Table 4 Sterol composition (mg/100g wet weight) of liver of Atlantic salmon smolt fed canola oil (CO), Echium oil (EO) and fish oil (FO) diets

Sterol	Initial (±SE)	CO (±SE)	EO (±SE)	FO (± SE)	*f*
Cholesterol	99.2 ± 7.0	222.5 ± 21.8	180.1 ± 16.8	151.4 ± 12.5	
Cholestanol	0.7 ± 0.2^{c}	0.1 ± 0.0^{a}	$0.2 \pm 0.1^{a,\ b}$	$0.4 \pm 0.1^{b,\ c}$	9.2
Brassicasterol	0.0 ± 0.0	0.5 ± 0.1	0.3 ± 0.1	0.4 ± 0.0	
24-Methylenecholesterol	0.3 ± 0.1^{a}	$1.7 \pm 0.1^{a,\ b}$	3.2 ± 0.8^{b}	0.9 ± 0.1^{a}	5.8
Campesterol	0.2 ± 0.1^{a}	4.6 ± 0.7^{b}	4.9 ± 0.9^{b}	0.7 ± 0.1^{a}	6.5
Stigmasterol	0.0 ± 0.0	0.1 ± 0.0	0.8 ± 0.3	0.3 ± 0.1	
β-sitosterol	0.0 ± 0.0^{a}	$0.1 \pm 0.1^{a,\ b}$	0.7 ± 0.2^{b}	0.0 ± 0.0^{a}	6.5
Isofucosterol	0.0 ± 0.0	0.2 ± 0.2	0.0 ± 0.0	0.0 ± 0.0	
Other minor sterols[d]	$0.3 \pm 0.0^{a,\ b}$	0.5 ± 0.0^{b}	0.9 ± 0.0^{c}	0.1 ± 0.0^{a}	6.4
Total phytosterols[e]	0.5 ± 0.2^{a}	$6.1 \pm 1.1^{b,c}$	7.5 ± 1.0^{c}	$3.3 \pm 0.4^{a,\ b}$	6.8

Systematic names for all sterols are contained in the footnote for Table 1

[a, b, c] Mean values across the row not sharing a common superscript were significantly different as determined by Tukey–Kramer HSD; $df = 3{,}36$, $P < 0.01$

[d] Other minor sterols including 24-ethyl-5α-cholest-7-en-3β-ol, lanosterol, and other undetermined sterols

[e] Includes all C_{28} and C_{29} sterols excluding 24-methylenecholesterol

There were no significant differences between the ADC of any phytosterol between the three diet treatments. Cholesterol has an ADC of 46.7–65.8% across the three diets. In general phytosterols had a lower ADC than cholesterol. Specifically, C_{28} phytosterols such as brassicasterol and campesterol had a relative absorption of 9.2–18.1%, three to sixfold lower than that of cholesterol. 24-Methylenecholesterol was excluded from the calculation as it is a metabolite of cholesterol and is usually not associated with plant phytosterols. C_{29} phytosterols including β-sitosterol, stigmasterol, and isofucosterol have a relative absorption of 1.1–7.1%, 7–60-fold lower than that of cholesterol**.**

Table 5 Apparent digestibility coefficients (ADC) (%) for the different sterols in canola oil (CO), Echium oil (EO) and fish oil (FO) diets fed to Atlantic salmon

ADC (%)	CO (±SE)	EO (±SE)	FO (±SE)
Cholesterol	57.5 ± 4.4	46.7 ± 5.4	65.8 ± 7.2
Cholestanol	ND	ND	52.7 ± 4.1
Brassicasterol	9.2 ± 8.0	ND	ND
24-Methylenecholesterol	12.4 ± 3.5	27.3 ± 5.2	17.0 ± 4.1
Campesterol	14.4 ± 2.2	15.2 ± 2.1	18.1 ± 1.6
Stigmasterol	4.7 ± 3.2	ND	ND
β-sitosterol	7.1 ± 2.1	4.1 ± 4.3	1.1 ± 2.0
Isofucosterol	7.6 ± 1.1	2.4 ± 2.7	8.5 ± 2.6
Other minor sterols[a]	3.4 ± 3.1	7.5 ± 3.3	5.2 ± 3.1

Systematic names for all sterols are contained in the footnote for Table 1

ND Not determined

[a] Other minor sterols including 24-ethyl-5α-cholest-7-en-3β-ol, lanosterol, and other undetermined sterols

Discussion

Due to the decreasing availability and increasing price of fish oil, renewable land plant based oils have been increasingly incorporated into aquafeeds, and the replacement of fish oil has become an industry priority. Plant based oils contain phytosterols which are not part of the natural diet of Atlantic salmon. Therefore it is important to investigate how natural abundances of phytosterols in replacement oils are digested and incorporated in different tissues of salmon. We demonstrated that both the liver and the white muscle accumulated significantly increased amounts of total phytosterols with both plant oil diets (CO and EO) compared to FO fed fish. Differences in the absolute abundances and relative levels of individual phytosterols were demonstrated in the liver and white muscle of fish fed plant oil diets compared to the FO and initial fish. This study indicates that small amounts of phytosterols can be digested and accumulated in both the white muscle and liver of fish when fed replacement plant oil over a 12 week period.

Digestibility of Phytosterols in Atlantic Salmon

Although cholesterol and phytosterols have similar structures, phytosterols have significantly reduced absorption compared to cholesterol and it has been shown that negligible amounts of phytosterol are absorbed by humans [18, 19]. There have been numerous studies looking at cholesterol and phytosterol adsorption in humans [20–23]. From these studies cholesterol has an absorption range of 33–60%, with phytosterols having reduced absorption, 2–10% for campesterol and 0.5–5% for β-sitosterol [20–23]. The digestibility of sterols and phytosterols in Atlantic salmon show similar patterns to those in humans. Our study demonstrates that cholesterol has an ADC of 46.7–65.8%. A reduced digestibility was demonstrated with phytosterols. An ADC of 14–18.1% for campesterol and 1.1–7.1% for β-sitosterol was observed across the diets. C_{29} phytosterols, such as β-sitosterol and isofucosterol, had reduced digestibility compared with that of C_{28} phytosterols such as 24-methylcholesterol. Phytosterols may be dealkylated to cholesterol which will reduce their ADC. Phytosterols and cholesterol are also likely to be metabolized by either internal and/or external microorganisms, or possibly by the smolt themselves. Both dealkylation and metabolism will also reduce the ADC, but the extent of these processes is yet to be assessed in Atlantic salmon. Phytosterols can be esterified with a mixture of fatty acids which are naturally occurring in small quantities in plants. The concentration of phytosterol esters can change rapidly in response to various types of stimuli. In this study, phytosterol esters were not detected in fish tissues by TLC–FID, however, small quantities occur in plant based replacement diets. It has been shown that in canola oil, 65% of the total phytosterols are present as free sterols and 35% as phytosterol esters [24]. Total phytosterols were measured in this trial and used in the calculation of digestibility. We have not defined the proportions of free phytosterols and phytosterol esters in the diets. However, the digestibility of total phytosterols was measured from saponified total solvent extract (TSE), which include both esters and free phytosterols. As no phytosterol esters were detected by TLC–FID in the fish muscle or liver this indicates that dietary phytosterol esters are hydrolyzed in the intestine or not digested [25]. Our study showed no difference in the digestibility of individual phytosterols across diets, which suggests that dietary concentration does not affect their digestibility by Atlantic salmon.

Accumulation of Phytosterols in Atlantic Salmon

We determined that 0.8–0.9 mg of total phytosterols per 100 g of tissue were accumulated in the white muscle and 6.1–7.5 mg/100 g in the liver of fish fed plant oil replacement diets over a 12 week period. Our experimental diets contained 100% replacement vegetable oil. This level of replacement would not be the case in commercial aquafeeds. Phytosterol accumulation is dependant on dietary concentration as they are unable to be in vivo biosynthesized. As phytosterols are lipid soluble, the higher the fat content of the fish or tissue will increase the amount of phytosterols it contains. The major phytosterols accumulated in the liver and white muscle were campesterol and β-sitosterol. Generally the relative concentrations of individual phytosterols in the liver and white muscle reflected that of their diet. However, C_{29} phytosterols had a reduced digestibility compared with C_{28} phytosterols and therefore lower amounts accumulated in the liver or white muscle in both the CO and EO fish.

Phytosterols are very expensive ingredients and therefore it would not be economically feasible for these ingredients to be added to aquafeeds. However, replacement plant oils, such a canola, contain phytosterols as minor components. Canola is a prime candidate for fish oil replacement as it contains high levels of $\omega 3$ PUFA, largely as α-linolenic acid (ALA, 18:3ω3) and is grown in sufficient quantities to meet future aquaculture demands. A recent study suggested that Echium oil also may be a candidate as it contains an unusual $\omega 3$ PUFA profile containing stearidonic acid (SDA, 18:4ω3), which was shown to maintain concentrations of important omega 3 long chain PUFA ($\omega 3$ LC-PUFA) in Atlantic salmon parr [7]. Both these plant oils have phytosterol compositions which are dependent on genotype, planting location and temperature [26–28].

In our study all the experimental diets had minor concentrations of phytosterols from the meal and oil sources. In the CO and EO diets the major source of phytosterols was the plant oil. All the diets contained plant based proteins, which consisted of soybean meal, casein and wheat gluten. As phytosterols occur in membranes and perhaps other parts of plant cells, the plant meals also will have residual concentrations of phytosterols. The FO diet contained 1.9 g/kg WW phytosterols, while the CO (6.8 g/kg WW) and the EO (5.6 g/kg WW) had 3.5 and 2.9 times the amount of total phytosterols (Table 1).

In the present study sterols represented only about 1% of the total lipid of salmon, and 92–99% of that 1% is present as cholesterol. Salmon smolt in this study had an average total white muscle lipid content of 28.3 and 39.6 mg/g in the liver. Therefore the amount of phytosterols in Atlantic salmon smolt compared to other lipids including cholesterol is relatively low. Phytosterols cannot be synthesized by humans or fish, therefore they are supplied in the diet. Phytosterols, due to their lipophilic nature, have been added to margarines and spreads which are known as "functional foods". Oily fish, such as Atlantic salmon, may provide another possible delivery source. Phytosterols in combination with the high levels of omega 3 long chain ($\geq C_{20}$) polyunsaturated fatty acids ($\omega 3$-LC PUFA) found in salmon may act in unison to deliver an enhanced benefit against coronary heart disease (CHD). Additionally and unlike $\omega 3$-LC PUFA, phytosterols are more stable compounds and are not as readily oxidised under severe conditions, such as deep frying.

Most human nutrition studies with phytosterols assessed an intake of 0.8–4.0 g of phytosterol as a daily dose which reduced the lower density lipoprotein (LDL) cholesterol between 6 and 15% which reduces the risk of CHD [2, 29]. Dietary intake of phytosterols ranges from 150 to 400 mg/day, with a typical composition of 65% β-sitosterol, 30% campesterol and 5% stigmasterol [2, 19]. The content of phytosterol from this experiment in white muscle of Atlantic salmon smolt is 0.8–0.9 mg/100 g which is well below the concentration range of dietary phytosterol generally being supplied in functional foods for CHD prevention. This result will be elevated in larger commercial cultured fish, where oil content (7–20%) of white muscle is markedly higher than observed in the smolt (2–3%) examined here. Due to use of extrusion technologies commercial salmon aquafeeds have an oil content of 30–40%. Our study used an inclusion of 20% oil which will underestimate the phytosterol content compared to commercial diet. It was not possible for this experiment to obtain the high lipid content of commercial aquafeeds. However, even at this lower inclusion, it was possible to demonstrate that phytosterols significantly accumulated in the tissues of Atlantic salmon. Our experiment was for a 12 week period. It is plausible to suggest that over a life time of replacement oil diets that Atlantic salmon will accumulate considerably more phytosterols. However, at this point it is yet to be determined to what concentrations Atlantic salmon will accumulate phytosterols. The phytosterol concentrations in the white muscle (0.8–0.9 mg/100 g) of plant oil fed fish is several orders of magnitude less than the recommended daily serving size of functional foods such as spreads and margarines (phytosterols total $\approx$ 200 mg/day) [30]. However, in a balanced diet, this additional amount of phytosterols (we estimated to be $\approx$20–50 mg/serve in a large commercial size fish) is a 10–25% increase in the average adult human dietary intake of phytosterols.

Environmental Effects of Phytosterols

Several studies have shown that phytosterols in effluent, in particular β-sitosterol, produced estrogenic effects in maturing fish as well as a reduced cholesterol level [8, 31, 32]. Cholesterol is a precursor of steroid hormones and therefore the presence of structurally similar molecules or the reduction of cholesterol may effect maturation in fish. Phytosterols, in particular β-sitosterol, are present in pulp and paper mill effluents and have been associated with different reproductive responses in fish including reduction in gonad size, delayed sexual maturation, and reduced expression of secondary sexual characteristics [31, 33, 34]. A recent study strongly suggested that cholesterol in Atlantic cod (*Gadus morhua*) liver is lowered by phytosterol rich soy based diet and is possibly involved in changes observed in gonad development [32]. It has also been suggested that increased sterol-like compounds may have contributed in the postponed spawning of Baltic cod in the Baltic Sea [32]. However, most farmed fish are harvested prior to maturation and a postponing of maturation may be advantageous to the aquaculture industry. Research has focused on the effect of phytosterols as a waterborne contaminant on fish health, reproduction and endocrine function [31, 33, 34]. The effects of dietary sources of phytosterols on fish have yet to be assessed, however, dietary concentrations are significantly lower than that of the effluent experiments.

There have been many well designed and executed experimental aquaculture trials with replacement oil, which have all shown no difference in growth, performance or health of fish [7, 35–40]. Further research looking at dietary phytosterol accumulation over a longer period and in particular reproductive and endocrine function such as the production of vitellogenin will provide insight on the accumulation and function of these ingredients. The use of vegetable oils in aquafeeds is now commonplace throughout the aquaculture industry and the small accumulation of phytosterols in Atlantic salmon that we have demonstrated will be advantageous to their continued use. However, Atlantic salmon require a dietary source of ω3 LC-PUFA which can presently only be provided by fish oil. Therefore, oil bends of plant and fish oils are commonly used throughout the aquaculture industry. While it has been shown that phytosterols in pulp mill effluent can be detrimental to fish health, low concentrations that occur in plant oils most likely will not affect health and performance of fish, and ultimately may provide health benefits to the consumer. Although the digestibility of phytosterols is low and their accumulation in fish of commercial size is likely to be at a level lower than used in functional food such as spreads and margarines, a small enhancement of dietary phytosterols along with the high content of ω3 LC-PUFA may give increased CHD protection to consumers.

Acknowledgments The authors gratefully acknowledge Keith Irwin and Nafisa Priti Sanga for technical assistance at UTAS, Danny Holdsworth for management of the CSIRO GC–MS facility, Rhys Hauler at Skretting Australia for the supply of feed ingredients and Springfield fisheries hatchery for the supply of fish.

References

1. Moreau RA, Whitaker BD, Hicks KB (2002) Phytosterols, phytostanols, and their conjugates in foods: structural diversity, quantitative analysis, and health-promoting uses. Prog Lipid Res 41:457–500
2. Ostlund RE (2002) Phytosterols in human nutrition. Annu Rev Nutr 22:533–549
3. Ostlund RE (2004) Phytosterols and cholesterol metabolism. Curr Opin Lipidol 15:37–41
4. Kritchevsky D, Chen SC (2005) Phytosterols—health benefits and potential concerns: a review. Nutr Res 25:413–428

5. Kuhlmann K, Lindtner O, Bauch A, Ritter G, Woerner B, Niemann B (2005) Simulation of prospective phytosterol intake in Germany by novel functional foods. Br J Nutr 93:377–385
6. Law M (2000) Plant sterol and stanol margarines and health. Br J Nutr 320:861–864
7. Miller MR, Nichols PD, Carter CG (2007) Replacement of dietary fish oil for Atlantic salmon parr (*Salmo salar* L.) with a stearidonic acid containing oil has no effect on omega-3 long-chain polyunsaturated fatty acid concentrations. Comp Biochem Physiol B 146:197–206
8. Tremblay L, Van der Kraak G (1998) Use of a series of homologous in vitro and in vivo assays to evaluate the endocrine modulating actions of beta-sitosterol in rainbow trout. Aqua Toxicol 43:149–162
9. Carter CG, Bransden MP, Lewis TE, Nichols PD (2003) Potential of thraustochytrids to partially replace fish oil in Atlantic salmon feeds. Mar Biotechnol 5:480–492
10. Wedemeyer GA (1996) Physiology of fish in intensive culture systems. Chapman & Hall, New York
11. Helland SJ, Grisdale-Helland B, Nerland S (1996) A simple method for the measurement of daily feed intake of groups of fish in tanks. Aquaculture 139:157–163
12. Carter CG, Lewis TE, Nichols PD (2003) Comparison of cholestane and yttrium oxide as digestibility markers for lipid components in Atlantic salmon (*Salmo salar* L.) diets. Aquaculture 225:341–351
13. Maynard LA, Loosli JK (1969) Animal nutrition. McGraw-Hill, New York
14. Bligh EG, Dyer WG (1959) A rapid method of total lipid extraction and purification. Can J Biochem Physiol 37:911–917
15. Volkman JK, Nichols PD (1991) Application of thin layer chromatography-flame ionization detection to the analysis of lipids and pollutants in marine environmental samples. J Planar Chromatogr 4:19–26
16. Miller MR, Nichols PD, Barnes J, Davies NW, Peacock EJ, Carter CG (2006) Regiospecificity profiles of storage and membrane lipids from the gill and muscle tissue of Atlantic salmon (*Salmo salar* L.) grown at elevated temperature. Lipids 41:865–876
17. Jones GJ, Nichols PD, Shaw PM (1994) Analysis of microbial sterols and hopanoids. In: Goodfellow M, O'Donnell AG (ed) Chemical methods in prokaryotic systematics. Wiley, New York
18. Rozner S, Garti N (2006) The activity and absorption relationship of cholesterol and phytosterols. Colloid Surf A 282:435–456
19. Trautwein EA, Duchateau G, Lin YG, Mel'nikov SM, Molhuizen HOF, Ntanios FY (2003) Proposed mechanisms of cholesterol-lowering action of plant sterols. Eur J Lipid Sci Technol 105:171–185
20. Ostlund RE, McGill JB, Covey DF, Stenson WF, Stearns JF, Spilburg CA (2002) Gastrointestinal absorption of soy sterols and soy stanols in human subjects. J Nutr 132:606S–607S
21. Ostlund RE, McGill JB, Zeng CM, Covey DF, Stearns J, Stenson WF, Spilburg CA (2002) Gastrointestinal absorption and plasma kinetics of Soy Δ(5)-phytosterols and phytostanols in humans. Am J Physiol Endocrinol Metab 282:E911–E916
22. Salen G Jr, Ahrens EH, Grundy M (1970) Metabolism of β-sitosterol in man. J Clin Invest 49:952
23. Heinemann T, Axtmann G, Vonbergmann K (1993) Comparison of intestinal-absorption of cholesterol with different plant sterols in man. Eur J Clin Invest 23:827–831
24. Gordon MH, Miller LAD (1997) Development of steryl ester analysis for the detection of admixtures of vegetable oils. J Am Oil Chem Soc 74:505–510
25. Normen L, Ellegard L, Janssen HG, Steenbergen H, Trautwein E, Andersson H (2006) Phytosterol and phytostanol esters are effectively hydrolysed in the gut and do not affect fat digestion in ileostomy subjects. Eur J Nutr 45:165–170
26. Gul MK, Seker M (2006) Comparative analysis of phytosterol components from rapeseed (*Brassica napus* L.) and olive (*Olea europaea* L.) varieties. Eur J Lipid Sci Technol 108:759–765
27. Hamama AA, Bhardwaj HL, Starner DE (2003) Genotype and growing location effects on phytosterols in canola oil. J Am Oil Chem Soc 80:1121–1126
28. Vlahakis C, Hazebroek J (2000) Phytosterol accumulation in canola, sunflower, and soybean oils: effects of genetics, planting location, and temperature. J Am Oil Chem Soc 77:49–53
29. Patel MD, Thompson PD (2006) Phytosterols and vascular disease. Atherosclerosis 186:12–19
30. Noakes M, Clifton PM, Doornbos AME, Trautwein EA (2005) Plant sterol ester-enriched milk and yoghurt effectively reduce serum cholesterol in modestly hypercholesterolemic subjects. Eur J Nutr 44:214–222
31. Tremblay L, Van der Kraak G (1999) Comparison between the effects of the phytosterol beta-sitosterol and pulp and paper mill effluents on sexually immature rainbow trout. Environ Toxicol Chem 18:329–336
32. Pickova J, Mørkøre T (2007) Alternate oils in fish feeds. Eur J Lipid Sci Technol 109:256–263
33. Munkittrick KR, Vanderkraak GJ, McMaster ME, Portt CB, Vandenheuvel MR, Servos MR (1994) Survey of receiving-water environmental impacts associated with discharges from pulp-mills. Gonad size, liver size, hepatic EROD activity and plasma sex steroid-levels in white sucker. Environ Toxicol Chem 13:1089–1101
34. McMaster ME, VanDerKraak GJ, Munkittrick KR (1996) An epidemiological evaluation of the biochemical basis for steroid hormonal depressions in fish exposed to industrial wastes. JGLRD 22:153–171
35. Bell JG, Henderson RJ, Tocher DR, Sargent JR (2004) Replacement of dietary fish oil with increasing levels of linseed oil: modification of flesh fatty acid compositions in Atlantic salmon (*Salmo salar*) using a fish oil finishing diet. Lipids 39:223–232
36. Bell JG, Dick JR, Sargent JR (1993) Effect of diets rich in linoleic or α-linolenic acid on phospholipid fatty acid composition and eicosanoid production in Atlantic salmon (*Salmo salar*). Lipids 28:819–826
37. Torstensen BE, Froyland L, Lie O (2004) Replacing dietary fish oil with increasing levels of rapeseed oil and olive oil—effects on Atlantic salmon (*Salmo salar* L.) tissue and lipoprotein lipid composition and lipogenic enzyme activities. Aquac Nutr 10:175–192
38. Miller MR, Nichols PD, Carter GC (2007) Replacement of fish oil with thraustochytrid *Schizochytrium* sp L. oil in Atlantic salmon parr (*Salmo salar* L.) diets. Comp Biochem Physiol A 148:382–392
39. Bransden MP, Carter CG, Nichols PD (2003) Replacement of fish oil with sunflower oil in feeds for Atlantic salmon (*Salmo salar* L.): effect on growth, performance, tissue fatty acid composition and disease resistance. Comp Biochem Physiol B 135:611–625
40. Tocher DR, Bell JG, McGhee F, Dick JR, Fonseca-Madrigal J (2003) Effects of dietary lipid level and vegetable oil on fatty acid metabolism in Atlantic salmon (*Salmo salar L.*) over the whole production cycle. Fish Physiol Biochem 29:193–209

Lipids (2008) 43:559–567
DOI 10.1007/s11745-008-3179-0

ORIGINAL ARTICLE

Unusual Fatty Acid Isomers of Triacylglycerols and Polar Lipids in Female Limpet Gonads of *Cellana grata*

Hideki Kawashima · Masao Ohnishi ·
Satoshi Ogawa · Kenji Matsui

Received: 9 January 2008 / Accepted: 3 April 2008 / Published online: 6 May 2008
© AOCS 2008

Abstract To investigate the occurrence of positional isomers of unsaturated fatty acids (FA) in triacylglycerols (TAG) and polar lipids (PL) in the female gonads of a dominant limpet, *Cellana grata*, fatty acid methyl esters (FAME) were fractionated according to the degree of their unsaturation by argentation thin-layer chromatography. Their structures were elucidated by gas chromatography–mass spectrometry of a combination of their FAME and picolinyl esters. A total of 125 different FA ranging from 12 to 24 carbon atoms were identified, and 105 unsaturated FA, including 34 nonmethylene-interrupted FA as minor components, were recognized. Although the major FA 16:0 and 18:1n-7, which accounted for more than 20 and 10%, respectively, of total FA, were present in TAG and PL, higher amounts of 20:4n-6 and 20:5n-3 were present in PL. Unsaturated FA consisting of more than five different positional isomers were 17:1, 19:1, 18:2, 19:2, 20:2, 21:2, 22:2, 20:3, and 22:3, most of which were present in TAG. Furthermore, a larger variety of nonmethylene-interrupted FA was found in TAG than in PL. This limpet gonad had a diverse assortment of unsaturated FA that comprised a wide range of unusual positional isomers with one to five double bonds.

Keywords *Cellana grata* · Limpet gonad · Nonmethylene-interrupted fatty acid · Positional isomer

Abbreviations

ECL	Equivalent chain length
FA	Fatty acid(s)
FAME	Fatty acid methyl ester(s)
GC-MS	Gas chromatography–mass spectrometry
GLC	Gas–liquid chromatography
NMI FA	Nonmethylene-interrupted fatty acid(s)
PL	Polar lipids
TAG	Triacylglycerols
TLC	Thin-layer chromatography

Introduction

Limpets, as intertidal gastropods, are abundant and familiar inhabitants of rocky shores and play an important role in littoral marine food webs [1–3]. Comparative biochemical research on the occurrence and distribution of FA in limpet gonads has been very limited, except for several studies examining the effects of environmental factors on FA composition of the gonads of limpet *Patella* species [4–6].

From the viewpoint of comparative biochemical interest, previous studies revealed that the significant differences between male and female gonads of two dominant limpet species, *Cellana grata* and *Collisella dorsuosa*, which are distributed in northern Japan, were characterized by their

H. Kawashima (✉)
Bioscience Laboratory, Miyako College, Iwate Prefectural University, Miyako 027-0039, Japan
e-mail: ajoe@iwate-pu.ac.jp

M. Ohnishi
Department of Agriculture and Life Science, Obihiro University of Agriculture and Veterinary Medicine, Obihiro 080-8555, Japan
e-mail: mohnishi@obihiro.ac.jp

S. Ogawa
Department of Chemical Engineering, Faculty of Engineering, Iwate University, Morioka 020-8551, Japan

K. Matsui
Center for Regional Collaboration in Research and Education, Iwate University, Morioka 020-8551, Japan

proportions of 16:0, 20:4n-6, and 20:5n-3 [7, 8], and their composition and proportions of unusual nonmethylene-interrupted (NMI) FA, whose physiological role and function are not fully understood. Furthermore, the positional isomers of unusual minor polyenoic FA with 24 carbon atoms have been also found in triacylglycerols (TAG) of the female gonads of *C. grata*, one of the commonest species, from the Sanriku coast, northern Japan [9]. Although mainly major FA and their characterization in limpet gonads have been investigated, the occurrence and unique structures of the unknown minor FA including NMI FA have yet not been well clarified. Therefore, as part of our continuing intensive investigation of gonad lipids from dominant species of Japanese limpets, positional isomers of FA with one to five double bonds in the female gonads of *C. grata* have been more completely clarified by detailed analysis of the FA mass spectra. This paper describes the occurrence and characterization of unusual positional isomers of unsaturated FA between TAG, the most abundant lipid class, and polar lipids (PL) in the gonads. The present results may provide new insights for a comparative biochemical study of marine gastropods of their gonads and the effects of ecological factors on their FA composition.

Materials and Methods

Reagents

Reagents and most standards were purchased from Sigma-Aldrich Co. (St Louis, MO, USA).

Sampling

The mean shell length of the limpet *C. grata* used for lipid and FA analysis was 34.1 ± 1.7 mm ($n = 25$). Limpets were collected from the coast waters of Miyako Bay, Iwate Prefecture, northern Japan, in July and August 2002. All individuals of *C. grata* were sexually mature. After sampling, all limpets were immediately frozen at −20 °C. The sex was determined by microscopic examination, and the gonads were distinguished as female or male.

Extraction and Fractionation of Lipids

Pooled female gonads (8.10 g wet weight, $n = 25$) of *C. grata* were suspended in a chloroform–methanol mixture (2:1, v/v) and homogenized for 1 min at $891 \times g$ using an IKA ULTRA-TURRAX T25 Basic (IKA Japan KK, Nara, Japan). Lipids were extracted using the method of Bligh and Dyer [10]. The extracted total lipids (488 mg) were fractionated into TAG (351 mg) and PL (103 mg) by preparative thin-layer chromatography (TLC) on Silica gel 60 (Merck KGaA., Darmstadt, Germany). The plates were developed with *n*-hexane/diethyl ether/acetic acid (80:30:1, v/v/v). The bands corresponding to TAG and PL were scraped off the plates and then extracted twice with a chloroform–methanol mixture (1:1, v/v). The solvent extracts were combined and dried under a gentle stream of nitrogen at room temperature. Each residue was dissolved in chloroform and stored at −20 °C until derivation prior to gas–liquid chromatography (GLC) and gas chromatography–mass spectrometry (GC–MS) analyses.

Preparation of FAME and Argentation TLC

Fatty acid methyl esters (FAME) were prepared with transesterification of TAG and PL with 14% BF_3 in methanol (GL Science, Tokyo, Japan) [11]. Five milliliters of the reagent was added to the fractionated lipids (40–60 mg) and refluxed at 90 °C for 60 min. The reaction was terminated by the addition of 2 mL of saturated NaCl solution. The FAME were extracted twice with 5 mL of *n*-hexane. The organic layer was dried over anhydrous sodium sulfate, filtered, and analyzed by TLC. The FAME were purified by preparative TLC and developed with the same solvent system that was used for the fractionation of TAG and PL. These samples were used for GLC and GC–MS analyses.

Fractionation of FAME by their double bond numbers and configuration of double bonds was performed using TLC plates on 5% (w/w) silver-impregnated layers of Kieselgel 60. The plates were developed twice with *n*-hexane/diethyl ether (80:20, v/v) and visualized at 366 nm after spraying with a solution of 2′,7′-dichlorofluorescein in ethanol (0.2%, w/v). The individual FAME bands corresponding to monoenoic, dienoic, trienoic, tetraenoic, and pentaenoic FA were separately scraped off and transferred to screw-capped tubes, and methanol (2 mL), *n*-hexane (2 mL), and an aqueous solution of NaCl (10% w/v, 1 mL) were successively added with thorough mixing after each addition. After standing for 1–2 min, the organic layer was withdrawn, and an aliquot of the solvent was evaporated to dryness under a gentle stream of nitrogen at room temperature. Then, the residues that were dissolved in dry dichloromethane were converted into picolinyl ester derivatives by the reaction with 3-potassiooxamethylpyridine, as a catalyst, as described below.

Catalytic Hydrogenation of Unsaturated FAME and Picolinyl Ester Derivatives

As previously described [12], an aliquot of unsaturated FAME was hydrogenated by stirring at room pressure and temperature for 40 min in methanol (5 mL) with catalytic amounts of palladium black (Wako Pure Chemical

Industries, Ltd, Osaka, Japan). The resulting mixture was analyzed by GLC and GC–MS as described below.

To further determine the double bond positions and methyl branching positions in FA detected in this study, FAME samples were converted into their picolinyl ester derivatives as previously described [13]. Briefly, a solution of potassium *tert*-butoxide (0.15 mL, 1.0 M in tetrahydrofuran) was added to 3-hydroxymethylpyridine (0.2 mL). After homogenization, the FAME (20–30 mg), fractionated by preparative argentation TLC, in dry dichloromethane (1 mL) was mixed with the reagent, and the mixture was held at 40 °C for 50 min in screw-capped tubes. After cooling to room temperature, distilled water (2 mL) and *n*-hexane (3 mL) were added to the reaction mixture, and the organic layer was collected, dried over anhydrous sodium sulfate, filtered, and evaporated to dryness under a gentle stream of nitrogen at room temperature. The residues were dissolved in *n*-hexane prior to structural determination of FA by GC–MS analysis.

GLC and GC–MS Analyses

Fatty acid methyl esters were analyzed by GLC with a Shimadzu GC-8A chromatograph (Shimadzu Seisakusho Co., Kyoto, Japan) equipped with a flame ionization detector (FID) and a Supelcowax^{TM}-10 capillary column (30 m × 0.25 mm i.d., 0.25 μm film thickness; Supelco Inc., Bellefonte, PA, USA). The column temperature was either isothermal at 200 °C for 30 min or programmed to increase from 180 to 250 °C at a rate of 3 °C/min and then hold at 250 °C for 10 min. The injector and detector temperatures were 260 and 270 °C, respectively. The carrier gas was helium, at a flow rate of 1.0 mL/min, and the injection split ratio was 1:50.

We identified the mass spectra of FAME and picolinyl ester derivatives by a Hewlett-Packard 6890 GC-5973N MSD. The GLC was equipped with an Omegawax^{TM}-320 capillary column (30 m × 0.32 mm i.d., 0.25 μm film thickness; Supelco Inc.) and used helium as the carrier gas with a constant flow of 1.5 mL/min. The oven temperature was held at 200 °C for 2 min, programmed to rise from 200 to 250 °C at a rate of 2 °C/min and then held for 90 min. The GC–MS analysis of FAME and picolinyl ester derivatives was recorded at an ionization energy of 70 eV by the electron impact mode. The split injection was performed with a split ratio of either 1:15 or 1:25. A scan range of 50–500 *m/z* was used. Most FA were identified by comparison of their mass spectra with those of authentic standards and published data [8, 9, 14]. In the absence of suitable standards, assignments were based on mass spectral fragments and on equivalent chain length (ECL) values for structurally analogous FA. The ECL values were determined by the same GLC apparatus with an FID, used for GLC analysis of FAME, using an Omegawax^{TM}-320 and a SAC^{TM}-5 (30 m × 0.25 mm i.d., 0.25 μm film thickness; Supelco Inc.) capillary columns. The column temperatures for an Omegawax^{TM}-320 and a SAC^{TM}-5 columns were isothermal at 200 and 250 °C, respectively. Except for the column temperatures, the GLC operating conditions were the same as described in GLC analysis of FAME. Gas–liquid chromatography analyses were performed in duplicate, and then mean values are reported here.

Results and Discussion

FA Composition of TAG and PL

The pooled female gonads of the limpet *C. grata* yielded 6.0% total lipids. The proportions of TAG, the most abundant lipid class, and PL were 72 and 21%, respectively. Among 53 different FA, accounting for more than 0.1% of total FA, including nine branched-chain FA and 2-hydroxyhexadecanoic acid, as shown in Table 1, the major FA 16:0 and 18:1n-7 each accounted for more than 20 and 10%, respectively, of total FA present in the TAG and PL of female gonads from *C. grata*. Both these fractions showed significantly higher amounts of 16:0 and 18:1n-7. Similar results of major FA have already been reported for those of the total lipids from female gonads of *C. grata* and *C. dorsuosa* [7]. More than 20 NMI FA were present as minor components in TAG rather than in PL. The present results were also shown to contain significantly higher amounts of 20:4n-6 and 20:5n-3 in PL, as compared with those in TAG. However, 22:6n-3, characteristic for marine lipids, was not detected in TAG and PL from the gonads.

To further clarify the characterization of the occurrence and detailed distribution of FA positional isomers with one to five double bonds between TAG and PL fractions in female gonads of *C. grata*, FAME were fractionated according to the degree of their unsaturation by preparative argentation TLC. Gas–liquid chromatography analyses of mono-, di-, tri-, tetra-, and pentanenoic FAME fractions generally showed a range of unknown minor peaks, some of which did overlap with those of other FA shown in Table 1. The structures of these minor FA newly found were identified by capillary GC–MS of their FAME and picolinyl esters. The results of FA positional isomers including minor ones (accounting for less than 0.1% of total FA) are shown in Tables 2, 3, 4, and 5.

Positional Isomers of Monoenoic FA

Table 2 lists the distribution of positional isomers of monoenoic FA. Among the 29 monoenoic FA identified, a

Table 1 FA composition (%) of triacylglycerols (TAG) and polar lipids (PL) in female gonads of the limpet *Cellana grata*

FA	TAG[a]	PL[b]
13:0	0.1	0.1
iso 14:0	0.1	0.1
anteiso 14:0	0.1	–
14:0	6.1	1.8
TMTD[c]	1.7	1.1
14:1n-7	0.1	–
14:1n-5	0.1	–
iso 15:0	0.2	0.2
anteiso 15:0	0.1	–
15:0	0.6	0.7
iso 16:0	0.3	–
16:0	23.4	20.0
16:1n-9	0.1	0.1
16:1n-7	0.6	0.5
iso 17:0	0.2	1.4
anteiso 17:0	1.4	0.6
17:0	1.6	1.2
17:1n-8	0.2	0.3
iso 18:0	0.3	0.5
18:0	4.1	5.2
18:1n-9	10.3	5.2
18:1n-7	10.9	12.1
18:2n-6	1.5	1.3
18:2n-4	0.9	0.5
18:3n-3	2.1	1.4
19:0	<0.1	0.2
19:1n-12	0.5	0.3
2-hydroxy 16:0	–	1.5
20:0	0.1	–
20:1n-13	4.0	1.9
20:1n-9	1.3	1.6
20:1n-7	0.9	0.4
20:2Δ5,11	<0.1	0.1
20:2Δ7,13	0.9	<0.1
20:2n-6	2.9	2.0
20:3Δ5,11,14	0.2	0.5
20:3n-6	1.5	0.8
20:3n-3	2.3	1.2
20:4n-6	5.1	17.1
20:5n-3	3.9	9.5
22:1n-15	0.6	0.3
22:2Δ5,9	<0.1	2.8
22:2Δ7,13	2.5	<0.1
22:2Δ7,15	0.8	0.3
22:3Δ7,13,16	1.4	0.5
22:3n-6	0.4	0.2
22:4n-6	2.2	1.6
22:4Δ7,13,16,19	0.3	0.1
22:5n-3	1.0	0.6
24:0	<0.1	0.1
24:2Δ5,9	<0.1	0.9
24:3Δ5,9,15	0.1	0.9
24:3Δ5,9,17	<0.1	0.3

[a] Minor FA (<0.1%), identified, such as 12:0, 16:1n-5, 18:1n-13, 18:2Δ5,9, 20:2Δ5,9, 20:2Δ5,13, 20:2n-3, 20:4Δ5,11,14,17, 22:1n-9, 22:2Δ9,15, 22:3Δ5,9,15, 22:4n-3, 24:2Δ9,15, 24:2Δ9,17, 24:3Δ9,15,18, 24:4Δ5,9,15,18, 24:4n-6, 24:5Δ5,9,15,18,21, and 24:5n-3 were excluded from Table 1

[b] Minor FA (<0.1%), identified, such as 16:1n-5, 18:1n-13, 18:2Δ5,9, 20:2Δ5,13, 20:2n-3, 20:4Δ5,11,14,17, 22:3Δ5,9,15, and 22:4n-3 were excluded from Table 1

[c] 4,8,12-Trimethyltridecanoic acid

number of unusual odd-numbered FA 17:1 and 19:1, which consisted of seven and six different positional isomers, respectively, were found in TAG, although 18:1n-7 and 18:1n-9 were present as the major monoenoic isomers. The isomer 15-methyl 16:1Δ9, together with other branched-chain FA, is present in mollusks, such as the marine sponges, *Aplysina fistularis* [15] *Hymeniacidon sanguinea* [16, 17], and *Plakortis halichondroides* [18], and the freshwater mussel, *Unio tumidus* [19], and also in the anaerobic sulfate bacterium of *Desulfovibrio* species [20]. However, the presence of 15-methyl 16:1Δ9 has not been reported in limpets and their gonads.

Positional Isomers of Dienoic FA

As shown in Table 3, a total of 42 dienoic FA with 16 and 18–24 carbon atoms were identified in this study, and the highly diverse NMI dienoic FA significantly differed between TAG and PL. The dienoic FA were 18:2, 19:2, 20:2, 21:2, and 22:2, which each consisted of more than five different positional isomers, and were mainly found in the TAG. Among these dienoic FA, the presence of both the odd-numbered FA 19:2 and 21:2 positional isomers including unusual NMI FA is very rare in living organisms.

As an interesting result of NMI dienoic FA, six different all-*cis*-Δ5,9-dienoic FA with 18 and 20–24 carbon atoms were identified by capillary GC–MS of their methyl ester (characteristic peaks at *m/z* 81 [parent ion], 109, 141, and $[M-49]^+$ for 5,9-double bonds) [14] and picolinyl ester (a characteristic abundant peak at *m/z* 219 for 5,9-double bonds) [14, 21] derivatives, whose mass spectral data were in agreement with literature data [14, 21–23]. (The mass spectra of picolinyl esters were also informative in identifying minor NMI polyenoic FA with a 5,9-double bond

Table 2 Distribution of positional isomers (%) of monoenoic FA in female gonads of the limpet *Cellana grata*

FA	TAG	PL
14:1n-7	57.1	–
14:1n-5	42.9	–
16:1n-9	19.1	15.5
16:1n-7	80.9	84.5
16:1n-5	<0.1	<0.1
15-Me-16:1Δ9	<0.1	–
17:1n-10	2.1	–
17:1n-8	25.5	23.0
17:1n-7	19.2	16.4
17:1n-6	15.4	13.6
17:1n-5	37.8	47.0
17:1n-3	–	<0.1
18:1n-13	<0.1	3.2
18:1n-9	46.1	28.3
18:1n-7	52.1	65.9
18:1n-5	1.8	2.6
19:1n-12	35.2	25.9
19:1n-10	32.6	5.8
19:1n-8	12.2	58.2
19:1n-6	5.2	2.9
19:1n-5	14.8	5.6
19:1n-4	<0.1	1.6
20:1n-13	55.6	49.1
20:1n-9	25.4	40.6
20:1n-7	19.0	10.3
20:1n-5	<0.1	–
22:1n-15	92.0	100
22:1n-9	8.0	<0.1
22:1n-7	<0.1	–

The proportion of each isomer was calculated from the total isomers

system, such as 22:3Δ5,9,15, 24:3Δ5,9,15, 24:3Δ5,9,17, 24:4Δ5,9,15,18, and 24:5Δ5,9,15,18,21, as described previously [8,9].) These Δ5,9-dienoic FA, some of which are frequently present in marine sponges [12, 17, 22, 24], were mainly detected in the TAG in small amounts. Although all-*cis*-Δ5,9-dienoic FA with 18 and 20 to 23 carbon atoms have been found in whole bodies of the sea anemone *Stoichactis helianthus* [23], the detailed distribution of both even- and odd-numbered all-*cis*-Δ5,9-dienoic FA occurring in marine gastropods and their gonads is reported here for first time. The identified dienoic FA, together with other unusual NMI FA, may be incorporated from the limpet's diet or may be biosynthesized by some of the limpet's symbiotic organisms including microorganisms, but the reason remains unclear. Some Δ5,9-dienoic FA are known to arise from a symbiotic relationship of associated bacteria with host cells of marine invertebrates [25].

Table 3 Distribution of positional isomers (%) of dienoic FA in female gonads of the limpet *Cellana grata*

FA	TAG	PL
16:2n-6	47.9	–
16:2n-4	52.1	–
18:2Δ5,9	3.1	2.3
18:2Δ5,11	2.1	–
18:2n-7	1.4	5.7
18:2n-6	55.8	92.0
18:2n-4	37.6	–
19:2Δ5,11	0.5	–
19:2Δ5,13	0.2	–
19:2n-9	2.5	–
19:2n-7	51.6	100
19:2n-6	16.9	–
19:2n-4	24.8	–
19:2n-3	3.5	–
20:2Δ5,9	<0.1	–
20:2Δ5,11	10.6	1.0
20:2Δ5,13	4.5	<0.1
20:2Δ7,13	17.3	0.5
20:2Δ9,13	<0.1	–
20:2n-7	1.7	–
20:2n-6	63.6	96.5
20:2n-5	0.3	–
20:2n-3	2.0	2.0
21:2Δ5,9	<0.1	–
21:2Δ7,13	38.1	25.3
21:2Δ7,15	3.8	10.1
21:2Δ7,16	37.4	64.6
21:2n-7	3.9	–
21:2n-6	13.5	–
21:2n-5	3.3	–
22:2Δ5,9	<0.1	89.8
22:2Δ7,13	68.4	1.0
22:2Δ7,15	29.6	9.2
22:2Δ7,17	<0.1	–
22:2Δ9,15	<0.1	–
22:2n-11	1.2	–
22:2n-9	0.8	–
22:2n-7	<0.1	–
23:2Δ5,9	100	–
24:2Δ5,9	1.0	–
24:2Δ9,15	55.8	–
24:2Δ9,17	43.2	100

The proportion of each isomer was calculated from the total isomers

Based on the results noted above, the large variety of positional isomer structures was of very special interest because it is first unique dienoic FA isomer composition

Table 4 Distribution of positional isomers (%) of trienoic FA in female gonads of the limpet *Cellana grata*

FA	TAG	PL
18:3n-6	<0.1	<0.1
18:3n-4	17.2	9.8
18:3n-3	82.8	90.2
20:3n-9	1.8	5.7
20:3Δ5,11,14	2.8	11.0
20:3n-6	35.1	26.9
20:3n-4	5.0	9.2
20:3n-3	55.3	47.2
21:3n-7	100	–
22:3Δ5,9,15	<0.1	6.0
22:3n-9	0.9	4.8
22:3Δ7,13,16	81.1	58.5
22:3n-6	12.5	30.7
22:3Δ8,14,18[a]	<0.1	–
22:3n-4	1.1	–
22:3n-3	4.4	–
23:3Δ7,13,16[b]	100	–
24:3Δ5,9,15	61.7	76.6
24:3Δ5,9,17	37.3	23.4
24:3Δ9,15,18	1.0	–

The proportion of each isomer was calculated from the total isomers

[a] Picolinyl ester, *m/z* (%); 92 (100), 164 (49), 220 (6), 246 (9), 302 (10), 328 (5), 356 (7), 382 (7), 425 (M^+, 41)

[b] Picolinyl ester, *m/z* (%); 92 (100), 164 (66), 206 (10), 232 (4), 288 (4), 314 (34), 328 (9), 354 (10), 439 (M^+, 37)

Table 5 Distribution of positional isomers (%) of tetraenoic and pentaenoic FA in female gonads of the limpet *Cellana grata*

FA	TAG	PL
18:4n-6	15.4	–
18:4n-3	84.6	–
20:4n-6	99.0	99.2
20:4Δ5,11,14,17	1.0	0.8
20:4n-3	<0.1	<0.1
22:4n-6	80.1	98.7
22:4Δ7,13,16,19	14.4	1.3
22:4n-3	5.5	–
24:4Δ5,9,15,18	16.3	–
24:4n-6	83.7	–
20:5n-3	100	100
22:5n-3	100	100
24:5Δ5,9,15,18,21	4.0	–
24:5n-3	96.0	–

The proportion of each isomer was calculated from the total isomers

found in gonads of marine gastropods. Although basic knowledge of the physiological activities of all-*cis*-Δ5,9-dienoic FA and their derivatives is very limited [26, 27], very long chain Δ5,9-dienoic FA possessing a cyclopropylidene group and 30:3Δ5,9,21 isolated from an Australian sponge, *Amphimedon* sp., and the known 27:2Δ5,9 and 28:2Δ5,9 isolated from marine sponges inhibit human DNA topoisomerase I. These findings suggest that an essential factor of the inhibition is the location of the 5,9-double bonds rather than the presence of a cyclopropylidene moiety [26]. Furthermore, a 1:2 mixture of 23:2Δ5,9 and 24:2Δ5,9 isolated from the Turkish sponge *Agelas oroides* inhibits the activity of an enoyl-acyl carrier protein reductase, which catalyzes the last step in each cycle of FA elongation, a key enzyme of FA biosynthesis, in *Plasmodium falciparum*, which causes malaria in humans, and in *Escherichia coli* [27]. Therefore, among the six different Δ5,9-dienoic FA identified in this study, some of them may play roles in a physiological activity in limpet gonads. This will be studied in the future in the physiology of limpet gonads.

Positional Isomers of Trienoic FA

Table 4 lists the distribution of positional isomers of trienoic FA, some of which were unusual NMI polyenoic FA with 23 and 24 carbon atoms. In this study, 16:3n-4, 16:3n-3, 16:4n-3, and 16:4n-1 were not detected, although these FA were found in the limpet gonads and soft bodies of *P. depressa* [5]. This difference may be linked to the limpet's diet and environmental conditions.

Among NMI trienoic FA, small amounts of 20:3Δ5,11,14, together with 20:4Δ5,11,14,17, are frequently present in gastropods and plants, such as the bivalves *Meretrix lusoria*, *Tapes philippinarum*, *Corbicula japonica*, *Crassostrea gigas*, and *Mytilus coruscus* [28], the algae of Phaeophyta [29], and seeds of Gymnospermae [30]. The most abundant isomer 22:3Δ7,13,16 of positional isomers of 22:3 together with 22:3Δ8,14,18, which was tentatively identified by capillary GC-MS of its picolinyl ester derivative (Table 4), and 22:3Δ5,9,15, were present in TAG. A very small amount of 22:3Δ7,13,16, together other NMI FA, has been reported for some marine invertebrates, such as the bivalves *Unio tumidus* [19], *Crassostrea gigas* [31], *Megangulus zyonoensis* [32], and *Ruditapes philippinarum* [33] and the sponge *Petrosia ficiformis* [34].

In this study, an unknown trienoic acid was detected in very small amounts in TAG. The methyl ester had an ECL of 23.71 on an Omegawax-320 column at 200 °C. The mass spectrum (MS) of this methyl ester showed a molecular ion peak at *m/z* 362 (relative intensity, 5%) and a characteristic ion peak at *m/z* 331 (relative intensity, 6%) due to a loss of OCH_3, suggesting a tricosatrienoic acid. The structure was confirmed by the disappearance of the

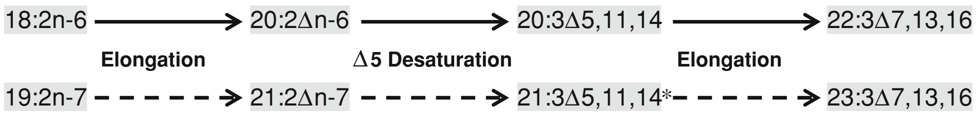

Fig. 1 Possible biosynthetic pathways for NMI trienoic FA

* Not found in this sample

corresponding GLC peak upon catalytic hydrogenation and by a molecular ion peak at *m/z* 368 for the corresponding methyl ester of *n*-tricosanoic acid. For further analysis of the double bond positions of this triene, the methyl tricosatrienoate was directly converted into its picolinyl ester derivative. The MS of the picolinyl ester gave a molecular ion at *m/z* 439, and the characteristic ions of the double bond positions, shown in Table 4, were in good agreement with those of the picolinyl ester 22:3Δ7,13,16 [14]. On the basis of the results described above, the triene detected in this study was determined to be 23:3Δ7,13,16, which was presumed to have all *cis* double bonds by comparison of its ECL values with those of all-*cis*-Δ7,13,16–22:3 using two different GLC columns, an Omegawax-320 and a SAC-5, and the same behavior of all-*cis*-Δ7,13,16–22:3 using argentation TLC. To the best of our knowledge, this is the first report of tentative identification of all-*cis*-Δ7,13,16–23:3 from living organisms. An interesting finding was the presence of a very unusual triene 23:3Δ7,13,16, together with 22:3Δ7,13,16, in the TAG of this species. However, compared with the even-numbered polyenoic FA occurring marine gastropods, which include bivalves, limpets, and their gonads, odd-numbered polyenoic FA with more than 21 carbon atoms, other than 21:5n-3, were not detected due to their very miniscule or small amounts. The biosynthesis of 23:3Δ7,13,16, like that of 22:3Δ7,13,16 as previously reported for marine bivalves [31, 35], may proceed by Δ5-desaturation followed by elongation (Fig. 1), but corroborating this hypothesis requires additional studies.

Positional Isomers of Tetraenoic and Pentaenoic FA

Table 5 lists the distribution of positional isomers of tetraenoic and pentaenoic FA. In this study, a total of 34 different NMI FA with 2–5 double bonds were identified, although the physiological role and function of these FA are unknown. Nonmethylene-interrupted fatty acids are present not only in invertebrates [36, 37] including marine gastropods and sponges, and also in plant seeds [30, 38], cellular slime mold [39], and fungus species [40].

As reported previously, positional isomers of unusual tri-, tetra-, and pentaenoic FA with 24 carbon atoms, 24:3Δ5,9,15, 24:3Δ5,9,17, 24:3Δ,9,15,18, 24:4Δ5,9,15,18, 24:5Δ5,9,15,18,21, 24:4n-6, and 24:5n-3, were present only in TAG in small amounts [9], but the reason is still unclear. Among these FA with 24 carbon atoms, both 24:4n-6 and 24:5n-3, which each accounted for less than 0.1% of total FA, together with minor n-6 and n-3 polyunsaturated FA with 24, 26, 28, and 30 carbon atoms, have been identified in three crustacean species of the order of Bathynellacea [41]. Small amounts of 24:4n-6, together with five minor NMI FA, 20:2Δ5,11, 22:2Δ7,13, 22:2Δ7,15, 20:3Δ5,11,14, and 20:4Δ5,11,14,17, were found in marine and freshwater gastropod species from the littoral zone of the Red Sea, Mediterranean Sea, and Sea of Galilee, mostly comprising less than 1% of total FA [42]. In contrast, 24:5n-3, 21:5n-3, and 22:5n-3, less than 1% of total FA, together with considerable amounts of 20:5n-3, were found in gonads of the oyster *Ostrea edulis* [43]. The differences in the polyenoic FA compositions among marine gastropod species may be due to different environmental conditions and dietary habits.

This study, together with previous studies [8, 9], showed that a large diversity of unsaturated FA and their positional isomers was present in the female gonad lipids of *C. grata*, especially in TAG, the most abundant lipid class, which consisted of 29 monoenoic FA, 42 dienoic FA, and 20 trienoic FA with both odd- and even-numbered chain lengths. Furthermore, a wide range of NMI dienoic FA with double bonds at Δ5,9, together with Δ5,11, Δ5,13, Δ7,13, Δ7,15, Δ7,16, Δ7,17, Δ9,13, Δ9,15, and Δ9,17, and NMI polyenoic FA (22:3Δ5,9,15, 24:3Δ5,9,15, 24:3Δ5,9,17, 24:4Δ5,9,15,18, and 24:5Δ5,9,15,18,21) with a 5,9-double bond system, were characterized by capillary GC–MS of their FA derivatives, although most of these FA were minor components. Expansion of our knowledge of the occurrence and structure of unusual minor FA as well as major FA in the marine environment and organisms may be linked to the clarification of their physiological roles in marine organisms and their tissues. The present results may provide valuable information for comparative biochemical studies of the occurrence and distribution of unsaturated FA of positional isomers in marine invertebrate gonads. Further studies are needed to investigate whether the FA compositions of limpet gonads are the effects of environmental factors or are related to the reproductive cycle.

Acknowledgments We are grateful to Dr. S. Budge for her helpful comments of the manuscript. This study was done as a cooperative research program (No. 107) with the International Coastal Research Center, Ocean Research Institute, The University of Tokyo.

References

1. Amino M (1963) A comparative embryology of marine gastropods with ecological consideration. J Shimonoseki Coll Fish 12:229–358
2. Branch GM (1985) Limpets: their role in littoral and sublittoral community dynamics. In: Moore PG, Seed R (eds) The ecology of rocky coasts. Hodder and Stoughton, London, pp 97–116
3. Liu JH (1994) The ecology of the Hong Kong limpets *Cellana grata* (Gould 1859) and *Patelloida pygmaea* (Dunker 1860): reproductive biology. J Moll Stud 60:97–111
4. Johns RB, Nichols PD, Perry GJ (1980) Fatty acid components of nine species of molluscs of the littoral zone from Australian waters. Comp Biochem Physiol B 65:207–214
5. Brazão S, Morais S, Boaventura D, Ré P, Narciso L, Hawkins SJ (2003) Spatial and temporal variation of the fatty acid composition of *Patella* spp. (Gastropoda: Prosobranchia) soft bodies and gonads. Comp Biochem Physiol B 136:425–441
6. Morais S, Boaventura D, Narciso L, Ré P, Hawkins SJ (2003) Gonad development and fatty acid composition of *Patella depressa* Pennant (Gastropoda: Prosobranchia) populations with different patterns of spatial distribution, in exposed and sheltered sites. J Exp Mar Biol Ecol 294:61–80
7. Kawashima H, Ohnishi M, Uchiyama H (2002) Sexual differences in gonad fatty acid compositions in dominant limpet species from the Sanriku coast in northern Japan. J Oleo Sci 51:503–508
8. Kawashima H (2005) Unusual minor nonmethylene-interrupted di-, tri-, and tetraenoic fatty acids in limpet gonads. Lipids 40:627–630
9. Kawashima H, Ohnishi M (2006) Occurrence of novel nonmethylene-interrupted C_{24} polyenoic fatty acids in female gonad lipids of the limpet *Cellana grata*. Biosci Biotechnol Biochem 70:2575–2578
10. Bligh EG, Dyer WJ (1959) A rapid method of total lipid extraction and purification. Can J Biochem Physiol 37:911–917
11. Morrison WR, Smith LM (1964) Preparation of fatty acid methyl esters and dimethylacetals from lipids with boron fluoride–methanol. J Lipid Res 5:600–608
12. Barnathan G, Kornprobst JM, Doumenq P, Miralles J (1996) New unsaturated long-chain fatty acids in the phospholipids from the *Axinellida* sponges *Trikentrion loeve* and *Pseudaxinella* cf. *lunaecharta*. Lipids 31:193–200
13. Destaillats F, Angers P (2002) One-step methodology for the synthesis of FA picolinyl esters from intact lipids. J Am Oil Chem Soc 79:253–256
14. Mass spectrometry of fatty acid derivatives (2007) The lipid library. http://www.lipidlibrary.co.uk/masspec.html. Accessed Dec 2007
15. Walkup RD, Jamieson GC, Ratcliff MR, Djerassi C (1981) Phospholipid studies of marine organisms: 2. Phospholipids, phospholipid-bound fatty acids and free sterols of the sponge *Aplysina fistularis* (Pallas) forma *fulva* (Pallas) (=*Verongia thiona*). Isolation and structure elucidation of unprecedented branched fatty acids. Lipids 16:631–646
16. Christie WW, Brechany EY, Marekov IN, Stefanov KL, Andreev SN (1994) The fatty acids of the sponge *Hymeniacidon sanguinea* from the Black Sea. Comp Biochem Physiol B 109:245–252
17. Nechev J, Christie WW, Robaina R, de Diego F, Popov S, Stefanov K (2004) Chemical composition of the sponge *Hymeniacidon sanguinea* from the Canary Islands. Comp Biochem Physiol A 137:365–374
18. Carballeira NM, Shalabi F (1990) Identification of naturally occurring *trans, trans* Δ5,9 fatty acids from the sponge *Plakortis halichondroides*. Lipids 25:835–840
19. Stefanov K, Seizova K, Brechany EY, Christie WW (1992) An unusual fatty acid composition for a fresh-water mussel, *Unio tumidus*, from Bulgaria. J Nat Prod 55:979–981
20. Boon JJ, de Leeuw JW, Hoek GJ, Vosjan JH (1977) Significance and taxonomic value of iso and anteiso monoenoic fatty acids and branched β–hydroxy acids in *Desulfovibrio desulfuricans*. J Bact 129:1183–1191
21. Dobson G, Christie WW (2002) Spectroscopy and spectrometry of lipids—part 2: mass spectrometry of fatty acid derivatives. Eur J Lipid Sci Technol 104:36–43
22. Christie WW, Brechany EY, Stefanov K, Popov S (1992) The fatty acids of the sponge *Dysideafragilis* from the Black Sea. Lipids 27:640–644
23. Carballeira NM, Medina JR (1994) New $\Delta^{5,9}$ fatty acids in the phospholipids of the sea anemone *Stoichactis helianthus*. J Nat Prod 57:1688–1695
24. Barnathan G, Genin E, Velosaotsy NE, Kornprobst JM, Al-Lihaibi S, Al-Sofyani A, Nongonierma R (2003) Phospholipid fatty acids and sterols of two *Cinachyrella* sponges from the Saudi Arabian Red Sea: comparison with *Cinachyrella* species from other origins. Comp Biochem Physiol B 135:297–308
25. Willenz P, Hartman WD (1989) Micromorphology and ultrastructure of Caribbean sclerosponges. I. *Ceratoporella nicholsoni* and *Stromatospongia norae* (Ceratoporellidae: Porifera). Mar Biol 103:387–401
26. Nemoto T, Yoshino G, Ojika M, Sakagami Y (1997) Amphimic acids and related long-chain fatty acids as DNA topoisomerase I inhibitors from an Australian sponge, *Amphimedon* sp.: Isolation, structure, synthesis, and biological evaluation. Tetrahedron 53:16699–16710
27. Tasdemir D, Topaloglu B, Perozzo R, Brun R, O'Neill R, Carballeira NM, Zhang X, Tonge PJ, Linden A, Rüedi P (2007) Marine natural products from the Turkish sponge *Agelas oroides* that inhibit the enoyl reductases from *Plasmodium falciparum*, *Mycobacterium tuberculosis* and *Escherichia coli*. Bioorg Med Chem 15:6834–6845
28. Takagi T, Itabashi Y, Kaneniwa M (1986) Fatty acid composition of bivalves from Japanese waters. J Jpn Oil Chem Soc 35:517–521
29. Kaneniwa M, Itabashi Y, Takagi T (1987) Unusual 5-olefinic acids in the lipids of algae from Japanese waters. Nippon Suisan Gakkaishi 53:861–866
30. Takagi T, Itabashi Y (1982) *cis*-5-Olefinic unusual fatty acids in seed lipids of Gymnospermae and their distribution in triacylglycerols. Lipids 17:716–723
31. Dunstan GA, Volkman JK, Barrett SM (1993) The effect of lyophilization on the solvent extraction of lipid classes, fatty acids and sterols from the oyster *Crassostrea gigas*. Lipids 28:937–944
32. Kawashima H, Ohnishi M (2004) Identification of minor fatty acids and various nonmethylene-interrupted diene isomers in mantle, muscle, and viscera of the marine bivalve *Megangulus zyonoensis*. Lipids 39:265–271
33. Kraffe E, Soudant P, Marty Y, Kervarec N (2005) Docosahexaenoic acid- and eicosapentaenoic acid-enriched cardiolipin in the Manila clam *Ruditapes philippinarum*. Lipids 40:619–625
34. Ayanoglu E, Walkup RD, Sica D, Djerassi C (1982) Phospholipid studies of marine organisms: III. New phospholipid fatty acids from *Petrosia ficiformis*. Lipids 17:617–625
35. Garrido JL, Medina I (2002) Identification of minor fatty acids in mussels (*Mytilus galloprovincialis)* by GC–MS of their 2-alkenyl-4,4-dimethyloxazoline derivatives. Anal Chim Acta 465:409–416
36. Ackman RG (1989) Fatty acids. In: Ackman RG (ed) Marine biogenic lipids, fats, and oils, vol 1. CRC Press, Boca Raton, FL, pp 103–137

37. Joseph JD (1989) Distribution and composition of lipids in marine invertebrates. In: Ackman RG (ed) Marine biogenic lipids, fats, and oils. vol 2. CRC Press, Boca Raton, FL, pp 51–143
38. Imbs AB, Pham LQ (1996) Fatty acids and triacylglycerols in seeds of Pinaceae species. Phytochemistry 42:1051–1053
39. Saito T, Ochiai H (1996) Identification of a novel all-*cis*-5,9,12-heptadecatrienoic acid in the cellular slime mold *Polysphondylium pallidum*. Lipids 31:445–447
40. Jareonkitmongkol S, Shimizu S, Yamada H (1993) Occurrence of two nonmethylene-interrupted Δ^5 polyunsaturated fatty acids in a Δ^6-desaturase-defective mutant of the fungus *Mortierella alpina* 1S-4. Biochim Biophys Acta 1167:137–141
41. Řezanka T, Dembitsky VM (1999) Very long chain polyunsaturated fatty acids in Crustacea of the order Bathynellacea. Biochem Syst Ecol 27:551–558
42. Go JV, Řezanka T, Strebnik M, Dembitsky VM (2002) Variability of fatty acid components of marine and freshwater gastropod species from the littoral zone of the Red Sea, Mediterranean Sea, and Sea of Galilee. Biochem Syst Ecol 30:819–835
43. Frolov AV, Pankov SL (1992) The reproduction strategy of oyster *Ostrea edulis* L. from the biochemical point of view. Comp Biochem Physiol B 103:161–182

Lipids (2008) 43:569–579
DOI 10.1007/s11745-008-3178-1

ORIGINAL ARTICLE

Fluorescence Anisotropy, FT-IR Spectroscopy and 31-P NMR Studies on the Interaction of Paclitaxel with Lipid Bilayers

Anand Babu Dhanikula ·
Ramesh Panchagnula

Received: 1 January 2008 / Accepted: 1 April 2008 / Published online: 6 May 2008
© AOCS 2008

Abstract To understand the bilayer interaction with paclitaxel, fluorescence polarization, Fourier transform infrared spectroscopy (FT-IR) and 31-phosphorus nuclear magnetic resonance (31P-NMR) studies were performed on paclitaxel bearing liposomes. Fluorescence anisotropy of three probes namely, 1,6-diphenyl-1,3,5-hexatriene (DPH), 12-(9-anthroyloxy) stearic acid (12AS) and 8-anilino-1-naphthalene sulfonate (ANS) were monitored as a function of paclitaxel concentration in the unsaturated bilayers. The incorporation of paclitaxel decreased anisotropy of 12AS and ANS probes, while slightly increased anisotropy of DPH. Paclitaxel has a fluidizing effect in the upper region of the bilayer whereas the hydrophobic core is slightly rigidized. FT-IR spectroscopy showed an increase in the asymmetric and symmetric methylene stretching frequencies, splitting of methylene scissoring band and broadening of carbonyl stretching mode. These studies collectively ascertained that paclitaxel mainly occupies the cooperativity region and interact with the interfacial region of unsaturated bilayers and induces fluidity in the headgroup region of bilayer. At higher loadings (>3 mol%), paclitaxel might gradually tend to accumulate at the interface and eventually partition out of bilayer as a result of solute exclusion phenomenon, resulting in crystallization; seed non-bilayer phases, as revealed by 31P-NMR, thereby destabilizing liposomal formulations. In general, any membrane component which has a rigidization effect will decrease, while that with a fluidizing effect will increase, with a bearing on headgroup interactions, partitioning of paclitaxel into bilayers and stability of the liposomes.

Keywords Paclitaxel · Bilayer · 31P-NMR · Fluorescence polarization · FT-IR · Interaction · Stability

Abbreviations

12AS	12-(9-Anthroyloxy) stearic acid
ANS	8-Anilino-1-naphthalene sulfonate
DPH	1,6-Diphenyl-1,3,5-hexatriene
FT-IR	Fourier transform infrared spectroscopy
31P-NMR	31-Phosphorus nuclear magnetic resonance
PC	Phosphatidylcholine
PG	Phosphatidylglycerol

Introduction

Paclitaxel has shown impressive performance in the clinic after its discovery due to its unique mechanism of action on microtubules and multiple pharmacological effects on rapidly dividing cells of tumor and its vasculature [1, 2]. In the clinic, paclitaxel is used for treatment of refractory breast and metastatic ovarian cancers, AIDS-related Kaposi's sarcoma, small and non-small cell lung, neck and colon cancers. This natural diterpenoid, a high molecular weight compound (854 Da) (Fig. 1), is extremely hydrophobic and has low aqueous solubility. After extensive formulation efforts, the final formulation selected for clinical use to deliver paclitaxel consisted of cremophor EL

A. B. Dhanikula · R. Panchagnula
Department of Pharmaceutics,
National Institute of Pharmaceutical Education and Research
(NIPER), S.A.S Nagar 160062, India

R. Panchagnula (✉)
Pharmaceutical R&D, VMPS, Pfizer Pharmaceutical India Pvt.
Ltd., Thane Belapur Road, Turbhe, K.U. Bazar Post, Navi
Mumbai 400 705, India
e-mail: Panchagnula@yahoo.com

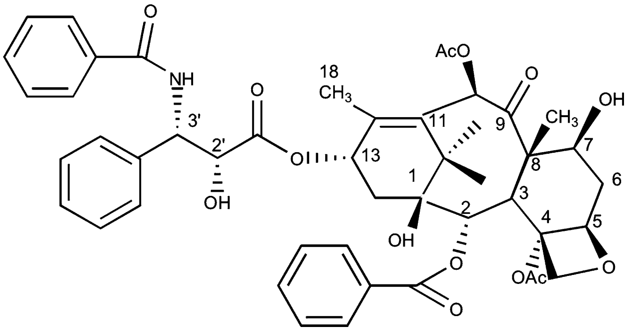

Fig. 1 Structure of paclitaxel

and ethanol. However, the former excipient has been responsible for causing hypersensitivity reactions in patients which necessitates concomitant administration of anti-histamines and steroidal anti-inflammatory drugs. In order to overcome the current drawbacks and improve the delivery of this promising antineoplastic agent, huge number of efforts are being made to develop alternative formulations of paclitaxel such as, emulsions, liposomes, micelles, nanoparticles, prodrugs, conjugates, etc. [1]. Among various approaches listed above, there are several advantages associated with the use of liposomal formulations for which reason liposomes have been extensively studied as carriers for anticancer drugs. For instance, encapsulation of antineoplastic drugs in liposomes has proved promising to increase therapeutic ratio of chemotherapeutic agents as well as to combat multidrug resistance in cancer chemotherapy [3, 4]. In this regard, liposomal formulations of paclitaxel have been prepared to reduce toxicity of free drugs and tested in animals and humans [5, 6].

Keeping in view the significant developments in liposomal paclitaxel delivery, it is pertinent to understand the nature of the interaction of paclitaxel with the liposomal bilayer. A comprehension of the location and depth of penetration into the bilayer of the molecule would be of immense value for successful formulation and in vivo delivery. Since paclitaxel possess no charge, it is anticipated that the hydrophobic nature promotes partitioning and location within the bilayer. The interaction of paclitaxel with bilayers has been previously investigated with the help of fluorescence polarization, circular dichroism, DSC, and FT-IR techniques [7–9] which indicate both fluidizing and rigidization effects of paclitaxel. In order to better anchor the molecule in bilayers, different 2′-acyl prodrugs of pacliatxel were synthesized which varied with respect to the acyl chain length (C-6, 12, 16) [10]. Based on DSC studies, they showed that taxane prodrugs were solvated to a greater degree in dimyristoyl PC bilayers than dipalmitoyl PC, distearoyl PC bilayers and, the association of these prodrugs was better than paclitaxel itself which further increased with the 2′-acyl chain length. In this work, it was also reported that the enthalpy of transition decreased with increasing amounts of paclitaxel within liposomes from which they related paclitaxel induced perturbation of bilayers to disruption of hydrogen bonding at lipid–water interface. Although a considerable number of reports point to the localization of paclitaxel at the membrane–water interface, to the best of our knowledge, so far, experimental evidence on the type of interaction and paclitaxel induced perturbation of interfacial region has not been substantial. In the present work, we make an attempt to further understand the interaction of paclitaxel with unsaturated lipid bilayers, and provide evidence for the interaction of paclitaxel with phospholipid headgroup region. Data acquired from spectroscopic studies comprising fluorescence anisotropy and FT-IR was useful in understanding the paclitaxel–bilayer interactions in terms of membrane dynamics and lipid acyl chain conformational changes. At the same time, 31P-NMR was employed as a more direct indicator of the effects induced in headgroup region as well as to detect type of perturbations imposed on the bilayer by paclitaxel.

Experimental Procedures

Materials

Paclitaxel was a sample donated by Dabur India Ltd. Soya phosphatidylcholine (PC) and phosphatidylglycerol (PG) *trans*-esterified from soya PC were kindly provided by Natterman Phospholipids (Germany). 1,6-Diphenyl-1,3,5-hexatriene (DPH), 12-(9-anthroyloxy) stearic acid (12AS) and 8-anilino-1-naphthalene sulfonate ammonium salt (ANS) were procured from Sigma-Aldrich (USA) and Fluka (Switzerland), respectively. Membrane filters were purchased from Millipore (USA). All other reagents were analytical or reagent grade. Water obtained from an ELGA purification unit (UK) was used throughout the study.

Preparation of Paclitaxel Liposomes

Liposomal dispersions of paclitaxel were prepared by the film-hydration method [11]. Appropriate quantities of paclitaxel, PC and PG stock solutions in chloroform were place in a round-bottomed flask and chloroform was removed under vacuum. In all cases the PC:PG mole ratio was 9:1. The drug–lipid mixture was re-dissolved in a cyclohexane-*tert*-butanol solvent system (0.5:1 v/v) and the organic phase was removed by rotary evaporation to obtain a drug–lipid film. The film was subjected to vacuum for an additional period of time in order to remove traces of solvent before hydration using a 0.9% (w/v) sodium chloride medium. After hydration of the film, the multilamellar vesicles obtained were extruded through polycarbonate filters of 0.4 μm pore size for further studies.

Analysis of Liposomal Components

The purity of the phospholipids used in the study was assessed by thin layer chromatography with two different mobile phases of different polarities and all samples exhibited a single spot. In addition, total lipid, PG in liposomal formulations were analyzed by the colorimetric methods described earlier [12, 13].

Steady-State Fluorescence Anisotropy Measurements

Both drug-containing and drug-devoid liposomes were prepared as mentioned in earlier section and labeled with fluorescent probes. The preparations contained lipids at 2 mg ml^{-1} concentration while the concentration of the drug was varied from 0.5 to 10 mol% with respect to the lipid. All liposomal preparations had a PC:PG mole ratio of 9:1 and were extruded through 0.4 μm membrane filters. The lipid to probe ratios of DPH, 12AS and ANS were 300:1, 200:1 and 100:1, respectively. Since the membrane probe concentrations are infinitesimally small, the lateral distributions of probes in liposomes primarily measure the dynamic component of membrane fluidity. DPH and 12AS stock solutions were prepared in tetrahydrofuran and added to extruded preparations while ANS was included in the medium for film hydration. After allowing a 2-h equilibration period in the dark, 75 μl of each formulation containing DPH or 12AS probe and 200 μl of formulation containing ANS were further diluted to 3 ml with saline for fluorescence anisotropy measurements. Fluorescence measurements were carried out on a Perkin Elmer LSB 50 spectrofluorimeter (UK) equipped with a circulating water bath and fluorescence anisotropy (r) was calculated according to the following equation:

$$r = \left(I_{\mathrm{p}} - I_{\mathrm{v}}\right) / \left(I_{\mathrm{p}} + 2I_{\mathrm{v}}\right) \quad (1)$$

where I_{p} and I_{v} are the fluorescence intensities of the emitted light polarized parallel and perpendicular to the excited light, respectively. "G" factor = 1. The excitation and emission slit widths were 5 and 10 nm while the excitation and emission wavelengths in nanometers of DPH, 12AS and ANS were as follows: (1) 380 and 430, (2) 370 and 450, (3) 380 and 480. During measurements, the temperature of the sample was controlled with an accuracy of ±0.2 °C of set temperature and, the phospholipid concentration was kept to <1 mg ml^{-1} to minimize interference from light scattering.

Attenuated Total Reflectance FT-IR Studies

Infrared spectra were measured at room temperature on a Bruker Vector 22 attenuated total reflectance FT-IR spectrometer (Bruker Optik GmbH, Ettlingen, Germany). To obtain the FT-IR spectra, 100 μl of liposome dispersions were placed on a germanium crystal and scanned in the range 600–3,000 cm^{-1}. A total of 100 scans were collected and coadded with a spectral resolution of 2 cm^{-1}. Background spectrum was always collected under identical conditions. The same liposomal preparations as described for NMR studies were used here.

31P-NMR Analysis

Liposomal formulations were prepared in a saline medium to obtain a final lipid concentration of 40 mg ml^{-1}. 31P-NMR spectra were recorded (phosphoric acid standard) on a Bruker 300 spectrometer operating at 121.45 MHz in a 5-mm broad band probe at 25 °C as previously reported [14]. Each sample was suspended in 10% D_2O and 5,000–5,200 transients were accumulated with a pulse length of 14 μs and 1 s relaxation delay. The free induction decays were processed using an exponential line broadening of 100 Hz prior to Fourier transformation.

Results

Liposomes containing paclitaxel were prepared at varying drug:lipid ratios at a fixed lipid composition (PC/PG:9/1) and the mean recoveries of total phospholipids and PG colorimetry were 95(±7.1) and 96(±5.5), respectively. In view of crystallization problems, formulations were also analyzed for paclitaxel content by a radiochemical method of analysis after centrifugation at 5,000 rpm for 5 min to sediment precipitated drug/lipids. The encapsulation of paclitaxel was always greater than 90% which shows the presence of pre-determined drug:lipid ratios in formulations during the time-frame of characterization. Subsequently, the sort of perturbations caused in bilayer physical properties were investigated by spectroscopic techniques to elucidate the interaction of paclitaxel with these unsaturated phospholipid membranes. By using fluorescent probes, it was possible to determine fluidity/rigidity of the lipid membrane due to paclitaxel as a function of depth within the bilayer. Further, the non-perturbing FT-IR spectroscopy technique allowed us to consolidate the findings of fluorescence polarization and to clarify the dynamics both in hydrocarbon and head-group regions. Finally, 31P-NMR shed light on the taxane induced generation of a non-bilayer phase that co-exists with the regular bilayer phase.

Steady-State Fluorescence Anisotropy Studies

For a given probe, the degree of fluorescence polarization depends on the rotation of the fluorophore relative to the direction of its emission transition moment [15]. The steady-state fluorescence anisotropy technique adopted here for examination of paclitaxel in the bilayer employed three probes, namely, DPH, 12AS and ANS which locate at different regions in the bilayer. Anisotropy measurements were done at 30 and 40 °C for liposomes at different paclitaxel loadings (Fig. 2). In general, anisotropy at 40 °C was observed to be lower when compared to 30 °C for all the probes at all drug loadings (as temperature is raised, more *gauche* rotamers are excited in the bilayer hydrocarbon) except for ANS where, the trend was reversed at greater than 3 mol% loadings (Fig. 2c). Barring this exception, anisotropy curves followed nearly identical trends for all probes at both temperatures.

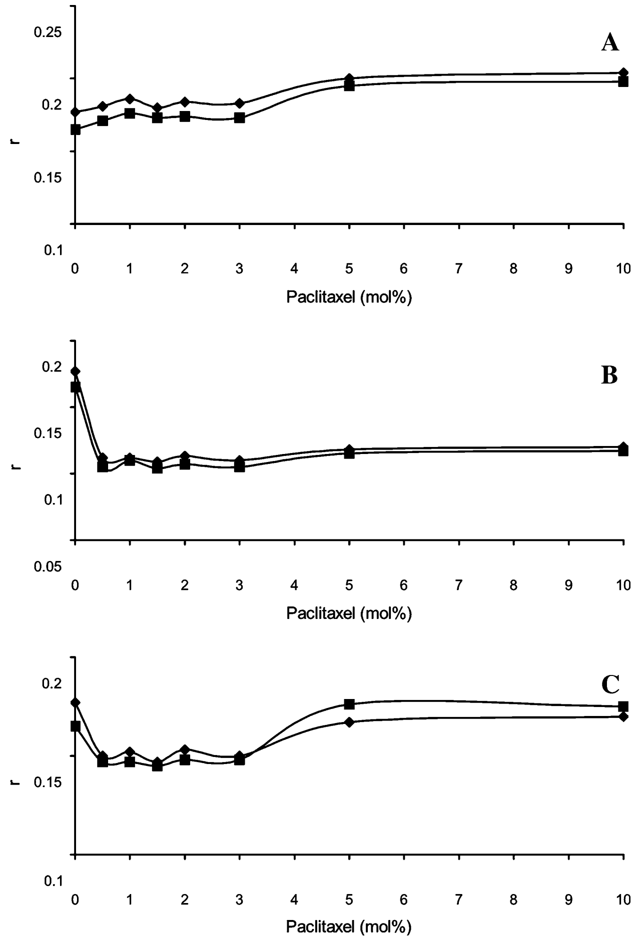

Fig. 2 The effect of paclitaxel on microviscosity of PC:PG = 9:1 (mol/mol) bilayers studied by steady-state fluorescence anisotropy (r) using membrane probes **a** DPH, **b** 12AS and **c** ANS. The lipid to probe ratios used were 300:1, 200:1 and 100:1 for DPH, 12AS and ANS. *Filled diamonds* 30 °C, *filled squares* 40 °C

At a given temperature, when the affect of paclitaxel on fluorescence anisotropy of DPH in soya PC:PG (9:1) bilayers was studied, the incorporation of paclitaxel caused a slight increase in anisotropy (Fig. 2a). It was also evident from Fig. 2 that at fixed temperature, the changes brought about in fluorescence anisotropy of DPH due to varying concentrations of paclitaxel were of considerably smaller magnitude than for the other two probes. Anisotropy values for DPH located in the hydrophobic core of bilayer increased slightly up to 1 mol% of paclitaxel after which a first plateau was observed till 3 mol%. Further increase in anisotropy was also seen with increase in drug loading from 3 to 5 mol% following which a second plateau was attained. In order to draw further information on the location of paclitaxel, 12AS was selected to understand the effects in the acyl chain region just above center of bilayer. The AS probes (2AS, 7AS and 12AS) have a stearic acid backbone that is intercalated parallel to fatty acid chains of the phospholipids with its charged carboxylic group anchored at interfacial region of the bilayer and 12AS probes region from the 8–9th to the 15–16th carbon [16]. In case of 12AS, the presence of paclitaxel even at lowest concentrations studied (0.5 mol%) decreased anisotropy values (Fig. 2b) and this was followed by a moderate increase thereafter with increasing paclitaxel concentrations (beyond 3 mol%).

Following anisotropy studies in the bilayer using DPH and 12AS probes, an attempt was also made to understand the interfacial phenomena exploring ANS probe. Since ANS is an interface probe, its anisotropic behavior physically reflects changes more on the bilayer surface morphology than in the lipid bilayer core. With increasing paclitaxel concentration, trends similar to that of 12AS were also observed in the case of ANS at both temperatures (Fig. 2c); the only points of difference being that the initial fall in anisotropy was less steep and a sudden increase was observed after 3 mol% loading. At 3 mol% of paclitaxel, anisotropy values were 0.183, 0.15 and 0.11 for DPH, ANS and 12AS, respectively, at 30 °C. The highest anisotropy values attained for the three probes at 30 °C were in the following order: DPH > 12AS > ANS (0.204 > 0.177 > 0.175). Clearly, the anisotropy curves for all probes showed no change at paclitaxel loadings greater than 5 mol% suggesting that at higher than optimal paclitaxel–lipid concentrations, the excess amounts may no longer be associated with the membrane interiors [17].

Attenuated Total Reflectance FT-IR Studies

FT-IR spectroscopy was employed to examine the effects of paclitaxel on the conformation of lipid acyl chains as well as headgroup and interfacial regions. Spectra of control and paclitaxel-loaded liposomes over the 3,000–800 cm^{-1}

range are shown in Fig. 3, and frequencies of selected absorption bands are listed in Table 1. Absorption bands considered to yield the most useful information on the analysis of FT-IR spectra are: methylene asymmetric and symmetric stretching, carbonyl stretching, phosphate asymmetric and symmetric stretching modes. In the hydrocarbon region, C–H stretching frequencies increase with increase in the number of *gauche* conformers while the bands broaden as a result of increasing motional freedom of methylene groups. In the spectral region of 3,000–2,800 cm^{-1} for control liposomes, the acyl chain methylene C–H bond asymmetric stretching v_{as} (CH_2) and symmetric stretching v_{s} (CH_2) were observed at 2,925 and 2,852 cm^{-1}, respectively. Due to paclitaxel, v_{as} (CH_2) stretch frequencies were unaltered while v_{s} (CH_2) frequency was $\sim$2,854 cm^{-1}. Though v_{as} (CH_2) was not affected due to paclitaxel, that of v_{s} (CH_2) stretch was substantially increased (2 cm^{-1}). Further, the methyl C–H bond asymmetric stretch v_{as} (CH_3) mode which was observed at 2,966 cm^{-1} for control liposomes, was less apparent in paclitaxel liposomes due to broadening. These changes were also accompanied by significant increases in band widths of v_{as} (CH_2) and v_{s} (CH_2) stretch frequencies (Fig. 3, inset) indicating to alteration of lipid acyl chain dynamics [18].

The other most useful information regarding acyl chain packing and inter-chain interactions is derived from CH_2 scissoring and wagging modes. For control liposomes a single sharp peak representing acyl CH_2 scissoring mode was observed at 1,456 cm^{-1} while for paclitaxel liposomes, it was observed with reduced intensity between 1,458 and 1,460 cm^{-1}. On the other hand, the acyl CH_2 wagging mode comprised multiple peaks in the spectra of control liposomes at 1,317, 1,289 and 1,261 cm^{-1} were not only shifted but also broadened by the incorporation of paclitaxel. The peak at 1,370 cm^{-1} observed in control liposomes which is considered to originate from the terminal δ_{s} (CH_3) symmetric bending mode, was found at 1,369–1,371 cm^{-1} for paclitaxel liposomes whose intensity lowered as a function of loading. The other weak bands corresponding to that of CH_2 scissoring adjacent to C=O group and terminal δ_{as} (CH_3) asymmetric bending modes were found at 1,422 and 1,432 cm^{-1}, respectively, in absence of paclitaxel. Upon incorporation of drug, these peaks merged into a single broad band and lacked sufficient resolution which did not allow assignment of frequencies to individual bands. Such characteristic changes in IR behavior of CH_2 adjacent to C=O are possibly reflective of conformational changes in the interface of bilayer which is in line with the changes observed for the carbonyl stretching band, as discussed below.

In the spectral region of 1,700–1,800 cm^{-1}, the phospholipid ester carbonyl stretching mode v (C=O) was observed as a sharp and symmetric peak at 1,741 cm^{-1} in the absence of paclitaxel in bilayers. However, there was a gradual broadening of the v (C=O) band with an increasing concentration of paclitaxel and the intensity of the peak was lost to the developing shoulder on the low frequency side leading to peak asymmetry. The other important feature in spectra at the interfacial region of lipid membranes is that representative of C–O stretching, namely v (OC–O) of esters of fatty acyl chains. This peak observed at 1,170 cm^{-1} (0 mol%) was broadened with paclitaxel concentration (1–2 mol%) but reappeared at 3 mol% as a weak signal. These observations are not only suggestive of unique interactions of the C=O group at the interface but

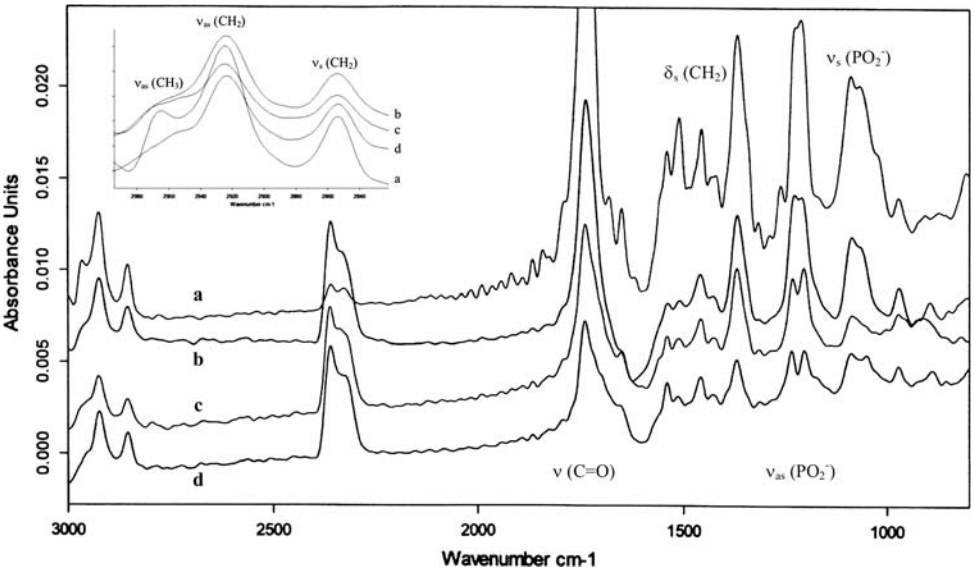

Fig. 3 FT-IR spectra of soya PC:PG=9:1 (mol/mol) liposomes in hydrated state containing 0 (*a*) 1 (*b*) 2 (*c*) and 3 (*d*) mol% pacliatxel. Spectra are plotted in absorbance mode. The *inset* on *left-top* shows acyl C–H stretch frequency bands. Also see Table 1 for designation and assignment of peaks. Note that C=O peak of *a* was truncated for clarity reasons

Table 1 Infrared absorption frequencies of acyl chain, interface and headgroup regions of soya PC/PG:9/1 liposomes at various loadings of paclitaxel

Assignment[a]	Wavenumber (cm^{-1})			
Paclitaxel concentration (mol%)	0	1	2	3
ν_{as} (CH$_3$) stretch	2,966	b	b	b
ν_{as} (CH$_2$) stretch	2,925	2,925	2,925	2,925
ν_s (CH$_2$) stretch	2,852	2,854	2,854	2,854
ν (^{12}C=O) stretch	1,741	1,740	1,742	1,742
ν (^{13}C=O) stretch	1,682	n	n	n
ν_{as} (N(CH$_3$)$_3$) bend	1,489	n	n	n
δ_s (CH$_2$) acyl scissoring	1,456	1,460	1,458	1,459
δ_s (CH$_2$) scissoring adjacent to C=O	1,422	b	b	b
δ_s (CH$_3$) bend	1,370	1,369	1,371	1,370
δ_s (CH$_2$) acyl wagging	1,317, 1,289, 1,267	1,315	1,315, 1,285	1,313, 1,283
ν_{as} (P=O) stretch (free)	1,226	1,228	1,232	1,234
ν_{as} (P=O) stretch (hydrogen bonded)	1,212	1,209	1,204	1,204
ν_s (OC–O) stretch	1,170	b	b	b
ν_s (P=O) stretch	1,089	1,087	1,087	1,088
ν (R–O–P–O–R′) stretch	1,067	1,061	1,055	1,049
ν (C–OP) stretch	1,019	n	n	n
ν_{as} (C–N$^+$–C) stretch	972	970	972	971
ν_{as} (O–P–O) stretch	810	b	b	b

Spectra are shown in Fig. 3

b Broad, *n* not prominent

[a] Peak assignments were done according to references [25–28, 32]

the reappearance of the C–O peak also indicates paclitaxel concentration being dependent on organizational differences of phospholipid molecules [19].

Besides the carbonyl group, the phosphate group is also sensitive to polarity changes in the headgroup region. When the effects of paclitaxel on the headgroup region were monitored via the asymmetric ν_{as} (P=O) and symmetric ν_s (P=O) stretch of phosphate, there were significant shifts in frequency of the former peak. In contrast to the usually observed single ν_{as} (P=O) peak for a given species of phospholipid, IR spectra here showed two well resolved peaks at 1,226 and 1,212 cm^{-1}; the former peak arising due to free phosphate and the latter from hydrogen bonded phosphate. This is considered as being possibly due to the presence of PG in the liposomes whose –OHs of glycerol moiety are known to form hydrogen bonds with phosphate thereby reducing the IR frequency [19, 20]. On this basis, ν_{as} (P=O) at 1,226 cm^{-1} for blank liposomes was assigned to free P=O, which was found to shift to 1,228, 1,232 and 1,234 cm^{-1}, respectively, at 1, 2 and 3 mol% paclitaxel loadings. On the other hand, ν_{as} (P=O) of hydrogen bonded phosphate moved in the opposite direction, i.e., from 1,212 cm^{-1} (0 mol% drug) to 1,209 cm^{-1} (1 mol%) and 1,204 cm^{-1} (3 mol%) as a result of which the 2 peaks were clearly resolved. Though paclitaxel shifted both n_{as} (P=O) stretch of free and hydrogen bonded wavenumbers in liposomes, n_s (P=O) stretch wavenumber was only slightly altered (1,089–1,887 cm^{-1}).

Other important changes include, a prominent shift in ν (R-O–P-O-R') stretch band from 1,067 cm^{-1} (control liposomes) to 1,061, 1,055 and 1,049 cm^{-1} for 1, 2 and 3 mol% paclitaxel loaded liposomes. Another peak distinctly observed in control liposomes but absent from paclitaxel liposomes was located at 1,019 cm^{-1}, and this peak was a result of C–OP stretch in phosphate ester region. Further, in the headgroup region, N(CH$_3$)$_3$ bending mode located at 1,489 cm^{-1} and n (P–O) phosphate ester stretch at 810 cm^{-1} were all considerably broadened upon incorporation of paclitaxel in liposomes. In addition to effect on n_{as} (P=O) vibration, concomitant changes recorded for the n (P–O) and n (C–OP) frequencies are also in support of paclitaxel mediated changes in the phosphate group. The broadening of n_s (P=O) and n (R-O–P-O-R') vibration bands indicating to greater mobility also is in agreement with increased fluidity due to paclitaxel in the headgroup region [20]. Further, in the headgroup region, broadening of the N(CH$_3$)$_3$ bending mode and n (P–O) phosphate ester stretch might confirm findings with the ANS probe, namely, increased fluidity. A further examination of headgroup conformational changes was based on 31P-NMR spectroscopy.

31P-NMR Studies

31P-NMR measurements were carried out with paclitaxel-loaded and paclitaxel-free liposomes to find out whether the drug was interacting with the headgroups. In the concentration range studied (1–3 mol%), all formulations showed an intermediate-type powder spectrum with a high-field peak at approx. −7 ppm and a low-field shoulder typical of bilayer arrangement of phospholipids within membrane (Fig. 4). The spectrum suggests that 400 nm sized vesicles undergo motional averaging due to a tumbling motion and the low intensity peak at 0 ppm superimposed on the main peak for control liposomes might be due to the presence of small vesicles [20, 21]. An important feature in the spectra following incorporation of paclitaxel is the emergence of a sharp isotropic signal at ~0 ppm which increased in intensity with increasing drug concentration (Fig. 4). Also, 31P-peak positions were observed to slightly shift towards isotropic signal indicating to fluidization of bilayers [22] and shapes were altered due to paclitaxel at the peak crest (Fig. 5). A closer inspection of NMR spectra discloses that liposomes containing paclitaxel present a small but distinct increase in the low field shoulder at the base (Fig. 5). The relation of paclitaxel concentration in liposomes to the overall peak shape and isotropic signal intensity at 0 ppm implies concentration-dependent effects of the molecule on PC:PG lipid bilayers.

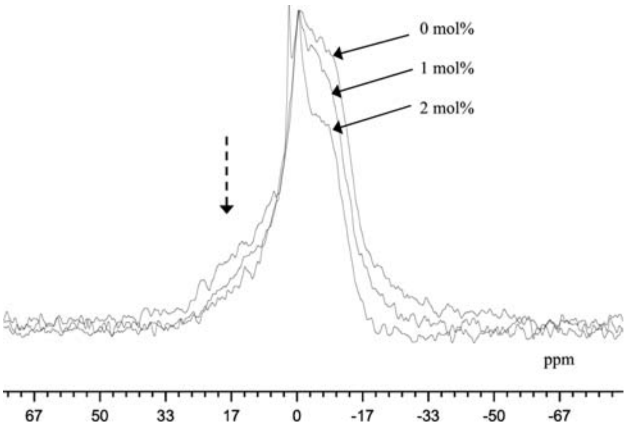

Fig. 5 An overlaid view of 31P-NMR spectra of soya PC:PG (9:1) liposomes with and without paclitaxel showing narrowing of peak width as a function of the taxane concentration. Liposomes at 3 mol% paclitaxel loading not shown here because of large isotropic signal. Note the gradually developing shoulder on low field with increasing paclitaxel concentration as indicated with *broken-line arrow*

Discussion

A number of reports exist in the literature dealing with the formulation of paclitaxel liposomes, which were shown to increase the biological half-life of drug [23] and retain antitumor properties of the molecule in cancer models [7]. In the clinical trials, liposomal paclitaxel was better tolerated than the cremophor formulation in the absence of standard premedication drugs even at higher doses [6]. Although paclitaxel is known to be located at the interface of the lipid bilayer, specific information about the nature of the interaction and the part of the phospholipid molecule involved is lacking. This information may help to better elucidate formulation aspects and the therapeutic efficacy of these delivery systems. Hence, in the current investigation an attempt was made to examine paclitaxel-bilayer interactions and results derived from fluorescence anisotropy, FT-IR and 31P-NMR techniques are presented.

Fig. 4 31P-NMR spectra of liposomes of composition soya PC:PG = 9:1 (mol/mol) prepared by film hydration and extrusion (400 nm). 0 (**a**), 1 (**b**), 2 (**c**) and 3 (**d**) mol% paclitaxel

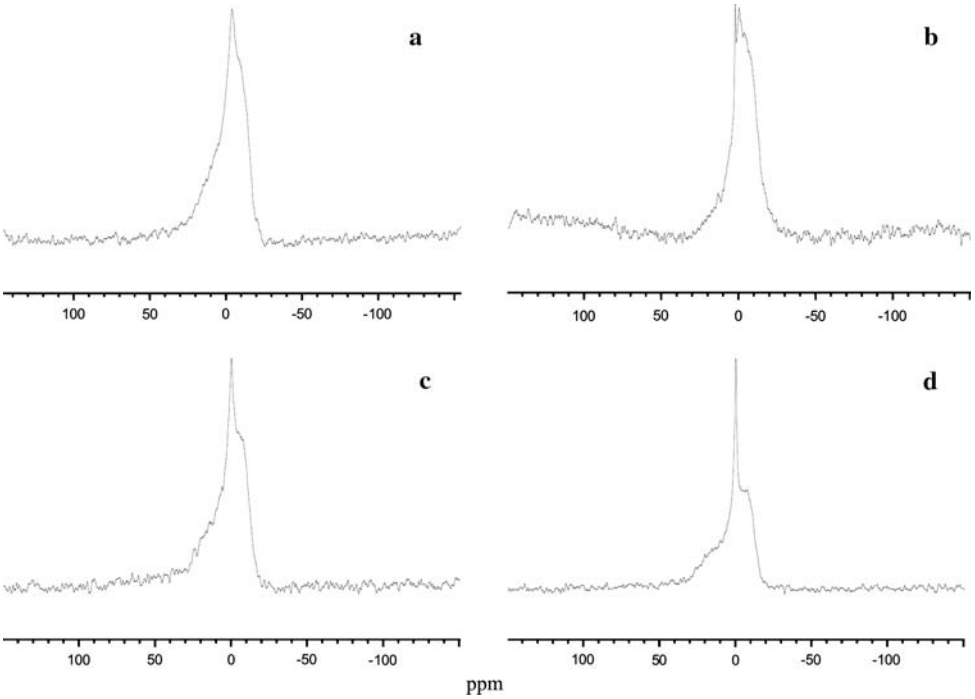

In fluorescence anisotropy studies, a decrease in anisotropy is explained by the increased fluidity of the bilayers [17]. If it is assumed that anisotropy of DPH reflects the average extent of acyl chain motion within the bilayer core by virtue of its location, the incorporation of paclitaxel has a weak rigidizing effect in the core of bilayer (towards the terminal methyl end of the lipid acyl chain, Fig. 1a). In contrast, the effect of paclitaxel in liposomes was quite different on 12AS and ANS probes where anisotropy of 12AS and ANS decreased at 0.5–3 mol% loading. The decrease in anisotropy of the 12AS probe was more dramatic (Fig. 2b) and the trend reflects the fluidizing effect of paclitaxel in the vicinity of this probe below 3 mol% incorporation. Moreover, the anisotropy of ANS was also found to decrease with the incorporation of paclitaxel in the concentration range of 0.5–3 mol% (Fig. 2c) and this decrease in anisotropy may also be related to increased fluidity at the interface. The variation in membrane fluidity, that is the occurrence of fluidity gradient across the bilayer, was also previously demonstrated for local anesthetics [24]. At > 3 mol% drug loading, an increase in ANS anisotropy was observed which might be attributed to onset of typical aggregation behavior of the taxane, as pointed out elsewhere [8]. At higher loadings, the aggregation of paclitaxel monomers into micro-clusters might occur at the interface resulting in partitioning of the ANS probe into these structures where the molecules experience higher anisotropy. Since the magnitude of anisotropy changes were maximally recorded for 12AS and ANS probes, it is anticipated that paclitaxel is located within the vicinity of these probes. In accordance with this assumption, paclitaxel is mainly located in the cooperativity region (towards the interface) with some part of the molecule extending into the headgroup region of the bilayer, as shown previously [10].

Further detailed understanding of intra- and intermolecular interactions occurring within lipid membranes was gained by FT-IR as a non-perturbing physical technique and these interpretations are classified into spectral features originating from the nonpolar hydrocarbon acyl chains, interfacial and headgroup regions (Table 1). Considering the acyl chain spectral features, the increase in frequency of the vibration of the ν_s (CH_2) band caused by paclitaxel (Fig. 3) is a reflection of the change in conformation of the lipid acyl chain from the ordered *trans* C–C structure to the disordered *gauche* C–C structures [25]. Also the conformational disorder caused by paclitaxel was accompanied by bandwidth increases leading to augmentation of rotational mobility of acyl chains [18]. This fact was also reinforced by the broadened and decreased intensity of CH_2 scissoring/wagging bands attributed to increased mobility and higher proportion of gauche conformers of methylene groups in acyl chains caused by paclitaxel [20]. This effect, when put together with decreased fluorescence anisotropy of 12AS, it may be regarded that paclitaxel induces an increased degree of disorderliness in bilayers and leads to increased fluidity of bilayers [26].

An idea about molecular organization in the interfacial regions can be drawn by monitoring the spectral properties of carbonyl (C=O). The C=O band stretching is sensitive to changes in the polarity of the local environment and is influenced by hydrogen bonding or other interactions occurring in the presence of interfacially placed molecules. Also, any change in the contours of the ν (C=O) band has often been understood in terms of structural and/or hydration changes at the bilayer interface [20]. In the present study, the typical alteration in the contour of the ν (C=O) stretch peak (low field shoulder; Fig. 3) by paclitaxel may be interpreted as conformational changes along with an increased rate of motion. This is coincident with the distinct changes generated each in the ν (OC–O) stretch mode and scissoring of CH_2 (adjacent to C=O) mode. In addition to the above-mentioned conformational changes, the broadening might also indicate to the possibility of involvement in hydrogen bonding for the population of carbonyl along the shoulder, since ν (C=O) stretch peak shoulder extended by about 10–20 cm^{-1} from the principal peak in the presence of paclitaxel [20]. Hydrogen bonding of water molecules to ν (C=O) group of phospholipid molecule was shown to shift the carbonyl stretch wavenumber to lower values resulting from a decrease in the double bond character [26–28]. In this regard, hydrogen bonding between the carbonyl of the phospholipids and the OH of water/paclitaxel is an immediate explanation in light of the decreased (C=O) bond strength. In order to arrive at a more plausible explanation in search of hitherto proposed hydrogen bonding, the incumbent evidence gathered from events occurring in headgroup region namely, ν_{as} (P=O), will be considered.

In the headgroup region of lipid vesicles, the most widely studied spectral feature is the IR absorption band of the phosphate because wavenumber of P=O mode is particularly sensitive to hydration/dehydration state of phosphate. Generally, ν_{as} (P=O) stretch mode is considered more sensitive and diagnostic of dehydration where, values around 1,220 cm^{-1} are reported for hydrated state and 1,235–1,250 cm^{-1} are observed for the dehydrated phosphate group [25]. In this context, an upward shift in the frequency of ν_{as} (P=O) indicates distinct effects of paclitaxel in the interfacial region arising from dehydration of phosphate due to the removal of water, because hydrogen bonding to the oxygen atom would have an opposite effect, i.e., a decrease in frequency due to weakening of the vibrational force constant [19]. Since this comprehension is strongly supported by relevant findings in literature and devoid of any ambiguity, it could be inferred that paclitaxel causes expulsion of water thereby decreasing the polarity in headgroup region, a condition favorable for association of hydrophobic taxane with bilayers at interface. A further extrapolation of this inference to C=O at interfacial region is that water is unavailable for hydrogen bonding with carbonyl of phospholipids thus indicating to the alternative possibility, i.e., the likely involvement of paclitaxel itself. In fact, previous studies claimed the location of paclitaxel in interfacial region of bilayer while the potential of 2′/7-OH groups of the molecule (Fig. 1) to engage in hydrogen bonding interactions was reported elsewhere [29]. From a consideration of structure of paclitaxel (Fig. 1), the involvement of 2′-OH in hydrogen bonding with phospholipid may be speculated based on geometrical and polarity constraints as this would obviate the need for placing the bulky taxane ring at the bilayer interface. There are other studies which indicate the existence of intermolecular interactions via C=O groups by means of hydrogen bonds in lipid membranes. Based on FTIR observations, it has been shown that melatonin interacts with dipalmitoyl PC through strong hydrogen bonding with (C=O) group [30]. Another publication reported on the extensive hydrogen bonding phenomenon between carbonyl ester of egg PC liposomes and OH of galactose moieties of digalactosyldiacylglycerol [31].

A special feature of PG-containing PC bilayers is the inter-molecular hydrogen bonding between headgroups [32] and the increased hydrophobicity of PC bilayers. Apart from interaction with the carbonyl, paclitaxel also seems to promote stronger hydrogen bonds between the hydroxyl of glycerol of PG and the phosphate of PC, i.e., following removal of water, the glycerol moiety of PG more closely interacts with P=O probably due to conformational changes in the headgroup region and steric factors. On extrapolating these properties of PG in lipid bilayers to paclitaxel liposomes, the simultaneous increase in hydrophobicity along with modification of bilayer headgroup with hydrogen bonding capacities could be held responsible for the observed favorable effects of PG, namely, promotion of formulation stability [3, 5].

31P-NMR spectroscopy provides valuable information on the organization of lipid bilayer vesicles due to sensitivity of the conformation and dynamics of the phosphate nucleus in the phospholipid headgroup to the surrounding environment. Differences in 31P-NMR line shapes/widths have been understood in terms of orientation of phospholipid headgroups and the motions that cause the related residual chemical shift anisotropy. Boulanger et al. [33] reported 8% change in the 31P-NMR basal line width in egg PC vesicles in the presence of charged tetracaine which preferably interacts with bilayers towards the interfacial region while such changes were absent with the uncharged form due to localization in the core of lipid membrane. Similarly, the interfacially interacting taxane altered 31P-NMR peak crest shapes (Fig. 5) because fluidity changes in bilayers could affect the motion of headgroups [20, 34]. To this end, the possibility of hydrogen bonding of paclitaxel with P=O of phosphate is ruled out since there is no distinct phosphorus peak associated with this event in 31P-NMR spectra (Fig. 4). Importantly, in the NMR spectra of liposomes there have been two major events associated with the incorporation of paclitaxel which were concentration dependent: the appearance of (1) a low field weak shoulder (increased basal line width) and (2)an isotropic peak. The shoulder albeit small due to low drug loadings and liquid crystalline nature of bilayers (Fig. 5), indicate to perturbations introduced in bilayer by paclitaxel. These perturbations might result from increased hydrogen bonding of phosphate with glycerol and the presence of paclitaxel-rich domains. While the former of the two possibilities has already been speculated on from FT-IR data and can be explained by reduced mobility of the phosphate thereby increasing 31P-NMR basal line widths, the latter event is based on non-homogeneous distribution of paclitaxel with lipids as a consequence of which such domains are formed and phase segregated from the rest of the membrane [8, 35]. These paclitaxel-rich domains, in contrast to the rest of the bilayer, would be featured with higher drug:lipid ratios with unique packing parameters.

An explanation for the isotropic peak is directed towards phospholipid molecules being present in non-bilayer phases (Fig. 5) within the lipid membrane and/or due to the formation of paclitaxel–phospholipid mixed micelles [36]. Owing to paclitaxel, a small fraction of lipid molecules participating in the bilayer phase are increasingly brought into the non-bilayer phase, for example, the hexagonal phase fostered by PG, whose phosphate headgroups are featured with rapid motion on the 31P-NMR time scale, thus exhibiting an isotropic signal [22, 36]. As reported earlier, the propensity of phospholipids to form non-bilayer phases followed by accumulation of paclitaxel aggregates into them is also thermodynamically favorable in view of reduced perturbation caused on bilayers in the aggregated state at higher concentrations [8]. Elsewhere, the ability of amitriptyline to transform egg PC bilayers into mixed micelles has been described [37–39]. It is highly probable that with increased loading, paclitaxel is gradually expelled out of the bilayer into a new non-bilayer transient phase and; the non-bilayer structures are involved in a fusion process that would promote coalescence of smaller vesicles to produce larger liposomes and increase the dispersion size on the shelf [39, 40].

Conclusion

The nature of the interaction of a guest molecule with the lipid bilayer depends not only on its hydrophobicity and conformation but also on the location of the molecule within the lipid membrane and the steric compatibility. Paclitaxel was predominantly observed to have a fluidizing effect on unsaturated phospholipid liposomal bilayers thereby influencing the acyl chain dynamics. However, the nature of paclitaxel interaction with the bilayer seems to be rather complex in that conformational changes are caused almost ovwe the whole stretch of the membrane as a consequence of which, its influences are felt from the headgroup to the acyl chain terminal regions within the the bilayer. Thus, it is considered that paclitaxel caused a significant alteration in the conformation of lipid acyl chains and the physical state of the bilayer. A further examination of these events by FT-IR spectroscopy revealed dehydrating effects of paclitaxel on phosphate groups as well its direct or mediated interaction with the carbonyl of the phospholipid. In addition, at higher concentrations of paclitaxel, phospholipid molecules tend to form non-bilayer structures and probably taxane-rich domains. Given these findings, the examination of molecular orientation of paclitaxel in bilayer and non-bilayer phases would be a subject of further interest.

References

1. Panchagnula R (1998) Pharmaceutical aspects of paclitaxel. Int J Pharm 172:1–15
2. Dhanikula AB, Panchagnula R (1999) Localized paclitaxel (Taxol) delivery. Int J Pharm 183:85–100
3. Dhanikula AB, Panchagnula R (2005) Preparation and characterization of water-soluble prodrug, liposomes and micelles of paclitaxel. Curr Drug Deliv 2:75–91
4. Dhanikula AB, Singh DR, Panchagnula R (2005) In vivo pharmacokinetic and tissue distribution studies in mice of alternative formulations for local and systemic delivery of paclitaxel: gel, film, prodrug liposomes and micelle. Curr Drug Deliv 2:35–44
5. Straubinger RM, Balasubramanian SV (2005) Preparation and characterization of taxane-containing liposomes. Methods Enzymol 391:97–117
6. Zhang JA, Anyarambhatla G, Ma L, Ugwu S, Xuan T, Sardone T, Ahmad I (2005) Development and characterization of a novel Cremophor EL free liposome-based paclitaxel (LEP-ETU) formulation. Eur J Pharm Biopharm 59:177–187
7. Campbell RB, Balasubramanian SV, Straubinger RM (2001) Influence of cationic lipids on the stability and membrane properties of paclitaxel-containing liposomes. J Pharm Sci 90:1091–1105
8. Belsito S, Bartucci R, Sportelli L (2005) Paclitaxel interaction with phospholipid bilayers: high-sensitivity differential scanning calorimetric study. Thermochim Acta 427:175–180
9. Zhao L, Feng SS (2004) Effects of lipid chain length on molecular interactions between paclitaxel and phospholipid within model biomembranes. J Coll Interface Sci 274:55–68
10. Ali S, Minchey S, Janoff A, Mayhew EAA (2000) Differential scanning calorimetry study of phosphocholines mixed with paclitaxel and its bromoacylated taxanes. Biophys J 78:246–256
11. Bangham AD (1978) Properties and uses of lipid vesicles: an overview. Ann N Y Acad Sci 308:2–7
12. Zhou X, Arthur G (1992) Improved procedures for the determination of lipid phosphorus by malachite green. J Lipid Res 33:1233–1236
13. Hope ML, Redelmeier TE, Wong KF, Rodrigueza W, Cullis PR (1989) Phospholipid asymmetry in large unilamellar vesicles induced by transmembrane pH gradients. Biochemistry 28:4181–4186
14. Frohlich M, Brecht V, Peschka-Suss R (2001) Parameters influencing the determination of liposome lamellarity by 31P-NMR. Chem Phys Lipids 109:103–112
15. Lentz BR (1993) Use of fluorescent probes to monitor molecular order and motions within liposome bilayers. Chem Phys Lipids 64:99–116
16. Thulborn KR, Tilley LM, Sawyer WH, Treloar FE (1979) The use of *n*-(9-anthroyloxy) fatty acids to determine fluidity and polarity gradients in phospholipid bilayers. Biochim Biophys Acta 558:166–178
17. Engelke M, Jessel R, Wiechmann A, Diehl HA (1997) Effect of inhalation anaesthetics on the phase behaviour, permeability and order of phosphatidylcholine bilayers. Biophys Chem 67:127–138
18. Lotta TI, Salonen SI, Virtanen JA, Eklund KK, Kinnunen PK (1988) Fourier transform infrared study of fully hydrated dimyristoylphosphatidylglycerol. Effects of Na+ on the *sn*-1′ and *sn*-3′ headgroup stereoisomers. Biochemistry 27:8158–8169
19. Hubner W, Blume A (1998) Interactions at the lipid–water interface. Chem Phys Lipids 96:99–123
20. Garidel P, Blume A, Hubner WA (2000) Fourier transform infrared spectroscopic study of the interaction of alkaline earth cations with the negatively charged phospholipid 1,2-dimyristoyl-*sn*-glycero-3-phosphoglycerol. Biochim Biophys Acta 1466:245–259
21. Traikia M, Warschawski DE, Recouvreur M, Cartaud J, Devaux PF (2000) Formation of unilamellar vesicles by repetitive freeze–thaw cycles: characterization by electron microscopy and 31P-nuclear magnetic resonance. Eur Biophys J 29:184–195
22. Tyteca D, Schanck A, Dufrene YF, Deleu M, Courtoy PJ, Tulkens PM, Mingeot MP (2003) The macrolide antibiotic azithromycin interacts with lipids and affects membrane organization and fluidity: studies on Langmuir–Blodgett monolayers, liposomes and J774 macrophages. J Membr Biol 192:203–215
23. Crosasso P, Ceruti P, Brusa M, Arpicco S, Dosio F, Cattel L (2000) Preparation, characterization and properties of sterically stabilized paclitaxel-containing liposomes. J Control Release 63:19–30
24. Yun I, Cho ES, Jang HO, Kim UK, Choi CH, Chung IK, Kim IS, Wood WG (2002) Amphiphilic effects of local anesthetics on rotational mobility in neuronal and model membranes. Biochim Biophys Acta 1564:123–132
25. Casal HL, Mantsch HI (1984) Polymorphic phase behaviour of phospholipid membranes studied by infrared spectroscopy. Biochim Biophys Acta 779:381–401
26. Umemura J, Cameron DG, Mantsch HH (1980) A Fourier transform infrared spectroscopic study of the molecular interaction of cholesterol with 1,2-dipalmitoyl-*sn*-glycero-3-phosphocholine. Biochim Biophys Acta 602:32–44
27. Blume A, Hubner W, Messner G (1988) Fourier transform infrared spectroscopy of ^{13}C=O-labeled phospholipids hydrogen bonding to carbonyl groups. Biochemistry 27:8239–8249
28. Hubner W, Mantsch HI (1991) Orientation of specifically 13C=O labeled phosphatidylcholine multilayers from polarized attenuated total reflection FT-IR spectroscopy. Biophys J 59:1261–1272
29. Balasubramanian SA, Straubinger RM (1994) Taxol–lipid interactions: taxol-dependent effects on the physical properties of model membranes. Biochemistry 33:8941–8947

30. Severcan F, Sahin I, Kazanci N (2005) Melatonin strongly interacts with zwitterionic model membranes-evidence of from FTIT and DSC. Biochim Biophys Acta 1668:215–222
31. Papova AV, Hincha DK (2003) Intermolecular interactions in dry and rehydrated pure and mixed bilayers of phosphatidylcholine and digalactosyl disacylglycerol: a Fourier transform infrared spectroscopy study. Biophys J 85:1682–1690
32. Lewis RNAH, McElhaney RN (1998) The structure and organisation of phospholipid bilayers as revealed by infrared spectroscopy. Chem Phys Lipids 96:9–21
33. Prenner EJ, Kiricsi M, Jelokhani-Niaraki M, Lewis RN, Hodges RS, McElhaney RN (2005) Structure–activity relationships of diastereomeric lysine ring size analogs of the antimicrobial peptide gramicidin S: mechanism of action and discrimination between bacterial and animal cell membranes. J Biol Chem 280:2002–2011
34. Boulanger Y, Schreier S, Smith IC (1981) Molecular details of anesthetic–lipid interaction as seen by deuterium and phosphorus-31 nuclear magnetic resonance. Biochemistry 20:6824–6830
35. Gjerde AU, Holmsen H, Nerdal W (2004) Chlorpromazine interaction with phosphatidylserines: a ^{13}C and ^{31}P solid-state NMR study. Biochim Biophys Acta 1682:28–37
36. Gao Z, Lukyanov AN, Chakilam AR, Torchillin VP (2003) PEG-PE/phosphatidylcholine mixed immunomicelles specifically deliver encapsulated taxol to tumor cells of different origin and promote their efficient killing. J Drug Target 11:87–92
37. Deo N, Somasundaran T, Somasundaran P (2004) Solution properties of amitriptyline and its partitioning into lipid bilayers. Colloids Surf B Biointerfaces 34:155–159
38. Yokouchi Y, Tsunoda T, Imura T, Yamauchi H, Yokoyama S, Sakai H, Abe M (2001) Effect of adsorption of bovine serum albumin on liposomal membrane characteristics. Colloids Surf B Biointerfaces 20:95–103
39. Schanck A, Deleers M (1993) ^{31}P NMR study of the parameters influencing the formation of non-bilayer phases in model membranes. Biochem Biophys Res Commun 195:654–658
40. Bernsdorff C, Reszka R, Winter R (1999) Interaction of the anticancer agent Taxol (paclitaxel) with phospholipid bilayers. J Biomed Mater Res 46:141–149

Lipids (2008) 43:581–588
DOI 10.1007/s11745-008-3189-y

ORIGINAL ARTICLE

2-Chlorohexadecanal and 2-Chlorohexadecanoic Acid Induce COX-2 Expression in Human Coronary Artery Endothelial Cells

Maria C. Messner · Carolyn J. Albert ·
David A. Ford

Received: 11 March 2008 / Accepted: 3 May 2008 / Published online: 21 May 2008
© AOCS 2008

Abstract 2-Chlorohexadecanal (2-ClHDA), a 16-carbon chain chlorinated fatty aldehyde that is produced by reactive chlorinating species attack of plasmalogens, is elevated in atherosclerotic plaques, infarcted myocardium, and activated leukocytes. We tested the hypothesis that 2-ClHDA and its metabolites, 2-chlorohexadecanoic acid (2-ClHA) and 2-chlorohexadecanol (2-ClHOH), induce COX-2 expression in human coronary artery endothelial cells (HCAEC). COX-2 protein expression increased in response to 2-ClHDA treatments at 8 and 20 h. 2-ClHA also increased COX-2 expression following an 8 h treatment. Quantitative PCR showed that 2-ClHDA treatment increased COX-2 mRNA over 8 h, while 2-ClHA treatment led to a modest increase by 1 h and those levels remained constant over 8 h. 2-ClHDA led to a significant increase in 6-keto-PGF$_{1\alpha}$ release (a measure of PGI$_2$ release) by HCAEC. These data suggest that 2-ClHDA and its metabolite 2-ClHA, which are produced during leukocyte activation, may alter vascular endothelial cell function by upregulation of COX-2 expression.

Keywords Myeloperoxidase · Reactive chlorinating species (RCS) · Fatty acid · Fatty alcohol · Plasmalogen · Prostacyclin

---

M. C. Messner · C. J. Albert · D. A. Ford
Department of Biochemistry and Molecular Biology,
St. Louis University Health Sciences Center,
St. Louis, MO 63104, USA

D. A. Ford (✉)
Department of Biochemistry and Molecular Biology,
St. Louis University School of Medicine,
1100 South Grand Boulevard, St. Louis, MO 63104, USA
e-mail: fordda@slu.edu

Abbreviations

RCS	Reactive chlorinating species
2-ClHDA	2-Chlorohexadecanal
2-ClHA	2-Chlorohexadecanoic acid
2-ClHOH	2-Chlorohexadecanol
HDA	Hexadecanal
COX-2	Cyclooxygenase-2
NF-κb	Nuclear factor kappa B
TNF-α	Tumor necrosis factor-alpha
HCAEC	Human coronary artery endothelial cells
MPO	Myeloperoxidase

Introduction

The inducible form of cyclooxygenase (COX-2) is highly expressed in atherosclerotic lesions and nearly absent in normal arterial tissue [1]. Both COX-1, which is constitutively active, and COX-2 catalyze the production of prostaglandin H$_2$ (PGH$_2$) from phospholipid-derived arachidonic acid [2, 3]. PGH$_2$ is subsequently converted by cell-specific isomerases into several structurally different eicosanoids. Activation of the coronary endothelium, leads to the production and release of PGI$_2$ [4, 5], which has vasodilatory and anti-atherogenic properties [6–8] that is partially mediated by upregulation of COX-2 [9].

Myeloperoxidase (MPO), highly expressed in atherosclerotic lesions [10], catalyzes the production of potent oxidants collectively termed reactive chlorinating species (RCS) [11]. The collateral damage caused by MPO-derived RCS to host tissue includes the formation of chlorinated tyrosine [12], cholesterol [12], and lipids [13–15]. Plasmalogens, a subclass of choline glycerophospholipids that contains a vinyl ether linkage between the *sn*-1 aliphatic chain and the glycerol backbone, are particularly abundant in the heart vasculature [16–18]. We have shown that RCS attack the vinyl ether bond of plasmenylcholine, resulting in the release of 2-ClHDA (2-chlorohexadecanal) [19], which accumulates in activated neutrophils [14], monocytes [20, 21], ischemic/reperfused myocardium [22] and atherosclerotic aorta [21]. Thus far, 2-ClHDA has been shown to reduce eNOS (endothelial nitric oxide synthase) expression in endothelial cells [23] and elicit neutrophil chemoattraction [14].

2-ClHDA is oxidized and reduced to 2-chlorohexadecanoic acid (2-ClHA) and 2-chlorohexadecanol (2-ClHOH), respectively [24]. Little is known about the signaling properties of this unique class of chlorinated lipids resulting from MPO-mediated RCS attack of plasmalogens. In this study, we examined the effect of 2-ClHDA, 2-ClHA, and 2-ClHOH to induce COX-2 expression in HCAEC. The results suggest that 2-ClHDA and 2-ClHA, but not 2-ClHOH, induce COX-2 protein expression and PGI_2 release by increasing COX-2 gene expression.

Experimental Procedures

Lipid Preparation

2-ClHDA was prepared by treating 1-O-hexadec-1′-enyl-glycero-3-phosphocholine (100 mg) with freshly prepared hypochlorous acid (final concentration 1.5 mM) in phosphate buffer (pH 4) for 5 min at 37°C [24]. Reactions were terminated by lipid extraction and the chloroform layer was collected [25]. 2-ClHDA was purified by HPLC utilizing a Dynamax Si column (21.4 mm × 250 mm; 8 μm), and gradient elution over 3 h with hexane as the initial mobile phase and chloroform as the final mobile phase at a flow rate of 8 ml/min. Purity of synthetic 2-ClHDA was confirmed by GC-MS, and quantified by acid methanolysis and GC-FID (HP 5890A) using arachidic acid as an internal standard. 2-ClHA was synthesized and purified as previously described [24]. To synthesize 2-ClHOH, 2-ClHDA was resuspended in 2 ml radical free ethyl ether and 0.5 ml benzene and treated with Red Al^{TM} reagent for 30 min at 37°C [24]. 2-ClHOH was purified by TLC (petroleum ether/ethyl ether/acetic acid (70/30/1 v/v/v) ($R_F = 0.41$).

Cell Culture

HCAEC (Cell Applications, San Diego, CA) were seeded onto 60-mm^2 or 35-mm^2 6-well polystyrene dishes and cultured in EGM-2-MV growth medium (Lonza, Walkersville, MD) at 37°C in a 5% CO_2 and 95% air atmosphere. Experiments were performed on confluent monolayers ($\sim 1 \times 10^6$ cells/60-mm^2 dish) between passages 5 and 9. HCAEC growth medium was replaced with growth medium containing 2% FBS for 4–6 h prior to experiments. Lipids were dried under a stream of nitrogen and reconstituted in ethanol to inject into culture medium at a final ethanol concentration of 0.1%. Lipids were mixed with basal medium and added to each dish by pipette for a final concentration of 50 μM. TNF-α was mixed with basal medium containing 0.1% ethanol and added to dishes for a final concentration of 50 ng/ml. Control conditions included incubations with basal medium containing a final ethanol concentration of 0.1%.

Western Blotting

Following each experimental condition, the medium was aspirated from the dishes and HCAEC monolayers were rinsed with PBS. Cells were scraped in SDS sample buffer, boiled, and protein was subjected to SDS-PAGE utilizing 10–12.5% polyacrylamide gels followed by transfer of proteins to polyvinylidene difluoride (PVDF)-plus membranes (GE Osmonics Inc., Trevose, PA) for Western blot analysis. Blots were probed with a monoclonal anti-COX-2 (1:1,000) (Zymed, San Francisco, CA) and an HRP-conjugated secondary antibody (1:7,000) (BioRad, Hercules, CA). Blots were stripped using 0.1 M glycine (pH 2.5) and, reprobed with a monoclonal anti-IκB (1:2,500) (BD Transduction Laboratories, San Jose, CA). Blots were stripped again and probed with a polyclonal β-Actin (1:5,000) (Abcam, Cambridge, MA) and probed with an HRP-conjugated goat-anti-rabbit (1:7,000) (Sigma, St. Louis, MO). Immunoreactive bands were visualized by exposure to autoradiographic film following incubation with enhanced chemiluminescence reagent (GE Healthcare, Piscataway, NJ). Densitometric analyses of immunoreactive bands were performed using ImageQuant software.

RNA Extraction, Reverse Transcription, and Quantitative PCR

RNA was extracted and purified using an RNeasy Mini Kit (Qiagen, Valencia, CA) by following the manufacturer's instructions. Less than half of the mRNA elute was incubated with 0.5 μg Oligo $(dT)_{12-18}$ primer (Invitrogen, Carlsbad, CA) at 70°C for 10 min to yield cDNA. RNA and reaction mixture (200 units M-MLV H^- reverse transcriptase (Promega, Madison, WI), buffer, dNTPs (Invitrogen, Carlsbad, CA), and 0.1 M DTT) were incubated at 42°C for 50 min and terminated at 70°C for 15 min. Reaction mix was incubated with 1U RNase H (Invitrogen, Carlsbad, CA) at 37°C for 20 min. Real-time PCR of the cDNA library was performed by mixing 1 μl cDNA, primers for COX-2 or GAPDH-1, dNTPs, TAQ polymerase, buffer, and SYBR Green fluorescence probe followed by quantitative RT-PCR (BioRad OpticonII) using the following parameters: 40 cycles of 95°C for 1 min, 56°C for 0.5 min, 72°C for 0.5 min, 87°C for 3 s. A melt curve from 80–96°C was performed. The COX-2 primer pairs (SuperArray, Frederick, MD) and the primer sequences (5′–3′) for GAPDH-1 are GCATCTTC-TTT TGCGTCGCC (forward), and GTCATTGATGGCAA-CAATATCC (reverse) were used. Data were analyzed using BioRad Opticon II software and COX-2 levels were normalized to GAPDH-1 levels for each sample. Fidelity of the PCR reaction was determined by melting temperature analysis and visualization of products on a 2% agarose gel.

6-keto-PGF$_{1\alpha}$ Quantification

Following experimental conditions, the medium from each 60-mm^2 HCAEC monolayer dish was removed and centrifuged. The internal standard d$_4$-6-keto-PGF$_{1\alpha}$ at 10 pg was added to each sample followed by acidification with HCl to 2.5 pH for 30 min. C-18 SPE columns (Supelco, Bellefonte, PA) were washed with acetonitrile and equilibrated with water prior to addition of samples. Following sample loading, columns were sequentially washed with acidic water (2.5 pH) and water/ethanol (85:15 v/v) prior to elution of prostaglandins with ethyl acetate. Samples were dried under a stream of nitrogen and derivatized by treatment with O-methoxamine and PFB-Br followed by BSTFA as described previously [26]. Samples were reconstituted in ethyl acetate for GC-MS analysis. PGI$_2$ was measured as its stable hydrolytic product 6-keto-PGF$_{1\alpha}$. Samples were analyzed by selected ion monitoring on a Hewlett Packard 6890 GC coupled to a Hewlett Packard 5973 MS as described previously [27].

Cell Death

Following experimental conditions, cell medium was removed from 60-mm^2 dishes, centrifuged, and assayed for general cell death using a lactate dehydrogenase release assay (Sigma, St. Louis, MO) following the manufacturer's instructions.

Data Analysis

Statistical analyses of data were performed by one-way ANOVA followed by a Dunnett post hoc test, as appropriate. $P \leq 0.05$ was considered statistically significant.

Results

Effects of TNF-α, 2-ClHDA and 2-ClHA on COX-2 Protein Expression

COX-2 expression in vascular endothelial cells is induced in response to several cytokines such as TNF-α and IL-1β [9, 28, 29] suggesting that COX-2 may be involved in the pathophysiology of inflammation [30]. Induction of COX-2 in the endothelium leads to the production and release of PGI$_2$ [31], which has vasodilatory and anti-atherogenic properties. A time course analysis of TNF-α-treated HCAEC monolayers shows an increase in COX-2 protein expression by 8 h, reaching maximal expression at 20 h (Figs. 1, 2a). In comparison to TNF-α at 20 h, 50 μM 2-ClHDA induced COX-2 expression to a lesser degree (Figs. 1, 2a). 2-ClHA increased COX-2 expression within 8 h, and returned to baseline by 20 h. 2-ClHDA, however, induced COX-2 expression above control at both 8 and 20 h (Figs. 1, 2a). Neither 2-ClHOH nor hexadecanal (HDA), the non-chlorinated aldehyde, induced COX-2 protein expression. Parallel experiments were performed showing that these chlorinated lipids did not cause significant cell death as determined by a lack of LDH release (Fig. 2b). Normal LDH concentrations fall between 100–350 U/ml, while elevated LDH concentrations occur above 500 U/ml. Treatment of 100 μM 4-hydroxy-2-nonenal (HNE), known to induce cell death, was used as a positive control.

Effects of TNF-α, 2-ClHDA and 2-ClHA on COX-2 Gene Expression

Quantitative PCR was performed to explore the effects of HCAEC monolayers treated with TNF-α, 2-ClHDA, 2-ClHA, or vehicle on COX-2 gene expression. Treatment with TNF-α led to a rapid 2.5-fold increase in mRNA expression by 1 h and levels returned to control levels by 2 h (Fig. 3). COX-2 mRNA expression following 2-ClHDA treatment increased by ~3 fold by 8 h. HCAEC treatment with 2-ClHA induced a 2-fold increase in COX-2 mRNA by 2 h and remained elevated by 8 h. In all treatment conditions, COX-2 mRNA levels returned to near control levels by 18 h (Fig. 3).

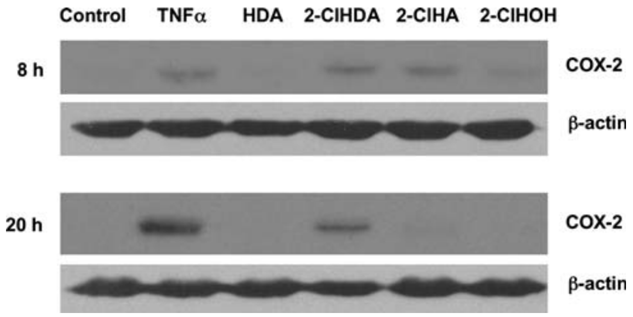

Fig. 1 2-Chlorohexadecanal and 2-chlorohexadecanoic acid induce COX-2 protein expression in HCAEC. Cell lysates were prepared from HCAEC treated with ethanol vehicle, 50 ng/ml TNF-α, or 50μM of hexadecanal (HDA), 2-chlorohexadecanal (2-ClHDA), 2-chlorohexadecanoic acid (2-ClHA), or 2-chlorohexadecanol (2-ClHOH) for 8 or 20 h as indicated. Samples were subjected to SDS-PAGE and western blotting for COX-2 expression

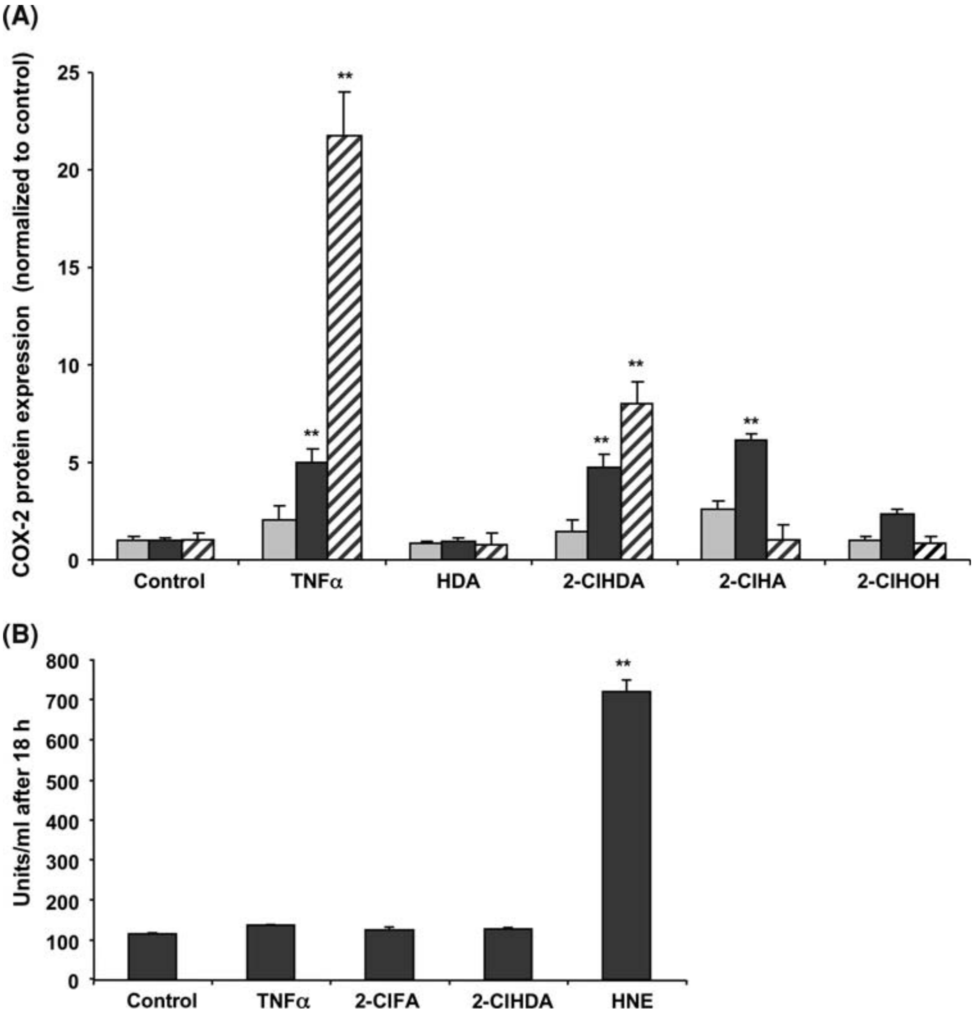

Fig. 2 Time course of 2-chlorohexadecanal and 2-chlorohexadecanoic acid elicited COX-2 protein expression in HCAEC. Cell lysates were prepared from HCAEC treated with ethanol vehicle, 50 ng/ml TNF-α, or 50μM of hexadecanal (HDA), 2-chlorohexadecanal (2-ClHDA), 2-chlorohexadecanoic acid (2-ClHA), or 2-chlorohexadecanol (2-ClHOH) for 2 h (*light grey bars*), 8 h (*black bars*), and 20 h (*striped bars*). Samples were subjected to SDS-PAGE and western blotting for COX-2 expression and analyzed by densitometry of immunoreactive bands (**a**). Following COX-2 analysis, blots were subsequently stripped and then subjected to western blotting for β-actin, which was used to normalize each experimental analysis of COX-2 expression. Cell medium was assayed for general cell death using a lactate dehydrogenase release assay (**b**). Values (mean ± SEM) are expressed as fold increase over control-treated cells for three independent determinations, ** represents $P < 0.01$

2-ClHDA and 2-ClHA Elicit PGI_2 Release

The predominant COX-derived arachidonic acid product in coronary endothelial cells is PGI_2 [4, 5, 7]. 6-keto-$PGF_{1\alpha}$, the stable hydrolytic product of PGI_2, was measured in cultured medium following solid phase extraction, derivatization, and GC-MS analysis [26, 27]. TNF-α treatment led to nearly a 2-fold increase in 6-keto-$PGF_{1\alpha}$, while 2-ClHDA, but not 2-ClHA at 20 h, led to lower but significant increases in 6-keto-$PGF_{1\alpha}$, (Fig. 4), analogous to the pattern seen in protein expression (Fig. 2a).

NF-κB Signaling Pathways by TNF-α, 2-ClHDA

NF-κB is normally sequestered in the cytosol by IκB under non-inflammatory conditions. Upon stimulation of the NF-κB pathway, IκB is targeted for degradation and NF-κB is free to translocate to the nucleus where it binds to NF-κB DNA sites in the promoter of various genes. It has been shown in several cell types that treatment with TNF-α leads to NF-κB binding to the COX-2 promoter and reporter gene expression [31–33]. In HCAEC, TNF-α and 2-ClHDA led to significant IκB protein disappearance at 20 h, while 2-ClHA or other tested lipids did not to lead to a significant decrease in IκB protein levels (Fig. 5a, b).

Discussion

Oxidative attack of plasmalogens by RCS leads to the production of reactive lipid aldehydes, such as 2-ClHDA [19]. Little is known about the possible signaling roles these naturally occurring halogenated lipids play. Marsche et al. [23] discovered that HDL treated with hypochlorous acid, a component of RCS, led to a reduction in eNOS expression in endothelial cells and, upon further investigation, found that 2-ClHDA was responsible for the reduction in eNOS. An abundant non-chlorinated lipid aldehyde, HNE, has been shown to induce COX-2 expression in RAW264.7 macrophages [34, 35] and in human osteoarthritic chondrocytes [35]. In the present study, we show that TNF-α, 2-ClHDA, and 2-ClHA, but not 2-ClHOH, induce an increase in COX-2

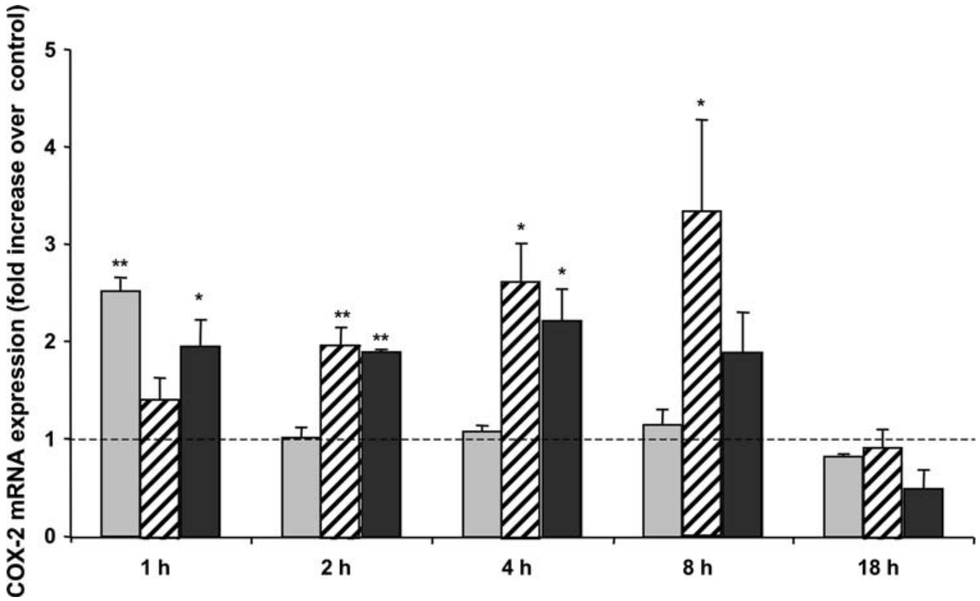

Fig. 3 2-Chlorohexadecanal and 2-chlorohexadecanoic acid induce COX-2 mRNA expression. HCAEC were treated with either ethanol vehicle, 50 ng/ml TNF-α (*light gray bars*), or 50 μM 2-chlorohexadecanal (2-ClHDA) (*striped bars*) or 50 μM 2-chlorohexadecanoic acid (2-ClHA) (*black bars*) for the times indicated. Cells were scraped in lysis buffer, cDNA was prepared from purified mRNA, and samples were analyzed by quantitative PCR using primers for COX-2. Values (mean ± SEM) were normalized to GAPDH and expressed as fold increase over control-treated cells at each time point for three independent determinations. SEM of control values was less than 5% of the mean at all time points and there was no significant increase in control values over time, * and ** represent $P < 0.05$ and $P < 0.01$, respectively

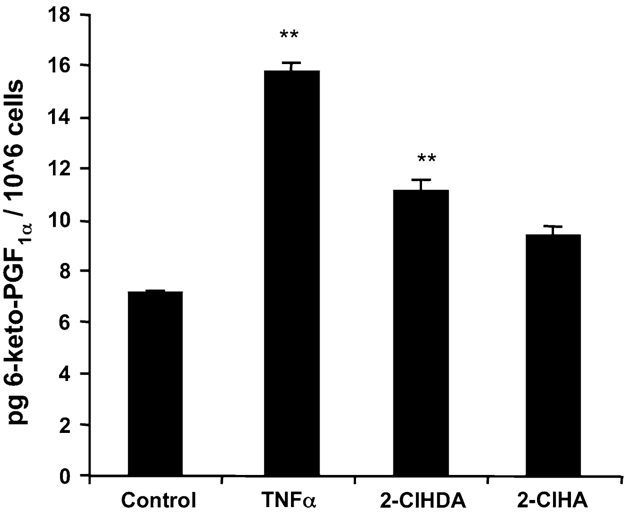

Fig. 4 2-Chlorohexadecanal and 2-chlorohexadecanoic acid lead to PGI_2 release at 20 h. HCAEC were treated with ethanol vehicle, 50 ng/ml TNFα, 50 μM 2-chlorohexadecanal (2-ClHDA), or 50 μM 2-chlorohexadecanoic acid (2-ClHA) for 20 h ($n = 4$ for each condition). Culture medium was removed and eicosanoids were purified by reverse SPE columns, converted to PFB esters, silylated using BSTFA, and analyzed by GC-MS, ** represents $P < 0.01$

protein expression in human coronary artery endothelial cells. 2-ClHDA is produced by the production of RCS from phagocyte-derived myeloperoxidase [19]. 2-ClHDA concentrations range from 25–100 μM in human neutrophils [14]. The concentration of 2-ClHDA used in these studies is within the range that is physiologically produced from activated leukocytes. Although 2-ClHDA has been shown to have pro-atherogenic properties by decreasing eNOS [23] and increasing neutrophil chemotaxis [14], we show that 2-ClHDA increases COX-2 and PGI_2 levels (as determined by increases in 6-keto-$PGF_{1\alpha}$ levels). Interestingly comparisons of the time course of 2-ClHDA and 2-ClHA elicited COX-2 expression show that 2-ClHDA has a sustained impact on COX-2 expression. This may reflect disparate half-lives of these chlorinated lipids. In fact, 2-ClHDA is the precursor of 2-ClHA [24]. Thus, over time while 2-ClHDA levels decrease, the sustained COX-2 expression may be elicited by the product of 2-ClHDA metabolism, 2-ClHA.

The increase in COX-2 protein expression from TNF-α, 2-ClHDA, and 2-ClHA appears to occur by increased transcription of the COX-2 gene demonstrated by the results from quantitative PCR. The COX-2 gene contains 17 copies of the AUUUA motif in its 3′-UTR and can be regulated post-transcriptionally by elements that bind the AU-rich regions in its messenger RNA [36, 37]. Previous studies have indicated that shear stress stabilizes COX-2 mRNA levels in HUVECs [37]. In this study, although we have shown that 2-ClHDA and 2-ClHA induce gene expression, we cannot rule out that 2-ClHDA and/or 2-ClHA also lead to a stabilization of COX-2 mRNA.

The human COX-2 promoter includes the NF-κB, cyclic AMP response element (CRE), activator protein-2 (AP2),

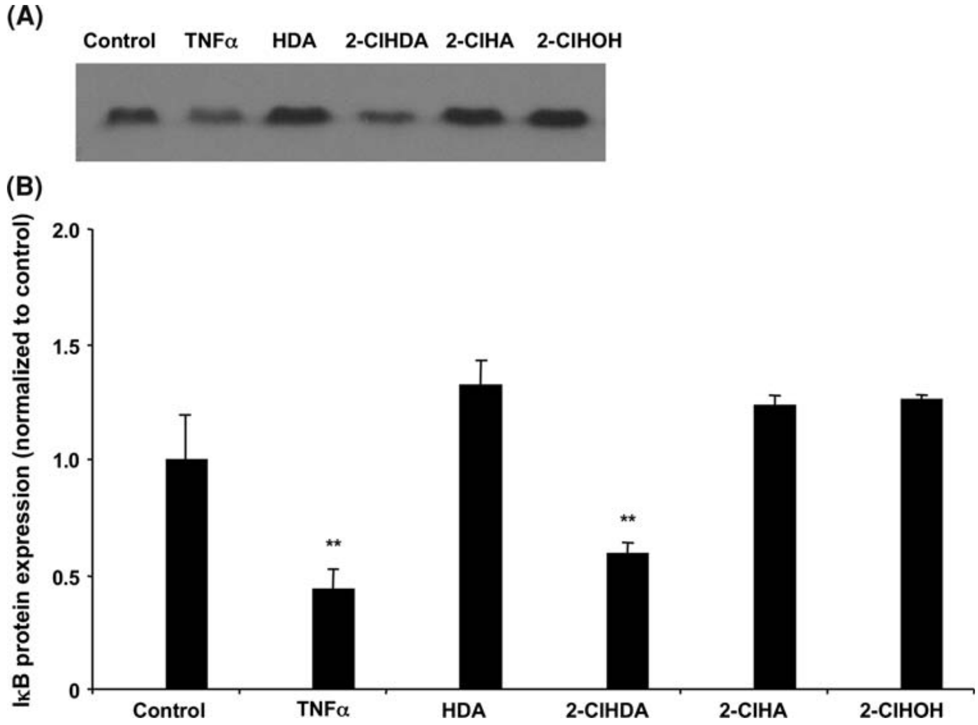

Fig. 5 2-Chlorohexadecanal decreases IκB protein expression. Cell lysates were prepared from HCAEC treated with ethanol vehicle, 50 ng/ml TNF-α, or 50 μM hexadecanal (HDA), 2-chlorohexadecanal (2-ClHDA), 2-chlorohexadecanoic acid (2-ClHA), 2-chlorohexadecanol (2-ClHOH) for 20 h. Samples were subjected to SDS-PAGE and western blotting for IκB expression (**a**) and analyzed by densitometry of immunoreactive bands (**b**). Values (mean ± SEM) are expressed as fold increase over control treated cell at each time point, ** is $P < 0.01$

signal transducers and activators of transcription (STAT3), SP1 and CCAAT/enhancer-binding protein (C/EBPb) [38–44]. The NF-κB pathway is considered to be a general inflammatory response pathway that can lead to gene transcription of various chemokines, adhesion molecules, and other pro-inflammatory molecules. In the present study we have shown that 2-chlorohexadecanal decreases IκB protein levels in HCAEC, suggesting that 2-ClHDA is signaling in part through the NF-κB pathway. Additionally it should be appreciated that COX-2 mRNA is elevated prior to IκB degradation in response to 2-chlorohexadecanal suggesting that additional pathways may play an important role in COX-2 expression in response to 2-chlorohexadecanal.

The release of 2-chloro fatty aldehydes from plasmalogens followed by its metabolism to 2-chloro fatty acids and 2-chloro fatty alcohols collectively suggest that a chlorinated lipidome is produced as a result of RCS attack of plasmalogens. It is now essential to determine the physiological role of these novel chlorinated lipids and their potential role in inflammation. The results herein demonstrate that 2-ClHA induces COX-2 expression and prostacyclin production in human coronary artery endothelial cells. Furthermore, the precursor of 2-ClHA, 2-ClHDA, also elicits COX-2 expression and prostacyclin production. It can be envisioned that the effect of these same chlorinated lipids on cells such as monocytes and neutrophils, which contain COX-2 associated isomerases that lead to pro-inflammatory eicosanoids, may have important roles in inflammation.

References

1. Schonbeck U, Sukhova GK, Graber P, Coulter S, Libby P (1999) Augmented expression of cyclooxygenase-2 in human atherosclerotic lesions. Am J Pathol 155:1281–1291
2. Masferrer JL, Seibert K, Zweifel B, Needleman P (1992) Endogenous glucocorticoids regulate an inducible cyclooxygenase enzyme. Proc Natl Acad Sci USA 89:3917–3921
3. Kraemer SA, Meade EA, DeWitt DL (1992) Prostaglandin endoperoxide synthase gene structure: identification of the transcriptional start site and 5′-flanking regulatory sequences. Arch Biochem Biophys 293:391–400
4. Whittaker N, Bunting S, Salmon J, Moncada S, Vane JR, Johnson RA, Morton DR, Kinner JH, Gorman RR, McGuire JC, Sun FF (1976) The chemical structure of prostaglandin X (prostacyclin). Prostaglandins 12:915–928
5. Moncada S, Gryglewski R, Bunting S, Vane JR (1976) An enzyme isolated from arteries transforms prostaglandin endoperoxides to an unstable substance that inhibits platelet aggregation. Nature 263:663–665
6. Dusting GJ, Moncada S, Vane JR (1977) Prostacyclin (PGX) is the endogenous metabolite responsible for relaxation of coronary arteries induced by arachindonic acid. Prostaglandins 13:3–15
7. Weksler BB, Marcus AJ, Jaffe EA (1977) Synthesis of prostaglandin I2 (prostacyclin) by cultured human and bovine endothelial cells. Proc Natl Acad Sci USA 74:3922–3926
8. Willems C, van Aken WG (1979) Production of prostacyclin by vascular endothelial cells. Haemostasis 8:266–273
9. Jones DA, Carlton DP, McIntyre TM, Zimmerman GA, Prescott SM (1993) Molecular cloning of human prostaglandin endoperoxide synthase type II and demonstration of expression in response to cytokines. J Biol Chem 268:9049–9054
10. Daugherty A, Dunn JL, Rateri DL, Heinecke JW (1994) Myeloperoxidase, a catalyst for lipoprotein oxidation, is expressed in human atherosclerotic lesions. J Clin Invest 94:437–444
11. Harrison JE, Schultz J (1976) Studies on the chlorinating activity of myeloperoxidase. J Biol Chem 251:1371–1374

12. Hazen SL, Hsu FF, Duffin K, Heinecke JW (1996) Molecular chlorine generated by the myeloperoxidase-hydrogen peroxide-chloride system of phagocytes converts low density lipoprotein cholesterol into a family of chlorinated sterols. J Biol Chem 271:23080–23088
13. Winterbourn CC, van den Berg JJ, Roitman E, Kuypers FA (1992) Chlorohydrin formation from unsaturated fatty acids reacted with hypochlorous acid. Arch Biochem Biophys 296:547–555
14. Thukkani AK, Hsu FF, Crowley JR, Wysolmerski RB, Albert CJ, Ford DA (2002) Reactive chlorinating species produced during neutrophil activation target tissue plasmalogens: production of the chemoattractant, 2-chlorohexadecanal. J Biol Chem 277:3842–3849
15. Messner MC, Albert CJ, Hsu FF, Ford DA (2006) Selective plasmenylcholine oxidation by hypochlorous acid: formation of lysophosphatidylcholine chlorohydrins. Chem Phys Lipids 144:34–44
16. Gross RW (1984) High plasmalogen and arachidonic acid content of canine myocardial sarcolemma: a fast atom bombardment mass spectroscopic and gas chromatography-mass spectroscopic characterization. Biochemistry 23:158–165
17. Han X, Gross RW (1994) Electrospray ionization mass spectroscopic analysis of human erythrocyte plasma membrane phospholipids. Proc Natl Acad Sci USA 91:10635–10639
18. Post JA, Verkleij AJ, Roelofsen B, Op de Kamp JA (1988) Plasmalogen content and distribution in the sarcolemma of cultured neonatal rat myocytes. FEBS Lett 240:78–82
19. Albert CJ, Crowley JR, Hsu FF, Thukkani AK, Ford DA (2001) Reactive chlorinating species produced by myeloperoxidase target the vinyl ether bond of plasmalogens: identification of 2-chlorohexadecanal. J Biol Chem 276:23733–23741
20. Thukkani AK, Albert CJ, Wildsmith KR, Messner MC, Martinson BD, Hsu FF, Ford DA (2003) Myeloperoxidase-derived reactive chlorinating species from human monocytes target plasmalogens in low density lipoprotein. J Biol Chem 278:36365–36372
21. Thukkani AK, McHowat J, Hsu FF, Brennan ML, Hazen SL, Ford DA (2003) Identification of alpha-chloro fatty aldehydes and unsaturated lysophosphatidylcholine molecular species in human atherosclerotic lesions. Circulation 108:3128–3133
22. Thukkani AK, Martinson BD, Albert CJ, Vogler GA, Ford DA (2005) Neutrophil-mediated accumulation of 2-ClHDA during myocardial infarction: 2-ClHDA-mediated myocardial injury. Am J Physiol Heart Circ Physiol 288:H2955–H2964
23. Marsche G, Heller R, Fauler G, Kovacevic A, Nuszkowski A, Graier W, Sattler W, Malle E (2004) 2-chlorohexadecanal derived from hypochlorite-modified high-density lipoprotein-associated plasmalogen is a natural inhibitor of endothelial nitric oxide biosynthesis. Arterioscler Thromb Vasc Biol 24:2302–2306
24. Wildsmith KR, Albert CJ, Anbukumar DS, Ford DA (2006) Metabolism of myeloperoxidase-derived 2-chlorohexadecanal. J Biol Chem 281:16849–16860
25. Bligh EG, Dyer WJ (1959) A rapid method of total lipid extraction and purification. Can J Biochem Physiol 37:911–917
26. Liu MC, Bleecker ER, Proud D, McLemore TL, Hubbard WC (1988) Profiling of bisenoic prostaglandins and thromboxane B2 in bronchoalveolar fluid from the lower respiratory tract of human subjects by combined capillary gas chromatography-mass spectrometry. Prostaglandins 35:67–79
27. Schweer H, Kammer J, Seyberth HW (1985) Simultaneous determination of prostanoids in plasma by gas chromatography-negative-ion chemical-ionization mass spectrometry. J Chromatogr 338:273–280
28. Eligini S, Stella Barbieri S, Cavalca V, Camera M, Brambilla M, De Franceschi M, Tremoli E, Colli S (2005) Diversity and similarity in signaling events leading to rapid Cox-2 induction by tumor necrosis factor-alpha and phorbol ester in human endothelial cells. Cardiovasc Res 65:683–693
29. Said FA, Werts C, Elalamy I, Couetil JP, Jacquemin C, Hatmi M (2002) TNF-alpha, inefficient by itself, potentiates IL-1beta-induced PGHS-2 expression in human pulmonary microvascular endothelial cells: requirement of NF-kappaB and p38 MAPK pathways. Br J Pharmacol 136:1005–1014
30. Wu KK (2005) Control of cyclooxygenase-2 transcriptional activation by pro-inflammatory mediators. Prostaglandins Leukot Essent Fatty Acids 72:89–93
31. Syeda F, Grosjean J, Houliston RA, Keogh RJ, Carter TD, Paleolog E, Wheeler-Jones CP (2006) Cyclooxygenase-2 induction and prostacyclin release by protease-activated receptors in endothelial cells require cooperation between mitogen-activated protein kinase and NF-kappaB pathways. J Biol Chem 281:11792–11804
32. Chen CC (2006) Signal transduction pathways of inflammatory gene expressions and therapeutic implications. Curr Pharm Des 12:3497–3508
33. Duque J, Diaz-Munoz MD, Fresno M, Iniguez MA (2006) Up-regulation of cyclooxygenase-2 by interleukin-1beta in colon carcinoma cells. Cell Signal 18:1262–1269
34. Kumagai T, Matsukawa N, Kaneko Y, Kusumi Y, Mitsumata M, Uchida K (2004) A lipid peroxidation-derived inflammatory mediator: identification of 4-hydroxy-2-nonenal as a potential inducer of cyclooxygenase-2 in macrophages. J Biol Chem 279:48389–48396
35. Vaillancourt F, Morquette B, Shi Q, Fahmi H, Lavigne P, Di Battista JA, Fernandes JC, Benderdour M (2007) Differential regulation of cyclooxygenase-2 and inducible nitric oxide synthase by 4-hydroxynonenal in human osteoarthritic chondrocytes through ATF-2/CREB-1 transactivation and concomitant inhibition of NF-kappaB signaling cascade. J Cell Biochem 100:1217–1231
36. Dixon DA, Kaplan CD, McIntyre TM, Zimmerman GA, Prescott SM (2000) Post-transcriptional control of cyclooxygenase-2 gene expression. The role of the 3′-untranslated region. J Biol Chem 275:11750–11757
37. Inoue H, Taba Y, Miwa Y, Yokota C, Miyagi M, Sasaguri T (2002) Transcriptional and posttranscriptional regulation of cyclooxygenase-2 expression by fluid shear stress in vascular endothelial cells. Arterioscler Thromb Vasc Biol 22:1415–1420
38. Allport VC, Slater DM, Newton R, Bennett PR (2000) NF-kappaB and AP-1 are required for cyclo-oxygenase 2 gene expression in amnion epithelial cell line (WISH). Mol Hum Reprod 6:561–565
39. Billack B, Heck DE, Mariano TM, Gardner CR, Sur R, Laskin DL, Laskin JD (2002) Induction of cyclooxygenase-2 by heat shock protein 60 in macrophages and endothelial cells. Am J Physiol Cell Physiol 283:C1267–C1277
40. Iniguez MA, Martinez-Martinez S, Punzon C, Redondo JM, Fresno M (2000) An essential role of the nuclear factor of activated T cells in the regulation of the expression of the cyclooxygenase-2 gene in human T lymphocytes. J Biol Chem 275:23627–23635
41. Inoue H, Yokoyama C, Hara S, Tone Y, Tanabe T (1995) Transcriptional regulation of human prostaglandin-endoperoxide synthase-2 gene by lipopolysaccharide and phorbol ester in vascular endothelial cells. Involvement of both nuclear factor for interleukin-6 expression site and cAMP response element. J Biol Chem 270:24965–24971
42. Kirtikara K, Raghow R, Laulederkind SJ, Goorha S, Kanekura T, Ballou LR (2000) Transcriptional regulation of cyclooxygenase-2 in the human microvascular endothelial cell line, HMEC-1: control by the combinatorial actions of AP2, NF-IL-6 and CRE elements. Mol Cell Biochem 203:41–51

43. Kosaka T, Miyata A, Ihara H, Hara S, Sugimoto T, Takeda O, Takahashi E, Tanabe T (1994) Characterization of the human gene (PTGS2) encoding prostaglandin-endoperoxide synthase 2. Eur J Biochem 221:889–897

44. Xu Q, Ji YS, Schmedtje JF Jr. (2000) Sp1 increases expression of cyclooxygenase-2 in hypoxic vascular endothelium. Implications for the mechanisms of aortic aneurysm and heart failure. J Biol Chem 275:24583–24589

Lipids (2008) 43:589–597
DOI 10.1007/s11745-008-3170-9

ORIGINAL ARTICLE

Hydroxy Radical, Hexanal, and Decadienal Generation by Autocatalysts in Autoxidation of Linoleate Alone and with Eleostearate

Makio Morita · Masako Tokita

Received: 25 January 2008 / Accepted: 27 February 2008 / Published online: 21 May 2008
© AOCS 2008

Abstract The formation of hydroxy radicals, hexanal, and 2,4-decadienal was demonstrated from the autocatalytic dimer peroxide which had been reported by us in autoxidizing linoleate (Morita and Tokita in Lipids 41:91–95, 2006). Then, autoxidizing linoleate containing eleostearate was investigated for new autocatalytic substances. The substances obtained were identified as peroxide-linked polymers consisting of both linoleate- and eleostearate-origin units with one hydroperoxy group, and also revealed activity of hydroxy-radical generation. The background of this study is as follows: the above paper reported this autocatalytic dimer peroxide as one of the real radical generators in linoleate autoxidation; this is a peroxide-linked dimer consisting of two linoleate moieties with two hydroperoxy groups, and was much more important than the main-product hydroperoxide in autocatalytic radical supply; its proposed decomposition mechanism has suggested the generation of hydroxy radicals, hexanal, and 2,4-decadienal; on the other hand, analogy to the formation mechanism of this dimer peroxide has predicted the formation of similar polymeric products from conjugated polyene components in lipids. In this study, these two predictions were successfully verified and a discussion is presented in connection with them.

Keywords Autocatalyst · Conjugated fatty acid · 2,4-Decadienal · Dimer · Eleostearate · Hexanal · Hydroxy radicals · Lipid autoxidation · Linoleate · Peroxide

M. Morita
Japan Women's University, Tokyo, Japan
e-mail: makio_morita@yahoo.co.jp

M. Tokita (✉)
Yamawaki Gakuen Junior College, 4-10-36, Akasaka,
Minato-ku, Tokyo 1078371, Japan
e-mail: m.asano@yamawaki-gakuen.ac.jp

Abbreviations

AutCat	Autocatalytic dimer peroxide
MLOOH	Main-product hydroperoxide of methyl linoleate
oxML	Autoxidizing methyl linoleate
MLOH	Hydroxy derivative from the main-product hydroperoxide of methyl linoleate
DNPH	2,4-Dinitrophenylhydrazone
Azo	2,2′-Azobis(4-methoxy-2,4-dimethylvaleronitrile)
equiv	equivalent

Introduction

The main product of lipid autoxidation is a type of hydroperoxide, and it has long been believed that the main-product hydroperoxide plays the main role both in autocatalytic supply of radicals and in forming aldehydes.

However, we have entertained a minority opinion [1–3] that this hypothesis is not necessarily valid, and as concerns aldehydes, we formerly obtained a clear result that they are not produced from the main-product hydroperoxide under usual mild conditions in linoleate autoxidation [4–5]. In our previous paper [6], the lack of autocatalytic activity was also clearly showed by using a highly rigorous and sensitive detecting method when the purified main-product hydroperoxide of methyl linoleate was examined under the usual storage conditions and at body temperature; in addition, a type of substance revealing potent autocatalytic activity was found in autoxidizing methyl linoleate.

The autocatalytic substances were isomeric mixtures possessing the structure of a peroxide-linked dimer with two hydroperoxy groups as shown in Scheme 1, which had been reported by Miyashita et al. [7–8] as oxidation products of both methyl linoleate and its main-product hydroperoxide.

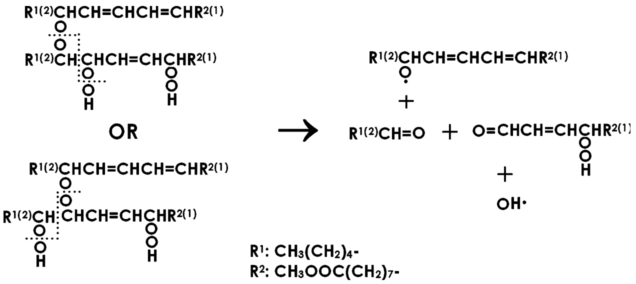

Scheme 1

We assumed [6] that the mechanism of their homolytic decomposition and radical supply is an energetically favorable concerted one as depicted also in Scheme 1. The mechanism predicted the formation of hydroxy radicals and hexanal as direct products of the homolysis, and the formation of 2,4-decadienal via the *β*-scission route from linoleate-skeleton alkoxy radicals. In the present paper, the prediction was successfully verified.

On the other hand, it was inferred that the formation mechanism of the autocatalytic substances is an addition of linoleate peroxy radicals to the conjugated diene of the main-product hydroperoxide followed by the usual addition of oxygen to the resultant dimer radicals and hydrogen abstraction from an unoxidized linoleate molecule. We predicted [6] that an analogous mechanism may result in the formation of addition products with peroxy radicals from minor components containing conjugated double bonds in lipids such as conjugated fatty acids and carotenoids. The present paper also verifies the formation of such products in autoxidizing methyl linoleate containing eleostearate, and their activity of autocatalyst and hydroxy radical generation.

Experimental Procedures

Preparation of Tung Oil Methyl Ester

Tung oil of industrial use was converted to the methyl ester by the usual transesterification with 1 M methanolic sodium methoxide at room temperature. A polar-impurity-free material was prepared by passing it through a silicic acid column with hexane. The α-eleostearate content was 83–85%.

Preparation of Autocatalytic Dimer Peroxide (AutCat)

Methyl linoleate (Tokyo Kasei Kogyo Ltd., Tokyo, Japan) containing 10^{-2} M 2,2′-azobis(4-methoxy-2,4-dimethylvaleronitrile) was allowed to stand at 20°C until the level of MLOOH reached 500–600 μmol/ml. The autoxidizing material (1 ml) was diluted to 4–5 ml with methanol and applied to a 1.35 × 120 cm Sephadex LH 20 column (Amersham Biosciences, Uppsala, Sweden) with methanol. Eluates were checked in TLC (Silicagel 60F$_{254}$, Merck, Darmstadt, Germany) with hexane/diethyl ether 2:1 by vol by detection under UV light. The elution range corresponding to the dimer was 105–115 ml. The dimer-containing eluates from three to five runs were combined and rechromatographed. The resultant sample was further chromatographed on a 1.35 × 120 cm Sephadex LH 20 column with chloroform. The eluates containing the main component group ranged from 108 to 135 ml. All the concentrated sample was then applied to a preparative HPLC on a 7.6 × 250 mm Nucleosil® 100-5 column (Agilent, Palo Alto, CA, USA) with hexane/diethyl ether, 80:20 by vol, at a flow rate of 3 ml/min, monitored at 234 nm absorbance. Although AutCat was eluted as a widely spread zone, owing to large excess loading, at retention time from 14 to 35 min, the AutCat material thus prepared was not inferior to the material reported in the previous paper [6] in purity on HPLC. The present procedure was more efficient and facile than before.

Preparation of oxML

One milliliter of methyl linoleate was spread on the bottom surface of a 300-ml beaker and was allowed to stand at 20°C until the level of MLOOH reached 500–600 μmol/ml.

Autoxidation of Linoleate Containing Tung Oil Methyl Ester and Separation of the Products

To methyl linoleate was added the methyl ester of tung oil and subjected to autoxidation at 20°C in the presence of 10^{-2} M 2,2′-azobis-(4-methoxy-2,4-dimethylvaleronitrile). Sephadex LH 20 chromatography with methanol was carried out as above. A reversed phase HPLC was carried out on a 7.6 × 250 mm Inertsil column (GL Science Inc.,Tokyo, Japan) with methanol at a flow rate of 3 ml/min, monitored at 234 nm absorbance.

Purification of MLOOH

Five microliters of oxML (600 μmol/ml) was applied to a 7.6 × 250 mm Nucleosil® 100-5 column with hexane/diethyl ether 92:8 by vol at a flow rate of 3 ml/min. The hydroperoxide was monitored at 234 nm absorbance and eluted from 9.4 to 12.5 min as a group of incompletely separated isomer peaks. The eluates were concentrated under reduced pressure below 30°C.

Analysis for Methyl α-Eleostearate

The concentration of α-eleostearate was determined by HPLC on a 4.6 × 150 mm Nucleosil® 100-5 column with hexane/diethyl ether 99.5:0.5 by vol at a flow rate of 1.5 ml/min, monitored at 270 nm absorbance.

Analysis for MLOOH

Main-product hydroperoxide of methyl linoleate was measured by HPLC on a 4.6 × 150 mm Nucleosil® 100-5 column with hexane/diethyl ether 88:12 by vol at a flow rate of 1.5 ml/min, monitored at 234 nm absorbance. It was eluted as four isomer peaks at retention time from 5.3 to 6.6 min and its concentration was calculated using an ε value of 2.7×10^{-4} as described [4].

Analysis for AutCat

AutCat was measured by HPLC on a 4.6 × 150 mm Nucleosil® 100-5 column with hexane/diethyl ether 70:30 by vol at a flow rate of 1.5 ml/min. AutCat was monitored at 234 nm absorbance, was eluted from 4.3 to 7.5 min as shown in Fig. 1, and the concentration was expressed as MLOOH equivalent using an ε value of 2.7×10^{-4}.

Analysis for Conjugated Diene

Molar quantity of conjugated diene in a product or a fraction was calculated tentatively on the assumption that the molar extinction at 234 nm was the same as that of main-product hydroperoxide of linoleate.

Autocatalytic Activity

Autocatalytic activity of samples was measured, and an expression for the activity, Azo equiv, was used according to the previous paper [6].

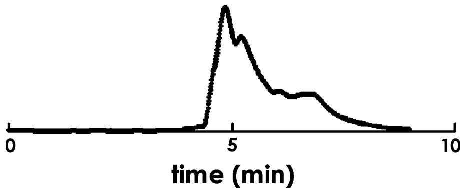

Fig. 1 Elution pattern of AutCat in HPLC. On a 4.6 × 150 mm Nucleosil®100-5 column using hexane/diethyl ether 70:30 by vol at a flow rate of 1.5 ml/min, monitored at 234 nm absorbance.

Analysis for Methyl Salicylate in the Presence of a Large Amount of Methyl Benzoate

Before analysis, the concentration of methyl benzoate was lowered below 0.5% by diluting samples with hexane. One hundred microliters of the hexane solution was applied to HPLC on a 4.6 × 150 mm Nucleosil® 100-5 column with hexane/2-methanol 99.95:0.05 by vol at a flow rate of 1.5 ml/min. The retention time of methyl salicylate was 2.8 min and its concentration was calculated from 305 nm absorbance.

Analysis for Hexanal and 2,4-Decadienal

A column (1.35 cm inner diameter) was packed with silica gel 3 cm thick (Wakogel® C-100, Wako Pure Chemical Industries, Ltd., Osaka, Japan). On top of this, a 2-cm layer of silica gel impregnated with aqueous 10% sulfuric acid solution containing 0.3% 2,4-dinitrophenylhydrazine was placed. The column was washed with hexane/diethyl ether 4:1 by vol. A hexane solution containing aldehydes was poured into the column. The column was flushed with 20 ml hexane/diethyl ether 4:1 by vol. The eluate was concentrated under reduced pressure. All the concentrate was applied to a 4.6 × 150 mm Nucleosil® 100-5 column with hexane/diethyl ether 70:30 by vol at a flow rate of 1.5 ml/min, monitored at 370 nm absorbance. A fraction (1.5–2.1 min) which could cover the elution region of both hexanal–DNPH and decadienal–DNPH was taken. The fraction was concentrated under reduced pressure and an aliquot of the concentrate was analyzed by HPLC on a 7.6 × 250 mm Inertsil column with methanol/water 90:10 by vol at a flow rate of 3 ml/min. The retention times of hexanal–DNPH and decadienal–DNPH were 6.8–7.8 and 13.0–14.5 min, respectively. The amounts of hexanal–DNPH and decadienal–DNPH were calculated from 358 to 389 nm absorbance, respectively.

Activity Forming Hydroxy Radicals and Aldehydes

AutCat, pure MLOOH, and oxML each were mixed with methyl benzoate in ratio of 0.6 μmol MLOOH (or MLOOH equivalent) to 1 μl methyl benzoate. The samples containing 2–5 μl methyl benzoate were treated at 50°C in Pyrex ampules sealed under a nitrogen atmosphere. After treatment, the contents of the ampules were diluted with hexane with a ratio of 1 μl of methyl benzoate to 0.2 ml hexane, and subjected to analysis for methyl salicylate and aldehydes.

Identification Procedures of Separated Products

Separated products from autoxidizing linoleate containing eleostearate were converted with triphenylphosphine and sodium borohydride, and by catalytic hydrogenation in a similar way to that for the autocatalytic substances reported [6].

GC–MS

The methyl salicylate formed from AutCat was identified after HPLC isolation by GC–MS (JEOL JMS600) with a DB-1MS capillary column (length, 60 m; ID, 0.25 mm; film thickness, 0.25 µm, J&W Scientific) at a flow rate of 1 ml/min from 50 to 300°C at a ramping rate of 16°C/min. GC–MS analysis of substances converted from the products of autoxidizing linoleate containing eleostearate was carried out as described [6].

Table 1 Formation of hydroxy radicals and aldehydes from autoxidation products of linoleate

Analysis item	Material tested						
	AutCat			MLOOH		oxML	
	0 h	6 h	19 h	0 h	6 h	0 h	6 h
Methyl salicylate	ND	0.58	0.32	ND	ND	ND	ND
Hexanal	0.2	5.7	9.0	0.4	0.2	0.4	0.4
Decadienal	ND	0.24	0.80	ND	ND	ND	ND
AutCat	100	52.0	9.8	–	–	–	–
MLOOH	–	–	–	100	71.1	100	102.2

Figures in Table are mol% based on the starting amount contained in each material tested

ND Not detected, – not analyzed

Results

The autocatalytic dimer peroxide (AutCat) previously reported by us [6] was examined for the activity of hydroxy radical and aldehyde formation. Methyl benzoate can scavenge hydroxy radicals to form methyl salicylate and we examined the formation of methyl salicylate. The AutCat sample after treatment at 50°C under a nitrogen atmosphere gave a peak at the position of methyl salicylate in HPLC, and GC–MS confirmed that the eluate corresponding to the peak actually contained methyl salicylate. Table 1 describes the yield of methyl salicylate from the AutCat sample after 6 or 19 h treatment at 50°C, and no detectable formation of methyl salicylate in the MLOOH and oxML samples after 6 h.

Table 1 also shows that hexanal and decadienal in the AutCat samples markedly increased after 6 and 19 h treatment at 50°C. In the MLOOH and oxML samples, each amount of hexanal at 0 h was low, and no increase after 6 h treatment was observed. Decadienal could not be detected both in the MLOOH and oxML samples.

The concentration of AutCat in the AutCat sample was decreased as treatment time advanced. In the MLOOH sample, the concentration of MLOOH decreased to some extent after 6 h treatment.

Then, autoxidizing linoleate containing eleostearate was searched for autocatalytic substances. In an autoxidizing linoleate containing 10% tung oil methyl ester, considerable amounts of products were observed by monitoring at 234 nm absorbance besides the main-product hydroperoxide of linoleate. Table 2 shows distribution of

Table 2 Autocatalytic activity of fractions from autoxidizing linoleate containing eleostearate

	Oxidation rate[a] (µmol/ml h)	Content[b] (%)	Retention time (min)	Component[c]
None	0.3			
fr.1	4.5	0.2	2.8–4.2	Azo[d]
fr.2	0.9	2.1	4.2–9.5	
fr.3	2.4	0.1	9.5–12.5	
fr.4	1.4	54.4	12.5–18.0	MLOOH
fr.5	2.8	21.7	18.0–23.0	ML[e] + MES[f]
fr.6	1.3	25.0	23.0–28.0	

The autoxidizing sample was fractionated by reversed phase HPLC on a 7.6 × 250 mm Inertsil column at a flow rate of 3 ml/min, monitored at 234 nm absorbance. After 14 min elution, the first solvent, methanol/water 85:15 by vol, was changed to methanol

[a] Autocatalytic activity was expressed as the formation rate of pentyl linoleate main-product hydroperoxide (oxidation rate) in autoxidation of pentyl linoleate in the presence of a sample to be tested for the activity [4]. Two microliters of pentyl linoleate with a sample of 0.13 µmol as conjugated diene was oxidized at 20°C for 20 h

[b] The amounts of fractions were expressed as conjugated diene, and their contents were described as % of the sum of all fractions

[c] Known components contained in fractions were shown here

[d] 2,2′-Azobis-(4-methoxy-2,4-dimethylvaleronitrile)

[e] Methyl linoleate

[f] Methyl eleostearate

autoxidation–accelerating activity among fractions separated by a reversed phase HPLC from the sample autoxidizing at a 5–600 μmol/ml level of main-product hydroperoxide. It was seen that the activity was widely spread over the fractions, although the intrinsic activity in fr.1 could not be evaluated owing to the residual Azo reagent.

A Sephadex LH20 gel filtration chromatography of the oxidized sample with methanol gave fractions eluted more rapidly than the main-product hydroperoxide of linoleate (Fig. 2). Frs.1, 2, and 3 in Fig. 2 each were further separated by reversed phase HPLC. Three main groups of components were obtained, P_3 from fr.1, P_2 from fr.2, and P_1 from fr.3. HPLC elution patterns of P_1, P_2, and P_3 are shown in Fig. 3 and the designation of P_1, P_2, and P_3 was based on the order of elution in the HPLC. P_1 was found in fr.5 in Table 2 and in fr.6 was contained P_2 and P_3. Table 3 summarizes the chromatographic behavior of P_1, P_2, and P_3, involving additionally that of related substances described in the later part. The elution position of P_1 in the Sephadex chromatography was similar to the previously reported dimer autocatalyst [6], which suggested that P_1 had a molecular size of a dimer. The sizes of P_2 and P_3 were, consequently, considered to be larger than a dimer size.

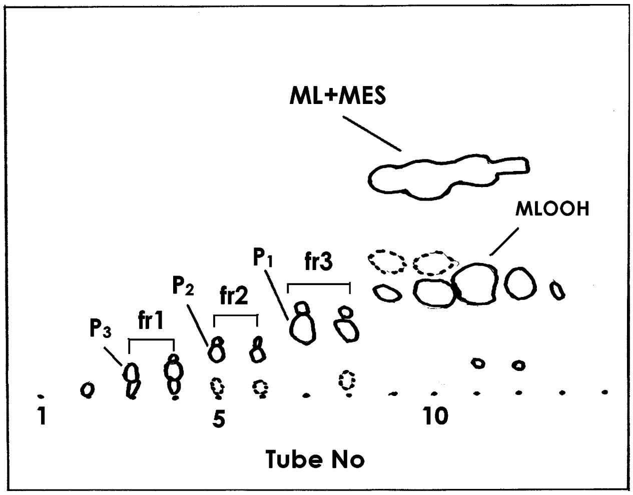

Fig. 2 Elution patterns of autoxidizing methyl linoleate containing tung oil methyl esters in Sephadex LH20 gel filtration chromatography with methanol. The autoxidizing material (0.3 ml) was diluted to 2 ml with methanol and applied to a 1.35 × 120 cm Sephadex LH 20 column. Eluates were separately collected in each 5 ml tube after 70 ml elution, and checked in TLC (Silicagel 60F_{254}) with hexane/diethyl ether 2:1 by vol by detecting under UV light. See text about P_1, P_2, and P_3

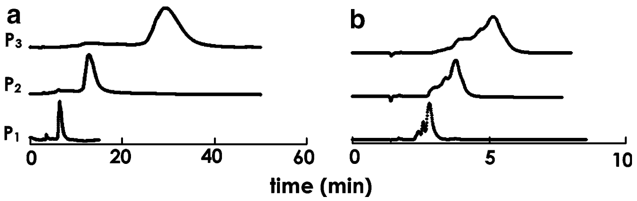

Fig. 3 Elution patterns of polymeric substances, P_1, P_2, and P_3 monitored at 234 nm absorbance. *Left side* chromatograms, **a** are on a 7.6 × 250 mm Inertsil column with methanol at a flow rate of 3 ml/min. *Right side* chromatograms, **b** are on a 4.6 × 150 mm Nucleosil®100-5 column with hexane/diethyl ether 75:25 by vol at a flow rate of 1.5 ml/min

Table 3 Chromatographic behavior of substances related with autoxidizing linoleate containing eleostearate

Materials[c]	Sephadex[a]	HPLC[b]			
		Reversed		Normal	
		M100	MW80:20	HE75:25	HE60:40
P_1	0.59	6.4		3.0–3.3	1.9
P_2	0.54	12.8		4.6	2.2
P_3	0.49	29.4		6.6	2.4
$P_1 + \Phi_3P$	0.59	6.4		6.5–8.3	2.7–3.1
$P_2 + \Phi_3P$	0.54	12.7		12.0	3.5
$P_3 + \Phi_3P$	0.49	26.4		15.5	4.2
ML[d]	0.67	6.5		1.5	1.4
MES[e]	0.67	6.0		1.5	1.4
MLOOH	0.70	3.5		2.2	1.7
MLOH	0.70	3.5	26.3–29.5	3.0–4.1	2.3–2.7
M_1	0.70	2.7	7.1		13.5
M_2	0.70	2.7	8.4		24.2
Azo[f]	0.70	2.6		5.4	

[a] A 13.5 mm × 120 cm Sephadex LH20 column with methanol was used, and figures in the Table are relative values of retention volumes when the bed volume of the column is taken as 1.0

[b] Reversed phase HPLC was carried out on a 7.6 × 250 mm Inertsil column with methanol only (M100) and methanol/water 80:20 by vol (MW75:25) at a flow rate of 3 ml/min. Normal phase HPLC was carried out on a 4.6 × 150 mm Nucleosil® 100-5 column with hexane/diethyl ether 75:25 by vol (HE75:25) and 60:40 by vol (HE60:40) at a flow rate of 1.5 ml/min. Elution was monitored at 234 nm absorbance, and figures in Table represent retention time (min)

[c] See text about P_1, P_2, P_3, M_1, and M_2. Samples obtained by treatment with triphenylphosphine are represented by addition of $+\Phi_3P$

[d] Methyl linoleate

[e] Methyl eleostearate

[f] 2,2′-Azobis-(4-methoxy-2,4-dimethylvaleronitrile)

A 1 ml autoxidizing sample at a 500 μmol/ml level of main-product hydroperoxide gave 46 μmol of P_1, 21 μmol of P_2, and 9 μmol of P_3 as conjugated diene. The autoxidation–accelerating activities of P_1, P_2, and P_3 were measured and expressed as Azo equiv of 3.7, 2.9, and 2.9×10^{-3}, respectively. On treatment of P_1 with methyl benzoate at 50°C for 19 h, hydroxy radicals from P_1 were detected as 0.58 mol% formation of methyl salicylate based on the starting amount of P_1, where the decrease in P_1 was 23%. Treatment of P_1 at 50°C gave no observable amounts of hexanal and 2,4-decadienal.

The reduction with triphenylphosphine brought about no change in molecular sizes of P_1, P_2, and P_3 as shown from their behavior in Sephadex LH20 chromatography (Table 3). In every case of P_1, P_2, and P_3, successive reduction with $NaBH_4$ gave, besides MLOH, two major products of a monomer size, M_1 and M_2 (Fig. 4). Both of them seemed to be di-OH compounds because of their lower mobilities in normal-phase HPLC as shown in Table 3. The substances M_1 and M_2 showed an absorption at 229 and 231 nm (in methanol) respectively, which suggested that they contained conjugated diene. Each of P_1, P_2, and P_3 was considered to consist of MLOH and the di-OH compounds. Absorbance ratios, $(M_1 + M_2)$/MLOH, at 234 nm in the $NaBH_4$ reduction products were increased in the order of 1.5 for P_1, 2.2 for P_2, and 3.3 for P_3. These ratios suggested that P_1 was a dimer consisting of one MLOH unit and one di-OH unit, P_2 was a trimer consisting of one MLOH unit and two di-OH units, and P_3 was a tetramer consisting of one MLOH unit and three di-OH units. After hydrogenation with platinum black under an atmospheric hydrogen, the converted substances from M_1 and M_2 showed no UV absorption, and their Rf values (0.08) on TLC (silica gel with hexane/diethyl ether 1:3 by detecting on charring) roughly resembled those of intact M_1 (0.14) and M_2 (0.10), suggesting that they were also di-OH compounds.

After trimethylsilylation, M_1, M_2, and their hydrogenated derivatives were subjected to GC–MS. The mass spectra of M_1 and M_2 were not distinguishable at all from each other, and the hydrogenated derivatives of M_1 and M_2 also gave indistinguishable spectra from each other. The lower spectrum in Fig. 5 was obtained from the hydrogenated derivatives, and its fragmentation was assigned undoubtedly to a structure of 9,14-dihydroxyoctadecanoic acid methyl ester, and in consideration of this result, the fragmentation of the upper spectrum indicated that M_1 and M_2 were 9,14-dihydroxy-10,12-octadecadienoic acid methyl ester, which had formerly reported by Hamberg [9] in a study on autoxidizing linoleic acid. M_1 and M_2 were probably two racemic pairs of diastereomeric isomers with 9- and 14-chiral centers.

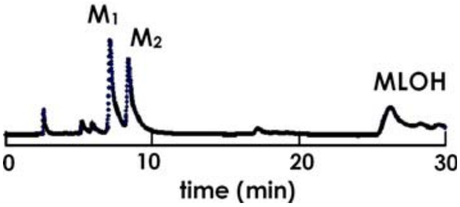

Fig. 4 Elution patterns of dihydroxy compounds, M_1 and M_2, from a 7.6 × 250 mm Inertsil column with methanol/water 80:20 by vol at a flow rate of 3 ml/min, monitored at 234 nm absorbance. MLOH also appears there

In the elution region of di-OH compounds, several minor peaks other than M_1 and M_2 were present as shown in Fig. 4, but the existence of 9,10- or 13,14-di-OH component was not recognized because the GC–MS of the hydrogenated products gave no component showing fragmentation characteristic of 9,10- or 13,14-di(trimethylsiloxy)octadecanoate.

Discussion

As expected, AutCat proved to be the source of hydroxy radicals. On the other hand, hydroxy radicals were not formed in the case of the purified MLOOH sample, which supported the hitherto accepted view that hydroxy-radical formation from homolytic cleavage of simple hydroperoxide is energetically unfavorable [10]. It is well known that hydroxy radicals are generated by the reaction of hydrogen peroxide with transition metals, e.g., the Fenton's reaction, but such a reaction seems unlikely in the lipid autoxidation products. From this point of view, it is a very important findings that AutCat, one of the products of lipid autoxidation, showed a clear activity of generating hydroxy radicals in the absence of transition metals.

The concentration of AutCat in the present oxML sample was too low to reveal observable hydroxy-radical generating activity. In this situation, the lack of observable activity in this sample indicated that there were not other potent sources of hydroxy radicals largely excelling AutCat.

The AutCat sample showed clear increases in hexanal and decadienal after 6 and 19 h treatment, while the oxML and MLOOH samples did not. Our former paper [4] has shown that MLOOH did not generate hexanal and decadienal under mild conditions. The present experiments were carried out in methyl benzoate, and the increases in hexanal and decadienal were also not observed, although the conditions were so different from the former ones that a large amount of parent unoxidized linoleate was present. The lack of the precursor activity of the oxML sample indicated that other potent precursors of hexanal and decadienal largely excelling AutCat were not present as well as hydroxy-radical generating sources.

In the AutCat sample, the formation of hydroxy radicals, hexanal, and decadienal demonstrated the presence of homolytic decomposition. The yield of hexanal was about 9 mol% when about 90% AutCat in the AutCat sample was decomposed after 19 h treatment. Theoretical yield of hexanal (R_1CHO) in Scheme 1 is expected to be 50 mol% of the amount of decomposed AutCat. So, a large part of AutCat seemed to disappear through other decomposition routes, probably being heterolytic ones, without giving radicals and aldehydes. The decrease in MLOOH observed

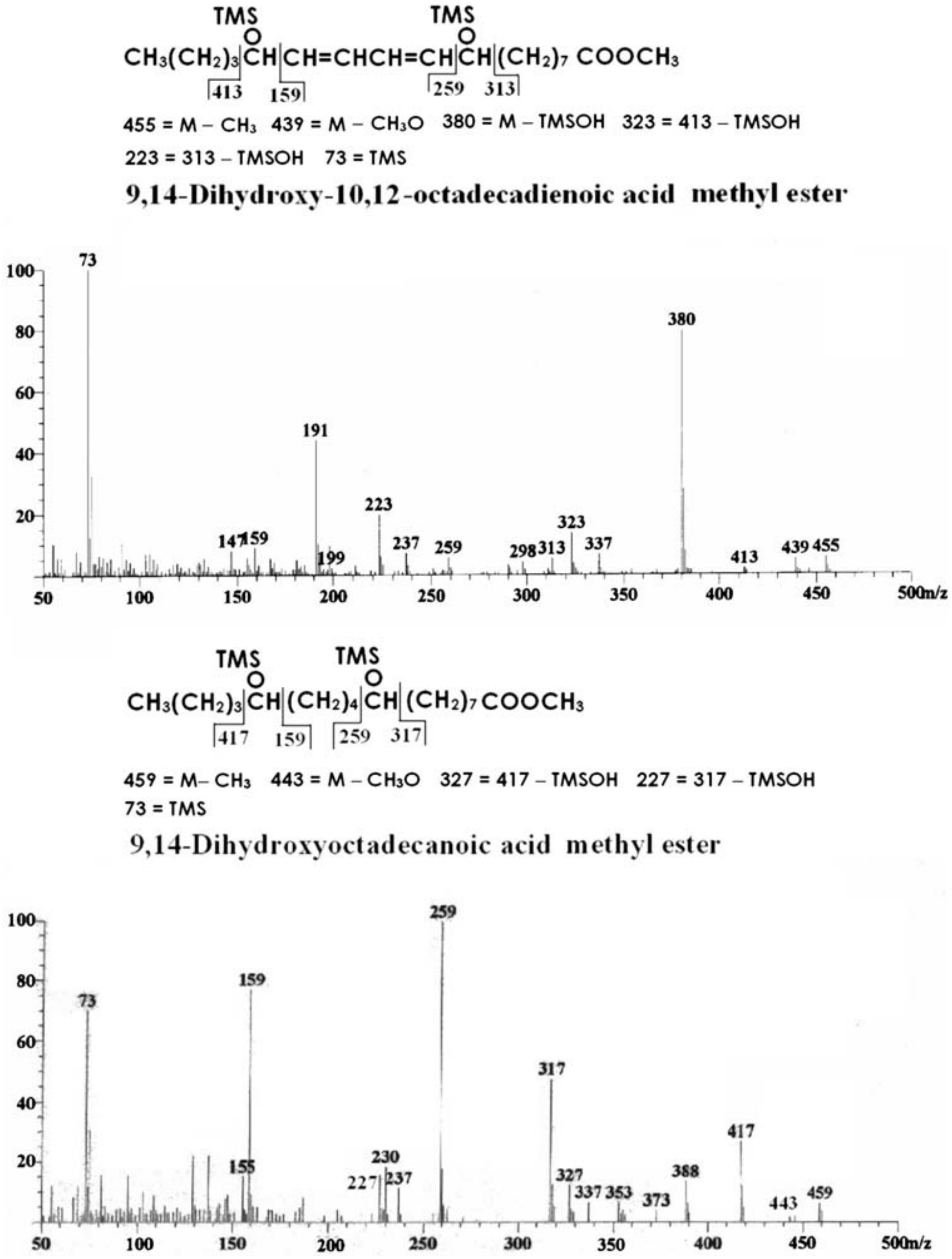

Fig. 5 Mass spectra of M_1 and M_2 (*upper*) and of their hydrogenated derivatives (*lower*). They were analyzed after trimethylsilylation. Identified structures and assignment for fragment ions are described

in the present MLOOH sample is presumably caused also by heterolytic routes. A smaller formation of decadienal than that of hexanal in the AutCat sample suggests that β-scission plays a relatively minor role in the fate of linoleate-skeleton alkoxy radicals shown in Scheme 1. The yield of methyl salicylate was much smaller than that of hexanal in the AutCat sample, which may suggest low efficiency of methyl benzoate as a scavenger of hydroxy radicals under the present conditions.

Formerly, we reported [2] that a potent autocatalyst and potent precursors of hexanal and decadienal were present in a polar fraction of autoxidizing methyl linoleate and, thereafter, we demonstrated more strictly [5] that hexanal and decadienal were formed through cumulative intermediates other than main-product hydroperoxide. The present AutCat is undoubtedly an important one of the substances suggested in these past papers.

To prove another prediction in our previous paper [6], attempts were made to search autoxidizing linoleate-containing conjugated polyene substances for other types of autocatalysts and hydroxy radical generators. In the present model experiments, we used an easily available material, tung oil, whose main constituent fatty acid is α-eleostearic acid, *cis*-9, *trans*-11, *trans*-13-octadecatrienoic acid. We planned experiments of autoxidation accelerated with 2,2′-azobis-(4-methoxy-2,4-dimethylvaleronitrile) in order to avoid the degradation of autocatalytic products during the long autoxidation time made necessary by the low oxidation rate.

In the case of 10% addition of tung oil methyl ester, the products of molecular sizes not less than dimer were found in considerably larger amounts than in the case of methyl linoleate alone. We could separate three groups of such products, P_1, P_2, and P_3, which each behaved as a single peak in reversed phase HPLC (Fig. 3). The derivatization and the following analyses of P_1, P_2, and P_3 suggested the structures shown in Structure 1. The structure implies that each of P_1, P_2, and P_3 consists of many isomers. Each of them was actually eluted as a set of incompletely separated peaks in normal phase HPLC (Fig. 3).

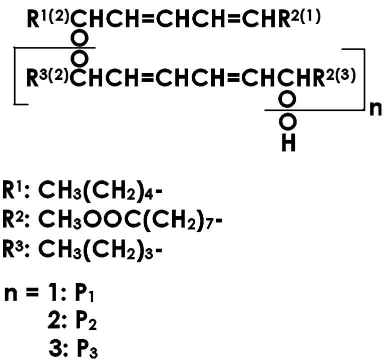

Structure 1

The structures of P_1, P_2, and P_3 suggest the following mechanism of formation: linoleate peroxy radicals are added to the conjugated triene of eleostearate followed by further addition of molecular oxygen as shown in Scheme 2; the fate of the resultant dimer peroxy radicals branches into two courses; one is the abstraction of hydrogen from linoleate giving P_1, and the other is further addition to eleostearate giving trimer radicals; the trimer radicals have similarly two sorts of fate; one gives P_2 and the other gives tetramer radicals; the tetramer radicals can give P_3 and enter a further polymer-generating sequence.

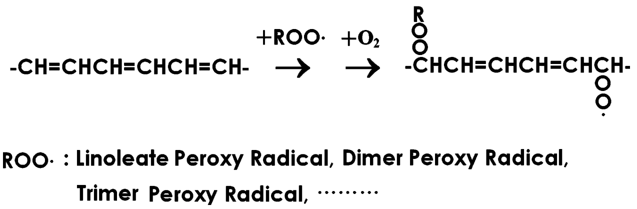
+ROO·
+O2
-CH=CHCH=CHCH=CH-
R
O
O
-CHCH=CHCH=CHCH-
O
O
·
ROO· : Linoleate Peroxy Radical, Dimer Peroxy Radical,
Trimer Peroxy Radical, ………

Scheme 2

As shown in this mechanism, there are many sorts of peroxy radicals, linoleate, dimer, trimer, and so on, and each of them enters two reactions, hydrogen abstraction from linoleate and addition to eleostearate, in a certain distribution ratio. If all the sorts of peroxy radicals have the same distribution ratio, the ratios of the formation rates for P_2 to P_1 and for P_3 to P_2 are expected to be equal. We can regard the yield ratio of P_1, P_2, and P_3 as a rough estimate for the ratio of their formation rates. Then, we will see the yield ratios. The molar ratio of the observed yields of P_1, P_2, and P_3 was 23:7.7:2.3, which was given from the ratio of 46:23:9 at 234 nm absorbance and the number of conjugated diene chromophores a molecule, two for P_1, three for P_2, and four for P_3. The yield ratio for P_2 to P_1 (7.7:23) approximated that for P_3 to P_2 (2.3:7.7). This agreement satisfactorily supports validity of the above argument.

In naturally occurring lipids, only such dimer products as P_1 are presumably important because low concentration of conjugated polyene compounds in general may lower the distribution of peroxy radicals to addition to such compounds, which is unfavorable to the formation of higher polymers than dimer.

Autocatalytic activity of autoxidizing linoleate containing eleostearate was not necessarily distributed only in higher-molecular-size fractions as shown in Table 2, but we focused the present survey on such higher-molecular-size products as P_1, P_2, and P_3. The autoxidation–accelerating activities as Azo equiv, 3.7×10^{-3} for P_1, 2.9×10^{-3} for P_2, and 2.9×10^{-3} for P_3 were comparable to 1.8×10^{-3} for the previously reported autocatalyst [6]. The hydroxy-radical-generating activity of P_1 (0.38 mol% yield of methyl salicylate) was also comparable to 0.3–0.6 mol% of this autocatalyst as shown in Table 1. These findings strongly suggested that conjugated polyene fatty acids which occur in lipid materials both as natural minor components and artificial products by heating, etc. can generate potent autocatalysts involving hydroxy radical generators such as the present substances. Activity generating hexanal and 2,4-decadienal was, however, not observed in P_1 unlike the previous autocatalyst. In the present investigation, we did not examine other aldehydes expected as products of eleostearate.

The previously reported autocatalytic substances have an α, β-diperoxy structure which is considered to undergo an energetically favorable concerted homolysis [6]. However, in the present system, polymeric products containing an α, β-diperoxy structure were not observed. The present substances, P_1, P_2, and P_3 possessed a 1,6-diperoxy-2,4-diene structure in which two peroxy groups are separated with conjugated diene, indicating that, after the addition of peroxy radicals to conjugated triene, the following addition of oxygen occurs only the remote position. It must be noted that, in autocatalytic activity and activity forming hydroxy radicals, the present substances are comparable to the previously reported autocatalysts in spite of different structural feature. On the other hand, the present substances clearly contrast with the main-product hydroperoxide of linoleate. The hydroperoxide shows no activity of autocatalysts [6] and forming hydroxy radicals as shown in Table 1, although its 1-peroxy-2,4-diene structure partly resembles the structure of the present substances. In consideration of these facts, it is suggested that the present substances are degraded through an unknown homolysis-assisting mechanism which may involve some interaction between two remote peroxy groups and may result in the cleavage to form radicals involving hydroxy radicals.

Acknowledgments One of the authors, M. Tokita, carried some of the experiments at Japan Women's University as a research fellow.

References

1. Morita M, Fujimaki M (1973) Non-hydroperoxy-type peroxides as autocatalysts of lipid autoxidation. Agric Biol Chem 37:1213–1214
2. Morita M, Fujimaki M (1973) Minor peroxide components as catalysts and precursors to monocarbonyls in the autoxidation of methyl linoleate. J Agric Food Chem 21:860–863
3. Morita M, Tanaka M, Takayama Y, Yamamoto Y (1976) Metal-requiring and non-metal-requiring catalysts in the autoxidation of methyl linoleate. J Am Oil Chem Soc 53:487–483
4. Morita M, Tokita M (1990) Evaluation of the role of hydroperoxides in the formation of aldehydes during linoleate autoxidation. Chem Phys Lipids 56:209–215
5. Morita M, Tokita M (1993) Courses of aldehyde formation during linoleate autoxidation and some information about precursors and mechanism. Chem Phys Lipids 66:13–22
6. Morita M, Tokita M (2006) The real radical generator other than main-product hydroperoxide in lipid autoxidation. Lipids 41:91–95
7. Miyashita K, Fujimoto K, Kaneda T (1984) Structural studies of polar dimers in autoxidizing methyl linoleate during the initial stages of autoxidation. Agric Biol Chem 48:2511–2515
8. Miyashita K, Hara N, Fujimoto K, Kaneda T (1985) Dimers formed in oxygenated methyl linoleate hydroperoxides. Lipids 20:578–587
9. Hamberg M (1983) Autoxidation of linoleic acid. isolation and structure of four dihydroxyoctadecadienoic acids. Biochim Biophy Acta, Lipids Lipid Metabolism 752:353–356
10. Chan H W-S (1987) The mechanism of autoxidation. In: Chan H W-S (ed) Autoxidation of unsaturated lipids. Academic Press, London, pp 10

Lipids (2008) 43:599–610
DOI 10.1007/s11745-008-3195-0

ORIGINAL ARTICLE

Autoxidation of Conjugated Linoleic Acid Methyl Ester in the Presence of α-Tocopherol: The Hydroperoxide Pathway

**Taina I. Pajunen · Mikael P. Johansson ·
Tapio Hase · Anu Hopia**

Received: 15 January 2008 / Revised: 6 April 2008 / Accepted: 13 May 2008 / Published online: 11 June 2008
© AOCS 2008

Abstract Autoxidation of conjugated linoleic acid (CLA) methyl ester follows at least partly Farmer's hydroperoxide theory. A mechanism for this hydroperoxide pathway has been proposed based on autoxidation of 9-*cis*,11-*trans*-CLA methyl ester. This investigation aims at confirming and further clarifying the mechanism by analyzing the hydroperoxides produced from 10-*trans*,12-*cis*-CLA methyl ester and by theoretical calculations. Five methyl hydroxyoctadecadienoates were isolated by HPLC and characterized by UV, GC-MS, and 1D- and 2D-NMR techniques. In addition, an HPLC method for the separation of the intact hydroperoxides was developed. The autoxidation of 10-*trans*,12-*cis*-CLA methyl ester in the presence of high amount of α-tocopherol (20%) was diastereoselective in favor of one geometric isomer, namely Me 9-OOH-10*t*,12*c*, and produced new positional isomers 10- and 14-hydroperoxides (Me 10-OOH-11*t*,13*t*; Me 14-OOH-10*t*,12*c*; and Me 14-OOH-10*t*,12*t*). Importantly, one of these new isomers, which was characterized as an intact hydroperoxide, had an unusual *cis,trans* geometry where the *cis* double bond is adjacent to the hydroperoxyl-bearing methine carbon. Further insight to the mechanism was provided by calculating the relative energies for different conformations of the precursor lipid, the allylic carbon–hydrogen bond dissociation enthalpies, and the spin distributions on the intermediate pentadienyl radicals. As a result, a better understanding of the isomeric distribution of the product hydroperoxides was achieved and a modified mechanism that accounts for these calculations is presented.

Key words Autoxidation · CLA ·
Bond dissociation enthalpy · Density functional theory ·
Free radical chain reaction · Hydroperoxide · NMR ·
Unpaired spin density

Abbreviations

BSTFA	Bis(trimethylsilyl)-trifluoroacetamide
COSY	Correlated spectroscopy
C–H BDE	Carbon–hydrogen bond dissociation enthalpy
DFT	Density functional theory
gHMBC	Gradient heteronuclear multiple bond correlation
gHSQC	Gradient heteronuclear single quantum coherence
LR-COSY	Long-range COSY
Me 9-OH-10*t*,12*c*	Methyl 9-(*R,S*)-hydroxy-10-*trans*,12-*cis*-octadecadienoate

---

T. I. Pajunen · T. Hase
Department of Chemistry, Laboratory of Organic Chemistry,
University of Helsinki, P.O. Box 55, A.I. Virtasen aukio 1,
Helsinki 00014, Finland

M. P. Johansson
Lundbeck Foundation Center for Theoretical Chemistry,
Aarhus University, 8000 Århus C, Denmark

M. P. Johansson
Department of Chemistry, Laboratory for Instruction in Swedish,
University of Helsinki, Helsinki 00014, Finland

A. Hopia
Department of Applied Chemistry and Microbiology,
Food Chemistry Division, University of Helsinki,
Helsinki 00014, Finland

T. I. Pajunen (✉)
Vuoritie 16, 02330 Espoo, Finland
e-mail: tainahamalainen@yahoo.co.uk

methyl linoleate	Methyl 9-*cis*,12-*cis*-octadecadienoate
TMCS	Trimethylchlorosilane
TOCSY	Total correlation spectroscopy

Introduction

Conjugated linoleic acid (CLA) is a generic name referring to a group of positional and geometric isomers of octadecadienoic acid with a 1,3-diene structure. Thus far, two CLA isomers, namely 9-*cis*,11-*trans*-CLA and 10-*trans*,12-*cis*-CLA, have been discovered to possess beneficial physiological properties [1]. The biochemical mechanisms of CLA action are unknown. These mechanisms, however, seem to include induction of fatty acid oxidation [2, 3]. Most oxidation studies on CLA are, despite the structure-specificity, performed with mixtures of isomers. Moreover, surprisingly little is known about the initial stages of CLA autoxidation. The early literature reported that CLA autoxidation differs from the autoxidation of linoleic acid (LA) and produces in the absence of antioxidants mainly relatively low molecular weight polymeric peroxides [4–7]. More recently, CLA has been proposed to autoxidize through two distinct pathways with unknown primary products [8] or speculated to yield products identical to those formed during singlet oxygen oxidation of CLA based on the analysis of secondary oxidation products [9, 10]. First in 2001, we discovered that hydroperoxides are one type of primary autoxidation product of CLA methyl ester formed in the presence and in the absence of α-tocopherol [11]. The hydroperoxides produced during autoxidation of 9-*cis*,11-*trans*-CLA methyl ester (Me 9*c*,11*t*-CLA) in the presence of 20% of α-tocopherol were isolated, reduced to the corresponding hydroxy derivatives, separated, and characterized [12]. This enabled us to propose a mechanism for the hydroperoxide pathway of CLA autoxidation, which occurs in agreement with kinetic data [5, 13] through an autocatalytic free radical chain reaction.

In continuation of our previous work [11, 12] we have now tested whether the mechanism proposed for the hydroperoxide pathway based on the autoxidation of Me 9*c*,11*t*-CLA correctly predicts the hydroperoxides and their isomeric distribution formed in the autoxidation of 10-*trans*,12-*cis*-CLA methyl ester (Me 10*t*,12*c*-CLA). To this end, Me 10*t*,12*c*-CLA was autoxidized under the same conditions as previously Me 9*c*,11*t*-CLA [12] in order to produce enough hydroperoxides for the characterization and to allow the comparison between the two studies. The hydroperoxides were isolated, reduced chemoselectively to hydroxy derivatives, and the separated hydroxy derivatives were characterized by UV, GC–MS, and 1D- and 2D-NMR techniques. Due to unsatisfactory separation of certain methyl hydroxyoctadecadienoates, an HPLC method for the separation of the intact hydroperoxides was developed. In addition, theoretical calculations were carried out to provide further insight to the initial stages of CLA autoxidation and to the distribution of the product hydroperoxides. A scheme for the hydroperoxide pathway of CLA autoxidation consistent with these calculations is presented.

Experimental Procedures

Materials

Me 10*t*,12*c*-CLA was purchased from Matreya Inc. (Pleasant Gap, PA, USA) and the presence of only one isomer was confirmed by ^{13}C NMR [14]. DL-α-Tocopherol was obtained from Calbiochem (Darmstadt, Germany). Isopropanol, heptane, and *tert*-butyl methyl ether (TBME) were from Rathburn Chemicals (Walkerburn, Scotland), bis(trimethylsilyl)-trifluoroacetamide and trimethylchlorosilane from Merck (Darmstadt, Germany), and calcium hydride, sodium borohydride, and platinum (IV) oxide from Fluka (Buchs, Switzerland). Isopropanol was dried by distillation over calcium hydride.

Autoxidation

Me 10*t*,12*c*-CLA (0.4 g, 1.4 mmol) was autoxidized in a glass vial (20 mL, $d = 2.0$ cm) for 16 days in the presence of α-tocopherol (20% per weight) under atmospheric oxygen at 40 °C in the dark. The yield of hydroperoxides based on TLC analysis and on peroxide value (PV = 193 mequiv O_2/kg) measured by the ferric thiocyanate method [15] was 6.3%. The hydroperoxides were isolated from the reaction mixture by SPE (2 g; Varian, Harbor City, CA, USA) using MTBE/heptane gradient (from 2.5 to 20%, v/v) as an eluent, and reduced to corresponding hydroxy derivatives using $NaBH_4$ in dry isopropanol at 0 °C according to the procedure reported previously [11]. The hydroperoxides and the hydroxy derivatives were stored as dilute heptane solutions at −20 °C under nitrogen.

Isocratic Normal-phase HPLC

The separation of five hydroxy-CLA methyl esters and six hydroperoxy-CLA methyl esters was achieved using a semi-preparative Merck silica column (Supelcosil LC-SI Semi-Prep, 25.0 × 1.0 cm I.D., particle size 5 μm) and isopropanol/TBME/heptane (0.05/5/95, v/v/v) and isopropanol/heptane (0.65/100, v/v) as an eluent, respectively, at 2.0 mL/min flow rate. Approximately 1 mg of the mixture of isomers was repeatedly injected. The fractions collected from non-baseline separated peaks were further purified using the semi-preparative column. The mixture and the separated isomers were analyzed by HPLC using a Supelco silica column (Supelcosil LC-SI, 25.0 cm × 2.1 mm I.D., particle size 5 μm) and isopropanol/TBME/heptane (0.05/4/95, v/v/v) or isopropanol/heptane (0.3/100, v/v) as an eluent at 0.4 mL/min flow rate. The columns were equipped with Waters 501 HPLC pump, Waters pump control module, Waters 717 plus autosampler, and Waters 996 photodiode array detector set at 234 nm.

UV Spectroscopy

The separated isomers were quantified by UV spectroscopy at $\lambda = 233$ nm for the *trans*,*trans* isomers and at $\lambda = 236$ nm *cis*,*trans* isomers. UV spectra were recorded in ethanol solution on a Perkin Elmer UV/vis spectrometer Lambda Bio (Ueberlingen, Germany). Molar absorbance (ε) values used in calculations are from [16]. The concentration of the isomers for which no ε value is available was approximated with the ε value of the nearest positional isomer with the appropriate diene geometry.

GC–MS

The hydroxy-CLA methyl esters were hydrogenated to hydroxystearates and derivatized to trimethylsilyl ethers according to the procedure described earlier [12]. The trimethylsilyl ethers were analyzed on an Agilent 5973 mass spectrometer (Palo Alto, CA, USA) connected to a Hewlett Packard gas chromatograph (HP 6890 Series GC System, Wilmington, DE, USA). GC was equipped with a Rtx-5MS (crossbond 5% diphenyl polysiloxane, 95% dimethyl polysiloxane) capillary column (60 m × 0.25 mm I.D., film thickness 0.1 μm, carrier gas: helium, 1.2 mL/min; Restek corporation, Bellefonte, PA, USA). Samples (0.1–1 μL) were injected using on-column injection. The column temperature program and other run parameters were as reported previously [12].

NMR Spectroscopy

^{1}H-, ^{13}C-, and 2D-NMR spectra, including correlated spectroscopy (COSY), long-range COSY (LR-COSY), gradient heteronuclear multiple bond correlation (gHMBC), gradient heteronuclear single quantum coherence (gHSQC) and total correlation spectroscopy (TOCSY), were recorded in deuterochloroform (contains 0.1% (v/v) tetramethylsilane, 99.8% ^{2}H; Aldrich, Milwaukee, WI, USA) on a Bruker DRX 500 spectrometer equipped with 5 mm broadband inverse probe with z-gradient (Fällanden, Switzerland) at 27 °C. Chemical shifts δ are given in parts per million (ppm) relative to tetramethylsilane (δ 0.00).

The 1D- and 2D-NMR data of methyl 9-(*R*,*S*)-hydroxy-10-*trans*,12-*cis*-octadecadienoate (Me 9-OH-10*t*,12*c*[1]; 97.4%, 31 mM) and that of methyl 13-(*R*,*S*)-hydroxy-9-*cis*,11-*trans*-octadecadienoate (Me 13-OH-9*c*,11*t*; 98.5%, 17 mM) agreed with published data [12].

Methyl 10-(*R*,*S*)-hydroxy-11-*trans*,13-*trans*-octadecadienoate (Me 10-OH-11*t*,13*t*; 94.3%, 16 mM) ^{1}H NMR δ 6.17 (*dd*, 1 H, H-12, $^3J_{12,11} = 15.2$ Hz, $^3J_{12,13} = 10.4$ Hz), 6.02 (*ddtd*, 1 H, H-13, $^3J_{13,14} = 15.1$ Hz, $|^4J_{13,15}| \approx 1.4$ Hz, $|^4J_{13,11}| \approx 0.9$ Hz), 5.70 (*dt*, 1 H, H-14, $^3J_{14,15} = 7.0$ Hz), 5.57 (*dd*, 1 H, H-11, $^3J_{11,10} = 7.0$ Hz), 4.10 (*dt*, 1 H, H-10, $^3J_{10,9} \approx 6.5$ Hz), 3.66 (*s*, 3 H, OCH$_3$), 2.30 (*t*, 2 H, H-2, $^3J_{2,3} = 7.6$ Hz), 2.08 (*tdd*, 2 H, H-15, $^3J_{15,16} \approx 7.3$ Hz), 1.61 (*quintet*, 2 H, H-3, $^3J_{3,4} = 7.3$ Hz), 1.59-1.52 (*m*, 1 H, H-9), 1.52-1.45 (*m*, 1 H, H-9′), 1.45-1.26 (*m*, 15 H, H-4 to H-8, H-16, H-17, OH), 0.90 (*t*, 3 H, H-18, $^3J_{18,17} = 7.2$ Hz).

Methyl 13-(*R*,*S*)-hydroxy-9-*trans*,11-*trans*-octadecadienoate (Me 13-OH-9*t*,11*t*; 99.6%, 31 mM) ^{1}H NMR δ 6.17 (*dd*, 1 H, H-11, $^3J_{11,12} = 15.2$ Hz, $^3J_{11,10} = 10.4$ Hz), 6.02 (*ddtd*, 1 H, H-10, $^3J_{10,9} = 15.1$ Hz, $|^4J_{10,8}| \approx 1.3$ Hz, $|^4J_{10,12}| \approx 0.6$ Hz), 5.68 (*dt*, 1 H, H-9, $^3J_{9,8} = 7.0$ Hz), 5.57 (*dd*, 1 H, H-12, $^3J_{12,13} = 7.0$ Hz), 4.11 (*dt*, 1 H, H-13, $^3J_{13,14} \approx 6.6$ Hz), 3.67 (*s*, 3 H, OCH$_3$), 2.30 (*t*, 2 H, H-2, $^3J_{2,3} = 7.6$ Hz), 2.07 (*dtd*, 2 H, H-8, $^3J_{8,7} \approx 6.9$ Hz), 1.62 (*quintet*, 2 H, H-3, $^3J_{3,4} = 7.4$ Hz), 1.60-1.53 (*m*, 1 H, H-14), 1.53-1.47 (*m*, 1 H, H-14′), 1.48-1.42 (br *s*, 1 H, OH), 1.42-1.25 (*m*, 14 H, H-4 to H-7, H-15, H-16, H-17), 0.89 (*t*, 3 H, H-18, $^3J_{18,17} = 6.9$ Hz).

Methyl 14-(*R*,*S*)-hydroxy-10-*trans*,12-*trans*-octadecadienoate (Me 14-OH-10*t*,12*t*; 98.0%, 17 mM) ^{1}H NMR δ 6.17 (*dd*, 1 H, H-12, $^3J_{12,13} = 15.2$ Hz, $^3J_{12,11} = 10.4$ Hz), 6.02 (*ddtd*, 1 H, H-11, $^3J_{11,10} = 15.1$ Hz, $|^4J_{11,9}| \approx 1.4$ Hz, $|^4J_{11,13}| \approx 0.6$ Hz), 5.69 (*dt*, 1 H, H-10, $^3J_{10,9} = 7.0$ Hz), 5.57 (*dd*, 1 H, H-13, $^3J_{13,14} = 7.0$ Hz), 4.11 (*dt*, 1 H, H-14, $^3J_{14,15} \approx 6.6$ Hz), 3.67 (*s*, 3 H, OCH$_3$), 2.30 (*t*, 2 H, H-2, $^3J_{2,3} = 7.6$ Hz), 2.07 (*dtd*, 2 H, H-9, $^3J_{9,8} \approx 6.9$ Hz), 1.61 (*quintet*, 2 H, H-3, $^3J_{3,4} = 7.3$ Hz), 1.62-1.54 (*m*, 1 H, H-15), 1.54-1.48 (*m*, 1 H, H-15′), 1.47-1.40 (br *s*, 1 H, OH), 1.42-1.25 (*m*, 14 H, H-4 to H-8, H-16, H-17), 0.90 (*t*, 3 H, H-18, $^3J_{18,17} = 7.0$ Hz).

Methyl 14-(*R*,*S*)-hydroperoxy-10-*trans*,12-*cis*-octadecadienoate (Me 14-OOH-10*t*,12*c*; 93.8%, 1 mM) ^{1}H NMR δ 7.76 (*s*, 1 H, OOH), 6.37 (*ddtd*, 1 H, H-11, $^3J_{11,10} = 14.9$ Hz, $^3J_{11,12} = 11.1$ Hz, $|^4J_{11,9}| \approx 1.3$ Hz, $|^4J_{11,13}| \approx 1.0$ Hz), 6.24 (*dd*, 1 H, H-12, $^3J_{12,13} \approx 11.0$ Hz), 5.78 (*dt*, 1 H,

---

[1] The CLA methyl ester hydroperoxides and their hydroxy derivatives are abbreviated in the following manner: Me 9-(O)OH-10*t*,12*c* stands for racemic methyl (hydroperoxy)hydroxyoctadecadienoate where the (hydroperoxyl) hydroxyl group is located at C-9 and the double bonds at C-10 and C-12. The geometry of the double bonds is denoted by *c* or *t* that refer to *cis* and to *trans* geometry.

H-10, $^3J_{10,9}$ = 7.1 Hz), 5.22 (*dd,* 1 H, H-13, $^3J_{13,14} \approx$ 9.0 Hz), 4.85 (*dt*, 1 H, H-14, $^3J_{14,15} \approx$ 6.7 Hz), 3.67 (*s*, 3 H, OCH_3), 2.30 (*t*, 2 H, H-2, $^3J_{2,3}$ = 7.5 Hz), 2.11 (*dtd*, 2 H, H-9, $^3J_{9,8} \approx$ 7.0 Hz), 1.71-1.65 (*m*, 1 H, H-15), 1.61 (*quintet*, 2 H, H-3, $^3J_{3,4} \approx$ 7.3 Hz), 1.48-1.42 (*m*, 1 H, H-15′), 1.42-1.25 (*m*, 14 H, H-4 to H-8, H-16, H-17), 0.90 (*t*, 3 H, H-18, $^3J_{18,17} \approx$ 7.0 Hz); ^{13}C NMR δ 138.33, 134.19, 126.93, 125.15 (C-10, C-11, C-12, C-13), 81.44 (C-14), 51.47 (OCH_3), 34.11 (C-2), 32.79, 32.42, 29.20, 29.16, 29.09, 29.07, 29.04, 27.36 (C-16), 24.92 (C-3), 22.66 (C-17), 13.95 (C-18).

Theoretical Calculations

All calculations have been performed at the density functional theory (DFT) level employing the hybrid B3LYP functional [17, 18] as implemented in the TURBOMOLE program package [19] version 5.91. The structures were optimized using the polarized split-valence def2-SVP basis set [20]. The conformations of Me 10*t*,12*c*-CLA were confirmed to be local minima on the potential energy surface by ensuring that the lowest vibrational mode was non-imaginary. Furthermore, it was made sure that the geometries were comparable. In particular, in the peroxyl radicals the O_2-group was always oriented in a similar manner facing the methine hydrogen, since the other local minimum with the O_2-group rotated to the opposite side of the chain lied ca. 0.8 kcal//mol higher in energy. Energies were evaluated using the larger, doubly polarized triple-zeta def-TZVPP basis set [20]. The environment was modeled using the COSMO continuum solvation model [21, 22] with a dielectric constant of methyl linoleate (3.4) which was considered as a typical value for this class of molecules [23]. Thermal enthalpy corrections at the autoxidation reaction temperature were calculated using the harmonic approximation via the (unscaled) vibrational frequencies calculated in gas-phase. An enthalpy correction of 5/2 *RT* was used for the hydrogen atom. The gross spin densities of the radicals were calculated as outlined in Reference [24]. This level of theoretical treatment has been found to be suitable in previous work [25–28]. Although bond dissociation energies are known to be slightly underestimated at B3LYP level, the error is systematic and thus relative energies are comparable [29]. This was further confirmed by using the described level of theory for calculating the dissociation energies and enthalpies at 298 K for the monoallylic C–H bond in methyl oleate and for the bisallylic C–H bond in methyl linoleate. The difference between the calculated dissociation energy (enthalpy at 298 K) values of 86.2 (79.1) and 74.2 (67.5) kcal/mol for mono- and bisallylic C–H bonds, respectively, compare well with the literature values of 88 and 75 kcal/mol [30].

Results and Discussion

The mechanism proposal developed for the hydroperoxide pathway of CLA autoxidation based on the autoxidation of Me 9*c*,11*t*-CLA [12] predicts that the autoxidation of Me 10*t*,12*c*-CLA is diastereoselective in favor of one geometric isomer, namely Me 9-OOH-10*t*,12*c*. In addition, the autoxidation should yield three types of geometric isomers and two new positional isomers *i.e.* 10- and 14-hydroperoxides. Importantly, one of these new positional isomers should have an unusual *cis*,*trans* geometry where the *cis* double bond is adjacent to the hydroperoxyl-bearing methine carbon. This type of geometric isomer is absent from the autoxidation of nonconjugated polyunsaturated fatty acids [31]. Analysis of the hydroperoxide mixture from autoxidation of Me 10*t*,12*c*-CLA confirmed that the mechanism predicts the formed isomers and the isomeric distribution correctly (see Scheme 1). The details of the mechanism, however, were altered based on the theoretical calculations.

Autoxidation, HPLC Separation, and Characterization of the Products

The autoxidation of CLA methyl ester differs from that of its nonconjugated counterpart, methyl linoleate, and produces mainly polymeric products [4–7, 32]. Moreover, only small amounts of peroxides accumulate during the autoxidation of CLA methyl ester compared to the autoxidation of methyl linoleate [4]. Therefore, in order to direct the autoxidation of CLA methyl ester from autoxidative polymerization toward hydroperoxide formation the

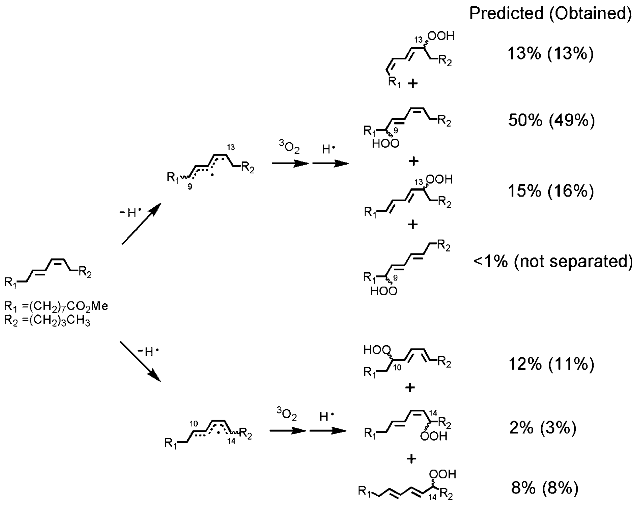

Scheme 1 Prediction of the hydroperoxide isomers and their isomeric distribution that will be formed during autoxidation of 10-*trans*,12-*cis*-CLA methyl ester based on autoxidation of 9-*cis*,11-*trans*-CLA methyl ester [12]

autoxidation must be performed in the presence of a good hydrogen atom donor [12]. Hence, Me 10*t*,12*c*-CLA was treated with 20% of α-tocopherol under atmospheric oxygen at 40 °C in the dark. Under these conditions, α-tocopherol does not exert its recognized antioxidant effect but allows the autoxidation to proceed quite rapidly to produce relatively good yield of monohydroperoxides. The separation and characterization of the Me 10*t*,12*c*-CLA hydroperoxides was attempted as their hydroxy derivatives. The separation of the hydroxy derivatives, however, proved to be more challenging than the separation of those from the autoxidation of Me 9*c*,11*t*-CLA. Indeed, only partial separation of the hydroxy derivatives was achieved when tested with mixtures of isopropanol/heptane, MTBE/heptane, and isopropanol/MTBE/heptane as an eluent. The best separation was obtained using isopropanol/MTBE/heptane (0.05/5/95, v/v/v) as an eluent and the elution order of five hydroxy derivatives was: Me 13-OH-9*c*,11*t*; Me 14-OH-10*t*,12*t*; Me 13-OH-9*t*,11*t*; Me 10-OH-11*t*,13*t*; and Me 9-OH-10*t*,12*c* (Fig. 1a). The separation of the intact Me 10*t*,12*c*-CLA hydroperoxides was, however, more successful and it was achieved using isopropanol/heptane (0.35/100, v/v) as an eluent as depicted in Fig. 1b. HPLC analysis of the mixture at λ = 234 nm gave the following elution order and area percentage composition for the hydroperoxides: Me 13-OOH-9*c*,11*t* (13%), Me 14-OOH-10*t*,12*c* (3%), Me 14-OOH-10*t*,12*t* (8%), Me 13-OOH-9*t*,11*t* (16%), Me 10-OOH-11*t*,13*t* (11%), and Me 9-OOH-10*t*,12*c* (49%). The 10- and 14-positional isomers were identified in the same manner as the hydroxy derivatives (*vide infra*) and the 9- and 13-hydroperoxides were identified by spiking the HPLC runs with pure hydroperoxides isolated from methyl linoleate autoxidation (i.e. Me 9-OOH-10*t*,12*c*; Me 9-OOH-10*t*,12*t*; Me 13-OOH-9*c*,11*t*; and Me 13-OOH-9*t*,11*t*). In particular, spiking with Me 9-OOH-10*t*,12*t* revealed that this isomer, which is the predicted seventh isomer that was not separated from the autoxidation mixture, was partly overlapping with the major product. This overlapping together with the expected small amount (<1%) explains why the separation of Me 9-OOH-10*t*,12*t* was not possible. Moreover, studies with methyl linoleate have established that this hydroperoxide isomer is formed through the β-scission pathway from Me 13-OOH-9*c*,11*t* and from Me 13-OOH-9*t*,11*t* [33–36] both of which were formed during the autoxidation of Me 10*t*,12*c*-CLA.

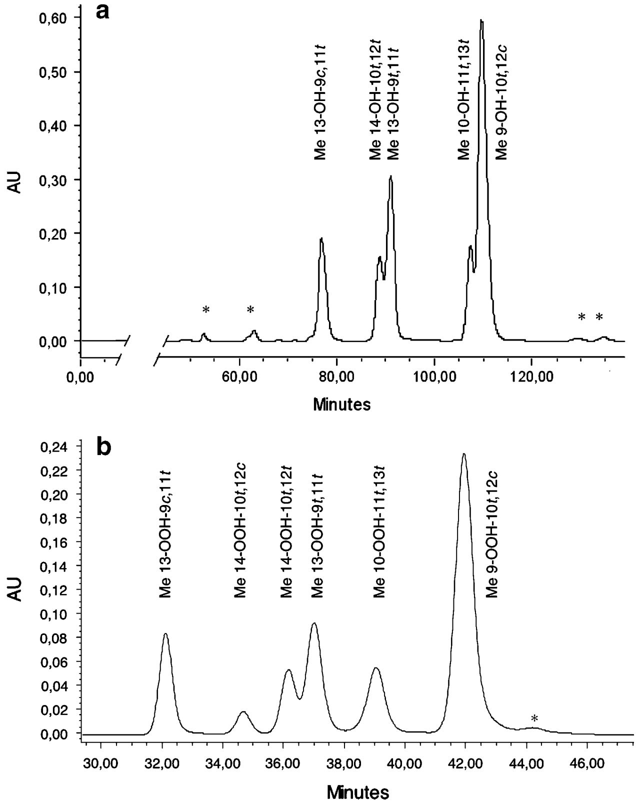

Fig. 1 Semi-preparative HPLC separation of **a** hydroxy-CLA methyl esters and **b** hydroperoxy-CLA methyl esters using Supelco silica column (Supelcosil LC-SI, 25.0 cm × 2.1 mm i.d., particle size 5 µm) and isopropanol/TBME/heptane (0.05/5/95, v/v/v) or isopropanol/heptane (0.35/100, v/v) as an eluent, respectively, at 2 mL/min flow rate with ultraviolet detection at 234 nm. For complete nomenclature of the compounds see Abbreviations. *Unknown compound without a conjugated diene structure

The separated isomers were analyzed by HPLC and UV spectra were recorded. In agreement with the findings of the autoxidation of Me 9*c*,11*t*-CLA, three different absorption maxima ($\lambda_{\max}$) values for the three types of geometric isomers were obtained: 230.9 nm for the *trans,trans* isomers, 232.1 nm for the new type of *cis,trans* isomer where the allylic methine is adjacent to the *cis* double bond, and 234.4 nm for the *cis,trans* isomers where the allylic methine is adjacent to the *trans* double bond.

The position of the hydroperoxyl or the hydroxyl group in the individual isomers was determined by GC-MS using trimethylsilyl ethers of the corresponding hydroxystearates, which gave two characteristic fragment ions in mass spectra: *m/z* 229, 259; *m/z* 215, 273; *m/z* 173, 315; and *m/z* 159, 329 for 9-, 10-, 13- and 14-hydroxystearate, respectively.

The position of the 1,3-diene system within the alkyl chain, i.e., whether the double bonds lie between the hydroxyl and the ester group or between the hydroxyl and the methyl group, was determined by a TOCSY experiment by establishing which one of the allylic resonances is closest to the methyl group. The ^{13}C-NMR spectra of the methyl hydroxyoctadecadienoates were assigned with the aid of the 2D-NMR spectra in a similar manner as described in detail previously [12, 37]. Because Me 10*t*,12*c*-CLA produces partly identical hydroperoxides with those from Me 9*c*,11*t*-CLA, only the unpublished

^{13}C-NMR data are listed in Table 1. Characteristic and easily recognizable signals, in addition to the carbonyl, C-2, C-3, methoxy carbon, C-17, and terminal methyl carbon, are the allylic methine at δ_C 72.89–72.91, allylic methylene at δ_C 32.32–32.61, and the olefinic carbons at δ_C 129.43–135.57. The existence of the unusual *cis*,*trans* geometry was evident both from the ^{1}H- and ^{13}C-NMR spectra of Me 14-OOH-10*t*,12*c*. In the ^{1}H-NMR spectrum, which was assigned with the aid of ^{1}H–^{1}H COSY and TOCSY experiments, the methine proton allylic to a *cis* double bond resonated at δ_H 4.85 and is thus ~0.5 ppm less shielded than those allylic to a *trans* double bond [11, 12]. In the ^{13}C-NMR spectrum of Me 14-OOH-10*t*,12*c*, the methine carbon resonated at δ_C 81.44. Thus, this allylic methine carbon adjacent to a *cis* double bond is ~5.3 ppm more shielded than those adjacent to a *trans* double bond. These findings agree with the ^{1}H- and ^{13}C-NMR data on *cis* and *trans* monoene allylic hydroperoxides from methyl oleate autoxidation [38–40]. A more detailed investigation on the NMR properties of the conjugated diene allylic monohydroperoxides produced from Me 10t,12*c*-CLA and also from Me 9c,11*t*-CLA including full assignments of the ^{13}C-NMR spectra is reported elsewhere [41].

Table 1 ^{13}C-NMR chemical shift values (in ppm) of methyl hydroxyoctadecadienoates in CDCl$_3$

Carbon Nucleus	Me 10-OH-11*t*,13*t*	Me 13-OH-9*t*,11*t*	Me 14-OH-10*t*,12*t*
C-1	174.33	174.32	174.34
C-2	34.12	34.10	34.12
C-3	24.94	24.93	24.94
C-4	a	a	a
C-5	a	a	a
C-6	a	a	a
C-7	a	a	a
C-8	25.40	32.59	a
C-9	37.32	135.39	32.61
C-10	72.89	129.53	135.49
C-11	133.60	130.91	129.48
C-12	130.99	133.72	130.95
C-13	129.43	72.91	133.68
C-14	135.57	37.32	72.91
C-15	32.32	25.14	37.05
C-16	31.39	31.80	27.63
C-17	22.24	22.61	22.65
C-18	13.92	14.05	14.04
OCH$_3$	51.45	51.46	51.45

The complete nomenclature is as follows: Methyl 10-(*R*,*S*)-hydroxy-11-*trans*,13-*trans*-octadecadienoate (Me 10-OH-11*t*,13*t*); Methyl 13-(*R*,*S*)-hydroxy-9-*trans*,11-*trans*-octadecadienoate (Me 13-OH-9*t*,11*t*); Methyl 14-(*R*,*S*)-hydroxy-10-*trans*,12-*trans*-octadecadienoate (Me 14-OH-10*t*,12*t*)

[a] Unassigned: Me 10-OH-11*t*,13*t* δ_C 29.12, 29.17, 29.35, 29.48; Me 13-OH-9*t*,11*t* δ_C 28.96, 29.08 (2 C), 29.13; Me 14-OH-10*t*,12*t* δ_C 29.10, 29.12, 29.18 (2 C), 29.26

Mechanism, Isomeric Distribution, and Theoretical Calculations

ESR studies have established that the first-formed pentadienyl radical in methyl linoleate autoxidation exists in the W-conformation [42] which is the most stable of the possible pentadienyl radical conformations. The W-conformation is also the only conformation detected at ambient temperature in the ESR studies with the pentadienyl radical itself [43, 44]. In our previous study [12], the most stable pentadienyl radicals were expected to be formed from the most extended conformation of Me 9*c*,11*t*-CLA and the proposed mechanism for the hydroperoxide pathway was drawn accordingly. In this study, the importance of the different conformations of the precursor lipid was estimated by calculating the energies for conformations A to D of Me 10*t*,12*c*-CLA (see Table 2). In these conformations, the allylic C–H bond that will undergo fragmentation in the hydrogen atom abstraction step is perpendicular or nearly so to the diene π system. This was considered important, because it enables the resonance stabilization to develop already in the transition state. The energy differences of the conformations with respect to conformation A together with the estimation of the distribution of these conformations using the Boltzmann equation are depicted in Table 2. The calculations agreed with our previous assumption that the extended conformation A is the most important contributor to the isomeric distribution of the product hydroperoxides. They also revealed that while the contribution of B is

Table 2 Calculated relative electronic energies (ΔE) at 0 K and enthalpies (ΔH) at 313 K (kcal/mol) of several conformations of 10-*trans*,12-*cis*-CLA methyl ester with respect to the most stable conformation A

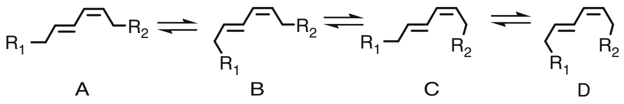

Conformation	ΔE (0 K)	ΔH (313 K)
A	0 (78.9%)	0 (79.3%)
B	+0.8 (20.8%)	+0.8 (20.4%)
C	+3.6 (0.23%)	+3.7 (0.19%)
D	+4.5 (0.06%)	+4.6 (0.05%)

Boltzmann distributions of the conformations based on the calculated energies are given in parenthesis. R_1 = (CH$_2$)$_7$CO$_2$Me, R_2 = (CH$_2$)$_3$CH$_3$

significant, that of C and D may be disregarded. Because the hydroperoxides formed from conformation B could theoretically arise from A (one directly and the other by the β-fragmentation pathway) these calculations proved crucial to our understanding of the autoxidation mechanism; it is now apparent that the six products isolated from the autoxidation of Me 10*t*,12*c*-CLA are kinetic hydroperoxides. This is supported by the obtained product distribution and the absence of conjugated diene hydroperoxides that may be formed by the β-fragmentation pathway. In addition, this agrees with our previous observation that the hydroperoxide mixture was slightly more complex in the absence than in the presence of high amount of α-tocopherol [11]. The experimental evidence also supported the result that conformations C and D are unimportant. For example, Me 10-OOH-11*t*,13*c*, a kinetic hydroperoxide that would theoretically arise from conformations C and D, was absent from the reaction mixture.

A modified mechanism for the hydroperoxide pathway of CLA methyl ester autoxidation in the presence of α-tocopherol (TocOH) that accounts for the theoretical calculations performed in this study is presented in Scheme 2. It is noteworthy, that all hydroperoxides are formed as racemic mixtures of enantiomers, *i.e.* the chiral center is formed without stereoselection. In the first step, the abstraction of one of the four allylic hydrogen atoms from CLA methyl ester leads to a formation of three distinct pentadienyl radicals **2A**, **2B**, and **3** (=**3A** + **3B**; Note: Radicals **3A** and **3B**, formed from conformations A and B by hydrogen atom abstraction from the allylic position adjacent to a *cis* double bond, are interconvertible conformations and thus, the subsequent steps are drawn only for **3A**). Peroxidation of the pentadienyl radicals followed by a fast hydrogen atom transfer from TocOH (ca. 10^6 M^{-1} s^{-1}; [45, 46]) explains the formation of five (**7**, **9**, **13**, **18**, and **21**) of the six conjugated diene allylic hydroperoxides isolated in this study. The most plausible pathway for the formation of the sixth hydroperoxide (**20**) is through rearrangement of the bisallylic peroxyl radical **15** into the conjugated diene peroxyl radical **17** followed by hydrogen atom abstraction.

In addition to conjugated diene hydroperoxides, the mechanism suggests the formation of three nonconjugated diene bisallylic hydroperoxides **8**, **12**, and **19**. These hydroperoxides are anticipated to be more unstable than the conjugated diene hydroperoxides based on the literature on products formed during singlet oxygen oxidation of conjugated dienes [47–49] and on kinetic studies with methyl linoleate [50, 51]. No attempts were made to isolate these hydroperoxides. HPLC analysis of the hydroperoxide mixture at $\lambda = 205$ nm revealed, however, three additional minor peaks that may correspond to these hydroperoxides. The formation of nonconjugated hydroperoxides during autoxidation of CLA has been suggested previously by Eulitz et al. [9] based on the analysis of secondary oxidation products. They speculate, however, that autoxidation and singlet oxygen oxidation of CLA would yield identical products and that the bisallylic hydroperoxides would form by way of a 1,3-addition reaction.

Scheme 2 illustrates that the key reactions governing the product distribution in the autoxidation of CLA in the presence of a good hydrogen atom donor are (1) the abstraction of one of the four allylic hydrogen atoms, (2) partitioning of oxygen on the resulted pentadienyl radicals, (3) hydrogen atom transfer from TocOH, and (4) β-fragmentation of the intermediate bisallylic peroxyl radicals. Since experimental and theoretical data on the latter two have been published [26, 45, 46, 50, 51], the first two key reactions were addressed by theoretical calculations.

It is generally accepted that the rate constant for hydrogen atom abstraction depends primarily on the strength of the C–H bond being broken [26, 52, 53]. Therefore, the bond dissociation enthalpies (BDEs) for the allylic C–H bonds of the precursor lipid in conformations A and B were calculated and the results are listed in Table 3. The calculated C–H BDEs values range between 73.7 and 75.0 kcal/mol and thus fall in between the monoallylic C–H BDE (79.2 kcal/mol) and the bisallylic C–H BDE (67.5 kcal/mol) values that were calculated at the same temperature and level of theory. It is of interest to note that hydrogen atom abstraction from an allylic position seems to be easier when adjacent to a *trans* double bond than when adjacent to a *cis* double bond. Of the two pentadienyl radicals derived from conformation A, **2A** (W-conformation) was 1.3 kcal/mol lower in energy than **3A** (Z-conformation). This is in relatively good agreement with the experimental values on W- and Z-pentadienyl radicals derived from 1,4-pentadiene [54]. Moreover, based on the results, the direct interconversion of **2A** and **2B** may be discounted on energetic grounds and by analogy with the pentadienyl radical itself [42, 55].

It is reasonable to expect that the addition of oxygen to the intermediate pentadienyl radicals occurs preferentially at centers having the highest spin density [26, 51]. Therefore, the unpaired spin density distribution was calculated for the pentadienyl radicals formed from conformations A and B and the results are illustrated in Fig. 2. The spin density occupies *p*-type orbitals with the lobes perpendicular to the plane of the conjugated system. The degree of spin polarization of the radicals is high and the two carbon atoms (C-10 and C-12 in **2A** and **2B**; C-11 and C-13 in **3A** and **3B**) between the three main spin centers possess a notable spin density of opposite sign. The gross spin density i.e. the sum of unpaired α and β spin amounts to ca. 1.6 electrons in the radicals studied. The spin contamination

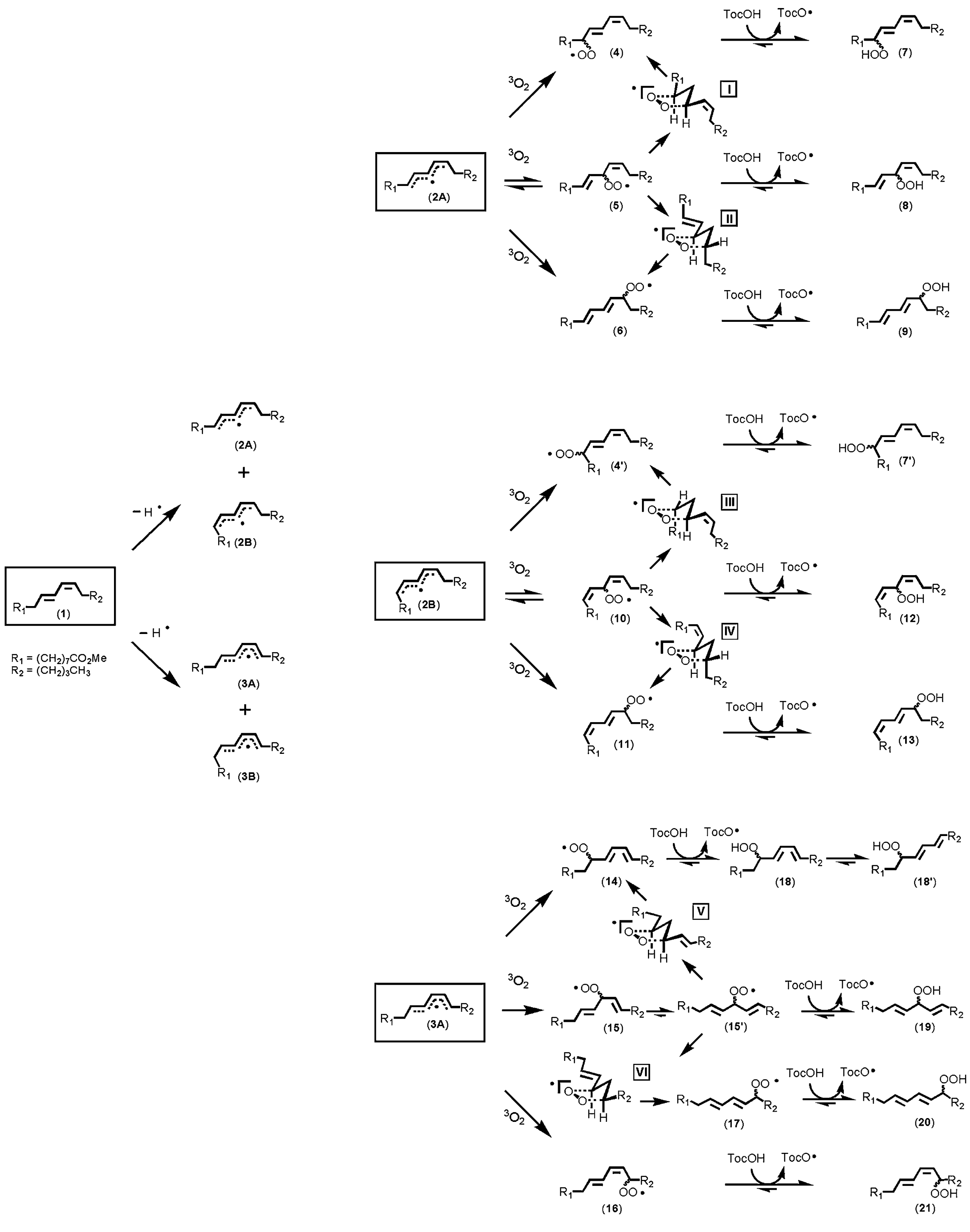
(1)
$R_1 = (CH_2)_7CO_2Me$
$R_2 = (CH_2)_3CH_3$
– H•
(2A)
(2B)
(3A)
(3B)
$^3O_2$
TocOH
TocO•
I
II
III
IV
V
VI
(4)
(5)
(6)
(7)
(8)
(9)
(4')
(7')
(10)
(11)
(12)
(13)
(14)
(15)
(15')
(16)
(17)
(18)
(18')
(19)
(20)
(21)

Scheme 2 A proposed mechanism for the hydroperoxide pathway of CLA autoxidation in the presence of α-tocopherol (TocOH)

was evaluated and found to be within acceptable limits; the $<S^2>$expectation value, which serves as a useful diagnostic also within DFT [56], was 0.79 for all radicals compared to the ideal non-spin polarized value of 0.75.

By coincidence, radicals **2A** and **2B** are identical to those formed by abstraction of a bisallylic hydrogen atom from Me 9*t*,12*c*-linoleate and from Me 9*c*,12*c*-linoleate, respectively. The calculated spin density values for **2A** and **2B** were slightly smaller than the experimental values obtained by ESR spectroscopy [42, 57] but comparable to those calculated by Pratt et al. for 1,5-dimethylpentadienyl radicals [26]. The calculations suggest that the central

Table 3 Calculated allylic C-H BDEs of 10-*trans*,12-*cis*-CLA methyl ester in conformations A and B as electronic energies (ΔE) at 0 K and as enthalpies (ΔH) at 313 K (kcal/mol), and the relative enthalpies ΔH (kcal/mol) of the conformations (reactants) and the pentadienyl radicals (products) with respect to the most stable conformation and pentadienyl radical (A and 2A, respectively)

Entry	BDE ΔE	BDE ΔH	ΔH (reactant)	ΔH (product)
1. 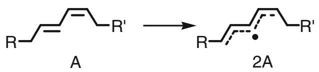	80.6	73.7	0	0
2. 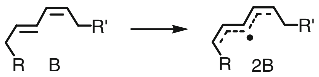	81.0	74.2	+0.8	+1.3
3. 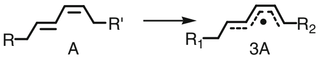	81.9	74.9	0	+1.3
4. 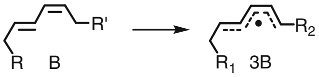	82.0	75.0	+0.8	+2.2

R_1 = $(CH_2)_7CO_2Me$, R_2 = $(CH_2)_3CH_3$

carbon atom of **2A** and **2B**, C-11, bears the highest spin density. Recent studies support this result; the bisallylic 11-hydroperoxides are the major oxidation products in the autoxidation of Me 9*t*,12*c*-linoleate and of Me 9*c*,12*c*-linoleate under kinetic conditions and at low conversion [50, 51].

According to the calculations there is a slightly higher spin density in **2A** at the *cisoid* end of the pentadienyl radical compared to the *transoid* end whereas in **2B** there is equal spin distribution at the two termini. The ESR measurements are consistent with this result [42, 57]. The calculations and the ESR both suggest that while the reaction of **2B** should lead to equal formation of **4′** and **11**, the *cisoid* end of **2A** should react faster with oxygen than the *transoid* end, leading to the preferential formation of peroxyl radical **6** over **4**. Subsequent hydrogen atom transfer from TocOH to **6** and **4** should produce more hydroperoxide **9** than **7**. This contradicts with our experimental results. Since the observed isomeric distribution of hydroperoxides in the autoxidation of Me 9*t*,12*c*-linoleate [36, 51] also contradicts with the calculations and ESR data, it seems apparent that the unpaired spin density alone does not control the partitioning of oxygen in geometrically unsymmetrical pentadienyl radicals such as **2A**. Tallman et al. [51] have proposed that the biased product distribution in the autoxidation of Me 9*t*,12*c*-linoleate results from rearrangement of the bisallylic peroxyl radicals into conjugated diene peroxyl radicals via intermediate radical-dioxygen complexes similar to allylic radical-dioxygen

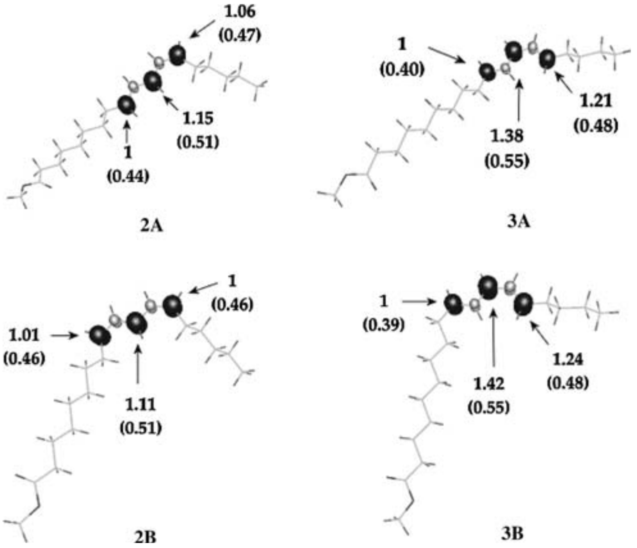

Fig. 2 Calculated relative Mulliken unpaired spin distribution in the pentadienyl radicals formed from conformations A and B of 10-*trans*,12-*cis*-CLA methyl ester (total Mulliken spin densities in parenthesis). *Dark gray* denotes excess α spin density, light gray excess *β* spin density. The numbering of the radicals corresponds to Scheme 2

complexes in the isomerization of allylic hydroperoxides. This is a plausible explanation also in the case of CLA autoxidation. Hence, the rearrangement of the bisallylic peroxyl radical **5** to conjugated diene peroxyl radicals **4** and **6** would occur through two distinct isomeric radical-dioxygen complexes, **I** and **II**. The formation of **I** derives from the rearrangement across the *trans* double bond and that of **II** across the *cis* double bond. The low-energy conformation of **I** would be a five-membered ring envelope structure where the substituents are both at equatorial positions and thus, is expected to be favored over the formation of **II** where one of the substituents is at equatorial and the other at axial position. As a consequence, the formation of the peroxyl radical **4** would be preferred over the peroxyl radical **6**, and thereafter the formation of the hydroperoxide **7** in accordance with our observations.

For radicals **3A** and **3B,** the calculations predict an even higher spin density at the central carbon atom of the pentadienyl radical than in **2A** and **2B**. In addition, the spin distribution at the two termini of **3A** and of **3B** is unequal. No ESR data on fatty acid pentadienyl radicals with this geometry have been reported. However, the ESR data for the Z-conformation of the pentadienyl radical itself [43, 55] reveals that the central carbon atom bears the highest spin density and it is comparable to our calculated values. Consequently, the major product in the peroxidation of **3A** should be the bisallylic peroxyl radical **15** that may rearrange through two distinct isomeric radical-dioxygen complexes, **V** and **VI**, to the conjugated diene peroxyl radicals **14** and **17**, and thereafter to equal amounts of the hydroperoxides **18** and **20**. Moreover, oxygen should not partition equally at the two termini of **3A** (or of **3B**). More peroxyl radical **16** than **14**, and thereafter more hydroperoxide **21** than **18** should be formed. Accordingly, slightly less hydroperoxide **21** was observed than what was expected. This might, however, result from the peroxyl radical **16** being more prone to isomerization and/or decomposition than the other peroxyl radicals because of its unusual *cis*,*trans* diene geometry.

As summarized in Scheme 2, the theoretical calculations provided an improved framework for understanding the formation of the isomeric distribution**.** The diastereoselectivity in favor of Me 9-OOH-10*t*,12*c* (**7**) may now be easily explained. Not only is this isomer formed in excess from **2A**, based on the analogy to the autoxidation of 9*t*,12c-methyl linoleate [51], but it is also formed from **2B**. Because the symmetrical radical **2B** is identical to that produced from 9*c*,12*c*-methyl linoleate [50], the reaction of **2B** leads to equal amounts of hydroperoxides **7** and **13** and thus, roughly one fourth of the main isomer **7** is formed through radical **2B**. Moreover, because the isolated products are kinetic products, it seems now apparent that *β*-fragmentations other than those of the bisallylic hydroperoxides are not important contributors to the isomeric distribution under these reaction conditions. The formation of a small amount of Me 13-OOH-9*t*,11*t* in the autoxidation of Me 9*c*,11*t*-CLA (corresponds to 9-OOH-10*t*,12*t*, which was not isolated in this study) through the *β*-fragmentation of a conjugated diene peroxyl radical is, however, highly plausible. In addition, as the isomerization of conjugated diene peroxyl radicals is so well established [33–36], it is safe to assume that three additional conjugated diene hydroperoxides, *i.e.* altogether nine conjugated diene hydroperoxides, are formed during autoxidation of Me 10*t*,12*c*-CLA in the absence of α-tocopherol. More research is needed to confirm the formation of the thermodynamic products.

The isomeric distribution of product hydroperoxides was expected to reflect the stability of the intermediate pentadienyl radicals. Calculations showed that **2A** was, as anticipated, the most stable (Table 3). Interestingly, the radicals **2B** and **3A** were of similar energy. Thus, more radicals **2A** + **2B** should be formed than radicals **3A** + **3B**. When only conformations A and B of the precursor lipid are considered significant, the ratio between radicals may be estimated based on the enthalpy differences (ΔHs) via the Boltzmann distribution. The calculated enthalpy difference between conformations A and B, 0.84 kcal/mol, gives an initial ratio A/B of 3.9/1. Considering the BDEs for the formation of the pentadienyl radicals the estimated ratio (**2A** + **2B**)/(**3A** + **3B**) becomes 6.6/1. Experimentally this ratio was roughly 3.5/1 based on the ratio (9- and 13-hydroperoxides)/(10- and 14-hydroperoxides) determined by HPLC. The difference between the theoretical and experimental ratio may be partly explained by noting that radicals **2A** and **2B** with their lower BDEs are more stable and thus less prone to undergo reaction [58]. To explore this, the reaction energies were calculated for the peroxidation and they are, indeed, *ca.* 1 kcal/mol less negative for **2A** and **2B** than for **3A** and **3B**, which would shift the distribution towards products formed from the latter two radicals. It must be emphasized, however, that the theoretical ratio is based merely on the ΔH values and it ignores all other factors such as reaction barriers and stereoelectronics that influence the course of the reactions.

Conclusions

The hydroperoxide pathway is one of the reaction pathways of CLA autoxidation in the presence of a good hydrogen atom donor. The mechanistic proposal developed for this pathway based on our previous work [11, 12] and this study serves as means for predicting the hydroperoxides and their isomeric distribution formed during autoxidation of yet another CLA isomer and it facilitates further investigations directed to a complete elucidation of the presented reaction mechanism. More research is required for example to establish the formation of the nonconjugated hydroperoxides as well as the details of the suggested isomerizations of the bisallylic peroxyl radicals. Knowledge of these initial steps is crucial for understanding the subsequent steps in the CLA autoxidation. In particular, it allows us to predict the structures of the oligomeric products that can be envisioned to be formed by addition of the peroxyl radicals to the double bond system of the oxidizing conjugated fatty acid ester. We anticipate that this addition reaction is the major pathway in the CLA autoxidation performed in the absence of a good hydrogen atom donor. However, in biological systems CLA is present only in small amounts and the likelihood of the autoxidative polymerization can be expected to be low. Therefore, the clarification of the reaction mechanism of the hydroperoxide formation can be considered to be of high importance when studying the biological significance of CLA isomers. This study offers now for the first time means of producing and separating intact CLA methyl ester hydroperoxides that may be used for evaluating their biological activity or for studying their secondary oxidation reactions.

Acknowledgments The authors wish to acknowledge funding support from the Finnish Cultural Foundation, the Emil Aaltonen Foundation, and the Orion Corporation Research Foundation. CSC—The Finnish IT Center for Science is acknowledged for providing computational resources.

References

1. Pariza MW, Park Y, Cook ME (2001) The biologically active isomers of conjugated linoleic acid. Prog Lipid Res 40:283–298
2. Belury MA (2002) Inhibition of carcinogenesis by conjugated linoleic acid: potential mechanisms of action. J Nutr 132:2995–2998
3. Evans ME, Brown JM, McIntosh MK (2002) Isomer-specific effects of conjugated linoleic acid (CLA) on adiposity and lipid metabolism. J Nutr Biochem 13:508–516
4. Allen RR, Jackson A, Kummerrow FA (1949) Factors which affect the stability of highly unsaturated fatty acids. I. Differences in the oxidation of conjugated and nonconjugated linoleic acid. J Am Oil Chem Soc 26:395–399
5. Kern W, Heinz AR, Stallman J (1955) Über die Autoxydation ungesättigter Verbindungen. IV. Die Autoxydation des 2,3-Dimethylbutadiens(1.3) und des 10,12-Octadecadiensäuremethylesters. Macromol Chem 16:21–35
6. Kern W, Heinz AR, Höhr D (1956) Über die Autoxydation ungesättigter Verbindungen. VI. Die Autoxydation des 9,11-Octadecadiensäuremethylesters. Macromol Chem 18/19:406–413
7. Privett OS (1959) Autoxidation and autoxidative polymerization. J Am Oil Chem Soc 36:507–512
8. Yurawecz MP, Sehat N, Mossoba MM, Roach JAG, Ku Y (1997) Oxidation products of conjugated linoleic acid and furan fatty acids. In: McDonald RE, Mossoba MM (eds) New techniques and applications in lipid analysis. AOCS Press, Champaign
9. Eulitz K, Yurawecz MP, Ku Y (1999) The oxidation of conjugated linoleic acid. In: Yurawecz MP, Mossoba MM, Kramer JKG, Pariza MW, Nelson GJ (eds) Advances in conjugated linoleic acid research, vol 1. AOCS Press, Champaign
10. Yurawecz MP, Delmonte P, Vogel T, Kramer JKG (2003) Oxidation of conjugated linoleic acid: initiators and simultaneous reactions: theory and practice. In: Sébédio J-L, Christie WW, Adlof R (eds) Advances in conjugated linoleic acid research, vol 2. AOCS Press, Champaign
11. Hämäläinen TI, Sundberg S, Mäkinen M, Kaltia S, Hase T, Hopia A (2001) Hydroperoxide formation during autoxidation of conjugated linoleic acid methyl ester. Eur J Lipid Sci Technol 103:588–593
12. Hämäläinen TI, Sundberg S, Hase T, Hopia A (2002) Stereochemistry of the hydroperoxides formed during autoxidation of CLA methyl ester in the presence of α-tocopherol. Lipids 37:533–540
13. Minemoto Y, Adachi S, Shimada Y, Nagao T, Iwata T, Yamauchi-Sato Y, Yamamoto T, Kometani T, Matsuno R (2003) Oxidation kinetics for cis-9, trans-11 and trans-10, cis-12 isomers of CLA. J Am Oil Chem Soc 80:675–678
14. Davis AL, McNeill GP, Caswell DC (1999) Analysis of conjugated linoleic acid isomers by ^{13}C NMR spectroscopy. Chem Phys Lipids 97:155–165
15. Ueda S, Hayashi T, Namiki M (1986) Effect of ascorbic acid on lipid autoxidation in a model food system. Agric Biol Chem 50:1–7
16. Chan HW-S, Levett G (1977) Autoxidation of methyl linoleate, separation and analysis of isomeric mixtures of methyl linoleate hydroperoxides and methyl hydroxylinoleates. Lipids 12:99–104
17. Becke AD (1993) Density-functional thermochemistry. III. The role of exact exchange. J Chem Phys 98:5648–5652
18. Lee C, Yang W, Parr RG (1988) Development of the Colle–Salvetti correlation-energy formula into a functional of the electron density. Phys Rev B 37:785–789
19. Ahlrichs R, Bär M, Häser M, Horn H, Kölmel C (1989) Electronic structure calculations on workstation computers: the program system TURBOMOLE. Chem Phys Lett 162:165–169
20. Weigend F, Ahlrichs R (2005) Balanced basis sets of split valence, triple zeta valence and quadruple zeta valence quality for H to Rn: design and assessment of accuracy. Phys Chem Chem Phys 7:3297–3305
21. Klamt A, Schüürmann G (1993) COSMO: a new approach to dielectric screening in solvents with explicit expressions for the screening energy and its gradient. J Chem Soc Perkin Trans 2:799–805
22. Schäfer A, Klamt A, Sattel D, Lohrenz JCW, Eckert F (2000) COSMO implementation in TURBOMOLE: extension of an efficient quantum chemical code towards liquid systems. Phys Chem Chem Phys 2:2187–2193
23. Lide DR (ed) (1999) CRC handbook of chemistry and physics, 80th edn. CRC Press, Boca Raton
24. Johansson MP, Sundholm D, Gerfen G, Wikström M (2002) The spin distribution in low-spin iron porphyrins. J Am Chem Soc 124:11771–11780
25. Bakalbassis EG, Chatzopulou A, Melissas VS, Tsimidou M, Tsolaki M, Vafiadis A (2001) Ab initio and density functional theory studies for the explanation of the antioxidant activity of certain phenolic acids. Lipids 36:181–191
26. Pratt DA, Mills JH, Porter NA (2003) Theoretical calculations of carbon-oxygen bond dissociation enthalpies of peroxyl radicals formed in the autoxidation of lipids. J Am Chem Soc 125:5801–5810
27. Lilienkampf A, Johansson MP, Wähälä K (2003) (*Z*)-1-Aryl-1-haloalkenes as intermediates in the Vilsmeier haloformylation of aryl ketones. Org Lett 5:3387–3390

28. Zhang W, Shi B, Shi J (2007) A theoretical study on autoxidation of unsaturated fatty acids and antioxidant activity of phenolic compounds. J Am Leather Chem Assoc 102:99–105
29. Fu Y, Liu L, Liu R, Guo Q-X (2005) Homolytic bond dissociation energies of 4-substituted bicyclo[2.2.2]octanyl compounds: inductive/field effects on the stabilities of organic radicals. J Phys Org Chem 18:529–538
30. Gardner HW (1989) Oxygen radical chemistry of polyunsaturated fatty acids. Free Radic Biol Med 7:65–86
31. Frankel EN (1998) Lipid oxidation, vol 10. The Oily Press, Dundee
32. Luna P, de la Fuente MA, Salvador D, Márquez-Ruiz G (2007) Differences in oxidation kinetics between conjugated and non-conjugated methyl linoleate. Lipids 42:1085–1092
33. Chan HW-S, Levett G, Matthew JA (1979) The mechanism of the rearrangement of linoleate hydroperoxides. Chem Phys Lipids 24:245–256
34. Porter NA, Weber BA, Weenen H, Khan JA (1980) Autoxidation of polyunsaturated lipids. Factors controlling the stereochemistry of product hydroperoxides. J Am Chem Soc 102:5597–5601
35. Porter NA, Lehman LS, Weber BA, Smith KJ (1981) Unified mechanism for polyunsaturated fatty acid autoxidation. Competition of peroxy radical hydrogen atom abstraction, β-scission, and cyclization. J Am Chem Soc 103:6447–6455
36. Porter NA, Wujek DG (1984) Autoxidation of polyunsaturated fatty acids, an expanded mechanistic study. J Am Chem Soc 106:2626–2629
37. Hämäläinen TI, Kamal-Eldin A (2005) Analysis of lipid oxidation products by NMR spectroscopy. In: Kamal-Eldin A, Pokornÿ J (eds) Analysis of lipid oxidation. AOCS Press, Champaign
38. Garwood RF, Khambay BPS, Weedon BCL, Frankel EN (1977) Allylic hydroperoxides from the autoxidation of methyl oleate. J Chem Soc Chem Commun pp 364-365
39. Frankel EN, Garwood RF, Khambay BPS, Moss GP, Weedon BCL (1984) Stereochemistry of olefin and fatty acid oxidation. Part 3. The allylic hydroperoxides from the autoxidation of methyl oleate. J Chem Soc Perkin Trans 1:2233–2240
40. Porter NA, Mills KA, Carter RL (1994) A mechanistic study of oleate autoxidation: competing peroxyl H-atom abstraction and rearrangement. J Am Chem Soc 116:6690–6696
41. Pajunen TI, Koskela H, Hase T, Hopia A (2008) NMR properties of conjugated linoleic acid (CLA) methyl ester hydroperoxides. Chem Phys Lipids. doi:10.1016/j.chemphyslip.2008.05.001
42. Bascetta E, Gunstone FD, Walton JC (1983) An electron spin resonance study of fatty acids and esters. Part 1. Hydrogen abstraction from oleic acid and acetylenic long chain esters. J Chem Soc Perkin Trans 2:603–613
43. Sustmann R, Schmidt H (1979) Pentadienyl-Radicale-Struktur und Spindichteverteilung. Chem Ber 112:1140–1447
44. Griller D, Ingold KU, Walton JC (1979) Two conformations of the pentadienyl radical. J Am Chem Soc 101:758–759
45. Burton GW, Hughes L, Ingold KU (1983) Antioxidant activity of phenols related to vitamin E. Are there chain-breaking antioxidants better than α-tocopherol? J Am Chem Soc 105:5950–5951
46. Burton GW, Doba T, Gabe EJ, Hughes L, Lee FL, Prasad L, Ingold KU (1985) Autoxidation of biological molecules. 4. Maximizing the antioxidant activity of phenols. J Am Chem Soc 107:7053–7065
47. Manring LE, Kanner RC, Foote CS (1983) Chemistry of singlet oxygen. 43. Quenching by conjugated olefins. J Am Chem Soc 105:4707–4710
48. Manring LE, Foote CS (1983) Chemistry of singlet oxygen. 44. Mechanism of photooxidations of 2,5-dimethylhexa-2,4-diene and 2-methyl-2-penten. J Am Chem Soc 105:4710–4717
49. O'Shea KE, Foote CS (1988) Chemistry of singlet oxygen. 51. Zwitterionic intermediates from 2,4-hexadienes. J Am Chem Soc 110:7167–7170
50. Tallman KA, Pratt DA, Porter NA (2001) Kinetic products of linoleate peroxidation: rapid β-fragmentation of nonconjugated peroxyls. J Am Chem Soc 123:11827–11828
51. Tallman KA, Roschek B Jr, Porter NA (2004) Factors influencing the autoxidation of fatty acids: effect of olefin geometry of the nonconjugated diene. J Am Chem Soc 126:9240–9247
52. Chan HW-S (1987) The mechanism of autoxidation. In: Chan HW-S (ed) Autoxidation of unsaturated lipids. Academic Press, London
53. Porter NA, Caldwell SA, Mills KA (1995) Mechanisms of free radical oxidation of unsaturated lipids. Lipids 30:277–290
54. Macinnes I, Walton JC (1985) Rotation barriers in pentadienyl and pent-2-en-4-ynyl radicals. J Chem Soc Perkin Trans 2:1073–1076
55. Davies AG, Griller D, Ingold KU, Lindsay DA (1981) An electron spin resonance study of pentadienyl and related radicals: homolytic fission of cyclobut-2-enylmethyl radicals. J Chem Soc Perkin Trans 2:633–641
56. Gräfenstein J, Cremer D (2001) On the diagnostic value of $<S^2>$ in Kohn–Sham density functional theory. Mol Phys 99:981–989
57. Bascetta E, Gunstone FD, Scrimgeour CM, Walton JC (1982) E.S.R. observation of pentadienyl and allyl radicals on hydrogen abstraction from unsaturated lipids. J Chem Soc Chem Commun pp 110–112
58. van Speybroeck V, Marin GB, Waroquier M (2006) Hydrocarbon bond dissociation enthalpies: from substituted aromatics to large polyaromatics. Chem Phys Chem 7:2205–2214

Lipids (2008) 43:611–618
DOI 10.1007/s11745-008-3187-0

ORIGINAL ARTICLE

Peroxisome Proliferator-Activated Receptor α Agonists Regulate Cholesterol Ester Transfer Protein

Thomas P. Beyer · Yanqun Chen · Regina K. Porter · Deshun Lu · Robert J. Schmidt · Nathan B. Mantlo · Robert J. Konrad · Guoqing Cao

Received: 28 January 2008 / Accepted: 22 April 2008 / Published online: 15 May 2008
© AOCS 2008

Abstract Peroxisome proliferator-activated receptor α (PPARα) belongs to the nuclear receptor superfamily that regulates multiple target genes involved in lipid metabolism. Cholesterol ester transfer protein (CETP) is a secreted glycoprotein that modifies high-density lipoprotein (HDL) particles. In humans, plasma CETP activity is inversely correlated with HDL cholesterol levels. We report here that PPARα agonists increase CETP mRNA, protein and accordingly its activity. In a human CETP transgenic animal model harboring the natural flanking regions (Jiang et al. in J Clin Investigat 90:1290–1295, 1992), both fenofibrate and a specific synthetic PPARα agonist LY970 elevated human CETP mRNA in liver, serum protein and CETP activity. In hamsters, the endogenous liver CETP mRNA level and the serum CETP activity were dose-dependently upregulated by fenofibrate. In addition Wy14643, a PPARα agonist, also significantly elevated CETP mRNA and activity. In a carcinoma cell line of hepatic origin, HepG2 cells, overexpression of PPARα resulted in increased CETP mRNA and agonist treatment further elevated CETP mRNA levels. We conclude that PPARα agonists upregulate CETP expression and activity and may play an important role in PPARα (agonist mediated HDL cholesterol homeostasis in humans.

Introduction

Peroxisome proliferator-activated receptor α (PPARα) together with PPARγ and PPARδ form a subfamily of nuclear receptors that play a critical role in mediating lipid homeostasis, inflammation and metabolism. PPARγ plays a key role in adipocyte differentiation and is the molecular target of anti-diabetic thiazolidinediones (TZD) [1]. PPARδ modulates lipid metabolism and inflammation in multiple tissues [2]. PPARα primarily regulates fatty acid oxidation and also regulates many target genes such as apolipoprotein AI (ApoAI) [3], apolipoprotein CIII (ApoCIII) [4], apolipoprotein AV (ApoAV) [5], phospholipid transfer protein (PLTP) [6] and scavenger receptor class B, type I (SR-BI) in liver [7] that are intimately involved in lipoprotein metabolism.

Cholesterol ester transfer protein (CETP) is a 74 KDa glycoprotein that is primarily synthesized in liver [8]. The secreted protein is mainly associated with high-density lipoprotein (HDL) and catalyzes the neutral lipid exchange (cholesterol ester from HDL to triglyceride-rich lipoprotein particles and TG vice versa) among lipoprotein particles. Increased plasma CETP activity is inversely associated with HDL cholesterol levels [9]. While convincing epidemiological data strongly suggest the protective role of HDL cholesterol in cardiovascular diseases, the exact role of CETP in coronary artery diseases, however, remains controversial. In recent years, CETP has emerged as a major therapeutic target to modulate HDL cholesterol levels and cardiovascular diseases. CETP inhibitor CP-529,414 (torcetrapib) dose-dependently inhibited plasma CETP activity, elevated HDL cholesterol and reduced low-density lipoprotein (LDL) cholesterol levels in recent clinical studies [10–12]. However, the phase III study of torcetrapib was halted because of significantly increased cardiovascular and

---

Thomas P. Beyer and Yanqun Chen contributed equally to this work.

T. P. Beyer · Y. Chen · R. K. Porter · D. Lu ·
R. J. Schmidt · N. B. Mantlo · R. J. Konrad · G. Cao (✉)
Cardiovascular Research, Lilly Research Laboratories,
Eli Lilly & Company, Indianapolis, IN 46285, USA
e-mail: guoqing_cao@lilly.com

total mortality [12]. While the exact reasons are being explored for the adverse mortality rate resulting from CETP inhibition using torcetrapib, torcetrapib was found to induce aldosterone levels and increase blood pressure in humans [12]. In addition, plasma electrolytes were also changed in patients treated with torcetrapib [12]. These observations on torcetrapib are believed to be off-target activity of torcetrapib, as other structurally divergent CETP inhibitors do not exhibit similar off-target activities [13, 14]. In addition, there have been no reports on blood pressure changes in human subjects with homozygous CETP deficiency.

To study the in vivo function of CETP, human CETP transgenic mice were generated using either metallothionein promoter [15] or its own genomic fragments (CETP minigene transgenic mice) [16]. The metallothionein promoter directed CETP transgenic mice did not have significant changes in HDL cholesterol although there was significant expression of human CETP under the basal condition. This was primarily due to the fact that CETP favors large HDL particles and in mice such HDL particles are relatively minor components of HDL [15]. The CETP minigene transgenic mice with its own natural flanking regions are responsive to diet-cholesterol, i.e. the increases in CETP transgene expression and its activity under hypercholesterolemic conditions [16]. A liver X receptor (LXR) basis was established recently for the observed cholesterol regulation of human CETP gene [17]. Synthetic LXR agonists thus regulate CETP expression in liver and possibly in adipose tissue as well [17].

Fatty acids are believed to be the natural ligands of PPARα. Fenofibrate as a hypolipidemic drug is also believed to act as a weak PPARα agonist [18]. In recent years, many potent synthetic pharmacological agonists have been made including LY970 that have demonstrated potent efficacy in reducing plasma triglyceride levels and elevating HDL cholesterol in an ApoAI transgenic animal model [19]. In humans, the fibrate class of drugs is known to effectively reduce plasma triglyceride levels but has only minimum to moderate effects in increasing HDL cholesterol levels [20, 21]. The modest change of HDL cholesterol mediated by PPARα agonists is thus intriguing in light of the combined regulations of ApoAI, PLTP and SR-BI that are expected to dramatically elevate HDL cholesterol levels. Human ApoAI transgenic mice have significantly elevated plasma HDL cholesterol [22]. PLTP is an HDL remodeling protein that contributes to PPARα agonist mediated HDL particle size increase [6] and SR-BI is an HDL receptor, reduced level of which leads to significantly elevated HDL cholesterol in mice [23].

We present evidence here in this report that PPARα agonists upregulate CETP. Because of the pleiotropic effects of PPARα agonists in regulating lipid homeostasis and also the limitation of the human CETP transgenic mice in studying the CETP activity link to its HDL cholesterol effect, it is difficult to assess the exact impact on HDL cholesterol homeostasis in our studies directly. However, based on the well established link of plasma CETP activity and HDL cholesterol levels in humans, our results suggest that this regulation may result in the attenuation of HDL cholesterol elevation mediated by PPARα agonists and thus may play a critical role in PPARα agonist mediated HDL cholesterol homeostasis in CETP species.

Methods

Materials

Fenofibrate, Wy14643, triolein and salts were obtained from Sigma-Aldrich (St Louis, MO). Cholesterol Oleate and POPC were obtained from Avanti Polar Lipids (Alabaster, AL). BODIPY-CE analogue was obtained from Molecular Probes (Eugene, OR). Purified human VLDL was obtained from Intracel (Frederick, MD). LY970, 2-(4-{3-[1-(3,4-Dimethyl-benzyl)-4-methyl-5-oxo-4,5-dihydro-1H-[1,2,4]triazol-3-yl]-propyl}-phenoxy)-2-methyl-propionic acid, was made at Lilly Research Laboratories as described [19].

Animals

All experiments involving animals were approved by the Institutional Animal Care and Use Committee of Eli Lilly and Company, Indianapolis, Indiana. The human CETP minigene transgenic mice were described previously [16]. Seven-week old male CETP human transgenic mice under the control of the natural human promoter were obtained from The Jackson Laboratory (Bar Harbor, ME, Stock No. 003904) and acclimated for 2 weeks prior to the start of the studies. Each study used 4–6 mice per group and the mice were individually caged. Light was controlled on a 12 h on 12 h off light/dark cycle. The mice were provided Purina 5001 chow ad libitum and had free access to water throughout the experiments. Compounds were dosed daily by oral gavage in CMC/Tween80 (1.0%/0.25%) vehicle for 7 days. The animals were sacrificed by CO_2 asphyxiation 3 h after the last dose. Blood samples for serum preparation were collected by cardiac puncture and livers were collected and frozen in liquid nitrogen. Eight-week old male Syrian Golden Hamsters (six per group) were obtained from Harlan Sprague Dawley (Indianapolis, IN) and acclimated 2 weeks prior to the start of the study. The hamsters were housed 5 per cage. Light was controlled on a 12 h on 12 h off light/dark cycle. The hamsters were provided Purina 36315 chow ad libitum and had free access to water throughout the experiments. Compounds were dosed daily by oral gavage in CMC/Tween80 (1.0%/0.25%) vehicle for 14 days. The animals were sacrificed by CO_2 asphyxiation 3 h after the last dose. Blood samples for serum preparation were collected by cardiac puncture and livers were collected and frozen in liquid nitrogen.

CETP Activity

A donor particle containing a fluorescent cholesterol ester analogue that self quenches its fluorescent signal was prepared similarly to what was described by Bisgaier et al. [24]. The particle contained 15 mol% BODIPY-CE analogue, 33 mol% cholesteryl oleate, 8 mol% triolein, and 44 mol% POPC. The donor particle was added to a Tris/NaCl buffer with an acceptor particle (purified human VLDL at final concentration of 25 μg/ml). Serum from the animals was added to the mixture and incubated 30 min at 37°C. Fluorescent signal at wavelengths 544 nm excitation, 595 nm emission with a 590 nm cutoff filter in a Gemini fluorescent plate reader (Molecular Devices, Sunnyvale, CA) represents CETP activity.

Plasma CETP Levels

An ELISA (Wako Diagnostics, Richmond, VA) was used to measure CETP protein concentration in mouse serum. The serum samples were serially diluted with PBS and the assay was performed as described according to the manufacturer's instructions.

Plasma Lipid Analysis

Serum triglyceride was measured in an automated clinical analyzer (Roche, Indianapolis, IN). Lipoproteins were analyzed by FPLC as described in Cao et al. [25].

mRNA Measurement

RNA was prepared with RNeasy Mini Kit (QIAGEN, Valencia, CA) or Total RNA Chemistry products for the ABI Prism 6100 Nucleic Acid PrepStation (PE Applied BioSystems, Foster City, CA, USA). Taqman real-time quantitative PCR (Q-PCR) was performed using an ABI Prism 7900 sequence detector (PE Applied BioSystems, Foster City, CA) with GAPDH as an internal control for HeG2 cells and 18S as an internal control for animal liver samples. Gene-specific primer probes were obtained from Applied BioSystems. Relative expression of the genes was determined by C_t method and calculated to fold induction against the controls.

Cell Culture Studies

Full length human PPARα cDNA was cloned from human liver and the sequence was confirmed by DNA sequencing. It was then subcloned into the mammalian expression vector pcDNA3.1(+) with *Kpn*I and *Not*I sites. The PPARα expression vector was used to establish a HepG2 Stable cell line in which PPARα was expressed at 80 fold (mRNA) over the basal expression level through standard Geneticin (G418, Invitrogen, Carlsbad, CA) selection procedure (800 μg/ml). HepG2 and HepG2 PPARα stable cells were grown in 3/1 DME/F12 + 10% FBS and seeded in 24-well plates at the density of 8×10^4 cells/well. Twenty-four hours later, the cells were treated with either DMSO or PPARα agonists for 48 h. RNAs were then prepared and analyzed as described above.

Statistics

Values are given as mean ± standard error of mean (SEM). Statistical differences, as defined as $P < 0.05$, from the vehicle control group were determined using Dunnett's test or *t* tests (JMP 5.1.1, SAS, Cary, NC).

Results

To explore whether PPARα agonists regulate CETP, we initially used a human CETP mini-gene transgenic mice. This mouse model utilized a DNA fragment containing the human CETP gene including coding regions, introns and flanking regulatory sequences to express the transgene product primarily in liver [16]. It has been shown previously that cholesterol rich diet induced hepatic CETP mRNA and activity in this model and the molecular basis for the observed regulation was traced to an LXR basis [16, 17]. We treated the animals ($n = 4$) using fenofibrate for 7 days and 3 h after the last dose, we sacrificed the animals and analyzed the data. Serum triglyceride level was reduced by 38% (Fig. 1a), suggesting the activation of PPARα in vivo. Serum CETP activity was assessed and demonstrated a significant increase (61%) (Fig. 1b). Measuring serum CETP protein levels using an ELISA indicated a 130% increase in serum CETP protein mass (Fig. 1c). A 2.7 fold increase in hepatic CETP mRNA was observed when liver samples were analyzed by the quantitative polymerase chain reaction (Fig. 1d). Next, we investigated specific PPARα mechanism by using a potent specific synthetic PPARα agonist LY970 that is structurally divergent from fenofibrate in the same model [19]. CETP mini-gene mice ($n = 4$–5) were treated with 1 mg/kg dose of LY970 for seven days and the serum lipid, protein and hepatic mRNA levels were analyzed similarly. As expected, LY970 reduced serum triglyceride level dramatically (75%, Fig. 2a), suggesting a very potent PPARα activation in this mouse model. Serum CETP activity was elevated 154% and the protein level increased 228% (Fig. 2b, c).

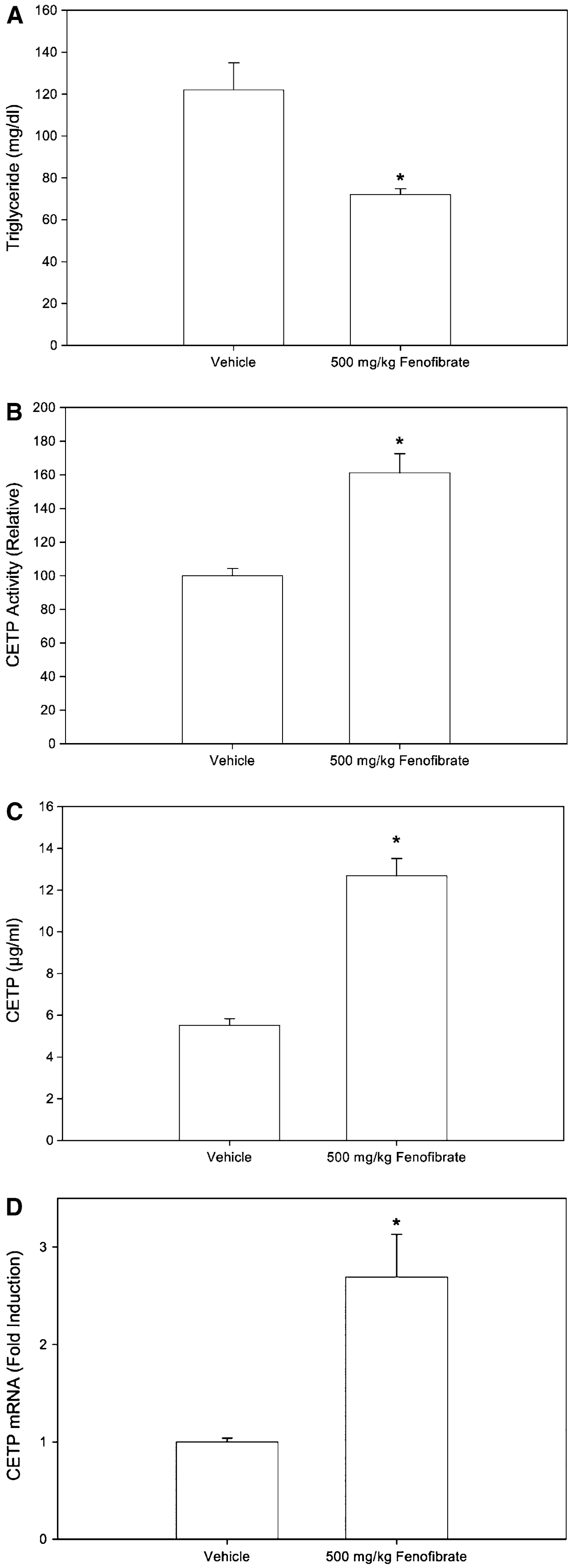

Fig. 1 Regulation of CETP by fenofibrate in CETP minigene ▶ transgenic mice. Four animals per group were dosed orally at 500 mg/kg for 7 days. Plasma and tissue samples were prepared 3 h after the last dose and analyzed as described in "Methods". **a** Fenofibrate reduced serum triglyceride levels. **b** Fenofibrate elevated CETP activity. Ex vivo CETP activity of serum samples was assessed with the assay described in "Methods". **c** Fenofibrate increased serum CETP protein mass. Serum CETP protein levels were measured by an ELISA kit for human CETP as described in "Methods". **d** Hepatic human CETP mRNA was increased upon PPARα activation by fenofibrate. Liver RNA was prepared and CETP mRNA level was assessed by the quantitative PCR as described in "Methods". $*P < 0.05$ versus vehicle (*t* test)

Hepatic mRNA was upregulated three fold as well (Fig. 2d). Significant reduction of total cholesterol (23%) that was attributable primarily to reductions of VLDL and LDL was observed. HDL cholesterol was not changed (data not shown).

To explore whether endogenous CETP could be regulated by PPARα agonists, we treated hamsters with increasing doses of fenofibrate or 10 mg/kg of Wy14634, a prototypic PPARα agonist for fourteen days and analyzed lipids, CETP mRNA and its activity. As were shown in Fig. 3, fenofibrate at the highest dose trended towards a reduction of serum triglyceride levels (nonsignificant, Fig. 3a). Fenofibrate elicited a dose-dependent increase in plasma CETP activity that was 221% at the highest dose compared to the vehicle group (Fig. 3b). Hepatic CETP mRNA was also dose-dependently elevated with the highest elevation around 60% with the highest fenofibrate dose and close to 90% increase with Wy14643 treatment (Fig. 3c). There was no significant change in HDL cholesterol levels as assessed by FPLC analysis (data not shown). Taken together, these data indicated that PPARα agonists upregulated CETP in vivo.

To explore the potential mechanisms of PPARα agonist regulation of CETP, we used a human liver carcinoma cell line HepG2 cells as a model. HepG2 cells have low PPARα expression [26] and not surprisingly, agonist treatment did not result in any significant change in CETP mRNA levels (Fig. 4b). We thus generated a stable cell line in which PPARα was overexpressed. PPARα overexpression led to an increase of more than 100% in CETP mRNA and a more than 5 fold elevation in carnitine palmitoyl transferase 1 (CPT1) mRNA as a control [27] (Fig. 4a). Treatment of the cells with PPARα agonists resulted in a further but moderate elevation in CETP mRNA compared to DMSO as the vehicle (20–60%, Fig. 4b). As controls, liver X receptor (LXR) agonist T0901317 robustly elevated CETP mRNA in these cells [17]. Thus, PPARα agonist regulation of CETP was direct on hepatocytes. In an attempt to map potential PPARα responsive elements within the regulatory regions of human CETP gene, we searched the promoter and intron one of the human CETP gene for potential direct

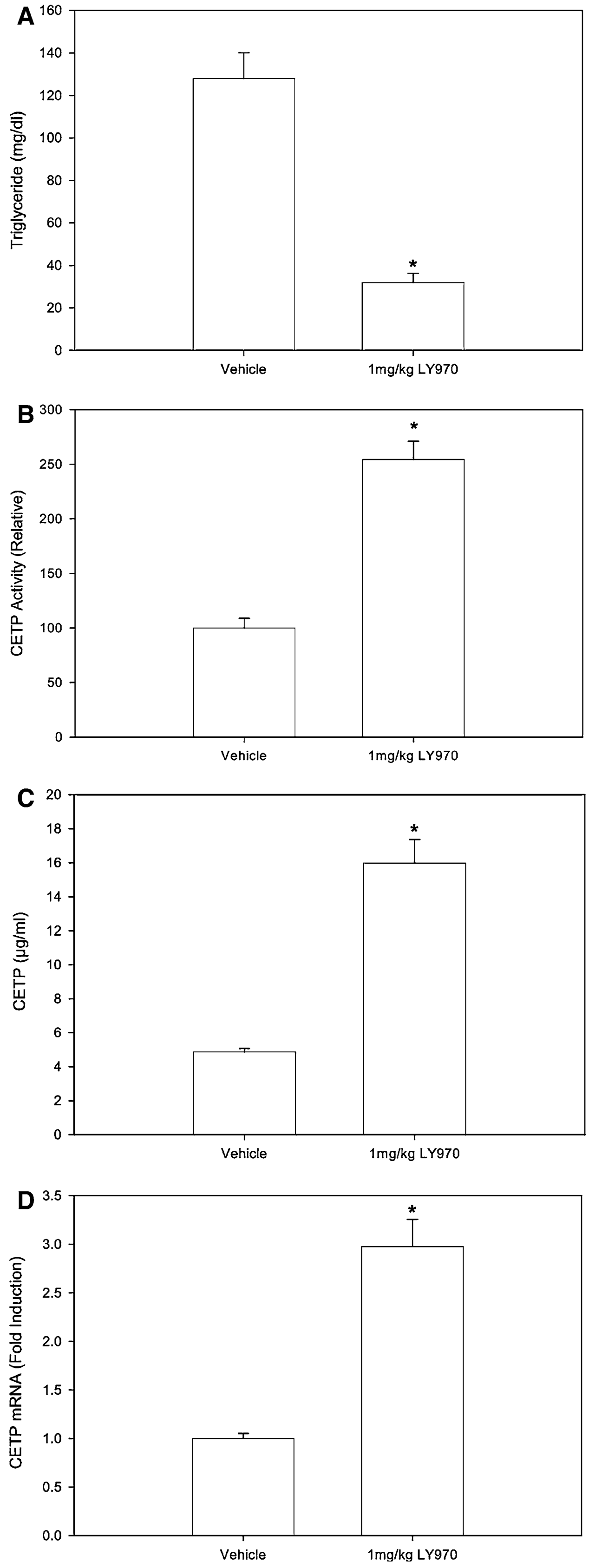

Fig. 2 Regulation of CETP by a specific synthetic PPARα agonist LY970 in CETP minigene transgenic mice. Five animals in vehicle group and four animals in compound group were treated with either vehicle or LY970 at 1 mg/kg for 7 days. Serum and tissue samples were prepared and analyzed similarly to "Methods" in Fig. 1. **a** Significant reduction of serum triglyceride levels. **b** Significant elevation of serum CETP activity. **c** Significant increase in serum CETP mass. **d** Significant increase in hepatic CETP mRNA levels by LY970. * $P < 0.05$ versus vehicle (*t*-test)

repeat of hormone responsive element AGGTCA separated by one nucleotide (DR1) and did not find any obvious DR1 elements (data now shown). Accordingly a five kilobase promoter fragment subcloned into a luciferase reporter did not show any PPARα agonist dependent increase in its reporter activity (data not shown). Thus, the molecular basis of PPARα agonist regulation of CETP remains to be defined.

Discussion

PPARα is a nuclear receptor that plays an important role in lipid homeostasis. Besides its major role in regulating ApoCIII [3], apoAV [5] and fatty acid oxidation [18], it has been well recognized that PPARα agonists regulate key molecular components involved in HDL cholesterol metabolism. Specifically, PPARα agonists upregulate human ApoAI [3] and PLTP [6] and reduce expression of SR-BI [7]. ApoAI is the major structural component of HDL particles and the amount of ApoAI is closely associated with HDL cholesterol levels. PPARα agonist treatment of human ApoAI transgenic mice resulted in dramatically elevated HDL cholesterol levels [3]. Although the role of PLTP in HDL metabolism is not entirely clear, it has been convincingly shown in rodent models that PLTP is essential for HDL biogenesis [28]. Further PPARα regulation of PLTP is necessary for PPARα agonist mediated HDL particle size increase in mice [6]. SR-BI is an HDL receptor, deficiency of which in mice leads to dramatically elevated plasma HDL cholesterol levels [23]. Despite the combined regulation of these important molecules involved in HDL cholesterol metabolism by PPARα agonists that are expected to raise HDL cholesterol level, the effect on HDL cholesterol by PPARα agonists in humans is minimum to modest [20, 21]. Although it has been suspected that potent synthetic PPARα agonists may elevate HDL cholesterol more dramatically, it has not been proven clinically and it appears that induction of HDL cholesterol by PPARα agonists may be bell-shaped [29]. A major missing link of PPARα regulation of ApoAI, PLTP and SR-BI and the associated impact on HDL cholesterol in humans versus

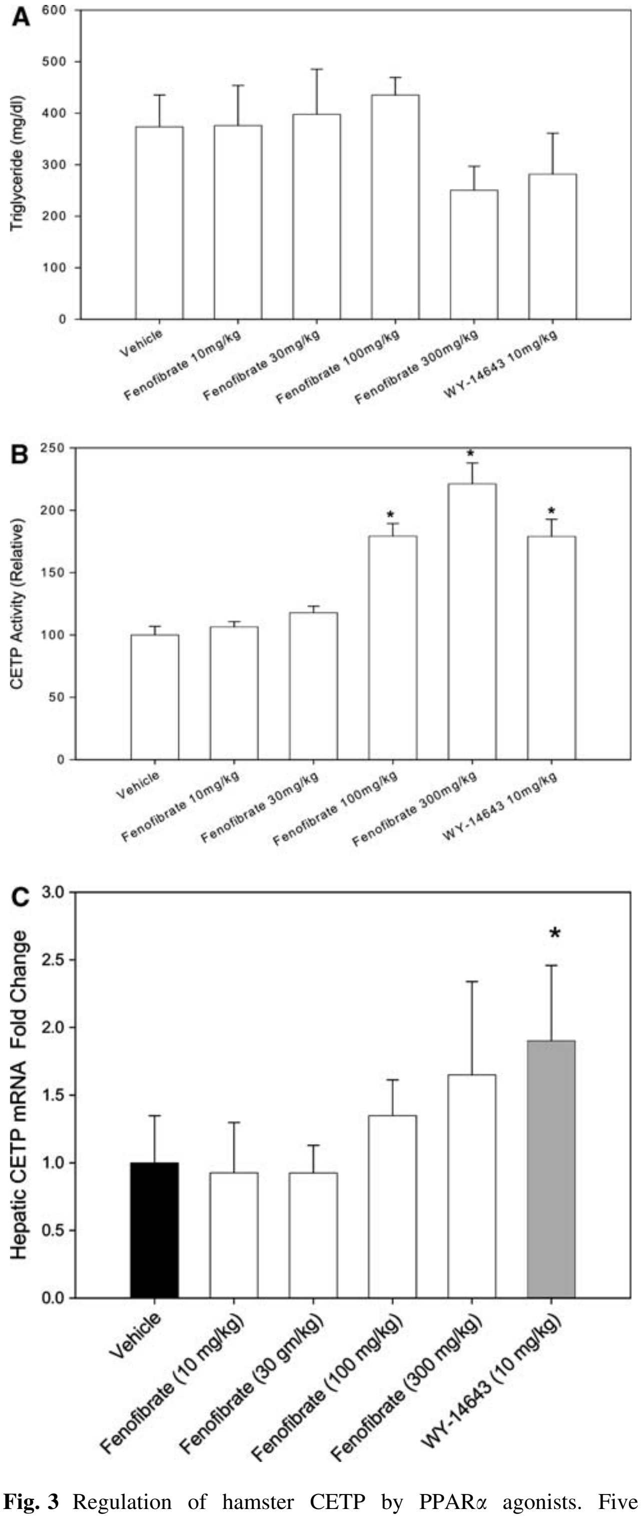

Fig. 3 Regulation of hamster CETP by PPARα agonists. Five animals per group were treated with either various doses of fenofibrate or Wy14643 at 10 mg/kg for 14 days. Serum lipid and CETP activity was analyzed similarly to the studies with CETP minigene transgenic mice. **a** Serum a triglyceride analysis. **b** Dose dependent increase in ex vivo CETP activity by fenofibrate and 10 mg/kg Wy14643. **c** Hepatic mRNA analysis by quantitative PCR. * $P < 0.05$ versus vehicle (Dunnett's)

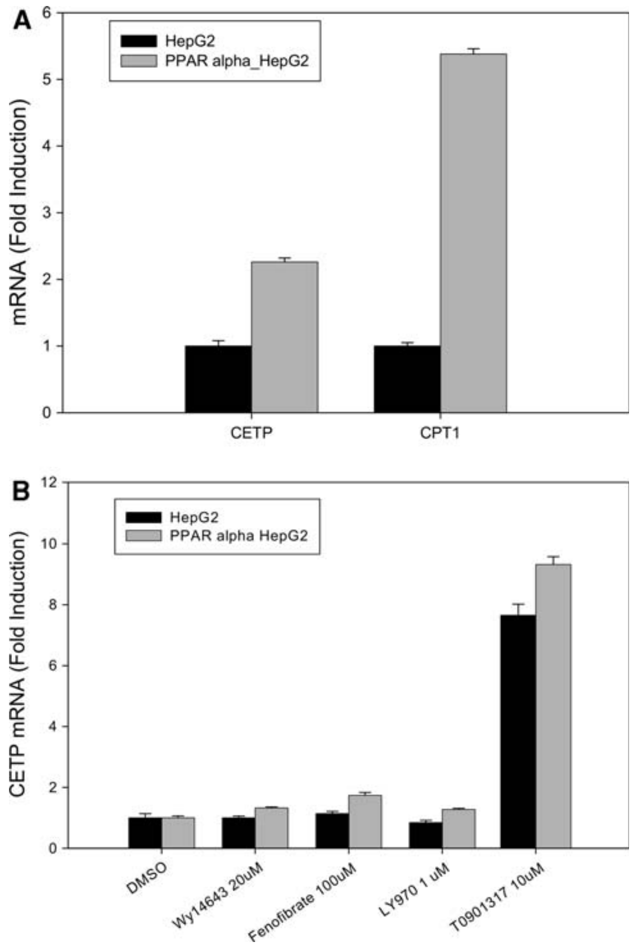

Fig. 4 Regulation of cellular CETP by PPARα. **a** Increased CETP expression by PPARα overexpression in HepG2 cells. A HepG2 stable cell line was established through stable overexpression of human PPARα driven by a CMV promoter. Relative CETP mRNA levels were assessed by quantitative PCR. **b** PPARα agonist regulation of CETP in hepatic cells. HepG2 stable cells overexpressing PPARα or the parental cell line were treated with different PPARα agonists. 48 h later, cells were lysed and mRNA levels were analyzed by the quantitative PCR. T0901317 was used as a control for LXR agonist mediated CETP regulation

the studies in mice is the presence of CETP in humans. CETP catalyzes the transfer of cholesterol ester from HDL particles to ApoB-containing lipoproteins in exchange for triglyceride. It has been well documented through extensive genetic studies with CETP deficiency and polymorphisms in humans that plasma CETP levels are inversely correlated with HDL cholesterol levels. Subjects with either heterozygous or homozygous CETP deficiency not only have significantly elevated HDL cholesterol levels but also have a significant increase in HDL particle size [30]. CETP has been shown to significantly attenuate or abolish completely lecithin cholesterol acyl-CoA acyltransferase (LCAT), or LXRα agonist mediated HDL cholesterol and particle size increase [31, 32]. Significant attenuation of PPARα agonist mediated HDL cholesterol increase by CETP in humans is thus conceivable and may at least partly explain the relative anemic elevation of HDL cholesterol induced by PPARα agonists. Our data indicate that PPARα agonists can increase CETP mRNA, serum proteins and activity and thus may provide a plausible explanation to the HDL cholesterol response clinically to PPARα agonists. In our animal models, it has been impossible to study the direct effect of the changes of CETP level to the changes of HDL cholesterol because of pleiotropic effects of PPARα agonists on HDL cholesterol homeostasis and the limitation of the human CETP transgenic mice [15]. Our attempt to study the clinical effect of PPARα agonists on CETP levels, unfortunately, was inconclusive primarily because of the variations of the baseline plasma CETP levels and the extremely limited number of samples that were available for the study (data not shown). Thus, the exact pharmacological impact of PPARα agonists on plasma CETP protein levels and its activity in humans awaits further investigation.

Our data are in stark contrast with van der Hoogt et al. [33], which reported a decrease in plasma CETP activity in CETP mini-gene transgenic mice with PPARα activation by fenofibrate. At the moment, we do not know exactly the basis for the apparent opposite findings. In our studies we have used three different PPARα agonists, each structurally divergent, to demonstrate the upregulation of CETP in mRNA, plasma protein and its activity. The experiment reported by van der Hoogt et al. was done with high fat diet in a hypercholesterolemic apoE3 Leiden transgenic background. Whether the presence of apoE3 Leiden transgene or the diet influenced the results they reported is not clear at the moment. Future studies will clarify the nature of the PPARα regulation on CETP and its impact on HDL cholesterol.

Acknowledgments We would like to thank Dr. Shuyu Li for help with bioinformatics and Youyan Zhang for editorial support. We are indebted to Richard Tielking, Jack Cochran and Patrick Forler for excellent technical assistance. This work is supported by Lilly Research Laboratories.

References

1. Lehmann JM, Moore LB, Smith-Oliver TA, Wilkison WO, Willson TM, Kliewer SA (1995) An antidiabetic thiazolidinedione is a high affinity ligand for peroxisome proliferator-activated receptor gamma (PPAR gamma). J Biol Chem 270:12953–12956
2. Barish GD, Narkar VA, Evans RM (2006) PPAR delta: a dagger in the heart of the metabolic syndrome. J Clin Invest 116:590–597
3. Berthou L, Duverger N, Emmanuel F, Langouet S, Auwerx J, Guillouzo A et al (1996) Opposite regulation of human versus mouse apolipoprotein A-I by fibrates in human apolipoprotein A-I transgenic mice. J Clin Invest 97:2408–2416
4. Staels B, Vu-Dac N, Kosykh VA, Saladin R, Fruchart JC, Dallongeville J et al (1995) Fibrates downregulate apolipoprotein C-III expression independent of induction of peroxisomal acyl coenzyme A oxidase. A potential mechanism for the hypolipidemic action of fibrates. J Clin Invest 95:705–712
5. Vu-Dac N, Gervois P, Jakel H, Nowak M, Bauge E, Dehondt H et al (2003) Apolipoprotein A5, a crucial determinant of plasma triglyceride levels, is highly responsive to peroxisome proliferator-activated receptor alpha activators. J Biol Chem 278:17982–17985
6. Bouly M, Masson D, Gross B, Jiang XC, Fievet C, Castro G et al (2001) Induction of the phospholipid transfer protein gene accounts for the high density lipoprotein enlargement in mice treated with fenofibrate. J Biol Chem 276:25841–25845
7. Mardones P, Pilon A, Bouly M, Duran D, Nishimoto T, Arai H et al (2003) Fibrates down-regulate hepatic scavenger receptor class B type I protein expression in mice. J Biol Chem 278:7884–7890
8. Tall AR, Jiang X, Luo Y, Silver D (2000) 1999 George Lyman Duff memorial lecture: lipid transfer proteins, HDL metabolism, and atherogenesis. Arterioscler Thromb Vasc Biol 20:1185–1188
9. Boekholdt SM, Thompson JF (2003) Natural genetic variation as a tool in understanding the role of CETP in lipid levels and disease. J Lipid Res 44:1080–1093 (Epub 2003 Mar 16)
10. Clark RW, Sutfin TA, Ruggeri RB, Willauer AT, Sugarman ED, Magnus-Aryitey G et al (2004) Raising high-density lipoprotein in humans through inhibition of cholesteryl ester transfer protein: an initial multidose study of torcetrapib. Arterioscler Thromb Vasc Biol 24:490–497 (Epub 2004 Jan 22)
11. Brousseau ME, Schaefer EJ, Wolfe ML, Bloedon LT, Digenio AG, Clark RW et al (2004) Effects of an inhibitor of cholesteryl ester transfer protein on HDL cholesterol. N Engl J Med 350:1505–1515
12. Barter PJ, Caulfield M, Eriksson M, Grundy SM, Kastelein JJ, Komajda M et al. (2007) Effects of torcetrapib in patients at high risk for coronary events. N Engl J Med 357:2109–2122 (Epub 007 Nov 5)
13. de Grooth GJ, Kuivenhoven JA, Stalenhoef AF, de Graaf J, Zwinderman AH, Posma JL et al (2002) Efficacy and safety of a novel cholesteryl ester transfer protein inhibitor, JTT-705, in humans: a randomized phase II dose-response study. Circulation 105:2159–2165
14. Krishna R, Anderson MS, Bergman AJ, Jin B, Fallon M, Cote J et al (2007) Effect of the cholesteryl ester transfer protein inhibitor, anacetrapib, on lipoproteins in patients with dyslipidaemia and on 24-h ambulatory blood pressure in healthy individuals: two double-blind, randomised placebo-controlled phase I studies. Lancet 370:1907–1914
15. Agellon LB, Walsh A, Hayek T, Moulin P, Jiang XC, Shelanski SA et al (1991) Reduced high density lipoprotein cholesterol in human cholesteryl ester transfer protein transgenic mice. J Biol Chem 266:10796–10801
16. Jiang XC, Agellon LB, Walsh A, Breslow JL, Tall A (1992) Dietary cholesterol increases transcription of the human cholesteryl ester transfer protein gene in transgenic mice. Dependence on natural flanking sequences. J Clin Invest 90:1290–1295
17. Luo Y, Tall AR (2000) Sterol upregulation of human CETP expression in vitro and in transgenic mice by an LXR element. J Clin Invest 105:513–520
18. Staels B, Dallongeville J, Auwerx J, Schoonjans K, Leitersdorf E, Fruchart JC (1998) Mechanism of action of fibrates on lipid and lipoprotein metabolism. Circulation 98:2088–2093

19. Xu Y, Mayhugh D, Saeed A, Wang X, Thompson RC, Dominianni SJ et al (2003) Design and synthesis of a potent and selective triazolone-based peroxisome proliferator-activated receptor alpha agonist. J Med Chem 46:5121–5124
20. Rubins HB, Robins SJ, Collins D, Fye CL, Anderson JW, Elam MB et al (1999) Gemfibrozil for the secondary prevention of coronary heart disease in men with low levels of high-density lipoprotein cholesterol. Veterans affairs high-density lipoprotein cholesterol intervention trial study group. N Engl J Med 341:410–418
21. Keech A, Simes RJ, Barter P, Best J, Scott R, Taskinen MR et al (2005) Effects of long-term fenofibrate therapy on cardiovascular events in 9795 people with type 2 diabetes mellitus (the FIELD study): randomised controlled trial. Lancet 366:1849–1861
22. Rubin EM, Ishida BY, Clift SM, Krauss RM (1991) Expression of human apolipoprotein A-I in transgenic mice results in reduced plasma levels of murine apolipoprotein A-I and the appearance of two new high density lipoprotein size subclasses. Proc Natl Acad Sci USA 88:434–438
23. Rigotti A, Trigatti BL, Penman M, Rayburn H, Herz J, Krieger M (1997) A targeted mutation in the murine gene encoding the high density lipoprotein (HDL) receptor scavenger receptor class B type I reveals its key role in HDL metabolism. Proc Natl Acad Sci USA 94:12610–12615
24. Bisgaier CL, Minton LL, Essenburg AD, White A, Homan R (1993) Use of fluorescent cholesteryl ester microemulsions in cholesteryl ester transfer protein assays. J Lipid Res 34:1625–1634
25. Cao G, Beyer TP, Yang XP, Schmidt RJ, Zhang Y, Bensch WR et al (2002) Phospholipid transfer protein is regulated by liver x receptors in vivo. J Biol Chem 277:39561–39565
26. Lawrence JW, Li Y, Chen S, DeLuca JG, Berger JP, Umbenhauer DR et al (2001) Differential gene regulation in human versus rodent hepatocytes by peroxisome proliferator-activated receptor (PPAR) alpha. PPAR alpha fails to induce peroxisome proliferation-associated genes in human cells independently of the level of receptor expression. J Biol Chem 276:31521–31527 (Epub 2001 Jun 19)
27. Mascaro C, Acosta E, Ortiz JA, Marrero PF, Hegardt FG, Haro D (1998) Control of human muscle-type carnitine palmitoyltransferase I gene transcription by peroxisome proliferator-activated receptor. J Biol Chem 273:8560–8563
28. Jiang XC, Bruce C, Mar J, Lin M, Ji Y, Francone OL et al (1999) Targeted mutation of plasma phospholipid transfer protein gene markedly reduces high-density lipoprotein levels. J Clin Invest 103:907–914
29. Nissen SE, Nicholls SJ, Wolski K, Howey DC, McErlean E, Wang MD et al (2007) Effects of a potent and selective PPAR-alpha agonist in patients with atherogenic dyslipidemia or hypercholesterolemia: two randomized controlled trials. Jama 297:1362–1373 (Epub 2007 Mar 25)
30. Yamashita S, Sprecher DL, Sakai N, Matsuzawa Y, Tarui S, Hui DY (1990) Accumulation of apolipoprotein E-rich high density lipoproteins in hyperalphalipoproteinemic human subjects with plasma cholesteryl ester transfer protein deficiency. J Clin Invest 86:688–695
31. Foger B, Chase M, Amar MJ, Vaisman BL, Shamburek RD, Paigen B et al (1999) Cholesteryl ester transfer protein corrects dysfunctional high density lipoproteins and reduces aortic atherosclerosis in lecithin cholesterol acyltransferase transgenic mice. J Biol Chem 274:36912–39920
32. Jiang XC, Beyer TP, Li Z, Liu J, Quan W, Schmidt RJ et al (2003) Enlargement of high density lipoprotein in mice via LXR activation requires apolipoprotein E and is abolished by cholesteryl ester transfer protein expression. J Biol Chem 28:28
33. van der Hoogt CC, de Haan W, Westerterp M, Hoekstra M, Dallinga-Thie GM, Romijn JA et al (2007) Fenofibrate increases HDL-cholesterol by reducing cholesteryl ester transfer protein expression. J Lipid Res 48:1763–1771 (Epub 2007 May 24)

Lipids (2008) 43:619–627
DOI 10.1007/s11745-008-3192-3

ORIGINAL ARTICLE

Farnesol Decreases Serum Triglycerides in Rats: Identification of Mechanisms Including Up-Regulation of PPARα and Down-Regulation of Fatty Acid Synthase in Hepatocytes

Robin E. Duncan · Michael C. Archer

Received: 20 March 2008 / Accepted: 5 May 2008 / Published online: 29 May 2008
© AOCS 2008

Abstract Obesity is associated with impaired fatty acid (FA) oxidation and increased de novo hepatic lipogenesis that may contribute to the development of hypertriglyceridemia, an important risk factor for the development of cardiovascular disease. Strategies to improve hepatocyte FA metabolism, including dietary interventions, are therefore important for the prevention of obesity-associated co-morbidities. Farnesol is consumed in the diet as a component of plant products. In the present study, we administered farnesol orally to rats for seven days and found significantly reduced serum triglyceride concentrations compared with controls. Potential mechanisms underlying the hypotriglyceridemic effect of farnesol were investigated using clone-9 cultured rat hepatocytes. Farnesol significantly upregulated expression of peroxisome proliferator-activated receptor alpha (PPARα) and the PPARα-regulated genes fatty acyl-CoA oxidase and carnitine palmitoyl transferase 1a, suggesting that increased hepatic FA oxidation may contribute to serum triglyceride lowering in rats. Farnesol did not change SREBP-1c mRNA levels, but significantly down-regulated fatty acid synthase (FAS) mRNA and protein levels and activity, indicating that attenuated lipogenesis may also contribute to hypotriglyceridemic effects of farnesol in vivo. Rescue experiments revealed that down-regulation of FAS by farnesol was not related to activation of PPARα, but rather was caused by a 9-*cis* retinoic acid mediated mechanism that involved down-regulation of retinoid X receptor β. Diets rich in plant products are associated with a lower risk of cardiovascular disease. Our findings suggest that farnesol may contribute to this protective effect by lowering serum TG levels.

Keywords Farnesol · Rat hepatocytes · Triglycerides ·
Fatty acid synthase ·
Peroxisome proliferator-activated receptor alpha ·
Fatty acyl-CoA oxidase ·
Carnitine palmitoyl transferase 1a ·
Sterol regulatory element binding protein 1c ·
Retinoid X receptor · 9-*cis* retinoic acid

Abbreviations

ACOX	Fatty acyl-CoA oxidase
CPT-1a	Carnitine palmitoyl transferase 1a
FA	Fatty acid
FAS	Fatty acid synthase
GAPDH	Glyceraldehyde-3-phosphate dehydrogenase
PPARα	Peroxisome-proliferator activated receptor alpha
RXRα	Retinoid X receptor alpha
RXRβ	Retinoid X receptor beta
SREBP-1c	Sterol regulatory element binding protein-1
TG	Triglycerides

R. E. Duncan · M. C. Archer (✉)
Department of Nutritional Sciences,
Faculty of Medicine, University of Toronto,
Fitzgerald Building, 150 College Street, Toronto,
ON M5S 3E2, Canada
e-mail: m.archer@utoronto.ca

M. C. Archer
Department of Medical Biophysics,
Faculty of Medicine, University of Toronto,
Toronto, ON M5S 3E2, Canada

Present Address:
R. E. Duncan
Department of Nutritional Sciences and Toxicology,
University of California, 220 Morgan Hall, Berkeley,
CA 94720, USA

Introduction

Dyslipidemia, including elevated circulating levels of atherogenic triglyceride (TG)-rich lipoproteins, is increasing in prevalence in Western populations where rates of obesity have risen dramatically [1]. Hepatic production of TG-rich lipoproteins is primarily regulated by availability of fatty acids (FA) as substrates for TG synthesis [2]. Obesity is associated with reduced hepatic catabolism of FA through down-regulation of peroxisome proliferator-activated receptor alpha (PPARα) and genes of FA oxidation [3], and increased hepatic lipogenesis resulting from elevated blood insulin levels that stimulate expression of sterol regulatory element binding protein-1c (SREBP-1c) and fatty acid synthase (FAS) [4–6]. Dietary interventions that increase FA oxidation and decrease FA synthesis in hepatocytes may, therefore, provide a useful strategy to limit hepatic production of atherogenic lipoproteins and thereby decrease cardiovascular disease risk.

Farnesol is produced endogenously in cells from farnesyl pyrophosphate, the precursor of squalene in the cholesterol biosynthetic pathway [7]. It is also consumed in the diet as a component of plant products [8] including fruits and berries such as apricots, peaches, plums, blueberries, cranberries, raspberries and strawberries, vegetables such as tomatoes [9] and herbs such as chamomile [10]. A number of studies have shown that farnesol affects lipid metabolism in hepatocytes and other cells, and may be of benefit in regulating serum lipid levels. Dietary farnesol lowers serum cholesterol in rats [11], and a role for farnesol in the feedback control of cholesterol biosynthesis through down-regulation of HMG-CoA reductase is well characterized [12]. Farnesol has also been shown to inhibit phosphatidylcholine biosynthesis in human leukemia cells [13] and fatty acid synthesis in CaCo-2 colonic epithelial cells [14]. De novo synthesis of triglycerides (TG) in primary rat hepatocytes has been shown to be inhibited by farnesol [15], although mechanisms underlying this effect have not previously been investigated. Furthermore, the effect of farnesol on serum TG in rats had not been tested.

In the present study we showed that Sprague–Dawley rats administered farnesol had significantly lower levels of serum TG. We hypothesized that changes in regulation of hepatocyte FA metabolism may mediate this effect. Using clone-9 cultured rat hepatocytes we showed that farnesol up-regulated PPARα and genes of FA oxidation. Although farnesol did not alter expression of the master lipogenic transcriptional regulator SREBP-1c, we showed for the first time that it significantly down-regulated FAS mRNA, protein, and activity levels, and that this was mediated by a 9-*cis* retinoic acid-dependent mechanism involving retinoid X receptor (RXR) β.

Materials and Methods

Materials

Unless otherwise indicated, all chemicals including *trans*,*trans*-farnesol were purchased from Sigma (Mississauga, ON, Canada).

Animals

Rats were cared for in accordance with the recommendations of the Canadian Council on Animal Care and the University of Toronto Animal Care Policies and Guidelines. The experimental protocol utilized in the present study was reviewed and received ethical approval by the University of Toronto Animal Care Committee. Nine male Sprague–Dawley rats 7 weeks of age were purchased from Charles River Laboratories (Wilmington, MA, USA) and acclimatized for 1 week prior to study commencement on a standard AIN-93G diet (Dyets, Bethlehem, PA, USA) that was used throughout. Rats were randomized into two groups and were gavaged once daily with cottonseed oil (vehicle control) or farnesol (500 mg/kg body weight) dissolved in cottonseed oil for 7 days. Body weights were monitored to ensure that treatments were well tolerated, and did not change over the course of the study. On day 7, following an overnight fast, rats were euthanized by CO_2 asphyxia followed by cervical dislocation and samples of blood were taken by cardiac puncture. Serum TG were analyzed according to the manufacturer's protocol using Infinity triglyceride reagent (Thermo, Melbourne, Australia).

Cell Culture

Clone-9 rat hepatocytes purchased from the American Type Cell Culture Collection (Manassas, VA, USA) were routinely cultured in DMEM in 150 dl flasks at 37 °C and 5% CO_2 in the presence of 1% penicillin/streptomycin with 10% fetal bovine serum (Hyclone, VWR, Mississauga, Canada). Farnesol and 9-*cis* RA were dissolved in DMSO immediately prior to use. Final concentrations of DMSO in both control and treatment medium were identical in all studies with a maximum level of 0.05%.

Immunoblotting

Cells were washed repeatedly with ice cold PBS, then scraped into RIPA lysis buffer (1× PBS, pH 7.4, 1% Nonidet P-40, 0.5% sodium deoxycholate, 0.1% SDS) containing 1% protease inhibitor cocktail and incubated on ice for 30 min with frequent vortexing then centrifuged for 20 min at $12{,}000 \times g$. Five to 40 μg of protein in supernatants were mixed with 2× Laemmli buffer, heated for 5 min at 95 °C, electrophoresed in 10% SDS-polyacrylamide gels and transferred to polyvinylidene difluoride membranes. Blots were blocked for 1 h then probed overnight at 4 °C, first with antibodies to FAS (BD Biosciences, Mississauga, ON, Canada) or RXRβ (Upstate Biotechnology Inc., Charlottesville, VA, USA), then with horseradish peroxidase conjugated anti-mouse or anti-rabbit secondary antibodies (Santa Cruz Biotechnology Inc., Santa Cruz, CA, USA). Signals were detected by enhanced chemiluminescence. Band densities were quantified in arbitrary units then expressed as relative density compared with untreated controls that were taken as 100%. Glyceraldehyde-3-phosphate dehydrogenase (GAPDH) (Abcam, Cambridge, MA, USA) was used as a loading control.

RNA Isolation, cDNA Synthesis, and PCR

Total RNA was isolated using TRI-Reagent. cDNA was synthesized from 5 μg of total RNA by oligo(dT) priming using the SuperScript^{TM} First-Strand Synthesis System for RT-PCR (Invitrogen, Burlington, ON, Canada). The cDNA was amplified under the following conditions: denaturation at 94°C for 5 min, followed by a pre-determined number of cycles of denaturation at 94 °C for 1 min, annealing at 62 °C for 1 min, and extension at 72 °C for 1 min, with the final extension at 72 °C for 10 min. The optimum cycle number for each primer set was determined so that the product was obtained during the exponential phase of the amplification (data not shown). Based on these preliminary studies cycle numbers, product size, and primer sets were used as outlined in Table 1. PCR products were electrophoresed on 1% agarose gels and stained with ethidium bromide. Band densities were measured and quantified by densitometry in arbitrary units under UV light using an Alpha Innotech Fluorochem with AlphaEase image quantification software (San Leandro, CA, USA). Densities of amplified cDNA were normalized to the density of the corresponding 36B4 band, and relative densities were expressed as a percentage of control values.

FAS Assay

Cells were assayed for FAS activity as previously described [16]. Briefly, cells were washed with PBS, harvested by scraping into 500 μl of PBS and pelleted by centrifugation for 5 min at 1,000×g. Cell pellets were resuspended in 50 μl of hypotonic buffer (20 mM Tris–HCl, 1 mM DTT, 1 mM EDTA, pH 7.5) for 15 min at room temperature and then centrifuged for 1 min at 12,000×g. Supernatants containing 15 μg of protein in 20 μl of hypotonic buffer were added to 125 μl of reaction buffer (100 mM potassium phosphate, 100 mM KCl, 0.5 mM NADPH, pH 7.0) and pre-warmed for 10 min at 37 °C. Reactions were started by the addition of 14 μl of a substrate mixture containing 25 nmol of acetyl-CoA, 25 nmol of malonyl-CoA, and 0.05 μCi of [2-^{14}C]malonyl-CoA (PerkinElmer Life Sciences, Boston, MA, USA). After 10 min, reactions were stopped by the addition of 1 ml of ice-cold 1 N HCl/methanol (6:4, v/v). Fatty acids were extracted with 1 ml of petroleum ether for 1 h and incorporation of radioactivity was measured by scintillation counting.

Statistical Analysis

All values shown are means ± SEM. For Western immunoblots, values represent means from at least four

Table 1 Primer sets, product size, and cycle number for PCR amplification of cDNA

Gene	For/Rev	Primers	Number of cycles	Size (bp)
36B4	Forward	5′-TGGGCTCCAAGCAGATGC-3′	20	413
	Reverse	5′-GGCTTCGCTGGCTCCCAC-3′		
SREBP-1c	Forward	5′-GGAGCCATGGATTGCACATT-3′	27	191
	Reverse	5′-AGGAAGGCTTCCAGAGAGGA-3′		
PPARα	Forward	5′-GGAGAGGAGAGTTCCGGAAG-3′	33	338
	Reverse	5′-CTGGCATTTGTTCCGGTTCT-3′		
ACOX	Forward	5′-CTTCAATCCGGAGTTGATCA-3′	28	304
	Reverse	5′-TCCTGCTGAGCAGTGGTGCC-3′		
CPT-1a	Forward	5′-CACTATGGAGTCCTGCAACT-3′	24	311
	Reverse	5′-TCATCGGCAACCGGCCCAAA-3′		
FAS	Forward	5′-GGCCTGGACTCGCTCATGGG-3′	20	514
	Reverse	5′-TGGGCCTGCAGCTGGGAGCA-3′		
RXRα	Forward	5′-CCGTGAGCAGCAGTGAGGAT-3′	25	379
	Reverse	5′-GGCACTGCTGGTGGACTCCA-3′		
RXRβ	Forward	5′-TGAGGGTCCCGGGGCCACCG-3′	25	339
	Reverse	5′-CCTCATGTCACGCATTTTGG-3′		

individual samples from two or more separate experiments with different cell preparations. Means for gene expression data were generated from five or more cell samples grown in three or more separate experiments. Differences between multiple treated groups and controls were analyzed by one-way ANOVA followed by Dunnett's post hoc test. Differences between treated and control FAS activity values were analyzed by Student's *t* test.

Results and Discussion

We began the present study by treating 8-week-old male Sprague–Dawley rats with farnesol (500 mg/kg) by gavage for 7 days. This dose has previously been shown to elevate hepatic farnesol levels in rats [17] and to be well tolerated, resulting in no changes in body weights, food intakes, or liver weights after 28 days [10]. In agreement with those results, we found that farnesol did not change rat body weights (Fig. 1a), indicating an absence of overt toxicity or malabsorption in treated animals. We found that serum TG concentration was reduced by ~40% in rats treated with farnesol compared with rats that received the vehicle control (Fig. 1b). To identify potential mechanisms underlying this effect, we next investigated the regulation of hepatocyte FA metabolism by farnesol using a rat hepatocyte cell line (clone-9 cells).

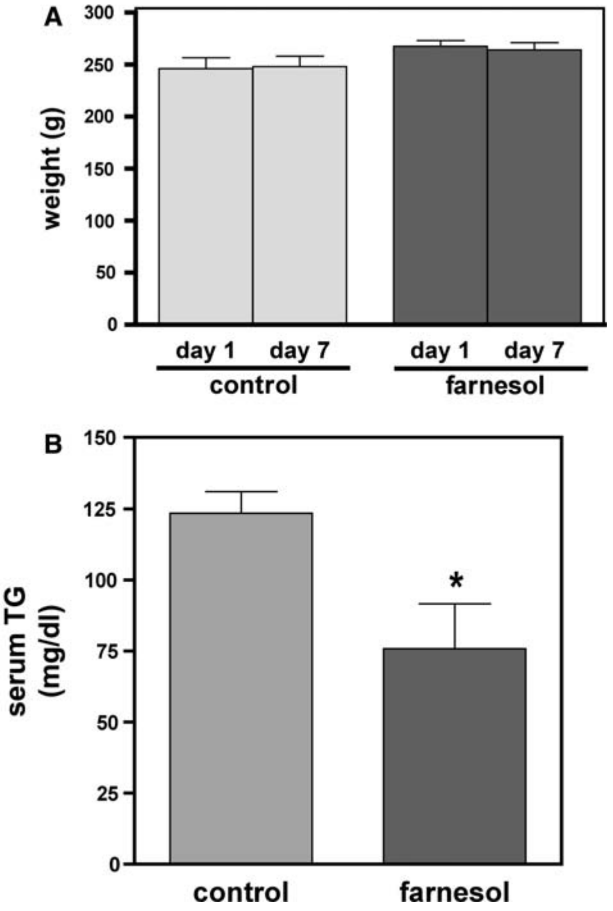

Fig. 1 Farnesol has no effect on body weights and decreases serum TG concentrations. Male Sprague Dawley rats were treated with cottonseed oil (control) or farnesol (500 mg/kg) by oral gavage once daily for 7 days. Rat body weights (**a**) and serum TG concentrations (**b**).*$P < 0.05$ versus control

In rodents, diet-induced obesity causes reduced hepatic expression of PPARα and genes of lipid oxidation [6]. Administration of PPARα agonists has been shown to upregulate the expression of genes related to the oxidation of fatty acids [18], to lower serum TG concentrations, and to reverse hepatic lipotoxicity in diabetic mice [19]. A preliminary concentration-response study showed a significant effect of 30 µM farnesol on expression of PPARα by 24 h (data not shown). A time-course analysis showed that PPARα was significantly induced by treatment with 30 µM farnesol at both 24 and 48 h (Fig. 2a), indicating an autoregulatory activation of PPARα transcription [20, 21] that has also been reported in HepG2 cells [22] and epidermal keratinocytes [23] treated with farnesol. PPARα regulates the expression of genes involved in lipid homeostasis, stimulating fatty acid oxidation and improving lipoprotein metabolism [24]. We found that farnesol significantly induced expression of fatty acyl-CoA oxidase (ACOX) (Fig. 2B), a PPARα-regulated gene involved in the peroxisomal beta-oxidation of very long chain FAs. Furthermore, farnesol stimulated expression of carnitine palmitoyl transferase 1a (CPT-1a), the rate-limiting enzyme in mitochondrial beta-oxidation of fatty acids (Fig. 2c). These results indicate that an increase in hepatic FA oxidation through activation of PPARα by farnesol may have contributed to the reduction of serum TG concentration that was observed in rats.

Obesity and insulin resistance are also associated with elevated hepatic FA synthesis, in addition to reduced levels of lipid oxidation [4–6]. Increased circulating levels of glucose can act as a substrate for de novo hepatic lipogenesis, while elevated insulin stimulates expression of SREBP-1c [25] that transactivates the FAS promoter to induce hepatic FA biosynthesis [26]. Previous work has shown that farnesol decreases the de novo synthesis of FA from acetate in CaCo-2 colonic epithelial cells, and that inhibition of HMG-CoA reductase, causing depletion of farnesol as well as other downstream metabolites in this pathway, induces FAS mRNA expression [14]. A direct effect of farnesol on FAS mRNA and protein levels and activity, however, has not previously been reported. Here we show in concentration-response experiments that FAS protein levels were significantly down-regulated in clone-9 hepatocytes at 48 h in cells treated with 30 µM farnesol (~40% reduction compared with controls) (Fig. 3a). A time-course analysis indicated that down-regulation of FAS

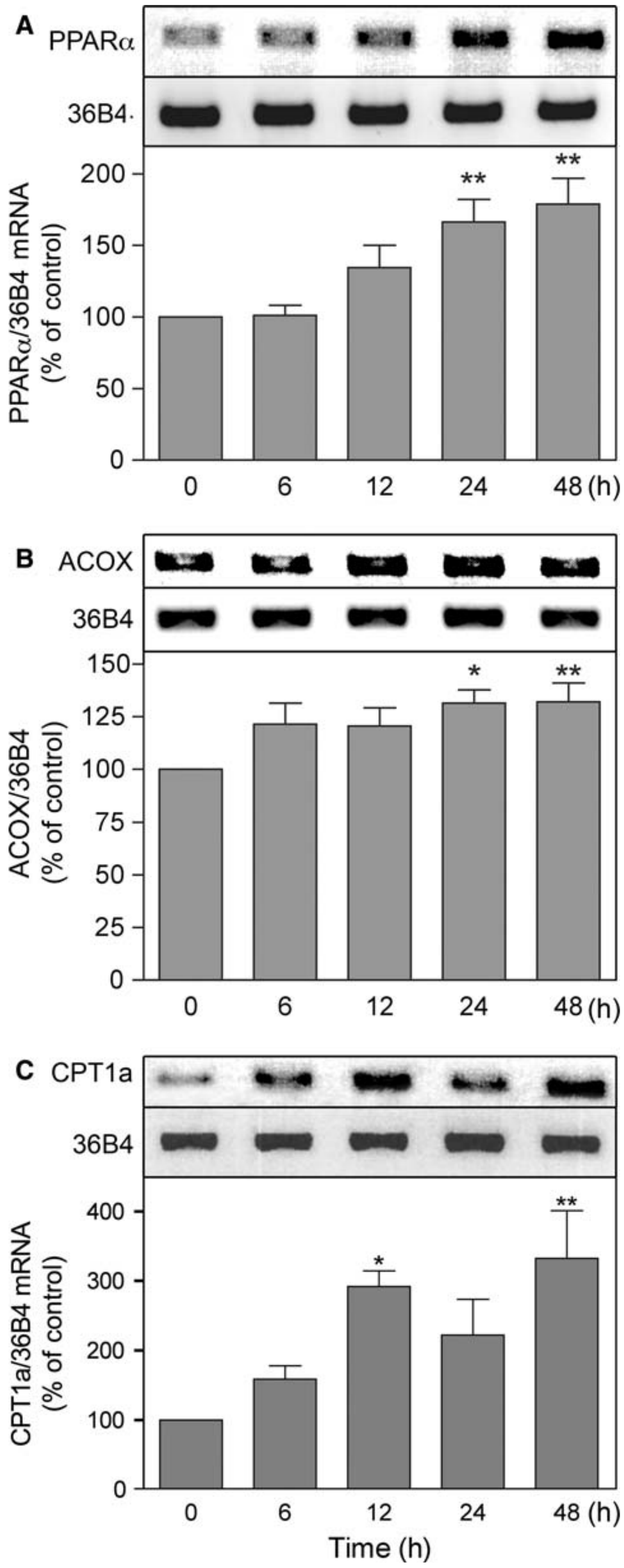

Fig. 2 Farnesol induces PPARα and genes of FA oxidation. Clone-9 rat hepatocytes were cultured with 30 μM farnesol or DMSO (*control*) for the time periods indicated prior to harvest and analysis for gene expression by RT-PCR. Expression of PPARα was significantly induced by farnesol (**a**), as was expression of the PPARα-regulated genes ACOX (**b**) and CPT1a (**c**). $*P < 0.05$; $**P < 0.01$ versus control

protein was not evident before 48 h (Fig. 3b). FAS mRNA levels were also significantly decreased at 48 h in cells treated with 30 μM farnesol (Fig. 3c). This decrease was evident by as early as 24 h (Fig. 3d), preceding the decrease in FAS protein and suggesting transcriptional regulation. Down-regulation of FAS protein by 30 μM farnesol resulted in a >50% decrease in activity of the enzyme after 48 h of treatment (Fig. 3e). FAS protein levels also tended to be lower in livers of rats given farnesol (Fig. 3f), although this effect did not reach significance ($P = 0.07$). These findings indicate that decreased hepatocyte FAS activity may contribute to hypotriglyceridemic effects of farnesol.

Interestingly, these findings may also explain several reports that the synthesis of fatty acids and triglycerides is modulated in response to changes in levels of metabolites derived from the cholesterol biosynthetic pathway [15, 27–30]. For example, statin drugs that deplete farnesol and other intermediates of the cholesterol biosynthetic pathway have been shown to increase TG synthesis in HepG2 hepatocarcinoma cells [29]. Conversely, squalene synthase inhibitors that increase cellular farnesol levels [31] have been shown to decrease the de novo synthesis of fatty acids and triglycerides in primary rat hepatocytes [15], and to lower serum triglyceride levels in several animal models [27, 28, 30]. Direct regulation of FAS by farnesol provides a unifying mechanism to explain these effects.

Mechanisms underlying the regulation of FAS expression by farnesol have not previously been investigated. Transcriptional regulation of the FAS promoter is complex. Multiple nuclear hormone receptors have been identified that can directly or indirectly modulate FAS transcription [26]. In an effort to understand the down-regulation of FAS by farnesol, we first tested whether farnesol caused any changes in expression of SREBP-1c, the major transcriptional regulator of lipogenesis [32]. SREBP-1c expression, however, did not change significantly in rat hepatocytes treated with farnesol (Fig. 4), in agreement with findings by Murthy et al. [14] who showed that SREBP-1c expression is not changed in CaCo-2 colonic epithelial cells treated with the farnesol precursor farnesyl-pyrophosphate. SREBP-1c is also regulated at the protein level by processing to an active form that translocates to the nucleus where it can regulate gene transcription [33]. While we did not measure protein levels of the nuclear form of SREBP-1c, we found no down-regulation of a number of genes that are controlled by this transcription factor (e.g., small heterodimer partner or ATP-binding cassette 1a (data not shown), or PPARα), indicating that a decrease in levels of the active form likely did not mediate down-regulation of FAS in the present study.

We next tested whether activation of PPARα could have mediated the down-regulation of FAS that we observed in

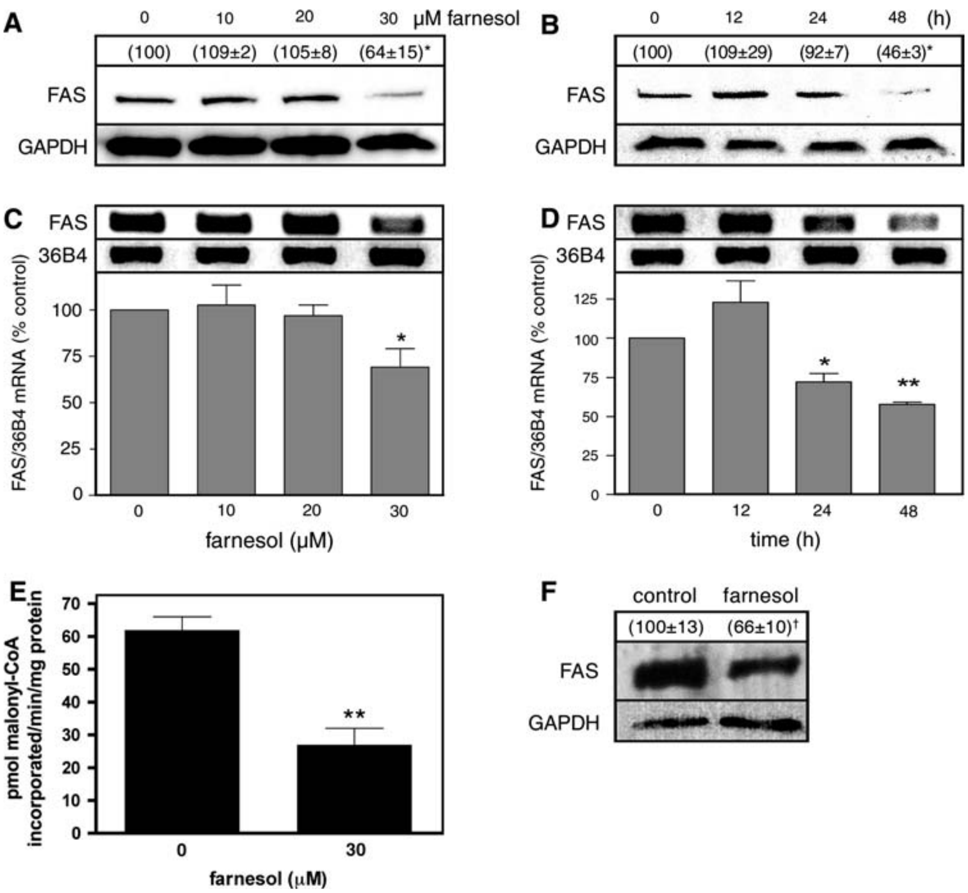

Fig. 3 Farnesol down-regulates FAS protein and mRNA expression and FAS activity in clone-9 cultured rat hepatocytes. **a** Representative immunoblot showing concentration-dependent effects of farnesol on FAS protein expression after 48 h. **b** Time-dependent effects of 30 µM farnesol on FAS protein levels. Numbers in parentheses are means ± SEM for relative band density measured as a percentage of the density of the control band. FAS mRNA expression was measured by densitometry and normalized to expression of 36B4 as outlined in "Materials and Methods". **c** Farnesol down-regulated FAS mRNA expression in a concentration-dependent manner in cells treated for 48 h. **d** Farnesol down-regulated FAS mRNA in a time-dependent manner in cells treated with 30 µM farnesol. **e** Treatment of rat hepatocytes for 48 h with 30 µM farnesol significantly decreased FAS activity. **f** FAS protein levels tended to be lower in livers of rats given farnesol by gavage. $^{\dagger}P = 0.07$; $^{*}P < 0.05$; $^{**}P < 0.01$ versus control

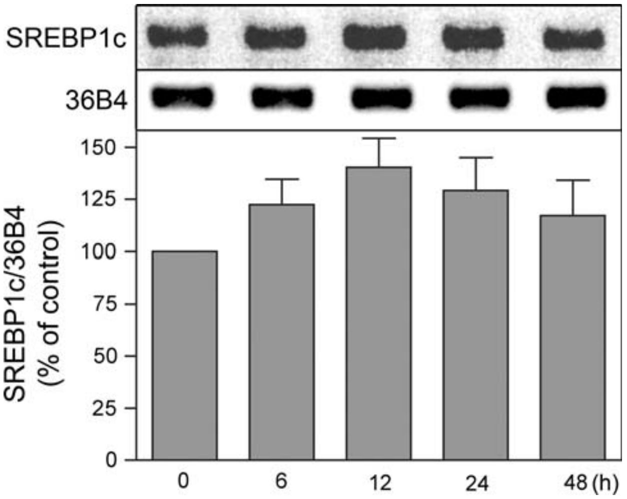

Fig. 4 Farnesol does not alter SREBP-1c mRNA expression. Expression of SREBP-1c mRNA in rat hepatocytes treated with 30 µM farnesol

clone-9 cells. However, when we treated cells with the potent PPARα agonist fenofibrate, there was a trend towards increased FAS mRNA expression (data not shown), indicating that decreased FAS in the present study is not explained by PPARα activation. We also treated cells with 9-*cis* retinoic acid (9-*cis* RA), a ligand activator of retinoid X receptors (RXRs) that heterodimerize with PPARs and other nuclear hormone receptors to form active complexes. Surprisingly, this compound alone completely restored FAS mRNA expression in the presence of farnesol (Fig. 5a). Ligand activation of RXRs by retinoids has previously been shown to induce FAS through a mechanism that does not appear to involve direct activation of a retinoic acid response element in the FAS promoter [34, 35]. Studies indicating induction of FAS by retinoids are normally performed under conditions in which the growth medium of cells has been treated to remove exogenous hormones and lipids from supplemental serum, or under

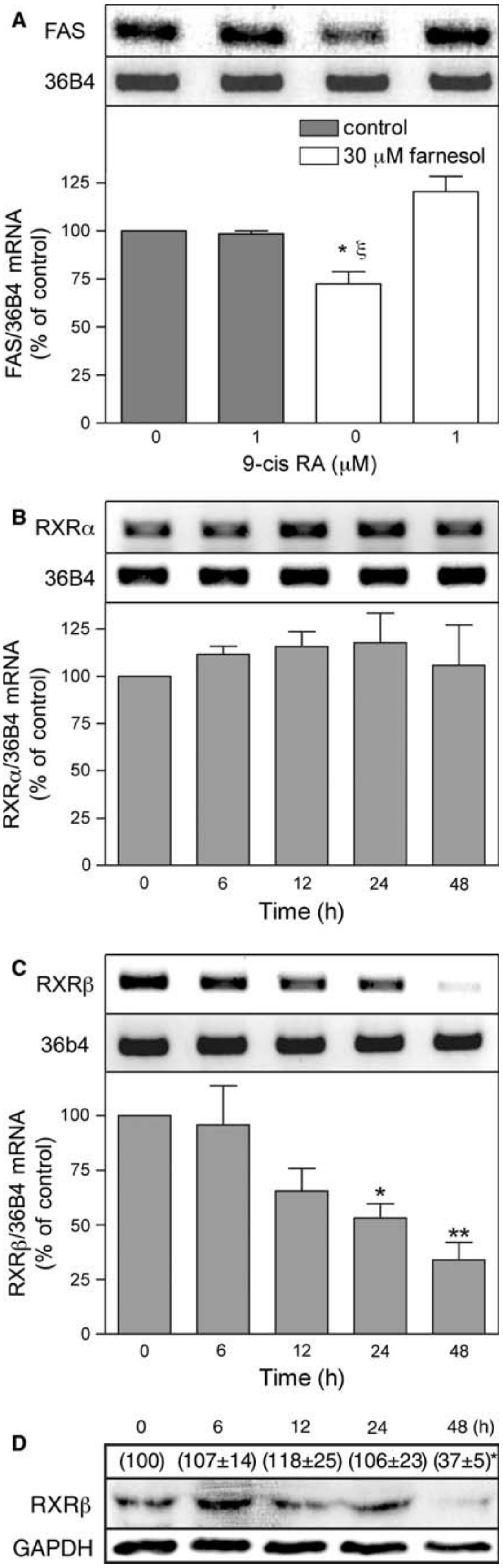

◀ **Fig. 5** Farnesol down-regulates FAS in clone-9 cells through a 9-*cis* RA dependent mechanism that may involve regulation of RXR*β*. Expression of FAS in cells treated with 30 μM farnesol was rescued by the addition of 1 μM 9-cis RA (**a**). Farnesol (30 μM) did not affect expression of RXR*α* (**b**), but significantly decreased mRNA expression of RXR*β* (**c**). Levels of RXR*β* protein were also significantly decreased by treatment with 30 μM farnesol (**d**). *Numbers in parentheses* are mean ±SEM for relative band density measured as a percentage of the density of the control band. *$P < 0.05$; **$P < 0.01$ versus control cells. $^{\xi}P < 0.01$ versus cells treated with farnesol + RA

serum-free conditions [34, 35]. In the present study we utilized complete medium containing 10% untreated FBS and found no change in FAS mRNA levels in cells treated with 9-*cis* RA in the absence of farnesol, precluding a non-specific stimulation of gene transcription by this ligand. Farnesol significantly down-regulated RXR*β* (Fig. 5c) but not RXR*α* (Fig. 5b). Western blotting indicated that RXR*β* protein levels were also down-regulated by farnesol (Fig. 5d), suggesting that decreased expression and activity of this transcription factor may play a role in mediating effects of farnesol on FAS. The discovery that RXR*β* is modulated by farnesol is novel and provides a new molecular pathway through, which farnesol may signal to regulate hepatocyte lipid metabolism.

In summary, we have shown that farnesol administered to rats significantly reduced serum TG concentration. Mechanisms that may mediate this effect include increased hepatocyte FA oxidation resulting from PPAR*α* activation and subsequent upregulation of genes involved in peroxisomal and mitochondrial beta-oxidation as well as down-regulation of hepatocyte FA synthesis resulting from decreased mRNA and protein levels and activity of FAS. Rescue experiments showed that down-regulation of FAS by farnesol involved a 9-*cis* retinoic acid mediated mechanism that involves down-regulation of RXR*β*. Diets rich in plant products, the principle source of farnesol, are generally associated with a reduced risk for the development of cardiovascular disease [36]. Our findings suggest that farnesol may contribute to this reduction in risk by not only helping to counter hypercholesterolemia, but also by lowering serum TG concentrations.

Acknowledgments This work was supported by a grant from the Natural Sciences and Engineering Research Council (NSERC) of Canada. R.E.D. is a recipient of an NSERC postdoctoral fellowship. The authors would like to thank Chris Lange for assistance.

References

1. Jacobson TA, Miller M, Schaefer EJ (2007) Hypertriglyceridemia and cardiovascular risk reduction. Clin Ther 29:763–777
2. Lewis GF (1997) Fatty acid regulation of very low density lipoprotein production. Curr Opin Lipidol 8:146–153

3. Marques-Lopes I, Ansorena D, Astiasaran I, Forga L, Martinez JA (2001) Postprandial de novo lipogenesis and metabolic changes induced by a high-carbohydrate, low-fat meal in lean and overweight men. Am J Clin Nutr 73:253–261
4. Diraison F, Dusserre E, Vidal H, Sothier M, Beylot M (2002) Increased hepatic lipogenesis but decreased expression of lipogenic gene in adipose tissue in human obesity. Am J Physiol Endocrinol Metab 282:E46–E51
5. Elam MB, Wilcox HG, Cagen LM, Deng X, Raghow R, Kumar P, Heimberg M, Russell JC (2001) Increased hepatic VLDL secretion, lipogenesis, and SREBP-1 expression in the corpulent JCR:LA-cp rat. J Lipid Res 42:2039–2048
6. Svegliati-Baroni G, Candelaresi C, Saccomanno S, Ferretti G, Bachetti T, Marzioni M, De Minicis S, Nobili L, Salzano R, Omenetti A, Pacetti D, Sigmund S, Benedetti A, Casini A (2006) A model of insulin resistance and nonalcoholic steatohepatitis in rats: role of peroxisome proliferator-activated receptor-alpha and n-3 polyunsaturated fatty acid treatment on liver injury. Am J Pathol 169:846–860
7. Meigs TE, Simoni RD (1997) Farnesol as a regulator of HMG-CoA reductase degradation: characterization and role of farnesyl pyrophosphatase. Arch Biochem Biophys 345:1–9
8. He L, Mo H, Hadisusilo S, Qureshi AA, Elson CE (1997) Isoprenoids suppress the growth of murine B16 melanomas in vitro and in vivo. J Nutr 127:668–674
9. Tatman D, Mo H (2002) Volatile isoprenoid constituents of fruits, vegetables and herbs cumulatively suppress the proliferation of murine B16 melanoma and human HL-60 leukemia cells. Cancer Lett 175:129–139
10. Horn TL, Long L, Cwik MJ, Morrissey RL, Kapetanovic IM, McCormick DL (2005) Modulation of hepatic and renal drug metabolizing enzyme activities in rats by subchronic administration of farnesol. Chemico Biol Interact 152:79–99
11. Ong TP, Heidor R, de Conti A, Dagli ML, Moreno FS (2006) Farnesol and geraniol chemopreventive activities during the initial phases of hepatocarcinogenesis involve similar actions on cell proliferation and DNA damage, but distinct actions on apoptosis, plasma cholesterol and HMGCoA reductase. Carcinogenesis 27:1194–1203
12. Meigs TE, Roseman DS, Simoni RD (1996) Regulation of 3-hydroxy-3-methylglutaryl-coenzyme A reductase degradation by the nonsterol mevalonate metabolite farnesol in vivo. J Biol Chem 271:7916–7922
13. Voziyan PA, Goldner CM, Melnykovych G (1993) Farnesol inhibits phosphatidylcholine biosynthesis in cultured cells by decreasing cholinephosphotransferase activity. Biochem J 295(Pt 3):757–762
14. Murthy S, Tong H, Hohl RJ (2005) Regulation of fatty acid synthesis by farnesyl pyrophosphate. J Biol Chem 280:41793–41804
15. Hiyoshi H, Yanagimachi M, Ito M, Yasuda N, Okada T, Ikuta H, Shinmyo D, Tanaka K, Kurusu N, Yoshida I, Abe S, Saeki T, Tanaka H (2003) Squalene synthase inhibitors suppress triglyceride biosynthesis through the farnesol pathway in rat hepatocytes. J Lipid Res 44:128–135
16. Swinnen JV, Esquenet M, Goossens K, Heyns W, Verhoeven G (1997) Androgens stimulate fatty acid synthase in the human prostate cancer cell line LNCaP. Cancer Res 57:1086–1090
17. Keller RK, Zhao Z, Chambers C, Ness GC (1996) Farnesol is not the nonsterol regulator mediating degradation of HMG-CoA reductase in rat liver. Arch Biochem Biophys 328:324–330
18. Ide T, Tsunoda M, Mochizuki T, Murakami K (2004) Enhancement of insulin signaling through inhibition of tissue lipid accumulation by activation of peroxisome proliferator-activated receptor (PPAR) alpha in obese mice. Med Sci Monit 10:BR388–BR395
19. Kim H, Haluzik M, Asghar Z, Yau D, Joseph JW, Fernandez AM, Reitman ML, Yakar S, Stannard B, Heron-Milhavet L, Wheeler MB, LeRoith D (2003) Peroxisome proliferator-activated receptor-alpha agonist treatment in a transgenic model of type 2 diabetes reverses the lipotoxic state and improves glucose homeostasis. Diabetes 52:1770–1778
20. Giguere V (1999) Orphan nuclear receptors: from gene to function. Endocr Rev 20:689–725
21. Pineda Torra I, Jamshidi Y, Flavell DM, Fruchart JC, Staels B (2002) Characterization of the human PPARalpha promoter: identification of a functional nuclear receptor response element. Mol Endocrinol 16:1013–1028
22. Takahashi N, Kawada T, Goto T, Yamamoto T, Taimatsu A, Matsui N, Kimura K, Saito M, Hosokawa M, Miyashita K, Fushiki T (2002) Dual action of isoprenols from herbal medicines on both PPARgamma and PPARalpha in 3T3-L1 adipocytes and HepG2 hepatocytes. FEBS Lett 514:315–322
23. Hanley K, Komuves LG, Ng DC, Schoonjans K, He SS, Lau P, Bikle DD, Williams ML, Elias PM, Auwerx J, Feingold KR (2000) Farnesol stimulates differentiation in epidermal keratinocytes via PPARalpha. J Biol Chem 275:11484–11491
24. Lefebvre P, Chinetti G, Fruchart JC, Staels B (2006) Sorting out the roles of PPAR alpha in energy metabolism and vascular homeostasis. J Clin Invest 116:571–580
25. Cagen LM, Deng X, Wilcox HG, Park EA, Raghow R, Elam MB (2005) Insulin activates the rat sterol-regulatory-element-binding protein 1c (SREBP-1c) promoter through the combinatorial actions of SREBP, LXR, Sp-1 and NF-Y *cis*-acting elements. Biochem J 385:207–216
26. Wang Y, Jones Voy B, Urs S, Kim S, Soltani-Bejnood M, Quigley N, Heo YR, Standridge M, Andersen B, Dhar M, Joshi R, Wortman P, Taylor JW, Chun J, Leuze M, Claycombe K, Saxton AM, Moustaid-Moussa N (2004) The human fatty acid synthase gene and de novo lipogenesis are coordinately regulated in human adipose tissue. J Nutr 134:1032–1038
27. Amin D, Rutledge RZ, Needle SN, Galczenski HF, Neuenschwander K, Scotese AC, Maguire MP, Bush RC, Hele DJ, Bilder GE, Perrone MH (1997) RPR 107393, a potent squalene synthase inhibitor and orally effective cholesterol-lowering agent: comparison with inhibitors of HMG-CoA reductase. J Pharmacol Exp Ther 281:746–752
28. Hiyoshi H, Yanagimachi M, Ito M, Saeki T, Yoshida I, Okada T, Ikuta H, Shinmyo D, Tanaka K, Kurusu N, Tanaka H (2001) Squalene synthase inhibitors reduce plasma triglyceride through a low-density lipoprotein receptor-independent mechanism. Eur J Pharmacol 431:345–352
29. Scharnagl H, Schinker R, Gierens H, Nauck M, Wieland H, Marz W (2001) Effect of atorvastatin, simvastatin, and lovastatin on the metabolism of cholesterol and triacylglycerides in HepG2 cells. Biochem Pharmacol 62:1545–1555
30. Ugawa T, Kakuta H, Moritani H, Matsuda K, Ishihara T, Yamaguchi M, Naganuma S, Iizumi Y, Shikama H (2000) YM-53601, a novel squalene synthase inhibitor, reduces plasma cholesterol and triglyceride levels in several animal species. Br J Pharmacol 131:63–70
31. Bradfute DL, Silva CJ, Simoni RD (1992) Squalene synthase-deficient mutant of Chinese hamster ovary cells. J Biol Chem 267:18308–18314
32. Shimano H, Horton JD, Shimomura I, Hammer RE, Brown MS, Goldstein JL (1997) Isoform 1c of sterol regulatory element binding protein is less active than isoform 1a in livers of transgenic mice and in cultured cells. J Clin Invest 99:846–854
33. Sato R, Yang J, Wang X, Evans MJ, Ho YK, Goldstein JL, Brown MS (1994) Assignment of the membrane attachment, DNA binding, and transcriptional activation domains of sterol

regulatory element-binding protein-1 (SREBP-1). J Biol Chem 269:17267–17273

34. Roder K, Zhang L, Schweizer M (2007) SREBP-1c mediates the retinoid-dependent increase in fatty acid synthase promoter activity in HepG2. FEBS Lett 581:2715–2720
35. Schweizer M, Roder K, Zhang L, Wolf SS (2002) Transcription factors acting on the promoter of the rat fatty acid synthase gene. Biochem Soc Trans 30:1070–1072
36. Key TJ, Fraser GE, Thorogood M, Appleby PN, Beral V, Reeves G, Burr ML, Chang-Claude J, Frentzel-Beyme R, Kuzma JW, Mann J, McPherson K (1999) Mortality in vegetarians and non-vegetarians: detailed findings from a collaborative analysis of 5 prospective studies. Am J Clin Nutr 70:516S–524S

Lipids (2008) 43:629–641
DOI 10.1007/s11745-008-3188-z

ORIGINAL ARTICLE

Fatty Acid Profile of Sunshine Bass: I. Profile Change is Affected by Initial Composition and Differs Among Tissues

Jesse T. Trushenski · Heidi A. Lewis ·
Christopher C. Kohler

Received: 28 March 2008 / Accepted: 4 May 2008 / Published online: 3 June 2008
© AOCS 2008

Abstract Fatty acid (FA) composition of fillet tissue can be tailored by transitioning fish from alternative lipid-based, low long-chain polyunsaturated fatty acid (LC-PUFA) grow-out feeds to high LC-PUFA "finishing" feeds. To address whether grow-out feed composition influences the responsiveness of fillet tissue to finishing, sunshine bass (SB, *Morone chrysops* × *M. saxatilis*) were reared to a submarketable size on grow-out feeds containing fish oil (FO) or a 50:50 blend of FO and coconut (CO), grapeseed (GO), linseed (LO), or poultry (PO) oil. For the final 8 weeks of the trial, fish were either maintained on assigned grow-out feeds or finished with the 100% FO feed. Production performance was unaffected by dietary lipid source, but fillet FA profile generally conformed to nutritional history. Regardless of grow-out regimen, finishing had a significant restorative effect on fillet FA composition; however, complete restoration of control levels of 20:5n-3, 22:6n-3, total LC-PUFA and n-3:n-6 FA ratio was achieved only among fish fed the CO-based grow-out feed. Saturated fatty acids (SFA) appear to be preferential catabolic substrates, whereas medium-chain and long-chain PUFA are selectively deposited in tissues. Provision of SFA in grow-out feeds appears to optimize selective FA metabolism and restoration of beneficial fillet FA profile during finishing.

Keywords Fish oil · Alternative lipid · Finishing feed · Fatty acid turnover/dilution · LC-PUFA · *Morone* spp.

J. T. Trushenski (✉) · H. A. Lewis · C. C. Kohler
Fisheries and Illinois Aquaculture Center and Department of Zoology, Southern Illinois University Carbondale, Carbondale, IL 62901-6511, USA
e-mail: saluski@siu.edu

Abbreviations

ANOVA	Analysis of variance
CO	Coconut oil
DHA	Docosahexaenoic acid, 22:6n-3
EPA	Eicosapentaenoic acid, 20:5n-3
FA	Fatty acid
FCR	Feed conversion ratio
FO	Fish oil
GO	Grapeseed oil
HSI	Hepatosomatic index
IPF	Intraperitoneal fat
IPFR	Intraperitoneal fat ratio
LC-PUFA	Long-chain polyunsaturated fatty acid(s)
LO	Linseed oil
MC-PUFA	Medium-chain polyunsaturated fatty acid(s)
MUFA	Monounsaturated fatty acid(s)
PO	Poultry oil
PUFA	Polyunsaturated fatty acid(s)
SB	Sunshine bass
SFA	Saturated fatty acid(s)

Introduction

Seafood represents an increasingly important food source for the human population, particularly in developing regions—seafood comprises 20% of animal protein intake for more than half of the world population [1]. In addition, seafood is the predominant dietary source of long-chain polyunsaturated fatty acids (carbon atoms $\geq$ 20, degree of unsaturation $\geq$ 3, LC-PUFA), such as eicosapentaenoic (EPA, 20:5n-3) and docosahexaenoic acids (DHA, 22:6n-3), that are critical to human health [2]. These fatty acids (FA) impart benefits beyond basic nutritive value, positively influencing neural, cardiac, vascular, immunological, reproductive, and oncogenetic health [3–8]. As a result, both nutritional and medical communities have recommended increasing human consumption of LC-PUFA to improve and maintain health of the American public [9].

With most traditional capture fisheries at sustainable harvest limits or in decline [10], seafood demand is increasingly met by aquaculture products. Currently, 45% of the fish consumed worldwide are cultured [1]. Assuming per capita seafood consumption is maintained, aquaculture production must double by 2030 to keep pace with human population growth over this time period [11]. Attendant to growth in the aquaculture sector is the further expansion of aquafeed manufacturing, an industry which relies on "reduction" fisheries for the production of fish meal and fish oil (FO) [12]. Recent peaks in the price of FO [13] reflect increasing competition for this resource among end-users and the inability of reduction fisheries to sustain further growth. In addition to economic and sustainability considerations, evidence linking FO in aquafeeds to elevated levels of environmental contaminants in cultured seafood [14–16] has motivated the aquaculture industry to identify alternatives to FO.

Fish oil replacement has been evaluated using a variety of plant- and animal-derived, alternative lipids in numerous aquaculture species, often with great success [17–20]. Although growth performance is typically unaffected by dietary lipid source, FA composition of fish tissues mirrors dietary content and is responsive to dietary change. Following a switch in dietary lipid source, fillet composition will change over time to more closely resemble the new dietary FA profile [21–24]. Thus, replacing FO with alternative lipid sources in aquafeeds results in the loss of nutritionally beneficial LC-PUFA within the resultant fillets and may, in turn, limit health benefits of cultured seafood to human consumers [25].

Based on the known plasticity of fillet composition, nutritionists have suggested the use of "finishing" feeds, high in LC-PUFA, to increase and/or restore high levels of these beneficial FA to the fillet prior to harvest. In this strategy, fish are raised on alternative lipid-based "grow-out" feeds for most of the production cycle and then transitioned to the finishing feed prior to harvest. Finishing feeds have been used to enhance fillet LC-PUFA content in a number of aquaculture species [26–34], however, the extent of LC-PUFA augmentation varies and complete restoration of FO-associated profile is infrequently reported [31, 34]. Fatty acid composition of the grow-out feed and pre-finishing fillet profile may contribute to differences in overall finishing success. Previous research suggested medium-chain polyunsaturated fatty acids (18 carbon, MC-PUFA) are resistant to "washout" or "dilution" during finishing [35], whereas saturated FA (SFA) are perhaps more labile in fish tissues [33]. Most finishing strategies have employed MC-PUFA-rich plant oils during the grow-out phase, but high levels of MC-PUFA may render fillets comparatively unresponsive to finishing and LC-PUFA augmentation. To address this hypothesis, we evaluated alternative lipid sources with distinct FA profiles in sunshine bass (SB, *Morone chrysops* × *M. saxatilis*) grow-out feeds and subsequently assessed the responsiveness of fillet tissue to LC-PUFA augmentation during finishing.

Methods and Materials

Diet Preparation and Analyses

Five feeds were manufactured based on a practical, reduced fish meal feed our group previously developed for SB culture ([36], Table 1). As originally formulated, this feed contained 9.8% FO (dry matter basis; menhaden-derived; Virginia Gold^{TM}, Omega Protein, Inc., Houston, TX, USA). In the present work, the original, FO-based formulation served as the control grow-out feed as well as the finishing feed. Four experimental grow-out feeds were derived from the basal formulation, with 50% of the FO replaced with poultry (PO, Tyson Foods, Inc., Robards, KY, USA), linseed (LO, Barlean's Organic Oils, Ferndale, WA, USA), grapeseed (GO, Kusha, Inc, Irvine, CA, USA), or coconut oil (CO, Spectrum Organic Products, Petaluma, CA, USA). These alternative lipids are predominantly comprised of a single FA class (monounsaturates [MUFA], n-3 MC-PUFA, n-6 MC-PUFA, and SFA, respectively) and were strategically chosen to generate distinct feed FA profiles for the purposes of hypothesis testing (Table 2). All feedstuffs were incorporated using a cutter–mixer (Model CM450, Hobart Corporation, Troy, OH, USA), pelleted using a food grinder, dried at room temperature to ~ 870 g kg^{-1} dry matter, and stored frozen (−20°C) throughout the duration of the study. Proximate analyses of triplicate diet samples were conducted according to standard methods for analysis of animal feeds [37, 38] to confirm diet composition (Table 1). Reserved crude lipid samples were analyzed for FA composition (Table 2) according to the procedures described by Lane et al. [33].

Experimental Design and Feeding Trial

Nine feeding regimens were developed to address influences of dietary lipid source and FA composition on production performance and subsequent finishing diet success in SB culture (Fig. 1). Eight experimental regimens represented feeding the grow-out feeds described above throughout the feeding trial (CO, LO, GO, and PO regimens) or with an 8-week finishing period (CO + Finish, LO + Finish, GO + Finish, and PO + Finish regimens). The control

Table 1 Formulation and proximate composition of experimental diets adapted from Lewis and Kohler [36]

Ingredient	Fish oil (FO)	Coconut oil (CO)	Grapeseed oil (GO)	Linseed oil (LO)	Poultry oil (PO)
Fish meal[a]	200	200	200	200	200
Fish oil[a]	98	49	49	49	49
Coconut oil[b]	–	49	–	–	–
Grapeseed oil[c]	–	–	49	–	–
Linseed oil[d]	–	–	–	49	–
Poultry oil[e]	–	–	–	–	49
Corn gluten meal[f]	140	140	140	140	140
Wheat middlings	201	201	201	201	201
Soybean meal	300	300	300	300	300
Carboxymethyl cellulose	20	20	20	20	20
Sodium phosphate monobasic	15	15	15	15	15
Calcium phosphate dibasic	15	15	15	15	15
Choline chloride	6	6	6	6	6
Mineral Premix[g]	1.5	1.5	1.5	1.5	1.5
Vitamin Premix[h]	1.5	1.5	1.5	1.5	1.5
Proximate composition					
Dry matter	88.0	87.8	88.3	84.7	85.7
Protein	41.1	41.5	41.0	40.5	39.4
Lipid	14.3	14.5	14.4	14.6	13.2
Ash	10.8	10.2	9.6	11.4	10.6

All proximate composition values are expressed as a mean in g/100g (%), dry matter basis. Formulation composition is expressed in g/kg

[a] Derived from menhaden *Brevoortia* spp., Omega Protein, Inc., Houston, TX, USA

[b] Spectrum Organic Products, Petaluma, CA, USA

[c] Kusha, Inc., Irvine, CA, USA

[d] Barlean's Organic Oils, Ferndale, WA, USA

[e] Tyson Foods, Inc., Robards, KY, USA

[f] Tate and Lyle, Decatur, IL, USA

[g] Formulated to contain: 7,000 mg $\mathrm{kg^{-1}}$ copper, 70,000 mg $\mathrm{kg^{-1}}$ iron, 100,000 mg $\mathrm{kg^{-1}}$ manganese, 200,000 mg $\mathrm{kg^{-1}}$ zinc, 0.24% iodine

[h] Formulated to contain: 99.8 mg $\mathrm{kg^{-1}}$ selenium, 2,200 mg $\mathrm{kg^{-1}}$ folic acid, 88,000 mg $\mathrm{kg^{-1}}$ niacin, 35,200 mg $\mathrm{kg^{-1}}$ pantothenic acid, 11,000 mg $\mathrm{kg^{-1}}$ vitamin B6, 13,200 mg $\mathrm{kg^{-1}}$ riboflavin, 11,000 mg $\mathrm{kg^{-1}}$ thiamin, 11,000 mg $\mathrm{kg^{-1}}$ vitamin B12, 66,000 mg $\mathrm{kg^{-1}}$ vitamin E, 4,400 mg $\mathrm{kg^{-1}}$ vitamin K, 4,400,000 IU $\mathrm{kg^{-1}}$ vitamin A, 2,200,000 IU $\mathrm{kg^{-1}}$ vitamin D, 100,000 mg $\mathrm{kg^{-1}}$ vitamin C

regimen represented feeding the FO control/finishing feed throughout the duration of the feeding trial (FO Control regimen). Juvenile SB [46 ± 1 g, mean ± SE; age 1 (~10 months); Keo Fish Farm, Keo AR] were group-reared on the grow-out feeds described above, then stocked into a recirculation system consisting of 30, 270-l fiberglass tanks with associated mechanical and biological filtration units for the final 12 weeks of the production cycle. Each experimental regimen was randomly assigned to three replicate tanks ($n = 3$), whereas the control regimen was assigned to six replicate tanks ($n = 6$). For all regimens, each replicate tank was stocked with six fish from the appropriate dietary group. Eight weeks prior to harvest, a subsample of one fish per tank was collected to determine baseline tissue FA profile prior to finishing (tissues collected as described in "Harvest, Sample Collection, and Production Performance"). After baseline sampling, remaining fish were finished with the 100% FO feed for the remaining 8 weeks of the feeding trial (CO + Finish, LO + Finish, GO + Finish, and PO + Finish regimens) or maintained on assigned grow-out feeds (FO Control, CO, LO, GO, and PO regimens). Throughout the 7-month culture period, fish were fed assigned feeds once daily to apparent satiation.

Temperature (YSI Model 55 Oxygen Meter, Yellow Springs, OH, USA) was measured daily, whereas dissolved oxygen (YSI Model 55 Oxygen Meter, Yellow Springs, OH, USA), ammonia-, nitrite-, and nitrate–nitrogen as well as alkalinity were measured periodically throughout the study period (Hach DR/2010 spectrophotometer, Hach Company, Loveland, CO, USA). All water quality parameters were maintained within ranges suitable for SB culture [39]. All culture and husbandry methods, as well as euthanasia and sample collection procedures described below, were conducted under the direction and approval of the Southern

Table 2 Dietary composition with respect to FA and FA classes

Fatty acid(s)	Fish oil (FO)	Coconut oil (CO)	Grapeseed oil (GO)	Linseed oil (LO)	Poultry oil (PO)
8:0	0.00 ± 0.05	1.83 ± 0.05	0.00 ± 0.05	0.00 ± 0.05	0.00 ± 0.05
10:0	0.00 ± 0.02	2.02 ± 0.02	0.00 ± 0.02	0.00 ± 0.02	0.00 ± 0.02
12:0	0.11 ± 0.02	17.59 ± 0.02	0.02 ± 0.02	0.04 ± 0.02	0.06 ± 0.02
14:0	7.65 ± 0.02	11.29 ± 0.02	4.41 ± 0.02	4.42 ± 0.02	4.68 ± 0.02
16:0	18.71 ± 0.02	15.12 ± 0.02	14.47 ± 0.02	13.45 ± 0.02	20.87 ± 0.02
18:0	3.50 ± 0.01	3.28 ± 0.01	3.58 ± 0.01	3.71 ± 0.01	4.48 ± 0.01
Total SFA[a]	31.90 ± 0.06	52.38 ± 0.06	23.90 ± 0.06	22.97 ± 0.06	31.40 ± 0.06
16:1n-7	9.84 ± 0.02	5.65 ± 0.02	5.62 ± 0.02	5.61 ± 0.02	7.85 ± 0.02
18:1n-7	2.90 ± 0.00	1.75 ± 0.00	1.98 ± 0.00	1.92 ± 0.00	2.45 ± 0.00
18:1n-9	7.74 ± 0.02	8.12 ± 0.02	13.62 ± 0.02	11.16 ± 0.02	19.67 ± 0.02
Total MUFA[b]	21.68 ± 0.03	16.20 ± 0.03	21.98 ± 0.03	19.40 ± 0.03	30.76 ± 0.03
18:2n-6	8.42 ± 0.08	8.85 ± 0.08	32.40 ± 0.08	14.68 ± 0.08	15.58 ± 0.08
20:4n-6	0.92 ± 0.01	0.58 ± 0.01	0.58 ± 0.01	0.58 ± 0.01	0.71 ± 0.01
n-6	10.12 ± 0.08	10.21 ± 0.08	33.45 ± 0.08	16.02 ± 0.08	16.92 ± 0.08
18:3n-3	2.14 ± 0.01	2.04 ± 0.01	1.59 ± 0.01	22.56 ± 0.01	1.82 ± 0.01
18:4n-3	3.49 ± 0.01	1.86 ± 0.01	1.86 ± 0.01	1.87 ± 0.01	1.82 ± 0.01
20:4n-3	1.49 ± 0.01	0.81 ± 0.01	0.84 ± 0.01	0.81 ± 0.01	0.81 ± 0.01
20:5n-3	11.46 ± 0.02	6.60 ± 0.02	6.53 ± 0.02	6.53 ± 0.02	6.52 ± 0.02
22:5n-3	2.11 ± 0.02	1.22 ± 0.02	1.28 ± 0.02	1.22 ± 0.02	1.21 ± 0.02
22:6n-3	12.73 ± 0.03	6.96 ± 0.03	6.86 ± 0.03	6.89 ± 0.03	7.04 ± 0.03
n-3	33.64 ± 0.05	19.60 ± 0.05	19.08 ± 0.05	40.02 ± 0.05	19.34 ± 0.05
Total PUFA[c]	46.42 ± 0.07	31.42 ± 0.07	54.12 ± 0.07	57.63 ± 0.07	37.84 ± 0.07
Total LC-PUFA[d]	29.13 ± 0.05	16.40 ± 0.05	16.33 ± 0.05	16.30 ± 0.05	16.59 ± 0.05
Total MC-PUFA[e]	14.72 ± 0.08	13.16 ± 0.08	36.26 ± 0.08	39.53 ± 0.08	19.69 ± 0.08
n-3:n-6	3.32 ± 0.02	1.92 ± 0.02	0.57 ± 0.02	2.50 ± 0.02	1.14 ± 0.02

Values represent least-square means ± SE of triplicate samples

[a] Saturated fatty acids—sum of all FA without double bonds

[b] Monounsaturated fatty acids—sum of all FA with a single double bond

[c] Polyunsaturated fatty acids—sum of all FA with ≥2 double bonds

[d] Long-chain PUFA—sum of all FA with chain length ≥ 20 carbon atoms and double bonds ≥ 3

[e] Medium-chain—sum of all PUFA with chain length of 18 carbon atoms; includes 18:3n-4 in addition to individually reported MC-PUFA

Illinois University Institutional Animal Care and Use Committee, protocol #07-008.

Harvest, Sample Collection, and Production Performance

After completion of the feeding trial, feed was withheld for 48 h prior to harvest. Fish within individual tanks were harvested and immediately anesthetized in an ice-water bath. Each anesthetized fish was individually weighed and euthanized by single cranial pithing prior to tissue sample collection. Boneless, skinless, J-cut (without belly flap) fillets were harvested by experienced filleters to calculate % dress-out [(weight of fillets/whole body weight) × 100]. Fillet subsamples were collected from a standardized dorso-anterior landmark (to isolate white muscle tissue), packaged in sterile, polyethylene bags (Whirl-pak®, Nasco, Fort Atkinson, WI, USA), and stored frozen (−80°C) prior to proximate and FA analyses. Additional fillet subsamples were packaged similarly and held refrigerated for analysis of oxidative stability. Livers and intraperitoneal fat (IPF) masses were dissected from the viscera to calculate hepatosomatic index [HSI; (liver weight/whole body weight) × 100] and intraperitoneal fat ratio [IPFR; (IPF weight/whole body weight) × 100] indices. Subsamples of hepatic and IPF tissue were packaged and stored in the same manner as fillet tissue for FA analysis. Survival, percent weight gain [((average individual weight$_{\text{final}}$ − average individual weight$_{\text{initial}}$)/average individual weight$_{\text{initial}}$) × 100], and food conversion ratio (FCR; average individual dry matter consumption/average individual gain) were calculated for each tank.

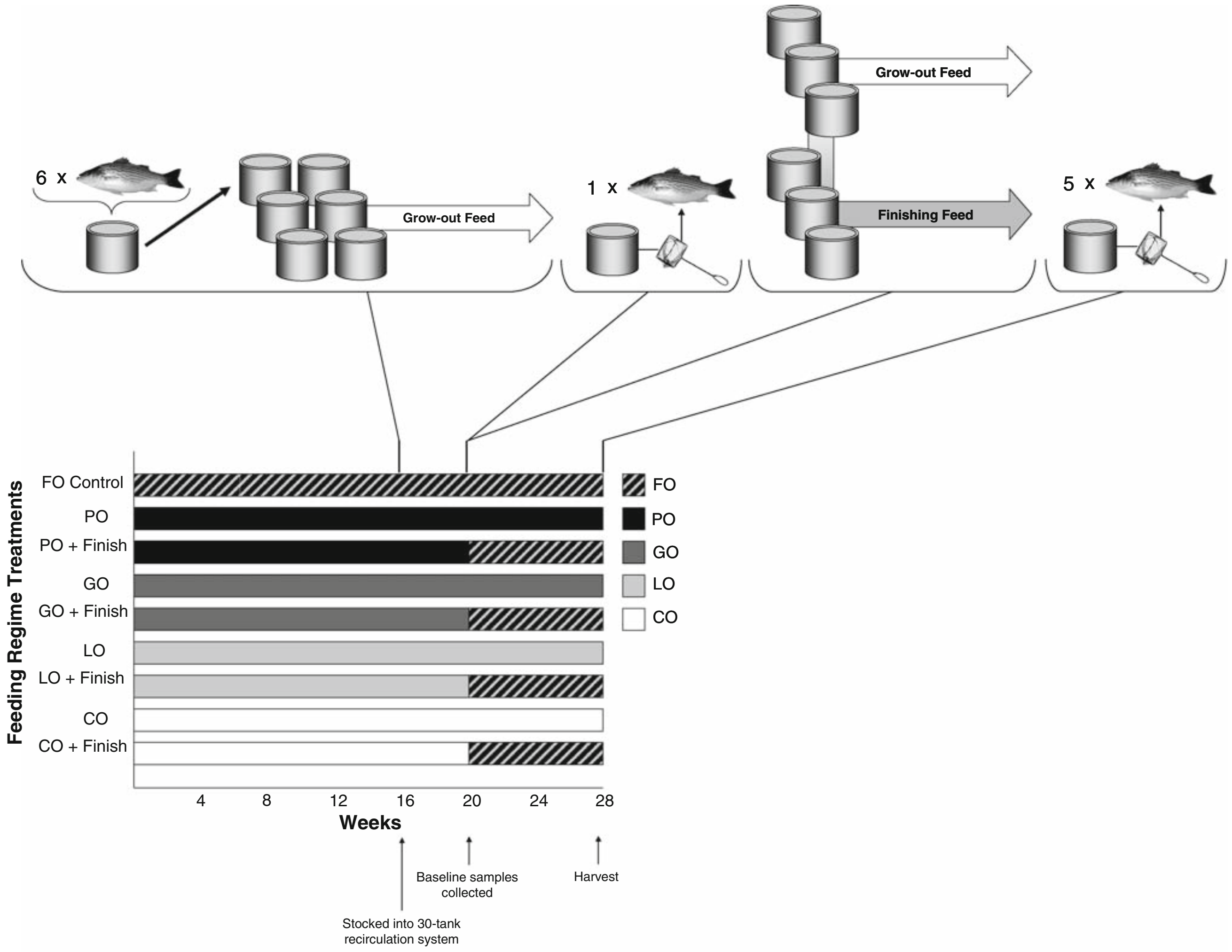
6 x
Grow-out Feed
1 x
Grow-out Feed
Finishing Feed
5 x
Feeding Regime Treatments
FO Control
PO
PO + Finish
GO
GO + Finish
LO
LO + Finish
CO
CO + Finish
▨ FO
■ PO
■ GO
■ LO
☐ CO
4
8
12
16
20
24
28
Weeks
Baseline samples collected
Harvest
Stocked into 30-tank recirculation system

Fig. 1 Schematic of experimental design and feeding trial. Groups of sunshine bass were group-reared on one of five grow-out feeds and then stocked into a recirculation system. Each grow-out group was assigned to six replicate tanks, each originally housing six fish. After 20 weeks of culture, baseline tissue samples were collected (1 fish per tank). Three replicate tanks within each grow-out group were transitioned to the FO-based finishing feed for the last 8 weeks of the trial, whereas the other tanks were maintained on assigned grow-out feeds. At harvest, production performance was assessed and tissue samples were collected from all remaining fish (5 fish per tank). FO, 100% fish oil feed; PO, 50:50 poultry/fish oil feed; GO, 50:50 grapeseed/fish oil feed; LO, 50:50 linseed/fish oil feed; CO, 50:50 coconut/fish oil feed

Tissue Composition

Fillet samples were analyzed according to standard methods [37, 38] for meat products to determine percent moisture, crude protein, crude lipid, and ash. All tissue samples were analyzed for FA composition in the same manner as diet samples (see “Diet Preparation and Analyses”).

Peroxidative Stability

Short-term fillet oxidative stability was assessed at 24 h post-harvest by analyzing refrigerated fillet samples for the presence of peroxides and aldehydes using the Peroxysafe^{TM} and Aldesafe^{TM} colorimetric assay kits (Saftest Incorporated, Tempe, AZ, USA).

Statistical Analyses

Although multiple individual fish were sampled from each tank, replicate tanks served as the experimental units for all statistical analyses ($n = 3$ for experimental regimens, $n = 6$ for control regimen). All data were analyzed by one-way analysis of variance (ANOVA) within the General Linear Model framework of the Statistical Analysis System, version 9.1 (SAS Institute, Cary, NC, USA) to determine significance of differences among feeding regimens. Tissue FA data was further analyzed by two-way ANOVA within the Mixed Model framework of the Statistical Analysis System to test for independent and interactive effects of feeding regimen and tissue type. In all cases, differences were considered significant at $P < 0.05$.

Results

Lipid source and FA profile of the grow-out feeds strongly influenced fillet FA profile and subsequent finishing success in SB culture. Feeding diets with different dietary lipid sources during the first 5 months of the feeding trial resulted in dramatic alterations of fillet FA composition, with baseline fillet profile (Table 3) generally mirroring dietary FA composition (Table 2). Expectedly, baseline fillet samples of fish fed the LO, GO, and PO feeds contained high levels of 18:3n-3, 18:2n-6, and total MUFA, respectively, whereas fillets of FO-fed fish were higher in LC-PUFA, particularly 20:5n-3 and 22:6n-3. However, baseline fillet samples of CO-fed fish did not reflect dietary prevalence of SFA or reduced LC-PUFA content, and prior to finishing, were largely equivalent to samples from the FO Control regimen.

Continued use of the alternative lipid-based grow-out feeds through harvest resulted in similar, though more pronounced deviations from the FO Control profile (Table 4). Nonetheless, in each of these unfinished regimens, fillet levels of LC-PUFA were exaggerated in comparison to dietary profile (Fig. 2). Finishing had a significant restorative effect on fillet FA profile, augmenting fillet levels of FO-associated FA, regardless of grow-out regimen (Table 4). However, complete restoration of FO Control levels of 20:5n-3, 22:6n-3, and LC-PUFA and n-3:n-6 FA ratio was achieved only in the CO + Finish group.

Liver and IPF FA composition were also significantly influenced by feeding regimen; however, comparison among fillet, liver, and IPF profiles revealed significant differences in how dietary FA were partitioned among the tissue types (Fig. 3). Saturated FA and MUFA were most abundant within the IPF, particularly when abundant in the feed. Conversely, levels of LC-PUFA, but not MC-PUFA, were consistently lower within the IPF compared to liver and fillet tissue ($P_{\mathrm{tissue\ type\ effect}} < 0.01$). Liver FA profile largely mirrored fillet composition, in that both tissue types typically contained lower levels of MUFA and higher levels of LC-PUFA compared to IPF tissue ($P_{\mathrm{tissue\ type\ effect}} < 0.01$). When tissue composition of the unfinished groups was standardized to dietary composition (Fig. 4), these distinctions were particularly apparent, indicating concentration of LC-PUFA within the liver and fillet tissues and concentration of MUFA within the IPF.

Fillet proximate composition did not vary, with the exception of fillet moisture content (Table 5), which showed slight, though significant, reductions for GO Control and PO + Finish treatments. Consumption, weight gain, FCR, HSI, and dress-out were unaffected by feeding regimen and acceptable in terms of production performance typically observed for SB (Table 6). LSI values were significantly lower among fish fed the CO- and GO feeds (Table 6). LSI tended to be higher among finished groups relative to their unfinished counterparts, though significant differences were only observed within the GO-fed groups. No mortalities occurred during the course of the feeding trial. Peroxide and aldehyde concentrations were below detection limits for all samples analyzed (data not shown).

Discussion

Although production performance and fillet crude lipid content were unaffected, feeding diets with different dietary lipid sources resulted in dramatic alterations of fillet total lipid FA composition. These findings are in agreement with previous investigations of CO [40], PO [41, 42], and LO [43], as well as the well-established paradigm of compositional plasticity of fish tissues with respect to FA profile. Finishing augments fillet nutritional quality among fishes raised on feeds containing FO alternatives [26–34]; however, complete restoration of FO-associated FA profile, specifically LC-PUFA content, is rarely observed [31–34]. For example, in Atlantic salmon *Salmo salar* fed linseed, palm, and/or rapeseed oil-based grow-out feeds, complete profile restoration was not observed after 20–24 weeks of finishing [27, 30, 32]. Similarly, 8–16 weeks of finishing were insufficient to completely restore the profile of Murray cod *Maccullochella peelii peelii* previously fed diets containing blends of linseed, olive, palm, sunflower, or rapeseed oils [34, 35]. Prior attempts to restore fillet LC-PUFA content of SB fed a corn-oil based, n-6 MC-PUFA-rich grow-out feed were unsuccessful after 12 weeks of finishing [33]. In the present work, restoration was incomplete among fish fed diets high in MC-PUFA. Fillet 20:5n-3, 22:6n-3, and LC-PUFA levels were considerably improved by finishing in the LO- and GO-fed fish, however, the magnitude of restoration was moderate compared to the CO- and PO-fed groups. Arguably, fillet profile could have been completely restored among the LO- and GO-fed fish, however, a longer finishing period would have been necessary to achieve complete FA profile restoration. Conversely, fish fed the CO feed needed little alteration to achieve the FO-associated composition, and fillet FA profile was successfully restored to control levels of LC-PUFA within 8 weeks of finishing.

Pre-finishing fillet FA profile influenced finishing success, and the inclusion of oils high in 18-carbon FA in grow-out feeds limited the effects of finishing feeds on SB fillet FA composition. Others have noted MC-PUFA, such as 18:2n-6 and 18:3n-3, deposited in the fillet are resistant to dietary modification and may be problematic in the context of LC-PUFA restoration during finishing. For

Table 3 Total lipid composition of baseline fillet samples with respect to predominant (>1% fatty acid methyl esters, FAME) fatty acid (FA) and FA classes

Fatty acid(s)	Fish (FO)	Coconut (CO)		Grapeseed (GO)		Linseed (LO)		Poultry (PO)	
	FO control	CO	CO + Finish	GO	GO + Finish	LO	LO + Finish	PO	PO + Finish
12:0	1.3 ± 0.4b	3.6 ± 0.5a	4.0 ± 0.6a	0.1 ± 0.5b	0.1 ± 0.5b	0.0 ± 0.5b	0.0 ± 0.5b	0.1 ± 0.5b	0.1 ± 0.5b
14:0	5.6 ± 0.3a	6.1 ± 0.4a	6.0 ± 0.5a	3.1 ± 0.4b	3.2 ± 0.4b	3.3 ± 0.4b	3.0 ± 0.4b	3.2 ± 0.4b	3.3 ± 0.4b
16:0	19.8 ± 0.5a	20.3 ± 0.7a	20.0 ± 0.9a	17.5 ± 0.7b	17.5 ± 0.7b	17.0 ± 0.7b	16.7 ± 0.7b	20.3 ± 0.7a	20.4 ± 0.7a
18:0	3.5 ± 0.3	4.8 ± 0.5	5.0 ± 0.6	3.9 ± 0.5	3.7 ± 0.5	4.2 ± 0.5	4.0 ± 0.5	4.2 ± 0.5	4.0 ± 0.5
Total SFA[a]	31.3 ± 0.5b	35.6 ± 0.7a	35.9 ± 0.9a	25.4 ± 0.7d	25.3 ± 0.7d	25.2 ± 0.7d	24.6 ± 0.7d	28.7 ± 0.7c	28.6 ± 0.7c
16:1n-7	8.7 ± 0.4a	5.9 ± 0.6bc	5.2 ± 0.7c	5.1 ± 0.6c	5.3 ± 0.5c	5.5 ± 0.6c	5.5 ± 0.6c	7.2 ± 0.6b	7.5 ± 0.6ab
18:1n-7	3.1 ± 0.0a	2.5 ± 0.1b	2.4 ± 0.1bc	2.2 ± 0.1c	2.2 ± 0.1c	2.3 ± 0.1bc	2.3 ± 0.1bc	2.7 ± 0.1b	2.7 ± 0.1b
18:1n-9	11.7 ± 0.6bc	10.5 ± 0.9c	10.3 ± 1.0c	13.3 ± 0.9b	13.8 ± 0.9b	13.2 ± 0.9b	13.6 ± 0.9b	18.8 ± 0.9a	19.3 ± 0.9a
Total MUFA[b]	24.2 ± 1.0b	19.5 ± 1.4c	18.5 ± 1.7c	21.1 ± 1.4bc	22.0 ± 1.4bc	21.7 ± 1.4bc	22.0 ± 1.4bc	29.5 ± 1.4a	30.3 ± 1.4a
18:2n-6	8.4 ± 0.4c	8.1 ± 0.6c	8.1 ± 0.7c	25.5 ± 0.6a	25.5 ± 0.6a	13.1 ± 0.6b	12.7 ± 0.6b	13.1 ± 0.6b	13.1 ± 0.6b
20:4n-6	1.2 ± 0.1ab	1.4 ± 0.1a	1.4 ± 0.1a	1.0 ± 0.1b	0.9 ± 0.1b	0.9 ± 0.1b	1.1 ± 0.1b	1.3 ± 0.1ab	1.2 ± 0.1ab
n-6[c]	10.4 ± 0.4c	10.4 ± 0.5c	10.5 ± 0.7c	27.7 ± 0.5a	27.8 ± 0.5a	14.9 ± 0.5b	14.7 ± 0.5b	15.4 ± 0.5b	15.3 ± 0.5b
18:3n-3	1.6 ± 0.3b	1.5 ± 0.5b	1.4 ± 0.6b	1.2 ± 0.5b	1.3 ± 0.5b	15.5 ± 0.5a	14.5 ± 0.5a	1.5 ± 0.5b	1.4 ± 0.5b
18:4n-3	1.8 ± 0.1a	1.1 ± 0.1b	0.9 ± 0.2b	0.9 ± 0.1b	0.9 ± 0.1b	1.0 ± 0.1b	0.9 ± 0.1b	1.0 ± 0.1b	1.0 ± 0.1b
20:5n-3	9.5 ± 0.3a	9.9 ± 0.5a	10.3 ± 0.6a	6.8 ± 0.5b	6.6 ± 0.5b	6.6 ± 0.5b	6.9 ± 0.5b	7.4 ± 0.5b	6.9 ± 0.5b
22:5n-3	2.4 ± 0.0a	2.2 ± 0.1a	2.2 ± 0.1a	1.7 ± 0.1bc	1.7 ± 0.1bc	1.6 ± 0.1c	1.9 ± 0.1b	1.8 ± 0.1bc	1.8 ± 0.1b
22:6n-3	17.2 ± 1.0ab	18.5 ± 1.4a	18.8 ± 1.6a	14.0 ± 1.4bc	13.2 ± 1.4c	12.3 ± 1.4c	13.3 ± 1.4c	13.6 ± 1.4c	13.6 ± 1.4c
n-3[d]	33.7 ± 1.1b	34.2 ± 1.6ab	34.8 ± 1.9ab	25.5 ± 1.6c	24.6 ± 1.6c	37.9 ± 1.6a	38.5 ± 1.6a	26.1 ± 1.6c	25.6 ± 1.6c
Total PUFA[e]	44.5 ± 0.8b	44.9 ± 1.2b	45.6 ± 1.4b	53.5 ± 1.2a	52.7 ± 1.2a	53.1 ± 1.2a	53.4 ± 1.2a	41.8 ± 1.2bc	41.1 ± 1.2c
Total LC-PUFA[f]	31.7 ± 1.3a	33.2 ± 1.8a	34.0 ± 2.2a	24.4 ± 1.8b	23.5 ± 1.2b	22.5 ± 1.8b	24.2 ± 1.8b	25.1 ± 1.8b	24.6 ± 1.8b
Total MC-PUFA[g]	12.1 ± 0.7c	11.0 ± 0.9c	10.8 ± 1.1c	27.9 ± 0.9a	28.0 ± 0.9a	29.8 ± 0.9a	28.4 ± 0.9a	15.9 ± 0.9b	15.7 ± 0.9b
n-3:n-6	3.3 ± 0.2a	3.3 ± 0.2a	3.4 ± 0.3a	0.9 ± 0.2d	0.9 ± 0.2d	2.5 ± 0.2b	2.6 ± 0.2ab	1.7 ± 0.2c	1.7 ± 0.2c

Values represent least-square means (relative area % of FAME) ± SE of a single individual sample from all tanks. Means within fatty acid(s) with common letter are not significantly different. Absence of letters indicates lack of statistical significance

[a] Saturated fatty acids—sum of all FA without double bonds; includes 15:0 and 17:0 in addition to individually reported SFA

[b] Monounsaturated fatty acids—sum of all FA with single double bond; includes 20:1n-9 in addition to individually reported MUFA

[c] Includes 20:2n-6 and 20:3n-6 in addition to individually reported n-6 FA

[d] Includes 20:3n-3 in addition to individually reported n-3 FA

[e] Polyunsaturated fatty acids—sum of all FA with double bonds ≥ 2; includes 18:3n-4, 20:3n-3, 20:4n-3, 20:2n-6, and 20:3n-6 in addition to individually reported PUFA

[f] Long-chain PUFA—sum of all PUFA with chain length ≥ 20 carbon atoms, double bonds ≥ 3; includes 20:3n-3, 20:4n-3, and 20:3n-6 in addition to individually reported LC-PUFA

[g] Medium-chain PUFA—sum of all PUFA with chain length of 18 carbon atoms; includes 18:3n-4 in addition to individually reported MC-PUFA

Table 4 Total lipid composition of harvest fillet samples with respect to predominant (>1% FAME) FA and FA classes

Fatty acid(s)	Fish oil (FO)	Coconut oil (CO)		Grapeseed oil (GO)		Linseed oil (LO)		Poultry oil (PO)	
	FO control	CO	CO + Finish	GO	GO + Finish	LO	LO + Finish	PO	PO + Finish
12:0	0.8 ± 0.1c	6.6 ± 0.1a	2.8 ± 0.1b	0.2 ± 0.1d	0.1 ± 0.1d	0.1 ± 0.1d	0.1 ± 0.1d	0.1 ± 0.1d	0.1 ± 0.1d
14:0	5.5 ± 0.1c	8.1 ± 0.1a	6.2 ± 0.1b	3.2 ± 0.1e	4.1 ± 0.1d	3.2 ± 0.1e	4.2 ± 0.1d	3.4 ± 0.2e	4.0 ± 0.1d
16:0	19.6 ± 0.1b	18.4 ± 0.2d	19.2 ± 0.2bc	17.2 ± 0.2f	18.7 ± 0.2cd	16.3 ± 0.2g	17.8 ± 0.2e	20.3 ± 0.2a	19.8 ± 0.2ab
18:0	3.7 ± 0.1	3.8 ± 0.1	3.6 ± 0.1	4.0 ± 0.1	3.8 ± 0.1	3.8 ± 0.1	3.7 ± 0.1	3.9 ± 0.1	4.0 ± 0.1
Total SFA	30.7 ± 0.2c	37.7 ± 0.2a	32.8 ± 0.2b	25.3 ± 0.2g	27.6 ± 0.2e	24.2 ± 0.2h	26.6 ± 0.2f	28.5 ± 0.3d	28.8 ± 0.3d
16:1n-7	8.9 ± 0.1a	6.8 ± 0.2d	8.0 ± 0.2b	5.4 ± 0.2e	7.1 ± 0.2d	5.6 ± 0.2e	7.3 ± 0.2cd	7.8 ± 0.2bc	8.0 ± 0.2b
18:1n-7	3.0 ± 0.0a	2.3 ± 0.0e	2.7 ± 0.0bc	2.2 ± 0.0f	2.6 ± 0.0cd	2.2 ± 0.0f	2.6 ± 0.0d	2.6 ± 0.0d	2.8 ± 0.0b
18:1n-9	10.7 ± 0.2g	11.4 ± 0.2ef	11.0 ± 0.2fg	13.9 ± 0.2b	12.1 ± 0.2d	13.0 ± 0.2c	11.8 ± 0.2de	19.7 ± 0.3a	14.6 ± 0.2b
Total MUFA	23.4 ± 0.3c	21.3 ± 0.4e	22.4 ± 0.4cde	22.2 ± 0.4de	22.6 ± 0.4cd	21.4 ± 0.4de	22.3 ± 0.4cde	30.9 ± 0.5a	26.1 ± 0.5b
18:2n-6	7.9 ± 0.1f	8.4 ± 0.2e	8.0 ± 0.2ef	25.2 ± 0.2a	16.3 ± 0.2b	12.8 ± 0.2c	10.4 ± 0.2d	13.2 ± 0.2c	10.2 ± 0.2d
20:4n-6	1.5 ± 0.0ab	1.4 ± 0.0c	1.6 ± 0.0a	1.2 ± 0.0d	1.4 ± 0.0bc	1.2 ± 0.0d	1.4 ± 0.0bc	1.4 ± 0.0abc	1.5 ± 0.0abc
n-6	10.2 ± 0.1e	10.6 ± 0.2e	10.4 ± 0.2e	27.8 ± 0.2a	18.7 ± 0.2b	14.9 ± 0.2c	12.6 ± 0.2d	15.5 ± 0.2c	12.5 ± 0.2d
18:3n-3	1.5 ± 0.1c	1.4 ± 0.2c	1.4 ± 0.2c	1.2 ± 0.2c	1.2 ± 0.2c	15.8 ± 0.2a	8.5 ± 0.2b	1.6 ± 0.2c	1.4 ± 0.2c
18:4n-3	1.5 ± 0.0a	1.1 ± 0.0d	1.3 ± 0.0b	0.8 ± 0.0f	1.1 ± 0.0cd	0.9 ± 0.0e	1.2 ± 0.0bc	0.9 ± 0.0ef	1.1 ± 0.0cd
20:5n-3	10.6 ± 0.1a	9.1 ± 0.2c	10.4 ± 0.2a	6.6 ± 0.2d	9.4 ± 0.2bc	6.9 ± 0.2d	9.3 ± 0.2bc	7.0 ± 0.2d	9.7 ± 0.2b
22:5n-3	2.7 ± 0.0a	2.4 ± 0.0c	2.6 ± 0.0b	2.0 ± 0.0d	2.3 ± 0.0c	2.0 ± 0.0d	2.5 ± 0.0bc	1.9 ± 0.1d	2.0 ± 0.0bc
22:6n-3	17.8 ± 0.4a	15.2 ± 0.5b	17.3 ± 0.5a	13.2 ± 0.6c	15.7 ± 0.5b	12.6 ± 0.5c	15.5 ± 0.5b	12.7 ± 0.6c	16.7 ± 0.6ab
n-3	35.3 ± 0.4b	30.1 ± 0.5d	34.1 ± 0.5b	24.5 ± 0.6e	30.8 ± 0.6cd	39.2 ± 0.6a	38.1 ± 0.5a	24.9 ± 0.7e	32.3 ± 0.6c
Total PUFA	45.9 ± 0.3d	41.0 ± 0.4e	44.8 ± 0.4d	52.5 ± 0.5b	49.8 ± 0.5c	54.3 ± 0.5a	51.0 ± 0.4c	40.7 ± 0.5e	45.1 ± 0.5d
Total LC-PUFA	34.0 ± 0.5a	29.2 ± 0.6d	33.1 ± 0.6ab	23.8 ± 0.7e	30.0 ± 0.7cd	23.8 ± 0.7e	30.0 ± 0.6cd	24.1 ± 0.8e	31.5 ± 0.7bc
Total MC-PUFA	11.3 ± 0.2g	11.2 ± 0.3g	11.0 ± 0.3g	27.5 ± 0.3b	19.0 ± 0.3d	29.8 ± 0.3a	20.4 ± 0.3c	15.9 ± 0.4e	13.0 ± 0.4f
n-3:n-6	3.5 ± 0.0a	2.8 ± 0.1c	3.3 ± 0.1a	0.9 ± 0.1f	1.6 ± 0.1e	2.6 ± 0.1cd	3.0 ± 0.1b	1.6 ± 0.1e	2.6 ± 0.1d

Values represent least-square means (relative area % of FAME) ± SE of multiple individuals (≥3) from all tanks. Means within fatty acid(s) with common letter are not significantly different. Absence of indicates lack of statistical significance

All abbreviations and other notations are as reported in Table 3

Fig. 2 Fatty acid (FA) composition of fillet total lipid expressed as a fraction of dietary FA composition for unfinished feeding regimes. Values were calculated from relative fatty acid methyl ester composition (%FAME) as $\%\mathrm{FAME}_{\mathrm{fillet}} \times \mathrm{FAME}_{\mathrm{feed}}^{-1}$. Based on this calculation, a value of 1 represents equality between fillet and dietary composition. All FA abbreviations are as reported in Table 3. Other abbreviations: FO, 100% fish oil feed; PO, 50:50 poultry/fish oil feed; GO, 50:50 grapeseed/fish oil feed; LO, 50:50 linseed/fish oil feed; CO, 50:50 coconut/fish oil feed

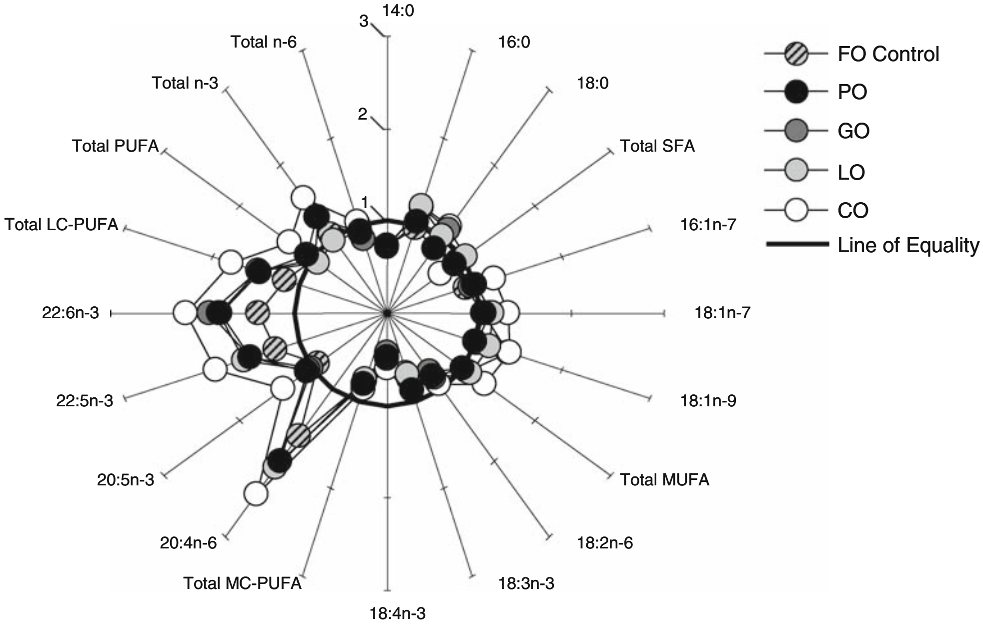

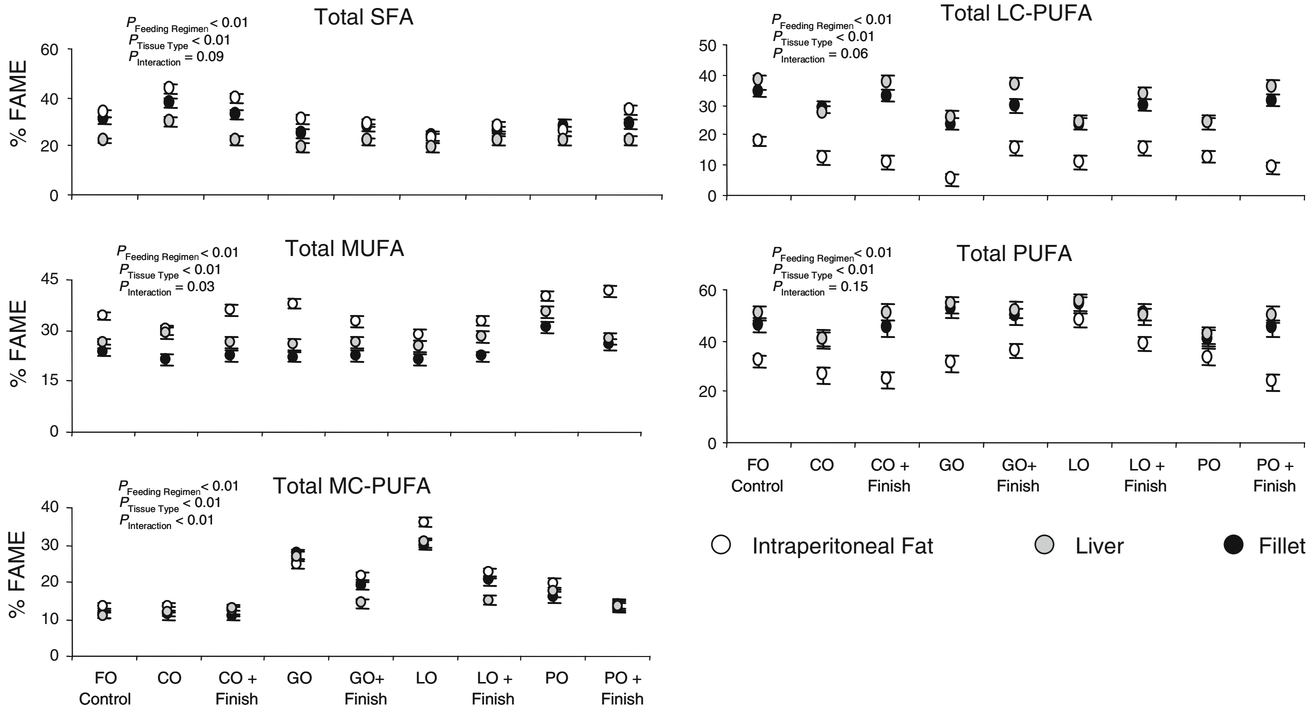

Fig. 3 Fatty acid composition of fillet, liver, and intraperitoneal fat tissue total lipid by feeding regimen. Error bars represent ±SE. All FA abbreviations are as reported in Table 3. Other abbreviations: FO, 100% fish oil feed; PO, 50:50 poultry/fish oil feed; GO, 50:50 grapeseed/fish oil feed; LO, 50:50 linseed/fish oil feed; CO, 50:50 coconut/fish oil feed

example, after finishing Murray cod raised on vegetable oil-based grow-out feeds, the most rapid and extensive restorative effects were observed in fish fed a low MC-PUFA grow-out feed compared to those fed a high MC-PUFA feed [35]. Menoyo et al. [43] indirectly evaluated the unresponsiveness of 18-carbon FA in Atlantic salmon tissues by using sunflower oil to spare either FO or LO, and noted ability of dietary sunflower oil to alter fillet composition was attenuated in the LO-fed groups. These authors attributed the differential response to reduced digestibility of the FO-based diets relative to the LO feeds; however, based on our findings, we suspect selective

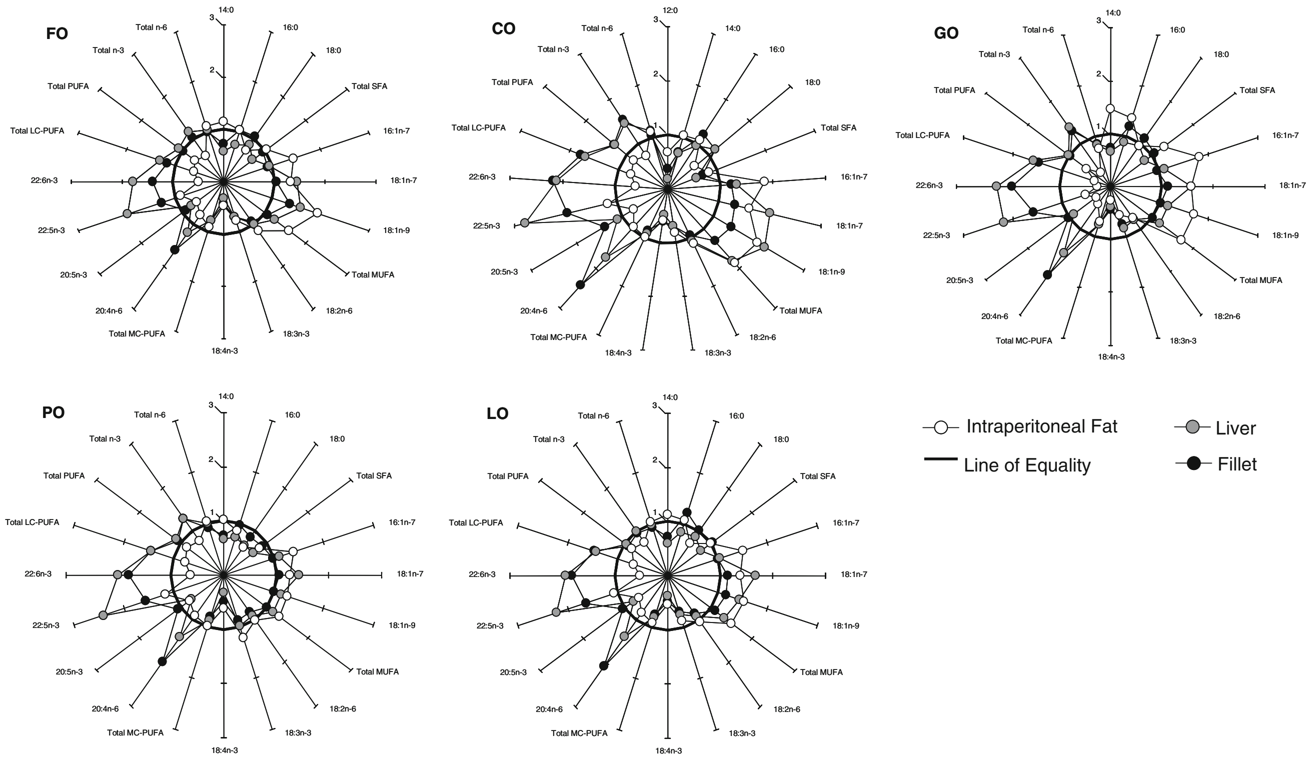

Fig. 4 Fatty acid composition of tissue total lipid expressed as a fraction of dietary FA composition for unfinished feeding regimes. Values were calculated from relative fatty acid methyl ester composition (%FAME) as $\%\mathrm{FAME}_{\mathrm{tissue}} \times \mathrm{FAME}_{\mathrm{feed}}{}^{-1}$. Based on this calculation, a value of 1 represents equality between fillet and dietary composition. All FA abbreviations are as reported in Table 3. Other abbreviations: FO, 100% fish oil feed; PO, 50:50 poultry/fish oil feed; GO, 50:50 grapeseed/fish oil feed; LO, 50:50 linseed/fish oil feed; CO, 50:50 coconut/fish oil feed

metabolism of certain FA may have been a contributing factor.

The process of FA profile change in fish tissues following a change in dietary lipid composition, often described as FA "dilution" or "washout", is relatively well-described by an asymptotic, simple dilution curve [21–23]. The simple dilution curve predicts temporal changes in tissue FA profile based on the relative disparity between dietary and tissue FA composition and the change in overall body mass or adiposity over time. By its definition, the dilution model assumes no selective processes of FA metabolism. Therefore, deviations from the dilution model are often interpreted as indicative of selective partitioning of specific FA, or FA classes, or catabolism via β-oxidation. Our group previously tested the dilution model by comparing the model's predictions to observed fillet FA profile of SB reared on corn-oil based feed after finishing [33]. This comparison revealed apparent selective retention of total n-3 FA, MC-PUFA, LC-PUFA, and n-3 LC-PUFA within fillet tissue. Conversely, total fillet SFA were significantly lower than the model's predictions, suggesting selective catabolism or storage of these FA in other lipid depots. The present work demonstrates dietary SFA are not proportionally reflected within fillet, liver, or IPF lipid of SB. Plausibly, consumed SFA may be elongated and/or desaturated to MUFA, for example, which are strongly partitioned into IPF lipid (Fig. 4). If this were the case, one would expect increased consumption of dietary SFA to result in increasing levels of MUFA within the tissues. However, given the lack of increasing levels of MUFA within any lipid depot of CO-fed fish (Fig. 3), and the generally poor ability of SB to biotransform FA in appreciable amounts [44], this scenario seems unlikely. Rather, levels of SFA were routinely lower than expected in all tissues analyzed, suggesting catabolism of these FA, not selective partitioning into storage lipid.

Evidence of selective FA metabolism has also been noted for Atlantic salmon [27, 45, 46], however, Bell and colleagues observed the FA composition of the dietary lipid seemed to influence the selective processes. Specifically, 22:6n-3 was selectively retained within fillet lipid in all three studies, illustrating the necessity of this FA for physiological function. Monounsaturated FA were selected against, indicating these FA are comparatively expendable, however, the strength of selective catabolism (magnitude of deviation from line of equality in tissue vs. dietary

Table 5 Fillet compositional characteristics at harvest by dietary/finishing treatment group

Parameter	Fish oil (FO)	Coconut oil (CO)		Grapeseed oil (GO)		Linseed oil (LO)		Poultry oil (PO)	
	FO control	CO	CO + Finish	GO	GO + Finish	LO	LO + Finish	PO	PO + Finish
Moisture (%)	76.0 ± 0.2ab	75.6 ± 0.3bc	76.0 ± 0.3ab	74.9 ± 0.3cd	76.2 ± 0.3ab	76.6 ± 0.3a	76.1 ± 0.3ab	75.3 ± 0.3bcd	74.6 ± 0.3d
Crude Protein[a] (%)	86.9 ± 1.0	84.5 ± 1.4	88.7 ± 1.4	84.2 ± 1.4	87.6 ± 1.4	87.2 ± 1.6	89.5 ± 1.4	83.5 ± 1.4	84.9 ± 1.5
Crude Lipid[a] (%)	8.1 ± 0.4	7.5 ± 0.6	6.9 ± 0.6	7.2 ± 0.6	7.3 ± 0.6	8.8 ± 0.6	8.4 ± 0.6	8.0 ± 0.6	6.8 ± 0.6
Ash[a] (%)	4.8 ± 0.3	4.60 ± 0.4	4.8 ± 0.4	5.4 ± 0.5	5.7 ± 0.5	6.0 ± 0.4	6.4 ± 0.4	4.6 ± 0.4	5.8 ± 0.4

Values represent least-square means ± SE of multiple individuals (≥3) within tanks. Means within parameters with common letter are not significantly different. Absence of letters indicates lack of statistical significance

[a] Dry matter basis

Table 6 Production performance by dietary/finishing treatment group

Production variable	Fish oil (FO)	Coconut oil (CO)		Grapeseed oil (GO)		Linseed oil (LO)		Poultry oil (PO)	
	FO control	CO	CO + Finish	GO	GO + Finish	LO	LO + Finish	PO	PO + Finish
Initial Weight[a] (g)	231 ± 7	209 ± 11	239 ± 11	206 ± 11	227 ± 11	221 ± 11	221 ± 11	206 ± 11	231 ± 11
Final Weight[a] (g)	548 ± 22	504 ± 32	551 ± 32	453 ± 32	531 ± 32	514 ± 32	512 ± 32	500 ± 32	538 ± 32
Weight Gain[b] (%)	137 ± 7	141 ± 10	131 ± 10	120 ± 10	134 ± 10	132 ± 10	132 ± 10	143 ± 10	133 ± 10
Consumption[b] (dry matter, g)	632 ± 20	707 ± 29	679 ± 29	656 ± 29	632 ± 29	581 ± 29	582 ± 29	632 ± 29	614 ± 29
Dress-out[a] (%)	30.5 ± 0.4	31.0 ± 0.7	30.1 ± 0.6	29.9 ± 0.6	30.0 ± 0.6	28.5 ± 0.6	29.0 ± 0.6	31.4 ± 0.7	30.4 ± 0.7
FCR[b,c]	2.0 ± 0.1	2.4 ± 0.2	2.2 ± 0.2	2.7 ± 0.2	2.1 ± 0.2	2.0 ± 0.2	2.1 ± 0.2	2.2 ± 0.2	2.1 ± 0.2
HSI[a,d]	1.1 ± 0.0	1.2 ± 0.1	1.1 ± 0.1	1.2 ± 0.1	1.1 ± 0.1	1.2 ± 0.1	1.1 ± 0.1	1.1 ± 0.1	1.1 ± 0.1
IPFR[a,e]	3.2 ± 0.1ab	2.5 ± 0.2c	2.8 ± 0.2bc	2.9 ± 0.2bc	3.4 ± 0.2a	3.1 ± 0.2ab	3.2 ± 0.2ab	3.3 ± 0.2ab	3.4 ± 0.2ab

Means within a production variable with common letter are not significantly different. Absence of letters indicates lack of statistical significance

[a] Values represent least-square means ± SE of multiple individuals (≥3) within tanks, tanks serving as experimental units

[b] Values represent least-square means ± SE of average individual performance criteria within tanks, tanks serving as experimental units

[c] Feed conversion ratio (consumption/weight gain)

[d] Hepatosomatic index [(liver mass/whole body mass) × 100]

[e] Intraperitoneal fat ratio [(intraperitoneal fat mass/whole body mass) × 100]

regressions) decreased with increasing availability of SFA. When SFA were abundant, these FA were more strongly selected for catabolism, and MUFA, given a "catabolic reprieve", were deposited to a greater extent in fillet tissue. Observations of selective FA metabolism in fish tissues are further supported by the preferential shunting of shorter chain FA into β-oxidation [47–50]. Oxidation of longer-chain and unsaturated FA appears to be a function of their relative abundance [51], and in the case of LC-PUFA, only substantial in vertebrates with a profusion of LC-PUFA stored in tissue [52].

Based on the various estimates of selective metabolism of FA in fishes, SFA appear to be the preferential catabolic substrate, whereas MC-PUFA and LC-PUFA are selectively deposited in tissues. Hence, attempts to spare LC-PUFA and optimize profile restoration during finishing may be enhanced by providing a largely saturated diet, with few MC-PUFA to compete with LC-PUFA for fillet deposition. Our work confirms this hypothesis in the context of SB culture. We demonstrated SB fillets with equivalent LC-PUFA content and associated nutritional value can be produced using a reduced FO grow-out feed followed by an 8-week finishing period. Using CO in the grow-out feed, the negative effects of FO replacement on SB fillet LC-PUFA content were rapidly reversed during finishing. The comprehensive profile restoration we observed among the CO-fed fish is unprecedented in SB culture. Low MC-PUFA feeds could be implemented in SB culture throughout a majority of grow-out, followed by implementation of an 8-week FO finishing period prior to harvest. Assuming the CO + Finish regimen and a conservative FCR (consumption/weight gain) of 2, fillets of equivalent LC-PUFA content and nutritional value could be produced with a 35% reduction in FO use over the course of the production cycle. This strategy offers a substantial reduction in marine-derived inputs to SB feeds and, potentially, a significant savings in feed cost. Furthermore, by restricting use of FO-rich feeds to the weeks immediately preceding harvest, cumulative dietary exposure of the livestock to FO-associated contaminants is reduced. We hypothesize other saturated lipids could be used to similar effect in SB and other cultured fishes. Compared to MC-PUFA-rich lipids, improved finishing success has been observed in Murray cod fed a blend of palm and olive oils, but after 16 weeks, LC-PUFA restoration was still incomplete [35]. Lack of comprehensive profile restoration may reflect a difference between Murray cod and SB as culture taxa (pure species vs. hybrid, marine vs. freshwater-reared euryhaline, medium-fat fleshed vs. lean-fleshed, etc.) or a difference between CO and palm and olive oils as lipid sources (mostly short-chain vs. medium-chain SFA and MUFA). Additional research will be necessary to resolve discrepancies in finishing success, and to identify appropriate strategies for all species. Regardless, use of a saturated grow-out feed coupled with finishing is an effective strategy to produce high quality cultured SB fillets and represents a considerable step forward in judicious use of limited marine resources in aquaculture.

Acknowledgments We thank Andrew Coursey, Adam Lohmeyer, Shawn Meyer, Quinton Phelps, John West, and John Zeigler for assisting in data collection, and James Garvey and Michael Arts for editorial advice provided during manuscript preparation. We also thank Tyson Foods, Omega Protein, and Tate and Lyle for the donation of feedstuffs used in the present work, and the National Science Foundation for provision of funding under grant #0227925.

References

1. Food and Agriculture Organization (2006) The state of world fisheries and aquaculture. Food and Agriculture Organization of the United Nations, Rome
2. Lands WEM (2005) Fish, omega-3, and human health, 2nd edn. AOCS Press, Urbana
3. Jump DB, Clarke SD, Thelen A, Liimatta M, Ren B, Badin MV (1997) Dietary fat, genes, and human health. Exp Med Biol 422:167–176
4. Williams CM (2000) Dietary fatty acids and human health. Ann Zootech 49:165–180
5. Duo L, Sinclair AJ (2002) Macronutrient innovations: the role of fats and sterols in human health. Asia Pac J Clin Nutr 11:155–162
6. Jahangiri A, Leifert WR, McMurchie EJ (2002) Omega-3 polyunsaturated fatty acids: recent aspects in relation to health benefits. Food Austral 54:74–77
7. Tapiero H, Ba GN, Couvreur P, Tew KD (2002) Polyunsaturated fatty acids (PUFA) and eicosanoids in human health and pathologies. Biomed Pharmacother 56:215–222
8. Duo L (2003) Omega-3 fatty acids and non-communicable diseases. Chin Med J 116:453–458
9. American Heart Association (AHA) (2004) Dietary guidelines: at-a-glance. http://www.americanheart.org/presenter.jhtml?identifier = 810. Accessed 18 Nov 2004
10. Pauly D, Watson D, Alder J (2005) Global trends in world fisheries: impacts on marine ecosystems and food security. Phil Trans R Soc B 360:5–12
11. Food and Agriculture Organization (2007) The role of aquaculture in sustainable development. http://www.fao.org/newsroom/en/news/2007/1000701/index.html. Accessed 19 Nov 2007
12. New MB, Wijkström UN (2002) Use of fishmeal and fish oil in aquafeeds: further thoughts on the fishmeal trap. Food and Agriculture Organization of the United Nations, Rome
13. Food and Agriculture Organization (2006) Fish oil market report—March 2006. http://www.globefish.org/index.php?id = 2759. Accessed 1 Apr 2006
14. Foran JA, Hites RA, Carpenter DO, Hamilton MC (2004) A survey of metals in tissues of farmed Atlantic and wild Pacific salmon. Environ Toxicol Chem 23:2108–2110
15. Hites RA, Foran JA, Carpenter DO, Hamilton MC, Knuth BA, Schwager SJ (2004) Global assessment of organic contaminants in farmed salmon. Science 303:226–229
16. Foran JA, Carpenter DO, Hamilton MC, Knuth BA, Schwager SJ (2005) Risk-based consumption advice for farmed Atlantic and wild Pacific salmon contaminated with dioxins and dioxin-like compounds. Environ Health Perspect 113:552–556

17. Bransden MP, Carter CG, Nichols PD (2003) Replacement of fish oil with sunflower oil in feeds for Atlantic salmon (*Salmo salar* L.): effect on growth performance, tissue fatty acid composition, and disease resistance. Comp Biochem Physiol B 135:611–625
18. Glencross BD, Hawkins WE, Curnow JG (2003) Restoration of the fatty acid composition of red seabream (*Pagrus auratus*) using a fish oil finishing diets after grow-out on plant oil based diets. Aquac Nutr 9:409–418
19. Wonnacott EJ, Lane RL, Kohler CC (2004) Influence of dietary replacement of menhaden oil with canola oil on fatty acid composition of sunshine bass. North Am J Aquac 66:243–250
20. Lewis HA, Kohler CC (2008) Minimizing fish oil and fish meal with plant-based alternatives in sunshine bass diets without negatively impacting growth and muscle fatty acid profile. J World Aquac Soc (in press)
21. Jobling M (2003) Do changes in Atlantic Salmon, *Salmo salar* L., fillet fatty acids following a dietary switch represent wash-out or dilution? Test of a dilution model and its application. Aquac Res 34:1215–1221
22. Jobling M (2004) Are modifications in tissue fatty acid profiles following a change in diet the result of dilution? Test of a simple dilution model. Aquaculture 232:551–562
23. Jobling M (2004) "Finishing" feeds for carnivorous fish and the fatty acid dilution model. Aquac Res 35:706–709
24. Robin JH, Regost C, Arzel J, Kaushik SJ (2003) Fatty acid profile of fish following a change in dietary fatty acid source: model of fatty acid composition with a dilution hypothesis. Aquaculture 225:283–293
25. Hunter BJ, Roberts DC K (2000) Potential impact of the fat composition of farmed fish on human health. Nutr Res 20:1047–1058
26. Regost C, Arzel J, Robin J, Rosenlund G, Kaushik SJ (2003) Total replacement of fish oil by soybean or linseed oil with a return to fish oil in turbot (*Psetta maxima*). 1. Growth performance, flesh fatty acid profile, and lipid metabolism. Aquaculture 217:465–482
27. Bell JG, Henderson RJ, Tocher DR, Sargent JR (2003) Replacement of dietary fish oil with increasing levels of linseed oil: modification of flesh fatty acid compositions in Atlantic salmon (*Salmo salar*) using a fish oil finishing diet. Lipids 39:223–232
28. Bell JG, Henderson RJ, Tocher DR, Sargent JR (2004) Replacement of dietary fish oil with increasing levels of linseed oil: modification of flesh fatty acid compositions in Atlantic salmon (*Salmo salar*) using a fish oil finishing diet. Lipids 39:223–232
29. Torstensen BE, Frǿyland L, Lie Ǿ (2004) Replacing dietary fish oil with increasing levels of rapeseed oil and olive oil—effects on Atlantic salmon (*Salmo salar* L) tissue and lipoprotein lipid composition and lipogenic enzyme activities. Aquac Nutr 10:175–192
30. Bell JG, McGhee F, Dick JR, Tocher DR (2005) Dioxin and dioxin-like polychlorinated biphenyls (PCBs) in Scottish farmed salmon (*Salmo salar*): effects of replacement of dietary marine fish oil with vegetable oils. Aquaculture 243:305–314
31. Izquierdo MS, Montero D, Robaina L, Caballero MJ, Rosenlund G, Ginéz R (2005) Alterations in fillet fatty acid profile and flesh quality in gilthead seabream (*Sparus aurata*) fed vegetable oils for a long term period. Recovery of fatty acid profiles by fish oil feeding. Aquaculture 250:431–444
32. Torstensen BE, Bell JG, Rosenlund R, Henderson RJ, Graff IE, Tocher DR, Lie Ǿ, Sargent JR (2005) Tailoring of Atlantic salmon (*Salmo salar* L.) flesh lipid composition and sensory quality by replacing fish oil with a vegetable oil blend. J Agric Food Chem 53:10166–10178
33. Lane RL, Trushenski JT, Kohler CC (2006) Modification of fillet composition and evidence of differential fatty acid turnover in sunshine bass *Morone chrysops* × *M. saxatilis* following change in dietary lipid source. Lipids 41:1029–1038
34. Turchini GM, Francis DS, De Silva SS (2006) Modification of tissue fatty acid composition in Murray cod (*Maccullochella peelii peelii*, Mitchell) resulting from a shift from vegetable oil diets to a fish oil diet. Aquac Res 37:570–585
35. Turchini GM, Francis DS, De Silva SS (2007) Finishing diets stimulate compensatory growth: results of a study on Murray cod, *Maccullochella peelii peelii*. Aquac Nutr 13:351–360
36. Lewis HA, Kohler CC (2008) Corn gluten meal partially replaces dietary fish meal without compromising growth or the fatty acid composition of sunshine bass. North Am J Aquac 70:50–60
37. Folch J, Lees M, Sloane-Stanley GH (1957) A simple method for the isolation and purification of total lipids from animal tissues. J Biol Chem 276:497–507
38. AOAC International (2003) Official methods of analysis. AOAC International, Arlington
39. Kohler CC (2000) Striped bass and hybrid striped bass culture. In: Stickney RR (ed) Encyclopedia of aquaculture. Wiley, New York, pp 898–907
40. Ballestrazzi R, Rainis S, Maxia M (2006) The replacement of fish oil with refined coconut oil in the diet of large rainbow trout (*Oncorhynchus mykiss*). Ital J Anim Sci 5:155–164
41. Higgs DA, Balfry SK, Oakes JD, Rowshandeli M, Skura BJ, Deacon G (2006) Efficacy of an equal blend of canola oil and poultry fat as an alternate dietary lipid source for Atlantic salmon (*Salmo salar* L.) in sea water. 1: Effects on growth performance, and whole body and fillet proximate and lipid composition. Aquac Res 37:180–191
42. Xue M, Luo L, Wu X, Ren Z, Gao P, Yu Y, Pearl G (2006) Effects of six alternative lipid sources on growth and tissue fatty acid composition in Japanese sea bass (*Lateolabrax japonicus*). Aquaculture 260:206–214
43. Menoyo D, Lopez-Bote CJ, Diez A, Obach A, Bautista JM (2007) Impact of n-3 fatty acid chain length and n-3/n-6 ratio in Atlantic salmon (*Salmo salar*) diets. Aquaculture 267:248–259
44. Nematipour GR, Gatlin DM (1993) Effects of different kinds of dietary lipid on growth and fatty acid composition of juvenile sunshine bass, *Morone chrysops* × *M. saxatilis*. Aquaculture 114:141–154
45. Bell JG, McEvoy J, Tocher DR, McGhee F, Campbell PJ, Sargent JR (2001) Replacement of fish oil with rapeseed oil in diets of Atlantic salmon (*Salmo salar*) affects tissue lipid compositions and hepatocyte fatty acid metabolism. J Nutr 131:1535–1543
46. Bell JG, Henderson RJ, Tocher DR, McGhee F, Dick JR, Porter A, Smullen RP, Sargent JR (2002) Substituting fish oil with crude palm oil in the diet of Atlantic salmon (*Salmo salar*) affect muscle fatty acid composition and hepatic fatty acid metabolism. J Nutr 132:222–230
47. Henderson RJ, Sargent JR (1985) Chain length specificities of mitochondrial and peroxisomal β-oxidation of fatty acids in livers of rainbow trout (*Salmo gairdneri*). Comp Biochem Phys B 82:79–85
48. Kiessling K-H, Keissling A (1993) Selective utilization of fatty acids in rainbow trout (*Oncorhynchus mykiss*, Walbaum) red muscle mitochondria. Can J Zool 71:248–251
49. Henderson RJ (1996) Fatty acid metabolism in freshwater fish with particular reference to polyunsaturated fatty acids. Arch Anim Nutr 49:5–22
50. Frǿyland L, Lie Ǿ, Berge RK (2000) Mitochondrial and peroxisomal β-oxidation capacities in various tissues from Atlantic Salmon, *Salmo salar*. Aquac Nutr 6:85–89
51. Torstensen BE, Frǿyland L, Ǿrnsrud R, Lie Ǿ (2004) Tailoring of a cardioprotective muscle fatty acid composition of Atlantic salmon (*Salmo salar*) fed vegetable oils. Food Chem 87:567–580
52. Crockett EL, Sidell BD (1993) Substrate selectivities differ for hepatic mitochondrial and peroxisomal β-oxidation in an Antarctic fish, *Notothenia gibberifrons*. Biochem J 289:427–433

Lipids (2008) 43:643–653
DOI 10.1007/s11745-008-3190-5

ORIGINAL ARTICLE

Fatty Acid Profile of Sunshine Bass: II. Profile Change Differs Among Fillet Lipid Classes

**Jesse T. Trushenski · Heidi A. Lewis ·
Christopher C. Kohler**

Received: 28 March 2008 / Accepted: 1 May 2008 / Published online: 30 May 2008
© AOCS 2008

Abstract Fatty acid (FA) profile of fish tissue mirrors dietary FA profile and changes in a time-dependent manner following a change in dietary FA composition. To determine whether FA profile change varies among lipid classes, we evaluated the FA composition of fillet cholesteryl esters (CE), phospholipids (PL), and triacylglycerols (TAG) of sunshine bass (SB, *Morone chrysops* × *M. saxatilis*) raised on feeds containing fish oil or 50:50 blend of fish oil and coconut, grapeseed, linseed, or poultry oil, with or without implementation of a finishing period (100% FO feed) prior to harvest. Each lipid class was associated with a generalized FA signature, irrespective of nutritional history: fillet PL was comprised largely of saturated FA (SFA), long-chain polyunsaturated FA (LC-PUFA), and total n-3 FA; fillet TAG was higher in MC-PUFA and total n-6 FA; and fillet CE was highest in monounsaturated FA (MUFA). Neutral lipids reflected dietary composition in a near-direct fashion; conversely, PL showed evidence of selectivity for MC- and LC-PUFA. Shorter-chain SFA were not strongly reflected within any lipid fraction, even when dietary availability was high, suggesting catabolism of these FA. FA metabolism in SB is apparently characterized by a division between saturated and unsaturated FA, whereby LC-PUFA are preferentially incorporated into tissues and SFA are preferentially oxidized for energy production. We demonstrated provision of SFA in grow-out feeds for SB, instead MC-PUFA which compete for tissue deposition, meets energy demands and allows for maximum inclusion of LC-PUFA within fillet lipids.

Keywords Fish oil · Alternative lipid · Finishing feed · Fatty acid turnover/dilution · LC-PUFA · *Morone* spp.

Introduction

Fish oil (FO) replacement has been investigated for a large number of aquaculture species, employing a variety of alternative lipid sources, such as corn, canola, soybean, linseed, and palm oils [1–4]. In general, these studies have demonstrated FO can be partially or completely replaced in aquafeeds without affecting growth performance of the livestock. We previously demonstrated canola, coconut, corn, grapeseed, linseed, and poultry oils are effective substitutes for FO in feeds for sunshine bass (SB, *Morone chrysops* × *M. saxatilis*) [3–5]. Unfortunately, FO replacement significantly alters the fatty acid (FA) composition of the resultant product and results in a corresponding decline in fillet long-chain polyunsaturated fatty acids (carbon atoms ≥20, degree of unsaturation ≥3, LC-PUFA), such as eicosapentaenoic (EPA, 20:5n-3) and docosahexaenoic acids (DHA, 22:6n-3). Fish tissues are plastic with respect to FA composition, and reflect recent nutritional history, that is, tissue FA profile mirrors dietary FA profile and changes in a time-dependent manner following modification of dietary composition [6–9]. Compared to FO, alternative oils are typically higher in monounsaturates (MUFA) and medium-chain polyunsaturated fatty acids (18 carbon, degree of unsaturation ≥2, MC-PUFA), whereas LC-PUFA are low or lacking altogether. Accordingly, fillets of fish fed alternative oil-based feeds reflect these differences: replacing LC-PUFA-rich FO with MC-PUFA-rich canola oil, for example, increases fillet 18:2n-6 and 18:3n-3 content at the expense of 20:5n-3 and 22:6n-3 [3, 4]. Although cultured seafood produced

J. T. Trushenski (✉) · H. A. Lewis · C. C. Kohler
Fisheries and Illinois Aquaculture Center and Department of Zoology, Southern Illinois University Carbondale, Carbondale, IL 62901-6511, USA
e-mail: saluski@siu.edu

using alternative lipids sources are attractive from sustainability and production cost standpoints, they are also substantially less valuable in terms of providing beneficial LC-PUFA to human consumers.

The inherent conflict between production of fillets with the greatest nutritional value (FO-based feeds) and the lowest feed costs (alternative lipid-based feeds) may be overcome through the use of "finishing" feeds to augment fillet LC-PUFA content of fish raised on alternative feeds prior to harvest. As mentioned above, fillet FA composition changes following dietary modification to more closely reflect the profile of the new feed. Finishing strategies exploit this process by implementing high-LC-PUFA content feeds at the end of the production cycle to restore fillet LC-PUFA content immediately prior to harvest. Employing FO-based finishing feeds, fillet LC-PUFA content of fish raised on alternative lipid-based grow-out feeds was augmented [10–18]; however, complete profile restoration has been achieved in very few studies [17, 18]. The process of FA profile change appears to differ among lipid classes [12, 17], leading some to attribute variation in finishing success to differences in fillet lipid content and class composition. We previously assessed production performance and finishing success of SB raised on multiple alternative lipid sources [5]. The purpose of the present work was to determine whether FA profile change varied among fillet lipid classes.

Methods and Materials

In the following sections, we describe our experimental design and provide a brief summary of the pertinent methods. Animal husbandry, sample collection, and analysis are described in detail in our previous paper [5]. All procedures were conducted under the direction and approval of the Southern Illinois University Institutional Animal Care and Use Committee, protocol #07-008.

Experimental Feeds

Five feeds were manufactured based on a practical, reduced fish meal feed our group had previously developed for SB culture [5]. As originally formulated, this feed contained 9.8% FO (dry matter basis; menhaden-derived; Virginia Gold™, Omega Protein, Inc., Houston, TX, USA). In the present work, the original, FO-based formulation served as the control grow-out feed as well as the finishing feed. Four experimental grow-out feeds were derived from the basal formulation, with 50% of the FO replaced with poultry (PO, Tyson Foods, Inc., Robards, KY, USA), linseed (LO, Barlean's Organic Oils, Ferndale, WA, USA), grapeseed (GO, Kusha, Inc, Irvine, CA, USA), or coconut oil (CO, Spectrum Organic Products, Petaluma, CA, USA). Dietary formulations and FA composition data are provided in Tables 1 and 2.

Experimental Design and Feeding Trial

Nine feeding regimens were developed to address influences of dietary lipid source and FA composition on production performance and subsequent finishing diet success in SB culture. Eight experimental regimens represented feeding the grow-out feeds described above throughout the feeding trial (CO, LO, GO, and PO regimens) or with an 8-week finishing period (CO + Finish, LO + Finish, GO + Finish, and PO + Finish regimens). The control regimen represented feeding the FO control/finishing feed throughout the duration of the feeding trial (FO Control regimen). Juvenile SB [46 ± 1 g, mean ± SE; age 1 (~10 months); Keo, Fish Farm, Keo AR] were fed the grow-out feeds for 20 weeks until they reached a submarketable size (328 ± 16 g). After 20 weeks, subsamples of fish were harvested to determine baseline tissue FA profile prior to finishing. After baseline sampling, remaining fish were finished with the 100% FO feed for the remaining 8 weeks of the feeding trial (CO + Finish, LO + Finish, GO + Finish, and PO + Finish regimens) or maintained on assigned grow-out feeds (FO Control, CO, LO, GO, and PO regimens). After completion of the feeding trial, all remaining fish were harvested. Survival and production performance criteria were assessed, and muscle samples were collected to determine fillet FA composition.

Lipid Class Separations and Fatty Acid Analysis

Total lipid was extracted from lyophilized fillet tissue as previously described [5]. Phospholipid (PL), cholesteryl ester (CE), and triacylglycerol (TAG) fractions were separated via solid-phase extraction according to Burdge et al. [19]. Briefly, ~75–100 mg of total lipid was suspended in chloroform and applied to amino-propyl silica columns (Supelclean™ LC-NH2 1 mL SPE columns, Supelco, Bellefonte, PA, USA) under gravity. The columns were washed with 2 mL of chloroform under a vacuum to elute a mixed TAG and CE fraction. The column was subsequently washed with 1 mL each of chloroform:methanol solution (3:2 v/v) and methanol to elute the phospholipid fraction. The mixed TAG and CE fraction was dried under nitrogen, resuspended in hexane, and applied to a fresh column (preconditioned with hexane). The column was washed with 2 mL of hexane followed by 2 mL of hexane:chloroform;ethyl acetate solution (100:5:5 v/v) to elute the CE and TAG fractions, respectively. Burdge et al. [19] also allows for separation of free fatty acids; however,

Table 1 Formulation and proximate composition of experimental feeds

Ingredient	Fish oil (FO)	Coconut oil (CO)	Grapeseed oil (GO)	Linseed oil (LO)	Poultry oil (PO)
Fish meal[a]	200	200	200	200	200
Fish oil[a]	98	49	49	49	49
Coconut oil[b]	–	49	–	–	–
Grapeseed oil[c]	–	–	49	–	–
Linseed oil[d]	–	–	–	49	–
Poultry oil[e]	–	–	–	–	49
Corn Gluten meal[f]	140	140	140	140	140
Wheat middlings	201	201	201	201	201
Soybean meal	300	300	300	300	300
Carboxymethyl cellulose	20	20	20	20	20
Sodium phosphate monobasic	15	15	15	15	15
Calcium phosphate Dibasic	15	15	15	15	15
Choline chloride	6	6	6	6	6
Mineral premix[g]	1.5	1.5	1.5	1.5	1.5
Vitamin premix[h]	1.5	1.5	1.5	1.5	1.5
Proximate composition					
Dry matter	88.0	87.8	88.3	84.7	85.7
Protein	41.1	41.5	41.0	40.5	39.4
Lipid	14.3	14.5	14.4	14.6	13.2
Ash	10.8	10.2	9.6	11.4	10.6

All proximate composition values are expressed as a mean in g/100g(%), dry matter basis. Formulation composition is expressed in g/kg

[a] Derived from menhaden *Brevoortia* spp., Omega Protein, Inc., Houston, TX, USA

[b] Spectrum Organic Products, Petaluma, CA, USA

[c] Kusha, Inc., Irvine, CA, USA

[d] Barlean's Organic Oils, Ferndale, WA, USA

[e] Tyson Foods, Inc., Robards, KY, USA

[f] Tate and Lyle, Decatur, IL, USA

[g] Formulated to contain: 7,000 mg kg^{-1} copper, 70,000 mg kg^{-1} iron, 100,000 mg kg^{-1} manganese, 200,000 mg kg^{-1} zinc, 0.24% iodine

[h] Formulated to contain: 99.8 mg kg^{-1} selenium, 2,200 mg kg^{-1} folic acid, 88,000 mg kg^{-1} niacin, 35,200 mg kg^{-1} pantothenic acid, 11,000 mg kg^{-1} vitamin B6, 13,200 mg kg^{-1} riboflavin, 11,000 mg kg^{-1} thiamin, 11,000 mg kg^{-1} vitamin B12, 66,000 mg kg^{-1} vitamin E, 4,400 mg kg^{-1} vitamin K, 4,400,000 IU kg^{-1} vitamin A, 2,200,000 IU kg^{-1} vitamin D, 100,000 mg kg^{-1} vitamin C

amounts recovered from fillet total lipid were extremely small (0.1–0.2 mg) and insufficient for subsequent FA analysis. Once separated, each lipid class was evaporated to dryness under nitrogen and weighed to determine total tissue PL, CE, and TAG content. All lipid samples were then resuspended in toluene, subjected to acid-catalyzed trans-methylation, and analyzed for FA composition as described in our previous paper [5].

Statistical Analysis

Although multiple individual fish were sampled from each tank, replicate tanks served as the experimental units for all statistical analyses ($n = 3$ for experimental regimens, $n = 6$ for control regimen). Lipid class data were analyzed by one-way analysis of variance (ANOVA) within the Mixed Model framework of the Statistical Analysis System, version 9.1 (SAS Institute, Cary, NC, USA) to determine significance of differences among feeding regimens. In all cases, differences were considered significant at $P < 0.05$.

Results

Across all lipid classes, FA profiles of unfinished groups generally reflected the FA composition of the grow-out feed (Tables 3, 4, 5). Increased levels of 12:0, 18:1n-9, 18:3n-3, and 18:2n-6 were associated with all lipid classes of the CO, PO, LO, and GO groups, respectively; however, the extent to which the tissue reflected the diet varied among individual lipid classes. Among unfinished groups, the TAG and CE fractions showed a strong correlation with dietary composition; whereas the PL fraction was less representative of dietary composition (Fig. 1). Comparing

Table 2 Dietary composition with respect to FA and FA classes

Fatty acid(s)	Fish oil (FO)	Coconut oil (CO)	Grapeseed oil (GO)	Linseed oil (LO)	Poultry oil (PO)	SEM
8:0	0.00	1.83	0.00	0.00	0.00	0.05
10:0	0.00	2.02	0.00	0.00	0.00	0.02
12:0	0.11	17.59	0.02	0.04	0.06	0.02
14:0	7.65	11.29	4.41	4.42	4.68	0.02
16:0	18.71	15.12	14.47	13.45	20.87	0.02
18:0	3.50	3.28	3.58	3.71	4.48	0.01
Total SFA[1]	31.90	52.38	23.90	22.97	31.40	0.06
16:1n-7	9.84	5.65	5.62	5.61	7.85	0.02
18:1n-7	2.90	1.75	1.98	1.92	2.45	0.00
18:1n-9	7.74	8.12	13.62	11.16	19.67	0.02
Total MUFA[2]	21.68	16.20	21.98	19.40	30.76	0.03
18:2n-6	8.42	8.85	32.40	14.68	15.58	0.08
20:4n-6	0.92	0.58	0.58	0.58	0.71	0.01
n-6	10.12	10.21	33.45	16.02	16.92	0.08
18:3n-3	2.14	2.04	1.59	22.56	1.82	0.01
18:4n-3	3.49	1.86	1.86	1.87	1.82	0.01
20:4n-3	1.49	0.81	0.84	0.81	0.81	0.01
20:5n-3	11.46	6.60	6.53	6.53	6.52	0.02
22:5n-3	2.11	1.22	1.28	1.22	1.21	0.02
22:6n-3	12.73	6.96	6.86	6.89	7.04	0.03
n-3	33.64	19.60	19.08	40.02	19.34	0.05
Total PUFA[3]	46.42	31.42	54.12	57.63	37.84	0.07
Total LC-PUFA[4]	29.13	16.40	16.33	16.30	16.59	0.05
Total MC-PUFA[5]	14.72	13.16	36.26	39.53	19.69	0.08
n-3:n-6	3.32	1.92	0.57	2.50	1.14	0.02

Values represent least-square means of triplicate samples

[1] Saturated fatty acids–sum of all FA without double bonds

[2] Monounsaturated fatty acids—sum of all FA with a single double bond

[3] Polyunsaturated fatty acids—sum of all FA with ≥2 double bonds

[4] Long-chain PUFA—sum of all FA with chain length ≥20 carbon atoms and double bonds ≥3

[5] Medium-chain—sum of all PUFA with chain length of 18 carbon atoms; includes 18:3n-4 in addition to individually reported MC-PUFA

the CO regimen with the FO Control regimen, the difference between 12:0 levels was greatest within the neutral TAG and CE fractions (1.1 vs. 9.5% for TAG, 1.0 vs. 8.6% for CE Tables 4 and 5) and minor, though statistically significant within the polar PL fraction (0.0 vs. 0.5%; Table 3). Differences in 18:1n-9 content between the FO Control and PO regimens were similarly partitioned among the neutral and polar lipid classes, with differences of the greatest magnitude observed within the TAG and CE. Although 18:3n-3 and 18:2n-6 enrichment within the LO and GO regimens was also greatest within the neutral lipid, substantial increases in these FA were also observed within the PL fraction.

Implementation of the 8-week finishing period reversed grow-out related changes in fillet FA composition to varying degrees (Tables 3, 4, 5). Absolute levels of LC-PUFA were increased in all lipid classes by finishing; however, differences between finished and unfinished groups were not statistically significant in all cases, particularly among the PL fraction (Tables 3, 4, 5). Among finished groups, increased levels of LC-PUFA were accompanied by decreased levels of MUFA and MC-PUFA. Reduced levels of MUFA and MC-PUFA in finished groups compared to unfinished groups were most noticeable among the PL fraction (Table 3).

Each lipid class was associated with a generalized FA signature, irrespective of nutritional history, which indicated differences in partitioning of dietary FA within the lipid classes. The PL fraction represented ~14% of the total fillet lipid (Table 3) and was comprised largely of SFA (specifically 16:0 and 18:0), LC-PUFA (specifically 20:4n-6, 20:5n-3, and 22:6n-3), and n-3 FA (Table 6). Conversely, the TAG fraction (~10% of total lipid, Table 5) contained greater amounts of MC-PUFA

Table 3 Fillet phospholipid fatty acid composition with respect to predominant (>1% fatty acid methyl esters, FAME) fatty acid (FA) and FA classes

Fatty acid(s)	Fish (FO)	Coconut (CO)		Grapeseed (GO)		Linseed (LO)		Poultry (PO)	
	FO Control	CO	CO + Finish	GO	GO + Finish	LO	LO + Finish	PO	PO + Finish
12:0	0.0 ± 0.0^{b}	0.5 ± 0.1^{a}	0.0 ± 0.0^{b}	0.0 ± 0.0^{b}	0.0 ± 0.0^{b}	0.0 ± 0.0^{b}	0.0 ± 0.0^{b}	0.0 ± 0.0^{b}	0.0 ± 0.0^{b}
14:0	1.7 ± 0.0^{b}	3.5 ± 0.1^{a}	1.9 ± 0.1^{b}	1.2 ± 0.0^{c}	1.6 ± 0.0^{b}	1.2 ± 0.0^{c}	1.7 ± 0.1^{b}	1.0 ± 0.1^{c}	1.6 ± 0.0^{b}
16:0	30.2 ± 0.5^{a}	28.6 ± 0.3^{abc}	30.2 ± 0.4^{a}	$27.4 \pm 0.8b^{c}$	29.4 ± 0.5^{abc}	27.0 ± 0.4^{c}	30.0 ± 0.7^{ab}	29.3 ± 0.3^{abc}	29.0 ± 0.2^{abc}
18:0	4.0 ± 0.1	4.1 ± 0.1	3.8 ± 0.1	4.0 ± 0.1	3.9 ± 0.1	4.1 ± 0.0	4.1 ± 0.1	3.7 ± 0.1	3.9 ± 0.1
SFA[1]	36.6 ± 0.6^{a}	37.4 ± 0.4^{a}	36.8 ± 0.4^{a}	33.3 ± 0.9^{bc}	35.7 ± 0.5^{abc}	33.0 ± 0.4^{c}	36.6 ± 0.8^{ab}	34.6 ± 0.3^{abc}	35.3 ± 0.2^{abc}
16:1n-7	2.4 ± 0.2^{a}	7.4 ± 0.2^{ab}	2.4 ± 0.1^{a}	1.5 ± 0.0^{c}	2.3 ± 0.1^{a}	1.6 ± 0.0^{c}	2.4 ± 0.1^{a}	1.9 ± 0.1^{bc}	2.4 ± 0.1^{a}
18:1n-7	2.4 ± 0.1^{a}	1.8 ± 0.1^{bc}	2.2 ± 0.1^{abc}	2.0 ± 0.1^{abc}	2.4 ± 0.1^{a}	1.7 ± 0.1^{c}	2.3 ± 0.1^{ab}	1.9 ± 0.1^{bc}	2.2 ± 0.1^{ab}
18:1n-9	7.8 ± 0.4^{c}	8.7 ± 0.3^{bc}	7.8 ± 0.3^{c}	9.4 ± 0.4^{b}	8.1 ± 0.2^{bc}	9.4 ± 0.1^{b}	8.6 ± 0.2^{bc}	11.2 ± 0.3^{a}	8.4 ± 0.1^{bc}
MUFA[2]	12.7 ± 0.2^{b}	12.9 ± 0.4^{b}	12.6 ± 0.3^{b}	13.1 ± 0.5^{b}	13.0 ± 0.4^{b}	12.9 ± 0.1^{b}	13.7 ± 0.2^{ab}	15.2 ± 0.4^{a}	13.2 ± 0.3^{b}
18:2n-6	4.2 ± 0.0^{e}	6.0 ± 0.1^{d}	4.6 ± 0.1^{e}	18.3 ± 0.3^{a}	7.4 ± 0.2^{c}	9.4 ± 0.1^{b}	6.2 ± 0.3^{d}	9.5 ± 0.3^{b}	5.6 ± 0.1^{d}
20:4n-6	3.0 ± 0.0^{a}	2.6 ± 0.0^{ab}	3.1 ± 0.2^{a}	2.3 ± 0.1^{b}	2.9 ± 0.1^{a}	2.6 ± 0.1^{ab}	2.9 ± 0.1^{a}	3.0 ± 0.1^{a}	3.1 ± 0.1^{a}
n-6[3]	7.8 ± 0.1^{g}	9.5 ± 0.1^{e}	$8.4 \pm 0.2\ ^{fg}$	21.9 ± 0.3^{a}	11.1 ± 0.1^{d}	12.8 ± 0.2^{c}	9.8 ± 0.3^{e}	13.3 ± 0.3^{b}	9.3 ± 0.1^{ef}
18:3n-3	0.4 ± 0.0^{c}	0.5 ± 0.0^{c}	0.4 ± 0.0^{c}	0.5 ± 0.0^{c}	0.4 ± 0.0^{c}	6.2 ± 0.1^{a}	1.8 ± 0.2^{b}	0.6 ± 0.0^{c}	0.4 ± 0.0^{c}
18:4n-3	0.3 ± 0.0^{ab}	0.3 ± 0.0^{a}	0.3 ± 0.0^{a}	0.2 ± 0.0^{d}	0.2 ± 0.0^{abc}	0.2 ± 0.0^{bcd}	0.3 ± 0.0^{a}	$0.2 \pm 0.0\ ^{cd}$	0.3 ± 0.0^{a}
20:5n-3	14.9 ± 0.3^{a}	15.6 ± 0.4^{a}	15.1 ± 0.3^{a}	9.9 ± 0.5^{b}	14.2 ± 0.3^{a}	11.6 ± 0.1^{b}	14.4 ± 0.6^{a}	12.8 ± 0.2^{b}	15.1 ± 0.3^{a}
22:5n-3	1.7 ± 0.0	1.7 ± 0.0	1.7 ± 0.1	1.5 ± 0.1	1.7 ± 0.1	1.5 ± 0.1	1.4 ± 0.3	1.6 ± 0.0	1.8 ± 0.1
22:6n-3	24.9 ± 0.6^{a}	21.5 ± 0.8^{ab}	24.0 ± 0.9^{a}	19.2 ± 1.0^{b}	23.0 ± 0.9^{ab}	21.2 ± 0.3^{ab}	21.5 ± 0.8^{ab}	21.3 ± 0.9^{ab}	23.9 ± 0.3^{ab}
n-3[4]	42.5 ± 0.7^{a}	40.0 ± 0.8^{ab}	41.9 ± 0.9^{ab}	31.5 ± 1.5^{c}	40.0 ± 0.7^{ab}	41.1 ± 0.3^{ab}	39.8 ± 1.2^{ab}	36.8 ± 0.9^{b}	41.9 ± 0.3^{ab}
PUFA[5]	50.5 ± 0.7	49.7 ± 0.8	50.5 ± 0.7	53.6 ± 1.3	51.2 ± 0.8	54.1 ± 0.3	49.9 ± 0.9	50.2 ± 0.7	51.5 ± 0.3
LC-PUFA[6]	45.0 ± 0.7^{a}	42.0 ± 0.9^{abc}	44.4 ± 0.8^{ab}	33.3 ± 1.5^{d}	42.3 ± 0.7^{abc}	37.5 ± 0.4^{cd}	40.9 ± 1.3^{abc}	39.2 ± 1.0^{bc}	44.5 ± 0.3^{ab}
MC-PUFA[7]	5.1 ± 0.0^{g}	7.1 ± 0.1^{de}	5.6 ± 0.1^{fg}	19.1 ± 0.4^{a}	8.3 ± 0.2^{d}	15.9 ± 0.2^{b}	8.4 ± 0.4^{d}	10.5 ± 0.3^{c}	6.5 ± 0.1^{ef}
n-3:n-6	5.5 ± 0.1^{a}	4.2 ± 0.1^{cd}	5.0 ± 0.2^{ab}	1.4 ± 0.1^{g}	3.6 ± 0.1^{de}	3.2 ± 0.1^{ef}	4.1 ± 0.2^{cd}	2.8 ± 0.1^{f}	4.5 ± 0.1^{bc}
Total phospholipids (% of total lipid)	14.1 ± 1.4	14.7 ± 2.0	14.8 ± 2.0	14.2 ± 2.0	12.6 ± 2.0	13.9 ± 2.0	13.3 ± 2.0	11.0 ± 2.0	$16.2.1 \pm 2.0$

Values represent least-square means (relative area % of FAME) ± SE of two individual samples from all tanks. Means within fatty acid(s) with common letter superscripts are not significantly different. Absence of superscripts indicates lack of statistical significance

[1] Saturated fatty acids—sum of all FA without double bonds; includes 15:0 and 17:0 in addition to individually reported SFA

[2] Monounsaturated fatty acids—sum of all FA with single double bond; includes 20:1n-9 in addition to individually reported MUFA

[3] Includes 20:2n-6 and 20:3n-6 in addition to individually reported n-6 FA

[4] Includes 20:3n-3 in addition to individually reported n-3 FA

[5] Polyunsaturated fatty acids—sum of all FA with double bonds ≥2; includes 18:3n-4, 20:3n-3, 20:4n-3, 20:2n-6, and 20:3n-6 in addition to individually reported PUFA

[6] Long-chain PUFA—sum of all PUFA with chain length ≥20 carbon atoms, double bonds ≥3; includes 20:3n-3, 20:4n-3, and 20:3n-6 in addition to individually reported LC-PUFA

[7] Medium chain PUFA—sum of all PUFA with chain length of 18 carbon atoms; includes 18:3n-4 in addition to individually reported MC-PUFA

Table 4 Fillet cholesteryl ester fatty acid composition with respect to predominant (>1% fatty acid methyl esters, FAME) fatty acid (FA) and FA classes

Fatty acid(s)	Fish (FO)	Coconut (CO)		Grapeseed (GO)		Linseed (LO)		Poultry (PO)	
	FO Control	CO	CO + Finish	GO	GO + Finish	LO	LO + Finish	PO	PO + Finish
12:0	1.0 ± 0.1^{c}	8.6 ± 0.5^{a}	3.3 ± 0.2^{b}	0.2 ± 0.0^{d}	0.1 ± 0.0^{d}	0.1 ± 0.0^{d}	0.0 ± 0.0^{d}	0.1 ± 0.0^{d}	0.3 ± 0.1^{d}
14:0	6.3 ± 0.1^{b}	9.5 ± 0.3^{a}	7.1 ± 0.2^{b}	3.8 ± 0.1^{e}	5.0 ± 0.1^{c}	3.8 ± 0.2^{de}	4.7 ± 0.1^{cd}	4.0 ± 0.1^{de}	5.2 ± 0.3^{c}
16:0	20.0 ± 0.1^{a}	18.7 ± 0.3^{bc}	19.7 ± 0.3^{ab}	16.7 ± 0.2^{d}	18.3 ± 0.2^{c}	16.6 ± 0.4^{d}	17.8 ± 0.3^{c}	20.4 ± 0.1^{a}	20.2 ± 0.3^{a}
18:0	3.5 ± 0.1	3.5 ± 0.3	3.7 ± 0.2	3.5 ± 0.1	3.4 ± 0.1	3.7 ± 0.3	3.5 ± 0.1	3.5 ± 0.1	3.7 ± 0.3
SFA[1]	31.9 ± 0.2^{c}	41.1 ± 0.3^{a}	34.7 ± 0.2^{b}	24.9 ± 0.2^{g}	27.6 ± 0.4^{f}	25.0 ± 0.5^{g}	27.0 ± 0.4^{f}	28.8 ± 0.1^{e}	30.3 ± 0.3^{d}
16:1n-7	10.4 ± 0.2^{a}	7.9 ± 0.3^{d}	9.1 ± 0.3^{bc}	6.3 ± 0.1^{e}	8.5 ± 0.2^{cd}	6.6 ± 0.3^{e}	8.4 ± 0.2^{cd}	9.2 ± 0.2^{bc}	9.8 ± 0.3^{ab}
18:1n-7	3.3 ± 0.0^{a}	2.5 ± 0.0^{d}	3.0 ± 0.0^{bc}	2.4 ± 0.0^{d}	2.9 ± 0.1^{c}	2.4 ± 0.0^{d}	2.9 ± 0.0^{c}	2.8 ± 0.0^{c}	3.2 ± 0.0^{ab}
18:1n-9	12.4 ± 0.2^{d}	12.7 ± 0.3^{d}	12.2 ± 0.3^{d}	15.7 ± 0.3^{b}	13.8 ± 0.3^{bcd}	14.8 ± 0.3^{bc}	13.3 ± 0.2^{cd}	22.4 ± 0.5^{a}	16.0 ± 0.9^{b}
MUFA[2]	26.9 ± 0.4^{c}	23.8 ± 0.6^{d}	25.1 ± 0.5^{cd}	25.1 ± 0.5^{cd}	26.0 ± 0.5^{cd}	24.5 ± 0.6^{cd}	25.3 ± 0.2^{cd}	35.4 ± 0.7^{a}	29.9 ± 1.0^{b}
18:2n-6	8.9 ± 0.2^{e}	8.8 ± 0.1^{e}	8.7 ± 0.1^{e}	27.8 ± 0.4^{a}	18.4 ± 0.6^{b}	13.7 ± 0.2^{c}	11.4 ± 0.4^{d}	14.3 ± 0.1^{c}	10.8 ± 0.4^{d}
20:4n-6	1.3 ± 0.1^{a}	1.1 ± 0.1^{ab}	1.4 ± 0.1^{a}	0.9 ± 0.0^{b}	1.1 ± 0.1^{ab}	0.9 ± 0.1^{c}	1.1 ± 0.0^{ab}	1.0 ± 0.1^{b}	1.2 ± 0.1^{ab}
n-6[3]	11.0 ± 0.2^{e}	10.7 ± 0.1^{e}	10.9 ± 0.1^{e}	30.1 ± 0.4^{a}	20.6 ± 0.6^{b}	15.6 ± 0.2^{c}	13.5 ± 0.3^{d}	16.1 ± 0.1^{c}	12.9 ± 0.4^{d}
18:3n-3	1.5 ± 0.0^{c}	1.4 ± 0.1^{c}	1.5 ± 0.1^{c}	1.3 ± 0.0^{c}	1.4 ± 0.0^{c}	16.4 ± 0.7^{a}	9.4 ± 0.7^{b}	1.6 ± 0.0^{c}	1.4 ± 0.1^{c}
18:4n-3	1.4 ± 0.1^{a}	1.1 ± 0.1^{bc}	1.2 ± 0.1^{ab}	0.8 ± 0.0^{c}	1.2 ± 0.0^{ab}	0.9 ± 0.1^{c}	1.2 ± 0.1^{ab}	1.0 ± 0.0^{bc}	1.3 ± 0.1^{ab}
20:5n-3	9.3 ± 0.1^{a}	7.6 ± 0.3^{b}	9.1 ± 0.2^{a}	5.6 ± 0.1^{c}	8.2 ± 0.2^{ab}	5.6 ± 0.2^{c}	8.1 ± 0.4^{ab}	5.8 ± 0.2^{c}	8.6 ± 0.3^{ab}
22:5n-3	2.2 ± 0.0^{a}	1.8 ± 0.1^{cd}	2.2 ± 0.1^{ab}	1.5 ± 0.0^{de}	2.0 ± 0.1^{bc}	1.5 ± 0.1^{de}	2.0 ± 0.1^{abc}	1.4 ± 0.0^{e}	2.0 ± 0.1^{abc}
22:6n-3	14.3 ± 0.6^{a}	11.3 ± 0.8^{bcd}	14.0 ± 0.6^{ab}	9.8 ± 0.6^{de}	11.7 ± 0.7^{bc}	9.3 ± 0.9^{de}	12.2 ± 0.3^{abc}	8.7 ± 0.5^{e}	12.4 ± 0.8^{abc}
n-3[4]	29.8 ± 0.5^{b}	24.1 ± 0.9^{d}	29.0 ± 0.5^{bc}	19.8 ± 0.6^{e}	25.4 ± 0.8^{d}	34.7 ± 0.5^{a}	33.9 ± 0.2^{a}	19.5 ± 0.8^{e}	26.7 ± 1.1^{cd}
PUFA[5]	41.1 ± 0.4^{c}	35.0 ± 0.9^{d}	40.2 ± 0.5^{c}	50.1 ± 0.3^{a}	46.3 ± 0.6^{b}	50.5 ± 0.5^{a}	47.7 ± 0.4^{ab}	35.8 ± 0.8^{d}	39.9 ± 0.8^{c}
LC-PUFA[6]	28.4 ± 0.6^{a}	22.8 ± 1.1^{cd}	27.8 ± 0.7^{ab}	18.7 ± 0.7^{de}	24.1 ± 0.9^{bc}	18.4 ± 1.2^{e}	24.6 ± 0.7^{bc}	18.0 ± 0.8^{e}	25.4 ± 1.1^{abc}
MC-PUFA[7]	12.1 ± 0.3^{d}	11.6 ± 0.2^{d}	11.3 ± 0.6^{d}	30.1 ± 0.5^{a}	21.3 ± 0.6^{b}	31.2 ± 1.0^{a}	22.3 ± 1.0^{b}	17.0 ± 0.2^{c}	13.8 ± 0.4^{d}
n-3:n-6	2.7 ± 0.1^{a}	2.2 ± 0.1^{bc}	2.7 ± 0.1^{ab}	0.7 ± 0.0^{e}	1.2 ± 0.1^{d}	2.2 ± 0.0^{bc}	2.5 ± 0.1^{abc}	1.2 ± 0.1^{d}	2.1 ± 0.2^{c}
Total cholesteryl esters (% of total lipid)[8]	65.1 ± 3.6	70.7 ± 5.0	69.8 ± 5.0	71.3 ± 5.0	70.5 ± 5.0	74.3 ± 5.0	68.9 ± 5.0	68.6 ± 5.0	72.2 ± 5.0

Values represent least-square means (relative area % of FAME) ± SE of two individual samples from all tanks. Means within fatty acid(s) with common letter superscripts are not significantly different. Absence of superscripts indicates lack of statistical significance

[1–7] All superscripts denote information provided as footnotes in Table 3

[8] The distribution of total fillet lipid among the lipid classes was somewhat surprising, specifically the high level of CE relative to PL and TAG. Previous research with SB has indicated CE contributes very little to total fillet lipid (<5% of total lipid) [37, 38]. However, each of these studies employed much smaller, juvenile fish (~30 g final weight), whose tissue composition is likely to differ from that of large (~500 g) fish nearing sexual maturity (well-developed gonadal tissue was observed in many of our fish at harvest). In this respect, one might expect the tissue composition of larger fish to be skewed toward increased levels of storage lipid, i.e., CE and TAG. Additionally, the previous studies by Gatlin and colleagues employed TLC-FID to quantify lipid classes, which may have underestimated CE content. Recovery of PL and TAG fractions with SPE methods is apparently equivalent to TLC; however, recovery of CE is significantly greater using SPE (19)

Table 5 Fillet triacylglycerol fatty acid composition with respect to predominant (>1% fatty acid methyl esters, FAME) fatty acid (FA) and FA classes

Fatty acid(s)	Fish (FO)	Coconut (CO)		Grapeseed (GO)		Linseed (LO)		Poultry (PO)	
	FO Control	CO	CO + Finish	GO	GO + Finish	LO	LO + Finish	PO	PO + Finish
12:0	1.1 ± 0.1^{c}	9.5 ± 0.3^{a}	3.6 ± 0.1^{b}	0.2 ± 0.0^{d}	0.1 ± 0.0^{d}	0.1 ± 0.0^{d}	0.0 ± 0.0^{d}	0.1 ± 0.0^{d}	0.1 ± 0.0^{d}
14:0	6.6 ± 0.1^{c}	10.0 ± 0.1^{a}	7.7 ± 0.1^{b}	4.0 ± 0.1^{e}	5.2 ± 0.1^{d}	3.8 ± 0.1^{e}	4.9 ± 0.2^{de}	4.3 ± 0.1^{e}	5.4 ± 0.1^{d}
16:0	15.5 ± 0.2^{bc}	14.5 ± 0.2^{cde}	15.4 ± 0.2^{bcd}	12.9 ± 0.1^{ef}	14.7 ± 0.2^{bcd}	12.1 ± 0.1^{f}	13.8 ± 0.6^{def}	17.4 ± 0.3^{a}	16.3 ± 0.2^{ab}
18:0	1.7 ± 0.0^{c}	1.6 ± 0.0^{c}	1.8 ± 0.1^{c}	1.9 ± 0.0^{bc}	1.9 ± 0.1^{bc}	1.9 ± 0.0^{bc}	1.8 ± 0.1^{bc}	2.3 ± 0.1^{a}	2.1 ± 0.1^{ab}
SFA[1]	25.8 ± 0.3^{c}	36.5 ± 0.4^{a}	29.4 ± 0.2^{b}	19.5 ± 0.2^{fg}	22.8 ± 0.2^{de}	18.5 ± 0.2^{g}	21.4 ± 0.7^{ef}	24.8 ± 0.5^{cd}	24.7 ± 0.4^{cd}
16:1n-7	11.1 ± 0.1^{a}	8.9 ± 0.0^{c}	10.5 ± 0.1^{ab}	7.0 ± 0.1^{d}	9.3 ± 0.1^{c}	6.8 ± 0.1^{d}	9.0 ± 0.3^{c}	10.1 ± 0.1^{b}	10.9 ± 0.1^{ab}
18:1n-7	2.9 ± 0.0^{a}	2.3 ± 0.1^{cd}	2.7 ± 0.0^{cd}	2.1 ± 0.0^{b}	2.5 ± 0.0^{c}	2.1 ± 0.0^{c}	2.5 ± 0.1^{cd}	2.7 ± 0.0^{ab}	2.9 ± 0.1^{a}
18:1n-9	9.1 ± 0.2^{d}	10.6 ± 0.1^{cd}	11.0 ± 0.5^{cd}	13.7 ± 0.2^{b}	11.7 ± 0.3^{c}	12.0 ± 0.2^{c}	11.3 ± 0.3^{cd}	20.4 ± 0.5^{a}	14.4 ± 0.2^{b}
MUFA[2]	24.5 ± 0.2^{cd}	22.4 ± 0.2^{cde}	24.9 ± 0.2^{c}	23.4 ± 0.2^{de}	28.0 ± 0.9^{de}	21.4 ± 0.3^{e}	23.3 ± 0.7^{de}	33.9 ± 0.6^{a}	28.9 ± 0.3^{b}
18:2n-6	9.1 ± 0.2^{e}	9.3 ± 0.0^{e}	9.3 ± 0.1^{e}	30.2 ± 0.3^{a}	19.5 ± 0.7^{b}	13.9 ± 0.1^{c}	11.9 ± 0.3^{d}	15.1 ± 0.1^{c}	11.9 ± 0.1^{d}
20:4n-6	0.9 ± 0.0^{a}	0.7 ± 0.0^{cd}	0.9 ± 0.0^{a}	0.6 ± 0.0^{d}	0.8 ± 0.0^{bc}	0.6 ± 0.0^{d}	0.7 ± 0.0^{cd}	0.7 ± 0.0^{bc}	0.9 ± 0.1^{ab}
n-6[3]	10.7 ± 0.2^{e}	10.8 ± 0.0^{e}	11.0 ± 0.2^{e}	32.0 ± 0.3^{a}	21.2 ± 0.6^{b}	15.4 ± 0.2^{c}	13.4 ± 0.3^{d}	16.7 ± 0.1^{c}	13.6 ± 0.1^{d}
18:3n-3	2.2 ± 0.0^{c}	2.3 ± 0.1^{c}	2.3 ± 0.0^{c}	2.1 ± 0.0^{c}	2.0 ± 0.0^{c}	23.7 ± 0.2^{a}	13.8 ± 1.2^{b}	2.4 ± 0.1^{c}	2.1 ± 0.1^{c}
18:4n-3	3.1 ± 0.1^{a}	2.4 ± 0.1^{b}	2.6 ± 0.1^{b}	1.8 ± 0.0^{d}	2.4 ± 0.1^{b}	1.7 ± 0.1^{d}	2.2 ± 0.1^{bc}	1.9 ± 0.1^{cd}	2.5 ± 0.1^{b}
20:5n-3	13.2 ± 0.1^{a}	10.0 ± 0.2^{d}	11.9 ± 0.2^{ab}	8.1 ± 0.1^{e}	11.3 ± 0.3^{bcd}	7.4 ± 0.2^{e}	10.2 ± 0.3^{cd}	7.8 ± 0.3^{e}	11.7 ± 0.3^{bc}
22:5n-3	3.1 ± 0.1^{a}	2.5 ± 0.2^{abc}	3.0 ± 0.1^{ab}	2.1 ± 0.1^{cd}	2.6 ± 0.1^{abc}	1.8 ± 0.1^{d}	2.5 ± 0.1^{bc}	1.9 ± 0.1^{d}	2.7 ± 0.1^{abc}
22:6n-3	15.3 ± 0.3^{a}	11.3 ± 0.2^{bcd}	12.7 ± 0.3^{b}	9.6 ± 0.3^{cde}	11.8 ± 0.4^{bc}	8.5 ± 0.3^{e}	11.2 ± 0.4^{bcd}	9.1 ± 0.5^{de}	11.9 ± 0.4^{bc}
n-3[4]	38.6 ± 0.6^{bc}	29.9 ± 0.5^{de}	34.2 ± 0.6^{cd}	24.8 ± 0.5^{ef}	31.5 ± 0.9^{d}	44.5 ± 0.7^{a}	41.5 ± 1.4^{ab}	24.2 ± 1.0^{f}	32.4 ± 0.7^{d}
PUFA[5]	49.7 ± 0.5^{cd}	41.1 ± 0.5^{ef}	45.7 ± 0.5^{def}	57.1 ± 0.4^{ab}	53.1 ± 0.5^{bc}	60.1 ± 0.5^{a}	55.3 ± 1.6^{ab}	41.2 ± 1.0^{f}	46.4 ± 0.6^{de}
LC-PUFA[6]	34.4 ± 0.6^{a}	26.2 ± 0.4^{b}	30.4 ± 0.5^{b}	21.7 ± 0.5^{c}	28.0 ± 0.9^{b}	19.8 ± 0.5^{c}	26.3 ± 0.5^{b}	20.9 ± 0.9^{c}	28.8 ± 0.6^{b}
MC-PUFA[7]	14.8 ± 0.2^{f}	14.4 ± 0.1^{f}	14.7 ± 0.5^{f}	34.4 ± 0.4^{b}	24.2 ± 0.6^{d}	39.6 ± 0.2^{a}	28.4 ± 1.4^{c}	19.7 ± 0.2^{e}	16.9 ± 0.1^{ef}
n-3:n-6	3.6 ± 0.1^{a}	2.8 ± 0.0^{bc}	3.1 ± 0.1^{b}	0.8 ± 0.0^{e}	1.5 ± 0.1^{d}	2.9 ± 0.1^{bc}	3.1 ± 0.1^{b}	1.4 ± 0.1^{d}	2.4 ± 0.1^{c}
Total triacylglycerols (% of total lipid)	10.3 ± 1.1	10.8 ± 1.6	11.5 ± 1.6	9.7 ± 1.6	8.4 ± 1.6	10.1 ± 1.6	8.0 ± 1.6	8.3 ± 1.6	11.6 ± 1.6

Values represent least-square means (relative area % of FAME) ± SE of two individual samples from all tanks. Means within fatty acid(s) with common letter superscripts are not significantly different. Absence of superscripts indicates lack of statistical significance

[1–7] All superscripts denote information provided as footnotes in Table 3

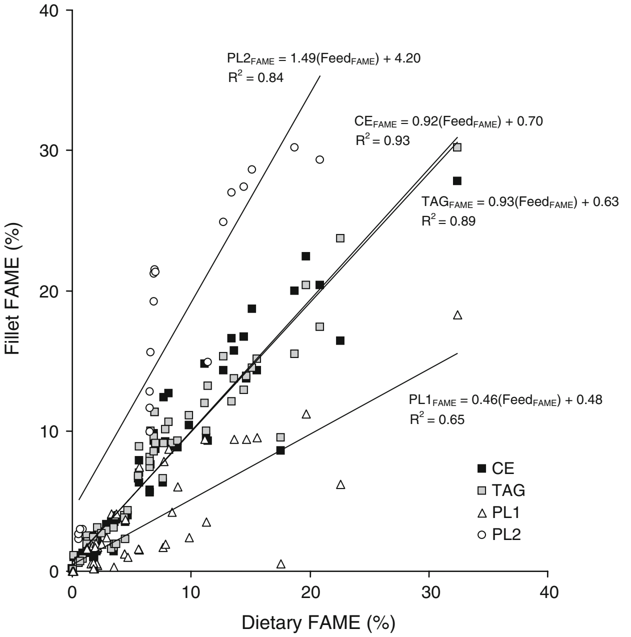

Fig. 1 Relationship between mean fatty acid composition (as relative % of fatty acid methyl esters) of feeds and fillet lipid classes. All fatty acids listed in Tables 1, 2, 3 are depicted. Abbreviations: *CE* cholesteryl esters, *TAG* triacylglycerols, *PL1* phospholipids, *16:0* 20:4n-6, 20:5n-3, 22:6n-3, *PL2* phospholipids, all other fatty acids. *Solid lines* represent best-fit linear regressions; equations and R^2 values are provided for each regression

(specifically 18:2n-6, 18:3n-3, and 18:4n-3) and n-6 FA (Table 6). CE was the most predominant lipid class represented within the fillet total lipid (~70% of total lipid, Table 4), and was highest in MUFA (specifically 18:1n-7 and 18:1n-9, Table 6).

Table 6 Fatty acid (FA) composition of fillet lipid classes, with respect to predominant (>1% fatty acid methyl esters, FAME) fatty acid (FA) and FA classes, pooled across feeding regimens

Fatty acid(s)	Lipid class		
	Cholesteryl esters	Phospholipids	Triacylglycerols
12:0	1.5 ± 0.0^{b}	0.1 ± 0.0^{c}	1.6 ± 0.0^{a}
14:0	5.5 ± 0.0^{b}	1.7 ± 0.0^{c}	5.8 ± 0.0^{a}
16:0	18.7 ± 0.1^{b}	29.0 ± 0.1^{a}	14.7 ± 0.1^{c}
18:0	3.5 ± 0.0^{b}	4.0 ± 0.0^{a}	1.9 ± 0.0^{c}
SFA[1]	30.1 ± 0.2^{b}	35.5 ± 0.2^{a}	24.8 ± 0.2^{c}
16:1n-7	8.4 ± 0.1^{b}	2.1 ± 0.1^{c}	9.3 ± 0.1^{a}
18:1n-7	2.8 ± 0.0^{a}	2.1 ± 0.0^{c}	2.5 ± 0.0^{b}
18:1n-9	14.8 ± 0.1^{a}	8.8 ± 0.1^{c}	12.8 ± 0.1^{b}
MUFA[2]	26.9 ± 0.2^{a}	13.3 ± 0.2^{c}	25.2 ± 0.2^{b}
18:2n-6	13.6 ± 0.1^{b}	7.9 ± 0.1^{c}	14.5 ± 0.1^{a}
20:4n-6	1.1 ± 0.0^{b}	2.8 ± 0.0^{a}	0.8 ± 0.0^{c}
n-6[3]	15.7 ± 0.1^{b}	11.5 ± 0.1^{c}	16.1 ± 0.1^{a}
18:3n-3	4.0 ± 0.1^{b}	1.2 ± 0.1^{c}	5.9 ± 0.1^{a}
18:4n-3	1.1 ± 0.0^{b}	0.2 ± 0.0^{c}	2.3 ± 0.0^{a}
20:5n-3	7.6 ± 0.1^{c}	13.7 ± 0.1^{a}	10.2 ± 0.1^{b}
22:5n-3	1.8 ± 0.0^{b}	1.6 ± 0.0^{c}	2.5 ± 0.0^{a}
22:6n-3	11.5 ± 0.2^{b}	22.3 ± 0.2^{a}	11.3 ± 0.2^{b}
n-3[4]	27.0 ± 0.3^{c}	39.5 ± 0.3^{a}	33.5 ± 0.3^{b}
PUFA[5]	43.0 ± 0.3^{c}	51.2 ± 0.3^{a}	50.0 ± 0.3^{b}
LC-PUFA[6]	23.1 ± 0.3^{c}	41.0 ± 0.3^{a}	26.3 ± 0.3^{b}
MC-PUFA[7]	19.0 ± 0.2^{b}	9.6 ± 0.2^{c}	23.0 ± 0.2^{a}
n-3:n-6	2.0 ± 0.0^{c}	3.8 ± 0.0^{a}	2.4 ± 0.0^{b}

Values represent least-square means

Standard errors less than ±0.1 are represented as ±0.0

[1–7] All superscripts denote information provided as footnotes in Table 3

Discussion

Fatty acid composition of fillet lipid classes was affected by feeding regimen, however, the extent to which tissue profile reflected dietary profile varied among lipid classes and feeding regimens. Fillet TAG and CE profiles of unfinished groups mirrored dietary FA composition in a direct relationship approaching unity (Fig. 1), indicating FA profile within these classes is plastic and suggests their composition is established via nonspecific processes. Accordingly, the neutral lipid classes were quite responsive to finishing, and overall, demonstrated a high level of finishing success, that is, restoration of the FO-associated FA profile. However, in terms of total LC-PUFA content within the CE, only the CO + Finish and the PO + Finish regimens were equivalent to the FO Control regimen. Of the experimental regimens, CO + Finish and PO + Finish were also the highest in LC-PUFA within the TAG fraction; however, within this lipid class they remained statistically different from the FO Control regimen.

Fillet PL composition was less responsive to dietary manipulations than the neutral lipid fractions, that is, the difference between finished and unfinished profiles was generally less noticeable within the PL fraction compared to the CE and TAG fractions. Although dietary FA composition was largely reflected within the PL, the relationship was more or less direct depending on the individual FA. For 16:0, 20:4n-6, 20:5n-3, and 22:6n-3, the relationship between dietary composition and tissue composition was greater than 1:1, suggesting selective incorporation of these FA within the PL fraction (Fig. 1). Conversely, for all other FA, the relationship was less than 1:1, suggesting exclusion of these FA from the PL fraction.

In comparing the finished and unfinished groups, it is interesting to note the pattern of change which did occur within the PL fraction. In the case of the GO-fed fish, the GO group displays a high level of 18:2n-6 enrichment within the PL, but the level of 18:2n-6 in the finished group is less than half that observed in the unfinished fish. In comparing the LO- and PO-fed regimens, we observe a similar PL enrichment in 18:3n-3 and 18:1n-9 among the LO and PO groups, respectively, and comparable reductions in these FA within the PL of the finished groups. Within the CO-fed fish, there is virtually no enrichment of 12:0 within the PL, and only a minor distinction between the final PL profiles of the CO and CO + Finish regimens. This suggests some level of plasticity within the PL fraction, but perhaps more importantly, a selectivity for certain FA which may drive profile change within this lipid class.

Phospholipids have been described as being less responsive to dietary manipulations than neutral lipids [6], but also as exhibiting more active FA turnover than neutral lipid [9, 20, 21]. The specificity of PL for FA of certain chain lengths and degrees of unsaturation has been documented [22], and may be responsible for the discrepancy between differing observations of unresponsiveness and active profile change within the PL fraction. Specificity of PL for certain FA moieties is thought to arise from FA selectivity occurring during two processes related to PL biosynthesis, specifically de novo phosphatidic acid synthesis and phospholipid FA remodeling. In terms of de novo phosphatidic acid synthesis, for example, mitochondrial glycerol-3-phosphate acyltransferase preferentially utilizes saturated FA acyl-coAs (acylated to the sn-1 position), whereas lysophosphatidic acid acyltransferase has a greater affinity for unsaturated FA acyl-coAs (acylated to the sn-2 position). Further, the FA binding proteins (FABP), which apparently direct this process via inhibitory/stimulatory effects on key enzymes and by regulating FA absorption and cellular uptake, also demonstrate FA selectivity. Fatty acid binding proteins, and their associated FA specificities, are also involved in the process of PL remodeling via deacylation-reacylation and transacylation reactions [22].

The FA composition of PL fractions in fishes may also be determined, in part, by the affinity of acyl transferases and/or FABPs for particular FA moieties. In fishes, the PL fraction is commonly associated with 16:0 and LC-PUFA, in a variety of tissues, including gametes [23, 24], and neural, optic, and immunocompetent cells [25], and our data are in agreement with these observations. In Atlantic salmon *Salmo salar* hepatocytes, 16:0, 20:4n-6, 20:5n-3, 22:6n-3 were preferentially incorporated into intra- and extracellular polar fractions relative to 18:1n-9, 18:2n-6, and 18:3n-3 [26]. Thus, the processes of FA incorporation and/or remodeling within the PL fraction of fish appear selective and similar to those observed in mammals. However, the prevalence of certain molecular "species" of PL is also influenced by FA availability, that is, dietary intake. Hvattum et al. [25] quantified the molecular species of PL within head kidney macrophages of Atlantic salmon reared on diets containing FO, soybean oil, or a 50:50 blend of these two lipids. Among fish fed the soybean oil diet, increasing dietary abundance of 18:2n FA (the analytical methods used in this study do not allow position of double bonds to be assigned, but the presumption is that 18:2n represents 18:2n-6, 20:5n represents 20:5n-3, 22:6n represents 22:6n-3, etc.) was reflected within the PL. Although some C_{20} and C_{22}-containing species decreased with increasing dietary soybean oil (e.g., 14:0/22:6 and 16:0/20:5n PC, 16:0/22:6n and 16:0/20:5n-3 PE, 16:0/20:5n and 16:0/22:6n PI, 16:0/20:5n and 16:0/22:6n PS, etc.) others increased (18:2n/20:5n and 18:2n/22:6n PE, 18:2/22:6n PS, etc.). This suggests that, despite decreasing dietary availability, 20:5n-3 and 22:6n-3 were being actively retained in the polar lipid, but increasingly paired with abundant 18:2n-6. Bell et al. [25] also noted conservation of LC-PUFA within the PL of salmon head kidney macrophages, but similar to Hvattum et al. [27], these authors observed substantial enrichment of 18:3n-3 and 18:2n-6 when this FA was abundant in the feed. Interestingly, the magnitude of 18:3n-3 enrichment was lower than that of 18:2n-6 despite roughly equivalent dietary levels [25]. We also observed 18:2n-6 enrichment within the PL (18.3% in GO-fed fish vs. 32.40% in GO feed) to exceed that of 18:3n-3 relative to dietary content (6.2% in LO-fed fish vs. 22.56% in LO feed), suggesting selective process(es) in PL metabolism have a greater affinity for 18:2n-6 than 18:3n-3.

Generally, composition of the neutral lipid classes demonstrates less specificity for certain FA moieties. Although many of the same enzymes and proteins involved in PL metabolism are also associated with TAG synthesis and remodeling, apparently TAG fractions are not as strongly affected by FA selectivity [24]. FA specificity may occur within biosynthesis of CE; however, lecithin:cholesterol acyltransferase, the enzyme responsible for esterifying FA to cholesterol, shows a preference for C_{14} and C_{16} FA [28]. The data available for fishes supports extension of these mammalian paradigms to piscine models. Although Stubhaug et al. [26] noted significant differences in incorporation of certain FA within the intracellular neutral lipid of Atlantic salmon hepatocytes, in general, this fraction showed less specificity for individual FA than the polar fraction [26]. Specificity was noted within the extracellular neutral lipid, but in this case, selection was for 16:0 and 18:0 within the sterol esters and TAG, respectively. In general, we did not observe enrichment of FA within the neutral lipid beyond dietary composition, and thus our data do not support a hypothesis of positive selection for certain FA within the CE or TAG fractions. However, the shorter-chain SFA (8:0, 10:0, 12:0, and 14:0) content of the CE and TAG fractions of fish fed the CO feed was lower than expected in all lipid classes, suggesting selection against deposition of these FA in fillet tissue.

High dietary levels of shorter-chain SFA in the CO feed were not proportionally reflected in fillet PL, TAG, or CE, or total lipid of other major lipid depots [5], which suggests either (1) impaired digestion/absorption or (2) catabolism of these FA. Lower digestibility of alternative lipids has been reported for cold-water marine species [29–32], and has been attributed to differences in melting points and PUFA content between the alternative lipid and FO. Reductions in growth are also observed in these cases, and dietary FA composition of poorly digested lipid is not reflected within the tissues [32]. Reduced digestibility of the CO feed seems an unlikely explanation for our results given the lack of growth differences and the limited, but significant, enrichment of CO-associated FA within the fillet and other tissues [5]. Sunshine bass can effectively utilize a wide-range of alternative lipids [3–5], as can other cool- and warm-water species, indicating lipid digestibility is primarily temperature-dependent, and issues of poor lipid digestion may be limited to cold-water species. Catabolism of shorter-chain SFA for energy production explains the low level of shorter-chain SFA enrichment observed in the CO-fed fish. Rates of β-oxidation have been determined for a variety of FA in several fish species, and these studies indicate SFA are preferred substrates for energy production [33–36].

The available data indicate selective processes govern the metabolic fate of FA in fishes. Although neutral lipids reflect dietary composition in a near-direct fashion, polar lipids show evidence of preference for certain FA. Medium-chain and LC-PUFA are preferred substrates for inclusion in polar lipid, whereas shorter-chain SFA are excluded. Although MC-PUFA appear to be somewhat inferior to LC-PUFA in terms of affinity, increased availability may overwhelm any enzymatic selectivity and result in high levels of incorporation of MC-PUFA within the PL fraction. Shorter-chain SFA are apparently poor substrates for the enzymes involved in PL synthesis and remodeling, and are not included within the PL fraction, even when availability is high. Conversely, SFA are preferentially used for energy production, whereas MC- and LC-PUFA are catabolized only when preferred substrates are absent. FA metabolism in fishes is characterized by a functional division between SFA and LC-PUFA, with MC-PUFA bridging the gap. Of the feeds we evaluated, the CO feed represented an ideal balance between providing preferred FA substrates for energy production (SFA) and tissue incorporation (LC-PUFA), and few MC-PUFA to compete within either process. We demonstrated provision of SFA in grow-out feeds for SB, instead of competing MC-PUFA, meets energy demands and allows for maximum inclusion of LC-PUFA within fillet lipid classes.

Acknowledgments We thank Andrew Coursey, Adam Lohmeyer, Shawn Meyer, Quinton Phelps, John West, and John Zeigler for assisting in data collection, and James Garvey and Michael Arts for editorial advice provided during manuscript preparation. We also thank Tyson Foods, Omega Protein, and Tate and Lyle for the donation of feedstuffs used in the present work, and the National Science Foundation for provision of funding under grant #0227925. This study was funded by the National Science Foundation under grant #0227925.

References

1. Bransden MP, Carter CG, Nichols PD (2003) Replacement of fish oil with sunflower oil in feeds for Atlantic salmon (*Salmo salar* L.): effect on growth performance, tissue fatty acid composition, and disease resistance. Comp Biochem Phys B 135:611–625
2. Glencross BD, Hawkins WE, Curnow JG (2003) Restoration of the fatty acid composition of red seabream (*Pagrus auratus*) using a fish oil finishing diets after grow-out on plant oil based diets. Aquac Nutr 9:409–418
3. Wonnacott EJ, Lane RL, Kohler CC (2004) Influence of dietary replacement of menhaden oil with canola oil on fatty acid composition of sunshine bass. North Am J Aquac 66:243–250
4. Lewis HA, Kohler CC (2008) Minimizing fish oil and fish meal with plant-based alternatives in sunshine bass diets without negatively impacting growth and muscle fatty acid profile. J World Aquac Soc (in press)
5. Trushenski JT, Lewis, HA, Kohler CC (XXXX) Restoring beneficial fatty acid profile of cultured sunshine bass *Morone chrysops* × *M. saxatilis*: I. Turnover is affected by initial composition and differs among tissues. *Lipids XX, XX-XX.*
6. Jobling M (2003) Do changes in Atlantic Salmon, *Salmo salar* L., fillet fatty acids following a dietary switch represent wash-out or dilution? Test of a dilution model and its application. Aquac Res 34:1215–1221
7. Jobling M (2004) Are modifications in tissue fatty acid profiles following a change in diet the result of dilution? Test of a simple dilution model. Aquaculture 232:551–562
8. Jobling M (2004) “Finishing” feeds for carnivorous fish and the fatty acid dilution model. Aquac Res 35:706–709
9. Robin JH, Regost C, Arzel J, Kaushik SJ (2003) Fatty acid profile of fish following a change in dietary fatty acid source: model of fatty acid composition with a dilution hypothesis. Aquaculture 225:283–293
10. Lane RL, Trushenski JT, Kohler CC (2006) Modification of fillet composition and evidence of differential fatty acid turnover in sunshine bass *Morone chrysops* × *M.* saxatilis following change in dietary lipid source. Lipids 41:1029–1038
11. Bell JG, Henderson RJ, Tocher DR, Sargent JR (2003) Replacement of dietary fish oil with increasing levels of linseed oil: modification of flesh fatty acid compositions in Atlantic salmon (*Salmo salar*) using a fish oil finishing diet. Lipids 39:223–232
12. Regost C, Arzel J, Robin J, Rosenlund G, Kaushik SJ (2003) Total replacement of fish oil by soybean or linseed oil with a return to fish oil in turbot (*Psetta maxima*). 1. Growth performance, flesh fatty acid profile, and lipid metabolism. Aquaculture 217:465–482
13. Bell JG, Henderson RJ, Tocher DR, Sargent JR (2004) Replacement of dietary fish oil with increasing levels of linseed oil: modification of flesh fatty acid compositions in Atlantic

salmon (*Salmo salar*) using a fish oil finishing diet. Lipids 39:223–232

14. Torstensen BE, Frøyland L, Lie Ǿ (2004) Replacing dietary fish oil with increasing levels of rapeseed oil and olive oil—effects on Atlantic salmon (*Salmo salar* L.) tissue and lipoprotein lipid composition and lipogenic enzyme activities. Aquac Nutr 10:175–192
15. Bell JG, McGhee F, Dick JR, Tocher DR (2005) Dioxin and dioxin-like polychlorinated biphenyls (PCBs) in Scottish farmed salmon (*Salmo salar*): effects of replacement of dietary marine fish oil with vegetable oils. Aquaculture 243:305–314
16. Torstensen BE, Bell JG, Rosenlund R, Henderson RJ, Graff IE, Tocher DR, Lie Ǿ, Sargent JR (2005) Tailoring of Atlantic salmon (*Salmo salar* L.) flesh lipid composition and sensory quality by replacing fish oil with a vegetable oil blend. J Agric Food Chem 53:10166–10178
17. Izquierdo MS, Montero D, Robaina L, Caballero MJ, Rosenlund G, Ginéz R (2005) Alterations in fillet fatty acid profile and flesh quality in gilthead seabream (*Sparus aurata*) fed vegetable oils for a long term period. Recovery of fatty acid profiles by fish oil feeding. Aquaculture 250:431–444
18. Turchini GM, Francis DS, De Silva SS (2006) Modification of tissue fatty acid composition in Murray cod (*Maccullochella peelii peelii*, Mitchell) resulting from a shift from vegetable oil diets to a fish oil diet. Aquac Res 37:570–585
19. Burdge GC, Wright P, Jones AE, Wootton SA (2000) A method for separation of phosphatidylcholine, triacylglycerol, non-esterified fatty acids and cholesterol esters from plasma by solid-phase extraction. Brit J Nutr 84:781–787
20. Sargent JR (1976) The structure, metabolism, and function of lipids in marine organisms. Biochem Biophys Perspect Mar BIol 3:149–212
21. Parker RS, Selivonchick DP, Sinnhuber RO (1980) Turnover of label from 1-^{14}C linolenic acid in phospholipids of coho salmon, *Oncorhychus kisutch*. Lipids 15:80–85
22. Jolly CA, Murphy EJ, Schroeder F (1998) Differential influence of rat liver fatty acid binding protein isoforms on phospholipids fatty acid composition: phosphatidic acid biosynthesis and phospholipids fatty acid remodeling. Biochim Biophys Acta 1390:258–268
23. Gallagher ML, Paramore L, Alves D, Rulifson RA (1998) Comparison of phospholipids and fatty acid composition of wild and cultured striped bass eggs. J Fish Biol 52:1218–1228
24. Bergey LL, Rulifson RA, Gallagher ML, Overton AS (2003) Variability of Atlantic coast striped bass egg characteristics. North Am J Fish Manage 23:558–572
25. Bell JG, Ashton I, Secombes CJ, Weitzel BR, Dick JR (1996) Dietary lipid affects phospholipids fatty acid compositions, eicosanoid production and immune function in Atlantic salmon (*Salmo salar*). Prostaglandins Leukot Essent Fatty Acids 54:173–182
26. Stubhaug I, Tocher DR, Bell JG, Dick JR, Torstensen BE (2005) Fatty acid metabolism in Atlantic salmon (*Salmo salar* L.) hepatocytes and influence of dietary vegetable oil. Biochim Biophys Acta 1734:277–288
27. Hvattum E, Røsjø Gjøen T, Rosenlund G, Ruyter B (2000) Effect of soybean oil and fish oil on individual molecular species of Atlantic salmon head kidney phospholipids determined by normal-phase liquid chromatography couple to negative ion electrospray tandem mass spectrometry. J Chromatogr B 748:137–149
28. Pownall HJ, Pao Q, Massey JB (1985) Acyl chain and headgroup specificity of human plasma lecithin:cholesterol acyltransferase. J Biol Chem 260:2146–2152
29. Lie Ǿ, Lied E, Lambertsen G (1987) Lipid digestion in cod (*Gadus morhua*). Comp Biochem Phys B 88:697–700
30. Olsen RE, Henderson RJ, Ringø E (1998) The digestion and selective absorption of dietary fatty acids in Arctic charr, *Salvelinus alpinus*. Aquac Nutr 4:13–21
31. Ng W-K, Sigholt T, Bell JG (2004) The influence of environmental temperature on the apparent nutrient and fatty acid digestibility in Atlantic salmon (*Salmo salar* L.) fed finishing diets containing different blends of fish oil, rapeseed oil, and palm oil. Aquac Res 35:1228–1237
32. Fonseca-Madrigal J, Karalazos V, Campbell PJ, Bell JG, Tocher DR (2005) Influence of dietary palm oil on growth, tissue fatty acid compositions, and fatty acid metabolism in liver and intestine in rainbow trout (*Oncorhynchus mykiss*). Aquac Nutr 11:241–250
33. Henderson RJ, Sargent JR (1985) Chain-length specificities of mitochondrial and peroxisomal beta-oxidation of fatty acids in livers of rainbow trout (*Salmo gairdneri*). Comp Biochem Phys B 82:79–85
34. Kiessling K-H, Kiessling A (1993) Selective utilization of fatty acids in rainbow trout (*Oncorhynchus mykiss* Walbaum) red muscle mitochondria. Can J Zool 71:248–251
35. Henderson RJ (1996) Fatty acid metabolism in freshwater fish with particular reference to polyunsaturated fatty acids. Arch Tierernahr 49:5–22
36. Frøyland L, Lie Ǿ, Berge RK (2000) Mitochondrial and peroxisomal β-oxidation capacities in various tissues from Atlantic salmon *Salmo salar*. Aquac Nutr 6:85–89
37. Gaylord TG, Gatlin DM (2000) Dietary lipid level but not L-carnitine affects growth performance of hybrid striped bass (*Morone chrysops* ♀ × *M. saxatilis* ♂). Aquaculture 190:237–246
38. Sealey WM, Craig SR, Gatlin DM (2001) Dietary cholesterol and lecithin have limited effects on growth and body composition of hybrid striped bass (*Morone chrysops* × *M. saxatilis*). Aquac Nutr 7:25–31

Lipids (2008) 43:655–662
DOI 10.1007/s11745-008-3185-2

ORIGINAL ARTICLE

Hydrolysis of Acyl-Homogeneous and Fish Oil Triacylglycerols Using Desalted Midgut Extract from Atlantic Salmon, *Salmo salar*

A. S. Bogevik · A. Oxley · R. E. Olsen

Received: 17 January 2008 / Accepted: 23 April 2008 / Published online: 21 May 2008
© AOCS 2008

Abstract Despite several studies aimed at evaluating the positional and fatty acid specificity of fish triacylglycerol (TAG) digestive lipases, there is still much uncertainty regarding these issues. The aim of the present study was therefore to address these questions in Atlantic salmon (*Salmo salar* L.). Crude luminal midgut extracts were collected from fed salmon and the hydrolysis studied for various substrates including triolein (Tri-18:1), trilinolein (Tri-18:2), trilinolenin (Tri-18:3), trieicosapentaenoin (Tri-20:5), tridocosahexaenoin (Tri-22:6) and natural fish oil TAG. Using Tri-18:1, in a time-curve model showed an initial high degree of *sn*-1 or *sn*-3 specificity where *sn*-1,2(2,3)-diacylglycerol (1,2(2,3)-DAG) and free fatty acid (FFA) were the main hydrolytic products up to 15 min. Lack of initial *sn*-2 specificity was confirmed by negligible *sn*-1,3-diacylglycerol (1,3-DAG) being produced. During the further hydrolysis of DAG, all positions appeared susceptible to attack causing a concomitantly small increase in *sn*-1(3)-monoacylglycerol (1(3)-MAG) and 2-MAG, but not at the level expected for an exclusively *sn*-1,3-specific lipase. Oleic acid (18:1n-9) and eicosapentaenoic acid (20:5n-3) were preferred substrates for hydrolysis using both fish oil and acyl-homogeneous TAGs with FFA as the main product of lipolysis. Hydrolysis of the natural fish oil TAG appeared slower yet produced proportionally more MAG and DAG after 5 min, and similar specificities, as for synthetic TAG substrates, were exhibited with 18:1n-9 and 20:5n-3 accumulating in the FFA fraction after 30 min. Notably, 16:0 was particularly conserved in MAG. As TAG resynthesis of absorbed lipid in salmon enterocytes proceeds preferably with 2-MAG as templates, the absorption of 2-MAG, produced during initial stages of TAG hydrolysis, would need to occur rapidly to be effectively utilised via the MAG pathway.

Keywords Gastrointestinal tract · Lipid hydrolysis · Triacylglycerol hydrolysis · Bile salt-dependent lipase · Intestine

Abbreviations

DAG	Diacylglycerol
FFA	Free fatty acid
FO	Fish oil
MAG	Monoacylglycerol
MGAT	Monoacylglycerol acyltransferase
Tri-18:1	Triolein
Tri-18:2	Trilinolein
Tri-18:3	Trilinolenin
Tri-20:5	Trieicosapentaenoin
Tri-22:6	Tridocosahexaenoin
PUFA	Polyunsaturated fatty acid
TAG	Triacylglycerol
TLC	Thin-layer chromatography

Introduction

In the pancreatic juice of mammals there are two major lipolytic enzymes responsible for neutral lipid digestion: pancreatic lipase (PL; E.C. 3.1.1.3.) and bile salt-dependent

A. S. Bogevik (✉) · A. Oxley · R. E. Olsen
Institute of Marine Research, Matre Aquaculture Research Station, 5984 Matredal, Norway
e-mail: andreb@imr.no

A. S. Bogevik
Department of Biology, University of Bergen, Bergen, Norway

lipase (BSDL; E.C. 3.1.1.1.). In the intestinal lumen, triacylglycerol (TAG) is mainly hydrolysed by PL. This enzyme has several distinctive characteristics. It possesses good activity towards lipid emulsions, yet is inhibited by the presence of bile salts and other amphipathic lipids. Inhibition is only overcome by the addition of colipase, which acts as an anchor for PL at the lipid droplet interface [1]. Furthermore, PL has a characteristic *sn*-1,3-specificity towards TAG producing free fatty acids (FFA) and *sn*-2-monoacylglycerols (2-MAG) for subsequent absorption.

In comparison, BSDL is dependent on bile salts for its hydrolytic activity towards TAG, cholesteryl esters, wax esters, vitamin esters, and phospholipids [2, 3]. BSDL is also less discriminatory, than PL, towards *sn*-fatty acyl position yielding mainly glycerol and FFA as hydrolytic products of TAG. Lower specificity is also apparent in that it has good activity towards all fatty acids including long chain polyunsaturated fatty acids (PUFA) that are not effectively hydrolysed by PL. Hence, intestinal BSDL is non-specific towards fatty acyl moiety and *sn*-position of TAG, displays a preference for micellar substrates, yet possesses 10–60 times less activity than PL in mammals. Thus, PL and BSDL appear to act sequentially where partial acylglycerols are released from lipid droplets by the PL-colipase complex for incorporation into mixed micelles and possible complete hydrolysis by BSDL [4, 5].

The advantage of producing 2-MAG during digestion, as is the case for PL, is that when absorbed into the enterocytes, resynthesis of TAG can proceed rapidly via the MAG pathway using 2-MAG as a template. This process is catalyzed by monoacylglycerol acyltransferase (MGAT) with relatively low expenditure of energy [6]. If TAG is completely hydrolysed to FFA and glycerol, TAG resynthesis in enterocytes must proceed through the slower and energy-consuming de novo glycerol-3-phosphate (G3P) pathway [7].

Dietary lipid for fish species in the marine environment is characteristically high in wax esters and TAG containing n-3 highly unsaturated fatty acids (HUFA) such as eicosapentaenoic (20:5n-3) and docosahexaenoic (22:6n-3) acids [8]. As PL does not possess wax ester hydrolytic activity and has low activity towards ester bonds containing pentaenoic and hexaenoic fatty acids, the predominant lipid-digesting enzyme in fish may be BSDL [2, 9]. This is furthermore evident in the failure to prove the existence of a PL-colipase system in fish [9, 10] and the cessation of all lipolytic activity upon removal of bile, that is subsequently restored by addition of bile salts in rainbow trout (*Oncorhynchus mykiss*), red sea bream (*Pagrus major*) and Atlantic salmon, *Salmo salar* [10–12].

Recent reports have however, shown the existence of MGAT in both Atlantic salmon [13, 14] and seabream, *Sparus aurata* [15], which is most likely required for a fast and efficient transfer of absorbed intestinal lipid to the blood as lipoproteins. This again indicates that the hydrolysis of luminal TAG may proceed through *sn*-1,3-specificity. This possibility is strengthened by the observation of some *sn*-1,3-specificity of digestive lipases in cod, *Gadus morhua* [16, 17] and rainbow trout [10, 18]. Furthermore, Gjellesvik [16] showed evidence of BSDL with *sn*-1,3-specificity using partially-purified caecal tissue from cod. This opens for the possibility that BSDL in fish may actually possess *sn*-1,3-specific lipase capability.

As previous studies in fish have shown both *sn*-1,3-specificity and complete hydrolysis of different TAG substrates, the present study was conducted to elucidate possible discrepancies in luminal lipase specificity with regard to *sn*-acyl position and fatty acid species. Complete hydrolysis to FFA and glycerol has especially been noted in fish if the fatty acid in *sn*-2 of TAG is PUFA [18–21]. Thus, we hypothesised that the luminal formation of 2-MAG is dependent on the species of fatty acid present at *sn*-2 position of TAG. The present study utilised a crude intestinal lipase preparation from the midgut lumen of Atlantic salmon as a model for studying TAG hydrolase activity [10, 12]. As BSDL activity is dependent on bile salt concentration [10], intestinal extracts were desalted and known concentrations added in the assay to avoid concentration dependent errors. Utilising synthetic acyl-homogeneous TAG substrates in the assay allowed for the relative determination of lipase *sn*-positional specificity, with respect to fatty acid species, by quantifying the isomeric products released. Furthermore, fish oil was also used to represent a natural TAG substrate, with a more typical distribution of fatty acids that salmon intestinal lipases would encounter.

Materials and Methods

Chemicals

Triolein (Tri-18:1), trilinolein (Tri-18:2), trilinolenin (Tri-18:3), trieicosapentaenoin (Tri-20:5), tridocosahexaenoin (Tri-22:6) and TLC standard (>99%) were all purchased from Nu-Chek Prep Inc. (Minnesota, USA). Chloroform, methanol, hexane, sulphuric acid, ethanol, acetone, sodium taurocholate, boric acid, 2,7-dichlorofluorescein were purchased from Sigma–Aldrich (St Louis, USA).

Substrate

The substrates of Tri-18:1, Tri-18:2, Tri-18:3, Tri-20:5 or Tri-22:6 were made to a concentration of 100 mg/mL in chloroform. Triacylglycerols from fish oil (Möllers Tran; MöllerCollett AS, Lysaker, Norway) were purified on TLC plates (20 × 20 cm × 0.5 mm, Merck 1.13894, Darmstadt, Germany) using hexane: diethyl ether: acetic acid (80:20:2) as developing solvent. Lipid classes were visualized using 0.1% (*w*/*v*) 2,7-dichlorofluorescein in 95% methanol. The TAG band was extracted from the silica with hexane: diethyl ether (1:1), evaporated under a stream of nitrogen and stored at −80 °C in chloroform. To prepare lipase substrates, 10 mg of the respective substrate was evaporated under a stream of nitrogen and the residue dissolved in 200 μL taurocholate (400 mM, 4 °C) and 1,800 μL of 100 mM potassium phosphate buffer (pH 8) containing 1 mM EDTA (ethylene diamine tetraacetic acid), 1 mM DTT (1,4-dithiothreitol) and 1 mM benzamidine (4 °C). The substrate mixture was stirred for 5 min, sonicated in ice-cold water for 2 min and vortexed for 1 min before use.

Enzyme

Atlantic salmon of 1,000 g, fed commercial diets (Biomar, Trondheim) 1 h twice a day, were anaesthetised in 4 g/kg benzocaine (Braine-Lálleud, Belgium) 1 hour after the last meal and killed by a sharp blow to the head. Four fish were weighed, and the intestinal tract dissected. Luminal contents were collected from the midgut, defined as the section from the last pyloric caeca to the start of the distal intestine, as recognised by its larger diameter [22]. The enzyme preparation was made once from pooling the intestinal contents from the four salmon. The pooled content were further diluted twofold (*w*/*v*) in 100 mM potassium phosphate buffer (pH 8) containing 1 mM EDTA, 1 mM DTT and 1mM benzamidine. The suspension was centrifuged at 3,220×*g* for 10 min at 4 °C. The lipid layer was aspirated from the surface and the infranatant collected and designated "crude extract". To remove endogenous bile salts, the extract was transferred to Zeba$^{\mathrm{TM}}$ Desalt Spin Columns (Pierce, Rockford, USA) and centrifuged at 200×*g* for 2 min at 4 °C. The protein contents of the desalted extract was analysed by the method of Lowry et al. [23] using an Ultrospec 4000 spectrophotometer (Pharmacia Biotech, Cambridge, England) and adjusted to 1.0 mg/mL. The enzyme preparation was then prepared in cryo tubes each containing materials for 1 day work and stored at −80 °C prior to use, as preliminary tests had shown no loss of activity when stored under these conditions. By this procedure, all experiments were carried out on the same enzyme preparation.

Incubation

The incubation assay was performed according to a modification of the method of Bogevik et al. [12]. In brief, 0.2 mL of the enzyme extract was added to 0.2 mL substrate suspension and incubated for 5–30 min at the ambient temperature of the fish (10 °C). The reaction was terminated by the addition of 8 ml chloroform. The tubes were vortexed for 15 s and centrifuged for 2 min at 300×*g* after which the upper aqueous layer was aspirated off and the lower chloroform layer evaporated under a stream of nitrogen. The residue was resuspended in 30–50 μL chloroform and applied to TLC plates (20 × 20 cm × 0.25 mm, Merck 1.05721, Darmstadt, Germany) pre-impregnated with 2.3% boric acid in ethanol:water (1:1) and developed in 50 ml chloroform:acetone (96:4), according to Thomas [24]. Lipid spots were detected by spraying the plate with 0.1% 2,7-dichlorofluorescein in 95% methanol and visualized under UV light.

Lipid Extraction

Two-hundred microlitres either of the pooled desalted midgut extract or the substrate suspension were added to 4 mL chloroform and extracted as above. The desalted midgut extract was separated into neutral lipid classes as described above.

Quantification of Lipid Classes

The lipid class bands representing 1(3)-MAG, 2-MAG, FFA, 1,2(2,3)-DAG, 1,3-DAG, and TAG were scraped into tubes, added internal standard (19:0) and subjected to acid-catalyzed transesterification using 1% (*v*/*v*) H_2SO_4 in methanol [25]. The resulting fatty acid methyl esters (FAME) were extracted and quantified by gas liquid chromatography using a HP 5890 gas chromatograph equipped with a J&N Scientific Inc. DB-23 fused silica column (30 m × 0.25 mm id). Hydrogen was used as carrier gas and temperature programming was from 50 to 150 °C at a rate of 40 °C/min, from 150 to 195 °C at 1.5 °C/min, and then to a final temperature of 205 °C at 0.5 °C/min. Individual components were identified by comparison with known standards.

Calculation and Statistics

The amount of fatty acids in neutral lipid classes were converted to the amount of lipid by a correction factor which takes into account the amount of glycerol [25]. The amount of lipid were converted into moles for the respective lipid classes. From this, individual lipid classes were calculated as a percentage of total lipid classes recovered from each substrate. Data is given as ±SD for replicate incubations. All statistical analysis was performed using STATISTICA 8.0 software for Windows (StatSoft. Inc., Tulsa, USA). The statistical significance of differences was tested using one-way ANOVA followed by the Tukey post hoc test for comparison of the different acyl-homogenous substrate in each lipid class after hydrolysis. Significance was accepted at $P < 0.05$. The fish oil TAG substrate contained different levels of each fatty acid, and the fatty acid profile in each lipid class was therefore compared to the original TAG substrate after hydrolysis.

Results

In order to test for possible interference from the lipid contained in the digesta, neutral lipid content of the desalted midgut extract was estimated. The distribution of lipid classes was: FFA (10 μg) > MAG (2 μg) > DAG (2 μg) > TAG (0.5 μg). The main fatty acids of the lipid classes were palmitic acid (16:0) in MAG (0.73 μg/200 μL), 1,2/2,3-DAG (0.40 μg/200 μL) and TAG (0.24 μg/200 μL), while 1,3-DAG had oleic acid, 18:1n-9 (0.79 μg/200 μL) and FFA had 20:5n-3 (2.84 μg/200 μL) as the major fatty acid (Table 1). However, the total amount of each of these fatty acids only accounted for a small fraction compared to the amount of substrate (1 mg) added in the incubation, and was subtracted from the fatty acids calculated in the lipid classes after hydrolysis.

The time course digestion of Tri-18:1 is shown in Fig. 1. The hydrolysis was very high over the first 5 min and then stabilized at a relative constant rate throughout. FFA was the major product reaching a 1:1 ratio of FFA and TAG after 20 min hydrolysis, and increased to account for almost 60% of the lipid classes at the termination of the study, showing a 10-times higher concentration than MAG and DAG. *Sn*-1,2(2,3)-DAG increased to a maximum of 14% of the lipid classes after 15 min followed by a reduction towards the termination of the study. Both 1(3)-MAG and 2-MAG increased slowly towards the end, but neither contributed to more than 9% of the lipids.

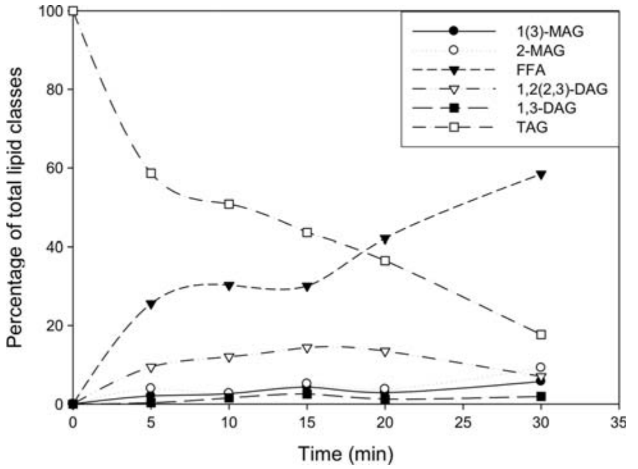

Fig. 1 The mol% of total lipid class hydrolysis of 1 mg tri-18:1 with desalted midgut extract (118 μg) from Atlantic salmon in 100 mM sodium phosphate-buffer (pH 8.0) and 20 mM sodium taurocholate at 0, 5, 10, 15, 20 and 30 min. Mean n = 3

The hydrolysis of various acyl-homogeneous TAGs was assessed after 5 (Fig. 2) and 30 min of incubation (Fig. 3). After 5 min, hydrolysis of Tri-18:1 and Tri-20:5 proceeded at a higher rate than the other synthetic TAG substrates. The main products were in both cases increased levels of FFA compared to the other TAG substrates. The 1,2(2,3)-DAG were the second largest hydrolysis products, while 1,3-DAG and various MAG products were in minute amounts. There was also a notable but non-significant tendency of more 2-MAG to be produced using Tri-18:1 and Tri-20:5 as substrates. The tendency of Tri-18:1 as the best substrate for lipolysis was verified after 30 min incubation where more than 80% was hydrolysed compared to less than 70% for the other substrates. The lowest rate of hydrolysis was found with Tri-22:6, where less than 50% was hydrolysed, which was significantly lower than for the other synthetic substrates (Fig. 3). In each case, FFA was the main product of hydrolysis, but there was also an increase in 1,2(2,3)-DAG and MAG isomers, particularly 2-MAG that reached around 10% of the lipid classes. Very low amounts of 1,3-DAG was produced regardless of substrate.

The hydrolysis of fish oil TAG appeared to progress at a different rate than for the structured substrates. After 5 min of hydrolysis, only 40% of the TAG remained with the main hydrolysis products being 1,2(2,3)-DAG (25%), 1(3)-MAG (15%) and 2-MAG (15%). Only 3% was found in FFA (Fig. 2). After 30 min of incubation, the FFA content

Table 1 Amount of fatty acids (μg/200 μL) in different lipid classes of the pooled desalted midgut extract

Lipid classes	Amount of fatty acids (μg) in 200 μL desalted midgut extract						
	16:0	18:1n-9	18:2n-6	18:3n-3	20:1n-9	20:5n-3	22:6n-3
1(3)-MAG	0.73	0.19	0.02	0.08	0.09	0.01	0.06
2-MAG	0.39	0.17	0.01	0.07	0.02	NT	0.03
FFA	1.45	2.55	0.94	0.37	0.27	2.84	1.87
1,2(2,3)-DAG	0.40	0.19	0.03	0.08	0.01	NT	0.07
1,3-DAG	0.25	0.79	0.05	0.15	NT	NT	NT
TAG	0.24	0.13	0.04	0.09	0.01	NT	0.03

NT not traceable

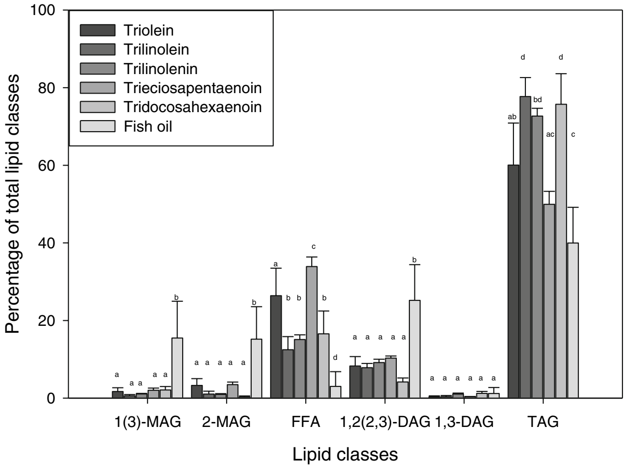

Fig. 2 The mol% of total lipid class upon 5 min hydrolysis of either 1 mg triolein (Tri-18:1), trilinolein (Tri-18:2), trilinolenin (Tri-18:3), trieicosapentaenoin (Tri-20:5), tridocosahexaenoin (Tri-22:6) with desalted midgut extract (118 μg) from Atlantic salmon in 100 mM sodium phosphate-buffer (pH 8.0) and 20 mM sodium taurocholate. The column represents the mean of 6 replicate incubations ±SD, values not having the same *superscript letter* are significantly different ($P < 0.05$) as determined by one-way-ANOVA

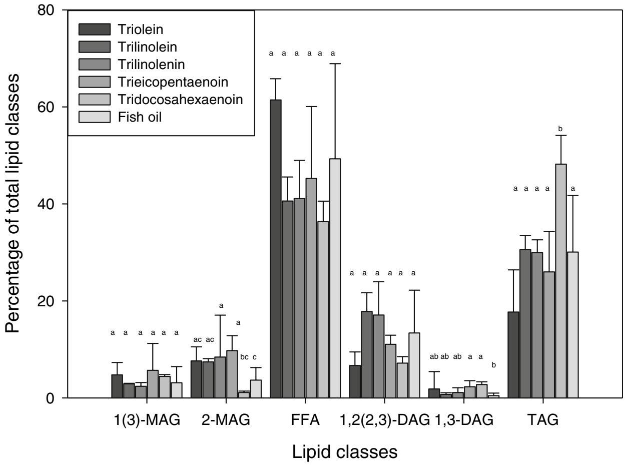

Fig. 3 The mol% of total lipid class hydrolysis of either 1 mg triolein (Tri-18:1), trilinolein (Tri-18:2), trilinolenin (Tri-18:3), trieicosapentaenoin (Tri-20:5), tridocosahexaenoin (Tri-22:6) with desalted midgut extract (118 μg) from Atlantic salmon in 100 mM sodium phosphate-buffer (pH 8.0) and 20 mM sodium taurocholate at 30 min. The column represents the mean of 6 replicate incubations ±SD, values not having the same *superscript letter* are significantly different ($P < 0.05$) as determined by one-way-ANOVA

had increased to 49% while the content of the different MAGs was notably decreased while the level of 1,2(2,3)-DAG was at 13% (Fig. 3).

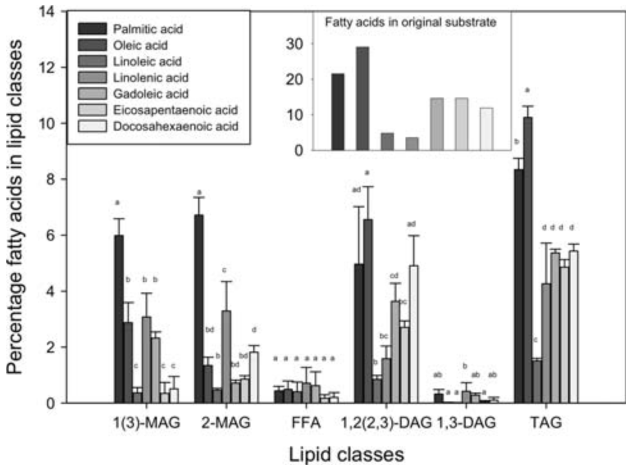

Fig. 4 Total fatty acid composition of the substrate and fatty acid specificity within each lipid class after hydrolysis of 1 mg of fish oil TAG with desalted midgut extract (118 μg) from Atlantic salmon in 100 mM sodium phosphate-buffer (pH 8.0) and 20 mM sodium taurocholate at 5 min (mol% fatty acid within each lipid class/1 mg TAG/118 μg desalted midgut extract/5 min). Means, n = 6 ± SD, values not having the same *superscript letter* are significantly different ($P < 0.05$) as determined by one-way-ANOVA

The fish oil TAG contained oleic acid (18:1n-9, 29.0%) as the major fatty acid followed by palmitic acid (16:0, 21.5%), the fatty acids of the 20-carbon series (gadoleic acid (20:1n-9), 14.6%), eicosapentaenoic acid (20:5n-3, 14.6%) and docosahexaenoic acid (22:6n-3, 11.9%). Linoleic acid (18:2n-6, 4.8%) and linolenic acid (18:3n-3, 3.5%) were only found in small amounts (Fig. 4).

After 5 min of incubation, the pattern of fatty acids in the remaining TAG was very similar to that of the substrate with the exception that the level of 20:5n-3 appeared to be somewhat reduced (Fig. 4). The fatty acid pattern in 1,2(2,3)-DAG had many similarities to that of TAG but with some notable differences. Firstly, the content of 22:6n-3 was increased to 5% of the fatty acids. Secondly, the content of 20:5n-3 was reduced further in relation to TAG. All MAGs were significantly altered compared to the substrate where 1(3)-MAG and 2-MAG were enriched in 16:0 by circa 6%. Furthermore, there was also a notable retention of 18:3n-3 in all MAGs, while the levels of 18:2n-6 and 20:5n-3 were very low. Comparing the different MAGs showed that 22:6n-3 accumulated somewhat in 2-MAG while 18:1n-9 and 18:3n-3 were higher in 1(3)-MAG. Of the minor lipid classes, FFA appeared to be enriched in 18:3n-3 and 20:1n-9 while 1,3-DAG was enriched in 16:0, 18:3n-3 and 20:1n-9.

After 30 min, unreacted TAG still had many similarities to the original substrate except for a lower content of 20:5n-3 and a tendency to increased levels of 22:6n-3 and 20:1n-9 (Fig. 5). In the FFA fraction, 18:1n-9 and 20:5n-3 was significantly increased in relation to the substrate while 22:6n-3 was reduced. As shown after 5 min, all MAGs were enriched in 16:0. In 2-MAG, there was still a clear accumulation of 22:6n-3. Docosahexaenoic acid (22:6n-3) was significantly increased in 1,2(2,3)-DAG compared to the substrate while the content of 18:1n-9 was reduced (Fig. 5).

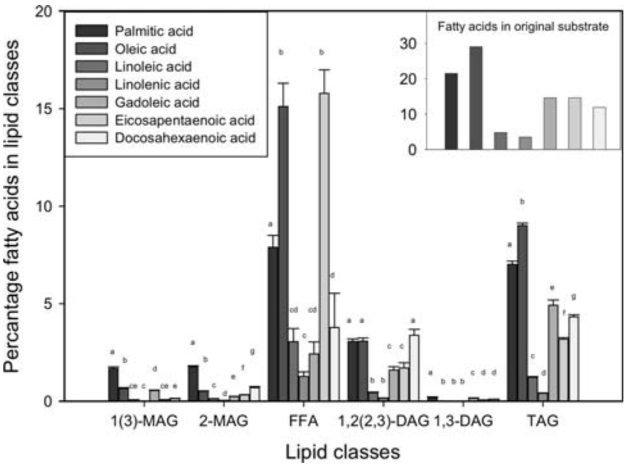

Fig. 5 Total fatty acid composition of the substrate and fatty acid specificity within each lipid class after hydrolysis of 1 mg of fish oil TAG with desalted midgut extract (118 µg) from Atlantic salmon in 100 mM sodium phosphate-buffer (pH 8.0) and 20 mM sodium taurocholate at 30 min (mol% fatty acid within each lipid class/1 mg TAG/118 µg desalted midgut extract/30 min). Means, n = 6 ± SD, values not having the same *superscript letter* are significantly different ($P < 0.05$) as determined by one-way-ANOVA

Discussion

Dietary lipid is well utilized in most fish species [9]. In order to accomplish this, fish require an efficient system for the intestinal digestion of TAG for absorption across the brush border membrane (BBM) and subsequent resynthesis of hydrolytic products in enterocytes for transportation. The MAG pathway has recently been established as the predominant pathway for TAG resynthesis in the intestine of Atlantic salmon [13, 14] and sea bream [15], which challenges the presence of a non-specific bile salt-dependent lipase (BSDL) as the major lipolytic enzyme of the luminal content in fish. There is a general assumption that BSDL does not discriminate towards *sn*-acyl position on the glycerol 'backbone' of TAG thus yielding glycerol and FFAs that must be resynthesized by the slower and more energetically-consuming glycerol-3-phosphate (G3P) pathway in enterocytes [6].

Therefore, there is some uncertainty as to which lipase system predominates in fish. Although several studies have attempted to verify the existence of a pancreatic *sn*-1,3-specific lipase, no such enzyme has ever been proven [9]. In most fish species studied so far, desalting appears to halt all lipolytic activity while it is regained by the addition of bile salts [10–12]. This clearly points to the prevalence of a bile salt dependent lipase (BSDL) in fish [9]. However, some studies have reported this lipase to be *sn*-1,3-specific [10, 16] which, concomitant with the presence of the MAG pathway in enterocytes, opens up the possibility that BSDL in fish may actually possess *sn*-1,3-specific hydrolytic activity. Furthermore, this specificity has especially been reported for Tri-18:1n-9 [16] and in the presence of shorter chain fatty acyl esters or saturated fatty acids [26].

The present study showed that the lipase has a high degree of *sn*-1 or *sn*-3 specificity initially where *sn*-1,2(2,3)-DAG and FFA were the main hydrolytic products of Tri-18:1n-9 up to 15 min, while *sn*-1,3-DAG was produced in minute amounts showing low activity towards the *sn*-2 position in the intermediate hydrolysis. During further hydrolysis of DAG, all *sn*-positions appeared to be susceptible to hydrolytic attack causing a concomitant small increase in *sn*-1(3)-MAG and *sn*-2-MAG in roughly equimolar concentrations. However, the occurrence of 1(3)-MAG could be an isomerisation product from 2-MAG due to the instability of 2-MAG in biological systems having a reported half-life of 2–10 min dependent on protein content and pH [27]. This does suggest the possibility for the existence of a 1,3-specific lipase. However, the total level of MAG (including 2-MAG) never reached the concentrations that would be expected with a 1,3-specific lipase (see Mattson and Volpenhein [4] and Gjellesvik et al. [16]) indicating that a step-wise hydrolysis from TAG through DAG and MAG will eventually proceed to glycerol and FFA as final products. In this respect, our data appear to comply with in vivo feeding studies of Atlantic salmon that has suggested that FFA and glycerol are the main hydrolysis products [28].

There was also an interesting difference in the rate of hydrolysis of synthetic substrates and fish oil. While the digestion of the synthetic substrates was faster producing mainly FFA, the natural substrate had a slower rate producing more intermediate products of MAG and DAG after 5 min. The reason for this could be the fatty acid complexity of the natural oil, where the enzyme will most likely prefer certain fatty acids in a certain position over another, as seen previously where complete hydrolysis to FFA and glycerol has especially been noted if the fatty acid in *sn*-2 position is a monounsaturated fatty acid [2, 18] or PUFA [18–21].

If the high activity of the MAG pathway is to be effective in the resynthesis of TAG, it is essential that the 2-MAG being produced at an early stage of hydrolysis is absorbed rapidly. In this respect it is interesting to note that the hydrolysis of fish oil over the first 5 min actually did produce substantial amounts of MAG. So even if salmon lipase does not have the traditional *sn*-1,3-specificity, the MAG pathway would still have sufficient material providing that the absorption is rapid. This would not be the case for the synthetic substrates where the hydrolysis seems to proceed to FFA and glycerol. Fish fed on these diets would consequently rely on the G3P pathway for TAG synthesis, and would probably have lower growth rates. Glycerol-3-phosphate (G3P) is normally produced from amino acids/pyruvate through pathways of glyceroneogenesis, or alternatively generated from glycerol via glycerol kinase, which has extremely low activity in mammalian intestine compared to adipose and has yet to be investigated in fish.

The salmon lipase in the present study also possessed some fatty acid specificity, at least during parts of the hydrolysis process. The most notable effect using synthetic substrates was the very rapid hydrolysis of Tri-18:1 and Tri-20:5n-3 over the first 5 min of incubation compared to the other substrates. This led to a significantly increase in FFA but not other acylglycerols. After 30 min of incubation all differences had evened out, and there was no significant difference between these substrates. This may indicate that FFA has a feedback inhibition on the lipase activity. The only notable effect after 30 min was the high level of Tri-22:6n-3 compared to the other substrates indicating low substrate specificity of the lipase. Fish oil was also very rapidly degraded over the first 5 min of incubation. But in this case, the main products were MAG and 1,2(2,3)-DAG with little occurring in FFA and 1,3-DAG. The build up of 22:6n-3 in 1,2(2,3)-DAG and 16:0 in the MAG fractions do however, show that these were difficult to digest by the lipase. At 30 min this tendency was maintained to some degree, although they were more hydrolysed to FFA, while the build up of 18:1n-9 and 20:5n-3 in the FFA fraction clearly demonstrates that these were preferred over the other fatty acids for hydrolysis.

These data do in some respects agree with previous results from fish. As in our study, Halldorsson et al. [29] showed that 16:0 accumulated in the DAG and MAG fractions while 20:5n-3 increased in the FFA fraction when caecal lipase was incubated with various fish oils. They did however, not observe a similar preference for 18:1n-9 as seen in the present study. Furthermore, they found a significant accumulation of 22:6n-3 in the FFA fraction that was not the case in the present study. Cod digestive lipase also seems to have many similarities with the salmon lipase in that there is a preference for unsaturated fatty acids, 20:5n-3 and a lower activity towards 22:6n-3 [17, 19, 25]. However, cod lipase also seems to have the same preference for shorter chain PUFA like 18:2n-6, which does not seem to be the case in salmon. It thus appears that although fish digestive lipases are similar with regard to preference for 20:5n-3, there are also notable differences. This may indicate some adaptations to natural habitats and the presence of different fatty acids in their natural diets.

However, it is also possible that some of the differences observed are due to variations in experimental conditions. In the present study for example, we used ambient temperature of the fish (10 °C) for incubations in order to mimic natural conditions. Other studies like that of Gjellesvik [26] and presumably Halldorsson et al. [29] used room temperature for their studies. As lipase specificity is known to change at higher temperatures, in cod lipase towards saturated fatty acids [26] this may explain some of the differences observed. Furthermore, assay conditions may also affect the specificities. This was elegantly shown using cod lipase where there was a dramatic change in specificity when the substrates were added in alcoholic or taurocholate solutions [26]. In the present study, we solubilised the TAG substrate in a taurocholate solution before use.

In conclusion, Atlantic salmon lipase does possess some specificity towards *sn*-1 or *sn*-3 fatty acyl positions on TAG, at least with Tri-18:1n-9 due to initial increases in 1,2(2,3)-DAG but not 1,3-DAG. However, this specificity is not as pronounced as for mammalian pancreatic lipase or as suggested for BSDL in other fish species. The lack of MAG as a major product of hydrolysis poses a problem for the MAG pathway for reconstituting TAG in the enterocytes when utilising acyl-homogeneous TAG substrates. However, by using natural TAG substrates in the present study, fairly large amounts of MAG were produced during the early stages of digestion that is not seen using synthetic substrates. Provided that MAG is absorbed rapidly, fish enterocytes may still be supplied with sufficient 2-MAG for the MAG pathway to function effectively. Atlantic salmon digestive lipases also have a clear specificity towards certain fatty acids like 20:5n-3 and 18:1n-9, regardless of their positional distribution. This lipase has therefore similarities to that found in other fish species like cod and rainbow trout [19, 29] but there are also some differences that may indicate species adaptations to specialized feed habitats, or simply variations in the in vitro experimental setup.

Acknowledgments This work was supported by the Norwegian Research Council (Grant no. 165051/S40). The authors are also grateful for the skillful assistance of Ivar Helge Matre, Institute of Marine Research, in looking after the fish.

References

1. Borgstrom B (1977) Action of bile-salts and other detergents on pancreatic lipase and interaction with colipase. Biochim Biophys Acta 488:381–391
2. Patton JS, Nevenzel JC, Benson AA (1975) Specificity of digestive lipases in hydrolysis of wax esters and triglycerides studied in anchovy and other selected fish. Lipids 10:575–583
3. Lombardo D (2001) Bile salt-dependent lipase: its pathophysiological implications. Biochim Biophys Acta 1533:1–28
4. Mattson FH, Volpenhein RA (1964) The digestion and absorption of triglycerides. J Biol Chem 239:2772–2777
5. Wang CS, Kuksis A, Manganaro F, Myher JJ, Downs D, Bass HB (1983) Studies on the substrate-specificity of purified human-milk bile salt-activated lipase. J Biol Chem 258:9197–9202
6. Lehner R, Kuksis A (1996) Biosynthesis of triacylglycerols. Prog Lipid Res 35:169–201
7. Johnston JM (1977) Gastrointestinal tissue. In: Snyder F (ed), Lipid metabolism in mammals, vol 1. Plenum Press, New York, pp 151–187
8. Cowey CB, Sargent JR (1977) Lipid nutrition in fish. Comp Biochem Physiol B Biochem Mol Biol 57:269–273

9. Olsen RE, Ringo E (1997) Lipid digestibility in fish: a review. Recent Res Dev Lipids Res 1:199–265
10. Tocher DR, Sargent JR (1984) Studies on triacylglycerol, wax ester and sterol ester hydrolases in intestinal ceca of rainbow-trout (*Salmo-Gairdneri*) fed diets rich in triacylglycerols and wax esters. Comp Biochem Physiol B Biochem Mol Biol 77:561–571
11. Iijima N, Tanaka S, Ota Y (1998) Purification and characterization of bile salt-activated lipase from the hepatopancreas of red sea bream, *Pagrus major*. Fish Physlog Biochem 18:59–69
12. Bogevik AS, Tocher DR, Waagbo R, Olsen RE (2008) Triacylglycerol-, wax ester- and sterol ester-hydrolases in midgut of Atlantic salmon (*Salmo salar*). Aquacult Nutr 14:93–98
13. Oxley A, Torstensen BE, Rustan AC, Olsen RE (2005) Enzyme activities of intestinal triacylglycerol and phosphatidylcholine biosynthesis in Atlantic salmon (*Salmo salar* L.). Comp Biochem Physiol B Biochem Mol Biol 141:77–87
14. Oxley A, Jutfelt F, Sundell K, Olsen RE (2007) *Sn*-2-monoacylglycerol, not glycerol, is preferentially utilised for triacylglycerol and phosphatidylcholine biosynthesis in Atlantic salmon (*Salmo salar* L.) intestine. Comp Biochem Physiol B Biochem Mol Biol 146:115–123
15. Caballero MJ, Gallardo G, Robaina L, Montero D, Fernandez A, Izquierdo M (2006) Vegetable lipid sources affect in vitro biosynthesis of triacylglycerols and phospholipids in the intestine of sea bream (*Sparus aurata*). Br J Nutr 95:448–454
16. Gjellesvik DR, Raae AJ, Walther BT (1989) Partial-purification and characterization of a triglyceride lipase from cod (*Gadus-Morhua*). Aquaculture 79:177–184
17. Gjellesvik DR, Lombardo D, Walther BT (1992) Pancreatic bile-salt dependent lipase from Cod (*Gadus-Morhua*)—purification and properties. Biochim Biophys Acta 1124:123–134
18. Leger C (1985) Digestion, absorption and transport of lipids. In: Cowey CB, Mackie AM, Bell JG (eds) Nutrition and feeding in fish. Academic Press, London, pp 299–331
19. Lie O, Lambertsen G (1985) Digestive lipolytic enzymes in cod (*Gadus-Morhua*)—fatty-acid specificity. Comp Biochem Physiol B Biochem Mol Biol 80:447–450
20. Lie O, Lied E, Lambertsen G (1987) Lipid digestion in cod (*Gadus-Morhua*). Comp Biochem Physiol B Biochem Mol Biol 88:697–700
21. Koven WM, Henderson RJ, Sargent JR (1994) Lipid Digestion in Turbot (*Scophthalmus-Maximus*). 1. Lipid class and fatty acid composition of digesta from different segments of the digestive-tract. Fish Physiol Biochem 13:69–79
22. Olsen RE, Myklebust R, Kaino T, Ringo E (1999) Lipid digestibility and ultrastructural changes in the enterocytes of Arctic char (*Salvelinus alpinus* L.) fed linseed oil and soybean lecithin. Fish Physiol Biochem 21:35–44
23. Lowry OH, Rosebrough NJ, Farr AL, Randall RJ (1951) Protein measurement with the folin phenol reagent. J Biol Chem 193:265–275
24. Thomas AE, Scharoun JE, Ralston H (1965) Quantitative estimation of isomeric monoglycerides by thin-layer chromatography. J Am Oil Chem Soc 42:789–792
25. Christie WW (2003) LIPID ANALYSIS: isolation, separation, identification and structural analysis of lipids. 3rd edn. The Oily Press, Bridgwater
26. Gjellesvik DR (1991) Fatty acid specificity of bile salt-dependent lipase—enzyme recognition and super-substrate effects. Biochim Biophys Acta 1086:167–172
27. Rouzer CA, Ghebreselasie K, Marnett LJ (2002) Chemical stability of 2-arachidonylglycerol under biological conditions. Chem Phys Lipids 119:69–82
28. Sigurgisladottir S, Lall SP, Parrish CC, Ackman RG (1992) Cholestane as a digestibility marker in the absorption of polyunsaturated fatty acid ethyl-esters in Atlantic salmon. Lipids 27:418–424
29. Halldorsson A, Kristinsson B, Haraldsson GG (2004) Lipase selectivity toward fatty acids commonly found in fish oil. Eur J Lipid Sci Technol 106:79–87

Lipids (2008) 43:663–671
DOI 10.1007/s11745-008-3184-3

ORIGINAL ARTICLE

Vitamin E Transfer from Lipid Emulsions to Plasma Lipoproteins: Mediation by Multiple Mechanisms

**M. Hacquebard · M. Vandenbranden ·
W. J. Malaisse · J. M. Ruysschaert ·
R. J. Deckelbaum · Y. A. Carpentier**

Received: 8 August 2007 / Accepted: 17 April 2008 / Published online: 29 May 2008
© AOCS 2008

Abstract The present study determined alpha-tocopherol mass transfer from an alpha-tocopherol-rich emulsion to LDL and HDL, and assessed the potential of different mechanisms to modulate alpha-tocopherol transfers. Emulsion particles rich in alpha-tocopherol were incubated in vitro with physiological concentrations of LDL or HDL. The influence of plasma proteins was assessed by adding human lipoprotein poor plasma (LPP) fraction with intact vs heat inactivated PLTP, or with a specific cholesteryl ester transfer protein (CETP) inhibitor, or by adding purified PLTP or pig LPP which lacks CETP activity. After 4 h incubation in absence of LPP, alpha-tocopherol content was increased by ~80% in LDL and ~160% in HDL. Addition of LPP markedly enhanced alpha-tocopherol transfer leading to 350–400% enrichment in LDL or HDL at 4 h. Higher (~10 fold) enrichment was achieved after 20 h incubation with LPP. Facilitation of alpha-tocopherol transfer was (i) more than 50% higher with human vs pig LPP (despite similar PLTP phospholipid transfer activity), (ii) reduced by specific CETP activity inhibition, (iii) not fully suppressed by heat inactivation, and (iv) not restored by purified PLTP. In conclusion, alpha-tocopherol content in LDL and HDL can be markedly raised by rapid transfer from an alpha-tocopherol-rich emulsion. Our results indicate that alpha-tocopherol mass transfer between emulsion particles and lipoproteins is mediated by more than one single mechanism and that this transfer may be facilitated not only by PLTP but likely also by other plasma proteins such as CETP.

Keywords Vitamin E · Alpha-tocopherol mass transfer · Lipid emulsions · LDL · HDL · PLTP · CETP

Abbreviations

CETP	Cholesteryl ester transfer protein
HDL	High density lipoproteins
LDL	Low density lipoproteins
LPP	Lipoprotein poor plasma
PLTP	Phospholipid transfer protein
TC	Total cholesterol
TG	Triglycerides
TGRP	Triglyceride-rich particles

Introduction

Vitamin E is a group of eight lipid soluble molecules including alpha-, beta-, gamma-, and delta-tocopherol as well as alpha-, beta-, gamma-, and delta-tocotrienols (Fig. 1). Alpha-tocopherol is the most abundant form of vitamin E in man due to the selective recognition and retention of this isoform by a specific binding protein present in the liver. Alpha-tocopherol is transported by plasma lipoproteins and plays an important role not only in

M. Hacquebard · W. J. Malaisse · Y. A. Carpentier (✉)
L. Deloyers Laboratory for Experimental Surgery,
Université Libre de Bruxelles, Avenue J. Wybran 40,
1070 Brussels, Belgium
e-mail: nutrisub@ulb.ac.be

M. Hacquebard
e-mail: Mirjam.Hacquebard@ulb.ac.be

M. Vandenbranden · J. M. Ruysschaert
Laboratory of Structure and Function of Biological Membranes-
Center of Structural Biology and Bioinformatics,
Université Libre de Bruxelles, Brussels, Belgium

R. J. Deckelbaum
Institute of Human Nutrition, Columbia University,
New York, USA

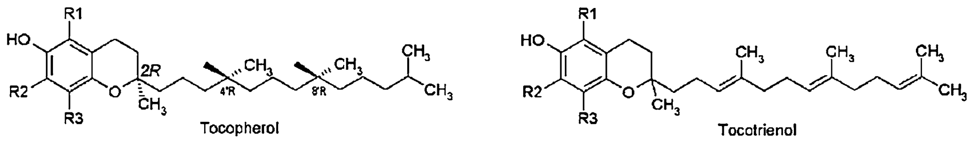

Isoforms of tocopherols and tocotrienols			
alpha-	R1=CH_3	R2=CH_3	R3=CH_3
beta-	R1=CH_3	R2=H	R3=CH_3
gamma-	R1=H	R2=CH_3	R3=CH_3
delta-	R1=H	R2=H	R3=CH_3

Fig. 1 The molecular structure of vitamin E is characterised by a chromanol ring substituted by an aliphatic side chain (C16), which is saturated for tocopherols and unsaturated for tocotrienols. The hydrophobic aliphatic side chain allows vitamin E to partition between membrane and lipoprotein lipids while presenting the chromanol ring with the hydroxyl group towards the aqueous phase. The four forms of tocopherols and tocotrienols vary in the number and the position of methyl groups on the chromanol ring

preventing lipid peroxidation but also in modulating several cell functions such as cell signaling and gene expression [1, 2]. Epidemiological studies have shown a better protection against cardiovascular diseases for individuals in the higher ranges of vitamin E status [3, 4]. However, the results of some large-scale clinical trials using supplementation with mega-doses (≥400 IU/day) vitamin E to general populations have not shown clear protection against cardiovascular diseases [5–8]. A recent meta-analysis even suggests that chronic supplementation with mega-doses of vitamin E may increase all-cause mortality [9]. Thus, many questions remain open notably with respect to potential indications, dosage as well as route of vitamin E supplementation for specific target populations.

Although alpha-tocopherol is transported by chylomicrons and very low density lipoproteins in the immediate and late postprandial phases, respectively, low density lipoproteins (LDL) and high density lipoproteins (HDL) are the main carriers of alpha-tocopherol in plasma and largely contribute to its delivery to cells and tissues [10]. Exchanges of alpha-tocopherol molecules occur between plasma lipoproteins and depend on the relative alpha-tocopherol content in each lipoprotein subpopulation [11, 12]. Alpha-tocopherol transfer between lipoproteins as well as between lipoproteins and cells may be facilitated by plasma proteins. Plasma phospholipid transfer protein (PLTP), member of the plasma lipid transfer protein family, has been reported to play a major role in the facilitation of alpha-tocopherol transfer between plasma lipoproteins as well as between lipoproteins and cells [13, 14], whereas the related cholesteryl ester transfer protein (CETP), has been reported not to facilitate alpha-tocopherol transfer [15].

Alpha-tocopherol exchanges may also occur, in both directions, between lipoproteins and intravenous lipid emulsion particles [16–18]. The relative importance of alpha-tocopherol net mass transfer from alpha-tocopherol rich lipid emulsion particles to LDL and HDL as well as the extent to which plasma factors facilitate these transfers have not been investigated in depth. In the present study, an in vitro model was used in which particles isolated from an alpha-tocopherol-enriched emulsion were incubated with total plasma or physiological concentrations of LDL or HDL in presence of non-lipid plasma fractions or purified transfer proteins. The aims were to determine: (i) the kinetics of alpha-tocopherol transfer from emulsion particles to plasma lipoproteins; (ii) the amount of alpha-tocopherol that can be acquired by LDL and HDL; (iii) the influence of proteins present in non-lipid plasma fractions on such alpha-tocopherol exchanges. Our data indicate that multiple mechanisms are involved in alpha-tocopherol mass transfer from lipid emulsions to plasma lipoproteins.

Material and Methods

Lipid Emulsion

A lipid emulsion (100 g triglycerides/l) containing a mixture of medium-chain triglycerides and long-chain triglycerides (1:1; w:w) with an elevated alpha-tocopherol content (10.70 ± 0.90 g/l) was prepared by B. Braun (Melsungen, Germany) for the purpose of this in vitro study. Since lipid emulsions contain a mixture of triglyceride-rich particles (TGRP) together with other particles formed from the excess of phospholipid emulsifier, the TGRP fraction was isolated by flotation in saline solution (NaCl 0.9%, EDTA 0.01%) through 3 × 30 min ultracentrifugation at 70,000 × *g* using a SW-41Ti rotor in a L8-55 ultracentrifuge (Beckman Instruments, Palo Alto, CA, USA). Approximately 90% of emulsion alpha-tocopherol content was recovered in the TGRP fraction. TGRP were stored overnight under nitrogen at 4 °C. In all incubation assays, TGRP were incubated at a triglyceride (TG) concentration of 100 mg/dL, a level commonly observed in the plasma of patients receiving parenteral nutrition with lipids [19].

Separation of LDL, HDL and Lipoprotein Poor Plasma Fraction

Lipoproteins (LDL and HDL) were separated from pooled normolipidemic human plasma by sequential ultracentrifugation [20] using a 50-2Ti rotor (Beckman, Palo Alto, CA, USA) in a L8-55 ultracentrifuge (Beckman). Plasma density was adjusted by addition of solid KBr at density ranges 1.025–1.055 and 1.070–1.18 g/mL for LDL and HDL, respectively. Plasma was centrifuged at 302,000 × *g* (5 °C) for 20 h for LDL and for another 40 h for HDL separation. The isolated lipoprotein fractions were then extensively dialysed against a saline solution (NaCl 0.9%, EDTA 0.01%, glycerol 10%, pH 7.4) and stored under nitrogen at −70 °C until incubation assays. Glycerol present in LDL and HDL fractions was removed by filtration on PD10 Sephadex columns (Amersham Pharmacia, Uppsala, Sweden) prior to incubation.

The lipoprotein poor plasma (LPP) fraction, containing the majority of plasma proteins, was also separated by sequential ultracentrifugation. Plasma density was adjusted at $d > 1.24$ g/mL and centrifuged during 40 h at 302,000 × *g* (5 °C) to remove all lipoproteins. After ultracentrifugation, the LPP fraction was extensively dialysed against a saline solution (NaCl 0.9%, EDTA 0.01%, pH 7.4) and stored under nitrogen at −20 °C until incubation assays.

Incubation Protocols

Alpha-tocopherol Mass Transfer from Lipid Emulsion Particles to LDL and HDL

To determine the kinetics of alpha-tocopherol net mass transfer from emulsion particles to plasma lipoproteins, TGRP (100 mg TG/dL) were incubated at 37 °C in presence of LDL (120 mg LDL-cholesterol/dL) or HDL (50 mg HDL-cholesterol/dL) over increasing time periods (0.5, 1, 2, 4 h) in a gently shaking water bath. Incubations were performed in absence or presence of human LPP (65 g protein/l). Furthermore, a few incubations were performed over 20 h in presence of LPP to determine the sub-maximal amount of alpha-tocopherol that can be acquired by LDL and HDL. Finally, TGRP were incubated in total plasma (with a LDL-cholesterol/HDL-cholesterol ratio of 1.2:1) to determine alpha-tocopherol partitioning between LDL and HDL. At the end of the incubation period, the TGRP fraction was isolated by flotation (ultracentrifugation of 45 min at 80,000 × *g* at 12 °C) from the infranatant containing the lipoproteins and LPP. After adjusting the density of the infranatant, individual lipoprotein fractions were isolated by sequential ultracentrifugation. Each collected fraction was stored at 4 °C for lipid analyses and aliquots of 300 µl were stored under nitrogen at −70 °C for vitamin E analyses performed within 2 weeks. Vitamin E content in LDL and HDL was expressed relative to particle lipid (total cholesterol + TG) content. Net alpha-tocopherol enrichment in LDL and HDL was calculated by comparison to data from control incubations of lipoproteins over the same time periods but without TGRP. Alpha-tocopherol content in lipoproteins was not significantly modified after control incubations over 4 and 20 h, whether in absence or presence of LPP.

Influence of Non-lipid Plasma Components on Alpha-tocopherol Transfer

To assess the influence of proteins present in the LPP plasma fraction on alpha-tocopherol exchanges, TGRP (100 mg TG/dL) were incubated at 37 °C with LDL (120 mg LDL-cholesterol/dL) or HDL (50 mg HDL-cholesterol/dL) for 2 h in the absence or presence of human LPP (65 g protein/l). To distinguish the effect of PLTP from that of CETP, experiments were carried out with LPP heated for 1 h at 58 °C to inactivate PLTP activity [13, 21, 22], or with addition of a potent CETP inhibitor (synthetised according to the patent application:WO2006013048; F. Hoffmann-La Roche, Basel, Switzerland) to LPP and to total plasma. CETP inhibitor was used at a concentration of 212 nM corresponding to four times the IC50 for a complete inhibition of CETP activity in plasma samples (personal communication, Roche Basel). In parallel, experiments were carried out with LPP (65 g protein/l) isolated from pig plasma, the latter being largely devoid of CETP [23, 24] but not of PLTP activity [25], Finally, incubations were also performed in absence of LPP but with albumin as the most abundant plasma protein (40 g/l fatty acid-free BSA, Sigma Aldrich, Steinheim, Germany), and with partially purified PLTP (5–10 µg/mL, Cardiovascular Targets Inc., NY, USA). After incubation, lipoproteins were isolated by ultracentrifugation and their alpha-tocopherol content analysed. The enhancing action of non-lipid plasma components upon alpha-tocopherol transfer from emulsion particles to LDL and HDL was obtained by subtracting spontaneous transfer measured in incubations with no proteins.

Analytical Measurements

Total cholesterol (TC) and TG concentrations were measured in LDL and HDL fractions using enzymatic kits CHOD-PAP (Roche Diagnostics GmbH, Mannheim, Germany) and Triglycerides Glycerol blanked (Roche Diagnostics GmbH), respectively. For alpha-tocopherol measurements in LDL and HDL [26, 27], lipoproteins were saponified at 70 °C with alcoholic KOH followed by alpha-tocopherol extraction with hexane. Hexane was dried and the extract was dissolved in methanol:water (95/5, w/w). Alpha-tocopherol content in the extract was then measured by reverse-phase HPLC (Merck-Hitachi Ltd, Tokyo, Japan) using a Lichrospher column 100 RP 18 (125 $m^2 \times 4\ m^3$; LxID; Merck, Darmstadt, Germany) and a mobile phase of methanol:water (95/5, w/w) at a flow rate of 1.5 mL/min; alpha-tocopherol was monitored at 292 nm by a UV detector [28].

Phospholipid Transfer Activity Assay

Phospholipid transfer activity was assessed by measuring the transfer of 1,2 di-[1-14C]palmitoyl phosphatidylcholine (100 mCi/mmol, Amersham Biosciences, Buckinghamshire, UK) from small unilamellar liposomes to HDL particles [29, 30]. In brief, labeled liposomes (125 nmol of phospholipids) were incubated with HDL (250 µg proteins) and LPP (10 µl) or partially purified PLTP (20 µg, Cardiovascular Targets Inc., NY, USA) in a final volume of 400 µl. The percentage of transferred radioactivity to HDL was calculated after correcting for background radioactivity. In this assay, partially purified PLTP induced a 19% transfer of total radiolabelled phospholipids, after correction for spontaneous transfer (7%).

Statistical Analysis

Results are expressed as mean values ± SEM. Statistical analyses were made by using Students' *t* test. The statistical significance of differences between values was assessed by paired comparison of data recorded within each individual experiment.

Results

Alpha-tocopherol Mass Transfer from Lipid Emulsion Particles to LDL and HDL

Kinetics of alpha-tocopherol transfer from emulsion particles to plasma lipoproteins, were assessed by incubating LDL and HDL with TGRP over increasing time periods (0.5–4 h) (Fig. 2). In the absence of LPP fraction, spontaneous transfer of alpha-tocopherol from TGRP to LDL progressively increased LDL alpha-tocopherol content over time leading to an 80 ± 6% enrichment after 4 h (5.26 ± 0.63 vs 2.91 ± 0.27 µmol/mmol in control LDL; $p < 0.001$). Spontaneous alpha-tocopherol transfer also occurred from TGRP to HDL particles and induced a 163 ± 36% enrichment after 4 h incubation (15.34 ± 0.41 vs 6.22 ± 0.79 µmol/mmol in control HDL; $p < 0.02$). Addition of LPP markedly enhanced alpha-tocopherol transfer to LDL particles leading to an alpha-tocopherol enrichment of 359 ± 4% after 4 h (13.57 ± 0.83 vs 2.96 ± 0.20 µmol/mmol in control LDL; $p < 0.0001$). Addition of LPP fraction also enhanced alpha-tocopherol transfer to HDL particles leading to an alpha-tocopherol enrichment of 393 ± 20% after 4 h (30.38 ± 2.67 vs 6.24 ± 0.62 µmol/mmol in control HDL; $p < 0.001$). Therefore, some factor(s) contained in LPP stimulate alpha-tocopherol transfer to cholesterol-rich particles.

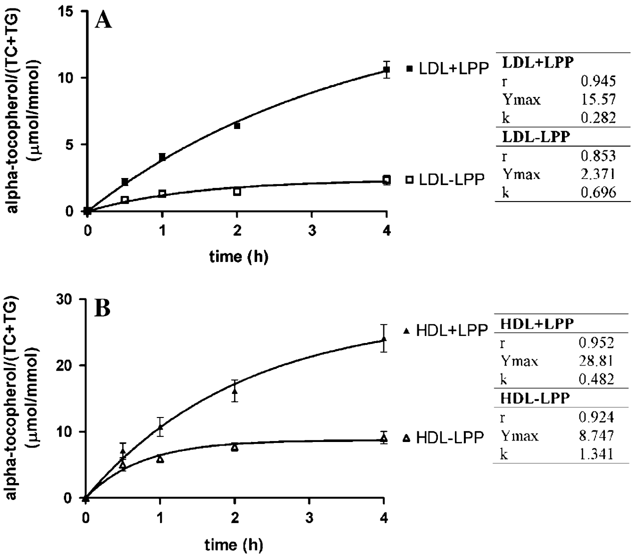

Fig. 2 The time course of alpha-tocopherol transfer over a 4 h incubation period from lipid emulsion particles to LDL (**a**) and HDL (**b**) in the absence and presence of human lipoprotein poor plasma fraction (LPP) was compatible with an exponential pattern according to the equation $Y = Y_{\max}(1 - e^{-kx})$. Equation in which Y represents the increment of alpha-tocopherol content compared to control conditions (lipoproteins incubated without TGRP), $Y_{\max}$ the maximal increment, k the rate constant and x the time (expressed as hours). In control incubations the absence vs presence of LPP did not modify the alpha-tocopherol content of control LDL (2.91 ± 0.27 vs 2.96 ± 0.2, $p > 0.8$) and HDL (6.22 ± 0.79 vs 6.24 ± 0.62, $p > 0.9$). Each point represents the mean ± SEM of 4 separate experiments. Also indicated is the correlation coefficient (r) between the mean experimental values and those derived from the above equation

As shown in Fig. 2, increases of LDL and HDL alpha-tocopherol content could be fitted to a single exponential equation, according to $Y = Y_{\max}(1 - e^{-kx})$, whether in presence or absence of LPP. The rate constant of alpha-tocopherol transfer was higher with HDL than with LDL, both in absence ($k = 0.48$ vs 0.28) and in presence of LPP ($k = 1.34$ vs 0.70). However, the enhancing effect of LPP on alpha-tocopherol transfer was more marked with LDL than with HDL (4.09 ± 0.59 fold for LDL and 2.09 ± 0.25 fold for HDL after 4 h incubation, $n = 16$; $p < 0.005$). Alpha-tocopherol enrichment in both LDL and HDL plateaud after 4 h incubation in absence but not in presence of LPP. When the incubation period was prolonged to 20 h in

Table 1 Alpha-tocopherol content of LDL and HDL after 20 h incubation

	Control (μmol/mmol)	20 h (μmol/mmol)
LDL + LPP	3.18 ± 0.21	27.53 ± 0.68
HDL + LPP	6.72 ± 0.28	47.37 ± 2.69

Alpha-tocopherol content of LDL and HDL particles after a 20 h incubation without (control) or with lipid emulsion particles and human lipoprotein poor plasma fraction (LPP). Alpha-tocopherol is expressed in relation to particles total cholesterol and triglyceride content (μmol/mmol). Results are means ± SEM of three separate experiments

Table 3 Phospholipid transfer activity

HDL + human LPP	22.5 ± 0.5
HDL + heated human LPP	5.3 ± 0.4
HDL + pig LPP	26.1 ± 0.2
HDL + heated pig LPP	20.7 ± 0.2

Lipoprotein poor plasma fraction (LPP) from human and pig plasma were compared for phospholipid transfer activity. Results are expressed as a percentage of total radiolabelled phospholipids (total count) which were transferred (after correcting for spontaneous transfer) from liposomes to HDL over a 30 min incubation period. Values are means ± SEM of two separate experiments

presence of LPP, alpha-tocopherol content further increased and led to an enrichment of 776 ± 83% in LDL and of 611 ± 73% in HDL ($p < 0.01$) (Table 1). In absolute values TGRP supplied 209 ± 9 μmol alpha-tocopherol in the incubation medium. After 4 h incubation in presence of LPP, ~15% of exogenous alpha-tocopherol was acquired by LDL (31 ± 3 μmol) or HDL (26 ± 2 μmol). After 20 h incubation in presence of LPP, the amount acquired by LDL (113 ± 16 μmol) or HDL (89 ± 7 μmol) corresponded to ~50% of exogenous alpha-tocopherol.

Finally, when TGRP were incubated in whole plasma for 4 h, a comparable alpha-tocopherol enrichment of ~75% was observed in both LDL (from 3.50 ± 0.14 to 6.06 ± 0.08 μmol/mmol, $n = 4$; $p < 0.0001$) and HDL (from 6.05 ± 0.11 to 10.72 ± 0.23 μmol/mmol, $n = 4$; $p < 0.0001$).

Influence of Non-lipid Plasma Components on Alpha-tocopherol Transfer

Since substantial alpha-tocopherol transfers to plasma lipoproteins were observed within 2 h incubation (and since the residence time of TG-rich emulsion particles in the circulation does not exceed 2 h), further experiments to characterise the influence of LPP proteins on alpha-tocopherol transfer were performed over 2 h.

Addition of human albumin did not facilitate alpha-tocopherol transfer from emulsion particles to LDL and HDL compared to spontaneous transfer ($p > 0.2$) (Table 2).

Heating the human LPP fraction at 58 °C for 1 h to inactivate PLTP activity almost completely abolished phospholipid-specific transfer activity as indicated by the transfer radioassay (Table 3). As shown in Fig. 2, alpha-tocopherol transfer from TGRP to LDL was lower in presence of heat-inactivated compared to normal LPP (6.20 ± 0.41 vs 8.94 ± 0.32 μmol/mmol; $n = 4$; $p < 0.01$). This suggests that 36 ± 6% of the enhancing action of human LPP on alpha-tocopherol transfer (calculated by subtracting spontaneous transfer from facilitated transfer) was due to heat sensitive factor(s), presumably PLTP. Alpha-tocopherol transfer from TGRP to HDL particles was also lower after heat inactivation of human LPP (11.35 ± 0.32 *vs* 13.46 ± 0.38 μmol/mmol; $n = 5$; $p < 0.005$); indicating that 27 ± 3% of the enhancing action of human LPP on alpha-tocopherol transfer to HDL was due to heat sensitive factor(s) (Fig. 3).

Addition of partially purified PLTP tended to increase alpha-tocopherol net transfer from TGRP to LDL (18.5 ± 8.5%; NS) and HDL (7.3 ± 2.8%; NS).

LPP fraction from pig plasma (devoid of functional CETP) induced comparable transfer of radiolabelled phospholipids as human LPP (Table 3); however, alpha-tocopherol mass transfer to LDL was lower with pig *vs* human LPP (5.29 ± 0.55 *vs* 7.94 ± 0.32 μmol/mmol; $n = 6$; $p < 0.001$). Hence, the enhancing effect of pig LPP on alpha-tocopherol transfer to LDL represented 55 ± 10% of that induced by human LPP. Surprisingly, heat inactivation had only a limited effect on reducing phospholipid specific transfer activity in pig LPP (Table 3). Consistently, prior heating of pig LPP did not significantly reduce alpha-tocopherol transfer ($p > 0.6$ by comparison to non-heated

Table 2 Influence of albumin on alpha-tocopherol transfer

	Control (μmol/mmol)	TGRP (μmol/mmol)	TGRP + albumin (μmol/mmol)	TGRP + LPP (μmol/mmol)
LDL	3.44 ± 0.14	5.30 ± 0.27	5.63 ± 0.19	12.20 ± 0.15
HDL	7.29 ± 0.07	13.94 ± 0.20	11.19 ± 1.32	18.80 ± 0.70

Alpha-tocopherol content of LDL and HDL particles incubated without (control) or with TGRP in presence of albumin or human lipoprotein poor plasma (LPP). Alpha-tocopherol is expressed in relation to particles total cholesterol and triglyceride content (μmol/mmol). Results are means ± SEM of three separate experiments

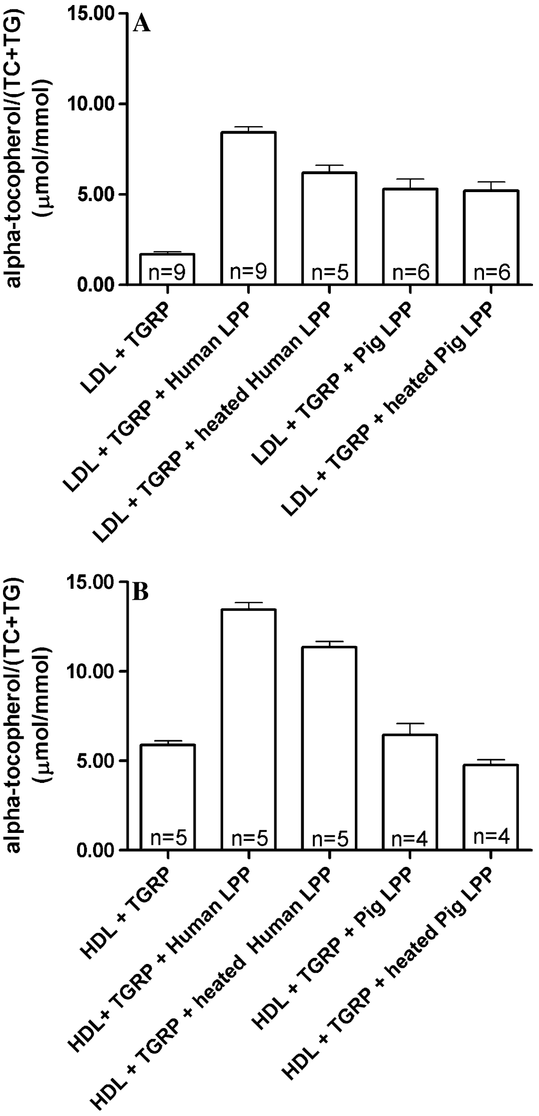

Fig. 3 Influence of lipoprotein poor plasma fraction (LPP) on alpha-tocopherol transfer from emulsion particles (TGRP) to LDL (**a**) and HDL (**b**). LDL (120 mg/dL) and HDL (50 mg/dL) were incubated for 2 h at 37 °C in absence and presence of human or pig LPP (65 g protein/l). All available values collected in each set of experiments are expressed as means ± SEM and represent the increment of alpha-tocopherol content compared to control conditions (lipoproteins incubated without TGRP). Compared to alpha-tocopherol facilitated transfer by human LPP substitution with heated human LPP ($p < 0.01$ for LDL and $p < 0.005$ for HDL), or with pig LPP ($p < 0.001$ for LDL and $p < 0.002$ for HDL), or with heated pig LPP ($p < 0.002$ for LDL and $p < 0.001$ for HDL) led to significantly reduced alpha-tocopherol transfer

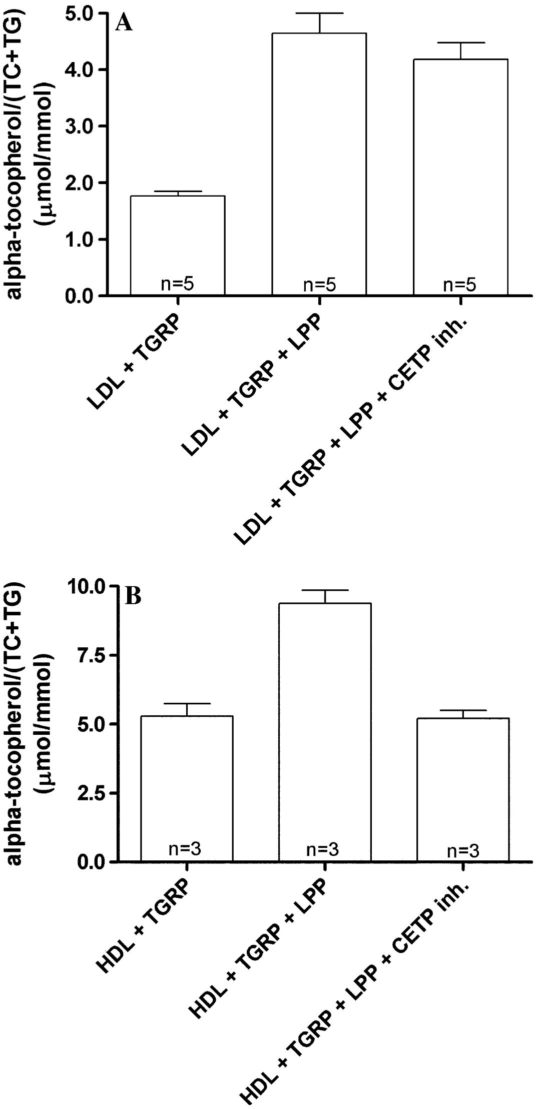

Fig. 4 Effect of a specific CETP inhibitor on alpha-tocopherol facilitated transfer from emulsion particles (TGRP) to LDL (**a**) and HDL (**b**). LDL (120 mg/dL) and HDL (50 mg/dL) were incubated for 2 h at 37 °C in absence or presence of human LPP (65 g protein/l) and CETP inhibitor (CETP inh. 212 nM). All available values collected in each set of experiments are expressed as means ± SEM and represent the increment of alpha-tocopherol content compared to control conditions (lipoproteins incubated without TGRP). Compared to alpha-tocopherol facilitated transfer by human LPP addition of CETP inhibitor significantly reduced alpha-tocopherol transfer to LDL ($p < 0.03$) or HDL ($p < 0.03$)

pig LPP; $n = 6$). In incubations of TGRP with HDL, alpha-tocopherol transfer was also much lower in presence of pig vs human LPP (6.44 ± 0.64 vs 13.59 ± 0.46 µmol/mmol; $n = 4$; $p < 0.002$). A limited enhancing action of pig LPP on alpha-tocopherol transfer was observed in only 3 out of 4 individual experiments. Even in these 3 experiments, this represented only 13.6 ± 2.9% of the facilitated transfer observed with human LPP within the same experiments ($p < 0.005$). Prior heating suppressed the modest enhancing action of pig LPP on alpha-tocopherol transfer to HDL particles ($p < 0.05$).

As shown in Fig. 4, addition of a specific CETP inhibitor to incubations of TGRP with LDL, reduced alpha-tocopherol facilitated transfer to LDL by ~11% (4.18 ± 0.30 vs 4.65 ± 0.35 µmol/mmol; $n = 5$; $p < 0.03$). In incubations with HDL, however, CETP inhibition markedly lowered

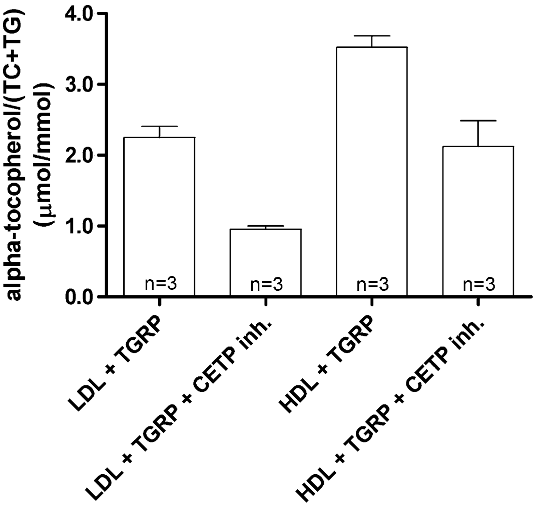

Fig. 5 Effect of a specific CETP inhibitor on alpha-tocopherol transfer from emulsion particles (TGRP) to LDL and HDL in total plasma. Total plasma (C) was incubated for 2 h at 37 °C in absence or presence of CETP inhibitor (CETP inh. 212 nM). At the end of the incubation period, LDL and HDL were isolated from total plasma. All available values collected in each set of experiments are expressed as means ± SEM and represent the increment of alpha-tocopherol content compared to control conditions (lipoproteins isolated from plasma that was incubated without TGRP). Addition of CETP inhibitor to total plasma significantly reduced alpha-tocopherol transfer to both LDL ($p < 0.03$) and HDL ($p < 0.04$)

alpha-tocopherol facilitated transfer to HDL (5.21 ± 0.30 vs 9.38 ± 0.48 µmol/mmol; $n = 3$; $p < 0.03$). Addition of CETP inhibitor to total plasma reduced by ~50% the transfer of alpha-tocopherol from TGRP to LDL (0.96 ± 0.05 vs 2.25 ± 0.16 µmol/mmol; $n = 3$; $p < 0.03$) and HDL (2.12 ± 0.36 vs 3.52 ± 0.16 µmol/mmol; $n = 3$; $p < 0.04$) (Fig. 5).

Discussion

Previous experiments studying alpha-tocopherol transfer between plasma lipoproteins have mainly used radiolabelled transfer assays and have generally focused on evaluating the effect of single mechanisms susceptible to facilitate alpha-tocopherol transfer [11, 13, 15]. The present study measures mass transfers of alpha-tocopherol from an artificial lipid emulsion to LDL and HDL and investigates the potential for several mechanisms to mediate such transfers. An in vitro model of incubation was used with an emulsion markedly enriched in alpha-tocopherol to avoid a rate-limiting availability of alpha-tocopherol when assessing mass transfers. In the different experiments, the emulsion lipid concentration was maintained at a relatively low level and lipoprotein concentration was comparable to that commonly found in the circulation. The range of incubation periods generally covered the residence time of emulsion particles in plasma.

In the first part of this study, alpha-tocopherol mass transfer from emulsion particles to lipoproteins was measured over increasing time periods. Incubations of alpha-tocopherol-rich emulsion particles together with either LDL or HDL resulted in a rapid net mass transfer of alpha-tocopherol to both plasma lipoprotein fractions. In absence of non-lipid plasma components, spontaneous alpha-tocopherol transfer was already detected after ≤1 h incubation and led to sub-maximal alpha-tocopherol enrichment after 4 h in LDL (+~80%) and HDL (+~160%). The higher spontaneous transfer to HDL may be related to the larger surface to volume ratio of HDL compared to LDL particles, which increases the available accepting surface for alpha-tocopherol molecules. To our knowledge, this is the first study to report such significant spontaneous alpha-tocopherol mass transfer from lipid emulsions to plasma lipoproteins. These observations differ from previous data of Desrumaux et al. [14] who did not detect spontaneous mass transfer between lipoproteins. However, these authors used for their transfer experiments lipoproteins depleted of alpha-tocopherol by oxidation, a procedure that may considerably modify particle surface and capacity for accommodating extra-alpha-tocopherol. Kostner et al. [13] who reported spontaneous transfer of radiolabelled alpha-tocopherol between plasma lipoproteins, showed that the addition of LPP accelerated alpha-tocopherol transfer without a net increase in lipoprotein alpha-tocopherol enrichment over spontaneous transfer. In our experiments, addition of LPP fraction not only accelerated but also increased the maximal amount of alpha-tocopherol transferred to LDL and HDL. In this condition, enrichment was not sub-maximal after 4 h incubation and alpha-tocopherol content could be further increased to almost 10 fold in both lipoproteins when incubation period was prolonged to 20 h.

Incubations with total plasma (containing LDL and HDL at a 1.2:1 cholesterol ratio) led to a comparable enrichment (~75% after 4 h) in both lipoprotein fractions, suggesting a competition between LDL and HDL fractions for alpha-tocopherol acquisition. All together, this data indicates that, at a fixed concentration of alpha-tocopherol provided by emulsion particles, the limiting factor for alpha-tocopherol enrichment is not the capacity of plasma lipoproteins to accommodate extra-amounts of alpha-tocopherol but rather the facilitating effect of non-lipid plasma components on alpha-tocopherol transfer, the residence time of emulsion particles and possibly the competition between different acceptor particles.

In the second part of this study the influence of individual or groups of proteins was assessed in relation to facilitating alpha-tocopherol transfer. Results of experiments using addition of heat inactivated LPP, of partially purified PLTP, of pig LPP and of CETP inhibitor suggest that the facilitating effect of LPP on alpha-tocopherol transfer from emulsion particles to plasma lipoproteins is not related to a single protein but rather to several non-lipid components present in the LPP fraction. This observation is at variance with previous papers suggesting an exclusive role for PLTP in enhancing vitamin E exchanges between plasma lipoproteins (together with surface phospholipids) [13], as well as between lipoproteins and cells [14]. Indeed, inactivation of PLTP activity by heating human LPP for 1 h at 58 °C reduced alpha-tocopherol transfer from emulsion particles by only ~40% in the case of LDL and ~30% in the case of HDL by comparison to experiments with non heated LPP. Moreover, addition to the incubation medium of partially purified PLTP (with maintained phospholipid-specific transfer activity) did not substantially increase alpha-tocopherol net mass transfer, although our model does not take into account alpha-tocopherol back transfers. Overall these results confirm a role for PLTP in alpha-tocopherol transfer facilitation but indicate that $\geq$50% of alpha-tocopherol transfer facilitation by human LPP is due to components other than heat-sensitive PLTP. This leads to question the role of heat-resistant lipid transfer proteins such as CETP. Granot et al. [15] who evaluated the role of purified CETP in alpha-tocopherol transfer between plasma lipoproteins did not report a facilitating effect of CETP. Nevertheless, this study used radiolabelled alpha-tocopherol which may not have distributed normally throughout the lipoprotein particles, did not assay for mass transfers and measured alpha-tocopherol transfer over relatively long incubation periods which would promote back transfers; these factors could explain the lack of effect of CETP. In our experiments using pig LPP with PLTP activity comparable to human LPP but deficient in CETP, alpha-tocopherol enrichment in LDL and HDL was much lower (~50%) than that facilitated by human LPP. This data again supports the point that alpha-tocopherol transfer from emulsion particles to plasma lipoproteins is facilitated not only by PLTP but also by other transfer proteins, and possibly CETP. Indeed, addition of a specific CETP inhibitor to incubation assays with LDL or HDL, or with total plasma, significantly reduced alpha-tocopherol transfer facilitated by human LPP. The reduction of alpha-tocopherol facilitated transfer was more marked for HDL when lipoproteins were incubated separately. However, addition of CETP inhibitor to total plasma, reduced by ~50% alpha-tocopherol transfer to both LDL and HDL particles. Hence, these experiments using a specific CETP inhibitor also support a role for CETP in alpha-tocopherol transfer from emulsion particles to plasma LDL and HDL. In addition to transfer proteins, lipoprotein lipase may facilitate alpha-tocopherol exchange between lipoproteins during the lipolytic process [27, 31]. This was not tested in the in vitro model used in the present study.

The present study demonstrates a very high capacity of LDL and HDL to accommodate extra-amounts of alpha-tocopherol by rapid transfer from an alpha-tocopherol enriched emulsion. Such increased alpha-tocopherol content in LDL and HDL may facilitate subsequent alpha-tocopherol delivery to cells and tissues. The emulsion used in this study was prepared for these in vitro experiments and not as a component of parenteral nutrition. However, similar alpha-tocopherol enriched preparations could be developed in view of intravenous bolus injections in patients with increased alpha-tocopherol requirements associated to acute conditions. If supported by evidence-based data, intravenous administration of emulsions with extra-alpha-tocopherol may find an indication in critically ill patients (injury, trauma, sepsis, ischemia, or severe inflammation) who consistently show reduced numbers of circulating LDL and HDL particles and are at high risk of oxidative tissue injury [32]. Furthermore, using intravenous emulsions as suppliers of alpha-tocopherol allows to bypass intestinal absorption which may be a limiting factor for alpha-tocopherol supplementation particularly in critically ill patients [33–35].

In conclusion, the present study demonstrates rapid and substantial mass transfer of alpha-tocopherol from an alpha-tocopherol rich lipid emulsion to plasma lipoproteins. Our data further indicates that alpha-tocopherol mass transfer is mediated by multiple mechanisms and that this transfer is largely facilitated not only by PLTP but also by other non-lipid factors present in plasma.

Acknowledgments M. Hacquebard is recipient of a fellowship from the Danone Institute, Belgium. Prof. R.J. Deckelbaum receives support from NIH grant #HL40404. The authors gratefully thank Dr. E. Niesor and Dr. C. Maugeais (F. Hoffmann-La Roche, Basel, Switzerland) for kindly providing CETP inhibitor and related information.

References

1. Traber MG, Packer L (1995) Vitamin E: beyond antioxidant function. Am J Clin Nutr 62:1501S–1509S
2. Ricciarelli R, Zingg JM, Azzi A (2002) The 80th anniversary of vitamin E: beyond its antioxidant properties. Biol Chem 383:457–465
3. Stampfer MJ, Hennekens CH, Manson JE, Colditz GA, Rosner B, Willett WC (1993) Vitamin E consumption and the risk of coronary disease in women. N Engl J Med 328:1444–1449
4. Rimm EB, Stampfer MJ, Ascherio A, Giovannucci E, Colditz GA, Willett WC (1993) Vitamin E consumption and the risk of coronary heart disease in men. N Engl J Med 328:1450–1456
5. Stephens NG, Parsons A, Schofield PM, Kelly F, Cheeseman K, Mitchinson MJ (1996) Randomised controlled trial of vitamin E in patients with coronary disease: Cambridge Heart Antioxidant Study (CHAOS). Lancet 347:781–786

6. Boaz M, Smetana S, Weinstein T, Matas Z, Gafter U, Iaina A, Knecht A, Weissgarten Y, Brunner D, Fainaru M, Green MS (2000) Secondary prevention with antioxidants of cardiovascular disease in endstage renal disease (SPACE): randomised placebo-controlled trial. Lancet 356:1213–1218
7. Yusuf S, Dagenais G, Pogue J, Bosch J, Sleight P (2000) Vitamin E supplementation and cardiovascular events in high-risk patients. The Heart Outcomes Prevention Evaluation Study Investigators. N Engl J Med 342:154–160
8. (1999) Dietary supplementation with n-3 polyunsaturated fatty acids, vitamin E after myocardial infarction: results of the GISSI-Prevenzione trial. Gruppo Italiano per lo Studio della Sopravvivenza nell'Infarto miocardico. Lancet 354:447–455
9. Miller ER 3rd, Pastor-Barriuso R, Dalal D, Riemersma RA, Appel LJ, Guallar E (2005) Meta-analysis: high-dosage vitamin E supplementation may increase all-cause mortality. Ann Intern Med 142:37–46
10. Behrens WA, Thompson JN, Madere R (1982) Distribution of alpha-tocopherol in human plasma lipoproteins. Am J Clin Nutr 35:691–696
11. Traber MG, Lane JC, Lagmay NR, Kayden HJ (1992) Studies on the transfer of tocopherol between lipoproteins. Lipids 27:657–663
12. Kayden HJ, Traber MG (1993) Absorption, lipoprotein transport, and regulation of plasma concentrations of vitamin E in humans. J Lipid Res 34:343–358
13. Kostner GM, Oettl K, Jauhiainen M, Ehnholm C, Esterbauer H, Dieplinger H (1995) Human plasma phospholipid transfer protein accelerates exchange/transfer of alpha-tocopherol between lipoproteins and cells. Biochem J 305(Pt 2):659–667
14. Desrumaux C, Deckert V, Athias A, Masson D, Lizard G, Palleau V, Gambert P, Lagrost L (1999) Plasma phospholipid transfer protein prevents vascular endothelium dysfunction by delivering alpha-tocopherol to endothelial cells. Faseb J 13:883–892
15. Granot E, Tamir I, Deckelbaum RJ (1988) Neutral lipid transfer protein does not regulate alpha-tocopherol transfer between human plasma lipoproteins. Lipids 23:17–21
16. Traber MG, Carpentier YA, Kayden HJ, Richelle M, Galeano NF, Deckelbaum RJ (1993) Alterations in plasma alpha- and gamma-tocopherol concentrations in response to intravenous infusion of lipid emulsions in humans. Metabolism 42:701–709
17. Steephen AC, Traber MG, Ito Y, Lewis LH, Kayden HJ, Shike M (1991) Vitamin E status of patients receiving long-term parenteral nutrition: is vitamin E supplementation adequate? JPEN J Parenter Enteral Nutr 15:647–652
18. Kelly FJ, Sutton GL (1989) Plasma and red blood cell vitamin E status of patients on total parenteral nutrition. JPEN J Parenter Enteral Nutr 13:510–515
19. Richelle M, Rubin M, Kulapongse S, Deckelbaum RJ, Elwyn DH, Carpentier YA (1993) Plasma lipoprotein pattern during long-term home parenteral nutrition with two lipid emulsions. JPEN J Parenter Enteral Nutr 17:432–437
20. Havel RJ, Eder HA, Bragdon JH (1955) The distribution and chemical composition of ultracentrifugally separated lipoproteins in human serum. J Clin Invest 34:1345–1353
21. Albers JJ, Tollefson JH, Chen CH, Steinmetz A (1984) Isolation and characterization of human plasma lipid transfer proteins. Arteriosclerosis 4:49–58
22. Jauhiainen M, Setala NL, Ehnholm C, Metso J, Tervo TM, Eriksson O, Holopainen JM (2005) Phospholipid transfer protein is present in human tear fluid. Biochemistry 44:8111–8116
23. Ha YC, Barter PJ (1982) Differences in plasma cholesteryl ester transfer activity in sixteen vertebrate species. Comp Biochem Physiol B 71:265–269
24. Speijer H, Groener JE, van Ramshorst E, van Tol A (1991) Different locations of cholesteryl ester transfer protein and phospholipid transfer protein activities in plasma. Atherosclerosis 90:159–168
25. Pussinen PJ, Olkkonen VM, Jauhiainen M, Ehnholm C (1997) Molecular cloning and functional expression of cDNA encoding the pig plasma phospholipid transfer protein. J Lipid Res 38:1473–1481
26. Hatam LJ, Kayden HJ (1979) A high-performance liquid chromatographic method for the determination of tocopherol in plasma and cellular elements of the blood. J Lipid Res 20:639–645
27. Traber MG, Olivecrona T, Kayden HJ (1985) Bovine milk lipoprotein lipase transfers tocopherol to human fibroblasts during triglyceride hydrolysis in vitro. J Clin Invest 75:1729–1734
28. Traber MG, Kayden HJ (1989) Preferential incorporation of alpha-tocopherol vs gamma-tocopherol in human lipoproteins. Am J Clin Nutr 49:517–526
29. Damen J, Regts J, Scherphof G (1982) Transfer of [14C]phosphatidylcholine between liposomes and human plasma high density lipoprotein. Partial purification of a transfer-stimulating plasma factor using a rapid transfer assay. Biochim Biophys Acta 712:444–452
30. Lagrost L, Athias A, Gambert P, Lallemant C (1994) Comparative study of phospholipid transfer activities mediated by cholesteryl ester transfer protein and phospholipid transfer protein. J Lipid Res 35:825–835
31. Tall AR, Krumholz S, Olivecrona T, Deckelbaum RJ (1985) Plasma phospholipid transfer protein enhances transfer and exchange of phospholipids between very low density lipoproteins and high density lipoproteins during lipolysis. J Lipid Res 26:842–851
32. Nathens AB, Neff MJ, Jurkovich GJ, Klotz P, Farver K, Ruzinski JT, Radella F, Garcia I, Maier RV (2002) Randomized, prospective trial of antioxidant supplementation in critically ill surgical patients. Ann Surg 236:814–822
33. Seeger W, Ziegler A, Wolf HR (1987) Serum alpha-tocopherol levels after high-dose enteral vitamin E administration in patients with acute respiratory failure. Intensive Care Med 13:395–400
34. Kelly FJ (1994) Vitamin E supplementation in the critically ill patient: too narrow a view? Nutr Clin Pract 9:141–145
35. Berger MM, Berger-Gryllaki M, Wiesel PH, Revelly JP, Hurni M, Cayeux C, Tappy L, Chiolero R (2000) Intestinal absorption in patients after cardiac surgery. Crit Care Med 28:2217–2223

Lipids (2008) 43:673–679
DOI 10.1007/s11745-008-3193-2

ORIGINAL ARTICLE

The ApoC-I Content of VLDL Particles is Associated with Plaque Size in Persons with Carotid Atherosclerosis

**Ann-Trude With Notø · Ellisiv Bøgeberg Mathiesen ·
Jan Brox · Johan Björkegren · John-Bjarne Hansen**

Received: 22 November 2007 / Accepted: 2 April 2008 / Published online: 29 May 2008
© AOCS 2008

Abstract Previous studies have shown that postprandial triglyceride-rich lipoproteins (TRLs) are enriched with apolipoprotein-C-I (apoC-I) in healthy individuals with increased intima-media thickness and in patients with coronary artery disease. The purpose of the present study was to determine apoC-I in TRL in persons with carotid atherosclerosis and its relation to plaque area. A population-based case ($n = 42$)-control ($n = 39$) study was conducted in persons with carotid atherosclerosis, assessed by B-mode ultrasound, and healthy controls. VLDL (Sf 20–400) was isolated in the fasting state and 4 h after ingestion of a standard fat meal. In the fasting state, persons with carotid atherosclerosis had increased number of apoC-I per VLDL-particle compared to persons without carotid atherosclerosis (8.6 ± 5.4 vs. 6.3 ± 4.2, $P = 0.018$). Total plaque area increased linearly ($P = 0.017$) across tertiles of apoC-I per VLDL-particle. In the postprandial state, a similar increase in the number of apoC-I per VLDL-particle occurred in both cases and controls ($P < 0.001$), but no significant difference was observed between groups. The number of apoC-I per VLDL-particle in the fasting state was accompanied by delayed clearance of TRL in the postprandial state, and associated with cholesterol enrichment of the VLDL-particles. Our findings support the concept that the number of apoC-I per VLDL-particle may be of importance for initiation and progression of atherosclerosis.

Key words Carotid arteries · Atherosclerosis · Plaque · Apolipoproteins · Lipids

Introduction

Elevated postprandial levels of triglyceride-rich lipoproteins (TRLs), i.e. chylomicrons (CM) and very low-density lipoproteins (VLDL) have been associated with both coronary [1] and carotid artery [2] atherosclerosis.

The metabolism of TRL particles is determined by their apolipoprotein (apo) and lipid composition, which affects their access to lipases and receptors [3, 4]. Hepatic removal of TRLs from the circulation is mediated by apoB100 and apoE [5], and lack of apoE leads to accumulation of chylomicron remnants [6]. Triglycerides in the core of TRL in circulating blood are hydrolyzed by the action of endothelial cell-bound lipoprotein lipase (LPL). Low LPL activity can be due to reduced mass or specific activity of LPL or its activator protein apoC-II. Low LPL activity, as encountered in patients with LPL deficiency, is associated with increased plasma levels of chylomicrons, [7] premature atherosclerosis and accelerated progression of atherogenesis [8].

A.-T. W. Notø · J.-B. Hansen (✉)
Department of Medicine, Center for Atherothrombotic Research in Tromsø, Institute of Clinical Medicine, University of Tromsø, 9037 Tromsø, Norway
e-mail: John.Bjarne.Hansen@unn.no

A.-T. W. Notø
e-mail: anntrude@fagmed.uit.no

E. B. Mathiesen
Department of Neurology, Institute of Clinical Medicine, University of Tromsø, Tromsø, Norway

J. Brox
Department of Clinical Chemistry, University of Tromsø, Tromsø, Norway

J. Björkegren
Department of Medicine, The Computational Medicine group, The Atherosclerosis Research Unit, Karolinska Institutet, Stockholm, Sweden

Members of the apolipoprotein-C family are of major importance for the metabolism of postprandial TRLs. ApoE-mediated binding of TRLs to receptors is inhibited by apoC-I and apoC-III, [9] and experimental studies have shown that apoC-I displaces apoE from TRL and thereby delays their hepatic uptake [10, 11]. Furthermore, apoC-II promotes and apoC-III attenuates the hydrolysis of TRLs by lipoprotein lipase (LPL) [12]. Enrichment of TRLs with apoC-I is associated with a proatherogenic composition of the particles by increasing the cholesterol/triglyceride ratio due to prolonged half-life of TRL remnants in the circulation [13].

Postprandial TRL is enriched with apoC-I in patients with coronary artery disease, [14] in healthy individuals with increased intima-media thickness (IMT) [15] and is an independent predictor for IMT in normolipidemic healthy middle-aged men [13]. These findings do suggest that the apoC-I content of TRL is a novel risk factor for early atherosclerosis and CAD. The purpose of the present study was to investigate the apoC-I in TRL in persons with carotid atherosclerosis and to determine the associations of the apoC-I in TRL with plaque area and morphology.

Material and Methods

Study Participants

The participants of the study were recruited from a population health study (the fifth survey of The Tromsø Study in 2001), which included ultrasound examination of the right carotid artery. Persons were eligible for the plaque group if they were aged 56–80 years and had one plaque or more in the carotid bifurcation or internal carotid artery at the screening with a plaque thickness of $\geq$2.5 mm. Persons in the same age groups without plaques in their carotid arteries were used as controls. Persons who responded positive to our invitation letter to participate in the study were invited to a screening visit. At the screening visit, a complete medical history, physical examination and blood samples were taken with special emphasis on exclusion criteria. A detailed interview on the occurrence of cerebrovascular and cardiovascular events, defined as prior or present transient ischemic attacks (TIA), stroke, amaurosis fugax, angina pectoris, myocardial infarction, peripheral vascular disease, and diabetes, smoking habits and drugs was obtained. Exclusion criteria were any of the following conditions: regular use of lipid-lowering drugs (HMG-CoA reductase inhibitors, resins or nicotinic acid derivates) or oral anticoagulants, cancer or other serious life- threatening medical conditions, hypothyroidism, renal, hepatic, or psychiatric disease, and current abuse of alcohol or drugs. Among eligible persons, 42 cases and 39 controls were invited to a second visit in which, an ultrasound examination of both carotid arteries was performed, and the participants were subjected to a fat tolerance test. Informed written consent was obtained from the participants, and the regional ethical committee approved the study. The study was performed at the Clinical Research Unit at the University Hospital of North-Norway.

Ultrasound Examination

At the population health screening, high-resolution B-mode and color Doppler/pulsed-wave Doppler ultrasonography of the right carotid artery was performed as described previously [16, 17]. A plaque was defined as a localized thickening of the vessel wall of more than 50% compared to the adjacent vessel wall thickness. As only the right carotid artery was examined at the screening, a new ultrasound examination of both carotid arteries was performed. These ultrasound examinations were performed by the same experienced examiner, and with the use of an Acuson Xp10 128 ART ultrasound scanner equipped with a linear array 5–7 MHz transducer.

Plaque morphology in terms of echogenicity was assessed by analysis of grey scale content of the plaques and calculation of grey scale median (GSM). Assessment of plaque size and morphology was made in all plaques present in the near and far walls of the common carotid, the bifurcation, and the internal carotid arteries on both sides (12 locations). All examinations and measurements of all plaques were recorded on videotapes. Stored B-mode images were subsequently transferred to a personal computer and digitized into frames of 768 × 576 pixels of 256 grey levels each (0 black and 256 white) with the use of a commercially available video grabber card (meteor II/Matrox Intellicam). Measurements of plaque area were made with the use of the Adobe Photoshop image-processing program (version 7.0.1), by tracing around the perimeter of each plaque with a cursor. The grey-level distribution and GSM of each plaque was calculated. Standardization of GSM was performed as previously described [18]. A fixed area of the lumen of the carotid artery (300 pixels), the brightest area of the innermost adventitia adjacent to the plaque (150 pixels), and the plaque were marked. The plaque image was normalized by adjusting linearly their grey tonal range so that the lumen was assigned a GSM of 1 and the adventitia 200. After standardization, the GSM of the plaques were recalculated. In persons with more than one plaque, the standardized GSM of the total plaque area was estimated as a weighted mean of the GSM value of each single plaque. The area of each plaque was divided by the total area of the plaques in each person, and this fraction was multiplied with each plaques normalized GSM value. All scores were added to calculate the total normalized GSM score for each person.

Fat Tolerance Test

A fat tolerance test was conducted using a test meal prepared from standard porridge cream containing 70% of calories from fat of which 66% saturated fat, 32% monounsaturated fat and 2% polyunsaturated fat. A weight-adjusted meal (1 g fat per kg body weight) was served at 8:00 a.m. and consumed over a 15 min period. The participants were allowed to drink 350 ml calorie-free beverages and eat an apple during the following 8 h. Blood samples for isolation of CM, VLDL, and serum- and plasma preparations were collected before the meal and every second hour during the next 8 h.

Blood Collection, Isolation of Triglyceride-rich Lipoproteins and Storage

Blood was drawn from an antecubital vein in the morning at 7:45 a.m. after 12 h overnight fasting and 2, 4, 6, and 8 h after the meal, using a 19 gauge needle in a vacutainer system with minimal stasis. Serum was prepared by clotting whole blood in a glass tube at room temperature for 1 h and then centrifuged at 2,000*g* for 15 min at 22 °C. Aliquots of 1 ml were transferred into sterile cryovials (Greiner laboratechnik, Nürtringen, Germany), flushed with nitrogen, and frozen at −70 °C until further analysis.

CM were isolated by over layering 8 ml EDTA plasma with 5 ml of NaCl solution (density 1.006 kg/L NaCl solution with 0.02% sodium azide and 0.01% EDTA) in a cellulose nitrate tube (Beckman Instruments Inc, CA, USA) and centrifuged in a Beckman SW40 Ti swinging bucket rotor at 20.000 rpm for 1 h at 4 °C. The CM, with Svedberg flotation (Sf) rates >400, were carefully removed by aspiration from the top of the tube. The baseline and 4 h plasma samples were relayered with 5 ml 1.006 kg/L NaCl solution and subjected to centrifugation at 40.000 rpm for 20 h at 20 °C. VLDL, with Sf 20−400, was carefully removed by aspiration from the top of the tube. TRL fractions were divided into three aliquots in cryovials, flushed with nitrogen, and frozen at −70 °C until further analysis.

Serum Lipid and Apolipoprotein Measurements

Serum lipids were analyzed on a Cobas Mira S (Roche Diagnostics, F. Hoffmann-La Roche Ltd, Basel, Switzerland) with reagents from ABX Diagnostics (Montpellier, France). Total cholesterol (CHOD-PAP) and triglycerides (GPO-PAP) were measured with enzymatic colorimetric methods. Low-density lipoprotein (LDL) and high-density lipoprotein cholesterol were measured by selective inhibition colorimetric assays (LDL cholesterol direct and HDL cholesterol direct, respectively, ABX Diagnostics). Serum apolipoprotein AI (apo-AI) and apolipoprotein-B (apo-B) were analyzed by turbidimetry on Cobas Mira S with reagents from ABX Diagnostics. Serum apolipoprotein E (apo E) was measured by an enzyme-linked immunosorbent assay, Apo-Tek ApoE^{TM} (PerImmune Inc., Rockville, MD, USA) and genotyping of Apo E was performed according to Hixson and Vernier [19] with slight modifications. An enzymatic immunoassay was used to measure apoC-I in isolated VLDL fractions [10].

Calculations and Statistics

The number of apoC-I per VLDL-particle was calculated by dividing apolipoprotein concentrations in density fraction S_f 20–400 by their respective molecular mass (apoB-100 = 549 kDa and apoC-I = 6.5 kDa). The fraction molarity of apoC-I was then divided by the corresponding molarity of apoB. Continuous variables were tested for normal distribution, and they were logarithmically transformed and expressed as geometric means if not normally distributed. Differences between the groups were analyzed by unpaired *t* test for continuous variables and χ^2 (Chi-square) tests for categorical variables. General linear models for univariate analysis of variance were used for adjustments. Pearson's correlation coefficients were used to examine correlations between continuous variables. Linear regression models were used to test linear trends. All analyses were performed using SPSS (SPSS Inc. Chicago, Illinois, USA) for windows software, version 14.0. Two-sided *P* values (<0.05) were considered statistically significant. Results are expressed as means ± 1 SD unless otherwise stated.

Results

Characteristics of the participants are shown in Table 1. Persons with carotid atherosclerosis were older ($P = 0.026$) and had a higher frequency of diabetes mellitus ($P = 0.006$), whereas the healthy controls tended to have higher BMI ($P = 0.075$). Fasting levels of total cholesterol, HDL cholesterol, triglycerides and apolipoproteins were not significantly different between groups, but LDL cholesterol ($P = 0.049$) and apolipoprotein-B ($P = 0.075$) tended to be higher in persons with carotid atherosclerosis. The frequencies of smoking, hypertension, presence of cardiovascular and cerebrovascular diseases and prescription of cardiovascular drugs were similar between groups. The apoE-genotype did not differ between groups, where 58% of the participants had the E3/3 isoform, 30% E3/4, 10% E2/3, 1% E4/4, 1% E2/4 and none had the E2/2 isoform.

Changes in concentrations of total and chylomicron triglycerides after ingestion of the test meal are shown in Fig. 1. Ingestion of a standard high fat meal caused a significant

Table 1 Baseline characteristics of persons with (n = 42) and without carotid atherosclerosis (n = 39) included in the study

Variables	Carotid stenosis	Controls	*P* values
Sex (% men)	60 (25)	51 (20)	0.51
Age (years)	70.7 ± 5.9	67.7 ± 6.3	0.026
Smoking (%)	19 (8)	23 (9)	0.79
Body mass index (kg/m^2)	25.8 ± 3.9	27.3 ± 3.6	0.075
Systolic blood pressure (mmHg)	129 ± 19	130 ± 17	0.86
Diastolic blood pressure (mmHg)	73 ± 10	75 ± 9	0.52
Total cholesterol (mmol/L)	6.54 ± 1.33	6.00 ± 1.19	0.058
HDL cholesterol (mmol/L)	1.80 ± 0.52	1.73 ± 0.44	0.51
LDL cholesterol (mmol/L)	4.16 ± 0.97	3.74 ± 0.90	0.049
Triglycerides (mmol/L)	1.20 ± 0.77	1.13 ± 0.49	0.61
Apolipoprotein-A1 (g/L)	1.42 ± 0.26	1.42 ± 0.22	0.91
Apolipoprotein-B (g/L)	1.12 ± 0.19	1.04 ± 0.21	0.075
Apolipoprotein-E (mg/L)	41.2 ± 14.9	44.6 ± 15.2	0.31
Hypertension (%)	40 (17)	38 (15)	1.00
Diabetes (%)	19 (8)	0 (0)	0.006
Coronary artery disease (%)	21 (9)	13 (5)	0.38
Cerebrovascular events (%)	7 (3)	5 (2)	1.00
Antihypertensive drugs (%)	38 (16)	33 (13)	0.82
Platelet inhibitors (%)	19 (8)	13 (5)	0.55
Omega-3FA (%)	43 (18)	59 (23)	0.18
Degree of stenosis (%)	39.4 ± 15.7		
Plaque thickness (mm)	3.15 ± 1.13		
Number of plaques	2.3 ± 1.6		
Total plaque area (mm^2)	6.1 ± 7.0		
Grey scale median (pixels)	63.5 ± 27.4		

Values are means ± 1SD or percentage with numbers in brackets

increase in total and chylomicron triglycerides, which peaked 4 h after the meal and returned to baseline levels after 8 h. Persons with carotid atherosclerosis had delayed clearance of total and chylomicron triglycerides 6 h (162.6 ± 89.1 μmol/L vs. 109.2 ± 83.7 μmol/L, $P = 0.028$) and 8 h (72.3 ± 52.7 μmol/L vs. 46.9 ± 38.0 μmol/L, $P = 0.017$) after the meal compared to persons without carotid atherosclerosis.

Plasma VLDL-particles, Sf 20–400, were isolated by preparative ultracentrifugation before and 4 h after intake of a standardized fat-enriched meal and analyzed for triglycerides, total cholesterol, apolipoprotein B and CI (Table 2). The fasting number of apoC-I per VLDL-particle was significantly higher in persons with carotid atherosclerosis compared to controls ($P = 0.013$). The difference between groups remained significant after adjustments for age, sex, BMI and diabetes mellitus ($P = 0.018$). Ingestion of the standard fat meal caused a significant increase in VLDL triglycerides ($P < 0.001$), VLDL cholesterol ($P < 0.001$), apoC-I concentration ($P < 0.001$) and the number of apoC-I molecules per VLDL-particle ($P < 0.001$) without differences between groups (Table 2). The number of apoC-I molecules per VLDL-particle at baseline was strongly correlated to the number of apoC-I molecules per VLDL-particle isolated four hrs after the meal both in persons with ($r = 0.53$, $P < 0.001$) and without ($r = 0.74$, $P < 0.001$) carotid atherosclerosis. Furthermore, significant correlations were found between the number of apoC-I molecules per VLDL-particle and VLDL cholesterol in the fasting state in persons with and without carotid atherosclerosis ($r = 0.64$, $P < 0.001$ and $r = 0.45$, $P = 0.006$, respectively) and in the postprandial state ($r = 0.41$, $P = 0.01$ and $r = 0.32$, $P = 0.03$, respectively). The levels of VLDL cholesterol and triglycerides at 4 h were not significantly different between groups.

Analyses of linear trends for change in total plaque area across tertiles of apoC-I per VLDL-particle showed that total plaque area ($P = 0.017$) increased with increasing number of apoC-I molecules per VLDL-particle, and this association remained significant after adjustments for age, sex, and BMI ($P = 0.012$) (Fig. 2). No relation was found between apoC-I per VLDL-particle and GSM.

Discussion

In the present study we found that the number of apoC-I per VLDL-particle in the fasting state was increased in persons with carotid atherosclerosis compared to persons

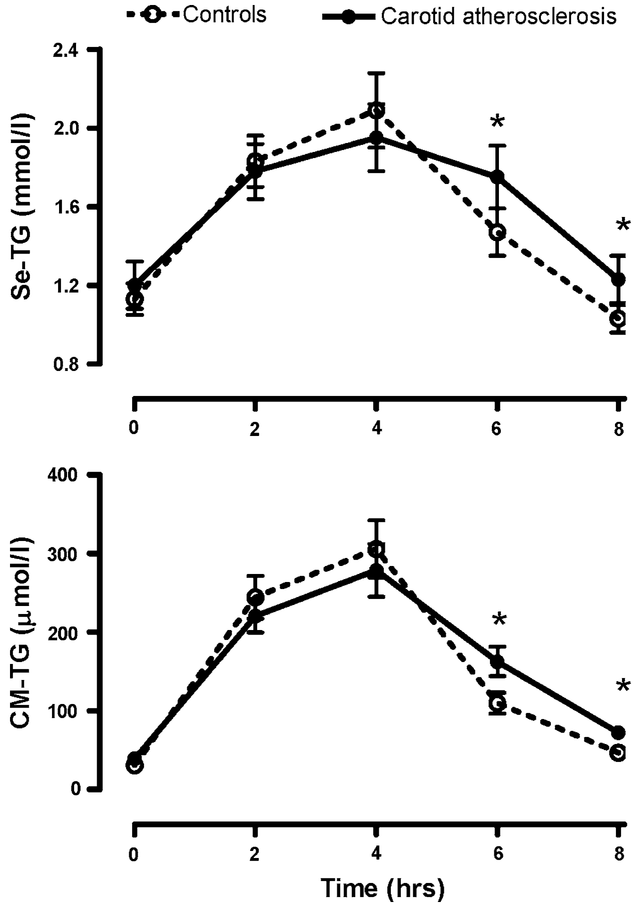

Fig. 1 *Line graph* showing postprandial concentrations of serum triglycerides (*upper panel*) and chylomicron triglycerides (*lower panel*) over time after a standard fat meal in persons with (n = 42) and without (n = 39) carotid atherosclerosis. Values are means ± SEM

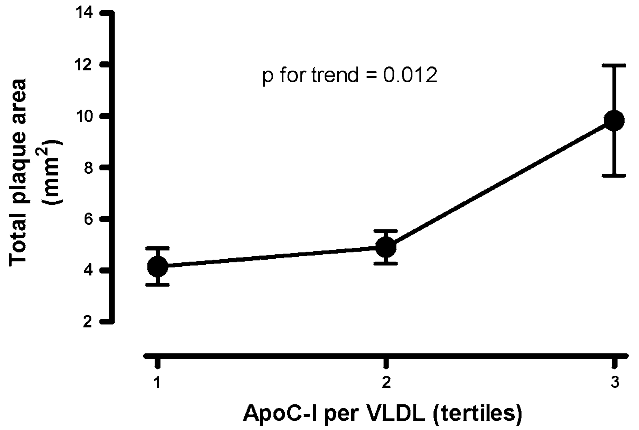

Fig. 2 *Line graph* showing the increase in total plaque area with increasing number of apoC-I per VLDL-particle under fasting condition in persons with (n = 42) and without (n = 39) carotid atherosclerosis. Values are means ± SEM. The number of apoC-I per VLDL-particle is divided in tertiles (mean, range); T1 (4.6, 3.1–5.7), T2 (6.9, 5.8–8.4), and T3 (14.3, 8.7–27.2)

without carotid atherosclerosis. Furthermore, within the atherosclerosis group, total plaque area was associated with the number of apoC-I per VLDL-particle. To the best of our knowledge, this is the first report that shows a significant linear relation between the number of apoC-I per VLDL-particle and carotid atherosclerotic plaques. These associations remained significant after adjustments for traditional atherosclerotic risk factors and the apoE-genotype. Our findings support the concept that the number of apoC-I per VLDL-particle may serve as an independent marker of carotid atherosclerosis and even play a pivotal role for initiation and progression of atherosclerosis.

In the fasting state, apoC-I is mostly associated with high-density lipoprotein and transferred to TRLs during the postprandial state [20]. In healthy volunteers, Björkegren and coworkers demonstrated a 75–150% transient increase of the number of apoC-I molecules per VLDL-particle, but not in chylomicron remnants, in the postprandial state [11]. In agreement with most studies in healthy individuals [11, 15] and patients with coronary artery disease [14], but not all, [13] we observed a pronounced increase in the number of apoC-I per VLDL-particle from the fasting to the postprandial state (Table 2). Furthermore, we found that the

Table 2 Composition of VLDL-particles isolated before and 4 h after intake of a standard high fat meal in persons with (n = 42) and without (n = 39) carotid atherosclerosis

Variables	Carotid atherosclerosis		Controls		Between groups (P values)	
	0 h	4 h	0 h	4 h	0 h	4 h
Triglycerides (mmol/L)	0.60 ± 0.51	0.94 ± 0.76***	0.48 ± 0.33	0.95 ± 0.58***	0.37	0.65
Cholesterol (mmol/L)	0.29 ± 0.23	0.34 ± 0.25**	0.26 ± 0.15	0.31 ± 0.15*	0.27	0.46
Apolipoprotein-B (mg/L)	45.1 ± 23.0	49.1 ± 27.8	44.6 ± 17.8	45.6 ± 20.1	0.44	0.50
Apolipoprotein CI (mg/L)	4.9 ± 3.2	7.3 ± 5.7***	3.3 ± 2.5	6.4 ± 4.7***	0.057	0.19
ApoC-I per VLDL-particle	8.6 ± 5.4	12.7 ± 6.9***	6.3 ± 4.2	11.5 ± 7.9***	0.018	0.27

Analyses of differences between groups were adjusted for age, gender, body mass index and presence of diabetes mellitus. Values are means ± 1 SD

Significance of difference within groups; *P < 0.05,**P < 0.01, ***P < 0.001

number of apoC-I per VLDL-particle in the fasting state was strongly correlated with the number of apoC-I per VLDL-particle in the postprandial state for both persons with and without carotid atherosclerosis. The latter observation may suggest that the number of apoC-I per VLDL-particle in the fasting state reflects the capacity for apoC-I transfer from high-density lipoprotein to VLDL in the postprandial state.

ApoC-I is known to inhibit apoE-mediated binding of TRLs to receptors, [9] and experimental studies have shown that apoC-I displaces apoE from TRL and thereby delays their hepatic uptake [10, 11]. Thus, delayed clearance of postprandial TRL in the present study and previous studies in patients with coronary and carotid atherosclerosis [1, 2, 14] may in part be explained by apoC-I enrichment of VLDL-particles. Delayed clearance of TRL will increase the time where CETP-mediated cholesterol ester-triglyceride exchange with HDL occur, and may thereby explain the present and previous [13–15] observed relation between apoC-I and cholesterol enrichment in these TRL particles.

Previous studies have shown a non-significant increase in the number of apoC-I per VLDL-particle in the fasting state of healthy individuals with increased intima-media thickness (IMT) [15] and in patients with coronary artery disease, [14] whereas our study showed a significant increase in the number of apoC-I per VLDL-particle in the fasting state in persons with carotid atherosclerosis. The reason for this apparent difference is unknown, but may in part be explained by differences in statistical power. The difference in the number of apoC-I per VLDL-particle was of similar magnitude in our and previous studies, but only 28–30 persons were included in the previous studies compared to 81 persons in the present study.

The most consistent and prominent finding in previous studies was that postprandial TRL was enriched with apo-C-I in patients with coronary artery disease, [14] in healthy individuals with increased intima-media thickness (IMT) [15] and was an independent predictor for IMT in normolipidemic healthy middle-aged men [13]. In contrast, we found a significant enrichment of VLDL with apoC-I in the fasting state among persons with carotid atherosclerosis, but only a tendency to enrichment of VLDL with apoC-I in the postprandial state. However, the total plaque area in persons with carotid atherosclerosis increased linearly with the number of apoC-I molecules per VLDL-particle both in the fasting and the postprandial state.

Many potential confounders may contribute to the apparent differences between our and previous findings. First, we isolated VLDL-particles from plasma 4 h after the meal in contrast to 6 h after the meal in those studies who reported an association between enrichment of TRL with apoC-I and IMT in the postprandial state. As delayed clearance [21] rather than increased peak levels [1, 2] of TRL are the most consistent finding in patients with atherosclerotic diseases in the postprandial state, isolation of VLDL-particles 4 h instead of 6 h after the meal may conceal potential differences between groups. Second, age, [22] BMI, [23] fasting triglycerides, [21, 23] apoE-genotype, [24] and severity of the atherosclerotic disease are all predictors for the increase in TRL in the postprandial state. We recruited participants with subclinical carotid plaques from a population-based survey in contrast to young myocardial infarction survivors and healthy individuals [13–15].In the previous studies [13–15] middle-aged men 45–55 years of age and only healthy males with the apoE3/E3 genotype were included. We recruited persons from an older age strata without predefined apoE-genotype criteria for inclusion. Furthermore, the difference in the number of apoC-I per VLDL-particle between groups and the linear relation between the number of apoC-I per VLDL-particle and plaque area remained significant after adjustments for traditional atherosclerotic risk factors and the apoE-genotype.

In conclusion, our study provides evidence for a pivotal role for the number of apoC-I per VLDL-particle in initiation and progression of atherosclerosis. Further experimental and clinical studies are warranted to elucidate the mechanism(s) by which enrichment of VLDL-particles with apoC-I affect the atherosclerotic process.

Acknowledgments The technical assistance of Hege Iversen Appelbom, Birgit Svensson and Kristin Sørensen is greatly appreciated. Ann-Trude With Notø was financed by a grant from the Norwegian Health Association. CART is supported by an independent grant from Pfizer AS. The study has received a grant from the Center for Research in Elderly in Tromsø.

References

1. Patsch JR, Miesenbock G, Hopferwieser T, Muhlberger V, Knapp E, Dunn JK, Gotto AM Jr, Patsch W (1992) Relation of triglyceride metabolism and coronary artery disease. Studies in the postprandial state. Arterioscler Thromb 12(11):1336–1345
2. Boquist S, Ruotolo G, Tang R, Bjorkegren J, Bond MG, de FU, Karpe F, Hamsten A (1999) Alimentary lipemia, postprandial triglyceride-rich lipoproteins, and common carotid intima-media thickness in healthy, middle-aged men. Circulation 100(7):723–728
3. Karpe F, Steiner G, Olivecrona T, Carlson LA, Hamsten A (1993) Metabolism of triglyceride-rich lipoproteins during alimentary lipemia. J Clin Invest 91(3):748–758
4. Bjorkegren J, Packard CJ, Hamsten A, Bedford D, Caslake M, Foster L, Shepherd J, Stewart P, Karpe F (1996) Accumulation of large very low-density lipoprotein in plasma during intravenous infusion of a chylomicron-like triglyceride emulsion reflects competition for a common lipolytic pathway. J Lipid Res 37(1):76–86
5. Mahley RW(1988) Apolipoprotein-E: cholesterol transport protein with expanding role in cell biology. Science 240(4852):622–630
6. Schaefer EJ, Gregg RE, Ghiselli G, Forte TM, Ordovas JM, Zech LA, Brewer HB Jr (1986) Familial apolipoprotein E deficiency. J Clin Invest 78(5):1206–1219

7. Brunzell JD, Miller NE, Alaupovic P, St Hilaire RJ, Wang CS, Sarson DL, Bloom SR, Lewis B (1983) Familial chylomicronemia due to a circulating inhibitor of lipoprotein lipase activity. J Lipid Res 24(1):12–19
8. Jukema JW, van Boven AJ, Groenemeijer B, Zwinderman AH, Reiber JH, Bruschke AV, Henneman JA, Molhoek GP, Bruin T, Jansen H, Gagne E, Hayden MR, Kastelein JJ (1996) The Asp9 Asn mutation in the lipoprotein lipase gene is associated with increased progression of coronary atherosclerosis. REGRESS Study Group, Interuniversity Cardiology Institute, Utrecht, The Netherlands. Regression Growth Evaluation Statin Study. Circulation 94(8):1913–1918
9. Jong MC, Hofker MH, Havekes LM (1999) Role of ApoCs in lipoprotein metabolism: functional differences between ApoC1, ApoC2, and ApoC3. Arterioscler Thromb Vasc Biol 19(3): 472–484
10. Bjorkegren J, Hamsten A, Milne RW, Karpe F (1997) Alterations of VLDL composition during alimentary lipemia. J Lipid Res 38(2):301–314
11. Bjorkegren J, Karpe F, Milne RW, Hamsten A (1998) Differences in apolipoprotein and lipid composition between human chylomicron remnants and very low-density lipoproteins isolated from fasting and postprandial plasma. J Lipid Res 39(7):1412–1420
12. LaRosa JC, Levy RI, Herbert P, Lux SE, Fredrickson DS (1970) A specific apoprotein activator for lipoprotein lipase. Biochem Biophys Res Commun 41(1):57–62
13. Hamsten A, Silveira A, Boquist S, Tang R, Bond MG, de FU, Bjorkegren J (2005) The apolipoprotein CI content of triglyceride-rich lipoproteins independently predicts early atherosclerosis in healthy middle-aged men. J Am Coll Cardiol 45(7):1013–1017
14. Bjorkegren J, Boquist S, Samnegard A, Lundman P, Tornvall P, Ericsson CG, Hamsten A (2000) Accumulation of apolipoprotein C–I-rich and cholesterol-rich VLDL remnants during exaggerated postprandial triglyceridemia in normolipidemic patients with coronary artery disease. Circulation 101(3):227–230
15. Bjorkegren J, Silveira A, Boquist S, Tang R, Karpe F, Bond MG, de FU, Hamsten A (2002) Postprandial enrichment of remnant lipoproteins with apoC-I in healthy normolipidemic men with early asymptomatic atherosclerosis. Arterioscler Thromb Vasc Biol 22(9):1470–1474
16. Joakimsen O, Bonaa KH, Stensland-Bugge E (1997) Reproducibility of ultrasound assessment of carotid plaque occurrence, thickness, and morphology. The Tromsø Study. Stroke 28(11): 2201–2207
17. Vik A, Mathiesen EB, Noto AT, Sveinbjornsson B, Brox J, Hansen JB (2006) Serum osteoprotegerin is inversely associated with carotid plaque echogenicity in humans. Atherosclerosis April 16
18. Fosse E, Johnsen SH, Stensland-Bugge E, Joakimsen O, Mathiesen EB, Arnesen E, Njolstad I (2006) Repeated visual and computer-assisted carotid plaque characterization in a longitudinal population-based ultrasound study: the Tromsø study. Ultrasound Med Biol 32(1):3–11
19. Hixson JE, Vernier DT (1990) Restriction isotyping of human apolipoprotein E by gene amplification and cleavage with HhaI. J Lipid Res 31(3):545–348
20. Havel RJ, Kane JP, Kashyap ML (1973) Interchange of apolipoproteins between chylomicrons and high density lipoproteins during alimentary lipemia in man. J Clin Invest 52(1):32–38
21. Schaefer EJ, Audelin MC, McNamara JR, Shah PK, Tayler T, Daly JA, Augustin JL, Seman LJ, Rubenstein JJ (2001) Comparison of fasting and postprandial plasma lipoproteins in subjects with and without coronary heart disease. Am J Cardiol 88(10):1129–1133
22. Cohn JS, McNamara JR, Cohn SD, Ordovas JM, Schaefer EJ (1988) Postprandial plasma lipoprotein changes in human subjects of different ages. J Lipid Res 29(4):469–79
23. Gronholdt ML, Nordestgaard BG, Wiebe BM, Wilhjelm JE, Sillesen H (1998) Echo-lucency of computerized ultrasound images of carotid atherosclerotic plaques are associated with increased levels of triglyceride-rich lipoproteins as well as increased plaque lipid content. Circulation 97(1):34–40
24. Weintraub MS, Eisenberg S, Breslow JL (1987) Dietary fat clearance in normal subjects is regulated by genetic variation in apolipoprotein E. J Clin Invest 80(6):1571–1577

Lipids (2008) 43:681–693
DOI 10.1007/s11745-008-3198-x

ORIGINAL ARTICLE

Photoaffinity Labeling and Mutational Analysis of 24-C-Sterol Methyltransferase Defines the AdoMet Binding Site

Pruthvi Jayasimha · W. David Nes

Received: 12 March 2008 / Accepted: 15 May 2008 / Published online: 18 June 2008
© AOCS 2008

Abstract Photolabeling and site-directed mutagenesis were performed on recombinant *Saccharomyces cerevisiae* 24-C-sterol methyltransferase (SMT) to elucidate the location and role of active site residues involved in AdoMet binding and catalysis. Bioinformatic analysis of the SMT revealed a ten amino acid segment, conserved between L124 and P133, associated with the Rossmann-like fold belonging to AdoMet-dependent methyltransferases. Irradiation of the SMT in the presence of [*methyl*-$^3H_3$]AdoMet directly photolabeled the protein. The specificity of photolabeling was demonstrated by inactivation experiments with structural analogs of AdoMet, including sinefungin. Trypsin digestion of the [*methyl*-$^3H_3$]AdoMet photolabeled Erg6p afforded a single radioactive band in SDS-PAGE gel of 4 kDa. HPLC purification of this material generated a single radioactive fraction. The corresponding ^{3}H-AdoMet-peptide adduct was subjected to Edman sequencing and the first fifteen residues gave a sequence Gly$_{120}$-Asp-Leu-Val-Leu-Asp-Val-Gly-Cys-Gly-Val-Gly-Gly-Pro-Ala$_{134}$ that contained the predicted AdoMet binding site. Amino acid residues in the tryptic digest fragment considered to bind covalently with the AdoMet at Asp125, Cys128, Pro133 and Tyr153 were replaced with leucine and analyzed kinetically and by photolabeling inactivation experiments. The results indicate that one or both of Cys128 and Pro133 are covalently bound to AdoMet.

Keywords Sterol methyltransferase · Rossmann fold · Mutagenesis · Zymosterol · *Saccharomyces cerevisiae* · AdoMet-dependent methyl transferase · Affinity labeling

Abbreviations

AdoHcy	*S*-adenosylhomocysteine
AdoMet	*S*-adenosyl-L-methionine
HEPES	*N*-(2-hydroxyethyl)piperazine-*N*′-(2-ethanesulfonic acid)
HPLC	High pressure liquid chromatography
MTase	Methyltransferase
MALDI-TOF	Matrix Assisted Laser Desorption-Time of Flight
SF	Sinefungin
SMT	24-C-sterol methyltransferase

Introduction

S-Adenosyl-L-methionine (AdoMet)-dependent methyltransferases (MTAses) are a large family of proteins involved in diverse methyl transfer reactions, including *N*-, *O*- and *C*-methyl transfer reactions [1]. Recently, these catalysts have been grouped into five distinct families based on their 3D structures [2, 3]. Kagan and Clarke reported several conserved regions aligned in the same order on the polypeptide chains and separated by comparable intervals; one of them possesses a consensus sequence (V/I/L)(L/V)(D/E)(V/I)G(G/C)G(T/P)G referred to as Motif II diagnostic for the MTases methylating small molecules such as sterol acceptors [4, 5]. In several instances, radiolabeled AdoMet and 8-azido AdoMet were shown to specifically label the MTase using UV radiation [6–11]. In addition, trypsin digestion of AdoMet-bound

---

Electronic supplementary material The online version of this article (doi:10.1007/s11745-008-3198-x) contains supplementary material, which is available to authorized users.

P. Jayasimha · W. D. Nes (✉)
Department of Chemistry and Biochemistry, Texas Tech University, Lubbock, TX 79409-1061, USA
e-mail: wdavid.nes@ttu.edu

proteins followed by chromatography to establish the peptide/amino acid-AdoMet adduct and site-directed mutagenesis experiments of amino acid residues predicted to be associated with the AdoMet binding site demonstrated the requirement for one or more conserved residues (i.e., Tyr, Cys or Pro) or motifs in MTase specific activity [12–14].

A major group of AdoMet-dependent methyltransferases for which no three-dimensional structure exists, yet are essential to the evolution of life through their contribution to the phytosterol (24-alkyl sterol) pathway of microbes and plants [15], are the 24-C-sterol methyltransferases (SMT). The SMTs operate C_1-and C_2-transfer activities of different reaction times to form single or multiple biomethyl products [16]. In humans, the 24-alkyl sterol pathway appears to have been lost (a TBLASTIN search of the SMT genome sequence in humans yielded no match for a SMT ortholog), although, human nutrition benefits from dietary supplements of plant sterols [17]. Interestingly, in the course of co-evolution of animals with certain microbes ergosterol-dependent diseases appeared for which the fungal/protozoan SMT is now considered a target of rational drug design and in chemotherapy [18–21]. Studies with a number of SMTs responsible for the formation of phytosterols of the ergostane (C24-methyl) (Fig. 1) and stigmastane (C24-ethyl) families have led to the formulation of a comprehensive proposal referred to as the steric-electric plug model for the stereochemical mechanism and substrate acceptability of SMT-catalyzed reactions [22].

Previous studies on SMT have focused on the biosynthetic function of the enzyme [15, 23–26] and, in particular, the substrate specificity and inhibitor potency of transition state analogs and mechanism-based inactivators designed to impair the SMT action involved with disrupting carbon flux to the final 24-alkyl sterols [18]. SMTs can be classified according to their specificity for the sterol acceptor, referred to as SMT1 for $\Delta^{24(25)}$-sterols or SMT2 for $\Delta^{24(28)}$-sterols [27]; or further categorized by the nature of the substrate nucleus for cycloartenol (E.C. 2.1.1.142), 24(28)-methylene lophenol (E.C. 2.1.1.143) or zymosterol (E.C. 2.1.1.41) [15]. Identification of the sterol binding site was demonstrated through primary structure comparisons, chemical affinity labeling and site-directed mutagenesis studies of fungal, plant and protozoan SMTs [28–34]. These studies unmasked multiple signature motifs that occur in all SMTs referred to as Regions I and III that stretch between Y81 and H90 and Y192 and P201, respectively in the Erg6p; directed mutations of select amino acids in the conserved domains were shown to affect catalytic competency and promote enzyme promiscuity. In contradistinction, a conserved motif of ten amino acids at L124 to Pro133 was detected in the SMT centered toward the N-terminus sandwiched between the catalytic sites of Regions I and III [34], considered to be the AdoMet-binding site.

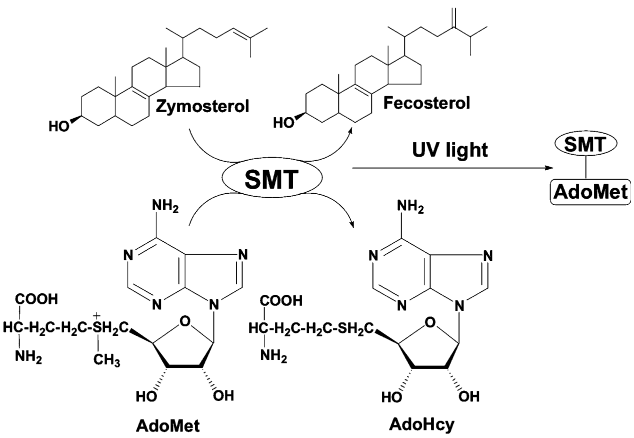

Fig. 1 *C*-methylation reaction catalyzed by the wild-type yeast 24-C-sterol methyltransferase (SMT) and photolabeling reaction to yield a SMT-AdoMet adduct

The ability of such a catalytically similar group of SMTs to utilize a shared methyl donor contrasts to the SMT recognition of different sterol acceptors involved with mono (fungi) and bifunctional (protozoa and plants) behavior [15]. On the one hand, these data suggest a common core that forms a structurally homologous active center of similar amino acids to contact the AdoMet and sterol in SMT1 and SMT2 isoforms. On the other hand, a sequence comparison of the relevant amino acids of the enzymes in the phytosterol pathway fail to reveal a motif or amino acid residue that reflects a common active site for sterol binding, nonetheless, in all cases these enzymes recognize similar sterol features, that is ca. 20 angstroms long, amphipatic and greasy. In related work, kinetic observations of AdoMet binding to the SMT support a single subsite [34], which is not the case for other enzymes that act on lipids where AdoMet can interact with multiple regions on the enzyme [12, 36]. Consequently, whether additional AdoMet binding region(s) exist in the SMT and the number and type of individual amino acids that contact the methyl donor in the active center remains enigmatic.

In this paper, we describe the further application of bioinformatics analysis with UV light-dependent photolinkage of [*methyl*-$^3H_3$]AdoMet to establish that a single motif corresponds to the conserved sequence considered to represent the AdoMet binding site of the SMT from *Saccharomyces cerevisiae*. The specificity of the photolinkage and essential nature of Cys128 and Pro133 contained in the covalently formed AdoMet-peptide adduct are demonstrated for the first time by a combination of sequence specific cleavage of the enzyme–ligand adduct with trypsin digestion followed by HPLC analysis of the trypsin digest fragments and site-directed mutagenesis experiments. The results reported here show close resemblance to motif-II of Class-I MTases with a typical sequence *GXGXG*, regarded as the hallmark of a nucleotide or AdoMet binding site [5]. In view of the high sequence similarity among several SMTs in this AdoMet binding region, the information generated in this study could potentially serve to reveal similar findings in the SMT family of proteins expressed in diverse species ranging from protozoa to fungi to plants.

Experimental Procedures

Materials

The sources and preparation of substrates of the wild-type yeast SMT catalyzed reaction are described in our earlier papers [28–34]: zymosterol, [3-^{3}H]zymosterol (sp. act. 9 µCi/µmol), AdoMet iodide salt, and [*methyl*-$^3H_3$]AdoMet (NEN, diluted with AdoMet to a sp. act. of 10 µCi/µmol). Sinefungin (SF), 5′-Deoxy-5′-(methylthio)adenosine (MTA), *S*-isobutyladenosine (SIBA) were from Sigma. H_2O_2 solution (50%) was from HACH Co. Ames, Iowa. Trypsin (proteomics-grade) was purchased from Sigma. Quick Change site-directed mutagenesis kit was purchased from Stratagene. Custom oligonucleotides were synthesized by Texas Tech Biotech Core Facility. Isopropyl *β*-D-thiogalactoside (IPTG) was purchased from Research Products International Corp. Bradford protein assay kit and protein electrophoretic supplies were obtained from Bio-Rad. All other reagents and chemicals were from Sigma or Fisher unless otherwise noted.

General Methods

General methods for cloning, expression of yeast-SMT (*ERG6*), and homogenate preparation were as described [32]. Protein concentration contained in the crude SMT enzyme was determined by Bradford method with bovine serum albumin (BSA) as the standard using commercial reagents from Bio-Rad. Otherwise, the determination of pure SMT concentration was measured at A_{280} using extinction coefficient of 58,370 cm^{-1} M^{-1} for the native SMT and considering the tetrameric composition of the native protein (ca. M_r 172 kDa).

SMT Activity Assays

The standard assay conditions for enzyme activity and kinetic analysis were as described [29–34]. To summarize, the standard assay for the wild-type or mutants of yeast-SMT enzyme was performed in 600 µL total volume, with 1 mg/mL total protein (100,000×*g* fraction) prepared by cell lysis (using French press) with saturating levels of co-substrates, zymosterol and [*methyl*-$^3H_3$]AdoMet. The reaction was quenched with an equal volume of methanolic KOH and methylated product was extracted with hexane (Fisher) three times and dried. The activity in each case was measured by liquid scintillation counting (Beckman) against a suitable blank. The initial velocity data was determined using Sigmaplot 2001 with the enzyme kinetics module software package. Data were fitted to the equation $v = V_{max}S/(K_m + S)$ using a nonlinear least-squares approach. Kinetic constants ± standard errors were never greater than 5% of the experimental measurement, and R^2 values were between 0.90 and 0.99. For k_{cat} analysis, partially purified SMT protein preparations from Q-Sepharose anion exchange chromatography (ca. 80% pure SMT) was used. Generally, the activity assay contained 0.3 µM SMT and varied amounts of zymosterol (5–100 µM) and a fixed [*methyl*-$^3H_3$]AdoMet concentration of 100 µM in buffer A (50 mM Tris–HCl, 2 mM $MgCl_2$, 2 mM 2-mercaptoethanol, and 20% (v/v) glycerol, pH 7.5). The assays were performed in triplicate with variation among the trials no greater than ± 5%. For reaction mixtures that generated activity, the experiment was repeated with saturating amounts of sterol and AdoMet and the product distribution examined by GC-MS according to the established protocol [29].

Binding Assays and Immunoblotting

Binding assays for AdoMet and zymosterol were performed using the equilibrium dialysis and filter-binding method respectively, as previously reported [29]. Varied concentrations of ligands-[*methyl*-$^3H_3$]AdoMet (0–40 µM); [3-^{3}H]zymosterol (0–28 µM), were incubated separately with purified SMT protein preparations in buffer A, pH 7.5 at 35 °C for the desired time on a shaking water bath. Nonspecific binding was estimated using 100,000×*g* supernatants of BL21(DE3) cells transformed with a pET(23a+) blank vector, the same expression system used in expressing SMT cDNA. In the case of the filter binding method, bound and free ligands were separated by filtration over Whatman GF/C filters (pretreated with 0.1%BSA) with ice cold buffer A. Binding parameters (K_d, B_{max}) were determined by nonlinear curve fitting for one-site ligand saturation. *Saccharomyces cerevisiae* SMT-specific antibody produced by Invitrogen® was purified using a Bio-Rad® IgG purification kit. For immunoblotting, Q-sepharose purified wild-type and mutant proteins resolved on a 12% SDS-PAGE gel were electrophoretically transferred on to a nitrocellulose membrane and SMT protein was detected using polyclonal anti-yeast SMT as a primary antibody (Invitrogen) and anti-Rabbit IgG-HRP conjugate as a secondary antibody with color development using a

HRP substrate kit (Bio-Rad) for appropriate time at room temperature.

AdoMet Photoaffinity Labeling

The wild-type yeast-SMT was semi-purified on a Q-Sepharose column previously equilibrated with HEPES Buffer [10 mM HEPES, 2 mM $MgCl_2$, 1 mM EDTA and 5% glycerol(v/v), pH 7.5]. The procedure for Q-Sepharose anion exchange chromatography remained the same as the earlier protocol [34] except for the change in the buffer system. The change in the buffer system is reported due to the observation of enhanced AdoMet photolabeling and enzyme activity in the case of HEPES buffer compared to the Tris buffered system used earlier. About 0.3 mg of Q-Sepharose semi-purified wild-type yeast-SMT protein (~80% pure, equivalent to 1.74 nmol) was made up to a 2.5 mL solution in HEPES Buffer, pH 7.5 and kept on ice. [*methyl*-$^3H_3$]AdoMet (10 Ci/mmol, Perkin Elmer) equivalent to 27.5 µCi or 18.34 nmol was dried under a low stream of N_2 to remove the sulfuric acid content, resuspended in 500 µL of HEPES Buffer, pH 7.5 to ensure the optimal pH conditions and added to the wild-type SMT protein solution prepared above. The mixture was incubated at 35 °C for 45 min in a shaking water-bath to allow the AdoMet to bind to SMT under steady-state conditions. The ice-cooled reaction mixture was transferred to a pre-chilled 96-well titer plate (Whatman®) with 100 µL of the sample placed in each well and illuminated with a UV lamp at short wavelength (254 nm) placed 1 cm above the sample for 45 min. The samples were mixed intermittently every 5 min. The irradiated samples were pooled and dialyzed using Slide-A-Lyser cassettes (Pierce) with HEPES Buffer, pH 7.5 at 4 °C to remove the unbound AdoMet. The samples were concentrated using a 10-kDa cut off ultrafiltration centrifugal device (Centricon) and stored at −20 °C until further use.

Fluorography

The AdoMet-bound SMT samples were resolved on a 12% SDS-PAGE. After staining (Coomassie Blue) and destaining, the gels were soaked in Fluoroenhancer solution (Kodak™, Perkin Elmer) and gently agitated for 30 min and dried on a gel dryer for 3–4 h. Films were developed by placing the dried gel over a blue sensitive X-ray film (Kodak X-Omat AR) in a cassette and incubated at −80 °C for 3 weeks or until the bands were visible.

Time-Dependent Inactivation and Inhibition Studies

The protocol involved similar photoaffinity labeling conditions as described above. Aliquots of 50 µL of the photolabeled mixture were siphoned out at different time intervals and assayed for enzyme activity at saturating concentrations of co-substrates, zymosterol and [*methyl*-$^3H_3$]AdoMet (100 µM each) under standard assay conditions. For data analysis, the dpm value obtained for the samples were transformed into % activity based on the sample at 0 min.

To test the AdoHcy analogs [Sinefungin (SF), 5′-Deoxy-5′-(methylthio)adenosine (MTA), *S*-isobutyladenosine (SIBA)] as inhibitors against AdoMet in a SMT catalyzed reaction, typical activity assays (in triplicates) were set up with varied [*methyl*-$^3H_3$]AdoMet concentration from 5 to 100 µM with a fixed zymosterol concentration of 100 µM and the inhibitor at a particular concentration (SF, 0.1–10 µM; MTA, 1–100 µM; SIBA, 1–100 µM), under standard assay conditions. The data were fitted into Michaelis–Menton equations for competitive [$v = V_{max}/\{1 + (K_m/S) \times (1 + I/K_i)\}$] or non-competitive [$v = V_{max}/\{(1 + I/K_i) \times (1 + K_m/S)\}$] or uncompetitive [$v = V_{max}/(1 + I/K_i + K_m/S)\}$] inhibition patterns to determine the most favorable kinetic pattern of inhibition for each inhibitor. Lineweaver-Burk plots were generated in each case using an enzyme kinetics module in Sigmaplot 2001 software. Minimal variation was detected in the experimentally determined kinetic constants with standard errors of 2–10% between the trials.

These inhibitors were also tested under AdoMet photolabeling to determine their effect on AdoMet photolabeling capabilities on the wild-type yeast-SMT enzyme. Under these conditions, the pre-incubated wild-type yeast-SMT samples with [*methyl*-$^3H_3$]AdoMet alone and AdoHcy analogs combined with [*methyl*-$^3H_3$]AdoMet were photo-irradiated for 45 min under the standardized conditions outlined above. The samples were dialyzed against HEPES Buffer, pH 7.5 to remove the unbound material and analyzed for radioactivity by liquid scintillation counting to establish the extent of binding in the presence and absence of each inhibitor.

H_2O_2 Digestion

The specific activity of the AdoMet photolabeled wild-type SMT protein resolved on a 12%-SDS-PAGE gel was determined separately using the H_2O_2 digestion procedure adapted from a previously reported protocol [9]. After staining and destaining, the bands corresponding to 43 kDa were excised from the gel, cut into 1 mm^2 pieces and transferred to a scintillation vial; 1 mL of chilled 50 % H_2O_2 solution was added and incubated at 70 °C for 20 h in a water bath and 5 mL of scintillation cocktail (Optiphase HiSafe 3, Perkin Elmer) was added to the vials and analyzed by liquid scintillation counting. A control was set up using a blank piece of gel that contained no protein.

Electroelution

The SMT bands corresponding to 43 kDa were electroeluted using Electro-Eluter Concentrator (C.B.S. Scientific Company, Inc. Del Mar, CA, USA) prior to trypsin digestion. The elution was carried out for a total duration of 15–20 h as per manufacturer's instruction. To determine the % recovery, an aliquot of electroeluted sample was counted for radioactivity. The yield was greater than 50% in the majority of the trials. The electroeluted SMT-AdoMet samples were pooled and concentrated using ultrafiltration centrifugal devices (Centricon, 10-kDa cut off membrane) and dialyzed with of 0.1 M NH_4HCO_3 Buffer, pH 8.5 suitable for further trypsin digestion.

Trypsin Digestion

The trypsin digestion of the enzyme–ligand adduct was initiated by addition of proteomics-grade trypsin (Sigma) solution (prepared in 1 mM HCl) to the electroeluted protein sample. The substrate to enzyme-S/E ratio for the tryptic digestion was 100–5 (w/w). The resulting reaction mixture was incubated for 8 h at 37 °C. A control was set up with trypsin in 0.1 M NH_4HCO_3 Buffer, pH 8.5 and incubated under similar conditions as above. The tryptic digestion was quenched by the addition of 5 μL of glacial acetic acid (HPLC grade) to the samples and rapid freezing of the reaction mixture in liquid N_2 and stored at −20 °C until use. The samples were resolved on a 20% SDS-PAGE gel and the radioactive peptides migrating in the gel identified either by fluorography and/or H_2O_2 digestion.

Radiolabeled Peptide Purification

As a primary step to get rid of most of the impurities, the trypsin-digested material was filtered using a 10-kDa cut off ultrafiltration centrifugal device (Sigma) to collect the pass through. The radiolabeled samples were resuspended in 0.1% Trifluoroacetic acid (TFA, HPLC grade, Biochemica) prior to HPLC purification. Preparative purification of the radiolabeled peptide was achieved by reverse-phase HPLC using C_{18} Vydac^{TM} (4.6 mm × 250 mm) with a solvent system comprising of 0.1% TFA in both water (A) and acetonitrile (B). The peptides were eluted with a linear gradient of 0–99% B at a constant flow rate of 0.5 mL/min with the column temperature maintained at 15 °C. The eluant was monitored using a multiple-diode array detector at 210, 240 and 280 nm. The radioactive peak fractions were identified by liquid scintillation counting of fractions collected every minute. The radioactive peak fractions were re-chromatographed under similar conditions until they were pure for further analysis.

MALDI-TOF Spectrometry

The samples were prepared by "dried-droplet" method. To obtain a better coverage of components in a mixture, spectra were acquired from the samples prepared with different matrix solution conditions [35]. The matrix solutions used were: 20 mg/mL α-cyano-4-hydroxy-*trans*-cinnamic acid (Sigma) or 20 mg/mL 2,5-dihydrobenzoic acid [DHB, Sigma] in 0.1% TFA in 50% acetonitrile in water solution. The matrix additive-1 mg/mL 2-methoxybenzoic acid (Sigma) was added to the DHB solution for detection of peptides larger than 3 kDa. A mixture of 1 μL each of matrix solution and peptide sample (1 pmol/μL) was applied to the gold target and air dried. A control was set up by using synthetic peptides (Biosynthesis Inc, Lewisville, TX, USA) with known molecular weights. For these purposes, peptides corresponding to Regions I (L63-R93, 3.7 kDa), II (G120-R135, 1.48 kDa) and a typical tryptic fragment (L203-K212, 1.2 kDa) of yeast-SMT were used as reference specimens. The individual mass was analyzed using laser intensity between 2,500 and 3,000 units. Minimal variations of 1–2% were observed in the experimental data compared to the established mass for peptide standards.

Site-Directed Mutagenesis of SMT

Site specific mutations at various positions along the pET23a(+)-*ERG*6 template were carried out using the QuickChange^{TM} (QC) site directed mutagenesis kit (Stratagene) as per manufacturers' instructions. The oligonucleotide primers used for mutagenesis are listed in Table 1. The relevant mutation was confirmed by automated sequencing at the Texas Tech Core facility. Routine screening of the mutants for activity assays are as previously described [34].

AdoMet Photolabeling of the Synthetic Peptide

The synthetic peptide corresponding to the 3.9-kDa peptide fragment obtained in this study was subjected to purification by HPLC on a C_{18} Vydac^{TM} (4.6 mm × 250 mm) instrument with a solvent system comprising of 0.1% TFA in both water (A) and acetonitrile (B). The peptide was eluted with a similar gradient system used for purification of radioactive peptide(s) mentioned before. The purified material was dried under N_2 to remove the solvent and resuspended in HEPES buffer, 7.5. [*methyl*-$^3H_3$]AdoMet was added in a stoichiometric ratio of peptide: AdoMet of 1:10 and the mixture was photo-irradiated under similar conditions outlined for wild-type Erg6p. The photolabeled sample was analyzed by HPLC radio-counting to determine the amount of photolabeling. The samples were

Table 1 DNA sequence of sense oligonucleotides used for site-directed mutagenesis of *ERG6* cDNA

Mutation	Sense oligonucleotide sequence (5′–3′)
Cys128Leu	5′-TAGTTCTCGACGTTGGT*TTG*GGTGTTGGGGGCCCA-3′
Cys128Ser	5′-GTTCTCGACGTTGGT*TCT*GGTGTTGGGGGCC-3′
Pro133Leu	5′-TGGTGTTGGGGGC*CTA*GCAAGAGAGATTGCA-3′
Tyr153Leu	5′-CAATAACGAT*TTA*CAAATTGCCAAGG-3′
Tyr153Phe	5′-GGTCTAAACAATAACGAT*TTC*CAAATTGCCAAGGCAA-3′

The mutagenic codons are in italics

finally resuspended in 0.1 M NH_4HCO_3 buffer, pH 8.5 in case to be subjected for further tryptic digestion. A similar sample prepared with cold-AdoMet was subjected to further analysis by MALDI/MS and/or Edman degradation (Macro Core Facility, Penn State College of Medicine, Hershey, PA, USA) to determine the derivatized amino acids within the synthetic peptide.

Results

Photoaffinity Labeling of Yeast-SMT with AdoMet

Preliminary photolabeling experiments, performed with the purified SMT and [*methyl*-$^3H_3$]AdoMet generated a covalently labeled enzyme–ligand adduct detected by fluorography (Fig. 2). The specificity of photolabeling was further demonstrated by inactivation experiments. Heat-inactivated enzyme preparations were used as negative controls in all experiments (data not shown) since irradiation of denatured SMT in the presence of [*methyl*-$^3H_3$]AdoMet did not generate any appreciable levels of photolabeling. During the course of our initial standardization procedures, we observed not only an increased specific activity for SMT catalysis but also AdoMet photolabeling efficiency by a factor of three when a buffer change was introduced to HEPES in our assays (data not shown). Therefore, we chose the HEPES buffer system for all the subsequent photoaffinity labeling treatments. The AdoMet photoaffinity labeled SMT from the Tris and HEPES buffered reaction mixtures resulted in similar outcomes in fluorography producing single radioactive band (data not shown).

In order to specify the optimal photo-irradiation time, we performed a time-dependent inactivation experiments with the wild-type yeast SMT. The photolabeled-SMT aliquoted under differing time periods was assayed in the presence of zymosterol using the standard assay conditions. Approximately 50% of the SMT activity was lost during the first 30 min of photo-irradiation and less than 10% of the activity was retained at the end of 60 min (Fig. 3). Based on these results, a 45 min of photo-irradiation time suited best for the routine-SMT photolabeling studies.

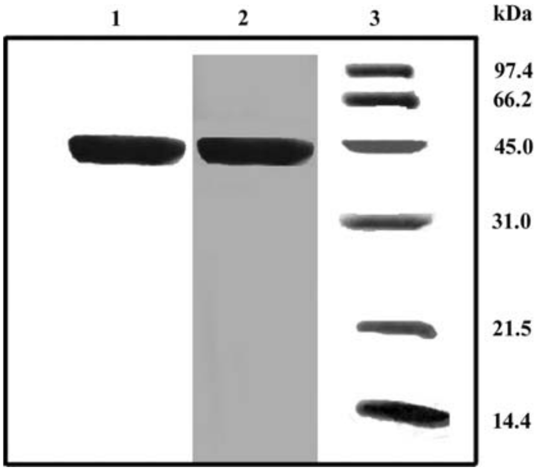

Fig. 2 SDS-PAGE analysis (12%) of AdoMet photolabeling of wild-type yeast SMT. *Lane 1* electroeluted sample of wild-type SMT species bound to [*methyl*-$^3H_3$]AdoMet; *Lane 2* fluorography of the sample as in *lane 1* showing single radioactive band corresponding to 43 kDa; *Lane 3* low molecular-weight range protein marker. The respective M.Wt in kDa is indicated

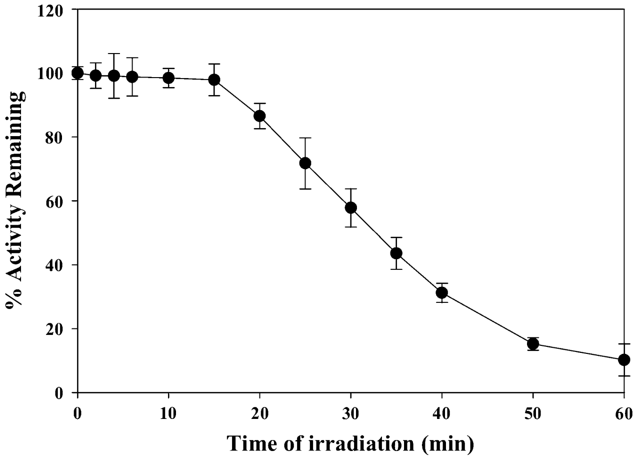

Fig. 3 Time-dependent inactivation of Wild-type Yeast-SMT against AdoMet photoirradiation time. The % activity values were normalized to the protein sample without AdoMet photolabeling (0 min of photolabeling). SMT activity in each reaction mixture was determined as per standard assay conditions using saturating concentrations (100 µM each) of co-substrates, zymosterol and [*methyl*-$^3H_3$]AdoMet. Each data point represents an average of three independent determinations with standard errors under 10%

Effect of AdoMet Analogs on Photolabeling

The AdoHcy analogs [SF, MTA, SIBA (Fig. 4)] were shown earlier to competitively inhibit the wild-type SMT [37]. Experiments were performed to determine the effect of these AdoMet analogs on photolabeling of the enzyme in the presence of AdoMet. Steady-state kinetic experiments revealed competitive-type inhibition kinetics against AdoMet with dissociations constants (K_i values) of 1.3 µM (SF), 22 µM (MTA) and 58 µM (SIBA) (Fig. 5). These observations are consistent with the expected behavior of the AdoMet analogs to compete for the same binding site on the enzyme surface. A similar trend was observed during the AdoMet photolabeling of the SMT enzyme. With the addition of SF, MTA or SIBA to the photolabeling mixture of [*methyl*-$^3H_3$]AdoMet and SMT, the percentage of reduction in the AdoMet photolabeling of SMT ranged from 85 to 50 (Fig. 6). There was a direct correspondence between the change in binding constants and the photolabeling results of the AdoMet analogs. These results agree with the proposed competitive nature of AdoHcy analogs against AdoMet [10, 37].

Limited Proteolysis of the SMT-AdoMet Adduct

In order to localize the AdoMet binding region in wild-type yeast-SMT, we subjected the electroeluted [*methyl*-$^3H_3$] AdoMet photolabeled samples of SMT protein to trypsin digestion to generate small peptide fragments that can be easily monitored on a 20% SDS-PAGE. For these studies, a procedure involving H_20_2 treatment of the excised SDS-PAGE gel slices was employed for the rapid detection of radioactivity associated with the peptide fragments. As shown in Fig. 7, more than 90% of the radioactivity applied to the SDS-PAGE gel electrophoresis was recovered and ca. 95% of the radioactivity migrates in a single zone at ca. 3.5–4 kDa. An independent experiment using fluorography confirmed that a single radioactive band migrates in the SDS-PAGE gel electrophoresis around 4 kDa (Fig. 7).

Identification of the Labeled Adduct

Since we had established above that a single AdoMet-peptide adduct of 4 kDa was formed by the limited proteolysis, we initially chose ultrafiltration with a 10 kDa cut off membrane to remove undigested material and other potential impurities larger than 10 kDa. The resulting peptide mixture was injected into the reverse-phase-HPLC eluted with the combination of acetonitrile and water as described in the "Experimental procedures". The radioactivity of individual fractions containing the peptide was determined, and the corresponding mass monitored by UV detection at 210 nm. Figure 8 (Panel A) shows a single radioactive peak fraction that elutes between 38 and 40 min, accounting for >80% of the total radioactivity injected into the HPLC. The elution profile remained consistent with several successive HPLC runs on the same column. A set of peptide standards were synthesized that ranged in size and corresponded to various segments of the SMT primary structure (Fig. 8, Panel B). A synthetic peptide was prepared that corresponded to the predicted composition of a yeast SMT peptide formed by limited trypsin digestion and that possesses a molecular weight of 3.9 kDa, close to the molecular weight of the adduct obtained from the 20% SDS-PAGE gel electrophoresis experiment. This synthetic peptide was photolabeled with AdoMet and the resulting adduct injected into the HPLC where the radioactive AdoMet-peptide adduct eluted at the same time as the synthetic peptide of 3.9 kDa (Fig. 8, Panel B).

To establish the exact mass of the radioactive AdoMet-peptide adduct, a separate experiment was performed to generate the non-radioactive adduct for MALDI-TOF analysis. Our initial MALDI-TOF analysis using α-cyano-4-hydroxy-*trans*-cinnamic acid as the matrix material did not show any mass for the peptide. It was not clear whether the recognition of no mass was due to our limits of detection or due to the hydrophobic nature of the peptide. On the other hand, the synthetic peptides corresponding to

Fig. 4 Structures of AdoMet analogs tested as inhibitors of the SMT

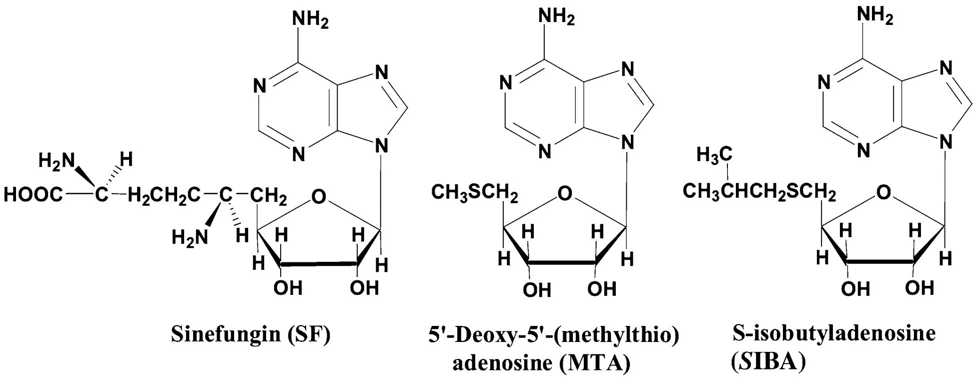

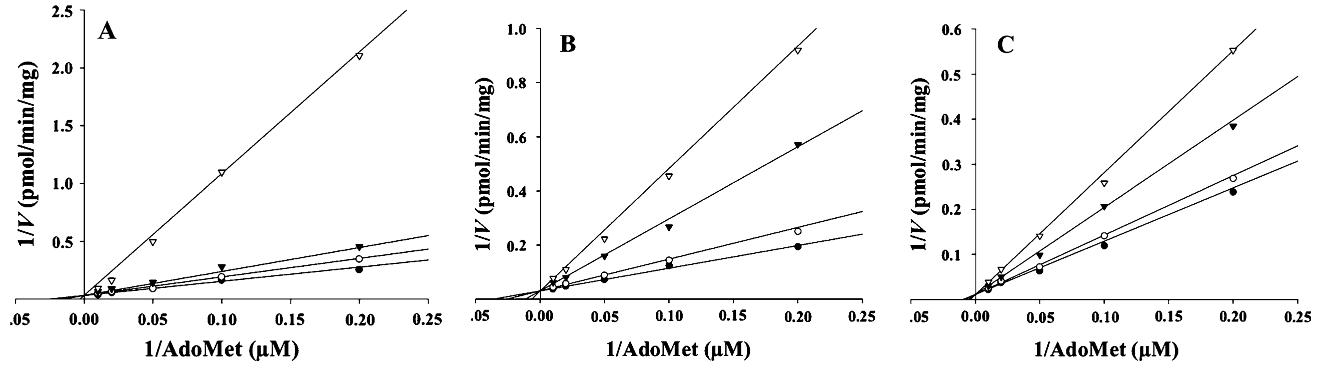

Fig. 5 Lineweaver-burk plots for the inhibition of yeast-SMT by AdoHcy analogs. **a** *SF* Sinefungin [0.1 μM (*filled circles*), 0.5 μM (*open circles*), 1 μM (*filled inverted triangles*), 10 μM (*open inverted triangles*)]; **b** *MTA* 5′-Deoxy-5′-(methylthio)adenosine [1 μM (*filled circles*), 10 μM (*open circles*), 50 μM (*filled inverted triangles*), 100 μM (*open inverted triangles*)]; **c** *SIBA* S-isobutyladenosine [1 μM (*filled circles*), 10 μM (*open circles*), 50 μM (*filled inverted triangles*), 100 μM (*open inverted triangles*)]. The kinetic pattern in all the cases was found to be competitive as determined by Sigma plot Enzyme kinetics module. Assays were performed as per standard conditions mentioned under "Experimental procedures" using fixed zymosterol of 100 μM and varied [*methyl*-$^3H_3$]AdoMet (5, 10, 20, 50, 100 μM) concentrations. Each data point represents a mean of three independent determinations with standard errors under 10%

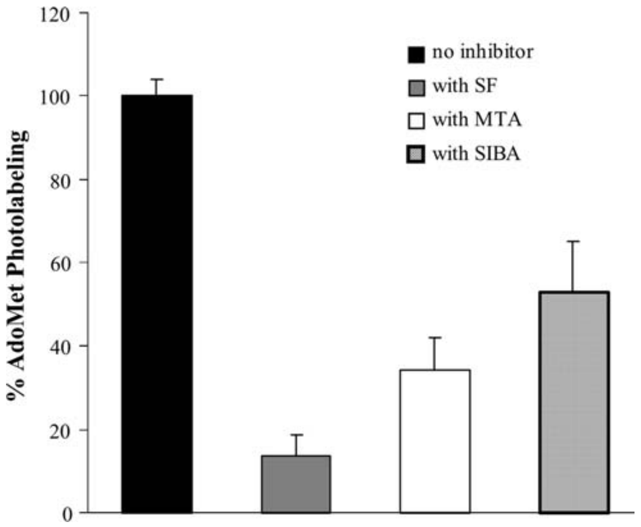

Fig. 6 Effect of AdoHcy analogs on AdoMet photolabeling efficiency of wild-type yeast-SMT. The % photolabeling values are based on the wild-type SMT protein samples labeled to AdoMet under normal photoaffinity labeling conditions. The concentration of inhibitor used are as follows: Sinefungin (SF), 100 μM; 5′-Deoxy-5′-(methylthio)adenosine (MTA), 200 μM; *S*-isobutyladenosine (SIBA), 200 μM. The values represent a mean of three independent determinations with standard errors between 4 and 12%

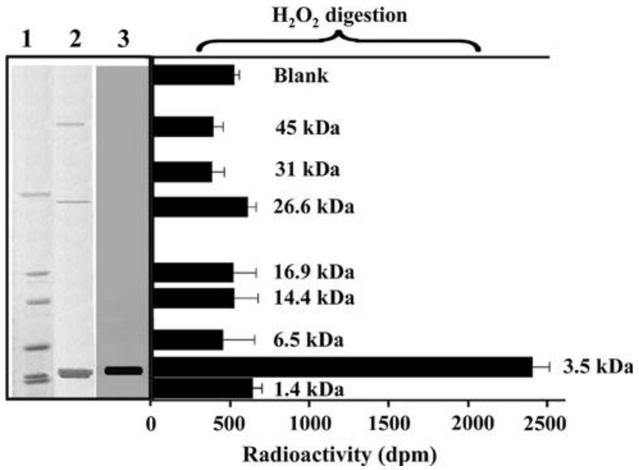

Fig. 7 SDS-PAGE analysis (20%) of AdoMet photolabeled tryptic digest fragments by H_2O_2 digestion and autoradiography. *Lane 1* polypeptide marker (kDa) in the order: 26.6, 16.9, 14.4, 6.5, 3.5 and 1.4; *Lane 2* tryptic digest sample of AdoMet photolabeled wild-type yeast SMT; *Lane 3* fluorography of the tryptic digested sample of SMT as in *lane 2*. The radioassay of gel samples by H_2O_2 digestion are indicated by histogram in the figure. The values from H_2O_2 digestion represent a mean of three independent determinations obtained from three successive SDS-PAGE runs with standard errors between 5 and 12%

different tryptic fragments of wild-type Erg6p, when concurrently used as peptide standards, under the similar conditions and similar concentrations revealed mass with less than 1% errors when compared to the respective established mass. Owing to the hydrophobic nature of the peptide, we decided to use 2,5-dihydrobenzoic acid (DHB) with the additive 2-methoxybenzoic acid as the matrix material for further analysis. This procedure allowed us to predict a mass of 3.9 kDa for the radioactive peptide, which is consistent with the 20% SDS-PAGE analysis; and for the synthetic peptide standards, the mass was identical to the previous determination, indicating similar level of accuracy (Supplementary Fig. 1).

Due to the large size of the AdoMet-peptide fragment adduct, Edman sequencing of the purified radioactive peak fraction was performed for the first fifteen cycles. This yielded a sequence NH_2-Gly-Asp-Leu-Val-Leu-Asp-Val-Gly-Cys-Gly-Val-Gly-Gly-Pro-Ala. When compared with the established primary and(or) cDNA sequence of Erg6p, the peptide sequence could be clearly assigned to residues

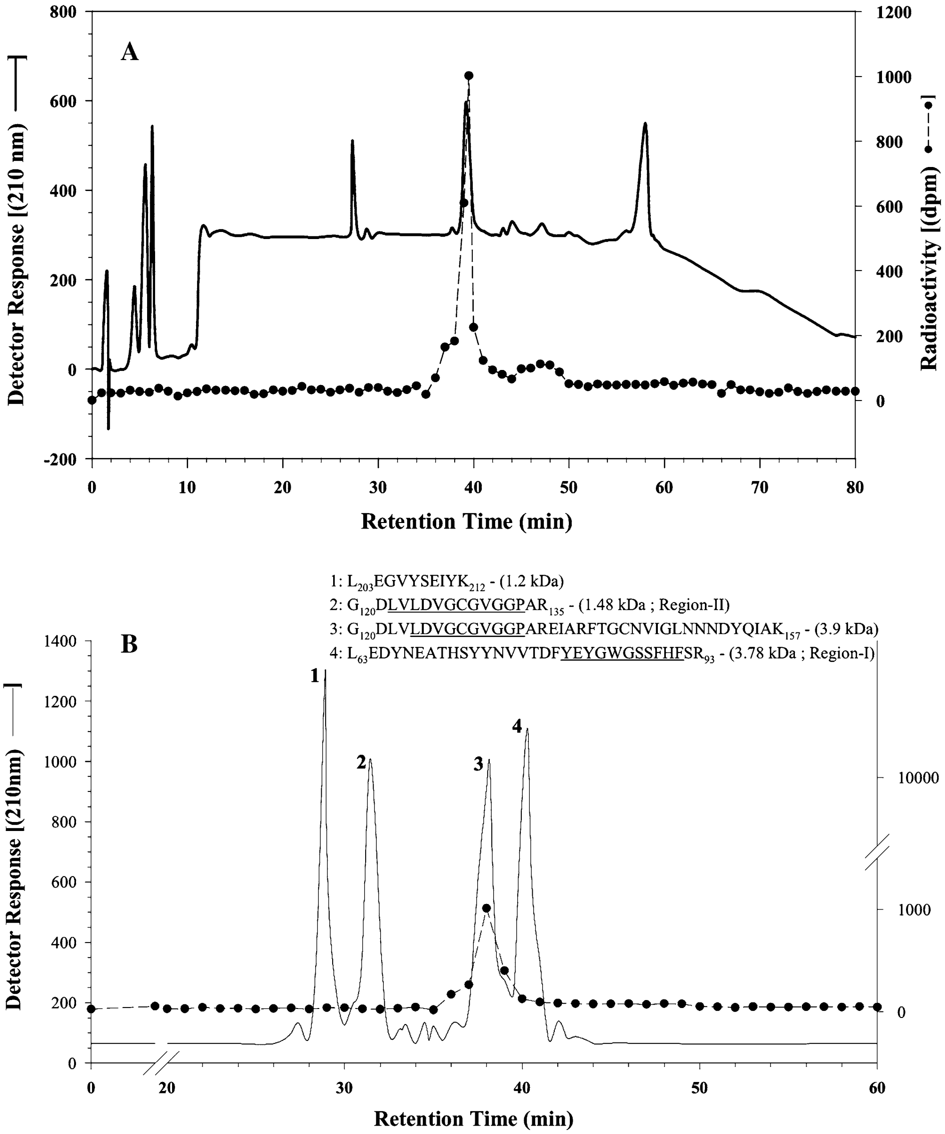

Fig. 8 HPLC of the tryptic digest of AdoMet Photolabeled wild-type yeast-SMT (**a**). The UV detector response was monitored at 210 nm. The fractions collected every minute were radioassayed by liquid scintillation counting. The radioactivity associated with each fraction is shown as a line and scattered plot. **b** HPLC of synthetic peptides used as reference specimens. The operating conditions of the HPLC in **b** were the same as the conditions used in the run shown in **a**

120–134. Due to unanticipated shortcomings, the specific amino acid residues derivatized in this peptide could not be established by means of radioassay of PTH derivative obtained from each cycle of Edman degradation. Yet, during the sequencing of the adduct, there was a huge drop in the amino acid yield starting from the second cycle which could only be attributed to the fact that the peptide fragment was bound to AdoMet. We were able to account for only 1.3 kDa for the first fifteen residues from the total of 3.9 kDa determined by MALDI-TOF spectrometry. Therefore, to get a complete peptide fragment length and taking into consideration the trypsin recognition sites and the mass from the AdoMet, we screened the downstream region of Erg6p starting from the 134th residue. Extension of peptide length to incorporate three immediate trypsin cut sites, the size of the peptide fragment exactly matched to 3.92 kDa, however the mass of the AdoMet could not be accounted for. One explanation for these results could be the elimination of AdoMet during the MALDI-TOF MS analysis. Based on these observations, the peptide fragment bound to AdoMet was determined to span the Erg6p from 120 to 157, a 38 residue segment with a highly conserved motif of L124 to P133 (Fig. 9).

Mutational Analysis of AdoMet Binding Region

Since Edman sequencing of the AdoMet-peptide adduct failed to establish the relevant amino acids covalently bound to AdoMet, we turned our efforts to site-directed mutagenesis of putative residues that might engage AdoMet during photolabeling. Sequence analysis of the Erg6p AdoMet binding domain compared with 17 different SMT species belonging to SMT1 and SMT2 type isoforms revealed several absolutely conserved amino acid residues

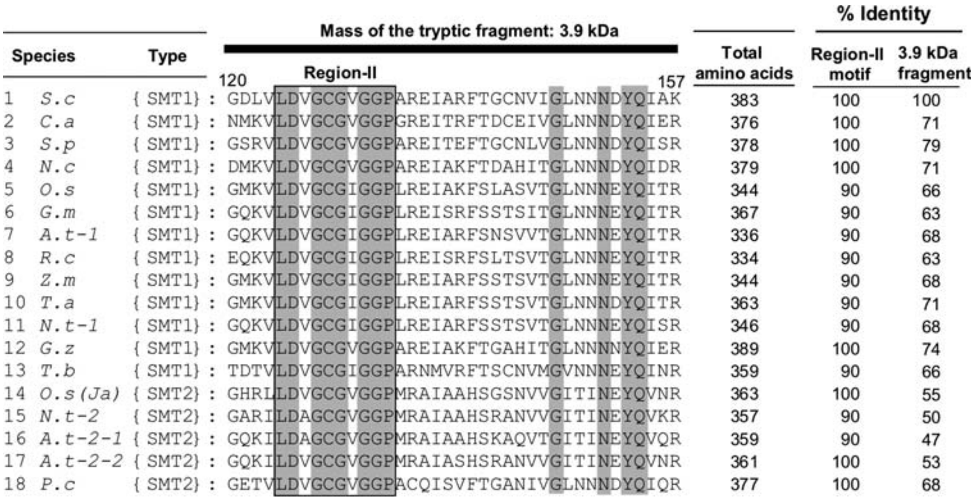

	Species	Type		Mass of the tryptic fragment: 3.9 kDa	Total amino acids	% Identity	
				120 Region-II 157		Region-II motif	3.9 kDa fragment
1	*S.c*	{ SMT1}	:	GDLVLDVGCGVGGPAREIARFTGCNVIGLNNNDYQIAK	383	100	100
2	*C.a*	{ SMT1}	:	NMKVLDVGCGVGGPGREITRFTDCEIVGLNNNDYQIER	376	100	71
3	*S.p*	{ SMT1}	:	GSRVLDVGCGVGGPAREITEFTGCNLVGLNNNDYQISR	378	100	79
4	*N.c*	{ SMT1}	:	DMKVLDVGCGVGGPAREIAKFTDAHITGLNNNDYQIDR	379	100	71
5	*O.s*	{ SMT1}	:	GMKVLDVGCGIGGPLREIAKFSLASVTGLNNNEYQITR	344	90	66
6	*G.m*	{ SMT1}	:	GQKVLDVGCGIGGPLREISRFSSTSITGLNNNEYQITR	367	90	63
7	*A.t-1*	{ SMT1}	:	GQKVLDVGCGIGGPLREIARFSNSVVTGLNNNEYQITR	336	90	68
8	*R.c*	{ SMT1}	:	EQKVLDVGCGIGGPLREISRFSLTSVTGLNNNEYQITR	334	90	63
9	*Z.m*	{ SMT1}	:	GMKVLDVGCGIGGPLREIARFSSTSVTGLNNNEYQITR	344	90	68
10	*T.a*	{ SMT1}	:	GMKVLDVGCGIGGPLREIARFSSTSVTGLNNNDYQITR	363	90	71
11	*N.t-1*	{ SMT1}	:	GQKVLDVGCGIGGPLREIARFSSTSVTGLNNNEYQISR	346	90	68
12	*G.z*	{ SMT1}	:	GMKVLDVGCGVGGPAREIAKFTGAHITGLNNNNYQIER	389	100	74
13	*T.b*	{ SMT1}	:	TDTVLDVGCGIGGPARNMVRFTSCNVMGVNNNEYQINR	359	90	66
14	*O.s(Ja)*	{ SMT2}	:	GHRLLDVGCGVGGPMRAIAAHSGSNVVGITINEYQVNR	363	100	55
15	*N.t-2*	{ SMT2}	:	GARILDAGCGVGGPMRAIAAHSRANVVGITINEYQVKR	357	90	50
16	*A.t-2-1*	{ SMT2}	:	GQKILDAGCGVGGPMRAIAAHSKAQVTGITINEYQVQR	359	90	47
17	*A.t-2-2*	{ SMT2}	:	GQKILDVGCGVGGPMRAIASHSRANVVGITINEYQVNR	361	100	53
18	*P.c*	{ SMT2}	:	GETVLDVGCGVGGPACQISVFTGANIVGLNNNDYQIQR	377	100	68

Fig. 9 Partial sequence alignments of 18 fungal and plant SMTs. The alignments are based on the sequence obtained from the Edman degradation of the [*methyl*-$^3H_3$]AdoMet wild-type yeast SMT peptide adduct. The appropriate amino acid numbering for the wild-type yeast-SMT peptide fragment is indicated. The 18 SMTs, indicated by the number are as follows: *1 Saccharomyces cerevisiae*, CAA52308; *2 Candida albicans*, AAC26626; *3 Schizosaccharomyces pombe*, CAB16897; *4 Neurospora crassa*, CAB97289; *5 Oryza sativa*, AAC34989; *6 Glycine max*, AAB04057; *7 Arabidopsis thaliana 1*, AAG28462; *8 Ricinus communis*, AAB62812; *9 Zea mays*, AAC04265; *10 Triticum aestivum*, AAB37769; *11 Nicotiana tabacum 1*, AAC34951; *12 Gibberella zeae*, EAA70778; *13 Trypanosoma brucei*, AAZ40214; *14 Oryza sativa sub sp. Japonica*, AAC34988; *15 Nicotiana tabacum* 2, T03848; *16 Arabidopsis thaliana 2-1*, CAA61966; *17 Arabidopsis thaliana 2–2*, AAB62809; *18 Pneumocystis carinii*, AAK54439. The type of each SMT, total length of the respective primary sequence and % identities within Region-II signature motif and in the 38 residue long partial fragment are indicated

(Fig. 9). Within the domain, a stretch of highly conserved residues is boxed and is referred to as Region-II to signify the similarities with GXGXG or GXG motif which is recognized as a hallmark of nucleotide (AdoMet) binding site in the Class-I type of AdoMet dependent methyltransferases superfamily of proteins [5]. The % identity within the Region-II motif ranged from 90 to 100% and 47–79% for the entire 3.9-kDa fragment relative to Erg6p sequence (Fig. 9). Overall, we were able to find 12 absolutely conserved amino acids within the 38 residue long Erg6p AdoMet binding segment. Thus, our plan was to determine which of the conserved residues in the adduct are directly involved with AdoMet binding. In other MTases, the AdoMet photoincorporation site has been established to be either a tyrosine, proline, aspartate (glutamate) or cysteine residue [6–12, 38], which are present in the radioactive tryptic fragment at Asp125, Cys128, Pro133, Asp152 and Tyr153. In this study, the relevant amino acids were replaced with leucine, phenylalanine or serine. The resulting proteins were expressed, partially purified and tested kinetically and via photo-incorporation.

Previously, through non-conservative mutagenesis experiments of conserved acidic residues in the SMT, the Asp125 and Asp152 were identified as key residues to AdoMet binding [34]. In similar fashion, to examine the role of Cys128 and Pro133, leucine, mutants were constructed and screened for SMT activity. These mutants exhibited no change either in protein purification process or native molecular weights compared to the wild-type yeast-SMT enzyme (data not shown). However, both Cys128Leu and Pro133Leu mutants turned out to be inactive (Table 2). The lack of catalytic competence was investigated further through binding studies for the two substrates which either showed AdoMet binding to be poor (Cys128) or no binding even at the highest concentration of AdoMet tested at 40 µM (Pro133). On the other hand, both mutants continued to bind zymosterol within the margin of acceptable binding for catalytic behavior. A second mutation of Cys128 to Ser was made to determine the importance of the thiol group to catalysis. The Cys128Ser mutant retained nearly 50% of the SMT activity compared to the wild-type (Table 2), suggesting that the Cys128 sulfur group is not essential to activity. In the C-terminal of this peptide fragment, the absolutely conserved Tyr residue (Tyr153) was replaced with phenylalanine or leucine. In both of the mutants, catalytic activity was retained (Table 2). Earlier, the mutational analysis of conserved acidics in the yeast-SMT suggested a potential role of Asp152 residue towards AdoMet binding [34]. The new results suggest that Cys128 and Pro133 can be important to AdoMet binding and ruled out Tyr153 as essential to activity. In further support to this proposal, none of the active mutants exhibited a gain in function where the zymosterol substrate was converted to fecosterol, which in turn can be converted to multiple 24-ethyl sterol products (data not shown), as reported for mutants of Region 1 [29, 30]. In order to examine these

Table 2 Effect of site-directed mutagenesis on AdoMet binding and photoaffinity labeling

Strain	K_m (μM)	k_{cat} (min^{-1})	K_d^a (μM) zymosterol	K_d^b (μM) AdoMet	% Photolabeled[c]
Wild-type	17.0	0.65 ± 0.01	4.0	4.0	100 ± 10
Asp125Leu[d]	NA	NA	6.0	12.0	30 ± 8
Cys128Leu	NA	NA	5.0	28.0	<1.0 ± 0.5
Cys128Ser	30.0	0.3 ± 0.01	5.0	8.0	ND
Pro133Leu	NA	NA	15.0	NB	<1.0 ± 0.5
Asp152Leu[d]	NA	NA	5.0	14.0	35 ± 6
Tyr153Leu	17.0	0.6 ± 0.01	4.0	4.0	ND
Tyr153Phe	16.0	0.2 ± 0.02	7.0	13.0	55 ± 10

All values represent an average of three independent determinations. The standard errors between the trials were 5 and 10%

k_{cat} the catalytic turnover value was determined from partially purified enzyme preparations using varied amounts of zymosterol and a fixed [*methyl*-$^3H_3$]AdoMet concentration of 100 μM as per standard assay conditions in buffer A, *NA* not active or not applicable, *NB* no binding, *ND* not determined

[a] Zymosterol binding was determined by filter binding assays with varied concentration of [3-^{3}H]zymosterol from 0 to 28 μM with the SMT protein concentration held at 0.25 μM in buffer A

[b] AdoMet binding was determined by equilibrium dialysis with varied concentration of [*methyl*-$^3H_3$]AdoMet from 0 to 40 μM and protein concentration held at 0.16 μM in buffer A

[c] % Photoaffinity labeling was determined by H_2O_2 digestion or equilibrium dialysis of photolabeled mixture

[d] The mutants were prepared and studied as in [34]

residues further as potential AdoMet photoincorporation site(s), we subjected the corresponding mutants to AdoMet photoaffinity labeling studies. Both Cys128Leu and Pro133Leu mutants failed to show any AdoMet labeling while the acidic mutants, Asp125Leu and Asp152Leu showed AdoMet photolabeling efficiencies of 30–40% and the Tyr153Phe mutant exhibited approximately 60% AdoMet photolabeling action compared to the native Erg6p (Table 2). These results indicate that one or both Cys128 and Pro133 can be covalently bound to the AdoMet during the photolabeling of the wild-type Erg6p.

Discussion

The SMTs are highly conserved sterol catalysts and differ from other phytosterol biosynthetic enzymes in the type and timing of the chemical reaction employed and differ kinetically from other MTases with respect to substrate recognition of the acceptor molecule. To date, no structural data is available for the yeast sterol methyltransferase that shows the AdoMet binding pocket. However, by employing a highly specific photoaffinity labeling procedure in the presence and absence of AdoHcy analogs, we observed high specificity of photolabeling of AdoMet to Erg6p, indicating AdoMet is covalently bound to the enzyme. Our research findings also revealed the first fifteen residues of the AdoMet-Erg6p peptide adduct are associated with a highly conserved (90–100%) motif among phylogenetically diverse SMTs (i.e., Region II) linked to the G*X*G*X*G motif of Class-I type MTases. From these observations, it would appear that the SMT is a Class-I type MTase with a AdoMet binding fold in the active site similar to related MTases [6–12, 38].

Although an exacting analysis of the peptide labeled species was not forthcoming from the initial work, subsequent functional analysis of key residues in the tryptic digest fragment by directed mutation indicated that two of them can interact with AdoMet after the photolabeling procedure. In a leucine scanning experiment, residues mutated at positions 125, 128, 133 and 152 and153, considered as possible contact amino acids in the peptide, were found to generate different activities that ranged from none to 100%. For the Cys128Leu and Pro133Leu mutants, catalytic competence was lost in conjunction with lost photolabeling activity, suggesting these resides contact AdoMet in the active site. Conservative replacement of Cys128 with Ser resulted in 50% of SMT activity and a slightly lower binding affinity (K_d) towards AdoMet relative to the native Erg6p, indicated that Cys128 interacts with AdoMet via hydrogen bonding interactions. On the other hand, the Tyr153 mutants behaved similarly to the wild-type Erg6p suggesting they are not in contact with AdoMet directly. The acidic residues mutated to leucine at Asp125 and Asp152 were inactive, yet reactive to photoaffinity labeling; they exhibited reduced photolabeling efficiency of 30–40% compared to the wild-type. Consequently, these residues are not likely attached to AdoMet upon photolabeling. Still unclear is which of these residues in the adduct bind AdoMet in covalent fashion. To resolve these anomalies, future experiments to unmask the catalytic amino acids bound to AdoMet after the photoaffinity labeling experiments are warranted.

SMTs have clearly been shown to be essential to normal growth and maturation of microbes and plants as well as a target for rational drug design in ergosterol-dependent diseases. This suggests that the family of SMTs may have particular importance to human health. Because there are no known 24-alkyl sterols synthesized in mammals, we believe that a thorough study of the distribution and enzyme properties of the SMT, including testing dual action inhibitors designed to disrupt the active center for methyl donor and acceptor is warranted. This investigation has enabled us to determine the potential roles of active site amino acids specifically in the Region-II (Erg6p nomenclature) of the yeast SMT. It is only a matter of time to the discovery of similar findings in other SMT types due to the highly conserved nature of this signature motif relative to Erg6p sequence. Deeper insights into the kind of interaction of AdoMet with the SMT should be possible from the three-dimensional structural data captured from covalently bound AdoMet and through affinity labeling of a suicide substrate, such as 26,27-dehydrozymosterol, where the AdoMet is part of the sterol covalently bound to the yeast-SMT. These investigations are underway.

Acknowledgments This work has been made possible by the following grants awarded to W.D.N.: National Science Foundation (MCB 0417436) and the Welch Foundation (D-1276). We are grateful to Dr. Julie Marshall for the technical assistance and advice of photolabeling techniques during the initial part of this investigation.

References

1. Faunam EB, Blumenthal RM, Cheng X (1999) Structure and evolution of AdoMet-dependent methyltransferases, in S-adenosylmethionine-dependent methyltransferases: structures and functions. In: Cheng X, Blumenthal RM (eds) World Scientific Publishing, Singapore, pp 1–38
2. Kozbial PZ, Mushegian AR (2005) Natural history of *S*-adenosylmethionine-binding proteins. BMC Struct Biol 5:19
3. Schubert HL, Blumenthal RM, Cheng X (2003) Many paths to methyltransfer: a chronicle of convergence. Trends Biochem Sci 28:329–335
4. Kagan RM, Clarke S (1994) Widespread occurrence of three sequence motifs in diverse *S*-adenosyl-L-methionine-dependent methyltransferases suggests a common structure for these enzymes. Arch Biochem Biophys 310:417–427
5. Malone T, Blumenthal RM, Cheng X (1995) Structure-guided analysis reveals nine sequence motifs conserved among DNA amino-methyltransferases, and suggests a catalytic mechanism for these enzymes. J Mol Biol 253:618–632
6. Syed SK, Kim S, Paik WK (1993) Identification of *S*-adenosyl-L-methionine binding site of protein carboxyl-*O*-methyltransferase using 8-azido-*S*-adenosyl-L-methionine. Biochemistry 32:2242–2247
7. Sumner J, Jencks DA, Khani S, Matthews RG (1986) Photoaffinity labeling of methylenetetrahydrofolate reductase with 8-azido-*S*-adenosyl-L-methionine. J Biol Chem 261:7697–7700
8. Som S, Friedman S (1990) Direct photolabeling of the *Eco*RII methyltransferase with *S*-adenosyl-L-methionine. J Biol Chem 265:4278–4283
9. Velkov T, Lawen A (2003) Photoaffinity labeling of the *N*-methyltransferase domains of cyclosporine synthetase. Photochem Photobiol 77:129–137
10. Subbaramaiah K, Simms SA (1992) Photolabeling of CheR methyltransferase with *S*-Adenosyl-L-methionine (AdoMet): studies on the AdoMet binding site. J Biol Chem 267:8636–8642
11. Velkov T, Lawen A (2003) Mapping and molecular modeling of *S*-adenosyl-L-methionine binding sites in *N*-methyltransferase domains of multifunctional polypeptide cyclosporin synthetase. J Biol Chem 278:1137–1148
12. Shields DJ, Altarejos JY, Wang X, Agellon LB, Vance DE (2003) Molecular dissection of the *S*-adenosylmethionine-binding site of phosphatidylethanolamine *N*-methyltransferase. J Biol Chem 278:35826–35836
13. Kornblatt J, Muzac I, Lim Y, Ahn JH, Ibrahim RK (2004) Role of Serine 286 in cosubstrate binding and catalysis of flavanol-*O*-methyltransferase. Biochem Cell Biol 82:531–537
14. Hacker C, Glinski M, Hornbogen T, Doller A, Zocher R (2000) Mutational analysis of the *N*-methyltransferase domain of the multifunctional enzyme enniatin synthetase. J Biol Chem 275:30826–30832
15. Nes WD (2005) Enzyme redesign and interactions of substrate analogues with sterol methyltransferase to understand phytosterol diversity, reaction mechanism and the nature of the active site. Biochem Soc Trans 33:1189–1196
16. Jayasimha P, Bowman CB, Pedroza JM, Nes WD (2006) Engineering pathway enzymes to understand the function and evolution of sterol structure and activity. Rec Adv Phytochem 40:212–251
17. Moreau RA, Whitaker BD, Hicks KB (2002) Phytosterols, phytostanols, and their conjugates in foods: structural diversity, quantitative analysis, and health promoting uses. Prog Lipid Res 41:457–500
18. Song Z, Nes WD (2007) Sterol biosynthesis inhibitors: potential for transition state analogs and mechanism-based inactivators targeted at sterol methyltransferase. Lipids 42:15–33
19. Burbiel J, Bracher F (2003) Azasteorids as antifungals. Steroids 68:587–594
20. Kaneshiro ES, Rosenfeld JA, Bassenlin-eiweida M, Stringer JR, Keely SP, Smulian AG, Giner J-L (2002) The *Pneumocystis carinii* drug target *S*-adenosyl-L-methionine: sterol C-24 methyltransferase has a unique substrate specificity. Mol Microbiol 44:989–999
21. Roberts CW, McLeod R, Rice DW, Ginger M, Chance ML, Goad LJ (2003) Fatty acid and sterol metabolism: potential antimicrobial targets in apicomplexan and trypanosomatid parasitic protozoa. Mole Biochem Parasitol 126:129–142
22. Nes WD (2000) Sterol methyltransferase: enzymology and inhibition. Biochim Biophys Acta 1529:63–88
23. Bloch KE (1983) Sterol structure and membrane function. CRC Crit Rev Biochem 14:47–82
24. Rodriquez RJ, Low C, Bottema CDK, Parks LW (1985) Multiple functions for sterols in *Saccharomyces cerevisiae*. Biochim Biophys Acta 837:336–343
25. Nes WD, Heupel RC (1986) Physiological requirement for biosynthesis of multiple 24β-methyl sterols in *Gibberella fujikuroi*. Arch Biochem Biophys 244:211–217
26. Schaller H (2004) New aspects of sterol biosynthesis in growth and development of higher plants. Plant Physiol Biochem 42:465–476
27. Bouvier-nave P, Husselstein T, Benveniste P (1998) Two families of sterol methyltransferases are involved in the first and second methylation steps of plant sterol biosynthesis. Eur J Biochem 256:88–96

28. Veeramachaneni PP (2005) Active site mapping of yeast recombinant sterol methyltransferase (Y81 W) from *Saccharomyces cerevisiae* and inhibition of ergosterol biosynthesis in *Candida albicans*. Master Thesis. Texas Tech University, Lubbock, pp 1–87
29. Nes WD, Marshall JA, Jia Z, Jaradat TT, Song Z, Jayasimha P (2002) Active site mapping and substrate channeling in the sterol methyltransferase pathway. J Biol Chem 277:42549–42556
30. Nes WD, Mc Court BS, Marshall JA, Ma J, Dennis AL, Lopez M, Li H, He L (1999) Site-directed mutagenesis of the sterol methyltransferase active site from *Saccharomyces cerevisiae* results in formation of novel 24-ethyl sterols. J Org Chem 64:1535–1542
31. Nes WD, Sinha A, Jayasimha P, Zhou W, Song Z, Dennis AL (2006) Probing the sterol binding site of soybean sterol methyltransferase by site-directed mutagenesis: functional analysis of conserved aromatic amino acids in Region 1. Arch Biochem Biophys 448:23–30
32. Zhou W, Lepesheva GI, Waterman MR, Nes WD (2006) Mechanistic analysis of a multiple product sterol methyltransferase implicated in ergosterol biosynthesis in *Trypanosoma brucei*. J Biol Chem 281:6290–6296
33. Nes WD, Song Z, Dennis AI, Zhou W, Nam J, Miller MM (2003) Biosynthesis of phytosterols. Kinetic mechanism for the enzymatic *C*-methylation of sterols. J Biol Chem 278:34505–34516
34. Nes WD, Jayasimha P, Zhou W, Kanagasabai R, Jin C, Jaradat TT, Shaw RW, Bujnicki JM (2004) Sterol methyltransferase. Functional analysis of highly conserved residues by site-directed mutagenesis. Biochemistry 43:569–576
35. Cohen SL, Chait BT (1996) Influence of matrix solution conditions on the MALDI-MS analysis of peptides and proteins. Anal Chem 68:31–37
36. Huang C-C, Smith CV, Glickman MS, Jacobs WR Jr, Sacchetini JC (2002) Crystal structure of mycolic acid cyclopropane synthases from *Mycobacterium tuberculosis*. J Biol Chem 277:11559–11569
37. McCammon MT, Parks LW (1981) Inhibition of sterol transmethylation by *S*-adenosylhomocysteine analogs. J Bacteriol 145:106–112
38. Chavan AJ, Ensor CM, Wu P, Haley BE, Tai HH (1993) Photoaffinity labeling of human placental NAD($^+$)-linked 15-hydroxyprostaglandin dehydrogenase with [α-^{32}P]^{2}N$_3$NAD$^+$. Identification of a peptide in the adenine ring binding domain. J Biol Chem 268:16437–16442

Lipids (2008) 43:695–702
DOI 10.1007/s11745-008-3191-4

ORIGINAL ARTICLE

Increase of Serum Cholesterol Levels by Heat-Moisture-Treated High-Amylose Cornstarch in Rats Fed a High-Cholesterol Diet

Haruhide Udagawa · Chika Kitaoka ·
Tatsuaki Sakamoto · Kazuo Kobayashi-Hattori ·
Yuichi Oishi · Soichi Arai · Toshichika Takita

Received: 24 October 2007 / Accepted: 25 April 2008 / Published online: 29 May 2008
© AOCS 2008

Abstract The effects of four cornstarches containing various contents of resistant starch on serum and liver cholesterol levels in rats fed a high-cholesterol diet were investigated. Male Sprague Dawley rats (aged 4 weeks) were divided into four groups ($n = 7$) and fed high-cholesterol diets containing 15% of cornstarch (CS), heat-moisture-treated CS (HCS), high-amylose CS (HA), or heat-moisture-treated HA (HHA) for 21 days. The results showed that the serum and hepatic level of total cholesterol, LDL-cholesterol, and triglyceride in rats of the HHA group and their arteriosclerosis index were significantly higher, suggesting that HHA increases the risk of arteriosclerosis under a high-cholesterol dietary condition. No significant between-group differences were noted in the levels of plasma mevalonic acid and hepatic HMG-CoA reductase mRNA, whereas fecal cholesterol excretion was significantly higher in the HHA group, indicating that the elevation of the serum and liver cholesterol levels was not due to the promotion of liver cholesterol synthesis and cholesterol absorption in the intestine.

Keywords High-cholesterol diet · Resistant starch · High-amylose cornstarch · Serum cholesterol · Rats

Abbreviations

RS	Resistant starch
CS	Cornstarch
HCS	Heat-moisture-treated cornstarch
HA	High-amylose cornstarch
HHA	Heat-moisture-treated high-amylose cornstarch

Introduction

Resistant starch (RS) is defined as "starch and partially degraded starch not absorbed by the healthy human small intestine" [1]. RS can be present in all starch-containing foods (grains, legumes and tubers) and is influenced by both botanical source and processing, and classified into three types: starch that cannot be physically exposed to digestive enzymes, raw starch not readily affected by digestive enzymes, and retrograded starch after cooking. In terms of such RS, there are many reports on the physiological functions. For instance, RS had a preventive effect against intestinal tumorigenesis due to the alteration of the colonic luminal environment by increasing the concentration of short chain fatty acid and lowering production of potentially harmful fermentation products [2]. In addition, RS has been shown to be fermented in the colon, and exhibit a dietary fiber-like effect [3]. Among the functions of RS, the noteworthy one is a hypocholesterolemic effect. The ingestion of RS contained in normal diets with no cholesterol loaded has been reported to decrease the serum cholesterol level, serum triglyceride level and epididymal fat weight [4–7]. In particular, HA and HHA, which have higher RS contents, are expected to exert the decreasing effect of serum cholesterol concentration. Liu et al. [8] showed that HA and HHA decreased the level of serum and liver cholesterol in ovariectomized rats. Vanhoof and Schrijver [9] have reported that the administration of retrograded high-amylose cornstarch (HA) to rats fed on a 1% cholesterol-containing diet decreased the serum cholesterol level. They have suggested that the promotion of coprostanol excretion

H. Udagawa (✉) · C. Kitaoka · T. Sakamoto ·
K. Kobayashi-Hattori · Y. Oishi · S. Arai · T. Takita
Department of Nutritional Science,
Faculty of Applied Bioscience, Tokyo University of Agriculture,
1-1-1 Sakuragaoka, Setagaya-ku, Tokyo 156-8502, Japan
e-mail: haruhideudagawa@ybb.ne.jp

by RS contained in HA was involved in the serum cholesterol-lowering action. We also reported that HHA was decreased serum cholesterol level in rats fed a diet with 0.1% cholesterol, 0.1% cholic acid and 10% lard [10].

However, little information is available about the function of RS under the condition of a high-cholesterol diet. Modern diets have high-levels of animal fat and cholesterol. Therefore, the increase in the level of serum cholesterol is becoming a concern because of increasing the concentration of serum LDL-cholesterol by ingestion of animal fat [11]. Consequently, it is necessary to investigate the physiological function of RS under high-cholesterol dietary conditions.

In this study, we made our study focused on heat-moisture-treated HA (HHA) whose RS content is increased more. Rats were fed a high-cholesterol diet constituted with four types of cornstarch, including HHA, to investigate their effects on the serum and liver cholesterol levels.

Materials and Methods

Materials

Cornstarch (CS), heat-moisture-treated CS (HCS) (Delicastar 200), high-amylose CS (HA), and heat-moisture-treated HA (HHA) (Amylogel HB450) were obtained from SANWA CORNSTARCH Co., Ltd (Nara, Japan). Determinar TC 555 kit was purchased from Kyowa Medex Co., Ltd (Tokyo, Japan). Triglyceride E test Wako and total bile acid test Wako kits were obtained from Wako Pure Chemical Industries Ltd (Osaka, Japan). Resistant starch measurement kit was purchased from Megazym (Sydney, Australia).

Resistant Starch Content of Various Types of Cornstarch

The RS content in samples was measured with a resistant starch measurement kit.

Animals and Diets

Four-week-old male Sprague Dawley rats were purchased from Clea Japan Co. (Tokyo, Japan). The rats were individually housed in stainless cages, and maintained in an animal room controlled at 23–25 °C and 50–56% humidity under a 12-h lighting cycle (light-on 8:00–20:00). The animals were made free access to food and drinking water. After acclimatization with a normal diet based on AIN-76 feed composition [12] for 1 week, animals were divided into four groups ($n = 7$): CS, HCS, HA, and HHA groups, and fed for 21 days on a high-cholesterol diet containing each of the starch samples. High-cholesterol diets containing each starch were prepared by replacing β-cornstarch with each cornstarch and adding 0.5% cholesterol, 0.25% cholic acid and 10% lard at the expense of sucrose (Table 1). The animals were dissected on the final day of experimental period under Nembutal anesthesia. Serum was prepared by centrifugation of the blood sample (3,000 rpm, 4 °C, 20 min), and used for the analysis of serum lipid and mevalonic acid. The liver was washed with physiological saline, rapidly frozen in liquid nitrogen, and then used for the analyses of liver lipids and HMG-CoA reductase mRNA. Feces were collected 3 days before dissection, weighed, and subjected to lipid analysis. Animal experiments in this study were performed in conformity to the guidelines for maintenance and handling of

Table 1 Composition of experimental diets

Ingredient	CS (g/kg diet)	HCS (g/kg diet)	HA (g/kg diet)	HHA (g/kg diet)
Casein	200.0	200.0	200.0	200.0
DL-methionine	3.0	3.0	3.0	3.0
Sucrose	442.5	442.5	442.5	442.5
Cornstarch	0.0	0.0	0.0	0.0
Cellulose powder	50.0	50.0	50.0	50.0
Lard	100.0	100.0	100.0	100.0
Mineral mixture[a]	35.0	35.0	35.0	35.0
Vitamin mixture[a]	10.0	10.0	10.0	10.0
Choline bitartrate	2.0	2.0	2.0	2.0
Cholic acid	2.5	2.5	2.5	2.5
Cholesterol	5.0	5.0	5.0	5.0
Various CS	150.0	150.0	150.0	150.0

CS cornstarch, *HCS* heat-moisture-treated cornstarch, *HA* high-amylose cornstarch, *HHA* heat-moisture-treated high-amylose cornstarch

[a] Based on AIN-76 mixture (Oriental Yeast Co., Tokyo, Japan)

experimental animals established by the Tokyo University of Agriculture Ethics Committee.

Lipid Analysis

The serum levels of total cholesterol (TC), HDL-cholesterol, LDL-cholesterol, triglyceride, and total lipid were measured using an automatic biochemical analyzer model 7450 (Hitachi Co., Tokyo, Japan). The arteriosclerosis index was calculated from the formula of (TC − HDL-cholesterol)/HDL-cholesterol.

Liver sample solutions were prepared as follows: 1.000 g of the excised liver was homogenized in a chloroform-methanol mixture, 2:1 (*v*/*v*), kept in a dark room for 1 day, and then filtered. The liver TC and triglyceride were measured with Determinar TC 555 kit and a Triglyceride E Test Wako kit, respectively. The phospholipid level was measured by molybdic acid colorimetry [13].

Fecal sample solutions were prepared as follows: freeze-dried feces were powdered, and 0.5 g of the powder was heat-extracted with a chloroform-methanol mixture, 2:1 (*v*/*v*), at 45 °C for 10 h. The fecal levels of TC and total bile acid were measured using a Determinar TC 555 kit and total bile acid test Wako kit, respectively. The RS level in feces was measured using a resistant starch measurement kit.

Organic Acid Analysis for Cecal Contents

The organic acid level in the cecal contents was measured by HPLC [14]. The sample solution was prepared as follows: a sample of the cecal contents (300 mg) was dissolved with 2 ml of 10 mM sodium hydroxide solution and centrifuged at 10,000×*g* for 15 min. Then, 1 ml of the supernatant was combined with 1 ml of chloroform and centrifuged. The supernatant was filtered through a 0.2-µm membrane filter before subjecting to HPLC. For HPLC analysis, two Shim-pack SCR-102H columns (8 mm i.d. × 300 mm, Shimadzu, Kyoto, Japan) and an electroconductivity detector (CDD-6A, Shimadzu) were used. The mobile phase for separation was 5 mM *p*-toluenesulfonic acid aqueous solution, and that for detection was 20 mM bis-(2-hydroxyethyl) iminotris (hydroxymethyl) methane (Bis–Tris) aqueous solution containing 5 mM *p*-toluenesulfonic acid aqueous solution and 100 µM EDTA. The HPLC was carried out at a flow rate of 0.8 ml/min and with a column temperature of 40 °C.

Plasma Mevalonic Acid Analysis

The plasma mevalonic acid (MVA) level was measured by HPLC by SRL Inc. (Tokyo, Japan).

RNA Extraction

RNA was extracted from the liver by the method reported by Chomczynski and Sacchi [15].

First-Strand cDNA Synthesis

cDNA was prepared from 5 µg of DNase I-treated total RNA using reverse transcriptase (Super-script III^{TM}, Invitrogen, CA, USA) following the instructions of the manufacturer.

Quantitative PCR

Quantitative PCR and hybridization primers were synthesized by Applied Biosystems (Foster, IN, USA). Oligonucleotide primers were designed to amplify rat HMG-CoA reductase nucleotide 1412–1503 (GenBank accession number NM013134) and β-actin nucleotide 2838–3041 (GenBank accession number V01217). The sequences of the primers are as follows : rat HMG-CoA reductase sense primer, 5′-AGA GAA AGG TGC GAA GTT CCT TAG T-3′ and HMG-CoA reductase antisense primer, 5′-CCA TGA GGG TTT CCA GTT TGT AG-3′; and β-actin sense primer, 5′-CCC TGG CTC CTA GCA CCA T-3′ and β-actin antisense primer, 5′-GAT AGA GCC ACC AAT CCA CAC A-3′.

The predicted PCR product sizes were 192 (rat HMG-CoA reductase) and 204 bp (β-actin). The amplification products obtained following the manufacturer's instructions were detected using a TaqMan universal PCR master mix core reagent kit (Applied Biosystems).

The rat HMG-CoA reductase hybridization probe was a nucleotide corresponding to 1452–1479, 5′-CAG TTG G TC AAT GCT AAG CAC ATC CCA G-3′, and the 5′ and 3′ ends were labeled with 6-carboxyfluorescein (FAM) and *N*,*N*,*N*′,*N*′-tetramethyl-6-carboxyrhodamine (TAMRA), respectively. The β-actin probe corresponded to 2865–2866 and 2991–3015 (2867–2990 corresponded to an intron), 5′-AGA TCA TTG CTC CTC CTG AGC GCA AGT-3′, and the 5′ and 3′ ends were labeled with VIC^{TM} and TAMRA, respectively. The mRNA level of HMG-CoA reductase was measured by quantitative PCR using an ABI Prism 7300 apparatus (Applied Biosystems), and presented as the relative value to the mRNA level of β-actin.

Statistical Analysis

A statistical analysis was performed with software, SPSS 15.0J. The statistically significant differences of the means among four groups were evaluated by non-parametric statistical analysis (Kruskal–Wallis) and individual comparisons were made by Tukey's multiple comparison test.

A statistically significant difference of the means between two groups was evaluated by the Mann–Whitney test.

Results

Resistant Starch Content of Various Types of Cornstarch

Figure 1 shows the RS contents of the four cornstarch samples used in this study. The RS content was significantly higher in HA and HHA than in the other types.

Food Intake and Body Weight

Table 2 shows the food intake and initial and final body weights in rats fed the high-cholesterol diets containing each of the starch samples. No significant between-group difference was found in terms of food intake. The final body weight was not significantly different between the CS and HCS groups or between the HA and HHA groups, but was significantly lowest in the HHA group whose RS content was higher than CS and HCS groups, showing that the high-RS diet was effective in reducing body weight.

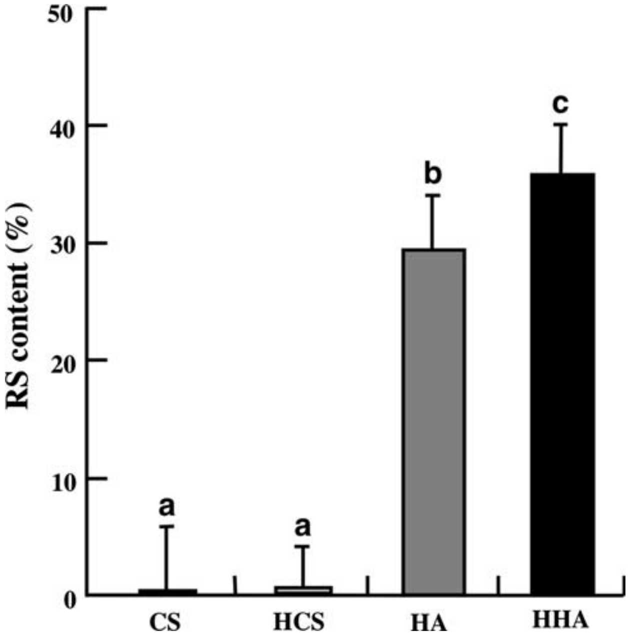

Fig. 1 Resistant starch contents in various types of cornstarch. Resistant starch contents in various types of cornstarch were measured with a resistant starch kit. *CS* cornstarch; *HCS* heat moisture treated cornstarch; *HA* high-amylose cornstarch; *HHA* heat-moisture-treated high-amylose cornstarch. Values are means ± SE ($n = 7$). *Bars* without a *common letter* represent significant differences at $P < 0.05$

Table 2 Effects of various types of cornstarch on food intake, and initial and final body weights in rats fed experimental diets

	CS	HCS	HA	HHA
Food intake (g/day)	20.6 ± 0.5	20.3 ± 0.4	21.1 ± 0.6	20.4 ± 0.6
Initial body weight (g)	147 ± 2	147 ± 2	149 ± 2	150 ± 2
Final body weight (g)	332 ± 7^{b}	321 ± 3^{b}	316 ± 2^{ab}	304 ± 2^{a}

Values are means ± SE ($n = 7$). Values within a row with different superscript letters denote that there are significant differences at $P < 0.05$. For abbreviations see Table 1

Serum Lipid Levels

Table 3 shows the serum lipid levels in rats fed the high-cholesterol diets containing each starch. The serum TC level was significantly higher in the HHA group than in the CS and HCS groups. The LDL-cholesterol level was significantly increased in the HA and HHA groups compared to the CS and HCS groups. No significant differences were observed in the level of HDL-cholesterol or total lipid level among the groups. The triglyceride level and arteriosclerosis index were significantly higher in the HHA group than in the CS, HCS, and HA groups.

Liver Tissue Weight and Liver Lipid Levels

Table 4 shows the liver weight and lipid levels in rats fed the high-cholesterol diets containing each starch. No significant difference was observed in the liver weight among the groups. The liver TC level was significantly higher in the HHA group than in the CS group. The levels of phospholipids and triglyceride in the test groups was similar to those in the control group.

Fecal Dry Weight, RS Content, and Lipid Levels

Table 5 shows the fecal dry weight, RS content, and lipid levels in rats fed the high-cholesterol diets containing each starch. The fecal dry weight was significantly higher in the HA and HHA groups, and increased as the RS level increased. In the RS content in feces, the HHA group was the highest of all groups, followed by HA, HCS, and CS groups, depending on the RS content of the diet. The fecal TC level was significantly higher in the HHA group than in the HCS group, showing that the TC level increased with an elevation in the RS content of the diet. The level of fecal bile acid was significantly increased in the HA and HHA groups compared to the HCS group.

Table 3 Effect of various types of cornstarch on serum lipid levels in rats fed experimental diets

	CS	HCS	HA	HHA
Total cholesterol (mmol/l)	5.67 ± 0.31^{a}	5.79 ± 0.34^{a}	6.52 ± 0.10^{ab}	7.40 ± 0.31^{b}
LDL-cholesterol (mmol/l)	3.93 ± 0.21^{a}	4.29 ± 0.26^{a}	5.71 ± 0.28^{b}	6.23 ± 0.26^{b}
HDL-cholesterol (mmol/l)	1.65 ± 0.09	1.73 ± 0.26	1.75 ± 0.05	1.58 ± 0.04
Triglycerides (mg/dl)	53.7 ± 9.5^{a}	52.0 ± 7.2^{a}	56.3 ± 6.7^{a}	87.2 ± 4.2^{b}
Total lipids (mg/dl)	523 ± 21	626 ± 61	616 ± 26	649 ± 44
Arteriosclerosis index	2.47 ± 0.21^{a}	2.42 ± 0.24^{a}	2.75 ± 0.11^{a}	3.74 ± 0.21^{b}

Values are means ± SE ($n = 7$). Values within a row with different superscript letters denote that there are significant differences at $P < 0.05$. For abbreviations see Table 1

Table 4 Effect of various types of cornstarch on liver weight and liver lipid levels in rats fed experimental diets

	CS	HCS	HA	HHA
Liver weight (g)	20.5 ± 1.1	18.3 ± 0.5	17.8 ± 0.2	17.7 ± 0.9
Liver lipids				
Total cholesterol (μmol/g)	175 ± 3^{a}	180 ± 5^{ab}	185 ± 8^{ab}	212 ± 14^{b}
Phospholipids (mg/g)	0.10 ± 0.01	0.17 ± 0.02	0.13 ± 0.05	0.19 ± 0.06
Triglyceride (mg/g)	87.0 ± 7.4	78.3 ± 3.3	71.4 ± 5.3	67.6 ± 2.7

Values are means ± SE ($n = 7$). Values within a row with different superscript letters denote that there are significant differences at $P < 0.05$. For abbreviations see Table 1

Table 5 Effects of various types of cornstarch on fecal parameters and fecal lipid levels in rats fed experimental diets

	CS	HCS	HA	HHA
Dry weight (g/day)	1.79 ± 0.15^{a}	1.64 ± 0.14^{a}	3.07 ± 0.11^{b}	3.60 ± 0.17^{b}
RS content (g/day)	0.01 ± 0.00^{a}	0.02 ± 0.00^{a}	0.64 ± 0.05^{b}	1.31 ± 0.08^{c}
Total cholesterol (μmol/day)	29.5 ± 1.5^{ab}	32.9 ± 1.9^{a}	35.6 ± 2.1^{ab}	38.6 ± 1.0^{b}
Total bile acid (mmol/day)	6.33 ± 0.57^{ab}	5.81 ± 0.30^{a}	8.16 ± 0.50^{c}	7.13 ± 0.37^{bc}

Values are means ± SE ($n = 7$). Values within a row with different superscript letters denote that there are significant differences at $P < 0.05$. For abbreviations see Table 1

Cecum Parameters

Table 6 shows the cecal tissue and content weights, pH, and organic acid level of the contents in rats fed the high-cholesterol diets containing each starch. The cecal tissue weight was significantly increased in the HHA group, compared to the CS group. No significant between-groups difference was found in the weight of cecal contents. The pH of the cecal contents was significantly lower in the HA and HHA groups. The maleic acid level of the cecal contents was significantly increased in the HA and HHA groups, compared to the CS and HCS groups. The level of succinic acid was higher in the HA and HHA groups than in the CS group. In the level of lactic acid and acetic acid, no significant difference was observed among the groups. The propionic acid and butyric acid levels were significantly lower in the HHA group than in the CS and HCS group.

Levels of Plasma Mevalonic Acid and Liver HMG-CoA Reductase mRNA

Figure 2 shows the plasma mevalonic acid and the liver mRNA levels of HMG-CoA reductase in rats fed the high-cholesterol diets containing each starch. The feeding of HHA did not change the plasma mevalonic acid level, an index of liver cholesterol synthesizing-enzyme activity, among the groups. The mRNA level of HMG-CoA reductase in the HHA group was similar to that in the CS group. The absence of significant differences in the mevalonic acid or mRNA level of HMG-CoA reductase in the liver was observed between the CS and HHA groups.

Table 6 Effect of various types of cornstarch on cecal parameters and organic acids in cecums of rats fed experimental diets

	CS	HCS	HA	HHA
Cecum				
Tissue weight (g)	0.45 ± 0.04^{a}	0.54 ± 0.04^{ab}	0.57 ± 0.01^{ab}	0.67 ± 0.04^{b}
Content weight (g)	2.35 ± 0.22	1.92 ± 0.18	2.25 ± 0.09	2.02 ± 0.14
pH	7.57 ± 0.09^{b}	7.45 ± 0.08^{b}	6.92 ± 0.06^{a}	6.88 ± 0.10^{a}
Organic acid (μmol/g wet cecal content)				
Maleic acid	1.38 ± 0.37^{a}	1.13 ± 0.21^{a}	2.78 ± 0.20^{bc}	3.37 ± 0.32^{c}
Succinic acid	0.59 ± 0.23^{a}	2.90 ± 0.61^{ab}	6.75 ± 1.22^{b}	6.87 ± 2.20^{b}
Lactic acid	1.02 ± 0.32	0.94 ± 0.11	1.43 ± 0.11	1.26 ± 0.16
Acetic acid	10.8 ± 1.6	9.82 ± 1.18	9.03 ± 1.36	7.16 ± 0.55
Propionic acid	2.31 ± 0.74^{b}	2.48 ± 0.49^{b}	2.27 ± 0.28^{ab}	1.65 ± 0.16^{a}
Butyric acid	1.17 ± 0.36^{b}	1.35 ± 0.20^{b}	0.92 ± 0.13^{ab}	0.45 ± 0.08^{a}

Values are means ± SE ($n = 7$). Values within a row with different superscript letters denote that there are significant differences at $P < 0.05$. For abbreviations see Table 1

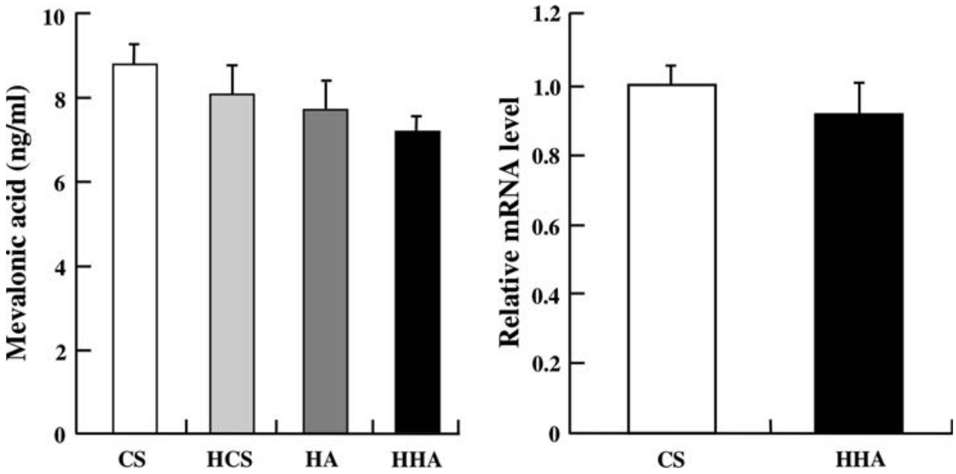

Fig. 2 Effects of various types of cornstarch on the levels of serum mevalonic acid and liver HMG-CoA reductase mRNA in rats fed a high-cholesterol diet. Mevalonic acid in serum was quantified by HPLC. The mRNA level of HMG-CoA reductase in the rat liver was measured by quantitative PCR. The mRNA level of HMG-CoA reductase was presented as the relative value to that of β-actin. *CS* cornstarch; *HCS* heat-moisture-treated cornstarch; *HA* high-amylose cornstarch; *HHA* heat-moisture-treated high-amylose cornstarch. Values are means ± SE ($n = 7$)

Discussion

In this study, we investigated the effect of HA and HHA, which have a high content of RS, on serum cholesterol levels in rats given a high-cholesterol diet. As a high-cholesterol diet, the diet containing 0.5% cholesterol, 0.25% cholic acid and 10% lard was used because such a diet increased serum cholesterol level in rats [16]. As a result, HHA increased the level of total cholesterol and triglyceride in serum, arteriosclerosis index and the level of cholesterol in the liver under the high-cholesterol diet condition (Table 3), although there are some reports that HHA decreased serum cholesterol level under the normal diet condition [4–7]. Similar to our results of HHA, HA increased the serum level of LDL-cholesterol. These increasing effects were not observed in rats fed a diet containing CS or HCS, suggesting that the high amylose content was a factor for the elevation of serum and liver cholesterol levels.

In this study, 0.5% cholesterol, 0.25% cholic acid and 10% lard in the high-cholesterol diet was added in order to increase the level of serum cholesterol. This diet condition was reported to lower the levels of HMG-CoA reductase activity and its mRNA level in the liver [17, 18]. In the present study, no significant differences were observed in the level of hepatic HMG-CoA reductase mRNA and the plasma level of mevalonic acid produced by hepatic HMG-CoA reductase [19] between the CS and HHA groups (Fig. 2). These results suggest that the promotion of cholesterol synthesis in the liver was not attributed to the serum and liver cholesterol-elevating effect by HHA ingestion.

In contrast, the lowering effect of resistant starch on the serum cholesterol level has previously been reported to be related to the promotion of bile acid excretion [20]. In addition, there is a report that the promotion of cholesterol uptake into the liver was a factor for the decreasing effect of resistant starch on the serum cholesterol level [21]. In this present study, no significant increase in bile acid excretion was apparent in any group fed on the HHA diet. Therefore, the promotion of bile acid excretion is not probably related to the increasing level of serum and liver cholesterol by HHA ingestion.

No information is still available on the elevation of serum level of cholesterol and triglyceride by intake of HA or HHA under the condition of a normal diet. Vanhoof and Schrijver [9] reported that retrograded HA lowered the serum cholesterol level in rats fed on 1% cholesterol- and 0.1% cholic acid-loading diet. However, their study differs from our study in view of the use of lard-unloaded diet and resistant starch contents used. Verbeek et al. [20] reported that the retrograded amylose decreased the serum cholesterol level in rats fed a cholesterol- and lard-loading diet. However, their study differs from our study in view of the use of cholic acid-unloaded diet. We investigated the effect of HHA on serum cholesterol level in rats fed a diet with 0–0.1% cholesterol, 0.1% cholic acid and 10% lard, and showed that HHA decreased serum cholesterol level in the rats fed a diet with 0.1% cholesterol [10]. In addition, our preliminary experiment of 0.25% instead of 0.1% cholic acid showed that a HHA had a lowering effect on the serum cholesterol level in rats fed on a 0.5% cholesterol and 10% lard diet (data not shown). Therefore, these results suggest that the serum level of the cholesterol- and triglyceride-elevating effect of HHA was dependent on the diet conditions, and the effect is highly likely to be caused by 0.5% cholesterol, 0.25% cholic acid and 10% lard in the diet.

Shibata et al. [16] showed that the level of serum cholesterol markedly increased in rats fed a diet with 0.5% cholesterol, 0.25% cholic acid and 10% lard, but no change in the activity for hepatic HMG-CoA reductase and CYP7a1, and a decrease in the level of LDL receptor mRNA was observed. Stanley et al. [22] reported that myristic, lauric and palmitic acids which are abundant in animal fats increased the level of serum cholesterol because the saturated fatty acids decreased the expression of the gene coding for the LDL receptor and increased expression of the gene coding for the VLDL particles released. Given that the serum level of cholesterol and triglyceride was increased by intake of high-cholesterol diet, HHA increased the serum level of LDL-cholesterol and triglyceride, a main lipid component in VLDL. This result suggests that intake of HHA affects factors involved in cholesterol metabolism.

However, it is unlikely that HHA itself increased the serum cholesterol and triglyceride levels, because HHA is not absorbed into the body due to being poorly digested. Thus, HHA may be indirectly involved in the serum cholesterol- and triglyceride-elevating effects. One of the possible reasons for the indirect action of HHA is organic acids in cecum contents. Hara et al. [23] have reported that a serum cholesterol-decreasing effect of feeding dietary fiber may be involved in the increased content of organic acids produced in the cecum of rats due to the inhibition of cholesterol synthesis in the liver. In this study, the concentration of maleic and succinic acids was elevated by HHA intake. There is a report that maleic acids decreased the level of serum cholesterol [24]. In addition, our preliminary experiment showed that the intake of maleic and succinic acids reduced the serum cholesterol-elevating effect using rats (data not shown). Therefore, maleic acid and succinic acid have little to do with the increase in the serum cholesterol level. In contrast, only propionic acid showed a significant decrease among organic acids in the cecum contents of HHA group. Interestingly, Chen et al. [25] have reported that the ingestion of propionate reduced the level of serum cholesterol in rats. Lin et al. [26] reported that propionate inhibited cholesterol and triglyceride synthesis in rat hepatocytes in a dose-dependent manner. It is possible that propionic acid produced by the intake of HHA caused the increase in serum cholesterol and triglyceride levels, due to low level of propionic acid in the cecum content.

In humans, although HA and HHA have been reported to lower the serum cholesterol level [27], no information is yet available about an increase in serum cholesterol level caused by ingestion of HHA. Our animal experiments showed that the intake of HHA in conjunction with a high-cholesterol/high-animal fat diet could increase serum cholesterol and triglyceride concentration in humans. However, since the metabolism of cholesterol and lipids in humans is different from that in rats, further studies on the effects of HHA in human and experimental animals will be required.

In conclusion, the intake of HHA elevated the serum and liver cholesterol levels and the arteriosclerosis index in association with a high-cholesterol diet. These results suggest that HHA, when consumed in conjunction with a high-cholesterol/high-animal fat diet, does not reduce serum cholesterol levels, but rather increases the risk of arteriosclerosis. Although the use of resistant starch has become popular in recent years, it is important to note that starch under severe conditions, such as in the case of heat-moisturing, has some undesirable effect on the target function of the body. Further experimentation will be needed to learn more about the effect of HHA at biochemical and physiological levels.

References

1. Englyst HN, Kingman SM, Cummings JH (1992) Classification and measurement of nutritionally important starch fractions. Eur J Clin Nutr 46:S33–S50
2. Le Leu RK, Brown IL, Hu Y, Morita T, Esterman A, Young GP (2007) Effect of dietary resistant starch and protein on colonic fermentation and intestinal tumourigenesis in rats. Carcinogenesis 28:240–245
3. De Deckere EAM, Kloots WJ, Van Amelsvoort JMM (1995) Both raw and retrograded starch decrease serum triacylglycerol concentration and fat accretion in the rat. Br J Nutr 73:287–298
4. Younes H, Levrat MA, Demigne C, Remesy C (1995) Resistant starch is more effective than cholestyramine as a lipid-lowering agent in the rat. Lipids 30:847–853
5. Hashimoto N, Ito Y, Han KH, Shimada K, Sekikawa M, Topping DL, Bird AR, Noda T, Chiji H, Fukushima M (2006) Potato pulps lowered the serum cholesterol and triglyceride levels in rats. J Nutr Sci Vitaminol 52:445–450
6. De Deckere EAM, Kloots WJ, Van Amelsvoort JMM (1993) Resistant starch decreases serum total cholesterol and triacylglycerol concentrations in rats. J Nutr 123:2142–2151
7. Englyst HN, Hudson GJ (1993) Dietary fiber and starch: classification and measurement. In: Spiller GA (ed) CRC handbook of dietary fiber in human nutrition, 2nd edn . CRC Press, London, pp 53–71
8. Liu X, Ogawa H, Ando R, Nakakuki T, Kishida T, Ebihara K (2007) Heat-moisture treatment of high-amylose corn starch increases dietary fiber content and lowers plasma cholesterol in ovariectomized rats. J Food Sci 72:S652–S658
9. Vanhoof KM, De Schrijver R (1997) Consumption of enzyme resistant starch and cholesterol metabolism in normo- and hypercholesterolemic rats. Nutr Res 17:1331–1340
10. Udagawa H, Kitaoka C, Sakamoto T, Hattori K, Oishi Y, Takita T (2008) Serum cholesterol-decreasing effect of heat-moisture-treated high-amylose cornstarch in cholesterol-loaded rats. Biosci Biotechnol Biochem 72(3):880–884
11. Turner JD, Le NA, Brown WV (1981) Effect of changing dietary fat saturation on low-density lipoprotein metabolism in man. Am J Physiol 241:E57–E63
12. American Institute of Nutrition (1977) Report of the American Institute of Nutrition ad hoc committee on standards for nutritional studies. J Nutr 107:1340–1348
13. Rouser G, Siakotos AN, Fleisher S (1966) Quantitative analysis of phospholipids by thin-layer chromatography and phosphorus analysis of spots. Lipids 1:85–86
14. Hoshi S, Sakata T, Mikuni K, Hashimoto H, Kimura S (1994) Galactosylsucrose and xylosylfructoside alter digestive tract size and concentrations of cecal organic acids in rats fed diets containing cholesterol and cholic acid. J Nutr 124:52–60
15. Chomczynski P, Sacchi N (1987) Single-step method of RNA isolation by acid guanidinium α-thiocyanate-phenol-chloroform extraction. Anal Biochem 162:156–159
16. Shibata S, Hayakawa K, Egashira Y, Sanada H (2007) Roles of nuclear receptors in the up-regulation of hepatic cholesterol 7α-hydroxylase by cholestyramine in rats. Life Sci 80:546–553
17. Moundras C, Behr SR, Remesy C, Demigne C (1997) Fecal losses of sterols and bile acids induced by feeding rats guar gum are due to greater pool size and liver bile acid secretion. J Nutr 127:1068–1076
18. Tomkins GM, Sheppard H, Chaikoff IL (1953) Cholesterol synthesis by liver III. Its regulation by ingested cholesterol. J Biol Chem 201:137–141
19. Yoshida T, Honda A, Tanaka N, Matsuzaki Y, He B, Osuga T, Kobayashi N, Ozawa K, Miyazaki H (1993) Simultaneous determination of mevalonate and 7α-hydroxycholesterol in human plasma by gas chromatography–mass spectrometry as indices of cholesterol and bile acid biosynthesis. J Chromatogr 613:185–193
20. Verbeek MJF, De Deckere EAM, Tijburg LBM, Van Amelsvoort JMM, Beynen AC (1995) Influence of dietary retrograded starch on the metabolism of neutral steroids and bile acids in rats. Br J Nutr 74:807–820
21. Han SH, Chung MJ, Lee SJ, Rhee C (2006) Digestion-resistant fraction from soybean [*Glycine max* (L.) Merrill] induces hepatic LDL receptor and CYP7A1 expression in apolipoprotein E-deficient mice. J Nutr Biochem 17:682–688
22. Stanley J (2005) How do saturated fatty acids raise the blood LDL-cholesterol level. Lipid Technol 17:159–161
23. Hara H, Haga S, Aoyama Y, Kiriyama S (1999) Short-chain fatty acids suppress cholesterol synthesis in rat liver and intestine. J Nutr 129:942–948
24. Izydore RA, Hall IH (1991) Hypolipidemic activity of aliphatic dicarboxylic acids in rodents. Acta Pharm Nord 3:141–146
25. Chen WJL, Anderson JW, Jennings D (1984) Propionate may mediate the hypocholesterolemic effects of certain soluble plant fibers in cholesterol-fed rats. Proc Soc Exp Biol Med 175:215–218
26. Lin Y, Vonk RJ, Slooff MJH, Kuipers F, Smit MJ (1995) Differences in propionate-induced inhibition of cholesterol and triacylglycerol synthesis between human and rat hepatocytes in primary culture. Br J Nutr 74:197–207
27. Nugent AP (2005) Health properties of resistant starch. Br Nutr Foundation Nutr Bull 30:27–54

Lipids (2008) 43:703–711
DOI 10.1007/s11745-008-3183-4

ORIGINAL ARTICLE

Long Chain Fatty Acid Uptake In Vivo: Comparison of [^{125}I]-BMIPP and [^{3}H]-Bromopalmitate

**Jane Shearer · Kimberly R. Coenen · R. Richard Pencek ·
Larry L. Swift · David H. Wasserman ·
Jeffrey N. Rottman**

Received: 21 January 2008 / Accepted: 17 April 2008 / Published online: 15 May 2008
© AOCS 2008

Abstract Insulin resistance is characterized by increased metabolic uptake of fatty acids. Accordingly, techniques to examine in vivo shifts in fatty acid metabolism are of value in both clinical and experimental settings. Partially metabolizable long chain fatty acid (LCFA) tracers have been recently developed and employed for this purpose: [9,10-^{3}H]-(*R*)-2-bromopalmitate ([^{3}H]-BROMO) and [^{125}I]-15-(ρ-iodophenyl)-3-*R*,*S*-methylpentadecanoic acid ([^{125}I]-BMIPP). These analogues are taken up like native fatty acids, but once inside the cell do not directly enter β-oxidation. Rather, they become trapped in the slower processes of ω and α-oxidation. Study aims were to (1) simultaneously assess and compare [^{3}H]-BROMO and [^{125}I]-BMIPP and (2) determine if tracer breakdown is affected by elevated metabolic demands. Catheters were implanted in a carotid artery and jugular vein of Sprague–Dawley rats. Following 5 days recovery, fasted animals (5 h) underwent a rest (n = 8) or exercise (n = 8) (0.6 mi/h) protocol. An instantaneous bolus containing both [^{3}H]-BROMO and [^{125}I]-BMIPP was administered to determine LCFA uptake. No significant difference between [^{125}I]-BMIPP and [^{3}H]-BROMO uptake was found in cardiac or skeletal muscle during rest or exercise. In liver, rates of uptake were more than doubled with [^{3}H]-BROMO compared to [^{125}I]-BMIPP. Analysis of tracer conversion by TLC demonstrated no difference at rest. Exercise resulted in greater metabolism and excretion of tracers with $\sim$37% and $\sim$53% of [^{125}I]-BMIPP and [^{3}H]-BROMO present in conversion products at 40 min. In conclusion, [^{3}H]-BROMO and [^{125}I]-BMIPP are indistinguishable for the determination of tissue kinetics at rest in skeletal and cardiac muscle. Exercise preferentially exacerbates the breakdown of [^{3}H]-BROMO, making [^{125}I]-BMIPP the analogue of choice for prolonged (>30 min) experimental protocols with elevated metabolic demands.

Keywords Tracer · Kinetics · Thin layer chromatography · Uptake · Clearance

Abbreviations

[^{125}I]-BMIPP	[^{125}I]-15-(ρ-Iodophenyl)-3-*R*,*S*-methylpentadecanoic acid
([^{3}H]-BROMO)	[9,10-3H]-(*R*)-2-Bromopalmitate
K_t	Tissue long chain fatty acid clearance
LCFA	Long chain fatty acid
NEFA	Nonesterified fatty acid
R_t	Index of tissue long chain fatty acid uptake
TLC	Thin layer chromatography

J. Shearer · K. R. Coenen · R. R. Pencek · D. H. Wasserman
Department of Molecular Physiology and Biophysics,
Vanderbilt University, Nashville, TN, USA

L. L. Swift
Department of Pathology, Vanderbilt University,
Nashville, TN, USA

J. N. Rottman
Department of Cardiology, Vanderbilt University,
Nashville, TN, USA

D. H. Wasserman · J. N. Rottman
The Mouse Metabolic Phenotyping Center,
Vanderbilt University, Nashville, TN, USA

J. Shearer (✉)
Departments of Kinesiology, Biochemistry and Molecular
Biology, University of Calgary, 2500 University Drive NW,
T2N 1N4 Calgary, AB, Canada
e-mail: jshearer@ucalgary.ca

Introduction

Abnormalities in lipid trafficking and uptake are a hallmark of numerous metabolic disease states including obesity, type 2 diabetes and atherosclerosis. To assess lipid kinetics in these states, partially metabolizable long chain fatty acid (LCFA) tracers have been developed for use in vivo [1–7]. Two such tracers are [9,10-^{3}H]-(*R*)-2-bromopalmitate ([^{3}H]-BROMO) and [^{125}I]-15-(ρ-iodophenyl)-3-*R*,*S*-methylpentadecanoic acid ([^{125}I]-BMIPP). Both analogues are taken up by tissues like native substrates however, once inside the cell, they become trapped in various stages of ω or α-oxidation. As a result, the analogues remain in the tissue allowing their quantification by specific activity.

Developed and extensively tested by Oakes et al. [8], [^{3}H]-BROMO shows excellent retention in the majority of tissues examined. Studies employing this tracer were the first to effectively show increased efficiency of tissue LCFA uptake in a model of dietary induced insulin resistance [9]. BMIPP was developed by Knapp et al. [10–12] and has been primarily used for cardiac imaging with an [^{123}I] label. Using single photon emission computed tomography (SPECT) defects in fatty acid uptake by the heart are imaged and are indicative of ischemia or tissue injury [5, 13–15]. Like [^{3}H]-BROMO, the tracer has also proven to be a powerful tool in evaluating various pharmacological treatments on cardiac metabolism [16–19].

To date, numerous studies have individually assessed the metabolism of these fatty acid tracers in vivo and some comparisons between different tracers have been reported [1]. However, studies directly comparing [^{125}I]-BMIPP and [^{3}H]-BROMO in specific tissues under varied metabolic conditions have not been performed. Therefore, the aim of the present study was to assess and compare [^{125}I]-BMIPP and [^{3}H]-BROMO in vivo. The effects of enhanced LCFA metabolism due to exercise on tissue retention of these tracers was examined. Together, these studies will provide needed information on the use of [^{125}I]-BMIPP and [^{3}H]-BROMO, and their applicability to the study of metabolism.

Experimental Methods

Animals

Male Sprague–Dawley rats (Harlan Industries, Indianapolis, IN) were housed individually and maintained at 23°C on a 0600–1800 hours light cycle. Rats were fed standard chow ad libitum (Purina, Nestlé, St Louis, MI) and given free access to water. The rats were housed under these conditions for ~1 week, by which time their weights had reached ~330 g. Following weight gain, rats were randomly divided into rest and exercise groups ($n = 8$ per group). All procedures were approved by the Vanderbilt University Animal Care and Use Subcommittee and followed National Institutes of Health guidelines for the care and use of laboratory animals.

Surgical Procedures

Surgical procedures were performed as previously described for arterial and venous catheterizations [20]. Briefly, animals were anaesthetized with a 50:5:1 vol/vol/vol mixture of ketamine, rompun, and acepromazine, and the left common carotid artery and right jugular vein were catheterized with PE50 catheters, which were exteriorized and secured at the back of the neck, filled with heparinized saline (150 U/ml), and sealed with a stainless steel plug. Immediately post-surgery, each animal received 75 mg/kg of ampicillin subcutaneously to prevent infection. After surgery, animal weights and food intake were monitored daily.

Isotopic Analogues

(ρ-iodophenyl)-3-*R*,*S*-methylpentadecanoic acid was a kind gift from Oak Ridge International Laboratories (Oak Ridge, TN). Radioiodination was performed according to the manufacturer's suggested protocol. Briefly, (ρ-iodophenyl)-3-*R*,*S*-methylpentadecanoic acid was heated in the presence of Na[^{125}I] solution (740 MBq/200 µl), propionic acid, and copper (II) sulfate. $Na_2S_2O_3$ was then added and the organic phase ether extracted and sequentially back extracted with saturated $NaHCO_3$ and water. After evaporation, the [^{125}I]-BMIPP was solubilized using sonication into ursodeoxycholic acid. The initial concentration of [^{125}I]-BMIPP was 1.05 µCi/µl. However, due to the short half life of [^{125}I]-BMIPP, the administered dose was volumetric. A dose of 100 µl was administered and the activity of the tracer was determined for each individual animal and corrected for any decay. To limit tracer decay, all studies were performed within 30 days of synthesis.

[^{3}H]-BROMO was prepared by American Radioactive Chemicals Co (St Louis, MO) from palmitic acid as previously described [8]. The final concentration was 1 µCi/µl. On the day of the experiment, 20 µl of [^{3}H]-BROMO was evaporated and reconstituted in 100 µl of saline containing 0.35 mg/ml rat albumin (Sigma Chemical, St Louis, MO). This solution was added to 100 µl of [^{125}I]-BMIPP in ursodeoxycholic acid. In total, [^{3}H]-BROMO, 19.5 µCi was administered to each animal. On the day of the experiment, 5 µl of infusate was retained for normalization of radioactivity while the remaining 195 µl was administered to the animal.

Resting Studies

On the morning of the study, rats were fasted for 5 h in a clear Tupperware (2 l) container lined with bedding. Approximately 1 h prior to the experiment, catheters were flushed with heparinized saline (10 U/ml) and connected to PE50 and Silastic tubing for infusions and sampling. Rats were then placed in the Tupperware container until the commencement of the experimental protocol. Throughout the experimental protocol rats were conscious and unrestrained. In total the experimental protocol was 40 min in duration. Prior to tracer infusions, a basal blood sample were obtained (100 μl) for the measurement of isotopic analogues, plasma glucose, insulin and nonesterified fatty acids (NEFA). To prevent declines in hematocrit, the erythrocytes taken prior to isotopic analogue infusion were washed in saline and re-infused shortly after each sample was taken. At 0 min, an instantaneous bolus of [^{125}I]-BMIPP and [^{3}H]-BROMO was administered and additional plasma samples (200 μl) were obtained at 2, 5, 10, 15, 25, and 40 min for the measurement of [^{125}I]-BMIPP, [^{3}H]-BROMO, NEFA and plasma glucose. Following the final blood sample, rats were anesthetized with pentobarbital sodium and skeletal muscle (gastrocnemius), liver, heart, brain and epididymal fat were rapidly excised, rinsed in saline to remove excess blood, freeze clamped in liquid nitrogen and frozen at −80°C until further analysis.

Exercise Studies

Two days prior to the protocol, rats in this treatment were acclimated by running on a motorized treadmill for 10 min at 0.6 mi/h. On the morning of the study, rats were fasted for 5 h in a clear Tupperware (2 l) container lined with bedding. Approximately 1 h prior to the experiment, catheters were flushed with heparinized saline (10 U/ml) and connected to PE50 and silastic tubing for infusions and sampling. Rats were then placed in the treadmill until the commencement of the experimental protocol. Following basal blood sampling, rats were run on the treadmill at 0.6 mi/h and samples were obtained as in the resting protocol. This exercise intensity is moderate for rats. At 40 min, rats were anesthetized and tissue samples were obtained as previously described.

Plasma Analysis

Plasma NEFAs were measured spectrophotometrically by an enzymatic colorimetric assay (Wako NEFA C kit, Wako Chemicals Inc., Richmond, VA). Plasma glucose concentrations were measured by the glucose oxidase method using an automated glucose analyzer (Beckman Instruments, Fullerton, CA). [^{125}I]-BMIPP and [^{3}H]-BROMO were measured in the same plasma sample (15 μl). Plasma was counted for [^{125}I]-BMIPP using a Beckman Gamma 5500 counter (Beckman Instruments, Fullerton, CA). Following this, 100 μl of 50% ethanol was added to the sample and ^{3}H radioactivity was counted after addition of fluor (10 ml; Ultimate Gold, Packard Bioscience, Boston, MA.) using a Packard Tri-Carb 2900TR Liquid Scintillation Analyzer (PerkinElmer, Boston, MA). In addition, plasma was also analyzed by thin layer chromatography (TLC) by methods that were derived from Kropp et al. [21]. Here, individual plasma time points were examined by TLC from a representative animal in each treatment group. TLC plates reflecting plasma samples were segmented into 1 cm sections and analyzed for tracer and tracer conversion products. Each plate was examined for radioactivity. Significant radioactivity appearing in minor lipid fractions over time was considered evidence of tracer breakdown, although the exact chemical nature of each product was not identified. Tracer conversion or breakdown was calculated as a ratio of total activity appearing on the plate for each time point.

Tissue Analysis

Total [^{125}I] radioactivity in tissues was determined on sections of whole tissue (~100 mg) using a Beckman Gamma 5500 counter (Beckman Instruments, Fullerton, CA). Following this, total lipid was extracted from the tissue using a modified Folch–Lees extraction [22]. The [^{125}I] radioactivity in this fraction was then reassessed before 10 ml of flour was added to samples and then ^{3}H radioactivity determined by liquid scintillation counting (Packard TRI-CARB 2900TR, Packard, Meriden, CT) with Ultima Gold (Packard) as scintillant. The relationship between gamma radioactivity and beta emissions using this specific process and counter has been previously established in our laboratory. This relationship was used to correct ^{3}H radioactivity for beta-emissions originating from [^{125}I] radioactivity in both tissue and plasma samples [3]. In addition, lipid was extracted from a portion of each tissue (~100 mg) from four rats in both the resting and exercise protocols using a Folch–Lees extraction [22]. Lipid fractions were then separated by TLC [23]. Plate segments were subsequently separated and individually counted. Tissues plates were separated based on lipid fraction (phospholipid, mono-diglyceride, free fatty acids and triglyceride).

Calculations

Plasma Kinetics

Identical equations were used for the determination of [^{125}I]-BMIPP and [^{3}H]-BROMO kinetics. Plasma tracer (p) kinetics are based on the disappearance of tracer from the plasma over time. Movement of the tracer out of the plasma pool into tissues is denoted by clearance (K_p, Eq. 1). When K_p is expressed in terms of tracee or mean LCFA concentration as measured by an enzymatic assay, the measure is termed uptake (R_p, Eq. 2). Finally, if K_p is expressed as a fraction of the original tracer dose administered (D), the resultant expression is metabolic clearance rate or MCR$_p$. Equations 1–3 are calculated independently for [^{125}I]-BMIPP and [^{3}H]-BROMO. Equations employed were defined as follows where $\int_0^t$ represents integral over the time between 2 and 40 min.

$$K_p = \int_0^t \left[[^{125}\mathrm{I}]\text{-BMIPP or } [^{3}\mathrm{H}]\text{-BROMO}\right] p\,\mathrm{d}t \quad (1)$$

$$R_p = K_p[\mathrm{LCFA}]p \quad (2)$$

$$\mathrm{MCR}_p = \frac{D}{\int_0^t \left[[^{125}\mathrm{I}]\text{-BMIPP or } [^{3}\mathrm{H}]\text{-BROMO}\right] p\,\mathrm{d}t} \quad (3)$$

Tissue Kinetics

Rates of tissue LCFA clearance (K_t, Eq. 4) and metabolic indices (R_t, Eq. 5) were calculated from the accumulation of [^{125}I]-BMIPP and [^{3}H]-BROMO in tissues (t) relative to the integral of the plasma (p) concentration following the instantaneous bolus. These measurements follow from Eqs. 1–3 and have been previously described [3, 9].

$$K_t = \frac{\left[[^{125}\mathrm{I}]\text{-BMIPP or } [^{3}\mathrm{H}]\text{-BROMO}\right] t}{\int_0^t \left[[^{125}\mathrm{I}]\text{-BMIPP or } [^{3}\mathrm{H}]\text{-BROMO}\right] p\,\mathrm{d}t} \quad (4)$$

$$R_t = K_t[\mathrm{LCFA}]p \quad (5)$$

A one-way repeated measures analysis of variance (ANOVA) was performed to compare differences between [^{125}I]-BMIPP and [^{3}H]-BROMO within specific tissues. To determine differences over time for blood glucose and NEFA, a two-way repeated measures ANOVA was performed. To establish differences within ANOVA, a Tukey post hoc test was used. Significance levels of $p \leq 0.05$ were employed, and data are reported as means ± standard error of the mean (SEM).

Results

Animal Characteristics

Baseline animal characteristics for both rest and exercise experiments are outlined in Table 1. Blood glucose remained stable in the rest group (7.7 ± 0.3 mM at 40 min) while it steadily increased in the exercise group to 11.5 ± 0.6 mM at the end of the protocol ($p < 0.05$). Plasma NEFA levels remained stable with average values of 0.63 ± 0.06 mM and 0.56 ± 0.05 mM for rest and exercise studies at the end of the experimental protocol ($p > 0.05$). All animals in the exercise protocol were able to successfully complete the required 40 min of exercise.

Metabolic Clearance and Uptake

Whole body metabolic clearance in the resting state was set to an arbitrary value of 1.0 for each tracer for comparison to the exercise treatment. Results show comparable increments in fatty acid clearance for each tracer with exercise (Fig. 1). Tissues (skeletal muscle, heart, liver, adipose tissue) were examined for rates of fatty acid uptake (R_t, μmol/100 g/min). Absolute values are shown in Fig. 2. No quantitative difference between [^{125}I]-BMIPP and [^{3}H]-BROMO R_t values were noted during the resting protocol with the exception of the liver. In the liver, rates of R_t calculated using [^{3}H]-BROMO was more than double that calculated using [^{125}I]-BMIPP.

Tracer Correlations

Correlations of tissue fatty acid uptake between [^{125}I]-BMIPP and [^{3}H]-BROMO are plotted in Fig. 3. R^2 values for resting and exercise samples are plotted individually, and an aggregate value also presented. Results of individual muscle types for rest and exercise studies were at least moderately correlated, with aggregate R^2 values of 0.39, 0.55, 0.26, and 0.56 for the soleus, vastus lateralis, gastrocnemius and heart respectively. In contrast, data from liver and adipose tissue are poorly correlated between tracers with both treatments.

Table 1 Baseline characteristics of animals in the sedentary and exercise experiments

	n	Weight (g)	Recovery (days)	Glucose (mM)	NEFA (mM)	Hct 0 (%)	Hct 40 (%)
Rest	8	330 ± 10	7.8 ± 0.9	7.3 ± 0.2	0.76 ± 0.11	47 ± 1	43 ± 1
Exercise	8	340 ± 12	8.3 ± 0.4	7.5 ± 0.2	0.73 ± 0.11	46 ± 1	41 ± 1

Recovery (days) reflects the number of days between surgery and the experiment. Basal plasma glucose (glucose) and non-esterified fatty acids (NEFA) are shown along with starting and ending hematocrit (Hct) levels

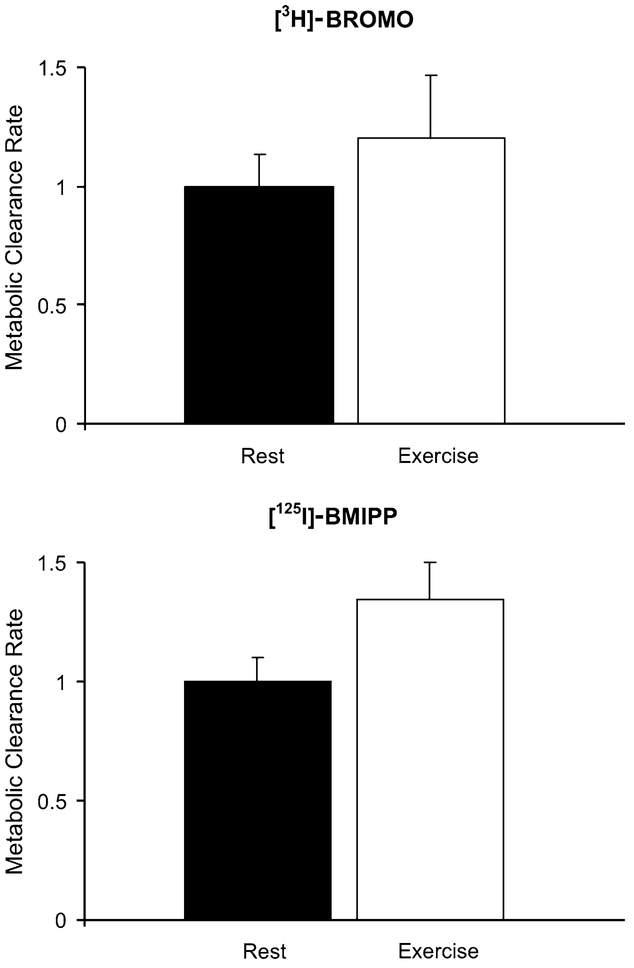

Fig. 1 Relative change in whole body LCFA clearance rates (MCR) for [^{3}H]-BROMO (*top panel*) and [^{125}I]-BMIPP (*bottom panel*) from rest to exercise. Calculations are based on the measurement of radioactivity in the plasma over time. As tracer moves from the plasma into tissues, the rate of decay for each tracer can be quantified. Resting values for each tracer were set to an arbitrary value of one. Values represent means ± SEM

Plasma Analysis

Analysis of tracer distribution in resting animals by TLC demonstrated no observable differences between [^{125}I]-BMIPP and [^{3}H]-BROMO at rest. Each tracer showed the expected exponential decay pattern and similar rates of fractional conversion in this state (Table 2). Analysis of fractional conversion during exercise was comparatively greater than exercise at all time points analyzed. Furthermore, results show conversion of [^{3}H]-BROMO to exceed that of [^{125}I]-BMIPP in the latter stages (>20 min) of the experiment (Table 2).

Tracer Tissue Distribution

The intracellular fate of tracers were analyzed by TLC. Results demonstrated tracers to reside in three distinct fractions (Table 3). The first fraction contained phospholipid, monoglyceride, and diglyceride (PL + MG + DG) while others analyzed free fatty acids (FFA), triglyceride (TG). Analysis showed the majority of radioactivity resided in the PL + MG + DG fraction followed by FFA and finally TG. Differences between tracer distributions were minimal. At rest, a lower fraction of [^{125}I]-BMIPP was found in TG in cardiac muscle. During exercise, lower [^{125}I]-BMIPP was found in cardiac FFA and skeletal muscle TG.

Discussion

The purpose of this study was to assess and compare [^{3}H]-BROMO and [^{125}I]-BMIPP during rest and a state of accelerated fatty acid metabolism (moderate exercise). Tracers were simultaneously administered so that direct comparisons of tissue fatty acid uptake could be made. Results show good agreement between [^{3}H]-BROMO and [^{125}I]-BMIPP for cardiac and skeletal muscle during rest and exercise. In contrast, liver and epididymal fat pads showed poor correlations under both conditions. At rest, rates of liver [^{3}H]-BROMO uptake were more than double those of [^{125}I]-BMIPP.

Conceptually, both agents are regarded as “generic” long chain fatty acid tracers. The close agreement between these tracers in muscle tissue is reassuring in terms of this usual simplification. There may be tissue specific differences related to precise molecular structure of both fatty acids and fatty acid tracers that are reflected in the differences in adipose and liver. An increase in hepatic extraction and breakdown of [^{3}H]-BROMO compared to [^{125}I]-BMIPP may also play a role. Evidence of increased hepatic [^{3}H]-BROMO breakdown has been previously reported [8]. Intravenous administration of [^{3}H]-BROMO to rodents found liver to have a retention rate of only 77% compared to skeletal muscle that retained over 90% of tracer during 16 min of infusion [8]. Given these and the present findings, it is reasonable to hypothesize that [^{125}I]-BMIPP retention rates may most closely reflect actual liver LCFA uptake. For epididymal fat, we show absolute rates of fatty acid uptake to be similar between tracers. However, correlation of individual animals between [^{3}H]-BROMO and [^{125}I]-BMIPP for this tissue yielded poor results. This discrepancy is likely due to the low rate of fatty acid uptake and tracer detection in this tissue.

To examine fractional conversion of each tracer by tissue, detailed analysis of tracer distribution in plasma over time was conducted by TLC. A known conversion product for [^{3}H]-BROMO is ^3H_2O. Previous analysis of the tracer show conversion to be ~5% of the dose at 16 min in sedentary rats [8]. This value compares favorably with the

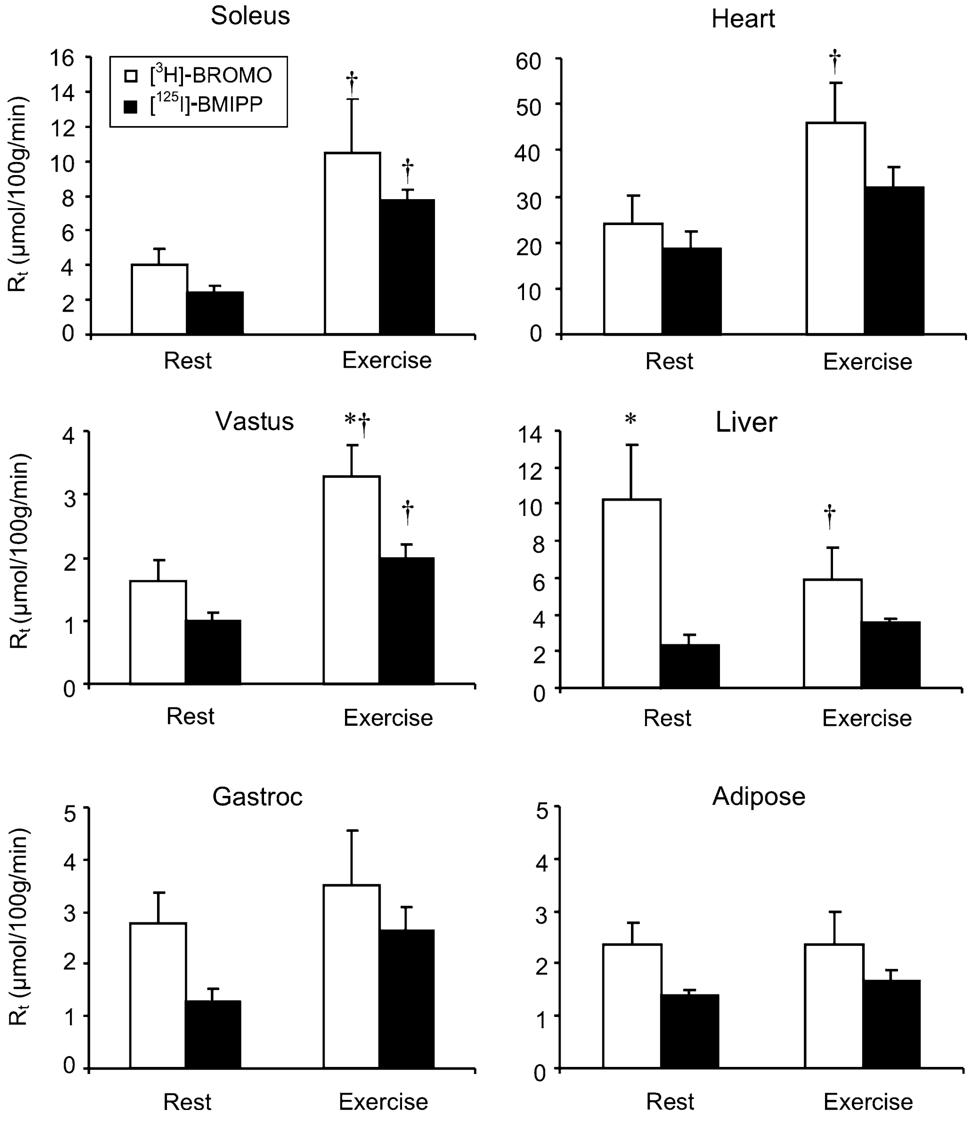

Fig. 2 Tissue fatty acid uptake (μmol/100 g/min) for [^{125}I]-BMIPP (*filled bars*) and [^{3}H]-BROMO (*empty bars*). Tissues were collected following 40 min of rest or moderate intensity exercise. * Indicates a significant difference between [^{3}H]-BROMO and [^{125}I]-BMIPP within an experimental protocol. † Indicates a significant difference between rest and exercise for a given tracer. Values represent means ± SEM

present study that estimates a conversion of ~4% at 15 min at rest. Like [^{3}H]-BROMO, [^{125}I]-BMIPP becomes trapped in α-oxidation [24]. End products of this reaction yield CO_2, a fatty acid shortened by one carbon and a methyl substitution at the second carbon, which in the case of [^{123}I]-BMIPP and [^{131}I]-BMIPP is 2-(ρ-iodophenyl) acetic acid (IPC_2) [21]. Previous analysis of fractional conversion of [^{123}I]-BMIPP show ~11% of injected dose is released at 60 min in humans while perfusion of isolated rat hearts have a conversion of ~12% following 3 h. In the present study, we show conversion of BMIPP to be ~12% of total radioactivity at 40 min. Comparison of [^{125}I]-BMIPP and [^{3}H]-BROMO during rest, show comparable levels of conversion over time. Given this, either tracer is suitable for resting studies.

Elevation of metabolic demands by moderate exercise resulted in increases fatty acid uptake in skeletal and cardiac muscle for both [^{125}I]-BMIPP and [^{3}H]-BROMO. Generally, tissue extraction of fatty acids doubled with exercise. This finding confirms previous observations of Oakes and colleagues [8] who have shown [^{3}H]-BROMO is not affected by metabolic (oxidative vs. nonoxidative) status in skeletal muscle. Of note, differences in liver fatty acid uptake at rest were not observed during exercise. This may be due to a diversion of blood flow away from this organ during exercise. In addition to increasing tracer tissue uptake, exercise also resulted in greater tissue excretion of tracers at all time points measured. At 40 min, 37 and 53% of the initial tracer dose were present in conversion products for [^{125}I]-BMIPP and [^{3}H]-BROMO respectively. This excretion is due to elevated α and ω-oxidation of fatty acids with exercise or simply back diffusion. However, despite increasing fractional conversion with exercise, we show good agreement between tracers in cardiac and skeletal muscle.

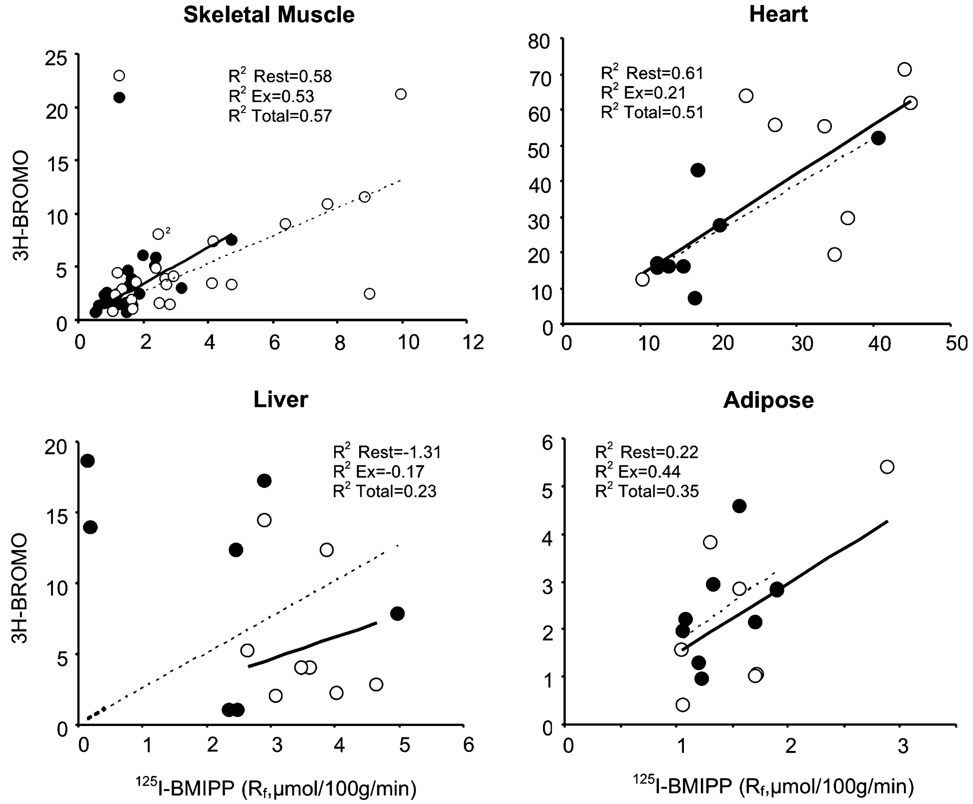

Fig. 3 Comparison of fatty acid uptake rates between [^{3}H]-BROMO (*y* axis) and [^{125}I]-BMIPP (*x* axis) for individual tissue measurements. Values for resting (*open circles*) and exercise (*closed circles*) are shown along with their corresponding R^2 values for rest, exercise and total aggregate are shown

Table 2 Estimated fractional tracer conversion of [^{3}H]-BROMO and [^{125}I]-BMIPP in plasma over time during rest and exercise

	2 (%)	5 (%)	10 (%)	15 (%)	25 (%)	40 (%)
Rest						
[^{125}I]-BMIPP	1.2	6.3	12.4	14.3	11.8	11.4
[^{3}H]-BROMO	1.0	4.0	9.2	12.7	10.5	10.4
Exercise						
[^{125}I]-BMIPP	4.6	10.4	14.6	17.3	24.7	37.0
[^{3}H]-BROMO	5.3	10.6	21.2	40.4	53.5	52.9

Results represent the % of radioactivity in breakdown products versus [^{3}H]-BROMO and [^{125}I]-BMIPP as assessed by thin layer chromatography

From a technical perspective, [^{3}H]-BROMO has advantages primarily related to the label-induced limitations of [^{125}I]-BMIPP. These include its shorter half-life, elevated biological risk and synthesis. [^{125}I]-BMIPP has a half life of 60 days compared to [^{3}H]-BROMO which is 12 years. Given this, corrections for tracer decay with [^{125}I]-BMIPP need to be considered, when studies extend over days to weeks. In the present study, a single batch of [^{125}I]-BMIPP was employed and studies occurred over a 1-month period. All results were scaled to include corrections for tracer decay. Another consideration involves the biological risk involved with working these isotopes. [^{125}I]-BMIPP is a gamma and X-ray emitter and although used in low doses, still poses a greater hazard than [^{3}H]-BROMO which is a lower energy beta emitter. Finally, the labelling for [^{3}H]-BROMO is complex but the compound is currently commercially available, while [^{125}I]-BMIPP is straightforward to label but requires specific precautions related to iodination, and currently must be performed in an institutional setting. Finally, in studies where multiple tracers are employed, there may be specific limitations related to other radioactive labeled compounds in concurrent use. These issues must be considered prior to commencing studies with either tracer.

In conclusion, this study directly compares isotopic analogs for the measurement of fatty acid kinetics in vivo. Results show both analogues are effective for the measurement of FFA uptake and clearance in plasma. We showed a high correlation between tracers for cardiac and skeletal muscle. However, in both the liver and adipose tissue, derived rates of uptake diverged depending on the specific tracer. As a result, studies employing these or other fatty acid tracers in these tissues must be interpreted with caution. Generally, technical considerations argue for [^{3}H]-BROMO. However, when studies are prolonged (>20 min) and employ experimental manipulations requiring elevated metabolism, we show the preferable analog to be [^{125}I]-BMIPP due to its lower rates of tissue excretion.

Table 3 Incorporation of [^{125}I]-BMIPP and [^{3}H]-BROMO into various lipid fractions in tissues at rest ($n = 5$) and exercise ($n = 5$) as determined by thin layer chromatography

Tissue	Lipid fraction	[^{3}H]-BROMO	[^{125}I]-BMIPP
Rest			
Heart	PL + MG + DG	45.5 ± 7.3$^{\#}$	49.3 ± 9.6$^{\#}$
	FFA	29.9 ± 8.7$^{\#}$	41.4 ± 10.1
	TG	32.7 ± 4.1	9.3 ± 2.3*
Skeletal muscle	PL + MG + DG	50.7 ± 10.9	45.0 ± 11.7
	FFA	36.7 ± 7.1	41.2 ± 13.0
	TG	15.6 ± 6.1	14.0 ± 4.3
Liver	PL + MG + DG	59.6 ± 6.3	37.9 ± 11.5
	FFA	22.2 ± 6.3	49.2 ± 13.3
	TG	19.2 ± 2.5	12.9 ± 2.6
Exercise			
Heart	PL + MG + DG	69.7 ± 8.9	83.4 ± 9.5
	FFA	13.0 ± 1.7	2.4 ± 1.0*
	TG	17.3 ± 7.6	11.2 ± 6.6
Skeletal muscle	PL + MG + DG	43.7 ± 6.1	67.4 ± 7.8
	FFA	34.9 ± 5.5	22.6 ± 5.7
	TG	24.4 ± 5.0	6.3 ± 1.5*
Liver	PL + MG + DG	54.0 ± 8.6	49.4 ± 15.4
	FFA	25.0 ± 8.7	39.4 ± 14.7
	TG	21.0 ± 8.8	11.2 ± 5.3

Values are expressed as a percentage of total radioactivity and represent means ± SEM.

PL phospholipid, *MG* monoglyceride, DG diglyceride, *FFA* free fatty acids, *TG* triglyceride.

* Represents a significant difference between [^{125}I]-BMIPP and [^{3}H]-BROMO within an experimental protocol

# Represents a significant difference with [^{125}I]-BMIPP or [^{3}H]-BROMO between rest and exercise protocols

Acknowledgments This work would not have been possible with the contribution of BMIPP from Dr. Russ Knapp, Nuclear Medicine Program, Oak Ridge National Laboratory, TN. The authors gratefully acknowledge his generosity and technical advice. JS holds salary support awards from the Alberta Heritage Foundation for Medical Research, the Heart and Stroke Foundation and the Canadian Diabetes Association. This work is supported by the CIHR (JS), Genome Canada (JS), NIDDK (DK-54902, U24-DK-59637). The authors wish to acknowledge the technical contributions of Wanda Sneed, Angela Slater, Carla Harris and Freyja James.

References

1. Renstrom B, Rommelfanger S, Stone CK, DeGrado TR, Carlson KJ, Scarbrough E, Nickles RJ, Liedtke AJ, Holden JE (1998) Comparison of fatty acid tracers FTHA and BMIPP during myocardial ischemia and hypoxia. J Nucl Med 39(10):1684–1689
2. Stone CK, Pooley RA, DeGrado TR, Renstrom B, Nickles RJ, Nellis SH, Liedtke AJ, Holden JE (1998) Myocardial uptake of the fatty acid analog 14-fluorine-18-fluoro-6-thia-heptadecanoic acid in comparison to beta-oxidation rates by tritiated palmitate. J Nucl Med 39(10):1690–1696
3. Rottman JN, Bracy D, Malabanan C, Yue Z, Clanton J, Wasserman DH (2002) Contrasting effects of exercise and NOS inhibition on tissue-specific fatty acid and glucose uptake in mice. Am J Physiol Endocrinol Metab 283(1):E116–E123
4. Coburn CT, Knapp FF Jr, Febbraio M, Beets AL, Silverstein RL, Abumrad NA (2000) Defective uptake and utilization of long chain fatty acids in muscle and adipose tissues of CD36 knockout mice. J Biol Chem 275(42):32523–32529
5. Zhao C, Shuke N, Okizaki A, Yamamoto W, Sato J, Ishikawa Y, Ohta T, Hasebe N, Kikuchi K, Aburano T (2003) Comparison of myocardial fatty acid metabolism with left ventricular function and perfusion in cardiomyopathies: by 123I-BMIPP SPECT and 99mTc-tetrofosmin electrocardiographically gated SPECT. Ann Nucl Med 17(7):541–548
6. Fujibayashi Y, Yonekura Y, Kawai K, Yamamoto K, Tamaki N, Konishi J, Yokoyama A, Torizuka K (1988) [Basic studies on I-123-beta-methyl-p-iodophenylpentadecanoic acid (BMIPP) for myocardial functional diagnosis: effect of beta-oxidation inhibitor]. Kaku Igaku 25(10):1131–1135
7. Verberne HJ, Sloof GW, Beets AL, Murphy AM, van Eck-Smit BL, Knapp FF (2003) 125I-BMIPP and 18F-FDG uptake in a transgenic mouse model of stunned myocardium. Eur J Nucl Med Mol Imaging 30(3):431–439
8. Oakes ND, Kjellstedt A, Forsberg GB, Clementz T, Camejo G, Furler SM, Kraegen EW, Olwegard-Halvarsson M, Jenkins AB, Ljung B (1999) Development and initial evaluation of a novel method for assessing tissue-specific plasma free fatty acid utilization in vivo using (R)-2-bromopalmitate tracer. J Lipid Res 40(6):1155–1169
9. Hegarty BD, Cooney GJ, Kraegen EW, Furler SM (2002) Increased efficiency of fatty acid uptake contributes to lipid accumulation in skeletal muscle of high fat-fed insulin-resistant rats. Diabetes 51(5):1477–1484
10. Knapp FF Jr., Goodman MM, Callahan AP, Kirsch G (1986) Radioiodinated 15-(p-iodophenyl)-3,3-dimethylpentadecanoic acid: a useful new agent to evaluate myocardial fatty acid uptake. J Nucl Med 27(4):521–531
11. Knapp FF Jr., Ambrose KR, Goodman MM (1986) New radioiodinated methyl-branched fatty acids for cardiac studies. Eur J Nucl Med 12(Suppl):S39–S44
12. Dudczak R, Schmoliner R, Angelberger P, Knapp FF, Goodman MM (1986) Structurally modified fatty acids: clinical potential as tracers of metabolism. Eur J Nucl Med 12(Suppl):S45–S48
13. Noriyasu K, Mabuchi M, Kuge Y, Morita K, Tsukamoto T, Kohya T, Kitabatake A, Tamaki N (2003) Serial changes in BMIPP uptake in relation to thallium uptake in the rat myocardium after ischaemia. Eur J Nucl Med Mol Imaging 30(12):1644–1650
14. Fujino T, Ishii Y, Takeuchi T, Hirasawa K, Tateda K, Kikuchi K, Hasebe N (2003) Recovery of BMIPP uptake and regional wall motion in insulin resistant patients following angioplasty for acute myocardial infarction. Circ J 67(9):757–762
15. Narita M, Kurihara T (2003) Is I-123-beta-methyl-p-iodophenyl-methylpentadecanoic acid imaging useful to evaluate asymptomatic patients with hypertrophic cardiomyopathy? I-123 BMIPP imaging to evaluate asymptomatic hypertrophic cardiomyopathy. Int J Cardiovasc Imaging 19(6):499–510
16. Yamauchi S, Takeishi Y, Minamihaba O, Arimoto T, Hirono O, Takahashi H, Miyamoto T, Nitobe J, Nozaki N, Tachibana H, Watanabe T, Fukui A, Kubota I (2003) Angiotensin-converting enzyme inhibition improves cardiac fatty acid metabolism in patients with congestive heart failure. Nucl Med Commun 24(8):901–906
17. Ito T, Hoshida S, Nishino M, Aoi T, Egami Y, Takeda T, Kawabata M, Tanouchi J, Yamada Y, Kamada T (2001) Relationship between evaluation by quantitative fatty acid myocardial

scintigraphy and response to beta-blockade therapy in patients with dilated cardiomyopathy. Eur J Nucl Med 28(12):1811–1816

18. Hegarty BD, Furler SM, Oakes ND, Kraegen EW, Cooney GJ (2004) PPAR activation induces tissue specific effects on fatty acid uptake and metabolism in vivo—a study using the novel PPAR {alpha}/{gamma} agonist Tesaglitazar. Endocrinology p en.2004-0260
19. Edgley AJ, Thalen PG, Dahllof B, Lanne B, Ljung B, Oakes ND (2006) PPAR[gamma] agonist induced cardiac enlargement is associated with reduced fatty acid and increased glucose utilization in myocardium of Wistar rats. Eur J Pharmacol 538(1–3):195
20. Petersen HA, Fueger PT, Bracy DP, Wasserman DH, Halseth AE (2003) Fiber type-specific determinants of Vmax for insulin-stimulated muscle glucose uptake in vivo. Am J Physiol Endocrinol Metab 284(3):E541–E548
21. Kropp J, Ambrose KR, Knapp FF Jr, Nissen HP, Biersack HJ (1992) Incorporation of radioiodinated IPPA and BMIPP fatty acid analogues into complex lipids from isolated rat hearts. Int J Rad Appl Instrum B 19(3):283–288
22. Folch J, Lees M, Sloane Stanley GH (1957) A simple method for the isolation and purification of total lipids from animal tissues. J Biol Chem 226(1):497–509
23. Morrison WR, Smith LM (1964) Preparation of fatty acid methyl esters and dimethylacetals from lipids with boron fluoride-methanol. J Lipid Res 53:600–608
24. Mannaerts GP, VVPP (1993) Metabolic role of mammalian peroxisomes, in peroxisomes: biology and importance in toxicology and medicine. In: Gibson G, Lake BG (eds) CRC, pp 39–50 (in press)

Lipids (2008) 43:713–722
DOI 10.1007/s11745-008-3180-7

ORIGINAL ARTICLE

Influence of Fatty Acid Profile of Total Parenteral Nutrition Emulsions on the Fatty Acid Composition of Different Tissues of Piglets

E. Amusquivar · M. Sánchez · M. J. Hyde · J. Laws · L. Clarke · E. Herrera

Received: 27 November 2007 / Accepted: 3 April 2008 / Published online: 9 May 2008
© AOCS 2008

Abstract Total parenteral nutrition (TPN) studies in human babies of very-low-birth-weight suggest that the lipid emulsions currently available are not optimum for neonatal nutrition. Since fatty acid metabolism in human and pigs is very similar, the present study examines how lipid emulsions used in clinical TPN (i.e. ClinOleic, Intralipid, Lipofundin or Omegaven), with different fatty acid compositions, administered to neonatal piglets for 7 days, influenced their tissue fatty acid composition as compared to those enterally fed with a sow milk replacer. A positive linear relationship was found between the proportion of all individual fatty acids in the lipid emulsions or in the milk replacer versus those in plasma, skeletal muscle, subcutaneous fat, liver, heart, pancreas, stomach or intestine total lipids or in brain phospholipids, the latter showing the lowest correlation coefficient. With the exception of brain, the proportion of either oleic acid or α-linolenic acid in the individual tissues was correlated with those present in the corresponding lipid emulsion or milk replacer, whereas the proportion of linoleic acid correlated significantly with all the tissues studied. With the exception of brain phospholipids, both eicosapentaenoic and docosahexaenoic acids were higher in the tissues of piglets receiving Omegaven than in all other groups. In conclusion, with the exception of the brain, fatty acid composition of plasma and different tissues in piglets are strongly influenced by the fatty acid profile of TPN emulsions. Fatty acid composition of brain phospholipids are, however, much less influenced by dietary composition, indicating an active and efficient metabolism that ensures its appropriate composition at this key stage of development.

Keywords Total parenteral nutrition · Fatty acid profile · Neonatal pig

Introduction

Total parenteral nutrition (TPN) has been used in routine nutritional care since the 1960s. The first lipid emulsion developed for TPN was a soybean oil-based lipid emulsion [1]. This lipid emulsion was marketed as Intralipid and is one of the most widely emulsions used in TPN administration [2]. Evidence has accumulated that, in addition to their nutritional role as energy source, lipid emulsions have numerous other biologic functions. In particular, it has been shown that the fatty acid composition of cell membranes is highly influenced by the fatty acid profile of dietary lipids [3], which may in turn affect their structural and regulatory properties [4]. Indeed, lipids can influence numerous physiological processes including some roles of the cellular membrane such as membrane permeability, receptor pathways and membrane-associated enzyme activities [5], and can also affect the immune function [6, 7].

Preterm infants often require a parenteral lipid emulsion in order to prevent essential fatty acid deficiency,

---

E. Amusquivar · M. Sánchez · E. Herrera (✉)
Facultades de Farmacia y Medicina,
Department of Biochemistry and Molecular Biology,
Universidad San Pablo-CEU, Crtra. Boadilla del Monte km
5.300, 28668 Boadilla del Monte (Madrid), Spain
e-mail: eherrera@ceu.es

M. J. Hyde · L. Clarke
Department of Biomedical Sciences, Imperial College London,
Wye Campus, Wye, Ashford, Kent TN26 2AH, UK

J. Laws
Department of Agricultural Sciences, Imperial College London,
Wye Campus, Wye, Ashford, Kent TN26 2AH, UK

particularly if an adequate energy and lipid intake cannot be achieved by enteral feeding. The adequacy of soybean lipid emulsions for the nutritional needs of newborn and premature infants has been questioned [8]. Soybean-oil-based lipid emulsions contain only minor amounts of the long chain polyunsaturated fatty acids (LCPUFA). These long chain fatty acids, in particular arachidonic acid (AA) and docosahexaenoic acid (DHA), have essential functions for early visual and neural development [9–11]. In addition, AA is the main precursor for eicosanoids [12, 13] and is known to play a key role in neonatal growth [14, 15]. The endogenous synthesis of LCPUFA from precursor essential fatty acids (EFA), linoleic acid (LA) and α-linolenic acid (ALA), involves Δ6 and Δ5 desaturases, constituting the n-6 and n-3 PUFA metabolic pathways, respectively [16, 17]. Although intake of PUFA is required to prevent any EFA deficiency, it is known that excessive intake has detrimental effects. Thus, excessive intake of LA may inhibit Δ6 desaturase resulting in a decrease in the formation of DHA from ALA [18]. An excess of n-3 fatty acids has also been demonstrated to inhibit Δ-6 desaturase activity [19], which is responsible for a major decline in AA concentrations in rats fed a fish oil diet [20]. Desaturase activities are limited in preterm and term infants [21], and the large amounts of LA and ALA in soybean oil emulsions may further impair LCPUFA formation through substrate inhibition. Furthermore, the high supply of PUFA in soybean oil emulsions may enhance lipid peroxidation [22], which is of particular concern in preterm infants as it may for example cause liver damage [23]. The lipid content must be balanced to provide the correct fatty acids for brain development whilst avoiding the dangers of oxidative damage.

Total parenteral nutrition studies in human babies of very-low-birth-weight suggest that lipid emulsions currently available are not optimum for nutrition of the neonate [8]. The new lipid emulsions for clinical use are differentiated by their content in polyunsaturated (n-3 and n-6), monounsaturated, and saturated fatty acids. Due to similarities in the fatty acid metabolism in human and pigs [24], and for obvious ethical reasons, a piglet model of such treatments has been successfully developed in this study, and has enabled the effects of the treatments on tissue composition to be determined.

Materials and Methods

Experimental protocols were carried out as defined by the regulations of the Animals (Scientific Procedures) Act 1986, under the appropriate Home Office Licence and all procedures were agreed by the local ethical review board.

Experimental Design

Sixteen nulliparous sows (25% Meishan, 12.5% Duroc and 62.5% Large White X Landrace) were entered into the study. A routine caesarean section was carried out under anaesthesia at 113 days of gestation (term = 115 days). Anaesthesia was induced by administration of 2–5 mg/kg ketamine i.v. (Ketaset, Fort Dodge, Southampton, UK) and maintained using isoflurane 4–6 % (Schering-Plough Animal Health, Harefield, UK) oxygen (BOC, Manchester, UK). Following delivery, the piglets were given oxygen and an intramuscular injection of vitamin K (0.25 ml, Konakion MM 10 mg ml^{-1}, Roche Products Ltd, Lewes, UK) to assist blood clotting and allowed to recover from anaesthesia.

Piglets were selected so as to balance experimental groups for sex, body weight at birth and maternal influences. Practically, each experimental group contained piglets from at least three sows and within each litter, male and female piglets were ranked according to weight, and any outliers removed. Within each gender, piglets were matched for weight, and randomly allocated to one of five treatment groups and fed either enterally (E) with a commercially-available sow milk replacer (4.5 kJ ml^{-1}, Primary Diets, Ripon, UK); or TPN solution (1,690 J/ml; 99.34 mg ml^{-1} glucose; 17.89 mg ml^{-1} amino acids; Portsmouth Hospital NHS Trust, Portsmouth, UK), plus one of the following commercially available lipid emulsions: Intralipid 20% (Fresenius Kabi Ltd., Runcorn, UK), ClinOleic 20% (Baxter Healthcare Ltd, Northampton, UK), Lipofundin 20% (Baxter Healthcare Ltd, Northampton, UK) or Omegaven 10% (Fresenius Kabi Ltd., Runcorn, UK). The fatty acid profile of the lipid emulsions is shown in Table 1. The TPN solution was formulated according to the prescription used by the local neonatal care centre (The William Harvey Hospital, Ashford, Kent). As humans and pigs have similar nutritional requirements [25] it is possible to provide adequate nutritional support in the pig using clinical TPN regimes, which is useful in establishing an animal model with clinical relevance [26].

At 2–4 h post-delivery, piglets of similar body weight were anaesthetized using isoflurane 0.5–2% (v:v; Schering-Plough Animal Health, Harefield, UK) and bilateral jugular catheters were inserted. One of these catheters was used for daily administration of TPN and the corresponding commercially available lipid emulsion, the other catheter was used to administer intravenous antibiotics, as required, and for blood sampling. The TPN solution was infused using a volumetric infusion pump (IVAC 598, Alaris medical, Basingstoke, UK) at 2.9 ml/h/kg. and lipid emulsion, via the same infusion line, using a syringe pump (IVAC P7000, Alaris medical, Basingstoke, UK) at 0.2 ml/h/kg for the

Table 1 Fatty acid profile in the lipid emulsions and the milk replacer

Fatty acid	Milk replacer	Clin oleic	Intralipid	Lipofundin	Omegaven
g/100 g fatty acid					
10:0	ND	ND	ND	21.7	ND
12:0	19.2	ND	ND	0.4	0.5
14:0	8.6	ND	0.1	0.1	5.8
16:0	23.2	13.0	12.3	9.8	13.0
18:0	6.5	3.8	3.6	3.9	2.5
18:1 (n-9)	33.3	60.3	23.5	17.9	16.0
18:2 (n-6)	6.5	18.4	52.8	39.6	3.3
18:3 (n-3)	0.9	2.1	5.6	4.8	1.3
20:4 (n-6)	ND	0.2	0.2	0.3	1.7
20:5 (n-3)	0.8	0.1	0.6	0.2	20.4
22:6 (n-3)	ND	0.1	0.2	0.1	17.5

All the analyses were carried out in triplicate, and data correspond to the mean values

ND non detectable

first 12 h. After 12 h the infusion rate of the TPN solution was increased to 5.8 ml/h/kg and lipid emulsion at 0.5 ml/h/kg and, after 24 h, piglets were receiving TPN solution at 5.8 ml/h/kg and lipid emulsion at 1.0 ml/h/kg. These rates were maintained throughout the remainder of the study. Other piglets, after recovering from surgery were fed enterally with a commercially-available sow milk replacer (Primary Diets, Ripon, UK). They were initially given 10 ml of milk replacer and subsequently supplied with 100 ml of milk at 4 h intervals, the volume of milk refused was recorded as a means of measuring intake. Piglets were weighed daily and given antibiotics i.v. (50 mg benzylpenicillin: Crystapen, Brittannia Ltd., Redhill, UK) twice daily.

On the final day of treatment (a few animals were slaughtered prior to the end of the study due to the varying ability of individual piglets to tolerate parenteral feeding), piglets were humanely slaughtered using pentobarbitone sodium (Euthatal, Rhone Merieux, Harlow, UK) and blood and tissue samples were taken. All tissue samples were frozen in liquid nitrogen and were kept at −80°C until analysis. Blood samples were taken into EDTA tubes (Teklab, Durham, UK) and centrifuged at 1,400 g in a bench centrifuge for 15 min at 4°C to produce plasma, which was stored at −20°C for subsequent analysis.

Processing of Samples

Fresh aliquots of each lipid emulsion as well as milk replacer, frozen plasma, liver, subcutaneous fat, brain, heart, pancreas, muscle, intestine and stomach were used for lipid extraction and purification [27]. To assess the fatty acid profile of the phospholipids in the brain, following the lipid extraction, lipids were separated by thin layer chromatography using Silicagel 60 F_{254} plates (Merck, Darmstadt, Germany) with *n*-heptane/diisopropyl ether/acetic acid (70:30:1 v/v/v) as the solvent system. The bands were visualized with 2′7′-dichlorofluorescein (Supelco, Bellafonte, PA, USA) and the phospholipid fractions were eluted from the plate. Total lipid or phospholipid fatty acids were simultaneously saponified and methylated following the method of Lepage and Roy [28, 29]. Fatty acid methyl esters were separated and quantified on a Perkin-Elmer gas chromatograph (Autosystem; Norwalk, CT, USA) with a flame ionisation detector and a 30 m × 0.25 mm Omegawax capillary column. Nitrogen was used as carrier gas, and the fatty acid methyl esters were compared with purified standards (Sigma Chemical Co., St. Louise, MO, USA). Individual fatty acids are expressed as percent of total fatty acids in the sample. Although all the fatty acids from 10:0 to 22:6 (n-3) were analyzed in every sample and used in calculating the corresponding proportions, in the tables and figures just those that have any significance due to their particular presence in the analyzed sample or are of interest due to their respective endogenous metabolism are given.

Statistical Analysis

Data are expressed as means ± SEM. Treatment effects (emulsions or enteral feeding) were analysed by one-way ANOVA with SPSS 12.0 for Windows. When treatment effects were significantly different ($P < 0.05$), means were tested by a Student–Newman–Keuls test. Linear regressions were calculated by the least-squares method [30]. To test the potential interrelationship in fatty acid composition between the emulsions given and the different tissues, correlations of the proportion of fatty acids in the emulsions and the mean value of individual fatty acids in each tissue were calculated.

Results

Plasma

The fatty acid profile of the plasma (Table 2) shows that the proportions of saturated and monounsaturated fatty acids were very similar between the groups with the only

Table 2 Fatty acid composition of plasma in piglets maintained on total parenteral nutrition (TPN) for up to 7 days (n = 5–9/group)

Fatty acid	Enteral	ClinOleic	Intralipid	Lipofundin	Omegaven
(g/100 g fatty acids)					
14:0	0.75 ± 0.27^{a}	0.60 ± 0.35^{a}	0.70 ± 0.26^{a}	1.22 ± 1.03^{a}	ND
16:0	18.15 ± 0.75^{ab}	17.05 ± 0.59^{ab}	17.78 ± 1.09^{ab}	14.58 ± 1.02^{b}	18.90 ± 0.67^{a}
18:0	10.07 ± 0.99^{a}	10.39 ± 0.35^{a}	10.40 ± 0.58^{a}	11.54 ± 1.31^{a}	11.01 ± 0.50^{a}
18:1 (n-9)	32.18 ± 2.04^{a}	32.63 ± 3.82^{a}	27.95 ± 2.79^{a}	21.12 ± 1.86^{a}	22.10 ± 1.07^{a}
18:2 (n-6)	17.95 ± 3.88^{a}	18.59 ± 2.29^{a}	24.05 ± 3.34^{a}	22.27 ± 9.38^{a}	15.26 ± 5.58^{a}
18:3 (n-3)	1.00 ± 0.50^{a}	0.98 ± 0.18^{a}	1.47 ± 0.40^{a}	0.80 ± 0.38^{a}	1.05 ± 0.67^{a}
20:4 (n-6)	9.17 ± 1.62^{a}	7.54 ± 0.74^{a}	7.41 ± 0.83^{a}	5.59 ± 2.20^{a}	5.77 ± 1.01^{a}
20:5 (n-3)	0.59 ± 0.11^{a}	0.96 ± 0.15^{a}	0.88 ± 0.24^{a}	3.92 ± 2.10^{b}	7.94 ± 2.02^{c}
22:6 (n-3)	3.06 ± 0.52^{a}	3.19 ± 0.61^{a}	2.49 ± 0.14^{a}	5.55 ± 3.49^{a}	12.19 ± 2.33^{b}

Values are expressed as means ± SEM. Student–Newman–Keuls test was used to determine differences between groups after ANOVA. Different superscripts in a row indicate significant differences ($P < 0.05$)

ND non detectable

exception being palmitic acid (16:0) which was the lowest in Lipofundin and highest in the Omegaven groups. The n-3 LCPUFA, eicosapentaenoic acid (EPA, 20:5 n-3) and also DHA (22:6 n-3) was higher in those animals given Omegaven compared to the other nutritional treatments (Table 2). AA (20:4 n-6) was almost non-detectable in the milk replacer and the lipid emulsions except for Omegaven (Table 1); however the plasma from all groups showed a considerable and similar proportion of AA (Table 2). There were no other changes observed in the PUFA between the groups, either in terms of the lipid of the nutrients supplied or in the plasma sampled from the animals.

Skeletal Muscle

The fatty acid composition of the skeletal muscle of piglets maintained on TPN with different lipid emulsions or enterally with milk replacer (Fig. 1) closely corresponded to the fatty acid composition of the TPN lipid emulsions or the milk replacer received by each group (Table 1). Of the saturated fatty acids the greatest proportion in all groups was palmitic acid and as it would be expected, myristic acid (14:0) was higher in the skeletal muscle of enterally fed piglets than in the TPN groups. Oleic acid (18:1n-9) was the predominant monounsaturated fatty acid in all the groups, being highest in the ClinOleic group, followed by the enterally fed group. Among n-6 fatty acids, linoleic acid (18:2 n-6) reached the greatest proportion in the Intralipid group followed by Lipofundin (Fig. 1), which fits with its larger proportion in these specific lipid emulsions (Table 1). The proportion of AA was similar in all the groups with a tendency of being slightly although not significantly higher in the Omegaven group than in the others. The proportion of α-linolenic acid (18:3n-3) in muscle, was greater in the Intralipid and Lipofundin groups than in the others (Fig. 1), in agreement with their higher proportion in the corresponding lipid emulsion. Concerning the long chain n-3 PUFA (EPA and DHA), their proportions in muscle were much higher in the Omegaven group than in any of the others.

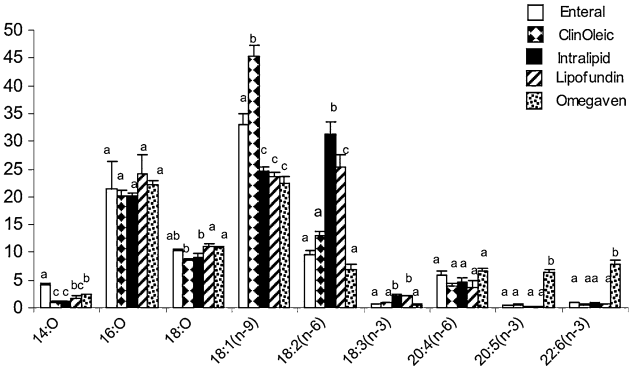

Fig. 1 Fatty acid profile (g/100 g fatty acids) of skeletal muscle in piglets maintained on total parenteral nutrition (TPN) for up to 7 days (n = 5–6/group). Values are expressed as means ± SEM. Student–Newman–Keuls test was used to determine differences between groups after ANOVA. *Different letters over each bar* indicate significant differences ($P < 0.05$)

Subcutaneous Adipose Tissue

As shown in Table 3, the fatty acid profile of subcutaneous fat also mirrored that of the milk replacer given enterally or the lipid emulsion given during TPN and was markedly different between the groups. No differences among the groups were seen for the saturated fatty acids, whereas the proportion of oleic acid was higher in both the enterally fed and the ClinOleic groups than in the others. The proportions of both linoleic and α-linolenic acids in subcutaneous adipose tissue were higher in the Intralipid and Lipofundin groups whereas no differences among the groups were

Table 3 Fatty acid composition of subcutaneous fat in piglets maintained on TPN for up to 7 days (n = 5–11/group)

Fatty acid	Enteral	ClinOleic	Intralipid	Lipofundin	Omegaven
(g/100 g fatty acids)					
14:0	2.52 ± 1.25^a	0.63 ± 0.23^a	0.47 ± 0.17^a	0.11 ± 0.04^a	0.15 ± 0.07^a
16:0	22.09 ± 2.89^a	22.87 ± 1.60^a	18.28 ± 1.50^a	20.34 ± 3.48^a	19.53 ± 1.70^a
18:0	12.40 ± 1.21^a	10.07 ± 0.38^a	10.01 ± 0.80^a	20.79 ± 1.03^b	12.92 ± 1.05^a
18:1 (n-9)	40.14 ± 3.89^a	46.42 ± 1.94^a	29.92 ± 1.13^b	26.83 ± 1.55^b	27.02 ± 1.72^b
18:2 (n-6)	6.14 ± 0.59^a	8.93 ± 0.43^b	29.06 ± 1.12^c	19.79 ± 1.11^d	2.41 ± 0.14^e
18:3 (n-3)	0.6 ± 0.09^a	0.84 ± 0.12^a	2.97 ± 0.11^b	2.40 ± 0.15^c	0.68 ± 0.04^a
20:4 (n-6)	2.11 ± 0.74^a	1.59 ± 0.40^a	1.49 ± 0.28^a	2.38 ± 0.42^a	2.58 ± 0.22^a
20:5 (n-3)	3.03 ± 0.93^a	0.32 ± 0.11^a	0.41 ± 0.23^a	0.25 ± 0.04^a	11.73 ± 0.41^b
22:6 (n-3)	0.64 ± 0.35^a	0.45 ± 0.11^a	0.43 ± 0.07^a	0.74 ± 0.14^a	11.22 ± 0.51^b

Values are expressed as means ± SEM. Student–Newman–Keuls test was used to determine differences between groups after ANOVA. Different superscripts in a row indicate significant differences ($P < 0.05$)

found for AA. Here again, the proportion of both EPA and DHA was greater in the Omegaven group than in any of the others.

Liver

In liver, the composition of the fatty acids differ from the other tissues (Fig. 2). The proportion of saturated fatty acid was similar among the groups except for stearic acid (18:0) that was higher in the enterally fed group than in any of the others. Oleic acid reached the largest proportion in liver of the ClinOleic group, which fits with being the lipid emulsion containing the highest proportion of this fatty acid. The proportion of linoleic acid was highest in the Intralipid and the lowest in the Omegaven group. The proportion of α-linolenic acid in liver was higher in the Intralipid and Lipofundin groups than in any of the others. With AA, its highest proportion was reached by the enterally fed piglets, whereas the rest of the groups showed a similar proportion including the Omegaven group, which on the other hand showed the greatest proportion of n-3 LCPUFA, EPA and DHA (Fig. 2).

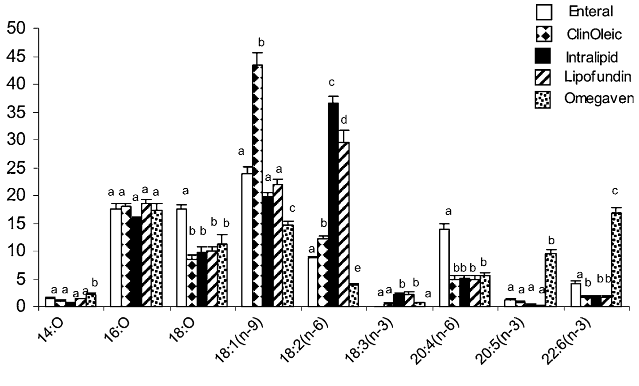

Fig. 2 Fatty acid profile (g/100 g fatty acids) of liver in piglets maintained on TPN for up to 7 days (n = 5–11/group). Values are expressed as means ± SEM. Student–Newman–Keuls test was used to determine differences between groups after ANOVA. *Different letters over each bar* indicate significant differences ($P < 0.05$)

Heart, Pancreas, Stomach and Intestine

Similar fatty acid profiles were found in heart (Table 4), pancreas (Table 5), and stomach (Table 6) and could be considered together: No major differences were detected for the saturated fatty acids, although values for stearic acid appeared lower in enterally fed and ClinOleic treated piglets than in the other groups in pancreas and stomach. Oleic acid tended to be higher in these tissues in the piglets receiving milk replacer enterally or the ClinOleic emulsion intravenously, than in the other groups. Both linoleic and α-linolenic acids were higher in these tissues in the groups given Intralipid and Lipofundin. AA showed a considerable proportion in these tissues in all the groups even though its proportion in the administered emulsions or enteral diet was very low, except for Omegaven. Piglets receiving the Omegaven emulsion showed the highest proportion of both EPA and DHA in these three tissues (Tables 4, 5, 6).

In the intestine there were some differences between the enterally fed piglets and those on TPN that require highlighting (Table 7). Higher proportions of lauric (12:0), myristic and oleic acid were found in the enterally fed group compared to any of the other groups. In contrast, proportions of stearic and AA were lower in the enterally fed piglets than in any of the other groups (Table 7). The Omegaven group also showed some differences in the intestine fatty acid profile compared to the other groups, with a lower proportion of both LA and ALA and a higher proportion of both EPA and DHA, all of which coincide with the relative proportions in the profile of the emulsion (Table 1).

Table 4 Fatty acid composition of heart in piglets maintained on TPN for up to 7 days ($n = 5$–6/group)

Fatty acid	Enteral	ClinOleic	Intralipid	Lipofundin	Omegaven
(g/100 g fatty acids)					
14:0	0.70 ± 0.09^{a}	0.27 ± 0.16^{b}	0.14 ± 0.02^{b}	0.15 ± 0.02^{b}	0.48 ± 0.16^{ab}
16:0	14.13 ± 0.46^{a}	13.15 ± 0.45^{ab}	12.98 ± 0.58^{ab}	12.19 ± 0.32^{b}	12.97 ± 0.32^{ab}
18:0	13.59 ± 0.36^{a}	13.12 ± 0.64^{a}	14.96 ± 0.59^{a}	15.72 ± 0.97^{a}	15.61 ± 0.46^{a}
18:1 (n-9)	24.91 ± 0.93^{ab}	27.62 ± 1.16^{a}	19.47 ± 2.52^{bc}	19.77 ± 1.49^{bc}	17.58 ± 0.45^{c}
18:2 (n-6)	16.16 ± 0.79^{a}	17.63 ± 0.84^{a}	30.28 ± 1.21^{b}	24.95 ± 2.35^{b}	12.64 ± 5.56^{a}
18:3 (n-3)	0.48 ± 0.08^{a}	0.56 ± 0.02^{a}	1.21 ± 0.02^{b}	1.02 ± 0.19^{b}	0.40 ± 0.04^{a}
20:4 (n-6)	14.29 ± 0.82^{a}	12.27 ± 0.66^{ab}	10.32 ± 0.90^{b}	11.56 ± 0.82^{ab}	12.85 ± 0.50^{ab}
20:5 (n-3)	0.42 ± 0.02^{a}	0.38 ± 0.01^{a}	0.31 ± 0.11^{a}	0.50 ± 0.15^{a}	11.08 ± 0.25^{b}
22:6 (n-3)	2.08 ± 0.43^{a}	1.88 ± 0.12^{a}	1.89 ± 0.37^{a}	1.91 ± 0.11^{a}	5.25 ± 1.30^{b}

Values are expressed as means ± SEM. Student–Newman–Keuls test was used to determine differences between groups after ANOVA. Different superscripts in a row indicate significant differences ($P < 0.05$)

Table 5 Fatty acid composition of pancreas in piglets maintained on TPN for up to 7 days ($n = 4$–7/group)

Fatty acid	Enteral	ClinOleic	Intralipid	Lipofundin	Omegaven
(g/100 g fatty acids)					
14:0	1.28 ± 0.46^{a}	0.18 ± 0.06^{a}	0.39 ± 0.09^{a}	0.37 ± 0.29^{a}	0.25 ± 0.21^{a}
16:0	22.74 ± 0.62^{b}	19.75 ± 0.58^{a}	21.04 ± 0.71^{ab}	23.35 ± 1.18^{b}	22.98 ± 0.66^{b}
18:0	10.70 ± 0.24^{a}	11.60 ± 0.42^{a}	13.75 ± 0.29^{b}	14.01 ± 0.90^{b}	13.83 ± 0.18^{b}
18:1 (n-9)	34.25 ± 1.20^{a}	32.68 ± 0.81^{a}	22.08 ± 0.63^{b}	22.05 ± 0.51^{b}	22.96 ± 0.30^{b}
18:2 (n-6)	11.57 ± 1.00^{a}	13.25 ± 0.71^{a}	22.58 ± 0.64^{b}	20.20 ± 1.48^{b}	7.25 ± 2.17^{c}
18:3 (n-3)	0.53 ± 0.06^{a}	0.37 ± 0.03^{a}	0.90 ± 0.08^{a}	0.85 ± 0.05^{a}	0.42 ± 0.07^{a}
20:4 (n-6)	7.74 ± 0.94^{a}	10.80 ± 0.37^{a}	8.90 ± 1.44^{a}	9.38 ± 0.69^{a}	9.40 ± 0.47^{a}
20:5 (n-3)	0.60 ± 0.07^{a}	0.88 ± 0.01^{a}	0.82 ± 0.03^{a}	0.84 ± 0.08^{a}	7.05 ± 1.54^{b}
22:6 (n-3)	1.36 ± 0.22^{a}	1.26 ± 0.10^{a}	1.37 ± 0.14^{a}	1.50 ± 0.41^{a}	3.74 ± 0.47^{b}

Values are expressed as means ± SEM. Student–Newman–Keuls test was used to determine differences between groups after ANOVA. Different superscripts in a row indicate significant differences ($P < 0.05$)

Table 6 Fatty acid composition of stomach in piglets maintained on TPN for up to 7 days ($n = 5$–11/group)

Fatty acid	Enteral	ClinOleic	Intralipid	Lipofundin	Omegaven
(g/100 g fatty acids)					
14:0	1.42 ± 0.16^{a}	0.31 ± 0.04^{b}	0.29 ± 0.02^{b}	0.38 ± 0.05^{b}	0.75 ± 0.13^{b}
16:0	20.99 ± 0.35^{a}	19.92 ± 0.67^{a}	18.69 ± 0.29^{a}	19.79 ± 0.56^{a}	21.71 ± 2.12^{a}
18:0	14.26 ± 0.34^{a}	14.73 ± 0.43^{a}	17.02 ± 0.56^{b}	16.81 ± 0.39^{b}	15.73 ± 0.87^{ab}
18:1 (n-9)	31.97 ± 0.47^{a}	32.60 ± 0.71^{a}	21.23 ± 0.29^{b}	21.46 ± 0.86^{b}	22.43 ± 0.49^{b}
18:2 (n-6)	10.28 ± 0.38^{a}	10.68 ± 0.51^{a}	19.53 ± 0.68^{b}	16.85 ± 1.20^{c}	4.78 ± 0.23^{d}
18:3 (n-3)	0.35 ± 0.04^{a}	0.36 ± 0.03^{a}	0.76 ± 0.10^{b}	0.65 ± 0.07^{b}	0.26 ± 0.02^{a}
20:4 (n-6)	10.19 ± 0.26^{a}	11.22 ± 0.31^{a}	10.94 ± 0.43^{a}	11.13 ± 0.15^{a}	9.93 ± 0.84^{a}
20:5 (n-3)	0.89 ± 0.03^{a}	0.87 ± 0.05^{a}	0.95 ± 0.03^{a}	1.07 ± 0.04^{a}	6.38 ± 0.38^{b}
22:6 (n-3)	2.05 ± 0.11^{a}	2.39 ± 0.14^{a}	2.59 ± 0.33^{a}	2.26 ± 0.15^{a}	5.04 ± 0.26^{b}

Values are expressed as means ± SEM. Student–Newman–Keuls test was used to determine differences between groups after ANOVA. Different superscripts in a row indicate significant differences ($P < 0.05$)

Brain

In relation to the fatty acid composition of brain phospholipids in piglets fed enterally or maintained on TPN (Fig. 3), it can be seen that there were no statistical differences in the proportions of the main saturated fatty acids (palmitic and stearic acids) between the different treatments. It is also interesting to notice that the proportion of

Table 7 Fatty acid composition of intestine in piglets maintained on TPN for up to 7 days (n = 5–11/group)

Fatty acid	Enteral	ClinOleic	Intralipid	Lipofundin	Omegaven
(g/100 g fatty acids)					
12:0	4.31 ± 1.13^{a}	0.06 ± 0.02^{b}	0.11 ± 0.05^{b}	0.05 ± 0.05^{b}	0.06 ± 0.04^{b}
14:0	3.21 ± 0.66^{a}	0.20 ± 0.03^{b}	0.22 ± 0.02^{b}	0.18 ± 0.05^{b}	0.52 ± 0.09^{b}
16:0	21.16 ± 0.54^{a}	20.28 ± 1.20^{a}	19.52 ± 0.48^{a}	17.25 ± 0.31^{b}	21.13 ± 0.69^{a}
18:0	12.05 ± 1.02^{a}	15.18 ± 1.04^{b}	17.38 ± 0.41^{bc}	19.39 ± 0.41^{c}	17.77 ± 0.77^{bc}
18:1 (n-9)	32.58 ± 0.88^{a}	28.59 ± 1.23^{b}	17.86 ± 0.41^{c}	18.70 ± 0.42^{c}	17.77 ± 0.73^{c}
18:2 (n-6)	13.11 ± 0.97^{a}	11.98 ± 0.60^{a}	22.10 ± 1.07^{b}	19.42 ± 1.16^{b}	4.51 ± 0.23^{c}
18:3 (n-3)	0.89 ± 0.07^{a}	0.46 ± 0.04^{b}	0.94 ± 0.10^{a}	1.00 ± 0.10^{a}	0.32 ± 0.02^{b}
20:4 (n-6)	6.15 ± 0.77^{a}	11.05 ± 0.84^{b}	10.83 ± 0.48^{b}	12.95 ± 0.69^{b}	11.30 ± 0.27^{b}
20:5 (n-3)	0.37 ± 0.04^{a}	0.51 ± 0.05^{a}	0.65 ± 0.06^{a}	0.52 ± 0.04^{a}	10.15 ± 0.29^{b}
22:6 (n-3)	1.45 ± 0.18^{a}	3.17 ± 0.27^{a}	3.08 ± 0.16^{a}	3.93 ± 0.21^{a}	8.49 ± 0.23^{b}

Values are expressed as means ± SEM. Student–Newman–Keuls test was used to determine differences between groups after ANOVA. Different superscripts in a row indicate significant differences ($P < 0.05$)

stearic acid seen in brain phospholipids of all the groups is higher than that present in plasma or in any of the other tissues studied. The proportion of oleic acid (18:1n-9) was also similar in all the groups despite the differences in the proportion of this fatty acid in the emulsions used. In relation with PUFA, linoleic acid proportions in all the groups were lower than in any of the other tissues studied, and values were higher in the Intralipid group, followed by Lipofundin, which may be related to the high proportion of this fatty acid in the emulsion's composition. The proportion of α-linolenic acid was practically undetectable in brain phospholipids from all the groups, despite its significant proportion in the corresponding emulsions. Despite major differences in the proportions of LCPUFA in the emulsions or milk replacer, the brain phospholipids showed similar proportions across the different groups, with the exception of DHA, which showed a large proportion in all the groups, although the Omegaven group showed its greatest proportion (Fig. 3).

Relationship Between Emulsions and Tissues

There were positive significant linear correlations between the proportion of the fatty acids in the emulsions and the proportions of the same fatty acids in each of the tissues studied, with brain phospholipids showing the lowest correlation coefficient (data not shown). Besides, by calculating the relationship of individual fatty acids for each tissue vs. their proportion in the milk replacer or lipid emulsions or even in plasma, it was found that in case of the saturated fatty acids the correlations did not reach statistical significance whereas the proportions of oleic acid, linoleic acid, α-linolenic acid, EPA or DHA were significantly correlated in case of skeletal muscle, subcutaneous fat, liver, heart, pancreas, stomach or intestine, but not in brain phospholipids (data not shown).

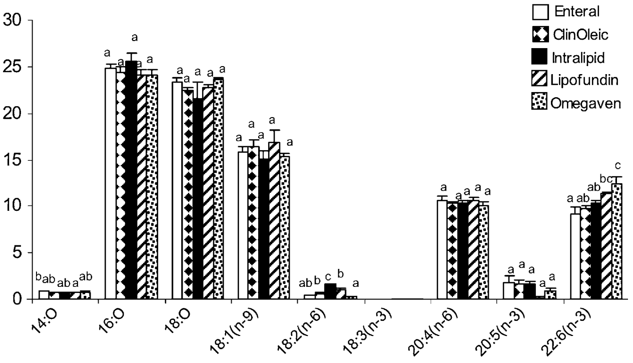

Fig. 3 Fatty acid profile (g/100 g fatty acids) of brain phospholipids in piglets maintained on TPN for up to 7 days (n = 4–11/group). Values are expressed as means ± SEM. Student–Newman–Keuls test was used to determine differences between groups after ANOVA. *Different letters over each bar* indicate significant differences ($P < 0.05$)

Discussion

Tissue Fatty Acid Profiles in Piglets on TPN Emulsions with Different FA Compositions

The present study shows that the fatty acid composition of the skeletal muscle and subcutaneous adipose tissue from piglets enterally fed a milk replacer or intravenously administered ClinOleic, Intralipid, Lipofundin or Omegaven emulsions—having different fatty acids composition—for 7 days from birth, is clearly influenced by the dietary fatty acid composition, and it is consistent with a previous report that indicates that fatty acid composition of adipose tissue and muscle of 7-day-old pigs reflects milk fatty acid composition [31]. This fits with the high lipoprotein lipase (LPL) activity that has been found in adipose tissue of these animals [31, 32], and although in muscle the LPL activity is lower, it has been found that there is no release of NEFA from skeletal muscle during high rates of LPL action, suggesting that in muscle LPL-derived fatty acids are effectively trapped in the tissue [33], which is in accordance with our results. Nevertheless, previous observations support the hypothesis that lipogenesis may be significant in adipose tissue of the neonatal pig [31, 34] and in our study the lack of difference in the proportion of palmitic acid in adipose tissue between the different groups studied, despite the fact that milk replacer contained nearly twofold the proportion of palmitic acid in the TPN emulsions, also supports this hypothesis.

In liver, the fatty acid composition must be modulated by in situ metabolism of fatty acids and the influx of fatty acids from the diet and/or from the de novo synthesis in the adipose tissue. Although it has been reported that the rate of lipogenesis in the liver of newborn piglets is low [35], a high rate of desaturase activities is found in the liver of piglets [19, 36]. As a result of this, and even though Omegaven emulsion is the only one that contains AA in its composition, all the groups produce high proportions of AA in liver. It is known that high proportions of long-chain n-3 fatty acids decrease Δ-6 desaturase activity [37, 38], the main enzyme responsible for the synthesis of AA from linoleic acid, but this effect could be compensated for by the presence of AA in the Omegaven emulsion, causing the Omegaven group to have a similar amount of AA in liver in comparison with the rest of the TPN fed groups. Moreover, it is important to point out that the highest proportion of AA in liver is observed in the enterally fed group, and the lower AA proportion in the TPN treated groups could be the result of lower rates of desaturation that have been already reported in other studies as a consequence of TPN treatments [39]. This lower proportion of AA following TPN occurs even after treatment with Intralipid, which contains the highest proportion of linoleic acid as compared to other emulsions and more than eight times higher than the milk replacer. It could well be that the high dietary intake of linoleic acid in this group inhibits AA synthesis or competes with AA for acylation, as it has been previously proposed [40]. Fatty acid composition of liver is also influenced by its LPL activity, allowing circulating triacylglycerols to be hydrolyzed and fatty acids to be taken up by the tissue. In contrast to what occurs in adults, the liver of the newborn in different species expresses LPL [41, 42] and the pig is not an exception [32]. In fact, we have previously shown that the piglets receiving TPN develop fatty liver, the effect being probably mediated by the action of LPL contributing to the tissue uptake of circulating fatty acids [32].

The fatty acid proportion in plasma must be the result of the influx of fatty acids from the emulsions, plus those from the metabolic changes taking place in liver and/or adipose tissue. The fact that no differences were found between the groups in oleic, linoleic, ALA and even AA in plasma, despite major differences in their respective proportion in the different lipid emulsions or milk replacers, would indicate that they represent a combination of these different sources. These metabolic changes also influence the fatty acid composition of other tissues such as heart, pancreas, stomach and intestine. Among them, the one that follows most closely the differences found in the lipid emulsions or milk replacer fatty acid composition is the heart, which has been reported not to exhibit desaturase activities [19, 43].

Relationship Between the Fatty Acid Profiles of the TPN Emulsions and in Different Tissues

In order to obtain an approximation of the influence of administered fatty acids, with the different emulsions or milk replacer, on the tissue fatty acid composition, linear correlations were made. Strong linear correlations were found between the fatty acids in the TPN emulsion given and the fatty acid composition of plasma and several tissues of piglets, the lowest correlation being found for brain phospholipids. In an attempt to analyze in more detail the influence that each fatty acid present in the emulsion has in its corresponding proportion in the different tissues, correlations were performed and it was found that the proportions of palmitic and stearic fatty acids, the main saturated fatty acids, did not correlate with their proportion in the TPN or in the milk replacer. This finding is consistent with the results found in other studies where it is observed that lipogenesis is significant in adipose tissue and muscle of neonatal pigs [31] and in developing brain [44, 45]. However, different to other tissues, oleic acid in brain phospholipids did not correlate with this fatty acid in the TPN emulsions or milk replacer, and its precursor, stearic acid shows the highest proportion in brain phospholipids than in any of the other tissues studied. Although we have not measured the actual rate of lipogenesis, these findings indicate an active elongase process in brain allowing the efficient conversion of palmitic acid into stearic acid, and the efficient Δ6 desaturation of the later, all of which agree with the active lipid metabolism known to take place in brain [46], and with the high stearoyl-CoA desaturase present in brain during the perinatal period [47]. The correlation between the proportion of tissue fatty acids and those present in the TPN emulsions and milk replacer were particularly significant for the PUFA, which agrees with similar previously described findings in adipose tissue [48]. EFA cannot be synthesized endogenously. The proportion of LA in the emulsions or milk replacer is strongly correlated with the proportion found in each of the tissues studied, including brain phospholipids. However, the LA derivative, AA, reach a proportion in different tissues that is independent of its presence (or absence) in the diets. This indicates an active endogenous synthesis of AA in all the studied tissues, including brain, where it has been described that is active during development [49]. Concerning the n-3 LCPUFA, present findings indicate that with exception of brain phospholipids, the presence of both EPA and DHA in the different tissues is very much dependent on their presence in the corresponding emulsion or milk replacer, since despite of the presence of their precursor in the diets and tissues both fatty acids reached significant proportions only in the tissues of the TPN-Omegaven group, indicating that their endogenous synthesis in the neonatal pig is relatively low. This situation completely differs in brain phospholipids, where the proportion of EPA did not differ in the piglets receiving Omegaven compared to any of the other groups and in case of DHA, its comparative proportion in brain of animals on Omegaven versus the rest of the groups is much smaller than for any of the other studied tissues. This occurs despite the brain having the lowest proportion of ALA in all the groups, suggesting a rapid and efficient conversion to their LCPUFA derivatives, EPA and DHA.

Final Considerations

It is not possible to directly compare present findings to the condition present in premature human neonates on TPN. However, the premature piglet has previously been used as a model for the premature infant [50–52], and by using an experimental design similar to that previously used, we have recently found that during TPN, the piglets show typical responses previously reported in human infants [32]. Thus, with the appropriate caution, the findings here reported can be used to understand some of the responses to TPN in human premature neonates.

In conclusion, with the exception of the brain, the fatty acid composition of plasma and of different tissues of piglets are strongly influenced by the fatty acid profile of TPN emulsions. However, fatty acid composition in brain phospholipids is much less dependent on dietary composition, indicating an active and efficient metabolism that ensures the appropriate composition in this key stage of its development. It is proposed that an appropriate availability of essential fatty acids, rather than synthesized LCPUFA is needed to ensure an appropriate fatty acid profile in the brain during its developmental stage.

Acknowledgments We thank Milagros Morante, Kate Perkins, Anne Corson, Jennie Litten, for their excellent technical assistance and the staff at Imperial College London's pig unit for the maintenance and supply of animals used in this study. Supported by grants from European Community (specific RTD programme "Quality of Life and Management of Living Resources", QLK1-2001—00138, PeriLip) and Ministerio de Educación y Ciencia (SAF2004-05998) of Spain. Matthew Hyde is funded by a BBSRC Doctoral studentship.

References

1. Schubert OWA (1961) Intravenous infusion of fat emulsion and phosphatides and emulsifying agents. Acta Chir Scan Suppl 278:1–21
2. Shamsuddin AF (2003) Brief history and development of parenteral nutrition support. Malaysian J Pharm 1:69–75
3. Hulbert AJ, Turner N, Storlien LH, Else PL (2005) Dietary fats and membrane function: implications for metabolism and disease. Biol Rev 80:155–169
4. Clandinin MT, Cheema S, Field CJ, Garg ML, Venkatraman J, Clandinin TR (1991) Dietary fat: exogenous determination of membrane structure and cell function. FASEB J 5:2761–2769
5. Hamosh M, Salem N (1998) Long-chain polyunsaturated fatty acids. Biol Neonate 74:106–120
6. Palmblad J (1991) Intravenous lipid emulsions and host defense: a critical review. Clin Nutr 10:303–308
7. Calder PC (1998) Dietary fatty acids and the immune system. Nutr Rev 56:570–583
8. Göbel Y, Koletzko B, Böhles HJ, Engelsberger I, Forget D, Le Brun A, Peters J, Zimmerman A (2003) Parenteral fat emulsions based on olive and soybean oils: a randomized clinical trial in preterm infants. J Pediatr Gastroenterol Nutr 37:161–167
9. Clandinin MT, Chapell JE, Leong S, Heim T, Swyer PR, Chance GW (1980) Intrauterine fatty acid accretion rates in human brain: Implications for fatty acid requirements. Early Hum Dev 120:121–130
10. Innis SM (2000) Essential fatty acids in infant nutrition: lessons and limitations from animal studies in relation to studies on infant fatty acid requirements. Am J Clin Nutr 71:238–244
11. Uauy R, Hoffman DR, Mena P, Llanos A, Birch E (2003) Term infant studies of DHA and ARA supplementation on neurodevelopment: results of randomized controlled trials. J Pediatr 143:17–25
12. Innis SM (1991) Essential fatty acids in growth and development. Prog Lipid Res 30:39–103
13. Benatti P, Peluso G, Nicolai R, Calvani M (2004) Polyunsaturated fatty acids: biochemical, nutritional and epigenetic properties. J Am Coll Nutr 23:281–302
14. Carlson SE, Werkman SH, Peeples JM, Cooke RJ, Tolley EA (1993) Arachidonic acid status correlates with first-year growth in preterm infants. Proc Natl Acad Sci USA 90:1073–1077
15. Amusquivar E, Ruperez FJ, Barbas C, Herrera E (2000) Low arachidonic acid rather than a-tocopherol is responsible for the delayed postnatal development in offspring of rats fed fish oil instead of olive oil during pregnancy and lactation. J Nutr 130:2855–2865
16. Cho HP, Nakamura M, Clarke SD (1999) Cloning, expression and nutritional regulation of the mammalian D-6 desaturase. J Biol Chem 274:471–477
17. Sprecher H (2000) Metabolism of highly unsaturated n-3 and n-6 fatty acids. Biochim Biophys Acta 1486:219–231
18. Al MDM, van Houwelingen AC, Badart-Smook A, Honstra G (1995) Some aspects of neonatal essential fatty acid status are altered by linoleic acid supplementation of women during pregnancy. J Nutr 125:2822–2830
19. de la Presa-Owens S, Innis SM, Rioux F (1998) Addition of Triglycerides with arachidonic acid or docosahexaenoic acid to

infant formula has tissue- and lipid class-specific effects on fatty acids and hepatic desaturase activities in formula-fed piglets. J Nutr 128:1376–1384
20. Amusquivar E, Herrera E (2003) Influence of changes in dietary fatty acids during pregnancy on placental and fetal fatty acid profile in the rat. Biol Neonate 83:136–145
21. Demmelmair H, Schenk U, Behrendt E, Sauerwald T, Koletzko B (1995) Estimation of arachidonic acid synthesis in full term neonates using natural variation of ^{13}C content. J Pediatr Gastr Nutr 21:31–36
22. Goulet O, de Potter S, Antébi H, Driss F, Colomb V, Béréziat G, Alcindor LG, Corriol O, Le Brun A, Dutot G, Forget D, Perennec V, Ricour C (1999) Long-term efficacy and safety of a new olive oil-based intravenous fat emulsion in pediatric patients: a double-blind randomized study. Am J Clin Nutr 70:338–345
23. Wang H, Khaoustov VI, Krishnan B, Cai W, Stoll B, Burrin D, Yoffe B (2006) Total parenteral nutrition induces liver steatosis and apoptosis in neonatal piglets. J Nutr 136:2547–2552
24. Innis SM (1993) The colostrum-deprived piglet as a model for study of infant lipid nutrition. J Nutr 123:386–390
25. Book S, Bustad L (1974) The fetal and neonatal pig in biomedical research. J Anim Sci 38:997–1002
26. Truskett PG, Shi ECP, Rose M, Sharp PA, Ham JM (1987) Model of TPN-associated hepatobiliary dysfunction in the young pig. Br J Surg 74:639–642
27. Folch J, Lees M, Sloane-Stanley GH (1957) A simple method for the isolation and purification of total lipids from animal tissues. J Biol Chem 226:497–509
28. Lepage G, Roy CC (1984) Improved recovery of fatty acid through direct transesterification without prior extraction and purification. J Lipid Res 25:1391–1396
29. Lepage G, Roy CC (1986) Direct transesterification of all classes of lipids in a one-step reaction. J Lipid Res 27:114–120
30. Quaresima V, Pizzi A, De Blasi RA, Ferrari A, Ferrari M (1996) Influence of the treadmill speed/slope on quadriceps oxygenation during dynamic exercise. Adv Exp Med Biol 388:231–235
31. Gerfault V, Louveau I, Mourot J, Le Dividich J (2000) Lipogenic enzyme activities in subcutaneous adipose tissue and skeletal muscle from neonatal pigs consuming maternal or formula milk. Reprod Nutr Dev 40:103–112
32. Hyde MJ, Amusquivar E, Laws J, Corson AM, Geering RR, Lean IJ, Putet G, Dodds PF, Herrera E, Clarke L (2008) The effects of lipid-supplemented total parenteral nutrition on fatty liver disease in a premature neonatal piglet model. Neonatology 93:77–86
33. Fielding BA, Frayn K (1998) Lipoprotein lipase and the disposition of dietary fatty acids. Br J Nutr 80:495–502
34. Smith DR, Knabe DA, Smith SB (1996) Depression of lipogenesis in swine adipose tissue by specific dietary fatty acids. J Anim Sci 74:975–983
35. Pégorier JP, Duée PH, Girard J, Peret J (1983) Metabolic fate of non-esterified fatty acids in isolated hepatocytes from newborn and young pigs. Evidence for a limited capacity for oxidation and increased capacity for esterification. Biochem J 212:93–97
36. Clandinin MT, Wong K, Hacker RR (1984) Synthesis of chain elongation-desaturation products of linoleic acid by liver and brain microsomes during development of the pig. Biochem J 226:305–309
37. Raz A, Kamin-Belsky N, Przedecki F, Obukowicz MG (1997) Fish oil inhibits D-6 desaturase activity in vivo: Utility in a dietary paradigm to obtain mice depleted of arachidonic acid. J Nutr Biochem 8:558–565
38. Garg ML, Thomson ABR, Clandinin MT (1990) Interactions of saturated, n-6 and n-3 polyunsaturated fatty acids to modulate arachidonic acid metabolism. J Lipid Res 6:51–62
39. Innis SM, Yuen DE (1988) Microsomal desaturation-elongation of linoleic acid following parenteral feeding with lipid emulsions in the rat. Lipids 23:546–550
40. Rioux F, Innis SM, Dyer R, Mackinnon MJ (1997) Diet-induced changes in liver and bile but not brain fatty acids can be predicted from differences in plasma phospholipid fatty acids in formula and milk-fed piglets. J Nutr 127:370–377
41. Ramírez I, Llobera M, Herrera E (1983) Circulating triacylglicerols, lipoproteins, and tissue lipoprotein lipase activities in rat mothers and offspring during the perinatal period: effect of postmaturity. Metabolism 32:333–341
42. Panadero MI, Bocos C, Herrera E (2006) Relationship between lipoprotein lipase and peroxisome proliferator-activated receptor-alpha expression in rat liver during development. J Physiol Biochem 62:171–180
43. Hagve TA, Sprecher H (1989) Metabolism of long-chain polyunsaturated fatty acids in isolated cardiac myocytes. Biochim Biophys Acta 1001:338–344
44. Edmond J, Higa TA, Korsak RA, Bergner EA, Paul Lee WN (1998) Fatty acid transport and utilization for the developing brain. J Neurochem 70:1227–1234
45. Marbois BN, Ajie HO, Korsak RA, Sensharma DK, Edmond J (1992) The origin of palmitic acid in brain of the developing rat. Lipids 27:587–592
46. Menkes JH (1971) Lipid metabolism of brain tissue in culture. Lipids 7:135–141
47. Cook HW, Spence MW (1973) Formation of monoenoic fatty acids by desaturation in rat brain homogenate. J Biol Chem 248:1793–1796
48. Innis SM, King JD, Dyer R, Quinlan P, Diersen-Schade D (1993) Adipose tissue fatty acids of piglets fed formulae varying in saturated and monounsaturated fatty acdis, linoleic acid and with longer chain n-3 fatty acids from fish oil. Nutr Res 13:929–940
49. Yehuda S, Rabinovitz S, Mostofsky DI (2005) Essential fatty acids and the brain: from infancy to aging. Neurobiol Aging 26S:98–102
50. Truskett PG, Shi ECP, Rose M, Sharp PA, Ham JM (1987) Model of TPN-associated hepatobiliary dysfunction in the young pig. Br J Surg 74:639–642
51. Mei J, Xu R (2003) The piglet as a model for studying parenteral nutrition. In: Xu R, Cranwell P (eds) The neonatal pig: gastrointestinal physiology and nutrition. Nottingham University Press, Nottingham, pp 309–335
52. Sangild P, Petersen Y, Schmidt M, Elnif J, Petersen T, Buggington R (2002) Preterm birth affects the intestinal response to parenteral and enteral nutrition in newborn pigs. J Nutr 132: 2673–2681

Lipids (2008) 43:723–732
DOI 10.1007/s11745-008-3203-4

ORIGINAL ARTICLE

Metabolic Syndrome Affects Fatty Acid Composition of Plasma Lipids in Obese Prepubertal Children

Mercedes Gil-Campos · Maria del Carmen Ramírez-Tortosa · Elvira Larqué · Javier Linde · Concepción M. Aguilera · Ramón Cañete · Angel Gil

Received: 13 January 2008 / Accepted: 5 June 2008 / Published online: 1 July 2008
© AOCS 2008

Abstract The aim of the present study was to assess the plasma fatty acid composition of the total plasma lipids and lipid fractions in obese prepubertal children with and without metabolic syndrome (MS). Thirty-four obese prepubertal children were recruited: 17 who met MS criteria and 17 who did not; and twenty prepubertal children of normal weight. MS characteristics, insulin resistance (by homeostasis model assessment [HOMA-IR]), and plasma adiponectin (by radioimmunoassay) were recorded. Separation of lipid fractions was performed by liquid chromatography and the concentration of fatty acids in total plasma lipids and fractions was determined by gas–liquid chromatography. Concentrations of 16:1n-7, 16:1n-9, 18:3n-3, 22:6n-3, and n-3 PUFA in total plasma lipids ($P < 0.05$) and of 16:0, 16:1n-7, 18:1n-9, 18:2n-6, and n-6 PUFA in triacylglycerols (TG) ($P < 0.05$) were significantly higher in obese MS versus normal-weight children. Increased risk of MS was positively associated with plasma concentration of 16:1n-7 and negatively associated with proportion of 20:4n-6 (OR 2.76; $P = 0.004$; OR 0.56, $P = 0.030$, respectively). Saturated FA in TG were associated with HOMA-IR ($R = 0.349$, $P = 0.017$) and 22:5n-6 with adiponectin ($R = 0.336$, $P = 0.05$). In conclusion, increased concentrations of 16:1n-7 and decreased proportions of 20:4n-6 and 22:5n-6 in plasma lipids appear to be early markers of MS in children at prepubertal age.

Keywords Insulin resistance · Metabolic syndrome · Childhood obesity · Plasma fatty acid composition · Plasma lipid fractions · Prepubertal children

Abbreviations

HOMA	Homeostatic assessment model
IR	Insulin resistance
FSH	Follicle-stimulating hormone
LC-PUFA	Long-chain polyunsaturated fatty acids
LH	Lutein hormone
MS	Metabolic syndrome
MUFA	Monounsaturated fatty acids
NEFA	Non-esterified fatty acids
NMS	Non-metabolic syndrome
SCD1	Stearoyl-coenzyme A desaturase 1
SFA	Saturated fatty acids
TG	Triacylglycerols
TFA	Total FA

Introduction

The prevalence of obesity in infancy has dramatically increased over the last few decades in both developed and developing countries [1]. Obese patients typically show a cluster of clinical and metabolic abnormalities known as metabolic syndrome (MS), characterised by insulin resistance (IR), hyperglycemia, high VLDL triacylglycerols

M. Gil-Campos · R. Cañete
Unit of Paediatric Endocrinology, Reina Sofia University Hospital, Cordoba, Spain

M. del Carmen Ramírez-Tortosa · J. Linde ·
C. M. Aguilera · A. Gil (✉)
Institute of Nutrition and Food Technology,
Department of Biochemistry and Molecular Biology II,
School of Pharmacy, University of Granada,
Campus de Cartuja, 18071 Granada, Spain
e-mail: agil@ugr.es

E. Larqué
Department of Physiology, School of Biology,
University of Murcia, Murcia, Spain

(TG), low HDL-cholesterol, and hypertension [2]. Changes in plasma concentrations of some hormones and adipokines, e.g., adiponectin, are also associated with MS [3]. Evidence is accumulating that IR induced by excess of fat may be a common link among clinical manifestations of MS [4–6]. MS has a high prevalence among children and adolescents, increases with worsening obesity, and is associated with an increased risk of cardiovascular disease [4, 7].

Very little research has been published on the association between childhood obesity or MS and possible changes in fatty acid profiles of plasma and its lipid fractions. Alterations in the proportions of saturated fatty acids (SFA) and some long-chain polyunsaturated fatty acids (LC-PUFA), mainly arachidonic acid (20:4n-6) have been reported in pubescent children with MS [8, 9]. More recently, plasma fatty acid composition was shown to be associated with MS and low-grade inflammation in overweight adolescents [10]. A search of the literature yielded no data on changes in plasma fatty acid composition related to obesity or MS in prepubertal children. The study of fatty acid composition in plasma of prepubertal children with and without MS may contribute to a better knowledge of the mechanisms involved in alterations of lipid metabolism related to early onset and development of obesity and MS. Therefore, the aim of the present study was to quantify and compare the plasma fatty acid composition of total plasma lipids and plasma lipid fractions PL, CE, TG and non-esterified fatty acids (NEFA) in obese prepubertal children with and without MS and in prepubertal children of normal weight.

Experimental Procedures

Subjects

Fifty-four Caucasian children aged 6–12 years, comprising 34 obese and 20 normal-weight children at prepubertal age (Tanner I) were selected, the clinical stage being confirmed with the determination of sexual hormones (FSH, LH, estradiol and testosterone). Children with Tanner II or III did not enter into the study and Tanner 1 with elevated levels of hormones that indicated starting puberty, were excluded. Most of the children that were 12 years old were boys.

Two recent papers by our group on the postprandial response of *trans* and other plasma fatty acids in the prepubertal obese children are based on the same population of the present report [11, 12]. The study was approved by the Human Investigation and Ethics Committees of the University of Granada and the Reina Sofia University Hospital of Cordoba (Spain). Written informed consent was obtained from parents and verbal approval from children.

Classification of Obese Children by Presence/Absence of Metabolic Syndrome

Although a new worldwide definition for the MS has been reported for adults [2], there has been no equivalent international agreement on the criteria for MS in childhood. Therefore, our classification of the obese children as non-MS (NMS) or MS was a modification of criteria established by the World Health Organisation [13] and the Adult Treatment Panel of the Cholesterol Education Program [14]. MS was diagnosed if three or more of the following criteria were met in relation to the age and sex of the child: BMI z score ≥ 2.0; plasma TG concentration >95th percentile; plasma HDL-cholesterol concentration <5th percentile; systolic or diastolic pressure >95th percentile; and impaired glucose tolerance, defined as a fasting plasma glucose concentration >6.1 mmol/L [15].

Dietary Assessment

Children and parents were interviewed on an individual basis to obtain information on lifestyle and dietary habits. Dietary intake was estimated by means of a food-frequency questionnaire and 72-h dietary survey, using a database of the composition of Spanish foods [16].

Anthropometric, Blood Pressure, and Sex Maturity Measurements

An initial examination was conducted by trained pediatric endocrinologists according to standardised methods. Measurements were taken of height, weight, tricipital and subscapular skinfolds, and waist and hip circumferences and the BMI (weight-[kg]/height^2 [m^2]) and waist-to-hip ratio were calculated. The BMI z score was calculated based on the averages and standard deviations of BMI for the Spanish children population, considering sex and age as published by Hernández et al. [17]. Blood systolic and diastolic pressures were measured using a standardised mercury sphygmomanometer and an adapted cuff size. Self-assessed Tanner stages and concentrations of plasma follicle-stimulating hormone (FSH), lutein hormone (LH), estradiol, and testosterone were recorded and used to estimate the sexual maturity of the children.

Blood sampling

Baseline blood samples were obtained from children at 9 a.m. after a 12-h overnight fast, using an indwelling venous line for the measurement of plasma glucose, insulin, sex hormones, lipids, total fatty acids, and fatty acid composition of lipid fractions. All samples were processed within 2 h of sampling, and were divided into aliquots for immediate processing or for long-term storage at −80 °C until their analysis.

Biochemical Analysis

Sex hormones, blood glucose, plasma insulin, adiponectin and lipids, as well as isolation, separation and quantitation of fatty acids in total plasma lipids and plasma lipid fractions were analysed as previously reported [3]. In brief, sex hormones (FSH: CV 3.6%; LH: CV 3.1%; testosterone: CV 2%; estradiol: CV 1.8%) were measured by chemiluminescence using an automatic analyser (Architet I4000, Abbott Laboratories Chicago, IL, USA). Glucose was analysed using the glucose oxidase method in an automatic analyser (CV 1%) (Roche-Hitachi Modular PyD Autoanalyser, Roche Laboratory Systems, Mannheim, Germany), and plasma insulin was analysed by radioimmunoassay (CV 2.6%) using an automatic analyser for microparticles (Axsym, Abbott Laboratories, Chicago, IL, USA). Insulin resistance was calculated by means of the homeostatic assessment model (HOMA-IR), as defined by the equation HOMA-IR = fasting glucose (G0) (mM) × fasting insulin (I0) (μU/mL)/22.5 [18].

Plasma TG (CV 1.5%) and HDL-cholesterol (CV 0.8%) were measured using an automatic analyser (Roche-Hitachi Modular PyD Autoanalyser, Roche Laboratory Systems, Mannheim, Germany). Plasma adiponectin was measured by radioimmunoassay (Human adiponectin RIA kit, Cat.#HADP-61HK, Linco Research Inc., St. Charles, MO, USA).

Statistical Analysis

The minimum sample size to detect an effect due to the presence of MS in obese children was estimated as 16 children per group; this figure allows a type I error $\alpha = 0.05$ and a type II error $\beta = 0.1$ (power 90%) for an estimated difference of 20% between groups in the mean value of major plasma fatty acids (oleic and linoleic acids), considering the variances obtained previously in plasma fatty acid analyses of children measured by gas–liquid chromatography [19].

All data for continuous variables are expressed as means ± SEM. Variables not following a normal distribution (insulin, HOMA, TG and fatty acid percentages) were logarithmically transformed before analysis. Comparisons of continuous variables among groups, with adjustments for age and sex, were assessed by general linear models of variance and post hoc Bonferroni tests. The association of fatty acid variables with variables considered in the definition of MS was analysed for the obese children by multivariable linear regression models. Logistic regression models were performed to identify fatty acids significantly related to the likelihood of having MS. All statistical analyses were performed with SPSS version 14.1 software (Statistical Package for Social Sciences, SPSS Inc. Chicago, IL, USA).

Results

Anthropometric, Metabolic, and Dietary Evaluation

Table 1 shows sex frequencies, age, and anthropometric and metabolic data adjusted for sex and age in the normal-weight, and NMS and MS obese prepubertal groups. Anthropometric and metabolic data, with the exception of the waist-to-hip ratio and glucose values, were significantly different in obese individuals than in controls, but did not differ between NMS and MS groups. However, insulin, HOMA-IR, and TG values were significantly higher, and adiponectin and cHDL significantly lower, in MS than in NMS groups. All anthropometric variables except for the waist-to-hip ratio were positively associated with MS. Blood pressure, insulin, HOMA-IR, and TG were also positively associated with MS whereas HDL-cholesterol was negatively associated with MS; fasting glucose was not associated with MS.

We previously reported that this group of obese children had a significant higher absolute daily intake of energy and all major nutrients compared with normal-weight children but the intake of energy and macronutrients to BMI ratios were significantly lower in the obese group [11]. No differences in the daily intake of energy and macronutrients as well as saturated, monounsaturated and polyunsaturated fat, were observed between the obese NMS and MS groups (Table 2).

Plasma Fatty Acids

Figure 1 shows the fasting plasma fatty acid concentrations of 16:1n-7, 16:1n-9, 18:3n-3, and 22:6n-3 by weight and MS status with significance adjusted for age, sex and BMI z score. Compared with the normal-weight group, obese MS children had significant higher concentrations of these fatty acids. 20:2n-6 and n-3 PUFA showed a trend to be significantly higher in the obese groups (20:2n-6 control: 5.4 ± 0.5, obese NMS: 7.3 ± 0.6 and obese MS: 7.0 ± 0.6, $P = 0.064$) (n-3 PUFA control: 80.5 ± 8.6, obese NMS: 88.3 ± 9.3 and obese MS: 118.1 ± 9.5, $P = 0.061$), and lower concentration of 22:5n-6 (control: 7.1 ± 0.6, obese NMS: 5.1 ± 0.5 and obese MS: 5.7 ± 0.6, $P = 0.086$).

Table 1 Anthropometric and metabolic characteristics of prepubertal control children and obese children with and without metabolic syndrome

Variables	Control ($n = 20$)	Obese NMS ($n = 17$)	Obese MS ($n = 17$)	P[1]
Sex, No. M:F (%)	11:9 (55:45)^{a}[2]	8:9 (47:53)^{a}	15:2 (88:12)^{b}	0.011
Age (years)	9.2 ± 0.5	9.6 ± 0.5	9.7 ± 0.4	0.649
BMI (kg/m^2)	16.8 ± 0.9^{a}	28.3 ± 1.0^{b}	30.1 ± 1.0^{b}	<0.001
BMI *z* score	−0.99 ± 0.40^{a}	3.84 ± 0.45^{b}	4.24 ± 0.44^{b}	<0.001
Tricipital skinfold (mm)	8.6 ± 1.1^{a}	26.4 ± 1.2^{b}	25.9 ± 1.1^{b}	<0.001
Subscapular skinfold (mm)	6.7 ± 1.4^{a}	29.0 ± 1.5^{b}	31.3 ± 1.4^{b}	<0.001
Waist circumference (cm)	59.4 ± 2.4^{a}	84.3 ± 2.6^{b}	92.6 ± 2.5^{b}	<0.001
Hip circumference (cm)	66.8 ± 2.7^{a}	93.4 ± 2.8^{b}	98.0 ± 2.7^{b}	<0.001
Waist- to-hip ratio (cm)	0.90 ± 0.03	0.91 ± 0.03	0.95 ± 0.03	0.365
Systolic blood pressure (mmHg)	94.7 ± 2.7^{a}	108.5 ± 3.3^{b}	112.7 ± 3.09^{b}	<0.001
Diastolic blood pressure (mmHg)	49.9 ± 2.1^{a}	59.4 ± 2.6^{b}	60.7 ± 2.4^{b}	0.002
Fasting glucose (mmol/L)	4.8 ± 0.1	4.8 ± 0.1	4.8 ± 0.1	0.460
Fasting insulin (pmol/L)[3]	33.5 ± 8.8^{a}	60.5 ± 9.9^{b}	105.2 ± 9.9^{c}	<0.001
HOMA-IR[3]	1.26 ± 0.32^{a}	2.11 ± 0.35^{b}	3.69 ± 0.35^{c}	<0.001
Triacylglycerols (mmol/L)[3]	0.58 ± 0.08^{a}	0.81 ± 0.09^{b}	1.17 ± 0.09^{c}	<0.001
HDL-cholesterol (mmol/L)	1.81 ± 0.06^{a}	1.42 ± 0.07^{b}	1.19 ± 0.07^{c}	<0.001
Adiponectin (mg/L)[3]	10.99 ± 0.73^{a}	8.06 ± 0.82^{b}	5.27 ± 0.82^{c}	<0.001

Values for sex are in proportions. Values for age and anthropometric and metabolic variables are expressed as means ± SEM. Metabolic variables are adjusted for age, sex and BMI *z* score. *NSM* non-metabolic syndrome, *MS* metabolic syndrome, *BMI* body mass index, *HOMA-IR* homeostasis model assessment: insulin resistance (calculated as the product of fasting plasma insulin (μU/mL) and glucose (mmol/L), divided by 22.5)

[1] Mantel-Haenszel chi-square test for sex proportions and general linear models of variance with post hoc Bonferroni tests for anthropometric and metabolic variables

[2] Mean values within a row with unlike superscript lowercase letters are significantly different

[3] Tested with log-transformed values

Table 2 Energy and nutrient daily intake in prepubertal obese children with and without metabolic syndrome and in a control group

Nutrient intake[1]	Control	Obese NMS	Obese MS	P[2]
Energy (kcal/day)	1,600 ± 82^{a}[3]	2,098 ± 86^{b}	1,967 ± 99^{b}	0.002
Protein (g/day)	64 ± 4^{a}	85 ± 4^{b}	82 ± 5^{b}	0.001
Carbohydrate (g/day)	181 ± 10^{a}	229 ± 14^{b}	214 ± 15^{b}	0.105
Lipids (g/day)	70 ± 4^{a}	96 ± 6^{b}	91 ± 5^{b}	0.006
SFA (g/day)	18.1 ± 1.2^{a}	23.0 ± 1.9^{ab}	24.4 ± 1.9^{b}	0.067
MUFA (g/day)	23.6 ± 1.6^{a}	38.1 ± 2.7^{b}	35.7 ± 2.6^{b}	<0.001
PUFA (g/day)	6.8 ± 0.5^{a}	11.8 ± 0.9^{b}	11.6 ± 0.8^{b}	<0.001
n-6 PUFA (g/day)	6.26 ± 0.42^{a}	10.84 ± 0.88^{b}	10.75 ± 0.72^{b}	<0.001
n-3 PUFA (g/day)	0.52 ± 0.03^{a}	0.90 ± 0.07^{b}	0.89 ± 0.06^{b}	<0.001
Cholesterol (mg/day)	198 ± 13^{a}	334 ± 29^{b}	269 ± 19^{b}	<0.001
Fibre (g/day)	11 ± 0.7^{a}	13 ± 0.9^{b}	15 ± 1.1^{b}	0.146

[1] All values expressed as means ± SEM. *NSM* non-metabolic syndrome, *MS* metabolic syndrome, *SFA* saturated fatty acids, *PUFA* polyunsaturated fatty acids, *MUFA* monounsaturated fatty acids

[2] General linear models of variance with adjustments for age, sex, and BMI *z* score with post hoc Bonferroni tests

[3] Mean values within a row with unlike superscript lowercase letters are significantly different

Table 3 shows the proportions of fatty acids in total plasma lipids by weight and MS status adjusted for age, sex and BMI *z* score. The proportion of 16:1n-7 was significantly higher in obese MS children compared with controls. In contrast, the proportion of 22:5n-6 was significantly lower in obese MS children than in controls. 16:1n-7 was significantly correlated with the carbohydrate dietary intake (16:1n-7 (mg/l), $r = 0.311$, $P = 0.042$;

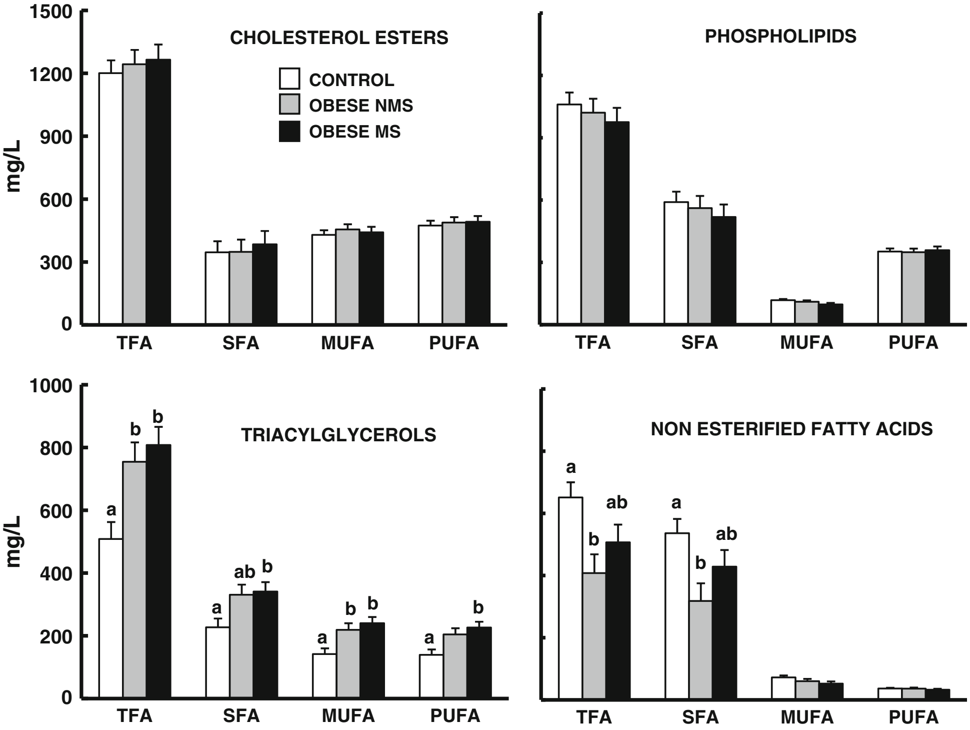

Fig. 1 Concentrations of selected fatty acid for total plasma lipids in prepubertal control children (n = 20) and obese children with (n = 17) and without metabolic syndrome (n = 17). *NSM* non-metabolic syndrome, *MS* metabolic syndrome. All values were expressed as means ± SEM adjusted for age and sex. Statistical analyses were done using general linear models of variance with adjustments for age, sex and BMI *z* score with post hoc Bonferroni tests. Values with different superscript letters are significantly different ($P < 0.05$)

16:1n-7(%), $r = 0.432$, $P = 0.004$). However, we did not find any association between plasma 20:5n-3 and 22:6n-3 and the estimated n-3 PUFA intake.

Fatty Acid Composition of Lipid Fractions

SFA, MUFA, and PUFA concentrations were higher in obese MS than in control children in plasma TG, but not in CE and PL; TFA and SFA concentrations in NEFA, were lower in NMS than in MS or control children (Fig. 2). 16:0, 16:1n-7, 18:1n-9, 18:2n-6 and n-6 PUFA were elevated in TG of obese children compared with controls; 16:1n-7 was higher in CE of obese MS than in normal weight children; 16:0 and 18:0 concentrations in NEFA were lower in obese NMS, but not in obese MS, compared with control children (Table 4).

Relationships Between Plasma Fatty Acid Concentrations and Metabolic Syndrome Features

Table 5 shows the multiple linear regression analysis of some plasma fatty acids and MS in obese prepubertal children. TFA, SFA and MUFA were associated with MS; particularly 16:0, 16:1n-9 and 22:5n-6 concentrations were highly associated to MS. As 16:1n-7 was correlated to the carbohydrate dietary intake we included this last variable as an additional exposure variable in the multivariate regression analysis for this fatty acid. Plasma 16:1n-7 both in concentration and percentage was positively associated with the MS. Particularly, for the plasma concentration of 22:5n-6 the partial correlation with adiponectin was significantly high ($\beta = 0.375$, $P = 0.009$). HOMA-IR and adiponectin were included among the risk factors associated with the MS in obese children because they were related to the risk of MS in the multiple logistic regression analysis (HOMA-IR: OR 2.28; 95% CI, 1.17–4.42; $P = 0.015$; Adiponectin: OR 0.593; 95% CI, 0.429–0.820; $P = 0.002$). Otherwise, after adjustment for sex and age, each unit increase in the concentration of total plasma 16:1n-7 was positively associated with a significant increase in the risk of MS (OR 2.76; 95% CI, 1.39–5.46, $P = 0.004$). Similarly, each 1.5 unit increase in the concentration of 16:1n-7 in TG was positively associated with a significant increase in the risk of MS (OR 4.70; 95% CI, 1.45–5.18, $P = 0.014$). Likewise, each half-unit decrease in the proportion of 20:4n-6 in plasma lipids was associated with a significant increase in the risk of MS (OR 0.56; 95% CI, 0.32–0.94, $P = 0.030$).

A significant negative association was found between presence of MS and the concentration of MUFA in PL fraction after adjustment for age and sex ($r = -0.307$, $P = 0.038$). In contrast, a positive association with MS presence was found for TFA ($r = 0.470$, $P = 0.003$), SFA ($r = 0.411$, $P = 0.011$), MUFA ($r = 0.402$, $P = 0.339$), PUFA ($r = 0.442$, $P = 0.006$), 16:0 ($r = 0.456$, $P = 0.014$), 16:1n-7 ($r = 0.339$, $P = 0.040$), 18:1n-9 ($r = 0.418$, $P = 0.010$), and 18:2n-6 ($r = 0.477$, $P = 0.003$) in plasma TG.

Table 3 Proportions of plasma fatty acids in prepubertal control and obese children with and without metabolic syndrome

FA type (percentage of total FA)	Total plasma lipids			
	Control (n = 20)	Obese NMS (n = 17)	Obese MS (n = 17)	P[1]
SFA	34.91 ± 0.46	35.77 ± 0.50	34.81 ± 0.50	0.295
14:0	1.25 ± 0.11	1.48 ± 0.12	1.43 ± 0.12	0.344
16:0	21.91 ± 0.37	22.82 ± 0.40	22.2 ± 0.41	0.197
18:0	9.65 ± 0.18	9.21 ± 0.20	8.85 ± 0.20	0.096
MUFA	21.13 ± 0.79	23.10 ± 0.85	22.10 ± 0.87	0.237
16:1n-7	1.17 ± 0.11[a2]	1.51 ± 0.12[ab]	1.60 ± 0.12[b]	0.037
16:1n-9	0.35 ± 0.02	0.38 ± 0.02	0.41 ± 0.02	0.236
18:1n-9	17.23 ± 0.73	18.95 ± 0.78	17.71 ± 0.79	0.264
PUFA	43.19 ± 0.86	40.53 ± 0.93	42.30 ± 0.94	0.079
18:2n-6	30.20 ± 0.84	28.65 ± 0.90	29.82 ± 0.92	0.151
20:2n-6	0.18 ± 0.01	0.22 ± 0.01	0.20 ± 0.01	0.210
18:3n-3	0.21 ± 0.03	0.28 ± 0.03	0.31 ± 0.03	0.104
20:3n-6	1.38 ± 0.08	1.51 ± 0.09	1.49 ± 0.09	0.341
20:4n-6	7.90 ± 0.39	6.84 ± 0.42	5.66 ± 0.43	0.185
20:5n-3	0.39 ± 0.09	0.43 ± 0.09	0.63 ± 0.10	0.460
22:5n-6	0.24 ± 0.02[a]	0.17 ± 0.02[b]	0.16 ± 0.02[b]	0.006
22:5n-3	0.36 ± 0.02	0.33 ± 0.02	0.38 ± 0.02	0.129
22:6n-3	1.63 ± 0.12	1.45 ± 0.13	1.87 ± 0.13	0.392
n-6 PUFA	40.41 ± 0.89	37.89 ± 0.96	37.87 ± 0.98	0.104
n-3 PUFA	2.78 ± 0.22	2.64 ± 0.23	3.42 ± 0.24	0.246
PUFA:SFA	1.24 ± 0.03	1.14 ± 0.04	1.22 ± 0.04	0.101
n-3: n-6 PUFA	15.46 ± 0.99[a]	15.21 ± 1.07[a]	11.07 ± 1.08[b]	0.150

All values expressed as means ± SEM adjusted for age and sex and tested with log-transformed values. *NSM* non-metabolic syndrome, *MS* metabolic syndrome, *TFA* total fatty acids, *SFA* saturated fatty acids, *MUFA* monounsaturated fatty acids, *PUFA* polyunsaturated fatty acids

[1] General linear models of variance with adjustments for age, sex and BMI z score with post hoc Bonferroni tests

[2] Mean values within a row with unlike superscript lowercase letters are significantly different

Discussion

The prevalence of MS in some studies that use several definitions, with moderate to substantial agreement between them, including that of Weiss et al. [4], ranges 25.7–57.4%. In a recent work to examine the prevalence of the MS using different pediatric definitions reported in the literature, regardless of the MS criteria used, its prevalence in obese Caucasian children and adolescents between 8 and 19 years was 51% [20]. The average prevalence of MS in children and adolescents aged 7–16 years with Weiss criteria is around 38.5% [21, 22], although there are no specific studies of prevalence in prepubertal children. In the present study, using the Weiss criteria, prepubertal obese children had a prevalence of MS about 50%. This high percentage may be due to the fact that our obese children were referred from primary health care centres to our specialised pediatric endocrinology unit because of the grade of obesity and suspicious of metabolic alterations.

The present study demonstrates that obese MS prepubertal children have higher concentrations of specific plasma fatty acids in comparison with prepubertal children of normal weight, related to the increased plasma TG in the former. Although studies in animal models of obesity [23] and in obese adult humans [24–29] have reported changes in fatty acid proportions in plasma lipid fractions and in adipose and hepatic tissue lipids, studies of plasma fatty acids in obese children have yielded controversial results [8, 10, 30–32].

Most studies of plasma fatty acids and obesity have been based on mixed populations of children and adolescents [9, 31–33] or preteen adolescents [10]. It has been proposed that puberty-related alterations should be investigated in homogeneous groups of children [32], and only prepubertal children were selected for the present investigation.

In contrast to most of previous reports, in the present study the concentrations of fatty acids were determined in total plasma lipids and in TG, PL, CE, and NEFA. This methodology was previously used in adults and children and, in comparison with measurement of proportions, provided a superior evaluation of metabolic and dietary changes related to effects of dietary long-chain PUFA supplementation in preterm infants [18] and related to certain diseases in adults e.g., liver cirrhosis [33] and inflammatory bowel disease [34].

Obesity and MS severely affects lipoprotein metabolism and especially TG synthesis and peripheral tissue utilisation, which are mediated by impaired insulin sensitivity [4, 35]. In the present study, the altered concentrations of some fatty acids in total plasma lipids of obese MS children are

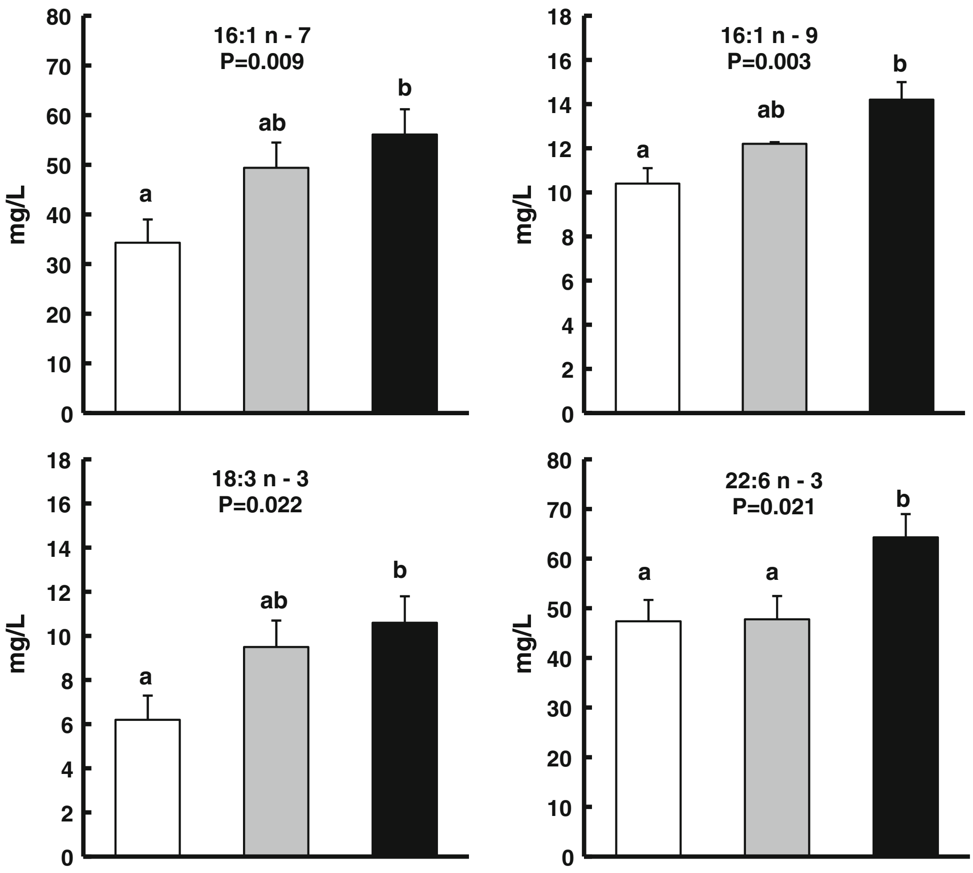

Fig. 2 Indices of fatty acid concentrations for plasma lipid fractions in prepubertal control children ($n = 20$) and obese children with ($n = 17$) and without metabolic syndrome ($n = 17$). *NSM* non-metabolic syndrome, *MS* metabolic syndrome, *TFA* total fatty acids, *SFA* saturated fatty acids, *MUFA* monounsaturated fatty acids, *PUFA* polyunsaturated fatty acids. All values were expressed as means ± SEM adjusted for age and sex. Statistical analyses were done using of variance with adjustments for age, sex and BMI *z* score with post hoc Bonferroni tests. Values with different superscript letters are significantly different ($P < 0.05$)

explained by the elevated concentrations of 16:0, 16:1n-7, 18:1n-9 and 18:2n-6 in TG compared with normal-weight children. SFA, and 16:0 were associated with MS, as also reported in obese adults [25, 29].

Palmitoleic acid (16:1n-7) and oleic acid (18:1n-9) are products of 16:0 and 18:0Δ-9 desaturation, respectively. Whereas oleic acid is present in most dietary fats, especially olive oil, 16:1n-7 is unusual in the human diet, but it is readily produced in humans by the enzyme stearoyl-CoA desaturase-1 (also called Δ-9 desaturase) [36]. Palmitoleic acid is a good marker for endogenous lipogenesis from carbohydrates and obese animals showed a significantly higher activity of liver stearoyl-coenzyme A desaturase 1 (SCD1) versus non-obese animals [37]. In addition, mice with targeted disruption of the *SCD1* gene were found to have decreased expression of lipogenesis genes and increased expression of lipid oxidative genes [38]. In the present study we have also documented a significant relationship between carbohydrate intake and plasma levels of 16:1n-7. Regardless of this fact, 16:1n-7 was highly associated with MS.

Significantly higher proportions of 16:1n-7 were reported in PL and CE of obese adolescents with MS compared with those without MS [9, 10]. The present study also found a higher concentration of this fatty acid in total plasma lipids and TG of the obese children with MS in comparison with the normal-weight children. However, no differences were found in its concentrations in PL, suggesting that 16:1n-7 is still not incorporated in this fraction during early stages of obesity. A study of 14 pairs of obese female monozygotic twins found that 16:1n-7 was present in adipose and serum TG and was associated with the BMI [27], as found in our study. Based on these findings, we hypothesise that this fatty acid is an early marker of lipid metabolic changes associated with obesity and MS.

Below-normal proportions of PL 20:4n-6 have been reported in serum from obese humans [24] and in liver from obese Zucker rats [39], suggesting an abnormality in Δ-6 desaturase activity or in the catabolism or distribution of 20:4n-6. A low proportion of 18:2n-6 has been described in obesity associated with insulin resistant states [24], and a reduced content of 18:2n-6 in TG, CE, and PL has been reported in obese adult patients [25]. However, a mixed population of children and adolescents showed a higher proportion of 20:4n-6 in the PL and CE of those with marked obesity, while no differences were found in 18:2n-6 [8, 30]. In a similar mixed population, the same group reported a lower proportion of 18:2n-6 in PL, and a higher proportion of 18:3n-6 and 20:3 n-6 in PL, TG and CE, in obese children with and without MS than in normal-weight

Table 4 Fatty acid concentrations for plasma lipid fractions in prepubertal control and obese children with and without metabolic syndrome

Fatty acid type (mg/L)	Cholesterol esters				Phospholipids			
	Control ($n = 20$)	Obese NMS ($n = 17$)	Obese MS ($n = 17$)	P^1	Control ($n = 20$)	Obese NMS ($n = 17$)	Obese MS ($n = 17$)	P
16:0	127.4 ± 62.3	132.2 ± 11.4	141.5 ± 7.8	0.798	303.8 ± 15.3	287.6 ± 14.5	321.5 ± 96.8	0.710
18:0	59.9 ± 78.8	57.0 ± 11.2	77.6 ± 5.4	0.159	205.5 ± 10.8	197.9 ± 14.1	226.5 ± 8.9	0.655
16:1n-7	12.4 ± 1.41	12.5 ± 2.1	15.5 ± 1.9	0.749	0.0 ± 0.0	0.0 ± 0.0	0.0 ± 0.0	0.708
18:1n-9	143.6 ± 13.0	144.3 ± 8.3	146.7 ± 7.3	0.954	67.6 ± 10.4	61.0 ± 8.5	76.1 ± 9.1	0.444
18:2n-6	443.0 ± 26.3	461.6 ± 26.7	437.3 ± 25.1	0.758	241.56 ± 14.8	235.3 ± 12.9	235.2 ± 12.6	0.916
18:3n-3	0.0 ± 0.0	0.0 ± 0.0	0.0 ± 0.0	0.842	0.0 ± 0.0	0.0 ± 0.0	0.0 ± 0.0	0.836
20:3n-6	0.9 ± 0.4	1.4 ± 0.4	1.3 ± 0.4	0.379	10.1 ± 0.7	10.9 ± 0.4	11.7 ± 0.7	0.401
20:4n-6	30.6 ± 2.1	33.7 ± 2.3	30.8 ± 1.8	0.819	61.3 ± 3.8	56.8 ± 2.1	57.9 ± 21.8	0.633
22:6n-3	0.0 ± 0.0	0.8 ± 0.8	0.5 ± 0.5	0.792	39.3 ± 3.9	42.2 ± 2.7	41.9 ± 2.4	0.444
n-6 PUFA	475.6 ± 28.5	496.8 ± 28.2	469.5 ± 25.8	0.752	312.9 ± 18.4	303.1 ± 14.9	304.9 ± 13.6	0.860
n-3 PUFA	0.0 ± 0.0	2.67 ± 1.93	0.51 ± 0.51	0.458	43.8 ± 4.1	46.9 ± 2.8	46.0 ± 3.2	0.325
PUFA:SFA	0.73 ± 0.87	0.77 ± 0.70	0.65 ± 0.27	0.525	0.60 ± 0.25	0.70 ± 0.56	0.62 ± 0.76	0.536
n-3: n-6 PUFA	0.0 ± 0.0	0.00 ± 0.07	0.00 ± 0.02	0.433	0.14 ± 0.22	0.15 ± 0.19	0.15 ± 0.23	0.555

Fatty acid type (mg/L)	Triacylglycerols				Non-esterified fatty acids			
	Control ($n = 20$)	Obese NMS ($n = 17$)	Obese MS ($n = 17$)	P	Control ($n = 20$)	Obese NMS ($n = 17$)	Obese MS ($n = 17$)	P
16:0	120.9 ± 95.0^{a2}	172.2 ± 17.4^{ab}	204.9 ± 25.4^{b}	0.045	212.8 ± 20.9^{a}	133.0 ± 13.2^{b}	206.2 ± 18.6^{a}	<0.001
18:0	69.3 ± 9.3	71.9 ± 13.5	93.1 ± 11.5	0.599	260.9 ± 27.4^{a}	159.4 ± 18.4^{b}	254.6 ± 24.8^{a}	<0.001
16:1n-7	6.9 ± 1.4^{a}	14.6 ± 1.8^{b}	14.1 ± 3.1^{b}	0.014	1.00 ± 0.72	0.0 ± 0.0	0.6 ± 0.6	0.862
18:1n-9	138.8 ± 13.8^{a}	215.4 ± 19.3^{b}	196.3 ± 25.1^{b}	0.006	66.0 ± 6.2	47.6 ± 17.8	66.8 ± 7.5	0.294
18:2n-6	117.1 ± 11.1^{a}	185.4 ± 21.1^{ab}	172.2 ± 21.9^{b}	0.029	35.7 ± 2.8	31.1 ± 11.6	32.6 ± 3.5	0.528
20:4n-6	9.6 ± 0.9	12.5 ± 0.9	14.6 ± 4.5	0.495	0.5 ± 2.4	1.7 ± 0.6	1.4 ± 0.7	0.509
n-6 PUFA	126.7 ± 11.8^{a}	197.9 ± 21.7^{b}	188.2 ± 23.7^{b}	0.028	37.2 ± 2.9	30.6 ± 3.4	34.3 ± 3.7	0.508
n-3 PUFA	18.9 ± 3.5	22.6 ± 4.7	27.8 ± 5.6	0.429	6.5 ± 5.1	1.4 ± 1.4	4.3 ± 3.5	0.674
PUFA:SFA	0.70 ± 0.09	0.75 ± 0.06	0.61 ± 0.16	0.030	0.12 ± 0.03	0.11 ± 0.02	0.08 ± 0.01	0.182
n-3: n-6 PUFA	0.18 ± 0.04	0.13 ± 0.03	0.15 ± 0.02	0.769	0.19 ± 0.13	0.02 ± 0.02	0.15 ± 0.12	0.819

All values expressed as means ± SEM adjusted for age and sex. *NSM* non-metabolic syndrome, *MS* metabolic syndrome, *SFA* saturated fatty acids, *PUFA* polyunsaturated fatty acids

[1] General linear models of variance with adjustments for age, sex and BMI z score with post hoc Bonferroni tests

[2] Values with different superscript letters are significantly different ($P < 0.05$)

Table 5 Relationships between plasma fatty acids and parameters associated with metabolic syndrome in prepubertal obese children

Relationships[a]	*R*	*P*
TFA (mg/L)	0.582	0.025
SFA (mg/L)	0.615	0.011
MUFA (mg/L)	0.559	0.042
16:0 (mg/L)	0.688	0.001
16:1n-7 (mg/L)	0.681	0.005
16:1n-7 (%)	0.603	0.041
16:1n-9 (mg/L)	0.670	0.002
22:5n-6 (mg/L)	0.628	0.008

[a] General multiple linear regression models with adjustments for MS features (BMI *z* score, arterial systolic blood pressure, triacylglycerols, HDL-cholesterol, homeostasis model assessment of insulin resistance and adiponectin) For 16:1n-7 we also included carbohydrate dietary intake as a variable in the regression analysis due to the fact that both concentration and percentage of this FA were correlated with the carbohydrate intake

TFA total plasma fatty acids, *SFA* saturated fatty acids, *MUFA* monounsaturated fatty acids

children [9]. In contrast to these findings by Decsi and coworkers, other authors found that obese children with MS had higher proportions of SFA and lower proportions of 22:6n-3 in plasma PL and CE and a lower proportion of 18:2n-6 in PL compared with children without MS [10]. The present series of prepubertal children with MS from Southern Spain showed higher concentrations of 22:6n-3 in total plasma lipids compared with those without MS and controls. This might be explained by a higher intake of n-3 PUFA. However, we did not found any difference in the estimated intake of n-3 PUFA between MS and NMS children. In addition, no correlation was found between n-3 PUFA intake and plasma 20:5n-3 and 22:6n-3. Nevertheless, the estimated ratio for the intake of n-3 to n-6 PUFA in our children was close to 10, which is considered an optimal figure to maintain an adequate status of n-3 PUFA in the body [40]. Although the low variance of fatty acids in GLC analysis allowed for a high statistical power in establishing differences between plasma fatty acid values for control and obese children, in the present study, the sample size (only 34 obese) is a limitation particularly when estimating the dietary intake. In addition, it was unfeasible to estimate the dietary intake of single fatty acids and then to evaluate the correlations between plasma fatty acid values and dietary fatty acid intakes.

No significant differences were found between obese and normal-weight children in concentrations or proportions of 18:2n-6, 20:4n-6 and 22:6n-3 in PL and CE. Therefore, it cannot be assumed that there is an enhanced activity of Δ-6 fatty acid desaturase in child obesity, as suggested by some authors [9], or a limitation of this activity, as proposed by others in adult obesity [38]. However, an inverse association was found between the proportion of 20:4n-6 in total plasma lipids and the risk of MS. In addition, lower levels of 22:5n-6, a metabolite of 20:4n-6, were associated with MS, and particularly with adiponectin. An association between circulating adiponectin, a component of the MS, and plasma fatty acid profile was recently reported in adults [41]. Indeed, the present results confirm that this adipokine appears to be an important feature of MS and is related to metabolic abnormalities that occur in obesity during the prepubertal period.

In conclusion, our findings suggest an altered plasma fatty acid profile in childhood obesity during the prepubertal period that is related to the main features of the MS. Elevated concentrations of 16:1n-7 and reduced proportions of 20:4n-6 and 22:5n-6 in plasma lipids appear to be early markers of MS in prepubertal children.

Acknowledgments Plan Nacional de Investigación Científica, Desarrollo e Innovación Tecnológica (I + D+I), Instituto de Salud Carlos III-Fondo de Investigación Sanitaria Project no. PI 020826 from the Spanish Ministry of Health and Consumption; FEDER; Fundación Salud 2000 and Hero España. S.A., Spain.

References

1. Haslam DW, James WPT (2005) Obesity. Lancet 366:1197–1209
2. Zimmet P, Magliano D, Matsuzawa Y, Alberti G, Shaw J (2005) The metabolic syndrome: a global public health problem and a new definition. J Atheroscler Thromb 12:295–300
3. Gil-Campos M, Cañete R, Gil A (2004) Adiponectin, the missing link in insulin resistance and obesity. Clin Nutr 24:963–974
4. Weiss R, Dziura J, Burgert TS, Tamborlane WV, Taksali SE, Yeckel CW, Allen K, Lopes M, Savoge M, Morrison J, Sherwin RS, Caprio S (2004) Obesity and the metabolic syndrome in children and adolescents. N Engl J Med 350:2362–2374
5. Reaven GM (2005) Why syndrome X? From Harold Himsworth to the insulin resistance syndrome. Cell Metab 1:9–13
6. Cañete R, Gil-Campos M, Gil A (2007) Development of insulin resistance and its relation to diet in the obese child. Eur J Nutr 46:81–187
7. Valle M, Gascón F, Martos R, Ruz FJ, Bermudo F, Morales R, Cañete R (2002) Metabolic cardiovascular syndrome in obese prepubertal children: the role of high fasting insulin levels. Metabolism 51:423–428
8. Decsi T, Molnár D, Koletzko B (1996) Long-chain polyunsaturated fatty acids in plasma lipids of obese children. Lipids 31:305–311
9. Decsi T, Csabi G, Torok K, Erhardt E, Minda H, Burus I, Molnar S, Molnar D (2000) Polyunsaturated fatty acids in plasma lipids of obese children with and without metabolic cardiovascular syndrome. Lipids 35:1179–1184
10. Klein-Platat C, Drai J, Oujaa M, Schlienger JL, Simon C (2005) Plasma fatty acid composition is associated with the metabolic syndrome and low-grade inflammation in overweight adolescents. Am J Clin Nutr 82:1178–1184
11. Larqué E, Gil-Campos M, Ramírez-Tortosa MC, Linde J, Cañete R, Gil A (2006) Postprandial response of trans fatty acids in prepubertal obese children. Int J Obes 30:1488–1493

12. Gil-Campos M, Larqué E, Ramírez-Tortosa MC, Linde J, Villada I, Cañete R, Gil A (2007) Changes in plasma fatty acid composition after intake of a standardised breakfast in prepubertal obese children. Br J Nutr 10:1–9
13. Alberti KG, Zimmet PZ (1998) Definitions, diagnosis and classification of diabetes mellitus and its complications. 1. Diagnosis and classification of diabetes mellitus provisional report of a WHO consultation. Diab Med 15:539–553
14. Third report of the National Cholesterol Education Program Expert Panel on Detection, Evaluation and Treatment of High Blood Cholesterol in Adults (Adult Treatment Panel III) (2001). Bethesda, Md.: National Heart, Lung, and Blood Institute (NIH publication no. 01-3670)
15. Cruz ML, Goran MI (2004) The metabolic syndrome in children and adolescents. Curr Diab Rep 4:53–62
16. Martínez-Victoria E, Mañas M (2002) Alimentación y Salud. Software nutricional (Spanish). (Feeding and Health. Nutritional software).Valencia, Spain: Instituto de Nutrición y Tecnología de los Alimentos, Universidad de Granada, and General Asde
17. Hernández M, Castellet J, Narvaiza JL, Rincón JM, Ruiz E, Sánchez E, Sobradillo B, Zurimendi A (2002) Curvas y tablas de crecimiento. Instituto de Investigación sobre crecimiento y desarrollo (Spanish) (Curves and tables of growth. Institute of Research on Growth and Development). Madrid, Spain: Fundación Faustino Orbegozo, Ed. Ergón
18. Matthews DR, Hosker JP, Rudenski AS, Naylor BA, Treacher DF, Turner RC (1985) Homeostasis model assessment: Insulin resistance and β-cell function from fasting plasma glucose and insulin concentrations in man. Diabetologia 28:412–419
19. Ramírez M, Gallardo EM, Souto AS, Weissheimer C, Gil A (2001) Plasma fatty-acid composition and antioxidant capacity in low-birth weight infants fed formula enriched with n–6 and n-3 long-chain polyunsaturated fatty acids from purified phospholipids. Clin Nutr 20:69–76
20. Lee S, Bacha F, Gungor N, Arslanian S (2008) Comparison of different definitions of pediatric metabolic syndrome: relation to abdominal adiposity, insulin resistance, adiponectin, and inflammatory biomarkers. J Pediatr 152:177–184
21. Reinehr T, Wunsch R, de Sousa G, Toschke AM (2007) Relationship between metabolic syndrome definitions for children and adolescents and intima-media thickness. Atherosclerosis. Epub ahead of print
22. Shaibi GQ, Goran MI (2008) Examining metabolic syndrome definitions in overweight Hispanic youth: a focus on insulin resistance. J Pediatr 152:171–176
23. Phinney SD, Fisler JS, Tang AB, Warden CH (1994) Liver fatty acid composition correlates with body fat and sex in a multigenic mouse model of obesity. Am J Clin Nutr 60:61–67
24. Phinney SD, Davis PG, Johnson SB, Holman RT (1991) Obesity and weight loss alter serum polyunsaturated lipids in humans. Am J Clin Nutr 53:831–838
25. Rossner S, Walldius G, Bjorvell H (1989) Fatty acid composition in serum lipids and adipose tissue in severe obesity before and after six weeks of weight loss. Int J Obes 13:603–612
26. Garaulet M, Pérez-Llamas F, Pérez-Ayala M, Martínez P, Sánchez de Medina F, Tébar FJ, Zamora S (2001) Site-specific differences in the fatty acid composition of abdominal adipose tissue in an obese population from a Mediterranean area: relation with dietary fatty acids, plasma lipid profile, serum insulin, and central obesity. Am J Clin Nutr 74:585–591
27. Kunesova M, Hainer V, Tvrzicka E, Phinney SD, Stich V, Parizkova J, Zak A, Stunkard AJ (2002) Assessment of dietary and genetic factors influencing serum and adipose fatty acid composition in obese female identical twins. Lipids 37:27–32
28. Vessby B (2003) Dietary fat, fatty acid composition in plasma and the metabolic syndrome. Curr Opin Lipidol 14:15–19
29. Tremblay AJ, Despres JP, Piche ME, Nadeau A, Bergeron J, Almeras N, Tremblay A, Lemieux S (2004) Associations between the fatty acid content of triglyceride, visceral adipose tissue accumulation, and components of the insulin resistance syndrome. Metabolism 53:310–317
30. Decsi T, Molnar D, Koletzko B (1998) The effect of under-and overnutrition on essential fatty acid metabolism in childhood. Eur J Clin Nutr 52:541–548
31. Agostoni C, Riva E, Bellu R, Vincenzo SS, Grazia BM, Giovannini M (1994) Relationships between the fatty acid status and insulinemic indexes in obese children. Prostaglandins Leukot Essent Fatty Acids 51:317–321
32. Scaglioni S, Verduci E, Salvioni M, Bruzzese MG, Radaelli G, Zetterstrom R, Riva E, Agostoni C (2006) Plasma long-chain fatty acids and the degree of obesity in Italian children. Acta Paediatr 95:964–969
33. Cabré E, Periago JL, Abad-Lacruz A, Gil A, González-Huix F, Sánchez-Medina F, Gasull MA (1988) Polyunsaturated fatty acid deficiency in liver cirrhosis: Its relation to associated protein-energy malnutrition (Preliminary report). Am J Gastroenterol 83:712–717
34. Esteve M, Ramírez M, Fernández-Bañares F, Abad-Lacruz A, Gil A, Cabré E (1992) Plasma polyunsaturated fatty acid pattern in active inflammatory bowel disease. Gut 33:1365–1369
35. Aguilera CM, Gil-Campos M, Cañete R, Gil A (2008) Alterations of plasma and tissue lipids associated with obesity and metabolic syndrome. Clin Sci 114:183–193
36. Phinney SD (2005) Fatty acids, inflammation and metabolic syndrome. Am J Clin Nutr 82:1151–1152
37. Hu CC, Qing K, Chen Y (2004) Diet-induced changes in stearoyl-CoA desaturase 1 expression in obesity-prone and -resistant mice. Obes Res 12:1264–1270
38. Sampath H, Ntambi JM (2006) Stearoyl-coenzyme A desaturase 1, sterol regulatory element binding protein-1c and peroxisome proliferator-activated receptor-alpha: independent and interactive roles in the regulation of lipid metabolism. Curr Opin Clin Nutr Metab Care 9:84–88
39. Phinney SD, Tang AB, Thurmond DC, Nakamura MT, Stern JS (1993) Abnormal polyunsaturated lipid metabolism in the obese Zucker rat, with partial metabolic correction by gamma-linolenic acid administration. Metabolism 42:1127–1140
40. Report of the joint WHO/FAO expert consultation Diet, nutrition and the prevention of chronic diseases WHO Technical Report Series, No. 916 (TRS 916), Rome (2003)
41. Fernández-Real JM, Vendrell J, Ricart W (2005) Circulating adiponectin and plasma fatty acid profile. Clin Chem 51:603–609

Lipids (2008) 43:733–740
DOI 10.1007/s11745-008-3204-3

ORIGINAL ARTICLE

Hepatic Lipase Gene −514*C*/*T* Polymorphism in the Guangxi Hei Yi Zhuang and Han Populations

Jinzhen Wu · Ruixing Yin · Weixiong Lin · Shangling Pan · Dezhai Yang

Received: 20 March 2008 / Accepted: 6 June 2008 / Published online: 1 July 2008
© AOCS 2008

Abstract Hei Yi Zhuang is an isolated subgroup of the Zhuang minority in China. This study was designed to compare the difference in the hepatic lipase gene (*LIPC*) −514*C*/*T* polymorphism and its association with lipid profiles between the Guangxi Hei Yi Zhuang and Han populations. Genotyping of the *LIPC* −514*C*/*T* was performed in 873 subjects of Hei Yi Zhuang and 867 participants of Han Chinese. The frequency of −514*T* allele was 43.47% in Hei Yi Zhuang, and 36.10% in Han ($P < 0.001$). The frequencies of *CC*, *CT* and *TT* genotypes were 30.01, 53.04 and 16.95% in Hei Yi Zhuang, and 40.95, 45.91 and 13.14% in Han ($P < 0.001$); respectively. Serum high-density lipoprotein cholesterol (HDL-C) and apolipoprotein B levels in both ethnic groups were higher in *LIPC* −514*T* carriers than in *C* carriers. In addition, serum triglyceride levels in Han were higher in *TT* genotype individuals than in *CC* genotype subjects ($P < 0.05$). Serum HDL-C levels were positively correlated with age, alcohol consumption and *LIPC* −514*C*/*T* genotypes, and negatively associated with hypertension and cigarette smoking in Hei Yi Zhuang ($P < 0.05$–0.01), whereas HDL-C levels were positively correlated with age, alcohol consumption and *LIPC* −514*C*/*T* genotypes, and negatively associated with body mass index and cigarette smoking in Han ($P < 0.05$–0.001). The differences in serum HDL-C levels between the two ethnic groups might partially attribute to the differences in the *LIPC* −514*C*/*T* polymorphism.

Keywords Lipids · Apolipoproteins · Hepatic lipase gene · Polymorphism

Abbreviations

ANCOVA	Analysis of covariance
Apo	Apolipoprotein
BMI	Body mass index
CHD	Coronary heart disease
DNA	Deoxyribonucleic acid
HDL-C	High-density lipoprotein cholesterol
HL	Hepatic lipase
LDL-C	Low-density lipoprotein cholesterol
LIPC	Hepatic lipase gene
PCR	Polymerase chain reaction
SNP	Single nucleotide polymorphisms
TC	Total cholesterol
TG	Triglyceride

J. Wu · R. Yin (✉)
Department of Cardiology, Institute of Cardiovascular Diseases,
the First Affiliated Hospital, Guangxi Medical University,
22 Shuangyong Road, 530021 Nanning, Guangxi,
People's Republic of China
e-mail: yinruixing@yahoo.com.cn

J. Wu
e-mail: yinrx2003@yahoo.com.cn

W. Lin · D. Yang
Department of Molecular Biology, Medical Scientific Research
Center, Guangxi Medical University, Nanning,
People's Republic of China
e-mail: lin78018@yahoo.com.cn

D. Yang
e-mail: ydz678@163.com

S. Pan
Department of Pathophysiology, School of Premedical Sciences,
Guangxi Medical University, Nanning,
People's Republic of China
e-mail: bitterlypan@yahoo.com.cn

Introduction

Epidemiological studies have shown that a low plasma concentration of high-density lipoprotein cholesterol (HDL-C) is associated with an increased risk of developing coronary heart disease (CHD) [1]. Plasma HDL-C concentration is modulated by both environmental and genetic factors. Family and twin studies have shown that genetic polymorphism could account for up to 60% of the interindividual variation in plasma HDL-C concentrations [2–4]. The polymorphism at the hepatic lipase gene (*LIPC*) −514*C*/*T* has been suggested to be a major cause of genetically determined variation in plasma HDL-C levels [4–6]. It can account for up to 25% of the variability in plasma HDL-C concentrations [4, 6]. Observational studies in the United States have demonstrated that CHD risk increases by 2–4% for every 1 mg/dL decrease in HDL-C levels [1].

Hepatic lipase (HL) is a lipolytic protein that catalyzes the hydrolysis of triglycerides (TG) and phospholipids in low-density lipoprotein cholesterol (LDL-C) and HDL particles and may also act as a ligand between these particles and receptors [7–9]. HL activity contributes to plasma HDL levels, as it promotes the conversion of large, buoyant HDL_2 to small, dense HDL_3 [10]. Increased HL activity is associated with reduced plasma HDL levels and reduced large, buoyant HDL_2 particles, thought to be the more anti-atherogenic subspecies of total HDL [11, 12].

The human *LIPC*, located on chromosome 15q21-q23 and composed of nine exons, is expressed in the liver. It spans more than 120 kb of deoxyribonucleic acid (DNA) and encodes a protein of 449 amino acids [13, 14]. Numerous common single nucleotide polymorphisms (SNPs) in the promoter region or in the coding region of the *LIPC* have been described [5, 15–17]. Four different promoter polymorphisms of the *LIPC* have been identified (*G*-250*A*, *C*-514*T*, *T*-710*C*, and *A*-763*G*), which are in complete linkage disequilibrium [16]. On a population level, the *LIPC* promoter polymorphism is quite common, but with different allele frequencies in diverse ethnic groups [5, 6, 18–20].

There are 56 ethnic groups in China. Han is the largest group, and Zhuang is the largest minority. Hei Yi (means black-worship and black dressing) Zhuang is the most conservative subgroup of the Zhuang minority. The population size is 51,655. Because of isolation from the other ethnic groups, the special customs and cultures including their clothing, intra-ethnic marriages, and dietary habits are still completely conserved to the present day. In a previous epidemiologic study, we showed that serum HDL-C concentrations were higher in Hei Yi Zhuang than in Han Chinese from the same region [21]. This ethnic difference in serum HDL-C concentrations cannot be accounted for by environmental factors. Although the genetic differences between the two ethnic groups are still not well known, we hypothesized that there may be significant differences in some gene polymorphisms between the two ethnic groups. Therefore, the aim of the present study was to determine the *LIPC* −514*C*/*T* polymorphism and its association with serum lipid profiles in the Guangxi Hei Yi Zhuang and Han populations.

Materials and Methods

Subjects

A total of 873 subjects of Hei Yi Zhuang residing in seven villages in Napo County, Guangxi Zhuang Autonomous Region were surveyed by a stratified randomized cluster sampling. The age of the subjects ranged from 16 to 80 years, with an average age of 46.15 ± 16.06 years. There were 452 men (51.78%) and 421 women (48.22%). All of them were peasants. During the same period, a total of 867 subjects of Han Chinese who lived in nine villages in Napo County were also surveyed by the same method. The mean age of the subjects was 45.58 ± 15.57 years (range 16–82). There were 449 males (51.79%) and 418 females (48.21%). All of them were also peasants. All study subjects were essentially healthy and had no evidence of any chronic illness, including hepatic, renal, thyroid, diabetes or CHD. None of them had been treated with β-adrenergic blocking agents and lipid-lowering drugs such as statins or fibrates. The present study was approved by the Ethics Committee of the First Affiliated Hospital, Guangxi Medical University. Informed consent was obtained from all subjects after they received a full explanation of the study.

Epidemiological Survey

The survey was carried out using internationally standardized methods, following a common protocol. Information on demographics, socioeconomic status, and lifestyle factors was collected with standardized questionnaires. Smoking status was categorized into groups of cigarettes per day: <10, 10–19, 20–39, and ≥40. Alcohol consumption was categorized into groups of grams of alcohol per day: <25, 25–49, 50–99, and ≥100. The physical examination included blood pressure, body height, and body weight etc., and body mass index (BMI) was calculated as weight (kg) divided by height (m) squared. Sitting blood pressure was measured three times with the use of a mercury sphygmomanometer after the subject rested for 5 min, and the average of the three measurements was used for the level of blood pressure. Systolic blood pressure was determined by the first Korotkoff sound, and diastolic blood pressure by the fifth Korotkoff sound.

Measurements of Lipids and Apolipoproteins

A venous blood sample of 8 mL was obtained from all subjects between 8 and 11 AM, after at least 12 h of fasting, from a forearm vein after venous occlusion for few seconds in a sitting position. 3 mL was collected into glass tubes and allowed to clot at room temperature, and used to determine serum lipid and apolipoprotein (apo) levels, and the remaining 5 mL was transferred to tubes with anticoagulant solution (4.80 g/L citric acid, 14.70 g/L glucose, and 13.20 g/L tri-sodium citrate) and used to extract DNA. Immediately following clotting serum was separated by centrifugation for 15 min at 3,000 rpm. The levels of total cholesterol (TC), TG, HDL-C, and LDL-C in samples were determined by enzymatic methods with commercially available kits, Tcho-1, TG-LH (RANDOX Laboratories Ltd., Ardmore, Diamond Road, Crumlin Co. Antrim, United Kingdom, BT29 4QY), Cholestest N HDL, and Cholestest LDL (Daiichi Pure Chemicals Co., Ltd., Tokyo, Japan), respectively. Serum apoA-I and apoB levels were detected by the immunoturbidimetric immunoassay using a commercial kit (RANDOX Laboratories Ltd.). All determinations were performed with an autoanalyzer (Type 7170A; Hitachi Ltd., Tokyo, Japan) in the Clinical Science Experiment Center of the First Affiliated Hospital, Guangxi Medical University [21].

Genotyping

Genomic DNA was isolated from peripheral blood leukocytes by the phenol-chloroform method as described in our previous reports [22]. Genotyping of the *LIPC* −514*C*/*T* was performed as described by Couture et al. [15]. A 285-bp sequence of the *LIPC* was amplified by polymerase chain reaction (PCR) by using oligonucleotide primers 5′-TCTAGGATCACCTCTCAATGGGTCA-3′ and 5′-GG TGGCTTCCACGTGG-CTGCCTAAG-3′. DNA templates were denatured at 95 °C for 3 min, and then each PCR was subjected to 35 cycles, each consisting of 1 min of denaturation at 95 °C, 0.5 min of annealing at 63 °C, and 0.5 min of extension at 72 °C. The PCR products were digested with 10 U of *Nla*III and the fragments separated by electrophoresis on a 1.5% agarose gel. After electrophoresis, the gel was treated with ethidium bromide for 20 min, and DNA fragments were visualized by UV illumination. The resulting fragments are 215 and 70 bp for the *T* allele and 285 bp for the uncut *C* allele. Genotypes were scored by an experienced reader blinded to epidemiological and lipid results.

Diagnostic Criteria

The normal values of serum TC, TG, HDL-C, LDL-C, apoA-I, apoB, and the ratio of apoA-I to apoB in our Clinical Science Experiment Center were 3.10–5.17, 0.56–1.70, 0.91–1.81, 1.70–3.20 mmol/L, 1.00–1.76, 0.63–1.14 g/L, and 1.00–2.50, respectively. The individuals with TC > 5.17 mmol/L and/or TG > 1.70 mmol/L were defined as hyperlipidemic [21]. Hypertension was defined as a systolic pressure of 140 mmHg or higher and/or a diastolic pressure of 90 mmHg or higher [23]. Overweight and obesity were defined according to the diagnostic criteria of the Cooperative Meta-analysis Group of China Obesity Task Force. Normal weight, overweight and obesity were defined as a BMI < 24, 24–28, and > 28 kg/m^2, respectively [24].

Statistical Analysis

Epidemiologic data were recorded on a pre-designed form and managed with Excel software. Levels of the quantitative variables are presented as mean ± standard deviation (SD). The difference of general characteristics between Hei Yi Zhuang and Han was tested by the Student's unpaired *t* test. The allelic and genotypic frequencies of *LIPC* −514*C*/*T* were estimated by counting alleles and genotypes and calculating sample proportions; the statistical significance of differences in frequencies between groups was compared by χ^2 test. The distribution of *LIPC* −514*C*/*T* polymorphism was tested for Hardy–Weinberg equilibrium using χ^2 goodness-of-fit test. The association of *LIPC* genotypes with lipid variables was tested by analysis of covariance (ANCOVA). The co-variables include sex, age, BMI, hypertension, alcohol consumption and cigarette smoking. In order to evaluate the association of HDL-C levels with ethnic group (Han Chinese = 0; Hei Yi Zhuang = 1), sex (male = 0; female = 1), age (year), BMI (kg/m^2), blood pressure (normotensives = 0; hypertensives = 1), alcohol consumption (nondrinkers = 0; <25 g/day = 1; 25–49 g/day = 2; 50–99 g/day = 3; ≥100 g/day = 4), cigarette smoking (nonsmokers = 0; <10 cigarettes/day = 1; 10–19 cigarettes/day = 2; 20–39 cigarettes/day = 3; ≥40 cigarettes/day = 4), or *LIPC* −514*C*/*T* genotype (*CC* = 1; *CT* = 2; *TT* = 3), unconditional logistic regression analysis was also performed in combined population of Hei Yi Zhuang and Han, Hei Yi Zhuang, and Han; respectively. The backward multiple logistic regression method was used to select the risk factors significantly associated with serum HDL-C levels. All statistical analyses were done with the statistical software package SPSS 11.5 (SPSS Inc., Chicago, Illinois). A *P* value of less than 0.05 was considered significant.

Results

General Characteristics and Serum Lipid Levels

Table 1 gives the general characteristics between the Hei Yi Zhuang and Han populations. Systolic blood pressure and pulse pressure levels were higher in Hei Yi Zhuang than in Han ($P < 0.001$ for each), whereas BMI was higher in Han than in Hei Yi Zhuang ($P < 0.001$). There were no significant differences in diastolic blood pressure levels, age structure, the percentages of subjects who consumed alcohol or smoked cigarettes, or the ratio of male to female between the two ethnic groups ($P > 0.05$). Serum TC, TG, LDL-C, and apoB levels were lower in Hei Yi Zhuang than in Han ($P < 0.01$–0.001), whereas HDL-C levels and the ratio of apoA-I to apoB were higher in Hei Yi Zhuang than in Han ($P < 0.001$). There were no significant differences in apoA-I levels between the two ethnic groups ($P > 0.05$).

Genotypic and Allelic Frequencies

The frequencies of the *LIPC* −514*C*/*T* alleles and genotypes are also shown in Table 1. The frequencies of *C* and *T* alleles were 56.53 and 43.47% in Hei Yi Zhuang, and 63.90 and 36.10% in Han ($P < 0.001$); respectively. The frequencies of *CC*, *CT* and *TT* genotypes were 30.01, 53.04 and 16.95% in Hei Yi Zhuang, and 40.95, 45.91 and 13.14% in Han ($P < 0.001$), respectively. There were no significant differences in the genotypic and allelic frequencies between males and females in the two ethnic groups ($P > 0.05$, Table 2).

The *LIPC* −514*C*/*T* Genotypes and Serum Lipid Levels

As shown in Table 3, there were significant differences in the serum HDL-C and apoB levels among three genotypes in the both ethnic groups after adjustment for all the covariates. Serum HDL-C and apoB levels were higher in

Table 1 Comparison of general characteristics, serum lipid levels, and genotypic and allelic frequencies between the Hei Yi Zhuang and Han populations

Parameters	Hei Yi Zhuang (n = 873)	Han Chinese (n = 867)	t (χ^2)	P value
Male/female	452/421	449/418	0.002	0.996
Age (year)	46.15 ± 16.06	45.58 ± 15.57	0.752	0.452
Body mass index (kg/m^2)	21.27 ± 2.30	22.56 ± 2.56	11.058	<0.001
Systolic blood pressure (mmHg)	125.96 ± 17.36	121.62 ± 16.35	5.367	<0.001
Diastolic blood pressure (mmHg)	77.11 ± 11.35	76.57 ± 10.73	1.020	0.308
Pulse pressure (mmHg)	49.36 ± 13.75	45.15 ± 11.24	6.990	<0.001
Cigarette smoking [n (%)]				
Nonsmoker	548 (62.77)	571 (65.86)		
<10 cigarettes/day	24 (2.75)	21 (2.42)		
10–19 cigarettes/day	153 (17.53)	128 (14.76)		
20–39 cigarettes/day	136 (15.58)	135 (15.57)		
≥40 cigarettes/day	12 (1.37)	12 (1.38)	2.880	0.578
Alcohol consumption [n (%)]				
Nondrinker	381 (43.64)	400 (46.14)		
<25 g /day	323 (37.00)	310 (35.76)		
25–49 g/day	91 (10.42)	89 (10.27)		
50–99 g/day	61 (6.99)	54 (6.23)		
≥100 g/day	17 (1.95)	14 (1.61)	1.447	0.836
Total cholesterol (mmol/L)	4.51 ± 0.96	4.77 ± 0.99	5.714	<0.001
Triglyceride (mmol/L)	1.15 ± 0.78	1.27 ± 0.84	3.088	0.002
HDL-C(mmol/L)	2.25 ± 0.62	2.13 ± 0.64	3.972	<0.001
LDL-C(mmol/L)	2.31 ± 0.62	2.47 ± 0.67	5.171	<0.001
Apolipoprotein (Apo) A-I(g/L)	1.45 ± 0.14	1.44 ± 0.15	1.438	0.151
ApoB(g/L)	0.87 ± 0.20	1.07 ± 0.21	20.344	<0.001
ApoA-I/apoB	1.67 ± 0.98	1.35 ± 0.79	7.496	<0.001
CC genotype [n (%)]	262 (30.01)	355 (40.95)***		
CT genotype [n (%)]	463 (53.04)	398 (45.91)**		
TT genotype [n (%)]	148 (16.95)	114 (13.14)*	23.317	<0.001
C allele [n (%)]	987 (56.53)	1,108 (63.90)		
T allele [n (%)]	759 (43.47)	626 (36.10)	19.711	<0.001

HDL-C high-density lipoprotein cholesterol; *LDL-C* low-density lipoprotein cholesterol

* $P < 0.05$, ** $P < 0.01$ and *** $P < 0.001$ in comparison with the same subgroup of Hei Yi Zhuang

Table 2 Comparison of the *LIPC* −514*C*/*T* genotypic and allelic frequencies between the Hei Yi Zhuang and Han populations according to sex

Genotypes/allele	Hei Yi Zhuang			Han Chinese		
	Male ($n = 452$)	Female ($n = 421$)	P value	Male ($n = 449$)	Female ($n = 418$)	P value
CC	145 (32.08)	117 (27.79)		186 (41.42)	169 (40.43)	
CT	233 (51.55)	230 (54.63)		205 (45.66)	193 (46.17)	
TT	74 (16.37)	74 (17.58)	0.384	58 (12.92)	56 (13.40)	0.950
C	523 (57.85)	464 (55.11)		577 (64.25)	531 (63.52)	
T	381 (42.15)	378 (44.89)	0.427	321 (35.75)	305 (36.48)	0.749

Table 3 Association of the *LIPC* −514*C*/*T* genotypes with serum lipid levels between the Hei Yi Zhuang and Han populations

Lipids	Hei Yi Zhuang				Han Chinese			
	CC (n = 262)	*CT* (n = 463)	*TT* (n = 148)	P value[e]	*CC* (n = 355)	*CT* (n = 398)	*TT* (n = 114)	P value[e]
TC(mmol/L)	4.52 ± 1.01	4.50 ± 0.93	4.52 ± 0.98	0.954	$4.75 \pm 1.02^{**}$	$4.78 \pm 0.95^{***}$	$4.80 \pm 0.99^{*}$	0.863
TG(mmol/L)	1.13 ± 0.67	1.15 ± 0.79	1.19 ± 0.81	0.744	1.21 ± 0.77	$1.28 \pm 0.79^{*}$	$1.42 \pm 0.86^{a*}$	0.046
HDL-C(mmol/L)	2.10 ± 0.59	2.28 ± 0.68^{b}	2.42 ± 0.71^{bc}	<0.001	2.06 ± 0.70	$2.14 \pm 0.74^{**}$	2.31 ± 0.63^{bc}	0.005
LDL-C(mmol/L)	2.33 ± 0.58	2.31 ± 0.65	2.28 ± 0.56	0.731	$2.45 \pm 0.65^{*}$	$2.47 \pm 0.68^{***}$	$2.53 \pm 0.66^{**}$	0.536
ApoA-I(g/L)	1.44 ± 0.14	1.46 ± 0.16	1.44 ± 0.15	0.154	1.43 ± 0.13	1.45 ± 0.15	1.44 ± 0.14	0.151
ApoB(g/L)	0.85 ± 0.19	0.87 ± 0.21	0.91 ± 0.22^{ac}	0.018	$1.03 \pm 0.20^{***}$	$1.09 \pm 0.22^{b***}$	$1.12 \pm 0.23^{b***}$	<0.001
ApoA-I/apoB	1.66 ± 1.12	1.68 ± 0.99	1.66 ± 0.94	0.959	$1.34 \pm 0.75^{***}$	$1.36 \pm 0.82^{***}$	$1.35 \pm 0.77^{**}$	0.941

TC total cholesterol; *TG* triglycerides; *HDL-C* high-density lipoprotein cholesterol; *LDL-C* low-density lipoprotein cholesterol; *apoA-I* apolipoprotein A-I; *apoB* apolipoprotein B; *apoA-I/apoB* the ratio of apolipoprotein A-I to apolipoprotein B

[*] $P < 0.05$, [**]$P < 0.01$ and [***]$P < 0.001$ in comparison with the same subgroup of Hei Yi Zhuang

[a] $P < 0.05$ in comparison with the CC genotype of the same ethnic group

[b] $P < 0.01$ in comparison with the CC genotype of the same ethnic group

[c] $P < 0.05$ in comparison with CT genotype of the same ethnic group

[d] $P < 0.01$ in comparison with CT genotype of the same ethnic group

[e] Analyses of covariate analysis, adjusted for sex, age, body mass index, hypertension, alcohol consumption and cigarette smoking

TT or *CT* genotype subjects than in *CC* genotype individuals. In addition, serum TG levels in Han were higher in *TT* genotype than in *CC* genotype subjects ($P < 0.05$). There were no significant differences in TC, LDL-C, apoA-I levels and the ratio of apoA-I to apoB among the three genotypes in the both ethnic groups ($P > 0.05$).

Correlative Factors for the HDL-C Levels

Multivariate logistic regression analysis showed that serum HDL-C levels were positively correlated with ethnic group (Hei Yi Zhuang), age, alcohol consumption, and the *LIPC* −514*C*/*T* genotypes, and negatively associated with BMI, hypertension and cigarette smoking in combined population of Hei Yi Zhuang and Han ($P < 0.05$–0.001). Serum HDL-C levels were positively correlated with age, alcohol consumption and *LIPC* −514*C*/*T* genotypes, and negatively associated with hypertension and cigarette smoking in Hei Yi Zhuang ($P < 0.05$–0.01). Serum HDL-C levels were positively correlated with age, alcohol consumption and *LIPC* −514*C*/*T* genotypes, and negatively associated with BMI and cigarette smoking in Han ($P < 0.05$–0.001). No association was found between serum HDL-C levels and sex in both ethnic groups ($P > 0.05$, Table 4).

Discussion

The present study shows that serum TC, TG, LDL-C and apoB levels were lower in Hei Yi Zhuang than in Han, whereas HDL-C levels and the ratio of apoA-I to apoB were higher in Hei Yi Zhuang than in Han. These findings are consistent with those of our previous studies in a large population [21]. It is well known that dyslipidemia is a complex trait caused by the interactions of multiple environmental and genetic factors. Hei Yi Zhuang is an isolated subgroups of the Zhuang minority in China. Strict intraethnic marriages have been performed in this population from time immemorial. But consanguineous marriages are forbidden in this ethnic subgroup. No one can marry to the

Table 4 Correlative factors for the HDL-C levels between the Hei Yi Zhuang and Han populations

Correlative factors	Regression coefficient	Standard error	Wald	*P* value	Odds ratio	95% Confidence interval
Han plus Hei						
Ethnic group	0.136	0.039	15.223	<0.001	1.883	1.363–2.631
Age	0.212	0.011	5.268	0.026	1.435	1.217–1.874
Body mass index	–0.353	0.008	5.764	0.021	1.613	1.273–2.033
Hypertension	−0.355	0.006	5.974	0.013	1.552	1.186–1.997
Alcohol consumption	0.218	0.025	7.773	0.007	1.676	1.233–2.139
Cigarette smoking	−0.210	0.017	8.542	0.005	1.729	1.096–2.248
LIPC −514*C*/*T* genotype	0.152	0.025	10.232	0.003	1.815	1.314–2.423
Hei Yi Zhuang						
Age	0.173	0.005	7.653	0.009	1.683	1.321–2.078
Hypertension	−0.205	0.002	9.950	0.003	1.795	1.331–2.362
Alcohol consumption	0.104	0.034	5.676	0.033	1.518	1.189–1.852
Cigarette smoking	−0.096	0.021	5.387	0.036	1.509	1.120–1.795
LIPC −514*C*/*T* genotype	0.271	0.025	13.121	0.002	1.788	1.335–2.516
Han Chinese						
Age	0.197	0.009	14.594	0.001	1.902	1.321–2.573
Body mass index	−0.161	0.010	7.534	0.011	1.564	1.228–1.981
Alcohol consumption	0.176	0.034	8.202	0.008	1.613	1.292–2.366
Cigarette smoking	−0.142	0.023	6.122	0.019	1.753	1.133–2.156
LIPC −514*C*/*T* genotype	0.126	0.031	5.323	0.024	1.677	1.212–1.882

direct descendant blood kin or the collateral branch blood kin in seven generations. Therefore, we hypothesized that the hereditary characteristic and genotypes of some lipid metabolism-related genes in this population may be different from those in Han Chinese.

In the present study, we show that the frequency of the *LIPC* −514*T* allele was higher in Hei Yi Zhuang than in Han. The frequencies *CT* and *TT* genotypes were also higher in Hei Yi Zhuang than in Han. There were no differences in the genotypic and allelic frequencies between males and females in both ethnic groups. The frequencies of the *LIPC* −514*T* allele and *TT* genotypes in Hei Yi Zhuang were also higher than those of previous studies in Chinese from America (Taiwanese-Chinese, *T* allele 37.5%) [20], Singapore (*TT* genotype 12.7%) [25], Taiwan (*TT* genotype 12.6%) [26], and Hong Kong (*TT* genotype 12.8–14.8%) [27]. Studies on the *LIPC* −514*C*/*T* polymorphism in several populations have demonstrated that the frequency of both −514*C*/*T* alleles varies highly among different ethnic populations [19, 27, 28]. The −514*C* allele is the most common allele in Caucasians, whereas the −514*T* allele is the major allele in black Americans. Asians have an intermediate frequency. The frequency of the −514*T* allele was 0.15–0.21, 0.45–0.53, and about 0.47 in Caucasians, African Americans, and Japanese Americans [5, 6, 17, 29], respectively. These variations in genotypic and allelic frequencies between the two ethnic groups may partially explain the observed higher HDL-C levels seen in the Hei Yi Zhuang populations. Several studies have shown that the −514*T* allele of the *LIPC* promoter appears to be associated with decreased HL activity, and increased HDL-C [6, 18].

The potential relationship between the *LIPC* −514*C*/*T* polymorphism and plasma or serum HDL-C levels in humans has been evaluated in a large number of studies. However, previous findings on the association of this polymorphism with the changes in plasma HDL-C levels are inconsistent. Jansen et al. [5], Couture et al. [15], and Murtomaki et al. [17] reported significant association between the *LIPC* polymorphisms and HDL-C levels, whereas Zambon et al. [18], Tahvanainen et al. [29], Hegele et al. [30], and Shohet et al. [31] failed to find a significant genetic effect on HDL-C concentrations. Zambon et al. [18] first reported that the promoter polymorphism significantly influenced HDL_2-C but not HDL-C levels, which is consistent with the previous report that HL activity is primarily associated with HDL_2-C but not with HDL_3-C [32, 33]. This result was also replicated on the basis of the data from the Framingham Offspring study [15]. However, only a few studies have reported an association between this polymorphism and plasma TG [14, 34]. In one study, carried out by Jansen et al. [34] in the European Atherosclerosis Research Study II, the *T* allele was associated with higher concentrations of plasma

TG, HDL-C, apoA-I and apoB. The effects of *LIPC* polymorphism on LDL-C and apoB are inconsistent; one study reported significantly higher LDL-C levels and borderline higher apoB levels in *TT* patients than in those with the *CC* genotype [35], whereas in other studies there were no differences in LDL-C and apoB levels with genotype [15, 29]. In the present study, we show that HDL-C and apoB levels in both ethnic groups were higher in *LIPC* −514*T* carriers than in noncarriers. In addition, serum TG levels in Han were higher in *TT* genotype individuals than in *CC* genotype subjects. These results suggest that there was an association between the *LIPC* −514*C*/*T* polymorphism and serum HDL-C and apoB levels.

In addition to the genetic factors, environmental factors such as obesity [36], physical inactivity [37], alcohol consumption [38], cigarette smoking [38, 39], diet [40], and hypertension [41] also influence plasma HDL-C levels. For example, heavy smokers have, on average, 9% lower HDL-C levels than matched nonsmokers [39]. Obesity is one of the most important factors in reducing HDL-C levels [36, 42]. In the present study, we also show that serum HDL-C levels were positively correlated with age and alcohol consumption, and negatively associated with hypertension and cigarette smoking in Hei Yi Zhuang. Serum HDL-C levels were also positively correlated with age and alcohol consumption, and negatively associated with BMI and cigarette smoking in Han. These findings suggest that environmental factors or the interactions of environmental and genetic factors may be involved in determining the difference in serum HDL-C concentrations between the two ethnic groups.

In conclusion, the results of the present study show that there were significant differences in genotypic and allelic frequencies of the *LIPC* −514*C*/*T* between the Hei Yi Zhuang and Han populations. An association between the *LIPC* −514*C*/*T* polymorphism and serum HDL-C and apoB levels was observed in both ethnic groups. Higher serum HDL-C and apoB levels were found in *LIPC* −514*T* carriers than in noncarriers. Serum HDL-C levels were positively correlated with *LIPC* −514*C*/*T* genotypes in both ethnic groups. The differences in serum HDL-C levels between the Hei Yi Zhuang and Han populations might partially attribute to the differences in the *LIPC* −514*C*/*T* genotypic and allelic frequencies.

Acknowledgments This study was supported by the National Natural Science Foundation of China (No: 30360038).

References

1. Gordon DJ, Probstfield JL, Garrison RJ, Neaton JD, Castelli WP, Knoke JD, Jacobs DR Jr, Bangdiwala S, Tyroler HA (1989) High-density lipoprotein cholesterol and cardiovascular disease. Four prospective American studies. Circulation 79:8–15
2. Heller DA, de Faire U, Pedersen NL, Dahlén G, McClearn GE (1993) Genetic and environmental influences on serum lipid levels in twins. N Engl J Med 328:1150–1156
3. Steinmetz J, Boerwinkle E, Gueguen R, Visvikis S, Henny J, Siest G (1992) Multivariate genetic analysis of high density lipoprotein particles. Atherosclerosis 92:219–227
4. Cohen JC, Wang Z, Grundy SM, Stoesz MR, Guerra R (1994) Variation at the hepatic lipase and apolipoprotein AI/CIII/AIV loci is a major cause of genetically determined variation in plasma HDL cholesterol levels. J Clin Invest 94:2377–2384
5. Jansen H, Verhoeven AJ, Weeks L, Kastelein JJ, Halley DJ, van den Ouweland A, Jukema JW, Seidell JC, Birkenhager JC (1997) A common C-to-T substitution at position 2480 of the hepatic lipase promoter associated with a lowered lipase activity in coronary artery disease patients. Arterioscler Thromb Vasc Biol 17:2837–2842
6. Guerra R, Wang J, Grundy SM, Cohen JC (1997) A hepatic lipase (LIPC) allele associated with high plasma concentrations of high density lipoprotein cholesterol. Proc Natl Acad Sci USA 94:4532–4537
7. Santamarina-Fojo S, Haudenschild C, Amar M (1998) The role of hepatic lipase in lipoprotein metabolism and atherosclerosis. Curr Opin Lipidol 9:211–219
8. Perret B, Mabile L, Martinez L, Tercé F, Barbaras R, Collet X (2002) Hepatic lipase: structure/function relationship, synthesis, and regulation. J Lipid Res 43:1163–1169
9. Deeb SS, Zambon A, Carr MC, Ayyobi AF, Brunzell JD (2003) Hepatic lipase and dyslipidemia: interactions among genetic variants, obesity, gender, and diet. J Lipid Res 44:1279–1286
10. Kuusi T, Saarinen P, Nikkilä EA (1980) Evidence for the role of hepatic endothelial lipase in the metabolism of plasma high density lipoprotein2 in man. Atherosclerosis 36:589–593
11. Salonen JT, Salonen R, Seppänen K, Rauramaa R, Tuomilehto J (1991) HDL, HDL2, and HDL3 subfractions, and the risk of acute myocardial infarction. A prospective population study in eastern Finnish men. Circulation 84:129–139
12. Lamarche B, Moorjani S, Cantin B, Dagenais GR, Lupien PJ, Després JP (1997) Associations of HDL2 and HDL3 subfractions with ischemic heart disease in men. Prospective results from the Québec Cardiovascular Study. Arterioscler Thromb Vasc Biol 17:1098–1105
13. Bensadoun A, Berryman DE (1996) Genetics and molecular biology of hepatic lipase. Curr Opin Lipidol 7:77–81
14. Cohen JC, Vega GL, Grundy SM (1999) Hepatic lipase: new insights from genetic and metabolic studies. Curr Opin Lipidol 10:259–267
15. Couture P, Otvos JD, Cupples LA, Lahoz C, Wilson PW, Schaefer EJ, Ordovas JM (2000) Association of the C-514T polymorphism in the hepatic lipase gene with variations in lipoprotein subclass profiles: the Framingham offspring study. Arterioscler Thromb Vasc Biol 20:815–822
16. vant Hooft FM, Lundahl B, Ragogna F, Karpe F, Olivecrona G, Hamsten A (2000) Functional characterization of 4 polymorphisms in promoter region of hepatic lipase gene. Arterioscler Thromb Vasc Biol 20:1335–1339
17. Murtomaki S, Tahvanainen E, Antikainen M, Tiret L, Nicaud V, Jansen H, Ehnholm C (1997) Hepatic lipase gene polymorphisms influence plasma HDL levels. Results from Finnish EARS participants. European atherosclerosis research study. Arterioscler Thromb Vasc Biol 17:1879–1884
18. Zambon A, Deeb SS, Hokanson JE, Brown BG, Brunzell JD (1998) Common variants in the promoter of the hepatic lipase gene are associated with lower levels of hepatic lipase activity,

buoyant LDL, and higher HDL2 cholesterol. Arterioscler Thromb Vasc Biol 18:1723–1729

19. Vega GL, Clark LT, Tang A, Marcovina S, Grundy SM, Cohen JC (1998) Hepatic lipase activity is lower in African American men than in white American men: effects of 5′ flanking polymorphism in the hepatic lipase gene (LIPC). J Lipid Res 39:228–232
20. Shohet RV, Vega GL, Bersot TP, Mahley RW, Grundy SM, Guerra R, Cohen JC (2002) Sources of variability in genetic association studies: insights from the analysis of hepatic lipase (LIPC). Hum Mutat 19:536–542
21. Yin R, Chen Y, Pan S, He F, Liu T, Yang D, Wu J, Yao L, Lin W, Li R, Huang J (2006) Effects of demographic, dietary and other lifestyle factors on the prevalence of hyperlipidemia in Guangxi Hei Yi Zhuang and Han populations. Eur J Cardiovasc Prev Rehabil 13:977–984
22. Yin R, Li R, Lin W, Yang D, Pan S (2006) Effect of the MTP −493 G/T polymorphism on the lipid profiles of the Guangxi Hei Yi Zhuang and Han populations. Eur J Lipid Sci Technol 108:561–568
23. Yin R, Yao L, Chen Y, Yang D, Lin W, Li M, He F, Wu J, Ye G, Nong Z (2006) Prevalence, awareness, treatment, control and risk factors of hypertension in the Guangxi Hei Yi Zhuang and Han populations. Hypertens Res 29:423–432
24. Cooperative Meta-analysis Group of China Obesity Task Force (2002) Predictive values of body mass index and waist circumference to risk factors of related diseases in Chinese adult population. Zhonghua Liu Xing Bing Xue Za Zhi 23:5–10
25. Tai ES, Corella D, Deurenberg-Yap M, Cutter J, Chew SK, Tan CE, Ordovas JM, Singapore National Health Survey (2003) Dietary fat interacts with the −514C>T polymorphism in the hepatic lipase gene promoter on plasma lipid profiles in a multiethnic Asian population: the 1998 Singapore National Health Survey. J Nutr 133:3399–3408
26. Ko YL, Hsu LA, Hsu KH, Ko YH, Lee YS (2004) The interactive effects of hepatic lipase gene promoter polymorphisms with sex and obesity on high-density-lipoprotein cholesterol levels in Taiwanese-Chinese. Atherosclerosis 172:135–142
27. Tan KC, Shiu SW, Chu BY (2001) Effects of gender, hepatic lipase gene polymorphism and type 2 diabetes mellitus on hepatic lipase activity in Chinese. Atherosclerosis 157:233–239
28. Nie L, Niu S, Vega GL, Clark LT, Tang A, Grundy SM, Cohen JC (1998) Three polymorphisms associated with low hepatic lipase activity are common in African Americans. J Lipid Res 39:1900–1903
29. Tahvanainen E, Syvanne M, Frick MH, Murtomaki-Repo S, Antikainen M, Kesaniemi YA, Kauma H, Pasternak A, Taskinen MR, Ehnholm C (1998) Association of variation in hepatic lipase activity with promoter variation in the hepatic lipase gene. The LOCAT study investigators. J Clin Invest 101:956–960
30. Hegele RA, Harris SB, Brunt JH, Young TK, Hanley AJ, Zinman B, Connelly PW (1999) Absence of association between genetic variation in the LIPC gene promoter and plasma lipoproteins in three Canadian populations. Atherosclerosis 146:153–160
31. Shohet RV, Vega GL, Anwar A, Cigarroa JE, Grundy SM, Cohen JC (1999) Hepatic lipase (LIPC) promoter polymorphism in men with coronary artery disease. Allele frequency and effects on hepatic lipase activity and plasma HDL-C concentrations. Arterioscler Thromb Vasc Biol 19:1975–1978
32. Applebaum-Bowden D, Haffner SM, Wahl PW, Hoover JJ, Warnick GR, Albers JJ, Hazzard WR (1985) Postheparin plasma triglyceride lipases. Relationships with very low density lipoprotein triglyceride and high density lipoprotein2 cholesterol. Arteriosclerosis 5:273–282
33. Després JP, Ferland M, Moorjani S, Nadeau A, Tremblay A, Lupien PJ, Thériault G, Bouchard C (1989) Role of hepatic-triglyceride lipase activity in the association between intra-abdominal fat and plasma HDL cholesterol in obese women. Arteriosclerosis 9:485–492
34. Jansen H, Chu G, Ehnholm C, Dallongeville J, Nicaud V, Talmud PJ (1999) The T allele of the hepatic lipase promoter variant C-480T is associated with increased fasting lipids and HDL and increased preprandial and postprandial LpCIII:B : European Atherosclerosis Research Study (EARS) II. Arterioscler Thromb Vasc Biol 19:303–308
35. Zambon A, Deeb SS, Brown BG, Hokanson JE, Brunzell JD (2001) Common hepatic lipase gene promoter variant determines clinical response to intensive lipid-lowering treatment. Circulation 103:792–798
36. Berns MA, de Vries JH, Katan MB (1989) Increase in body fatness as a major determinant of changes in serum total cholesterol and high density lipoprotein cholesterol in young men over a 10-year period. Am J Epidemiol 130:1109–1122
37. Durstine JL, Grandjean PW, Davis PG, Ferguson MA, Alderson NL, DuBose KD (2001) Blood lipid and lipoprotein adaptations to exercise: A quantitative analysis. Sports Med 31:1033–1062
38. Criqui MH, Cowan LD, Tyroler HA, Bangdiwala S, Heiss G, Wallace RB, Cohn R (1987) Lipoproteins as mediators for the effects of alcohol consumption and cigarette smoking on cardiovascular mortality: results form the Lipid Research Clinics Follow-up Study. Am J Epidemiol 126:629–637
39. Craig WY, Palomaki GE, Haddow JE (1989) Cigarette smoking and serum lipid and lipoprotein concentrations: an analysis of published data. BMJ 298:784–788
40. Mann JI (1997) Dietary effects on plasma LDL and HDL. Curr Opin Lipidol 8:35–38
41. Zhang X, Sun Z, Zheng L, Li J, Liu S, Xu C, Li J, Zhao F, Hu D, Sun Y (2007) Prevalence of dyslipidemia and associated factors among the hypertensive rural Chinese population. Arch Med Res 38:432–439
42. Park HS, Yun YS, Park JY, Kim YS, Choi JM (2003) Obesity, abdominal obesity, and clustering of cardiovascular risk factors in South Korea. Asia Pac J Clin Nutr 12:411–418

Lipids (2008) 43:741–748
DOI 10.1007/s11745-008-3202-5

ORIGINAL ARTICLE

Anti-Tumor Effect of Orally Administered Spinach Glycolipid Fraction on Implanted Cancer Cells, Colon-26, in Mice

**Naoki Maeda · Yasuo Kokai · Seiji Ohtani · Hiroeki Sahara ·
Yuko Kumamoto-Yonezawa · Isoko Kuriyama · Takahiko Hada ·
Noriyuki Sato · Hiromi Yoshida · Yoshiyuki Mizushina**

Received: 5 November 2007 / Accepted: 4 June 2008 / Published online: 2 July 2008
© AOCS 2008

Abstract We succeeded in purifying a major glycolipid fraction from a green vegetable, spinach. This fraction consists mainly of three glycolipids: monogalactosyl diacylglycerol (MGDG), digalactosyl diacylglycerol (DGDG), and sulfoquinovosyl diacylglycerol (SQDG). In a previous study, we found that the glycolipid fraction inhibited DNA polymerase activity, cancer cell growth and tumor growth with subcutaneous injection. We aimed to clarify oral administration of the glycolipid fraction, suppressing colon adenocarcinoma (colon-26) tumor growth in mice. A tumor graft study showed that oral administration of 20 mg/kg glycolipid fraction for 2 weeks induced a 56.1% decrease in the solid tumor volume ($P < 0.05$) without any side-effects, such as loss of body weight or major organ failure, in mice. The glycolipid fraction induced the suppression of colon-26 tumor growth with inhibition of angiogenesis and the expression of cell proliferation marker proteins such as Ki-67, proliferating cell nuclear antigen (PCNA), and Cyclin E in the tumor tissue. These results suggest that the orally administered glycolipid fraction from spinach could suppress colon tumor growth in mice by inhibiting the activities of neovascularization and cancer cellular proliferation in tumor tissue.

Keywords Glycolipid · Spinach · Anti-tumor activity · Anti-angiogenesis activity · Anti-cancer cell growth activity

Abbreviations

MGDG	Monogalactosyl diacylglycerol
DGDG	Digalactosyl diacylglycerol
SQDG	Sulfoquinovosyl diacylglycerol

N. Maeda · Y. Kumamoto-Yonezawa · I. Kuriyama ·
H. Yoshida · Y. Mizushina (✉)
Laboratory of Food and Nutritional Sciences,
Department of Nutritional Science,
Kobe-Gakuin University, Nishi-ku,
Kobe, Hyogo 651-2180, Japan
e-mail: mizushin@nutr.kobegakuin.ac.jp

N. Maeda · I. Kuriyama
Japan Society for the Promotion of Science,
Kobe-Gakuin University, Nishi-ku, Kobe,
Hyogo, Japan

Y. Kokai · S. Ohtani
Biomedical Research Center Laboratory of Biomedical
Engineering, Sapporo Medical University School of Medicine,
Chuo-ku, Sapporo 060-8556, Japan

H. Sahara
Marine Biomedical Institute,
Sapporo Medical University School of Medicine,
Oshidomari, Rishirifujij, Hokkaido 097-0101, Japan

T. Hada
Hada Giken Co. Ltd,
Yamaguchi-shi, Yamaguchi 753-0047, Japan

N. Sato
Pathology and Chemistry,
Sapporo Medical University School of Medicine,
Chuo-ku, Sapporo 060-8556, Japan

H. Yoshida · Y. Mizushina
Cooperative Research Center of Life Sciences,
Kobe-Gakuin University, Nishi-ku, Kobe,
Hyogo 651-2180, Japan

PBS	Phosphate-buffered saline
PCNA	Proliferating cell nuclear antigen
vWF	von Willebrand Factor
MVD	Microvessel density

Introduction

We have been screening for inhibitors of eukaryotic DNA polymerase for more than 10 years, and we and other researchers have reported previously that major plant glycolipids [1] such as monogalactosyl diacylglycerol (MGDG), digalactosyl diacylglycerol (DGDG), and sulfoquinovosyl diacylglycerol (SQDG) have potential anticancer functions as follows: DNA polymerase inhibition [2–7], suppression of cancer cell proliferation [4–6, 8, 9], anti-angiogenesis [10], and anti-tumor promotion [11, 12]. In animals, glycolipids are contained in a minute amount in the brain [13] and in sea urchin [14, 15]. Comparing various vegetables, we found that glycolipids were highest in spinach, which is especially rich in SQDG [16]. In our previous study, we developed a method to purify a glycolipid fraction from spinach and found that this fraction had anti-tumor activity in a subcutaneous solid tumor model [17, 18].

We eat vegetables, grains, and so on every day; however, the anti-cancer effect of orally administered glycolipids has not been ascertained, and the functional role of glycolipids is not well understood. In addition, a few studies have suggested that some of these glycolipids are digested and not absorbed in an in vivo rat model [19, 20], in vitro human pancreatic lipolytic enzyme, and duodenal contents model [21].

We investigated the orally administered glycolipid fraction of spinach for anti-tumor function in a colon solid tumor mouse model, and then evaluated anti-angiogenesis and anti-proliferation effects in tumor tissue using histopathological analysis.

Experimental Procedure

Materials

Spinach (*Spinacia oleracea* L.) was purchased from a supermarket (Co-operation Union Co., Kobe, Hyogo prefecture, Japan). Rabbit polyclonal antibodies of anti-Ki-67 (NB500-170), Cyclin E (ab7959) and von Willebrand Factor (vWF, AB7356) were obtained from Novus Biologicals, Inc. (CO, USA), Abcam, Inc. (MA, USA) and Chemicon International, Inc. (CA, USA), respectively. Mouse anti-proliferating cell nuclear antigen (PCNA) monoclonal antibody (sc-56) was purchased from Santa Cruz Biotechnology, Inc. (CA, USA). Peroxidase-conjugated forms of goat anti-rabbit or anti-mouse IgGs (i.e., secondary antibodies) were obtained from Nichirei Biosciences Inc. (Tokyo, Japan). All reagents were analytical grade and were purchased from Merck Ltd (Tokyo, Japan).

Purification Methods of the Glycolipid Fraction from Spinach

Water-soluble substances were extracted from dried spinach (20 g) with 1,000 mL of water at 60 °C. The tissue cake was added to 1,000 mL of 100% ethanol at 60 °C, and substances containing glycolipids were extracted. The 100% ethanol extract was diluted to a 70% ethanol solution with water. The solution was subjected to Diaion HP-20 (Mitsubishi Chemical Inc., Tokyo, Japan) column chromatography, hydrophobic-type chromatography, washed with 1,000 mL of 70% ethanol, and then eluted using 95% ethanol. The 95% ethanol-eluted solution was the glycolipid fraction (1.3 g). This fraction was stored at −20 °C until used for an experiment and contained the three major glycolipids: MGDG, DGDG, and SQDG [6], the chemical structures of which are shown in Fig. 1. By fatty acid analysis of each spinach glycolipid by gas chromatography,

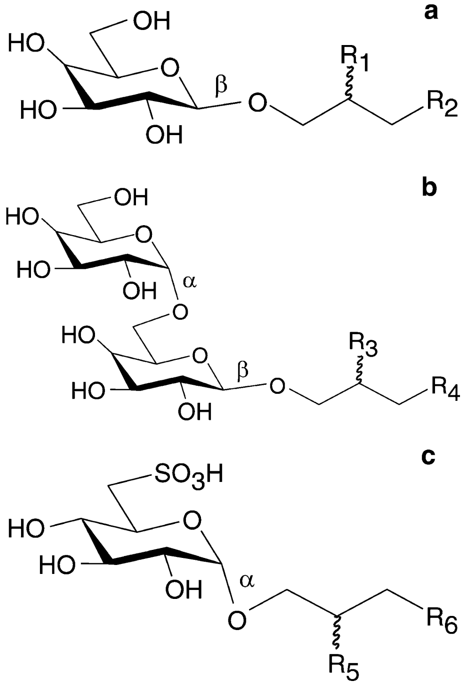

Fig. 1 Chemical structures of the major glycolipids in the fraction from spinach. **a** Monogalactosyl diacylglycerol (MGDG). **b** Digalactosyl diacylglycerol (DGDG). **c** Sulfoquinovosyl diacylglycerol (SQDG). R_1–R_6 = in these structures are fatty acids

the major fatty acids of MGDG were stearic acid (18:0) and oleic acid (18:1), DGDG contained mostly palmitic acid (16:0) and oleic acid (18:1), and SQDG mostly consisted of palmitic acid (16:0) and linolenic acid (18:3) [6].

Cell Culture and Cell Growth Inhibition Assay

The mouse colon adenocarcinoma cell line, colon-26 [22] was provided by the Cell Resource Center for Biomedical Research (Tohoku University, Sendai, Japan), and human cancer cell lines, A549 (lung cancer), BALL-1 (B cell acute lymphoblastoid leukemia), HeLa (cervical cancer), Molt-4 (T cell acute lymphoblastic leukemia), and NUGC-3 (stomach cancer), were obtained from the Health Science Research Bank (Osaka, Japan). These cancer cells were cultured in RPMI 1640 (Nissui Pharmaceutical Co., Ltd, Tokyo, Japan) supplemented with 10% fetal bovine serum (Equitech-Bio, Inc., Texas, USA), penicillin (100 units/mL), and streptomycin (100 µg/mL). The cells were cultured under an atmosphere of 95% air and 5% CO_2 at 37 °C. The cancer cells (5×10^3) were seeded onto a 96-well plate ($n = 5$) and allowed to adhere overnight. The culture was then washed and added to the medium or to the medium containing different concentrations (0–100 µg/mL) of the glycolipid fraction of spinach dissolved in each medium. After 24 h, cell-growth activity was determined by the 3-(4,5-dimethylthiazol-2-yl)-2,5-diphenyl-2*H*-tetrazolium bromide (MTT) assay [23].

Animals

Specific pathogen-free female BALB/c mice (5 weeks of age, 14–19 g) were purchased from Japan SLC, Inc. (Shizuoka, Japan). The laboratory standard diet for mice (code: MF) was purchased from Oriental Yeasts Co., Ltd (Osaka, Japan). The mice were housed and acclimated in the animal research facilities for a least 1 week before being used in the present study. They were kept in isolation rooms at a controlled temperature and had free access to laboratory standard diet (contents by weight %: water-soluble non-nitrogen compounds 52.3%, protein 24.6%, water 8%, ash 6.4%, fat 5.6%, and fiber 3.1%) and water. All animal studies were approved by the Kobe-Gakuin University Animal Committee, according to the guidelines for the “Care and Use of Laboratory Animals” of the University.

Implantation of Mouse Cancer Cells and Anti-Tumor Growth Assay

For anti-tumor experiments in vivo, colon-26 cells [1×10^6 cells/mouse in 100 µL of phosphate-buffered saline (PBS)] were subcutaneously inoculated into BALB/c mice (18–21 g). Five days after the start of inoculation, we observed the engraftment of tumor cells, which reached a volume of 20–30 mm^3; tumors were measured with a caliper at each administration, and tumor volumes were calculated using the formula: volume $= a \times b \times b/2$, where a and b are the length and width diameters. The mice were divided randomly into three groups: a control group ($n = 5$) with orally administered PBS alone, and two experimental groups (each $n = 5$) with the orally administered glycolipid fraction dissolved in PBS. All mice were orally administered 100 µL of the fraction dissolved in PBS at dose of 10, 20 mg/kg or PBS only every day using a gastric feeding needle, and tumor volume was measured from the beginning of administration for 2 weeks (total of 15 administrations). After the anti-tumor assay (i.e., 19 days after implantation), the mice were killed and the histopathological features of the tumors were observed with gross diagnosis of major organs, the lung, heart, spleen, stomach, liver, pancreas, kidney, intestine, and brain.

Preparation of Mouse Tissue Samples

In the significantly decreased tumor volume group, we evaluated the tumor tissue. For hematoxylin and eosin (H&E) staining and immunohistochemical procedures, tumor tissues from killed mice were fixed with 10% formalin in PBS (pH 7.2) and processed for paraffin embedding. The sections, 3 µm thick, were stained with H&E or appropriate antigens for immunohistochemistry. For immunohistochemical staining, all antibodies were reacted with deparaffinized antigen-retrieved sections.

Histopathological and Immunohistochemical Analysis of Cell Proliferation in Tumor Tissues

The sections were histopathologically analyzed using the mitotic index [number of mitoses/high power field (HPF)] of five to eight random non-necrotic areas by H&E stain at 400× magnification. The expressions of cell proliferation marker proteins such as Ki-67, PCNA, and Cyclin E [24–26] were determined by immunohistochemistry. The sections were incubated overnight at 4 °C with the primary antibodies such as 1:50 dilution of anti-Ki-67, 1:500 dilution of anti-PCNA, or 1:1,000 of anti-Cyclin E. The sections were then rinsed three times with PBS and incubated for 10 or 30 min with the peroxidase-conjugated secondary antibody at room temperature. The positive reaction was visualized by incubating the sections with 3,3′-diaminobenzidine (DAB) for 5–10 min. The sections were then washed with water and counterstained with hematoxylin. To assess the average proteins of proliferation markers in entire tumor sections, four to six areas, were chosen from the stained section in each tumor, and high expression spots at 400× magnification were counted.

Vessel Count within Tumor Tissue

Deparaffinized sections were incubated overnight with 1:1,000 dilution of anti-vWF at 4 °C. The sections were rinsed three times with PBS and incubated for 30 min with the peroxidase-conjugated secondary antibody at room temperature. The positive reaction was visualized by incubating the sections with DAB for 5–10 min. The sections were then washed with water and counterstained with hematoxylin. Vessel counts were based on the criteria of Weidner et al. [27] and were performed at 200× magnification ($0.785\ \mathrm{mm}^2$ per field). To assess average vascularization in entire tumor sections, three areas were chosen from the stained section of each tumor, and the number of vessel markers with a high expression in the field was counted.

Statistical Analysis

Statistical analyses were performed using the Steel–Dwass test for in vitro experiments and the Mann–Whitney *U* test for in vivo experiments, using the software package KyPlot 5.0 (Kyens Lab., Inc., Tokyo, Japan) for Windows.

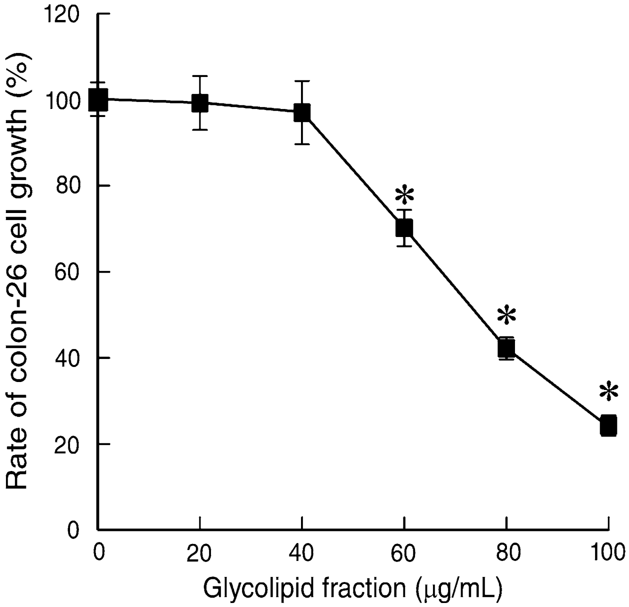

Fig. 2 Dose–response curve of the glycolipid fraction for cancer cell growth inhibition. Colon-26 cells (mouse colon adenocarcinoma) were incubated with 0–100 μg/mL of the glycolipid fraction of spinach for 24 h. The rate of cultured cell growth inhibition was determined by MTT assay [23]. *Bars* indicate the mean ± SEM of five independent experiments. *Different from the control, $P < 0.05$

Results

Inhibitory Effect of the Glycolipid Fraction on Cancer Cell growth

The glycolipid fraction from spinach was incubated with mouse colon-26 cell lines for 24 h, and cellular proliferation was inhibited in a dose-dependent manner, with an IC_{50} value of 74.5 μg/mL (Fig. 2). At 100 μg/mL, the growth inhibition rate of colon-26 cells decreased to 75.7% compared with the control ($P < 0.05$).

We also investigated whether this fraction could inhibit the growth of other cancer cell lines from humans, and the IC_{50} values are shown in Table 1. The glycolipid fraction also suppressed the growth of all human cancer cell lines by 24 h incubation, and the range of IC_{50} values were 58.5–81.7 μg/mL. The inhibitory effect of 48 h culture was as strong as with 24 h incubation (data not shown). The cancer cell line from mice (i.e., colon-26) showed almost the same cell growth inhibitory results as cancer cell lines from humans; therefore, we used mouse colon-26 cells in the latter part of this study.

Suppression of Tumor Growth in BALB/c Mice

Five days after cancer cell implantation, daily oral administration of the glycolipid fraction at 20 mg/kg significantly suppressed the growth of colon-26 solid tumor in mice ($n = 5$), and treatment with the glycolipid fraction resulted in a 56.1% inhibition of tumor growth compared with the control group ($P < 0.05$) on the final day (i.e., 19 days after implantation) (Fig. 3). However, oral administration of 10 mg/kg glycolipid fraction did not

Table 1 Inhibitory effect of the glycolipid fraction from spinach on cultured cancer cell growth

Cell line	Type of cancer	IC_{50} values (μg/mL)
Colon-26	Mouse colon	74.5 ± 9.0
A549	Human lung cancer	81.7 ± 9.9
BALL-1	Human B cell acute lymphoblastoid leukemia	59.0 ± 7.1
HeLa	Human cervix cancer	57.2 ± 6.9
Molt-4	Human T cell acute lymphoblastic leukemia	58.5 ± 7.1
NUGC-3	Human stomach cancer	79.8 ± 9.6

Mouse cancer cells, such as colon-26, and human cancer cells, such as A549, BALL-1, HeLa, Molt-4 and NUGC-3, were incubated with the glycolipid fraction for 24 h. The rate of cell growth inhibition was determined by MTT assay [23]. Data are expressed as the mean ± SEM of five independent experiments

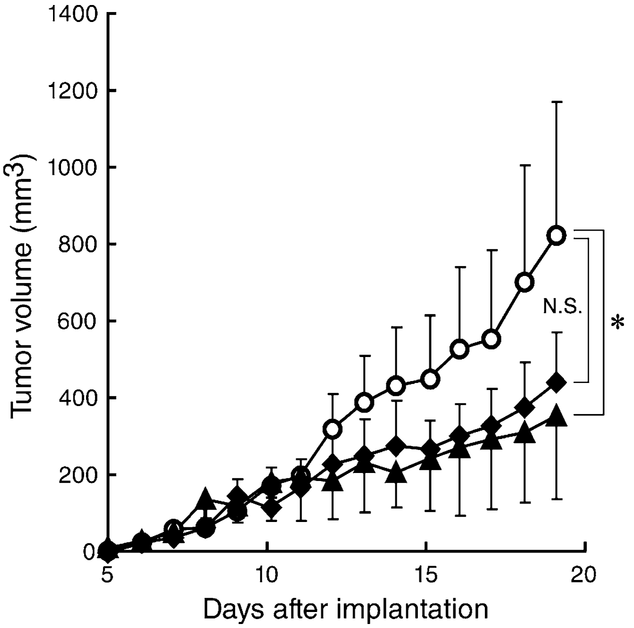

Fig. 3 Effect of the glycolipid fraction on tumor growth in mice. Mice with solid tumors were orally administered 100 μL of PBS as a control group ($n = 5$) (*open circles*) and the glycolipid fraction in 100 μL of PBS at dose of 10 mg/kg ($n = 5$, *closed diamonds*) and 20 mg/kg ($n = 5$, *closed triangles*) as experimental groups. All data are shown as the means ± SEM of five independent animals. *Different from the control, $P < 0.05$

significantly decrease the solid tumor volume on the final day compared with the control group ($P = 0.42$). The body and major organ weights in the experimental group with the orally administered glycolipid fraction were almost the same as in the control group with orally administered PBS, and there was no drug-related animal death.

Suppression of the Expression of Mitosis and Cell Proliferation Marker Proteins in Tumor Tissues

After the tumor formation experiment in mice ($n = 3$–5), paraffin sections of tumor tissues were made for H&E staining and immunohistochemical staining of cell proliferation marker proteins such as Ki-67, PCNA, and Cyclin E. The results of histopathological analysis for the proliferation of tumor cells are shown in Table 2. First, the mitotic index, which indicates the rate of cell division, of the administered glycolipid fraction was approximately 1.8-fold lower than that of the control mitotic index. Second, the immunohistochemical assay showed that the number of high expression spots in positive cells treated with the glycolipid fraction in tumor tissues decreased compared with the control, and the reduction rates of Ki-67, PCNA, and Cyclin E were 18.7, 17.6, and 14.4%, respectively. These results suggest that the glycolipid fraction could inhibit cell proliferation in tumor tissue.

Inhibition of Anti-Angiogenic Activity in Tumor Tissues

As shown in Fig. 4a and b, daily oral administration of 20 mg/kg glycolipid fraction decreased the number of microvessels compared with the control. Microvessel density (MVD) was measured by positive staining of vessels with vWF antibody per 1 mm^2. Mice ($n = 4$–5) treated with the glycolipid fraction (11.3 ± 1.8) induced 56.4% inhibition of vessel formation compared with the control (25.8 ± 5.3, $P < 0.05$, Fig. 4c). These results suggest that the glycolipid fraction of spinach could lead to a significant decrease of MVD, and this phenomenon must increase necrosis of colon-26 tumors (Fig. 5). Since the value of MVD is closely related to angiogenesis formation, the glycolipid fraction could be considered as having anti-angiogenic activity.

Discussion

We prepared the glycolipid fraction of spinach, and showed that it has anti-tumor activity with oral administration. This fraction consists of three glycolipids: MGDG, DGDG, and SQDG, but it is too difficult to purify each glycolipid separately from the fraction. We consider that the fraction containing glycolipids, which is easy to purify from spinach, could be a functional foodstuff with anti-cancer effects.

We found that oral administration of 20 mg/kg glycolipid fraction of spinach suppressed the formation of colon tumor in mice with no adverse drug reaction (Fig. 3). The

Table 2 Histopathological analysis of the sections of colon-26 cells in mouse tumor tissue

	Mitosis (/HPF)	Ki-67 (%)	PCNA (%)	Cyclin E (%)
Control	16.6 ± 1.3	86.7 ± 4.7	78.6 ± 1.4	57.1 ± 2.0
Spinach glycolipid fraction	9.4 ± 1.7*	70.5 ± 3.0*	64.8 ± 1.3*	48.9 ± 1.0*

Mice were orally administered PBS (control) or the glycolipid fraction from spinach in PBS at a dose of 20 mg/kg. Mitotic index and immunohistochemical proliferative analysis were calculated at a high magnification field (400×). Data are shown as the means ± SEM of four to six areas per mouse ($n = 3$–5)

* Different from the control, $P < 0.05$

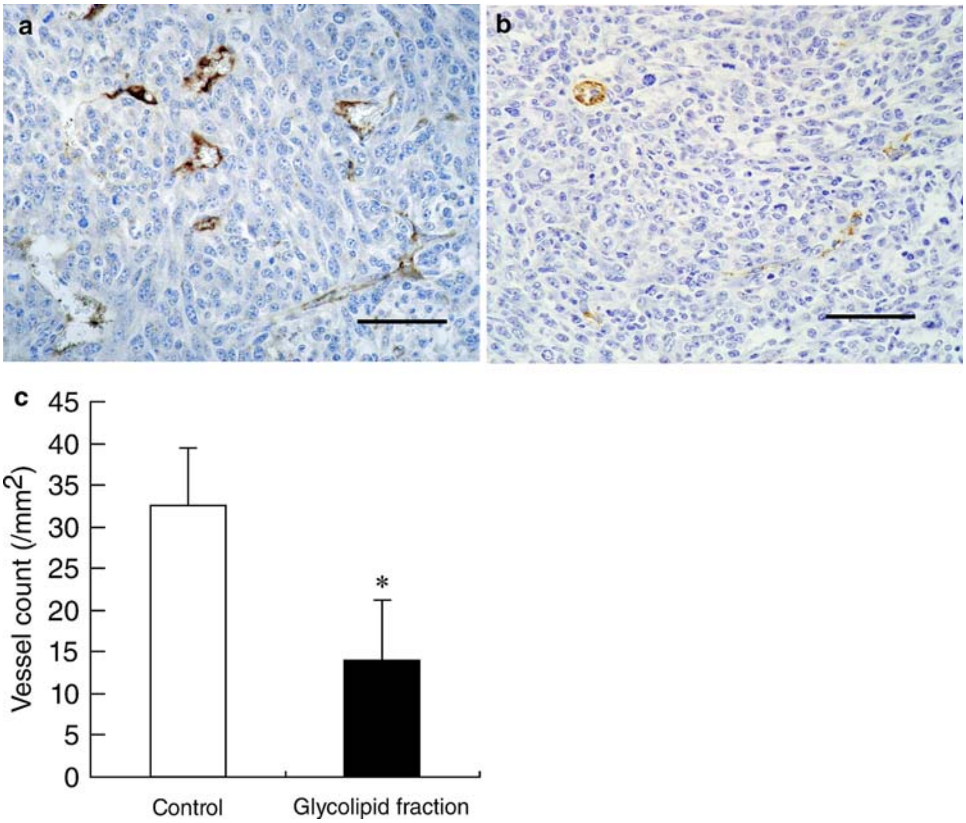

Fig. 4 Effect of the glycolipid fraction on tumor angiogenesis in mice 19 days after implantation. Tumor tissues were sectioned and stained with anti-vWF antibody. **a**, **b** MVD of the administered PBS control group (**a**) and the administered glycolipid fraction group at a dose of 20 mg/kg (**b**). *Bars* are 50 μm. (**c**) Numbers of microvessels are indicated by vWF-positive objects per 1 mm^2. All data are shown as the means ± SEM of three areas of the sections per mouse ($n = 4$–5). *Different from the control, $P < 0.05$

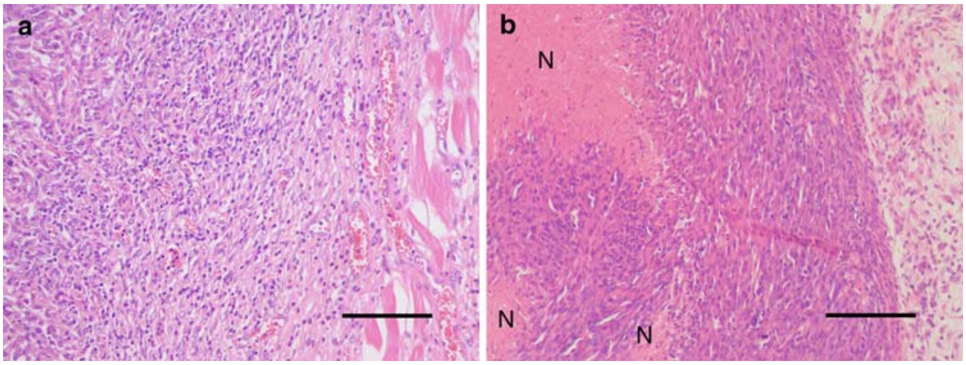

Fig. 5 Histopathological examination of the colon tumors of mice treated with the glycolipid fraction at a dose of 20 mg/kg 19 days after implantation. Tumor sections were stained with H&E. Mice were orally administered PBS as a control group (**a**) or the glycolipid fraction in PBS at a dose of 20 mg/kg as the experimental group (**b**). *N* necrosis. *Bars* are 100 μm

content (weight %) of fat in the laboratory standard diet of mice is 81.0% triglycerides, 17.4% phospholipids and 1.6% cholesterol. This diet hardly consists of glycolipids; therefore, glycolipids must be important for anti-tumor activity. Generally, tumor growth depends on angiogenesis [28, 29], and oral administration of the glycolipid fraction inhibited angiogenesis in tumor tissues (Fig. 4). The formation of tumors treated with the glycolipid fraction decreased MVD to 56.5% (Fig. 4c). These results showed that the inhibition of angiogenesis might cause tumor shrinkage and widespread necrosis (Fig. 5). In addition, since MVD relates to tumor development, malignancy, and metastasis [30–32], the glycolipid fraction could influence these phenomena.

The spinach glycolipid fraction induced a significant decrease of the expression of cell proliferation marker proteins such as Ki-67, PCNA, Cyclin E, and the index of tumor mitosis in tumor tissues (Table 2). The expression of Ki-67 occurs continuously in all cycling cells of G_1, S, G_2, and M phases, but not in resting cells in the G_0 phase. PCNA and Cyclin E are positive in the nuclear cell cycle of G_1 and S phases. Therefore, this fraction could arrest the cell cycle, and reduce the cell proliferation in the tumor cells. In addition, these cell proliferation marker proteins have negative effects on other indicators such as tumor prognosis, malignancy and metastasis [31, 33–35]. We have observed that glycolipids inhibited the activity of DNA polymerases [2–7]. Tumors have high DNA polymerase activity; therefore, the dual activities of anti-proliferation of cancer cells and inhibition of DNA polymerases must suppress the turnover and division of tumor cells.

On the other hand, a rat intake study and human duodenal contents study shows that glycolipids are digested or not absorbed [19–21]; however, the present study indicated that glycolipids might be absorbed and affect anti-tumor activity, similar to previous studies [7, 17]. Glycolipids, especially MGDG and SQDG, are hydrolyzed and yield monogalactosyl monoacylglycerol (MGMG) and sulfoquinovosyl monoacylglycerol (SQMG), respectively, and MGMG and SQMG increased the inhibition of DNA polymerase activity, anti-proliferation of cancer cells [36] and tumor suppression more than MGDG and SQDG [17].

In conclusion, this study shows that 20 mg/day of the orally administered spinach glycolipid fraction can effectively suppress mouse colon tumor growth, influenced by the anti-angiogenesis and anti-proliferation of tumor cells without side-effects. The glycolipid fraction suppressed the growth of cancer cells from humans and mice (Table 1; Fig. 2); therefore, glycolipids are suggested as preventing human cancer disease, and this spinach fraction could become a functional foodstuff with anti-cancer effects.

Acknowledgments This investigation was supported by a Grant-in-Aid for JSPS Fellows (N. M.), a Grant-in-Aid for Kobe-Gakuin University Joint Research (A) (H. Y. and Y. M.) and a “Life Science Center for Cooperative Research” Project for Private Universities: matching fund subsidy from MEXT (Ministry of Education, Culture, Sports, Science and Technology), 2006–2010 (H. Y. and Y. M.). Y. M. acknowledges a Grant-in-Aid for Young Scientists (A) (No. 19680031) from MEXT, and Grant-in-Aids from the Nakashima Foundation (Japan) and the Foundation of the Oil & Fat Industry kaikan (Japan).

References

1. Roughan PG, Batt RD (1969) The glycerolipid composition of leaves. Phytochemistry 8:363–369
2. Ohta K, Mizushina Y, Hirata N, Takemura M, Sugawara F, Matsukage A, Yoshida S, Sakaguchi K (1998) Sulfoquinovosyldiacylglycerol, KM043, a new potent inhibitor of eukaryotic DNA polymerases and HIV-reverse transcriptase type 1 from a marine red alga, *Gigartina tenella*. Chem Pharm Bull (Tokyo) 46:684–686
3. Mizushina Y, Watanabe I, Ohta K, Takemura M, Sahara H, Takahashi N, Gasa S, Sugawara F, Matsukage A, Yoshida S, Sakaguchi K (1998) Studies on inhibitors of mammalian DNA polymerase alpha and beta: sulfolipids from a pteridophyte, *Athyrium niponicum*. Biochem Pharmacol 55:537–541
4. Ohta K, Hanashima S, Mizushina Y, Yamazaki T, Saneyoshi M, Sugawara F, Sakaguchi K (2000) Studies on a novel DNA polymerase inhibitor group, synthetic sulfoquinovosylacylglycerols: inhibitory action on cell proliferation. Mutat Res 467:139–152
5. Hanashima S, Mizushina Y, Ohta K, Yamazaki T, Sugawara F, Sakaguchi K (2000) Structure–activity relationship of a novel group of mammalian DNA polymerase inhibitors, synthetic sulfoquinovosylacylglycerols. Jpn J Cancer Res 91:1073–1083
6. Murakami C, Kumagai T, Hada T, Kanekazu U, Nakazawa S, Kamisuki S, Maeda N, Xu X, Yoshida H, Sugawara F, Sakaguchi K, Mizushina Y (2003) Effects of glycolipids from spinach on mammalian DNA polymerases. Biochem Pharmacol 65:259–267
7. Maeda N, Hada T, Yoshida H, Mizushina Y (2007) Inhibitory effect on replicative DNA polymerases, human cancer cell proliferation, and in vivo anti-tumor activity by glycolipids from spinach. Curr Med Chem 14:955–967
8. Quasney ME, Carter LC, Oxford C, Watkins SM, Gershwin ME, German JB (2001) Inhibition of proliferation and induction of apoptosis in SNU-1 human gastric cancer cells by the plant sulfolipid, sulfoquinovosyldiacylglycerol. J Nutr Biochem 12:310–315
9. Hossain Z, Kurihara H, Hosokawa M, Takahashi K (2005) Growth inhibition and induction of differentiation and apoptosis mediated by sodium butyrate in Caco-2 cells with algal glycolipids. In Vitro Cell Dev Biol Anim 41:154–159
10. Matsubara K, Matsumoto H, Mizushina Y, Mori M, Nakajima N, Fuchigami M, Yoshida H, Hada T (2005) Inhibitory effect of glycolipids from spinach on in vitro and ex vivo angiogenesis. Oncol Rep 14:157–160
11. Morimoto T, Nagatsu A, Murakami N, Sakakibara J, Tokuda H, Nishino H, Iwashima A (1995) Anti-tumor-promoting glyceroglycolipids from the green alga, *Chlorella vulgaris*. Phytochemistry 40:1433–1437
12. Colombo D, Franchini L, Toma L, Ronchetti F, Nakabe N, Konoshima T, Nishino H, Tokuda H (2005) Anti-tumor-promoting activity of simple models of galactoglycerolipids with branched and unsaturated acyl chains. Eur J Med Chem 40:69–74
13. Inoue T, Dehmukh DS, Pieringer RA (1971) The association of the galactosyl diglycerides of brain with myelination. I: changes in the concentration of monogalactosyl diglyceride in the somal and myelin fractions of brain of rats during development. J Biol Chem 246:5688–5694
14. Nagai Y, Isono Y (1965) Occurrence of animal sulfolipid in the gametes of sea urchins. Jpn J Exp Med 35:315–318
15. Kitagawa I, Hamamoto Y, Kobayashi M (1979) Sulfonoglycolipid from the sea urchin *Anthocidaris crassispina* A. Agassiz. Chem Pharm Bull (Tokyo) 27:1394–1397
16. Kuriyama I, Musumi K, Yonezawa Y, Takemura M, Maeda N, Iijima H, Hada T, Yoshida H, Mizushina Y (2005) Inhibitory effects of glycolipids fraction from spinach on mammalian DNA polymerase activity and human cancer cell proliferation. J Nutr Biochem 16:594–601
17. Maeda N, Hada T, Murakami-Nakai C, Kuriyama I, Ichikawa H, Fukumori Y, Hiratsuka J, Yoshida H, Sakaguchi K, Mizushina Y (2005) Effects of DNA polymerase inhibitory and antitumor activities of lipase-hydrolyzed glycolipid fractions from spinach. J Nutr Biochem 16:121–128
18. Maeda N, Kokai Y, Ohtani S, Sahara H, Hada T, Ishimaru C, Kuriyama I, Yonezawa Y, Iijima H, Yoshida H, Sato N, Mizushina Y (2007) Anti-tumor effects of the glycolipids fraction from spinach which inhibited DNA polymerase activity. Nutr Cancer 57:216–223
19. Ohlsson L, Blom M, Bohlinder K, Carlsson A, Nilsson A (1998) Orally fed digalactosyldiacylglycerol is degraded during absorption in intact and lymphatic duct cannulated rats. J Nutr 128:239–245
20. Sugawara T, Miyazawa T (2000) Digestion of plant monogalactosyldiacylglycerol and digalactosyldiacylglycerol in rat alimentary canal. J Nutr Biochem 11:147–152
21. Andersson L, Bratt C, Arnoldsson KC, Herslof B, Olsson NU, Sternby B, Nilsson A (1995) Hydrolysis of galactolipids by human pancreatic lipolytic enzymes and duodenal contents. J Lipid Res 36:1392–1400
22. Corbett TH, Griswold DP Jr, Roberts BJ, Peckham JC, Schabel FM Jr (1975) Tumor induction relationships in development of

transplantable cancers of the colon in mice for chemotherapy assays, with a note on carcinogen structure. Cancer Res 35:2434–2439

23. Mosmann T (1983) Rapid colorimetric assay for cellular growth and survival: application to proliferation and cytotoxicity assays. J Immunol Methods 65:55–63
24. Gerdes J, Lemke H, Baisch H, Wacker HH, Schwab U, Stein H (1984) Cell cycle analysis of a cell proliferation-associated human nuclear antigen defined by the monoclonal antibody Ki-67. J Immunol 133:1710–1715
25. Kubben FJ, Peeters-Haesevoets A, Engels LG, Baeten CG, Schutte B, Arends JW, Stockbrugger RW, Blijham GH (1994) Proliferating cell nuclear antigen (PCNA): a new marker to study human colonic cell proliferation. Gut 35:530–535
26. Dong Y, Sui L, Tai Y, Sugimoto K, Hirao T, Tokuda M (2000) Prognostic significance of cyclin E overexpression in laryngeal squamous cell carcinomas. Clin Cancer Res 6:4253–4258
27. Weidner N, Semple JP, Welch WR, Folkman J (1991) Tumor angiogenesis and metastasis-correlation in invasive breast carcinoma. N Engl J Med 324:1–8
28. Folkman J (1971) Tumor angiogenesis: therapeutic implications. N Engl J Med 285:1182–1186
29. Folkman J (1985) Tumor angiogenesis. Adv Cancer Res 43:175–203
30. Bossi P, Viale G, Lee AK, Alfano R, Coggi G, Bosari S (1995) Angiogenesis in colorectal tumors: microvessel quantitation in adenomas and carcinomas with clinicopathological correlations. Cancer Res 55:5049–5053
31. Takahashi Y, Kitadai Y, Bucana CD, Cleary KR, Ellis LM (1995) Expression of vascular endothelial growth factor and its receptor, KDR, correlates with vascularity, metastasis, and proliferation of human colon cancer. Cancer Res 55:3964–3968
32. Takahashi Y, Bucana CD, Liu W, Yoneda J, Kitadai Y, Cleary KR, Ellis LM (1996) Platelet-derived endothelial cell growth factor in human colon cancer angiogenesis: role of infiltrating cells. J Natl Cancer Inst 88:1146–1151
33. Keyomarsi K, Tucker SL, Buchholz TA, Callister M, Ding Y, Hortobagyi GN, Bedrosian I, Knickerbocker C, Toyofuku W, Lowe M, Herliczek TW, Bacus SS (2002) Cyclin E and survival in patients with breast cancer. N Engl J Med 347:1566–1575
34. Dobashi Y, Jiang SX, Shoji M, Morinaga S, Kameya T (2003) Diversity in expression and prognostic significance of G1/S cyclins in human primary lung carcinomas. J Pathol 199:208–220
35. Hotta K, Shimoda T, Nakanishi Y, Saito D (2006) Usefulness of Ki-67 for predicting the metastatic potential of rectal carcinoids. Pathol Int 56:591–596
36. Mizushina Y, Maeda N, Kawasaki M, Ichikawa H, Murakami C, Takemura M, Xu X, Sugawara F, Fukumori Y, Yoshida H, Sakaguchi K (2003) Inhibitory action of emulsified sulfoquinovosyl acylglycerol on mammalian DNA polymerases. Lipids 38:1065–1074

Lipids (2008) 43:749–755
DOI 10.1007/s11745-008-3207-0

ORIGINAL ARTICLE

Characteristics of High α-Linolenic Acid Accumulation in Seed Oils

Suryadevara Rao · Mohammed Abdel-Reheem ·
Resham Bhella · Charles McCracken ·
David Hildebrand

Received: 6 March 2008 / Accepted: 3 June 2008 / Published online: 3 July 2008
© AOCS 2008

Abstract Modern diets are often deficient in ω-3 fatty acids and additional dietary sources of ω-3 fatty acids are useful. In order to investigate the molecular basis of the high accumulation of the ω-3 fatty acid, α-linolenic acid (18:3), in three different plants, flax (*Linum usitatissimum)*, *Dracocephalum moldavica*, and *Perilla frutescens* ω-3 desaturase activity, transcript levels, and 18:3 in-vivo synthesis were examined. The 18:3 content was found to be higher at the later developmental stage of *D. moldavica* (68%) compared with *P. frutescens* (59%) and flax (45%) cotyledons. The 18:3 and 18:2 contents in both PC and TAG were determined during various stages of seed development for all three plants in addition to soybean (*Glycine max*). Northern blot analysis data of three different stages of *D. moldavica*, flax, and *P. frutescens* compared with moderately low 18:3 producers, soybean (*Glycine max*), and *Arabidopsis thaliana* and *Brassica napus*, (8–10% 18:3) at a stage of zygotic embryo development of high triglyceride synthesis showed that ω-3 desaturase mRNA levels were higher in all three high 18:3 producers, flax, *D. moldavica* and *P. frutescens*. This indicates that the high level of α-linolenic acid in TAG may be largely controlled by the level of ω-3 desaturase gene expression. However, the PC versus TAG fatty acid composition data suggested that along with ω-3 desaturase other enzymes also play a role in 18:3 accumulation in TAG, and the high accumulators have a selective transfer of α-linolenic acid into TAG.

Keywords Fatty acid · Lipids · Omega-3 · Flax · Perilla

Abbreviations

ACP	acyl carrier protein
ALA	α-linolenic acid
DAG	diacylglycerol
DGAT	diacylglycerol acyl transferase
DHA	docosohexaenoic acid
EFA, EPA	eicosapentaenoic acid
ER	endoplasmic reticulum
FFAP, PC	phosphatidylcholine
PUFA	polyunsaturated fatty acid
TAG	triacylglycerol

Introduction

The diets of people in some countries come close to the apparent ω-3/ω-6 fatty acid ratio of diet during human evolution: such as the traditional diets of Greece and Japan. In both countries the rate of death due to cardiovascular disease is among the lowest. It is now recognized that there is a need to return ω-3 fatty acids into the food supply, both for normal growth and development and for the prevention and management of chronic diseases [1]. Human beings evolved on a diet in which the ratio of omega-6/omega-3 EFA was about 1, whereas in the western diets the ratio is 15/1 to 16.7/1. Increased use of certain plant oils and modern day agriculture has led to a decrease in omega-3

S. Rao · M. Abdel-Reheem · R. Bhella · C. McCracken · D. Hildebrand
Plant Biochemistry/Physiology/Molecular Biology Program,
University of Kentucky, 445 Plant Sci. Bldg.,
Lexington, KY 40546-0312, USA

D. Hildebrand (✉)
403 Plant Science Building 0312,
Lexington, USA
e-mail: dhild@uky.edu

fatty acids and increases in omega-6 fatty acids [2–4] Linoleic acid and α-linolenic acid are not interconvertible in animals and compete for the rate limiting delta-6 desaturase in the synthesis of long chain PUFA. Among the cardiovascular benefits of increased omega-3 fatty acids in the diet is the prevention of cardiac arrhythmias [4]. Already eggs high in omega-3 fatty acids are available on the market [5]. All these factors increase proportionally with an increase in the omega-3 fatty acid intake, including either ALA or EPA, but especially DHA.

Seed oils are composed primarily of triacylglycerols (TAGs), which are glycerol esters of fatty acids. The primary fatty acids in the TAGs of oilseed crops are 16–18 carbons in length and contain 0–3 double bonds. Palmitic acid (16:0), oleic acid (18:1), linoleic acid (18:2), and linolenic acid (18:3) predominate. In this study we used soybean (*G. max*) as a moderate linolenic acid producer and three different high linolenic acid producers: flax (*Linum usitatissimum*) which has a high content of linolenic acid in the triacylglycerol (TAG), normally more than 45% of the total fatty acid content [6–8], *Perilla frutescens* oil contains 50–64% of 18:3 [9–11], and *Dracocephalum moldavica* contains 59–68% 18:3 [9, 12, 13].

Flax (*L. usitatissimum*) oil content ranges from 40 to 52% and 40 to 64% of this oil is linolenic acid depending on the flax variety [6–8]. *D. moldavica* contains 25–30% oil and 59–68% of it is 18:3 [9, 12, 13]. The oil content of *P. frutescens* is 35–45%, and contains 50–64% of 18:3 [9–11] It is known that ω-3 fatty acids are synthesized from ω-6 fatty acid precursor membrane lipids in plastids and the ER by ω-3 desaturases [14].

The objective of this study was to investigate the biochemical basis of α-linolenic acid accumulation in developing seeds of flax (*L. usitatissimum*), *D. moldavica* and *P. frutescens* as high linolenate accumulators compared to the moderate accumulators soybeans and canola.

Materials and Methods

Plant Materials

Soybean (*G. max*) cv. 'Jack', *Brassica napus* cv. 'Westar', flax (*L. usitatissimum*) cv. 'NorLin', *P. frutescens* and *D. moldavica* plants were grown in the greenhouse at the University of Kentucky, Lexington. Dicot embryogenesis is divided into five general stages: globular, heart, cotyledon, maturation, and dormancy. By the end of the cotyledon stage and during maturation primary storage products including lipids accumulate in preparation for seed germination later [15]. In this study we focused on cotyledon to maturation stages and classified them to six different stages based on seed size, color, and weight. Seed coats were carefully removed; embryo length and fresh weight were measured. Samples were frozen in liquid N_2, lyophilized and the dry weight was measured.

Fatty Acid and Lipid Analysis

The overall fatty acid composition of seed tissues of different cotyledon developmental stages of the investigated plants were analyzed by modifications of the procedure of [16]. About 1–10 mg lyophilized seed samples with added heptadecanoic acid (17:0) were placed into 2 mL of 2% (v/v) H_2SO_4 in methanol. The samples were ground finely, and then heated at 80 °C until the volume was reduced to approximately 0.5 mL (2 h). One and one-half milliliters of hexane containing 0.001% butylated hydroxytoluene (BHT) were added and the mixture was vortexed vigorously. The fatty acid methyl esters in the hexane layer were separated by gas chromatography on a Hewlett-Packard 0.25 mm I.D. × 0.33 mm × 10 m FFAP column and quantified using a flame ionization detector. A Hewlett-Packard 5890A gas chromatograph was programmed for an initial temperature of 140 °C for 1 min followed by increases of 12 °C/min to 210 °C and to 235 °C. The final temperature was maintained for 8 min. The injector and detector temperatures were 220 and 250 °C, respectively. Helium was used as the carrier gas with a flow rate of 10 mL/min. Total lipids were extracted from seed tissue as described by [17]. Individual lipids were separated by one-dimensional thin layer chromatography 20 × 20 cm TLC plate (LK60 silica gel 60 A°, Whatman) by the method of [18]. TLC plates were developed in two solvent systems. Phospholipids and glycolipids were separated in chloroform:methanol:water (65:25:4, v/v). Neutral lipids were separated in hexane:diethyl ether:acetic acid (100:100:2, v/v) [17, 19]. Lipids were located by spraying the plates with a solution of 0.005% primulin in 80% acetone, followed by visualization under UV light. In order to determine the fatty acid composition of individual lipids, ten µg of 19:0 was added to the silica gel of each lipid band before scraping, transferred to a tube containing 2 mL of 2% (v/v) H_2SO_4 in methanol, and fatty acid methyl esters were prepared and analyzed as described above. Radiolabeled 18:2 CoA was synthesized using ^{14}C linoleic acid and co-enzyme A by the method described by [20].The labeled ^{14}C 18:2-CoA was fed to the embryos on a µL (0.0028 µCi/µL) per gram fresh weight basis and incubated for 90 min in light as described by [8]. After incubation the embryos were washed to remove unabsorbed radioactivity and crushed in chloroform/methanol (2:1) to extract lipids. Reverse phase chromatography was used to separate the 18:2 from 18:3. The free fatty acids were methylated by diazomethane and the esterified fatty acids by sodium methoxide. The samples along with the standards were loaded on to a KV18 silica gel plate and ran in a solvent system consisting of acetonitrile/acetic acid/water (70:10:10). The image was developed in a phosphorimager. The standards were identified and thus used to identify the location of the radioactivity, by placing the plate into an iodine chamber.

RNA Isolation

RNA was isolated using the Trizol Reagent (Life Technologies, GibcoBrl). 50–100 mg seed tissues of different cotyledon developmental stages of tested plants were frozen in liquid N_2, homogenized in 1 mL Trizol reagent, transferred into microcentrifuge tubes and incubated for 5 min at room temperature. 0.2 mL chloroform per 1 mL of Trizol was added; tubes were vigorously shaken for 15 s and incubated at room temperature for 3 min. Samples were centrifuged at 12,000×*g* for 15 min at 2–8 °C. The upper aqueous phase containing RNA was collected in fresh tubes; RNA was precipitated with 0.5 mL of isopropyl alcohol and samples incubated at room temperature for 10 min. Samples were centrifuged at 12,000×*g* for 10 min, and the RNA pellet was washed once with 1 mL of 75% ethanol. Samples were vortexed and centrifuged at 7,500×*g* for 5 min. The RNA pellet was air-dried, then dissolved in RNase-free water and incubated for 10 min at 60 °C. The concentration of RNA was estimated by reading the absorbance at 260 nm. The 260/280 ratio of the RNA was 1.9–2.0. The quality of RNA was checked using 1.2% agarose gels. Samples were stored at −80 °C until used.

Northern Blotting

RNA samples (30 µg) were prepared by adding 2.0 µL of 5× formaldehyde gel-running buffer, 3.5 µL 12.3 M formaldehyde, 10 µL formamide, and incubated 15 min at 65 °C. The samples were chilled in ice for 3 min. Samples were immediately loaded on a pre-run denaturing 1% agarose-formaldehyde gel, the electrophoresis was carried out in the presence of 1× formaldehyde gel-running buffer. The gel was washed with 0.05 N NaOH for 20 min, rinsed with RNase-free water, followed by 10× SSC for 45 min. Blotting and transfer of RNA onto the 6× SSC pre-soaked nylon membrane was carried out according to the standard procedure [21]. RNA was fixed to the Zeta-probe nylon membrane by UV cross-linking (UV stratalinker 1800, Stratagene). The *B. napus* ω-3 desaturase probe was labeled with [α-^{32}P] dCTP using the random priming method. Pre-hybridization and hybridization were carried out at 42 °C following the instructions for using the Zeta-Probe Membrane (Bio-Rad) as outlined by the manufacturer. After hybridization a PhosphorImager system (Molecular Dynamis, 445 SI) was used to visualize the bands obtained. The radioactive probes were stripped by washing the blots three times with 0.1% SDS in 2× SSC at 95 °C, 10 min each.

Results

Fatty Acid Composition in Different Oil Seeds of Moderate and High Linolenate Accumulators During Maturation

The percentage of total fatty acids in flax seeds at different cotyledon developmental stages were analyzed (Fig. 1). Linolenic acid (18:3) accumulated during seed

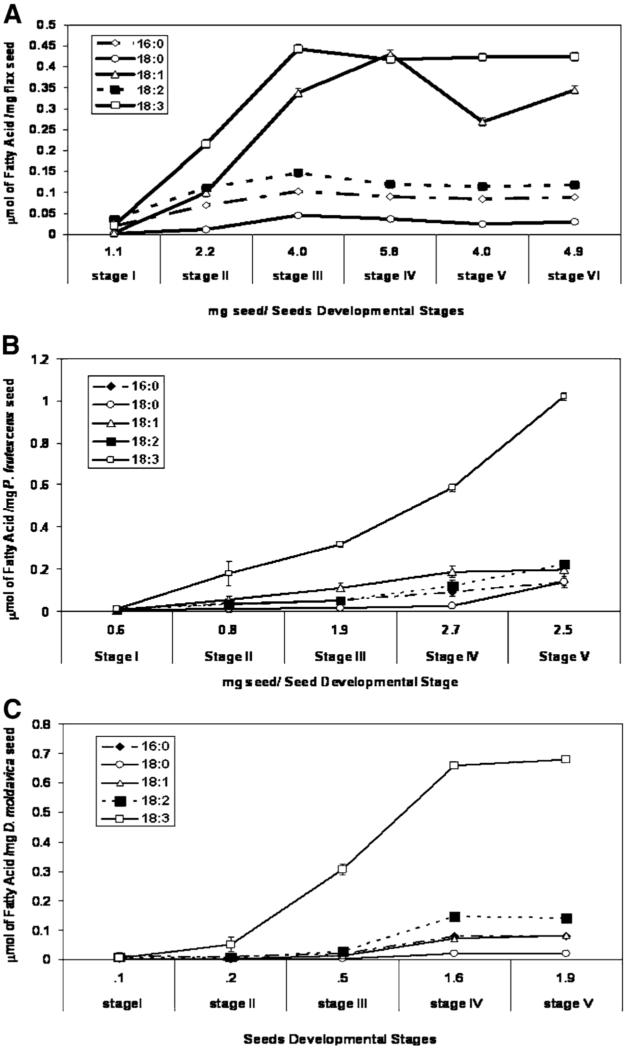

Fig. 1 Accumulation of fatty acids in developing flax seeds (**a**), *P. frutescens* seeds (**b**), *D. moldavica* seeds (**c**). µmol of fatty acid/mg seed dry weight were calculated during different stages of cotyledon development. Data points are the means of six replications ± standard errors

development and reached 46% by the end of maturation, oleic acid increased during maturation until stage IV at 40% and then become steady until the end of the maturation. 18:2 was found to be 45% at the first stage and dropped dramatically during the rest of the developmental stages to reach 10% by the end of the maturation process. Also 16:0 dropped from 25% at the beginning of the cotyledon maturation stage to 10% by the end of seed maturation.

The synthesis of 18:3 takes place rapidly at the beginning of cotyledon development in *P. frutescens*. The level of 18:2 declines with the increase in 18:3 while the 18:1 content slightly increased during seed maturation but its level remained relatively lower than the case of flax seed. This suggests that Δ-12 desaturase is more efficient in desaturating 18:1–18:2 in *P. frutescens* than in flax. *P. frutescens* seed has a high content of α-linolenate (57%) [10, 22, 23] and other fatty acid contents were also similar to reported values. The percentage ratio for both 18:2 and 18:3 in *P. frutescens* seed during maturation indicates that ω-3 desaturase is very active at the beginning of cotyledon development. However, the 18:3 content reached a steady state at the third stage and remained constant thereafter until the end of seed maturation (Fig. 1). The amount of 18:3 (μmol/mg dry weight) increased during cotyledon developmental stages to reach 1.15 μmol/mg dry weight at the maturation stage.

The accumulation of 18:3 in *D. moldavica* increased gradually to 68% by the end of seed maturation (Fig. 1). The 18:2 and 18:1 levels are lower at maturity. This suggests that both Δ12 and Δ15 (ω-3) desaturases are very active in desaturation of 18:1 and 18:2 and are largely responsible for the high level of 18:3 in *D. moldavica*. The accumulation of other FA including 18:1 is minimal as in *P. frutescens* unlike the accumulation of 18:1 in flax during seed maturation. In all high 18:3 accumulators, the linolenic acid content starts at a moderate level. The percentage of 18:3 is higher at a very early cotyledon developmental stage (first stage) of *P. frutescens* (35%) compared with flax (25%) and *D. moldavica* (15%). α-Linolenic acid gradually accumulated in developing cotyledons of all three plants. However, 18:3 content was found to be higher at the late mature developmental stage of *D. moldavica* (68%) compared with *P. frutescens* (59%) and flax (45%) cotyledons under our greenhouse growth conditions (Fig. 1).

The ratio of 18:2 and 18:3 in TAG in developing soybean seeds is the opposite to that in the three high 18:3 accumulators previously mentioned, which suggests that the level of desaturation of 18:2 into 18:3 decreases in soybean as the seeds mature (Fig. 2). The unsaturated fatty acid levels in PC remain almost constant throughout seed maturation. The increase in lipid content in soybean seed is accompanied by a shift in lipid composition from PC (membrane lipids) to TAG accumulation (storage lipids) during seed maturation [24, 25]. Figure 2 shows the amount of 18:3 in flax seed increases during cotyledon maturation stages in TAG in comparison to the 18:3 content in PC.

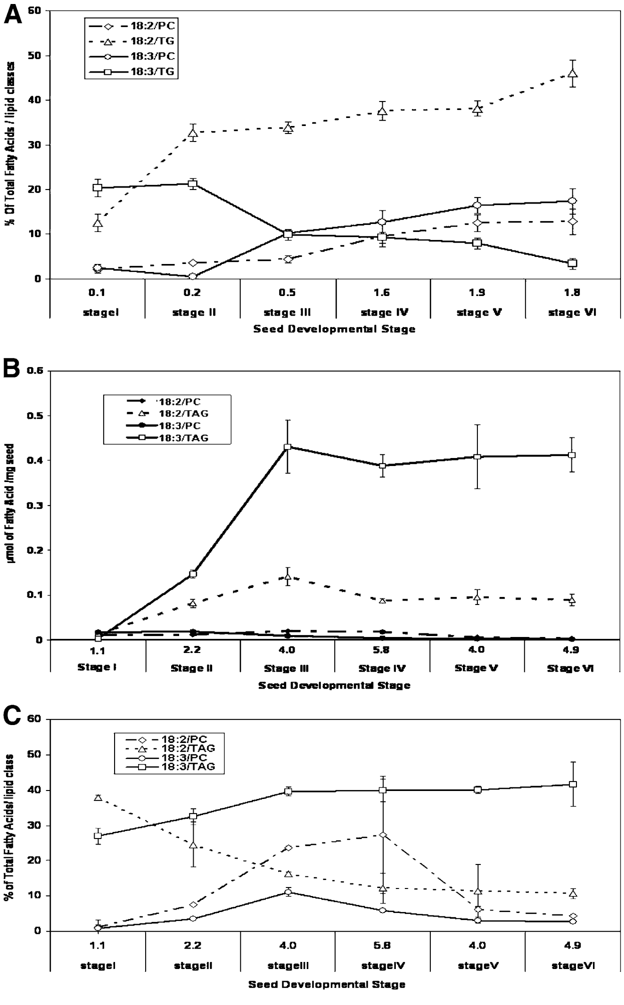

Fig. 2 Linoleic and linolenic acids in PC versus TAG in developing soybean seeds (**a**), Flax seeds (**b**), *P. frutescens* seeds (**c**)

The level of 18:3 in *P. frutescens* TAG is much higher than in PC, also compared with flax (Fig. 2) the 18:2 levels in *P. frutescens* is lower in PC, which agree with the fact that 18:3 level in TAG of *P. frutescens* seed (Fig. 2) is much higher.

A slightly higher 18:3 amount was found in PC of flax seed in the first three stages of cotyledon development compared to the amount of 18:3 in PC of *P. frutescens* seeds (Fig. 2). However, the percentage of 18:3 in *P. frutescens* PC was slightly higher (6%) in the first two stages compared to the first two stages in flax PC (0.9–3%). Unlike TAG, the 18:3 content was low in PC throughout seed development in flax and *P. frutescens* (Fig. 2). An increase in 18:3 content was observed in TAG of developing seeds in both flax and *P. frutescens*, however, flax seeds showed a gradual increase of 18:3 in TAG throughout all stages of development, while on the other hand a dramatic increase of 18:3 in TAG of *P. frutescens* seeds was observed during the later stages of development (from 0.15 μmol/mg seed at the second stage up to 0.9 μmol/mg seed at seed maturation). It was found that the second stage of cotyledon development is the optimum stage for monitoring ω-3 desaturase activity so this stage was used for northern blots.

The 18:3 levels are much higher in TAG compared to its level in PC in *D. moldavica* developing cotyledons while the level of 18:2 is lower in TAG but in PC the amount of 18:2 (μmol/mg seed) is relatively higher during second to third stages of cotyledon development (data not shown). The 18:2 level in PC dropped by the end of maturation of the seed.

ω-3 Desaturase Activity

To investigate whether higher ω-3 desaturase activity is responsible for the higher synthesis of 18:3 fatty acid, which in turn is incorporated in to TAG in higher amounts, the ω-3 desaturase of flax and two moderate accumulators *Arabidopsis* and soybean were assayed. Feeding studies with ^{14}C labeled 18:2-CoA showed that developing embryos of flax have higher ω-3 desaturase activity compared to *Arabidopsis* and soybean (Fig. 3). Stage II flax seeds have much higher activity compared to the stage V flax seeds. During stage II 18:3 accumulation is linear and in stage V embryos 18:3 reaches a plateau (Fig. 1).

Microsomal ω-3 Desaturase Transcript Levels

The ω-3 desaturase transcripts levels in stage II flax embryos are much higher compared to soybean embryos of both stages and stage V flax embryos (Fig. 4). These results were also in line with 18:3 fatty acid accumulation in flax seeds (Fig. 1) and also indicated by the ω-3 desaturase activity assay (Fig. 3). The activity assay results show that stage II flax embryos had much higher activity than both stages of soybean embryos and stage V flax. Northern blot analysis data also show developing embryos of *P. frutescens* have much higher ω-3 desaturase transcript levels than soybean and *Arabidopsis* (Fig. 5). When three different stages of *D. moldavica*, *P. frutescens* and flax, were compared with the moderately low 18:3 producers (8–10%), soybean and *Arabidopsis*, and *B. napus*, ω-3 desaturase mRNA levels were also higher in all three high 18:3 producers, flax, *D. moldavica* and *P. frutescens* compared with the moderately low 18:3 producers (figure not shown for *D. moldavica)*. However among high 18:3 producer plants, the ω-3 desaturase transcript level was found to be much higher in *D. moldavica* than in *P. frutescens*, which in turn has a higher transcription level than flax (Fig. 5).

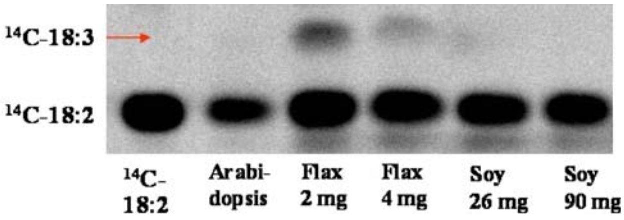

Fig. 3 ω-3 desaturase assays: 14C–18:2 CoA was fed to developing embryos of high 18:3 accumulating flax and moderate 18:3 accumulators soybean and *Arabidopsis*. Lipids were extracted, methylated, and separated on a reverse phase C18 TLC plate and then read on a phosphorimager

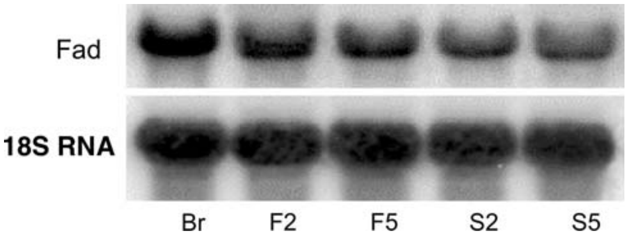

Fig. 4 Northern blot analyses of ω-3 desaturase expression in developing embryos of flax and soybean. RNA was extracted from: *B. napus* (Br), the second and fifth developmental stage of flax cotyledons (F1, F5) and the second and fifth developmental stage of soybean cotyledons (S2, S5). (*Above*) *B. napus* ω-3 desaturase (FAD3) cDNA was used as a probe to check the expression of FAD3 gene (*Below*) to confirm the amount of RNAs loaded were equal 18S ribosomal DNA was used as probe to measure 18S rRNA expression. Equal RNA loading was also confirmed by measuring RNA concentration spectroscopically at 260 nm

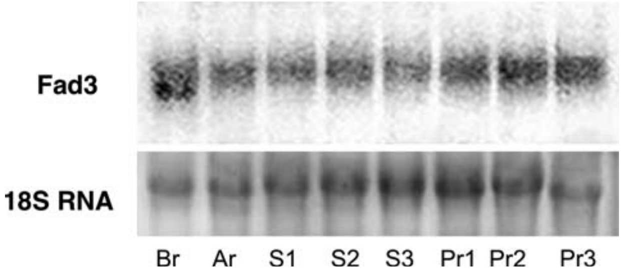

Fig. 5 Northern blot analyses of ω-3 desaturase gene expression in developing embryos of *B. napus*, *Arabidopsis*, soybean and *P. frutescens*. RNA was extracted from *B. napus* (Br), *Arabidopsis* seed (Ar), soybean seed cotyledon developmental stages 5–6 mm (S1), 7–9 mm (S2), 9–11 mm (S3), Pr1, Pr2, Pr3, are *P. frutescens* cotyledon at developmental stages (based on size, color, and seed weight) 1, 2 and 3?. (*Above*) RNAs were blotted on a nylon membrane and probed with *B. napus* ω-3 desaturase cDNA to check the ω-3 desaturase gene expression (*Below*) To confirm the amount of RNAs loaded were equal 18S ribosomal DNA was used as probe to measure 18S rRNA expression. Equal RNA loading was also confirmed by measuring RNA concentration spectroscopically at 260 nm

The lipid content and compositions of soybean seeds changes considerably as the embryo progress from the early stages of development to the maturation stage [26]. In soybean the level of 18:3 is higher at the beginning of the cotyledon maturation stage and begins to decline toward the late maturation stages while the 18:2 concentration increases. The opposite is found in all high 18:3 accumulators, with levels of 18:3 increasing during the maturation stages while the 18:2 levels decreased .

In flax (Fig. 3), ω-3 desaturase is highly active in converting 18:2-CoA to 18:3 compared to *Arabidopsis* and soybean.

Discussion

During the first three stages of cotyledon development, in all high 18:3 producers, linear increases in 18:3 levels were found. This suggests that these stages have the highest ω-3 desaturase activity. The 18:1 levels in both flax and *P. frutescens* (Fig. 1 and 2) suggests that Δ-12 desaturase is more active in desaturating 18:1–18:2 in *P. frutescens* than in flax. In *D. moldavica* 18:3 levels was very high compared with other fatty acids levels suggesting that lipid metabolism in this plant is optimally adjusted for 18:3 accumulation. The level of 18:3 in *P. frutescens* TAG is much higher than in PC, also compared with flax (Fig. 2) the 18:2 levels in *P. frutescens* is lower in PC, which is consistent with the high 18:3 level in TAG of *P. frutescens* seed (Fig. 2). This suggests that desaturation of 18:2– 18:3 by ω-3 desaturase is more efficient in *P. frutescens* than in flax, which in turn is much higher than in soybean.

The changes in lipid concentration are accompanied by a shift in lipid composition from polar lipids to storage lipids [24]. In soybean the 18:2 levels in TG increase while 18:3 levels decrease. Acyltransferase enzymes catalyze the incorporation of fatty acids into the glycerol backbone to produce different glycerolipids classes including PC and TG [25, 27–29], so that from our data (e.g., Fig. 2) and the selective accumulation of 18:2 in TG of soybeans we can suggest that acyltransferases are selective with 18:2 over 18:3 in soybean seed. However, the absolute amount (μ mol/mg seed) of 18:3 in high producing plants suggests that the incorporation rate into TG is very high which in turn indicates that acyltransferases may selectively incorporate 18:3 into storage lipids.

Northern blot data shows that the ω-3 desaturase gene expression level is higher in high 18:3 producing plants compared to low producers. This indicates that the level of ω-3 desaturase gene expression may largely control the level of α-linolenic acid in TAG, although as mentioned above acyltransferases also appear to be involved. High accumulation of 18:3 correlates with ω-3 desaturase mRNA levels which suggests transcriptional control of fatty acid desaturase genes [30, 31]. However, the PC versus TAG fatty acid composition data suggest that ω-3 desaturase is not the only factor in 18:3 accumulation in TAG, and the high accumulators appear to have a selective transfer of α-linolenic acid into TAG which in turn suggested that certain acyltransferases or transacylases may play an important role in 18:3 accumulation in triacylglycerols. Another possible factor is the speed of flux from phospholipid to TAG as this can compete with 18:2–18:3 desaturation. It was shown in flax cultivars AC Emerson and Vimy that diacylglycerol acyltransferase (DGAT) prefers 18:3-CoA as substrate [32]. The data from both lipid analysis and Northern blot highly suggest that the reduced linolenic acid content in soybean compared with high 18:3 accumulators is mainly due to the lower transcript level of ω-3 desaturase. Byrum et al. [33] found that the reduced 18:3 concentration in the soybean genotype A5 was at least partially the result of a microsomal ω-3 desaturase gene with a reduced activity. Collectively, these results indicate that one can obtain *B. napus*, soybeans or other oilseed crops that accumulate high ω-3 fatty acid levels simply by increasing expression of the ω-3 desaturase gene by use of a strong promoter or trans-activation. Acyltransferases with specificity for 18:3 are likely to be needed for very high ω-3 fatty acid accumulation, for example, >80%.

Acknowledgments This work was supported by a graduate fellowship from Ain Shams University in Cairo Egypt to Mohammed Abdel-Reheem, the United Soybean Board and the KY Agricultural Experiment Station.

References

1. de Lorgeril M, Salen P (2003) Dietary Prevention of coronary heart disease: Focus on omega-6/omega-3 essential fatty acid balance. In: Simpolus A, Cleland L (eds) Omega-6/omega-3 essential fatty acid ratio: the scientific evidence. Basel, Karger, pp 37–56
2. Trautwein EA (2001) n-3 Fatty acids—physiological and technical aspects for their use. Eur J Lipid Sci Technol 103:45–55
3. Sprecher H (2002) The roles of anabolic and catabolic reactions in the synthesis and recycling of polyunsaturated fatty acids. Prostaglandins Leukot Essent Fatty Acids 67:79–83
4. de Lorgeril M, Salen P (2004) Alpha-linolenic acid and coronary heart disease. Nutr Metab Cardiovasc Dis 14(3):162–169
5. Lewis NM, Seburg S, Flanagan NL (2000) Enriched eggs as a source of N-3 polyunsaturated fatty acids for humans. Poult Sci 79(7):971–974
6. Kuznetsova NV (1978) Variability of fatty acid contents in seed oil of fiber flax cultivars of different origin. Byulleten Vsesoyuznogo Ordana 59:30–36
7. Yarosh NP, Megorskaya OM, Ivanova ON (1980) Dynamics of fatty acids in the free and bound lipids in ripening seeds of linseed and flax. Trudy po Prikladnoi Botanike, Genetike i Selektsii 66(3):28–36

8. Stymne S, Tonnet ML, Green AG (1992) Biosynthesis of linolenate in developing embryos and cell-free preparations of high-linolenate linseed (*Linum usitatissimum*) and low-linolenate mutants. Arch Biochem Biophys 294(2):557–563
9. Hagemann JM, Earle FR, Wolff IA (1967) Search for new industrial oils. XIV. Seed oils of labiatae. Lipids 2(5):371–380
10. Hwang SZ, Ko YS (1982) Studies on the constituents of Korean edible oils and fats, 5: analysis of fatty acids in sesame and perilla oil by high performance liquid chromatography. Korean J Nutr 15(1):15–21
11. Lee JI et al (1986) Study on the evaluation of oil quality and the differences of fatty acids composition between varieties in perilla (*Perilla frutescens* Britton var. japonica Hara). Korean J Breed (Korean R.) 18(3):228–233
12. Domokos J, Peredi J, Halasz-Zelnik K (1994) Characterization of seed oils of dragonhead (*Dracocephalum moldavica* L.) and catnip (Nepeta cataria var. citriodora Balb). Ind Crops Prod 3(1–2):91–94
13. Matthaus B (1997) Antinutritive compounds in different oilseeds. Fett-Lipid 99(5):170–174
14. Toyoaki A, Tomoko Yamada, Takehito Kinoshita, Shaikh M. Rahman, Yutaka Takagi (2005) Identification of corresponding genes for three low-α-linolenic acid mutants and elucidation of their contribution to fatty acid biosynthesis in soybean seed. Plant Sci 168:1615–1623
15. Norby SW, Adams CA, Rinne RW (1984) An ultrastructural study of soybean seed development. in American Soy Association Monograph. University of Ilinois Press, Champagne Urbana, IL
16. Dahmer ML et al (1989) A rapid screening technique for determining the lipid composition of soybean seeds. J Am Oil Chem Soc 66(4):543–548
17. Miquel M, Browse JA (1992) Arabidopsis mutants deficient in polyunsaturated fatty acid synthesis. Biochemical and genetic characterization of a plant oleoyl-phosphatidylcholine desaturase. J Biol Chem 267(3):1502–1509
18. Khan MU, Williams JP (1977) Improved thin-layer chromatographic method for the separation of major phospholipids and glycerolipids from plant lipid extracts and phosphatidylglycerol and bis (monoacylglyceryl) phosphate from animal lipid extracts. J Chromatogr 140:179–185
19. Lightner J, Wu J, Browse J (1994) A mutant of Arabidopsis with increased levels of stearic acid. Plant Physiol 106:1443–1451
20. Taylor DC, Weber N, Hogge LR, Underhill EW (1990) A simple enzymatic method for the preparation of radiolabeled erucoyl-CoA and other long-chain fatty acyl-CoAs and their characterization by mass spectrometry. Anal Biochem 184(2):311–316
21. Stymne S, Lorraine Tonnet M, Green AG (1992) Biosynthesis of linolenate in developing embryos and cell-free preparations of high-linolenate linseed (*Linum usitatissimum*) and low-linolenate mutants. Arch Biochem Biophys 294(2):557–563
22. Karcher SJ (1995) Molecular biology: a project approach. Academic Press, Inc., San Diego, CA
23. Longvah T, Deosthale YG (1991) Chemical a nutritional studies on Hanshi (Perilla frutescens) a traditional oil seed from northeast India. J Am Oil Chem Soc 68:781–784
24. Longvah T, Deosthale YG, Kumar PU (2000) Nutritional and short term toxicological evaluation of perilla seed oil. Food Chem 70(1):13–16
25. Privett OS et al (1973) Studies on the lipid composition of developing soybean seeds. J Am Oil Chem Soc 50:516–520
26. Suh MC, Schultz DJ, Ohlrogge TB (2002) What limits production of unusual monoenoic fatty acids in transgenic plants? Planta 215:584–595
27. Wilson RF (1987) Soybean: improvement, production and uses. In: Wilcox JR (ed) Seed metabolism. American Society of Agronomy, Madison, WI, pp 643–686
28. Ohlrogge JB, Browse J (1995) Lipid biosynthesis. Plant Cell 7:957–970
29. Topfer R, Martini N, Schell J (1995) Modification of plant lipid synthesis. Science 268:681–686
30. Thomaeus S, Carlsson AS, Stymne S (2001) Distribution of fatty acids in polar and neutral lipids during seed development in Arabidopsis thaliana genetically engineered to produce acetylenic, epoxy and hydroxyl fatty acids. Plant Sci 161(5):997–1003
31. Horiguchi G, Kodama H, Iba K (2001) Characterization of Arabidopsis mutants that are associated with altered C18 unsaturated fatty acid metabolism. Plant Sci 161:1117–1123
32. O'Hara P, Slabas AR, Fawcett T (2002) Fatty acid and lipid biosynthetic genes are expressed at constant molar ratios but different absolute levels during embryogenesis. Plant Physiol 129:310–320
33. Sorensen B, Furukawa-Stoffer TL, Marshall KS, Page EK, Mir Z, Forster RJ, Weselake RJ (2005) Storage lipid accumulation and acyltransferase action in developing flax seed. Lipids 40:1043–1049
34. Byrum JR et al (1997) Alteration of the ω-3 fatty acid desaturase gene is associated with reduced linolenic acid in the A5 soybean genotype. Theor Appl Genet 94(3–4):356–359

Lipids (2008) 43:757–763
DOI 10.1007/s11745-008-3196-z

COMMUNICATION

Metabolic Kinetics of *tert*-Butylhydroquinone and Its Metabolites in Rat Serum after Oral Administration by LC/ITMS

Wen Huang · Hai Niu · Yinchun Gu

Received: 27 February 2008 / Accepted: 14 May 2008 / Published online: 13 June 2008
© AOCS 2008

Abstract Liquid chromatography–ion trap mass spectrometry (LC/ITMS) was employed for a metabolic kinetics study of *tert*-butylhydroquinone (TBHQ) and its metabolites in rat serum after oral administration. The mean serum concentration–time data of TBHQ and its four metabolites (M1–M4) in both male and female rats after oral administration of TBHQ at dosages of 7, 350 and 700 mg/kg were all best-fitted by a two-compartment model with first-order absorption. TBHQ was rapidly absorbed, distributed and metabolized. The metabolites were also distributed rapidly except M2, but eliminated more slowly than TBHQ. At the doses of 350 and 700 mg/kg, the total concentrations of TBHQ and its metabolites in serum were much higher for male than female rats during the metabolic process ($P < 0.01$). In addition, the serum concentrations of M1, M3 and M4 were all much higher for males than for females ($P < 0.01$) during the metabolic process, while no significant differences between male and female rats were found ($P > 0.05$) for TBHQ and M2, at the doses of 350 and 700 mg/kg. The exploratory assessment of dose proportionality for TBHQ and its metabolites by the power model indicated that the TBHQ exposure increased in a more-than-dose-proportional manner, but the exposures of the metabolites M1–M4 increased in a less-than-dose-proportional manner, across the dose of 7–700 mg/kg.

Keywords *tert*-Butylhydroquinone (TBHQ) · Liquid chromatography–ion trap mass spectrometry (LC/ITMS) · Metabolic kinetics

Introduction

Prevention of lipid peroxidation has long become an important issue, since oils and fats, essential to our diets, tend to encounter problems of oxidation and rancidity, which affect food quality and may endanger our health [1]. Among various modern methods for preventing lipid peroxidation, the addition of antioxidants is preferentially considered [2, 3]. Most of the commonly used antioxidants are synthetic compounds such as tertiary butylhydroquinone (TBHQ) because of its chemical stability, low cost and availability. However, the safety of the antioxidant was questioned due to its potential risk [4–7]. In order to evaluate the safety of TBHQ, several methods have been carried out to measure TBHQ in body fluids as well as foods [8–10]. Most methods require long analysis time and laborious techniques for the treatment of samples which also have low resolution. Meanwhile, it is found that they are limited in study of biological samples, such as analyses of metabolites, which is very important to study the pharmacokinetics and toxicology of TBHQ. HPLC coupled with mass spectrometry is a currently developed unique

W. Huang (✉)
Institute for Nanobiomedical Technology and Membrane Biology, State Key Lab of Biotherapy of Human Diseases, Cancer Center, West China Hospital,
West China Medical School, Sichuan University,
No 1, Keyuan 4 Lu, Gaopeng Dadao, Gaoxing Qu,
Chengdu 610041, China
e-mail: hwpharm@tom.com

H. Niu
Mathematical College, Sichuan University, Chengdu 610064, China

Y. Gu
School of Light Industry and Food, Sichuan University,
Chengdu 610065, China

technique for monitoring antioxidant content and studying compound structure [11]. In particular, MS/MS triple quadrupole mass spectrometry in the multiple reaction monitoring modes (MRM) provides surpassing speed, sensitivity and selectivity. But, there is very little information regarding the metabolites of TBHQ and its metabolic kinetics using liquid chromatography–ion trap mass spectrometry (LC/ITM).

In our previous study, we established a rapid, sensitive, precise and accurate quantitative method for the measurement of TBHQ in commercial edible oil as well the determination of TBHQ and its metabolites in rat serum after oral administration by liquid chromatography/tandem mass spectrometry (LC/MS/MS) [12, 13]. Mass spectral analysis of TBHQ and its metabolites peaks in rat serum indicated four major ionic parent masses $[M–H]^-$ at *m*/*z* 245 (M1), *m*/*z* 305 (M2), *m*/*z* 327 (M3) and *m*/*z* 341 (M4) [13]. M1 and M4 were found to be a TBHQ-sulfate (3-*tert*-butyl-4-hydroxyphenyl hydrogen sulfate) and a TBHQ-glucuronide [6-(3-*tert*-butyl-4-hydroxyphenoxy)-3,4,5-trihydroxytetrahydro-2*H*-pyran-2-carboxylic acid] and two TBHQ-sulfate-derived substances named M2 and M3 in further identifying work) by LC/MS/MS [13]. In this study, the LC/MS/MS method was applied to metabolic kinetics studies of TBHQ and its metabolites in rat serum following oral administration of TBHQ at three different dosage levels.

Experimental Procedure

Reagents

The purity of TBHQ (IUPAC compliant name: 2-(1, 1-dimethylethyl)-1,4-benzenediol, CAS No.: 1948-33-0) from J & K chemica, Augsburg, Germany was better than 98%. Methanol and acetonitrile (Fisher Scientific, Pittsburgh, PA) were of HPLC grade. Absolute ethyl alcohol, aqua ammonia and acetic acid (Beijing Chemical Reagent Co., Beijing, China) were of analytic grade. Water was purified using a Milli-Q gradient system (Millipore Corporation, Genay Cedex, France).

Animals

Adult Sprague–Dawley (SD) rats, weighing 160 ± 10 g, were obtained from Department of Laboratory Animal Science of Peking University (Beijing, China). The animals in this study received humane care according to the guidelines set forth in the principles of the care and use of laboratory animals formulated by the General Administration of National Quality Supervision, Inspection and Quarantine of the People's Republic of China (GB14923-2001).

Animal Handling and Sample Collection

The procedures for animal handling and sample collection were described in the previous paper [10, 13]. On the study of metabolic kinetics, SD rats used were divided into four groups (six male and six female rats/group). Rats in group 1, as control group, were assigned to receive corn oil at a gavage dose of 1 mL, respectively. Rats in Group 2, 3 and 4 were given TBHQ dissolved in corn oil at gavage doses of 7, 350 and 700 mg/kg, respectively. Blood samples from rat tail vein were collected in EP (epoxy epoxide) tubes (0.25 mL of blood sample/rat) at times of 0.08, 0.25, 0.5, 1, 2, 3, 5, 7, 9, 12, 24 and 48 h after oral administration and following centrifugation of the blood samples at 13,225 g-force for 20 min, each serum sample was collected and stored at −20 °C until analyzed [13].

Quantitative Analyses of TBHQ and Its Metabolites

The procedures for quantitative analysis of TBHQ and its metabolites in rat serum were described in the previous paper [13]. TBHQ's MS^2 characteristic product ion and its MS^1 product ions based on extracted ion chromatograms (EICs) were employed for quantitation of free TBHQ and semi-quantitation of its metabolites in rat serum.

The concentration of TBHQ in rat serum was quantified using an external standard prepared in a blank matrix. The calibration curve was obtained by plotting the peak area of EIC *m*/*z* 149 (MS^2) against the concentration of TBHQ. The calibration curve ($Y = 401.22X + 39958.87$) showed good linearity over the concentration range of 49–5,030 μg/L with the coefficient (r^2) of 0.99. The detection limit of TBHQ for serum sample was 14 μg/L ($S/N = 3$). To evaluate accuracy and precision, six serum samples, where each contains three different concentrations of TBHQ (328, 998, 1,969 μg/L), were prepared and analyzed. The recoveries of TBHQ in serum ($n = 6$) were 96.08 ± 11.85, 93.43 ± 6.65 and $95.50 \pm 9.44\%$. The intra-day relative standard deviations (RSDs) ($n = 6$) were 14.82, 10.31 and 7.74% and the inter-day RSDs over three consecutive days were 20.60, 14.39 and 8.26%. The results show that the method could be used for quantifying TBHQ in rat serum.

Under the adopted LC/ITMS conditions, peaks of TBHQ and its metabolites appear with retention times of 5.3 and 3–4 min, respectively. The nearness of their chromatographic retention times suggests that the polarities of TBHQ and its metabolites are quite similar. The MS^1 response of a compound is decided by its polarity to some extent. So, using TBHQ standards, the semi-quantification of its metabolites was acceptable for metabolic kinetics study. In the research, the MS^1 responses of per unit concentration were defined to be equivalent for TBHQ and its metabolites; the calibration curve was obtained by plotting the peak area of EIC m/z 165 against the concentration of TBHQ. The coefficient (r^2) of the calibration curve ($Y = 817.23X - 74268.46$) was 0.98, suggesting that the curve could work well for semi-quantifying the metabolites of TBHQ in rat serum.

Metabolic Kinetics Analysis

The most common method of evaluating the metabolic kinetics of a chemical is to assume that the chemical concentration–time data can be described by one of several compartment models. The model was selected on the basis of the residual sum of squares and minimum Akaike's information criterion (AIC) value [14, 15]. AIC is a criterion for selecting the best model among a number of candidate models, and the model that yields the smallest value of AIC is considered the best. The Practical Pharmacokinetic Program was usually used for metabolic kinetics analysis [16–19]. In our study, the metabolic kinetics parameters were calculated using Practical Pharmacokinetic Program-Version 97 (3P97) published by the Chinese Pharmacological Association (Beijing, China). The metabolic kinetics parameters include those such as the hybrid rate constant for the distribution phase (α), the hybrid rate constant for the elimination terminal phase (β), the first-order absorption rate constant (k_a), absorption half-life ($T_{1/2}k_a$), half-life of α phase ($T_{1/2\alpha}$), half-life of β phase ($T_{1/2\beta}$), distribution rate constant for transfer of the chemical from the central to the peripheral compartment and from the peripheral to the central compartment (K_{12} and K_{21}), the elimination rate constant (K_{10}), area under the curve from time zero to last time of sampling (AUC_{0-t}), area under the curve from time zero to infinity ($\mathrm{AUC}_{0-\infty}$), maximum chemical concentration after oral administration ($C_{\max}$), and the interval (time) from oral administration until $C_{\max}$ were obtained ($T_{\max}$).

Statistical Analysis

Data are presented as means ± SD. The results were statistically analyzed by analysis of variance (ANOVA) followed by Fisher's test. Differences were considered significant at $P < 0.01$.

Results and Discussion

The mean serum concentration–time courses of TBHQ and its four metabolites (M1–M4) after oral gavage of TBHQ at dosages of 7, 350 or 700 mg/kg were investigated in previous research [13]. According to ACI value, the mean serum concentration–time data of TBHQ and its metabolites M1–M4 could all best-fitted by a two-compartment model with first-order absorption as serum concentration $C = Ae^{\alpha t} + Be^{\beta t} - (A + B)e^{-k_a t}$. The metabolic kinetics parameters based on the serum concentration–time data of TBHQ and its metabolites M1–M4 were automatically simulated with the aid of Practical Pharmacokinetic Program 3P97. The metabolic kinetics parameters were listed in Tables 1, 2, 3.

After oral administration, TBHQ was rapidly absorbed with a mean $T_{\max}$ between 0.12 and 0.23 h (male, ♂), 0.16–0.27 h (female, ♀). A rapid distribution phase and a slower elimination phase were also observed, with a half-life of distribution α phase ($T_{1/2\alpha}$) of 0.12–0.35 h (♂), 0.21–0.48 h (♀) and a half-life of elimination β phase ($T_{1/2\beta}$) of 10.27–14.39 h (♂), 3.51–10.73 h (♀). When administered orally, TBHQ was rapidly metabolized to M1, M3 and M4, with a mean $T_{\max}$ of 0.17–0.57 h (♂) and 0.18–0.61 h (♀) for M1, 0.30–0.60 h (♂) and 0.22–0.66 h (♀) for M3, 0.29–0.74 h (♂) and 0.23–0.46 h (♀) for M4, respectively. However, the metabolic reaction from TBHQ to M2 was a bit slower, with a mean $T_{\max}$ of 5.29–8.95 h (♂) and 4.50–9.74 h (♀) for M2. The distribution half-lives ($\mathrm{T}_{1/2\alpha}$) of the metabolites were very short, like TBHQ, 0.35–0.63 h (♂) and 0.32–1.11 h (♀) for M1, 0.10–0.28 h (♂) and 0.27–0.51 h (♀) for M2, 0.38–0.77 h (♂) and 0.98–1.62 h (♀) for M3, 0.26–2.60 h (♂) and 1.07–1.66 h (♀) for M4, respectively. But the elimination half-lives ($\mathrm{T}_{1/2\beta}$) of the metabolites were longer than TBHQ, 12.69–45.57 h (♂) and 11.75–24.54 h (♀) for M1, 7.75–17.64 h (♂) and 8.96–28.62 h (♀) for M2, 43.61–66.71 h (♂) and 29.82–68.38 h (♀) for M3, 9.94–65.78 h (♂) and 21.98–36.00 h (♀) for M4, respectively. This reveals that the metabolites of TBHQ are transported to tissues or organs from blood almost as rapidly as TBHQ, but cleared more slowly from blood than TBHQ, which is consistent with the results reported by Ikeda et al. [10] to a certain extent. Ikeda et al. [10] found that the distribution of [^{14}C] TBHQ in various tissues was biphasic, consisting of a rapid component and a slower component.

The plots of $C_{\max}$ versus dose are presented in Fig. 1. In previous study, it was found that the concentration of free TBHQ in the serum samples at the dose of 7 mg/kg was lower than the limit of detection [13], therefore, $C_{\max}$ of free TBHQ at the dose is regarded as 0 μmol/L (Fig. 1a). With TBHQ across a dosage range of 7–700 mg/kg, significant increases of $C_{\max}$ were found for TBHQ (both ♂ and ♀), M1 (♀) and M4 (both ♂ and ♀). For M1 (♂) and M3 (both ♂ and ♀), $C_{\max}$ increased when the dosage of TBHQ was raised, but apparent saturations in $C_{\max}$ were observed at doses higher than 350 mg/kg. An almost sustained $C_{\max}$ value was observed for M2 (both ♂ and ♀). Furthermore, the exploratory assessment of dose proportionalities for TBHQ and its metabolites was performed by fitting the power model: $\ln C_{\max} = a + b \ln dose$, where the slope $b = 1$ indicates dose-proportionality. The *dose*-proportionality constant for

Table 1 Metabolic kinetic parameters of M1–M4 in rat serum after a single oral dose of 7 mg/kg TBHQ

Parameters	M1		M2		M3		M4	
	♂	♀	♂	♀	♂	♀	♂	♀
A (μmol/L)	59.95 ± 9.52	20.23 ± 5.83	–3.40 ± 0.56	−7.89 ± 1.35	3.34 ± 0.71	3.83 ± 0.59	6.60 ± 0.50	3.43 ± 0.78
α (h^{-1})	3.34 ± 0.39	1.12 ± 0.05	5.57 ± 0.13	13.62 ± 1.82	1.61 ± 0.09	1.39 ± 0.28	1.75 ± 0.25	1.75 ± 0.61
B (μmol/L)	3.40 ± 0.75	3.39 ± 0.61	8.95 ± 1.94	52.08 ± 4.73	2.24 ± 0.52	3.01 ± 0.28	3.02 ± 0.92	3.00 ± 0.59
β (h^{-1})	0.03 ± 0.01	0.02 ± 0.01	0.04 ± 0.01	0.08 ± 0.03	0.01 ± 0.00	0.01 ± 0.00	0.02 ± 0.01	0.03 ± 0.01
k_a (h^{-1})	15.84 ± 1.77	29.06 ± 2.69	0.20 ± 0.02	0.38 ± 0.08	11.52 ± 3.90	21.39 ± 5.97	8.95 ± 1.98	16.33 ± 2.47
$T_{1/2\alpha}$ (h)	0.32 ± 0.02	0.63 ± 0.12	0.24 ± 0.02	0.51 ± 0.14	0.77 ± 0.15	1.62 ± 0.57	0.26 ± 0.08	1.07 ± 0.29
$T_{1/2\beta}$ (h)	24.54 ± 1.30	45.57 ± 6.28	17.64 ± 2.93	8.96 ± 1.65	66.71 ± 7.92	68.58 ± 9.50	50.69 ± 8.43	24.42 ± 6.33
$T_{1/2}k_a$ (h)	0.24 ± 0.02	0.04 ± 0.03	4.72 ± 0.83	3.01 ± 0.17	0.06 ± 0.02	0.04 ± 0.01	0.08 ± 0.02	0.36 ± 0.13
K_{21} (h^{-1})	0.53 ± 0.13	0.25 ± 0.08	0.36 ± 0.08	1.91 ± 0.90	0.74 ± 0.13	0.50 ± 0.11	1.21 ± 0.27	0.40 ± 0.12
K_{10} (h^{-1})	0.29 ± 0.03	0.08 ± 0.03	0.78 ± 0.67	0.42 ± 0.06	0.02 ± 0.00	0.02 ± 0.01	0.04 ± 0.02	0.16 ± 0.01
K_{12} (h^{-1})	2.55 ± 0.23	0.93 ± 0.50	4.46 ± 4.22	11.37 ± 5.83	0.86 ± 1.01	0.87 ± 0.06	1.88 ± 0.50	1.39 ± 0.29
AUC_{0-t} (μmol h/L)	65.84 ± 7.20	126.25 ± 17.81	139.18 ± 18.38	372.56 ± 21.78	48.67 ± 6.27	113.05 ± 12.59	108.24 ± 13.27	71.03 ± 4.44
$AUC_{0-\infty}$ (μmol h/L)	99.16 ± 9.56	368.08 ± 40.31	174.11 ± 22.89	389.11 ± 22.37	161.82 ± 32.82	314.51 ± 32.19	214.83 ± 35.08	107.37 ± 23.50
T_{max} (h)	0.18 ± 0.08	0.17 ± 0.02	6.12 ± 1.57	4.50 ± 0.37	0.31 ± 0.09	0.22 ± 0.07	0.23 ± 0.08	0.29 ± 0.06
C_{max} (μmol/L)	17.72 ± 5.62	16.91 ± 4.94	4.23 ± 0.33	14.20 ± 6.75	4.04 ± 0.89	5.53 ± 0.94	6.01 ± 1.33	7.43 ± 0.51

A and *B*: mathematical coefficients. ♂ denotes male rat and ♀ denotes female rat. Data represent mean ± SD for six rats

Table 2 Metabolic kinetic parameters of TBHQ and its metabolites M1–M4 in rat serum after a single oral dose of 350 mg/kg TBHQ

Parameters	TBHQ		M1		M2		M3		M4	
	♂	♀	♂	♀	♂	♀	♂	♀	♂	♀
A (μmol/L)	41.62 ± 4.41	42.43 ± 5.74	768.61 ± 45.43	1475.04 ± 203.12	−8.65 ± 1.87	−7.01 ± 1.02	22.03 ± 2.19	21.00 ± 3.40	226.55 ± 19.49	48.35 ± 5.14
α (/h)	5.83 ± 0.95	3.67 ± 0.40	2.31 ± 0.40	1.15 ± 0.84	9.57 ± 1.08	10.42 ± 2.40	0.66 ± 0.13	1.07 ± 0.78	2.62 ± 0.88	0.56 ± 0.11
B (μmol/L)	2.38 ± 0.67	6.34 ± 1.05	245.00 ± 31.03	69.52 ± 6.59	30.60 ± 4.11	77.04 ± 7.18	11.25 ± 4.27	7.48 ± 1.27	37.86 ± 6.58	6.86 ± 0.47
β (h^{-1})	0.08 ± 0.03	0.22 ± 0.07	0.06 ± 0.00	0.06 ± 0.02	0.04 ± 0.01	0.10 ± 0.05	0.02 ± 0.01	0.03 ± 0.01	0.07 ± 0.01	0.03 ± 0.01
k_a (h^{-1})	27.94 ± 3.15	34.70 ± 4.50	5.14 ± 0.96	5.39 ± 0.87	0.10 ± 0.01	0.25 ± 0.09	12.62 ± 7.45	18.29 ± 4.17	10.95 ± 2.31	5.18 ± 1.36
$T_{1/2\alpha}$ (h)	0.12 ± 0.02	0.21 ± 0.07	0.35 ± 0.16	0.53 ± 0.17	0.10 ± 0.02	0.46 ± 0.43	0.38 ± 0.26	1.10 ± 0.88	0.29 ± 0.10	1.66 ± 0.80
$T_{1/2\beta}$ (h)	10.27 ± 3.48	3.51 ± 0.58	12.69 ± 0.67	11.75 ± 4.12	16.49 ± 3.02	9.43 ± 0.97	42.82 ± 4.89	29.82 ± 5.25	9.94 ± 1.34	21.98 ± 6.92
$T_{1/2}k_a$ (h)	0.03 ± 0.01	0.03 ± 0.01	0.14 ± 0.02	0.15 ± 0.08	7.07 ± 0.44	3.12 ± 0.98	0.07 ± 0.04	0.07 ± 0.06	0.12 ± 0.07	0.18 ± 0.02
K_{21} (h^{-1})	0.58 ± 0.07	0.77 ± 0.14	0.91 ± 0.19	0.24 ± 0.01	0.24 ± 0.02	0.73 ± 0.07	0.26 ± 0.01	0.40 ± 0.03	1.00 ± 0.40	0.13 ± 0.02
K_{10} (h^{-1})	1.01 ± 0.63	1.06 ± 0.24	0.15 ± 0.06	0.45 ± 0.15	1.76 ± 0.51	0.98 ± 0.26	0.03 ± 0.02	0.09 ± 0.04	0.20 ± 0.07	0.17 ± 0.05
K_{12} (h^{-1})	4.31 ± 0.79	2.06 ± 0.11	1.18 ± 0.57	0.81 ± 0.19	7.62 ± 0.82	8.82 ± 1.79	0.37 ± 0.12	0.63 ± 0.19	1.48 ± 0.75	0.29 ± 0.08
AUC_{0-t} (μmol h/L)	19.54 ± 8.31	35.05 ± 6.03	5200.18 ± 390.07	1472.02 ± 429.01	432.21 ± 42.89	262.72 ± 46.57	513.11 ± 85.01	227.23 ± 50.12	583.76 ± 47.01	260.76 ± 72.93
$AUC_{0-\infty}$ (μmol h/L)	37.40 ± 9.07	40.03 ± 9.10	5509.15 ± 548.17	1515.36 ± 207.56	575.92 ± 35.51	289.78 ± 57.50	854.09 ± 26.90	329.11 ± 83.52	615.28 ± 50.63	291.14 ± 80.65
T_{max} (h)	0.12 ± 0.02	0.16 ± 0.02	0.45 ± 0.12	0.44 ± 0.07	8.95 ± 1.22	4.80 ± 0.59	0.41 ± 0.10	0.26 ± 0.15	0.40 ± 0.19	0.67 ± 0.28
C_{max} (μmol/L)	20.84 ± 8.82	31.82 ± 6.29	400.68 ± 93.51	353.17 ± 57.80	11.92 ± 3.51	11.30 ± 4.13	25.08 ± 3.39	21.16 ± 5.90	75.43 ± 9.53	34.80 ± 6.30

A and *B*: mathematical coefficients. ♂ denotes male rat and ♀ denotes female rat. Data represent mean ± SD for six rats

Table 3 Metabolic kinetic parameters of TBHQ and its metabolites M1–M4 in rat serum after a single oral dose of 700 mg/kg TBHQ

Parameters	TBHQ		M1		M2		M3		M4	
	♂	♀	♂	♀	♂	♀	♂	♀	♂	♀
A (μmol/L)	1344.72 ± 974.90	171.84 ± 39.29	3976.63 ± 354.44	2813.05 ± 341.93	−6.09 ± 1.01	−2.24 ± 0.13	69.43 ± 8.62	71.72 ± 8.83	209.85 ± 83.31	209.13 ± 23.56
α (h^{-1})	2.25 ± 0.06	1.46 ± 0.14	2.42 ± 0.61	0.86 ± 0.21	9.62 ± 0.72	10.94 ± 3.81	1.76 ± 0.86	0.89 ± 0.37	0.35 ± 0.12	0.70 ± 0.09
B (μmol/L)	2.85 ± 0.22	2.31 ± 0.09	251.49 ± 46.01	87.22 ± 8.19	61.44 ± 5.04	16.80 ± 5.28	16.74 ± 4.43	10.63 ± 3.50	23.22 ± 2.78	18.77 ± 5.60
β (h^{-1})	0.18 ± 0.13	0.15 ± 0.08	0.06 ± 0.01	0.04 ± 0.01	0.09 ± 0.01	0.03 ± 0.00	0.02 ± 0.00	0.02 ± 0.01	0.01 ± 0.00	0.02 ± 0.01
k_a (h^{-1})	15.94 ± 3.30	15.05 ± 1.03	3.49 ± 1.00	6.44 ± 0.31	0.20 ± 0.04	0.26 ± 0.06	3.43 ± 0.81	10.02 ± 2.01	19.51 ± 7.85	6.08 ± 1.68
$T_{1/2\alpha}$ (h)	0.35 ± 0.05	0.48 ± 0.04	0.40 ± 0.05	1.11 ± 0.21	0.28 ± 0.02	0.27 ± 0.08	0.48 ± 0.05	0.98 ± 0.17	2.60 ± 0.51	1.42 ± 0.05
$T_{1/2\beta}$ (h)	14.39 ± 1.58	10.73 ± 7.26	12.70 ± 2.43	18.66 ± 6.48	7.75 ± 0.85	28.62 ± 9.96	43.61 ± 10.06	40.24 ± 6.06	65.78 ± 8.85	36.00 ± 2.96
$T_{1/2}k_a$ (h)	0.08 ± 0.02	0.06 ± 0.03	0.26 ± 0.05	0.24 ± 0.07	4.51 ± 0.28	2.78 ± 0.55	0.25 ± 0.03	0.26 ± 0.08	0.12 ± 0.01	0.28 ± 0.06
K_{21} (h^{-1})	0.23 ± 0.16	0.17 ± 0.08	0.72 ± 0.09	0.14 ± 0.05	0.79 ± 0.21	2.93 ± 0.28	0.71 ± 0.13	0.28 ± 0.08	0.06 ± 0.02	0.13 ± 0.02
K_{10} (h^{-1})	1.50 ± 0.18	1.15 ± 0.22	0.32 ± 0.05	0.26 ± 0.07	0.86 ± 0.04	0.08 ± 0.04	0.05 ± 0.01	0.08 ± 0.06	0.08 ± 0.02	0.15 ± 0.07
K_{12} (h^{-1})	0.69 ± 0.19	0.23 ± 0.02	1.44 ± 0.16	0.50 ± 0.04	8.06 ± 0.90	7.96 ± 0.52	1.02 ± 0.37	0.56 ± 0.10	0.22 ± 0.04	0.45 ± 0.08
AUC_{0-t} (μmol h/L)	93.44 ± 4.54	125.55 ± 18.34	5963.28 ± 296.02	2741.46 ± 443.16	254.66 ± 24.76	399.47 ± 12.03	575.44 ± 11.64	351.76 ± 58.47	1307.69 ± 558.10	768.41 ± 44.81
$AUC_{0-\infty}$ (μmol h/L)	105.28 ± 32.02	128.14 ± 17.41	6352.02 ± 472.23	3152.69 ± 411.75	265.25 ± 30.56	650.64 ± 23.01	1047.36 ± 78.09	597.07 ± 72.55	1989.32 ± 366.12	1011.41 ± 482.48
T_{max} (h)	0.23 ± 0.10	0.27 ± 0.07	0.57 ± 0.05	0.61 ± 0.11	5.29 ± 0.14	9.74 ± 1.71	0.60 ± 0.14	0.66 ± 0.04	0.46 ± 0.06	0.74 ± 0.03
C_{max} (μmol/L)	81.27 ± 8.38	109.60 ± 9.59	632.12 ± 98.71	418.51 ± 59.17	9.83 ± 1.84	11.70 ± 3.23	28.73 ± 6.38	23.55 ± 2.15	141.56 ± 13.33	87.72 ± 5.11

A and *B*: mathematical coefficients. ♂ denotes male rat and ♀ denotes female rat. Data represent mean ± s.d. for six rats

C_{max} is estimated as 1.19 (♂) and 1.25 (♀) for TBHQ, 0.83 (♂) and 0.78 (♀) for M1, 0.21 (♂) and −0.04 (♀) for M2, 0.44 (♂) and 0.33 (♀) for M3, 0.64 (♂) and 0.51 (♀) for M4, respectively. The dose-proportionality constants for C_{max} are in the order of TBHQ > 1 > M1 > M4 > M3 > M2. The results of power model show that as determined by C_{max}, TBHQ exposure increases in a more-than-dose-proportional manner, but the exposures of the metabolites M1–M4 increase in a less-than-dose-proportional manner, across the dose of 7–700 mg/kg. It seems that the metabolic reactions from TBHQ to M1–M4 are likely to be restricted by enzymes or substrates connecting with those reactions to different extents, and metabolic saturations would occur at TBHQ doses higher than 350 mg/kg.

The serum concentrations of M1, M3 and M4 were all much higher for males than for females ($P < 0.01$) during the metabolic process, while no significant differences between male and female rats were found ($P > 0.05$) for TBHQ and M2, at the doses of 350 and 700 mg/kg. The sex difference in the metabolism of TBHQ and its metabolites might be attributed to differences in the expressed levels of cytochrome P-450 (CYP-450) and other metabolizing enzymes [20–22]. A differentiated pattern of hormone release in females and males [23] contributes to different levels of CYP-450 expression, influencing their metabolic capability [24], which could result in differences of metabolic kinetics between TBHQ and its metabolites.

In this work, the LC/ITMS was used for investigating the metabolic kinetics of TBHQ and its metabolites in rat serum after oral doses of 7, 350 and 700 mg/kg. It was found that the TBHQ exposure increases in a more-than-dose-proportional manner, but the exposures of the metabolites M1–M4 increase in a less-than-dose-proportional manner, across the dose of 7–700 mg/kg. TBHQ were rapidly absorbed, distributed and metabolized. The metabolites except M2 appear to be rapidly absorbed and distributed as TBHQ, but they were observed to be eliminated more slowly than TBHQ. Moreover, apparent sex difference in the metabolism of TBHQ was found. After oral administration, TBHQ seems to be more completely absorbed and biotransformed by males than females and the serum concentrations of M1, M3 and M4 also appear significantly higher for males than females. The results suggest that TBHQ may result in higher acute oral toxicity for males than for females. The sex differences of metabolic kinetics and the toxicities of TBHQ and its metabolites, which might be resulted from the differences of expressed levels of CYP-450 and other metabolizing enzymes between male and female, should be further investigated. These findings suggest that although rat is a useful animal model for clarifying the mechanisms underlying TBHQ adverse actions after oral administration and to optimize its usages, sex differences should be

Fig. 1 Plots of peak serum concentration (C_{max}) of TBHQ and its metabolites versus dose after oral administration. **a** for TBHQ, **b** for M1, **c** for M2, **d** for M3, and **e** for M4

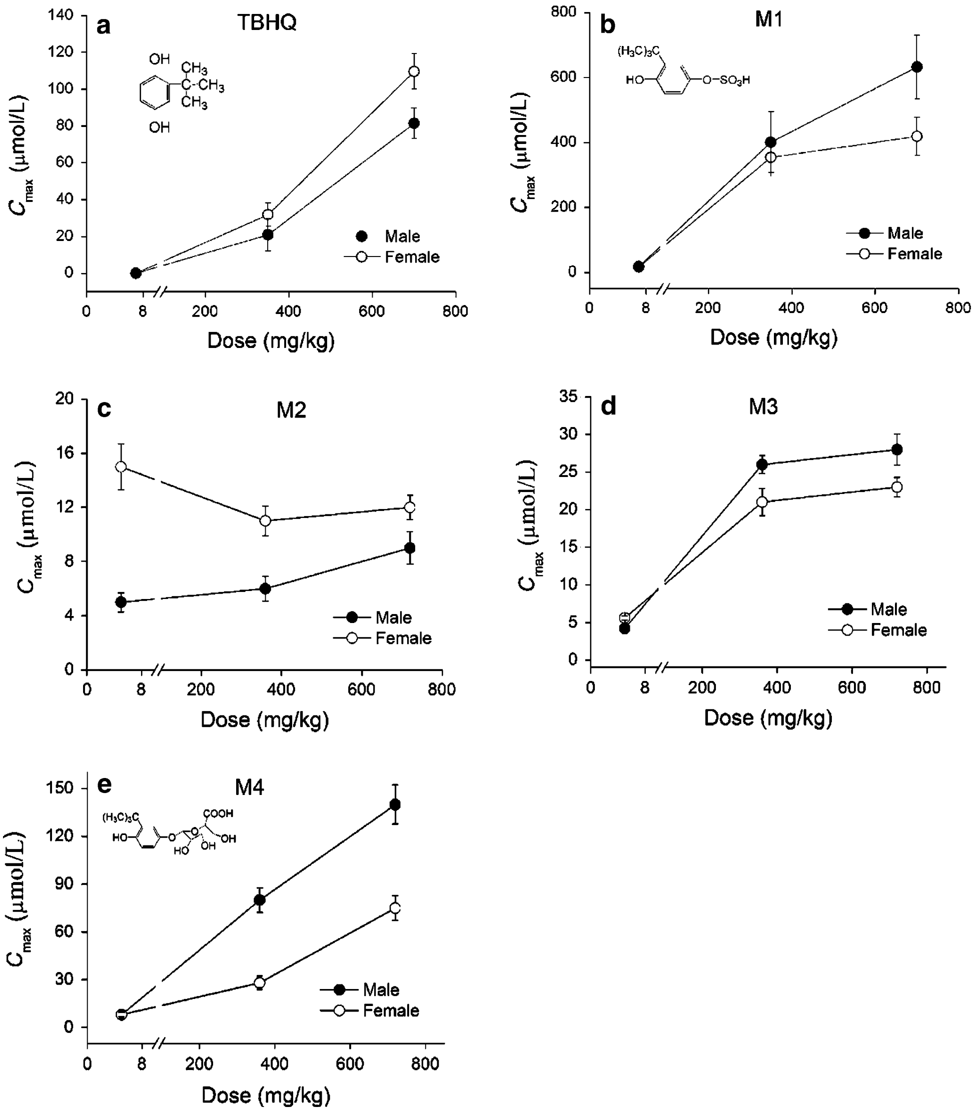

carefully considered especially when extrapolating metabolic kinetic profile and the safety results of TBHQ from rat to human. The research is not only favorable for enhancing the understanding of the metabolic mechanism of TBHQ, but also for facilitating finding additional targets such as its metabolites for evaluation of TBHQ safety.

Acknowledgments This study was partly supported by the key special S&T project number 2001BA804A21 on food safety initiated by the Ministry of Science and Technology of the People's Republic of China. The authors wish to sincerely thank their colleagues for their valuable experimental assistance.

References

1. Rojas M, Brewer M (2007) Effect of natural antioxidants on oxidative stability of cooked, refrigerated beef and pork. J Food Sci 72:282–288
2. Gámez-Mezaa B, Noriega-Rodrígueza J, Medina-Juáreza LA, Ortega-Garcíaa J, Cázarez-Casanovaa R, Angulo-Guerrerob O (1999) Antioxidant activity in soybean oil of extracts from Thompson Grape Bagasse. J Am Oil Chem Soc 76:1445–1447
3. Min DB, Schweizer D (1983) Gas chromatographic determination of butylated hydroxyanisole, butylated hydroxytoluene and tertiary butyl hydroquinone in soybean oil. J Food Sci 48:73–74
4. Okubo T, Yokoyama Y, Kano K, Kano I (2003) Cell death induced by the phenolic antioxidant tert-butylhydroquinone and its metabolite tert-butylquinone in human monocytic leukemia U937 cells. Food Chem Toxicol 41:679–688
5. Hirokazu H, Mitsuhiro O, Kiyoe O, Sadako K, Tetsuo A (2003) Increase of antioxidative potential by tert-butylhydroquinone protects against cell death associated with 6-hydroxydopamine-induced oxidative stress in neuroblastoma SH-SY5Y cells. Mol Brain Res 119:125–131
6. Mohamed H, Abdel W (2003) Testicular toxicity of dibromoacetonitrile and possible protection by tertiary butylhydroquinone. Pharmacol Res 47:509–515
7. Peter MMCG, Lau SS, Dulik D, Murphy D, Van OB, Van BPJ, Monks TJ (1996) Metabolism of tert-Butylhydroquinone to S-

substituted conjugates in the Male Fischer 344 Rat. Chem Res Toxicol 9:133–139
8. Christian P, Liliane M (2002) Quantification of synthetic phenolic antioxidants in dry foods by reversed-phase HPLC with photodiode array detection. Food Chem 77:93–100
9. Yang MH, Lin HJ, Choong YM (2002) A rapid gas chromatographic method for direct determination of BHA, BHT and TBHQ in edible oils and fats. Food Res Int 35:627–633
10. Ikeda GJ, Sapienza PP, Ross IA (1998) Distribution and excretion of radiolabelled tert-butylhydroquinone in Fischer 344 rats. Food Chem Toxicol 36:907–914
11. Romsted LS, Zhang J (2002) Kinetic method for determining antioxidant distributions in model food emulsions: distribution constants of t-butylhydroquinone in mixtures of octane, water and a nonionic emulsifier. J Agric Food Chem 50:3328–3336
12. Huang W, Niu H, Shi B, Yang ML, Jiang XJ (2008) HPLC coupled to ion trap-ms/ms for analysis of tertiary-butylhydroquinone in edible oil samples. J Food lipids 15:1–12
13. Huang W, Gu YC, Niu H (2008) Determination of tertiary-butylhydroquinone and its metabolites in rat serum by liquid chromatography–ion trap mass spectrometry. Lipids 43:281–288
14. Zhao HY, Zheng JM, Jiang ZM (2001) Pharmacokinetics of thrombinlike enzyme from venom of Agkistrodon halys ussuriensis Emelianov determined by ELISA in the rat. Toxicon 39: 1821–1826
15. Guo LQ, Xie ZH, Lin XC, Wu XP, Qiu B, Zhang YB, You HN, Chen GN (2005) Pharmacokinetics of ciprofloxacin in eels by high-performance liquid chromatography with fluorescence detection. Anal Biochem 341:275–279
16. Liu Z, Sha YF, Huang TM, Yang B, Duan GL (2005) High-performance liquid chromatographic determination of vertilmicin in rat plasma using sensitive fluorometric derivatization. J Chromatogr B 828:2–8
17. Wu GH, Meng Y, Zhu XH, Huang C (2006) Pharmacokinetics and tissue distribution of enrofloxacin and its metabolite ciprofloxacin in the Chinese mitten-handed crab Eriocheir sinensis. Anal Biochem 358:25–30
18. Xiao YY, Song YM, Chen ZP, Ping QN (2006) The preparation of silybin-phospholipid complex and the study on its pharmacokinetics in rats. Int J Pharm 307:77–82
19. Zhang LJ, Xing DM, Wang W, Wang RF, Du LJ (2006) Kinetic difference of baicalin in rat blood and cerebral nuclei after intravenous administration of Scutellariae Radix extract. J Ethnopharmacol 103:120–125
20. Kato R (1974) Sex-related differences in drug metabolism. Drug Metab Rev 3:1–32
21. Mugford CA, Kedderis GL (1998) Sex-dependent metabolism of xenobiotics. Drug Metab Rev 30:441–498
22. Kato R, Yamazoe Y (1992) Sex-specific cytochrome P450 as a cause of sex- and species-related differences in drug toxicity. Toxicol Lett 64–65:661–667
23. Furukawa T, Manabe S, Watanabe T, Sharyo S, Mori Y (1999) Sex difference in the daily rhythm of hepatic P450 monooxygenase activities in rats is regulated by growth hormone release. Toxicol Appl Pharmacol 161:219–224
24. Alessandra MH, Howard PH, Elizabeth ML, Gentrya WB, Owens SM (2005) Sex- and dose-dependency in the pharmacokinetics and pharmacodynamics of (+)-methamphetamine and its metabolite (+)-amphetamine in rats. Toxicol Appl Pharmacol 209:203–213

Lipids (2008) 43:765–774
DOI 10.1007/s11745-008-3199-9

ORIGINAL ARTICLE

Structural Characterization of α,β-Unsaturated Aldehydes by GC/MS is Dependent upon Ionization Method

Eric K. Long · Irina Smoliakova · Ales Honzatko · Matthew J. Picklo Sr.

Received: 5 October 2007 / Accepted: 10 May 2008 / Published online: 1 July 2008
© AOCS 2008

Abstract α,β-unsaturated aldehydes are toxic products of lipid peroxidation. Detection and characterization of these aldehydes is important in many human disease states as well as in the food industry. Our study shows that electron ionization-mass spectrometry (EI-MS) and positive-ion chemical ionization-mass spectrometry (PICI-MS), but not electron capture negative ionization-mass spectrometry (ECNI-MS), can be used to detect the C4-hydroxylation state of α,β-unsaturated aldehydes derivatized with pentafluorobenzyl hydroxylamine alone. EI-MS and PICI-MS spectra of 4-hydroxy-2-alkenals contained a fragment with *m*/*z* 252, whereas spectra of 2-alkenals contained a fragment with *m*/*z* 250. These fragments are consistent with fragmentation between C3 and C4 with transfer of two hydrogens from C4 and the C4 hydroxyl group in the case of 4-hydroxy-2-alkenals. In addition, EI-MS and PICI-MS were able to distinguish 4-hydroxy-2-alkenals and 2-alkenals from 4-keto-2-alkenals and 4-hydroxyalkanals. On the other hand, ECNI-MS provided complex spectra regarding C4-hydroxylation state. Furthermore, the *syn*- and *anti*-configurations of PFB-oximes had different resultant spectra using ECNI-MS, but not with EI-MS or PICI-MS. These data indicate that EI-MS and PICI-MS are more amenable for structural analysis of α,β-unsaturated aldehydes than ECNI-MS.

Keywords Lipid peroxidation · Oxidized lipids · Arachidonic acid · Docosahexaenoic acid

Abbreviations

HNE	*trans*-4-Hydroxy-2-nonenal
HHE	*trans*-4-Hydroxy-2-hexenal
HNA	4-Hydroxynonanal
4-ONE	*trans*-4-oxo-2-nonenal
d_{11}-HNE	*trans*-4-Hydroxy-2-nonenal-5,5,6,6,7,7,8,8,9,9,9-d_{11}
d_1-HNE	*trans*-4-Hydroxy-2-nonenal-4-d_1
MDA	Malondialdehyde
HNDE	*trans* 4-Hydroxy-2,6-nonadienal
EI	Electron ionization
PICI	Positive-ion chemical ionization
ECNI	Electron-capture negative-ionization
GC/MS	Gas chromatography/mass spectrometry
ESI	Electrospray ionization
PFBHA	*O*-(2,3,4,5,6-pentafluorobenzyl) hydroxylamine
DHA	Docosahexaenoic acid 226n-3
RIC	Reconstructed ion chromatogram

Introduction

Lipid peroxidation is important in the food industry [1] and is implicated in many disease states such as Alzheimer's disease [2], atherosclerosis [3], and amyotrophic lateral sclerosis [4]. Lipid peroxidation of n-3 and n-6 fatty acids leads to the formation of multiple keto and aldehyde species, including α,β-unsaturated aldehydes. These α,β-unsaturated aldehydes include *trans*-4-hydroxy-2-alkenals, such as *trans*-4-hydroxy-2-nonenal (HNE), *trans*-4-

---

E. K. Long (✉) · A. Honzatko · M. J. Picklo Sr.
Department of Pharmacology, Physiology, and Therapeutics,
University of North Dakota, Grand Forks, ND 58202-9024, USA
e-mail: elong@medicine.nodak.edu

I. Smoliakova · M. J. Picklo Sr.
Department of Chemistry, University of North Dakota,
Grand Forks, ND 58202-9024, USA

hydroxy-2-hexenal (HHE), *trans*-4-oxo-2-alkenals such as *trans*-4-oxo-2-nonenal (4-ONE) and *trans*-4-oxo-2-hexenal, and 2-alkenals, such as *trans*-2-hexenal [5–9].

Structural and quantitative analyses of α,β-unsaturated aldehydes are performed using gas chromatography (GC) coupled to various forms of ionization methods, such as electron ionization-mass spectrometry (EI-MS) and electron capture negative ionization-mass spectrometry (ECNI-MS). Typically, samples are derivatized with O-(2,3,4,5,6-pentafluorobenzyl)-hydroxylamine (PFBHA) [10–12]. PFB-derived aldehydes containing hydroxyl groups may be further derivatized using *N*,*O*-bis(trimethylsilyl) acetamide [5, 6].

During development of an analytical method for quantifying α,β-unsaturated aldehydes using GC/EI-MS, we observed mass spectral differences between 4-hydroxy-2-alkenals and 2-alkenals when derivatized with PFBHA alone. 4-Hydroxy-2-alkenal spectra contained an abundant *m/z* 252 fragment whereas spectra of 2-alkenals contained an abundant *m/z* 250 fragment (Fig. 1).

Based on these initial data, the goals of this study are to determine the mechanism by which these fragments are produced and determine if other ionization methods produce results similar to those seen using GC/EI-MS. Our results demonstrate that hydrogen transfer is involved in the fragmentation difference observed between C4-hydroxylated and unsubstituted 2-alkenals using GC/EI-MS. The fragmentation pattern observed for 4-hydroxy-2-alkenals requires both a 4-hydroxyl group and a C2, C3 double bond. GC/positive-ion chemical ionization-mass spectrometry (PICI-MS) yielded results similar to those of EI-MS, and provided the $[M + H]^+$ ion in the case of 2-alkenals and the

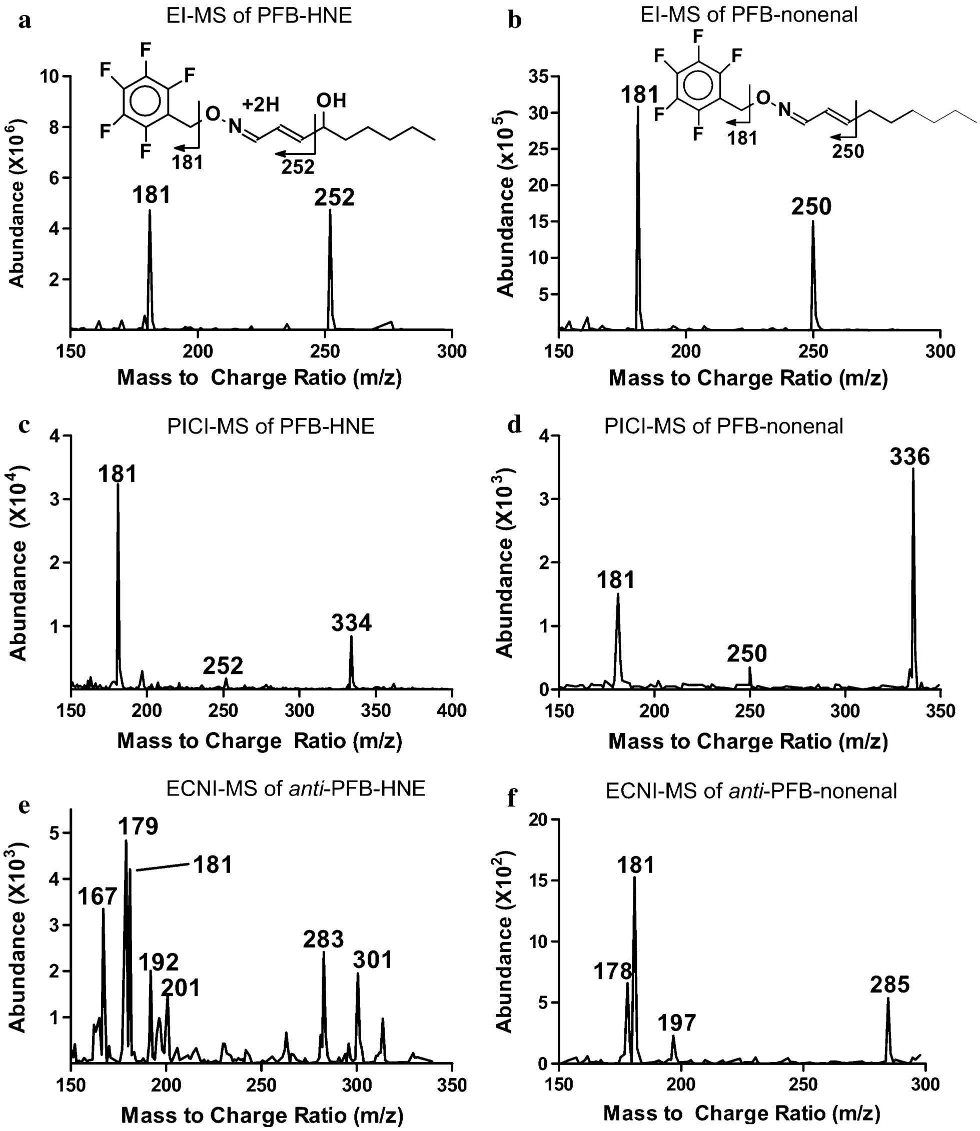

Fig. 1 EI-MS spectra of PFB-HNE (**a**) and PFB-nonenal contain fragments with *m/z* 252 and *m/z* 250, respectively. In addition, both contain *m/z* 181, characteristic of PFB-oximes. The PICI-MS spectrum of PFB-HNE (**c**) contains a fragment with *m/z* 334 corresponding to $[M + H–H_2O]^+$, in addition to fragments with *m/z* 181 and 252. The PICI-MS spectrum of PFB-Nonenal (**d**) contains a fragment with *m/z* 336 corresponding to $[M + H]^+$, in addition to fragments with *m/z* 181 and 250. The ECNI-MS spectrum of PFB-HNE contains a complex mixture of spectra, which include *m*/z 192, specific to 4-hydroxy-2-alkenals, and m/z 301 which corresponds to $[M–CF_2]^-$. The ECNI-MS spectrum of PFB-nonenal include m/z 197, specific to 2-alkenals, and m/z 285, which corresponds to $[M–CF_2]^-$

$[M + H-H_2O]^-$ ion for 4-hydroxy-2-alkenals. However, ECNI-MS yielded less clear structural information in regards to α,β-unsaturated aldehydes. Despite the different information provided by each ionization method, our results also demonstrate that these techniques can be used for complementary characterization and identification of α,β-unsaturated aldehydes.

Materials and Methods

Materials

HHE was purchased from Cayman Chemical Company (Ann Arbor, MI). *O*-(2,3,4,5,6-pentafluorobenzyl) hydroxylamine (PFBHA) was purchased from Alpha Aesar (Ward Hill, MA). Sodium borodeuteride ($NaBD_4$) and 1,1,3,3-tetramethoxypropane were purchased from Sigma (St Louis, MO). *trans*-4-Hydroxy-2-nonenal-5,5,6,6,7,7,8,8,9,9,9-d_{11} (d_{11}-HNE) dimethyl acetal (stated isotopic purity >99%) was purchased from CDN Isotopes (Pointe-Claire, QC, Canada). *trans*-2-Nonenal was purchased from Aldrich (Milwaukee, WI). *trans*-2-Hexenal and diisobutyl aluminum hydride (DIBAL-H) were purchased from Acros Organics (NJ, USA). Docosahexaenoic acid and arachidonic acid were purchased from Nu-Chek Prep, Inc. (Elysian, MN). HNE and HNE dimethyl acetal were synthesized in our laboratory [13, 14].

Methods

Synthesis of 4-Hydroxynonanal (HNA)

HNA was synthesized from γ-nonalactone via a method similar to that of Bloch and Gilbert [15]. Six grams of γ-nonalactone was added to 400 mL toluene and cooled to −78 °C under argon. 60 mL of 1 M DIBAL-H was added dropwise for 1 h. The reaction was stirred for 3.5 h at −78 °C. Excess DIBAL-H was destroyed by addition of 30 mL isopropyl alcohol (2 M) in toluene. One milliliter of water was added, followed by 100 mL tetrahydrofuran, then 15 g of silica gel with 30 g magnesium sulfate, with 30 min between each addition. This reaction was filtered, and the residue was washed with 100 mL THF and 100 mL dichloromethane. The filtrate and washes were combined and dried twice over magnesium sulfate. HNA was purified from the filtrate via flash chromatography with silica solid phase and 70:30 hexane:isopropanol mobile phase, dried, weighed and suspended in hexane. The structure of HNA was confirmed using ESI-MS (positive mode) as evidenced by a peak with m/z 159 corresponding to $[M + H]^+$. Also present were peaks corresponding to $[M-17]^+$ which corresponds to addition of a hydrogen followed by loss of water, and $[M + 23]^+$, which corresponds to the sodium adduct. ESI-MS/MS was done using a Perkin-Elmer/Sciex API 3000 triple quadrupole mass spectrometer (Concord, ON, Canada). We also compared HNA to HNE and 4-ONE via HPLC-UV analysis and determined that HNA did not coelute with HNE or 4-ONE (data not shown). The yield from this reaction was 17.4 mg HNA.

^{1}H-NMR spectra of HNA were recorded in $CDCl_3$ using TMS as an internal standard on an Avance 500 Bruker spectrometer. ^{1}H-NMR spectrum (500 MHz, $CDCl_3$, δ): 0.89 t (3H, $J = 6.6$ Hz, CH_3), 1.25–2.17 m (12H, six CH_2 groups), 2.97 and 3.06 two d (1H, $J = 2.5$ Hz, OH), 3.97 and 4.20 two m [1H, H(4)], 5.47 and 5.55 two m [1H, H(1)]. According to the ^{1}H-NMR spectrum of HNA in $CDCl_3$, the compound exists in the solution as a cyclic hemiacetal. The ratio of the integration curves for the trace signal at δ 9.80 ppm [assigned to the H(1) of the linear form] and two signals at 5.47 and 5.55 ppm (assigned to the H(1) of the cyclic form), suggests that the amount of the linear form in the solution does not exceed 1%. As expected, some signals [e.g., the OH, CH(4), and CH(1) signals] assigned to the hemiacetal, are doubled due to the presence of two chiral centers. ^{1}H-NMR spectra showed no evidence of a carbon-carbon double bond.

Synthesis of trans-4-Hydroxy-2-nonenal-4-d_1 (d_1-HNE)

d_1-HNE was synthesized according to the method for synthesis of ^{3}H-HNE by Chandra and Srivastava [13]. Two hundred and thirty-seven milligrams of pyridinium chlorochromate, 265 mg sodium acetate and 7.3 mL CH_2Cl_2 were mixed together and stirred. To this mixture, 112 mg HNE-dimethylacetal was added and stirred for 30 min. This reaction was monitored by TLC. Forty millilitres of ether was added to the mixture, decanted, filtered, and evaporated, resulting in 4-ONE dimethylacetal. Ten milligrams of 4-ONE dimethylacetal was added to 5 mL ethanol with 8 mg $NaBD_4$ and stirred for 2 h. This resulted in the reduction of the 4-keto group yielding a C4 deuterium and a C4-hydroxyl group. The reaction was evaporated and added to 50 mL water acidified to pH 2 with phosphoric acid to remove the protecting groups. The reaction was then extracted three times into CH_2Cl_2, evaporated, weighed, and raised in hexane. The product coeluted with non-deuterated HNE during HPLC-UV analysis using a Waters Spherisorb ODS2 reverse phase column. The solvent system was 65:35 water:acetonitrile with a flow rate of 1.5 mL/min. Absorbance was monitored using a photodiode array detector scanning from 200 to 300 nm. The absorbance maximum for HNE and d_1-HNE was 223 nm (data not shown). No other compounds were detected. The yield of this reaction was 3.54 mg.

ESI-MS analysis (in positive mode) of the resulting d_1-HNE resulted in four main m/z peaks at 157 (relative percentage of 20.7%), 158 (70.5%), 159 (8.2%), and 160 (0.6%). The m/z 157 corresponds to the $[M + H]^+$ of non-deuterated HNE. The m/z 158 corresponds to the $[M + H]^+$ of d_1-HNE. Given the natural abundance of ^{13}C (1.1%), the m/z 159 and m/z 160 likely correspond to the $[M + H]^+$ of d_1-HNE containing one and two atoms of ^{13}C, respectively. Taking into consideration the abundance of ^{13}C, approximately 2% of the m/z 159 is non-deuterated HNE. From these data, we conclude that the isotopic purity of d_1-HNE is 77%.

Comparison of ^1H-NMR spectra of the resulting d_1-HNE and non-deuterated HNE was used to confirm the C4 deuterium of d_1-HNE. For non-deuterated HNE, ^1H NMR ($CDCl_3$, δ, ppm): 0.90 t (3H, $^3J = 7.0$ Hz, CH_3), 1.30–1.70 m (6H, three CH_2 groups), 1.81 m (1H, OH), 4.43 m (1H, HC(4)O), 6.31 ddd (1H, $^4J_1 = 6.3$, $^3J_2 = 7.8$, $^3J_3 = 15.6$ Hz, HC(2)), 6.82 dd (1H, $^3J_1 = 4.7$, $^3J_2 = 15.6$ Hz, HC(3)), 9.59 d (1H, $J = 7.8$ Hz, H–C=O). The ^1H-NMR spectra of both d_1-HNE and non-deuterated HNE in $CDCl_3$ have the signals of the C(3)H=C(2)H–HC(1)=O and $CH_3CH_2CH_2CH_2$ fragments. However, in the spectrum of d_1-HNE, the signal at d 4.43 ppm, assigned to the hydrogen bonded to the C4 OH group in the spectrum of the non-deuterated HNE, is greatly reduced. These data confirm that the deuterium of d_1-HNE is localized to C4, and that there is some non-deuterated HNE present.

Synthesis of 4-oxo-2-nonenal (4-ONE)

Seventy-five milligrams of 4-ONE dimethyl acetal was deprotected in 50 mL pH 2 water acidified with phosphoric acid to form 4-ONE. The product was confirmed as 4-ONE via comparison during synthesis by TLC to 4-ONE standard purchased from Cayman Chemical Company (Ann Arbor, MI) with a solvent system of 80:20 hexane:ethyl acetate. The standard and the reaction product were both reactive towards dinitrophenylhydrazine and chromatographed identically. The product and the standard had the same λ_{max} of 228 nm in ethanol. The product had a mass consistent with a bis-PFBHA oxime derivative of 4-ONE by GC-MS (see Table 2). The yield of this reaction was approximately 65 mg of 4-ONE.

Preparation of d_{11}-HNE

d_{11}-HNE dimethyl acetal was added to 50 mL water acidified to pH 2 with phosphoric acid to yield d_{11}-HNE. The reaction was extracted three times into CH_2Cl_2, evaporated, weighed, and raised in hexane. Molecular mass was confirmed by ESI-MS/MS. The yields of this reaction were typically over 90%.

Synthesis of Malondialdehyde

Malondialdehyde (MDA) was synthesized by deprotection of 1,1,3,3-tetramethoxypropane in 1 M HCl according to the method of Hjelle and Petersen [16]. This reaction consisted of 1 mL of 1 M HCl containing 567 mM 1,1,3,3-tetramethoxypropane. The reaction was allowed to proceed for 2 h at 37 °C. After incubation, the reaction mixture was diluted to approximately 10 mL final volume with 50 mM sodium phosphate buffer set to pH 7.4. The final stock was set to pH 7.4 using 1 M NaOH. The final concentration was determined using spectrophotometric analysis at λ_{max} 265 nm using $\varepsilon = 31{,}800\ M^{-1}\ cm^{-1}$.

Preparation of PFB-Oximes

Aldehydes at 10 μM concentrations were added to an equal volume of 50 mM PFBHA in 50 mM sodium acetate buffer at pH 5.0 for 30 min. Following derivatization, reaction mixtures were acidified using sulfuric acid to precipitate unreacted PFBHA·HCl. Previous work by Luo et al. [17] shows that acidification aided in the removal of excess PFBHA. Samples were extracted three times into methylene chloride and dried over sodium sulfate and evaporated under nitrogen. The samples were then raised to their original volume (1 mL) in methylene chloride.

Gas Chromatography/Mass Spectrometry

GC/MS analyses were performed using a ThermoElectron Corp (Waltham, MA) GC/MS with a Trace GC, a PolarisQ ion trap mass spectrometer and an AS3000 autosampler. This system was coupled to a Dell PC and data was analyzed using Xcalibur version 1.3 software. We used a J&W Scientific 30 m DB5-MS capillary column. Our method used a 1 μL splitless injection. The inlet temperature was held at 250 °C. The oven temperature was held at 50 °C for 1 min followed by an increase of 20 °C/min up to 320 °C, which was held for 10 min. The transfer line temperature was 300 °C and the ion source temperature was maintained at 250 °C for all analyses. Total ion current was measured from 5 to 24 min using a 70 eV ionization energy for EI analyses. Chemical ionization analyses used the same method as above with the addition of methane reagent gas (3.0 mL/min). Samples were analyzed using both PICI-MS and ECNI-MS using total ion current.

Oxidation of Docosahexaenoic Acid and Arachidonic Acid

DHA and arachidonic acid oxidation reactions were prepared separately at concentrations of 10 mM in 10 mL of 50 mM sodium phosphate buffer at pH 7.4 in the presence of 1 mM ascorbic acid and 50 µM iron(II) chloride [18]. The reaction mixtures were heated to 37 °C for 6 h. After incubation, 1 mL of the reaction mixtures was taken and added to 1 mL 50 mM PFBHA derivatization solution for 1 h. After derivatization, derivatives were extracted three times with dichloromethane and dried under nitrogen. Samples were then reconstituted in 1 mL of dichloromethane and subjected to GC/MS analysis.

Statistical Analyses

Linear regression was performed using Prism 4 software (Graphpad Software, Inc., San Diego, CA).

Results

As shown in Fig. 1, derivatization of α,*β*-unsaturated aldehydes with PFBHA followed by analysis using GC/EI-MS produced clear spectra that distinguished the C4-hydroxylation state of α,*β*-unsaturated aldehydes. Spectra of all aldehydes contained fragments with *m/z* 181 corresponding to $[C_6H_2F_5]^+$, a common indicator of PFB-oximes produced by EI-MS [15]. In addition to *m/z* 181, spectra of 4-hydroxy-2-alkenals (HNE and HHE) contained fragments with *m/z* 252 (Fig. 1;Table 1) whereas unsubstituted 2-alkenals (*trans*-2-nonenal and *trans*-2-hexenal) contained fragments with *m/z* 250 (Fig. 1; Table 1). Both of these fragments are consistent with fragmentation between C3 and C4 with the 2 mass unit difference resulting from hydrogen transfer to the charged fragment.

In order to determine the origin of the hydrogens transferred during analysis of 4-hydroxy-2-alkenals, we employed d_{11}-HNE, deuterated on C5–C9. Our EI-MS spectrum of PFB-derivatized d_{11}-HNE contained a fragment with *m/z* 252, showing that the deuteria remained on the deuterocarbon tail during fragmentation (Table 1). We synthesized d_1-HNE, which contained a C4 deuterium to determine if one of these hydrogens originated from C4. The EI-MS spectrum of PFB-d_1-HNE contained a fragment with *m/z* 253 (Table 1). These data indicate that the transfer of a hydrogen from C4 accounts in part for the *m/z* 252 fragment observed with the 4-hydroxy-2-alkenals.

To determine the necessity of the C2, C3 double bond to produce *m/z* 252 or 250 using EI-MS, we synthesized HNA, a known metabolite of HNE, and derivatized it with PFBHA [19]. Spectra of PFB-HNA contained *m/z* 181 and *m/z* 251 fragments, resulting from fragmentation at the C3–C4 bond with a subsequent loss of a proton (Table 1). This result indicates that the *m/z* 252 fragment seen in 4-hydroxy-2-alkenal spectra requires a C2–C3 double bond.

In order to determine if the fragmentation differences seen using EI-MS are a property of general C4-substitution or specific to C4-hydroxylation we analyzed PFB-4-ONE to determine if an aldehyde with a 4-keto group would produce the same fragmentation pattern as those of PFB-HNE and PFB-HHE. This resulted in different fragmentation as

Table 1 EI-MS fragmentation of PFBHA-derived aldehydes

PFBHA-Derived Aldehydes	Fragments (m/z)
HNE/HHE 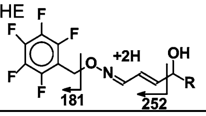 HHE: R=C_2H_5 (MW 309 g/mol) HNE: R=C_5H_{11} (MW 351 g/mol) d_{11}-HNE: R=C_5d_{11} (MW 362 g/mol)	181 252
trans-2-nonenal/*trans*-2-hexenal 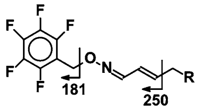 Hexenal: R=C_2H_5 (MW 293 g/mol) Nonenal: R=C_5H_{11} (MW 335 g/mol)	181 250
4-ONE (MW 544 g/mol) 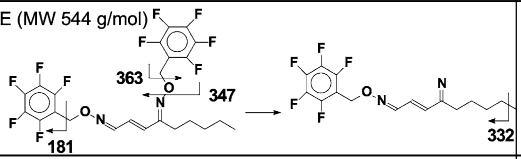	181 332 347 363
HNA (MW 353 g/mol) 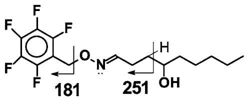	181 236 251
d_1-HNE (MW 353 g/mol) 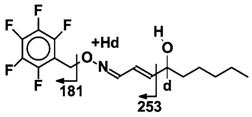	181 253

4-ONE formed a bis-PFB-oxime at the aldehyde and ketone moieties. The characteristic *m/z* 181 fragment was accompanied by *m/z* 363 $[M–C_7H_2F_5]^+$, *m/z* 347 $[M–C_7H_2F_5O]^+$, and *m/z* 332 $[M–C_8H_5F_5O]^+$ (Table 1). This pattern was different from EI-MS fragments of both 4-hydroxy-2-alkenals and 2-alkenals, thus differentiating these aldehydes from 4-keto-α,*β*-unsaturated aldehydes.

Chemical ionization is also widely used for characterization and quantification of α,*β*-unsaturated aldehydes. Analysis of PFB-oximes via PICI-MS yielded results similar to those seen using EI-MS. A fragment corresponding to *m/z* 181 was seen for all aldehydes and the *m/z* 252 versus *m/z* 250 distinction was preserved (Fig. 1; Table 2). PICI-MS also provided information about molecular mass and hydroxylation state in the form of $[M + H]^+$ fragments for 2-alkenals and $[M + H–H_2O]^+$ for 4-hydroxy-2-alkenals (Fig. 1; Table 2).

PICI-MS spectra of PFB-4-ONE were similar to EI-MS spectra of PFB-4-ONE with two exceptions: (1) the *m/z* 363 peak seen using EI-MS was absent and (2) a $[M + H]^+$ (*m/z* 545) peak was detected (Table 2). These data show that the fragmentation patterns of PFB-HNE and PFB-HHE using PICI-MS were specific to the presence of a C4-hydroxyl group. In contrast, the fragmentation pattern seen for 4-HNA was different with PICI-MS than EI-MS. The characteristic *m/z* 181 peak was present, but the *m/z* 251 peak was absent. The other prominent peak observed at *m/z* 350 is presumably associated with $[M + CH_5–H_2–H_2O]^+$ (Table 2).

ECNI-MS of α,*β*-unsaturated aldehydes yielded spectra different than EI-MS and PICI-MS. ECNI-MS produced two spectra associated with either *syn*-PFB-oximes or *anti*-PFB-oximes that are separated chromatographically [10]. Spectra of *anti*-PFB-oximes provided information regarding structural characteristics; 4-hydroxy-2-alkenals contained a fragment with *m/z* 192 corresponding to $[C_7H_2F_4NO]^-$ and 2-alkenals contained a fragment *m/z* 197 corresponding to $[C_7H_2F_5O]^-$ (Fig. 1; Table 3). These fragments were not found in spectra of PFB-4-ONE or PFB-HNA (Fig. 1; Table 3), suggesting that they are specific to 4-hydroxy-2-alkenals and 2-alkenals, respectively. In addition, spectra of *anti*-PFB-4-hydroxy-2-alkenals contained fragments with *m/z* 167 $[C_6F_5]^-$, 179, 181 $[C_6H_2F_5]^-$, 201, $[M-C_2H_7FO]^-$, and $[M-CF_2]^-$. Spectra of *anti*-PFB-2-alkenals contained fragments with *m/z* 178, 181, and $[M–CF_2]^-$ in addition to the aforementioned *m/z* 197. Spectra of *syn*-PFB-oximes did not provide specific structural information regarding C4-hydroxylation state of α,*β*-unsaturated aldehydes, as fragments with *m/z* 197, in the case of 2-alkenals, and *m/z* 192, in the case of 4-hydroxy-2-alkenals, were not present. The fragments observed are shown in Fig. 1d, e and listed in Table 3. Spectra of syn-PFB-HNE are similar to previously described results [10].

Comparison of limits of quantitation of α,*β*-unsaturated aldehydes for each ionization method is essential for the determination of their utility in analyses of complex mixtures. Limits of quantitation for PFB-derivatives of α,*β*-unsaturated aldehydes were determined for each ionization method using d_{11}-HNE as an internal standard. EI-MS yielded limits of quantitation below 100 fmol for 2-alkenals and 250 fmol for 4-hydroxy-2-alkenals using *m/z* 250 and *m/z* 252 for quantitation, respectively (Fig. 2a, b). Calibration curves were linear from 100 fmol to 2.5 pmol with an r^2 value of 0.992 for 2-alkenals and from 250 fmol to 2.5 pmol

Table 2 PICI-MS fragmentation of PFBHA-derived aldehydes

PFBHA-Derived Aldehydes	Fragments (m/z)
HNE/HHE HHE: R=C_2H_5 (MW 309 g/mol) HNE: R=C_5H_{11} (MW 351 g/mol) 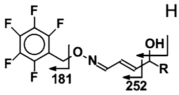	181 252 292 (HHE) $[M+H-H_2O]^+$ 334 (HNE) $[M+H-H_2O]^+$
trans-2-nonenal/*trans*-2-hexenal Hexenal: R=C_2H_5 (MW 293 g/mol) Nonenal: R=C_5H_{11} (MW 335 g/mol) 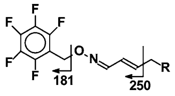	181 250 294 (Hexenal) $[M+H]^+$ 336 (Nonenal) $[M+H]^+$
4-ONE (MW 544 g/mol) 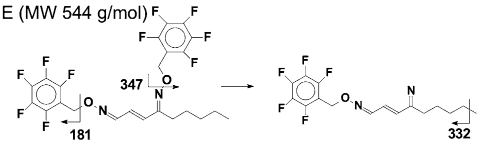 F F F F F O N 347 F F F F F O N 181 F F F F F O N N 332	181 332 347 545 $[M+H]^+$
HNA (MW 353 g/mol) 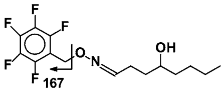	181 350 $[M+CH_5^+-H_2-H_2O]^+$

Table 3 ECNI-MS fragmentation of PFBHA-derived aldehydes

PFBHA-Derived Aldehydes	***Syn*- fragments (m/z)**	***Anti*- fragments (m/z)**
HNE/HHE 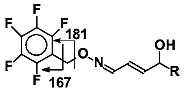 HHE: R=C_2H_5 (MW 309 g/mol) HNE: R=C_5H_{11} (MW 351 g/mol)	167 170 181 201 110 (HHE) $[M\text{-}C_7H_4F_5O]^-$ 241 (HHE) $[M\text{-}CF_2\text{- }H_2O]^-$ 259 (HHE) $[M\text{-}CF_2]^-$ 152 (HNE) $[M\text{-}C_7H_4F_5O]^-$ 283 (HNE) $[M\text{-}CF_2\text{- }H_2O]^-$ 301 (HNE) $[M\text{-}CF_2]^-$	167 179 181 192 201 241 (HHE) $[M\text{-}CF_2\text{-}H_2O]^-$ 259 (HHE) $[M\text{-}CF_2]^-$ 283 (HNE) $[M\text{-}CF_2\text{-}H_2O]$- 301 (HNE) $[M\text{-}CF_2]^-$
trans-2-nonenal/*trans*-2-hexenal 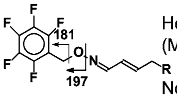 Hexenal: R=C_2H_5 (MW 293 g/mol) Nonenal: R=C_5H_{11} (MW 335 g/mol)	181 243 (Hexenal) $[M\text{-}CF_2]^-$ 285 (Nonenal) $[M\text{-}CF_2]^-$	178 181 197 243 (Hexenal) $[M\text{-}CF_2]^-$ 285 (Nonenal) $[M\text{-}CF_2]^-$
4-ONE (MW 544 g/mol) 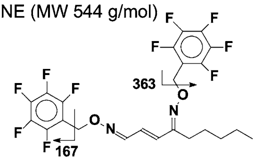 F F F F F 363 O N F F F F F O N 167	167 363	167 363
HNA (MW 353 g/mol) 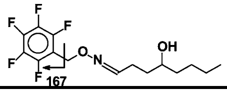 	167 178 316 $[M\text{-}H_2FO]^-$ 333 $[M\text{-}HF]^-$	167 178 316 $[M\text{-}H_2FO]^-$ 333 $[M\text{-}HF]^-$

with an r^2 value of 0.998 for 4-hydroxy-2-alkenals. PICI-MS yielded limits of quantitation below 250 fmol for 2-alkenals and 500 fmol for 4-hydroxy-2-alkenals, using $[M + H]^+$ and $[M + H–H_2O]^-$ for quantitation, respectively (Fig. 2c, d). Calibration curves were linear from 250 fmol to 2.5 pmol for 2-alkenals with an r^2 value of 0.995 and from 500 fmol to 10 pmol for 4-hydroxy-2-alkenals with an r^2 value of 0.997. Fragments with m/z 250 or 252 were not used for quantitation in PICI-MS analyses because they were not suitable for quantitation below 2.5 pmol. ECNI-MS yielded limits of quantitation below 100 fmol for 2-alkenals and 250 fmol for 4-hydroxy-2-alkenals using $[M–CF_2]^-$ for both classes of α,β-unsaturated aldehydes (Fig. 2e, f). Calibration curves were linear from 100 fmol to 10 pmol for 2-alkenals with an r^2 value of 0.999 and from 250 fmol to 10 pmol for 4-hydroxy-2-alkenals with an r^2 value of 1.00.

In order to show the role of each ionization method for characterization of α,β-unsaturated aldehydes in complex mixtures, we oxidized DHA and arachidonic acid. Using reconstructed ion chromatograms (RIC) of EI-MS spectra using m/z 250 or m/z 252 we were able to determine the presence of 4-substituted and unsubstituted α,β-unsaturated aldehydes. RIC of DHA and arachidonic acid oxidations using m/z 250 showed peaks corresponding to acrolein (RT 6.53 min) and MDA (RT 11.00 and 11.14 min) (Fig. 3a, b). The identity of these peaks was confirmed by comparison to pure standards. In addition, RIC of arachidonic acid with m/z 250 also showed peaks that likely correspond to *trans*-2-heptenal (RT 9.01 and 9.07) and *trans*-2-octenal (RT 9.48 and 9.64), the latter of which was identified as a product of arachidonic acid by Mlakar and Spiteller [20] (Fig. 3b, inset). The identity of these analytes was deduced using the $[M + H]^+$ ion (m/z 308 for *trans*-2-heptenal and m/z 322 for *trans*-2-heptenal) provided by PICI-MS analysis and the $[M–CF_2]^-$ ion (m/z 257 for trans-2-heptenal and m/z 271 for trans-2-octenal) provided by ECNI-MS analysis. RIC of arachidonic acid oxidations using m/z 252 contained one major peak corresponding to PFB-HNE (RT 11.06 and 11.17), consistent with previous evidence that HNE is the major 4-hydroxy-2-alkenal product of n-6 fatty acid oxidation [9]. RIC of DHA oxidations produced similar results in that the major peak represented by m/z 252 corresponded to PFB-HHE (RT 9.59 and 9.64) (Fig. 3c, d). However, there was an additional peak present in the DHA RIC that corresponded to the PFB-derivative of 4-hydroxy-2,6-nonadienal (RT 11.01 and 11.13), a product of DHA oxidation previously identified by Beckman et al. [5]. The structure of this analyte was deduced using the $[M + H–H_2O]^-$ (m/z 338) ion provided by PICI-MS and the $[M–CF_2]^-$ (m/z303) ion provided by ECNI-MS.

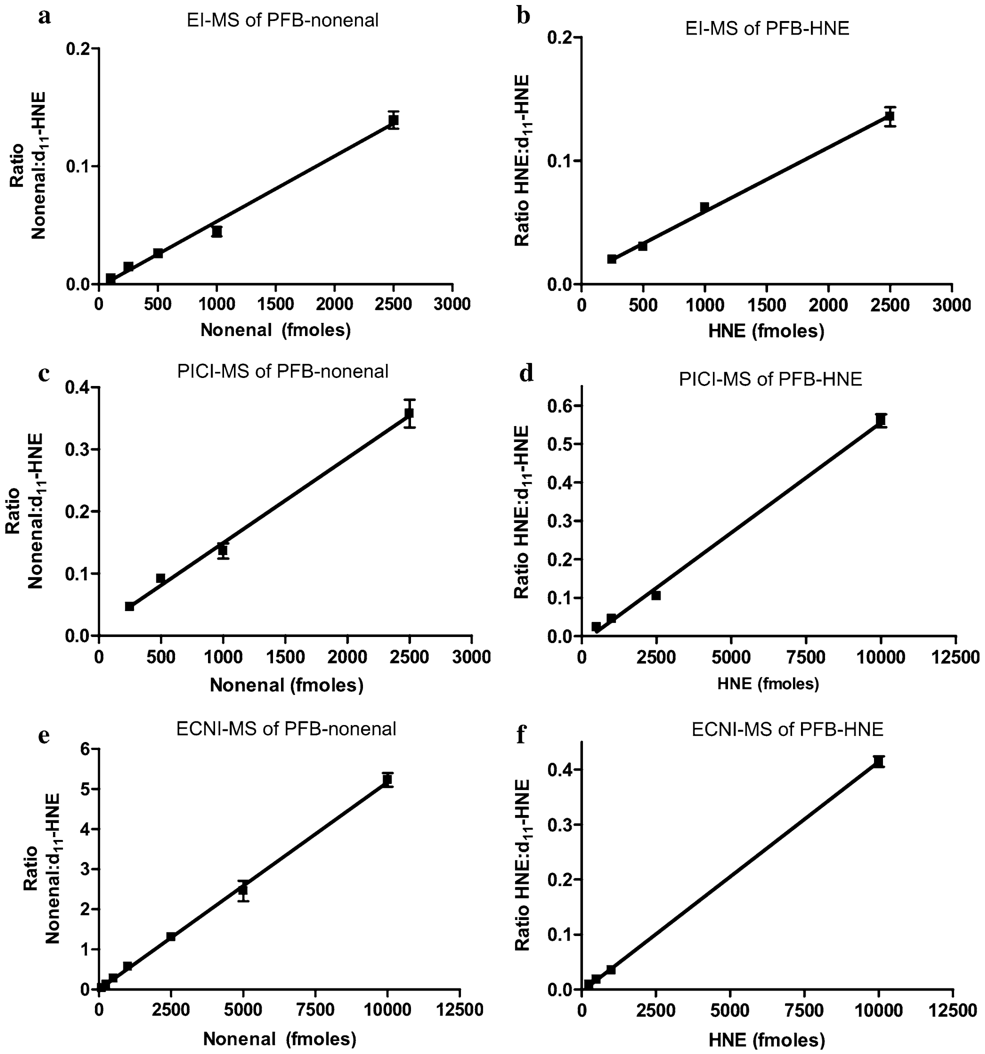

Fig. 2 Plots of linear regression analyses show the linear range in fmol for EI-MS, PICI-MS, and ECNI-MS. Linear ranges for EI-MS PFB-nonenal using *m*/*z* 250 and PFB-HNE using *m*/*z* 252 are represented by (**a**) and (**b**), respectively. Linear ranges for PICI-MS of PFB-nonenal using *m*/*z* 336 and PFB-HNE using *m*/*z* 334 are represented by (**c**) and (**d**), respectively. Linear ranges for ECNI-MS of PFB-nonenal using *m*/*z* 285 and PFB-HNE using *m*/*z* 301 are represented by (**e**) and (**f**), respectively

Discussion

Previous studies have catalogued the utility of derivatization with PFBHA for detection and quantification of biologically relevant molecules such as α,β-unsaturated aldehydes [10, 17]. In studies examining 4-hydroxylated aldehydes, PFBHA derivatization is often followed by trimethylsilylation. However, one study demonstrated that PFBHA derivatization alone can be used to detect and quantify known 4-hydroxy-2-alkenals in biological samples in the absence of trimethylsilylation using GC/ECNI-MS [10].

Our study demonstrates that EI-MS and PICI-MS produce simple and clear information regarding the C4-hydroxylation state of α,β-unsaturated aldehydes. In the case of 4-hydroxylated or unsubstituted α,β-unsaturated aldehydes, spectra contain either a *m*/*z* 252 or *m*/*z* 250 fragment, respectively. These fragments are the result of cleavage of the C3, C4 bond. The *m*/*z* 252 fragment is consistent with the transfer of two hydrogens during the fragmentation process. As fragmentation occurred between C3 and C4 with the PFB-containing fragment becoming positively charged, the hydrogens likely originate from either the C4/C4-hydroxyl moiety or from the C5–C9 hydrocarbon tail. As spectra of PFB-d_{11}-HNE, which is deuterated at the C5–C9 tail, contained a fragment with *m*/*z* 252 we concluded that deuteria were not transferred from this moiety. A possible origin of the hydrogens transferred during fragmentation are C4 and the C4-hydroxyl group. Analysis of the PFB-oxime of d_1-HNE resulted in a fragment with *m*/*z* 253 and indicates that the C4 deuterium along with another hydrogen of undefined origin were transferred to the charged fragment.

ECNI-MS is often used for the analysis of α,β-unsaturated aldehydes. However, ECNI-MS spectra of PFBHA-derived α,β-unsaturated aldehydes are complex in that they contain a number of peaks that are not easily related to structure of the analyte in question. Furthermore, ECNI-MS analysis is complicated by differences in the *syn*- and *anti*-configuration spectra [10]. These differences in

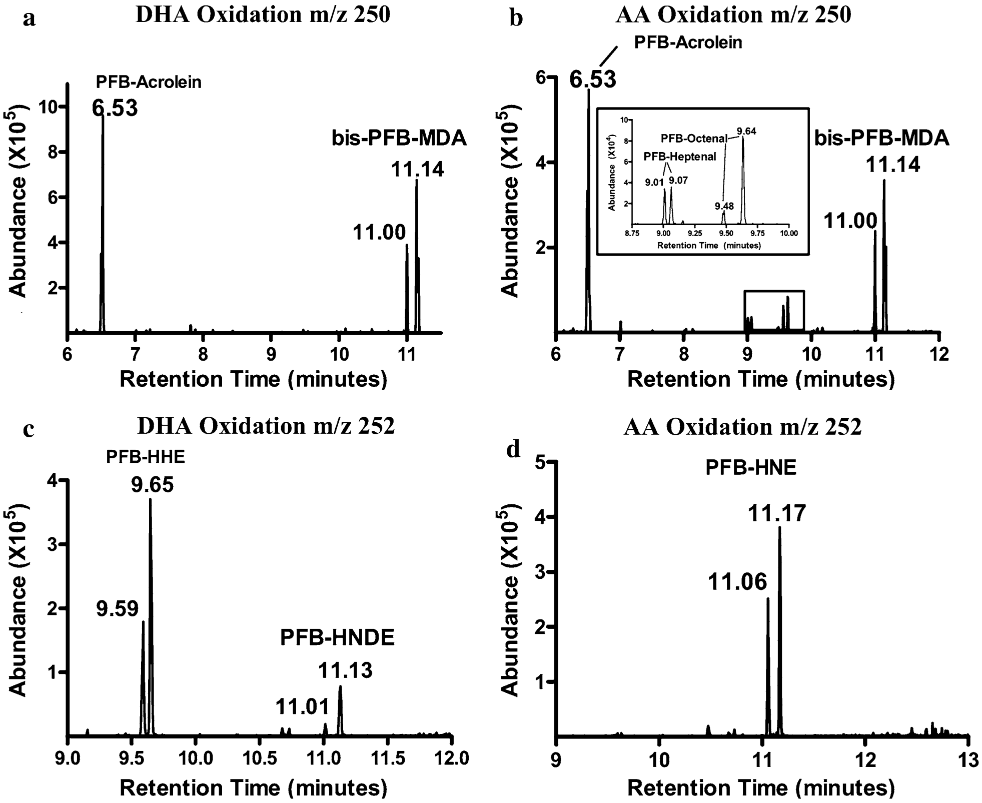

Fig. 3 A reconstructed ion chromatogram (RIC) of EI-MS analysis of an oxidation reaction of DHA using *m/z* 250 (**a**) resulted in two major peaks corresponding to PFB-acrolein and bis-PFB-malondialdehyde. RIC of EI-MS analysis of an oxidation reaction of arachidonic acid (AA) using *m/z* 250 (**b**) resulted in four peaks corresponding to PFB-acrolein, *trans*-2-heptenal (inset), *trans*-2-octenal (*inset*), and bis-PFB-MDA. RIC of EI-MS analysis of an oxidation reaction of DHA using *m/z* 252 (**c**) resulted in peaks corresponding to PFB-HHE and PFB-4-hydroxy-2,6-nonadienal. RIC of an EI-MS analysis of an oxidation reaction of arachidonic acid (AA) using *m/z* 252 (**d**) resulted in one peak corresponding to PFB-HNE

syn- and *anti*-spectra were not present when using EI-MS or PICI-MS. This complexity makes ECNI-MS a difficult method to utilize for structural characterization of unknown α,β-unsaturated aldehydes in complex biological mixtures.

Using pure standards, we were able to show that the three ionization methods used in this study were comparable in terms of sensitivity. ECNI-MS and EI-MS were equally sensitive, with PICI-MS being slightly less sensitive. Due to this similarity in sensitivity, these methods can be used in combination for characterization and identification of α,β-unsaturated aldehydes. The EI-MS spectra are useful because of the abundance of the *m/z* 250 and 252 fragments, which allows for characterization of 4-hydroxyl-substitution. PICI-MS is useful for determination of the molecular ion in the case of 2-alkenals, and the ion corresponding to addition of hydrogen and loss of water for 4-hydroxy-2-alkenals. Finally, ECNI-MS can be used to confirm the results obtained by EI-MS and PICI-MS using the $[M\text{-}CF_2]^-$ ion.

Each ionization technique utilized in our work can be used for quantitation of a known analyte as determined by comparison to pure standard. However, in the case of an unknown, none of these methods alone is sufficient for identification without corroboration from another source. We show that combinations of EI-MS, PICI-MS, and ECNI-MS can effectively be used to characterize and identify unknown α,β-unsaturated aldehydes produced by oxidation of DHA and arachidonic acid in the absence of pure standard. These results highlight the potential application of this combination of analyses to characterization and identification of α,β-unsaturated aldehydes in foods, supplements, and biological samples (Figs. 2, 3).

Acknowledgments This study was made possible by NIH grant P20 RR17699-01 COBRE from the NCRR. We thank Dr. Alena Kubatova for her training in the use of gas chromatography/mass spectrometry instrumentation. We thank Dr. Mikhail Golovko of the UND Mass Spectrometry Core Facility for performing the ESI-MS analyses.

References

1. St Angelo AJ (1996) Lipid oxidation on foods. Crit Rev Food Sci Nutr 36:175–224
2. Volkel W, Sicilia T, Pahler A, Gsell W, Tatschner T, Jellinger K, Leblhuber F, Riederer P, Lutz WK, Gotz ME (2006) Increased brain levels of 4-hydroxy-2-nonenal glutathione conjugates in severe Alzheimer's disease. Neurochem Int 48:679–686
3. Salomon RG, Kaur K, Podrez E, Hoff HF, Krushinsky AV, Sayre LM (2000) HNE-derived 2-pentylpyrroles are generated during oxidation of LDL, are more prevalent in blood plasma from patients with renal disease or atherosclerosis, and are present in atherosclerotic plaques. Chem Res Toxicol 13:557–564
4. Shibata N, Yamada S, Uchida K, Hirano A, Sakoda S, Fujimura H, Sasaki S, Iwata M, Toi S, Kawaguchi M, Yamamoto T, Kobayashi M (2004) Accumulation of protein-bound 4-hydroxy-2-hexenal in

spinal cords from patients with sporadic amyotrophic lateral sclerosis. Brain Res 1019:170–177

5. Beckman JK, Howard MJ, Greene HL (1990) Identification of hydroxyalkenals formed from omega-3 fatty acids. Biochem Biophys Res Commun 169:75–80
6. Kawai Y, Takeda S, Terao J (2007) Lipidomic analysis for lipid peroxidation-derived aldehydes using gas chromatography-mass spectrometry. Chem Res Toxicol 20:99–107
7. Porter NA, Caldwell SE, Mills KA (1995) Mechanisms of free radical oxidation of unsaturated lipids. Lipids 30:277–290
8. Gardner HW (1989) Oxygen radical chemistry of polyunsaturated fatty acids. Free Radic Biol Med 7:65–86
9. Esterbauer H, Schaur RJ, Zollner H (1991) Chemistry and biochemistry of 4-hydroxynonenal, malonaldehyde and related aldehydes. Free Radic Biol Med 11:81–128
10. Selley ML (1997) Determination of the lipid peroxidation product (E)-4-hydroxy-2-nonenal in clinical samples by gas chromatography—negative-ion chemical ionisation mass spectrometry of the *O*-pentafluorobenzyl oxime. J Chromatogr B Biomed Sci Appl 691:263–268
11. van Kuijk FJ, Thomas DW, Stephens RJ, Dratz EA (1986) Occurrence of 4-hydroxyalkenals in rat tissues determined as pentafluorobenzyl oxime derivatives by gas chromatography-mass spectrometry. Biochem Biophys Res Commun 139:144–149
12. Loidl-Stahlhofen A, Kern W, Spiteller G (1995) Gas chromatographic-electron impact mass spectrometric screening procedure for unknown hydroxyaldehydic lipid peroxidation products after pentafluorobenzyloxime derivatization. J Chromatogr B Biomed Appl 673:1–14
13. Chandra A, Srivastava SK (1997) A synthesis of 4-hydroxy-2-trans-nonenal and 4-(3H) 4-hydroxy-2-trans-nonenal. Lipids 32:779–782
14. Honzatko A, Brichac J, Murphy TC, Reberg A, Kubatova A, Smoliakova IP, Picklo MJ Sr (2005) Enantioselective metabolism of *trans*-4-hydroxy-2-nonenal by brain mitochondria. Free Radic Biol Med 39(7):913–924
15. Bloch R, Gilbert L (1987) Synthesis of both enantiomers of 4-substituted α,β-unsaturated 4-lactones. J Org Chem 52:4603–4605
16. Hjelle JJ, Petersen DR (1983) Metabolism of malondialdehyde by rat liver aldehyde dehydrogenase. Toxicol Appl Pharmacol 70:57–66
17. Luo XP, Yazdanpanah M, Bhooi N, Lehotay DC (1995) Determination of aldehydes and other lipid peroxidation products in biological samples by gas chromatography-mass spectrometry. Anal Biochem 228:294–298
18. Kawai Y, Fujii H, Okada M, Tsuchie Y, Uchida K, Osawa T (2006) Formation of Nε-(succinyl)lysine in vivo: a novel marker for docosahexaenoic acid-derived protein modification. J Lipid Res 47:386–398
19. Kubatova A, Murphy TC, Combs C, Picklo MJ Sr (2006) Astrocytic biotransformation of *trans*-4-hydroxy-2-nonenal is dose-dependent. Chem Res Toxicol 19:844–851
20. Mlakar A, Spiteller G (1996) Previously unknown aldehydic lipid peroxidation compounds of arachidonic acid. Chem Phys Lipids 79:47–53

Lipids (2008) 43:775–782
DOI 10.1007/s11745-008-3201-6

ORIGINAL ARTICLE

Calcium-Independent Phospholipase A_2 in Rabbit Ventricular Myocytes

Caroline S. Beckett · Jane McHowat

Received: 17 January 2008 / Accepted: 30 May 2008 / Published online: 24 June 2008
© AOCS 2008

Abstract We have previously reported that the majority of phospholipase A_2 (PLA_2) activity in rabbit ventricular myocytes is membrane-associated, calcium-independent ($iPLA_2$), selective for arachidonylated plasmalogen phospholipids and inhibited by the $iPLA_2$-selective inhibitor bromoenol lactone (BEL). Here, we identified the presence of $iPLA_2$ in rabbit ventricular myocytes, determined the full length sequences for rabbit $iPLA_2\beta$ and $iPLA_2\gamma$ and compared their homology to the human isoforms. Rabbit $iPLA_2\beta$ encoded a protein with a predicated molecular mass of 74 kDa that is 91% identical to the human $iPLA_2\beta$ short isoform. Full length $iPLA_2\gamma$ protein has a predicated molecular mass of 88 kDa and is 88% identical to the human isoform. Immunoblot analysis of $iPLA_2\beta$ and γ in membrane and cytosolic fractions from rabbit and human cardiac myocytes demonstrated a similar pattern of distribution with both isoforms present in the membrane fraction, but no detectable protein in the cytosol. Membrane-associated $iPLA_2$ activity was inhibited preferentially by the R enantiomer of bromoenol lactone [(*R*)-BEL], indicating that the majority of activity is due to $iPLA_2\gamma$.

Keywords Bromoenol lactone · Phospholipase A_2 · Myocardium · Plasmalogens · Arachidonic acid

Abbreviations

BEL	Bromoenol lactone
$iPLA_2$	Calcium-independent phospholipase A_2
MAFP	Methyl arachidonyl fluorophosphonate
PKC	Protein kinase C
PLA_2	Phospholipase A_2

Introduction

Phospholipase A_2 (PLA_2) catalyzes the hydrolysis of the fatty acid at the *sn*-2 position of membrane phospholipids, resulting in the generation of multiple biologically-active, membrane phospholipid-derived metabolites (for review, see [1]). The family of PLA_2 enzymes has been classified into 15 groups and several subgroups based on the catalytic mechanism, functional and structural features, and sequence homology [1].

We reported previously that the majority of PLA_2 activity in rabbit ventricular myocytes is membrane-associated, calcium-independent ($iPLA_2$) and selective for arachidonylated plasmalogen phospholipids [2]. Activation of this membrane-associated $iPLA_2$ occurs when ventricular myocytes are incubated with phorbol 12-myristate 13-acetate, suggesting that activation of $iPLA_2$ is regulated by protein kinase C [3]. We have also demonstrated that rabbit ventricular myocyte membrane-associated $iPLA_2$ is activated in response to either thrombin stimulation [4] or the presence of hypoxia [5]. Multiple types of $iPLA_2$ have been identified in cytosolic, microsomal and mitochondrial fractions from mammalian myocardium [6, 7], but to date there is no data concerning the specific $iPLA_2$ isoform that may be present and activated in rabbit ventricular myocytes. Our previous data indicate that rabbit ventricular myocyte $iPLA_2$ activity is inhibited by bromoenol lactone (BEL) but not by methyl arachidonyl fluorophosphonate (MAFP) [2], suggesting that it is either $iPLA_2\beta$ or $iPLA_2\gamma$.

C. S. Beckett · J. McHowat (✉)
Department of Pathology, Saint Louis University School of Medicine, 1402 S. Grand Blvd., St. Louis, MO 63104, USA
e-mail: jane.mchowat@tenethealth.com

The iPLA$_2\beta$ isoform is predominantly a cytosolic isoform and highly homologous cDNAs have been cloned from the hamster, mouse, rat and human (approximately 95% identity). In addition, several splice variants of human iPLA$_2\beta$ have been identified [8]. However, in COS-7 cells overexpressing iPLA$_2\beta$, Larsson Forsell et al demonstrated a 5.5-fold increase in membrane-associated iPLA$_2$ activity [8], and membrane-associated iPLA$_2\beta$ has also been found in rat vascular smooth muscle cells [9].

More recently, a novel membrane associated iPLA$_2$ (iPLA$_2\gamma$) has been identified [7] which possesses several of the properties demonstrated in our previous studies using rabbit ventricular myocytes, including the optimum pH for activity, sensitivity to BEL and a tight association with the membrane fraction. Homology between iPLA$_2\beta$ and iPLA$_2\gamma$ is confined to the ATP binding motif, the serine lipase site and a region of nine amino acids for which, as yet, there is no known functional significance [7]. The human iPLA$_2\gamma$ gene contains 4 possible translation codons that result in proteins of 63, 74, 77 and 88 kDa [10]. When first described, iPLA$_2\gamma$ was proposed to be localized to peroxisomes due to the presence of a C-terminal SKL signal sequence and recent studies have confirmed that the peroxisomal iPLA$_2\gamma$ is the 63-kDa protein [11]. More recent studies have demonstrated higher molecular weight isoforms of iPLA$_2\gamma$ in mitochondria and endoplasmic reticulum [6].

This study was designed to identify the presence of iPLA$_2\beta$ and iPLA$_2\gamma$ in rabbit ventricular myocytes and to determine the similarity of these isoforms to those identified previously.

Experimental Procedures

Rabbit Ventricular Myocyte Isolation and Culture

Adult rabbits of either sex weighing 2–3 kg were anesthetized with intravenous pentobarbitone sodium (50 mg/kg) and the heart rapidly removed. The heart was mounted on a Langendorff perfusion apparatus and perfused for 5 min with a Tyrode solution containing (mmol/l) NaCl 118, KCl 4.8, CaCl$_2$ 1.2, MgCl$_2$ 1.2, NaHCO$_3$ 24, KH$_2$PO$_4$ 1.2 and glucose 11; the Tyrode solution was saturated with 95%O$_2$/5%CO$_2$ to yield a pH of 7.4. This was followed by a 4-min perfusion with a Ca-free Tyrode solution containing EGTA (100 μM) and a final perfusion for 20 min with the Tyrode solution containing 100 μM Ca and 0.033% collagenase. The heart was removed from the perfusion apparatus, the atria were removed and the remaining ventricles were cut into small pieces and incubated in fresh 0.033% collagenase solution at 37 °C in a shaking water bath for 4 successive harvests of 20 min. Individual myocytes were washed with a HEPES buffer containing (mmol/l): NaCl 133.5, KCl 4.8, MgCl$_2$ 1.2, CaCl$_2$ 0.3, KH$_2$PO$_4$ 1.2, glucose 10 and HEPES 10 (pH 7.4). Extracellular Ca was increased to 1.2 mM in three stages at intervals of 20 min. Myocytes were incubated overnight in M199 medium with 10% fetal calf serum at 37 °C and then washed three times with 1.2 mM Ca HEPES solution.

Culture of Human Cardiac Myocytes

Human adult cardiac myocytes (Sciencell, San Diego, CA) were cultured in cardiac myocyte medium consisting of 500 ml of basal medium, 25 ml of fetal bovine serum, 5 ml of cardiac myocyte growth supplement and 5 ml of penicillin/streptomycin solution (Sciencell, San Diego, CA).

Generation of iPLA$_2$ Clones

Total RNA for use in all cloning steps was isolated with the Versagene Cell Kit (Gentra Systems, Minneapolis, MN); 5′ and 3′ end sequences of rabbit ventricular myocyte iPLA$_2$ were obtained by rapid amplification of cDNA ends following the manufacturer's instructions for the GeneRacer Kit from Invitrogen (Carlsbad, CA). Briefly, total RNA was dephosphorylated, decapped and ligated to the GeneRacer RNA Oligo to form template for first strand RACE-ready cDNA synthesis. Following cDNA amplification with the appropriate GeneRacer Oligo and gene specific Oligo, 5′ and 3′ end PCR fragments were cloned into the pCR4-TOPO vector and sequenced by automated DNA sequencing with BigDye chemistry. This sequence was conceptually translated and Oligos were designed to yield a full-length amplicon corresponding to the longest open reading frame for each isoform. Oligo dT primed first strand cDNA was generated from total RNA using the Thermoscript RT-PCR System (Invitrogen) and used as template for PCR amplification of full-length iPLA$_2$ clones. These products were cloned into the pCR-XL-TOPO vector and five independent clones of each isoform, β and γ, were sequenced. Sequence analysis and assembly was performed using the Vector NTI Suite 9.0.0 (Invitrogen) and the BLAST server at NCBI. Sequence assembly was performed using the ContigExpress program (Invitrogen) and the full-length cDNA sequences were deposited into Genbank (iPLA$_2\beta$—Accession # AY744674, iPLA$_2\gamma$—Accession # AY738591).

Production of iPLA$_2\gamma$ Antibody

A custom-made chicken antibody was obtained from Aves Labs, Inc. (Tigard, OR). Hens were injected four times with a KLH conjugate of the peptide CZSKYIERNEHKMK

KVAK and immune eggs were collected for 10–15 days after the final injection. The IgY fractions were purified and passed over an affinity column, the column washed and antibody eluted. The final concentration of affinity-purified antibody in the eluant was 0.6 mg/ml.

HPLC Separation of (*R*)- and (*S*)-Enantiomers of BEL

(*R*)- and (*S*)-enantiomers of BEL were isolated from racemic BEL (Calbiochem) using a chirex 3,5-dinitrobenzoyl-(*R*)-phenylglycine chiral HPLC column (Phenomenex Inc., Torrance, CA) and previously published methods [17]. The column was equilibrated with hexane/dichloroethane/ethanol (150:15:1, by vol) and the optical enantiomers eluted isocratically at 2 ml/min. Elution of (*R*)- and (*S*)-BEL was monitored by UV absorbance at 280 nm. Under these conditions the retention times (R_t) for (*R*)- and (*S*)-BEL differ by almost 1 min with the $\mathrm{R_t}$ for (*S*)-BEL being 11.1 min and 12.2 min for (*R*)-BEL [12]. Peaks corresponding to these R_t were collected, dried under N_2, and stored at −20 °C. The concentration of each enantiomer was determined spectrophotometrically based on its UV absorbance [12].

Immunoblot Analysis of iPLA$_2$ Isoforms

Myocytes were suspended in lysis buffer containing (mmol/l) HEPES 20 (pH 7.6), sucrose 250, dithiothreitol 2, EDTA 2, EGTA 2, β-glycerophosphate 10, sodium orthovanadate 1, phenylmethylsulfonyl fluoride 2, leupeptin 20 µg/ml, aprotinin 10 µg/ml and pepstatin A 5 µg/ml (buffer 2). Cells were sonicated on ice for 6 bursts of 10 s and centrifuged at 10,000×*g* at 4 °C for 20 min to remove cellular debris and nuclei. Cytosolic and membrane fractions were separated by centrifuging the supernatant at 100,000×*g* for 60 min. The pellet was resuspended in lysis buffer and the suspension centrifuged at 100,000×*g* for 60 min twice to minimize contamination of the membrane fraction with cytosolic protein. The final pellet was resuspended in lysis buffer containing 0.1% Triton X-100. Protein (cytosol or membrane) was mixed with an equal volume of SDS sample buffer and heated at 95 °C for 5 min prior to loading onto a 10% polyacrylamide gel. Protein was separated by SDS/PAGE at 200 V for 35 min and electrophoretically transferred to PVDF membranes (Bio-Rad, Richmond, CA) at 100 V for 1 h. Non-specific sites were blocked with Tris buffered solution containing 0.05% (v/v) Tween-20 (TBST) and 5% (w/v) nonfat milk for 1 h at room temperature. The blocked PVDF membrane was incubated with primary antibodies to iPLA$_2\beta$ (1 in 1,000 dilution, Cayman Chemical Company, Ann Arbor, MI) or iPLA$_2\gamma$ (1 in 1,000 dilution, Aves Labs Inc., Tigard, OR), followed by horseradish peroxidase-conjugated secondary antibodies. Regions of antibody binding were detected using enhanced chemiluminescence (Amersham, Arlington Heights, IL) after exposure to film (Hyperfilm, Amersham). Multiple exposures of film to the blots were developed.

Phospholipase A$_2$ Activity

Myocytes were suspended in 1 ml buffer containing (mmol/l): Sucrose 250, KCl 10, imidazole 10, EDTA 5, dithiothreitol (DTT) 2 with 10% glycerol, pH 7.8 (buffer 1). The suspension was sonicated on ice six times for 10 s (using a microtip probe at 20% power output, 500 Sonic Dismembrator, Fisher Scientific) and the sonicate centrifuged at 20,000×*g* for 20 min to remove cellular debris and nuclei. The supernatant was then centrifuged at 100,000×*g* for 60 min to separate the membrane fraction (pellet) from the cytosolic fraction (supernatant). The pellet was washed twice to minimize contamination of the membrane fraction with cytosolic protein by resuspending in buffer1, and centrifuging at 100,000×*g* for 60 min. The final pellet was resuspended in buffer 1. PLA$_2$ activity in cytosolic and membrane fractions was assessed by incubating enzyme (8 µg membrane protein) with 100 µM (16:0, [^{3}H]18:1) plasmenylcholine substrate in assay buffer containing (mmol/l): Tris 10, EGTA 4, 10% glycerol, pH 7.0 at 37 °C for 5 min in a total volume of 200 µl. The radiolabeled phospholipid substrate was introduced into the incubation mixture by injection in 5 µl ethanol to initiate the assay. Reactions were terminated by the addition of 100 µl butanol and released radiolabeled fatty acid was isolated by application of 25 µl of the butanol phase to channeled Silica Gel G plates, development in petroleum ether/diethyl ether/acetic acid (70/30/1, v/v) and subsequent quantification by liquid scintillation spectrometry. Protein content of each sample was determined by the Lowry method utilizing freeze dried bovine serum albumin as the protein standard. Radiolabeled (16:0, [^{3}H]18:1) plasmenylcholine was synthesized using [9,10-^{3}H] oleic acid and lysoplasmenylcholine as described in detail previously [4].

Statistical Analysis

Statistical comparison of values was performed by Student's *t* test. All results are expressed as mean ± SEM. Statistical significance was considered to be $P < 0.05$.

Results

iPLA$_2\beta$ cDNA was amplified, cloned and sequenced from freshly isolated rabbit ventricular myocytes, (GenBank accession No. 744674), and the amino acid sequence was determined (Fig. 1). The longest open reading frame of iPLA$_2\beta$ was found to encode a protein of 665 amino acids in length with a predicted molecular mass of 74 kDa that a BLAST analysis of the non-redundant protein database reveals is 91% identical to the human short isoform. The sequences are highly conserved except for a divergent segment at the N-terminus which is 128 amino acids long in the human and 42 amino acids in the rabbit. Immunoblot analysis of cytosolic and membrane fractions isolated from rabbit and human cardiac myocytes demonstrated an

Fig. 1 Full-length rabbit iPLA2β cDNA sequence. *Underlines* indicate the conserved ATP-binding and lipase active sites. Potential transmembrane domains were predicted using the TMpred server and are indicated with boldface type. Potential PKC-phosphorylation sites were predicted using the NetPhosK 1.0 Server and are boxed

```
atgcctcccagctgccgcccttctacgagagctccgtccaggtcctgcacgttgaggtcctgcagcacc
M  P  P  S  C  R  P  S  T  R  A  P  S  R  S  C  T  L  R  S  C  S  T
tgtccgacctcatccgcaaccaccccagctggtcggtggcgcacctggccgtggagactggggatccgt
C  P  T  S  S  A  T  T  P  A  G  R  W  R  T  W  P  W  R  L  G  I  R
gagtgcttccaccacagccgcatcatcagctgtgccaacagcacggagaatgaggagggctgcactccc
E  C  F  H  H  S  R  I  I  S  C  A  N  S  T  E  N  E  E  G  C  T  P
ctgcacctggcctgccgcaagggagacggggagattcttctggagctggtgcagtactgccacgcccag
L  H  L  A  C  R  K  G  D  G  E  I  L  L  E  L  V  Q  Y  C  H  A  Q
atggacgtcaccgacaacaaggggaaaccgccttccactacgctgtgcagggtgacaactcgcaggtg
M  D  V  T  D  N  K  G  E  T  A  F  H  Y  A  V  Q  G  D  N  S  Q  V
ctgcagctcctaggaaagaacgcgtcgacgggtgtgaaccaggtgaacagccaaggcctgaccccgctg
L  Q  L  L  G  K  N  A  S  T  G  V  N  Q  V  N  S  Q  G  L  T  P  L
cacctggcctgccagatgggcaagcaggagatggtccgcgtgctgctgctgtgcaacgcccgctgcaac
H  L  A  C  Q  M  G  K  Q  E  M  V  R  V  L  L  L  C  N  A  R  C  N
atcctggggcccgaaggctaccccatccacacggccatgaagttctcccagaggggtgtgctgagatg
I  L  G  P  E  G  Y  P  I  H  T  A  M  K  F  S  Q  R  G  C  A  E  M
atcatcagcatggacagcaaccagatccacagcaaagaccctcgctatggagccagcccctgcactgg
I  I  S  M  D  S  N  Q  I  H  S  K  D  P  R  Y  G  A  S  P  L  H  W
gccaagaatgcggagatggctcgcttgctgctgaagcgaggctgcgacgtgaacagcaccagctcctcg
A  K  N  A  E  M  A  R  L  L  L  K  R  G  C  D  V  N  S  T  S  S  S
gggtacacagccttgcacgtggccgtgatgcgcaaccgattcgagtgcgtcatggtgctgctcacctac
G  Y  T  A  L  H  V  A  V  M  R  N  R  F  E  C  V  M  V  L  L  T  Y
ggcgccaacgccgatgcccgcggcgagcacggcaacaccccgctgcacctggccgtgtcgaaagacaac
G  A  N  A  D  A  R  G  E  H  G  N  T  P  L  H  L  A  V  S  K  D  N
gtgganatggtcaaggccctcatcgtgtttggggcagaggtggacacacccaatgatttcggggagact
V  X  M  V  K  A  L  I  V  F  G  A  E  V  D  T  P  N  D  F  G  E  T
cctgccttcatagcctccaagatcagcaaacaactgcaggatgtcatgcacatctcccgggcccggaag
P  A  F  I  A  S  K  I  S  K  Q  L  Q  D  V  M  H  I  S  R  A  R  K
ccggcgtttatcctgagctccctgagggacgagaagcggacccatgaccacctgctctgcctggacggc
P  A  F  I  L  S  S  L  R  D  E  K  R  T  H  D  H  L  L  C  L  D  G
gggggcgtgaaaggcctcgtcatcatccagctcctcatcgccatcgagaaggcctcaggcgtggccacc
G  G  V  K  G  L  V  I  I  Q  L  L  I  A  I  E  K  A  S  G  V  A  T
aaggacctcttcgactgggtggcagggaccagcactggcggcatcctggccctggccatcctacacagt
K  D  L  F  D  W  V  A  G  T  S  T  G  G  I  L  A  L  A  I  L  H  S
aagtccatggcctacatgcgtggcgtgtacttccgcatgaaggatgaggtgttccggggctcgcggccc
K  S  M  A  Y  M  R  G  V  Y  F  R  M  K  D  E  V  F  R  G  S  R  P
tatgagtcggggcccctggaggagttcctgaagcgggagttcggggagcacaccaagatgacagacgtc
Y  E  S  G  P  L  E  E  F  L  K  R  E  F  G  E  H  T  K  M  T  D  V
aagaaacccaaggtgatgctgacggggacactgtctgaccggcagccggccgagctccacctcttccgc
K  K  P  K  V  M  L  T  G  T  L  S  D  R  Q  P  A  E  L  H  L  F  R
aattacgacgctccagagtccgtgcgggagcctcgcttcagcccgaacatcaacctgaagcccctgact
N  Y  D  A  P  E  S  V  R  E  P  R  F  S  P  N  I  N  L  K  P  L  T
cagccctcagaccagctggtgtggcgggcagcccggagcagtggggcggcccccacctacttccggcct
Q  P  S  D  Q  L  V  W  R  A  A  R  S  S  G  A  A  P  T  Y  F  R  P
aatgggcgcttcctggacggcgggctgctggccaacaaccccacgctggacgccatgaccgagatccac
N  G  R  F  L  D  G  G  L  L  A  N  N  P  T  L  D  A  M  T  E  I  H
gagtacaaccaggacctgatccgcaagggtcagagcgaaagggtgaagaaactctccatcgttgtctct
E  Y  N  Q  D  L  I  R  K  G  Q  S  E  R  V  K  K  L  S  I  V  V  S
ctggggacagggaggtccccgcaggtgcccgtgacctgcgtggacgtcttccgccccagcaacccctgg
L  G  T  G  R  S  P  Q  V  P  V  T  C  V  D  V  F  R  P  S  N  P  W
gagctggccaagactgtttttggggccaaggaacttggcaagatggtggtggactgttgcacggatccc
E  L  A  K  T  V  F  G  A  K  E  L  G  K  M  V  V  D  C  C  T  D  P
gacgggcgggccgtggaccgcgcgcgggcctggtgcgagatggtcggcatccagtacttcaggctgaac
D  G  R  A  V  D  R  A  R  A  W  C  E  M  V  G  I  Q  Y  F  R  L  N
ccccagctgggcgcggacatcatgctggacgaggtcagcgacgccgtgctggtcaacgccctctgggag
P  Q  L  G  A  D  I  M  L  D  E  V  S  D  A  V  L  V  N  A  L  W  E
accgaggtctacatctacgagcaccgagagcagttccagaaactcatccagctgctgctgtcaccatga
T  E  V  Y  I  Y  E  H  R  E  Q  F  Q  K  L  I  Q  L  L  L  S  P  -
```

iPLA$_2\beta$ immunoreactive band that ran just below the 80-kDa molecular mass marker (Fig. 3a). The human and rabbit immunoreactive bands ran at a similar molecular weight and were present in the membrane fraction only. No immunoreactive band was detected with iPLA$_2\beta$ antibody in the cytosolic fraction of human or rabbit myocytes (Fig. 3a).

Rabbit ventricular myocyte iPLA$_2\gamma$ was also cloned and sequenced, and is predicted to encode a full-length protein of 786 amino acids (Fig. 2) with a molecular mass of 88 kDa that was found by BLAST analysis to be 88% identical to the human form. It has been reported previously that the human iPLA$_2\gamma$ sequence contains multiple alternative start sites for translation, which correspond to protein products of 88, 77, 74 and 63 kDa [10]. We analyzed the amino acid sequence for iPLA$_2\gamma$ in rabbit ventricular myocytes and identified 6 methionine residues upstream of the active site which could encode functional PLA$_2$. In addition to the 88-, 77-, 74-, and 63-kDa isoforms found in the human isoform, we also identified two single amino acid substitutions which could encode alternative start sites for 58 and 49 kDa proteins. Immunoblot analysis of rabbit ventricular myocytes detected immunoreactive bands corresponding to the 88- and 73-kDa isoenzymes in the membrane fraction of isolated rabbit ventricular myocytes. Immunoblot analysis of human cardiac myocytes revealed a single band corresponding to the 73-kDa isoform of iPLA$_2\gamma$ in the membrane fraction (Fig. 3b). No bands were detected in the cytosolic fractions from either rabbit or human myocytes (Fig. 3b).

Since we detected both iPLA$_2\beta$ and γ in isolated rabbit ventricular myocytes and the majority of iPLA$_2$ activity is membrane-associated, we incubated isolated membrane fractions with (*R*)-BEL, (*S*)-BEL or racemic BEL. Previous studies have indicated that (*S*)-BEL is approximately an order of magnitude more selective for iPLA$_2\beta$ in

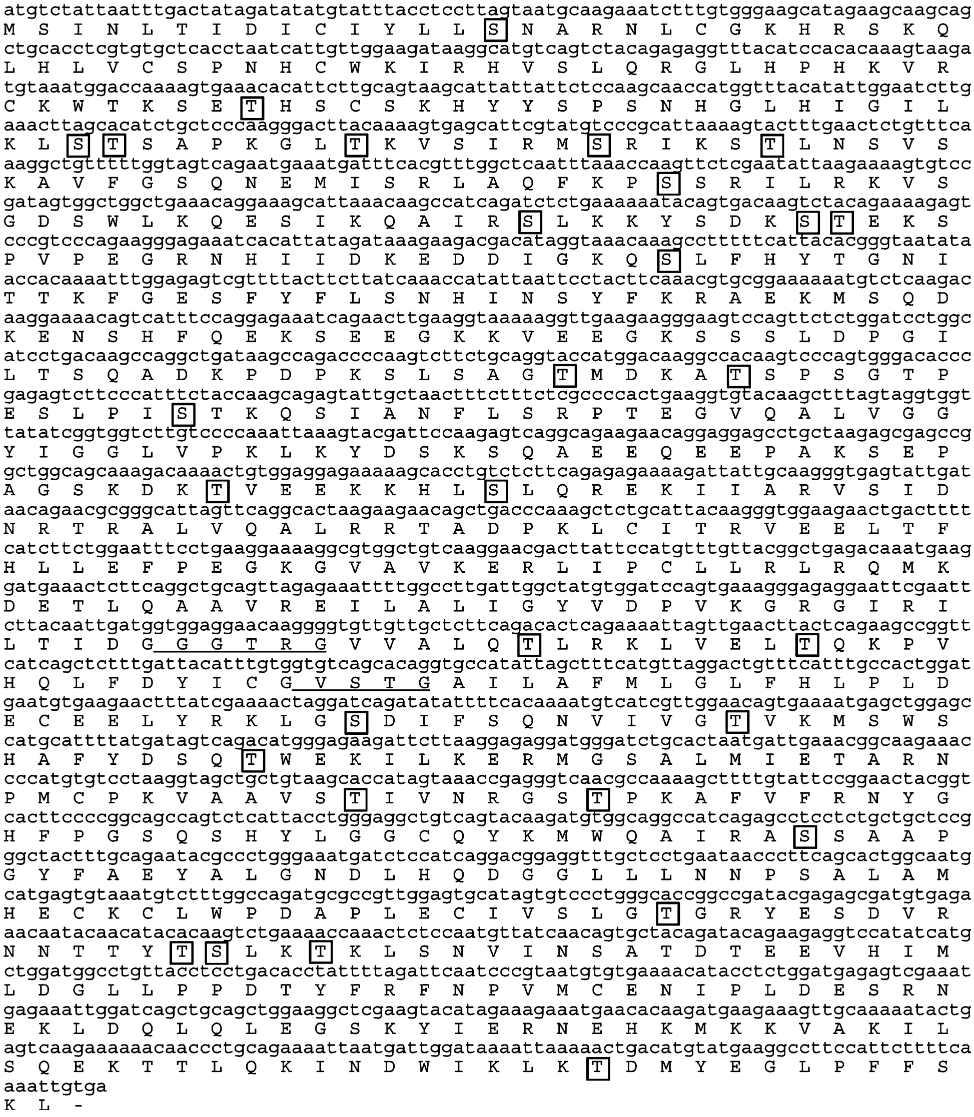

```
atgtctattaatttgactatagatatatgtatttacctccttagtaatgcaagaaatctttgtgggaagcatagaagcaagcag
M  S  I  N  L  T  I  D  I  C  I  Y  L  L  S  N  A  R  N  L  C  G  K  H  R  S  K  Q
ctgcacctcgtgtgctcacctaatcattgttggaagataaggcatgtcagtctacagagaggtttacatccacacaaagtaaga
L  H  L  V  C  S  P  N  H  C  W  K  I  R  H  V  S  L  Q  R  G  L  H  P  H  K  V  R
tgtaaatggaccaaaagtgaaacacattcttgcagtaagcattattattctccaagcaaccatggtttacatattggaatcttg
C  K  W  T  K  S  E  T  H  S  C  S  K  H  Y  Y  S  P  S  N  H  G  L  H  I  G  I  L
aaacttagcacatctgctcccaagggacttacaaaagtgagcattcgtatgtcccgcattaaaagtactttgaactctgtttca
K  L  S  T  S  A  P  K  G  L  T  K  V  S  I  R  M  S  R  I  K  S  T  L  N  S  V  S
aaggctgttttggtagtcagaatgaaatgatttcacgtttggctcaatttaaaccaagttctcgaatattaagaaaagtgtcc
K  A  V  F  G  S  Q  N  E  M  I  S  R  L  A  Q  F  K  P  S  S  R  I  L  R  K  V  S
gatagtggctggctgaaacaggaaagcattaaacaagccatcagatctctgaaaaaatacagtgacaagtctacagaaaagagt
G  D  S  W  L  K  Q  E  S  I  K  Q  A  I  R  S  L  K  K  Y  S  D  K  S  T  E  K  S
cccgtcccagaagggagaaatcacattatagataaagaagacgacataggtaaacaaagcctttttcattacacgggtaatata
P  V  P  E  G  R  N  H  I  I  D  K  E  D  D  I  G  K  Q  S  L  F  H  Y  T  G  N  I
accacaaaatttggagagtcgttttacttcttatcaaaccatattaattcctacttcaaacgtgcggaaaaaatgtctcaagac
T  T  K  F  G  E  S  F  Y  F  L  S  N  H  I  N  S  Y  F  K  R  A  E  K  M  S  Q  D
aaggaaaacagtcatttccaggagaaatcagaacttgaaggtaaaaaggttgaagaagggaagtccagttctctggatcctggc
K  E  N  S  H  F  Q  E  K  S  E  E  G  K  K  V  E  E  G  K  S  S  S  L  D  P  G  I
atcctgacaagccaggctgataagccagaccccaagtcttctgcaggtaccatggacaaggccacaagtcccagtgggacaccc
L  T  S  Q  A  D  K  P  D  P  K  S  L  S  A  G  T  M  D  K  A  T  S  P  S  G  T  P
gagagtcttcccatttctaccaagcagagtattgctaactttctttctcgccccactgaaggtgtacaagctttagtaggtggt
E  S  L  P  I  S  T  K  Q  S  I  A  N  F  L  S  R  P  T  E  G  V  Q  A  L  V  G  G
tatatcggtggtcttgtccccaaattaaagtacgattccaagagtcaggcagaagaacaggaggagcctgctaagagcgagccg
Y  I  G  G  L  V  P  K  L  K  Y  D  S  K  S  Q  A  E  E  Q  E  E  P  A  K  S  E  P
gctggcagcaaagacaaaactgtggaggagaaaaagcacctgtctcttcagagagaaaagattattgcaagggtgagtattgat
A  G  S  K  D  K  T  V  E  E  K  K  H  L  S  L  Q  R  E  K  I  I  A  R  V  S  I  D
aacagaacgcgggcattagttcaggcactaagaagaacagctgacccaaagctctgcattacaagggtggaagaactgactttt
N  R  T  R  A  L  V  Q  A  L  R  R  T  A  D  P  K  L  C  I  T  R  V  E  E  L  T  F
catcttctggaatttcctgaaggaaaaggcgtggctgtcaaggaacgacttattccatgtttgttacggctgagacaaatgaag
H  L  L  E  F  P  E  G  K  G  V  A  V  K  E  R  L  I  P  C  L  L  R  L  R  Q  M  K
gatgaaactcttcaggctgcagttagagaaattttggccttgattggctatgtggatccagtgaaagggagaggaattcgaatt
D  E  T  L  Q  A  A  V  R  E  I  L  A  L  I  G  Y  V  D  P  V  K  G  R  G  I  R  I
cttacaattgatggtggaggaacaaggggtgttgttgctcttcagacactcagaaaattagttgaacttactcagaagccggtt
L  T  I  D  G  G  G  T  R  G  V  V  A  L  Q  T  L  R  K  L  V  E  L  T  Q  K  P  V
catcagctctttgattacatttgtggtgtcagcacaggtgccatattagctttcatgttaggactgtttcatttgccactggat
H  Q  L  F  D  Y  I  C  G  V  S  T  G  A  I  L  A  F  M  L  G  L  F  H  L  P  L  D
gaatgtgaagaactttatcgaaaactaggatcagatatatttcacaaaatgtcatcgttggaacagtgaaaatgagctggagc
E  C  E  E  L  Y  R  K  L  G  S  D  I  F  S  Q  N  V  I  V  G  T  V  K  M  S  W  S
catgcattttatgatagtcagacatgggagaagattcttaaggagaggatgggatctgcactaatgattgaaacggcaagaaac
H  A  F  Y  D  S  Q  T  W  E  K  I  L  K  E  R  M  G  S  A  L  M  I  E  T  A  R  N
cccatgtgtcctaaggtagctgctgtaagcaccatagtaaaccgagggtcaacgccaaaagcttttgtattccggaactacggt
P  M  C  P  K  V  A  A  V  S  T  I  V  N  R  G  S  T  P  K  A  F  V  F  R  N  Y  G
cacttccccggcagccagtctcattacctgggaggctgtcagtacaagatgtggcaggccatcagagcctcctctgctgctccg
H  F  P  G  S  Q  S  H  Y  L  G  G  C  Q  Y  K  M  W  Q  A  I  R  A  S  S  A  A  P
ggctactttgcagaatacgccctgggaaatgatctccatcaggacggaggtttgctcctgaataacccttcagcactggcaatg
G  Y  F  A  E  Y  A  L  G  N  D  L  H  Q  D  G  G  L  L  L  N  N  P  S  A  L  A  M
catgagtgtaaatgtctttggccagatgcgccgttggagtgcatagtgtccctgggcaccggccgatacgagagcgatgtgaga
H  E  C  K  C  L  W  P  D  A  P  L  E  C  I  V  S  L  G  T  G  R  Y  E  S  D  V  R
aacaatacaacatacacaagtctgaaaaccaaactctccaatgttatcaacagtgctacagatacagaagaggtccatatcatg
N  N  T  T  Y  T  S  L  K  T  K  L  S  N  V  I  N  S  A  T  D  T  E  E  V  H  I  M
ctggatggcctgttacctcctgacacctatttagattcaatcccgtaatgtgtgaaaacatacctctggatgagagtcgaaat
L  D  G  L  L  P  P  D  T  Y  F  R  F  N  P  V  M  C  E  N  I  P  L  D  E  S  R  N
gagaaattggatcagctgcagctggaaggctcgaagtacatagaaagaaatgaacacaagatgaagaaagttgcaaaaatactg
E  K  L  D  Q  L  Q  L  E  G  S  K  Y  I  E  R  N  E  H  K  M  K  K  V  A  K  I  L
agtcaagaaaaaacaaccctgcagaaaattaatgattggataaaattaaaaactgacatgtatgaaggccttccattcttttca
S  Q  E  K  T  T  L  Q  K  I  N  D  W  I  K  L  K  T  D  M  Y  E  G  L  P  F  F  S
aaattgtga
K  L  -
```

Fig. 2 Full-length rabbit iPLA$_2\gamma$ cDNA sequence. *Underlines* indicate the conserved ATP-binding and lipase active sites. Potential PKC-phosphorylation sites were predicted using the NetPhosK 1.0 Server and are boxed

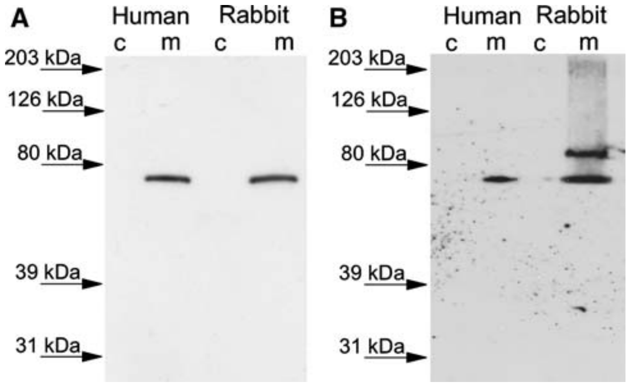

Fig. 3 Immunoblot analysis of the localization of iPLA$_2\beta$ (*Panel* **A**) and iPLA$_2\gamma$ (*Panel* **B**) in the cytosolic (*C*) and membrane (*M*) subcellular fractions isolated from rabbit and human cardiac myocytes. Proteins were separated by SDS-PAGE and transferred to polyvinylidene difluoride membranes. Membranes were probed with anti-iPLA$_2\beta$ or anti-iPLA$_2\gamma$ antibodies (1:1,000 dilution) and incubated with horseradish peroxidase-linked secondary antibody (1:50,000 dilution). Immunoblots were detected with enhanced chemiluminescence and exposure to film

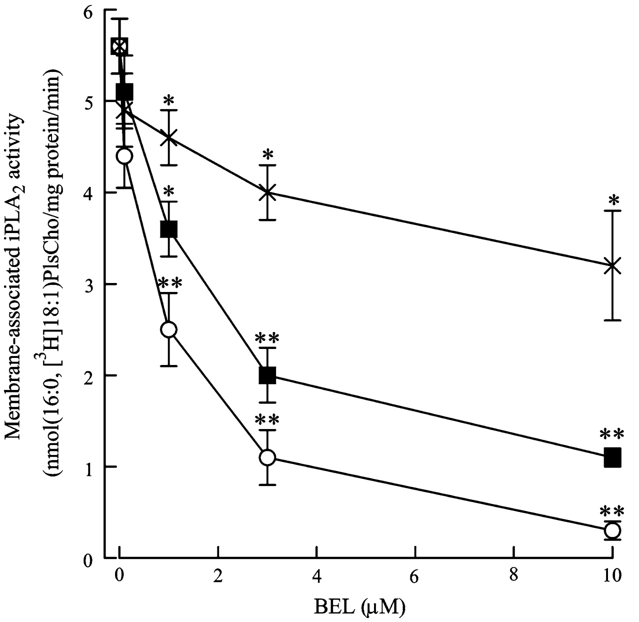

Fig. 4 Membrane-associated iPLA$_2$ activity measured in the absence or presence of bromoenol lactone (BEL). Isolated membrane fractions were incubated with increasing concentrations of (*R*)-BEL (*open circles*), (*S*)-BEL (X) or racemic BEL (*filled squares*) for 10 min prior to assay of PLA$_2$ activity. PLA$_2$ activity was measured using 100 μM (16:0, [^{3}H]18:1) plasmenylcholine (PlsCho) in the absence of Ca (4 mM EGTA). Values are mean ± SEM for independent results from six separate animals. *$P < 0.05$, **$P < 0.01$ when compared to activity in the absence of BEL

comparison to iPLA$_2\gamma$ [12]. Conversely, (*R*)-BEL is approximately an order of magnitude more selective for iPLA$_2\gamma$ in comparison to iPLA$_2\beta$ [12]. After pretreatment with BEL for 10 min, membrane-associated iPLA$_2$ activity was significantly decreased with concentrations of (*R*)-BEL greater than 0.1 μM (Fig. 4). At 10 μM, (*R*)-BEL inhibited iPLA$_2$ activity by 90%, whereas (*S*)-BEL inhibited iPLA$_2$ activity by approximately 50% (Fig. 4).

Discussion

Myocardial iPLA$_2$ activity in the rabbit was first described by Ford et al. [13]. They described a tenfold increase in microsomal, plasmalogen-selective iPLA$_2$ activity during myocardial ischemia [13]. We have demonstrated increases in membrane-associated, plasmalogen-selective iPLA$_2$ activity in isolated rabbit ventricular myocytes in response to thrombin [14] and hypoxia [5]. The activation of iPLA$_2$ and accelerated plasmalogen phospholipid hydrolysis lead to the production of lysoplasmenylcholine [5, 14], an amphipathic metabolite that can have direct effects on the function of integral membrane proteins. We have shown that lysoplasmenylcholine produces action potential derangements in cardiac myocytes at much lower concentrations than that previously demonstrated for lysoplasmenylcholine [5]. The action potential derangements caused by lysoplasmenylcholine occur as a result of its action on multiple membrane currents [15].

Although several studies have described iPLA$_2$ activation in rabbit ventricular myocytes, this is the first study to sequence iPLA$_2\beta$ and iPLA$_2\gamma$ and to demonstrate that iPLA$_2\gamma$ is the major isoform in the rabbit myocardium. Our immunoblot analysis data suggest that the vast majority of iPLA$_2$ is membrane-associated, and this agrees with our previous data measuring iPLA$_2$ activity [2]. In previously reported studies, iPLA$_2\beta$ has been demonstrated to be primarily cytosolic. It was originally purified from the cytosol of the mouse macrophage cell line P388D$_1$ [16] and its cDNA was later identified in P388D$_1$ and Chinese hamster ovary cells [17] and human B lymphocytes [18]. In humans the difference between the membrane-associated and cytosolic isoforms is the presence of 54 amino acid residues that may lead to a membrane-associated protein [8]. While we did not identify a similar sequence in the rabbit isoform, TMpred analysis suggests that rabbit iPLA$_2\beta$ contains a potential transmembrane domain (indicated by the boldface type in Fig. 1).

In a previous study, we have identified the presence of multiple iPLA$_2$ isoforms in several tissues and species [6]. The role of myocardial iPLA$_2$ isoforms has been investigated in several recent studies using mouse models. iPLA$_2$ activity in murine heart is less than 5% of that in human myocardium, suggesting that the mouse could be a species-specific knockdown model of human ischemia-induced arrhythmogenesis [19]. Accordingly, Mancuso et al. [19] generated transgenic mice that expressed amounts of iPLA$_2\beta$ activity comparable to that present in human myocardium and demonstrated malignant ventricular arrhythmias, increased fatty acid release in venous effluents and increased lysophospholipid content in the ischemic zone in response to ischemia. These data demonstrate the role of myocardial iPLA$_2\beta$ in the hydrolysis of membrane phospholipids and arryhthmogenesis in response to ischemia. Transgenic mice expressing iPLA$_2\gamma$ in cardiac myocytes demonstrated a marked loss of mitochondrial phospholipids accompanied by mitochondrial dysfunction [20]. In a subsequent study, mice null for iPLA$_2\gamma$ displayed growth retardation, cold intolerance, reduced exercise endurance and abnormal mitochondrial function [21]. In particular, iPLA$_2\gamma$ knockout mice were more susceptible to sudden death following transverse aortic constriction, indicating the importance of iPLA$_2\gamma$ in the ability of the myocardium to respond to stress [21].

We have previously reported that incubation of isolated membrane fractions from rabbit ventricular myocytes demonstrate increased iPLA$_2$ activity when incubated with phorbol 12-myristate 13-acetate in the absence of Ca [3]. These data suggests that a membrane-associated novel PKC isoform modulates iPLA$_2$ activity. Increased iPLA$_2$ activity required the presence of ATP, suggesting that the enzyme is phosphorylated by PKC [3]. Sequence analysis of rabbit ventricular myocyte iPLA$_2\beta$and γ isoforms reveals the presence of several predicted PKC phosphorylation sites that are indicated by the boxes in Figs. 1 and 3.

In conclusion, we have identified and sequenced iPLA$_2\beta$and iPLA$_2\gamma$ from isolated rabbit ventricular myocytes. These isoforms possess a high degree of sequence homology between rabbit and human and there is a similar protein expression pattern when comparing rabbit and human cardiac myocytes. Both isoforms have several putative PKC phosphorylation sites and our previous studies suggest that membrane-associated iPLA$_2$ is activated directly by a membrane-associated novel PKC isoform [3]. Finally, our data obtained using (*R*)- and (*S*)-enantiomers of the iPLA$_2$-selective inhibitor BEL, suggest that the majority of membrane-associated iPLA$_2$ activity is iPLA$_2\gamma$.

Acknowledgments This research was supported in part by National Heart, Lung and Blood Institute Grant HL 68588 (JM). The authors would like to thank Dr. Brian Cummings for the separation of (*R*)- and (*S*)-enantiomers of BEL.

References

1. Schaloske RH, Dennis EA (2006) The phospholipase A$_2$ superfamily and its group numbering system. Biochim Biophys Acta 1761:1246–1259
2. McHowat J, Creer MH (1998) Calcium-independent phospholipase A$_2$ in isolated rabbit ventricular myocytes. Lipids 33:1203–1212
3. Steer SA, Wirsig KC, Creer MH, Ford DA, McHowat J (2002) Regulation of membrane-associated iPLA$_2$ activity by a novel PKC in ventricular myocytes. Am J Physiol 283:C1621–C1626
4. McHowat J, Creer MH (1998) Thrombin activates a membrane-associated calcium-independent PLA$_2$ in ventricular myocytes. Am J Physiol 274:C447–C454
5. McHowat J, Liu SJ, Creer MH (1998) Selective hydrolysis of plasmalogen phospholipids by Ca^{2+}-independent PLA$_2$ in hypoxic ventricular myocytes. Am J Physiol 274:C1727–C1737
6. Kinsey GR, Cummings BS, Beckett CS, Saavedra G, Zhang W, McHowat J, Schnellmann RG (2005) Identification and distribution of endoplasmic reticulum iPLA$_2$. Biochem Biophys Res Commun 327:287–293
7. Mancuso DJ, Jenkins CM, Gross RW (2000) The genomic organization, complete mRNA sequence, cloning, and expression of a novel human intracellular membrane-associated calcium-independent phospholipase A$_2$. J Biol Chem 275:9937–9945
8. Larsson Forsell PK, Kennedy BP, Claessen HE (1999) The human calcium-independent phospholipase A$_2$ gene multiple enzymes with distinct properties from a single gene. Eur J Biochem 262:575–585
9. Miyake R, Gross RW (1992) Multiple phospholipase A$_2$ activities in canine vascular smooth muscle. Biochim Biophys Acta 1165:167–176
10. Mancuso DJ, Jenkins CM, Cohen JM, Sims HF, Yang J, Gross RW (2004) Complex transcriptional and translational regulation of iPLA$_2\gamma$ resulting in multiple gene products containing dual competing sites for mitochondrial or peroxisomal localization. Eur J Biochem 271:4709–4724
11. Yang J, Han X, Gross RW (2003) Identification of hepatic peroxisomal phospholipase A$_2$ and characterization of arachidonic acid-containing choline glycerophospholipids in hepatic peroxisomes. FEBS Lett 546:247–250
12. Jenkins CM, Han X, Mancuso DJ, Gross RW (2002) Identification of calcium-independent phospholipase A$_2$ (iPLA$_2$) β, and not iPLA$_2\gamma$, as the mediator of arginine vasopressin-induced arachidonic acid release in A-10 smooth muscle cells. Enantioselective mechanism-based discrimination of mammalian iPLA$_2$s. J Biol Chem 277:32807–32814
13. Ford DA, Hazen SL, Saffitz JE, Gross RW (1991) The rapid and reversible activation of a calcium-independent plasmalogen-selective phospholipase A$_2$ during myocardial ischemia. J Clin Invest 88:331–335
14. McHowat J, Creer MH (2000) Selective plasmalogen substrate utilization by thrombin-stimulated Ca^{2+}- independent PLA$_2$ in cardiomyocytes. Am J Physiol 278:H1933–H1940
15. Liu SJ, Creer MH, Kennedy RH, McHowat J (2003) Alterations in Ca^{2+} cycling by lysoplasmenylcholine in adult rabbit ventricular myocytes. Am J Physiol 284:C826–C838
16. Ackermann EJ, Kempner ES, Dennis EA (1994) Ca^{2+}-independent cytosolic phospholipase A$_2$ from macrophage-like P388D$_1$ cells. Isolation and characterization. J Biol Chem 269:9227–9233
17. Balboa MA, Balsinde J, Jones SS, Dennis EA (1997) Identity between the Ca^{2+}-independent phospholipase A$_2$ enzymes from P388D$_1$ macrophages and CHO cells. J Biol Chem 272:8576–8580
18. Larsson PK, Claesson HE, Kennedy BP (1998) Multiple splice variants of the human calcium-independent phospholipase A$_2$ and their effect on enzyme activity. J Biol Chem 273:207–214
19. Mancuso DJ, Abendschein DR, Jenkins CM, Han X, Saffitz JE, Schuessler RB, Gross RW (2003) Cardiac ischemia activates calcium-independent phospholipase A$_2\beta$, precipitating ventricular tachyarrhythmias in transgenic mice: rescue of the lethal

electrophysiologic phenotype by mechanism-based inhibition. J Biol Chem 278:22231–22236

20. Mancuso DJ, Han X, Jenkins CM, Lehman JJ, Sambandam N, Sims HF, Yang J, Yan W, Yang K, Green K, Abendschein DR, Saffitz JE, Gross RW (2007) Dramatic accumulation of triglycerides and precipitation of cardiac hemodynamic dysfunction during brief caloric restriction in transgenic myocardium expressing human calcium-independent phospholipase $A_2\gamma$. J Biol Chem 282:9216–9227

21. Mancuso DJ, Sims HF, Han X, Jenkins CM, Guan SP, Yang J, Moon SH, Pietka T, Abumrad NA, Schlesinger PH, Gross RW (2007) Genetic ablation of calcium-independent phospholipase $A_2\gamma$ leads to alterations in mitochondrial lipid metabolism and function resulting in a deficient mitochondrial bioenergetic phenotype. J Biol Chem 282:34611–34622

Lipids (2008) 43:783–791
DOI 10.1007/s11745-008-3211-4

ORIGINAL ARTICLE

Dietary Conjugated Linoleic Acid Renal Benefits and Possible Toxicity vary with Isomer, Dose and Gender in Rat Polycystic Kidney Disease

Malcolm R. Ogborn · Evan Nitschmann · Aviva Goldberg · Neda Bankovic-Calic · Hope A. Weiler · Harold M. Aukema

Received: 26 November 2007 / Accepted: 18 June 2008 / Published online: 16 July 2008
© AOCS 2008

Abstract Conjugated linoleic acid (CLA) is anti-proliferative and anti-inflammatory in the Han:SPRD-*cy* rat model of kidney disease. We used different doses of CLA and examined effects on renal histological benefit, the renal PPARγ system and hepatic and renal levels of CLA isomers. Male and female offspring of Han:SPRD-*cy* heterozygotes were fed diets with 0, 1 or 2% CLA isomer mixture for 12 weeks before dual-energy X-ray absorptiometry, harvest of renal and hepatic tissue for histologic and lipid analysis. Both CLA diets reduced body fat content in both genders but did not change lean body mass. CLA produced a dose dependent reduction in female renal cystic change. CLA reduced fibrosis, but this reduction was significantly less with higher dose in males. CLA reduced macrophage infiltration, tissue oxidized LDL content and proliferation of epithelial cells. Serum creatinine rose significantly in female animals fed CLA diets. CLA treatment did not change PPARγ activation. A significant negative correlation with renal content of the 18:2 c9,t11 isomer and the sum of histologic effects was identified. CLA reduces histologic renal injury in the Han:SPRD-*cy* rat model probably inversely proportionate to c9,t11 renal content. Possible functional CLA toxicity at high dose in female animals warrants further exploration.

Keywords Polycystic kidney disease · Conjugated linoleic acid · Inflammation · Rat · Nutrition · Body composition

Abbreviations

ARA	Arachidonic acid
ALA	α-linolenic acid
CLA	Conjugated linoleic acid
CO	Corn oil
DHA	Docosahexaenoic acid
DXA	Dual-energy X-ray absorptiometry
EPA	Eicosapentaenoic acid
GC	Gas chromatography
LNA	Linoleic acid
ox-LDL	Oxidized low density lipoprotein
PCNA	Proliferating cell nuclear antigen
PGE_2	Prostaglandin E_2
PKD	Polycystic kidney disease
PPAR	Peroxisome proliferator-activated receptor
PUFA	Polyunsaturated fatty acid

Introduction

Conjugated linoleic acid (CLA) refers to a group of positional and geometric isomers of linoleic acid produced by bacterial action in the gastrointestinal tract of ruminants [1, 2] that are significant dietary components in humans on

---

M. R. Ogborn · E. Nitschmann · A. Goldberg ·
N. Bankovic-Calic · H. M. Aukema
Department of Pediatrics and Child Health,
University of Manitoba, JBRC513-715 McDermot Avenue,
Winnipeg, MB R3C 3P4, Canada

M. R. Ogborn · H. M. Aukema
Department of Human Nutritional Sciences,
University of Manitoba, Winnipeg, MB, Canada

H. A. Weiler
School of Dietetics and Human Nutrition,
McGill University, Montreal, QC, Canada

M. R. Ogborn (✉)
9-386 3333 University Way, Prince George,
BC V2N 4Z9, Canada
e-mail: ogborn@unbc.ca

hunter-gatherer or primitive agrarian diets, but exposure is much lower in modern urban diets [3]. CLA has been shown to have a dose dependent effect on tumor development or growth in skin, prostate, mammary and colonic tumors [2, 4, 5]. CLA feeding has demonstrated beneficial effects in a murine model of lupus nephritis [6]. CLA produces tissue specific alteration in production of eicosanoids [7, 8], and decreases release of arachidonic acid (ARA) or prostaglandin E_2 (PGE_2) in different tissue types or cell lines [9–12]. CLA has been associated with improved outcome in experimental porcine colitis [13], and is capable of exerting an anti-inflammatory effect without compromising resistance to infection [14]. CLA has been identified as a ligand for PPARα, through which effects on lipid and carbohydrate metabolism may be modified [15], and PPARγ, through which anti-inflammatory and anti-proliferative effects may be modulated [16].

In a previous study, we demonstrated that dietary supplementation with a mixture of CLA isomers was effective in reducing histologic injury and renal PGE_2 production in male animals with the Han:SPRD-*cy* form of polycystic kidney disease [11]. The Han:SPRD-*cy* model of polycystic kidney disease (PKD), characterized by autosomal dominant inheritance with marked sexual dimorphism in expression, has proved an excellent system in which to explore the modification of chronic renal injury, including by dietary means. Epithelial proliferation and progressive dilatation of nephrons, marked interstitial inflammation and fibrosis characterize the disease [17]. Oxidant injury has been implicated in its pathogenesis [18]. It can be ameliorated with methylprednisolone [19], angiotensin blockade or converting enzyme inhibition [20, 21], and lovastatin [22]. Amelioration occurs with dietary soy protein substitution [23], protein restriction [21], flaxseed, flax oil or flax lignans [24–28] and citrate supplementation [29].

Although this model is amenable to dietary modification, a recent study we performed with flax derivatives demonstrated that gender influenced the extent of the dietary benefit [27], with female animals with an earlier stage of the disease demonstrating greater beneficial changes in renal histology. This study was therefore undertaken to explore if the observed benefits of CLA supplementation could be increased with a higher level of supplementation and as well as whether this response was influenced by animal gender. As secondary objectives, we explored if histologic benefits were associated with reduction in renal PPARγ activation and whether benefit could be correlated with tissue level changes in specific CLA isomers. We also explored previously reported effects of CLA on body composition to see if they are reproduced in animals with renal disease, and if these showed any relationship to renal histologic and functional change.

Methods

Animals

All animal procedures and care were approved by the University of Manitoba Committee on Animal Use and were within the guidelines of the Canadian Council on Animal Care. Surviving offspring of known Han:SPRD-*cy* heterozygotes from our own breeding colony were randomly assigned to groups fed 7% by weight corn oil as the lipid source alone, 6% corn oil and 1% CLA concentrate, or 5% corn oil and 2% CLA concentrate ad libitum at weaning at 3 weeks of age. CLA concentrate was a gift of Bioriginal, Saskatoon, Canada, and was diluted into the oil fraction of the diet to achieve the target concentrations. Animals were killed after 12 weeks on the diet and kidney, liver and serum collected for analysis. Animals found not to have PKD at necropsy, approximately one-third of the total, were excluded from further analysis. Diets were based on the formula from prior studies [11, 27] using casein as the protein source (20% by weight) supplemented with 0.3% methionine, corn starch (52% by weight) and dextrose (13% by weight) as the carbohydrate sources and lipid sources as described. The detailed analysis of the dietary fatty acid content is summarized in Table 1. The animals were fed ad libitum, as our prior studies have not found differences in intake related to disease status in animals in the earlier stages of disease progression [11, 23, 28, 30].

Table 1 Lipid analysis of CLA diets

Lipid	Control	1% CLA	2% CLA
C13:0	ND	1.9	2.5
C16:0	10.6	9.6	10.2
C18:0	0.1	1.6	1.8
C18:1 c9	28.6	26.1	27.7
C18:1 c11	ND	0.50	0.53
C18:2 9c,12c	56.3	57.3	52.7
C18:2 9c,11t	ND	0.45	1.25
C18:2 10t,12c	ND	0.45	1.26
C18 :2 10t,12t	ND	0.14	0.20
C18:3 n6	0.4	0.19	ND
C18:3 n3	1.1	0.74	0.85
C20:0	ND	0.36	0.39
C20:1	ND	0.21	0.30
C22:0	0.1	0.11	0.11
C20:3 n6	0.2	0.13	n.d.
C22:2	ND	0.11	0.15

ND not detected

Results expressed as mol% total lipid

DXA Scanning

Animals were anesthetized after 12 weeks of study using sodium pentobarbital (65 mg/kg, i.p.), followed by measurement of whole body weight and body composition including bone mass using dual-energy X-ray absorptiometry and the small animal software (QDR 4500A, Hologic Inc, Waltham, MA). This technology has been validated for use in rodents [31].

Histology and Immunohistochemistry

Tissue from the left kidney was processed using our previously described methods [11, 26] for histologic and immunohistochemical analysis. These studies included hematoxylin and eosin, Sirius red staining for fibrosis, PCNA (M 0879, Dako A/S, Glostrup, Denmark) and macrophages (MAB1435, Chemicon International, Temecula, CA). Oxidized LDL (ox-LDL) staining was used as a marker of oxidant injury [27, 32], using a polyclonal antibody (AB3230, Chemicon, Temecula, CA). Animals were classified as affected by one of two experienced observers (N.B.C., M.R.O.), blinded to dietary intervention on the basis of the characteristic cystic and inflammatory pathology of this disease.

Image Analysis

Image analysis procedures were performed with a system consisting of a Spot Junior CCD camera mounted on an Olympus BX60 microscope. The captured images from random stage movement through the sections were subsequently analyzed using Image Pro version 4.5 Package (Media Cybernetics, Silver Spring, MD). The observer was blinded to dietary treatment, although disease status is obvious upon microscopic examination. Raw analysis data were processed as previously described [23] to give objective measures of cystic change, fibrosis, interstitial macrophage infiltration and extent of ox-LDL staining. Measurements of fibrosis and cellular markers were corrected to solid-tissue areas of sections so that the presence of empty cystic areas on the section did not lead to an underestimation of these parameters.

Chemistry

Biochemical measurements were performed by an observer blinded to disease status and dietary intervention (E.N.). Serum and urine creatinine, and serum cholesterol were determined by spectrophotometric methods using Sigma kits (Sigma Chemical Co., St Louis, MO). Urine protein was measured by the brilliant Coomassie Blue method of Bradford.

Gas Chromatography

Lipids were extracted for gas chromatographic analysis using a modified Folch extraction procedure, as we have previously described [23, 26, 33]. Liver tissue was examined in addition to kidney as our previous studies have shown this tissue to be a more sensitive and consistent marker to confirm absorption and incorporation of the ingested PUFA. Prior to analysis, samples were redissolved in 1 ml of dry toluene, mixed with 2.0 ml of 0.5 M sodium methoxide and heated to 50 °C for 10 min, then mixed with 0.1 ml of glacial acetic acid, 5 ml of distilled H_2O, and 5 ml of hexane. This method was selected as being reliable for the methylation of the CLA isomers which were primary interest in tissue analysis in this study [34]. After vortexing, the mixture was centrifuged at $2{,}500\times g$ for 10 min and the hexane fraction removed. Fresh hexane is added to the remaining solution and the previous steps repeated. The hexane fractions were dried under anhydrous sodium sulfate, evaporated under nitrogen and the lipid esters redissolved in 1 ml hexane. Gas chromatography (GC) was performed on a Varian Chrompack 3800 instrument, using a Varian CP-Sil 88 100 meter column (Varian, Walnut Creek, CA). Total $\omega6{:}\omega3$ ratio was calculated from the sum of proportions of linoleic acid (LNA, 18:2 c9,c12), γ-linolenic acid (GLA), 20:3 $\omega6$ and ARA divided by the sum of α-linolenic acid (ALA), 20:3 $\omega3$, eicosapentaenoic acid (EPA), and docosahexaenoic acid (DHA). The ratio of ARA:LNA was calculated as an indicator of Δ-6 desaturase activity. The ratio of 18:1 c9 (oleic acid) to 18:0 (stearic acid) was calculated as an indicator of Δ-9 desaturase activity.

PPARγ Activation

PPARγ activation was measured using a commercial ELISA assay (Panomics EK1211, Fremont, CA) of in-vitro binding to a specific DNA promoter sequence, after extraction of nuclear material according the manufacturer's specifications. Results were expressed as percentage of activity of a positive control standard provided by the manufacturer.

Statistical Analysis

Results were analyzed using two-way and three-way analyses of variance (ANOVA) with Tukey's post hoc comparisons, using SAS version 9.1 software packages as appropriate. The model detected differences between main effects by diet, and sex as applicable. The model also reported interaction effects between diet and sex which were considered significant at $P < 0.05$. Log and square root transformations were done for the variables which were not distributed in a Gaussian fashion. To measure the degree of relationship between histology measures with renal contents of specific fatty acids, canonical correlation analysis was performed using the SAS version 9.1 software package.

Results

A total of 54 female and 47 male animals who were found to be Han:SPRD-*cy* heterozygotes were included in the analysis. Animal weight was found to be significantly influenced by gender, but not by diet, with females being smaller as expected (Fig. 1). Serum creatinine, as a marker of renal function, was also significantly influenced by gender, again consistent with the known slower progression of the disease in female animals (Fig. 2), but serum creatinine actually increased significantly with increasing dose of CLA in female animals.

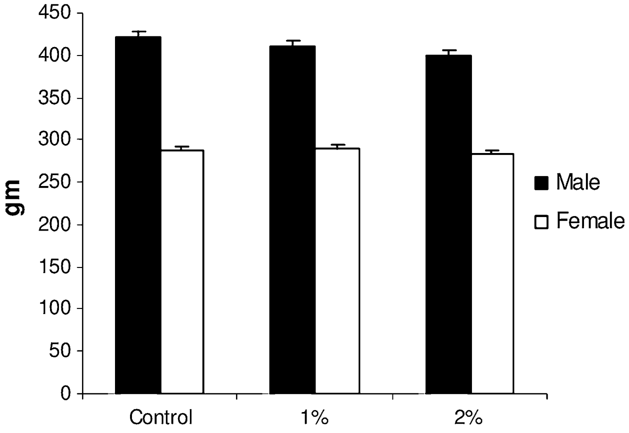

Fig. 1 Animal weight at conclusion of feeding period (g). A main effect of gender only is significant ($P < 0.001$)

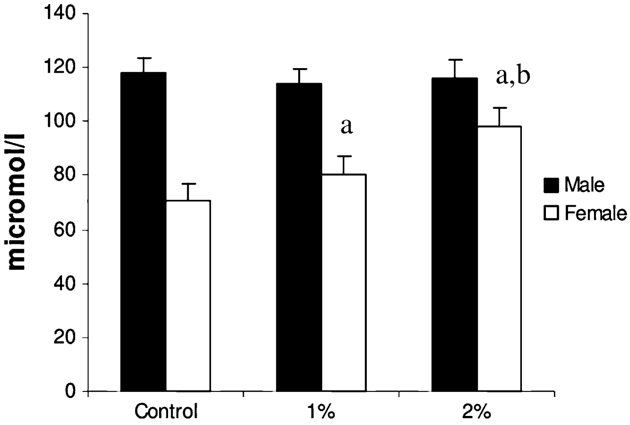

Fig. 2 Serum creatinine at conclusion of study (μmol/l). A significant major dietary effect was seen. *a* Significant difference from control diet, same gender in post hoc testing. *b* Significant difference between 1% and 2% CLA, same gender in post hoc testing

When results of all densitometric indices of histologic injury are considered, diet ($P < 0.01$) and gender ($P < 0.001$) had significant effect on reducing relative cyst area which was found to be dose dependent for diet, although in post hoc analysis, significant differences between dietary groups in female animals accounted for the observed effect (Fig. 3a). As gender difference is inherent to the model, post hoc comparisons between genders, which were significant for all histologic outcome measures

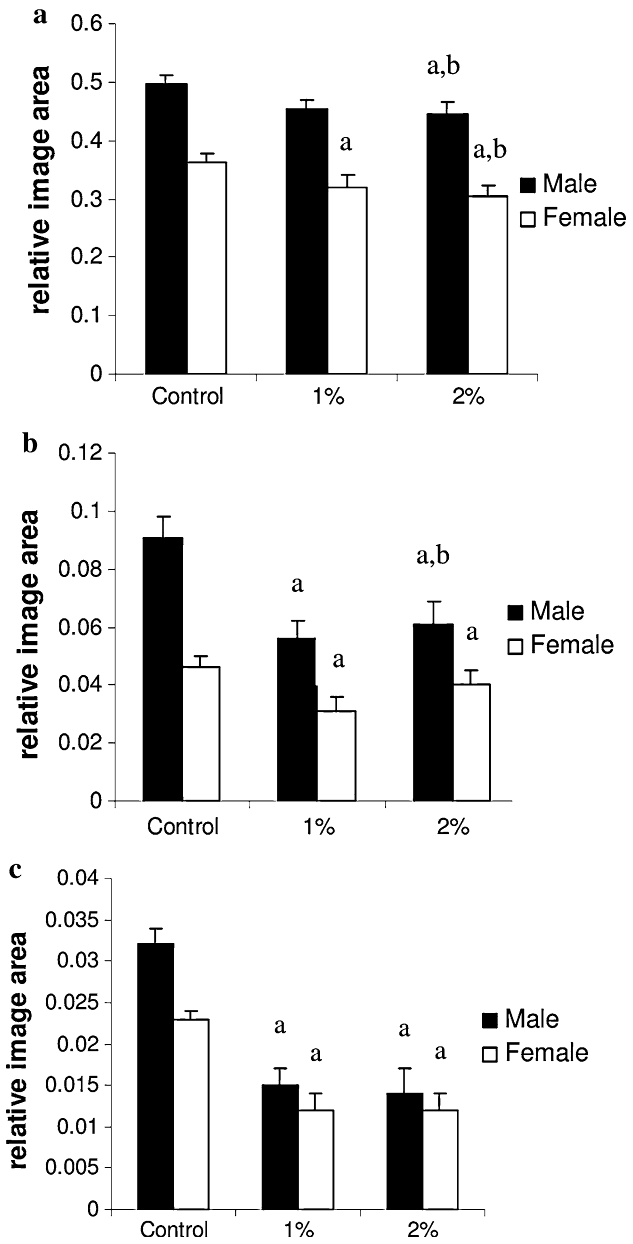

Fig. 3 Densitometric analysis of renal cystic change (**a**) fibrosis (**b**) and Ox-LDL (**c**) (fraction image area, fibrosis and ox-LDL are corrected to solid-tissue area). A significant major dietary effect was seen for all histologic measures. *a* Significant difference from control diet, same gender in post hoc testing. *b* Significant difference between 1 and 2% CLA, same gender in post hoc testing

and serum creatinine, are not further reported here. A similar dose dependent effect of diet ($P < 0.001$) and effect of gender ($P < 0.001$) was observed with fibrosis (Fig. 3b) Diet also had dose dependent effects on ox-LDL measurement ($P < 0.001$, Fig. 3c) with marginal gender interactions manifest as lower values in female animals (diet × gender, $P = 0.05$). Major diet effects were also observed upon macrophage content and PCNA count ($P < 0.001$, Fig. 4) due entirely to highly significant differences between control and both dietary interventions in post hoc testing. The small differences between the 1 and 2% CLA dietary groups within genders did not achieve significance in post hoc testing for these parameters.

Neither diet nor gender had a statistically significant effect on PPARγ activation (Fig. 5).

Diet significantly elevated renal levels of all detected CLA isomers in kidney and liver as expected and decreased levels of LNA in both organs. The levels found in both organs, however, were in different proportions to the diet (Table 2). Both diet and gender were likely to influence fatty acid composition of liver more than that of kidney. Levels of 18:1 c9 were significantly lower in liver but not kidney tissue in both genders, as was Δ-9 desaturase activity. ARA content did not differ with diet in renal and hepatic tissue and Δ-6 desaturase activity was significantly increased in liver from animals of both genders (Table 2). Female animals demonstrated higher hepatic content of the anti-inflammatory PUFA, DHA. Canonical correlation between renal content of CLA isomers and a total histologic score pooled across both genders derived by addition of the numeric values of all histologic variables revealed a significant negative correlation only between the renal content of 18:2 c9, t11 and histologic indices (standardized canonical coefficient = −0.63, $P < 0.001$). There was no significant correlation between the renal level of any CLA isomer and serum creatinine in the whole group; however, if the analysis was restricted to only female animals with PKD, the correlation between serum creatinine and the renal levels of the t10, t12 isomer approached significance ($r^2 = 0.27$, $P = 0.067$).

Gender was associated with expected changes in bone mineral content, body fat and lean body mass (Table 3). Diet only had a significant effect in reducing % body fat in both genders compared to controls of the same gender in post hoc testing. Increases in lean body mass in animals receiving CLA diets did not achieve significance. Lean body mass did not correlate with serum creatinine in either gender (males $r^2 = -0.139$, females $r^2 = 0.299$, $P =$ ns).

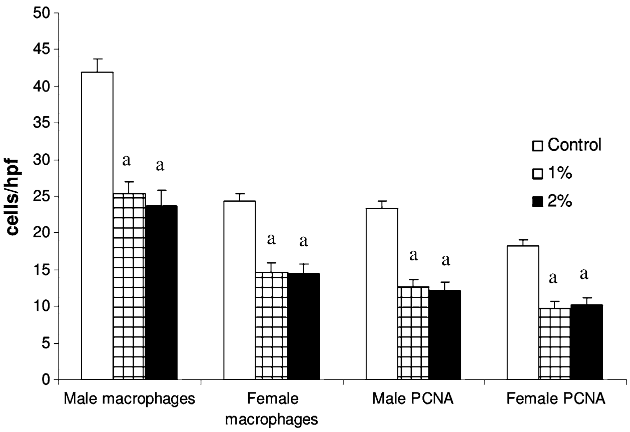

Fig. 4 Cell count analysis of renal macrophages and PCNA positive renal epithelial cells (cells per high power field, corrected to solid-tissue area). A significant major dietary effect was seen, *a* significant difference from control diet, same gender in post hoc testing

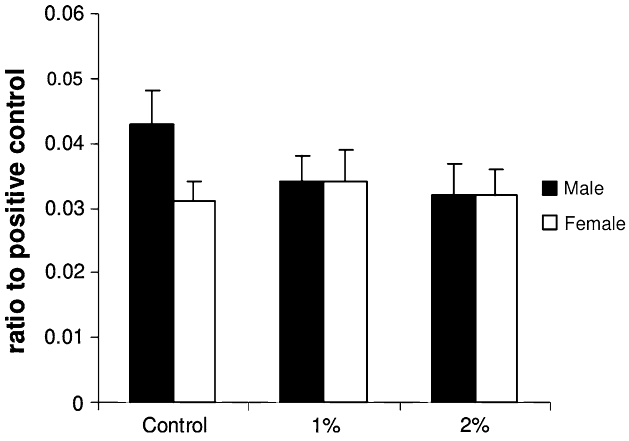

Fig. 5 PPARγ activation in renal tissue homogenates expressed as a ratio to the manufacturer's positive control

Discussion

The results reported here reinforce the findings of our previous studies with respect to a possible therapeutic role for CLA in inflammatory renal disease [11]. This study, however, is the first to explore the role of animal gender in the response to CLA in this context, and, as with our recent study with flax derivatives, gender does influence the outcome of this type of dietary intervention. Indeed, we have not been able to identify any prior study exploring gender differences in CLA response in any system.

CLA isomers may compete with linoleic acid at the level of desaturases and elongases, thus influencing ARA content [35]. CLA reduces the expression of the gene for stearoyl-CoA reductase, the initial Δ9-desaturase step in the formation of monoenoic fatty acids [36], a finding confirmed by our results. Δ6-desaturase inhibition by CLA has been reported in a transfected yeast system [37], and by the t10, c12 isomer specifically in human hepatoma cells [38], whereas our study found no such effect in kidney and possibly the opposite

Table 2 Renal and hepatic lipid content

Gender and tissue	Female kidney			Male kidney			*P* diet	*P* gender
Diet	Control	1% CLA	2% CLA	Control	1% CLA	2% CLA		
18:0	14.9 (1.9)	19.3 (2.2)	15.1 (2.1)	15.5 (0.9)	15.2 (0.8)	16.6 (0.8)	ns	ns
18:1 c9	14.3 (1.1)	10.1 (1.4)	11.9 (1.3)	11.9 (1.1)	11.5 (1.0)	9.9 (1.0)	ns	ns
18:2 c9,c12	18.3 (1.0)	13.8 (1.2)	14.4 (1.2)	14.2 (1.1)	15.7 (1.0)	13.1 (1.0)	ns	ns
18:2 c9, t11	0.3 (0.2)^{c}	0.9 (0.3)^{c}	2.1 (0.3)^{c}	0.0 (0.3)^{c}	1.2 (0.2)^{b}	1.7 (0.2)^{b}	0.001^{a}	0.005^{a}
18:2 t10,c12	0.1 (0.1)^{f,g}	0.5 (0.1)^{f}	1.1 (0.1)$^{b-d}$	0.0 (0.2)^{f,g}	0.7 (0.2)^{b}	1.0 (0.2)^{b,c}	<0.001	ns
18:2 t10,t12	0.1 (0.1)^{f,g}	0.2(0.1)^{f}	0.5 (0.1)$^{b-d}$	0.0 (0.1)^{f,g}	0.3 (0.1)	0.4 (0.1)^{b,c}	<0.001	ns
18:3 n3	0.09 (0.02)	0.03 (0.02)	0.07 (0.02)	0.09 (0.03)	0.05 (0.02)	0.02 (0.02)	0.031	ns
20:4	22.4 (1.7)	25.4 (2.0)	24.0 (1.9)	26.7 (1.9)	24.2 (1.7)	26.1 (1.9)	ns	ns
22:6 n3	1.18 (0.12)	0.97 (0.14)	0.97 (0.14)	0.60 (0.04)	0.50 (0.04)	0.52 (0.04)	ns	ns
Δ-9 desaturase	1.21 (0.17)	0.77 (0.20)	0.94 (0.19)	0.88 (0.17)	0.87 (0.15)	0.66 (0.15)	ns	ns
Δ-6 desaturase	1.49 (0.18)	2.05 (0.22)	1.79 (0.21)	2.10 (0.21)	1.72 (0.19)	2.10 (0.20)	ns	ns
Gender and tissue	Female liver			Male liver			*P* diet	*P* gender
18:0	20.4 (0.4)^{c,e,f}	21.6 (0.5)^{b}	24.0 (0.5)^{b,c,g}	14.2 (0.3)$^{c-e,g}$	17.9 (0.3)^{b,c,g}	20.1 (0.4)^{b,g}	<0.001^{a}	<0.001^{a}
18:1 c9	10.4 (0.3)^{e,f}	9.1 (0.4)^{e,g}	8.2 (0.3)^{b,c}	9.7 (0.3)^{d,f,g}	7.1 (0.3)^{b,c,e}	6.7 (0.3)^{b,c,e,g}	<0.001	<0.001
18:2 c9,c12	16.9 (0.5)^{c,e,g}	15.8 (0.5)^{e,g}	12.5 (0.5)^{b,c,g}	22.1 (0.4)$^{c-f,g}$	19.9 (0.4)^{b,c,e,g}	17.7 (0.5)^{b,g}	<0.001	<0.001
18:2 c9, t11	0.0 (0.1)$^{d-g}$	1.2 (0.1)^{b,c,f,g}	2.1 (0.1)$^{b-d,f,g}$	0.0 (0.1)$^{d-g}$	1.2 (0.1)^{b,c,f,g}	2.2 (0.1)$^{b-e,g}$	<0.001	ns
18:2 t10,c12	0.0 (0.02)$^{d-f,g}$	0.5 (0.03)^{b,c,f,g}	0.9 (0.03)$^{b-e}$	0.0 (0.04)$^{d-g}$	0.6 (0.04)^{b,c,f,g}	1.0 (0.04)^{b,c,f,g}	<0.001	0.011
18:2 t10,t12	0.0 (0.02)$^{d-g}$	0.4 (0.02)^{b,c,f,g}	0.7 (0.02)^{b,c,e,g}	0.0 (0.03)$^{d-f,g}$	0.4 (0.03)^{b,c,f,g}	0.8 (0.04)^{b,c,f,g}	<0.001	0.04
18:3 n3	0.10 (0.01)^{f,g}	0.08 (0.01)^{b,g}	0.05 (0.01)$^{b-e}$	0.11 (0.01)$^{d-g}$	0.08 (0.01)^{b,g}	0.06 (0.01)^{b,c}	<0.001	0.017
20:4	21.7 (0.4)^{c,e,g}	20.6 (0.4)^{c,e,g}	21.2 (0.4)^{c,e,g}	24.0 (0.5)^{c,e,g}	24.7 (0.5)^{c,e,g}	24.4 (0.6)^{c,e,g}	ns	<0.001
22:6 n3	3.70 (0.09)$^{b,d-g}$	3.16 (0.10)^{b,c,e,g}	3.12 (0.09)^{b,c,e,g}	2.26 (0.09)^{b,c,e,f,g}	1.94 (0.09)^{c,e,g}	2.01 (0.10)^{c,e,g}	<0.001	<0.001
Δ-9 desaturase	0.51 (0.03)^{b,f,g}	0.44 (0.03)^{c}	0.34 (0.03)^{b,c}	0.70 (0.03)$^{c-g}$	0.40 (0.03)^{b}	0.34 (0.03)^{b,c}	<0.001	ns
Δ-6 desaturase	1.30 (0.06)^{f}	1.35 (0.06)^{c,f}	1.72 (0.06)^{b,c,e,g}	1.10 (0.05)$^{e-g}$	1.25 (0.05)^{g}	1.40 (0.05)^{b,g}	<0.001	<0.001

[a] Significant interaction between diet and gender, $P < 0.01$,

[b] Significantly different from control diet in same gender group in post host testing, $P < 0.05$

[c] Significantly different from control diet in opposite gender group in post host testing $P < 0.05$

[d] Significantly different from 1% CLA diet in same gender group in post host testing $P < 0.05$

[e] Significantly different from 1%CLA diet in opposite gender group in post host testing $P < 0.05$

[f] Significantly different from 2% CLA diet in same gender group in post host testing $P < 0.05$

[g] Significantly different from 2% CLA diet in opposite gender group in post host testing $P < 0.05$

Table 3 Bone and body composition data from DXA scanning

	Control	1% CLA	2% CLA	*P* gender	*P* diet
Male bone mineral content (gm)	11.0 (0.16)	10.8 (0.16)	10.5 (0.18)	<0.001	ns
Female bone mineral content (gm)	8.7 (0.15)	8.8 (0.16)	8.5 (0.16)		
Male bone mineral density (gm/cm^2)	0.16 (0.001)	0.16 (0.001)	0.16 (0.001)	ns	ns
Female bone mineral density (gm/cm^2)	0.16 (0.001)	0.16 (0.001)	0.16 (0.001)		
Male % body fat	9.1 (0.48)	7.0 (0.48)^{a}	6.6 (0.55)^{a}	<0.001	<0.001
Female % body fat	15.1 (0.45)	10.4 (0.52)^{a}	10.1 (0.50)^{a}		
Male lean body mass (gm)	359 (4.7)	356 (4.8)	349 (5.4)	<0.001	ns
Female lean body mass (gm)	230 (4.5)	237 (4.9)	242 (5.1)		

Figures in parentheses are standard errors of the means; no significant interactions were detected between diet and gender

[a] Significantly different from control diet, same gender in post hoc testing

effect in liver. In a prior study using a soy protein based diet, we found an association between inhibition of Δ6-desaturase and histologic improvement in this model [23], but this is clearly not the mechanism here. Although found to have benefits in the areas of carbohydrate metabolism, cholesterol metabolism and atherosclerosis [39], the major health related interest in CLA has been as an anti-carcinogen [2]. CLA enhances lymphocyte proliferative responses to phytohemaglutinin, but not to LPS or concanavalin A [40], implying a positive or negative immunomodulatory role under differing circumstances. Our results demonstrating decreased macrophage infiltration and fibrosis might be interpreted as a specific effect on the inflammatory response or may be a non-specific response based on inhibition of cell proliferation.

Most CLA preparations are a mixture of isomers, with the precise mix a function of both the substrate oil and the manufacturing process [41]. Our statistical association of benefit with the renal concentration of the c9-t11 isomer, while a novel approach to the issue of identifying the active lipid, is supported by studies using pure isomers. Jensen et al. [4] have associated antiproliferative effects of CLA with the c9-c11 isomer. Yang and Cook [42] have demonstrated that the release of anti-inflammatory cytokines essential to the innate immune response is inhibited by the c9-t11 isomer. Conversely, the t10-t12 isomer has been associated with pro-inflammatory effects [43], may have adverse effects on lipid metabolism [44], and may play a larger prostaglandin inhibition mediated effects of CLA [38].

Our finding of a different distribution of CLA isomers in tissue compared to the diet and differing proportions in differing organs is consistent with previous reports. Kramer et al. [45] have reported similar findings in a piglet model and speculate that the cause is related to differing metabolism of different isomers, which is supported by Tsuzuki et al. [46] who failed to demonstrate differences in absorption as a basis for such differences in a rat model. The basis for the observed differences remains to be elucidated. In this inflammatory model, the content and role of fatty acids in the inflammatory cell population that may migrate into the kidney from a circulating pool would be extremely difficult to measure and yet may be extremely important in elucidating the precise relationships between this nutritional intervention and histologic change and toxicity.

The role of CLA as a ligand for the PPARγ system suggests a direct pathway that might mediate the observed effects [15]. This pathway has been specifically implicated in the regulation of inflammatory response [16]. Our results do not demonstrate a dietary effect on PPARγ activation, thus cannot at this stage support this as the relevant pathway. It is, however, possible, that as we based our measurements upon whole tissue homogenates, we would not have had sufficient sensitivity to detect activation that is specific to individual cell types such as macrophages and fibroblasts. In-vitro studies of separated cells may offer insight into this question.

The new finding of a rise in serum creatinine in female animals is a serious concern. CLA has been associated with an increase in lean body mass [47–49], which may increase serum creatinine without change in renal function [50]. In this study, however, very small changes in lean body mass that did not achieve significance and were proportionately much less than the change in serum creatinine were observed. In a previous study, we demonstrated that a 1% CLA diet reduced renal PGE_2 production [11]. It is plausible that at even higher doses, a more generalized effect of prostaglandin inhibition on glomerular tubular balance, combined with the loss of urinary concentrating ability that is an early clinical feature of this disease my result in disturbed renal function in a manner analogous to the adverse effects of non-steroidal anti-inflammatory drugs [51]. Sullivan et al. [52] have described gender dimorphism with higher expression of prostaglandin synthase and renal production of prostaglandins in female spontaneously hypertensive rats, but the relationship of this observation to renal functional homeostasis is not known. It is possible that their observation implies that more prostaglandin synthesis is required for homeostasis in females; inhibition of the pathway would therefore create a larger functional disturbance. Our finding of a diminution of the antifibrotic effect at higher doses of the CLA mixture in males may also be cautionary and could reflect a shift in the balance of beneficial versus harmful effects of the two predominant isomers [43]. As with an earlier study with flax oil and lignan [27], we did detect relatively subtle qualitative differences in the profile of histologic effects between genders. The magnitude of these differences may not be of clinical significance but the finding underlines the importance of considering gender as a variable in functional food studies.

Proportions of CLA in plasma, adipose tissue and red blood cell membranes are low in adult patients with chronic renal failure managed without dialysis, but increase in dialysis patients [53]. It is likely that changes in dietary intake, with severe restriction of dairy products mandated to maintain serum phosphate in an acceptable range, are a major factor. Our study suggests that CLA, and in particular the c9-t11 isomer, may warrant further exploration as an anti-inflammatory functional food that may influence renal injury. Our results, however, also caution that the unconditional recommendation of CLA supplements of variable composition and quality in this high risk population is not only premature but carries a credible risk of harm.

Acknowledgments This work was supported by a grant from Dairy Farmers of Canada and performed in facilities of the Manitoba Institute of Child Health, a division of the Children's Hospital Foundation of Manitoba, Inc. The assistance of Dr Rasheda Rabbani with the statistical analysis and of Heather Kovacs with the DXA scanning is gratefully acknowledged.

References

1. Parodi PW (1997) Cows' milk fat components as potential anticarcinogenic agents. J Nutr 127:1055–1060
2. Parodi PW (1999) Conjugated linoleic acid and other anticarcinogenic agents of bovine milk fat. J Dairy Sci 82:1339–1349
3. Cordain L, Watkins BA, Florant GL, Kelher M, Rogers L, Li Y (2002) Fatty acid analysis of wild ruminant tissues: evolutionary implications for reducing diet-related chronic disease. Eur J Clin Nutr 56:181–191
4. Jensen RG, Lammi-Keefe C (2001) The anticarcinogenic conjugated fatty acid c9, t11–c18:2, or rumenic acid, in human milk: amounts and effects. Adv Exp Med Biol 501:153–156
5. Cesano A, Visonneau S, Scimeca JA, Kritchevsky D, Santoli D (1998) Opposite effects of linoleic acid and conjugated linoleic acid on human prostatic cancer in SCID mice. Anticancer Res 18:1429–1434
6. Yang M, Pariza MW, Cook ME (2000) Dietary conjugated linoleic acid protects against end stage disease of systemic lupus erythematosus in the NZB/W F1 mouse. Immunopharmacol Immunotoxicol 22:433–449
7. Whigham LD, Cook EB, Stahl JL, Saban R, Bjorling DE, Pariza MW, Cook ME (2001) CLA reduces antigen-induced histamine and PGE(2) release from sensitized guinea pig tracheae. Am J Physiol Regul Integr Comp Physiol 280:R908–R912
8. Whigham LD, Higbee A, Bjorling DE, Park Y, Pariza MW, Cook ME (2002) Decreased antigen-induced eicosanoid release in conjugated linoleic acid-fed guinea pigs. Am J Physiol Regul Integr Comp Physiol 282:R1104–R1112
9. Harris MA, Hansen RA, Vidsudhiphan P, Koslo JL, Thomas JB, Watkins BA, Allen KG (2001) Effects of conjugated linoleic acids and docosahexaenoic acid on rat liver and reproductive tissue fatty acids, prostaglandins and matrix metalloproteinase production. Prostaglandins Leukot Essent Fatty Acids 65:23–29
10. Miller A, Stanton C, Devery R (2001) Modulation of arachidonic acid distribution by conjugated linoleic acid isomers and linoleic acid in MCF-7 and SW480 cancer cells. Lipids 36:1161–1168
11. Ogborn MR, Nitschmann E, Bankovic-Calic N, Weiler HA, Fitzpatrick-Wong S, Aukema HM (2003) Dietary conjugated linoleic acid reduces PGE2 release and interstitial injury in rat polycystic kidney disease. Kidney Int 64:1214–1221
12. Watkins BA, Seifert MF (2000) Conjugated linoleic acid and bone biology. J Am Coll Nutr 19:478S–486S
13. Hontecillas R, Wannemeulher MJ, Zimmerman DR, Hutto DL, Wilson JH, Ahn DU, Bassaganya-Riera J (2002) Nutritional regulation of porcine bacterial-induced colitis by conjugated linoleic acid. J Nutr 132:2019–2027
14. Turnock L, Cook M, Steinberg H, Czuprynski C (2001) Dietary supplementation with conjugated linoleic acid does not alter the resistance of mice to Listeria monocytogenes infection. Lipids 36:135–138
15. Moya-Camarena SY, Belury MA (1999) Species differences in the metabolism and regulation of gene expression by conjugated linoleic acid. Nutr Rev 57:336–340
16. Yu Y, Correll PH, Vanden Heuvel JP (2002) Conjugated linoleic acid decreases production of pro-inflammatory products in macrophages: evidence for a PPAR gamma-dependent mechanism. Biochim Biophys Acta 1581:89–99
17. Gretz N, Ceccherini I, Kranzlin B, Kloting I, Devoto M, Rohmeiss P, Hocher B, Waldherr R, Romeo G (1995) Gender-dependent disease severity in autosomal polycystic kidney disease of rats. Kidney Int 48:496–500
18. Maser RL, Vassmer D, Magenheimer BS, Calvet JP (2002) Oxidant stress and reduced antioxidant enzyme protection in polycystic kidney disease. J Am Soc Nephrol 13:991–999
19. Gattone VHII, Cowley BD Jr, Barash BD, Nagao S, Takahashi H, Yamaguchi T, Grantham JJ (1995) Methylprednisolone retards the progression of inherited polycystic kidney disease in rodents. Am J Kidney Dis 25:302–313
20. Keith DS, Torres VE, Johnson CM, Holley KE (1994) Effect of sodium chloride, Enalapril, and Losartan on the development of polycystic kidney disease in. Am J Kidney Dis 24:491–498
21. Ogborn MR, Sareen S (1995) Amelioration of polycystic kidney disease by modification of dietary protein intake in the rat. J Am Soc Nephrol 6:1649–1654
22. Gile RD, Cowley BD Jr, Gattone VHII, O'Donnell MP, Swan SK, Grantham JJ (1995) Effect of lovastatin on the development of polycystic kidney disease in the Han:SPRD rat. Am J Kidney Dis 26:501–507
23. Ogborn MR, Nitschmann E, Weiler HA, Bankovic-Calic N (2000) Modification of polycystic kidney disease and fatty acid status by soy protein diet. Kidney Int 57:159–166
24. Ogborn MR, Nitschmann E, Bankovic-Calic N, Buist R, Peeling J (1998) The effect of dietary flaxseed supplementation on organic anion and osmolyte content and excretion in rat polycystic kidney disease. Biochem Cell Biol 76:553–559
25. Ogborn MR, Nitschmann E, Bankovic-Calic N, Weiler H, Aukema H (2005) Flax and soy phytoestrogen effects on renal injury and lipid content in experimental polycystic kidney disease. JANA 8:26–32
26. Ogborn MR, Nitschmann E, Weiler H, Leswick D, Bankovic-Calic N (1999) Flaxseed ameliorates interstitial nephritis in rat polycystic kidney disease. Kidney Int 55:417–423
27. Ogborn MR, Nitschmann E, Bankovic-Calic N, Weiler HA, Aukema HM (2006) Effects of flaxseed derivatives in experimental polycystic kidney disease vary with animal gender. Lipids 41:1141–1149
28. Ogborn MR, Nitschmann E, Bankovic-Calic N, Weiler HA, Aukema H (2002) Dietary flax oil reduces renal injury, oxidized LDL content, and tissue n-6/n-3 FA ratio in experimental polycystic kidney disease. Lipids 37:1059–1065
29. Tanner GA (1998) Potassium citrate/citric acid intake improves renal function in rats with polycystic kidney disease. J Am Soc Nephrol 9:1242–1248
30. Ogborn M, Bankovic-Calic N, Shoesmith C, Buist R, Peeling J (1998) Soy protein modification of rat polycystic kidney disease, *Am J Physiol* 274 (Renal Physiol 43):F541–F549
31. Bertin E, Ruiz JC, Mourot J, Peiniau P, Portha B (1998) Evaluation of dual-energy X-ray absorptiometry for body-composition assessment in rats. J Nutr 128:1550–1554
32. Bosmans JL, Holvoet P, Dauwe SE, Ysebaert DK, Chapelle T, Jurgens A, Kovacic V, Van Marck EA, De Broe ME, Verpooten GA (2001) Oxidative modification of low-density lipoproteins and the outcome of renal allografts at 1 1/2 years. Kidney Int 59:2346–2356
33. Uauy RD, Birch DG, Birch EE, Tyson JE, Hoffman DR (1990) Effect of dietary omega-3 fatty acids on retinal function of very-low-birth-weight neonates. Pediatr Res 28:485–492
34. Kramer JK, Fellner V, Dugan ME, Sauer FD, Mossoba MM, Yurawecz MP (1997) Evaluating acid and base catalysts in the methylation of milk and rumen fatty acids with special emphasis on conjugated dienes and total trans fatty acids. Lipids 32:1219–1228
35. Sebedio J, Juaneda P, Dobson G, Ramilison I, Martin J, Chardigny J, Christie W (1997) Metabolites of conjugated isomers of linoleic acid (CLA) in the rat. Biochim Biophys Acta 1345:5–10
36. Bretillon L, Chardigny JM, Gregoire S, Berdeaux O, Sebedio JL (1999) Effects of conjugated linoleic acid isomers on the hepatic microsomal desaturation activities in vitro. Lipids 34:965–969

37. Chuang LT, Thurmond JM, Liu JW, Kirchner SJ, Mukerji P, Bray TM, Huang YS (2001) Effect of conjugated linoleic acid on fungal delta6-desaturase activity in a transformed yeast system. Lipids 36:139–143
38. Eder K, Slomma N, Becker K (2002) Trans-10, cis-12 conjugated linoleic acid suppresses the desaturation of linoleic and alpha-linolenic acids in HepG2 cells. J Nutr 132:1115–1121
39. Sebedio JL, Gnaedig S, Chardigny JM (1999) Recent advances in conjugated linoleic acid research. Curr Opin Clin Nutr Metab Care 2:499–506
40. Wong MW, Chew BP, Wong TS, Hosick HL, Boylston TD, Shultz TD (1997) Effects of dietary conjugated linoleic acid on lymphocyte function and growth of mammary tumors in mice. Anticancer Res 17:987–993
41. Yang L, Huang Y, Wang H, Chen Z (2002) Production of conjugated linoleic acids through KOH-catalyzed dehydration of ricinoleic acid. Chem Phys Lipids 119:23
42. Yang M, Cook ME (2003) Dietary conjugated linoleic acid decreased cachexia, macrophage tumor necrosis factor-alpha production, and modifies splenocyte cytokines production. Exp Biol Med (Maywood) 228:51–58
43. Riserus U, Basu S, Jovinge S, Fredrikson GN, Arnlov J, Vessby B (2002) Supplementation with conjugated linoleic acid causes isomer-dependent oxidative stress and elevated C-reactive protein: a potential link to fatty acid-induced insulin resistance. Circulation 106:1925–1929
44. Roche HM, Noone E, Sewter C, Mc Bennett S, Savage D, Gibney MJ, O'Rahilly S, Vidal-Puig AJ (2002) Isomer-dependent metabolic effects of conjugated linoleic acid: insights from molecular markers sterol regulatory element-binding protein-1c and LXR-alpha. Diabetes 51:2037–2044
45. Kramer J, Sehat N, Dugan M, Mossoba M, Yurawecz M, Roach J, Eulitz K, Aalhus J, Schaefer A, Ku Y (1998) Distributions of conjugated linoleic acid (CLA) isomers in tissue lipid classes of pigs fed a commercial CLA mixture determined by gas chromatography and silver ion-high-performance liquid chromatography. Lipids 33:549–558
46. Tsuzuki T, Ikeda I (2007) Slow absorption of conjugated linoleic acid in rat intestines, and similar absorption rates of 9c, 11t-conjugated linoleic acid and 10t, 12c-conjugated linoleic acid. Biosci Biotechnol Biochem 71:2034–2040
47. Weiler H, Austin S, Fitzpatrick-Wong S, Nitschmann E, Bankovic-Calic N, Mollard R, Aukema H, Ogborn M (2004) Conjugated linoleic acid reduces parathyroid hormone in health and in polycystic kidney disease in rats. Am J Clin Nutr 79:1186S–1189S
48. Burr LL, Taylor CG, Weiler HA (2006) Dietary conjugated linoleic acid does not adversely affect bone mass in obese fa/fa or lean Zucker rats. Exp Biol Med (Maywood) 231:1602–1609
49. Kelly GS (2001) Conjugated linoleic acid: a review. Altern Med Rev 6:367–382
50. Smith SA (1988) Estimation of glomerular filtration rate from the serum creatinine concentration. Postgrad Med J 64:204–208
51. Taber SS, Mueller BA (2006) Drug-associated renal dysfunction. Crit Care Clin 22:357–374, viii.
52. Sullivan JC, Sasser JM, Pollock DM, Pollock JS (2005) Sexual dimorphism in renal production of prostanoids in spontaneously hypertensive rats. Hypertension 45:406–411
53. Lucchi L, Banni S, Melis MP, Angioni E, Carta G, Casu V, Rapana R, Ciuffreda A, Corongiu FP, Albertazzi A (2000) Changes in conjugated linoleic acid and its metabolites in patients with chronic renal failure. Kidney Int 58:1695–1702

Lipids (2008) 43:793–804
DOI 10.1007/s11745-008-3214-1

ORIGINAL ARTICLE

HDL Composition Regulates Displacement of Cell Surface-Bound Hepatic Lipase

**Naghmeh Rouhani · Elizabeth Young ·
Cynthia Chatterjee · Daniel L. Sparks**

Received: 2 April 2008 / Accepted: 8 July 2008 / Published online: 1 August 2008
© AOCS 2008

Abstract HDL is able to displace cell surface-bound hepatic lipase (HL) and stimulate vascular triglyceride (TG) hydrolysis, much like heparin. Displacement appears to be a result of a high-affinity association of HL and apoA-I. HDL varies in its ability to displace HL, and therefore experiments were undertaken to evaluate the impact of HDL composition and structure on HL displacement from cell surface proteoglycans. HDL apolipoprotein and lipid composition directly affect HL displacement. ApoA-II and apoC-I significantly increase HL displacement from the cell surface. While changes in HDL cholesteryl ester and fatty acid content have no effect on HL displacement, increases in HDL phospholipid and TG content significantly inhibit HL displacement. HDL fractions from hyperlipidemic patients are unable to displace HL from the cell surface. These results indicate that the structure and composition of HDL particles in plasma are central to regulation of HL displacement and the hydrolytic activity of HL.

Keywords Proteoglycans · Triglycerides · Apolipoproteins · Phospholipids · Cholesteryl ester · Fatty acids

Abbreviations

apoA-I	Apolipoprotein A-I
apoA-II	Apolipoprotein A-II
apoE	Apolipoprotein E
DPPC	Dipalmitoyl phosphatidylcholine
HL	Hepatic lipase
CETP	Cholesteryl ester transfer protein
CHD	Coronary heart disease
HSPG	Heparan sulfate proteoglycan
LPL	Lipoprotein lipase
LCAT	Lecithin:cholesterol acyl transferase
PLA_2	Phospholipase A
PC	Phosphatidylcholine
PA	Phosphatidic acid
PS	Phosphatidylserine
PI	Phosphatidylinositol
rHDL	Reconstituted HDL
TG	Triacylglyceride
VLDL	Very low-density lipoprotein

Introduction

Heparin promotes the displacement of hepatic lipase (HL) and lipoprotein lipase (LPL) from the liver and vascular endothelium and stimulates lipolytic activity and plasma triglyceride (TG) clearance [3, 28, 46]. The enzymatic activity of HL is undetectable in the plasma, and activity is usually measurable only after intravenous injection of heparin (post-heparin HL activity). Increased post-heparin HL activity is associated with low HDL-cholesterol (HDL-C) levels [22, 27, 35] and an abundance of small, dense LDL particles in the plasma [6, 11, 49]. A number of clinical studies show that these conditions are concomitant with increased coronary heart disease (CHD) risk in the patients. Lower HDL-C levels in postmenopausal women and similarly aged men, and a higher incidence of CHD in these groups compared to the premenopausal women, are related to higher post-heparin HL activity [14]. Similarly,

---

N. Rouhani · E. Young · C. Chatterjee · D. L. Sparks (✉)
Lipoprotein and Atherosclerosis Research Group,
University of Ottawa Heart Institute,
40 Ruskin Street, H452, Ottawa, ON, Canada K1Y 4W7
e-mail: dsparks@ottawaheart.ca

conditions related to the higher risk of heart disease, such as smoking [19], visceral obesity [16], and sedentary lifestyle [31], are known to be associated with elevated post-heparin HL activity. In addition, combined familial hyperlipidemic [39] and type 2 diabetic patients [47], who are at a higher risk for CHD, have elevated levels of post-heparin HL activity and an atherogenic lipoprotein profile (small dense LDL particles, decreased HDL-C, and increased TG levels) [1, 4, 5].

Accumulating evidence suggests that an increase in post-heparin HL lipolytic activity may be representative of an increased inactive pool of cell-associated HL in the liver. In vitro experiments have shown that proteoglycan-bound HL is inactive [37]. Displacement of HL from the cell surface increases hydrolytic activity and stimulates TG hydrolysis. In vivo experiments [10] have confirmed that an increase in circulating HL increases plasma HL lipolytic activity. In the mouse model, expression of a mutant human HL, which is unable to bind liver cells, elevates pre-heparin HL activity and leads to enhanced lipid hydrolysis and lipoprotein catabolism. An increased post-heparin HL activity may therefore be indicative of a reduced ability of liver-bound HL to be displaced and activated. As such, a high post-heparin HL activity would be expected to result in decreased vascular lipolysis and may be related to increased plasma TG levels.

Similar to heparin, both apoA-I and HDL stimulate HL displacement from the cell surface proteoglycans of CHO and HepG2 cells [36, 37]. Specific subclasses of HDL have different effects on HL displacement. The larger and more buoyant HDL_2 causes more HL to be displaced from the cell surface, while the smaller dense HDL_3 is unable to displace HL [36, 37]. The differential ability of HDL particles to liberate lipases from cell surface proteoglycans appears to influence lipid hydrolysis and clearance. Abnormalities in HDL structure and lipase displacement ability may therefore be related to perturbations in TG metabolism.

In this study, the relationship between HDL structure and HL displacement was evaluated. It was shown that both the lipid and protein components of HDL affect HL displacement. The results provide new insights into the regulation of HL metabolism and demonstrate how the lipid and protein composition of HDL controls HL displacement. Evidence suggests that HDL isolated from hyperlipidemic patients may have an impaired ability to promote HL displacement. Perturbations in HL displacement may therefore be partly causative of the abnormal clearance of plasma TG.

Materials

TG diagnostic kits were purchased from Roche Diagnostics (Laval, PQ, Canada). Anti-mouse IgG horseradish peroxidase (HRP)-linked whole antibody (isolated from goat), broad-range molecular weight markers, protein-G Sepharose 4 Fast Flow beads, HiTrap heparin HP columns, and native gradient Phast gels were purchased from Amersham Biosciences (Baie d'Urfé, PQ, Canada). Super Signal West Pico Chemiluminescent Substrate was purchased from Pierce Chemical Co. (Rockford, IL). Agarose Paragon® lipogels and the lipid stains were obtained from Beckman Coulter Inc. (Fullerton, CA). Novex polyacrylamide mini-gels, Ham's F12 medium, Dulbecco's modified Eagle's medium (DMEM), Geneticin® Selective Antibiotic (G418 sulfate), L-glutamine, and penicillin/streptomycin (pen/strep) were obtained from Invitrogen (Burlington, ON, Canada). Fetal bovine serum (FBS) and heparin (from porcine intestine) were purchased from Sigma Chemical Co. (St. Louis, MO). 1-Palmitoyl-2-oleoylphosphatidylcholine (POPC) was purchased from Avanti Polar Lipids (Alabaster, AL). CHO and HepG2 cell lines were obtained from ATCC (Manassas, VA). The polyclonal anti-human apolipoprotein A-I antibody from rabbit was purchased from Calbiochem Biosciences Inc. (La Jolla, CA). The monoclonal anti-human HL XHL3-6a antibody from mouse and monoclonal anti-human apoA-I (5F6 and 4H1) antibody from mouse were obtained from Drs. Bensadoun and Marcel, respectively. The polyclonal anti-human HL antibody from rabbit was obtained from Santa Cruz (Santa Cruz, CA). All other reagents were of analytical grade.

Methods

Isolation of Lipoproteins by Sequential Ultracentrifugation

Blood was donated from human subjects with informed consent of the participants and approval from the University of Ottawa Heart Institute Research Ethics Board. Blood samples from fasting normolipidemic and hyperlipidemic subjects were collected in Vacuette® tubes. VLDL, LDL, and HDL fractions were isolated from the plasma by sequential ultracentrifugation within the density ranges of $\rho < 1.006$ g/ml, $\rho = 1.019-1.063$ g/ml, and $\rho = 1.063-1.21$ g/ml, respectively, as previously described [23]. The isolated lipoprotein fractions were dialyzed extensively against PBS (50 mM sodium phosphate, 150 mM NaCl, pH 7.2) at 4 °C. Protein concentrations of lipoproteins were determined by the modified Markwell Lowry method [30]. Cholesterol and TG concentrations were measured enzymatically, using the commercial diagnostic kits (Roche Diagnostics, Laval, PQ). The homogeneity of the lipoprotein fractions was determined by agarose gel electrophoresis using pre-made Paragon® Lipogels.

HL Purification

HL was purified from post-heparin human plasma by heparin affinity chromatography as previously described [17, 36, 37]. Post-heparin human plasma was collected from normolipidemic subjects, and a 20% TG emulsion (Intralipid 20%, Pharmacia & Upjohn Inc., Missassauga, ON, Canada) was added to the plasma. Lipid cakes were harvested centrifugally and delipidated. The resuspended aqueous solution of crude HL was loaded onto a heparin-Sepharose CL-6B column and eluted with linear salt gradient of 0.15–1.5 M NaCl in 5 mM sodium barbital, pH 7.4, 20% glycerol, and the pooled fractions stored at −80 °C until use. HL activity was characterized using a TG emulsion and quantified into units of enzyme activity (where 1 unit = 1 µmol of fatty acid hydrolyzed/h). The protein concentration of the purified HL was 0.114 mg/ml, and the specific activity was determined to be 19,455 units/mg protein. SDS-PAGE and immunochemical analysis using the HL monoclonal antibody, XHL3-6a, showed a single band with an apparent molecular mass of 66 kDa.

Preparation of reconstituted HDL (rHDL) Particles

Purified apoA-I, apoA-II, and apoC-I were isolated from delipidated HDL by anion exchange chromatography [43]. Apolipoproteins were resolubilized in a 6 M guanidine HCl, 10 mM Tris (pH 7.2) solution, and dialyzed extensively against PBS (pH 7.2). Reconstituted HDL complexes were prepared by sonicating POPC with a mixture of apolipoproteins (apoA-I, A-II, C-I) with or without additional amounts of TG (triolein), FFA (oleic acid), or CE (cholesteryl oleate) (molar ratio of 1 mol protein: 60 mol lipids) as previously described [8]. The molar concentration of apolipoproteins in rHDL was determined by chemical crosslinking with dimethylsuberimidate [8] (Tables 1, 2). Briefly, POPC (3.2 mg) and other lipids in chloroform were dried under nitrogen in a 12 × 75-mm test tube, and 800 µl of PBS, pH 7.4 was added. The lipid-buffer solution was initially sonicated for 1 min in a 15 °C water bath using a Branson 450 sonicator. The suspension was then incubated in a sealed tube for 30 min at 37 °C and sonicated again for 5 min using a 95% duty cycle. ApoA-I (3 mg of a 1.8 mg protein/ml PBS, pH 7.4) or other apolipoproteins were added to the lipid suspension, and the protein–lipid mixture was sonicated for 4 × 1 min punctuated by 1-min cooling periods. All rHDL complexes were filtered through a 0.22-µm syringe tip filter. The size and homogeneity of rHDL complexes were estimated by non-denaturing gel electrophoresis on precast 8–25% acrylamide Phastgels (Amersham Biosciences) after protein staining. The protein concentration was determined by the modified Markwell Lowry method.

Table 1 Reconstituted HDL apolipoprotein composition

rHDL particle[a]	POPC (mol)	apoA-I (mol)	apoA-II (mol)	apoC-I (mol)	apoHDL (mol)	rHDL protein:lipid[b] (mol:mol:mol)
ApoA-I/POPC	60	1.0	0.0	0.0	0.0	2:120
ApoA-I/A-II/POPC	60	0.33	0.66	0.0	0.0	1:2:120
ApoA-I/C-I/POPC	60	0.33	0.0	0.66	0.0	1:2:120
ApoHDL[c]/POPC	60	0.0	0.0	0.0	1.0	Nd

[a] rHDL particles were prepared by cosonication with the indicated compositions as described

[b] rHDL prepared from apoA-I alone contained 2 mol of apoA-I/particle, while those prepared with apolipoprotein mixtures contained 1 mol of apoA-I, and 2 mol of the test apolipoprotein

[c] apoHDL was prepared from delipidated HDL and contained apoA-I, apoA-II, apoC-I, apoC-II, and apoC-III

Table 2 Reconstituted HDL lipid composition

rHDL particle[a]	ApoA-I (mol)	POPC (mol)	CE (mol)	TG (mol)	FFA (mol)	rHDL protein:lipid[b] (mol:mol:mol)
ApoA-I/POPC	1.0	60.0	0.0	0.0	0.0	2:120
ApoA-I/POPC/CE	1.0	60.0	15.0	0.0	0.0	2:120:30
ApoA-I/POPC/TG	1.0	60.0	0.0	15.0	0.0	2:120:30
ApoA-I/POPC/FFA	1.0	60.0	0.0	0.0	15.0	2:120:30

[a] rHDL particles were prepared by cosonication with the indicated compositions as described

[b] rHDL particles contain 2 mol of apoA-I/particle

Preparation of Lipid-enriched HDL

Phosphatidylinositol (PI) and phosphatidylcholine (PC) vesicles were prepared by sonication in PBS and then incubated with native HDL. Briefly, 3 mg of each lipid in chloroform was dried under nitrogen. PBS (1 ml) was added, and the lipid-PBS mixture was sonicated for 1 min at constant duty cycle in a 15 °C water bath and incubated at 37 °C for 15 min. The mixture was then sonicated for 5 min at 95% duty cycle. The lipid vesicles (0.2 mg) were incubated per 1 mg fresh HDL protein for 48 h at 4 °C. Under these conditions, essentially the entire exogenous lipid was assimilated into the HDL particles. HDL charge was determined by electrophoretic mobilities on 0.6% agarose Paragon lipogels (Beckman, Coulter) as previously described [42].

Preparation of Apolipoprotein-enriched HDL

Freshly isolated HDL (1 ml; 5.8 mg protein/ml) from a fasting normolipidemic subject was incubated with 1.35 ml of purified and dialyzed apoA-II (2.4 mg protein/ml) for 30 min at room temperature with constant stirring. At the end of the incubation, the free apoA-I and apoA-II were separated from HDL by ultracentrifugation. The apoA-I/apoA-II mass ratio of HDL was estimated by SDS-PAGE on 12% precast Novex minigels followed by silver staining. The apoA-II content of HDL was also approximated by subtraction of apoA-I concentration from total protein. The apoA-I protein concentration of HDL was determined by ELISA (enzyme-linked immunosorbent assay) and calculated relative to an apoA-I standard curve. The ratio of apoA-I/apoA-II was similar using both measurements.

HL Displacement Assay in CHO and HepG2 Cells

CHO cells stably transfected with human HL (CHO-hHL) were plated in Ham's F12 medium containing 10% FBS, 500 µg/ml G418, 1% glutamine, and 1% penicillin/streptomycin in six-well plates. HepG2 cells were plated and grown to confluency in DMEM medium containing 10% FBS, 1% glutamine, and 1% penicillin/streptomycin in six-well plates. Once confluent, cells were washed with PBS and incubated with fresh medium in the absence of FBS overnight. The next day, the medium was aspirated, and the cells were washed 2× with FBS-free medium. Following the washes, the cells were incubated with FBS-free medium containing HDL or rHDL samples at a concentration of 150 µg/ml for 30 min at 37 °C. The media was collected into microcentrifuge tubes and stored at −80 °C. Cell lysates were prepared by washing the cells twice with PBS and incubation with 100 µl of sample buffer (62.5 mM Tris-HCl, pH 6.8, 20% glycerol, 2% SDS, 0.5% (w/v) bromophenol blue) for 30 min at 37 °C. The cell lysates were transferred into microcentrifuge tubes, heated for 10 min at 90 °C, and kept at −20 °C until it was electrophoresed. The frozen medium was lyophilized overnight, resolubilized in 200 µl of sample buffer, and heated at 90 °C for 10 min.

SDS-PAGE and Immunochemical Analysis

The cell lysate and media samples were electrophoresed on 8% polyacrylamide gels under denaturing conditions and transferred onto a nitrocellulose membrane. The membrane was incubated with blocking solution (PBS containing 1% BSA and 0.2% Tween-20) at room temperature for 1 h and then with the monoclonal anti-human HL XHL3-6a antibody from mouse (1:5,000) in blocking solution containing 0.02% NaN_3 at 4 °C overnight. Following three washes in PBS-0.2% Tween-20, a goat anti-mouse IgG HRP-linked whole antibody was used as the secondary antibody. After 1 h incubation with secondary antibody, the membrane was washed in PBS-0.2% Tween-20 and visualized by chemiluminescence following a 5-min incubation with the Pierce Super Signal West Pico substrate. The membrane was exposed to film, and the molecular mass of the cell surface-associated HL as well as the HL liberated into the medium was determined using broad-range molecular weight markers as a reference. The film was subsequently scanned, and the mass of HL that had been displaced into the media, by various types of HDL, was determined relative to standard rHDL by densitometry.

Non-denaturing Gradient Gel Electrophoresis Analysis

Conditioned media samples were electrophoresed using 4–20% Tris-Glycine precast gels under non-denaturing conditions overnight for 2000Vh at 4 °C. The gel was then incubated in a 0.1% SDS solution for 15 min to ensure the proteins had enough negative charge to transfer unidirectionally toward the anode. The gel was transferred for 4 h at 125 V at 4 °C (Tris-Glycine transfer buffer with 20% methanol) onto a PVDF membrane. The membrane was cut in half, and each half was incubated with either an HL blocking solution (TBS containing 1% BSA and 0.2% Tween-20) or an apoA-I blocking solution (TBS containing 5% skim milk and 0.2% Tween-20) overnight at 4 °C. The membranes were then incubated with either the monoclonal anti-human HL XHL3-6a antibody from mouse (1:5,000) or the monoclonal anti-human apoA-I 4H1 (2–8) and 5F6 (118–141) antibody from mouse (1:5,000) in blocking solution. Following three washes in TBS-0.2% Tween-20, both membranes were incubated for 1 h with a goat anti-mouse IgG HRP-linked whole antibody as the secondary antibody. The membranes were washed in TBS-0.2% Tween-20 and visualized by chemiluminescence following a 5-min incubation with the Pierce Super Signal West Dura substrate. The molecular weight and the densitometry profiles were generated using AlphaEase© software (AlphaInnotech Corp., San Leandro, CA).

HL Immunoprecipitation

Purified HDL (100 μg) from human plasma was mixed with 20 μl of purified HL (114 μg protein/ml) and 10 μl of polyclonal anti-human HL antibody and incubated overnight at 4 °C on a rotating wheel. A 10% protein-G Sepharose bead suspension (200 μl) (2% BSA in PBS) was added to the samples and incubated at 4 °C on a rotating wheel for 2 h. The samples were centrifuged at maximum speed in a microcentrifuge for 3 min. The supernatant was discarded, and following two gentle washes with PBS, SDS sample buffer was added to remove proteins from the beads with heating. The samples were either electrophoresed on a 12% polyacrylamide gel and probed for human apoA-I or electrophoresed on a 8% gel and probed for human HL.

Statistical Analyses

The significance of the difference between group mean values was calculated by the Student's *t*-test or one-way ANOVA and Dunnett post-test analysis using SigmaStat® Software (Version 3.0) (Systat Software Inc., San Jose, CA).

Results

Displacement of HL by Heparin and HDL in CHO-hHL Cells

Experiments show that HDL and heparin affect the cell surface association of HL and release it into the media of the human HL transfected CHO (CHO-hHL) cells (Fig. 1). There is very little HL normally released into the media when the cells are cultured in FBS-free medium alone, but similar to heparin, HDL readily displaces HL. Displacement of HL by heparin or HDL is time and dose dependent, and the maximal HL displacement into the incubation media occurs with 200 IU of heparin/ml or 150 μg of HDL protein/ml of media (Fig. 1). Both HDL and heparin increased the displacement of HL over the 2 h time course (data not shown). The molecular weight of HL released into the media (HSPG-bound HL) is estimated to be 66 kDa, which is similar to that for purified human HL (Fig. 2) [37].

Displacement of Cell Surface-Bound HL by HDL in HepG2 Cells

To compare the effect of HDL on HL displacement in transfected CHO-hHL cells and cells that express HL endogenously (HepG2), both cell lines were grown and treated with HDL, heparin, or FBS-free medium alone for 30 min. The results of immunochemical analysis by anti-HL mAb show two distinctive bands in the total extract of the CHO cells corresponding to the intra- and extra-cellular forms of overexpressed HL (Fig. 2a) [36]. Addition of HDL or heparin to the incubation medium results in the appearance of a 66 kDa HL band in the incubation media of CHO and HepG2 cells (Fig. 2b, d).

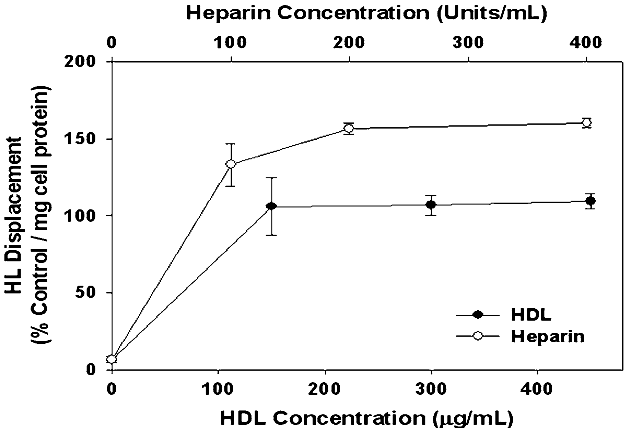

Fig. 1 Concentration-dependent displacement of cell surface-bound HL in CHO-hHL cells by HDL and heparin: CHO-hHL cells were grown to confluency and incubated with increasing concentrations of HDL protein or heparin for 30 min at 37 °C. The media was collected and analyzed by Western blots to determine the amount of HL released. HL release into medium was calculated relative to control incubations with apoA-I and normalized to total cell protein. These values are the mean ± SD of triplicate determinations from one assay and are representative of two separate experiments

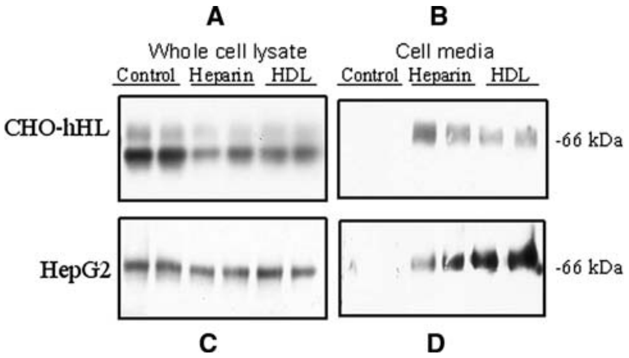

Fig. 2 Displacement of cell surface-bound HL from CHO-hHL (*panel a* and *b*) and HepG2 cells (*panel c* and *d*): CHO-hHL and HepG2 cells were grown to confluency and incubated with FBS-free media (control), heparin, and HDL for 30 min at 37 °C. The incubating media was collected, lyophilized, and resolubilized in SDS sample buffer. The cells were washed twice with PBS and solubilized in SDS sample buffer. Immunochemical analysis followed to detect the amounts of HL associated with the cells (CHO-hHL cells: *panel a*, HepG2 cells: *panel c*) and released into the medium (CHO-hHL cells: *panel b*, HepG2 cells: *panel d*). The duplicate images are from one analysis and are representative of three separate experiments for each cell line

Association of HDL and HL In Vitro

In order to evaluate whether a direct interaction occurs between HDL and HL, both non-denaturing electrophoretic Western blots and co-immunoprecipitation studies were undertaken. Non-denaturing gradient gel electrophoresis (NGGE) was performed on normolipidemic HDL samples that had been incubated with CHO-hHL cells. The proteins were transferred to PVDF membrane and probed for both apoA-I and HL (Fig. 3). NGGE probed for apoA-I showed the expected profile for a normolipidemic HDL, with the large, 11-nm HDL_2 class and smaller 8.0-nm HDL_3 class. NGGE probed for HL had almost an identical profile as shown for apoA-I (Fig. 3). HL appears to be associated with all classes of apoA-I containing HDL particles. Similar results were observed for HDL preparations from three different subjects. In co-immunoprecipitation studies, mixtures of pure HL and HDL were immunoprecipitated with a polyclonal anti-human HL Ab. The immunoprecipitate was electrophoresed and analyzed by Western blots to detect both apoA-I and HL. Blots probed for human apoA-I showed that HDL particles are immunoprecipitated when pure human HL is added to the HDL preparation (data not shown). These results confirm our earlier chromatographic work [8, 9], which showed that HL tightly interacts with HDL particles in solution.

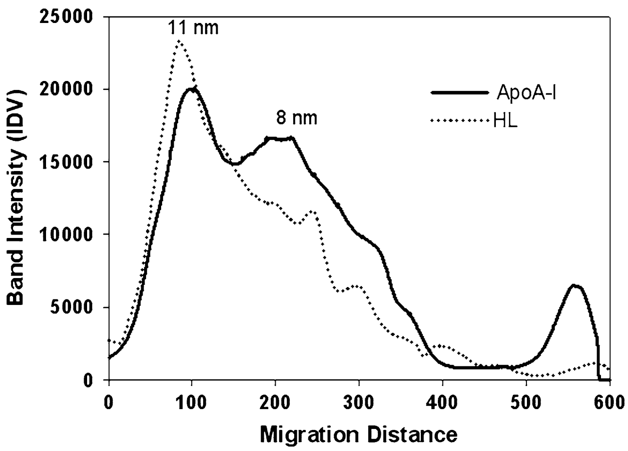

Fig. 3 Non-denaturing gradient gel electrophoresis of HL displaced from CHO-hHL cells by HDL: CHO-hHL cells were grown to confluency and incubated with 150 µg/ml of HDL for 30 min at 37 °C. The cell medium was collected and analyzed by non-denaturing gradient gel electrophoresis on 4–20% polyacrylamide gels. Proteins were transferred to PVDF and immunoblotted with anti-apoA-I and anti-HL antibodies. Densitometric profiles of apoA-I and HL blots are shown. The profiles are from one experiment undertaken with HDL from a single normolipidemic subject. Profiles are similar to that observed from separate experiments with HDL isolated from three different subjects

Displacement of Cell Surface-Bound HL by Synthetic HDL

The ability of native and synthetic HDL particles to displace HL was determined by incubating CHO-hHL cells with native HDL from normolipidemic subjects, rHDL (apoA-I and POPC), heparin, and FBS-free medium. rHDL displaces HL similar to heparin, while the ability of HDL is variable (60–90%) and dependent on the batch/donor of HDL (data not shown). This is consistent with previous work showing that pure apoA-I is more effective at displacing cell surface-associated HL than HDL [36].

HL Displacement by HDL Enriched with apoA-II

Normolipidemic HDL was enriched with pure apoA-II and ultracentrifuged to separate free apolipoproteins from the mixture. The apoA-I and apoA-II content of HDL was determined from silver-stained PAGE gels. The mass ratio of apoA-I to apoA-II decreased by 50% in apoA-II-enriched HDL.

HL displacement from CHO-hHL cells by HDL or HDL-apoA-II is shown in Fig. 4. Percent HL displacement was calculated relative to that for a control rHDL (apoA-I:POPC) particle. Incorporation of apoA-II into HDL causes a 2.5-fold increase in HL displacement from the cell surface. These data suggest that apoA-II is a structural component of HDL that plays a significant role in displacing cell surface-bound HL. The work appears

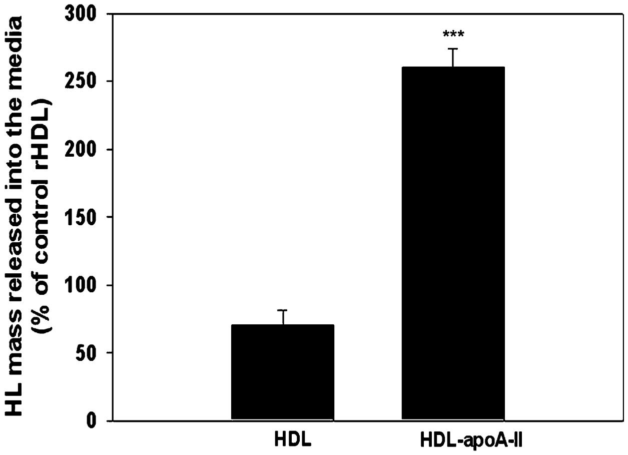

Fig. 4 HL displacement in CHO-hHL cells by HDL and apoA-II-enriched HDL: CHO-hHL cells were grown to confluency and incubated with 150 µg/ ml of HDL or apoA-II-enriched HDL for 30 min at 37 °C. The cell medium was collected and analyzed to determine the mass of liberated HL by HDL or HDL-apoA-II relative to a control rHDL (apoA-I/POPC) particle. The concentration of HL in the media is mean value ± SD of triplicate determinations from one assay and is representative of two separate displacement experiments. (The significance of difference relative to control HDL was determined by Student's *t*-test, ***$p < 0.0001$.)

consistent with previous work showing that apoA-II enhances association of HL with HDL particles [8].

HL Displacement by rHDL Particles Enriched with Apolipoproteins

To confirm that apoA-II has a specific impact on HL displacement and to estimate the role of other structural apolipoproteins of HDL in HL displacement, various HDL particles were reconstituted with different apolipoprotein mixtures. Purified apolipoproteins apoA-I, A-II, and C-I were isolated from delipidated HDL by anion exchange chromatography and used to generate rHDL complexes. rHDLs were also prepared from a full compliment of HDL apolipoproteins (apoHDL) that was prepared by delipidation of HDL. The molar ratio of the lipid and protein components of each particle is shown in Table 1.

Figure 5 presents the percent HL release into the media by various kinds of rHDL particles and heparin, relative to the standard rHDL particle (apoA-I/POPC). The figure indicates that apoA-I/apoA-II/POPC particles increase HL displacement by more than twofold relative to control rHDL. This confirms the results of the previous experiment with apoA-II-enriched native HDL. ApoA-I/apoC-I/POPC particles also increase HL displacement by 1.5-fold compared to the control. This suggests that both apoC-I and apoA-II are able to stimulate HL displacement. HDL apolipoproteins (apoHDL) were resolubilized after HDL extraction and shown to contain primarily apoA-I, apoA-II, apoC-I, apoC-II, and apoC-III. ApoHDL/POPC particles were less able to promote HL displacement (25% of control rHDL).

HL Displacement by HDL Enriched with Phospholipids

Normolipidemic HDL was enriched with various phospholipid vesicles (PI and POPC), and the impact of the increased phospholipid content of HDL on HL displacement was studied. Agarose gel electrophoresis of HDL-PI showed that PI enrichment of HDL increases lipoprotein net negative charge, while PC had the opposite effect (data not shown). HL displacement with native HDL, HDL-PI, and HDL-POPC, followed by immunoblotting of the incubation media, reveals that both phospholipids decrease HL displacement relative to native HDL or heparin (~50% that of control rHDL) (Fig. 6).

HL Displacement by rHDL Particles Enriched with Specific Lipids

Different kinds of rHDL particles were prepared enriched in cholesterol ester (CE), TG, and free fatty acid (FFA) to evaluate the impact of HDL lipid composition on HL displacement. These particles contained apoA-I, POPC, and

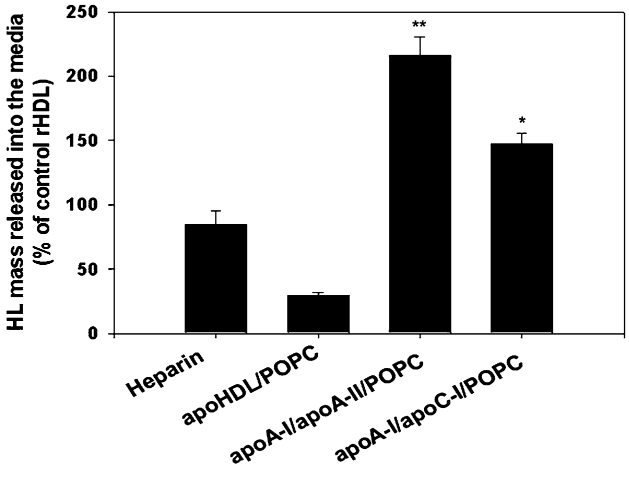

Fig. 5 HL displacement by rHDL particles containing various apolipoproteins: CHO-hHL cells were grown to confluency and incubated with 150 μg/ml of various synthetic rHDL particles: apoA-I/POPC, apoA-I/apoA-II/POPC, apoA-I/apoC-I/POPC, and apoHDL/POPC, for 30 min at 37 °C. The incubating media was analyzed by Western blots to determine the mass of HL released into the media. HL mass in the media was calculated relative to the control rHDL (apoA-I/POPC). The values of HL are mean ± SD of triplicate determinations from one assay and represent three displacement experiments. (The significance of difference relative to heparin was determined by one-way ANOVA, **$p < 0.001$, *$p < 0.01$)

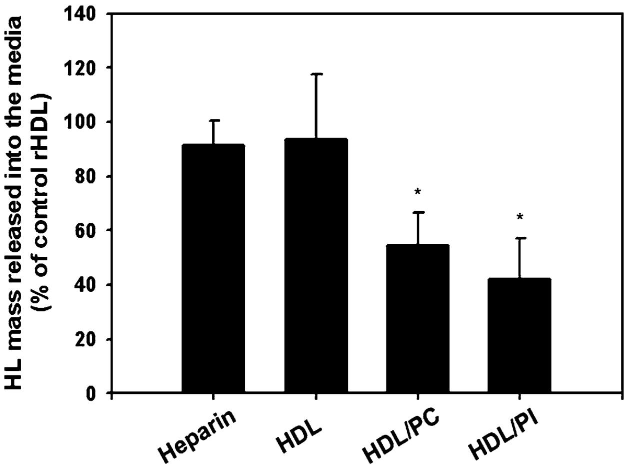

Fig. 6 HL displacement by phospholipid-enriched HDL: HDL obtained from normolipidemic subjects was enriched with phosphatidylcholine (PC) or phosphotidylinositol (PI) as described. CHO-hHL cells were grown to confluency and incubated with 100 IU/ml of heparin or 150 μg/ml of HDL, HDL/PC, or HDL/PI for 30 min at 37 °C. The incubating media was analyzed by Western blots to determine the mass of HL released into the media. The values of HL in the medium were calculated relative to the control rHDL particle (apoA-I/POPC). These values are mean ± SD of triplicate determinations from one assay and are representative of three different experiments. (The significance of difference relative to heparin was determined by one-way ANOVA, *$p < 0.01$)

the test lipid (starting ratios are shown in Table 2). HL displacement from CHO-hHL cells (Fig. 7) demonstrates that CE-enriched particles slightly increase HL displacement (1.2-fold), whereas rHDL enriched with FFA has a modest inhibitory effect in HL displacement. Enrichment with TG significantly decreases HL displacement to 25% of the control. These results suggest that the TG component of HDL is an important inhibitor of HL displacement from the cell surface.

HL Displacement by HDL Fractions from Hypercholesterolemic Patients

To determine whether HDL from hypercholesterolemic patients has an altered ability to displace cell surface HL, displacement experiments were performed with HDL isolated from hypercholesterolemic patient plasma and normolipidemic plasma. The plasma sample from the hypercholesterolemic patient had a total cholesterol of 5.9 mM, a TG of 1.22 mM, and an HDL cholesterol of 1.33 mM. The HDL–TG levels were significantly higher in the hypercholesterolemic than the normolipidemic subject. The HDL_2 and HDL_3 fractions were isolated from plasma samples ultracentrifugally ($d = 1.063-1.125$ g/ml and 1.125–1.21 g/ml, respectively). HL levels were low and barely detectible in isolated HDL fractions. CHO-hHL cells were treated with total HDL, HDL_2, and HDL_3 fractions and the incubation media analyzed for HL content. The Western blots of the cell media (Fig. 8, upper blot) reveal that HDL from the normolipidemic subject was able to displace HL into the media. As previously shown [36, 37], the HDL_2 fraction (lanes 8 and 9) was more effective at displacing HL than the HDL_3 fraction (lanes 5, 6, and 7). In contrast, none of the HDL fractions from the hypercholesterolemic patient (lower blot) were able to displace cell surface HL. Similar observations have been made with HDL isolated from three other hypercholesterolemic patients, with similar lipid profiles (data not shown).

Discussion

Previous work has shown that HDL and apoA-I can displace HL from purified HSPG [37] and cell surface proteoglycans [36] and increase VLDL–TG hydrolysis. HL displacement by infused heparin and the consequent increase in plasma HL activity (post-heparin HL activity) was demonstrated as early as 1972 [28]. Intravenous injection of heparin to both humans [26] and animal models [2] results in the displacement of HL from the hepatic endothelium and increases HL activity in the bloodstream. The data cumulatively suggest that hepatic-bound HL is inactive and HL displacement is required for

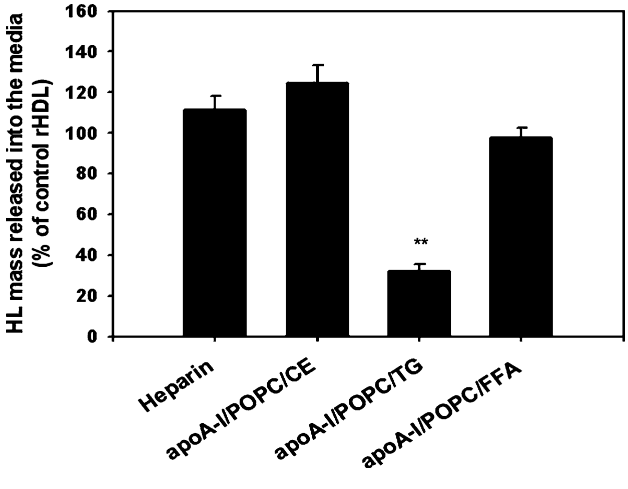

Fig. 7 HL displacement by rHDL particles prepared with different lipids: Confluent CHO-hHL cells were incubated with 100 IU/ml of heparin or 150 µg/ml of different rHDL particles: apoA-I/POPC, apoA-I/POPC/CE, apoA-I/POPC/TG, and apoA-I/POPC/FFA, for 30 min at 37 °C. The incubating media was then analyzed immunochemically to determine the mass of HL released into the media. The values of HL in the media were calculated relative to the control rHDL particle (apoA-I/POPC). These values are mean ± SD of triplicate determinations from one set of particles and are representative of three different experiments. (The significance of difference relative to heparin was determined by one-way ANOVA, $^{**}p < 0.001$)

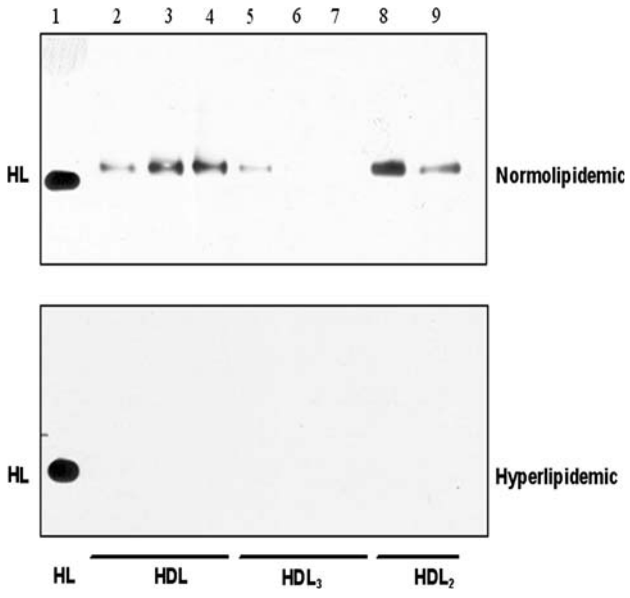

Fig. 8 HL displacement by normal and hyperlipidemic HDL: HDL subfractions from a normolipidemic and a hyperlipidemic subject were incubated (150 µg/ml) with confluent CHO-hHL cells for 30 min at 37 °C. The incubating medium was then analyzed by Western blots to determine the mass of HL released into the medium. The images are from one analysis and are similar to that observed from separate experiments with HDL isolated from three different hyperlipidemic patients

TG hydrolytic activity [37]. In vivo evidence that supports this view [10] also comes from mice expressing a mutant human HL that had decreased binding to liver HSPG. While wild-type human HL transfected animals had no increase in plasma activity and no overt phenotype, the animals expressing the mutant HL had elevated pre-heparin HL activity and decreased plasma lipid and apolipoprotein levels. The increase in lipid hydrolysis and clearance resulting from increased circulating HL activity suggests that hepatic-bound HL is minimally active and activity is linked to displacement. Therefore, a high post-heparin HL activity may reflect the size of the storage/inactive pool of HL in the liver.

Post-heparin HL activity in familial low HDL patients is higher than in normal subjects [40]. This supports the view that plasma HDL plays a role in displacement and activation of HL. Cell culture studies have shown that the larger, more buoyant subfractions of HDL have the greatest ability to displace cell surface-bound HL [36]. This suggests that composition and structural properties of HDL may be important regulatory factors in HL displacement. Interestingly, related studies have demonstrated that both the apolipoprotein and lipid components of HDL also directly regulate HL activity and VLDL–TG hydrolysis by directly affecting HL association with HDL [8, 9]. These data suggest that plasma HDL regulates HL at two stages: (1) displacement of cell surface-bound HL and (2) modulation of the activity of displaced HL by binding to it and inhibiting VLDL–TG hydrolysis. Activity and displacement are regulated independently. Tight associations with HDL appear critical to inhibiting the activity of circulating HL. The activity of HL is activated by lipoprotein electrostatic properties [9], but HL displacement is controlled by lipid and protein composition of HDL particles.

Heparin has a well-documented role in displacing HL and LPL. Tagashira et al. [48] reported that heparin may act through protein kinase-dependent signaling pathways to stimulate the release of HL. However, it is generally thought that heparin directly interacts with the lipase or competes with it to bind to the binding sites on the cell surface HSPG [2]. It has been suggested that the interaction of heparin with lipases or other biological molecules such as antithrombin-III is due to the association of charged groups of heparin with unique sequences of amino acid residues that are potentially involved in heparin binding [2, 12]. Endogenous heparin levels may impact lipid metabolism. Individuals with lower endogenous circulating heparin activity have more serum lipid abnormalities and are more susceptible to atherosclerosis [20].

Low HDL levels are also associated with an increased post-heparin plasma HL activity, aberrant TG metabolism, and increased atherosclerotic risk [13, 15, 21, 38]. HDL may regulate HL displacement, and evidence suggests that HDL may displace cell surface HL by directly binding to the enzyme. HL binds to HDL with a high affinity interaction, and studies show that HL is primarily found in the plasma compartment associated with HDL particles [8, 9, 33]. Co-immunoprecipitation studies confirm the association of HL with HDL and Western blots of NGGE show that HL is associated with all classes of HDL containing apoA-I. NGGE densitometric profiles for apoA-I and HL were almost identical (Fig. 3). In contrast, NGGE probed for other apoproteins (i.e., apoA-II) showed completely different profiles from that shown for HL (data not shown).

HDL composition directly affects HL displacement, and HDL apolipoproteins play an important role. The effect of apoA-II on apoA-I conformation and HDL structure has been described previously [8]. ApoA-II significantly increases the binding of HL with HDL particles [8, 33]. Thus, one may conclude that HDL structural alterations caused by apoA-II directly enhance HDL and HL association. Previous work, however, has shown that apoA-II also inhibits VLDL–TG hydrolysis by HL [8]. The increased binding of HL to HDL may therefore increase HL displacement but decrease activity by blocking the ability of HL to shuttle between the lipoprotein substrates and hydrolyze them. HDL_2 has a greater capacity to displace HL, while HDL_3 is poor at displacing HL from the cell surface [36]. This observation is consistent with the inverse relationship reported between plasma HDL_2 levels and magnitude of post-prandial lipemia [34]. However, HDL_2 contains lower relative amounts of apoA-II [23], and therefore apoA-II content cannot directly account for the increased displacement ability of HDL_2.

ApoC-I also increases HL displacement, but to a lesser extent than apoA-II. Since this apolipoprotein is readily exchangeable between VLDL and HDL (more than apoA-II) [18], it is conceivable that apolipoprotein exchanges during a post-prandial response render HDL more able to displace cell surface HL (Fig. 9, Steps 1 and 2). HDL is known to lose other apoC proteins post-prandially [18], and since apoHDL containing rHDL was poor at displacing HL, it is also conceivable that a loss of apoC-II and apoC-III from HDL could directly enhance HL displacement.

The HDL lipid components also regulate HL displacement. Phospholipid-enrichment of HDL particles blocks the displacement of HL from the CHO-hHL cells. The electrostatic charge of the HDL particle does not appear to directly affect HL displacement, as opposite changes in charge (HDL–PI = negative, HDL–PC = positive) both inhibit HL displacement. This suggests that phospholipid components of HDL affect its structure and function in a manner independent of charge modifications. Phospholipids have also been shown to increase the hydrolytic activity of HL by reducing the binding affinity of HL for HDL [9]. It is known that during a post-prandial response, remnant

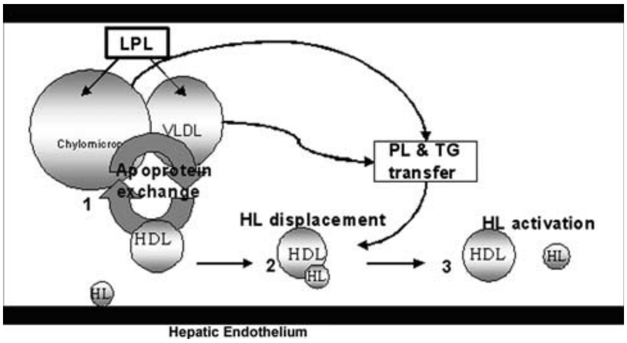

Fig. 9 Proposed model of HL displacement and activation by HDL: Alterations in HDL composition may control the displacement and activation of HL. Apolipoprotein exchange between HDL and chylomicron/VLDL particles occurs during a post-prandial response (Step 1). Assimilation or loss of apolipoprotein molecules from/to HDL stimulates HL displacement by promoting a direct binding of HL to HDL (Step 2). Enrichment of HDL with remnant PL and TG causes HL to dissociate from HDL (Step 3). Dissociation of HL from HDL activates HL-mediated lipid hydrolysis

phospholipids are absorbed into the HDL pool. This may have the function to block additional HL displacement and liberate HL from HDL for increased VLDL hydrolysis.

The TG content of HDL is also an inhibitor of HL displacement. While the free fatty acid and cholesteryl ester contents of HDL have only modest effects on HL displacement, small changes in TG content block HL displacement. Modifications in the neutral lipid content of HDL give rise to unique changes in the structure of apoA-I and stability of the particle. A decrease in CE/TG ratios in reconstituted HDL particles decreases the integrity of the particle and stability of apoA-I α-helical segments [43]. This kind of alteration in the composition and structure of HDL has been observed in the plasma of hyperlipidemic subjects [18, 45]. Abnormalities in HDL composition directly affect the physiological functions of HDL by altering the interaction of HDL with LCAT [44], CETP [32], and cell surfaces [24]. An increase in the TG content of HDL would be expected to disrupt the stability of the complex, which may directly impact HL displacement. Conversely, apoA-II increases HDL structural stability [8] and enhances HL displacement. It is believed that the core TG enrichment and CE depletion of HDL associated with conformational changes of apoA-I may be related to acceleration of atherosclerosis in metabolic diseases [25]. Thus, an increased CE/TG content of HDL seems to be essential for proper function of HDL. This perspective appears to be consistent with enhancement of HL displacement by larger classes of HDL, which contain increased CE/TG in their core [7].

HDL from dyslipidemic patients appears unable to displace HL. This may support the view that the TG content of HDL plays a role in regulation of HL displacement. This could be a normal phenomenon during a post-prandial response that has negative consequences in dyslipidemic subjects. Several hours after a meal, plasma TG levels reach a peak, the magnitude and duration of which is dependent on TG hydrolytic rates. During this period, the exchange of core lipids and apolipoproteins between circulating lipoproteins is increased [29]. Lipemia is prolonged in hyperlipidemic conditions and results in TG enrichment of LDL and HDL particles [29]. The expected consequence would be less HL displacement and higher post-heparin HL activity. Elevated post-heparin HL activity is common in hyperlipidemia and therefore suggests that abnormal HL displacement may result in high blood TG levels.

Figure 9 summarizes the view that HL displacement and activation are regulated by structural modifications of HDL during a post-prandial response. Apolipoprotein exchanges between HDL and the apoB lipoproteins may act to initiate HL displacement (Step 1). An increase in HDL apoC-I, apoA-II, and/or loss of apoC-II, apoC-III may act to promote HL displacement from the liver (Step 2). High-affinity association of HL with HDL inhibits lipolytic activity [8, 9], and therefore the displaced circulating HL would be initially inactive. As VLDL and chylomicrons are degraded by LPL, remnant fatty acids and PL are transferred to HDL, which act to liberate HL and stimulate HL-mediated lipolysis (Step 3). HL can then return to its storage location in the liver. Chronic hypertriglyceridemia would be expected to give rise to alterations in HDL structure and block Steps 1 and 2, which would leave higher levels of cell-associated HL in the liver. Elevated post-heparin HL activities in hyperlipidemic patients are in fact a hallmark of perturbations in TG clearance and are directly associated with increased CHD risk [41].

Acknowledgments This work was supported by a grant from the Heart and Stroke Foundation of Canada. We would also like to thank Dr. A. Bensadoun and Dr. Y. Marcel for the monoclonal anti-HL and the anti-apoA-I antibodies, respectively.

References

1. Allayee H, Dominguez KM, Aouizerat BE, Krauss RM, Rotter JI, Lu J, Cantor RM, de Bruin TW, Lusis AJ (2000) Contribution of the hepatic lipase gene to the atherogenic lipoprotein phenotype in familial combined hyperlipidemia. J Lipid Res 41(2):245–252
2. Assmann G, Krauss RM, Fredrickson DS, Levy RI (1973) Characterization, subcellular localization, and partial purification of a heparin-released triglyceride lipase from rat liver. J Biol Chem 248(6):1992–1999
3. Assmann G, Krauss RM, Fredrickson DS, Levy RI (1973) Positional specificity of triglyceride lipases in post-heparin plasma. J Biol Chem 248(20):7184–7190
4. Austin MA, Breslow JL, Hennekens CH, Buring JE, Willett WC, Krauss RM (1988) Low-density lipoprotein subclass patterns and risk of myocardial infarction. JAMA 260(13):1917–1921

5. Austin MA, King MC, Vranizan KM, Krauss RM (1990) Atherogenic lipoprotein phenotype. A proposed genetic marker for coronary heart disease risk. Circulation 82(2):495–506
6. Auwerx JH, Marzetta CA, Hokanson JE, Brunzell JD (1989) Large buoyant LDL-like particles in hepatic lipase deficiency. Arteriosclerosis 9(3):319–325
7. Barter PJ (2002) Hugh Sinclair lecture: the regulation and remodelling of HDL by plasma factors. Atheroscler Suppl 3(4):39–47
8. Boucher J, Ramsamy TA, Braschi S, Sahoo D, Neville TA, Sparks DL (2004) Apolipoprotein A-II regulates HDL stability and affects hepatic lipase association and activity. J Lipid Res 45(5):849–858
9. Boucher JG, Nguyen T, Sparks DL (2007) Lipoprotein electrostatic properties regulate hepatic lipase association and activity. Biochem Cell Biol 85:696–708
10. Brown RJ, Gauthier A, Parks RJ, McPherson R, Sparks DL, Schultz JR, Yao Z (2004) Severe hypoalphalipoproteinemia in mice expressing human hepatic lipase deficient in binding to heparan sulfate proteoglycan. J Biol Chem 279(41):42403–42409
11. Campos H, Dreon DM, Krauss RM (1995) Associations of hepatic and lipoprotein lipase activities with changes in dietary composition and low density lipoprotein subclasses. J Lipid Res 36(3):462–472
12. Cardin AD, Weintraub HJ (1989) Molecular modeling of protein-glycosaminoglycan interactions. Arteriosclerosis 9(1):21–32
13. Carr MC, Ayyobi AF, Murdoch SJ, Deeb SS, Brunzell JD (2002) Contribution of hepatic lipase, lipoprotein lipase, and cholesteryl ester transfer protein to LDL and HDL heterogeneity in healthy women. Arterioscler Thromb Vasc Biol 22(4):667–673
14. Colvin PL Jr, Auerbach BJ, Case LD, Hazzard WR, Applebaum-Bowden D (1991) A dose-response relationship between sex hormone-induced change in hepatic triglyceride lipase and high-density lipoprotein cholesterol in postmenopausal women. Metabolism 40(10):1052–1056
15. Deeb SS, Zambon A, Carr MC, Ayyobi AF, Brunzell JD (2003) Hepatic lipase and dyslipidemia: interactions among genetic variants, obesity, gender, and diet. J Lipid Res 44(7):1279–1286
16. Despres JP, Ferland M, Moorjani S, Nadeau A, Tremblay A, Lupien PJ, Theriault G, Bouchard C (1989) Role of hepatic-triglyceride lipase activity in the association between intra-abdominal fat and plasma HDL cholesterol in obese women. Arteriosclerosis 9(4):485–492
17. Ehnholm C, Kuusi T (1986) Preparation, characterization, and measurement of hepatic lipase. Methods Enzymol 129:716–738
18. Eisenberg S (1984) High density lipoprotein metabolism. J Lipid Res 25(10):1017–1058
19. Eliasson B, Mero N, Taskinen MR, Smith U (1997) The insulin resistance syndrome and postprandial lipid intolerance in smokers. Atherosclerosis 129(1):79–88
20. Engelberg H (2001) Endogenous heparin activity deficiency: the ‘missing link’ in atherogenesis? Atherosclerosis 159(2):253–260
21. Glaser DS, Yost TJ, Eckel RH (1992) Preheparin lipoprotein lipolytic activities: relationship to plasma lipoproteins and postheparin lipolytic activities. J Lipid Res 33(2):209–214
22. Haffner SM, Applebaum-Bowden D, Wahl PW, Hoover JJ, Warnick GR, Albers JJ, Hazzard WR (1985) Epidemiological correlates of high density lipoprotein subfractions, apolipoproteins A-I, A-II, and D, and lecithin cholesterol acyltransferase. Effects of smoking, alcohol, and adiposity. Arteriosclerosis 5(2):169–177
23. Havel RJ, Eder HA, Bragdon JH (1955) The distribution and chemical composition of ultracentrifugally separated lipoproteins in human serum. J Clin Invest 34(9):1345–1353
24. Johnson WJ, Mahlberg FH, Rothblat GH, Phillips MC (1991) Cholesterol transport between cells and high-density lipoproteins. Biochim Biophys Acta 1085(3):273–298
25. Kontush A, Chapman MJ (2006) Functionally defective high-density lipoprotein: a new therapeutic target at the crossroads of dyslipidemia, inflammation, and atherosclerosis. Pharmacol Rev 58(3):342–374
26. Krauss RM, Levy RI, Fredrickson DS (1974) Selective measurement of two lipase activities in postheparin plasma from normal subjects and patients with hyperlipoproteinemia. J Clin Invest 54(5):1107–1124
27. Kuusi T, Kinnunen PK, Nikkila EA (1979) Hepatic endothelial lipase antiserum influences rat plasma low and high density lipoproteins in vivo. FEBS Lett 104(2):384–388
28. LaRosa JC, Levy RI, Windmueller HG, Fredrickson DS (1972) Comparison of the triglyceride lipase of liver, adipose tissue, and postheparin plasma. J Lipid Res 13(3):356–363
29. Lopez-Miranda J, Perez-Martinez P, Marin C, Moreno JA, Gomez P, Perez-Jimenez F (2006) Postprandial lipoprotein metabolism, genes and risk of cardiovascular disease. Curr Opin Lipidol 17(2):132–138
30. Markwell MA, Haas SM, Bieber LL, Tolbert NE (1978) A modification of the Lowry procedure to simplify protein determination in membrane and lipoprotein samples. Anal Biochem 87(1):206–210
31. Marniemi J, Peltonen P, Vuori I, Hietanen E (1980) Lipoprotein lipase of human postheparin plasma and adipose tissue in relation to physical training. Acta Physiol Scand 110(2):131–135
32. Morton RE (1988) Free cholesterol is a potent regulator of lipid transfer protein function. J Biol Chem 263(25):12235–12241
33. Mowri HO, Patsch JR, Gotto AM Jr, Patsch W (1996) Apolipoprotein A-II influences the substrate properties of human HDL2 and HDL3 for hepatic lipase. Arterioscler Thromb Vasc Biol 16(6):755–762
34. Patsch JR, Karlin JB, Scott LW, Smith LC, Gotto AM Jr (1983) Inverse relationship between blood levels of high density lipoprotein subfraction 2 and magnitude of postprandial lipemia. Proc Natl Acad Sci USA 80(5):1449–1453
35. Patsch JR, Prasad S, Gotto AM Jr, Patsch W (1987) High density lipoprotein2. Relationship of the plasma levels of this lipoprotein species to its composition, to the magnitude of postprandial lipemia, and to the activities of lipoprotein lipase and hepatic lipase. J Clin Invest 80(2):341–347
36. Ramsamy TA, Boucher J, Brown RJ, Yao Z, Sparks DL (2003) HDL regulates the displacement of hepatic lipase from cell surface proteoglycans and the hydrolysis of VLDL triacylglycerol. J Lipid Res 44(4):733–741
37. Ramsamy TA, Neville TA, Chauhan BM, Aggarwal D, Sparks DL (2000) Apolipoprotein A-I regulates lipid hydrolysis by hepatic lipase. J Biol Chem 275(43):33480–33486
38. Rashid S, Watanabe T, Sakaue T, Lewis GF (2003) Mechanisms of HDL lowering in insulin resistant, hypertriglyceridemic states: the combined effect of HDL triglyceride enrichment and elevated hepatic lipase activity. Clin Biochem 36(6):421–429
39. Seed M, Mailly F, Vallance D, Doherty E, Winder A, Talmud P, Humphries SE (1994) Lipoprotein lipase activity in patients with combined hyperlipidaemia. Clin Investig 72(2):100–106
40. Soderlund S, Soro-Paavonen A, Ehnholm C, Jauhiainen M, Taskinen MR (2005) Hypertriglyceridemia is associated with prebeta-HDL concentrations in subjects with familial low HDL. J Lipid Res 46(8):1643–1651
41. Soro A, Jauhiainen M, Ehnholm C, Taskinen MR (2003) Determinants of low HDL levels in familial combined hyperlipidemia. J Lipid Res 44(8):1536–1544
42. Sparks DL, Davidson WS, Lund-Katz S, Phillips MC (1993) Effect of cholesterol on the charge and structure of apolipoprotein A-I in recombinant high density lipoprotein particles. J Biol Chem 268(31):23250–23257

43. Sparks DL, Davidson WS, Lund-Katz S, Phillips MC (1995) Effects of the neutral lipid content of high density lipoprotein on apolipoprotein A-I structure and particle stability. J Biol Chem 270(45):26910–26917
44. Sparks DL, Pritchard PH (1989) The neutral lipid composition and size of recombinant high density lipoproteins regulates lecithin:cholesterol acyltransferase activity. Biochem Cell Biol 67(7):358–364
45. Sparks D, Frohlich JJ, Pritchard PH (1991) Lipid transfer proteins, hypertriglyceridemia, and reduced high-density lipoprotein cholesterol. Am Heart J 122(2):601–607
46. Swaney JB, Orishimo MW (1989) Effects of heparin-induced lipolytic activity on the structure of rat high-density lipoprotein. Biochim Biophys Acta 1002(3):338–347
47. Syvanne M, Ahola M, Lahdenpera S, Kahri J, Kuusi T, Virtanen KS, Taskinen MR (1995) High density lipoprotein subfractions in non-insulin-dependent diabetes mellitus and coronary artery disease. J Lipid Res 36(3):573–582
48. Tagashira H, Nakahigashi S, Kerakawati R, Motoyashiki T, Morita T (2005) Involvement of Ca2+/calmodulin-dependent protein kinase II in heparin-stimulated release of hepatic lipase activity from rat hepatocytes. Biol Pharm Bull 28(3):409–412
49. Zambon A, Austin MA, Brown BG, Hokanson JE, Brunzell JD (1993) Effect of hepatic lipase on LDL in normal men and those with coronary artery disease. Arterioscler Thromb 13(2):147–153

Lipids (2008) 43:805–811
DOI 10.1007/s11745-008-3215-0

ORIGINAL ARTICLE

Stearidonic Acid-Enriched Soybean Oil Increased the Omega-3 Index, an Emerging Cardiovascular Risk Marker

William S. Harris · Shawna L. Lemke · Susan N. Hansen · Daniel A. Goldstein · Maureen A. DiRienzo · Hong Su · Margaret A. Nemeth · Mary L. Taylor · Gulam Ahmed · Cherian George

Received: 6 June 2008 / Accepted: 10 July 2008 / Published online: 6 August 2008
© AOCS 2008

Abstract A plant source of omega-3 fatty acid (FA) that can raise tissue eicosapentaenoic acid (EPA) and/or docosahexaenoic acid (DHA) is needed. A soybean oil (SBO) containing approximately 20% stearidonic acid [SDA; the delta-6 desaturase product of alpha-linolenic acid (ALA)] derived from genetically modified soybeans is under development. This study compared the effects of EPA to SDA-SBO on erythrocyte EPA + DHA levels (the omega-3 index). Overweight healthy volunteers ($n = 45$) were randomized to SDA-SBO (24 ml/day providing ~3.7 g SDA) or to regular SBO (control group) without or with EPA ethyl esters (~1 g/day) for 16 weeks. Serum lipids, blood pressure, heart rate, platelet function and safety laboratory tests were measured along with the omega-3 index. A per-protocol analysis was conducted on 33 subjects (11 per group). Compared to baseline, average omega-3 index levels increased 19.5% in the SDA group and 25.4% in the EPA group ($p < 0.05$ for both, vs. control). DHA did not change in any group. Relative to EPA, SDA increased RBC EPA with about 17% efficiency. No other clinical endpoints were affected by SDA or EPA treatment (vs. control). In conclusion, SDA-enriched SBO significantly raised the omega-3 index. Since EPA supplementation has been shown to raise the omega-3 index and to lower risk for cardiac events, SDA-SBO may be a viable plant-based alternative for providing meaningful intakes of cardioprotective omega-3 FAs.

Keywords Omega-3 fatty acids · Stearidonic acid · Cardiovascular disease · Risk factors · Soybean oil · Genetically modified organisms

Introduction

Evidence from large clinical trials confirms that diets enriched with long-chain omega-3 (n-3) fatty acids (eicosapentaenoic acid, EPA, or C20:5n-3 and docosahexaenoic acid, DHA, or C22:6n-3) are advantageous to cardiovascular health [1]. Although most studies have been done with both EPA and DHA (provided as fish oils), the largest clinical trial with major coronary heart disease (CHD) endpoints, the Japan EPA lipid intervention study [2], was done with EPA alone and was shown to reduce the risk of these events by 19%. EPA supplementation raises membrane phospholipid EPA content, and elevated omega-3 fatty acid (FA) membrane levels alter cellular metabolism in a number of ways beneficial to cardiovascular health [3]; therefore, it is reasonable to conclude that raising tissue levels of EPA can reduce the risk for CHD. A new marker for tissue omega-3 content is the "omega-3 index," which is the sum of EPA and DHA in erythrocyte membranes [4]. This metric has been shown to reflect human myocardial EPA and DHA content [5, 6], and has been proposed as a novel risk factor for death from CHD [7].

The American Heart Association has recommended that all adults strive to consume at least two servings of fish (preferably oily) per week to reduce the risk for CHD [8]. Western diets are typically low in EPA and DHA because

---

Electronic supplementary material The online version of this article (doi:10.1007/s11745-008-3215-0) contains supplementary material, which is available to authorized users.

W. S. Harris (✉) · S. N. Hansen
Sanford Research/USD, 1100 East 21st Street, Suite 700,
Sioux Falls, SD 57105, USA
e-mail: harrisw@sanfordhealth.org

S. L. Lemke · D. A. Goldstein · M. A. DiRienzo · H. Su ·
M. A. Nemeth · M. L. Taylor · G. Ahmed · C. George
Product Safety Center, Monsanto Company,
800 North Lindbergh Boulevard, St Louis, MO, USA

the primary source of these FAs is oily fish (such as salmon, mackerel, albacore tuna, and sardines), and consumption of these is minimal [9]. If such advice were actually heeded, there is serious doubt that the world's oceans could support such a shift in dietary consumption patterns [10]. Accordingly, a new and sustainable source of long-chain omega-3 FAs is needed. Currently, land-based sources of omega-3 FAs include flaxseed, canola, and soybean oils, which contain alpha-linolenic acid (C18:3n-3, ALA). ALA can be converted in vivo via desaturation and elongation pathways to EPA [11]. However, this conversion has a very low efficiency, converting somewhere between 0.01 and 8% of ALA to EPA and less to DHA [11, 12]. The rate-limiting step in the conversion of ALA to EPA is the delta-6 desaturase, and the product of this reaction is stearidonic acid (C18:4n-3, SDA). SDA is more readily converted to EPA than is ALA [13]. Hence, another strategy for raising tissue EPA levels with a plant-based omega-3 FA is to consume foods containing SDA. SDA is found in low concentrations (up to 4% w/w of total fatty acids) in fish oils (which also provide EPA and DHA), but also in some plant oils that are consumed as dietary supplements (e.g., echium). Recently, soybean plants have been genetically modified to produce oil containing a substantial amount of SDA (15–30% w/w of total fatty acids) [14]. This study was designed to test the hypothesis that increased SDA intake would favorably impact the omega-3 index.

Subjects and Methods

Study Participants

Healthy male or female adult volunteers between the ages of 21 and 70 with a body mass index (BMI) of 25–40 kg/m^2, an initial omega-3 index of $\leq$5%, and with an average resting heart rate >69 bpm were recruited. Individuals who were pregnant or lactating, current smokers, or had a history of significant cardiac, renal, hepatic, gastrointestinal, pulmonary, biliary or endocrine disorder, as well as any persons with diagnosed cancer, psychiatric disorders, diabetes mellitus, peripheral arterial disease, symptomatic coronary artery disease, a history of stroke or transient ischemic attack were excluded. Persons on specific medications or supplements that affected heart rate, blood pressure, serum lipids or platelet function were also excluded, as were those on weight-loss medications. Individuals taking dietary supplements that could alter tissue omega-3 fatty acids, such as fish oil, flaxseed or flaxseed oils, were excluded. Finally, persons with untreated hypertension, those who had taken any investigational agent in the prior 30 days and premenopausal females not on an effective birth control regimen were excluded.

Design

This was a randomized, double-blind, placebo-controlled study, conducted between January and October 2007. Subjects were randomized into one of three treatment groups. The control group was given packets and capsules containing regular SBO; the EPA group was given regular SBO packets plus capsules of EPA ethyl esters (2 × 500 mg); the SDA group was given packets of SBO derived from plants genetically modified to produce SDA (SDA-SBO; 16.6% SDA) plus SBO capsules. The fatty acid composition of the test oils is given in Table 1. In addition to SDA, SDA-SBO also contains 5% gamma-linolenic acid (GLA, which is not found in regular SBO) and somewhat higher amounts of ALA. The oils were provided in single-use, tear-open packets, and subjects were instructed to keep their packets in the refrigerator at home. They were instructed to consume the contents of three 8-ml packets (total dispensed oil averaged 7.4 g/packet) daily by pouring them onto foods and to take two 500-mg capsules per day. The total daily intake of SDA was ~3.66 g/day in the SDA group, and the intake of EPA was 0.98 g/day in the EPA group. ALA intake from the test oils was 1.7 g/day in the control and EPA groups, and 2.42 g/day in the SDA group. The study lasted for 16 weeks. All participants were instructed to maintain a

Table 1 Fatty acid composition of regular and SDA soybean oils (% weight)

Fatty acid	Regular soy oil	SDA soy oil
Saturated fats		
Myristic acid	0.05	0.07
Palmitic acid	9.96	11.18
Stearic acid	4.08	4.61
Arachidic acid	0.32	0.39
Behenic acid	0.36	0.06
Lignoceric acid	0.11	0.06
Monounsaturated fats		
Palmitoleic acid	0.10	0.11
Oleic acid	21.89	18.12
Eicosenoic acid	0.22	0.22
Polyunsaturated fats		
Omega-6 fatty acids		
Linoleic acid	54.65	31.48
γ-Linolenic acid	ND	5.38
Omega-3 fatty acids		
α-Linolenic acid	7.60	10.59
Stearidonic acid	ND	16.56
Other fatty acids	0.70	1.20

ND Not detected; defined as <0.05%

consistent lifestyle (diet, exercise, alcohol intake, sleep habits, etc.) and to avoid intake of fatty fish (including salmon, mackerel, albacore tuna, herring and sardines) for the duration of the study. Compliance with the treatment regimen was measured by counting unused oil packets and capsules. Non-compliance was defined as consumption of less than 80% of the experimental oils and/or capsules. The study was approved by the Copernicus Group Institutional Review Board, and all subjects gave informed consent prior to participation.

Laboratory Methods

The primary endpoint of the study was EPA + DHA as a percent of total red blood cell (RBC) FAs (the omega-3 index). Secondary endpoints were EPA, DHA and SDA alone (all as a percent of total RBC FAs), fasting lipids (cholesterol, triglycerides, LDL and HDL cholesterol), whole blood platelet aggregation, blood pressure and heart rate.

Omega-3 Index

Fasting venous blood samples were collected into ethylenediaminetetraacetic acid-containing vacutainer tubes. After centrifugation for 5 min at 10 g, plasma and buffy coats were removed, and an aliquot of the RBC pellet was stored at −80°C until analyzed. RBC samples were thawed and placed in a reaction vial containing 14% boron trifluoride (BF_3) in methanol (one part RBC to ten parts methanol) and heated at 100°C for 10 min. After cooling, hexane and distilled water (same volumes as BF_3 methanol) were added, and the tube was shaken and centrifuged to separate layers. An aliquot of the hexane supernatant was analyzed by flame ionization gas chromatography using a GC2010 (Shimadzu Corporation, Columbia, MD) equipped with a 100-m capillary column (SP-2560, Supelco, Bellefonte, PA). FAs were identified and response factors adjusted (assuming palmitic acid = 1.0) using a standard FA mixture (GLC-727, Nuchek Prep, Elysian, MN). FAs are reported as a percent of total identified FAs in the RBC sample.

Platelet Aggregation Analysis

Fresh venous blood was collected into 3.8% (w/v) citrated vacuutainer tubes and analyzed using a Chronolog 4 Channel Whole Blood Aggregometer (Model 590-4D) within 30–60 min as described by Riess et al. [15]. Whole blood was mixed 1:1 with isotonic saline, placed in a cuvette and stirred prior to the addition of agonists. Collagen (5 μg) or ADP (1 μg) was added to separate aliquots to stimulate aggregation. The change in impedance as platelets adhered to the electrode was recorded over the subsequent 5–8 min, and the peak impedance was recorded.

Lipid Analysis and Serum Chemistry

Blood samples were collected after a 12-h fast into serum separator tubes and assayed for total cholesterol (C), high density lipoprotein (HDL)-C and low density lipoprotein (LDL)-C, and triacylglycerol using enzymatic methodologies in the clinical laboratory at Sanford USD Medical Center. Standard serum safety tests were performed at baseline and study end.

Other Measurements

Body weight was measured at each visit, and subjects who gained weight between visits were offered additional dietetic counseling to reinforce calorie substitution advice. Heart rate and blood pressure were measured at each study visit by averaging multiple values taken after the subjects had rested quietly for at least 5 min.

Statistical Analysis

Data were analyzed for both intention-to-treat (ITT) and per-protocol (PP) populations. The ITT analysis utilized the missing-at-random method to account for missing values. Analysis of covariance (ANCOVA) was used for each of the efficacy endpoints to examine the treatment effect after 16 weeks. This method takes into account group differences in baseline measurements and demographics (age, sex and BMI). ANCOVA results represent an estimate of what the mean values at the end of the study would have been if all groups had had the same baseline values and demographic profiles. To control type I error, Holm's step-down Bonferroni method was used to adjust p-values for comparisons among treatment groups. Fisher's exact test was used to test for differences between treatments for number of adverse events by body system category and by severity. For all analyses, a two-tailed p-value of <0.05 was required for statistical significance.

Results

Of the 64 subjects who were screened and gave informed consent, 45 were enrolled and 33 completed the study. Reasons for early discontinuation are described below under "Adverse events and safety". The ITT analysis was conducted on all 45 subjects and the PP analysis on 33. As there were no differences between the two, only the PP efficacy results are presented. There were no significant differences between treatment groups at baseline with

Table 2 Baseline characteristics for per-protocol subjects

Characteristic	Control	EPA	SDA
Number of subjects	11	11	11
Female (%)	6 (55.5)	7 (63.6)	6 (55.5)
Age (years)	42.3 ± 12.1	47.8 ± 9.9	38.4 ± 9.8
Body mass index (kg/m^2)	31.1 ± 3.8	31.3 ± 3.4	30.0 ± 4.0

respect to demographics or laboratory or clinical metrics (Tables 2, 3, 4).

Omega-3 Index and Other RBC Fatty Acids

The omega-3 index was increased (relative to the control group) in the EPA ($p = 0.026$) and the SDA ($p = 0.042$) groups (Table 3). There was no difference between the omega-3 index in the EPA and SDA groups ($p = 0.69$). The %EPA in RBCs was significantly increased by EPA ($p < 0.0001$) and SDA ($p = 0.0005$), relative to the control group, but there was no difference between the two omega-3 groups ($p = 0.07$). There were no effects on DHA. SDA increased RBC EPA with about 17% of the efficacy of EPA, whereas the efficiency of the additional ALA provided in the control SBO group was about 0.1% (Table 5). Low endogenous levels of SDA were detected in RBCs in all treatment groups at baseline. The %SDA in RBCs was increased by SDA treatment ($p = 0.0002$), but final levels remained less than 0.05%.

Table 3 Effects of treatment on fatty acid endpoints ($n = 11$ per group; per protocol)

Characteristic	Control	EPA	SDA
Omega-3 index (%)			
Initial	4.36 ± 0.95	4.07 ± 0.86	4.02 ± 0.90
Final	4.21 ± 0.81	5.10 ± 0.82	4.80 ± 1.00
Adjusted final	4.11	5.00*	4.87*
% EPA in RBCs			
Initial	0.52 ± 0.22	0.47 ± 0.21	0.42 ± 0.13
Final	0.52 ± 0.18	1.73 ± 0.44	1.21 ± 0.59
Adjusted final	0.50	1.64**	1.27**
% DHA in RBCs			
Initial	3.84 ± 0.83	3.60 ± 0.80	3.59 ± 0.81
Final	3.70 ± 0.66	3.37 ± 0.67	3.59 ± 0.71
Adjusted final	3.60	3.37	3.60
% SDA in RBCs			
Initial	0.007 ± 0.007	0.008 ± 0.0051	0.010 ± 0.006
Final	0.008 ± 0.007	0.007 ± 0.0045	0.044 ± 0.030
Adjusted final	0.008	0.006	0.046**

*Differs significantly (p-value < 0.05) from the control group

**Differs significantly (p-value < 0.01) from the control group

Summary statistics for initial and final are expressed as mean ± SD (standard deviation). Adjusted final is the estimate of mean from ANCOVA model after adjustment for the baseline, sex, age and BMI

Table 4 Effects of treatment on non-fatty acid endpoints ($n = 11$ per group; per protocol)

Characteristic	Control	EPA	SDA
Body weight (kg)			
Initial	91.2 ± 14.7	89.7 ± 12.0	89.3 ± 19.8
Final	91.4 ± 16.5	91.1 ± 13.5	89.7 ± 21.1
Adjusted final	90.0	91.2	90.5
Heart rate (bpm), resting			
Initial	74.0 ± 2.7	73.9 ± 2.5	75.3 ± 5.0
Final	69.7 ± 6.9	68.9 ± 5.1	71.0 ± 4.9
Adjusted final	69.6	69.8	69.6
Systolic blood pressure, mmHg			
Initial	117.0 ± 15.1	122.5 ± 9.7	118.3 ± 13.0
Final	112.9 ± 12.8	116.4 ± 13.0	118.0 ± 17.3
Adjusted final	115.0	113.1	120.5
Diastolic blood pressure, mmHg			
Initial	72.5 ± 9.7	75.0 ± 6.6	72.1 ± 7.7
Final	69.5 ± 12.0	75.3 ± 6.9	70.2 ± 9.0
Adjusted final	70.1	73.5	72.3
Total cholesterol (mg/dl)			
Initial	204 ± 46	202 ± 35	190 ± 27
Final	205 ± 41	207 ± 27	192 ± 24
Adjusted final	203	205	199
HDL cholesterol (mg/dl)			
Initial	47.5 ± 10.0	56.9 ± 17.4	55.6 ± 20.8
Final	50.1 ± 16.5	60.4 ± 17.1	55.1 ± 14.8
Adjusted final	54.9	55.2	53.6
LDL cholesterol (mg/dl)			
Initial	126.7 ± 40.3	120.5 ± 34.8	117 ± 29
Final	127 ± 36	123 ± 27	120 ± 30
Adjusted final	123	122	126
Triglycerides (mg/dl)			
Initial	149.8 ± 68.5	122.7 ± 83.7	90 ± 40
Final	142 ± 94	116 ± 76	84 ± 33
Adjusted final	123	130	101

Summary statistics for initial and final are expressed as mean ± SD (standard deviation). Adjusted final is the estimate of mean from ANCOVA model after adjustment for the baseline, sex, age and BMI

Physiological, Biochemical and Platelet Function Endpoints

No significant differences were noted for any of the physiological (heart rate, blood pressure, body weight) or lipid endpoints (Table 4). Similarly, there was no effect on platelet function in any treatment group (data not shown).

Adverse Events and Safety Laboratory Tests

No serious adverse events were reported. Non-serious adverse events were summarized by severity and category (i.e., body system) and evaluated by Fisher's exact test in

Table 5 Relative enrichment of RBC EPA from dietary ALA and SDA vs. dietary EPA

	Dose (g/day)	Baseline (%)	End (%)[a]	Absolute change (%)	Increase per g n-3 FA (%)	Efficiency relative to EPA (%)	Inverse
EPA	0.98	0.47	1.73	1.27	129	100.00	1
SDA	3.66	0.42	1.21	0.78	21.4	16.6	6.0
ALA	1.7	0.515	0.517	0.002	0	0.09	>1000
Data from James et al. [16]							
EPA	1.125	0.810	2.56	1.75	155.6	100.00	1
SDA	1.125	0.960	1.44	0.48	42.7	27.43	3.6
ALA	1.125	0.880	1.01	0.13	11.6	7.43	13.5

[a] Actual means, not ANCOVA estimates

the ITT population. There were no significant associations between the category or the severity of adverse events and treatments. Likewise, there were no clinically significant changes in laboratory safety tests (all adverse event and clinical laboratory safety data are provided in Tables 1, 2, 3 in the Online Supplement). Non-serious adverse events related to gastrointestinal distress (e.g., diarrhea, abdominal cramps) were evenly distributed across all three groups and contributed to early study discontinuation in four subjects. Other reasons for discontinuation from the study included abscess (1), acid reflux (1), throat swelling (1), fatigue (1), asthma exacerbation (1), mouth sores (1), use of excluded medication (1) and change in family circumstances (1).

Discussion

SDA-enriched SBO significantly increased the omega-3 index in overweight subjects. On a mass basis, six parts of SDA raised RBC EPA levels to the same extent as one part of EPA. The efficiency of conversion (relative to EPA) of SDA in this study (about 17%) was less than the 27% seen by James et al. [16] when calculated based on changes in RBC EPA levels. This discrepancy may relate to the different chemical forms of SDA used (triglyceride vs. ethyl ester), the differences in study duration (16 vs. 6 weeks) or the types of subjects included (BMIs were 31 vs. 26 kg/m^2). Although there were differences in background linoleic acid intakes (about 7% of total energy in James and about 10% in the present study, data not shown), this is not a likely explanation for the difference in response because linoleic acid would not be expected to impair the conversion of SDA to EPA like it would inhibit the more upstream conversion of ALA to SDA (by competing for delta-6-desaturase).

Based on the lack of any change in RBC EPA in the control group that received an additional 1.7 g of ALA per day, it is not possible to calculate a percent conversion and can only estimate that, under these conditions, it would take over 1,000 parts of ALA to produce the same effect. The lack of change in RBC EPA in the control group in this study indicates that none of the rise in RBC EPA seen in the SDA group can be attributed to the ALA contained in the SDA-enriched SBO. The virtual lack of conversion of ALA to EPA seen in this study has been reported by others using different methods. Pawlosky et al. used stable isotope tracers and multi-compartmental modeling to track ALA conversion to EPA and reported a conversion of 0.2% [17]. On the other hand, Goyens and colleagues used a similar approach and found approximately 8% conversion [18]. Neither of these studies calculated conversion relative to that produced by EPA or based on RBC fatty acid pattern changes; hence, their results cannot be directly compared with the present study. Both of those studies did, however, confirm the fact that ALA conversion to EPA is significantly reduced by higher background dietary linoleic acid levels, presumably because these two essential fatty acids compete for the delta-6 desaturase [12].

Higher omega-3 indexes have been associated with a reduction in risk for sudden cardiac death both prospectively and cross-sectionally [19, 20], and the EPA and DHA content of RBC membranes is highly correlated with that of the human heart [5]. Further, there is evidence that a 1% change in the omega-3 index (e.g., from 4 to 5%) could have a significant impact on risk for sudden cardiac death [21]. Thus, if SDA consumption could materially raise RBC and heart EPA content, as suggested in this study, the impact is likely to be clinically significant.

Increasing the omega-3 index can be easily accomplished by eating oily fish species [22] or fish oil [4], but many populations around the world are not significant fish consumers (e.g. the USA and UK), and changing population taste preferences is typically difficult. In addition, over-fishing is depleting stocks of some species [10], intensifying the need for new sources. Thus, alternative, readily available dietary sources of omega-3 fatty acids are needed. Currently available plant sources, such as soybean, canola and flax seed oils, contain ALA. Although epidemiological data support the hypothesis that ALA favorably affects heart health [23–25], few randomized trials with clinically important endpoints have been conducted with ALA. In those that have been done, clear conclusions have been difficult to reach, but overall consensus at this time is that ALA does not have a demonstrated benefit on cardiovascular disease outcomes [1, 26].

The western diet contains very little SDA, but there are natural sources, notably fish oils, which contain up to 4% SDA (w/w of total fatty acids) [14]. Oil derived from *Echium plantagineum*, a plant that grows wild in Australia, contains about 8–12% SDA [27]. Echium oil raised the EPA content of peripheral blood mononuclear cell phospholipids [28, 29], and, when fed at 15 g/day for 4 weeks, significantly increased EPA and DPA, but not DHA, in plasma and neutrophils in 11 hypertriglyceridemic humans [30]. In the same trial, echium was reported to lower serum triglyceride concentrations by 21%, but these findings need to be confirmed in randomized, blinded and placebo-controlled trials. Compared to canola or soybean oil, which are in large-scale commercial production and approved for human consumption, echium oil is very limited in abundance, and its use is currently limited to dietary supplements in the USA. Other minor sources of SDA are also limited in availability (e.g., evening primrose, borage and black currant seed oils). The genetically enhanced SBO used in this study contained about 17% SDA [14], but other cultivars can approach 30% and hence could provide a substantial amount of omega-3 fatty acids in the human diet.

The Japan EPA lipid intervention study (JELIS) provided strong evidence for cardioprotective effects of EPA alone [2]. In this randomized clinical trial, over 18,000 statin-treated patients were assigned to either 1.8 g of EPA ethyl esters/day in their diet or to usual care, and followed for major adverse cardiac events for 4.5 years. Although EPA treatment reduced overall risk by 19% ($p = 0.01$), the interpretation and extrapolation of these results to the context of the western diets is complicated by the relatively high usual intake of EPA and DHA (about 1 g/day) in this Japanese population [31]. Median intakes of EPA and DHA in the USA are about 100–150 mg/day [3]. Nevertheless, the results of the JELIS trial indicate that increasing already high tissue levels of omega-3 FA with additional EPA confers additional protection against cardiovascular disease and that these benefits can be achieved in patients on statin therapy.

In conclusion, a marker of omega-3 biostatus, the omega-3 index, was increased by feeding SDA-enriched SBO for 16 weeks. The impact of dose and duration of SDA intake on the omega-3 index and the degree to which such alterations in the omega-3 index affect risk for CHD and other chronic diseases need to be further defined.

Acknowledgments The authors express their appreciation to Karla Reilly, RN, for study coordination and to Andrew Christianson and Brenda Collison–Schmidt for the RBC analyses. In addition, we wish to thank our research volunteers, without whom this study would not have been possible. This study was funded by Monsanto Company.

References

1. Wang C, Harris WS, Chung M et al (2006) n-3 fatty acids from fish or fish-oil supplements, but not alpha-linolenic acid, benefit cardiovascular disease outcomes in primary- and secondary-prevention studies: a systematic review. Am J Clin Nutr 84:5–17
2. Yokoyama M, Origasa H, Matsuzaki M et al (2007) Effects of eicosapentaenoic acid on major coronary events in hypercholesterolaemic patients (JELIS): a randomised open-label, blinded endpoint analysis. Lancet 369:1090–1098
3. Kris-Etherton PM, Taylor DS, Yu-Poth S et al (2000) Polyunsaturated fatty acids in the food chain in the United States. Am J Clin Nutr 71:179S–188S
4. Harris WS, von Schacky C (2004) The omega-3 index: a new risk factor for death from coronary heart disease? Prev Med 39:212–220
5. Harris WS, Sands SA, Windsor SL et al (2004) Omega-3 fatty acids in cardiac biopsies from heart transplant patients: correlation with erythrocytes and response to supplementation. Circulation 110:1645–1649
6. Metcalf RG, James MJ, Gibson RA et al (2007) Effects of fish-oil supplementation on myocardial fatty acids in humans. Am J Clin Nutr 85:1222–1228
7. Harris WS (2007) Omega-3 fatty acids and cardiovascular disease: a case for omega-3 index as a new risk factor. Pharmacol Res 55:217–223
8. Kris-Etherton PM, Harris WS, Appel LJ (2002) Fish consumption, fish oil, omega-3 fatty acids, and cardiovascular disease. Circulation 106:2747–2757
9. Gebauer SK, Psota TL, Harris WS, Kris-Etherton PM (2006) n-3 fatty acid dietary recommendations and food sources to achieve essentiality and cardiovascular benefits. Am J Clin Nutr 83:1526S–1535S
10. Worm B, Barbier EB, Beaumont N et al (2006) Impacts of biodiversity loss on ocean ecosystem services. Science 314:787–790
11. Brenna JT (2002) Efficiency of conversion of alpha-linolenic acid to long chain n-3 fatty acids in man. Curr Opin Clin Nutr Metab Care 5:127–132
12. Plourde M, Cunnane SC (2007) Extremely limited synthesis of long chain polyunsaturates in adults: implications for their essentiality and use as supplements. Appl Physiol Nutr Metab 32:619–634
13. Yamazaki K, Fujikawa M, Hamazaki T, Yano S, Shono T (1992) Comparison of the conversion rates of alpha-linolenic acid (18:3(n-3)) and stearidonic acid (18:4(n-3)) to longer polyunsaturated fatty acids in rats. Biochim Biophys Acta 1123:18–26
14. Ursin VM (2003) Modification of plant lipids for human health: development of functional land-based omega-3 fatty acids. J Nutr 133:4271–4274
15. Riess H, Braun G, Brehm G, Hiller E (1986) Critical evaluation of platelet aggregation in whole human blood. Am J Clin Pathol 85:50–56
16. James MJ, Ursin VM, Cleland LG (2003) Metabolism of stearidonic acid in human subjects: comparison with the metabolism of other n-3 fatty acids. Am J Clin Nutr 77:1140–1145

17. Pawlosky RJ, Hibbeln JR, Novotny JA, Salem NJ (2001) Physiological compartmental analysis of alpha-linolenic acid metabolism in adult humans. J Lipid Res 42:1257–1265
18. Goyens PL, Spilker ME, Zock PL, Katan MB, Mensink RP (2006) Conversion of alpha-linolenic acid in humans is influenced by the absolute amounts of alpha-linolenic acid and linoleic acid in the diet, and not by their ratio. Am J Clin Nutr (in press)
19. Siscovick DS, Raghunathan TE, King I et al (1995) Dietary intake and cell membrane levels of long-chain n-3 polyunsaturated fatty acids and the risk of primary cardiac arrest. J Am Med Assoc 274:1363–1367
20. Albert CM, Campos H, Stampfer MJ et al (2002) Blood levels of long-chain n-3 fatty acids and the risk of sudden death. N Engl J Med 346:1113–1118
21. Harris WS, von Schacky C (2008) Omega-3 fatty acids, acute coronary syndrome and sudden death. Curr Hypertens Rep 2:161–166
22. Sands SA, Reid KJ, Windsor SL, Harris WS (2005) The impact of age, body mass index, and fish intake on the EPA and DHA content of human erythrocytes. Lipids 40:343–347
23. Albert CM, Oh K, Whang W et al (2005) Dietary alpha-linolenic acid intake and risk of sudden cardiac death and coronary heart disease. Circulation 112:3232–3238
24. Djousse L, Arnett DK, Carr JJ et al (2005) Dietary linolenic acid is inversely associated with calcified atherosclerotic plaque in the coronary arteries: the NHLBI family heart study. Circulation 111:2921–2926
25. Ascherio A, Rimm EB, Giovannucci EL, Spiegelman D, Stampfer M, Willett WC (1996) Dietary fat and risk of coronary heart disease in men: cohort follow up study in the United States. BMJ 313:84–90
26. Harris WS (2005) Alpha-linolenic acid—a gift from the land? Circulation 111:2872–2874
27. Whelan J, Rust C (2006) Innovative dietary sources of n-3 fatty acids. Annu Rev Nutr 26:75–103
28. Miles EA, Banerjee T, Dooper MM, M’Rabet L, Graus YM, Calder PC (2004) The influence of different combinations of gamma-linolenic acid, stearidonic acid and EPA on immune function in healthy young male subjects. Br J Nutr 91:893–903
29. Miles EA, Banerjee T, Calder PC (2004) The influence of different combinations of gamma-linolenic, stearidonic and eicosapentaenoic acids on the fatty acid composition of blood lipids and mononuclear cells in human volunteers. Prostaglandins Leukot Essent Fatty Acids 70:529–538
30. Surette ME, Edens M, Chilton FH, Tramposch KM (2004) Dietary echium oil increases plasma and neutrophil long-chain (n-3) fatty acids and lowers serum triacylglycerols in hypertriglyceridemic humans. J Nutr 134:1406–1411
31. Iso H, Kobayashi M, Ishihara J et al (2006) Intake of fish and n-3 fatty acids and risk of coronary heart disease among Japanese: the Japan public health center-based (JPHC) study cohort I. Circulation 113:195–202

Lipids (2008) 43:813–827
DOI 10.1007/s11745-008-3208-z

ORIGINAL ARTICLE

Dietary n-3 HUFA Affects Mitochondrial Fatty Acid β-Oxidation Capacity and Susceptibility to Oxidative Stress in Atlantic Salmon

**M. A. Kjær · M. Todorčević · B. E. Torstensen ·
A. Vegusdal · B. Ruyter**

Received: 19 March 2008 / Accepted: 3 June 2008 / Published online: 10 July 2008
© AOCS 2008

Abstract Atlantic salmon (*Salmo salar*) (90 g) were fed four different diets for 21 weeks (final weight 344 g). The levels of n-3 highly unsaturated fatty acids (HUFA) ranged from 11% of the total fatty acids (FA) in the low n-3 diet to 21% in the intermediate n-3 diet, to 55 and 58% in the high n-3 diets. The high n-3 diets were enriched with either docosahexaenoic acid (DHA) or eicosapentaenoic acid (EPA). Increasing dietary levels of n-3 HUFA led to increasing percentages (from 31 to 52%) of these FA in liver lipids. The group fed the highest level of DHA had higher expressions of peroxisome proliferator-activated receptor (PPAR) β and the FA β-oxidation genes acyl-CoA oxidase (ACO) and carnitine palmitoyltransferase (CPT)-II, compared to the low n-3 groups. The high n-3 groups had reduced activity of mitochondrial cytochrome c oxidase and β-oxidation capacity, together with increased activities of superoxide dismutase (SOD) and caspase-3 activities. In the group fed the highest level of n-3 HUFA, decreased percentages of major phospholipids (PL) in the mitochondrial and microsomal membranes of the liver were also apparent. The percentage of mitochondrial cardiolipin (Ptd_2Gro) was 3.1 in the highest n-3 group compared to 6.6 in the intermediate group. These data clearly show an increased incidence of oxidative stress in the liver of fish fed the high n-3 diets.

Keywords Lipid metabolism · Lipid peroxidation · Gene expression · Fish oil · n-3 fatty acids · n-6 fatty acids

Abbreviations

ACO	Acyl-CoA oxidase
BSA	Bovine serum albumin
CoA	Coenzyme A
CPT	Carnitine palmitoyltransferase
DHA	Docosahexaenoic acid
DTT	Dithiothreitol
EDTA	Ethylene diamine tetra-acetic acid
EF1-α_β	Elongation factor 1-α beta isoform
EGTA	Ethylene glycol tetra-acetic acid
EPA	Eicosapentanoic acid
FA	Fatty acid
FAD	Flavin adenine dinucleotide
FBS	Fetal bovine serum
FO	Fish oil
HPTLC	High-performance thin-layer chromatography
HUFA	Highly unsaturated fatty acid
L-15	Leibowitz-15 medium
NAD	Nicotinamide adenine dinucleotide
PBS	Phosphate-buffered saline
PL	Phospholipid
PPAR	Peroxisome proliferator-activated receptor
PtdCho	Phosphatidyl-choline
PtdEtn	Phosphatidyl-ethanolamine
Ptd_2Gro	Cardiolipin
PtdIns	Phosphatidyl-inositol
RO	Rapeseed oil
ROS	Reactive oxygen species

M. A. Kjær (✉) · M. Todorčević · A. Vegusdal · B. Ruyter
Nofima, NO-1432 Ås, Norway
e-mail: marte.kjaer@nofima.no

M. A. Kjær · M. Todorčević
Department of Animal and Aquacultural Sciences,
Norwegian University of Life Sciences, 1432 Ås, Norway

B. E. Torstensen
NIFES, National Institute of Nutrition and Seafood Research,
5817 Bergen, Norway

SOD	Superoxide dismutase
TAG	Triacylglycerol

Introduction

Atlantic salmon (*Salmo salar*) have traditionally been fed diets rich in fish oil (FO) containing relatively high levels of the essential highly unsaturated fatty acids (HUFA) eicosapentaenoic acid (EPA, 20:5n-3) and docosahexaenoic acid (DHA, 22:6n-3). Dietary n-3 HUFA play a prominent role in fish nutrition, providing essential FA that are vital constituents of cell membranes, being necessary for the normal membrane structure and function [1]. However, recent trends in the fish industry include replacing these FO in the diet by more available vegetable oils, having lower n-3 HUFA levels. This change in dietary regimes has resulted in a major research focus on how this reduction in the essential FA affect FA metabolism. The tissues capacity of β-oxidation may be affected by changes in dietary FA, as demonstrated by decreased liver β-oxidation capacity when salmon were fed dietary vegetable oils [2–4]. In addition, both high dietary EPA and an increase in the n-3/n-6 ratio of FA in the diet induce mitochondrial proliferation [5–8]. Furthermore, Jordal et al. [9] found that dietary rapeseed oil (RO), which has a lower level of n-3 HUFA, induced a significant down-regulation of several mitochondrial genes in Atlantic salmon liver. In addition, salmonids fed a diet scarce in n-3 FA generally have higher activities of Δ5- and Δ6-desaturases than fish fed an n-3 FA rich diet [10–13]. They also express higher mRNA levels of the gene for Δ5-desaturase [9, 14].

There has been much focus on the effects of reduced levels of n-3 HUFA, however, less is known about the effects of n-3 HUFA levels above those normally obtained when salmon are fed commercial cod liver oil diets. The South American FO for instance, is generally a rich source of these n-3 HUFA. The HUFA are highly susceptible to peroxidation due to their high number of double bonds [15]. Peroxidation products may influence the HUFA in membrane phospholipids (PL), and thereby impair cell and organelle membrane structure and functions [1]. HUFA taken into the body are mostly delivered to liver cells in mammals [16]. The liver is thus one of the principal targets of HUFA peroxidative effects. Lipid peroxidation generally results in a decrease in membrane fluidity, an increase in the permeability of the membrane, and inactivation of membrane-bound enzymes [17, 18]. These effects can eventually lead to a complete loss of membrane integrity and cause apoptosis. The proteins cytochrome c and cytochrome c oxidase located in the mitochondrial membrane of healthy mammalian cells, function in the respiratory chain interacting with the membrane PL cardiolipin (Ptd_2Gro) [19]. Decline in cytochrome c oxidase activity can be ascribed to a loss in Ptd_2Gro content [20]. Further, both cytochrome c and Ptd_2Gro decrease in mitochondria has been shown as an initial step in the pathway of apoptosis in mammals [21, 22]. Whether these mechanisms are the same in fish or not remains to be studied.

The present study had two primary goals; firstly to study how the mitochondrial and peroxisomal FA β-oxidation and its regulatory genes were affected by increasing levels of n-3 HUFA in the diet. Secondly to determine whether increasing dietary levels of n-3 HUFA affect the composition of membrane PL—both in cells and their organelles, cell morphology, intracellular oxidative stress and apoptosis.

Materials and Methods

Materials

Metacain (MS-222) was obtained from Norsk Medisinaldepot (Oslo, Norway). The radioactive isotope [1-^{14}C]-palmitoyl coenzyme A, (40–60 mCi/mmol) was obtained from American Radiolabeled Chemicals, Inc. (St. Louis, MO, USA). Sodium chloride, sulfuric acid, perchloric acid, diethyl ether, methyl acetate, hexane, copper acetate, phosphoric acid and benzene were purchased from Merck (Darmstadt, Germany). Ethylene glycol tetra-acetic acid (EGTA) was bought from AppliChem (Darmstadt, Germany). Cell flasks and cell scrapers were obtained from Nalge Nunc International (Rochester, NY, USA). Glutaraldehyde, Epon resin, copper grids, uranyl acetate, osmium tetroxide, sodium cacodylate and lead citrate were supplied by Electron Microscopy Science (Fort Washington, PA, USA). RNeasy Mini Kit and QIAshredder columns were purchased from Qiagen (Valencia, CA, USA). The TaqMan® Gold RT-PCR kit and the ABI Prism 7000 sequence detection system were bought from Applied Biosystems (Foster City, CA, USA). Insta gel II plus was obtained from Packard Instruments (Downers Grove, IL, USA). Chloroform, methanol and acetic acid were obtained from VWR International (West Chester, PA, USA). Total protein kit, cytochrome c oxidase (EC 1.9.3.1) assay kit, acid phosphatase (EC 3.1.3.2) assay kit, Leibowitz-15 medium (L-15), phosphate-buffered saline (PBS), fetal bovine serum (FBS), bovine serum albumin (BSA), sucrose, ethylene diamine tetra-acetic acid (EDTA), antibiotics, HEPES, L-glutamine, collagenase type 1 (EC 3.4.24.3), trypsin, sodium bicarbonate solution, trypan blue, laminin, potassium ferrocyanide, NaOH, nicotinamide adenine dinucleotide (NAD), dithiothreitol (DTT), flavin adenine dinucleotide (FAD), Triton-X 100, L-Carnitine, Coenzyme

A (CoA), Imidazole buffer, Palmitoyl CoA, Tris base, Peroxidase type II (EC 1.11.1.7), HCl, 2,2-dimethoxypropane, 2’,7’-dichlorofluorescein and silica gel 60 glass-backed TLC plates were all supplied by Sigma-Aldrich (St. Louis, MO, USA). Primers for the real-time PCR analysis were ordered from Invitrogen Ltd (Paisley, UK). The superoxide dismutase (SOD, EC 1.15.1.1) assay kit was purchased from Cayman Chemicals (Ann Arbor, MI, USA) and the Caspase-3 (EC 3.4.22.56) colorimetric assay kit was from R&D Systems, Inc. (Minneapolis, MN, USA). Hydrogen peroxide and titanium oxysulfate were obtained from Riedel-de Haën (Seelze, Germany). *O*-Nitrophenyl acetate was purchased from MP Biomedicals (Solon, OH, USA). Ethanol and isopropanol were obtained from Arcus (Oslo, Norway). 2’,7’-dichlorofluorescine was bought from Eastman Kodak Company (Rochester, NY, USA).

Feeding Trial and Sampling

The feeding trial was carried out at Nofima’s research station, Sunndalsøra, Norway. Four diets with approximately 50% (of dry matter, by weight) crude protein and 23% (of dry matter, by weight) crude lipid contained 13.5% (g/100 g feed) oils with increasing levels of n-3 HUFA (Table 1). The diets contained 11, 21, 55 and 58% n-3 HUFA (of total FA), and they were named low n-3 diet, intermediate n-3 diet, high n-3 DHA diet and high n-3 EPA diet, respectively. The high n-3 EPA diet and high n-3 DHA diet were both characterized by high percentages of n-3 HUFA and low percentages of n-6 FA (Table 2). In contrast, the low n-3 diet contained almost four times more n-6 FA than the intermediate n-3 diet, and 2.5 times more n-6 FA than the high n-3 EPA and high n-3 DHA diets. Four groups of post-smolt Atlantic salmon (*Salmo salar*), with an initial average weight of 90 g were distributed into three cylinder-conical tanks (flow through system, 0.85 m diameter) per diet, and fed one of the four diets for 21 weeks. The fish were not fasted prior to the final sampling. The average fish weight was 344 g at the end of the growth period, with no significant differences in the growth (total weight) between the dietary groups.

Isolation of Hepatocytes

Five fish per diet (randomly taken from the three tanks) were used for the isolation of hepatocytes at the end of the growth period. The fish were anaesthetized with metacain (MS-222) and their individual weights and lengths determined. The abdominal cavity was exposed and the vena portae cannulated. The liver was perfused following a two-step collagenase procedure developed by Seglen [23] and modified by Dannevig and Berg [24], in order to isolate hepatocytes. The hepatocytes were isolated after collagenase digestion by gentle shaking of the digested liver in L-15 medium. The suspension of parenchymal cells was filtered through a 100 µm mesh nylon filter. Hepatocytes

Table 1 Formulation and chemical composition of the diets

	Diets			
	Low n-3	Intermediate n-3	High n-3 DHA	High n-3 EPA
Formulation (% of total)				
Fish meal, LT	67.9	67.9	67.9	67.9
Rapeseed oil	13.5			
Fish oil		13.5		
DHA[a]			13.5	
EPA[b]				13.5
Wheat	17.1	17.1	17.1	17.1
Vitamin premix[c]	1.0	1.0	1.0	1.0
Mineral premix[c]	0.4	0.4	0.4	0.4
Yttrium oxide[d]	0.01	0.01	0.01	0.01
Carophyll Pink[e] (8%)	0.064	0.064	0.064	0.064
Chemical composition				
Dry matter (%)	92.2	92.3	92.2	93.0
Percentage of dry matter				
Protein	54.6	55.4	54.4	55.1
Fat	23.0	22.5	23.3	22.7
Ash	9.9	9.5	9.7	9.5
Energy (MJ/kg)	23.9	23.8	23.8	23.6

The EPA-enriched oil used in the high n-3 EPA diet, the DHA-enriched oil used in the high n-3 DHA diet and the rapeseed oil used in the low n-3 diet were added 150 ppm butylated hydroxytoluene (BHT) before coated onto the feed

[a] Incromega DHA 500TG SR, Croda Chemicals Europe Ltd., Goole, England

[b] Incromega EPA 500TG SR, Croda Chemicals Europe Ltd., Goole, England

[c] As described by Mundheim et al. [58]

[d] Inert marker, Y_2O_3, Sigma

[e] Hoffman-LaRoche, Basel, Switzerland

Table 2 Fatty acid compositions of diets

Fatty acids (% of total)	Diet			
	Low n-3	Intermediate n-3	High n-3 DHA	High n-3 EPA
14:0	1.99	6.88	2.22	2.09
16:0	7.58	12.87	5.36	4.91
18:0	1.53	1.46	1.50	0.62
20:0	0.44	3.66	0.39	4.57
22:0	0.30	0.07	ND	0.07
24:0	0.08	0.03	0.47	0.12
Σ Saturated[a]	12.19	25.85	10.27	12.68
16:1n-7	1.23	4.26	1.37	1.27
18:1n-7	2.77	1.67	1.14	0.88
18:1n-9	40.22	7.84	5.26	3.73
20:1n-9	4.27	9.96	5.18	3.65
22:1n-11	0.19	15.76	6.59	5.28
Σ Monounsaturated[b]	49.87	43.07	23.83	18.37
18:2n-6	14.09	2.70	1.61	2.20
18:3n-3	7.27	1.71	0.91	1.02
18:3n-6	ND	0.11	0.52	0.31
20:3n-6	0.19	0.40	1.34	2.35
20:4n-3	0.45	1.04	0.67	0.65
20:4n-6	0.06	ND	0.32	0.12
20:5n-3	4.95	7.12	8.68	42.87
22:5n-3	0.29	0.76	3.27	1.58
22:5n-6	2.56	0.39	0.53	1.29
22:6n-3	4.96	12.18	41.73	12.36
Σ Polyunsaturated[c]	36.14	28.14	63.23	66.63
Σ n-3	18.79	23.34	56.13	59.38
Σ n-6	17.05	4.50	6.61	6.80
∑ n-3 HUFA	11.37	21.32	54.79	57.92
EPA + DHA	9.91	19.30	50.41	55.23

nd not detected

[a] Includes 15:0, 17:0, 19:0

[b] Includes 14:1n-5, 16:1n-9, 17:1n-7, 18:1n-11, 20:1n-7, 22:1n-7, 22:1n-9, 24:1n-9

[c] Includes 16:2n-3, 16:2n-6, 16:3n-4, 18:3n-4, 18:4n-3, 20:2n-6, 20:3n-3, 21:5n-3, 22:4n-6

were washed three times in L-15 medium and sedimented by spinning for 2 min at 50×*g*. The hepatocytes were resuspended in L-15 culture medium containing 10% FBS, 1% bicarbonate, 1% L-glutamine, 1% penicillin-streptomycin solution and 5 mM HEPES. Cell viability was assessed by staining with Trypan Blue (0.4%). Approximately 1 × 10^7 hepatocytes were plated onto 25 cm^2 cell flasks coated with laminin, and left to attach overnight at 12 °C. Two hepatocyte flasks per fish were used for transmission electron microscopy and one flask for the isolation of RNA.

Preparation of Hepatocytes for Transmission Electron Microscopy

The cells were washed in PBS and harvested in 1.5 ml of fixative solution (2% glutaraldehyde in 0.1 M cacodylate buffer, pH = 7.4). Then, the cells were washed twice in 0.1 M cacodylate buffer, and post-fixed for 1 h in 0.1 M cacodylate buffer containing 2% osmium tetroxide and 1.5% potassium ferrocyanide. The specimens were stained for 30 min in 1.5% uranyl acetate, dehydrated in a series of ethanol solutions (70, 90, 96 and 100%), and embedded in epon resin. The resin was polymerized at 60 °C for at least 12 h. Ultra-thin sections were prepared and stained with lead citrate. EM specimens were examined using a Philips CM100 transmission electron microscope (80 V) (FEI, Acht, The Netherlands).

Liver Homogenization

A further three fish per diet (one from each tank) were used for liver homogenization. The fish were anaesthetized with metacain (MS-222) and their weights and lengths determined. They were killed by a blow to the head, and the livers were dissected out and weighed. The hepato-somatic indexes (HSI: liver weight/body weight × 100) were 1.00 ± 0.11, 1.06 ± 0.08, 0.88 ± 0.04 and 0.88 ± 0.03

for low n-3, intermediate n-3, high n-3 DHA and high n-3 EPA dietary groups, respectively, with no significant differences between the groups. The tissue was homogenized in a sucrose buffer (0.25 mM sucrose, 15 mM HEPES, 1 mM EDTA and 1 mM EGTA) by using a glass Dounce homogenizer powered by a drill.

Analysis of Fatty Acid Composition

Liver homogenate from three fish in each dietary group (one from each tank) was used for the analysis of FA composition. The total FA profiles in the diets (Table 2) and the livers (Table 4) were determined. Lipids were extracted using the Folch method [25]. The chloroform phase was dried under N_2 and the residual lipid extract was redissolved in benzene, and then transmethylated overnight with 2,2-dimethoxypropane and methanolic HCl at room temperature, as described by Mason and Waller [26] and by Hoshi et al. [27]. The methyl esters of FA thus formed were separated in a gas chromatograph (Hewlett Packard 6890) with a split injector, SGE BPX70 capillary column (length 60 m, internal diameter 0.25 mm and thickness of the film 0.25 μm) flame ionization detector and the results analysed using HP Chem Station software. The carrier gas was helium. The injector and detector temperatures were 280 °C. The oven temperature was raised from 50 °C to 180 °C at the rate of 10 °C/min, and then raised to 240 °C at the rate of 0.7 °C/min. The relative quantity of each FA present was determined by measuring the area under the peak corresponding to that FA.

Lipid Class Analysis

The lipid class compositions in different liver fractions (total homogenate, mitochondria and microsomes) were quantified using high-performance thin-layer chromatography (HPTLC). Ten microgram total lipid was applied using an automatic sample applicator (ATS4, CAMAG, Muttenz, Switzerland) onto a 10 × 20 cm HPTLC plate that had been pre-run in hexane/diethyl ether (1:1, by vol.) and activated at 110 °C for 30 min. The plates were developed for the first 5.5 cm in methyl acetate/isopropanol/chloroform/methanol/0.25% aqueous KCl (25:25:25:10:9, by vol.) to separate PL classes with neutral lipids running at the solvent front [28] using an automatic developing chamber (AMD2, CAMAG, Muttenz, Switzerland). After drying, the plates were developed fully in hexane/diethyl ether/acetic acid (80:20:2, by vol.) to separate neutral lipids and cholesterol. Lipid classes were visualized by charring at 160 °C for 15 min after dipping the plate into a glass tank with 3% copper acetate (w/v) in 8% (v/v) phosphoric acid. The lipid classes were identified by comparison with commercially available standards, and quantified by scanning densitometry using a CAMAG TLC Scanner 3. Scan lines were analysed using an integrator (WinCATS-Planar Chromatography, Version 1.3.3). Further, the weight of each lipid class per gram of tissue was determined by establishing standard equations for each lipid class within a linear area, and a standard mix of all the lipid classes was included on each HPTLC plate to correct for between plate variations.

Subcellular Fractionation

Subcellular fractions were separated by differential centrifugation first described by de Duve [29]. The homogenate was centrifuged at 1,000×*g* for 10 min to separate out the nuclear fraction. The pelleted nucleus was re-homogenized in 1 ml of homogenization buffer. Mitochondria and peroxisomes were then isolated by two differential centrifugation steps for 10 min at 2,000×*g* and 25,000×*g*, respectively, in a fixed-angle rotor 70-Ti (Beckman). Each mitochondrial and peroxisomal pellet recovered was resuspended in 1.5 and 1 ml of the buffer, respectively. The remaining supernatant was the microsomal fraction. The different organelles in the fractions were identified by measuring the activities of subcellular marker enzymes in the diluted pellets and supernatant.

The presence of mitochondria was assessed by a Sigma kit based on the method of Storrie and Madden [30]. The amounts of mitochondria were determined by measuring the activity of cytochrome c oxidase. Total cytochrome c oxidase activity was measured by observing the decrease in absorbance at 550 nm of Fe^{2+}-cytochrome c caused by its oxidation to Fe^{3+}-cytochrome c by cytochrome c oxidase in mitochondria (measured at room temperature for 3 min). Further, the cytochrome c oxidase assay allowed us to measure the integrity of the outer mitochondrial membrane, by measuring the cytochrome c oxidase activity in the presence and in the absence of the detergent *n*-dodecyl *β*-D-maltoside. This detergent allows the maintenance of the cytochrome c oxidase dimer in solution. Absorbance was measured in a GBC UV/VIS 918 spectrophotometer (GBC Scientific Equipment, Victoria, Australia).

The presence of peroxisomes was assessed by the activity of catalase (EC 1.11.1.6), using a method based on that of Baudhuin et al. [31]. The substrate hydrogen peroxide, produced in peroxisomes, is broken down by catalase to oxygen and water. This reaction is stopped by the addition of a saturated solution (0.45%) of titanium oxysulfate in 2 N sulfuric acid. Titanium oxysulfate reacts with the amount of hydrogen peroxide that remains to give a yellow solution of peroxy titanium sulfate. The amount of the product was measured spectrophotometrically at 405 nm in a Victor 3 1420 Multilabel counter spectrophotometer (PerkinElmer, CT, USA).

Acid phosphatase is an acid hydrolase that normally resides in lysosomes. This enzyme was assayed as described by Bergmeyer [32], using an acid phosphatase assay kit to identify the lysosomes. The measurement was based on the hydrolysis of 4-nitrophenyl phosphate by acid phosphatase. The samples were mixed with 4-nitrophenyl phosphate and citrate buffer solution (0.09 M, pH 4.8), and incubated for 20 min at room temperature. The reaction was stopped by NaOH (0.5 N). The color formed was measured spectrophotometrically at 405 nm in a Victor 3 1420 Multilabel counter spectrophotometer (PerkinElmer, CT, USA).

Esterase (EC 3.1.1.1) was first assayed by Beaufay et al. [33]. Esterase is a marker enzyme for microsomes, and catalyzes the production of o-nitrophenol from o-nitrophenyl acetate. To 2.7 ml of medium containing 20 mM potassium phosphate buffer (pH 7.4), 1 mM EDTA, 0.1% Triton X-100 and 0.25 ml of sample were added. The changes in absorbance were measured at 420 nm for 3 min in a GBC UV/VIS 918 spectrophotometer (GBC Scientific Equipment, VIC, Australia).

Beta-Oxidation Assay

Mitochondrial β-oxidation was measured in freshly isolated mitochondria by the method of Lazarow [34]. This assay determines the amounts of acid-soluble products in mitochondrial fractions. Acid-insoluble ^{14}C-palmitoyl-CoA is converted to acid soluble ^{14}C-acetyl-CoA. Incubation media contained 50 mM Tris–HCl (pH 8.0), 20 mM NAD, 0.33 M DTT, 1.5% BSA, 10 mM CoA, 1 mM FAD, 5 mM palmitoyl-CoA and ^{14}C-palmitoyl-CoA (60 Ci/mol, 20 µCi/ml), 0.25 M sucrose and 1 mM L-carnitine. The samples were incubated for 30 min at room temperature. Reactions were stopped by adding ice-cold 6% perchloric acid. A zero-time control was used in which perchloric acid was added to the reaction mixture before the addition of organelle. This control established the acid stability of ^{14}C-palmitoyl-CoA, as virtually all unchanged substrate was precipitated by acid. The radioactivity in 500 µl of the supernatant was determined by liquid scintillation spectrometry.

Acyl-CoA Oxidase Assay

Acyl-CoA oxidase (ACO, EC 1.3.3.6) activity was assayed in peroxisomes by determining the rate at which hydrogen peroxide was produced, coupled to the oxidation of 2’,7’-dichlorofluorescine, essentially as described by Small et al. [35]. The oxidation of 2’,7’-dichlorofluorescine by hydrogen peroxide to 2’,7’-dichlorofluorescein was followed spectrophotometrically at 502 nm in a GBC UV/VIS 918 spectrophotometer (GBC Scientific Equipment). The reaction mixture contained 0.1 M Tris-HCl (pH 8.5), 0.05 M 2’,7’-dichlorofluorescine, 50 µM horseradish peroxidase type II, 0.015 mM FAD, 60 mg/ml BSA and 0.02% Triton-X 100, and was started with 60 µM palmitoyl-CoA. All concentrations are given as final values. The reaction mixture contained 30–85 µg of protein in a total volume of 1 ml at 20 °C. The ACO activity was calculated as total activity per gram liver.

Protein Measurements

Protein concentrations were determined using a total protein kit (Micro Lowry/Peterson’s modification) based on the method of Lowry [36] and modified by Peterson [37]. Standards (BSA) were prepared by diluting 400 µg/ml of BSA in water. Sodium chloride (final concentration of 0.1 M) was added in order to reduce ampholyte interference. Proteins were precipitated by adding 0.1% trichloroacetic acid in the presence of 0.15% deoxycholate. Color was measured at 500 nm in a Wallac 1420 VICTOR$^{3\text{TM}}$ Multilabel counter spectrophotometer (PerkinElmer, CT, USA).

Superoxide Dismutase Assay

The SOD catalyzes the reduction of superoxide to oxygen and hydrogen peroxide. A cell that has a high level of SOD has probably increased production of this enzyme in order to deal with high levels of superoxide. The kit uses a tetrazolium salt to detect superoxide radicals generated by xantine oxidase and hypoxanthine. One unit of SOD is defined as the amount of enzyme needed to achieve 50% dismutation of the superoxide radical. Color was measured at 405 nm in a Titertek Multiskan PLUS MKII (Labsystems, Helsinki, Finland) plate reader.

Caspase-3 Assay

Caspases are a group of cysteine proteases that exist as proenzymes, becoming activated during the cascade of events associated with apoptosis. The caspase-3 colorimetric assay kit detects the increased enzymatic activities of the caspase-3 classes of proteases in apoptotic cells by a colorimetric reaction. Cells are first lysed to release their intracellular contents. The cell lysate can then be tested for protease activity by the addition of a caspase-specific peptide that conjugates to a color reporter molecule, *p*-nitroanaline. The cleavage of the peptide by the caspase releases the chromophore *p*-nitroanaline, which can be quantified spectrophotometrically. Color was measured at 405 nm in a Titertek Multiskan PLUS MKII (Labsystems, Helsinki, Finland) plate reader.

RNA Isolation

Total RNA was isolated from hepatocytes from three fish in each dietary group using an RNeasy® Mini Kit. Samples were first lysed in RNeasy lysis buffer and then homogenized using QIAshredder columns. Ethanol was added to the lysate to provide ideal binding conditions. The lysate was then loaded onto the RNeasy silica-gel membrane. The RNA bound to the membrane, while all contaminants were efficiently washed away. Pure, concentrated RNA was eluted in water. Residual amounts of remaining DNA were removed using an RNase-Free DNase set during the RNeasy procedure. The total RNA concentrations were determined by spectrophotometry.

Sequence Information, Primer Design and Real-Time PCR

The designs of the PCR primers and TaqManMGB probes were based on published sequences from Atlantic salmon or comparative species. The forward and reverse primers and probes are listed in Table 3. RT-PCR efficiency was monitored using two-fold dilution curves of RNA. Four concentrations were used for the two-fold dilution curve (starting at 250 ng total RNA). For analysis of gene expression (separate 96 well plates) three parallels were used at a total RNA concentration of 125 ng (± 5%). The following conditions were used for the amplification of cDNA: 2 min at 50 °C, followed by denaturation for 10 min at 95 °C, followed by 50 cycles of 15 s at 95 °C and finally 1 min at the annealing temperature listed in Table 3. Thermal cycling and fluorescence detection was done using an ABI Prism 7000 sequence detection system.

Data Analysis and Statistical Analysis of Gene Expression Data

Each assay was tested on different samples from the same plate to determine how reproducible the results were. QGene was used to normalize and calculate relative expression data [38]. QGene takes into account the PCR efficacy, calculated on the basis of two-fold dilution curves, and obtains, in this way, normalized expression data. The gene expression levels were normalized against a reference gene. Two different reference genes, β-actin and elongation factor 1-alpha beta isoform (EF1-α_β) [39], were measured for all dietary treatments. Results based on the use of β-actin as reference gene had a higher variation between replicates of hepatocytes, and thus EF1-α_β was used for the final calculations of relative gene expression in hepatocytes. Gene expressions from fish in the intermediate n-3 dietary group were set to 1, and the expression of each target gene for the experimental groups low n-3, high n-3 EPA and high n-3 DHA was expressed relative to this. Significant differences ($P \leq 0.05$) in normalized gene expression levels between dietary treatments were detected by one-way analysis of variance (ANOVA) (Statistica, version 6.1; Statsoft, Tulsa, USA).

Statistical Analysis

All data, except for gene expression data, were subjected to one-way ANOVA for the factor “diet”, and differences were ranked by Duncan’s multiple range test. We used the software package UNISTAT (London, England). The significance level was set to $P \leq 0.05$.

Results

Fatty Acid Composition

The percentages of n-3 HUFA in the fish livers increased with increasing level of n-3 HUFA in the diet, while the percentages of n-6 FA decreased (Table 4). The main contributor to n-3 FA in the intermediate n-3 and high n-3 DHA dietary groups was 22:6n-3, while 20:5n-3 and 22:5n-3 also contributed in the high n-3 EPA dietary group. In contrast, the livers from fish fed the low n-3 diet contained more than twice as much n-6 FA as those from the other three dietary groups, with 18:2n-6 being the dominating n-6 FA. In addition, the low n-3 group contained approximately 20% 18:1n-9, whereas the intermediate n-3, high n-3 EPA and high n-3 DHA dietary groups all contained less than 8% of this FA. The percentage of 22:6n-3 in the liver lipids was the same in fish fed the low n-3 diet as in the fish fed the high n-3 EPA diet, despite a threefold higher 22:6n-3 level in the latter diet. The percentage of the elongation product 22:5n-3 was significantly higher in livers from the high n-3 EPA group.

Lipid Classes

There were between 33 and 53% polar lipids in the total liver homogenate, and between 47 and 66% neutral lipids (Table 5). TAG was the major lipid class followed by phosphatidyl-choline (PtdCho) and then cholesterol and phosphatidyl-ethanolamine (PtdEtn) in the total liver homogenate. The fraction of polar lipids was significantly lower in the high n-3 EPA group than in the other groups, and the fraction of neutral lipids higher. Ptd_2Gro was present almost exclusively in mitochondria. Fish from the high n-3 EPA dietary group contained less Ptd_2Gro than fish from the intermediate n-3 group. The amount of PtdCho in microsomes was slightly higher than in the mitochondria. Phosphatidyl-inositol (PtdIns) was present in

Table 3 TaqMan assays. All sequences are presented as 5′–3′

Gene	Accession number	Direction	Primer sequence	MGB probe	Annealing temperature	Amplicon size
CPTI	AM230810	F	CTTTGGGAAGGGCCTGATC	AGTGTCGTACCAGCCC	60	121
		R	CATGGACGCCTCGTACGTTA			
CPTII	BG934647	F	TGCTCAGCTAGCGTTCCATATG	AGGCAGTATGGGCAGACA	54	75
		R	AGTGCTGCAGGACTCGTATGTG			
ACO	DQ364432	F	CACTGCCAGGTGTGGTGGTA	AGGACCCAAGTTTG	54	92
		R	GGAATTGTACGTTCTCCAATTTCA			
ACAD	CB511813	F	GCCAAGTACTGGGCGTCTGA	AGTACCCCATCGCCAAG	54	127
		R	TGGGCTGGATACGGGAATC			
PPARβ	AJ416953	F	AAGTCTCATGACGAAGAGGTTGTG	AGCAGGAGCAAGAGG	58	71
		R	GTGGCTGTTACTATTCCCCTTCTC			
PPARγ	AJ416952, AJ416951, AJ292963, AJ292962	F	GCCTCAGGCTTCCACTATGG	CTGCAAGGGATTCTTC	60	78
		R	CAGTTTTAACCGCACGGTTCTG			
D5D	AF478472	F	GGAACCACAAACTGCACAAGT	CAGAGGCACCCTTTAGGTG	60	83
		R	GTGCTGGAAGTGACGATGGT			
D6D	AY458652	F	GGGATTTAATCCATCGCATATTAACT	TGTGAACAGAGATAGTTTCCCCAGACGTTTG	60	87
		R	CGTCACAACAAAATACAGCATCTG			
β-actin	BG933897	F	CCAAAGCCAACAGGGAGAAG	TGACCCAGATCATGTTT	60	91
		R	AGGGACAACACTGCCTGGAT			
EF1-α_β	BG933853	F	TGCCCCTCCAGGATGTCTAC	CCAATACCGCCGATTTT	60	59
		R	CACGGCCCACAGGTACTG			

CPTI, II carnitin palmitoyl transferase I, II, *ACO* acyl-CoA oxidase, *ACAD* acyl-CoA dehydrogenase, *PPARβ, γ* peroxisome proliferating activating receptor β, γ, *D5D* Δ5-desaturase, *D6D* Δ6-desaturase, *EF1-α*$_\beta$ elongation factor 1-α_β, *F* forward, *R* reverse

Table 4 FA compositions of the livers

Fatty acids (% of total)	Low n-3	Intermediate n-3	High n-3 DHA	High n-3 EPA
14:0	1.3 ± 0.06^{b}	2.5 ± 0.19^{a}	1.7 ± 0.08^{b}	1.8 ± 0.29^{b}
16:0	11.9 ± 0.92^{ab}	14.8 ± 0.84^{a}	12.3 ± 0.96^{ab}	10.8 ± 0.99^{b}
18:0	4.6 ± 0.04^{b}	4.1 ± 0.15^{a}	5.0 ± 0.14^{b}	4.8 ± 0.16^{b}
∑ Saturated[a]	21.6 ± 0.59	22.2 ± 1.04	21.4 ± 1.23	19.4 ± 1.67
16:1 n-7	0.9 ± 0.15^{b}	1.8 ± 0.27^{a}	1.1 ± 0.08^{ab}	1.5 ± 0.27^{ab}
18:1 n-7	1.9 ± 0.08^{a}	1.8 ± 0.09^{a}	1.5 ± 0.06^{b}	1.4 ± 0.06^{b}
18:1 n-9	21.1 ± 0.88^{b}	8.4 ± 1.25^{a}	7.7 ± 0.45^{a}	7.5 ± 0.15^{a}
18:1 n-11	1.2 ± 0.13^{b}	2.4 ± 0.17^{a}	1.6 ± 0.28^{b}	1.6 ± 0.10^{b}
20:1 n-9	2.7 ± 0.03^{ab}	3.3 ± 0.30^{a}	2.7 ± 0.29^{ab}	2.2 ± 0.26^{b}
22:1 n-7	0.8 ± 0.04^{ab}	1.3 ± 0.17^{a}	0.7 ± 0.11^{b}	2.6 ± 0.32^{c}
22:1 n-11	0.5 ± 0.07^{b}	1.4 ± 0.10^{a}	1.2 ± 0.22^{ab}	1.5 ± 0.33^{a}
∑ Monounsaturated[b]	30.4 ± 1.10^{b}	22.3 ± 2.29^{a}	18.6 ± 1.51^{a}	20.5 ± 0.64^{a}
18:2 n-6	5.6 ± 0.32^{b}	1.6 ± 0.09^{a}	1.5 ± 0.04^{a}	1.7 ± 0.03^{a}
18:3 n-3	1.3 ± 0.11^{b}	0.5 ± 0.02^{a}	0.2 ± 0.05^{a}	0.5 ± 0.12^{a}
20:2 n-6	2.9 ± 1.57	1.7 ± 1.22	0.7 ± 0.03	0.4 ± 0.04
20:3 n-6	2.4 ± 0.11^{c}	0.3 ± 0.05^{ab}	0.1 ± 0.02^{b}	0.4 ± 0.04^{a}
20:4 n-6	2.6 ± 0.23^{b}	1.9 ± 0.08^{a}	3.6 ± 0.19^{c}	3.0 ± 0.04^{b}
20:5 n-3	4.3 ± 0.28^{b}	6.0 ± 0.67^{a}	5.1 ± 0.47^{ab}	18.6 ± 0.47^{c}
22:4 n-6	ND	ND	1.3 ± 0.03	ND
22:5 n-3	1.4 ± 0.10^{a}	2.6 ± 0.56^{a}	3.1 ± 0.22^{a}	9.3 ± 1.60^{b}
22:6 n-3	25.4 ± 1.77^{b}	34.7 ± 1.10^{a}	41.7 ± 1.27^{c}	23.4 ± 0.89^{b}
∑ Polyunsaturated[c]	46.0 ± 0.70^{a}	49.9 ± 1.22^{a}	58.2 ± 0.77^{b}	58.3 ± 2.11^{b}
∑ n-3	32.4 ± 1.85^{b}	44.3 ± 2.02^{a}	50.9 ± 0.63^{c}	52.5 ± 2.03^{c}
∑ n-6	13.6 ± 1.20^{b}	5.6 ± 1.15^{a}	7.3 ± 0.14^{a}	5.8 ± 0.08^{a}
EPA + DHA	29.8 ± 1.86^{b}	40.7 ± 1.77^{a}	46.7 ± 0.83^{c}	42.0 ± 1.25^{ac}

The FA composition was measured in homogenate of the livers from fish fed four different diets. The quantity of each fatty acid is given as the percentage of total fatty acids. The values given are means ± SEM ($n = 3$). Different letters indicate significant differences ($P \leq 0.05$) between the different dietary treatments within each lipid class

nd not detected

[a] Includes: 12:0, 17:0, 22:0

[b] Includes: 14:1n-5, 16:1n-5, 16:1n-9, 17:1n-7, 20:1n-7, 20:1n-11, 22:1n-7, 22:1n-9, 24:1n-9

[c] Includes: 16:2n-6, 18:3n-4, 18:3n-6, 18:4n-3, 20:3n-3, 20:4n-3

all tissue fractions, but the highest percentage was found in microsomes.

Fatty Acid β-Oxidation

The β-oxidation capacity in the high n-3 EPA and high n-3 DHA dietary groups were significantly lower than the capacity in the intermediate n-3 and low n-3 dietary groups (Fig. 1). There were no significant differences between the intermediate n-3 and the low n-3 groups. There were no significant differences in the total liver ACO activity between the dietary groups. However, a tendency toward higher ACO activity in the high n-3 DHA group was evident (Fig. 2).

Gene Expression

The relative expressions of genes involved in lipid metabolism are shown in Fig. 3. Fish fed the low n-3 diet had significantly higher expression of both Δ5-desaturase and Δ6-desaturase genes than fish fed the high n-3 DHA diet. The relative expressions of genes involved in peroxisomal β-oxidation (ACO), mitochondrial β-oxidation [carnitine palmitoyltransferase (CPT) II, acyl-CoA dehydrogenase (ACAD)] and the transcription factor PPARβ were all up-regulated in livers from fish fed the high n-3 DHA diet. These genes showed the lowest expression levels in livers from fish fed the lowest n-3 HUFA diet.

Oxidative Stress Markers

Cytochrome c oxidase measurements showed that its activity was greatly reduced in the mitochondrial membranes, by a factor of 2–3, in the high n-3 EPA and high n-3 DHA dietary groups than in the group with the lowest level of n-3 HUFA (Fig. 4). Caspase-3 activity, an apoptosis marker, was also significantly different between the dietary groups (Fig. 5a). Caspase activity was significantly higher in the high n-3 EPA group than in all other groups, increasing by 100–200%. The activity of SOD, as well, was significantly different between the dietary groups (Fig. 5b). The activities were lowest in fish fed low n-3 and intermediate n-3 diets, and significantly higher in fish from the two high n-3 groups. EM pictures of representative cells from the low n-3 HUFA dietary group (6a), and the high n-3 EPA group (6b) are shown in Fig. 6. Cells from fish given high n-3 EPA diet had an abnormal morphology. The nuclear chromatin in these

Table 5 Lipid class distribution in liver organelle fractions

	Mitochondria				Microsomes				Total homogenate			
	Low n-3	Intermediate n-3	High n-3 DHA	High n-3 EPA	Low n-3	Intermediate n-3	High n-3 DHA	High n-3 EPA	Low n-3	Intermediate n-3	High n-3 DHA	High n-3 EPA
Percentage distribution												
LPC	2.3 ± 0.24^{a}	1.9 ± 0.26^{a}	2.4 ± 0.29^{a}	1.1 ± 0.09^{b}	0.0 ± 0.0	0.7 ± 0.69	0.0 ± 0.0	0.7 ± 0.67	0.0 ± 0.0^{a}	0.5 ± 0.52^{a}	2.1 ± 0.28^{b}	0.4 ± 0.41^{a}
SM	4.4 ± 1.55	4.7 ± 1.19	3.4 ± 0.39	3.8 ± 2.10	6.8 ± 0.89	5.7 ± 0.89	5.4 ± 0.07	6.0 ± 0.51	3.5 ± 0.28	4.1 ± 0.87	4.5 ± 0.24	2.9 ± 0.39
PtdCho	22.5 ± 1.02^{ab}	28.1 ± 2.51^{a}	23.5 ± 2.89^{ab}	16.1 ± 2.82^{b}	29.0 ± 2.24	29.3 ± 1.36	29.6 ± 3.38	23.0 ± 0.94	25.0 ± 1.29^{a}	26.9 ± 1.85^{a}	23.3 ± 1.65^{a}	16.1 ± 2.72^{b}
PtdSer	0.0 ± 0.0^{a}	0.0 ± 0.0^{a}	1.0 ± 0.50^{b}	0.0 ± 0.0^{a}	2.3 ± 0.17^{a}	2.0 ± 0.14^{a}	1.8 ± 0.17^{ab}	1.4 ± 0.16^{b}	1.4 ± 0.11^{ab}	1.7 ± 0.13^{a}	1.6 ± 0.08^{ab}	1.0 ± 0.30^{b}
PtdIns	4.1 ± 0.32^{ab}	4.3 ± 0.77^{ab}	5.2 ± 0.57^{b}	2.3 ± 0.59^{a}	6.6 ± 0.69	6.1 ± 0.85	6.1 ± 0.48	4.6 ± 0.18	5.3 ± 0.21^{a}	5.7 ± 0.78^{a}	4.9 ± 0.46^{ab}	3.6 ± 0.39^{b}
Ptd_2Gro	5.1 ± 0.31^{ab}	6.6 ± 0.96^{a}	5.1 ± 0.63^{ab}	3.1 ± 0.61^{b}	0.0 ± 0.0^{b}	0.6 ± 0.36^{a}	0.0 ± 0.0^{b}	0.0 ± 0.0^{b}	1.8 ± 0.18	1.7 ± 0.18	1.8 ± 0.18	1.4 ± 0.21
PtdEtn	11.7 ± 0.12^{ab}	14.6 ± 0.99^{a}	11.2 ± 1.23^{ab}	8.9 ± 1.46^{b}	11.5 ± 1.03^{ab}	12.6 ± 0.16^{a}	9.6 ± 1.02^{c}	8.7 ± 0.25^{bc}	10.9 ± 0.62^{a}	11.8 ± 0.72^{a}	9.7 ± 0.62^{ab}	7.5 ± 1.34^{b}
DAG	1.5 ± 0.10^{a}	1.3 ± 0.23^{a}	1.8 ± 0.18^{ab}	2.5 ± 0.39^{b}	1.5 ± 0.12^{ab}	1.7 ± 0.13^{a}	1.6 ± 0.13^{a}	1.1 ± 0.13^{b}	1.6 ± 0.04^{b}	2.1 ± 0.20^{a}	1.8 ± 0.06^{ab}	1.8 ± 0.05^{ab}
CHOL	7.5 ± 0.27	8.9 ± 1.03	9.0 ± 0.97	5.7 ± 1.35	11.6 ± 1.05^{ab}	13.5 ± 1.77^{a}	11.8 ± 1.00^{ab}	8.9 ± 0.49^{b}	10.8 ± 0.88^{ab}	13.3 ± 0.47^{a}	11.1 ± 0.72^{ab}	8.4 ± 1.53^{b}
FFA	16.4 ± 0.34^{a}	13.6 ± 1.65^{ab}	11.0 ± 0.82^{b}	13.4 ± 0.33^{ab}	6.4 ± 0.47	8.6 ± 1.25	7.7 ± 0.67	6.4 ± 0.05	14.0 ± 0.25	14.0 ± 1.27	11.2 ± 1.29	13.4 ± 0.51
TAG	20.5 ± 1.52^{a}	13.3 ± 2.87^{a}	24.6 ± 7.26^{ab}	41.3 ± 7.20^{b}	24.0 ± 5.67^{ab}	18.0 ± 3.97^{a}	26.3 ± 6.08^{ab}	39.2 ± 1.52^{b}	25.7 ± 3.12^{ab}	17.7 ± 4.10^{a}	27.1 ± 5.49^{ab}	42.7 ± 7.29^{b}
$\sum$ PL	54.1 ± 1.10^{ab}	62.9 ± 5.74^{a}	53.6 ± 5.98^{ab}	37.1 ± 5.96^{b}	56.5 ± 4.17^{ab}	58.3 ± 3.92^{a}	52.5 ± 4.83^{ab}	44.3 ± 0.96^{b}	47.9 ± 2.12^{a}	53.0 ± 3.31^{a}	48.9 ± 3.61^{a}	33.7 ± 5.39^{b}
$\sum$ NL	45.9 ± 1.10^{ab}	37.1 ± 5.74^{a}	46.4 ± 5.98^{ab}	62.9 ± 5.96^{b}	43.5 ± 4.17^{ab}	41.7 ± 3.92^{a}	47.5 ± 4.83^{ab}	55.7 ± 0.96^{b}	52.1 ± 2.12^{a}	47.0 ± 3.31^{a}	51.1 ± 3.61^{a}	66.3 ± 5.39^{b}

The lipid class composition was measured in total homogenate, microsomes and mitochondria in liver from fish fed four different diets. The quantity of each lipid class is given as the percentage of total lipids. The values given are means ± SEM ($n = 3$). Different letters indicate significant differences ($P \leq 0.05$) between the different dietary treatments within each lipid class, within each fraction

LPC lyso-phosphatidyl-choline, *SM* sphingomyelin, *PtdCho* phosphatidyl-choline, *PtdSer* phosphatidyl-serine, *PtdIns* phosphatidyl-inositol, *Ptd_2Gro* cardiolipin, *PtdEtn* phosphatidyl-ethanolamine, *DAG* diacylglycerol, *CHOL* cholesterol, *FFA* free fatty acids, *TAG* triacylglycerol, *PL* polar lipids, *NL* neutral lipids

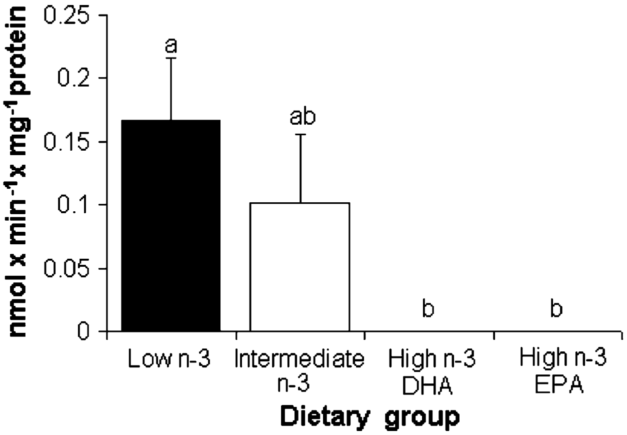

Fig. 1 Mitochondrial β-oxidation activity. β-oxidation was measured in the mitochondrial fraction. Data are means ± SEM ($n = 3$). *Different letters* indicate significant differences ($P \leq 0.05$)

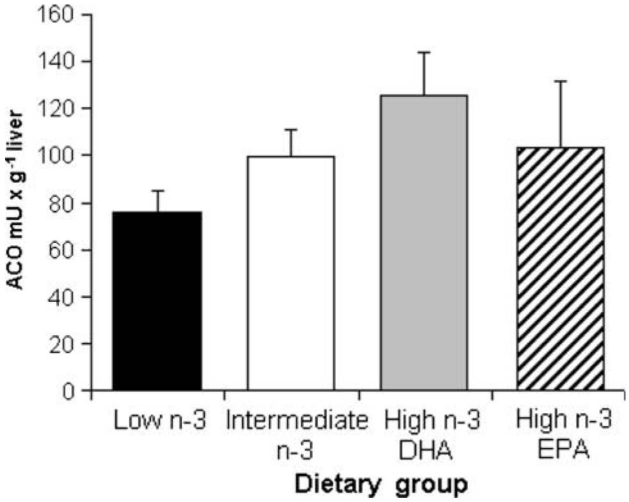

Fig. 2 ACO enzyme activity. ACO activity was measured in the peroxisomal fractions, and is displayed here as the total activity per gram liver tissue. Data are means ± SEM ($n = 3$). *Different letters* indicate significant differences ($P \leq 0.05$)

cells was condensed, and the cellular contents seemed to be released.

Discussion

Feeding Atlantic salmon diets having major differences in the n-3 HUFA content affected the FA composition of the liver. N-3 HUFA in the liver increased with increasing dietary level of these FA. However, even though the level of 22:6n-3 in the low n-3 diet was less than half of the 22:6n-3 level in the high n-3 EPA diet, the percentages of 22:6n-3 recovered in the liver lipids were the same in these two dietary groups. One explanation for this relatively low percentage of 22:6n-3 recovered in liver of fish fed the high n-3 EPA diet may be explained by a lower capacity to produce 22:6n-3 than in those fed a diet with low levels of n-3 HUFA. In addition, the livers of the fish fed the high n-3 EPA diet had significantly higher percentages of 22:5n-3, indicating that the further conversion of 22:5n-3 to 22:6n-3, which involves a Δ6-desaturation step, is inhibited. These findings are further supported by the lower expression of genes for both Δ5-desaturase and Δ6-desaturase in the liver tissue from fish fed the two high-level n-3 HUFA diets. It has previously been shown that Atlantic salmon fed diets containing plant oils have significantly higher desaturation enzyme activity [10–13] and higher expressions of hepatic Δ5-desaturase and Δ6-desaturase genes than those fed FO diets [9, 14]. An alternative explanation to the relatively high 22:6n-3 level in the tissue of fish fed low n-3 diet could be selective utilization of shorter chain, less unsaturated FA, and a more highly conservation of 22:6n-3 in the liver PL of fish fed low n-3 HUFA levels. This is in agreement with what was found in fish fed an essential FA free diet [40]. We have recently shown that feeding salmon diets rich in EPA increases the number of mitochondria in the liver [8]. We know that the shorter chained FA are mainly oxidized within mitochondria [41], and that the longer chained FA, like 22:6n-3, are very poor substrates for mitochondrial FA β-oxidation [42]. The finding that several mitochondrial and peroxisomal genes, involved in FA β-oxidation, were up-regulated in fish fed high levels of dietary 22:6n-3 may then support the last explanation. An unexpected result was therefore that the mitochondrial β-oxidation capacities were dramatically lower in isolated liver mitochondria from fish fed the diets with the high levels of n-3 HUFA, than they were in liver mitochondria from fish fed low n-3 and intermediate n-3 diets. Though not well studied in fish, the mitochondrial membrane is found to be a very sensitive target for lipid peroxidation in mammals [43]. The low FA β-oxidation capacity in our study, seen in livers of fish fed the high n-3 HUFA diets may be the result of an extensive lipid peroxidation of the mitochondrial membranes. This assumption is further supported by the loss of cytochrome c oxidase activity and mitochondrial membrane PL found in livers of fish fed high levels on n-3 HUFA. The higher SOD levels found in both high n-3 EPA and high n-3 DHA dietary groups compared to the two groups with lower level of n-3 HUFA further support the theory that the mitochondrial function has been damaged due to oxidative stress. The decreased percentages of PL, especially Ptd$_2$Gro, in the high n-3 EPA mitochondrial membranes may also be consistent with a higher level of apoptosis in this group. It has been suggested in mammalian studies that Ptd$_2$Gro is required for the activity of cytochrome c oxidase [19], and that the Ptd$_2$Gro content in mitochondria decreases during

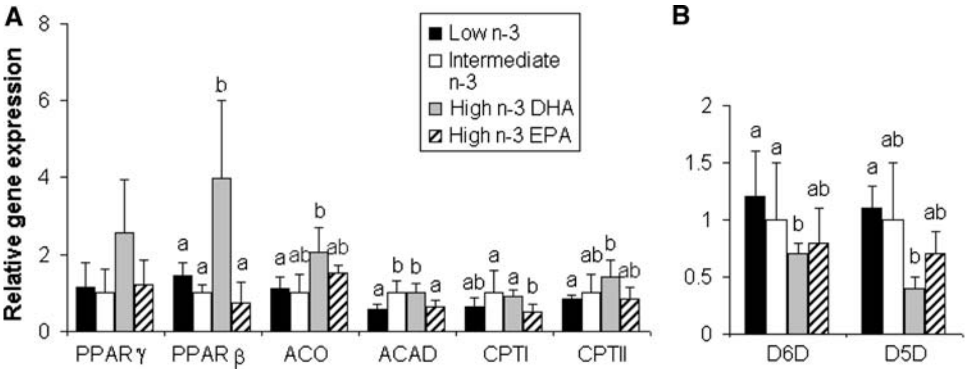

Fig. 3 Relative gene expressions of lipid-related genes. **3a** Gene expressions were measured using isolated mRNA from hepatocytes. Genes involved in gene regulation (PPARs), peroxisomal β-oxidation (ACO) and mitochondrial β-oxidation (ACAD, CPTI, CPTII) were measured. **3b** Δ6-desaturase and Δ5-desaturase activity. Data are presented as means ± SD ($n = 3$). *Different letters* indicate significant differences between dietary groups within each gene. Significance level is set at $P \leq 0.05$. *PPAR* peroxisome proliferator-activated receptor, *ACO* acyl-CoA oxidase, *ACAD* acyl-CoA dehydrogenase, *CPT I, II* carnitine palmitoyltransferase I, II, *D6D* delta 6 desaturase, *D5D* delta 5 desaturase

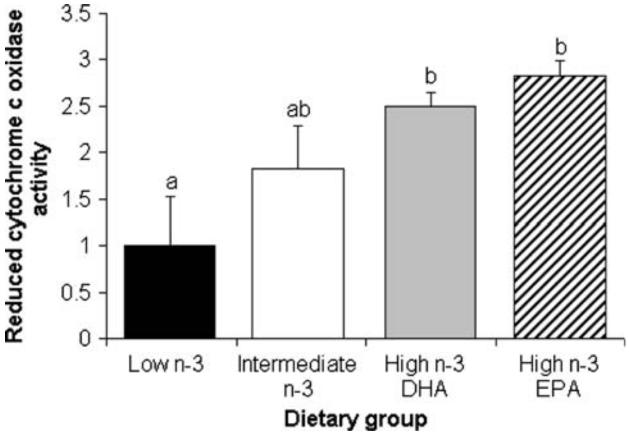

Fig. 4 Cytochrome c oxidase activity. The activity of cytochrome c oxidase was measured in mitochondrial fractions with and without dodecyl. The difference in activity between preparations with and without dodecyl measured in the low n-3 HUFA group was set to 1, and the differences in the other dietary groups are expressed relative to this. Data are means ± SEM ($n = 3$). *Different letters* indicate significant differences ($P \leq 0.05$)

apoptosis [44]. Oxidative stress in mitochondria is known to mediate the apoptotic signalling pathway in mammals [45], and caspases, in particular caspase-3, play a central role. The activity of caspase-3 increased in the high n-3 EPA dietary group. These results are further confirmed by our EM pictures showing abnormal morphology of hepatocytes from fish fed the high n-3 EPA diet. Nuclear chromatin was more highly condensed in these cells, and cellular contents were released [46]. Although not studied in such detail, similar results were found in grass carp (*Ctenopharyngodon idella*), which show decreased growth performance, increased blood lipid peroxidation, altered lipoprotein synthesis and impaired FA β-oxidation capacity when fed a diet with high lipid level, especially high HUFA levels [47, 48]. These results led us to yet another possible explanation for the lower level of 22:6n-3 found in the high n-3 EPA dietary group relative to the level found in the low n-3 HUFA group. The cause could be increased breakdown of 22:6n-3 due to peroxidation.

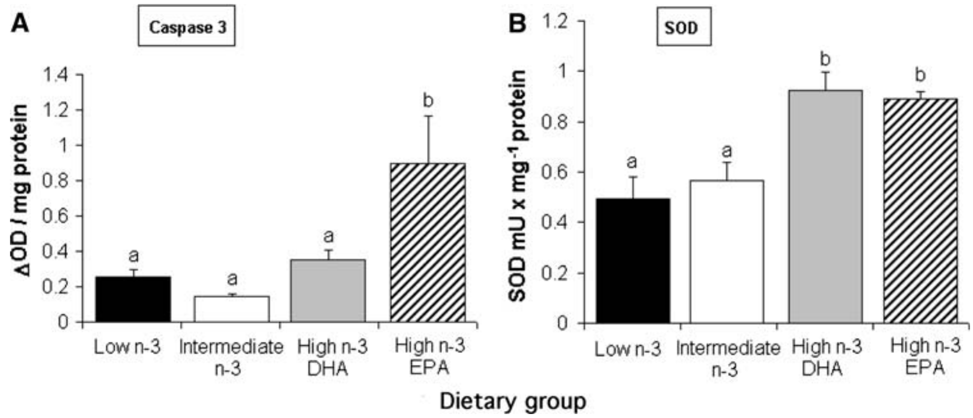

Fig. 5 Enzyme activities. Caspase-3 (5a) and SOD (5b) activity was measured in total homogenates. Data are means ± SEM ($n = 3$). *Different letters* indicate significant differences ($P \leq 0.05$)

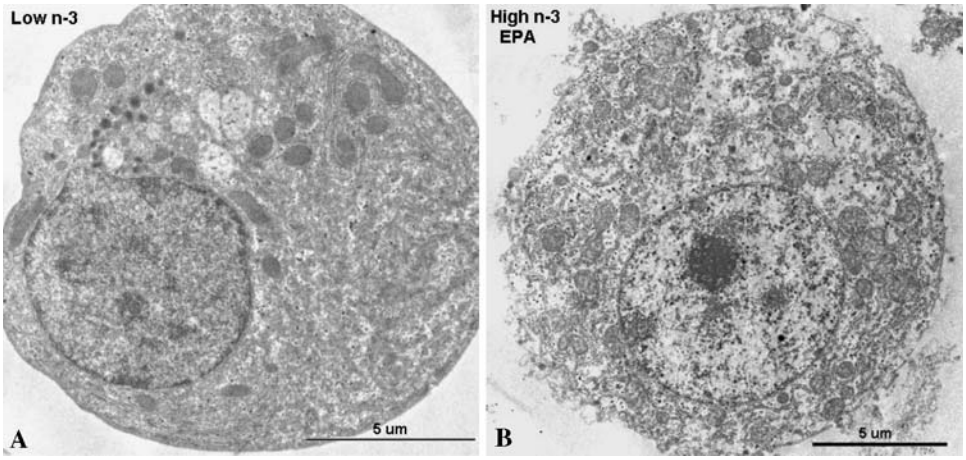

Fig. 6 Electron micrographs of hepatocytes. The images shown are representative cells for fish fed the low n-3 diet (**a**) and fish fed the high n-3 EPA diet (**b**). *Bars* 5 µm

In the present study we fed fish with diets containing high levels (55% of total FA) of n-3 HUFA, and these high values of n-3 rich lipids clearly led to oxidative stress in the liver. In our study, cases of damage were apparent despite of added antioxidants (160 ppm Vitamin E and 150 ppm BHT). This show the importance of protecting high n-3 HUFA feed with proper antioxidants and proper storage in order to minimize the peroxidation of FAs both prior to feeding and in fish after feeding. Stephan et al. [49] demonstrated that a FO-enriched diet fed to turbot (*Scophthalmus maximus*), increased the susceptibility to FA peroxidation. They found that increased levels of dietary and tissue HUFA require increased dietary supplementation with antioxidants to prevent the occurrence of oxidative damage. A correlation between increased dietary HUFA and antioxidant requirement has been found in other fish species as well [50–52], including Atlantic salmon [53]. More research is needed in order to increase the knowledge about suitable antioxidants and concentrations of these in fish diets, in order to protect FA from oxidative damages both in the feed and in the fish.

In this study, we have shown that the expressions of genes encoding proteins involved in lipid metabolism differ between the low n-3 HUFA group and the groups with the highest n-3 HUFA levels. We do not know whether it is peroxidative damage due to the increased level of HUFA, or the HUFA themselves that are involved in the regulation of these genes. Some studies have suggested that the inhibitory effect of HUFA on lipogenic genes is linked to cytotoxic effects, due to the peroxidative mechanism [54, 55]. On the other hand, other studies have shown that lipid-related genes are altered due to the direct transcriptional effect of HUFA themselves, not to peroxidative damage [56, 57].

In conclusion, we have shown that the expressions of several genes related to hepatic lipid metabolism in Atlantic salmon change in response to changes in dietary HUFA. These genes include those for Δ5-desaturase and Δ6-desaturase and several genes whose gene products are involved in mitochondrial functions such as FA β-oxidation. The observed increased production of SOD and caspases, and loss of cytochrome c oxidase and Ptd_2Gro in the membranes of fish fed high levels of n-3 HUFA may be a result of increased dietary HUFA levels in the membranes, and subsequent increased oxidative breakdown of FA rich in double bonds. Clearly, the presence of lipids vulnerable to oxidation may be involved in oxidation processes that can have toxic consequences for fish, whether they arise from dietary input or from deficiencies in essential antioxidant nutrients. These results reveal new elements in favor of greater sensitivity of n-3 FAs to peroxidation in fish. Nevertheless, it is important to appreciate that n-3 FA have both adverse and beneficial effects, to adequately evaluate the consequences of membrane enrichment with these lipids.

Acknowledgments We wish to thank Inger Ø. Kristiansen and Målfrid T. Bjerke (Nofima) for skillful technical assistance. This work was carried out with support from the Norwegian Research Council.

References

1. Sargent JR, Tocher DR, Bell JG (2002) The lipids. In: Halver JE, Hardy RW (eds) Fish nutrition. Academic Press, New York, pp 181–257
2. Stubhaug I, Froyland L, Torstensen BE (2005) Beta-Oxidation capacity of red and white muscle and liver in Atlantic salmon (*Salmo salar* L.)—effects of increasing dietary rapeseed oil and olive oil to replace capelin oil. Lipids 40:39–47
3. Stubhaug I, Lie O, Torstensen BE (2006) Beta-oxidation capacity in liver increases during parr-smolt transformation of Atlantic salmon fed vegetable oil and fish oil. J Fish Biol 69:504–517
4. Stubhaug I, Lie O, Torstensen BE (2007) Fatty acid productive value and beta-oxidation capacity in Atlantic salmon (*Salmo salar* L.) fed on different lipid sources along the whole growth period. Aquacult Nutr 13:145–155
5. Vegusdal A, Gjoen T, Berge RK, Thomassen MS, Ruyter B (2005) Effect of 18:1n–9, 20:5n–3, and 22:6n–3 on lipid accumulation and secretion by Atlantic salmon hepatocytes. Lipids 40:477–486

6. Willumsen N, Vaagenes H, Lie O, Rustan AC, Berge RK (1996) Eicosapentaenoic acid, but not docosahexaenoic acid, increases mitochondrial fatty acid oxidation and upregulates 2,4-dienoyl-CoA reductase gene expression in rats. Lipids 31:579–592
7. Vamecq J, Vallee L, de la Porte PL, Fontaine M, de Craemer D, van den Branden C, Lafont H, Grataroli R, Nalbone G (1993) Effect of various n-3/n-6 fatty acid ratio contents of high fat diets on rat liver and heart peroxisomal and mitochondrial [beta]-oxidation. Biochim Biophys Acta 1170:151–156
8. Kjaer MA, Vegusdal A, Gjoen T, Rustan AC, Todorcevic M, Ruyter B (2008) Effect of rapeseed oil and dietary n-3 fatty acids on triacylglycerol synthesis and secretion in Atlantic salmon hepatocytes. Biochim Biophys Acta 1781:112–122
9. Jordal AE, Torstensen BE, Tsoi S, Tocher DR, Lall SP, Douglas SE (2005) Dietary rapeseed oil affects the expression of genes involved in hepatic lipid metabolism in Atlantic salmon (Salmo salar L.). J Nutr 135:2355–2361
10. Bell JG, McEvoy J, Tocher DR, McGhee F, Campbell PJ, Sargent JR (2001) Replacement of fish oil with rapeseed oil in diets of Atlantic salmon (Salmo salar) affects tissue lipid compositions and hepatocyte fatty acid metabolism. J Nutr 131:1535–1543
11. Moya-Falcon C, Thomassen MS, Jakobsen JV, Ruyter B (2005) Effects of dietary supplementation of rapeseed oil on metabolism of [1–14C]18:1n–9, [1–14C]20:3n-6, and [1–14C]20:4n-3 in Atlantic salmon hepatocytes. Lipids 40:709–717
12. Ruyter B, Thomassen MS (1999) Metabolism of n-3 and n-6 fatty acids in Atlantic salmon liver: stimulation by essential fatty acid deficiency. Lipids 34:1167–1176
13. Tocher DR, Bell JG, Dick JR, Crampton VO (2003) Effects of dietary vegetable oil on Atlantic salmon hepatocyte fatty acid desaturation and liver fatty acid compositions. Lipids 38:723–732
14. Zheng X, Tocher DR, Dickson CA, Bell JG, Teale AJ (2004) Effects of diets containing vegetable oil on expression of genes involved in highly unsaturated fatty acid biosynthesis in liver of Atlantic salmon (*Salmo salar*). Aquaculture 236:467–483
15. Gray J (1978) Measurement of lipid oxidation: a review. J Am Oil Chem Soc 55:539–546
16. Nilsson A, Hjelte L, Strandvik B (1992) Incorporation of dietary [14C]arachidonic acid and [3H]eicosapentaenoic acid into tissue lipids during absorption of a fish oil emulsion. J Lipid Res 33:1295–1305
17. Winston GW, Di Giulio RT (1991) Prooxidant and antioxidant mechanisms in aquatic organisms. Aquat Toxicol 19:137–161
18. Halliwell B, Gutteridge J (1999) Free radicals in biology and medicine, 3 edn. Oxford University Press, Oxford
19. Schlame M, Rua D, Greenberg ML (2000) The biosynthesis and functional role of cardiolipin. Prog Lipid Res 39:257–288
20. Paradies G, Petrosillo G, Pistolese M, Di Venosa N, Serena D, Ruggiero FM (1999) Lipid peroxidation and alterations to oxidative metabolism in mitochondria isolated from rat heart subjected to ischemia and reperfusion. Free Radical Bio Med 27:42–50
21. Ostrander DB, Sparagna GC, Amoscato AA, McMillin JB, Dowhan W (2001) Decreased cardiolipin synthesis corresponds with cytochrome c release in palmitate-induced cardiomyocyte apoptosis. J Biol Chem 276:38061–38067
22. Petrosillo G, Ruggiero FM, Pistolese M, Paradies G (2001) Reactive oxygen species generated from the mitochondrial electron transport chain induce cytochrome c dissociation from beef-heart submitochondrial particles via cardiolipin peroxidation. Possible role in the apoptosis. FEBS Lett 509:435–438
23. Seglen PO (1976) Preparation of isolated rat liver cells. Methods Cell Biol 13:29–83
24. Dannevig BH, Berg T (1985) Endocytosis of galactose-terminated glycoproteins by isolated liver cells of the rainbow trout (Salmo gairdneri). Comp Biochem Physiol B 82:683–688
25. Folch J, Lees M, Sloane Stanley GH (1957) A simple method for the isolation and purification of total lipids from animal tissues. J Biol Chem 226:497–509
26. Mason ME, Waller GR (1964) Dimethoxypropane induced transesterification of fats + oils in preparation of methyl esters for gas chromatographic analysis. Anal Chem 36:583–586
27. Hoshi M, Williams M, Kishimoto Y (1973) Esterification of fatty acids at room temperature by chloroform-methanolic HCl-cupric acetate. J Lipid Res 14:599–601
28. Vitiello F, Zanetta JP (1978) Thin-layer chromatography of phospholipids. J Chromatogr 166:637–640
29. De Duve C, Pressman BC, Gianetto R, Wattiaux R, Appelmans F (1955) Tissue fractionation studies. 6. Intracellular distribution patterns of enzymes in rat-liver tissue. Biochem J 60:604–617
30. Storrie B, Madden EA (1990) Isolation of subcellular organelles. Methods Enzymol 182:203–225
31. Baudhuin P, Beaufay H, Rahman-Li Y, Sellinger OZ, Wattiaux R, Jacques P, De DC (1964) Tissue fractionation studies. 17. Intracellular distribution of monoamine oxidase, aspartate aminotransferase, alanine aminotransferase, D-amino acid oxidase and catalase in rat-liver tissue. Biochem J 92:179–184
32. Bergmeyer HU, Gawehn K, Grassl M (1974) Methods of enzymatic analysis, 2nd edn. Academic Press, Inc., New York, pp 495–496
33. Beaufay H, Amar-Costesec A, Feytmans E, Thines-Sempoux D, Wibo M, Robbi M, Berthet J (1974) Analytical study of microsomes and isolated subcellular membranes from rat liver: I. Biochemical methods. J Cell Biol 61:188–200
34. Lazarow PB (1981) Assay of peroxisomal beta-oxidation of fatty acids. Methods Enzymol 72:315–319
35. Small GM, Burdett K, Connock MJ (1985) A sensitive spectrophotometric assay for peroxisomal acyl-CoA oxidase. Biochem J 227:205–210
36. Lowry OH, Rosebrough NJ, Farr AL, Randall RJ (1951) Protein measurement with the Folin phenol reagent. J Biol Chem 193:265–275
37. Peterson GL (1977) A simplification of the protein assay method of Lowry et al. which is more generally applicable. Anal Biochem 83:346–356
38. Simon P (2003) Q-Gene: processing quantitative real-time RT-PCR data. Bioinformatics 19:1439–1440
39. Olsvik P, Lie K, Jordal AE, Nilsen T, Hordvik I (2005) Evaluation of potential reference genes in real-time RT-PCR studies of Atlantic salmon. BMC Mol Biol 6:21–29
40. Ruyter B, Rosjo C, Einen O, Thomassen MS (2000) Essential fatty acids in Atlantic salmon: time course of changes in fatty acid composition of liver, blood and carcass induced by a diet deficient in n-3 and n-6 fatty acids. Aquacult Nutr 6:109–117
41. Mannaerts GP, Debeer LJ, Thomas J, De Schepper PJ (1979) Mitochondrial and peroxisomal fatty acid oxidation in liver homogenates and isolated hepatocytes from control and clofibrate-treated rats. J Biol Chem 254:4585–4595
42. Madsen L, Froyland L, Dyroy E, Helland K, Berge RK (1998) Docosahexaenoic and eicosapentaenoic acids are differently metabolized in rat liver during mitochondria and peroxisome proliferation. J Lipid Res 39:583–593
43. Vladimirov YA, Olenev VI, Suslova TB, Cheremisina ZP (1980) Lipid peroxidation in mitochondrial membrane. Adv Lipid Res 17:173–249
44. Nomura K, Imai H, Koumura T, Kobayashi T, Nakagawa Y (2000) Mitochondrial phospholipid hydroperoxide glutathione peroxidase inhibits the release of cytochrome c from mitochondria by suppressing the peroxidation of cardiolipin in hypoglycaemia-induced apoptosis. Biochem J 351:183–193
45. Shimizu S, Eguchi Y, Kamiike W, Waguri S, Uchiyama Y, Matsuda H, Tsujimoto Y (1996) Retardation of chemical

hypoxia-induced necrotic cell death by Bcl-2 and ICE inhibitors: possible involvement of common mediators in apoptotic and necrotic signal transductions. Oncogene 12:2045–2050

46. Otsuki Y, Li Z, Shibata MA (2003) Apoptotic detection methods—from morphology to gene. Prog Histochem Cytochem 38:275–339
47. Du ZY, Clouet P, Zheng WH, Degrace P, Tian LX, Liu YJ (2006) Biochemical hepatic alterations and body lipid composition in the herbivorous grass carp (Ctenopharyngodon idella) fed high-fat diets. Br J Nutr 95:905–915
48. Du ZY, Clouet P, Huang LM, Degrace P, Zheng WH, He JG, Tian LX, Liu YJ (2008) Utilization of different dietary lipid sources at high level in herbivorous grass carp (Ctenopharyngodon idella): mechanism related to hepatic fatty acid oxidation. Aquacult Nutr 14:77–92
49. Stephan G, Guillaume J, Lamour F (1995) Lipid peroxidation in turbot (Scophthalmus maximus) tissue: effect of dietary vitamin E and dietary n-6 or n-3 polyunsaturated fatty acids. Aquaculture 130:251–268
50. Puangkaew J, Kiron V, Satoh S, Watanabe T (2005) Antioxidant defense of rainbow trout (Oncorhynchus mykiss) in relation to dietary n-3 highly unsaturated fatty acids and vitamin E contents. Comp Biochem Physiol C 140:187–196
51. Roem AJ, Kohler CC, Stickney RR (1990) Vitamin E requirements of the blue tilapia, *Oreochromis aureus* (Steindachner), in relation to dietary lipid level. Aquaculture 87:155–164
52. Watanabe T, Takeuchi T, Wada M, Uehara R (1981) The relationship between dietary-lipid levels and alpha-tocopherol requirement of rainbow-trout. Bull Jpn Soc Sci Fish 47:1463–1471
53. Waagboe R, Sandnes K, Sandvin A, Lie O (1991) Feeding three levels of *N*-3 polyunsaturated fatty acids at two levels of vitamin E to Atlantic salmon (*Salmo salar*). Growth and chemical composition, Fiskeridir Skr (Ernaering) vol 4, no 1, pp 51–63, 51–63
54. Foretz M, Foufelle F, Ferré P (1999) Polyunsaturated fatty acids inhibit fatty acid synthase and spot-14-protein gene expression in cultured rat hepatocytes by a peroxidative mechanism. Biochem J 341:371–376
55. Mikkelsen L, Hansen HS, Grunnet N, Dich J (1993) Inhibition of fatty acid synthesis in rat hepatocytes by exogenous polyunsaturated fatty acids is caused by lipid peroxidation. Biochim Biophys Acta 1166:99–104
56. Eder K, Kirchgessner M (1998) The effect of dietary vitamin E supply and a moderately oxidized oil on activities of hepatic lipogenic enzymes in rats. Lipids 33:277–283
57. Kim H, Choi S, Lee HJ, Lee JH, Choi H (2003) Suppression of fatty acid synthase by dietary polyunsaturated fatty acids is mediated by fat itself, not by peroxidative mechanism. J Biochem Mol Biol 36:258–264
58. Mundheim H, Aksnes A, Hope B (2004) Growth, feed efficiency and digestibility in salmon (Salmo salar L.) fed different dietary proportions of vegetable protein sources in combination with two fish meal qualities. Aquaculture 237:315–331

Lipids (2008) 43:829–841
DOI 10.1007/s11745-008-3205-2

ORIGINAL ARTICLE

Physico-Chemical Characterisation of Lipids from *Mytilus galloprovincialis* (L.) and *Rapana venosa* and their Healing Properties on Skin Burns

Diana L. Badiu · Alina M. Balu · Lucica Barbes · Rafael Luque · Roxana Nita · Marius Radu · Ecaterina Tanase · Natalia Rosoiu

Received: 5 March 2008 / Accepted: 3 June 2008 / Published online: 10 July 2008
© AOCS 2008

Abstract Black Sea molluscs and gastropods are the most studied organisms from the Romanian littoral zone. In particular, those from the Mytilidae species are of great interest because biochemical investigations have shown that they can be sources of biological active substances which can have different applications (e.g. food additives). We report here the extraction of lipids from two different species of molluscs (*Mytilus galloprovincialis* L., Mediterranean mussel) and gastropods (*Rapana venosa*, hard-shell clam). The extracts were evaluated in terms of antioxidant and composition properties and their healing properties were tested on skin burns in Wistar rats. Our studies proved that the two lipid extracts contained a relatively complex distribution of compounds, in terms of characteristic indices, polyunsaturated fatty acids (PUFA) and vitamins E and D. The presence of such compounds rendered the extracts very efficient in healing induced skin burns in Wistar rats. The histological analysis showed a reduction in the time of healing (12–13 and 13–15 days for the *Mytilus galloprovincialis* (L.) *Rapana venosa* extracts, respectively) compared to 20–22 for untreated animals, based on results from tissues and blood samples. Our investigations have been proved to be promising in terms of future potential applications of the extracts as skin-care products, cosmetics and/or pharmaceutical preparations owing to their dermorestitutive properties.

Keywords Lipid extracts · *Mytilus galloprovincialis* (L.) · *Rapana venosa* · Neopreol · Wound healing

Introduction

Prospecting marine resources for biotechnological use, particularly in drug discovery, is a relatively recent activity.

D. L. Badiu (✉)
Department of Biology-Biochemistry,
Faculty of Natural and Agricultural Sciences, "Ovidius"
University of Constanza, Constanza, Romania
e-mail: dianabadiu@yahoo.com

A. M. Balu
Institute of Physical Chemistry "Ilie Murgulescu",
Romanian Academy, Bucharest, Romania

L. Barbes
Department of Chemistry, Faculty of Physics, Chemistry,
Electronics and Petroleum Technology, "Ovidius"
University of Constanza, Constanza, Romania

R. Luque (✉)
Green Chemistry Centre of Excellence,
The University of York, Heslington, York YO10 5DD, UK
e-mail: rla3@york.ac.uk; q62alsor@uco.es

R. Nita
Laboratory of Physico-Chemical Analyses,
S·C. Biotehnos S.A., Bucharest, Romania

M. Radu
Department of Biology, Faculty of Natural and Agricultural
Sciences, "Ovidius" University of Constanza,
Constanza, Romania

E. Tanase
Histo-pathology Laboratory,
Veterinary and Health Centre, Constanza, Romania

N. Rosoiu
Department of Biochemistry, Faculty of Medicine,
"Ovidius" University of Constanza, Constanza, Romania

The ocean is a rich source of biological and chemical diversity. It covers more than 70% of the earth's surface and hosts more than 300,000 described species of plants and animals to date [http://blacksea.orlyonok.ru/e2-1.shtml]. This diversity has been the source of unique chemical compounds with potential for industrial development as pharmaceuticals, cosmetics, nutritional supplements, molecular probes, enzymes, and agrochemicals [1–4].

Focussing on the Black Sea, molluscs are very important species [http://blacksea.orlyonok.ru/e2-1.shtml]. These marine resources have not been industrially exploited in any form so far, with a few exceptions in the food industry [5].

Many compounds can potentially be obtained from marine organisms such as *Mytilus galloprovincialis* (L.) (Mediterranean mussel) and *Rapana venosa* (hard-shell clam) including polyunsaturated omega 3 (ω-3) and omega 6 (ω-6) fatty acids (FA) and liposoluble vitamins (A, D and E) [6–10]. However, few reports dealing with applications of these lipid extracts can be found (apart from supplements in nutrition) mainly due to the low efficiency (in terms of quantities) in their extraction and unknown effects that did not encourage further investigations of these useful and promising extracts [11–14].

Long chain ω-3 and ω-6 polyunsaturated fatty acids (PUFA) including eicosapentaenoic (EPA, 20:5n-3), docosahexenoic (DHA, 22:6n-3) and arachidonic acids (AA, 20:4n-6) have been recognised as effective compounds in human health and nutrition, especially in the prevention of cardiovascular diseases [15–17] and to alleviate various inflammation conditions [18–23].

In addition to the reported anti-inflammatory effects of ω-3 and ω-6, these compounds have been shown to have immune enhancing benefits, improving resistance to infection, inhibiting platelet function and reducing thrombosis [24–26]. However, how these substances can affect cutaneous wound healing is still under debate [27–29].

In the present work, the physico-chemical characterisation of two lipid extracts from *Mytilus galloprovincialis* (L.) and *Rapana venosa* was carried out. The two species were especially chosen as they have a trophic relationship, being the gastropod *Rapana venosa* a common predator of the mollusc *Mytilus galloprovincialis* (L.)

Based on the rich polyunsaturated fatty acids content (in particular ω-3 and ω-6) that is expected to be found on the lipid extracts [8, 30, 31], this study aimed to investigate their wound healing properties on skin burns and comparing them to those of a commercially available ointment (Neopreol, Iasi Medicals) with fish oil as a bioactive substance as the control sample.

Materials and Characterisation

Samples Characterisation

The samples (from different sizes ranging from 2 to 5 cm) were collected from the Baia Mamaia zone–Park (Latitude, 44°10′N, Longitude 28°41′E, Romanian sector of the Black Sea), from Constanza. We are aware of the variabilities due to the sampling season as reported by other authors [8, 30, 31]. In this regard, molluscs were collected in May (2006 and 2007) as spring is ideal due to the accumulation of bioactive (lipids) and structural compounds (proteins) as the marine organisms prepare for reproduction as well as to the maximum concentrations of organic substances in plankton [30, 32].

The two *Mytilus galloprovincialis* (L.) and *Rapana venosa* lipid extracts were obtained according to the Christie method [33]. Total organ lipid content [13, 14] and total body fatty acid contents [33] were determined. The tissue was dried at 50 °C, homogenised and the samples subsequently extracted in chloroform: methanol 1:2 (v/v). The mixture was then filtered off and the organic phase was kept. The final extract was concentrated on a rotary evaporator under vacuum at room temperature and lyophilised (−20 °C) to avoid any oxidation due to thermal treatment.

Several physico-chemical properties of the lipid extracts [34, 35] were investigated including the relative density, refractive index, acidity, iodine, saponification indexes and unsaponified substances [36]. Olive oil was also investigated and analysed for comparison purposes following the Reg CEE 796/2002 directive.

The relative density of the samples was determined using a picnometer, and 1 mL of extract.

The refractive index was obtained using an ABBE Refractometer (Carl Zeiss, Jena, 389820 type) from the Physico-optics laboratory (Ovidius University of Constanza). The extracts were solubilised in ethanol (0.25 mg/25 mL ethanol) and then the refractive index was measured.

The acidity index was measured by titration of the lipid extracts with KOH, after their solubilisation in ethanol/ether mixture 1:2 (v/v).

The iodine index was determined as follows: 0.11 g sample (*Mytilus galloprovincialis* (L.), *Rapana venosa* lipid extracts and olive oil) were dissolved in 10 mL $CHCl_3$ and subsequently stirred in 25 mL of Hannus solution [IBr in acetic acid], keeping the mixture in a dark place for 1 h at room temperature. Then, 20 mL of a KI solution in 100 mL water was added and 6 mL $Na_2S_2O_3$ in the presence of 1 mL starch solution until disappearance of the blue colour. Blank samples were analysed in parallel using the same quantities and procedure.

The saponification index was also determined. A 2 g sample were stirred in 25 mL KOH and the excess of the mixture was then titrated with a HCl 0.5 N solution using phenolphthalein as indicator.

The unsaponified substances were also analysed. 5 g lipid extract, 2.5 g KOH and 40 mL ethanol were heated under reflux for 2 h. The ethanol was then distilled and the residue was extracted twice in a separating funnel with 50 mL hot water (25 + 25 mL). Then, the organic substances were extracted with 50 mL ether (twice) and after separation of the organic phase, the extract was concentrated in a rotary evaporator and subsequently dried. The quantity of the unsaponified substances was reported for 100 g [27].

The extracts were characterised using different techniques including Infrared (FTIR), UV-Vis spectroscopy and Gas Chromatography-Mass Spectrometry (GC–MS).

FTIR spectra were recorded on a BRUKER-VEKTOR 33 instrument equipped with a liquid N_2 cooled MCT detector. Attenuation Total Reflectance (ATR) spectra were obtained using a methodology devised by the Romanian Spectroteam and Arena Group from Bucharest. 1 g extract was dissolved in *n*-hexane 1:2 (v/v) and then the measurement was performed. The spectra were collected in the 3,900–450 cm^{-1} range.

UV-Vis absorption measurements were performed on a GBC CINTRA 5 Spectrophotometer, using a few drops of sample diluted in *n*-hexane to a 1:2 (v/v), in 10 mm quartz cells.

Lipid extracts were analysed by GC–MS using an Agilent GC 6890N model (1 μL sample injected, split 1:50 column flow 1.6 mL/min., program temp. 100–290 °C (rate 10 °C/min) coupled with a quadrupolar MS 5973. Samples were injected after derivatisation for the complete identification of all existing compounds in the lipid extracts. The derivatisation of the extracts to investigate the total body fatty acid content was carried out by methylation. Bis-(trimethylsilyl)-trifluoroacetamide (BSFTA) was employed as derivatising agent to determine the quantities of sterols present in the extracts.

The methylation comprises several steps: 1 g extract (*Mytilus galloprovincialis* (L.), *Rapana venosa* lipid extracts or olive oil) dissolved in 10 mL MeOH (0.2 ml KOH were also added to the mixture) was heated under reflux for 15 min, cooled down and extracted with 5 mL heptane and 10 mL saturated NaCl solution. The organic phase was dried on Na_2SO_4 and subsequently analysed by GC and GC–MS.

The derivatisation using BSFTA was carried out as follows: 0.5 mL BSFTA (per 0.055 g sample) after heating the mixture of the sample and the BSFTA in heptane (5 mL) at 90 °C for 1 h. The resulting solution was allowed to cool down and subsequently analysed by GC and GC–MS.

Animals and Experimental Design

The study was carried out on adult male Wistar rats, weighing 250 ± 10 g. The animals were individually housed in thermostated (22 ± 2 °C) windowless plexiglass cages with constant humidity and controlled lighting conditions (12 h of light and 12 h of darkness per day) as well as with free access to tap water. They were fed under standard laboratory conditions.

The experiment was carried out in accordance with the Helsinki Declaration and guidelines of the Ethics Committee of the International Association for The Study of Pain. They were approved by the Animal Care Committee of the Faculty of Natural and Agricultural Sciences, “Ovidius” University, Romania.

Each animal was firstly anaesthetised with an intraperitoneal (IP) injection of 5% ketamine (Narkamon inj., Leciva, Czech Republic) in a dose of 90 mg/kg. The hair of the dorsum (around 2.5 cm diameter skin area) was deeply shaved with an electric razor and the wound was subsequently induced with hot water (90 °C, 5 s) on the shaved area, resulting in a clearly distinguished burn.

Fifteen male Wistar rats were randomly divided into five groups, according to the treatment, as follows:

Group 1 (control), ($n = 3$): Rats with an induced skin burn without any treatment.
Group 2 ($n = 3$): Rats with an induced skin burn treated with the *Mytilus galloprovincialis* (L.) lipid extract, (0.2 mg/kg, twice a day).
Group 3 ($n = 3$): Rats with an induced skin burn treated with the *Rapana venosa* lipid extract (0.2 mg/kg, twice a day).
Group 4 ($n = 3$): Rats with an induced skin burn treated with a mixture of the *Mytilus galloprovincialis* (L.): *Rapana venosa* lipid extracts (1:1 ratio, w/w) (0.2 mg/kg, twice a day).
Group 5 ($n = 3$): Rats with an induced skin burn treated with the specific ointment Neopreol (Iasi Medicals, Romania), (0.2 mg/kg, twice a day).

Experiments were terminated after 22 days, after achieving comparable healed wounds between the untreated animals (control) and the animals treated with both *Mytilus galloprovincialis* (L.) and *Rapana venosa* lipid extract, as observed from the histological results and established through different scores.

Sample Preparation

Samples were periodically taken from tissues and blood to be analysed. The animals were anaesthetised using IP injections of 90 mg/kg ketamine and 15 mg/kg xylazine

(Rometar inj., Leciva, Czech Republic) and blood and tissue samples from the wounded area were taken.

Tissue samples were homogenised in 10% formaldehyde solution and lyophilised at −20 °C. Blood samples were taken by aorta puncture and collected into tubes containing ethylenediamine tetraacetic acid (EDTA), subsequently frozen and stored −25 °C until analysis.

The microscope employed in the samples analysis was a Leica DM L 32 and the visualisation was with 20 × 10 for the tissues and 10 × 100 for the blood.

Tissue sections (5 µm) were stained with a Mayer haematoxylin solution in ethanol (15 min) and an eosin solution in ethanol (10 s) (H&E) for general histology [37]. After subsequent washing with ethanol and distilled water, the tissues were eventually mounted in Canada balsam.

The blood was stained according to the May Grunwald Giemsa protocol: the sections were covered with a certain quantity of May Grunwald solution and subsequently washed with distilled water for 1 min. The mixture was then removed without washing and the sections were immersed in a Giemsa solution ex tempore (20–30 min). The sections were eventually washed with water and mounted in Canada balsam [38].

Statistical Analysis

Statistical comparisons were performed by one-way analysis of variance (ANOVA). In the case of the identification of statistical differences using ANOVA, the Student Newmal-Keuls test was used to compare the groups. Probability values <0.05 were considered to indicate significant difference. Data in Fig. 7 are presented as mean values ± standard deviation (SD, error bar depicted in the figure).

Results and Discussion

Physico-Chemical Properties of the Extracts

The results of the physico-chemical characteristics of the lipid extracts of *Mytilus galloprovincialis* (L.) (dark brown colour) and *Rapana venosa* (orangish colour), compared to those of olive oil, are summarised in Table 1.

Several interesting differences could be found between the extracts. The two extracts had similar values of relative density, refractive index and unsaponified substances compared to olive oil, which demonstrates the purity of the obtained extracts. Moreover, a significant difference was showed for unsaponified substances (Table 1, entry 6) when the olive oil was compared to *Mytilus galloprovincialis* (L.) lipid extract ($P = 0.005$). It is worth mentioning at this stage that the olive oil employed in all measurements was commercially refined oil.

Interestingly, there were differences in density between the two extracts, being the *Mytilus galloprovincialis* (L.) more dense compared to *Rapana venosa.* This interesting fact led us to think that there will be differences between the two extracts in terms of compounds present in the mixture, as we will see later on. The refractive index of the lipid extracts were also within the XRF and EECC limits established for food and pharmaceutical oils.

A remarkable difference was found in acidity index in the lipid extracts compared to olive oil (Table 1, entry 3). The molluscs' extracts were close to 20 times higher in acidity than olive oil. This suggested the presence of important quantities of free fatty acids in the mixtures. Nevertheless, the 5 mL KOH/g difference between the *Mytilus galloprovincialis* (L.) and *Rapana venosa* extracts suggested that there may not be major differences between the two species in terms of quantities of free fatty acids present in the extracts. A significant difference was observed when olive oil was compared with *Rapana venosa* lipid extract ($P = 0.005$).

The iodine index (Table 1, entry 4) is characteristic of the content of (poly)unsaturated lipids/fatty acids [39] and it is also an indicative of the physiological condition of the marine organisms. The value of the iodine index is also greatly influenced by the position of the double bond(s) with respect to the carboxylic group. Interesting differences were also found for the two lipid extracts compared to olive oil. The higher iodine index in the *Mytilus galloprovincialis* (L.) and *Rapana venosa* extracts (83 and 87 mL $Na_2S_2O_3$/g, respectively) compared to olive oil (66 mL

Table 1 Physico-chemical characteristics of the *Mytilus galloprovincialis* (L.) and *Rapana venosa* lipid extracts compared to olive oil

Entry	Physical-chemical characteristics	*Mytilus galloprovincialis* (L.)	*Rapana venosa*	Olive oil
1	Relative density (d^{20}_{20}, g/mL)	1.03	0.83	0.91
2	Refraction index (n^{20}D)	1.48	1.49	1.47
3	Acidity index (mL KOH/g)	44	39	2
4	Iodine index (mL $Na_2S_2O_3$/g)	83	87	66
5	Saponification index (mL HCl/g)	281	140	112
6	Unsaponification substances (%g)	2.77	2.44	2.00

$Na_2S_2O_3$/g) suggested a higher content of (poly)unsaturated lipids in our extracts, which is extremely important in terms of nutritive value. Also, significant differences were found when olive oil was compared with both lipid extracts ($P = 0.007$ and 0.004 for *Mytilus galloprovincialis* (L.) and *Rapana venosa*, respectively). The presence of these unsaturated compounds is slightly higher in the *Rapana venosa* species compared to *Mytilus galloprovincialis* (L.).

The saponification index (Table 1, entry 5) indicates the average molecular weight of the fatty acids in fats/lipids, which are related to their organoleptic properties (firmness, taste and flavour) [39]. The measurements provided extremely interesting results in the particular case of the *Mytilus galloprovincialis* (L.) lipid extract which showed a remarkably high saponification index (281 mL HCl/g) compared to *Rapana venosa* (140 mL HCl/g, respectively). This suggested the presence of a higher content of low molecular weight fatty acids in the *Mytilus galloprovincialis* (L.) extract compared to *Rapana venosa*. A significant difference could also be observed when olive oil was compared to the lipid extract from *Rapana venosa* ($P = 0.0007$).

All values obtained for our lipid extracts were within the allowed minimum-maximum range as established in the XRF and EECC regulations (EEC/2568/91 and EEC/2472/97) of the European Union Commission.

Identification of the Different Compounds Present in the Extracts

UV-VIS Absorption Measurements

The UV-Vis spectra of the *Mytilus galloprovincialis* (L.) and *Rapana venosa* lipids extracts compared to olive oil are included in Fig. 1. The experiments were run after dilution of the extracts in *n*-hexane. The most relevant data that can be extracted from the UV-spectra is summarised in Table 2.

The *Mytilus galloprovincialis* (L.) diluted extract UV-spectra showed 4 significant bands at 271, 281, 412 and 670 nm. The bands were attributed to the presence of different compounds as detailed in Table 2. The most interesting chromophore in the mixture was the E-vitamin (α-tocopherol), which was identified by its characteristic absorption bands at 223 and 292 nm [40, 41]. Peaks at 223 and 292 nm, were found only in the concentrated extract (UV-spectra not shown), although a slight shoulder could be observed for the diluted spectra (Fig. 1). This shoulder was also present (in a significantly higher concentration) in the olive oil sample.

The UV-spectra of the *Rapana venosa* diluted extract exhibited a similar profile to that of the *Mytilus galloprovincialis* (L.) but various distinctive bands were present in the spectra. The 200–350 nm range was pretty similar to both species and may be attributed to the absorption of unsaturated fatty acids in the extracts. The 400–600 nm range (missing in the olive oil spectra) was significantly different. In particular, the absence of the broad absorption band at 400–450 nm was correlated to the absence of various chromophores. The UV-Vis spectra of the *Rapana venosa* concentrated extract (not showed) also revealed the presence of an absorption band at 264 nm, characteristic of different components/complexes of vitamin D and another interesting band at ca. 1,100 nm that could be attributed to *trans*-C_6H_5–$(CH=CH)_n$-C_6H_5 poly-enes and/or carboxylic organic compounds that absorbed at higher wavelengths. In any case, UV results provided enough data to demonstrate the presence of different characteristic chromophores.

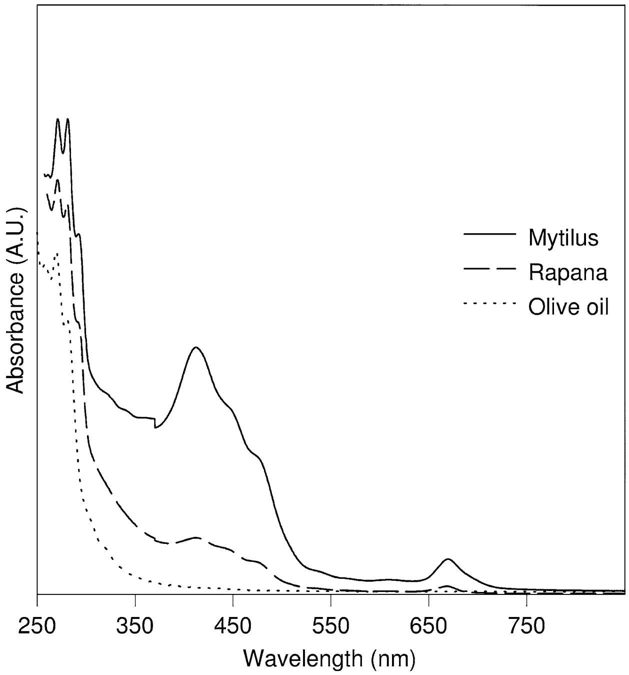

Fig. 1 UV-VIS spectra of *Mytilus galloprovincialis* (L.) (*solid line*) and *Rapana Venosa* (*dashed line*) lipid extract compared to olive oil (*dotted line*)

IR Experiments

Figure 2 includes the IR spectra of the *Mytilus galloprovincialis* (L.) (a) and *Rapana venosa* (b) lipid extracts compared to olive oil (c). Interesting differences were found in the spectra. The three mixtures showed a similar IR profile in the 3,500–2,000 cm^{-1} range, that is, bands below 3,000 cm^{-1} that are attributed to the saturated part from the compounds and a small peak over 3,000 cm^{-1}, due to unsaturations. No alkyne bands were found at 3,300–3,500 cm^{-1}. However, the *Rapana venosa* extract had a very broad peak in the 3,400–3,600 cm^{-1} range that

Table 2 Relevant UV-data of the two diluted lipid extracts (1:2 dilution in hexane) from *Mytilus galloprovincialis* (L.) and *Rapana venosa* lipid extracts compared to olive oil

Mytilus galloprovincialis (L.)		*Rapana venosa*		Olive oil	
λ (wavelength)	Chromophore	λ (wavelength)	Chromophore	λ (wavelength)	Chromophore
271	Poly-enes/sterol derivatives	270.5	Poly-enes	271	Poly-enes/sterol derivatives
281	E-vitamin (α-tocopherol)	281	E-vitamin (α-tocopherol)	281	E-vitamin (α-tocopherol)
412	$C_6H_5(CH{=}CH)_5–C_6H_5$-*trans*	412	$C_6H_5(CH{=}CH)_5–C_6H_5$-*trans*		
670	$(CH_3)_3C–NO$, n-π	608	R–NO, n-π		
		668	$(CH_3)_3C–NO$, n-π		
		Around 1,100	Organic acids $C_6H_5–(CH{=}CH)n–C_6H_5$ *trans*		

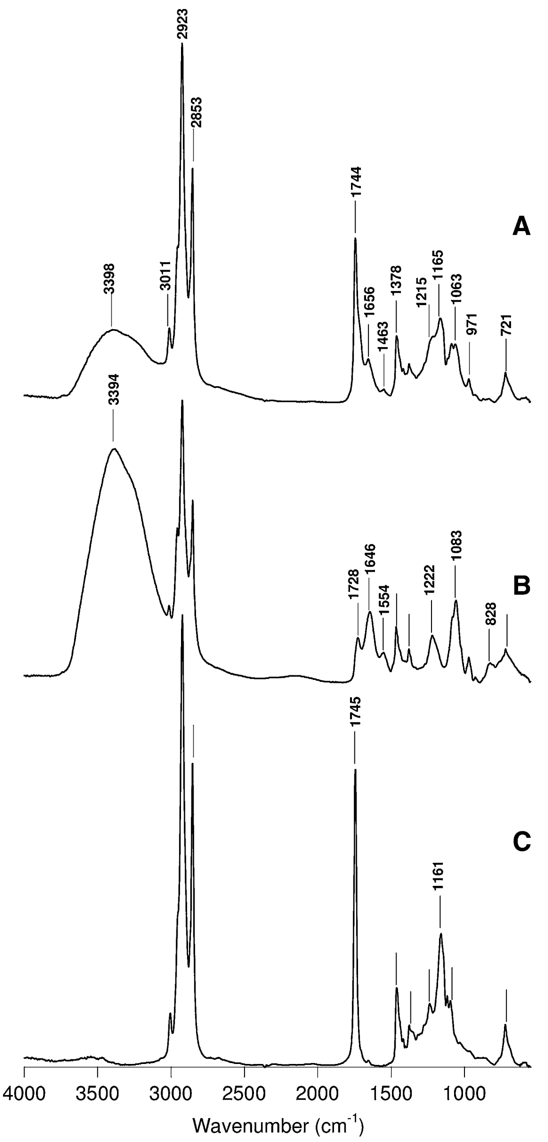

Fig. 2 IR spectra of **a** *Mytilus galloprovincialis* (L.), **b** *Rapana venosa* and **c** Olive oil

could be attributed to OH groups coming from alcohol groups presumably from the fatty acids in the mixture and/or water traces in the extract. The most interesting part of the spectra is probably the 1,800–1,000 cm^{-1} range.

A very intense and sharp peak at ca. 1,744 cm^{-1} was found for the *Mytilus galloprovincialis* (L.) sample whereas there was no peak at 1,744 cm^{-1} in the *Rapana venosa* extract. This peak is likely to be due to C=O bands arising from α,β-unsaturated carboxylic acids. Only a small peak at ca. 1,728 cm^{-1} was found for the *Rapana venosa* extract, implying a significant difference in nature of the fatty acids and compounds with C=O present in the sample. Moreover, a peak at 1,646 and 1,656 cm^{-1} was found for the *Mytilus galloprovincialis* (L.) and the *Rapana venosa* extracts, respectively. These are likely to be due to C=O bands in aromatic acids and/or compounds in which intermolecular interactions are present. Peaks at 1,500–1,300 cm^{-1} were attributed to CH_3-CH_2- alkyl chains and were present in all samples. Moreover, the peaks at 971 and 973 cm^{-1} for the *Mytilus galloprovincialis* (L.) and the *Rapana venosa* extracts have been attributed to specific γ-CH *trans* vibrational modes as they were not present in olive oil.

Interestingly, a peak due to monosubstituted aromatics (C–H bending, 828 cm^{-1}, only one band) was found for the *Rapana venosa* lipid extract, in good agreement with the UV-Vis results that were indicating the potential presence of monosubstituted aromatics in the extract.

Gas Chromatography–Mass Spectrometry (GC/MS) Analysis

Qualitative and quantitative GC/MS analysis of the lipid extracts were performed in order to identify the different compounds in the extracts following a similar methodology to that reported by Christie [42]. Some examples of the chromatograms are shown in Figs. 3 and 4, respectively.

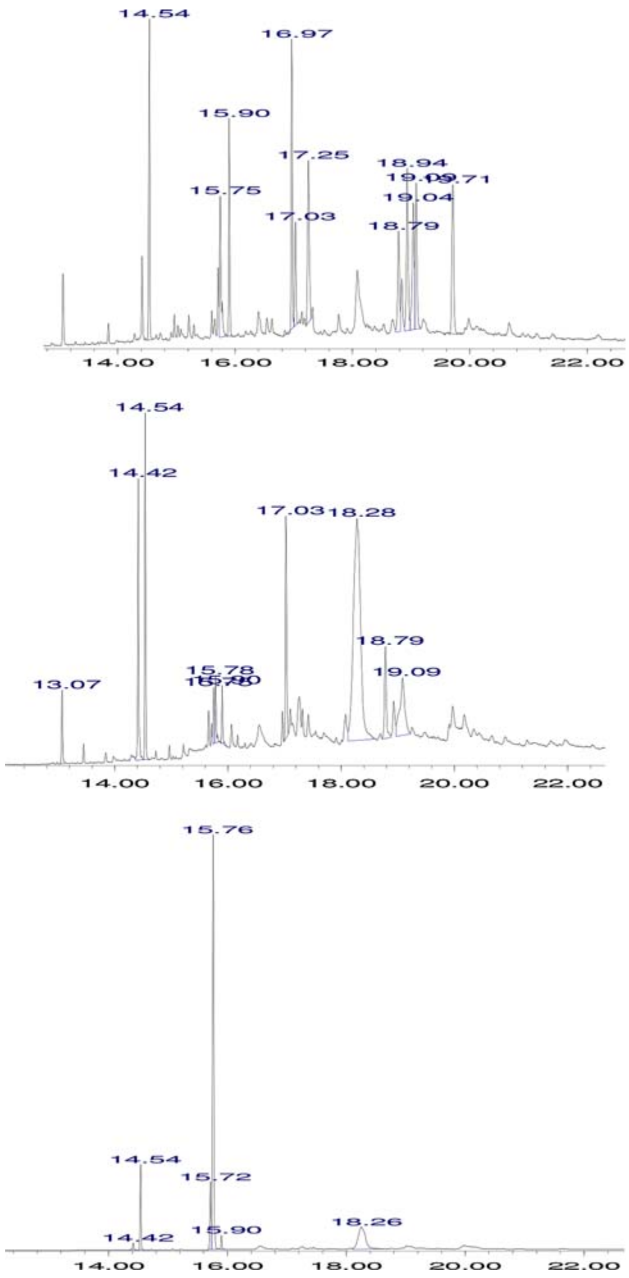

Fig. 3 GC–MS product distribution of the fatty acids from *Rapana venosa* (*top*) and *Mytilus galloprovincialis Lmk*. (*middle*) lipid extracts compared to olive oil (*bottom*) using the derivatisation by methylation

Several products were identified and quantified. The relative proportions of the components in the extract were obtained for both fatty acids (Table 3) and sterols (Table 4) after derivatisations by methylation and using BSFTA, respectively, as method of analysis. Cholesterol was found to account for over 50% weight of the extracts. Data included in Table 3 were recalculated removing such 50% cholesterol contribution to further clarify future discussions about the application of the lipid extracts.

Various saturated, mono-, di and polyunsaturated fatty acids were present in the extracts. Saturated fatty acids including 14:0, 16:0, 18:0 were found in different quantities in the lipid extracts but accounting for a similar saturated fatty acid content (around 35% of the total FA content). Similarly, monounsaturated acids (16:1n-7, 18:1n-9 and n-10, 20:1n-9) content was also analogous (around 30% of the total FA content) for both marine species.

Nevertheless, the differences between samples in terms of content and distribution of PUFA were significant. Thus, the *Mytilus galloprovincialis* (L.) extract had up to a 31% (of the total FA content) by weight of PUFA with a 2:1 EPA:DHA ratio (Table 3, entries 13 and 14). The *Rapana venosa* extract had a striking 40% by weight of PUFA including a 17 and 20 wt% of ω-3 and ω-6 FA, respectively (Table 3, entries 12–14). Interestingly, no ω-6 FA were found in the *Mytilus galloprovincialis* (L.) extract. The unsaturated/saturated FA ratio in our extracts was close to 2:1 in good agreement with reported results for *Mytilus galloprovincialis* (L.) [8, 30, 31] and *Rapana venosa* [9]. Furthermore, the sum of quantities of EPA and DHA was similar to that of AA [9]. EPA and DHA inhibit competitively the utilisation of AA [43].

Further investigations were performed to identify the sterols distribution in the lipid extracts through derivatisation using BSFTA. Various sterols have been identified in various species from marine invertebrates [9, 44, 45]. Up to five different compounds in different quantities were clearly identified in the lipid extracts (Table 4, entries 2–6), accounting for about 30–35% in *Mytilus galloprovincialis* (L.) and *Rapana venosa*, in agreement with previous reports of identified sterols in molluscs [9, 45]. The difference to 100 corresponds to other compounds including 7 and 8-dehydrocholesterols, cholesterilene and related substances [9, 45].

α-tocopherol (14 μg mL^{-1} extract) and D-vitamin (40 U.I) were also found and quantified in the concentrated samples.

Studies of Regenerative Properties of the Extracts

The potential healing activity of the lipid extracts was then investigated in their application to induced skin burns in rats. Table 5 summarises the main scoring employed for the histological features of the wound tissue samples. A summary of the main results is presented in Figs. 5, 6 and 7 and Table 6.

A summary of the microscopic properties of the different blood and tissue samples extracted from the wounds are presented in Figs. 6 and 7. Blood samples for treated rats presented the normal constituents including leucocytes, lymphocytes and so on (Fig. 5c–f, groups 2 to 5).

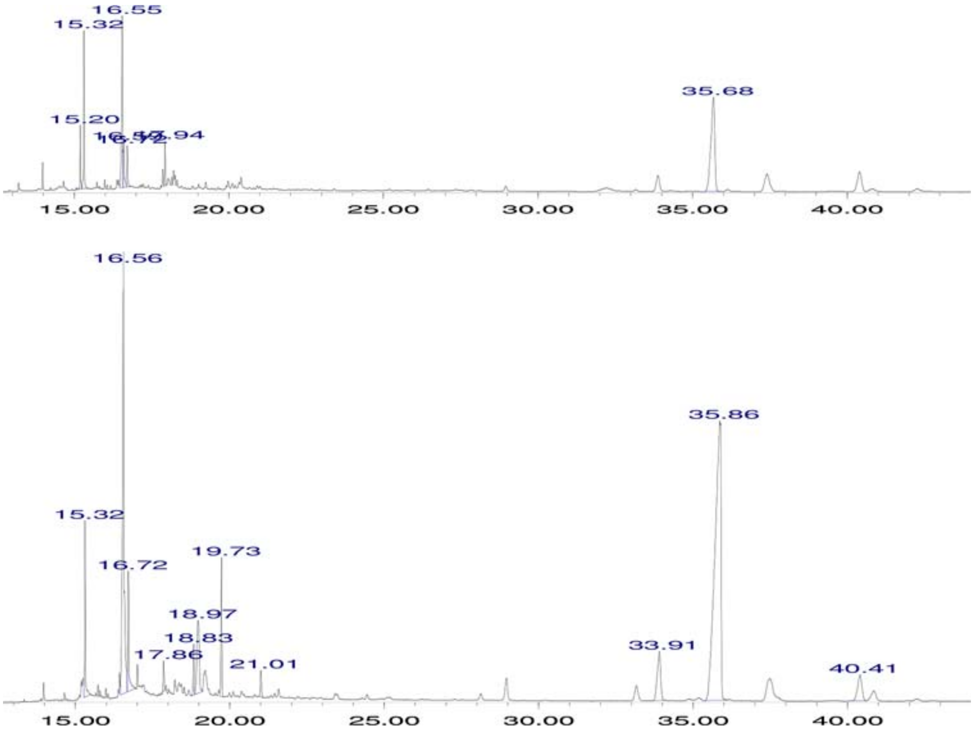

Fig. 4 GC–MS product distribution of the sterols identified from *Rapana venosa* (*top*) and *Mytilus galloprovincialis Lmk.* (*bottom*) lipid extracts using BSFTA as derivatising agent

Table 3 GC–MS product distribution and relative proportions (wt% of total fatty acids) of the fatty acids from *Mytilus galloprovincialis* (L.) and *Rapana venosa* lipid extracts compared to olive oil (in wt % dry weight lipid extract) using methylation as derivatisation method

Entry	Fatty acid	*Mytilus galloprovincialis* (L.)	*Rapana venosa*	Olive oil
1	10:0 (4,8,12-trimethyldecanoic acid)	1.30	–	–
2	14:0 (myristic acid)	5.57	4.40	–
3	16:0 (palmitic acid)	22.71	16.45	9.84
4	16:1n-7 (palmitoleic acid)	17.9	4.57	0.88
5	17:0 iso 16-methyl (16-methyl-heptadecanoic acid)	–	1.71	–
6	18:0 (stearic acid)	6.23	12.33	1.93
7	18:1n-9 (oleic acid)	5.28	10.98	60.12
8	18:1n-10 (10-octadecenoic acid)	7.00	–	–
9	18:2n-6 (linoleic acid)	2.04	–	8.10
10	20:0 (arachidic acid)	–	–	18.81
11	20:1n-9 (*cis*-11-eicosenoic acid)	–	13.51	–
12	20-4n-6 (arachidonic acid)	–	18.90	–
13	20:5n-3 (all-*cis*-5,8,11,14,17-eicosapentaenoic acid, EPA)	20.65	8.19	–
14	22:6n-3 (all-*cis*-4,7,10,13,16,19-docosahexaenoic acid, DHA)	11.18	8.90	–
15	Others	0.14	0.06	0.32

Untreated animals exhibited a leucocyte afflux with increasing quantities of constituents (leucocytes, lymphocytes, eosinophyles and monocytes) compared to normal blood (Fig. 5a, Group 1).

Microscope examination of the tissues of treated mice disclosed moderate to complete re-epithelialisation, minimal intercellular or subepithelial oedema, without crusting (++ to +++ scoring, Table 6, Fig. 6). In general, granulation tissue was characterised by dense collagen matrix deposition, slight oedema, and few scattered inflammatory infiltrates mainly confined in deep dermis and to the wound margins. The capillaries were significantly bigger than those found in untreated Wistar rats with no evidence of fibrin deposition, haemorrhage or vascular congestion.

Table 4 GC–MS product distribution and relative proportions (wt% of total sterol content) of the sterols identified from *Mytilus galloprovincialis* (L.) and *Rapana venosa* dry weight lipid extracts

Entry	Sterols	*Mytilus galloprovincialis* (L.)	*Rapana venosa*
1	Cholesterol	51.87	71.52
2	(22E)-24-norcholesta-5, 22-dien-3β-ol	7.89	6.11
3	(22E)-5α-ergosta-7,22-dien-3β-ol	11.12	7.75
4	25-hydroxy-24-methylcholesterol	12.93	5.20
5	5α-cholesta-8, 24-dien-3β-ol (zymosterol)	–	3.77
6	5α-ergosta-7,24-dien-3β-ol	–	4.29
7	Others (7 and 8 dehydrocholesterols, cholesterilene)	16.19	1.36

Table 5 Criterion to evaluate the histological features of the tissue samples

Score	Epidermal and dermal regeneration	Granulation tissue thickness	Angiogenesis
+	Little epidermal and dermal regeneration	Thin granular layer	High degree of oedema, haemorrhage and occasionally congestion and thrombosis
++	Moderate epidermal and dermal regeneration	Moderate granulation layer	Moderate degree of oedema and haemorrhage. Few newly formed capillary vessels
+++	Complete regeneration of epidermis and dermis	Thick granulation layer	Moderate degree of perivascular and interstitial oedema, absence of haemorrhage, newly formed capillary vessels
		Very thick granulation layer	Well-structured capillary vessels at the wound margins. Low degree of oedema

Skeletal muscle cells form a border zone between normal and wounded tissue, notably in Groups 3 and 5 (Fig. 6d, f). However, some scar tissue was still visible for groups 3, 4 and 5. In the particular case of the use of neopreol, the epidermis was indeed not completely recovered (Fig. 6f).

Compared to most treated animals, those treated with the lipid extracts from *Mytilus galloprovincialis* (L.). and the mixture *Mytilus galloprovincialis* (L.)/*Rapana venosa* exhibited an almost complete regenerated skin including epidermis, dermis and hypodermis (Fig. 6c and e, Groups 2 and 4, +++ scoring). New epithelium was being laid down and newly formed vessels, collagen fibres, and basal membrane could be visualised in provisional fibrin matrix. The inner epithelial layer was almost completely remodelled by day 12 and granulation tissue thickened close to the base of the wound (Fig. 6c, e).

In contrast, untreated animals presented only a partially recovered skin (Fig. 6b, Group 1) with abundant scar tissue, oedematous and inflamated granulation tissue with little epithelial covering (Fig. 6b, right side of the image). Few newly and immature formed vessels along with fibrin deposition, haemorrhage, interstitial oedema and evidence of generalised vascular congestion were also observed. Undeveloped collagenous connective tissue stroma and moderate granulation tissue accumulation with minimal adipose tissue substitution could also be seen.

The results pointed out the untreated wounds required a time to heal of approximately 3 weeks (20–22 days) to achieve a ++ score (Fig. 7, Table 6). The use of the lipid extracts was found to remarkably reduce such time of healing to 12–13 days (with a daily treatment with the *Mytilus galloprovincialis* (L.) extract) and 13–15 days (daily treatment with the *Rapana venosa* extract) to achieve +++ and ++ score, respectively. Interestingly, the mixture of the two lipid extracts did not significantly improve the time of healing (14–15 days, Fig. 7, group 4), although a better score was awarded due to the almost complete regeneration of the skin (Table 6). The commercial ointment neopreol also gave very similar results (Fig. 7, group 5, Table 6).

Discussion Along the Wound Healing Properties of the Extracts

Wound healing is a complex and continuous sequence of cellular and molecular processes including inflammation, cell migration, angiogenesis, synthesis of provisional matrix, collagen deposition and re-epithelialisation [27, 29, 46]. Nevertheless, the initial inflammatory phase has been reported as the most critical [27]. In this regard, the proven anti-inflammatory and immunomodulatory benefits of ω-3 and ω-6 FA seemed to have a positive effect on the wound healing as demonstrated in Fig. 7. Our results are in conflict with those reported by Cardoso et al. that reported the topical administration of ω-3 and ω-6 essential FA significantly delayed the wound closure process [47], in a

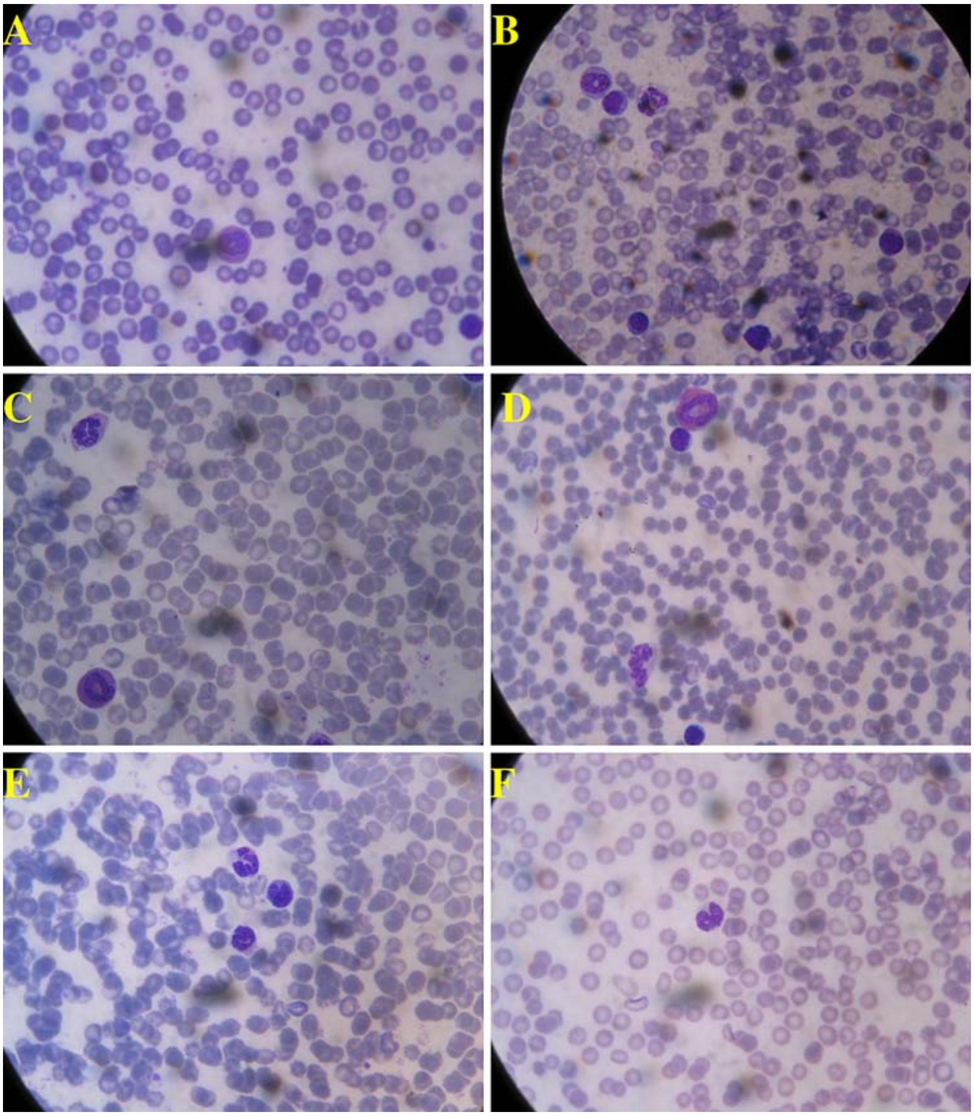

Fig. 5 Microscopy images (10 × 100, MGG) of the blood sections of **a** healthy rats; **b** untreated rats with skin burns after 21 days (Group 1); **c** rats with skin burns treated with the *Mytillus galloprovinciallis* (L.) lipid extract after 12 days (Group 2); **d** rats with skin burns treated with *Rapana venosa* lipid extract after 14 days (Group 3); **e** rats with skin burns treated with *Mytilus galloprovincialis* Lmk.:*Rapana venosa* lipid extracts after 13 days (Group 4); **f** rats with skin burns treated with Neoprenol after 14 days (Group 5)

similar way to results reported by Albina et al. that suggested the use of a ω-3 enriched diet might negatively affect the wound healing process by altering the fibroblastic or maturational phases [48].

Despite our controversial findings, other authors have observed that both ω-3 and ω-6 do not seem to have a harmful effect on wound healing in mice [9].

With regards to the potentially active compounds involved in the healing process, we believe the ω-3 (EPA and DHA) and ω-6 (AA) essential FA actively take part possibly via reduction of the initial inflammatory phase and consequent facilitation of the subsequent wound healing steps through stimulation of dermal and epidermal regeneration, proliferation of fibroblasts and formation of new well-structured capillary vessels. Furthermore, the higher content of ω-3 (EPA and DHA) essential FA and improved healing properties of the *Mytilus galloprovincialis* (L.) and mixture *Mytilus galloprovincialis* (L.)/*Rapana venosa* extracts compared to those of *Rapana venosa* led us to infer the direct involvement of EPA and DHA in the wound healing process.

In conclusion, we have investigated two different lipid extracts from two molluscs species from the Black Sea. The mixtures analysed were found to be very complex, containing overall a high cholesterol content and interesting quantities of several saturated and PUFA including ω-3 (EPA and DHA) and ω-6 (AA).

The activities of the lipid extracts were then investigated on induced cutaneous burns in Wistar rats.

The extracts were found to accelerate the time of healing in the wounds from 20–22 days (untreated animals) to 12–16 days (treated animals), showing some improvements with respect to results obtained using neopreol. We believe the AA and, in particular, the EPA and DHA essential FA are directly involved in the healing process, reducing the initial inflammatory phase and promoting the recovery of the damaged tissue.

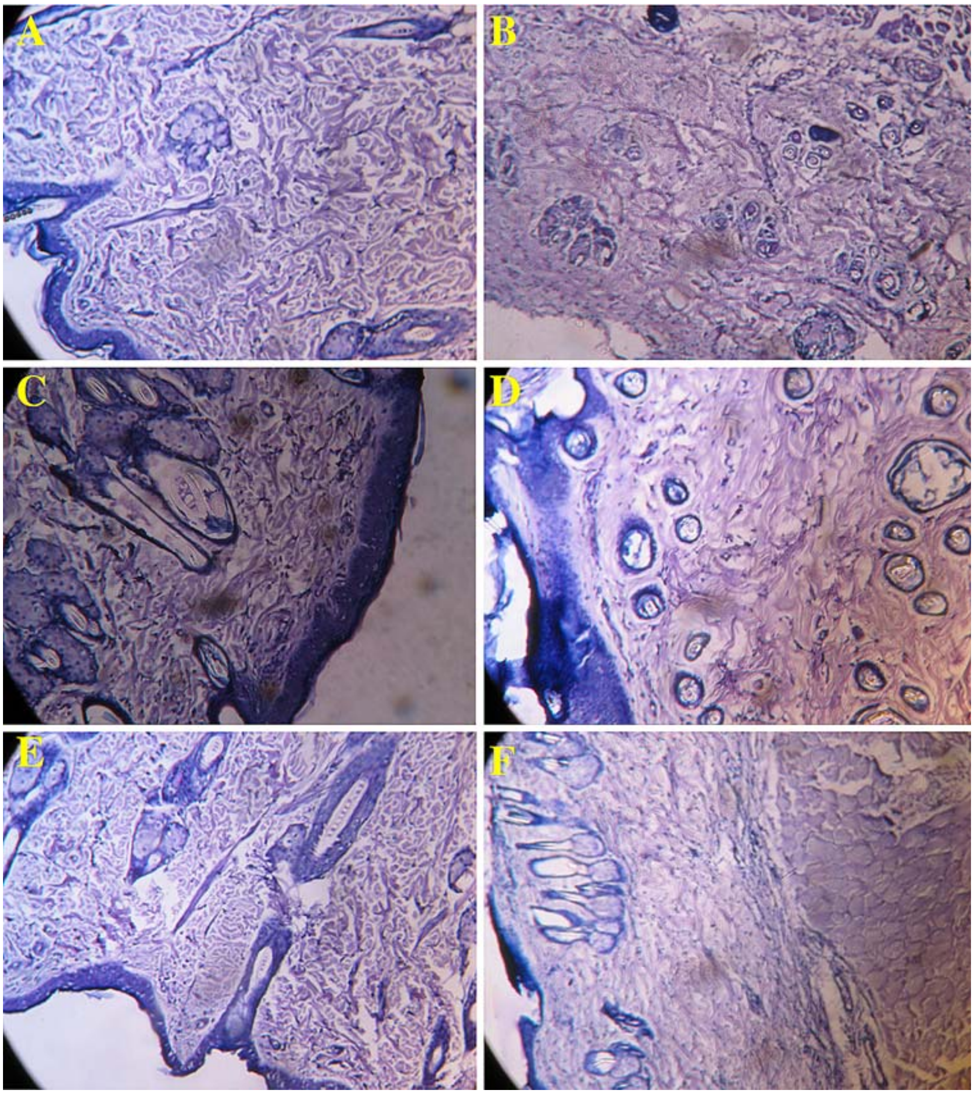

Fig. 6 Microscopy images (20 × 10, HE) of the tissue sections of **a** healthy rats before the skin burn was induced; **b** untreated rats with skin burns after 21 days (Group 1); **c** rats with skin burns treated with the *Mytillus galloprovinciallis* (L.) lipid extract after 12 days (Group 2); **d** rats skin burns treated with *Rapana venosa* lipid extract after 14 days (Group 3); **e** rats skin burns treated with *Mytilus galloprovincialis* Lmk.: *Rapana venosa* = 1:1 lipid extract after 13 days; **f**) rats with skin burns treated with Neoprenol after 14 days (Group 5)

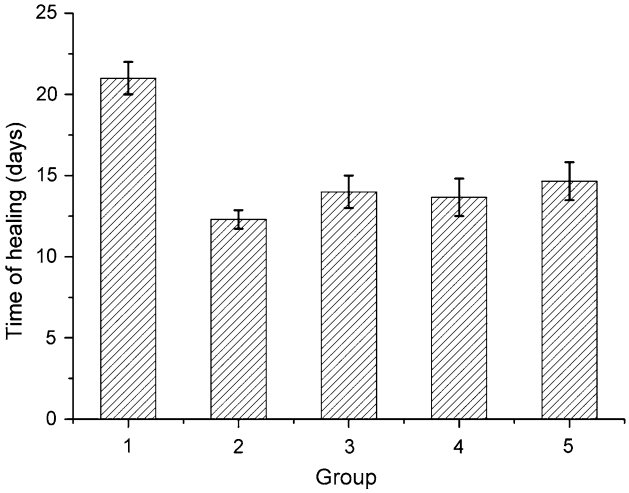

Fig. 7 Healing time (days) of the skin burns for the five groups of Wistar rats: *1* untreated animals; *2* treated with *Mytilus galloprovincialis* (L.); *3* treated with *Rapana venosa*; *4* treated with a *Mytilus galloprovincialis* (L.):*Rapana venosa* 1:1 mixture*;* *5* treated with neopreol

Table 6 The histological score of the five groups of Wistar rats

Groups	Histological score
1 (Control)	++
2	+++
3	++
4	+++
5	++

These results pointed out the lipid extracts have an outstanding potential to be used as active compounds in ointments and skin-care products with potential benefits on burns, inflammations etc.

References

1. Biodiversity II: Understanding and protecting our biological resources (1997) Reaka-Kudla ML, Wilson DE, Wilson EO (eds). Joseph Henry Press, ISBN 0309055849
2. Borowitzka MA (1995) Microalgae as sources of pharmaceuticals and other biologically active compounds. J Appl Phycol 7:235–242

3. Mayer AMS, Hamann MH (2005) Marine pharmacology in 2001–2002: Marine compounds with antihelmintic, antibacterial, anticoagulant, antidiabetic, antifungal, antiinflammatory, antimalarial, antiplatelet, antiprotozoal, antituberculosis and antiviral activities, affecting the cardiovascular, immune and nervous systems and other miscellaneous mechanisms of action. Comp Biochem Physiol C: Toxicol Pharmacol 3–4(140):265–286
4. Roşoiu N (1985) Studies on the use of the marine biological resources for pharmaceutical purposes, ALFLUTOP- the first original Romanian drug created in the Roumanian marine research institute from small fish species. Marine Researches, INCDM 18:235–255
5. Gomoiu MT (1984) Sur le stock de moules (*Mytilus galloprovincialis* L.) de plateau continental Roumain de la Mer Noire". Res Mar 17:143–163
6. Roşoiu N (1998) Donne biochimiques chez *Mytilus galloprovincialis* L. du littoral Roumain de la Mer Noire. "Ovidius" University Annals, Medical Sciences Series 3:158–161
7. Mârza M (1972) Data about the proteins and amino acids contained in some Black Sea molluscs. Marine Researches, INCDM 4:205–210
8. Vernocchi P, Maffei M, Lanciotti R, Suzzi G, Gardini F (2007) Characterisation of Mediterranean mussels (*Mytilus Galloprovinciallis*) harvested in Adriatic Sea (Italy). Food Control 18:1575–1583
9. Guven KC, Yazici Z, Akinci S, Okus E (1999) Fatty acids and sterols of *Rapana venosa*. J Shellfish Res 18(2):601–604
10. Freites L, Fernandez-Reiriz MJ, Labarta U (2002) Lipid classes of mussel seeds *Mytillus Galloprovincialis* of subtidal and rocky shore origin. Aquaculture 207:97–111
11. Bomba A, Jonecová Z, Koščová J, Nemcová R, Gancarčíková S, Mudroňová D, Sciranková L, Buleca V, Lazar G, Pošivák J, Kaštel R, Mareková M (2006) The improvement of probiotics efficacy by synergistically acting components of natural origin: a review. Biologia 61:712–729
12. Isanga J, Zhang G-N (2007) Biologically Active Components and Nutraceuticals in Peanuts and Related Products: Review. Food Rev Int 23:123–129
13. Roşoiu N, Serban M (1981) Quelques donnes biochimiques chez *Rapana thomasiana* Grosse. Rapp Comm Int Mer Med 27:3–31
14. Roşoiu N, Serban M (1992) Biological active substances from marine organisms. Romanian Academy Ed., Bucharest
15. Harris WS (2004) Fish oil supplementation: evidence for health benefits. Clev Clin J Med 71(3):208–210, 212, 215–218.
16. Astorg P, Guesnet P, Alessandri JM, Galan P, Lavialle M (2006) Omega-3 polyunsaturated fatty acids and health: a mini-review of current knowledge. Sci Aliments 26:8–28
17. Angerer P, von Schacky C (2000) n-3 polyunsaturated fatty acids and the cardiovascular system. Curr Opin Lipidol 11(1):57–63
18. Calder PC (2003) Long-chain n-3 fatty acids and inflammation: potential application in surgical and trauma patients. Braz J Med Biol Res 36(4):433–446
19. Suzuki R, Shimizu T, Kudo T, Ohtsuka Y, Yamashiro Y, Oshida K (2002) Effects of n-3 polyunsaturated fatty acids on dermatitis in NC/Nga mice. Int Bibliogr Inf Diet Suppl 66(4):435–440
20. Belluzzi A, Boschi S, Brignola C, Munarini A, Cariani C, Miglio F (2000) Polyunsaturated fatty acids and inflammatory bowel disease. Am J Clin Nutr 71:339S–342S
21. Gibson SLM, Gibson RG (1998) The treatment of arthritis with a lipid extract of *Perna canaliculus*: a randomized trial. Complement Ther Med 6:122–126
22. Blok WL, Katan MB, Van der Meer JW (1996) Modulation of inflammation and cytokine production by dietary (n-3) fatty acids. J Nutr 126(6):1515–1533
23. Storlien LH, Jenkins AB, Chisholm DJ, Pascoe WS, Khouri S, Kraegen EW (1991) Influence of dietary fat composition on development of insulin resistance in rats. Relationship to muscle triglyceride and omega-3 fatty acids in muscle phospholipids. Diabetes 40(2):280–289
24. Giamarellos-Bourboulis EJ, Grecka P, Dionyssiou-Asteriou A, Giamarellou H (2000) Impact of n-6 polyunsaturated fatty acids on growth of multidrug-resistant *Pseudomonas aeruginosa*: interaction with amikacin and ceftazidime. Antimicrob Agents Chemother 44:2187–2189
25. Kirsch C, Takamiya-Wik M, Reinold S, Hahlbrock K, Somssich IE (1997) Rapid, transient, and highly localized induction of plastidial ω-3 fatty acids desaturase mRNA at fungal infection sites in *Petroselinum crispum*. Proc Natl Acad Sci USA 94:2079–2084
26. Aiko S, Yoshizumi Y, Tsuwano S, Shimanouchi M, Sugiura Y, Maehara T (2005) The effects of immediate enteral feeding with a formula containing high levels of omega-3 fatty acids in patients alter surgery for esophageal cancer. JPEN J Parenter Enteral Nutr 29:141–147
27. Gercek A, Yildirim O, Konya D, Bozkurt S, Ozgen S, Kilic T, Sav A, Pamir N (2007) Effects of parenteral fish-oil emulsion (Omegaven) on cutaneous wound healing in rats treated with dexamethasone. JPEN J Parenter Enteral Nutr 31:161–166
28. Parrelli JM, Meisler N, Cutroneo KR (1998) Identification of a glucocorticoid response element in the human transforming growth factor beta 1 gene promoter. Int J Biochem Cell B 30:623–627
29. Altavilla D, Saitta A, Cucinotta D, Galeano M, Deodato B, Colonna M, Torre V, Russo G, Sardella A, Urna G, Campo GM, Cavallari V, Squadrito G, Squadrito F (2001) Inhibition of lipid peroxidation restores impaired vascular endothelial growth factor expression and stimulates wound healing and angiogenesis in the genetically diabetic mouse. Diabetes 50:667–674
30. Ventrella V, Pirini M, Pagliarani A, Trombetti F, Manuzzi MP, Borgatti AR (2008) Effect of temporal and geographical factors on fatty acid composition of *M. galloprovincialis* from the Adriatic sea. Comp Biochem Physiol B 149:241–250
31. Pirini M, Manuzzi MP, Pagliarani A, Trombetti F, Borgatti AR, Ventrella V (2007) Changes in fatty acid composition of *Mytilus galloprovincialis* (Lmk) fed on microalgal and wheat germ diets. Comp Biochem Physiol B 147:616–626
32. Trigari G, Pirini M, Pagliarani A, Manuzzi MP, Ventrella V (2001) High levels of NMID fatty acids in molluscs. Ital J Biochem 50:41–46
33. Christie W (1982) Isolation, separation, identification and structural analysis of lipids. Pergamon Press, NY
34. Keates M (1986) Techniques in lipidology: isolation analysis and identification of lipids. 2nd edn. Amsterdam, Elsevier Press Maid&BL, Olsen
35. Wilson K, Walker JM (1994) Principles and techniques of practical biochemistry, 4th edn. Cambridge University Press, London
36. A X-A Farmacopeea Romana (1993, Suppl. 2004), Editura Medicala, Bucuresti, http://www.anm.ro/home_anm.asp
37. PS L 56 (2006) Histological processing technique of the tissue samples, Histo-pathology Laboratory technique, Veterinary and Health Centre, Constanza, Romania
38. Onet E, Constantinescu V (1978) The laboratory diagnostic in veterinary medicine- The May Grunwald Giemsa Method, Ceres Ed., Bucharest, p 238
39. Padilla FC, Liendo R, Quintana A (2000) Characterization of cocoa butter extracted from hybrid cultivars of Theobroma cacao L. ALAN, 50:200–205. ISSN 0004-0622
40. Frampton VL, Skinner WA, Bailey PS (1952) The production of tocored upon the oxidation of dl-α-tocopherol with ferric chloride. J Am Chem Soc 76:282–284
41. Van Haaften RIM, Evelo CTA, Haenen GRMM, Bast A (2001) No reduction of alpha-tocopherol quinone by glutathione in rat liver microsomes. Biochem Pharmacol 61:715–719

42. Christie WW (1998) Gas chromatography-mass spectrometry methods for structural analysis of fatty acids. Lipids 33:343–353
43. Dyerberg J, Bang HO, Stoffersen G, Moncada S, Vane JR (1978) Eicosapentenoic acid and prevention of thrombosis and arteriosclerosis. Lancet 2:117–119
44. Tsujimoto M, Koyanagi H (1934) The sterol in marine invertebrates: composition, biosynthesis and metabolites. J Soc Chem Ind Jpn 37:436B
45. Kanazawa A (2001) Sterols in marine invertebrates. Fish Sci 67:997–1007
46. Clark RAF (1985) Cutaneous wound repair: basic biologic considerations. J Am Acad Dermatol 13:701–705
47. Cardoso CR, Souza MA, Ferro EA, Favoreto S Jr, Pena JD (2004) Influence of topical administration of n-3 and n-6 essential and n-9 nonessential fatty acids on the healing of cutaneous wounds. Wound Repair Regen 12:235–243
48. Albina JE, Gladden P, Walsh WR (1993) Detrimental effects of an omega-3 fatty acid enriched diet on wound healing. JPEN J Parenter Enteral Nutr 17:519–521

Lipids (2008) 43:843–851
DOI 10.1007/s11745-008-3206-1

ORIGINAL ARTICLE

Multiply Methyl-Branched Fatty Acids and Diacids in the Polar Lipids of a Microaerophilic Subsurface Microbial Community

David B. Hedrick · Aaron D. Peacock ·
Philip Long · David C. White

Received: 13 January 2008 / Accepted: 6 June 2008 / Published online: 9 July 2008
© AOCS 2008

Abstract A previously unreported series of di- and trimethylated fatty acids, as well as saturated and monounsaturated diacids were identified in polar lipids isolated from environmental subsurface sediment samples. Mechanisms are proposed for their formation, but their origin and role in cell membranes remains unknown.

Keywords Branched fatty acids · Lipid analysis · Environmental samples

Abbreviations

PLFA	Polar lipid fatty acids
ECL	Equivalent chain length

D.C. White: deceased.

Electronic supplementary material The online version of this article (doi:10.1007/s11745-008-3206-1) contains supplementary material, which is available to authorized users.

D. B. Hedrick (✉)
Microbial Insights, Inc., 2340 Stock Creek Blvd.,
Rockford, TN 37853-3044, USA
e-mail: davidhedrick@earthlink.net

A. D. Peacock
Haley & Aldrich, 465 Medford St., Ste. 2200, Boston,
MA 02129-1400, USA

P. Long
Pacific Northwest National Laboratory, Richland,
WA 99352, USA

D. B. Hedrick · A. D. Peacock · D. C. White
Center for Biomarker Analysis, University of Tennessee,
10515 Research Dr., Ste. 300, Knoxville, TN 37932-2567, USA

Introduction

Polar lipid fatty acid (PLFA) analysis is a powerful method in microbial ecology, providing information on the biomass, community structure, and metabolic status of the viable microbial community [1, 2]. To extract the maximum information from environmental samples, it is important to identify unusual PLFA, which may be of low abundance, and for which there are often no standards available.

As part of a study on biological immobilization of uranium by reduction from soluble U^{6+} to insoluble U^{4+} [3, 4], sediment samples were analyzed for their PLFA content. An unusually large number of unknown fatty acid methyl esters were detected by gas chromatography–mass spectroscopy, a few of which had been seen previously in samples from other environments. Their mass spectra were those of saturated fatty acid methyl esters (74 and 87, or 88 and 101 for 2-methyl, or 74 and 101 for 3-methyl fatty acid methyl esters, M+, M-31, and the alkyl loss series), but their retention times were too early for straight-chain or singly branched fatty acids. The pattern of their appearance in other samples sets had been suggestive of some component of the microbial community, but could not be proven not to be a new contaminant. Their number and abundance in this sample set presented the opportunity for their identification, but the samples had already been analyzed and the chance to use the more informative picolinyl or DMOX derivatives was past. Using mass spectral and equivalent chain length analyses, and relying heavily on the lipid literature, 21 multiply branched saturated fatty acids, 4 diacids, and 3 monounsaturated diacids were identified as their methyl esters.

Materials and Methods

Study Site

The Old Rifle site is a former uranium processing facility near Rifle, CO, USA. Within the sampling area and near the time of sampling, groundwater analysis found U^{6+} from 0.5 to 1.3 μM, nitrate 0.1–0.3 mM, Fe^{2+} 0.03–0.05 μM, sulfate 5.3–6.8 mM, sulfide 6–33 μg/L, pH 6.7–7.0, and oxygen from 0.2 to 0.5 mg/L. Sediment samples were collected from the saturated zone of the aquifer, between 4 and 5.2 m below land surface. Subsurface sediment samples were collected aseptically using a rotosonic drilling rig (Boart Longyear, Environmental Drilling Division, Little Falls, MN, USA) and were kept frozen until analysis, as described [4]. As part of the overall experiment, ^{13}C-labeled acetate was injected into the aquifer, but only control samples collected before ^{13}C-labeled acetate injection were used for the identification of unknowns.

Polar Lipid Fatty Acid Analysis

The total lipid was extracted from subsurface sediment samples by the method of Bligh and Dyer [5] as modified [6] utilizing a single-phase mixture of chloroform, methanol, and phosphate buffer. The polar lipid fraction was separated from neutral lipids and glycolipids by silicic acid column chromatography, and transesterified to fatty acid methyl esters by a mild alkaline methanolysis [7]. Gas chromatography–mass spectroscopy was performed on an Agilent 6890 series gas chromatograph with a 50 m HP-1 nonpolar column (0.2 mm I.D., 0.11 μm film thickness), and a temperature program of 100 °C initial temperature, 10 °C/min to 150 °C, hold for a minute, 3 °C/min to 282 °C, and hold for 5 min. The injector and detector temperatures were 270 and 290 °C, respectively. The carrier gas was hydrogen. Peak quantitation and mass spectral acquisition was by an Agilent 5973 mass-selective detector.

Equivalent Chain Length Analysis

Equivalent chain lengths (ECL) of fatty acid methyl esters were calculated by linear interpolation between the normal saturates, rather than the more commonly used linear or non-linear regression across the entire chromatogram. The untransformed retention times were regressed against carbon number for the 12 normal saturates, in order to test for outlier retention times. Pearson's R^2 for the regression was generally greater than 0.95. The high abundance of 16:0 gave non-ideal behavior in some samples. Due to the method used, the ECLs of the normal saturates are by definition equal to their chain lengths (Table 1).

Equivalent chain lengths for the multiply branched fatty acid methyl esters identified by mass spectroscopy were estimated by considering them as isomers of a normal saturate, each methyl branch lowering the ECL by some fraction, depending upon position and chain length (Fig. 1 of the Electronic Supplementary Material). This is expected to give reasonable estimates of the ECLs when the methyls are well-separated on the carbon chain, so that interaction between the methyl groups is not significant. The fractional ECL for a fatty acid methyl ester X, $\mathrm{f(ECL)}_X$, was calculated by

$$\mathrm{f(ECL)}_X = \mathrm{ECL}_X - \mathrm{ECL}_\mathrm{I} + 1$$

where ECL_I is the ECL of the isomeric normal saturate. Since a methyl branch nearer the carboxylate end of the molecule affects the retention time more than one further away, the calculated ECL is based on the ECL of the isomeric mono-methyl FAME at the first position, and then adjusted for the methyl closer to the aliphatic end. Using the equation

$$\mathrm{ECL} = \mathrm{ECL}_{n,1} + \mathrm{f(ECL)}_{n,2} - 1$$

where n is the carbon number of the dimethyl fatty acid and 1 and 2 represent the methyl positions closer to and further from the carboxylate, respectively. If the f(ECL) of the second methyl branch varies strongly with chain length, the following equation is more accurate.

$$\mathrm{ECL} = \mathrm{ECL}_{n,1} + \mathrm{f(ECL)}_{n-1,2} + \left\{ \mathrm{f(ECL)}_{n,1} \times \left[\mathrm{f(ECL)}_{n-1,2} - \mathrm{f(ECL)}_{n,2} \right] \right\} - 1$$

Results

Table 1 lists 86 polar lipid fatty acid methyl esters detected in this microaerophilic microbial community and Fig. 1 gives some of the structures. The 12 normal saturates detected from 14:0 to 26:0 showed a strong even carbon number dominance and a bimodal distribution centered on 16:0 and 22:0. The 6 terminally branched fatty acids had the even- and odd-numbered *iso*-branched and odd-numbered *anteiso*-branched fatty acids expected of bacterial lipids [8]. Both the 15- and 17-carbon terminally branched fatty acids had more of the *anteiso*- than *iso*-branched isomer, as is often found in actinomycetes [9–11]. The ECLs of the terminally branched fatty acids were consistent internally and with published values [12].

The three 2-methyl fatty acid methyl esters (2Me16:0, 2Me17:0, and 2Me18:0) had fragments at $m/z = 88$, 101, M+, and M −31. They showed the alkyl loss series (101, 115, … M − 15) similar to normal saturates but with lower

Table 1 Polar lipid fatty acid methyl esters, average of 11 subsurface sediment samples

Fatty Acid	MW	ECL	Percent
i14:0	242	13.64	0.26
14:0	242	14.00	0.74
neo15:0	256	14.18	–
3Me14:0	256	14.39	–
8Me14:0	256	14.46	0.16
9Me14:0	256	14.49	–
10Me14:0	256	14.52	0.38
11Me14:0	256	14.59	–
i15:0	256	14.63	3.14
a15:0	256	14.72	4.24
15:1	254	14.81	0.04
2,10diMe14:0	270	14.87	–
15:0	256	15.00	0.46
3Me-i15:0	270	15.03	0.20
8Me-i15:0	270	15.07	0.33
10Me-i15:0	270	15.10	0.36
3Me-a15:0	270	15.10	
6Me-a15:0	270	15.14	0.02
neo16:0	270	15.19	–
i16:1w5c	268	15.41	0.13
10Me15:0	270	15.48	0.39
12Me15:0	270	15.58	0.31
i16:0	270	15.64	1.73
16:1w9c	268	15.72	0.71
16:1w7c	268	15.76	5.25
16:1w7t	268	15.81	0.43
16:1w5c	268	15.86	1.82
16:0	270	16.00	13.01
3Me-i16:0	284	16.03	–
10Me-i16:0	284	16.07	0.87
2Me16:0	284	16.35	0.22
i17:1	282	16.37	1.12
3Me16:0	284	16.38	–
10Me16:0	284	16.45	10.75
11Me16:0	284	16.48	1.26
12Me16:0	284	16.52	0.42
i17:0	284	16.64	1.58
a17:0	284	16.73	2.69
2,10diMe16:0	298	16.78	0.47
3,10diMe16:0	298	16.82	0.43
Cy17:0	282	16.84	3.09
2,12diMe16:0	298	16.86	0.01
3,12diMe16:0	298	16.91	0.07
2Me-i17:0	298	16.97	–
17:0	284	17.00	0.71
10Me-i17:0	298	17.06	1.92
10Me-a17:0	298	17.12	0.78
2Me17:0	298	17.36	0.06
2,10diMe-i17:0	312	17.39	0.31
10Me17:0	298	17.43	0.71
18:2w6	294	17.63	1.90
18:3w3	292	17.67	0.36
18:1w9c	296	17.72	4.25
18:1w7c	296	17.77	4.67
18:1w7t	296	17.81	0.71
18:1w5c	296	17.87	0.26
18:0	298	18.00	2.97
br19:1a	310	18.06	0.29
br19:1b	310	18.10	0.77
2Me18:0	312	18.35	0.15
10Me18:0	312	18.41	1.33
12Me18:0	312	18.44	0.84
10,12diMe-i18:0	326	18.62	0.36
16:1diacid	312	18.66	0.98
2,8diMe18:0	326	18.71	–
2,10diMe18:0	326	18.74	0.35
2,12diMe18:0	326	18.78	0.38
Cy19:0	310	18.86	5.34
19:0	312	19.00	0.17
16:0dioic	314	19.10	2.06
10Me-a19:0	326	19.16	0.10
9,10epox18:0	326	19.39	0.06
20:1w9c	324	19.71	0.31
20:1w7c	324	19.77	0.06
20:0	326	20.00	0.78
2oh19:1	326	20.06	0.17
18:0dioic	342	21.12	1.31
22:0	354	22.00	2.08
20:1dioic	368	22.74	0.32
23:0	368	23.00	0.58
20:0dioic	370	23.12	0.64
24:0	382	24.00	1.12
22:1dioic	396	24.78	0.46
25:0	396	25.00	0.23
22:0dioic	398	25.13	0.51
26:0	410	26.00	0.39

MW molecular weight of the methyl ester, *ECL* equivalent chain length, and *Percent* average mole percent

and more equal abundance [13]. The ECLs of all three are consistent with 2Me fatty acids [12, 14]. Two 3-methyl fatty acids were detected (3Me14:0 and 3Me16:0), with major fragments at $m/z = 74$ and 101, and mass spectra otherwise similar to 2-methyl fatty acids [13].

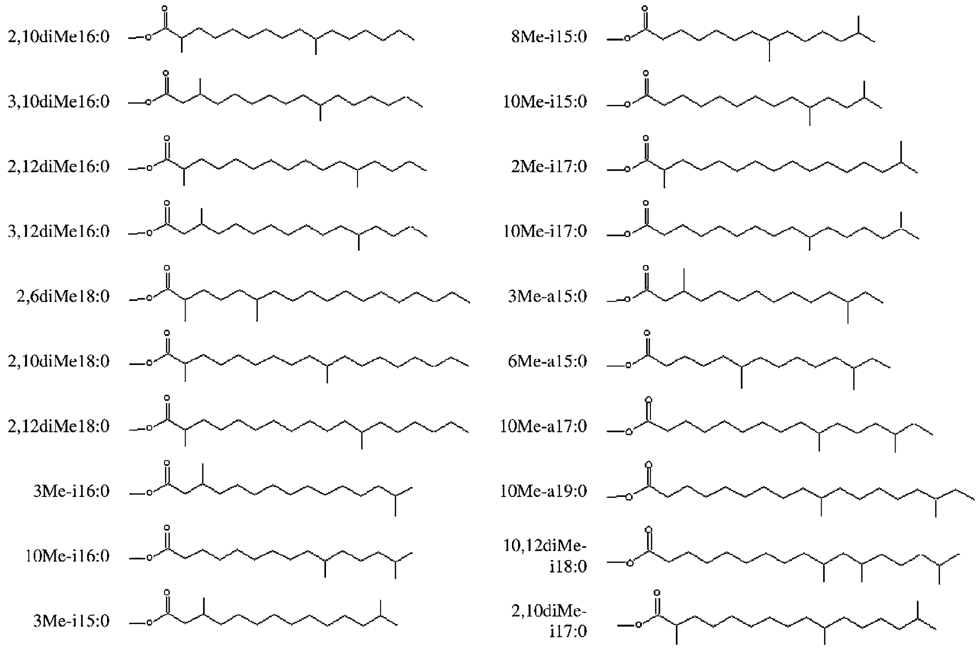

Fig. 1 Some novel polar lipid fatty acids

The 12 mid-chain branched fatty acid methyl esters identified (Table 1) showed the expected order of elution times 2Me < 3Me < 8Me < 10Me < 11Me < 12Me < *iso*-branched < *anteiso*-branched [15], and the expected decrease in fractional ECL with increasing carbon number. Saturated mid-chain branched fatty acid methyl esters were identified by comparison with the isomeric normal saturate (Fig. 2), which is characterized by fragments at $m/z = 74$, 87, M+, M – 31, the alkyl loss series (87, 101, 115, … M – 15) [13]. A mid-chain branched fatty acid methyl ester always has a retention time earlier than its *iso*-branched isomer. Single mid-chain methyl groups were located by the absence or lower abundance of the alkyl loss fragment at the methyl position, and the enhanced alkyl loss fragments from cleavage at either side of the methyl branch (Fig. 2). Other characteristic fragments with much lower abundance are the loss of methanol (loss of 32) from the alkyl loss fragments at either side of the branch and methanol + water (loss of 50) from the longer fragment [13] (Fig. 2). Their ECLs were also consistent with earlier work in this laboratory and with literature values [15, 16].

There were 21 multiply methyl-branched saturated fatty acid methyl esters identified in these samples with fragmentograms as described above for 2-methyl, 3-methyl, or mid-chain branched fatty acids, but ECLs less than the isomeric 2-methyl fatty acid methyl esters (Table 2). Nineteen of these were dimethyl fatty acids, and two had three methyl groups.

Five fatty acids with mid-chain and terminal branches were identified by the fragmentations typical of mid-chain branched fatty acids (above), M – 29 > M – 31 for *anteiso*-branched fatty acids, ECLs much lower than possible for a single methyl branch, and by eliminating all other possibilities. The estimated ECLs were correct to within ±4% of a methylene unit.

There were eight dimethyl fatty acids with a mid-chain branch and the other methyl group on the second or third carbon identified (Table 2).

Two trimethyl fatty acids were also identified in these samples—10,12diMe-i18:0 and 2,10diMe-i17:0. There were other multiply branched fatty acids seen in these samples which could not be completely identified including 3Me-br14:0, ECL = 14.03; 8Me-br14:0, 14.09; 3Me-br17:0, 17.03; 2Me-br19:0, 18.79; br20:0, 19.16; 2Me-br21:0, 20.71; 2Me-br22:0, 21.02; 2Me-br23:0, 22.68; and 2Me-br24:0, 22.97.

Four long chain diacids and 3 monounsaturated diacids were identified in these samples by their mass spectra (NBS75K library, Hewlett-Packard, Palo Alto, CA, USA) and retention times. An *n*-carbon saturated diacid dimethyl ester elutes soon after the $(n + 3)$-carbon normal saturate methyl ester [17]. For example, 16:0dioic elutes soon after 19:0 at an ECL of 19.10. The monounsaturated diacid dimethyl esters eluted about as much earlier than the corresponding saturate as an ω7c monounsaturated methyl ester eluted earlier than its corresponding normal saturate.

Discussion

Mass Spectral and Equivalent Chain Length Analyses

The multiply branched fatty acids identified in this work had mass spectra typical of saturated fatty acid methyl

Table 2 Multiply branched polar lipid fatty acid methyl esters in subsurface sediment samples

Name	%	ECL	Est.	Err.	Grp.	IUPAC
Dimethyl branched						
2,10diMe14:0	–	14.87	14.88	0.01	e	2,10-dimethyl-tetradecanoate
2,10diMe16:0	0.34	16.78	16.81	0.02	e	2,10-dimethyl-hexadecanoate
3,10diMe16:0	0.22	16.82	16.84	0.02	e	3,10-dimethyl-hexadecanoate
2,12diMe16:0	–	16.86	16.88	0.02	e	2,12-dimethyl-hexadecanoate
3,12diMe16:0	0.02	16.91	16.92	0.01	e	3,12-dimethyl-hexadecanoate
2,8diMe18:0	–	18.71	18.72	0.01	e	2,8-dimethyl-octadecanoate
2,10diMe18:0	0.34	18.74	18.74	0.00	e	2,10-dimethyl-octadecanoate
2,12diMe18:0	0.38	18.78	18.80	0.01	e	2,12-dimethyl-octadecanoate
3Me-i16:0	–	16.02	16.02	0.00	ei	3,14-dimethyl-pentadecanoate
10Me-i16:0	0.83	16.07	16.09	0.03	ei	10,14-dimethyl-pentadecanoate
3Me-i15:0	0.18	15.03	15.03	−0.01	oi	3,13-dimethyl-tetradecanoate
8Me-i15:0	0.28	15.07	15.07	0.01	oi	8,13-dimethyl-tetradecanoate
10Me-i15:0	0.34	15.10	15.11	0.01	oi	10,13-dimethyl-tetradecanoate
2Me-i17:0	–	16.97	17.00	0.03	oi	2,15-dimethyl-hexadecanoate
10Me-i17:0	1.84	17.06	17.06	0.00	oi	10,15-dimethyl-hexadecanoate
3Me-a15:0	–	15.10	15.11	0.01	a	3,12-dimethyl-tetradecanoate
6Me-a15:0	–	15.14	15.12	–0.02	a	6,12-dimethyl-tetradecanoate
10Me-a17:0	0.80	17.12	17.15	0.03	a	10,14-dimethyl-hexadecanoate
10Me-a19:0	0.11	19.16	19.14	–0.02	a	10,16-dimethyl-octadecanoate
Trimethyl branched						
10,12diMe-i18:0	0.18	18.62	18.46	**–0.16**	ei	10,12,16-trimethyl-heptadecanoate
2,10diMe-i17:0	0.33	17.39	17.40	0.01	oi	2,10,15-trimethyl-hexadecanoate

Bold value indicates that it is the exception to the high accuracy of the ECL calculation, due the methyl groups being close to each other on the carbon chain

% mole percent, *ECL* equivalent chain length, *Est.* estimated ECL, *Err.* Est.–ECL, *Grp.* fatty acid biosynthetic group (*e* even, *ei* even *iso*, *oi* odd *iso*, *a anteiso*), and *IUPAC* fatty acid name according to the rules of the International Union of Pure and Applied Chemists

esters, as illustrated with the mass spectra of the isomers 16:0, 12Me15:0, and 10Me-i15:0 (Fig. 2). The two most abundant peaks are at 74 and 87, or 88 and 101 for 2-methyl fatty acids, or 74 and 101 for 3-methyl fatty acids. The molecular ion, M+, and M – 32 (loss of methanol) are usually apparent, though M – 32 may not be seen in longer-chain fatty acid methyl esters. Consideration of the major ions and molecular weight eliminated unsaturated, hydroxylated, keto, or methoxyl fatty acids, as well as various possible nitrogen, sulfur, or halogen substitutions. Ethyl-branches would give rise to an M – 28 ion [18], which was not observed. By similar arguments, larger alkyl branches or cyclic saturates were eliminated as possibilities.

The effect of methyl substitution on the mass spectrum of a fatty acid methyl ester is greatest at the two position, and decreases as the position of the substitution proceeds down the carbon chain, to the *iso*-branched fatty acid which can rarely be distinguished from the normal saturate isomer by its mass spectrum [13]. In multiply methyl branched saturated fatty acid methyl esters, the methyl nearer the carboxyl end of the molecule somewhat suppresses ions due to the methyl further away. Identification of these minor fatty acids by subtle differences in their mass spectra required analysis of multiple chromatograms and extensive use of background subtraction and extracted ion chromatograms.

ECL analysis can support a proposed structure, but is not proof. The great power of ECL analysis is in eliminating a proposed structure. Once a structure was deduced from the mass spectral analysis, it was tested by ECL analysis. All structures reported here were supported by both methods.

Elimination of Known Multi-Methyl Fatty Acid Methyl Esters

The mass spectra and ECLs of several other types of multiply branched fatty acids were compared with these multi-methyl branched fatty acids, but did not match. The mycocerosates found in *Mycobacteria* have methyl groups at the even-numbered carbons near the carboxyl terminus. Examples include (with ECLs) 2,4diMe14:0 (14.56),

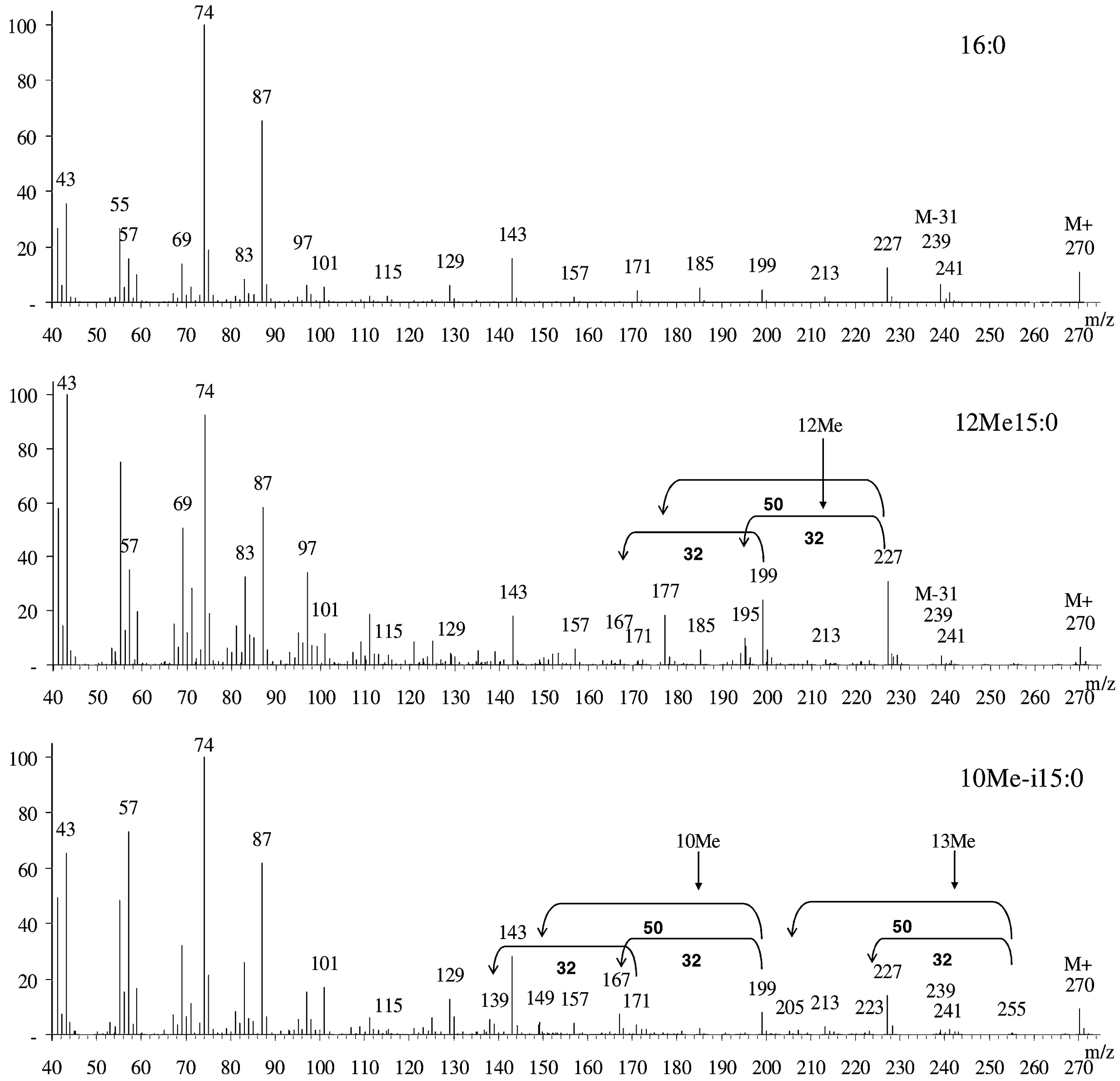

Fig. 2 Mass spectra of the isomers 16:0, 12Me15:0, and 10Me-i15:0

2,4diMe16:0 (16.59), 2,4diMe20:0 (20.67), 2,4,6triMe22:0 (22.82), 2,4diMe24:0 (24.67) [14, 15]. None of these compounds were found. Their retention times are earlier than the multiply branched fatty acids found in this study with the same molecular weight and degree of methylation due to the crowding of their methyl groups near the carboxy-terminus. Their mass spectra are characterized by major fragments at $m/z = 88$ and 101 (due to the 2-methyl), and 129 (due to the 4-methyl) [19–21], which do not match any compounds found in these samples. Certain 2-hydroxy-alkanes found in the membrane lipids of *Mycobacteria* were also not found in these samples—2-hydroxy-octadecane and 2-hydroxy-eicosane [14].

Another source of multiply branched fatty acids is the degradation of isoprenoids from chlorophyll or archaebacterial ether lipids. However, the multiply branched saturated FAME's found in these samples do not appear at the published retention times for these products, nor do the mass spectra match [22–24]. For some of the isoprenoid fatty acids, multiple ECLs were reported for a single structure, which is most likely due to variation in the stereochemistry of the methyl groups [25]. These include 3,7diMe-i13:0 (ECL = 13.44), 4,8diMe-i14:0 (14.16, 14.53), 5,9diMe-i15:0 (15.49), 2,6,10triMe-i16:0 (15.80, 16.61), 3,7,11triMe-i17:0 (17.04, 17.29, 17.72), and 4,8,12triMe-i18:0 (18.34) [25–31].

Another possibility is sub-terminal carboxylation (addition of carboxylic acid to the second carbon of an alkane to produce a 2-methyl fatty acid) which has been seen in some anaerobic bacteria [32, 33]. However, for this mechanism to be relevant requires abundant alkanes, which were not reported in this environment. Also, the typical distribution of alkanes from industrial or natural sources would produce a large envelope of small overlapping peaks, which was not seen. And further, most of the multiply branched fatty acids found were *iso*- or *anteiso*-branched, which would require unusually high levels of *iso*- and *anteiso*-branched alkanes as substrate.

A similar series of multiply methyl branched fatty acids have been found in a halophilic *Bacillus*, including 4,11diMe12:0, 4,10diMe12:0, 2,13diMe14:0, 2,12diMe14:0, and 4,13diMe14:0 [34]. While the 4-methyl branched fatty acids from this *Bacillus* were not found in these sediments, 2,12diMe14:0 is a shorter chain homolog of 2,12diMe16:0 and 2,12diMe18:0 which were found in these sediments.

Are These Membrane Fatty Acids?

There are several lines of evidence that these multiply branched and dioic fatty acids are membrane fatty acids produced by some organism, probably a bacterium, living in these subsurface sediments.

When ^{13}C-acetate was injected into the subsurface sediment (as part of a test of a bioremediation program), the label appeared in several of the multiply branched fatty acids (A. D. Peacock et al. in preparation). This is very strong support for biosynthesis of multiply branched fatty acids in the subsurface environment.

Second, this is a well-studied site with an active program of experimental bioremediation [3, 4; and references therein], but there is no mention of organic contaminants at this site which might be the source for these compounds.

Third, the total viable microbial biomass over these samples averaged 238 pmol/g with a standard deviation of 102 pmol/g ($n = 11$), and the percent of multiply branched fatty acids averaged 7.3% of the total with a standard deviation of 1.3%, similar to other fatty acid groups. If these compounds were independent of microbial biomass, their percentage would be expected to be more variable than the other fatty acid groups. Rather the amount of multiply branched fatty acids closely followed the amount of total PLFA. A similar pattern was seen for the diacids.

Fourth, some of these multiply methyl branched fatty acids have been detected but not identified before in PLFA from environmental samples, but not in procedural blanks. However, due to their very low abundance and lack of identification, they were not reported.

Fifth, the multiply branched fatty acids were detected as methyl esters and the diacids as dimethyl esters. The mild alkaline methanolysis used transesterified ester-bound carboxylic acids, but does not efficiently form methyl esters from free fatty acids. Therefore, these compounds were ester-linked in some complex polar lipid in the sample. Complex polar lipids are essential components of all cellular membranes, but polar lipid anthropogenic contaminants are very rare.

Sixth, while an extensive literature search revealed no previous report of several of these compounds, this is probably due to them not being recognized as authentic membrane components. These multiply branched fatty acids and diacids were minor components in these samples, but more abundant in these samples than any others in our experience. 2-Methyl or 3-methyl fatty acid methyl esters might not be recognized if they were not expected, and if the compounds were very minor components, because they do not have the signature $m/z = 74$ and 87 typical of fatty acid methyl esters. The mass spectra of diacid dimethyl esters are similar to those of fatty acid methyl esters, and may have been confused with the normal saturates or a hydrocarbon contaminant series which elute near them. Alternatively, the increasing background noise due to the chromatographic temperature program could have obscured the diacid peaks, or the temperature program might not have been run long enough to elute the diacids.

And finally, seventh, these multiply branched fatty acids and diacids could be synthesized by extension of known microbial lipid biosynthetic pathways. For most of the multiply branched fatty acids found, there are fatty acids in this sample with a single methyl group at each of those positions. A fatty acid can be converted into a diacid by the same oxidation mechanisms that convert alkanes to acids [35, 36].

The Origin of Multiply Branched Fatty Acids

While a strong argument can be made that these are biosynthesized membrane lipids, the organism(s) responsible for their synthesis and their role in the cell are unknown. The three main mechanisms for methyl group addition to bacterial fatty acids are (1) *iso*- and *anteiso*-branched fatty acids synthesized by using a branched volatile fatty acid as the primer in fatty acid biosynthesis in place of acetate [8], (2) mid-chain branched fatty acids formed by addition of a methyl group from *S*-adenosyl-methionine to an unsaturation [37, 38], and (3) 2-methyl fatty acids and mycocerosates are made by *Mycobacteria* by substituting methyl malonyl-CoA for acetate in chain elongation [39]. The multiply branched fatty acids found in these samples could have been formed by the successive action of these 3 methylation mechanisms, but the 2- and 3-methyl fatty acids found in these samples do not match to those produced by *Mycobacteria*.

Dioic Fatty Acids

In this sample set, 4 diacids and 3 monounsaturated diacids of chain length from 16 to 22 carbons were found in the polar lipid fraction (Table 1). The only example in the literature of a long-chain diacid in membrane lipids is diabolic acid, found in a few eubacterial extremophiles [40]. But diabolic acid has 30 carbons including 2 methyl groups near the center of the molecule, while the diacids found in this work were shorter and unbranched. Dembitsky found several dioics in methanolysates of total lipids from a red alga [41], but they were only from 7 to 11 carbons long, and they could have been neutral or complex lipids.

Diacids are major components of plant waxes such as cutin. For example, diacids from 14 to 22 carbons long, including a monounsaturated diacid, were found in samples of pine, fig, and oak bark [42]. Diacids from 20 to 28 were found in whole soil methanolysates, which probably originated from plant waxes [43]. While the diacids found in this sample were most similar to plant wax diacids, there is no source of plant waxes in this subsurface environment. Furthermore, plant waxes would not appear in the polar lipid fraction.

These multiply branched and dioic fatty acids are biologically reasonable in terms of known lipid biosynthetic pathways, and are unlikely to be anthropogenic contaminants esterified in the polar lipid fraction. They probably have been unreported from earlier PLFA analyses of environmental samples because they were unexpected, minor components.

These multiply branched fatty acids are similar in degree of methylation to fatty acids from bird preen gland lipids [12, 18], and the dioics are like plant wax lipids in chain-length distribution and the presence of a monounsaturation [42]. Bird preen gland lipids and plant waxes are both protective hydrophobic barriers. Perhaps these unusual membrane lipids are a defense against aqueous toxins, such as sulfide and metals found at this site.

Acknowledgments This research was funded by the Natural and Accelerated Bioremediation Research program, Biological and Environmental Research, U.S. Department of Energy (grants DE-FG02-0ER62985 and DE-FG02-97ER62475).

References

1. Hedrick DB, Peacock A, White DC (2005) Interpretation of fatty acid profiles of soil microorganisms, Chap. 12. In: Margesin R, Schinner F (eds) Manual for soil analysis—monitoring and assessing soil bioremediation. Springer-Verlag, Berlin Heidelberg New York
2. Hedrick DB, Peacock AD, White DC (2007) Lipid analyses for viable microbial biomass, community composition, metabolic status, and in situ metabolism, Chap. 10. In: Hurst CJ, Crawford RL, Garland JL, Lipsom DA, Mills AL, Stetzenbach LD (eds) ASM manual of environmental microbiology, 3rd edn. American Society for Microbiology Press, Washington
3. Anderson RT, Vrionis HA, Ortiz-Bernad I, Resch CT, Long PE, Dayvault R, Karp K, Marutzky S, Metzler DR, Peacock A, White DC, Lowe M, Lovley DR (2003) Stimulating the in situ activity of *Geobacter* species to remove uranium from the groundwater of a uranium-contaminated aquifer. Appl Environ Microbiol 69:5884–5891
4. Vrionis HA, Anderson RT, Ortiz-Bernad I, O'Neill KR, Resch CT, Peacock AD, Dayvault R, White DC, Long PE, Lovley DR (2005) Microbiological and geochemical heterogeneity in an in situ uranium bioremediation field site. Appl Environ Microbiol 71:6308–6318
5. Bligh EG, Dyer WJ (1954) A rapid method of total lipid extraction and purification. Can J Biochem Physiol 37:911–917
6. White DC, Stair JO, Ringelberg DB (1996) Quantitative comparisons of in situ microbial biodiversity by signature biomarker analysis. J Ind Microbiol 17:185–196
7. Guckert JB, Antworth CP, Nichols PD, White DC (1985) Phospholipid, ester-linked fatty acid profiles as reproducible assays for changes in prokaryotic community structure of estuarine sediments. FEMS Microbiol Ecol 31:147–158
8. Kaneda T (1977) Fatty acids of the genus *Bacillus*: an example of branched-chain preference. Bacteriol Rev 41:391–418
9. Wauters G, Charlier J, Janssens M, Delmée M (2000) Identification of *Arthrobacter oxydans, Arthrobacter luteolus* sp. nov., and *Arthrobacter albus* sp. nov., isolated from human clinical specimens. J Clin Microbiol 38:2412–2415
10. Bernard K, Bellefeuille M, Hollis DG, Daneshvar MI, Moss CW (1994) Cellular fatty acid composition and phenotypic and cultural characterization of CDC Fermentative Coryneform groups 3 and 5. J Clin Microbiol 32:1217–1222
11. Kroppenstedt TM (1985) Fatty acid and menaquinones analysis of actinomycetes and related organisms. In: Goodfellow M, Minnikin DE (eds) Chemical methods in bacterial systematics. Academic Press, London
12. Jacob J (1976) Bird waxes, Chap. 4. In: Kolattukudy PE (ed) Chemistry and biochemistry of natural waxes. Elsevier, Amsterdam
13. Ryhage R, Stenhagen E (1959) Mass spectrometric studies IV. Esters of mono-methyl substituted long chain fatty acids. Arkiv Für Kemi 15:291–315
14. Luquin M, Ausina V, López Calahorra F, Belda F, García Barceló M, Celma C, Prats G (1991) Evaluation of practical chromatographic procedures for identification of clinical isolates of Mycobacteria. J Clin Microbiol 29:120–130
15. Springer B, Tortoli E, Richter I, Grűnewald R, Rűsch-Gerdes S, Uschmann K, Suter F, Collins MD, Kroppenstedt RM, Bőttger EC (1995) *Mycobacterium conspicuum* sp. nov., a new species isolated from patients with disseminated infections. J Clin Microbiol 33:2805–2811
16. Raederstorff D, Shu AYL, Thompson JE, Djerassi C (1987) Biosynthetic studies of marine lipids. 11. Synthesis, biosynthesis, and absolute configuration of the internally branched demospongic acid, 22-methyl-5, 9-octacosadienoic acid. J Org Chem 52:2337–2346
17. Pulchan KJ, Helleur R, Abrajano TA (2003) TMAH thermochemolysis characterization of marine sedimentary organic matter in a Newfoundland fjord. Organic Geochem 34:305–317
18. Jacob J (1978) Hydrocarbon and multibranched ester waxes from the uropygial gland secretion of grebes (Podicipediformes). J Lipid Res 19:148–153
19. Hunter SW, Murphy RC, Clay K, Goren MB, Brennan PJ (1983) Trehalose-containing lipooligosaccharides: a new class of species-specific antigens from Mycobacterium. J Biol Chem 258:10481–10487
20. Chatterjee D, Bozic CM, Knisley C, Cho S-N, Brennan PJ (1989) Phenolic Glycolipids of *Mycobacterium bovis*: new structures and synthesis of a corresponding seroreactive neoglycoprotein. Infect Immune 57:322–330
21. Ryhage R, Stenhagen E (1960) Mass spectrometry in lipid research. J Lipid Res 1:361–390

22. Rontani JF, Aubert C (2003) Electron ionization mass spectral fragmentation of C19 isoprenoid aldehydes and carboxylic acid methyl and trimethylsilyl esters. Rapid Commun Mass Spectrom 17:949–956
23. Hansen RP, Morrison JD (1964) The Isolation and Identification of 2, 6, 10, 14-tetramethylpentadecanoic Acid from Butterfat. Biochem J 93:225–228
24. McKenna EJ, Kallio RE (1971) Microbial metabolism of the isoprenoid alkane pristane. Proc Nat Acad Sci USA 68:1552–1554
25. Ackman RG (1968) Prediction of retention times in the GLC of diastereoisomers of methyl-branched fatty acids. J Chromatog 34:165–173
26. Ackman RG (1967) Calculation of ECL values in the gas-liquid chromatography of multiple-branched fatty acids. J Chromotog 23:225–231
27. Ackman RG, Hansen RP (1967) The occurrence of diastereomers of phytanic and pristanic acids and their determination by gas–liquid chromatography. Lipids 2:357–362
28. Awad NE, Selim MA, Saleh MM, Matloub AA (2003) Seasonal variation of the lipoidal matters and hypolipidaemic activity of the red alga *Corallina Officinalis* L. Phytother Res 17:19–25
29. Kates M, Hancock AJ, Ackman RG, Hooper SN (1972) Preparation and characterization of the DDD(RRR)-stereoisomer of 4, 8, 12, 16-tetramethylheptadecanoic and 5, 9, 13, 17-tetramethyloctadecanoic acid. Chem Phys Lipids 8:32–41
30. Harris HM, Applegarth DA, Clarke LA, Wong J (1989) Phytanic acid, pristanic acid, and very-long-chain fatty acid methyl esters measured simultaneously by capillary gas chromatography. Clin Chem 35:703–704
31. Nechev J, Christie WW, Robaina R, de Diego F, Popov S, Stefanov K (2002) Lipid composition of the sponge *Verongia aerophoba* from the Canary Islands. Eur J Lipid Sci Technol 104:800–807
32. So CM, Young LY (1999) Initial reactions in anaerobic alkane degradation by a sulfate reducer, strain AK-01. Appl Environ Microbiol 65:5532–5540
33. Rabus R, Wilkes H, Behrends A, Armstroff A, Fischer T, Pierik AJ, Widdell F (2001) Anaerobic initial reaction of n-alkanes in a denitrifying bacterium: evidence for (1-methylpentyl)succinate as initial product and for involvement of an organic radical in n-hexane metabolism. J Bacteriol 183:1707–1715
34. Carballeira NM, Miranda C, Lozano CM, Nechev JT, Ivanova A, Ilieva M, Tzvetkova I, Stefanov K (2001) Characterization of novel methyl-branched chain fatty acids from a halophilic *Bacillus* species. J Nat Prod 64:256–259
35. Craft DL, Madduri KM, Eshoo M, Wilson CR (2003) Identification and characterization of the CYP52 family of *Candida tropicalis* ATCC 20336, important for the conversion of fatty acids and alkanes to alpha, omega-dicarboxylic acids. Appl Environ Microbiol 69:5983–5991
36. Kester AS, Foster JW (1963) Diterminal oxidation of long-chain alkanes by bacteria. J Bacteriol 85:859–869
37. K Fujii, Fukui S (1970) Hydrocarbon-utilizing microorganism. Relationship of fatty acid composition and biosynthesis to hydrocarbon substrate and to vitamin B_{12} level in *Corynebacterium simplex*. Eur J Biochem 17:552–560
38. Ramakrishnan T, Murthy PS, Gopinathan KP (1972) Intermediary metabolism of Mycobacteria. Bacteriol Rev 36:65–108
39. Rainwater DL, Kolattukudy PE (1985) Fatty acid biosynthesis in *Mycobacterium tuberculosis* var. *bovis Bacillus Calmette-Guerin*. Purification and characterization of a novel fatty acid synthase, mycocerosic acid synthase, which elongates n-fatty acyl-CoA with methylmalonyl-CoA. J Biol Chem 260:616–623
40. Hazlewood GP, Northrop AJ, Dawson RM (1981) Diabolic acids: occurrence and identification in natural products and their metabolism by simple-stomached and ruminant animals. Br J Nutr 45:159–165
41. Dembitsky VM, Srebnik M (2002) Use of serially coupled capillary columns with different polarity of stationary phases for the separation of the natural complex volatile mixture of the marine red alga *Corallina elongata*. Biochemistry (Moscow) 67:1068–1074
42. Matzke K, Riederer M (1991) A comparative study into the chemical constitution of cutins and suberins from *Picea abies* (L.) Karst., *Quercus robur* L., and *Fagus sylvatica* L. Planta 185:233–245
43. Chefetz B, Tarchitzky J, Deshmukh AP, Hatcher PG, Chen Y (2002) Structural characterization of soil organic matter and humic acids in particle-size fractions of an agricultural soil. Soil Sci Soc Am J 66:129–141

Lipids (2008) 43:853–865
DOI 10.1007/s11745-008-3210-5

ORIGINAL ARTICLE

Significance of Coprophagy for the Fatty Acid Profile in Body Tissues of Rabbits Fed Different Diets

**Florian Leiber · Janina S. Meier · Bettina Burger ·
Hans-Rudolf Wettstein · Michael Kreuzer ·
Jean-Michel Hatt · Marcus Clauss**

Received: 15 April 2008 / Accepted: 17 June 2008 / Published online: 15 July 2008
© AOCS 2008

Abstract Four groups of eight New Zealand hybrid rabbits were fattened with ad libitum access to the following pelleted experimental diets: ryegrass meal or alfalfa meal fed either alone or with oats meal in a ratio of 1:1. After 25 weeks they were slaughtered and dissected. Fatty acid (FA) profiles of caecotrophs (re-ingested fermentation products of the caecum), perirenal adipose tissue and intramuscular fat in the *Musculus quadriceps* were determined. With high proportions of branched-chain FA (BFA) and *trans* FA, and increased proportions of saturated FA relative to the diets, the caecotroph FA profile showed a clear fingerprint of anaerobe microbial lipid metabolism including biohydrogenation. By contrast, the FA profiles of adipose and lean tissue comprised high proportions of polyunsaturated FA (PUFA), whilst BFA and *trans* FA occurred in much lower proportions compared to the caecotrophs. Thus, coprophagy did not substantially modify the FA composition of the tissues investigated. Use of forage-only diets, compared to the oats supplemented diets, led to extraordinary high proportions of n-3 PUFA (including 18:3 and long-chain n-3) in the fat of adipose (21.3 vs. 6.7%) and lean tissue (15.4 vs. 5.7%). The forage type diet (grass vs. alfalfa) had smaller effects on the FA profiles. Indications of diet effects on endogenous desaturation, chain elongation and differential distribution of functional FA between the two tissues investigated were found.

Keywords Rabbit · Coprophagy · Caecum · Meat · Microbial lipid metabolism · Branched chain fatty acids · *trans*-Fatty acids · N-3 fatty acids · Forage · Oats

Abbreviations

ALA	α-linolenic acid
BFA	Branched chain fatty acids
CLA	Conjugated linoleic acids
FA	Fatty acids
FAME	Fatty acid methyl ester
MUFA	Monounsaturated fatty acids
PUFA	Polyunsaturated fatty acids
SFA	Saturated fatty acids
TVA	*trans*-Vaccenic acid 11*trans*-18:1

Introduction

The significance of microbial lipid digestion in rabbits and other small herbivores with significant microbial fermentation in the hindgut (caecum) [1], is not yet well known. Information on the effect of the microbial influence on lipids in the digestive tract mostly comes from ruminant animals with their large forestomach [2, 3]. The microbial fermentation of the ingested feed is associated with biohydrogenation and isomerisation of unsaturated FA. This results in the production of considerable amounts of several *trans*-FA, conjugated linolenic acids (CLA) and stearic acid [2, 4]. Another particularity of ruminal digestion is the de novo synthesis of branched-chain FA [3]. Therefore, microbial digestion results in characteristic FA profiles in

F. Leiber (✉) · J. S. Meier · H.-R. Wettstein · M. Kreuzer
Department of Agricultural and Food Science, ETH Zurich,
Universitätstrasse 2, 8092 Zurich, Switzerland
e-mail: fleiber@ethz.ch

B. Burger · J.-M. Hatt · M. Clauss
Clinic for Zoo Animals, Exotic Pets and Wildlife,
Vetsuisse Faculty, University of Zurich,
Winterthurerstrasse 260, 8057 Zurich, Switzerland

the tissues of ruminants, which were subject to extensive research work aimed to improve the nutritional quality of animal products [2, 4–8]. In rabbits, digestive fermentation takes place in the hindgut, namely the caecum. Ingesta undigested so far—predominantly plant cell walls—are fermented and relevant nutrients including B vitamins and protein are anaerobically synthesised by the hindgut microbes [1, 9]. Because nutrient absorption from the hindgut is limited, these animals produce a particular kind of soft feces in the caecum, the caecotrophs, which are re-ingested [9, 10]. In wild living rabbits, the main part of the unabsorbed ingesta is recycled by this way [9].

Lipids produced by bacteria in the caecum should share the typical microbial FA profile as described for the foregut of ruminants. Potentially, such lipids could reach the duodenum and the blood via coprophagial re-ingestion. High amounts of *trans*-FA and branched-chain FA (BFA), as found in the tissues of beavers [11, 12], could be explained by this behavior. However, in-depth research on the FA profile of caecotrophs and an evaluation of its influence on the endogenous FA metabolism of such animals has not yet been performed. This could be useful in comparative physiological research on wild animals in order to develop a marker for coprophagy [10]. It could also elucidate the significance of coprophagy for the endogenous metabolism of the animal and, consequently, for the use of rodents and rabbits, as animal models in lipid metabolism research. These species could, by coprophagy alone, ingest an uncontrolled amount of these FA in experimental studies, which may cause particular metabolic responses [13], thus partially questioning their use to simulate potential effects of *trans* FA and BFA in humans. Finally, coprophagy could influence the nutritional value of rabbit meat if the ingested hindgut microbe-derived FA result in a substantial modification of the tissue lipids. This context has not yet been investigated.

Another important question is how the diets fed to rabbits interact with the microbial metabolism in the caecum resulting in a specific pattern of FA supply. In comparison, n-3 PUFA and 9*c*,11*t*-18:2 CLA in meat and milk from ruminants increase when animals are fed diets containing high proportions of forage and only low proportions of cereal or legume grain crops [6–8], i.e. diets which are relatively close to the natural feeding behavior of these species. A similar situation might be found in rabbits which are grazing animals as well [14]. Accordingly, in the tissues of wild rabbits, concentrations of ALA and long-chain n-3 PUFA were found [15] to be clearly higher than those reported from rabbits fattened on farm [16]. Rabbits in agricultural production systems are commonly fed diets which largely differ from that of wild rabbits because they contain high cereal proportions [17–19]. The question remains whether the nutritional quality of the rabbit meat lipids could be increased with high-forage diets which are closer to the natural diets, and to which extent an interaction with coprophagy is relevant. Although a number of publications on the fat quality of rabbit meat exist [15–17, 19–23], no reports on controlled studies of the effects of high-forage diets are available. Diet type, especially the proportion of concentrate, was shown to influence the amount of caecotroph formation [18, 24] and, thus, indirectly the ingestion of microbially modified FA. Finally, the forage type might be important in this respect. From ruminant research, there are indications that legumes such as alfalfa, although having lower ALA proportions in the lipids than ryegrass [25], could inhibit microbial biohydrogenation [2, 5] and thus could increase supply with ALA. In case caecotrophy substantially influences FA intake, such an effect could be important in rabbits, too.

The hypotheses to be tested by an experiment with growing rabbits included: (1) that the profile of long-chain FA in rabbit's caecotrophs closely resembles the FA profile of ruminant digesta, (2) that traces or larger amounts of those FA which are typical for microbial fermentation can be recovered in the body tissue of rabbits, (3) that high-forage diets have a direct (more ALA) or caecotrophy-mediated (more 9*c*,11*t*-18:2 CLA and TVA) influence on tissue FA composition, and (4) that a leguminous forage type has a significant influence in this respect.

Experimental Procedure

Four groups of eight New Zealand hybrid type rabbits were fattened on different diets for 25 weeks. The four diets were pelleted, consisting either of pure ryegrass meal (G), pure alfalfa meal (A), grass meal and oats meal 1:1 (GO) or alfalfa meal and oats meal 1:1 (AO). The composition of the main dietary nutrients as analyzed according to Naumann and Bassler [26] is given in Table 1, and their FA profile in Table 2. The rabbits originated from one breeding facility for meat rabbits. At the beginning of treatment feeding, they were between 5 and 6 weeks old with a body mass between 1,124 and 1,930 g. Groups proportionately consisted of female and castrated male animals, and allocation to treatment was balanced with respect to the average of and variation in initial body mass. Animals of each group were kept together on woodchips in enclosures of 5.4 m^2, fitted with a sleeping box of 0.59 m^2. Feed and water was provided with ad libitum access. Daily intake was recorded as the average per group. Feed consumption of the groups was monitored daily by weighing the feed refusals before filling the troughs for the next day. No measures were taken to prevent coprophagy in the animals. The animals were also weighed before slaughter.

Table 1 Nutrient composition of the experimental diets as well as food intake and body masses development in the experimental groups (means)

Diets[a]	G	A	GO	AO
Dry matter (DM; g/100 g as fed)	89.5	90.4	90.8	89.4
Nutrients (g/100 g DM)				
Organic matter	85.3	85.5	90.8	91.8
Crude protein	18.1	16.4	13.5	14.6
Ether extract	4.0	1.9	5.1	3.5
Neutral detergent fibre	45.8	46.3	33.3	38.2
Food intake (g as fed/animal/day)[b]	274 ± 60[c]	283 ± 58	210 ± 54	211 ± 46
Initial body mass (g)	1,493 ± 209[d]	1,525 ± 209	1,474 ± 233	1,482 ± 199
Body mass at slaughter (g)	4,776 ± 364[d]	4,637 ± 315	5,286 ± 425	5,206 ± 375
Dressed carcass mass (g)[e]	2,320 ± 258[d]	2,259 ± 165	2,517 ± 182	2,495 ± 131

[a] *G* grass only; *A* alfalfa only; *GO* grass and oats 1:1; *AO* alfalfa and oats 1:1

[b] Average over the complete feeding period; data obtained as total intake per group

[c] SD based on between day variation

[d] SD based on between animal variation

[e] Body mass minus feet, head, skin, internal organs, and discrete adipose tissue

Immediately after slaughter, the animals were dissected, and samples of abdominal (perirenal) fat and of the central quadriceps muscle of the left hind leg were taken. Additionally, the gastrointestinal tract was dissected, opened, and controlled for the presence of caecotrophs. In the colon, caecotrophs can be differentiated from hard faeces based on their smaller size, and softer and moister consistency [1]. Due to a tough mucoprotein membrane, which resists digestion in the stomach for several hours [9], re-ingested caecotrophs can be identified from shape, form and consistency. Therefore, we assumed that caecotrophs in the stomach that still were not disintegrated were equal in composition to caecotrophs from the caecum and colon. No caecotrophs were collected from the small intestine. Samples of adipose and muscle tissue and caecotrophs were immediately sealed in plastic bags and stored at −20°C until analysis.

Lipid Extraction from the Samples

Lipids from feeds and caecotrophs were extracted by accelerated solvent extraction (ASE 200; Dionex Corp., Sunnyvale CA) using hexane/isopropanol (2:1 vol/vol) and transformed into FA methyl esters (FAME) according to Wettstein et al. [27]. The FAME were dissolved in hexane and purified on a silica gel column.

Lipid extraction from lean and adipose tissue was performed after homogenisation of the samples. Lipids from *M. quadriceps* were extracted by dissolving 1 g of homogenisate in 5 ml hexane-isopropanol (3:2). The lipids from adipose tissue were extracted from 0.2 g homogenisate with 12 ml hexane. Both solvents contained triundecanin and phosphatidylcholin (Fluka Chemie, Buchs, Switzerland) as internal standards. Subsequently, the fatty acids in the extracts were converted to methyl esters according to the official IUPAC method [28] with slight modifications (2 ml 0.5 M methanolic NaOH boiled for 3 min in a reaction tube, 3 ml 1.3 M boron trifluoride boiled for 4 min). A cleaning step was carried out to prevent artifacts caused by cholesterol when analyzing the *trans*-FA isomers. The FAME were sprayed onto a thin layer chromatography glass plate coated with silica gel 60 F_{254} (Merck KGaA, Darmstadt, Germany). Subsequently, the plates were run in a chamber saturated with a solution of hexane, diethylether and acetic acid in a ratio of 85:15:0.2 for 30 min until the solvent had reached the upper border of the plate. The FAME were identified and marked in UV light (440 nm) after having sprayed the plate with a fluorescent dye (2′,7′-Dichlorofluorescein, Fluka, Sigma-Aldrich Chemie GmbH, Buchs, Switzerland). The identified zone was scratched off, dissolved with a 1:1 mixture of chloroform and hexane and filtered through a silica gel column.

Fatty Acid Analysis

All samples were analyzed for individual FAME on a gas chromatograph (HP 6890, Agilent Technologies Inc., Wilmington, DE) equipped with an FID detector and a Supelcowax^{TM} 10 capillary column (30 m × 0.32 mm, 0.25 μm film thickness; Supelco, Bellefonte, PA). An amount of 1 μl was injected by split injection (1:30, split temperature 260°C). Hydrogen was used as a carrier gas at a flow rate of 2.2 ml/min and a pressure of 55.8 kPa. The initial oven temperature was 160°C for 0.5 min. The temperature program was as follows; increase of 20°C/min up

Table 2 Total amount and individual proportions of FAME (g/100 g FAME) in the experimental diets (means of duplicate analyses; deviation always below 0.05)

Diets[a]	G	A	GO	AO
FAME, g/100 g diet	3.34	1.55	4.35	3.20
Total SFA	19.3	27.0	21.4	24.8
12:0	0.18	0.27	0.07	0.11
14:0	0.45	0.82	0.44	0.71
15:0	0.11	0.20	0.07	0.18
16:0	13.7	18.2	16.7	18.7
17:0	0.14	0.34	0.13	0.19
18:0	2.78	3.58	2.87	3.67
20:0	0.49	0.86	0.37	0.39
22:0	0.73	1.06	0.33	0.36
24:0	0.63	1.41	0.38	0.47
Total MUFA	19.8	8.3	34.2	29.2
16:1n-7	0.44	0.65	0.33	0.61
17:1	0.13	0.19	0.09	0.10
9*c*-18:1	17.4	6.5	32.2	26.7
*t*18:1[b]	1.41	0.72	0.96	1.12
20:1n-9	0.39	0.23	0.63	0.65
Total PUFA	58.9	61.9	43.0	44.6
18:2n-6	25.5	21.8	29.4	31.9
18:3n-3	32.9	39.2	13.3	12.0
20:2n-6	0.11	0.33	0.07	0.14
20:3n-3	0.05	0.10	0.03	0.03
20:5n-3	0.16	0.26	0.13	0.31
22:6n-3	0.22	0.16	0.09	0.18
Total n-6 FA	25.6	22.1	29.4	32.0
Total n-3 FA	33.3	39.7	13.6	12.6
n-6/n-3 ratio	0.77	0.56	2.17	2.55

FAME fatty acid methyl esters; *SFA* saturated fatty acids; *MUFA* monounsaturated fatty acids; *PUFA* polyunsaturated fatty acids

[a] *G* grass only, *A* alfalfa only; *GO* grass and oats; *AO* alfalfa and oats

[b] Not fully separated peaks of *t*10- and *t*11- 18:1

to 190°C; increase of 7°C/min up to 230°C; isotherm at 230°C for 5.3 min; increase of 20°C/min up to 250°C; isotherm for 6 min. The detector temperature was 270°C. For a clearer separation of *trans* and *cis*18:1 isomers, extracts from caecotrophs, adipose and lean tissue were further analyzed on a 200 m × 0.25 mm size CP7421 capillary column (Varian Inc., CA, USA). An amount of 1 μl was split injected (1:50; split temperature 270°C). Again hydrogen was used as a carrier gas, and gas flow was 1.7 ml/min for 59 min and, subsequently, 1.3 ml/min for 42 min. The initial temperature was 181°C for 60 min. Subsequently the temperature was increased by 5°C/min up to 230°C; isotherm for 32 min, then increase by 5°C/min up to 250°C, then kept isothermic for 12 min. The detector temperature was 300°C.

Statistical Evaluation

Linear multivariate ANOVA was carried out with the SPSS© 14.0 software. Fixed factors were oats supplementation (− vs. + oats) and forage type (ryegrass vs. alfalfa), and the model included the interaction of both factors.

Results

Alfalfa contained less lipids than the ryegrass. The SFA were higher and MUFA were lower in alfalfa compared to ryegrass. The PUFA proportions were similar in both forages. (Tables 1, 2). By contrast, the addition of oats increased the ether extract content of the diets and massively shifted the FA profile from ALA to monounsaturated FA. BFA occurred for all diets only at the detection threshold in feed and are therefore not given in Table 2. *trans*18:1 FA occurred at a low level. Due to the higher energy density (less fibre) in the oats supplemented diets, voluntary food intake was lower while gains and dressing percentage (48.2% on average) remained similar. Differences found in body mass at slaughter between the groups were mostly due to variations of discrete adipose tissue. Caecotrophs were found with similar frequency in all groups (in 4, 4, 4 and 3 animals of groups G, A, GO and AO, respectively).

Fatty Acid Profile of the Caecotrophs and Effects of Diet

In the caecotrophs, the saturated FA (SFA) represented the most abundant group of FA, followed by monounsaturated FA (MUFA) and PUFA (Table 3). The proportion of the branched-chain saturated FA (BFA) was also rather high, ranging from 7 to 13 g/100 g FAME on average. The FA 15:0a (anteiso) and 16:0i (iso) contributed clearly more than half of all BFA. Oats supplementation had significant effects on proportions of various FA in the caecotrophs. With diets GO and AO, total SFA were significantly higher compared to diets G and A, due to higher proportions of 18:0, while BFA, *trans*18:1 FA and n-3 PUFA were lower. Overall total MUFA, PUFA and n-6 PUFA were not affected ($P > 0.05$) by dietary oats. Among the two most abundant 18:1 FA, 9*c*-18:1 was higher, while *trans*-vaccenic acid (11*t*-18:1; TVA) was lower ($P < 0.05$) when feeding oats. With diets GO and AO, the proportion of 9*c*,11*t*-CLA in the caecotroph FAME was reduced to below 0.1 g/100 g. The largest proportionate reduction with oats was found in 18:3n-3 leading to a significant increase of the n-6/n-3 ratio from about one to 2–4. The use of alfalfa instead of grass meal led to significantly lower proportions of 18:0 both in diets with and without oats. Most of the

Table 3 Concentration of total FAME (g/100 g wet weight) and fatty acid profile (g/100 g total FAME) in the caecotrophs of rabbits fed different diets ($n = 4$ for groups G, A, GO; $n = 3$ for group AO)

	Diets[a]					*P* levels[b]		
	G	A	GO	AO	SEM[c]	O	F	O × F
Total FAME	1.03	0.39	1.05	0.83	0.172	ns	<0.05	ns
Total SFA	49.8	54.8	63.9	53.1	2.01	<0.05	ns	<0.01
12:0	0.523	0.892	0.573	0.717	0.0549	ns	<0.01	ns
13:0	0.180	0.406	0.215	0.235	0.0433	ns	<0.05	<0.05
14:0	2.21	3.81	1.92	2.87	0.224	<0.05	<0.001	ns
15:0	4.35	5.37	2.84	3.08	0.377	<0.001	ns	ns
16:0	18.5	22.2	21.2	22.7	1.554	ns	ns	ns
17:0	1.010	2.308	0.962	1.073	0.1345	<0.01	<0.001	<0.01
18:0	19.0	12.1	33.1	18.8	2.059	<0.001	<0.001	ns
19:0	0.177	0.343	0.084	0.117	0.0431	<0.01	<0.05	ns
20:0	0.998	2.188	0.994	1.108	0.1160	<0.01	<0.001	<0.01
22:0	1.53	2.66	1.05	1.18	0.131	<0.001	<0.01	<0.01
23:0	0.333	0.986	0.277	0.344	0.0624	<0.001	<0.001	<0.01
24:0	1.55	2.89	1.20	1.45	0.135	<0.001	<0.001	<0.01
Total BFA	9.18	13.06	6.64	9.48	0.757	<0.01	<0.01	ns
14:0i	1.31	1.85	1.05	1.28	0.158	<0.05	<0.05	ns
15:0i	1.137	1.824	0.863	1.302	0.1370	<0.05	<0.01	ns
15:0a	2.61	4.21	1.87	3.15	0.380	<0.05	<0.01	ns
16:0i	3.06	3.65	2.20	2.89	0.285	<0.05	ns	ns
17:0i	0.650	0.813	0.269	0.360	0.0466	<0.001	<0.05	ns
17:0a	0.417	0.710	0.385	0.485	0.0682	ns	<0.05	ns
Total MUFA	21.0	16.8	18.6	22.3	1.11	ns	ns	<0.01
15:1	0.896	1.871	0.496	0.948	0.1686	<0.01	<0.01	ns
16:1n-7	0.512	0.678	0.253	0.353	0.0902	<0.05	ns	ns
17:1	0.430	0.632	0.367	0.407	0.0840	ns	ns	ns
5*t* -18:1	0.057	0.138	0.026	0.049	0.0063	<0.001	<0.001	<0.01
6*t*/8*t*-18:1[d]	0.191	0.130	0.135	0.151	0.0208	ns	ns	ns
9*t*-18:1	0.197	0.270	0.164	0.187	0.0123	<0.01	<0.01	ns
10*t*-18:1	0.157	0.137	0.129	0.121	0.0132	ns	ns	ns
11*t*-18:1	7.39	5.48	3.61	4.19	0.775	<0.05	ns	ns
12*t*-18:1	0.312	0.283	0.260	0.279	0.0200	ns	ns	ns
13*t*/14*t*-18:1[e]	0.483	0.388	0.419	0.429	0.0233	ns	ns	ns
16*t*-18:1	0.234	0.249	0.136	0.167	0.0191	<0.01	ns	ns
9*c*/15*t*-18:1[e]	7.15	4.63	10.06	11.77	0.940	<0.01	ns	ns
11*c*-18:1	1.544	0.842	0.812	0.985	0.1299	ns	ns	<0.05
12*c*-18:1	0.639	0.350	0.886	1.362	0.0778	<0.001	ns	<0.01
13*c*-18:1	0.073	0.172	0.067	0.073	0.0248	ns	ns	ns
14*c*-18:1	0.264	0.245	0.307	0.227	0.0313	ns	ns	ns
15*c*-18:1	0.113	0.156	0.032	0.064	0.0140	<0.001	<0.05	ns
20:1n-9	0.246	0.155	0.321	0.482	0.0586	<0.01	ns	ns
22:1	0.063	0.004	0.067	0.029	0.0221	ns	ns	ns
24:1	0.030	0.000	0.043	0.011	0.0192	ns	ns	ns
Total PUFA	15.6	10.2	8.8	12.2	1.38	ns	ns	<0.05
18:2n-6	7.24	5.75	6.09	9.53	0.840	ns	ns	<0.05
9*c*11*t*-18:2	0.115	0.183	0.059	0.088	0.0302	<0.05	ns	ns
18:3n-6	0.050	0.051	0.170	0.067	0.0445	ns	ns	ns

Table 3 continued

	Diets[a]					*P* levels[b]		
	G	A	GO	AO	SEM[c]	O	F	O × F
18:3n-3	7.33	4.78	2.15	2.12	0.715	<0.001	<0.05	<0.05
20:3n-6	0.000	0.000	0.012	0.000	0.0061	ns	ns	ns
20:3n-3	0.036	0.014	0.012	0.010	0.0091	ns	ns	ns
20:4n-3	0.078	0.090	0.183	0.319	0.1836	ns	ns	ns
20:5n-3	0.040	0.021	0.022	0.015	0.0142	ns	ns	ns
22:6n-3	0.076	0.000	0.092	0.021	0.0460	ns	ns	ns
Total n-3	7.67	4.89	2.46	2.49	0.715	<0.001	ns	ns
Total n-6	7.29	5.80	6.27	9.60	0.680	ns	ns	<0.05
n-6/n-3	0.95	1.18	2.55	3.86	0.203	<0.001	<0.001	0.0300

FAME fatty acid methyl esters; *SEM* standard error of means; *SFA* saturated fatty acids; *BFA* branched-chain fatty acids; *MUFA* monounsaturated fatty acids; *PUFA* polyunsaturated fatty acids

[a] *G* grass only; *A* Alfalfa only; *GO* grass and oats 1:1; *AO* alfalfa and oats 1.1

[b] *O* oats effect (with vs. without); *F* forage type effect (grass vs. alfalfa)

[c] Average SEM within groups

[d] These fatty acids are co-eluting

[e] Sum of two peaks containing unidentified 18:2 isomers

BFA and some minor SFA were significantly higher with the pure alfalfa diet, but this was reversed for the SFA in the presence of the oats (O × F interaction, $P < 0.01$). Interactions among the two dietary factors were also found for total MUFA and PUFA with the result that no clear overall forage type effect remained. Alfalfa resulted in a lower 18:3n-3 proportion than the grass ($P < 0.05$), but only in the non supplemented diets.

Fatty Acid Profile of the Body Tissues and Effects of Diet

In the perirenal adipose tissue, total SFA, MUFA and PUFA occurred at relatively similar levels. BFA, TVA and CLA, indicative for microbial lipid sources, occurred at very low proportions (Table 4). Most of the FA were significantly influenced by oats supplementation. For the SFA, this effect was marginal, while MUFA were clearly elevated by oats. This resulted mainly from higher values of the 9*c*-18:1/15*t*-18:1 peak ($P < 0.001$); but also 16:1n-7 was considerably higher ($P < 0.01$) with the oats diets. Total PUFA declined with diets GO and AO compared to G and A, exclusively resulting from a highly significant drop in n-3 PUFA. Thus, the average n-6/n-3 ratio increased from 0.7 with G and O to 2.7 with GO and AO ($P < 0.001$). The proportions of total and individual BFA were lower by about half with oats diets ($P < 0.001$). Total SFA significantly increased and total MUFA and PUFA significantly declined with the alfalfa compared to the grass diet, but this effect occurred mainly in the diets without oats. Total and some individual BFA were significantly higher in proportion with alfalfa instead of the grass, while 18:3n-3 was lower ($P < 0.01$). Alfalfa significantly increased long chain n-3 PUFA; this, however, at a low level.

The FA profile of the intramuscular fat and its variation with diet were relatively similar in nature to those found in the adipose tissue (Table 5). However, particularly for individual PUFA, the effects of oats addition were not as distinct, and significant effects of alfalfa were absent. Intramuscular lipids proportion of 18:3n-3 was considerably lower, and the long-chain PUFA (>3 double bonds) occurred with five- to ten-fold higher proportions than in the FAME of the adipose tissue. Particularly arachidonic acid (20:4n-6) and docosapentaenoic acid (22:5n-3) made up a considerable proportion of total PUFA in intramuscular fat, which was not the case in perirenal adipose tissue.

Differences in Fatty Acid Profiles of Food, Caecotrophs and Body Tissues

In contrast to the body tissue lipids, caecotroph lipids contained comparably high proportions of BFA and *trans*-18:1 FA. These FA occurred only in traces or low amounts in feeds and body tissues. Although the diet effects on BFA were similar in direction in the caecotrophs and in the body tissues, the relative proportions between the individual BFA in caecotrophs differed. The relative proportions of 17:0i and 17:0a within BFA were clearly higher in the body tissues than in the caecotrophs. A second property,

Table 4 Concentration of FAME (g/100 g wet weight) and fatty acid profile (g/100 g total FAME) in the perirenal adipose tissue of rabbits fed different diets ($n = 8$ per group)

	Diets[a]					*P* levels[b]		
	G	A	GO	AO	SEM[c]	O	F	O × F
Total SFA	34.0	41.6	36.2	37.1	0.59	ns	<0.001	<0.001
10:0	0.019	0.023	0.015	0.016	0.0020	<0.01	ns	ns
12:0	0.066	0.075	0.053	0.057	0.0032	<0.001	ns	ns
14:0	2.11	2.79	2.42	2.72	0.086	ns	<0.001	<0.05
15:0	0.555	0.990	0.397	0.502	0.0248	<0.001	<0.001	<0.001
16:0	23.5	28.5	25.8	26.6	0.49	ns	<0.001	<0.001
17:0	0.670	1.097	0.493	0.591	0.0154	<0.001	<0.001	<0.001
18:0	6.60	7.62	6.73	6.33	0.288	ns	ns	<0.05
19:0	0.205	0.247	0.140	0.150	0.0055	<0.001	<0.001	<0.01
20:0	0.183	0.185	0.134	0.111	0.0035	<0.001	<0.01	<0.01
22:0	0.022	0.028	0.008	0.008	0.0012	<0.001	<0.01	<0.01
24:0	0.048	0.049	0.027	0.022	0.0023	<0.001	ns	<0.05
Total BFA	0.713	0.957	0.499	0.524	0.0219	<0.001	<0.001	<0.001
14:0i	0.051	0.065	0.036	0.032	0.0028	<0.001	ns	<0.01
15:0i	0.097	0.136	0.072	0.062	0.0130	<0.01	ns	ns
15:0a	0.117	0.168	0.065	0.080	0.0048	<0.001	<0.001	<0.01
16:0i	0.207	0.303	0.150	0.157	0.0103	<0.001	<0.001	<0.001
17:0i	0.064	0.067	0.043	0.043	0.0017	<0.001	ns	ns
17:0a	0.170	0.208	0.127	0.143	0.0044	<0.001	<0.001	<0.05
Total MUFA	26.21	23.52	37.91	37.27	0.66	<0.001	<0.05	ns
15:1	0.136	0.419	0.066	0.119	0.0090	<0.001	<0.001	<0.001
16:1n-7	4.02	4.55	5.29	5.73	0.418	<0.01	ns	ns
17:1	0.416	0.576	0.310	0.386	0.0080	<0.001	<0.001	<0.001
5*t* -18:1	0.000	0.009	0.000	0.000	0.0033	ns	ns	ns
6*t*/8*t*-18:1[d]	0.033	0.037	0.023	0.020	0.0033	<0.001	ns	ns
9*t*-18:1	0.062	0.047	0.059	0.059	0.0044	ns	ns	ns
10*t*-18:1	0.046	0.023	0.017	0.018	0.0046	<0.01	<0.05	<0.05
11*t*-18:1	0.183	0.134	0.131	0.109	0.0092	<0.001	<0.001	ns
12*t*-18:1	0.025	0.021	0.021	0.024	0.0042	ns	ns	ns
13*t*/14*t*-18:1[e]	0.068	0.065	0.035	0.053	0.0041	<0.001	ns	<0.05
16*t*-18:1	0.028	0.032	0.022	0.022	0.0014	<0.001	ns	ns
9*c*/15*t*-18:1[e]	19.1	15.9	29.5	28.4	0.38	<0.001	<0.001	<0.05
11*c*-18:1	0.99	0.72	1.05	1.22	0.038	<0.001	ns	<0.001
12*c*-18:1	0.095	0.093	0.089	0.084	0.0052	ns	ns	ns
13*c*-18:1	0.074	0.068	0.067	0.086	0.0051	ns	ns	<0.05
14*c*-18:1	0.015	0.019	0.014	0.016	0.0009	ns	<0.01	ns
15*c*-18:1	0.008	0.008	0.004	0.004	0.0008	<0.001	ns	ns
19:1	nd	nd	nd	nd				
20:1n-9	0.212	0.145	0.360	0.351	0.0053	<0.001	<0.001	<0.001
22:1	0.012	0.008	0.022	0.017	0.0011	<0.001	<0.001	ns
Total PUFA	38.48	33.51	24.89	24.47	0.77	<0.001	<0.01	<0.01
18:2n-6	15.8	12.6	17.5	17.8	0.42	<0.001	<0.01	<0.001
9*c*11*t*-18:2	0.072	0.060	0.056	0.066	0.0036	ns	ns	<0.01
18:2[c]	0.080	0.071	0.045	0.048	0.0021	<0.001	ns	<0.01
18:3n-3	21.64	19.50	6.94	5.87	0.500	<0.001	<0.01	ns
20:3n-6	0.033	0.035	0.040	0.041	0.0015	<0.001	ns	ns

Table 4 continued

	Diets[a]					*P* levels[b]		
	G	A	GO	AO	SEM[c]	O	F	O × F
20:3n-3	0.230	0.245	0.088	0.088	0.0090	<0.001	ns	ns
20:4n-6	0.107	0.104	0.113	0.120	0.0035	<0.01	ns	ns
20:4n-3	0.043	0.037	0.022	0.020	0.0014	<0.001	<0.01	ns
20:5n-3	0.086	0.106	0.037	0.055	0.0035	<0.001	<0.001	ns
22:4n-6	0.022	0.027	0.016	0.011	0.0008	<0.001	ns	<0.001
22:5n-3	0.202	0.238	0.094	0.112	0.0114	<0.001	<0.05	ns
22:6n-3	0.070	0.072	0.017	0.051	0.0042	<0.001	<0.001	<0.001
Total n-3	22.13	20.44	7.19	6.20	0.457	<0.001	<0.01	ns
Total n-6	16.15	12.92	17.57	18.14	0.403	<0.001	<0.01	<0.001
n-6/n-3	0.73	0.63	2.45	2.93	0.036	<0.001	<0.001	<0.001

For footnotes see Table 3

characterising the caecotrophs vs. the tissue lipids, was the high proportion of SFA (including most individual SFA). The proportion of SFA in total FAME was clearly above 50 g/100 g for caecotrophs and below 40 g/100 g for the perirenal adipose and intramuscular fat. Complementary, PUFA were distinctly higher in the investigated tissues than in the caecotrophs.

Discussion

Characteristics of the Caecotroph Fatty Acid Profile, and Effects of Diet Type

In general, comparing the FA profiles of the caecotroph lipids with those of the corresponding feeds indicated an active anaerobe microbial lipid metabolism. A first crude indicator was the ratio of SFA, in particular 18:0, to PUFA, being higher in caecotrophs than in the diets. As described for the forestomach of ruminant animals [2], 18:0 is the terminal product of microbial biohydrogenation of dietary 18:3 and 18:2. A second indicator was the high concentration of *trans* FA, mainly 11*trans*18:1, found in the caecotrophs. These FA are also the result of microbial lipid metabolism in the digestive tract [2, 29]. Finally, the substantial proportions of BFA and odd-chain FA found in the caecotroph lipids support the same conclusion [3].

High proportions of forages in the diet are known to increase BFA formation in ruminant digestion [3]. In the caecotrophs, the same effect was indicated by the elevated proportions of BFA and odd-chain FA found in the rabbits receiving the forage-only diets (G and A). Alfalfa diets obviously did not have the inhibitory effect on ALA biohydrogenation anticipated from replacing grass by legumes [2, 5]. By contrast, when feeding the pure alfalfa diet the reduction of the ALA proportion was even more pronounced than with the ryegrass diet, suggesting increased biohydrogenation and isomerisation. Higher BFA proportions with the alfalfa diets suggest increased microbial activity, too, contrasting to what is known from ruminants [5, 30].

However, an increased biohydrogenation should not only reduce ALA or linoleic acid proportions, but also increase CLA, octadecanoic MUFA and 18:0 [2]. In this respect, the results on the caecotroph FA profiles were apparently inconsistent because neither 18:1 nor 18:0 were higher with diet A compared to G. A confounding between discriminating absorption in the duodenum and biohydrogenation in the caecum cannot be excluded. The interactions of the two dietary factors give no clear picture for SFA, MUFA and PUFA in the caecotrophs, either. Significant interactions of the sums of FA groups have no corresponding counterpart in interactions in all single FA. They appear rather to be artifacts. Thus, the clearest information about diet effects on microbial activity in the caecum apparently may be obtained from BFA which are synthesised de novo. This is reflected by the fact that the diet effects on all FA of this group were almost parallel.

Signature of the Caecotroph FA Profile as Found in the Body Tissues

FA profiles typical for microbial fermentation are found in both ruminating and non-ruminating foregut-fermenting herbivores, e.g. kangaroos [2, 31–33]. By contrast, monogastric herbivores have no forestomach with microbial fermentation; instead, microbial digestion occurs in the caecum and the colon of such species. In most aspects, the bacterial fermentation in the hindgut is comparable to that in the rumen [34] and similar effects of microbial lipid metabolism were demonstrated in the hindgut and the faeces, as e.g. by Hartman et al. [31] for horse faeces.

Table 5 Concentration of FAME (g/100 g wet weight) and fatty acid profile (g/100 g total FAME) in the intramuscular fat of the *M. quadriceps* of rabbits fed different diets ($n = 8$ per group)

	Diets[a]					*P* levels[b]		
	G	A	GO	AO	SEM[c]	O	F	O × F
Total FAME	2.15	2.93	3.15	2.56	0.302	ns	ns	<0.05
Total SFA	35.2	39.2	35.7	36.2	0.52	<0.05	<0.001	<0.01
10:0	0.032	0.036	0.029	0.028	0.0038	ns	ns	ns
12:0	0.059	0.067	0.060	0.058	0.0037	ns	ns	ns
14:0	2.02	2.47	2.51	2.52	0.111	<0.05	<0.05	ns
15:0	0.427	0.700	0.317	0.371	0.0217	<0.001	<0.001	<0.001
16:0	23.3	25.9	24.9	25.0	0.453	ns	<0.01	<0.01
17:0	0.598	0.898	0.389	0.462	0.0217	<0.001	<0.001	<0.001
18:0	8.36	8.52	7.04	7.26	0.295	<0.001	ns	ns
19:0	0.282	0.307	0.233	0.256	0.0120	<0.001	ns	ns
20:0	0.116	0.132	0.089	0.083	0.0064	<0.001	ns	ns
22:0	0.051	0.104	0.064	0.083	0.0135	ns	<0.05	ns
24:0	0.023	0.027	0.021	0.015	0.0040	ns	ns	ns
Total BFA	0.477	0.622	0.351	0.362	0.0217	<0.001	<0.01	<0.01
14:0i	0.033	0.042	0.027	0.022	0.0028	<0.001	ns	<0.05
15:0i	0.056	0.069	0.040	0.041	0.0026	<0.001	<0.05	<0.05
15:0a	0.072	0.102	0.045	0.051	0.0040	<0.001	<0.001	<0.01
16:0i	0.147	0.205	0.107	0.109	0.0089	<0.001	<0.01	<0.01
17:0i	0.048	0.053	0.037	0.040	0.0021	<0.001	ns	ns
17:0a	0.122	0.152	0.095	0.099	0.0051	<0.001	<0.01	<0.05
Total MUFA	28.5	26.8	37.0	35.8	1.23	<0.001	ns	ns
15:1	0.088	0.259	0.050	0.079	0.0082	<0.001	<0.001	<0.001
16:1n-7	5.28	5.58	7.49	7.42	0.568	<0.01	ns	ns
17:1	0.405	0.557	0.330	0.374	0.0161	<0.001	<0.001	<0.01
5*t* -18:1	0.036	0.042	0.053	0.051	0.0100	ns	ns	ns
6*t*/8*t*-18:1[d]	0.006	0.018	0.005	0.011	0.0037	ns	<0.05	ns
9*t*-18:1	0.063	0.039	0.039	0.037	0.0106	ns	ns	ns
10*t*-18:1	0.056	0.057	0.044	0.064	0.0137	ns	ns	ns
11*t*-18:1	0.121	0.107	0.090	0.062	0.0134	<0.05	ns	ns
12*t*-18:1	0.047	0.022	0.017	0.027	0.0068	ns	ns	<0.05
13*t*/14*t*-18:1[e]	0.036	0.061	0.034	0.030	0.0040	<0.001	<0.05	<0.01
16*t*-18:1	0.110	0.165	0.191	0.181	0.0226	<0.05	ns	ns
9*c*/15*t*-18:1[e]	20.3	18.3	26.4	24.6	0.741	<0.001	<0.05	ns
11*c*-18:1	1.23	0.95	1.39	1.58	0.058	<0.001	ns	<0.001
12*c*-18:1	0.066	0.062	0.062	0.054	0.0038	ns	ns	ns
13*c*-18:1	0.046	0.068	0.082	0.089	0.0099	<0.01	ns	ns
14*c*-18:1	0.042	0.018	0.011	0.009	0.0060	<0.01	<0.05	ns
15*c*-18:1	0.008	0.009	0.003	0.008	0.0018	ns	ns	ns
19:1	0.112	0.091	0.068	0.063	0.0033	<0.001	<0.001	<0.05
20:1n-9	0.141	0.099	0.242	0.221	0.0112	<0.001	<0.05	ns
22:1	0.017	0.020	0.022	0.018	0.0040	ns	ns	ns
Total PUFA	34.8	32.4	25.8	26.4	1.08	<0.001	ns	ns
18:2n-6	14.9	12.8	15.2	15.7	0.46	<0.01	ns	<0.05
9*c*11*t*-18:2	0.078	0.065	0.071	0.072	0.0038	ns	ns	ns
18:2[c]	0.071	0.067	0.047	0.063	0.0111	ns	ns	ns
18:3n-3	11.48	12.37	4.41	3.40	0.456	<0.001	ns	<0.05

Table 5 continued

	Diets[a]					*P* levels[b]		
	G	A	GO	AO	SEM[c]	O	F	O × F
20:3n-6	0.368	0.321	0.293	0.361	0.0351	ns	ns	ns
20:3n-3	0.185	0.216	0.079	0.076	0.0066	<0.001	ns	<0.05
20:4n-6	3.60	2.78	3.14	4.10	0.437	ns	ns	ns
20:4n-3	0.056	0.061	0.032	0.030	0.0047	<0.001	ns	ns
20:5n-3	0.596	0.604	0.156	0.205	0.0382	<0.001	ns	ns
22:4n-6	0.186	0.167	0.381	0.532	0.0365	<0.001	ns	<0.05
22:5n-3	2.10	1.83	1.16	1.30	0.170	<0.001	ns	ns
22:6n-3	0.694	0.539	0.242	0.464	0.0493	<0.001	ns	<0.001
Total n-3	15.11	15.62	6.07	5.39	0.379	<0.001	ns	ns
Total n-6	19.2	16.3	19.2	20.5	0.87	<0.05	ns	<0.05
n-6/n-3	1.28	1.04	3.16	3.79	0.098	<0.001	ns	<0.001

For footnotes see Table 3

However, as these processes in monogastric animals occur after the digesta has passed the duodenum, the major site of absorption for lipids, they do not have a major influence on the lipid composition of body tissues. This is reflected by higher proportions of PUFA in the tissues of horses, pigs and other hindgut fermenters as compared to ruminants and non-ruminant foregut fermenters [35–38].

Due to this dichotomy—absorption of 'ruminant-specific' FA in foregut fermenters, no absorption of such FA in hindgut fermenters—the endogenous presence of 'ruminant specific' FA has been considered as an indicator of foregut fermentation [39]. Thus, Käkela et al. [11] interpreted the endogenous presence of BFA and *trans* FA in tissue lipids of beavers (*Castor canadensis*) as an indication of a 'ruminant-like' bacterial fermentation in the gastrointestinal tract. However, the same research group [12] described PUFA levels in beaver tissues exceeding those found in ruminants by far. The beaver, therefore, shares similarities with ruminants with respect to BFA and *trans* FA and with hindgut-only fermenters concerning PUFA. This phenomenon could be explained by the digestive strategy of coprophagy of rodents and other small herbivores [9]. Coprophagy has been studied particularly well in rabbits [18, 24, 40, 41]. Hirakawa [9] describes that wild rabbits recycle almost the entire undigested matter in the form of caecotrophs. Based on the values published by Belenguer et al. [24], coprophagy could have made up approximately 10% of nutrient intake in our study. The proportion of total lipid absorption covered by coprophagy is not clear from the literature.

One central question of the present study was to which extent coprophagy can alter rabbit tissue FA composition. If the microbial lipids contain functional FA like CLA, even a proportion of 10% of the absorbed FA would be valuable in terms of the nutritional quality of the meat. If, on the other hand, with a more natural feeding strategy, coprophagy would be intensified [9, 24], the related increase of SFA might counterbalance such positive effects. The results show that both were only marginally the case. With its extraordinary high proportions of PUFA, the rabbits' tissues had nothing in common with those of ruminants, which consistently comprise much lower proportions of PUFA [4, 6–8, 29, 30]. It seems likely that a high proportion of dietary FA was absorbed in the small intestine before any biohydrogenation processes could take place in caecum and colon. This is consistent with the reduction found in total FAME from diets to caecotrophs, which was in the magnitude of 2/3. In this respect, the rabbits of this experiment were not only able to corroborate some previous findings on tissue PUFA content in rabbits [15, 19], but also the observations of the high PUFA content in beaver tissues [12].

However, certain amounts of BFA, odd-chain FA and *trans*18:1 FA were still found in the rabbits' tissues. Although endogenous BFA synthesis cannot be excluded, this is expected to take place to a low extent [3]. It seems reasonable to assume that the majority of BFA found in the tissues are of caecotroph origin. Compared to that reported for sheep [42], the BFA content of intramuscular fat was only approximately three times lower. Considering the high impact of ruminal processes on the endogenous FA metabolism in sheep [2], the amounts of BFA in the rabbits' tissues indicate that the contribution of microbially modified lipids to the total dietary lipids was not negligible. The considerably higher BFA proportions in tissues of the groups fed without oats are obviously a reflection of the diet effects on caecotrophs. With increasing dietary fibre proportions, the caecal microbial fermentation in rabbits and their intake of microbially fermented matter increases [18, 24]. Based on what is known from ruminant digestion [3], it seems likely that the increased BFA proportions in the tissues are an indicator of increased coprophagial activity by the rabbits fed forage-only diets. In this context, the increase in SFA in the tissues of the forage-only groups compared to the oats-groups could be explained by an enhanced intake of caecotrophs as these contained proportionately more SFA than the diets. By contrast, the low and insignificant amounts of *trans*-FA found in the tissues do not allow the same conclusion.

We conclude that, although on a low level, FA originating from the caecotrophs are traceable in the rabbits' metabolism, but to a different degree for individual FA. Provided these results are confirmed with other diets and under different conditions, markers for the occurrence of coprophagy in wild animals could be developed on the basis of certain BFA and *trans* FA. Under free-ranging conditions, on a less consistent supply of high-quality forage, coprophagy might contribute even more to the animal's nutrient intake. This would lead to higher tissue proportions of the discussed FA. For example, the higher proportions of *trans* FA in free-ranging beavers [12], as compared to the rabbits of the present study, could indicate a higher proportionate intake of caecotrophs.

Influence of Excluding Concentrate on the FA Profile of the Body Tissues

Feeding the forage-oats diets resulted in a recovery of the characteristically high MUFA content of oats. It also led to high concentrations of n-3 PUFA, particularly of 18:3n-3, in the lipids of perirenal adipose and muscle tissue. These concentrations were in the upper range of data reported in the majority of other studies about rabbit meat quality [16, 17, 21–23]. By feeding a high n-3 oil supplement, Dal Bosco et al. [43] achieved n-3 PUFA concentrations in the range found in the present study with the oats diets. Cobos et al. [15] found such values in wild rabbits and hares from central Spain. For long chain n-3 PUFA in intramuscular lipids, comparable or higher values were described by Forrester-Anderson et al. [19] for grazing rabbits consuming an unknown amount of additional concentrate. Comparably high n-3 FA proportions in the rabbit meat had never been achieved in the other studies reviewed. Those studies always used dietary forage proportions of less than 50%, the lowest value applied in the present investigation.

When increasing the forage proportion from 50 to 100% in the present study, the 18:3n-3 proportions were significantly higher and amounted to 15.4 and 21.3% of the intramuscular and the adipose fat of the rabbits, respectively. This reflects the favorably high 18:3n-3/18:2n-6 ratio in diets G and A, and illustrates the limited role coprophagy played for the FA composition of the rabbits' tissues. Positive effects of the forage-only diets were also noted on the proportions of the long-chain n-3 PUFA, particularly in the intramuscular lipids. This indicates considerable chain elongation processes, converting ingested 18:3n-3 into long-chain n-3 PUFA. Elongation of 18:2n-6 and 18:3n-3 competes for the same enzymes and depends on the respective concentration of both substrates [44]. Thus, the effects of diets G and A on n-3 PUFA confirmed our anticipation. The expected decrease of 20:4n-6, however, was lacking. The efficiency of endogenous elongation is crucial for the estimation of health effects of dietary 18:3n-3 in human diets [45], and the findings are controversial in this respect [46, 47]. The present data show that the endogenous concentrations of long-chain n-3 PUFA may depend considerably on the intake of 18:3n-3, at least in rabbits. An open question is whether the source of dietary 18:3n-3, other dietary factors or both have a confounding influence on the elongation processes.

In a broad range of animal species, body tissues were found to have higher proportions of n-3 PUFA under free-ranging conditions as compared to animals kept in captivity [48]. Our data, as well as data for cattle [8, 29], suggest that this 'wilderness effect' can be mimicked in domesticated herbivore species by high-forage diets. Overall, the present data show that a forage-only diet increases the sum of n-3 PUFA in rabbit meat to a level similarly high as that found in free-ranging conspecifics [15]. Compared to domesticated animals, including ruminants [36], free-range grazing pigs [49] and the horse [36], the enhancement of total of n-3 PUFA by a forage-only diet was particularly high in the rabbits of the present study. Even under extensive organic feeding conditions neither pork [49, 50] nor beef [8] reached these concentrations. Provided these results can be generalised for various rabbit rearing conditions, meat from forage-only fed rabbits could represent a particularly healthy food. Although feed conversion efficiency is lower with forage-only diets due to the high contents of indigestible fibre [24], the economic success of forage-only feeding systems could be substantial, if the nutritional value of such a high n-3 meat is paid for.

Another significant effect of the forage-only compared to the oats-supplemented diets was the lower proportion of 9*c*-16:1. Since this MUFA only occurred in traces in feeds and caecotrophs, it is likely that the high tissue level was caused by endogenous δ-9-desaturation [51]. This would imply that forage-only diets might reduce tissue desaturase activity. One explanation for this phenomenon could be the higher exogenous intake of dietary PUFA making endogenous desaturation less important.

Influence of the Forage Type on the FA Profile of the Body Tissues

The comparison of alfalfa versus grass as dietary forages did not reveal substantial effects on tissue FA profiles. Besides the influence on BFA, which was discussed above, the most obvious effect of dietary alfalfa compared to ryegrass was a small but significant reduction in 18:3n-3 and an increase in long-chain n-3 PUFA. This suggests a positive effect of alfalfa on the endogenous chain elongation. This effect only occurred in adipose tissue. The distribution of n-3 PUFA across the entire organism depends on several factors as described for other small herbivores [46], pigs [47], and humans [45]. Thus, any explanation for the alfalfa effect on adipose n-3 PUFA remains speculative. It is, however, interesting to note that total n-3 PUFA did not differ much between grass- and alfalfa-fed rabbits although total lipid and, accordingly, total n-3 content of the alfalfa-containing diets was lower by a factor of two than with the grass.

Conclusion

1. The FA profiles of caecotroph lipids of rabbits showed typical properties of an anaerobic microbial lipid metabolism comparable to that occurring during ruminal digestion.
2. Small amounts of BFA and *trans*-FA from caecotrophs are obviously ingested and metabolised. This could have significance for the evaluation of FA digestion and metabolism with small herbivore animal models. It seems possible to develop markers for the occurrence of significant levels of coprophagy in non-ruminant herbivores particularly on the basis of BFA and *trans*18:1 FA.
3. Considering the nutritive value of rabbit meat, the contribution of coprophagy to the tissue FA profiles appears to be marginal. This holds true for SFA concentrations, which are more similar to horse meat than to beef, as well as for CLA, which were nearly absent in the tissues of the rabbits in the present study.
4. The endogenous FA metabolism, with respect to chain elongation, desaturation and distribution between different tissues, to some extent depends on dietary factors such as proportions and type of forage.
5. The effect of high dietary forage proportions on the n-3 contents of rabbit meat is so substantial that it seems worthwhile confirming these data with various forages and developing forage-based feeding strategies for rabbit meat production.

Acknowledgments This project was partly funded by the Vetsuisse Faculty, University of Zurich, Switzerland; Grant No. ZH12/05. We are grateful to Seher Ayra for her support in the fatty acid analyses.

References

1. Carabano R, Piquer J (1998) The digestive system of the rabbit. In: de Blas C, Wiseman J (eds) The nutrition of the rabbit. CABI Publishing, New York, pp 1–16
2. Chilliard Y, Glasser F, Ferlay A, Bernard L, Rouel J, Doreau M (2007) Diet, rumen biohydrogenation and nutritional quality of cow and goat milk fat. Eur J Lipid Sci Technol 109:828–855
3. Vlaeminck B, Fievez V, Cabrita ARJ, Fonseca AJM, Dewhurst RJ (2006) Factors affecting odd- and branched-chain fatty acids in milk: a review. Anim Feed Sci Technol 131:389–417
4. Dugan MER, Kramer JKG, Robertson WM, Meadus WJ, Aldai N, Rolland DC (2007) Comparing subcutaneous adipose tissue in beef and muskox with emphasis on *trans* 18:1 and conjugated linoleic acids. Lipids 42:509–518
5. Dewhurst RJ, Shingfield KJ, Lee MRF, Scollan ND (2006) Increasing the concentrations of beneficial polyunsaturated fatty acids in milk produced by dairy cows in high-forage systems. Anim Feed Sci Technol 131:168–206
6. Leiber F, Kreuzer M, Nigg D, Wettstein HR, Scheeder MRL (2005) A study on the causes for the elevated n-3 fatty acids in cows' milk of alpine origin. Lipids 40:191–202
7. Leiber F, Scheeder MRL, Wettstein HR, Kreuzer M (2004) Milk fatty acid profile of cows under the influence of alpine hypoxia and high mountainous forage quality. J Anim Feed Sci 13(Suppl 1):693–696
8. Razminowicz RH, Kreuzer M, Scheeder MRL (2006) Quality of retail beef from two grass-based production systems in comparison with conventional beef. Meat Sci 73:351–361
9. Hirakawa H (2001) Coprophagy in leporids and other mammalian herbivores. Mammal Rev 31:61–80
10. Clauss M, Besselmann D, Schwarm A, Ortmann S, Hatt JM (2007) Demonstrating coprophagy with passage markers? The example of the plains viscacha (*Lagostomus maximus*). Comp Biochem Physiol A 147:453–459
11. Käkelä R, Hyvärinen H, Vainiotalo P (1996) Unusual fatty acids in the depot fat of the Canadian beaver (*Castor Canadensis*). Comp Biochem Physiol B 113:625–629
12. Käkelä R, Hyvärinen H (1996) Fatty acids in extremity tissues of Finnish beavers (*Castor canadensis* and *Castor fiber*) and muskrats (*Ondathra zibeticus*). Comp Biochem Physiol B 113:113–124
13. Tagiri M, Endo Y, Fujimoto K, Suzuki T (1994) The digestibility of branched-chain triacylglycerols and their effects on plasma and hepatic lipid levels in the rat. Biosci Biotech Biochem 58:1093–1096
14. Martins H, Milne JA, Rego F (2002) Seasonal and spatial variation in the diet of the wild rabbit (*Oryctolagus cuniculus* L.) in Portugal. J Zool 258:395–404
15. Cobos A, Delahoz L, Cambero MI, Ordonez JA (1995) Chemical and fatty-acid composition of meat from Spanish wild rabbits and hares. Z Lebensm-Untersuch Forsch 200:182–185
16. Combes S (2004) Nutritional value of rabbit meat: a review. Prod Anim 17:373–383
17. Pla M, Hernandez P, Arino B, Ramirez JA, Diaz I (2007) Prediction of fatty acid content in rabbit meat and discrimination between conventional and organic production systems by NIRS methodology. Food Chem 100:165–170
18. de Arruda AMV, Lopes DC, Ferreira WM, Rostagno HS, de Queiroz AC, Pereira ES, da Silva JF, Jham GN (2003) Caecal

microbial activity and caecotrophy nutritional contribution in rabbits fed diets with different starch levels and fiber sources. Rev Bras Zootec 32:891–902

19. Forrester-Anderson IT, McNitt J, Way R, Way M (2006) Fatty acid content of pasture-reared fryer rabbit meat. J Food Comp Anal 19:715–719
20. Griffiths TW, Gandemer G, Viau M, Vedrenne P (1988) Polyunsaturated fatty acid (PUFA) content of rabbit meat: a potential source of PUFA for human nutrition. Proc Nutr Soc 48:5A
21. Corino C, Lo Fiego DP, Macchioni P, Pastorelli G, Di Giancamillo A, Domeneghini C, Rossi R (2007) Influence of dietary conjugated linoleic acids and vitamin E on meat quality, and adipose tissue in rabbits. Meat Sci 76:19–28
22. Cambero MI, de la Hoz L, Sanz B, Ordóñez J (1991) Lipid and fatty acid composition of rabbit meat: Part 1. Apolar fraction. Meat Sci 29:153–166
23. Marongiu ML, Bovera F, Moniello G, Nizza A, Pinna W (2005) Influence of weaning age (28 *vs.* 63 d) on quantitative and qualitative carcass traits of rabbits. Ital J Anim Sci 4 (Suppl 2):547–549
24. Belenguer A, Balcells J, Fondevila M, Torre C (2002) Caecotrophs intake in growing rabbits estimated either from urinary excretion of purine derivatives or from direct measurement using animals provided with a neck collar: effect of type and level of dietary carbohydrate. Anim Sci 74:135–144
25. Boufaied H, Chouinard PY, Tremblay GF, Petit HV, Michaud R, Belanger G (2003) Fatty acids in forages. I. Factors affecting concentrations. Can J Anim Sci 83:501–511
26. Naumann K, Bassler R (1997) Chemical Analysis of Feed. VdLUFA-Verlag, Darmstadt
27. Wettstein HR, Scheeder MRL, Sutter F, Kreuzer M (2001) Effect of lecithins partly replacing rumen-protected fat on fatty acid digestion and composition of cow milk. Eur J Lipid Sci Technol 103:12–22
28. IUPAC, International Union of Pure and Applied Chemistry (1987) Preparation of the fatty acid methyl esters. In: Dieffenbacher A, Pocklington WD (eds) IUPAC standard methods for the analysis of oils, fats and derivates. Blackwell, Oxford, UK, pp 123–129
29. Scollan N, Hocquette JF, Nuernberg K, Dannenberger D, Richardson I, Moloney A (2006) Innovations in beef production systems that enhance the nutritional and health value of beef lipids and their relationship with meat quality. Meat Sci 74:17–33
30. Lourenco M, Van Ranst G, De Smet S, Raes K, Fievez V (2007) Effect of grazing pastures with different botanical composition by lambs on rumen fatty acid metabolism and fatty acid pattern of longissimus muscle and subcutaneous fat. Animal 1:537–545
31. Hartman L, Shorland FB, McDonald IRC (1955) The *trans*-unsaturated acid contents of fats of ruminants and non-ruminants. Biochem J 61:603–607
32. Wolff RL, Precht D, Nasser B, El Kebbaj MS (2001) *trans*- and *cis*-octadecenoic acid isomers in the hump and milk lipids from *Camelus dromedarius*. Lipids 36:1175–1178
33. Engelke CF, Siebert BD, Gregg K, Wright ADG, Vercoe PE (2004) Kangaroo adipose tissue has higher concentrations of *cis* 9, *trans* 11-conjugated linoleic acid than lamb adipose tissue. J Anim Feed Sci 13(Suppl 1):689–692
34. Stevens CE, Hume ID (1998) Contributions of microbes in vertebrate gastrointestinal tract to production and conservation of nutrients. Physiol Rev 78:393–427
35. He ML, Ishikawa S, Hidari H (2005) Fatty acid profiles of various muscles and adipose tissues from fattening horses in comparison with beef cattle and pigs. Asian-Aust J Anim Sci 18:1655–1661
36. Paleari MA, Moretti VM, Beretta G, Mentasti T, Bersani C (2003) Cured products from different animal species. Meat Sci 63:485–489
37. Pelizzola V, Contarini G, Povolo M, Giangiacomo R (2006) Chemical-physical characteristics and fatty acid composition of mare's milk. Milchwissenschaft 61:33–36
38. Clauss M, Grum C, Hatt JM (2008) Polyunsaturated fatty acid content in adipose tissue in foregut and hindgut fermenting mammalian herbivores: a literature survey. Mammal Biol (in press). doi:10.1016/j.mambio.2008.04.004
39. Duncan WRH, Garton GA (1968) The fatty acid composition and intramolecular structure of triglycerides from adipose tissue of the hippopotamus and the African elephant. Comp Biochem Physiol 25:319–325
40. Thacker EJ, Brandt CS (1955) Coprophagy in the rabbit. J Nutr 55:375–385
41. Hirakawa H, Okada A (1995) Hard faeces reingestion and the passage and recycling of large food particles in the Japanese hare (*Lepus brachyurus*). Mammalia 59:237–247
42. Santercole V, Mazzette R, De Santis EPL, Banni S, Goonewardene L, Kramer JKG (2007) Total lipids of Sarda sheep meat that include the fatty acid and alkenyl composition and the CLA and *trans*-18:1 isomers. Lipids 42:361–382
43. Dal Bosco A, Castellini C, Bianchi L, Mugnai C (2004) Effect of dietary α-linolenic acid and vitamin E on the fatty acid composition, storage stability and sensory traits of rabbit meat. Meat Sci 66:407–413
44. Contreras MA, Rapoport SI (2002) Recent studies on interactions between n-3 and n-6 polyunsaturated fatty acids in brain other tissues. Curr Opin Lipidol 13:267–272
45. Sinclair AJ, Attar-Bashi NM, Li D (2002) What is the role of α-linolenic acid for mammals? Lipids 37:1113–1123
46. Fu Z, Sinclair AJ (2000) Increased α-linolenic acid intake increases tissue α-linolenic acid content and apparent oxidation with little effect on tissue docosahexaenoic acid in the guinea pig. Lipids 35:395–400
47. Kloareg M, Noblet J, van Milgen J (2007) Deposition of dietary fatty acids, de novo synthesis and anatomical partitioning of fatty acids in finishing pigs. Br J Nutr 97:35–44
48. Clauss M, Grum C, Hatt JM (2007) Fatty acid status of captive wild animals: a review. Zool Garten N F 76:382–401
49. Ventanas S, Ventanas J, Tovar J, Garcia C, Estevez M (2007) Extensive feeding versus oleic acid and tocopherol enriched mixed diets for the production of Iberian dry-cured hams: Effect on chemical composition, oxidative status and sensory traits. Meat Sci 77:246–256
50. Hogberg A, Pickova J, Andersson K, Lundstrom K (2003) Fatty acid composition and tocopherol content of muscle in pigs fed organic and conventional feed with different n6/n3 ratios, respectively. Food Chem 80:177–186
51. Fievez V, Vlaeminck B, Dhanoa MS, Dewhurst RJ (2003) Use of principal component analysis to investigate the origin of heptadecenoic and conjugated linoleic acids in milk. J Dairy Sci 86:4047–4053

Lipids (2008) 43:867–875
DOI 10.1007/s11745-008-3209-y

ORIGINAL ARTICLE

Nystatin Interferes with the Effects of *N*-Methyl-*N*′-nitro-*N*-nitrosoguanidine on Sphingolipid Metabolism in Human FL Cells

**Guangyi Liu · Weimin Wang · Gongping Sun ·
Xiaoqiong Ma · Ziyang Liu · Jun Yang**

Received: 18 February 2008 / Accepted: 16 June 2008 / Published online: 15 July 2008
© AOCS 2008

Abstract Previously we have shown that an alkylating agent *N*-methyl-*N*′-nitro-*N*- nitrosoguanidine (MNNG) can induce receptor clustering and the activation of a downstream signal molecule NF-κB, and that the receptor clustering is associated with changes in sphingolipids metabolism. On the other hand, the polyene antibiotic nystatin can block MNNG-induced receptor clustering. In this study, using a lipidomic approach, we further evaluated whether nystatin influenced the effects of MNNG on sphingolipids metabolism. It was found that nystatin itself induced changes in the sphingolipids profile in human amnion FL cells to a certain extent, including an increase or decrease of some sphingolipid species. Interestingly, nystatin can block, at least partially, the changes of sphingolipids-induced by MNNG. In addition, nystatin can also partially inhibit the activation of NF-κB induced by MNNG. Neither MNNG nor nystatin affects the mRNA levels of serine palmitoyltransferase, acid sphingomyelinase (ASM), and sphingomyelin synthase, key enzymes in the sphingolipids biosynthesis pathway. However, MNNG can activate ASM and neutral sphingomyelinase, while nystatin preincubation inhibits the activation. Taken together, these data suggested that nystatin interferes with the effects of MNNG, and might elicit its function through altered sphingolipids metabolism.

Keywords Nystatin · Sphingolipids · Lipidomics · Mass spectrometry · MNNG

Introduction

Besides serving as structural materials to provide a physical barrier for cells and providing a platform (the so-called lipid raft) for membrane protein–protein interaction, many lipids also have distinct cellular functions. Sphingolipids are the second largest group of membrane lipids as well as the major components of the lipid raft. In the sphingolipid metabolism pathway, ceramide is on the center stage; it can be generated from simple molecules by a de novo synthesis pathway, or from the hydrolysis of more complex sphingolipids (Fig. 1) [1, 2]. Now it is clear that sphingolipids and their metabolites are involved in many important signal transduction pathways which regulate many cellular events such as cell cycle arrest or apoptosis, proliferation, calcium homeostasis, cancer development, multidrug resistance, or even viral or bacterial infection processes [1, 3]. Clearly, the importance of this group of lipids should not be underestimated.

However, the study of lipids goes far behind those of genes and proteins, and the major problem is the lack of high-throughput technologies for lipid analysis. Only after the coming of "lipidomics", in which the individual lipid components can be analyzed by the mass spectrometric (MS) technique, have vast amounts of information been generated regarding the changes of lipid metabolism under

---

Guangyi Liu and Weimin Wang contributed equally to this work.

G. Liu · G. Sun · X. Ma · J. Yang (✉)
Department of Toxicology, Zhejiang University School of Public Health, 388 Yu-Hang-Tang Road, Hangzhou,
Zhejiang 310058, China
e-mail: gastate@zju.edu.cn

W. Wang
College of Life Science, China Jiliang University,
Hangzhou, China

Z. Liu
Department of Chemistry, College of Science,
Zhejiang University, Hangzhou, China

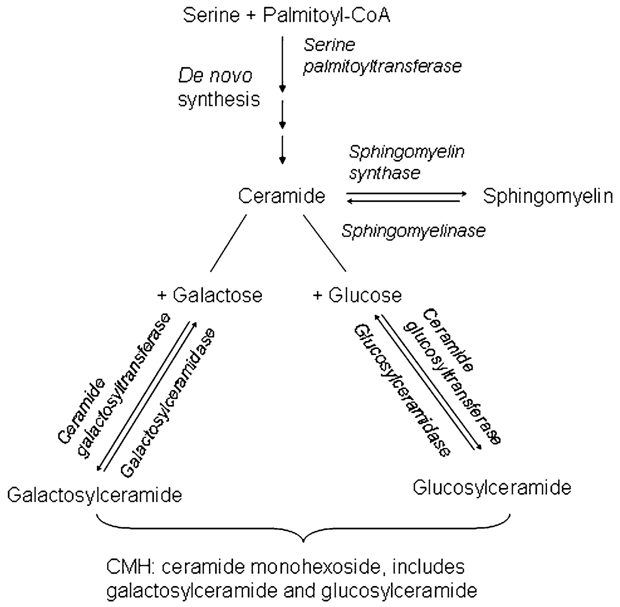

Fig. 1 The metabolic pathways of sphingolipids

various conditions [3–5]. Compared with traditional methods, such as thin-layer chromatography (TLC) and high-performance liquid chromatography (HPLC), MS analysis is more accurate, less labor-intensive and can identify the molecular species of each class of lipids [6, 7].

For lipid studies, the ability to perturb lipid metabolism is essential to understanding the metabolic pathways of lipids. Nystatin is a polyene antibiotic that is routinely used to interfere with cellular lipid rafts, by depleting cholesterol from lipid rafts thus leading to their disruption [8–10]. Previously, we have found that an alkylating agent *N*-methyl-*N*′-nitro-*N*-nitrosoguanidine (MNNG) can induce the clustering of membrane receptors, including epidermal growth factor receptor (EGFR) and tumor necrosis factor α receptor (TNFR), as well as the activation of the downstream signal molecule NF-κB [11, 12]. By using TLC and matrix-assisted laser desorption ionization-time of flight (MALDI-TOF) MS techniques, it was further shown that MMNG affected sphingolipid metabolism, including changes in ceramide and sphingomyelin species, and that sphingolipids are involved in MNNG-induced receptor clustering [13–15]. On the other hand, nystatin can block MNNG-induced receptor clustering [13]. Although the disruption of the lipid raft by nystatin could contribute to the inhibition of receptor clustering, however, it was not clear whether nystatin had any other influence on MNNG-induced changes in cells, such as altered sphingolipids metabolism and the activation of NF-κB. Therefore, in the present study, using the lipidomic approach, the effects of nystatin on MNNG-induced sphingolipid changes were evaluated. In addition, the effects of various treatments on the activation of NF-κB and the expression of key enzymes in sphingolipids metabolism were examined.

Experimental Procedures

Cellular Culture, Reagents, and Treatment

Human amnion FL cells were cultured in Eagle's Minimum essential medium (EMEM, Invitrogen, Carlsbad, CA) containing 10% fetal bovine serum, and supplemented with 100 U/ml penicillin, 100 U/ml streptomycin and 0.03% L-glutamine in a humidified incubator at 37 °C with 5% CO_2. MNNG (Sigma, St Louis, MO) was dissolved in dimethylsulfoxide (DMSO) as a 10 mM stock. Nystatin (Sigma) was also dissolved in DMSO as a 1 mg/ml stock. To evaluate the effects of nystatin on MNNG, cells were pre-incubated with 100 μg/ml nystatin for 30 min, and then treated with 0.2 μM MNNG for another 8 h. C_2-ceramide was purchased from Sigma, and cells were treated with 100 μg/ml for 8 h as positive control.

Sphingolipid Extraction and MALDI-TOF MS

Sphingolipids were extracted as described before [2]. In short, approximately 4×10^7 cells were dissolved in 500 μl chloroform:methanol (2:1, V/V). One milliliter H_2O was then added to each sample. The mixed samples were centrifuged at 4,770×*g* for 15 min, and the lower phase was dried by vacuum centrifugation in a centrifugal evaporator (Speed-Vac, Thermo Savant, Holbrook, NY). Then, 500 μl of methanol containing 0.1 M NaOH was added into each tube and held at 55 °C for 1 h to decompose glycerophospholipids. After neutralization with 100 μl methanol containing 1 M HCl, 500 μl hexane and one drop of water were added to each sample. The mixture was then centrifuged again at 4,770×*g* for 15 min, and the lower phase was dried in a centrifugal evaporator after the upper phase was removed. The residue was mixed with 0.8 ml theoretical lower phase (chloroform:methanol:water, 86:14:1, V/V) and 0.2 ml theoretical upper phase (chloroform:methanol:water, 3:48:47, V/V) for Folch partition, and centrifuged in a centrifugal evaporator after removing the upper phase to discard the salt. The residual crude sphingomyelin was stored at −70 °C.

For MALDI-TOF MS analysis, each sample was dissolved in 5 μl chloroform:methanol (2:1, V/V), followed by the addition of 5 μl matrix solution (ethyl acetate containing 0.5 M 2,5-dihydroxyl-benzoic acid (2,5-DHB, Sigma) and 0.1% TFA) in a 0.5 ml Eppendorf tube. The tube was agitated vigorously on a vortex mixer then centrifuged in a microcentrifuge for 1 min. One microliter of mixture was directly applied to the sample plate and rapidly dried under a moderately warm stream of air in order to remove the organic solvent within seconds.

All samples were analyzed using a Voyager-DE STR MALDI-TOF mass spectrometer (ABI Applied Biosystem, Framingham, MA) with a 337 nm N_2 UV laser. The mass spectra of the sample were obtained in positive ion mode. Mass/charge (*m*/*z*) ratios were measured in the reflector/delayed extraction mode with an accelerating voltage of 20 kV, grid voltage of 67% and delay time of 100 ns. C_2-dihydroceramide (MW 343.6) was used to calibrate the instrument. All sample lipid spectra were acquired using a low-mass gate at 400 Da. For each sample 7 spectra were obtained.

Establishment of Reference Mass Spectrum and Relative Quantification

For analyzing sphingolipids, the "reference mass spectrum" (RMS) method established in this laboratory was applied to deal with the problem of intra-sample variation, as well as the problem associated with the poor quantification capability of MALDI-TOF-MS [2]. The basic principle is that only those peaks present in at least 5 mass spectra collected from the same sample were chosen for entry into the RMS. By doing so, the intra-sample variation could be minimized. Since it is difficult to quantify the amount of each sphingolipid species using MALDI-TOF-MS, a relative quantification method was also created by comparing the ratio of different sphingolipid species instead of the absolute amount of each species. It was found in all the mass spectra obtained, peak 506.9, was always given the relative intensity of 100%. Thus, the relative intensities of other peaks were calculated by comparing to peak 506.9. Then the mean and standard deviation of the relative intensity of each peak was computed for each sample. Combining these data, a final RMS was established for these samples, and the particular lipid giving rise to the peak was identified by comparing their validated masses in our database (http://lipid.zju.edu.cn). All the comparisons were then conducted using the RMS.

NF-κB p65 Activity Analysis

Nuclear protein was extracted using the Nuclear Extract Kit (Active Motif, Carlsbad, CA) following the manufacturer's instructions. Briefly, cells in a 75 cm^2 flask were washed with ice-cold PBS, then scraped off the flask into 10 ml of ice-cold PBS and transferred into a pre-chilled 15 ml tube and spun at 300×*g* for 5 min at 4 °C. The pellet was resuspended in 1 ml of ice-cold hypotonic buffer by gentle pipetting and then transferred into a pre-chilled 1.5 ml tube. After swelling on ice for 15 min, 50 μl 10% Nonidet P-40 was added and mixed by gentle pipetting. The homogenate was centrifuged for 30 s at 4 °C in a microcentrifuge. The nuclear pellet was resuspended in 50 μl complete lysis buffer and gently rocked on ice for 30 min on a shaking platform. The mixture was centrifuged for 10 min at 14,000×*g* at 4 °C, and the supernatant (nuclear cell extract) was then stored at −80 °C for further analysis. The protein concentration was determined by using the Bradford assay.

NF-κB activity was measured using the TransAM NF-κB p65 Kit (Active Motif). In short, 30 μl of complete binding buffer was added to each well of the 96-well plate provided by the kit, and then 20 μl of the nuclear protein extracts were added. After 1 h incubation at room temperature, the wells were washed with buffer for three times, and 100 μl NF-κB antibody (1:1,000) was added for another 1 h incubation at room temperature. The plate was then washed for three times, and HRP-conjugated secondary antibody (1:10,000) was added and incubated for another 1 h. Finally, the chemiluminescent working solution was added, and chemiluminescence was read at 450 nm by the Infinite 200 multifunctional microplate reader (Tecan, Austria).

RNA Isolation and RT-PCR

The mRNA levels of three enzymes, e.g., serine palmitoyltransferase (SPT), acid sphingomyelinase (ASM), and sphingomyelin synthase (SMS), were analyzed by RT-PCR following various treatments. Total RNA was prepared using TRIzol reagents (Invitrogen) according to the manufacturer's instruction. RNA samples were dissolved with diethylpyrocarbonate (DEPC) -treated water and stored at −80 °C. For reverse transcription, the complementary DNA (cDNA) was generated using 5 μg of total RNA, N6 primer, and RevertAid^{TM} M-MuLV Reverse transcriptase (Fermentas, Glen Burnie, MD) following the manufacturer's instructions. The subsequent PCR was carried out in a 20-μl mixture containing 1 μl cDNA, 2 μl 10× PCR buffer [100 mM Tris–HCl (pH 8.3), 500 mM KCl, 15 mM $MgCl_2$], 0.5 μl of 2.5 mM of each dNTPs, 0.5 μl of each primer (20 mM), and 2.5 U Taq DNA polymerase (Takara Biotech. Inc., Dalian, China). The following primers were used in the PCR reaction:

1. SPT: sense 5′-GGGCT TCATC ATCTA TGG-3′ and anti-sense 5′-TCAGT AGCTG AGGCA ATGTC-3′;
2. ASM: sense 5′-CTCTG TCTGA CTCTC GGGTT C-3′ and anti-sense 5′-GCTTC GGCAC AGTAG GC-3′;
3. SMS: sense 5′-GTAAA CCCAA GAGCT TATCCA-3′ and anti-sense 5′-GCCCA TTTCA CCCTA TCA-3′;
4. *β*-Actin: sense 5′-CATGT ACGTT GCTAT CCAGG C-3′ and anti-sense 5′-CTCCT TAATG TCACG CACGAT-3′.

Amplification was performed with an initial denaturation step at 94 °C for 5 min followed by 30 cycles of denaturation for 30 s, annealing at optimum temperature (ASM and SMS at 60 °C, SPT at 55 °C) for 30 s and extension at 72 °C for 45 s. A final extension was carried out at 72 °C for 8 min. PCR amplification was performed in an automated heat block thermal cycler (GeneAmp PCR System 9700, ABI). The products were run on a 1% agarose gel and stained with ethidium bromide. The gels were then scanned with GelDoc-It^{TM} Imaging System (UVP Inc., Upland, CA) and quantified using VisionWorksLS Image Acquisition and Analysis Software (UVP). The percentage of surface area under the peak of each band was normalized to that of the corresponding β-actin band.

Sphingomyelinase Activity Measurement

Sphingomyelinase activity was measured by Amplex Red sphingomyelinase assay kit (Molecular Probe, Invitrogen, UK). In short, 10^6 cells were collected and resuspended in 40 µl ice-cold buffer (150 mM NaCl, 5 mM EGTA, 10 mM Tris–HCl, pH 7.5, for neutral sphingomyelinase (NSM); 50 mM sodium acetate, 5 mM EGTA, pH 5.0, for ASM) containing 1% Triton X-100 and 100 µg/ml phenylmethylsulfonyl fluoride. After shaking on ice for 30 min, cells were frozen and thawed three times with liquid nitrogen. Cellular debris was removed by centrifugation at 14,000 rpm for 30 min. Then the supernatant was diluted with reaction buffer (pH 7.4, 100 mM Tris–HCl for NSM and pH 5.0 NaAc for ASM), and the SMase activity was measured according to the manufacturer's instruction. The samples were read in an Infinite M200 multifunctional microplate reader (Tecan, Austria) with the excitation and emission wavelength set at 530 and 585 nm, respectively.

Statistical Analysis

Each experiment was conducted at least three times. Statistical analysis was performed Student's *t*-test. A probability level of $P < 0.05$ was considered significant. Data are presented as mean ± SD.

Results

Nystatin Inhibits MNNG-induced Changes in Sphingolipid Profiles

Previously, we have shown that MNNG can induce dramatic changes in ceramide and sphingomyelin [13, 14]. On the other hand, although nystatin is routinely used to interfere with the cellular lipid metabolism, little is known about its effect on sphingolipids. Therefore, we first analyzed the sphingolipid profile using MALDI-TOF MS in cells treated with nystatin (Fig. 2). To establish the RMS, peak 506.9 was chosen as the internal standard and assigned a relative intensity of 100%. The final RMS obtained was shown in Fig. 3, and the ions characterized, as well as the values of their relative intensities, are listed in Table 1.

As shown in Figs. 2 and 3, it was found that nystatin could induce changes in sphingolipid profile, such as the decrease of intensities of ions *m*/*z* 701.5 and 831.2, while the intensity of *m*/*z* 617.7 was significantly increased. On the other hand, nystatin had little effect on ceramide-monohexoside (CMH). In contrast, the effects of MNNG were more profound, including the generation of many new sphingolipid species.

However, when cells were first incubated with nystatin and then treated with MNNG, it was found that most of the effects of MNNG on sphingolipids were suppressed. For example, for ceramides, the intensity of *m*/*z* 645.6 was returned to basal levels, while *m*/*z* 589.2 and 683.9 disappeared again as in controls. Similarly, MNNG-induced increase of sphingomyelin and CMH were also inhibited. Together, these data indicated that nystatin can reverse the effects of MNNG on sphingolipid metabolism.

Nystatin Partially Inhibits the Activation of NF-κB by MNNG

Previously, we have shown that MNNG can induce the activation of NF-κB [11, 12], which is a downstream molecule effector in both EGFR- and TNFR-mediated signaling pathway [16, 17]. Since nystatin can influence the effects of MNNG on sphingolipids, it was also of interest to know whether nystatin can affect the activation of NF-κB by MNNG. Therefore, cells were preincubated with nystatin, followed by MNNG treatment, and the activation of NF-κB was measured using the NF-κB activity kit. As shown in Fig. 4, nystatin preincubation indeed, although not completely, inhibited the MNNG-induced NF-κB activation.

Neither Nystatin nor MNNG Affect the Expression of mRNA of Key Enzymes in the Sphingolipid Metabolism Pathway

Sphingolipid metabolism is regulated by various enzymes. For example, serine palmitoyltransferase (SPT) is the rate-limiting enzyme in the de novo synthesis pathway for ceramide, while acid sphingomyelinase (ASM) and sphingomyelin synthase (SMS) control the balance between ceramide and sphingomyelin (Fig. 1). Since nystatin and MNNG can both induce changes in sphingolipid profile, we were interested to know whether these agents affected the

Fig. 2 Representative MALDI-TOF mass spectra of FL cells following different treatments. DMSO was used as solvent control. *M+N* cells were pretreated with nystatin (100 μg/ml) for 30 min followed by MNNG (0.2 μM) treatment for 8 h

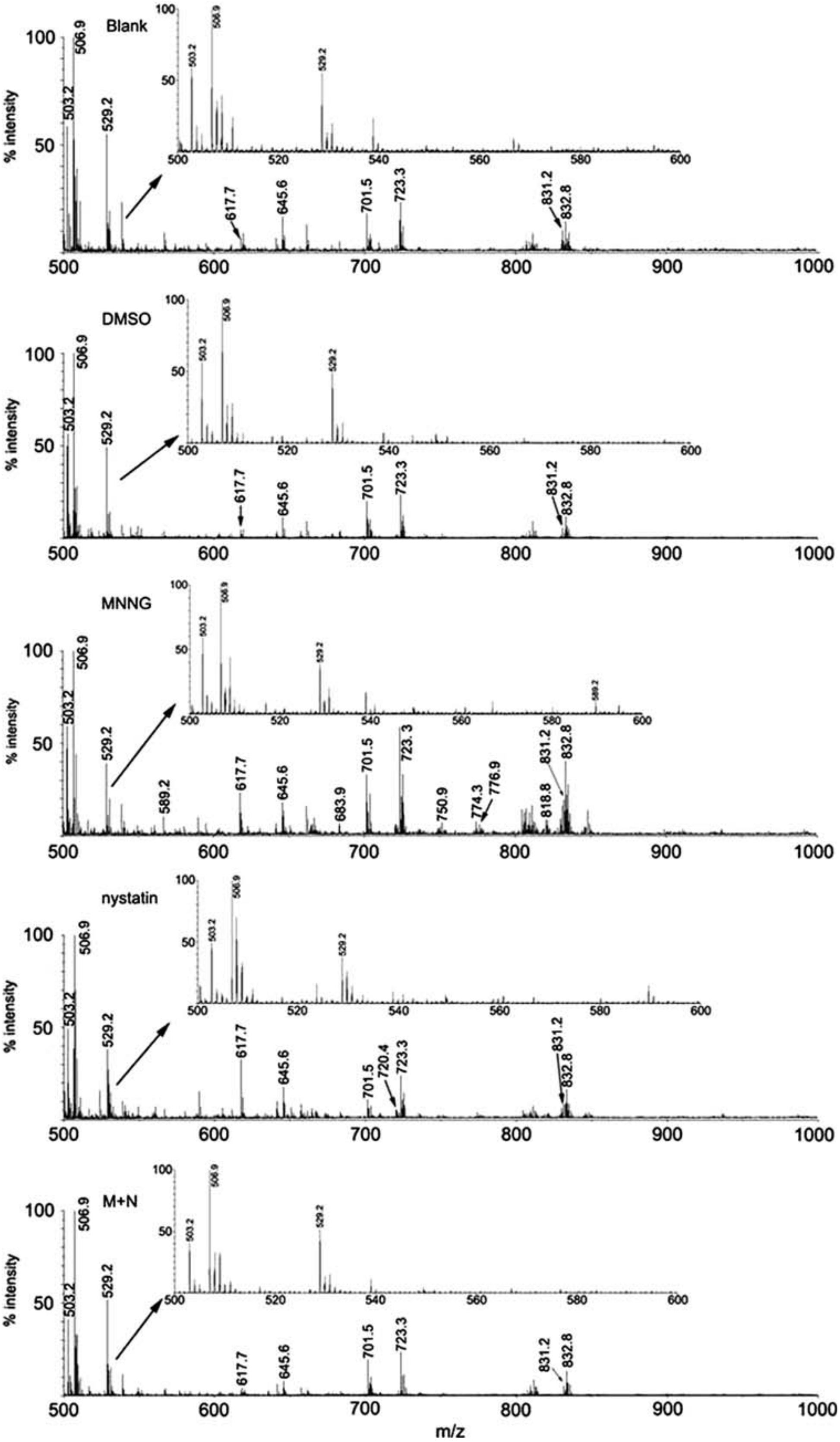

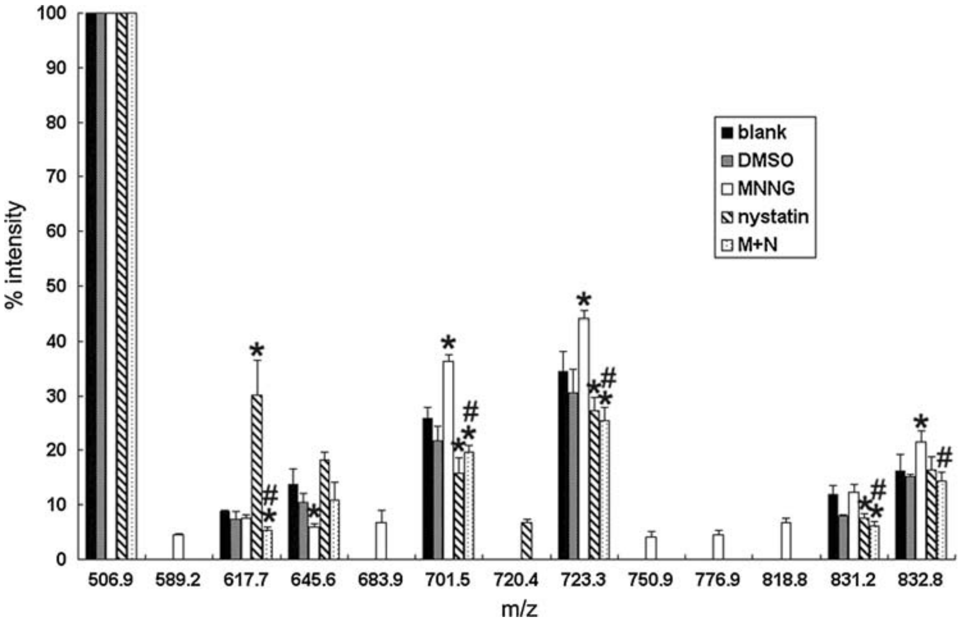

Fig. 3 Reference mass spectra of sphingolipids in cells following different treatments. *M+N* MNNG with nystatin preincubation. * $P < 0.05$, compared to blank; # $P < 0.05$, compared to MNNG, student's *t*-test

transcription of genes of these key enzymes. Therefore, mRNA from cells with different treatments was extracted and subjected to RT-PCR to examine transcription of SPT, ASM, and SMS genes, with β-actin as an internal standard. As shown in Fig. 5, neither nystatin or MNNG treatment alone, nor nystatin plus MNNG treatment significantly affects the expression of mRNA of these three enzymes.

MNNG Activates both ASM and NSM while Preincubation with Nystatin Inhibits such Activation

Since neither MNNG nor nystatin affected the mRNA levels of these enzymes, we were interested to know if they can affect their activities. Thus, the activities of both ASM and NSM were examined after different treatments. As shown in Fig. 6, it was found that MNNG indeed can increase the activities of both ASM and NSM. In contrast, nystatin did not induce the activation of neither ASM nor NSM. On the other hand, 30 min preincubation with nystatin almost completely inhibited the activation of NSM, but only partially inhibited the activation of ASM.

Discussion

In our laboratory MNNG is used as a model chemical to investigate characteristics of DNA damage by environmental toxins. However, during the study some phenomena independent of nuclear DNA damage were also observed, and one such phenomenon was the clustering of cell surface receptors EGFR and TNFR that occur on lipid rafts [12, 13]. Further analysis revealed that sphingolipids are involved in this process, and that MNNG can induce profound changes in sphingolipid metabolism [13, 14]. It has also been demonstrated that nystatin, which can disrupt lipid rafts, also inhibits receptor clustering [13].

The polyene antibiotics including nystatin and filipin have long been used to interfere with lipid rafts due to their ability to interact with cholesterol [10, 18]. However, to date there had been no information regarding their effects on another important class of lipid raft components, the sphingolipids. Here for the first time, using a lipidomic approach, we have shown that nystatin also influences sphingolipid metabolism, although the effects were less profound than those of MNNG (Table 1). More importantly, it is shown that nystatin could partially inhibit the effects of MNNG. Therefore, we postulated that nystatin might also inhibit MNNG-induced, lipid raft-mediated receptor clustering through perturbation of sphingolipid metabolism.

Once receptor clustering is disrupted, it likely follows that the downstream signaling would also be disrupted. Thus, we further evaluated the activation of NF-κB, a known downstream signaling molecule of both EGFR and TNFR [16, 17]. Although nystatin itself did not affect the activation status of NF-κB, it can inhibit the activation of NF-κB by MNNG (Fig. 4). Hence, based on these data, it is suggested that nystatin could target lipid raft, presumably through the combined action of cholesterol depletion and altered sphingolipid metabolism, and at least partially, interfere with the function of MNNG (Fig. 7).

Sphingolipid metabolism is a very complex process, involving the regulation of many enzymes (Fig. 1). As nystatin and MNNG can both alter the sphingolipid profile, we also examined the expression levels of some key metabolic enzymes in the sphingolipid synthesis pathway, which might be responsible for the sphingolipid changes

Table 1 The average relative intensity of sphingolipids in blank and cells with different treatments

Characteristic sphingolipid ions (*m/z*)	Blank (mean ± SD)	DMSO (mean ± SD)	MNNG (mean ± SD)	Nystatin (mean ± SD)	M+N (mean ± SD)
589.2					
Cer[d18:1C18:0+Na]$^+$			4.55 ± 0.12		
Cer[d18:0C18:1+Na]$^+$					
617.7					
Cer[d18:1C19h:0+Na]$^+$	8.77 ± 0.19	7.41 ± 1.46	7.54 ± 0.75	30.07 ± 6.39*	5.29 ± 0.76$^{*\#}$
Cer[d18:1C20:0+Na]$^+$					
645.6					
Cer[d18:1C22:0+Na]$^+$	13.77 ± 2.83	10.35 ± 1.77	5.87 ± 0.72*	18.15 ± 1.52	10.77 ± 3.41
Cer[d18:0C22:1+Na]$^+$					
Cer[d16:1C24:0+Na]$^+$					
683.9					
Cer[d18:2C24:1+K]$^+$			6.74 ± 2.18		
Cer[d18:1C25:1+Na]$^+$					
701.5					
SM[d18:1C16:1+H]$^+$	25.83 ± 2.14	21.66 ± 2.81	36.37 ± 1.10*	15.77 ± 2.88*	19.57 ± 1.32$^{*\#}$
SM[d18:2C16:0+H]$^+$					
720.4					
SM[d18:1C16h:0+H]$^+$				6.86 ± 0.48	
SM[d18:0C26:0+H_2O+Na]$^+$					
723.3					
SM[d18:1C16:1+Na]$^+$	34.42 ± 3.61	30.61 ± 4.31	44.07 ± 1.36*	27.27 ± 2.35*	25.49 ± 2.35$^{*\#}$
SM[d18:2C16:0+Na]$^+$					
750.9					
CMH[d18:1C18:0+Na]$^+$			4.06 ± 1.03		
776.9					
CMH[d18:1C20:1+Na]$^+$			4.6 ± 0.79		
818.8					
CMH[d18:1C22h:0+H_2O+H]$^+$			6.69 ± 0.96		
CMH[d18:1C23:1+Na]$^+$					
831.2					
SM[d18:1C24h:0+H]$^+$	11.88 ± 1.61	7.97 ± 0.21	12.25 ± 1.47	7.66 ± 0.70*	6.25 ± 0.70$^{*\#}$
832.8					
CMH[d18:1C24:1+Na]$^+$	16.27 ± 3.04	15.11 ± 0.43	21.54 ± 2.02*	16.38 ± 2.48	14.25 ± 1.79$^{\#}$

Cer ceramide; *SM* sphingomyelin; *CMH* ceramide-monohexoside; *d* dihydroxy-sphingosine; *h* hydroxyl group in side chain, $n = 7$; *M+N* MNNG with nystatin

* $P < 0.05$ (compared with blank)

$^{\#}$ $P < 0.05$ (compared with MNNG); student's *t*-test

induced by these treatments. However, our results demonstrated that the various treatments did not affect the expression of these enzymes at the mRNA level (Fig. 5). Therefore, it is more likely that changes in enzyme activity rather than changes in enzyme quantity might be the reason for altered sphingolipid metabolism. Indeed, our results showed that MNNG can activate both ASM and NSM, while nystatin can inhibit the effects of MNNG (Fig. 6).

Lipidomics is a fast growing research area, which has already been applied in biomarker discovery, drug development, signaling pathway analysis, as well as disease mechanistic studies [19–23]. MS has been adopted as the instrumental platform of choice to investigate lipidomics by the lipid metabolites and pathways strategy (LIPID MAPS) initiative [24]. Our study, in particular, has utilized MALDI-TOF MS. Although MALDI-TOF MS has its own advantages, however, compared to other types of MS such as liquid chromatography-electrospray ionization-tandem MS (LC-ESI-MS/MS), it suffers from the poor quantification. To overcome this problem, we had developed the

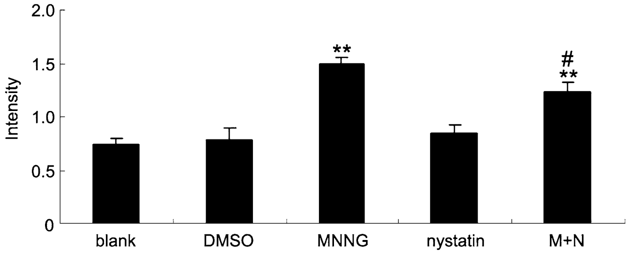

Fig. 4 The activation of NF-κB in FL cells following various treatments. After different treatments, the activity of NF-κB was measured by TransAM NF-κB p65 Kit. *M+N* MNNG with nystatin preincubation; ** $P < 0.01$, compared to blank; # $P < 0.05$, compared to MNNG, student's *t*-test

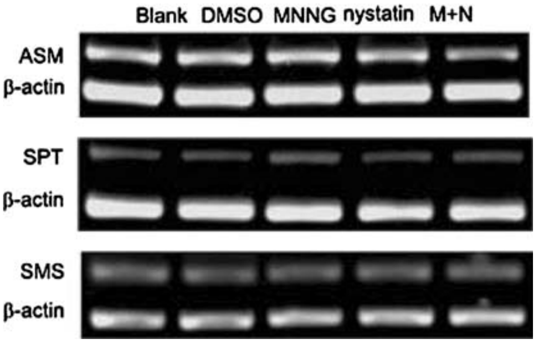

Fig. 5 mRNA levels corresponding to key enzymes in the sphingolipid metabolic pathway. After various treatments, the expression of mRNA of serine palmitoyltransferase (SPT), acid sphingomyelinase (ASM), and sphingomyelin synthase (SMS) was measured by RT-PCR. β-Actin was used as an internal control. *M+N* MNNG with nystatin preincubation

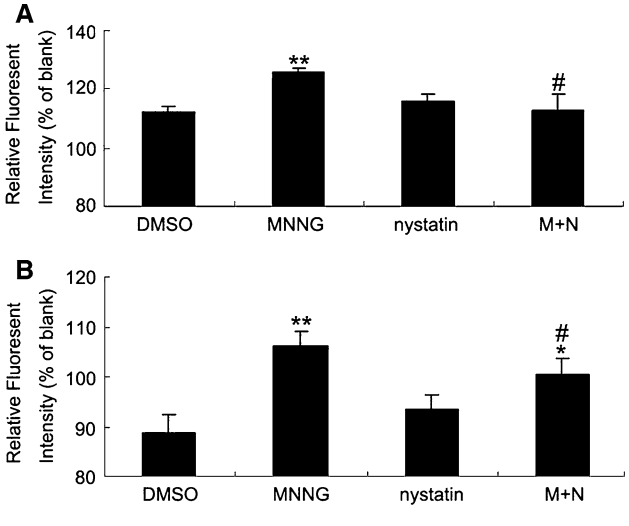

Fig. 6 The activity of NSM and ASM after different treatments. (**a**) NSM, (**b**) ASM. * $P < 0.05$, compared to DMSO; ** $P < 0.01$, compared to DMSO; # $P < 0.05$, compared to MNNG, student's *t*-test

RMS method to quantify the sphingolipids relative to a single, commonplace sphingolipid and, thus to facilitate comparisons among separate experiments [2]. In this study, RMS was also established for the sphingolipid profile of human FL cells, although the defined internal reference (*m/z* 506.0) was not the same as that for mice brain tissues (*m/z* 753.6) [2]. This could be the result of different sphingolipid composition of different species. Nonetheless, this poses a problem when comparing results from different samples/experiments, especially across species. Recently, Fujiwaki et al. [25] used sphingosylphosphorylcholine (SPC) as an internal standard to quantitatively evaluate sphingolipids in human patients. As SPC is physiologically nonexistent in normal human tissues or body fluids except as an artifact [25], it is believed that SPC might be a better choice as externally added standard for quantification purpose.

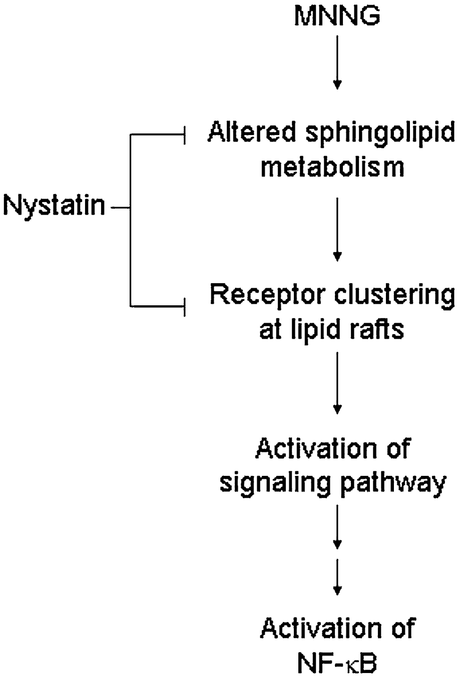
MNNG
Altered sphingolipid metabolism
Nystatin
Receptor clustering at lipid rafts
Activation of signaling pathway
Activation of NF-κB

Fig. 7 Illustration of proposed action of nystatin to interfere with the effects of MNNG

There are also problems faced by the lipidomic study. For example, during the extraction of sphingolipids, there is the possibility of potential degradation of sphingolipids and artifact during base methanolysis, which should be recognized. Also, the assignments for sphingolipid molecule solely based on the mass determined by MALDI-TOF/MS may not be accurate, and only by further MS/MS analysis could the definite molecular structures be assigned. Still, in the present study, we first demonstrated that the polyene antibiotic nystatin can affect sphingolipid metabolism. In addition, it can inhibit the biological effects of MNNG (such as the activation of NF-κB), probably through the altered sphingolipid metabolism.

Acknowledgments This work was supported in part by grants from the National Natural Science Foundation of China (No. 30500413) to

W. Wang; NNSF China (No. 30771826), New Century Excellent Talent Program of Ministry of Education (NCET-05-0520), Fok Ying Tung Education Foundation (No. 101036), Zhejiang Provincial Program for the Cultivation of High-level Innovative Health Talents, and Zhejiang Provincial Health Bureau (2006QN020) to J. Yang. The authors are grateful to Dr. R. Wohlhueter, recently retired from the Centers for Disease Control and Prevention (CDC, Atlanta, GA), for his editorial assistance.

References

1. Yang J, Yu Y, Sun S, Duerksen-Hughes PJ (2004) Ceramide and other sphingolipids in cellular responses. Cell Biochem Biophys 40:323–350
2. Ma X, Liu G, Wang S, Chen Z, Lai M, Liu Z, Yang J (2007) Evaluation of sphingolipids changes in brain tissues of rats with pentylenetetrazol-induced kindled seizures using MALDI-TOF-MS. J Chromatogr B Analyt Technol Biomed Life Sci 859:170–177
3. van Meer G (2005) Cellular lipidomics. EMBO J 24:3159–3165
4. Kolter T (2006) Lipids and lipidomics. Angew Chem Int Ed Engl 45:5910–5911
5. Wenk MR (2005) The emerging field of lipidomics. Nat Rev Drug Discov 4:594–610
6. Han X, Gross RW (2005) Shotgun lipidomics: multidimensional MS analysis of cellular lipidomes. Expert Rev Proteomics 2:253–264
7. Han X, Gross RW (2003) Global analyses of cellular lipidomes directly from crude extracts of biological samples by ESI mass spectrometry: a bridge to lipidomics. J Lipid Res 44:1071–1079
8. Coutinho A, Silva L, Fedorov A, Prieto M (2004) Cholesterol and ergosterol influence nystatin surface aggregation: relation to pore formation. Biophys J 87:3264–3276
9. Silva L, Coutinho A, Fedorov A, Prieto M (2006) Nystatin-induced lipid vesicles permeabilization is strongly dependent on sterol structure. Biochim Biophys Acta 1758:452–459
10. Grassme H, Jekle A, Riehle A, Schwarz H, Berger J, Sandhoff K, Kolesnick R, Gulbins E (2001) CD95 signaling via ceramide-rich membrane rafts. J Biol Chem 276:20589–20596
11. Wang G, Yu Y, Chen X, Xie H (2001) Low concentration *N*-methyl-*N*′-nitro-*N*-nitrosoguanidine activates DNA polymerase-beta expression via cyclic-AMP-protein kinase A-cAMP response element binding protein pathway. Mutat Res 478:177–184
12. Wang Z, Wang G, Yang J, Guo L, Yu Y (2003) Activation of protein kinase A and clustering of cell surface receptors by *N*-methyl-*N*′-nitro-*N*-nitrosoguanidine are independent of genomic DNA damage. Mutat Res 528:29–36
13. Huang Y, Yang J, Shen J, Chen FF, Yu Y (2005) Sphingolipids are involved in *N*-methyl-*N*′-nitro-*N*-nitrosoguanidine-induced epidermal growth factor receptor clustering. Biochem Biophys Res Commun 330:430–438
14. Huang Y, Shen J, Wang T, Yu YK, Chen FF, Yang J (2005) A lipidomic study of the effects of *N*-methyl-*N*′-nitro-*N*-nitrosoguanidine on sphingomyelin metabolism. Acta Biochim Biophys Sin (Shanghai) 37:515–524
15. Yang J, Duerksen-Hughes PJ (2001) Activation of a p53-independent, sphingolipid-mediated cytolytic pathway in p53-negative mouse fibroblast cells treated with *N*-methyl-*N*-nitro-*N*-nitrosoguanidine. J Biol Chem 276:27129–27135
16. Sethi G, Ahn KS, Chaturvedi MM, Aggarwal BB (2007) Epidermal growth factor (EGF) activates nuclear factor-kappaB through IkappaBalpha kinase-independent but EGF receptor-kinase dependent tyrosine 42 phosphorylation of IkappaBalpha. Oncogene 26:7324–7332
17. McFarlane SM, Pashmi G, Connell MC, Littlejohn AF, Tucker SJ, Vandenabeele P, MacEwan DJ (2002) Differential activation of nuclear factor-kappaB by tumour necrosis factor receptor subtypes. TNFR1 predominates whereas TNFR2 activates transcription poorly. FEBS Lett 515:119–126
18. Awasthi-Kalia M, Schnetkamp PP, Deans JP (2001) Differential effects of filipin and methyl-beta-cyclodextrin on B cell receptor signaling. Biochem Biophys Res Commun 287:77–82
19. Wolf C, Quinn PJ (2008) Lipidomics: practical aspects and applications. Prog Lipid Res 47:15–36
20. Han X (2007) An update on lipidomics: progress and application in biomarker and drug development. Curr Opin Mol Ther 9:586–591
21. Gross RW, Han X (2007) Lipidomics in diabetes and the metabolic syndrome. Methods Enzymol 433:73–90
22. Serhan CN, Lu Y, Hong S, Yang R (2007) Mediator lipidomics: search algorithms for eicosanoids, resolvins, and protectins. Methods Enzymol 432:275–317
23. Wakelam MJ, Pettitt TR, Postle AD (2007) Lipidomic analysis of signaling pathways. Methods Enzymol 432:233–246
24. Schmelzer K, Fahy E, Subramaniam S, Dennis EA (2007) The lipid maps initiative in lipidomics. Methods Enzymol 432:171–183
25. Fujiwaki T, Tasaka M, Takahashi N, Kobayashi H, Murakami Y, Shimada T, Yamaguchi S (2006) Quantitative evaluation of sphingolipids using delayed extraction matrix-assisted laser desorption ionization time-of-flight mass spectrometry with sphingosylphosphorylcholine as an internal standard. Practical application to cardiac valves from a patient with Fabry disease. J Chromatogr B Analyt Technol Biomed Life Sci 832:97–102

Lipids (2008) 43:877–886
DOI 10.1007/s11745-008-3218-x

ORIGINAL ARTICLE

Physico-Chemical Characterization of Sesame Oil Derivatives

**Iacopo Zanardi · Valter Travagli · Alessandro Gabbrielli ·
Luisa Chiasserini · Velio Bocci**

Received: 14 May 2008 / Accepted: 15 July 2008 / Published online: 5 August 2008
© AOCS 2008

Abstract Ozone treatment of commercially available vegetable oils gives rise to the formation of chemical species that are responsible for the therapeutic properties of ozonated oil derivatives in dermatological diseases. In the last years, these products have been successfully used as a topical disinfectant in a number of serious skin affections. The medical application of empirically prepared ozonated oil has yielded striking improvements with unexpected and rapid healing, compelling us to begin a long-range study aiming first to define the main characteristics of the most common ozonated vegetable oils, about which there is usually no medical consensus because of the lack of standardization of their technological parameters. Sesame oil was selected because of its great amount of polyunsaturated acyl groups, as well as natural antioxidants. Moreover, we have determined the kinetics and optimal conditions of ozonation (e.g., ozone concentrations, time of exposure, temperature) for obtaining an ozonated oil characterized by well-established technological and physico-chemical properties, namely an accurate peroxide value determination. On the basis of the results, we have gained an understanding of the modifications of the vegetable oils during the ozonation process.

Keywords Oxidized lipids · PUFAs · Analytical techniques

I. Zanardi · V. Travagli (✉) · A. Gabbrielli · L. Chiasserini
Dipartimento Farmaco Chimico Tecnologico,
Università degli Studi di Siena, Via Aldo Moro,
2-53100 Siena, Italy
e-mail: travagli@unisi.it

V. Bocci
Dipartimento di Fisiologia, Università degli Studi di Siena,
Via Aldo Moro, 2-53100 Siena, Italy

Abbreviations

4-HNE	4-Hydroxynonenal
AV	Acid value
IV	Iodine value
PV	Peroxide value
OE	Ozonation efficiency
PUFAs	Polyunsaturated fatty acids
SO	Sesame oil
TAG	Triacylglicerides

Introduction

From many years the medical use of ozone has represented a challenging topic [1–5]. The parenteral autohemotherapy—namely the method of exposing ex vivo human blood to oxygen–ozone for a few minutes in an ozone-resistant glass bottle and successive, prompt reinfusion in the donor patient—is still the object of controversial findings [6]. It has been reported that ozonetherapy is very useful in many pathologies, such as chronic osteomyelitis, pleural empyema, abscesses with intractable fistulae, infected wounds, bed sores, chronic ulcers and initial gangrene, necrotizing fasciitis, diabetic foot, skin, mouth, vaginal and rectal bacterial as well as viral infections and burns [7], especially when in combination with topical therapy by ozonated oils [8, 9]. Rapid healing is attributable to the disinfectant properties of ozone and to an enhanced cell proliferation allowed by an improved oxygenation and metabolism [10]. Thus, the antimicrobial properties of ozone derivatives like ozonated oils represent an interesting pharmaceutical approach to the management of a variety of dermatological pathologies [10, 11]. Unsaturated vegetable oils react with ozone at the level of double bonds to form ozonoid compounds that have sustained germicidal actions, as well as retaining the properties of stimulating tissue regeneration and repair.

The chemical reactions of ozone when bubbled into an oil are very complex. The analyses of these reactions provide information on the functional group changes during ozonation as well as the identification of the products without prior separation techniques, according to the well-known Criegee mechanism regarding the formation of ozonides from alkenes and ozone [12]. The peroxidic species are one of the most important products formed. This group includes hydroperoxides, hydrogen peroxides, polymeric peroxides, and other organic peroxides [13–15]. The yield of ozonated derivatives from unsaturated oils depends on reaction conditions (e.g., temperature, time, ozone generator, reactor type, stirring conditions, applied ozone dose). Therefore, an understanding of the physico-chemical properties of ozonated vegetable oils has great importance for their characterization and identification. For determining the quality of ozonated products, analytical methods such as peroxide, acidity, and iodine values are usually carried out [10, 13, 15].

Referring to ozonation of vegetable raw materials, theobroma fats [16] as well as olive, soybean and sunflower oils have been the most investigated [17–19]. The aim of the present study was to extend knowledge of pharmaceutical interest to other vegetable oil products, with particular emphasis on sesame oil (SO). It is expressed from the seeds of *Sesamum indicum*. SO is used in the pharmaceutical, cosmetic, and food industries. The major use of SO in pharmaceutical formulations is as a solvent in the preparation of sustained-release intramuscular or subcutaneous injections [20, 21] as well as an auxiliary substance in the preparation of oral capsules, disperse systems, and topical ointments [22, 23]. SO has been selected for our investigation because it is a convenient starting material, with a high concentration of olefinic double bonds. SO is composed principally of triacylglicerides (TAG). The predominant unsaturated fatty acids in SO are oleic acid (45.4%) and linoleic acid (40.4%). However, these acyl groups are not distributed randomly across the glycerol positions. The saturated acyl groups are almost exclusively in the 1 and 3 positions, and unsaturated acyl groups are predominantly in the 2 position [24]. Furthermore, SO presents significant proportions of natural antioxidants, which protect it against natural oxidation [25, 26] and could play a significant role during the ozonation process. Our goal is to investigate the doses of ozone, which, at appropriate experimental conditions, can react with oils leading to biologically active derivatives without any deleterious effect in terms of toxicity and stability. Moreover, attention should be paid to a correct quantification of the peroxide value, because of the great number and stability properties of the various peroxidic species generated during ozone treatment [14] as well as the underestimated values obtained using official methodology.

We consider our results useful to determine technological aspects that are necessary for the optimization of ozonated oil quality.

Experimental Procedure

Materials

Chemicals were purchased from Sigma-Aldrich and used without further purification. In particular, the SO was obtained from the seeds of *S. indicum* (batch number S3547). 4-Hydroxynonenal (4-HNE) was obtained from Cayman Chemical Co. and stored at −80°C.

Ozonation Method

Ozone was generated by the O_3 generator (Model Ozonosan PM 100 K, Hansler GmbH, Iffezheim, Germany) from medical-grade oxygen (O_2) as feed gas using electrical corona arc discharge. The gas flow rate and O_3 concentration have been controlled in real time by both photometric and iodometric determinations, as recommended by the Standardization Committee of the International O_3 Association. The O_3 flow rate was kept constant at 1.5 l/min in all experiments, and ozone concentration was 55 mg/l. The ozone/oxygen mixture was bubbled in Drechsel bottles containing 40 ml of SO for different times comprising between 15 and 120 min (SO15, SO30, SO60, SO90 and SO120), and corresponding to about 1,240, 2,480, 4,950, 7,450 and 9,900 mg of O_3 dose, respectively. Gas inlet was performed by using a Drechsel bottle with a sintered filter at the bottom (porosity 145–174 μm), unless otherwise stated. Furthermore, we have carried out blank tests under the same conditions bubbling only oxygen for the same time (see above).

FT–IR Spectroscopy

Ozonated SO samples were used for FT–IR spectroscopy measurement (Perkin–Elmer Spectrum BX). About 2 μl of sample were deposited between two disks of KBr, avoiding air bubble formation [27], then the transmittance % was measured in the range 4,000–800 cm^{-1}. Spectra were obtained using a 16-scan summation at a minimal resolution of 4 cm^{-1}.

NMR Spectroscopy

^{1}H and ^{13}C NMR spectroscopy was performed on a Bruker Avance 400-MHz Spectrometer; 100 µl of each sample was placed into 5-mm tubes and dissolved in $CDCl_3$ (750 µl). To obtain information on the production of toxic aldehydes like 4-HNE as by-products of ozonation, a neat SO sample was cured with 5 µl of 4-HNE, and the ^{1}H NMR was recorded.

Iodine Value

The iodine value (IV) is a measure of the total number of double bonds present in the sample. It represents the quantity of iodine (in grams) that will react with the double bonds in 100 g of sample. IV was determined according to the European Pharmacopoeia [28]. The IV was calculated by means of the following equation:

$$\mathrm{IV} = \frac{1.269 \times (n_1 - n_2)}{m} \quad (1)$$

where n_1 is the volume in ml of thiosulphate solution used for carry out a blank test, n_2 is the volume in ml of thiosulphate solution used for the titration, and m the quantity, in grams, of substance.

Acid Value

The acid value (AV) is the number that expresses, in mg, the quantity of potassium hydroxide required to neutralize the free acids present in 1 g of the substance [29]. The AV was calculated by means of the following equation:

$$\mathrm{AV} = \frac{5.610 \times n}{m} \quad (2)$$

where n is the volume in ml of titrant and m the quantity, in grams, of substance.

Peroxide Value and Method Evaluation

The peroxide value (PV) represents the quantity of peroxide expressing in milliequivalents of active oxygen contained in 1,000 g of the sample.

PV was determined introducing changes, unless otherwise stated, into the method described in the official monograph [30], as recently evidenced by some authors in the case of materials characterized by a high peroxide content and slow iodide reactivity with dialkylperoxides [14, 31]. In particular, we are able to obtain reproducible and/or realistic results only by modifying both the temperature and the reaction time with respect to the monograph conditions. Briefly, 2 g of SO were weighed in a 250-ml conical flask, and 30 ml of chloroform/glacial acetic acid (2:3) were added. Then, 3.0 ml of saturated potassium iodide solution was added. The flask was stirred at reflux temperature (60° C) for various times (0–180 min). After this time, the solution was cooled, and 25 ml of water was added. Solutions of sodium thiosulphate at the appropriate concentration (0.0001–0.1 M) were used for the titration. The PV was calculated by means of the following equation:

$$\mathrm{PV} = \frac{1,000 \times (V_1 - V_0) \times c}{m} \quad (3)$$

where V_1 is the volume in ml of thiosulphate solution used for the titration, V_0 is the volume in ml of thiosulphate solution used for carry out a blank, c the thiosulphate concentration, and m the quantity of substance.

All samples carried out by peroxide value titration were treated in order to evaluate the reaction process. Briefly, the organic layer of titrated mixture was dried over sodium sulfate and evaporated under reduced pressure to give a yellow oil, which was analyzed by both FT–IR and ^{1}H-NMR spectroscopies (see above).

Moreover, the ozonation efficiency (OE%) was calculated. It represents the % ratio of the amount of peroxidation due to the ozonation process, as estimated by PV value, to the amount of total ozone applied to the system.

Viscosity Measurements

Viscosity measurements were carried out with an innovative torsional-oscillation viscometer [32] (Viscomate VM-10AL, CBC Europe). Briefly, this instrument measures viscosity by sensing a change in oscillation amplitude of a liquid-immersed detector, based on constant input voltage. The detector oscillation amplitude with no resistance is 1 µm. Angular acceleration of the detector is measured and reported as dynamic viscosity with a declared range of 0.400–1,000 mPa s and a precision equal to ±5%. All the determinations were conducted in polystyrene Technicon® sample cups (Kartell, nominal capacity 2 ml). Temperature control was accurately monitored during the experiments (22.0 ± 0.1 or 35.0 ± 0.1 C). Viscosity values were recorded until equilibrium (data collection every 5 s) by PC connection through a RS-232 port.

In the present study all the physico-chemical characterizations were repeated at least three times.

Results

FT–IR Spectroscopy

For the IR spectroscopy of SO we have focused our attention on the wave numbers characterizing the double bond, C=C stretching (1,654 cm^{-1}) and =C–H stretching (3,009 cm^{-1}) [33], as well as the ozonide CO stretching (the 1,105 cm^{-1}) by unsaturated fatty acid moieties [34, 35]. As expected, the intensity of the bands corresponding to the double bond decreases and the band identifying the formation of the ozonide increases with respect to time of ozone treatment (Fig. 1). Apparently, when we have the maximum ozone dose, all double bond signals disappeared. As can be seen, the peaks reported above reveal the chemical changes occurring in the fatty acid chain during the reaction.

NMR Spectroscopy

The ^{1}H NMR and ^{13}C NMR assignment to principal peaks of SO are listed in Table 1. The proton and carbon resonances were assigned according with literature data, as obtained for similar vegetable oils [25, 34]. The ^{1}H NMR spectrum of SO is shown in Fig. 2, top. NMR analyses confirmed the structural changes undergone by oil during the ozonation (Fig. 2, bottom). The new signals found in ozonated oil are summarized in Table 2. In ^{1}H NMR spectra of ozonated SO, new signal at 5.15 ppm appears, attributed to the ring proton of 1,2,4-trioxolane. Such evidence was confirmed by the appearance of signal in ^{13}C NMR spectra at 104.33 ppm assigned by Wu et al. [36] as the ring carbon in the same structure. Moreover, the decrease of multiplet at 5.20–5.38 ppm and of signals at 128.06–130.16 ppm was observed in the ^{1}H and ^{13}C NMR spectra, respectively, due to olefinic moiety. Furthermore, a new signal at 5.56 ppm, assigned as protons directly bonded to sp^2-hybridized carbons, appeared at the early stage of ozonation (until 60 min) to gradually decrease, in agreement with previous results obtained for transesterified sunflower oil [34].

The protons of the methylene group α to the sp^2–hybridized carbons resonated at 2.00 and 2.71 ppm before the ozonation and shifted to 1.36 and 1.65 ppm after formation of 1,2,4-trioxolane [37]. ^{1}H NMR spectra of ozonated SO showed peaks at 9.69 and 2.42 ppm attributable to the aldehydic proton and the methylene proton α to the carbonil carbon, respectively. In ^{13}C NMR, the carbonil carbon, and the carbon α to it, resonated at 202.58 and 44.02 ppm, respectively.

Iodine, Acid and Peroxide Values

In Table 3 the IV, AV, PV as well as the ozonation efficiency are reported. As far as IV is concerned, it decreases as the insufflated ozone dose increases, leaving from the value of 113.65 (according to certificate of analysis limits, 103–116) to 13.39 with the greater ozone dose used (9,900 mg). Such a value is indicative that about all of the unsaturated group in SO reacted with ozone, according to the double bond disappearance.

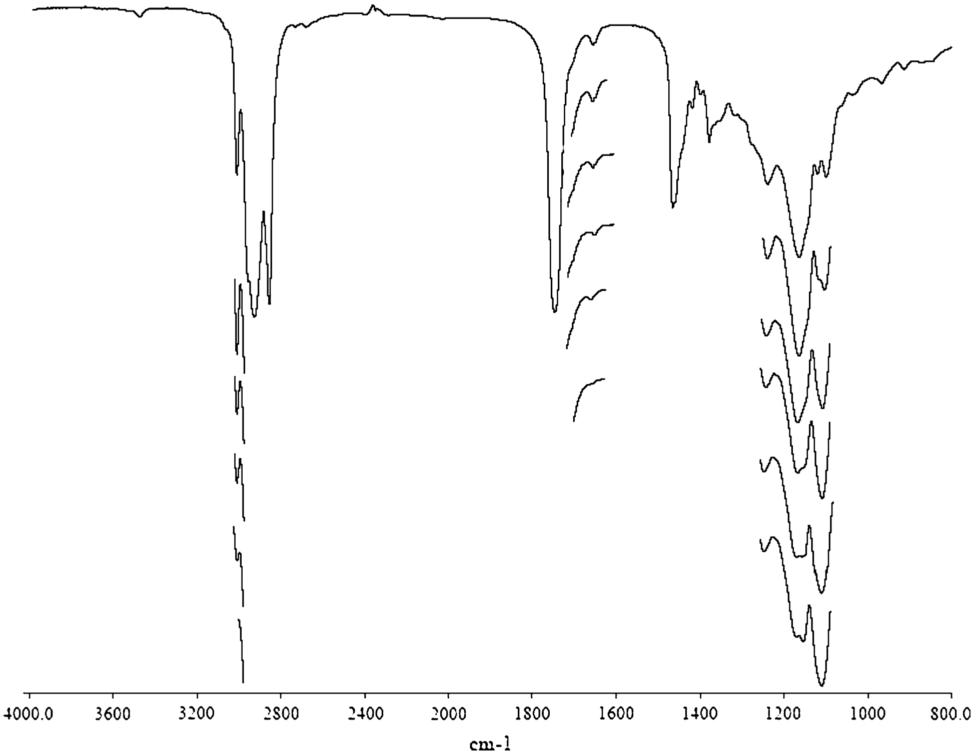

Fig. 1 FT–IR spectroscopy of the samples after exposure to progressively increasing ozone amounts

Table 1 ^{1}H and ^{13}C NMR assignments of neat sesame oil (SO)

Chemical shift (ppm)		Functional group
^{1}H	^{13}C	
0.83	14.28	**–CH$_3$**
1.27	29.15–31.89	–**(CH$_2$)**$_n$–
1.60	24.84	**–CH$_2$–**CH$_2$–OCO–
2.00	27.18	**–CH$_2$**–CH=CH–**CH$_2$**–
2.30	34.08	**–CH$_2$**–OCO–
2.71	25.62	–CH=CH–**CH$_2$**–CH=CH–
4.05–4.35	173.07	**–CH$_2$**–OCOR
5.20–5.26	172.73	>**CH**–OCOR
5.20–5.38	128.06–130.16	–CH$_2$–**CH=CH–**CH$_2$–
–	172.98	**–OCO**–

An increase in both acidity and peroxidation values was observed. In detail, about 18- and 34-fold grow-up with respect to the initial value and ozonation time was obtained, respectively (see Table 3). In the first ozonation phase (SO30, 2,480 mg of ozone) the increase was fast, followed by a decrease in rate, until the plateau of about 3,800 was obtained in terms of peroxide value (SO120, 9,900 mg of ozone). These results were expected because, in preliminary experiments, we noted only a partial reaction of ozone in the oil compartment, as evidenced by an increased amount of ozone recovered in a suitable iodide trap that was posed after the vessel. Such a phenomenon is justified if we consider that a substantial portion of the unsaturation became slow reacting with time, because of probabilistic and steric conditions [38]. This behavior might be due to formation of polymeric peroxides, which are responsible for viscous mass achieved after massive ozonation.

In Table 3, ozonation efficiency was also reported. It represents an estimation of the amount of ozonated compound, evaluated by PV, to the amount of the applied ozone. As expected, the reaction yield decreases because of the double bond disappearance with time.

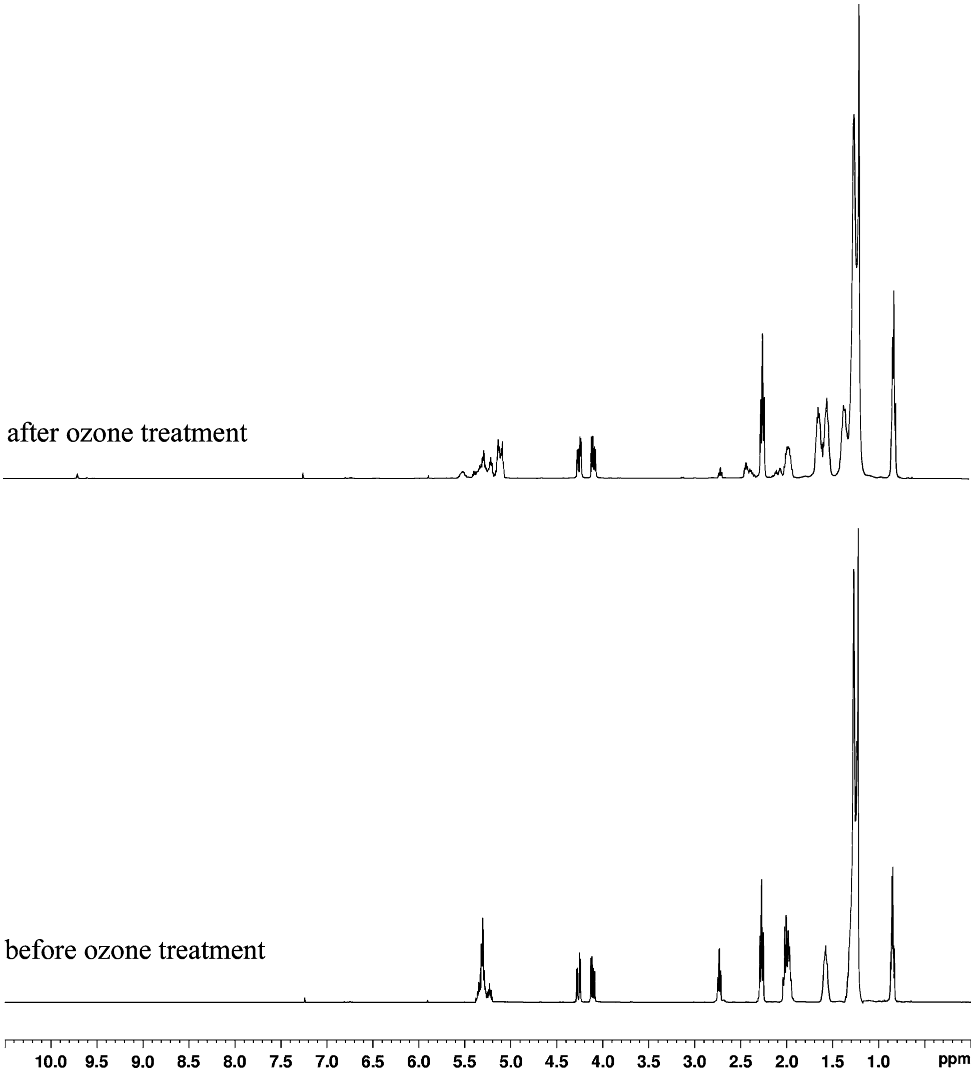

Fig. 2 ^{1}H NMR spectra: neat sesame oil (before ozone treatment) and ozonated sesame oil (after ozone treatment, 90 min)

Method Evaluation of the Peroxide Value

The PV determination according to the European Pharmacopoeia [30] leads to an underestimation of O_3 reacting with unsaturated substrates. In fact, these values are very low with regard to the O_3 dose insufflated ($PV < 350$, see Fig. 3). The difference between values among the various treatment times is minimal, even if statistically significant ($P < 0.001$), in all cases except between SO90 and SO120.

Table 2 ^{1}H and ^{13}C NMR new signals of ozonated sesame oil

Chemical shift (ppm)		Functional group
^{1}H	^{13}C	
5.15	104.33	1,2,4-trioxolane
1.36	–	$-\mathbf{CH_2}-CH=CH-\mathbf{CH_2}-$
1.65	–	$-CH=CH-\mathbf{CH_2}-CH=CH-$
2.42	44.02	α-Methylene group
9.69	202.58	Aldehyde

FT–IR spectra of titrated samples confirm this assumption: ozonide CO stretching (1,105 cm^{-1}) was unchanged between the control sample and the sample titrated according to Pharmacopoeia (Fig. 4). Such a result was also validated by the signal at 5.15 ppm in NMR spectra (data not shown).

The behavior is different if the sample was stirred at reflux temperature: PV considerably increases already after 10 min (about 2,800 for SO120), corresponding to a decrease in the CO stretching band. The full titration was carried out for 180 min at reflux. The plateau, defined as the absence of statistically significant differences between two successive points, was reached after 120 min for SO15, SO30, and SO60, whereas the samples SO90 and SO120 required minor reflux times (30 min).

The data were confirmed by NMR spectroscopy analysis carried out on oil recovered from the titration, where the 5.15 ppm signal disappears.

It should be noted that the heat treatment does not change the FT–IR transmittance band of the SO control sample (Fig. 4, left side).

Table 3 Iodine value (IV), acid value (AV) and peroxide value (PV) of the samples after exposure to progressively increasing ozone amounts

Sample	Ozone dose (mg)	IV (g/100 g)	AV (mg KOH/g)	PV (mEq/1,000 g)	OE (%)
SO	0	113.65 (±1.50)	0.70 (±0.01)	104 (±3)	–
SO15	1,240	92.20 (±1.60)	2.30 (±0.08)	1,480 (±70)	96
SO30	2,480	79.65 (±4.80)	3.19 (±0.08)	2,503 (±101)	84
SO60	4,950	52.65 (±1.10)	7.40 (±0.18)	3,100 (±93)	52
SO90	7,425	37.10 (±1.00)	9.80 (±0.30)	3,440 (±89)	38
SO120	9,900	13.90 (±0.50)	12.6 (±0.35)	3,800 (±179)	31

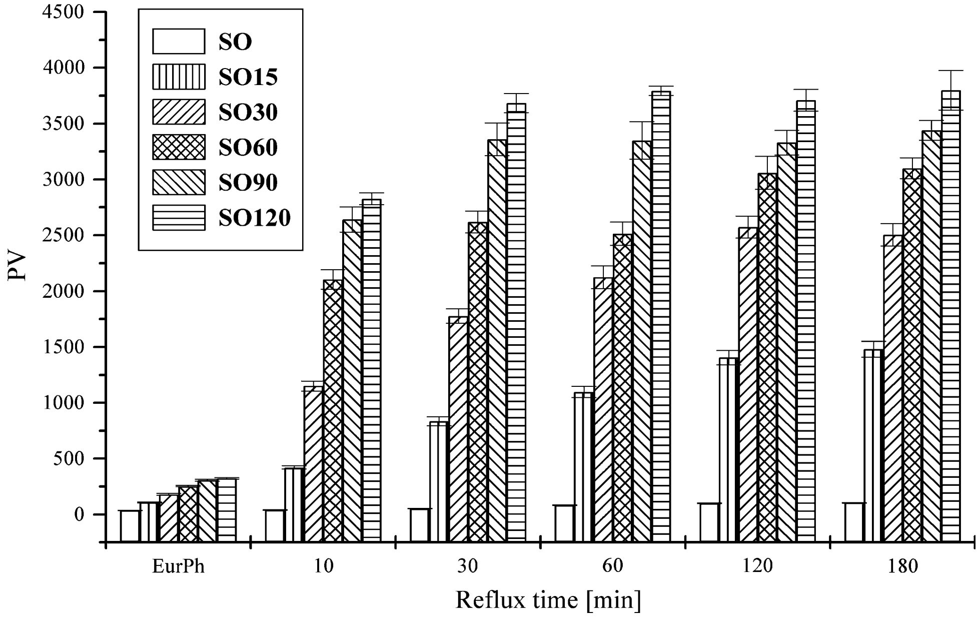

Fig. 3 Peroxide values at the different conditions adopted (see text for explanation)

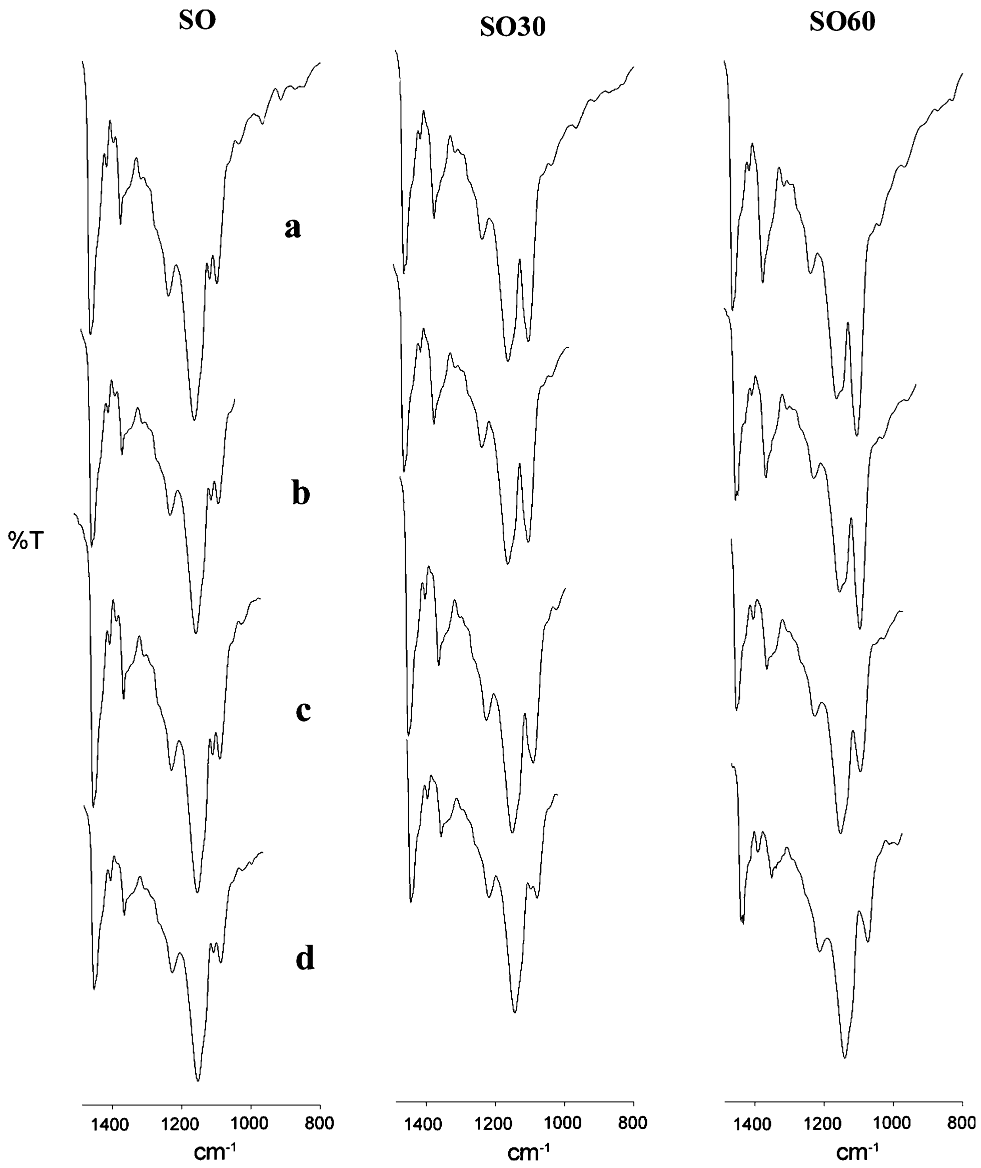

Fig. 4 FT–IR spectroscopy of titration samples (SO, SO30 and SO60): **a** control, **b** titration in agreement with the European Pharmacopoeia monograph, **c** reflux time 10 min, **d** reflux time 60 min

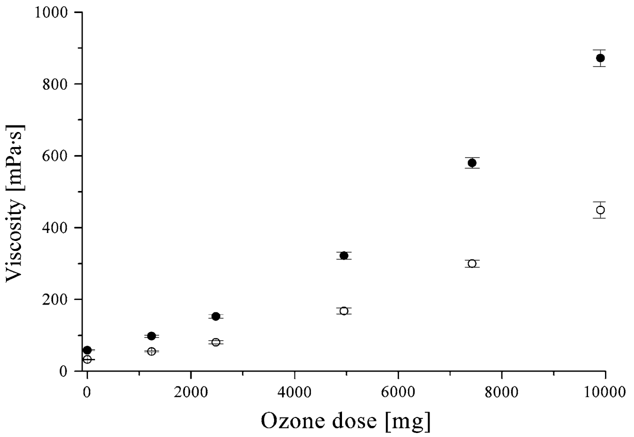

Fig. 5 Viscosity measurements of the samples after exposure to progressively increasing ozone amounts: open circle and solid circle refer to 35 °C and room temperature, respectively

As expected, the OE% is almost quantitative (>96%) and anyhow high (>80%) for SO15 and SO30, respectively. After this time, it is possible to observe a reduction in the ozone yield (until 31%, SO120) due to a lack in the number of available double bonds for the reaction (Table 3).

Viscosity Measurement

An increase of the ozonation time leads to an exponential trend in the increase of the sample viscosity, as shown in Fig. 5. Ozonated SO reached viscosity values up to 900 and 400 mPa s, depending to the temperature of determination (22 and 35 °C, respectively).

It is noteworthy that when ozone inlet was performed by using a Drechsel bottle with Drechsel bottle heads in the absence or in the presence of a sintered filter disk, analogous results in terms of IV, PV NMR and FT–IR characterization as well as viscosity determination were always obtained. Moreover, when oxygen inlet instead of ozone was performed as control, no differences were observed with respect to the native SO characteristics.

Eventually, the stability of the ozonated oil was monitored over a period of at least 1 year. No appreciable changes in the physico-chemical profile of the derivatives was observed if they were stored at room temperature in the dark.

Discussion

SO represents a valuable matrix to obtain derivatives useful in treating dermatological affections. SO was selected because this vegetable product is often used in pharmaceutical formulations, but it was never characterized in terms of its reactivity with ozonation processes. Our proposed accurate methods to check the oxidative processes and status are important factors in terms of sample stability.

Specific bibliographic information on the spectroscopic characterization (FT–IR and NMR) of SO derivatives generated by ozonation is absent. Ozone concentration and time of reaction are important for the ozonation reaction. The appreciable change in the FT–IR spectra between 3,300 and 3,600 cm^{-1} broad peak, indicating the presence of hydroxyl groups in the ozonated oil different from SO [35], was not evidenced in our study.

The extent of ozonation had very little effect on the aldehyde-to-ozonide ratio obtained from NMR spectra. These results indicate that, as expected, also for SO the NMR spectroscopy can provide valuable information about the amount of reaction compounds during ozone treatment. ^{1}H-NMR spectra of neat oil samples and ozone-treated oil showed peaks due to methyl protons from fatty acids. It was also evidenced from NMR spectra that the double bond peak decreased in intensity after ozonation. Moreover, the appearance of new peaks at 2.42 and 9.69 ppm for the ozonated oils is comparable with analogous derivatives obtained for similar substances (2.50 and 9.75 ppm). These results can be explained by the decomposition of all the peroxidic compounds present in the different equilibriums into the same reaction system. One example of these is the formation of carboxylic acid from peroxidic compounds. Besides, SO has a high proportion of unsaturated fatty acid, leading to a very complex ozonated system where the peroxidic compound decomposition to acid is very high.

As far as formation of several secondary oxidation products is concerned, aldehydes are of peculiar concern in terms of their cytotoxic and genotoxic potentiality [39]. In particular, among the reactive species produced upon lipid peroxidation, 4-HNE is one of the most abundant aldehydes when ozone reacts with olefins in the presence of water [40]. In the overall spectra, it was observed that the specific region of this compound (9.57–9.59 ppm) was free of signals, leading us to conclude that 4-HNE is not a secondary product of SO ozonation.

During ozonation reaction, ozone reacted with the vegetable oils that have high levels of polyunsaturated fatty acids (PUFAs). This aspect was evidenced by the IV decrease in relation to applied ozone dosage, representing a measure of the residual double bonds. Almost all unsaturated groups reacted with ozone, even if the condensation of peroxides led to a thickening of the system that could limit the whole double bond accessibility [19, 24].

The reaction of ozone with PUFAs present in SO, as well as in other unsaturated substrates, produces different types of peroxidic compounds as described by the Criegee mechanism, and the peroxide value represents the method generally employed to determine total peroxidic compounds formed. However, the official monographs report standard methods based on iodometric characterization with a reaction time of 1 min to analyze the samples. It should be observed that these assays apply well only to samples at low content of peroxidic compounds. In fact, ozonated SO as well as other unsaturated oils contains a great amount and diversity of peroxides. For these reason, different conditions could be necessary to determine its correct peroxide content. In particular, the prescribed reaction time of 1 min is insufficient for determining all kinds of long-chain peroxides [14, 31].

Acids are directly formed both during ozonation and because of peroxide decomposition. However, at these conditions, a high acidity value does not directly indicate that the oil quality has diminished and is at risk of becoming rancid.

Viscosity represents an evaluation of the peroxides species that are generated during the SO ozonation process, giving information about: (1) the increase of the van der Waals interactions due to the disappearance of the double bonds, indicating that the double bonds in the oil molecules reacted with ozone to form a more bulky molecule; (2) the modification of the unsaturated acyl chains ozonation kinetic, affecting the mobility and the reactivity of the species involved in the reaction. This aspect is of particular importance in terms of product characterization and evaluation of the ozonation reaction. Furthermore, our proposed method represents a useful online instrumentation that doesn't require periodic recalibration or frequent maintenance while providing continuous data logging during both ozonation reaction and storage time.

It could be considered that, when ozone inlet was performed by using the Drechsel bottle with Drechsel bottle heads in the absence or in the presence of sintered filter disk, a large vortex is always formed, resulting in significant mixing of the liquid phase and high ozone dispersion and reactivity, leading to a high efficiency of the various systems.

In conclusion, these results suggest that physico-chemical properties can provide valuable information about the ozonation level of SO and its potential applicability in dermatological infective pathologies. The evaluation of the oxygenated compound derived by ozonation processes is necessary in order to deepen the mechanism of action of these products. The future objectives will be the ongoing preclinic studies of both their antimicrobial properties and in vivo assessment of nontoxicity/allergenicity as well as the therapeutic activity of ozonated SO at different concentrations in a variety of chronic skin ulcers of patients with peripheral obstructive arterial diseases.

Acknowledgments The linguistic revision by Mrs. H. Carter is gratefully acknowledged.

References

1. Stoker G (1916) The surgical use of ozone. Lancet 188:712
2. Sweet F, Kao MS, Lee SC, Hagar WL, Sweet WE (1980) Ozone selectively inhibits growth of human cancer cells. Science 209:931–933
3. Bocci V (1994) Autohemotherapy after treatment of blood with ozone. A reappraisal. J Int Med Res 22:131–144
4. Andreula CF, Simonetti L, de Santis F, Agati R, Ricci R, Leopardi M (2003) Minimally invasive oxygen-ozone therapy for lumbar disk herniation. Am J Neuroradiol 24:996–1000
5. Stübinger S, Sader R, Filippi A (2006) The use of ozone in dentistry and maxillofacial surgery: a review. Quintessence Int 37:353–359
6. Travagli V, Zanardi I, Silvietti A, Bocci V (2007) A physicochemical investigation on the effects of ozone on blood. Int J Biol Macromol 41:504–511
7. Bocci VA (2006) Scientific and medical aspects of ozone therapy. State of the art. Arch Med Res 37:425–435
8. Sechi LA, Lezcano I, Nuñez N, Espim M, Dupre I, Pinna A (2001) Antibacterial activity of ozonized sunflower oil (OLEOZON). J Appl Microbiol 90:279–284
9. Menéndez S, Falcón L, Simón DR, Landa N (2002) Efficacy of ozonized sunflower oil in the treatment of tinea pedis. Mycoses 45:329–332
10. Valacchi G, Fortino V, Bocci V (2005) The dual action of ozone on the skin. Br J Dermatol 153:1096–1100
11. Rae ID (2006) Ozonised oils as disinfectants. Ambix 53:3–20
12. Criegee R (1975) Mechanism of ozonolysis. Angew Chem Int Edit 14:745–752
13. Mirabal JM, Menendez Cepero SA, Diaz Rubi VF, Garcia LAF, Ledea Lozano OE, Diaz Gomez MF, Lezcano Lastre ID. Method for obtaining ozonized oils and vegetable fats and use of said products for pharmaceutical and cosmetic purposes, WO 03/085072 A1
14. Martinez Tellez G, Lozano LO, Diaz Gomez MF (2006) Measurement of peroxidic species in ozonized sunflower oil. Ozone Sci Eng 28:181–185
15. Sadowska J, Johansson B, Johannessen E, Friman R, Broniarz-Press L, Rosenholm JB (2008) Characterization of ozonated vegetable oils by spectroscopic and chromatographic methods. Chem Phys Lipids 151:85–91
16. Díaz Gómez MF, Téllez GM, Cruz MA, Mancheño RG (2006) Chemical analysis of ozonized theobroma fat. J Am Oil Chem Soc 83:943–946
17. Diaz M, Lezcano I, Molerio J, Hernandez F (2001) Spectroscopic characterization of ozonides with biological activity. Ozone Sci Eng 23:35–40
18. Soriano NU Jr, Migo VP, Matsumura M (2006) Ozonized vegetable oil as pour point depressant for neat biodiesel. Fuel 85:25–31
19. Díaz MF, Hernández R, Martínez G, Vidal G, Gómez M, Fernández H, Garcés R (2006) Comparative study of ozonized olive oil and ozonized sunflower oil. J Braz Chem Soc 17:403–407
20. Schultz K, Møllgaard B, Fisher AN, Illum L, Larsen C (1998) Intramuscular rate of disappearance of oily vehicles in rabbits investigated by gamma-scintigraphy. Int J Pharm 169:121–126
21. Larsen SW, Rinvar E, Svendsen O, Lykkesfeldt J, Friis GJ, Larsen C (2001) Determination of the disappearance rate of iodine-125 labelled oils from the injection site after intramuscular and subcutaneous administration to pigs. Int J Pharm 230:67–75
22. Cable CG, Cable CG ((2006)) Sesame oil. In: Rowe RC, Sheskey PJ, Owen SC (eds) Handbook of pharmaceutical excipients, 5th edn edn. The Pharmaceutical Press, London, pp 646–648
23. Martindale (2007) The complete drug reference. 35th Edn. In: Sweetman SC (ed) Pharmaceutical Press, London, p 2162
24. Scrimgeour C (2005) Chemistry of fatty acids. In: Shahidi F (ed) Bailey's industrial oil and fat products, vol 1, 6th edn, Hoboken, pp 1–43
25. Guillén MD, Ruiz A (2004) Formation of hydroperoxy and hydroxyalkenals during thermal oxidative degradation of sesame oil monitored by proton NMR. Eur J Lipid Sci Tech 106:680–687
26. Yoshida H, Tanaka M, Tomiyama Y, Mizushina Y (2007) Regional distribution in the fatty acids of triacylglycerols and phospholipids of sesame seeds (*Sesamum indicum*). J Food Lipids 14:189–201
27. Guillén MD, Goicoechea E (2007) Detection of primary and secondary oxidation products by fourier transform infrared spectroscopy (FTIR) and 1H nuclear magnetic resonance (NMR) in sunflower oil during storage. J Agric Food Chem 55:10729–10736
28. European pharmacopoeia (2004) Iodine value. Council of Europe, 5th edn. Strasbourg Cedex, France, pp 127–128
29. European pharmacopoeia (2004) Acid value. Council of Europe, 5th edn. Strasbourg Cedex, France, p 127
30. European pharmacopoeia (2004) Peroxide value. Council of Europe, 5th edn. Strasbourg Cedex, France, pp 128–129
31. Richaud E, Farcas F, Fayolle B, Audouin L, Verdu J (2006) Hydroperoxide titration by DSC in thermally oxidized polypropylene. Polym Test 25:829–838
32. Travagli V, Zanardi I, Boschi L, Gabbrielli A, Mastronuzzi V, Cappelli R, Forconi S (2008) Comparison of blood viscosity using a torsional oscillation viscometer and a rheometer. Clin Hemorheol Micro 38:65–74
33. Vlachos N, Skopelitis Y, Psaroudaki M, Konstantinidou V, Chatzilazarou A, Tegou E (2006) Applications of Fourier transform–infrared spectroscopy to edible oils. Anal Chim Acta 573–574:459–465
34. Soriano NU Jr, Migo VP, Matsumura M (2003) Functional group analysis during ozonization of sunflower oil methyl esters by FT–IR and NMR. Chem Phys Lipids 126:133–140
35. John J, Bhattacharya M, Raynor PC (2004) Emulsions containing vegetable oils for cutting fluid application. Colloids Surf A 237:141–150

36. Wu M, Church DF, Mahier TJ, Barker SA, Pryor WA (1992) Separation and spectral data of the six isomeric ozonides from methyl oleate. Lipids 27:129–135
37. Anachlov MP, Rakovski SK, Stefanova RV (2000) Ozonolysis of 1, 4-cis-polyisoprene and 1, 4-trans-polyisoprene in solution. Polym Degrad Stab 67:355–363
38. Razumovskii SD, Zaikov GE (1980) Kinetics and mechanism of the reaction of ozone with double bonds. Russ Chem Rev 49:1163–1180
39. Esterbauer H, Schaur RJ, Zollner H (1991) Chemistry and biochemistry of 4-hydroxynonenal, malonaldehyde and related aldehydes. Free Radic Biol Med 11:81–128
40. Pryor WA, Porter NA (1990) Suggested mechanisms for the production of 4-hydroxy-2-nonenal from the autoxidation of polyunsaturated fatty acids. Free Radic Biol Med 8:541–543

Lipids (2008) 43:887–894
DOI 10.1007/s11745-008-3217-y

REVIEW

Biological Functions and Metabolism of Oleoylethanolamide

Clémentine Thabuis · Delphine Tissot-Favre · Jean-Baptiste Bezelgues · Jean-Charles Martin · Cristina Cruz-Hernandez · Fabiola Dionisi · Frédéric Destaillats

Received: 25 March 2008 / Revised: 11 July 2008 / Accepted: 14 July 2008 / Published online: 13 August 2008
© AOCS 2008

Abstract The present review is focused on the metabolism and the emerging roles of oleoylethanolamide (OEA) with emphasis on its effects on food intake control and lipid metabolism. The biological mechanism of action, including a non-genomic effect mediated through peroxisome proliferator-activated receptor alpha (PPAR-α) and transient receptor potential vanilloid type 1 (TRPV1) receptor, is discussed. The research related to fatty acid ethanolamides has been focused until recently on anandamide and its interaction with cannabinoid receptor subtype 1. The roles of other *N*-acyl ethanolamine fatty acid derivatives have been neglected until it was demonstrated that OEA can modulate food intake control through interaction with PPAR-α. Further investigations demonstrated that OEA modulates lipid and glucose metabolism, and recent study confirmed that OEA is an antagonist of TRVP1. It has been demonstrated that OEA has beneficial effects on health by inducing food intake control, lipid β-oxidation, body weight loss and analgesic effects. The investigation of the mechanism of action revealed that OEA activates PPAR-α and stimulates the vagal nerve through the capsaicin receptor TRPV1. Pre-clinical studies showed that OEA remains active when administered orally.

Keywords *N*-acyl fatty acid ethanolamine · Food intake · Oleoylethanolamide · Energy metabolism · Lipid metabolism

Introduction

Fatty acid ethanolamides belong to a family of lipids naturally found in both plant and animal tissues. These fatty acid derivatives appear to have biological properties. Indeed, palmitoylethanolamide (PEA, derived from palmitic acid) has anti-nociceptive and anti-inflammatory properties [1]. Within this family, anandamide (derived from arachidonic acid) has been of great interest. In the last decade, it was discovered that anandamide is an endogenous ligand for cannabinoid receptor subtype 1 (CB1). Activating CB1, anandamide increases food intake. Another interesting fatty acid amide is oleoylethanolamide (OEA), formed from oleic acid and phosphatidylethanolamine. Biological functions of OEA, such as anorexigenic or body fat loss properties, have been extensively studied over the past decade. This molecule is naturally present at low concentrations in food products, such as cocoa powder (up to 2 μg/g), oatmeal or nuts [2, 3]. Biologically, the OEA function is to regulate food intake via a synthesis/degradation balance, which occurs mainly in the enterocytes (brush border). The present review is focused on these recently discovered biological functions of OEA, its metabolism and analysis.

C. Thabuis · J.-C. Martin
UMR1260 «Nutriments Lipidiques et Prévention des Maladies Métaboliques», INRA, Marseille 13385, France

C. Thabuis · J.-C. Martin
U476, INSERM, Marseille 13385, France

C. Thabuis · J.-C. Martin
Faculté de Médecine, IPHM-IFR 125,
University Aix-Marseille 1, University Aix-Marseille 2,
Marseille 13385, France

D. Tissot-Favre · J.-B. Bezelgues · C. Cruz-Hernandez ·
F. Dionisi · F. Destaillats (✉)
Nestlé Research Center, Vers-chez-les-Blanc,
P.O. Box 44, 1000 Lausanne 26, Switzerland
e-mail: frederic.destaillats@rdls.nestle.com

Biological Functions of Oleoylethanolamide

Effect of Oleoylethanolamide on Food Intake Control

Oleoylethanolamide is synthesized in the small intestine of various vertebrate species, where its level decreases during food deprivation and increases upon re-feeding [2, 4, 5]. The increased level of plasmatic OEA after feeding could be due to the presence of OEA in food [2, 3], but OEA concentrations in food products are really low (under 2 µg/g of food), suggesting that one part of the increased level of OEA is linked to an activated endogenous synthesis. Indeed, food intake may stimulate *N*-acyltransferase (NAT) activity, and biosynthesized OEA can trigger satiety signals [2, 4, 5]. In brain, the anandamide concentration significantly increases upon severe food restriction. The level of this endocannabinoid is modulated in the brain structures according to the feeding status and depending on specific localization in the brain. Anandamide levels do not change in the hypothalamus, but increase in the limbic forebrain [6]. Anandamide and OEA were shown to be active through two distinct pathways. Thus, anandamide activates cannabinoid receptor CB1 mainly in the mesolimbic system [6], leading to an increase of food intake, whereas intestinal OEA induces a satiety signal, leading to a decrease of food intake. Similarly to anandamide, the natural levels of OEA change with respect to the nutritional status, leading to a precise control of food intake. This control is central to induce food intake and peripheral to induce satiety [5].

Pharmacological studies have been performed to better understand how a very simple fatty acid derivative can control food intake. A significant decrease of food intake was observed for 4 h after intraperitoneal (ip) injection of OEA at 5 mg/kg of body weight and for all of the 9 days of the experiment in rats [7]. The same treatment also lowered the body weight gain compared to the control [7]. Intracerebroventricular administration of OEA did not induce any effects underlying the peripheral action of OEA [4]. Various OEA doses have been tested with ip administration from 5 to 20 mg/kg of body weight, always leading to a dose-dependent decrease of food intake. Compared to the control (animals injected with vehicles), the percentages of food intake decrease were 32, 24 and 14%, respectively, for 20, 10 and 5 mg of OEA/kg bw on the 24 h following the injection [8, 9]. These measures were performed in a 24-h experiment. The effects of OEA on food intake were reproducible for 14 days. Indeed, subchronic intraperitoneal administration of 5 mg OEA/kg bw induced a global diminution of food consumption. Cumulative food intake was significantly decreased over the 14 days of the experiment, but the daily food intake was not significantly lower compared to controls among these experimental periods. Nevertheless, the subchronic OEA administration, with a daily injection of 5 mg OEA/kg bw, induced a 3% significant decrease of body weight for all of the experiment [10].

Further studies looking at the oral administration effect of OEA confirmed that OEA acts peripherally [11]. When OEA was administrated by gavage at different concentrations, a significant decrease of food intake on 24 h was observed at 200 mg/kg of oral OEA [11]. When OEA was administrated in pH-protective capsules (releasing OEA at pH 6), a similar effect was observed at a fourfold lower level (50 mg/kg bw) [12]. The effects of OEA capsules were significantly different from controls 5 h after administration, which corresponds to the time for the capsules to go from the stomach to the small intestine. All together, these results suggest that OEA reduces food intake by acting at a local site within the small intestine [12]. Several meal parameters have also been monitored and demonstrated that OEA induced a delay of the first meal, a decrease of the size of the first meal and an increase of the post-meal intervals [12]. It has been shown that ethanolamine and oleic acid, the degradation products of OEA, did not have any influence on food intake when administrated orally [11]. A bioavailability study, using radiolabeled OEA administrated to rats by gavage (10 mg/kg of body weight), has been performed to assess OEA degradation in the gastrointestinal tract [11]. This treatment increased the OEA level to about 11 times in intestinal tissue. However, only 0.48% of the given dose was found unchanged in the tissue. The ratio of intact OEA to hydrolyzed OEA decreased along the gastrointestinal tract, showing that OEA is progressively catabolized [11].

In parallel, studies have been performed to establish whether OEA has any influence on the synthesis of satiety signaling biomarkers, such as glucagon-like peptide-1 (GLP-1), cholecystokinin (CCK) and peptide YY (PYY), which have satietogenic effects, and ghrelin, which stimulates appetite. These molecules act along the gastrointestinal tract and are secreted separately depending on the nutritional status. The satietogenic peptides GLP-1, CCK and PYY are released during the post-prandial period, whereas the ghrelin plasma level is increased under starvation. The alternative release of these different biomarkers contributes strongly to food consumption regulation. Intraperitoneal injection of OEA was shown to reduce the ghrelin level, but not the GLP-1 concentration in rats [13], whereas CCK and PYY remained unaffected [8]. The anorectic effects of OEA do not imply the modulation of the secretion of satiety signals [8, 13].

Satietogenic properties of OEA can also be partially explained by its action on the gastrointestinal tract itself. Indeed, OEA delays gastric emptying [14] and slows down intestinal motility [15]. The delay of these parameters has a strong influence on nutrient absorption and thus on food intake control. All together, these results suggest that OEA plays a role in the peripheral control of food intake that has to be integrated with the nervous and hormonal control of satiety. Nevertheless, more studies are necessary to confirm that OEA properties that were observed in in vitro studies or in animal models are applicable to humans for therapeutic metabolic health.

Effects of Oleoylethanolamide on Lipid Metabolism

The modulation of lipid metabolism by OEA was initially demonstrated by Rodriguez de Fonseca et al. [4]. Indeed, OEA treatment induced a higher reduction of body weight gain than the one observed in the pair-fed group, demonstrating that the effect on body weight is not only due to the decrease of food intake, but also to a direct effect on lipid metabolism [4]. Intraperitoneal administration of 5 mg/kg of OEA in rats increased the expression of FAT/CD36 (fatty acid translocase) in adipose tissues [4]. Following this observation, the OEA effect was tested on cell cultures of enterocytes and adipocytes. In adipocytes, OEA induced an increase of the FAT/CD36 expression and of the fatty acid release, suggesting an increased lipolysis [7]; it is also an agonist of the capsaicin receptor transient receptor potential vanilloid type 1 (TRPV1) that is expressed in preadipocytes. Once activated, this receptor inhibits differentiation of preadipocytes and adipogenesis [16]. In enterocytes, an increase of FAT/CD36 expression and of fatty acid uptake was demonstrated after OEA treatment [7]. These observations suggest that the increased fatty acid uptake in enterocytes is due to the decreased food intake and body weight gain. OEA would enhance the utilization of nutrients in the small intestine. These findings support the fact that OEA would play an important role in lipid metabolism by increasing the lipolysis in adipocytes and, simultaneously, increasing fatty acid uptake in the intestine, partially implicating the modulation of FAT/CD36 expression [7]. These results on lipolysis were previously demonstrated in vivo, suggesting a role of peroxisome proliferator-activated receptor alpha (PPAR-α) in fatty acid β-oxidation in muscle through a study performed on PPAR-α null mice [17], but also in obese rats, as OEA treatment can reduce the accumulation of lipid droplets in the liver and significantly decrease plasma cholesterol and triglyceride levels [10].

These results suggest that OEA has lipolytic properties through the inhibition of adipogenesis in adipose tissue [16] and the activation of lipid β-oxidation in muscle [17]. Nevertheless, OEA concentration was not decreased during preadipocyte differentiation after the negative control of leptin or PPAR-γ, contrary to the level of its anti-inflammatory analogue PEA [16]. These last findings do not favor the local action of OEA on preadipocyte differentiation through the activation of TRPV1 [18]. Consequently, the major action of OEA on lipid metabolism would be essentially an increased lipid β-oxidation in muscle and a better fat utilization through a higher lipolysis in mature adipocytes. These results would have to be confirmed in humans through clinical trials.

Oleoylethanolamide Acts Peripherally

It has been demonstrated that in some of the OEAs observed, peripheral anorexic effects [4] are mediated by the activation of peroxisome proliferator-activated receptor alpha (PPAR-α) [19] with a relatively high affinity ($K_d = 37.4$ nM) compared to other potential endogenous ligands of PPAR-α present in partially digested food, such as free fatty acids [20]. A study has been performed in wild-type and PPAR-α knock-out mice to understand how OEA, which is a potent endogenous PPAR-α agonist, can regulate food intake and body weight gain [10]. This study showed that OEA reduces food intake, inhibits body-weight gain and lowers plasma cholesterol levels in wild-type mice, whereas it does not have such effects in PPAR-α mutant mice [10]. This implication of PPAR-α in the OEA mechanism of action has also been confirmed with some in vitro gene reporter assays on cell cultures [21].

In addition to its interaction with PPAR-α, OEA has been shown to be an agonist of TRPV1. At submicromolar concentrations, OEA activates native TRPV1 in rodents on perivascular sensory nerves and elicits whole cell currents and fluorometric calcium response in human cell lines expressing TRPV1 [22]. TRPV1 activation leads to the excitation of peripheral vagal sensory nerves involved in the nervous control of food intake [23]. TRPV1 is expressed in both nociceptive neurons, where it is involved in the detection of noxious chemicals and thermal stimuli, and in visceral sensory neurons and brain, where it could have a role on food intake control. OEA was shown to indirectly regulate the activity of TRPV1 and the excitation of sensory nerves expressing TRPV1. Indeed, if TRPV1 is phosphorylated by the protein kinase C, it becomes more sensitive to OEA activation [23]. To confirm TRPV1 involvement in OEA effects on food intake, normal mice and TRPV1-null mice were injected with OEA (12.5 mg/kg bw). Short-term feeding was significantly reduced in the control group, but not in the TRPV1-null group, showing the role of this receptor in feeding regulation [22, 24]. Another study was performed in vivo and in vitro to establish the relationship between the rat TRPV1 receptor and OEA, employing measurement of $^{45}Ca^{2+}$ uptake in TRPV1 receptor-transfected cells. OEA showed agonist properties on TRPV1 receptor by stopping $^{45}Ca^{2+}$ uptake in cells expressing TRPV1 [25]. The mechanism of action of OEA on TRPV1 is linked to a Ca^{2+} concentration modulation inside the cell, inducing an effect on vagal sensory nerves and, consequently, on food intake regulation.

Furthermore, a protein-G coupled receptor (GPR119) having affinity with OEA (OEA activates GPR119 with an EC_{50} superior to 30 μM) has been recently identified in intestinal and pancreatic cells [26, 27]. This receptor is mainly expressed in the gastrointestinal tract and in the pancreas. A specific agonist of GPR119, named PSN632408, has been identified. The satietogenic efficiency of PSN632408 was investigated in vivo through intraperitoneal administration (100 mg/kg bw). It induced a 30% decrease of food intake, strongly associated to GPR119 activation. As GPR119 is activated by OEA, it could partially participate in OEA satietogenic effects [26]. However, although the implication of GPR119 in food intake regulation has been demonstrated, it is still uncertain whether it can be activated in vivo by OEA [28].

In Fig. 1, a tentative mechanism of action of OEA on the control of food intake is proposed. Fatty acids and derivatives such as OEA are PPAR-α ligands (Kd = 37.4 nM for OEA) [19, 29]. OEA can activate intestinal PPAR-α, inducing the activation of other nuclear receptors such as RXR. Indeed, PPAR-α and RXR can form a heterodimer that can bind to response elements, leading to the activation of target gene transcription [29, 30]. These expression modulations would be involved in food intake and lipid metabolism regulation. In addition to this intestinal effect, circulating OEA could block TRPV1 receptors on neuronal cells. This mechanism would modify the electrical status of the Ca^{2+} channel, inducing small depolarization [24]. Thus, the vagal sensory nerves would be excited, directly influencing food intake regulation.

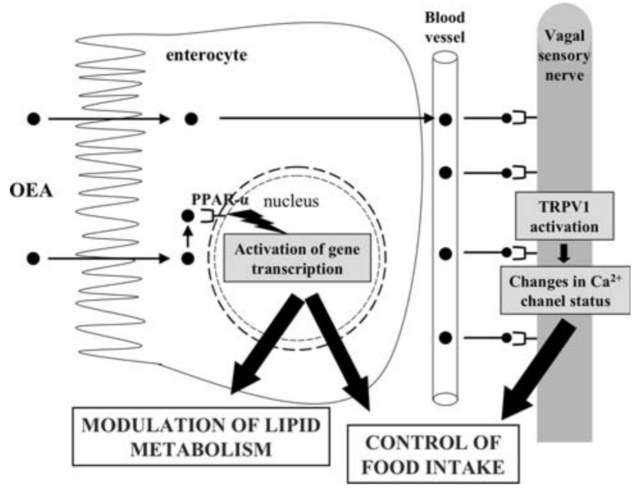

Fig. 1 Mechanism of action of oleoylethanolamide. PPAR-α and TRPV1 stand respectively for peroxisome proliferator-activated receptor α and transient receptor potential vanilloid 1

Effects of Oleoylethanolamide on Glucose Metabolism

Rats, intraperitoneally treated with OEA, showed a glucose intolerance compared to control without decreasing the insulin level [31]. The effects of OEA on the plasma glucose management were tested in vivo by performing glucose tolerance tests [31]. OEA-treated animals had significantly higher plasma glucose after 30 min of glucose load, but no other significant differences in any other time points have been noticed, indicating an impairing effect on glucose tolerance in the short term rather than a diabetogenic effect [31].

Some experiments performed on isolated adipocytes showed that OEA induces a 30% inhibition of insulin-stimulated glucose uptake and inhibits insulin action [31]. These observations cannot totally explain the glucose intolerance observed in rats in vivo [31], because, on one hand, the glucose transport inhibition due to OEA in adipocytes is really low, and, on the other hand, only part of the glucose clearance from the blood happens in adipocytes; the liver and the skeletal muscles strongly contribute to this phenomenon. Moreover, in another study, OEA administration did not induce modification of blood glucose levels at any time point [10], and it has been reported that OEA can trigger phosphorylation of the glucose transporter GLUT4, which could counterbalance the observed OEA inhibition of insulin-stimulated glucose transport [31]. Indeed, glucose transport activity has been reported to be mediated by phosphorylation and dephosphorylation of transporters such as GLUT4.

Oleoylethanolamide effects on glucose metabolism seem to depend on the tissue; further studies need to be performed, including a glucose tolerance test on hepatic cells.

Metabolism of Oleoylethanolamide in Animals

In mammalian tissue, the synthesis/degradation of OEA occurs mainly in specific cells, such as enterocytes (brush border) [32–40]; nevertheless, OEA biosynthesis has also been observed in adipose tissue and in insulinoma β-cells [41]. OEA biosynthesis involves two steps, which are catalyzed by two different enzymes called NAT and *N*-acyl-phosphatidylethanolamine phospholipase D (NAPE-PLD) (Fig. 2) [42, 43]. The first step, catalyzed by NAT, consists of the *N*-acylation of an oleic acid residue from membrane phosphatidylcholine (PC) to a phosphatidylethanolamine (PE). Different pathways have been proposed for the formation of *N*-acyl-phosphatidylethanolamine (NAPE) by inter- or intra-molecular N-acylation from PE, PC, lyso-PC or cardiolipin (Fig. 3) [43]. OEA, together with a phosphatidic acid molecule, is released from the

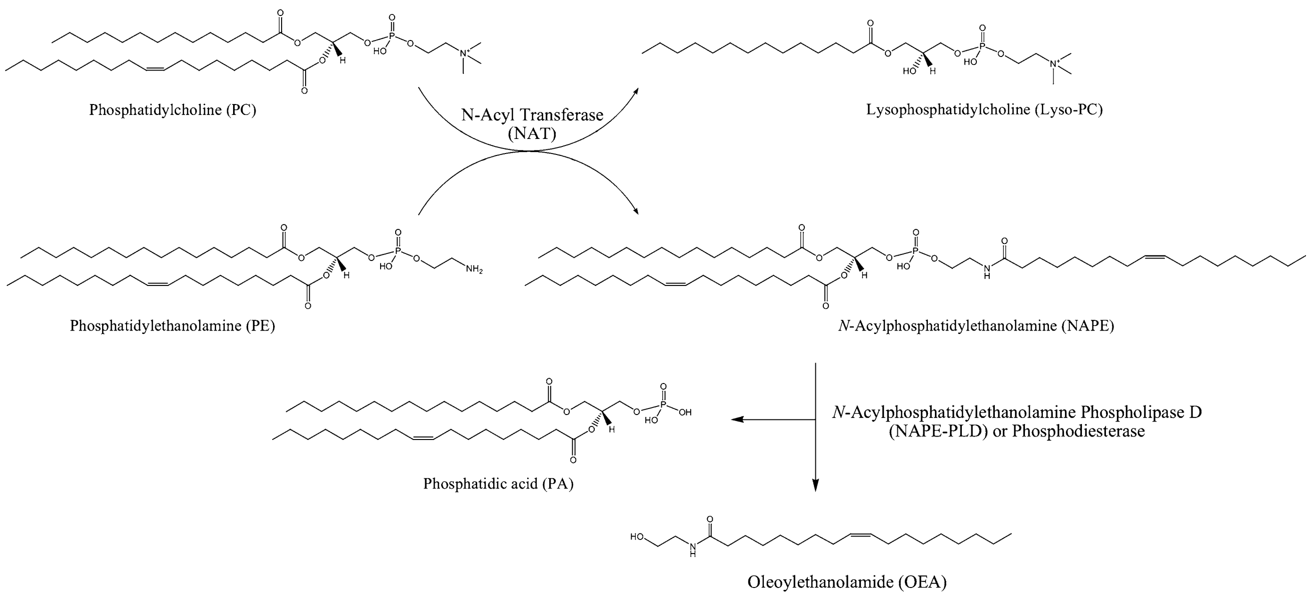
Phosphatidylcholine (PC)
N-Acyl Transferase (NAT)
Lysophosphatidylcholine (Lyso-PC)
Phosphatidylethanolamine (PE)
N-Acylphosphatidylethanolamine (NAPE)
Phosphatidic acid (PA)
N-Acylphosphatidylethanolamine Phospholipase D (NAPE-PLD) or Phosphodiesterase
Oleoylethanolamide (OEA)

Fig. 2 Metabolism of oleoylethanolamide (adapted from LoVerme et al. [42] and Schmid [43])

NAPE formed by NAPE-PLD-catalyzed hydrolysis. Alternatively, hydrolysis can be catalyzed by phosphodiesterase. OEA can be broken down into oleic acid and ethanolamine by two different hydrolases: fatty acid amide hydrolase (FAAH) or *N*-acylsphingosine amidohydrolase-like protein (ASAH like-protein) [44]. FAAH is specific for fatty acid amides and mainly responsible of OEA degradation according to high levels of plasma OEA in FAAH-null mice [15], and ASAH like-protein is a more ubiquitous amidase (Fig. 4) [42].

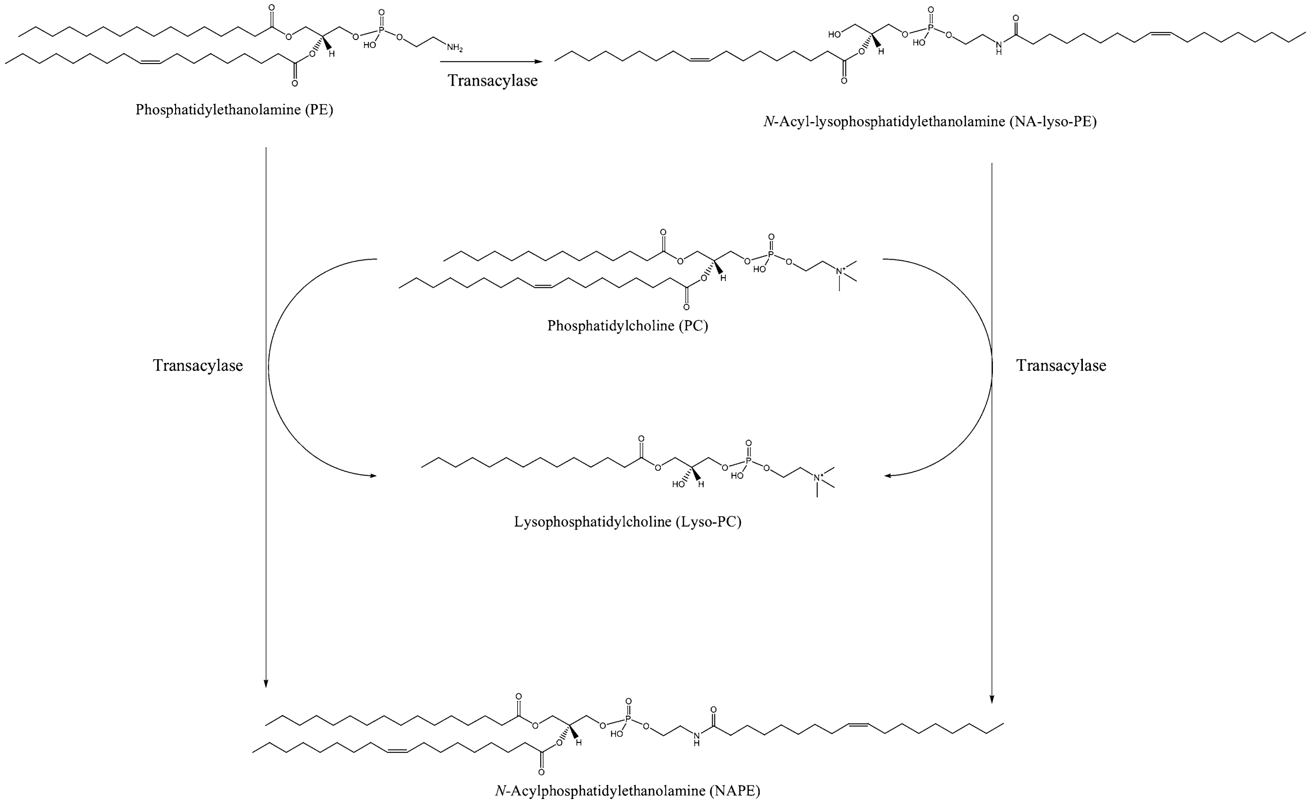
Phosphatidylethanolamine (PE)
Transacylase
N-Acyl-lysophosphatidylethanolamine (NA-lyso-PE)
Phosphatidylcholine (PC)
Transacylase
Transacylase
Lysophosphatidylcholine (Lyso-PC)
N-Acylphosphatidylethanolamine (NAPE)

Fig. 3 Inter- and intra-molecular N-acylation of PE from PC (adapted from Schmid [43])

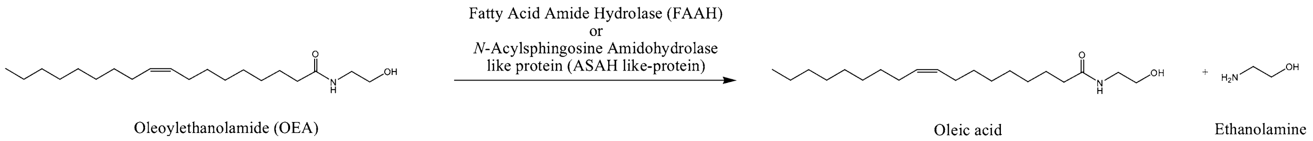
Fatty Acid Amide Hydrolase (FAAH)
or
N-Acylsphingosine Amidohydrolase
like protein (ASAH like-protein)
Oleoylethanolamide (OEA)
Oleic acid
Ethanolamine

Fig. 4 Catabolism of oleoylethanolamide, adapted from LoVerme et al. [42]

Moreover, the link between OEA and food intake regulation has been shown by Fu et al. [45]; indeed, feeding stimulates OEA mobilization in the mucosal layer of rat duodenum and jejunum by increasing NAPE-PLD activity and expression and by decreasing amido-hydrolase (FAAH) activity and expression. Nutrient availability regulates OEA mobilization in the mucosa of the proximal intestine through a concerted regulation of OEA biosynthesis and degradation [45].

Astarita et al. [2] examined whether feeding-induced OEA mobilization can be observed in Burmese pythons (*Python molurus*), which consume huge meals after months of fasting. Their way of feeding seems to depend on changes in gastrointestinal hormonal release and gut morphology. A nearly 300-fold increase in OEA levels in the small intestine of fed compared to fasted animals has been observed [2]. NAPE species increase simultaneously with OEA in situ; therefore, NAPEs can be considered as potential biosynthetic precursors for OEA.

OEA synthesis in the intestinal mucosa has been extensively studied; less is known about the regulation of OEA synthesis in other tissues. In adipocytes, OEA levels do not vary during differentiation, contrary to PEA levels [41], whereas in insulinoma β-cells, OEA levels are decreased under “high glucose” conditions [41]. In “high glucose” conditions, OEA biosynthesis is activated by glucose and insulin [41]. In addition, diabetes type II patients are characterized by a higher OEA level in their plasma after food consumption [41]. All together, these results suggest that OEA biosynthesis is downregulated under transient hyperglycemia [41].

Conclusion and Perspectives

Oleoylethanolamide is a very promising molecule; the simple derivative of oleic acid is a transient endogenous signaling lipid formed from PE and PC through the actions of NAT and NAPE-PLD. After ingestion, OEA has a short lifetime and is cleaved into acid oleic and ethanolamine by the FAAH or the ASAH-like protein in many tissues, including the gastrointestinal tract. The core biological functions of OEA are (1) to control food intake through activation of peripheral PPAR-α, (2) to promote lipid utilization and (3) to modulate lipid storage in liver and circulating plasma lipids (triglycerides and cholesterol). However, the effects of chronic oral administration of OEA on lipid metabolism and satiety have not been extensively studied to date. The gap between the science and the potential applications in weight management is important, and studies evaluating long-term effects and safety are necessary.

References

1. Lambert DM, Vandevoorde S, Jonsson KO, Fowler CJ (2002) The palmitoylethanolamide family: a new class of anti-inflammatory agents? Curr Med Chem 9:663–674
2. Astarita G, Rourke BC, Andersen JB, Fu J, Kim JH, Bennett AF, Hicks JW, Piomelli D (2006) Postprandial increase of oleoylethanolamide mobilization in small intestine of the Burmese python (*Python molurus*). Am J Physiol Regul Integr Comp Physiol 290:R1407–R1412
3. Di Marzo V, Sepe N, De Petrocellis L, Berger A, Crozier G, Fride E, Mechoulam R (1998) Trick or treat from food endocannabinoids? Nature 396:636–637
4. Rodriguez de Fonseca F, Navarro M, Gomez R, Escuredo L, Nava F, Fu J, Murillo-Rodriguez E, Giuffrida A, LoVerme J, Gaetani S, Kathuria S, Gall C, Piomelli D (2001) An anorexic lipid mediator regulated by feeding. Nature 414:209–212
5. Petersen G, Sorensen C, Schmid PC, Artmann A, Tang-Christensen M, Hansen SH, Larsen PJ, Schmid HH, Hansen HS (2006) Intestinal levels of anandamide and oleoylethanolamide in food-deprived rats are regulated through their precursors. Biochim Biophys Acta 1761:143–150 discussion 141–142
6. Kirkham TC, Williams CM, Fezza F, Di Marzo V (2002) Endocannabinoid levels in rat limbic forebrain and hypothalamus in relation to fasting, feeding and satiation: stimulation of eating by 2-arachidonoyl glycerol. Br J Pharmacol 136:550–557
7. Yang Y, Chen M, Georgeson KE, Harmon CM (2006) Mechanism of acylethanolamides (OEA) on fatty acid uptake in small intestine after food intake and body weight reduction. Am J Physiol Regul Integr Comp Physiol
8. Proulx K, Cota D, Castaneda TR, Tschop MH, D’Alessio DA, Tso P, Woods SC, Seeley RJ (2005) Mechanisms of oleoylethanolamide-induced changes in feeding behavior and motor activity. Am J Physiol Regul Integr Comp Physiol 289:R729–R737
9. Gaetani S, Oveisi F, Piomelli D (2003) Modulation of meal pattern in the rat by the anorexic lipid mediator oleoylethanolamide. Neuropsychopharmacology 28:1311–1316
10. Fu J, Oveisi F, Gaetani S, Lin E, Piomelli D (2005) Oleoylethanolamide, an endogenous PPAR-alpha agonist, lowers body weight and hyperlipidemia in obese rats. Neuropharmacology 48:1147–1153
11. Nielsen MJ, Petersen G, Astrup A, Hansen HS (2004) Food intake is inhibited by oral oleoylethanolamide. J Lipid Res 45:1027–1029

12. Oveisi F, Gaetani S, Eng KT, Piomelli D (2004) Oleoylethanolamide inhibits food intake in free-feeding rats after oral administration. Pharmacol Res 49:461–466
13. Cani PD, Montoya ML, Neyrinck AM, Delzenne NM, Lambert DM (2004) Potential modulation of plasma ghrelin and glucagon-like peptide-1 by anorexigenic cannabinoid compounds, SR141716A (rimonabant) and oleoylethanolamide. Br J Nutr 92:757–761
14. Aviello G, Matias I, Capasso R, Petrosino S, Borrelli F, Orlando P, Romano B, Capasso F, Di Marzo V, Izzo AA (2008) Inhibitory effect of the anorexic compound oleoylethanolamide on gastric emptying in control and overweight mice. J Mol Med 86:413–422
15. Capasso R, Matias I, Lutz B, Borrelli F, Capasso F, Marsicano G, Mascolo N, Petrosino S, Monory K, Valenti M, Di Marzo V, Izzo AA (2005) Fatty acid amide hydrolase controls mouse intestinal motility in vivo. Gastroenterology 129:941–951
16. Matias I, Gonthier MP, Petrosino S, Docimo L, Capasso R, Hoareau L, Monteleone P, Roche R, Izzo AA, Di Marzo V (2007) Role and regulation of acylethanolamides in energy balance: focus on adipocytes and beta-cells. Br J Pharmacol 152:676–690
17. Guzman M, Lo Verme J, Fu J, Oveisi F, Blazquez C, Piomelli D (2004) Oleoylethanolamide stimulates lipolysis by activating the nuclear receptor peroxisome proliferator-activated receptor alpha (PPAR-alpha). J Biol Chem 279:27849–27854
18. Zhang LL, Yan Liu D, Ma LQ, Luo ZD, Cao TB, Zhong J, Yan ZC, Wang LJ, Zhao ZG, Zhu SJ, Schrader M, Thilo F, Zhu ZM, Tepel M (2007) Activation of transient receptor potential vanilloid type-1 channel prevents adipogenesis and obesity. Circ Res 100:1063–1070
19. Fu J, Gaetani S, Oveisi F, Lo Verme J, Serrano A, Rodriguez De Fonseca F, Rosengarth A, Luecke H, Di Giacomo B, Tarzia G, Piomelli D (2003) Oleylethanolamide regulates feeding and body weight through activation of the nuclear receptor PPAR-alpha. Nature 425:90–93
20. Lambert DM, Muccioli GG (2007) Endocannabinoids and related *N*-acylethanolamines in the control of appetite and energy metabolism: emergence of new molecular players. Curr Opin Clin Nutr Metab Care 10:735–744
21. Astarita G, Di Giacomo B, Gaetani S, Oveisi F, Compton TR, Rivara S, Tarzia G, Mor M, Piomelli D (2006) Pharmacological characterization of hydrolysis-resistant analogs of oleoylethanolamide with potent anorexiant properties. J Pharmacol Exp Ther 318:563–570
22. Movahed P, Jonsson BA, Birnir B, Wingstrand JA, Jorgensen TD, Ermund A, Sterner O, Zygmunt PM, Hogestatt ED (2005) Endogenous unsaturated C18 *N*-acylethanolamines are vanilloid receptor (TRPV1) agonists. J Biol Chem 280:38496–38504
23. Ahern GP (2003) Activation of TRPV1 by the satiety factor oleoylethanolamide. J Biol Chem 278:30429–30434
24. Wang X, Miyares RL, Ahern GP (2005) Oleoylethanolamide excites vagal sensory neurones, induces visceral pain and reduces short-term food intake in mice via capsaicin receptor TRPV1. J Physiol 564:541–547
25. Almasi R, Szoke E, Bolcskei K, Varga A, Riedl Z, Sandor Z, Szolcsanyi J, Petho G (2008) Actions of 3-methyl-*N*-oleoyldopamine, 4-methyl-*N*-oleoyldopamine and *N*-oleoylethanolamide on the rat TRPV1 receptor in vitro and in vivo. Life Sci
26. Overton HA, Babbs AJ, Doel SM, Fyfe MC, Gardner LS, Griffin G, Jackson HC, Procter MJ, Rasamison CM, Tang-Christensen M, Widdowson PS, Williams GM, Reynet C (2006) Deorphanization of a G protein-coupled receptor for oleoylethanolamide and its use in the discovery of small-molecule hypophagic agents. Cell Metab 3:167–175
27. Sakamoto Y, Inoue H, Kawakami S, Miyawaki K, Miyamoto T, Mizuta K, Itakura M (2006) Expression and distribution of Gpr119 in the pancreatic islets of mice and rats: predominant localization in pancreatic polypeptide-secreting PP-cells. Biochem Biophys Res Commun 351:474–480
28. Brown AJ (2007) Novel cannabinoid receptors. Br J Pharmacol 152:567–575
29. Desvergne B, Wahli W (1999) Peroxisome proliferator-activated receptors: nuclear control of metabolism. Endocr Rev 20:649–688
30. Michalik L, Auwerx J, Berger JP, Chatterjee VK, Glass CK, Gonzalez FJ, Grimaldi PA, Kadowaki T, Lazar MA, O'Rahilly S, Palmer CN, Plutzky J, Reddy JK, Spiegelman BM, Staels B, Wahli W (2006) International Union of Pharmacology. LXI. Peroxisome proliferator-activated receptors. Pharmacol Rev 58:726–741
31. Gonzalez-Yanes C, Serrano A, Bermudez-Silva FJ, Hernandez-Dominguez M, Paez-Ochoa MA, Rodriguez de Fonseca F, Sanchez-Margalet V (2005) Oleylethanolamide impairs glucose tolerance and inhibits insulin-stimulated glucose uptake in rat adipocytes through p38 and JNK MAPK pathways. Am J Physiol Endocrinol Metab 289:E923–E929
32. Ueda N, Tsuboi K, Lambert DM (2005) A second *N*-acylethanolamine hydrolase in mammalian tissues. Neuropharmacology 48:1079–1085
33. Hogestatt ED, Jonsson BA, Ermund A, Andersson DA, Bjork H, Alexander JP, Cravatt BF, Basbaum AI, Zygmunt PM (2005) Conversion of acetaminophen to the bioactive *N*-acylphenolamine AM404 via fatty acid amide hydrolase-dependent arachidonic acid conjugation in the nervous system. J Biol Chem 280:31405–31412
34. Di Marzo V (1999) Biosynthesis and inactivation of endocannabinoids: relevance to their proposed role as neuromodulators. Life Sci 65:645–655
35. Di Marzo V, Fontana A, Cadas H, Schinelli S, Cimino G, Schwartz JC, Piomelli D (1994) Formation and inactivation of endogenous cannabinoid anandamide in central neurons. Nature 372:686–691
36. Cadas H, Gaillet S, Beltramo M, Venance L, Piomelli D (1996) Biosynthesis of an endogenous cannabinoid precursor in neurons and its control by calcium and cAMP. J Neurosci 16:3934–3942
37. Cadas H, di Tomaso E, Piomelli D (1997) Occurrence and biosynthesis of endogenous cannabinoid precursor, *N*-arachidonoyl phosphatidylethanolamine, in rat brain. J Neurosci 17:1226–1242
38. Kuwae T, Shiota Y, Schmid PC, Krebsbach R, Schmid HH (1999) Biosynthesis and turnover of anandamide and other N-acylethanolamines in peritoneal macrophages. FEBS Lett 459:123–127
39. Khan SH, Kaphalia BS, Ansari GA (2005) In vitro conjugation of ethanolamine with fatty acids by rat liver subcellular fractions. J Toxicol Environ Health A 68:667–676
40. Bisogno T, Delton-Vandenbroucke I, Milone A, Lagarde M, Di Marzo V (1999) Biosynthesis and inactivation of *N*-arachidonoylethanolamine (anandamide) and *N*-docosahexaenoylethanolamine in bovine retina. Arch Biochem Biophys 370:300–307
41. Matias I, Petrosino S, Racioppi A, Capasso R, Izzo AA, Di Marzo V (2008) Dysregulation of peripheral endocannabinoid levels in hyperglycemia and obesity: effect of high fat diets. Mol Cell Endocrinol
42. LoVerme J, Guzman M, Gaetani S, Piomelli D (2006) Cold exposure stimulates synthesis of the bioactive lipid oleoylethanolamide in rat adipose tissue. J Biol Chem 281:22815–22818
43. Schmid HH (2000) Pathways and mechanisms of *N*-acylethanolamine biosynthesis: can anandamide be generated selectively? Chem Phys Lipids 108:71–87

44. Sun YX, Tsuboi K, Zhao LY, Okamoto Y, Lambert DM, Ueda N (2005) Involvement of *N*-acylethanolamine-hydrolyzing acid amidase in the degradation of anandamide and other *N*-acylethanolamines in macrophages. Biochim Biophys Acta 1736:211–220
45. Fu J, Astarita G, Gaetani S, Kim J, Cravatt BF, Mackie K, Piomelli D (2007) Food intake regulates oleoylethanolamide formation and degradation in the proximal small intestine. J Biol Chem 282:1518–1528

Lipids (2008) 43:895–902
DOI 10.1007/s11745-008-3233-y

ORIGINAL ARTICLE

Substrate Preferences of a Lysophosphatidylcholine Acyltransferase Highlight Its Role in Phospholipid Remodeling

Michael Kazachkov · Qilin Chen · Liping Wang · Jitao Zou

Received: 11 June 2008 / Accepted: 20 August 2008 / Published online: 10 September 2008
© AOCS 2008

Abstract An important enzyme involved in phospholipid turnover is the acyl-CoA: lysophosphatidylcholine acyltransferase (LPCAT). Here, we report characterization of a newly discovered human LPCAT (LPCAT3), which has distinct substrate preferences strikingly consistent with a role in phosphatidylcholine (PtdCho) remodeling and modulating fatty acid composition of PtdCho. LPCAT3 prefers lysophosphatidylcholine (lysoPtdCho) with saturated fatty acid at the *sn-1* position and exhibits acyl donor preference towards linoleoyl-CoA and arachidonoyl-CoA. Furthermore, LPCAT3 is active in mediating 1-*O*-alkyl-*sn*-glycero-3-phosphocholine acylation with long chain fatty acyl-CoAs to generate 1-*O*-alkyl-phosphatidylcholine, another very important constitute of mammalian membrane systems. These properties are precisely the known attributes of LPCAT previously ascribed to the isoform involved in Lands' cycle, and thus strongly suggest that LPCAT3 is involved in phospholipids remodeling to achieve appropriate membrane lipid fatty acid composition.

Keywords LPCAT · Phospholipid · Arachidonic acid · PtdCho turnover

Abbreviations

DAG	Diacylglycerol
CDP-choline	Cytidine 5′-diphosphocholine
CDP-DAG	Cytidine 5′-diacylglycerol
EUROSCARF	European *Saccharomyces cerevisiae* archive for functional analysis
LPCAT3	Human acyl-CoA: lysophosphatidylcholine acyltransferase
LCA1	Yeast lysophosphatidylcholine acyltransferase
LysoPA	Lysophosphatidic acid
LPCAT	Acyl-CoA: lysophosphatidylcholine acyltransferase
LysoPtdCho	Lysophosphatidylcholine
LysoPtdEtn	Lysophosphatidylethanolamine
LysoPtdGro	Lysophosphatidylglycerol
MBOAT	Membrane-bound *O*-acyltransferase
PAF	Platelet-activating factor
PtdCho	Phosphatidylcholine

Introduction

Phosphatidylcholine (PtdCho) is one type of glycerolipid molecule that is present in almost all cellular membrane systems. An important aspect of PtdCho metabolism first discovered by Lands almost a half century ago was that PtdCho synthesized through the de novo pathways undergoes extensive remodeling [1–4]. The remodeling process, which concerns the turnover of about half of the PtdCho molecules, involves the deacylation of PtdCho

---

M. Kazachkov · Q. Chen · L. Wang · J. Zou (✉)
Plant Biotechnology Institute,
National Research Council Canada,
110 Gymnasium Place, Saskatoon,
SK S7N OW9, Canada
e-mail: Jitao.zou@nrc-cnrc.gc.ca

M. Kazachkov
Genome Prairie, 101-111 Research Drive,
Saskatoon, SK S7N 3R2, Canada
e-mail: Michael.Kazachkov@nrc-cnrc.gc.ca

M. Kazachkov
Institute of Bioorganic Chemistry and Petrochemistry,
National Academy of Science of Ukraine,
1 Murmanskaya str, Kiev-94 02660, Ukraine

to lysophosphatidylcholine (lysoPtdCho), followed by reacylation of lysoPtdCho to PtdCho. It has since become apparent that the process of PtdCho remodeling concerns a wide range of cellular activities because fatty acids derived from PtdCho can be precursors for the biosynthesis of other lipid-related molecules, and that any change in the balance of the deacylation/reacylation processes may have a direct consequence to membrane lipid composition. One key enzymatic component involved in PtdCho remodeling is acyl-CoA: lysophosphatidylcholine acyltransferase (LPCAT), which is detected in many different types of mammalian cells [4].

Fatty acyltransferases are integral membrane proteins recalcitrant to purification, and often exhibit promiscuity in regards to substrate specificity. Recently, identifications of several LPCAT enzymes have been reported; they all mediate the *sn-2* acylation of lysoPtdCho, but also have their own distinct functionalities. For example, LPCAT1 identified from lung alveolar type II cells was responsible for lung surfactant PtdCho production [5, 6]. An isoform with lyso-platelet-activating factor (lysoPAF) and lysoPtdCho dual substrate acyltransferase was reported as involved in inflammatory process in inflammatory cells [7]. Another isoform particularly important for PtdCho biosynthesis in human red blood cells was also identified [8]. With regard to structure, all these enzymes exhibit high sequence similarity to the previously identified *sn-2* lysophosphatidic acid acyltransferase family, which is characterized by four highly conserved motifs [9].

We and others have recently reported a new lysophosphatidylcholine acyltransferase (LCA1) from yeast that is predominant in mediating lysoPtdCho acylation [2, 10–13]. Structurally, the yeast LPCAT is closely related to the membrane-bound *O*-acyltransferase (MBOAT) family and does not possess the conserved motifs of the previously studied *sn-2* acyltransferases [9]. The present study was conducted to examine the biochemical function of LCA1 close homologs from mammals. Data presented in this report extend the latest reports from Zhao et al. [14] and Hishikawa et al. [15] on the LPCAT activity of this class of enzyme, but we conducted our study through heterologous expression in a yeast LPCAT knockout mutant that had a very low LPCAT background, and hence ideal for substrate specificity characterization. Our results serve to emphasize the properties that draw attention to its role in PtdCho remodeling and modulating the fatty acid compositions of PtdCho. We also show that, in addition to acylating lysoPtdCho, this enzyme is active in mediating 1-*O*-alkyl-*sn*-glycero-3-phosphocholine (also known as lyso-platelet-activating factor, lysoPAF) acylation to generate 1-*O*-alkyl-phosphatidylcholine. Its distinct substrate preferences and wide distribution of transcript strongly suggest that this isoform is a key component of the Land's cycle, and hence important in modulating the fatty acid composition of membrane lipids.

Materials and Methods

Strains and Reagents

Yeast strains: BY4741 (WT, *MATa hisΔ1 leuΔ0 metΔ0 uraΔ0*) and Y02431 (*lca1Δ*, *MATa his3Δ1 leu2Δ0 met15Δ0 ura3Δ0* YOR175c::KanX4) were purchased from European *Saccharomyces cerevisiae* archive for functional analysis (EUROSCARF). Various lysophospholipids and acyl-CoAs were obtained from Avanti Polar Lipids (Alabaster, AL). [^{14}C] oleoyl-CoA, [^{14}C] palmitoyl-CoA, [^{14}C] arachidonoyl-CoA, [^{14}C] palmitoyl lysoPtdCho were purchased from American Radiolabeled Chemicals Inc. and Moravek Biochemicals, Inc. Yeast extract, Yeast Nitrogen Base, Bacto-peptone, and Bacto-agar were purchased from Difco™, D-glucose, D-galactose and D-raffinose were from Sigma. SC minimal medium and plates was prepared according to Invitrogen's recipe described for the pYES2.1 TOPO TA Cloning Kit.

Gene Expression Vector Construction and Yeast Transformation

Full-length cDNAs of human genes (NM_005768, NM_024298) and mouse genes (NM_145130, NM_029934) were purchased from Openbiosystem (Huntsville, USA). The cDNAs were PCR amplified with primer pairs listed in Table 1 and cloned into yeast expression vector pYES2.1 using pYES2.1TOPO TA Expression Kit. Correctly-oriented plasmids were identified by mini-prep and further verified through DNA sequencing. The plasmid was subsequently introduced into yeast strain Y02431, of which the MBOAT lysophosphatidylcholine acyltransferase-encoding gene *LCA1* was disrupted.

Microsomal Preparation

Yeast strains were first grown in 15 ml of SC-Ura medium containing 2% glucose. Protein expression induction was carried out as described in the manufacturer manual (Invitrogen). After 24 h of growth in SC + 2% galactose + 1% raffinose, the cells were washed sequentially with distilled water and homogenization buffer [50 mM Tris–HCl, 1 mM EDTA, 0.6 M sorbitol, pH 7.4, 1 mM dithiothreitol (DTT)]. After centrifugation at 4,000 rpm (Eppendorf centrifuge 5145C), the cells were resuspended in 1 ml homogenization buffer containing 10 µl yeast protease cocktail (Sigma), and shaken vigorously

Table 1 Primer pairs used in PCR amplification of cDNAs of human and mouse LPCAT candidate genes

Protein	Gene	Forward primer	Reverse primer
NP_005759	NM_005768	GGGGGTGAAGCGATAGCGTT	GCACAGGCCACCAGGGAAAT
NP_077274	NM_024298	TCATACACATACGATTTAGGT	CTGGCAGAGGGAGCGTCGT
NP_660112	NM_145130	GGGGGCGCCCGCAGTTA	CTCGGCCACCAGGGAAAGA
NP_084210	NM_029934	CGAAAAGGAGCTCCGCAGTT	CAAACAAAAACCCCAAACAAACA

(1 min × 2 times) in the presence of acid-washed glass beads (diameter 0.5 mm). The resultant homogenate was centrifuged at 12,000 rpm for 10 min at 4 °C. The decanted supernatant was further centrifuged at 100,000×*g* for 90–120 min at 4 °C. The supernatant was discarded, and the pellet was resuspended in homogenization buffer containing 20% glycerol and frozen at −80 °C until use. Protein concentration was measured using a Bio-Rad Protein Assay Kit for final enzyme activity calculation.

In Vitro Assay of LPCAT Activity

LPCAT substrate specificity was determined by measuring incorporation of [^{14}C] lysoPtdCho or [^{14}C] Acyl-CoA into PtdCho. All assays were performed at least twice. In order to reduce the influence of endogenous acyl-CoAs two different concentrations of microsomal proteins were used. For lysophospholipid substrate specificity assessment, 1.0 ml HEPES (pH 7.4, 0.1 M) buffer contained 0.5 µg microsomal protein, 5.6 µM of lysophospholipid substrates and 13.5 µM [^{14}C] arachidonoyl-CoA (20 nCi/nmol). For acyl-CoA substrate selectivity analysis, 1.0 ml HEPES reaction buffer (pH 7.4, 0.1 M) contained 20 µg microsomal proteins, 11.25 µM acyl-CoA and 5.6 µM [^{14}C] palmitoyl lysoPtdCho (1.35 nCi/nmol). Reaction was allowed to proceed for 10 min at 30 °C with 100 rpm shaking. For determination of K_m and V_{max}, 20 µg microsomal protein was used in a 0.8 ml HEPES reaction buffer (pH 7.4, 0.1 M) with different concentrations of acyl-CoA and 5.6 µM [^{14}C] palmitoyl-lysoPtdCho (1.35 nCi/nmol). All reactions were linear in 1 h range. The reaction products were extracted with chloroform/methanol (2/1, v/v) and separated with Merck silica G60 TLC plates. Spots corresponding to different phospholipid species products were scraped off and ^{14}C incorporation were scintillation counted.

1-*O*-Alkyl-*sn*-Glycero-3-Phosphocholine Sensitivity

Yeast strains Y02431 expressing NM_005768 cDNA or harboring empty vector were first grown in 15 ml of SC-Ura medium containing 2% glucose then transferred to SC-Ura + 2% galactose and 1% raffinose. After 12 h gene expression induction, the culture was diluted to correspond to OD_{600} value of 0.5, 1, 2 and 4. A measure of 5 µl of each dilution was spotted to YPD plate supplemented with varying concentrations of 1-hexadecyl-*sn*-glycero-3-phosphocholine. The plates were incubated at 28 °C for 2 days.

Northern Blot

The premade human Northern blot (Cat.#:HN-MT-1) was purchased from ZYAGEN laboratories. A 1.5 kb fragment of *LPCAT3* (NM_005768) cDNA was PCR amplified with primer pairs described in Table 1 and purified for probe preparation. The ^{32}P-labeled probe was purified with NICK column (Amersham), denatured by incubation at 100 °C for 5 min and then added to the hybridization tube containing 25 ml hybridization solution (0.5 M Sodium Phosphate buffer pH 7.5, 7% SDS, 1 mM EDTA, 1% BSA). After overnight hybridization at 60 °C, the membrane was washed twice using 40 mM sodium phosphate buffer and 1% SDS and exposed to X-ray film in Saran wrap for 1 week.

Results

Identification of LPCAT3

We previously established that the yeast MBOAT protein YOR175cp (LCA1) is a LPCAT and plays a significant role in PtdCho turnover. A BLAST [16] search using YOR175cp identified several homologs from human (MBOAT1 NP_001073949, XP_001131044, MBOAT2 NP_620154, MBOAT4 XP_001125855, MBOAT5 NP_005759, MBOAT7, NP_077274) and mouse (MBOAT1 NP_705774, XP_134120, MBOAT2 isoform b NP_001076810, MBOAT2 isoform a NP_080313, MBOAT5 NP_660112, MBOAT7 NP_084210). Sequence alignment indicated that human proteins NP_077274, NP_005759, and mouse proteins NP_660112, NP_084210 had the highest sequence similarity to YOR175p (Fig. 1). Consequently, these four proteins were selected as human and mouse LPCAT candidates in this study.

The cDNAs of the four candidate genes were cloned into the yeast expression vector pYES2.1 and subsequently introduced into the yeast host strain *lca1Δ*. The *lca1Δ* strain has a very low LPCAT background activity, and thus functionality of LPCAT orthologs can be readily tested in

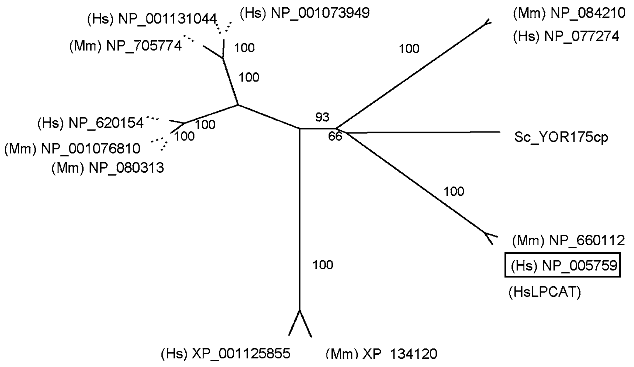

Fig. 1 Unrooted phylogenetic tree based on yeast LPCAT (YOR175cp) and its related proteins in human and mouse. An alignment analysis of all the selected protein sequences was performed with ClustalW of Molecular Evolutionary Genetics Analysis software (Mega 4) with default parameters: gap opening penalty = 10; gap extension penalty = 0.2. The phylogenetic tree was constructed by neighbor-joining method using default settings

this host strain. The calculation of the enzyme activity was based on the difference between the *lca1Δ* strain harboring the human cDNAs and that of an empty vector. Preliminary enzyme assays using microsomal fractions with palmitoyl-lysoPtdCho as acyl acceptor, and either oleoyl-CoA (18:1) or arachidonoyl-CoA (20:4) as acyl donor, showed that *lca1Δ* expressing NP_005759 and NP_660112 displayed LPCAT activity (Fig. 2). But repeated assays failed to detect significant increase of LPCAT enzyme activity in *lca1Δ* strains expressing the other two closely related homologs, NP_077274 and NP_084210. NP_077274 was recently shown to have LPIAT activity [17]. Since both NP_005759 and NP_660112 appeared to have similar enzyme property, we subsequently conducted detailed biochemical characterization on the human protein NP_005759. We followed the nomenclature proposed by Zhao et al. [14], and designated this enzyme as LPCAT3.

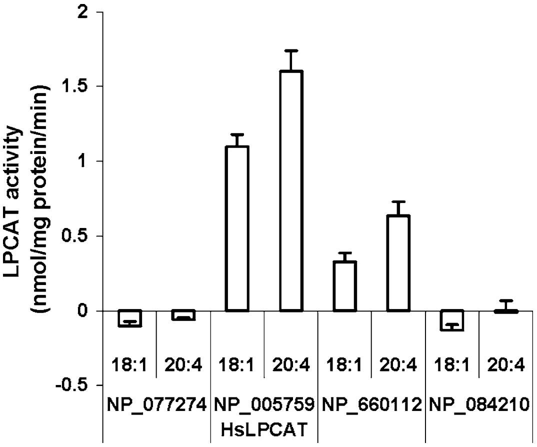

Fig. 2 LPCAT activity of selected human and mouse LPCAT orthologs. Assays were performed with 5.6 μM [^{14}C] palmitoyl-lysoPtdCho (1.35 nCi/nmol), 11.25 μM acyl-CoA (18:1/20:4) and 20 μg microsomal protein prepared from *lca1Δ* strains expressing human proteins NP_077274, NP_005759, mouse proteins NP_660112 and NP_084210. Empty vector transformant (EV) was used as control. The enzyme reactions were allowed to proceed for 15 min at 30 °C. The results were presented as means ± SD of differences between empty vector and LPCAT3 transformants

LPCAT3 Displays Acyl-Acceptor Preference Towards 18:0-lysoPtdCho

In light of observations that acyltransferases are often promiscuous in substrate specificity [5, 7, 18], we performed acyltransferase assays with various lysophospholipid substrates to assess acyl acceptor preference of LPCAT3. Based on previous reports that selective acylation of lysophospholipids tends to occur only at very low concentration of substrates [19] and enzyme activity could be inhibited by high levels of acyl acceptors [3], the concentration of lysophospholipid substrate in our assays was provided at 5.6 μM. Based on existing literature showing that PC in many tissues was predominant by 20:4 at the *sn-2* position [20], we used [^{14}C] arachidonoyl-CoA (20:4-CoA) as acyl donor at 11.25–13.5 μM, a concentration much lower than reported level (50–130 μM) of long chain acyl-CoA known to be present in human tissue [19]. As shown in Fig. 3, the yeast strain expressing *LPCAT3* exhibited a dramatic increase in acylation activity with lysoPtdCho. Efficient LysoPtdEtn acylation was also evident. But no significant activity of acylation was detected when 16:0-lysoPtdGro was used as substrate. Acylation rate for lysoPA was less than 1% of the LPCAT activity. Thus, similar to the yeast LCA1[2] LPCAT3 exhibited the highest activity with lysoPtdCho.

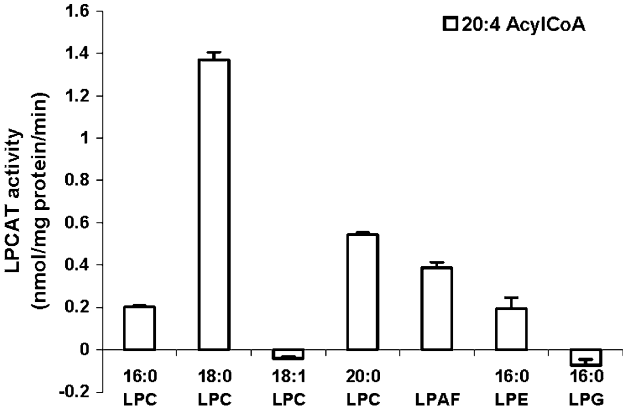

Fig. 3 LysoPtdCho substrate preference assessment of LPCAT3. Assay mixture contained 13.5 μM [^{14}C] arachidonoyl-CoA (20 nCi/nmol), 5.6 μM lysophospholipid and 0.5 μg microsomal protein extracted from *lca1Δ* harbouring empty vector or expressing *LPCAT3*. The reaction mixture was incubated for 1 h at 25 °C. The results were presented as means ± SD of differences between empty vector and LPCAT3 transformants

To investigate if the *sn-1* fatty acid species of the lysophospholipid acceptor affected LPCAT3 activity, assays were also performed using 1-palmitoyl-lysoPtdCho (16:0-lysoPtdCho), 1-stearoyl-lysoPtdCho (18:0-lysoPtdCho), 1-oleoyl-lysoPtdCho (18:1-lysoPtdCho), 1-arachidonyl-lysoPtdCho (20:0-lysoPtdCho), as well as the ether-linked lysoPtdCho analog of 1-hexadecyl-*sn*-glycero-3-phosphocholine, arachidonoyl-CoA (20:4-CoA) was provided as acyl donor. The LPCAT3 could efficiently use 16:0-lysoPtdCho, 18:0-lysoPtdCho and 20:0-lysoPtdCho, but apparently not the 18:1-lysoPtdCho (Fig. 3). LPCAT3 could also efficiently mediate 16:0-lysoPAF acylation. Based on our assay using arachidonoyl-CoA as acyl donnor, LPCAT3 exhibited substrate preferences in the order of 18:0-lysoPtdCho > 20:0-lysoPtdCho ≈ 16:0-lyso-PAF > 16:0-lysoPtdCho. It must be noted, however, as we show later in Fig. 4 that 18:2-CoA is the most preferable acyl donor, the question of whether 18:2-CoA would affect the order of acyl acceptor preferences requires future investigation.

LPCAT3 is Most Active in Utilizing 18:2-CoA as Acyl Donor

To characterize LPCAT3 acyl-CoA substrate preference, we incubated yeast microsomal fraction with 16:0-lysoPtdCho and acyl-CoAs of different chain length and various degrees of unsaturation (Fig. 4). LPCAT3 exhibited activity with all acyl-CoAs tested. However, the activity with linoleoyl-CoA (18:2) at a concentration of 11.25 μM was several folds higher than that with other acyl-CoAs. The degree of unsaturation seemed not to be the only determinant of lysoPtdCho acylation activity, since the utilization rate of other acyl-CoAs was found in the order of 16:0-CoA ≈ 20:4-CoA > 18:1-CoA > 18:0-CoA. The effect of increasing concentrations of two acyl donors, 18:1-CoA and 20:4-CoA, on LPCAT activity is shown in Fig 5. At lower acyl-CoA concentrations the enzyme was more active with 18:1-CoA. However, at concentrations higher than 3 μM, the enzyme was more active with 20:4-CoA. The V_{max} was calculated as 7.4 pmol/min/μg protein for 18:1-CoA and 12.4 pmol/min/μg protein for 20:4-CoA. The apparent K_m was 0.45 ± 0.01 μM and 5.1 ± 1.2 μM for 18:1-CoA and 20:4-CoA, respectively. Since the reported physiological acyl-CoA concentration was 5–160 μM [21, 22], our results suggest that under physiological conditions the LPCAT3 could effectively acylate lysoPtdCho into PtdCho, especially using 20:4-CoA as acyl donor.

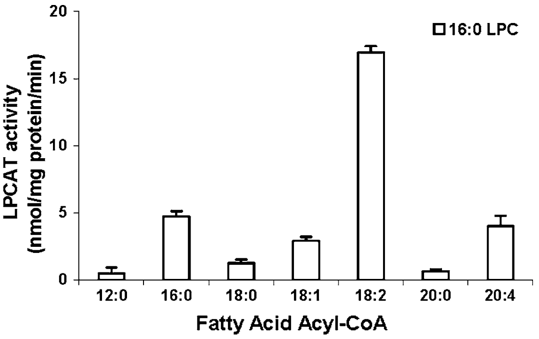

Fig. 4 Acyl-CoA substrate preference assessment of LPCAT3. Assays were preformed with 5.6 μM [^{14}C] palmitoyl-lysoPtdCho (1.35 nCi/nmol), 11.25 μM acyl-CoA as indicated and 20 μg microsomal protein from *lca1Δ* yeast cells harbouring empty vector or expressing LPCAT3. The reaction mixtures were incubated for 10 min at 30 °C. Results were presented as means ± SD of differences between empty vector and LPCAT3 transformants

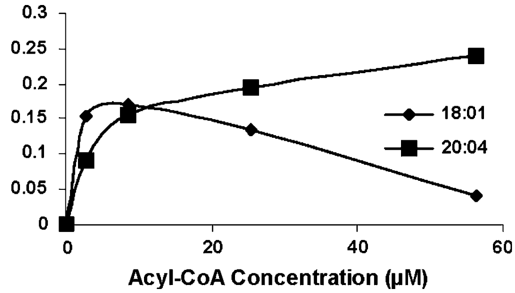

Fig. 5 LPCAT3 activity dependence on acyl-CoA concentration. Assays were performed with 5.6 μM [^{14}C] palmitoyl-lysoPtdCho (1.35 nCi/nmol), 18:1-CoA or 20:4-CoA of various concentrations, 20 μg microsomal proteins prepared from *lca1Δ* yeast cells harbouring empty vector or expressing *LPCAT3*. The enzyme reaction was allowed to proceed for 10 min at 30 °C

LPCAT3 Acylates 1-*O*-Alkyl-*sn*-Glycero-3-Phosphocholine with Arachidonyl-CoA but not Acetyl-CoA

Since LPCAT3 could efficiently acylate 1-*O*-alkyl-*sn*-glycero-3-phosphocholine with long chain fatty acid, particularly 20:4-CoA (Fig. 4), we then tested if LPCAT3 could acylate this ether lipid with acetyl-CoA, which would generate the platelet-activating factor (PAF). Our result showed that acetylation of 1-*O*-alkyl-*sn*-glycero-3-phosphocholine was negligible (Fig. 6). It is known that 1-*O*-alkyl-*sn*-glycero-3-phosphocholine can be effectively taken up and reacylated by yeast [23], and that the *lca1Δ* yeast strain was hypersensitive to 1-*O*-alkyl-*sn*-glycero-3-phosphocholine [2], likely caused by the detergent effect of this ether lipid when it is not reacylated. To examine if LPCAT3 could detoxify 1-*O*-alkyl-*sn*-glycero-3-phosphocholine when expressed in yeast, the *LPCAT3* transformant and vector-only transformant of *lca1Δ* yeast strain were spotted onto media supplemented with varying concentration of 1-*O*-alkyl-*sn*-glycero-3-phosphocholine. Both strains could grow reasonably well with 5 μg/ml 1-*O*-alkyl-*sn*-glycero-3-phosphocholine but failed to grow at a concentration beyond 20 μg/ml. However, when transferred to

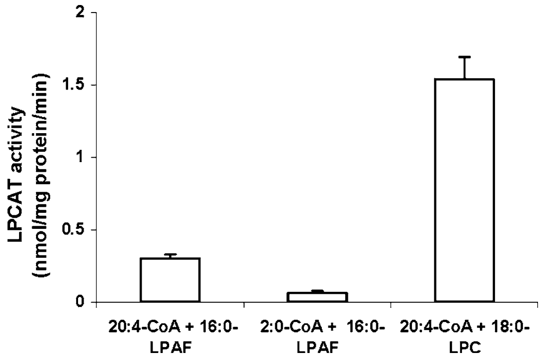

Fig. 6 Comparative assessment of LPCAT3 substrate preference towards lysoPtdCho and lyso-PAF. Assays were performed with 5.6 µM lysophospholipids, 13.5 µM [^{14}C] radiolabeled acyl-CoA (20 nCi/nmol) and 0.5 µg microsomal protein extracted from *lca1Δ* harbouring empty vector or expressing *LPCAT3*. The reaction mixture was incubated for 1 h at 25 °C. Results were presented as means ± SD of differences between empty vector and LPCAT3 transformants

media supplemented with 10 µg/ml 1-*O*-alkyl-*sn*-glycero-3-phosphocholine, *LPCAT3* transformant evidently grew better as compared with the vector-only transformant (Fig. 7). This result further corroborated our in vitro assay data that LPCAT3 possessed the ability to transfer an acyl group to *sn-2* position of 1-*O*-alkyl-*sn*-glycero-3-phosphocholine.

Transcript of LPCAT3 Is Widely Distributed

We examined the *LPCAT3* gene expression profile in different human tissues through Northern blot hybridization. *LPCAT3* was highly expressed in lung and thymus but also expressed at a significant level in testis, heart, kidney and pancreas (Fig. 8a). Since Northern blot analysis would not allow an accurate quantitative assessment of the transcript level, we also retrieved *LPCAT3* expression pattern from Genevestigator (https://www.genevestigator.ethz.ch), which contained *LPCAT3* expression data from many tissues and cell cultures not included in our northern blot. A considerable high expression level was detected in adipocyte cell (Fig. 8b). Taken together, these results indicated a wide distribution of *LPCAT3* transcript in human tissues.

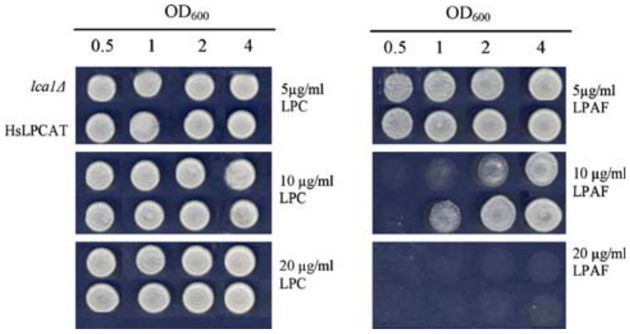

Fig. 7 1-*O*-alkyl-*sn*-glycero-3-phosphocholine sensitivity test of *lca1Δ* harbouring empty vector and *lca1Δ* strain expressing LPCAT3. Cells were grown first in SC-Ura + 2% glucose media overnight then in protein expression induction media for 6 h. Cultures were diluted to OD_{600} = 0.5, 1, 2, 4, respectively. A measure of 5 µl of each dilution was inoculated (from *left* to *right*) onto YPD plate containing 16:0-lysoPtdCho and 1-hexadecyl-*sn*-glycero-3-phosphocholine of varying concentration. The *plates* were incubated at 28 °C for 36 h

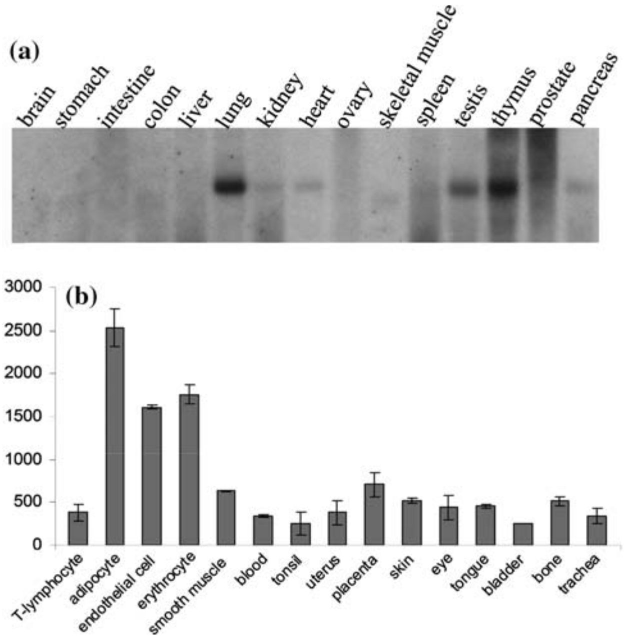

Fig. 8 *LPCAT3* expression profile in different human tissues **a** Northern blot hybridization **b** relative expression in different cells and tissues based on Genevestigator human gene expression data

Discussion

There is usually an asymmetric distribution of acyl groups in phospholipids, with saturated fatty acids esterified at the *sn-1* position of the glycerol backbone, whereas the unsaturated fatty acids are normally found at the *sn-2* position. It has been accepted as truism that the appropriate fatty acid composition in membrane systems is achieved through extensive PtdCho remodeling after de novo synthesis [3, 4], and that the Lands cycle represents a major route through which "tailoring" of the PtdCho takes place. However, understanding of the mechanistic details has been hindered by the lack of a molecular handle.

Upon testing different lysoPtdCho substrates we found that LPCAT3 had a lysoPtdCho species preference in the order of 18:0-lysoPtdCho > 20:0-lysoPtdCho > 16:0-lysoPtdCho. Strikingly, lysoPtdCho with unsaturated fatty acid residue (18:1-lysoPtdCho) was not able to sustain detectable acylation by this enzyme. Such an acyl acceptor preference is remarkably consistent with the stereo-specific distribution of fatty acids in PtdCho because 18:0 and 16:0 fatty acyl moieties occupy the *sn-1* position in more than 80% of PtdCho molecules in most tissues [24–26]. In this respect, this mammalian LPCAT is different from that reported for a plant LPCAT, which was shown to display equal utilization rate to 16:0, 18:0 and 18:1-lysoPtdCho [27]. With regard to acyl donors, LPCAT3 is very active in incorporating unsaturated 18:2-CoA. Indeed, in animal cells, the most prevalent fatty acid found at the *sn-2* position of the PtdCho is 18:2 [24–26]. LPCAT in Lands' cycle is also believed to play a role in mediating the replacement of the fatty acid at the *sn-2* position of PtdCho with arachidonic acid, which is stored until it is required for the generation of signal molecules including prostaglandins, prostacyclins, thromboxanes and leucotrienes. Depending on tissues, PtdCho containing an arachidonoyl moiety at the *sn-2* position represents as much as a third of total PtdCho. Interestingly, we found that LPCAT3 was very efficient in incorporating 20:4 into PtdCho. Taken together, these substrate preferences, presumably reflecting its properties in vivo, strongly suggest that LPCAT3 is a key enzymatic agent controlling the fatty acid composition of PtdCho in membrane systems [28].

It was also significant that LPCAT3 was capable of acylating 1-*O*-alkyl-*sn*-glycero-3-phosphocholine. The substrate specificity of this LPCAT leads to the expectation that it is a radyl-lysophosphocholine acyltransferase that does not distinguish the type of bond at the *sn-1* position of phospholipids. A minimal interpretation of these results is that LPCAT3 may play a role in generating 1-*O*-alkyl-phosphatidylcholine, which, depending on tissues, can represent a significant portion of membrane lipid constituent. However, different from the recently identified lysoPtdCho/lysoPAF dual substrate enzyme [15], it is clear that LPCAT3 is not directly involved in PAF biosynthesis because LPCAT3 did not display any activity in mediating acetylation of lyso-PAF with acetyl-CoA to generate PAF [29] (Fig. 6).

It must be noted that it is enzyme substrate specificity and supply of acyl donor substrates that collectively account for the phospholipid profiles of membrane systems. Concentrations of different fatty acyl-CoAs under physiological condition are at about 5–150 μM in a variety of the tissues [21, 22]. Moreover, different tissues may have variable intracellular acyl-CoA concentrations that can be fluctuating within a wide range [30]. The K_m of LPCAT3 for acyl-CoAs was found to be well below physiological levels. Thus, LPCAT3 may mediate a metabolic step that allows changes in acyl-CoA pool size to influence PtdCho composition. Another aspect of LPCAT3 being able to potentially exert regulatory input to PtdCho composition is the observation that higher 18:1-CoA concentration could in fact inhibit its acylation activity. The curve of the substrate dependence for 18:1-CoA exhibited a typical shape of an enzymatic reaction with substrate inhibition. It is unclear if this inhibitory effect has any significance in vivo, but clearly it was not caused by micelle formation since micelle formation would typically require fatty acyl-CoAs in a range of 10–30 μM [31, 32]. Intriguingly, 20:4-CoA did not appear to exert inhibitory effects to LPCAT3.

Our assessment on the transcript distribution from both RNA blot analysis and the public available microarray data indicated that *LPCAT3* was widely distributed in different tissues. This finding is somewhat different from the results of a previous report in which LPCAT3 was shown to be primarily expressed in metabolic active tissues [14]. We are unable to explain this apparent discrepancy, but tissue conditions and/or physiological conditions may have contributed to this. It should be noted that the mouse *mLPCAT3* was also found in a wide range of tissues.

Conclusions

The turnover of phospholipids and the remodeling of fatty acid composition have direct effects on membrane structure and intracellular trafficking in the secretory and endocytic pathways. The different kinetics mechanisms, substrate selectivity of LPCAT3 for both acyl acceptors (lysoPtdCho species) and acyl donors (acyl-CoAs) may play an important role in modulating the fatty acid composition of PtdCho in mammalian membrane systems. Our results also show that LPCAT3 is sensitive to acyl-CoA level and thus this enzyme provide a basis for metabolic variables to influence fatty acid compositions of PtdCho. That the *LPCAT3* gene is widely expressed in different tissues offers the prospect of it being a novel platform for studying Lands' cycle and PtdCho remodeling.

Acknowledgments We are grateful to Dr. Zhifu Zheng and Dr. Olga Kharchenko for helpful discussion and suggestions. We thank Drs. Patrick Covello and Meng Zhang for critical reading of the manuscript. This research is support in part by Genome Prairie and Genome Canada, a not-for-profit organization that is leading Canada's national strategy on genomics. This is National Research Council Canada publication # 50106.

References

1. Carman GM, Henry SA (1999) Phospholipid biosynthesis in the yeast Saccharomyces cerevisiae and interrelationship with other metabolic processes. Prog Lipid Res 38:361–399
2. Chen Q, Kazachkov M, Zheng Z, Zou J (2007) The yeast acylglycerol acyltransferase LCA1 is a key component of Lands cycle for phosphatidylcholine turnover. FEBS Lett 581:5511–5516

3. Choy PC, Skrzypczak M, Lee D, Jay FT (1997) Acyl-GPC and alkenyl/alkyl-GPC:acyl-CoA acyltransferases. Biochim Biophys Acta 1348:124–133
4. Lands WE (1960) Metabolism of glycerolipids. 2. The enzymatic acylation of lysolecithin. J Biol Chem 235:2233–2237
5. Chen X, Hyatt BA, Mucenski ML, Mason RJ, Shannon JM (2006) Identification and characterization of a lysophosphatidylcholine acyltransferase in alveolar type II cells. Proc Natl Acad Sci USA 103:11724–11729
6. Nakanishi H, Shindou H, Hishikawa D, Harayama T, Ogasawara R, Suwabe A, Taguchi R, Shimizu T (2006) Cloning and characterization of mouse lung-type acyl-CoA:lysophosphatidylcholine acyltransferase 1 (LPCAT1). Expression in alveolar type II cells and possible involvement in surfactant production. J Biol Chem 281:20140–20147
7. Shindou H, Hishikawa D, Nakanishi H, Harayama T, Ishii S, Taguchi R, Shimizu T (2007) A single enzyme catalyzes both platelet-activating factor production and membrane biogenesis of inflammatory cells. Cloning and characterization of acetyl-CoA:LYSO-PAF acetyltransferase. J Biol Chem 282:6532–6539
8. Soupene E, Fyrst H, Kuypers FA (2008) Mammalian acyl-CoA:lysophosphatidylcholine acyltransferase enzymes. Proc Natl Acad Sci USA 105:88–93
9. Lewin TM, Wang P, Coleman RA (1999) Analysis of amino acid motifs diagnostic for the sn-glycerol-3-phosphate acyltransferase reaction. Biochemistry 38:5764–5771
10. Benghezal M, Roubaty C, Veepuri V, Knudsen J, Conzelmann A (2007) SLC1 and SLC4 encode partially redundant acyl-coenzyme A 1-acylglycerol-3-phosphate O-acyltransferases of budding yeast. J Biol Chem 282:30845–30855
11. Jain S, Stanford N, Bhagwat N, Seiler B, Costanzo M, Boone C, Oelkers P (2007) Identification of a novel lysophospholipid acyltransferase in Saccharomyces cerevisiae. J Biol Chem 282:30562–30569
12. Riekhof WR, Wu J, Jones JL, Voelker DR (2007) Identification and characterization of the major lysophosphatidylethanolamine acyltransferase in Saccharomyces cerevisiae. J Biol Chem 282:28344–28352
13. Tamaki H, Shimada A, Ito Y, Ohya M, Takase J, Miyashita M, Miyagawa H, Nozaki H, Nakayama R, Kumagai H (2007) *LPT1* encodes a membrane-bound *O*-acyltransferase involved in the acylation of lysophospholipids in the yeast *Saccharomyces cerevisiae*. J Biol Chem 282:34288–34298
14. Zhao Y, Chen Y, Bonacci TM, Bredt DS, Li S, Bensch WR, Moller DE, Kowala M, Konrad RJ, Cao G (2008) Identification and characterization of a lysophosphatidylcholine acyltransferase that is primarily expressed in metabolic tissues. J Biol Chem 283:8258–8265
15. Hishikawa D, Shindou H, Kobayashi S, Nakanishi H, Taguchi R, Shimizu T (2008) Discovery of a lysophospholipid acyltransferase family essential for membrane asymmetry and diversity. Proc Natl Acad Sci USA 105:2830–2835
16. Altschul SF, Gish W, Miller W, Myers EW, Lipman DJ (1990) Basic local alignment search tool. J Mol Biol 215:403–410
17. Lee HC, Inoue T, Imae R, Kono N, Shirae S, Matsuda S, Gengyo-Ando K, Mitani S, Arai H (2008) Caenorhabditis elegans mboa-7, a member of the MBOAT family, is required for selective incorporation of polyunsaturated fatty acids into phosphatidylinositol. Mol Biol Cell 19:1174–1184
18. Yen CL, Monetti M, Burri BJ, Farese RV Jr (2005) The triacylglycerol synthesis enzyme DGAT1 also catalyzes the synthesis of diacylglycerols, waxes, and retinyl esters. J Lipid Res 46:1502–1511
19. Okuyama H, Lands WE (1972) Variable selectivities of acyl coenzyme A: monoacylglycerophosphate acyltransferases in rat liver. J Biol Chem 247:1414–1423
20. Yamashita A, Sugiura T, Waku K (1997) Acyltransferases and transacylases involved in fatty acid remodeling of phospholipids and metabolism of bioactive lipids in mammalian cells. J Biochem 122:1–16
21. Faergeman NJ, Knudsen J (1997) Role of long-chain fatty acyl-CoA esters in the regulation of metabolism and in cell signalling. Biochem J 323(Pt 1):1–12
22. Larson TR, Graham IA (2001) Technical advance: a novel technique for the sensitive quantification of acyl CoA esters from plant tissues. Plant J 25:115–125
23. Zaremberg V, McMaster CR (2002) Differential partitioning of lipids metabolized by separate yeast glycerol-3-phosphate acyltransferases reveals that phospholipase D generation of phosphatidic acid mediates sensitivity to choline-containing lysolipids and drugs. J Biol Chem 277:39035–39044
24. Kuksis A, Breckenridge WC, Marai L, Stachnyk O (1969) Molecular species of lecithins of rat heart, kidney, and plasma. J Lipid Res 10:25–32
25. Marai L, Kuksis A (1969) Molecular species of lecithins from erythrocytes and plasma of man. J Lipid Res 10:141–152
26. Wood R, Harlow RD (1969) Structural studies of neutral glycerides and phosphoglycerides of rat liver. Arch Biochem Biophys 131:495–501
27. Furukawa-Stoffer TL, Boyle RM, Thomson AL, Sarna MA, Weselake RJ (2003) Properties of lysophosphatidylcholine acyltransferase from *Brassica napus* cultures. Lipids 38:651–656
28. Waku K, Lands WE (1968) Control of lecithin biosynthesis in erythrocyte membranes. J Lipid Res 9:12–18
29. Waku K, Lands WE (1968) Acyl coenzyme A:1-alkenyl-glycero-3-phosphorylcholine acyltransferase action in plasmalogen biosynthesis. J Biol Chem 243:2654–2659
30. Veloso D, Veech RL (1974) Stoichiometric hydrolysis of long chain acyl-CoA and measurement of the CoA formed with an enzymatic cycling method. Anal Biochem 62:449–450
31. Brecher P The interaction of long-chain acyl CoA with membranes. http://www.ncbi.nlm.nih.gov/entrez/query.fcgi?cmd=Retrieve&db=PubMed&dopt=Citation&list_uids=6358858, Accessed 1 57
32. Powell GL, Grothusen JR, Zimmerman JK, Evans CA, Fish WW (1981) A re-examination of some properties of fatty acyl-CoA micelles. J Biol Chem 256:12740–12747

Lipids (2008) 43:903–912
DOI 10.1007/s11745-008-3216-z

ORIGINAL ARTICLE

Effect of CLA and Other C18 Unsaturated Fatty Acids on DGAT in Bovine Milk Fat Biosynthetic Systems

Brent M. Sørensen · E. Chris Kazala · Gordon K. Murdoch · Aileen F. Keating · Cristina Cruz-Hernandez · Jochen Wegner · John J. Kennelly · Erasmus K. Okine · Randall J. Weselake

Received: 20 January 2008 / Accepted: 9 July 2008 / Published online: 13 August 2008
© AOCS 2008

Abstract Production of dairy products with increased amounts of nutraceutic FA such as conjugated linoleic acid (CLA) represents a recent approach for dairy producers and processors to increase the value of their products. The effect of CLA and other FA on the expression of *diacylglycerol acyltransferase-1* (*DGAT-1*) and *DGAT-2*, and DGAT activity were investigated in bovine mammary gland epithelial (MAC-T) cells. DGAT gene expression analyses were also conducted using bovine mammary gland tissue from dairy cows. In the studies with MAC-T cells, there were no significant effects of CLA isomers or other FA on *DGAT1* expression, whereas all FA tested showed enhanced *DGAT2* expression ($P < 0.05$ to $P < 0.001$), with α-linolenic acid (α-18:3) having the greatest effect. Additionally, *DGAT2* expression was coordinated with expression of *lysophosphatidic acid acyltransferase* (*LPAAT*), an observation that was also apparent in mammary gland from lactating dairy cows. In contrast, treatment of MAC-T cells with *trans*-10, *cis*-12 18:2 or α-18:3 resulted in a significant ($P < 0.05$) decrease in overall DGAT enzyme activity, although the mechanisms resulting in these effects are unclear. Competition assays using microsomes from bovine mammary gland tissue and 1-[^{14}C]oleoyl-CoA suggested that DGAT activity was more selective for oleoyl (*cis*-9 18:1)-CoA than *cis*-9, *trans*-11 18:2-, *trans*-10, *cis*-12 18:2- or *cis*-9, *cis*-12 18:2-CoA. Collectively, the results suggest the relationship between *trans*-10, *cis*-12 18:2 and reduced TAG production in bovine milk is not linked to the production of DGAT1 or DGAT2 transcripts, but probably involves effects of this CLA isomer at events beyond transcription, such as post-translational and/or enzyme activity effects.

Keywords Conjugated linoleic acid · Diacylglycerol acyltransferase · Gene expression · Milk fat depression · Cattle · Dairy

Abbreviations

ACAT	Acyl-CoA:cholesterol acyltransferase
DGAT	Diacylglycerol acyltransferase
GAPDH	Glyceraldehyde-3-phosphate dehydrogenase
GPAT	*sn*-glycerol-3-phosphate acyltransferase
LPAAT	Lysophosphatidic acid acyltransferase
MFD	Milk fat depression
QRT-PCR	Quantitative real-time polymerase chain reaction
SCD	Stearoyl-CoA desaturase

Introduction

Conjugated linoleic acid (CLA) is a naturally abundant component in ruminant milk fat. These positional and geometric isomers of octadecadienoic acid occur as intermediates during the biohydrogenation of dietary fatty acids (i.e., linoleic and linolenic acid) by rumen microbes. Several isomers, most notably *cis*-9, *trans*-11 18:2 and *trans*-10, *cis*-12 18:2, have demonstrated nutraceutic properties,

---

B. M. Sørensen · E. Chris Kazala · G. K. Murdoch ·
A. F. Keating · C. Cruz-Hernandez · J. J. Kennelly ·
E. K. Okine · R. J. Weselake (✉)
Department of Agricultural, Food and Nutritional Science,
University of Alberta, 4-10 Agriculture/Forestry Centre,
Edmonton, AB T6G 2P5, Canada
e-mail: randall.weselake@ualberta.ca

J. Wegner
Research Institute for the Biology of Farm Animals,
18196 Dummerstorf, Germany

including decreased cancer incidence [1] and body weight [2]. Endogenous synthesis in the mammary gland is estimated to account for up to 78% of *cis*-9, *trans*-11 18:2 in milk from cows on total mixed ration diets [3, 4] and for up to 91% of milk CLA from pasture-fed cows [5].

Dairy producers wish to market products enriched in CLA so that consumers may benefit from these properties. The content of CLA isomers can be readily increased in milk fat by supplementing cattle diets with oilseeds or plant oils enriched in linoleic acid (*cis*-9, *cis*-12 18:2) [6, 7]. Another strategy is to supplement cattle with synthetic mixtures of CLA isomers protected from the rumen microflora by abomasal infusion [8]. The ionophore monensin may also be supplemented to the diet to prevent CLA isomers from being altered through rumem biohydrogenation [9].

In many cases, strategies resulting in elevated milk CLA content have also been shown to result in net milk fat depression (MFD). *Trans*-10, *cis*-12 18:2 has been suggested as the isomer responsible for this phenomenon [10, 11]. Cattle fed diets resulting in increased milk *trans*-10, *cis*-12 18:2 content coinciding with MFD also had decreased mRNA levels representing lipogenic genes, including those encoding *sn*-glycerol-3-phosphate acyltransferase (GPAT, EC 2.3.1.15), and lysophosphatidic acid acyltransferase (LPAAT, EC 2.3.1.51) [12]. GPAT and LPAAT catalyze the first and second acyl-CoA-dependent acylations of the glycerol backbone, respectively, in the Kennedy pathway leading to TAG [13].

Diacylglycerol acyltransferase (DGAT, EC 2.3.1.20) catalyzes the transfer of an acyl moiety from acyl-CoA to *sn*-1,2 diacylglycerol to form triacylglycerol (TAG) [13]. cDNAs encoding two isoforms of this enzyme (DGAT1 and DGAT2), which do not share amino acid sequence, have been isolated [14, 15]. An early study suggested that the level of DGAT activity in fat-forming tissues may have a substantial effect on the flow of carbon into TAG [16]. Indeed, over-expression of *DGAT1* and *DGAT2* in mouse liver has been shown to result in a 2.0- and 2.4-fold increase, respectively, in tissue TAG content [17]. In contrast, female mice with an inactivated DGAT1 gene ($DGAT^{-/-}$) are unable to lactate [18] and have impaired mammary gland development [19]. Additionally, a missense mutation in *DGAT1* has been shown to result in decreased milk fat content in dairy cows [20]. Hamsters supplemented with CLA isomers in the diet have been shown to display decreased intestinal acyl-CoA: cholesterol acyltransferase (ACAT EC 2.3.1.26) activity [21], suggesting that CLA may act to down regulate ACAT activity. Since DGAT1 shares some sequence homology with ACAT [14], CLA might regulate both enzymes in a similar fashion. In another study, murine primary preadipocyte cultures (3T3-L1) treated with arachidonic acid (all-*cis*-5,8,11,14 20:4) has been shown to result in repressed DGAT activity [22]. In addition, rats fed mixtures of CLA have been shown to display decreased hepatic DGAT activity compared with control rats fed the same amount of FA [22]. Earlier studies had found no difference in DGAT activity in rats fed similar amounts of *cis*-9 18:1 versus 18:0 [23].

Given the association of *trans*-10, *cis*-12 18:2 with MFD, we hypothesized that *DGAT* expression and/or DGAT activity might be affected by this CLA isomer. The effect of CLA isomers, including *cis*-9, *trans*-11 18:2 and *trans*-10, *cis*-12 18:2, and other FA, on *DGAT1*, *DGAT2*, and *LPAAT* expression levels, and DGAT activity were examined in cultured bovine mammary gland epithelial cells (MAC-T cells). Other FAs tested included *trans*-11 18:1, a substrate of mammalian Δ-9 desaturase, and FA commonly found in dietary plant oils ingested by dairy cattle. In addition, expression of *DGAT1*, *DGAT2*, and *LPAAT* were examined in mammary gland tissue from lactating dairy cows. Furthermore, the direct effects of CLA isomers on DGAT activity were investigated using microsomes prepared from bovine mammary gland tissue.

Materials and Methods

Animals

All procedures involving the use of animals were approved by the University of Alberta Animal Policy and Welfare Committee. Cows were housed in tie-stalls with water available at all times. The diets were fed once per day at 09:00 as total mixed rations consisting of 60% (w/w) forage and 40% (w/w) concentrate. Feed intake was recorded daily and adjusted to maintain 5–10% orts (feed remaining). Diets for the primiparous and multiparous lactating Holstein cows are described elsewhere [24]. Samples of mammary gland tissue were taken from six cows supplemented with safflower oil and monensin and six cows not receiving this treatment using a method adapted from Knight et al. [25]. The animals were sedated by administration of xylazine hydrochloride (10 mg/50 kg body weight) and ketamine (2 mg/kg body weight) via jugular catheter. The animals were maintained in a state of sedation with an intravenous drip of glycerol guaiacolate and ketamine [50 g glycerol guaiacolate, 1,000 mg ketamine, 1,000 ml 50% (w/v) dextrose and 900 ml sterile water]. The drip rate was set at 20 ml/min and maintained during surgery. The udder was shaved around the biopsy site and swabbed with iodine and 70% (v/v) ethanol. A region of the basal portion of the udder free of major subcutaneous blood vessels was chosen for the biopsy site. The area was anesthetized locally by injection of lidocaine (10–30 ml of 2% v/v lidocaine with epinephrine). An 8-cm incision was made in the skin; a 5–10-g piece of mammary gland tissue was excised using a scalpel and snap frozen in liquid nitrogen and then stored at −80°C.

Chemicals

Both *cis*-9, *trans*-11 18:2 and *trans*-10, *cis*-12 18:2 were obtained from Matreya (Pleasant Gap, PA). [1-^{14}C] *cis*-9 18:1 was from GE Healthcare (Baie d'Urfé, Quebec, Canada). Fatty acyl-CoA was prepared from the above FA as described by Taylor et al. [26]. Silica gel 60 H was from VWR Canlab (Missisauga, Ontario, Canada). Solvents (HPLC grade) were from Fisher Scientific (Ottawa, Ontario, Canada). Ecolite(+) biodegradable scintillation cocktail was from ICN Biomedicals (Irvine, CA). *sn*-1,2 Diolein was from Nu Chek Prep Inc. (Elysian, MN). Dulbecco's Modified Eagle Media (DMEM), fetal bovine serum (FBS), TRIzol® reagent, M-MLV reverse transcriptase, oligo (dT)12–18 primer, Rnase OUT Rnase inhibitor, dNTPs, 5X first strand buffer, and custom primers were from Invitrogen (Burlington, Ontario, Canada). rDNase, 10X buffer, and DNase inactivation agent were included in the Ambion DNA-*free*™ kit (catalog no. 1906, Austin, TX). FAM and VIC labeled probes and TaqMan® Universal PCR Mastermix were from Applied Biosystems (Foster City, CA). All other chemicals were from Sigma (Oakville, Ontario, Canada).

Maintenance and Treatment of Cultured Mammary Gland Epithelial Cell Line

MAC-T cells were originally established by Huynh et al. [27] and were kindly provided by Nicholas Lemee of Nexia Biotechnologies, Inc. (Montreal, Quebec, Canada). Cells were maintained essentially as described by Keating et al. [28]. The cells were cultured in high glucose (4.5 g/l) DMEM containing L-glutamine, sodium pyruvate, and pyroxidine-HCl and supplemented with 10% (v/v) FBS and 5 µg bovine insulin/ml. FAs used to treat MAC-T cells were complexed to BSA as potassium salts. Twelve milligrams of FA was treated with 1 ml of 0.1 M KOH. The solution was vortexed and incubated at 50°C, and then added dropwise to 9 ml of 7.5% (w/v) BSA. The resulting FA-BSA stock solution was incubated at room temperature for 3 h and then overnight at 4°C, and finally stored in small aliquots at −20°C. FA-BSA stock solution was added to DMEM to produce the final FA concentration used in FA treatment experiments. Cells were maintained in a humidified incubator at 37°C and 5% CO_2.

RNA Isolation, Reverse Transcription, and Quantitative Real-Time Polymerase Chain Reaction (QRT-PCR)

Total RNA was extracted from confluent MAC-T cells treated for 24 h with various exogenous FA and from the mammary gland tissue using TRIzol® reagent as described in the manufacturer's protocol. The total RNA was then treated with DNAase using the DNA-*free*™ kit from Ambion. cDNA was synthesized from 1 µg of total RNA in a 20-µl reaction volume with a final concentration of 0.5 mM dNTP mix, 0.5 µg Oligo $(dT)_{12–18}$, 5 µM DTT, 4 µl 5X first strand buffer, 40 U RNase out RNase inhibitor, and 200 U of M-MLV reverse transcriptase. The reaction mixture was incubated at 37°C for 60 min and then at 70°C for 15 min.

QRT-PCR was performed using the ABI Prism® 7900HT FAST QRT-PCR system with 9600 Emulation (Applied Biosystems) in a total volume of 25 µl reaction mixture following the manufacturer's protocol, using TaqMan® 2X Universal PCR Mastermix, 0.1 µM each of forward and reverse primer, and 0.2 µM of probe. Primers and TaqMan–MGB probes were designed against mRNA sequences specific for *DGAT1* (GenBank NM_174693), *DGAT2* (NM_205793), *LPAAT* (NM_177518), and *glyceraldehyde-3-phosphate dehydrogenase (GAPDH)* (NM_001034034) from *Bos taurus* using Primer Express® 3.0 Software (Applied Biosystems; Table 1).

Relative gene expression for *DGAT1*, *DGAT2*, or *LPAAT* was normalized to a calibrator that was chosen to be the basal condition (BSA control) for each treatment. Results were calculated with the $2_T^{-\Delta\Delta C}$ method [29] where $\Delta\Delta C_\mathrm{T} = (C_\mathrm{T,\ Target} - C_\mathrm{T,\ GAPDH})_\mathrm{Time\ \mathit{x}} - (C_\mathrm{T,\ Target} - C_\mathrm{T,\ GAPDH})_\mathrm{Time\ 0}$ and expressed as n-fold differences in gene expression relative to GAPDH mRNA and calibrator (BSA). Standard errors of the average $C_\mathrm{T,\ Target}$ and average $C_\mathrm{T,\ GAPDH}$ were pooled. C_T is defined as the number of cycles required until the specific dye-reporter emission reached the defined intensity threshold.

Extraction of Lipid from MAC-T Cells and Analysis of FA Composition

MAC-T cells were grown in 75-cm^2 flasks in DMEM containing 20 µM FA-BSA and incubated at 37°C. Upon confluence, cells were treated with trypsin-EDTA and harvested and transferred to acid-washed glass tubes. The vials were centrifuged at 1,500×*g*. The supernatant was removed, and the cells were resuspended in 1 ml phosphate buffered saline. The resuspended cells were probe sonicated for 30 s, and a sample was removed for protein determination. Lipids were extracted using a modified Folch [30] protocol. The following were added in sequence to the cell suspension, mixing by vortex for 30 s after each

Table 1 Primer and probe sequences for real-time polymerase chain reaction

Primers/detection probes	Sequence
DGAT1 forward primer	5′-GAACTCCGAGTCCATCACCTACTT-3′
DGAT1 reverse primer	5′-TCTGATGCACCACTTGTGAACA-3′
DGAT1 detection probe	5′-6FAM-TGGCAGAACTGGAACAT-MGBNFQ-3
DGAT2 forward primer	5′-GCCCTGCGCCATGGA-3′
DGAT2 reverse primer	5′-TACACCTCATTCTCCCCAAAGG-3′
DGAT2 detection probe	5′-6FAM-CCTGGTTCCCACCTAC-MGBNFQ-3
LPAAT forward primer	5′-GGACGCAACGTCGAGAACA-3′
LPAAT reverse primer	5′-CCGTACAGGTATTTGATGTGGAGTA-3′
LPAAT detection probe	5′-6FAM-AAGATCTTGCGTCTGATG-MGBNFQ-3
GAPDH forward primer	5′-TGCCGCCTGGAGAAACC-3′
GAPDH reverse primer	5′-CGCCTGCTTCACCACCTT-3′
GAPDH detection probe	5′-6FAM-CCAAGTATGATGAGATCAA-MGBNFQ-3

addition: 0.1 M KCl to bring suspension to total volume of 1.6 ml, 0.8 ml methanol, 2 ml chloroform/methanol (1:1, v/v), 2.7 ml chloroform, and 2.5 ml chloroform/methanol (2:1, v/v). The samples were incubated overnight at 4°C. Phase separation was achieved by centrifugation, and the chloroform layer was transferred to a glass vial and dried under N_2 (g). Prior to extraction, 100 μg of tritricosanoin (tri-23:0) was added to the cell suspension as an internal standard.

Production and GC analysis of FAME was based on methods described by Cruz-Hernandez et al. [31]. To the dried extract was added 100 μg of trinonadecanoin (tri-19:0), 1.7 ml of hexane, 40 μl of methyl acetate, and 100 μl of $NaOCH_3$ (0.5 M in methanol) followed by mixing for 2 min and incubation at room temperature for 20 min. The vial was then cooled at −20°C for 20 min, and 60 μl of oxalic acid (saturated in diethyl ether) was added. The vials were centrifuged to collect the oxalate precipitate, and the supernatant was spotted to a TLC plate. The plate was developed in one ascension of hexane/diethyl ether (80:20, v/v) using methyl-oleate as a standard. The plates were then visualized by spraying with 0.2% (w/v) 2,7’ dichlorofluorescein. The area corresponding to methyl-oleate was scraped and transferred to a column containing sodium sulfate. The FAMEs were eluted using 2 ml of chloroform, and 50 μg of methyl-hexacosanoate (methyl-26:0) was added.

FAMEs were analyzed by GC with a Varian 3800 GC (Varian Inc., Mississauga, Ontario, Canada), equipped with splitless injection port flushed after 0.3 s, a flame ionization detector (FID), autosampler (Model 8200, Varian Inc.), 100-m CP-Sil 88 fused capillary column (Varian Inc.), and a Hewlett-Packard ChemStation software system (version A.07). Operating conditions included: injector and detector temperatures both at 250°C; H_2 as carrier gas (1 ml/min) and for the FID (40 ml/min), N_2 (g) as makeup gas (100 ml/min), and purified air (250 ml/min). The initial temperature of 45°C was held for 4 min, increased at a rate 13°C/min to 175°C, and held for 27 min, and finally increased at a rate 4°C/min to 215°C and held for 35 min. FAMEs were identified by comparison with a reference standard.

Assay of DGAT Activity in MAC-T Cells

DGAT activity was measured in MAC-T cells based on the protocol described by Geelen [32]. MAC-T cells were grown in DMEM containing 20 μM FA-BSA. Confluent cells were treated with trypsin-EDTA and centrifuged for 10 min at 1,500 × *g*. The pelleted cells were incubated in 96 mM MES (pH 6.5) containing 9.6 mM EDTA, 1.9 mM DTT, 125 mM NaCl, 15 μM [1-^{14}C]*cis*-9 18:1-CoA, 30 μg BSA, and 18 μg of digitonin for 10 min at 37°C. The reaction was quenched with 10 μl of 12.4 M HCl, and lipids were extracted as described by Bligh and Dyer [33]. Lipids were spotted to silica gel 60 H TLC plates, which were developed with a single ascension of hexane/diethyl ether (80:20, v/v) using triolein as a standard. Standards were visualized using iodine vapor, and corresponding areas were scraped into vials followed by the addition of scintillant and the determination of [1-^{14}C] *cis*-9 18:1 incorporated into TAG. The protein content of sonically disrupted cells was determined using the Bio-Rad protein microassay based on the method of Bradford [34] using BSA as a standard.

Assay of DGAT Activity in Microsomes from Mammary Gland Tissue

Microsomes were prepared from bovine mammary gland tissue as previously described for muscle and adipose tissue [35], and DGAT was assayed as described in Lozeman et al. [36] with a final concentration of 15 μM [1-^{14}C] *cis*-9 18:1-CoA (56 Ci/mol) in the reaction mixture. Reactions were allowed to proceed for 10 min at 30°C in the presence of increasing concentrations (0–20 μM) of unlabeled *cis*-9, *trans*-11 18:2-; *trans*-10, *cis*-12 18:2-; *cis*-9, *cis*-12 18:2- or *cis*-9 18:1-CoA.

Statistical Analysis

For effect of exogenous FA treatment on expression of genes encoding lipogenic enzymes in cultured MAC-T cells, statistical analysis was performed using the mixed procedure in SAS (version 9.1), with variance components covariance structure and Kenward-Roger adjustment for the denominator degrees of freedom. The statistics are based on duplicates from three independent trials. Gene and FA treatments were considered fixed effects, and the trial was considered as a random effect in the mixed model analysis. For the effect of various FA treatments on the mole percentages of various FA in the acyl lipid of MAC-T cells, the mixed procedure (SAS) was used, with FA treatment as fixed effect. Spearman's rho correlation coefficients (JMP® IN statistical software, version 4, Duxbury Press, Toronto, ON, Canada) were generated for *DGAT1*, *DGAT2*, and *LPAAT* expression data for mammary gland tissue obtained from lactating Holstein cows. For the experiment measuring the effect of increasing concentrations of various unlabeled acyl-CoA species on the incorporation of radiolabeled-18:1 (from radiolabeled-18:1-CoA) into TAG using bovine mammary gland microsomes, statistical analysis was performed using the mixed procedure in SAS using a diagonal covariance structure and residual degrees of freedom method, considering substrate and substrate concentration as fixed effects in the model.

Results

Effect of Exogenous FA on Expression of Genes Encoding Lipogenic Enzymes in MAC-T Cells

Results from QT-PCR of *DGAT1*, *DGAT2*, and *LPAAT* expression are shown in Fig. 1. None of the FA isomers had a substantial effect on *DGAT1* expression relative to the control, and none resulted in significant change in the expression of *DGAT1*. Treatment with oleic acid (*cis*-9 18:1), vaccenic acid (*trans*-11 18:1); linoleic acid (*cis*-9, *cis*-12 18:2); *cis*-9, *trans*-11 18:2; *trans*-10, *cis*-12 18:2; or α-linolenic acid (α-18:3), however, resulted in increases in *DGAT2* expression ($P < 0.01$, $P < 0.001$, $P < 0.01$, $P < 0.05$, $P < 0.05$, and $P < 0.001$, respectively). CLA isomers, *cis*-9, *trans*-11 18:2 and *trans*-10, *cis*-12 18:2 did not have a differential effect on *DGAT1* versus *DGAT2* expression, but *trans*-11 18:1 treatment resulted in more enhanced *DGAT2* expression ($P < 0.05$) than for treatment with *cis*-9, *trans*-11 18:2. All FA tested for enhanced *LPAAT* expression ($P < 0.001$) in the MAC-T cells.

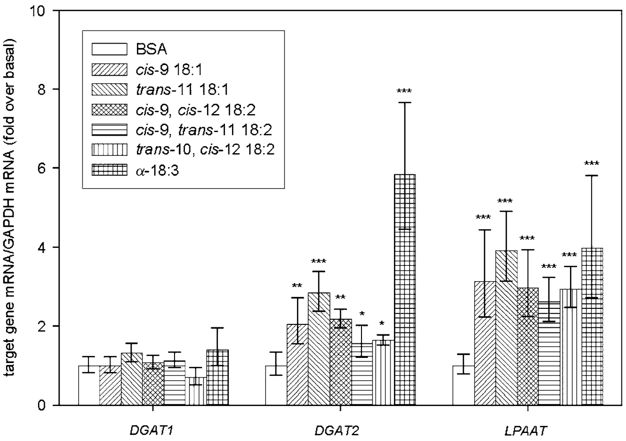

Fig. 1 Expression of genes encoding lipogenic enzymes in MAC-T cells treated with exogenous FA. Data points were calculated using the $2_T^{-\Delta\Delta CT}$ method [30]. Duplicates from three separate trials were used. *Error bars* represent upper and lower intervals. *, **, *** represent significant differences between treatment and control *($P < 0.05$), **($P < 0.01$), ***($P < 0.001$)

Expression of Genes Encoding Lipogenic Enzymes in Mammary Gland

Spearman rho coefficients for *DGAT1*, *DGAT2*, and *LPAAT* expression in mammary gland samples from 12 lactating cows are shown in Table 2. Expression of *DGAT2* demonstrated significant positive correlation to that of *LPAAT*.

Effect of Exogenous FA on Lipid Accumulation and DGAT Activity in MAC-T Cells

None of the exogenous FA tested affected lipid accumulation in MAC-T cells (Fig. 2). The FA composition of lipid extracted from treated MAC-T cells is shown in Table 3. SFA, MUFA, and PUFA proportions are shown

Table 2 Spearman ρ coefficients for expression[a] of genes encoding lipogenic enzymes from mammary gland tissue of lactating Holstein cows ($n = 12$)

	DGAT2	*LPAAT*
DGAT1	0.37	0.37
DGAT2		0.59*

DGAT-1 diacylglycerol acyltransferase-1, *DGAT-2* diacylglycerol acyltransferase-2, *GAPDH* glyceraldehyde-3-phosphate dehydrogenase, *LPAAT* lysophosphatidic acid acyltransferase

*$P < 0.05$

[a] ΔC_T value (i.e., $C_{T\ \mathrm{Target}} - C_{T\ \mathrm{GAPDH}}$)

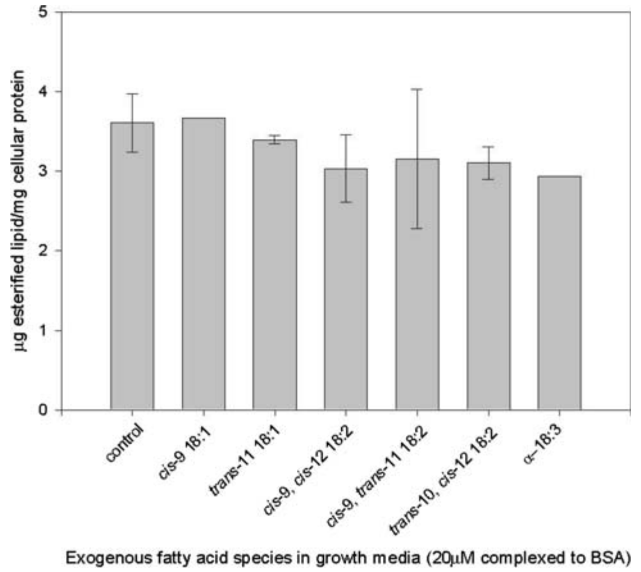

Fig. 2 Acyl lipid content of MAC-T cells treated with exogenous FA. Esterified lipid (fatty acyl lipid) content was obtained from the FA composition. Mean values are presented for the results of two experiments

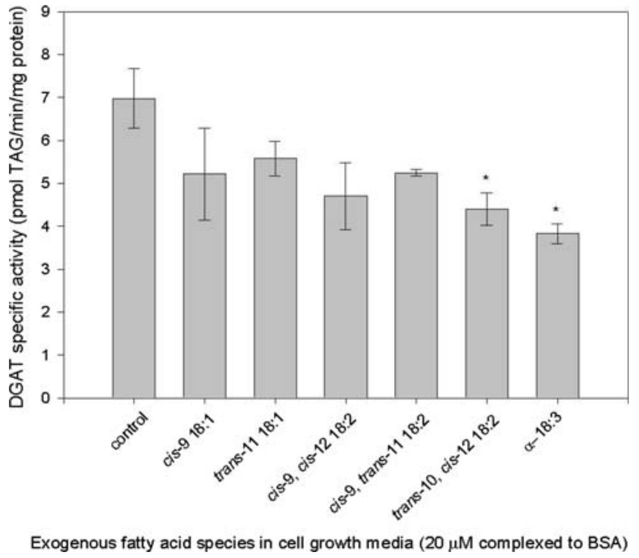

Fig. 3 DGAT activity of MAC-T cells treated with exogenous FA. Values represent means ± SEM ($n = 6$). *Values are significantly different from control ($P < 0.05$)

along with specific proportions for C18 FA. In each case, there was an enhanced incorporation of exogenous FA into the cellular lipid. Treatment of the cells with *trans*-10, *cis*-12 18:2 resulted in increased proportions of saturated FA and stearic acid (18:0) ($P < 0.01$) and a decreased proportion of *cis*-9 18:1.

The effect of exogenous FA on DGAT-specific activity in MAC-T cells is shown in Fig. 3. Compared to control cells (treated only with BSA), the DGAT-specific activities of cells treated with *trans*-10, *cis*-12 18:2, and α-18:3 were decreased ($P < 0.05$).

Competition Assays of DGAT Activity Using Mammary Gland Microsomes

The effect of increasing concentrations of unlabeled molecular species of acyl-CoA on the incorporation of [1-^{14}C] *cis*-9 18:1 from radiolabeled *cis*-9 18:1-CoA is shown in Fig. 4. Incorporation of [1^{14}-C]18:1 into TAG was decreased at all concentrations of *cis*-9, *trans*-11 18:2-; *trans*-10, *cis*-12 18:2- or *cis*-9, *cis*-12 18:2-CoA into TAG was decreased ($P < 0.001$) compared to *cis*-9 18:1-CoA.

Table 3 FA composition (mole %) of acyl lipid extracted from MAC-T-cells treated with exogenous FA

	Treatment						
	BSA	*cis*-9 18:1	*cis*-9, *cis*-12 18:2	α-18:3	*trans*-11 18:1	*cis*-9, *trans*-11 18:2	*trans*-10, *cis*-12 18:2
SFA	38.4 ± 1.1	38.5 ± 0.7	39.9 ± 0.4	45.7 ± 2.7*	37.8 ± 2.0	40.6 ± 0.8	52.2 ± 1.1***
MUFA	42.2 ± 2.4	43.9 ± 0.7	19.9 ± 1.1***	26.5 ± 2.6**	45.5 ± 1.8	34.9 ± 1.2*	25.4 ± 1.5**
PUFA	19.3 ± 1.7	17.7 ± 1.0	40.2 ± 0.7***	27.8 ± 0.6**	16.6 ± 1.2	24.6 ± 0.8*	22.4 ± 2.1
18:0	12.3 ± 1.0	10.0 ± 0.5	12.0 ± 0.5	14.6 ± 1.2	10.6 ± 1.9	11.6 ± 0.3	17.7 ± 0.4**
cis-9 18:1	25.0 ± 1.4	32.1 ± 0.3**	10.9 ± 0.5***	14.7 ± 1.0**	21.4 ± 1.0	20.0 ± 0.5*	15.6 ± 1.4**
cis-9, *cis*-12 18:2	4.2 ± 0.6	4.0 ± 0.3	24.1 ± 0.2***	4.4 ± 0.4	3.4 ± 0.1	3.9 ± 0.1	3.1 ± 1.0
α-18:3	0.4 ± 0.3	0.1 ± 0.0	0.1 ± 0.0	9.2 ± 1.7***	0.1 ± 0.0	0.1 ± 0.0	0.1 ± 0.0
cis-9, *trans*-11 18:2	0.4 ± 0.2	0.3 ± 0.1	0.2 ± 0.1	0.4 ± 0.2	1.9 ± 0.7	3.6 ± 1.7	0.3 ± 0.0
trans-10, *cis*-12 18:2	0.1 ± 0.0	0.1 ± 0.0	0.1 ± 0.0	0.1 ± 0.0	0.1 ± 0.0	0.1 ± 0.0	3.0 ± 1.5

Values represent means ± SEM ($n = 4$)

*, **, *** Represent significant differences between treatment and control (BSA) within a row, *($P < 0.05$); **($P < 0.01$); ***($P < 0.001$)

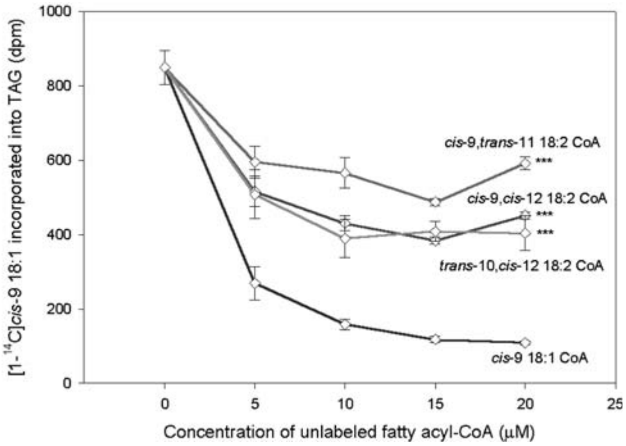

Fig. 4 Effect of increasing concentrations of various unlabeled acyl-CoA species on the incorporation of [1-^{14}C] *cis*-9 18:1 from [1-^{14}C] *cis*-9 18:1-CoA into TAG using bovine mammary gland microsomes. Values represent mean ± SEM ($n = 3$). ***Represents significant differences between *cis*-9 18:1-CoA and other acyl donors at all concentrations, ***($P < 0.001$)

Discussion

In an early study, Hansen and Knudsen [37] found that the addition of long chain FA, namely 18:0 and *cis*-9, *cis*-12 18:2, inhibited the incorporation of FA into the TAG of mammary gland epithelial cells. Peterson et al. [12] reported that treating MAC-T cells with *trans*-10, *cis*-12 18:2 resulted in reduced lipid synthesis. In the current study, this CLA isomer had no effect on lipid accumulation in cultured MAC-T cells (Fig. 2). Peterson et al. [12], however, measured lipid synthesis by monitoring the incorporation of [^{14}C] acetate into total lipid and noted inhibition of lipid accumulation at increasing concentrations of *trans*-10, *cis*-12 18:2. The effects of other isomers of CLA were not investigated. Our studies of lipid accumulation in MAC-T cells were based on the methods used in the recent report by Keating et al. [28] to study bovine mammary cell growth, apoptosis, and stearoyl-CoA (SCD) gene expression. In this recent report, various concentrations of CLA and other FA were applied to MAC-T-cells for 48 h. CLA (*cis*-9, *trans*-11 18:2 and *trans*-10, *cis*-12 18:2) concentrations of 30 µM or greater resulted in MAC-T-cell apoptosis. Twenty micromolar CLA was the highest concentration that could be applied before the cells began to do poorly. In the current study, a 20-µM FA treatment for 24 h was used to minimize the chances of apoptosis. The MAC-T cell line presents limitations for the study of a functioning mammary gland as it has abnormal characteristics in vitro. The in vitro data of Keating et al. [28], however, may help to clarify the effect of relatively high doses of fatty acids in vivo on the mammary gland. Eventually these investigations could be extended to evaluate the effects of CLA on differentiated mammary gland cells in vitro, such as the bovine mammary epithelial cell collagen cell culture system [38].

In the current study, treatment of MAC-T-cells with *trans*-10, *cis*-12 18:2 resulted in an increased proportion of 18:0 and decreased proportion of *cis*-9, 18:1 in total lipid compared to the control treatment (Fig. 3). This is consistent with evidence that this CLA isomer results in decreased expression and activity of SCD [39]. The decreased production of *cis*-9 18:1 and ultimately *cis*-9 18:1-CoA, a readily utilized substrate of DGAT, might be a factor in the MFD effect. The ability of DGAT to effectively utilize *cis*-9 18:1-CoA is confirmed in our competition studies using mammary gland microsomes where radiolabeled *cis*-9 18:1-CoA was incubated separately with unlabeled *cis*-9 18:1-; *cis*-9, *trans*-11 18:2-; *trans*-10, *cis*-12 18:2- or *cis*-9, *cis*-12 18:2.-CoA (Fig. 4).

Degrace et al. [40] have reported that feeding *trans*-10, *cis*-12 18:2 to mice increases the abundance of hepatic DGAT1 mRNA. All mice received control diet for 1 week and then control verus CLA isomer diets for 4 weeks. In the current study, treating of MAC-T-cells with various FA, however, had no effect on the expression of *DGAT1*. Peterson et al. [12] reported that cattle fed a MFD-inducing diet (i.e., high concentrate/low forage) resulted in decreased expression of *LPAAT*, whereas our data indicate that that *trans*-10, *cis*-12 18:2 increased expression of this gene to the same extent as any other FA tested. In the current study, incubation of MAC-T cells with *trans*-10, *cis*-12 18:2 or α-18:3 resulted in decreases ($P < 0.05$) in DGAT activity. In the competitive assay, however, the addition of *cis*-9 18:1-CoA decreased the incorporation of radiolabeled [1-^{14}C] *cis*-9 18:1 into TAG more than for other acyl-CoA tested. Although *cis*-9 18:1 may be preferentially used by DGAT, it is possible that one or more of the other molecular species of acyl-CoA tested is inhibitory. For example, *trans*-10, *cis*-12 18:2 might inhibit microsomal DGAT activity and not serve as an effective substrate for the enzyme. Berge et al. [41] incubated rat liver microsomes in the presence of various acyl-CoA derivatives, including *cis*-9, *cis*-12 18:2-CoA in the presence of 20 µM *cis*-9 18:1-CoA, and demonstrated that TAG synthesis was decreased. Eicosapentaenoyl-CoA (all *cis*-5,8,11,14,17 20:5-CoA) has also been shown to cause a substantial decrease in hepatic DGAT activity, but other acyl-CoAs tested were not inhibitory [42].

Although DGAT activity was decreased in the MAC-T cells as a result of incubation with *trans*-10, *cis*-12 18:2 or α-18:3, it is unclear how DGAT production may have been affected. Application of all FA types led to increased expression of *DGAT2* (Fig. 1), suggesting that the effect of *trans*-10, *cis*-12 and α-18:3 in decreasing DGAT activity production was post-transcriptional in nature. Exogenous application of α-18:3 did not influence lipid accumulation in the MAC-T cells (Fig. 1), even though treatment of the cells with this FA appeared to have the greatest effect on enhancing *DGAT2* expression (Fig. 2).

Furthermore, treatment with α-18:3 resulted in a decrease in microsomal DGAT-specific activity (Fig. 3). A number of studies have shown that dietary α-18:3 leads to enhanced β-oxidation and reduced fat accumulation [43–46]. The increased *DGAT2* expression brought about by treatment of MAC-T cells with α-18:3 and other FAs suggests that DGAT2 mRNA levels probably do not reflect the activity of this isoenzyme of DGAT in promoting fat accumulation in this system. The occurrence of DGAT2 transcript in the bovine mammary gland, however, is consistent with the previous discovery of this transcript in human mammary gland [15]. CLA may not directly affect the activity of DGAT, but rather the apparent *trans*-10, *cis*-12 18:2-mediated decrease in DGAT activity may be the result of the action of this isomer on other lipogenic enzymes that generate substrates for DGAT. Cattle treated by abomasal infusion of purified *trans*-10, *cis*-12 18:2 emulsified in skim milk have been shown to exhibit a decrease in the expression of *SCD* [47]. In $SCD^{-/-}$ mice, decreased SCD activity has been shown to result in the accumulation of saturated FA, which had an inhibitory effect on acetyl-CoA carboxylase [48]. In turn, decreased acetyl-CoA carboxylase activity has been shown to result in a decrease in the production of malonyl-CoA, and ultimately a decrease in FA synthesis would result in less acyl-CoA available for DGAT. In cattle fed a MFD-inducing diet (i.e., high concentrate/low forage), Peterson et al. [12] also noted a decrease in the abundance of mRNA encoding FA binding protein. In another study, Brown et al. [49] have shown that treatment of human primary preadipocytes with *trans*-10, *cis*-12 18:2 results in a decrease in the expression of acyl-CoA binding protein. Thus, a decrease in the cellular content of these proteins might affect the availability of substrate for DGAT.

It is also possible that *trans*-10, *cis*-12 18:2 may influence the splicing of DGAT mRNA. Indeed, Grisart et al. [50] have shown using a baculovirus expression system that a K232A mutation in DGAT1 increases the occurrence of an alternative splicing variant of *DGAT1* that produces a DGAT1 isoform that is devoid of DGAT activity.

In addition, *trans*-10, *cis*-12 may have caused alterations in the phospholipid composition of the ER of the MAC-T cells leading to changes in the physical properties of the membrane. Ma et al. [51] have shown that *trans*-10, *cis*-12 18:2 is rapidly incorporated into the membrane phospholipid of MDA-MB-123 cells. Changes in SCD activity induced by *trans*-10 *cis*-12 18:2 also resulted in altered membrane composition. Since DGAT is membrane-bound, changes in the membrane environment may affect the activity of the enzyme. Indeed, Mathur et al. have shown that varying the phospholipid composition in incubations of rat liver microsomes alters ACAT activity [52].

In the present study, the fact that *DGAT2* and *LPAAT* showed similar expression patterns in response to the application of various exogenous FAs (Fig. 1) suggests that the two acyltransferases may be coordinated at the transcriptional level. As well, the expression of *DGAT2* and *LPAAT* showed a significant positive correlation in mammary gland tissue obtained from 12 dairy cows (Table 2). A similar association was observed by Kazala et al. [53] who previously reported a significant positive correlation between microsomal DGAT and LPAAT activity in bovine *pars costalis diaphragmitis* muscle tissue. The results reported here suggest this relationship is also reflected at the transcript level. Although Cases et al. [15] were able to differentiate between the activity of murine DGAT1 and DGAT2 by altering the concentration of $MgCl_2$ in the reaction mixture, we were unable to replicate this technique using MAC-T cells or bovine mammary gland tissue. At this point, it remains unclear to which extent DGAT2 contributes to the overall DGAT activity.

In conclusion, *trans*-10, *cis*-12 18:2 does not appear to mediate MFD by decreasing the expression of either *DGAT1* or *DGAT2*. Instead, the results of this study suggest that, upon exposure to *trans*-10, *cis*-12 18:2 or α-18:3, DGAT activity in MAC-T-cells is decreased, but the mechanism is unclear. *Trans*-10, *cis*-12 18:2 may inhibit DGAT activity either directly or indirectly as a result of altered substrate pools that in turn are a result of the action of *trans*-10, *cis*-12 18:2 on enzymes that are located upstream of DGAT in the lipid biosynthetic pathway. MFD caused by the *trans*-10, *cis*-12 CLA isomer probably affects a number of lipogenic enzymes including possible effects on DGAT production and/or activity.

Acknowledgments The authors acknowledge the financial support of the Alberta Agricultural Research Institute, Animal Health Division of Eli Lilly Canada, Inc., Dairy Farmers of Canada, Natural Sciences and Engineering Research Council of Canada, and the Canada Research Chairs Program. As well, the authors thank Dr. David Glimm for assistance in procuring bovine mammary gland biopsy samples. B.M.S. and C.C.H. held an Alberta Ingenuity Scholarship and Alberta Ingenuity Post-doctoral Fellowship, respectively.

References

1. Corl BA, Barbano DM, Bauman DE, Ip C (2003) *cis*-9, *trans*-11 CLA derived endogenously from *trans*-11 18:1 reduces cancer risk in rats. J Nutr 133:2893–2900
2. Park Y, Storkson JM, Albright KJ, Liu W, Pariza MW (1999) Evidence that the *trans*-10, *cis*-12 isomer of conjugated linoleic acid induces body composition changes in mice. Lipids 34:235–241

3. Griinari JM, Corl BA, Sh Lacy, Shouinard PY, Nurmela KVV, Bauman DE (2000) Conjugated linoleic acid is synthesized endogenously in lactating cows by delta-9 desaturase. J Nutr 130:2285–2291
4. Corl BA, Baumgard LH, Dwyer DA, Griinari JM, Phillips BS, Bauman DE (2001) The role of delta-9 desaturase in the production of *cis*-9, *trans*-11 CLA. J Nutr Biochem 12:622–630
5. Kay Mackle TR, Auldist MJ, Thomson NA, Bauman DE (2004) Endogenous synthesis of *cis*-9, *trans*-11 conugated linoleic acid in dairy cows fed fresh pasture. J Dairy Sci 87:369–378
6. Lock AL, Bauman DE (2004) Modifying milk fat composition of dairy cows to enhance fatty acids beneficial to human health. Lipids 39:1197–1206
7. Dhiman TR, Nam SH, Ure AL (2005) Factors affecting conjugated linoleic acid content in milk and meat. Crit Rev Food Sci Nutr 45:463–482
8. Chouinard PY, Corneau L, Barbano DM, Metzger LE, Bauman DE (1999) Conjugated linoleic acids alter milk fatty acid composition and inhibit milk fat secretion in dairy cows. J Nutr 129:1579–1584
9. Dhiman TR, Anand GR, Satter LD, Pariza MW (1999) Conjugated linoleic acid content of milk from cows fed different diets. J Dairy Sci 82:2146–2156
10. Baumgard LH, Corl BA, Dwyer DA, Saebo A, Bauman DE (2000) Identification of the conjugated linoleic acid isomer that inhibits milk fat synthesis. Am J Physiol Regul Integr Comp Physiol 278:R179–R184
11. Piperova LS, Teter BB, Bruckental I, Sampugna J, Mills SE, Yurawecz MP, Fritsche J, Ku K, Erdman RA (2000) Mammary lipogenic enzyme activity, *trans* fatty acids and conjugated linoleic acids are altered in lactating dairy cows fed a milk fat-depressing diet. J Nutr 130:2568–2574
12. Peterson DG, Matitashvili EA, Bauman DE (2003) Diet-induced milk fat depression in dairy cows results in increased *trans*-10, *cis*-12 CLA in milk fat and coordinate suppression of mRNA abundance for mammary enzymes involved in milk fat synthesis. J Nutr 133:3098–3102
13. Kennedy EP (1961) Biosynthesis of complex lipids. Fed Proc Am Soc Exp Biol 20:934–940
14. Cases S, Smith SJ, Zheng YW, Myers HM, Lear SR, Sande E, Novak S, Collins C, Welch CB, Lusis AJ, Erickson SK, Farese RV Jr (1998) Identification of a gene encoding an acyl CoA:diacylglycerol acyltransferase, a key enzyme in triacylglycerol synthesis. Proc Natl Acad Sci USA 95:13018–13023
15. Cases S, Stone SJ, Zhou P, Yen E, Tow B, Lardizabal KD, Voelker T, Farese RV Jr (2001) Cloning of DGAT2, a second mammalian diacylglycerol acyltransferase, and related family members. J Biol Chem 276:38870–38876
16. Mayorek N, Grinstein I, Bar-Tana J (1989) Triacylglycerol synthesis in cultured rat hepatocytes.The rate-limiting role of diacylglycerol acyltransferase. Eur J Biochem 182:395–400
17. Millar JS, Stone SJ, Tietge UJ, Tow B, Billheimer JT, Wong JS, Hamilton RL, Farese RV Jr, Rader DJ (2006) Short-term overexpression of DGAT1 or DGAT2 increases hepatic triglyceride but not VLDL triglyceride or apoB production. J Lipid Res 47:2297–2305
18. Smith SJ, Cases S, Jensen DR, Chen HC, Sande E, Tow B, Sanan DA, Raber J, Eckel RH, Farese RV (2000) Obesity resistance and multiple mechanisms of triglyceride synthesis in mice lacking Dgat. Nat Genet 25:87–90
19. Cases S, Zhou P, Shillingford JM, Wiseman BS, Fish JD, Angel CS, Hennighausen L, Werb Z, Farese RV (2004) Development of the mammary gland requires DGAT1 expression in stromal and epithelial tissues. Development 131:3047–3055
20. Grisart B, Coppieters W, Farnir F, Karim L, Ford C, Berzi P, Cambisano N, Mni M, Reid S, Simon P, Spelman R, Georges M, Snell R (2002) Positional candidate cloning of a QTL in dairy cattle: identification of a missense mutation in the bovine *DGAT1* gene with major effect on milk yield and composition. Genome Res 12:222–231
21. Thomas-Yeung CH, Yang L, Huang Y, Wang J, Chen ZY (2000) Dietary conjugated linoleic acid mixture affects the activity of intestinal acyl coenzyme A: cholesterol acyltransferase in hamsters. Br J Nutr 84:935–941
22. Giudetti AM, Beynen AC, Lemmens AG, Gnoni GV, Geelen MJ (2005) Hepatic lipid and carbohydrate metabolism in rats fed a commercial mixture of conjugated linoleic acids (Clarinol G-80). Eur J Nutr 44:33–39
23. Giudetti AM, Beynen AC, Lemmens AG, Gnoni GV, Geelen MJ (2003) Hepatic fatty acid metabolism in rats fed diets with different contents of C18:0, C18:1 *cis* and C18:1 *trans* isomers. Br J Nutr 90:887–893
24. Bell JA, Griinari JM, Kennelly JJ (2006) Effect of safflower oil, flaxseed oil, monensin and vitamin E on concentration of conjugated linoleic acid in bovine milk fat. J Dairy Sci 89:733–748
25. Knight CH, Hillerton JE, Teverson RM, Winter A (1992) Biopsy of the bovine mammary gland. Br Vet J 148:129–132
26. Taylor DC, Weber N, Hogge LR, Underhill EW (1990) A simple enzymatic method for the preparation of radiolabeled erucoyl-CoA and other long-chain fatty acyl-CoAs and their characterization by mass spectrometry. Anal Biochem 184:311–316
27. Huynh HT, Robitaille G, Turner JD (1991) Establishment of bovine mammary epithelial cells (MAC-T): an in vitro model for bovine lactation. Exp Cell Res 197:191–199
28. Keating AF, Zhao F-Q, Finucane KA, Glimm DR, Kennelly JJ (2008) Effect of conjugated linoleic acid on bovine mammary cell growth, apoptosis and stearoyl Co-A desaturase gene expression. Domest Anim Endocrinol 34:284–292
29. Livak KJ, Schmittgen TD (2001) Analysis of relative gene expression data using real-time quantitative PCR and the $2_{\mathrm{T}}^{-\Delta\Delta C}$ method. Methods 25:402–408
30. Folch J, Lees M, Stanley GHS (1957) Preparation of lipid extracts from brain tissue. J Biol Chem 226:497–509
31. Cruz-Hernandez C, Deng Z, Zhou J, Hill AR, Yurawecz MP, Delmonte P, Mossoba MM, Dugan MER, Kramer JKG (2004) Methods for analysis of conjugated linoleic acids and trans-18:1 isomers in dairy fats by using a combination of gas chromatography, silver-ion thin-layer chromatography/gas chromatography, and silver-ion liquid chromatography. J AOAC Int 87:545–562
32. Geelen MJ (2003) Measurement of diacylglycerol acyltransferase activity in isolated hepatocytes. Anal Biochem 322:264–268
33. Bligh EG, Dyer WJ (1959) A rapid method of total lipid extraction and purification. Can J Biochem Physiol 37:911–917
34. Bradford MM (1976) A rapid and sensitive method for the quantitation of microgram quantities of protein utilizing the principle of protein-dye binding. Anal Biochem 72:248–254
35. Middleton CK, Kazala EC, Lozeman FJ, Hurly TA, Mir PS, Bailey DRC, Jones SDM, Weselake RJ (1998) Evaluation of diacylglycerol acyltransferase as an indicator of intramuscular fat content in beef cattle. Can J Anim Sci 78:265–270
36. Lozeman FJ, Middleton CK, Deng J, Kazala EC, Verhaege C, Mir PS, Laroche A, Bailey DRC, Weselake RJ (2001) Characterization of microsomal diacylglycerol acyltransferase activity from bovine adipose and muscle tissue. Comp Biochem Physiol B Biochem Mol Biol 130:105–115
37. Hansen HO, Knudsen J (1987) Effect of exogenous long-chain fatty acids on lipid biosynthesis in dispersed ruminant mammary gland epithelial cells: esterification of long-chain exogenous fatty acids. J Dairy Sci 70:1344–1349
38. Collier RJ, Steining CM, Pollard BC, VanBaale MJ, Baumgard LH, Gentry PC, Coussens PM (2006) Use of gene expression

microarrays for evaluating environmental stress tolerance at the cellular level in cattle. J Anim Sci 84:Suppl E1–E13
39. Perfield JW 2nd, Lock AL, Pfeiffer AM, Bauman DE (2004) Effects of amide-protected and lipid-encapsulated conjugated linoleic acid supplements on milk fat synthesis. J Dairy Sci 87:3010–3016
40. Degrace P, Demizieux L, Gresti J, Chardigny JM, Sébédio JL, Clouet P (2004) Hepatic steatosis is not due to impaired fatty acid oxidation capacities in C57BL/6 J mice fed the conjugated *trans*-10, *cis*-12-isomer of linoleic acid. J Nutr 134:861–867
41. Berge RK, Madsen L, Vaagenes H, Tronstad KJ, Gottlicher M, Rustan AC (1999) In contrast with docosahexaenoic acid, eicosapentaenoic acid and hypolipidaemic derivatives decrease hepatic synthesis and secretion of triacylglycerol by decreased diacylglycerol acyltransferase activity and stimulation of fatty acid oxidation. Biochem J 343(Pt 1):191–197
42. Rustan AC, Nossen JO, Christiansen EN, Drevon CA (1988) Eicosapentaenoic acid reduces hepatic synthesis and secretion of triacylglycerol by decreasing the activity of acyl-coenzyme A:1, 2-diacylglycerol acyltransferase. J Lipid Res 29:1417–1426
43. Ide T, Murata M, Sugano M (1996) Stimulation of the activities of hepatic fatty acid oxidation enzymes by dietary fat rich in α-linolenic acid in rats. J Lipid Res 37:448–463
44. Ide T, Kobayashi H, Ashakumary L, Rouyer IA, Takahashi Y, Aoyama T, Hashimoto T, Mizugaki M (2000) Comparative effects orf perilla and fish oils on the activity and gene expression of fatty acid oxidation enzymes in rat liver. Biochim Biophys Acta 1485:23–35
45. Murase T, Aoki M, Tokimitsu I (2005) Supplementation with α-linolenic acid-rich diacylglycerol suppresses fatty liver formation accompanied by an up-regulation of β-oxidation in Zucker fatty rats. Biochim Biophys Acta 1733:224–231
46. Ferrini G, Baucells MD, Esteve-García E, Barroeta AC (2008) Dietary polyunsaturated fat reduces skin fat as well as abdominal fat in broiler chickens. Poult Sci 87:528–535
47. Baumgard LH, Matitashvili E, Corl BA, Dwyer DA, Bauman DE (2002) *trans*-10, *cis*-12 conjugated linoleic acid decreases lipogenic rates and expression of genes involved in milk lipid synthesis in dairy cows. J Dairy Sci 85:2155–2163
48. Ntambi JM, Miyazaki M, Stoehr JP, Lan H, Kendziorski CM, Yandell BS, Song Y, Cohen P, Friedman JM, Attie AD (2002) Loss of stearoyl-CoA desaturase-1 function protects mice against adiposity. Proc Natl Acad Sci USA 99:11482–11486
49. Brown JM, Boysen MS, Jensen SS, Morrison RF, Storkson J, Lea-Currie R, Pariza M, Mandrup S, McIntosh MK (2003) Isomer-specific regulation of metabolism and PPARgamma signaling by CLA in human preadipocytes. J Lipid Res 44:1287–1300
50. Grisart B, Farnir F, Karim L, Cambisano N, Kim JJ, Kvasz A, Mni M, Simon P, Frere JM, Coppieters W, Georges M (2004) Genetic and functional confirmation of the causality of the DGAT1 K232A quantitative trait nucleotide in affecting milk yield and composition. Proc Natl Acad Sci USA 101:2398–2403
51. Ma DW, Field CJ, Clandinin MT (2002) An enriched mixture of *trans*-10, *cis*-12-CLA inhibits linoleic acid metabolism and PGE2 synthesis in MDA-MB-231 cells. Nutr Cancer 44:203–212
52. Mathur SN, Simon I, Lokesh BR, Spector AA (1983) Phospholipid fatty acid modification of rat liver microsomes affects acylcoenzyme A:cholesterol acyltransferase activity. Biochim Biophys Acta 751:401–411
53. Kazala EC, Lozeman FJ, Mir PS, Aalhus JL, Schmutz SM, Weselake RJ (2006) Fatty acid composition of muscle fat and enzymes of storage lipid synthesis in whole muscle from beef cattle. Lipids 41:1049–1057

Lipids (2008) 43:913–923
DOI 10.1007/s11745-008-3226-x

ORIGINAL ARTICLE

Conjugated Linoleic Acid Isomers Reduce Cholesterol Accumulation in Acetylated LDL-Induced Mouse RAW264.7 Macrophage-Derived Foam Cells

Robert Ringseis · Gaiping Wen · Daniela Saal · Klaus Eder

Received: 19 May 2008 / Accepted: 13 August 2008 / Published online: 4 September 2008
© AOCS 2008

Abstract Synthetic activators of peroxisome proliferator-activated receptors (PPAR)-α and -γ are capable of reducing macrophage foam cell cholesterol accumulation through the activation of genes involved in cholesterol homeostasis. Since conjugated linoleic acids (CLA) were also demonstrated to activate PPARα and PPARγ in vivo and in vitro, we tested the hypothesis that CLA are also capable of reducing macrophage foam cell cholesterol accumulation. Thus, mouse RAW264.7 macrophage-derived foam cells were treated with CLA isomers, *c*9*t*11-CLA and *t*10*c*12-CLA, and linoleic acid (LA), as reference fatty acid, and analyzed for the concentrations of free and esterified cholesterol, cholesterol efflux and expression of genes involved in cholesterol homeostasis (CD36, ABCA1, LXRα, NPC-1, and NPC-2). Treatment with *c*9*t*11-CLA and *t*10*c*12-CLA, but not LA, lowered cholesterol accumulation, stimulated acceptor-dependent cholesterol efflux, and increased relative mRNA concentrations of CD36, ABCA1, LXRα, NPC-1, and NPC-2 ($P < 0.05$). In conclusion, the present study showed that CLA isomers reduce cholesterol accumulation in RAW264.7 macrophage-derived foam cells presumably by enhancing lipid acceptor-dependent cholesterol efflux.

Keywords Conjugated linoleic acid · Peroxisome proliferator-activated receptors · Cholesterol accumulation · Cholesterol efflux · Macrophage foam cell · Atherosclerosis

R. Ringseis (✉) · G. Wen · D. Saal · K. Eder
Institute of Agricultural and Nutritional Sciences,
Martin-Luther-University of Halle-Wittenberg,
Emil-Abderhalden-Strasse 26,
06108 Halle (Saale), Germany
e-mail: robert.ringseis@landw.uni-halle.de

Abbreviations

ABCA1	ATP-binding cassette transporter A1
AcLDL	Acetylated LDL
CLA	Conjugated linoleic acid
HDL	High-density lipoprotein
LA	Linoleic acid
LDL	Low-density lipoprotein
LXRα	Liver X receptor α
NPC	Niemann Pick type C
PPAR	Peroxisome proliferator-activated receptor

Introduction

Atherosclerosis, the principle cause of coronary heart disease and stroke, is responsible for more than 40% of all deaths in Europe and the US [1]. Macrophages are centrally involved in the initiation and progression of atherosclerosis and are the predominant cellular component of atherosclerotic lesions [2]. When concentrations of low-density lipoprotein (LDL) are elevated, macrophages accumulate lots of LDL-derived cholesterol through scavenger receptor-dependent pathways, and, then transform into cholesterol-enriched foam cells. Development of macrophage-derived foam cells is considered to be a critical step in atherogenesis, since foam cells account for the development of fatty streaks which represent the initial stage of atherosclerosis [3].

Recent in-vitro studies indicated that synthetic activators of PPARα and PPARγ induce cholesterol removal from macrophage foam cells through the induction of genes involved in cholesterol homeostasis [4, 5]. Although PPARγ ligands increase expression of CD36 scavenger receptors [6, 7], which mediate uptake of modified LDL, concomitant induction by PPARα and PPARγ ligands of liver X receptor α (LXRα) and cholesterol exporters of the ATP-binding cassette (ABC) family, ABCA1 and ABCG1, results in a net increase in cholesterol efflux from macrophage foam cells [4, 5, 8, 9]. ABCA1 in particular plays a key role in cellular cholesterol efflux from macrophages to apo-AI, the first step in reverse cholesterol transport. This has been demonstrated in patients with a mutated ABCA1 gene, where cholesterol efflux and reverse cholesterol transport are impaired and development of atherosclerosis is accelerated [10–12]. Recent studies also demonstrated that PPARα activators up-regulate proteins involved in intracellular cholesterol trafficking, namely Niemann Pick type C (NPC) proteins-1 and -2 [13], which mediate cholesterol transport from the lysosome to the plasma membrane [14, 15]. Increased expression of NPC-1 and NPC-2 by PPARα activators increases cholesterol content of the plasma membrane, and, the efflux of cholesterol to extracellular acceptors such as apo-AI [13]. These in vitro-effects of PPARs also explain, at least partially, that treatment with PPARα and PPARγ ligands exerts anti-atherogenic effects in vivo [16, 17]. Similarly to synthetic agents, conjugated linoleic acids (CLA), a group of positional and geometric isomers of linoleic acid naturally occurring in food derived from ruminants such as milk and milk products, were also demonstrated to activate PPARα and PPARγ [18–20], and inhibited atherosclerosis in animal feeding experiments [21–23]. Although the effects of CLA on plasma lipid concentrations as a surrogate marker of atherosclerosis in human studies are very inconsistent [24], there is at least some evidence that specific CLA isomers exert beneficial effects on plasma lipids in humans as well [25]. This suggests that CLA might stimulate cholesterol removal from macrophage foam cells through activation of PPARα and PPARγ, but a recent study by Weldon et al. [26] revealed no effects of CLA on molecular markers of cholesterol homeostasis in human THP-1 macrophage-derived foam cells. Although the lack of effect might be explained by the relatively poor accumulation of CLA isomers in THP-1 cells [26] when compared to other cell types [27–29], cell type-specific actions of CLA, e.g. on PPARγ expression [30, 31], might also account for this.

Thus, in the present study we aimed to test the hypothesis that CLA isomers have an impact on cholesterol homeostasis in RAW264.7 macrophage-derived foam cells. These cells have been reported to show pronounced biological activities, partially mediated by a PPARγ-dependent mechanism, in response to treatment with CLA [19, 28]. Moreover, these cells are a widely used model to study macrophage foam cell cholesterol homeostasis [32]. RAW264.7 macrophages were transformed to foam cells by treatment with acetylated LDL (acLDL). AcLDL is a well-recognized ligand for multiple scavenger receptors (SR) including CD36 and SR-A [33–36], and causes excessive uptake of lipoprotein-associated cholesterol in an unregulated fashion, leading to foam cell formation in vitro [37]. Kunjathoor et al. [36] have demonstrated that CD36 and SR-A account for 75–90% of the total amount of acLDL degraded by macrophages. Cholesterol loading by acLDL is further increased because acLDL dramatically increases CD36 expression in macrophages [38, 39]. In contrast, other SR involved in the uptake of acLDL such as SREC-I play only a minor role for acLDL uptake in both non-stimulated as well as stimulated macrophages [40]; according to [40] the contribution of SREC-I to the overall uptake and degradation of acLDL is only 5% in the non-stimulated and 6% in the stimulated condition. As parameters of cholesterol homeostasis, we considered the concentrations of free and esterified cellular cholesterol, and mRNA and/or protein expression levels of PPARα and PPARγ as well as important genes involved in the regulation of cholesterol homeostasis (CD36, ABCA1, LXRα, NPC-1, and NPC-2) in acLDL-induced macrophage foam cells. Cholesterol removal from macrophage foam cells was estimated by measurement of high-density lipoprotein (HDL)-dependent cholesterol efflux. As isomers *cis*-9, *trans*-11 (*c*9*t*11)-CLA, which contributes to more than 90% of total CLA in natural foods such as milk, dairy products, and meat of ruminants [41], and *trans*-10, *cis*-12 (*t*10*c*12)-CLA, which is a minor isomer in natural foods but one of the main isomers in chemically produced CLA mixtures, were used. Linoleic acid (LA) was used as reference fatty acid.

Experimental Procedure

Materials and Reagents

The CLA isomers *c*9*t*11-CLA (≥96% pure) and *t*10*c*12-CLA (≥98% pure) were purchased from Cayman Chemicals (Ann Arbor, MI). LA (≥99% pure) was obtained from Sigma-Aldrich (Taufkirchen, Germany).

Cell Culture and Treatments

Mouse RAW264.7 cells, obtained from LGC Promochem (Wesel, Germany), were grown in DMEM medium (Gibco/Invitrogen, Karlsruhe, Germany) supplemented with 10% fetal calf serum, 4 mmol/L L-glutamine, 4.5 g/L glucose, 1 mmol/L sodium pyruvate, 1.5 g/L sodium bicarbonate and 0.5% gentamicin. For experiments RAW264.7 cells were plated in 24-well plates at a density of 2×10^5/well. After reaching 80% confluence, cells were treated with 50 µmol/L of either *c*9*t*11-CLA, *t*10*c*12-CLA or LA for 24 h. To induce foam cell transformation, cells were incubated with fatty acids and 50 µg/mL human acLDL for an additional 24 h, as established in the literature [42]. Cells treated without additional fatty acids but with the vehicle (ethanol) were used as controls. Incubation media containing fatty acids were prepared by diluting the fatty acid stock solutions (100 mmol/L fatty acid in ethanol) with DMEM medium to the concentration indicated. Incubation media of control cells contained the same vehicle (ethanol) concentration of 0.05% (v/v). Preliminary experiments revealed no differences between vehicle controls and non-vehicle controls (data not shown). Experiments were performed between passages 5 and 20.

Cell Viability

The viability of cells after treatment with fatty acids was examined by the MTT assay [43].

Fatty Acid Analysis of Cell Total Lipids

After treatment of cells as indicated above, cells were washed with PBS and total lipids were extracted with hexane/isopropanol (3:2 v/v). Aliquots of the lipid extracts were dried under nitrogen, and total lipids of the extracts were transmethylated with trimethylsulfonium hydroxide as recently described in detail [44]. In brief, fatty acid methyl esters (FAME) were separated by gas chromatography using a gas chromatographic system (Hp 5890; Hewlett Packard, Waldbronn, Germany) fitted with an automatic split injection system, a flame ionization detector and a FFAP fused silica capillary column (30 m × 0.53 mm i.d.; Macherey and Nagel, Düren, Germany). FAME were identified by comparing their retention times with those of individual purified standards.

Isolation and Acetylation of LDL

LDL was isolated from fresh human serum by sequential gradient ultracentrifugation [45]. Afterwards LDL was dialyzed for 24 h at 4 °C against a buffer containing 0.15 mol/L NaCl and 0.3 mmol/L EDTA, pH 7.4. Acetylation of LDL was performed according to the method of Fraenkel-Conrad [46]. In brief, 1 mL of 0.15 mol/L NaCl containing 3 mg LDL protein was added to 1 mL of a saturated sodium acetate solution, and stirred in an ice water bath. Acetic anhydride (Sigma) was added slowly in small aliquots (2 µL/2 min) equal to 1.5 times the mass of LDL protein, and the mixture was stirred for an additional 30 min. Subsequently, the acLDL was dialyzed for 24 h at 4 °C against a buffer containing 0.15 mol/L NaCl and 0.3 mmol/L EDTA, pH 7.4, filter-sterilized, and stored at 4 °C.

Cholesterol Analysis

After treatment of cells as indicated above, cells were washed twice with PBS, cellular lipids extracted with a mixture of hexane and isopropanol (3:2 v/v), and lipid extracts dried under a stream of nitrogen. Total cholesterol and free cholesterol concentrations were determined using enzymatic assays (Wako Chemicals GmbH, Germany). The concentration of esterified cholesterol was determined by subtraction of the concentration of free cholesterol from that of total cholesterol. Cholesterol concentrations were related to cellular protein as determined by the BCA protein assay kit (Pierce, Rockford, IL). Cellular protein was obtained by lysis of cells in 0.2 mol/L NaOH after extraction of cellular lipids. Results are expressed as lipids/mg cellular protein.

RNA Isolation and Real-Time RT-PCR

After treatment of cells as indicated above, total RNA of the cells was extracted using Trizol reagent (Invitrogen, Karlsruhe, Germany) according to the manufacturer's instructions. RNA concentration and purity were estimated from the optical density at 260 and 280 nm, respectively. cDNA synthesis and real-time RT-PCR were performed as described recently in detail [47]. Mouse-specific primer sequences were as follows (forward, reverse): β-Actin (5′-ACG GCC AGG TCA TCA CTA TTG-3′, 5′-CAC AGG ATT CCA TAC CCA AGA AG-3′), CD36 (5′-GAA CCT ATT GAA GGC TTA CAT CC-3′, 5′-CCC AGT CAC TTG TGT TTT GAA C-3′), PPARα (5′-CGG CCC CAT ACA GGA GAG CAG-3′, 5′-GGG TGG CAG GAA GGG AAC AGA C-3′), PPARγ (5′-GGC GAG GGC GAT CTT GAC AG-3′, 5′-GGG CTT CCG CAG GTT TTT GAG-3′), ABCA1 (5′-TGC CAG CAA GAC GAA ACA GAC G-3′, 5′-GAC CAG GGC AAT GCA AAC AAA GAC-3′), LXRα (5′-GTA CAA CCC CGG CAG TGA GAG C-3′, 5′-GCA GGC GAA GGG CAA ACA C-3′), NPC-1 (5′-GGG GCA TCA GTT ACA ATG CT-3′, 5′-AAA CAC CGC ACT TCC CAT AG-3′), NPC-2 (5′-GAA ATC AGA CCC GAA ATG GA-3′, 5′-CAT CCT GTC TGG TGG AAC CT-3′).

Western Blot Analysis

After treatment of cells as indicated above, cells were lysed with RIPA lysis buffer (50 mmol/L Tris pH 7.5, 150 mmol/L NaCl, 1 mmol/L EDTA, 1% Triton X-100, 1% sodium deoxycholate, 0.1% SDS) containing protease inhibitor cocktail (Sigma), and protein concentrations of lysates determined by the BCA assay. Equal amounts of protein were electrophoresed by 7.5% SDS-PAGE for ABCA1 and 10% SDS-PAGE for LXRα, PPARγ, and β-Actin, and transferred to a nitrocellulose membrane. The membranes were blocked overnight at 4 °C in blocking solution (5% skim milk in Tris buffered saline with Tween-20 [TBS-T]: 50 mmol/L Tris, 150 mmol/L NaCl, pH 7.5, 0.1% Tween-20), and then incubated with primary antibodies against PPARγ (1:1,000, Upstate), ABCA1 (1:1,000, Novus Biologicals), LXRα (1:500, Affinity Bioreagents), and β-Actin (1:1,000, Novus Biologicals) for 1.5 h at room temperature. The membranes were washed with TBS-T, and incubated with a horseradish peroxidase conjugated secondary anti-mouse IgG antibody (1:2,000, Amersham Biosciences) or anti-rabbit IgG antibody (1:10,000, Amersham Biosciences) for 1.5 h at room temperature. Afterwards blots were developed using ECL Plus (Amersham Biosciences). The signal intensities of specific bands were detected with a Bio-Imaging system (Biostep) and quantified using TotalLab TL100-Quick Start analysis software (nonlinear dynamics).

Cholesterol Efflux Measurement

Cholesterol efflux assays were performed as described with minor modifications [32]. Twenty-four hours after plating, RAW264.7 macrophages were pre-treated with medium containing 10% low density lipoprotein-deficient serum for 24 h. Subsequently, RAW264.7 cells were incubated with fatty acids in the absence or presence of acLDL (50 μg/mL) and 1 μCi ^{3}H-cholesterol (Amersham-Biosciences) per well in a medium containing 0.2% bovine serum albumin for 24 h. After incubation, the medium was aspirated, cells were washed two times with PBS, and incubated with fatty acids in a medium containing 0.2% bovine serum albumin for a further 8 h. Cells were washed again with PBS, and incubated in the presence or absence of 50 μg/mL HDL as cholesterol acceptor for 4 h. After incubation, the medium was collected and cells were lysed using 0.2 M NaOH, and the medium and lysates were checked for ^{3}H-activity. Cholesterol efflux was calculated as the percentage of ^{3}H-activity in the medium from the total ^{3}H-activity in the medium and lysate as described in [48].

Statistical Analysis

Data were subjected to one-way ANOVA using the Minitab Statistical Software (Minitab, State College, PA, USA). For statistically significant F values, individual means of the treatment groups were compared by Fisher's multiple range. Means were considered significantly different for $P < 0.05$. Significant effects are denoted with superscript letters. Bars marked with different superscript letters significantly differ.

Results

Effects of Treatment on Viability of RAW264.7 Macrophage-Derived Foam Cells

Treatment with 50 μmol/L of either *c*9*t*11-CLA, *t*10*c*12-CLA or LA had no affect on the viability of RAW264.7 cells compared to vehicle control treatment; cell viabilities after treatment with *c*9*t*11-CLA, *t*10*c*12-CLA or LA were in the range between 97 and 103% relative to vehicle controls (=100%).

Effects of Treatment on Fatty Acid Composition of RAW264.7 Macrophage Total Lipids

Incubation of RAW264.7 macrophages with 50 μmol/L of either *c*9*t*11-CLA, *t*10*c*12-CLA or LA resulted in a marked incorporation of the respective fatty acids into the total cell lipids compared to vehicle controls (Table 1). However, the increase in the proportion of C18:2*c*9*t*11 after treatment with *c*9*t*11-CLA was less pronounced than the increase in the proportions of C18:2*t*10*c*12 and C18:2(n-6) after treatment with *t*10*c*12-CLA and LA, respectively. The incorporation of the respective fatty acids was accompanied by a concomitant marked decrease in the proportions of C16:1 and C18:1 when compared to vehicle controls. Other major fatty acids such as C16:0 and C18:0 were similar between treatment groups. The proportion of C14:0 was slightly increased by treatment with *c*9*t*11-CLA and *t*10*c*12-CLA relative to vehicle controls. Moreover, the proportion of C22:6(n-3) was decreased by treatment with *c*9*t*11-CLA and *t*10*c*12-CLA, whereas the

Table 1 Fatty acid composition (g/100 g total FAME) of total lipids of RAW264.7 macrophages cultured in the absence (control) or presence of 50 μmol/L of *c*9*t*11-CLA, *t*10*c*12-CLA or LA for 24 h

Treatment	Control	*c*9*t*11-CLA	*t*10*c*12-CLA	LA
Fatty acid				
C14:0	2.5 ± 0.1	3.1 ± 0.1	3.1 ± 0.1	2.5 ± 0.1
C16:0	22.6 ± 0.2	24.3 ± 0.1	24.9 ± 0.1	22.3 ± 0.2
C16:1	10.2 ± 0.1	5.3 ± 0.1	3.9 ± 0.1	3.3 ± 0.1
C18:0	15.4 ± 0.1	14.8 ± 0.1	15.3 ± 0.1	15.0 ± 0.1
C18:1	32.6 ± 0.5	23.1 ± 0.2	18.8 ± 0.2	17.5 ± 0.3
LA (C18:2n-6)	1.4 ± 0.1	2.2 ± 0.3	2.1 ± 0.1	13.0 ± 0.6
*c*9*t*11-CLA	<0.1	9.2 ± 0.5	0.1 ± 0.1	<0.1
*t*10*c*12-CLA	<0.1	0.1 ± 0.1	13.3 ± 0.5	<0.1
C20:4(n-6)	4.5 ± 0.1	4.2 ± 0.1	4.2 ± 0.1	8.4 ± 0.3
C20:5(n-3)	2.9 ± 0.1	2.4 ± 0.1	2.9 ± 0.1	2.7 ± 0.1
C22:4(n-6)	0.5 ± 0.1	0.7 ± 0.1	0.7 ± 0.1	3.1 ± 0.1
C22:6(n-3)	2.8 ± 0.1	2.3 ± 0.1	2.3 ± 0.1	2.4 ± 0.1

[a] Values are mean ± SEM of two independent experiments ($n = 2$). Data were not subjected to statistical analysis due to the low amount of experiments

proportion of C20:5(n-3) was only decreased by treatment with *c*9*t*11-CLA compared to vehicle controls. Treatment with LA increased the proportions of C20:4(n-6) and C22:4(n-6) when compared to vehicle controls.

Effects of Treatment on Cholesterol Concentrations in RAW264.7 Macrophage-Derived Foam Cells

Treatment of acLDL-induced RAW264.7 macrophage-derived foam cells with either *c*9*t*11-CLA or *t*10*c*12-CLA lowered concentrations of esterified cholesterol but not of free cholesterol compared to vehicle control cells ($P < 0.05$; Fig. 1). Treatment with LA had no effect on the concentrations of free or esterified cholesterol in acLDL-induced RAW264.7 macrophage-derived foam cells when compared to vehicle controls. However, the effect of CLA isomers on the concentration of esterified cholesterol did not differ from that of LA.

Effects of Treatment on Relative mRNA Concentrations of Genes Involved in Cholesterol Homeostasis in RAW264.7 Macrophage-Derived Foam Cells

Relative mRNA concentrations of CD36, ABCA1, and LXRα were significantly increased by both *c*9*t*11-CLA and *t*10*c*12-CLA compared to vehicle control cells and LA ($P < 0.05$; Fig. 2), whereas those of NPC-1 and NPC-2 were only increased by *t*10*c*12-CLA compared to vehicle control cells and LA ($P < 0.05$). Treatment of RAW264.7 macrophage-derived foam cells with LA did not alter mRNA concentrations of the genes investigated compared to vehicle controls ($P < 0.05$). Relative mRNA concentration of PPARα in RAW264.7 macrophage-derived foam cells was not altered by treatment with either fatty acid. Relative mRNA concentration of PPARγ in RAW264.7 macrophage-derived foam cells was significantly elevated by incubation with *c*9*t*11-CLA compared to vehicle controls and LA ($P < 0.05$). Incubation with *t*10*c*12-CLA or LA had no effect on the relative mRNA concentration of PPARγ in RAW264.7 macrophage-derived foam cells compared to vehicle controls.

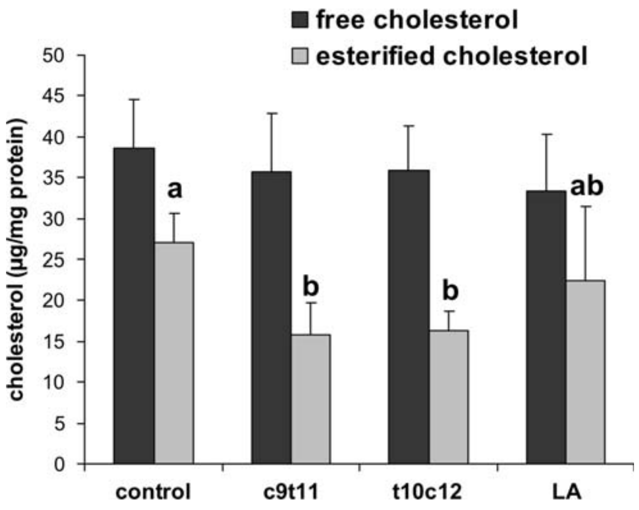

Fig. 1 Effect of treatment with 50 µmol/L of either *c*9*t*11-CLA, *t*10*c*12-CLA or LA on free and esterified cholesterol concentrations in acLDL-induced RAW264.7 macrophage-derived foam cells. Cells treated without fatty acids were used as controls. Data represent mean ± SEM of at least three independent experiments ($n \geq 3$). Results from statistical analysis (one-way ANOVA followed by Fisher's test) are indicated: Significant effects are denoted with superscript letters. *Bars* marked without a common superscript letter significantly differ ($P < 0.05$)

Effects of Treatment on Relative Protein Concentrations of ABCA1, LXRα and PPARγ in RAW264.7 Macrophage-Derived Foam Cells

Since mRNA data indicated an induction of genes involved in cholesterol efflux by CLA we also determined relative protein concentrations of ABCA1 and its transcriptional activator LXRα in western blot experiments. PPARγ protein was also considered because of the marked effect of *c*9*t*11-CLA on its mRNA concentration. Our western blot experiments revealed that the protein concentration of ABCA1 was significantly increased by *t*10*c*12-CLA compared to vehicle controls and LA ($P < 0.05$; Fig. 3a, b), whereas *c*9*t*11-CLA tended to increase the protein concentration of ABCA1. Relative protein concentration of LXRα was not altered by treatment with either CLA isomers or LA. The relative protein concentration of PPARγ was significantly increased by *c*9*t*11-CLA compared to vehicle controls and LA ($P < 0.05$). Treatment with LA even decreased the relative protein concentration of PPARγ compared to vehicle controls ($P < 0.05$).

Effects of Treatment on Cholesterol Efflux from RAW264.7 Macrophage-Derived Foam Cells

In the presence of HDL, cholesterol efflux from acLDL-induced RAW264.7 macrophage-derived foam cells was significantly increased by *c*9*t*11-CLA and *t*10*c*12-CLA compared to vehicle control treatment ($P < 0.05$; Fig. 4), but not by LA. The effect of *c*9*t*11-CLA and *t*10*c*12-CLA, however, did not differ from that of LA. In the absence of HDL, cholesterol efflux was not different between vehicle control cells and cells treated with fatty acids.

Discussion

Pharmacological PPARα and PPARγ ligands have been demonstrated to induce cholesterol removal from

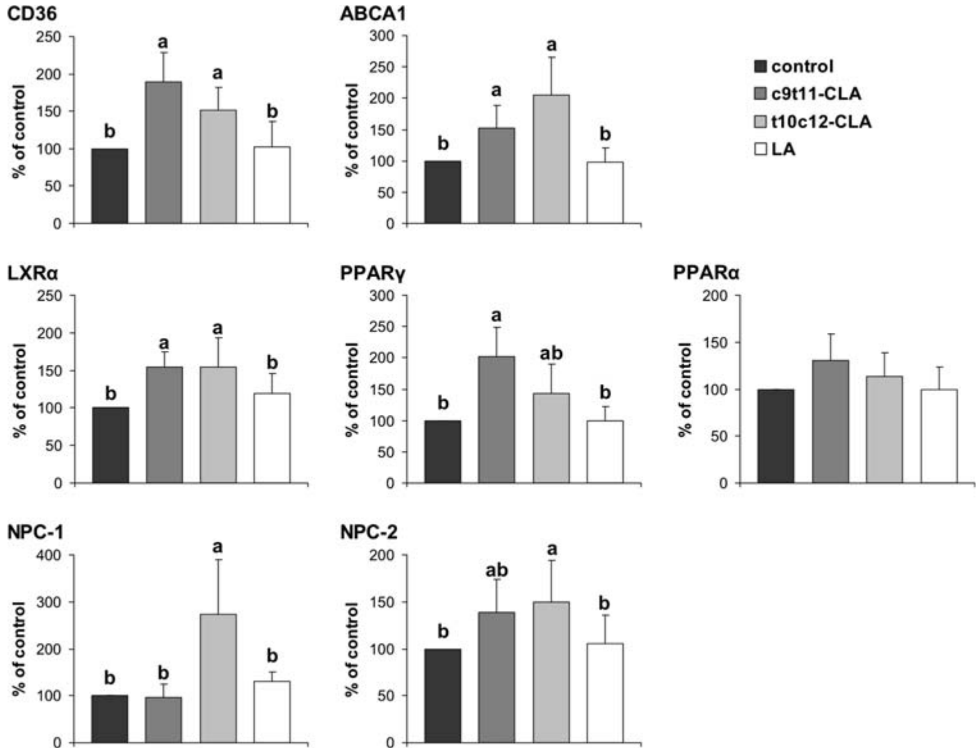

Fig. 2 Effect of treatment with 50 µmol/L of either *c*9*t*11-CLA, *t*10*c*12-CLA or LA on relative mRNA concentrations of genes involved in cholesterol homeostasis in acLDL-induced RAW264.7 macrophage-derived foam cells. Cells treated without fatty acids were used as controls. Data represent mean ± SEM of at least three independent experiments ($n \geq 3$) and are expressed as percentage of mRNA abundance of controls (=100 ± 0%). Results from statistical analysis (one-way ANOVA followed by Fisher's test) are indicated: Significant effects are denoted with superscript letters. *Bars* marked without a common superscript letter significantly differ ($P < 0.05$)

macrophage foam cells through alterations in the expression of genes involved in cholesterol homeostasis [4, 5, 8, 9, 13]. Since CLA are also well-known activators of PPARα and PPARγ [18–20], the present study aimed to test the hypothesis that CLA isomers have an impact on cholesterol homeostasis in RAW264.7 macrophage-derived foam cells. For the incubation experiments, we used concentrations of CLA of 50 µmol/L. This concentration is similar to what has been typically used in cell culture studies dealing with CLA's mechanisms of action [20, 26–31]. However, based on the observation that incubating RAW264.7 cells with 50 µmol/L of CLA resulted in concentrations of CLA in cell lipids of up to 13 g/100 g of total fatty acids, this concentration of CLA must be considered as rather high. In contrast, humans supplemented with 3 g per day of a CLA mixture for 6 weeks had plasma concentrations of *c*9*t*11-CLA of only about 0.8 g/100 g total fatty acids [49]. Nevertheless, our study shows that the concentration of CLA isomers in macrophage cells can be extremely elevated as also observed in several other cell lines [20, 29] while the cells still have normal morphological appearance and growth characteristics. This opens up the possibility of studying the influence of high concentrations of CLA on diverse functional properties of cells and of addressing mechanistic questions. This cell culture study, thus, must be considered as a model study that cannot be directly extrapolated to humans. As expected, the incorporation of the CLA isomers into macrophage total lipids was accompanied by concomitant changes in the proportions of other fatty acids. Most important, the proportions of C16:1 and C18:1 were markedly reduced by treatment with CLA isomers, and the proportions of polyunsaturated fatty acids (PUFA) like C22:6(n-3) and C20:5(n-3) were slightly decreased by CLA isomers. This indicates that the effects observed in the present study cannot solely be ascribed to the incorporation of CLA isomers but also, at least partially, to changes in fatty acid composition. However, since the proportions of PUFA, which are known PPAR ligands [50], were even decreased by treatment with CLA isomers, we are confident that activation of PPARs in response to CLA treatment was primarily caused by the added CLA isomers.

The present study clearly demonstrated that *c*9*t*11-CLA and *t*10*c*12-CLA lowered concentrations of esterified cholesterol, the storage form of cholesterol in macrophage-foam cells, and stimulated HDL-dependent cholesterol efflux in mouse RAW264.7 macrophage-derived foam cells when compared to control cells treated without additional fatty acids. The reduction of cholesterol accumulation by CLA isomers in RAW264.7 macrophage-derived foam cells was evidenced by a decline in the concentration of esterified cholesterol. Thus, the finding that lowering of macrophage cholesterol accumulation and induction of HDL-dependent cholesterol removal could be observed with CLA isomers, which has also been reported in response to pharmacological PPAR ligands [4, 5, 8, 9, 13], strengthens our hypothesis that CLA isomers are capable of affecting macrophage foam cell cholesterol

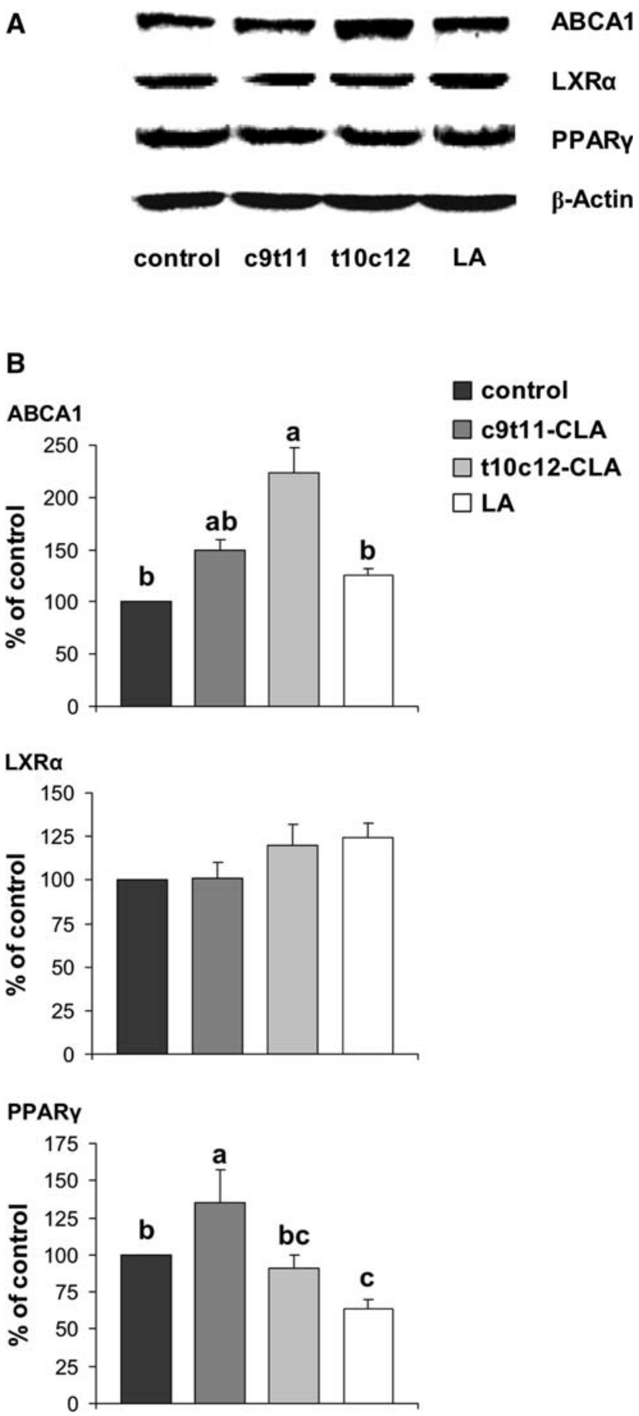

Fig. 3 Effect of treatment with 50 µmol/L of either *c*9*t*11-CLA, *t*10*c*12-CLA or LA on relative protein concentrations of ABCA1, LXRα, and PPARγ in acLDL-induced RAW264.7 macrophage-derived foam cells. Cells treated without fatty acids were used as controls. **a** Representative immunoblots specific to ABCA1, LXRα, PPARγ, and β-Actin which was used for normalization are shown. **b** Graphs represent data from densitometric analysis and represent mean ± SEM of at least three independent experiments ($n \geq 3$). Data are expressed as percentage of protein concentration of controls (=100 ± 0%). Results from statistical analysis (one-way ANOVA followed by Fisher's test) are indicated: significant effects are denoted with superscript letters. *Bars* marked without a common superscript letter significantly differ ($P < 0.05$)

homeostasis through their potential to activate PPARs. In connection with recent findings that treatment with CLA isomers failed to reduce cholesterol accumulation in human THP-1 macrophage-derived foam cells [26], the results from the present study may indicate that the effect of CLA on macrophage cholesterol accumulation is cell type- or species-specific. The reason for these divergent effects of CLA cannot be definitely ruled out, but differences in the cellular uptake and incorporation of CLA isomers between RAW264.7 and THP-1 cells might be causative. Whereas in THP-1 macrophages only a poor incorporation of CLA isomers in total cell lipids after treatment with CLA isomers has been reported [26], treatment of RAW264.7 macrophage foam cells with CLA isomers in the present study resulted in a marked incorporation of CLA isomers. However, since up-regulation of CD36 by CLA isomers has been observed in that recent report [26] other reasons such as differences in the expression pattern of PPAR-subtypes between these two cell lines might also apply [18, 51]. Nevertheless, to resolve these contradictory results between RAW264.7 and THP-1 cells with certainty further research is required.

On the molecular level, reduction of cholesterol accumulation in cultured macrophages by PPARα and PPARγ activators has been explained by increased expression of LXRα, which in turn activates expression of LXRα target genes such as macrophage cholesterol exporters, namely ABCA1 and ABCG1, and, thereby, stimulates cholesterol efflux to extracellular acceptors for reverse cholesterol transport [4, 5, 8, 9]. A recent study further demonstrated that PPARα activation stimulates postlysosomal mobilization of cholesterol by induction of gene expression of NPC-1 and NPC-2 [13]. Both proteins control intracellular trafficking of cholesterol from the late endosomal compartment and lysosome, respectively, to the plasma membrane [14, 15]. It has been suggested [13] that this results in an enrichment of cholesterol in the plasma membrane and an enhanced availability of cholesterol at the cell membrane, which also contributes to increased macrophage cholesterol efflux and reverse cholesterol transport by PPARα activators. Hence, the increased mRNA abundance of ABCA1, LXRα, NPC-1, and NPC-2 in response to CLA isomers as observed in the present study is associated with the reduced cholesterol accumulation in RAW264.7 macrophage-derived foam cells. The induction of ABCA1 by CLA isomers could also be observed at the protein level although this effect was only significant for *t*10*c*12-CLA whereas *c*9*t*11-CLA only showed a tendency towards an increased ABCA1 protein concentration. However, this observation is in the line

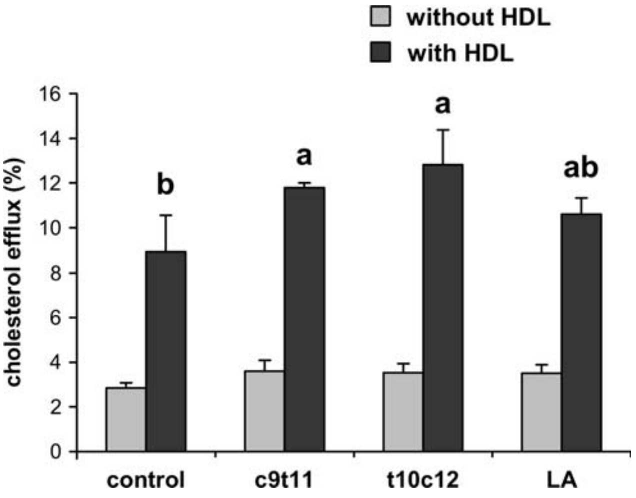

Fig. 4 Effect of treatment with 50 μmol/L of either *c*9*t*11-CLA, *t*10*c*12-CLA or LA on cholesterol efflux in acLDL-induced RAW264.7 macrophage-derived foam cells in the presence and absence of HDL. Cells treated without fatty acids were used as controls. Efflux is expressed as counts media/(counts media + counts lysate) × 100. Data represent mean ± SEM of at least three independent experiments ($n \geq 3$). Results from statistical analysis (one-way ANOVA followed by Fisher's test) are indicated: significant effects are denoted with superscript letters. *Bars* marked without a common superscript letter significantly differ ($P < 0.05$)

with the more pronounced effect of *t*10*c*12-CLA on the elevation of ABCA1 mRNA concentration compared with *c*9*t*11-CLA. We have no explanation for the slightly stronger effect of *t*10*c*12-CLA on ABCA1 mRNA concentration compared with *c*9*t*11-CLA. However, this might be related to the slightly higher incorporation of *t*10*c*12-CLA into the macrophage total lipids when compared to *c*9*t*11-CLA, which in turn resulted in an increased PPAR ligand availability, thereby, causing a stronger LXRα and ABCA1 induction. Surprisingly, we could not detect an increased protein concentration of LXRα in response to *t*10*c*12-CLA or *c*9*t*11-CLA although both CLA isomers elevated the mRNA concentration of this transcription factor. Although we do not know the exact reason for this discrepancy it has to be considered that the elevation of LXRα mRNA concentration by CLA isomers was only about 50%, a degree that can hardly be demonstrated in western blot experiments. In addition, it should be kept in mind that CLA isomers might have also stimulated LXRα transactivation without influencing protein levels of this transcription factor. This, however, has to be elucidated in further studies. Nevertheless, collectively the present data suggest that reverse cholesterol transport is presumably stimulated by natural PPAR ligands deriving from food like CLA. The observation from a recent study that plasma HDL cholesterol concentrations and ABCA1 gene expression were increased in the aorta of hamsters fed *c*9*t*11-CLA is indeed indicative of the potential of CLA to increase the capacity for reverse cholesterol transport [52].

We cannot exclude the possibility that CLA isomers might also had an effect on genes regulating cholesterol esterification in macrophage-derived foam cells such as acyl-CoA:cholesterol acyltransferase (ACAT), which catalyzes cholesteryl ester formation from cholesterol and fatty acyl-CoA, and cholesteryl ester hydrolase (CEH), which is responsible for hydrolysis of stored cholesterol esters in macrophage foam cells and release of free cholesterol for high-density lipoprotein-mediated efflux. Indeed, Hirakata et al. [53] have demonstrated that reduction of cholesteryl ester accumulation by pharmacological PPARγ ligands in THP-1 macrophages was accompanied by enhanced CEH mRNA expression and inhibited ACAT-1 mRNA expression. Since free cholesterol mobilized from hydrolysis of cholesteryl esters by increased expression of CEH is also partially diffusing through the plasma membrane as shown by the cholesterol efflux observed in the absence of added HDL, we suggest that this stimulation of "passive" cholesterol efflux is at least in part responsible for the reduced cholesteryl ester levels observed during incubation without extracellular cholesterol acceptors (Fig. 1). Therefore, downregulation of ACAT-1 and upregulation of CEH by CLA isomers might have also contributed to the reduced cholesteryl ester concentrations as observed in the present study. However, this deserves further investigation.

The present study revealed that the inhibitory effect of CLA isomers on macrophage foam cell cholesterol accumulation was only significant when compared to vehicle control cells treated without additional fatty acids. However, when compared to LA, a frequently used reference fatty acid when studying the effects of CLA [26, 54], the inhibitory effect of CLA isomers on cholesterol accumulation was not significant. In part, this might be due to the fact that the standard variation of measured values in the LA group (e.g. esterified cholesterol) was quite high whereas that in the vehicle control group was comparatively low, therefore, explaining that the effect of CLA was not different from LA. Since the present study further shows that treatment with LA had no effect on mRNA abundance of genes involved in cholesterol homeostasis in RAW264.7 macrophage-derived foam cells, we suggest that LA had no effect on macrophage foam cell cholesterol accumulation and, thus, clearly differs from CLA in its action on the parameters investigated herein. This indicates that the inhibitory effect of CLA isomers on macrophage foam cell cholesterol accumulation is dependent on the specific conjugated dienoic structure of CLA. In part the lack of effect of LA might be explained by the fact that LA is a weaker PPARα and PPARγ activator than *c*9*t*11-CLA or *t*10*c*12-CLA [18]. Consistent with this finding is the observation that LA, in contrast to *c*9*t*11-CLA or *t*10*c*12-CLA, did not induce the PPARγ target gene CD36 in RAW264.7 and THP-1 macrophage-derived foam cells [26]. Similar observations have been reported from Yu et al. [19] using RAW264.7 macrophages.

In conclusion, the present study shows that *c*9*t*11-CLA and *t*10*c*12-CLA reduce cholesterol accumulation in RAW264.7 macrophage-derived foam cells probably by stimulating HDL-dependent cholesterol efflux. The CLA-induced increase in cholesterol efflux from macrophage foam cells is presumably explained by the up-regulation of ABCA1, which operates on cholesterol export to extracellular acceptors such as apo-AI/HDL. Up-regulation of NPC-1 and NPC-2 as evidenced by increased transcript levels of NPC-1 and NPC-2 in response to treatment with CLA isomers probably also contributes to the observed lowering of cholesterol accumulation in RAW264.7 cells, since both proteins mediate intracellular cholesterol transport to the plasma membrane and increase the availability of cholesterol for efflux through extracellular acceptors. Since treatment with CLA isomers also caused an increase in the transcript levels of CD36, which mediates cholesterol uptake from modified LDL particles [55], we suggest that the concomitant up-regulation of ABCA1, which mediates cholesterol removal from cells, was probably more pronounced leading to a net efflux of cholesterol. Because extensive accumulation of cholesterol by macrophage foam cells in the arterial wall leads to atherosclerosis, the present findings in connection with other beneficial effects of CLA in macrophages [19, 26, 56, 57] might in part explain the anti-atherogenic actions of CLA as observed in animal models of experimental atherosclerosis [21–23].

References

1. Rosamond W, Flegal K, Friday G, Furie K, Go A, Greenlund K, Haase N, Ho M, Howard V et al (2007) Heart disease and stroke statistics—2007 update: a report from the American Heart Association Statistics Committee and Stroke Statistics Subcommittee. Circulation 115:e69–e171
2. Gerrity RG, Naito HK (1980) Ultrastructural identification of monocyte-derived foam cells in fatty streak lesions. Artery 8:208–214
3. Glass CK, Witztum JL (2001) Atherosclerosis: the road ahead. Cell 104:503–516
4. Chinetti G, Lestavel S, Bocher V, Remaley AT, Neve B, Torra IP, Teissier E, Minnich A, Jaye M et al (2001) PPAR-α and PPAR-γ activators induce cholesterol removal from human macrophage foam cells through stimulation of the ABCA1 pathway. Nat Med 7:53–58
5. Chinetti G, Lestavel S, Fruchart JC, Clavey V, Staels B (2003) Peroxisome proliferator-activated receptor α reduces cholesterol esterification in macrophages. Circ Res 92:212–217
6. Nagy L, Tontonoz P, Alvarez JG, Chen H, Evans RM (1998) Oxidized LDL regulates macrophage gene expression through ligand activation of PPARγ. Cell 93:229–240
7. Tontonoz P, Nagy L, Alvarez JG, Thomazy VA, Evans RM (1998) PPARγ promotes monocyte/macrophage differentiation and uptake of oxidized LDL. Cell 93:241–252
8. Chawla A, Boisvert WA, Lee CH, Laffitte BA, Barak Y, Joseph SB, Liao D, Nagy L, Edwards PA et al (2001) PPARγ-LXR-ABCA1 Pathway in macrophages is involved in cholesterol efflux and atherogenesis. Mol Cell 7:161–171
9. Moore KJ, Rosen ED, Fitzgerald ML, Randow F, Andersson LP, Altshuler D, Milstone DS, Mortensen RM, Spiegelman BM, Freeman MW (2001) The role of PPAR-γ in macrophage differentiation and cholesterol uptake. Nat Med 7:41–47
10. Bodzioch M, Orsó E, Klucken J, Langmann T, Böttcher A, Diederich W, Drobnik W, Barlage S, Büchler C et al (1999) The gene encoding ATP-binding cassette transporter 1 is mutated in Tangier disease. Nat Genet 22:347–351
11. Brooks-Wilson A, Marcil M, Clee SM, Zhang LH, Roomp K, van Dam M, Yu L, Brewer C, Collins JA et al (1999) Mutations in ABC1 in Tangier disease and familial high-density lipoprotein deficiency. Nat Genet 22:336–345
12. Rust S, Rosier M, Funke H, Real J, Amoura Z, Piette JC, Deleuze JF, Brewer HB, Duverger N et al (1999) Tangier disease is caused by mutations in the gene encoding ATP-binding cassette transporter 1. Nat Genet 22:352–355
13. Chinetti-Gbaguidi G, Rigamonti E, Helin L, Mutka AL, Lepore M, Fruchart JC, Clavey V, Ikonen E, Lestavel S, Staels B (2005) Peroxisome proliferator-activated receptor α controls cellular cholesterol trafficking in macrophages. J Lipid Res 46:2717–2725
14. Carstea ED, Morris JA, Coleman KG, Loftus SK, Zhang D, Cummings C, Gu J, Rosenfeld MA, Pavan WJ et al (1997) Niemann-Pick C1 disease gene: homology to mediators of cholesterol homeostasis. Science 277:228–231
15. Strauss JF III, Liu P, Christenson LK, Watari H (2002) Sterols and intracellular vesicular trafficking: lessons from the study of NPC1. Steroids 67:947–951
16. Li AC, Binder CJ, Gutierrez A, Brown KK, Plotkin CR, Pattison JW, Valledor AF, Davis RA, Willson TM et al (2004) Differential inhibition of macrophage foam-cell formation and atherosclerosis in mice by PPARα, β/δ, and γ. J Clin Invest 114:1564–1576
17. Collins AR, Meehan WP, Kintscher U, Jackson S, Wakino S, Noh G, Palinski W, Hsueh WA, Law RE (2001) Troglitazone inhibits formation of early atherosclerotic lesions in diabetic and nondiabetic low density lipoprotein receptor-deficient mice. Arterioscler Thromb Vasc Biol 21:365–371
18. Moya-Camarena SY, Vanden Heuvel JP, Blanchard SG, Leesnitzer LA, Belury MA (1999) Conjugated linoleic acid is a potent naturally occurring ligand and activator of PPARα. J Lipid Res 40:1426–1433
19. Yu Y, Correll PH, Vanden Heuvel JP (2002) Conjugated linoleic acid decreases production of pro-inflammatory products in macrophages: evidence for a PPARγ-dependent mechanism. Biochim Biophys Acta 1581:89–99
20. Ringseis R, Müller A, Herter C, Gahler S, Steinhart H, Eder K (2006) CLA isomers inhibit TNFα-induced eicosanoid release from human vascular smooth muscle cells via a PPARγ ligand-like action. Biochim Biophys Acta 1760:290–300
21. Toomey S, Harhen B, Roche HM, Fitzgerald D, Belton O (2006) Profound resolution of early atherosclerosis with conjugated linoleic acid. Atherosclerosis 187:40–49
22. Kritchevsky D, Tepper SA, Wright S, Tso P, Czarnecki SK (2000) Influence of conjugated linoleic acid (CLA) on establishment and progression of atherosclerosis in rabbits. J Am Coll Nutr 19:472S–477S

23. Mitchell PL, Langille MA, Currie DL, McLeod RS (2005) Effect of conjugated linoleic acid isomers on lipoproteins and atherosclerosis in the Syrian Golden hamster. Biochim Biophys Acta 1734:269–276
24. Tricon S, Burdge GC, Williams CM, Calder PC, Yaqoob P (2005) The effects of conjugated linoleic acid on human health-related outcomes. Proc Nutr Soc 64:171–182
25. Tricon S, Burdge GC, Kew S, Banerjee T, Russell JJ, Jones EL, Grimble RF, Williams CM, Yaqoob P, Calder PC (2004) Opposing effects of cis-9, trans-11 and trans-10, cis-12 conjugated linoleic acid on blood lipids in healthy humans. Am J Clin Nutr 80:614–620
26. Weldon S, Mitchell S, Kelleher D, Gibney MJ, Roche HM (2004) Conjugated linoleic acid and atherosclerosis: no effect on molecular markers of cholesterol homeostasis in THP-1 macrophages. Atherosclerosis 174:261–273
27. Agatha G, Voigt A, Kauf E, Zintl F (2004) Conjugated linoleic acid modulation of cell membrane in leukemia cells. Cancer Lett 209:87–103
28. Cheng WL, Lii CK, Chen HW, Lin TH, Liu KL (2004) Contribution of conjugated linoleic acid to the suppression of inflammatory responses through the regulation of the NF-κB pathway. J Agric Food Chem 52:71–78
29. Ringseis R, Müller A, Düsterloh K, Schleser S, Eder K, Steinhart H (2006) Formation of conjugated linoleic acid metabolites in human vascular endothelial cells. Biochim Biophys Acta 1761:377–383
30. Cimini A, Cristiano L, Colafarina S, Benedetti E, Di Loreto S, Festuccia C, Amicarelli F, Canuto RA, Cerù MP (2005) PPARγ-dependent effects of conjugated linoleic acid on the human glioblastoma cell line (ADF). Int J Cancer 117:923–933
31. Kang K, Liu W, Albright KJ, Park Y, Pariza MW (2003) Trans-10, cis-12 CLA inhibits differentiation of 3T3-L1 adipocytes and decreases PPARγ expression. Biochem Biophys Res Commun 303:795–799
32. Venkateswaran A, Laffitte BA, Joseph SB, Mak PA, Wilpitz DC, Edwards PA, Tontonoz P (2000) Control of cellular cholesterol efflux by the nuclear oxysterol receptor LXRα. Proc Natl Acad Sci USA 97:12097–12102
33. Calvo D, Gómez-Coronado D, Lasunción MA, Vega MA (1997) CLA-1 is an 85-kD plasma membrane glycoprotein that acts as a high-affinity receptor for both native (HDL, LDL, and VLDL) and modified (OxLDL and AcLDL) lipoproteins. Arterioscler Thromb Vasc Biol 17:2341–2349
34. Calvo D, Gómez-Coronado D, Suárez Y, Lasunción MA, Vega MA (1998) Human CD36 is a high affinity receptor for the native lipoproteins HDL, LDL, and VLDL. J Lipid Res 39:777–788
35. Endemann G, Stanton LW, Madden KS, Bryant CM, White RT, Protter AA (1993) CD36 is a receptor for oxidized low density lipoprotein. J Biol Chem 268:11811–11816
36. Kunjathoor VV, Febbraio M, Podrez EA, Moore KJ, Andersson L, Koehn S, Rhee JS, Silverstein R, Hoff HF, Freeman MW (2002) Scavenger receptors class A-I/II and CD36 are the principal receptors responsible for the uptake of modified low density lipoprotein leading to lipid loading in macrophages. J Biol Chem 277:49982–49988
37. Araki N, Horiuchi S, Rahim AT, Takata K, Morino Y (1990) Microquantification of cholesterol and cholesteryl esters in rat peritoneal macrophages by reverse-phase high-performance liquid chromatography. Anal Biochem 185:339–345
38. Han J, Hajjar DP, Febbraio M, Nicholson AC (1997) Native and modified low density lipoproteins increase the functional expression of the macrophage class B scavenger receptor, CD36. J Biol Chem 272:21654–21659
39. Devaraj S, Hugou I, Jialal I (2001) Alpha-tocopherol decreases CD36 expression in human monocyte-derived macrophages. J Lipid Res 42:521–527
40. Tamura Y, Osuga J, Adachi H, Tozawa R, Takanezawa Y, Ohashi K, Yahagi N, Sekiya M, Okazaki H et al (2004) Scavenger receptor expressed by endothelial cells I (SREC-I) mediates the uptake of acetylated low density lipoproteins by macrophages stimulated with lipopolysaccharide. J Biol Chem 279:30938–30944
41. Steinhart H, Rickert R, Winkler K (2003) Identification and analysis of conjugated linoleic acid isomers (CLA). Eur J Med Res 8:370–372
42. Lorenzi I, von Eckardstein A, Cavelier C, Radosavljevic S, Rohrer L (2008) Apolipoprotein A-I but not high-density lipoproteins are internalised by RAW macrophages: roles of ATP-binding cassette transporter A1 and scavenger receptor BI. J Mol Med 86:171–183
43. Vistica DT, Skehan P, Scudiero D, Monks A, Pittman A, Boyd MR (1991) Tetrazolium-based assays for cellular viability: a critical examination of selected parameters affecting formazan production. Cancer Res 51:2515–2520
44. Eder K, Brandsch C (2002) Effect of fatty acid composition of rapeseed oil on plasma lipids, fatty acid composition of tissues and susceptibility of low-density lipoprotein to lipid peroxidation in cholesterol-fed hamsters. Eur J Lipid Sci Technol 104:3–13
45. Hojnacki JL, Nicolosi RJ, Hoover G, Liansa N, Ershow RG, El Lozy M, Haycs KG (1978) Comparison of two ultracentrifugation procedures for separation of nonhuman primate lipoproteins. Anal Biochem 88:485–494
46. Fraenkel-Conrad H (1957) In: Colowick SP, Kaplan NO (eds) Methods in Enzymology, vol 4. Academic Press, New York, pp 247–269
47. Ringseis R, Muschick A, Eder K (2007) Dietary oxidized fat prevents ethanol-induced triacylglycerol accumulation and increases expression of PPARα target genes in rat liver. J Nutr 137:77–83
48. Westerterp M, Van Eck M, de Haan W, Offerman EH, Van Berkel TJ, Havekes LM, Rensen PC (2007) Apolipoprotein CI aggravates atherosclerosis development in ApoE-knockout mice despite mediating cholesterol efflux from macrophages. Atherosclerosis 195:e9–e16
49. Noone EJ, Roche HM, Nugent AP, Gibney MJ (2002) The effect of dietary supplementation using isomeric blends of conjugated linoleic acid on lipid metabolism in healthy human subjects. Br J Nutr 88:243–251
50. Bocos C, Göttlicher M, Gearing K, Banner C, Enmark E, Teboul M, Crickmore A, Gustafsson JA (1995) Fatty acid activation of peroxisome proliferator-activated receptor (PPAR). J Steroid Biochem Mol Biol 53:467–473
51. Ricote M, Li AC, Willson TM, Kelly CJ, Glass CK (1998) The peroxisome proliferator-activated receptor-gamma is a negative regulator of macrophage activation. Nature 391:79–82
52. Valeille K, Ferezou J, Parquet M, Amsler G, Gripois D, Quignard-Boulange A, Martin JC (2006) The natural concentration of the conjugated linoleic acid, cis-9, trans-11, in milk fat has antiatherogenic effects in hyperlipidemic hamsters. J Nutr 136:1305–1310
53. Hirakata M, Tozawa R, Imura Y, Sugiyama Y (2004) Comparison of the effects of pioglitazone and rosiglitazone on macrophage foam cell formation. Biochem Biophys Res Commun 323:782–788
54. Schleser S, Ringseis R, Eder K (2006) Conjugated linoleic acids have no effect on TNFα-induced adhesion molecule expression, U937 monocyte adhesion, and chemokine release in human aortic endothelial cells. Atherosclerosis 186:337–344

55. Febbraio M, Podrez EA, Smith JD, Hajjar DP, Hazen SL, Hoff HF, Sharma K, Silverstein RL (2000) Targeted disruption of the class B scavenger receptor CD36 protects against atherosclerosis lesions development in mice. J Clin Invest 105:1049–1056
56. Stachowska E, Dziedziejko V, Safranow K, Gutowska I, Adler G, Ciechanowicz A, Machalinski B, Chlubek D (2007) Inhibition of phospholipase A2 activity by conjugated linoleic acids in human macrophages. Eur J Nutr 46:28–33
57. Stachowska E, Baśkiewicz-Masiuk M, Dziedziejko V, Adler G, Bober J, Machaliński B, Chlubek D (2007) Conjugated linoleic acids can change phagocytosis of human monocytes/macrophages by reduction in Cox-2 expression. Lipids 42:707–716

Lipids (2008) 43:925–936
DOI 10.1007/s11745-008-3222-1

ORIGINAL ARTICLE

Women and Smokers Have Elevated Urinary F_2-Isoprostane Metabolites: A Novel Extraction and LC–MS Methodology

Alan W. Taylor · Richard S. Bruno ·
Maret G. Traber

Received: 21 January 2008 / Accepted: 31 July 2008 / Published online: 27 August 2008
© AOCS 2008

Abstract F_2-Isoprostanes (F_2-IsoPs), regio- and stereoisomers of prostaglandin $F_{2\alpha}$ ($PGF_{2\alpha}$), and urinary F_2-IsoP metabolites including 2,3-dinor-5,6-dihydro-8-*iso*-$PGF_{2\alpha}$ [2,3-dinor-8-*iso*-$PGF_{1\alpha}$ (2,3-dinor-F1)] and 2,3 dinor-8-*iso*-$PGF_{2\alpha}$ (2,3-dinor-F2), have all been used as biomarkers of oxidative stress. A novel method was developed to measure these biomarkers using a single solid phase extraction (SPE) cartridge, separation by HPLC, and detection by negative mode selected reaction monitoring (SRM) mass spectrometry (MS), using authentic standards of $PGF_{2\alpha}$; 8-*iso*-$PGF_{2\alpha}$; 2,3-dinor-F1 and 2,3-dinor-F2 to identify specific chromatographic peaks. The method was validated in a population of healthy, college-aged nonsmokers ($n = 6$ M/8F) and smokers ($n = 6$ M/5F). Urinary F_2-IsoP concentrations were ~0.2–1.5 µg/g creatinine, 2,3-dinor-F1 was ~1–3 µg/g and 2,3-dinor-F2 was ~3–5 µg/g. Additional F_2-IsoPs metabolites were identified using SRM. The sum of all urinary F_2-IsoP metabolites was 50–100 µg/g creatinine indicating their greater abundance than F_2-IsoPs. Women had higher F_2-IsoP metabolite concentrations than did men (MANOVA, main effect $P = 0.003$); cigarette smokers had higher concentrations than did nonsmokers (main effect $P = 0.036$). For men or women, respectively, smokers had higher metabolite concentrations than did nonsmokers ($P < 0.05$). Thus, our method simultaneously allows measurement of urinary F_2-IsoPs and their metabolites for the determination of oxidative stress.

Keywords Oxidative stress · LC–MS · F_2-Isoprostanes · F_2-Isoprostane metabolites · Prostaglandin $F_{2\alpha}$ ($PGF_{2\alpha}$) · Cigarette smoking · Gender difference · 2,3-dinor-5,6-dihydro-8-*iso*-$PGF_{2\alpha}$ · 2,3 dinor-8-*iso*-$PGF_{2\alpha}$

Abbreviations

CE	Collision energies
F_2-IsoPs	F_2-Isoprostanes
GC–MS	Gas chromatography-mass spectrometry
LC–MS	Liquid chromatography-mass spectrometry
SPE	Solid phase extraction
SRM	Selected reaction monitoring
2,3 dinor-F1	2,3-dinor-5,6-dihydro-8-*iso*-$PGF_{2\alpha}$, or 2,3-dinor-8-*iso*-$PGF_{1\alpha}$
2,3 dinor-F2	2,3-dinor-8-*iso*-$PGF_{2\alpha}$

Introduction

F_2-Isoprostanes (F_2-IsoPs, Fig. 1) are regio- and stereoisomers of prostaglandin $F_{2\alpha}$ ($PGF_{2\alpha}$) formed by the free radical-mediated oxidation of arachidonic acid [1]. Thus, F_2-IsoPs, particularly the 15-series regioisomer, 8-*iso*-$PGF_{2\alpha}$, are often used as biomarkers of oxidative stress [2, 3], and have been measured using well-established GC–MS and ELISA methods [4]. Recent advances in LC–MS methods have allowed faster and simpler sample preparation [4, 5].

Plasma or tissue F_2-IsoPs concentrations provide a "snap-shot" assessment of oxidative stress. However, concerns have arisen due to the potential for artifacts

A. W. Taylor · M. G. Traber (✉)
Linus Pauling Institute, Oregon State University,
Corvallis, OR 97331-6512, USA
e-mail: maret.traber@oregonstate.edu

R. S. Bruno
Department of Nutritional Sciences, University of Connecticut,
Storrs, CT 06269-4017, USA

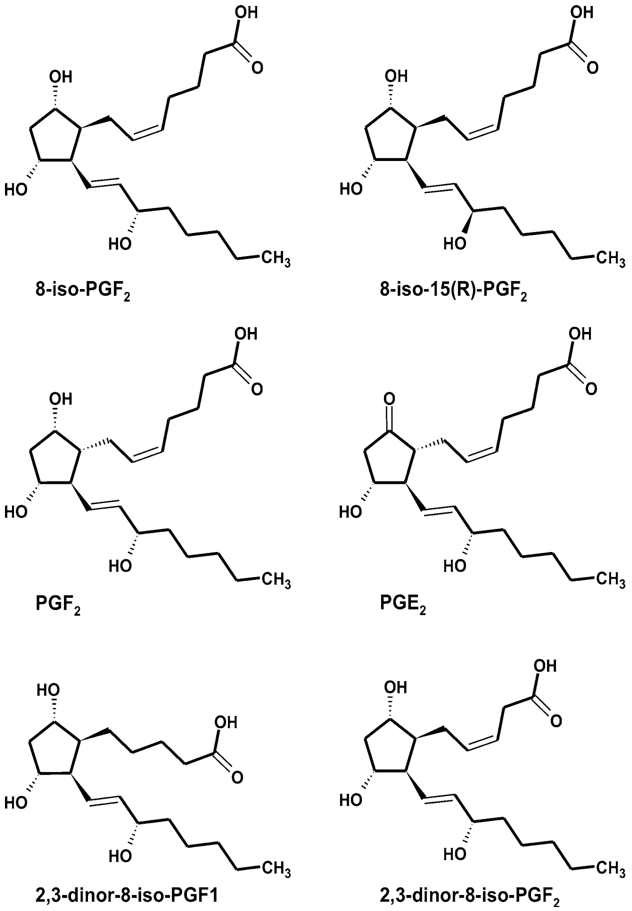

Fig. 1 Structures of F_2-Isoprostanes (F_2-isoPs) and metabolites

arising from in vitro lipid oxidation changes during sample preparation [6]. Thus, measurement of urinary F_2-IsoPs was proposed to be more reliable and less prone to artifactual increases in measured products thereby allowing for the more reliable assessment of oxidative stress in vivo. [6]. Urine also contains appreciable levels of F_2-IsoP metabolites [4, 6, 7], which could be measured simultaneously to bolster urinary F_2-IsoP results. Additionally, urine can be collected non-invasively from humans. Thus, urinary F_2-IsoPs may provide a better assessment of oxidative stress than samples from other biological materials, such as plasma.

Potentially, urinary F_2-IsoP metabolites may be better biomarkers of oxidative stress [4, 6, 7]. Roberts et al. [6] determined that 2,3-dinor-5,6-dihydro-8-*iso*-PGF$_{2\alpha}$ (2,3-dinor-F1, Fig. 1) was the major metabolite of 8-*iso*-PGF$_{2\alpha}$. Chiabrando et al. [4] also identified 2,3-dinor-8-*iso*-PGF$_{2\alpha}$ (2,3-dinor-F2) as an additional urinary 8-*iso*-PGF$_{2\alpha}$ metabolite. Interestingly, both 2,3-dinor-F1 and -F2 were present in similar urinary concentrations. Although both groups developed GC–MS procedures for the identification of these compounds [4, 8], the GC–MS methodology described by Nourooz-Zadeh et al. [7] facilitated the simultaneous measurement of these metabolites along with the parent compound, 8-*iso*-PGF$_{2\alpha}$. Importantly, there is consensus among these investigators that the F_2-IsoPs metabolites, 2,3-dinor-F1 and -F2, are present in significantly greater urinary concentrations than is 8-*iso*-PGF$_{2\alpha}$, suggesting that the metabolites may be more easily measured biomarkers. Moreover, F_2-IsoP metabolism may be important in decreasing adverse consequences of oxidative stress and increasing removal of oxidatively damaged lipids [9].

LC–MS methodologies for the determination of these metabolites have been developed [5, 10]. These methods stressed high sample throughput by using short HPLC columns (e.g. rocket method) and reported a single value for the F_2-IsoP metabolites. However, the metabolites from the 64 possible isomers of F_2-IsoPs are likely to be numerous. Moreover, it is unlikely that all species from a biological sample having the same molecular-ion-to-product-ion reaction are derived from a single parent compound. Thus, the evaluation of F_2-IsoP metabolites resolved by prolonged HPLC separation, as we described for plasma F_2-IsoPs [11], may be more advantageous than existing rocket methods because quantitation of specific biomarkers could potentially provide information concerning metabolism of specific precursors.

To this end, we developed a method that uses one solid phase extraction (SPE) cartridge, followed by prolonged gradient HPLC–MS-MS, to identify and quantitate urinary F_2-IsoPs and their metabolites, specifically including 2,3-dinor-F1 and -F2. Additionally, we have identified several other potential F_2-IsoP metabolites using selected reaction monitoring (SRM). The procedure was validated by assessing urinary F_2-IsoPs and their metabolites from a cohort of otherwise healthy nonsmokers and smokers, described previously [12]. Free F_2-IsoPs were measured previously in the plasma from these individuals [12], as were total (free + esterified) 15-series F_2-IsoPs [11]. While mean F_2-IsoP concentrations were numerically higher among smokers compared to nonsmokers, the differences were not statistically significant for any measured analyte due to large within-group variation. Thus, the simultaneous quantitation of urinary F_2-IsoPs and their metabolites from this same cohort will assess the utility of measuring F_2-IsoPs in urine versus plasma as well as measuring F_2-IsoP metabolites versus parent F_2-IsoPs in urine.

Experimental Procedures

Materials

HPLC grade solvents and reagents were obtained from VWR (West Chester, PA). Purified water was obtained

Table 1 Participant characteristics

Gender	Group	Age (years)	BMI (kg/m^2)	Serum lipids			Cotinine (ng/ml)	Cigarettes/day
				TG (mg/dl)	Cholesterol (mg/dl)	HDL-cholesterol (mg/dl)		
Women	Non-smoker	22.4 ± 0.7	24.3 ± 1.0^{a}	71 ± 12	164 ± 4	76 ± 5^{a}	28 ± 5^{b}	0^{c}
	Smoker	20.2 ± 0.7	$23.4 \pm 2.2^{a,b}$	92 ± 18	161 ± 13	$72 \pm 15^{a,b}$	$1{,}473 \pm 263^{a}$	8 ± 1^{b}
Men	Non-smoker	23.0 ± 0.7	26.6 ± 0.9^{a}	81 ± 17	160 ± 18	48 ± 5^{b}	23 ± 5^{b}	0^{c}
	Smoker	22.5 ± 1.3	20.9 ± 0.4^{b}	84 ± 18	155 ± 9	$64 \pm 5^{a,b}$	$3{,}037 \pm 708^{a}$	14 ± 2^{a}
Statistical summary (MANOVA)								
Gender		NS	NS	NS	NS	0.03	NS	0.022
Smoking		NS	0.014	NS	NS	NS	<0.0001	<0.0001
Interaction		NS	NS	NS	NS	NS	NS	0.022

Participant characteristics (mean ± SE) were analyzed using MANOVA and Tukey's post hoc where appropriate for pair-wise comparisons. Main effects are listed in the table and pair-wise comparisons not sharing the same superscript are significantly different ($P < 0.05$)

BMI body mass index (body weight (kg)/height (m^2)

from a Millipore Milli-Q apparatus (Billerica, MA). Authentic samples of 8-*iso*-prostaglandin F$_{2\alpha}$ (8-*iso*-PGF$_{2\alpha}$), PGF$_{2\alpha}$, PGE$_2$, 2,3-dinor-8-*iso*-PGF$_{1\alpha}$, and 2,3-dinor-8-*iso*-PGF$_{2\alpha}$, and the deuterated internal standards 8-*iso*-PGF$_{2\alpha}$-d$_4$ and PGE$_2$-d$_4$ were obtained commercially (Cayman Chemical; Ann Arbor, MI).

Study Design and Sample Collection

The study protocol for assessing vitamin E pharmacokinetics and oxidative stress markers in smokers and nonsmokers was reported previously [12]. The protocol was approved by the Institutional Review Board for the protection of human subjects at Oregon State University. At the time of the study, participants consented to the use of archived specimens for the continued assessment of oxidative stress biomarkers.

In brief, healthy, 18–35-year old male and female non-smokers ($n = 6$ M/8F) and smokers ($n = 6$ M/5F; 10–20 cigarettes/day) were recruited from the university area [12]. Participants were not nutritional supplement users (>6-months) and they maintained normal exercise patterns (<7 h/week aerobic exercise). The study was designed as a randomized, double-blind, placebo-controlled vitamin C intervention study in which participants received vitamin C (500 mg; twice daily) or matching placebo for 17 days. On day 14, participants received an equimolar mixture of deuterium-labeled α- and γ-tocopherols (~50 mg each d$_6$-α- and d$_2$-γ-tocopheryl acetates) on a single occasion and blood was collected in regular intervals from 0 to 72 h following labeled-tocopherol administration. Urine was collected in 8-h intervals from 0 to 24 h, aliquoted, and subsequently stored at −20 °C. The last 8 h collection (16–24 h) contained the first void on the second day of the trial. At the completion of the trial, all participants underwent a 3-month washout period, and subsequently returned to the study center to complete the alternate arm of the study as described. During each supplementation period, participants were instructed to follow a low ascorbic acid diet; plasma ascorbic acid was reported previously [12].

Plasma unesterified F$_2$-IsoPs were measured previously using GC–MS [12]. Plasma samples were analyzed previously for total (free + esterified) F$_2$-IsoPs by HPLC–MS-MS [11]. The data reported herein from 24 h urine collections are limited to those participants who completed the vitamin C intervention and respective placebo trial and provided complete urine samples from each 8 h collection period. Thus, the present investigation is limited to non-smokers ($n = 6$ M/8F) and smokers ($n = 6$ M/5F). Smokers had lower body mass indexes (BMI) than non-smokers and higher cotinine concentrations; women had higher high density lipoprotein (HDL) cholesterol concentrations (Table 1). Otherwise, there were no major differences between genders or smoking status groups.

Sample Preparation

Urine was thawed at room temperature, mixed by inversion, and centrifuged (200*g*, 5 min). The supernatant (600 μl) was mixed with 500 μl methanol, internal standards (IS, 12 ng 8-*iso*-PGF$_{2\alpha}$-d$_4$ and 3 ng PGE$_2$-d$_4$ in 24 μl 1:1 methanol:water) added, followed by addition of buffer (2.0 ml 0.02 M bis-tris-HCl) with mixing at each step. The diluted sample pH was then adjusted using H$_3$PO$_4$ or KOH to pH 6.0 ± 0.05.

Strata X-AW cartridges (100 mg/3 ml, Phenomenex, Torrance, CA) were each pre-conditioned with 2 ml 98:2 methanol:formic acid (v:v) and subsequently equilibrated with 2 ml water. Diluted urine samples were loaded, the cartridges washed with 2 ml water, followed by 4 ml 25% methanol, 2 ml acetonitrile, and cartridges dried under a gentle vacuum (~5 mm Hg, 30 s). Cartridges were then eluted 3-times with 1 ml methanol, and the eluants from each cartridge pooled and collected into glass tubes. Samples were dried under nitrogen gas, reconstituted in 200 µl methanol containing 0.1% formic acid (v:v), and injected onto the LC–MS-MS.

Chromatography and Mass Spectrometry

Separation was carried out using a Shimadzu HPLC system (Columbia, MD) consisting of two LC-10ADvp pumps, a DGU-14A degasser, a SIL-HTc autosampler-system controller maintained at 10 °C, and a CTO-10Avp column oven (35 °C) with a Synergi Hydro-RP column (250 × 2 mm i.d., 4 µm) equipped with a SecurityGuard C_{18} guard cartridge (4 × 2 mm; both from Phenomenex; Torrance, CA). Mobile phases A (water) and B (methanol) contained 0.01% acetic acid (v/v) and were delivered at a total flow of 200 µl/min using the following gradient scheme: 5 min equilibration at 30% B prior to injection, 30% B from 0–0.5 min, followed by a linear gradient over 1 min to 58% B, a linear gradient over 13.5 min to 66% B, a linear gradient over 7 min to 69% B, then to 100% B over 2 min which was held until the completion of the run at 32 min.

The HPLC system was coupled to a triple quadrupole mass spectrometer with TurboIon Spray source operated with both mass analyzers set at unit resolution in negative mode (Applied Biosystems/MDS Sciex API 3000, Foster City, CA). Nebulizer, curtain, and collision (CAD) gas parameters were set at 12, 10, and 7, respectively. Heater gas was supplied at 6 l/min at 425 °C. All gases were high purity nitrogen supplied by a custom liquid nitrogen system (Polar Cryogenics, Portland, OR). The ionizing voltage was −4,000 V, and the declustering, focusing, entrance, and exit potentials were −50, −250, −8, −35, and −11 V, respectively.

To identify chromatographic peaks, product ion spectra of authentic standards of 8-*iso*-$PGF_{2\alpha}$, $PGF_{2\alpha}$, 2,3-dinor-F1, and 2,3-dinor-F2 were acquired at collision energies (CE, see below) that produced a molecular ion intensity of 30–80% of the most abundant fragment ion. Then, each standard was analyzed by gradient HPLC and detected by selected reaction monitoring (SRM) experimentation based on the major fragment ions in the corresponding product ion spectrum, thereby creating a multi-trace profile for each compound. Next, a human urine sample was analyzed similarly to identify corresponding chromatographic peaks eliciting identical SRM characteristics to each specific standard.

Analytes were detected and quantified using SRM of seven reactions:

15-series PGFs, *m/z* 353–193, CE −35 V.
8-*iso*-$PGF_{2\alpha}$-d_4 internal standard, *m/z* 357–197, CE −35 V.
PGE_2, *m/z* 351–189, CE −27 V; PGE_2-d_4, *m/z* 355–193, CE −27 V.
2,3-dinor-F1, *m/z* 327–283, CE −28 V.
2,3-dinor-F2, *m/z* 325–237, CE −22 V.

Standard curves were constructed at 8 concentrations for 8-*iso*-$PGF_{2\alpha}$, $PGF_{2\alpha}$, PGE_2 (100–4,000 pg/ml), 2,3-dinor-F1 (1,250–50,000 pg/ml), and 2,3-dinor-F2 (2,500–100,000 pg/ml). 8-*iso*-$PGF_{2\alpha}$-d_4 was used as the IS for all analytes with the exception that PGE_2-d_4 was used for PGE_2. Quantitation was performed using the Analyst 1.41 software (Applied Biosystems/MDS Sciex). The Analyst software calculated signal to noise (S/N) ratios for 2,3-dinor-F1 (*m/z* 327–283) ranging from 6 to 50 (15–20 as the mode values), when a representative, non-zero background region of a urine sample chromatogram (at 4–6 min) was chosen as the reference background.

Accuracy and Precision

Assay accuracy was evaluated by standard addition experiments conducted in urine and methanol. Known quantities of 8-*iso*-$PGF_{2\alpha}$, $PGF_{2\alpha}$, PGE_2, 2,3-dinor-F1, and 2,3-dinor-F2 were spiked, in duplicate, into urine or methanol. Spiked urine was extracted as described above and spiked methanol was analyzed by LC–MS without prior extraction. Intra-day- and between-day precision was determined by analyzing five aliquots of urine on five separate occasions throughout a month.

Statistical Analysis

Data are expressed as mean ± SE. Repeated measures MANOVA was performed using JMP Statistical Discovery Software (SAS Institute, Cary, NC) to evaluate effects attributed to smoking status, gender, and with-in subject vitamin C treatment effects and time effects from urine samples collected in three 8-h intervals over 24 h (0–8, 8–16, and 16–24 h). For the analysis of repeated measures (multiple samples from the same subject), the natural logarithm of the dependent variables (urine concentration at the three time points in each study period, or vitamin C treatment) was used to minimize the correlation between the mean and variance of the data. Results were considered to be statistically significant at $P < 0.05$. Vitamin C had no effect on the oxidative stress parameters studied, as has been observed previously [13], so data from time points were averaged, as indicated. Similarly, when other parameters did not reach statistical significance, the values from each subject were averaged and the statistical analysis was repeated using matched pairs or MANOVA with repeated measures, as appropriate. It should be noted that as the numbers of data points decreased the statistical power decreased.

Results

Precision and Accuracy of the SPE Extraction and LC–MS Analyses

The intra-day and inter-day precision of the SPE extraction and LC–MS analyses were evaluated from five aliquots of a single urine specimen analyzed over one month on five separate occasions. For the five analytes for which standards are available (8-*iso*-PGF$_{2\alpha}$; PGF2$_{2\alpha}$; PGE$_2$; 2,3-dinor-F1 and 2,3-dinor-F2), the intra-day coefficients of variation (CV) for each of the standards ranged from 6 to 9%, while the inter-day CVs for each ranged from 10 to 14%.

Assay accuracy was determined by comparing the ratio of the slopes of the line determined from measured amounts recovered from spiked human urine samples (standard addition) with the slope generated from spiked methanol. Standard addition experiments indicated that the accuracy of the assay was 101% for 8-*iso*-PGF$_{2\alpha,}$ 104% for PGF$_{2\alpha}$, 102% for PGE$_2$, 59% for 2,3-dinor-F1, and 86% for 2,3-dinor-F2. Because the measured concentrations of 2,3-dinor-F1 and F2 were within the quantitative range of the standard curves, the lower accuracy for these analytes was apparently the result of lower extraction recoveries. Therefore, the extraction protocol was optimized for maximum recovery of 2,3-dinor-F1 and -F2.

The standard addition regression estimates were linear in the range of 0, 20, 50, and 100% of standard mix added (equivalent to a urinary concentration of 8-*iso*-PGF$_{2\alpha}$, 1,000 pg/ml; PGF$_{2\alpha}$ and PGE$_2$, 2,000 pg/ml; 2,3-dinor-F1, 5,000 pg/ml, and 2,3-dinor-F2 10,000 pg/ml at 100%). The standard curves used for quantitation were linear from 0 to 4,000 pg/ml for 8-*iso*-PGF$_{2\alpha}$, PGF$_{2\alpha}$, and PGE$_2$; 0–40 ng/ml for 2,3-dinor-F1; and 0–80 ng/ml for 2,3-dinor-F2.

Identification of Metabolites with SRM Patterns Similar to 2,3-dinor-F1 and 2,3-dinor-F2

Identification of biomarkers of lipid peroxidation is difficult due to the variety of lipid oxidation products, which potentially may be metabolized to an even greater variety of products. In addition, few authentic standards are available commercially. To circumvent these potential limitations, we used a prolonged HPLC gradient to separate multiple peaks from human urine samples and identified those peaks with product ion spectra matching those of available standards.

F$_2$-IsoPs in human urine were identified tentatively as 8-*iso*-15(*R*)-PGF$_{2\alpha}$, 8-*iso*-PGF$_{2\alpha}$, and PGF$_{2\alpha}$ because they had retention times identical to those of the standards and they had SRM profiles matching the authentic standards, 8-*iso*-PGF$_{2\alpha}$ and PGF$_{2\alpha}$ (data not shown).

Product ion spectra of the 2,3-dinor-F1 and -F2 standards (Figs. 2A, 3A, respectively) were similar to those reported previously by others [5, 10]. The retention times shown from the HPLC-SRM tracings of the 2,3-dinor-F1 and -F2 standards were 11.7 and 11.9 min, respectively (Figs. 2B, 3B, respectively). However, when urine sample extracts were analyzed, additional, sometimes larger, peaks had the same SRM profiles as these standards. Three peaks (identified as 2, 3 and 4 in Fig. 2C), had SRM profiles that matched 2,3-dinor-F1 (Fig. 2B, identified as 1 in Fig. 2C). Similarly, three peaks (identified as 1, 3 and 4 in Fig. 3C) had SRM profiles that matched 2,3-dinor-F2 (Fig. 3B, identified as 2 in Fig. 3C).

Peaks are named according to their metabolite class and retention time (e.g. F1-12 from a 2,3-dinor-F1 SRM match eluting at 12 min).

F$_2$-IsoPs in Urine from Smokers and Nonsmokers

The method described herein allows the simultaneous measurement of both F$_2$-IsoPs and F$_2$-IsoP metabolites in a single extraction and LC/MS separation. Urinary F$_2$-IsoPs (Fig. 4), specifically 8-*iso*-PGF$_{2\alpha}$, 8-*iso*-15(*R*)-PGF$_{2\alpha}$ and PGF$_{2\alpha}$, were measured in three separate urine specimens collected in 8 h intervals over 24 h from smokers and nonsmokers who completed placebo and vitamin C supplementation trials [12]. Thus, six samples were analyzed for each subject. Remarkably, neither the time of day, nor vitamin C supplementation had any effect on the urinary excretion of any of the three F$_2$-IsoPs measured ($P > 0.05$, MANOVA). The consistency of the methodology described herein is readily apparent in that the urinary concentrations for each of the subjects did not vary widely for any of the three F$_2$-IsoPs measured (Fig. 4).

In contrast to our expectation that cigarette smoking would increase all of the urinary F$_2$-IsoPs identified, we found that only 8-*iso*-PGF$_{2\alpha}$ concentrations were significantly increased in smokers ($P = 0.012$, MANOVA, main effect of smoking). However, women compared with men (MANOVA, main effect of gender) excreted significantly greater 8-*iso*-PGF$_{2\alpha}$ ($P = 0.02$), 8-*iso*-15*(R)*-PGF$_{2\alpha}$ ($P = 0.04$), and PGF$_{2\alpha}$ ($P = 0.015$) concentrations.

Given the lack of statistical significance in the F$_2$-IsoP concentrations between time points, or with vitamin C supplementation, the concentrations for each of the six samples were then averaged for each subject (three collections for each of the two supplements) and the statistical analyses repeated. Nonsmoking men had the lowest

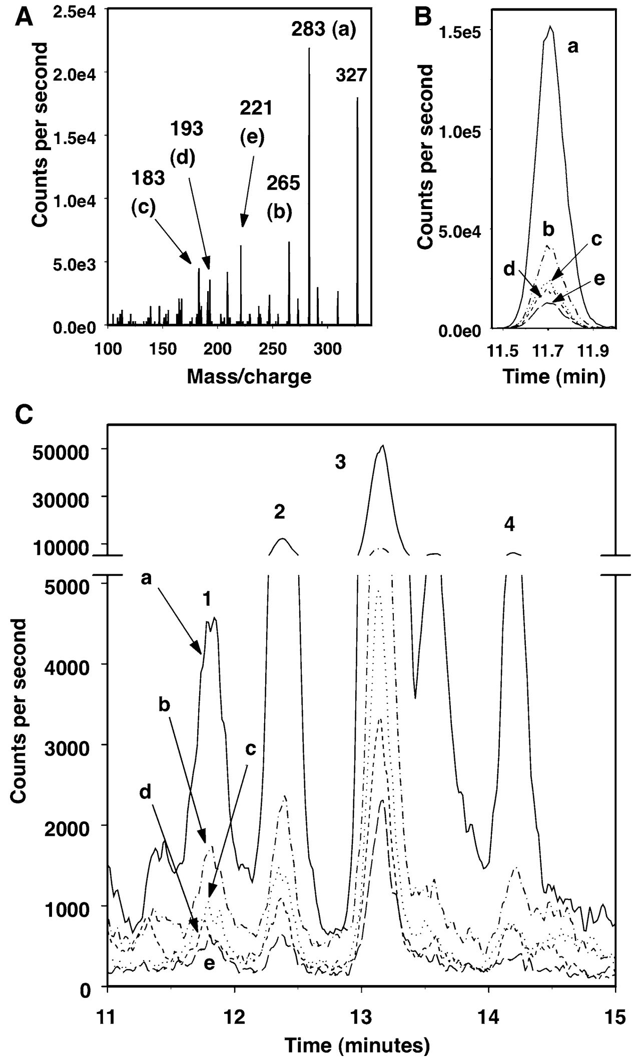

Fig. 2 LC–MS identification of 2,3-dinor-PGF$_{1\alpha}$. **A** Fragmentation pattern of 2,3-dinor-PGF$_{1\alpha}$ standard, *m/z* 327–283 (*a*), 265 (*b*), 183 (*c*), 193 (*d*) or 221 (e). **B** LC–MS chromatogram of 2,3-dinor-PGF$_{1\alpha}$ standard showing tracings of each of the fragments (*a–e*) identified in **A**. **C** LC–MS chromatogram of a urine extract with tracings of peaks identified with SRM profiles showing each of the fragments (*a–e*, identified in **A**) that matched those of 2,3-dinor-PGF$_{1\alpha}$ (2,3-dinor-F1, retention time same as the standard, *labeled 1*; F1-12, *labeled 2*; F1-13, *labeled 3*, and F1-14 *labeled 4*)

F$_2$-IsoP concentrations, while women smokers had the highest concentrations (Table 2). In general, urinary PGF$_{2\alpha}$ concentrations were approximately double those of either 8-*iso*-PGF$_{2\alpha}$ or 8-*iso*-15*(R)*-PGF$_{2\alpha}$. Although PGF$_{2\alpha}$ is the largest of the 15-series peaks in our samples, it is likely a mixture of PGF$_{2\alpha}$ and *ent*-PGF$_{2\alpha}$ that we cannot resolve, based on the findings by Yin et al. [14], who used a chiral column and showed that the major portion of PGF$_{2\alpha}$ in human urine is the enantiomer (*ent*) form of PGF$_{2\alpha}$. Thus, this peak is called PGF$_{2\alpha}$ + *ent*-PGF$_{2\alpha}$.

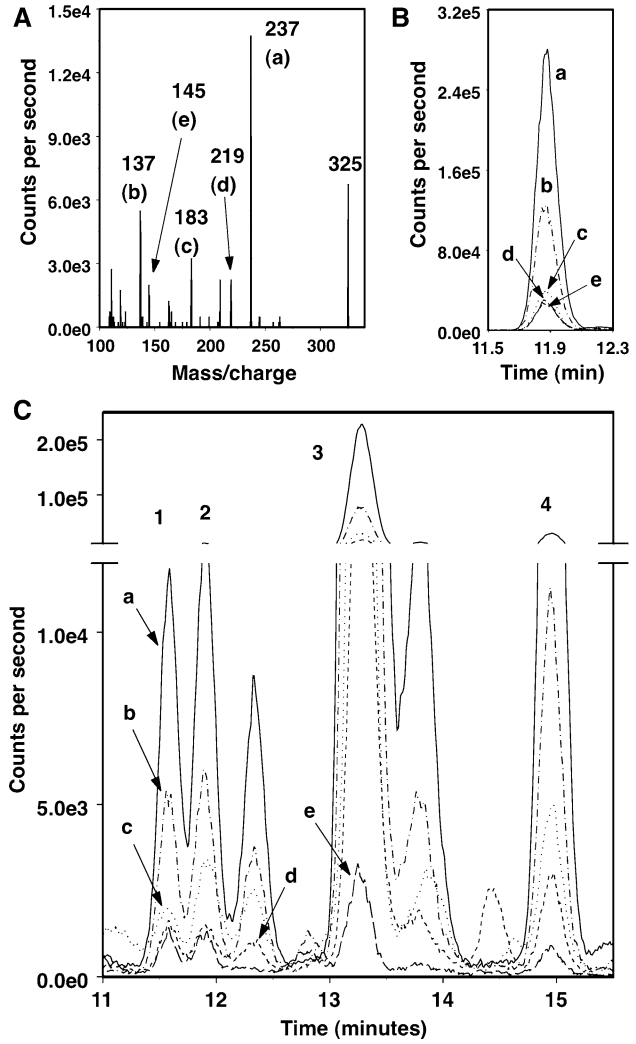

Fig. 3 LC–MS identification of 2,3-dinor-PGF$_{2\alpha}$. **A** Fragmentation pattern of 2,3-dinor-PGF$_{2\alpha}$ standard, *m/z* 325–237 (*a*), 137 (*b*), 183 (*c*), 219 (*d*) or 145 (*e*). **B** LC–MS chromatogram of 2,3-dinor-PGF$_{2\alpha}$ standard showing tracings of each of the fragments (*a–e*) identified in **A**. **C** LC–MS chromatogram of a urine extract with tracings of peaks identified with SRM profiles showing each of the fragments (*a–e*, identified in **A**) that matched those of 2,3-dinor-PGF$_{2\alpha}$ (2,3-dinor-F2, retention time same as the standard, *labeled 2*; F2-12, *labeled 1*; F2-13, *labeled 3*, and F2-15 *labeled 4*)

2,3-dinor-F1 and 2,3-dinor-F2 in Urine from Smokers and Nonsmokers

The urinary F$_2$-IsoPs metabolites, 2,3-dinor-F1 and -F2, were measured in the same extract and during the same HPLC analyses as described above for the urinary F$_2$-IsoPs. Similar to the F$_2$-IsoPs data, no significant effects of vitamin C supplementation on urinary 2,3-dinor-F1 or -F2 concentrations were observed (data not shown). The consistency of the 2,3-dinor-F1 and 2,3-dinor-F2 measurements is readily apparent in the concentrations (averages for each time point

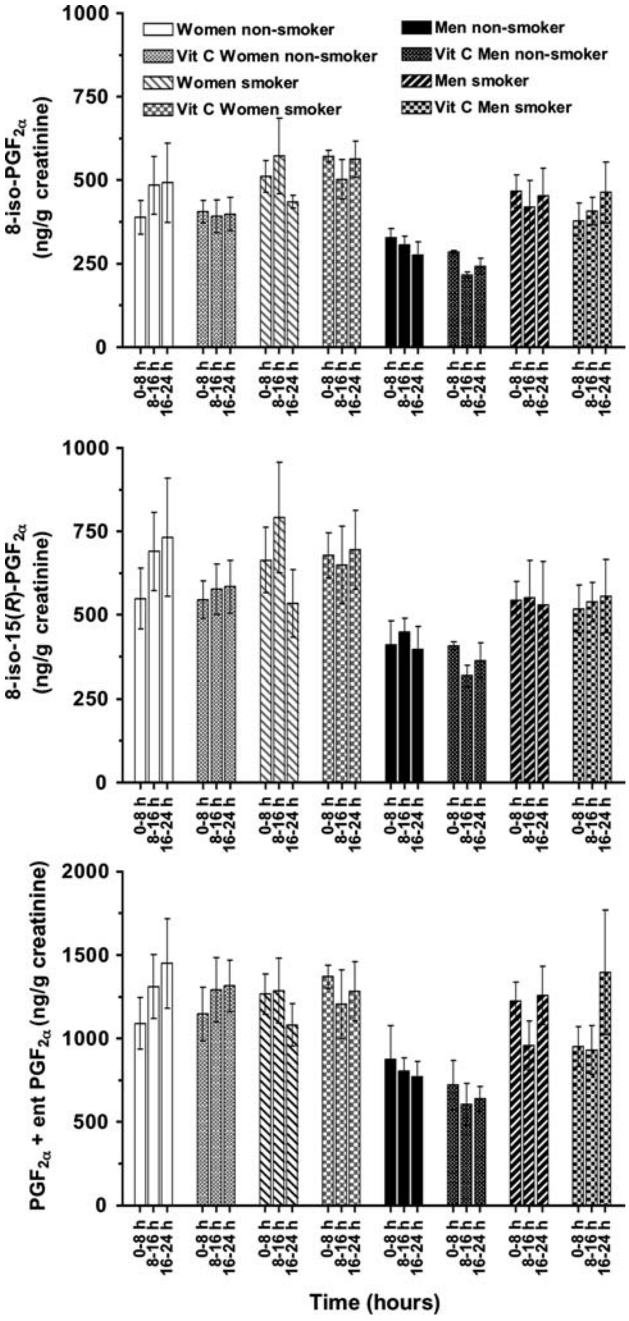

Fig. 4 Urinary F$_2$-isoPs determined over 24 h in smokers and nonsmokers. The urinary F$_2$-isoPs: 8-*iso*-PGF$_{2\alpha}$, 8-*iso*-15(*R*)-PGF$_{2\alpha}$ and PGF$_{2\alpha}$, were quantified both during placebo and vitamin C supplementation in smokers and nonsmokers from three separate urine collections (0–8, 8–16, and 16–24 h after taking deuterated α-tocopherol during a vitamin E kinetics study [12]). Neither the time of day, nor the supplementation with vitamin C had any effect on the urinary excretion of each of the three F$_2$-isoPs measured ($P > 0.05$, MANOVA). 8-*iso*-PGF$_{2\alpha}$ concentrations were significantly increased in smokers ($P = 0.012$, MANOVA, main effect of smoking). Women compared with men excreted significantly (MANOVA, main effect of gender) higher concentrations of 8-*iso*-PGF$_{2\alpha}$ ($P = 0.02$), 8-*iso*-15(*R*)-PGF$_{2\alpha}$ ($P = 0.04$), and PGF$_{2\alpha}$ + *ent*-PGF$_{2\alpha}$ ($P = 0.015$)

obtained during the vitamin C and placebo trials) shown for the three time points for each group (Fig. 5a, b).

Women excreted more 2,3-dinor-F1 than did men (MANOVA, main effect of gender, $P = 0.025$); cigarette smokers also excreted more 2,3-dinor-F1 than did nonsmokers (main effect of smoking $P = 0.039$, Fig. 5a). When 2,3-dinor-F1 concentrations were averaged over the six time points for each subject, women smokers had significantly higher concentrations ($P < 0.05$, 2.3 ± 0.3 μg/g creatinine) than did nonsmokers (women 1.6 ± 0.3, or men 1.2 ± 0.1), or male smokers (1.5 ± 0.3).

Women also excreted more 2,3-dinor-F2 than did men (MANOVA, main effect of gender $P = 0.0012$). Similarly, cigarette smokers excreted more 2,3-dinor-F2 than did nonsmokers (main effect of smoking $P = 0.013$, Fig. 5b). However, 2,3-dinor-F2 concentrations varied with time (main effect, $P = 0.006$). When the 2,3-dinor-F2 data were analyzed separately for men and women, interesting differences were apparent. Women smokers excreted more 2,3-dinor-F2 (4.6 ± 0.5 μg/g creatinine) than did nonsmokers (3.2 ± 0.4 μg/g, $P = 0.036$), but concentrations did not vary significantly with the time of day. In contrast, cigarette smoking had no significant effect on the 2,3-dinor-F2 excretion in men. However, men excreted greater 2,3-dinor-F2 concentrations (3.0 ± 0.3 μg/g creatinine) during the overnight collection (16–24 h) compared with 8–16 h (2.3 ± 0.2, $P = 0.001$). The collections taken during the day 0–8 h (2.6 ± 0.3 μg/g creatinine) were also greater than during 8–16 h ($P = 0.03$). These latter data suggest that men may have increased F$_2$-IsoPs metabolism and excretion overnight into morning.

Additional Urinary F$_2$-IsoPs Metabolites in Smokers and Nonsmokers

In addition to 2,3-dinor-F1 and -F2, we identified using SRM several other potential urinary F$_2$-IsoP metabolites (Figs. 2, 3, respectively). Pair-wise correlations between all data ($n = 144$) showed that F1-12 and F1-13 concentrations were correlated with 2,3-dinor-F1 ($r > 0.9$, $P < 0.0000$); F2-12, F2-13 and F2-15 concentrations were correlated with 2,3-dinor-F2 ($r = 0.7$–0.9, $P < 0.0000$); while F1-14 had lower correlation coefficients with concentrations of either 2,3-dinor-F1 or -F2 ($r < 0.4$, Table 3). Of particular interest, F1-14 was not correlated ($P > 0.05$) with 8-*iso*-15*(R)*-PGF$_{2\alpha}$ suggesting that it has a different precursor than do the other metabolites.

Given that all of the "identified" urinary F$_2$-IsoPs metabolite concentrations (except F1-14) were correlated, the concentrations calculated for each metabolite were summed for each subject at each time point and then

Table 2 Urinary F_2-isoprostanes in smokers and nonsmokers

Gender	Group	8-*iso*-$PGF_{2\alpha}$ (μg/g creatinine)	8-*iso*-15*(R)*-$PGF_{2\alpha}$ (μg/g creatinine)	$PGF_{2\alpha}$ + *ent*-$PGF_{2\alpha}$ (μg/g creatinine)
Women	Nonsmoker	0.43 ± 0.06^{a}	$0.61 \pm 0.09^{a,b}$	1.27 ± 0.16^{a}
	Smoker	0.52 ± 0.03^{a}	0.65 ± 0.09^{a}	1.24 ± 0.08^{a}
Men	Nonsmoker	0.28 ± 0.01^{b}	0.39 ± 0.03^{b}	0.74 ± 0.09^{b}
	Smoker	0.43 ± 0.06^{a}	$0.54 \pm 0.09^{a,b}$	1.12 ± 0.15^{a}

Statistical summary (MANOVA)	*P*-value		
Gender	0.019	0.04	0.015
Smoking	0.012	NS	NS
Interaction	NS	NS	NS

No significant differences were observed for vitamin C supplementation or for each 8-h collection interval; therefore, urinary F_2-IsoPs were averaged within each participant over time and vitamin C supplementation. Urinary F_2-IsoPs were analyzed using MANOVA and Tukey's post hoc where appropriate for pair-wise comparisons. Main effects are listed in the table and pair-wise comparisons within a column not sharing the same superscript are significantly different ($P < 0.05$)

averaged for the six time points within each subject. Women had higher F_2-IsoPs metabolite concentrations than did men (MANOVA, main effect $P = 0.0033$), while cigarette smokers had higher concentrations than did nonsmokers (main effect $P = 0.036$, Fig. 6). Women smokers had higher metabolite concentrations than did men ($P < 0.05$); nonsmoking men had lower concentrations than did women ($P < 0.05$).

Although F1-14 concentrations were not used in the above estimation of F_2-IsoPs metabolites, the SRM characteristics of the peaks were consistent with the F_2-IsoPs metabolite standards, 2,3-dinor-F1 and -F2. F1-14 concentrations (averaged over the six time points for each subject) showed that smokers had higher F1-14 concentrations than did nonsmokers ($P = 0.025$, Fig. 7). Unlike all of the other biomarkers of lipid peroxidation that were evaluated and reported herein, there was no statistically significant effect of gender on F1-14 concentrations even when all six data points per subject (rather than averages) were evaluated.

Discussion

The strategy used in the current study was to identify multiple biomarkers of oxidative stress in human urine. Rather than using a rapid passage through the HPLC column to obtain a single peak containing various F_2-IsoPs or their metabolites, the separation was prolonged to resolve individual peaks of interest. Our hypothesis was that some biomarkers may be more sensitive to oxidative stress than others. Our strategy has been effective in that significant differences in urinary F_2-IsoPs were detected between women and men, nonsmokers and smokers (~10 cigarettes/day); differences that our plasma F_2-IsoP assay was unable to detect in these same subjects [11]. Perhaps more

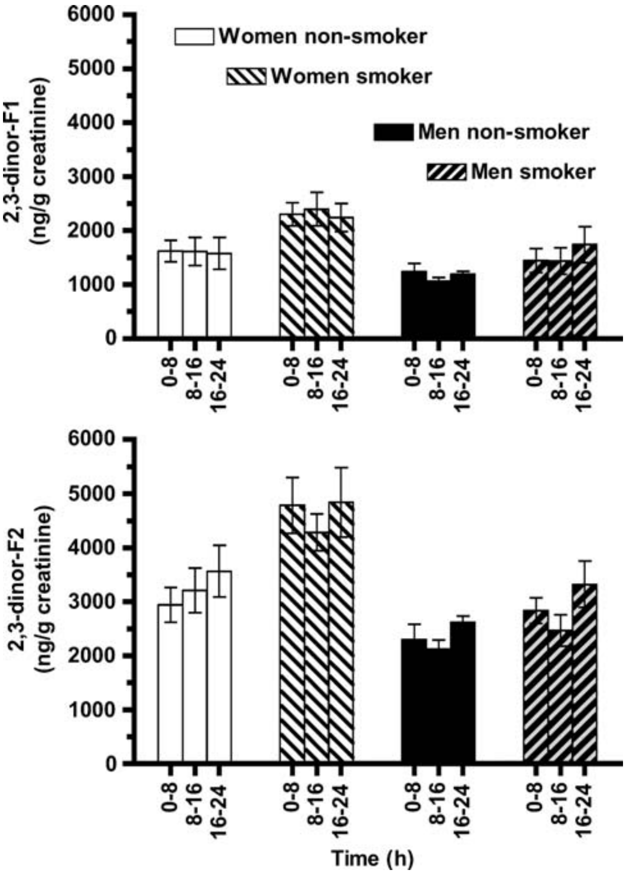

Fig. 5 Urinary isoprostane metabolites excreted by smokers and nonsmokers. Urinary 2,3 dinor F1 (**a**) and 2,3 dinor F2 (**b**) concentrations, respectively, were averaged for the vitamin C and placebo supplementation trials at each of the three time points. **a** Women excreted higher 2,3-dinor-F1 concentrations than did men (MANOVA, main effect of gender $P = 0.025$); cigarette smokers excreted higher concentrations than did non-smokers (main effect of smoking $P = 0.039$). **b** Women excreted more 2,3-dinor-F2 than did men (MANOVA, main effect of gender $P = 0.0012$); cigarette smokers excreted higher concentrations than did non-smokers (main effects of smoking $P = 0.013$). 2,3-dinor-F2 concentrations also varied with time (main effect, $P = 0.006$)

Table 3 Pair-wise correlations between F_2-IsoPs and their putative metabolites

	8-*iso*-$PGF_{2\alpha}$	8-*iso*-15*(R)*-$PGF_{2\alpha}$	$PGF_{2\alpha}$ + *ent*-$PGF_{2\alpha}$	2,3-dinor-F1	F1-12	F1-13	F1-14	2,3-dinor-F2	F2-12	F2-13	F2-15
8-*iso*-$PGF_{2\alpha}$	1.0000	0.9066	0.7938	0.6008	0.5641	0.5797	0.2407	0.6317	0.6360	0.5143	0.4448
8-*iso*-15*(R)*-$PGF_{2\alpha}$		1.0000	0.7263	0.4304	0.3834	0.4474	0.1090	0.4629	0.4678	0.4286	0.3674
$PGF_{2\alpha}$ + *ent*-$PGF_{2\alpha}$			1.0000	0.3280	0.3307	0.3458	0.3046	0.4434	0.4372	0.4294	0.4987
2,3-dinor-F1				1.0000	0.9292	0.9399	0.4010	0.8555	0.8552	0.6641	0.4483
F1-12					1.0000	0.9367	0.5028	0.8336	0.8192	0.6879	0.4841
F1-13						1.0000	0.3794	0.8628	0.8729	0.7539	0.4982
F1-14							1.0000	0.2894	0.2636	0.2343	0.3642
2,3-dinor-F2								1.0000	0.9700	0.8790	0.7298
F2-12									1.0000	0.8763	0.7129
F2-13										1.0000	0.8767
F2-15											1.0000

All pair-wise correlations are statistically significant ($P < 0.0001$) with the exception of the correlation of F1-14 with 8-*iso*-$PGF_{2\alpha}$ ($P = 0.0037$), 8-*iso*-15*(R)*-$PGF_{2\alpha}$ (not significant), $PGF_{2\alpha}$ + *ent*-$PGF_{2\alpha}$ ($P = 0.0002$), 2,3-dinor-F2 ($P = 0.0004$), F2-12 ($P = 0.0014$), and F2-13 ($P = 0.0047$)

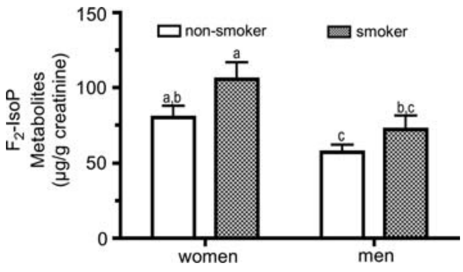

Fig. 6 Urinary total isoprostane metabolites excreted by men and women smokers and nonsmokers. Urinary F_2-isoP metabolite concentrations (identified as shown in Figs. 2 and 3, except F1-14) were individually calculated, summed for each subject at each time point and then averaged for the six time points for each subject. Women had higher F_2-isoP metabolite concentrations than did men (MANOVA, main effect $P = 0.0033$), while cigarette smokers had higher concentrations than did nonsmokers (main effect $P = 0.036$). *Bars not sharing the same letter* are significantly different by Tukey's pair-wise comparisons ($P < 0.05$)

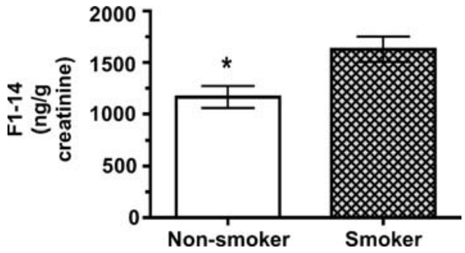

Fig. 7 Urinary F1-14 excreted by smokers and nonsmokers. F1-14 (identified in Fig. 2C) concentrations were averaged over the six time points for each subject. Smokers had higher F1-14 concentrations than did nonsmokers ($P = 0.025$). There were no significant effects of gender on F1-14 concentrations

importantly, we have identified a series of metabolites that have mass spectral characteristics of the relatively low abundance 2,3-dinor-F1 and -F2, but when summed together, these apparent metabolites are excreted in quantities 50–100 times greater than the two metabolites for which we have commercially available standards. The urinary F_2-IsoPs were found at concentrations of about 0.2–1.5 µg/g creatinine (Fig. 4), while urinary 2,3-dinor-F1 was about 1–3 µg/g and 2,3-dinor-F2 was about 3–5 µg/g (Fig. 5). In contrast, the sum of the various F_2-IsoP metabolites was in the range of 50–100 µg/g (Fig. 6). Thus, these urinary F_2-IsoPs metabolite concentrations are supportive of rapid F_2-IsoP metabolism [15] and the excretion of the metabolites as potentially important in ameliorating the adverse effects of oxidative stress.

To identify F_2-IsoPs and F_2-IsoPs metabolites, we first acquired product ion spectra of the individual standards. We then used these results to design an SRM program for each class of analyte. For example, authentic 2,3-dinor-F1 had a molecular ion of *m/z* 327 (negative mode), and major products ions, in order of abundance, of *m/z* 283, 265, 209, 183, 193, and 221 (Fig. 2). The SRM program detected these ions as *m/z* 327 products during an HPLC separation of authentic 2,3-dinor-F1 and also during analysis of a human urine extract. The peaks in the urine extract chromatogram that had SRM profiles resembling those of authentic 2,3-dinor-F1, were likely to have a similar chemical structure, but perhaps with stereochemical differences. Once specific peaks were identified based on SRM profiles as likely members of a particular analyte type, we integrated only those peaks. Note that that Figs. 2C and 3C also show peaks in the urine extract that did not have the appropriate SRM profile, thus, were not included in our analyses.

Previous methods have utilized mass spectrometry to identify and quantify components with the same single molecular ion-to-product ion reaction as that of available standards with minimal HPLC separation. We found that human urine chromatograms contained a peak, F1-14, with a product ion spectrum similar to that of 2,3-dinor-F1; however, the amounts were not correlated with F_2-IsoP concentrations (Table 3). These findings suggest that peak F1-14 is not derived from the F_2-IsoPs that we quantitated. Moreover, analyses based solely on tandem MS detection with minimal or no HPLC separation may not provide accurate results. Importantly, unlike every other F_2-IsoP and metabolite we detected, there was no gender effect, just increased F1-14 concentrations in smokers (Fig. 7). Without the prolonged HPLC separation we used, this very interesting biomarker would have escaped discovery. F1-14 likely has a molecular structure similar to that of 2,3-dinor-F1, but with perhaps different stereochemistry. Clearly, further investigation is needed to characterize this molecule(s).

The SPE method described is a new innovation compared with previously published methods by others. We sought to extend our LC–MS-MS assay for plasma 15-series F_2-IsoPs [11] for use with urine samples and to simultaneously measure urinary F_2-IsoPs metabolites. However, our initial efforts using liquid-liquid extraction or published SPE protocols [5, 10] yielded poor recoveries (∼25–50% of spiked internal standard) from urine samples. A generic anion exchange SPE protocol (including a methanol wash, then elution with acidified methanol) using mixed-mode weak anion exchange-reverse phase cartridges gave satisfactory recovery of the internal standard, 8-*iso*-$PGF_{2\alpha}$-d_4, when added to water, but not when added to urine. Moreover, when the internal standard was added to an extracted urine sample, only half the expected increase in peak area was observed, suggesting a matrix effect, possibly ion suppression in the mass spectrometer. In the course of developing a new F_2-IsoP extraction method, we observed that when urine samples were loaded on mixed-mode reverse phase-weak anion exchange cartridges at ∼1 pH unit above the typical carboxylic acid pK_a (e. g., *n*-butyric, pH 4.81), the protic solvent, methanol (but not acetonitrile) was capable of eluting F_2-IsoPs and F_2-IsoP metabolites, indicating ionic forces still contributed to F_2-IsoP binding to the cartridge at the lower pH. Acetonitrile could then be used to wash any neutral, nonpolar compounds from the cartridge, as well as any residual water. Good recoveries of F_2-IsoPs and F_2-IsoP metabolites were achieved with neutral methanol elution, while agents that caused ion suppression in the MS were eluted with acidified solvents. These findings explain the low recoveries of urinary F_2-IsoPs and F_2-IsoP metabolites when we used conventional anion exchange methods, in which samples are usually loaded at greater than or equal to 2 pH units higher than the pK_a of the analyte of interest, which in turn, is eluted with acidified solvents.

Intra- and inter-day precision of the final assay compare satisfactorily with previously published methods, and the accuracy of measurements of the F_2-IsoPs was nearly 100%. However, the accuracies of 2,3-dinor-F1 and -F2 were lower. We believe the lower accuracy is due to lower rates of recovery of these analytes from urine. The SPE procedure was more robust for variations in the loading pH and elution volumes when determining recoveries of 8-*iso*-$PGF_{2\alpha}$, $PGF_{2\alpha}$, and PGE_2 than for 2,3-dinor-F1 and -F2. As a consequence, attention was focused on achieving as good recovery as possible of the latter without compromising the recovery of the F_2-IsoPs. Our accuracy of 59% for 2,3-dinor-F1 and 86% for 2,3-dinor-F2 is not as high as the 80% reported for the former [5] or the 98–99% reported for the latter [10]. Nevertheless, the recoveries were reproducible and were linear over a large range, allowing the use of our protocol in analyzing a set of samples collected from college-age subjects, some of them light smokers and others nonsmokers. Bohnstedt et al. [16] previously reported that reverse phase SPE was unsatisfactory for urine sample preparation; they then developed a liquid-liquid extraction method for F_2-IsoPs. Herein we report a SPE procedure using a different stationary phase chemistry that was satisfactory for both F_2-IsoPs and their metabolites. Bohnstadt et al. [16] reported urinary concentrations of iPF2a from control subjects (216 pg/mg creatinine) that were similar to those we observed of 8-*iso*-$PGF_{2\alpha}$ (the same compound) from nonsmoking male subjects (280 pg/mg creatinine), while we report higher concentrations in female smokers (530 pg/mg creatinine). Welsh et al. [17] also report satisfactory recoveries of F_2-IsoPs and their metabolites using SPE technology.

In the present study, we observed that smokers had greater urinary 8-*iso*-$PGF_{2\alpha}$ concentrations than did nonsmokers, but cigarette smoking did not significantly increase urinary 8-*iso*-15*(R)*-$PGF_{2\alpha}$ or $PGF_{2\alpha}$ concentrations. We previously reported plasma F_2-IsoPs measured from a similar cohort of otherwise healthy college-aged nonsmokers and smokers. Utilizing GC–MS [12] or LC–MS [11] approaches, smokers had numerically higher plasma F_2-IsoPs but without statistical significance between the groups. In a separate study, plasma F_2-IsoPs were significantly higher among smokers, but their smoking history and frequency (>30 cigarettes/day) were substantially greater than observed in the participants from the present study [18, 19]. Also, proposed biomarkers of oxidative stress are often tested with a strong stress such as CCl_4 poisoning [20]. Thus, significantly greater urinary 8-*iso*-$PGF_{2\alpha}$ in smokers supports the well-established literature indicating that smoking enhances oxidative stress [21, 22] and supports the hypothesis of the present work that specific F_2-IsoPs may be more sensitive biomarkers of oxidative stress in vivo. The latter is important for studies conducted in populations that are otherwise healthy, young, and with a limited history (<5 years) and frequency (~10 cigarettes/day) of smoking, that is, subjects with a relatively low magnitude of oxidative stress, where decreased variability in the methodology would allow increased sensitivity to detect differences between subjects.

It should be noted that our method also allows quantitation of PGE_2. In general, PGE_2 is formed enzymatically [23], but there is evidence that non-enzymatic generation can also occur [24]. Given our interest in oxidative stress markers, and the non-specific origin of PGE_2, this molecule was not quantitated for smokers and non-smokers.

Of particular interest is that plasma F_2-IsoP turnover is rapid [15]; therefore, blood levels may vary widely over time with transient oxidative stress. Thus, urinary F_2-IsoPs and their metabolite concentration would be expected to provide a more reliable index of systemic oxidative stress with less variability than that of circulating concentrations. Indeed, our measurements confirmed this notion (Table 2) and demonstrated the significance of measuring these biomarkers in urine.

Consistent with the notion of enhanced oxidative stress in smokers, we observed significantly higher urinary 2,3-dinor-F1 and -F2 concentrations in smokers compared with nonsmokers (Fig. 5), as were urinary total F_2-IsoP metabolites (Fig. 6). However, to our surprise, we observed that women compared with men had higher urinary concentrations of all F_2-IsoPs measured (Table 2; Fig. 4), as well as urinary F_2-IsoP metabolites (Figs. 5, 6) despite men and women having similar characteristics (Table 1). Gender effects on lipid peroxidation or oxidative stress biomarkers have been addressed in clinical studies only to a limited extent and the results have been equivocal. Men had higher urinary F_2-IsoPs and plasma thiobarbituric acid-reactive substances (TBARS) than did women [25], as well as higher plasma malondialdehyde (MDA) [26]. However, in a study with nearly 300 men and women, Block et al. [27] demonstrated that women had significantly higher plasma MDA and F_2-IsoPs than did men. Moreover, the gender effect was maintained despite efforts to adjust for BMI which would potentially control for differences in adiposity. In the present study, F_2-IsoPs and F_2-IsoP metabolite concentrations were not correlated with any parameter shown in Table 1, including BMI (data not shown). Coudray et al. [28] also observed significantly greater evidence of lipid peroxidation in women compared with men in a cohort of nearly 1,400 participants. Clearly, additional study is needed to further characterize gender differences on oxidative stress as well as to potentially unravel the mechanism leading to such effect.

Acknowledgments The study authors would like to thank Katie Payne for excellent technical assistance, Dr. Clifford Pereira and Cody Olsen for statistical consultations, and Phenomenex for the donation of SPE cartridges used during method development. The project described was supported by grants to MGT (R01DK059576 and R01DK067930 from the National Institute of Diabetes and Digestive and Kidney Diseases and the Office of Dietary Supplements) and to the Environmental Health Sciences Center at Oregon State University from the National Institute of Environmental Health Sciences (NIH P30 ES00210). The content is solely the responsibility of the authors and does not necessarily represent the official views of the National Institute of Diabetes and Digestive and Kidney Diseases or the National Institutes of Health.

References

1. Morrow JD, Harris TM, Roberts LJ 2nd (1990) Noncyclooxygenase oxidative formation of a series of novel prostaglandins: analytical ramifications for measurement of eicosanoids. Anal Biochem 184:1–10
2. Lawson JA, Rokach J, FitzGerald GA (1999) Isoprostanes: formation, analysis and use as indices of lipid peroxidation in vivo. J Biol Chem 274:24441–24444
3. Roberts LJII, Morrow JD (2000) Measurement of F2-isoprostanes as an index of oxidative stress in vivo. Free Radic Biol Med 28:505–513
4. Chiabrando C, Valagussa A, Rivalta C, Durand T, Guy A, Zuccato E, Villa P, Rossi J-C, Fanelli R (1999) Identification and measurement of endogenous B-oxidation metabolites of 8-epi-prostaglandin F2a. J Biol Chem 274:1313–1319
5. Davies SS, Zackert W, Luo Y, Cunningham CC, Frisard M, Roberts LJ 2nd (2006) Quantification of dinor, dihydro metabolites of F(2)-isoprostanes in urine by liquid chromatography/tandem mass spectrometry. Anal Biochem 348:185–191
6. Roberts LJII, Moore KP, Zackert WE, Oates JA, Morrow JD (1996) Identification of the major metabolite of the F2-isoprostane 8-iso-prostaglandin F2alpha in humans. J Biol Chem 271:20617–20620
7. Nourooz-Zadeh J, Cooper MB, Ziegler D, Betteridge DJ (2005) Urinary 8-epi-pgf2a and its endogenous B-oxidation products (2, 3-dinor and 2, 3-dinor–5, 6-dihydro) as biomarkers of total body oxidative stress. Biochem Biophys Res Comm 330:731–736
8. Morrow JD, Zackert WE, Yang JP, Kurhts EH, Callewaert, Oates JA, Roberts LJ, II (1999) Quantification of the major urinary metabolite of 15-F2t-isoprostane (8-iso-pgf2a) by a stable isotope dilution mass spectrometric assay. Anal Biochem 269:326–331
9. Blumberg JB, Frei B (2007) Why clinical trials of vitamin E and cardiovascular diseases may be fatally flawed. commentary on “the relationship between dose of vitamin E and suppression of oxidative stress in humans”. Free Radic Biol Med 43:1374–1376
10. Liang Y, Wei P, Duke RW, Reaven PD, Harman SM, Cutler RG, Heward CB (2003) Quantification of 8-iso-prostaglandin-F2alpha and 2, 3-dinor-8-iso-prostaglandin-F2alpha in human urine using liquid chromatography-tandem mass spectrometry. Free Radic Biol Med 34:409–418
11. Taylor AW, Bruno RS, Frei B, Traber MG (2006) Benefits of prolonged gradient separation for high-performance liquid

chromatography-tandem mass spectrometry quantitation of plasma total 15-series F2-isoprostanes. Anal Biochem 350:41–51

12. Bruno RS, Leonard SW, Atkinson JK, Montine TJ, Ramakrishnan R, Bray TM, Traber MG (2006) Faster vitamin E disappearance in smokers is normalized by vitamin C supplementation. Free Radic Biol Med 40:689–697
13. Levine M, Wang Y, Padayatty S, Morrow J (2001) A new recommended dietary allowance of vitamin C for healthy young women. Proc Natl Acad Sci USA 98:9842–9846
14. Yin H, Gao L, Tai H-H, Murphey LJ, Porter NA, Morrow JD (2007) Urinary prostaglandin F2a is generated from the isoprostane pathway and not the cyclooxygenase in humans. J Biol Chem 282:329–336
15. Basu S, Helmersson J (2005) Factors regulating isoprostane formation in vivo. Antioxid Redox Signal 7:221–235
16. Bohnstedt KC, Karlberg B, Wahlund LO, Jonhagen ME, Basun H, Schmidt S (2003) Determination of isoprostanes in urine samples from Alzheimer patients using porous graphitic carbon liquid chromatography-tandem mass spectrometry. J Chromatogr B Analyt Technol Biomed Life Sci 796:11–19
17. Welsh TN, Hubbard S, Mitchell CM, Mesiano S, Zarzycki PK, Zakar T (2007) Optimization of a solid phase extraction procedure for prostaglandin E2, F2 alpha and their tissue metabolites. Prostaglandins Other Lipid Mediat 83:304–310
18. Morrow JD, Frei B, Longmire AW, Gaziano JM, Lynch SM, Shyr Y, Strauss WE, Oates JA, Roberts LJII (1995) Increase in circulating products of lipid peroxidation (F2-isoprostanes) in smokers. Smoking as a cause of oxidative damage. N Engl J Med 332:1198–1203
19. Reilly NDM, Delanty N, Lawson JA, FitzGerald GA (1996) Modulation of oxidant stress in vivo in chronic cigarette smokers. Circulation 94:19–25
20. Morrow JD, Awad JA, Kato T, Takahashi K, Badr KF, Roberts LJ 2nd, Burk RF (1992) Formation of novel non-cyclooxygenase-derived prostanoids (F2-isoprostanes) in carbon tetrachloride hepatotoxicity. an animal model of lipid peroxidation. J Clin Invest 90:2502–2507
21. Bruno RS, Traber MG (2005) Cigarette smoke alters human vitamin E requirements. J Nutr 135:671–674
22. Bruno RS, Traber MG (2006) Vitamin E biokinetics, oxidative stress and cigarette smoking. Pathophysiology 13:143–149
23. Hao CM, Breyer MD (2008) Physiological regulation of prostaglandins in the kidney. Annu Rev Physiol 70:357–377
24. Gao L, Zackert WE, Hasford JJ, Danekis ME, Milne GL, Remmert C, Reese J, Yin H, Tai HH, Dey SK et al (2003) Formation of prostaglandins E2 and D2 via the isoprostane pathway: a mechanism for the generation of bioactive prostaglandins independent of cyclooxygenase. J Biol Chem 278:28479–28489
25. Ide T, Tsutsui H, Ohashi N, Hayashidani S, Suematsu N, Tsuchihashi M, Tamai H, Takeshita A (2002) Greater oxidative stress in healthy young men compared with premenopausal women. Arterioscler Thromb Vasc Biol 22:438–442
26. Nielsen F, Mikkelsen BB, Nielsen JB, Andersen HR, Grandjean P (1997) Plasma malondialdehyde as biomarker for oxidative stress: reference interval and effects of life-style factors. Clin Chem 43:1209–1214
27. Block G, Dietrich M, Norkus EP, Morrow JD, Hudes M, Caan B, Packer L (2002) Factors associated with oxidative stress in human populations. Am J Epidemiol 156:274–285
28. Coudray C, Roussel AM, Mainard F, Arnaud J, Favier A (1997) Lipid peroxidation level and antioxidant micronutrient status in a pre-aging population; correlation with chronic disease prevalence in a French epidemiological study (Nantes, France). J Am Coll Nutr 16:584–591

Lipids (2008) 43:937–943
DOI 10.1007/s11745-008-3223-0

ORIGINAL ARTICLE

Glucose-Sensitive Liposomes Incorporating Hydrophobically Modified Glucose Oxidase

Seong-Min Jo · Hyeon Yong Lee · Jin-Chul Kim

Received: 9 April 2008 / Accepted: 4 August 2008 / Published online: 27 August 2008
© AOCS 2008

Abstract Glucose-sensitive liposomes were prepared by incorporating hydrophobically modified glucose oxidase (EC 1.1.3.4.) into the liposomal bilayer of dioleoylphosphatidylethanolamine and cholesteryl hemisuccinate. For the release test, calcein, a fluorescence marker, was entrapped in the liposomes. The liposomes were stable under neutral conditions in terms of calcein release but an extensive release was observed under acidic conditions. In the experiment of glucose concentration-dependent calcein release, no release was observed for 180 min when the suspension of liposome was free of glucose. With a glucose concentration of 50 mg/dL, no appreciable amount of calcein was released for the first 20 min, and then the release rate was accelerated. At 200 mg/dL glucose concentration which is diagnostic and indicative for insulin-dependent diabetes, the lag time of calcein release became shorter and a faster response was obtained. When glucose concentration further increased to 400 mg/dL, the calcein release rate and the degree of release in 180 min were almost the same as the values when the glucose concentration was 200 mg/dL. The glucose concentration-dependent release is due to pH change, since the suspension of liposomes became acidic during the release experiments.

Keywords Glucose oxidase · Liposomes · Glucose-sensitive release

Introduction

Much attention has been paid to stimuli-sensitive drug delivery systems, since they can control drug release in response to environmental stimuli such as change in pH [1, 2], temperature [3–8] and biochemical concentration [9]. One of extensive research areas is glucose-sensitive systems for the treatment of type I diabetes. Glucose-sensitive polymer membranes were prepared using immobilized glucose oxidase (GOD; EC 1.1.3.4.) in pH-sensitive polymers [10–15]. Glucose was converted to gluconic acid and hydrogen peroxide by the enzymatic reaction of GOD. In turn, the pH of release medium decreased with time, since the concentration of gluconic acid increases as the enzymatic reaction progresses. Accordingly, release is triggered by the swelling and the deswelling of the pH-sensitive hydrogels. Other glucose-sensitive systems were based on the competitive binding of glycosylated insulin and free glucose to concanavalin A (Con A). One example is that glycosylated insulin bound to Con A was immobilized either in polymer beads or in membranes [16–21]. When the concentration of free glucose is abnormally high, glycosylated insulin is detached from Con A and is released from the beads or the membranes. Another example takes advantage of the competitive binding of glucose attached to a polymer and free glucose to Con A [16–21]. Depending on the concentration of glucose, a sol–gel transition of the polymer system occurs and the insulin release is controlled. In previous studies, synthetic polymers were used for insulin carriers. However, the synthetic polymers are, in general, toxic and not tolerated in the human body. In this study, liposomes were designed as a glucose-sensitive carries. A liposome is defined as a phospholipid bilayer vesicle and it is known to be non-toxic and non-immunogenic in human body [22]. Liposomes can be

---

S.-M. Jo · H. Y. Lee · J.-C. Kim (✉)
School of Biotechnology and Bioengineering and Institute of Bioscience and Biotechnology, Kangwon National University, 192-1, Hyoja 2-dong, Chunchon, Kangwon-do 200-701, South Korea
e-mail: jinkim@kangwon.ac.kr

functionalized by modifying the surface with environment-responsive molecules. The specific functions of liposomes are induced by direct interaction with targets sites [23, 24], environmental pH [1, 2] and temperature changes [3–8]. Target-sensitive liposomes were proposed by modifying the surface of dioleoylphosphatidylethanolamine (DOPE) liposomes with an antibody [23, 24]. Specific interaction between a ligand immobilized on the liposomal membrane and a receptor on a target cell leads to the destabilization of DOPE liposomes. On the other hand, pH-sensitive liposomes were prepared by combining DOPE with *N*-succinyl-1,2-phosphatidylethanolamine, cholesteryl hemisuccinate (CHEMS), fatty acid and its derivatives, and palmitoyl homocysteine [26, 27]. Since the molecule of DOPE is conical and its packing parameter is greater than one, the phospholipids tend to form a non-bilayer structure in a physiological condition [26, 27]. In order to form a bilayer, it needs complementary molecules which fill the space among the head groups of DOPE [25–27]. It is a weakly acidic amphiphile and could stabilize DOPE bilayers at neutral pH. Among pH-sensitive complementary molecules, CHEMS has been the most frequently used [28–33]. It is also a weakly acidic amphiphilic molecule and could stabilize DOPE bilayers at physiological pH.

In this study, a novel glucose-sensitive liposome was developed by modifying the surface of pH-sensitive liposomes with hydrophobically modified glucose oxidase (HmGOD). As the concentration of glucose increases, the pH of the liposomal suspension decreases due to the increased amount of gluconic acid, which is produced by the enzymatic reaction. Accordingly, release is triggered by pH change of the liposomal suspension. Our idea was to develop a glucose-sensitive liposome. DOPE and CHEMS were used as the lipid components of the pH-sensitive liposome. To immobilize GOD onto the surface of the liposome, GOD was hydrophobically modified by covalently attaching alkyl chains to the amino groups of the enzyme. The DOPE/CHEMS liposome incorporating HmGOD was prepared by a detergent removal method and the glucose-sensitive release of the liposome was investigated.

Experimental

Materials and Methods

DOPE was purchased from Fluka (Buchs, Switzerland). Deoxycholate (DOC), CHEMS, GOD from *Aspergillus niger* Type X, palmitic acid *N*-hydroxysuccinimide ester, 4-(2-hydroxyethyl)-1-piperazineethanesulfonic acid (HEPES), calcein, sodium phosphate, sodium acetate trihydrate, sodium citrate, citric acid, horseradish peroxidase, β-D-glucose, *o*-dianisidine dihydrochloride, sodium lauryl sulfate (SLS), Bradford reagent and amino acid standard were purchased from Sigma Chemical Co (St. Louis, MO, USA). Trinitrobenzene sulfonic acid (TNBS, 5% methanol solution) was provided by PIERCE (Rockford, IL, USA). All other reagents were of analytical grade.

Modification of GOD

GOD was hydrophobically modified as described in a previous report [34]. First of all, 0.24 g of DOC was dissolved in 12 mL of phosphate buffer (pH 8.8, 0.16 M) and then, 0.081 g of GOD was added to the solution. In parallel, 0.0228 g of palmitic acid *N*-hydroxysuccinimide ester was dissolved in 2 mL of dry dioxane. The 0.4 mL of ester solution was added to the GOD solution by adding one of four portions of 0.1 mL every 2 h. Therefore, the molar ratio of GOD to the palmitic acid ester was 1:40. The reaction was done at 30 °C for 10 h with gently stirring. To remove insoluble byproducts, the reaction mixture was filtered through a syringe filter (0.45 μm) and then, the filtrate was dialyzed against 1 L of phosphate buffer (pH 8.0, 0.02 M) for 12 h with four exchanges of the buffer. Further dialysis was performed for 12 h with two exchanges of phosphate buffered saline (pH 7.4, 0.15 M). Finally, the dialyzed solution was filtered through a syringe filter (0.22 μm) and lyophilized for 3 days.

Determination of the Number of Palmitic Acid Residues Conjugated to GOD

The number of palmitic acid residues conjugated to GOD was determined by the TNBS method [34, 35]. A measure of 0.025 g of SLS was dissolved in 50 mL of phosphate buffer (pH 8.9, 0.01 M). A TNBS solution (0.03%) was prepared by adding 0.5 mL of TNBS to 83 mL of the SLS solution. One milliliter of each SLS and TNBS solution were mixed with 0.5 mL of HmGOD solution (3.55 mg/mL) in a 10 mL vial and the reaction was carried out at 50 °C for 1 h. Then, 1.9 mL of HCl solution (0.21 M) was added to the reaction mixture and the vial was kept at room temperature for 30 min. Finally the absorbance of the reaction was measured at 335 nm. A standard curve was prepared following the same procedure as described above except various concentrations of amino acid standard solutions were used instead of HmGOD. The number of palmitic acid residues conjugated to GOD was determined by comparing the absorbance of enzyme solutions with the standard curve.

Determination of Enzymatic Activity

A measure of 0.173 mL of 10% glucose solution in HEPES buffer (pH 7.5, 10 mM HEPES and 150 mM sodium chloride) and 0.827 mL of *o*-dianisidine dihydrochloride solution (0.21 mM) in HEPES buffer were mixed together. And then, 0.033 mL of horseradish peroxidase solution in HEPES buffer (0.33 mg/mL, 60 purpurogallin units/mL) was added to the solution. Finally, 0.1 mL of enzyme solution in distilled water (0.0488 mg/mL) was added to the previous solution. The concentration of the enzyme was determined using Bradford method [36]. The products of the enzymatic reaction are gluconic acid and hydrogen peroxide. Hydrogen peroxide oxidizes *o*-dianisidine dihydrochloride to the oxidized form with the aid of the catalytic action of horseradish peroxidase. The characteristic wavelength of the oxidized form is around 500 nm. Thus, the absorbance is a measure of the enzymatic activity. Since the amount of hydrogen peroxide increases with reaction time, the absorbance was proportional to time elapse. The absorbance value was converted to units/mg enzyme by using the millimolar extinction coefficient of oxidized o-dianisidine dihydrochloride at 500 nm. HEPES buffer of free enzyme was used as a control.

Preparation of DOPE/CHEMS Liposome Incorporating HmGOD

DOPE (10 mg/mL) and CHEMS (6.53 mg/mL) solutions in chloroform were put into a 50 mL round bottom flask so that the molar ratio of DOPE to CHEMS is 7:3 and the total amount of lipids is 18 mg. The solvent was evaporated in a rotary evaporator at reduced pressure to obtain a mixed dry film of DOPE and CHEMS. The dry film was dispersed into 2 mL of HEPES buffer (pH 8.2) containing calcein (50 mM), and DOC (0.09%). HmGOD was added to the dispersion so that the molar ratio of lipid to HmGOD is 10,000:1. The mixture was sonicated for 20 min with a bath-type sonicator (Ultrasonic processor, VCX 500, SONIX, USA). The liposomal suspensions were allowed to stand at room temperature for 4–5 h. DOC, unentrapped calcein and unbound enzyme were removed by gel permeation chromatography using a Sephadex G-75 column (1.6 cm × 40 cm). The final concentrations of lipids were adjusted to 2 mg/mL.

pH-Dependent Calcein Release

The calcein-containing liposome suspensions of 0.1 mL, 2 mg lipid/mL in HEPES (pH 8.2), were injected into a fluorescence cell containing 2.9 mL of HEPES buffer or sodium citrate buffer, pre-adjusted to pH ranging from 5.0 to 8.0. The change in fluorescence was monitored at 524 nm with excitation at 494 nm. The percentage release of calcein was determined as follows.

$$\% \text{ Release} = (F_t - F_i)/(F_f - F_i) \times 100$$

where F_t is the intensity of fluorescence at a given pH and F_i is the initial intensity at pH 8.2. F_f is the total fluorescence after adding DOC so that the final concentration is 0.2%. The fluorescence intensity at various pHs should be converted to the intensity at pH 8.2, since the release experiment was performed at various pHs, which is different from the pH of liposome preparation (pH 8.2). The calibration curves of calcein fluorescence were obtained at various pHs, where the degree of release was observed. The slope of each curve decreased with decreasing pH. It means that the intensity of fluorescence is suppressed at acidic pHs. Using these curves, fluorescence intensities were corrected.

Glucose-Dependent Calcein Release and Change in pH by Enzymatic Reaction

The 1.724 mL of liposome suspension was put into 50 mL of glucose solution in isotonic saline (adjusted to pH 7.5 with 0.001 M NaOH). The final concentrations of glucose were 0, 50, 200 and 400 mg/dL. The percent release of calcein was determined as described in the section of pH-dependent calcein release. In parallel, the change in pH of the liposomal suspensions containing varying amounts of glucose was measured during the release experiment.

Results and Discussion

Determination of Number of Palmitic Acid Residue Conjugated to GOD

The amino acid standard curve was expressed as $A_{335} = 0.572\ \text{M} + 0.0062$ ($R^2 = 0.9994$), where A_{335} is absorbance at 335 nm and M is μmol of amino acids. Since the TNBS method detects reactive amino groups, the absorbance of enzyme solutions is directly related to the number of reactive lysine residues of the enzymes. Under our experimental conditions, the absorbance of native GOD was 0.165, corresponding to 25.02 reactive amino groups per native GOD molecule. On the other hand, the absorbance of HmGOD was 0.127, calculated to be 19.03 reactive amino groups per the modified GOD molecule. This means that six palmitic acids were covalently attached to one GOD molecule by amide bonds formation with reactive lysine residues. In a previous report where GOD from *Aspergillus niger* (Type VII-S) was hydrophobized using palmitic acid *N*-hydroxysuccinimide ester, the number of reactive amino groups in native GOD was reported to be around 24 and the average number of covalently attached alkyl chains per GOD molecule was around 5 ± 1 [34].

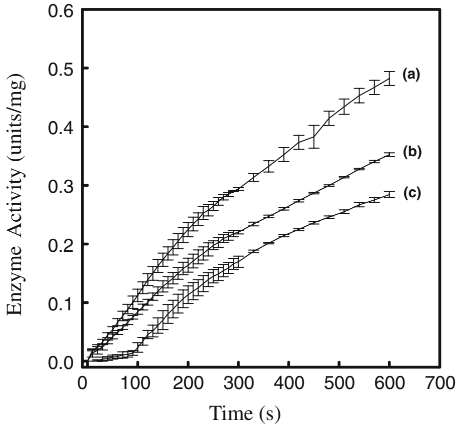

Fig. 1 Activity of native GOD **a,** HmGOD **b,** and HmGOD incorporated into liposomal membrane **c**

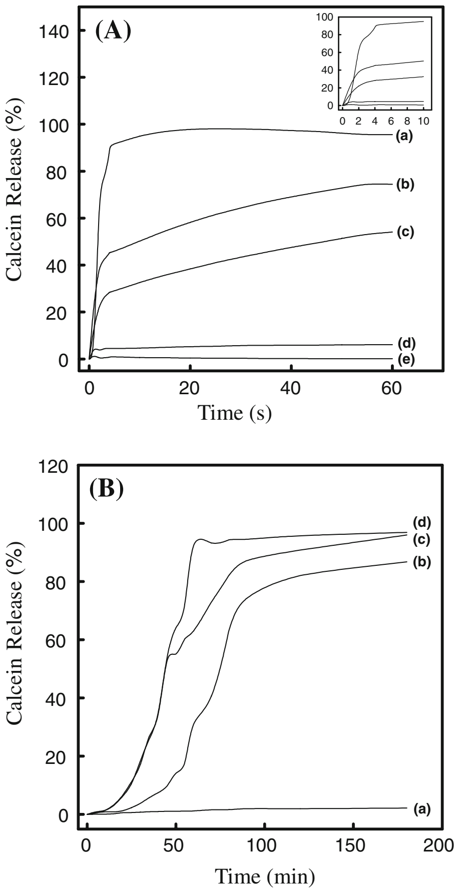

Fig. 2 pH-Dependent calcein release (panel *a*) and glucose-triggered calcein release (panel *b*) from liposome composed of DOPE/CHEMS /HmGOD. Inset in panel *a* is pH-dependent calcein release for 10 s labels for panel *a* : pH 5.0 **a**, pH 5.6 **b**, pH 6.0 **c**, pH 7.0 **d**, pH 8.2 **e** labels for panel *b* : 0 mg glucose/dL **a**, 50 mg glucose/dL **b**, 200 mg glucose/dL **c** and 400 mg glucose/dL **d**

Determination of Enzymatic Activity

Figure 1 shows the enzymatic activities of native GOD, HmGOD and HmGOD incorporated into liposomal membranes. According to the data, the activity of HmGOD was 60–65% of that of native GOD. The covalent attachment of alkyl chains to lysine residues has a great effect on the enzymatic activity, possibly because of the enzyme deformation caused by the modification. In addition, HmGOD is likely to aggregate since it has six alkyl chains attached. In this circumstance, active sites could be sequestered, resulting in an attenuated enzymatic activity. In the case of HmGOD immobilized in the liposomal membrane, the activity is slightly less than that of free HmGOD. The mobility of HmGOD immobilized in liposomal membranes would be less than that of free HmGOD. Accordingly, the formation of a substrate/enzyme complex would be somewhat restricted, resulting in reduced activity. Another reason is that some of HmGOD would be entrapped in the inner aqueous phase of liposome and the amount of HmGOD available for the enzymatic reaction might decrease.

pH-Dependent Calcein Release

Figure 2a shows the pH-dependent calcein release from the liposome composed of DOPE/CHEMS/HmGOD (7/3/0.0007 in molar ratio). There was no significant release in 60 s at pH 8.2 and pH 7.0 whereas, the release became extensive at pH 5.6 and pH 6.0, and the degrees of release in 60 s were 51 and 73%, respectively. Almost 100% of release was observed at pH 5.0. Several studies have been done on the pH-dependent fluorescent dye release from DOPE/CHEMS (6/4–7/3 in molar ratio) [33, 37–39]. According to their results, no significant release was observed in neutral pH range, whereas almost 100% of release was observed around pH 4.5–5.0. These previous results are in a good agreement with results obtained in this study. Since the p*K* value of carboxylic acid of CHEMS is 5.8, the carboxylic acid would be ionized above the pH, such as pH 7.0 and 8.2, so that the head group was large enough to stabilize DOPE bilayers. On the other hand, when pHs were below the p*K* value, such as pH 5 and pH 5.6, carboxylic acid would be deionized and the size of head group of CHEMS could decrease. Accordingly, the DOPE bilayer would be destabilized into non-bilayer structures, giving a rise to a higher release. At pH 5.6 and 6.0, a fast release was observed for the first 5 s and then subsequently a slow release. Those pHs are the values around p*K* and accordingly the deionization of CHEMS would occurs gradually at those pHs. This may account for the slow release at the latter stage. At pH 5.0, the initial rate of release was faster [see initial slope of plot (a)], so the release was completed in 5 s. Because pH 5.0 was less than p*K*, CHEMS could be deionized at a burst. This may explain the earlier completion of the release at pH 5.0.

Glucose-Triggered Calcein Release and Change in pH Caused by the Enzymatic Reaction

Figure 2b shows glucose-triggered calcein release from liposomes incorporating HmGOD. In case of the suspension of liposome without glucose, there was no release observed for 180 min. When the concentration of glucose was 50 mg/dL, no appreciable amount of calcein released for the first 20 min, and then the release rate accelerated for the next 70 min. Thereafter, the rate of acceleration was reduced and the degree of release was approximately 80% in 180 min. Glucose is converted to gluconic acid and hydrogen peroxide by the enzymatic reaction of HmGOD. Thus, the pH of liposomal suspension would decrease with time because the concentration of gluconic acid increases as the enzymatic reaction goes on. Thus, it is believed that the release was triggered by the pH change of liposomal suspension. When the concentration of glucose was 50 mg/dL, the concentration of gluconic acid was thought not to be high enough to trigger the release for the first 20 min. That is, the lag time of 20 min is possibly due to the lower concentration of glucose and gluconic acid. When the concentration of glucose increased to 200 mg/dL, which is diagnostic and indicative for insulin-dependent diabetes, the release pattern was similar to that of 50 mg/dL. But the lag time became shorter, and a faster response was obtained. This is because higher concentration of glucose produces more gluconic acid. In addition, the rate of release was higher and the degree of release within 180 min was more extensive (about 95%). When glucose concentration further increased to 400 mg/dL, the release rate for the first 40 min and the degree of release within 180 min were almost the same as the values when the glucose concentration was 200 mg/dL. The release was, however, completed in 60 min and the completion of release was earlier than in case of 200 mg/dL. On the other hand, liposomes without HmGOD exhibited only 2% of release over 180 min even at a glucose concentration of 400 mg/dL. Therefore, the calcein release from liposomes incorporating HmGOD was not due to osmotic pressure but due to the acidification caused by the enzymatic reaction. To investigate whether the glucose-dependent release is triggered by pH change or not, the pH of liposomal suspension was measured with time (Fig. 3). When glucose was not added, the pH remained almost constant. When the glucose concentration was 50 mg/dL, pH decreased steadily for the first 60 min and the decreasing rate of pH was accelerated for the next 30 min. Thereafter, the rate of the decrease in pH was reduced. The pH of the liposomal suspension was around 4.3 after 180 min had elapsed.

When the glucose concentration was 50 mg/dL, it took about 20 min to reach pH 7 (Fig. 3). In 20 min when pH was 7, there was no appreciable amount of calcein released at the same concentration of glucose (Fig. 2b). At pH 7, no appreciable amount was released (Fig. 2a). For another example, when the glucose concentration was 50 mg/dL, it took about 70 min to reach pH 6 (Fig. 3). In 70 min when pH was 6, the degree of release was about 45% at the same concentration of glucose (Fig. 2b). At pH 6, the degree of completed release was about 50% (Fig. 2a), not significantly different from 45%. In similar manner, the comparisons of Figs. 2a, b and 3 were also applicable when the glucose concentrations are 200 and 400 mg/dL. Therefore, it is reasonable that the release could be caused by pH change, which is due to the conversion of glucose to gluconic acid.

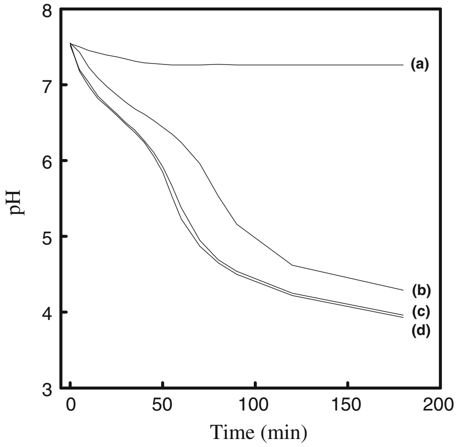

Fig. 3 Change in pH of the suspensions of liposomes incorporating HmGOD over time. The concentrations of glucose in liposomal suspensions were 0 mg/dL **a**, 50 mg/dL **b**, 200 mg/dL **c** and 400 mg/dL **d**

Insulin might be encapsulated in the liposomes incorporating HmGOD for the treatment of type I diabetes. Unfortunately, the release from liposomes occurred when the glucose concentration was less than the indicative concentration for diabetes. That is one of the handicaps to be overcome. In order to use the liposome as an insulin carrier for diabetes, the carrier should retain its content when glucose concentration is in the normal range (80–140 mg/dL) and it should release timely when the glucose concentration is more than 200 mg/dL. In addition, calcein release from the liposome in this study was achieved in distilled water. Hence, the glucose-induced release of calcein would be irrelevant in a pH-buffered medium. However, the pH near the location of the enzyme immobilization on the liposome surface could be changed for an instant even in a pH-buffered medium. Hence, the glucose-induced release would also occur even in buffer solution. In fact, Traitel and his coworkers prepared glucose-sensitive hydrogel using GOD and poly(2-hydroxyethyl methacrylate-*co*-*N*,*N*-dimethylaminoethyl methacrylate), and they investigated the release of insulin in phosphate-buffered saline (pH 7.4) at glucose concentrations of 0, 100, and 500 mg/dL [40]. According to their results, a significant insulin release occurred at the concentration of 500 mg/dL. Although the concentration triggering the release was higher than in the present study, the results obviously showed a possibility that the glucose-sensitive system would work in a buffered milieu. On the other hand, an on–off type of release could hardly be observed under our experimental conditions. It might be obtained by varying the amounts of CHEMS and HmGOD in the liposomal membrane. However, it would be hard to avoid the leakage at normal glucose concentrations (80–140 mg/dL) because the amount of deionized CHEMS at those concentrations might be already enough to destabilize DOPE bilayers. One of more practical approaches to suppress the undesirable release is to shift the triggering glucose concentration. For that purpose, other complement molecules could be used instead of CHEMS. Their titratable groups p*K* values should be quite different from that of carboxylic acid of CHEMS. The most important thing for practical use is that compounds involved in the glucose-sensitive liposomes should be non-toxic in the human body. CHEMS is believed to increase immunogenicity of tumor cells and no toxicity profiles about CHEMS have been reported [41]. GOD is known to be antibiotic because hydrogen peroxide, produced by the enzymatic reaction of GOD, exhibits antibacterial activity [42]. Hydrogen peroxide causes oxidative stress in the human body. As a result, degeneration of DNA, membrane lipid and protein, and enzyme may occur, leading to various pathological conditions [43]. To circumvent the side effect of hydrogen peroxide, catalase has been frequently used when GOD is included in glucose-sensitive insulin delivery systems [44].

Conclusion

Glucose-sensitive release was obtained by incorporating hydrophobically modified GOD into the membrane of pH-sensitive liposomes. Although a clear-cut release pattern could hardly be obtained, the degree and the rate of release from DOPE/CHEMS liposomes incorporating HmGOD were strongly dependent on the concentration of glucose. The liposome is thought to have a potential as a carrier for diabetes treatment.

Acknowledgments This work was supported by a grant (20070101033021) from a Special Agricultural Research Program, Rural Development Administration, Republic of Korea.

References

1. Choi M-J, Han H-S, Kim H (1992) pH-sensitive liposomes containing polymerized phosphatidylethanolamine and fatty acid. J Biochem 112:694–699
2. Maeda M, Kumano A, Tirrell DA (1988) H^+-Induced release of contents of phosphatidylcholine vesicles bearing surface bound polyelectrolyte chains. J Am Chem Soc 110:7455–7459
3. Yatvin MB, Weinstein JN, Dennis WH, Blumenthal R (1978) Design of liposomes for enhanced local release of drugs by hyperthermia. Science 202:1290–1293
4. Weinstein JN, Magin RL, Cysyl RL, Zaharko DS (1980) Treatment of solid L1210 murine tumors with local hyperthermia and temperature-sensitive liposomes containing methotrexate. Cancer Res 40:1388–1395
5. Hayashi H, Kono K, Takagishi T (1996) Temperature-controlled release property of phospholipid vesicles bearing a thermo-sensitive polymer. Biochim Biophys Acta 1280:127–134
6. Kim J-C, Bae SK, Kim J-D (1997) Temperature-sensitivity of liposomal lipid bilayers mixed with poly(N-isopropylacrylamide-co-acrylic acid). J Biochem 121:15–19
7. Kono K, Nakai R, Morimoto K, Takagishi T (1999) Thermosensitive polymer-modified liposomes that release contents around physiological temperature. Biochim Biophys Acta 1416:239–250
8. Kono K, Henmi A, Yamashita H, Hayashi H, Takagishi T (1999) Improvement of temperature-sensitivity of poly(N-iso-propyl-acrylamide)-modified liposomes. J Control Release 59:63–75
9. Chu L-Y, Liang Y-J, Chen W-M, Ju X-J, Wang H-D (2004) Preparation of glucose-sensitive microcapsules with a porous membrane and functional gates. Colloid Surf B-Biointerfaces 37:9–14
10. Horbett T, Kost J, Ratner B (1983) Swelling behavior of glucose sensitive membranes. Am Chem Soc. Div Polym Chem 24:34–35
11. Horbett T, Kost J, Ratner B (1984) Swelling behavior of glucose sensitive membranes. In: Shakaby S, Hoffman A, Horbett T, Ratner B (eds) Polymers as Biomaterials. Plenum, New York
12. Kost J, Horbett T, Ratner B, Singh M (1985) Glucose sensitive membranes containing glucose oxidase: activity, swelling and permeability studies. J Biomed Mater Res 19:1117–1133
13. Albin G, Horbett T, Ratner B (1985) Glucose sensitive membranes for controlled delivery of insulin: insulin transport studies. J Control Release 2:153–164
14. Albin G, Horbett T, Miller S, Ricker N (1987) Theoretical and experimental studies of glucose sensitive membranes. J Control Release 6:267–291
15. Albin G, Horbett T, Ratner B (1990) Glucose-sensitive membranes for controlled release of insulin. In: Kost J (ed) Pulsed and self-regulated drug delivery. CRC Press, Boca Raton
16. Kim SW, Jeong SY, Sato S, McRea JC, Feijen F (1984) Self regulating insulin delivery system-a chemical approach. In: Anderson JM, Kim SW (eds) Recent advances in drug delivery systems. Plenum, New York
17. Jeong SY, Kim SW, Eenink MJD, Feijen J (1984) Self-regulating insulin delivery systems I. Synthesis and characterization of glycosylated insulin. J Control Release 1:57–66
18. Sato S, Jeong SY, McRea JC, Kim SW (1984) Self-regulating insulin delivery systems II. In vitro studies. J Control Release 1:67–77
19. Jeong SY, Kim SW, Holemberg D, McRea JC (1985) Self-regulating insulin delivery systems III. In vivo studies. J Control Release 2:143–152
20. Sato S, Jeong SY, McRea JC, Kim SW (1984) Glucose stimulated insulin delivery system. Pure Appl Chem 56:1323–1328
21. Seminoff L, Kim SW (1990) A self-regulating insulin delivery system based on competitive binding of glucose and glycosylated insulin. In: Kost J (ed) Pulsed and self-regulated drug delivery. CRC Press, Boca Raton
22. New RRC (1990) Introduction. In: New RRC (ed) Liposomes: a practical approach. IRL Press, New York
23. Lee EO, Kim JG, Kim J-D (1992) Induction of vesicle-to-micelle transition by bile salts for DOPE vesicles incorporating immunoglobulin G. J Biochem 112:671–676

24. Huang A, Tsao YS, Kennel SJ, Huang L (1983) Characterization of antibody covalently coupled to liposomes. Biochim Biophys Acta 716:140–150
25. Taraschi TF, van der Steen AT, de Kruijff B, Tellier C, Verkleij AJ (1982) Lectin-receptor interactions in liposomes: Evidence that binding of wheat germ agglutinin to glycoprotein-phosphatidylethanolamine vesicles induced nonbilayer structure. Biochemistry 21:5756–5764
26. New RRC, Black CDV, Parker RJ, Puri A, Scherphof GL (1990) Liposomes in biological systems. In: New RRC (ed) Liposomes: a practical approach. IRL Press, New York
27. Schubert R, Peschka-Suess R (2003) pH-Sensitive liposomes. In: Torchilin VP, Weissig V (eds) Liposomes second edition: a practical approach. Oxford University Press, New York
28. Straubinger RM, Du”zgu”nes N, Papahadjopoulos D (1984) pH-Sensitive liposomes mediate cytoplasmic delivery of encapsulated macromolecules. FEBS Lett 179:148–154
29. Liu D, Huang L (1990) pH-sensitive, plasma-stable liposomes with relatively prolonged residence in circulation. Biochim Biophys Acta 1022:348–354
30. Litzinger DC, Huang L (1992) Phosphatidylethanolamine liposomes: drug delivery, gene transfer and immunodiagnostic applications. Biochim Biophys Acta 1113:201–227
31. Ellens H, Bentz J, Szoka FC (1984) pH-Induced destabilization of phosphatidyl ethanolamine-containing liposomes: role of bilayer contact. Biochemistry 23:1532–1538
32. Cullis PR, Kruijff BD (1979) Lipid polymorphism and the functional roles of lipids in biological membranes. Biochim Biophys Acta 559:399–420
33. Van Bambeke F, Kerkhofs A, Schanck A, Remacle C, Sonveaux E, Tulkens PM, Mingeot-Leclercq MP (2000) Biophysical studies and intracellular destabilization of pH-sensitive liposomes. Lipids 35:213–223
34. Baszkin A, Boissonnade MM, Rosilio V, Kamyshny A, Magdassi S (1997) Adsorption of hydrophobized glucose oxidase at solution/air interface. J Colloid Interface Sci 190:313–317
35. Hermanson G (1996) Bioconjugate technigues. Academic Press, San Diego
36. Bradford MM (1976) A rapid and sensitive for the quantitation of microgram quantitites of protein utilizing the principle of protein-dye binding. Anal Biochem 72:248–254
37. Sudimack JJ, Guo W, Tjarks W, Lee RJ (2002) A novel pH-sensitive liposome formulation containing oleyl alcohol. Biochim Biophys Acta 1564:31–37
38. Kim M-J, Lee HJ, Lee I-A, Kim I-Y, Lim S-K, Cho H-A, Kim J-S (2008) Preparation of pH-sensitive, long-circulating and EGFR-targeted immunoliposomes. Arch Pharm Res 31:539–546
39. Ishida T, Okada Y, Kobayashi T, Kiwada H (2006) Development of pH-sensitive liposomes that efficiently retain encapsulated doxorubicin (DXR) in blood. Int J Pharm 309:94–100
40. Traitel T, Cohen Y, Kost J (2000) Characterization of glucose-sensitive insulin release systems in simulated in vivo conditions. Biomaterials 21:1679–1687
41. Ding W-X, Qi X-R, Li P, Maitani Y, Nagai T (2005) Cholesteryl hemisuccinate as a membrane stabilizer in dipalmitoylphosphatidylcholine liposomes containing saikosaponin-d. Int J Pharm 300:38–47
42. Tiina M, Sandholm M (1989) Antibacterial effect of the glucose oxidase-glucose system on food-poisoning organisms. Int J Food Microbiol 8:165–174
43. Hussin M, Abdul-Hamid A, Mohamad S, Saari N, Ismail M, Bejo MH (2007) Protective effect of *Centella asiatica* extract and powder on oxidative stress in rats. Food Chem 100:535–541
44. Sisak C, Csanádi Z, Rónay E, Szajáni B (2006) Elimination of glucose in egg white using immobilized glucose oxidase. Enzyme Microb Tech 39:1002–1007

Lipids (2008) 43:945–950
DOI 10.1007/s11745-008-3227-9

ORIGINAL ARTICLE

Circulating Levels of Lectin-Like Oxidized Low-Density Lipoprotein Receptor-1 are Associated with Inflammatory Markers

Valter Lubrano · Serena Del Turco ·
Giuseppina Nicolini · Pietro Di Cecco ·
Giuseppina Basta

Received: 3 June 2008 / Accepted: 29 July 2008 / Published online: 10 September 2008
© AOCS 2008

Abstract Lectin-like oxidized-low-density lipoprotein receptor-1 (LOX-1) is increasingly linked to atherosclerotic plaque formation and the soluble form of this receptor may reflect activities of disease. We investigated the associations among levels of sLOX-1, oxidized-low-density lipoprotein (ox-LDL), cytokines and the extension of atherosclerosis in patients with coronary artery disease (CAD). Lipid, TNF-α, IL-6, C reactive protein (CRP), ox-LDL, peroxy radical and sLOX-1 levels were measured in 29 controls and 60 patients with CAD, 30 of which with one or two vessels involved (group 1), and 30 patients with three or four vessels involved (group 2). The serum levels of sLOX-1 were significantly and progressively higher in group 1 [611 (346–1,313) pg/ml, median (interquartile range)] and in group 2 [2,143 (824–3,201) pg/ml] than in control subjects [268 (111–767) pg/ml]. LOX-1 levels positively correlated with IL-6 ($r = 0.38$, $P = 0.0042$), TNF-α ($r = 0.38$, $P = 0.0037$), CRP levels ($r = 0.32$, $P = 0.027$) and age ($r = 0.25$, $P = 0.048$). In the multivariate analysis TNF-α resulted the only independent determinant of LOX-1 serum levels (β-value $= 0.304$, $P = 0.017$). These findings suggest that sLOX-1 levels are up-regulated during CAD progression and are associated with inflammatory markers. The measurement of the circulating soluble form of this receptor may be potentially useful in predicting CAD progression in humans.

Keywords Cytokines · Lipoprotein receptors · Cholesterol oxidation · Coronary artery disease · Inflammation

Introduction

Lectin-like oxidized-low-density lipoprotein receptor-1 (LOX-1) was initially identified as the major receptor for ox-LDL (oxidized low-density lipoprotein) in endothelial cells and was later found also to have an inducible expression in macrophages and smooth muscle cell [1, 2]. Besides ox-LDL, LOX-1 can recognize apoptotic/aged cells, activated platelets, and bacteria, implying versatile physiological functions as a "scavenger" receptor. LOX-1 activation by ox-LDL binding stimulates intracellular signalling, gene expression and production of superoxide radicals [3, 4]. In vivo, its expression is enhanced in pro-atherogenic settings including, hypertension, hyperlipidemia, diabetes, and atherosclerosis. Transgenic mouse models for LOX-1 overexpression or gene knockout suggests that LOX-1 contributes to atherosclerotic plaque formation and progression [5, 6]. Besides being involved in the activation of endothelial cells, LOX-1 is also involved in the transformation of smooth muscle cells, and accumulation of lipids in macrophages, resulting in cell injury that facilitates the development of atherosclerosis.

Like many cell-surface receptors with a single transmembrane domain, LOX-1 can be cleaved at the juxtamembrane region, most likely by serine proteases, and secreted in a soluble form [7]. Since elevated levels of soluble receptors in plasma may reflect increased expression of membrane-bound receptors and disease activities, circulating soluble LOX-1 (sLOX-1) is increasingly viewed as a vascular disease biomarker and

---

V. Lubrano · S. Del Turco · G. Nicolini · P. Di Cecco ·
G. Basta (✉)
Institute of Clinical Physiology CNR and G. Monasterio foundation, Via Moruzzi, 1, 56124 Pisa, Italy
e-mail: lapina@ifc.cnr.it

a potential therapeutic target in heart attack and stroke prevention [8].

Serum sLOX-1 have been shown to be increased early in patients with acute coronary syndrome, suggesting that it may reflect vulnerable unstable atherosclerotic plaques with enhanced proinflammatory and protease activities [9]. Recently, it has been shown that sLOX-1 correlated with oxidative stress markers in stable coronary artery disease [10]. However, the association of circulating sLOX-1 with the extension of CAD and inflammatory markers has not been properly addressed. We therefore attempted to clarify the link between sLOX-1 with plasma ox-LDL, cytokines and the extension of coronary atherosclerosis in patients affected by CAD.

Methods

The study included 60 patients admitted to our Institute because of documented or suspected ischemic heart disease and who, after undergoing coronary angiography, were diagnosed as being affected by coronary artery disease (CAD). Our controls were 29 healthy subjects who had not undergone coronary angiography. Physical examination and routine laboratory tests excluded the presence of other major disease (e.g. diabetes, hypertension, renal or liver diseases, infectious, chronic inflammatory or immunologic diseases, or malignancies). Exclusion criteria were any acute cardiovascular events during the last 3 months before hospitalization, and assumption of statins, other hypolipemic therapy, vitamins or antioxidant dietary supplements. Prior to drawing blood, patients were taken off antianginal medication, while sublingual nitrates were allowed only in the case chest pain were to persist for more than 3 minutes. Of the initial patients, 4 required sublingual nitrates and were therefore excluded from the study. All other medication, except antiplatelets, was suspended 7 days before taking the blood sample.

All subjects gave written informed consent for their participation in the study which was approved by the local ethics committee and conforms to the principles outlined in the Declaration of Helsinki.

Of the 60 patients enrolled, 17 had a reduced lumen diameter in one coronary artery, 14 patients had two arteries involved, 15 patients had three arteries involved and 14 patients had four arteries involved; in each case the mean reduction lumen was at least about 50%.

Analytical Methods

All blood samples were collected at 4 °C the day before the cardiac catheterization and were immediately centrifuged. Plasma or serum samples were stably stored at −80 °C for no more than 15 days. Plasma concentrations of TC, HDL and Triglycerides (Tg) were determined by standard laboratory methods. The concentration of LDL was calculated using the Friedewald equation.

To measure the generation of peroxy radicals—the initial products of the reaction between free radicals and oxygen—a colorimetric method (D-Roms test, Diacron international, Italy) was used as previously described [11]. This test is based on the ability of transition metals to catalyze in the presence of peroxides with the generation of free radicals that are trapped by an alchilamine whose reaction yields a colored radical detectable at 505 nm. The results are expressed as Carratelli Units (UC) (1 UC = 0.08 mg H_2O_2/dl).

High sensitivity (hs)-IL-6 and hs-TNFα were quantified using sandwich ELISA kits (Biosource International, CA) according to the manufactures' instructions. Inter-assay coefficients of variation was 7.8%.

High sensitivity C reactive protein (hs-CRP) was measured by the Immulite System (Diagnostic Products Corporation, CA).

Ox-LDL was assessed by a sandwich ELISA kit (Mercordia AB, Sweden) according to the manufactures' instructions. The inter-assay coefficient of variation was 4.7%.

Serum LOX-1 levels were measured by an in-house double-sandwich ELISA kits. Briefly, 96-well microplates (Nunc-Immuno Plates Maxisorp, Nunk, Roskilde, Denmark) were coated with monoclonal anti-human LOX-1 antibody (R & D systems, Minneapolis, MN) (0.25 μg/ml) in coating buffer (10 mmol/l PBS, pH 7.2) and incubated overnight at room temperature (RT). The serum specimens were initially inactivated at 56 °C for 30 min to block non-specific protein binding sites. Four rinses with washing buffer (PBS containing 0.05% Tween 20, PBST) followed each incubation step. After blocking with reagent buffer (1% BSA in PBS) at RT for 1 h, 100 μl of heat-inactivated sample (diluted 1:2 in reagent diluent) was added, and incubated at RT for 2 h. Recombinant human LOX-1 (R & D systems) was used as the standard in a concentration range of 100–10,000 pg/ml. Then, 100 μl of polyclonal goat anti-human LOX-1 antibody (R & D systems) (0.25 μg/ml) was added and incubated at RT for 2 h. Next, 100 μl of rabbit antigoat-HRP antibody (Santa Cruz Biotechnology, Inc., CA) (diluted 1:400) was added and incubated for 1 h at RT. Finally, 100 μl of tetramethylbenzidine substrate (Sigma-Aldrich, St. Louis, MO) was added. After 5–15 min, 50 μl of 2 mol/l sulphuric acid was added to stop the reaction, and optical density at 450 nm determined by an ELISA plate reader. The inter-assay coefficient of variation value was 7.2%. The lower limit of detection for LOX-1 was 30 pg/ml.

Statistical Analysis

Data are given as the mean ± SD. Variables with a skewed distribution are expressed as median and interquartile range. Appropriate variable transformations were made to reduce the skewness of the data, such as natural logarithmic transformation for sLOX-1, TNF-α, IL-6 etc. Differences among different groups of patients and controls were evaluated by one-way ANOVA followed by Bonferroni post hoc test for continuous variables and by X^2 test for noncontinuous variables. Relationships between serum sLOX-1 and other factors were assessed by Pearson correlation analysis. In order to evaluate the factors affecting sLOX-1 levels, all variables significantly associated with sLOX-1 were included in the multiple regression analysis, plus gender and BMI as confounding factors. A P value lower than 0.05 was considered statistically significant.

Results

To determine whether the circulating parameters varied with the severity of the disease, we divided the patients into two groups. Patients with one or two vessels involved were clustered in group 1, while patients with three or four vessels involved were clustered in group 2. Table 1 summarizes age, gender and lipid profiles in each group of patients and controls. Controls and patients were comparable for sex, age, BMI, pressure, glycemia and triglycerides, while HDL values were more elevated in controls than in patients. Instead, total cholesterol and LDL values resulted significantly lower in the group 2 compared to the controls (Table 1).

Circulating sLOX-1, as well as peroxy radical, CRP, TNF-α, IL-6 levels resulted significantly higher in patients than controls and tended to increase with the severity of CAD (values of group 2 were higher than values of group 1) (Table 2). Instead, ox-LDL values were significantly higher in group 1, while those of the group 2 resulted comparable to control values (Table 2).

As shown in the Fig. 1a–d, LOX-1 serum levels positively correlated with TNF-α ($r = 0.38$, $P = 0.0037$), IL-6 ($r = 0.38$, $P = 0.0042$), CRP levels ($r = 0.32$, $P = 0.027$) and age ($r = 0.25$, $P = 0.048$), and did not correlate with peroxy radicals, ox-LDL, and with all the other parameters reported in Table 1. The multivariate analysis revealed that, after correction for confounding factors, TNF-α was the only determinant of LOX-1 levels (β-value $= 0.304$, $P = 0.017$).

Discussion

Atherosclerosis is associated with oxidative stress, inflammation, and upregulation of LOX-1. We found that sLOX-1 is significantly more elevated in patients affected by CAD than in controls and that this increase correlated with the number of affected vessels.

This increase raises the question of the cell source and the triggers for this soluble receptor. Although we do not know whether the measured sLOX-1 levels in serum are related to tissue LOX-1 values, some studies have highlighted that circulating concentrations of this receptor are indicative of endothelial-surface bound receptor levels [9, 12]. In vitro, the cell-surface expression of LOX-1 is induced by many inflammatory cytokines, oxidative stress,

Table 1 Biochemical and clinical features of study subjects

	Controls	Patients		P
		Group 1	Group 2	
Age (years)	62.0 ± 13.6	65.8 ± 13.0	67.9 ± 12.5	n.s.
Gender (female, male)	8/21	7/24	4/25	n.s.
BMI (kg/m^2)	26.3 ± 0.9	26.8 ± 4.2	25.0 ± 5.7	n.s.
Systolic pressure	130.0 ± 19.8	127.7 ± 23.9	121.6 ± 21.5	n.s.
Diastolic pressure	85.0 ± 9.5	68.7 ± 10.6	70.9 ± 8.5	n.s.
Glycemia (mg/dl)	98.96 ± 30.9	86.6 ± 11.7	107.4 ± 34.4	n.s.
Triglycerides (mg/dl)	90.8 ± 41.9	117.6 ± 43.2	111.3 ± 62.8	n.s.
Total cholesterol (mg/dl)	194.0 ± 24.6	186.6 ± 33.2	155.1 ± 45.8*,§	0.0007
HDL (mg/dl)	50.7 ± 15.9	38.3 ± 8.9§	35.4 ± 11.7**	0.0001
LDL (mg/dl)	124.1 ± 18.2	124.5 ± 28.7	97.4 ± 36.7$^{\#,\dagger}$	0.0017

Group 1 patients with one- or two-vessel coronary artery disease; *Group 2* patients with three- or four-vessel coronary artery disease; *BMI* body mass index; *HDL* high density lipoprotein; *LDL* low density lipoprotein

* $P < 0.01$ versus Group 1; § $P < 0.001$ versus controls; ** $P < 0.0001$ versus controls; $^{\#}$ $P < 0.05$ versus controls; † $P < 0.01$ versus Group 1

Table 2 Oxidative and inflammatory parameters of study subjects

	Controls	Patients		*P*
		Group 1	Group 2	
LOX-1 (pg/ml)	268 (111–767)	611 (346–1,313)*	2,143 (824–3,201)§,**	0.0015
Peroxy radicals (UC)	315 ± 92	345 ± 90	410 ± 110$^{\S,\#}$	0.0018
CRP (mg/dl)	0.09 (0.06–0.29)	0.25 (0.12–0.53)*	0.43 (0.18–1.57)§,**	0.0038
TNF-α (pg/ml)	1.07 (0.09–1.8)	1.74 (0.62–3.52)*	2.00 (0.91–3.97)§	0.032
IL-6 (pg/ml)	0.18 (0.04–0.61)	0.79 (0.23–2.17)†	1.2 (0.4–3.0)§	0.0059
ox-LDL (U/l)	72.5 (58.6–154.1)	143 (79.7–272.3)*	77.7 (32.8–157.2)$^{\#}$	0.0073

Group 1 patients with one or two diseased vessels; *Group 2* patients with three or four diseased vessels; *LOX-1* lectin-like oxidised lipoprotein receptor-1; *CRP* C reactive protein; *TNF-α* tumor necrosis factor; *IL-6* Interleukin-6; *ox-LDL* oxidized low density lipoprotein

* $P < 0.05$ versus controls; § $P < 0.001$ versus controls; ** $P < 0.05$ versus Group 1; $^{\#}$ $P < 0.01$ versus Group 1; † $P < 0.01$ versus controls

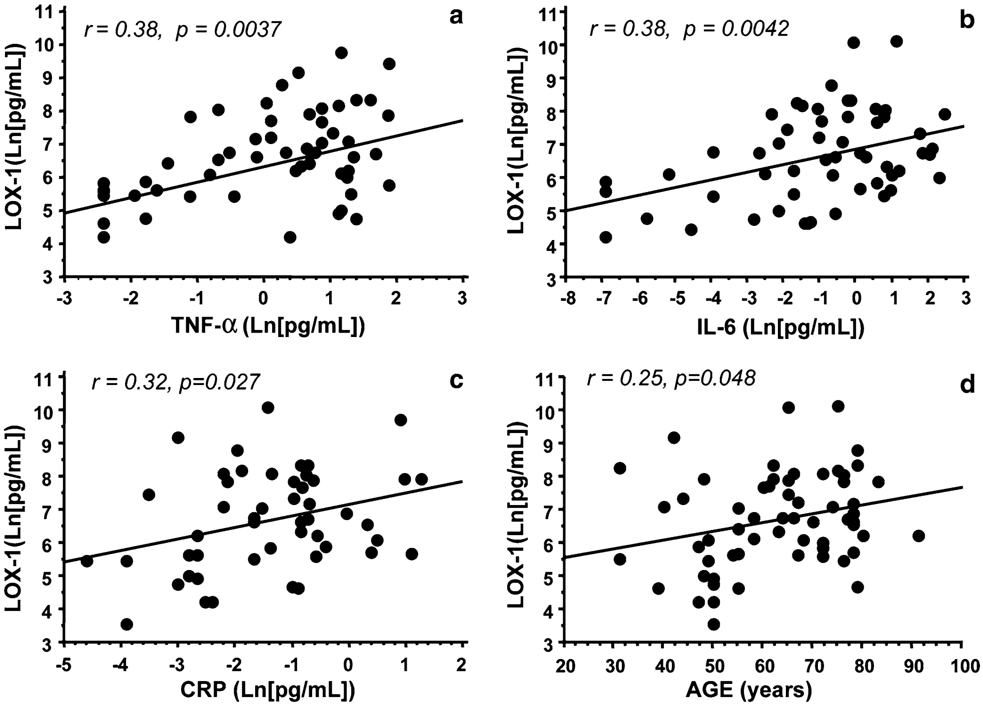

Fig. 1 Correlations between serum sLOX-1 concentrations and TNF-α (**a**), IL-6 (**b**), CRP (**c**) and age (**d**) in all subjects of the study

hemodynamic stimuli [13, 14]. Expression of LOX-1 can be induced after macrophage-like differentiation in vitro in human peripheral blood monocytes [15]. In endothelial cells activated by TNF-α, the cell-surface expression of LOX-1 precedes soluble LOX-1 production [7], suggesting that the regulation of LOX-1 cleavage is correlated to LOX-1 cell expression. Our present study clearly shows a positive correlation between circulating sLOX-1 and TNF-α plasma concentrations, indicating this latter as independent determinant and possible trigger of the s-LOX-1 increase. Likewise, CRP and IL-6 enhance, in a dose- and time-dependent manner, endothelial LOX-1 mRNA and protein expression [14]. In line with this finding, we found a significant relationship between circulating sLOX-1 and CRP or IL-6. However, our results do not agree with those of other authors [9, 10] who have reported no correlation between sLOX-1 and CRP or IL-6. This discrepancy with our results probably stems from a difference in the selection of patients. Contrary to them, we excluded patients with diabetes, hypertension, and/or under the respective therapy that could influence the results. Another explanation for this discrepancy could be the higher sensitivity of our method (10-fold more sensible) that is able to reveal correlations with the other parameters which could have remained hidden with the less sensitive methodology used in the above-mentioned studies.

Similarly to other studies [16, 17], our data confirm the link between CAD and elevated plasma concentrations of peroxy radicals, cytokines, and CRP, and between their levels and the severity of the disease.

However in our study, contrary to expectations, ox-LDL plasma levels were higher in less severe patients (group 1) and lower in more severe patients (group 2).

We can assume that, the reduced levels of ox-LDL in more severely affected patients, could be due to increased uptake of ox-LDL by sLOX-1 which are present in high levels in this group. In support to this hypothesis, some studies have shown that soluble membrane receptors can modulate disease activity by binding to its ligand and preventing ligand uptake by the receptor at the cell-surface [18–20]. For instance, the soluble TNF receptors, whose shedding is induced by TNF itself as well as other cytokines [18], have extracellular regulatory functions affecting local or systemic TNF bioavailability. Circulating sLOX-1 could hence be an important regulator of plasma ox-LDL levels. To explore whether the antibodies used in our ELISA could bind the complex ox-LDL ↔ sLOX-1 in serum as well, we performed a sLOX-1 assay in the presence of exogenously added high levels of ox-LDL; no interference of this ligand was observed in sLOX-1 detection (data not shown). Alternatively, we performed an ox-LDL assay in the presence of high levels of sLOX-1. Also in this case, the adding of sLOX-1 did not interfere with the assay (data not shown). Thus, we can speculate that, cytokines, ox-LDL and the soluble form of its receptor constitute a complex network, which interactively influence the development of the atherosclerotic vascular lesion. However, unlike the inflammatory cytokines and ox-LDL that have a clear pathogenetic role in the atherosclerotic process, little is known about the regulation of sLOX-1 shedding, the biological mechanisms underlying the kinetics of sLOX-1 production and removal and the complex interaction between the soluble receptor and its ligands in health and disease states.

Conclusion

The measurement of sLOX-1 in serum may be potentially useful in predicting atherosclerotic disease progression in humans. Nevertheless, in order to have a clear picture of the pathophysiological roles of sLOX-1 and establish the diagnostic value of sLOX-1 in atherogenesis and vascular diseases, further studies are required.

Acknowledgments The authors thank Manuela Walker for the reviewing of the English language.

References

1. Sawamura T, Kume N, Aoyama T, Moriwaki H, Hoshikawa H, Aiba Y, Tanaka T, Miwa S, Katsura Y, Kita T, Masaki T (1997) An endothelial receptor for oxidized low-density lipoprotein. Nature 386:73–77
2. Yoshida H, Kondratenko N, Green S, Steinberg D, Quehenberger O (1998) Identification of the lectin-like receptor for oxidized low-density lipoprotein in human macrophages and its potential role as a scavenger receptor. Biochem J 334(Pt 1):9–13
3. Khan BV, Parthasarathy SS, Alexander RW, Medford RM (1995) Modified low density lipoprotein and its constituents augment cytokine-activated vascular cell adhesion molecule-1 gene expression in human vascular endothelial cells. J Clin Invest 95:1262–1270
4. Inoue M, Itoh H, Tanaka T, Chun TH, Doi K, Fukunaga Y, Sawada N, Yamshita J, Masatsugu K, Saito T, Sakaguchi S, Sone M, Yamahara K, Yurugi T, Nakao K (2001) Oxidized LDL regulates vascular endothelial growth factor expression in human macrophages and endothelial cells through activation of peroxisome proliferator-activated receptor-gamma. Arterioscler Thromb Vasc Biol 21:560–566
5. Inoue K, Arai Y, Kurihara H, Kita T, Sawamura T (2005) Overexpression of lectin-like oxidized low-density lipoprotein receptor-1 induces intramyocardial vasculopathy in apolipoprotein E-null mice. Circ Res 97:176–184
6. Mehta JL, Sanada N, Hu CP, Chen J, Dandapat A, Sugawara F, Satoh H, Inoue K, Kawase Y, Jishage K, Suzuki H, Takeya M, Schnackenberg L, Beger R, Hermonat PL, Thomas M, Sawamura T (2007) Deletion of LOX-1 reduces atherogenesis in LDLR knockout mice fed high cholesterol diet. Circ Res 100:1634–1642
7. Murase T, Kume N, Kataoka H, Minami M, Sawamura T, Masaki T, Kita T (2000) Identification of soluble forms of lectin-like oxidized LDL receptor-1. Arterioscler Thromb Vasc Biol 20:715–720
8. Dunn S, Vohra RS, Murphy JE, Homer-Vanniasinkam S, Walker JH, Ponnambalam S (2008) The lectin-like oxidized low-density-lipoprotein receptor: a pro-inflammatory factor in vascular disease. Biochem J 409:349–355
9. Hayashida K, Kume N, Murase T, Minami M, Nakagawa D, Inada T, Tanaka M, Ueda A, Kominami G, Kambara H, Kimura T, Kita T (2005) Serum soluble lectin-like oxidized low-density lipoprotein receptor-1 levels are elevated in acute coronary syndrome: a novel marker for early diagnosis. Circulation 112:812–818
10. Kamezaki F, Yamashita K, Tasaki H, Kume N, Mitsuoka H, Kita T, Adachi T, Otsuji Y (2008) Serum soluble lectin-like oxidized low-density lipoprotein receptor-1 correlates with oxidative stress markers in stable coronary artery disease. Int J Cardiol. doi: 10.1016/j.ijcard.2007.12.069
11. Lubrano V, Vassalle C, L'Abbate A, Zucchelli G (2002) A new method to evaluate oxidative stress in humans. Immunoanalyse Biologie Specialisée 17:172–175
12. Tan KC, Shiu SW, Wong Y, Leng L, Bucala R (2008) Soluble lectin-like oxidized low density lipoprotein receptor-1 in type 2 diabetes mellitus. J Lipid Res 49(7):1438–1444
13. Kume N, Murase T, Moriwaki H, Aoyama T, Sawamura T, Masaki T, Kita T (1998) Inducible expression of lectin-like oxidized LDL receptor-1 in vascular endothelial cells. Circ Res 83:322–327
14. Li L, Roumeliotis N, Sawamura T, Renier G (2004) C-reactive protein enhances LOX-1 expression in human aortic endothelial cells: relevance of LOX-1 to C-reactive protein-induced endothelial dysfunction. Circ Res 95:877–883
15. Moriwaki H, Kume N, Kataoka H, Murase T, Nishi E, Sawamura T, Masaki T, Kita T (1998) Expression of lectin-like oxidized low density lipoprotein receptor-1 in human and murine macrophages: upregulated expression by TNF-alpha. FEBS Lett 440:29–32
16. van der Wal AC, Becker AE, van der Loos CM, Das PK (1994) Site of intimal rupture or erosion of thrombosed coronary atherosclerotic plaques is characterized by an inflammatory process

irrespective of the dominant plaque morphology. Circulation 89:36–44

17. Levine GN, Frei B, Koulouris SN, Gerhard MD, Keaney JF Jr, Vita JA (1996) Ascorbic acid reverses endothelial vasomotor dysfunction in patients with coronary artery disease. Circulation 93:1107–1113
18. Aderka D (1996) The potential biological and clinical significance of the soluble tumor necrosis factor receptors. Cytokine Growth Factor Rev 7:231–240
19. Huang L, Wang Z, Li C (2001) Modulation of circulating leptin levels by its soluble receptor. J Biol Chem 276:6343–6349
20. Ge H, Huang L, Pourbahrami T, Li C (2002) Generation of soluble leptin receptor by ectodomain shedding of membrane-spanning receptors in vitro and in vivo. J Biol Chem 277:45898–45903

Lipids (2008) 43:951–959
DOI 10.1007/s11745-008-3197-y

ORIGINAL ARTICLE

Brain Mitochondrial Lipid Abnormalities in Mice Susceptible to Spontaneous Gliomas

**Michael A. Kiebish · Xianlin Han · Hua Cheng ·
Jeffrey H. Chuang · Thomas N. Seyfried**

Received: 9 April 2008 / Accepted: 19 May 2008 / Published online: 17 June 2008
© AOCS 2008

Abstract Alterations in mitochondrial function have long been considered a hallmark of cancer. We compared the lipidome and electron transport chain activities of non-synaptic brain mitochondria in two inbred mouse strains, the C57BL/6J (B6) and the VM/Dk (VM). The VM strain is unique in expressing a high incidence of spontaneous brain tumors (1.5%) that are mostly gliomas. The incidence of gliomas is about 210-fold greater in VM mice than in B6 mice. Using shotgun lipidomics, we found that the mitochondrial content of ethanolamine glycerophospholipid, phosphatidylserine, and ceramide was higher, whereas the content of total choline glycerophospholipid was lower in the VM mice than in B6 mice. Total cardiolipin content was similar in the VM and the B6 mice, but the distribution of cardiolipin molecular species differed markedly between the strains. B6 non-synaptic mitochondria contained 95 molecular species of cardiolipin that were symmetrically distributed over 7 major groups based on mass charge. In contrast, VM non-synaptic mitochondria contained only 42 molecular species that were distributed asymmetrically. The activities of Complex I, I/III, and II/III enzymes were lower, whereas the activity of complex IV was higher in the mitochondria of VM mice than in B6 mice. The high glioma incidence and alterations in electron transport chain activities in VM mice compared to B6 mice could be related to the unusual composition of mitochondrial lipids in the VM mouse brain.

Introduction

Mitochondria are necessary for the maintenance of brain metabolism supporting neurological function. Alterations in brain mitochondria can impair bioenergetic efficiency resulting in disease pathology or neurological impairment [1–3]. Although such alterations can exist at the DNA or protein level, little attention has been focused on the role of mitochondrial lipids in neurological function. Mitochondrial membrane lipids can regulate numerous functions to include electron transport chain (ETC) activities, membrane fluidity, mitochondrial protein import, and ATP synthesis [4–8]. Non-synaptic (NS) brain mitochondria are derived from the cell bodies of neurons and glia and represent the predominant mitochondrial population in brain [9]. Alterations in the NS mitochondrial lipid composition could influence ETC activities resulting in a change in neural cell metabolism.

Shotgun lipidomics, using electrospray ionization mass spectrometry (ESI/MS), can now determine the total content and composition mitochondrial lipids (the lipidome) [10]. Using this approach, we recently characterized the lipid composition of mouse brain mitochondria [11]. The mitochondrial specific lipid cardiolipin (1,3-diphosphatidyl-*sn*-glycerol, Ptd_2Gro), contains nearly 100 different molecular species in the C57BL/6J (B6) mouse brain [11].

Electronic supplementary material The online version of this article (doi:10.1007/s11745-008-3197-y) contains supplementary material, which is available to authorized users.

M. A. Kiebish · J. H. Chuang · T. N. Seyfried (✉)
Biology Department, Boston College, Chestnut Hill, MA, USA
e-mail: thomas.seyfried@bc.edu

M. A. Kiebish
e-mail: kiebish@bc.edu

X. Han · H. Cheng
Department of Internal Medicine,
Washington University School of Medicine,
St Louis, MO, USA

Moreover, these molecular species are symmetrically distributed in seven major groups when arranged according to mass to charge ratios [11]. This distribution in B6 mice is similar to that in several other mammalian species and reflects a conserved cardiolipin remodeling process for brain [12].

Our objective was to compare and contrast the lipidome of NS mitochondria and ETC activities in mice of the B6 and the VM/Dk (VM) strains. B6 mice are often used as a control strain for many existing neurological mutations that alter CNS function [13, 14]. VM mice are unique in expressing a relatively high incidence (1.5%) of spontaneous brain tumors, which occur over a broad age range between 4 and 18 months [15]. Most of these brain tumors were characterized as astrocytomas, but microgliomas and neural stem tumors also occur [15–17]. Indeed, the incidence of spontaneous brain tumor formation is about 210-fold greater in VM mice than in B6 mice. Although altered mitochondrial energy metabolism has long been connected to tumorigenesis (Warburg theory) [18–21], the role of mitochondrial lipids in this connection remains unclear. Ours is the first comparative analysis of the NS brain mitochondria lipidome in two mouse strains that differ in susceptibility to spontaneous gliomas.

Experimental Procedures

Animals

The VM mice were obtained from Professor H. Fraser, University of Edinburgh. The B6 mice were obtained from the Jackson Laboratory (Bar Harbor, ME). Mice of both strains were matched for age (4 months) and sex (males) and were propagated under similar conditions at the Boston College Animal Facility. Mice were housed in plastic cages with filter tops containing Sani-Chip bedding (P.J. Murphy Forest Products Corp., Montville, NJ, USA). The room was maintained at 22 °C on a 12 h light/dark cycle. Food (Prolab RMH 3000; PMI LabDiet, Richmond, IN, USA) and water were provided ad libitum. This study was conducted with the National Institutes of Health Guide for the Care and Use of Laboratory Animals and was approved by the Institutional Animal Care Committee.

Non-synaptic Brain Mitochondrial Isolation

We recently described an improved procedure for isolation and purification of NS mitochondria from mouse brain for the purpose of lipid analysis and biochemical analysis of ETC activities [11]. Briefly, the B6 and VM mice were sacrificed by cervical dislocation and the cerebral cortex was dissected. Mitochondria were isolated in a cold room (4 °C) and all reagents were kept on ice. The isolation procedure employed a combination of gradients and strategies as previously described [22–28] (Fig. 1). The cerebral cortexes (a pool of 6/sample) were diced on an ice cold metal plate and then placed in 12 mL of mitochondria isolation buffer [MIB; 0.32 M sucrose, 10 mM Tris–HCl, and 1 mM EDTA-K (pH 7.4)]. The pooled cerebral cortexes were homogenized using a Potter Elvehjem homogenizer with a Teflon coated pestle attached to a hand-held drill. Samples were homogenized using 15 up and down strokes at 500 rpm. The homogenate was centrifuged at 1,000×*g* for 5 min. The supernatant was collected and the pellet was washed twice by centrifugation, collecting the supernatants each time. The supernatants were pooled and centrifuged at 1,000×*g* for 5 min. The collected supernatant was then spun at 14,000×*g* for 15 min. The supernatant was discarded and the pellet, which contained primarily NS mitochondria, synaptosomes and myelin, was resuspended in 12 mL MIB and was layered on a 7.5/12% discontinuous Ficoll gradient. Each Ficoll gradient layer contained 12 mL for a total volume of 36 mL. The Ficoll gradients were made from a 20% Ficoll stock with MIB. The gradient was centrifuged at 73,000×*g* for 36 min (4 °C) in a Sorvall SW 28 rotor with slow acceleration and deceleration (Optima L-90K Ultracentrifuge). The centrifugation time used permitted sufficient acceleration and deceleration to achieve maximum *g* force and to prevent synaptosomal contamination of the mitochondrial fraction below the 12% Ficoll layer [27]. Crude myelin collected at the MIB/7.5% Ficoll interface was discarded. The Ficoll gradient purified NS mitochondria (FM) were collected as a pellet below the 12% Ficoll.

The FM pellet, containing NS mitochondria, was resuspended in MIB containing 0.5 mg/mL bovine serum albumin (BSA) and was centrifuged at 12,000×*g* for 15 min. The resulting pellet was collected and resuspended in 6 mL of MIB. The resuspended FM pellet was layered on a discontinuous sucrose gradient containing 0.8/1.0/1.3/1.6 M sucrose. The volumes for the sucrose gradient were 6/6/10/8 mL, respectively. The gradients were made from a 1.6 M sucrose stock containing 1 mM EDTA-K and 10 mM Tris–HCl (pH 7.4). The discontinuous sucrose gradient was centrifuged at 50,000×*g* for 2 h (4 °C) in a Sorvall SW 28 rotor using slow acceleration and deceleration to prevent disruption of the gradient. Purified NS mitochondria were collected at the interface of 1.3 and 1.6 M sucrose. NS mitochondria were collected and resuspended in (1:3, v/v) TE buffer (1 mM EDTA-K and 10 mM Tris–HCl, pH 7.4) containing 0.5 mg/mL BSA and centrifuged at 18,000×*g* for 15 min. The pellet was then resuspended in MIB and centrifuged at 12,000×*g* for 10 min. The pellet was again resuspended in MIB and centrifuged at 8,200×*g* for 10 min.

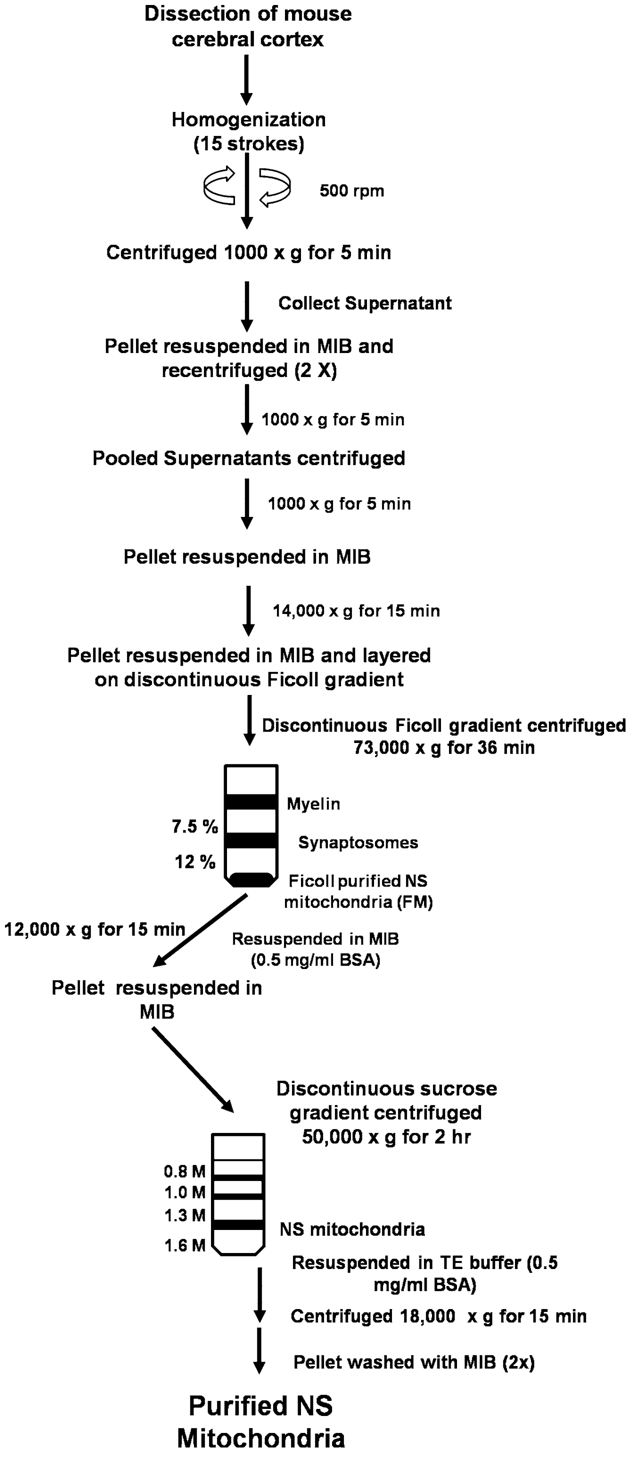
Dissection of mouse cerebral cortex
Homogenization (15 strokes)
500 rpm
Centrifuged 1000 x g for 5 min
Collect Supernatant
Pellet resuspended in MIB and recentrifuged (2 X)
1000 x g for 5 min
Pooled Supernatants centrifuged
1000 x g for 5 min
Pellet resuspended in MIB
14,000 x g for 15 min
Pellet resuspended in MIB and layered on discontinuous Ficoll gradient
Discontinuous Ficoll gradient centrifuged 73,000 x g for 36 min
Myelin
7.5 %
Synaptosomes
12 %
Ficoll purified NS mitochondria (FM)
12,000 x g for 15 min
Resuspended in MIB (0.5 mg/ml BSA)
Pellet resuspended in MIB
Discontinuous sucrose gradient centrifuged 50,000 x g for 2 hr
0.8 M
1.0 M
1.3 M
1.6 M
NS mitochondria
Resuspended in TE buffer (0.5 mg/ml BSA)
Centrifuged 18,000 x g for 15 min
Pellet washed with MIB (2x)
Purified NS Mitochondria

Fig 1 Procedure used for the isolation and purification of NS mitochondria from mouse cerebral cortex

Materials for Mass Spectrometry

Synthetic phospholipids including 1,2-dimyristoleoyl-*sn*-glycero-3-phosphocholine (14:1-14:1 PtdCho), 1,2-dipalmitoleoyl-*sn*-glycero-3-phosphoethanolamine (16:1-16:1 PtdEtn), 1,2-dipentadecanoyl-*sn*-glycero-3-phosphoglycerol (15:0-15:0 PtdGro), 1,2-dimyristoyl-*sn*-glycero-3-phosphoserine (14:0-14:0 PtdSer), *N*-lauroryl sphingomyelin (N12:0 CerPCho), 1,1′,2,2′-tetramyristoyl cardiolipin (T14:0 Ptd_2Gro), heptadecanoyl ceramide (N17:0 Cer), 1-heptadecanoyl-2-hydroxy-*sn*-Glycero-3-phosphocholine (17:0 LysoPtdCho) were purchased from Avanti Polar Lipids, Inc. (Alabaster, AL, USA). It should be noted that the prefix "N" denotes the amide-linked acyl chain. All the solvents were obtained from Burdick and Jackson (Honeywell International Inc., Burdick and Jackson, Muskegon, MI, USA). All other chemicals were purchased from Sigma-Aldrich (St. Louis, MO, USA).

Sample Preparation for Mass Spectrometric Analysis

An aliquot of the mitochondrial preparation was transferred to a disposable culture borosilicate glass tube (16 × 100 mm). Internal standards were added based on protein concentration and included 16:1-16:1 PtdEtn (100 nmol/mg protein), 14:1-14:1 PtdCho (45 nmol/mg protein), T14:0 Ptd_2Gro (3 nmol/mg protein), 15:0-15:0 PtdGro (7.5 nmol/mg protein), 14:0-14:0 PtdSer (20 nmol/mg protein), 17:0 LysoPtdCho (1.5 nmol/mg protein), N12:0 CerPCho (20 nmol/mg protein), N17:0 Cer (5 nmol/mg protein). This allowed the final quantified lipid content to be normalized to the protein content and eliminated potential loss from the incomplete recovery. The molecular species of internal standards were selected because they represent $<0.1\%$ of the endogenous cellular lipid mass as demonstrated by ESI/MS lipid analysis.

A modified Bligh and Dyer procedure was used to extract lipids from each mitochondrial preparation as previously described [29]. Each lipid extract was reconstituted with a volume of 500 μL/mg protein (which was based on the original protein content of the samples as determined from protein measurement) in $CHCl_3$/MeOH (1:1, v/v). The lipid extracts were flushed with nitrogen, capped, and stored at −20 °C for ESI/MS analysis. Each lipid solution was diluted approximately 50-fold immediately prior to infusion and lipid analysis.

Instrumentation and Mass Spectrometry

A triple-quadrupole mass spectrometer (Thermo Scientific TSQ Quantum Ultra, Plus, San Jose, CA, USA), equipped with an electrospray ion source and Xcalibur system software, was utilized as previously described [30]. The first and third quadrupoles serve as independent mass analyzers using a mass resolution setting of peak width 0.7 Th while the second quadrupole serves as a collision cell for tandem MS. The diluted lipid extract was directly infused into the ESI source at a flow rate of 4 μL/min with a syringe pump.

Typically, a 2-min period of signal averaging in the profile mode was employed for each mass spectrum. For tandem MS, a collision gas pressure was set at 1.0 mTorr, but the collision energy varied with the classes of lipids as described previously [10, 30]. Typically, a 2- to 5-min period of signal averaging in the profile mode was employed for each tandem MS spectrum. All the mass spectra and tandem MS spectra were automatically acquired by a customized sequence subroutine operated under Xcalibur software. Data processing of 2D MS analyses including ion peak selection, data transferring, peak intensity comparison, and quantitation was conducted using self-programmed Microsoft Excel macros [30].

Electron Transport Chain Enzyme Activities

Purified mitochondrial samples were freeze–thawed three times before use in enzyme analysis to give substrate access to the inner mitochondrial membrane. All assays were performed on a temperature controlled SpectraMax M5 plate reader (Molecular Devices) and were done in triplicate. Specific enzyme activities were calculated using ETC complex inhibitors in order to subtract background activities.

Complex I (NADH-ubiquinone oxidoreductase) activity was determined by measuring the decrease in the concentration of NADH at 340 nm as previously described [31, 32]. The assay was performed in buffer containing 50 mM potassium phosphate (pH 7.4), 2 mM KCN, 5 mM $MgCl_2$, 2.5 mg/mL BSA, 2 μM antimycin, 100 μM decylubiquinone, and 0.3 mM K_2NADH. The reaction was initiated by adding purified mitochondria (20 μg). The enzyme activity was measured for 5 min and values were recorded 30 s after the initiation of the reaction. Specific activities were determined by calculating the slope of the reaction in the linear range in the presence or absence of 1 μM rotenone (Complex I inhibitor).

Complex II (succinate decylubiquinone DCIP oxidoreductase) activity was determined by measuring the reduction of 2,6-dichloroindophenol (DCIP) at 600 nm as previously described [32, 33]. The Complex II assay was performed in buffer containing 25 mM potassium phosphate (pH 7.4), 20 mM succinate, 2 mM KCN, 50 μM DCIP, 2 μg/mL rotenone, and 2 μg/mL antimycin. Purified mitochondria (10 μg) were added prior to initiation of the reaction. The reaction was initiated by adding 56 μM decylubiquinone. Specific activities were determined by calculating the slope of the reaction in the linear range in the presence or absence of 0.5 mM Thenoyltrifluoroacetone (Complex II inhibitor).

Complex III (ubiquinol cytochrome *c* reductase) activity was determined by measuring the reduction of oxidized cytochrome *c* at 550 nm. The Complex III assay was performed in buffer containing (25 mM potassium phosphate (pH 7.4), 1 mM EDTA, 1 mM KCN, 0.6 mM dodecyl maltoside, 32 μM oxidized cytochrome *c*) using purified mitochondria (2.5 μg). The reaction was initiated by adding 35 μM decylubiquinol. The reaction was measured following the linear slope for 1 min in the presence or absence of 2 μM antimycin (Complex III inhibitor). Decylubiquinol was made by dissolving decylubiquinone (10 mg) in 2 mL acidified ethanol (pH 2) and using sodium dithionite as a reducing agent. Decylubiquinol was further purified by cyclohexane [31, 32, 34].

Complex IV (cytochrome *c* oxidase) activity was determined by measuring the oxidation of reduced ferrocytochrome *c* at 550 nm. The Complex IV assay was performed in buffer containing [10 mM Tris–HCl and 120 mM KCl (pH 7.0)] using purified mitochondria (5 μg). The reaction was initiated by adding 11 μM reduced ferrocytochrome *c* and monitoring the slope for 30 s in the presence or absence of 2.2 mM KCN (Complex IV inhibitor) [32, 35].

Complex I/III (NADH cytochrome *c* reductase) activity was determined by measuring the reduction of oxidized cytochrome *c* at 550 nm. The Complex I/III assay was performed in buffer [50 mM potassium phosphate (pH 7.4), 1 mM EDTA, 2 mM KCN, 32 μM oxidized cytochrome *c*, and 105 μM K_2NADH] and was initiated by adding purified mitochondria (10 μg). The reaction was measured for 30 s with a linear slope in the presence or absence of 1 μM rotenone and 2 μM antimycin (Complex I and III inhibitors) [31, 32, 34].

Complex II/III (succinate cytochrome *c* reductase) activity was measured following the reduction of oxidized cytochrome *c* at 550 nm. The Complex II/III assay was performed in buffer [25 mM potassium phosphate (pH 7.4), 20 mM succinate, 2 mM KCN, 2 μg/mL rotenone] using purified mitochondria (10 μg). The reaction was initiated by adding 40 μM oxidized cytochrome *c* in the presence or absence of 2 μM antimycin (Complex III inhibitor) [31, 32].

Results

Lipid Composition of B6 and VM NS Brain Mitochondria

The differences between the B6 and VM mice for the content NS mitochondrial lipids are shown in Table 1. The lipid classes were listed according to their relative abundance. The mass content of phosphatidylinositol (PtdIns), phosphatidylserine (PtdSer), and ceramide (Cer) was higher, whereas the content of total choline glycerophospholipids (ChoGpl), in particular phosphatidylcholine (PtdCho), was lower in VM mice than in B6 mice. Plasmenylethanolamine (plasmalogen, PlsEtn) was significantly higher in VM mice than in B6 mice. Plasmanylethanolamine (PakEtn) was detected

Table 1 Lipid composition of non-synaptic brain mitochondria in B6 and VM mice

Lipid	B6	VM
Ethanolamine glycerophospholipids	187.4 ± 12.1	264.0 ± 4.8*
Phosphatidylethanolamine	164.9 ± 10.0	186.1 ± 5.9
Plasmenylethanolamine	22.5 ± 2.2	72.2 ± 3.7*
Plasmanylethanolamine	ND	5.7 ± 0.9*
Choline glycerophospholipids	129.9 ± 7.7	87.9 ± 12.9*
Phosphatidylcholine	119.6 ± 5.3	74.9 ± 13.2*
Plasmenylcholine	1.2 ± 0.1	4.2 ± 4.2
Plasmanylcholine	9.1 ± 3.2	8.8 ± 4.1
Cardiolipin	52.7 ± 4.5	50.0 ± 2.4
Phosphatidylinositol	9.3 ± 0.8	12.5 ± 0.8*
Phosphatidylglycerol	7.1 ±0.5	8.2 ± 0.5
Sphingomyelin	5.3 ± 1.2	2.7 ± 0.2
Phosphatidylserine	4.6 ± 1.5	18.6 ± 2.0**
Lysophosphatidylcholine	2.7 ± 0.6	4.7 ± 0.9
Ceramide	0.7 ± 0.2	2.0 ± 0.1*
Total	399.7 ± 29.1	450.6 ± 24.6

Values are expressed as nmol/mg protein ± SDM of three independent samples

ND Not detected

Asterisks indicate that the value in VM mice differ from B6 mice at $*P < 0.02$; $**P < 0.001$ as determined from the two-tailed *t*-test

only in the NS mitochondria of VM mice and not in B6 mitochondria. No differences were found between the strains for the mass content of phosphatidylethanolamine (PtdEtn), Ptd_2Gro, sphingomyelin (CerPCho), plasmenylcholine (PlsCho), or plasmanylcholine (PakCho). Previously, it was reported that the ratios of ChoGpl/EtnGpl and CerPCho/EtnGpl were accurate indicators of a change in mitochondrial membrane fluidity. Bangur et al. [36] showed that differences in these ratios were correlated with changes in membrane fluidity as determined by fluorescence polarization. The ratio of ChoGpl to EtnGpl in the B6 and VM mice was 0.693 and 0.333, respectively, whereas the ratio of CerPCho to EtnGpl in these strains was 0.028 and 0.010, respectively. Myelin-enriched lipids, sulfatides and cerebrosides, were not detected in B6 or VM NS mitochondria (data not shown). Our previous findings also showed that gangliosides are not present in NS mitochondria from B6 mice [11]. Corresponding lipid molecular species mass content can be found in Supplementary Tables 4, 5, 6, 7, 8, 9, 10, 11 and 12.

Cardiolipin Molecular Species Distribution in B6 and VM NS Brain Mitochondria

B6 mice contained 95 molecular species of cardiolipin, whereas VM mice contained only 45 molecular species (Supplementary Table 6). In addition, some cardiolipin molecular species found in the VM mice (18:1-16:1-16:1-16:1, 18:1-16:1-16:1-16:0, 18:1-16:1-16:0-16:0, 18:2-18:1-16:1-16:1) were not found in the B6 mice. The cardiolipin species found in VM mice may represent newly synthesized forms based on chain lengths and degree of unsaturation [11]. These fatty acids were also similar to those found in PtdGro, the precursor of cardiolipin (Supplementary Table 8). When expressed as mole percentages of mass charge values, the cardiolipin molecular species in B6 NS mitochondria formed a unique pattern consisting of seven major groups (Fig. 2). Group I had the shortest fatty acid chain lengths and the least degree unsaturation, whereas group VII had the longest chain lengths and the greatest unsaturation [11]. The cardiolipin pattern found for VM mice differed markedly from that of B6 mice (Fig. 2; Supplementary Table 6). Cardiolipin in VM mice had elevated amounts of short chain fatty acids and lacked the molecular species found in groups IV, V, and VII. These groups are enriched in 20:4 and 22:6 fatty acids in the B6 brain cardiolipin. These fatty acids were reduced in VM cardiolipin molecular species likely due to the loss of these cardiolipin groups (Table 2). The content of the 16:0, 16:1, 16:2, and 18:1 in brain cardiolipin molecular species was higher in the mitochondria of VM mice than in B6 mice (Table 2). More variation in the distribution of mitochondrial EtnGpl fatty acids was found in the VM mice than in the B6 mice. The content of 22:6 fatty acids in brain ChoGpl was lower in VM mitochondria than in the B6 mitochondria.

ETC Activities in NS Mitochondria of B6 and VM Mice

The activities of the unlinked ETC complexes (Complex I, II, III, and IV) as well as those of the linked enzyme complexes (Complex I/III and II/III) are shown in (Table 3). The activities of Complex I, I/III, and II/III were 22, 51, and 25% lower and Complex IV was 22% higher in VM mitochondria than in B6 mitochondria (Table 3).

Discussion

We found that the NS mitochondrial lipidome differed markedly between the B6 and VM mice. Mitochondrial membrane lipids are known to influence membrane fluidity/permeability, ETC activities, membrane fusion, calcium homeostasis, and ATP synthesis [4, 6, 37, 38]. EtnGpl and ChoGpl were the most abundant phospholipids in the NS mitochondria of both mouse strains. Previous studies showed that changes in the ChoGpl/EtnGpl ratio and the CerPCho/EtnGpl ratio could significantly influence mitochondrial membrane fluidity [36]. We found that these lipid

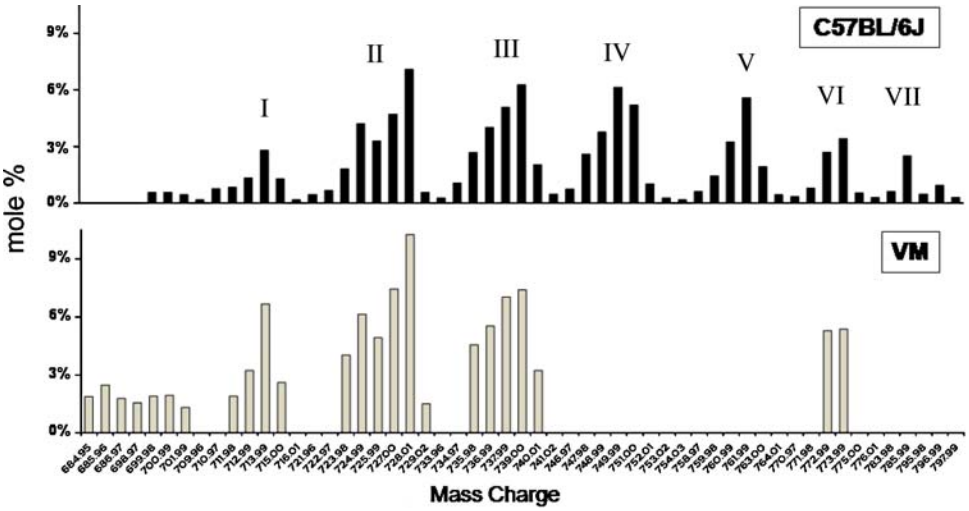

Fig 2 Distribution of brain cardiolipin molecular species in B6 NS (*black bar*) and VM NS (*gray bar*) mitochondria. Cardiolipin molecular species were arranged according to mass to charge ratios. Corresponding molecular species mass content can be found in Supplementary Table 6. Molecular species can be arranged into seven groups (I–VII) based on chain length and degree of unsaturation

Table 2 Fatty acid percent distribution in phospholipids involved in cardiolipin remodeling

Fatty Acid	B6			VM		
	EtnGpl	ChoGpl	Ptd_2Gro	EtnGpl	ChoGpl	Ptd_2Gro
14:0	ND	0.2 ± 0.1	ND	0.7 ± 0.3	2.6 ± 3.8	ND
14:1	ND	0.6 ± 0.1	ND	0.1 ± 0.0	0.7 ± 0.5	ND
16:0	12.3 ± 0.3	34.3 ± 1.7	3.9 ± 0.0	13.7 ± 0.1**	32.8 ± 2.4	7.1 ± 0.5**
16:1	ND	0.7 ± 0.1	5.4 ± 0.0	1.7 ± 0.1**	2.1 ± 2.5	11.5 ± 1.1*
16:2	ND	ND	0.2 ± 0.0	0.1 ± 0.0	ND	0.4 ± 0.0***
18:0	20.8 ± 0.2	7.6 ± 0.2	2.0 ± 0.0	17.3 ± 0.2***	10.7 ± 2.2	1.9 ± 0.3
18:1	17.0 ± 0.1	18.0 ± 0.7	44.7 ± 1.0	19.2 ± 0.3**	15.9 ± 1.9	51.3 ± 0.9***
18:2	1.3 ± 0.1	16.1 ± 0.4	8.2 ± 0.2	4.3 ± 0.2***	13.3 ± 2.2	7.9 ± 0.1
18:3	ND	0.1 ± 0.0	0.3 ± 0.0	ND	0.1 ± 0.0	ND
20:0	2.6 ± 0.1	3.2 ± 1.1	ND	3.0 ± 0.4	3.5 ± 1.4	ND
20:1	ND	0.1 ± 0.0	0.1 ± 0.0	3.0 ± 0.3**	0.2 ± 0.1	ND
20:2	1.5 ± 0.2	2.7 ± 0.5	ND	1.1 ± 0.2	1.4 ± 1.0	ND
20:3	1.9 ± 0.3	0.4 ± 0.1	2.7 ± 0.1	3.7 ± 0.1**	0.5 ± 0.6	1.9 ± 0.0***
20:4	7.8 ± 0.2	11.1 ± 0.3	21.0 ± 0.3	7.7 ± 0.4	6.9 ± 2.5	12.9 ± 1.5*
22:2	ND	ND	ND	0.6 ± 0.3	ND	ND
22:3	2.7 ± 0.3	ND	ND	0.9 ± 0.2**	ND	ND
22:4	7.2 ± 0.1	ND	0.1 ± 0.0	3.9 ± 0.1***	ND	ND
22:5	11.3 ± 0.2	1.4 ± 0.3	0.2 ± 0.1	7.9 ± 0.8*	2.1 ± 0.9	ND
22:6	13.6 ± 0.3	3.5 ± 0.5	11.4 ± 0.4	11.1 ± 0.8*	7.2 ± 1.0*	5.1 ± 0.5***

Values represented as the mean mole percentage distribution of fatty acids ± SDM from three independent analyses as determined by electrospray MS

EtnGpl glycerophospholipids, *ChoGpl* choline glycerophospholipids, *Ptd2Gro* cardiolipin, *ND* Not detected

Significantly different values from B6 NS mitochondria at $*P < 0.05$; $**P < 0.01$; $***P < 0.001$ as determined by the two-tailed *t*-test

ratios were markedly lower in the VM NS mitochondria than in the B6 mitochondria indicating that mitochondrial membrane fluidity is greater in VM mice than in B6 mice.

The most remarkable difference in NS mitochondrial lipid composition found between the strains was for the distribution of cardiolipin molecular species. While B6 mice expressed 95 cardiolipin molecular species that were symmetrically distributed over 7 major groups based on mass charge, the VM mice expressed only 45 cardiolipin molecular species that were asymmetrically distributed with three major groups missing. The distribution of brain cardiolipin molecular species in B6 NS mitochondria was similar to that in the brains of other mammalian species indicating that the distribution in B6 mitochondria is

Table 3 Electron transport chain activities of non-synaptic brain mitochondria

	B6	VM
Complex I: NADH ubiquinone oxidoreductase	975 ± 64	761 ± 48**
Complex II: succinate DCIP oxidoreductase	292 ± 18	316 ± 42
Complex III: ubiquinol cytochrome *c* oxidoreductase	437 ± 71	308 ± 46
Complex IV: cytochrome *c* oxidase	179 ± 25	230 ± 19*
Complex I/III: NADH cytochrome *c* oxidoreductase	269 ± 59	133 ± 26*
Complex II/III: succinate cytochrome *c* reductase	309 ± 30	230 ± 8*

Enzyme activities are expressed as (nmol/min/mg protein) ± SDM. ($N = 3$–4)

Significantly different values from B6 NS mitochondria at*$P < 0.05$; **$P < 0.01$ as determined from the two-tailed *t*-test

conserved [12]. It is also important to mention that the distribution of cardiolipin molecular species in brain differs significantly from the distribution in non-neural tissues, which contain predominantly tetralinoleic cardiolipin (18:2-18:2-18:2-18:2) [39]. Newly synthesized cardiolipin is extensively remodeled using donor fatty acyl groups from the *sn*-2 position of ChoGpl and EtnGpl to form mature cardiolipin (Fig. 3) [40]. The unusual cardiolipin distribution in VM brain mitochondria could result from a strain difference in the activities or specificities of phospholipases and/or acyltransferases, which regulate cardiolipin remodeling. This would alter the normal remodeling process involving random incorporation of fatty acids as occurs in B6 mice [11]. We propose that the asymmetrical distribution of cardiolipin molecular species in VM mice arises in part through abnormalities in the remodeling process.

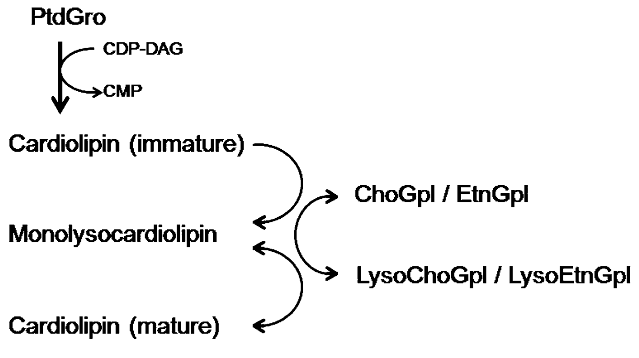

Fig 3 Cardiolipin synthesis and remodeling. Cardiolipin is synthesized by the condensation of phosphatidylglycerol (PtdGro) and CDP-DAG to form immature cardiolipin. Immature cardiolipin is then deacylated to form monolysocardiolipin, which uses the deacylated *sn*-2 position fatty acid tails of choline (ChoGpl) and ethanolamine (EtnGpl) glycerophospholipids for the reacylation of monolysocardiolipin. This remodeling process forms mature cardiolipin with specific fatty acid molecular species

The lipid differences in NS mitochondria found between the strains would lead to differences in mitochondrial function. Support for this comes from finding significant differences in the ETC enzyme activities between the strains. Changes in cardiolipin molecular speciation can influence the activity of complex I and may affect the mitochondrial membrane environment influencing linked enzyme activities (I/III and II/III) or supercomplex formation [5, 41–44]. Alterations in supercomplex formation would result in a decrease in efficiency of respiration [43, 45]. Increased docosahexaenoic (DHA) containing cardiolipin results in decreased complex IV activity [46–48]. A loss of DHA containing cardiolipin might therefore produce increased Complex IV activity as we found in the VM strain. Previous studies suggest that cardiolipin does not significantly influence Complex II activity [41]. This is interesting since we found that Complex II activity was similar in the B6 and VM mitochondria. As mitochondrial membrane lipids can influence ETC activities [4, 5, 42, 49], it is likely that the differences in lipid composition underlie the differences in ETC activities.

Alterations in brain mitochondrial lipid composition should affect mitochondrial energy production and neurological function. Additionally, disturbances in the brain mitochondrial lipidome could produce a bioenergetic state conducive to brain tumorigenesis. Warburg indicated that respiratory damage was the cause of most tumors [19]. However, the type of respiratory damage was not specified. It is possible that the lipidomic abnormalities expressed in the VM brain mitochondria could contribute to a respiratory defect that enhances the incidence of spontaneous brain tumors. Further studies will be needed to determine if the differences in brain mitochondrial lipid composition between the B6 and VM mouse strains are related to the differences between these strains for the incidence of spontaneous brain tumors.

Acknowledgments We would like to thank Purna Mukherjee, Rena Baek, and John Mantis for helpful discussions. This work was supported by grants from NIH (HD39722), NCI (CA102135), and NIA (AG23168).

References

1. Bowling AC, Beal MF (1995) Bioenergetic and oxidative stress in neurodegenerative diseases. Life Sci 56:1151–1171
2. Calabrese V, Scapagnini G, Giuffrida Stella AM, Bates TE, Clark JB (2001) Mitochondrial involvement in brain function and dysfunction: relevance to aging, neurodegenerative disorders and longevity. Neurochem Res 26:739–764
3. Pope S, Land JM, Heales SJ (2008) Oxidative stress and mitochondrial dysfunction in neurodegeneration: cardiolipin a critical target? Biochim Biophys Acta. doi:10.1016/j.bbabio.2008.030011
4. Daum G (1985) Lipids of mitochondria. Biochim Biophys Acta 822:1–42

5. Hoch FL (1992) Cardiolipins and biomembrane function. Biochim Biophys Acta 1113:71–133
6. Petrushka E, Quastel JH, Scholefield PG (1959) Role of phospholipids in oxidative phosphorylation and mitochondrial structure. Can J Biochem Physiol 37:989–998
7. Shinzawa-Itoh K, Aoyama H, Muramoto K, Terada H, Kurauchi T, Tadehara Y, Yamasaki A, Sugimura T, Kurono S, Tsujimoto K, Mizushima T, Yamashita E, Tsukihara T, Yoshikawa S (2007) Structures and physiological roles of 13 integral lipids of bovine heart cytochrome *c* oxidase. EMBO J 26:1713–1725
8. Jiang F, Ryan MT, Schlame M, Zhao M, Gu Z, Klingenberg M, Pfanner N, Greenberg ML (2000) Absence of cardiolipin in the crd1 null mutant results in decreased mitochondrial membrane potential and reduced mitochondrial function. J Biol Chem 275:22387–22394
9. Davey GP, Clark JB (1996) Threshold effects and control of oxidative phosphorylation in nonsynaptic rat brain mitochondria. J Neurochem 66:1617–1624
10. Han X, Gross RW (2005) Shotgun lipidomics: multidimensional MS analysis of cellular lipidomes. Expert Rev Proteomics 2:253–264
11. Kiebish MA, Han X, Cheng H, Lunceford A, Clarke CF, Moon H, Chuang JH, Seyfried TN (2008) Lipidomic analysis and electron transport chain activities in C57BL/6J mouse brain mitochondria. J Neurochem. doi:10.1111/j.1471-4159.2008.05383.x
12. Cheng H, Mancuso DJ, Jiang X, Guan S, Yang J, Yang K, Sun G, Gross RW, Han X (2008) Shotgun lipidomics reveals the temporally dependent, highly diversified cardiolipin profile in the mammalian brain: temporally coordinated postnatal diversification of cardiolipin molecular species with neuronal remodeling. Biochemistry 47:5869–5880
13. Bedell MA, Jenkins NA, Copeland NG (1997) Mouse models of human disease. Part I: techniques and resources for genetic analysis in mice. Genes Dev 11:1–10
14. Bedell MA, Largaespada DA, Jenkins NA, Copeland NG (1997) Mouse models of human disease. Part II: recent progress and future directions. Genes Dev 11:11–43
15. Fraser H (1971) Astrocytomas in an inbred mouse strain. J Pathol 103:266–270
16. Huysentruyt LC, Mukherjee P, Banerjee D, Shelton LM, Seyfried TN (2008) Metastatic cancer cells with macrophage properties: Evidence from a new murine tumor model. Int J Cancer 123:73–84
17. Fraser H (1986) Brain tumours in mice, with particular reference to astrocytoma. Food Chem Toxicol 24:105–111
18. Warburg O (1931) The metabolism of tumours. Richard R. Smith Inc, New York
19. Warburg O (1956) On the origin of cancer cells. Science 123:309–314
20. Cavalli LR, Liang BC (1998) Mutagenesis, tumorigenicity, and apoptosis: are the mitochondria involved? Mutat Res 398:19–26
21. Augenlicht LH, Heerdt BG (2001) Mitochondria: integrators in tumorigenesis? Nat Genet 28:104–105
22. Lai JC, Clark JB (1976) Preparation and properties of mitochondria derived from synaptosomes. Biochem J 154:423–432
23. Lai JC, Walsh JM, Dennis SC, Clark JB (1977) Synaptic and non-synaptic mitochondria from rat brain: isolation and characterization. J Neurochem 28:625–631
24. Mena EE, Hoeser CA, Moore BW (1980) An improved method of preparing rat brain synaptic membranes. Elimination of a contaminating membrane containing 2′, 3′-cyclic nucleotide 3′-phosphohydrolase activity. Brain Res 188:207–231
25. Dagani F, Gorini A, Polgatti M, Villa RF, Benzi G (1983) Synaptic and non-synaptic mitochondria from rat cerebral cortex. Characterization and effect of pharmacological treatment on some enzyme activities related to energy transduction. Farmaco (Sci) 38:584–594
26. Rendon A, Masmoudi A (1985) Purification of non-synaptic and synaptic mitochondria and plasma membranes from rat brain by a rapid Percoll gradient procedure. J Neurosci Methods 14:41–51
27. Battino M, Bertoli E, Formiggini G, Sassi S, Gorini A, Villa RF, Lenaz G (1991) Structural and functional aspects of the respiratory chain of synaptic and nonsynaptic mitochondria derived from selected brain regions. J Bioenerg Biomembr 23:345–363
28. Brown MR, Sullivan PG, Geddes JW (2006) Synaptic mitochondria are more susceptible to Ca^{2+} overload than nonsynaptic mitochondria. J Biol Chem 281:11658–11668
29. Cheng H, Guan S, Han X (2006) Abundance of triacylglycerols in ganglia and their depletion in diabetic mice: implications for the role of altered triacylglycerols in diabetic neuropathy. J Neurochem 97:1288–1300
30. Han X, Yang J, Cheng H, Ye H, Gross RW (2004) Toward fingerprinting cellular lipidomes directly from biological samples by two-dimensional electrospray ionization mass spectrometry. Anal Biochem 330:317–331
31. Birch-Machin MA, Turnbull DM (2001) Assaying mitochondrial respiratory complex activity in mitochondria isolated from human cells and tissues. Methods Cell Biol 65:97–117
32. Ellis CE, Murphy EJ, Mitchell DC, Golovko MY, Scaglia F, Barcelo-Coblijn GC, Nussbaum RL (2005) Mitochondrial lipid abnormality and electron transport chain impairment in mice lacking alpha-synuclein. Mol Cell Biol 25:10190–10201
33. King TE (1967) Preparation of succinate dehydrogenase and reconstitution of succinate oxidase. In: Estabrook RW, Pullman ME (eds) Methods enzymol. Academic Press, New York, pp 322–331
34. Degli Esposti M (2001) Assessing functional integrity of mitochondria in vitro and in vivo. Methods Cell Biol 65:75–96
35. Yonetan T (1967) Cytochrome oxidase: beef heart. In: Estabrook RW, Pullman ME (eds) Methods enzymol. Academic Press, New York pp, 332–335
36. Bangur CS, Howland JL, Katyare SS (1995) Thyroid hormone treatment alters phospholipid composition and membrane fluidity of rat brain mitochondria. Biochem J 305(Pt 1):29–32
37. Brand MD, Turner N, Ocloo A, Else PL, Hulbert AJ (2003) Proton conductance and fatty acyl composition of liver mitochondria correlates with body mass in birds. Biochem J 376:741–748
38. Fleischer S, Brierley G, Klouwen H, Slautterback DB (1962) Studies of the electron transfer system. 47. The role of phospholipids in electron transfer. J Biol Chem 237:3264–3272
39. Schlame M, Ren M, Xu Y, Greenberg ML, Haller I (2005) Molecular symmetry in mitochondrial cardiolipins. Chem Phys lipids 138:38–49
40. Schlame M (2007) Cardiolipin synthesis for the assembly of bacterial and mitochondrial membranes. J Lipid Res. doi: 10.1194/JLR.R700018JLR200
41. Chicco AJ, Sparagna GC (2007) Role of cardiolipin alterations in mitochondrial dysfunction and disease. Am J Physiol Cell Physiol 292:C33–C44
42. Fry M, Green DE (1981) Cardiolipin requirement for electron transfer in complex I and III of the mitochondrial respiratory chain. J Biol Chem 256:1874–1880
43. Pfeiffer K, Gohil V, Stuart RA, Hunte C, Brandt U, Greenberg ML, Schagger H (2003) Cardiolipin stabilizes respiratory chain supercomplexes. J Biol Chem 278:52873–52880
44. Zhang M, Mileykovskaya E, Dowhan W (2002) Gluing the respiratory chain together. Cardiolipin is required for supercomplex formation in the inner mitochondrial membrane. J Biol Chem 277:43553–43556

45. McKenzie M, Lazarou M, Thorburn DR, Ryan MT (2006) Mitochondrial respiratory chain supercomplexes are destabilized in Barth Syndrome patients. J Mol Biol 361:462–469
46. Kraffe E, Soudant P, Marty Y, Kervarec N, Jehan P (2002) Evidence of a tetradocosahexaenoic cardiolipin in some marine bivalves. Lipids 37:507–514
47. Yamaoka S, Urade R, Kito M (1988) Mitochondrial function in rats is affected by modification of membrane phospholipids with dietary sardine oil. J Nutr 118:290–296
48. Fry M, Blondin GA, Green DE (1980) The localization of tightly bound cardiolipin in cytochrome oxidase. J Biol Chem 255:9967–9970
49. Gohil VM, Hayes P, Matsuyama S, Schagger H, Schlame M, Greenberg ML (2004) Cardiolipin biosynthesis and mitochondrial respiratory chain function are interdependent. J Biol Chem 279:42612–42618

Lipids (2008) 43:961–970
DOI 10.1007/s11745-008-3219-9

ORIGINAL ARTICLE

A Striking Parallel Between Cardiolipin Fatty Acid Composition and Phylogenetic Belonging in Marine Bivalves: A Possible Adaptative Evolution?

E. Kraffe · J. Grall · M. Le Duff · P. Soudant · Y. Marty

Received: 26 April 2008 / Accepted: 14 July 2008 / Published online: 21 August 2008
© AOCS 2008

Abstract Thirty-five species of marine mollusk bivalves were analyzed for their fatty acid (FA) composition of cardiolipin (Ptd_2Gro). All species showed a Ptd_2Gro with strong selectivity for only a few polyunsaturated fatty acids, but three characteristic FA profiles emerged, with clear parallels to bivalve phylogeny. A first group of 12 species belonging to the Eupteriomorphia subgroup (Filibranchia) was characterized by a Ptd_2Gro almost exclusively composed of 22:6n-3, whereas in the four Filibranchia Pteriomorph species analyzed, this FA was combined with substantial proportions of 18:2n-6 and 18:3n-3. Finally, a third group of 20 species, all belonging to the Heterodonta subclass, possessed Ptd_2Gro containing predominantly both 22:6n-3 and 20:5n-3. Polyunsaturated FA moieties and arrangements in the Ptd_2Gro of some marine species investigated in other classes of the mollusk phylum (Gastropoda, Polyplacophora) were found to be different. The present results suggest that the specific Ptd_2Gro FA compositions in bivalves are likely to be controlled and conserved in species of the same phylogenetic group. Functional significances of the evolution of this mitochondrial lipid structure in bivalves are discussed.

Keywords Cardiolipin · DHA · EPA · Bivalves · Phylogeny · Mitochondria

E. Kraffe (✉) · Y. Marty
Unité Mixte CNRS 6521, Université de Bretagne Occidentale,
C.S. 93837, 29238 Brest Cedex, France
e-mail: Edouard.Kraffe@univ-brest.fr

J. Grall · M. Le Duff · P. Soudant
Unité Mixte CNRS 6539, IUEM,
Université de Bretagne Occidentale,
29280 Plouzané, France

Introduction

Cardiolipin (Ptd_2Gro) is an anionic phospholipid with a unique dimeric phosphatidyl lipid moiety. This phospholipid is predominantly distributed in bacterial plasma membranes and in eukaryotic mitochondrial inner membranes [1]. Ptd_2Gro has been shown to be a key factor in the control of major mitochondrial membrane protein activity, such as ADP–ATP and pyruvate carriers, but also of the large complexes involved in oxidative phosphorylation, including complex I (NADH–CoQ reductase), III (ubiquinol:cytochrome *c* oxydoreductase), complex IV (cytochrome *c* oxidase), and V (F_0F_1-ATP synthase) [2–6]. Ptd_2Gro plays a central role in higher order organization of complexes III and IV of the respiratory chain in mitochondria [7–9], as well as in optimal coupling of oxidative phosphorylation [10]. There is also evidence that Ptd_2Gro regulates membrane binding of the mitochondrial peripheral membrane protein cytochrome *c* [11] and is a critical component in the apoptotic cell-death program [12].

One of the intriguing aspects of eukaryotic Ptd_2Gro is the unique acyl composition of its four FA residues [2, 13, 14]. Only C_{16}–C_{18} monounsaturated or diunsaturated fatty acyl chains are usually selected for the assembly of Ptd_2Gro [14, 15]. For instance, in many mammalian tissues, Ptd_2Gro has a strong preference for 18:2n-6, constituting up to 85 mol% of the total FA of Ptd_2Gro [4, 6]. This specific hydrophobic part appears to be an important structural requirement for the high binding affinity of Ptd_2Gro with proteins, and appropriate molecular composition of Ptd_2Gro may be critical for optimum mitochondrial respiratory performance [16]. Indeed, in mammals, dietary manipulations affecting 18:2n-6 levels in Ptd_2Gro (corresponding to a Ptd_2Gro enriched in 22:6n-3) is associated with a decrease of the O_2 consumption rate of mitochondria isolated from rat heart, a decrease of the activity of cytochrome *c* oxidase [17–20], but an increase of the activity of F_1F_0-ATPase [17]. Selection of a limited number of molecular species also appears to be an important feature for Ptd_2Gro protein interactions influencing enzymatic activities [16]. This common feature was found among Ptd_2Gro from diverse eukaryotic organisms having different FA compositions [14]. This led to structural uniformity and to a high proportion of molecules with symmetric FA distribution [14]. It is argued that tafazzin (TAZ gene product), a phospholipid acyltransferase, is involved in this acyl-specific modeling of Ptd_2Gro [16, 21].

Recently, we characterized a Ptd_2Gro containing more than 80 mol% of 22:6n-3 in three commercial marine bivalve species, the scallop *Pecten maximus*, the oyster *Crassostrea gigas*, and the mussel *Mytilus edulis* [22]. Thereafter, a new highly unsaturated Ptd_2Gro was discovered in the Manila clam, *Ruditapes philippinarum*, which had two main FA (20:5n-3 and 22:6n-3) found in approximately equal proportions [23]. In this study, we reported a symmetrical structure with 20:5n-3 and 22:6n-3 predominating at *sn*-1 and *sn*-2 positions, respectively. Interestingly, 22:6n-3-enriched Ptd_2Gro and 20:5n-3/22:6n-3-enriched Ptd_2Gro, respectively, in scallops, oysters, mussels, and Manila clams are conserved between organs [23]. The replacement of the 22:6n-3 chain in *sn*-1 positions by the 20:5n-3 for the Manila clams, when compared to mussel, oyster, and scallop, is puzzling. It appeared that these characteristic Ptd_2Gro FA compositions were species specific rather than dietary dependent for the analyzed bivalve species, and it was speculated that these structures could be essential for optimal energy and respiratory metabolisms of mitochondria between bivalve species. These observations raised the questions of the importance and significance of such highly unsaturated long-chain FA and composition specificities in bivalve Ptd_2Gro.

To begin to address these questions, we investigated the FA composition of Ptd_2Gro in 35 different species of marine mollusk bivalves belonging to the three most important subclasses in terms of number of species: Filibranchia Pteriomorpha, Filibranchia Eupteriomorphia, and Eulamellibranch Heterodonta (including Anomalodesmata). Investigated species covered 17 of the 94 existing families (20% of family diversity) and 8 of the 13 orders. Ptd_2Gro FA compositions of some marine species in other classes of the mollusk phylum (Gastropoda, Polyplacophora) were also investigated. Specific objectives were: (1) to assess whether 22:6n-3/20:5n-3-enriched Ptd_2Gro and 22:6n-3-dominant Ptd_2Gro are the most representative patterns in bivalves, or whether other FA patterns of Ptd_2Gro exist, and (2) to determine if chemotaxonomic relationships exist between Ptd_2Gro FA composition and bivalve phylogeny. The possible functional implications of the FA patterns found in Ptd_2Gro also were considered.

Materials and Methods

Reagents

Boron trifluoride [BF_3, 10% (by wt) in methanol] was obtained from Supelco (St. Quentin Fallavier, France). Other reagents and solvents were purchased from Merck (Darmstadt, Germany).

Bivalve Species

The locations and sampling date of the bivalves species studied are presented in Table 1. For the purpose of the present table, bivalve species are listed according to the taxonomic subclass to which they belong. We followed a recent combined morphological, anatomical, and molecular study in a total evidence framework that resumed a clear pattern of bivalve phylogeny [24]. This classification also includes the two subgroups in the subclass Filibranchia: the Pteriomorphia and the Eupteriomorphia [25].

Sample Preparation and Lipid Extraction

For all the species analyzed, the digestive tract was removed before whole animals were pooled and homogenized with a Dangoumeau homogenizer at −180°C. Lipids were extracted from tissue homogenates according to the method described by Folch et al. [26]. To ensure complete extraction of tissue lipids, a solvent-to-tissue ratio of 70:1 was used as described by Nelson [27]. After removing the organic phase, the residue was washed with a mixture of $CHCl_3$/MeOH (2:1, *v*/*v*) to avoid any solvent retention. The final extract was stored at −20°C under nitrogen atmosphere with 0.01wt% BHT (antioxidant).

Separation of Polar Lipids by Silica Gel Microcolumn

An aliquot of the lipid extracts was evaporated to dryness, and lipids were recovered with three washings of 500 µl of $CHCl_3$/MeOH (98/2, *v*/*v*) and deposited at the top of a silica gel micro-column (30 × 5 mm ID, packed with Kieselgel 60 70-230 mesh previously heated at 450°C and deactivated with 5 wt% H_2O) [28]. Neutral lipids were eluted with 10 ml of $CHCl_3$/MeOH (98/2 *v*/*v*). The polar lipid fraction was recovered with 15 ml of MeOH and

Table 1 Systematic list, sampling location, and time of collection of the bivalve species used in the analysis (following [24, 25])

Class: Bivalvia	Order	Family	Species	Origin	Time of collection
Subclass: Filibranchia					
Pteriomorphia	Arcoida	Arcidae	*Arca lactea* (5)	France (B)	March
		Glycymerididae	*Glycymeris glycymeris* (4)	France (B)	March
	Mytiloida	Mytilidae	*Modiolus barbuatus* (4)	France (B)	March
			Mytilus edulis (3)	France (B)	October
Eupteriomorphia	Pteroida	Pectinidae	*Placopecten magellanicus* (3)	Canada (MI)	June
			Zygochlamys patagonica (2)	Argentine	June
			Aequipecten opercularis (3)	France (B)	July
			Mizuhopecten yessoensis (3)	Japan	July
			Chlamys distorta (5)	France (B)	March
			Nodipecten subnodosus (2)	Mexico (BC[c])	May
			Mimachlamys varia (3)	France (B)	May
			Pecten maximus (3)	France (B)	October
		Anomiidae	*Anomia ephippium* (8)	France (B)	March
	Ostreida	Ostreidae	*Crassostrea gigas* (3)	France (M)	March
			Crassostrea virginica (4)	USA (East coast)	August
Subclass: Heterodonta	Veneroida	Ungulinidae	*Diplodonta rotundata* (1)	France (B)	March
		Cardidae	*Laevicardium crassum* (4)	France (B)	April
			Parvicardium ovale (2)	France (B)	April
			Cerastroderma edule (3)	France (D)	April
		Mactridae	*Spisula subtruncata* (4)	France (B)	October
			Mactra corallina (3)	France (B)	March
			Lutraria lutraria (2)	France (B)	March
			Acanthocardia paucicostata (2)	France (D)	March
		Solenidae	*Ensis ensis* (4)	France (B)	April
		Solecurtidae	*Pharus legumen* (2)	France (B)	April
		Tellinidae	*Tellina tenuis* (4)	France (D)	March
		Scrobiculariidae	*Scrobicularia plana* (4)	France (B)	March
		Veneroidae	*Dosinia exoleta* (1)	France (B)	March
			Ruditapes decussatus (3)	France (B)	October
			Ruditapes philippinarum (3)	France (D)	October
			Venus verucosa (3)	France (B)	April
			Mercenaria mercenaria (2)	France (B)	March
		Petricolidae	*Petricola lithophaga* (3)	France (N)	October
	Myoida	Myoidae	*Mya arenaria* (2)	France (B)	October
Subclass: Anomalodesmata	Pholadomyoida	Thraciidae	*Thracia phaseolina* (2)	France (D)	June

The list includes 35 species. Number of individuals pooled for analysis is given within brackets

B Brittany/Bay of Brest, *MI* Madeleine Islands, *BC* Baja California, *M* Marenne-Oléron, *D* Brittany/Bay of Douarnenez

stored at −20°C for later phospholipid class separation by HPLC and FA composition analysis by GC.

Separation of Phospholipid Classes and Ptd_2Gro—Fatty Acid Analysis

Separation of the phospholipid classes followed a method previously described [23], using a Waters (Milford, MA, USA) HPLC system (UV detection at 206 nm). The Ptd_2Gro fraction as well as the other glycerophospholipid classes were identified (i.e., phosphatidylethanolamine, phosphatidylcholine, phosphatidylserine, phosphatidylinositol, ceramide aminoethylphosphonate, and natural lysophosphatidylcholine), collected, and analyzed for FA composition using GC after transesterification ($MeOH/BF_3$) [29]. Phosphatidylglycerol (PtdGro) was not detected in the analyzed species and is likely to be absent or only present in trace amounts in marine bivalve tissues [22].

Statistics

A hierarchical cluster analysis using the Bray–Curtis similarity index values was accomplished on Ptd$_2$Gro FA composition of the 35 bivalve species using Arcsinus transformation of the percentage data (“R” software). Simple linear regressions between neutral lipid (NL) and Ptd$_2$Gro FA compositions were carried out using StatGraphics Plus 5.1 (Sigma Plus Inc., Toulouse, France). FA for which results are shown were considered significantly correlated when $P \leq 0.05$.

Table 2 FA composition of cardiolipin (Ptd$_2$Gro) in the 35 bivalve species

Species	18:2n-6	18:3n-3	20:4n-6	20:5n-3	22:6n-3
Cardiolipin type 1					
Mytilus edulis (3)	1.7	5.9	0.9	1.9	82.6
Placopecten magellanicus (3)	–	–	2..0	3.4	76.2
Zygochlamys patagonica (2)	–	–	1.3	4.8	85.6
Aequipecten opercularis (3)	0.1	0.2	0.8	2.3	77.9
Mizuhopecten yessoensis (3)	–	–	0.2	0.3	86.8
Chlamys distorta (5)	–	–	0.1	0.1	87.1
Nodipecten subnodosus (2)	–	–	2.5	2.1	81.3
Mimachlamys varia (3)	–	–	3.5	6.0	73.2
Pecten maximus (3)	–	0.1	0.8	2.5	77.7
Anomia ephippium (8)	0.8	–	–	1.4	82.2
Crassostrea gigas (3)	0.2	0.2	0.8	2.3	85.5
Crassostrea virginica (4)	–	–	1.0	1.8	81.1
Cardiolipin type 2					
Arca lactea (5)	16.9	11.2	4.8	4.8	38.0
Glycymeris glycymeris (4)	19.7	9.1	3.5	3.7	39.5
Modiolus barbuatus (4)	5.7	11.6	3.7	6.2	40.3
Cardiolipin type 3					
Diplodonta rotundata (1)	–	–	2.6	29.9	54.5
Laevicardium crassum (4)	0.4	0.7	3.2	35.4	43.6
Parvicardium ovale (2)	–	–	2.0	44.2	46.2
Cerastroderma edule (3)	–	–	6.6	50.7	28.4
Spisula subtruncata (4)	–	0.4	2.0	49.9	34.8
Mactra corallina (3)	0.3	0.5	3.5	47.6	31.4
Lutraria lutraria (2)	–	–	16.6	44.6	17.0
Acanthocardia paucicostata (2)	–	–	2.5	48.7	34.1
Ensis ensis (4)	–	1.2	1.1	36.5	43.5
Pharus legumen (2)	–	3.2	6.9	25.2	34.7
Tellina tenuis (4)	0.2	0.4	2.2	38.3	49.4
Scrobicularia plana (4)	1.1	1.6	9.4	36.7	29.3
Dosinia exoleta (1)	–	0.6	4.6	34.8	31.4
Ruditapes decussatus (3)	0.2	0.5	8.7	42.5	39.3
Ruditapes philippinarum (3)	0.1	0.1	6.8	34.9	37.9
Venus verucosa (3)	–	–	4.0	36.4	36.3
Mercenaria mercenaria (2)	0.2	2.1	1.3	44.4	32.2
Petricola lithophaga (3)	0.9	–	13.1	25.7	36.5
Mya arenaria (2)	–	0.3	6.8	60.4	21.8
Thracia phaseolina (2)	–	–	5.4	42.7	40.8

Only predominant PUFA are depicted (saturated FA and monounsaturated FA were always found lower than 15 and 10%, respectively). Results are expressed in mol% of the total FA of the class

Results

Taxonomic Sampling

The two most important recognized subclasses of the class Bivalvia were well represented with 20 species belonging to the subclass Heterodonta (+Anomalodesmata) and 15 to the Filibranchia. Two subgroups were distinguished in the subclass of Filibranchia: Pteriomorph (4 species) and Eupteriomorph (11 species) (Table 1). Species investigated covered 17 of the 94 existing families (20% of family diversity) and 8 of the 13 orders of mollusk bivalves.

FA Composition of Ptd_2Gro

Tissues of all bivalve species tested were dominated by only a few polyunsaturated FA (PUFA) (22:6n-3, 20:5n-3, 20:4n-6, 18:3n-3, and 18:2n-6), representing 76–96% of the total FA of Ptd_2Gro, while saturated FA (16:0 and 18:0) (<15%), and monounsaturated FA (mainly 18:1n-9 and 18:1n-7) (<10%) were always found in low proportions.

Table 2 reports the proportions of the five main PUFA found in the Ptd_2Gro of the 35 bivalve species. Three "types" of FA composition were characterized. In 12 species, Ptd_2Gro was dominated by 22:6n-3, representing 73.2–87.1% of total FA (cardiolipin type 1). The other PUFA, 20:5n-3 and 20:4n-6, were minor components (<6% individually). In three other species, *Arca lactea*, *Glycymeris glycymeris*, and *Modiolus barbuatus*, 22:6n-3 represented 38.0–40.3% of total FA, and 18:2n-6 and 18:3n-3 were found in fairly high proportions in the Ptd_2Gro of these species. This specificity was considered as a second type of Ptd_2Gro (cardiolipin type 2). The other PUFA, 20:5n-3 and 20:4n-6, were also found in low proportions in these species (<6.2%). In the last 20 species, 22:6n-3 (ranging from 17 to 54.5%) and 20:5n-3 (ranging from 30 to 60.4%) were found to be the two predominant PUFA in Ptd_2Gro, defining a third type of Ptd_2Gro (cardiolipin type 3). In these species, although 20:4n-6 was still a minor component, there is an evident trend that this FA reached higher levels than in species having Ptd_2Gro of type 1 or type 2. The 18:2n-6 and 18:3n-3 FA were always lower than 3.2% in type 3 species.

To investigate if the FA compositions found in bivalves are representative of FA in Ptd_2Gro from the mollusk phylum in general, FA compositions of Ptd_2Gro from species belonging to other classes of mollusk were investigated. In the three gastropods and one polyplacophor species analyzed, Ptd_2Gro revealed neither the same type of FA moieties nor the same arrangements (Table 3). Ptd_2Gro had a mixed FA pattern with three or more kinds of FA. Nevertheless, as in bivalves, saturated FA (16:0 and 18:0) were found in small proportions (<15%) in these species.

Total FA compositions of Ptd_2Gro of the 35 bivalve species were submitted to statistical analysis based upon Bray–Curtis similarity index values (Fig. 1). The hierarchical cluster dendrogram obtained clearly shows three main groups corresponding to the three types of Ptd_2Gro FA composition described above. The overall similarity between type 1 and type 3 and between type 2 and type 3 is less than 40%, while it is close to 50% for types 1 and 2. Comparison between the cluster results and bivalve phylogeny [24, 25] enabled establishing a strong correlation between the three different types of Ptd_2Gro FA composition and marine bivalves subclass and subgroup belonging. Indeed, all species in group 1 (12 species),

Table 3 FA composition of cardiolipin (Ptd_2Gro) in four species belonging to non-bivalve marine mollusk classes (Gastropoda and Polyplacophora)

	Patella vulgata (Archeogastropoda)	*Crepidula fornicata* (Caenogastropoda)	*Littorina littorea* (Caenogastropoda)	*Acanthochitona fascicularis* (Polyplacophora)
Fatty acids				
16:0	7.3	3.1	0.9	6.5
18:0	7.2	1.8	0.8	2.4
18:1n-7	3.4	0.3	–	19.8
18:2n-6	1.5	25.5	16.3	0.7
18:3n-3	2.1	10.6	49.7	2.0
20:2n-6	22.4	1.7	0.9	14.7
20:3n-3	16.6	–	–	–
20:4n-6	18.5	6.6	2.2	15.8
20:5n-3	–	12.8	5.1	32.4
22:5n-3	–	11.0	17.8	0.7
22:6n-3	13.0	4.0	–	1.0
Total SFA	15.2	8.1	2.2	8.9
Total MUFA	10.0	6.2	1.0	22.6
Total PUFA	74.9	85.7	96.8	68.5

Only predominant PUFA are depicted. Results are expressed in mol% of the total FA of the class which have 22:6n-3-enriched Ptd_2Gro (type 1), belong to the Eupteriomorphia (Filibranchia) group. Species in group 3 (20 species) having Ptd_2Gro with a strong preference for both 22:6n-3 and 20:5n-3 (type 3) were members of the Heterodonta and Anomalodesmata subclasses. In the second group (three species, type 2), species are all Filibranchia Pteriomorph. One exception is observed for *M. edulis*, which associated with Ptd_2Gro of type 1, and thus the Filibranchia Eupteriomorph cluster, although this species is considered to be phylogenetically related to Filibranchia Pteriomorph. Nevertheless, the 18:2n-6 and 18:3n-3 proportions found in *M. edulis* (1.7 and 5.9%, respectively) were much higher than in the Ptd_2Gro of all the other "true" Filibranchia Eupteriomorph species. This discrepancy between *M. edulis* phylogenetic position and its Eupteriomorph Filibranchia Ptd_2Gro FA composition was confirmed by the Bray–Curtis analysis, which partitioned *M. edulis* into an isolated subcluster within the type 1 cluster.

FA Composition of Neutral Lipids

To check for the possible dietary effect on FA in Ptd_2Gro, FA composition of the neutral lipid fraction (NL), which carries a strong imprint of dietary FA in bivalves, was analyzed in 20 species among the 35 sampled species. Seven species were representatives of Ptd_2Gro of type 1, three of type 2, and ten of type 3. These data showed a constant abundance of both 20:5n-3 and 22:6n-3 FA in NL of all species analyzed (Table 4). Linear correlations were tested between NL and Ptd_2Gro for the major PUFA of Ptd_2Gro (18:2n-6, 18:3n-3, 20:4n-6, 20:5n-3, 22:6n-3). From these statistical analyses, it clearly appeared that 18:2n-6, 18:3n-3, and 20:5n-3 contents in Ptd_2Gro were independent of those FA in the NL as no significant correlation could be established between these two lipid fractions for any of these FA. 20:4n-6 and 20:5n-3 showed lower P values ($P < 0.1$). Nevertheless, only a weak correlation could be noted for both FA with their content in

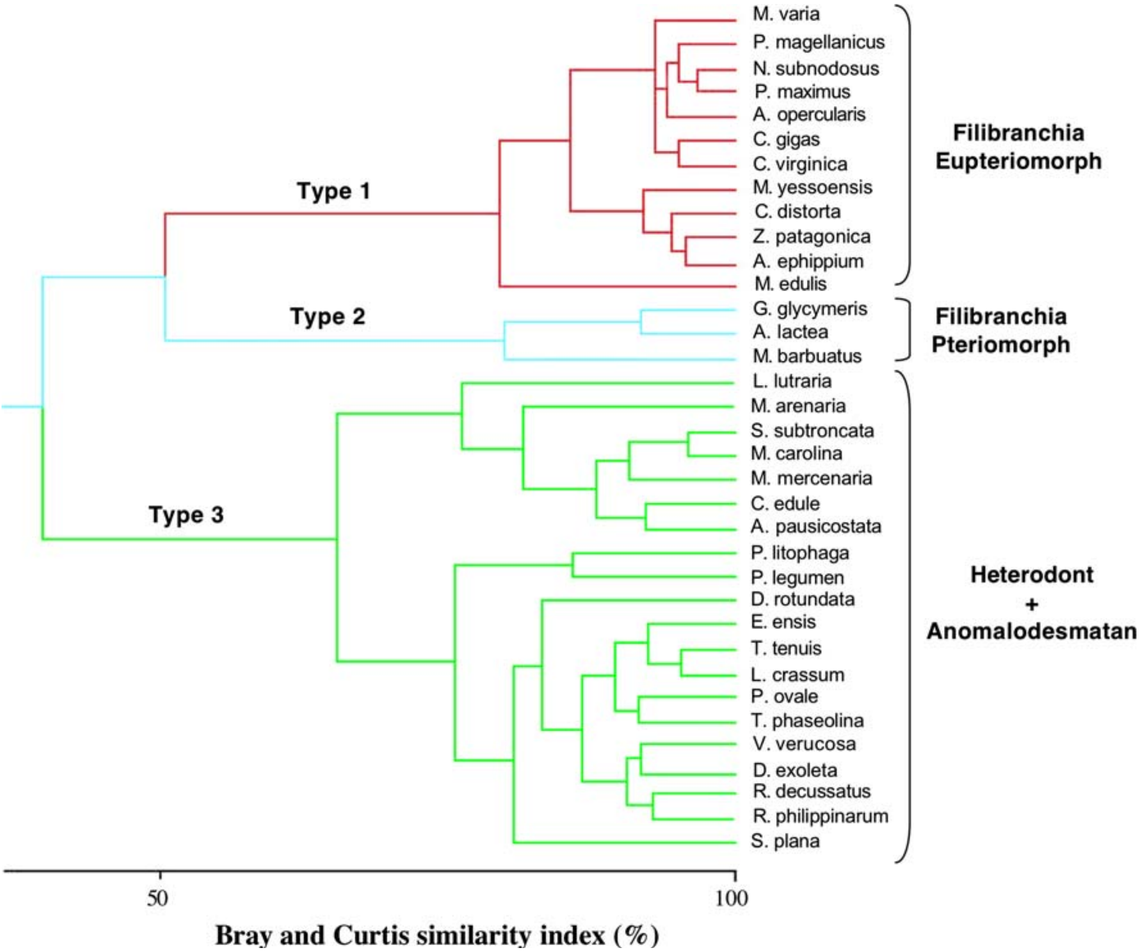
M. varia
P. magellanicus
N. subnodosus
P. maximus
A. opercularis
C. gigas
C. virginica
M. yessoensis
C. distorta
Z. patagonica
A. ephippium
M. edulis
G. glycymeris
A. lactea
M. barbuatus
L. lutraria
M. arenaria
S. subtroncata
M. carolina
M. mercenaria
C. edule
A. pausicostata
P. litophaga
P. legumen
D. rotundata
E. ensis
T. tenuis
L. crassum
P. ovale
T. phaseolina
V. verucosa
D. exoleta
R. decussatus
R. philippinarum
S. plana
Type 1
Type 2
Type 3
Filibranchia Eupteriomorph
Filibranchia Pteriomorph
Heterodont + Anomalodesmatan
50
100
Bray and Curtis similarity index (%)

Fig. 1 Hierarchical cluster dendrogram based on Bray and Curtis similarity index values showing relationship of total FA composition of Ptd_2Gro and bivalve species. Established using Arcsinus transformation of the percentage (mol%) of total FA

Table 4 FA compositions of neutral lipids (NL)

Species	18:2(n-6)	18:3(n-3)	20:4(n-6)	20:5(n-3)	22:6(n-3)	DHA/EPA
Cardiolipin type 1 (Filibranchia Eupteriomorph)						
Placopecten magellanicus	0.4	0.3	1.6	17.8	16.8	0.9
Zygochlamys patagonica	2.1	0.5	1.4	5.7	10.3	1.8
Aequipecten opercularis	1.9	2.9	1.5	15.4	13.8	0.9
Nodipecten subnodosus	1.2	0.7	7.4	6.6	16.7	2.5
Mimachlamys varia	2.0	3.2	1.8	11.6	15.8	1.4
Crassostrea gigas	1.5	2.1	1.9	18.6	8.9	0.5
Mytilus edulis	1.5	2.6	1.4	13.5	12.8	0.9
Cardiolipin type 2 (Filibranchia Pteriomorph)						
Arca lactea	1.9	1.8	3.5	10.4	20.6	2.0
Glycymeris glycymeris	1.0	1.2	5.3	11.0	13.1	1.2
Modiolus barbuatus	2.7	2.2	5.3	16.7	11.1	0.7
Cardiolipin type 3 (Heterodont)						
Laevicardium crassum	1.2	1.3	2.5	16.5	15.0	0.9
Cerastroderma edule	–	–	7.4	13.9	7.6	0.5
Spisula subtruncata	0.8	1.5	1.4	16.4	7.4	0.45
Mactra carolina	0.7	1.1	2.4	16.0	8.0	0.5
Lutraria lutraria	1.9	2.2	3.7	13.7	13.7	1
Acanthocardia pausicostata	0.7	0.4	4.4	7.8	6.7	0.9
Pharus legumen	0.4	0.5	7.6	19.5	9.6	0.5
Scrobicularia plana	0.7	0.6	8.6	7.3	4.8	0.7
Ruditapes philippinarum	0.5	0.7	1.4	17.1	6.5	0.4
Venus verrucosa	0.5	0.4	4.9	11.2	10.1	0.9
R^2*	0.005	0.007	0.19	0.0007	0.15	
P	0.36	0.26	0.055	0.74	0.09	

For comparison, only PUFA predominating in Ptd_2Gro are depicted. Results are expressed in mol% of the total FA

* Correlations between FA in NL and the same FA associated to Ptd_2Gro in the 20 species analyzed. FA for which results are shown were considered significantly correlated when $P \leq 0.05$

NL explaining only 19 and 15% of their respective proportion in Ptd_2Gro.

Discussion

FA compositions of Ptd_2Gro were characterized in 35 marine bivalve species and were found to be related to the 3 major bivalve subclasses/subgroups: Filibranchia Pteriomorphia, Filibranchia Eupteriomorphia, and Heterodonta + Anomalodesmata. Ptd_2Gro of Filibranchia Eupteriomorphia species was almost exclusively composed of 22:6n-3. For the species belonging to the Heterodonta subclasses, Ptd_2Gro was characterized by the predominance of 20:5n-3 and 22:6n-3, even though inter-species variability in their proportions could be observed. The only species analyzed thus far in the Anomalodesmata subclass (*Thracia phaseolina*) has a Ptd_2Gro FA composition very similar to those found in Heterodonta species. Interestingly, this corroborates the recent inclusion of this subclass within Heterodonta [24]. In addition to these two Ptd_2Gro FA patterns described previously in *P. maximus*, *C. gigas*, and *M. edulis* for Filibranchia Eupteriomorph species [22] and in *R. philippinarum* for Heterodonts [23], a new FA composition was found for Ptd_2Gro of Filibranchia Pteriomorph. Indeed, also predominated by 22:6n-3 as the Ptd_2Gro of Filibranchia Eupteriomorph bivalves, this FA is combined in this subgroup with substantial proportions of 18:2n-6 and 18:3n-3.

Ptd_2Gro analysis of some marine species in other mollusk classes (Gastropoda, Polyplacophora) revealed neither the same unsaturated FA nor the same arrangements. The characteristic Ptd_2Gro FA compositions within bivalve classes and groups may therefore be considered as an interesting chemotaxonomic marker. In addition, the uniformity of FA patterns observed across Pteriomorph, Eupteriomorph, and Heterodont + Anomalodesmatan bivalves suggests that FA composition of Ptd_2Gro is possibly associated with genotypic evolution in these phylogenetic groups. Nevertheless, before one can definitively associate a specific FA composition of Ptd_2Gro with evolutionary patterns, the possible role played by environmental conditions in the modeling of Ptd_2Gro FA composition must be considered. Among environmental factors, the diet is generally supposed to have a profound effect on the FA composition of the lipids in bivalves [30–

35]. Bivalves have low, limited, or no ability for synthesis of C_{20}–C_{22} PUFA with more than three double bonds. Thus, bivalves must acquire these from diets [36–38] rich in $C_{20–22}$ PUFA, including particularly 20:5n-3 and 22:6n-3 [39]. In other words, one can argue that the 22:6n-3-enriched Ptd_2Gro of Filibranchia Eupteriomorph, jointly with 18:2n-6 and 18:3n-3 for Pteriomorph and 22:6n-3 + 20:5n-3-enriched Ptd_2Gro of Heterodonta (+Anomalodesmatan), can reflect dietary differences in the availability of certain FA between these bivalve groups. For Ptd_2Gro, dietary modification is known to affect FA composition significantly in mammals [4, 18, 40]. In contrast, even though there is not as much knowledge concerning the FA composition sensitivity of Ptd_2Gro in marine animals, a relatively consistent 22:6n-3 content in Ptd_2Gro was found in both female and male gonads of scallops *P. maximus* (Fillibranchia Eupteriomorph) despite large differences in 22:6n-3 and 20:5n-3 contents in their diets [33, 34]. Another argument that refutes the possibility of a FA dietary imbalance between groups of bivalves is the examination of the FA compositions of NL (storage lipids) in bivalves. NL containing FA (mainly triacylglycerols) provides a good signature of dietary quality, in terms of FA [39, 41]. It appeared that there was no correlation for 22:6n-3 and 20:5n-3 contents between Ptd_2Gro and NL of the bivalve species analyzed. Similarly, levels of 18:2n-6 and 18:3n-3 in Ptd_2Gro were independent of those FA in NL. A clear example is the high proportions of 18:2n-6 and 18:3n-3 found in Ptd_2Gro of Filibranchia Pteriomorph bivalves that could not be related to enrichment in their diets, as NL of these species contained as low levels of these FA as those found in the Filibranchia Eupteriomorph and Heterondont species.

Environmental factors such as temperature or salinity are also known to influence the FA composition of membrane lipids of ectotherms in order to defend membrane function from the effects of their fluctuations [42–45]. Whether Ptd_2Gro FA compositions could show phenotypic or genotypic modifications in response to differences in these environmental factors is still unresolved for bivalves. Nevertheless, when considering that phylogenetically close species (Pectinids) such as *Nodipecten subnodosus*, *P. maximus* [origin France or Norway/south of Bergen (data not shown)], and *Placopecten magellanicus* inhabiting, respectively, sub-tropical, temperate, and sub-Antarctic regions, possess a Ptd_2Gro fairly uniform in terms of FA composition, it is unlikely for FA composition of Ptd_2Gro to be markedly influenced by latitudinal adaptations, i.e., different thermal environments. In addition, clear differences of composition between 22:6n-3-enriched Ptd_2Gro of Filibranchia Eupteriomorph, 18:2n-6- and 18:3n-3-enriched Ptd_2Gro of Pteriomorph, and 22:6n-3 + 20:5n-3 enriched Ptd_2Gro of Heterodont (+Anomalodesmatan) were found among species growing in similar habitats and sampled at the same period of the year. One exception concerned the peppery furrow shell, *Scrobicularia plana* (da Costa), which is commonly found in estuarine conditions with low salinities [46]. Nevertheless, a similar Ptd_2Gro FA composition was found in this Heterodont species in comparison to the other "truly" marine species. Obviously, taking these observations into account, these specific FA patterns in Ptd_2Gro of bivalves are likely to be related to different evolutionary positions rather than to environmental factors. This supports the above hypothesis that Ptd_2Gro FA patterns should be genetically controlled.

The high proportion of PUFA found in bivalve Ptd_2Gro is a unique, but common feature for most eukaryotic species [6, 14]. To date, in eukaryotes only one or two FA were usually reported for the assembly of Ptd_2Gro, particularly C_{16}–C_{18} monounsaturated or diunsaturated acyl chains [14, 15]. For instance, in many mammalian tissues, Ptd_2Gro has a strong preference for 18:2n-6, constituting up to 90 mol% of total FA of Ptd_2Gro in heart tissue [4, 6]. The fact that bivalve Ptd_2Gro shows selective incorporation of a very small number of PUFA may reflect an ancestral characteristic of this intriguing structural aspect of eukaryote Ptd_2Gro. Interestingly, we previously showed that molecular symmetry occurs in the Ptd_2Gro of the Heterodont species *R. philippinarum* (20:5n-3 and 22:6n-3 predominating at *sn*-1 and *sn*-2 positions, respectively) [23] and obviously in the Ptd_2Gro of the Eupteriomorph species, *P. maximus*, *M. edule*, and *C. gigas*, as this group contains only a single type of FA (22:6n-3) [22]. Then, although the type of FA in Ptd_2Gro varied according to phyla and within the bivalve phylum, a high proportion of molecules with structural uniformity and symmetric FA distribution may also emerge as a common feature, as recently suggested for Ptd_2Gro of various eukaryotes and organs in mammals [14]. Several acyltransferases, such as Tafazzin (TAZ gene product), acyl-CoA:monolysocardiolipin acyltransferase, and acyl-CoA:dilysocardiolipin acyltransferase (ALCAT gene product), as well as other enzymes, such as scramblase-3, are argued to be involved in this acyl-specific remodeling of Ptd_2Gro [16, 47–50]. Homologs of these acyltransferases have been reported in the genomes of diverse eukaryotes [16]. Molecular mechanisms and existence of genes that encode for these enzymes remain to be established in bivalves. But from the present and previous data, the differences in FA specificity found in Ptd_2Gro may be attributable to the existence of multiple and different remodeling acyltransferases, or gene isoforms, between Eupteriomorph, Pteriomorph and Heterondont + Anomalodesmatan species.

The functional significance of such specificity of Ptd_2Gro FA composition among Eupteriomorph, Pteriomorph, and Hetrodont + Anomalodesmatan species has yet to be addressed. However, Ptd_2Gro is now clearly recognized to play several key roles in mitochondria related to energy metabolism [5, 6, 21, 51], membrane integrity [3, 9, 52], but also apoptosis [12, 53] and ROS-induced damaging processes [54]. In mammals, as well as in ectotherms, the specific hydrophobic part (i.e., the fatty acid) of the Ptd_2Gro appeared to be structurally important for the lipid–protein interactions with proteins involved in oxidative metabolism, such as the cytochrome *c* oxidase [19, 20, 55, 56] and F_0F_1-ATPase [17], but also complex I and III [6, 54]. An appropriate molecular symmetry of Ptd_2Gro species may also be critical for optimal mitochondrial respiratory performance [14]. This notion was supported recently by the discovery that Barth syndrome (BTHS), an X-linked human disease, is associated with striking abnormalities in Ptd_2Gro molecular species leading to changes in mitochondrial architecture and function [21, 57–59]. Thus far, there is no evidence of altered mitochondrial functionality among bivalve phylogenetic groups. However, taking into account all these observations, it may be considered that the specialized Ptd_2Gro FA compositions found in these groups could be required for optimal functional activation of inner mitochondrial membrane proteins involved in oxidative phosphorylation.

Conclusion

This work utilized marine bivalve phylogeny to explore the distribution, structure, and evolution of Ptd_2Gro FA composition in 35 different species. The emerging picture suggests a parallel between FA composition and bivalve taxons. The consequences to mitochondrial function and mechanisms that underlie such unusual Ptd_2Gro FA compositions remain to be explained. However, in the light of functions associated to the FA moieties of Ptd_2Gro in mitochondria, we hypothesize that genotypic changes in Ptd_2Gro FA composition during evolution could constitute an adaptive "strategy" of mitochondrial oxidative phosphorylation processes linked to prevailing conditions in different environmental habitats. Indeed, it is intriguing to note that bivalve species belonging to Eulamellibranch (Heterodonta subclass) containing 20:5n-3 with 22:6n-3 in Ptd_2Gro are all burrowing bivalves, while those belonging to Filibranch (Pteriomorph and Eupteriomorph subclass), which have very low levels of 20:5n-3 in their Ptd_2Gro, are epifaunal animals (lying on the surface of the sea bed).

Many questions remain unanswered, but the bivalve Ptd_2Gro model could be an interesting field of study for the understanding of some of the intriguing aspects of the atypical Ptd_2Gro acyl composition in eukaryotes.

Acknowledgments We would like to thank A. Wacker, E. Palacios, and A. Druinker for supply of some bivalve species. This work was supported by a grant from "Ministère de l'Education Nationale de la Recherche et de la Technologie" (M.E.N.R.T., France).

References

1. Daum G (1985) Lipids of mitochondria. Biochim Biophys Acta 822:1–42
2. Robinson NC, Zborowski J, Talbert LH (1990) Cardiolipin-depleted bovine heart cytochrome *c* oxidase: binding stoichiometry and affinity for cardiolipin derivatives. Biochemistry 29:8962–8969
3. Hoch FL (1992) Cardiolipins and biomembrane function. Biochem Biophys Acta 1113:71–133
4. Berger A, German JB, Gershwin ME (1993) Biochemistry of CL: sensitivity to dietary fatty acids. In: Kissela JE (ed) Advances in food and nutrition research, vol 37. Academic Press, San Diego, pp 259–338
5. McAuley KE, Fyfe PK, Ridge JP, Isaacs NW, Cogdell RJ, Jones MR (1999) Structural details of an interaction between cardiolipin and an integral membrane protein. Proc Natl Acad Sci 96:14706–14711
6. Schlame M, Rua D, Greenberg ML (2000) The biosynthesis and functional role of cardiolipin. Prog Lipid Res 39:257–288
7. Zhang M, Mileykovskaya E, Dowhan W (2002) Gluing the respiratory chain together: cardiolipin is required for supercomplex formation in the inner mitochondrial membrane. J Biol Chem 277:43553–43556
8. Pfeiffer K, Gohil VM, Stuart JA, Hunte C, Brandt U, Greenberg ML, Schägger H (2003) Cardiolipin stabilizes respiratory chain supercomplexes. J Biol Chem 278:52873–52880
9. Boekema EJ, Braun H-P (2006) Supramolecular structure of the mitochondrial oxidative phosphorylation system. J Biol Chem 282:1–4
10. Koshkin V, Greenberg ML (2000) Oxidative phosphorylation in cardiolipin-lacking yeast mitochondria. Biochem J 347:687–691
11. Tuominen EKJ, Carmichael CJA, Kinnunen PKJ (2002) Phospholipid–cytochrome *c* interaction. J Biol Chem 277:8822–8826
12. Orrenius S, Zhivotovsky B (2005) Cardiolipin oxidation sets cytochrome *c* free. Nat Chem Biol 1:188–189
13. Robinson NC (1982) Specificity and binding affinity of phospholipids to the high-affinity cardiolipin sites of beef heart cytochrome *c* oxidase. Biochemistry 21:184–188
14. Schlame M, Ren M, Xu Y, Greenberg ML, Haller I (2005) Molecular symmetry in mitochondrial cardiolipins. Chem Phys Lipids 138:38–49
15. Schlame M, Brody S, Hostetler K (1993) Mitochondrial CL in diverse eukaryotes. Comparison of biosynthetic reactions and molecular acyl species. Eur J Biochem 212:727–735
16. Schlame M, Ren M (2006) Barth syndrome, a human disorder of cardiolipin metabolism. FEBS Lett 580:5450–5455
17. Yamaoka S, Urade R, Kito M (1988) Mitochondrial function in rats is affected by modification of membrane phospholipids with dietary sardine oil. J Nutr 118:290–296
18. Yamaoka S, Urade R, Kito M (1990) Cardiolipin molecular species in rat heart mitochondria are sensitive to essential fatty acid-deficient dietary lipids. J Nutr 120:415–421
19. Yamaoka-Koseki S, Urade R, Kito M (1991) Cardiolipins from rats fed different dietary lipids affect bovine heart cytochrome c oxidase activity. J Nutr 121:956–958
20. Watkins SM, Lin TY, Davis RM, Ching JR, DePeters EJ, Halpern GM, Walzem RL, German JB (2001) Unique phospholipid metabolism in mouse heart in response to dietary docosahexaenoic or alpha-linoleic acids. Lipids 36:247–254

21. Xu Y, Sutachan JJ, Plesken H, Kelley RI, Schlame M (2005) Characterization of lymphoblast mitochondria from patients with Barth syndrome. Lab Invest 85:823–830
22. Kraffe E, Soudant P, Marty Y, Kervarec N, Jehan P (2002) Evidence of a tetradocosahexaenoic cardiolipin in some marine bivalves. Lipids 37:507–514
23. Kraffe E, Soudant P, Marty Y, Kervarec N (2005) Docosahexaenoic and eicosapentaenoic enriched cardiolipin in the Manila clam *Ruditapes philippinarum*. Lipids 40(6):619–625
24. Giribet G, Wheeler WC (2002) On bivalve phylogeny: a high-level analysis of the Bivalvia (Mollusca) based on combined morphology and DNA sequence data. Invertebr Biol 121:271–324
25. Waller TR (1998) Origin of the molluscan class bivalvia and a phylogeny of major groups. In: Johnston PA, Haggart JW (eds) Bivalves: an eon of evolution—paleobiological studies honoring Norman D. Newell. University of Calgary Press, Calgary, pp 1–45
26. Folch J, Lees M, Sloane-Stanley GH (1957) A simple method for the isolation and purification of total lipides from animal tissues. J Biol Chem 226:497–509
27. Nelson GJ (1993) Isolation and purification of lipids from biological matrices. In: Perkins EG (ed) Analyse of fats, oils and derivatives. AOCS Press, Champaign, pp 20–89
28. Marty Y, Delaunay F, Moal J, Samain JF (1992) Changes in the fatty acid composition of the scallop *Pecten maximus* (L.) during larval development. J Exp Mar Biol Ecol 163:221–234
29. Soudant P, Marty Y, Moal J, Masski H, Samain JF (1998) Fatty acid composition of polar lipid classes during larval development of scallop *Pecten maximus* (L.). Comp Biochem Phys A 121:279–288
30. Napolitano GE, Ackman RG (1993) Fatty acid dynamics in sea scallops *Placopecten magallanicus* (Gmelin, 1791) from Georges Bank, Nova Scotia. J Shell Res 12:267–277
31. Delaunay F, Marty Y, Moal J, Samain JF (1993) The effect of monospecific algal diets on growth and fatty acid composition of *Pecten maximus* (L.) larvae. J Exp Mar Biol Ecol 173:163–179
32. Soudant P, Marty Y, Moal J, Robert R, Quéré C, Le Coz JR, Samain JF (1996) Effect of food fatty acids and sterol quality on *Pecten maximus* gonad composition and reproduction process. Aquaculture 143:361–378
33. Soudant P, Moal J, Marty Y, Samain JF (1996) Impact of the quality of dietary fatty acids on metabolism and the composition of polar lipid classes in female gonads of *Pecten maximus* (L.). J Exp Mar Biol Ecol 205:149–163
34. Soudant P, Moal J, Marty Y, Samain JF (1997) Composition of polar lipid classes in male gonads of *Pecten maximus* (L.). Effect of nutrition. J Exp Mar Biol Ecol 215:103–114
35. Pernet F, Tremblay R, Bourget E (2003) Biochemical indicator of sea scallop (*Placopecten magellanicus*) quality based on lipid class composition. Part I: Broodstock conditionning and young larvae performance. J Shell Res 22:365–376
36. De Moreno JEA, Moreno VJ, Brenner RR (1976) Lipid metabolism of the yellow clam, *Mesodesma mactroïdes*: 2—polyunsaturated fatty acid metabolism. Lipids 11:561–566
37. Chu FLE, Webb KL (1984) Polyunsaturated fatty acids and neutral lipids in developing larvae of the oyster, *Crassostrea virginica*. Lipids 19:815–820
38. Waldock MJ, Holland DL (1984) Fatty acid metabolism in young oysters, *Crassostrea gigas*: polyunsaturated fatty acids. Lipids 19:332–336
39. Ackman RG (1983) Fatty acid metabolism of bivalves. In: Proceedings of the second international conference on aquaculture nutrition. Special Publication 2, pp 358–375
40. Clandinin MT, Field CJ, Hargraves K, Morson L, Zsigmond E (1985) Role of diet fat in subcellular structure and function. Can J Physiol Pharmacol 63:546–556
41. Napolitano GE, Ratnayake WMN, Ackman RG (1988) Fatty acid components of larval *Ostrea edulis* (L.): importance of triacylglycerols as a fatty acid reserve. Comp Biochem Phys 90B:875–883
42. Leray C, Chapelle S, Duportail G, Florentz A (1984) Changes in fluidity and 22:6(n-3) content in phospholipids of trout intestinal bruxh-border membrane as related to environmental salinity. Biochim Biophys Acta 7711:233–238
43. Hazel JR (1988) Homeoviscous adaptation in animal cell membranes. In: Aloia RC, Curtain CC, Gordon LM (eds) Physiological regulation of membrane fluidity. A.R. Liss, New York, pp 149–188
44. Hazel JR (1995) Thermal adaptation in biological membranes: is homeoviscous adaptation the explanation? Annu Rev Physiol 57:19–42
45. Glémet HC, Ballantyne JS (1995) Influences of environmental salinity on the structure and function of gill mitochondria membranes of an osmoconforming invertebrate, *Crassostrea virginica*. Mar Biol 121:673–683
46. Green J (1957) The growth of *Scrobicularia plana* (da Costa) in the gwendraeth estuary. J Mar Biol Assoc UK 36:41–47
47. Xu Y, Kelley RI, Blanck TJJ, Schlame M (2003) Remodeling of cardiolipin by phospholipid transacylation. J Biol Chem 278:51380–51385
48. Xu Y, Malhotra A, Ren M, Schlame M (2006) The enzymatic function of tafazzin. J Biol Chem 281:39217–39224
49. Cao J, Liu Y, Lockwood J, Burn P, Shi Y (2004) A novel cardiolipin-remodeling pathway revealed by a gene encoding an endoplasmic reticulum-associated acyl-CoA:lysocardiolipin acyltransferase (ALCAT1) in mouse. J Biol Chem 279:31727–31734
50. Van Q, Liu J, Lu B, Feingold KR, Shi Y, Lee RM, Hatch GM (2007) Phospholipid scramblase-3 regulates cardiolipin de novo biosynthesis and its resynthesis in growing HeLa cells. Biochem J 401:103–109
51. Gohil VM, Hayes P, Matsuyama S, Schägger H, Schlame M, Greenberg ML (2004) Cardiolipin biosynthesis and mitochondrial respiratory chain function are interdependent. J Biol Chem 279:42612–42618
52. Hoch FL (1998) Minireview: cardiolipins and mitochondrial proton-selective leakage. J Bioenerg Biomembr 30:511–532
53. Gonzalvez F, Gottlieb E (2007) Cardiolipin: setting the beat of apoptosis. Apoptosis 12:877–885
54. Paradies G, Petrosillo G, Pistolese M, Ruggiero FM (2002) Reactive oxygen species affect mitochondrial electron transport complex I activity through oxidative cardiolipin damage. Gene 286:135–141
55. Wodtke E (1981) Temperature adaptation of biological membranes. Compensation of the molar activity of cytochrome *c* oxidase in the mitochondrial energy-transducing membrane during thermal acclimation of the carp (*Cyprinus carpio* L.). Biochim Biophys Acta 640:710–720
56. Kraffe E, Marty Y, Guderley H (2007) Changes in mitochondrial oxidative capacities during thermal acclimation of rainbow trout *Oncorhynchus mykiss*: roles of membrane proteins, phospholipids and their fatty acid compositions. J Exp Biol 210:149–165
57. Valianpour F, Wanders RJA, Overmars H, Vreken P, van Gennip AH, Baas F, Plecko B, Santer R, Becker K, Barth PG (2002) Cardiolipin deficiency in X-linked cardioskeletal myopathy and neutropenia (Barth syndrome, MIM 302060): a study in cultured skin fibroblast. J Pediatr 141:729–733
58. Schlame M, Towbin JA, Heerdt PM, Jehle R, DiMauro S, Blank TJJ (2002) Deficiency of tetralinoleyl-cardiolipin in Barth syndrome. Ann Neurol 51:634–637
59. Ma L, Vaz FM, Gu Z, Wanders RJA, Greenberg ML (2004) The human *TAZ* gene complements mitochondrial dysfunction in the yeast *taz*1D mutant. Implications for Barth syndrome. J Biol Chem 279:44394–44399

Lipids (2008) 43:971–976
DOI 10.1007/s11745-008-3212-3

ORIGINAL ARTICLE

An Improved Method for Separating Cardiolipin by HPLC

Gwendolyn Barceló-Coblijn · Eric J. Murphy

Received: 15 March 2008 / Accepted: 24 June 2008 / Published online: 18 July 2008
© AOCS 2008

Abstract Herein we report an improved method to separate cardiolipin (Ptd_2Gro) from tissue total lipid extracts using a biphasic solvent system combined with high performance liquid chromatography. This method uses a normal phase silica column and two mobile phases: mobile phase A that was *n*-hexane:2-propanol (3:2 by vol) and mobile phase B that was *n*-hexane:2-propanol:water (56.7:37.8:5.5 by vol). The initial solvent conditions were 95% A and 5% B, with a flow rate of 1.5 mL/min. The samples were from non-derivatized aliquots of liver, heart, or brain lipid extracts. The peak corresponding to Ptd_2Gro appeared at 31 min, was well defined and did not overlap with neighboring peaks. The adjacent peak corresponded to ethanolamine glycerophospholipids and the remaining phospholipids were eluted in a single peak. The identity of the phospholipids separated by this method was verified by thin layer chromatography (TLC) and fatty acid analysis, which confirmed that the Ptd_2Gro was well resolved from other phospholipids. This method is useful to separate and quantify Ptd_2Gro from small tissue samples thereby avoiding the variability associated with TLC methods.

Keywords High Performance liquid Chromatography · Cardiolipin · Phospholipids · Brain · Liver · Heart · Separation

Abbreviations

ARA	Arachidonic acid
DHA	Docosahexaenoic acid
EtnGpl	Ethanolamine glycerophospholipids
FAME	Fatty acid methyl esters
GLC	Gas liquid chromatography
HPLC	High performance liquid chromatography
TLC	Thin layer chromatography
Ptd_2Gro	Cardiolipin

Introduction

Cardiolipin (Ptd_2Gro) is a unique phospholipid that contains three glycerol molecules, two phosphate groups, and four fatty acids. Ptd_2Gro is synthesized in mitochondria where it represents 12% of the total mitochondrial phospholipids [1]. In rat heart and liver, it represents approximately 7% of total phospholipids, while the brain contains substantially less Ptd_2Gro, where it represents only 2.5% of the total brain phospholipids [2]. While Ptd_2Gro is found in bacteria, in mammals it is found almost exclusively in the inner mitochondrial membrane and at intermembrane contact sites [3, 4]. Ptd_2Gro is essential for the optimal function of numerous mitochondrial enzymes involved in energy metabolism, such as cytochrome *c* oxidase. It binds tightly to the cytochrome *c* oxidase complex and this interaction is required for efficient electron transport activity [5]. In addition, alterations in the content or structure of Ptd_2Gro have been observed in aging [6, 7] and in a variety of diseases as, for example,

---

G. Barceló-Coblijn · E. J. Murphy (✉)
Department of Pharmacology, Physiology, and Therapeutics,
School of Medicine and Health Sciences,
University of North Dakota, 501 N. Columbia Road,
Room 3700, Grand Forks, ND 58202-9037, USA
e-mail: emurphy@medicine.nodak.edu

E. J. Murphy
Department of Chemistry, University of North Dakota,
Grand Forks, ND 58202-9037, USA

Present Address:
G. Barceló-Coblijn
Department of Biology, University of the Balearic Islands,
Illes Balears, Palma de Mallorca, Spain

Barth's syndrome, a rare genetic disorder in which the synthesis of Ptd_2Gro is deficient and mitochondrial function is impaired [8]. Although these observations imply a critical function for Ptd_2Gro, the exact role in mitochondria is still not clear.

There are different techniques available for isolating and analyzing Ptd_2Gro content (for review see [9]). It can be separated using one- or two-dimensional thin layer chromatography (TLC) [10–12], by column chromatography [13] or by high performance liquid chromatography (HPLC) [14]. However, separations using TLC are subject to variability in resolution based upon humidity and the fatty acids are subject to oxidation, both of which are minimized using an HPLC separation. In addition, Ptd_2Gro can be measured spectrofluorimetrically using a Ptd_2Gro specific dye *n*-nonyl acridine orange (NOA) [15]. Because there are concerns regarding the specificity of NOA to Ptd_2Gro [16] and its dependency on membrane potential [17, 18], the reliability of this dye to be used to quantify Ptd_2Gro is questionable. While this technique is not sufficient to analyze Ptd_2Gro molecular species, such analysis can be achieved by GC–MS, but this method involves several derivatization steps. In order to avoid sample manipulation and any chromatographic separation using GC–MS, shotgun lipidomics has been used to analyze Ptd_2Gro molecular species and mass using an approach utilizing multidimensional mass spectroscopy [19].

Here we have developed a HPLC method to isolate Ptd_2Gro from total lipid extracts using a solvent system and column matrix that we routinely use to separate major phospholipids. The reason for improving our current method was that although it is able to separate minor phospholipids such as lysophosphatidylethanolamine and lysophosphatidylcholine, it does not separate Ptd_2Gro [20]. Although we have used TLC methods in the past [21, 22], we found these separations to be highly dependent on environmental conditions and required multiple runs per sample to verify values, with the need for such repetition being the driving force for the development of our new HPLC based method. This new method allows a clear separation of Ptd_2Gro from the rest of phospholipids even from tissues with low Ptd_2Gro content, such as brain.

Methods

Animals

Male mice (25–30 g) 9-months old were maintained on standard laboratory chow diet and water ad libitum. All mice used in this study were killed by head-focused microwave irradiation (2.8 kW, 1.35 s; Cober Electronics, Inc., Norwalk, CT, USA). This study was conducted in accordance with the National Institutes of Health Guidelines for Care and Use of Laboratory Animals (NIH Publication 80-23) and under an animal protocol approved by the IACUC at the University of North Dakota (Protocol 0110-1).

Lipid Extraction

Livers, hearts, and brains were rapidly removed from mice post-mortem, the tissue immediately frozen in liquid nitrogen, and then pulverized under liquid nitrogen temperatures to a fine homogeneous powder. Lipids were extracted using *n*-hexane/2-propanol (3:2 vol/vol) from approximately 100 mg of frozen tissue [23, 24]. Tissue extracts were centrifuged at 1,000×*g* to pellet debris. The lipid-containing liquid phase was decanted, placed in a screw top test tube, overlaid with a nitrogen atmosphere, and stored at −80 °C until analysis.

Thin Layer Chromatography

Individual phospholipid classes were separated by TLC using Whatman silica gel-60 plates (20 cm × 20 cm, 250 μm) that were heat-activated at 110 °C for 1 h. Samples streaked onto plates and the phospholipids were separated using chloroform:methanol:acetic acid:water (55:37.5:3:2 by vol) [10]. This method separates all major phospholipids, including Ptd_2Gro, phosphatidic acid, and phosphatidylglycerol. Ptd_2Gro was identified using bovine heart Ptd_2Gro (catalog number 99054; Avanti Polar Lipids, Alabaster, AL, USA) as a standard. Mass was determined by assaying for the lipid phosphorus content [25] and converted to moles of using a standard curve. Moles of Ptd_2Gro were calculated by dividing the total moles of lipid phosphorus by 2.

Fatty Acid Analysis

The liver, heart, and brain Ptd_2Gro and EtnGpl fractions collected from the HPLC separation were subjected to base-catalyzed transesterification, converting the phospholipid acyl chains to fatty acid methyl esters (FAME). To each fraction, 2 mL of 0.5 M KOH dissolved in anhydrous methanol were added [26]. FAME were extracted from the methanol using 2 mL of *n*-hexane and the *n*-hexane phase containing the FAME was removed. The lower phase was re-extracted two more times with 3 mL of *n*-hexane and these washes were combined with the original aliquot.

Individual fatty acids were separated by gas liquid chromatography (GLC) using an SP-2330 column (0.32 mm ID × 30 m length) and a Trace GLC (ThermoElectron, Austin, TX, USA) equipped with dual autosamplers and dual flame ionization detectors. Fatty acids were quantified using a standard curve from commercially purchased standards (NuChek Prep, Elysian, MN) and 17:0 was used as the internal standard.

HPLC Method

Prior to phospholipid analysis, the lipid extracts were dried under nitrogen and redissolved in a known volume of *n*-hexane/2-propanol/water (56.7:37.8:5.5, by vol). The separation method for Ptd_2Gro used a biphasic solvent system with a step gradient and a Selectosil column (4.6 × 250 mm, 5 µm, Phenomenex, Torrance, CA, USA). Solvents used were HPLC grade *n*-hexane and 2-propanol from EMD and purchased from VWR (Chicago, IL, USA). The HPLC system consisted of a Beckman 126 pump and a 166 UV/Vis detector, the eluant was monitored at 205 nm.

The solvent system consisted of a combination of two mobile phases: Mobile phase A was *n*-hexane:2-propanol (3:2 by vol) and mobile phase B was *n*-hexane:2-propanol:water (56.7:37.8:5.5 by vol). The step gradient was as follows (1) initial conditions mobile phase A was 95%; (2) at 5 min mobile phase A was decreased to 90% and maintained for 5 more minutes; (3) at 10 min mobile phase A was decreased to 85% and maintained for 10 min; and (4) at 20 min mobile phase decrease to 0% A maintained for 30 min. The final step ensured that all possible phospholipids remaining on the column were removed. To return the column to stable starting conditions, mobile phase A was increased to 95% and maintained for 5 min. The method program is summarized in Table 1. The total run time was 55 min and the flow rate was 1.5 mL/min.

Results

Separation of Ptd_2Gro by HPLC

Total lipids were extracted by *n*-hexane:2-propanol (3:2, by vol) from 100 mg of liver, heart, or brain tissue. An aliquot of each tissue extract corresponding to 5% of heart and liver lipid extract and 10% of brain lipid extract, was injected onto the HPLC column. Our previous experience for using TLC to separate phospholipid have indicated that brain Ptd_2Gro is present in a lower concentration compared to heart and liver Ptd_2Gro, necessitating injecting twice the amount of brain total lipid in order to approximate the amount used in the analysis of heart and liver lipid extracts. The elution profile shows three major peaks for each tissue analyzed (Fig. 1). We collected the first two peaks for analysis by TLC and fatty acid composition analysis by GLC. The first peak (*peak 1*), which we hypothesized was Ptd_2Gro, eluted at 31 min, while the second peak (*peak 2*), which we hypothesized could correspond mainly to EtnGpl, eluted at 33 min. Note that the peak corresponding to Ptd_2Gro was a well defined peak that did not overlap

Table 1 Step gradient of the new HPLC method for Ptd_2Gro separation

Time (min)	Mobile phase A (%)	Mobile phase B (%)
0	95	5
5	90	10
10	85	15
20	0	100
50	95	5

Mobile phase A was *n*-hexane:2-propanol (3:2 by vol); mobile phase B was *n*-hexane:2-propanol:water (56.7:37.8:5.5 by vol)

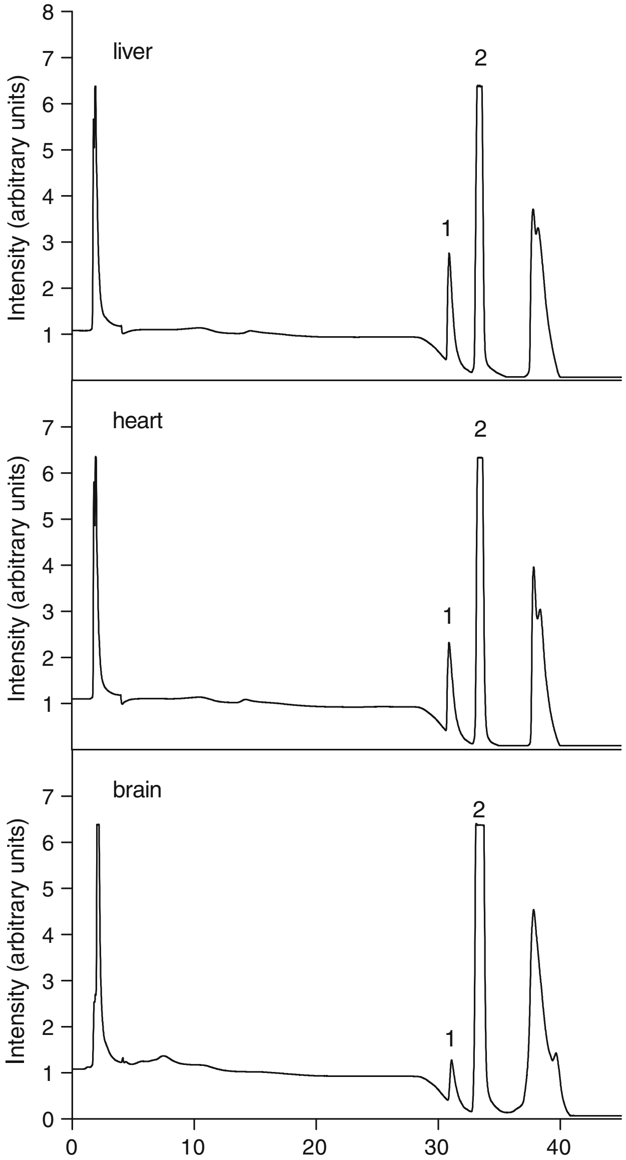

Fig. 1 High performance liquid chromatography elution profile of liver, heart, and brain total lipids. *Peak 1* corresponds to Ptd_2Gro while *peak 2* contains mainly EtnGpl

with neighboring peaks. *Peak 1* appears clearly in all tissues, even in brain where Ptd_2Gro level is low compared to liver and heart.

Analysis of the Ptd_2Gro Fraction by TLC

To verify that the fraction named as *peak 1* was indeed Ptd_2Gro, we applied this peak to a TLC plate and resolved it via the solvent system described previously [10]. *Peak 1* or the putative Ptd_2Gro fraction (F) collected from each of the tissues was spotted next to its corresponding total lipid extract (T) (Fig. 2). In Fig. 2, it is clear that only one phospholipid was detected in the lane corresponding to *peak 1* after visualization with iodine. In addition, this phospholipid ran to the same height as the Ptd_2Gro of the total lipid extract and as the Ptd_2Gro standard (st). Visualization with 6-*p*-toluidino-2-naphthalenesulfonic acid, a very sensitive fluorescent indicator dye [27], also demonstrated no contamination of the Ptd_2Gro with other phospholipids or neutral lipids, e.g., triacylglycerols, cholesteryl esters (data not shown). Thus, the apparent baseline separation of *peak 1* from *peak 2*, was confirmed by TLC and the identity of *peak 1* was Ptd_2Gro as compared to authentic standards.

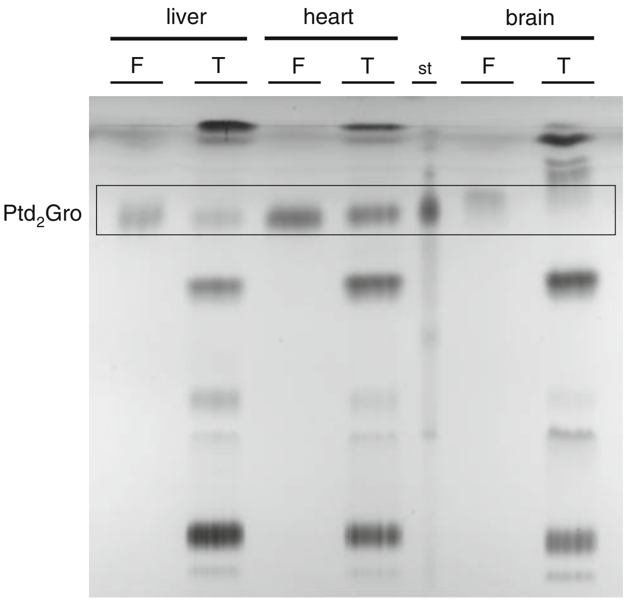

Fig. 2 Thin layer chromatography (TLC) separation of isolated *peak 1* from the HPLC separation. Ptd_2Gro fractions (F) obtained by the new HPLC method (labelled as *Peak 1*) and total lipid extracts (E) from liver, heart and brain were separated by one-dimensional TLC as described in materials and methods. *St* commercial Ptd_2Gro standard. Phospholipid fractions were visualized by exposing the plate to iodine vapors. Other bands on the TLC plate correspond to, beginning at bottom of the plate, sphingomyelin, choline glycerophospholipid, phosphatidylserine, phosphatidylinositol, and ethanolamine glycerophospholipid (EtnGpl)

Fatty Acid Analysis of the Ptd_2Gro Fraction

The main fatty acid in liver Ptd_2Gro is linoleic acid (LNA, 18:2n-6) representing 70% of total Ptd_2Gro fatty acids [28] while in bovine heart, Ptd_2Gro contains about 80–90% LNA [29]. We took advantage of this characteristic fatty acid composition, to verify that *peak 1* corresponded to Ptd_2Gro. Thus, we analyzed both *peak 1* and *peak 2* fatty acid composition by gas chromatography (Table 1). The fraction corresponding to liver and heart Ptd_2Gro contained a very high percentage of LNA, 65 and 87%, respectively, confirming that the peak was indeed Ptd_2Gro. Interestingly, brain Ptd_2Gro fatty acid composition differed considerably, containing oleic acid (18:1n-9) as the predominant fatty acid (34.4%) and a much lower level of LNA (9%), results that agree with published data [30, 31]. In addition, brain Ptd_2Gro contained higher amounts of longer and more unsaturated fatty acids such as arachidonic acid (ARA, 20:4n-6, 18.6%) and docosahexaenoic acid (DHA, 22:6n-3, 11.1%), consistent with previously published data [22]. In addition, brain The fatty acid composition of *peak 2* was clearly different as compared to *peak 1*, being highly enriched in ARA and DHA, a composition which is characteristic of the EtnGpl [2]. The lack of high amounts of ARA and DHA in the liver Ptd_2Gro, adds additional evidence that the Ptd_2Gro separated by HPLC was indeed well separated from *peak 2*, which was EtnGpl.

Intersample Variability

We compared mouse brain Ptd_2Gro mass obtained by TLC and by HPLC from the same seven mice. While mass of Ptd_2Gro separated by TLC was 573 ± 88 nmol/g ww ($n = 7$), mass of Ptd_2Gro separated by HPLC was 739 ± 97 nmol/g ww ($n = 7$). While the relative standard deviation between these two methods was similar 15.3 and 13.1%, there was a significant difference between the mass ($p = 0.0057$, two-way, unpaired Student's *t*-test), indicating that some Ptd_2Gro was lost when brain lipids are separated by TLC (see Sect. 'Discussion').

Discussion

In mammals, as in other eukaryotes, Ptd_2Gro is a minor phospholipid present only in mitochondrial membranes [3, 4], with levels corresponding to the amount of mitochondria found in any given tissue. Thus, in mitochondria rich tissues such as heart and liver, Ptd_2Gro is found at higher levels as compared with brain [2, 21, 22]. While we routinely use TLC to separate brain phospholipids, when brain lipids are separated using this method, Ptd_2Gro appears as a disperse and blurry band, mainly due to its diverse fatty acid composition (Table 2) [22]. For this reason we sought an alternative method to separate and isolate Ptd_2Gro, modifying a previous HPLC method designed to separate major phospholipids and minor phospholipids as lysophosphatidylcholine and lysophosphatidylethanolamine [20].

This new method is based on the combination of two mobile phases. Mobile phase A is formed by *n*-hexane:2-propanol (3:2 by vol), while mobile phase B is formed by *n*-hexane:2-propanol:water (56.7:37.8:5.5 by vol) where water was added to increase the polarity of the solvent system. As observed in the HPLC eluting profile (Fig. 1) and in the TLC separation (Fig. 2), our new method allowed a clear separation of Ptd_2Gro and the resolution was not sensitive to different concentrations of total lipid extracts commonly used for such analysis (Fig. 3). We spotted the eluted *peak 1* on a TLC plate (F lane) and it clearly ran to the same position as the Ptd_2Gro standard (Fig. 2). F lane did not present with any additional spots and consequently we considered that this was a first demonstration that the eluted *peak 1* contained only Ptd_2Gro. In addition, we developed the TLC plate with a fluorescent dye (6-*p*-toluidino-2-naphthalenesulfonic acid), which is more sensitive than iodine [27]. Even under these conditions, no additional bands appeared F lanes.

For further confirmation, we analyzed the fatty acid composition of *peak 1* and *peak 2* (Fig. 1). The results of these analysis confirmed that the peak eluting at 31 min was Ptd_2Gro (Table 2). Heart and liver Ptd_2Gro fatty acid composition was highly enriched in LNA [32, 33], while brain Ptd_2Gro fatty acid composition differ from previous tissues [22]. This different fatty acid composition is consistent with the fact that brain contains extremely low concentrations of LNA [2, 34]. The role that the unique brain Ptd_2Gro fatty acid composition has with regard to function remains elusive, although recent evidence indicates that changes in these fatty acids alters the membrane environment in a manner that can alter mitochondrial function [22].

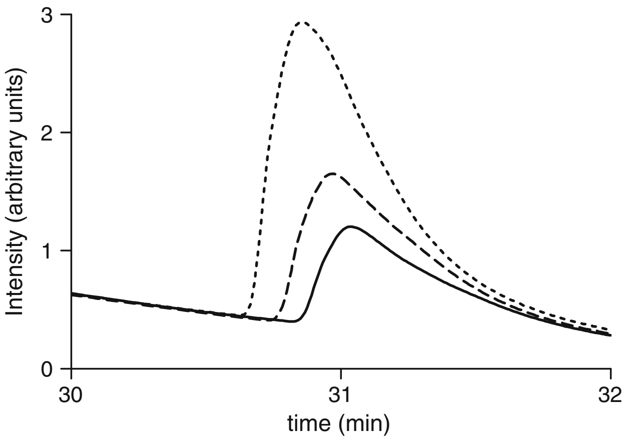

Fig. 3 The effect of total lipid concentration on the resolution of Ptd_2Gro and EtnGpl was determined. We injected 100 nmol of total heart phospholipids containing approximately 10 nmol of Ptd_2Gro (*continuous line*), 200 nmol of total heart phospholipids containing approximately 20 nmol of Ptd_2Gro (*dashed line*), and 300 nmol of total heart phospholipids containing approximately 30 nmol of Ptd_2Gro (*dotted line*)

Table 2 Liver, heart, and brain fatty acid composition of *peak 1* and *peak 2* separated by the new HPLC method

FAME	Liver		Heart		Brain	
	Peak 1	Peak 2	Peak 1	Peak 2	Peak 1	Peak 2
16:0	3.4	18.0	1.7	5.6	5.6	5.0
16:1	1.8	0.5	ND	ND	2.9	0.2
18:0	1.5	19.9	0.9	27.4	4.6	22.5
18:1n-9	9.8	4.8	5.3	4.1	34.4	13.0
18:1n-7	8.5	3.8	2.1	2.3	7.9	3.6
18:2n-6	68.2	9.3	87.3	13.3	12.0	0.6
18:3n-3	0.7	0.3	ND	0.3	ND	0.3
20:1n-9	ND	ND	ND	ND	0.7	4.1
20:2n-6	0.9	ND	ND	ND	ND	ND
20:3n-6	2.1	0.6	0.5	0.2	2.2	0.4
20:4n-6	1.7	26.4	0.8	20.4	18.6	15.1
20:5n-3	ND	0.4	ND	0.2	ND	ND
22:4n-6	ND	1.2	ND	0.9	ND	6.1
22: 5n-6	ND	0.3	ND	0.6	ND	0.4
22:5n-3	0.6	2.4	0.6	2.9	ND	0.3
22:6n-3	0.8	12.1	0.6	21.8	11.1	28.5

Values are expressed as percentage of total fatty acid (mol%). Values are *n* = 1 for each tissue

ND non detected fatty acid

Because the main problem in our studies was to adequately separate and isolate brain Ptd_2Gro, we compared the mass of brain Ptd_2Gro in the same cohort of seven mice separated by either TLC (573 ± 88 nmol/g ww, $n = 7$) or by HPLC (739 ± 97 nmol/g ww, $n = 7$). The results clearly showed that we obtained 1.3-fold more Ptd_2Gro when we separated total lipids by HPLC, although the relative standard deviation was similar. One explanation accounting for this difference is the diffuse nature of the brain Ptd_2Gro band (Fig. 2), more than likely due to the diverse fatty acid composition of brain Ptd_2Gro. This diffuse nature could lead to the inadequate removal of the band from the TLC plate.

Using the same solvent system of Dugan et al. [20] is an advantage because it permits the separation all the phospholipids with no need to change systems, but would require modifying the step gradient program after the elution of the Ptd_2Gro. An additional advantage of this method is that Ptd_2Gro is separated directly from the total lipid extract with no need for derivatization. In conclusion, this new HPLC method is a simple method which allows a good separation of Ptd_2Gro with no need of derivatization, previous separation of neutral lipids, is compatible with different tissues, and it is highly compatible with a HPLC method that can be used to separate the remaining phospholipid classes.

Acknowledgments This work was funded in part as a project to EJ Murphy on a COBRE grant from the NIH 1P20 RR117699.

References

1. de Kroon A, Dolis D, Mayer A, Lill R, de Kruijff B (1997) Phospholipid composition of highly purified mitochondrial outer membranes of rat liver and *Neurospora crassa*. Is cardiolipin present in the mitochondrial outer membrane? Biochim Biophys Acta 1325:108–116
2. Barcelo-Coblijn G, Collison LW, Jolly CA, Murphy EJ (2005) Dietary alpha-linolenic acid increases brain but not heart and liver docosahexaenoic acid levels. Lipids 40:787–798
3. Ardail D, Privat JP, Egret-Charlier M, Levrat C, Lerme F, Louisot P (1990) Mitochondrial contact sites. Lipid composition and dynamics. J Biol Chem 265:18797–18802
4. Hovius R, Lambrechts H, Nicolay K, de Kruijff B (1990) Improved methods to isolate and subfractionate rat liver mitochondria. Lipid composition of the inner and outer membrane. Biochim Biophys Acta 1021:217–226
5. Nicolay K, de Kruijff B (1987) Effects of Adriamycin on respiratory chain activities in mitochondria from rat liver, rat heart and bovine heart. Evidence for a preferential inhibition of complex III and IV. Biochim Biophys Acta 892:320–330
6. Paradies G, Ruggiero FM, Gadaleta MN, Quagliariello E (1992) The effect of aging and acetyl-L-carnitine on the activity of the phosphate carrier and on the phospholipid composition in rat heart mitochondria. Biochim Biophys Acta 1103:324–326
7. Paradies G, Ruggiero FM, Petrosillo G, Gadaleta MN, Quagliariello E (1994) The effect of aging and acetyl-L-carnitine on the function and on the lipid composition of rat heart mitochondria. Ann N Y Acad Sci 717:233–243
8. Kawasaki K, Kuge O, Chang SC, Heacock PN, Rho M, Suzuki K, Nishijima M, Dowhan W (1999) Isolation of a Chinese hamster ovary (CHO) cDNA encoding phosphatidylglycerophosphate (PGP) synthase, expression of which corrects the mitochondrial abnormalities of a PGP synthase-defective mutant of CHO-K1 cells. J Biol Chem 274:1828–1834
9. Schlame M (2007) Assays of cardiolipin levels. Methods Cell Biol 80:223–240
10. Jolly C, Hubbell T, Behnke WD, Schroeder F (1997) Fatty acid binding protein: stimulation of microsomal phosphatidic acid formation. Arch Biochem Biophys 341:112–121
11. Wolff R, Combe NA, Entressangles B (1985) Positional distribution of fatty acids in cardiolipin of mitochondria from 21-day-old rats. Lipids 20:908–914
12. Fine J, Sprecher H (1982) Unidimensional thin-layer chromatography of phospholipids on boric acid-impregnated plates. J Lipid Res 23:660–663
13. Yabuuchi H, O'Brien JS (1968) Brain cardiolipin: isolation and fatty acid positions. J Neurochem 15:1383–1390
14. Lesnefsky E, Stoll MS, Minkler PE, Hoppel CL (2000) Separation and quantitation of phospholipids and lysophospholipids by high-performance liquid chromatography. Anal Biochem 285:246–254
15. Petit J, Maftah A, Ratinaud MH, Julien R (1992) 10N-nonyl acridine orange interacts with cardiolipin and allows the quantification of this phospholipid in isolated mitochondria. Eur J Biochem 209:267–273
16. Gohil VM, Gvozdenovic-Jeremic J, Schlame M, Greenberg ML (2005) Binding of 10-N-nonyl acridine orange to cardiolipin-deficient yeast cells: implications for assay of cardiolipin. Anal Biochem 343:350–352
17. Jacobson J, Duchen MR, Heales SJ (2002) Intracellular distribution of the fluorescent dye nonyl acridine orange responds to the mitochondrial membrane potential: implications for assays of cardiolipin and mitochondrial mass. J Neurochem 82:224–233
18. Keij JF, Bell-Prince C, Steinkamp JA (2000) Staining of mitochondrial membranes with 10-nonyl acridine orange, MitoFluor Green, and MitoTracker Green is affected by mitochondrial membrane potential altering drugs. Cytometry 39:203–210
19. Han X, Yang K, Yang J, Cheng H, Gross RW (2006) Shotgun lipidomics of cardiolipin molecular species in lipid extracts of biological samples. J Lipid Res 47:864–879
20. Dugan L, Demediuk P, Pendley CEII, Horrocks LA (1986) Separation of phospholipids by high-performance liquid chromatography: all major classes, including ethanolamine and choline plasmalogens, and most minor classes, including lysophosphatidylethanolamine. J Chromatogr 378:317–327
21. Barcelo-Coblijn G, Golovko MY, Weinhofer I, Berger J, Murphy EJ (2007) Brain neutral lipids mass is increased in alpha-synuclein gene-ablated mice. J Neurochem 101:132–141
22. Ellis C, Murphy EJ, Mitchell DC, Golovko MY, Scaglia F, Barcelo-Coblijn GC, Nussbaum RL (2005) Mitochondrial lipid abnormality and electron transport chain impairment in mice lacking alpha-synuclein. Mol Cell Biol 25:10190–10201
23. Hara A, Radin NS (1978) Lipid extraction of tissues with a low-toxicity solvent. Anal Biochem 90:420–426
24. Radin N (1988) Lipid extraction. In: Boulton AA, Baker GB, Horrocks LA (eds) Neuromethods lipids and related compounds. Humana, Clifton
25. Rouser G, Siakotos AN, Fleischer S (1966) Quantitative analysis of phospholipids by thin-layer chromatography and phosphorus analysis of spots. Lipids 1:85–86
26. Brockerhoff H (1975) Determination of the positional distribution of fatty acids in glycerolipids. Methods Enzymol 35:315–325
27. Jones M, Keenan RW, Horowitz P (1982) Use of 6-p-toluidino-2-naphthalenesulfonic acid to quantitate lipids after thin-layer chromatography. J Chromatogr 237:522–524
28. Schlame M, Brody S, Hostetler KY (1993) Mitochondrial cardiolipin in diverse eukaryotes. Comparison of biosynthetic reactions and molecular acyl species. Eur J Biochem 212:727–735
29. Keenan T, Awasthi YC, Crane FL (1970) Cardiolipin from beef heart mitochondria: fatty acid positioning and molecular species distribution. Biochem Biophys Res Commun 40:1102–1109
30. Bayir H, Tyurin VA, Tyurina YY, Viner R, Ritov V, Amoscato AA, Zhao Q, Zhang XJ, Janesko-Feldman KL, Alexander H, Basova LV, Clark RS, Kochanek PM, Kagan VE (2007) Selective early cardiolipin peroxidation after traumatic brain injury: an oxidative lipidomics analysis. Ann Neurol 62:154–169
31. Cheng H, Mancuso DJ, Jiang X, Guan S, Yang J, Yang K, Sun G, Gross RW, Han X (2008) Shotgun lipidomics reveals the temporally dependent, highly diversified cardiolipin profile in the mammalian brain: temporally coordinated postnatal diversification of cardiolipin molecular species with neuronal remodeling. Biochemistry 47:5869–5880
32. Hoch F (1992) Cardiolipins and biomembrane function. Biochim Biophys Acta 1113:71–133
33. Hostetler K (1982) Polyglycerolphospholipids. In: Hawthorne JN, Ansell GB (eds) Phospholipids. Elsevier, Amsterdam
34. Castagnet P, Golovko MY, Barcelo-Coblijn GC, Nussbaum RL, Murphy EJ (2005) Fatty acid incorporation is decreased in astrocytes cultured from alpha-synuclein gene-ablated mice. J Neurochem 94:839–849

Lipids (2008) 43:977
DOI 10.1007/s11745-008-3213-2

ERRATUM

A Whole Body, In Vivo, Fatty Acid Balance Method to Quantify PUFA Metabolism (Desaturation, Elongation and Beta-oxidation)

**Giovanni M. Turchini · David S. Francis ·
Sena S. De Silva**

Published online: 19 August 2008
© AOCS 2008

**Erratum to: Lipids (2007) 42:1065–1071
DOI 10.1007/s11745-007-3105-x**

Page 1068–1070, in "Computation Example", "Discussion" and also in Table 1: there has been a mistake in reporting the unit measure. In all instances in which in the text it was reported mmol (millimoles) it should be written μmol (micromoles).

Page 1066, right column, line 15: "(=FA accumulation − FA intake − FA excretion)" should be "[=FA accumulation − (FA intake − FA excretion)]".

Page 1068, left column, Eq. 13:

1. in the text: "per day" should be "per total no. of days".
2. The reported equation contains two mistakes. "Gram of BW day^{-1} = (initial body weight + final body weight) × 2^{-1} × no. of days^{-1}" should be "Gram of BW day = (initial body weight + final body weight) × 2^{-1} × no. of days".
3. On the right side of the equation the indication of the Eq. (13) is missing.

Page 1068, left column, Eqs. 14, 15 and 16: "(gram of BW day^{-1})" should be "(gram of BW day)" and similarly on pp. 1069–1070, where the same equations were reported in the "Computation Example"

Page 1065, right column, line 6: "18:3" should be "18:3n-3".

The online version of the original article can be found under doi:10.1007/s11745-007-3105-x.

G. M. Turchini (✉) · D. S. Francis
School of Life & Environmental Sciences, Deakin University,
PO Box 423, Warrnambool, VIC 3280, Australia
e-mail: giovanni.turchini@deakin.edu.au

S. S. De Silva
Network of Aquaculture Centers in Asia-Pacific, PO Box 1040,
Kasetsart Post Office, Bangkok 10903, Thailand

Introduction

The abundance of linoleic acid (C18.2ω6) and linolenic acid (C18.3ω3) in higher plants coincides with the occurrence of multiple lipoxygenase (LOX) enzymes that specifically oxygenate these polyunsaturated fatty acids. Linoleic acid has only two available positions for LOX-catalyzed oxygenation, at C-9 or C-13, and all LOX activities in plants target one position or the other, or both. Although LOX activities abound in plant tissues, and LOX-encoding genes have been identified in dozens of plant species, the positional specificity of the vast majority of plant *LOX* genes remains to be determined [1]. One issue addressed here concerns the identification of a specific *9-LOX* gene in *Arabidopsis* (AtLOX1) and tomato (LOXA). An accompanying manuscript by Andreou et al. [2] details a 9-LOX characterization from potato.

Currently there is no direct evidence showing how LOX enzymes catalyze their specific oxygenations [3]. The amino acid sequences in the gene family are well conserved, indicating that in general terms the arrangement of the catalytic machinery is conserved. A single atom of non-heme iron is held in place by well-conserved amino acid ligands comprised mainly of histidines and the carboxyl group of the C-terminal amino acid, usually an isoleucine. Within this conserved structural framework, individual LOX enzymes are known to oxygenate at specific positions on the fatty acid and in either the *R* or *S* stereoconfiguration. To accommodate all the known activities within the well conserved enzyme structures, one of the variables proposed in individual enzymes is a change in the head-to-tail orientation of the bound fatty acid substrate. This was proposed originally in 1972 as the logical explanation for how corn 9*S*-LOX and soybean 13*S*-LOX abstract the 11*R* and 11*S* hydrogen respectively from linoleic acid in forming their 9*S*-HPODE and 13*S*-HPODE products (Fig. 1a) [4]. Other lines of circumstantial evidence point to 13*S* oxygenation being associated with the "tail-first" mode of fatty acid binding. For example, 13-LOX can oxygenate very large esters such as linoleoylphosphatidylcholine in the same way as free linoleic acid (e.g., ref. [5]). This suggests that 13*S* oxygenation involves tail-first entry of the fatty acid into the active site, as it is hard to imagine a carboxyl esterified to phosphatidylcholine entering the LOX active site.

Substrate binding orientation in 9*S*-LOX has been deduced in different ways in the literature. In contrast to the earlier conclusion of carboxyl-first substrate binding (Fig. 1a) [4], two separate observations lead logically to a contrary conclusion [6, 7]. The first relates to a known activity of several plant 9-LOX, namely that the main product of arachidonic acid oxygenation is the 5*S*-hydroperoxide. van Zadelhoff et al. [6] reported that when arachidonate ethanolamide (anandamide) is metabolized by purified barley or tomato 9-LOX, the main specific oxygenation produces the 11*S*-hydroperoxide. This suggests that the carbon chain has slipped into a different alignment in the active site, and given the presence of the bulky anandamide moiety at the carboxyl end, it is hard to see why this would force the fatty acid deeper into the active site. Therefore, the investigators drew the opposite conclusion, that the fatty acid binds tail-first in 9-LOX [6]. Butovich and Reddy observed that 1-linoleoyl-glycerol is metabolized similarly to linoleic acid by potato 9-LOX (to the 9-hydroperoxide), and as this would seem to be incompatible with carboxyl end-first binding, they also came to the logical conclusion that the fatty acid substrate binds tail-first in 9-LOX.

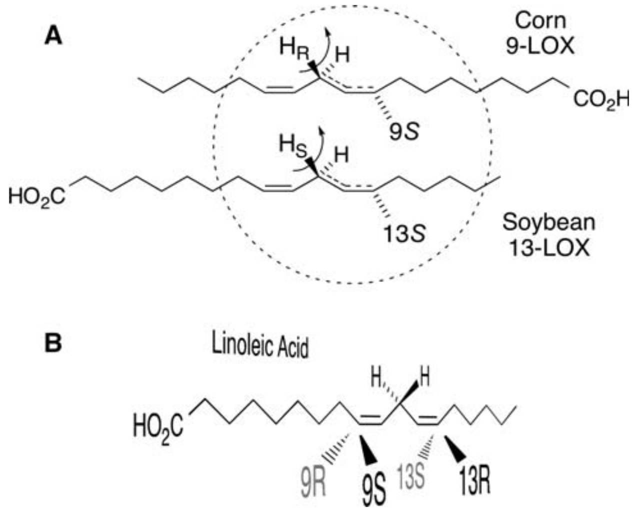

Fig. 1 Stereochemistry of linoleic acid oxygenation. *Panel a*: Stereospecific hydrogen abstraction and specific oxygenation of linoleic acid retain the same spatial relationship in corn 9-LOX and soybean 13-LOX if the substrates adopt reversed orientations in the respective enzyme active sites. Adapted from ref. [35]. *Panel b*: A drawing in perspective illustrating potential oxygenation of linoleic acid at each end of the pentadiene. Note that 9*S* and 13*R* oxygenations are on the same face of the molecule, and 9*R*/13*S* on the other face. Adapted from ref. [3]

Herein we address the issue of substrate binding in 9-LOX by testing a model that predicts reaction specificity and the formation of *R* or *S* configuration products in LOX enzymes [8]. A single active site amino acid was found to exert a major influence over *R* or *S* oxygenation [9]. This key determinant is conserved as an Ala in *S* lipoxygenases and a Gly in *R* lipoxygenases. An Ala allows oxygenation deep in the active site cavity and gives *S*-hydroperoxides while a change to Gly switches the position of oxygenation across the face of the reacting pentadiene and gives *R*-hydroperoxide stereochemistry. The model predicts that linoleic acid 9*S*-LOX (which naturally have Ala in the key position), should switch to forming 13*R*-hydroperoxide after the appropriate Ala-to-Gly mutation (see Fig. 1b).

Given that the model fits with many different LOX enzymes with different predicted orientations of fatty acid binding, the model is also only compatible with the carboxyl end-first substrate orientation in plant 9-LOX.

Experimental Procedures

Materials

Fatty acids were purchased from NuChek Prep Inc. (Elysian, MN). [1-^{14}C]linoleic, and [1-^{14}C]arachidonic acids were purchased from Perkin Elmer Life Sciences. Standards of racemic HPODEs and HODEs were prepared by vitamin E-controlled autoxidation [10]. 9*S*-H(P)ODE was prepared using the 9-LOX activity in potato tuber extracts, and 13*S*-H(P)ODE using soybean lipoxygenase (Sigma type V) [11]. 1-Palmitoyl-2-linoleoyl-*sn*-glycero-3-phosphatidylcholine (C_{16}/LA-PC) and 1-palmitoyl-2-arachidonoyl-*sn*-glycero-3-phosphatidylcholine (C_{16}/AA-PC) were purchased from Avanti Polar Lipids, Inc. (Alabaster, AL).

Construction of Expression Vectors

A full-length At*LOX1* cDNA [12] as kindly provided by Dr. Kaye Peterman (Wellesley College). A PCR-based strategy was used to construct an expression vector for production of AtLOX1 with an N-terminal $(His)_6$-tag. Forward and reverse primers that amplify the cDNA contained *NdeI* and *Xho*I restriction sites, respectively. The sequence of the forward primer was 5′-GGAATTCCATA TGTTCGGAGAACTTAG-3′ and that of the reverse primer 5′-CCGCTCGAGTCAGATAGAGACGCTATTT-3′. PCR amplification of At*LOX1* yielded a 2.7-kb product that was subsequently cut with *Nde*I and *Xho*I and subcloned into the same sites of the expression vector pET-14b (Novagen, Madison, WI). The resulting construct produced a $(His)_6$-tagged AtLOX1 protein in which 20 amino acids (MGSSHHHHHHSSGLVPRGSH) were added to the initiator Met of the LOX1 enzyme. This construct was introduced into *E. coli* host strain BL21 (DE3) for protein expression.

The tomato (*Solanum lycopersicum*) *LOXA* cDNA was obtained by RT-PCR using an Enhanced Avian RT-PCR kit (Sigma Aldrich). The reverse transcription reaction contained 2 µg of total RNA isolated from 9-day-old tomato seedlings (cv. Castlemart) and an oligo $(dT)_{23}$ primer. The PCR reaction was performed with *LOXA*-specific primers 5′-CGGGATCCATGTTAGGTGAACTTGTGGG TG-3′ and 5′-CCGAGCTCACATGTGTACTCAAAACTC TTC-3′, which included *BamH*I and *Sac*I restriction sites, respectively. The resulting PCR product was cloned into *BamH*I and *Sac*I sites of pBlueScript. The nucleotide sequence of this tomato cDNA exactly matched the tomato *LOXA* sequence (GenBank accession number U09026) reported by Ferrie et al. [13].

A PCR-based strategy was used to construct an expression vector for production of an N-terminally $(His)_6$-tagged LOXA enzyme. Following amplification with primers 5′-CGGGATCCGGTGGGTGGATTAATTGGTG-3′ and 5′-CGGGATCCCTATATTGACACACTGTTT-3′, this PCR fragment was cloned into the *BamH*I site of pET14b. The N-terminal amino acid sequence of the resulting $(His)_6$-tagged LOXA enzyme is MGSSHHHH HHSSGLVPRGSHMLEDPVGGL. The subcloning procedure resulted in a three amino acid change (GLD → EDP, underlined) in the N terminus of the native LOXA protein.

Expression of Recombinant LOX in *E. coli*

Wild-type and mutant LOX were expressed in *E. coli* BL21 (DE3) as $(His)_6$-tagged proteins using the protocol described for coral 8*R*-LOX [14] with the following modifications. The expressed proteins were recovered using Bugbuster (Novagen) with added 1 µl/ml Benzonase (Novagen) and 1 mM PMSF. The supernatants were purified on Ni-NTA agarose (Qiagen) according to manufacturer instructions. Fractions collected from the affinity column were assayed by SDS/PAGE and fractions containing recombinant lipoxygenases were dialyzed against 50 mM phosphate pH 7.0, 150 mM NaCl buffer containing 20% glycerol.

Fractions of 0.5 ml were collected from the affinity column and 10 µl aliquots analyzed using SDS-PAGE. Protein was determined using the Bio-Rad protein assay with bovine serum albumin as standard. Fractions containing the highest concentrations of protein were pooled and dialyzed against a buffer of 50 mM Tris (pH 7.5), 300 mM NaCl to remove imidazole.

Quantitation of LOX Protein

The LOX proteins were quantified using a specific in-gel assay in which the LOX band on a stained SDS-PAGE gel is compared in intensity to the protein bands in a series of quantified albumin standards run in other lanes. Aliquots of the dialyzed protein from the Ni-NTA column were run on a 20–4% SDS-PAGE gel, and a second gel was run with aliquots of bovine albumin in concentrations ranging from 0.25 to 15 µg. The gels were stained with Bio-Safe Coomassie stain (Bio-Rad) and rinsed repeatedly with water. The protein bands at ~97 kDa representing the LOX protein were then quantified with the Odyssey Infrared Imaging System (Li-Cor Biosciences, Lincoln, NE), using the known amount of protein in the BSA bands to generate a standard curve.

Site Directed Mutagenesis

Site directed mutagenesis of AtLOX1 and LOXA was performed using the QuikChange® site directed mutagenesis kit (Stratagene) using overlapping mismatching oligonucleotides as primers designed according to the manufacturer's instructions. The His-tagged Arabidopsis AtLOX1 and tomato LOXA in the pET14b expression vector were used as templates. The primer sequences (55-mers) were, for Arabidopsis LOX1, 5′-GTGATACGATGAATATCAATGCACTTGGTAGGCAAATCTTGATCAATGGTGGTGG, and 5′-CCACCACCATTGATCAAGATTTGCCTACCAAGTGCATTGATATTCATCGTATCAC, and for tomato LOXA, 5′-GGGACACAATGAATATTAATGCTTTGGGAAGACAGATCCTAATCAATGCTGGTGG, and 5′-CCACCAGCATTGATTAGGATCTGTCTTCCCAAAGCATTAATATTCATTGTGTCCC. PCR reactions and transformation of *Escherichia coli* XL1-Blue cells were performed according to the manufacturer's instructions (Stratagene). Correctly mutated clones were identified by DNA sequencing.

Enzyme Reactions, Incubation and Extraction

Enzymatic activity of the Nickel column-purified enzymes was determined by monitoring the increase of the signal at 235 nm using a Perkin-Elmer Lambda-35 UV–Vis spectrophotometer. Rates of reaction were calculated from the initial linear part of the curve. Rates at varying pH values were compared using 50 μM linoleic acid with phosphate buffers (pH 5.0, 6.0. 7.0 and 8.0) and borate buffer (pH 9.0). Products from reaction at pH 6 were extracted without pH change into dichloromethane or using a 1 ml Oasis HLB cartridge (Waters).

Incubations with anandamide were conducted in 1 ml of 100 mM sodium phosphate (pH 6) using 2 μg of LOX protein; anandamide (50 μM final concentration) was added in 5 μl ethanol. After a 5 min incubation at room temperature, the reactions were extracted using a 1-ml Oasis HLB cartridge (Waters).

Incubations with C_{16}/$C_{18.2}$-phosphatidylcholine were conducted at pH 7.5 in the presence of sodium deoxycholate (final concentration, 4 mM) to help solubilize the substrate. The reactions were extracted using the Bligh and Dyer procedure [15] then transesterified using sodium methoxide [5] and the methyl esters subsequently analyzed by normal phase HPLC.

HPLC Analysis

Reaction products of the two LOX enzymes and mutants with [1-^{14}C]linoleic acid or [1-^{14}C]arachidonic acid were analyzed on an Agilent 1100 HPLC equipped with a diode array detector connected online to a Radiomatic FLO-ONE A-100 radioactive detector. Straight-phase HPLC analysis used a Beckman Ultrasphere silica column (25 × 0.46 cm) eluted at a flow rate of 1 ml/min with hexane/isopropanol/acetic acid (100/2/0.1, v/v/v) with UV detection at 205, 220, 235 and 270 nm. Reversed-phase HPLC used a Waters Symmetry C18 5-μm column eluted at 1 ml/min with a solvent of methanol/water/acetic acid (80/20/0.01, v/v/v), and finally with methanol to elute unreacted substrate. Chiral analysis was performed on HODE methyl esters using a Daicel Chiralpak AD column (25 × 0.46 cm) eluted with hexane/methanol (100/2, v/v) at a flow rate of 1 ml/min, with UV detection at 235 nm [16].

Results

Expression and Purification

The cDNAs in the bacterial expression vector were prepared with an added N-terminal (His)$_6$-tag as described in Methods. The two LOX enzymes expressed well in *E. coli* (2–5 mg LOX protein per 100 ml culture) and were partially purified by nickel affinity chromatography (Fig. 2). The *Arabidopsis* Ala562Gly mutant expressed at lower levels, although sufficient for evaluation of its activity and for analysis of products. In other SDS-PAGE analyses in which the LOX protein band was not overloaded (in contrast to Fig. 2), each LOX protein band at ~97 kD was quantified by in-gel assay (Odyssey Imaging Systems, see "Methods"), and this specifically quantified LOX protein was used in the calculation of activity turnover numbers.

Catalytic Activity and pH-Activity Profile

The pH dependence of AtLOX1 reacting with linoleic acid as substrate showed very similar rates over the pH range of 5–9, maximal at pH 6 (310 turnovers/s). For tomato LOXA activity was optimal around pH 6 (390 turnovers/s) and

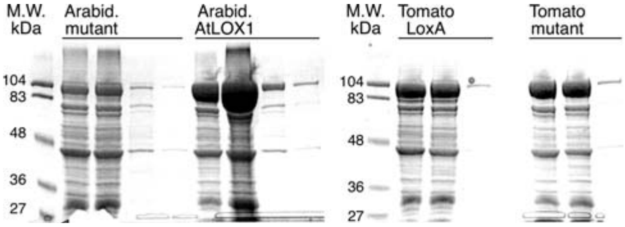

Fig. 2 SDS-PAGE gel analysis of LOX enzymes expressed in *E. coli*. The mutants refer to the AtLOX1 Ala562Gly and tomato LOXA Ala564Gly mutants. The *three lanes* for each sample represent aliquots (10 μl) from the first three 0.5 ml fractions collected from the nickel NTS column purification. Proteins were detected using Coomassie staining. *MW* molecular weight

was maintained at least 30 and 15% of this optimal activity at pH 8 and pH 9, respectively. SP-HPLC analysis of the products from linoleic acid at pH 6 showed that 9*S*-HPODE accounted for over 95% of the products of both enzymes (Table 1; Figs. 3a, 4c). α-Linolenic acid reacted at similar rates and similarly formed almost exclusively the 9-hydroperoxide. For comparison to the reactions at the optimal pH 6, the distribution of products from a reaction with linoleic acid conducted at pH 9 was also analyzed by SP-HPLC. Remarkably, the product pattern was indistinguishable from the reaction products at pH 6, i.e., 9*S*-HPODE accounted for >95% of the products (data not shown). This is in contrast to the properties of soybean LOX-1, which is specific for 13*S* oxygenation at its optimal pH 9-10, but changes at lower pH (pH 6 or 7) to producing a mixture of 9- and 13-hydroperoxide products with both *trans–trans* and *cis–trans* conjugated dienes [17].

Effects of Active Site Ala–Gly Mutation

By alignment with other LOX enzymes, the residue equivalent to the Ala that has a major influence on reaction stereospecificity [9] is Ala562 in *Arabidopsis* 9-LOX and Ala564 in tomato 9-LOX. This Ala was changed to Gly by site-directed mutagenesis and the expressed enzymes were reacted with linoleic acid. Following reduction of the hydroperoxides, two similar-sized peaks of hydroxy product were obtained by normal phase HPLC (Fig. 3b), identified as 13-HODE and 9-HODE by co-chromatography with standards and by their characteristic identical UV spectra with lambda max 234 nm (cf. ref. [18]). Chiral analysis showed the two products were almost purely the 13*R*-HODE and 9*S*-HODE enantiomers, respectively (Fig. 4d, e).

Table 1 Linoleic acid products formed by *A. thaliana* AtLOX1 and tomato LOXA

Enzyme	9-HPODE (%)	13-HPODE (%)		
A. thaliana WT	98.8	1.2		
A. thaliana A562G	68.9	31.1		
Tomato WT	99.1	0.9		
Tomato A564G	59.9	40.1		
	Chiral analysis (%)			
	9*R*	9*S*	13*R*	13*S*
A. thaliana WT	0.4	99.6	71.7[a]	28.3
A. thaliana A562G	0.7	99.3	98.4	1.6
Tomato WT	0.3	99.7	67.7[a]	32.3
Tomato A564G	0.9	99.1	98.6	1.4

[a] Note that, as shown above, WT produces 13-HPODE as only ~1% of products

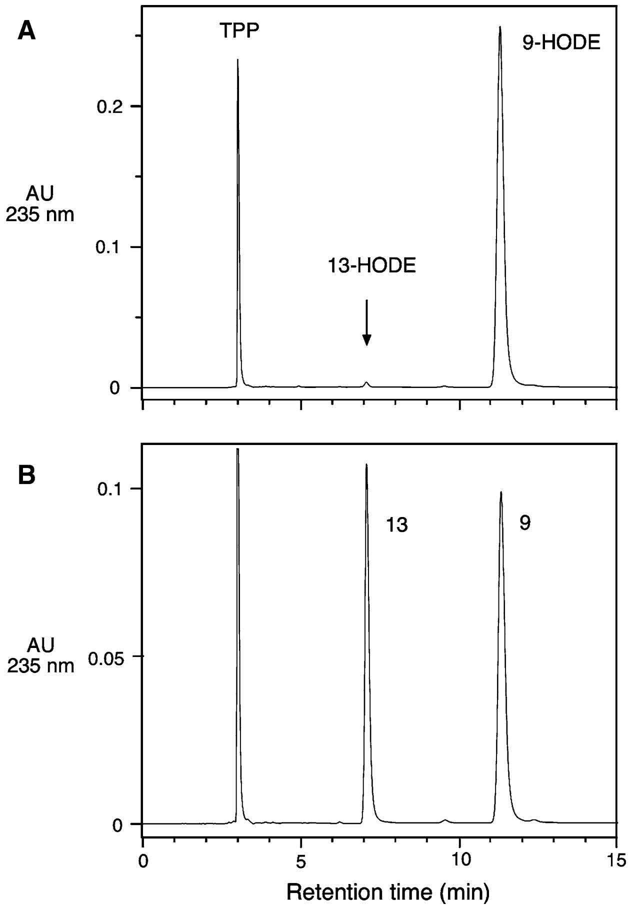

Fig. 3 Normal phase HPLC analysis of linoleic acid products. Panel a: Wild-type tomato LOXA product profile. Panel b: Tomato LOXA Ala564Gly product profile. A Beckman Ultrasphere silica column (5 μm, 25 × 0.46 cm) was eluted at 1 ml/min with hexane/isopropanol/glacial acetic acid (100/2/0.1, v/v/v) with UV detection at 235 nm. *TPP* triphenylphosphine

Arachidonic Acid Metabolism

Plant 9-LOX tend to form a mixture of chiral hydroperoxides when arachidonic acid (an unnatural substrate for a plant) is used as substrate (e.g., ref. [19, 20]). 9-LOX purified from potato tubers and one of the recombinant potato LOX isozymes give 5*S*-HPETE as the major hydroperoxide [21, 22]. Some other plant 9-LOX are reported to give 11*S*-HPETE as the major product [23]. As measured by the radioactive products formed from [^{14}C]arachidonic acid (after $NaBH_4$ reduction of the HPETEs to HETEs), we found that AtLOX1 formed 11-HETE as the major product (accounting for 47% of the total HETEs), together with half as much 5-HETE (23%), and in order of abundance also 9-HETE (11%), 12-HETE (9%), and 8-HETE and 15-HETE (4.5% each). Tomato LOXA formed 11-HETE and 5-HETE in essentially equal amounts (38–39% each), and also 8-HETE (11%), 12-HETE (4%), 15-HETE (3%) and 9-HETE (2%). The

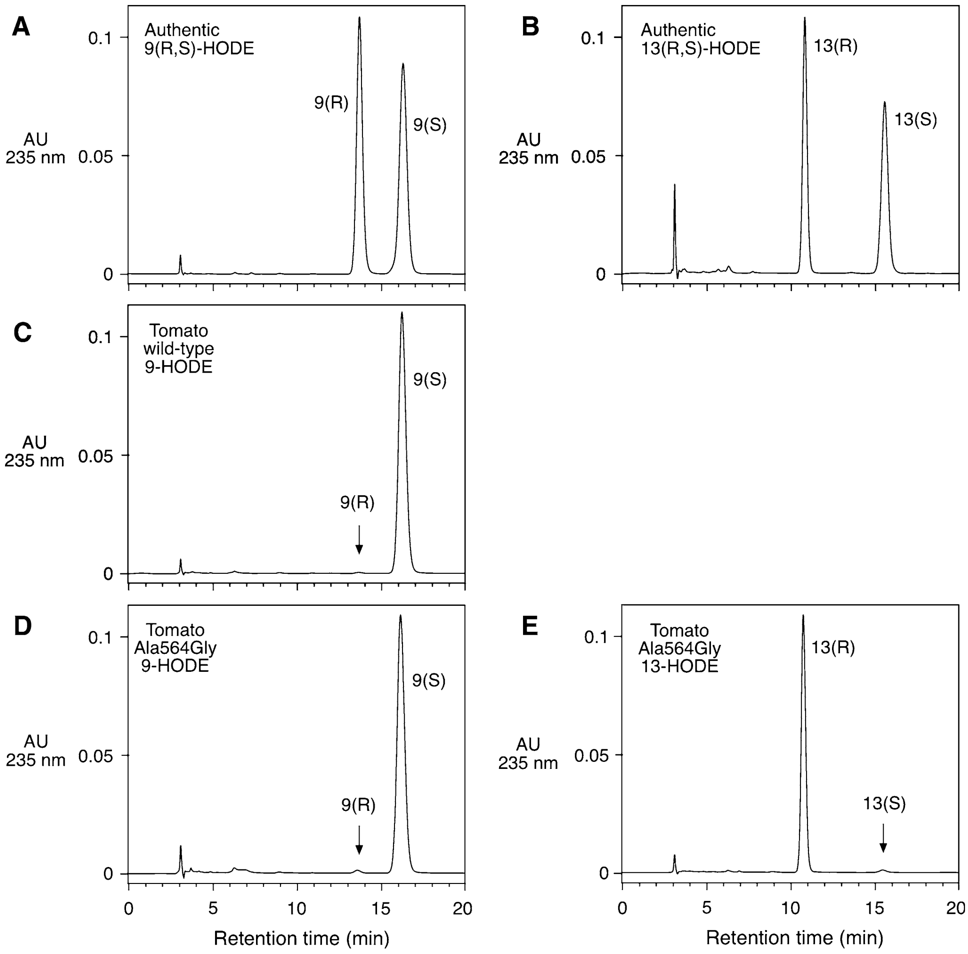

Fig. 4 Chiral phase HPLC analysis of HODE methyl ester derivatives. Panels a and b: resolution of 9*RS*-HODE and 13*RS*-HODE, respectively. Panel c: 9-HODE from wild-type tomato LOXA. *Panel D* 9-HODE from tomato LOXA Ala564Gly. *Panel E*: 13-HODE from tomato LOXA Ala564Gly. A Diacel Chiralpak AD column (5 µm, 25 × 0.46 cm) was eluted at 1 ml/min with hexane/methanol (100/2, v/v) with UV detection at 235 nm

pattern of hydroperoxide products for the tomato LOXA is similar to that illustrated previously for a 9-LOX purified from tomato [6]. We also found that the product profiles for each wild-type 9-LOX with arachidonic acid as substrate were essentially the same at pH 7 and 9; this contrasts with the results shown for a recombinant rice 9-LOX isozyme in which the 5-HPETE product almost disappeared at high pH [24].

Catalytic Activity with Other Substrates

Our results using arachidonate ethanolamide (anandamide) as substrate with the two recombinant 9-LOX enzymes are summarized in Table 2. The chiral analyses were performed after reduction to the hydroxy form, HANA, on a reversed-phase Chiralpak AD-RH column in which H(P)ETEs and their methyl ester derivatives are known to run with the *R* enantiomer eluting before the *S* enantiomer [25]. The same appeared to be true for anandamide derivatives, as confirmed using an authentic standard of 15*S*-HPANA prepared using soybean LOX-1, and from the fact that 11*S*-HPANA is the known product of purified 9-LOX from barley and tomato [6]. The most significant findings were that wild-type AtLOX1 converted anandamide mainly to 11*S*-HPANA (99.4% 11*S*, and accounting for 91% of the total HPANA products). The AtLOX1 Ala562Gly mutant formed 11*S*-HPANA (98.3% 11*S*) plus an additional prominent product, 15*R*-HPANA (93% 15*R*) in a 3:2 ratio in favor of 11-HPANA. Wild-type tomato LOXA also formed mainly 11*S*-HPANA (99.0% 11*S*, accounting for 71% of total HPANA products) plus 16% 5*S*-HPANA (89% 5*S*). The tomato LOXA Ala564Gly mutant formed two additional prominent products, 15*R*-HPANA (93% 15*R*, accounting for 34% of HPANA products) and 9-HPANA (19% of products). On chiral analysis the 9-HANA product chromatographed as one main peak with no definite minor enantiomer, so it was not possible to determine order of elution and infer chirality.

We also tested 1-palmitoyl-2-linoleoylphosphatidycholine as a potential substrate for AtLOX1 using the bile salt deoxycholate as detergent, a condition that achieves reaction with plant 13-LOX [26], coral 8R-LOX [9], as well as several mammalian arachidonate 12-LOX and 15-LOX [27–30]. However, we could detect no reaction with the recombinant 9-LOX, in agreement with a result reported for a purified tomato 9-LOX [20].

Table 2 Distribution of 9-LOX products from anandamide (2A) and the chirality of selected products (2B)

2A

Enzyme	H(P)ANA products (% of total)					
	15	11	12	8	9	5
Tom WT	5.5	71.8	1.8	3.6	1.3	15.9
Tom Mut	19.6	18.2	2.5	1.3	18.9	39.5
Arab WT	4.7	90.8	0.6	0.2	0.9	2.9
Arab Mut	34.1	59.4	1.1	0.3	1.7	3.5

2B

Enzyme	Chirality of 15-, 11- and 5-HANA (%)					
	15*R*	15*S*	11*R*	11*S*	5*R*	5*S*
Soybean[a]	2.5	97.5	15.5	84.5	–[b]	–
Tomato WT	53	47	1	99	11	89
Tom Mut	85	15	4	96	1.3	98.7
Arab WT	62	38	0.6	99.4	2.5	97.5
Arab Mut	93	7	1.7	98.3	6.6	93.4

[a] Relative proportions of products with soybean LOX1:15-HANA, 92%; 11-HANA, 5.5%; 5-HANA, 1%

[b] Not analyzed

Discussion

The *Arabidopsis* genome contains six *LOX* genes (Table 3) and there are at least five *LOX* genes in tomato (Table 4). Although tomato has long been used as a source of 9-LOX [31], to our knowledge, the positional specificity, as determined by direct characterization of LOX reaction products, has not been reported for any recombinant *Arabidopsis* or tomato LOX. Our experimental analysis of purified recombinant AtLOX1 and tomato LOXA showed that both proteins function as specific linoleate 9-LOX. This finding is consistent with phylogenetic analysis showing that AtLOX1 and tomato LOXA are closely related members of the plant LOX family (Fig. 5), and further predicts that other members of this subgroup are 9-LOX as well. In an accompanying paper, Andreou et al. [2] characterize the activity of a related sequence from potato also as a linoleate 9-LOX.

The notion that AtLOX1 and tomato LOXA are homologous proteins is supported by similarities in their expression pattern. Both genes, for example, are expressed to relatively high levels in germinating seedlings [13, 32]. Our results thus support the hypothesis that 9-LOX activity plays a physiological role during the early stages of seedling growth. Plant 9-LOX has been implicated in a variety of developmental and stress-related processes [1, 33]. Recently, oxylipins derived from the 9-LOX pathway were shown to play a role in lateral root development and pathogen defense in *Arabidopsis* [34]. Our data are in agreement with the proposal by Vellosillo and co-workers that 9-LOX activity in *Arabidopsis* roots can be attributed to LOX1/LOX5 [34].

Using the AtLOX1 and tomato LOXA we re-examined the debated issue of the mode of substrate binding orientation in the active site of 9-LOX, and how this relates to formation of specific chiral products. According to the model we outlined in the Introduction [35], linoleic acid should bind with a carboxyl end-first orientation in the active site of linoleate 9*S*-LOX, the same conclusion as originally inferred from the hydrogen abstraction results of 1972 with corn 9*S*-LOX (cf. Fig. 1a) [4]. The model predicts that the Ala-to-Gly switch in 9*S*-LOX should produce a new product, 13*R*-HPODE, formed on the same face of the molecule as 9*S*-HPODE (cf. Fig. 1b). This is exactly what was observed (Figs. 3, 4; Table 1).

Table 3 *Arabidopsis thaliana* LOX genes

Designation	GenBank access. no.	AGI no.[a]	No. of amino acids	MW (Da)	N-terminal sequence	Positional specificity	References
AtLOX1	NM_104376	AT1G55020	859	98,045	MFGELRDLLT	9	[12], this paper
AtLOX2	NM_114383	AT3G45140	870	99,036	MYCRESLSSL	13	[36]
AtLOX3	NM_101603[b]	AT1G17420	919	103,710	MALAKELMGY	13	Feussner, 2nd 13-LOX (GenBank AJ249794)[c]
AtLOX4	AJ302042	AT1G72520	926	104,813	MALANEIMGS	13	Feussner, 3rd 13-LOX, chloroplastic, leaves[c]
AtLOX5	NM_113137[d]	AT3G22400	886	101,058	MIHTDIAEIL	9	Feussner, 2nd 9-LOX[c]
AtLOX6	NM_105423	AT1G67560	917	104,514	MFVASPVKTN	13	Feussner, plastid 13-LOX[c]

[a] Gene designation at http://www.arabidopsis.org

[b] GenBank entry AC007843 has 7 less N-terminal amino acids

[c] Designations given in the GenBank entry

[d] GenBank entry AJ302043 is the same sequence with 32 less N-terminal amino acids

We also re-examined the 9-LOX metabolism of anandamide, and also the consequences of the Ala-to-Gly

Table 4 Tomato (*Lycopersicon esculentum*/*Solanum lycopersicum*) LOX genes

Designation	GenBank Access. no.	No. of amino acids	MW (Da)	N-terminal sequence	Positional specificity	References
LOXA	U09026	860	96,764	MLGQLVGGLI	9S	Cloned by [13], this paper
LOXB	U09025	859	97,122	MSLGGIVDAI	13S	Cloned by [13]
LOXC	U37839	896	101,744	MLKPQFQQST	NS	[37]
LOXD	U37840	908	102,292	MALAKEIMGI	NS	[37]
LOXE	AY008278	862	97,505	MILNKIVDSI	NS	[38]

Genome sequencing currently in progress (2008)

NS not specified

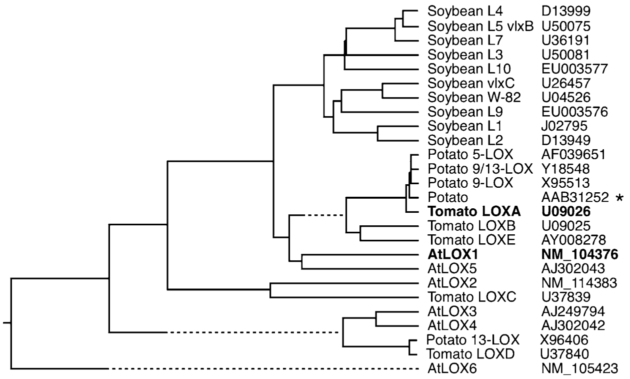
Soybean L4 D13999
Soybean L5 vlxB U50075
Soybean L7 U36191
Soybean L3 U50081
Soybean L10 EU003577
Soybean vlxC U26457
Soybean W-82 U04526
Soybean L9 EU003576
Soybean L1 J02795
Soybean L2 D13949
Potato 5-LOX AF039651
Potato 9/13-LOX Y18548
Potato 9-LOX X95513
Potato AAB31252 *
Tomato LOXA U09026
Tomato LOXB U09025
Tomato LOXE AY008278
AtLOX1 NM_104376
AtLOX5 AJ302043
AtLOX2 NM_114383
Tomato LOXC U37839
AtLOX3 AJ249794
AtLOX4 AJ302042
Potato 13-LOX X96406
Tomato LOXD U37840
AtLOX6 NM_105423

Fig. 5 Phylogenetic tree of selected plant LOX enzymes. The enzymes include the six LOX in the *Arabidopsis*, the current five reported for tomato, ten soybean enzymes, and five sequences from potato. The enzymes studied in the present paper are shown in *bold* type. The *asterisk* marks a potato LOX studied in an accompanying paper [2]. GenBank accession numbers are shown

mutation on the distribution of products. As noted in the Introduction, purified barley and tomato 9-LOX were reported to convert anandamide mainly to 11*S*-HPANA (11*S*-hydroperoxyanandamide), in contrast to their products with arachidonic acid, which were largely 5-HPETE for barley 9-LOX and 5-HPETE/11-HPETE mixtures for tomato 9-LOX. And, because it appears that the additional functional moiety at the carboxyl end has pushed oxygenation further down the carbon chain, these observations were used to infer that the substrate binding orientation in plant 9-LOX is tail end-first [6]. Although this is a reasonable conclusion, we offer a different interpretation. Whereas van Zadelhoff et al. [6] placed an emphasis on the conversion of arachidonic acid to 5*S*-HPETE by the linoleate 9-LOX, we note that formation 11*S*-HPETE is equally common with several of the wild-type enzymes (cf. refs. [6, 20, 23] and the “Results” section above). With anandamide, the balance of oxygenation products tips in favor of 11*S*-HPANA and in some cases 5*S*-HPANA remains prominent. Significantly, the Ala-to-Gly mutation induces the formation of 15*R*-HPANA along with the 11*S*-HPANA, and 9-HPANA along with 5-HPANA (“Results”, Table 3). These new findings fit perfectly with the orientation model that predicts carboxyl end-first binding of the substrate. Admittedly, this will require the “extra” ethanolamide moiety at C-1 to be accommodated in the 9-LOX active site, but our surmise is that this is the most straightforward interpretation of the available data.

Butovich and Reddy used the observation that linoleate 9-LOX can metabolize 1-linoleoyl-glycerol to the 9-hydroperoxide to propose the tail-first binding orientation [7]. As an extension of this conjecture, we tested 1-palmitoyl-2-linoleoyl-phosphatidylcholine and could find no reaction. While caution is warranted in interpretation of negative results, this lack of reaction classifies the linoleate 9-LOX along with other LOX enzymes that are predicted to exhibit carboxyl end-first binding and that show no reaction with very large phospholipid esters (arachidonate 8*S*-LOX and 5*S*-LOX) [9, 28]. (By contrast, all the LOX enzymes that have predicted tail-first substrate binding do react specifically with phospholipid ester substrates [5, 9, 26–30]). Again, our interpretation is that the 9*S*-LOX active site can accommodate substrates with C-1 appendages of the size of ethanolamide or glycerol, and that overall, the carboxyl end-first binding is the most satisfactory model for oxygenations by linoleate 9*S*-LOX enzymes.

Acknowledgments We thank Kaye Peterman (Wellesley College) for kindly proving the *AtLOX1* cDNA. This work was supported by NIH grants GM-53638 and GM-074888 (to ARB) and by the US Department of Energy Grant DE-FG02-91ER20021 (to GAH).

References

1. Feussner I, Wasternack C (2002) The lipoxygenase pathway. Annu Rev Plant Biol 53:275–297
2. Andreou A, Hornung E, Rosahl S, Feussner I (2008) On the substrate binding of a 9-LOX from potato. Lipids (submitted)
3. Schneider C, Pratt DA, Porter NA, Brash AR (2007) Control of oxygenation in lipoxygenase and cyclooxygenase catalysis. Chem Biol 14:473–488
4. Egmond MR, Vliegenthart JFG, Boldingh J (1972) Stereospecificity of the hydrogen abstraction at carbon atom n-8 in the

oxygenation of linoleic acid by lipoxygenases from corn germs and soya beans. Biochem Biophys Res Commun 48:1055–1060
5. Brash AR, Ingram CD, Harris TM (1987) Analysis of a specific oxygenation reaction of soybean lipoxygenase-1 with fatty acids esterified in phospholipids. Biochemistry 26:5465–5471
6. van Zadelhoff G, Veldink GA, Vliegenthart JFG (1998) With anandamide as substrate plant 5-lipoxygenases behave like 11-lipoxygenases. Biochem Biophys Res Commun 248:33–38
7. Butovich IA, Reddy CC (2001) Enzyme-catalyzed and enzyme-triggered pathways in dioxygenation of 1-monolinoleoyl-rac-glycerol by potato tuber lipoxygenase. Biochim Biophys Acta 1546:379–398
8. Coffa G, Imber AN, Maguire BC, Laxmikanthan G, Schneider C, Gaffney BJ, Brash AR (2005) On the relationships of substrate orientation, hydrogen abstraction and product stereochemistry in single and double dioxygenations by soybean lipoxygenase-1 and its Ala542Gly mutant. J Biol Chem 280:38756–38766
9. Coffa G, Brash AR (2004) A single active site residue directs oxygenation stereospecificity in lipoxygenases: stereocontrol is linked to the position of oxygenation. Proc Natl Acad Sci USA 101:15579–15584
10. Peers KF, Coxon DT (1983) Controlled synthesis of monohydroperoxides by α-tocopherol inhibited autoxidation of polyunsaturated lipids. Chem Phys Lipids 32:49–56
11. Brash AR, Song W-C (1996) Detection, assay, and isolation of allene oxide synthase. Meth Enzymol 272:250–259
12. Melan MA, Dong X, Endara ME, Davis KR, Ausubel FM, Peterman TK (1993) An *Arabidopsis thaliana* lipoxygenase gene can be induced by pathogens, abscisic acid, and methyl jasmonate. Plant Physiol 101:441–450
13. Ferrie BJ, Beaudoin N, Burkhart W, Bowsher CG, Rothstein SJ (1994) The cloning of two tomato lipoxygenase genes and their differential expression during fruit ripening. Plant Physiol 106:109–118
14. Boutaud O, Brash AR (1999) Purification and catalytic activities of the two domains of the allene oxide synthase-lipoxygenase fusion protein of the coral *Plexaura homomalla*. J Biol Chem 274:33764–33770
15. Bligh EG, Dyer WJ (1959) A rapid method of total lipid extraction and purification. Can J Biochem Physiol 37:911–917
16. Schneider C, Boeglin WE, Brash AR (2000) Enantiomeric separation of hydroxy-eicosanoids by chiral column chromatography: effect of the alcohol modifier. Anal Biochem 287:186–189
17. Gardner HW (1989) Soybean lipoxygenase-1 enzymically forms both (9*S*)- and (13*S*)-hydroperoxides from linoleic acid by a pH-dependent mechanism. Biochim Biophys Acta 1001:274–281
18. Ingram CD, Brash AR (1988) Characterization of HETEs and related hydroxy-dienes by UV spectroscopy. Lipids 23:340–344
19. Heydeck D, Wiesner R, Kühn H, Schewe T (1991) On the reaction of wheat lipoxygenase with arachidonic acid and its oxygenated derivatives. Biomed Biochim Acta 50:11–15
20. Regdel D, Kühn H, Schewe T (1994) On the reaction specificity of the lipoxygenase from tomato fruits. Biochim Biophys Acta 1210:297–302
21. Shimizu T, Rådmark O, Samuelsson B (1984) Enzyme with dual lipoxygenase activities catalyzes leukotriene A_4 synthesis from arachidonic acid. Proc Natl Acad Sci USA 81:689–693
22. Chen X, Reddanna P, Reddy GR, Kidd R, Hildenbrandt G, Reddy CC (1998) Expression, purification, and characterization of a recombinant 5-lipoxygenase from potato tuber. Biochem Biophys Res Commun 243:438–443
23. Reddy GR, Reddanna P, Reddy CC, Curtis WR (1992) 11-Hydroperoxyeicosatetraenoic acid is the major dioxygenation product of lipoxygenase isolated from hairy root cultures of *Solanum tuberosum*. Biochem Biophys Res Commun 189:1349–1352
24. Zhang LY, Hamberg M (1996) Specificity of two lipoxygenases from rice: unusual regiospecificity of a lipoxygenase isoenzyme. Lipids 31:803–809
25. Schneider C, Yu Z, Boeglin WE, Zheng Y, Brash AR (2007) Enantiomeric separation of hydroxy and hydroperoxy eicosanoids by chiral column chromatography. Meth Enzymol 433:145–157
26. Eskola J, Laakso S (1983) Bile salt-dependent oxygenation of polyunsaturated phosphatidylcholines by soybean lipoxygenase-1. Biochim Biophys Acta 751:305–311
27. Schewe T, Halangk W, Hiebsch C, Rapoport SM (1975) A lipoxygenase in rabbit reticulocytes which attacks phospholipids and intact mitochondria. FEBS Lett 60:149–153
28. Jung G, Yang DC, Nakao A (1985) Oxygenation of phosphatidylcholine by human polymorphonuclear leukocyte 15-lipoxygenase. Biochem Biophys Res Commun 130:559–566
29. Murray JJ, Brash AR (1988) Rabbit reticulocyte lipoxygenase catalyzes specific 12(*S*) and 15(*S*) oxygenation of arachidonyl–phosphatidylcholine. Arch Biochem Biophys 265:514–523
30. Takahashi Y, Glasgow WC, Suzuki H, Taketani Y, Yamamoto S, Anton M, Kühn H, Brash AR (1993) Investigation of the oxygenation of phospholipids by the porcine leukocyte and human platelet arachidonate 12-lipoxygenases. Eur J Biochem 218:165–171
31. Matthew JA, Chan HW-S, Galliard T (1977) A simple method for the preparation of pure 9-D-hydroperoxide of linoleic acid and methyl linoleate based on the positional specificity of lipoxygenase in tomato fruit. Lipids 12:324–326
32. Melan MA, Enriquez A, Peterman TK (1994) The LOX1 gene of *Arabidopsis* is temporally and spatially regulated in germinating seedlings. Plant Physiol 105:385–393
33. Howe GA, Schilmiller AL (2002) Oxylipin metabolism in response to stress. Curr Opin Plant Biol 5:230–236
34. Vellosillo T, Martínez M, López MA, Vicente J, Cascón T, Dolan L, Hamberg M, Castresana C (2007) Oxylipins produced by the 9-lipoxygenase pathway in *Arabidopsis* regulate lateral root development and defense responses through a specific signaling cascade. Plant Cell 19:831–846
35. Coffa G, Schneider C, Brash AR (2005) A comprehensive model of positional and stereo control in lipoxygenases. Biochem Biophys Res Commun 338:87–92
36. Bell E, Mullet JE (1993) Characterization of an *Arabidopsis* lipoxygenase gene responsive to methyl jasmonate and wounding. Plant Physiol 103:1133–1137
37. Heitz T, Bergey DR, Ryan CA (1997) A gene encoding a chloroplast-targeted lipoxygenase in tomato leaves is transiently induced by wounding, systemin, and methyl jasmonate. Plant Physiol 114:1085–1093
38. Chen G, Hackett R, Walker D, Taylor A, Lin Z, Grierson D (2004) Identification of a specific isoform of tomato lipoxygenase (TomloxC) involved in the generation of fatty acid-derived flavor compounds. Plant Physiol 136:2641–2651

NADPH	Nicotinamide adenine dinucleotide phosphate-oxidase
PCR	Polymerase chain reaction
PPAR	Peroxisome proliferator-activated receptors
PUFA	Polyunsaturated fatty acid
SD	Standard deviation

Introduction

Sesamin is a known lipid modulator well investigated in mammalian systems [1–3]. To our knowledge it has never been investigated in fish. As lipid modulation can be of importance to improve the value of vegetable oil in fish diets in relation to aquaculture, we wanted to explore the physiological effects of sesamin in fish. The demand for fish oil for the aquaculture industry from natural pelagic fish populations is expected to outstrip current supply within the next decade [4, 5]. Partial replacement of marine oils with vegetable oils in fish feed is possible and is practiced. This requires new insights that consider the effects of a wide range of bioactive minor lipid components naturally present in the vegetable oils [6]. So far, studies have mostly focused on the production yield when fish are grown on feeds with a partial replacement of fish oil with vegetable oils, e.g. soybean and rapeseed oils. It was shown that up to 50% replacement of fish oils with a number of vegetable oils does not alter fish growth [7]. Thus, feeds with a replacement of 10–25% of fish oil by soybean and rapeseed oil are frequently commercialized [8]. A natural drawback of feeding vegetable oils to fish is decreased amounts of the highly unsaturated fatty acids (HUFA) eicosapentaenoic acid (20:5n-3, EPA), docosapentaenoic acid (22:5n-3, DPA), docosahexaenoic acid (22:6n-3, DHA) and to some extent arachidonic acid (20:4n-6, ARA) and increased amounts of the n-6 fatty acids, mainly linoleic acid (18:2n-6, LA), in the fish muscle. Depending on species, fish have different capabilities to elongate and desaturate fatty acids. In rainbow trout (*Oncorhynchus mykiss)* and salmon (*Salmo salar*), the steps in the elongation and desaturation from alpha-linolenic acid (18:3n-3, ALA) to DHA are well described [9–11]. Thus, new strategies leading to increased levels of n-3 HUFA in fish farmed with feed containing vegetable oils are needed. The increased levels of n-3 HUFA in farmed fish will contribute to positive health effects of the fish and also provide marketing advantages of farmed fish [12].

Sesamin, a minor component of sesame oil, is known to affect fatty acid desaturation and significantly increases the activity of enzymes involved in β-oxidation and expression of these enzymes in rats [2, 3]. Even though confirmation still is required, Ashakumary et al. [2] suggested, that the underlying mechanism include the expression of peroxisome proliferator-activated receptors (*PPAR*s).

Sesamin inhibits cholesterol absorption and synthesis, and tocopherol hydroxylation and urinary excretion by Cytochrome P450 in rats and humans [1, 13–15]. The methylenedioxyphenyl group of sesamin is known to affect cytochrome P450-dependent drug oxidation [16]. Cytochrome P450 (CYP) enzymes are known to play a central role in the oxidative metabolism and biotransformation of a wide range of endogenous and exogenous compounds [17]. Among the numerous CYP families identified, primarily CYP 1-3 are involved in biotransformation of xenobiotics. The CYP 1A subfamily is reported to be expressed in the liver of both mammals and fish [16, 18]. Due to the role of CYP1A isoenzymes in the metabolism and bioactivation of foreign compounds, alteration of the expression of hepatic CYP1A may affect the potential risk of xenobiotics [19]. CYP1A is readily inducible by aryl hydrocarbon (Ah) receptor agonist, thus the activity of CYP1A, measured as ethoxyresorufin O-deethylase (EROD) activity, is used as a biomarker for exposure to xenobiotic compounds in fish.

This study designed to investigate the physiological response of fish to sesamin in combination with vegetable oils with particular emphasis on n-3 HUFA and the n-3 desaturation index. We were especially interested in the physiological effects of sesamin at different n-6/n-3 ratios in the diet provided by either a mixture of linseed and sunflower oil or linseed oil solely. Further, we studied the expression of *PPAR*s in liver, and sesamin content in liver and muscle lipid as well as response of total CYP content and CYP1A catalytic activity in liver.

Materials and Methods

Chemicals and Reagents

The sesamin/episesamin mixture (1:1, w/w) was a kind gift from Takemoto Oil and Fat Co., Ltd. (Gamagori Aichi, Japan). Fatty acid peaks were identified by comparison with the standard mixture GLC-68 A (Nu-check Prep, Inc, Elysian, MO). All solvents and other chemicals used for analysis were purchased from Merck and were used without further purification. All reagents and other chemicals for total CYP and EROD analysis were purchased from the Sigma Chemical Co. (St. Louis, MO).

Animals and Diets

Rainbow trout (*Oncorhynchus mykiss*) were fed four different experimental diets. Prior to the study the fish were fed a commercial feed (Nutra Parr, Skretting AB, Västra

Table 1 The lipid content and relative fatty acid composition (%) in the experimental diets

	MO	MO + S	LO	LO + S
Lipid content	16.3	16.7	17.4	19.8
SAFA	10.4	10.6	10.0	10.1
MUFA	21.7	21.5	17.6	17.6
18:2n-6	33.2	31.9	15.0	14.7
18:3n-3	31.7	32.4	53.4	52.5
20:5n-3	0.2	0.2	0.2	0.3
22:6n-3	0.4	0.5	0.4	0.5
n-3 PUFA/n-6 PUFA	1.0	1.0	3.6	3.6

SAFA saturated fatty acids (14:0, 16:0, 18:0, 20:0, 22:0, 24:0); *MUFA* monounsaturated fatty acids (16:1, 18:1n-9, 18:1n-7, 20:1, 22:1, 24:1); *PUFA* polyunsaturated fatty acids; *MO* mixed oil; *MO + S* mixed oil + sesamin; *LO* linseed oil; *LO + S* linseed oil + sesamin

Frölunda, Sweden). Experimental diets were prepared according to the method of Sanchez-Vazquez et al. [20] and contained casein (18.6%), calcium sulphate (4%), gelatine (3.1%), defatted fish meal (TripleNine, Esbjerg, Denmark) (21.8%), dextrin (9.8%), vegetable oil (21.8%), vitamin and mineral mixture (0.3%), starch (15%) and sodium alginate (4%). An equi-mixture of (+)-sesamin and (−)-episesamin was added at 0.58 g 100 g^{-1} feed, in this paper we will refer to this equi-mixture as sesamin. The level of added sesamin was decided from the natural concentration of lignan in sesame oil, i.e. up to 2.5%. In a diet containing 20% sesame oil, this corresponds to 0.58 g 100 g^{-1} feed. The four experimental diets used were: (1) mixed oil (linseed oil:sunflower oil, 6:4, by vol) (MO), (2) MO with sesamin addition (MO + S), (3) linseed oil (LO), and (4) LO with sesamin addition (LO + S). The fatty acid compositions of the experimental diets are shown in Table 1. Eight juvenile rainbow trout in each group (initial weight 34 g) were kept in tanks with a water temperature of 10 °C and fed ad libitum for 35 days. This number of fish was used as replicates to study the physiological response of pure sesamin in fish diet, as sesamin has been shown to have individual physiological response in rats (see above). At harvest (average fish weight 53 g), tissues from all fish were dissected, frozen in liquid nitrogen and stored at −80 °C until analyzed.

Lipid Analysis

Tissues and diets were extracted following the method of Hara and Radin [21]. Total lipids of tissues were separated into phospholipids and triacylglycerols according to Pickova et al. [22]. Total lipids in the diets, and the phospholipids and triacylglycerols of tissues were methylated following the procedure of Appelqvist [23] and the fatty acids were analyzed with a gas chromatograph CP3800 (Varian AB, Stockholm, Sweden) equipped with flame ionisation detector (FID) and split injector and fitted with a fused silica capillary column BPX 70 (SGE, Austin, Tex.), length 50 m. id. 0.22 mm, 0.25 µm film thickness. The column temperature was programmed to start at 158 °C held 5 min and then increased by 2 °C/min up to 220 °C where it remained for 8 min. The carrier gas was helium (0.8 ml/min) and the make up gas was nitrogen. The injector and detector temperatures were 230 and 250 °C respectively. Fatty acids were identified by comparison with the standard fatty acid mixture GLC-68 and retention times. Peak areas were integrated using Star chromatography workstation software version 5.5 (Varian AB, Stockholm, Sweden). For each group six samples were analyzed in duplicate.

Sesamin and Episesamin Analyses

For the analysis of sesamin and episesamin, the lipid extracts of tissues and feed were dissolved in hexane and analysed with high performance liquid chromatography (HPLC) [15]. The mobile phase used was hexane/1,4-dioxane (94:4, by vol). The HPLC system was equipped with a Bischoff HPLC pump (Bischoff Analysentechnik und Geräte GmbH, Leonberg, Germany), and an Agilent 1100 series fluorescence detector (Agilent Technologies, Waldbronn, Germany). The HPLC column was Alltech SI 5U silica column (4.6 × 250 mm; Alltech Associates Inc., Deerfield, IL). The fluorescence detector was operated at an excitation wavelength of 296 nm and an emission wavelength of 324 nm. Identification and quantification was achieved by comparison to external standards. For each group six samples were analyzed in duplicate.

Total Content of CYP and EROD Activity in Liver

For the analysis of total CYP content and EROD activity, only a few samples were available and therefore we choose to only compare the physiological response of sesamin regardless if the oil was MO or LO. For the total CYP analysis, samples also had to be pooled due to technical reasons in the analytical steps (insufficient amount of microsome suspension). For the CYP analysis, three samples from the control group and two from the sesamin group were analyzed. For the EROD analysis six samples from the control group and four from the sesamin group were analyzed.

The liver tissue was homogenized in ice-cold homogenization buffer (0.25 M sucrose and 0.1 mM EDTA in 0.01 M TRIS buffer, pH 7.4) using a Potter-Elvehjem homogeniser. The homogenate was centrifuged for 15 min at 10,000*g* (4 °C) and the resulting supernatant was spun down for 1 h at 105,000*g* (4 °C). The microsomal pellets were resuspended in the homogenization buffer and stored at −80 °C until used. The total CYP content was determined spectrophotometrically by the Co- and dithionite difference method (Shimanzu UV-1601PC, Columbia, USA) according to Omura and Sato [24].

Hepatic EROD activity was determined according to a modified method by Jönsson et al. [17]. Standard solutions of resorufin (0–50 μM) and protein (BSA; 1 mg BSA ml^{-1}) were prepared in HEPES-Cortland (HC) buffer pH 8. The HC buffer was prepared by dissolving 0.38 g KCl, 7.74 g NaCl, 0.23 g $MgSO_4{\cdot}7H_2O$, 0.23 g $CaCl_2{\cdot}2H_2O$, 0.41 g $NaH_2PO_4{\cdot}H_2O$, 1.43 g HEPES, and 1 g glucose in 1 l of distilled water. Microsome suspensions were further diluted in the same buffer (1:5 and 1:10). Aliquots of the microsome suspensions (50 μl) and of the standard solutions (40 μl of resorufin and 10 μl of BSA) were added in duplicate wells in 96-well plate. A 160 μl aliquot of 7-ethoxyresorufin (12.7 μM) and NADPH (2.1 mM) in HC buffer was rapidly added to all wells. The plate was then immediately placed in a microplate reader (Wallac 1420 VICTOR^2, Turku, Finland) and the resorufin fluorescence was monitored for 10 min by repeated measurements at 544 nm (ex) and 590 nm (em). EROD activity was calculated and expressed as pmol of resorufin formed per mg protein per minute. The protein contents of the microsomes were assayed by the method of Smith et al. [25], adapted for microplate readers.

RNA Analysis

Total RNA was purified from three livers from each group and analyzed in duplicate, using Trizol® (invitrogene), followed by DNase treatment (TURBO DNA-free, Ambion). All protocols were according to the manufacture's instructions. RNA quality and quantity were determined Spectrophotometrically ($A_{260/280}$) by using NanoDrop® (ND-1000 Spectrophotometer, NanoDrop Technologies, Wilmington, DE). Samples were stored in RNase-free water at −80 °C.

The cDNA was synthesized following a modified protocol from the Taq Man Reverse Transcription Reagents kit (Applied Biosystems). The Oligo $d(T)_{16}$ primers were used. The reaction was performed by incubating the samples at 25 °C for 10 min, 48 °C for 6 min, 95 °C for 50 min and was terminated by reducing the temperature to 10 °C. Primers for Real-Time PCR analysis (Table 2) were designed using the Primer Express® software based on available salmon sequences in the GenBank® and purchased from Invitrogene (CA, USA). Real-Time PCR was performed in a Prism® 7000 system by using gene-specific primers. A 2× SYBR® Green PCR Mastermix (ABI) was used in the PCR reaction mix of 25 μl with 1 μl primers (final concentration of 0.5 μM), and 5 μl cDNA. All samples were analyzed in duplicate with a non-template control on each plate. The reference gene used was elongation factor 1α (EF1A). The reaction was preformed by incubating the samples at 50 °C for 2 min, 95 °C 10 min and 50 cycles of 95 °C for 10 s and 60 °C for 15 s. Standard curves were made for each primer pair and efficiencies (E) were calculated $E = 10^{(-1/\mathrm{slope})}$.

Data Analysis

Fatty acids, and sesamin and episesamin data are presented as mean values ± standard deviation (SD). The General Linear Model (GLM) of SAS (SAS Institute Inc., Cary, NC, version 8.2) was used to compare the physiological responses of the different diets. The model included the fixed effect of treatment and random effect of individual. Relative expression of the different genes, in relation to housekeeping genes were determined using the Relative Expression Software Tool (REST-384©-version 1).

Results

Growth Measures

No mortality occurred during the experiment. There was no difference in starting weight, final weight or daily growth coefficient (DGC) among the four fish groups (Table 3). The DGC were calculated as: $DGC = 100 \times (W_2^{1/3} - W_1^{1/3})\ D^{-1}$ with W_2 being final weight, W_1 the starting weight and *D* the number of days [26]. The fat contents of the muscle tissues and liver were also similar among treatments (Table 3).

Fatty Acid Composition

Some of the white muscle fatty acids were significantly affected by the presence of sesamin in the feed (Table 4). The presence of sesamin in the feed increased the

Table 2 Primers for quantitative real-time PCR analysis

Target gene	Forward promer (5′–3′)	Reverse primer (5′–3′)	Primer efficiency	GenBank Acc. no.
EF1A	CACCACCGGCCATCTGATCTACAA	TCAGCAGCCTCCTTCTCGAACTTC	1.97	AF321836
PPARα	TCCTGGTGGCCTACGGATC	CGTTGAATTTCATGGCGAACT	1.99	DQ294237
PPARβ	GAGACGGTCAGGGAGCTCAC	CCAGCAACCCGTCCTTGTT	2.07	AJ416953
PPARγ	CATTGTCAGCCTGTCCAGAC	ATGTGACATTCCCACAAGCA	2.04	AJ416951

Table 3 Initial, final weight (g) and daily growth coefficient (DGC) of the fish and lipid content (%) in white and red muscles and livers of fish fed diets based on different vegetable oils, mean values ± SD ($n = 8$ for weight and DGC, $n = 6$ for lipid content)

	MO	MO + S	LO	LO + S
Initial weight	31.7 ± 10.2	36.6 ± 9.07	30.4 ± 8.18	32.9 ± 6.35
Final weight	50.0 ± 12.5	57.6 ± 12.2	$51.6 \pm 16.\ 2$	53.9 ± 13.5
DGC	1.55 ± 0.28	1.55 ± 0.42	1.69 ± 0.74	1.60 ± 0.47
Lipid content (%)				
White muscle	2.0 ± 0.5	2.0 ± 0.3	2.8 ± 0.7	2.1 ± 0.5
Red muscle	10.5 ± 2.2	13.3 ± 1.7	13.7 ± 4.6	13.7 ± 2.5
Liver	4.2 ± 0.3	4.4 ± 0.9	3.8 ± 0.4	4.6 ± 0.6

For abbreviations see Table 1

proportion of DHA ($P = 0.02$) in the MO + S group and decreased that of 18:3n-3 ($P = 0.05$) in the LO + S group (Fig. 1; Table 4) with a tendency to increase the desaturation index (n-3 HUFA/18:3n-3) ($P = 0.06$) in MO + S group (Table 4). Sesamin addition also decreased the proportion of 18:2n-6 in the MO + S group ($P < 0.01$). The total percentage of polyunsaturated fatty acids (PUFA) was significantly decreased in triacylglycerols of MO + S group. The content of DHA was significantly increased ($P < 0.02$) in phospholipid fraction in both MO + S and LO + S group. The proportions of EPA ($P = 0.04$) and total n-3 fatty acids ($P < 0.01$) were significantly increased and that of 18:3n-3 ($P = 0.02$) decreased in the LO + S group phospholipid fraction. The fatty acid composition of the liver and red muscle was not significantly altered by the addition of sesamin in the diet (data not shown).

Sesamin and Episesamin

The mixture of sesamin fed to fish was found in white and red muscle and liver with the episesamin levels being higher than the sesamin levels (Table 5). A significantly higher level of sesamin and episesamin in red muscle ($P = 0.04$) and of sesamin in liver ($P = 0.05$) was found in the in the LO + S fed group compared to the MO + S group. The sesamin/episesamin ratio did not differ between the oils within the tissues, but the ratio was significantly

Table 4 White muscle fatty acid composition (the storage lipid fraction, triacylglycerols and membrane lipid fraction, phospholipids), expressed as percentage of total fatty acids, mean values ± SD, $n = 6$ in all groups

Fatty acid	Triacylglycerol				Phospholipids			
	MO	MO + S	LO	LO + S	MO	MO + S	LO	LO + S
18:2n-6	21.8 ± 6.2^{a}	16.0 ± 4.1^{b}	10.4 ± 0.7^{c}	9.8 ± 1.2^{c}	6.2 ± 2.0^{a}	4.8 ± 1.0^{b}	3.2 ± 0.2^{c}	2.8 ± 0.2^{c}
18:3n-3	13.2 ± 4.2^{a}	9.7 ± 3.5^{a}	23.4 ± 3.6^{b}	19.0 ± 4.4^{c}	5.1 ± 1.2^{a}	5.0 ± 1.0^{a}	9.9 ± 1.0^{b}	8.4 ± 0.9^{c}
18:4n-3	3.2 ± 0.8^{a}	2.3 ± 0.2^{b}	3.3 ± 0.2^{a}	3.2 ± 0.4^{a}	1.0 ± 0.3^{a}	0.7 ± 0.1^{b}	1.0 ± 0.1^{a}	0.9 ± 0.1^{a}
20:2n-6	0.5 ± 0.1^{a}	0.4 ± 0.1^{a}	0.3 ± 0.0^{b}	0.3 ± 0.0^{b}	0.5 ± 0.2^{a}	0.4 ± 0.1^{ac}	0.3 ± 0.0^{bc}	0.2 ± 0.1^{b}
20:3n-6	0.4 ± 0.1^{a}	0.3 ± 0.1^{b}	0.2 ± 0.0^{c}	0.2 ± 0.0^{c}	0.6 ± 0.3^{a}	0.5 ± 0.1^{b}	0.3 ± 0.0^{c}	0.2 ± 0.0^{c}
20:4n-6	0.3 ± 0.1	0.3 ± 0.0	0.2 ± 0.0	0.2 ± 0.0	1.0 ± 0.3^{a}	0.8 ± 0.1^{b}	0.6 ± 0.0^{c}	0.7 ± 0.1^{bc}
20:3n-3	0.3 ± 0.1^{ac}	0.3 ± 0.1^{a}	0.6 ± 0.1^{b}	0.4 ± 0.1^{bc}	0.4 ± 0.1^{a}	0.4 ± 0.2^{a}	0.8 ± 0.1^{b}	0.6 ± 0.1^{c}
20:4n-3	2.8 ± 1.9^{ab}	4.3 ± 1.2^{c}	3.1 ± 0.4^{bc}	4.0 ± 0.8^{bc}	1.3 ± 0.3^{a}	1.4 ± 0.2^{a}	1.8 ± 0.1^{b}	1.7 ± 0.2^{b}
20:5n-3	2.2 ± 0.9^{ab}	2.8 ± 0.5^{a}	2.4 ± 0.4^{bc}	2.8 ± 0.4^{c}	5.5 ± 0.5^{ab}	5.1 ± 0.4^{a}	5.2 ± 0.2^{a}	5.6 ± 0.4^{b}
22:5n-3	0.7 ± 0.3	0.9 ± 0.3	0.7 ± 0.1	0.9 ± 0.1	1.2 ± 0.1	1.2 ± 0.1	1.2 ± 0.1	1.3 ± 0.1
22:6n-3	5.7 ± 2.4^{a}	7.8 ± 1.6^{b}	6.2 ± 0.7^{ab}	7.5 ± 1.0^{b}	40.9 ± 3.3^{a}	43.9 ± 0.7^{b}	38.6 ± 2.6^{a}	43.7 ± 1.7^{b}
SAFA*	15.8 ± 2.0^{a}	19.2 ± 1.9^{b}	17.2 ± 1.3^{ab}	18.0 ± 1.8^{b}	26.3 ± 1.6^{ac}	27.1 ± 3.8^{ac}	27.1 ± 2.7^{ac}	24.9 ± 0.7^{a}
MUFA**	28.4 ± 2.8^{ab}	29.9 ± 2.0^{a}	26.3 ± 1.2^{b}	27.4 ± 1.8^{b}	8.5 ± 0.8^{c}	7.6 ± 0.6^{ab}	8.1 ± 0.3^{bc}	7.3 ± 0.6^{a}
PUFA	50.9 ± 5.8^{a}	45.1 ± 4.6^{b}	50.7 ± 2.7^{a}	48.4 ± 3.8^{ab}	63.7 ± 1.5^{ac}	64.0 ± 2.9^{ac}	62.7 ± 3.0^{c}	66.2 ± 1.1^{b}
n-3	28.0 ± 0.9^{a}	28.1 ± 1.2^{a}	39.6 ± 2.1^{b}	37.9 ± 2.7^{b}	55.4 ± 1.4^{b}	57.5 ± 1.7^{ab}	58.4 ± 2.8^{a}	62.2 ± 1.2^{c}
n-6	22.9 ± 6.2^{a}	17.0 ± 4.2^{b}	11.1 ± 0.7^{c}	10.5 ± 1.2^{c}	8.3 ± 2.7^{a}	6.5 ± 1.2^{b}	4.3 ± 0.3^{c}	4.0 ± 0.3^{c}
n-3/n-6	1.3 ± 0.4^{a}	1.7 ± 0.4^{b}	3.58 ± 0.0^{c}	3.62 ± 0.2^{c}	7.2 ± 2.3^{a}	$9.0 \pm 1.\ 6^{b}$	13.2 ± 0.7^{c}	15.4 ± 1.3^{d}
n-3 HUFA/18:3n-3	1.3 ± 0.7^{ab}	2.2 ± 11.2^{a}	0.7 ± 0.2^{b}	1.1 ± 0.5^{b}	10.4 ± 3.0^{a}	10.9 ± 2.2^{a}	5.0 ± 0.6^{b}	6.5 ± 0.8^{b}
n-6 HUFA/18:2n-6	0.06 ± 0.0^{a}	0.06 ± 0.01^{ab}	0.06 ± 0.01^{ab}	0.07 ± 0.02^{b}	0.34 ± 0.03^{a}	0.3 ± 0.03^{a}	0.36 ± 0.03^{b}	0.40 ± 0.03^{b}

HUFA highlyunsaturated fatty acids (18:4n-3, 20:2n-6, 20:3n-6, 20:4n-6, 20:3n-3, 20:4n-3, 20:5n-3, 22:5n-3, 22:6n-3), for others see Table 1

$^{a-d}$ Mean values across the row and lipid class not sharing a common superscript were significantly different as determined by $P < 0.05$

* SAFA includes 14:0, 16:0, 18:0, 20:0, 22:0, 24:0

** MUFA includes 16:1, 18:1n-9, 18:1n-7, 20:1, 22:1, 24:1

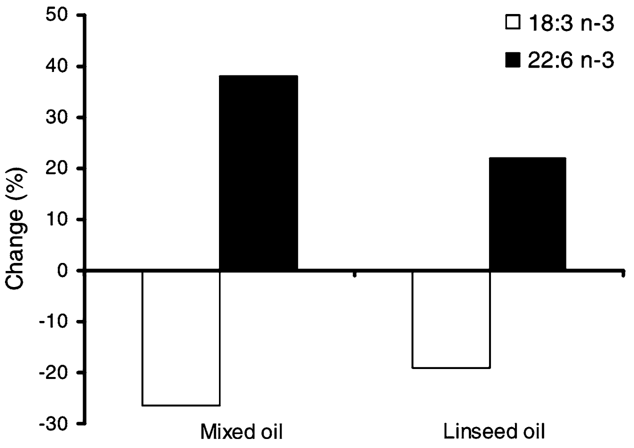

Fig. 1 Changes of α-linolenic acid (18:3n-3) and docosahexaenoic acid (22:6n-3) in white muscle triacylgycerols after addition of sesamin in the mixed oil and linseed oil diet respectively (*zero line* represents sesamin free diet). For the significance of the effect see Table 5

Table 5 Contents of sesamin and episesamin in tissue lipids (mg/100 g lipid) and the ratio of sesamin/episesamin

Diet	Sesamin	Episesamin	Sesamin/episesamin
White muscle			
MO	–	–	–
MO + S	19.5 ± 3.3	26.9 ± 5.4	0.73 ± 0.05^{a}
LO	–	–	–
LO + S	24.1 ± 8.2	34.1 ± 12.0	0.71 ± 0.02^{a}
Red muscle			
MO	–	–	–
MO + S	19.5 ± 3.3^{a}	28.3 ± 5.4^{a}	0.69 ± 0.02^{b}
LO	–	–	–
LO + S	24.3 ± 3.2^{b}	35.5 ± 5.1^{b}	0.69 ± 0.01^{b}
Liver			
MO	–	–	–
MO + S	17.0 ± 5.3^{a}	25.1 ± 6.5	0.75 ± 0.05^{a}
LO	–	–	–
LO + S	23.5 ± 3.3^{b}	32.2 ± 4.3	0.73 ± 0.04^{a}

For abbreviations see Table 1

[a,b] Mean values across the column and tissue not sharing a common superscript were significantly different as determined by $P < 0.05$, $n = 6$ in all groups

higher in liver compared to red muscle ($P < 0.01$) and in white muscle compared to red muscle ($P = 0.03$).

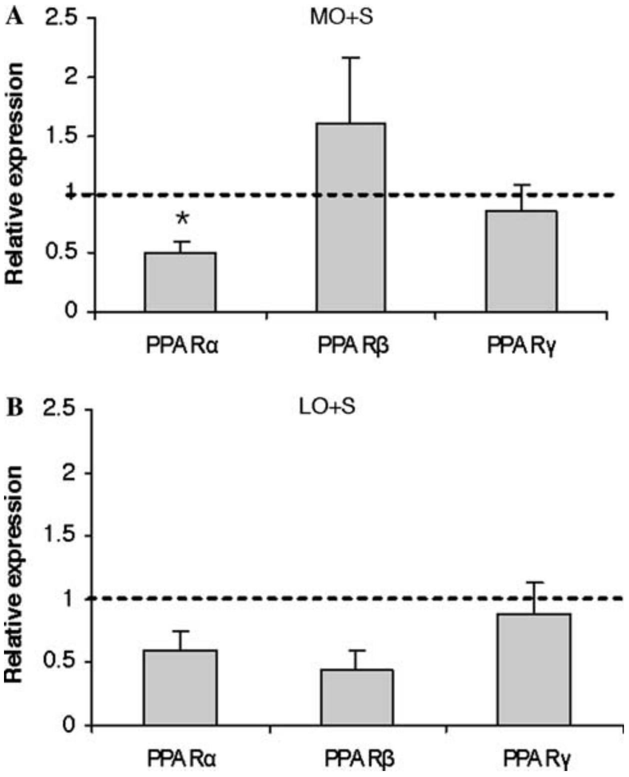

Fig. 2 Relative expression of PPARs in liver of mix oil based diets (**a**) and of linseed based oil diets (**b**). *Asterisk* denotes significant difference from vegetable oil diet without sesamin ($P < 0.05$), $n = 3$. *PPARα, β, γ* peroxisome proliferator-activated receptor alpha, beta, gamma

Gene Expression

The expression of *PPARα* was significantly down regulated in liver of fish fed MO + S diet (Fig. 2). In fish fed LO + S diet, *PPARα* was also reduced, albeit not significantly. Expression of *PPARβ* and *PPARγ* was not significantly affected by the inclusion of sesamin (Fig. 2).

Total Content of CYP and EROD Activity

The total amount of cytochrome P450 (CYP) was significantly higher ($P < 0.01$) in the experimental group MO + S (0.117 nmol mg^{-1} protein) when compared with mean level of CYP in the experimental group MO (0.086 nmol mg^{-1} protein) (Fig. 3). Further, hepatic EROD activity was also higher ($P < 0.01$) in MO + S experimental group (535.8 pmol mg^{-1} protein min^{-1}), when compared with experimental group MO (535.8 pmol mg^{-1} protein min^{-1}). Total CYP content and EROD activity were increased by the factors 1.4 and 8 in sesamin fed fish, respectively (Fig. 3).

Discussion

This study aimed to investigate the physiological effects of sesamin on fatty acid composition in rainbow trout fed vegetable oils. We were interested to study the effects of sesamin in diets containing different n-6/n-3 fatty acid ratio and different amount of 18:3n-3 substrate for elongation

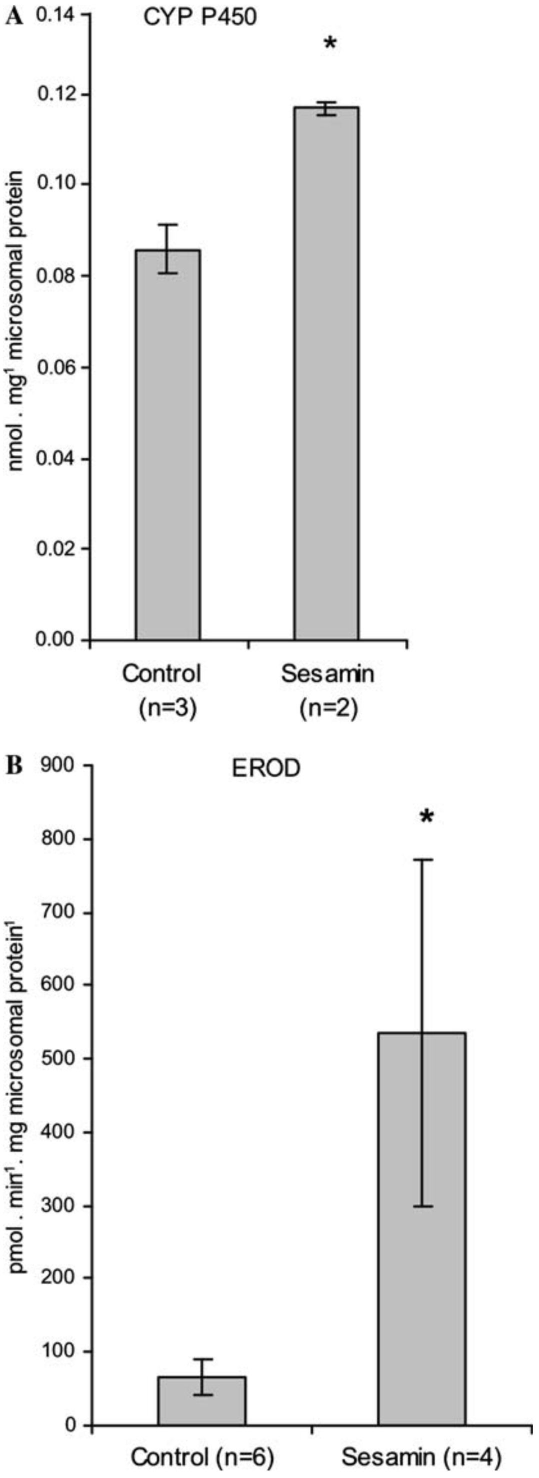

Fig. 3 Total amount of CYP, $n = 6$ for control group and $n = 4$ for sesamin group (**a**) and EROD activity, $n = 3$ for control group and $n = 2$ for sesamin group (**b**) in liver. *Asterisk* denotes significant difference from vegetable oil diet without sesamin ($P < 0.01$)

and desaturation. Therefore, we used linseed oil diet (LO) with the n-3/n-6 fatty acid ratio 3.6 and a mixed linseed oil/sunflower oil diet (MO) with the n-3/n-6 fatty acid ratio 1.0. In general, sesamin had the greatest physiological effect when it was fed in combination with the MO diet, having the higher n-6/n-3 ratio of these two diets. Also in combination with the MO diet, lower levels of sesamin were found in the tissues.

Previously, sesamin has been reported to increase the rate of both peroximal and mitochondrial β-oxidation in rats [2, 14]. Even if the β-oxidation rate is low in the white muscle of fish, it is important as the white muscle contributes a lager part of the total body weight [27]. Peroximal β-oxidation is involved in the shortening of long-chain fatty acids (including synthesis of DHA from 24:6n-3) [28], in contrast to mitochondrial β-oxidation where saturated fatty acids are preferred substrates [29]. Thus increased β-oxidation at both mitochondria and peroxisomes by sesamin may explain the lower proportion of total PUFA and the increased percentage of DHA in the white muscle triacylglycerol fraction. This is in agreement with results from our in vitro study [30].

The increase in DHA corresponds well to decreased percentages of 18:3n-3 (Fig. 1; Table 4) and increased desaturation index (n-3 HUFA/18:3n-3) (Table 4). The addition of sesamin also significantly decreased the proportion of 18:2n-6 in the MO + S group phospholipid and triacylglycerol fraction (Table 4). In rats, it has been shown that sesamin has effects on the fatty acid composition with especially increased proportions of n-6 fatty acids [13]. The results from this study show more effects on the n-3 fatty acids in fish. An important difference between fish and rat diets is the higher lipid content and also content of 18:3n-3 in the fish diet [13]. One could argue that the amount of substrate (18:3n-3) is one of the reasons for the results obtained in this study. Another possibility is the difference in capacity for elongation and desaturation between species [9].

A slightly higher (non significant) percentage of DHA in phospholipids was found in the MO-fed fish than in the LO-fed fish, which could be due to the higher percentage of 18:3n-3 in the LO diet, in agreement with the suggestion by Tocher et al. [31] that linseed oil results in lower amounts of DHA than rapeseed oil. However in contradiction, in the triacylglycerol fraction DHA is higher in the LO group than in the MO group (non significant). In the white muscle, approximately 75% of the lipids belong to the triacylglycerol fraction (compared to fish of similar stage as in [32]). The triacylglycerol fraction of the white muscle, which is the fraction mostly affected in this study, is the important fraction in terms of the fatty acid composition of fish muscle as human food. The possibility that sesamin can be added to feeds containing vegetable oils with eighteen carbon polyunsaturated fatty acids (e.g. rapeseed oil and linseed oil) to improve their elongation and desaturation in fish towards HUFA, especially DHA, is beneficial in relation to nutrition of both fish and human. It might increase the efficacy of alternate vegetable oil partial replacement to the fish oil needed in aquaculture production. The fact that the fatty acid composition of the livers was unchanged may be positive in terms of fish welfare.

In fish fed the mixture of sesamin/episesamin, these lignans were found in all tissues analyzed (Table 5) in contrast to rats [33] and humans where mostly the catecol metabolites are found [15]. The ratio sesamin/episesamin was similar in the fish tissues but was lower than in the feed. This finding is in agreement with a study in rats, showing twice as high level of episesamin than sesamin, even though the sesamin/episesamin ratio was one in the diet [34]. This could be caused by different absorption or by different rate of catabolism between the two isomers. The higher sesamin/episesamin ratio in the liver and white muscle compared to red muscle could indicate that sesamin is metabolized and deposited at different rates in the tissues, assuming that the tissues were exposed to the same ratio of sesamin/episesamin. To our knowledge, there are no studies on how fish metabolize sesamin and related compounds. The in vivo administrations of sesamin like compounds (methylenedioxyphenyl compounds) to rats and mammals exhibits a biphasic effect on CYP and microsomal oxidation activity that consist of a transient inhibitory phase and a subsequent phase of induction [16]. The level of total CYP and the EROD activity elevation in MO + S fish, indicates induction of cytochrome system in sesamin exposed fish. This indicates that sesamin in fish is recognized as a xenobiotic compound, however the pooled samples and the low power of statistics make it difficult to make any clear conclusions. No other toxic responses by the fish were recognized. In contrast, in vitro studies in humans show that sesamin inhibits cytochromes P450 [35].

Many studies in rats have shown effects of sesamin on the target genes or enzymes regulated by *PPAR*s [2, 3]. In this study we demonstrate a relative down regulation of *PPAR*α in liver of the MO + S group ($P = 0.04$) and a non significant down regulation in the LO + S group. This effect on gene expression indicates a different response in fish compared to rats. In rats, it has been shown that sesamin stimulates up regulation of genes involved in β-oxidation and metabolism of xenobiotic substances [36]. Similar to sesamin, expression of *PPAR*α has been reported to be down regulated in salmon fed 3-thia fatty acids [37], compounds that have also been associated with up regulation of *PPAR*s in mammals [38, 39]. The effects of sesamin on gene expression are further investigated in an in vitro study on Atlantic salmon hepatocytes [30].

Conclusion

The addition of sesamin/episesamin to vegetable oil-based diets increased the amount of DHA in the muscle of rainbow trout. Both sesamin and episesamin were found in the analyzed muscle and liver and were present at higher levels in fish fed linseed oil than the mixed oil. The addition of sesamin to the diet of fish fed vegetable oils may enhance the nutritional value of the fish muscle, in particular the fatty acid quality. Studies in large scale, with market-sized fish and sesamin of feed grade would be interesting to do in order to evaluate the commercial use of sesamin in aquaculture production. Dose-response studies in larger scale are needed in order to achieve information of the economical viability of sesamin in aquaculture feeds. Sesamin could play an important role in enhancing the fatty acid quality in fish fed vegetable oils to complement the limited amounts of fish raw materials.

Acknowledgments This study was financed by the Swedish research councils, Vetenskapsrådet and FORMAS, and the European Union Structural Funding for Fisheries. The authors like to thank Anne-Lise Rishovd at University of Oslo for valuable and skillful technical assistance.

References

1. Mizukuchi A, Umeda-Sawada R, Igarashi O (2003) Effect of dietary fat level and sesamin on the polyunsaturated fatty acid metabolism in rats. J Nutr Sci Vitaminol 49:320–326
2. Ashakumary L, Rouyer I, Takahashi Y, Ide T, Fukuda N, Aoyama T, Hashimoto T, Mizugaki M, Sugano M (1999) Sesamin, a sesame lignan, is a potent inducer of hepatic fatty acid oxidation in the rat. Metabolism 48:1303–1313
3. Ide T, Hong DD, Ranasinghe P, Takahashi Y, Kushiro M, Sugano M (2004) Interaction of dietary fat types and sesamin on hepatic fatty acid oxidation in rats. Biochim Biophys Acta 1682:80–91
4. Tacon AGJ (2008) State of information on salmon aquaculture feed and the environment. Report prepared for the WWF US Initiated Salmon Aquaculture Dialogue, 80p. http://www.westcoastaquatic.ca/Aquaculture_feed_environment.pdf (Accessed March 2008)
5. FAO (2007) FAOSTAT. http://faostat.fao.org/ (Accessed Nov 2007)
6. Kamal-Eldin A (2005) Minor components of vegetable oils. In: Shahidi F (ed) Bailey′s industrial oil and fat products. Wiley, Sussex
7. Torstensen BE, Bell JG, Rosenlund G, Henderson RJ, Graff IE, Tocher DR, Lie O, Sargent JR (2005) Tailoring of Atlantic salmon (*Salmo salar* L.) flesh lipid composition and sensory quality by replacing fish oil with a vegetable oil blend. J Agric Food Chem 53:10166–10178
8. Romarheim OH, Skrede A, Gao YL, Krogdahl A, Denstadli V, Lilleeng E, Storebakken T (2006) Comparison of white flakes and toasted soybean meal partly replacing fish meal as protein source in extruded feed for rainbow trout (*Oncorhynchus mykiss*). Aquaculture 256:354–364
9. Tocher DR (2003) Metabolism and functions of lipids and fatty acids in teleost fish. Rev Fish Sci 11:107–184
10. Bell JG, Tocher DR, Farndale BM, Cox DI, McKinney RW, Sargent JR (1997) The effect of dietary lipid on polyunsaturated fatty acid metabolism in Atlantic salmon (*Salmo salar*) undergoing Parr-Smolt transformation. Lipids 32:515–525

11. Buzzi M, Henderson RJ, Sargent JR (1997) Biosynthesis of docosahexaenoic acid in trout hepatocytes proceeds via 24-carbon intermediates. Comp Biochem Physiol B Biochem Mol Biol 116:263–267
12. Ackman RG (1996) DHA: can it benefit salmon marketing? J Aquatic Food Prod Tech 5:7–26
13. Fujiyama-Fujiwara Y, Umeda-Sawada R, Kuzuyama M, Igarashi O (1995) Effects of sesamin on the fatty acid composition of the liver of rats fed n–6 and n-3 fatty acids-rich diet. J Nutr Sci Vitaminol 41:217–225
14. Jeng KCG, Hou RCW (2005) Sesamin and sesamolin: nature's therapeutic lignans. Current enzyme Inhibition 1:11–20
15. Moazzami A, Kamal-Eldin A (2006) Sesame seed is a rich source of dietary lignans. J Am Oil Chem Soc 83:719–723
16. Murray M (2000) Mechanisms of inhibitory and regulatory effects of methylenedioxyphenyl compounds on cytochrome P450-dependent drug oxidation. Curr Drug Met 1:67–84
17. Nelson DR, Koymans L, Kamataki T, Stegeman JJ, Feyereisen R, Waxman DJ, Waterman MR, Gotoh O, Coon MJ, Estabrook RW, Gunsalus IC, Nebert DW (1996) P450 superfamily: update on new sequences, gene mapping, accession numbers and nomenclature. Pharmacogenetics 6:1–42
18. Jönsson M, Abrahamson A, Brunström B, Brandt I (2006) Cytochrome P4501A induction in rainbow trout gills and liver following exposure to waterborne indigo, benzo(a)pyrene and 3, 3′, 4′, 5-pentachlorobiphenyl. Aquat Toxicol 79:226–232
19. Williams DE, Lech JJ, Buhler DR (1998) Xenobiotics and xenoestrogens in fish: modulation of cytochrome P450 and carcinogenesis. Mutat Res Fund Mol Mech Mut 399:179–192
20. Sanchez-Vazquez FJ, Yamamoto T, Akiyama T, Madrid JA, Tabata M (1999) Macronutrient self-selection through demand-feeders in rainbow trout. Physiol Behav 66:45–51
21. Hara A, Radin NS (1978) Lipid extraction of tissue with low toxicity solvent. Anal Biochem 90:420–426
22. Pickova J, Dutta PC, Larsson PO, Kiessling A (1997) Early embryonic cleavage pattern, hatching success, and egg-lipid fatty acid composition: comparison between two cod (*Gadus morhua*) stocks. Can J Fish Aquat Sci 54:2410–2416
23. Appelqvist L (1968) Rapid methods of lipid extractions and fatty acid methyl ester preparation for seed and leaf tissue with special remarks on preventing the accumulation of lipids contaminants. R Swedish Acad Sci 28:551–570
24. Omura T, Sato R (1964) The carbon monoxide-binding pigment of liver microsomes. II. Solubilization, purification, and properties. J Biol Chem 239:2379–2385
25. Smith PK, Krohn RI, Hermansson GT, Malilia AK, Gartner FH, Provenzano MD, Fujimito EK, Goeke NM, Olson BJ, Klenk DC (1985) Measurement of protein using bicinchoninic acid. Anal Biochem 150:76–85
26. Brännäs E, Chaix T, Nilsson J, Eriksson LO (2005) Has a 4-generation selection programme affected the social behaviour and growth pattern of Arctic charr (*Salvelinus alpinus*)? Appl Anim Behav Sci 94:165–178
27. Froyland L, Lie O, Berge RK (2000) Mitochondrial and peroxisomal beta-oxidation capacities in various tissues from Atlantic salmon *Salmo salar*. Aquac Nutr 6:85–89
28. Voss A, Reinhart M, Sankarappa S, Sprecher H (1991) The metabolism of 7, 10, 13, 16, 19-docosapentaenoic acid to 4, 7, 10, 13, 16, 19-docosahexaenoic acid in rat-liver is independent of a 4-desaturase. J Biol Chem 266:19995–20000
29. Kiessling KH, Kiessling A (1993) Selective utilization of fatty-acids in rainbow-trout (*Oncorhynchus-Mykiss Walbaum*) red muscle mitochondria. Can J Zool 71:248–251
30. Trattner S, Ruyter B, Østbye TK, Gjøen T, Zlabek V, Kamal-Eldin A, Pickova J (2008) Sesamin increases alpha-linolenic acid conversion to docosahexaenoic acid in Atlantic salmon (*Salmo salar* L.) hepatocytes: role of altered gene expression. Lipids. doi: 10.1007/s11745-008-3229-7
31. Tocher DR, Fonseca-Madrigal J, Bell JG, Dick JR, Henderson RJ, Sargent JR (2002) Effects of diets containing linseed oil on fatty acid desaturation and oxidation in hepatocytes and intestinal enterocytes in Atlantic salmon (*Salmo salar*). Fish Physiol Biochem 26:157–170
32. Kiessling A, Pickova J, Johansson L, Asgard T, Storebakken T, Kiessling KH (2001) Changes in fatty acid composition in muscle and adipose tissue of farmed rainbow trout (*Oncorhynchus mykiss*) in relation to ration and age. Food Chem 73:271–284
33. Nakai M, Harada M, Nakahara K, Akimoto K, Shibata H, Miki W, Kiso Y (2003) Novel antioxidative metabolites in rat liver with ingested sesamin. J Agric Food Chem 51:1666–1670
34. Umeda-Sawada R, Ogawa M, Igarashi O (1999) The metabolism and distribution of sesame lignans (sesamin and episesamin) in rats. Lipids 34:633–637
35. Von Moltke LL, Weemhoff JL, Bedir E, Khan IA, Harmatz JS, Goldman P, Greenblatt DJ (2004) Inhibition of human cytochromes P450 by components of Ginkgo biloba. J Pharma Pharmacol 56:1039–1044
36. Kiso Y, Tsuruoka N, Kidokoro A, Matsumoto I, Abe K (2005) Sesamin ingestion regulates the transcription levels of hepatic metabolizing enzymes for alcohol and lipids in rats. Alcohol Clin Exp Res 29:116S–120S
37. Kleveland EJ, Ruyter B, Vegusdal A, Sundvold H, Berge RK, Gjoen T (2006) Effects of 3-thia fatty acids on expression of some lipid related genes in Atlantic salmon (*Salmo salar* L.). Comp Biochem Physiol B 145:239–248
38. Berge K, Tronstad KJ, Flindt EN, Rasmussen TH, Madsen L, Kristiansen K, Berge RK (2001) Tetradecylthioacetic acid inhibits growth of rat glioma cells ex vivo and in vivo via PPAR-dependent and PPAR-independent pathways. Carcinogenesis 22:1747–1755
39. Raspe E, Madsen L, Lefebvre AM, Leitersdorf I, Gelman L, Peinado-Onsurbe J, Dallongeville J, Fruchart JC, Berge R, Staels B (1999) Modulation of rat liver apolipoprotein gene expression and serum lipid levels by tetradecylthioacetic acid (TTA) via PPAR alpha activation. J Lipid Res 40:2099–2110

TAG	Triacylglycerols
TLC	Thin-layer chromatography
VLDL	Very low-density lipoprotein
Δ5	Δ5 Desaturase
Δ6	Δ6 Desaturase

Introduction

Due to a shortage of fish oil and an expected increase in aquaculture production, research is focussing on replacement of aqua feeds with increasing amounts of vegetable oils [1, 2]. It is well known that substitution of fish oil with vegetable oils decreases the content of n-3 long chain polyunsaturated fatty acids (LCPUFA) in the fish tissues [3]. In terms of the consumer's health, it would be beneficial to maintain as high as possible amounts of n-3 LCPUFA in fish muscle [4]. In a previous study from our group, we have shown that sesamin in vegetable oil based fish feed increased the percentage of DHA in the white muscle of rainbow trout (*Oncorhynchus mykiss*). This result indicates that vegetable-based ingredients may have beneficial effects in preserving the healthy fatty acid profile of fish muscle [5].

Sesamin is the main lignan in sesame seed and has been associated with several effects on lipid metabolism in mammals [6]. Although very little is known for fish, sesamin was shown to increase β-oxidation [7, 8] and affect elongation and desaturation of fatty acids in rats [9]. Sesamin was also shown to lower serum levels of triacylglycerols (TAG) and cholesterol in rats and humans [7, 10, 11]. A wide range of enzymes involved in the desaturation and β-oxidation of fatty acids are affected by sesamin, both at activity and mRNA levels (e.g., acyl-CoA oxidase and carnitin palmitoyl transferase) [6, 7, 10]. Many of these effects are presumed to be caused through the activation of peroxisome proliferator-activated receptors (PPARs) and inhibition of sterol regulatory element-binding protein-1 (SREBP-1) [8, 12].

In this study, we aimed to investigate the metabolic effects of sesamin on β-oxidation, elongation, desaturation, fatty acid profile and the expression of some lipid-related genes in hepatocytes isolated from Atlantic salmon (*Salmo salar* L.).

Materials and Methods

Chemicals and Reagents

The radiolabelled fatty acid [1-^{14}C] 18:3n-3 (specific radioactivity 50 mCi/mmol) was obtained from American Radiolabeled Chemicals (St. Louis, MO, USA). The non-labelled 18:3n-3, essential fatty acid free bovine serum albumin (BSA), fetal bovine serum (FBS), Leibovitz-15 (L-15), 2′,7′-dichlorfluorescein, 2′,7′- dichlorfluorescein and collagenase, Phosphate buffer saline (PBS), phenylethylamine and 4-(2-hydroxyethyl)-1-piperazineethanesulfonic acid (HEPES), ethylenediaminetetraacetic acid (EDTA), sodium bicarbonate solution, L-glutamine, were obtained from Sigma Chemical Co. (St. Louis, MO, USA) and metacain MS-222 from Norsk Medisinaldepot (Norway). Sesamin (sesamin/episesamin mixture, 1:1, w/w) was a kind gift from Takemoto Oil and Fat Co., Ltd. (Gamagori Aichi, Japan). Fatty acid peaks were identified by comparison with the standard mixture GLC-68 A (Nu-check Prep, Inc, Elysian, Minnesota, USA). Ammonium dihydrogenphosphate, perchloric acid ($HClO_4$), thin-layer chromatography (TLC)-plates, all solvents and other chemicals for fatty acid and sesamin analysis were purchase from Merck (Darmstadt, Germany).

General Description

Hepatocytes isolated from Atlantic salmon were incubated with radiolabelled and non-radiolabelled α-linolenic acid (18:3n-3) in the presence and absence of sesamin. For the experiment with non-radiolabelled fatty acid fatty acid composition and expression of some lipid related genes were measured. The radiolabelled 18:3n-3 was used to measure changes in fatty acid metabolism, desaturation and β-oxidation. The details of the different methodological and analytical steps are described below.

Isolation of Hepatocytes

Atlantic salmon of approximately 800 g (NIVAs Research Station, Drøbak, Norway) were kept in seawater at 10 °C and fed on a commercial diet prior to isolation of hepatocytes. Hepatocytes were isolated from three fish at three different time points and used for three experiments: (1) Effects of sesamin (0.05 mM) on fatty acid β-oxidation, elongation, desaturation and fatty acid profile, (2) dose response study (0, 0.005, 0.05, 0.075 and 0.11 mM sesamin final concentration in the medium) on the effect on gene expression, (3) time course study over a 72 h time period and the effect of gene expression. The livers were perfused following the two-step collagenase procedure developed by Seglen [13] and modified by Dannevig and Berg [14] and conducted as per Kjær et al. [15]. At each time point, the hepatocytes were pooled from three livers and incubated as described below.

Incubation of Hepatocytes with Linolenic Acid 18:3n-3

The isolated hepatocytes were incubated with 35 nmol, 2.5 µCi of [1-^{14}C] 18:3n-3 as well as non radiolabelled

18:3n-3, final fatty acid concentration of 7 μM, in 5 ml of L-15 culture medium without FBS. The radiolabelled fatty acid was added to the medium as potassium salt bound to BSA. To each experimental flask (four radiolabelled and seven with non-radiolabelled 18:3n-3), dimethyl sulfoxide (7.4 μl/5 ml) without or with sesamin (final concentration 0.05 mM) was added and to control and treatment flasks (each four radiolabelled and seven with non-radiolabelled 18:3n-3) and in other two flasks sesamin but no fatty acid was added. The cells were incubated at 12 °C for 48 h. The radiolabelled experiment flasks with and without sesamin (four each) were washed and harvested in PBS for further analysis of *β*-oxidation, radiolabelled lipid classes and radiolabelled cellular fatty acids. The cells in the two flasks with no fatty acid substrate added were denaturated after the incubation and thereafter added radiolabelled substrate in order to be used as a negative control for the acid soluble products (ASP) measurements and high pressure liquid chromatography analyses. In the non-labelled study, control and sesamin flask (four each) were washed in PBS prior to isolation of mRNA according to the protocol RNeasy® Mini Kit for gene expression analysis and three flasks of each control and sesamin were washed and harvested in PSB for fatty acid and sesamin analysis.

Incubation of Hepatocytes for Dose Response and Time Course Study

The cells for the dose response study were washed in PBS 24 h after seeding and incubated in L-15 culture medium with 10% FBS (the fatty acid composition of L-15 + FBS was: 14:0 = 8.4%; 14:1 = 0.6%; 15:0 = 2.3%; 16:0 = 31.7%; 16:1 = 4,1%; 18:0 = 31.7%; 18:1 n-9 = 14.9%; 18:1n-7 = 2.7%; 18:2n-6 = 3.7%; 18:3n-3 = 1.0%; 20:3 n-6 = 0.8%; 20:4n-6 = 2.4%; 20:5n-3 = 0.5%; 22:5n-3 = 0.9%; 22:6n-3 = 1.2%) and with five different concentrations of sesamin. Sesamin dissolved in dimethyl sulfoxide (7.4 μl/5 ml medium) was added at final concentrations of 0.005 mM, 0.05 mM, 0.075 mM and 0.11 mM to duplicate flasks of cells in a regression design and incubated for 42 h at 12 °C. For the time course study, a final concentration of 0.05 mM sesamin in culture medium was added to the hepatocytes in duplicate flasks. The cells were incubated for 0, 18, 24, 42, 48, 66 and 72 h. As a control in both the dose response study and the time course study, dimethyl sulfoxide (7.4 μl/5 ml medium) was added to the cells without sesamin. After incubation, the cells were washed in PBS prior to isolation of mRNA according to the protocol RNeasy® Mini Kit for gene expression analysis.

Analysis of Lipids in Cells and Medium

Lipids from cells and medium incubated with [1-^{14}C] 18:3n-3 were extracted according to Folch et al. [16] and the fatty acid composition of the cells was determined by reversed phase high pressure liquid chromatography as described by Narce et al. [17]. The mobile phase was acetonitrile:water (85:15 v/v) at a flow rate of 1 ml/min and a temperature of 30 °C. The column used was a symmetry 3.5 μm C_{18} column and the fatty acids were detected with a radioactive detector A-100 (Radiomatic Instrument & Chemicals, Tampa, FL, USA). The fatty acids were identified by comparison of their retention times with those of external standards. The lipids extracted from the medium were separated on TLC-plates into various classes using a mixture of petroleum ether, diethyl ether and acetic acid (113:20:2 v/v/v). The separated lipid classes, phospholipids (PL), monoglycerides (MG) free fatty acids (FFA) and triacylglycerols (TAG) were visualised by spraying with 0.2% 2′,7′-dichlorofluorescein in methanol and identified by comparison to standards under UV-light. The lipid classes were scraped off and dissolved in scintillation fluid for scintillation counting (TRI-CARB 1900 TR, Packard Instruments). The esterified fatty acids, PL, MG and TAG fractions within the media will be denoted as secreted fatty acids.

Lipids from the non-radioactive cells and the medium used for the dose response and the time course studies were extracted by using hexane:isopropanol (3:2 v/v) [18]. Total lipids were converted to fatty acid methyl esters by using 20% boron trifluoride–methanol complex according to Appelqvist [19] and analysed with Gas Chromatograph CP3800 (Varian AB, Stockholm, Sweden) according to Fredriksson et al. [20].

Measurements of *β*-Oxidation

The capacity of *β*-oxidation was measured by determination of the ^{14}C-containing oxidation products, ASP and CO_2 as described by Christiansen et al. [21]. ^{14}C-CO_2 produced during the incubation of the cells was measured by transferring 1.5 ml of the medium to glass vials sealed with a rubber stop and a central well containing a Whatman filter paper with 0.3 ml phenylethylamine/methanol (1:1 v/v). The medium were acidified with 0.3 ml 1 M $HClO_4$ and ^{14}C-CO_2 was trapped for 1 h. Then the filter papers were placed in vials and dissolved in 8 ml of scintillation fluid for scintillation counting (Radiomatic Instrument & Chemicals, Tampa, FL, USA). The amount of ^{14}C-ASP was determined by adding 0.5 ml ice cold 2 M $HClO_4$ to the incubation medium and incubated at 4 °C for 1 h, then the samples were centrifuged at 17,950×g for 10 min at 10 °C and 200 µl of the supernatant was collected for scintillation counting (Radiomatic Instrument & Chemicals, Tampa, FL, USA). The remaining supernatant was neutralised with NaOH and the different ASPs were detected by using high pressure liquid chromatography equipped with a ChromSep Inertsil C8-3 column (250 × 4.6 mm stainless steel), an UV-detector at 210 nm and radioactive detector A-100 (Radiomatic Instrument & Chemicals, Tampa, FL, USA) coupled to the UV detector. The mobile phase was 0.1 M ammonium dihydrogenphosphate adjusted with phosphoric acid to pH 2.5, the flow rate was 1 ml/min. The components were identified by comparison to external standards and retention times.

Protein Determination and Acyl-CoA Oxidase (ACO) Activity

The protein content of the cells was determined by using the total protein kit (Micro Lowry/Peterson's modification) [22, 23] and measured at 540 nm in a 96 well plate reader Titertek, Multiscan (Labsystem, Finland). The ACO activity was determined according to Small et al. [24]. The oxidation of 2,7 dichlorofluorescein (LDCF) was measured with a GBC UV/VIS 98 spectrophotometer (502 nm; GBC Scientific equipment, PTY, LTD, Melborne, Victoria, Australia) during 3 min. The assay mixture contained 10 µl LDCF, 50 µl peroxidase type II in 0.1 M Tris, 10 µl BSA (60 mg/ml), 10 µl FAD, 0.15 mg protein and H_2O up to 1 ml. The reaction was started with 10 µl PalmCoA (6 mg/ml 0.1 M TRIS).

Total RNA Extraction, cDNA Synthesis and Real Time PCR

Total RNA was isolated from the cells using the RNeasy® Mini Kit with on-column Rnase free DNase set (Qiagen, MD, USA). All protocols were according to the manufacture's instructions. Purity and density were measured by optical density (NanoDrop® ND-1000 Spectrophotometer, NanoDrop Technologies, Wilmington, Delaware, USA) and samples were stored in RNase-free water (Eppendorf, Hamburg, Germany) at −70 °C.

The cDNA was synthesised following a modified protocol from the Taq Man Reverse Transcription Reagents kit (Applied Biosystems). The Oligo $d(T)_{16}$ primers were used. The reaction was performed by incubating the samples at 25 °C for 10 min, 48 °C for 6 min, 95 °C for 50 min and was terminated by reducing temperature to 10 °C.

Primers for Real-Time PCR analysis (Table 1) were designed based on available salmon sequences in the GenBank® using the Primer Express® software and ordered from Invitrogene (CA, USA). Real-Time PCR for the dose response study was performed in a Prism® 7000 system with gene-specific primers for scavenger receptor type B (SRB-I), PPARα, β, γ and cluster of differentiation 36 (cd36) (Table 1). A 2× SYBR® Green PCR Mastermix (ABI) was used in the PCR reaction mix of 25 µl with 1 µl primers (final concentration of 0.5 µM), and 5 µl cDNA. All samples were analyzed in duplicate with non-template control on each plate. Elongation factor 1α (EF1A) and RNA polymerase II polypeptide (RPL2) were used as reference genes. The reaction was performed by incubating the samples at 50 °C for 2 min, 95 °C 10 min and 50 cycles of 95 °C for 10 s and 60 °C for 15 s. Standard curves were made for each primer pair and primer efficiency (E) calculated [$E = 10^{(-1/\mathrm{slope})}$]. The Real-Time PCR for the time study and the cells incubated with non radiolabelled 18:3n-3 was performed in a LightCycler® 480 system using SYBR® Green PCR Mastermix (Roche, Oslo, Norway) and gene-specific primers for SRB-I, Δ5 desaturase, Δ6 desaturase, PPARα, β, γ, cd36, acyl-CoA

Table 1 Sequence of primers

Primer	Forward primer (5′–3′)	Reverse primer (5′–3′)	GenBank Acc. no.	Efficiency
RPL2	TAACGCCTGCCTCTTCACGTTGA	ATGAGGGACCTTGTAGCCAGCAA	CA049789	1.95
EF1A	CACCACCGGCCATCTGATCTACAA	TCAGCAGCCTCCTTCTCGAACTTC	AF321836	1.97
PPARα	CGTTGAATTTCATGGCGAACT	TCCTGGTGGCCTACGGATC	DQ294237	1.90
PPARβ	CCAGCAACCCGTCCTTGTT	GAGACGGTCAGGGAGCTCAC	AJ416953	2.04
PPARγ	CATTGTCAGCCTGTCCAGAC	ATGTGACATTCCCACAAGCA	AJ292963	1.95
SRB-I	AACTCAGTGAAGAGGCCAAACTTG	TGCGGCGGTGATGATG	DQ266043	1.79
cd36	GGATGAACTCCCTGCATGTGA	TGAGGCCAAAGTACTCGTCGA	AY606034	1.76
Δ5	GAGAGCTGGCACCGACAGAG	GAGCTGCATTTTTCCCATGG	AF478472	1.77
Δ6	AGAGCGTAGCTGACACAGCG	TCCTCGGTTCTCTCTGCTCC	AY458652	1.90
ACO	CCTTCATTGTACCTCTCCGCA	CATTTCAACCTCATCAAAGCCAA	DQ364432	2.00
CPT1	GTACCAGCCCCGATGCCTTCAT	TCTCTGTGCGACCCTCTCGGAA	AM230810	1.90

RPL2 RNA polymerase II polypeptide, *EF1A* elongation factor 1α, PPAR peroxisome proliferator-activated receptor, *SRB-I* scavenger receptor type B, *cd 36* cluster of differentiation 36, *Δ5* Δ5 desaturase, *Δ6* Δ6 desaturase, *ACO* acyl-CoA oxidase, *CPT1* carnitin palmitoyl transferase I

oxidase (ACO) and carnitine palmitoyl transferase I (CPT1) (Table 1). The PCR reaction mix (10 μl) consisted of 1 μl forward and reverse primer (final concentration of 0.5 μM), 4 μl cDNA and 5 μl mastermix. All samples were analysed in duplicate with non-template control on each plate and for each gene. RPL2 was used as a reference gene. The reaction was incubated at 95 °C for 5 min, 45 cycles of 95 °C for 10 s, 60 °C for 15 s and 72 °C for 15 s. Standard curves were made and the primer efficiency (*E*) was calculated for each primer pair using the LightCycler$^{\circledR}$ 480 software.

Statistical Analysis

Relative expressions of the different genes, in relation to housekeeping genes, were determined using the Relative Expression Software Tool (REST-384$^{\copyright}$-version 1). For all other data, the student t-test in Microsoft Office Excel 2003 was used. The number of experimental replicates was three for the non-radiolabelled experiment [except the dose response and the time course study ($n = 2$)] and was four for the radiolabelled experiment. Differences were considered as significant at $P < 0.05$.

Results

Lipid Content and Fatty Acid Profiles in Hepatocytes Incubated with 18:3n-3

The total mean lipid content of the control cells (1.7 mg = 1.3%) was not different from that of cells incubated with sesamin (1.4 mg = 1.0%). Table 2 shows the fatty acid profiles of the hepatocytes incubated with non-radiolabelled 18:3n-3 in the absence and presence of sesamin. The addition of sesamin significantly reduced saturated fatty acids (SAFA, $P < 0.01$) and monounsaturated fatty acids (MUFA, $P < 0.02$) and elevated n-3 polyunsaturated fatty acids (n-3 PUFA, $P < 0.01$). Especially, the proportion of DHA was significantly increased in the sesamin-incubated hepatocytes, from 27.2 to 36.0% ($P < 0.01$) while the proportion of eicosapentaenoic acid (20:5n-3, EPA) did not change. The desaturation index (n-3 LCPUFA/18:3n-3) was increased from 27.0 to 33.8 in the presence of sesamin ($P < 0.05$).

Table 2 Fatty acid composition in total lipid fraction (% of total fatty acids) in the hepatocytes, ($n = 3$ in control and sesamin group)

	Control	Sesamin	*P*-value*
14:0	1.8 ± 0.41	1.3 ± 0.02	0.10
15:0	0. 5 ± 0.17	0.3 ± 0.01	0.14
16:0	21.4 ± 1.73	16.6 ± 0.84	0.01
16:1	1.3 ± 0.31	1.2 ± 0.05	0.58
18:0	4.8 ± 0.50	4.3 ± 0.28	0.20
18:1n-9	14.9 ± 0.56	12.6 ± 0.60	0.01
18:1n-7	2.1 ± 0.08	1.9 ± 0.09	0.02
18:2n-6	4.2 ± 0.28	3.9 ± 0.23	0.16
18:3n-3	1.7 ± 0.09	1.6 ± 0.12	0.28
18:4n-3	0.3 ± 0.04	0.3 ± 0.04	0.73
20:1	1.1 ± 0.06	1.0 ± 0.05	0.15
20:2n-6	0.5 ± 0.04	0.5 ± 0.03	0.54
20:3n-6	0.5 ± 0.06	0.5 ± 0.04	0.74
20:4n-6	2.3 ± 0.87	2.8 ± 0.24	0.43
22:1	1.0 ± 0.11	1.1 ± 0.14	0.68
20:5n-3	7.9 ± 0.50	7.7 ± 0.49	0.69
22:5n-3	2.6 ± 0.33	2.8 ± 0.19	0.60
22:6n-3	27.2 ± 2.43	36.0 ± 2.76	0.01
n-3 PUFA	39.6 ± 2.90	48.3 ± 1.95	0.01
n-6 PUFA	7.5 ± 0.82	7.6 ± 0.49	0.92
SAFA	28.7 ± 1.73	22.7 ± 1.12	0.01
MUFA	20.5 ± 0.87	17. 8 ± 0.87	0.02
PUFA	47.2 ± 3.11	55.9 ± 1.51	0.01
n-3 LCPUFA/18:3n-3	27.2 ± 2.74	34.1 ± 2.75	0.04

SAFA saturated fatty acids, *MUFA* monounsaturated fatty acids, *PUFA* polyunsaturated fatty acids, *n-3LCPUFA* 20:5n-3 + 22:5n-3 + 22:6n-3

* *P*-value present comparison of sesamin and control group

The proportions of radioactive fatty acids in the hepatocytes incubated with ^{14}C 18:3n-3 in the presence or absence of sesamin are shown in Table 3. The percentage of ^{14}C DHA was significantly higher in the sesamin treated group than in the control group, 20.2 versus 10.5%, respectively ($P < 0.001$). Sesamin also increased the percentage of ^{14}C 18:4n-3 ($P = 0.04$) and the total amount of ^{14}C LCPUFA ($P = 0.01$). Notably, the percentage of ^{14}C EPA was higher in the control than in the sesamin group, 12.3 versus 7.5%, respectively ($P < 0.01$). As with the non-labelled 18:3n-3 experiment, the desaturation index (^{14}C LCPUFA/18:3n-3) was significantly higher in the sesamin group ($P = 0.03$).

Distribution of radioactive products from ^{14}C 18:3n-3 substrate in cellular and secreted lipids, lipid classes and *β*-oxidation products.

The total amount of ^{14}C 18:3n-3 in cells and medium and the distribution of radiolabelled fatty acids in cellular, secreted lipids (i.e., all esterified lipid classes including phospholipids (PL), monoglyceride (MG), triacylglycerol (TAG) and free fatty acids), as well as the amount of radiolabelled fatty acids in the *β*-oxidation products (ASP, CO_2 and total *β*-oxidation products = ASP + CO_2) are shown in Table 4. Significantly more ^{14}C 18:3n-3 have been taken up into the sesamin-incubated hepatocytes than into the control hepatocytes, 3.2 and 2.8 nmol fatty acids mg protein^{-1}, respectively ($P < 0.01$). In contrast, the

Table 3 The proportion of radioactive fatty acid (from ^{14}C 18:3n-3, expressed as % of total identified fatty acids) in hepatocytes ($n = 4$ in each group)

Fatty acid	Control	Sesamin	*P*-value
16:0	2.5 ± 0.33	2.4 ± 0.52	0.54
18:3n-3	57.7 ± 0.27	52.8 ± 4.57	0.07
18:4n-3	2.0 ± 0.35	2.7 ± 0.38	0.04
20:3n-3	11.6 ± 0.37	10.6 ± 1.21	0.15
20:4n-3	2.7 ± 0.20	2.5 ± 0.28	0.32
20:5n-3	12.3 ± 0.85	7.5 ± 0.93	<0.01
24:5n-3	0.6 ± 0.25	1.4 ± 0.28	0.01
22:6n-3	10.5 ± 0.10	20.2 ± 2.05	<0.01
n-3 LCPUFA/18:3n-3	0.49 ± 0.01	0.66 ± 0.12	0.03

n-3 LCPUFA = 18:4n-3 + 20:4n-3 + 20:5n-3 + 24:5n-3 + 22:6n-3

amount of secreted lipids (PL + TAG + MG) tended to be lower in sesamin treated cells than the control cells (0.10 ± 0.02 and 0.20 ± 0.07, respectively, $P = 0.09$), mainly the TAG content decreased in the medium (Table 4). The addition of sesamin increased the total β-oxidation (ASP + CO_2), ($P < 0.01$) of 18:3n-3 and especially the amount of ASP increased from 0.03 ± 0.02 to 0.08 ± 0.02 ($P < 0.01$). The compound increased by sesamin in the ASP fraction was acetate representing 53.5% of ASP in the control group and 72.6% of ASP in the sesamin group ($P < 0.01$). Oxaloacetate and malate decreased correspondingly (Fig. 1). No significant differences in the enzymatic activity of acyl-CoA oxidase between the groups were found. The acyl-CoA oxidase activity was 0.35 ± 0.08 and 0.39 ± 0.02 m unit mg protein^{-1} in control and sesamin cells, respectively.

Gene Expression

In the dose response experiment the relative expression of SRB-I, PPARα, PPARγ and cd36 were significantly ($P < 0.05$) downregulated at 0.05 mM sesamin and were downregulated at all concentrations of sesamin above (Fig. 2). In the cells incubated with sesamin (0.05 mM) and 18:3n-3, the expression of CTP1 was significantly upregulated by a factor 3.8 ($P < 0.01$) and expression of PPARγ was down-regulated by a factor 2.2 ($P < 0.01$, Fig. 3). In the time study, significant effects ($P < 0.05$) of sesamin (0.05 mM) on the relative expression of Δ6 and Δ5 desaturases were found after 24 and 42 h incubation, respectively (Fig. 4). Both Δ6 and Δ5 desaturases followed the same pattern of relative expression.

Discussion

In this study, we demonstrated clear effects of sesamin on fatty acid metabolism in salmon hepatocytes. An overview of the findings from this study is presented in Fig. 5. In the hepatocytes incubated with nonradioactive 18:3n-3 and sesamin, the percentage of DHA ($P < 0.01$) and PUFA ($P = 0.01$) and the desaturation index (LCPUFA/18:3n-3) ($P = 0.04$) were significantly increased, and the percentage of 16:0 was significantly decreased ($P < 0.01$). In both the sesamin and the control cells incubated with ^{14}C 18:3n-3, elongation and desaturation occurred. Strikingly 18:4n-3 and DHA increased while 18:3n-3 and EPA decreased in cells incubated with sesamin. This can be explained by the increase in activity of Δ6 desaturase and β-oxidation by sesamin leading to increased conversion of 18:3n-3 to DHA. In addition, as the level of DHA in the liver cells has not reached the levels found before [15], it is unlikely that DHA would be β-oxidised to EPA.

The proportion of acetate in the acid soluble product (ASP) fraction increased by sesamin addition (Fig. 1, $P < 0.01$). Previously, sesamin has been reported to increase the rate of both peroxisomal and mitochondrial β-oxidation in rats [7, 8]. In rat hepatocytes, acetate has been defined as the main product of peroxisomal β-oxidation [25]. However, we do not know if this is the case in salmon. The analysis of enzymatic activity of acyl-CoA oxidase did not show any significant differences between

Table 4 Distribution of radioactivity in the cells and the medium after incubation of hepatocytes with ^{14}C18:3n-3 in the presence and absence of sesamin, ($n = 4$ in each group)

	Control	Sesamin	*P*-value
Total fatty acids in cells and medium (nmol)	23.63 ± 0.53	24.16 ± 0.28	0.13
Cellular lipids (nmol mg protein^{-1})	2.80 ± 0.10	3.19 ± 0.03	<0.01
CO_2 in medium (nmol mg protein^{-1})	0.007 ± 0.001	0.006 ± 0.000	0.06
Acid soluble fraction in medium (nmol mg protein^{-1})	0.032 ± 0.017	0.080 ± 0.020	<0.01
Total β-oxidation products (nmol mg protein^{-1})	0.039 ± 0.017	0.087 ± 0.016	<0.01
Free fatty acids in medium (nmol mg protein^{-1})	0.11 ± 0.05	0.11 ± 0.04	0.94
Secreted lipids in medium (nmol mg protein^{-1})[a]	0.20 ± 0.07	0.10 ± 0.02	0.09

[a] Secreted = triacylglycerols, monoglycerides and phospholipids in the medium

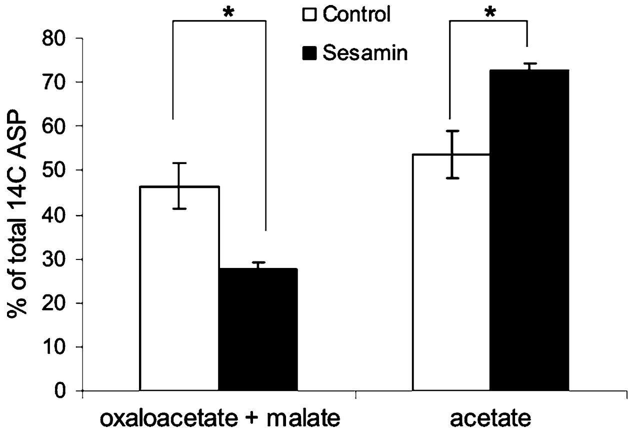

Fig. 1 Percentage distribution of radiolabelled oxaloacetate + malate and acetate in the acid soluble fraction (*ASP*) from ^{14}C 18:3n-3 oxidation. The control cells are illustrated with *white bars* and the sesamin cells are illustrated with *black bars*. Data are shown as mean values ± standard deviation. *Asterisk* indicate significant difference ($P < 0.01$), ($n = 4$)

the groups, but a slight increase in the sesamin group. The peroxisomal acyl-CoA oxidase activity in rat liver was significantly increased by dietary sesamin [7, 8, 12]. The peroxisomal β-oxidation is also involved in the synthesis of DHA (shortening of 24:6n-3 to 22:6n-3) [26]. Therefore, the increased DHA levels in this study and the previous study [5] could also result from increased peroxisomal β-oxidation. On the other hand, the increased gene expression of CPT1 indicates that mitochondrial β-oxidation is also influenced by sesamin addition. Since sesamin increased the production of radio labelled acetate and not oxaloacetate and malate β-oxidation, one can suggest that 18:3n-3 and its elongated and desaturated products were mainly oxidised in the peroxisomes and that β-oxidation of other fatty acids mainly occurs in the mitochondria as evidenced by the increase expression of CPT1. Kiessling et al. [27] showed that SAFA are the preferred substrate for selective β-oxidation in mitochondria in rainbow trout. In the sesamin treated cells incubated with non-radiolabelled 18:3n-3, lower percentage of 16:0 was found, a possible result of increased mitochondrial β-oxidation.

Sesamin tended to decrease the amount of secreted lipids in the medium by ~50% from 0.20 to 0.10 nmol mg protein^{-1}, the most decreased lipid class was TAG. This suggests lower levels of very low-density lipoprotein (VLDL) secreted from the liver. This result is in agreement with studies on rats, which show that sesamin lowers the levels of VLDL and TAG in plasma and serum [7, 10, 11, 28]. Increased levels of n-3 fatty acids are also shown to decrease the secretion of TAG in salmon [15, 29]. The reduced TAG level can also be an effect of the increased content of n-3 LCPUFA in this study.

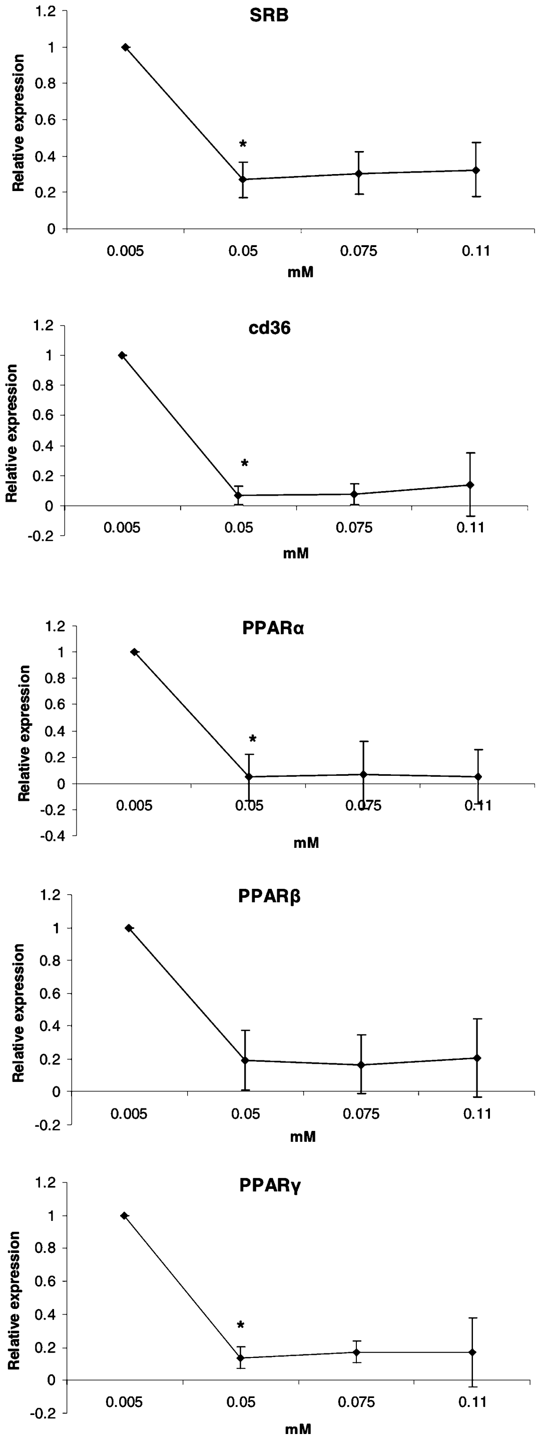

Fig. 2 Relative expression of SRB-I, cd36, PPARα,β,γ in the four concentrations 0.005, 0.05, 0.075, 0.11 mM compared to the control group incubated with out sesamin, significant differences between the groups at the different concentrations are denoted with *Asterisk* ($n = 2$)

Kushiro et al. [10] suggests that the serum lipid lowering effects of sesamin are primary a response to decreased activity of lipogenic enzymes. In this study, we showed a

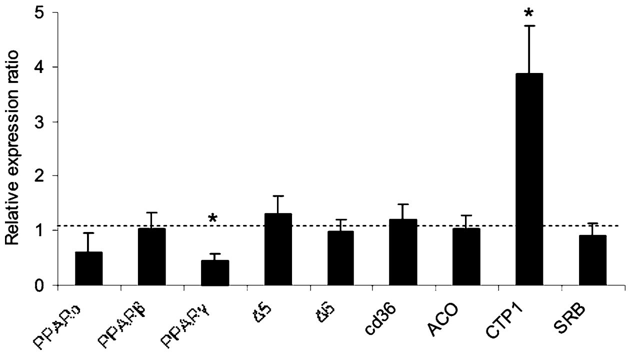

Fig. 3 Relative expression of some lipid related genes in salmon hepatocytes incubated with 0.05 mM sesamin for 48 h. *Asterisk* indicate significant difference between control group and sesamin group ($P < 0.05$). *PPARα, β, γ* peroxisome proliferator-activated receptor alpha, beta, gamma, Δ*5* Δ5 desaturase, Δ*6* Δ6 desaturase, *cd36* cluster of differentiation 36, *ACO* acyl-CoA oxidase, *CTP1* Carnitine palmitoyltransferase I, *SRB-I* scavenger receptor type B ($n = 3$)

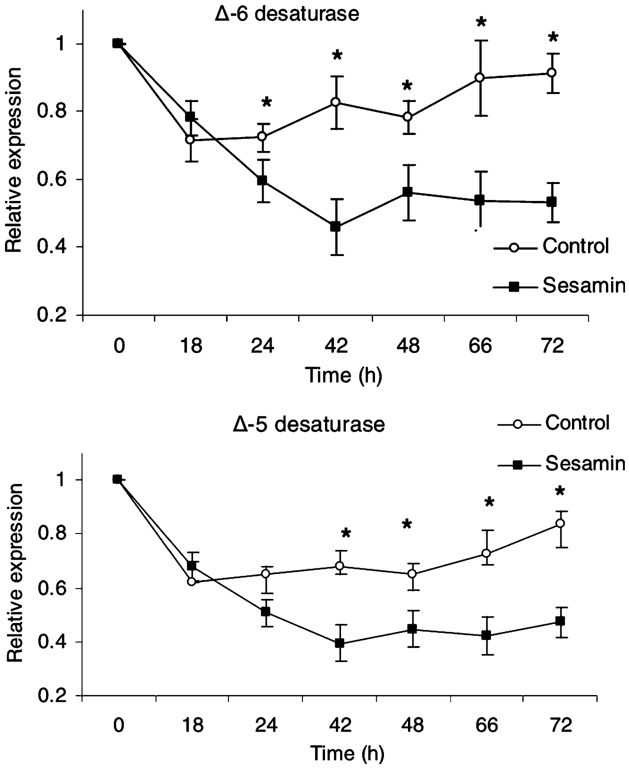

Fig. 4 Relative expression of Δ5 and Δ6 desaturase during the 72 h time course study, significant difference between the control and sesamin groups at the different time-points is denoted with *Asterisk* ($P < 0.05$), ($n = 2$)

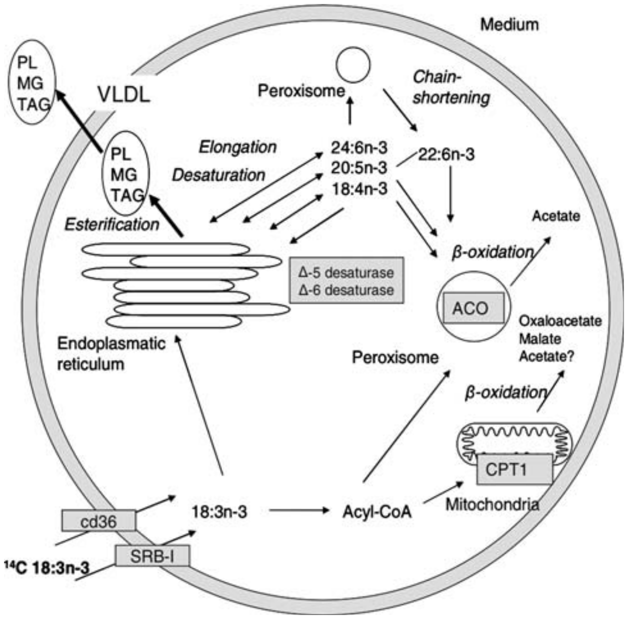

Fig. 5 Schematic drawing of the metabolic pathways of ^{14}C 18:3n-3 fatty acid analyzed in the hepatocytes in this study. Analyzed genes are shown in *grey boxes* and biochemical reactions are written in *italics*, all fatty acids shown in the figure are products of ^{14}C 18:3n-3. For abbreviations of genes see Table 1, *PL* phospholipids, *MG* monoglycerides, *TAG* triacylglycerols, *VLDL* very low-density lipoprotein

downregulation of PPARγ, which may indicate a reduced lipid synthesis. PPARγ is highly expressed in adipose tissue in rodents, humans and Atlantic salmon where it, among other functions, is involved in lipid synthesis [30–33]. The expression of cd36, a gene involved in lipid storage and uptake is regulated by PPARγ [34] and was also downregulated in the dose-response study at 0.05 and 0.075 mM sesamin. This may also affect the content of TAG in secreted lipids.

The relative expression of both Δ5 and Δ6 desaturases was significantly downregulated by sesamin at several time points. Our first expectation was that the expression of these desaturase would be upregulated. However, at all time points from 42 to 72 h the relative expression of Δ5 and Δ6 desaturase was lower in the sesamin cells compared to the control cells (Fig. 4). One could speculate that the lower levels of mRNA are due to increased translation at a higher rate than the transcription rate. Interestingly, the curve for both Δ5 and Δ6 desaturases in the sesamin cells follow the same pattern over time and is different compared to the control cells. At this stage, we can not explain exactly how sesamin is affecting the expression of Δ5 and Δ6 desaturase. We know that there is a clear effect on the expression of Δ5 and Δ6 desaturase and that sesamin significantly increases the desaturation and elongation from 18:3n-3 to DHA. However, the present study can not explain whether that is due to increased transcription or translation or whether there are other mechanisms involved.

This study provides strong evidence that sesamin is a potent modulator of fatty acid metabolism in Atlantic salmon hepatocytes. In agreement with the results of our in vivo study [5] sesamin increased desaturation and elongation of 18:3n-3 towards DHA. The β-oxidation of lipids was clearly increased as well as the expression of CPT1, a gene involved in β-oxidation. Furthermore, sesamin has an effect on several lipid related genes such as genes for $\Delta5$ and $\Delta6$ desaturase. It decreases secretion of lipid from hepatocytes, affecting in particular the TAG-levels. This knowledge can be of interest within aquaculture production in order to improve fish muscle quality by increasing its DHA levels.

Acknowledgments This study was financed by the Swedish research councils, Vetenskapsrådet and FORMAS, and the European Union Structural Funding for Fisheries. The authors like to thank Inger Ø Kristiansen at A.S. Nofima for valuable and skillful technical assistance.

References

1. Tacon AGJ (2008) State of information on salmon aquaculture feed and the environment. Report prepared for the WWF US Initiated Salmon Aquaculture Dialogue, p 80, http://www.westcoastaquatic.ca/Aquaculture_feed_environment.pdf(accessed March 2008)
2. FAO (2007) Faostat, http://www.faostat.fao.org/ (accessed November 2007)
3. Torstensen BE, Bell JG, Rosenlund G, Henderson RJ, Graff IE, Tocher DR, Lie O, Sargent JR (2005) Tailoring of Atlantic salmon (*Salmo salar* L.) flesh lipid composition and sensory quality by replacing fish oil with a vegetable oil blend. J Agri Food Chem 53:10166–10178
4. Ackman RG (1996) DHA: can it benefit salmon marketing? J Aquatic Food Prod Tech 5:7–26
5. Trattner S, Kamal-Eldin A, Brännäs E, Moazzami A, Zlabek V, Larsson P, Ruyter B, Gjøen T, Pickova J (2008) Sesamin supplementation increases white muscle docosahexaenoic acid (DHA) levels in rainbow trout (*Oncorhynchus mykiss*) fed high alpha-linolenic acid (ALA) containing vegetable oil: metabolic actions. Lipids. doi:10.1007/s11745-008-3228-8
6. Kiso Y, Tsuruoka N, Kidokoro A, Matsumoto I, Abe K (2005) Sesamin ingestion regulates the transcription levels of hepatic metabolizing enzymes for alcohol and lipids in rats. Alcohol Clin Exp Res 29:116S–120S
7. Jeng KCG, Hou RCW (2005) Sesamin and sesamolin: nature's therapeutic lignans. Curr Enzym Inhib 1:11–20
8. Ashakumary L, Rouyer I, Takahashi Y, Ide T, Fukuda N, Aoyama T, Hashimoto T, Mizugaki M, Sugano M (1999) Sesamin, a sesame lignan, is a potent inducer of hepatic fatty acid oxidation in the rat. Metabolism 48:1303–1313
9. Fujiyama-Fujiwara Y, Umeda-Sawada R, Kuzuyama M, Igarashi O (1995) Effects of sesamin on the fatty acid composition of the liver of rats fed n-6 and n-3 fatty acids-rich diet. J Nutr Sci Vitaminol 41:217–225
10. Kushiro M, Masaoka T, Hageshita S, Takahashi Y, Ide T, Sugano M (2002) Comparative effect of sesamin and episesamin on the activity and gene expression of enzymes in fatty acid oxidation and synthesis in rat liver. J Nutri Biochem 13:289–295
11. Kamal-Eldin A, Frank J, Razdan A, Tengblad S, Basu S, Vessby B (2000) Effects of dietary phenolic compounds on tocopherol, cholesterol, and fatty acids in rats. Lipids 35:427–435
12. Ide T, Hong DD, Ranasinghe P, Takahashi Y, Kushiro M, Sugano M (2004) Interaction of dietary fat types and sesamin on hepatic fatty acid oxidation in rats. Biochim Biophys Acta 1682:80–91
13. Seglen PO (1976) Preparation of isolated rat liver cells. Methods Cell Biol 13:29–83
14. Dannevig BH, Berge T (1985) Endocytosis of galactose-terminated glycoproteins by isolated liver cells of the rainbow trout (*Salmo gairdneri*). Comp Biochem Physiol B 82:683–688
15. Kjaer MA, Vegusdal A, Gjoen T, Rustan AC, Todorcevic M, Ruyter B (2008) Effect of rapeseed oil and dietary n-3 fatty acids on triacylglycerol synthesis and secretion in Atlantic salmon hepatocytes. Biochim Biophys Acta 1781:112–122
16. Folch J, Lees M, Stanley SG H (1957) A simple method for the isolation and purification of total lipids from animal tissues. J Biol Chem 226:497–509
17. Narce M, Gresti J, Bezard J (1988) Method for evaluating the bioconversion of radioactive polyunsaturated fatty acids by use of reversed-phase liquid chromatography. J Chromatogr A 448:249–264
18. Hara A, Radin NS (1978) Lipid extraction of tissue with low toxicity solvent. Anal Biochem 90:420–426
19. Appelqvist L (1968) Rapid methods of lipid extractions and fatty acid methyl ester preparation for seed and leaf tissue with special remarks on preventing the accumulation of lipids contaminants. R Swedish Acad of Sci 28:551–570
20. Fredriksson S, Elwinger K, Pickova J (2006) Fatty acid and carotenoid composition of egg yolk as an effect of microalgae addition to feed formula for laying hens. Food Chem 99:530–537
21. Christiansen R, Borrebaek B, Bremer J (1976) The effect of (-)carnitine on the metabolism of palmitate in liver cells isolated from fasted and refed rats. FEBS Lett 62:313–317
22. Lowry OH, Rosebrough NJ, Farr AL, Randall RJ (1951) Protein measurement with the folin phenol reagent. J Biol Chem 193:265–275
23. Peterson GL (1977) A simplification of the protein assay method of Lowry et al. which is more generally applicable. Anal Biochem 83:346–356
24. Small GM, Burdett K, Connock MJ (1985) A sensitive spectrophotometric assay for peroxisomal acyl-CoA oxidase. Biochem J 227:205–210
25. Leighton F, Bergseth S, Rortveit T, Christiansen EN, Bremerll J (1989) Free acetate production by rat hepatocytes during peroxisomal fatty acid and dicarboxylic acid oxidation. J Biol Chem 264:10347–10350
26. Voss A, Reinhart M, Sankarappa S, Sprecher H (1991) The metabolism of 7, 10, 13, 16, 19-docosapentaenoic acid to 4, 7, 10, 13, 16, 19-docosahexaenoic acid in rat-liver is independent of a Δ4-Desaturase. J Biol Chem 266:19995–20000
27. Kiessling KH, Kiessling A (1993) Selective utilization of fatty-acids in rainbow-trout (*Oncorhynchus-Mykiss Walbaum*) red muscle mitochondria. Can J Zool 71:248–251
28. Umeda-Sawada R, Ogawa M, Igarashi O (1998) The metabolism and n-6/n-3 ratio of essential fatty acids in rats: effect of dietary arachidonic acid and mixture of sesame lignans (sesamin and episesamin). Lipids 33:567–572
29. Vegusdal A, Ostbye TK, Tran TN, Gjoen T, Ruyter B (2004) Beta-oxidation, esterification, and secretion of radiolabeled fatty acids in cultivated Atlantic salmon skeletal muscle cells. Lipids 39:649–658
30. Ferre P (2004) The biology of peroxisome proliferator—activated receptors—relationship with lipid metabolism and insulin sensitivity. Diabetes 53:S43–S50
31. Ruyter B, Andersen O, Dehli A, Farrants AKO, Gjoen T, Thomassen MS (1997) Peroxisome proliferator activated receptors in Atlantic salmon (*Salmo salar*): effects on PPAR transcription and acyl-CoA oxidase activity in hepatocytes by peroxisome proliferators and fatty acids. Biochim Biophys Acta 1348:331–338

32. Andersen Ø, Eijsink VGH, Thomassen M (2000) Multiple variants of the peroxisome proliferator-activated receptor (PPAR) [gamma] are expressed in the liver of Atlantic salmon (*Salmo salar*). Gene 255:411–418
33. Todorčević M, Vegusdal A, Gjøen T, Sundvold H, Torstensen EB, Kjær AM, Ruyter B (2008) Changes in fatty acids metabolism during differentiation of Atlantic salmon preadipocytes; Effects of n-3 and n-9 fatty acids. Biochim Biophys Acta 1781:326–335
34. Lee CH, Olson P, Evans RM (2003) Minireview: lipid metabolism, metabolic diseases, and peroxisome proliferator-activated receptors. Endocrinology 144:2201–2207

various ray fish liver oils to the Pacific white shrimp *Litopenaeus vannamei*, the species of greatest commercial importance in the Americas.

Experimental Procedure

Source of Shrimp

Postlarvae at PL18 stage were obtained from the shrimp larviculture laboratory ‘Syaqua-Mexico S.A. de C.V.’, Coast of Hermosillo, Sonora, Mexico. They were transported to the Kino Bay Experiment Station (KBES), University of Sonora at Kino Bay, Sonora, Mexico, and maintained in an outdoor 6-m^3 circular (2.9-m diameter) fiberglass tank filled with seawater. Animals were maintained here for approximately one month and fed a commercial feed (Camaronina, Agribrands Purina®, Ciudad Obregon, Sonora, Mexico) with a protein content of 40% until initiation of the experiment, at an overall mean (±SD) wet body weight of 1.01 ± 0.04 g.

Experimental Systems

The experiment was conducted at the Wet Laboratory of Aquaculture Nutrition and Biotechnology of the KBES, using two identical recirculating experimental culture systems, each system composed of 50 30-cm diameter circular polyethylene tanks (bottom area of 0.07 m^2 and 19-L capacity), a 1,100-L sump tank, a biofilter, a 19″ sand filter (Jacuzzi, Model L-190-7, Little Rock, AR, USA), a 1.5-HP pump (Jacuzzi, Model 150MF-T, Little Rock, AR, USA), a 20-μm pore size cartridge filter (Pentek, Model Big Blue PL5010BB, Sheboygan, WI, USA), a 120-W ultraviolet light chamber (Rainbow Lifeguard, Model UV97, El Monte, CA, USA), a 1,500-W in-line heater (Aquatic Ecosystems, Model DE-6115, Apopka, FL, USA), and a 1/2 HP in-line chiller (Aquatic Ecosystems, Model AE62B, Apopka, FL, USA). Aeration for both culture systems was provided by a 1.0-HP blower (Fuji, Model VFC40, Saddle Brook, NJ, USA). Seawater recirculation rate in each tank was 1.9 L/min (14,400% exchange in 24 h), and 5–10% daily replacement with fresh-filtered seawater was applied. The culture systems were interconnected with each other, i.e., they shared the same water quality. Shrimp were stocked into tanks at a rate of four individuals/tank (56 shrimp/m^2).

Extraction of Ray Fish Liver Oil

Livers were obtained from four different ray fish species, two from the Gulf of California, stingray (*Dasyatis brevis*) and golden cownose ray (*Rhinoptera steindachneri*), and two from the Gulf of Mexico, spotted ray (*Aetobatus narinari*) and cownose ray (*R. bonasus*). Livers were removed from the fishes immediately after landing, frozen and transported to the Nutrition laboratory at the University of Sonora’s main campus, Hermosillo, Sonora, Mexico, to perform oil extraction. Livers were homogenized for 2 min and incubated for 1 h in a water bath at 35 °C. Anhydrous sodium sulfate was added (30%, w/w) and the homogenate was mixed for 3 min and then centrifuged at 1,150×*g* for 20 min at 25 °C [11].

Experimental Treatments

Four feeds were prepared according to a basal experimental feed formulation (Table 1). Each dietary treatment was prepared with a different ray fish liver oil. A fifth experimental feed, included as a control treatment, was prepared with Menhaden fish oil (MP Biomedicals Inc., Solon, OH, USA). Feeds were prepared by cold extrusion using a Hobart mixer (Model A-200, Hobart, Troy, OH, USA). They were dried overnight at 40 °C, ground to appropriate size and stored frozen until use. Shrimp were fed to slight excess, with the daily ration divided into two equal amounts, one feed at 0800 and one at 1700. Faeces, exuviae and excess feed were siphoned out of all tanks each morning. Treatments were assigned randomly to at least 16 replicate tanks.

Water Quality

A multi-function oxygen meter (YSI, Model Y85, Yellow Springs, OH, USA) was employed to measure water temperature, dissolved oxygen, and salinity each day. Weekly measurements of the concentrations of ammonia, nitrite, and nitrate were performed according to standard chemical procedures [12, 13].

Proximate Composition of Feeds and Fatty Acid Analysis

Proximate composition of feeds was determined according to standard procedures (procedures 984.13, 920.85, 925.09, and 923.03 for protein, crude fat, moisture, and ash, respectively) [14]. For fatty acid analysis, lipids were extracted from feeds and abdominal shrimp muscle [15]. Quantification was performed by a gravimetric method after drying an aliquot under nitrogen. Fatty acids (FA) were transesterified using boron trifluoride (14% boron trifluoride in methanol, Sigma, St Louis, MO, USA). Fatty acid methyl esters (FAME) were analyzed with a gas chromatograph (Varian, Model CP 3800, Walnut Creek, CA, USA) equipped with a 30 m × 0.25 mm fused silica capillary column (Model CP WAX 52CB, Varian Inc., Palo Alto, CA, USA), and a flame-ionization detector [16]. They were identified by comparison of retention times to those of known standards

Table 1 Ingredient composition of the basal experimental feed for *L. vannamei*

Ingredient	% of dry weight
Wheat starch[a]	37.86
Soybean protein concentrate[b]	24.79
Casein (vitamin-free)[c]	6.63
Mineral premix[d]	6.00
Wheat gluten[a]	6.00
Sodium alginate[c]	2.00
Sodium hexametaphosphate[c]	1.00
Calcium phosphate monobasic[c]	2.53
Squid meal[e]	4.00
Cholesterol[f]	0.50
Vitamin premix[g]	0.50
Methionine[c]	0.35
Lysine[h]	0.15
Arginine[h]	0.02
Ascorbic acid[c]	0.60
Zinc sulphate[c]	0.06
Cupric chloride[c]	0.01
Soybean lecithin[i]	2.00
Test oil	5.00

[a] Gluten y Almidones Industriales, S.A. de C.V., Mexico City, Mexico

[b] Sumilab S.A. de C.V., Mazatlán, Sinaloa, Mexico

[c] Faga Lab S.A. de C.V., Mazatlán, Sinaloa, Mexico

[d] MP Biomedicals Inc., Solon, OH, USA, g/100 g premix: cobalt chloride 0.004, cupric sulfate pentahydrate 0.250, ferrous sulfate 4.0, magnesium sulfate heptahydrate 28.398, manganous sulfate monohydrate 0.650, potassium iodide 0.067, sodium selenite 0.010, zinc sulfate heptahydrate 13.193, filler 53.428

[e] Selecta de Guaymas, S.A. de C.V., Guaymas, Sonora, Mexico

[f] Hycel de México, S.A. de C.V., Mexico City, Mexico

[g] MP Biomedicals Inc., Solon, OH, USA, g/kg premix/kg premix: thiamin HCl 0.5, riboflavin 3.0, pyridoxine HCl 1.0, DL Ca-Pantothenate 5.0, nicotinic acid 5.0, biotin 0.05, folic acid 0.18, vitamin B12 0.002, inositol 5.0, menadione 2.0, vitamin A acetate (20,000 IU/g) 5.0, vitamin D3 (400,000 IU/g) 0.002, dl-alpha-tocopheryl acetate (250 IU/g) 8.0, Alpha-cellulose 865.266

[h] Jalmek Científica, S.A. de C.V., San Nicolás de los Garza, Nuevo León, Mexico

[i] Impulsora Golden, S.A. de C.V., Mexico City, Mexico

and quantified using heptadecanoic acid (17:0) as an internal standard [17]. Triplicate composite muscle samples were processed for fatty acid analysis, each composite sample consisted of tissue from the last abdominal segment of four individuals at intermolt stage taken from different tanks.

Statistical Analysis

Growth, survival (arcsine-transformed, untransformed data are shown), and shrimp muscle fatty acid content data were analyzed by one-way ANOVA with a significance level of $P \leq 0.05$. Mean separation was applied using Tukey's Honestly Significant Difference (HSD) method. All statistical analyses were performed using Statistical Analysis System software (SAS Institute Inc. 1999-2000, Software Release 8.1, Cary, NC, USA).

Results

Water Quality

Mean values (±SD) for water temperature, dissolved oxygen, salinity, pH, ammonia, nitrite, and nitrate were 31.7 ± 0.18 °C, 5.87 ± 0.12 mg/L, 38.7 ± 2.25‰, 8.0 ± 0.0, 0.12 ± 0.03 mg NH_4–N/L, 0.04 ± 0.01 mg NO_2–N/L, and 3.16 ± 0.53 mg NO_3–N/L, respectively.

Proximate Composition of Feeds

Proximate composition of the various feeds was characterized by homogeneous mean values for protein, crude fat, moisture and ash content (Table 2).

Shrimp Growth and Survival

No significant differences in growth or survival of shrimp were observed among treatments at the end of the experiment (Table 3).

Fatty Acid Analysis of Oils and Feeds

PUFA and HUFA represented the largest proportion of identified FAME of all ray fish liver oils, as well as of Menhaden fish oil and their respective feeds, ranging from 293.73 to 375.61 mg/g oil and from 8.4 to 14.52 mg/g feed (Tables 4, 5). Spotted ray liver oil and the feed prepared with it contained the highest amount of saturated fatty acids (197.86 mg/g oil and 11.02 mg/g feed, respectively). Monounsaturated fatty acids were more abundant in Menhaden fish oil and feed (174.47 mg/g oil and 8.35 mg/g feed) (Tables 4, 5). In the case of specific fatty acids, the content of arachidonic acid (ARA) was highest in spotted ray liver oil and feed. Spotted ray liver oil also contained the greatest amount of linoleic acid (LOA) and linolenic acid (LNA) (Table 4), but, in the feeds, the greatest content of these fatty acids corresponded to that prepared with Menhaden fish oil (Table 5). Eicosapentaenoic acid (EPA) and docosahexaenoic acid (DHA) were more abundant in Menhaden fish oil and in its respective feed (Tables 4, 5).

Table 2 Proximate composition of feeds containing different ray fish liver oils and Menhaden fish oil

Composition (%)	Treatment (oil source)				
	Golden cownose ray	Spotted ray	Cownose ray	Stingray	Menhaden fish oil
Protein	28.00 ± 0.18	28.21 ± 0.11	27.77 ± 0.08	28.18 ± 0.49	27.66 ± 0.56
Crude fat	6.78 ± 0.24	7.66 ± 0.15	7.20 ± 0.05	6.98 ± 0.18	6.56 ± 0.23
Moisture	5.94 ± 0.06	5.92 ± 0.03	5.26 ± 0.02	5.69 ± 0.01	5.10 ± 0.12
Ash	9.40 ± 0.05	9.70 ± 0.02	9.50 ± 0.01	9.69 ± 0.02	9.72 ± 0.01

Values are means (±SD) of duplicate samples

Table 3 Growth and survival of *L. vannamei* fed diets containing different ray fish liver oils and Menhaden fish oil

Treatment (oil source)	Initial weight (g)	Final weight (g)	Weight gain (g)	Survival (%)
Golden cownose ray	1.00 ± 0.03	1.71 ± 0.14	0.71 ± 0.12	80.6 ± 16.2
Spotted ray	1.00 ± 0.05	1.82 ± 0.17	0.82 ± 0.17	82.8 ± 17.6
Cownose ray	1.01 ± 0.03	1.72 ± 0.19	0.71 ± 0.19	71.9 ± 20.2
Stingray	1.02 ± 0.03	1.78 ± 0.29	0.75 ± 0.27	70.8 ± 23.1
Menhaden fish oil	1.03 ± 0.03	1.86 ± 0.26	0.83 ± 0.25	76.6 ± 23.2

Values are means (±SD) of 16 or 18 replicates

Table 4 Fatty acid composition (mg/g oil) of ray fish liver oils and Menhaden fish oil

Fatty acid	Treatment (oil source)				
	Golden cownose ray	Spotted ray	Cownose ray	Stingray	Menhaden fish oil
16:0	104.00	166.16	106.98	84.76	93.33
18:0	17.44	12.15	30.46	19.39	14.94
18:1	58.38	47.70	64.72	77.57	59.76
18:2n-6	127.41	147.95	121.16	104.60	90.63
18:3n-3	8.01	21.39	7.06	8.63	13.92
20:4n-6	25.57	52.16	21.74	19.28	8.33
20:5n-3	62.87	16.82	64.67	61.53	99.64
22:6n-3	81.01	9.45	101.64	64.91	108.09
Saturates[a]	136.18	197.86	177.95	115.56	151.17
Monounsaturates[b]	94.88	109.28	114.29	132.87	174.47
PUFA + HUFA[c]	369.32	293.73	375.61	306.80	354.04
Total n-3[d]	176.24	68.40	194.03	152.47	240.89
Total n-6[e]	155.25	201.21	144.93	125.55	100.77

Values are means of duplicate samples

[a] Saturates: 12:0, 14:0, 16:0, 18:0, 20:0, 22:0

[b] Monounsaturates: 16:1, 18:1, 20:1, 22:1

[c] PUFA + HUFA: 16:3, 16:4, 18:2n-6, 18:3n-3, 20:2, 20:3n-6, 20:4n-6, 20:3n-3, 20:5n-3, 22:2, 22:3, 22:4, 22:5n-3, 22:6n-3

[d] Total n-3: 18:3n-3, 20:3n-3, 20:5n-3, 22:5n-3, 22:6n-3

[e] Total n-6: 18:2n-6, 20:3n-6, 20:4n-6

Total Lipid and Fatty Acid Analysis of Shrimp Muscle Tissue

Total lipid in shrimp muscle tissue ranged from 1.03 to 1.37% of wet weight, with no significant differences among treatments at the end of the feeding trial (Table 6).

Similarly to what was observed for oils and feeds, fatty acids of shrimp muscle tissue were mainly composed of PUFA and HUFA (Table 6). LOA, LNA, EPA, and DHA, more abundant in the feed containing Menhaden fish oil, were also more abundant in muscle tissue of shrimp receiving this dietary treatment. Specifically, the

Table 5 Fatty acid composition[f] (mg/g feed) of feeds containing different ray fish liver oils and Menhaden fish oil

Fatty acid	Treatment (oil source)				
	Golden cownose ray	Spotted ray	Cownose ray	Stingray	Menhaden fish oil
16:0	5.50 ± 1.02	9.19 ± 1.15	5.09 ± 0.45	5.55 ± 1.80	6.63 ± 0.96
18:0	1.48 ± 0.16	1.34 ± 0.13	1.62 ± 0.07	1.66 ± 0.55	1.02 ± 0.17
18:1	4.96 ± 0.84	5.28 ± 0.72	3.43 ± 0.38	4.93 ± 1.57	4.14 ± 0.61
18:2n-6	4.10 ± 0.81	3.83 ± 0.32	3.48 ± 0.28	4.20 ± 1.11	4.87 ± 0.64
18:3n-3	0.61 ± 0.25	0.46 ± 0.06	0.61 ± 0.07	0.79 ± 0.25	1.05 ± 0.11
20:4n-6	0.83 ± 0.10	1.85 ± 0.13	0.66 ± 0.03	0.82 ± 0.23	0.31 ± 0.04
20:5n-3	1.93 ± 0.28	0.38 ± 0.01	2.10 ± 0.09	2.59 ± 0.73	3.57 ± 0.56
22:6n-3	2.58 ± 0.41	0.35 ± 0.01	2.99 ± 0.12	2.56 ± 0.67	3.59 ± 0.61
Saturates[a]	7.44 ± 1.25	11.02 ± 1.35	7.43 ± 0.56	7.74 ± 2.54	9.15 ± 1.41
Monounsaturates[b]	6.44 ± 1.04	7.13 ± 0.92	4.31 ± 0.45	7.08 ± 2.15	8.35 ± 1.17
PUFA + HUFA[c]	11.89 ± 2.10	8.40 ± 0.49	11.37 ± 0.57	12.79 ± 3.43	14.52 ± 2.17
Total n-3[d]	5.69 ± 1.03	1.83 ± 0.10	6.11 ± 0.19	6.58 ± 1.80	8.76 ± 1.39
Total n-6[e]	5.03 ± 0.91	5.75 ± 0.44	4.20 ± 0.32	5.10 ± 1.37	5.26 ± 0.69

[a–e] See footnotes of Table 4 for explanation

[f] Values are means (±SD) of duplicate samples

Table 6 Fatty acid composition (mg/g wet weight) and total lipid content (% wet weight) of muscle of *L. vannamei* fed diets containing different ray fish liver oils and Menhaden fish oil

Fatty acid	Treatment (oil source)				
	Golden cownose ray	Spotted ray	Cownose ray	Stingray	Menhaden fish oil
16:0	5.87 ± 0.39^{a}	7.81 ± 0.77^{b}	7.38 ± 1.14^{b}	9.46 ± 0.27^{c}	7.70 ± 0.31^{b}
18:0	2.51 ± 0.46	3.03 ± 0.07	3.01 ± 0.45	2.70 ± 0.22	2.54 ± 0.16
18:1	5.12 ± 0.32	6.04 ± 0.56	5.31 ± 0.51	5.70 ± 0.31	5.91 ± 0.76
18:2n-6	3.83 ± 0.59^{ab}	4.82 ± 0.40^{bc}	4.13 ± 0.76^{abc}	3.45 ± 0.88^{a}	5.17 ± 0.16^{c}
18:3n-3	0.32 ± 0.12	0.36 ± 0.09	0.30 ± 0.06	0.25 ± 0.05	0.46 ± 0.01
20:4n-6	2.19 ± 0.20^{b}	4.11 ± 0.34^{c}	2.22 ± 0.44^{b}	1.54 ± 0.04^{a}	1.40 ± 0.07^{a}
20:5n-3	4.43 ± 0.49^{ab}	4.02 ± 0.32^{ab}	5.05 ± 1.01^{bc}	3.47 ± 0.12^{a}	5.93 ± 0.35^{c}
22:6n-3	2.78 ± 0.50^{abc}	2.52 ± 0.26^{ab}	3.13 ± 0.68^{bc}	2.01 ± 0.13^{a}	3.45 ± 0.20^{c}
Saturates[a]	7.61 ± 2.23^{a}	11.10 ± 0.81^{b}	10.70 ± 1.53^{b}	12.47 ± 0.26^{b}	10.56 ± 0.46^{b}
Monounsaturates[b]	5.68 ± 0.39	6.96 ± 0.68	6.23 ± 0.48	6.59 ± 0.26	7.08 ± 0.90
PUFA + HUFA[c]	14.29 ± 1.90^{b}	16.89 ± 1.37^{b}	15.49 ± 3.04^{b}	10.61 ± 0.47^{a}	17.15 ± 0.79^{b}
Total n-3[d]	7.68 ± 1.11^{ab}	7.31 ± 0.63^{ab}	8.59 ± 1.70^{bc}	5.75 ± 0.26^{a}	9.98 ± 0.52^{c}
Total n-6[e]	6.02 ± 0.72^{b}	8.93 ± 0.73^{c}	6.36 ± 1.19^{b}	4.49 ± 0.22^{a}	6.57 ± 0.23^{b}
Total lipid	1.06 ± 0.10	1.06 ± 0.11	1.04 ± 0.11	1.37 ± 0.32	1.03 ± 0.08

Values are means (±SD) of triplicate samples. Means with similar superscripts in the same row are not significantly different ($P > 0.05$)

[a–e] See footnotes of Table 4 for explanation

concentration of EPA in muscle tissue of shrimp fed the diet with Menhaden fish oil (5.93 mg/g muscle wet weight) was significantly greater than those of shrimp receiving feeds prepared with stingray, golden cownose ray, and spotted ray oil (3.47, 4.43, and 4.02 mg/g muscle wet weight, respectively), but not significantly greater than that of shrimp fed the diet with cownose liver oil (5.05 mg/g muscle wet weight). In the case of DHA, muscle tissue of shrimp fed the treatment with Menhaden fish oil (3.45 mg/g muscle wet weight) was significantly more concentrated than those of shrimp fed diets with stingray and spotted ray liver oil (2.01 and 2.52 mg/g muscle wet weight, respectively), but not statistically more concentrated than those of the treatments with cownose ray and golden cownose ray liver oil (3.13 and 2.78 mg/g muscle wet weight, respectively) (Table 6).

Discussion

Water Quality

Adequate water quality was maintained throughout the study, for all physico-chemical parameters and levels of nitrogenous wastes were always kept within levels considered optimal for shrimp culture [18–21].

Proximate Composition of Feeds

The homogeneity and small variability in the proximate composition of protein, crude fat, moisture and ash of the various feeds confirmed their isolipidic and isoproteic nature, and thus, their adequate preparation.

Shrimp Growth and Survival

The lack of significant differences in final weight, weight gain or survival of shrimp revealed that the four ray fish liver oils evaluated were as efficient in promoting growth and survival of *L. vannamei* as Menhaden fish oil, an ingredient known for its adequate nutritional value to shrimp and fish [5]. These results effectively illustrate a practical application of a locally available resource that is currently being wasted. In this respect, it would be of interest to explore the use of the other parts of the ray fish body, i.e., the complete head and trunk with all other viscera, which like the liver, are discarded on shore or directly into the sea. On the other hand, the incorporation of ray fish liver oils into shrimp feeds represents only one of the many possible applications that, as other fish oils, they may have. For example, the preparation of the "so-called" omega-3-rich supplements for human consumption, their use in food products like baked goods and baking mixes, meat products, gravies, and sauces, among others [22].

Fatty Acid Analysis of Oils and Feeds

Although added at a moderate level (5% of feed dry weight), the fatty acid composition of the oils undoubtedly influenced that of the resulting feeds, as illustrated by the higher levels of ARA found in spotted ray liver oil (52.16 mg/g oil) and its respective feed (1.85 mg/g feed), as well as by the greater levels of EPA and DHA of Menhaden fish oil (99.64 and 108.09 mg/g oil, respectively), also greater in the feed prepared with it (3.57 and 3.59 mg/g feed, respectively) (Tables 4, 5).

In the same way as Menhaden fish oil, used as a control treatment, the most prominent aspect of the ray fish liver oils evaluated was their high content of HUFA. In fact, all four liver oils were higher in ARA (ranging from 19.28 to 52.16 mg ARA/g oil) than Menhaden fish oil (8.33 mg ARA/g oil) (Table 4). Menhaden fish oil had the highest concentration of EPA and DHA (99.64 and 108.09 mg/g oil, respectively) (Table 4), results that were consistent with previous data for this oil. For example, an EPA and a DHA content of 140 and 80 mg/g oil, respectively [22] or an EPA and a DHA content of 11.0 and 9.1% of total fatty acids [23] versus 14.7 and 15.9% of total fatty acids in this study. These fatty acids also were found in considerable concentrations in cownose ray, golden cownose and stingray liver oil (an EPA content ranging from 61.53 to 64.67 mg/g oil and a DHA content from 64.91 to 101.64 mg/g oil, respectively) but in moderately low concentrations in spotted ray liver oil (16.82 and 9.45 mg/g oil, respectively) (Table 4). However, spotted ray liver oil had a particularly high concentration of ARA (52.16 mg ARA/g oil), more than six times greater than that of Menhaden fish oil. Regardless of the family they belong to (n-3 or n-6 family), *L. vannamei* is reported to have a nutritional requirement for HUFA and not for PUFA [24, 25]. In this context, the fatty acid profile of the ray fish liver oils evaluated seems to adequately satisfy such requirement, and at the same time, explains their growth-promoting effect on *L. vannamei*, comparable to that of world renowned Menhaden fish oil.

Few other studies of the fatty acid profile of ray fish liver are available. EPA and DHA concentrations of 48.4 and 55.7 mg/g oil, respectively, have been reported for liver oil from golden cownose ray [11], as compared to 62.87 and 81.01 mg/g oil, respectively, for the same species in this study (Table 4). In liver oil of stingray, an EPA content of 53 mg/g oil and a DHA content of 48 mg/g oil have been reported [26], while in the present study this species had 61.53 and 64.91 mg/g oil, respectively (Table 4). EPA and DHA contents of 59.0 and 100.0 mg/g oil, respectively, were reported in *Gymnura marmorata* [26]. Levels of EPA and DHA in liver of the ray fishes *R. marginata. D. marmorata*, and *Rhinobatos cemiculus* have been reported to range from 1.88 to 5.01% and from 5.64 to 13.4% of total fatty acids, respectively [9]. In this study, the levels of these fatty acids varied from 2.8 to 11.08% and 1.57 to 13.49% of total fatty acids, respectively. In general, results of previous studies and of the present investigation are comparable not only in terms of PUFA and HUFA comprising the major fraction of identified fatty acids, but also in terms of the relatively high concentration of HUFA like EPA and DHA [9, 27].

Total Lipid and Fatty Acid Analysis of Shrimp Muscle Tissue

Total lipid found in shrimp muscle tissue varied from 1.03 to 1.37% of wet weight, agreeing with data reported for *L. vannamei* (ranging from 0.71 to 2.10% of wet weight) [28, 29]. Although dietary lipid level is known to influence muscle total lipid [30], the lack of significant differences among treatments in this study can be explained by the isolipidic nature of the feeds.

To a large extent, fatty acids of shrimp muscle tissue reflected the dietary fatty acid profile. The direct influence of dietary fatty acids on the fatty acid profile of shrimp tissues has been demonstrated a number of times in the past [28–35]. In this study, differences in dietary fatty acids elicited significant differences in the fatty acid content of muscle tissue among some dietary treatments, e.g., muscle tissue of shrimp fed the diet with Menhaden fish oil was significantly higher in EPA than muscle of shrimp fed diets with stingray, golden cownose ray or spotted ray liver oil. Shrimp fed Menhaden fish oil had a muscle tissue concentration of DHA statistically greater than muscle of shrimp fed stingray or spotted ray liver oil (Tables 5, 6). However, these differences were not reflected in shrimp growth or survival, supporting the earlier observation that the four ray fish liver oils evaluated seem to satisfy the dietary fatty acid requirements of *L. vannamei*.

In conclusion, PUFA and HUFA content of liver oils of the ray fishes evaluated were of comparable magnitude to that of Menhaden fish oil, an ingredient known for its adequate nutritional quality to shrimp and fish. When incorporated into shrimp feeds, the oils evaluated were as efficient as Menhaden fish oil in promoting growth and survival of *L. vannamei* and demonstrated one of the many possible applications of a locally available resource that is currently being wasted.

References

1. Tacon AGJ, Hasan MR, Subasinghe RP (2006) Use of fishery resources as feed input for aquaculture development: trends and policy implications. FAO Fisheries Circular No. 1018, Rome, Italy
2. Food and Agriculture Organization (2006) The state of world fisheries and aquaculture. Rome, Italy, 162 p
3. Al-Owafeir MA, Belal IE (1996) Replacing palm oil for soybean oil in tilapia, *Oreochromis niloticus* (L.), feed. Aquacult Res 27:221–224
4. Bell JG, Henderson RJ, Tocher DR, McGhee F, Dick JR, Porte RA, Smullen RP, Sargent JR (2002) Substituting fish oil with crude palm oil in the diet of Atlantic salmon (Salmo salar) affects muscle fatty acid composition and hepatic fatty acid metabolism. J Nutr 132:222–230
5. Ng WK, Sigholt T, Bell JG (2004) The influence of environmental temperature on the apparent nutrient and fatty acid digestibility in Atlantic salmon (*Salmo salar* L.) fed finishing diets containing different blends of fish oil, rapeseed oil and palm oil. Aquacult Res 35:1228–1237
6. Rosenlund G, Obach A, Sandberg MG, Standal H, Tveit K (2001) Effect of alternative lipid sources on longterm growth performance and quality of Atlantic salmon (*Salmo salar* L.). Aquacult Res 32:323–328
7. Viegas EMM, Contreras ESG (1994) Effect of dietary crude palm oil and a deodorization distillate of soybean oil on growth of tambaqui (*Colossoma macropomum*) fingerlings. Aquaculture 124:128
8. Perez-Velazquez M, González-Félix ML, Valenzuela-Escalante E, Navarro-García G (2008) Nutritional evaluation of various rayfish liver oils for penaeid shrimp. Book of Abstracts. Aquaculture America 2008. Lake Buenavista, Florida, USA. 9–12 February, pp 291
9. El Kebir MVO, Barnathan G, Gaydou EM, Siau Y, Miralles J (2007) Fatty acids in liver, muscle and gonad of three tropical rays including non-methylene-interrupted dienoic fatty acids. Lipids 42:525–535
10. Secretaría de Agricultura, Ganadería, Desarrollo Rural, Pesca y Alimentación (2006) Carta Nacional Pesquera. Diario Oficial, Mexico City, Mexico
11. Navarro-García G, Bringas-Alvarado L, Pacheco-Aguilar R, Ortega-García J (2004) Oxidative resistance, carotenes, tocopherols and lipid profile of liver of the ray *Rhinoptera steindechneri*. J Food Comput Anal 17:699–706
12. Solarzano L (1969) Determination of ammonia in natural waters by the phenolhypochlorite method. Limnol Oceanogr 14:799–801
13. Spotte S (1979) Fish and invertebrate culture: water management in closed systems, 2nd edn. Wiley, New York
14. Association of Official Analytical Chemists (AOAC) (1999) Official methods of analysis. 16th edn. Gaithersburg, Maryland, USA
15. Folch J, Lees M, Sloane-Stanley CH (1957) A simple method for the isolation and purification of total lipids from animal tissues. J Biol Chem 226:477–509
16. Lochman RT, Gatlin DM III (1993) Essential fatty acid requirements of juvenile red drum (*Sciaenops ocellatus*). Fish Physiol Biochem 12:221–235
17. González-Félix ML, Perez-Velazquez M, Quintero-Álvarez JM, Davis DA (2008) Effect of various dietary levels of docosahexaenoic and arachidonic acid and different n-3/n-6 ratios on biological performance of Pacific white shrimp, *Litopenaeus vannamei* raised in low salinity. J World Aquacult Soc (in press)
18. Jiang DH, Lawrence AL, Neill WH, Grant WH, Gong H (1999) Lethal effect of ammonia to postlarval *Penaeus vannamei* at two temperatures, 25 and 30°C. Book of Abstracts, American Aquaculture Society Annual Conference, Tampa, Florida, USA, 27-30 January, pp 77
19. Lin YC, Chen JC (2001) Acute toxicity of ammonia on *Litopenaeus vannamei* Boone juveniles at different salinity levels. J Exp Mar Biol Ecol 259:109–119
20. Lin YC, Chen JC (2003) Acute toxicity of nitrite on *Litopenaeus vannamei* (Boone) juveniles at different salinity levels. Aquaculture 224:193–201
21. Tsai SJ, Chen JC (2002) Acute toxicity of nitrate on *Penaeus monodon* juveniles at different salinity levels. Aquaculture 213:163–170
22. U.S. Food and Drug Administration (2002) Center for food safety and applied nutrition, Office of food additive safety, Agency response letter. GRAS notice No. GRN 000109, 4 December 2002
23. Nichols PD (2007) Fish oil sources. In: Breivik H (ed) Long-chain omega-3 specialty oils. The Oily Press, Bridgwater
24. González-Félix ML, Lawrence AL, Glatlin DMIII, Perez-Velazquez M (2003) Nutritional evaluation of fatty acids for the open thelycum shrimp, *Litopenaeus vannamei*: I. Effect of dietary linoleic and linolenic acids at different concentrations and ratios on juvenile shrimp growth, survival and fatty acid composition. Aquacult Nutr 9:107–113
25. González-Félix ML, Glatlin DMIII, Lawrence AL, Perez-Velazquez M (2003) Nutritional evaluation of fatty acids for the open

thelycum shrimp, *Litopenaeus vannamei*: II. Effect of dietary n-3 and n-6 polyunsaturated and highly unsaturated fatty acids on juvenile shrimp growth, survival and fatty acid composition. Aquacult Nutr 9:115–112

26. Navarro-García G, Pacheco-Aguilar R, Bringas-Alvarado L, Ortega-García J (2004) Characterization of the lipid composition and natural antioxidants in the liver oil of *Dasyatis brevis* and *Gymnura marmorata* rays. Food Chem 87:89–96
27. El Kebir MVO, Barnathan G, Siau Y, Miralles J, Gaydou EM (2003) Fatty acid distribution in muscle, liver, and gonads of rays (*Dasyatis marmorata, Rhinobatos cemiculus*, and *Rhinoptera marginata*) from the East tropical Atlantic ocean. J Agric Food Chem 51:1942–1947
28. González-Félix ML, Lawrence AL, Gatlin DM III, Perez-Velazquez M (2002) Growth, survival and fatty acid composition of juvenile *Litopenaeus vannamei* fed different oils in the presence and absence of phospholipids. Aquaculture 205:325–343
29. González-Félix ML, Gatlin DM III, Lawrence AL, Perez-Velazquez M (2002) Effect of dietary phospholipid on essential fatty acid requirements and tissue lipid composition of *Litopenaeus vannamei* juveniles. Aquaculture 207:151–167
30. González-Félix M, Gatlin DM III, Lawrence AL, Perez-Velazquez M (2002) Effect of various dietary lipid levels on quantitative essential fatty acid requirements of juvenile pacific white shrimp *Litopenaeus vannamei*. J World Aquacult Soc 33:330–340
31. Colvin PM (1976) The effect of selected seed oils on the fatty acid composition and growth of *Penaeus indicus*. Aquaculture 8:81–89
32. Guary JC, Kayama M, Murakami Y, Ceccaldi HJ (1976) The effects of a fat-free diet and compounded diets supplemented with various oils on molt, growth and fatty acid composition of prawn, Penaues japonicus Bate. Aquaculture 7:245–254
33. Deering MJ, Fielder DR, Hewitt DR (1997) Growth and fatty acid composition of juvenile leader prawns, *Penaeus monodon*, fed different lipids. Aquaculture 151:131–141
34. Kayama M, Hirata M, Kanazawa A, Tokiwa S, Saito M (1980) Essential fatty acids in the diet of prawn: III. Lipid metabolism and fatty acid composition. Bull Jpn Soc Sci Fish 46:483–488
35. Millamena OM (1989) Effect of fatty acid composition of broodstock diet on tissue fatty acid patterns and egg fertilization and hatching in pond reared *Penaeus monodon*. Asian Fish Sci 2:127–134

2005 the fish export earnings had replaced the traditional coffee as the leading export [3].

Lipids and fatty acids (FAs) have been studied in tissues of freshwater fish from all parts of the world [4]. This has led to the recognition of a so-called freshwater pattern, in contrast to a marine pattern, where the freshwater fish are able to convert the essential FAs 18:2n-6 and 18:3n-3 to longer FAs and physiologically important, highly unsaturated FAs [4, 5]. In this manner algae and plants with low nutritional value as food for herbivore fish will be converted into food with higher nutritional value. It is established that lipid and FA contents vary both within and between species [4], apparently more in tropical freshwater fish than in fish from colder waters [6]. Many factors may be responsible for the variation, i.e. internal factors like genetic variation, age, sex, condition, starvation, reproductive cycle, and external factors like diet, season, temperature.

A plethora of feeding experiments, particularly on salmon (*Salmo salar*) and Nile tilapia, two of the most common species in fish farming, have been conducted to study the influence of the diet on the FA composition of the edible tissue of the fish. Heavy impact of the FA composition of the diet on the FA composition of the fish tissue is evident, e.g in salmon [7] and in Nile tilapia [8]. In line with this, studies on freshwater tropical fish in the wild have indicated the importance of the diet for the FA composition of the fish tissue [6, 9]. However, recently investigations reluctant to the heavy dietary control of the tissue FA composition and leaning more towards genetic control have surfaced [10, 11]. Indeed, tissue FA composition has been used for identification of stocks of marine fish [12].

Only two of the many species of fish inhabiting the lakes Victoria and Kyoga, Nile tilapia and Nile perch, have been investigated for tissue FAs [11]. Differences in the FA compositions were found between these two species and populations. The differences were even greater compared with Nile tilapia from other African lakes [13], and compared with this species collected in other parts of the world. It was of general interest to determine the tissue FA composition of other fish species used for consumption from lakes Victoria and Kyoga, and also to study if the pattern of species and population differences were of the same magnitude as in Nile tilapia and Nile perch. The heart tissue was chosen since it has been extensively used in identification of fish stocks [12]. It is a well defined tissue, easy to subsample, and the lipids are dominated by phospholipids.

In the present investigation tropical freshwater fish from seven different species were collected from three different sites, one at Lake Victoria and two at Lake Kyoga. The objectives were to detect how the FA composition/profiles of the lipids in white muscle and heart tissue varied with species and populations, to explore the importance of diet and genetics for the tissue FA composition, and to report on the nutritional value of the muscle tissue.

Materials and Methods

Sample Collection

Specimens of Nile perch (*L. niloticus*), Nile tilapia (*O. niloticus*), marbled lungfish (*P. aethiopicus*), African catfish (*C. gariepinus*), Lake Victoria squeaker (*S. victoriae*), *B. docmas*, and *T. zilli* were caught in Bukungu on Lake Kyoga in October 2005, in Lwampanga on Lake Kyoga in December 2005, and in Napoleon Gulf in Lake Victoria in November 2005 (Fig. 1; Table 1). Three fleets of graded multifilament gillnets of mesh size 1–7 inches at an interval of 0.5 inches were set every evening and retrieved in the morning the following day. At each landing site a fleet would be located inshore, mid-shore and offshore, about 100, 100–200 and 200–300 m from the shore, respectively, at a water depth of 10 m or less. Fish specimen were identified according to Greenwood [20] and only mature specimen with a total length greater than: 28 cm for *O. niloticus*, 60 cm for *L. niloticus*, 73 cm for *P. aethiopicus*, 50 cm for *C. gariepinus*, 35 cm for *B. docmas*, 13 cm for *S. victoriae* and 13 cm for *T. Zilli* were selected. The fish

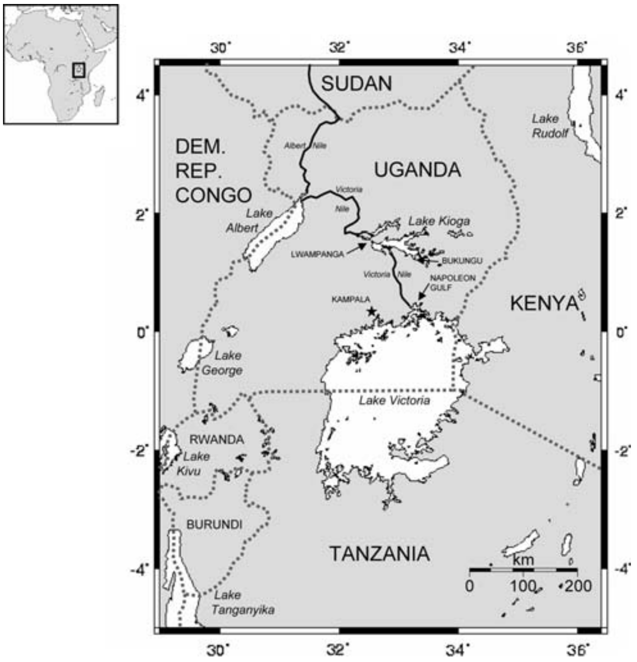

Fig. 1 The fish were collected in Napoleon Gulf (V) in Lake Victoria, and Bukungu (B) and Lwampanga (L) at Lake Kyoga

Table 1 Food groups and major food items of the seven investigated species

Species	Feeding habit/life stage	Major food items	References
Oreochromis niloticus (Nile tilapia)	<5 cm	Zooplankton	[14]
	TL > 10 cm	Bivalves, *C. nilotica* or oligochaetes.	[15, 16]
	All size groups	Algae, fish and plant material phytoplankton and bottom detritus, rarely/occasionally ingest crustaceans, insect larvae and zooplankton	
Lates niloticus (Nile perch)	<20 cm	Mainly on invertebrates, especially the prawn *Caridina nilotica*, zooplankton, chironomids.	[17]
	Adult Nile perch	Shifts to a fish diet with increasing size, like *Rastrineobola argentea*, Tilapinnes and juvenile Nile perch.	
Protopterus aethiopicus (marbled lungfish)	Omnivorous	Detritus, algae, Odonata, molluscs and small fish especially haplochromines.	[1] [18]
Synodontis victoriae (Lake Victoria squeaker)	Omnivorous Matures 13–21 cm	Chronomid larvae, Ostracods, Odonata, fish remains, Povilla, insect remains and higher plant material.	[18]
Clarias gariepinus (African catfish)	Omnivorous	Small fishes, insects' larvae (Chironomid larvae and pupae), molluscs and plants (zooplankton).	[1] [19]
Bagrus docmas	Carnivorous	Mainly insect larvae (Odonata and terrestrial insects (cricket), crustaceans and small fishes especially haplochromines.	[18]
Tilapia zilli	Omnivorous Matures 13–15 cm	Higher plants and ingest bottom deposits	[1]

were brought to the laboratory on ice and immediately deep frozen at −20°C until analysis after 2–4 weeks.

Laboratory Methods

The FAs were determined in sub-samples of the tissues, weighing approximately 30–50 mg. The heart was carefully washed in water to remove blood and dried on filter paper, and the subsample was cut from the tip. From the white dorsal muscle the subsample was cut from the side about 2/5 of the distance from snout to tail, carefully avoiding red muscle, skin and bone. The subsamples were transferred to 15-mL thick-walled glass tubes containing an accurately determined amount of internal standard (19:0). After addition of 1 mL of anhydrous methanol containing 2 M HCl and exchange of the atmosphere in the tubes with nitrogen gas, the tubes were securely closed with Teflon-lined screw caps and placed in an oven for 2 h at 90°C for complete methanolysis.

After cooling to room temperature, the tubes were opened and the methanol evaporated down to about 0.5 mL by a stream of nitrogen gas and 0.5 mL distilled water was added to reduce the solubility of the formed FA methyl esters (FAME) which were extracted with 2 × 1 mL hexane.

One microliter of the combined hexane extracts were injected splitless (the split was opened after 4 min), and chromatographed on a 25 m × 0.25 mm (i.d.) fused silica column with polyethylene–glycol (PEG) as stationary phase, with a thickness of 0.2 μm (CP-WAX 52CB Chrompack) and helium at 20 psi as mobile phase. The column was mounted in Hewlett-Packard 5890A gas chromatograph equipped with a Hewlett-Packard 7673A autosampler and a flame-ionisation detector (FID). The injector temperature was set at 260°C and the detector temperature at 330°C. The oven was programmed as follows: 90°C for 4 min, 30°C/min to 165°C, then 3°C/min to 225°C, where it was left isothermally for 10.5 min before cooling for the next run. The FID signal was A/D converted, recorded, stored and treated in Chromeleon 6.60 software.

The chromatographic peaks were identified by comparison with a chromatogram of a standard mixture of 20 FAME, GLC reference standard 68D from Nu-Chek-Prep (Elysian, Minn., USA), and by chromatographing selected samples under identical conditions with mass-spectrometric detection on Fison 800 GC–MS.

To monitor the performance of the column in the gas chromatograph, the standard mixture of FAME was chromatographed at regular intervals for each tenth sample. Empirical response factors relative to 18:0 were computed for the 20 FAME present in known amounts in the standard mixture. The response factors for each of the FAME not present in the standard mixture were estimated by comparison with the standard FAME which resembled them most closely in terms of chain length and number of double bonds. The areas of the FAME peaks were corrected with the response factors, and the relative amount of each FA in a sample was expressed as a percentage of the sum of all FAs in the sample. The total amount of FAs in the tissue was determined by relating the total area of all FAME peaks to the area of the peak of the internal standard, 19:0.

A response factor for determination of the level of cholesterol from the sum of the areas of two peaks representing degradation products of cholesterol was obtained from calibration curves based on four different concentrations of cholesterol and cholesteryl stearate, respectively, together with known amounts of the internal standard 19:0, carried through methanolysis and gas chromatography. The response factor was found to be 0.27 ± 0.02 relative to 19:0.

In the area of the chromatograms between 14:0 and 18:0 two peaks of methyl alkenyl ethers, i.e. *cis* and *trans* derived from plasmalogen with 18:0 side chain, and five peaks of dimethyl acetals derived from plasmalogens with 16:0, 17:0, 18:0, 18:1n-9 and 18:1n-7 side chains, respectively, were identified by mass spectrometry. The areas of these peaks were summed up. An average molecular weight of these seven components of 310 and an average weight of the parent plasmalogens of 750 gave a response factor of 0.4.

Statistical Methods

Corrected areas of chromatographic peaks were subjected to multivariate statistics using principal component analysis (PCA) available in the SIRIUS 7.0 software package [21]. The relative values (i.e. percentage of the sum) of the FAs were logarithmically transformed, thereby leveling out the quantitative differences among FAs. With each sample positioned in the multi-dimensional space described by the log-transformed variables (FA), new coordinates (principal components, PCs) in the directions of the largest and second largest variance among the samples were computed using SIRIUS [21]. In this manner the relationship between the samples could be described in much fewer dimensions than the original, retaining the systematic variation among the samples. The relative positions of the samples were displayed by projecting them on a plane defined by two new coordinates, i.e. PC1 and PC2, resulting in PC-plots.

The PC-plots are only qualitative displays of the relationship among the samples, they do not cover the total variation among them. Quantitative measures of the difference among the samples were obtained in two ways. Based on the average values for the fish from each species and location for the 14 most abundant FAs the five first PCs covered 91% of the total variance among the samples, as calculated from the normalized and log-transformed values. A hierarchical cluster analysis was then performed on the Euclidean distances between the samples in the 5D space based on the five PCs.

The other method for quantifying, Soft Independent Modeling of Class Analogy (SIMCA) [22] available in the software package SIRIUS [21], was used to determine the differences between the seven species. This computation was based on the 35 most abundant FAs. The normalized values were standardized within each species, i.e. by dividing the values for each FA by the standard deviation of that FA within each species. PCs were then fitted to the samples of each species and cross validation analysis [23] was done to get the best PC(s) that adequately describe the species. Space-filling models were then constructed around the PC(s) with an outer 95% confidence limit, RSD_{max}. The distance to the model, RSD, of each fish was determined. A fish belongs to a species when its RSD is lower than the RSD_{max} of the model.

Results

Regardless of tissue, species, population (site) the most abundant saturated FA (SAFA) was palmitic acid (16:0) followed by stearic acid (18:0) (Tables 2 and 3). Odd number SAFA pentadecanoic acid (15:0) and margaric acid (17:0) were present in small levels.

The dominating monounsaturated FA (MUFA) was oleic acid (18:1n-9) in all species except in *P. aethiopicus* (lungfish), where it was exceeded by vaccenic acid (18:1n-7). The level of 18:1n-9 was higher in the muscle tissue (4–18%) than in the heart tissue (4–13%)

Among the polyunsaturated FAs (PUFA) docosahexaenoic acid (DHA) 22:6n-3 and arachidonic acid (AA) 20:4n-6 were dominating in both muscle and heart tissue. PUFA was the dominating group, with MUFA the group present in the lowest levels, i.e. PUFA > SAFA > MUFA. The ratio $n-3/n-6$ was 0.5–3 in the muscle and 0.4–1.6 in the heart tissue. In the heart tissue the n-6 PUFA was generally present in higher amounts than in the muscle tissue. The rather high standard deviations indicate large individual differences within each species.

Two components with longer retention times than that of 24:1n-9 appeared in higher amounts in the heart tissue than in the muscle tissue. The two components were identified by GC-MS as two isomeric degradation products of cholesterol, $m/z = 368$, cholesta-3,5-diene and cholesta-2,5-diene [24, 25]. It has turned out that the decomposition of cholesterol is reproducible, and these two peaks were used to determine the level of cholesterol in the tissue sample. The muscle tissue contained around 50 mg cholesterol per 100 g tissue, and the heart tissue contained from three to ten times as much, Tables 2 and 3.

The total amount of dimethylacetals and methyl alkenyl ethers amounted to 0.09–0.60 mg/g in the muscle tissue and 0.42–2.66 mg/g in the heart tissue.

Table 2 Fatty acids in white muscle of seven species of fish from Lakes Victoria and Kyoga

	Oreochromis niloticus			*Lates niloticus*			*Protopterus aethiopicus*			*Synodontis victoriae*		*Clarias gariepinus*		*Bagrus docmas*		*Tilapia zilli*		
fatty acids	V N = 6	B N = 8	L N = 8	V N = 6	B N = 4	L N = 5	V N = 4	B N = 8	L N = 5	V N = 6	B N = 7	L N = 6	B N = 5	V N = 8	L N = 8	V N = 6	B N = 5	L N = 8
14:0	1.9 ± 0.4	1.9 ± 0.3	2.1 ± 0.4	1.3 ± 0.1	1.1 ± 0.2	0.8 ± 0.1	2.9 ± 0.6	3.0 ± 0.5	2.2 ± 0.2	1.1 ± 0.2	1.6 ± 0.2	1.5 ± 0.1	1.7 ± 0.3	1.0 ± 0.1	1.8 ± 0.2	0.8 ± 0.1	1.2 ± 0.1	1.0 ± 0.1
iso15:0	0.17 ± 0.01	0.2 ± 0.1	0.2 ± 0.1	0.17 ± 0.01	0.19 ± 0.05	0.14 ± 0.02	0.6 ± 0.1	0.4 ± 0.1	0.5 ± 0.1	0.23 ± 0.03	0.18 ± 0.05	0.3 ± 0.1	0.4 ± 0.1	0.2 ± 0.1	0.2 ± 0.1	0.5 ± 0.2	0.24 ± 0.01	0.3 ± 0.1
15:0	0.37 ± 0.04	0.4 ± 0.1	0.4 ± 0.1	0.4 ± 0.1	1.3 ± 0.2	0.4 ± 0.1	0.5 ± 0.1	0.6 ± 0.1	0.7 ± 0.2	0.7 ± 0.1	0.5 ± 0.1	0.6 ± 0.1	0.74 ± 0.04	0.5 ± 0.1	0.5 ± 0.1	0.5 ± 0.1	0.6 ± 0.1	0.5 ± 0.1
16:0	22.0 ± 1.0	22.2 ± 2.6	22.3 ± 1.5	19.3 ± 1.7	18.8 ± 1.5	20.5 ± 0.3	12.0 ± 0.5	16 ± 1	13.7 ± 1.2	23.0 ± 1.7	23.8 ± 2.1	23.1 ± 0.9	22.0 ± 0.3	20.8 ± 0.8	21.5 ± 1.1	21.4 ± 1.9	21.1 ± 1.7	19.7 ± 2.0
iso17:0	0.4 ± 0.1	0.5 ± 0.1	0.4 ± 0.1	0.5 ± 0.1	0.5 ± 0.2	0.34 ± 0.02	1.0 ± 0.3	0.7 ± 0.1	0.47 ± 0.02	1.2 ± 0.3	0.8 ± 0.1	1.1 ± 0.1	0.4 ± 0.1	0.5 ± 0.1	0.3 ± 0.1	0.82 ± 0.03	0.6 ± 0.1	0.8 ± 0.1
17:0	1.7 ± 0.1	1.0 ± 0.2	0.84 ± 0.05	0.9 ± 0.1	2.1 ± 0.5	0.9 ± 0.1	1.1 ± 0.1	1.24 ± 0.03	1.4 ± 0.2	1.7 ± 0.3	0.9 ± 0.1	1.21 ± 0.01	1.2 ± 0.3	1.6 ± 0.2	1.3 ± 0.1	1.6 ± 0.1	1.7 ± 0.4	1.5 ± 0.3
18:0	9.4 ± 1.0	9.8 ± 0.6	11.0 ± 1.2	10.3 ± 0.5	11.7 ± 0.9	10.8 ± 0.4	10.4 ± 0.7	10.6 ± 1.4	12.6 ± 1.2	9.6 ± 0.5	11.4 ± 0.7	10.1 ± 1.0	8.9 ± 0.3	10.3 ± 0.8	10.8 ± 0.5	11.5 ± 0.8	10.6 ± 1.1	11.8 ± 0.4
20:0	0.25 ± 0.04	0.24 ± 0.04	0.3 ± 0.1	0.3 ± 0.1	0.3 ± 0.1	0.28 ± 0.04	0.3 ± 0.1	0.24 ± 0.02	0.44 ± 0.01	0.2 ± 0.1	0.24 ± 0.04	0.21 ± 0.04	0.2 ± 0.1	0.20 ± 0.04	0.14 ± 0.02	0.3 ± 0.1	0.3 ± 0.1	0.30 ± 0.02
22:0	0.5 ± 0.1	0.7 ± 0.1	0.6 ± 0.1	0.4 ± 0.1	0.4 ± 0.1	0.4 ± 0.1	0.8 ± 0.4	0.6 ± 0.1	0.53 ± 0.01	0.21 ± 0.01	0.35 ± 0.04	0.23 ± 0.04	0.34 ± 0.05	0.23 ± 0.04	0.29 ± 0.05	0.4 ± 0.1	0.6 ± 0.1	0.70 ± 0.03
24:0	0.6 ± 0.1	0.4 ± 0.1	0.5 ± 0.2	0.4 ± 0.1	0.3 ± 0.1	0.4 ± 0.2	0.9 ± 0.1	0.2 ± 0.1	0.3 ± 0.1	0.2 ± 0.1	0.2 ± 0.1	0.3 ± 0.2	0.2 ± 0.1	0.2 ± 0.1	0.3 ± 0.1	0.3 ± 0.1	0.6 ± 0.1	0.6 ± 0.1
14:1 n5	0.05 ± 0.01	0.01 ± 0.01	0.1 ± 0.01	0.02 ± 0.01	0.01 ± 0.01	0.01 ± 0.01	0.1 ± 0.1	0.04 ± 0.01	0.04 ± 0.04	0.02 ± 0.01	0.01 ± 0.01	0.03 ± 0.02	0.02 ± 0.02	0.04 ± 0.01	0.02 ± 0.02	0.05 ± 0.07	0.01 ± 0.01	0.02 ± 0.02
16:1n11	0.2 ± 0.1	0.2 ± 0.1	0.2 ± 0.1	0.08 ± 0.03	0.13 ± 0.02	0.1 ± 0.1	0.1 ± 0.1	0.07 ± 0.02	0.07 ± 0.01	0.2 ± 0.1	0.4 ± 0.1	0.3 ± 0.2	0.4 ± 0.1	0.10 ± 0.03	0.1 ± 0.1	0.14 ± 0.03	0.2 ± 0.1	0.10 ± 0.03
16:1n9	0.4 ± 0.1	0.2 ± 0.1	0.3 ± 0.1	0.3 ± 0.1	0.3 ± 0.1	0.2 ± 0.1	0.8 ± 1.2	0.34 ± 0.04	0.5 ± 0.1	0.4 ± 0.1	0.6 ± 0.1	0.5 ± 0.1	0.5 ± 0.1	0.33 ± 0.05	0.3 ± 0.1	0.3 ± 0.1	0.6 ± 0.1	0.4 ± 0.2
16:1 n7	3.6 ± 0.1	4.8 ± 1.4	3.2 ± 1.1	2.4 ± 0.6	1.4 ± 0.1	1.6 ± 0.2	4.1 ± 0.5	6.5 ± 0.8	1.9 ± 0.2	3.1 ± 0.6	3.4 ± 0.7	2.2 ± 0.6	3.1 ± 0.8	1.7 ± 0.3	1.6 ± 0.3	3.3 ± 0.6	2.3 ± 0.3	1.4 ± 0.2
16:1n5	0.24 ± 0.03	0.6 ± 0.2	0.26 ± 0.05	0.3 ± 0.1	0.16 ± 0.02	0.17 ± 0.02	0.6 ± 0.2	0.6 ± 0.1	0.3 ± 0.1	0.2 ± 0.0	0.2 ± 0.1	0.3 ± 0.1	0.24 ± 0.05	0.21 ± 0.03	0.20 ± 0.01	0.6 ± 0.1	0.23 ± 0.03	0.3 ± 0.1
17:1n9	0.4 ± 0.2	0.2 ± 0.1	0.3 ± 0.1	0.5 ± 0.1	0.4 ± 0.1	0.7 ± 0.1	0.3 ± 0.1	0.4 ± 0.1	0.4 ± 0.0	0.6 ± 0.2	0.4 ± 0.1	0.38 ± 0.03	0.5 ± 0.1	0.3 ± 0.1	0.3 ± 0.1	0.5 ± 0.1	0.4 ± 0.1	0.4 ± 0.1
18:1n11	0.3 ± 0.1	0.20 ± 0.04	0.3 ± 0.1	0.34 ± 0.03	0.19 ± 0.02	0.28 ± 0.03	0.4 ± 0.2	0.22 ± 0.03	0.2 ± 0.1	0.2 ± 0.1	0.2 ± 0.1	0.3 ± 0.1	0.18 ± 0.03	0.2 ± 0.1	0.2 ± 0.1	0.3 ± 0.1	0.19 ± 0.04	0.32 ± 0.05
18:1 n9	5.2 ± 1.0	4.7 ± 1.2	5.4 ± 1.2	8.7 ± 0.9	7.0 ± 0.8	8 ± 1	4.9 ± 0.9	6 ± 1	5.0 ± 0.6	19.3 ± 1.7	13.8 ± 1.1	7.9 ± 1.0	7.1 ± 2.1	5.9 ± 0.9	5.9 ± 0.6	7.1 ± 0.6	5.5 ± 0.4	6.6 ± 1.2
18:1 n7	2.6 ± 0.9	3.8 ± 0.6	2.7 ± 0.3	4.0 ± 0.4	3.1 ± 0.6	4.7 ± 1.1	6.5 ± 0.2	7.8 ± 0.7	8.0 ± 0.2	2.5 ± 0.5	3.9 ± 0.4	4.6 ± 0.2	6.1 ± 0.1	4.4 ± 0.5	6.3 ± 0.3	3.7 ± 0.7	2.7 ± 0.4	2.9 ± 0.6
18:1n5	0.16 ± 0.02	0.3 ± 0.1	0.2 ± 0.1	0.3 ± 0.1	0.16 ± 0.03	0.2 ± 0.1	0.3 ± 0.1	0.27 ± 0.04	0.1 ± 0.1	0.3 ± 0.1	0.2 ± 0.1	0.1 ± 0.1	0.14 ± 0.01	0.16 ± 0.03	0.08 ± 0.02	0.3 ± 0.1	0.2 ± 0.1	0.18 ± 0.03
20:1n11	0.7 ± 0.1	0.5 ± 0.1	0.5 ± 0.2	0.9 ± 0.4	0.46 ± 0.03	0.53 ± 0.04	1.9 ± 0.4	0.6 ± 0.1	0.8 ± 0.1	0.8 ± 0.2	0.7 ± 0.2	1.31 ± 0.04	0.5 ± 0.1	0.4 ± 0.1	0.5 ± 0.1	0.7 ± 0.1	0.5 ± 0.1	0.5 ± 0.1
20:1 n9	0.17 ± 0.01	0.20 ± 0.02	0.2 ± 0.1	0.3 ± 0.1	0.26 ± 0.03	0.2 ± 0.1	0.2 ± 0.1	0.28 ± 0.04	0.17 ± 0.01	0.6 ± 0.3	0.7 ± 0.2	0.38 ± 0.04	0.3 ± 0.1	0.25 ± 0.05	0.21 ± 0.03	0.4 ± 0.2	0.3 ± 0.1	0.16 ± 0.01
22:1n11	0.05 ± 0.01	0.07 ± 0.03	0.03 ± 0.03	0.04 ± 0.02	0.07 ± 0.03	0.02 ± 0.02	0.1 ± 0.1	0.06 ± 0.02	0.04 ± 0.01	0.06 ± 0.02	0.08 ± 0.01	0.1 ± 0.1	0.04 ± 0.03	0.02 ± 0.01	0.01 ± 0.01	0.04 ± 0.01	0.01 ± 0.01	0.04 ± 0.03
22:1 n9	0.08 ± 0.05	0.13 ± 0.01	0.06 ± 0.03	0.03 ± 0.03	0.12 ± 0.02	0.05 ± 0.01	0.01 ± 0.01	0.08 ± 0.01	0.01 ± 0.01	0.06 ± 0.02	0.08 ± 0.01	0.02 ± 0.01	0.01 ± 0.01	0.02 ± 0.02	0.01 ± 0.01	0.05 ± 0.03	0.1 ± 0.1	0.06 ± 0.01
24:1 n9	0.8 ± 0.1	0.3 ± 0.1	0.8 ± 0.1	1.0 ± 0.1	1.1 ± 0.1	0.8 ± 0.1	0.8 ± 0.2	0.3 ± 0.1	0.28 ± 0.02	0.3 ± 0.1	0.5 ± 0.1	0.6 ± 0.1	0.4 ± 0.1	0.4 ± 0.1	0.6 ± 0.1	0.5 ± 0.1	0.5 ± 0.2	0.5 ± 0.1
16:2n6	0.15 ± 0.02	0.2 ± 0.1	0.2 ± 0.2	0.1 ± 0.1	0.03 ± 0.05	0.05 ± 0.03	0.04 ± 0.03	0.23 ± 0.04	0.04 ± 0.01	0.11 ± 0.05	0.1 ± 0.1	0.04 ± 0.01	0.08 ± 0.04	0.02 ± 0.01	0.03 ± 0.01	0.08 ± 0.05	0.06 ± 0.03	0.03 ± 0.01
18:2 n6	2.0 ± 0.5	2.3 ± 0.4	3.5 ± 0.6	2.1 ± 0.5	2.4 ± 0.4	3.1 ± 0.4	1.0 ± 0.1	2.4 ± 0.3	2.5 ± 0.5	1.7 ± 0.4	2.2 ± 0.4	3.8 ± 0.7	5.5 ± 0.7	2.1 ± 0.1	2.2 ± 0.2	3.1 ± 1.5	2.9 ± 0.2	3.8 ± 0.7
18:2n4	0.1 ± 0.1	0.18 ± 0.02	0.1 ± 0.1	0.09 ± 0.04	0.06 ± 0.04	0.12 ± 0.03	0.06 ± 0.04	0.26 ± 0.03	0.12 ± 0.03	0.3 ± 0.1	0.14 ± 0.03	0.1 ± 0.1	0.14 ± 0.04	0.10 ± 0.02	0.06 ± 0.03	0.12 ± 0.04	0.1 ± 0.1	0.09 ± 0.03
18:3n6	0.2 ± 0.1	0.19 ± 0.02	0.3 ± 0.1	0.2 ± 0.1	2.4 ± 0.1	0.20 ± 0.05	0.08 ± 0.03	0.12 ± 0.02	0.07 ± 0.01	0.08 ± 0.03	0.10 ± 0.02	0.15 ± 0.03	0.20 ± 0.05	0.06 ± 0.02	0.10 ± 0.03	0.1 ± 0.1	0.3 ± 0.2	0.3 ± 0.1
18:3 n3	2.1 ± 0.1	1.8 ± 0.5	2.1 ± 0.5	1.6 ± 0.2	1.8 ± 0.1	1.2 ± 0.1	0.43 ± 0.04	0.5 ± 0.3	1.0 ± 0.1	1.5 ± 0.3	0.7 ± 0.1	1.7 ± 0.3	2.5 ± 0.4	1.1 ± 0.1	1.2 ± 0.1	2.1 ± 0.6	2.5 ± 0.7	1.6 ± 0.4
18:4n3	0.2 ± 0.1	0.18 ± 0.05	0.2 ± 0.1	0.1 ± 0.1	0.05 ± 0.02	0.10 ± 0.01	0.03 ± 0.01	0.13 ± 0.03	0.1 ± 0.1	0.1 ± 0.1	0.12 ± 0.04	0.3 ± 0.3	0.18 ± 0.01	0.05 ± 0.02	0.06 ± 0.02	0.11 ± 0.03	0.3 ± 0.1	0.3 ± 0.3
20:2 n6	0.2 ± 0.1	0.32 ± 0.05	0.3 ± 0.1	0.36 ± 0.05	0.5 ± 0.1	0.4 ± 0.1	0.63 ± 0.03	0.5 ± 0.1	0.7 ± 0.1	0.7 ± 0.1	0.5 ± 0.1	0.8 ± 0.1	0.6 ± 0.2	0.5 ± 0.1	0.53 ± 0.05	0.8 ± 0.1	0.4 ± 0.1	0.4 ± 0.1
20:3n6	0.7 ± 0.2	0.5 ± 0.2	0.5 ± 0.1	0.5 ± 0.1	0.6 ± 0.1	0.68 ± 0.03	0.6 ± 0.1	0.8 ± 0.1	1.5 ± 0.1	0.5 ± 0.1	0.8 ± 0.2	1.8 ± 0.5	1.4 ± 0.1	0.4 ± 0.1	0.9 ± 0.1	0.7 ± 0.1	0.6 ± 0.1	0.8 ± 0.2
20:4 n6	6 ± 2	6.8 ± 1.9	6.2 ± 0.8	9.5 ± 0.8	11.9 ± 1.6	13.0 ± 0.4	21.1 ± 1.5	13.1 ± 1.5	15.2 ± 0.5	5.0 ± 1.2	6.7 ± 1.5	8.0 ± 0.6	8.5 ± 1.4	6.4 ± 0.9	8.5 ± 0.8	10.4 ± 1.6	5.7 ± 1	9.1 ± 0.9
20:3 n3	0.7 ± 0.3	0.6 ± 0.2	0.5 ± 0.1	0.7 ± 0.1	0.3 ± 0.1	0.4 ± 0.1	0.4 ± 0.1	0.3 ± 0.1	0.8 ± 0.02	0.6 ± 0.1	0.3 ± 0.1	0.4 ± 0.1	0.51 ± 0.03	0.9 ± 0.1	0.5 ± 0.1	0.8 ± 0.2	0.7 ± 0.2	0.5 ± 0.2
20:4n3	0.4 ± 0.1	0.4 ± 0.1	0.4 ± 0.1	0.28 ± 0.03	0.2 ± 0.1	0.3 ± 0.1	0.14 ± 0.02	0.4 ± 0.1	1.4 ± 0.3	0.26 ± 0.01	0.3 ± 0.1	0.8 ± 0.1	0.38 ± 0.01	0.27 ± 0.02	0.4 ± 0.1	0.44 ± 0.03	0.5 ± 0.1	0.9 ± 0.5
20:5 n3	4.6 ± 0.4	5.5 ± 1.0	3.9 ± 0.6	3.4 ± 0.2	2.1 ± 0.7	3.0 ± 0.7	2.3 ± 0.2	4.7 ± 1.1	2.5 ± 0.5	3.5 ± 0.6	3.7 ± 0.8	4.8 ± 0.4	6.4 ± 0.4	5.0 ± 0.5	3.6 ± 0.5	3.0 ± 0.6	5.1 ± 0.7	4.6 ± 0.2
21:5n3	0.3 ± 0.2	0.2 ± 0.1	0.3 ± 0.3	0.3 ± 0.2	0.6 ± 0.4	0.2 ± 0.2	0.6 ± 0.2	0.2 ± 0.1	0.1 ± 0.1	0.4 ± 0.1	0.19 ± 0.05	0.0 ± 0.1	0.2 ± 0.1	0.2 ± 0.1	0.03 ± 0.02	0.2 ± 0.2	0.3 ± 0.2	0.1 ± 0.1
22:4n6	1.8 ± 0.3	1.3 ± 0.2	0.9 ± 0.2	1.6 ± 0.2	2.5 ± 0.7	2.5 ± 0.7	7.3 ± 2.2	3.0 ± 0.7	5.3 ± 0.2	1.3 ± 0.2	1.7 ± 0.3	1.3 ± 0.1	0.81 ± 0.05	0.9 ± 0.1	0.89 ± 0.05	2.0 ± 0.3	1.5 ± 0.3	1.1 ± 0.3
22:5n6	2.0 ± 0.6	1.8 ± 0.4	1.3 ± 0.1	2.2 ± 0.5	3.2 ± 0.3	2.4 ± 0.6	1.8 ± 0.2	0.7 ± 0.1	0.9 ± 0.1	1.5 ± 0.1	1.5 ± 0.2	0.9 ± 0.1	0.8 ± 0.1	2.0 ± 0.1	1.8 ± 0.6	2.2 ± 0.4	2.3 ± 0.4	2.3 ± 0.7
22:5n3	5.6 ± 0.6	8.2 ± 1.1	5.7 ± 1.0	5.4 ± 0.8	4.3 ± 0.2	4.9 ± 0.1	4.2 ± 0.7	6.3 ± 0.8	6.3 ± 0.3	2.6 ± 0.3	3.7 ± 0.3	3.4 ± 0.4	3.6 ± 0.3	3.2 ± 0.2	2.9 ± 0.6	5.2 ± 0.9	6.1 ± 1.4	6.7 ± 0.4
22:6 n3	20.4 ± 2.2	15.8 ± 2.1	20.4 ± 1.3	18.1 ± 1.0	15.4 ± 1.4	14.4 ± 0.8	7.8 ± 2.7	8.5 ± 1.1	11.0 ± 0.4	12.8 ± 1.4	12.0 ± 2.2	13.9 ± 2.1	12.6 ± 1.9	26.7 ± 2.0	22.8 ± 1.5	12.4 ± 1.9	19.6 ± 1.4	16.3 ± 1.3
∑SAFA	37.2 ± 0.5	37.4 ± 0.8	38.7 ± 0.5	34.1 ± 0.5	36.7 ± 0.5	35.0 ± 0.1	30.5 ± 0.2	34.0 ± 0.5	32.7 ± 0.5	38.2 ± 0.5	40.0 ± 0.6	38.7 ± 0.4	36.1 ± 0.1	35.5 ± 0.3	37.1 ± 0.3	38.3 ± 0.6	37.4 ± 0.6	37.2 ± 0.6
∑MUFA	14.9 ± 0.4	16.1 ± 0.4	14.5 ± 0.4	19.2 ± 0.3	14.9 ± 0.2	18.1 ± 0.3	21.1 ± 0.3	23.6 ± 0.3	17.7 ± 0.1	28.8 ± 0.4	25.1 ± 0.3	19.0 ± 0.3	19.5 ± 0.6	14.4 ± 0.2	16.3 ± 0.2	17.9 ± 0.2	13.7 ± 0.1	13.8 ± 0.3
∑PUFA	47.8 ± 0.6	46.4 ± 0.6	46.8 ± 0.4	46.7 ± 0.3	48.4 ± 0.5	46.9 ± 0.3	48.4 ± 0.8	42.4 ± 0.5	49.6 ± 0.3	33.0 ± 0.4	34.9 ± 0.6	42.3 ± 0.5	44.4 ± 0.5	50.0 ± 0.5	46.6 ± 0.4	43.8 ± 0.6	48.9 ± 0.5	49.0 ± 0.4
∑n3	32 ± 1	31.2 ± 0.7	31.4 ± 0.4	27.4 ± 0.4	22.8 ± 0.5	22.7 ± 0.3	14 ± 1	19.5 ± 0.5	21.2 ± 0.3	21.0 ± 0.5	19.6 ± 0.7	24 ± 1	24.6 ± 0.6	35 ± 1	29.2 ± 0.5	22.3 ± 0.6	33 ± 1	29.0 ± 0.4
∑n6	13 ± 1	12.8 ± 0.6	12.3 ± 0.3	15.2 ± 0.3	22 ± 1	20.9 ± 0.3	29 ± 1	19 ± 1	23.9 ± 0.2	10.6 ± 0.4	12.8 ± 0.5	15.7 ± 0.3	16.9 ± 0.5	11.9 ± 0.3	13.9 ± 0.3	18 ± 1	12.9 ± 0.3	16.6 ± 0.4
n3:n6	2.5	2.4	2.5	1.8	1.1	1.1	0.5	1.0	0.9	2.0	1.5	1.5	1.5	3.0	2.1	1.3	2.6	1.7
TOTAL FA mg/g	1.9 ± 0.5	3.7 ± 1.1	3.5 ± 2.3	3.5 ± 1.1	3.3 ± 0.5	2.8 ± 0.1	2.7 ± 0.7	4.6 ± 1.3	2 ± 0.2	5 ± 2	5.8 ± 1	3.2 ± 0.7	4 ± 1	2.6 ± 1.2	2.8 ± 0.3	3.8 ± 0.7	3.7 ± 0.9	2.7 ± 0.1
Cholesterol mg/100g	49 ± 18	41 ± 17	32 ± 7	60 ± 2	57 ± 5	53 ± 19	39 ± 12	62 ± 7	29 ± 3	29 ± 11	65 ± 3	34 ± 0	40 ± 12	47 ± 21	39 ± 17	64 ± 20	45 ± 7	52 ± 25
Plasmalogens mg/g	0.11 ± 0.02	0.14 ± 0.02	0.15 ± 0.02	0.17 ± 0.03	0.20 ± 0.02	0.11 ± 0.01	0.60 ± 0.04	0.40 ± 0.03	0.24 ± 0.01	0.25 ± 0.03	0.36 ± 0.03	0.29 ± 0.02	0.24 ± 0.01	0.18 ± 0.02	0.22 ± 0.02	0.27 ± 0.03	0.16 ± 0.03	0.09 ± 0.01

[1] Mean relative amounts as % of sum ± SD
V: Napoleon gulf in Lake Victoria, B: Bukungu at Lake Kyoga, L: Lwampanga at Lake Kyoga,
SAFA: saturated fatty acids, MUFA: monounsaturated fatty acids, PUFA: polyunsaturated fatty acids
TOTAL FA: total amount of fatty acids, in mg/g wet weight,
cholesterol in mg/100g wet weight
plasmalogens in mg/g wet weight

Table 3 Fatty acids in heart tissue of seven species of fish from Lakes Victoria and Kyoga

	Oreochromis niloticus			*Lates niloticus*			*Protopterus aethiopicus*			*Synodontis victoriae*		*Clarias gariepinus*		*Bagrus docmas*		*Tilapia zilli*		
fatty acids	V N = 6	B N = 9	L N = 6	V N = 6	B N = 6	L N = 4	V N = 4	B N = 6	L N = 5	V N = 7	B N = 6	B N = 5	L N = 5	V N = 5	L N = 4	V N = 6	B N = 4	L N = 4
14:0	1.9 ± 0.4	1.6 ± 0.2	1.7 ± 0.5	0.9 ± 0.1	1.3 ± 0.1	1.4 ± 0.02	2.8 ± 0.5	2.2 ± 0.1	2.2 ± 0.3	1.2 ± 0.2	1.9 ± 0.6	1.1 ± 0.1	1.5 ± 0.2	1.44 ± 0.33	1.61 ± 0.04	1.4 ± 0.3	1.5 ± 0.3	1.2 ± 0.1
iso 15:0	0.24 ± 0.05	0.2 ± 0.1	0.22 ± 0.04	0.2 ± 0.1	0.22 ± 0.04	0.2 ± 0.05	0.4 ± 0.1	0.3 ± 0.03	0.5 ± 0.1	0.2 ± 0.1	0.2 ± 0.0	0.2 ± 0.1	0.4 ± 0.1	0.32 ± 0.09	0.19 ± 0.03	0.4 ± 0.03	0.3 ± 0.04	0.3 ± 0.1
15:0	0.4 ± 0.1	0.4 ± 0.1	0.3 ± 0.1	0.4 ± 0.1	0.6 ± 0.1	0.3 ± 0.1	1.0 ± 0.1	0.5 ± 0.02	0.7 ± 0.2	0.4 ± 0.1	0.4 ± 0.1	0.5 ± 0.1	0.6 ± 0.2	0.6 ± 0.1	0.6 ± 0.2	0.6 ± 0.1	0.4 ± 0.1	0.4 ± 0.1
16:0	14.9 ± 0.5	15.6 ± 1.5	17.0 ± 1.4	14.2 ± 1.2	17 ± 1	14.6 ± 0.8	12.9 ± 0.5	16.9 ± 0.2	11.9 ± 0.9	22.3 ± 2.9	23.6 ± 2.4	17.4 ± 0.9	18.2 ± 2.2	14.1 ± 1.0	13.9 ± 1.6	12.7 ± 1.1	11.8 ± 0.6	12.1 ± 1.1
iso 17:0	0.5 ± 0.1	0.4 ± 0.1	0.24 ± 0.04	0.43 ± 0.04	0.6 ± 0.1	0.4 ± 0.1	1.6 ± 0.2	0.6 ± 0.1	0.6 ± 0.2	1.8 ± 0.2	1.4 ± 0.2	0.4 ± 0.1	0.9 ± 0.6	0.5 ± 0.1	0.3 ± 0.1	0.7 ± 0.1	0.5 ± 0.1	0.4 ± 0.1
17:0	1.3 ± 0.2	0.8 ± 0.1	0.7 ± 0.1	1.1 ± 0.2	0.9 ± 0.1	0.8 ± 0.1	1.7 ± 0.2	1.01 ± 0.03	1.3 ± 0.2	1.8 ± 0.5	1.4 ± 0.3	1.3 ± 0.2	1.8 ± 0.1	1.8 ± 0.5	1.3 ± 0.2	1.2 ± 0.1	1.2 ± 0.5	1.5 ± 0.2
18:0	12.3 ± 1.5	13 ± 1	13.0 ± 1.1	11.9 ± 0.2	12.6 ± 0.6	12.2 ± 0.7	14.0 ± 1.3	16.3 ± 1.5	15.3 ± 1.4	12.3 ± 1.3	12.5 ± 1.3	14.0 ± 0.4	12.3 ± 0.7	14.0 ± 1.3	15.0 ± 1.1	12.6 ± 1.1	14.3 ± 1.1	15.6 ± 0.9
20:0	0.33 ± 0.04	0.3 ± 0.1	0.3 ± 0.1	0.37 ± 0.04	0.38 ± 0.05	0.3 ± 0.1	0.2 ± 0.1	0.23 ± 0.03	0.3 ± 0.1	0.3 ± 0.1	0.4 ± 0.1	0.30 ± 0.04	0.2 ± 0.1	0.4 ± 0.1	0.3 ± 0.1	0.29 ± 0.02	0.4 ± 0.1	0.5 ± 0.1
22:0	0.8 ± 0.1	1.1 ± 0.1	0.8 ± 0.2	0.7 ± 0.1	0.8 ± 0.1	0.8 ± 0.1	0.49 ± 0.04	0.8 ± 0.1	0.69 ± 0.05	0.33 ± 0.05	0.5 ± 0.1	0.9 ± 0.1	0.5 ± 0.1	0.42 ± 0.09	0.46 ± 0.01	0.7 ± 0.1	1.0 ± 0.1	1.0 ± 0.2
24:0	0.3 ± 0.1	0.4 ± 0.1	0.3 ± 0.1	0.6 ± 0.2	0.7 ± 0.1	0.6 ± 0.1	0.15 ± 0.01	0.3 ± 0.1	0.2 ± 0.1	0.2 ± 0.2	0.3 ± 0.1	0.6 ± 0.1	0.4 ± 0.1	0.26 ± 0.22	0.59 ± 0.01	0.3 ± 0.1	0.4 ± 0.1	0.5 ± 0.0
14:1 n5	0.04 ± 0.01	0.01 ± 0.01	0.05 ± 0.02	0.01 ± 0.01	0.01 ± 0.01	0.01 ± 0.01	0.08 ± 0.03	0.02 ± 0.03	0.04 ± 0.01	0.02 ± 0.02	0.02 ± 0.01	0.01 ± 0.01	0.01 ± 0.01	0.02 ± 0.01	0.01 ± 0.01	0.03 ± 0.01	0.02 ± 0.02	0.01 ± 0.01
16:1n11	0.10 ± 0.02	0.08 ± 0.01	0.10 ± 0.01	0.1 ± 0.1	0.18 ± 0.03	0.17 ± 0.02	0.07 ± 0.01	0.09 ± 0.01	0.08 ± 0.02	0.13 ± 0.02	0.18 ± 0.04	0.27 ± 0.04	0.21 ± 0.06	0.17 ± 0.02	0.21 ± 0.04	0.10 ± 0.03	0.14 ± 0.02	0.11 ± 0.02
16:1n9	0.3 ± 0.1	0.18 ± 0.03	0.17 ± 0.03	0.23 ± 0.03	0.3 ± 0.1	0.25 ± 0.03	0.23 ± 0.05	0.32 ± 0.05	0.6 ± 0.1	0.5 ± 0.1	0.6 ± 0.1	0.4 ± 0.1	0.6 ± 0.3	0.4 ± 0.1	0.5 ± 0.1	0.2 ± 0.1	0.42 ± 0.05	0.4 ± 0.3
16:1 n7	4.0 ± 1.0	4.8 ± 1.4	2.5 ± 0.9	1.3 ± 0.1	1.3 ± 0.01	1.2 ± 0.1	4.2 ± 0.5	6 ± 1	2.7 ± 0.2	3.2 ± 0.8	3.9 ± 0.7	2.0 ± 0.6	2.3 ± 0.6	2.3 ± 0.6	1.5 ± 0.1	1.6 ± 0.4	3.1 ± 0.7	1.5 ± 0.2
16:1n5	0.31 ± 0.02	1.4 ± 0.5	0.23 ± 0.05	0.3 ± 0.1	0.3 ± 0.1	0.3 ± 0.1	0.44 ± 0.02	0.6 ± 0.2	0.4 ± 0.1	0.2 ± 0.1	0.24 ± 0.05	0.2 ± 0.1	0.3 ± 0.1	0.22 ± 0.04	0.17 ± 0.02	0.5 ± 0.2	0.3 ± 0.1	0.2 ± 0.1
17:1n9	0.5 ± 0.1	0.3 ± 0.1	0.4 ± 0.2	0.4 ± 0.1	0.4 ± 0.1	0.3 ± 0.01	0.7 ± 0.2	0.30 ± 0.03	0.6 ± 0.1	0.7 ± 0.1	0.5 ± 0.2	0.5 ± 0.1	0.6 ± 0.2	0.5 ± 0.1	0.7 ± 0.3	0.4 ± 0.2	0.4 ± 0.1	0.4 ± 0.1
18:1n11	0.2 ± 0.2	0.16 ± 0.03	0.1 ± 0.0	0.1 ± 0.03	0.2 ± 0.1	0.1 ± 0.1	0.3 ± 0.1	0.2 ± 0.1	0.09 ± 0.02	0.1 ± 0.1	0.2 ± 0.1	0.1 ± 0.0	0.2 ± 0.1	0.1 ± 0.1	0.1 ± 0.1	0.2 ± 0.1	0.1 ± 0.1	0.10 ± 0.03
18:1 n9	8.2 ± 0.6	7.0 ± 1.2	9.1 ± 1.2	5.4 ± 0.4	6.2 ± 0.3	4.8 ± 0.4	5.8 ± 0.3	5.3 ± 0.4	5 ± 1	13.4 ± 2.5	13.4 ± 1.2	7.0 ± 0.3	8.1 ± 0.8	8.3 ± 1.1	9.0 ± 0.6	6.6 ± 0.7	6.4 ± 0.8	8.4 ± 0.4
18:1 n7	4.9 ± 0.6	4 ± 1	4.5 ± 0.9	4.6 ± 0.5	4.3 ± 0.7	4.3 ± 0.5	11.5 ± 0.1	9.1 ± 0.5	11.6 ± 0.3	3.8 ± 0.5	5.1 ± 0.6	7.7 ± 0.4	6.2 ± 0.5	4.7 ± 0.6	5.5 ± 1.4	3.8 ± 0.7	5 ± 1	5.0 ± 0.7
18:1n5	0.20 ± 0.03	0.3 ± 0.1	0.2 ± 0.1	0.13 ± 0.02	0.1 ± 0.02	0.1 ± 0.01	0.34 ± 0.04	0.3 ± 0.1	0.17 ± 0.04	0.2 ± 0.1	0.2 ± 0.1	0.07 ± 0.02	0.16 ± 0.05	0.18 ± 0.05	0.08 ± 0.03	0.2 ± 0.1	0.1 ± 0.1	0.12 ± 0.02
20:1n11	0.2 ± 0.1	0.3 ± 0.1	0.13 ± 0.03	0.2 ± 0.1	0.2 ± 0.1	0.2 ± 0.04	0.7 ± 0.2	0.5 ± 0.2	0.6 ± 0.2	1.64 ± 0.03	0.7 ± 0.2	0.2 ± 0.1	0.4 ± 0.2	0.31 ± 0.11	0.49 ± 0.01	0.5 ± 0.1	0.3 ± 0.1	0.19 ± 0.03
20:1 n9	0.24 ± 0.02	0.17 ± 0.04	0.2 ± 0.1	0.24 ± 0.03	0.3 ± 0.1	0.2 ± 0.03	0.4 ± 0.1	0.28 ± 0.04	0.2 ± 0.1	0.8 ± 0.2	1.3 ± 0.1	0.2 ± 0.1	0.5 ± 0.3	0.29 ± 0.08	0.28 ± 0.08	0.3 ± 0.1	0.7 ± 0.1	0.3 ± 0.04
22:1n11	0.05 ± 0.02	0.05 ± 0.01	0.03 ± 0.01	0.04 ± 0.01	0.09 ± 0.01	0.1 ± 0.03	0.1 ± 0.1	0.04 ± 0.01	0.05 ± 0.03	0.07 ± 0.04	0.10 ± 0.02	0.06 ± 0.03	0.2 ± 0.1	0.09 ± 0.04	0.04 ± 0.02	0.05 ± 0.02	0.03 ± 0.02	0.04 ± 0.02
22:1 n9	0.10 ± 0.03	0.11 ± 0.03	0.05 ± 0.01	0.08 ± 0.01	0.06 ± 0.01	0.04 ± 0.02	0.08 ± 0.03	0.10 ± 0.01	0.02 ± 0.01	0.08 ± 0.01	0.08 ± 0.03	0.04 ± 0.01	0.04 ± 0.01	0.07 ± 0.03	0.02 ± 0.02	0.06 ± 0.03	0.1 ± 0.0	0.05 ± 0.03
24:1 n9	0.5 ± 0.1	0.4 ± 0.1	0.5 ± 0.1	1.6 ± 0.2	1.6 ± 0.2	1.6 ± 0.2	0.40 ± 0.02	0.3 ± 0.2	0.3 ± 0.1	0.5 ± 0.1	0.5 ± 0.1	0.6 ± 0.1	0.7 ± 0.1	0.7 ± 0.1	1.0 ± 0.1	0.6 ± 0.2	0.5 ± 0.2	0.4 ± 0.2
16:2n6	0.13 ± 0.04	0.2 ± 0.1	0.1 ± 0.1	0.06 ± 0.04	0.03 ± 0.01	0.07 ± 0.03	0.01 ± 0.01	0.2 ± 0.1	0.1 ± 0.1	0.1 ± 0.1	0.1 ± 0.1	0.07 ± 0.02	0.06 ± 0.01	0.1 ± 0.1	0.01 ± 0.01	0.04 ± 0.02	0.07 ± 0.04	0.03 ± 0.01
18:2 n6	2.9 ± 0.4	2.2 ± 0.3	4.3 ± 1.2	2.7 ± 0.6	3.7 ± 0.9	3.8 ± 0.3	1.6 ± 0.2	2.1 ± 0.2	3.6 ± 0.7	2.5 ± 0.6	2.2 ± 0.5	5 ± 1	3.9 ± 0.8	1.7 ± 0.4	2.2 ± 0.3	3.2 ± 0.2	3.6 ± 0.4	4.1 ± 0.9
18:2n4	0.19 ± 0.02	0.18 ± 0.03	0.2 ± 0.1	0.11 ± 0.03	0.1 ± 0.02	0.14 ± 0.02	0.15 ± 0.01	0.31 ± 0.04	0.3 ± 0.1	0.3 ± 0.1	0.2 ± 0.1	0.15 ± 0.04	0.2 ± 0.1	0.13 ± 0.01	0.07 ± 0.03	0.12 ± 0.02	0.13 ± 0.02	0.08 ± 0.02
18:3n6	0.5 ± 0.7	0.2 ± 0.1	0.3 ± 0.1	0.07 ± 0.02	0.1 ± 0.02	0.09 ± 0.02	0.04 ± 0.01	0.09 ± 0.01	0.07 ± 0.04	0.06 ± 0.02	0.08 ± 0.02	0.3 ± 0.4	0.1 ± 0.1	0.08 ± 0.03	0.08 ± 0.01	0.10 ± 0.02	0.15 ± 0.05	0.14 ± 0.02
18:3 n3	2.7 ± 0.6	1.7 ± 0.4	2.2 ± 0.3	1.0 ± 0.1	0.7 ± 0.1	1.0 ± 0.1	1.7 ± 0.1	1.4 ± 0.2	1.8 ± 0.3	2.1 ± 0.6	1.4 ± 0.2	1.23 ± 0.03	1.4 ± 0.4	1.2 ± 0.2	1.8 ± 0.3	1.6 ± 0.3	3.4 ± 0.5	1.1 ± 0.1
18:4n3	0.19 ± 0.03	0.1 ± 0.1	0.2 ± 0.1	0.05 ± 0.01	0.05 ± 0.01	0.05 ± 0.01	0.04 ± 0.01	0.10 ± 0.02	0.2 ± 0.1	0.17 ± 0.04	0.1 ± 0.1	0.07 ± 0.01	0.2 ± 0.2	0.09 ± 0.03	0.04 ± 0.01	0.07 ± 0.02	0.2 ± 0.1	0.2 ± 0.2
20:2 n6	0.6 ± 0.2	0.3 ± 0.1	0.3 ± 0.1	0.5 ± 0.1	0.6 ± 0.2	0.6 ± 0.2	1.6 ± 0.2	0.5 ± 0.1	0.9 ± 0.3	1.4 ± 0.2	0.5 ± 0.1	0.6 ± 0.2	0.8 ± 0.2	0.6 ± 0.1	0.6 ± 0.0	1.3 ± 0.1	0.5 ± 0.1	0.5 ± 0.1
20:3n6	1.5 ± 0.3	0.6 ± 0.1	1.1 ± 0.2	1.0 ± 0.1	1.6 ± 0.3	0.91 ± 0.02	0.7 ± 0.1	1.1 ± 0.1	1.7 ± 0.2	0.8 ± 0.1	0.7 ± 0.1	1.7 ± 0.2	1.7 ± 0.3	0.7 ± 0.1	1.5 ± 0.2	0.9 ± 0.1	1.2 ± 0.3	1.6 ± 0.2
20:4 n6	11.8 ± 2.1	13.1 ± 2.2	9.8 ± 0.8	21.5 ± 1.1	22.1 ± 1.9	22.7 ± 0.8	13.9 ± 0.6	10.1 ± 0.3	14.0 ± 1.8	5.3 ± 1.4	6.1 ± 0.8	13.2 ± 1.4	11.9 ± 1.7	10.5 ± 0.8	11.2 ± 1.4	21.8 ± 0.9	16.4 ± 0.6	19.8 ± 1.5
20:3 n3	0.9 ± 0.2	0.5 ± 0.2	0.7 ± 0.2	0.38 ± 0.03	0.29 ± 0.05	0.27 ± 0.04	0.29 ± 0.04	0.3 ± 0.1	0.5 ± 0.1	0.6 ± 0.1	0.3 ± 0.1	0.40 ± 0.03	0.5 ± 0.1	0.7 ± 0.1	0.6 ± 0.2	0.7 ± 0.1	1.0 ± 0.2	0.5 ± 0.1
20:4n3	0.7 ± 0.2	0.40 ± 0.05	0.6 ± 0.1	0.20 ± 0.02	0.16 ± 0.02	0.19 ± 0.01	0.15 ± 0.03	0.5 ± 0.0	1.7 ± 0.4	0.4 ± 0.1	0.3 ± 0.1	0.4 ± 0.1	0.6 ± 0.1	0.3 ± 0.1	0.4 ± 0.1	0.27 ± 0.04	0.6 ± 0.2	0.34 ± 0.03
20:5 n3	4.9 ± 0.5	7.1 ± 1.2	7.4 ± 1.1	3.2 ± 0.8	1.7 ± 0.4	1.9 ± 0.6	1.7 ± 0.4	4.2 ± 0.6	1.7 ± 0.6	3.3 ± 0.7	1.6 ± 0.2	3.6 ± 0.5	2.8 ± 0.4	4.5 ± 0.7	3.9 ± 0.4	1.6 ± 0.3	3.6 ± 1.2	2.6 ± 0.4
21:5n3	0.4 ± 0.5	0.18 ± 0.04	0.2 ± 0.1	0.13 ± 0.02	0.2 ± 0.1	0.16 ± 0.04	1.9 ± 1.1	0.3 ± 0.1	0.3 ± 0.2	0.5 ± 0.3	0.1 ± 0.1	0.2 ± 0.2	0.08 ± 0.01	0.2 ± 0.1	0.04 ± 0.01	0.4 ± 0.2	0.1 ± 0.1	0.11 ± 0.04
22:4n6	1.0 ± 0.2	1.1 ± 0.4	0.7 ± 0.1	1.2 ± 0.3	2.3 ± 0.8	2.0 ± 0.5	8.3 ± 1.2	3.6 ± 0.3	7.1 ± 1.3	1.3 ± 0.3	1.4 ± 0.3	0.9 ± 0.2	0.9 ± 0.1	1.5 ± 0.1	3.5 ± 0.8	1.9 ± 0.4	0.9 ± 0.1	1.3 ± 0.2
22:5n6	1.4 ± 0.5	1.3 ± 0.3	0.9 ± 0.1	4.1 ± 0.5	3.0 ± 0.7	3.7 ± 1.1	1.5 ± 0.2	1.1 ± 0.1	1.1 ± 0.4	1.0 ± 0.2	1.4 ± 0.2	0.8 ± 0.2	0.9 ± 0.1	2.1 ± 0.2	1.9 ± 0.8	3.1 ± 0.7	3.1 ± 0.7	2.9 ± 0.4
22:5n3	5.9 ± 0.5	7 ± 1	5.6 ± 0.6	3.0 ± 0.6	3.2 ± 0.7	2.9 ± 0.5	2.9 ± 0.4	4.1 ± 0.3	2.8 ± 0.5	3.1 ± 0.3	2.8 ± 0.4	2.8 ± 0.3	2.5 ± 0.4	3.0 ± 0.6	2.8 ± 0.4	5.3 ± 0.2	5 ± 1	4.7 ± 0.2
22:6 n3	11.5 ± 1.2	10.4 ± 1.5	12.6 ± 1.2	15.3 ± 1.6	9.7 ± 1.1	14.4 ± 1.1	3.2 ± 0.5	7.5 ± 0.6	5.7 ± 0.8	10.7 ± 1.9	11.0 ± 1.6	13 ± 2	14.2 ± 1.5	20 ± 4	15.5 ± 1.4	11.5 ± 2.5	10.4 ± 0.7	9.0 ± 0.9
Σ SAFA	33.0 ± 0.5	34.1 ± 0.5	34.6 ± 0.5	30.9 ± 0.4	34.8 ± 0.3	31.6 ± 0.3	35.2 ± 0.4	39.2 ± 0.4	33.8 ± 0.4	40.9 ± 1	42.6 ± 0.8	36.7 ± 0.3	36.9 ± 0.6	33.7 ± 0.4	34.2 ± 0.5	30.8 ± 0.4	32.1 ± 0.3	33.6 ± 0.4
Σ MUFA	20.0 ± 0.3	19.5 ± 0.5	18.3 ± 0.4	14.7 ± 0.1	15.7 ± 0.2	13.5 ± 0.2	25.2 ± 0.1	23.3 ± 0.3	22.7 ± 0.2	25.4 ± 0.6	27.0 ± 0.3	19.4 ± 1	20.5 ± 0.2	18.3 ± 0.3	19.6 ± 0.4	15.3 ± 0.2	17.8 ± 0.3	17.4 ± 0.2
Σ PUFA	47.1 ± 0.5	46.3 ± 0.6	47.2 ± 0.4	54.4 ± 0.5	49.5 ± 0.5	54.9 ± 0.4	39.6 ± 0.4	37.5 ± 0.2	43.6 ± 0.5	33.7 ± 0.5	30.4 ± 0.4	43.9 ± 0.6	42.7 ± 0.5	48.0 ± 1	46.2 ± 0.5	53.9 ± 0.6	50.1 ± 0.3	49.1 ± 0.4
Σn3	24.8 ± 0.4	25.0 ± 0.6	27.3 ± 0.5	20.6 ± 0.6	14.2 ± 0.4	19.0 ± 0.4	10.8 ± 0.4	17.0 ± 0.3	13.8 ± 0.2	20.1 ± 0.6	16.4 ± 0.5	18.9 ± 0.7	20.3 ± 0.5	28 ± 1	22.4 ± 0.4	22.5 ± 0.4	19 ± 1	17.4 ± 0.3
Σn6	18.1 ± 0.6	17 ± 1	16.2 ± 0.4	27.6 ± 0.4	29.6 ± 0.6	30.6 ± 0.4	25.4 ± 0.4	17.4 ± 0.1	26.4 ± 0.6	12.3 ± 0.4	11.7 ± 0.3	19.9 ± 0.5	18.5 ± 0.6	15.9 ± 0.3	18.8 ± 0.5	24.0 ± 0.3	29.1 ± 0.3	28.4 ± 0.5
n3:n6	1.4	1.4	1.7	0.7	0.5	0.6	0.4	1.0	0.5	1.6	1.4	0.9	1.1	1.8	1.2	0.7	0.9	0.6
TOTAL FA mg/g	15.6 ± 3.3	12.2 ± 1.2	12.4 ± 1.5	16.1 ± 1.9	14.3 ± 2.5	13.3 ± 0.3	7.4 ± 2.2	14.8 ± 1.6	8.6 ± 1	25.6 ± 8.4	23.5 ± 4.7	21.9 ± 1.4	10.3 ± 2.2	13.5 ± 1.4	13.4 ± 1.3	29 ± 4.7	17.9 ± 5.1	11.4 ± 2
Cholesterol mg/100g	242 ± 66	164 ± 18	131 ± 9	193 ± 92	266 ± 57	219 ± 19	88 ± 11	165 ± 53	72 ± 4	180 ± 67	298 ± 66	427 ± 67	236 ± 88	328 ± 76	171 ± 46	507 ± 21	310 ± 37	152 ± 55
Plasmalogens mg/g	1.16 ± 0.2	1.11 ± 0.1	1.02 ± 0	1.09 ± 0.1	1.53 ± 0	1.45 ± 0.1	1.49 ± 0.1	1.26 ± 0.1	1.2 ± 0	1.38 ± 0.1	0.84 ± 0.1	2.66 ± 0.1	0.98 ± 0.08	1.09 ± 0.1	0.42 ± 0.02	2.21 ± 0.1	1.51 ± 0.2	1.08 ± 0.1

---

[1] Mean relative amounts as % of sum ± SD
V: Napoleon gulf in Lake Victoria, B: Bukungu at Lake Kyoga, L: Lwampanga at Lake Kyoga,
SAFA: saturated fatty acids, MUFA: monounsaturated fatty acids, PUFA: polyunsaturated fatty acids
TOTAL FA: total amount of fatty acids, in mg/g wet weight,
cholesterol in mg/100g wet weight
plasmalogens in mg/g wet weight

A monovariate approach, i.e. evaluating one FA in Tables 2 and 3 at a time, makes it impossible to compare all the seven species sampled at the three different sites/locations. To extract the total information from the average values of the 14 most abundant FAs in the seven species collected at the three sites, we employed multivariate principal component analyses. The FA composition of the lungfish is distinct from those of the other species for both muscle and heart tissue (Fig. 2a, c). Since all samples in these PC-plots influence the position of each other, the lungfish samples, being the most distinct, are squeezing the other samples together. Recalculation without the lungfish samples reveals that the other six species also have distinct, species specific FA compositions of the tissues (Fig. 2b, d).

Separate PCA on each of the seven species, including each fish, shows that the FA composition in both tissues is distinctly different between the three landing sites (Fig. 3).

The PC-plots in Figs. 2 and 3 are, however, only a qualitative display of the differences, and cover only parts of the total variation among the samples. To obtain a quantitative measure where the total variation is taken into account, space filling models for each species, pooling the samples from the three (two) landing sites, were carried out using SIMCA [22] available in software package SIRIUS [21] based on 35 most abundant FAs. The average distances expressed as RSD of all fish to the seven models for each of the heart and muscle tissues were calculated, Table 4. The vast majority of the fish were correctly allocated to their own species with only 15% not classified. No fish were wrongly classified. For the heart tissue, one fish (*O. niloticus*), and for the muscle tissue, four fish (*O. niloticus* and *T. Zilli*) were allocated to another species in addition to their own.

Discussion

The results are characterized by large variations in the FA composition. A large individual variation is obvious from the large SD of the FA values, Tables 2 and 3. In spite of this, there is a systematic difference within each species between fish from the three locations, Figs. 3 and 4. Furthermore, differences between the species were even greater than the differences within the species, Fig. 2. Variations, both within and between species have been a commonplace observation for fresh water fish [11, 26]. Various factors such as diet, genetic variation, temperature, age, size and season are responsible for variability in FA composition of the tissues of fresh water fish [4]. Of these factors, diet is supposed to be dominating [27, 28]. Zenebe et al. [6] found a remarkably large variation in the lipid and

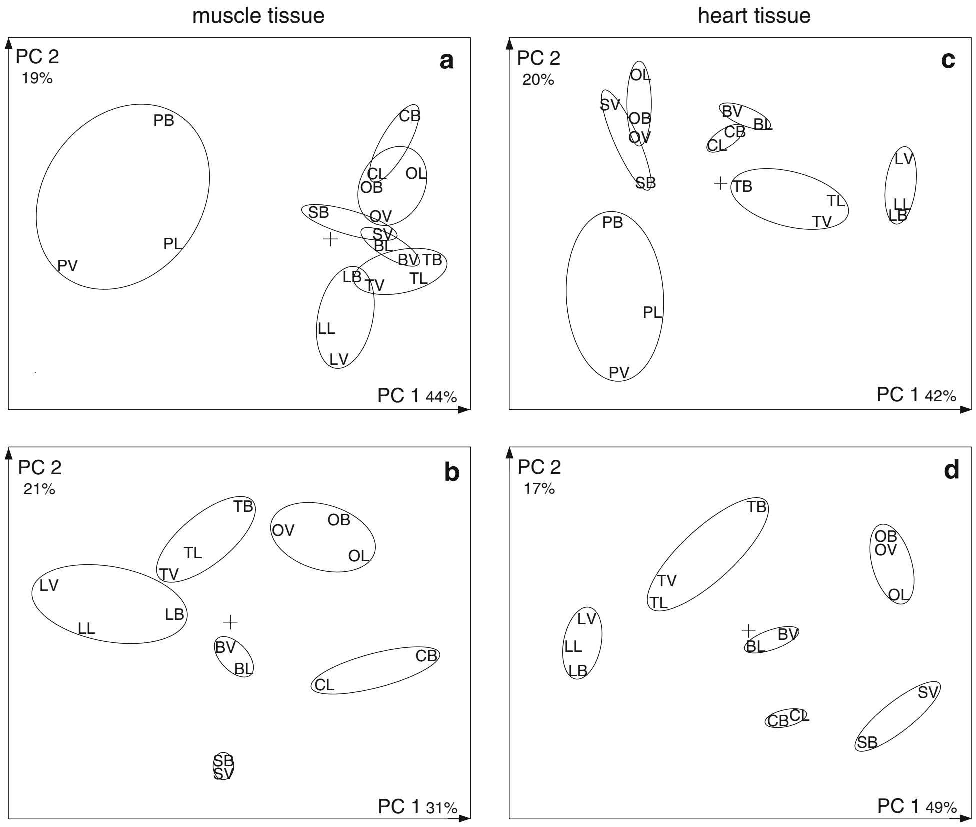

Fig. 2 PC-plots of the average samples of fish from the respective species and locations based on the 14 most abundant FAs. The *first letter* in the code indicates the species: *L L. niloticus*, *O O. niloticus*, *P P. aethiopicus*, *C C. gariepinus*, *S S. victoriae*, *B B. docmas*, *T T. zilli.* The *second letter* indicates the location where they were caught: *V* Napoleon Gulf in Lake Victoria, *B* Bukungu at Lake Kyoga, *L* Lwampanga at Lake Kyoga. **a** muscle tissue with all species, **b** muscle tissue without *P. aethiopicus*, **c** heart tissue with all species, **d** heart tissue without *P. aethiopicus.* The percentage of the total variation among the samples along each of the two PC's is given

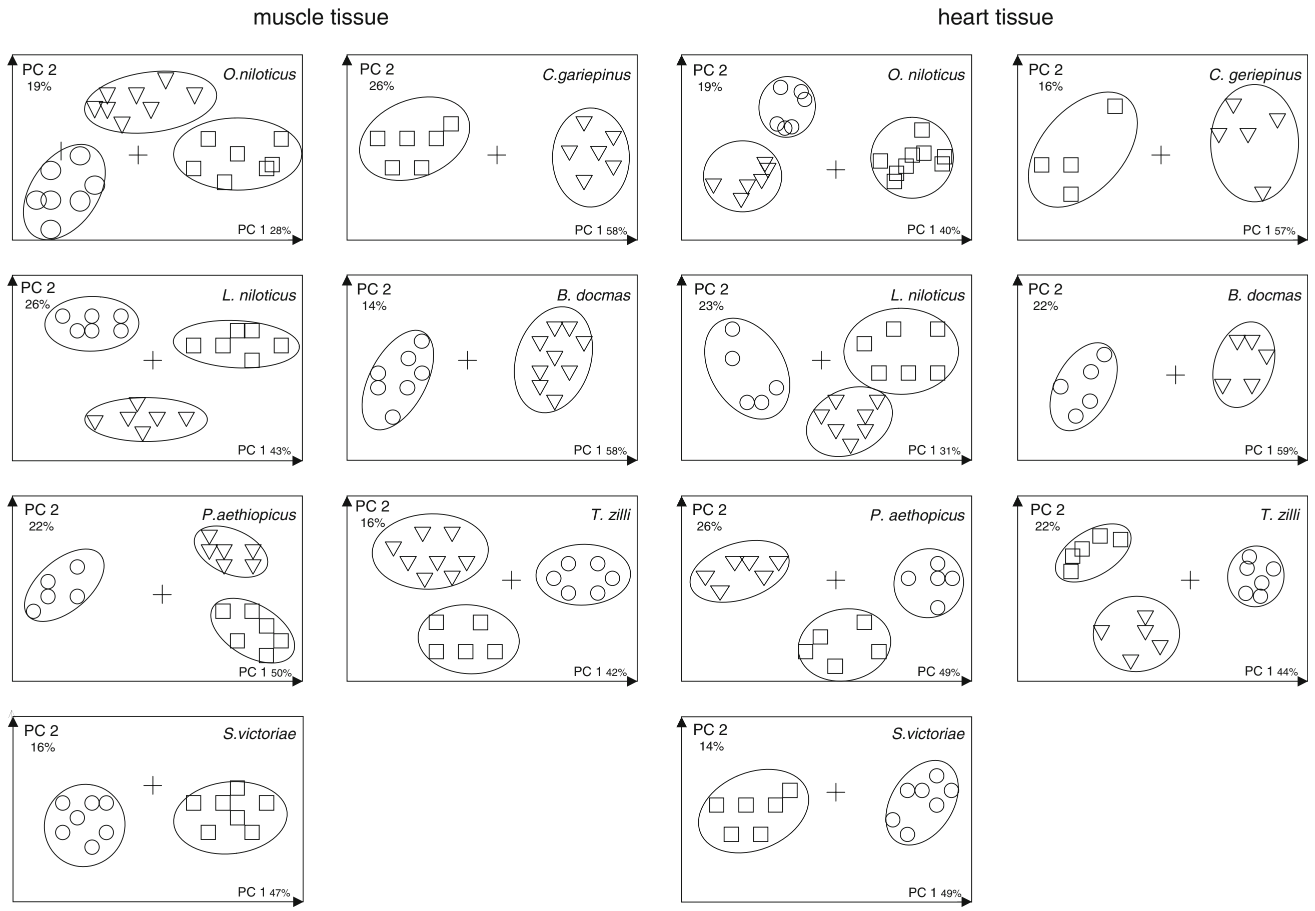

Fig. 3 PC-plots based on 35 FAs of samples of muscle tissue and heart tissue from each fish from each location: *triangles* Lwampanga at Lake Kyoga, *circles* Napoleon Gulf in Lake Victoria, *squares* Bukungu at Lake Kyoga. The percentage of the total variation among the samples along each of the two PC's is given

FA contents of the herbivorous *O. niloticus* in five Ethiopian lakes. They concluded that the FA content reflects the food quality of the fish feed, indicating that the statement "You are what you eat" applies particularly well to herbivores. They maintained that a species specific FA pattern can hardly be detected.

However, some doubts about how important the diet is for the composition of the FAs in the tissues have recently been expressed. Bahurmiz and Ng [29] state that the deposition of FAs in the fillet of red hybrid tilapia was influenced primarily by the FA composition of the experimental diets. Still, they found that the concentrations of 16:0 were generally high in the fillet regardless of dietary treatments, and that total MUFA were maintained somewhat constant at 33–37%. Ng et al. [30] have found a relatively uniform concentration of 16:0 in Nile tilapia despite being fed diets with a difference of about 20% in the level of this FA. They also found high levels of DHA even with low levels in the experimental diet, i.e. 20% vs. 5%. Ng et al. [31] fed tilapia palm oil-based diets with 47% and 76%, respectively, of SAFA but did not detect a significant increase in the deposition of SAFA in fish muscle compared to fish fed a cod-liver oil based diet with 16% SAFA. Other researchers have also found that dietary SAFA tend to be incorporated into fish fillets within narrowly defined physiological levels. Francis et al. [32] found no correlation between the amount of SAFA in the diet and the SAFA in the fillet of Murray cod. Olsen et al. [33] have shown that tilapias have the ability to bio-convert C18 FA to highly unsaturated FA. The FA content of the food had slightly influenced the FA content of the dorsal muscle tissue of Nile tilapia [10]. The dominance of long-chained PUFA in the fish tissue, particularly DHA which was absent in both the algal and commercial diets (the control), indicated that the elongation and desaturation enzymes were very effective in the herbivorous *O. niloticus*. The temperature had little influence on the PUFA content of *O. niloticus*. These researchers, contrary to their earlier anticipations [8, 13], now state that *Oreochromis* seems to have a rather great capacity to modify FA, found in algal food, into their own species specific FA pattern.

Table 4 The average relative distance of the fish from each species from all sites expressed as residual standard deviations (RSD) to the respective statistical models

Models based on muscle tissue

	O. niloticus $\mathrm{RSD}_{\max} = 1.10$ $N = 24(5,1)$	*L. niloticus* $\mathrm{RSD}_{\max} = 0.91$ $N = 15(2,0)$	*P. ethiopicus* $\mathrm{RSD}_{\max} = 0.82$ $N = 17(1,0)$	*S. victoriae* $\mathrm{RSD}_{\max} = 0.85$ $N = 13(0,0)$	*C. gariepinus* $\mathrm{RSD}_{\max} = 1.00$ $N = 11(2,0)$	*B. docmas* $\mathrm{RSD}_{\max} = 0.90$ $N = 17(2,0)$	*T. zilli* $\mathrm{RSD}_{\max} = 1.04$ $N = 19(2,3)$
O. niloticus	**0.89 ± 0.21**	2.19 ± 0.54	3.15 ± 1.20	2.82 ± 0.56	2.45 ± 0.32	1.59 ± 0.16	1.85 ± 0.83
L. niloticus	2.22 ± 0.53	**0.74 ± 0.12**	4.32 ± 1.04	2.78 ± 0.73	3.23 ± 0.53	2.07 ± 0.28	2.79 ± 1.71
P.aethiopicus	1.93 ± 0.33	2.30 ± 0.33	**0.66 ± 0.18**	2.44 ± 0.38	1.62 ± 0.11	1.92 ± 0.30	1.90 ± 0.30
S. victoriae	2.41 ± 0.41	2.04 ± 0.52	5.13 ± 2.51	**0.41 ± 0.09**	2.50 ± 0.24	2.14 ± 0.42	3.01 ± 2.07
C.gariepinus	3.11 ± 0.75	3.99 ± 1.02	4.30 ± 1.51	2.43 ± 0.42	**0.80 ± 0.22**	2.85 ± 0.62	3.60 ± 0.83
B. docmas	3.61 ± 0.99	4.18 ± 1.13	9.04 ± 3.80	4.28 ± 0.67	3.21 ± 0.40	**0.73 ± 0.14**	3.73 ± 1.05
T. zilli	1.55 ± 0.33	1.91 ± 0.41	3.05 ± 0.80	2.38 ± 0.32	2.11 ± 0.18	1.68 ± 0.33	**0.85 ± 0.17**

Models based on heart tissue

	O. niloticus $\mathrm{RSD}_{\max} = 1.09$ $N = 21(2,1)$	*L. niloticus* $\mathrm{RSD}_{\max} = 1.20$ $N = 16(2,0)$	*P. aethiopicus* $\mathrm{RSD}_{\max} = 0.82$ $N = 15(2,0)$	*S. victoriae* $\mathrm{RSD}_{\max} = 1.02$ $N = 13(2,0)$	*C. gariepinus* $\mathrm{RSD}_{\max} = 0.87$ $N = 10(4,0)$	*B. docmas* $\mathrm{RSD}_{\max} = 1.10$ $N = 9(1,0)$	*T. zilli* $\mathrm{RSD}_{\max} = 1.03$ $N = 14(3,0)$
O. niloticus	**0.89 ± 0.19**	2.58 ± 0.24	3.54 ± 1.33	4.35 ± 0.33	2.03 ± 0.68	2.49 ± 0.74	2.01 ± 0.32
L. niloticus	6.01 ± 1.40	**0.98 ± 0.22**	8.62 ± 3.12	6.65 ± 0.84	3.53 ± 1.23	3.52 ± 0.58	3.64 ± 1.53
P.aethiopicus	1.83 ± 0.34	3.12 ± 0.28	**0.66 ± 0.17**	3.37 ± 0.48	2.12 ± 0.34	3.09 ± 0.96	2.22 ± 0.37
S. victoriae	3.87 ± 1.20	4.64 ± 0.48	4.81 ± 1.27	**0.83 ± 0.16**	3.57 ± 0.52	3.79 ± 1.43	3.84 ± 0.44
C.gariepinus	2.94 ± 0.66	3.28 ± 0.54	6.44 ± 2.65	2.70 ± 0.33	**0.65 ± 0.30**	2.79 ± 1.00	2.98 ± 0.51
B. docmas	3.52 ± 2.00	2.73 ± 0.35	3.37 ± 0.88	3.54 ± 0.49	2.42 ± 0.53	**0.86 ± 0.18**	2.70 ± 0.32
T. zilli	1.66 ± 0.44	2.13 ± 0.21	2.76 ± 0.76	2.94 ± 0.40	2.08 ± 0.46	2.87 ± 1.38	**0.83 ± 0.20**

Maximum allowed distances of the models based on 95% confidence limits, are given as $\mathrm{RSD}_{\max}$. Averages which fall within a model are shown in bold. The first number in parentheses after the total number of fish for each species indicates the number of fish which do not fall into their own model, i.e. nonclassifed. The second number in the parentheses indicates the number of fish which fall into both their own model and into another model, i.e. biclassified

The seven species we have studied belong to six families (Fig. 4) with 270 genera and more than two thousand species and numerous undescribed forms. A fast emergence of morphological changes and new species has been observed in Lake Victoria [34]. These fish are also rather stationary, e.g. *Tilapia spp*. movements in Lake Victoria were typically short (<1 km), and there were no systematic shifts in centres of gravity of populations [35]. The East African lakes contain closely spaced patches of habitat [36]. This may lead to different patterns of gene expression, i.e. differences in the transcriptomes, among the various populations [37], resulting in differences in the FA composition of the membrane lipids.

There is poor correlation between feeding habits of the fish species and FA composition of their tissues. This may infer that there is a low dietary effect on the FA composition. For example *T. zilli*, feeding on higher plants and bottom deposits and *L. niloticus* feeding primarily on fish, Table 1, have the smallest difference in FA composition (Fig. 5). *O. niloticus*, with algal and plant material as the major food items, is grouped together with *C. gariepinus,* which are omnivorous, feeding mostly on insects and small fishes (Fig. 5).

The marbled lungfish, *P. aethiopicus*, belongs, according to the traditional morphologically based classification, to a different class than all the six other species (Fig. 4). The classification based on FA composition of the white muscle tissue shows the same distinction (Fig. 5). The further classsification of three catifsh species in one order, Siluriformes, and the three others in a different order, namely Perciformes, (Fig. 4) is, however, not paralleled by the FA classification (Fig. 5). Here the cichlid Nile tilapia is grouped together with the two catfish species *S. victoriae* and *C. gariepinus*, and the catfish *B. docmas* is grouped together with the two Perciformes *T. zilli* and *L. niloticus*. As discussed above, this deviation from the traditional classification cannot be explained by differences/similarities in diet.

The fish species studied here are very lean having between 2 and 6 mg total FAs per gram of muscle tissue, average 3.4 mg/g. This means that there are only small amounts of storage lipids and then mostly membrane lipids

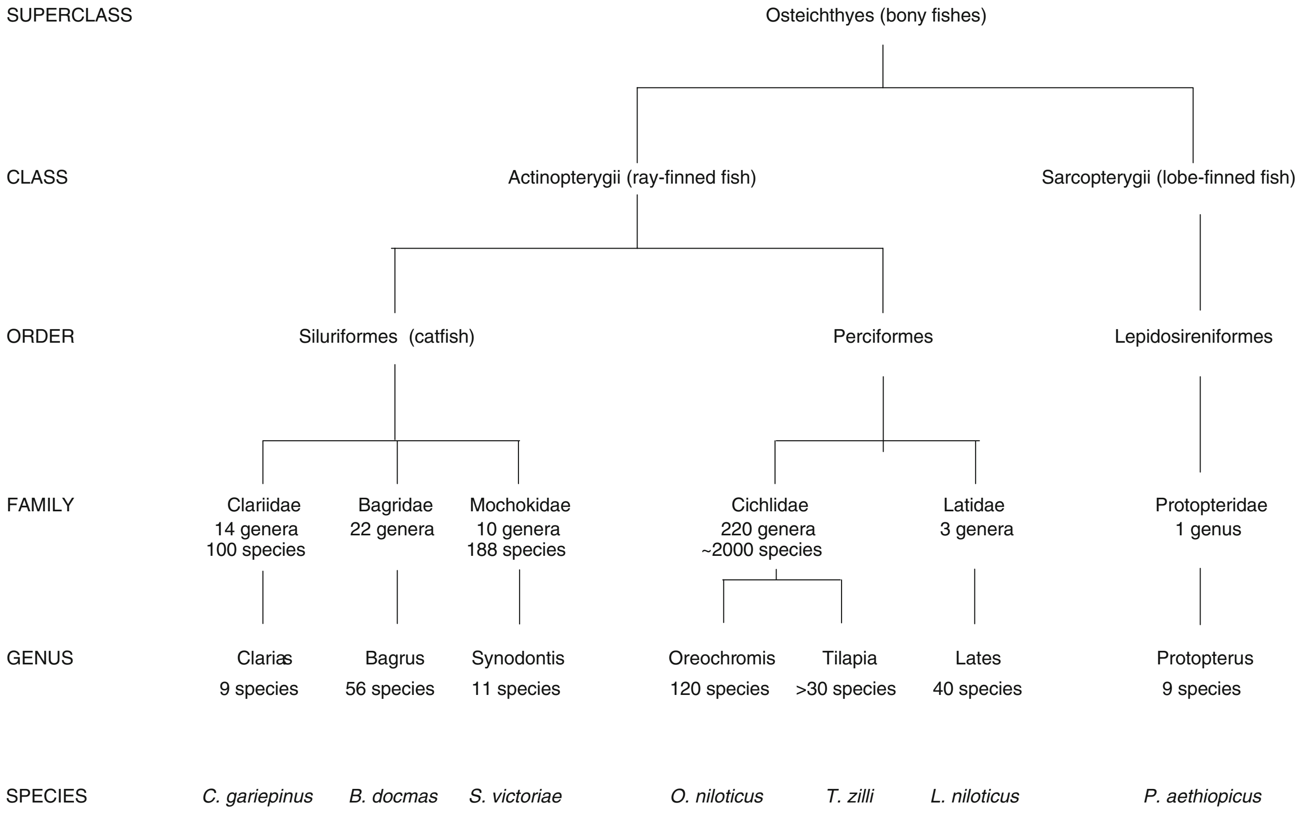
SUPERCLASS
Osteichthyes (bony fishes)
CLASS
Actinopterygii (ray-finned fish)
Sarcopterygii (lobe-finned fish)
ORDER
Siluriformes (catfish)
Perciformes
Lepidosireniformes
FAMILY
Clariidae
14 genera
100 species
Bagridae
22 genera
Mochokidae
10 genera
188 species
Cichlidae
220 genera
~2000 species
Latidae
3 genera
Protopteridae
1 genus
GENUS
Clarias
9 species
Bagrus
56 species
Synodontis
11 species
Oreochromis
120 species
Tilapia
>30 species
Lates
40 species
Protopterus
9 species
SPECIES
C. gariepinus
B. docmas
S. victoriae
O. niloticus
T. zilli
L. niloticus
P. aethiopicus

Fig. 4 Classification of the seven species according to Greenwood [20] and Okaronon et al. [57]. The numbers of genera and species are obtained from Wikipedia

Fig. 5 Hierarchical cluster analysis of average samples of fish from the respective species and locations. The clustering is based on the 14 FAs present at the highest levels in the muscle samples. Five principal components were determined, describing 91% of the total variation among the samples, and the Euclidean distances between the samples positioned in the 5D space was the basis for the cluster analysis. The codes are explained in Fig. 2

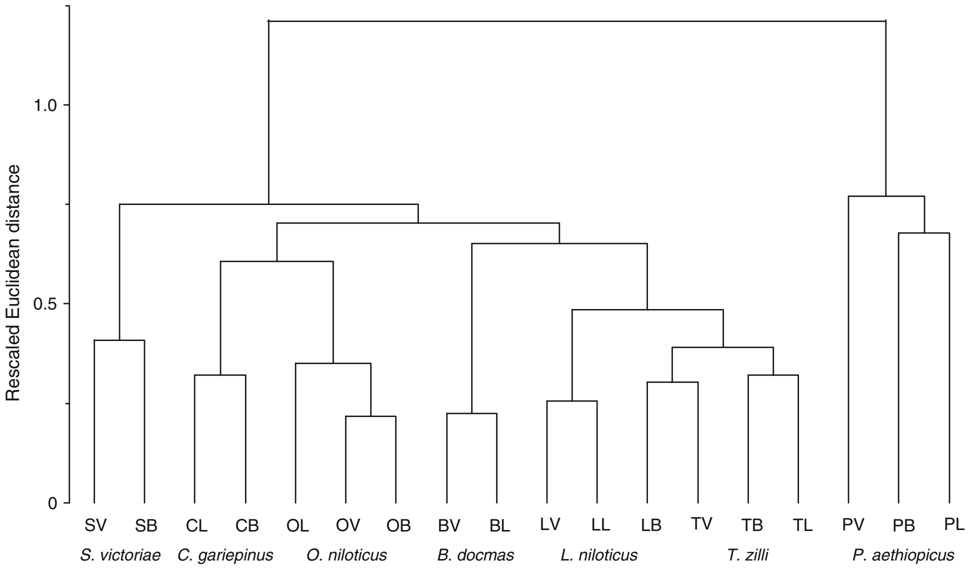

in the cells. The general assumption is that the FA composition of the neutral, storage lipids reflect trophic influences much better than the physiologically more important phospholipids [38]. The formation of the phospholipids of the membranes are subjected to genetic control [39]. This suggests that the species differences in FA composition (Fig. 4) are genetically determined. Furthermore, it suggests that the observed differences within the species among fish from the different locations (Fig. 3) are also of genetic character and not results of differences in foraging strategy.

The lipid level in the heart tissue is about five times higher than in the muscle tissue, i.e. with an average content of total FAs of 15.5 mg/g tissue, spanning from 7 to 29 mg/g

(Tables 2 and 3). There is no correlation between the total FA content of the muscle and heart tissues from fishes from the various species/locations. The cells in the heart tissue do not contain storage lipids. They are much smaller than the cells in white muscle tissue, about one fifth in diameter, and contain many more mitochondria than the muscle cells [40]. Therefore there are much larger amounts of membrane lipids on a tissue weight basis in the heart. This explains the higher levels of total FAs.

There is also a qualitative difference between the lipids in the heart and white muscle cells, with a different FA composition, i.e. lower levels of SAFA and higher levels of MUFA, but about the same levels of PUFA. Within the PUFA there are less n-3 and more n-6 FAs in the heart tissue, giving an average n-3/n-6 ratio of 1.0 ± 0.4, that is significantly, $P < 0.01$ (student's *t*), lower than the ratio in the muscles, 1.7 ± 0.7. The large difference in FA composition between the polar lipids of the heart and white muscles emphasizes the low importance of the dietary lipids on the composition of the FA in the tissues.

The n-3/n-6 ratios are typical for freshwater fish, where the ratio lies in the interval 0.5–3.8, compared to the interval 4.7–14.4 for marine fish [4]. From a nutritional point of view the ratio is close to the recommended ideal value of between 0.5 and 1 [41]. However, these species are so lean that it will be impossible to cover the daily recommended intake of 500 mg 20:5n-3 and 22:6n-3 by eating fish alone [42].

Cholesterol

As a natural component of membranes, regulating their fluidity, cholesterol is found in all tissues. The method of direct methanolysis of tissue samples used in the present investigation allows for quantitative determination of cholesterol since the cholestdiene derivatives that are formed during workup and chromatographic procedure are detected in the gas chromatograph [25]. We found between 30 and 60 mg cholesterol per 100 g muscle tissue with an average of 46 mg/100 g. The few data available on freshwater fish show approximately the same values: Three Brazilian farmed freshwater species were reported by Moreira et al. [43] to contain approximately 50 mg/100 g. Francis et al. [44] found approximately 60 mg/100 g, and Siddhuraju and Becker [45] approximately 70 mg/100 g cholesterol in Nile tilapia in feeding experiments. Piironen et al. [46] found cholesterol contents in the range 50–100 mg/100 g of the edible parts of fish from Finnish waters. Mathew et al. [47] found between 22 and 148 mg/100 g cholesterol in 97 species of Indian fish with the majority between 45 and 65 mg/100 g. In the freshwater species the cholesterol content was found to be lower than in their marine counter-parts. This is in contrast to Oehlenschläger [48], who reported that the cholesterol content of the edible part of freshwater fish was found to be generally higher than the cholesterol content of marine fish species. Our results tend to support the finding of a lower level of cholesterol in freshwater fish.

Being largely of interest from a nutritional viewpoint, most cholesterol determinations have been carried out on the edible tissue of fish, and also in liver samples caused by studies of cholesterol synthesis. The present investigation is probably the first report on quantitative determination of cholesterol in fish hearts. It showed about five times higher levels in the heart tissue than in the muscle tissue, i.e. an average of 46 mg/100 g in the muscle tissue and 230 mg/100 g in the heart tissue.

Oehlenschläger [48] showed that the cholesterol content decreased the fattier the fish was. This was explained by the fact that cholesterol is a component of the phospholipids of cell membranes and not of depot fat within the cells, and the number of cells does not increase with an increase in the amount of depot fat. Francis et al. [49], on the other hand, suggested that higher muscle cholesterol content can be related to higher carcass lipid content. Both cholesterol and FA levels are five times higher in the heart than in the muscle tissue in the present case. This shows that the lipids in these tissues are predominantly phospholipids. In the heart tissue, where the levels are highest, the correlation between cholesterol and total FAs was fair, i.e. $R^2 = 0.75$, $P = 7 \times 10^{-6}$, but in the muscle tissue the correlation was poorer, $R^2 = 0.29$, $P = 0.025$.

Cholesterol has earlier been qualitatively determined in heart tissue from cod, where it was important for the discrimination between two populations [24]. It therefore appears that the tissue level of cholesterol may be genetically controlled. Genetic control of the cholesterol content was also suggested by Mathew et al. [47] who found significant differences among families of Indian fish. The variations detected here may therefore be species and population dependent.

Plasmalogens

The phospholipids in membranes normally have two FAs esterified to the glycerol molecule with the phosphoric acid moiety esterified in the third position. However, a substantial portion of the phospholipids have an alkyl chain with 16 or 18 carbons bound by a vinyl ether bond to the first position of the glycerol backbone. These alkenyl-acyl-phospholipids are called plasmalogens and are present in all tissues [51]. They were first detected in marine organisms in 1960 [53].

The plasmalogens are unstable towards acid [51]. Under the conditions we use for methanolysis of the tissue lipids, the vinyl ether group is cleaved to give an aldehyde which is methanolysed to a dimethyl acetal. They are gas chromatographed together with the FAMEs, although some loss of methanol occurs in the injector, giving methyl alkenyl ethers, which also give nice peaks in the chromatogram [52]. The plasmalogens make out 7–8% of the amount of total FAs (Tables 2 and 3), with about five times as much in the heart tissue as in the muscle tissue. The higher amount in heart tissue correlates with the higher amount of phospholipids, measured as total FAs.

There are few reports on plasmalogens in freshwater fish. They have been studied in carp, *Cyprinus carpio*, and rainbow trout, *Oncorhynchus mykiss* [55, 56]. They are structural components of cell membranes, reducing their fluidity, and may have a number of other functions. When the environmental temperature is increased membrane permeability can be expected to increase and the plasmalogens can be raised to regulate this phenomenon. Kraffe et al. [54] found that total plasmalogen increased in warm acclimated rainbow trout, which might explain the relatively high values in fish from the tropical waters of lakes Victoria and Kyoga.

In the present investigation we have found large differences in FA composition of muscle and heart tissue among seven tropical freshwater fish species. We have demonstrated that the FA compositions are species specific and appear to be independent of the dietary intake, thus questioning the traditional view on the important dietary impact. The fish appear to belong to local populations as manifested by systematic differences in the tissue FA composition. We have shown how cholesterol and plasmalogens can be determined simultaneously with the FA by our analytical method of acid catalysed transesterification followed by gas chromatography.

References

1. Ogutu-Ohwayo R, Wandera SB (2002) The fishes and fisheries of Uganda: their Biology, Ecology, Exploitation and Management. NARO – FIRRI Report, p 1–9.
2. MAAIF (2003) Report on information on fisheries management in Uganda December 2003. Annual Fish Production 2001. Ministry of Agriculture, Animal Industry and Fisheries, Department of Fisheries Resources, Uganda, p 3
3. OECD (2006) Africa economic outlook, Uganda AfDB/OECD 2006 report p 511
4. Henderson RJ, Tocher DR (1987) The lipid composition and biochemistry of freshwater fish. Prog Lipid Res 26:281–347
5. Linares F, Henderson RJ (1991) Incorporation of 14C-labelled polyunsaturated fatty acids by juvenile turbot, *Scophthalmus maximus* (L.), in vivo. J Fish Biol 38:335–347
6. Zenebe TG, Ahlgren G, Boberg M (1998) Fatty acid content of some freshwater fish of commercial importance from tropical lakes in the Ethiopian Rift Valley. J Fish Biol 53:987–1005
7. Ng W-K, Tocher DR, Bell JG (2007) The use of palm oil in aquaculture feeds for salmonid species. Eur J Lipid Sci Technol. 109:394–399
8. Tocher DR, Agaba M, Hastings N, Bell JG, Dick JR, Teale AJ (2002) Nutritional regulation of hepatocyte fatty acid desaturation and polyunsaturated fatty acid composition in zebrafish (*Danio rerio*) and tilapia (*Oreochromis niloticus*). Fish Physiol Biochem 24:309–320
9. Kuusipalo L, Käkelä R (2000) Muscle fatty acids as indicators of niche and habitat in Malawian cichlids. Limnol Oseanogr 45:996–2000
10. Zenebe TG, Boberg M, Sonesten L, Ahlgren G (2003) Effects of algal diets and temperature on the growth and fatty acid content of the cichlid fish *Oreochromis niloticus* L. A laboratory study. Aquatic Ecol 37:169–182
11. Kwetegyeka J, Mpango G, Grahl-Nielsen O (2006) Fatty acid composition of muscle and heart tissue of Nile perch, Lates niloticus, and Nile tilapia, *Oreochromis niloticus*, from various populations in Lakes Victoria and Kyoga, Uganda. Afri J Aquat Sci 31:297–304
12. Grahl-Nielsen O (2004) Fatty acid profiles as natural marks for stock identification. In: Cadrin SX, Friedland KD, Waldman JR (eds) Stock identification methods. Academic Press, NY, pp 239–261
13. Zenebe T, Ahlgren G, Gustafsson I-G, Boberg G (1998) Fatty acid and lipid content of *Oreochromis niloticus* L. in Ethiopian lakes—dietary effects of phytoplankton. Ecol Freshw Fish 7:146–158
14. Njiru M, Okeyo-Owuor JB, Muchiri M, Cowx IG (2004) Shifts in the food of Nile tilapia, *Oreochromis niloticus* (L.) in Lake Victoria, Kenya. Afr J Ecol 42:163–170
15. Getabu A (1994) A comparative study on the feeding habits of *Oreochromis niloticus* (Linnaeus) in Nyanza Gulf, Lake Victoria and sewage fish ponds. In: Okemwa E, Wakwabi EO, Getabu A (eds) Proceedings of the 2nd EEC Regional Seminar on Recent Trends of Research on Lake Victoria Fisheries. ICIPE Science, Nairobi, pp 93–103
16. Balirwa J S (1998) Lake Victoria wetlands and the ecology of the Nile Tilapia, *Oreochromis niloticus.* PhD Thesis. Agric. University, Wageningen. Published as a book with 9 chapters. A. Balkema, Rotterdam, NL; Brookfield, 247 pp ISBN 90–95104112
17. Mkumbo OC, Ligtvoet W (1992) Changes in the diet of Nile perch, *Lates niloticus* (L.) in the Mwanza Gulf, Lake Victoria. Hydrobiologia 232:79–83
18. Mbabazi D, Ogutu-Ohwayo R, Wandera SB, Kiziito Y (2004) Fish species and trophic diversity of haplochromine cichlids in the Kyoga satellite lakes (Uganda) African. J Ecol 42:59–68
19. Rinne JN, Wanjala B (1983) Maturity, fecundity and breeding seasons of the major catfishes (Suborder: Siluroidae) in Lake Victoria East Africa. J Fish Biol 23:357–363
20. Greenwood PH (1958) The fishes of Uganda. The Uganda Society, Kampala, p 124
21. Kvalheim OM, Karstang TV (1987) A general purpose program for multivariate data analysis. Chemometr Intell Lab Syst 2:235–237
22. Wold S, Sjostrom S (1977) SIMCA: a method for analyzing chemical data in terms of similarity and analogy. In: Kowalski BR (ed) Chemometrics: theory and applications, vol 52, American Chemical Society Symposium Series, pp 243–282
23. Wold S (1978) Cross validation estimation of the number of components in factor and principal models. Technometrics 20:397–406
24. Joensen H, Steingrund P, Fjallstein I, Grahl-Nielsen O (2000) Discrimination between two reared stocks of cod (*Gadus morhua*) from the Faeroe Islands by chemometry of the fatty acid composition in the heart tissue. Mar Biol 136:573–580
25. Meier S, Mjøs S, Joensen H, Grahl-Nielsen O (2006) Validation of a one-step extraction/methylation method for determination of fatty acids and cholesterol in marine tissues. J Chromatogr A 1104:291–298

26. Ahlgren G, Blomquist P, Boberg M, Gustafsson I-B (1994) Fatty acid content of the dorsal muscle—an indicator of fat quality in freshwater fish. J Fish Biol 45:131–157
27. Steffens W (1997) Effect of variation in essential fatty acid in fish feeds on nutritive value of freshwater fish for humans. Aquaculture 151:97–119
28. Justi KC, Hayashi C, Visentainer JV, de Souza NE, Matsushita M (2003) The influence of feed supply time on the fatty acid profile of Nile tilapia (*Oreochromis niloticus*) fed on a diet enriched with n-3 fatty acids. Food Chem 80:489–493
29. Bahurmiz OM, Ng W-K (2007) Effects of dietary palm oil source on growth, tissue fatty acid composition and nutrient digestibility of red hybrid tilapia *Oreochromis* sp., raised from stocking to marketable size. Aquaculture 262:382–392
30. Ng W-K, Koh C-B, Din ZB (2006) Palm oil-laden spent bleaching clay as a substitute for marine fish oil in the diets of Nile tilapia, *Oreochromis niloticus*. Aquac Nutr 12:459–468
31. Ng W-K, Lim P-K, Sidek H (2001) The influence of a dietary lipid source on growth, muscle fatty acid composition and erythrocyte osmotic fragility of hybrid tilapia. Fish Physiol Biochem 25:301–310
32. Francis DS, Turchini GM, Jones PL, DeSilva SS (2006) Effects of dietary oil on growth and fillet fatty acid composition of Murray cod, *Maccullochella peelii peelii*. Aquaculture 253:547–556
33. Olsen RE, Henderson RJ, McAndrew BJ (1990) The conversion of linoleic and linolenic acid to longer chain polyunsaturated fatty acids by Tilapia (*Oreochromis nilotecus*) in vivo. Fish Physiol Biochem 8:261–277
34. Witte F, Wanink JH, Kishe-Machumu M (2007) Species distinction and biodiversity crisis in Lake Victoria. Trans Am Fish Soc 136:1146–1159
35. Rinne JN, Wanjala B (1982) Observations on movement patterns of Tilapia spp. in Nyanza Gulf, Lake Victoria, East Africa. J Fish Biol 20:317–322
36. Markert JA, Danley PD, Arnegard ME (2001) New markers for new species: microsatellite loci and the East African ciclides. Trends Ecol Evol 16:100–107
37. Liu ZJ (2007) Fish genomics and analytical genetic technologies, with examples of their potential applications in management of fish resources. In: Bartley DM, Harvey BJ, Pullin RSV (eds) FAO Fisheries Proceedings 5. Workshop on status and trends in aquatic genetic resources. FAO Rome 2007, ISBN 978-92-5-105818-3
38. Dalsgaard J, St. John M, Kattner G, Müller-Navarra D, Hagen W (2003) Fatty acid trophic markers in the pelagic marine environment. Adv Mar Biol 46:225–340
39. Olsen Y (1999) Lipids and essential fatty acids in aquatic food webs: What can freshwater ecologists learn from mariculture? In: Arts MT, Wainman BC (eds) Lipids in freshwater ecosystems. Springer, New York, pp 161–202. ISBN 0-387-98505-0
40. Bone Q, Marshall NB, Blaxter JHS (1995) Biology of fishes. Blackie, London
41. Simopoulos AP, Leaf A, Salem N (1999) Essentiality and recommended dietary intakes for omega-6 and omega-3 fatty acids. Ann Nutr Metabol 43:127–130
42. ISSFAL (2004) International society for the study of fatty acids and lipids. Report on dietary intake of essential fatty acids. Recommendations for intake of polyunsaturated fatty acids in healthy adults. June 2004, p7
43. Moreira AB, Visentainer JV, de Souza NE, Matsushita M (2001) Fatty acids and cholesterol contents of three Brazilian *Brycon* freshwater fishes. J Food Compost Anal 14:565–574
44. Francis G, Levavi-Sivan B, Avitan A, Becker K (2002) Effects of long term feeding of *Quillaja* saponins on sex ratio, muscle and serum cholesterol and LH levels in Nile tilapia (*Oreochromis niloticus* (L.). Comp Biochem Physiol C 133:593–603
45. Siddhuraju P, Becker K (2003) Comparative nutritional evaluation of differentially processed mucuna seeds (*Mucuna pruriens* (L.) DC. var. *utilis* (Wall ex Wight) Baker ex Buck) on growth performance, feed utilization and body composition in Nile tilapia (*Oreochromis niloticus* L.). Aquac Res 34:487–500
46. Piironen V, Toivo J, Lampi A-M (2002) New data for cholesterol contents in meat, fish, milk, eggs and their products consumed in Finland. J Food Compost Anal 15:705–713
47. Mathew S, Ammu K, Nair PGV, Devadasan K (1999) Cholesterol content of Indian fish and shellfish. Food Chem 66:455–461
48. Oehlenschläger J (2006) Cholesterol content in seafood, data from the last decade A: review. In: Luten JB, Jacobsen C, Bekaert K, Saebø A, Oehlenschläger J A (eds) Seafood research from fish to dish. Wageningen Academic Publishers, Wageningen, pp 41–57
49. Francis G, Makkar HPS, Becker K (2001) Effects of *Quillaja* saponins on growth, metabolism, egg production and muscle cholesterol in individually reared Nile tilapia (*Oreochromis niloticus*). Comp Biochem Physiol C 129:105–114
50. Ackman RG (1999) Comparison of lipids in marine and freshwater organisms. In: Arts MT, Wainman BC (eds) Lipids in freshwater ecosystems. Springer, New York, pp 263–298. ISBN 0-387-98505-0
51. Chapelle S (1987) Plasmalogens and *O*-alkylglycerophospholipids in aquatic animals. Comp Biochem Physiol B 88:1–6
52. Brosche T, Platt D, Vostorowsky O (1985) Methyl enol ethers as artefacts in capillary gas chromatographic profiles of aldehyde dimethyl acetals. J Chromatogr 345:219–227
53. Yamaguchi T, Miyamoto K, Yagi S, Horigane A, Sato M, Takeuchi M (2000) Detection of plasmalogen from plasma low density lipoprotein in carp, *Cyprinus carpio*, and rainbow trout, *Oncorhynchus mykiss*. Comp Biochem Physiol A 127:339–346
54. Kraffe E, Marty Y, Guderley H (2007) Changes in mitochondrial oxidative capacities during thermal acclimation of rainbow trout *Oncorhynchus mykiss*: roles of membrane proteins, phospholipids and their fatty acid compositions. J Exp Biol 210:149–165
55. Okaronon JO, Katunzi EF B, Asila (1997) Fish species identification guide for Lake Victoria. Lake Victoria Research Project Phase II. Sept 1997, Kampala pp 39

EPA	Eicosapentaenoic acid
HAM-D	Hamilton Depression Rating Scale
JBD	Juvenile bipolar disorder
LCn-3PUFA	Long-chain omega-3 polyunsaturated fatty acid
MDD	Major depressive disorder
TMRS	Tripartite Mood Rating Scale
YMRS	Young Mania Rating Scale

Introduction

The diagnosis of juvenile bipolar disorder (JBD) in children and adolescents is becoming increasingly well accepted in research literature and by clinicians [1, 2]. The lifetime prevalence of JBD is approximately 1% during adolescence and 2% during young adulthood [3, 4], similar to that found in adults [5]. On average there is a 10–15 year delay between the time that patients report having symptoms of JBD until their diagnosis and treatment which suggests that patients with JBD may have had the disease for many years, when they were children or adolescents, prior to treatment [6].

There is growing evidence that a deficiency in long-chain omega-3 polyunsaturated fatty acids (LCn-3PUFA) may be involved in the aetiology of bipolar disorder (BD) and major depressive disorder (MDD). The rate of fish consumption in western diets is negatively related to the occurrence of BD [7] and MDD [8]. Red blood cell (RBC) membrane concentrations of docosahexaenoic acid (DHA) are reportedly lower in adults with BD [9] and plasma eicosapentaenoic acid (EPA) [10] and DHA [11] lower in adults with MDD compared with normal controls. Although lower concentrations of LCn-3PUFA have been reported in adults, no past studies have examined blood concentrations of LCn-3PUFA in JBD.

One of the main criticisms of studies examining blood concentrations of LCn-3PUFA has been a lack of control for LCn-3PUFA intake [12]. Intake of LCn-3PUFA is closely related to blood concentrations of LCn-3PUFA, with plasma phospholipid concentrations representing intake over the last 1–2 weeks [13] and RBC concentrations reflecting intake in the previous 14–120 days [14].

The present study is the first to assess LCn-3PUFA intake and blood concentrations in children and adolescents with JBD compared with healthy controls. It was predicted that blood concentrations of LCn-3PUFA would be significantly lower in children and adolescents diagnosed with JBD compared with healthy controls after controlling for family socio-economic status (SES) and LCn-3PUFA intake.

Materials and Methods

All experimental procedures were approved by the Hunter New England Area Health Service Research Ethics Committee and the University of Newcastle Human Research Ethics Committee. The study was conducted with cognisance of the following principles and guidelines: the Declaration of Helsinki [15, 16]; the National Statement on Ethical Conduct in Research Involving Humans [17] and the International Committee of Harmonisation Good Clinical Practice (GCP) guidelines [18]. All participants' parents/guardians gave written informed consent and participants gave informed assent prior to inclusion in the study. The study was also registered with the Australian Clinical Trials Registry (http://www.actr.org.au) ACTRN: ACTRN012606000440527.

Participants

Participants with JBD were referred to The Bipolar Program (Hunter New England Area Health Service) and assessed prior to study admission through a clinical interview by a clinical psychologist and child and adolescent psychiatrist and during a structured interview using the Washington University at St Louis Schedule for Affective Disorders and Schizophrenia (WASH-U-K-SADS) [19]. One of the authors (TH) had been trained to administer and interpret this instrument. Psychological histories were obtained from the young person as well as their parent or carer.

Participants with JBD were included in the study if they satisfied the following criteria: met diagnostic criteria for either BD I, BD II or BD Not Otherwise Specified (BD NOS) as specified in the DSM-IV-TR [20]; had an episode of mania, hypomania, mixed mania or major depression in the preceding 6 months; were currently being prescribed a mood stabiliser, an atypical antipsychotic or a combination of both medications and were stabilised for at least 4 weeks prior to the study; and were aged between 8 and 18 years. Participants were excluded if they had a primary medical or neurological cause of their mood disorder or had a comorbid diagnosis of Autistic Spectrum Disorder or clinically evident mental retardation.

Participants were not excluded if they had a co-morbid substance abuse, as comorbidity can be up to 17.6% [21]. Substance induced hypomania was not an exclusion criteria [22], as this disorder was automatically excluded when a diagnosis of JBD was confirmed. Inclusion and exclusion criteria took into account previous guidelines [10, 23].

Healthy age and sex-matched controls were recruited from the general community and were excluded if they fulfilled any of the following criteria: had previously been diagnosed with any DSM-IV disorder or JBD according to the WASH-U-K-SADS; had a family history of mental illness in first degree relatives; had ever been prescribed psychotropic medication or had a history of substance abuse.

In addition, participants with JBD or healthy controls were excluded from the study if they satisfied any of the following common criteria: had a diagnosis of a significant medical disorder, such as active hepatic or renal disease, dementia, serious head injury or active cancer, Non-Insulin Dependent Diabetes Mellitus (NIDDM)—type 2 diabetes, cardiovascular, haematological or gastrointestinal disease; had taken fish oil (LCn-3PUFA) as supplements within the previous 6 weeks; were taking medication affecting lipid metabolism, such as HMG-CoA inhibitors or high-dose niacin; were pregnant; had a body mass index (BMI) less than 16 or greater than 30; or finally, were actively consuming a low fat diet.

Measurements

Fasting blood samples were collected on one occasion for analysis of fatty acids. Following collection and separation of plasma by centrifugation, RBC membranes were washed with saline [24] and centrifuged again prior to being frozen at −80 °C pending further analysis. LCn-3PUFA intake was assessed using a Food Frequency Questionnaire (FFQ). Development and preliminary validation of the FFQ will be reported separately.

SES was assessed in all participants by asking parents/guardians about their occupation, highest education level achieved and income [25, 26]. Parental occupation was rated according to the ANU3_2 occupational status scale [27].

Psychological and Behavioural Tests and Observations in Participants with JBD

Psychological measures assessed at the time of blood collection included clinician reported mania (Young Mania Rating Scale, YMRS [4, 28]) parent reported mania (P-YMRS, and clinician reported depression (Hamilton Depression Rating Scale, HAM-D [29]). Overall severity of symptoms (mania and depression) was assessed using the Clinical Global Impressions scale (CGI [30, 31]). Higher scores on these measures represent a higher severity of illness. Global functioning was assessed using the Global Assessment Scale for Children (C-GAS [32]), where a higher score represents a higher level of functioning. The Child Behaviour Checklist (CBCL [33]) was completed by parents or guardians and participant behaviour was self-assessed using The Beck Youth Inventories (BYI [34]). Higher scores on these measures also reflect more severe illness.

Average mood was rated by patients and clinicians on the Tripartite Mood Rating Scale (Client Version [35]), which incorporates a 3-pronged Likert scale for the moods depression, euphoric mania and dysphoric mania (anger), with higher scores representing a worsening of mood.

Fatty Acid Analysis

Total fatty acids were determined in plasma and RBC using the method established by Lepage and Roy [36] and validated for RBC [37]. Briefly, following extraction and methylation of fatty acids using methanol:toluene and acetyl chloride, fatty acids were quantified using a Hewlett Packard Series Gas Chromatograph with a flame ionization detector in comparison to a standard mixture of genuine fatty acid methyl esters (Nu Chek Prep, Elysian, MN USA). Details of the methods have been described previously [38].

Statistical Analysis

Prior to analysis, data were assessed for homoscedasticity and normality assumptions using the Scatterplot and Explore options of the Statistical Package for Social Sciences (SPSS) version 14.0 for Windows [39]. Differences in RBC fatty acid concentrations between groups were analysed using the MIXED Model procedure in the SAS program [40, 41] with subject pair as the individual experimental unit and pair within gender as a random effect. Data were analysed for main effects of group and gender as well as the interaction between main effects. SES and intake of LCn-3PUFA were analysed as co-variates and, where significant, were included in the final model. Psychological test score in participants with JBD were also correlated with plasma and RBC concentrations of LCn3PUFA by Pearson correlation using SPSS.

Results

Fifteen participants with JBD (9 female, mean age = 15.0 ± 0.95 year; 6 male, mean age = 13.6 ± 1.29 year) and fifteen age and sex-matched controls (female mean age = 14.7 ± 1.12 year; male mean age = 13.8 ± 1.30 year) were enrolled in the study. Participants with JBD were diagnosed with BD I ($n = 7$), BD II ($n = 3$) or BD NOS ($n = 5$) and were all receiving mood stabilising medication. No participants had taken LCn-3PUFA supplements within 12 weeks prior to the study.

The reported intake of LCn-3PUFA was significantly lower for participants with JBD compared with healthy controls (Table 1). Prior to adjusting for intake, RBC concentrations of EPA and DHA were significantly lower in participants with JBD compared with healthy controls

Table 1 Mean reported daily intakes of LCn-3PUFA in children and adolescents in Australia diagnosed with JBD compared with healthy controls

LCn-3PUFA[b]	Fatty acid intake (mg/day)[a]		*P*-values
	Control	Bipolar	
EPA	39 (±3)	19 (±3)	<0.001
DPA	31 (±4)	23 (±4)	0.152
DHA	70 (±6)	28 (±7)	<0.001
LCn-3PUFA	139 (±11)	69 (±11)	<0.001

[a] Values are least squares means ± standard error of the least squares mean for 15 age and sex-matched pairs, $n = 6$ males (mean age = 13.6 years) and $n = 9$ females (mean age = 15.0 years)

[b] *EPA* eicosapentaenoic acid (C20:5n-3), *DPA* docosapentaenoic acid (C22:5n-3), *DHA* docosahexaenoic acid (C22:6n-3)

(Table 2). However RBC EPA (r (30) = 0.65, $P < 0.001$) and DHA (r (30) = 0.63, $P < 0.001$) were significantly correlated to EPA and DHA intake, respectively and, after controlling for LCn-3PUFA intake as a co-variate in the analysis, RBC concentrations of EPA and DHA were not significantly different between participant groups.

RBC DHA concentration was negatively related to clinician ratings of depression using the CGI (r (15) = −0.55, $P = 0.044$) and participant ratings of aggression using the BYI (r (15) = −0.55, $P = 0.043$). Plasma EPA (% of total fatty acids) was significantly positively associated with symptoms of mania and externalising and disruptive behaviour (Table 3).

RBC EPA (2.83 ± 0.38 versus 3.17 ± 0.44, $P = 0.584$), DHA (15.67 ± 2.82 versus 23.08 ± 3.28, $P = 0.123$) and arachidonic acid (AA; 70.15 ± 9.82 versus 82.53 ± 12.03, $P = 0.440$) were not significantly different between participants with JBD receiving either lithium or valproate as their primary mood stabilising medication. Similarly, RBC concentrations of LCn-3PUFA were not significantly related to smoking, alcohol consumption or BMI.

Discussion

Red blood cell membrane concentrations of EPA and DHA were significantly lower in children and adolescents diagnosed with JBD compared with healthy controls. However, reported intakes of EPA and DHA were also lower in participants with JBD and significantly related to RBC concentrations. Therefore, after controlling for reported intakes of EPA and DHA, RBC concentrations of EPA and DHA were not significantly different between participants with JBD compared with controls. This is the first study to report RBC concentrations of LCn-3PUFA in JBD compared with healthy controls and one of the first to report RBC LCn-3PUFA in mental illness after adequately controlling for intake in the statistical analysis.

A genetically determined metabolic abnormality of LCn-3PUFA metabolism such as a specific deficiency of fatty acid CoA ligase 4 and/or Type IV phospholipase A_2, resulting in reduced incorporation of LCn-3PUFA into phospholipids and lower concentrations of LCn-3PUFA in RBC, in particular, is proposed in patients with BD and MDD [42, 43]. However, LCn-3PUFA intake was not assessed in several studies linking reduced LCn-3PUFA with BD [9] or MDD [10, 11, 23], so differences between the effects of intake and metabolism cannot be determined.

In addition, intakes of fish or LCn-3PUFA were reported in several studies, but inadequate design and statistical methods mean that their results cannot be easily interpreted. For example, RBC membrane EPA and DHA were significantly lower in adults with MDD compared with healthy controls [44]. Although intake of LCn-3PUFA was estimated using a 7-day weighed food record, differences in blood LCn-3PUFA were analysed using a 2-sample (non-paired) *t*-test, meaning intake could not be included as a co-variate in the analysis. As the correlation between

Table 2 Red blood cell LCn-3PUFA concentration (μg/mL) in children and adolescents diagnosed with JBD compared with healthy controls

LCn-3PUFA[b]	RBC concentration (μg/mL)[a]		*P*-values	
	Control	JBD	Co-variate	No co-variate
EPA	3.69 (±0.266)	3.37 (±0.260)	0.458	0.016
DPA	15.05 (±1.221)	11.23 (±1.200)	–	0.062
DHA	24.61 (±2.384)	22.08 (±2.234)	0.528	0.014
LCn-3PUFA	64.01 (±5.116)	38.12 (±5.036)	–	0.010
n-6:n-3 ratio	3.19 (±0.317)	3.94 (±0.311)	–	0.152
Omega-3 index	4.72 (±0.353)	4.11 (±0.348)	–	0.152

[a] Values are least squares means ± standard error of the least squares mean adjusted for LCn-3PUFA intake as a co-variate for 15 age and sex-matched pairs, $n = 6$ males (mean age = 13.6 years) and $n = 9$ females (mean age = 15.0 years)

[b] *EPA* eicosapentaenoic acid (C20:5n-3), *DPA* docosapentaenoic acid (c22:5n-3), *DHA* docosahexaenoic acid (C22:6n-3), n-6:n-3 ratio of total n-6:total n-3 fatty acids, Omega-3 index = RBC EPA% + DHA% total fatty acids [58], High risk of disease = 0–4%, medium risk of disease = 4–8%, low risk of disease >8%

Table 3 Relationship between plasma and red blood cell (RBC) EPA and DHA (% total fatty acids) and ratings of mood and behaviour in children and adolescents diagnosed with JBD

	Clinician ratings		Parent ratings		Participant ratings	
	YMRS	CGI-mania	P-YMRS	CBCL-external	BDBI-Y	TMRS-mania
Plasma EPA	0.48*	0.71***	0.42	0.71***	0.59**	0.61**
Plasma DHA	0.33	0.50*	0.11	0.39	0.02	0.01
RBC EPA	0.24	0.49*	0.21	0.23	0.04	−0.02
RBC DHA	0.17	0.32	0.05	0.14	−0.28	−0.39

YMRS Young Mania Rating Scale, *CGI-mania* clinical global improvements mania scale, *P-YMRS* parent version of the Young Mania Rating Scale, *CBCL* Child Behaviour Checklist, *BDBI-Y* disruptive behaviour inventory on the Beck Youth Inventories, *TMRS* tripartite mood rating scale. NB. $n = 15$ for all correlations

* $P < 0.10$, ** $P < 0.05$, *** $P < 0.01$

reported intake and RBC % LCn-3PUFA were significant [44], it is likely that intake would have been significant as co-variate in the analysis and this may have significantly altered the outcome. In addition, it is unlikely that 14 controls and 10 patients with MDD could be matched on all criteria specified in the study. Similar problems matching criteria with control participants and not using intake as a co-variate in statistical analyses also occurred in other studies of attempted suicide [45] and ADHD [46].

As blood concentrations were related to LCn-3PUFA intake and not significantly different between participants with JBD and controls after controlling for intake, data from the current study suggest that there was not a genetic abnormality in LCn-3PUFA incorporation into RBC in participants with JBD. However, there are still several possible hypotheses linking LCn-3PUFA intake and JBD incidence.

Firstly, as there is a strong genetic component to BD, participants with JBD are more likely to be from families with a higher incidence of BD and, subsequently, lower SES. Participants with JBD in the current study had a strong family history of depression and BD and family SES was lower for these participants than controls (data to be presented in more detail separately). These results agree with previous research linking lower SES to increased incidence of mental illness [47–49]. Therefore, a secondary effect from having JBD may be reduced SES, reduced family capacity to purchase food containing high concentrations of LCn-3PUFA (such as fresh oily fish which is expensive) and, therefore, RBC concentrations merely reflect lower intake. SES is significantly positively associated with fish consumption [50, 51] and serum phospholipid EPA % [26].

Secondly, lower intakes of LCn-3PUFA may precede the onset of JBD and lower blood concentrations may be involved in the aetiology of JBD through several mechanisms previously reviewed [52]. Finally, it is possible there is a combination of effects, if participants with JBD are from a lower SES, they consume less LCn-3PUFA, blood concentrations are lower and this contributes to an additive decline in brain functioning and a worsening of symptoms (Fig. 1).

Increasing the consumption of LCn-3PUFA through fish or seafood high in LCn-3PUFA or by using supplements may break this negative cycle and lead to an improvement of symptoms separate to other pharmacological treatment. This strengthens the hypothesis to include LCn-3PUFA supplements as an adjunct to normal pharmacological treatment. Symptoms of JBD may be improved without altering pharmaceutical doses or similar symptom control

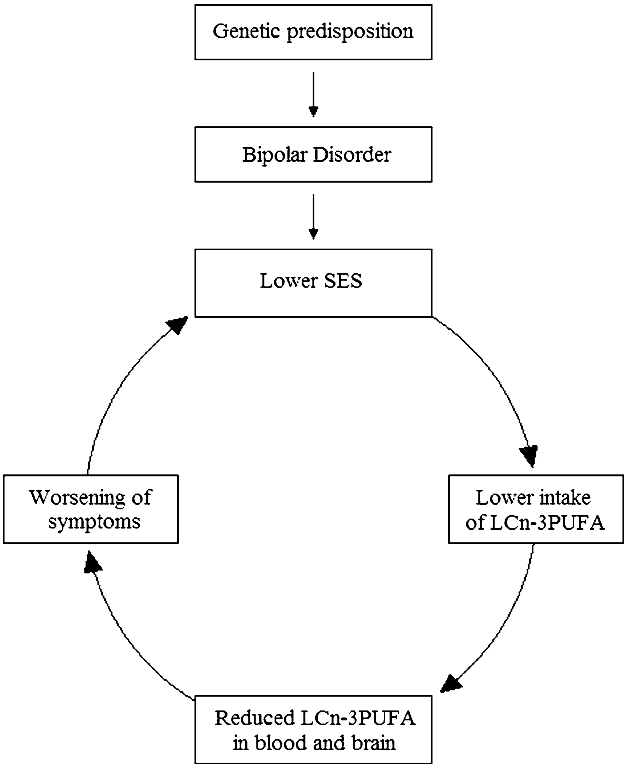

Fig. 1 Theoretical cycle linking SES, intake of LCn-3PUFA and symptom severity in JBD

may be achieved with lower doses of pharmaceuticals and, therefore, lower unwanted side-effects.

RBC concentrations of DHA in the current study were negatively related to clinician ratings of depression and participant ratings of aggression. Lower LCn-3PUFA is related to increased depression and aggression in rats [53] and supplementation with DHA reduces aggression induced by stress [54]. Plasma EPA%, which reflects recent intake [55], was positively related to clinician ratings of mania, parent ratings of externalising symptoms and participant ratings of disruptive behaviour, while RBC EPA was not significantly related to any psychological measures. Future research should further distinguish differences between short-term intake and blood concentrations and long-term intake with state and trait measures of mood and behaviour. LCn-3PUFA supplementation is proposed to be more effective for depression than mania [56, 57] and DHA may be the preferred target treatment for depression and aggression.

The omega-3 index (RBC EPA + DHA%) [58] was not significantly different between groups. However, the omega-3 index of all participants was in the range considered to be a "Medium Risk" for cardiovascular disease (0–4% High Risk, 4–8% Medium Risk, >8% Low risk), indicating that all the participants in the current study had relatively low RBC EPA and DHA compared with recommended levels.

Although the effect of mood stabilising medication on RBC membrane LCn-3PUFA concentrations has not previously been studied, lithium [59, 60] and sodium valproate [61] are associated with decreased arachidonic acid (AA) turnover in the brain of rats without altering the turnover of DHA. In the current study, RBC concentrations of EPA and DHA (after controlling for intake) and AA were not significantly different between participants with JBD who were prescribed lithium compared with those prescribed sodium valproate. Antidepressants [11], haloperidol and diazepam [62] do not alter RBC LCn-3PUFA levels, so it seems unlikely that pharmaceutical treatment would explain further variation in blood concentrations. Therefore, LCn-3PUFA supplements could be effective in addition to standard pharmacotherapy for the treatment of JBD. Previous research has indicated that adjunct supplementation may be beneficial in the treatment of BD in adults [63–65]. Future clinical studies should monitor the interaction between medications and blood LCn-3PUFA.

There are obvious limitations to conducting a study with small numbers of participants. The results should be treated with caution and require replication. However, given the significant relationship between intake and RBC membrane concentrations of LCn-3PUFA, the methods used in the current study appear to be valid.

Conclusions

Red blood cell membrane concentrations of EPA and DHA were not significantly different in participants with JBD compared with healthy controls after controlling for intake. However, lower intakes and subsequent blood concentrations in participants with JBD may contribute to worsening of symptoms, as RBC concentrations of DHA were negatively related to symptoms of depression. Therefore, supplementation with LCn-3PUFA to break the cycle of lower intake and to increase blood concentrations may be of benefit in alleviating symptoms of JBD.

Acknowledgments We thank the expert technical assistance of Robert Blake for advice on LCn-3PUFA analysis and Melinda Phang for assistance in conducting analyses. We also thank staff from the Hunter Area Pathology Service for assistance with blood collection and Dr Trent Watson for advice on the preparation of this manuscript. This study was conducted without dedicated external funding. This study was supported from in-kind donations from the Nutraceuticals Research Group and Hunter New England Area Health Service. Dr Clayton, Dr Hanstock, Mr Hirneth, Dr Kable, Professor Garg and Professor Hazell have previously received in-kind donations of omega-3 capsules from NuMega Ingredients Pty Ltd. The authors do not have any other financial interests or potential conflicts of interest in connection with this manuscript.

References

1. Geller B, Luby J (1997) Child and adolescent bipolar disorder: a review of the past 10 years. J Am Acad Child Adolesc Psychiatry 36(9):1168–1176
2. Reddy YC, Srinath S (2000) Juvenile bipolar disorder. Acta Psychiatr Scand 102(3):162–170
3. Lewinsohn PM, Klein DN, Seeley JR (2000) Bipolar disorder during adolescence and young adulthood in a community sample. Bipolar Disord 2(3):281–293
4. Youngstrom EA, Gracious BL, Danielson CK, Findling RL, Calabrese J (2003) Toward an integration of parent and clinician report on the young mania rating scale. J Affect Disord 77(2):179–190
5. Lewinsohn PM, Klein DN, Seeley JR (1995) Bipolar disorders in a community sample of older adolescents: prevalence, phenomenology, comorbidity, and course. J Am Acad Child Adolesc Psychiatry 34(4):454–463
6. Lish JD, Dime-Meenan S, Whybrow PC, Price RA, Hirschfeld RM (1994) The national depressive and manic-depressive association (DMDA) survey of bipolar members. J Affect Disord 31(4):281–294
7. Noaghiul S, Hibbeln JR (2003) Cross-national comparisons of seafood consumption and rates of bipolar disorders. Am J Psychiatry 160(12):2222–2227
8. Hibbeln JR (1998) Fish consumption and major depression. Lancet 351(9110):1213
9. Chiu CC, Huang SY, Su KP et al (2003) Polyunsaturated fatty acid deficit in patients with bipolar mania. Eur Neuropsychopharmacol 13(2):99–103
10. Maes M, Christophe A, Delanghe J, Altamura C, Neels H, Meltzer HY (1999) Lowered omega-3 polyunsaturated fatty acids in serum phospholipids and cholesteryl esters of depressed patients. Psychiatr Res 85(3):275–291

11. Peet M, Murphy B, Shay J, Horrobin D (1998) Depletion of omega-3 fatty acid levels in red blood cell membranes of depressive patients. Biol Psychiatry 43(5):315–319
12. Sontrop J, Campbell MK (2006) Omega-3 polyunsaturated fatty acids and depression: a review of the evidence and a methodological critique. Prev Med 42(1):4–13
13. Sztern MI, Harris WS (1991) Short-term effects of fish oil on human plasma lipid levels. J Nutr Biochem 2(5):255–259
14. Brown AJ, Pang E, Roberts DC (1991) Persistent changes in the fatty acid composition of erythrocyte membranes after moderate intake of n-3 polyunsaturated fatty acids: study design implications. Am J Clin Nutr 54(4):668–673
15. World Medical Association (1964) Declaration of Helsinki. BMJ 313(7070):1448–1449
16. World Medical Association (1997) World Medical Association declaration of Helsinki. Recommendations guiding physicians in biomedical research involving human subjects. JAMA 277(11): 925–926
17. NHMRC (2001) National statement on ethical conduct in research involving humans. National health and medical research council act 1992
18. ICH (1996) Good clinical practice: consolidated guidance. In: International conference on harmonisation of technical requirements for registration of pharmaceuticals for human use E6, April, 1996
19. Geller B, Williams M, Zimerman B, Frazier J (1996) Washington University in St. Louis kiddie schedule for affective disorders and schizophrenia (WASH-U-KSADS). Washington University, St Louis
20. APA (2000) Diagnostic and statistical manual of mental disorders (text revised). 4th edn. American Psychiatric Association, Washington
21. Findling RL, Gracious BL, McNamara NK et al (2001) Rapid, continuous cycling and psychiatric co-morbidity in pediatric bipolar I disorder. Bipolar Disord 3(4):202–210
22. Post RM, Luckenbaugh DA (2003) Unique design issues in clinical trials of patients with bipolar affective disorder. J Psychiatr Res 37(1):61–73
23. Maes M, Smith R, Christophe A, Cosyns P, Desnyder R, Meltzer H (1996) Fatty acid composition in major depression: decreased omega 3 fractions in cholesteryl esters and increased C20: 4 omega 6/C20:5 omega 3 ratio in cholesteryl esters and phospholipids. J Affect Disord 38(1):35–46
24. Wirfalt E, Vessby B, Mattisson I, Gullberg B, Olsson H, Berglund G (2004) No relations between breast cancer risk and fatty acids of erythrocyte membranes in postmenopausal women of the Malmo Diet Cancer cohort (Sweden). Eur J Clin Nutr 58(5):761–770
25. Western J, McMillan J, Durrington D (1998) Differential access to higher education: the measurement of socioeconomic status, rurality and isolation. Department of Employment, Education, Training and Youth Affairs, Brisbane
26. Crowe FL, Skeaff CM, Green TJ, Gray AR (2007) Serum phospholipid n-3 long-chain polyunsaturated fatty acids and physical and mental health in a population-based survey of New Zealand adolescents and adults. Am J Clin Nutr 86(5):1278–1285
27. McMillan J, Jones FL (2000) The ANU3_2 scale: a revised occupational status scale for Australia. J Sociol 36(1):64–80
28. Young RC, Biggs JT, Ziegler VE, Meyer DA (1978) A rating scale for mania: reliability, validity and sensitivity. Br J Psychiatry 133:429–435
29. Hamilton M (1960) A rating scale for depression. J Neurol Neurosurg Psychiatry 23(2):56–62
30. Guy W (1976) Clinical global impressions. New clinical drug evaluation unit (ECDEU). Assessment Manual for Psychopharmacology, pp 218–222
31. Spearing MK, Post RM, Leverich GS, Brandt D, Nolen W (1997) Modification of the clinical global impressions (CGI) scale for use in bipolar illness (BP): the CGI-BP. Psychiatr Res 73(3):159–171
32. Shaffer D, Gould MS, Brasic J et al (1983) A children's global assessment scale (CGAS). Arch Gen Psychol 40(11):1228–1231
33. Achenbach TM, Rescorla LA (2001) Manual for the ASEBA school-age forms and profiles. VT University of Vermont, Research Centre and Children, Youth and Families, Burlington
34. Beck J, Beck A, Jolly J (2001) Beck youth inventories of emotional and social impairment manual. TX Psychological Corporation, San Antonio
35. Hanstock TL, Clayton EH, Hunt SA, Hazell PL (2006) The tripartite mood rating scale (TMRS): a new self-report mood instrument for children and adolescents with bipolar. In: Biederman J (ed) NIMH paediatric bipolar conference, Chicago
36. Lepage G, Roy CC (1986) Direct transesterification of all classes of lipids in a one-step reaction. J Lipid Res 27(1):114–120
37. Rodriguez-Palmero M, Lopez-Sabater MC, Castellote-Bargallo AI, De la Torre-Boronat MC, Rivero-Urgell M (1997) Comparison of two methods for the determination of fatty acid profiles in plasma and erythrocytes. J Chromatogr A 778(1–2):435–439
38. Garg ML, Blake RJ, Clayton EH et al (2007) Consumption of an n-3 polyunsaturated fatty acid-enriched dip modulates plasma lipid profile in subjects with diabetes type II. Eur J Clin Nutr 61(11):1312–1317
39. Coakes SJ, Steed LG (2001) SPSS: analysis without anguish: Version 10.0 for windows. Wiley, Sydney
40. SAS Institute Inc (1997) SAS/STAT software: changes and enhancements through release 6.12. SAS Institute Inc, Carey
41. Littell RC, Henry PR, Ammerman CB (1998) Statistical analysis of repeated measures data using SAS procedures. J Anim Sci 76:1216–1231
42. Horrobin DF, Bennett CN (1999) Depression and bipolar disorder: relationships to impaired fatty acid and phospholipid metabolism and to diabetes, cardiovascular disease, immunological abnormalities, cancer, ageing and osteoporosis. Possible candidate genes. Prost Leukotr Essent Fatty Acids 60(4):217–234
43. Ross BM (2007) Omega-3 fatty acid deficiency in major depressive disorder is caused by the interaction between diet and a genetically determined abnormality in phospholipid metabolism. Med Hypotheses 68(3):515–524
44. Edwards R, Peet M, Shay J, Horrobin D (1998) Omega-3 polyunsaturated fatty acid levels in the diet and in red blood cell membranes of depressed patients. J Affect Disord 48(2–3): 149–155
45. Huan M, Hamazaki K, Sun Y et al (2004) Suicide attempt and n-3 fatty acid levels in red blood cells: a case control study in China. Biol Psychiatry 56(7):490–496
46. Colter AL, Cutler C, Meckling KA (2008) Fatty acid status and behavioural symptoms of attention deficit hyperactivity disorder in adolescents: a case-control study. Nutr J 7(1):8
47. Eachus J, Williams M, Chan P et al (1996) Deprivation and cause specific morbidity: evidence from the Somerset and Avon survey of health. BMJ 312(7026):287–292
48. Lehtinen V, Joukamaa M (1994) Epidemiology of depression: prevalence, risk factors and treatment situation. Acta Psychiatr Scand Suppl 377:7–10
49. Skapinakis P, Weich S, Lewis G, Singleton N, Araya R (2006) Socio-economic position and common mental disorders. Longitudinal study in the general population in the UK. Br J Psychiatry 189:109–117
50. Galobardes B, Morabia A, Bernstein MS (2001) Diet and socioeconomic position: does the use of different indicators matter? Int J Epidemiol 30(2):334–340

51. Barberger-Gateau P, Jutand MA, Letenneur L, Larrieu S, Tavernier B, Berr C (2005) Correlates of regular fish consumption in French elderly community dwellers: data from the Three-City study. Eur J Clin Nutr 59(7):817–825
52. Clayton EH, Hanstock TL, Garg ML, Hazell PL (2007) Long-chain omega-3 polyunsaturated fatty acids in the treatment of psychiatric illnesses in children and adolescents. Acta Neuropsych 19(2):92–103
53. DeMar JC Jr, Ma K, Bell JM, Igarashi M, Greenstein D, Rapoport SI (2006) One generation of n-3 polyunsaturated fatty acid deprivation increases depression and aggression test scores in rats. J Lipid Res 47(1):172–180
54. Hamazaki T, Sawazaki S, Itomura M et al (1996) The effect of docosahexaenoic acid on aggression in young adults. J Clin Invest 97(4):1129–1133
55. Bjerve KS, Brubakk AM, Fougner KJ, Johnsen H, Midthjell K, Vik T (1993) Omega-3 fatty acids: essential fatty acids with important biological effects, and serum phospholipid fatty acids as markers of dietary omega 3-fatty acid intake. Am J Clin Nutr 57(5 Suppl):S801–S805
56. Lin PY, Su KP (2007) A meta-analytic review of double-blind, placebo-controlled trials of antidepressant efficacy of omega-3 fatty acids. J Clin Psychiatry 68(7):1056–1061
57. Ross BM, Seguin J, Sieswerda LE (2007) Omega-3 fatty acids as treatments for mental illness: which disorder and which fatty acid? Lipids Health Dis 6(1):21
58. Harris WS (2007) Omega-3 fatty acids and cardiovascular disease: a case for omega-3 index as a new risk factor. Pharmacol Res 55(3):217–223
59. Chang MC, Grange E, Rabin O, Bell JM, Allen DD, Rapoport SI (1996) Lithium decreases turnover of arachidonate in several brain phospholipids. Neurosci Lett 220(3):171–174
60. Chang MC, Bell JM, Purdon AD, Chikhale EG, Grange E (1999) Dynamics of docosahexaenoic acid metabolism in the central nervous system: lack of effect of chronic lithium treatment. Neurochem Res 24(3):399–406
61. Chang MC, Contreras MA, Rosenberger TA, Rintala JJ, Bell JM, Rapoport SI (2001) Chronic valproate treatment decreases the in vivo turnover of arachidonic acid in brain phospholipids: a possible common effect of mood stabilizers. J Neurochem 77(3):796–803
62. Fehily AMA, Bowey OAM, Ellis FR, Meade BW, Dickerson JWT (1981) Plasma and erythrocyte membrane long chain polyunsaturated fatty acids in endogenous depression. Neurochem Int 3(1):37–42
63. Keck PE, Freeman MP, McElroy SL et al (2002) A double-blind, placebo-controlled trial of eicosapentanoic acid in rapid cycling bipolar disorder. Bipolar Disord 4(Suppl 1):26–27
64. Osher Y, Bersudsky Y, Belmaker RH (2005) Omega-3 eicosapentaenoic acid in bipolar depression: report of a small open-label study. J Clin Psychiatry 66(6):726–729
65. Frangou S, Lewis M, McCrone P (2006) Efficacy of ethyl-eicosapentaenoic acid in bipolar depression: randomised double-blind placebo-controlled study. Br J Psychiatry 188:46–50

Typical changes in the insulin resistant state are an increased fat mass due to adipocyte hyperplasia and hypertrophy [1–4], liver steatosis and triacylglycerol (TAG) accumulation in skeletal muscle [5–8], as well as fasting and postprandial hyperlipidemia [9–11]. Previous studies have provided convincing evidence that an excessive amount of fatty acids is an important etiological factor in the development of these pathologies. Systemic insulin resistance can be induced in humans and in animal models by high fat diets (HFDs) [12–14] or by systemic elevation of fatty acids through lipid infusion [6, 15–17]. Alteration of fatty acid fluxes by transgenic intervention or by pharmacological means were demonstrated to modulate insulin sensitivity in disease models [18–22], adding further evidence to the notion that an excess of fatty acids causes insulin resistance.

In addition to overall fatty acid quantities, composition of tissue fatty acid pools is an important aspect of metabolic disease. Observational studies established that certain fatty acids are frequently associated with insulin resistance, suggesting that they may have a pathogenic role. For example, in human plasma, palmitate (C16:0), palmitoleate (C16:1), oleate (C18:1) and dihomo-γ-linolenate (C20:3n-6) were found to be increased in insulin resistant subjects, while linoleate (C18:2) negatively correlated with metabolic disease in many cross-sectional and prospective studies (see [23] for review). Direct evidence that some fatty acid species or classes are more pathogenic than others was generated in dietary intervention studies. Diets enriched in SFA and MUFA were shown to induce insulin resistance in rodents [13, 24–26] while n-6 PUFA showed more variable effects [13, 27] and dietary fats enriched in n-3 PUFA unequivocally showed strong weight-reducing and insulin sensitizing effect in diet-induced obesity rodent models [24, 25]. In humans, a diet enriched in SFA but not one enriched in MUFA induced insulin resistance in healthy subjects [14]. In contrast to rodents, dietary intervention studies in humans using fish oils rich in n-3 PUFA found no positive effect on insulin action [14, 28–31], although muscle phospholipid n-3 PUFA content was found to correlate with insulin sensitivity [32, 33].

The fatty acid composition in the body is determined not only by dietary intake but also by fatty acid synthesis and processing of dietary fatty acids. One important pathway is the synthesis of SFA and MUFA including de novo synthesis of C16:0 by fatty acid synthase (FAS), elongation by fatty acid elongases (ELOVL1-6) and Δ9-desaturation by stearoyl-CoA desaturase (SCD), enzymes highly expressed in the major lipogenic tissues liver and adipose tissue. Among the lipogenic enzymes SCD1 is an especially well studied example. Its activity is essential for induction of other lipogenic genes, liver steatosis and weight gain after HFD feeding of mice [34]. Genetic deficiency of SCD1 and long-term knockdown using antisense RNA technology led to protection from insulin resistance and obesity [35, 36]. Importantly, short-term inhibition of SCD1 improved insulin signaling, however, was not accompanied by reduced obesity or liver steatosis, suggesting a direct insulin sensitizing effect on liver [37]. SCD1 activity has also been implicated in human obesity and insulin resistance. Δ9-desaturase (Δ9D) indices, calculated from products and precursors of the SCD1 reaction, were frequently increased in obesity, insulin resistance and other parameters of metabolic disease suggesting that SCD1 is also an important mediator of human insulin resistance [23, 38, 39].

Fatty acid profiling in humans revealed that insulin resistance is also frequently associated with alterations in activity indices of Δ6-desaturase (FADS2) and Δ5-desaturase (FADS1), which are essential for synthesis of PUFA from essential fatty acids. Apparent activity of FADS2 is typically increased in metabolic disease while FADS1 is decreased [23]. In rodent models of obesity and insulin resistance alterations of FADS1 and FADS2 has been studied only in a few insulin resistant models [40, 41]. Compared to SCD1, less is known about causal links to metabolic disease. Even less is known about the role of fatty acid elongases in insulin resistance. Interestingly, the isoform ELOVL6, using fatty acids with chain length below C_{18} as substrate, was recently shown to promote liver insulin resistance [42].

HFD-induced obesity in the C57Bl/6 mouse [12] is one of the most widely used mouse models of insulin resistance exhibiting many aspects of the metabolic syndrome in humans such as impaired glucose tolerance, hypertension, diminished immune function and a propensity for atherosclerosis [43]. The strain is susceptible to diet-induced obesity on different HFDs with the exception of diets rich in n-3 PUFA [25]. Despite the frequent use, especially for genetic studies, alterations in fatty acid profiles in relation to insulin resistance have not been studied extensively in this model. Therefore, we set out to perform a comprehensive lipid profiling experiment using a lard-based HFD to induce different degrees of insulin resistance. We observed profound changes in fatty acid content and composition. Some of these changes occurred even in a very early insulin resistant state while others were only apparent in fully developed insulin resistance.

Materials and Methods

Animal Diet Regimens and Necropsy

Age-matched male C57Bl/6 mice (Taconic, Germantown, NY) on distinct diets were used as models of insulin resistance and as the respective controls. Healthy control mice were fed a normal chow diet (Chow, Purina 5001). Insulin resistance was induced by a lard-based, diabetogenic HFD (Bio-Serv S3282; proximate nutrient profile by weight: 35.5% lard, 20% casein, 14% sucrose, 18.6% maltose dextrin). As shown in Supplemental Figure 1, one group was made profoundly insulin resistant by feeding the HFD for a period of 16 weeks starting at weaning (16w-HFD). Another group was designed to be mildly insulin resistant and received the HFD only 1 week before necropsy (1w-HFD), after randomization at 19 weeks of age with the Chow-fed controls for fasting plasma insulin and glucose. At 20 weeks of age, blood and organs were collected from the mice for metabolic profiling. Before necropsy each feeding group was divided into two subgroups, mice fasted overnight for 16 h (Fasted) and mice fasted overnight with subsequent access to the HFD for 4 h (Refed).

The animals were anesthetized with isoflurane and cardiac stick was performed to collect blood as EDTA plasma (Li-heparin for NMR) from the right ventricle of the heart. After bleeding, the animals were perfused (10 U/L heparinized saline) through the right ventricle of the heart, allowing the blood to exit through a cut in the caudal vena cava. Organs and blood were taken and snap frozen in liquid nitrogen for storage at −80 °C.

Animals were maintained on a 12-h light, 12-h dark cycle and received tap water ad libitum. All animals were maintained in accordance with the Institutional Animal Use and Care Committee of Eli Lilly and Company and the NIH Guide for the Use and Care of Laboratory Animals.

Plasma Parameters

Plasma insulin was determined using Rat/Mouse Insulin Assay kit (Mesoscale Discovery, Gaithersburg, MD) and Mouse Endocrine Lincoplex kit (Millipore, St. Charles, MO) for randomization and final study, respectively. Glucose was measured using a Hitachi 912 clinical chemistry analyzer (Roche, Indianapolis, IN). Adiponectin was determined using an ELISA from R&D Systems (Minneapolis, MN). Blood lipid measurements including FPLC analysis were performed as described [44].

Metabolite Quantification by NMR

Li-heparin plasma samples were transferred into 1-mm NMR sample tubes and stored for a maximum duration of 2 h at 4 °C prior to NMR data acquisition. T2-filtered ^{1}H-NMR spectra were recorded at 300 K on a Bruker 600 MHz AVANCE spectrometer using a 1-mm TXI micro probe head equipped with *z*-gradient system. A standard 1D CPMG (Carr–Purcell–Meiboom–Gill) pulse sequence [45] with 2 s presaturation delay ($\gamma B_1 = 50$ Hz) and 80 echo cycles of 800 µs duration resulting in a total echo time of 64 ms was employed. 256 scans of 32,768 data points covering 12019 Hz were recorded and zero filled to 65,536 points. An exponential window function with a line-broadening factor of 2.0 Hz was applied prior to Fourier transformation. All spectra were manually phased and baseline corrected and referenced to the CH_3 signal of lactate (1.33 ppm). The relative 3-hydroxybutyrate, acetone and glycerol concentrations were determined by manual deconvolution of the spectra using reference data of the corresponding compounds recorded at 4 mM concentration in 0.067 mM phosphate buffer (pH 7.4). Reference data were recorded using the first time increment of the 2D NOESY experiment [46] with presaturation ($\gamma B_1 = 50$ Hz) during 2 s relaxation delay and 100 ms mixing time, respectively. Other parameters were as above except 64 scans were accumulated and data were referenced according to internal TSP at a concentration of 0.4 mM. The determined relative concentrations are given in relative units since the values were not corrected for attenuation of the signals caused by relaxation during the T2 filter delay and rapid pulsing saturation effects.

Liver Total Lipid Quantification

In homogenized liver samples, basal lipid values are high enough to measure efficiently and specifically total lipid content by standard colorimetric assays without any extraction. For lipid quantification, 50-mg pieces of frozen liver were homogenized in lysis buffer (2 mM $CaCl_2$, 80 mM NaCl, 1% TritonX-100, 50 mM *Tris*/HCl, pH 8.0). TAG and cholesterol were determined using commercial kits (Roche/Hitachi, Mannheim, Germany). Protein concentrations were measured by a Lowry method, which was modified for lipid containing samples by addition of 0.1% SDS.

Western Blot Analysis

Liver lysates were generated by homogenizing tissue in lysis buffer (50 mM Tris, 250 mM mannitol, 1 mM EDTA, 1 mM EGTA, 20 mM $Na_4P_2O_7$, 2 mM Na_3VO_4, 1 mM DTT, 50 mM NaF, protease inhibitors (COMPLETE, Roche, Mannheim, Germany), phosphatase inhibitor cocktail (Sigma, Munich, Germany), 1% Triton X-100) with subsequent clarification by centrifugation at 13,000 rpm for 30 min. Protein concentrations were determined using the BCA protein assay (Perbio, Bonn, Germany). Proteins were separated by SDS-polyacrylamide gel electrophoresis (4–12% acrylamide, NuPAGE system, Invitrogen, Karlsruhe, Germany) under denaturing conditions and transferred to Protran nitrocellulose membranes. Immunodetection was performed with antibodies against IRS1 (Upstate, Schwalbach, Germany) and IRS2 (Santa Cruz, Heidelberg, Germany) using standard procedures. The signals were quantified by normalization to beta-tubulin using an antibody from Sigma (Munich, Germany).

Total RNA Extraction and Real-time Quantitative PCR

Total RNA from frozen liver samples was extracted using the TissueLyser and RNeasy system (Qiagen, Hilden, Germany) according to the manufacturer's instructions. DNA contaminants were removed via column DNase treatment (RNase-Free DNase set; Qiagen). 1 μg of RNA was reverse transcribed in 50 μl reaction mixture using the High Capacity cDNA Archive Kit (Applied Biosystems, Darmstadt, Germany) according to the manufacturer's instructions. Real-time RT-PCR was performed as described previously [47].

For all other genes Assay-on-Demand primer/probe sets supplied by Applied Biosystems were used (Assay IDs are available upon request). Relative expression was calculated by normalization to selected housekeeper mRNA (TBP) by ΔΔCt method [48]. Data are reported as copy number relative to housekeeper.

Fatty Acid Analysis

All chemicals were of analytical grade. Fatty acid methyl ester standards were obtained from Restek, (Bad Homburg, Germany), Cayman (IBL, Hamburg) and Supelco (Sigma). Total lipids from liver, subcutaneous adipose tissue and skeletal muscle were extracted essentially as described by Folch et al. [49]. Briefly, 250 μl of butylhydroxytoluene (0.1 mol/l in methanol) and 6 ml of chloroform/methanol (2:1) were added to 50 mg of tissue. After homogenization using an Ultraturrax homogenizer the samples were heated to 50 °C for 30 min and centrifuged (1800 g, 5 min). Lipid class separation of liver tissue was performed according to the method of Hamilton and Comai [50] using prepacked silica columns (Separtis, Grenzach-Wyhlen, Germany). Separated lipid fractions were evaporated and redissolved in methanol/toluene (4:1). Fatty acid methyl esters were prepared based on the method of Lepage and Roy [51] except that toluene was used instead of benzene. Briefly, 10 μl of plasma (or 100 μl of tissue extract), 2 ml methanol/toluene (4:1), 50 μl heptadecanoic acid (200 μg/ml in methanol/toluene, 4:1) and 200 μl acetyl chloride were heated in a capped tube for 1 h at 100°C. After cooling to room temperature 5 ml of 6% sodium carbonate was added. The mixture was centrifuged (1800 g 5 min.) and 150–200 μl of the upper layer were transferred to auto sampler vials. For liver extracts dilutions were made by adding 1.6 ml of toluene preliminarily to the sodium carbonate. Gas chromatography analyses were performed using an HP 5890 gas chromatograph (Hewlett Packard) equipped with flame ionization detectors (Stationary phase: DB-225 30 m × 0.25 mm id., film thickness 0.25 μm; Agilent, Böblingen, Germany). Peak identification and quantification was performed by comparing retention times and peak areas, respectively, to standard chromatograms. All calculations are based on fatty acid methyl esters values. Composite Δ9D index was calculated as the sum of the fractional contents of all MUFA divided by the sum of the fractional contents of both MUFA and SFA.

Statistical Analysis

Unless indicated otherwise two-tailed Student's *t*-test was used to assess statistical significance between groups. Pearson's correlation test was used to evaluate the degree and the significance of association between plasma lipids and obesity or insulin resistance parameters.

Results

Short- and Long-Term Feeding of High Fat Diet Results in Progressive Insulin Resistance

Insulin sensitivity and metabolic status of the HFD-fed mice and control mice was determined by measuring plasma concentrations of glucose and insulin, as well as adipokines and lipids in the fasted and in the refed state (Supplemental Table 1). Feeding the HFD for 1 week resulted in a mild but significant insulin resistance as shown by higher fasting glucose and insulin in 1w-HFD mice vs. Chow mice (Fig. 1). Also, a significant rise in body weight and plasma leptin (Supplemental Table 1, Figure 1) was observed. As expected, 16 weeks HFD led to more pronounced overweight and insulin resistance compared to 1w-HFD mice, as reflected by fasting glucose, insulin and leptin levels. Fasting plasma adiponectin was decreased by HFD feeding, however, only in the 16w-HFD group (Fig. 1).

In the refed state, plasma glucose and insulin were elevated compared to fasted state in each dietary group, as expected. While in the refed state, glucose was still significantly higher in the 1w-HFD group vs. control mice, refed insulin levels were equal in both groups (Fig. 1). Consistent with the observation that leptin secretion is stimulated by high metabolic fuel availability [52, 53], plasma leptin was profoundly increased in the refed vs. the fasted state in controls and the 1w-HFD group. In the 16w-HFD group this regulation was lost and leptin was actually lower in refed vs. fasted animals. Interestingly, adiponectin

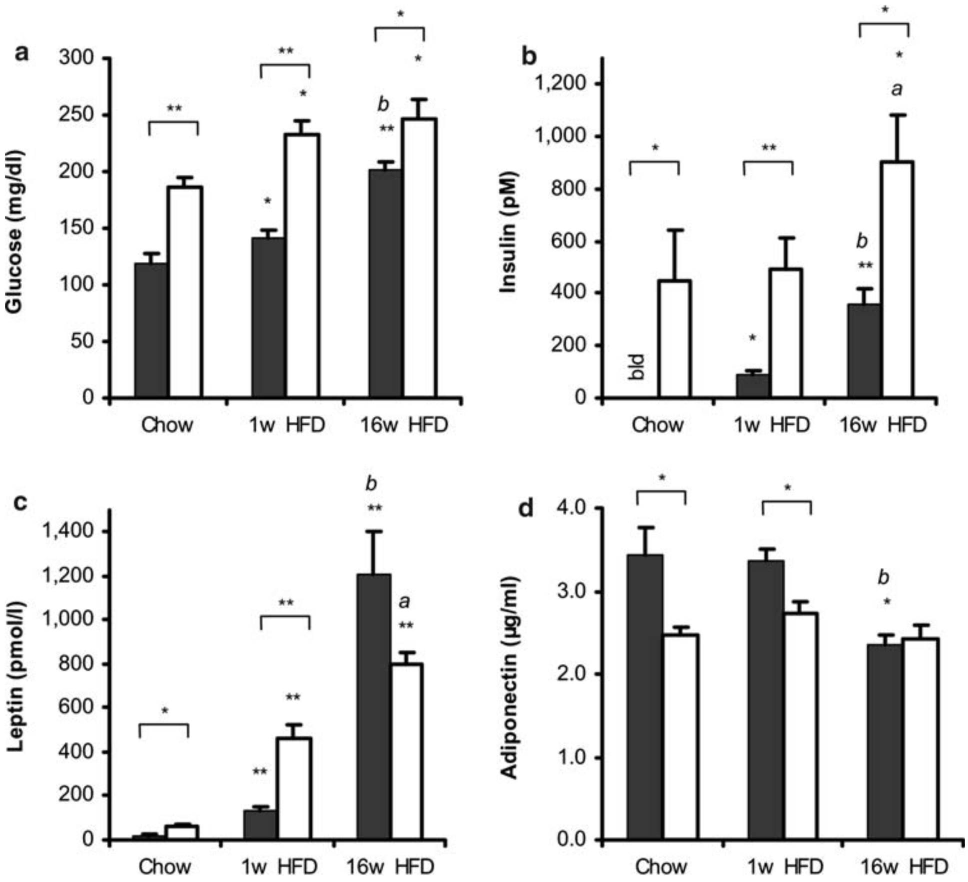

Fig. 1 Plasma parameters related to insulin resistance. Plasma glucose **a** insulin **b** leptin **c** and adiponectin **d** levels in mice fed either control diet (Chow), control diet for 15 weeks and HFD for 1 week (1w-HFD), and HFD for 16 weeks (16w-HFD), respectively. Bar graphs are presented as mean ± SEM. *Closed bars*, fasted state; *open bars*, refed state. T-Test HFD vs. Chow: * $p < 0.05$; ** $p < 0.001$; T-Test 16w-HFD vs. 1w-HFD: *a*: $p < 0.05$; *b*: $p < 0.001$. Mann–Whitney U-Test was used for insulin since most fasted Chow values were below detection limit (bld, 56 pmol/l)

levels in the refed state were no longer different between the feeding groups (Fig. 1).

High Fat Diet Induces Plasma Hyperlipidemia while Reducing Ketone Bodies

HFD feeding increased levels of plasma lipids, as expected (Supplemental Table 1). The lipid levels correlated positively with measures of obesity and insulin resistance, cholesterol having the highest scores (Pearson correlation coefficients for fasting plasma cholesterol: insulin, $r = 0.899$; glucose, $r = 0.823$; leptin, $r = 0.854$; $p < 0.001$). In order to characterize the observed hyperlipidemia in more detail we assessed the lipoprotein profiles of the insulin resistant mice by FPLC. The size of the HDL peak (fractions 22–28) increased moderately after 1 week of HFD feeding and increased further after 16 weeks of HFD (Fig. 2), as observed previously in mice [54]. A more dramatic change upon HFD feeding was observed for a peak eluting before HDL (fractions 15–20). This peak contained apolipoproteins B, E and C (data not shown) and, therefore, probably corresponded to LDL and/or apoE-containing HDL. The peak correlated with the degree of insulin resistance and was barely detectable in the Chow controls (Fig. 2). TAG-rich lipoproteins (fractions 7–11) were increased in both the 1w-HFD and 16w-HFD group in the fasted state, whereas no increase compared to the control group was present in the refed insulin resistant animals. Similar levels of free glycerol (fractions 36–40) were measured in all experimental groups in the fasted state, as could be confirmed independently by NMR quantification (Supplemental Table 1). As expected, upon refeeding, the peak was strongly suppressed in Chow controls, presumably reflecting suppression of adipocyte lipolysis by insulin. Interestingly, this regulation was completely lost in the 16w-HFD group, indicating strong adipose tissue insulin resistance. In the 1w-HFD group, the suppression was partially lost, suggesting that adipocyte insulin signaling was already impaired at this early stage of the disease.

We quantified plasma ketone bodies as measures of liver ketone synthesis and, indirectly, of fatty acid oxidation. 3-hydroxybutyrate and acetone, the degradation product of the ketone body acetoacetate, were detectable by NMR. As expected, the ketones were much higher in fasted compared to refed animals, reflecting higher flux of fatty acids from adipose tissue to the liver. In agreement with previous reports describing reduction of ketone bodies in non-diabetic insulin resistant states [55–57], fasted ketones were significantly lower (60%) in the 16w-HFD group relative to Chow controls (Supplemental Table 1), while in the 1w-

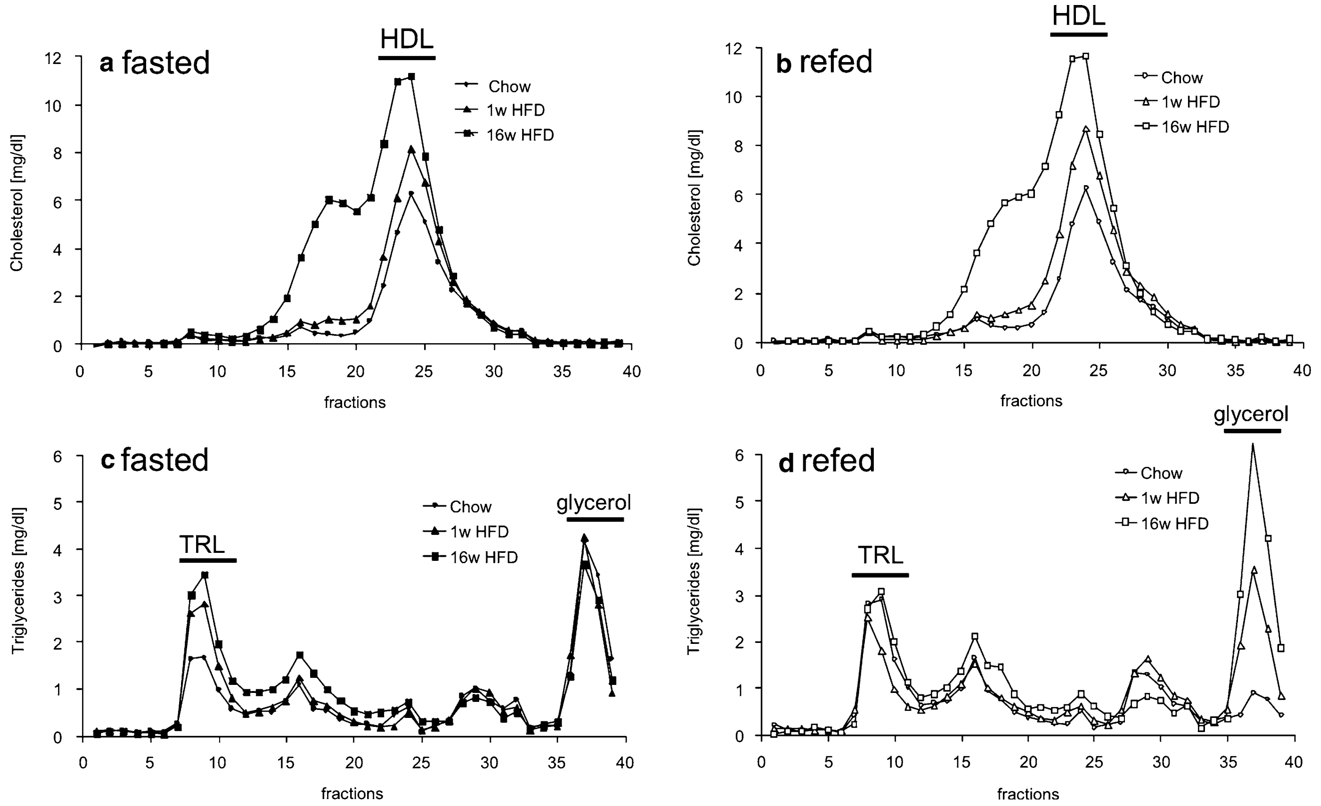

Fig. 2 Plasma lipoprotein profiles. Lipoprotein profiles of individual mice were determined by FPLC using samples from **a**, **c** fasted and **b**, **d** refed animals. **a**, **b** Cholesterol and **c**, **d** TAG in each fraction were determined using standard enzymatic lipid measurements. The means of eight animals per group are shown. Peaks corresponding to HDL, TAG-rich lipoproteins (TRL) and free glycerol are marked

HFD group acetone but not 3-hydroxybutyrate was significantly decreased.

HFD-Induced Changes in Fatty Acid Composition Correspond to Δ9-Desaturase Indices and Liver Lipid Concentration

We determined fasting state plasma and liver fatty acid profiles by gas chromatography to correlate alterations in fatty acid metabolism with insulin resistance after short-term and chronic HFD feeding.

As shown in Fig. 3, profound alterations in fatty acid profiles were observed, among others for the major C16 and C18 fatty acid species. The fractional content of C16:1 was decreased in the HFD-fed animals in plasma and liver already after 1 week HFD (Fig. 3). More moderate changes were observed for C16:0, most noteworthy a small increase in liver after 16 weeks of HFD feeding, as opposed to a decrease in plasma (Fig. 3).

A divergent pattern was observed for stearate (C18:0) and C18:1. The plasma content of C18:0 had significantly increased and that of C18:1 had decreased in both insulin resistant groups compared to Chow controls. In liver there was a profound rise in C18:0 and a complementary drop in C18:1 after 1 week HFD while the opposite pattern was present after 16 weeks of HFD (Fig. 3).

The observed divergent regulation of C16 and C18 SFA and MUFA suggested liver regulation of SCD1, the Δ9D important for metabolic control in humans and mice. Therefore, we calculated Δ9D activity indices using substrate/product ratios (Fig. 4). Surprisingly, the product vs. substrate ratios of the two predominant Δ9D reactions, the C16:1/C16:0 ratio and the C18:1/C18:0 ratio, showed a converse pattern. Whereas the C16:1/C16:0 ratio showed a progressive decrease in liver and plasma, the C18:1/C18:0 ratio showed a distinct temporal pattern in liver, namely a drop in the 1w-HFD group and a subsequent increase, resulting in a higher ratio compared to Chow controls (Fig. 4). In plasma the C18:1/C18:0 ratio was equally decreased compared to Chow in the 1w-HFD and the 16w-HFD group. Calculation of a composite Δ9D index taking into account the sums of all MUFA and SFA (see “Materials and Methods”) resulted in a pattern similar to the C18:1/C18:0 ratio in liver (Fig. 4). The composite Δ9D index as well as the C18:1/C18:0 ratio in liver correlated with the expression of *Scd1*, which showed a non-significant dip after 1w-HFD and a significant increase after 16w-HFD (Fig. 4). Since increased Δ9D activity and SCD1

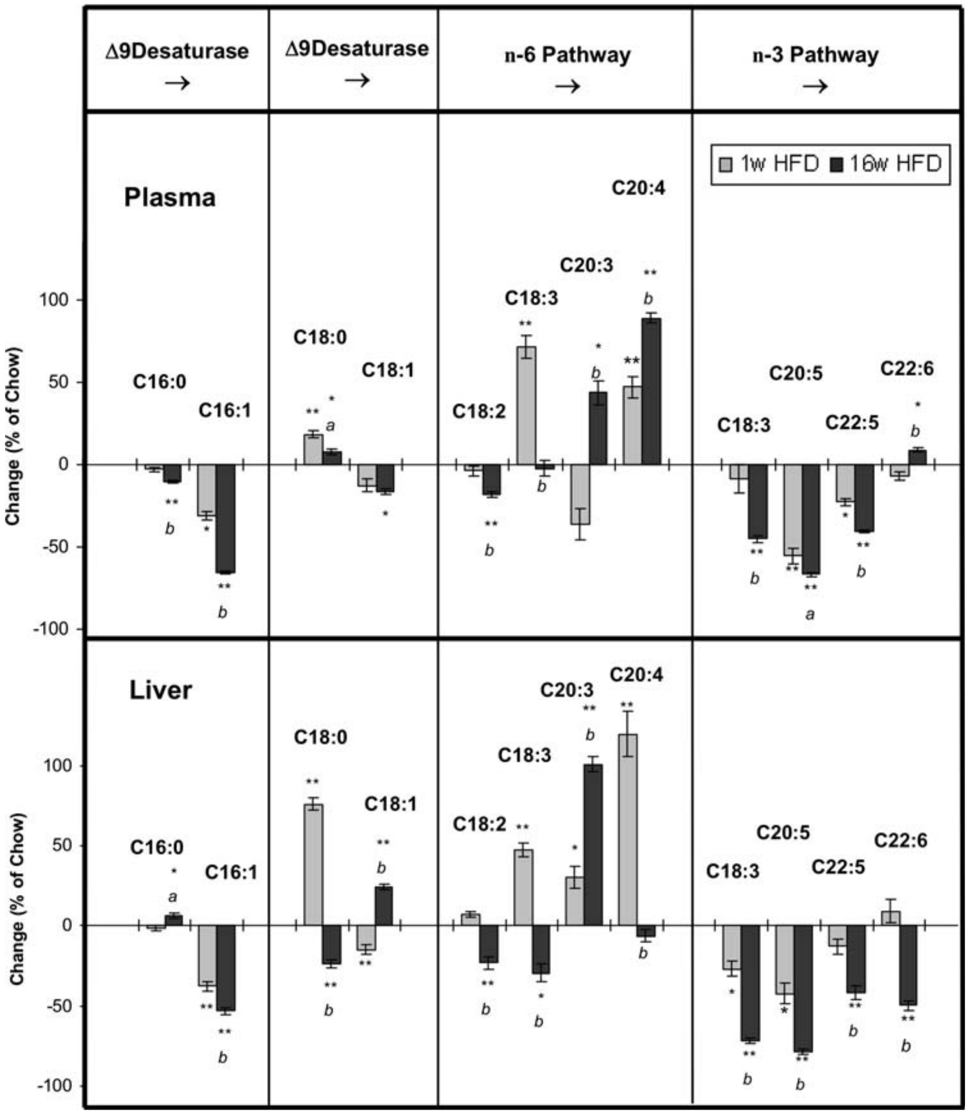

Fig. 3 Changes in plasma and liver fatty acids. Changes in fractional content of fatty acids representing selected synthesis pathways. Total lipid fatty acids were determined in plasma and liver of fasted animals. Data are presented as percent change (mean ± SEM) in 1w-HFD and 16w-HFD groups compared to Chow controls. T-Test HFD vs. Chow: * $p < 0.05$; ** $p < 0.001$; T-Test 16w-HFD vs. 1w-HFD: *a*: $p < 0.05$; *b* $p < 0.001$

expression is typically associated with liver steatosis, we measured TAG and cholesterol content of the liver. After 1 week of HFD there was a strong decrease in fasted liver TAG content while after 16 weeks HFD liver TAG was significantly increased compared to Chow (Fig. 5). For liver cholesterol a similar, however less pronounced, pattern was observed (Fig. 5). To investigate whether decreased liver lipid content is associated with a corresponding increase in peripheral organs, we measured total fatty acid content in plasma, liver, skeletal muscle and subcutaneous adipose tissue (Fig. 5). Fatty acid content in the liver was decreased after 1 week HFD whereas in plasma, muscle and subcutaneous adipose tissue fatty acid levels per tissue wet weight was increased. In addition, the total weight of subcutaneous fat pads was profoundly increased already after 1 week HFD (Chow: 97 ± 26 mg; 1w-HFD: 506 ± 77 mg and 16w-HFD: 1325 ± 52 mg; $p < 0.001$). Despite the lower total liver lipid levels in the 1w-HFD group, mechanisms related to hepatic insulin resistance may already have been initiated at this stage, as suggested by decreased protein levels of the insulin receptor substrate (IRS) isoforms. The protein content of IRS1 and IRS2 were further diminished in the 16w-HFD group (Fig. 5).

Taken together, the C18:1/C18:0 ratio as well as the composite Δ9D index correlated with liver SCD-1 mRNA and with liver TAG content, however, not with early insulin resistance after 1w-HFD feeding.

HFD Increases Plasma and Hepatic Arachidonate

Arachidonate (C20:4) as the precursor of eicosanoids plays an important part in inflammation and may, therefore, be important for insulin resistance. For this reason we analyzed the content of C20:4 in plasma and liver. In plasma, a progressive increase in C20:4 was observed upon HFD

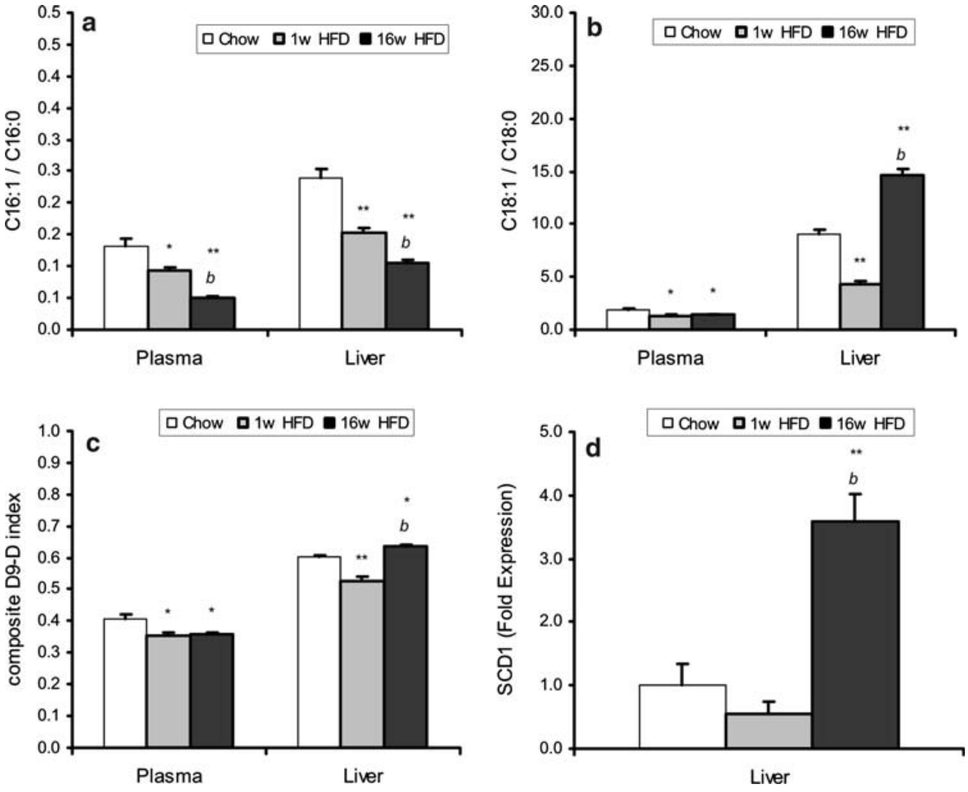

Fig. 4 Δ9D activity indices and Scd1 expression. Δ9D indices **a**, **b**, **c** calculated from fatty acid fractional contents in plasma and liver of fasted HFD-fed and control mice. Scd1 expression determined by real-time quantitative PCR **d** in liver of fasted HFD-fed and control mice. Data are presented as mean ± SEM. T-Test HFD vs. Chow: * $p < 0.05$; ** $p < 0.001$; T-Test 16w-HFD vs. 1w-HFD: *a* $p < 0.05$; *b* $p < 0.001$

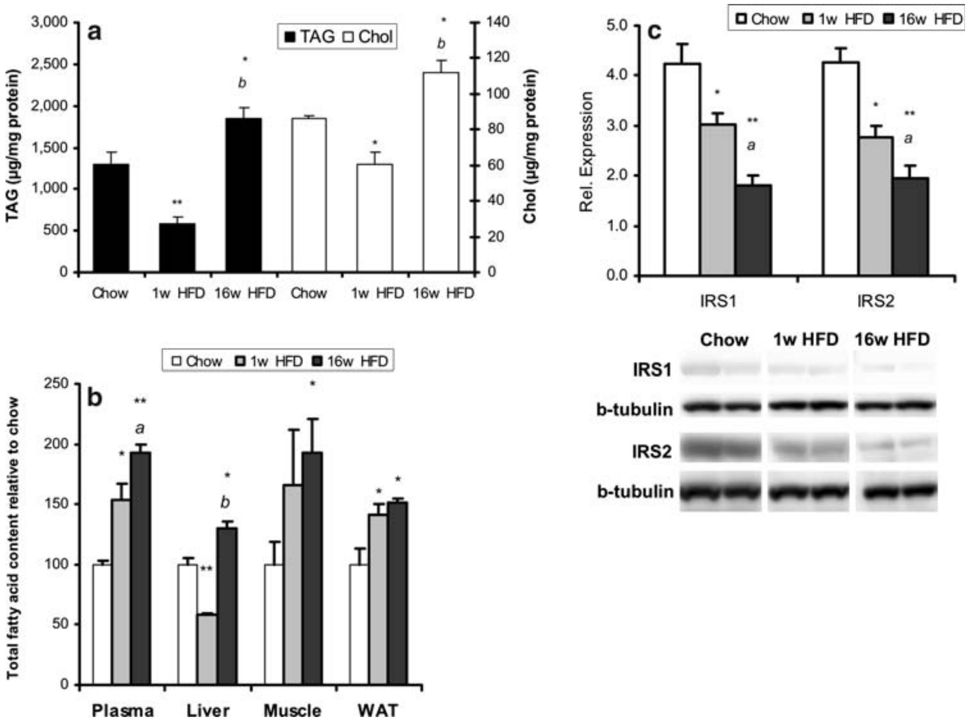

Fig. 5 Liver lipid, tissue fatty acid and liver IRS protein content. Fasting state **a** total TAG and cholesterol content, tissue **b** total fatty acid content and **c** liver IRS protein expression. Total tissue fatty acid content was determined by lipid extraction and quantitative gas chromatography. IRS protein bands were quantified by densitometry and normalized to beta-tubulin. Data are presented as mean ± SEM. T-Test HFD vs. Chow: * $p < 0.05$; ** $p < 0.001$; T-Test 16w-HFD vs. 1w-HFD: *a* $p < 0.05$; *b* $p < 0.001$

feeding while at the same time the precursor C18:2 did not rise, actually decreased after 16 weeks of HFD (Fig. 3). In liver a similar pattern was present in the 1w-HFD group, however, after 16 weeks HFD feeding the hepatic C20:4 content returned to Chow level (Fig. 3).

C20:4, like other PUFA, is enriched in PL and exerts its most important biological functions from that lipid pool. In order to further characterize the changes in C20:4 content in liver we separated liver lipids into TAG, cholesteryl esters (CE), PL and free fatty acids (FFA), and determined total fatty acid content as well as fractional content of C20:4 and other fatty acids in these subclasses (Fig. 6). As expected, C20:4 in the TAG and CE fractions, which are the most abundant lipids in liver showed a pattern similar to that found with total liver lipids (Fig. 3). In contrast, the PL and FFA fractions exhibited a significant increase in C20:4 after 1 week HFD feeding which did not further increase in the 16w-HFD group (Fig. 6, Supplemental Table 2).

Docosahexaenoate is Preserved in Plasma and Liver Phospholipid of Insulin Resistant Mice

Reduction of the final product of the n-3 PUFA synthesis pathway, docosahexaenoate (C22:6), has been mechanistically implicated in insulin resistance [13]. Therefore, we quantified C22:6 as well as its precursors. C22:6 showed little change in plasma, while it was profoundly downregulated in the liver of 16w-HFD but not 1w-HFD mice (Fig. 3). Interestingly, when C22:6 was quantified in liver lipid subclasses, it became apparent that the decrease in total C22:6 was due to a decrease in the CE and TAG compartment while in PL, the compartment most important for PUFA function, C22:6 was preserved and the fractional content was actually increased in the 16w-HFD group (Fig. 6, Supplemental Table 2). A different scenario was found for the precursors of C22:6. The first molecule in the n-3 synthesis pathway, the essential fatty acids α-linolenate (C18:3n-3), and the n-3 intermediates eicosapentaenoate (C20:5) and docosapentaenoate (22:5), were reduced in insulin resistant mice in both plasma and liver (Fig. 3).

Hepatic Expression of Genes Regulating Fatty Acid Synthesis

The profound alterations in fatty acid profiles and liver lipid contents prompted us to look for potential mechanisms involving expression of key genes of lipogenesis and fatty acid metabolism in liver (Table 1). Genes important for lipogenesis (*Acc1*, *Fas*, *Gpat1*, *Dgat2*) were increased in the 16w-HFD group but not in the 1w-HFD group, consistent with the observed increase in liver TAG content in 16w-HFD mice. To understand the increase of C20:4 and C22:6 content in liver we quantified the key genes of PUFA synthesis. The expression of the two elongases important for PUFA elongation, *Elovl5* and *Elovl2*, was moderately decreased in the 16w-HFD group. In contrast, an increase in the expression of the two desaturases essential for PUFA synthesis, *Fads1* and *Fads2*, was observed already after 1 week of HFD, indicating that up-

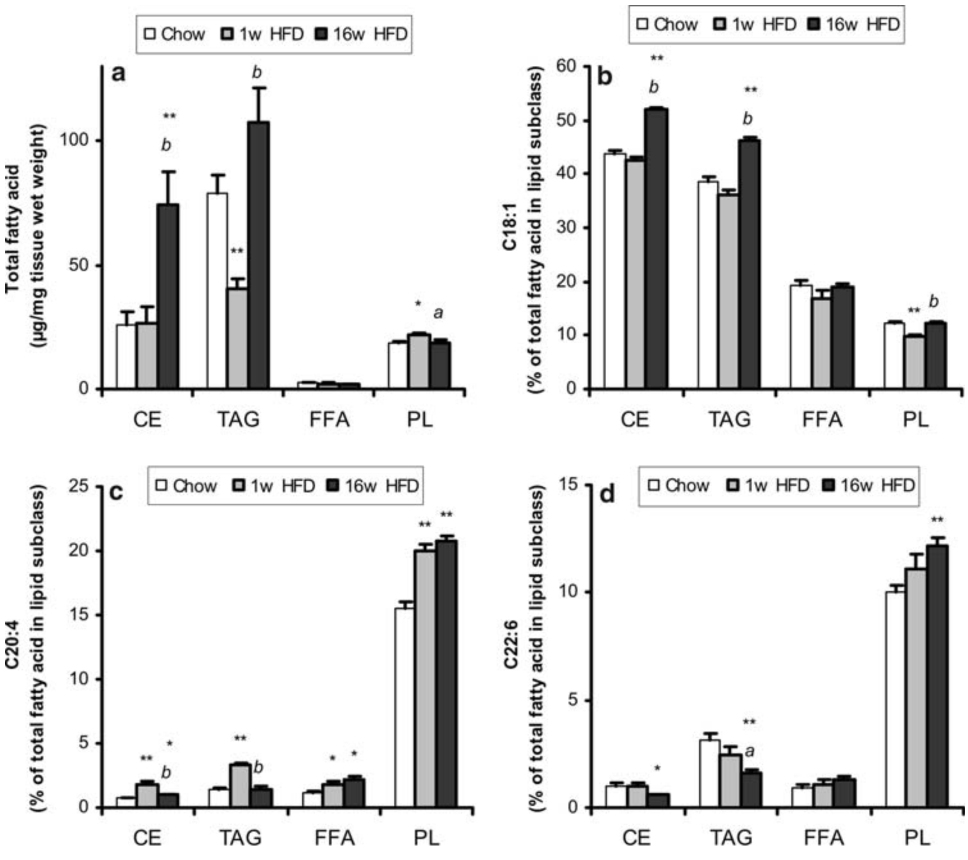

Fig. 6 Fatty acid content in liver lipid subclasses. **a** Total fatty acid content and fractional content of selected fatty acids **b**, **c**, **d** in cholesteryl ester (CE), triacylglycerol (TAG), free fatty acid (FFA) and phospholipid (PL) fractions in livers of fasted mice. Data are presented as mean ± SEM. T-Test HFD vs. Chow: * $p < 0.05$; ** $p < 0.001$; T-Test 16w-HFD vs. 1w-HFD: *a* $p < 0.05$; *b* $p < 0.001$

Table 1 Liver gene expression

	Chow	1w-HFD	16w-HFD
De novo fatty acid synthesis and lipogenesis			
Acc1	2.68 ± 0.38	2.34 ± 0.31	3.96 ± 0.34*^{a}
Fas	3.52 ± 0.34	3.67 ± 0.59	4.85 ± 0.42*
Gpat1	5.84 ± 0.22	6.10 ± 0.51	7.88 ± 0.37**^{a}
Dgat2	32.29 ± 1.53	45.26 ± 4.39*	83.53 ± 3.65**^{b}
Fatty acid elongation			
Elovl2	63.31 ± 4.73	61.43 ± 3.75	27.35 ± 1.55**^{b}
Elovl5	109.59 ± 19.51	116.16 ± 10.90	78.52 ± 8.07^{a}
Elovl6	0.83 ± 0.11	0.77 ± 0.14	0.94 ± 0.15
Fatty acid desaturation			
Scd1 (Δ9D)	102.66 ± 34.77	55.47 ± 20.82	367.38 ± 44.38**^{b}
Fads1 (Δ5D)	23.33 ± 1.32	32.50 ± 4.30	41.33 ± 2.39**
Fads2 (Δ6D)	49.79 ± 2.28	92.61 ± 8.03**	64.05 ± 3.78*^{a}

Gene expression determined by TaqMan real-time PCR was calculated as copy numbers per copy TBP mRNA. Data are mean ± SEM ($n = 6$)

T-Test HFD vs. Chow: * $p < 0.05$; ** $p < 0.001$

T-Test 16w-HFD vs. 1w-HFD: ^{a} $p < 0.05$; ^{b} $p < 0.001$

regulation of these enzymes may be a cause for the observed increase in C20:4 and preservation of C22:6 in liver phospholipids and plasma.

Discussion

The approach of this study was to generate detailed lipid and fatty acid profiles in mice made insulin resistant by means of a HFD. Mild and profound insulin resistance were induced in the mice by feeding HFD for 1 and 16 weeks, respectively. Subsequently, the observed metabolic alterations compared to chow-fed controls were related to the degree of insulin resistance in order to identify novel causative processes and biomarkers. As shown in Fig. 1 and Supplemental Table 1, fasting plasma levels of glucose and insulin were already increased after feeding the HFD for 1 week and were further increased in the chronically HFD-fed group, as expected. Body weight, plasma leptin and plasma total lipids were also significantly increased in the 1w-HFD group compared to the chow-fed controls, and further increased in the 16w-HFD group. Thus, the experimental groups used in this study displayed distinct degrees of insulin resistance, obesity and dyslipidemia and could be used for correlation with multiple lipid parameters.

In order to identify novel lipid markers and mechanisms in diet-induced insulin resistance, we determined fatty acid profiles in plasma and in liver. One striking observation was profound quantitative changes of the most abundant C16 and C18 fatty acids. Surprisingly, the fractional content of C16:1 was decreased in plasma and liver of both HFD-fed groups (Fig. 3) despite higher content of this fatty acid in the diet (Supplemental Table 3). C16:0 content was also decreased, however, only in plasma of the 16w-HFD group (Fig. 3). This observation is in strong contrast to previous human studies, but also to rat experiments, which almost unequivocally found an increase in the fractional content of both C16:0 and C16:1 in insulin resistant states [23, 58]. The reason for this difference is not clear. The mechanisms proposed for humans, namely increased dietary intake of C16:0 and increased Δ9D activity (see below), were also present in our study. Therefore, alternative explanations must be chosen, such as increased conversion to longer fatty acids by fatty acid elongases. Intriguingly, a very recent paper using *Elovl6* knockout mice found that this elongase isoform is rate-limiting for elongation of C16 fatty acids as revealed by accumulation of C16 fatty acids in knockout liver. Furthermore, the knockout conferred protection from HFD-induced liver insulin resistance [42]. In our study we observed the opposite, namely a decrease of fatty acid substrates of ELOVL6 (C12-C16 fatty acids) in plasma and liver (data not shown). Therefore, although liver *Elovl6* mRNA expression was not altered in our study (Table 1) it is possible that flux through Elovl6 or a related elongase was increased in the HFD-fed mice and did contribute to insulin resistance. Quantitative flux studies in metabolic disease models and humans as well as elongase gain of function studies will be needed to clarify the role of Elovl6 and other elongases in the development of insulin resistance.

In the analysis of the fatty acid profiles we also addressed the potential involvement of SCD1, the predominant Δ9D converting SFA to MUFA by calculating a composite Δ9D activity index. The Δ9D index, like the C18:1/C18:0 ratio, exhibited an early and persistent decline in plasma, whereas in liver a transient drop in the 1w-HFD group and a subsequent increase was observed (Fig. 4). Unlike reported in many human studies [23], the C16:1/C16:0 ratio in our study decreased progressively with insulin resistance. The mechanism underlying the decreased ratio is not clear. It may be related to the reduced content of both C16 fatty acids, possibly caused by increased elongation of C16 fatty acids, as discussed above. More studies, taking into account de novo synthesis, elongation and desaturation of C16:0 are warranted to understand why the C16:1/C16:0 ratio behaves differently in mice and humans, and how this is related to insulin resistance.

Given the known strong link between SCD1 activity and lipogenesis, the Δ9D results in liver suggested that lipogenesis was suppressed in the 1w-HFD group and elevated in the 16w-HFD group. Indeed, we found that total TAG and cholesterol content in liver was suppressed after 1 week of HFD feeding and elevated after 16 weeks of HFD feeding (Fig. 5). Surprisingly, despite the suppression of liver lipids after 1 week of HFD, protein levels of IRS1 and IRS2 were already significantly reduced (Fig. 5) suggesting but not proving that liver insulin resistance mechanisms were initiated at this stage. The mechanism underlying these dynamic TAG changes is unclear. Although we observed a downward trend for Scd1 expression in the 1w-HFD group, correlating with the Δ9D index, other lipogenic genes were not down-regulated in the 1w-HFD group. This could mean that lipogenesis is suppressed through posttranscriptional mechanisms. Alternatively, increased, compensatory VLDL secretion could take place in the 1w-HFD group, triggered for example by increased leptin signaling which is likely to be present in the 1w-HFD animals (Fig. 1, [59–61]). Clearly, additional experiments are needed in order to identify the mechanisms causing the drop in liver lipids after short-term HFD feeding and also, to assess their relationship with the initiation of insulin resistance.

The plasma fatty acid profiling in our study revealed profound changes in PUFA content. Fractional content of C20:4, the end product of the n-6 fatty acid synthesis pathway, was increased by about 50% after 1 week of HFD, and doubled after 16 weeks of HFD (Fig. 3). In liver there was an early and persistent increase of C20:4 in PL (Fig. 6, Supplemental Table 2). As a potential mechanism for the C20:4 elevation in liver we identified induction of the two fatty acid desaturases participating in PUFA synthesis, *Fads1* and *Fads2*, which were increased already after 1 week of HFD (Table 1). Elevated C20:4 content and induction of Fads1 or Fads2 in liver has been observed in a few previous studies using insulin resistant rats and mice [40, 41, 54]. However, it is unclear if induction of the C20:4 synthesis pathway does occur in insulin resistance in general, as other animal and human metabolic disease studies have yielded variable results regarding C20:4 content [23, 58]. On the other hand, in most human insulin resistance studies decreased plasma content of the n-6 pathway precursor C18:2 and increased plasma content of the intermediate C20:3 was reported [23], suggesting increased flux through the PUFA synthesis pathway. In any event, our data indicate that n-6 fatty acid synthesis is induced in liver leading to progressively increased C20:4 efflux from liver on the HFD feeding regimen while in liver PL, C20:4 content reaches saturation level at an earlier time point.

The accumulation of C20:4 may have a functional impact on insulin resistance through several mechanisms. For instance, increased availability of C20:4 as a precursor of leukotrienes and other pro-inflammatory eicosanoids may support chronic inflammation, which is known to be one of the causes of insulin resistance [62]. In support of this notion, we observed up-regulation of several inflammatory markers in both liver and adipose tissue already after 1 week of HFD feeding [63]. Alternatively, increased availability of C20:4 may affect insulin signaling directly, for example through activating PKC as shown in a rat liver cell line [64]. On the other hand, low PUFA content in phospholipids has been proposed as an insulin resistance mechanism (see below). Therefore, the induction of C20:4 could also be a mechanism counteracting insulin resistance. Intervention studies using inhibitors of desaturases critical for PUFA synthesis [65] or genetic knockdown studies would be suitable to address the role of C20:4 in the development of insulin resistance.

With respect to n-3 PUFA we found a decrease of C18:3n-3, C20:5 and C22:5 in plasma and liver. Interestingly, in liver the final product of the pathway, C22:6, was markedly reduced in the storage lipid classes (TAG and CE) but not in the PL compartment where it was actually increased after HFD feeding (Fig. 6). Because in plasma, C22:6 was also increased it is reasonable to assume that C22:6 was also not decreased in the PL membranes of the peripheral tissues, for example in skeletal muscle. These findings demonstrate the physiological capability of selectively preserving PUFA in PL membranes. Also, it is in conflict with several studies concluding that in insulin resistance there is a reduction in PUFA content in insulin target tissues and that this does contribute to impaired insulin signaling [13, 32, 33]. At least in the HFD-fed mouse model this does not appear to be the case.

In summary, we performed a comprehensive lipid profiling experiment in HFD-fed mice and confirmed previous reports showing a close correlation of plasma lipids with the degree of insulin resistance and hyperglycemia. Surprisingly, in liver, the 1w-HFD group had lower apparent Δ9D activity as well as markedly reduced TAG and cholesterol content, despite significant insulin resistance. This may indicate a compensatory mechanism directing excessive fat away from liver and into adipose tissue and muscle after short-term HFD feeding. Furthermore, we observed an early induction of desaturases important for PUFA synthesis accompanied by increased C20:4 content, which may play a role in the initiation of insulin resistance. The content of C22:6 was also increased in liver PL and in plasma. These findings indicate that lack of PUFA in cell membranes seems not to be responsible for the induction of insulin resistance in HFD-fed mice, as it has been postulated for other animal models.

Acknowledgments We would like to thank Sandra Ehret for excellent technical assistance, Alexander Bleeck for providing support with the FPLC measurements, Anna Opalek for Western blot analysis and Bernard Vanrossomme for preparation of the NMR samples. This work was supported by grants from the Juergen-Rickertsen-Stiftung and the City of Hamburg (Norgenta).

References

1. Hirsch J, Batchelor B (1976) Adipose tissue cellularity in human obesity. Clin Endocrinol Metab 5:299–311
2. Weyer C, Foley JE, Bogardus C, Tataranni PA, Pratley RE (2000) Enlarged subcutaneous abdominal adipocyte size, but not obesity itself, predicts type II diabetes independent of insulin resistance. Diabetologia 43:1498–1506
3. Lundgren M, Svensson M, Lindmark S, Renstrom F, Ruge T, Eriksson JW (2007) Fat cell enlargement is an independent marker of insulin resistance and 'hyperleptinaemia'. Diabetologia 50:625–633
4. Jernas M, Palming J, Sjoholm K, Jennische E, Svensson PA, Gabrielsson BG, Levin M, Sjogren A, Rudemo M, Lystig TC, Carlsson B, Carlsson LM, Lonn M (2006) Separation of human adipocytes by size: hypertrophic fat cells display distinct gene expression. FASEB J 20:1540–1542
5. Seppala-Lindroos A, Vehkavaara S, Hakkinen AM, Goto T, Westerbacka J, Sovijarvi A, Halavaara J, Yki-Jarvinen H (2002) Fat accumulation in the liver is associated with defects in insulin suppression of glucose production and serum free fatty acids independent of obesity in normal men. J Clin Endocrinol Metab 87:3023–3028
6. Kim JK, Fillmore JJ, Sunshine MJ, Albrecht B, Higashimori T, Kim DW, Liu ZX, Soos TJ, Cline GW, O'Brien WR, Littman DR, Shulman GI (2004) PKC-theta knockout mice are protected from fat-induced insulin resistance. J Clin Invest 114:823–827
7. Utzschneider KM, Kahn SE (2006) Review: the role of insulin resistance in nonalcoholic fatty liver disease. J Clin Endocrinol Metab 91:4753–4761
8. McGarry JD (2002) Banting lecture 2001: dysregulation of fatty acid metabolism in the etiology of type 2 diabetes. Diabetes 51:7–18
9. Taskinen MR (2005) Type 2 diabetes as a lipid disorder. Curr Mol Med 5:297–308
10. Chahil TJ, Ginsberg HN (2006) Diabetic dyslipidemia. Endocrinol Metab Clin North Am 35:491–510
11. Karpe F (1999) Postprandial lipoprotein metabolism and atherosclerosis. J Intern Med 246:341–355
12. Surwit RS, Kuhn CM, Cochrane C, McCubbin JA, Feinglos MN (1988) Diet-induced type II diabetes in C57BL/6 J mice. Diabetes 37:1163–1167
13. Storlien LH, Jenkins AB, Chisholm DJ, Pascoe WS, Khouri S, Kraegen EW (1991) Influence of dietary fat composition on development of insulin resistance in rats. Relationship to muscle triglyceride and omega-3 fatty acids in muscle phospholipid. Diabetes 40:280–289
14. Vessby B, Unsitupa M, Hermansen K, Riccardi G, Rivellese AA, Tapsell LC, Nalsen C, Berglund L, Louheranta A, Rasmussen BM, Calvert GD, Maffetone A, Pedersen E, Gustafsson IB, Storlien LH (2001) Substituting dietary saturated for monounsaturated fat impairs insulin sensitivity in healthy men and women: the KANWU study. Diabetologia 44:312–319
15. Roden M, Price TB, Perseghin G, Petersen KF, Rothman DL, Cline GW, Shulman GI (1996) Mechanism of free fatty acid-induced insulin resistance in humans. J Clin Invest 97:2859–2865
16. Ferrannini E, Barrett EJ, Bevilacqua S, DeFronzo RA (1983) Effect of fatty acids on glucose production and utilization in man. J Clin Invest 72:1737–1747
17. Thiebaud D, DeFronzo RA, Jacot E, Golay A, Acheson K, Maeder E, Jequier E, Felber JP (1982) Effect of long chain triglyceride infusion on glucose metabolism in man. Metabolism 31:1128–1136
18. Ferreira LD, Pulawa LK, Jensen DR, Eckel RH (2001) Overexpressing human lipoprotein lipase in mouse skeletal muscle is associated with insulin resistance. Diabetes 50:1064–1068
19. Kim JK, Fillmore JJ, Chen Y, Yu C, Moore IK, Pypaert M, Lutz EP, Kako Y, Velez-Carrasco W, Goldberg IJ, Breslow JL, Shulman GI (2001) Tissue-specific overexpression of lipoprotein lipase causes tissue-specific insulin resistance. Proc Natl Acad Sci USA 98:7522–7527
20. Maeda K, Cao H, Kono K, Gorgun CZ, Furuhashi M, Uysal KT, Cao Q, Atsumi G, Malone H, Krishnan B, Minokoshi Y, Kahn BB, Parker RA, Hotamisligil GS (2005) Adipocyte/macrophage fatty acid binding proteins control integrated metabolic responses in obesity and diabetes. Cell Metab 1:107–119
21. Bajaj M, Suraamornkul S, Romanelli A, Cline GW, Mandarino LJ, Shulman GI, DeFronzo RA (2005) Effect of a sustained reduction in plasma free fatty acid concentration on intramuscular long-chain fatty Acyl-CoAs and insulin action in type 2 diabetic patients. Diabetes 54:3148–3153
22. Ahren B (2001) Reducing plasma free fatty acids by acipimox improves glucose tolerance in high-fat fed mice. Acta Physiol Scand 171:161–167
23. Vessby B, Gustafsson IB, Tengblad S, Boberg M, Andersson A (2002) Desaturation and elongation of fatty acids and insulin action. Ann NY Acad Sci 967:183–195
24. Buettner R, Parhofer KG, Woenckhaus M, Wrede CE, Kunz-Schughart LA, Scholmerich J, Bollheimer LC (2006) Defining high-fat-diet rat models: metabolic and molecular effects of different fat types. J Mol Endocrinol 36:485–501
25. Ikemoto S, Takahashi M, Tsunoda N, Maruyama K, Itakura H, Ezaki O (1996) High-fat diet-induced hyperglycemia and obesity in mice: differential effects of dietary oils. Metabolism 45:1539–1546
26. Tsunoda N, Ikemoto S, Takahashi M, Maruyama K, Watanabe H, Goto N, Ezaki O (1998) High-monounsaturated fat diet-induced obesity and diabetes in C57BL/6J mice. Metabolism 47:724–730
27. Lee JS, Pinnamaneni SK, Eo SJ, Cho IH, Pyo JH, Kim CK, Sinclair AJ, Febbraio MA, Watt MJ (2006) Saturated, but not n-6 polyunsaturated, fatty acids induce insulin resistance: role of intramuscular accumulation of lipid metabolites. J Appl Physiol 100:1467–1474
28. Browning LM, Krebs JD, Moore CS, Mishra GD, O'Connell MA, Jebb SA (2007) The impact of long chain n-3 polyunsaturated fatty acid supplementation on inflammation, insulin sensitivity and CVD risk in a group of overweight women with an inflammatory phenotype. Diabetes Obes Metab 9:70–80
29. Mostad IL, Bjerve KS, Bjorgaas MR, Lydersen S, Grill V (2006) Effects of n-3 fatty acids in subjects with type 2 diabetes: reduction of insulin sensitivity and time-dependent alteration from carbohydrate to fat oxidation. Am J Clin Nutr 84:540–550
30. Friedberg CE, Janssen MJ, Heine RJ, Grobbee DE (1998) Fish oil and glycemic control in diabetes. A meta-analysis. Diabetes Care 21:494–500
31. Giacco R, Cuomo V, Vessby B, Uusitupa M, Hermansen K, Meyer BJ, Riccardi G, Rivellese AA (2007) Fish oil, insulin sensitivity, insulin secretion and glucose tolerance in healthy people: is there any effect of fish oil supplementation in relation to the type of background diet and habitual dietary intake of n-6 and n-3 fatty acids? Nutr Metab Cardiovasc Dis 17:572–580
32. Borkman M, Storlien LH, Pan DA, Jenkins AB, Chisholm DJ, Campbell LV (1993) The relation between insulin sensitivity and the fatty-acid composition of skeletal-muscle phospholipids. N Engl J Med 328:238–244

33. Pan DA, Lillioja S, Milner MR, Kriketos AD, Baur LA, Bogardus C, Storlien LH (1995) Skeletal muscle membrane lipid composition is related to adiposity and insulin action. J Clin Invest 96:2802–2808
34. Sampath H, Miyazaki M, Dobrzyn A, Ntambi JM (2007) Stearoyl-CoA desaturase-1 mediates the pro-lipogenic effects of dietary saturated fat. J Biol Chem 282:2483–2493
35. Ntambi JM, Miyazaki M, Stoehr JP, Lan H, Kendziorski CM, Yandell BS, Song Y, Cohen P, Friedman JM, Attie AD (2002) Loss of stearoyl-CoA desaturase-1 function protects mice against adiposity. Proc Natl Acad Sci USA 99:11482–11486
36. Jiang G, Li Z, Liu F, Ellsworth K, Dallas-Yang Q, Wu M, Ronan J, Esau C, Murphy C, Szalkowski D, Bergeron R, Doebber T, Zhang BB (2005) Prevention of obesity in mice by antisense oligonucleotide inhibitors of stearoyl-CoA desaturase-1. J Clin Invest 115:1030–1038
37. Gutierrez-Juarez R, Pocai A, Mulas C, Ono H, Bhanot S, Monia BP, Rossetti L (2006) Critical role of stearoyl-CoA desaturase-1 (SCD1) in the onset of diet-induced hepatic insulin resistance. J Clin Invest 116:1686–1695
38. Stumvoll M (2004) Control of glycaemia: from molecules to men. Minkowski lecture 2003. Diabetologia 47:770–781
39. Sjogren P, Sierra-Johnson J, Gertow K, Rosell M, Vessby B, de Faire U, Hamsten A, Hellenius ML, Fisher RM (2007) Fatty acid desaturases in human adipose tissue: relationships between gene expression, desaturation indexes and insulin resistance. Diabetologia 51(2):328–335
40. Brenner RR, Rimoldi OJ, Lombardo YB, Gonzalez MS, Bernasconi AM, Chicco A, Basabe JC (2003) Desaturase activities in rat model of insulin resistance induced by a sucrose-rich diet. Lipids 38:733–742
41. Wang Y, Botolin D, Xu J, Christian B, Mitchell E, Jayaprakasam B, Nair MG, Peters JM, Busik JV, Olson LK, Jump DB (2006) Regulation of hepatic fatty acid elongase and desaturase expression in diabetes and obesity. J Lipid Res 47:2028–2041
42. Matsuzaka T, Shimano H, Yahagi N, Kato T, Atsumi A, Yamamoto T, Inoue N, Ishikawa M, Okada S, Ishigaki N, Iwasaki H, Iwasaki Y, Karasawa T, Kumadaki S, Matsui T, Sekiya M, Ohashi K, Hasty AH, Nakagawa Y, Takahashi A, Suzuki H, Yatoh S, Sone H, Toyoshima H, Osuga J, Yamada N (2007) Crucial role of a long-chain fatty acid elongase, Elovl6, in obesity-induced insulin resistance. Nat Med 13:1193–1202
43. Collins S, Martin TL, Surwit RS, Robidoux J (2004) Genetic vulnerability to diet-induced obesity in the C57BL/6J mouse: physiological and molecular characteristics. Physiol Behav 81:243–248
44. Heeren J, Niemeier A, Merkel M, Beisiegel U (2002) Endothelial-derived lipoprotein lipase is bound to postprandial triglyceride-rich lipoproteins and mediates their hepatic clearance in vivo. J Mol Med 80:576–584
45. Nicholson JK, Foxall PJ, Spraul M, Farrant RD, Lindon JC (1995) 750 MHz 1H and 1H-13C NMR spectroscopy of human blood plasma. Anal Chem 67:793–811
46. Price WS (1999) Water signal suppression in NMR spectroscopy. Annu Rep NMR Spectrosc 38(38):289–354
47. Zitzer H, Wente W, Brenner MB, Sewing S, Buschard K, Gromada J, Efanov AM (2006) Sterol regulatory element-binding protein 1 mediates liver X receptor-beta-induced increases in insulin secretion and insulin messenger ribonucleic acid levels. Endocrinology 147:3898–3905
48. Livak KJ, Schmittgen TD (2001) Analysis of relative gene expression data using real-time quantitative PCR and the 2(-Delta Delta C(T)) method. Methods 25:402–408
49. Folch J, Lees Ascolli M, Ascolli I, Meath JA, LeBaron N (1951) Preparation of lipide extracts from brain tissue. J Biol Chem 191:833–841
50. Hamilton JG, Comai K (1988) Rapid separation of neutral lipids, free fatty acids and polar lipids using prepacked silica Sep-Pak columns. Lipids 23:1146–1149
51. Lepage G, Roy CC (1986) Direct transesterification of all classes of lipids in a one-step reaction. J Lipid Res 27:114–120
52. Levy JR, Lesko J, Krieg RJ Jr, Adler RA, Stevens W (2000) Leptin responses to glucose infusions in obesity-prone rats. Am J Physiol Endocrinol Metab 279:E1088–E1096
53. Bradley RL, Cheatham B (1999) Regulation of ob gene expression and leptin secretion by insulin and dexamethasone in rat adipocytes. Diabetes 48:272–278
54. Biddinger SB, Almind K, Miyazaki M, Kokkotou E, Ntambi JM, Kahn CR (2005) Effects of diet and genetic background on sterol regulatory element-binding protein-1c, stearoyl-CoA desaturase 1, and the development of the metabolic syndrome. Diabetes 54:1314–1323
55. Inokuchi T, Orita M, Imamura K, Takao T, Isogai S (1992) Resistance to ketosis in moderately obese patients: influence of fatty liver. Intern Med 31:978–983
56. Vice E, Privette JD, Hickner RC, Barakat HA (2005) Ketone body metabolism in lean and obese women. Metabolism 54:1542–1545
57. Azain MJ, Ontko JA (1989) An explanation for decreased ketogenesis in the liver of the obese Zucker rat. Am J Physiol 257:R822–R828
58. Fukuchi S, Hamaguchi K, Seike M, Himeno K, Sakata T, Yoshimatsu H (2004) Role of fatty acid composition in the development of metabolic disorders in sucrose-induced obese rats. Exp Biol Med (Maywood) 229:486–493
59. Huang W, Dedousis N, Bandi A, Lopaschuk GD, O'Doherty RM (2006) Liver triglyceride secretion and lipid oxidative metabolism are rapidly altered by leptin in vivo. Endocrinology 147:1480–1487
60. Huang W, Dedousis N, O'Doherty RM (2007) Hepatic steatosis and plasma dyslipidemia induced by a high-sucrose diet are corrected by an acute leptin infusion. J Appl Physiol 102:2260–2265
61. Lin S, Thomas TC, Storlien LH, Huang XF (2000) Development of high fat diet-induced obesity and leptin resistance in C57Bl/6 J mice. Int J Obes Relat Metab Disord 24:639–646
62. Hotamisligil GS (2006) Inflammation and metabolic disorders. Nature 444:860–867
63. Scheja L, Heese B, Zitzer H, Michael MD, Siesky AM, Pospisil H, Beisiegel U, Seedorf K (2008) Acute-phase serum amyloid A as a marker of insulin resistance in mice. Exp Diabetes Res 2008 (article ID 230837)
64. Puljak L, Pagliassotti MJ, Wei Y, Qadri I, Parameswara V, Esser V, Fitz JG, Kilic G (2005) Inhibition of cellular responses to insulin in a rat liver cell line. A role for PKC in insulin resistance. J Physiol 563:471–482
65. Obukowicz MG, Welsch DJ, Salsgiver WJ, Martin-Berger CL, Chinn KS, Duffin KL, Raz A, Needleman P (1998) Novel, selective delta6 or delta5 fatty acid desaturase inhibitors as anti-inflammatory agents in mice. J Pharmacol Exp Ther 287:157–166

Introduction

Bdellovibrios (*Bdellovibrio* and like organisms; BALO) are fast swimming, small, comma- or crescent-shaped delta-proteobacteria that prey on larger Gram-negative bacteria [1–6]. After collision and attachment to the surface the predator penetrates the host cell then proliferates in the intraperiplasmic space of the prey producing large, rounded bdelloplasts [7, 8]. The parasitic phase is characterized by degradation of host macromolecules and uptake of the products into *Bdellovibrio*, which grows as a filament [9–13]. The filament forms septa and individual progeny cells are released during lysis of the host cell. BALO are ubiquitous and live in a wide range of water and soil habitats [2, 14, 15]. Because of their predatory and parasitic life style, it has been suggested that these bacteria might prove useful in treating environmental pollution, purifying drinking water systems, disrupting biofilms, and serving as potential agents for clearing bacterial infections [14, 16–18].

Bdellovibrio bacteriovorus is the major experimental system for studying predatory and parasitic bacteria [4, 14] and the genome of this bacterium has been sequenced [3]. Previous radiotracer studies showed that this bacterium mainly utilizes host fatty acids during intraperiplasmic growth but that it also has the capacity to synthesize some of its own [19–21]. However, details such as the identification of the bacterium's phospholipid classes are lacking. In contrast, much more is known about the lipids of the facultative predatory strain UKi2 of *Bacteriovorus stolpii* [22] (formerly also referred to as *Bdellovibrio bacteriovorus* [6, 23] and *Bdellovibrio stolpiii* UKi2 [23]), which can be grown axenically. Once thought to be closely related, *Bdellovibrio* and *Bacteriovorus* were designated as separate genera in 2000 and various species were reassigned after genotyping data showed these organisms represented distant phylogenetic backgrounds [23, 24]. In 1973, Steiner et al. [22] reported that *B. stolpii* UKi2 contained several sphingophosphonolipids (SPNL). More recently, the structural identities of 18 molecular species of *B. stolpii* UKi2 SPNL were elucidated by mass spectrometry (MS) and nuclear magnetic resonance (NMR) spectroscopy techniques [25, 26].

Host-independent (HID) *B. bacteriovorus* strains are readily derived from host-dependent (HD) strains [27–30] and these facultative predators grow in axenic cultures. Since the biochemical makeup of axenically grown HID bacteria would not be complicated by the presence of compounds scavenged by parasitizing prey cells, such organisms can be analyzed and compared to the lipids of axenically grown *B. stolpii* UKi2. In the present study the major glycerophospholipids and fatty acids were identified in *Bdellovibrio bacteriovorus* strain HID5 providing new data on the biochemical nature of this important predatory and parasitic bacterium.

Experimental Procedures

Organisms

Bdellovibrio bacteriovorus host-independent strain (HID5) was obtained from Carey Lambert and Elizabeth Sockett (University of Nottingham, UK), which was fully capable of predatory behavior and exhibited parasitic growth at the time of these studies. Cultures were grown in axenically in PY medium (1% yeast extract and 0.3% peptone) for four days at 29 °C in a shaker at 200 rpm. 50-ml cultures in 250 ml Erlenmeyer flasks or 500-ml in Fernbach flasks were grown for analyses. Organisms were harvested by centrifugation at 10,000*g* for 10 min at 4 °C. The supernatant was discarded and the pellet was washed three times with double-distilled water (ddH$_2$0) and the final pellet was extracted for lipids.

Strain HD100 cultures, the parental strain of HID5, were maintained in liquid or agar plate cultures with *Escherichia coli* (K12). For mass cultures, an overnight culture of *E. coli* was grown at 37 °C in a shaking incubator at 200 rpm in YT medium (1.6% tryptone, 1% yeast extract, 0.5% NaCl). HD100 and *E. coli* cells were washed in a buffered solution containing 20 mM HEPES and 2.5 mM CaCl$_2$, pH 7.4 (Ca/HEPES buffer) then combined. The mixed cell suspension was incubated at 29 °C on a shaker at 200 rpm for 1–2 days and aliquots were microscopically monitored for complete lysis of the *E. coli* cells by *B. bacteriovorus* HD100.

Lipid Extraction and Analysis

All organic solvents were redistilled before use. Butylated hydroxytoluene (BHT, Shell Chemical Co., NY, USA) was added to all solvents at a final concentration of 8 µg/ml and dried lipid samples were stored under N$_2$ atmosphere to prevent oxidation of the lipids. BHT was excluded from solvents during the preparation of fatty acid methyl esters (FAME) for gas–liquid chromatographic (GLC) analysis.

The cell pellet was extracted for total lipids with CHCl$_3$:methanol (MeOH):ddH$_2$O (1:2:0.75, v/v/v) [31] for 24 h at room temperature. The lipids were purified by biphasic partitioning [32] then fractionated by adsorption column chromatography (Unisil, Clarkson Chromatography Products Inc., South Williamsport, PA, USA). The neutral lipid fraction was eluted with CHCl$_3$, and polar lipids were eluted with MeOH. Sample volumes were reduced on a rotary evaporator, redissolved in CHCl$_3$:MeOH (2:1, v/v), transferred into 4 dram screw-capped shell vials and were dried down under a stream of N_2 and quantified gravimetrically.

Thin-Layer Chromatography

The polar lipids were separated into individual phospholipid classes by thin-layer chromatography (TLC). Lipids on TLC plates were initially identified by the stain formulated by Dittmer and Lester [33] for phospholipids, Draggendorf for choline [34], ninhydrin for primary amines [34]. Iodine vapor, H_2O and UV illumination were non-destructive methods used for visualizing the separated lipid classes. Authentic phosphatidylethanolamine (PE), phosphatidylcholine (PC), phosphatidylserine (PS), phosphatidylinositol (PI), cardiolipin (CL) (all from Avanti Polar Lipids, Inc., Alabaster, AL) and phosphatidylglycerol (PG) (Sigma Chemical Co, St Louis, MO, USA) served as standards.

Preparative 1-D TLC for isolating individual lipids was performed on 500 µm-thick Silica H plates (Analtech, Newark, DE, USA) using $CHCl_3$:MeOH:acetic acid:water (170:25:25:6, v/v/v/v; SS #1). This system separated lipids into three distinct bands (from the origin to the solvent front), band 1 (PG); band 2 (PS and PE); and band 3 [CL and *N*-acylphosphatidylethanolamine (NAPE)]. After recovering material in band 2, PE and PS were resolved on Silica 60 HPTLC plates (Merck KGaA, Darmstadt, Germany) developed in *n*-propanol:*n*-propylamine:ddH_2O (80:15:5, v/v/v; SS #2) [25, 26]. Similarly, CL and NAPE recovered from band 3 by 1-D TLC were also separated using SS #2.

Analytical 2-D HPTLC Silica 60 plates were used to quantify individual phospholipids using $CHCl_3$:MeOH:H_2O (65:35:8, v/v/v; SS#3) in the first dimension. After the plate was dried, it was redeveloped in the same direction using $CHCl_3$:MeOH:acetic acid (90:2:8, v/v/v; SS#4). After drying overnight, the plate was developed in the second dimension using SS #2 and stained for phosphorus [33]. Stained plates were scanned at 200 dpi (HP Scanjet 5590, Hewlett-Packard, L.P.) and quantified by image analysis (Metamorph2, Universal Imaging Corp., West Chester, PA, USA).

Analysis for Sphingolipids

To test whether sphingophosphonolipids were present in *B. bacteriovorus*, the total polar lipid fraction and individual TLC-purified phospholipid classes were subjected to mild alkaline hydrolysis [35]. The products were recovered and analyzed by TLC in SS#1 and stained for phosphorus [33].

Fatty Acids

Individual TLC-purified phospholipid classes were subjected to mild alkaline methanolysis to produce fatty acid methyl esters (FAME). Alternatively, fatty acids were hydrolyzed then subjected to online derivatization in the GLC injection port according to the micro-method of MacGee and Allen [36]. Briefly, lipid components separated by TLC were saponified in 0.5 ml of 15% KOH–MeOH, phosphoric acid was added then the fatty acids were extracted into hexane. Fatty acids were then extracted from the hexane and concentrated into 10 µl of Meth-Prep I (Alltech Associates Inc, Deerfield, IL, USA) and injected with methylpropionate:methanol (1:2, v/v) into the gas chromatograph.

Gas-Liquid Chromatography

FAME were separated and quantified using a Hewlett-Packard 5890 gas chromatograph equipped with a 30 m × 0.32 mm DB-1 fused silica capillary column (J&W Scientific, Folsom, CA, USA). The instrument was operated isothermally with 180 °C oven temperature. Injection port was set at 225 °C and the flame ionization detector (FID) temperature was set at 290 °C. Helium was the carrier gas at a flow rate of 1 ml/min. Initial identification of the fatty acids were made by comparing retention times with those of authentic standards (various mixtures from Matreya, Pleasant Gap, PA, USA, and Alltech) and confirmed by GC–MS. Peaks on chromatograms that did not correspond to available authentic standards were identified by GC–MS.

Dimethyl Disulfide Derivatization and GC/MS

Dimethyl disulfide derivatives of the *B. bacteriovorus* FAME were prepared by adding 200 µl of dimethyl disulfide to the FAME samples [37]. A small iodine crystal of iodine was added and the solution was heated to 50 °C for 2 h. After cooling, 800 µl of a sodium thiosulfate solution (0.9541 g $Na_2S_2O_3 \cdot 5H_2O$ in 10 ml of water) was added. The derivatization procedure adds dimethyl disulfide across double bonds resulting in dithiomethoxy derivatives. The dithiomethoxy methyl esters were extracted with 600 µl of hexane. Nitrogen gas was used to concentrate the methyl esters by evaporating the hexane.

After dimethyl disulfide derivatization, analyses of the methyl esters derived from the phospholipids were performed using a Waters Micromass GCT^{TM} GC/MS mass spectrometer. The gas chromatographic portion of the GCT^{TM} was an Agilent Technologies model 6890 N gas chromatograph. Separation was performed using a J&W Scientific DB-XLB column (length: 30 m; ID 0.25 mm; film: 0.25 µm). Samples were injected under splitless conditions at 290 °C with helium as the carrier gas. The temperature was held at 120 °C for 1 min and increased at 10 °C/min to 290 °C and held for the remainder of the

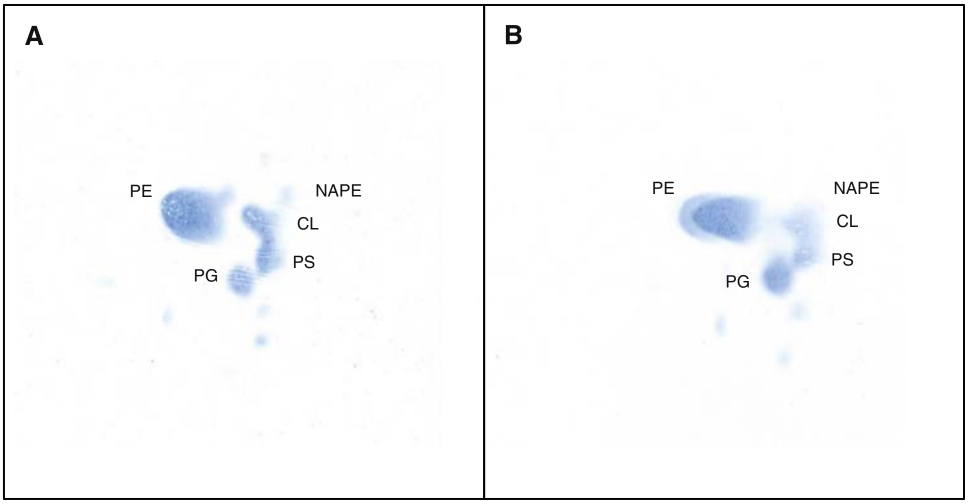

Fig. 1 Two-dimensional HPTLC separations of *B. bacteriovorus* strain HID5 (**a**) and strain HD100 (**b**) phospholipids stained for phosphorus. *PE* phosphatidylethanolamine, *CL* cardiolipin, *PG* phosphatidylglycerol, *PS* phosphatidylserine, *NAPE N*-acylphosphatidylethanolamine. These same major phospholipid classes were present in both strains

45-min analysis. Electron ionization (EI) mass spectrometry was performed using 70 eV electrons with a 200 μA trap current. The mass spectrometer's source was held at 180 °C.

Nanospray Mass Spectrometry

Analyses of the separated phospholipids were performed in a Thermo Finnigan LTQ-FT^{TM} MS using the static nanospray source. New Objective PicoTip^{TM} emitters (2 μm tip) were used for sample introduction. Nanospray solutions were prepared by dissolving the dried samples in $CHCl_3$ followed by adding an equal volume of either MeOH or MeOH with 0.1 N NH_4OH. The source voltage was held at 1.70 kV with a capillary temperature of 175 °C. Capillary, tube lens, and other voltages varied and were optimized prior to data collection. High mass accuracy measurements of both the nanosprayed ions and product ions arising from collisional-induced dissociation, was performed in the Fourier transform ion cyclotron resonance (FT-ICR) portion of the LTQ-FT^{TM}. FT-ICR data were acquired with the resolution set at 100,000. Collision-induce dissociation (MS^n) was performed in the linear ion trap portion of the LTQ-FT^{TM} with a normalized collision energy of 25. Automatic gain control (AGC) was used during data acquisition with the following settings: LTQ full scan 3e4; LTQ Selective Ion Monitoring (SIM) 1e4; LTQ MS^n 1e4; FT full scan 5e5; FT SIM 5e5; FT MS^n 1e5.

Results

Total extractable lipids and phospholipid composition of *B. bacteriovorus* HID5. Stationary phase cultures (500 ml) yielded 27 mg total extractable lipids (±2 SEM, $n = 3$). The neutral and polar lipid fractions accounted for 17 and 83%, respectively, of the total lipids (97% recovery). Approximately 8–10 phosphorus-positive spots were resolved and detected by 2-D HPTLC in the polar lipid fraction (Fig. 1). Five major components were tentatively identified by TLC migrations and staining properties compared to those of authentic standards. PE, PS and NAPE were phosphorus- and ninhydrin-positive; no spot stained with the Dragendorff reagent hence choline lipids were not detected. The relative percentages of the five identified phospholipid classes quantified by 2-D HPTLC separations and visualized by staining for phosphorus indicated the relative abundance of the phospholipid classes was $PE > PS = PG = CL \gg NAPE$ (Table 1). However, as the lipids were stained for phosphorus and since CL contains two atoms of phosphorus, the moles of CL would be approximately half and the estimated moles of CL present in both strains were less than those estimated for PS and PG (Table 1).

After saponification, no detectable phosphorus-positive components were detected by 1-D HPTLC using SS #1 and by 2-D HPTLC using the same solvent systems described above. Thus alkaline-stable sphingolipids were not detectable among the phospholipids of *B. bacteriovorus* under the experimental conditions and analytical methods used in the present study. These analyses did not rule out the possible presence of free ceramides in the bacterium.

Mass spectrometric identification of B. bacteriovorus *HID5 phospholipids.* The identities of the five major phospholipid components in *B. bacteriovorus* HID5 were determined by accurate mass (Fig. 2; Table 2) and tandem MS procedures. The dominant phospholipid was PE and PS, PG and CL were also readily detected and identified. We were able to identify a minor phospholipid class in *B. bacteriovorus* by MS as the relatively rare phospholipid NAPE.

FT-ICR provided exceptional mass accuracy, typically less than 500 ppb, resulting in confident assignments of elemental composition (Fig. 2; Table 2). Ions were

Table 1 The major phospholipid classes of *B. bacteriovorus*

Strain	PE	CL	PG	PS	NAPE
HID5	54.3 ± 5.1	13.0 ± 1.2	14.3 ± 1.8	18.0 ± 3.8	<1
HD100	60.3 ± 1.8	8.3 ± 0.8	17.7 ± 1.2	13.7 ± 1.7	<1

Phospholipids were separated by 2-D HPTLC, stained for phosphorus, scanned, and quantified by image analysis. Values are expressed as percent of total identified phospholipids

observed in the negative ion mode and represented the deprotonated form of the molecular species. The data was acquired at 100,000 mass resolution for *m/z* 400. This high resolution characteristic of an FT instrument was necessary to separate isobaric species including complications arising from isotopic contributions. While the FT-ICR data assigned elemental compositions, tandem mass spectrometry or MS^n data from the linear ion trap, provided structural information.

Multiple stages of tandem MS up to MS^4, were used to characterize the phospholipids. Negative ion MS/MS clearly identified the fatty acid components of phospholipids by product ions resulting from ketene loss, carboxylic acid loss, or directly as illustrated by the observed carboxylate anions. The observed product ions for the PG anions corresponded well with the literature [38]. Transferring the MS/MS product ions to the FT-ICR portion of the

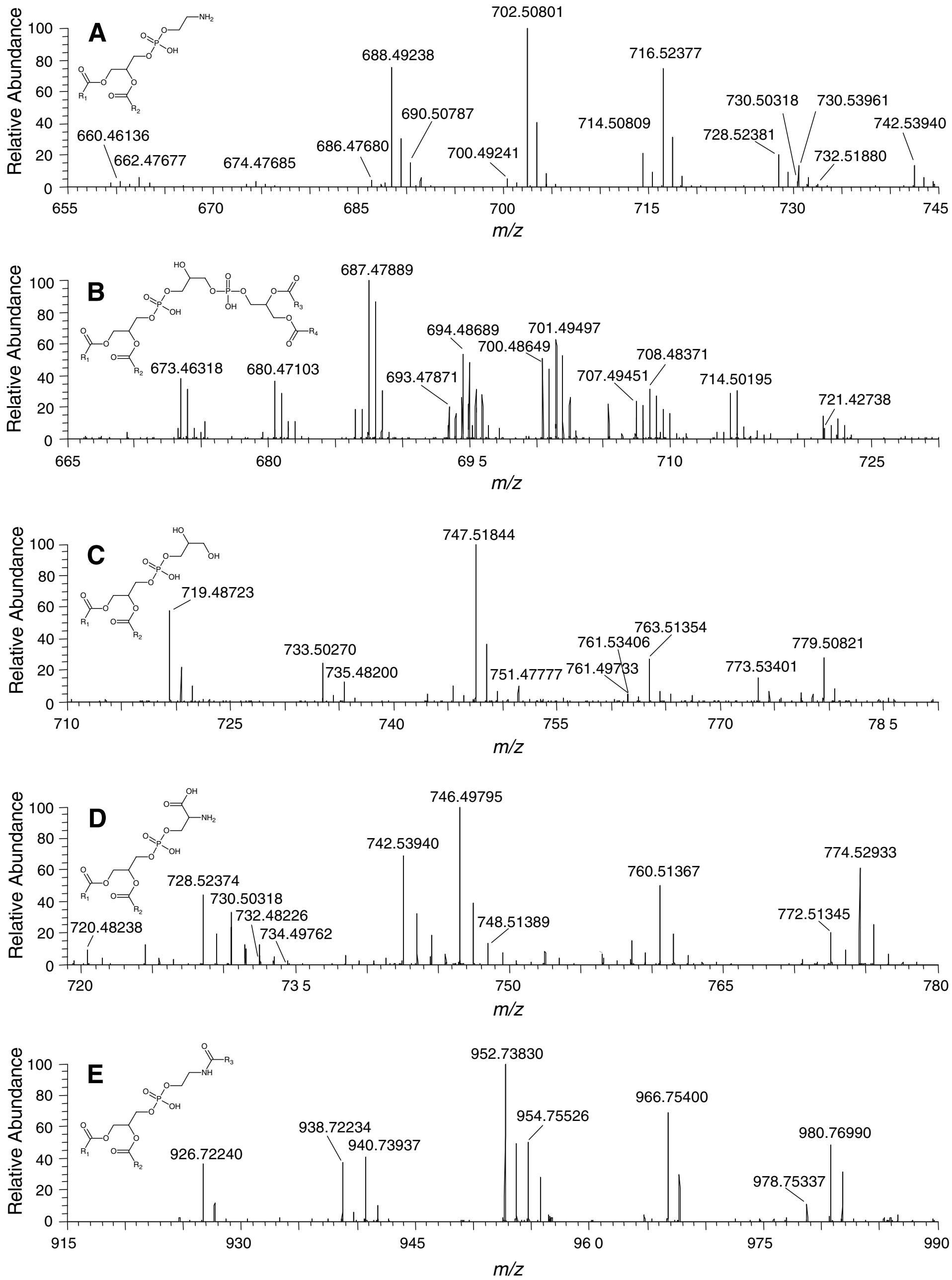

Fig. 2 Nanospray ionization high mass accuracy mass spectra of the major glycerophospholipids identified in *B. bacteriovorus* HID5. Phosphatidylethanolamine (**a**); cardiolipin (diphosphatidylglycerol) (**b**); phosphatidylglycerol (**c**); Phosphatidylserine (**d**); *N*-acylphosphatidylethanolamine (**e**). Ions were acquired in the negative ion mode and represent the deprotonate form of the molecular species

Table 2 Accurate mass MS identification of isolated intact *B. bacteriovorus* HID5 phospholipids

Ion mass (*m/z*)	Elemental composition	Error (ppb)	Major fatty acids[a]
Phosphatidylethanolamines			
660.46136	$C_{35}H_{67}NO_8P^-$	575	–[b]
662.47677	$C_{35}H_{69}NO_8P^-$	211	C14:0/C16:0
674.47685	$C_{36}H_{69}NO_8P^-$	325	C15:0/C16:1; C14:0/C17:1[c]
676.45188	$C_{36}H_{71}NO_8P^-$	−592	–
686.47680	$C_{37}H_{69}NO_8P^-$	247	–
688.49238	$C_{37}H_{71}NO_8P^-$	144	C16:0/C16:1
690.50787	$C_{37}H_{73}NO_8P^-$	−88	C16:0/C16:0
700.49241	$C_{38}H_{71}NO_8P^-$	185	–
702.50801	$C_{38}H_{73}NO_8P^-$	113	C16:0/C17:1[c]
704.48740	$C_{37}H_{71}NO_9P^-$	291	–
714.50809	$C_{39}H_{73}NO_8P^-$	223	C16:1/C18:1
716.523677	$C_{39}H_{75}NO_8P^-$	264	C16:1/C18:0
728.52381	$C_{40}H_{75}NO_8P^-$	315	C17:1[c]/C18:1
730.50312	$C_{39}H_{73}NO_9P^-$	376	(C16:1/ C18:1) + O[d,e]
730.53961	$C_{40}H_{77}NO_8P^-$	519	C16:0/C19:1[c]
732.51880	$C_{39}H_{75}NO_9P^-$	416	–
742.53940	$C_{41}H_{77}NO_8P^-$	228	C18:1/C18:1
744.51878	$C_{40}H_{75}NO_9P^-$	382	(C17:1[c]/ C18:1) + O[f]
Phosphatidylserines			
720.48238	$C_{37}H_{71}NO_{10}P^-$	375[g]	C15:0/C16:0
732.48226	$C_{38}H_{71}NO_{10}P^-$	205[g]	C16:0/C16:1
734.49762	$C_{38}H_{73}NO_{10}P^-$	−190[g]	C16:0/C16:0; C15:0/C17:0
746.49795	$C_{39}H_{73}NO_{10}P^-$	255	C16:1/C17:0
748.51389	$C_{39}H_{75}NO_{10}P^-$	641[g]	C16:0/C17:0
760.51367	$C_{40}H_{75}NO_{10}P^-$	342	C16:0/C18:1
772.51345	$C_{41}H_{75}NO_{10}P^-$	52	C16:1/C19:1[c]; C17:1[c]/C18:1
774.52933	$C_{41}H_{77}NO_{10}P^-$	349	C16:0/C19:1[c]; C17:0/C18:1
N-Acylphosphatidylethanolamines			
926.72240	$C_{53}H_{101}NO_9P^-$	490	–
938.72234	$C_{54}H_{101}NO_9P^-$	419	–
940.73937	$C_{54}H_{103}NO_9P^-$	1,885[g]	–
952.73830	$C_{55}H_{103}NO_9P^-$	739	–
954.75526	$C_{55}H_{105}NO_9P^-$	2,109	–
966.75400	$C_{56}H_{105}NO_9P^-$	779	–
978.75337	$C_{57}H_{105}NO_9P^-$	126	–
980.76990	$C_{57}H_{107}NO_9P^-$	1,023	–
Phosphatidylglycerols			
719.48723	$C_{38}H_{72}O_{10}P^-$	513	C16:0/C16:1
733.50270	$C_{39}H_{74}O_{10}P^-$	258	C16:0/C17:1[c]
735.48200	$C_{38}H_{72}O_{11}P^-$	305	C16:0/ (C16:1 + O)
747.51844	$C_{40}H_{76}O_{10}P^-$	373	C16:0/C18:1
751.47777	$C_{38}H_{72}O_{12}P^-$	1,400[g]	–
761.49733	$C_{40}H_{74}O_{11}P^-$	−126	–
761.53406	$C_{41}H_{78}O_{10}P^-$	327	–
763.51354	$C_{40}H_{76}O_{11}P^-$	608	C16:0/(C18:1 + O)
779.50821	$C_{40}H_{76}O_{12}P^-$	282	–
Cardiolipins			
673.46318	$C_{73}H_{136}O_{17}P_2^{-2}$	−13	C16:0/C16:0/ C16:1/C16:1
680.47103	$C_{74}H_{138}O_{17}P_2^{-2}$	24	C16:0/C16:0/ C16:1/C17:1[c]
687.47889	$C_{75}H_{140}O_{17}P_2^{-2}$	74	C16:0/C16:0/ C16:1/C18:1
693.47871	$C_{76}H_{140}O_{17}P_2^{-2}$	−186	C16:0/C16:1/ C17:1[c]/C18:1
694.48689	$C_{76}H_{142}O_{17}P_2^{-2}$	326	C16:0/C16:0/ C17:1[c]/C18:1
700.48647	$C_{77}H_{142}O_{17}P_2^{-2}$	−248	–
701.49497	$C_{77}H_{144}O_{17}P_2^{-2}$	686[g]	C16:0/C16:0/ C18:1/C18:1
707.49451	$C_{78}H_{144}O_{17}P_2^{-2}$	30	C16:0/C17:1[c]/ C18:1/C18:1
708.48371	$C_{77}H_{142}O_{18}P_2^{-2}$	−580[h]	–
713.49395	$C_{79}H_{144}O_{17}P_2^{-2}$	−755	–
714.50195	$C_{79}H_{146}O_{17}P_2^{-2}$	−509	C16:0/C18:1/ C18:1/C18:1
721.49176	$C_{79}H_{144}O_{18}P_2^{-2}$	−258	–
722.49898	$C_{79}H_{146}O_{18}P_2^{-2}$	1,095[g]	–

[a] Minor components may also be present but are not shown in this table; e.g. PE *m/z* 702 has C15:0/C18:1

[b] Indicates that ions were too low in abundance or spectra too complex due to isotopic or multiple species

[c] GC/MS analysis indicated that C17:1 and C19:1 may be present as cyclopropyl fatty acids

[d] Unsaturated fatty acid with "+O" indicates an oxidized fatty acid possibly as an epoxide

[e] Both (C16:1 + O)/C18:1 and C16:1/(C18:1 + O) were observed

[f] Both (C17:1 + O)/C18:1 and C17:1/(C18:1 + O) were observed

[g] Overlapped with another phospholipid ion

instrument allowed for accurate mass assignments for the product ions. For example, as illustrated in Fig. 3, the deprotonated C16:0/C18:1 PG anion at *m/z* 747.5 produced the following products ions including their elemental composition, mass error from the theoretical mass, and ion structural description: 509.28832 ($C_{24}H_{46}O_9P^-$, −344 ppb, ketene loss from the C16:0 group), 491.27774 ($C_{24}H_{44}O_8P^-$, −388 ppb, fatty acid loss from the C16:0 group), 483.27265 ($C_{22}H_{44}O_9P^-$, −404 ppb, ketene loss

Fig. 3 MS/MS of PG *m/z* 747 on the LTQ-FT. Linear trap detection (**a**); FT-ICR detection (**b**)

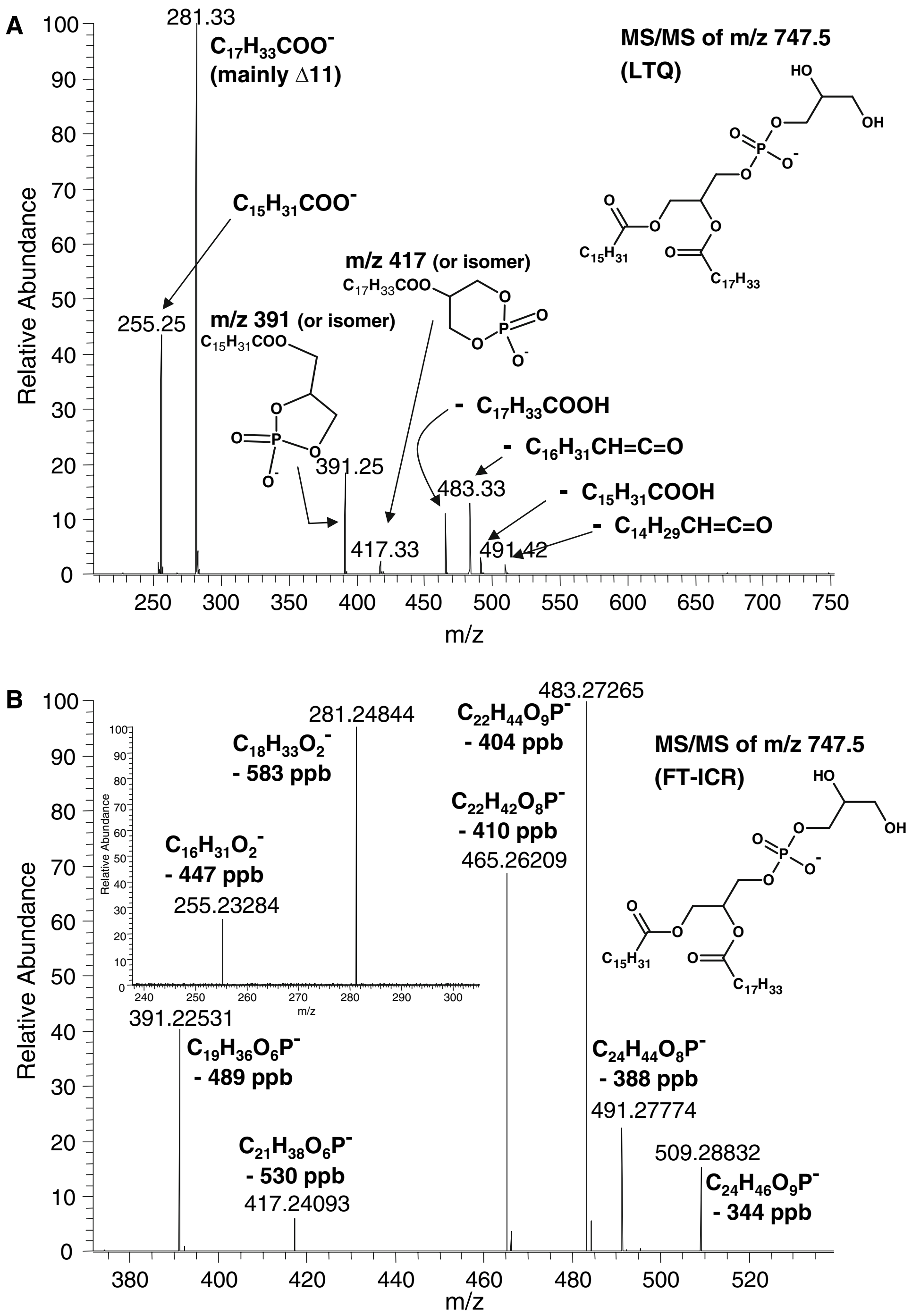

from the C18:1 group), 465.26209 ($C_{22}H_{42}O_8P^-$, −410 ppb, fatty acid loss from the C18:1 group), 417.24093 ($C_{21}H_{38}O_6P^-$, −530 ppb; see Fig. 3), 391.22531 ($C_{19}H_{36}O_6P^-$, −489 ppb, see Fig. 3), 281.24844 ($C_{18}H_{33}O_2^-$, −583 ppb, C18:1 carboxylate anion), and 255.23284 ($C_{16}H_{31}O_2^-$, −447 ppb, carboxylate anion). Relative ion intensities show a preference for the C18:1 ketene and acid losses and the C18:1 carboxylate formation, which favors the C18:1 group in the *sn*-2 position and the C16:0 group in the *sn*-1 position [38]. While it may be difficult with many isobaric species being analyzed simultaneously (e.g., *m/z* 719 is predominantly C16:0/C16:1 but also has significant C14:0/C18:1), it appears that the *sn*-2 position favors the unsaturated group. It has been shown in the literature that the relative intensity of the loss corresponds more to position and not degree of unsaturation [38].

Oxidized phospholipids were also observed and characterized. While every effort was made to avoid oxidizing the phospholipid samples (see "Experimental Procedures"), the possibility must be considered. Nonetheless, identification of these species is possible. Some of these species have been identified as containing epoxy-fatty acids. An example of an oxidized PG is the deprotonated anion at *m/z* 763. Collision-induced dissociation of *m/z* 763 coupled with FT-ICR mass accuracy measurements yielded an MS/MS product ion of *m/z* 297.24356 and an elemental composition of $C_{18}H_{33}O_3^-$ (−164 ppb mass error). Further dissociation of the *m/z* 297 product ion or MS^3 and accurate mass measurements, resulted in two subsequent product ions at *m/z* 199.13393 ($C_{11}H_{19}O_3^-$, −192 ppb) and *m/z* 183.13905 ($C_{11}H_{19}O_2^-$, −19 ppb); these ions are indicative of an epoxy group primarily at the Δ^{11} position. MS^2 results on *m/z* 297 from an epoxy acid standard further supported the identification.

Fatty Acids

The total cellular fatty acid composition of *B. bacteriovorus* HID5, was dominated by 16:0 (Table 3). No polyunsaturated acids were detected and only monounsaturated acids with either 16, 17 or 18 carbons were present. However, several isomers with different double bond positions were identified among these monounsaturated fatty acids. The double bond position, determined by the addition of dimethyl disulfide across the double bond of unsaturated fatty acids and separation of the different isomers by GLC of their methyl ester derivatives. Electron ionization spectra for these derivatized compounds clearly indicated the location of the double bond prior to dimethyl disulfide derivatization [37].

The methyl ester of the cyclopropane fatty acid 9,10-Mt C16:0 (cyC17:0) was identified by MS. This component had a mass identical to the methyl ester of a 17:1 fatty acid and it did not react with dimethyl disulfide. Incomplete derivatization of 17:1 was ruled out as underivatized 16:1 and 18:1, which are fatty acids that are present at higher concentration, were not detected. Furthermore, the spectrum of the *B. bacteriovorus* cyC17:0 is the same as those of two entries in the National Institute of Standards and Technology registry of mass spectra (NIST 13093 and NIST 111346) reported for authentic standards of this fatty acid (cyclopropaneoctanoic acid, 2-hexyl-, methyl ester) (Fig. 4).

Table 3 Fatty acid composition of *B. bacteriovorus* strain HID5 total lipids and its major glycerophospholipids and the total lipid fatty acid composition of *B. bacteriovorus* HD100 and *E. coli* prey cells

Fatty acid[a]	Total lipids						
	HID5	PE	PS	PG	CL	HD100	*E. coli*
14:0	2.1 ± 1.4	0.7 ± 0.6	0.8 ± 0.3	1.0 ± 0.04	Trace	0.7 ± 0.3	5.2 ± 1.3
15:0[b]	2.6 ± 2.0	5.1 ± 0.4	0.9 ± 0.4	1.6 ± 0.2	Trace	1.9 ± 0.1	2.9 ± 0.8
16:0	45.8 ± 6.2	49.7 ± 1.4	50.4 ± 2.2	43.9 ± 0.8	40.9 ± 2.9	40.2 ± 1.1	50.0 ± 4.6
16:1	12.5 ± 3.4	0.4 ± 0.01	8.5 ± 3.1[c]	15.8 ± 1.9[d]	14.1 ± 1.3	8.3 ± 0.1	7.7 ± 1.0
17:0	1.1 ± 0.7	1.5 ± 0.2	2.0 ± 0.0	1.5 ± 0.1	2.1 ± 0.8	4.5 ± 0.1	1.6 ± 1.6
9,10-Mt C16:0[e]	16.3 ± 4.8	35.8 ± 2.2	23.3 ± 1.1	4.7 ± 0.2	0.7 ± 0.4	12.2 ± 0.2	16.5 ± 0.9
18:0	2.2 ± 1.3	1.7 ± 0.9	0.3 ± 0.1	1.4 ± 0.2	1.9 ± 0.6	Trace	Trace
18:1	12.4 ± 1.5	3.1 ± 0.9	13.3 ± 0.3[f]	29.2 ± 1.2[g]	28.5 ± 1.4	31.6 ± 0.5	14.3 ± 2.2
U/S[h]	0.33	0.04	0.28	0.82	0.75	0.67	0.29
U + C/S[i]	0.86	0.71	0.84	1.03	1.22	1.10	0.64

Total extracted lipids of strain HID5 and its major phospholipid classes and total extracted lipids of strain HD100 and its prey *E. coli* (percent of total ± SEM; $n = 3$). Fatty acids were identified and quantified by a combination of GLC analyses of FAME and by GC/MS (TIC) of DMDS derivatives. Fatty acids of *N*-acylphosphatidylethanolamine and other minor unidentified phospholipid components were not analyzed in this study

[a] Number of carbons:number of double bonds

[b] Includes iso-branched and normal acids

[c] $16{:}1^{\Delta 9}$ was the only isomer detected by MS in PS

[d] $16{:}1^{\Delta 7}$ represented 4.3%, $16{:}1^{\Delta 9}$ was 92.8%, and $16{:}1^{\Delta 11}$ comprised 2.9% of the total 16:1 fatty acids in PG as determined by MS analysis

[e] 9,10 Indicates location of ring in the chain; Mt, methano; C16:0, cyclopropane fatty acid with 16 carbons in the straight portion of the chain (also designated as cyC17:0)

[f] $18{:}1^{\Delta 11}$ was the only isomer detected in PS by MS

[g] $18{:}1^{\Delta 9}$ comprised 1.0%, $18{:}1^{\Delta 11}$ was 30.9%, and $18{:}1^{\Delta 13}$ was 1.0% of the total 18:1 fatty acids in PG as determined by MS

[h] Unsaturation index (% total unsaturated fatty acids/% total saturated fatty acids)

[i] Lipid bilayer fluidity index (% total unsaturated + cyclopropane fatty acids/% total normal saturated fatty acids)

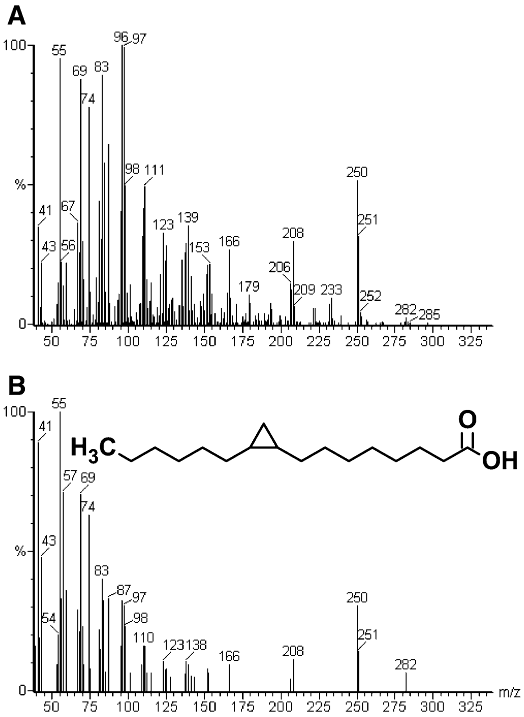

Fig. 4 Electron ionization (EI) GC/MS of the major cyclopropane fatty acid in *B. bacteriovorus* HID5 identified as 9,10-Mt C16:0. The mass spectrum of *B. bacteriovorus* 9,10-Mt C16:0 (**a**); mass spectrum library entry for 9,10-Mt C16:0 (**b**). Some differences in ion intensities are the result of background subtraction which was required to remove the contribution of the perfluorinated tributylamine standard. This standard was continuously introduced during the chromatographic run to provide a "lock mass" that enhanced mass accuracy

Analyses of individually isolated phospholipid classes of *B. bacteriovorus* strain HID5 indicated that there were similarities in the fatty acid profiles between PE and PS and between PG and CL. PE and PS had high percentages of cyC17:0 compared to PG and CL whereas PG and CL were enriched in the monounsaturated acids 16:1 and 18:1.

There was insufficient amount of *B. bacteriovorus* NAPE isolated in the present study and only few of the major acids were detectable by GLC. Therefore, quantitative analysis of the fatty acid composition of this phospholipid class was not performed.

Discussion

This is the first report on the glycerophospholipids of the predatory and parasitic delta-protobacterium *Bdellovibrio bacteriovorus*. With respect to general lipid classes, PE, PS, CL, and PG identified in HID5 were those commonly found among most organisms. Preliminary studies on the parental host-dependent *B. bacteriovorus* strain HD100 cultured with prey *E. coli* indicated that the same major glycerophospholipid classes were also present in this strain (Table 1).

Although the glycerophospholipid NAPE is usually found as minor membrane components of plant and animal cells [39–41] and is developmentally regulated in the cellular slime mold *Dictyostelium discoideum* [42], these are very rare among prokaryotes. This lipid was detected in another bacterium, the anaerobic ovine rumen bacterium *Butyrivibrio fibrisolvens* [43]. The present study suggests the possibility that NAPEs might also be more commonly distributed among prokaryotes than previously thought. These lipids might not have been identified because NAPEs might represent only minor lipid components of bacterial cells as they are in eukaryotic cells. The property of having an additional fatty acid in NAPE is expected to enhance insertion of the amphipathic phospholipid molecule into membrane lipid bilayers.

Although there is evidence suggesting that a transacylation reaction between two PE molecules produces NAPE and lysoPE in *Butyrivibrio*, it remains unclear whether *O*-linked fatty acyl groups of PE or other lipids can be deacylated and used in transacylation reactions to produce the *N*-acylation of PE [43]. Studies on the biosynthesis of NAPE or any glycerophospholipid in *Bdellovibrio* are lacking. In a study of *Bacteriovorus stolpii* UKi2, cells metabolically radiolabeled with serine indicated PS, PE and a spot in TLC plates corresponding to the migration of NAPE were radioactive [44]. Whether this minor lipid component in *B. stolpii* UKi2 is NAPE remains to be determined by additional experiments.

As many organisms, especially parasites, scavenge lipids and other molecules from their environment (in the environment, culture medium or host cytoplasm) *B. bacteriovorus* was shown to gain most of its fatty acids from the host cell during intraperiplasmic growth [19]. However, the present analysis of *B. bacteriovorus* HID5 grown axenically in the absence of prey host cells demonstrates it has the ability to synthesize de novo its own fatty acids producing its distinct fatty acid profile. Like *B. bacteriovorus*, the culture medium is enriched in 16:0 but other components in the bacterium such as cyclopropane fatty acids are not found in the medium [25] and hence must be synthesized by the bacterium. The fatty acid composition of *E. coli* strain K12 identified in the present study was similar to those recently reported by Oursel et al. [45] on the lipids of strain LM3118. These workers employed liquid chromatography and tandem MS/MS with electrospray ionization that are comparable state of art techniques used in the present study. The total lipid fatty acid compositions of strains HD100 and HID5 might differ (Table 3) qualitatively (e.g. 18:0) and in the proportions of individual components. However, definitive conclusions on HD100 fatty acid compositions cannot yet be made. In this initial analysis of HD100 cells, elimination of *E. coli* cell debris by extensive purification procedures were not included to prevent starvation conditions and other physiological and potentially biochemical changes in the *B. bacteriovorus* HD100 cells. Hence some *E. coli* cell debris might have been included in the HD100 cell preparations analyzed. Nonetheless, the major fatty acids in HD100, *E. coli* and axenically grown HID5 were 16:0, cy17:0 (not detected in the culture medium), 18:1, and 16:1 (Table 3).

Initial studies earlier reported on the total ester-linked fatty acids in *B. stolpii* UKi2 grown in a peptone and yeast extract medium indicated that the major components were those with 15 carbons (iso-branch, monousaturated, or saturated); no cyclopropane fatty acids were detected [22]. The fatty acids in isolated glycerophospholipids of *B. stolpii* were not analyzed in that study. In contrast, the present study on *B. bacteriovorus* clearly demonstrated that this bacterium has ester-linked fatty acid distinct from that of *B. stolpii* UKi2 and that fatty acid synthesis in *B. stolpii* UKi2 and *B. bacteriovorus* are quite different. Fifteen-carbon acids in *B. bacteriovorus* total glycerolipids and in each isolated phospholipid class analyzed were only present in low proportions. The dominant fatty acid was 16:0 as previously reported [19]. Analysis of individual glycerophospholipids demonstrated that the monounsaturated acids 16:1 and 18:1 were found high in PG and CL and low in PE and PS whereas the cyclopropane fatty acid cyC17:0 was high in PE and PS and low in PG and CL. These data suggest that CL is produced from two PG molecules and PE from the decarboxylation of the PS headgroup.

Unsaturation index comparing unsaturated to saturated fatty acids is commonly examined as an indication of membrane bilayer fluidity (Table 3). However, both double bonds and the bulk of the cyclopropane ring contribute to loosening of lipid bilayer packing. If only double bonds are considered to contribute to fluidity, it would then appear that *B. bacteriovorus* HID5 membrane bilayers are tightly packed but when combining unsaturated and cyclopropane fatty acids and then comparing those values to normal saturated fatty acids, the unsaturation index values are close to 1. Since *B. bacteriovorus* is ubiquitous in nature and grows in a broad range of temperatures [2, 4, 15, 46] it should have the ability to alter membrane bilayer packing like other poikilothermic organisms. Thus, it is expected that the fatty acid composition would differ from that reported here if the bacterium is grown at a temperature different from that used in this study.

Sphingophosphonolipids were not detected in *B. bacteriovorus* and the presence in its genome of the gene coding for serine:fatty acyl transferase is not apparent. Therefore the correlation previously made between the presence of these lipids and predation in *B. stolpii* UKi2 (and their absence in non-predatory UKi1 and other strains) does not appear applicable to *B. bacteriovorus*. Furthermore, it was recently shown that myriocin-treated *B. stolpii* UKi2 can exhibit predation and parasitism in the absence of sphingophosphonolipids albeit their locomotory behavior was affected [44]. On the other hand, the presence of sphingolipids in *B. bacteriovorus* cannot yet be ruled out; they might be present in concentrations not detectable by protocols used in the present study. While we have identified PG and CL in the present study, only the gene coding for cardiolipin synthase in the *B. bacteriovorus* HD100 was identified (National Center for Biotechnology Information, NCBI, #2735852); annotation for most genes coding for enzyme proteins in phospholipid synthesis is not yet available. This initial study on the extractable lipids of *B. bacteriovorus* indicate that there are other minor lipids present in this bacterium. Hence it would be good if future studies were conducted to identify the other lipid components present in *B. bacteriovorus*. Nonetheless the differences found so far between the lipids of these two predatory bacteria *Bdellovibrio bacteriovorus* and *Bacteriovorus stolpii* are consistent with the assignment of them to separate genera.

Acknowledgments We thank Carey Lambert and R. Elizabeth Sockett, Nottingham University for providing cultures of *B. bacteriovorus*, and Stephen Macha for assistance with mass spectrometer analyses. Supported in part by a grant from the University of Cincinnati Research Council, NIH RO1 AI064084, and NIH RR019900.

References

1. Davidov Y, Jurkevitch E (2004) Diversity and evolution of *Bdellovibrio*-and-like organisms (BALOs), reclassification of *Bacteriovorax starrii* as *Peredibacter starrii* gen. nov., comb. nov., and description of the *Bacteriovorax-Peredibacter* clade as *Bacteriovoracaceae* fam. nov. Int J Syst Bacteriol 54:1439–1452
2. Pineiro SA, Stine OC, Chauhan A, Steyert SR, Smith R, Williams HN (2007) Global survey of diversity among environmental saltwater Bacteriovoracaceae. Environ Microbiol 9:2441–2450
3. Rendulic S, Jagtap P, Rosinus A, Eppinger M, Baar C, Lanz C, Keller H, Lambert C, Evans KJ, Goesmann A, Meyer F, Sockett RE, Schuster SC (2004) A predator unmasked: life cycle of *Bdellovibrio bacteriovorus* from a genomic perspective. Science 303:689–692
4. Ruby EG (1981) The genus *Bdellovibrio*. In: Balows A, Truper HG, Dworkin M, Harder W, Schleifer KH (eds) The prokaryotes, 2nd edn. Springer, New York, pp 3400–3415
5. Starr MP, Baigent NL (1966) Parasitic interaction of *Bdellovibrio bacteriovorus* with other bacteria. J Bacteriol 91:2006–2017
6. Stolp H, Starr MP (1963) *Bdellovibrio bacteriovorus* gen. et sp. n., a predatory ectoparasitic and bacteriolytic microorganism. Antonie van Leeuwenhoek J Microbiol Serol 29:217–248
7. Abram D, Castro J, Melo E, Chou D (1974) Penetration of *Bdellovibrio bacteriovorus* into host cells. J Bacteriol 118:663–680
8. Evans KJ, Lambert C, Sockett RE (2007) Predation by *Bdellovibrio bacteriovorus* HD100 requires type IV pili. J Bacteriol 189:4850–4859
9. Beck S, Schwudke D, Strauch E, Appel B, Linscheid M (2004) *Bdellovibrio bacteriovorus* strains produce a novel major outer

membrane protein during predacious growth in the periplasm of prey bacteria. J Bacteriol 186:2766–2773

10. Engelking HM, Seidler RJ (1974) The involvement of extracellular enzymes in the metabolism of *Bdellovibrio*. Arch Mikrobiol 95:293–304
11. Gray KM, Ruby EG (1990) Prey-derived signals regulating duration of the developmental growth phase of *Bdellovibrio bacteriovorus*. J Bacteriol 172:4002–4007
12. Hespell RB (1978) Intraperiplasmic growth of *Bdellovibrio bacteriovorus* on heat-treated *Escherichia coli*. J Bacteriol 33:1156–1162
13. Hespell RB, Miozzari GF, Rittenberg SC (1975) Ribonucleic acid destruction and synthesis during intraperiplasmic growth of *Bdellovibrio bacteriovorus*. J Bacteriol 123:481–491
14. Jurkevitch E (2000) The genus *Bdellovibrio*. In: Dworkin M, Falkow S, Rosenberg E, Schleifer KH, Stackebrandt E (eds) The prokaryotes, Springerg, New York, 33 pp. http://141:150.157.117:8080/prokPUB/index.htm
15. Kelley JL, Turng BF, Williams HN, Baier M (1997) Effect of temperature, salinity, and substrate on the colonization of surfaces in situ by aquatic bdellovibrios. Appl Environ Microbiol 6:84–90
16. Sockett RE, Lambert C (2004) *Bdellovibrio* as therapeutic agents: a predatory renaissance? Nat Rev Microbiol 2:669–675
17. Wand H, Vacca G, Kuschk P, Krüger M, Kästner M (2007) Removal of bacteria by filtration in planted and non-planted sand columns. Water Res 41:159–167
18. Yair S, Yaacov D, Susan K, Jurkevitch E (2003) Small eats big: ecology and diversity of *Bdellovibrio* and like organisms, and their dynamics in predator-prey interactions. Agronomie 23:433–439
19. Kuenen JG, Rittenberg SC (1975) Incorporation of long-chain fatty acids of the substrate organism by *Bdellovibrio bacteriovorax* during intraperiplasmic growth. J Bacteriol 121:1145–1157
20. Nelson DR, Rittenberg SC (1981) Incorporation of substrate cell lipid A components into the lipopolysaccharide of intraperiplasmically grown *Bdellovibrio bacteriovorus*. J Bacteriol 147:860–868
21. Nelson DR, Rittenberg SC (1981) Partial characterization of lipid A of intraperiplasmically grown *Bdellovibrio bacteriovorus*. J Bacteriol 147:869–874
22. Steiner S, Conti SF, Lester RL (1973) Occurrence of phosphonosphingolipids in *Bdellovibrio bacteriovorus* strain UKi2. J Bacteriol 116:1199–1211
23. Baer ML, Ravel J, Chun J, Hill RT, Williams HN (2000) A proposal for the reclassification of *Bdellovibrio stolpii* and *Bdellovibrio starrii* into a new genus, *Bacteriovorax* gen. nov. as *Bacteriovorax stolpii* comb. nov. and *Bacteriovorax starrii* comb. nov., respectively. Int J Syst Evol Microbiol 50:219–224
24. Snyder AR, Williams HN, Baer ML, Walker KE, Stine OC (2002) 16S rDNA sequence analysis of environmental *Bdellovibrio*-and-like organisms (BALO) reveals extensive diversity. Int J Syst Evol Microbiol 52:2089–2094
25. Jayasimhulu K, Hunt SM, Watanabe Y, Giner J-L, Kaneshiro ES (2007) Detection and identification of *Bacteriovorax stolpii* UKi2 sphingophosphonolipid molecular species. J Am Soc Mass Spectrom 18:394–403
26. Watanabe Y, Nakajima M, Hoshino T, Jayasimhulu K, Brooks EE, Kaneshiro ES (2001) A novel sphingophosphonolipid head group 1-hydroxy-2-aminoethyl phosphonate in *Bdellovibrio stolpii*. Lipids 36:513–519
27. Cotter TW, Thomashow MF (1992) Identification of a *Bdellovibrio bacteriovorus* genetic locus, *hit*, associated with the host-independent phenotype. J Bacteriol 174:6018–6024
28. Gordon RF, Stein MA, Diedrich DL (1993) Heat shock-induced axenic growth of *Bdellovibrio bacteriovorus*. J Bacteriol 175:2157–2161
29. Ishiguro EE (1973) A growth initiation factor for host-independent derivatives of *Bdellovibrio bacteriovorus*. J Bacteriol 115:243–252
30. Seidler RJ, Starr MP (1969) Isolation and characterization of host-independent bdellovibrios. J Bacteriol 100:69–785
31. Bligh EG, Dyer WJ (1959) A rapid method of total lipid extraction and purification. Can J Biochem Physiol 37:911–917
32. Folch J, Lees M, Sloane-Stanley GH (1957) A simple method for the isolation and purification of total lipids from animal tissues. J Biol Chem 226:497–509
33. Dittmer JC, Lester RL (1964) A simple, specific spray for the detection of phospholipids on thin-layer chromatograms. J Lipid Res 5:126–127
34. Kates M (1986) Techniques of lipidology: isolation, analysis and identification of lipids. In: Work TS, Work E (ed), Laboratory techniques in biochemistry and molecular biology, 2nd edn. Elsevier, Amsterdam, pp 220–223
35. Ferguson KA, Conner RL, Mallory FB, Mallory CW (1972) α-Hydroxy fatty acids in sphingolipids of *Tetrahymena*. Biochim Biophys Acta 270:111–116
36. MacGee J, Allen KG (1974) Microanalysis of fatty acids of a small number of whole cells. J Chromatogr 100:35–42
37. Vincenti M, Guglielmetti G, Cassani G, Tonini C (1987) Determination of double bond position in diunsaturated compounds by mass spectrometry of dimethyl disulfide derivatives. Anal Chem 59:694–699
38. Pulfer M, Murphy RC (2003) Electrospray mass spectrometry of phospholipids. Mass Spectrom Rev 22:332–364
39. Cadas H, DiThomaso E, Piomellil D (1997) Occurrence and biosynthesis of endogenous cannabinoid precursor, *N*-arachidonyl phosphatidylethanolamine, in rat brain. J Neurosci 17:1226–1242
40. Chapman KD, Moore TS Jr (1993) *N*-acylphosphatidylethanolamine synthesis in plants: occurrence, molecular composition, and phospholipid origin. Arch Biochem Biophys 301:21–33
41. Schmid HHO, Schmid PC, Nataranjan V (1990) *N*-acylated glycerophospholipids and their derivatives. Prog Lipid Res 29:1–43
42. Ellingson JS (1980) Identification of *N*-acylethanolamine phosphoglycerides and acylphosphatidylglycerol as the phospholipids which disappeared as *Dictyostelium dicoideum* cells aggregate. Biochemistry 19:6176–6182
43. Hazlewood GP, Dawson RMC (1975) Intermolecular transacylation of phosphatidylethanolamine by a *Butyrivibrio* sp. Biochem J 150:521–525
44. Kaneshiro ES, Hunt SM, Watanabe Y (2008) *Bacteriovorax stolpii* proliferation and predation without sphingophosphonolipids. Biochem Biophys Res Commun 367:21–25
45. Oursel D, Loutelier-Bourhis C, Orange N, Chevalier S, Norris V, Lange CM (2007) Lipid composition of membranes of *Escherichia coli* by liquid chromatography/tandem mass spectrometry using negative electrospray ionization. Rapid Comm Mass Spectrom 21:1721–1728
46. Jurkevitch E, Minz D, Ramati B, Barel G (2000) Prey range characterization, ribotyping, and diversity in soil and rhizosphere *Bdellovibrio* spp. isolated on phytopathogenic bacteria. Appl Environ Microbiol 66:2365–2371

dioxygenases. Lipoxygenases catalyse the addition of molecular oxygen to polyunsaturated fatty acids with a (*cic,cis*)-1-4-pentadiene system to give an unsaturated fatty acid hydroperoxide [10]. However, an oxygenation of monounsaturated fatty acids such as oleic [11–14] and octadec-*cis*-12-enoic [14] acids by such enzymes has also been reported. These reactions produce mainly hydroxy, hydroperoxy or oxoacids. Lipoxygenases are widely distributed in plants, fungi and animals [15]; however, these enzymes have also been detected in bacteria [12, 16]. The fungal heme enzyme linoleate 8-dioxygenase abstracts allylic hydrogen and introduces molecular oxygen in an antarafacial way at C-8 leading to the formation of 8*R*-hydroperoxylinoleic acid [17, 18]. It is interesting to note that the allylic oxygenation induced by this enzyme, which also oxygenates oleic, α-linolenic and ricinoleic acids [17], presents some analogies with the regiospecific allylic oxygenation of *cis*-vaccenic acid at C-10 previously observed [8, 9].

In the present work, we intended to re-examine the strain *Erythrobacter* sp. MG3 in order to try to determine the growth conditions favouring this peroxidation of *cis*-vaccenic acid and to elucidate the behaviour of the 10-hydroperoxyoctadec-11(*cis*)-enoic acid thus formed.

Experimental Procedures

Organism

Erythrobacter sp. strain MG3 was isolated in December 2000 from the surface of SE Atlantic/W Indian Ocean (41°06′N, 72°27′W). The strain is phylogenetically related to *Erythrobacter longus* and exhibits the typical features of members of the *Erythrobacter* genus [2]. The cultures were grown in Erlenmeyer flasks on a rotary shaker at 23 °C. The illumination was provided by a bank of luminescent tubes giving ~200 μmol quanta m^{-2} s^{-1} with a 12:12 h light/dark cycle. Generally the cells were grown in an enriched seawater medium supplemented by 0.5 g peptone and 0.1 g yeast extract per litre [2]. For nutrient limitation studies the cultures were grown on artificial seawater media as described in [2] and supplemented by glucose as the sole source of carbon. The carbon limited medium contained 1 mM glucose, 2.5 mM ammonium sulfate and 0.3 mM phosphate. For the phosphorus limitation condition, the medium was supplemented by 10 mM glucose and the phosphate content was reduced to 0.03 mM. In the case of nitrogen limitation, the ammonium sulfate content was reduced to 0.1 mM and supplemented by 10 mM glucose and 0.3 mM phosphate. The cultures were harvested in steady-state phase by centrifugation (10,000 × g).

Alkaline Hydrolysis

Saponification was carried out on both reduced and non-reduced cells. After reduction, 25 ml of water and 2.8 g of potassium hydroxide were added and the mixture was directly saponified by refluxing for 2 h. In the case of non-reduced samples, an additional 25 ml of methanol was added before saponification. After cooling, the contents of the flask were extracted three times with *n*-hexane. The combined *n*-hexane extracts were dried over anhydrous Na_2SO_4, filtered and concentrated to give the unsaponified fraction. The aqueous phase was then acidified with hydrochloric acid (pH 1) and subsequently extracted three times with dichloromethane. Treatment of the combined dichloromethane extracts as described above gave the saponified fraction.

Reduction

Hydroperoxides were reduced to the corresponding alcohols in methanol (25 ml) by excess $NaBH_4$ or $NaBD_4$ (10 mg/mg of extract) using magnetic stirring (15 min at 0 °C). During this treatment, ketones are also reduced and the possibility of some ester cleavage cannot be excluded. After reduction, a saturated solution of NH_4Cl (10 ml) was added cautiously to destroy the excess reagent, the pH was adjusted to 1 with dilute HCl (2 N) and the mixture was shaken and extracted with hexane:$CHCl_3$ (4:1, v/v; x3). The combined extracts were dried as described above and evaporated to dryness under a stream of nitrogen.

Catalytic Hydrogenation

Lipid extracts were hydrogenated overnight under magnetic stirring in methanol with Pd/$CaCO_3$ (10–20 mg/mg of extract) (Aldrich) as a catalyst. After hydrogenation, the catalyst was removed by filtration and the filtrate was concentrated by rotary evaporation.

Osmium Tetroxide Oxidation

Lipid extracts and OsO_4 (1:2, w:w) were added to a pyridine-dioxane mixture (1:8, v/v; 5 ml) and incubated for 1 h at room temperature. Then, 6 ml of Na_2SO_3 suspension (16% Na_2SO_3 in water-methanol, 8.5:2.5, v/v) was added and the mixture was again incubated for 1.5 h. The resulting mixture was gently acidified (pH 3) with HCl and extracted three times with dichloromethane (5 ml). The combined dichloromethane extracts were subsequently dried over anhydrous Na_2SO_4, filtered and concentrated.

Methylation

Lipid extracts were taken up in 2 ml of BF_3/methanol (14%) and heated at 80 °C for 1 h. After cooling, an excess of water was added and methyl esters were extracted three times with hexane, dried over anhydrous Na_2SO_4, filtered and concentrated using rotary evaporation.

Silylation

After evaporation of the solvent, each residue was taken up in 300 µl of a mixture of anhydrous pyridine and BSTFA (Supelco) (2:1, v/v) and silylated for 1 h at 50 °C. After evaporation to dryness under nitrogen, the residue was redissolved in ethyl acetate (2 ml/mg) and BSTFA (0.1 ml) (in order to avoid desilylation of fatty acids) and then analysed by GC–EIMS.

Gas Chromatography–Electron Impact Mass Spectrometry (GC–EIMS)

GC–EIMS analyses were carried out with an Agilent 6890 gas chromatograph connected to an Agilent 5973 Inert mass spectrometer. The following conditions were employed: 30 m × 0.25 mm (i.d.) fused silica capillary column coated with SOLGEL-1 (SGE; 0.25 µm film thickness); oven temperature programmed from 70 to 130 °C at 20 °C min^{-1}, from 130 to 250 °C at 5 °C min^{-1} and then from 250 to 300 °C at 3 °C min^{-1}; carrier gas (He) maintained at 0.69 bar until the end of the temperature program and then programmed from 0.69 to 1.49 bar at 0.04 bar min^{-1}; injector (on column with retention gap) temperature, 50 °C; electron energy, 70 eV; source temperature, 190 °C; cycle time, 1.99 cycles s^{-1}, scan range, 50–800.

Structural assignments were based on the interpretation of mass spectrometric fragmentations and confirmed by comparison of retention times and mass spectra with those of authentic compounds, when these were available.

Standard Compounds

Classical fatty acids and 2-hydroxy acids were purchased from Sigma (St. Quentin Fallavier, France). Fe^{++}/ascorbate induced autoxidation [19] of *cis*-vaccenic acid produced a mixture of allylic hydroperoxides containing significant amounts of *cis*- and *trans*-10-hydroperoxyoctadec-11-enoic and 12-hydroperoxyoctadec-10-enoic acids [20]. Subsequent reduction of these different allylic hydroperoxides in methanol with excess $NaBH_4$ afforded the corresponding hydroxy acids. Oxoacids were obtained by dehydration of the corresponding hydroperoxides in a mixture of pyridine and acetic anhydride [20]. Hydrogenation of hydroxy acids and oxoacids was carried out in methanol with $Pd/CaCO_3$ as catalyst [20].

Results and Discussion

Characterisation of the Main Lipidic Components of *Erythrobacter sp.* strain *MG3*

The unsaponified lipidic fraction obtained after alkaline hydrolysis of cells of *Erythrobacter sp.* strain *MG3* is dominated by a single component, assigned by GC/EIMS as phytol. This isoprenoid alcohol arises from the hydrolysis of bacteriochlorophyll-a, which constitutes with erythroxanthin sulfate the major pigments of this phototrophic bacterium [2]. Though present in large amounts in this fraction, erythroxanthin sulfate was non-amenable to gas chromatography with the operating conditions used.

As previously described [8], the corresponding saponified fraction obtained after $NaBH_4$ reduction is dominated by *cis*-vaccenic acid and also contain $C_{12:0}$, $C_{14:0}$, $C_{15:0}$, $C_{16:1\omega7}$, $C_{16:0}$, $C_{18:2\omega7,13}$, $C_{18:0}$, 11-methyl$C_{18:1\omega6}$ fatty acids and some 2-hydroxy acids, which are classical components of sphingolipids of *Erythrobacter*-related strains. As expected, we detected *cis* and *trans* 10-hydroxyoctadec-11-enoic acid trimethylsilyl derivatives (Table 1). These two isomers exhibit exactly similar mass spectra [9] and their identification is based on comparison of their retention times with standards. Deuterium labelling allowed previously to prove that these compounds resulted from the reduction during the treatment of a mixture of the corresponding hydroperoxyacids, oxoacids and hydroxy acids [8]. Surprisingly, the proportion of 10-hydroxyoctadec-11(*cis*)-enoic acid after reduction, which constituted previously only 1% of the parent *cis*-vaccenic acid during the stationary phase of growth [8], is now of 48 % (Table 1). We also detected small amounts of *trans* 12-hydroxyoctadec-10-enoic acid deriving from allylic rearrangement of the 10-hydroperoxyoctadec-11-enoic acid. In addition to all these previously described compounds, we observed the production of five new interesting compounds (7,10-epoxyoctadec-11-enoic, 11-hydroxyoctadecanoic, 12-hydroxyoctadecanoic, 10-hydroxyoctadecanoic and 10-hydroxyoctadeca-5,11-enoic acids) (Table 1).

Mass spectra of the methyl and trimethylsilyl esters of 7,10-epoxyoctadec-11-enoic acid appeared to be poorly informative (Fig. 1). The position of the tetrahydrofuran (THF) ring of this compound was determined after hydrogenation of the corresponding methyl ester (in the presence of Pd as catalyst) and subsequent GC–EIMS analysis (Fig. 2b). The mass spectrum thus obtained exhibits a molecular peak at *m/z* 312 (instead of *m/z* 310 for the non-hydrogenated methyl ester) (Fig. 1a) and two

Table 1 Fatty acid composition (relative percentage) of *Erythrobacter* sp. strain MG3 cells collected at different phases of growth

	Exponential phase	Late exponential phase	Steady state phase
Dodecanoic acid	0.3	0.1	0.6
Tetradecanoic acid	0.9	0.3	1.0
Pentadecanoic acid	0.6	0.1	0.3
Hexadec-9-enoic acid	1.1	0.6	0.5
2-Hydroxytetradecanoic acid	1.3	1.3	3.6
Hexadecanoic acid	3.7	1.5	4.9
Octadeca-5,11-dienoic acid	4.8	5.0	12.1
2-Hydroxyhexadecanoic acid	0.5	0.4	0.5
Octadec-11(*cis*)-enoic acid (*cis* vaccenic acid)	57.7	56.6	37.2
Octadecanoic acid	1.2	0.4	2.4
11-Methyloctadec-12-enoic acid	0.9	2.5	3.0
7,10-Epoxyoctadec-11-enoic acid	2.0	6.4	11.5
10-Hydroxyoctadeca-5,11-dienoic acid	0.4	1.0	1.8
10-Hydroxyoctadec-11(*cis*)-enoic acid	22.3	21.6	18.1
10-Hydroxyoctadec-11(*trans*)-enoic acid	1.6	1.6	1.4
12-Hydroxyoctadec-10-enoic acid	0.3	0.2	0.2
10- + 11- + 12-Hydroxyoctadecanoic acids	0.4	0.4	0.9

prominent ions at *m/z* 183 and 199 corresponding to the two strongly favoured α-cleavages relative to the ionised oxygen of the THF ring. These two fragments then undergo losses of water or methanol affording ions at *m/z* 149, 165, 167 and 181. The presence of the fragment ion at *m/z* 172 resulting from a THF-specific cleavage initiated by an initial hydrogen transfer from the carbon 7 to the ester group [21] also confirms the position of the THF ring relative to the ester group. The position of the double bond was determined after OsO_4 oxidation of the methyl ester and subsequent silylation. The mass spectrum of the bis-trimethylsilyloxy derivative thus obtained (Fig. 2a) exhibited two fragment ions at *m/z* 187 and 301 resulting from the cleavage of the bond between the two carbon atoms bearing the trimethylsilyloxy groups. Due to the involvement of subsequent loss of methanol (*m/z* 269) and different cleavages induced by the THF ring or the ester group, the fragment ion at *m/z* 301 is weaker than this at *m/z* 187. The useful ion at *m/z* 374 resulting from trimethylsilyl transfer towards the ester group [22, 23] (and this at *m/z* 284 formed after an additional loss of trimethylsilanol) confirmed that the fragment ion at *m/z* 301 contains the ester group. This proved the presence of a double bond in position 11 in the parent fatty acid and allowed us to identify this compound as 7,10-epoxyoctadec-11-enoic acid. If the presence of furan fatty acids in several marine bacteria [24, 25] and crayfish [26] was previously described; to our knowledge, this is the first report of a natural fatty acid containing a THF cycle.

Reduction with $NaBD_4$ instead of $NaBH_4$ allowed to show that the 11-hydroxyoctadecanoic and 12-hydroxyoctadecanoic acids detected arise from the reduction of 11,12-epoxyoctadecanoic acid during the treatment (Fig. 3a, b). The presence of this epoxide could be confirmed in non-reduced samples. Deuterium labelling also allowed us to demonstrate that the 10-hydroxyoctadecanoic acid detected results from the reduction of the corresponding oxoacid during the treatment.

The mass spectrum of the silylated derivative of 10-hydroxyoctadeca-5,11-enoic acid is given in Fig. 3c. It exhibits a molecular peak at *m/z* 440 (instead of *m/z* 442 in the case of the silylated 10-hydroxyoctadec-11-enoic acid) [9] and a strong fragment ion at *m/z* 213 corresponding to the cleavage at the carbon bearing, $OSiMe_3$ group. The presence of this compound is very interesting. Indeed, it shows that the regiospecific enzymatic peroxidation of the allylic position 10 is not restricted to *cis*-vaccenic acid but seems to act on all the fatty acids possessing a double bond at the position 11.

Behaviour of 10-Hydroperoxyoctadec-11-enoic Acid in Cells of *Erythrobacter* sp. strain MG3

Hydroperoxides are extremely cytotoxic and cause damage to membranes and proteins in particular [27]. Several enzymatic processes causing further reactions of the hydroperoxides and avoiding their accumulation have been previously described. These processes involve: (1) reduction to the corresponding hydroxy acids [27], (2) homolytic cleavage of the O-O bond resulting in the formation of oxoacids [15], (3) dehydration to allene oxides and subsequent hydrolysis of these unstable intermediates [28], and (4) direct cleavage of the hydroperoxides to aldehydes

Fig. 1 EI mass spectra of 7,10-epoxyoctadec-11-enoic acid methyl (**a**) and trimethylsilyl (**b**) esters

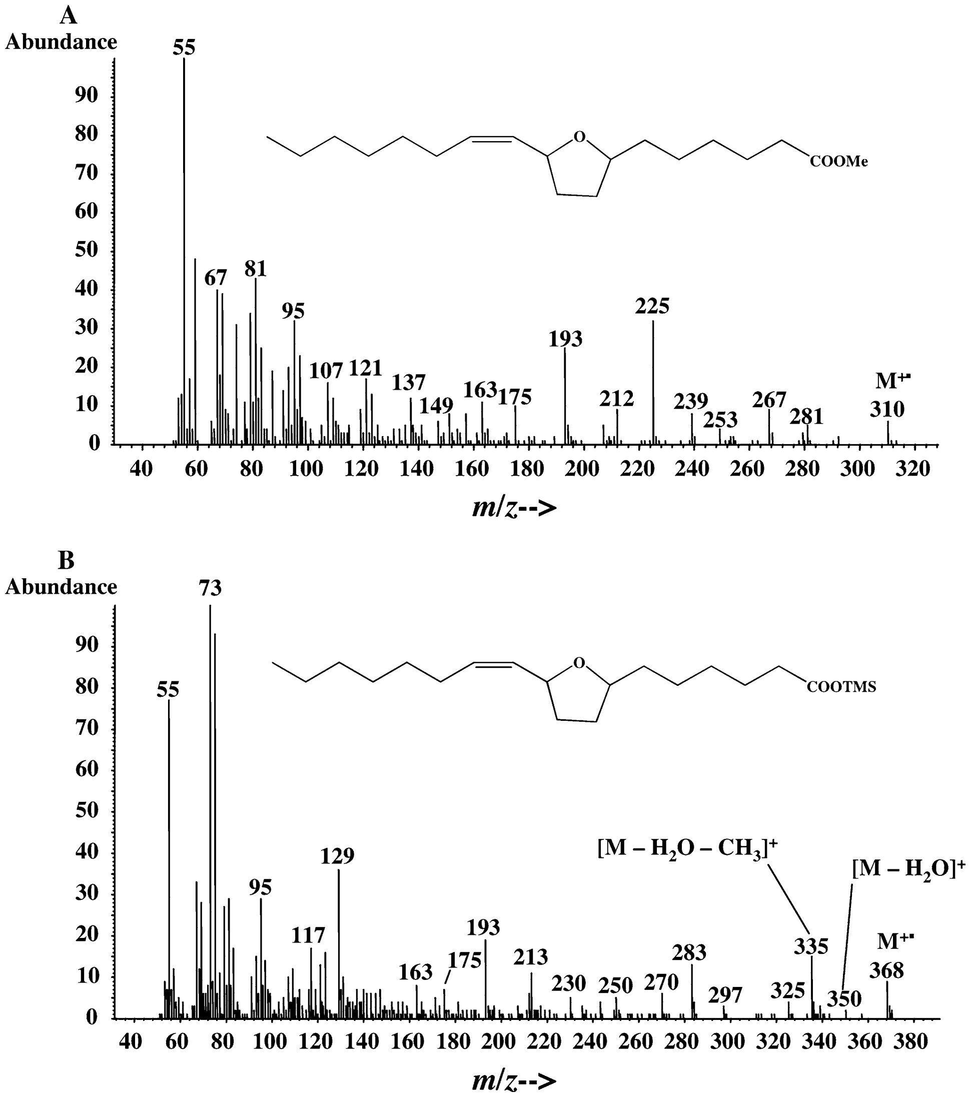

and oxoacids [29]. Only the two first processes seem to act in strain MG3. The reduction of hydroperoxyacids to the corresponding hydroxy acids is generally attributed to dioxygenases themselves [27]. However, the presence of 11,12-epoxyoctadecanoic acid in strain MG3 (see above) allowed us to attribute the reduction of 10-hydroperoxyoctadec-11-enoic acid to the corresponding alcohol to the involvement of a peroxygenase. Indeed, this enzyme catalyses an intermolecular transfer of oxygen from hydroperoxides to the double bonds of fatty acids yielding alcohols and epoxides (Fig. 4) [30, 31]. Conversion of hydroperoxyacids to oxoacids is induced by lipohydroperoxidases [32].

Allylic hydroperoxides are not stable and may also undergo highly stereoselective free radical allylic rearrangement [33]. These processes, which can act on both *cis* and *trans* allylic hydroperoxides, affords only *trans* configurations [33]. Allylic rearrangement of 10-hydroperoxyoctadec-11(*cis*)-enoic acid results to the formation of 10-hydroperoxyoctadec-11(*trans*)-enoic and 12-hydroperoxyoctadec-10(*trans*)-enoic acids; these isomeric hydroperoxyacids being then also converted to the corresponding hydroxyacids and oxoacids (Fig. 4).

The *cis* and *trans* 10-oxooctadec-11-enoic acids formed undergoes subsequent saturation to 10-oxooctadecanoic acid (Fig. 4). The saturation of unsaturated fatty acids in the gut of some animals has been long recognised [34]. This biohydrogenation is brought about by the mixed culture of rumen bacteria and involves several enzyme catalysed steps. It was previously demonstrated that anaerobic incubation of oleic and elaidic acids with strained rumen contents lead to their saturated counterpart (stearic acid) and to a lesser extent to the isomerisation of each monounsaturated fatty acid to its geometric isomer [35]. Consequently, the formation of 10-oxooctadec-*trans*-11-enoic acid may be also attributed to the isomerisation of its geometrical isomer during the biohydrogenation (Fig. 4).

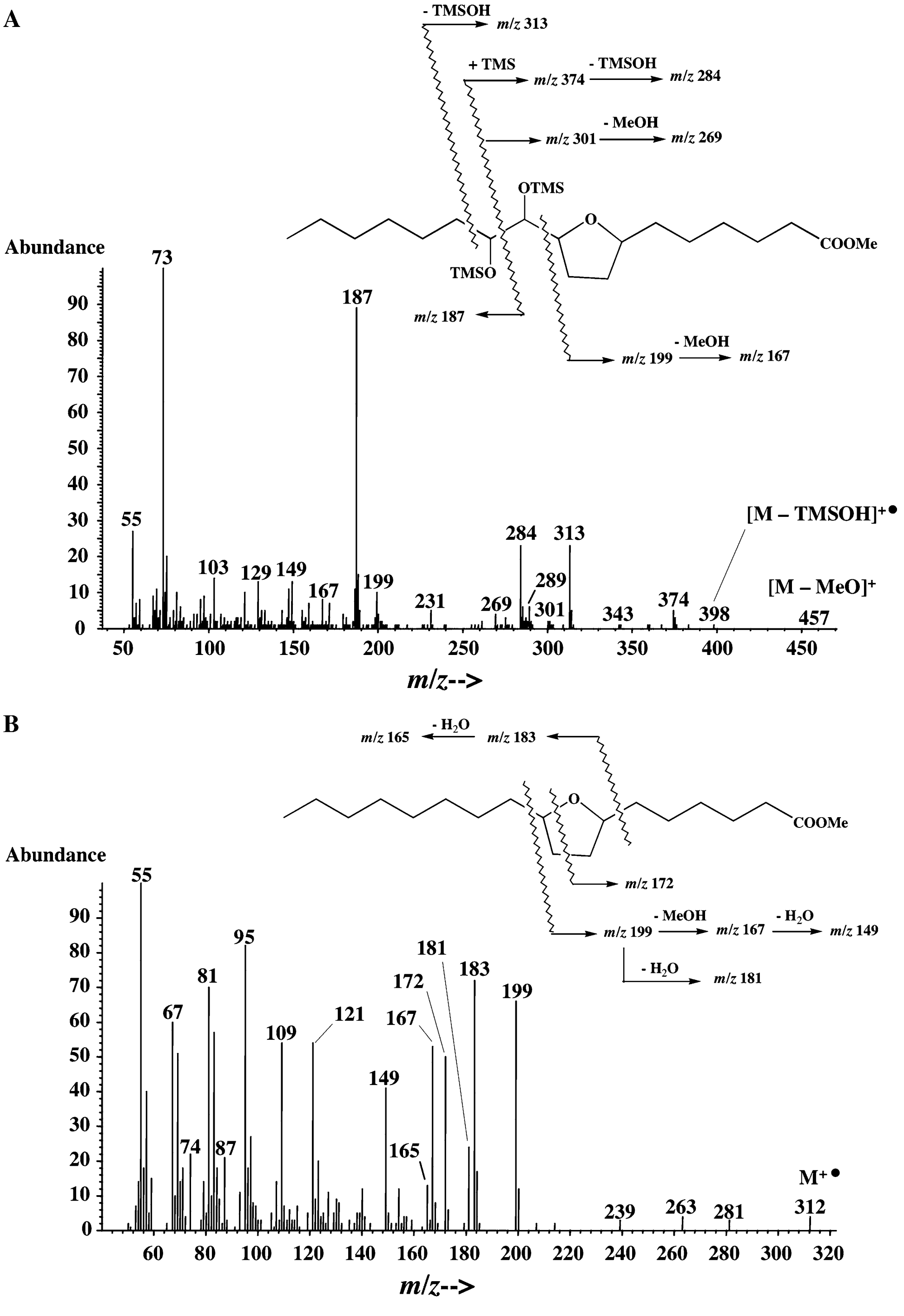

Fig. 2 EI mass spectra of the silylated OsO_4 (**a**) and hydrogenated (**b**) derivatives of 7,10-epoxyoctadec-11(*cis*)-enoic acid methyl ester

In parallel to enzymatic conversion, hydroperoxides may also undergo chemical decomposition under mild conditions. The majority of these decomposition reactions involve free radicals and are promoted by heat, photolysis, metal ions and metalloproteins. The very distinct proportions of hydroperoxyacids, hydroxy acids and oxoacids observed in the case of the *cis* and *trans* isomers [8] allowed us to exclude the involvement of such abiotic processes during the degradation of *cis* and *trans* 10-hydroperoxyoctadec-11-enoic acid to the corresponding hydroxyacids and oxoacids. In contrast, we proposed the abiotic formation pathways described in Fig. 5 for the formation of 7,10-epoxyoctadec-11-enoic acid. These pathways involve the cyclisation of the alkoxyl radical deriving from homolytic cleavage of 10-hydroperoxyoctadec-11-enoic acid. A similar cyclisation process (involving

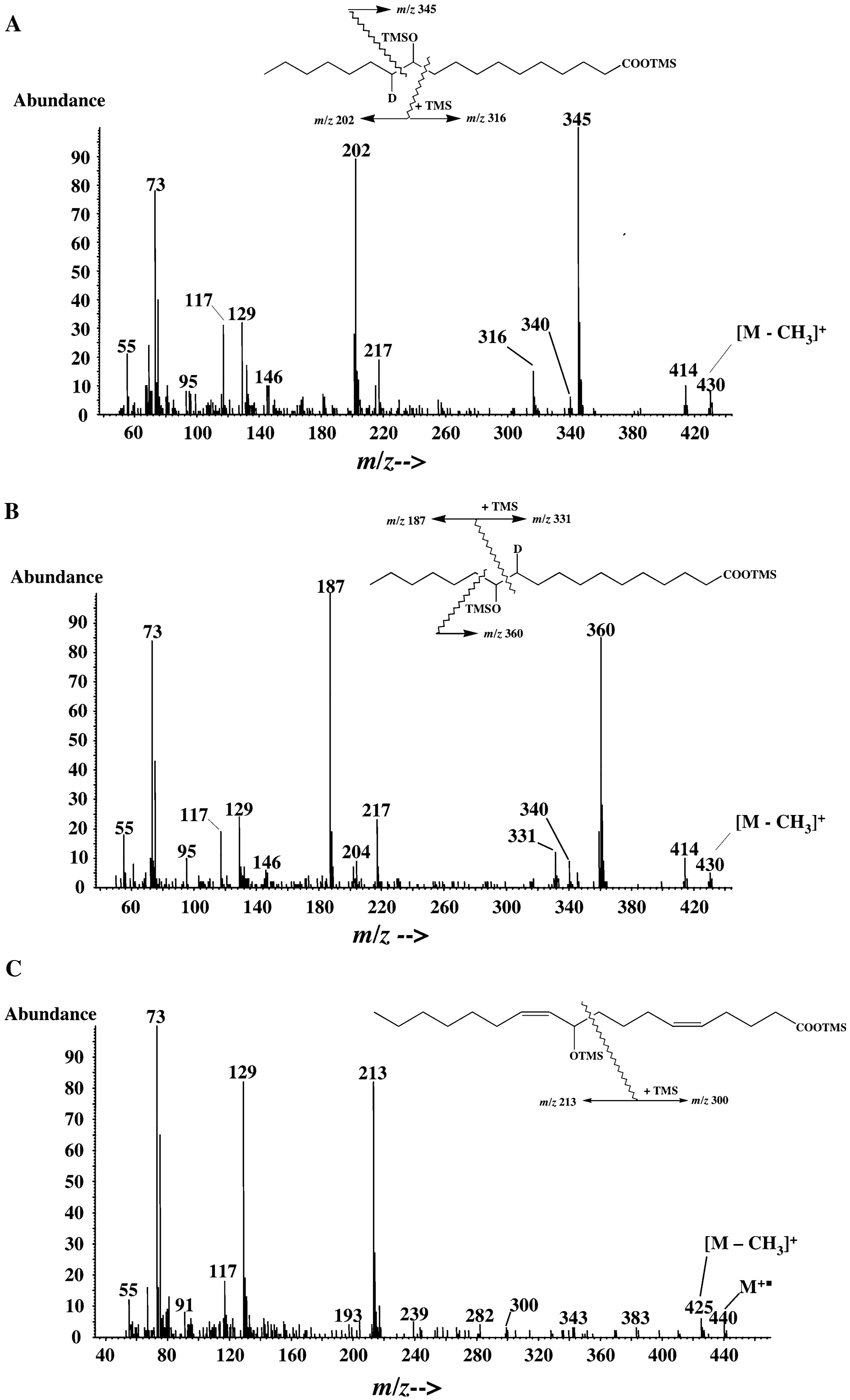

Fig. 3 EI mass spectra of (11-D_1)-12-hydroxyoctadecanoic (**a**), (12-D_1)-11-hydroxyoctadecanoic (**b**) and 10-hydroxyoctadeca-5,11-dienoic (**c**) acid trimethylsilyl derivatives

the passing through alkoxyl radicals) was previously proposed to explain the formation of THF rings during the treatment of monohydroxyalcohols with lead tetraacetate [36]. The strong increase of the ratio 7,10-epoxyoctadec-11-enoic acid / 10-hydroxyoctadec-11(*cis*)-enoic acid observed during the growth (Table 1) well supports a

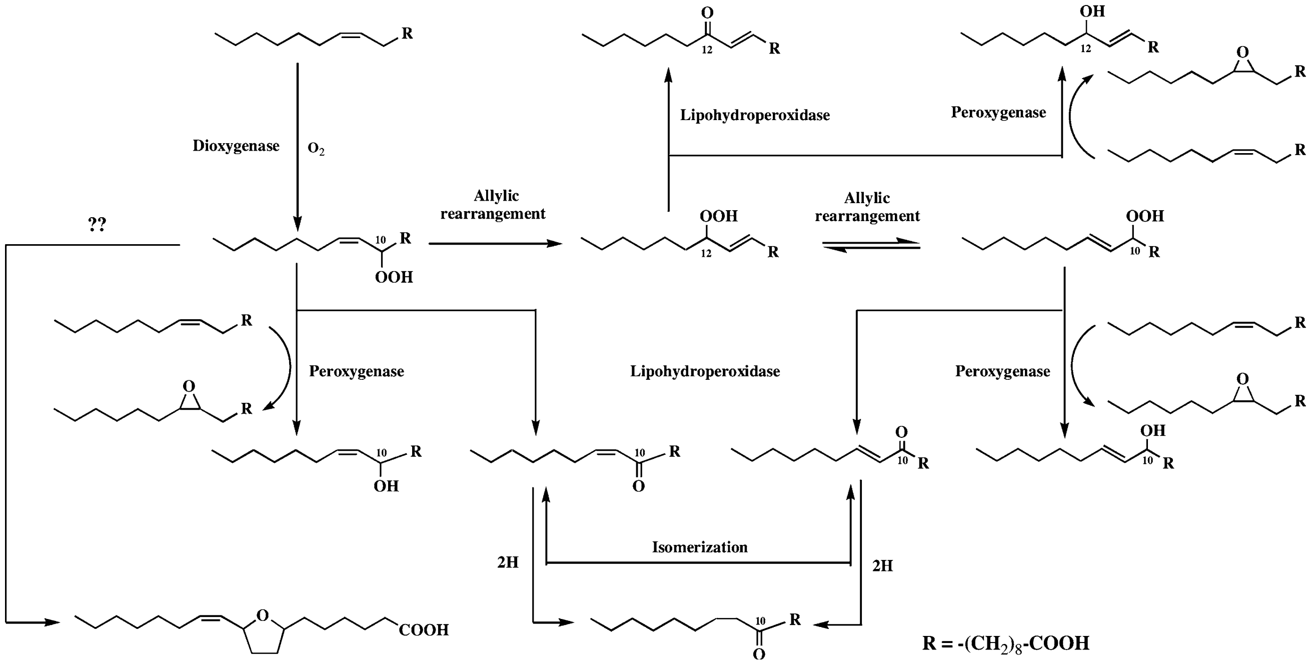
Dioxygenase
O2
??
Allylic rearrangement
Allylic rearrangement
Lipohydroperoxidase
Lipohydroperoxidase
Peroxygenase
Peroxygenase
Peroxygenase
OOH
OH
O
10
12
R
Isomerization
2H
2H
COOH
R = -(CH2)8-COOH

Fig. 4 Proposed pathways for the regiospecific enzymatic oxygenation of the allylic carbon 10 of *cis*-vaccenic acid in MG3 cells

formation of this cyclic compound by such a degradative process. The detection of diastereoisomeric 7,10-epoxy-octadecanoic acids after catalytic hydrogenation of the double bond (Fig. 6) allowed us to exclude the involvement of a stereospecific enzymatic cyclisation process. It may be noted that abstraction of a hydrogen atom on another molecule by the intermediate alkoxyl and alkyl radicals involved in this cyclisation process may also constitute an additional source of 10-hydroxyoctadec-11(*cis*)-enoic acid (Fig. 5).

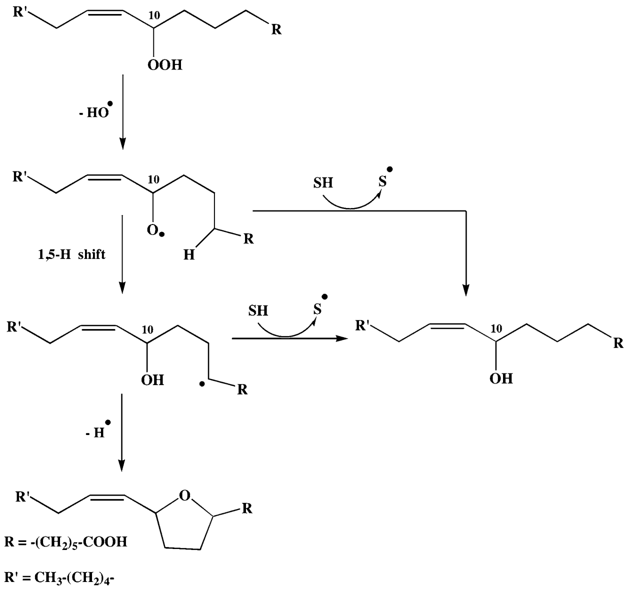
R'
10
R
OOH
- HO•
SH
S•
1,5-H shift
O•
H
OH
- H•
O
R = -(CH2)5-COOH
R' = CH3-(CH2)4-

Fig. 5 Proposed pathways for the formation of 7,10-epoxyoctadec-11(*cis*)-enoic acid from 10-hydroperoxyoctadec-11(*cis*)-enoic acid

Influence of Growth Conditions Upon the Regiospecific Peroxidation of Vaccenic Acid

The very strong variation in the proportion of 10-hydroxy-octadec-11(*cis*)-enoic acid observed between our previous examination of this strain [8] and this work suggests that the induction of the regiospecific peroxidation of the allylic carbon 10 of *cis*-vaccenic acid strongly depends on the physiological status of the cells. To investigate this phenomenon, the fatty acid composition was analysed in MG3 cultures harvested in exponential, late exponential and steady-state (7 days in steady-state) growth phases. The very strong increase in the proportion of 10-hydroperoxyoctadec-11(*cis*)-enoic acid and its degradation products (7,10-epoxyoctadec-11-enoic, 10-hydroxyoctadec-11(*cis*)-enoic, 10-hydroxyoctadec-11(*trans*)-enoic, 12-hydroxyoctadec-10-enoic, 10-hydroxyoctadecanoic, 11-hydroxyoctadecanoic and 12-hydroxyoctadecanoic acids) observed during the growth (47% during the exponential phase, 54% during the late exponential phase and 87% during the steady state phase) readily supports this hypothesis.

Additional tests were performed with *Erythrobacter* sp. strain MG3 cultures grown under different nutrient limitation and light conditions. The experiments have shown that carbon limitation enhances the amount of 10-hydroperoxy-octadec-11(*cis*)-enoic acid and its degradation products, but light does not seem to have an effect. Interestingly, the lipid

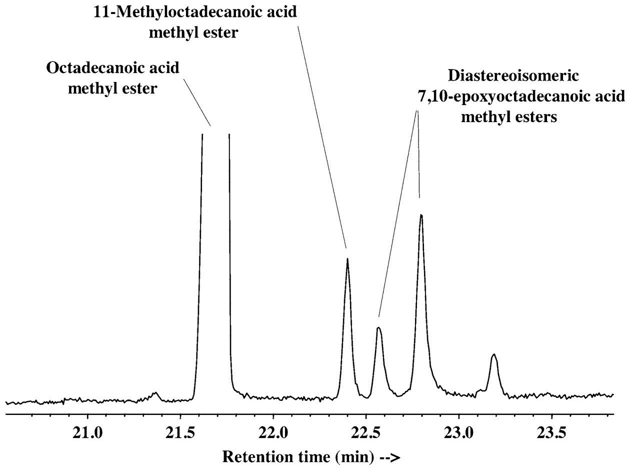

Fig. 6 Partial total ion chromatogram showing the presence of diastereoisomeric 7,10-epoxyoctadecanoic acids after catalytic hydrogenation of methylated lipid extracts obtained from *Erythrobacter* sp. strain MG3 (steady-state phase)

peroxidation appeared to be strongly enhanced in all the cultures grown at low (7 °C) temperature (Table 2).

Re-examination of the fatty acid content of *Erythrobacter* sp. strain MG3 cells (dominated by *cis*-vaccenic acid) allowed us to confirm the involvement of an unusual regiospecific enzymatic peroxidation of the allylic carbon 10 of *cis*-vaccenic acid, which seems to be a characteristic of aerobic and anaerobic phototrophic bacteria. A peroxidation of the allylic carbon 10 of octadeca-5,11-dienoic acid, which is also present in this strain [4], could also be observed showing that this enzymatic attack is not restricted to *cis*-vaccenic acid but can act on all the acids possessing a double bond at the position 11. Enzymatic degradation of 10-hydroperoxyoctadec-11(*cis*)-enoic acid resulting from the peroxidation of *cis*-vaccenic acid mainly involves reduction to the corresponding hydroxy acid (probably catalysed by peroxygenases) and cleavage to the corresponding oxoacid, which is then biohydrogenated. In parallel to these enzymatic processes, 10-hydroperoxyoctadec-11(*cis*)-enoic acid also undergoes abiotic allylic rearrangement to 10-hydroperoxyoctadec-11(*trans*)-enoic and 12-hydroperoxyoctadec-10(*trans*)-enoic acids and cyclisation to the very unusual 7,10-epoxyoctadec-11-enoic acid. The proportion of products resulting from this enzymatic peroxidation strongly increases at low temperature and in carbon limited steady-state cultures.

Table 2 Percentage (relative to residual *cis*-vaccenic acid) of compounds resulting from the enzymatic attack of the allylic position 10 (Sum of 7,10-epoxyoctadec-11-enoic, 10-hydroxyoctadec-11(*cis*)-enoic, 10-hydroxyoctadec-11(*trans*)-enoic, 12-hydroxyoctadec-10-enoic, 10-hydroxyoctadecanoic, 11-hydroxyoctadecanoic and 12-hydroxyoctadecanoic acids) in *Erythrobacter* sp. strain MG3 cultivated at different growth conditions

Growth conditions	Percentage
C-limited 22 °C light/dark	7.1
N-limited 22 °C light/dark	2.6
P-limited 22 °C light/dark	3.0
C-limited 22 °C dark	7.5
N-limited 22 °C dark	3.2
P-limited 22 °C dark	2.3
C-limited 7 °C dark	36.5
N-limited 7 °C dark	36.5

Acknowledgments This work was supported by grants from the Centre National de la Recherche Scientifique (CNRS) and the Université de la Méditerranée. This research was also supported by the Czech GAČR project 206/07/0241 and the Inst. research concepts MSM6007665808 and AV0Z50200510. Two anonymous reviewers are acknowledged for their useful and constructive comments.

References

1. Yurkov VV, Beatty JT (1998) Aerobic anoxygenic phototrophic bacteria. Microbiol Mol Biol Rev 62:695–724
2. Koblížek M, Béjà O, Bidigare RR, Christensen S, Benetiz-Nelson B, Vetriani C et al (2003) Isolation and characterization of *Erythrobacter* sp strains from the upper ocean. Arch Microbiol 180:327–338
3. Kolber ZS, Plumley FG, Lang AS, Beatty JT, Blankenship RE, VanDover CL et al (2001) Contribution of aerobic photoheterotrophic bacteria to the carbon cycle in the ocean. Science 292:2492–2495
4. Mašín M, Zdun A, Stoń-Egiert J, Nausch M, Labrenz M, Moulisová V, Koblížek M (2006) Seasonal changes and diversity of aerobic anoxygenic phototrophs in the Baltic Sea. Aquat Microbial Ecol 45:247–254
5. Jiao N, Zhang Y, Zeng Y, Hong N, Liu R, Chen F, Wang P (2007) Distinct distribution pattern of abundance and diversity of aerobic anoxygenic phototrophic bacteria in the global ocean. Environ Microbiol 9:3091–3099
6. Mašín M, Nedoma J, Pechar L, Koblížek M (2008) Distribution of aerobic anoxygenic phototrophs in temperate freshwater systems. Environ Microbiol 10:1988–1996
7. Koblížek M, Mašín M, Ras J, Poulton AJ, Prášil O (2007) Rapid growth rates of aerobic anoxygenic phototrophs in the ocean. Environ Microbiol 9:2401–2406
8. Rontani J-F, Christodoulou S, Koblížek M (2005) GC–MS structural characterization of fatty acids from marine aerobic anoxygenic phototrophic bacteria. Lipids 40:97–107
9. Marchand D, Grossi V, Hirschler-Réa A, Rontani J-F (2002) Regiospecific enzymatic oxygenation of *cis*-vaccenic acid during aerobic senescence of the halophilic purple sulphur bacterium *Thiohalocapsa halophila*. Lipids 37:541–548
10. Kühn H, Schewe T, Rapoport SM (1986) The stereochemistry of the reactions of lipoxygenases and their metabolites. Proposed nomenclature of lipoxygenases and related enzymes. Adv Enzymol 58:273–311
11. Wang T, Yu WG, Powell WS (1992) Formation of monohydroxy derivatives of arachidonic acid, linoleic acid, and oleic acid during oxidation of low density lipoprotein by copper ions and endothelial cells. J Lipid Res 33:525–537

12. Guerrero A, Casals I, Busquets M, Leon Y, Manresa A (1997) Oxidation of oleic acid to (*E*)-10-hydroperoxy-8-octadecenoic and (*E*)-10-hydroxy-8-octadecenoic acids by *Pseudomonas* sp. 42A2. Biochim Biophys Acta 1347:75–81
13. Oliw EH, Su C, Skogstrom T, Benthin G (1998) Analysis of novel hydroperoxides and other metabolites of oleic, linoleic and linolenic acids by liquid chromatography-mass spectrometry. Lipids 33:843–852
14. Clapp CH, Senchak SE, Stover TJ, Potter TC, Findeis PM, Novak MJ (2001) Soybean lipoxygenase-mediated oxygenation of monounsaturated fatty acids to enones. J Am Chem Soc 123:747–748
15. Schewe T, Rapoport SM, Kühn H (1986) Enzymology and physiology of reticulocyte lipoxygenase: comparison with other lipoxygenases. Adv Enzymol 58:191–272
16. Porta H, Rocha-Sosa M (2001) Lipoxygenase in bacteria: a horizontal transfer event. Microbiology 147:3199–3200
17. Su C, Oliw EH (1996) Purification and characterization of linoleate 8-dioxygenase from the fungus *Gaeumannomyces graminis* as a novel hemoprotein. J Biol Chem 271:14112–14118
18. Brodowsky ID, Oliw EH (1993) Biosynthesis of 8R-hydroperoxylinoleic acid by the fungus *Laetisaria arvalis*. Biochem Biophys Acta 1168:68–72
19. Loidl-Stahlhofen A, Spiteller G (1994) α-Hydroxyaldehydes, products of lipid peroxidation. Biochim Biophys Acta 1211:156–160
20. Marchand D, Rontani J-F (2001) Characterisation of photooxidation and autoxidation products of phytoplanktonic monounsaturated fatty acids in marine particulate matter and recent sediments. Org Geochem 32:287–304
21. Porter QN (1985) Mass spectrometry of heterocyclic compounds. Taylor EC, Weissberger A (eds) Wiley, New York, pp 47–51
22. Capella P, Zorzut CM (1968) Determination of double bond position in monounsaturated fatty acid esters by mass spectrometry of their trimethylsilyloxy derivatives. Anal Chem 40:1458–1463
23. de Leeuw JW, van der Meer JW, Rijpstra WIC, Schenck PA (1980) On the occurrence and structural identification of long chain ketones and hydrocarbons in sediments. In: Douglas AG, Maxwell JR (eds) Advances in organic geochemistry 1979. Pergamon, Oxford, pp 211–217
24. Shirasaka N, Nishi K, Shimizu S (1995) Occurrence of a furan fatty acid in marine bacteria. Biochim Biophys Acta 1258:225–227
25. Shirasaka N, Nishi K, Shimizu S (1997) Biosynthesis of furan fatty acids (F-acids) by a marine bacterium, *Shewanella putrefaciens*. Biochim Biophys Acta 1346:253–260
26. Ishii K, Okajima H, Koyamatsu T, Okada Y, Watanabe H (1988) The composition of furan fatty acids in the crayfish. Lipids 23:694–700
27. Galliard T, Chan HWS (1980) Lipoxygenases. In: Stumpf PK, Conn EE (eds) The biochemistry of plants: a comprehensive treatise. Academic Press, New York, vol 4, pp 131
28. Hamberg M (1987) Mechanism of corn hydroperoxide isomerase: detection of 12, 13(S)-oxido-9(Z), 11-octadecadienoic acid. Biochim Biophys Acta 920:76–84
29. Galliard T, Matthew JA, Fishwick MJ, Wright AJ (1976) The enzymatic degradation of lipids resulting from physical disruption of cucumber (*Cucumis sativus*) fruit. Phytochemistry 15:1647–1650
30. Blée E (1998) Biosynthesis of phytooxylipins: the peroxygenase pathway. Fett Lipid 4–5:121–127
31. Blée E, Schuber F (1990) Efficient epoxidation of unsaturated fatty acids by a hydroperoxide-dependent oxygenase. J Biol Chem 265:12887–12894
32. Kühn H, Eggert L, Zabolotsky OA, Myagkowa GI, Schewe T (1991) Keto fatty acids not containing doubly allylic methylenes are lipoxygenase substrates. Biochemistry 30:10269–10273
33. Porter NA, Caldwell SE, Mills KA (1995) Mechanisms of free radical oxidation of unsaturated lipids. Lipids 30:277–290
34. Hammond RC (1988) Enzymatic modification at the mid-chain of fatty acids. Fat Sci Technol 1:18
35. Morris LJ (1970) Mechanism and stereochemistry in fatty acid metabolism. Biochem J 118:681
36. Paredes MD, Alonso R (1999) Oxidation of α-hydroxysilanes by lead tetraacetate. Tetrahedron Lett 40:3973–3976

domain and sheds a soluble form [3, 4]. CXCL16 promotes interactions between macrophages/DC and CD8 T cells and guides effector T cell trafficking in lymphoid organs and some nonlymphoid tissues [3, 5, 6]. The membrane bound CXCL16 also mediates the firm adhesion of CXCR6-expressing T cells [6]. Recent reports indicated that the elevated CXCL16 mediated a unique pathogenic role in chronic inflammatory diseases such as rheumatoid arthritis, cardiac vascular atherosclerosis, and cancers [7–9]. CXCL16 is not exclusively expressed on the cell surface. It is also found as a soluble molecule that is constitutively generated by proteolytic cleavage of its transmembrane variant, a process called shedding [10].

LysoPtdOH is a serum-borne lysophospholipid that signals through the cognate G protein-coupled receptors to evoke a great variety of responses in numerous cell types. In addition to stimulating cell proliferation and survival, lysoPtdOH might regulate the trafficking, cytokine production, and T cell-activating functions of DC [11–13]. Reports have indicated that lysoPtdOH receptors might also appear on the human macrophage surface, however, influences of lysoPtdOH on cytokines/chemokines production in macrophages/DC have been controversial [14–16]. The effect of lysoPtdOH on CXCL16 expression in macrophages/DC has never been explored. Using monocyte-derived macrophages/DC (MoDC), we investigated how lysoPtdOH regulate CXCL16 production and shedding. The increased production of CXCL16 stimulated by lysoPtdOH in macrophages/MoDC may involve multiple signaling transduction pathways including $G_{i/o}$, Rho, and NF-κB, which would affect the chemotactic activity of macrophages/MoDC as well.

Materials and Methods

Reagents

The endotoxin content of the sodium salt of 18:1 lysoPtdOH (1-oleoyl-2-hydroxy-*sn*-glycero-3-phosphate; Avanti Polar Lipids) in working solution was <50 pg/ml. Pertussis toxin (PTx), lipopolysaccharide (LPS), and pyrrolidine dithiocarbamate (PDTC) were purchased from Sigma (St Louis, MO). The C3 exoenzyme (exoC3) was purchased from Cytoskeleton (Denver, CO). Anti-lysoPtdOH receptor antibodies, anti-CXCL16 antibody, and isotype-matched control were from BD Pharmingen (San Diego, CA).

Cell Source and Culture

$CD14^+$ monocytes were purified from heparinized peripheral blood mononuclear cells (PBMC), which were either purchased from BRT Laboratory (Baltimore, MD) or healthy donors using immunomagnetic selection according to the manufacturer's instructions (Miltenyi Biotec, Auburn, CA). All donors (both male and female, 20–50 year old) provided written informed consent according to federal, state and institutional guidelines. Monocyte-derived macrophages were obtained by culturing $CD14^+$ monocytes (0.5×10^6 cells/ml) in complete RPMI-1640 (Invitrogen, Carlsbad, CA) with 10% human serum (Sigma, MO) in the presence of GM-CSF (50 ng/ml, R&D Systems, Minneapolis, MN) for 6 days. MoDC were generated by supplementing with GM-CSF and IL-4 (50 ng/ml, each) for over 6 days. Macrophages/MoDC were washed and incubated with LPS (100 ng/ml, Sigma Chemicals) for 24 h to induce cytokine secretion. To determine whether lysoPtdOH affect macrophages/MoDC activation or modulate the effects of LPS, macrophages/MoDC were incubated with and without lysoPtdOH or LPS.

Flow Cytometry Analysis

Cells were counted (2×10^6) and stained with fluorescence-labeled antibodies against lysoPtdOH receptors and CXCL16 for 30 min, washed and analyzed by flow cytometry (FACS, Becton Dickenson Immunocytometry Systems, San Jose, CA). Gated on live cells, expression of LPA1, LPA2, LPA3, and CXCL16 was analyzed in comparison with isotype-match controls. Mean fluorescence intensities (MFI) were analyzed with CellQuest software (Becton Dickenson Immunocytometry Systems).

Qualitative RT-PCR

Cells were lysed using TRIzol Reagents. Total RNA was precipitated from the aqueous phase using isopropyl alcohol after separation by chloroform. After DNase I treatment, cDNA was synthesized from 1 μg total RNA using MLV-Reverse Transcriptase (Invitrogen, Carlsbad, CA) according to the manufacturer's directions. RT-PCR profiled as followed: 48 °C for 45 min, 94 °C for 2 min, 30 cycles (94 °C for 30 s, 60 °C for 1 min, 68 °C for 2 min), 68 °C for 5 min. Primer sequences used in RT-PCR were 5′-CGGAGACTGACTGTCAGCAC-3′ and 5′-GGTCCAGAACTATGCCGAGA-3′ for LPA1 mRNA; 5′-TGGCCTACCCTCTTCCTCATGTTCCA-3′, 5′-GGGTCCAGCACACCACAAATGCC-3′ for LPA2 mRNA; 5′-GGACACCCATGAAGCTAAT-3′ and 5′-TCTGGGTTCTCCTGAGAGAA-3′ for LPA3 mRNA [17, 18]. β-actin primer sequences were described previously [19]. To analyze the reactions, 10 μl of each reaction was subjected to electrophoresis on a 1% agarose gel and DNA was detected by ethidium bromide staining.

ELISA

CXCL16 concentrations in the spent culture supernatant were measured by ELISA kits purchased from R&D Systems (Minneapolis, MN). Briefly, the capture antibody in the working concentration was diluted and coated in a 96-well microplate overnight at 4 °C. After washing and blocking, 100 µl of the sample or standard in appropriate diluents were added and incubated for 2 h at room temperature following the manufacturer's protocol. The detection antibody conjugated with biotin in the working concentration was added after washing for 2 h, then streptavidin conjugated with HRP was incubated for 1 h. Color was developed by adding substrates for 20 min and the optical density of each well was determined using a microplate reader set to 650 nm. CXCL16 concentrations were calculated according to the standard controls.

Real-time PCR

Cells were lysed, total RNA was purified and cDNA was synthesized as above. RT-PCR was set up in a 96-well plate using a TaqMan® Universal PCR Master Mix kit from Applied Biosystems (Foster City, CA). The reactions were run on an ABI PRISM® 7300 Sequence Detection System and compared to the actin control. Prevalidated primers and probes specific for CXCL16 (Hs00222859_m1) and *β*-actin (Hs00194811_m1) were purchased from Applied Biosystems. After normalization RNA amplified from different cells was exported as TIFF files.

T cells Activation and Migration Assay

$CD3^+$ T cells were purified from normal donor PBMC as above by positive selection (Miltenyi Biotec, Auburn, CA). Purified $CD3^+$ T cells were stimulated with anti-CD3/CD28 coated beads for 5 days before analysis or migration assay [20]. Activated $CD3^+$ cells were loaded into the top chamber of a trans-well (5.0 µm pore size, Costar, New York, NY). In the bottom well, a total of 500 µl spent culture supernatant or fresh media as control were plated. Anti-CXCL16 blocking antibody was purchased from R&D Systems. Migration was allowed to proceed for 2 h. Then cells that had migrated to the bottom wells were counted and the absolute numbers of migrated cells were calculated. Some macrophages were pretreated with different inhibitors PTx (1 µg/ml), exoC3 (1 µg/ml), or PDTC (200 µM), then treated with lysoPtdOH/LPS, spent culture supernatant were collected and plated in the bottom wells [13, 21].

Statistics

One-way ANOVA with Dunnett's post test was performed using GraphPad InStat version 3.05 to compare the averages of different experiment groups. $P < 0.05$ was accepted as being significant.

Results

Macrophages and MoDC Express LysoPtdOH Receptors

Macrophages and MoDC were derived from $CD14^+$ monocytes from normal donor PBMC without age or gender discrimination. FACS confirmed the cell surface expression of LPA1 and LPA2, but not LPA3 on macrophages/MoDC, as well as their precursors $CD14^+$ monocytes (Fig. 1a). Similar results were observed when analyzing mRNA expression of lysoPtdOH receptors by qualitative RT-PCR, where expression of both LPA1 and LPA2 mRNA was readily detectable (Fig. 1b).

Macrophages and MoDC Express and Secrete CXCL16

FACS confirmed macrophages and MoDC expressed CXCL16 on the cell surface. A few monocytes expressed CXCL16 on their cell surface, almost all macrophages acquired CXCL16 after differentiation, MoDC expressed CXCL16 with the highest intensity on the cell surface (Fig. 2a). ELISA showed both macrophages and MoDC secreted soluble CXCL16, while macrophages released more CXCL16 into their spent culture supernatants (Fig. 2b).

LysoPtdOH Stimulates CXCL16 Production from Macrophages

To examine the effect of lysoPtdOH on CXCL16 expression, we cultured macrophages, stimulated them with LPS to trigger chemokine release. We observed that lysoPtdOH at 10 µM significantly increased the production and release of CXCL16 from macrophages by more than twofold as detected by ELISA (Fig. 3a). LysoPtdOH did not affect CXCL16 cell surface presentation shown by FACS (Fig. 3b). Quantitative real-time PCR showed lysoPtdOH upregulated CXCL16 mRNA expression in macrophages also (Fig. 3c). Control macrophages had basal CXCL16 mRNA (detectable at cycle 35), lysoPtdOH increased CXCL16 mRNA (detectable at cycle 32), LPS induced CXCL16 mRNA (detectable at cycle 28), however, lysoPtdOH and LPS synergized in CXCL16 mRNA transcription (detectable at cycle 22). By calculating the cycle

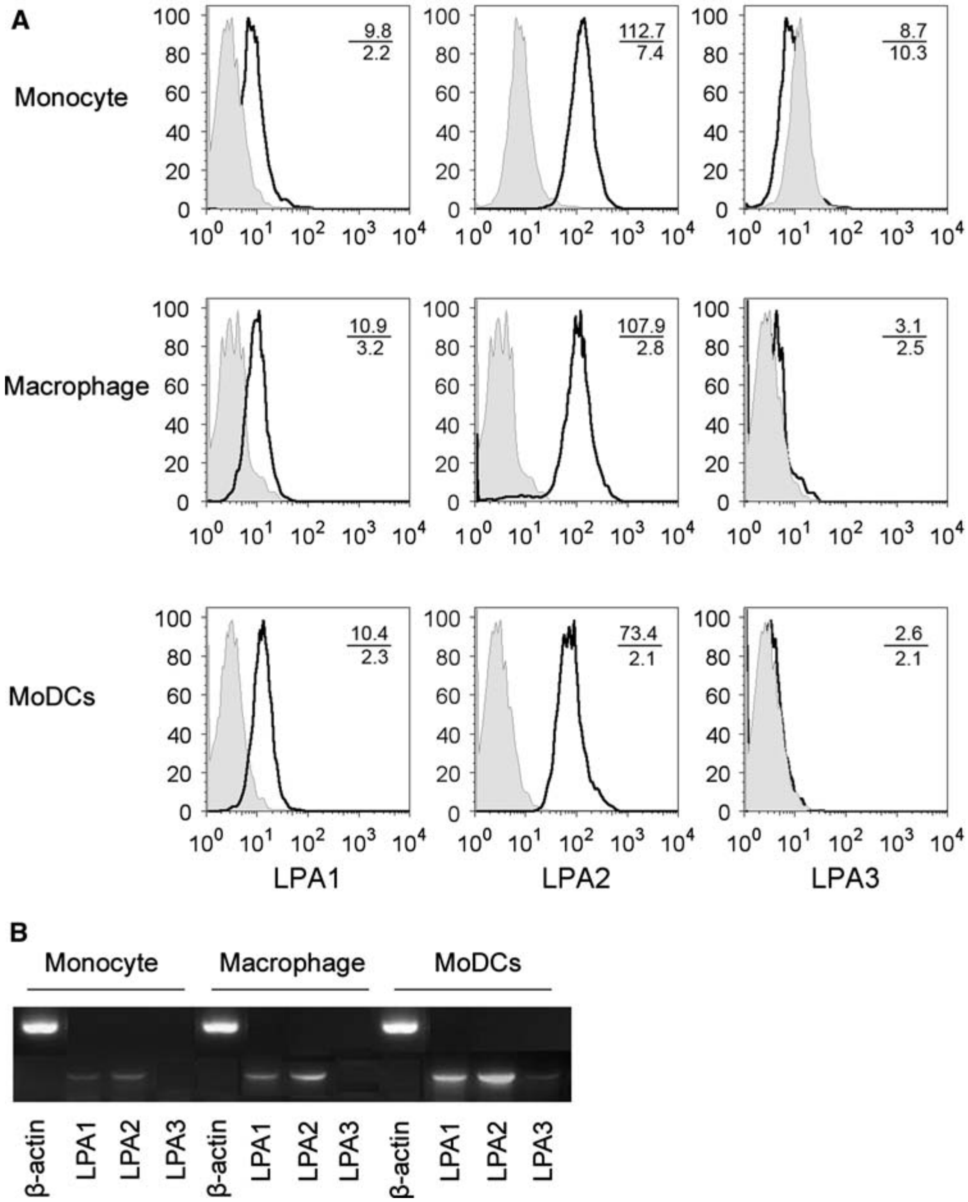

Fig. 1 **a** Expression of lysoPtdOH receptors on the cell surface of macrophages and MoDC. Macrophages and MoDC were derived from $CD14^+$ monocytes by culturing with GM-CSF or GM-CSF+IL-4 for 6 days. Cells were harvested and stained with PE labeled anti-LPA antibodies. Cells were washed and analyzed by FACS. *Filled curves* show results from cells stained with isotype-matched control mAbs. *Curves with just lines* show results from cells stained with specific antibodies. The *numbers* shown in each histogram represent MFI of LPA, LPA_2 or LPA_3 over control. *Graphs* shown are representative of three independent experiments. **b** RT-PCR analysis of mRNAs encoding lysoPtdOH receptors in macrophages and MoDC

threshold (CT) values of each sample and ΔCT, we found that lysoPtdOH enhanced CXCL16 mRNA transcription by 64-fold.

Signaling Pathways Regulating CXCL16 Production Enhanced by LysoPtdOH

By binding to specific LPA receptors, lysoPtdOH activates complex cell signaling including PTx sensitive and insensitive G proteins depending on cell types, triggering tyrosine phosphorylation and regulating rho-dependent actin reorganization [19, 22]. PTx, a specific inhibitor of $G_{i/o}$ proteins, which has been shown to inhibit $G_{i/o}$-dependent lysoPtdOH effects in different cell systems. Pretreatment of macrophages with 10 ng/ml of PTx for 16 h before lysoPtdOH suppressed CXCL16 protein production stimulated by LPS. In addition, pretreatment with 1 μg/ml of exoC3, a specific inhibitor of Rho and 200 μM of PDTC, an inhibitor of the NF-κB-dependent pathway significantly decreased lysoPtdOH enhanced CXCL16 protein production from macrophages, suggesting that the enhancement of lysoPtdOH on CXCL16 production are $G_{i/o}$, Rho, and NF-κB dependent (Fig. 4). Similar results were also observed at the RNA level as detected by RT-PCR.

LysoPtdOH Enhances Chemotactic Activity of Macrophages

Macrophages play an important role in immune cell trafficking into inflammation and tumor sites. To investigate

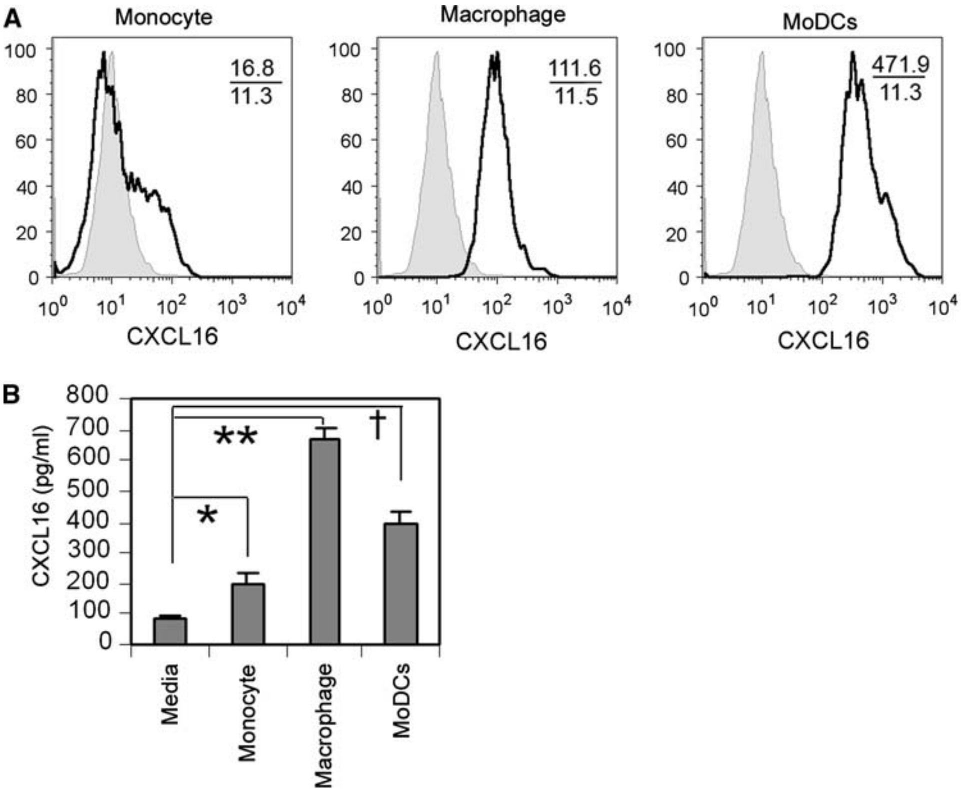

Fig. 2 **a** Macrophages and MoDC express CXCL16 on the cell surface. Macrophages and MoDC were cultured as above and stained with anti-CXCL16-PE and analyzed by FACS. *Filled curves* represent cells stained with isotype-matched control mAb. *Curves consisting of lines alone* were from cells stained with anti-CXCL16. The *numbers* shown in each histogram were MFI of CXCL16 over control. The data shown are representative of five repeated experiments. **b** Macrophages and MoDC secrete soluble CXCL16. Cells were washed on day 5, resuspended at 5 × 10^5/ml and cultured. The spent culture supernatants were harvested after 24 h. The concentrations of CXCL16 were measured by ELISA. Data shown are means ± SE of three experiments with duplicates. Compare to the media control, monocytes secrete basal level CXCL16 ($*P < 0.06$); macrophages give the highest level of CXCL16 ($**P < 0.01$); while MoDC shed the median level of CXCL16 ($\dagger P < 0.05$)

CXCL16 production stimulated by lysoPtdOH would functionally attract more T lymphocyte migration, chemotactic activity of spent culture supernatant collected from lysoPtdOH/LPS treated macrophages was tested in a trans-well system. Results showed that spent culture supernatant from lysoPtdOH/LPS stimulated macrophages significantly increased $CD3^+$ T cells migration, and pre-incubation the spent culture supernatant with 10 µg/ml blocking antibody against human CXCL16 significantly blocked $CD3^+$ cells migration. In contrast, normal mouse IgG (10 µg/ml) had no effects on $CD3^+$ cell migration, implying the enhanced chemotactic activity of macrophages stimulated by lysoPtdOH was mediated through the increased production of soluble CXCL16 (Fig. 5a). Consistent with the ELISA results of CXCL16 production regulated by lysoPtdOH through several signaling transduction pathways above, the chemotactic activity of macrophages was also mediated through $G_{i/o}$-, Rho-, and NF-κB-dependent pathways, since $CD3^+$ cells migration toward to spent culture supernatant collected from macrophages were blocked by pretreatment macrophages with PTx, exoC3, or PDTC (Fig. 5b). LysoPtdOH and LPS alone did no significantly enhance $CD3^+$ cells migration.

Discussion

Chemokines play an important role as paracrine and autocrine mediators in healthy and diseased skin. They have been implicated in wound healing, inflammatory processes and tumors [23, 24]. CXCL16 has been linked with different biological activities. As a surface-expressed molecule CXCL16 functions as a scavenger receptor for oxidized low-density lipoprotein [25], binds to CXCR6 expressed on leukocytes and establishes firm cell to cell contact [5]. The constitutively proteolytic soluble form CXCL16 functions as a chemoattractant for CXCR6-expressing cells such as T cells [26–28]. CXCL16 has been detected in wound fluids, acute and chronic inflammation sites and tumor tissues, implicating its important roles in broad physiological and pathological situations [10, 24].

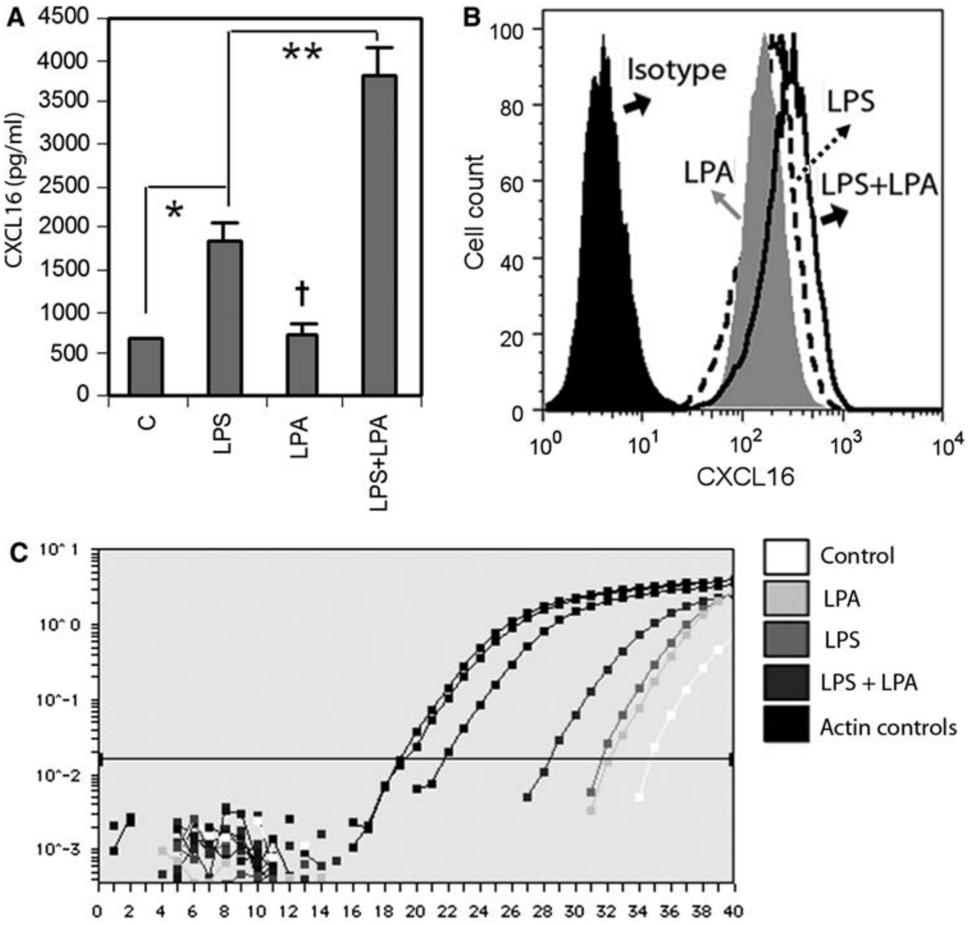

Fig. 3 **a** LysoPtdOH increases CXCL16 production and shedding in macrophages. Macrophages were prepared as above. Cells were treated with LPS, lysoPtdOH or lysoPtdOH plus LPS for 16 h, levels of CXCL16 in spent culture supernatant were measured by ELISA. Data presented as the mean ± SE of five experiments with similar results. Compare to macrophage control supernatant, LPS induced CXCL16 release from macrophage ($*P < 0.01$); LysoPtdOH increased CXCL16 production and shedding from macrophage stimulated by LPS ($**P < 0.05$); while lysoPtdOH alone had no effect on CXCL16 secretion ($\dagger P > 0.05$). **b** LysoPtdOH lead to undetectable change on CXCL16 cell surface presentation in macrophages. Above macrophages were stained with anti-CXCL16-PE and analyzed by FACS. *Black filled curve* represent cells stained with isotype-matched control mAb. *Gray filled curve* was for cells stained with anti-CXCL16 after lysoPtdOH stimulation. *Broken line curve* was for cells stained with anti-CXCL16 after LPS activation. *Solid line curve* was for cells stained with anti-CXCL16 after lysoPtdOH and LPS treatment. Data shown are representative of three repeatable experiments. **c** LysoPtdOH upregulated CXCL16 mRNA expressions in macrophages shown by real-time PCR. The same number of cells treated as above were lysed, RNA was purified, cDNA was synthesized and the same amount of cDNA was used for RT-PCR

Lipids have long since been recognized as signaling molecules that have the capacity to control important cellular processes, including cell proliferation, apoptosis, metabolism and migration and trigger profound physiological responses [29]. The same signaling lipid can provoke different cellular responses, depending on the precise cell type and underlying signaling network present in the target cell. LysoPtdOH, a natural occurring water-soluble phospholipid was originally identified as a key molecule in lipid biosynthesis. It is stored within the cell at concentrations up to 60 µM and may accumulate in extracellular fluids such as in the inflammatory exudate at concentrations as high as 10 µM [22]. Both lysoPtdOH and CXCL16 have been detected in the wound fluid in multiple tissues upon injury with the similar kinetics [24, 30–32], which may allow the coordinated skin repair with subsequent cell infiltrations [33, 34]. The instrumental role of disintegrin-like metalloproteinase ADAM10 on CXCL16's proteolytic shedding has been introduced recently [10, 24], and lysoPtdOH has been reported to affect the production and shedding of several transmembrane proteins [35, 36], here we have shown that lysoPtdOH treatment significantly increased the production and shedding of CXCL16 stimulated by LPS as well, supporting the important roles of lysoPtdOH in multiple cellular systems by regulating macrophages/MoDC's chemotactic activity toward to T

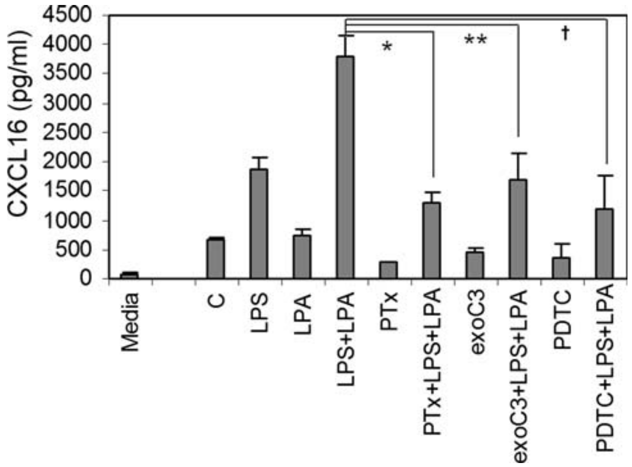

Fig. 4 Signaling transductions regulating CXCL16 shedding stimulated by LysoPtdOH. Macrophages prepared as above were pretreated with different inhibitors for 16 h before lysoPtdOH and/or LPS stimulations, concentrations of CXCL16 in spent culture supernatant were measured by ELISA. Data were presented as the mean ± SE from three experiments with similar results. Compare to spent supernatant from lysoPtdOH/LPS treated macrophages, CXCL16 secretion in supernatant collected from PTx, exoC3, or PDTC pretreated macrophages were significantly inhibited (*$P < 0.01$; **$P < 0.05$; †$P < 0.01$)

cells. The correlated expression of CXCL16 and its protease ADAM-10 within the synovium and cultured macrophages has been reported recently [37], which may explain why the change of cell surface presentation of CXCL16 affected by lysoPtdOH was undetectable by FACS in our culture system.

Playing an important role in innate immunity, macrophages detect the invading pathogens through Toll-like receptors (TLR). LPS, a major cell wall component of gram-negative bacteria, binds to mainly TLR4 and other cell surface molecules such as HSP70, HSP90, chemokine receptor 4 (CXCR4), and growth differentiation factor 5, as well as some cytoplasm molecules then lead to mainly activation of NF-κB [38–42]. Therefore, whether the involvement of NF-κB in lysoPtdOH-enhanced CXCL16 production stimulated by LPS was solely induced by lysoPtdOH from LPS cannot be decided in this experimental setting. Meanwhile activation of $G_{i/o}$-, Rho- in lysoPtdOH and LPS stimulated macrophages is more likely through LPA receptors binding and signaling [19, 43–45].

LysoPtdOH has been indicated as promoting early T cell migration to tissue sites of immune responses and regulating T cell proliferation and secretion of numerous cytokines [46, 47]. LysoPtdOH has also been reported to regulate the differentiation and activation of monocytes/macrophages and their further interactions with endothelial cells [48, 49]. However, this is the first demonstration that lysoPtdOH increases CXCL16 production and shedding in addition to other inflammatory cytokines [21, 50, 51],

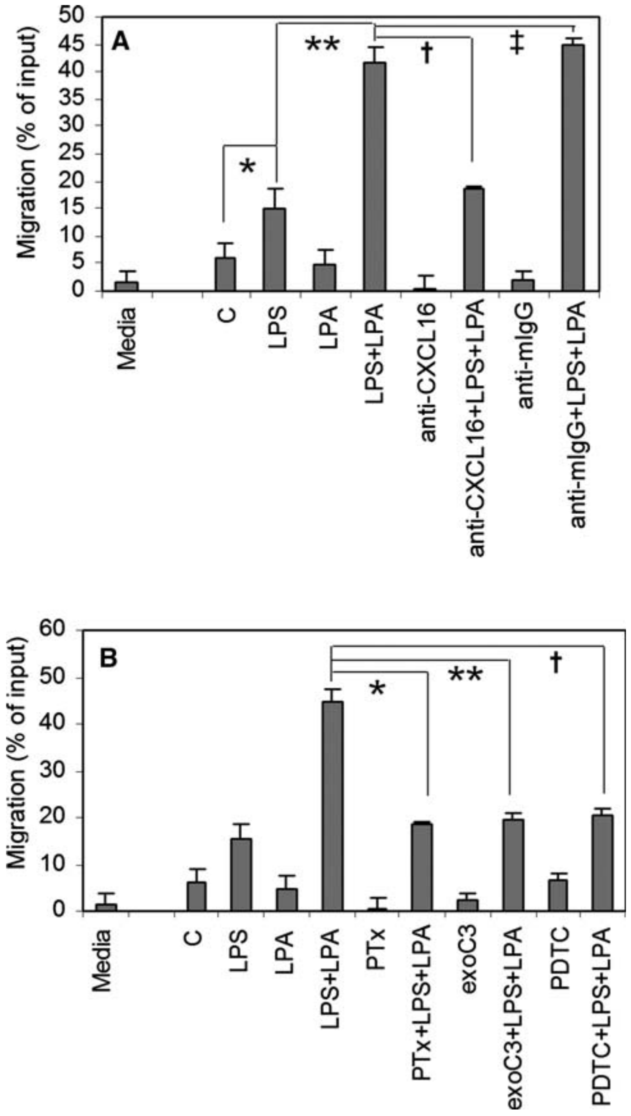

Fig. 5 **a** LysoPtdOH increased chemotactic activity of macrophages. Spent culture supernatant was put in the bottom well of a trans-well system and activated $CD3^+$ T cells were loaded into the top chambers of the trans-well system. Migration was allowed for 2 h, and cells that had migrated to the bottom wells were collected and counted. Data are presented as the mean ± SE of five experiments with similar results. Compared to the supernatant from control macrophages, supernatant collected from LPS treated cells slightly induced $CD3^+$ T cells migration (*$P < 0.05$); supernatant collected from LPA/LPS treated cells macrophages attracted more $CD3^+$ T cells migration (**$P < 0.01$), which was significantly blocked by preincubation supernatant with anti-CXCL16 blocking antibody (†$P < 0.01$); non-specific mIgG antibody had no effect on the chemotactic activity of supernatant collected from LPA/LPS treated macrophages (‡$P > 0.05$). **b** Signaling pathways regulating chemotactic activity of macrophages. Spent culture supernatant collected from macrophages treated with different inhibitors was also placed in the bottom wells of a trans-well system and migration of $CD3^+$ T cells was calculated. Data presented as the mean ± SE of three experiments with similar results. Compare to spent supernatant from LPA/LPS treated macrophages, migration of $CD3^+$ T cells toward supernatant collected from PTx, exoC3, or PDTC pretreated macrophages were significantly blocked (*$P < 0.01$; **$P < 0.01$; †$P < 0.01$)

therefore directing more activated T cells to the inflammation and tumor sites to develop functional immune responses [13, 52]. Since most of CXCL16 binding CXCR6 expressing cells in blood are IFN-secreting helper T cells, cytotoxic T cells, or CD56$^+$ T cells that are enriched for effector functions, thus upregulation of CXCL16 by lysoPtdOH in macrophages and MoDC most likely leads to the (T helper 1) Th1 and cytotoxic effector function in inflammation and tumor sites. The direct effect of lysoPtdOH on MoDC maturation and the ability of DC to influence Th1 cell polarization has been investigated [16], this study elucidated its role in CXCL16 production in macrophages as a focus. We hope this mechanic link between lysoPtdOH and chemokines advances our knowledge of lipid mediated immune responses.

Acknowledgments We thank all the healthy blood donors provided written informed consent according to federal, state and institutional guidelines. The authors declare no conflicting and commercial interest.

References

1. Zlotnik A, Yoshie O (2000) Chemokines: a new classification system and their role in immunity. Immunity 12:121
2. Balkwill F (2004) Cancer and the chemokine network. Nat Rev Cancer 4:540
3. Matloubian M, David A, Engel S, Ryan JE, Cyster JG (2000) A transmembrane CXC chemokine is a ligand for HIV-coreceptor Bonzo. Nat Immunol 1:298
4. Wilbanks A, Zondlo SC, Murphy K, Mak S, Soler D, Langdon P, Andrew DP, Wu L, Briskin M (2001) Expression cloning of the STRL33/BONZO/TYMSTRligand reveals elements of CC, CXC, and CX3C chemokines. J Immunol 166:5145
5. Shimaoka T, Nakayama T, Fukumoto N, Kume N, Takahashi S, Yamaguchi J, Minami M, Hayashida K, Kita T, Ohsumi J, Yoshie O, Yonehara S (2004) Cell surface-anchored SR-PSOX/CXC chemokine ligand 16 mediates firm adhesion of CXC chemokine receptor 6-expressing cells. J Leukoc Biol 75:267
6. Tabata S, Kadowaki N, Kitawaki T, Shimaoka T, Yonehara S, Yoshie O, Uchiyama T (2005) Distribution and kinetics of SR-PSOX/CXCL16 and CXCR6 expression on human dendritic cell subsets and CD4+ T cells. J Leukoc Biol 77:777
7. Nanki T, Shimaoka T, Hayashida K, Taniguchi K, Yonehara S, Miyasaka N (2005) Pathogenic role of the CXCL16-CXCR6 pathway in rheumatoid arthritis. Arthritis Rheum 52:3004
8. Yamauchi R, Tanaka M, Kume N, Minami M, Kawamoto T, Togi K, Shimaoka T, Takahashi S, Yamaguchi J, Nishina T, Kitaichi M, Komeda M, Manabe T, Yonehara S, Kita T (2004) Upregulation of SR-PSOX/CXCL16 and recruitment of CD8+ T cells in cardiac valves during inflammatory valvular heart disease. Arterioscler Thromb Vasc Biol 24:282
9. Wagsater D, Hugander A, Dimberg J (2004) Expression of CXCL16 in human rectal cancer. Int J Mol Med 14:65
10. Ludwig A, Schulte A, Schnack C, Hundhausen C, Reiss K, Brodway N, Held-Feindt J, Mentlein R (2005) Enhanced expression and shedding of the transmembrane chemokine CXCL16 by reactive astrocytes and glioma cells. J Neurochem 93:1293
11. Moolenaar WH (1999) Bioactive lysophospholipids and their G protein-coupled receptors. Exp Cell Res 253:230
12. Moolenaar WH (2000) Development of our current understanding of bioactive lysophospholipids. Ann N Y Acad Sci 905:1
13. Panther E, Idzko M, Corinti S, Ferrari D, Herouy Y, Mockenhaupt M, Dichmann S, Gebicke-Haerter P, Di Virgilio F, Girolomoni G, Norgauer J (2002) The influence of lysophosphatidic acid on the functions of human dendritic cells. J Immunol 169:4129
14. Fueller M, Wang DA, Tigyi G, Siess W (2003) Activation of human monocytic cells by lysophosphatidic acid and sphingosine-1-phosphate. Cell Signal 15:367
15. Oz-Arslan D, Ruscher W, Myrtek D, Ziemer M, Jin Y, Damaj BB, Sorichter S, Idzko M, Norgauer J, Maghazachi AA (2006) IL-6 and IL-8 release is mediated via multiple signaling pathways after stimulating dendritic cells with lysophospholipids. J Leukoc Biol 80:287
16. Chen R, Roman J, Guo J, West E, McDyer J, Williams MA, Georas SN (2006) Lysophosphatidic acid modulates the activation of human monocyte-derived dendritic cells. Stem Cells Dev 15:797
17. Kaneyuki U, Ueda S, Yamagishi S, Kato S, Fujimura T, Shibata R, Hayashida A, Yoshimura J, Kojiro M, Oshima K, Okuda S (2007) Pitavastatin inhibits lysophosphatidic acid-induced proliferation and monocyte chemoattractant protein-1 expression in aortic smooth muscle cells by suppressing Rac-1-mediated reactive oxygen species generation. Vascul Pharmacol 46:286
18. Budnik LT, Brunswig-Spickenheier B (2005) Differential effects of lysolipids on steroid synthesis in cells expressing endogenous LPA2 receptor. J Lipid Res 46:930
19. Kang S, Luo R, Smicun Y, Fishman DA, Meng Y (2006) Selective induction of cyclooxygenase-2 plays a role in lysophosphatidic acid regulated Fas ligand cell surface presentation. FEBS Lett 580:443
20. Grossman WJ, Verbsky JW, Barchet W, Colonna M, Atkinson JP, Ley TJ (2004) Human T regulatory cells can use the perforin pathway to cause autologous target cell death. Immunity 21:589
21. Lin CI, Chen CN, Chen JH, Lee H (2006) Lysophospholipids increase IL-8 and MCP-1 expressions in human umbilical cord vein endothelial cells through an IL-1-dependent mechanism. J Cell Biochem 99:1216
22. Goetzl EJ, Lynch KR (2000) Preface: the omnific lysophospholipid growth factors. Ann N Y Acad Sci 905:xi
23. Gillitzer R, Goebeler M (2001) Chemokines in cutaneous wound healing. J Leukoc Biol 69:513
24. Scholz F, Schulte A, Adamski F, Hundhausen C, Mittag J, Schwarz A, Kruse ML, Proksch E, Ludwig A (2007) Constitutive expression and regulated release of the transmembrane chemokine CXCL16 in human and murine skin. J Invest Dermatol 127:1444
25. Shimaoka T, Kume N, Minami M, Hayashida K, Kataoka H, Kita T, Yonehara S (2000) Molecular cloning of a novel scavenger receptor for oxidized low density lipoprotein, SR-PSOX, on macrophages. J Biol Chem 275:40663
26. Abel S, Hundhausen C, Mentlein R, Schulte A, Berkhout TA, Broadway N, Hartmann D, Sedlacek R, Dietrich S, Muetze B, Schuster B, Kallen KJ, Saftig P, Rose-John S, Ludwig A (2004) The transmembrane CXC-chemokine ligand 16 is induced by IFN-gamma and TNF-alpha and shed by the activity of the disintegrin-like metalloproteinase ADAM10. J Immunol 172:6362
27. Gough PJ, Garton KJ, Wille PT, Rychlewski M, Dempsey PJ, Raines EW (2004) A disintegrin and metalloproteinase 10-mediated cleavage and shedding regulates the cell surface expression of CXC chemokine ligand 16. J Immunol 172:3678
28. Geissmann F, Cameron TO, Sidobre S, Manlongat N, Kronenberg M, Briskin MJ, Dustin ML, Littman DR (2005) Intravascular immune surveillance by CXCR6+ NKT cells patrolling liver sinusoids. PLoS Biol 3:e113

29. Wymann MP, Schneiter R (2008) Lipid signalling in disease. Nat Rev Mol Cell Biol 9:162
30. Mazereeuw-Hautier J, Gres S, Fanguin M, Cariven C, Fauvel J, Perret B, Chap H, Salles JP, Saulnier-Blache JS (2005) Production of lysophosphatidic acid in blister fluid: involvement of a lysophospholipase D activity. J Invest Dermatol 125:421
31. Watsky MA, Griffith M, Wang DA, Tigyi GJ (2000) Phospholipid growth factors and corneal wound healing. Ann N Y Acad Sci 905:142
32. Li C, Dandridge KS, Di A, Marrs KL, Harris EL, Roy K, Jackson JS, Makarova NV, Fujiwara Y, Farrar PL, Nelson DJ, Tigyi GJ, Naren AP (2005) Lysophosphatidic acid inhibits cholera toxin-induced secretory diarrhea through CFTR-dependent protein interactions. J Exp Med 202:975
33. Ishii I, Fukushima N, Ye X, Chun J (2004) Lysophospholipid receptors: signaling and biology. Annu Rev Biochem 73:321
34. Sano T, Baker D, Virag T, Wada A, Yatomi Y, Kobayashi T, Igarashi Y, Tigyi G (2002) Multiple mechanisms linked to platelet activation result in lysophosphatidic acid and sphingosine 1-phosphate generation in blood. J Biol Chem 277:21197
35. Fishman DA, Liu Y, Ellerbroek SM, Stack MS (2001) Lysophosphatidic acid promotes matrix metalloproteinase (MMP) activation and MMP-dependent invasion in ovarian cancer cells. Cancer Res 61:3194
36. Meng Y, Kang S, Fishman DA (2005) Lysophosphatidic acid stimulates fas ligand microvesicle release from ovarian cancer cells. Cancer Immunol Immunother 54:807
37. van der Voort R, van Lieshout AW, Toonen LW, Sloetjes AW, van den Berg WB, Figdor CG, Radstake TR, Adema GJ (2005) Elevated CXCL16 expression by synovial macrophages recruits memory T cells into rheumatoid joints. Arthritis Rheum 52:1381
38. Hugot JP, Chamaillard M, Zouali H, Lesage S, Cezard JP, Belaiche J, Almer S, Tysk C, O'Morain CA, Gassull M, Binder V, Finkel Y, Cortot A, Modigliani R, Laurent-Puig P, Gower-Rousseau C, Macry J, Colombel JF, Sahbatou M, Thomas G (2001) Association of NOD2 leucine-rich repeat variants with susceptibility to Crohn's disease. Nature 411:599
39. Medzhitov R, Preston-Hurlburt P, Janeway CA Jr (1997) A human homologue of the Drosophila Toll protein signals activation of adaptive immunity. Nature 388:394
40. Ogura Y, Bonen DK, Inohara N, Nicolae DL, Chen FF, Ramos R, Britton H, Moran T, Karaliuskas R, Duerr RH, Achkar JP, Brant SR, Bayless TM, Kirschner BS, Hanauer SB, Nunez G, Cho JH (2001) A frameshift mutation in NOD2 associated with susceptibility to Crohn's disease. Nature 411:603
41. Triantafilou K, Triantafilou M, Dedrick RL (2001) A CD14-independent LPS receptor cluster. Nat Immunol 2:338
42. Takeda K, Kaisho T, Akira S (2003) Toll-like receptors. Annu Rev Immunol 21:335
43. Anliker B, Chun J (2004) Lysophospholipid G protein-coupled receptors. J Biol Chem 279:20555
44. Gardell SE, Dubin AE, Chun J (2006) Emerging medicinal roles for lysophospholipid signaling. Trends Mol Med 12:65
45. Meyer zu Heringdorf D, Jakobs KH (2007) Lysophospholipid receptors: signalling, pharmacology and regulation by lysophospholipid metabolism. Biochim Biophys Acta 1768:923
46. Graler MH, Goetzl EJ (2002) Lysophospholipids and their G protein-coupled receptors in inflammation and immunity. Biochim Biophys Acta 1582:168
47. Huang MC, Graeler M, Shankar G, Spencer J, Goetzl EJ (2002) Lysophospholipid mediators of immunity and neoplasia. Biochim Biophys Acta 1582:161
48. Goetzl EJ (2004) Immunoregulatory lysophospholipids: new stars in the mast cell constellation. Curr Allergy Asthma Rep 4:175
49. Lee H, Liao JJ, Graeler M, Huang MC, Goetzl EJ (2002) Lysophospholipid regulation of mononuclear phagocytes. Biochim Biophys Acta 1582:175
50. Wiesend CL, Elsner P, Ziemer M (2007) Masked melanocytic nevus: histopathologic difficulties in diagnosing melanocytic nevi coexisting with underlying dermatoses. Am J Clin Dermatol 8:187
51. Banchereau J, Steinman RM (1998) Dendritic cells and the control of immunity. Nature 392:245
52. Lanzavecchia A, Sallusto F (2000) Dynamics of T lymphocyte responses: intermediates, effectors, and memory cells. Science 290:92

eicosapentaenoic acid (20:5ω3; EPA) and DHA, as well as the principal 'competing' ω6 fatty acid—arachidonic acid (20:4ω6; ARA) [4]. Because the level of 'free' (non-esterified) plasma DHA and ARA is thought to be important for their uptake by the brain [5], those data are provided as both percentages and concentrations.

Methods

All procedures reported here were approved by the Human Ethics Research Committee of the Health and Social Sciences Center—Sherbrooke University Geriatrics Institute, which is the committee mandated to oversee human experimentation at our institution.

Compliance Methodology

In addition to capsule counts and a checklist completed by the subjects, we independently verified compliance by adding a small amount of carbon-13-labeled glucose (^{13}C; Cambridge Isotopes Limited, Andover, USA) to the ω3 fatty acid capsules used in the metabolic study. This was done only during the third week of the study. With 10 mg/capsule of ^{13}C-glucose, we established in preliminary tests that if breath ^{13}C value during the supplementation period did not exceed 2.5 times the baseline ^{13}C value, the subject was non-compliant on that day. Non-compliance on more than one day/week led to exclusion of the subject's data from the final analysis.

ω3 Fatty Acid Supplementation

Following informed written consent, the participants' medical histories were taken by a registered nurse and 12 h fasting blood chemistries were assessed. Inclusion criteria were: 18–29 years old or 70–79 years old, thyroid stimulating hormone (0.35–7.0 mI U/L), glucose (3.3–6.1 mmol/L), cholesterol (3.3–4.6 mmol/L in the young and 3.3-6.2 mmol/L in the elderly), triglycerides (0.6–2.3 mmol/L), and hemoglobin A_{1c} (4.0–6.0 mmol/L). Exclusion criteria were: smokers, pregnancy/lactation, <18 years old or between 30 and 70 years old or >70 years old, or use of medication for diabetes, liver disease, renal disease, hypertension, anemia or low serum albumin or other evidence of malnutrition. An upper limit of 3.0% DHA in plasma total lipids was set to exclude those individuals who were probably already consuming ω3 fatty acid supplements or relatively high amounts of fish.

A dose of ω3 fatty acids (EPA and DHA) was provided that was calculated to be four to five times the average intake in Quebec of ω3 fatty acids from fish or seafood [6]. One lot of an encapsulated commercially available brand of fish oil was purchased in sufficient quantity to supply all the participants for the duration of the study (Genuine Health, O3mega + Think, Toronto, Canada). According to our measurements, two capsules/day provided 1,070 mg of ω3 fatty acids: 3 mg α-linolenic acid (18:3ω3), 64 mg docosapentaenoic acid (22:5ω3), 323 mg of eicosapentaenoic acid (20:5ω3; EPA) and 680 mg of DHA (Table 1). Participants consumed the two capsules each morning for 3 week, followed by a 2 week wash-out during which no capsules were consumed. Participants were told to take the capsules in the morning at breakfast and to take duplicate breath samples not less than 2 and not more than 4 h later. Fasting blood samples were collected once weekly between 7–8 a.m. They were anti-coagulated in EDTA and the plasma removed by centrifugation and stored at −20 °C.

Analytical Methodology

For fatty acid analysis, total lipids from 0.5 ml plasma was extracted into chloroform-methanol, internal standards added, the lipid classes separated by neutral lipid thin layer chromatography, and fatty acid methyl esters prepared and analyzed as previously described [7]. Glucose, triglycerides, total cholesterol, and free fatty acids were measured by an automated analyzer (Xpand, Dade-Behring, Mississauga, ON).

Table 1 Baseline characteristics of the two groups

Group	Young ($n = 9$)	Elderly ($n = 10$)
Age	24 ± 2	74 ± 4*
Male/female	5/4	5/5
Weight (kg)	71.1 ± 18.1	75.0 ± 13.4
Body mass index (kg/m^2)	24.5 ± 4.1	28.0 ± 4.3
Free fatty acids (mmol/L)	0.48 ± 0.21	0.62 ± 0.24
Phospholipids (mmol/L)	0.72 ± 0.21	0.84 ± 0.17
Triglycerides (mmol/L)	1.0 ± 0.4	1.3 ± 0.4
Cholesterol (mmol/L)	4.4 ± 0.6	5.5 ± 0.9*
Fatty acids** (%)		
Sum Saturates	28.9 ± 2.5	29.5 ± 2.5
Sum Monounsaturates	24.7 ± 3.8	27.6 ± 2.6*
Linoleate	34.3 ± 3.1	28.8 ± 3.2*
Arachidonate	6.6 ± 0.9	7.5 ± 1.0*
α-Linolenate	1.0 ± 0.5	0.8 ± 0.3
Eicosapentaenoate	0.6 ± 0.3	1.0 ± 0.3*
Docosapentaenoate	0.4 ± 0.2	0.5 ± 0.1
Docosahexaenoate	1.5 ± 0.5	1.6 ± 0.6

Mean ± SD

* $P < 0.05$, Mann–Whitney

** Plasma total lipids

Statistics

Using DHA values in plasma total lipids analyzed in our laboratory as a benchmark, power analysis showed that 9–10 subjects/group would be sufficient to demonstrate a significant effect of the supplement. Data are shown as means ± SD. Fatty acid values were not normally distributed so the non-parametric Mann-Whitney test was used (SPSS; Chicago, IL, USA) with the cut-off for statistical significance set at $P < 0.05$. Freidman's test was used to verify whether the young and elderly groups differed when there was no effect of the supplement.

Results

Compliance

Based on the rise in ^{13}C in breath CO_2 from the ^{13}C-glucose on the capsules, we observed that one young participant was non-compliant on two occasions and another was non-compliant on six of the seven days tested, leaving $n = 9$ in the young group. Lack of change in plasma $\omega3$ fatty acids in the least compliant participant supported the ^{13}C compliance data. All 10 elderly participants who started the supplementation study were included in the final analyses.

$\omega3$ Fatty Acid Supplementation

DHA in plasma total lipids was not different between the two groups at baseline. After 3 week supplementation, in the elderly, plasma DHA stabilized 46% higher than baseline ($P < 0.05$), a rise that was 42% higher than in the young group. During the wash-out, plasma DHA declined to a similar value in both groups (Fig. 1). After the supplementation, EPA in plasma total lipids rose similarly in both groups. In both groups, whereas % DHA rose in plasma phospholipids during the supplementation period, EPA was largely unaffected in phospholipids, and neither changed significantly in plasma triglycerides (data not shown). Other $\omega3$ fatty acids (α-linolenic acid, $\omega3$ docosapentaenoic acid) remained statistically unchanged during supplementation and did not differ between the two groups.

Expressed as percentage of the plasma free (non-esterified) fatty acid pool, free DHA did not differ between the two groups and also did not change significantly during either the supplementation or the wash-out phase of the study. The plasma concentration of free DHA also did not change during fish oil supplementation, but owing to the higher concentration of plasma total free fatty acids in the elderly, the plasma concentration of free DHA averaged over both phases of the study was 82% higher in the elderly (data not shown). EPA was largely undetectable in plasma free fatty acids so the few values that were recorded could not be compiled and are not reported here.

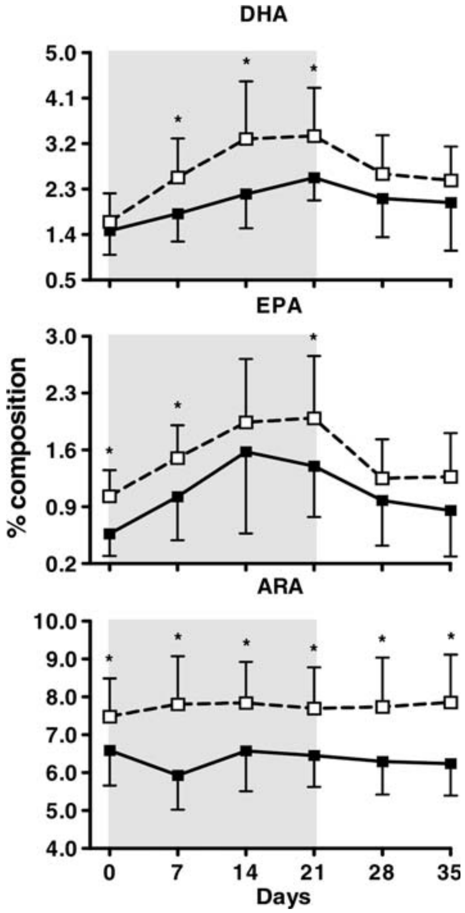

Fig. 1 Docosahexaenoic acid (*DHA*), eicosapentaenoic acid (*EPA*) and arachidonic acid (*ARA*) in plasma total lipids (%) during 3 weeks supplementation and 2 weeks follow up in nine young and ten elderly subjects. *Black squares* young adults, *White squares* elderly adults: mean ± SD, *$P < 0.05$

In the elderly, plasma total ARA started and remained about 20% higher throughout the supplementation and wash-out periods ($P < 0.00004$; Fig. 1).

The higher percentage of ARA in plasma of the elderly seen both at baseline and throughout the study was a function of higher ARA in both phospholipids and triglycerides but not free fatty acids (data not shown). When expressed as a percentage of the total free fatty acid pool, free ARA did not differ between the two groups at any time point. When expressed as a concentration (mg/dL), free ARA differed between the two groups at a couple of time points but not overall (data not shown).

There was no treatment effect on the plasma concentration of the main plasma lipid classes during the supplementation period or during the wash-out. Hence, during the overall study period, the elderly averaged 9%

higher phospholipids, 19% higher triglycerides, and 64% higher free fatty acids; all $P < 0.05$). The significant difference in plasma total cholesterol between the two groups seen at baseline was unaffected during the supplementation and wash-out periods (data not shown).

Discussion

This study shows that compared to young adults, healthy, free-living elderly from our region of Québec have a somewhat higher response of plasma DHA to a short-term daily fish oil supplement. This result contradicts our initial hypothesis that the plasma response to a fish oil supplement would be significantly dampened in the healthy elderly. Higher baseline plasma EPA in our elderly group (Table 1) confirms observations reported previously for plasma EPA [8, 9] and red cell ω3 PUFA [10, 11]. In 30-year old women, plasma EPA tends to rise more quickly than DHA during short term supplementation with fish oil and fall more quickly after the supplementation period [12].

Despite raising DHA intake by four to five fold compared to average intake in Quebec [6] and approximately doubling plasma total DHA during the supplementation period, in neither group did plasma *free* DHA rise significantly during the supplementation period nor fall during the wash-out (whether expressed as percentage or as mg/dL). The higher concentration of free plasma DHA in our elderly subjects was clearly a function of a larger plasma free fatty acid pool and not due to higher percentage DHA in plasma free fatty acids. No change in % DHA in plasma free fatty acids has previously been reported during a 3 week supplementation with 750 mg/day of DHA but no EPA [13]. However, in that study, plasma free DHA did rise significantly after the 6th week of supplementation or when a 1,500 mg daily dose of DHA was given. We focused on plasma free DHA because of its purported role as a precursor to brain DHA [5]. Given the emerging though still controversial link between low DHA status and increased risk of cognitive decline in the elderly [3], it was therefore not anticipated that the pool of plasma free DHA would be higher in the elderly than in our young subjects. If, as proposed by Lagarde's group, a lysophosphatidylcholine form of DHA is the carrier of DHA to the brain [14], then the larger pool of plasma free DHA in the elderly would have no direct bearing on their susceptibility to cognitive decline.

In all plasma lipid classes we evaluated, ARA was statistically unaffected by an intake of about 1,000 mg/day of ω3 fatty acids, given mostly as EPA and DHA. Higher baseline ARA in our elderly group contrasts somewhat with the results of Rees et al. [9] but their elderly group was 15 years younger than ours. Rees et al. [9] also used a higher dose of EPA and DHA and for a longer period but otherwise both our studies agree that raising EPA and DHA intake by up to tenfold does not seem to significantly affect plasma ARA.

Incomplete compliance is one potential confounder that was not a factor in the results of the present study. Our stable isotope-based method was relatively non-invasive and well tolerated. It was a good independent measure of compliance but because of cost, labor-intensiveness and the need for specialized equipment to analyze ^{13}C in breath CO_2, it perhaps not widely applicable.

We conclude that during short-term supplementation with fish oil capsules, healthy aging is associated with significantly higher DHA incorporation into plasma lipids. This result contributes to the emerging literature suggesting that subtle but potentially important changes in ω3 PUFA metabolism occur during healthy aging. The possible relevance of these aging-related changes in ω3 PUFA metabolism to risk of chronic disease, particularly cognitive decline, remains to be established.

Acknowledgments Financial assistance was provided by the Canadian Institutes for Health Research, Natural Sciences and Engineering Research Council of Canada, the Canada Research Chairs (SCC), the Canadian Foundation for Innovation, and FORMSAV (MV). Excellent technical assistance was provided by Mary Ann Ryan, Julie Desgagné and Martine Fisch.

References

1. van Gelder BM, Tijhuis M, Kalmijn S, Kromhout D (2007) Fish consumption, n-3 fatty acids, and subsequent 5-y cognitive decline in elderly men: the Zutphen Elderly Study. Am J Clin Nutr 85:1142–1147
2. Gillette-Guyonnet S, Abellan Van Kan G, Andrieu S et al (2007) IANA task force on nutrition and cognitive decline with aging. J Nutr Health Aging 11:132–152
3. Plourde M, Fortier M, Vandal M, Tremblay-Mercier J, Freemantle E, Begin M, Pifferi F, Cunnane SC (2007) Unresolved issues in the link between docosahexaenoic acid and Alzheimer's disease. Prostaglandins Leukot Essent Fatty Acids 77:301–308
4. Lands WE (2005) Learning how membrane fatty acids affect cardiovascular integrity. J Membr Biol 206:75–83
5. Rapoport SI, Rao JS, Igarashi JM (2007) Brain metabolism of nutritionally essential polyunsaturated fatty acids depends on both diet and the liver. Prostaglandins Leukot Essent Fatty Acids 77:151–161
6. Nkondjock A, Shatenstein B, Ghadirian P (2003) A case-control study of breast cancer and dietary intake of individual fatty acids and antioxidants in Montreal, Canada. Breast 12:128–135
7. McCloy U, Ryan MA, Pencharz PB, Ross RJ, Cunnane SC (2004) A comparison of the metabolism of eighteen-carbon 13C-unsaturated fatty acids in healthy women. J Lipid Res 45:474–485
8. Meydani M, Natiello F, Goldin B et al (1991) Effect of long-term fish oil supplementation on vitamin E status and lipid peroxidation in women. J Nutr 121:484–491
9. Rees D, Miles EA, Banerjee T et al (2006) Dose-related effects of eicosapentaenoic acid on innate immune function in healthy

humans: a comparison of young and older men. Am J Clin Nutr 83:331–342

10. Caprari P, Scuteri A, Salvati AM et al (1999) Aging and red blood cell membrane: a study of centenarians. Exper Gerontol 34:47–57
11. Carver JD, Benford VJ, Han B, Cantor AB (2001) The relationship between age and the fatty acid composition of cerebral cortex and erythrocytes in human subjects. Brain Res Bull 56:79–85
12. Hodge J, Sanders K, Sinclair AJ (1993) Differential utilization of eicosapentaenoic acid and docosahexaenoic acid in human plasma. Lipids 28:525–531
13. Conquer JA, Holub BJ (1998) Effect of supplementation with different doses of DHA on the levels of circulating DHA as non-esterified fatty acid in subjects of Asian Indian background. J Lipid Res 39:286–292
14. Lagarde M, Bernoud N, Brossard N, Lemaitre-Delaunay D, Thiès F, Croset M, Lecerf J (2001) Lysophosphatidylcholine as a preferred carrier form of docosahexaenoic acid to the brain. J Mol Neurosci 16:201–204

Lipids (2008) 43:1091–1093
DOI 10.1007/s11745-008-3262-6

Recent Advances in Sterol Research Presented at the 99th AOCS Annual Meeting & Expo in Seattle Washington, May 2008

Robert A. Moreau · W. David Nes · Thomas J. Bach · Edward J. Parish · Jerzy Zawistowski

Received: 15 October 2008 / Accepted: 21 October 2008 / Published online: 25 November 2008
© AOCS 2008

Since 1970, AOCS has been a regular host to the sterol symposia. Table 1 summarizes the history of the AOCS Sterol Symposium Series. The pioneers who established the AOCS Sterol Symposium during its first decade include Dr. Henry W. Kircher (University of Arizona, an expert on natural product chemistry and insect-sterol ecology), Dr. James W. Hendrix (University of Kentucky, an expert on fungal sterols), Dr. John L. Laseter (University of New Orleans, an expert on the analysis of sterols by gas chromatography), Dr. William R. Nes (Drexel University, a bioorganic chemist and an expert on the structure, function and evolution of sterols, and whose research accomplishments were commemorated in Steroids 53:261–648, 1989), and Dr. Erich Heftmann (Western Regional Research Center, USDA, ARS, a biochemist and an expert on the chromatography and biosynthesis of plant sterols, and whose research accomplishments were commemorated in J Chromatogr A 452, 1–634, 1988). Throughout the years the sterol symposia have focused on current research in the areas of sterol structure, biosynthesis, chemistry, regulation, and function.

The 2008 Sterol Symposium, “Recent Advances in Sterol Research,” was held at the AOCS Annual Meeting in Seattle, Washington. This year the symposium held special significance, for it hosted the presentation of the fourth G. J. Schroepfer Jr. Award for sterol research. The Award was established to honor the memory of Dr. George J. Schroepfer Jr., a prominent sterol biochemist and chemist who made major and lasting contributions to the sterol field. Much of his research dealt with the biosynthesis of cholesterol and its regulation. In addition, he maintained a strong organic synthesis program to support his biochemical studies. A biography describing many of Dr. Schroepfer’s contributions can be found in this journal (Wilson, W. K. Lipids 35, 242, 2000). Dr. Schroepfer was scheduled to be the keynote speaker at the sterol symposium in Orlando, Florida, in 1999, but unfortunately, he passed away on 11 December 1998. The three previous recipients of the Schroepfer Award were Professor Geoffrey Gibbons (2002), Professor Jan Sjövall (2004) and Professor Ingemar Björkhem (2006).

The fourth recipient of the G. J. Schroepfer Jr. Award for sterol research was Professor Michel Rohmer from the Institute of Chemistry at the University Louis Pasteur/CNRS in Strasbourg, France. Professor Rohmer, a member of the French Academy of Sciences, has made major contributions to the sterol field and we were pleased when we learned that he had been chosen to receive this

---

R. A. Moreau (✉)
Eastern Regional Research Center, USDA,
ARS, Wyndmoor, PA 19038, USA
e-mail: robert.moreau@ars.usda.gov

W. D. Nes
Department of Chemistry and Biochemistry,
Texas Tech University, Lubbock, TX 79409, USA

T. J. Bach
Centre National de la Recherche Scientifique,
Institut de Biologie Moléculaire des Plantes,
67083 Strasbourg, France

E. J. Parish
Department of Chemistry, Auburn University,
Auburn, AL 36849, USA

J. Zawistowski
Food, Nutrition and Health,
University of British Columbia,
Vancouver, BC, Canada

Table 1 History of AOCS sterol symposia

Year	Location	Organizers	Schroepfer Award recipients
1970	New Orleans	H. Kircher	
1971	Houston	J. Hendrix	
1973	New Orleans	J. L. Laseter	
1974	Philadelphia	H. Kircher	
1978	St. Louis	W. R. Nes, E. Heftmann	
1980	New York	H. Kircher, E. Heftmann	
1981	New Orleans	H. Kircher, W. R. Nes	
1985	Philadelphia	W. D. Nes, L. W. Parks	
1986	Honolulu	G. W. Patterson	
1990	Baltimore	J. D. Weete, G. W. Patterson	
1994	Atlanta	W. D. Nes, E. J. Parish	
1996	Indianapolis	W. D. Nes, R. A. Norton	
1997	Seattle	E. J. Parish, W. D. Nes	
1999	Orlando	J. D. Weete, E. J. Parish, W. D. Nes	
2002	Montreal	E. J. Parish, W. D. Nes, J. R. Williams	G. F. Gibbons
2004	Cincinnati	E. J. Parish, R. A. Moreau, I. Ikeda, W. D. Nes, J. R. Williams	J. Sjövall
2006	St. Louis	E. J. Parish, R. A. Moreau, T. J. Bach, W. D. Nes, J. R. Williams	I. Björkhem
2008	Seattle	R. A. Moreau, W. D. Nes, T. J. Bach, E. J. Parish, J. Zawistowski	M. Rohmer
2010	Phoenix		

prestigious award. Professor Rohmer is well known for research on the discovery of bacterial hopanoids and on the elucidation of the mevalonate-independent methylerythritol phosphate (MEP) biosynthetic pathway (sometime called the non-mevalonate pathway), a second pathway for the biosynthesis of terpenes. Although it was previously thought that all terpenes were synthesized via the mevalonate (MVA) pathway, the research of Professor Rohmer and his collaborators established that terpenoids are synthesized by the alternative MEP route in most bacteria (e.g. triterpenes of the hopane series, the prenyl chains of ubiquinone), in unicellular green algae (all terpenoids including the sterols), as well as in the chloroplasts in plants (carotenoids, the phytol portion of chlorophyll, the prenyl chain of plastoquinone). The same pathway was shown to be involved in the formation of other terpene series in plant plastids (hemi-, mono- and diterpenes), whereas the cytoplasmic MVA pathway is involved in the biosynthesis of sterols and the prenyl chain of ubiquinone. Professor Rohmer's research accomplishments are described in detail in the first paper in this issue and were also summarized in a recent article that he has authored (Rohmer, M. Nonprogrammed research: discovery of the mevalonate-independent methylerythritol phosphate pathway for the formation of isoprene units in bacteria and plants. Inform 19, 482–485, 2008).

Professor Michel Rohmer

In this year's Sterol Symposium, Professor Michael Waterman from Vanderbilt University was also honored for his long and productive career and for his significant contributions to the field of steroid biochemistry, especially for his pioneering research into the role of various cytochrome P450 enzymes in the steroid biosynthetic pathway. Several of Professor Waterman's colleagues (students, postdocs, and other collaborators) were invited to present seminars describing their individual accomplishments and the positive influence that Professor Waterman had on their careers. The colleagues included I. Pikuleva (Case Western Reserve University), M. Sewer (Georgia Institute of Technology), R. Bernhardt (Universität des Saarlandes), S. K. Kelley (Swansea University), R. Peters (Iowa State University), J. Noel (The Salk Institute) and G. Lepesheva (Vanderbilt University).

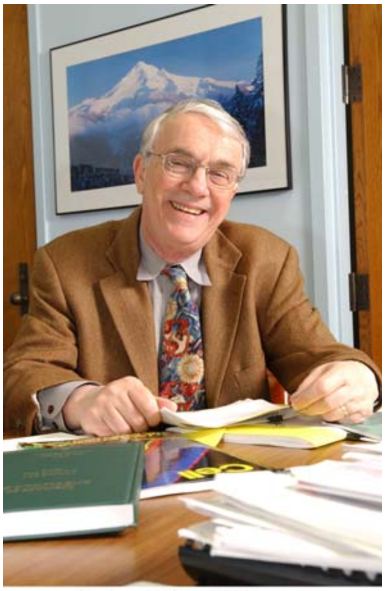

Professor Michael Waterman

As with past sterol symposia, we are indebted to our corporate partners who helped make the symposium a success. This year, Forbes Medi-Tech generously supported our symposium. We appreciate their contribution and look forward to their continued support of our symposium series. We also appreciate the support of the Biotechnology Division of AOCS for their long commitment to support the AOCS Sterol Symposium. We are looking forward to the next sterol symposium which will be held at the 101st Annual Meeting and Expo of the American Oil Chemists' Society, 16–19 May 2010, in Phoenix, Arizona.

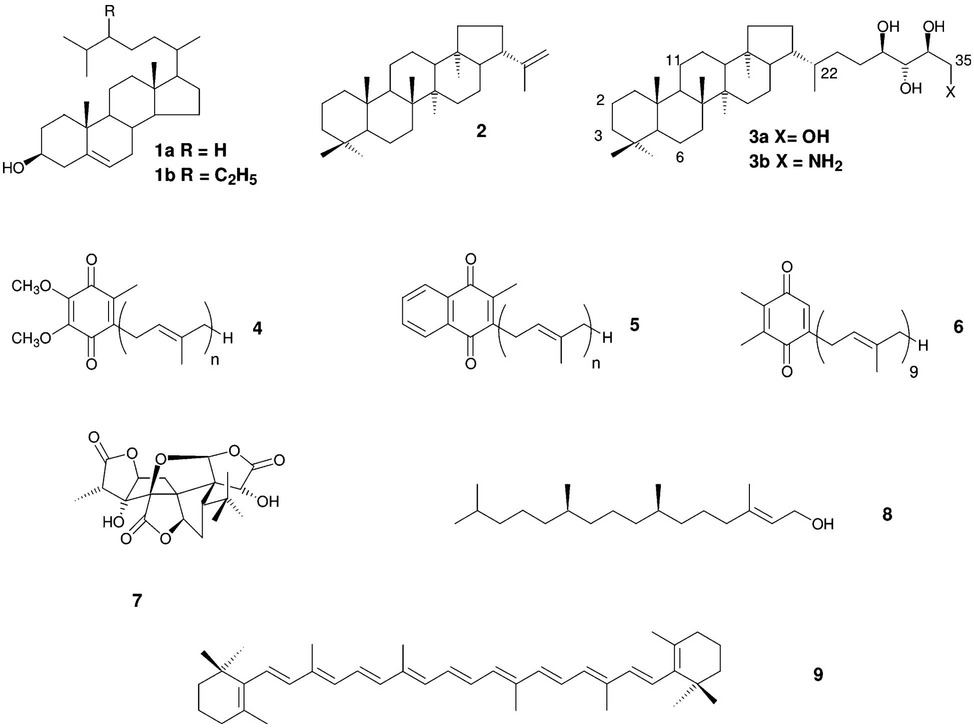

Fig. 1 Isoprenoids. **1a** cholesterol, **1b** sitosterol, **2** diploptene, **3a** bacteriohopanetetrol, **3b** aminobacteriohopanetriol, **4** ubiquinone, **5** menaquinone, **6** plastoquinone, **7** ginkgolide, **8** phytol, **9** β-carotene

Bacterial Biohopanoids

Geohopanoids probably represent the most abundant natural products on earth. This pentacyclic triterpenoid series is found in the organic matter of all sediments, independent of their age, origin or nature [11]. They represent the molecular fossils of a long overlooked family of bacterial metabolites. Triterpenes of the hopane series are rarely found in plants. They are more common in lichens, mosses and especially ferns. In contrast to the higher plant hopanoids, which are derived from the cyclization of oxidosqualene and possess an oxygenated function at C-3, hopanoids from lower eukaryotes are mostly derived from the direct cyclization of squalene and are accordingly devoid of such an oxygen function. Diploptene **2** (Fig. 1), a simple C_{30} hopanoid, was the first triterpene found in bacteria in the early 1970s. The major triterpenoids in all bacteria producing hopanoids were, however, always the C_{35} bacteriohopane derivatives (e.g. **3a**, **3b**, Fig. 1) [12]. Their discovery was rather fortuitous, by looking at the compounds responsible for the alignment of the cellulose microfibrils secreted by '*Acetobacter xylinum*' [13, 14]. This family of natural products, proved to be first precursors for the ubiquitous geohopanoids, presented an unique feature in natural product chemistry: an additional polyfunctionalized C_5 *n*-alkyl side-chain is linked by a carbon/carbon bond to one of the methyl group of isopropyl group of the hopane skeleton [15]. A huge structural diversity characterizes the bacterial biohopanoids. Modifications of the triterpene hopane skeleton include the introduction of double-bonds at C-6 and/or C-11 [16, 17], of an additional methyl group at C2β, C-2α or C-3β [18–21] or the presence of the two diastereomers at C-22 [15]. The side chains may differ by the number of the hydroxy groups, the replacement by the terminal C-35 hydroxy group by an amino group, the presence of polar moieties linked to the terminal hydroxy group (hexose derivatives linked via a glycosidic bond or carbapseudopentose linked via an ether bond) or to the terminal amino group (amino-acids or fatty acids via a peptide bond) [22]. Usually hopanoids are present in eubacterial cells in concentrations similar to those found for sterols in eukaryotes [12] and suitable for ^{13}C-NMR biosynthetic studies.

Like cholesterol **1a** (Fig. 1), biohopanoids are amphiphilic molecules with a flat, rigid skeleton due to the all *trans* ring junctions of the pentacyclic triterpene ring system and a length corresponding to the half of the thickness of a phospholipid bilayer. Such structural similarities suggested similar physiological roles. Indeed, in membrane models, hopanoids behave much like sterols, modulating the fluidity and the permeability of phospholipid mono and bilayers [23, 24]. This interpretation is corroborated by in vivo data. The hopanoid concentration increases with temperature in the thermoacidophile *Alicyclobacillus acidocaldarius*, counterbalancing the destabilizing effect of temperature [25]. In *Zymomonas mobilis*, a bacterium that can tolerate high ethanol concentrations up to 13% in its culture medium [26], the extremely high hopanoid concentrations (30 mg/g, dry weight) has been proposed as being involved in the membrane stabilization in the presence of the solvent. Other roles may be assigned to hopanoids. In the cyst cells of the nitrogen-fixing *Frankia* sp., the high hopanoid concentrations may protect the sensitive nitrogenase from degradation by atmospheric oxygen [27]. In *Streptomyces coelicolor*, hopanoid biosynthesis is strongly linked to aerial growth and sporulation, these triterpenoids being nearly undetectable under vegetative growth conditions in submersed cultures [28].

The chemistry and biochemistry of the bacterial hopanoids turned out to be a rich topic. Hopanoid biosynthesis is a mine of yet undisclosed enzyme reactions involved in the linkage of the side-chain to the triterpene moiety and in the methylation of the A ring. The most surprising consequence was however, the non-programmed and non-programmable discovery of a novel pathway for the formation of the isoprene units.

The biosynthesis of isopentenyl diphosphate (IPP **18**, Fig. 2) and dimethylallyl diphosphate (DMAPP **19**), the universal precursors of isoprene units had already been elucidated in the 1950s, essentially using systems prepared from liver and from yeast, and resulted in the description of the mevalonate (MVA **15**) pathway (Fig. 2b). This pathway is also involved in the formation of plant triterpenoids, including sterols. MVA was believed to be the universal precursor of isoprene units despite many contradictory observations in the field of the biosynthesis of the isoprenoids from bacteria and especially plants (e.g. the biosynthesis of mono and diterpenes, carotenoids) [29].

Hopanoid Biosynthesis: First ^{13}C-Labeling Experiments and Discovery of the Methylerythritol Phosphate (MEP) Pathway

The first incorporations of ^{13}C-labeled precursors into bacterial hopanoids were designed in order to determine the origin of the C_5 side-chain linked to the triterpenes moiety [30]. For this purpose, selected bacteria were grown on a synthetic mineral medium with acetate as the sole carbon and energy source. These growth conditions differed from those of most former experiments where the labeled carbon source was usually administered in a complex medium in the presence of many other sources of carbon. Under such growth conditions, there is no competition for the utilization of different carbon sources. The cells are obliged to use the labeled substrate via known probable metabolic routes. Starting from the ^{13}C-labeled position and their isotope abundance, a retro-biosynthetic scheme, we expected to be able to deduce the enzyme reactions involved in the metabolism of the carbon source. Such experiments were first made on bacteria capable of utilizing acetate as the sole carbon and energy source: *Rhodopseudomonas palustris*, which is characterized by very simple hopanoid content, synthesizing only aminobacteriohopanetriol **3b** (Fig. 1), and *Methylobacterium organophilum*, which produces bacteriohopanetetrol **3a** (Fig. 1) derivatives and has a better versatility in the utilization of carbon sources, a feature which later proved interesting.

These first experiments showed that the bacteriohopane side-chain is indeed a D-pentose, derived from the non-oxidative pentose phosphate pathway and linked via its C-5 carbon atom to the hopane isopropyl group [30, 31]. The most striking result was, however, found on the triterpene moiety. The labeling pattern of the hopane isoprene units (Fig. 3) was not in accordance with the expected one from the MVA pathway. At the time of these early investigations, there was no reason to reject the universally accepted MVA pathway. Results were interpreted in the frame of this metabolic route, expecting that MVA had to be formed from two distinct acetyl-CoA pools, although a completely different pathway could not be excluded [30].

Incorporation of ^{13}C-Labeled Glucose Isotopomers into the Hopanoids of *Zymomonas mobilis*: The Origin of the Carbon Atoms of Isoprene Units in the MEP Pathway

Zymomonas mobilis is a good hopanoid producer [32] and possesses minimal enzymatic equipment, utilizing only hexoses (mainly glucose) as a carbon and energy source and having no complete tricarboxylic acid cycle. These properties made this bacterium an interesting target for the further investigations that we performed in collaboration with the group of Hermann Sahm (Forschungszentrum Jülich, Germany). Incorporation of ^{13}C-labeled D-glucose isotopomers into the hopanoids of the bacterium *Zymomonas mobilis* (with labeling either at C-1, C-2, C-3, C-5 or C-6) gave the first insights into an alternative metabolic route for the formation of isoprene units [33]. The carbon atoms of IPP **18** (for IPP skeleton numbering, cf. Fig. 2c) could be divided into two subgroups. C-3 and C-5 had a dual origin, being respectively equally derived from C-2 or C-5 of glucose for the former and C-3 and C-6 of glucose for the second one, whereas C-1, C-2 and C-4 of IPP had a single origin, being respectively derived from C-6, C-5 and C-4 of glucose. This labeling pattern characterizes the glucose catabolism via the Entner–Doudoroff pathway in *Z. mobilis*. The first subgroup corresponds to the C-2 and C-3 carbon atoms of pyruvate **11**, and the second one to the complete carbon skeleton of D-glyceraldehyde-3-phosphate **10** (Fig. 2). This interpretation requires a rearrangement allowing the insertion of the two-carbon subunit derived from pyruvate (by decarboxylation) between the carbon atoms from D-glyceraldehyde-3-phosphate derived from

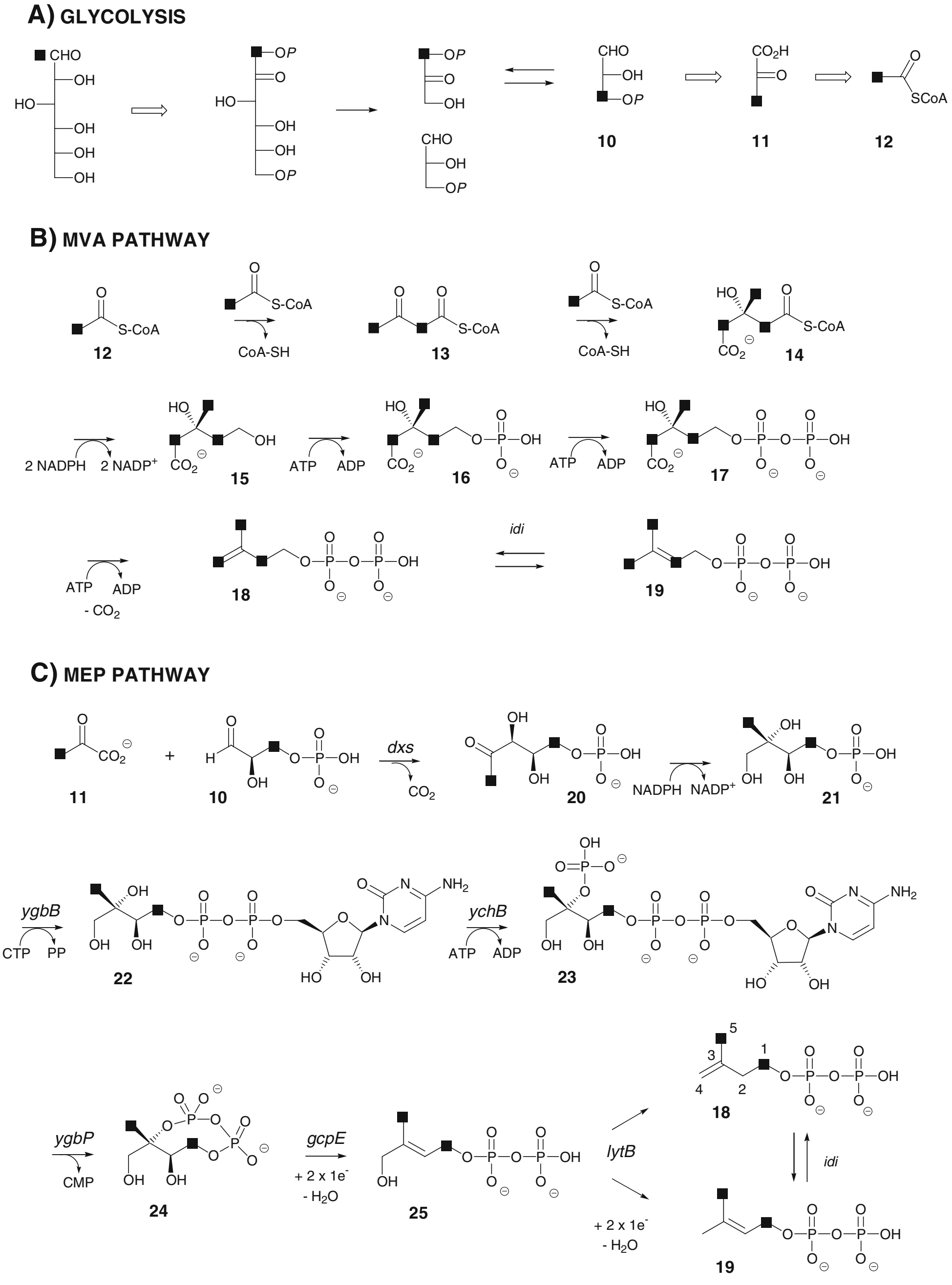

Fig. 2 Biosynthesis of isoprene units. **a** Labeling from [1-^{13}C] glucose of glyceraldehyde phosphate **10** and pyruvate **11**, the precursors of the methylerythritol phosphate (MEP) pathway, and of acetyl-CoA **12**, the precursor of the mevalonate (MVA) pathway. **b** Mevalonate pathway. **12** acetyl-CoA, **13** acetoacetyl-CoA, **14** hydroxymethylglutaryl-CoA, **15** MVA, **16** phosphoMVA, **17** diphosphoMVA, **18** IPP, **19** DMAPP. **c** Methylerythritol phosphate pathway. **10** D-glyceraldehyde 3-phosphate, **11** pyruvate, **20** 1-deoxy-D-xylulose 5-phosphate, **21** 2-*C*-methyl-D-erythritol 4-phosphate, **22** 4-diphosphocytidyl-2-*C*-methyl-D-erythritol, **23** 4-diphosphocytidyl-2-*C*-methyl-D-erythritol 2-phosphate, **24** 2-*C*-methyl-D-erythritol 2,4-cyclodiphosphate, **25** (*E*)-4-hydroxy-3-methylbut-2-enyl diphosphate, **18** IPP, **19** DMAPP. Adapted from reference [117]

C-4 and C-5 of glucose. Incorporation of doubly labeled [4,5-$^{13}C_2$] glucose showed in the isoprene units of the bacteriohopanetetrol derivatives and of 2*β*-methyldiplopterol characteristic $^2J^{13}C/^{13}C$ coupling constants, indicating that C-4 and C-5 from glucose are introduced into the isoprene units via a single precursor molecule and representing the signature of the previously described rearrangement. Confirmation of the role of pyruvate and D-glyceraldehyde-3-phosphate was obtained after incorporation of uniformly labeled [U-$^{13}C_6$] glucose into the hopanoids of *Z. mobilis* and the incorporation of [1-^{13}C] glucose into the prenyl chain of ubiquinone in *E. coli* mutants, each lacking an enzyme of the triose phosphate metabolism inter converting glycerol and pyruvate [34]. Evidence for an alternative biosynthetic route was later obtained for other bacterial isoprenoid series. In *Escherichia coli*, which do not synthesize hopanoids, the same labeling pattern was obtained in the isoprene units of the prenyl chain of ubiquinone upon feeding with ^{13}C-labeled acetate as in the hopanoids from *R. palustris* and *M. organophilum*. Upon feeding with [1-^{13}C] glucose, the labeling distribution could be analyzed in the same way as

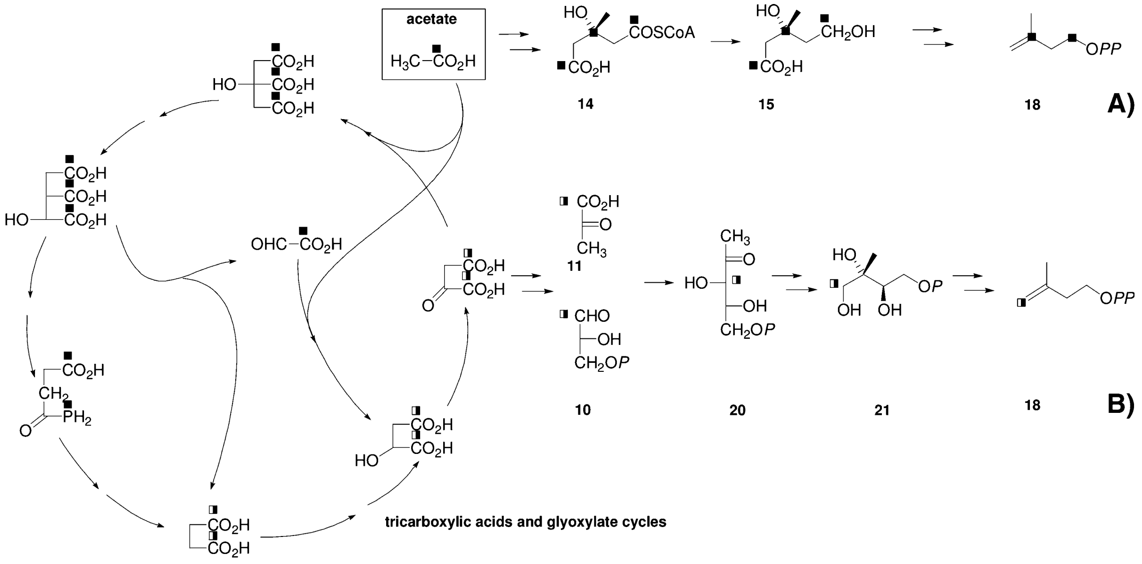

Fig. 3 Incorporation of [1-^{13}C] acetate for isoprene unit biosynthesis into the MVA pathway (***A***) or via the tricarboxylic acids and the glyoxylate cycles into the MEP pathway (***B***). For the sake of simplicity, cofactors have been omitted in the tricarboxylic acids and glyoxylate cycles. Only the carbon skeletons of the metabolites have been represented

those obtained for the formation of isoprene units in *Z. mobilis*, but in the frame of the glycolysis, which is utilized by *E. coli* for glucose catabolism [33].

All these features are inconsistent with the MVA pathway and a novel biosynthetic route had to be imagined [33, 34]. This was proposed by analogy with known enzymatic and chemical reactions. The pyruvate-derived two-carbon subunit is obtained from pyruvate decarboxylation by a thiamine diphosphate enzyme, much like the reactions catalyzed by pyruvate decarboxylase or pyruvate dehydrogenase, yielding (hydroxyethylidene) thiamine diphosphate. The later intermediate is a nucleophile that can be added onto the carbonyl group of glyceraldehyde-3-phosphate in a reaction resembling the reaction catalyzed by a transketolase and yielding a 1-deoxypentulose phosphate identified as 1-deoxy-D-xylulose 5-phosphate (DXP, **20**, Fig. 2c). A further step is the intramolecular rearrangement mentioned above, followed by the concomitant reduction of the resulting aldehyde intermediate. It was thought to be an acid-catalyzed rearrangement of a α-ketol resembling the rearrangement involved in the formation of the carbon skeleton of the branched amino-acids, but was later characterized by analysis of the isotope effects induced by the presence of a deuterium atom either at C-3 or at C-4 in the substrate as a retro-aldol/aldol reaction [35]. The reaction product is 2-*C*-methyl-D-erythritol 4-phosphate (MEP, **22**, Fig. 2C), a tetrol already presenting the branched isoprene skeleton. In contrast with DXP, which is also in *E. coli* a precursor of thiamine diphosphate and pyridoxal phosphate, no other function than that of an isoprenoid precursor is known for MEP. Accordingly, the pathway was proposed to be named after this intermediate.

The first two candidates for the C_5 precursors of this novel MVA-independent pathway are the phosphates of already known natural products. 1-Deoxy-D-xylulose (DX, **26**, Fig. 4) was previously isolated from the fermentation broth of a *Streptomyces* sp. and was known as a precursor of pyridoxal phosphate thiamine diphosphate in *E. coli*, and 2-*C*-methyl-D-erythritol (ME, **27**, Fig. 4) is accumulated in many plants, often in stress conditions [29, 36]. Incorporation of deuterium-labeled isotopomers of 1-deoxy-D-xylulose by the group of Duilio Arigoni [37] and of 2-*C*-methyl-D-erythritol [38–40] by our group into the prenyl chain of ubiquinone **4** and menaquinone **5** (Fig. 1) from *Escherichia coli* confirmed that these compounds are involved in an isoprenoid biosynthetic pathway.

The odd labeling patterns obtained with the first ^{13}C-labeled acetate incorporations [30] can now be easily interpreted. One has only to find out how glyceraldehyde-3-phosphate **10** and pyruvate **11** are synthesized from acetate via the tricarboxylic acid and the glyoxylate cycles, which are utilized by bacteria when acetate is the only carbon and energy source (Fig. 3).

Isoprenoid Biosynthesis in Plant Plastids

While we were carrying out our investigations on the biosynthesis of bacterial hopanoids, the group of Duilio Arigoni (ETH, Zürich, Switzerland) was investigating

Fig. 4 IPP **18** and DMAPP **19** as precursors of isoprene units in the MEP pathway. Tracing the origin of the isoprene units by incubation of [4-^{2}H]DX **26** or [3-^{2}H]ME **27**. Adapted from reference [98] and reproduced with permission

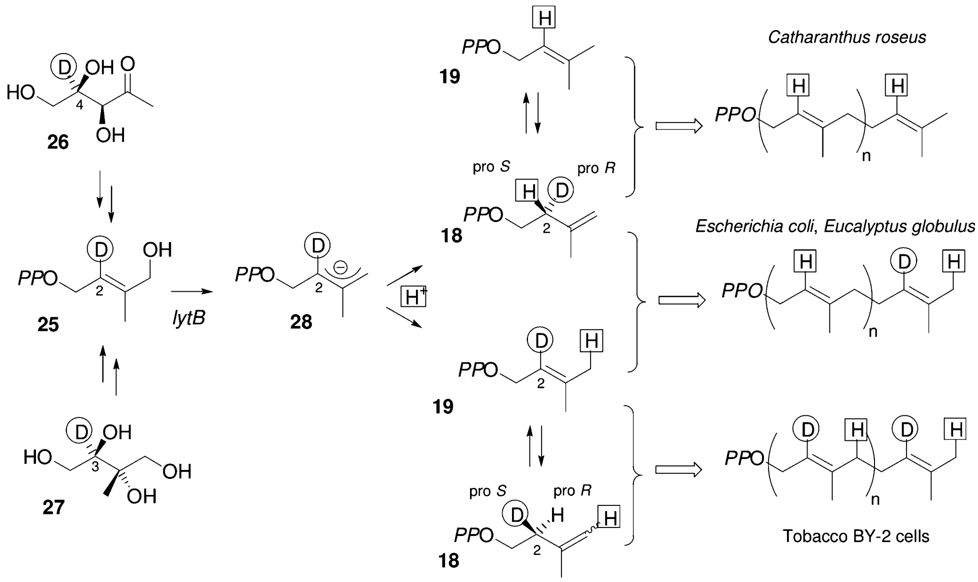

independently and nearly simultaneously the biosynthesis of diterpenoids of the ginkgolide series **7** (Fig. 1) in *Ginkgo biloba* embryos [41, 42]. In this study, and again in contrast with former work on plant isoprenoid biosynthesis where ^{13}C-labeled acetate was utilized, labeling experiments were performed with ^{13}C-labeled glucose. Results were straightforward. Labeling patterns determined in the diterpenoid isoprene units did not correspond to those expected from the MVA pathway. They corresponded to those described for the bacterial MEP pathway. Isoprene units were synthesized from pyruvate and GAP, both derived from labeled glucose via glycolysis [41].

Interestingly, this study on ginkgo embryos showed for the first time the dichotomy characterizing isoprenoid biosynthesis in plants: sitosterol **1b** (Fig. 1) is synthesized in the cytoplasm as expected via the MVA pathway whereas diterpenoids, which are plastid isoprenoids, are derived from the alternative MEP route [41, 42].

We later extended this observation in collaboration with the group of Hartmut K. Lichtenthaler (University of Karlsruhe, Germany) to algae [43–46] and to other plants and to the normal isoprenoid constituents of the photosynthetic apparatus. Incubation of barley seedlings, an axenic duckweed culture or a carrot tissue culture with [1-^{13}C] glucose all showed the same dichotomy: the cytoplasmic phytosterols are synthesized via the MVA pathway and phytol **8** (Fig. 1) from chlorophyll, carotenoids **9** and the prenyl chain of plastoquinone **6** via the MEP route [47]. Confirmation of such a compartmentation was obtained for many other systems. The key to the success for all these experiments was the utilization of ^{13}C-labeled glucose for in vivo incubation in the place of labeled acetate. Hemiterpenes (such as isoprene and 2-methylbut-3-en-2-ol) [48, 49], monoterpenes [50, 51], diterpenes [52–54] and carotenoids [47, 55], are mainly synthesized in the plastids and derived from MEP pathway. This intracellular localization of the MEP pathway was later corroborated by the presence of a plastid targeting sequence for all enzymes involved in this metabolic route [56, 57].

Molecular Biology: The Key for the Full Elucidation of the MEP Pathway

When the MEP pathway was discovered, no bacterial genome was completely sequenced. The formation of DXP was thought to be catalyzed by a thiamine diphosphate enzyme with a transketolase resembling mechanism. Indeed, deoxyxylulose phosphate synthase shares sequence similarities with transketolases and was thus rapidly identified in the genomes of *E. coli* [58, 59] and peppermint [60]. Once ME was shown to be incorporated into the isoprenoids of *E. coli*, the search for auxotrophic mutants requiring this tetrol for growth led to the identification of the DXP reductoisomerase [61, 62], an enzyme which catalyzes as expected the reversible rearrangement of DXP into 2-*C*-methyl-D-erythrose phosphate [63] and the concomitant NADPH-dependent reduction of the latter aldehyde into MEP.

In the meantime, more and more bacterial genomes were sequenced facilitating the search for the MEP pathway genes among unannotated genes. The next genes were detected by genome mining. Incubation of ^{3}H-labeled MEP with crude cell-free extracts from *E. coli* led to the isolation of a radioactive compound when the reaction mixture contained ATP. Yields were improved in the presence of CTP, and radioactivity was incorporated from [α-^{32}P]CTP, but not from [γ-^{32}P]CTP, suggesting that the detected product is a MEP adduct to a nucleoside derivative. This compound could not be further purified and characterized by chemical methods. The search for the gene of an enzyme catalyzing the coupling of a polyol phosphate to a nucleotide triphosphate resulted in the finding of the recently described *acs1* gene from *Haemophilus influenzae* encoding a bifunctional enzyme, which catalyzes the conversion of ribulose 5-phosphate into ribitol 5-phosphate and the further coupling of ribitol 1-phosphate to CTP yielding the CDP adduct of ribitol [64]. This *acs1 H. influenzae* gene presents homologies with the unannotated *ygbP* gene from *E. coli*, and the cognate protein catalyzes the conversion of MEP into 4-diphosphocytidyl-2-*C*-methyl-D-erythritol **22** (Fig. 2c) in the presence of CTP [65]. The next two genes belong, with the former one, to a small cluster in the *E. coli* genome. They were consecutively identified, and the corresponding enzymes characterized. The unannotated *ychB* and *ygbB* genes of *E. coli* were revealed by bacterial genomics. Their distribution in bacterial genomes was identical with that of the already known genes of the MEP pathway, and the corresponding recombinant proteins catalyzed the next steps: the phosphorylation of the tertiary hydroxy group yielding 4-diphosphocytidyl-2-*C*-methyl-D-erythritol 2-phosphate **23** [66], followed by the elimination of UMP yielding 2-*C*-methyl-D-erythritol 2,4-cyclodiphosphate (MEcPP) **24** [67] (Fig. 2c). The two latter compounds were incorporated into carotenoids by isolated *Capsicum annuum* chromoplast and were thus established as intermediates of the MEP pathway. Sequence homologies led to the identification of the corresponding genes in *Arabidopsis thaliana* and tomato [68, 69].

Isoprenoid biosynthesis is an essential metabolic pathway. Any deletion of a MEP pathway gene is therefore lethal. Another approach for the identification of MEP pathway genes was the deletion of genes in an *E. coli* construct capable of utilizing exogenous MVA as isoprenoid precursor after the insertion of all genes required for the conversion of MVA into IPP (MVA kinase, phosphoMVA kinase and diphosphoMVA decarboxylase, Fig. 2a) [70, 71]. Growth after deletion of a MEP pathway gene is thus restored by addition of exogenous MVA to the culture medium. This approach was independently utilized for the characterization of the genes encoding the three enzymes responsible for the conversion of MEP into MEcPP **24** [70, 72, 73].

The last steps correspond to the reduction of a tetrol derivative, MEcPP **24**, into a primary allylic (DMAPP, **19**) and/or homoallylic (IPP, **18**) alcohol diphosphate (Fig. 2c). This implies unprecedented elimination as well as reduction steps, i.e. the involvement of an associated reduction system. The genes corresponding to these last steps were found by bacterial genome mining. The search for the genes accompanying the already known MEP pathway genes led to the identification of two unannotated genes in *E. coli gcpE* and *lytB*. Their involvement in isoprenoid biosynthesis was shown using the *E. coli* mutants capable of utilizing MVA described above: the lethal deletion of *gcpE* or *lytB* was rescued by the addition of exogenous MVA [74, 75]. In vivo incorporation of [U-$^{13}C_6$]DX by *E. coli* constructs overexpressing MEP pathway genes followed by ^{13}C-NMR analysis of the resulting crude cell extracts afforded interesting clues about the respective role of the GcpE and LytB proteins [76, 77]. Overexpression of all genes upstream of GcpE was followed by the accumulation of MEcPP **24** (Fig. 2c). Additional overexpression of *gcpE* resulted in the accumulation of (*E*)-4-hydroxy-3-methylbut-2-enyl diphosphate (HMBPP, **25**, Fig. 2), and of *gcpE* and *lytB* in the accumulation of IPP **18** as well as DMAPP **19** in a ca. 5:1 ratio, identifying MEcPP and HMBPP as substrates of respectively GcpE and LytB, and HMBPP and IPP as well as DMAPP as the reaction products of the same enzymes.

Characterization of the corresponding enzymatic activities was rather tricky. The first hints of the role of GcpE were obtained in vivo with an *E. coli* strain with a deleted *dxr* gene, engineered for the utilization of exogenous MVA and overexpressing *gcpE*: in the presence of a cocktail of cofactors (including those required for reduction reactions), ^{3}H-labeled ME was converted into MEcPP **24** (Fig. 2c), suggesting that the cyclodiphosphate is the substrate of GcpE [78]. Further, a crude cell free-system from an *E. coli* strain overexpressing *gcpE* converted MEcPP into (*E*)-methylbut-2-ene-1,4-diol in the presence of a phosphatase [79] or into HMBPP **25** (Fig. 2c) in the presence of fluoride as phosphatase inhibitor [80]. In contrast, in a MVA utilizing and *lytB*-deficient *E. coli* strain HMBPP **25** was accumulated in sufficient amounts for direct spectroscopic characterization, indicating that this allylic diol diphosphate is most probably the substrate of LytB [81].

Improvements in the enzyme assay methods were only possible once the real nature of the GcpE and LytB proteins was recognized. GcpE and LytB share with [4Fe–4S] cluster enzymes three conserved cysteins serving as anchors for such a cluster [79, 80, 82]. Most of these enzymes are quite oxygen sensitive, losing their prosthetic group and consequently their activity in the presence of air. They usually require handling under an inert atmosphere in a glove box as well as reconstitution of their prosthetic group in the presence of Fe^{3+}, sulfide and dithiothreitol. This observation opened up new possibilities for the investigations on the last two steps of the MEP pathway. When bacterial [4Fe–4S] cluster enzymes are involved in a reducing process, they are associated in vivo to flavodoxin/flavodoxin reductase/NADPH for the regeneration of the reduced state of the prosthetic group. The former biological system can be replaced in an enzyme assay by the semiquinone radical obtained by photoreduction of deazaflavin. This approach proved fruitful. Reconstituted recombinant GcpE enzyme from *E. coli* [83] or the native as-isolated protein [84] converted in the presence of the biological or of the chemical reducing system MEcPP **24** into HMBPP **25** (Fig. 2c). Even dithionite was an effective reducing agent with the *Thermus thermophilus* GcpE [85]. Binding of intermediates to the cluster was suggested by EPR for the GcpE from *E. coli* [86].

Similarly, the last enzyme encoded by the *lytB* gene was also found to be a [4Fe–4S] enzyme converting HMBPP **25** (Fig. 4) into either IPP **18** or DMAPP **19** in a ca. 1:5 ratio [82] in the presence of the same associated biological reducing systems for the *E. coli* enzyme [87], and even in the presence of dithionite in the case of the *Aquifex aeolicus* enzyme [88]. Protonation of an allylic anion intermediate **28** (Fig. 4) is the most likely final step of the LytB catalyzed reaction (Fig. 4) [89].

Characterization of the cluster was performed by EPR spectroscopy of the LytB enzyme from *E. coli* with the cluster in its reduced $[4Fe–4S]^{1+}$ form from *E. coli* obtained upon dithionite reduction [87]. The as-isolated enzyme presented the signal of a $[3Fe–4S]^{2+}$ cluster, which represented about 10% of the protein and was most likely derived from the degradation by oxygen [87]. The same signal was also reported from the spectrum of LytB isolated under an inert atmosphere [90]. Mössbauer spectroscopy allowed the characterization of the GcpE/IspG from *E. coli* and *Arabidopsis thaliana* in the oxidized $[4Fe–4S]^{2+}$ form upon reconstitution with ^{57}Fe [91].

In plants and other organisms phylogenetically related to phototrophic phyla, the MEP pathway is localized in the plastids where flavodoxin is absent. GcpE interacts with ferredoxin in the cyanobacterium *Thermosynechococcus elongatus* [92] and in the malaria parasite *Plasmodium falciparum* [93], and activity was characterized in the presence of the associated reducing system ferredoxin/ferredoxin reductase/NADPH. In higher plants, the electrons required for the reduction converting MEcPP **24** into HMBPP **25** are derived also from ferredoxin. Indeed, a preparation containing *Arabidopsis thaliana* GcpE and purified spinach thylakoids afforded upon illumination, and in the absence of any reducing cofactor, HMBPP **25** from MEcPP **24** (Fig. 2c) [94], showing that the electron flow derived from the photo-oxidation of water can be directly diverted via photosystems I and II towards isoprenoid biosynthesis. In the dark (or in roots), the electron flow must come from catabolic processes, and ferredoxin is associated with the NADPH-dependent ferredoxin reductase under these conditions [94].

Conclusion: Further Developments

The MEP pathway for the biosynthesis of isoprene units in bacteria and plant plastids is now completely elucidated. All genes and enzymes are known. Many structural features of the enzymes as well as mechanistic aspects of the catalyzed reactions have, however, still to be deciphered. The discovery of this new metabolic pathway opened additional unexplored fields in plant and bacterial metabolism.

IPP and/or DMAPP as Precursor of the Isoprene Units?

The origin of the hydrogen atoms found in the isoprene units derived from MEP pathway was followed by incorporation of ^{2}H-labeled DX or ME. If the hydrogen atoms corresponding to those located at C-1, C-4 and C-5 of MEP are integrally retained in the isoprene units, quite striking observations were made on the retention or the loss of the hydrogen atom at C-4 of DXP corresponding to the hydrogen atom at C-3 of MEP. Three labeling patterns were described for isoprene units upon feeding of DX **26** or ME **27** (Fig. 4) with ^{2}H labeling at C-4 or C-3 respectively: (i) quantitative loss in all isoprene units wherever they are derived from IPP or from DMAPP as found in the carotenoids and phytol from a plant cell culture of *Catharanthus roseus* [95], (ii) quantitative retention in the DMAPP derived unit and quantitative loss in those derived from IPP in the prenyl chains of ubiquinone and menaquinone from the bacterium *Escherichia coli* [40, 96] or significant retention in the DMAPP derived unit and nearly complete loss in that derived from IPP in the monoterpene cineol from *Eucalyptus globulus* [97] and finally (iii) retention of deuterium in all isoprene units derived either from IPP or from DMAPP as observed for phytoene and the prenyl chain of plastoquinone from a tissue culture of tobacco BY-2 [98] (Fig. 4). Such apparently contradictory observations may in fact be explained, keeping in mind that IspH/LytB, the last enzyme of the MEP pathway, affords two reaction products, IPP **18** or alternatively DMAPP **19**. Taking into account the stereoselectivity of the introduction of the proton on the allylic anionic intermediate and of the elimination of the pro-*R* proton of IPP by the IPP isomerase and the *trans*-prenyl transferase, each labeling pattern reflects the origin of the isoprene units, the presence of deuterium representing the signature of a DMAPP origin, and its absence the signature of an IPP origin [36, 98] (Fig. 4).

Cross-Talk Between Cytoplasmic and Plastidial Compartments in Plant Cells

In plant cells, two pathways contribute to isoprenoid biosynthesis: the MVA pathway localized in the cytoplasm and the MEP pathway found in the plastids. The origin of the isoprene unit precursors, IPP and/or DMAPP is, however, scrambled by exchanges of intermediates between these two cell compartments. This aspect is well illustrated by the labeling patterns observed after incorporation of [1-^{13}C] glucose into plant isoprenoids, and was already clearly documented in the first study on ginkgolide biosynthesis. From the labeling pattern observed in the diterpenes skeleton of ginkgolides, it was deduced that most of the geranylgeranyl diphosphate (ca. 98%) was made from isoprene units uniquely derived from the MEP pathway. A small but significant part of the C_{20} skeleton has a composite origin: a C_{15} farnesyl diphosphate chain synthesized from isoprene units derived from the MVA pathway is completed by a fourth unit solely derived from the MEP pathway [41]. This shows that an acyclic C_{15} precursor, most probably farnesyl diphosphate, is carried from the cytoplasm to the plastids. Similar observations describing a dual origin for isoprene units were later reported for many other systems from higher plants [41, 55, 99–101], liverwort [102] and hornwort [103], illustrating the possibility of exchanges of C_5, C_{10} and C_{15} intermediates between cytoplasm and plastids. A striking example is given by the tobacco BY-2 cell culture where MEP and MVA pathways can complement each other [104]. Upon inhibition of the MVA pathway by a sublethal dose of mevinolin, phytosterol in the cytoplasm are synthesized via the MEP pathway from exogenous DX. Similarly, upon inhibition of the MEP pathway by fosmidomycin, the prenyl chain of the plastidial plastoquinone is synthesized from MVA, like the isoprene units of sterols [104].

The simultaneous presence of two independent pathways opens new understanding of plant physiology at the level of the regulation of isoprenoid biosynthesis. For instance, the emission of volatile plant defense terpenoid is dependent on both pathways: sesquiterpenoids being preferentially derived from the MVA route whereas monoterpenoids are synthesized via the MEP pathway [105, 106]. In addition, a nycthemeral rhythm (corresponding to the succession of day and night) has been pointed out for the MEP pathway in snapdragon flowers. Emission of volatile terpenoid synthesized via the MEP pathway occurs essentially during the day and is controlled by the circadian clock. Both plastidial monoterpenes and the cytosolic sesquiterpene nerolidol are derived from MEP pathway, suggesting a unidirectional trafficking of precursor(s) from plastids towards the cytoplasm [107].

MEP Pathway Enzymes as Targets for Antibacterial Drugs

The MEP pathway is the major metabolic route for isoprenoid biosynthesis in eubacteria. It is present in most bacterial taxa, including many obligate pathogens as well as opportunistic pathogens responsible for hospital-acquired diseases [108, 109]. In addition, some eukaryotes phylogenetically related to photosynthetic phyla, possess the MEP pathway, among them the *Plasmodium* spp. responsible for malaria [110].

The MEP pathway is absent in humans and animals, and isoprenoid biosynthesis is an essential metabolic route in all living organisms. Inhibition of any enzyme of this pathway has lethal consequences. This means that all enzymes of the MEP represent unexplored targets for the design of antibacterial or antiparasitic drugs [109–111]. This aspect is particularly interesting to overcome the widespread resistance towards most current commercial antibiotics. The concept has already been validated. Indeed, despite poor pharmacokinetic properties, a rapid elimination in urine [112] and the fast appearance of bacterial resistance, fosmidomycin, a natural antibiotic and a potent inhibitor of the second enzyme of the MEP pathway, the DXP reducto-isomerase [113], is quite effective against bacterial growth [112, 114] or against simple *Plasmodium* infections in rodents and in man [110, 115, 116].

Acknowledgments This work was partly supported by a grant from the "Agence Nationale de la Recherche" (grant Nb ANR-05-BLAN-0217-02).

References

1. Bruan B, Shey J, Gerst N, Wilson WK, Schroepfer GJ Jr (1996) Silver ion high pressure liquid chromatography provides unprecedented separation of sterols: application to the enzymatic formation of cholesta-5,8-dien-3β-ol. Proc Natl Acad Sci USA 93:11603–11608
2. Rohmer M, Brandt RD, Ourisson G (1972) Hydrosoluble complexes of sterols, sterol esters and their precursors in *Zea mays*. Eur J Biochem 36:172–179
3. Rohmer M, Brandt RD (1973) Les stérols et leurs précurseurs chez *Astasia longa* Pringsheim. Eur J Biochem 36:446–454
4. Rohmer M, Ourisson G, Benveniste P, Bimpson T (1975) Sterol biosynthesis in heterotrophic plant parasites. Phytochemistry 14:727–730
5. Whiters N, Kokke WCMC, Fennical WH, Rohmer M, Djerassi C (1979) Isolation of sterols with cyclopropane containing side-chains from a cultured marine alga. Tetrahedron Lett 3605–3608
6. Rohmer M, Kokke WCMC, Fennical WH, Djerassi C (1980) Isolation of two new C_{30} sterols, (24*E*)-24-*n*-propylidenecholesterol and 24-*n*-propylcholesterol from a cultured marine Chrysophyte. Steroids 35:219–231
7. Kho E, Imagawa DK, Rohmer M, Kashman Y, Djerassi C (1981) 22. Isolation and structure elucidation of conicasterol and theonellasterol, two new 4-methylenesterols from the Red Sea

sponge *Theonella conica* and *Theonella swinhoei*. J Org Chem 46:1836–1839

8. Raederstorff D, Rohmer M (1987) The action of systemic fungicides tridemorph and fenpropimorph on sterol biosynthesis by the soil amoeba *Acanthamoeba polyphaga*. Eur J Biochem 164:421–426
9. Raederstorff D, Rohmer M (1987) Sterol biosynthesis via cycloartenol and other biochemical features related to photosynthetic phyla in the amoebae *Naegleria lovaniensis* and *Naegleria gruberi*. Eur J Biochem 164:427–434
10. Hoehn-Thierry P (1992) Lipides et biosynthèse de stérols chez le mildiou, *Plasmopara viticola*, parasite strict de la vigne. PhD Thesis, Université de Haute Alsace, Mulhouse, France
11. Ourisson G, Albrecht P (1992) Hopanoids. 1. Geohopanoids: the most abundant natural products on earth? Acc Chem Res 25:398–402
12. Rohmer M, Bouvier-Navé P, Ourisson G (1984) Distribution of hopanoid triterpenes in prokaryotes. J Gen Microbiol 130:1137–1150
13. Förster HJ, Biemann K, Haigh WG, Tattrie NH, Colvin JR (1973) The structure of novel C_{35} pentacyclic terpenes from *Acetobacter xylinum*. Biochem J 135:133–143
14. Haigh WG, Förster HJ, Biemann K, Tattrie NH, Colvin JR (1973) Induction of orientation of bacterial cellulose microfibrils by a novel terpenoid from *Acetobacter xylinum*. Biochem J 135:145–149
15. Rohmer M, Ourisson G (1976) Structure des bactériohopanetétrols d'*Acetobacter xylinum*. Tetrahedron Lett 3633–3636
16. Rohmer M, Ourisson G (1976) Dérivés du bactériohopane: variations structurales et répartition. Tetrahedron Lett 3637–3640
17. Rohmer M, Ourisson G (1986) Unsaturated bacteriohopanepolyols from *Acetobacter aceti* ssp. *xylinum*. J Chem Res (S) 356–357; (M) 3037–3059
18. Rohmer M, Ourisson G (1976) Méthylhopanes d'*Acetobacter xylinum* et d'*Acetobacter rancens*. Tetrahedron Lett 3633–3636
19. Zundel M, Rohmer M (1985) Prokaryotic triterpenoids. 1. 3β-Methylhopanoids from *Acetobacter* species and *Methylococcus capsulatus*. Eur J Biochem 150:23–27
20. Bisseret P, Zundel M, Rohmer M (1985) Prokaryotic triterpenoids. 2. 2β-Methylhopanoids from *Methylobacterium organophilum* and *Nostoc muscorum*, a new series of prokaryotic triterpenoids. Eur J Biochem 150:29–34
21. Stampf P, Herrmann D, Bisseret P, Rohmer M (1991) 2α-Methylhopanoids: first recognition in the bacterium *Methylobacterium organophilum* and obtention via sulphur induced isomerization of 2β-methylhopanoids. An account for their presence in sediments. Tetrahedron 47:7081–7090
22. Rohmer M (1993) The biosynthesis of triterpenoids of the hopane series in Eubacteria: a mine of new enzyme reactions. Pure Appl Chem 65:1293–1298
23. Rohmer M, Bouvier P, Ourisson G (1979) Molecular evolution of biomembranes: structural equivalents and phylogenetic precursors of sterols. Proc Natl Acad Sci USA 76:847–851
24. Ourisson G, Rohmer M, Poralla K (1987) Prokaryotic hopanoids and other polyterpenoid sterol surrogates. Annu Rev Microbiol 41:301–333
25. Poralla K, Härtner T, Kannenberg E (1984) Effect of temperature and pH on the hopanoid content of *Bacillus acidocaldarius*. FEMS Microbiol Lett 23:253–256
26. Hermans MAF, Neuss B, Sahm H (1991) Content and composition of hopanoids in *Zymomonas mobilis* under various growth conditions. J Bacteriol 173:5592–5595
27. Berry AM, Harriott OT, Moreau RA, Osman SF, Benson DR, Jones AD (1993) Hopanoid lipids compose the *Frankia* vesicles envelope, presumptive barrier of oxygen diffusion to nitrogenase. Proc Natl Acad Sci USA 90:6091–6094
28. Poralla K, Muth G, Härtner T (2000) Hopanoids are formed during transition from substrate to aerial hyphae in *Streptomyces coelicolor* A3(2). FEMS Microbiol Lett 189:93–95
29. Rohmer M (1999) A mevalonate-independent route to isopentenyl diphosphate. In: Cane DE (ed) Comprehensive natural products chemistry, isoprenoids including steroids and carotenoids, vol 2. Pergamon, Oxford, pp 45–68
30. Flesch G, Rohmer M (1988) Prokaryotic triterpenoids. The biosynthesis of the bacteriohopane skeleton: formation of isoprenic units from two distinct acetate pools and a novel type of carbon/carbon linkage between a triterpene and D-ribose. Eur J Biochem 175:405–411
31. Rohmer M, Sutter B, Sahm H (1989) Bacterial sterol surrogates. Biosynthesis of the side-chain of bacteriohopanetetrol and of a carbocyclic carbapseudopentose from ^{13}C-labelled glucose in *Zymomonas mobilis*. J Chem Soc Chem Commun 1471–1472
32. Renoux JM, Rohmer M (1985) Prokaryotic triterpenoids. New bacteriohopanetetrol cyclitol ethers from the methylotrophic bacterium *Methylobacterium organophilum*. Eur J Biochem 151:405–410
33. Rohmer M, Knani M, Simonin P, Sutter B, Sahm H (1993) Isoprenoid biosynthesis in bacteria: a novel pathway for the early steps leading to isopentenyl diphosphate. Biochem J 295:517–524
34. Rohmer M, Seemann M, Horbach S, Sahm H (1996) Glyceraldehyde 3-phosphate and pyruvate as precursors of isoprenic units in an alternative non-mevalonate pathway for terpenoid biosynthesis. J Am Chem Soc 118:2564–2566
35. Wong U, Cox RJ (2007) The chemical mechanisms of D-1-deoxyxylulose 5-phosphate reductoisomerase from *Escherichia coli*. Angew Chem Int Ed 46:4926–4929
36. Rohmer M (2007) Diversity in isoprenoid biosynthesis: the methylerythritol phosphate pathway in plastids and plants. Pure Appl Chem 79:739–751
37. Broers STJ (1994) I Über die frühen Stufen der Biosynthese von Isoprenoiden in *Escherichia coli*. II. Beitrag zur Aufklärung der Biosyntheses von Vitamin B12 in *Propionibacterium shermanii*. PhD Thesis Nb 10978, Eidgenössische Technische Hochschule, Zürich, Switzerland
38. Duvold T, Bravo JM, Pale-Grosdemange C, Rohmer M (1997) Biosynthesis of 2-*C*-methyl-D-erythritol, a putative C_5 intermediate in the mevalonate-independent pathway for isoprenoid biosynthesis. Tetrahedron Lett 38:4769–4772
39. Duvold T, Cali P, Bravo JM, Rohmer M (1997) Incorporation of 2-*C*-methyl-D-erythritol, a putative intermediate in the mevalonate independent pathway, into ubiquinone and menaquinone of *Escherichia coli*. Tetrahedron Lett 38:6181–6184
40. Charon L, Hoeffler JF, Pale-Grosdemange C, Lois LM, Campos N, Boronat A, Rohmer M (2000) Deuterium labeled isotopomers of 2-*C*-methyl-D-erythritol 4-phosphate pathway for isoprenoid biosynthesis. Biochem J 346:737–742
41. Schwarz M (1994) Terpen-Biosynthese in *Ginkgo biloba*: eine überraschende Geschichte. PhD Thesis Nb 10951, Eidgenössische Technische Hochschule, Zürich, Switzerland
42. Schwarz M, Arigoni D (1999) Ginkgolide biosynthesis. In: Cane DE (ed) Comprehensive natural products chemistry, isoprenoids including steroids and carotenoids, vol 2. Pergamon, Oxford, pp 367–400
43. Schwender J, Seemann M, Lichtenthaler HK, Rohmer M (1996) Biosynthesis of isoprenoids (carotenoids, sterols, prenyl side-chains of chlorophylls and plastoquinone) via a novel pyruvate/glyceraldehyde 3-phosphate non-mevalonate pathway. Biochem J 316:73–80

44. Disch A, Schwender J, Muller C, Lichtenthaler HK, Rohmer M (1998) Distribution of the mevalonate and glyceraldehyde phosphate/pyruvate pathways for isoprenoid biosynthesis in unicellular algae and the cyanobacterium *Synechocystis* PCC 6714. Biochem J 333:381–388
45. Schwender J, Zeidler J, Gröner R, Müller C, Focke M, Braun S, Lichtenthaler FW, Lichtenthaler HK (1997) Incorporation of 1-deoxy-D-xylulose into isoprene and phytol by higher plants and algae. FEBS Lett 414:129–134
46. Schwender J, Gemünden C, Lichtenthaler HK (2001) Chlorophyta exclusively use the 1-deoxyxylulose 5-phosphate/2-*C*-methylerythritol 4-phosphate pathway for the biosynthesis of isoprenoids. Planta 212:416–423
47. Lichtenthaler HK, Schwender J, Disch A, Rohmer M (1996) Biosynthesis of isoprenoids in higher plant chloroplasts proceeds via a mevalonate-independent pathway. FEBS Lett 400:271–274
48. Zeidler JG, Lichtenthaler HK, May HU, Lichtenthaler FW (1996) Is isoprene emitted by plants synthesized via the novel isopentenyl pyrophosphate pathway? Z Naturforsch 52c:15–23
49. Zeidler J, Lichtenthaler HK (2001) Biosynthesis of 2-methyl-3-buten-2-ol emitted from needles of *Pinus ponderosa* via the non-mevalonate DOXP/MEP pathway for isoprenoid biosynthesis. Planta 213:323–326
50. Eisenreich W, Sagner S, Zenk MH, Bacher A (1997) Monoterpenoid essential oils are not of mevalonoid origin. Tetrahedron Lett 38:3889–3892
51. Adam KP, Thiel R, Zapp J, Becker H (1998) Involvement of the mevalonic acid pathway and the glyceraldehyde phosphate-pyruvate pathway in terpenoid biosynthesis of the liverworts *Ricciocarpos natans* and *Conocephalum conicum*. Arch Biochem Biophys 354:181–187
52. Eisenreich W, Menhard B, Hylands PJ, Zenk MH, Bacher A (1997) Studies on the biosynthesis of taxol: the taxane carbon skeleton is not of mevalonoid origin. Proc Natl Acad Sci USA 93:6431–6436
53. Knöss W, Reuter B, Zapp J (1997) Biosynthesis of the labdane diterpene marrubiin in *Marrubium vulgare* via a non-mevalonate pathway. Biochem J 326:449–454
54. Hayashi T, Asai T, Sankawa U (1999) Mevalonate-independent biosynthesis of bicyclic and tetracyclic diterpenes of *Scoparia dulcis* L. Tetrahedron Lett 40:8239–8243
55. Arigoni D, Sagner S, Latzel C, Eisenreich W, Bacher A, Zenk MH (1997) Terpenoid biosynthesis from 1-deoxy-D-xylulose in higher plants by an intramolecular skeletal rearrangement. Proc Natl Acad Sci USA 94:10600–10605
56. Rodríguez-Concepción M, Boronat A (2002) Elucidation of the methylerythritol phosphate pathway for isoprenoid biosynthesis in bacteria and plastids. A metabolic milestone achieved through genomics. Plant Physiol 130:1079–1089
57. Eisenreich W, Bacher A, Arigoni D, Rohdich F (2004) Biosynthesis of isoprenoids via the non-mevalonate pathway. Cell Mol Life Sci 61:1401–1426
58. Sprenger GA, Schörken U, Wiegert T, Grolle S, de Graaf A, Taylor SV, Begley TP, Bringer-Meyer S, Sahm H (1998) Identification of a thiamin-dependent synthase in *Escherichia coli* required for the formation of the 1-deoxy-D-xylulose 5-phosphate precursor to isoprenoids, thiamin and pyridoxol. Proc Natl Acad Sci USA 94:12857–12862
59. Lois LM, Campos N, Rosa-Putra S, Danielsen K, Rohmer M, Boronat A (1998) Cloning and characterization of a gene from *Escherichia coli* encoding a novel transketolase-like enzyme that catalyzes the synthesis of D-1-deoxyxylulose 5-phosphate, a common precursor for isoprenoid, thiamin and pyridoxol biosynthesis. Proc Natl Acad Sci USA 95:2105–2110
60. Lange BM, Wildung MW, McCaskill D, Croteau R (1998) A family of transketolases that directs isoprenoid biosynthesis via a mevalonate-independent pathway. Proc Natl Acad Sci USA 95:2100–2104
61. Kuzuyama T, Shimizu T, Takahashi S, Seto H (1998) Direct formation of 2-*C*-methyl-D-erythritol 4-phosphate from 1-deoxy-D-xylulose 5-phosphate reductoisomerase: a novel enzyme in the non-mevalonate pathway to isopentenyl diphosphate. Tetrahedron Lett 39:4509–4512
62. Takahashi S, Kuzuyama T, Watanabe H, Seto H (1998) A 1-deoxy-D-xylulose 5-phosphate reductoisomerase catalyzing the formation of 2-*C*-methyl-D-erythritol 4-phosphate in an alternative nonmevalonate pathway for isoprenoid biosynthesis. Proc Natl Acad sci USA 95:9879–9884
63. Hoeffler JF, Tritsch D, Grosdemange-Billiard C, Rohmer M (2002) Isoprenoid biosynthesis via the methylerythritol phosphate pathway: mechanistic investigations on the 1-deoxy-D-xylulose 5-phosphate synthase. Eur J Biochem 269:446–4457
64. Follens A, Veiga-da-Cunha M, Merckx R, Van Schaftingen E, Van Eldere J (1999) *acs1*of *Haemophilus influenzae* type a capsulation locus region II encodes a bifunctional ribulose 5-phosphate reductase-CDP-ribitol pyrophosphorylase. J Bacteriol 181:2001–2007
65. Rohdich F, Wungsintaweekul J, Fellermeier M, Sagner S, Herz S, Kis K, Eisenreich W, Bacher A, Zenk MH (1999) Cytidine 5′-triphosphate-dependent biosynthesis of isoprenoids: YgbP protein of *Escherichia coli* catalyzes the formation of 4-diphosphocytidyl-2-*C*-methylerythritol. Proc Natl Acad Sci USA 96:11758–11763
66. Lüttgen H, Rohdich F, Herz S, Wungsintaweekul J, Hecht S, Schuhr CA, Fellermeier M, Sagner S, Zenk MH, Bacher A, Eisenreich W (2000) Biosynthesis of terpenoids: YchB protein of *Escherichia coli* phosphorylates the 2-hydroxy group of 4-diphosphocytidyl-2C-methyl-D-erythritol. Proc Natl Acad Sci USA 97:1062–1067
67. Herz S, Wungsintaweekul J, Schuhr C, Hecht S, Lüttgen Sagner S, Fellermeier M, Eisenreich W, Zenk MH, Bacher A, Rohdich F (2000) Biosynthesis of terpenoids: YgbB protein converts 4-diphosphocytidyl-2C-methyl-D-erythritol 2-phosphate into 2C-methyl-D-erythritol-2, 4-cyclodiphosphate. Proc Natl Acad Sci USA 97:2486–2490
68. Rohdich F, Wungsintaweekul J, Eisenreich W, Richter G, Schuhr CA, Hecht S, Zenk MH, Bacher A (2000) Biosynthesis of terpenoids: 4-diphosphocytidyl-2C-methyl-D-erythritol synthase of *Arabidopsis thaliana*. Proc Natl Acad Sci USA 97:6451–6456
69. Rohdich F, Wungsintaweekul J, Lüttgen Fischer M, Eisenreich W, Schuhr CA, Fellermeier M, Schramek N, Zenk MH, Bacher A (2000) Biosynthesis of terpenoids: 4-diphosphocytidyl-2-*C*-methyl-D-erythritol kinase from tomato. Proc Natl Acad Sci USA 97:8251–8256
70. Kuzuyama T, Takagi M, Kaneda K, Dairi T, Seto H (2000) Formation of 4-(cytidine 5′-diphospho)-2-*C*-methyl-D-erythritol from 2-*C*-methyl-D-erythritol 4-phosphate by 2-*C*-methyl-D-erythritol 4-phosphate cytidylyl transferase, a new enzyme of the nonmevalonate pathway. Tetrahedron Lett 41:703–706
71. Campos N, Rodríguez-Concepción M, Sauret-Güeto S, Gallego F, Lois LM, Boronat A (2001) *Escherichia coli* engineered to synthesize isopentenyl diphosphate and dimethylallyl diphosphate from mevalonate: a novel system for the genetic analysis of the 2-*C*-methyl-D-erythritol 4-phosphate pathway for isoprenoid biosynthesis. Biochem J 353:59–67
72. Kuzuyama T, Takagi M, Kaneda K, Watanabe H, Dairi T, Seto H (2000) Studies on the nonmevalonate pathway: conversion of 4-(cytidine 5′-diphospho)-2-*C*-methyl-D-erythritol to its

2-phospho derivative by 4-(cytidine 5′-diphospho)-2-*C*-methyl-D-erythritol kinase. Tetrahedron Lett 41:2925–2928

73. Takagi M, Kuzuyama T, Kaneda K, Watanabe H, Dairi T, Seto H (2000) Studies on the nonmevalonate pathway: formation of 2-*C*-methyl-D-erythritol 2, 4-cyclodiphosphate from 2-phospho-4-(cytidine 5′-diphospho)-2-C-methyl-D-erythritol. Tetrahedron Lett 41:3395–3398
74. Campos N, Rodríguez-Concepción M, Seemann M, Rohmer M, Boronat A (2001) Identification of *gcpE* as a novel gene of the 2-*C*-methyl-D-erythritol 4-phosphate pathway for isoprenoid biosynthesis in *Escherichia coli*. FEBS Lett 488:170–173
75. Altincicek B, Kollas AK, Eberl M, Wiesner J, Sanderbrand S, Hintz M, Beck E, Jomaa H (2001) *LytB*, a novel gene of the 2-*C*-methyl-D-erythritol 4-phosphate pathway of isoprenoid biosynthesis in *Escherichia coli*. FEBS Lett 499:37–40
76. Hecht S, Eisenreich W, Adam P, Amslinger S, Kis K, Bacher A, Arigoni D, Rohdich F (2001) Studies on the nonmevalonate pathway to terpenes: the role of GcpE (IspG) protein. Proc Natl Acad Sci USA 98:14837–14842
77. Rohdich F, Hecht S, Gärtner K, Adam P, Krieger C, Amslinger S, Arigoni D, Bacher A, Eisenreich W (2002) Studies on the nonmevalonate terpene biosynthetic pathway: metabolic role of IspH (LytB) protein. Proc Natl Acad Sci USA 99:1158–1163
78. Seemann M, Campos N, Rodríguez-Concepción M, Hoeffler JF, Grosdemange-Billiard C, Boronat A, Rohmer M (2002) Isoprenoid biosynthesis via the methylerythritol phosphate pathway: accumulation of 2-*C*-methyl-D-erythritol 2,4-cyclodiphosphate in a gcpE deficient mutant of *Escherichia coli*. Tetrahedron Lett 43:775–778
79. Seemann M, Campos N, Rodríguez-Concepción M, Ibañez E, Duvold T, Tritsch D, Boronat A, Rohmer M (2002) Isoprenoid biosynthesis via the methylerythritol phosphate pathway: enzymatic conversion of methylerythritol cyclodiphosphate into a phosphorylated derivative of (*E*)-methylbut-2-ene-1, 4-diol. Tetrahedron Lett 43:1413–1415
80. Wolff M, Seemann M, Grosdemange-Billiard C, Tritsch D, Campos N, Rodríguez-Concepción M, Boronat A, Rohmer M (2002) Isoprenoid biosynthesis via the methylerythritol phosphate pathway. (*E*)-4-Hydroxy-3-methylbut-2-enyl diphosphate: chemical synthesis and formation from methylerythritol cyclodiphosphate by a cell-free system from *Escherichia coli*. Tetrahedron Lett 43:2555–2559
81. Hintz M, Reichenberg A, Bahr U, Gschwind R, Kollas AK, Beck E, Wiesner J, Eberl M, Jomaa H (2001) Identification of (*E*)-4-hydroxy-3-methyl-but-2-enyl pyrophosphate as major activator for human $\gamma\delta$ T cells in *Escherichia coli*. FEBS Lett 509:317–322
82. Adam P, Hecht S, Eisenreich W, Kaiser J, Gräwert T, Arigoni D, Bacher A, Rohdich F (2002) Biosynthesis of terpenes: studies on 1-hydroxy-2-methyl-2-(*E*)-butenyl 4-diphosphate reductase. Proc Natl Acad Sci USA 99:12108–12113
83. Seemann M, Tse Sum Bui B, Wolff M, Tritsch D, Campos N, Boronat B, Marquet A, Rohmer M (2002) Isoprenoid biosynthesis via the methylerythritol phosphate pathway: the (*E*)-4-hydroxy-3-methylbut-2-enyl diphosphate synthase (GcpE) is a [4Fe–4S] protein. Angew Chem Int Ed Engl 114:4513–4515
84. Rohdich F, Zepeck F, Adam P, Hecht S, Kaiser J, Laupitz R, Gräwert T, Amslinger S, Eisenreich W, Bacher A, Arigoni D (2003) The deoxyxylulose phosphate pathway of isoprenoid biosynthesis: studies on the mechanisms of the reactions catalyzed by the IspG and IspH protein. Proc Natl Acad Sci USA 100:1586–1591
85. Kollas AK, Duin EC, Eberl M, Altincicek B, Hintz M, Reichenberg A, Henschker D, Henne A, Steinbrecher I, Ostrovsky DN, Hedderich R, Beck E, Jomaa H, Wiesner J (2002) Functional characterization of GcpE, an essential enzyme of the non-mevalonate pathway of isoprenoid biosynthesis. FEBS Lett 532:432–436
86. Adedeji D, Hernandez H, Wiesner J, Köhler U, Jomaa H, Duin EC (2007) Possible direct involvement of the active-site [4Fe–4S] cluster of the GcpE enzyme from *Thermus thermophilus* in the conversion of MEcPP. FEBS Lett 581:279–283
87. Wolff M, Seemann M, Tse Sum Bui B, Frapart Y, Tritsch D, Garcia-Estrabot A, Rodríguez-Concepción M, Boronat A, Marquet A, Rohmer M (2003) Isoprenoid biosynthesis via the methylerythritol phosphate pathway: the (*E*)-4-hydroxy-3-but-2-enyl diphosphate reductase (LytB/IspH) from *Escherichia coli* is a [4Fe–4S] protein. FEBS Lett 541:115–120
88. Altincicek B, Duin CE, Reichenberg A, Hedderich R, Kollas AK, Hintz M, Wagner S, Wiesner J, Beck E, Jomaa H (2002) LytB protein catalyzes the terminal step of the 2-*C*-methyl-D-erythritol-4-phosphate pathway of isoprenoid biosynthesis. FEBS Lett 532:437–440
89. Laupitz R, Gräwert T, Rieder C, Zepeck F, Bacher A, Arigoni D, Rohdich F, Eisenreich W (2004) Stereochemical studies on the making and unmaking of isopentenyl diphosphate in different biological systems. Chem Biodiv 1:1367–1376
90. Gräwert T, Kaiser J, Zepeck F, Laupitz R, Hecht S, Amslinger S, Schramek N, Schleicher E, Weber S, Haslbeck M, Buchner J, Rieder C, Arigoni D, Bacher A, Eisenreich W, Rohdich F (2004) IspH protein of *Escherichia coli*: studies on iron-sulfur cluster implementation and catalysis. J Am Chem Soc 126:12847–12855
91. Seemann M, Wegner P, Schünemann V, Tse Sum Bui B, Wolff M, Marquet A, Trautwein AX, Rohmer M (2005) Isoprenoid biosynthesis via the methylerythritol phosphate pathway: the (*E*)-4-hydroxy-3-methylbut-2-enyl diphosphate synthase (GcpE) from *Arabidopsis thaliana* is a [4Fe–4S] protein. J Biol Inorg Chem 10:131–137
92. Okada K, Hase T (2005) Cyanobacterial non-mevalonate pathway: (*E*)-4-hydroxy-3-methylbut-2-enyl diphosphate synthase interacts with ferredoxin in *Thermosynechococcus elongatus* BP-1. J Biol Chem 280:20672–20679
93. Röhrich RC, Englert N, Troschke K, Reichenberg A, Hintz M, Seeber F, Balconi E, Aliverti A, Zanetti A, Köhler U, Pfeiffer M, Beck E, Jomaa H, Wiesner J (2005) Reconstitution of an apicoplast-localised electron transfer pathway involved in the isoprenoid biosynthesis of *Plasmodium falciparum*. FEBS Lett 579:6433–6438
94. Seemann M, Tse Sum Bui B, Wolff M, Miginiac-Maslow M, Rohmer M (2006) Isoprenoid biosynthesis in plant chloroplasts via the MEP pathway: direct thylakoid/ferredoxin-dependent photoreduction of GcpE/IspG. FEBS Lett 580:1547–1552
95. Arigoni D, Eisenreich W, Latzel C, Sagner S, Radykewicz T, Zenk MH, Bacher A (1999) Dimethylallyl pyrophosphate is not the committed precursor of isopentenyl diphosphate during terpenoid biosynthesis from 1-deoxyxylulose in higher plants. Proc Natl Acad Sci USA 96:1309–1314
96. Giner JL, Jaun B, Arigoni D (1998) Biosynthesis of isoprenoids in *Escherichia coli*: the fate of the 3-H and 4-H atoms of 1-deoxy-D-xylulose. J Chem Soc Chem Commun 1857–1858
97. Rieder C, Jaun B, Arigoni D (2000) On the early steps of cineol biosynthesis in *Eucalyptus globulus*. Helv Chim Acta 83:2504–2513
98. Hoeffler JF, Hemmerlin A, Grosdemange-Billiard C, Bach TJ, Rohmer M (2002) Isoprenoid biosynthesis in higher plants and in *Escherichia coli*: on the branching in the methylerythritol phosphate pathway and the independent synthesis of isopentenyl diphosphate and dimethylallyl diphosphate. Biochem J 366:573–582
99. Adam KP, Zapp J (1998) Biosynthesis of the isoprene units of chamomile sesquiterpenes. Phytochemistry 48:953–959

100. De-Eknamkul W, Potduang B (2003) Biosynthesis of β-sitosterol and stigmasterol in *Croton sublyratus* proceeds via a mixed origin of isoprene units. Phytochemistry 62:389–398
101. Schuhr CA, Radykewicz T, Sagner S, Latzel C, Zenk MH, Arigoni D, Bacher A, Rohdich F, Eisenreich W (2003) Quantitative assessment of crosstalk between two isoprenoid biosynthesis pathways in plants by NMR spectroscopy. Phytochemistry Rev 2:3–16
102. Nabeta K, Ishikawa T, Okuyama H (1995) Sesqui- and di-terpene biosynthesis from ^{13}C labelled acetate and mevalonate in cultured cells of *Heteroscyphus planus*. J Chem Soc [Perkin 1] 3111–3115
103. Itoh D, Karunagoda RP, Fushie T, Katoh K, Nabeta K (2000) Nonequivalent labeling of the phytyl side chain of chlorophyll *a* in callus of the hornwort *Acanthoceros punctatus*. J Nat Prod 63:1090–1093
104. Hemmerlin A, Hoeffler JF, Meyer O, Tritsch D, Kagan IA, Grosdemange-Billiard C, Rohmer M, Bach TJ (2003) Cross-talk between the cytosolic mevalonate and the plastidial methylerythritol phosphate pathways in tobacco bright yellow-2 cells. J Biol Chem 278:26666–26676
105. Piel J, Donath J, Bandemer K, Boland W (1998) Mevalonate-independent biosynthesis of terpenoid volatiles in plants: induced and constitutive emission of volatiles. Angew Chem Int Ed 37:2478–2481
106. Jux A, Gleixner G, Boland W (2001) Classification of terpenoids according to the methylerythritol phosphate or the mevalonate pathway with natural ^{12}C:^{13}C isotope ratios: dynamic allocation of resources in induced plants. Angew Chem Int Ed 40:2091–2093
107. Dudareva N, Andersson S, Orlova I, Gatto N, Reichelt M, Rhodes D, Boland W, Gershenzon J (2005) The nonmevalonate pathway supports both monoterpene and sesquiterpene in snapdragon flowers. Proc Natl Acad Sci USA 102:933–938
108. Rosa-Putra S, Disch A, Bravo JM, Rohmer M (1998) Distribution of mevalonate and glyceraldehyde phosphate/pyruvate routes to isoprenoid biosynthesis in some gram-negative bacteria and mycobacteria. FEMS Microbiol Lett 164:169–175
109. Rohmer M, Grosdemange-Billiard C, Seemann M, Tritsch D (2004) Isoprenoid biosynthesis as a novel target for antibacterial and antiparasitic drugs. Curr Opin Invest Drugs 5:154–162
110. Jomaa H, Wiesner J, Sanderbrand S, Altincicek B, Weidemeyer C, Hintz M, Türbachova I, Eberl M, Zeidler J, Lichtenthaler HK, Soldati D, Beck E (1999) Inhibitors of the nonmevalonate pathway of isoprenoid biosynthesis as antimalarial drugs. Science 285:1573–1576
111. Singh N, Chevé G, Avery MA, McCurdy CR (2007) Targeting the methylerythritol phosphate (MEP) pathway for novel antimalarial, antibacterial and herbicidal drug discovery: inhibition of 1-deoxy-D-xylulose-5-phosphate reductoisomerase (DXR) enzyme. Curr Pharm Des 13:1161–1177
112. Kuemmerle HP, Murakawa T, Sakamoto H, Sato N, Konishi T, De Santis F (1985) Fosmidomycin, a new phosphonic acid antbiotic Part II 1. Human pharmacokinetics 2. Preliminary early phase II a clinical studies. Int J Clin Pharmacol Ther Toxicol 23:521–528
113. Kuzuyama T, Shimizu T, Takahashi S, Seto H (1998) Fosmidomycin, a specific inhibitor of 1-deoxy-D-xylulose-5-phosphate reductoisomerase in the nonmevalonate pathway for terpenoid biosynthesis. Tetrahedron Lett 39:7913–7916
114. Shigi Y (1989) Inhibition of bacterial isoprenoid synthesis by fosmidomycin, a phosphonic acid-containing antibiotic. J Antimicrob Chemother 24:131–145
115. Lell B, Ruangweerayut R, Wiesner J, Anoumou Missinou M, Schindler A, Baranek T, Hintz M, Hutchinson D, Jomaa H, Kremsner PG (2003) Fosmidomycin, a novel chemotherapeutic for malaria. Antimicrob Agents Chemother 47:735–738
116. Oyakhirome S, Issifou S, Pongratz P, Barondi F, Ramharter M, Kun J, Lell B, Kremsner P (2007) Fosmidomycin–clindamycin versus sulfadoxine-pyrimethamine in the treatment of *Plasmodium falciparum* malaria: a randomized controlled trial. Antimicrob Agents Chemother 51:1869–1871
117. Rohmer M (2008) Non-programmed research: discovery of the mevalonate-independent methylerythritol phosphate pathway for the formation of isoprene units in bacteria and plants. Inform 19:482–485

aspects of the factors that control hormone production are unknown. For example, steroid hormone biosynthesis is a step-wise process that requires several enzymes that are compartmentalized in mitochondria and the endoplasmic reticulum (ER) (Fig. 1). However, the molecular mechanisms underlying inter-organelle substrate delivery are largely unexplored. Research carried out over the past several decades have provided evidence for a key role of the cytoskeleton in mediating steroidogenesis. The goal of this review is to provide a brief summary of studies investigating the role of components of the cytoskeleton in controlling steroidogenic capacity.

The Cytoskeleton

The cytoskeleton plays a key role in varied cellular processes, including motility and migration, organelle and vesicular transport, cell–cell communication and gap junction formation, mitosis and meiosis, and maintenance of cellular morphology. In eukaryotic cells there are three major cytoskeleton components: microfilaments, intermediate filaments, and microtubules. Microfilaments are comprised of polymerized actin and are integral in the formation of cleavage furrows during cytokinesis and in cytoplasmic streaming. Intermediate filaments are larger in diameter than microfilaments and serve to maintain cellular structural architecture and spatial distribution of organelles. Intermediate filaments are comprised of lamins (form the nuclear envelope), keratin, and vimentins. Microtubules are formed when tubulin polymerizes and the dynamic assembly and disassembly of these fibers is largely regulated by the hydrolysis of GTP. Consistent with the role of GTP in microtubule function, these polymers are typically associated with motor proteins such as kinesin and dynein. Microtubules play a well-established role in the formation of cilia and flagella and are gaining much attention for their role in the intracellular transport of vesicles and organelles, particularly mitochondria in neurons.

Due to the multifaceted roles of cytoskeletal proteins in general cellular processes, it is not difficult to ascribe functions for these proteins in the biosynthesis of steroid hormones in the adrenal cortex and gonads. In fact, four decades ago observations made on Y1 mouse adrenal cells that underwent morphological changes in response to adrenocorticotropin (ACTH) provided clues into the role of the cytoskeleton architecture in controlling the response of steroidogenic cells to trophic hormone stimulation [3, 4]. These marked changes in steroidogenic cell morphology have been confirmed by several researchers [5–7] and have been subsequently attributed to cAMP-dependent rapid dephosphorylation of the focal adhesion protein paxillin [8, 9].

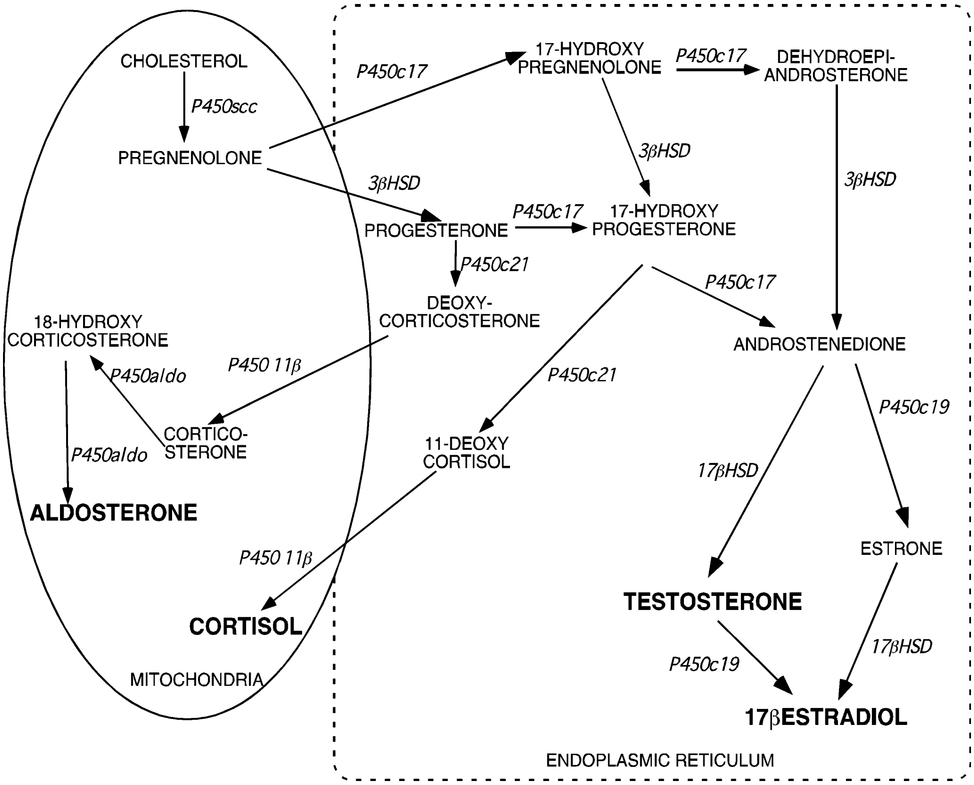
CHOLESTEROL
P450scc
PREGNENOLONE
P450c17
17-HYDROXY PREGNENOLONE
P450c17
DEHYDROEPI-ANDROSTERONE
3βHSD
3βHSD
3βHSD
PROGESTERONE
P450c17
17-HYDROXY PROGESTERONE
P450c21
DEOXY-CORTICOSTERONE
P450c17
ANDROSTENEDIONE
18-HYDROXY CORTICOSTERONE
P450aldo
P450 11β
CORTICO-STERONE
P450aldo
ALDOSTERONE
P450c21
11-DEOXY CORTISOL
P450c19
17βHSD
ESTRONE
P450 11β
CORTISOL
TESTOSTERONE
P450c19
17βHSD
17βESTRADIOL
MITOCHONDRIA
ENDOPLASMIC RETICULUM

Fig. 1 Steroidogenic biosynthetic pathways

Cholesterol Trafficking

The first and rate-limiting step in steroid hormone biosynthesis is the delivery of the substrate cholesterol to the inner mitochondrial membrane, the site of the first enzymatic reaction. Efficient delivery of cholesterol requires the coordination of several steps. First, two receptors, low-density lipoprotein receptor (LDLR) and scavenger receptor BI (SR-BI), import lipoprotein particles containing esterified cholesterol molecules into steroidogenic cells. In humans, the primary source of cholesterol for steroid hormone production is LDL, which is imported via LDLR. However, SR-BI has been shown to be a major provider of cholesterol for hormone biosynthesis, particularly in the rodent [10, 11]. Unlike lipoproteins imported by SR-BI, both LDL and LDLR are internalized and transported to lysosomes for processing.

Studies carried out by Crivello and Jefcoate three decades ago indicated a role for cytoskeletal proteins in adrenocortical steroidogenesis [12]. Various chemical inhibitors of microfilament and microtubule formation have been shown to inhibit corticosterone biosynthesis in rat adrenal glands [12]. Notably, these studies also found that inhibitors of microtubule and microfilament polymerization decreased the delivery of cholesterol to P450 side chain cleavage enzyme (P450scc), suggesting that cytoskeleton proteins regulate steroidogenesis by facilitating the trafficking of substrate to mitochondria. A role for microtubules in steroidogenesis was also shown by Rajan and Menon where lipoprotein-stimulated progesterone synthesis was found to be inhibited by the tubulin polymerization inhibitors colchicine and nocodazole [13]. Significantly, the authors demonstrated that microtubule polymerization inhibitors decreased the degradation of radiolabeled LDL and high density lipoprotein (HDL) in cultured rat luteal cells. The role of the cytoskeleton in facilitating the uptake of HDL for steroidogenesis was also demonstrated in studies using cytochalasin B, an inhibitor of actin polymerization [14] and also in experiments using the endonuclease DNase I [15].

In a series of elegant experiments employing laser scanning coherent anti-Stokes Raman scattering (CARS) microscopy it was recently shown that lipid droplets move along microtubule tracts in Y1 mouse adrenal cells [16]. Interestingly, when CARS and two-photon fluorescence microscopy were simultaneously used to image lipid droplets and mitochondria, the investigators found that the mitochondria interacted with lipid droplets that were highly motile. In contrast to these studies establishing a role for microtubules in cholesterol transport in steroidogenic cells, it has also been found that while colchicine disrupts both lipid droplet capsules and microtubules, it stimulates corticosterone biosynthesis in rat adrenocortical cells [17]. Colchicine has also been found to stimulate corticosterone secretion from wild type Y1 protein kinase A (PKA) deficient kin-8 mouse adrenal cell lines [18], suggesting that preventing microtubule polymerization promotes steroidogenesis in a cAMP/PKA-independent manner. These studies also showed that taxol, an agent that stabilizes microtubules, inhibits ACTH- and colchicine-stimulated corticosterone biosynthesis [18].

A role for actin polymerization into microfilaments has also been demonstrated in Y1 murine adrenal cells. Treatment of Y1 cells with acrylamide to disrupt microfilaments stimulates corticosterone production in a cAMP-independent manner [19]. The stimulatory effect of acrylamide on adrenal steroidogenesis was shown to be mediated at a step prior to the conversion of cholesterol to pregnenolone [19], thus implicating the cytoskeleton in assuring efficient substrate delivery.

After lipoproteins are processed, cholesterol movement out of lysosomes is facilitated by Niemann-Pick type C1 (NPC). NPC1 is localized in late endosomes along with the lipid transfer proteins MLN64 and NPC2 that travel along microtubules tracks [20, 21]. Thus, the cytoskeleton plays a key role in directing the positioning of cholesterol in steroidogenic cells. The processing of stored cholesterol esters is mediated by hormone sensitive lipase (HSL), a neutral cholesterol ester hydrolase that cleaves the ester bonds to form free cholesterol substrate [22]. While HSL trafficking has not been studied in steroidogenic cells, the lipase is rapidly translocated to the surface of lipid droplets in 3T3-L1 adipocytes upon treatment with the beta-adrenergic receptor agonist isoproteranol [23]. This translocation, however, is not dependent on microtubules and microfilaments [23]. Collectively, these studies demonstrate the pivotal role that the cytoskeleton plays in assuring efficient uptake, processing, and transport of cholesterol in steroidogenic cells.

Steroid Hormone Biosynthesis

As mentioned above, upon delivery of cholesterol to the inner mitochondrial membrane of human adrenocortical cells, this substrate is subjected to the sequential actions of several steroid hydroxylases (cytochrome P450s) and 3β-hydroxysteroid dehydrogenase (3βHSD) leading to the production of steroid hormones (Fig. 1). In the human adrenal cortex, production of these steroid hormones occurs in specific zones, where aldosterone is formed in the outermost zone (glomerulosa), cortisol in the zona fasciculata (middle zone), and adrenal androgens in the zona reticularis (inner zone). As shown in Fig. 1, three P450s are localized in mitochondria (P450scc, P450 11β, P450aldo), while P450c17, P450c21, and P450c19 are expressed in the ER, and 3βHSD expressed in both organelles.

In the first enzymatic process, P450scc (encoded by CYP11A1) catalyzes the conversion of 27-carbon cholesterol to a 21- carbon pregnenolone. Once pregnenolone is formed, it enters the ER where it can be hydroxylated on carbon-17 by P450c17 (encoded by CYP17) to form 17-hydroxy pregnenolone or converted to progesterone by 3βHSD (Fig. 1). Importantly, optimal steroid hormone production requires the movement of pregnenolone out of mitochondria and into the ER. However, the factors that regulate inter-organelle delivery of pregnenolone to the ER are largely unexplored.

In the ER P450c17 also catalyzes a 17,20 lyase reaction to form the adrenal androgens dehydroepiandrosterone (DHEA) and androstenedione. Also, both progesterone and 17-hydroxy progesterone can be hydroxylated at the 21-carbon by P450c21 to yield deoxycorticosterone and 11-deoxycortisol, respectively (Fig. 1). The final reactions in adrenocortical steroid hormone biosynthesis occur in mitochondria, where 11-deoxycortisol and deoxycorticosterone are converted to cortisol and corticosterone, respectively, by P450 11β hydroxylase (encoded by CYP11B1). As is the case for the movement of pregnenolone into the ER, regulated transport of deoxycorticosterone and 11-deoxycortisol is also required for glucocorticoid and mineralocorticoid biosynthesis. While inter-organelle trafficking of metabolites produced in the ER back to mitochondria plays a key role in the biosynthesis of glucocorticoids and mineralocorticoids, adrenal androgens only depend on the movement of pregnenolone out of mitochondria and to ER. In the human adrenal cortex, expression of P450aldo (encoded by CYP11B2) in the zona glomerulosa allows for the conversion of corticosterone to aldosterone in a series of hydroxylation steps. In the gonads, all reactions except the initial conversion of cholesterol to pregnenolone, which takes place in the inner mitochondrial membrane, occur in the ER (Fig. 1).

Regulation of Steroid Hormone Production by the Cytoskeleton

The relationship between steroidogenesis and the cytoskeleton has been studied in several laboratories that have used microtubule depolymerization agents to demonstrate that steroid hormone production is impaired [13, 18, 24–28]. Immunostaining of microtubules in sheep follicles has revealed decreases in the amount of polymerized tubulin prior to ovulation followed by subsequent increases in microtubule formation as progesterone biosynthesis increases [29]. Moreover, colchicine prevents increased progesterone production in these follicular cells [29], providing support for the importance of dynamic changes in microtubule structure in response to changing demands for steroid hormone production. In contrast to the inhibitory effect of colchicine on progesterone production in sheep [29], this microtubule polymerization inhibitor has been shown to stimulate progesterone biosynthesis in porcine luteal cells [30]. Stabilization of microtubules in porcine granulosa cells using taxol suppresses both basal and human choriogonadotropin-stimulated progesterone and 17β-estradiol [31].

In human adrenocortical slices, preventing microtubule polymerization has been shown to reduce ACTH-stimulated cortisol biosynthesis [32]. However, Benis and Mattson have also found that stabilizing microtubules inhibits ACTH-stimulated steroidogenesis in cultured murine adrenocortical cells [27, 28]. While collectively the studies described have demonstrated an integral role for cytoskeletal proteins in controlling hormone biosynthesis, the use of chemical inhibitors to manipulate cytoskeletal protein polymer formation has resulted in conflicting results being found with regard to the specific role of these proteins. Although it is likely that many of these inconsistencies can be attributed to species and cell specific differences, further investigation is needed to resolve these conflicting findings. Additionally, more detailed interrogation of each of the steps involved in steroidogenesis is warranted to determine if the cytoskeleton also regulates processes in hormone production that occur after cholesterol uptake and transport.

Regulation of Organelle Positioning by the Cytoskeleton

As discussed earlier, components of the cytoskeleton function in a wide variety of cellular processes. Extensive research has provided compelling evidence for the critical roles of microtubules and microfilaments in cholesterol transport and steroid hormone secretion [33, 34], however, less is known about the role of cytoskeletal proteins in the transport of substrates (pregnenolone, deoxycorticosterone, and 11-deoxycortisol) between mitochondria and the ER or increasing the proximity of mitochondria and ER.

Given the well-established role of mitochondrial transport in neurons [35–38], we sought to characterize the role of dynamic mitochondrial movements in steroidogenesis. Mitochondria have been visualized in association with microfilaments [35], microtubules [39, 40], and intermediate filaments [41, 42] in various cells types. Further, mitochondria-bound motor proteins, such as kinesins, facilitate the movement of these organelles along cytoskeletal fibers [43–47].

We postulated that components of the cytoskeleton facilitate steroidogenesis by promoting inter-organelle substrate delivery. We envisioned that agents that induce steroid hormone biosynthesis might regulate a discrete set of factors that act to promote the transport of substrates between mitochondria and the ER. To begin examining these processes, we employed time-lapsed video microscopy of H295R human adrenocortical cells. H295R cells were plated onto cover slips, labeled with MitoTracker Red, and mounted into a chamber for microscopic analysis. Cells were then treated with the bioactive lipid sphingosine-1-phosphate (S1P). S1P was used because we have previously demonstrated that S1P increases CYP17 gene expression and steroidogenesis in H295R human adrenocortical cells [48]. Several other laboratories have also shown that S1P stimulates hormone secretion from various steroidogenic cell types [49–52]. Further, S1P is a well-established inducer of cell migration [53–57] and chemotaxis [58, 59].

As shown in Fig. 2a, administration of S1P to H295R cells resulted in a 3-fold increase in the rate of mitochondrial movement. The increase in S1P-stimulated mitochondrial movement was attenuated when cells were pre-treated with colchicine, indicating that microtubule polymerization is required for S1P-dependent mitochondrial trafficking. In addition to an increase in the rate of mitochondrial trafficking, S1P also promoted cell migration (Fig. 2b).

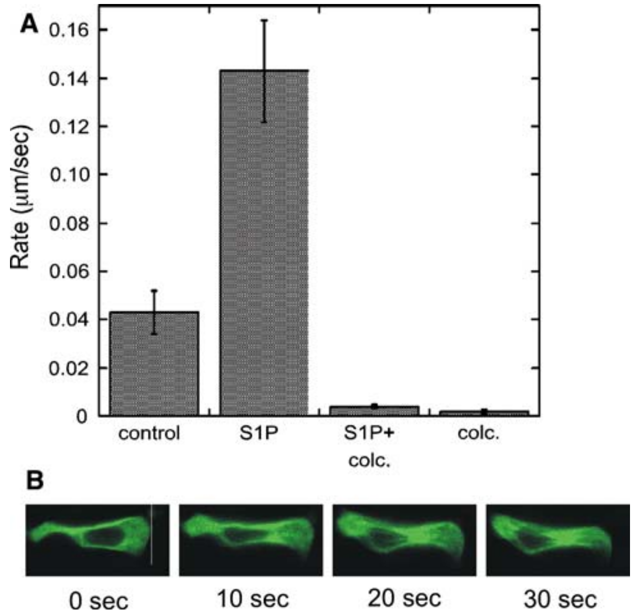

Fig. 2 S1P stimulates mitochondrial movement and cell migration. **a** H295R cells were cultured on cover slips, incubated with MitoTracker Red (Invitrogen), and then placed in a chamber for time lapsed video microscopy. Cells were treated with S1P (1 μM) and/or 1 μM colchicine (colc.) and data was collected for 1 h using an LSM510 confocal microscope system (Carl Zeiss Inc., Thornwood, NY) equipped with a krypton-equipped with a helium-neon Coherent laser with an excitation wavelength of 543 nm MitoTracker Red. Emissions were collected with a C-apochromast 40 1.3 NA oil immersion objective (Zeiss) using a 560-nm long pass filter. **b** Cells expressing GFP-labeled tubulin were monitored by time lapsed video microscopy. Shown are frames during time course after exposure to 1 μM S1P

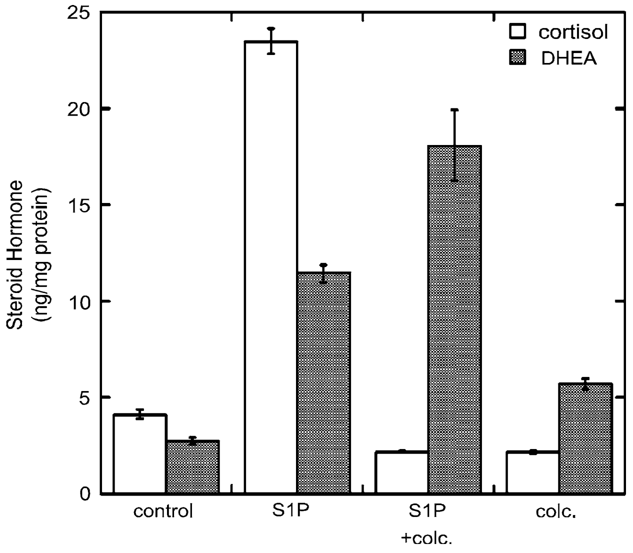

Fig. 3 Colchicine alters the ratio of cortisol and DHEA secreted in response to S1P. Media was collected from cells treated with S1P (1 μM) and/or colc. (1 μM) and cortisol and DHEA released determined in triplicate against standards made up in DME/F12 medium using a 96-well plate enzyme-linked immune assay (Diagnostic Systems Corporation, Houston, TX). Results are expressed as nanomoles per milligram cellular protein

We also determined the effect of S1P and colchicine on the secretion of cortisol and DHEA into the cell culture media. S1P increased the amounts of cortisol and DHEA produced by the H295R cells while colchicine prevented this increase (Fig. 3). Interestingly, colchicine did not decrease the amount of DHEA secreted into the media, suggesting that the increase in the rate of mitochondrial trafficking evoked by S1P is dependent on microtubule polymerization and required for S1P-induced cortisol secretion. Studies are underway to determine the effect of ACTH and other agents known to stimulate adrenocortical steroidogenesis on the positioning of mitochondria in adrenal cells. Ongoing experiments are also aimed at defining the precise molecular mechanism by which S1P (and other inducers of steroidogenesis) promote mitochondrial trafficking and at identifying the factors involved in controlling the microtubule-dependent mitochondrial movement.

Conclusions and Future Directions

Significant advances have been made in understanding the complex and multi-faceted mechanisms used to control steroid hormone biosynthesis. Further, the use of chemical agents that perturb the polymerization of cytoskeletal proteins has shed light on a key role for microfilaments and microtubules in regulating the uptake and transport of cholesterol in steroidogenic cells. Our data presented herein describing that S1P induces rapid increases in the trafficking of mitochondria in a manner that is dependent on microtubules suggests that the cytoskeleton is also involved in steroid hormone production at steps subsequent to cholesterol delivery to mitochondria. It is tempting to speculate that the increased rate of mitochondrial movement in response to S1P promotes cortisol biosynthesis by bringing mitochondria in close proximity to the ER, thereby maximizing the delivery of 11-deoxycortisol to mitochondria for the final step of steroidogenesis. However, further studies are required to elucidate the precise role of mitochondrial trafficking in steroidogenesis. Additionally, it is equally likely that a macromolecular complex containing an unidentified 11-deoxycortisol binding transport protein may mediate this response. The use of approaches such as RNA interference, mass spectrometry, and time-lapsed video microscopy are likely to provide insight into the precise molecular parameters that underlie the role cytoskeletal proteins play in steroid hormone biosynthesis.

Acknowledgments This work is supported by the National Institutes of Health/National Institute of General Medical Sciences (GM073241) and by a CAREER award from the National Science Foundation (MCB0347682).

References

1. Sewer MB, Dammer EB, Jagarlapudi S (2007) Transcriptional regulation of adrenocortical steroidogenic gene expression. Drug Metab Rev 39:371–388
2. Sewer MB, Waterman MR (2003) ACTH modulation of transcription factors responsible for steroid hydroxylase gene expression in the adrenal cortex. Microsc Res Tech 61:300–307
3. Yasumura Y, Buonassisi V, Sato G (1966) Clonal analysis of differentiated function in animal cell cultures. I. Possible correlated maintenance of differentiated function and the diploid karyotype. Cancer Res 26:529–535
4. Yasumura Y (1968) Retention of differentiated function in clonal animal cell lines, particularly hormone-secreting cultures. Am Zool 8:285–305
5. Cuprak LJ, Lammi CJ, Bayer RC (1977) Scanning electron microscopy of induced cell rounding of mouse adrenal cortex tumor cells in culture. Tissue Cell 9:667–680
6. Mattson P, Kowal J (1978) The ultrastructure of functional mouse adrenal cortical tumor cells in vitro. Differentiation 11:75–88
7. Voorhees H, Aschenbrenner J, Carnes J, Mrotek J (1984) Rounding and steroidogenesis of enzyme- and ACTH-treated Y-1 mouse adrenal tumor cells. Cell Biol Int Rep 8:483–497
8. Han JD, Rubin CS (1996) Regulation of cytoskeleton organization and paxillin dephosphorylation by cAMP. J Biol Chem 271:29211–29215
9. Whitehouse BJ, Gyles SL, Squires PE, Sayed SB, Burns CJ, Persaud SJ, Jones PM (2002) Interdependence of steroidogenesis and shape changes in Y1 adrenocortical cells: studies with inhibitors of phosphoprotein phosphatases. J Endocrinol 172: 583–593
10. Connelly MA, Williams DL (2004) SR-BI and HDL cholesteryl ester metabolism. Endocr Res 30:697–703
11. Azhar S, Leers-Sucheta S, Reaven E (2003) Cholesterol uptake in adrenal and gonadal tissues: the SR-BI and “selective” pathway connection. Front Biosci 8:998–1029
12. Crivello JF, Jefcoate CR (1978) Mechanisms of corticotropin action in rat adrenal cells. I. The effects of inhibitors of protein synthesis and of microfilament formation on corticosterone synthesis. Biochem Biophys Res Commun 542:315–329
13. Rajan VP, Menon KM (1985) Involvement of microtubules in lipoprotein degradation and utilization for steroidogenesis in cultured rat luteal cells. Endocrinology 117:2408–2416
14. Cortese F, Wolff J (1978) Cytochalasin-stimulated steroidogenesis from high density lipoproteins. J Cell Biol 77:507–516
15. Osawa S, Betz G, Hall PF (1984) Role of actin in the responses of adrenal cells to ACTH and cyclic AMP: inhibition by DNase I. J Cell Biol 99:1335–1342
16. Nan X, Potma EO, Xie XS (2006) Nonperturbative chemical imaging of organelle transport in living cells with coherent anti-strokes Raman scattering microscopy. Biophysical J 91:728–735
17. Lee LJ, Chen JS, Ko TL, Wang SM (2001) Mechanism of colchicine-induced steroidogenesis in rat adrenocortical cells. J Cell Biochem 81:162–171
18. Sackett DL, Wolff J (1986) Cyclic AMP-independent stimulation of steroidogenesis in Y-1 adrenal tumor cells by antimitotic agents. Biochim Biophys Acta 888:163–170
19. Shiver TM, Sackett DL, Knipling L, Wolff J (1992) Intermediate filaments and steroidogenesis in adrenal Y-1 cells: acrylamide stimulation of steroid production. Endocrinology 131:201–207
20. Strauss JF 3rd, Liu P, Christenson LK, Watari H (2002) Sterols and intracellular vesicular trafficking: lessons from the study of NPC1. Steroids 67:947–951
21. Zhang M, Liu P, Dwyer NK, Christenson LK, Fujimoto T, Martinez F, Comly M, Hanover JA, Blanchette-Mackie EJ, Strauss JF 3rd (2002) MLN64 mediates mobilization of lysosomal cholesterol to steroidogenic mitochondria. J Biol Chem 277:33300–33310
22. Kraemer FB, Shen WJ (2002) Hormone-sensitive lipase: control of intracellular tri-(di-)acylglycerol and cholesteryl ester hydrolysis. J Lipid Res 43:1585–1594
23. Brasaemle DL, Levin DM, Adler-Wailes DC, Londos C (2000) The lipolytic stimulation of 3T3-L1 adipocytes promotes the translocation of hormone-sensitive lipase to the surfaces of lipid storage droplets. Biochim Biophys Acta 1483(2):251–262
24. Denkova R, Ivanov I, Dimitrova M (1992) Microtubules and regulation of granulosa cell steroidogenesis by porcine granulosa cell conditioned medium. Endocr Regul 26:195–199
25. Carnegie JA, Tsang BK (1987) Microtubules and the calcium-dependent regulation of rat granulosa cell steroidogenesis. Biol Reprod 36:1007–1015
26. Carnegie JA, Dardick I, Tsang BK (1987) Microtubules and the gonadotropic regulation of granulosa cell steroidogenesis. Endocrinology 120:819–828
27. Benis R, Mattson P (1989) Microtubules, organelle transport, and steroidogenesis in cultured adrenocortical tumor cells. 1. An ultrastructural analysis of cells in which basal and ACTH-induced steroidogenesis was inhibited by taxol. Tissue Cell 21:479–494
28. Benis R, Mattson P (1989) Microtubules, organelle transport, and steroidogenesis in cultured adrenocortical tumor cells. 2. Reversibility of taxol’s inhibition of basal and ACTH-induced steroidogenesis is unaccompanied by reversibility of taxol-induced changes in cell ultrastructure. Tissue Cell 21:687–698
29. Murdoch WJ (1996) Microtubular dynamics in granulosa cells of periovulatory follicles and granulosa-derived (large) lutein cells

of sheep: relationships to the steroidogenic folliculo-luteal shift and functional luteolysis. Biol Reprod 54:1135–1140

30. Gregoraszczuk EL, Stlomczynska M (1996) The cytoskeleton proteins and LH-regulated steroidogenesis of porcine luteal cells. Folia Histochem Cytobiol 34:35–39
31. Chen TT, Massey PJ, Caudle MR (1994) The inhibitory action of taxol on granulosa cell steroidogenesis is reversible. Endocrinology 134:2178–2183
32. Feuilloley M, Contesse V, Lefebvre H, Delarue C, Vaudry H (1994) Effects of selective disruption of cytoskeletal elements on steroid secretion by human adrenocortical slices. Am J Physiol 266:E202–E210
33. De Loof A, Vanden J, Janssen I (1996) Hormones and the cytoskeleton of animals and plants. Int Rev Cytol 166:1–58
34. Hall PF, Almahbobi G (1997) Roles of microfilaments and intermediate filaments in adrenal steroidogenesis. Microsc Res Tech 36:463–479
35. Morris RL, Hollenbeck PJ (1995) Axonal transport of mitochondria along microtubules and F-actin in living vertebrate neurons. J Cell Biol 131:1315–1326
36. Morris RL, Hollenbeck PJ (1993) The regulation of bidirectional mitochondrial transport is coordinated with axonal outgrowth. J Cell Sci 104:917–927
37. Davis AF, Clayton DA (1996) In situ localization of mitochondrial DNA replication in intact mammalian cells. J Cell Biol 135:883–893
38. Chada SR, Hollenbeck PJ (2004) Nerve growth factor signaling regulates motility and docking of axonal mitochondria. Curr Biol 14:1272–1276
39. Ball EH, Singer SJ (1982) Mitochondria are associated with microtubules and not with intermediate filaments in cultured fibroblasts. Proc Natl Acad Sci 79:123–126
40. Yi M, Weaver D, Hajnoczky G (2004) Control of mitochondrial motility and distribution by the calcium signal: a homeostatic circuit. J Cell Biol 167:661–672
41. Summerhayes IC, Wong D, Chen LB (1983) Effect of microtubules and intermediate filaments on mitochondrial distribution. J Cell Sci 61:87–105
42. Stromer MH, Bendayan M (1990) Immunocytochemical identification of cytoskeletal linkages to smooth muscle cell nuclei and mitochondria. Cell Motil Cytoskeleton 17:11–18
43. Tanaka Y, Kanai Y, Okada Y, Nonaka S, Takeda S, Harada A, Hirokawa N (1998) Targeted disruption of mouse conventional kinesin heavy chain, kif5B, results in abnormal perinuclear clustering of mitochondria. Cell 93:1147–1158
44. Miki H, Okada Y, Hirokawa N (2005) Analysis of the kinesin superfamily: insights into the structure and function. Trends Cell Biol 15:467–476
45. Kwok BH, Kapoor TM (2007) Microtubule flux: drivers wanted. Curr Opin Cell Biol 19:36–42
46. Hollenbeck PJ, Saxton WM (2005) The axonal transport of mitochondria. J Cell Sci 118:5411–5419
47. Gross SP (2004) Hither and yon: a review of bi-directional microtubule-based transport. Phys Biol 1:R1–R11
48. Ozbay T, Rowan A, Leon A, Patel P, Sewer MB (2006) Cyclic adenosine 5′-monophosphate-dependent sphingosine-1-phosphate biosynthesis induces human CYP17 gene transcription by activating cleavage of sterol regulatory element binding protein 1. Endocrinology 147:1427–1437
49. Rabano M, Pena A, Brizuela L, Marino A, Macarulla JM, Trueba M, Gomez-Munoz A (2003) Sphingosine-1-phosphate stimulates cortisol secretion. FEBS Lett 535:101–105
50. Cai Z, Kwintkiewicz J, Young M, Stocco D (2007) Prostaglandin E2 increases CYP19 expression in rat granulosa cells: implication of GATA-4. Mol Cell Endocrinol 263:181–189
51. Brizuela L, Rabano M, Pena A, Gangoiti P, Macarulla JM, Trueba M, Gomez-Munoz A (2006) Sphingosine-1-phosphate: a novel stimulator of aldosterone secretion. J Lipid Res 47:1238–1249
52. Brizuela L, Rabano M, Gangoiti P, Narbona N, Macarulla JM, Trueba M, Gomez-Munoz A (2007) Sphingosine-1-phosphate stimulates aldosterone secretion through a mechanism involving the PI3 K/PKB and MEK/ERK1/2 pathways. J Lipid Res 48:2264–2274
53. Goparaju SK, Jolly PS, Watterson KR, Bektas M, Alvarez S, Sarkar S, Mel L, Ishii I, Chun J, Milstien S, Spiegel S (2005) The S1P2 receptor negatively regulates platelet-derived growth factor-induced motility and proliferation. Mol Cell Biol 25:4237–4249
54. Spiegel S, Milstien S (2003) Sphingosine-1-phosphate: an enigmatic signalling lipid. Nat Rev Mol Cell Biol 4:397–407
55. Sarkar S, Maceyka M, Hait NC, Paugh SW, Sankala H, Milstien S, Spiegel S (2005) Sphingosine kinase 1 is required for migration, proliferation and survival of MCF-7 human breast cancer cells. FEBS Lett 579:5313–5317
56. Hait NC, Sarkar S, Le Stunff H, Mikami A, Maceyka M, Milstien S, Spiegel S (2005) Role of sphingosine kinase 2 in cell migration toward epidermal growth factor. J Biol Chem 280:29462–29469
57. Rosenfeldt HM, Hobson JP, Maceyka M, Olivera A, Nava VE, Milstien S, Spiegel S (2001) EDG-1 links the PDGF receptor to Src and focal adhesion kinase activation leading to lamellipodia formation and cell migration. FASEB J 15:2649–2659
58. Le Stunff H, Mikami A, Giussani P, Hobson JP, Jolly PS, Milstien S, Spiegel S (2004) Role of sphingosine-1-phosphate in epidermal growth factor-induced chemotaxis. J Biol Chem 279:34290–34297
59. Jolly PS, Bektas M, Olivera A, Gonzalez-Espinosa C, Proia RL, Rivera J, Milstien S, Spiegel S (2004) Transactivation of sphingosine-1-phosphate receptors by FcepsilonRI triggering is required for normal mast cell degranulation and chemotaxis. J Exp Med 199:959–970

sterol biosynthetic pathway exists in all eukaryotic kingdoms and is even found in some bacteria [6]. At the stage of squalene 2,3-epoxide cyclase the pathway bifurcates into two branches (Fig. 1a). The cycloartenol route is typical for photosynthetic organisms, while nonphotosynthetic progenitors and their descendants possess a lanosterol-based pathway [7]. Further conversions of sterol precursors include C14 and C4 demethylations, introduction of double bond(s) into the B ring and, in plants, fungi and protists, modification of the side chain to form cholesterol (animals), ergosterol (fungi) and a variety of 24 alkylated and olefinated products in plants and protists. Sterols stabilize the membranes, determine their fluidity and permeability and also serve as precursors for biologically active molecules essential for regulation of growth and development.

In view that humans consume cholesterol from the diet thereby downregulating sterol biosynthesis, the microbial ergosterol biosynthetic pathway can serve as a potential selective target for the treatment of human infections with ergosterol biosynthetic inhibitors such as itraconazole. The majority of currently used clinical antifungal drugs (azoles) are aimed at inhibiting the fungal sterol 14α-demethylase (CYP51). Many of them have also been proven experimentally to be effective against human infections involving protozoa [8–11]. However, due to low amino acid identity of CYP51s across these two biological kingdoms (about 22–24% in average) without direct characterization of protozoan sterol 14α-demethylases it has been difficult to predict the potential efficiency of the antifungal drugs against protozoan infections and impossible to conduct directed search for new more potent compounds.

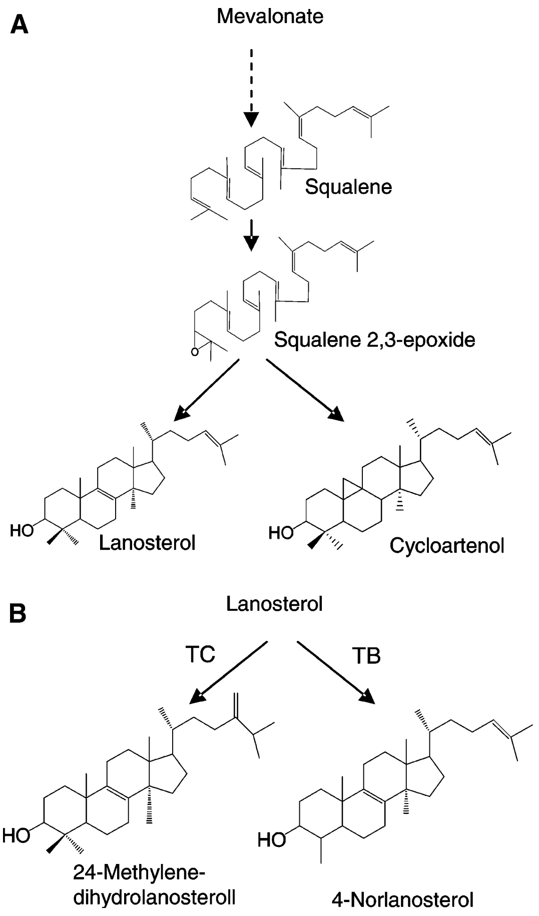

Fig. 1 Divergence in sterol biosynthesis: **a** in photosynthetic (cycloartenol) and non-photosynthetic (lanosterol) eukaryotes; **b** in *Trypanosomatidae*

Using heterologously expressed (*E. coli*) and highly purified CYP51 orthologs from *Trypanosoma cruzi* (TC) and *Trypanosoma brucei* (TB), we studied inhibition of their activity in vitro, in reconstituted enzyme reactions, followed by testing the effects of the most promising compounds on trypanosomal cells. Both of these protozoan parasites are human pathogens, the origin of endemic diseases that are deadly and so far very difficult to cure. TC is the causative agent of Chagas disease, or American trypanosomiasis; while TB species cause sleeping sickness, or African trypanosomiasis. The organisms belong to the same family of lower eukaryotes (*Trypanosomatidae*), both having complex life-cycles that include insect and mammalian stages which are significantly different between the trypanosomes. TB and TC differ in their insect vectors, preferred mammalian hosts (though both infect humans), localization in the host organism, and symptomatic manifestation. From our studies, the most interesting differences between the two trypanosomes lie in their sterol requirements. While TC produces endogenous sterols at all life stages, the TB in the mammalian (bloodstream) stage was shown to be able to use host cholesterol. Since sterols are known to play a dual role in eukaryotic organisms [12], we used TC as a model to study the effect of inhibition of the production of structural (most abundant) sterols, while TB was a model to test the possible importance of so called functional (sparking) sterols, which are synthesized at hormonal levels, and might be important for the parasite development and life cycle regulation. In both cases direct correlation between CYP51 inhibition and antiparasitic effect in trypanosomal cells has been observed.

Experimental Procedures

Expression and purification of TB, TC, human and *Candida albicans* CYP51 and use of cytochrome P450 reductase as their electron donor partner, reconstitution of enzymatic activity in vitro, and inhibition of enzymatic reaction were performed as described previously [13–15]. Inhibitory potencies of the tested compounds were compared as molar ratio inhibitor/enzyme which causes a twofold decrease in the enzyme activity (I/E_2) expressed either as a turnover number (initial rate, I/E_2, 5 min) or, for the most potent inhibitors, as percentage of substrate conversion per 1 h reaction (I/E_2, 60 min) [16]. Imidazole derivatives were from Novartis Research Institute (Vienna, Austria). Optical high throughput screening (HTS) of a 20,000 compound library of bioactive molecules (http://www.fmp-berlin.de/kries/index1.html) against TB and TC CYP51s took advantage of the P450 property to change the Soret band absorbance maximum upon ligand binding [16]. It was carried out at the Screening Unit, Leibniz Institute for Molecular Pharmacology (Berlin, Germany) and the details of screening will be described elsewhere. Web search for structural similarity to reactive molecules from the screening was done using ChemDiv data base (http://chemdiv.emolecules.com). Structure of substrate analogs, YNE and MCP, was confirmed by MS and NMR data. TB and TC cellular growth and inhibition experiments, extraction of TC cellular sterols and TLC analysis were carried out as described [16, 17]. Scanning electron microscopy of TC amastigotes grown in Brain Heart Infusion Medium +10% FBS exposed or not to CYP51 inhibitors was performed using a Hitachi 2700 scanning electron microscope [18].

Results and Discussion

TB and TC CYP51s Differ in their Substrate Preferences

Trypanosomatidae, like other non-photosynthetic eukaryotes (Fig. 1a), cyclize squalene 2,3-epoxide into lanosterol and not into cycloartenol [19, 20]. In TC, prior to the CYP51 reaction, lanosterol is converted to form 24-methylenedihydrolanosterol (Fig. 1b), suggesting that the postsqualene portion of sterol biosynthesis in this protozoa is similar to the pathway in filamentous fungi except that the major sterol products in TC are not limited to ergosterol [21]. TBCYP51, on the contrary, has strict preference toward the C4 monomethylated sterols as substrates [14]. In the reconstituted enzyme reaction in vitro the TBCYP51 turnover of obtusifoliol (the substrate of CYP51s from plants) and norlanosterol (C4-monomethylated analog of lanosterol) are more than 100-fold faster than the 14α-demethylation of lanosterol, 24-dihydrolanosterol or 24-methylenedihydrolanosterol. We have shown earlier that the differences in the substrate preferences of TB and TC CYP51 are connected with a phyla-specific residue in the B′-helix (plant-specific F105 in TB and other CYP51s from *Trypanosomatidae* as opposed to animal/fungi-like I105 in TCCYP51) [15]. The same TB-like preference for C4-mononmethylated sterol substrates have been observed for CYP51 from *Leishmania infantum* (NCBI accession number EF192938) (unpublished). Based on the catalytic properties of TB sterol methyl transferase [22], detailed analysis of TB sterols [23] and information from the literature on sterol composition of *Leishmania* species [12], 31-norlanosterol rather than obtusifoliol appear to be the natural substrate of TBCYP51 and most likely of all other CYP51s from *Trypanosomatidae* except for TC (Fig. 1b). This finding strongly suggests that *Trypanosomatidae* developed a unique postsqualene portion of the sterol biosynthetic pathway.

Functionally Irreversible Inhibitory Effect of β-Phenyl Imidazoles is Specific for Trypanosomal CYP51s

Since TB and TC CYP51 share 83% amino acid sequence identity, it is not surprising that, regardless of the differences in their substrate preferences, they both were found to be strongly inhibited by the same groups of imidazole derivatives (example structures are shown in Table 1). The strongest inhibition was observed for the β-phenyl imidazoles. Several such compounds produced a functionally irreversible effect with complete inhibition of TB and TC CYP51 activity at equimolar ratio inhibitor/enzyme [16]. At the same binding parameters ($K_d < 0.1$ μM) the inhibitory effect of the α-phenyl azoles on the initial rate of TB and TC CYP51 reaction was similarly strong ($I/E_2 < 1$), but reversible, the compounds being easily replaced by the excess of substrate upon long-term enzymatic reaction. Thus the difference in the I/E_2 values per 5 min and per 1 h for the α-phenyl azole shown in Table 1 is more than 10-fold for TCCYP51 and more than 35-fold in the case of TBCYP51. Finally, imidazoles without an aromatic group between the azole ring and the amide portion of the molecule were weakly binding ligands and weak inhibitors.

Proving the importance of detailed preliminary knowledge about target enzyme inhibition for further drug development, direct correlation between the α- and β-phenyl azole potencies as CYP51 inhibitors and their antiparasitic effects in trypanosomal cells was observed [16]. The β-phenyl azole inhibitor shown in Table 1 produces EC_{50} values (effective concentration, inhibitor concentration in growth media which causes 50% cellular growth inhibition) of 7 and 1.3 μM, respectively, in procyclic (insect stage) and bloodstream (mammalian stage) TB and $EC_{50} < 1$ μM in trypomastigotes (extracellular form) and amastigotes (intracellular form) of TC, while the EC_{50} values for the strongest α-phenyl azole inhibitor, are 16 and 14 μM in procyclic and bloodstream TB; 8 and 20 μM in trypomastigotes and amastigotes of TC. Though the effect in TB is weaker than in TC, it strongly suggests that functional sterols must be important in the bloodstream form of the parasite and that inhibitors of sterol biosynthesis should be envisaged as potential anti-sleeping

Table 1 Inhibitory effect of azoles on CYP51 from different organisms

CYP51	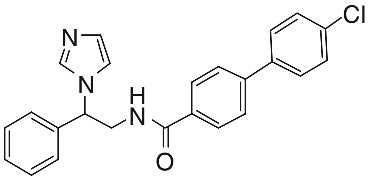 α-Phenyl (SDZ285428)		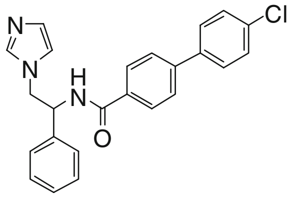 β-Phenyl (SDZ285604)	
	I/E_2[a] (5 min)	I/E_2 (60 min)	I/E_2 (5 min)	I/E_2 (60 min)
T. cruzi	<1	9	<1	<1
T. brucei	<1	35	<1	<1
H. sapiens	>100	>100	100	>100
C. albicans	>100	>100	<1	8

Numbers are averages of duplicate determinations and varied by not more than 10%

[a] Molar ratio inhibitor/enzyme which causes a twofold decrease in the activity

sickness drugs. For the comparison, published EC_{50} values in TC cells for benznidazole, one of the two drugs currently used for clinical treatment of TC infections, were reported to be within 25–50 μM [24–26]. Much lower values from our work suggest using the *β*-phenyl azoles as lead structures for anti-trypanosomal chemotherapy.

Scanning electron microscopy of the TC cells shows that treatment with 1 μM CYP51 inhibitor affects the topology of the TC plasma membrane (Fig. 2a). Ultrastructural alterations include the formation of blebs at the plasma membrane, membrane disorganization and alterations in the parasite shape. Analysis of the sterol composition of TC amastigotes treated with this azole confirmed that the parasite membranes are lacking C14-demethylated sterols (Fig. 2b; TLC of TC epimastigotes and GC–MS analysis of their cellular sterols can be found in [16]).

Interestingly, extremely potent, functionally irreversible inhibition by the *β*-phenyl imidazoles demonstrated by TB and TC CYP51 appears to be specific for trypanosomal sterol 14α-demethylases (Table 1). The effect of SDZ 285604 on the fungal CYP51 ortholog (from *C. albicans*) is still strong but reversible (I/E_2 per 60 min = 8), while the activity of human CYP51 is only slightly affected by the presence of up to 100-fold molar excess of both the α- and *β*-phenyl azoles. The data indicate that development of species-specific drugs based on the comparative analysis of the drug target enzyme inhibition in vitro is possible.

Benznidazole as CYP51 Inhibitor

Despite >40 years of its clinical use as an anti-chagasic drug, the mechanism(s) of action of benznidazole have remained elusive. It has been proposed that in trypanosomes, the drug mediates parasite killing by inducing oxidative stress [27–29] or that it works as a prodrug activated by TC nitroheterocycle reductases which reduce the nitro-group leading to covalent binding or other types of interaction between nitroreduction intermediates and various cellular

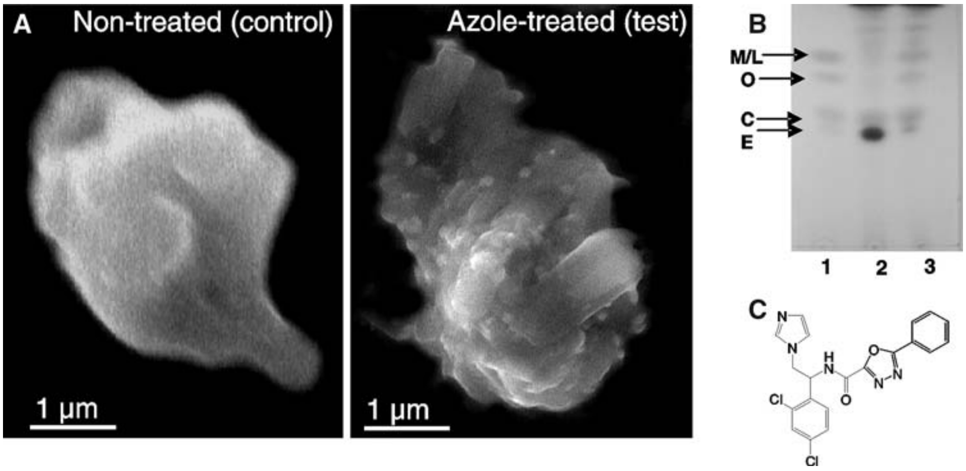

Fig. 2 Cellular effects of SDZ284692 (1 μM) on TC amastigotes. **a** Scanning electron microscopy. **b** TLC analysis of extracted sterols. Sterol standards: 24-methylenedihydrolanosterol (M), lanosterol (L), obtusifoliol (O), cholesterol (C) and ergosterol (E), 5 nmol each (lane 1). Sterols from untreated amastigotes (lane 2) and amastigotes incubated for 120 h with SDZ284692 (lane 3). **c** Structural formula of the inhibitor

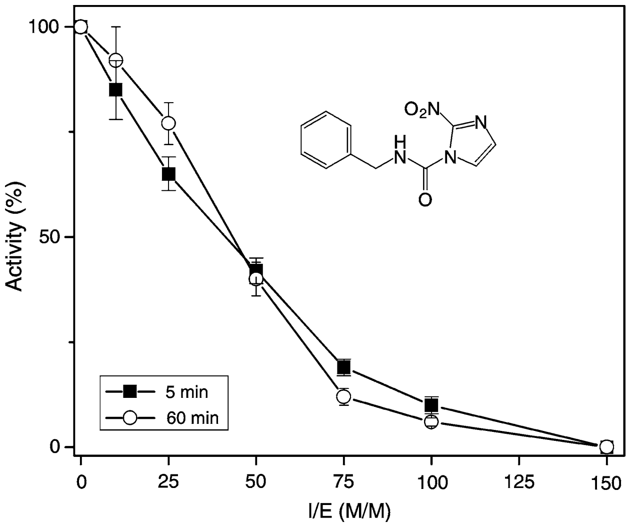

Fig. 3 Inhibitory effect of benznidazole on TCCYP51 activity. *I/E* inhibitor enzyme ratio

components, like DNA, lipids and proteins [30–32]. It has been shown experimentally that nitroaromatic compounds can be reduced by lipoamide dehydrogenase and trypanothione reductase from TC in vitro, as well as by other known electron transfer proteins including cytochrome P450 reductase [33].

Since benznidazole is an azole derivative, we tested it in our reconstituted TCCYP51 reaction to see whether the anti-chagasic activity of the drug might involve a sterol biosynthesis inhibitory component. The results show that benznidazole inhibits TCCYP51 with $I/E_2 = 42$ (5 min) and, surprisingly, $I/E_2 = 45$ (1 h) (Fig. 3). The rather high I/E_2 value for inhibition of the initial rate of the reaction is most likely due to low affinity of the binding (benznidazole does not induce spectral changes in TCCYP51 so the binding parameters can not be estimated by spectral titration). The comparable I/E_2 for the long-term inhibitory effect suggests that the drug might act as an irreversible CYP51 inhibitor, the nitro-group being reduced by cytochrome P450 reductase and then covalently bound to the P450 protein moiety. This hypothesis needs to be tested in more detail but it is not excluded that introduction of a nitro-group into the structures of some known CYP51 inhibitors might lead to the development of new, more potent drugs.

Search for CYP51 Inhibitors other than Azoles

It is known that azoles, at least those currently used as clinical and agricultural fungicides, upon long-term treatment often can cause resistance. The mechanism(s) for the resistance remain unclear, but the three most often suggested reasons are: increase in the sterol flow; mutations in the target enzyme, or accelerated azole efflux from the cells [34]. In order to investigate alternative options for the development of new sets of CYP51 targeted anti-trypanosomal drugs, optical HTS of TB and TC CYP51 for binding ligands other than azoles has been undertaken and several compounds producing type 1 (substrate-like) or type 2 (azole-like) spectral responses in the cytochrome P450 Soret band were identified [best HTS hits are shown in Table 2(A)]. The most potent inhibitor, *N*-(4-pyridyl)-formamide, compound **3**, has K_ds of 0.8 and 0.5 μM and I/E_2 (5 min) of 7 and 10 for TB and TC CYP51, respectively. It probably coordinates to the heme iron through the pyridyl nitrogen. This has been supported by results of a web-database search for structural similarity using compound **3** as template. The strongest ligands from the web search [Table 2(B)] have bulky structures attached to the *N*-(4-pyridyl)-amide moiety, suggesting influence of the configuration of the non-coordinated portion of the ligand molecule, which (similar to azole inhibitors) might enhance the inhibitory effect by forming interactions with amino acid residues in the CYP51 substrate binding cavity. Having strong but reversible inhibitory effect on TCCYP51, comparable with the effects of the α-phenyl azoles, compound **5** has potential to serve as a lead for the design of novel non-azole CYP51 inhibitors. It has been tested in TC cells and produced the EC_{50} values of 5 μM in amastigotes and 8 μM in trypomastigotes.

Substrate Analogs

The idea of using substrate analogs as inhibitors of sterol 14α-demethylase has been explored as an attempt to develop new hypocholesterolemic agents. It has been found that 7-oxo, 15-keto 15-keto, 15-oxime, 15-hydroxy, 26-oxo derivatives of lanosterol have potential to inhibit cholesterol biosynthesis in humans [35–37]. The advantages of use of substrate analogs as CYP51 inhibitors arise from their strict specificity for the target enzyme, better cellular permeability, longer lifetime in aqueous solutions in comparison to many azoles, and it is quite likely that being similar to endogenous sterols they would not cause resistance. The major problem, however, appears to be connected with very strict requirements that CYP51 enzymes have towards their substrates so that minor alterations in the structure of the sterol molecule can affect binding and inhibitory potency. Recently we have shown that two 14α-methylamino derivatives of lanosterol [4,4-dimethyl-14α-aminomethyl-cholest-7-en-3*β*-ol (AL7) and 4,4-dimethyl-14α-aminomethyl-cholest-8-en-3*β*-ol (AL8)] show inhibitory effect on CYP51 from TC and *C. albicans*, the I/E_2 values for the initial rate of TCCYP51 catalysis being 11 and 14 for AL7 and AL8, respectively [15].

In this study two other 14α-derivatized sterols, Δ7-14α-methylene cyclopropyl didydrolanosterol (MCP) and Δ7,

Table 2 Binding and inhibition of trypanosomal CYP51 activity with the HTS hits (A), web-search findings (B) and substrate analogs (C) (Numbers are averages of duplicate varied by not more than 10% determinations and varied by not more than 10%)

Inhibitor structure			TBCYP51			TCCYP51		
			K_d (μM)	I/E_2 (5 min)	I/E_2 (60 min)	K_d (μM)	I/E_2 (5 min)	I/E_2 (60 min)
A	1	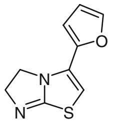	14	45	>100	9	28	>100
	2	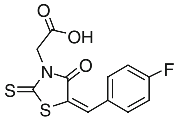	45[a]	>50	ND	38[a]	>50	ND
	3	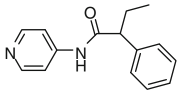	0.8	7	>100	0.5	10	>100
B	4	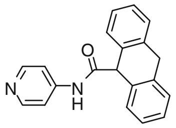	0.4	<1	40	0.8	14	65
	5	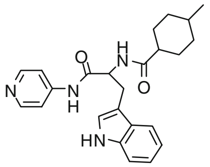	0.6	<1	25	0.2	<1	20
C	YNE	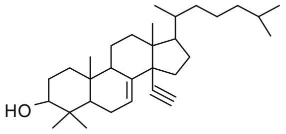	1.2	46	>100	1.3	4	25
	MCP	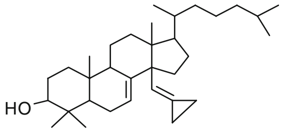	0.5	7	28	0.5	2	6

ND not determined

[a] Type 1 spectral response

14α-yne-dihydrolanosterol (YNE), were studied as potential TC and TB CYP51 inhibitors (Table 2C). Contrary to the amino-derivatized AL7 and AL8 which induce type 2 spectral responses in TCCYP51, binding of MCP and YNE cause typical type 1 spectral response (Soret band maximum 393 nm) (Fig. 4a). Titration with YNE leads to 35–40% low to high spin transition in the heme iron of TB and TC CYP51 (not shown) while upon addition of MCP the high spin content in TBCYP51 reaches 85%, the highest currently observed for a CYP51 enzyme. Under the same conditions maximal high spin content in TCCYP51 is only 41%. Since TBCYP51 does not respond spectrally to the C4-double-methylated CYP51 sterol substrates, including dihydrolanosterol [14], the fact that structures longer than the methyl group at the 14α-position (methyl-yne- and especially methyl-cyclopropyl) having such a profound influence on the binding parameters was quite unexpected. To test whether these differences in the maximum spectral response are connected with the phyla-specific residue in the trypanosomal CYP51s described above, binding of MCP to the TBCYP51-like I105F mutant of TCCYP51 [15] was tested and 87% high spin form was reached.

Despite of the amplitude of the spectral responses and the calculated apparent binding parameters, both MCP and YNE were found to inhibit TCCYP51 activity much more strongly than they inhibit TBCYP51 (Table 2C). Based on the fact that in the case of MCP the I/E_2 values for the initial rate of the reaction and long-term inhibitory effect are comparable (2 and 6, respectively), it is not excluded that MCP might act as a mechanism based inhibitor. Thus, the bulky phenyl residue in the B'-helix portion of the

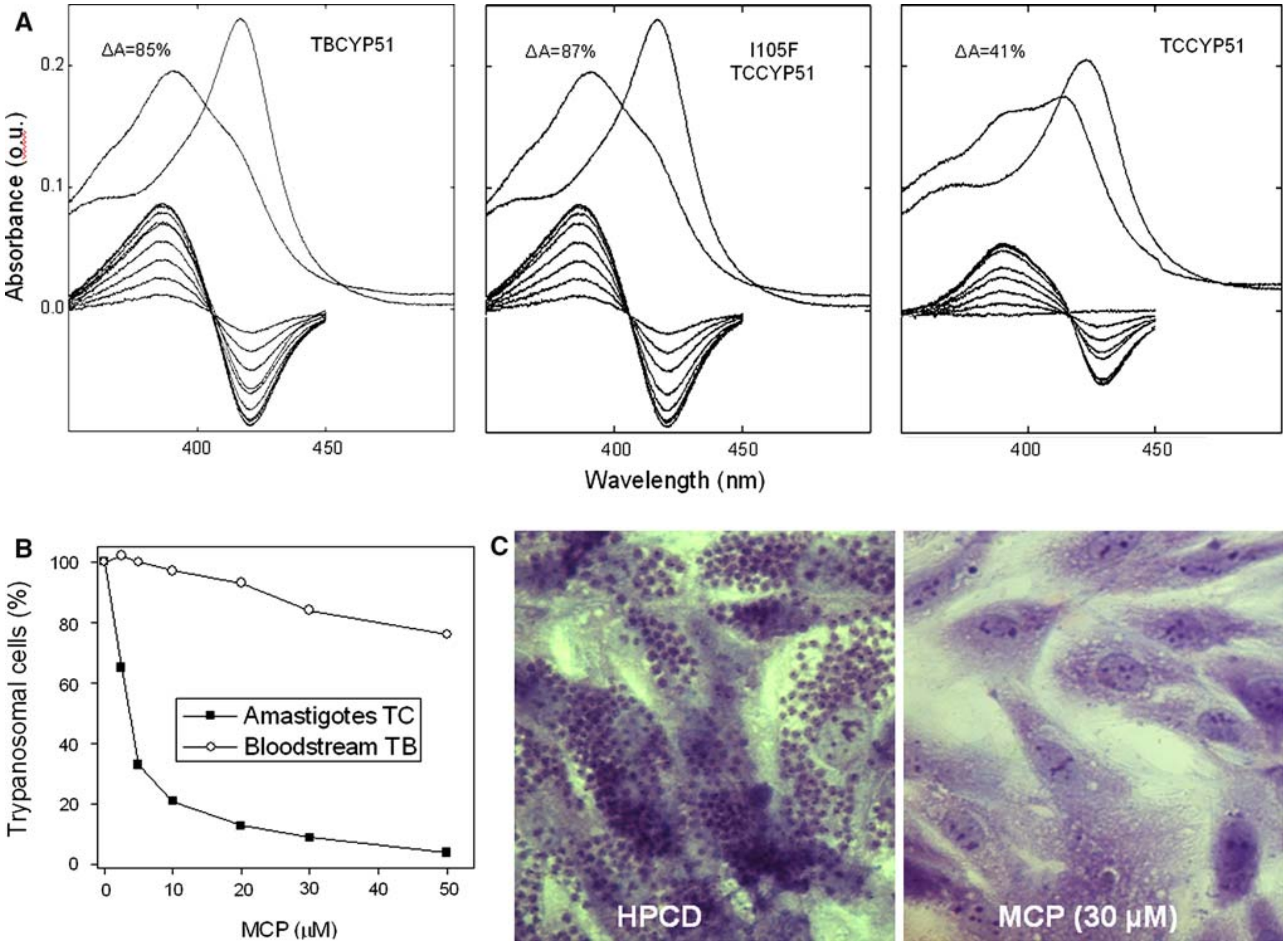

Fig. 4 MCP as a CYP51 inhibitor. **a** MCP induced type 1 spectral responses in TB and TC CYP51 and in the I105F mutant of TCCYP51. **b** Dose–response curves of trypanosomal cell growth inhibition. **c** Microscopic observation of the inhibition of TC multiplication by 30 μM MCP within cardiomyoblasts at 72 h. TC pre-treated with control HPCD (used to dissolve MCP) showed high levels of parasite multiplication, whereas cells exposed to trypanosomes pre-incubated with MCP showed dramatic decrease in the number of intracellular parasites

CYP51 substrate binding cavity promotes displacement of the water molecule from the heme iron coordination sphere upon binding of MCP or YNE. However, it does not strengthen the enzyme-ligand interaction and both C4-double-methylated inhibitors, similar to the preferred substrates, remain selective for TCCYP51. This conclusion was confirmed by the results from MCP-treated trypanosomal cells: while EC_{50} for TB was higher than 50 μM, 50% cell growth inhibition of TC was reached at 3 μM (Fig. 4b), more than 90% of the parasite cells being cleared from TC infected cardiomyoblasts upon treatment with 30 μM MCP (Fig. 4c).

Conclusions

- First, the fact that the *β*-phenyl imidazoles are strong, functionally irreversible inhibitors of trypanosomal but not fungal or human CYP51 opens an opportunity for the development of species specific CYP51 inhibitors;
- Second, introduction of additional chemically reactive functional groups (e.g. nitro group) into the structure of known CYP51 inhibitors might strengthen their potency;
- Third, optical HTS followed by web-search for structurally similar compounds is a useful method to find new CYP51 inhibitors;
- Fourth, since so far TCCYP51 is the only trypanosomal sterol 14α-demethylase with animal/fungal-like substrate preferences, C4-monomethylated substrate based inhibitors are likely to demonstrate selectivity towards CYP51 s from TB and all other *Trypanosomatidae* sequenced to date;
- We surmise that detailed knowledge of specific inhibition toward CYP51 might provide treatment for deadly human infections with protozoan parasites.

Acknowledgments This work was supported by grants from the American Heart Association (0535121 N to G.I.L), the National Institutes of Health (GM067871 to M.R.W and G.I.L., GM 081168 and AI 080580 to F.V. and GM63477 to W.D.N), and from the Robert A. Welch Foundation (D-1276 to W.D.N.).

We thank Dr. Inge Schuster (Institute of Pharmaceutical Chemistry, University Vienna, Oesterreich, Austria) and Novartis Research Institute (Vienna, Austria) for imidazole derivatives and Dr. Jens P. von Kries (Unit and Department of Medicinal Chemistry, Leibniz Institute for Molecular Pharmacology, Berlin, Germany) or HTS measurements.

References

1. Volkman JK (2005) Sterols and other triterpenoids: source specificity and evolution of biosynthetic pathways. Org Geochem 36:139–159
2. Nes WR, McKean MR (1977) Biochemistry of steroids and other isopentenoids. University Park Press, Baltimore
3. Ourisson G, Rohmer M, Poralla K (1987) Prokaryotic hopanoids and other polyterpenoid sterol surrogates. Annu Rev Microbiol 41:301–333
4. Nes WR (1974) Role of sterols in membranes. Lipids 9:596–612
5. Nes WR, Nes WD (1980) Lipids in evolution. Plenum, New York, pp 71–81
6. Lepesheva GI, Waterman MR (2007) Sterol 14alpha-demethylase cytochrome P450 (CYP51), a P450 in all biological kingdoms. Biochim Biophys Acta 1770:467–477
7. Nes WD, Norton RA, Crumley FG, Madigan SJ, Katz ER (1990) Sterol phylogenesis and algal evolution. Proc Natl Acad Sci USA 87:7565–7569
8. Docampo R, Moreno SN, Turrens JF, Katzin AM, Gonzalez-Cappa SM, Stoppani AO (1981) Biochemical and ultrastructural alterations produced by miconazole and econazole in *Trypanosoma cruzi*. Mol Biochem Parasitol 3:169–180
9. Lazardi K, Urbina JA, de Souza W (1990) Ultrastructural alterations induced by two ergosterol biosynthesis inhibitors, ketoconazole and terbinafine, on epimastigotes and amastigotes of *Trypanosoma (Schizotrypanum) cruzi*. Antimicrob Agents Chemother 34:2097–2105
10. Urbina JA (2001) Specific treatment of Chagas disease: current status and new developments. Curr Opin Infect Dis 6:733–741
11. Croft SL, Barrett MP, Urbina JA (2005) Chemotherapy of trypanosomiases and leishmaniasis. Trends Parasitol 21:508–512
12. Roberts CW, McLeod R, Rice DW, Ginger M, Chance ML, Goad LJ (2003) Fatty acid and sterol metabolism: potential antimicrobial targets in apicomplexan and trypanosomatid parasitic protozoa. Mol Biochem Parasitol 126:129–142
13. Lepesheva GI, Virus C, Waterman MR (2003) Conservation in the CYP51 family. Role of the B' helix/BC loop and helices F and G in enzymatic function. Biochemistry 42:9091–9101
14. Lepesheva GI, Nes WD, Zhou W, Hill GC, Waterman MR (2004) CYP51 from *Trypanosoma brucei* is obtusifoliol-specific. Biochemistry 43:10789–10799
15. Lepesheva GI, Zaitseva NG, Nes WD, Zhou W, Arase M, Liu J, Hill GC, Waterman MR (2006) CYP51 from *Trypanosoma cruzi*: a phyla-specific residue in the B' helix defines substrate preferences of sterol 14α-demethylase. J Biol Chem 281:3577–3585
16. Lepesheva GI, Ott RD, Hargrove TY, Kleshchenko YY, Schuster I, Nes WD, Hill GC, Villalta F, Waterman MR (2007) Sterol 14α-demethylase as a potential target for antitrypanosomal therapy: enzyme inhibition and parasite cell growth. Chem Biol 11:1283–1293
17. Villalta F, Kierszenbaum F (1982) Growth of isolated amastigotes of *Trypanosoma cruzi* in cell-free medium. J. Protozool 29:570–576
18. Madison MN, Kleshchenko YY, Nde PN, Simmons KJ, Lima MF, Villalta F (2007) Human defensin α–1 causes *Trypanosoma cruzi* membrane pore formation and induces DNA fragmentation, which leads to trypanosome destruction. Infect Immun 75:4780–4791
19. Buckner FS, Griffin JH, Wilson AJ, Van Voorhis WC (2001) Potent anti-*Trypanosoma cruzi* activities of oxidosqualene cyclase inhibitors. Antimicrob Agents Chemother 45:1210–1215
20. Joubert BM, Buckner FS, Matsuda SP (2001) Trypanosome and animal lanosterol synthases use different catalytic motifs. Org Lett 3:1957–1960
21. Lepesheva GI, Hargrove TY, Ott RD, Nes WD, Waterman MR (2006) Biodiversity of CYP51 in trypanosomes. Biochem Soc Trans 34(Pt 6):1161–1164
22. Zhou W, Lepesheva GI, Waterman MR, Nes WD (2006) Mechanistic analysis of a multiple product sterol methyltransferase implicated in ergosterol biosynthesis in *Trypanosoma brucei*. J Biol Chem 281:6290–6296
23. Zhou W, Cross GA, Nes WD (2007) Cholesterol import fails to prevent catalyst-based inhibition of ergosterol synthesis and cell proliferation of *Trypanosoma brucei*. J Lipid Res 48:665–673
24. Faundez M, Pino L, Letelier P, Ortiz C, López R, Seguel C, Ferreira J, Pavani M, Morello A, Maya JD (2005) Buthionine sulfoximine increases the toxicity of nifurtimox and benznidazole to *Trypanosoma cruzi*. Antimicrob Agents Chemother 49:126–130
25. de Castro SL, de Meirelles Mde N (1987) Effect of drugs on *Trypanosoma cruzi* and on its interaction with heart muscle cell "in vitro". Mem Inst Oswaldo Cruz 82:209–218
26. Saraiva J, Vega C, Rolon M, da Silva R, E Silva ML, Donate PM, Bastos JK, Gomez-Barrio A, de Albuquerque S (2007) In vitro and in vivo activity of lignan lactones derivatives against *Trypanosoma cruzi*. Parasitol Res 100:791–795
27. Docampo R, Mason RP, Mottley C, Muniz RP (1981) Generation of free radicals induced by nifurtimox in mammalian tissues. J Biol Chem 256:10930–10933
28. Docampo R (1990) Sensitivity of parasites to free radical damage by antiparasitic drugs. Chem Biol Interact 73:1–27
29. Viodé C, Bettache N, Cenas N, Krauth-Siegel RL, Chauvière G, Bakalara N, Périé J (1999) Enzymatic reduction studies of nitroheterocycles. Biochem Pharmacol 57:549–557
30. Revelli S, Le Page C, Piaggio E, Wietzerbin J, Bottasso O (1999) Benznidazole, a drug employed in the treatment of Chagas' disease, down-regulates the synthesis of nitrite and cytokines by murine stimulated macrophages. Clin Exp Immunol 118:271–277
31. Diaz de Toranzo EG, Castro JA, Franke de Cazzulo BM, Cazzulo JJ (1988) Interaction of benznidazole reactive metabolites with nuclear and kinetoplastic DNA, proteins and lipids from *Trypanosoma cruzi*. Experientia 44:880–881
32. Wilkinson SR, Taylor MC, Horn D, Kelly JM, Cheeseman I (2008) A mechanism for cross-resistance to nifurtimox and benznidazole in trypanosomes. Proc Natl Acad Sci USA 105:5022–5027
33. Viodé C, Bettache N, Cenas N, Krauth-Siegel RL, Chauvière G, Bakalara N, Périé J (1999) Enzymatic reduction studies of nitroheterocycles. Biochem Pharmacol 57:549–557
34. Lupetti A, Danesi R, Campa M, Del Tacca M, Kelly S (2002) Molecular basis of resistance to azole antifungals. Trends Mol Med 8:76–81
35. Aoyama Y, Yoshida Y, Sonoda Y, Sato Y (1987) 7-Oxo-24,25-dihydrolanosterol: a novel lanosterol 14 α-demethylase (P-45014DM) inhibitor which blocks electron transfer to the oxyferro intermediate. Biochim Biophys Acta 922:270–277

36. Frye LL, Leonard DA (1999) Lanosterol analogs: dual-action inhibitors of cholesterol biosynthesis. Crit Rev Biochem Mol Biol 34:123–140
37. Trzaskos JM, Ko SS, Magolda RL, Favata MF, Fischer RT, Stam SH, Johnson PR, Gaylor JL (1995) Substrate-based inhibitors of lanosterol 14α-methyl demethylase: I. Assessment of inhibitor structure-activity relationship and cholesterol biosynthesis inhibition properties. Biochemistry 34:9670–9676

sterol 27-hydroxylase that catalyzes cholesterol 27-hydroxylation in many extrahepatic tissues. In addition, CYP27A1 also metabolizes bile acid intermediates in the liver and vitamin D_3 in the kidney [3]. Partial or complete lack of CYP27A1 activity results in a disease cerebrotendinous xanthomatosis manifested by a variety of phenotypes including tendon xanthomas, bilateral cataracts, premature atherosclerosis, osteoporosis, neurological and neuropsychiatric abnormalities [4]. Unlike CYP27A1, expression of CYP11A1 is limited to steroidogenic tissues and the brain, where it catalyzes the conversion of cholesterol to pregnenolone, the first step in overall steroid hormone biosynthesis [5]. Partial or complete lack of CYP11A1 activity results in a disorder of steroidogenesis in which cholesterol accumulates within the steroidogenic tissues, and the synthesis of all adrenal and gonadal steroids is impaired [2]. Several different approaches have been used previously to study membrane topology of mitochondrial P450s [6–10]. Ou et al. treated mitochondria from the bovine adrenal cortex with trypsin and digested CYP11A1 present in these mitochondria into two fragments. Mitochondria were then washed with sodium carbonate followed by evaluation of the association of the two fragments with the membrane [6]. Usanov et al. [7] studied the interaction of the mitochondrion-associated CYP11A1 with antibodies to the whole enzyme and its fragments. We investigated CYPs 27A1 and 11A1 by combining heterologous expression in *E. coli* and site-directed mutagenesis [8, 11]. Residues in the F-G loop, a putative site of the interaction with the membrane, were mutated, the mutant P450s expressed in *E. coli* and their subcellular distribution and catalytic activities compared with those of the wild type enzyme. Simultaneously with our studies, Headlam et al. [10] investigated the F-G loop as well as several other regions in CYP11A1 by utilizing cysteine mutagenesis followed by fluorescent labeling of the mutated residues and measurements of the changes in the fluorescence upon association of the mutant P450 with phospholipid vesicles. The N- and C-terminal truncated variants of CYP11A1 were also generated. Both groups suggested that the F-G loop is the site of interaction of mitochondrial P450s with the membrane. In the present investigation we continued elucidation of the membrane topology of mitochondrial P450s. We tested whether we can identify membrane-interacting areas in mitochondrial P450s other than the F-G loop by combining the methodologies of heterologous expression and proteolytic digestion with advances in mass spectrometry. CYPs 11A1 and 27A1 were expressed in *E. coli, the E. coli* membranes isolated and treated with trypsin. Peptides remaining after extensive washes of the trypsin-treated membranes with sodium carbonate were extracted and identified by MALDI MS. The data obtained suggest that not only the F-G loop but also a part of the G helix is embedded in the membrane in mitochondrial P450s.

Experimental Procedure

Materials

Sequencing grade modified trypsin was from the Promega Corp. (Madison, WI, USA). All other chemicals were purchased from Sigma-Aldrich (St. Louis, MO, USA).

Membrane Fractionation

Recombinant human CYP27A1 and bovine CYP11A1 were expressed in *E. coli* as described [12, 13]. Cells were harvested by centrifugation at 10,000 *g* for 10 min, resuspended in 10 mM HEPES (pH 7.8) containing 10% sucrose, and treated with 0.2 mg/ml lysozyme on ice for 30 min. Spheroplasts were pelleted at 10,000 *g* for 10 min, resuspended in 10 mM HEPES (pH 7.8) containing 10% sucrose and sonicated using six 10-s pulses at 40% duty cycle (Sonifier 450, Branson Ultrasonics Corp., Dandury, CT). The suspension was then layered over a cushion of 55% sucrose topped with 10% sucrose in 10 mM HEPES (pH 7.8) and subjected to centrifugation in a Ti70 rotor at 35,000 rpm for 60 min. The total membrane fraction was recovered from the 55% sucrose interface, washed twice with 25 mM NH_4HCO_3 (pH 7.9), and placed in pre-weighed tubes.

Trypsin Treatment

The wet membrane pellet (5 mg) was resuspended in 1 ml of 25 mM NH_4HCO_3 (pH 7.9) followed by addition of 10 µg of sequencing grade modified trypsin. The suspension was sonicated as described above and left for proteolysis for 15 h at 37 °C. The sample was then subjected to 106,000 *g* centrifugation for 20 min in Optima TLX ultracentrifuge (Beckman Instruments, Inc., Fullerton, CA, USA). The pellet was collected and washed sequentially with 100 mM Na_2CO_3 (pH 11.5) containing 0.3 M NaCl (5 times) and with water (1 time). Traces of water from the wet pellet were removed by adding 0.2 ml of methanol/chloroform mixture (4/1, *v/v*) and drying the sample in a Vacufuge (Eppendorf AG, Hamburg, Germany). The dried pellet was then vortexed with 0.2 ml of chloroform, the organic phase discarded, and the membranes dried again. Extraction of peptides from the dried membranes was carried out with 100 µl of 50% acetonitrile/0.1% trifluoroacetic acid (TFA). The extracted sample was further purified using ZipTip C_{18} (Millipore Corporation, Bedford, MA, USA) according to the manufacture protocol.

Mass Spectrometry Analysis

Peptide samples after ZipTip purification were dried, dissolved in 5 mg/ml α-cyano-4-hydroxycinnamic acid in 50% acetonitrile containing 0.1% TFA, and manually spotted onto the ABI 01-192-6-AB target plate. Mass spectrometry (MS) analyses were performed using an AB4700 Proteomics Analyzer (Applied Biosystems, Framingham, MA, USA). MS-mode acquisitions consisted of 1,000 laser shots averaged from 20 sample positions. In the MS/MS-mode acquisitions, 6,000 laser shots were averaged from 60 sample positions for PSD fragments. Automated acquisition of MS and MS/MS data was controlled by 4000 Series Explorer software 3.0.

Computational Analysis

Free energy of transfer from water to bilayer interface (ΔG_{WW}) was computed using Totalizer module of MPEx (http://blanco.biomol.uci.edu/mpex) based on the Wimley-White hydrophobicity scale. A function of "no end groups" as a subsequence of a longer sequence was used for this calculation. Hydrophobic moment (μ_{H}) was also computed using the Totalizer module of MPEx.

Results

Identification of the Membrane-Interacting Peptides in CYP27A1 and CYP11A1

A representative MS spectrum of the extract derived from trypsin-treated CYP27A1-containing *E. coli* membranes is shown in Fig. 1a. Manual analysis revealed 4 peptides with *m/z* $[\mathrm{M + H}]^+$ values expected for the CYP27A1 hydrolysis with trypsin. Two of these peptides with *m/z* $[\mathrm{M + H}]^+$ values 1329.72 and 1485.81 are labeled in Fig. 1a. Signals for two other peptides with *m/z* $[\mathrm{M + H}]^+$ values 1645.78 and 1929.95 were very small and could be seen only after zooming (not shown). In the MALDI experiment, signal intensity does not linearly correlate with the concentration of analyte, therefore very small peaks were annotated as well. A summary of all the peptides identified in CYP27A1 is given in Table 1. The expected *m/z* $[\mathrm{M + H}]^+$ values were calculated using MASCOT software and rounded to two decimal places. The accuracy of mass measurement in *ppm* was calculated as a difference between the expected and observed values divided by the observed value. Without the internal calibration, the observed *m/z* $[\mathrm{M + H}]^+$ values for these peptides deviate from the expected *m/z* $[\mathrm{M + H}]^+$ values in a range of 40 ppm. Figure 1b shows the MS/MS spectrum for the peptide ion with *m/z* $[\mathrm{M + H}]^+$ value 1329.72. This spectrum has an immonium ion for Trp and various *y*- and *b*-type fragment ions that collectively confirm the correct assignment of the amino acid sequence. The MS analysis of the CYP11A1 sample revealed two CYP11A1 peptides. One of them with *m/z* $[\mathrm{M + H}]^+$ value 1675.80 is labeled in Fig. 1c. The zoomed spectrum for the second peptide with *m/z* $[\mathrm{M + H}]^+$ value 1107.59 is shown in Fig. 1d. The intensity for this peptide was very low.

Analysis of the Identified Peptides

Membrane-interacting protein sequences usually possess a unique combination of hydrophobicity and amphiphilicity. Therefore, the identified peptides were evaluated for two parameters that render peptides "membrane-seeking": free energy of transfer from water to the bilayer interface and hydrophobic moment. Free energy of transfer (ΔG_{WW}) is a measure of solubility in the non-polar phase with the positive value of ΔG_{WW} being unfavorable for partitioning the peptide sequence into the membrane interface. Hydrophobic moment (μ_{H}) detects periodicities in the hydrophobicity of amino acid sequences and is a measure of the amphiphilicity of a protein fragment [14, 15]. The ΔG_{WW} and μ_{H} values of the CYP27A1 and CYP11A1 peptides are shown in Table 1. All of the identified peptides except one, ^{238}AEKYTEIFYQDLR^{250}, have negative values of ΔG_{WW} and values of μ_{H} from 1.98 to 6.12. This is consistent with the fact that they were extracted from the membrane. The ^{238}A-R^{250} peptide has a positive ΔG_{WW} value but a high μ_{H} value which strongly increases the chances for this sequence to interact with the membrane. Trypsin cannot cleave amino acid residues embedded in the membrane. Therefore, the identified peptides contain both membrane-bound and soluble regions. If the soluble region is too long, this may affect the calculated ΔG_{WW}, and could be the case with the ^{238}A-R^{250} peptide.

In addition to the computational analysis, peptides were examined for the presence of the missed cleavage sites. One may assume that the missed cleavage sites are located either in the membrane or close to the membrane surface, and therefore resistant to proteolysis. Two peptides in CYP27A1, ^{227}W-R^{237} and ^{238}Y-K^{251}, and one peptide in CYP11A1, ^{238}A-R^{250}, contain one missed cleavage site, and one peptide in CYP11A1, ^{218}L-R^{225}, has two missed cleavage sites. Also, the CYP27A1 peptides with *m/z* $[\mathrm{M + H}]^+$ values 1329.72 and 1485.81 represent the same sequence without and with the trypsin missed cleavage site, respectively.

The position of the membrane-interacting peptides in the primary and secondary sequences of CYPs 27A1 and 11A1 is shown in Fig. 2. Peptides in CYP27A1 represent a contiguous portion of the polypeptide chain comprising the

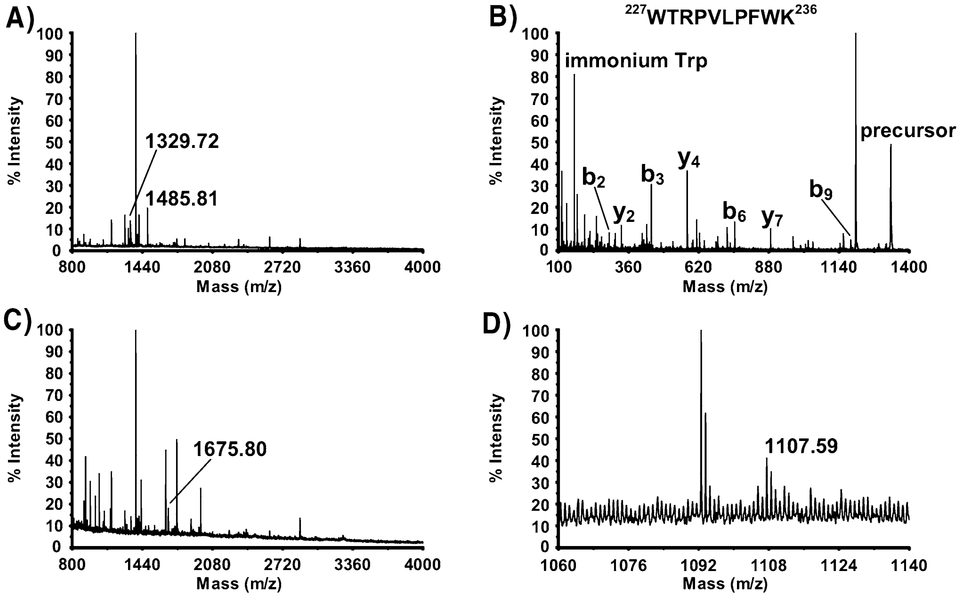

Fig. 1 Membrane-interacting peptides in CYP27A1 and CYP11A1. **a** MS spectrum of the extract from the trypsin-treated CYP27A1-containing *E. coli* membranes. Peptides with *m/z* [M + H]$^+$ values 1329.72 and 1485.81 correspond to CYP27A1, all the other peptides are of the *E. coli* origin. **b** MS/MS spectrum of the peptide ion with *m/z* [M + H]$^+$ value 1329.72 that corresponds to the ^{227}WTRPVLPFWK^{236} peptide in CYP27A1. Multiple fragment ions matching to this sequence are labeled as follows: b_2, WT; b_3, WTR; b_6, WTRPVL; b_9, WTRPVLPFW; y_2, WK; y_4, PFWK; and y_7, PVLOFWK. **c** and **d** Regular and zoomed MS spectrum of the extract from the trypsin-treated CYP11A1-containing *E. coli* membrane. Peptides with *m/z* [M + H]$^+$ value 1675.80 and 1107.59 correspond to CYP11A1

Table 1 Membrane-interacting peptides in CYPs 27A1 and 11A1

Peptide	[M + H]$^+$ expected	[M + H]$^+$ observed	Δ (ppm)	ΔG_{WW} (kcal mol^{-1})[a]	Hydrophobic moment (μ_H)[a]
CYP27A1					
^{210}SIGLMFQNALYATFLPK^{226}	1930.01	1929.95	31	−2.36	1.98
^{227}WTRPVLPFWK^{236}	1329.75	1329.72	23	−2.48	5.25
^{227}WTRPVLPFWKR^{237}	1485.85	1485.81	27	−1.67	5.59
^{238}YLDGWNAIFSFGKK^{251}	1645.84	1645.78	36	−1.97	6.12
CYP11A1					
^{218}LFRTKTWR^{225}	1107.64	1107.59	45	−0.65	1.39
^{238}AEKYTEIFYQDLR^{250}	1675.83	1675.80	18	4.08	6.11

Missed cleavage sites are underlined

[a] Free energy of transfer from water to the bilayer interface based on the Wimley-White hydrophobicity scale (ΔG_{WW}) and hydrophobic moment (μ_H) were computed using the Totalizer module of MPEx (http://blanco.biomol.uci.edu/mpex)

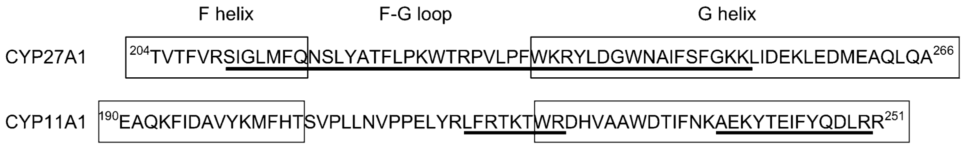
F helix
F-G loop
G helix
CYP27A1
204TVTFVRSIGLMFQNSLYATFLPKWTRPVLPFWKRYLDGWNAIFSFGKKLIDEKLEDMEAQLQA266
CYP11A1
190EAQKFIDAVYKMFHTSVPLLNVPPELYRLFRTKTWRDHVAAWDTIFNKAEKYTEIFYQDLRR251

Fig. 2 Location of the membrane-interacting peptides (*underlined*) in the primary and secondary structures of CYPs 27A1 and 11A1. Boxes indicate putative F and G helices. The secondary structure consensus prediction program (http://npsa-pbil.ibcp.fr/cgi-bin/npsa_automat.pl?page=/NPSA/npsa_seccons.html) was used to identify these structural elements

putative F-G loop and flanking portions of the F and G helixes. In CYP11A1, the ^{218}L-R^{225} peptide is located in the F-G loop and the ^{238}A-R^{250} peptide in the C-terminal portion of the G helix.

Discussion

In the current study, we used CYP27A1- and CYP11A1-containing *E. coli* membranes as a model system to study membrane topology of these mitochondrial enzymes. Previously, we developed *E. coli* expression for both proteins, showed that they stay associated with the membrane fraction when expressed in *E. coli*, and are catalytically active in the *E. coli* membranes [8, 9, 12, 13]. The membrane topology of CYPs 27A1 and 11A1 was then studied by selecting a hydrophobic region in their primary sequence, the F-G loop, and evaluating how mutations within this region affect binding to the membrane and activity of the mutant P450s [8, 9]. Weakened binding of some the mutants indicated that the F-G loop indeed interacts with the membrane. Mitochondrial P450s are suggested as having a peripheral association with the membrane [16, 17]. However, it is not currently clear whether one or several segments of the primary sequence are associated with the membrane. Headlam and colleagues began to address this question by investigating three regions in CYP11A1, the F-G loop, A' helix, and the 14 amino acid residue-segment at the C-terminus [10]. These regions were selected based on hydrophobicity profiling and secondary and tertiary structure predictions. The data obtained indicate the involvement of the F-G loop and possibly A' helix, but not the C-terminus of CYP11A1, in the interactions with the membrane. Thus, although the computational analysis provided a reasonable prediction, not all of the putative membrane-interacting regions were then validated by other methods. In the present study a principally different approach was undertaken. It includes the protease degradation of the solution-exposed portion of the membrane-associated CYPs 27A1 and 11A1 and subsequent MS analysis of the recovered membrane-bound peptides. Consistent with previous studies, peptide(s) from the F-G loop were extracted from the membrane in CYPs 27A1 and 11A1. Identification of these peptides lends support to the validity of our approach and serves as additional evidence for the role of the F-G loop. We also identified one peptide in CYP27A1 (^{238}Y-K^{251}) and one peptide in CYP11A1 (^{238}A-R^{250}) that are located outside the F-G loop, in the N- and C-terminal parts of the G helix, respectively. The N-terminal part of the G helix represents a continuation of the F-G loop. Therefore identification of the ^{238}Y-K^{251} peptide in CYP27A1 is not an unexpected finding. In fact, it provides an explanation of our previous observation that CYP27A1 is associated more tightly with the *E. coli* membrane than CYP11A1 [8]. A longer stretch of amino acid residues in the F-G loop region seem to interact with the membrane in CYP27A1 than in CYP11A1. Identification of the ^{238}A-R^{250} peptide in CYP11A1 is a more interesting finding because the C-terminal part of the G helix has never been considered as a potential membrane-binding site in CYP11A1. Further studies are required to confirm this unexpected finding. As any method, the MS-based approach has a limitation. This limitation is hidden in the procedure of analysis. Certain classes of long peptides with high hydrophobicity can escape MS analysis [18], therefore a set of identified peptides may never reach a full completeness. For example, when purified CYPs 27A1 and 11A1 are digested with trypsin in solution, we usually obtain peptides covering about 54% of the primary sequence. If each of the P450s is subjected to SDS PAGE and digested in gel, the coverage of the primary sequence by the identified peptides is ~46%. When combined, tryptic peptides from solution and in-gel digestion cover ~65% of the primary sequence. Thus, MS studies with purified CYPs 27A1 and 11A1 raise a possibility that not all of the membrane-interacting peptides in CYPs 27A1 and 11A1 were identified in the present study. Nevertheless, our approach provided a further insight into the membrane topology of CYPs 27A1 and 11A1 and is a valuable addition to the other methods in the field.

Acknowledgments This research was supported in part by the grants from the National Institutes of Health GM062882 and AG024336 (to I.A.P.). Certain commercial materials, instruments, and equipment are identified in this manuscript in order to specify the experimental procedure as completely as possible. In no case does such identification imply a recommendation or endorsement by the National Institute of Standards and Technology (NIST) nor does it imply that the materials, instruments, or equipment identified is necessarily the best available for the purpose

References

1. Omura T (2006) Mitochondrial P450s. Chem Biol Interact 163:86–93
2. Pikuleva IA (2006) Cholesterol-metabolizing cytochromes P450. Drug Metab Dispos 34:513–520
3. Pikuleva IA (2006) Cytochrome P450s and cholesterol homeostasis. Pharmacol Ther 112:761–773
4. Bjorkhem I, Boberg KM, Leitersdorf E (1995) Inborn errors in bile acid biosynthesis and storage of sterols other than cholesterol. In: Scriver AL, Beaudet AL, Sly WS, Valle D, Childs B, (eds) The metabolic and molecular bases of inherited disease. vol 2, 7th edn. McGraw-Hill, New York, 2073–2099
5. Stone D, Hechter O (1954) Studies on ACTH action in perfused bovine adrenals: site of action of ACTH in corticosteroids. Arch Biochem Biophys 51:457–469
6. Ou WJ, Ito A, Morohashi K, Fujii-Kuriyama Y, Omura T (1986) Processing-independent in vitro translocation of cytochrome P-450(SCC) precursor across mitochondrial membranes. J Biochem 100:1287–1296
7. Usanov SA, Chernogolov AA, Chashchin VL (1990) Is cytochrome P-450scc a transmembrane protein? FEBS Lett 275:33–35
8. Murtazina D, Puchkaev AV, Schein CH, Oezguen N, Braun W, Nanavati A, Pikuleva IA (2002) Membrane-protein interactions contribute to efficient 27-hydroxylation of cholesterol by mitochondrial cytochrome P450 27A1. J Biol Chem 277:37582–37589
9. Pikuleva IA (2004) Putative F-G loop is involved in association with the membrane in P450scc (P450 11A1). Mol Cell Endocrinol 215:161–164

10. Headlam MJ, Wilce MC, Tuckey RC (2003) The F-G loop region of cytochrome P450scc (CYP11A1) interacts with the phospholipid membrane. Biochim Biophys Acta 1617:96–108
11. Pikuleva IA, Puchkaev A, Bjorkhem I (2001) Putative helix F contributes to regioselectivity of hydroxylation in mitochondrial cytochrome P450 27A1. Biochemistry 40:7621–7629
12. Pikuleva IA, Mackman RL, Kagawa N, Waterman MR, Ortiz de Montellano PR (1995) Active-site topology of bovine cholesterol side-chain cleavage cytochrome P450 (P450scc) and evidence for interaction of tyrosine 94 with the side chain of cholesterol. Arch Biochem Biophys 322:189–197
13. Pikuleva IA, Bjorkhem I, Waterman MR (1997) Expression, purification, and enzymatic properties of recombinant human cytochrome P450c27 (CYP27). Arch Biochem Biophys 343:123–130
14. Eisenberg D, Weiss RM, Terwilliger TC (1982) The helical hydrophobic moment: a measure of the amphiphilicity of a helix. Nature 299:371–374
15. Eisenberg D, Weiss RM, Terwilliger TC (1984) The hydrophobic moment detects periodicity in protein hydrophobicity. Proc Natl Acad Sci USA 81:140–144
16. von Wachenfeldt C, Johnson EF (1995) Structures of eukaryotic cytochrome P450 enzymes. In: Ortiz de Montellano PR (ed) Cytochrome P450: structure, mechanism, and biochemistry. Plenum Press, New York, pp 183–244
17. Williams PA, Cosme J, Sridhar V, Johnson EF, McRee DE (2000) Mammalian microsomal cytochrome P450 monooxygenase: structural adaptations for membrane binding and functional diversity. Mol Cell 5:121–131
18. Eichacker LA, Granvogl B, Mirus O, Muller BC, Miess C, Schleiff E (2004) Hiding behind hydrophobicity. Transmembrane segments in mass spectrometry. J Biol Chem 279:50915–50922

cytochromes P450 interact with electron transfer proteins. The cytochromes P450 are divided into ten classes depending on the nature of their redox partners [3]. In general, the soluble bacterial cytochromes P450 are more stable than the membrane bound P450s and therefore easier to express and to purify.

Besides playing an important role in physiological processes, e.g. steroid and vitamin D biosynthesis, drug biotransformation and degradation of xenobiotics, cytochromes P450 are important for biotechnology [1]. In particular, steroid-converting cytochromes P450 are useful in the steroid producing industry. The complex steroid molecule structure requires complicated, multi-step schemes for the chemical synthesis of respective steroid compounds. The preparation of intermediates with protection groups and their subsequent removal is often necessary, making the chemical synthesis expensive and time consuming. Furthermore, the basic ring structure of some steroid derivatives is sensitive to cleavage by a wide variety of chemicals. Chemical synthesis also requires the use of reagents that are hazardous to the health of production staff, and constitute a serious environmental disposal problem [4]. Currently, chemical and biochemical processes are often combined in the production of steroids. Biochemical reactions in the steroid industry are usually performed by whole-cell systems to avoid the costs of enzyme isolation, purification, stabilization, and to solve the problem of the NAD(P)H co-factor regeneration [4, 5]. The corresponding biochemical processes are used to produce various steroidogenic compounds, including 11β-, 11α-, 15α- and 16α-hydroxylated products. These compounds are mainly used for the production of adrenal cortex hormones and their analogues [4, 6, 7]. They have a broad therapeutic application in contraceptives, anti-inflammatory, immunosuppressive, anabolic, and diuretic drugs.

Although biochemical processes are well established in the production process of steroids, there is still need for improvement of the product yield. Needed improvements include the hydroxylation specificity so as to have fewer by products, introduction of new hydroxylation sites into a known substrate or adaptation of the enzyme to a new substrate. The function of enzymes can be modified by replacing amino acids on positions responsible for the enzyme activity. Therefore, a basic knowledge of the structure–function relationship is required. For a predominant number of enzymes, little or nothing is known about the structure–function relationship. Directed evolution can be used to solve this problem. Herein, a number of random mutants in the whole gene or in parts of the gene are generated, and this library of mutants is screened using an appropriate test system to select a protein with the desired function. Thus, enzymes with an improved function (e.g. higher activity) or a completely new protein function can be generated.

The difficult part of the directed evolution process is creation of an efficient screening system. The screening system should allow selection of protein variants with a specific function. Development of a screening system for some selection processes is easy. Evolution of antibiotic resistance [8] or protein solubility [9] are examples of simple screening systems. In contrast, conventional detection methods for steroids, like HPLC and GC-MS, are time consuming and quite expensive. Appel et al. [10] presented a simple detection method for steroids. They used a fluorescence based test system to determine the conversion rate of 11-deoxycortisol to cortisol of a CYP11B1 expressing *Schizosaccharomyces pombe* culture. We established an adaptation of this method to micro titer plate format, and used it to measure the activity of the steroid hydroxylating CYP106A2 [11]. CYP106A2 was isolated from *Bacillus megaterium* ATCC 13368. This soluble cytochrome P450 is able to hydroxylate steroids such as progesterone, 11-deoxycortisol, and testosterone. It hydroxylates specifically 3-oxo-Δ^4-steroids, whereas 3β-hydroxy-Δ^5-steroids will not be converted. CYP106A2 hydroxylates mainly in the 15β position. Other hydroxylation positions described are 6β, 9α and 11α, when using progesterone as substrate [12, 13]. The expression yield in *Escherichia coli* is high (8.000 pmol P450/mg total protein, 13.700 nmol/l culture) [14]. Activity in vitro is achieved using the bovine adrenodoxin (Adx) and adrenodoxin reductase (AdR) as electron transfer partners [15, 16]. In a previous publication we described the co-expression of Adx and AdR together with CYP106A2 in *E. coli* to allow an in vivo activity of CYP106A2 [11]. In this paper, we demonstrate, (1) functionality of a fluorescence based test system for the directed evolution of a steroid hydroxylating enzyme, CYP106A2, (2) improvement of the activity of CYP106A2, and (3) application of the CYP106A2 model in order to understand the function of the identified randomly changed amino acid residues.

Materials and Methods

Reagents and Chemicals

11-deoxycortisol (RSS) and progesterone (P) were from Sigma Chemicals Co (St Louis, MO, USA). All other chemicals were from standard sources and of the highest purity available.

Random Mutagenesis of CYP106A2

Random mutagenesis of CYP106A2 in pACYC_FHH2_8 was performed by error-prone-PCR using the GeneMorph random mutagenesis kit (Stratagene, La Jolla, CA, USA).

An average mutation frequency of 0–3 mutations per kb was achieved according to the manufacturer's protocol. After cutting the fragment ends with *Nco*I/*Hind*III and ligation with the vector pACYC, the resulting plasmids were introduced into electrocompetent *E. coli* Top10F$'$, due to its better transforming efficiency. A 100-ml culture containing ampicillin (100 µg/ml) was inoculated, incubated 16 h at 37 °C and used for plasmid isolation.

The second mutant generation, with a mutation frequency of 0–4.5 mutations per kb, was obtained using GeneMorph II random mutagenesis kit (Stratagene). It was generated using mutant A106T/R409L as template.

Co-transformation, Co-expression and Screening for Improved activity

Co-expression of adrenodoxin, adrenodoxin reductase and CYP106A2 wild type enzyme or its mutants in *E. coli* is described in [11]. The screening procedure in micro titer plates is based on the method published previously [11].

Expression and Purification CYP106A2, CYP106A2 Mutants, and Adrenodoxin Reductase and Adrenodoxin

Expression of CYP106A2 wild type and mutants, located on pACYC_FHH2_8, was performed as described in Simgen et al. [16]. Purification was performed according to Lisurek et al. [13].

Recombinant bovine adrenodoxin reductase and a truncated form of bovine adrenodoxin (4–108) were expressed and purified according to Sagara et al. [17] and Uhlmann et al. [18].

In Vitro Catalytic Activity

Enzyme activity of CYP106A2 wild type, and mutants was measured in a reconstituted system with a final volume of 500 µl at 30 °C for 1 min in 50 mM Hepes buffer, pH 7.4 with 0.05% Tween 20. The reconstituted system contained 0.5 µM adrenodoxin reductase, 5 µM adrenodoxin (4–108), 0.25 µM CYP106A2, a NADPH-generating system (1 mM $MgCl_2$, 5 mM glucose-6-phosphate, 1U glucose-6-phosphate-dehydrogenase, and 0.1 mM NADPH), and 25–750 µM of the substrate 11-deoxycortisol. Reactions with progesterone were performed using 140 µM substrate and stopped after 1 min incubation time by addition of chloroform. Steroids were extracted twice with 500 µl chloroform, organic phases were combined and evaporated. The remnant was dissolved in methanol and subjected to HPLC analysis.

A reversed phase Waters Nova Pak Nukleosil C18 (4 µm, 3.9 × 150 mm) (Waters, Milford, MA, USA), using acetonitrile:water = 35:65 as mobile phase at a flow rate of 1 ml/min at 25 °C, was used for HPLC analysis.

The relative amounts of the products were determined using the relative peak area of the internal standard DOC, and the respective hydroxylation activity was calculated. Each reaction was performed a minimum of three times. Data were fitted by hyperbolic regression using Sigma Plot (Rockware, Golden, CO, USA).

Molecular Modeling of CYP106A2

The WebLab ViewerLite 4.2 program (Accelrys) was chosen to map substituted residues in the published model of CYP106A2 [19]. The Swiss Pdb-Viewer program [20] was used to simulate H bonds in CYP106A2 mutants.

Results

Development of a Screening System for CYP106A2 Activity

Fast and reliable assay systems are crucial for directed evolution, so we established a screening system for our purposes. We decided to use a fluorescence assay due to its high sensitivity and ease of handling. For this the previously described activity assay [10, 11] was adopted to micro titer plates and high-throughput conditions. Tests were performed to assess the general usability of the fluorescence assay for our purposes (Fig. 1). *E. coli* was co-transformed with plasmids pACYC_FHH2_8 and

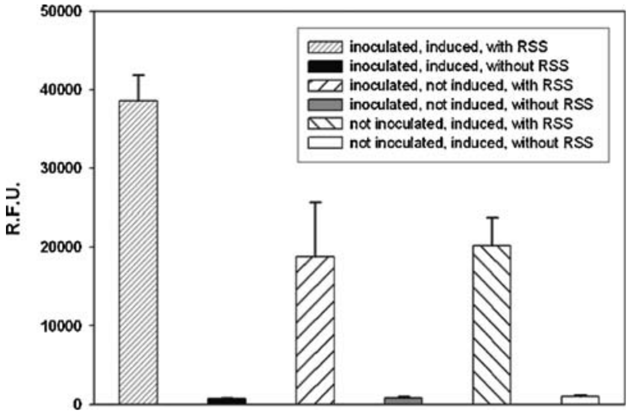

Fig. 1 To show the reliability of the fluorescence assay, some wells of a micro titer plate were inoculated with the *E. coli* culture and later the expression was induced by added IPTG. Steroid hydroxylation takes place only after expression of a functional hydroxylase system ("inoculated and induced"). The fluorescence intensity of the 11-deoxycortisol hydroxylating cultures is almost two times higher than of cultures without 11-deoxycortisol conversion (culture media in the wells are not inoculated or no expression of the hydroxylase system)

pBar_Twin allowing the co-expression of CYP106A2, AdR, and Adx. To the *E. coli* cultures in the micro titer plate, 1 mM IPTG and/or 400 μM RSS were added. The measured fluorescence of cultures containing IPTG and RSS was compared with *E. coli* cultures with induced protein expression (IPTG presence) but without RSS to estimate the background fluorescence caused by other compounds secreted by *E. coli*. Conversion of RSS in cultures with a functional hydroxylase system yielded a twofold higher fluorescence than of cultures without RSS conversion due to a non-expressed hydroxylase system (IPTG not present). Cultures with RSS conversion exhibit the highest fluorescence in this assay, whereas cultures without RSS show only minimum fluorescence (Fig. 1). The difference between unspecific and specific fluorescence is twofold, therefore the assay is sufficiently specific to be used as a reliable screening system.

For the screening, three positions on each 96-well plate were inoculated with clones expressing CYP106A2 wild type and AdR/Adx. The fluorescence intensity of these clones was used as a reference to select mutants with higher activity towards RSS or P. As shown in Fig. 2, about 25% of mutants exhibit a higher fluorescence intensity than wild type CYP106A2 in the RSS hydroxylation assays. Only 30% of the mutants display a lower fluorescence intensity than wild type CYP106A2 indicating lower or no enzyme activity. The majority of the clones display a fluorescence intensity similar to the wild type controls. For further studies clones were selected which showed a clear increase in fluorescence intensity (at least 1.5- to 2-fold) compared to the wild type control (Fig. 2). Approximately 2.100 clones of the first mutant generation were screened using the substrate RSS and about 1.900 clones using P as substrate. Six CYP106A2 clones were selected using RSS as substrate and four clones were selected using P as substrate. Sequencing revealed that three of the clones from the screening with RSS contained the same A106T/R409L replacement, the other three mutants were A106T, D153V/I214F, or D217V replacements. Two of the four clones selected with P as substrate showed the A106T/R409L double mutation. A106T and F165I replacements were detected in the two other mutants.

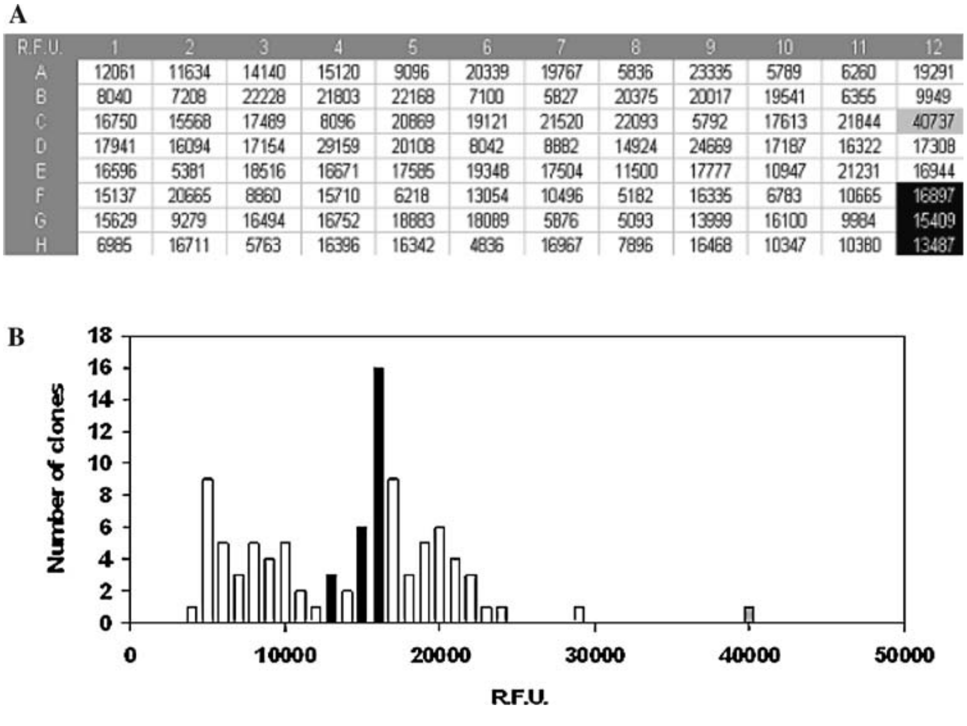

A

R.F.U.	1	2	3	4	5	6	7	8	9	10	11	12
A	12061	11634	14140	15120	9096	20339	19767	5836	23335	5789	6260	19291
B	8040	7208	22228	21803	22168	7100	5827	20375	20017	19541	6355	9949
C	16750	15568	17489	8096	20869	19121	21520	22093	5792	17613	21844	40737
D	17941	16094	17154	29159	20108	8042	8882	14924	24669	17187	16322	17308
E	16596	5381	18516	16671	17585	19348	17504	11500	17777	10947	21231	16944
F	15137	20665	8860	15710	6218	13054	10496	5182	16335	6783	10665	16897
G	15629	9279	16494	16752	18883	18089	5876	5093	13999	16100	9984	15409
H	6985	16711	5763	16396	16342	4836	16967	7896	16468	10347	10380	13487

Fig. 2 Analysis of fluorescence formation of first generation CYP106A2 mutants After 48 h incubation cultures in the micro titer plates were harvested by centrifugation. The steroids were extracted with methyl isobutyl ketone (MIBK). The MIBK phase was transferred into another micro titer plate and treated with a sulfuric acid/acetic acid mixture. The developing fluorescence was measured in a micro titer plate reader (λ_{ex} 485 nm, λ_{em} 535 nm) (RFU relative fluorescence units). **a** Example of fluorescence values of one micro titer plate after RSS conversion. Positions 12F, 12G, and 12H (*black background*) were inoculated with wild type CYP106A2 giving an average fluorescence value for wild type CYP106A2. Position 12C (*gray background*) shows a mutant with more than twofold increase in fluorescence. **b** Distribution analysis of the measured fluorescence intensities of this micro titer plate. The measured fluorescence intensities were divided into groups (e.g. RFU of 13.487, 13.054, and 13.999 were combined in the 13.000 RFU group) and plotted versus the number of clones in this group. The distribution analysis shows that approximately one-third of the clones are less active or even inactive as indicated by a lower measured fluorescence intensity and one-fourth are more active than the CYP106A2 wild type. *Black bars* indicate groups that include the RFU values of the wild type

The A106T/R409L mutant with five detections was the most common mutation found in the screening, followed by A106T with two detections. Mutant A106T/R409L, which has the highest RSS hydroxylation rate of all first generation mutants, was chosen to generate the second mutant generation. In the screening assay of the second generation, where RSS was used as substrate, again about 2.100 clones were tested. The differences between the fluorescence intensities of the control (mutant A106T/R409L), and the highest measured fluorescence intensities were lower compared to the results of the first generation screening. Seven variants with an 1.2- to 1.5-fold increased fluorescence intensity were picked. One of these seven clones showed a A106T/Q189K/T399S/R409L mutation whereas the other six clones had an identical sequence as the template (mutant A106T/R409L). Furthermore, two additional silent mutations were found in A106T/R409L, as well as in the derived quadruple mutant A106T/Q189K/T399S/R409L.

After separation of the plasmid pACYC_FHH2_8 carrying the sequence of the cytochrome P450 from Adx and AdR containing plasmid pBar_Twin, the P450 mutants were expressed in JM109 *E. coli* cells. The CYP106A2 wild type expressed with a yield of 453 nmol/l culture. The expression level of the mutants ranges from 17% (A106T) to 60% (D217V) of the wild type (Table 1). The double mutant A106T/R409L shows a slightly increased expression yield (+28 %), compared to the A106T single mutant. Purification of the proteins was done as described under "Materials and methods". Spectra of the purified proteins ranged from 250 to 700 nm for the oxidized protein, and from 400 to 500 nm for the reduced versus reduced and CO-bound state. Spectra showed the characteristic absorption of oxidized cytochromes P450 with peaks at 280, 358, 417, 534 and 568 nm. The proteins were in low spin state. The CO difference spectra showed all P450 characteristics expected with maxima at around 450 nm. The correct size of the P450 mutants was checked by SDS-PAGE. SDS-PAGE analysis show high purity of the proteins after purification (Fig. 3).

Table 1 Expression level of CYP106A2 and mutants in JM109 cells transformed with pACYC_FHH2_8 plasmid after 48 h incubation at 30 °C in TB media in the presence of 0.5 mM 5-amino levulinic acid and 1 mM IPTG

	CYP content (nmol/l culture)
CYP106A2-WT	453.0
D153V/I214F	211.0
A106T/R409L	127.4
D217V	276.0
A106T	77.7
A106T/Q189K/T399S/R409L	273.3
F165I	87.5

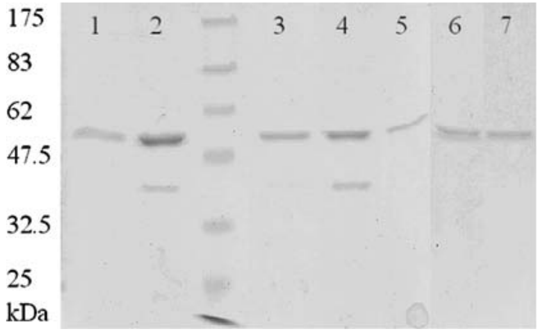

Fig. 3 SDS-PAGE analysis of purified CYP106A2 wild type and mutant proteins. Purified proteins were separated on a 10 % SDS-PAGE: *Lane 1*, D153V/I214F; *Lane 2*, A106T/R409L; *Lane 3*, D217V; *Lane 4*, A106T; *Lane 5*, CYP106A2 wild type; *Lane 6*, A106T/Q189K/T399S/R409L; *Lane 7*, F165I

Kinetic Investigation of the Mutants

The activity of the purified CYP106A2 mutants was tested with the substrates RSS and P in vitro. The test system contained 0.25 μM P450, 0.5 μM AdR, and 5 μM Adx. The apparent V_{max} and K_m values of the RSS conversion were determined. Activity of the mutants with P was calculated as the percentage of progesterone conversion after 1 min incubation time in the presence of 140 μM substrate.

The apparent K_m value of the RSS conversion for all tested mutants was lower (36.9–67.5 μM) than the K_m of the CYP106A2 wild type (93.4 μM) reflecting an improved substrate binding of the mutants (Fig. 4, Table 2). Also, the

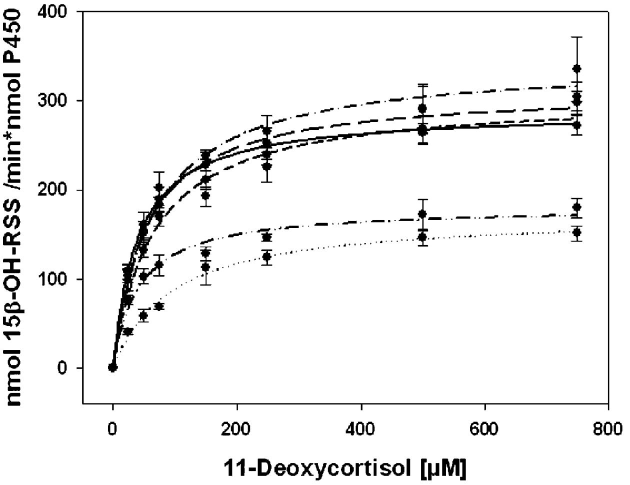

Fig. 4 Kinetics of the selected CYP106 mutants. Apparent V_{max} (nmol 15*β*-OH-RSS/min*nmol P450) (*dotted*, CYP106A2 WT; *dash-dot-dot*, D153V/I214F; *short dash*, D217V; *solid*, A106T/Q189K/T399S/R409L; *dash-dot*, A106T/R409L; *long dash*, A106T) is blotted versus 11-deoxycortisol concentration. The standard deviation was calculated from three independent experiments

Table 2 Kinetic parameters of the 11-deoxycortisol conversion of CYP106A2 wild type and mutants. (*) This CYP106A2 mutant was obtained of the second mutant generation when screened with RSS as substrate

	Apparent K_m (μM)	Apparent V_{max} (nmol 15β-OH-RSS/nmol P450/min)	Apparent k_{cat}/K_m (M^{-1} s^{-1}) × 10^3	Increase to WT
CYP106A2-WT	93.4 ± 8.8	172.1 ± 4.9	30.7 ± 3.0	1
D153V/I214F	37.3 ± 6.7	181.8 ± 7.6	81.2 ± 15.0	2.64
A106T/R409L	67.5 ± 5.4	374.1 ± 8.8	92.4 ± 7.7	3
D217V	65.9 ± 5.9	325.2 ± 8.5	82.3 ± 7.7	2.68
A106T	58.8 ± 3.6	343.4 ± 5.9	97.3 ± 6.3	3.17
A106T/Q189K/T399S/R409L*	36.9 ± 5.4	294.1 ± 9.9	132.6 ± 19.9	4.32

maximal RSS hydroxylation rate is improved as indicated by an increased apparent V_{max} value. When calculating the catalytic efficiency k_{cat}/K_m, the differences between the CYP106A2 wild type and the mutants are more dramatic. For CYP106A2 wild type, an apparent k_{cat}/K_m of 30.7 × 10^3 (M^{-1} s^{-1}) of the 15β-OH-RSS production was calculated. Mutant A106T/R409L shows a number of 92.4 × 10^3 (M^{-1} s^{-1}), a threefold increase. The activity of these mutants towards P is similar to RSS hydroxylation activity. Mutants A106T and A106T/R409L show the highest progesterone conversion after 1 min incubation time (Table 3). The second generation mutant A106T/Q189K/T399S/R409L has an apparent V_{max} of 294.1 nmol 15β-OH-RSS/nmol P450*min, which is lower than the apparent V_{max} of the double mutant A106T/R409L used as template (374.1 nmol 15β-OH-RSS/nmol P450*min), but still significantly higher than the wild type with 172.1 nmol 15β-OH-RSS/nmol P450*min. Despite the lowered V_{max} this mutant shows an increased apparent k_{cat}/K_m due to an improved K_m. Therefore, the catalytic efficiency of CYP106A2 towards RSS could be improved in two mutant generations by more than a factor of four. In addition, also the conversion of P improved in these mutants.

Table 3 Progesterone conversion of the CYP106A2 mutants compared to the wild type. The in vitro reactions were stopped after 1 min incubation time and the conversion of P was estimated by the percentage of total peak area (P and the hydroxylated progesterone products 11α-, 9α-, 6β-, and 15β-OH-progesterone) minus the peak area of the remaining P. The concentration of P was 140 μM. (*) This CYP106A2 mutant was obtained from the second mutant generation when screened with RSS as substrate. F165I was obtained exclusively in the screening with P as substrate

	Progesterone conversion after 1 min (%)	Increase to WT
CYP106A2 WT	34.8 ± 2.1	1
D153V/I214F	32.4 ± 1.5	0.93
A106T/R409L	49.9 ± 0.8	1.43
D217V	41.4 ± 1.6	1.18
A106T	50.0 ± 0.5	1.43
A106T/Q189K/T399S/R409L*	39.2 ± 0.1	1.13
F165I	43.5 ± 0.2	1.25

Discussion

CYP106A2 has application for biotechnological purposes. This enzyme is soluble, easy to express, and is one of the few known bacterial CYPs with steroid hydroxylation capability. Our intent was to improve the steroid hydroxylation activity of CYP106A2 using directed evolution. Previously, we described a method to obtain steroid conversion in CYP106A2 and redox partner protein expressing *E. coli* cells [11]. The in vivo activity of CYP106A2 in *E. coli* was obtained by co-transformation with plasmid pBar_Twin carrying adrenodoxin and adrenodoxin reductase sequence, and with plasmid pACYC_FHH2_8 carrying the CYP106A2 sequences and subsequent expression of all three proteins. The use of two plasmids allows an easier mutagenesis of CYP106A2 as well as an easier expression of selected CYP106A2 mutants for further characterization. Both plasmids, pBar_Twin and pACYC_FHH2_8, can be easily separated, and after transformation of pACYC_FHH2_8 into the *E. coli* expression host only the CYP106A2 mutants can be expressed.

This in-vivo steroid-converting recombinant *E. coli* system was used as a high-throughput screening system for our directed evolution studies. Directed evolution requires a fast screening system with high sensitivity and accuracy. Established steroid analysis methods are GC-MS, LC-MS, and immunosorbent assays [21–24]. The drawbacks of these methods are a lack of fast performance, high costs, and in the case of immunoassays, cross reactivities of the antibodies. For example, monoclonal cortisol antibodies show a cross reactivity of 19% with RSS [23]. We used a fluorescence assay based on a method described by Appel et al. [10]. Steroids exhibit fluorescence in acidic environment in which the intensity of the fluorescence depends on the numbers of hydroxyl groups [25]. This fact is also true for the steroid pair 11-deoxycortisol and cortisol [10, 11]. The results of our work show that the 11-deoxycortisol and progesterone products of CYP106A2 hydroxylation give a higher fluorescence intensity than their precursors. CYP106A2 hydroxylates mainly in the 15β position. Using progesterone as substrate, hydroxylations in 6β, 9α and 11α positions can be observed as side reactions [12, 13]. The mechanism of the fluorescence formation is not completely understood. However, steroids with keto groups, side chain on C17, and α configuration of their hydroxyl groups exhibit a stronger fluorescence in an acidic milieu than other steroids [10].

Our work shows the functionality of the assay as a sensitive, accurate and reliable screening method. After screening of the first mutant generation, six mutants with higher 11-deoxycortisol hydroxylation rate, and four mutants with higher progesterone hydroxylation rate were selected. After further testing, A106T was identified as the best mutant. In comparison to A106T/R409L with an apparent k_{cat}/K_m of $92.4 \times 10^3(M^{-1}\ s^{-1})$, A106T showed a slightly better apparent k_{cat}/K_m of the RSS hydroxylation of $97.3 \times 10^3\ (M^{-1}\ s^{-1})$ (Table 2). However, this single mutant seems to be less stable than the double mutant as indicated by a lower expression level, and by the number of selected clones carrying this single mutation. Only one clone with a A106T mutation could be selected out of six clones from the screening of the first mutant generation with 11-deoxycortisol and only one out of four in the screening with progesterone. Because of higher expression yield, mutant A106T/R409L was chosen as the template sequence to generate the second mutant generation. A106T/Q189K/T399S/R409L was selected in the screening of the second mutant generation with 11-deoxycortisol as substrate. It shows a lower apparent V_{max} value than A106T/R409L. However, due to a lower apparent K_m, this second generation mutant displays a much better apparent k_{cat}/K_m than the first generation mutant A106T/R409L (Table 2). Furthermore, A106T/Q189K/T399S/R409L can be expressed with an even higher yield of about 273 nmol/l.

In conclusion, evolution over two generations led to a 4.3-fold improved catalytic activity of CYP106A2 towards RSS. The estimated progesterone hydroxylation rate of the mutants is similar to that of the 11-deoxycortisol hydroxylation activity (Tables 2, 3). Here, mutants A106T and A106T/R409L hydroxylate the progesterone 1.4-fold faster than the wild type. A106T/R409L converts the progesterone and the 11-deoxycortisol 1.3-fold faster than A106T/Q189K/T399S/R409L. These results are expected since the structures of progesterone and 11-deoxycortisol differ only in additional hydroxyl groups on C17 and C21 of the 11-deoxycortisol.

We assume that the Q189 K and/or T399S mutations might have an influence on the flexibility of structure of the catalytically improved CYP106A2 mutants. The CYP106A2 model [19] predicts location of Q189 in the G helix (Fig. 5a). The predicted location of T399 is in the β4-1/β4-2 loop which is positioned above the heme (Fig. 5b).

The F and G helices form a flexible loop. The F/G loop is part of the substrate access channel. In several P450s, the substrate free protein shows an open conformation, and after substrate binding, the F/G loop moves towards the

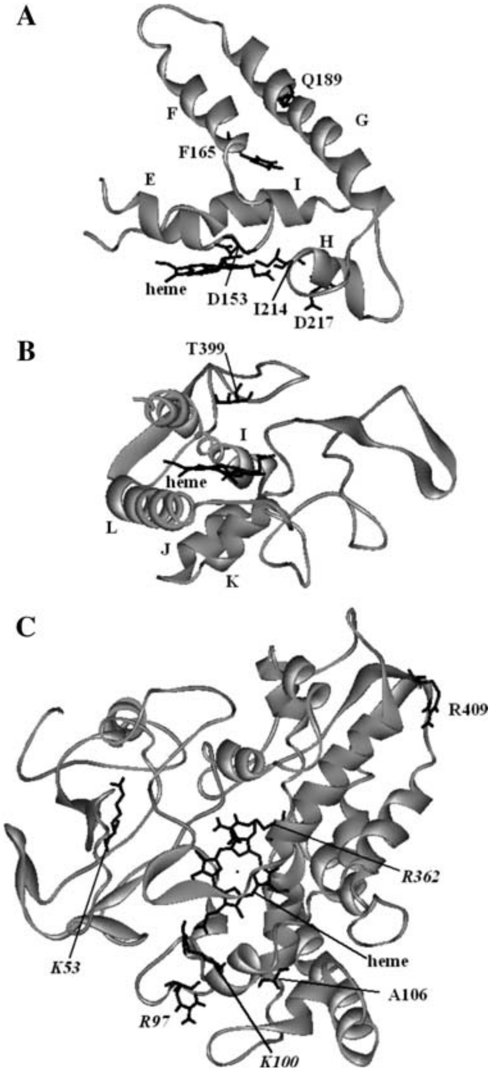

Fig. 5 Mapping of substitutions in the CYP106A2 model. The CYP106A2 model was obtained from Lisurek et al. [19]. Residues substituted in the catalytically improved CYP106A2 mutants are marked. **a** Residues D153, F165, Q189, I214, and D214 are associated to the F/G loop. D153 is located at the C terminus of the E helix, F165 in the F helix, Q189 in the G helix, I214 and D217 in the H helix. **b** Residue T399 is located in the β4-1/β4-2 loop above the heme. **c** CYP106A2 structure as seen from the proximal site. Residue A106 presumably associated with adrenodoxin interaction is mapped. *Italic letters* indicate corresponding residues of CYP101 responsible for the putidaredoxin binding. Mutation of residue R409 might cause conformational changes of the *N*-terminus of CYP106A2

I helix in order to close the access channel. This movement was observed in CYP101 [26] and in CYP119 [27]. In CYP101 movement of the H and I helices upon substrate binding was shown, too. Activating effects of mutations in this regions of CYP106A2 suggest that the F/G loop in CYP106A2 undergoes significant conformational changes upon substrate binding. With I214F and D217V, two mutated residues located in the H helix of the CYP106A2 model could be identified (Fig. 5a). Furthermore, the loop between the E and F helix could act as a "hinge". Residue D153, located in that region, might have influence on the flexibility of the F/G loop.

Comparison with the CYP101 structure suggests a function of A106 in CYP106A2 in the interaction with the redox partner adrenodoxin. Experimental evidence suggested that negatively charged amino acids on the electron donor [28–32] interact with positively charged residues at the proximal site of the cytochrome P450, which is usually centered over the cysteine-pocket of all bacterial cytochromes P450 that interact with ferredoxins [33, 34]. Three surface arginine residues on the proximal site of CYP101 are necessary for successful electron transfer from putidaredoxin [35]. These residues are R72 in the B-helix, R109 and R112 [36–38] in the C-helix. R112 could be involved in electron transfer [39]. There are corresponding positively charged residues in the CYP106A2 model, namely K53, R97 and R100. Additionally, R364 in the L-helix of CYP101 could contribute to putidaredoxin binding [40]. The corresponding position in CYP106A2 is an arginine (R362). A106 lies in close proximity to the residues R97 and R100 in or next to the C helix as shown by the CYP106A2 model (Fig. 5c). This fact and the nature of the substitution from a non polar alanine to a polar threonine imply a function of the mutant A106T in the binding of adrenodoxin. The effect of changed redox partner-cytochrome P450 binding on the activity of the P450 was previously also shown for the couple adrenodoxin/CYP11A1 [41].

Mutation R409L is most likely not involved in the interaction with adrenodoxin due to the distance from the charged residues in the proximal site (Fig 5c). R409 is connected via H bonds to H378, K377 in the 3-3 sheet, and to D131 in the β3-1 sheet. Simulations of the CYP106A2 model show that L409 builds H bonds to H378 and to F376, both are located in the β3-3 sheet (not shown). This might result in a minimal conformational change of the *N*-terminal part of CYP106A2.

In summary, increase of catalytic activity of CYP106A2 by more than a factor of four, proves the functionality of the screening system. It also demonstrates the usability of directed evolution as a tool to improve significantly the activity of this steroid hydroxylating P450. This assay system has great potential since it is easy to perform and not limited to a specific hydroxylation position, making this test applicable for other steroid hydroxylating enzymes. The assay may be modified by reducing the incubation time and/or reducing the substrate concentration, which would elevate the selection pressure towards improved K_m values.

Acknowledgments The authors thank Wolfgang Reinle for excellent purification of adrenodoxin reductase and adrenodoxin. A grant of the Fonds der Chemischen Industrie to R.B. is acknowledged.

References

1. Bernhardt R (2006) Cytochromes P450 as versatile biocatalysts. J Biotechnol 124:128–145
2. Isin EM, Guengerich FP (2007) Complex reactions catalyzed by cytochrome P450 enzymes. Biochim Biophys Acta 1770:314–329
3. Hannemann F, Bichet A, Ewen KM, Bernhardt R (2007) Cytochrome P450 systems-biological variations of electron transport chains. Biochim Biophys Acta 1770:330–344
4. Fernandes P, Cruz A, Angelova B, Pinheiro HM, Cabral JMS (2003) Microbial conversion of steroid compounds: recent developments. Enzyme Microb Technol 32:688–705
5. Chefson A, Auclair K (2006) Progress towards the easier use of P450 enzymes. Mol Biosyst 2:462–469
6. Mahato SB, Garai S (1997) Advances in microbial steroid biotransformation. Steroids 62:332–345
7. Jekkel A, Ilkóy É, Horváth G, Pallagi I, Süto J, Ambrus G (1998) Microbial hydroxylation of 13β-ethyl-4-gonene-3, 17-dione. J Mol Catal B Enzym 5:385–387
8. Orencia MC, Yoon JS, Ness JE, Stemmer WP, Stevens RC (2001) Predicting the emergence of antibiotic resistance by directed evolution and structural analysis. Nat Struct Biol 8:238–242
9. Hart DJ, Tarendeau F (2006) Combinatorial library approaches for improving soluble protein expression in *Escherichia coli*. Acta Crystallogr D Biol Crystallogr 62:19–26
10. Appel D, Schmid RD, Dragan CA, Bureik M, Urlacher VB (2005) A fluorimetric assay for cortisol. Anal Bioanal Chem 383:182–186
11. Hannemann F, Virus C, Bernhardt R (2006) Design of an *Escherichia coli* system for whole cell mediated steroid synthesis and molecular evolution of steroid hydroxylases. J. Biotechnol 124:172–181
12. Berg A, Gustafsson JA, Ingelman-Sundberg M (1976) Characterization of a cytochrome P-450-dependent steroid hydroxylase system present in *Bacillus megaterium*. J Biol Chem 251:2831–2838
13. Lisurek M, Kang MJ, Hartmann RW, Bernhardt R (2004) Identification of monohydroxy progesterones produced by CYP106A2 using comparative HPLC and electrospray ionisation collision-induced dissociation mass spectrometry. Biochem Biophys Res Commun 319:677–682
14. Virus C, Lisurek M, Simgen B, Hannemann F, Bernhardt R (2006) Function and engineering of the 15beta-hydroxylase CYP106A2. Biochem Soc Trans 34:1215–1218
15. Berg A, Ingelman-Sundberg M, Gustafsson JA (1979) Purification and characterization of cytochrome P-450meg. J Biol Chem 254:5264–5271
16. Simgen B, Contzen J, Schwarzer R, Bernhardt R, Jung C (2000) Substrate binding to 15beta-hydroxylase (CYP106A2) probed by FT infrared spectroscopic studies of the iron ligand CO stretch vibration. Biochem Biophys Res Commun 269:737–742

17. Sagara Y, Wada A, Takata Y, Waterman MR, Sekimizu K, Horiuchi T (1993) Direct expression of adrenodoxin reductase in *Escherichia coli* and the functional characterization. Biol Pharm Bull 16:627–630
18. Uhlmann H, Beckert V, Schwarz D, Bernhardt R (1992) Expression of bovine adrenodoxin in *E. coli* and site-directed mutagenesis of/2 Fe-2S/cluster ligands. Biochem Biophys Res Commun 188:1131–1138
19. Lisurek M, Simgen B, Antes I, Bernhardt R (2008) Theoretical and experimental evaluation of a CYP106A2 low homology model and production of mutants with changed activity and selectivity of hydroxylation. Chembiochem 9:1439–1449
20. Guex N, Peitsch MC (1997) SWISS-MODEL and the Swiss-PdbViewer: an environment for comparative protein modeling. Electrophoresis 18:2714–2723
21. Volin P (1995) High-performance liquid chromatographic analysis of corticosteroids. J Chromatogr B 671:319–340
22. Shimada K, Mitamura K, Higashi T (2001) Gas chromatography and high-performance liquid chromatography of natural steroids. J Chromatogr A 935:141–172
23. Lewis JG, Manley L, Whitlow JC, Elder PA (1992) Production of a monoclonal antibody to cortisol: application to a direct enzyme-linked immunosorbent assay of plasma. Steroids 57:82–85
24. Mirasoli M, Deo SK, Lewis JC, Roda A, Daunert S (2002) Bioluminescence immunoassay for cortisol using recombinant aequorin as a label. Anal Biochem 306:204–211
25. Goldzieher JW, Bodenchuk JM, Nolan P (1954) Fluorescence reactions of steroids. Anal Chem 26:853–856
26. Dunn AR, Dmochowski IJ, Bilwes AM, Gray HB, Crane BR (2001) Probing the open state of cytochrome P450cam with ruthenium-linker substrates. Proc Natl Acad Sci USA 98:12420–12425
27. Park SY, Yamane K, Adachi S, Shiro Y, Weiss KE, Maves SA, Sligar SG (2002) Thermophilic cytochrome P450 (CYP119) from *Sulfolobus solfataricus*: high resolution structure and functional properties. J Inorg Biochem 91:491–501
28. Geren LM, O'Brien P, Stonehuerner J, Millett F (1984) Identification of specific carboxylate groups on adrenodoxin that are involved in the interaction with adrenodoxin reductase. J Biol Chem 259:2155–2160
29. Geren L, Tuls J, O'Brien P, Millett F, Peterson JA (1986) The involvement of carboxylate groups of putidaredoxin in the reaction with putidaredoxin reductase. J Biol Chem 261:15491–15495
30. Bernhardt R, Makower A, Jänig G-R, Ruckpaul K (1984) Selective chemical modification of a functionally linked lysine in cytochrome P-450LM2. Biochim Biophys Acta 785:186–190
31. Bernhardt R, Pommerening K, Ruckpaul K (1987) Modification of carboxyl groups on NADPH-cytochrome P-450 reductase involved in binding of cytochromes c and P-450LM2. Biochem Int 14:823–832
32. Coghlan VM, Vickery LE (1991) Site-specific mutations in human ferredoxin that affect binding to ferredoxin reductase and cytochrome P450scc. J Biol Chem 266:18606–18612
33. Stayton PS, Sligar SG (1990) The cytochrome P-450cam binding surface as defined by site-directed mutagenesis and electrostatic modeling. Biochemistry 29:7381–7386
34. Wada A, Waterman MR (1992) Identification by site-directed mutagenesis of two lysine residues in cholesterol side chain cleavage cytochrome P450 that are essential for adrenodoxin binding. J Biol Chem 267:22877–22882
35. Pochapsky TC, Lyons TA, Kazanis S, Arakaki T, Ratnaswamy G (1996) A structure-based model for cytochrome P450cam-putidaredoxin interactions. Biochimie 78:723–733
36. Koga H, Sagara Y, Yaoi T, Tsujimura M, Nakamura K, Sekimizu K, Makino R, Shimada H, Ishimura Y, Yura K et al (1993) Essential role of the Arg112 residue of cytochrome P450cam for electron transfer from reduced putidaredoxin. FEBS Lett 331:109–113
37. Nakamura K, Horiuchi T, Yasukochi T, Sekimizu K, Hara T, Sagara Y (1994) Significant contribution of arginine-112 and its positive charge of *Pseudomonas putida* cytochrome P-450cam in the electron transport from putidaredoxin. Biochim Biophys Acta 20:40–48
38. Unno M, Shimada H, Toba Y, Makino R, Ishimura Y (1996) Role of Arg112 of cytochrome p450cam in the electron transfer from reduced putidaredoxin. Analyses with site-directed mutants. J Biol Chem 271:17869–17874
39. Roitberg A, Holden M, Mayhew M, Kurnikov IV, Beratan DN, Vilker V (1998) Binding and electron transfer between putidaredoxin and cytochrome P450cam. Theory and experiments. J Am Chem Soc 120:8927–8932
40. Stayton PS, Poulos TL, Sligar SG (1989) Putidaredoxin competitively inhibits cytochrome b5-cytochrome P-450cam association: a proposed molecular model for a cytochrome P-450cam electron-transfer complex. Biochemistry 28:8201–8205
41. Bichet A, Hannemann F, Rekowski M, Bernhardt R (2007) A new application of the yeast two-hybrid system in protein engineering. Protein Eng Des Sel 20:117–123

CYP enzymes are the main catalysts involved in the oxidation of drugs, steroids, and carcinogens and in many biosynthetic pathways producing sterols, steroids, prostaglandins, secondary metabolites. The reactions catalyzed usually require an external source of reducing equivalents, NADH or NADPH, and auxiliary proteins to transfer the electrons to the CYP to catalyze molecular splitting of atmospheric oxygen. CYP51 (EC1.14.13.70) is regarded as an ancestral CYP from which other CYPs evolved [9] and is an important enzyme (C14-demethylase) in the sterol biosynthesis pathway of most organisms. In yeasts CYP51 catalyzes the 14 α-demethylation of lanosterol, whilst in filamentous fungi CYP51 catalyzes the 14 α-demethylation of eburicol.

Recently CYP63s A1, A2 and A3 in *P. chrysosporium* have been characterized [10, 11] and CYP53 [12] following heterologous expression in *E. coli*. In the present study we describe the expression and characterization of CYP51 (GenBank FJ174578) as a prelude to further characterization of the CYPome of *P. chrysosporium*.

Experimental Procedure

Cloning *CYP51* into pGEMT-Easy vector™, pCWori$^+$ and pYES2.1 TOPO Vectors

A Lambda ZAP II cDNA library for *Phanerochaete chrysosporium* was constructed using Strategene reagents (La Jolla, CA, USA) from total RNA extracted from 3 day-old cultures of *P. chrysosporium* ATCC24725. Primer design was based on information provided by Dr. David Nelson (http://drnelson.utmem.edu/whiterot.html). Primers against the *CYP51* gene were designed to incorporate an *Nde*I site in the forward primer (5′-CATCGCCATATGTCTCTCAGCCAGTACGGG-3′) and a 4-His tag and *Hin*dIII site in the reverse primer (5′-ACTGCTAAGCTTCTAGTGATGGTGATGGTCGAAGTTACGCCGCCT-3′). PCR was performed using an annealing temperature of 56 °C using Expand High Fidelity™ DNA polymerase (Roche, UK). The *CYP51* gene (FJ174578) was cloned into pGEMT-Easy vector™ (Promega, Southampton, UK). Positive recombinants were fully sequenced to establish integrity of each clone. The *CYP51* gene was excised and cloned into pCWori$^+$ vector by digestion with *Nde*I and *Hin*dIII followed by ligation with T4 DNA ligase (Roche, UK). Positive recombinants were sequenced to establish integrity prior to expression studies.

Forward (5′-ACCATGTCTCTCAGCCAGTA-3′) and reverse (5′-GTCGAAGTTACGCCGCCT-3′) primers were designed against the *CYP51* gene for use with the pYES2.1 TOPO (Invitrogen, Renfrew, UK) vector system. PCR was performed as described above and the PCR product used to transform TOPO10 *E. coli* cells. The plasmids from positive clones were verified by sequencing and used to transform yeast AH22Δura3 cells using the lithium acetate TRAFO method [13].

Heterologous Expression in *E. coli* and Isolation of Recombinant *CYP51*

The *CYP51*-pCWori$^+$ construct was transformed into *E. coli* strain DH5α using ampicillin selection. Overnight cultures (10 ml) of *CYP51* transformants were used to inoculate one litre volumes of Terrific Broth supplemented with 20 g l^{-1} peptone and 0.1 mg ml^{-1} sodium ampicillin. Cultures were grown at 37 °C, 230 rpm for 6 h prior to induction with 1 mM IPTG and expression at 25 °C, 190 rpm for 18 h in the presence of 1 mM 5-aminolevulinic acid. CYP51 protein was isolated according to the method of Arase et al. [14] except that 2% (w/v) sodium cholate and no Tween20 were used in the sonication buffer. The solubilized CYP51 protein was purified by affinity chromatography using Ni^{2+}-NTA agarose as previously described [15] with the modification that 0.1% (w/v) L-histidine in 50 mM sodium phosphate, pH 7.5, 25% (w/v) glycerol was used to elute non-specifically bound *E. coli* proteins after the NaCl washes and elution of CYP51 was achieved with 1% (w/v) L-histidine in 50 mM sodium phosphate, pH 7.5, 25% (w/v) glycerol. Protein purity was assessed by SDS polyacrylamide gel electrophoresis [16]. Isolated CYP51 protein fractions were stored at −80 °C.

Heterologous Expression in *S. cerevisiae* and Isolation of Recombinant CYP51

Overnight cultures of *CYP51* transformants were prepared in 10 ml of 1.34% (w/v) yeast nitrogen base (YNB) containing 2% (w/v) glucose, 0.005% (w/v) histidine and grown at 30 °C, 200 rpm. These were used to inoculate one litre volumes of media containing 1.34% (w/v) YNB, 2% (w/v) glucose, 0.05% (w/v) leucine and 0.005% (w/v) histidine. The cells were grown for 20 h at 30 °C and 200 rpm prior to harvesting and washing under sterile conditions. The harvested cells were resuspended in fresh one litre volumes of media containing 1.34% (w/v) YNB, 3% (w/v) galactose, 0.05% (w/v) leucine and 0.005% (w/v) histidine. Galactose dependent expression of the CYP proteins was achieved by incubation at 25 °C, 120 rpm for 20 h.

All the following operations were performed at 4 °C. Following centrifugation at 1,500×*g*, pelleted cells were resuspended in 0.1 M potassium phosphate buffer, pH 7.4 and homogenized using a C5 emulsiflex homogenizer (Glen Creston, Stanmore, Middlesex, UK) at 250,000 kPa pressure. The homogenates were centrifuged for 10 min at

3,000×g to remove cell debris and then twice at 20,000×g for 20 min to remove mitochondria. The microsomal fractions were recovered by ultracentrifugation at 100,000×g for 1 h. Microsomal pellets were resuspended in 0.1 M potassium phosphate buffer, pH 7.4, 20% (v/v) glycerol and frozen at −80 °C.

Spectral Determination of CYP51 Protein Concentrations

Cytochrome P450 concentration was determined by reduced carbon monoxide difference spectra according to Omura and Sato [17] with carbon monoxide being passed through the CYP51 solution prior to the addition of sodium dithionite. The extinction coefficient of 91 $\mathrm{mM}^{-1}\,\mathrm{cm}^{-1}$ was used for the calculation of P450 concentration from the difference in absorbance units between 450 and 490 nm. Absolute spectra were determined as previously described [15] between 250 and 700 nm in 50 mM sodium phosphate, pH 7.5, 25% (w/v) glycerol for the oxidized protein, the sodium dithionite reduced protein and the reduced carbon monoxide-P450 complex. Total protein concentrations were determined by the bicinchoninic acid method using bovine serum albumin standards. Spectral determinations were made using a Hitachi U-3310 UV/VIS spectrophotometer (San Jose, CA, USA).

Azole-binding Spectral Determinations

Binding of azole antifungal agents to CYP51 was performed as previously described [18, 19]. Stock 0.1 mg ml^{-1} solutions of clotrimazole, fluconazole, itraconazole, ketoconazole and voriconazole were prepared in dimethylsulfoxide (DMSO). Azole was progressively titrated against Ni^{2+}-NTA agarose purified *P. chrysosporium* CYP51 (1.8 µM, 0.138 mg ml^{-1} total protein) to a maximum DMSO concentration of 1.5% (v/v) with the spectral difference $\Delta A_{430\text{–}412}$ determined after each incremental addition of azole. Each azole titration experiment was repeated in triplicate with the mean values and associated standard errors being used in subsequent data analyzes. Clotrimazole concentrations of 0.29, 0.58, 0.87, 1.16, 1.45, 1.74, 2.32, 2.90, 3.48, 4.35 and 5.80 µM were used. Fluconazole concentrations of 0.33, 0.65, 0.98, 1.31, 1.63, 1.96, 2.29, 2.61, 3.27, 3.92 and 4.90 µM were used. Itraconazole concentrations of 0.14, 0.28, 0.43, 0.57, 0.71, 0.85, 0.99, 1.13, 1.42, 1.70 and 2.13 µM were used. Ketoconazole concentrations of 0.19, 0.38, 0.56, 0.75, 0.94, 1.13, 1.32, 1.51, 1.88, 2.26 and 2.82 µM were used. Voriconazole concentrations of 0.29, 0.57, 0.86, 1.14, 1.43, 1.72, 2.00, 2.29, 2.86, 3.43, 4.29 and 5.72 µM were used. The k_d values for each azole were determined by non-linear regression (Levenberg–Marquardt algorithm) of $\Delta \mathrm{A}_{430\text{–}412}$ against azole concentration using the Hill equation $[\Delta A = \Delta A_{\max}/(1 + k_d/[\mathrm{Azole}]^n)]$ [20]. The k_d is defined here as the dissociation constant of the non-productive enzyme–azole complex. Curve-fitting was performed using the program ProfFit 5.0.1 (Quantumsoft, Zurich). The $[\mathrm{Azole}]_{0.5}$ values were determined directly from the plot of $\Delta A_{430\text{–}412}$ against azole concentration and are defined as the azole concentration required to obtain half the observed $\Delta A_{430\text{–}412}$ maximum value.

Complementation of Yeast YUG37 Mutant by *P. chrysosporium* CYP51

The *CYP51*: pYES2.1 plasmid was re-engineered by PCR so that *CYP51* retained a stop codon but did not have the 6-His tag of the pYES2.1 plasmid. The forward and reverse primers used were 5′-ACCATGTCTCTCAGCCAGTA-*3*′ and 5′-CTAGTCGAAGTTACGCCG-*3*′, respectively. The *S. cerevisiae* strain YUG37 with the *CYP51* gene placed under the control of the doxycycline regulatable *tet-O*$_7$-*CYC*1 promoter was used in this study. The promoter down-regulates the endogenous *CYP51* gene in the presence of doxycycline and expresses transcripts to levels comparable to those observed with the strong *GAL*1 promoter (pYES2.1) in the absence of doxycycline [21, 22]. This mutant allowed the study of *P. chrysosporium* CYP51: pYES2.1 complementation by induction in a doxycycline down-regulated growth condition. Growth rates of cultures were measured with a Bioscreen C$^{\mathrm{TM}}$ instrument (Labsystems, Finland) by measuring the optical density at 600 nm in a working volume of 100 µl. An overnight culture was grown in 1.34% (w/v) YNB, 2% (w/v) raffinose, 3% (w/v) galactose and 0.01% (w/v) tryptophan from a single colony. The culture was diluted tenfold and 50 µl of diluted cells used to inoculate the Bioscreen$^{\mathrm{TM}}$ plates with or without 100 µg ml^{-1} doxycycline in the same media. The YUG37 strain requires an additional supplement of 0.01% (w/v) uracil.

Data Analysis

Construction and analysis of the *CYP51* gene and protein sequences were performed using the computer programs Chromas version 1.45 (http://www.technelysium.com.au/chromas14x.html), ClustalX version 1.8 (ftp://ftp-igbmc.u-strasbg.fr/pub/) and BioEdit version 5.0.6. (http://www.mbio.ncsu.edu/BioEdit/bioedit.html). The genomic DNA sequence for the *P. chrysosporium CYP51* gene was extracted from scaffold 44 deposited in the JGI white-rot fungus database (http://genome.jgi-psf.org/whiterot1/whiterot1.home.html) using the initial predictions of Dr. David Nelson (http://drnelson.utmem.edu/whiterot.fasta.html). Phylogenic trees were prepared using ClustalX version 1.8 and Treeview version 1.6.1 (http://taxonomy.zoology.gla.ac.uk/rod/treeview.html). The online BLOCK MAKER program (http://blocks.fhcrc.org/blocks/make_blocks.html) was used to identify conserved ungapped 'MOTIF' segments between nine basidiomycete CYP51 sequences. The online SignalP 3.0 (http://www.cbs.dtu.dk/services/SignalP/) and TargetP 1.1 (http://www.cbs.dtu.dk/services/TargetP/) were used to predict of the N-terminal membrane anchor region of *P. chrysosporium* CYP51. Predotor 1.03 (http://urgi.versailles.inra.fr/predotar/test.seq) and TargetP 1.1 were used to predict the subcellular location of *P. chrysosporium* CYP51. The analyzes of the Bioscreen C^{TM} data were performed using ProFit 5.01 (QuantumSoft, Zurich, Switzerland).

Chemicals

All chemicals, including fluconazole, itraconazole and ketoconazole, were obtained from Sigma Chemical Company (Poole, UK), unless otherwise stated. Voriconazole was supplied by Discovery Fine Chemicals (Bournemouth, UK). DIFCO growth media were obtained from Becton Dickinson UK Ltd (Cowley, UK).

Results and Discussion

Characterization of *P. chrysosporium CYP51* Gene Organization

CYP51 was isolated by PCR from the cDNA library and cloned into the pGEMT-Easy vector^{TM}. The full gene sequence of *CYP51* was constructed using the Chromas 1.45, Clustal X 1.8 and BioEdit 5.0.6 computer programs with the genomic DNA as the template (Fig. 1). The 1,956 bp DNA sequence of the *CYP51* cDNA clone, coding for a protein 550 amino acids long of 62,327 molecular weight and theoretical pI of 6.27, was compared against the predicted sequence (http://drnelson.utmem.edu/whiterot.html) and to a previously deposited predicted sequence Q68HC3 [23] for the *P. chrysosporium CYP51* gene. The *CYP51* cDNA clone was free of any nucleotide changes from the genome sequence and utilized the same strain. The *CYP51* cDNA isolated was identical to the predicted sequence by Dr David Nelson (http://drnelson.utmem.edu/whiterot.html) except for one amino acid (T531A) found at the last intron-exon boundary. *CYP51* was found to contain 7 exons and 6 introns compared to the 6 exons and 5 introns of the predicted Q68HC3 sequence. The extra intron was located close to the 3′ end of the gene (1,839–1,893 bp). The stop codon of the *CYP51* cDNA clone was a further 10 bases downstream of the predicted *CYP51* sequence. The start codon of the Q68HC3 sequence is 67 bases downstream from the start codon in the *CYP51* cDNA clone and Q68HC3 has a 9-base shorter exon 3 coding region than that observed for the experimental *CYP51* cDNA clone. In addition, the *CYP51* cDNA clone contained an extra 3 amino acid sequence (126-VYG-128).

These observed differences in the cDNA sequences translate into differences in the protein sequences in this, the first experimentally determined CYP51 sequence. The N-terminal anchor region, as predicted by SignalP and TargetP, extended to the same serine residue at position 40 of the *CYP51* cDNA. TargetP predicted that *P. chrysosporium* CYP51 would be secretory and Predator 1.1 predicted CYP51 would be targeted to the endoplasmic reticulum. *P. chrysosporium* CYP51 expressed in *E. coli* during this study was localized in the membrane fraction, confirming the presence of a N-terminal membrane anchor. The extra intron found in the *CYP51* cDNA clone between base pairs 1839 and 1893 was responsible for the last 20 amino acids of the *CYP51* cDNA clone being different to those previously predicted, utilizing an alternate downstream TAG termination site. This 20 amino acid C-terminal region of *P. chrysosporium* CYP51 was found to have a high homology against the C-terminus of two basidiomycete CYP51 proteins with 55% identity against A8DBU6 (*A. cinnamomea*) and 60% identity against A8NUS3 (*C. cinerea*) and lesser homology (10 to 25%) to other basidiomycete CYP51s.

The presence of two possible ATG start codons suggests that alternate initiation sites for translation might exist. The existence of possible splice variants was investigated by PCR using the original forward primer (5′-CATCGCCATATGTCTCTCAGCCAGTACGGG-*3*′) and a modified reverse primer (5′-ACT GCT AAG CTT CTA GTG ATG GTG ATG CGC CGC CTG TAG AGA ATG-3′) designed to prime against the alternate stop codon (10 bases upstream) as previously predicted. The PCR products were cloned into pGEMT-Easy vector^{TM}. Sequencing these revealed the presence of the same 7 exons and 6 introns as observed previously with no splice variants present.

Phylogenetic Analysis of *P. chrysosporium* CYP51

Phylogenetic analysis of *P. chrysosporium* CYP51 was performed against other selected basidiomycete and ascomycete CYP51 proteins. Analysis of the primary amino acid sequences using Clustal X and Treeview programs (Fig. 2) established that *P. chrysosporium* CYP51 had greatest homology towards other basidiomycete CYP51 proteins with identities of 65, 65, 64, 57, 56, and 51% with *C. cinereus*, *C. cinerea*, *A. cinnamomea*, *M. globosa*, *C. neoformans* and *U. maydis* CYP51 proteins, respectively. However, *P. chrysosporium* CYP51 only had

```
DNA          ATGTCTCTCAGCCAGTACGGGCCCATCGCG GGCCTCGTCGGCCAGGCCTACGACGCCCTG  GCATCCATGTCCACCTCACGTCTCGTCCTC    90
Protein       M  S  L  S  Q  Y  G  P  I  A   G  L  V  G  Q  A  Y  D  A  L    A  S  M  S  T  S  R  L  V  L     30

DNA          TTCCTCCTCATCAACATTCCTATCCTTTCT GTTGTGTGCAACGTCATCTACCAGCTGgtg  cgtatgcgaacttgaacatccgtttacgcg   180
Protein       F  L  L  I  N  I  P  I  L  S   V  V  C  N  V  I  Y  Q  L                                        49

DNA          tgctcaacgtctctcagTTGCCCAAGGAC  AAGTCTCTGCCTCCCGTGGTCTGGCATTGG  TTCCCGTGGTTCGGCTCTGCAGCGGCATAC   269
Protein                        L  P  K  D    K  S  L  P  P  V  V  W  H  W    F  P  W  F  G  S  A  A  A  Y     73

DNA          GGAGAGGATCCTATCAAGTTCTTCTTTGAC TGCAAGGAGAAGgtgtgtcatcttctgtaac ctttcgtgctcgtactaacaatgtacagTAC  361
Protein       G  E  D  P  I  K  F  F  F  D   C  K  E  K                                                  Y    88

DNA          GGCAATGTGTTCACGTTCATCCTGATGGGA CGCAAGGTTACGGTCGCGCTCACGCCAGCT  GGCAACAACTTCATCATGGGCGGGAAGCAC   451
Protein       G  N  V  F  T  F  I  L  M  G   R  K  V  T  V  A  L  T  P  A    G  N  N  F  I  M  G  G  K  H    118

DNA          ACGACCTTCTCCGCTGAGGAGGTGTACGGG gtgcgtttcgttcaacgcacgcccattctg  cgtgactgacgcgtttaacagGGTTTGACG   541
Protein       T  T  F  S  A  E  E  V  Y  G                                                        G  L  T    131

DNA          ACCCCCGTCTTCGGCAAGGACGTCGTATAC GACTGCCCGAACGAGCTGCTCATGGAGCAG  AAGAAGTTCGTTAAGTTCGGTCTCTCAACA   631
Protein       T  P  V  F  G  K  D  V  V  Y   D  C  P  N  E  L  L  M  E  Q    K  K  F  V  K  F  G  L  S  T    161

DNA          GAGAACTTCCGCCAATACGTCGGCATGATT GAGGAGGAGGTCCTCCAATTTATGCGGAAC  GATGCTAGCTTCAAGATTTACCAGATGAAC   721
Protein       E  N  F  R  Q  Y  V  G  M  I   E  E  E  V  L  Q  F  M  R  N    D  A  S  F  K  I  Y  Q  M  N    191

DNA          GACATTAACGAATGGGGCGCCTTCGATGTT CTGAAGGTCATGTCCGAAATCACAATCCTC  ACCGCTTCCCGGACACTGCAAGGCAAGGAA   811
Protein       D  I  N  E  W  G  A  F  D  V   L  K  V  M  S  E  I  T  I  L    T  A  S  R  T  L  Q  G  K  E    221

DNA          GTTCGCGCAAACATCACCAAGGACTACGCT CAGGTCTACAACGACTTGGACGGTGGTTTC  ACTCCCTTGCACTTCATGTTCCCCAACCTT   901
Protein       V  R  A  N  I  T  K  D  Y  A   Q  V  Y  N  D  L  D  G  G  F    T  P  L  H  F  M  F  P  N  L    251

DNA          CCTCTCGAGTCGTACCGTAAGCGCGACGCC GCGCACAAGAAGATCAGTGACTTCTACATT  AGCATCATCCGCAAGCGTAGGGAGAACCCT   991
Protein       P  L  E  S  Y  R  K  R  D  A   A  H  K  K  I  S  D  F  Y  I    S  I  I  R  K  R  R  E  N  P    281

DNA          GGCCAGgttcgtatcctccagaatgtcagc agcagttttctgactagttgtttagGAGGAA GAGCACGACATGATTGCGGCTCTCATGAAC  1083
Protein       G  Q                                                   E  E   E  H  D  M  I  A  A  L  M  N    295

DNA          CAGAAGTACCGTGTCGGTCGCCCACTTAAG GATCACGAAATCGCCCACATCATGATCGCT  CTTCTCATGGCTGGTCAGCACACAAGTTCC  1173
Protein       Q  K  Y  R  V  G  R  P  L  K   D  H  E  I  A  H  I  M  I  A    L  L  M  A  G  Q  H  T  S  S    325

DNA          GCCACCGGCTCCTGGGCACTGCTGCACATT GCCGACCGTCCGGATGTCGCgtgagtattc  tcattgaatacgtgtacagttccctaacgcg 1264
Protein       A  T  G  S  W  A  L  L  H  I   A  D  R  P  D  V  A                                             342

DNA          aacattctagTGAGGCTTTGTATGAGGAG  CAGGTCAAGCACTTCCGTCAATCTGACGGC  TCCTGGCGCACTCCCGAATACGAGGAATTG  1352
Protein                  E  A  L  Y  E  E    Q  V  K  H  F  R  Q  S  D  G    S  W  R  T  P  E  Y  E  E  L    368

DNA          AAGGAGCTTCCTGTCCTCGACTCGGTCATC CGTGAGACTCTCCGTATCCACCCGCCCATT  CACAGCATCATGCGTGCCGTACGTGAGGAT  1442
Protein       K  E  L  P  V  L  D  S  V  I   R  E  T  L  R  I  H  P  P  I    H  S  I  M  R  A  V  R  E  D    398

DNA          GTCGTCGTCCCGCCTACACTCGCTGCTCCG TCGGAGGACGGTCGCTACGTCATTCCCAAA  GGCCACGTCGTACTGTCGTCCGCAGCCATC  1532
Protein       V  V  V  P  P  T  L  A  A  P   S  E  D  G  R  Y  V  I  P  K    G  H  V  V  L  S  S  A  A  I    428

DNA          AGTCAGGTTGATCCGATGCTTTGGAAGAAT GCCAACGACTGGGATCCCTCGCGCTGGTCA  GATCCCGAGGGTGTCGCTGCGCAGGCGTAC  1622
Protein       S  Q  V  D  P  M  L  W  K  N   A  N  D  W  D  P  S  R  W  S    D  P  E  G  V  A  A  Q  A  Y    458

DNA          AAGCAGTACGACGACGCCGAGGGCGCCAAG GTTGACTTTGGCTTTGGTCTCGTCAGCAAG  GGTACCGACAGCCCGTATCAGCCTTTCGGC  1622
Protein       K  Q  Y  D  D  A  E  G  A  K   V  D  F  G  F  G  L  V  S  K    G  T  D  S  P  Y  Q  P  F  G    488

DNA          GCCGGTCGCCACAGGTGCATCGGCGAGCAG TTCGCATATCTCCAGCTCGGCACGATCATC  TCGACCTTTGTTCGCCATGTCGAGATGCGT  1802
Protein       A  G  R  H  R  C  I  G  E  Q   F  A  Y  L  Q  L  G  T  I  I    S  T  F  V  R  H  V  E  M  R    518

DNA          CTGCCTGAAACTGGTGTGCCTCCGCCGAAC TACCACgtacgttcccatacccgtatattg  aggctggtttgtgctgacgtggcatctgcag 1893
Protein       L  P  E  T  G  V  P  P  P  N   Y  H                                                            530

DNA          ACGATGATCACACTCCCGAAGGCGCCTCGC AACATTCTCTACAGGCGGCGTAACTTCGAC  TAG                             1956
Protein       T  M  I  T  L  P  K  A  P  R   N  I  L  Y  R  R  R  N  F  D    *                              550
```

Fig. 1 *Phanerochaete chrysosporium CYP51* gene structure. The DNA sequence of the *CYP51* cDNA clone (GenBank FJ174578) was compared against the JGI genomic DNA sequence (http://genome.jgi-psf.org/whiterot1/whiterot1.home.html) using the programs Clustal X 1.8 and BioEdit 5.0.6. The genomic DNA sequence contains both exons (*upper-case*) and introns (*lower-case*). The exon–intron boundaries were determined by sequencing the *CYP51* cDNA clone. The possible alternate 'start' and 'stop' sites are underlined. The *P. chrysosporium CYP51* gene is comprised of 7 exons and 6 introns

44–46% identity to the remaining fungal CYP51 proteins and identities of 39, 37 and 30% to rat (Q64654), human (Q16850) and sorghum (P93846) CYP51 proteins, respectively.

Expression of *P. chrysosporium* CYP51 in *E. coli*

Expression of CYP51 protein in *E. coli* resulted in the isolation of 62 nmol CYP51 per litre culture in the

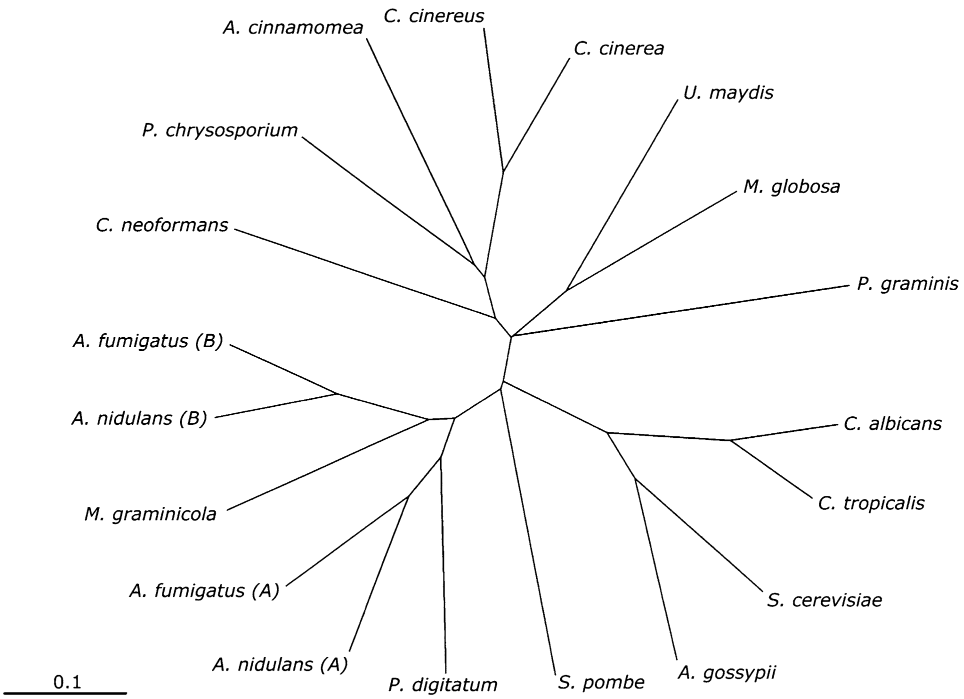

Fig. 2 Phylogenetic tree of basidiomycete and ascomycete CYP51 proteins. ClustalX 1.8 and Treeview 1.6.1 computer programs were used to construct the phylogenetic tree from selected basidiomycete and ascomycete CYP51 protein sequences. Basidiomycete sequences included were *Phanerochaete chrysosporium* (FJ174578), *Cryptococcus neoformans* (AAF35366), *Ustilago maydis* (P49602), *Antrodia cinnamomea* (A8DBU6), *Coprinus cinereus* (Q68HC4), *Coprinopsis cinerea* (A8NUS3), *Malassezia globosa* (A8Q3I7) and *Puccinia graminis* (PGTG07202: http://www.broad.mit.edu/annotation/genome/puccinia_graminis). Ascomycete sequences included were *Candida albicans* (P10613), *Candida tropicalis* (P14263), *Schizosaccaromyces pombe* (Q09736), *Saccharomyces cerevisiae* (P10614), *Penicillium digitatum* (Q9P340), *Ashbya gossypii* (Q759W0), *Mycosphaerella graminicola* (C_100070; http://genome.jgi.doe.gov/Mycgr1/Mycgr1.home.html), *Aspergillus fumigatus* CYP51A (B0Y5N0), *Aspergillus fumigatus* CYP51B (B0YC83), *Aspergillus nidulans* CYP51A (AN1901—http://www.broad.mit.edu/annotation/genome/aspergillus_group/MultiHome.html) and *Aspergillus nidulans* CYP51B (AN8283: http://www.broad.mit.edu/annotation/genome/aspergillus_group/MultiHome.html)

solubilized cellular protein fraction. Native CYP51 accounted for 1.1% of the total protein isolated in the solubilized fraction. Purification of CYP51 on Ni^{2+}-NTA agarose increased the purity of the CYP51 preparation by 71-fold, with native CYP51 now accounting for 81.1% of the total protein and a 55% recovery of active CYP51 relative to the original solubilized fraction.

The purified CYP51 fraction gave characteristic absolute and reduced carbon monoxide difference spectra (Fig. 3a) of a P450 monooxygenase. The ferric-P450 form existed in the low-spin state, characterized by a heme Soret γ band at 417 nm in addition to α, β and δ bands at 565, 535 and 355 nm, respectively. An additional spectral peak was observed in the near ultraviolet at 293 nm. One electron reduction of CYP51 with sodium dithionite resulted in small blue-shift of the Soret γ band from 417 to 415 nm. Reduction of CYP51 to the ferrous form also caused the α and β bands to merge with an absorption maximum of 550 nm. Binding of carbon monoxide to the dithionite-reduced ferrous-P450 resulted in a typical red-shift of the Soret γ band from 415 to 445 nm in the formation of the CO-ferrous P450 complex. A significant amount of P420 was also observed when carbon monoxide was bound to the dithionite-reduced form of the protein, suggesting instability in the presence of dithionite. This was supported by the observation that the carbon dioxide difference spectra obtained (Fig. 3b) contained no visible P420 as dithionite was added last just prior to the measurement of the absorbance spectrum.

SDS polyacrylamide gel electrophoresis indicated that the Ni^{2+}-NTA agarose purified CYP51 protein was over 90% pure with an apparent molecular weight of 63 kDa.

Azole-binding to *P. chrysosporium* CYP51

Spectral titrations of Ni^{2+}-NTA agarose purified CYP51 protein (1.8 μM) against the five azole antifungal compounds clotrimazole, fluconazole, itraconazole, ketoconazole and voriconazole were performed in triplicate. Figure 4 shows the Type II spectral titration (Fig. 4a) obtained with fluconazole and the associated binding saturation curve (Fig. 4b). Similar Type II titrations and azole

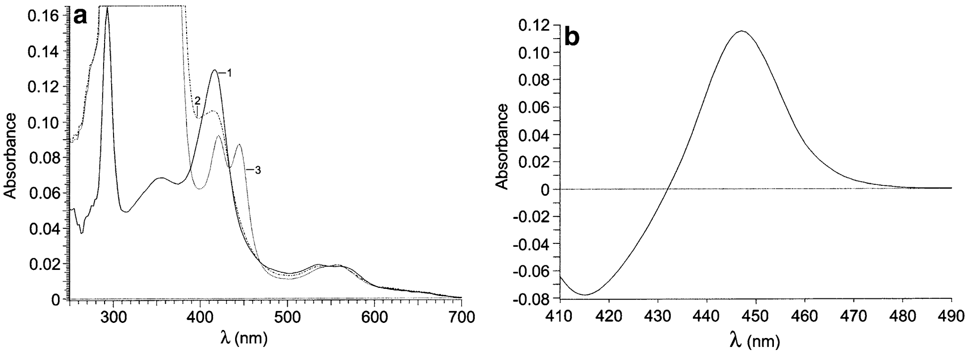

Fig. 3 Absolute and reduced carbon monoxide difference spectra of *P. chrysosporium* CYP51. The absolute spectrum of CYP51 was determined between 250 and 700 nm (**a**) in the absence (trace 1) and presence (trace 2) of 5 μM sodium dithionite and in the presence of 5 μM sodium dithionite saturated with carbon monoxide (trace 3). A reduced carbon monoxide difference spectrum (**b**) was obtained using Ni^{2+}-NTA agarose purified *P. chrysosporium* CYP51 expressed in *E. coli* (2.6 μM and 0.2 mg ml^{-1} total protein) as previously described by Omura and Sato [17] with the sample and reference cuvettes saturated with carbon monoxide prior to addition of dithionite to the sample cuvette only. The extinction coefficient was 91 mM^{-1} cm^{-1}

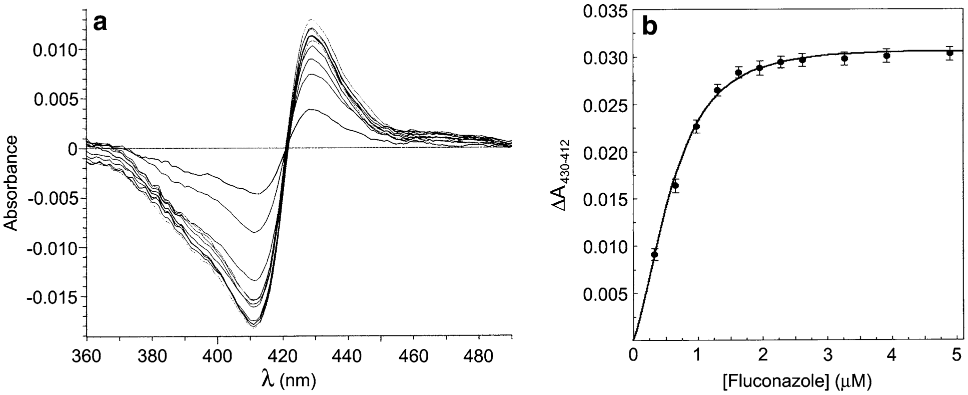

Fig. 4 Spectral titration of fluconazole against *P. chrysosporium* CYP51. Fluconazole was progressively titrated against Ni^{2+}-NTA agarose purified *P. chrysosporium* CYP51 (1.8 μM, 0.138 mg ml^{-1} total protein) to a maximum DMSO concentration of 1.5% (v/v) with the spectral difference $\Delta A_{430-412}$ determined after each incremental addition of azole (**a**). Fluconazole concentrations of 0.33, 0.65, 0.98, 1.31, 1.63, 1.96, 2.29, 2.61, 3.27, 3.92 and 4.90 μM were investigated. The spectral titration was repeated in triplicate with the mean values and associated standard errors being used to construct the fluconazole saturation curve (**b**). Non-linear regression (Levenberg–Marquardt algorithm) of the Hill equation [$\Delta A = \Delta A_{max}/(1 + k_d/[Azole]^n)$] was used to analyze the data

binding saturation curves were also obtained for clotrimazole, itraconazole, ketoconazole and voriconazole (not shown) indicative of the co-ordination of the triazole N-3 with the heme as a sixth ligand [24]. The binding of azoles to CYP51 was found to be sigmoidal obeying the Hill equation [$\Delta A = \Delta A_{max}/(1 + k/[Azole]^n)$] [20]. The k_d values (±SD) obtained for clotrimazole, fluconazole, itraconazole, ketoconazole and voriconazole were 0.25 μM (±0.05), 0.35 μM (±0.04), 0.45 μM (±0.06), 0.40 μM (±0.02) and 0.28 μM (±0.04), respectively, indicating that *P. chrysosporium* CYP51 bound all five azoles with equal affinity. Apparent Hill numbers (±SD) of 2.19 (±0.22), 1.85 (±0.12), 1.59 (±0.09), 1.62 (±0.05) and 2.27 (±0.14) were obtained for clotrimazole, fluconazole, itraconazole, ketoconazole and voriconazole, respectively. The $[Azole]_{0.5}$ values obtained for clotrimazole, fluconazole, itraconazole, ketoconazole and voriconazole were 0.54, 0.56, 0.51, 0.56 and 0.49 μM, respectively, equating to 27–31% of the 1.8 μM CYP51 protein present. The $[Azole]_{0.5}$ values obtained were comparable to those previously obtained with *Candida albicans* [25, 26] at 0.13 μM (33% of 0.4 μM P450 present) for ketoconazole and 0.11 μM (60% of the 0.2 μM P450 present) for fluconazole.

Only one azole molecule can bind to the heme group at the P450 enzyme active site (one to one binding) as the sixth co-ordinated ligand to produce the characteristic type II binding spectra observed. Therefore there are two possible causes of the positive cooperativity observed for the binding of azoles to *P. chrysosporium* CYP51. Firstly, two or more specific azole binding sites exist on the cytochrome P450 molecule with positive cooperativity being exerted between the binding sites (multiple site cooperativity) with only one azole molecule directly coordinated as the sixth ligand of the heme prosthetic group and the other azole molecule acting as a positive allosteric effector/regulator. Secondly, cytochrome P450 molecules aggregate in vitro to form oligomers which then display positive cooperativity between the monomers during azole binding (multimer cooperativity).

Ouellet et al. [20] have observed similar positive cooperative binding with clotrimazole and econazole to *Mycobacterium tuberculosis* CYP130. They established that for CYP130 the binding of econazole did not involve multiple binding sites within a single CYP130 molecule by determining a 1:1 stoichiometry for bound azole using econazole and miconazole, a structurally similar azole that exhibited no cooperativity. Ouellet et al. [20] managed to abolish the observed binding cooperativity towards econazole by the inclusion of 50 mM KCl, suggesting that the observed cooperativity may have arisen from protein–protein interactions between CYP130 molecules that were disrupted by the inclusion of the ionic KCl.

The azole binding buffer used for the *P. chrysosporium* CYP51 studies contained 92 mM sodium cations from the 50 mM sodium phosphate, pH 7.5 present and strong positive cooperative allosterism was observed for all five azoles, especially clotrimazole and voriconazole. The addition of an additional 0.5 M NaCl to the binding buffer did not dissipate the positive allosterism towards clotrimazole and voriconazole binding (data not shown). Both the k_d and apparent Hill number values did not significantly alter in the presence of 0.5 M NaCl, although the observed A_{max} values decreased by 10–12%. Therefore, the observed azole binding allosterism with *P. chrysosporium* CYP51 was not disrupted by the inclusion of 0.5 M NaCl, suggesting that the allosterism was not due to electrostatic protein–protein interactions between CYP51 molecules. However, the azole binding buffers used did not contain any detergent. Therefore the possibility that the allosteric azole-binding observed was caused by hydrophobic protein–protein interactions could not be excluded. Further investigations are required to confirm the origins of the observed allosterism for azole binding to *P. chrysosporium* CYP51 which exhibited a high affinity for all five azole antifungals examined in this study.

Expression and Functional Analysis of *P. chrysosporium* CYP51 in *S. cerevisiae*

CYP51 protein was successfully expressed using the pYES2.1 vector in *Saccharomyces cerevisiae*, although overall protein yields were low at 1.5 nmol CYP51 per litre of culture in an AH22 host strain. In *S. cerevisiae* (yeast), the deletion of the *CYP51* (*ERG11*) gene has been shown to be lethal to the cell [27, 28]. Complementation studies were performed using a yeast CYP51 mutant *YUG37:erg11*, which carries a doxycycline repressible *tet-O$_7$-CYC1* promoter upstream of the native *CYP51* (*ERG11*) gene, in the absence and presence of 100 μg ml^{-1} doxycycline. Control experiments in the presence and absence of pYES2 and addition of doxycycline caused a distinctive decrease in the growth levels (Fig. 5c, d) while complementation by the pYES2.1 *P. chrysosporium CYP51* construct (Fig. 5b) was observed under the same conditions. The wild type parent *YUG37* yeast strain (Fig. 5a), was insensitive to doxycycline. These results confirm the ability of the *P. chrysosporium* CYP51 protein to couple with the native yeast cytochrome P450 reductase (CPR) in vivo to catalyze the 14α-demethylation of lanosterol to 4, 4-dimethylergosta-8, 14, 24-trienol when transcription of native CYP51 is down-regulated.

Other Properties of *P. chrysosporium* CYP51

A comparison of the nine basidiomycete CYP51 proteins using the BLOCKMAKER program identified nine conserved 'MOTIF' regions (Table 1). Only three of these nine basidiomycete CYP51s have been demonstrated to be functionally active (*P. chrysosporium* [this study]; *C. neoformans* [23]; *U. maydis* [29]). Blocks A, C, E and H are highly conserved with 46, 41, 44 and 43%, respectively, of the amino acid residues conserved among all nine fungal species. Blocks D, F and G are moderately conserved with 33, 33, and 29%, respectively, of the residues being absolutely conserved amongst all nine species. Block B was highly conserved (42%) for eight of the nine basidiomycete CYP51 sequences, with the exception of *P. graminis* CYP51 (PGTG07202.2) where block B appeared to be largely missing. Block B contains the B'helix–B'C loop region of the CYP51 molecule. The reason for the absence of this region in *P. graminis* CYP51 appears to be an incorrect assignment of the intron/exon boundaries in the genomic database, as within the designated 'intron 2' the amino acid sequence 'LATPVFGTKMVYDVPNAILMRPK' can be deduced, which has a high homology (70% to A8Q3I7) to the first 23 residues of block B (Table 1). The DNA sequence deposited for 'intron 2' also contains a long run of unknown nucleotides (N) suggesting that this region was the end of a sequencing run leading to the remainder of block B being missing from the current deposited sequence.

Comparing the fungal CYP51 proteins with the published crystal structure for *M. tuberculosis* CYP51 [30], the heme and fluconazole binding domains could be identified. Block H contained the main C-terminal heme-binding domain PFGXGRHRCXGEXFAY. The other heme-binding domains PXHSXXR, AGQHTS, and AEEXYXXLTTPVFGKXVVYDCPNXXLMEQKKFVKXGL are present in

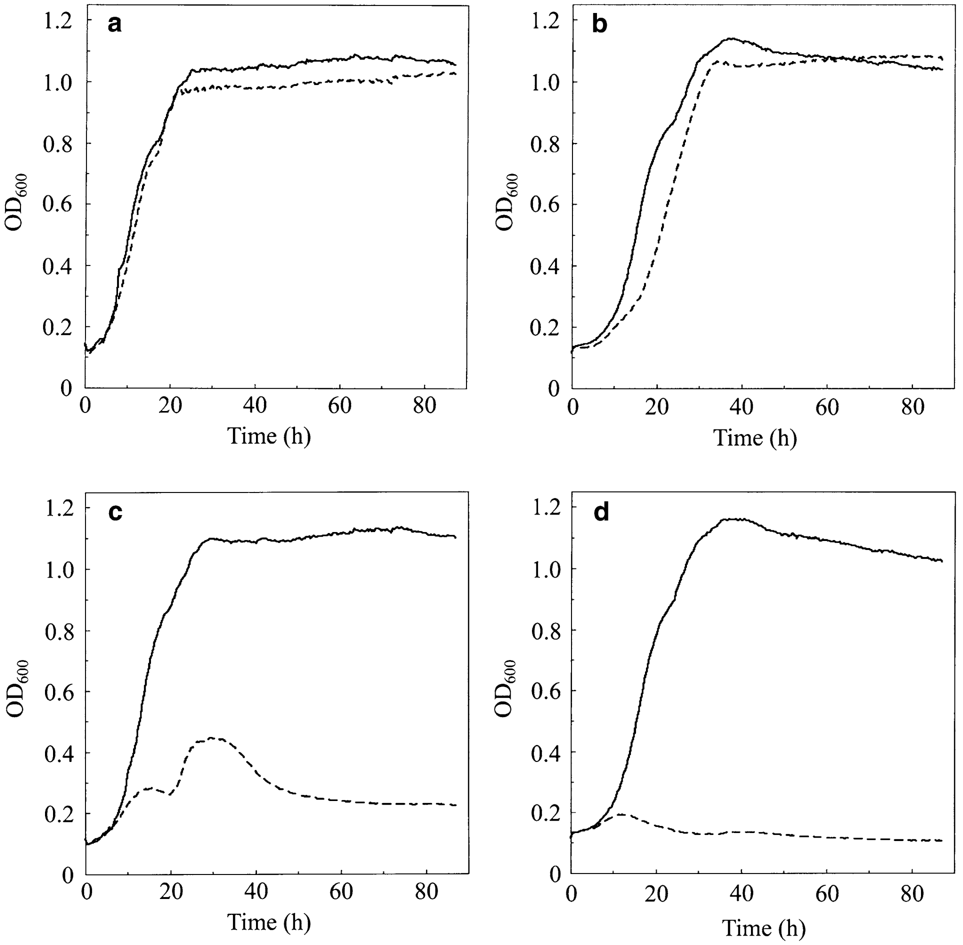

Fig. 5 Growth curves for the *YUG37:erg11* yeast strain measured using a Bioscreen C^{TM} instrument in the absence (*solid line*) and in the presence of 100 µg ml^{-1} doxycycline (*dashed line*). The sample frequency was 20 min. The response to doxycycline treatment of the wild-type *YUG37* strain (**a**), *YUG37:erg11* carrying the pYES2.1 plasmid with *P. chrysosporium* CYP51 (**b**), *YUG37:erg11* (**c**) and *YUG37:erg11* carrying the control pYES2.1 plasmid (**d**) was investigated

Table 1 Identification of conserved regions in basidiomycete CYP51 proteins

Block	Residues	Block sequence
A	55	51 P*****PP*VFH**P**GSA**YG*DP**F***CR*KYG**FTF*L*G***TVAL
B	53	130 LTTPVFGK*VVYD*PN***M*QK*F*K*G***E****Y***I**E***F****
C	46	206 *E**ILTASRTLQG*EVR**L***FA**Y*DLD*G*TP**F**PNL
D	27	252 PL*S***RD*A****S*FY**I***R*
E	39	308 *IAH*MIALLMAGQHTSSAT*SW**L*LA**P*****L*
F	43	371 *P**D**I*ETLR*H*PIHSI*R*V**D**VP**L********
G	34	414 Y*IPKG****A*P**SQ*DP*IW*******P*RW
H	44	469 D*G*G**S*G**SPY*PFGAG*HRC*GEQFAY*Q*********R

The on-line program BLOCKMAKER (http://blocks.fhcrc.org/blocks/make_blocks.html) was used to identify conserved ungapped 'MOTIF' regions of amino acid residues between *P. chrysosporium* CYP51 cDNA (FJ174578) and eight other basidiomycete CYP51 proteins from *Puccinia graminis* (PTGT07202 http://www.broad.mit.edu/annotation/genome/puccinia_graminis), *Coprinopsis cinerea* okayama7#130 (A8NUS3), *Antrodia cinnamomea* (A8DBU6), *Coprinus cinereus* (Q68HC4), *Cryptococcus neoformans* var. grubbi (Q870D1), *Cryptococcus neoformans* var. neoformans (Q9P8P1), *Malassezia globosa* CBS7966 (A8Q3I7) and *Ustilago maydis* (P49602). Amino acid residues conserved between eight of the nine sequences are listed and non-conserved amino acid residues are represented by a star symbol. The conserved sequence of block B does not include data from *P. graminis* CYP51, as this region (B' helix–B'C loop) appeared to be absent from the assembled sequence PTGT07202. The amino acid sequence of block B therefore represents the conserved residues of seven out of the eight remaining sequences. The residue numbers of each block relates to the start position in the *P. chrysosporium* CYP51 protein

blocks F, E and B, respectively. Blocks B, E and F contain the binding sites for fluconazole and other azole drugs. The residues through which the azoles interact appear less conserved than those of the heme-binding sites, allowing differences in azole specificity amongst CYP51 proteins from different species.

An alignment of deposited full length CYP51 sequences in the EXPASY (http://expasy.org/) and NCBI (http://www.ncbi.nlm.nih.gov/Genbank/) databases (93 sequences including 10 mammalian, 14 other animal, 42 yeast and fungal, 17 bacterial, 10 plant) and recently elucidated CYP51 sequences for *Mycobacterium avium*, Wheat, Poplar, Tomato, *Arabidopsis thaliana*, Dog, *Monosiga ovata*, *Aspergillus nidulans*, *Trypanosoma brucei* and *Aspergillus niger* was created using the computer program ClustalX. This alignment identified ten conserved amino acid residues amongst all the CYP51 proteins. For *P. chrysosporium* CYP51, the ten conserved residues corresponded to 219G, 380E, 383R, 393R, 446R, 488G, 490G, 492H, 494C and 496G. The amino acid residue 219G was located in block C and residues 380E, 383R and 393R were located in block F, which participates in binding azole antifungal agents. Residue 446R was located in block G and residues 488G, 490G, 492H, 494C and 496G were located in block H, the main C-terminal heme-binding region of *P. chrysosporium* CYP51. The eight conserved amino acids within blocks F and H confirms the importance of these two regions in correct CYP51 function. Many recently deposited CYP51 sequences have been identified from automated DNA sequencing results generated during genome mapping projects. In most cases functionality of 'putative' CYP51s have not been demonstrated by cloning and expression studies. Once more CYP51 sequences have been verified by cloning and expression, the number of conserved CYP51 residues may rise above 10 when only reliable CYP51 sequences are aligned.

Further studies on CYP51 and other CYPs present in *P. chrysosporium* are required to unravel the biological functions of this complex CYPome. Our study indicates the importance of analyzing actual transcript and protein when studying and comparing the annotated or unannotated cytochromes P450 sequences of genome projects such as for *P. chrysosporium* as well as in comparisons between the sequences of CYP51s across the Kingdoms of Life.

Acknowledgments We are grateful to the Biotechnology and Biological Science Research Council of the UK for support.

References

1. Pszczynski A, Crawford RL (1995) Potential for bioremediation of xenobiotic compounds by the white-rot fungus *Phanerochaete chrysosporium*. Biotechnol Prog 11:368–379
2. Juhasz A, Naidu R (2000) Bioremediation of high molecular weight polycyclic aromatic hydrocarbons: a review of the microbial degradation of benzo(a)pyrene. Int Biodeter Biodegrad 45:57–88
3. Bumpus JA, Aust SD (1987) Biodegradation of DTT [1, 1, 1-trichloro-2, 2-bis(4-chlorophenyl)ethane] by the white rot fungus *Phanerochaete chrysosporium*. Appl Environ Microbiol 53:2001–2008
4. Reddy CA (1995) The potential for white-rot fungi in the treatment of pollutants. Curr Opin Biotechnol 6:320–328
5. Masaphy S, Levanon D, Henis Y, Venkateswarlu K, Kelly SL (1996) Evidence for cytochrome P450 and P450-mediated benzo(a)pyrene hydroxylation in the white-rot fungus *Phanerochaete chrysosporium*. FEMS Lett 135:51–55
6. Doddapaneni H, Chakraborty R, Yadav JS (2005) Genome-wide structural and evolutionary analysis of the P450 monooxygenase genes (P450ome) in the white rot fungus *Phanerochaete chrysosporium*: evidence for gene duplications and extensive gene clustering. BMC Genomics 6:92
7. Yadav JS, Loper JC (2000) Cytochrome P450 oxidoreductase gene and its differentially terminated cDNAs from the white-rot fungus *Phanerochaete chrysosporium*. Curr Genet 37:65–73
8. Martinez D, Larrondo LF, Putnam N, Gelpke MD, Huang K, Chapman J, Helfenbein KG, Ramaiya P, Detter JC, Larimer F, Coutinho PM, Henrissat B, Berka R, Cullen D, Rokhsar D (2004) Genome sequence of the lignocellulose degrading fungus *Phanerochaete chrysosporium* strain RP78. Nat Biotechnol 22:695–700
9. Kelly SL, Lamb DC, Jackson CJ, Warrilow AGS, Kelly DE (2003) The biodiversity of microbial cytochromes P450. Adv Microb Physiol 47:131–186
10. Doddapaneni V, Subramanian V, Yadav JS (2005) Physiological regulation, xenobiotic induction, and heterologous expression of P450 monooxygenase gene *pc-3* (CYP63A3), a new member of the CYP63 gene cluster in the white-rot fungus *Phanerochaete chrysosporium*. Curr Microbiol 50:292–298
11. Doddapaneni H, Yadav JS (2004) Differential regulation and xenobiotic induction of tandem P450 monoxygenase genes *pc-1* (CYP63A1) and *pc-2* (CYP63A2) in the white-rot fungus *Phanerochaete chrysosporium*. Appl Microbiol Biotechnol 65:559–565
12. Matsuzaki F, Wariishi H (2005) Molecular characterization of cytochrome P450 catalyzing hydroxylation of benzoates from the white-rot fungus *Phanerochaete chrysosporium*. Biochem Biophys Res Commun 334:1184–1190
13. Gietz RD, Schiestl RH (1991) Application of high efficiency lithium acetate transformation of intact yeast cells using single-stranded nucleic acids as carrier. Yeast 7:253–263
14. Arase M, Waterman MR, Kagawa N (2006) Purification and characterization of bovine steroid 21-hydroxylase (P450c21) efficiently expressed in *Escherichia coli*. Biochem Biophys Res Commun 344:400–405
15. Bellamine A, Mangla AT, Nes WD, Waterman MR (1999) Characterization and catalytic properties of the sterol 14 alpha-demethylase from *Mycobacterium tuberculosis*. Proc Natl Acad Sci USA 96:8937–8942
16. Laemmli UK (1970) Cleavage of structural proteins during the assembly of the head of bacteriophage T_4. Nature 227:680–685
17. Omura T, Sato R (1964) The carbon monoxide-binding pigment of liver microsomes. I. Evidence for its hemoprotein nature. J Biol Chem 239:2370–2378
18. Lamb DC, Kelly DE, Schunck WH, Shyadehi AZ, Akhtar M, Lowe DJ, Baldwin BC, Kelly SL (1997) The mutation T315A in *Candida albicans* sterol 14alpha-demethylase causes reduced enzyme activity and fluconazole resistance through reduced affinity. J Biol Chem 272:5682–5688
19. Lamb DC, Kelly DE, Venkateswarlu K, Manning NJ, Bligh HF, Schunck WH, Kelly SL (1999) Generation of a complete, soluble, and catalytically active sterol 14 alpha-demethylase–reductase complex. Biochemistry 38:8733–8738
20. Ouellet H, Podust LM, Ortiz de Montellano PR (2008) *Mycobacterium tuberculosis* CYP130: crystal structure, biophysical characterization, and interactions with antifungal azole drugs. J Biol Chem 283:5069–5080

21. Hegemann J (1998) Essential genes and gene families. EUROFAN, Interim Report 1, pp 33–34
22. Groenveld P, Rolley N, Kell DB, Kelly SL, Kelly DE (2002) Metabolic control analysis and engineering of the yeast sterol biosynthetic pathway. Mol Biol Rep 29:27–29
23. Revankar SG, Fu J, Rinaldi MG, Kelly SL, Kelly DE, Lamb DC, Keller SM, Wickes BL (2004) Cloning and characterization of the lanosterol 14α-demethylase (ERG11) gene in *Cryptococcus neoformans*. Biochem Biophys Res Commun 324:719–728
24. Kelly SL, Arnoldi A, Kelly DE (1993) Molecular genetic analysis of azole antifungal mode of action. Biochem Soc Trans 98:1034–1038
25. Lamb DC, Kelly DE, Waterman MR, Stromstedt M, Rozman D, Kelly SL (1999) Characteristics of the heterologously expressed human lanosterol 14α-demethylase (other names: P45014DM, CYP51, P45051) and inhibition of the purified human and *Candida albicans* CYP51 with azole antifungal agents. Yeast 15:755–763
26. Kelly SL, Lamb DC, Loeffler J, Einsele H, Kelly DE (1999) The G464S amino acid substitution in *Candida albicans* sterol 14α-demethylase causes fluconazole resistance in the clinic through reduced affinity. Biochem Biophys Res Commun 262:174–179
27. Kalb VF, Loper JC, Dey CR, Woods CW, Sutter TR (1986) Isolation of a cytochrome P450 structural gene from *Saccharomyces cerevisiae*. Gene 45:237–245
28. Kalb VF, Woods CW, Turi TG, Dey CR, Sutter TR, Loper JC (1987) Primary structure of the P450 lanosterol demethylase gene from *Saccharomyces cerevisiae*. DNA 6:529–537
29. Lamb DC, Kelly DE, Manning NJ, Hollomon DW, Kelly SL (1998) Expression, purification, reconstitution and inhibition of *Ustilago maydis* sterol 14α-demethylase (CYP51; $P450_{DM}$). FEMS Microbiol Lett 169:369–373
30. Podust LM, Poulos TL, Waterman MR (2001) Crystal structure of cytochrome P450 14α-sterol demethylase (CYP51) from *Mycobacterium tuberculosis* in complex with azole inhibitors. Proc Natl Acad Sci USA 98:3068–3073

absorption and circulatory concentrations of non-cholesterol sterols. Berge et al. observed that lower baseline PS concentrations were associated with two common sequence variations, 145 G > C (D19H) and 1289 C > A (T400 K) of the *ABCG8* half-transporter gene [11]. Other researchers found that variations in T400 K may explain cross-sectional differences in plasma PS concentrations and determine the responsiveness for changes in plasma PS concentrations [12]. Further, variations in D19H may be associated with responsiveness to atorvastatin therapy [6]. In addition, these SNPs may also explain the inter-individual responsiveness to dietary PS [12] or cholesterol [3, 13] interventions in humans. Such findings implicate SNP variations in *ABCG5/G8* as playing key roles in regulating circulatory sterol concentrations. It remains nevertheless unclear whether *ABCG5/G8* polymorphisms could also affect sterol absorption and synthesis kinetics in response to PS intervention.

The NPC1L1 protein is a key modulator of cholesterol influx from micelles into intestinal mucosal cells [1, 4, 14]. Variations in the *NPC1L1* gene have been shown to be associated with an improved LDL-C lowering effect [4], and may explain inter-individual variations in LDL-C level response to ezetimibe treatment [1, 15, 16]. Several rare genotype variations in *NPC1L1* are associated with reductions in sterol absorption and circulatory LDL-C concentrations [1]. Some common SNPs in *NPC1L1* such as 872 C > G (L272L) have shown to be associated with inter-individual variation in ezetimibe response [1, 16]. In terms of PS supplementation, however, human trials have yet to be performed to address whether *NPC1L1* polymorphisms play a role in the cholesterol lowering responsiveness.

Moreover, no data are currently available to identify the combined effects of the *ABCG5/G8* and *NPC1L1* genotype SNP variations on changes in sterol absorption, cholesterol synthesis and plasma sterol concentrations in context of PS intervention. Subsequently, the aim of the present study was to investigate in 82 hypercholesterolemic men whether the SNP variations in *ABCG5/G8* and *NPC1L1* are individually or mutually associated with (1) basal absorption and circulatory concentrations of cholesterol and PS, (2) with changes in absorption and circulatory concentrations of cholesterol and PS after supplementation with 2 g/day of PS, and (3) with inter-individual variation in cholesterol lowering response to PS intervention.

Experimental Procedure

PS Enriched Diet Intervention and Blood Lipid Analyses

A randomized, crossover design was employed with two 4-week intervention phases, separated by a 4-week washout period in 82 hypercholesterolemic men characterized by high vs. low basal plasma PS concentrations. The experimental protocol was approved by the Ethics Committee of the Faculty of Medicine at McGill University. Details of volunteer recruitment, study diet, blood collection and analysis for testing serum concentrations of total cholesterol (TC), high density lipoprotein (HDL), LDL, triacylglycerol (TG) as well as plasma PS concentrations have been previously described by Houweling et al. [17].

Analyses of Sterol Absorption and Synthesis

On day 25, subjects were randomly designated to receive a single bolus of either 100 mg of D_7-campesterol ($n = 43$) or D_7-sitosterol ($n = 39$) within a 10 g aliquot of margarine in order to measure campesterol or sitosterol absorption. Simultaneously, 75 mg of $^{13}C_2$-cholesterol was orally given to all subjects for measurement of cholesterol absorption. On day 28, subjects also received a 25 g oral dose of D_2O (isotope purity > 99%), to measure cholesterol synthesis rate during the following 24-h period. All isotope chemicals were purchased from CDN Isotope, Pointe-Claire, Quebec, Canada.

The absorption indices of campesterol, sitosterol and cholesterol in the red blood cell (RBC) free sterol pool were assessed using a single stable isotope tracer method, which has been validated previously [18]. Total sterols were extracted and separated with the method as reported previously [19]. Free cholesterol ^{13}C enrichments were measured by differential isotope ratio mass spectrometry (IRMS), using an automated dual-inlet system (SIRA 12; Isomass, Cheshire, UK). Free PS deuterium (D) enrichments were measured by differential IRMS, using a dual-inlet system (VG Isomass 903 D; Cheshire, England). The absorption indices of campesterol and sitosterol were expressed as the averaged D enrichments between 24–72 h over baseline (0 h), relative to standard mean ocean water, in the RBC free sterol pool. The absorption index of cholesterol was expressed as the averaged ^{13}C enrichments between 24 and 96 h above the baseline level (0 h) in the RBC free sterol pool. Cholesterol fractional synthesis rate (FSR) was defined as the rate of incorporation of D from body water into RBC free cholesterol during the last 24 h of each treatment phase, and expressed as FSR in pools per day (pool per day) as previously described [19, 20].

Analyses of *ABCG5/G8* and *NPC1L1* Genotype SNPs

The *ABCG5/G8* polymorphisms, 1950 G > C (Q604E), 145 G > C (D19H), 1289 C > A (T400 K) and 1572 (A632 V), as well as the *NPC1L1* polymorphisms, 872 C > G (L272L) and 3929 G > A (Y1291Y), were screened from the published SNP data demonstrating an established functional significance for cholesterol modulation. DNA was extracted from 0.5 to 1.0 mL of plasma by QIAamp DNA Blood Mini Kit (Qiagen Inc, Canada). SNPs in *ABCG5/G8* and *NPC1L1* were determined using PCR-based TaqMan allele discrimination assays (Applied Biosystems, Foster City, CA, USA). The primers used for PCR have been described previously [6, 21–23]. A 7500 Real Time PCR thermal-cycler (Applied Biosystems, Foster City, CA, USA) was used for PCR analysis. Reactions were initially subjected to 92 °C for 10 min, and then 40 cycles, each of which was started at 95 °C for 15 s and 60 °C for 1 min for absolute quantification and then 60 °C for 1 min for allelic discrimination.

Statistical Analyses

Subjects were classified according to the criteria of (1) the screening sum of basal circulatory plasma PS concentrations (campesterol + sitosterol) into a high PS group (>50th percentile, $n = 41$) and a low PS group (<50th percentile, $n = 41$), or (2) responsiveness in serum lipid profiles to PS intervention into PS responders and non-responders. Subjects demonstrating a placebo adjusted reduction in both TC and LDL in response to PS intake were classified as responders; they were otherwise classified as non-responders. The SNP variations whose allele frequencies were abiding by the Hardy–Weinberg distribution equation were included in the statistical analysis. Prior to the analysis of diet–SNP interaction, the minor homozygous variants (mutant homozygote, $n \leq 4$) were collapsed to the heterozygote group. Similarly, in analyzing the combined effect of two transporter genes, due to the limited number of participating subjects and the similarity in phenotypes in terms of cholesterol metabolism, *NPC1L1* haplotypes with either or both heterozygous L272L and Y1921Y were combined into one heterozygous category. For serum TC, LDL-C, HDL-C and TG concentrations, data at baseline (day 1) and endpoint (day 29) of each phase were compared by performing analysis of covariance (ANCOVA) of proc mixed linear mode (SAS 9.1, Cary, NC, USA) to identify treatment effects and their interactions with high vs. low basal plasma PS concentrations and genotype variations. When treatment effect was identified as significant, Duncan's post hoc tests were utilized at particular time points. The normality distribution was evaluated with Shapiro–Wilk test ($p > 0.05$). Unpaired one-tailed *t*-test or one-way ANOVA was employed between individuals with high and low basal plasma PS concentrations or among the different common polymorphisms within the same phase where appropriate. A two-way ANOVA was employed to examine the interaction of metabolic parameters with different common polymorphisms. The distribution patterns of two factors were analyzed by chi-square test followed by one-sided Fisher's exact test. All data are expressed as mean ± standard error of the mean. The level of significance was established at $\alpha = 0.05$, unless otherwise noted.

Results

Responders and Non-Responders to PS Intake

Eighty-two hypercholesterolemic men completed the crossover study with consumption of a placebo spread or a spread delivering 2 g/day of PS. Responders were those who showed a reduction (placebo adjusted) in both TC and LDL-C; otherwise they were classified as non-responders in that at least one of TC and LDL-C was not reduced. Responders ($n = 51$, 62%) and non-responders ($n = 31$, 38%) clearly manifested differing serum cholesterol responses to PS intervention for both TC (−12.7 ± 1.2% vs. 4.42 ± 1.2%, respectively, $p < 0.0001$) and LDL-C (−18.3 ± 2.0% vs. 9.41 ± 2.5%, respectively, $p < 0.0001$) (Table 1).

Absorption indices of campesterol, sitosterol and cholesterol did not differ among responders and non-responders (Table 2). In terms of cholesterol synthesis rate expressed as FSR, responders demonstrated a 20.7% lower FSR (4.68 ± 0.27% vs. 5.65 ± 0.43%, $p < 0.05$) in comparison to non-responders during the control phase. In the phase of PS intake, however, the difference in FSR values between responders and non-responders became very narrow (6.30 ± 0.37% vs. 6.64 ± 0.48%), because the responders achieved a greater percentage increase in FSR (38.5 ± 4.8% vs. 24.3 ± 5.9%, $p < 0.05$) than did non-responders.

Table 2 also indicates that subjects with low basal PS plasma concentrations were characterized as possessing low sterol absorption and high cholesterol FSR, a pattern that was reversed in subjects with high basal plasma PS concentrations. We also noticed a trend ($p = 0.086$, chi-square test, followed by Fisher's exact test) of responders converging in the high basal PS group vs. non-responders in the low basal PS group. Among responders there were less individuals categorized with low basal PS (43% of total 51 responders) than identified with high basal PS concentrations. Inversely, in the group of non-responders, there were more individuals possessing low basal PS levels (61% of total 31 non-responders).

Relation of *ABCG5/G8* Gene Polymorphism Variations with Responsiveness to PS Intake

The genotype frequencies of *ABCG5/G8* common polymorphisms, T400 K, D19H and A632 V, were identified to abide with Hardy–Weinberg equilibrium [24]. As listed in

Table 1 Baseline and endpoint plasma concentrations of plant sterols and lipid profiles between responders vs. non-responders

Subjects	Phases	Plasma plant sterol concentrations (μmol/L)[a]		Plasma lipid concentrations (mmol/L)[a]			
		Campesterol	Sitosterol	TC	LDL	HDL	TG
Responder[a]	*Control*						
	Baseline (day 1)	20.06 ± 1.49	12.50 ± 1.13	5.73 ± 0.14	3.68 ± 0.12	1.18 ± 0.03	2.02 ± 0.15
	Endpoint (day 29)	17.09 ± 1.28	10.10 ± 0.96	5.45 ± 0.14	3.61 ± 0.12	1.10 ± 0.03	1.68 ± 0.11
	%Change[b]	−5.5 ± 5.5%	−38.7 ± 10.9%***	−4.3 ± 1.4%	−0.5 ± 2.3%	−5.1% ± 1.7%*	−10.0 ± 3.7%
	PS intake						
	Baseline (day 1)	19.03 ± 1.65	11.63 ± 1.36	6.05 ± 0.14	3.95 ± 0.11	1.22 ± 0.04	2.06 ± 0.16
	Endpoint (day 29)	20.95 ± 1.42	12.26 ± 1.01	5.01 ± 0.13	3.20 ± 0.11	1.07 ± 0.03	1.65 ± 0.12
	%Change[b]	24.9 ± 7.6%	34.4 ± 12.9%	−17.0 ± 1.2%***	−18.8 ± 1.5%***	−11.8 ± 1.6%***	−14.7 ± 4.0%*
	Inter-phase difference[c]	30.0 ± 6.9%	71.9 ± 13.2%	−12.7 ± 1.2%	−18.3 ± 2.0%	−6.73 ± 1.7%	−4.73 ± 5.0%
Non-responder[a]	*Control*						
	Baseline (day 1)	17.01 ± 1.64	12.50 ± 1.95	5.77 ± 0.14	3.61 ± 0.12	1.21 ± 0.05	2.18 ± 0.22
	Endpoint (day 29)	14.48 ± 1.72	9.61 ± 1.37	4.85 ± 0.15	3.05 ± 0.11	1.02 ± 0.04	1.73 ± 0.13
	%Change[b]	−2.37 ± 13.3%	−40.1 ± 11.0%**	−15.8 ± 1.8%***	−14.7 ± 2.0%**	−15.4 ± 2.2%**	−11.2 ± 6.7%*
	PS intake						
	Baseline (day 1)	16.91 ± 1.80	13.98 ± 2.30	5.40 ± 0.14	3.20 ± 0.11	1.18 ± 0.05	2.30 ± 0.18
	Endpoint (day 29)	18.01 ± 1.23	13.30 ± 1.92	4.78 ± 0.16	3.02 ± 0.13	1.03 ± 0.05	1.62 ± 0.12
	%Change[b]	26.6 ± 10.2%	20.5 ± 11.5%	−11.4 ± 1.7%**	−5.2 ± 2.5%	−12.4 ± 2.2%*	−23.6 ± 4.8%**
	Inter-phase difference[c]	24.2 ± 17.8%	60.6 ± 16.9%	4.42 ± 1.2%	9.41 ± 2.5%	2.98 ± 1.9%	−12.5 ± 7.3%

Values are means ± SEM

[a] Responders are those subjects who showed a reduction (placebo adjusted) in both TC and LDL-C; otherwise they were classified as non-responders (at least one of TC and LDL-C was not reduced)

[b] %Change is percentage change of endpoint value (day 29) over that of baseline (day 1). Differences between two values were analyzed by paired *t*-test, the significance was expressed as * $p < 0.05$, ** $p < 0.01$, *** $p < 0.001$

[c] Inter-phase differences were the values of %change of PS intake phase subtracted by %change of control phase

Table 3, individuals with high and low basal plasma PS concentrations were almost equally distributed across the majority of the wild type homozygote SNP cohorts examined. However, in the heterozygote SNP cohorts, individuals with low basal PS out-numbered those with high basal PS concentrations. In terms of responsiveness to PS intervention, non-responders of heterozygous individuals were predominantly clustered within the low basal PS, but not within the high basal PS group. Most typically, for the *ABCG8* T400 K polymorphisms, TT and TK/KK, individuals with high and low basal PS concentrations were differently distributed ($p < 0.05$). Among homozygote (TT) carriers, 61 and 39% were categorized as high and low basal PS individuals, respectively. Among heterozygote (TK/KK) carriers, this distribution was reversed to be 33 and 67% in individuals with high and low basal PS concentrations, respectively.

In view of the distribution of responders and non-responders among different *ABCG8* T400 K polymorphisms, the numbers of responders and non-responders were not different ($p = 0.38$) among the high vs. low basal PS groups possessing TT polymorphism. However, for the TK/KK polymorphism, 10 of 11 non-responders were concentrated in the low basal PS group and only one non-responder was characterized as having a high basal PS concentration ($p < 0.05$; Fig. 1). This pattern was consistently reflected in cholesterol response to PS intake. Individuals carrying the TT genotype manifested a similar cholesterol response among the high vs. low basal PS groups (Fig. 2). In the individuals carrying TK/KK genotypes, those in the high basal PS group presented a 2.5-fold greater response in TC (−10.4 ± 2.3% vs. −3.0 ± 3.4%, $p < 0.05$) and a 3.9-fold greater response in LDL-C (−16.6 ± 6.3% vs. −3.4 ± 5.7%, $p < 0.05$) as compared with those in the low basal PS group.

ABCG8 T400 K polymorphisms were also identified to be associated with variations in basal plasma PS concentration. With the T400 K polymorphism, TT carriers presented higher plasma concentrations of campesterol (12.2 ± 0.8 μmol/L vs. 9.7 ± 0.9 μmol/L, $p < 0.05$), sitosterol (6.5 ± 0.4 μmol/L vs. 5.1 ± 0.5 μmol/L, $p < 0.05$) and sum of campesterol and sitosterol (18.7 ± 1.2 μmol/L vs. 14.8 ± 1.4 μmol/L, $p < 0.05$), respectively, as compared with TK/KK carriers (Fig. 3).

Table 2 Sterol kinetic profiles in response to PS intake in hypercholesterolemic men with high and low basal PS concentrations

Subjects	Phases	Absorption index (per mL)[3]		Cholesterol synthesis rate (% pool per day)[3]
		Campesterol or sitosterol	Cholesterol	
Responder[1]	*Control*			
	All ($n = 51$)[2]	60.1 ± 6.8	5.47 ± 0.21	4.68 ± 0.27^{a}
	H_PS ($n = 29$)[2]	74.8 ± 10.0	5.61 ± 0.30	4.47 ± 0.36^{a}
	L_PS ($n = 22$)[2]	40.8 ± 7.0^{a}	5.29 ± 0.27	4.98 ± 0.43^{a}
	PS intake			
	All[2]	36.4 ± 5.3 (−40.8 ± 3.5%)[4]	3.52 ± 0.16 (−34.0 ± 2.7%)[4]	6.30 ± 0.37 (38.5 ± 4.8%)[4, b]
	H_PS[2]	46.9 ± 8.3 (−40.8 ± 4.7%)[4]	3.66 ± 0.22 (−32.6 ± 3.6%)[4]	6.39 ± 0.56 (44.6 ± 6.4%)[4, b]
	L_PS[2]	22.4 ± 3.9 (−40.9 ± 5.4%)[4, b]	3.33 ± 0.22 (−35.9 ± 4.0%)[4]	6.18 ± 0.44 (29.9 ± 6.9%)[4, b]
Non-responder	*Control*			
	All ($n = 31$)[2]	64.3 ± 8.3	5.06 ± 0.29	5.65 ± 0.42
	H_PS ($n = 12$)[2]	65.7 ± 14.6	5.46 ± 0.58	4.34 ± 0.46
	L_PS ($n = 19$)[2]	63.5 ± 10.5^{a}	4.83 ± 0.32	6.52 ± 0.56
	PS intake			
	All[2]	39.1 ± 5.0 (−32.9 ± 5.4%)[4]	3.26 ± 0.23 (−34.7 ± 3.1%)[4]	6.64 ± 0.48 (24.3 ± 5.9%)[4]
	H_PS[2]	41.8 ± 9.3 (−26.7 ± 11.5%)[4]	3.92 ± 0.46 (−27.0 ± 6.2%)[4]	5.14 ± 0.37 (26.9 ± 10.7%)[4]
	L_PS[2]	37.5 ± 6.1 (−36.7 ± 5.2%)[4, b]	2.88 ± 0.21 (−39.2 ± 3.2%)[4]	7.64 ± 0.69 (22.5 ± 7.3%)[4]

Values are means ± SEM. Different superscript letters represent significant inter-phase differences ($p < 0.05$)

[1] For description of responders and non-responders, see Table 1

[2] H_PS and L_PS represent high (>50th percentile, $n = 41$) and low (<50th percentile, $n = 41$) sum of PS (campesterol + sitosterol) concentrations at screening, respectively. All represents total subjects ($n = 82$). The distribution of responders and non-responders among H_PS and L_PS groups was analyzed using chi-square test, followed by one-side Fisher's exact test

[3] Absorption indices and synthesis rates were the endpoint values of each phase

[4] The values in parentheses are the percentage change of values in PS intake phase over that in control phase

Table 3 Distribution of *ABCG5/G8* and *NPC1L1* gene polymorphisms in hypercholesterolemic men with high vs. low basal PS levels

SNP name	SNP type	SNP subjects numbers							
		By responsiveness[a]						By basal plasma plant sterol concentrations[b]	
		Responder[a]			Non-responder[a]			H_PS[b]	L_PS[b]
		H_PS[b]	L_PS[b]	H + L_PS[b]	H_PS[b]	L_PS[b]	H + L_PS[b]		
ABCG8									
A632 V	AA (68)	27 (59%)[c]	19 (41%)[c]	46	10 (45%)[c]	12 (55%)[c]	22	37 (54%)[c]	31 (46%)[c]
	VA (11)	2 (40%)[c]	3 (60%)[c]	5	2 (33%)[c]	4 (67%)[c]	6	4 (36%)[c]	7 (64%)[c]
T400 K*	TT (51)	20 (59%)[c]	14 (41%)[c]	34	11 (65%)[c]	6 (35%)[c]	17	31 (61%)[c]	20 (39%)[c]
	TK/KK (28)	9 (53%)[c]	8 (47%)[c]	17	1 (9%)[c]	10 (91%)[c]	11	11 (39%)[c]	17 (61%)[c]
D19H	DD (70)	25 (57%)	19 (43%)	44	12 (46%)	14 (54%)	26	37 (53%)	33 (47%)
	DH (9)	4 (57%)	3 (43%)	7	0 (0 %)	2 (100%)	2	4 (44%)	5 (56%)
NPC1L1									
L272L	G/G (43)	15 (58%)	11 (42%)	26	7 (41%)	10 (59%)	17	22 (51%)	21 (49%)
	G/C,C/C (36)	14 (56%)	11 (44%)	25	5 (45%)	6 (55%)	11	19 (53%)	17 (47%)
Y1291Y	G/G (55)	19 (54%)	16 (46%)	35	7 (35%)	13 (65%)	20	26 (47%)	29 (53%)
	G/A,A/A (24)	10 (63%)	6 (37%)	16	5 (63%)	3 (37%)	8	15 (63%)	9 (37%)

Distributions of responders and non-responders among subjects with high and low basal PS levels at different SNPs were analyzed by chi-square test, followed by one-side Fisher's exact test, significant was considered at * $p < 0.05$

[a, b] For description of responders vs. non-responders and H_PS ($n = 41$) and L_PS ($n = 38$), see Table 1

[c] Percentage in parenthesis represents the % of the stated subject numbers over the total subject numbers

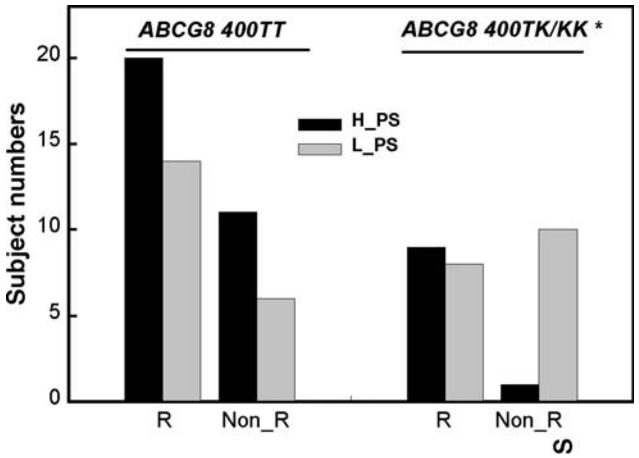

Fig. 1 Number of responders and non-responders with high and low basal plasma PS concentrations among different *ABCG8* T400 K polymorphisms *R* responder, *Non-R* non-responder. For description of H_PS and L_PS groups, see Table 2. Subject distributions between basal PS levels (H_PS vs. L_PS) and responsiveness (*R* vs. *Non-R*) in different SNP variations (TT vs. TK/KK) were analyzed by Chi-square test, followed by one-side Fisher's exact test (SAS 9.1). Significance of difference was set at * $p < 0.05$

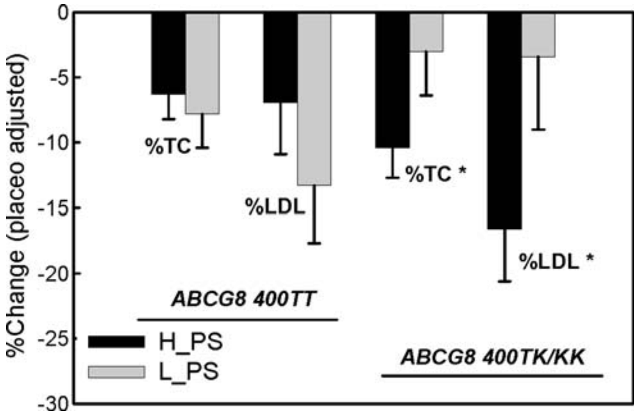

Fig. 2 Changes in plasma TC and LDL in response to PS intervention among subjects with different *ABCG8* T400 K polymorphisms. Analysis of covariance with mix linear mode (SAS 9.1) was used to analyze the interaction of PS levels and SNP variation in response to PS intervention. Main treatment $p < 0.0001$, interaction of SNP and PS levels (H_PS vs. L_PS), $p = 0.079$ for TC and $p = 0.016$ for LDL. Significance of difference in %TC and %LDL (both placebo adjusted) was set at * $p < 0.05$

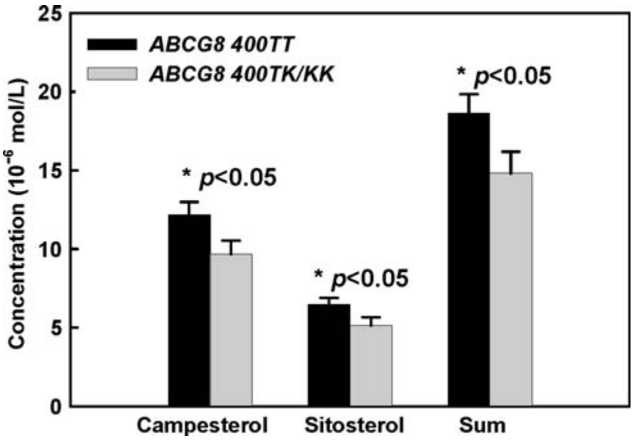

Fig. 3 Basal plasma PS concentrations among subjects with different *ABCG8* T400 K polymorphisms. Unpaired *t*-test for differences among polymorphisms, significance of the difference was set at * $p < 0.05$

Relation of *NPC1L1* Gene Polymorphism Variations with Cholesterol Responsiveness to PS Intake

Two sets of *NPC1L1* common polymorphisms, L272L and Y1291Y, were identified to abide with Hardy–Weinberg equilibrium and thus further analyzed. Results show that these SNPs were not related to basal cholesterol concentrations, nor with PS or cholesterol absorption indices (data not shown). Moreover, the numbers of responders and non-responders possessing different SNP variations were not statistically different (Table 4). However, heterozygous carriers demonstrated a trend of an enhanced cholesterol lowering effect in response to PS intervention, as compared to homozygous counterparts. With L272L polymorphisms, the mutant G allele carriers ($n = 37$) showed a trend of a greater reduction in TC (−9.8 ± 2.0% vs. −4.1 ± 1.6%, $p = 0.057$) and LDL-C (−14.5 ± 3.3% vs. −4.4 ± 2.5% $p = 0.082$) in comparison with their wild type counterparts (C/C, $n = 42$). Similarly, for the Y1291Y polymorphism, carriers of the mutant A allele ($n = 24$) showed a trend toward a greater TC lowering effect (−9.4 ± 2.1% vs. −5.6 ± 1.6%, $p = 0.073$) compared with their wild type counterparts ($n = 55$).

In terms of haplotypes of L272L and Y1291Y, individuals with either heterozygous L272L or heterozygous Y1291Y manifested a similar trend ($0.05 < p < 0.1$, two-way ANOVA) of greater reductions in TC and LDL-C as compared to their homozygous counterparts (Table 4). Subsequently, all haplotypes with any heterozygous SNPs were merged into one heterozygote category. TC concentrations in these individuals were lowered 1.3-fold more (−9.3 ± 1.8% vs. −4.1 ± 1.7%, $p < 0.05$) than those of homozygous subjects. Similarly, LDL-C was reduced 2.4-fold more (−13.4 ± 3.0 vs. −3.9 ± 2.9, $p < 0.05$).

Interactions of *ABCG8* and *NPC1L1* Polymorphism Variations with Cholesterol Responsiveness to PS Intake

Since the functions of *ABCG5/G8* and *NPC1L1* transporters are counter-opposing, when the two genotype variations coexist in one subject, the contribution of an individual SNP variation to phenotype cannot be correctly appreciated unless background effects are adjusted. Subjects were hence categorized into four subgroups according to the

Table 4 Single nuclear polymorphisms and haplotypes of *NPC1L1* on lipid in response to PS intake

SNP type	Allele loci and names		Plasma lipid changes (%, placebo adjusted)			
	+872 C > G (L272L)	+3929 G > A (Y1291Y)	TC	LDL	HDL	TG
Wild type[a]	C/C		−4.1 ± 1.6	−4.4 ± 2.5	−1.8 ± 1.9	−4.9 ± 6.2
Mutant allele[b]	C/G, G/G		−9.8 ± 2.0	−14.5 ± 3.3	−4.8 ± 2.1	−7.0 ± 5.3
p-Value main effect[c]			<0.0001	<0.0001	<0.0001	<0.0001
p-Value SNP effect[c]			0.057	0.082	NS	NS
Wild type[a]		G/G	−5.6 ± 1.6	−8.3 ± 2.7	−3.9 ± 1.7	−2.1 ± 5.3
Mutant allele[b]		G/A, A/A	−9.4 ± 2.1	−10.9 ± 2.9	−1.7 ± 2.6	−14.5 ± 5.5
p-Value, main effect[c]			<0.0001	<0.0001	<0.05	<0.0001
p-Value, SNP effect[c]			0.073	NS	NS	NS
Haplotypes						
Homozygote ($n = 38$)	C/C	G/G	−4.1 ± 1.7	−3.9 ± 2.9	−2.9 ± 2.0	−6.1 ± 7.2
Heterozygote ($n = 41$)	C/G, C/C, C/G	G/G, G/A, G/A	−9.3 ± 1.8	−13.4 ± 3.0	−3.9 ± 2.1	4.8 ± 5.8
p-Value, main effect[c]		<0.0001	<0.0001	<0.0001	<0.0001	−20.2 ± 6.4
p-Value, SNP effect[c]			<0.05	<0.05	NS	NS

NS not significant

[a] Wild type: homozygote with major allele

[b] Mutation variant: mutation heterozygote and minor homozygous allele

[c] Analysis of covariance with using baseline value as a covariate, the results were adjusted by the factor of SNPs

heterozygosity of polymorphisms and phenotype characteristics: (1) Ho_Ho *(ABCG8* T400T + *NPC1L1* homozygote); (2) He_Ho (*ABCG8* T400 K + *NPC1L1* homozygote); (3) Ho_He (*ABCG8* T400T + *NPC1L1* heterozygote); (4) He_He (*ABCG8* T400 K + *NPC1L1* heterozygote) (Table 5).

These four subgroups showed an overall difference in PS induced alterations in plasma LDL-C concentration ($p < 0.05$, two-way ANOVA). It was further revealed that individuals with *ABCG8* T400 K heterozygous genotypes against homozygous *NPC1L1* background (He_Ho) were the most refractory cohort to PS intervention, exhibiting a minimal change in LDL-C. Indeed, LDL-C levels in these individuals were slightly increased (+1.6 ± 7.2%) as a result of PS intake. In contrast, individuals with *NPC1L1* heterozygous genotypes against homozygous *ABCG8* background (Ho_He) displayed the most pronounced LDL-C lowering effect (−13.6 ± 4.0%). The LDL-C response in these two subgroups presented a striking contrast ($p < 0.05$). A similar difference ($p < 0.05$) was also seen for TC. As He_Ho classified individuals demonstrated a limited reduction in TC (−1.9 ± 4.4%), whereas Ho_He individuals showed a more enhanced reduction in TC concentrations (−9.3 ± 2.5%).

Table 5 Interaction of *ABCG8* T400 K SNP and *NPC1L1* L272 and/or Y1291Y haplotypes for responsiveness of PS intake

ABCG8	*NPC1L1*	Basal plasma plant sterol concentrations (μmol/L)		Absorption index (%change)[3]		Synthesis rate (%change)[3]	Plasma lipid change (%, placebo adjusted)[4]			
T400 K[1]	L272L/ Y1291Y[2]	Campesterol	Sitosterol	Campesterol or sitosterol	Cholesterol	Cholesterol	TC	LDL-C	HDL-C	TG
Ho	Ho	12.1 ± 1.0	6.5 ± 0.6	−33.2 ± 5.4	−33.8 ± 4.2	33.0 ± 7.5	−4.8 ± 1.8	−5.7 ± 3.0[ab]	−4.4 ± 2.2	−6.4 ± 9.0
He	Ho	10.0 ± 1.6	5.7 ± 1.0	−37.4 ± 8.7	−42.9 ± 4.7	37.5 ± 11.7	−1.9 ± 4.4	+ 1.6 ± 7.2[a]	1.4 ± 4.9	−5.3 ± 10.1
Ho	He	12.3 ± 1.3	6.4 ± 0.6	−37.6 ± 5.7	−27.7 ± 3.8	34.5 ± 6.7	−9.3 ± 2.5	−13.6 ± 4.0[b]	−3.2 ± 3.1	−5.1 ± 6.1
He	He	11.0 ± 1.6	5.6 ± 0.9	−38.7 ± 6.9	−38.0 ± 6.9	30.3 ± 8.5	−8.7 ± 2.5	−13.3 ± 4.1[b]	−3.7 ± 2.5	6.4 ± 7.4

Different superscript letters indicate the difference among the subgroups

[1, 2] *Ho*: homozygote, *He*: heterozygote; For *ABCG8 T400 K*, Ho (TT), He (TK/KK); for *NPC1L1*, Ho (872 C > G + 3929 G/G); He (872 C > G + 3929 G/G, 872 C/C + 3929 G > A, 872 C/G + 3929 G > A)

[3] %Change of kinetic values of PS intake phase over that of control phase

[4] %Change of values in PS intake phase subtracted by values of control phase. A two-way ANOVA, with adjustment for SNP effects, significance was set at $p < 0.05$

Discussion

The present work represents the first investigation of the relationship between genotype polymorphism variations in two important sterol transporter genes, *ABCG5/G8* and *NPC1L1*, and their response in cholesterol absorption and synthesis kinetics, as well as serum cholesterol concentrations, to dietary PS intervention. Results indicate that variations in both *ABCG5/G8* and *NPC1L1* polymorphisms have a profound effect on inter-individual responsiveness of cholesterol concentrations.

Inter-individual variation in PS-induced cholesterol response exists as a re-occurring problem encountered in clinical trials [1–4]. In this trial approximately one third of subjects (38%) were non-responders. It has been postulated that genetic predispositions could be attributable for response variations. *ABCG5/G8* transporters have been suggested to limit sterol absorption by both pumping the sterol back to the intestinal lumen and promoting biliary secretion from the liver [9, 10]. The results of the current study with hypercholesterolemic men indicate that different SNP profiles of *ABCG5/G8* are related to varying serum cholesterol response. Our results exemplify that homozygous carriers of *ABCG8* T400 K polymorphisms are more likely to be responders, whereas carriers of heterozygous polymorphisms showed a trend to be classified as non-responders. *ABCG8* T400 K was previously suggested by Plat et al. [12] to explain the inter-individual variation in PS metabolism in healthy volunteers after consumption of PS esters. These investigators observed that TT carriers possessed higher plasma campesterol and sitosterol concentrations in comparison to TK/KK carriers, a finding consistent with the results observed in the present study. In view of polymorphism distribution, it was further noticed that individuals with high basal plasma PS concentrations were more likely to possess the TT polymorphism, whereas individuals with low basal PS were predominantly carrying the TK/KK polymorphism. In terms of cholesterol response to PS intervention, our study further revealed that the varying cholesterol response among carriers with T400 K polymorphisms were likely associated with basal plasma PS concentrations. A poor responsiveness to PS intervention is associated with heterozygous polymorphism (TK/KK) of *ABCG8* T400 K in addition to a low basal plasma PS concentration.

NPC1L1 is another important sterol transporter protein that plays a critical role in intestinal uptake of both PS and cholesterol [14, 24]. NPC1L1 protein is also the postulated target for ezetimibe intervention, by which cholesterol absorption is suppressed [2]. Previously, Hegele et al. observed that *NPC1L1* haplotype variations were associated with inter-individual differences in plasma LDL-C response to ezetimibe [1]. However, whether *NPC1L1* polymorphism variations also explain the suppression in cholesterol absorption and plasma concentration as a result of PS intake remains unclear. The present study reveals the trends indicating that polymorphisms in *NPC1L1* L272L and Y1291Y augment the extent of PS-induced cholesterol lowering in comparison to wild type counterparts. There is an understanding that under certain circumstances, haplotypes may be a useful way to reduce the complexity of the candidate-gene association analyses [25], which is consistent with our findings that haplotypes of two SNP L272L and Y1291Y mutant alleles elicited a similar response to PS intervention. Obviously, our results are consistent with *NPC1L1* being closely involved in inter-individual variation in response to PS intervention, as it has been observed with ezetimibe therapy [1].

Another novel finding of the present study is the description of the combined effect of *ABCG8* and *NPC1L1* transporter genotype variations on the response to PS intervention. Kajinami et al. suggested that combined analysis of different polymorphisms is more informative than single locus analysis for defining the responsiveness of a patient to statin therapy [6]. These authors found that polymorphisms in *ABCG8* and *CYP7A1*, both of which are functionally significant in the secretion of cholesterol from the liver into bile, interact in an allele-cumulative manner in atorvastatin-treated subjects. However, in the present study, the combined actions of *ABCG8* T400 K and *NPC1L1* haplotypes of L272L/Y1291Y seem more complex than simply being cumulative; the phenotype expression of each individual polymorphism may interfere with the concurrence of two counteracting transporter gene polymorphisms. To more specifically expose the characteristics of target SNP variations, we singled out target SNP variants and pooled in common wild type background polymorphisms to more specifically portray the characteristics of target SNP variations.

Very recently, a case–control study by Rudkowska et al. [26] also tested the same sets of SNPs in *ABCG5/G8* and *NPC1L1* among 26 hyperlipidemic subjects after PS intervention, but small sample size in their study design made the results ineligible for statistical analysis. In extending of Rudkowska et al.'s [26] work, our trial recruited more subjects, and plasma lipid response was analyzed in context of background adjusted SNPs of *ABCG8* and *NPC1L1*. Subsequently, the results of the present trial managed to unravel that heterozygous *ABCG8* T400 K genotypes attenuate the cholesterol lowering response, while heterozygous haplotypes of *NPC1L1* L272L/Y1291Y enhance cholesterol lowering response to PS, in comparison with their respective wild type homozygous counterparts.

Limitations of this study include the fact that SNPs represent the most frequent form of polymorphism in the human genome [24]. According to the National Center for Biotechnology Information database, so far, 280 of *ABCG5/G8* and 70 of *NPC1L1* common polymorphism variations have been identified in the human genome. This study involves less than ten common polymorphism candidates that have known or predicted functional consequences with sterol metabolism based on previous studies [1, 4, 12, 13, 15]. Whether these individual or combined common polymorphisms are adequate to fully explain inter-individual variations of sterol metabolism cannot be fully identified from previous [1, 4, 12, 13, 15] and the present studies.

In conclusion, this study examined the role of *ABCG5/G8* and *NPC1L1* transporter gene common polymorphisms in explaining inter-individual responsiveness to PS intervention in the context of their impact on cholesterol absorption and synthesis. In the *ABCG8* T400 K polymorphism, heterozygous carriers with low basal plasma PS concentrations showed a minimal cholesterol reduction as compared to homozygote carriers. In contrast, among *NPC1L1* L272L/Y1291Y haplotypes, heterozygous carriers manifested a maximal cholesterol reduction as compared to homozygote carriers. Such a pattern was more obviously demonstrated after background SNP adjustment. Results suggest that common polymorphisms of sterol transporter genes, together with basal circulating plasma PS concentrations, are indicative of the expected cholesterol lowering effect induced by dietary PS intake.

Acknowledgments This project was supported by grants from Unilever R&D, Vlaardingen, the Netherlands, and by the Canadian Institutes of Health Research—Provincial Partnership Program. The authors thank Brian Sithoo for his technical support in SNP analysis and Iwona Rudkowska for her comments on discussion.

References

1. Hegele RA, Guy J, Ban MR, Wang J (2005) NPC1L1 haplotype is associated with inter-individual variation in plasma low-density lipoprotein response to ezetimibe. Lipids Health Dis 4:16
2. Wang J, Williams CM, Hegele RA (2005) Compound heterozygosity for two non-synonymous polymorphisms in NPC1L1 in a non-responder to ezetimibe. Clin Genet 67:175–177
3. Herron KL, McGrane MM, Waters D, Lofgren IE, Clark RM, Ordovas JM, Fernandez ML (2006) The ABCG5 polymorphism contributes to individual responses to dietary cholesterol and carotenoids in eggs. J Nutr 136:1161–1165
4. Cohen JC, Pertsemlidis A, Fahmi S, Esmail S, Vega GL, Grundy SM, Hobbs HH (2006) Multiple rare variants in NPC1L1 associated with reduced sterol absorption and plasma low-density lipoprotein levels. Proc Natl Acad Sci USA 103:1810–1815
5. Sehayek E, Nath C, Heinemann T, McGee M, Seidman CE, Samuel P, Breslow JL (1998) U-shape relationship between change in dietary cholesterol absorption and plasma lipoprotein responsiveness and evidence for extreme interindividual variation in dietary cholesterol absorption in humans. J Lipid Res 39:2415–2422
6. Kajinami K, Brousseau ME, Nartsupha C, Ordovas JM, Schaefer EJ (2004) ATP binding cassette transporter G5 and G8 genotypes and plasma lipoprotein levels before and after treatment with atorvastatin. J Lipid Res 45:653–656
7. Gylling H, Hallikainen M, Pihlajamaki J, Agren J, Laakso M, Rajaratnam RA, Rauramaa R, Miettinen TA (2004) Polymorphisms in the ABCG5 and ABCG8 genes associate with cholesterol absorption and insulin sensitivity. J Lipid Res 45:1660–1665
8. Field FJ, Born E, Mathur SN (2004) Stanol esters decrease plasma cholesterol independently of intestinal ABC sterol transporters and Niemann-Pick C1-Like 1 protein gene expression. J Lipid Res 45:2252–2259
9. Bhattacharyya AK, Connor WE (1974) Beta-sitosterolemia and xanthomatosis. A newly described lipid storage disease in two sisters. J Clin Invest 53:1033–1043
10. Klett EL, Patel S (2003) Genetic defenses against noncholesterol sterols. Curr Opin Lipidol 14:341–345
11. Berge KE, von Bergmann K, Lutjohann D, Guerra R, Grundy SM, Hobbs HH, Cohen JC (2002) Heritability of plasma noncholesterol sterols and relationship to DNA sequence polymorphism in ABCG5 and ABCG8. J Lipid Res 43:486–494
12. Plat J, Bragt MC, Mensink RP (2005) Common sequence variations in ABCG8 are related to plant sterol metabolism in healthy volunteers. J Lipid Res 46:68–75
13. Weggemans RM, Zock PL, Tai ES, Ordovas JM, Molhuizen HO, Katan MB (2002) ATP binding cassette G5 C1950G polymorphism may affect blood cholesterol concentrations in humans. Clin Genet 62:226–229
14. Davis HR Jr, Zhu LJ, Hoos LM, Tetzloff G, Maguire M, Liu J, Yao X, Iyer SP, Lam MH, Lund EG et al (2004) Niemann-Pick C1 Like 1 (NPC1L1) is the intestinal phytosterol and cholesterol transporter and a key modulator of whole-body cholesterol homeostasis. J Biol Chem 279:33586–33592
15. Simon JS, Karnoub MC, Devlin DJ, Arreaza MG, Qiu P, Monks SA, Severino ME, Deutsch P, Palmisano J, Sachs AB et al (2005) Sequence variation in NPC1L1 and association with improved LDL-cholesterol lowering in response to ezetimibe treatment. Genomics 86:648–656
16. Temel RE, Tang W, Ma Y, Rudel LL, Willingham MC, Ioannou YA, Davies JP, Nilsson LM, Yu L (2007) Hepatic Niemann-Pick C1-Like 1 regulates biliary cholesterol concentration and is a target of ezetimibe. J Clin Invest 117:1968–1978
17. Houweling AH, Vanstone CA, Trautwein EA, Duchateau GSMJE, Jones PJH (2007) Baseline plasma plant sterol concentrations do not predict changes in serum lipids, C-reactive protein (CRP) and plasma plant sterols following intake of a plant sterol-enriched food. Eur J Clin Nutr. Epub ahead of print. doi: 10.1038/sj.ejcn.1602969
18. Wang Y, Vanstone CA, Parsons WD, Jones PJ (2004) Validation of a single-isotope-labeled cholesterol tracer approach for measuring human cholesterol absorption. Lipids 39:87–91
19. Jones PJ, Raeini-Sarjaz M, Ntanios FY, Vanstone CA, Feng JY, Parsons WE (2000) Modulation of plasma lipid levels and cholesterol kinetics by phytosterol versus phytostanol esters. J Lipid Res 41:697–705
20. Jeske DJ, Dietschy JM (1980) Regulation of rates of cholesterol synthesis in vivo in the liver and carcass of the rat measured using [3H]water. J Lipid Res 21:364–376
21. McGuigan FE, Ralston SH (2002) Single nucleotide polymorphism detection: allelic discrimination using TaqMan. Psychiatr Genet 12:133–136
22. McGuigan F, Salmon K (2005) Pre-event discussion and recall of a novel event: how are children best prepared? J Exp Child Psychol 91:342–366

23. Hubacek JA, Berge KE, Cohen JC, Hobbs HH (2001) Mutations in ATP-cassette binding proteins G5 (ABCG5) and G8 (ABCG8) causing sitosterolemia. Hum Mutat 18:359–360
24. Altmann SW, Davis HR Jr, Zhu LJ, Yao X, Hoos LM, Tetzloff G, Iyer SP, Maguire M, Golovko A, Zeng M et al (2004) Niemann-Pick C1 Like 1 protein is critical for intestinal cholesterol absorption. Science 303:1201–1204
25. Carlson CS, Eberle MA, Rieder MJ, Yi Q, Kruglyak L, Nickerson DA (2004) Selecting a maximally informative set of single-nucleotide polymorphisms for association analyses using linkage disequilibrium. Am J Hum Genet 74:106–120
26. Rudkowska I, Abumweis SS, Nicole C, Jones PJ (2008) Association between non-responsiveness to plant sterol intervention and polymorphisms in cholesterol metabolism genes: a case-control study. Appl Physiol Nutr Metab 33(4):728–734

Introduction

Cholesterol is required for the proper structure and function of multiple transport and signaling pathways in mammalian membranes, especially plasma membranes [1–9]. Furthermore, cholesterol is also a required substrate for peroxisomal enzymes involved in the synthesis of bile acids (for intestinal lipid absorption) and for the synthesis of steroids—potent hormones that regulate glucose metabolism, lipid metabolism, reproduction, etc. Conversely, accumulation of excess cholesterol results in formation of cholesterol crystals in membranes [10–12] and lysosomes [13–15]. Accumulation of excess cholesterol in the plasma membranes inhibits numerous intracellular functions (mitochondrial ATP–ADP exchange, microsomal UDP-glucuronyltransferase, Na^+–Ca^{2+} exchange in heart sarcoplasmic reticulum) but also plasma membrane functions such as ion transport (Na^+, K^+-ATPase, anion transport), receptor function (acetylcholine receptor, insulin receptor), nutrient transport (glucose), proteins involved in transmembrane signaling (adenylate cyclase), and others [13, 16, 17]. Formation of intracellular cholesterol crystals is cytotoxic [13, 18] and can result in formation of atherosclerotic plaques [19–26]. It is thought that excess cholesterol-induced death of macrophages is the main cell type that undergoes necrosis near the lipid cores of atherosclerotic lesions [13]. Thus, excess cholesterol is associated with significant pathologies including atherosclerosis, cardiovascular disease, Niemann-Pick C disease, Alzheimer's disease, as well as others.

While enhanced free cholesterol efflux, increased esterification, and decreased cholesteryl ester droplet hydrolysis have been considered as serving protective roles against cholesterol-induced macrophage cytotoxicity [13]), some early studies suggest a potential role for intracellular sterol binding/carrier proteins such as sterol carrier protein-2 (SCP-2). SCP-2 has been detected in macrophages and arteries [27, 28]. Furthermore, incubation of rat peritoneal macrophages with acetylated LDL (AcLDL) resulted in a dose- and time-dependent increase not only in cellular cholesterol, but also in both SCP-2 protein and mRNA which were upregulated as much as 2.6-fold [15, 29]. In contrast, hepatic SCP-2 and SCP-x (product of alternate transcription site of the SCP-2 gene) were both deficient in adult Niemann-Pick C mice, a murine model sharing similar pathologies and lysosomal cholesterol accumulation as observed in human NPC disease [30, 31]. Finally, hepatic SCP-2 protein levels were reduced 60% in mildly and 90% in severely hypercholesterolemic diabetic rats [32]. Taken together, these data suggest a potential protective role for SCP-2 in accumulation of crystalline cholesterol and cytotoxicity. However, the mechanism(s) whereby SCP-2 may be protective is as yet unclear. However, both in vitro and intact cell studies indicate that SCP-2 dramatically enhances cholesterol transport from a variety of model and biological membranes, including lysosomal membranes [1–3, 33, 34]. While these studies suggest that SCP-2 similarly facilitate removal of cholesterol from cholesterol crystals, this possibility remains to be examined.

Because cholesterol is not readily visualized in real-time, either in vitro or in living cells, the availability of a fluorescent sterol with properties closely mimicking those of cholesterol represents a major technological advance for elucidating the mechanism(s) of protein-mediated sterol crystal dissolution, sterol organization in membranes, sterol dynamics, and sterol-protein interactions. Since the discovery of dehydroergosterol (DHE) in membranes of eukaryotes such as yeast *Candida tropicalis* [35] and Red Sea sponge *Biemna fortis* [36], DHE has been studied in model membranes [37–40], biological membranes of various intracellular organelles including plasma membrane sub-fractions [1–3, 9, 34, 41–43]), lipoproteins [44–47], cholesterol binding protein-sterol complexes [48–50], and annular cholesterol surrounding hormone receptors [51, 52]. These studies have shown DHE to be an excellent probe molecule with structural and functional properties that closely mimic those of cholesterol. More recent studies involve fluorescence resonance energy transfer (FRET) from DHE [3, 41, 53] to other sterols or to protein aromatic amino acid residues to determine intermolecular interaction distances [48, 54–56]. DHE has provided direct visualization of sterol in living cells by early confocal [41], multiphoton [41], and video [57] studies. Three-photon excitation laser scanning microscopy has enhanced real-time visualization of DHE in sterol-rich and –poor domains in the plasma membrane of living cells [38, 58, 59] while improved video imaging allowed resolution of DHE in larger structures such as microvilli/filopodia in living cells [60, 61].

Because of these properties of DHE and the propensity of DHE to form microcrystals in aqueous buffers [39, 48, 54] at very similar concentrations as cholesterol [19, 20, 62, 63], DHE was used in the present investigation to: (1) elucidate the crystal structure of DHE monohydrate, (2) examine spontaneous transfer from DHE microcrystals, (3) determine if SCP-2 enhances DHE transfer from DHE microcrystals to acceptor cholesterol crystals, model membranes, plasma membranes, and sub-fractionated vesicles, (4) examine the real-time intracellular effects of SCP-2 on microcrystalline DHE within living cells by multi-photon laser scanning imaging microscopy (MPLSM).

Materials and Methods

Materials

Ergosterol (Fig. 1a) was used to synthesize dehydroergosterol (Fig. 1b) as described previously [38, 64] The ergosterol (98% pure) was purchased from Steraloids (Wilmington, NH). Materials used in the synthesis included Burdick-Jackson (Muskegon, MI) "Purified Plus" solvents (methanol, chloroform, ethyl ether) and JT Baker (Mallinckrodt Baker, Phillipsburg, NJ) "Baker Analyzed" glacial acetic acid (99 + % pure), acetic anhydride (99+% pure) from VWR (Atlanta, GA), and anhydrous mercuric acetate from Fisher Scientific (Pittsburgh, PA) in order to obtain the highest purity of DHE (>99%) determined as described [65, 66]. Human recombinant 13.2 kDa SCP-2 was isolated and purified as described earlier [67]. Lipids including 1-palmitoyl-2-oleoyl-*sn*-glycero-3-phosphocholine (POPC), 1,2-dioleoyl-*sn*-glycero-3-[phospho-L-serine] (DOPS), and cholesterol were purchased from Avanti Polar Lipids (Alabaster, AL).

Crystal Growth

Colorless needle shaped crystals of DHE were grown by slow evaporation of a saturated 95% ethanol solution. A Bausch and Lomb 10 × microscope was used to identify a suitable colorless needle 0.2 mm × 0.2 mm × 0.05 mm from a representative sample of crystals of the same habit. The crystal was coated in a cryogenic protectant (mineral oil), and was then fixed to a glass fiber which in turn was fashioned to a copper mounting pin. The mounted crystal was then placed in a cold nitrogen stream (Oxford) maintained at 110 K.

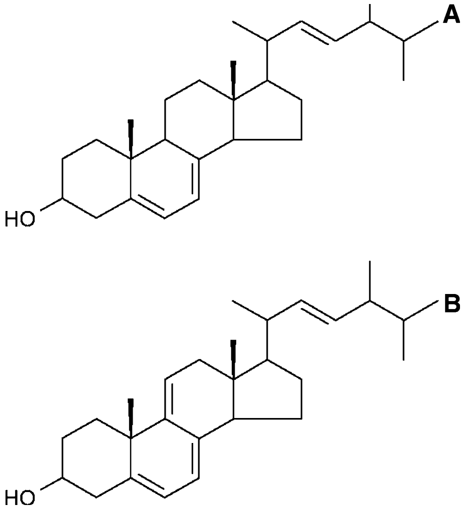

Fig. 1 The structural differences between ergosterol and fluorescent reduced ergosterol (DHE). **a** Ergosterol (ergosta-5,7,22-trien-3β-ol) contains three double bonds. **b** Reduced ergosterol (ergosta-5,7,9(11),22-tetraen-3β-ol) contains an additional double bond located between carbon 9 and carbon 11 of the third ring, forming a conjugated triene system

Crystallography

A BRUKER SMART 1000 X-ray three-circle diffractometer was employed for crystal screening, unit cell determination, and data collection (Bruker-AXS, Madison, WI). The goniometer was controlled using the SMART Software Suite, version 5.056 (Microsoft NT operating system). The sample was optically centered with the aid of a video camera so that no translations were observed as the crystal was rotated through all positions. The detector was set at 5.0 cm from the crystal sample (CCD-PXL-KAF2, SMART 1000, 512 × 512 pixel). The X-ray radiation employed was generated from a Mo-sealed X-ray tube ($K_\alpha = 0.70173$ Å with a potential of 50 kV and a current of 40 mA) and filtered with a graphite monochromator in the parallel mode (175 mm collimator with 0.5 mm pinholes).

Dark currents were obtained for the appropriate exposure time 30 s and a rotation exposure was taken to determine crystal quality and the X-ray beam intersection with the detector. The beam intersection coordinates were compared to the configured coordinates and changes were made accordingly. The rotation exposure indicated acceptable crystal quality and the unit cell determination was undertaken. Sixty data frames were taken at widths of 0.3° with an exposure time of 30 s. Over 200 reflections were centered and their positions were determined. These reflections were used in the auto-indexing procedure to determine the unit cell. A suitable cell was found and refined by nonlinear least squares and Bravais lattice procedures (Table 1). The unit cell was verified by examination of the *hkl* overlays on several frames of data, including zone photographs. No super-cell or erroneous reflections were observed. After careful examination of the unit cell, a standard data collection procedure was initiated. This procedure consists of collection of one hemisphere of data collected using omega scans, involving the collection 1201 0.3° frames at fixed angles for ϕ, 2θ, and χ ($2\theta = -28°$, $\chi = 54.73°$), while varying omega. Each frame was exposed for 30 s and contrasted against a 30 s dark current exposure. The total data collection was performed for duration of approximately 13 h at 110 K. No significant intensity fluctuations of equivalent reflections were observed.

Analysis of Crystal Structure

The structure of dehydroergosterol was solved by standard direct methods and further refined employing

Table 1 Comparison of low temperature structure (173 K) of ergosterol and the low temperature structure (110 K) of dehydroergosterol (reduced ergosterol)

Formula	$C_{28}H_{44}O_1$ H_2O	$C_{28}H_{42}O_1$ H_2O
Formula weight	414.6	412.6
Space group	$P2_1$	$P2_1$
Cell constants		
A	9.902 (1)	9.975 (1) Å
B	7.518 (1)	7.4731 (9) Å
C	34.657 (7)	34.054 (4) Å
β	94.25 (3)	92.970 (2)°
V	2,572.9 (5)	2,535.1 (5) $Å^3$
Z	4	4
D_{cal}	1.071	1.081
$R_f[I > 2\sigma(I)]$	6.8	6.9

Lobkovsky (2000) private communication (ergosterol). This work (reduced ergosterol)

SHELXS and SHELX97 [68]. CCDC 639255 contains the supplementary crystallographic data for this paper. These data can be obtained free of charge from the Cambridge Crystallographic Data Centre via http://www.ccdc.cam.ac.uk/data_request/cif. Since chirality is known, reflections were merged since the configuration would be determined. In this file, the hydrogen atoms of the water molecules were disordered and therefore omitted. A large ratio of U_{eqmax}/U_{eqmin} was due to terminal CH_3 groups that may be dynamically disordered and as such was not modeled.

Dehydroergosterol Donors: Microcrystals in Aqueous Buffer

DHE microcrystal dispersions were formed by adding small amounts of DHE from ethanolic stock solutions to a buffered solution of PIPES, pH 7.4 as described earlier [38, 66]. No filtering was performed and the microcrystals were observed previously to exist in irregular shapes with sizes ranging up to several microns when created by this technique [38, 54].

Cholesterol Acceptors: Microcrystals in Aqueous Buffer

Cholesterol acceptor microcrystal dispersions were formed by adding small amounts of cholesterol from ethanolic stock solutions to a buffered solution of PIPES, pH 7.4 similarly as described for DHE earlier [38, 66]. The resultant solution of microcrystals was not filtered.

Membrane Acceptors: Large Unilamellar Vesicles

Large unilamellar vesicles composed of POPC: DOPS: cholesterol (55:10:30 molar ratio) were formed exactly as described earlier [38, 69, 70].

Membrane Acceptors: Plasma Membrane, Caveolin-1 and Cholesterol-Rich Sub-Fraction (CAVCR), and Non-caveolin-1 and Cholesterol-Poor Sub-Fraction(non-CAVCP)

Madin-Darby canine kidney (MDCK, American Type Culture Collection) cells were grown as described previously [71] for 72 h at 37 °C and 5% CO_2 in the presence of Dulbecco's Modification of Eagle's medium (D-MEM) (Cellgrow/Mediatech, Herndon, VA). The high glucose medium was supplemented with 2 mM L-glutamine, 1 mM sodium pyruvate, 0.25 µg/L Fungizone, 100 units/L penicillin, 100 µg/L streptomycin, and 5% serum supreme from (Bio-Whittaker/Canbrex, East Rutherford, NJ) as well as 0.1 mM nonessential amino acids (Cellgrow/Mediatech, Herndon, VA), and 43.9 mM sodium bicarbonate (Invitrogen, Carlsbad, CA). Following washing with phosphate buffered saline (PBS), the cells were covered with serum-free medium and incubated with DHE (20 µg/ml) added directly to the media from a stock solution derived from absolute ethanol and containing <1 mol% butylated hydroxytoluene (BHT) that was originally stored at −80 °C. The amount of ethanol added was kept below 0.3% to prevent any deleterious effects on the cells. CAVCR (binding fraction) and non-CAVCP (non-binding fraction) were resolved by concanavalin-A affinity chromatography from purified plasma membranes [42, 43, 71–73]. Purity of the plasma membrane, binding, and non-binding fractions was determined as described in the cited papers using western blotting of a panel of protein markers for plasma membranes (Na^+K^+-ATPase, SRB1), caveolae (caveolin-1 and GM1), and non-caveolae (Na^+K^+-ATPase).

Excitation and Emission Anisotropy of DHE

Measurements of the wavelength dependence of anisotropy for both the excitation and emission of DHE were performed using a Cary Eclipse spectrofluorometer (Varian, Palo Alto, CA) with a Peltier temperature controlled holder kept at 24 °C. The slits of both the excitation and emission monochromators were set to 5 nm bandwidths with scan speed set at 120 nm/min. The emission scan of anisotropy was performed with an excitation wavelength of 324 nm. Two excitation scans of anisotropy were made with the fluorescence emission collected at 375 nm and 425 nm.

Measurement of DHE Fluorescence Anisotropy During Exchange Assays

All measurements of fluorescence anisotropy over time (~4 h) were made using a T-format of an ISS PC1 spectrofluorometer (ISS Instruments, Champaign, IL) with rotating cuvette turrets as well as with UV-grade Glan-Thompson excitation and emission polarizers. The excitation wavelength was set at 324 nm and the emission was collected using a Schott KV389 cutoff filter (Schott Optics, Duryea, PA). Baseline DHE fluorescence anisotropy of the donor microcrystals (2.5 μM 10 mM PIPES buffer, pH = 7.4) was measured for 20 min to ensure a stable baseline and obtain initial DHE anisotropy. After addition of 10-fold excess of acceptor (contains no DHE), DHE anisotropy was recorded at 20 s intervals for 4 h to monitor sterol transfer between DHE microcrystal donors and acceptor cholesterol microcrystals or membranes. Residual light scatter contributions were corrected using controls and subtracting the residual fluorescence anisotropy from all experimental data. To prevent inner filter artifacts, absorbance of sample solutions at the excitation wavelengths were <0.15. The equations $r = \frac{I_{\text{pl}} - I_{\text{pd}}}{I_{\text{pl}} + 2I_{\text{pd}}}$ was where r is the anisotropy, I_{pl} and I_{pd} is the emission intensity measure with polarizers parallel and perpendicular, respectively, to the excitation polarizer set vertically, and I_{T} is total emission intensity [74].

Determination of Sterol Exchange: Polarization Assay

Sterol exchange between DHE microcrystal donors and acceptor cholesterol microcrystals, large unilamellar vesicles, plasma membranes, binding fraction, or non-binding fractions was determined by using a fluorescent sterol (DHE) exchange assay as previously established [42, 43, 71, 75]. Time dependent anisotropy changes was modeled with the equation

$$r(t) = f_{\text{d}}(t)r_{\text{d}}(t) + f_{\text{a}}(t)r_{\text{a}}(t) \tag{1}$$

where *r(t)* was the measured anisotropy over time, $f_{\text{d}}(t)$ was the fractional intensity resulting from the donor, $f_{\text{a}}(t)$ was the fractional intensity resulting from DHE transfer into the acceptor, $r_{\text{d}}(t)$ was the donor anisotropy, and $r_{\text{a}}(t)$ was the acceptor anisotropy for the membrane. Crystalline donor anisotropy ($r_{\text{d}} = 0.09$) was constant for microcrystalline DHE and approximately independent of the concentration of crystals. DHE crystalline anisotropy was highly depolarized as compared to the anisotropy of DHE within membrane vesicles, which varied depending upon concentration as a result of self-quenching effects as seen in other studies [76–79]. The acceptor anisotropy was typically derived from the a standard curve that must be measured from varying dehydroergosterol mole fractions ($X_{\text{a}} = C_{\text{a}}/C_{\text{T}}$) of the particular acceptor and fit to the equation

$$r_{\text{a}}(X_{\text{a}}) = r_0 + b_1^* X_{\text{a}} + b_2^* (X_{\text{a}})^2 \tag{2}$$

where r_0 is the anisotropy at infinite dilution [71]. However, since for 10-fold dilution $0 < X_{\text{a}} < 0.1$ and $\frac{\mathrm{d}r}{\mathrm{d}X_a} \sim 0$, the effect of self-quenching would be minimal so that $r_{\text{a}}(t)$ was fixed to r_0 of each acceptor membrane type.

The fractional intensity contribution to the anisotropy of the DHE in the acceptor was described by the following equation:

$$f_{\text{a}}(t) = f_1(1 - e^{-at}) + f_2(1 - e^{-bt}) \tag{3}$$

where f_1 and f_2 are related to the fractional pool sizes of easily exchangeable cholesterol within the acceptor membrane vesicle with half-times

$$t_{1/2}^1 = \frac{\ln(2)}{a} \quad \text{and} \quad t_{1/2}^2 = \frac{\ln(2)}{b} \tag{4}$$

The donor fractional intensity is related to the acceptor contribution by the following equation:

$$f_{\text{d}}(t) = 1 - f_{\text{a}}(t) \tag{5}$$

Combining these concepts formulated the equation, $r(t) = (1 - f_a(t))r_{\text{d}} + f_{\text{a}}(t)r_{\text{a}}$ which is further simplified:

$$r(t) = r_{\text{d}} + \left[f_1(1 - e^{-at}) + f_2\left(1 - e^{-bt}\right)\right](r_{\text{a}} - r_{\text{d}}) \tag{6}$$

The anisotropy curves were plotted and fitted by nonlinear regression to Eq. 5 using Sigma Plot 8.0 (Systat Software, San Jose, CA) and the half-times were calculated using Eq. 3. The initial rates of the exchange of sterol from the microcrystalline form of DHE to membrane vesicles was calculated from the derivative of *r(t)* evaluated at *t* = 0.

$$\frac{\mathrm{d}r(t)}{\mathrm{d}t}\Big|_{t=0} = [f_1 a + f_2 b](r_{\text{a}} - r_{\text{s}}) \tag{7}$$

DHE Spectra at the Beginning and at the End of Exchange Assays

Steady state fluorescence emission spectra of DHE excited at 324 nm were obtained with a PC1 Photon Counting Fluorometer (ISS Instr., Champaign, IL). Light scatter was minimized by use of narrow excitation slits, low concentration, and cutoff filters. Residual Raman scattering was subtracted. Absorbance at the excitation wavelength was maintained below 0.15 to avoid potential inner filter effects. Spectra were analyzed with Grams32 (Thermo Galactic, Salem, NH).

Cell Culture of Control and SCP-2 Overexpressing L-cells

Murine L cells and L-cells transfected with cDNA corresponding to the 15-kDa pro-SCP-2 protein were cultured on Lab-Tek Chambered coverglass (Nunc, Naperville, IL) at 37 °C and 5% CO_2 overnight in Higuchi medium [80], supplemented with 10% fetal bovine serum (Hyclone, Logan, UT), as described earlier [42]. The cells with transfected cDNA overexpressed SCP-2 protein so that it comprised 0.036% of the total cytosolic proteins while the level in the control mock transfected L-cells was negligible. Subsequently, the cells were washed with PBS followed by the addition of serum-free medium containing DHE (20 μg/ml) added directly from the ethanolic stock solution previously described (<0.3% ethanol added). The cells on the cover glass was incubated for 24 h and washed with PBS followed by the addition of serum containing media. Cells were removed for imaging at approximately 12 h time points.

Multi-Photon Laser Scanning Microscopy (MPSLM) of Dehydroergosterol

A Bio-Rad MRC-1024 MP (Zeiss, Thornwood, NY) laser scanning confocal/multi-photon microscopic imaging system was used to obtain images of the fluorescence emission of the structural distribution of DHE within living cells over the 60-h time period. The MRC-1024 MP was coupled to a Zeiss Axiovert 135 inverted microscope (Zeiss, Thornwood, NY) with heated incubator and stage. A Zeiss 40 × Plan-Apochromat (1.4 N.A.) was used for real-time imaging from $t = 0$ to $t = 60$ h. The cells on chambered cover glass were maintained in a 37 °C CO_2 incubator between imaging time points. Imaging software, MetaMorph 4.5 (Molecular Devices, Downingtown, PA), was used to determine the mean integrated intensities from labeled cells (both control and SCP-2 overexpressing L-cells) at each time point from collective measurements of $\sim$50 cells while mean integrated intensities of autofluorescence were obtained similarly using unlabeled cells (both control and SCP-2 overexpressing L-cells). Multiphoton excitation of the DHE was provided by a pulsed mode-locked Coherent Mira 900F (Coherent, Palo Alto, CA) tuned to 900 nm. Two photomultipliers of an external detector system (Dr. Zipfel, Cornell University, Ithaca, NY) was used in combination with two emission filters (Chroma Technology, Rockingham, VT), 375/50 nm and 455/30 nm, to simultaneously collect the emission in two distinct spectral regions. The ratio of the integrated measurements collected from the two channels was used to determine the intracellular monomeric versus crystalline distributions of DHE.

Data and Statistical Analyses

Curve-fitting and non-linear regression analyses were performed within the scientific data and analysis and graphing software, SigmaPlot v.8 (Systat Software, Inc., San Jose, CA).

Results

Dehydroergosterol Monohydrate Crystal Structure Solution and Refinement

DHE monohydrate crystal screening, unit cell determination, and data collection on a suitable cell were performed as described in "Materials and Methods". The data was reduced (SAINT, Bruker-AXS, Madison, WI) and merged. The structure of DHE was solved by standard direct methods and further refined using software developed by G.M. Sheldrick as described in "Materials and Methods". The crystal refinement results were provided in Table 2.

A dehydroergosterol monohydrate crystal was grown from saturated 95% ethanol solution to the dimensions $0.20 \times 0.20 \times 0.10$ mm^3 along the a, b, c axes. The dehydroergosterol monohydrate symmetry of diffraction was found to be monoclinic (Note: the cholesterol monohydrate has an apparent monoclinic symmetry, but close inspection of the twinned crystals revealed triclinic symmetry; [81, 82]). The space group was thus $P2_1$, with reduced cell parameters $a = 9.9747(11)$ Å, $b = 7.4731(9)$ Å, $c = 34.054(4)$ Å, $\alpha = 90°$, $\beta = 92.970°(2)$, $\gamma = 90°$. The DHE unit cell is smaller than that reported by Bernal [83] who reported an A2 structure of eight molecules in the unit cell with $a = 9.5$ Å, $b = 7.5$ Å, $c = 75.2$ Å, $\beta = 96°$ from data recorded with photographic film from an impure crystal. In this case the cell reported by Bernal in 1940 was a superstructure of the cell reported in this manuscript. The volume of the dehydroergosterol monohydrate crystal unit cell was 2535.1(5) Å^3, with a density of 1.081 mg/m^3, in agreement with that calculated from the assuming the unit cell contained $4(C_{28}H_{44}O_2)\cdot 4H_2O$. A dimer unit of two $(C_{28}H_{44}O_2)\cdot H_2O$ forms the asymmetric volume of the unit cell with four molecules of $(C_{28}H_{44}O_2)\cdot H_2O$ in the unit cell (Fig. 2a, b) similar to ergosterol monohydrate, while cholesterol monohydrate has eight molecules in its unit cell. From the 32,269 reflections collected, only 8,865 with intensity $I > 2\sigma(I)$ were obtained and used for resolving the structure. Large amplitudes of atomic thermal vibrations primarily accounted for the high proportion of weak reflections. All 64 (only asymmetric volume atoms are detected, the remainder are generated by symmetry) n-hydrogen atoms were detected in electron density maps. A full-matrix least-squares on F^2 revealed goodness of fit of 1.041, final R indices $[I > 2\sigma(I)]$ of $R1 = 0.0688$ and

Table 2 Crystal data and structure refinement for dehydroergosterol

Empirical formula	$C_{28}H_{44}O_2$
Formula weight	412.63
Temperature	110 (2) K
Wavelength	0.71073 Å
Crystal system	Monoclinic
Space group	$P2_1$
Unit cell dimensions	$a = 9.9747$ (11) Å, $\alpha = 90°$
	$b = 7.4731$ (9) Å, $\beta = 92.970(2)°$
	$c = 34.054$ (4) Å, $\gamma = 90°$
Volume	2,535.1 (5) Å^3
Z	4
Density (calculated)	1.081 Mg/m^3
Absorption coefficient	0.065 mm^{-1}
F(000)	912
Crystal size	0.20 × 0.20 × 0.10 mm^3
Theta range for data collection	2.10–24.99°
Index ranges	$-11 \leq h \leq 11$, $-8 \leq k \leq 8$, $-40 \leq l \leq 40$
Reflections collected	32,269
Independent reflections	8,865 [R(int) = 0.0563]
Completeness to theta = 24.99°	99.4%
Absorption correction	None
Max. and min. transmission	0.9935 and 0.9870
Refinement method	Full-matrix least-squares on F^2
Data/restraints/parameters	8,865/1/542
Goodness-of-fit on F^2	1.041
Final R indices [$I > 2\sigma(I)$]	$R1 = 0.0688$, w$R2 = 0.1766$
R indices (all data)	$R1 = 0.1180$, w$R2 = 0.2142$
Absolute structure parameter	0 (3)
Largest diff. peak and hole	0.505 and −0.331 e Å^{-3}

w$R2 = 0.1766$, and R indices (all data) $R1 = 0.0688$ and w$R2 = 0.1766$.

The molecules are packed in staggered layers (Fig. 2a, b) with the intermolecular separation of 5.50(1) Å between the centroids of the molecules. The hydrophilic ends of the DHE molecules are located inward toward the water molecules while the hydrophobic ends of the molecules are directed outward toward the hydrophobic ends of the adjacent DHE molecules. The hydrogen atoms apart of the water molecules were disordered and have not been included (Fig. 2a, b). The ring system of the DHE molecule (Fig. 1b) is approximately planar where the ring A had a chair conformation, ring B was significantly planar, ring C was formed a partial chair structure with that was planar except for the last carbon joining ring D, and ring D was a distorted. The DHE molecules stack in a parallel mode normal to the diagonal of the a and c axes.

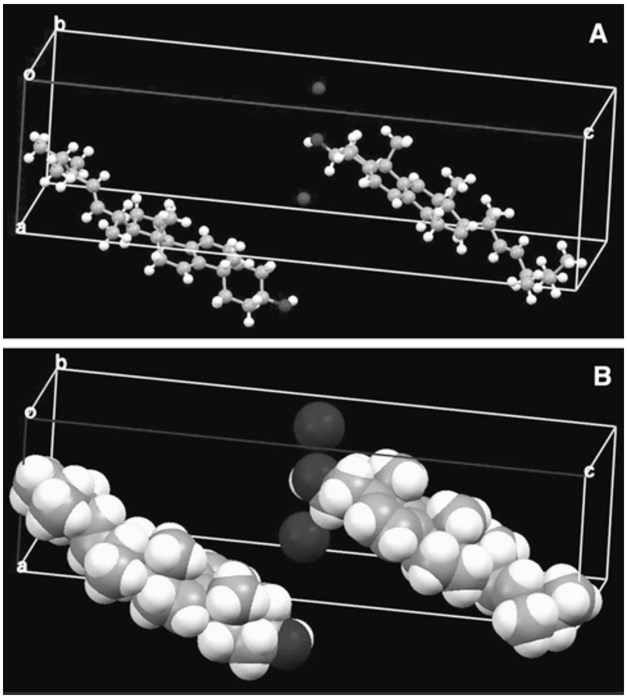

Fig. 2 Crystal structure of dehydroergosterol monohydrate. The unit cell consists of four dehydroergosterol monohydrate molecules, two (**a**, **b**) of which are unrelated by crystal symmetry. **a** 3-D ball and stick representation of the orientation of the **a** and **b** molecules in the crystallographic unit cell. The hydrogen atoms on the water molecules were disordered and are not shown. **b** 3-D space-filling representation of the orientation of the **a** and **b** molecules in the crystallographic unit cell. Molecules of oxygen are shown in dark gray, hydrogen in white, and carbon in light gray

The Effect of Excitation and Emission Wavelength on Anisotropy of Aqueous Dispersions of Microcrystalline Dehydroergosterol

Anisotropy excitation spectra were acquired as described in the "Materials and Methods" and graphed as shown in Fig. 3a. The open circles represent the excitation anisotropy spectrum acquired with the emission monochromator fixed to 375 nm with a 5 nm bandwidth. This spectrum revealed that the anisotropy was relatively constant across much of the excitation wavelengths with only a slight increase in anisotropy at the longer wavelengths. Typically this observation has been made when transition moments are near collinear which occurs when the emission originates from the same state as the absorption band. The closed circles (Fig. 3a) represent the excitation anisotropy spectrum acquired with the emission monochromator fixed to 425 nm with a 5 nm bandwidth wherein the greatest enhancement in emission arises under crystal formation. In this spectrum, the anisotropy was relatively constant across the shortest wavelengths but decreased gradually at the longer wavelengths indicative of a larger displacement of

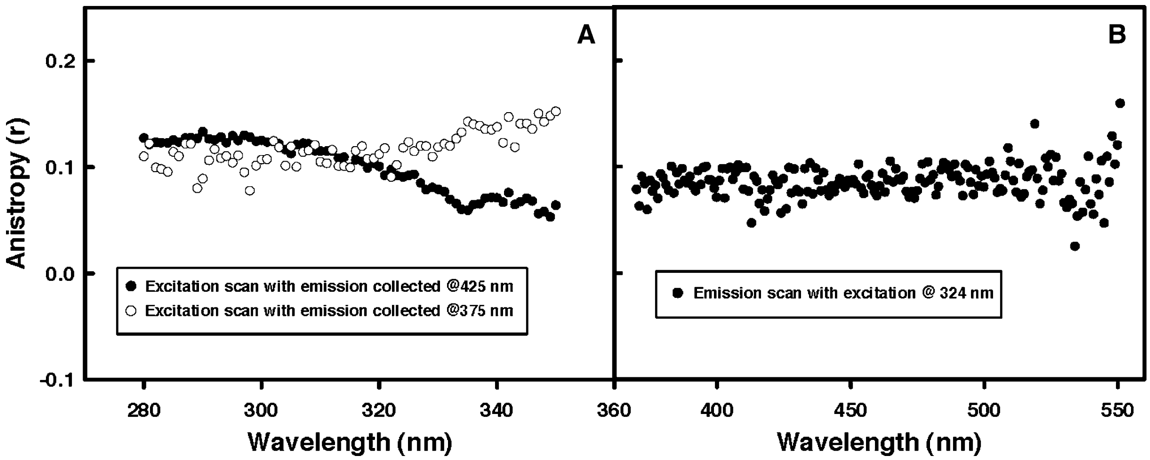

Fig. 3 Excitation and emission anisotropy of DHE. **a** Plots of the anisotropy versus excitation wavelength over the region 280–350 nm for emission collected at 375 nm (*open circles*) and 425 nm (*closed circles*). **b** Plot of emission anisotropy over the region 370–550 nm, resulting from excitation at 324 nm. Bandwidths were 5 nm for both excitation and emission monochromators

transition moments. Due to the restrictive environment within the crystal and the observed higher quantum yield, this was suggestive of an involvement in a different state possibly the result of formation of an excited state dimer rather than simple homotransfer or self-quenching that has been observed in vesicles [38, 54]. Despite the different states involved in the fluorescence emission, the emission anisotropy spectrum (Fig. 3b), acquired with excitation wavelength fixed to 324 nm and a 5 nm bandwidth, showed very little dependence upon wavelength. This was in agreement with the excitation anisotropy measured at 324 nm (Fig. 3a) where only a slight difference existed using the acquisition emission wavelengths of 375 nm and 425 nm.

Sterol Exchange Between Donors and Acceptors

DHE has proven to be a useful probe for cholesterol transfer because it is a naturally-occurring fluorescent sterol [35, 36] exhibiting structural and functional properties closely resembling those of cholesterol as detailed in the Introduction [1, 2, 38, 39, 45, 51, 75, 84–87]. The theoretical basis for the DHE exchange assay has been previously established with respect for exchange of sterol from donor membranes to acceptor membranes [42, 43, 71, 76, 77, 88, 89]. Briefly, at high concentrations of DHE in membranes, significant depolarization or decrease in anisotropy occurs as a result of resonance energy transfer (RET) between DHE molecules. Upon addition of 10-fold excess (by sterol) acceptor cholesterol microcrystals or acceptor membranes, the donor DHE microcrystal exchanges DHE one-for-one with cholesterol in the acceptor, resulting in release of DHE from self-quenching, thereby increasing polarization or anisotropy. Typically, a standard curve is determined by measuring the polarization or anisotropy as a function of the mole fraction of the fluorescent sterol within donor and acceptor (if different membrane type). Thus, a determination is made from the standard curve of the mol percent of DHE that has been exchanged. However, in this study, the donor consists of microcrystalline DHE with low anisotropy ($r \sim 0.09$) that remains constant until the amount of aqueous DHE falls below the critical micelle concentration (CMC) which is quite low (~30 nM). By implication, sterol exchange observed by increasing anisotropy would be the result of increasing localization of sterol within the acceptor. Because of the 10-fold excess of acceptors, the acceptor anisotropy occurs between $r(X_a = 0) = r_0$ (anisotropy at infinite dilution) to $r(X_a = 0.1) \approx r_0$. This approximation implies that only the fractional contributions of the anisotropy depend upon the sterol mole fractions (see “Materials and Methods”).

Effect of Cholesterol Transfer Proteins on the Sterol Exchange Between Crystalline Dehydroergosterol and Crystalline Cholesterol

Sterol exchange between dehydroergosterol microcrystals and cholesterol microcrystals was determined with a fluorescence polarization assay as described in “Materials and Methods”. Baseline anisotropy of DHE microcrystals in buffer alone was essentially unchanged over a 4 h time period (Fig. 4a). At the end of this incubation period, the emission spectrum of DHE microcrystals (excited at 324 nm) was obtained. As shown in Fig. 4b, the raw emission spectra exhibited four major peaks near 355, 373, 397, and 426 nm. After correction for background, the ratios of emission peaks as 426 nm/355 nm and 426 nm/

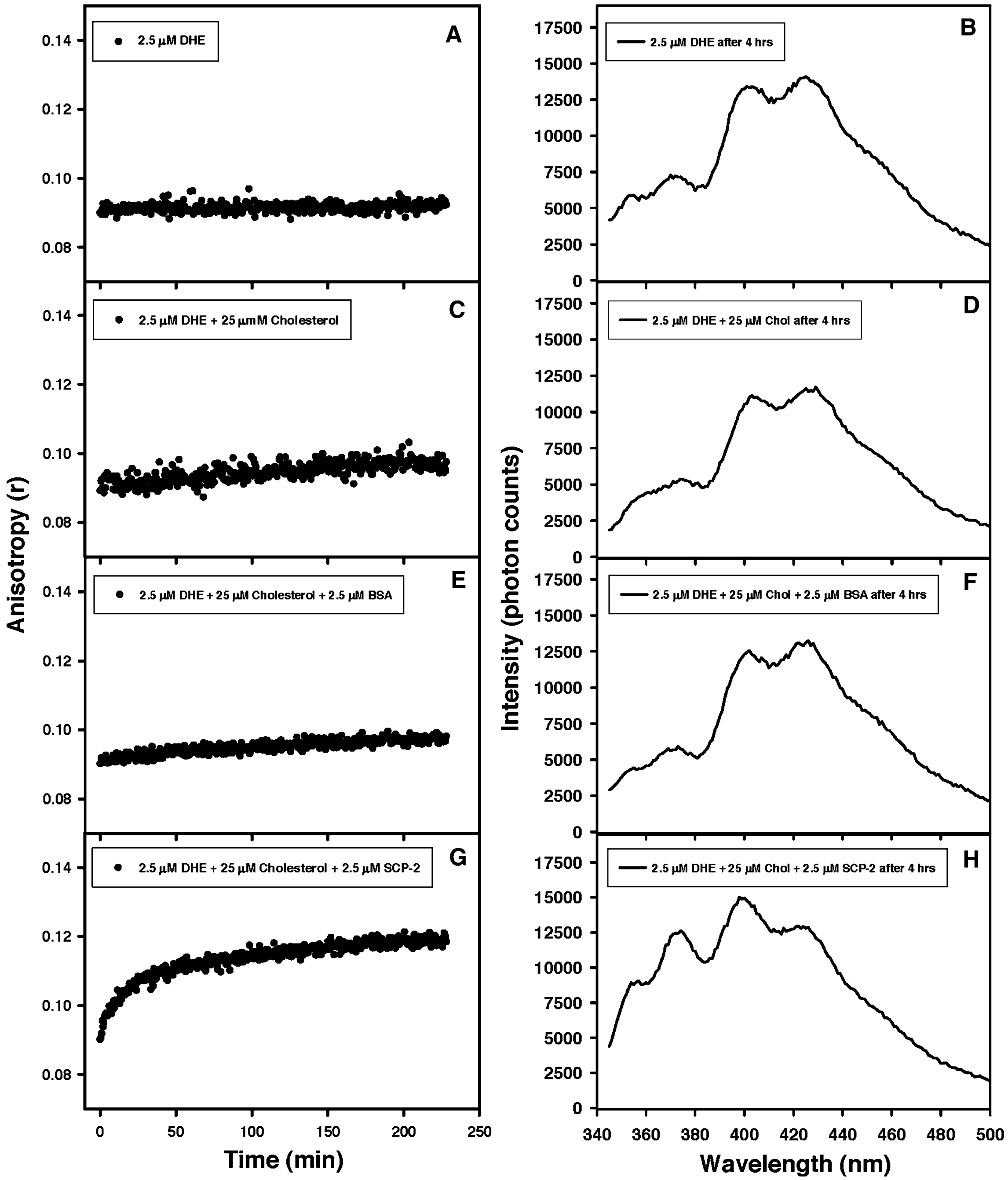

Fig. 4 Anisotropy and spectral measurements of microcrystal disruption involving DHE and cholesterol. Exchange of sterol was monitored using polarized light as described in the "Materials and Methods" with excitation at 324 nm. **a** 2.5 µM DHE was added to buffered 10 mM PIPES (pH 7.2) to form microcrystals. The polarization was monitored for 225 min and converted to anisotropy. This curve represents the donor only curve and remains flat over the time period. **b** Emission spectrum of the DHE microcrystals after baseline anisotropy measurement of (**a**), approximately 4 h. **c** Time-dependent changes in anisotropy involving donor 2.5 µM DHE as a result of the addition of 25 µM cholesterol to the solution as a 10-fold excess of acceptor. **d** Emission spectrum after measurement of the spontaneous sterol exchange in (**c**), at approximately 4 h. **e** Sterol exchange between a donor 2.5 µM DHE microcrystal dispersion in the presence of 25 µM cholesterol microcrystal dispersion with the addition of 2.5 µM BSA. **f** Emission spectrum acquired after the sterol exchange in (**e**) at approximately 4 h. **g** Sterol exchange between a 2.5 µM DHE microcrystal dispersion (donors) in the presence of 25 µM cholesterol microcrystal dispersion (acceptors) with the addition of 2.5 µM SCP-2. **h** Emission spectrum of the combination in (**g**) acquired at 4 h

373 nm were 3.7 and 2.5, respectively—consistent with DHE being localized primarily in crystalline structures as described earlier [38, 48, 54]. The ratio of 455 nm/375 nm was 1.5 at the endpoint.

To examine spontaneous sterol exchange between donor and acceptor microcrystals, 10-fold excess acceptor cholesterol microcrystals were added to donor DHE microcrystals in aqueous buffer. The DHE anisotropy increased slowly (Fig. 4c), consistent with one-for-one exchange of DHE in the donor DHE microcrystals and cholesterol in the cholesterol microcrystal acceptors. Analysis as described in "Materials and Methods" revealed that the anisotropy change best fit a single component with a long half-time $t_1^{1/2} = 130$ min and a very low exchangeable fraction of 0.057 of the total donor sterol (Table 3). After correction for background, the ratio of 455 nm/375 nm was 1.4—again consistent with DHE being localized primarily in crystalline environment. These findings suggested that very little DHE had transferred to the cholesterol microcrystal and the environment basically exhibited similar properties as that in DHE microcrystals determined by spectral analysis.

To determine if proteins known to enhance lipid transfer between membranes might also facilitate DHE exchange between microcrystals, the effects of two classic cholesterol transfer proteins were tested: (1) An extracellular cholesterol transfer protein (bovine serum albumin, BSA); (2) An intracellular cholesterol transfer protein (SCP-2). Addition of albumin or SCP-2 to DHE microcrystal donors alone did not significantly alter the anisotropy or spectral properties (not shown). Addition of bovine serum albumin to DHE microcrystal donors in the presence of 10-fold excess cholesterol microcrystal acceptors (Fig. 4e) significantly decreased the half-time of transfer (Table 3). The initial rate did not change significantly and the overall exchangeable fraction, though slightly lower, was similar to the spontaneous (Table 3) as corroborated by the spectral properties (Fig. 4f) where the ratio of 455 nm/375 nm was 1.3. In contrast, SCP-2 rapidly increased the DHE anisotropy with increasing time of DHE exchange between DHE microcrystal donors and cholesterol microcrystal acceptors (Fig. 4g). Analysis of the exchange curves as described in "Materials and Methods" indicated that they optimally fit two components: (1) the contribution $t_1^{1/2} = 74 \pm 4$ min with a total exchangeable fraction of 0.0867 ± 0.0003 and (2) the contribution $t_2^{1/2} = 6.1 \pm 0.3$ min with a total exchangeable fraction of 0.0732 ± 0.0006. The first fraction was increased only about 1.5-fold more than the spontaneous (Table 3), but the 2.5 μM SCP-2 significantly reduced the half-time $t_1^{1/2}$ of DHE exchange by 2.2-fold which was similar to the 2.5 μM BSA (Table 3). Furthermore, SCP-2 induced the formation of a second component, nearly as large as the first. The half-time $t_2^{1/2}$ of the new component induced by SCP-2 was very short, near 6 min or a nearly 22-fold faster exchange (Table 3) which contributed to an initial rate increase of 29-fold over the spontaneous. Finally, SCP-2 significantly altered the emission spectra of DHE at the end of the exchange process (Fig. 4h). After correction for background, the ratio of 455 nm/375 nm was 0.6—consistent with a significant amount of transferred DHE being localized in a less crystalline/more disordered region of the acceptor cholesterol microcrystals.

In summary, spontaneous DHE exchange between DHE microcrystals and cholesterol microcrystals was best fit by a single, very slow component. While BSA only decreased

Table 3 Initial rates and kinetic multi-exponential analysis of molecular sterol exchange

Donor-acceptor	Protein added	Initial rate (pmol/min)	$t_1^{1/2}$ (min)	f_1	$t_2^{1/2}$ (min)	f_2
DHE-Chol	None	0.3 ± 0.06	130 ± 20	0.057 ± 0.001	–	–
	BSA	0.45 ± 0.03	60 ± 2	0.0400 ± 0.0002	–	–
	SCP-2	8.8 ± 0.7	74 ± 4	0.0867 ± 0.0003	6.1 ± 0.3	0.0732 ± 0.0006
DHE-LUV	None	0.435 ± 0.002	813 ± 1	1[a]	–	–
	SCP-2	40 ± 10	133 ± 1	0.8684 ± 0.0007	0.31 ± 0.07	0.0314 ± 0.0002
DHE-PM	None	–	–	–	–	–
	SCP-2	4.67 ± 0.06	72.9 ± 0.6	0.9431 ± 0.0006	–	–
DHE-CAVCR	None	–	–	–	–	–
	SCP-2	3.9 ± 0.1	270 ± 20	0.299 ± 0.003	3.7 ± 0.3	0.0453 ± 0.0002
DHE- non-CAVCP	None	–	–	–	–	–
	SCP-2	–	–	–	–	–

Fluorescence polarization exchange curves for DHE sterol transfer from DHE donor to cholesterol crystals and membrane vesicles. The exchanges involving LUV, PM, CAVCR, and non-CAVCP were measured in the absence or presence of SCP-2 (1.5 μM) followed by determination of initial rates and kinetic analysis as described in "Materials and Methods". Half times $t_1^{1/2}$ and $t_2^{1/2}$ were in minutes with the corresponding fractions, f_1 and f_2, representing the fractions due to the exchangeable components. Values represent the mean ± SE ($n = 3$–4)

[a] Value was fixed during fit

the half-time of the slow component of DHE exchange without inducing a rapid exchangeable component, the intracellular cholesterol transport protein SCP-2 dramatically facilitated DHE exchange by decreasing the half-time over twofold and inducing the formation of a second DHE pool with very short, nearly 22-fold shorter, half-time, thereby nearly tripling the total fraction of sterol available for exchange under the experimental conditions.

Effect of SCP-2 on Sterol Exchange Between Crystalline Dehydroergosterol and Model Membranes of Large Unilamellar Vesicles

Large unilamellar vesicles consisting of 55 mol% POPC: 35 mol% Chol: 10 mol% PS were made by extrusion as described in the "Materials and Methods". The exchange assay previously described was used to examine the ability of SCP-2 to enhance sterol exchange from out of a crystalline domain with that of model membrane associated cholesterol. DHE was added to 10 mM PIPES buffer at pH 7.2 to form a 1.5 µM solution of DHE. The aqueous dispersion of microcrystalline DHE (not shown) gave a baseline anisotropy of $r = 0.09$ and remain unchanged over a 4 h period similar to Fig. 4a. This experiment was repeated in the presence of 1.5 µM SCP-2 (not shown), which also was unchanged over a 4 h time period. However, when the 55:35:10 (POPC:CHOL:PS) LUVs were added in 10-fold excess to the 1.5 µM DHE microcrystalline dispersion, the anisotropy began to slowly rise with time indicative of sterol exchange as observed in Fig. 5a (closed circles). After 4 h, a spectrum of the solution was acquired which revealed a significant drop in the amount of crystalline DHE (Fig. 5b) as revealed by the ratio of 455 nm/375 nm = 0.82. As shown in Table 3 a single half-time component of 813 ± 1 min was calculated with the fraction fixed to 1 at infinitely long time. This was justified by the near linear slope of the curve over the 4 h time period. The initial rate calculated was very close to that of the BSA mediated and spontaneous DHE to cholesterol crystal exchange. Another solution of 1.5 µM DHE microcrystalline dispersion was made in PIPES buffer, after 10 min the acceptors (10 × LUVs) was added along with SCP-2 for a final protein concentration of 1.5 µM. This created a significant increase in anisotropy over the period of the 4 h as seen in Fig. 5a (open circles) with a corresponding increase in monomeric DHE content as seen in the emission spectrum (Fig. 5c) acquired immediately after the exchange time period. This spectrum showed very little excimeric emission as demonstrated by the low ratio of 455 nm/375 nm = 0.18. As shown in Table 3, a long half-time component of 133 ± 1 and an extremely short half-time of 0.31 ± 0.07 were calculated. The respective fractions of 0.8684 ± 0.0007 and 0.0314 ± 0.0002 revealed that the majority of the exchangeable sterol was in the slower fraction but 3% was located in a rapid exchangeable fraction which contributed to an initial rate of 40 ± 10 pmol/min. The addition of SCP-2 to the sterol

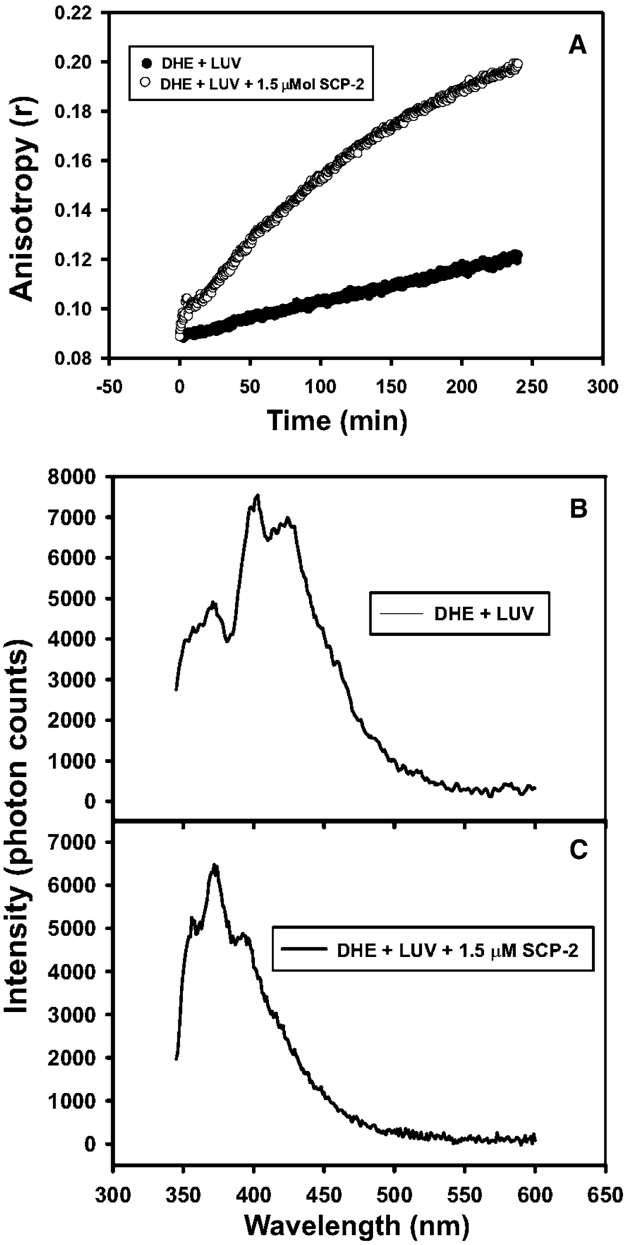

Fig. 5 Sterol exchange between donor DHE microcrystals and large unilamellar vesicles (LUVs). Large unilamellar vesicles (55 mol % POPC: 35 mol % cholesterol: 10 mol % PS) were prepared as described in the "Materials and Methods". **a** Spontaneous and SCP-2 mediated exchange of sterol between a 1.5 µM solution of DHE microcrystals (donor) and a 10-fold excess of LUVs (acceptors) in PIPES buffer were monitored by anisotropy measurements with excitation at 324 nm. **b** Spectrum acquired after 4 h of the spontaneous exchange (DHE + 10-fold access LUV). **c** Spectrum acquired after 4 h of the SCP-2 mediate exchange (DHE + 10-fold access LUV + 1.5 µM SCP-2)

exchange involving DHE microcrystals and LUVs boosted the initial rate 92-fold. The overall exchangeable sterol was 90% of the total sterol, which was clearly evident of the spectrum acquired after 4 h (Fig. 5c).

Effect of SCP-2 on Nonfluorescent Mechanisms in Mixtures of Crystalline Cholesterol and Model Membranes of Large Unilamellar Vesicles

In order to determine if the time-dependent enhancement of anisotropy was independent of the fluorescent sterol DHE and potentially a result of changes in residual scatter, several control experiments were performed using the same experimental and instrumental parameters but with cholesterol crystal donors. First, the anisotropy of cholesterol crystals in PIPES buffer was monitored for 4 h. Second, the anisotropy of the mixture of cholesterol crystal donors in the presence of 10-fold excess of LUV cholesterol acceptors was monitored for 4 h. Last, the anisotropy of the mixture of cholesterol crystal donors in the presence of 10-fold excess of LUV acceptors and SCP-2 was monitored for 4 h as shown in Fig. 6. In all three cases, the anisotropy of the weak residual light scatter leaking through the KV389 filter remained constant over time implying that the changes in anisotropy in the case of DHE were not a scatter artifact involving crystals, LUVs, and the protein.

Effect of SCP-2 on Sterol Exchange Between Crystalline Dehydroergosterol and Biological Membranes of Three Types: Plasma Membranes as well as the Sub-Fractions: CAVCR and Non-CAVCP

Biological membranes in the form of vesicles were isolated by previously established methods and used to determine the significance of crystalline sterol domain exchange in complex systems. The plasma membranes of MDCK cells were isolated using differential (Percoll) centrifugation with subsequent sub-fractionation into two portions, CAVCR and non-CAVCP, through the use of concanavalin A affinity purification technique as described in "Materials and Methods" and characterized in studies involving diverse cell types [42, 71–73, 90]. The cholesterol-rich sub-fraction (CAVCR) also contained proteins such as caveolin-1 and GM1 gangliosides as opposed to the cholesterol-poor sub-fraction (non-CAVCP). They were also highly purified and relatively free of contamination from endoplasmic reticulum.

Baseline anisotropy of DHE microcrystals in buffer alone was again essentially unchanged over a 4-h time period. The anisotropy of the 1.5 μM DHE microcrystals in the presence of 10-fold excess of MDCK PM acceptor membrane vesicles showed no change over 4 h (Fig. 7a) and the spectrum acquired after the 4 h showed almost no change in the spectrum (not shown). However, with the same conditions and including 1.5 μM SCP-2 at the time of addition of acceptors changed the dynamics completely (Fig. 7a). The anisotropy increased rapidly in nearly 4 h, corresponding to a single large exchangeable fraction of 0.9431 ± 0.0006 with a half-time of 72.9 ± 0.6 min (Table 3). The emission spectrum at 4 h (Fig. 7d) revealed mostly monomeric type emission as evidenced by the emission ratio of 455 nm/375 nm = 0.2. The CAVCR sub-fraction of the MDCK PM also exhibited enhanced exchange in the presence of 1.5 μM SCP-2 as shown in Fig. 7b (closed circles) albeit with the introduction of two components, one slow and one fast. The slow component resulted in a half-time of 270 ± 20 min with an exchangeable fraction of 0.299 ± 0.003 and the fast component in a half-time of 3.7 ± 0.3 min albeit a small fraction of 0.0453 ± 0.0002. No changes were evident in the spontaneous exchange of the CAVCR sub-fraction without SCP-2 as shown in Fig. 7b (open circles). As previously observed in the PM, the spectrum after the exchange in the presence of SCP-2 was that of mostly monomeric DHE with an emission ratio of 455 nm/375 nm = 0.3 (Fig. 7e). Sterol exchange, whether spontaneous or with SCP-2, was nonexistent in the non-CAVCP sub-fraction of the PM (Fig. 7c) with the spectrum (Fig. 7f) revealing a crystalline type emission with an emission ratio of 455 nm/375 nm = 1.5. Herein SCP-2 provided greater enhancement of sterol transfer within the first hour as compared to an earlier study using CAVCR membrane vesicles containing DHE as donors to similarly obtained cholesterol containing acceptors [71]. Also, SCP-2 did not

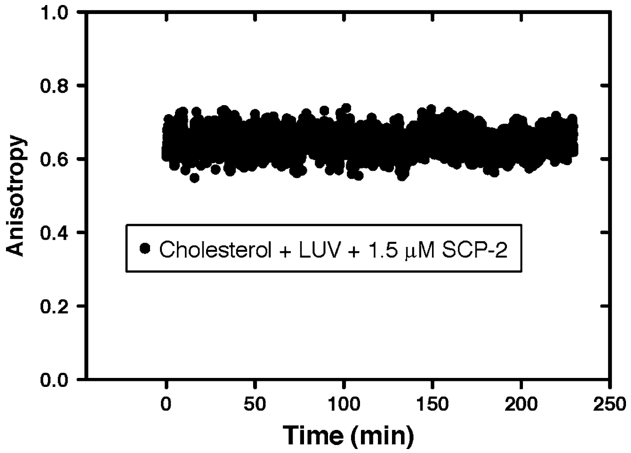

Fig. 6 Time dependent anisotropy measurements of cholesterol microcrystals with large unilamellar vesicles (LUVs). Large unilamellar vesicles (55 mol % POPC: 35 mol % cholesterol: 10 mol % PS) were prepared as described in the "Materials and Methods". **a** Using the same instrumental setup for measuring the anisotropy of DHE (Fig. 4), residual scatter was monitored for approximately 4 h using a 1.5 μM solution of cholesterol microcrystals (donor) and a 10-fold excess of LUVs (acceptors) in PIPES buffer

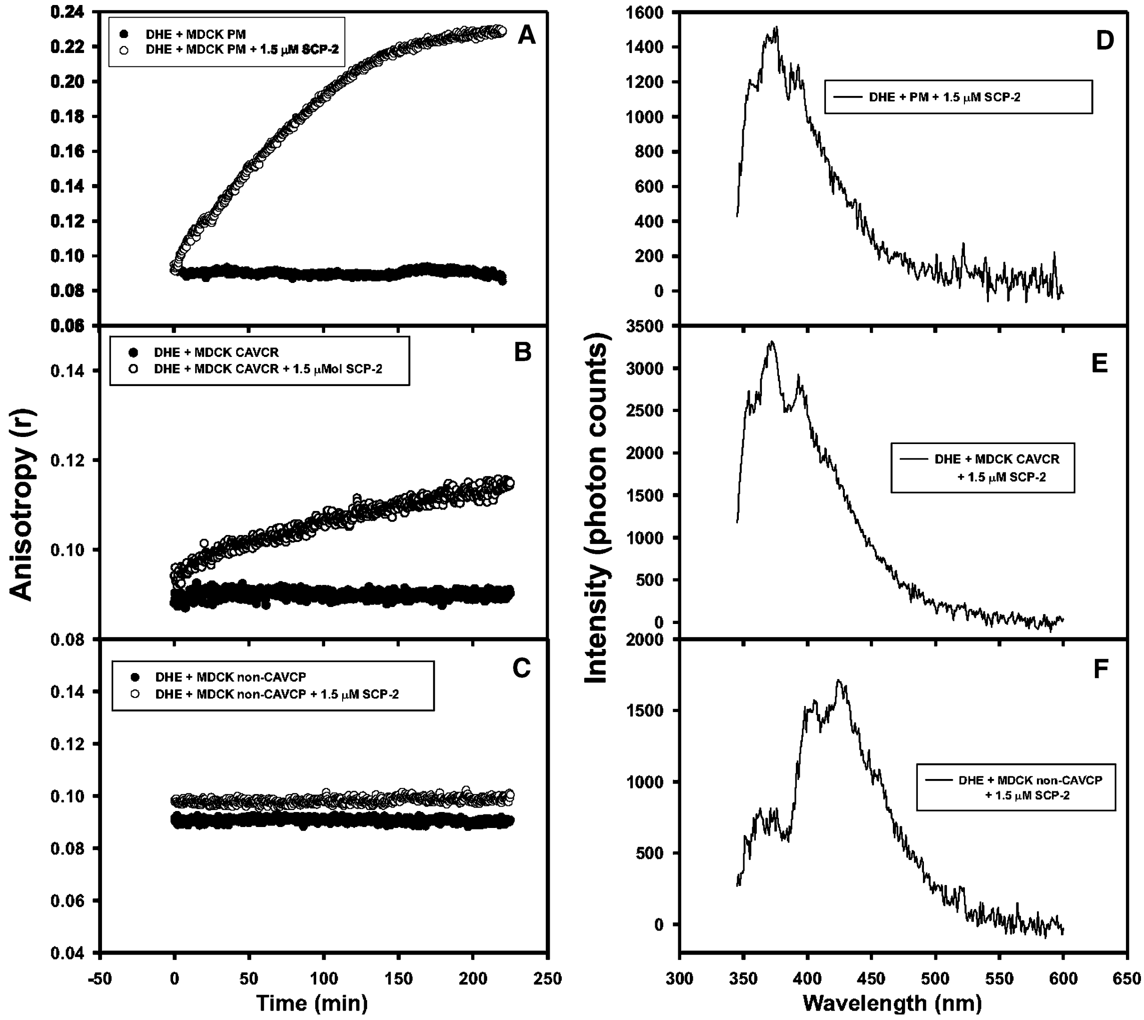

Fig. 7 Sterol exchange between donor DHE microcrystals and acceptors of biological plasma membrane fractions and sub-fractions. Plasma membranes were isolated from Madin-Darby canine kidney (MDCK) cells followed by sub-fractionation of the plasma membrane isolation, to yield CAVCR and non-CAVCP vesicles as described in the "Materials and Methods". Sterol exchanges were performed in a quartz cuvette with a 1.5 μM solution of DHE microcrystals as donors and a 10-fold excess of acceptor membrane vesicles in 10 mM PIPES buffer at pH 7.2. The anisotropy was measured with an ISS PC1 spectrofluorometer using excitation at 324 nm and the kinetic curves plotted for the spontaneous and SCP-2 mediated exchange of sterol from the donor DHE microcrystals to the following acceptors: **a** plasma membrane; **b** CAVCR; and **c** non-CAVCP. After a 4 h sterol exchange assay, spectra were acquired at 324 nm excitation to determine the structural form of the DHE. Spectra were plotted for the SCP-2 mediated exchanges (DHE donor microcrystals + 10-fold access acceptors + 1.5 μM SCP-2) for the following acceptors: **d** plasma membrane after 4 h showing mostly monomeric DHE; **e** CAVCR after 4 h showing mostly monomeric DHE; **f** non-CAVCP after 4 h showing microcrystalline DHE

significantly enhance sterol exchange between DHE containing donor non- CAVCP acceptor vesicles [71].

Multi-Photon Laser Scanning Microscopy of Dehydroergosterol Monohydrate

DHE in a solution of 90% ethanol and 10% water was evaporated at room temperature on chambered cover glass and imaged by multi-photon laser scanning microscopy using the instrumental setup described in the "Materials and Methods". Many microcrystals of DHE monohydrate were formed as seen by the small fluorescent plate structures (Fig. 8). Changes in shape and sizes occurred depending upon conditions such as concentration, temperature, and water content and subsequently rate of evaporation. DHE in anhydrous ethanol evaporated under nitrogen, typically formed longer structures as observed in cholesterol [20].

Multi-Photon Imaging of Crystalline Dehydroergosterol Disappearance in SCP-2 Overexpressing Cells as Compared to Control L-cells

L-cells and L-cells overexpressing SCP-2 were cultured as described in the "Materials and Methods". After supplementing the cells with crystalline DHE for 24 h, cells were

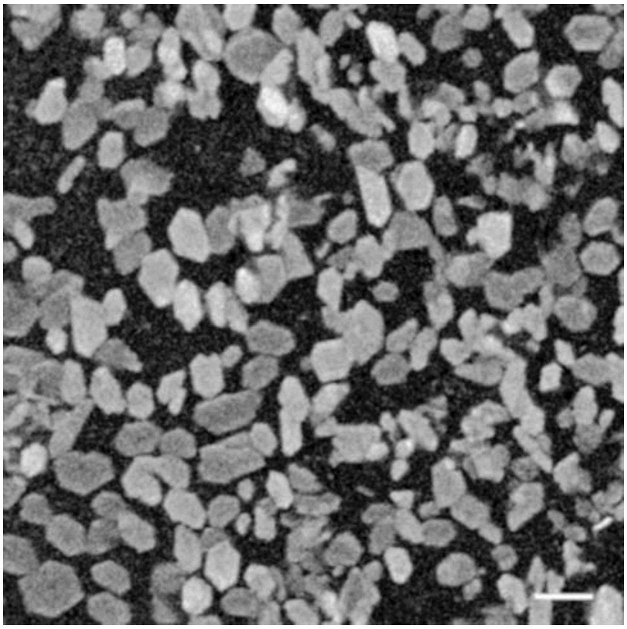

Fig. 8 Multi-photon laser scanning microscopy of DHE monohydrate microcrystals. The microcrystals were formed by evaporation from a solution of DHE in 90% ethanol and 10% water onto a chambered cover glass. The microcrystals were then imaged through a Zeiss 63X plan-Apochromat 1.4 NA oil immersion objective using a Bio-Rad MRC-1024 MP laser scanning microscopy imaging system with a Coherent titanium:sapphire femto-second mode-locked laser tuned to an excitation wavelength of 900 nm. This grayscale image of the plate-like structures represents the DHE crystalline enhanced fluorescence filtered through a Chroma Technology 455/30 nm dichroic filter. *White scale bar in the lower right-hand corner of the image* represents 4 μm

washed and serum containing media was added. Both control and SCP-2 overexpressing cells with phagocytosed crystals of DHE were immediately imaged by multi-photon microscopy using dual channel detection as described in the "Materials and Methods" at time $t = 0$. Power, gain, and black level were adjusted initially to minimize photobleaching, saturation, and dynamic range and maintained throughout the time based experiment. After the instrumental acquisition parameters were set appropriately, images of the autofluorescence of L-cells were acquired. Due to the brightness of the emission of microcrystalline DHE, no autofluorescence was observable in either the blue channel (Fig. 9a) or UV channel (Fig. 9b). Similar images (not shown) of the SCP-2 overexpressing cells were acquired. Images of the DHE emission from microcrystals of DHE in control cells and cells overexpressing SCP-2 were obtained by collecting the fluorescence in the blue and UV channels at $t = 0$. Figure 9c, d were multiphoton images acquired of the microcrystalline DHE in L-cells overexpressing SCP-2 at the initial time point. Subsequently, cells on several chambered cover glass were imaged at 12 h increments using multi-photon laser scanning microscopy using both channels. Representative images acquired from the blue (Fig. 9e) and UV channels (Fig. 9f) reveal the character of the remaining DHE in L-cells overexpressing SCP-2 after 60 h. Integrated intensity measurements were made of the dual channel acquisition images of cells across multiple regions of each slide and the mean integrated intensity was plotted as a function of time for both SCP-2 overexpressing and control cells (Fig. 10a). The rate of disappearance of DHE crystalline fluorescence (Fig. 10a) appeared linear over the period of 60 h for both cell types and did not appear significantly different between cell types due to large variability especially in the control L-cells. The SCP-2 overexpressing cells took up more microcrystals and trended toward faster disappearance as compared to the control cells. The emission at in the UV channel (375 nm) also decreased more rapidly even than that of the blue channel (455 nm) as seen in the graph of the ratio of the blue channel to UV channel (455 nm emission/375 nm emission) over time (Fig. 10b); which implied that at longer time points, monomeric DHE was distributed faster throughout the cellular membranes with a substantial portion effluxed out of the cell [89].

Discussion

Excess cholesterol is cytotoxic and can result in deleterious accumulation of crystalline cholesterol within the cell [10–12]. While increased excretion, intracellular esterification of cholesterol, and reduced hydrolysis of cholesteryl esters can in part prevent toxicity due to excess cholesterol [13], other factors may exist to enhance dissolution of crystalline cholesterol and transport from the cell. Early studies with macrophages, NPC fibroblasts, and hypercholesterolemic rats suggested a potential role for intracellular sterol binding/carrier proteins such as SCP-2 [15, 30–32]. In fact SCP-2 has been shown to enhance transfer of DHE out of microcrystals and exchange with cholesterol within intact lysosomal membranes [38]. This was somewhat surprising since even though DHE microcrystals appeared in large quantities of lysosomes as determined by fluorescence imaging/colocalization and isolation of intact lysosomes, SCP-2 has been observed in only very small amounts within lysosomes. Since cells can accumulate excess cholesterol in microcrystalline patches within the plasma membrane [10], a part of the current study was undertaken with dehydroergosterol, a naturally-occurring fluorescent sterol analog, and purified SCP-2 to determine if this protein enhanced the transfer/exchange of sterol between crystals and between crystals and membrane acceptors, especially plasma membranes and associated membrane domains. Together the data presented herein provide new

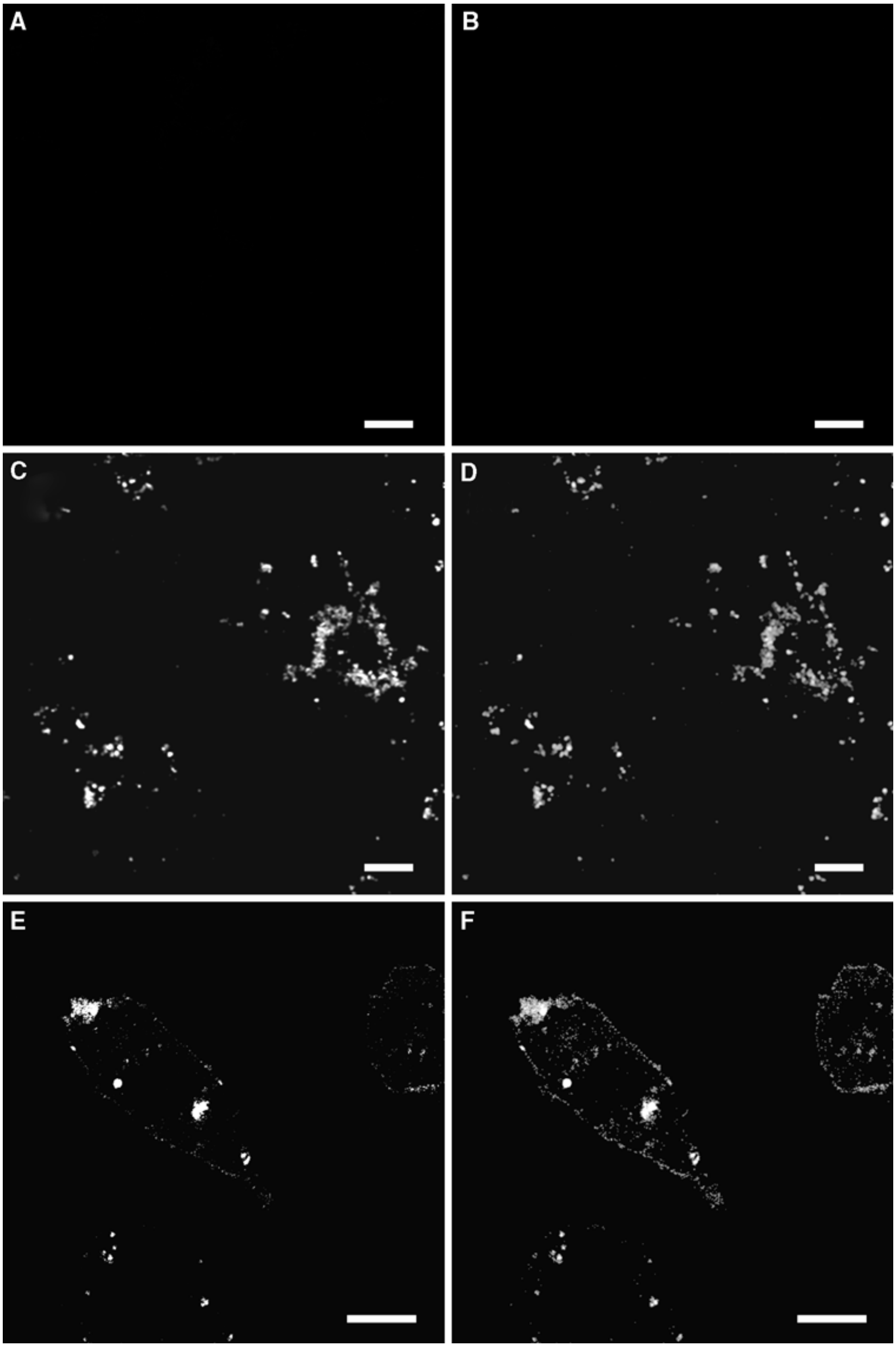

Fig. 9 The effect of SCP-2 overexpression on DHE microcrystals in living cells. Living cells on chambered cover glass were incubated with DHE microcrystals for 24 h. Cells were washed with PBS three times and the replaced with serum containing media. The cells were immediately imaged at $t = 0$ using multi-photon laser scanning microscopy imaging. Multi-photon excitation of the DHE was accomplished at 900 nm with simultaneously mostly crystalline DHE fluorescence emission was collected using a D455/30 nm filter (blue channel) and mostly monomeric DHE fluorescence emission was collected using a D375/50 nm filter (UV channel). The cells on chambered cover glass were returned to the incubator and subsequently imaged every 12 h up to 60 h. Image of L-cells without DHE labeling (autofluorescence) collected using the blue channel **a** and the UV channel **b**. The gain and black levels were adjusted to reduce the autofluorescence to near zero as seen in the images (**a**, **b**). Fluorescence emission of DHE microcrystals in living cells overexpressing SCP-2 as imaged in the blue channel **c** and UV channel **d** at time $t = 0$. Fluorescence emission of DHE microcrystals in living cells overexpressing SCP-2 as imaged in the blue channel **e** and UV channel **f** at time $t = 60$ h. *Scale bar in lower right corner* represents 10 μm

insights on the potential role of SCP-2 in dissolution of crystalline sterol and transfer of crystal derived sterol to cellular derived membrane fractions of enriched cholesterol and caveolin-1.

At the outset, the crystal structure of dehydroergosterol monohydrate was determined for the first time from DHE synthesized with a purity >99%. Comparison with the crystal structure of cholesterol monohydrate reveals overall similarities such as its organization into a bilayer system albeit with subtle differences, suggesting that it would be a suitable donor for SCP-2-mediated sterol transfer. Similar to ergosterol monohydrate, dehydroergosterol monohydrate crystallizes in the space group $P2_1$ with two molecules in the asymmetric unit while cholesterol monohydrate crystallizes in the space group P1 with four molecules in the asymmetric unit. If the unit cell of dehydroergosterol

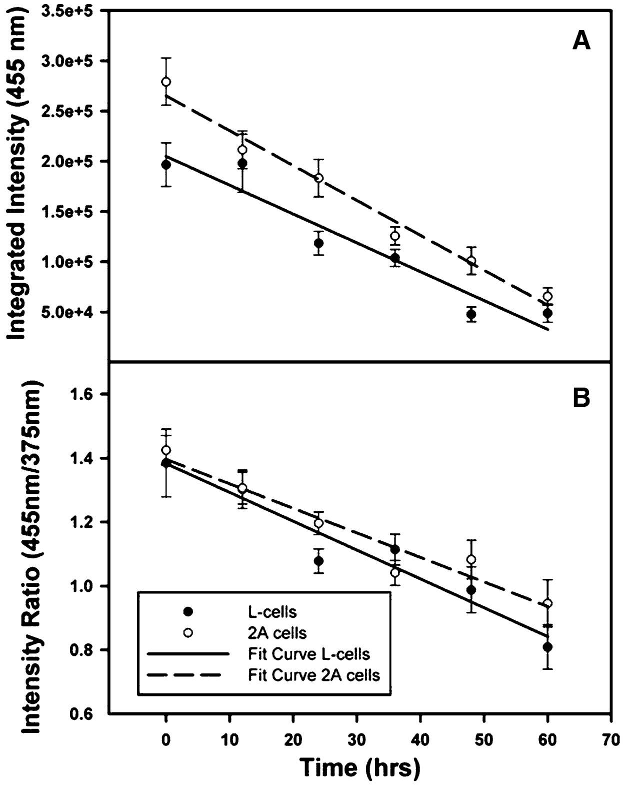

Fig. 10 Disappearance of microcrystalline DHE from L-cells and L-cells overexpressing SCP-2. **a** The background corrected integrated intensities obtained from images of DHE emission collected through the D455/30 nm filter (blue channel) were plotted for both control L-cells and cells overexpressing SCP-2. **b** The ratio of the background corrected integrated intensities of monomer to crystalline that were acquired using the D455/30 nm filter (blue channel) and the D375/50 nm filter (UV channel) were plotted for both control L-cells and L-cells overexpressing SCP-2. Each point was derived from mean integrated intensities obtained from collective measurements of ~50 cells and corrected for residual background autofluorescence; the *error bars* represent the standard error

monohydrate was doubled and the space group reduced to P1 then the transformed unit cell of dehydroergosterol monohydrate would be comparable to cholesterol monohydrate. Although, cholesterol monohydrate has triclinic symmetry, it does have some pseudo-symmetry such that the cholesterol monohydrate can easily be mistaken for monoclinic [81, 82]. The low temperature monohydrate crystalline structure of ergosterol was quite similar to the reduced form (Table 1) where the main effect of the addition of the two double bonds (Fig. 1) forming the conjugated system brought about the shortening of the longest axis c and with the decrease in the angle β bringing it closer to approximating an orthorhombic system. The space group reduced cell parameters of dehydroergosterol monohydrate measured to be slightly smaller (a = 9.9747(11) Å, b = 7.4731(9) Å, c = 34.054(4) Å, α = 90°, β = 92.970°[2], γ = 90°) than those of cholesterol monohydrate (a = 12.39 Å, b = 12.41 Å, c = 34.36 Å, α = 91.9°, β = 98.1°, γ = 100.8°) as reported previously [81]. In comparing dehydroergosterol monohydrate to the cholesterol monohydrate reported by Craven [81, 82] the intermolecular distance between the centroids of the staggered ring system for dehydroergosterol monohydrate [5.50(1)Å] was significantly shorter than cholesterol monohydrate [6.33(1) Å]. Consistent with previous measurements of force-area isotherms of monolayers formed using mixtures of either high mol% dehydroergosterol or cholesterol with POPC, the density of dehydroergosterol monohydrate ($\rho_{\mathrm{DHE}} = 1.081$ mg/m^3) was slightly larger, with a ratio of $\rho_{\mathrm{DHE}}/\rho_{\mathrm{Chol}} = 1.034$, than that of cholesterol monohydrate ($\rho_{\mathrm{Chol}} = 1.045$ mg/m^3) [38, 81]. Taken together, these data would suggest that dehydroergosterol was arranged in a slightly closer packed configuration than cholesterol.

DHE in its crystalline form yields enhanced red shifted emission reminiscent of the excimeric emission of pyrene although with much less increase in fluorescence and some spectral structure. Pyrene forms crystals that are monoclinic with four molecules in a unit cell and belong to the space group $P2_1/a$ such that the pyrene molecules are arranged as sandwich dimers, forming the basis of the excimer. Such a parallel arrangement observed of the stacking of parallel dehydroergosterol molecules could also form the basis of excimeric sandwich dimers although at interplanar distances ~1.5-fold greater than in pyrene crystals. The larger distance in the DHE crystal could explain the lower amount of enhanced emission from monomer to excimer as compared to the pyrene crystal. Also, the vibrational level structure observed in the difference spectra (crystalline-monomer) could indicate a somewhat longer-lived ground state dissociative dimer. At the present time, the enhanced red-shifted emission seems to be relegated to the crystalline form as this spectral characteristic has not been observed in highly concentrated solutions (not saturated and with no observable crystals) of DHE in ethanol. As such the existence of such enhancement in emission has proven to be a very useful tool to detect the existence of crystalline form in biological systems [91, 92].

Kinetic experiments, utilizing anisotropy measurements of aqueous dispersions of DHE microcrystals in the vicinity of 10-fold excess of acceptors, suggested that the addition of SCP-2, but not albumin, significantly enhanced disruption of the DHE microcrystalline structure when in the presence of excess cholesterol. Of greater significance, in experiments with model membranes containing POPC, cholesterol, and DOPS, SCP-2 enhanced exchange of sterol between microcrystals and LUVs nearly 92-fold more in the initial rate than the spontaneous exchange, even affecting two dynamic pools of cholesterol within the model membrane acceptors. The question remains, however, whether model membrane system studies would reflect the DHE transfer between microcrystals and biological membranes such as the plasma membrane.

The plasma membranes of many types of cells contain specialized cholesterol-rich microdomains [13, 18]. The localization of the protein caveolin to these regions can result in membrane invaginations (50–100 nm) which are morphological features visualized by electron microscopy and defined as caveolae. By selectively partitioning specific lipids and proteins, these membrane regions represent a nexus organizing multiple cell membrane functions such as reverse cholesterol transport, cell recognition, signaling, immune function, and potocytosis [4, 9, 93–97]. Although plasma membrane cholesterol-rich microdomains such as caveolae are important not only in normal cell physiology, aberrant microdomains are associated with metabolic diseases (cardiovascular, diabetes, obesity, Niemann-Pick C disease, Alzheimer's disease, as well as others) [19–26], pathogen entry, and the action of many bacterial and viral toxins [98–104]. In order to better understand the potential role of such microdomains in the removal of crystalline sterol, kinetic experiments were repeated with vesicles derived from the plasma membrane of MDCK cells: (1). plasma membrane acceptors and (2). affinity-purified acceptors consisting of CAVCR and non-CAVCP membrane vesicles sub-fractionated from plasma membrane isolation. Although the CAVCR sub-fraction was previously shown to contain proteins such as caveolin-1 and GM1 that are typically considered caveolae proteins and the non-CAVCP were shown to be void of these proteins, the argument remains at the edge of the definitive due to the invasive nature of the isolation [71, 73, 105]. Whether or not the cholesterol-rich vesicles can truly be considered to behave similarly to intact caveolar membranes, the two sub-fractions, respectively represent biological derived membrane substrates with and without a complement of active proteins thought to be involved in sterol uptake/efflux [9, 106]. As such, these fractions were used to characterize the interaction of crystalline sterol and active proteins in a biologically relevant lipid microsystem. In the plasma membrane fraction, a rather large amount (94%) of the sterol was exchangeable with a half-time on the order of 73 min, a value somewhat faster than that of MDCK membrane fractions but typical of other organellar types [71, 107]. Due to the large size of this rapid exchangeable pool and variability in isolations, it is possible that a much smaller fast component was obscured. Noticeably, in the binding sub-fraction (CAVCR) of the MDCK plasma membrane, a significantly faster component emerged that represented about 5% of the total sterol and 13% of the total exchangeable pool. However, only about 35% of the total sterol was exchangeable compared to approximately 58% when using plasma membrane binding fraction donors as well [71]. Similar to the plasma membrane vesicles, in LUVs almost all of the sterol was available for exchange in both the spontaneous and the SCP-2 enhanced. Two dynamic pools were observed wherein the majority (87%) pool had exchange rates on the order of a typical cholesterol-rich microdomain sub-fraction and a small pool (3%) had a very fast exchange rate (half-time on the order of s). Significant enhancement, as a result of the addition of SCP-2, occurred for the transfer of DHE out of microcrystals into membranes vesicles, both model and cellular except for the non-CAVCP, as might be expected at the outset. Although the largest bulk transfer occurred from plasma membrane vesicles, the CAVCR showed significant decrease in half-time but with less exchangeable sterol availability, possibly due to an intrinsic protein-cholesterol binding interaction (e.g., caveolin).

Multi-photon laser scanning microscopy with its optical sectioning capability has proven indispensable in observing naturally occurring fluorophores like DHE that absorb in ultraviolet wavelengths. With this technique, microcrystals of DHE have been observed to incorporate into L-cells [38]. This was not surprising since L-cells have been shown to take up latex beads nearly 2 μm in diameter [108]. Noninvasive spectroscopic imaging measurements revealed that living cells work to reduce the amount of intracellular crystalline sterol and showed that lysosomes play a major role in this process but little was known about whether SCP-2 might aid in the intracellular dissolution process [38]. L-cells overexpressing SCP-2 were used to determine the rate of disappearance of microcrystalline DHE monohydrate in real-time as compared to control cells. Cellular monomeric DHE that remained within the cell localized in lipid storage droplets and intracellular membranes with substantial accumulation in the plasma membrane as formerly observed in L-cells [38, 58].

Previous studies have demonstrated the ability of protein interaction in facilitating uptake of aqueous dispersions of cholesterol aggregates. In cells overexpressing the scavenger receptor class B type I (SR-BI) it was shown that SR-BI effected uptake of free radiolabeled cholesterol ([^{3}H] cholesterol) to stimulate cholesterol esterification after a 5 h incubation period with similar effectiveness as lipoproteins [109]. Moreover, SR-BI was shown to facilitate uptake of cholesterol from mixed bile salt micelles [110].

In conclusion, not only the low solubility of cholesterol in aqueous media but also the build up of crystalline patches in cellular membranes presents many challenges to biological systems. However, small lipid binding proteins such as SCP-2 in combination with specialized regions of lipid-protein systems can facilitate and mediate the exchange of sterol though sequestered in microcrystalline form in order to adequately transport and access the sterol for further utilization. Therefore the observed enhanced transfer effects with SCP-2 reveal the possibility of lipid-protein processes to remediate cholesterol aggregation within the cell. This was demonstrated herein through the use of the naturally occurring fluorescent cholesterol analog, DHE, in monohydrate crystalline structures somewhat resembling that of cholesterol monohydrate but with unique fluorescent spectral properties.

Acknowledgments This work was supported in part by the by the USPHS, NIH GM31651 (FS, ABK), DK70965(BPA), and Mentored Quantitative Research Career Development Award (K25) DK062812 (AMG).

References

1. Schroeder F, Jefferson JR, Kier AB, Knittell J, Scallen TJ, Wood WG, Hapala I (1991) Membrane cholesterol dynamics: cholesterol domains and kinetic pools. Proc Soc Exp Biol Med 196:235–252
2. Schroeder F, Frolov AA, Murphy EJ, Atshaves BP, Jefferson JR, Pu L, Wood WG, Foxworth WB, Kier AB (1996) Recent advances in membrane cholesterol domain dynamics and intracellular cholesterol trafficking. Proc Soc Exp Biol Med 213:150–177
3. Schroeder F, Gallegos AM, Atshaves BP, McIntosh A, Petrescu AD, Huang H, Chao H, Yang H, Frolov A, Kier AB (2001) Recent advances in membrane microdomains: rafts, caveolae and intracellular cholesterol trafficking. Exp Biol Med 226:873–890
4. Smart EJ, van der Westhuyzen DR (1998) Scavenger receptors, caveolae, caveolin, and cholesterol trafficking. In: Chang TY, Freeman DA (eds) Intracellular cholesterol trafficking. Kluwer, Boston, pp 253–272
5. Fielding CJ (1991) Reverse cholesterol transport. Curr Opin Lipidol 2:376–378
6. Fielding PE, Fielding CJ (1991) Dynamics of lipoprotein transport in the circulatory system. In: Vance DE, Vance J (eds) Biochemistry of lipids, lipoproteins, and membranes, vol 20. Elsevier, New York, pp 427–459
7. Fielding PE, Fielding CJ (2002) Dynamics of lipoprotein transport in the human circulatory system. In: Vance DE, Vance J (eds) Biochemistry of lipids, lipoproteins and membranes, vol 36. Elsevier, New York, pp 527–552
8. Yancey PG, Bortnick AE, Kellner-Weibel G, de la Llera-Moya M, Phillips MC, Rothblat GH (2003) Importance of different pathways of cellular cholesterol efflux. Arterioscler Thromb Vasc Biol 23:712–719
9. Schroeder F, Atshaves BP, Gallegos AM, McIntosh AL, Liu JC, Kier AB, Huang H, Ball JM (2005) Lipid rafts and caveolae organization. In: Frank PG, Lisanti MP (eds) Advances in molecular and cell biology, vol 36. Elsevier, Amsterdam, pp 3–36
10. Tulenko TN, Chen M, Mason PE, Mason RP (1998) Physical effects of cholesterol on arterial smooth muscle membranes: evidence of immiscible cholesterol domains and alterations in bilayer width during atherogenesis. J Lipid Res 39:947–956
11. Chen M, Mason RP, Tulenko TN (1995) Atherosclerosis alters the composition, structure and function of arterial smooth muscle cell plasma membranes. Biochim Biophys Acta 1272:101–112
12. Gleason MM, Medow MS, Tulenko TN (1991) Excess membrane cholesterol alters calcium movements, cytosolic calcium levels, and membrane fluidity in arterial smooth muscle cells. Circ Res 69:216–227
13. Tabas I (1997) Free cholesterol-induced cytotoxicity. Trends Cardiovasc Med 7:256–263
14. McConathy WJ, Koren E, Stiers DL (1989) Cholesterol crystal uptake and metabolism by P388D1 macrophages. Atherosclerosis 77:221–225
15. Tangirala RK, Jerome WG, Jones NL, Small DM, Johnson WJ, Glick JM, Mahlberg FH, Rothblat GH (1994) Formation of cholesterol monohydrate crystals in macrophage-derived foam cells. J Lipid Res 35:93–104
16. Luly P, Shinitzky M (1979) Gross structural changes in isolated liver cell plasma membranes upon binding of insulin. Biochemistry 18:445–450
17. Sweet WD, Schroeder F (1988) Lipid domains and enzyme activity. In: Aloia RC, Cirtain CC, Gordon LM (eds) Advances in membrane fluidity: lipid domains and the relationship to membrane function. Alan R Liss Inc, New York, pp 17–42
18. Warner GJ, Stoudt G, Bamberger M, Johnson WJ, Rothblat GH (1995) Cell toxicity induced by inhibition of acyl coenzyme A: cholesterol acyltransferase and accumulation of unesterified cholesterol. J Biol Chem 270:5772–5778
19. Small DM, Shipley GG (1974) Physical-chemical basis of lipid deposition in atherosclerosis. Science 185:222–229
20. Loomis CR, Shipley GG, Small DM (1979) The phase behavior of hydrated cholesterol. J Lipid Res 20:525–535
21. Small DM (1988) Progression and regression of atherosclerotic lesions. Insights from lipid physical chemistry. Arteriosclerosis 8:103–129
22. Guo W, Morrisett JD, Lawrie GM, DeBakey ME, Hamilton JA (1998) Identification of different lipid phases and calcium phosphate deposits in human carotid artery plaques by MAS NMR spectroscopy. Magn Reson Med 39:184–189
23. Guo W, Morrisett JD, DeBakey ME, Lawrie GM, Hamilton JA (2000) Quantification in situ of crystalline cholesterol and calcium phosphate hydroxyapatite in human atherosclerotic plaques by solid-state magic angle spinning NMR. Arterioscler Thromb Vasc Biol 20:1630–1636
24. Vanier MT, Pentchev PG, Rodriguez-Lafrasse C, Rousson R (1991) Niemann-Pick disease type C: an update. J Inherit Metab Dis 14:580–595
25. Blanchette-Mackie EJ, Pentchev P (1998) Cholesterol distribution in Golgi, lysosomes, and endoplasmic reticulum. In: Chang TY, Freeman DA (eds) Intracellular cholesterol trafficking. Kluwer, Boston, pp 53–73
26. Sokol J, Blanchette-Mackie EJ, Kruth HS, Dwyer NK, Amende LM, Butler JD, Robinson E, Patel S, Brady RO, Comly ME, Vanier MT, Pentchev P (1988) Type C Niemann-Pick disease: lysosomal accumulation and defective intracellular mobilization of LDL cholesterol. J Biol Chem 263:3411–3417
27. Hirai A, Kino T, Tokinaga K, Tahara K, Tamura Y, Yoshida S (1994) Regulation of sterol carrier protein 2 (SCP2) gene expression in rat peritoneal macrophages during foam cell formation. A key role for free cholesterol content. J Clin Invest 94:2215–2223
28. Ban T, Hirai A, Kino T, Oeda T, Fujiki Y, Tamura Y, Yoshida S (1991) Sterol carrier protein$_2$ (SCP$_2$)-like protein in rat aorta. Artery 18:54–70
29. Tangirala RK, Mahlberg FH, Glick JM, Jerome WG, Rothblat GH (1993) Lysosomal accumulation of unesterified cholesterol in model macrophage foam cells. J Biol Chem 268:9653–9660
30. Roff CF, Pastuszyn A, Strauss JFI, Billheimer JT, Vanier MT, Brady RO, Scallen TJ, Pentchev PG (1992) Deficiencies in sex-regulated expression and levels of two hepatic sterol carrier proteins in a murine model of Niemann-Pick type C disease. J Biol Chem 267:15902–15908
31. Pentchev PG, Brady RO, Blanchette-Mackie EJ, Vanier MT, Carstea ED, Parker CC, Goldin E, Roff CF (1994) The

Niemann-Pick C lesion and its relationship to the intracellular distribution and utilization of LDL cholesterol. Biochim Biophys Acta 1225:235–243

32. McLean MP, Billheimer JT, Warden KJ, Irby RB (1995) Differential expression of hepatic sterol carrier proteins in the streptozotocin-treated diabetic rat. Endocrinology 136:3360–3368
33. Schoer J, Gallegos A, Starodub O, Petrescu A, Roths JB, Kier AB, Schroeder F (2000) Lysosomal membrane cholesterol dynamics: role of sterol carrier protein-2 gene products. Biochemistry 39:7662–7677
34. Gallegos AM, Atshaves BP, Storey SM, Schoer J, Kier AB, Schroeder F (2002) Molecular and fluorescent sterol approaches to probing lysosomal membrane lipid dynamics. Chem Phys Lipids 116:19–38
35. Sica D, Boniforti L, DiGiacomo G (1982) Sterols of candida tropicalis grown on *n*-alkanes. Phytochemistry 21:234–236
36. Delseth C, Kashman Y, Djerassi C (1979) Ergosta-5, 7, 9(11), 22-tetraen-3beta-ol and its 24epsilon-ethyl homolog, two new marine sterols from the red sea sponge Biemna fortis. Helv Chim Acta 62:2037–2045
37. Nemecz G, Fontaine RN, Schroeder F (1988) A fluorescence and radiolabel study of sterol exchange between membranes. Biochim Biophys Acta 943:511–521
38. McIntosh A, Gallegos A, Atshaves BP, Storey S, Kannoju D, Schroeder F (2003) Fluorescence and multiphoton imaging resolve unique structural forms of sterol in membranes of living cells. J Biol Chem 278:6384–6403
39. Schroeder F (1984) Fluorescent sterols: probe molecules of membrane structure and function. [Review]. Prog Lipid Res 23:97–113
40. Smutzer G, Crawford BF, Yeagle PL (1986) Physical properties of the fluorescent sterol probe dehydroergosterol. Biochim Biophys Acta 862:361–371
41. Schroeder F, Frolov A, Schoer J, Gallegos A, Atshaves BP, Stolowich NJ, Scott AI, Kier AB (1998) Intracellular sterol binding proteins, cholesterol transport and membrane domains. In: Chang TY, Freeman DA (eds) Intracellular cholesterol trafficking. Kluwer, Boston, pp 213–234
42. Atshaves BP, Gallegos A, McIntosh AL, Kier AB, Schroeder F (2003) Sterol carrier protein-2 selectively alters lipid composition and cholesterol dynamics of caveolae/lipid raft vs non-raft domains in L-cell fibroblast plasma membranes. Biochemistry 42:14583–14598
43. Gallegos AM, McIntosh AL, Atshaves BP, Schroeder F (2004) Structure and cholesterol domain dynamics of an enriched caveolae/raft isolate. Biochem J 382:451–461
44. Schroeder F, Goh EH, Heimberg M (1979) Regulation of the surface physical properties of the very low density lipoprotein. J Biol Chem 254:2456–2463
45. Bergeron RJ, Scott J (1982) Cholestatriene and ergostatetraene as in vivo and in vitro membrane and lipoprotein probes. J Lipid Res 23:391–404
46. Smutzer G (1988) A fluorescent sterol probe study of human serum low density lipoproteins. Biochim Biophys Acta 958:323–333
47. Yeagle PL, Bensen J, Greco M, Arena C (1982) Cholesterol behavior in human serum lipoproteins. Biochemistry 21:1249–1254
48. Fischer RT, Cowlen MS, Dempsey ME, Schroeder F (1985) Fluorescence of delta 5, 7, 9(11), 22-ergostatetraen-3 beta-ol in micelles, sterol carrier protein complexes, and plasma membranes. Biochemistry 24:3322–3331
49. Schroeder F, Frolov A, Starodub O, Russell W, Atshaves BP, Petrescu AD, Huang H, Gallegos A, McIntosh A, Tahotna D, Russell D, Billheimer JT, Baum CL, Kier AB (2000) Pro-sterol carrier protein-2: role of the N-terminal presequence in structure, function, and peroxisomal targeting. J Biol Chem 275:25547–25555
50. Martin GG, Hostetler HA, Tichy SE, Russell DH, Berg JM, Woldegiorgis G, Spencer TA, Ball JA, Kier AB, Schroeder F (2008) Structure and function of the sterol carrier protein-2 (SCP-2) N-terminal pre-sequence. Biochemistry 47:5915–5934
51. Gimpl G, Fahrenholz F (2000) Human oxytocin receptors in cholesterol-rich vs cholesterol-poor microdomains of the plasma membrane. Eur J Biochem 267:2483–2497
52. Burger K, Gimpl G, Fahrenholz F (2000) Regulation of receptor function by cholesterol. Cell Mol Life Sci 57:1577–1592
53. Stolowich NJ, Petrescu AD, Huang H, Martin G, Scott AI, Schroeder F (2002) Sterol carrier protein-2: structure reveals function. Cell Mol Life Sci 59:193–212
54. Loura LMS, Prieto M (1997) Dehydroergosterol structural organization in aqueous medium and in a model system of membranes. Biophys J 72:2226–2236
55. Kubelt JK, Muller P, Wustner D, Hermann A (2002) Rapid transbilayer movement of the fluorescent sterol dehydroergosterol in lipid membranes. Biophys J 83:1525–1534
56. Schroeder F, Butko P, Nemecz G, Scallen TJ (1990) Interaction of fluorescent delta 5, 7, 9(11), 22-ergostatetraen-3β-ol with sterol carrier protein-2. J Biol Chem 265:151–157
57. Mukherjee S, Zha X, Tabas I, Maxfield FR (1998) Cholesterol distribution in living cells:fluorescence imaging using dehydroergosterol as a fluorescent cholesterol analog. Biophys J 75:1915–1925
58. Zhang W, McIntosh A, Xu H, Wu D, Gruninger T, Atshaves BP, Liu JCS, Schroeder F (2005) Structural analysis of sterol distribution in the plasma membrane of living cells. Biochemistry 44:2864–2984
59. McIntosh A, Atshaves BP, Huang H, Gallegos AM, Kier AB, Schroeder F, Xu H, Zhang W, Liu S (2007) Multiphoton laser scanning microscopy and spatial analysis of dehydroergosterol distributions on plasma membranes of living cells. In: McIntosh T (ed) Lipid rafts. Humana, Totowa, pp 85–105
60. Wustner D (2005) Improved visualization and quantitative analysis of fluorescent membrane sterol in polarized hepatic cells. J Microsc 220:47–64
61. Wustner D (2007) Plasma membrane sterol distribution resembles the surface topography of living cells. Mol Biol Cell 18:211–228
62. Haberland ME, Reynolds JA (1973) Self-association of cholesterol in aqueous solution. Proc Natl Acad Sci 70:2313–2318
63. Renshaw PF, Janoff AS, Miller KW (1983) On the nature of dilute aqueous cholesterol suspensions. J Lipid Res 24:47–51
64. Ruyle WV, Jacob TA, Chemerda JM, Chamberlin EM, Rosenburg DW, Sita GE, Erickson RL, Aliminosa LM, Tishler M (1953) The preparation of delta7, 9(11)-allo-steroids by the action of mercuric acetate on delta7-allo steroids. J Am Chem Soc 75:2604–2609
65. McIntosh AL, Atshaves BP, Huang H, Gallegos AM, Kier AB, and Schroeder F (2008) Fluorescence techniques using dehydroergosterol to study cholesterol trafficking. Lipids
66. Fischer RT, Stephenson FA, Shafiee A, Schroeder F (1985) Structure and dynamic properties of dehydroergosterol, delta 5, 7, 9(11), 22-ergostatetraen-3 beta-ol. J Biol Phys 13:13–24
67. Frolov A, Cho TH, Billheimer JT, Schroeder F (1996) Sterol carrier protein-2, a new fatty acyl coenzyme A-binding protein. J Biol Chem 271:31878–31884
68. Sheldrick GM (1997) SHELXS-97 Program for crystal structure solution. Institute fur Anorganishe Chemie der Universität, Gottingen

69. Huang H, Ball JA, Billheimer JT, Schroeder F (1999) Interaction of the N-terminus of sterol carrier protein-2 with membranes: role of membrane curvature. Biochem J 344:593–603
70. Huang H, Ball JA, Billheimer JT, Schroeder F (1999) The sterol carrier protein-2 amino terminus: a membrane interaction domain. Biochemistry 38:13231–13243
71. Gallegos AM, Storey SM, Kier AB, Schroeder F, Ball JM (2006) Structure and cholesterol dynamics of caveolae/raft and nonraft plasma membrane domains. Biochemistry 45:12100–12116
72. Atshaves BP, McIntosh AL, Payne HR, Gallegos AM, Landrock K, Maeda N, Kier AB, Schroeder F (2007) Sterol carrier protein-2/sterol carrier protein-x gene ablation alters lipid raft domains in primary cultured mouse hepatocytes. J Lipid Res 48:2193–2211
73. Storey SM, Gallegos AM, Atshaves BP, McIntosh AL, Martin GG, Landrock K, Kier AB, Ball JA, Schroeder F (2007) Selective cholesterol dynamics between lipoproteins and caveolae/lipid rafts. Biochemistry 46:13891–13906
74. Lakowicz JR (1983) Principles of fluorescence spectroscopy. In: Lakowicz JF (ed) Plenum, New York
75. Gallegos AM, Atshaves BP, Storey SM, Starodub O, Petrescu AD, Huang H, McIntosh A, Martin G, Chao H, Kier AB, Schroeder F (2001) Gene structure, intracellular localization, and functional roles of sterol carrier protein-2. Prog Lipid Res 40:498–563
76. Gallegos AM, McIntosh AL, Kier AB, Schroeder F (2008) Membrane domain distributions: analysis of fluorescent sterol exchange kinetics. Curr Anal Chem 4:1–7
77. Butko P, Hapala I, Nemecz G, Schroeder F (1992) Sterol domains in phospholipid membranes: dehydroergosterol polarization measures molecular sterol transfer. J Biochem Biophys Methods 24:15–37
78. Frolov A, Woodford JK, Murphy EJ, Billheimer JT, Schroeder F (1996) Spontaneous and protein-mediated sterol transfer between intracellular membranes. J Biol Chem 271:16075–16083
79. Schoer J, Peterson S, Gonzalez A, and Schroeder F (1998) Lysosomal membrane sterol transfer. Contribution of lipoproteins to intermembrane sterol transfer
80. Higuchi K (1970) An improved chemically defined culture medium for strain L mouse cells based on growth responses to graded levels of nutrients including iron and zinc. J Cell Physiol 75:65–72
81. Craven BM (1976) Crystal structure of cholesterol monohydrate. Nature 260:727–729
82. Craven BM (1979) Pseudosymmetry in cholesterol monohydrate. Acta Crystallogr B35:1123–1128
83. Bernal J (1940) *Philos. Trans. R. Soc. London B239*, 135
84. Schroeder F, Nemecz G (1990) Transmembrane cholesterol distribution. In: Esfahami M, Swaney J (eds) Advances in cholesterol research. Telford, Caldwell, pp 47–87
85. Hale JE, Schroeder F (1982) Asymmetric transbilayer distribution of sterol across plasma membranes determined by fluorescence quenching of dehydroergosterol. Eur J Biochem 122:649–661
86. Schroeder F, Gallegos AM, Atshaves BP, Storey SM, McIntosh A, Petrescu AD, Huang H, Starodub O, Chao H, Yang H, Frolov A, Kier AB (2001) Recent advances in membrane cholesterol microdomains: rafts, caveolae, and intracellular cholesterol trafficking. Exp Biol Med 226:873–890
87. Bergeron RJ, Scott J (1982) Fluorescent lipoprotein probe. Anal Chem 119:128–134
88. Hapala I, Kavecansky J, Butko P, Scallen TJ, Joiner C, Schroeder F (1994) Regulation of membrane cholesterol domains by sterol carrier protein-2. Biochemistry 33:7682–7690
89. Gallegos AM, Atshaves BP, Storey S, McIntosh A, Petrescu AD, Schroeder F (2001) Sterol carrier protein-2 expression alters plasma membrane lipid distribution and cholesterol dynamics. Biochemistry 40:6493–6506
90. Atshaves BP, Jefferson JR, McIntosh AL, McCann BM, Landrock K, Kier AB, Schroeder F (2007) Effect of sterol carrier protein-2 expression on sphingolipid distribution in plasma membrane lipid rafts/caveolae. Lipids 42:871–884
91. Camerman A, Trotter J (1065) The crystal and molecular structure of pyrene. Acta Crystallogr 18:636–643
92. Birks JB (1975) Excimers. Rep Prog Phys 38:903–974
93. Anderson R (1998) The caveolae membrane system. Ann Rev Biochem 67:199–225
94. Lavie Y, Liscovitch M (2000) Changes in lipid and protein constituents of rafts and caveolae in multidrug resistant cancer cells and their functional consequences. Glycoconj J 17:253–259
95. Everson WV, Smart EJ (2001) Influence of caveolin, cholesterol, and lipoproteins on nitric oxide synthase. TCM 11:246–250
96. Brown DA, London E (2000) Structure and function of sphingolipid- and cholesterol-rich membrane rafts. J Biol Chem 275:17221–17224
97. Anderson RGW, Jacobson K (2002) A role for lipid shells in targeting proteins to caveolae, rafts, and other lipid domains. Science 296:1821–1825
98. Abrami L, Liu S, Cosson P, Leppla SH, van der Groot FG (2003) Anthrax toxin triggers endocytosis of its receptor via a lipid raft-mediated clathrin-independent process. J Cell Biol 160:321–328
99. Sandvig K, van Deurs B (1999) Endocytosis and intracellular transport of ricin: recent discoveries. FEBS Lett 452:67–70
100. Bavari S, Bosio CM, Wiegand E, Ruthel G, Will AB, Geisbert TW, Hevey M, Schmaljohn C, Aman MJ (2002) Lipid raft microdomains. A gateway for compartmentalized trafficking of Ebola and Marburg viruses. J Exp Med 195:593–602
101. Marjomaki V, Pietiainen V, Upla P, Ivaska J, Nissinen L, Reunanen H, Huttunen P, Hyypia T, Heino J (2002) Internalization of Echovirus 1 in caveolae. J Virol 76:1856–1865
102. Sieczkarski SB, Whittaker GR (2002) Dissecting virus entry via endocytosis. J Gen Virol 83:1535–1545
103. Shin J-S, Abraham SN (2002) Caveolae as portals of entry for microbes. Microbes and Infect 3:755–761
104. Norkin LC (2001) Caveolae in the uptake and targeting of infectious agents and secreted toxins. Adv Drug Deliv Rev 49:301–315
105. Storey SM, Gibbons TF, Williams CV, Parr RD, Schroeder F, Ball JM (2007) Full-length, glycosylated NSP4 is localized to plasma membrane caveolae by a novel raft isolation technique. J Virol 81:5472–5483
106. Everson WV, Smart EJ (2005) Caveolae and the regulation of cellular cholesterol homeostasis. In: Lisanti MP, Frank PG (eds) Caveolae and lipid rafts: roles in signal transduction and the pathogenesis of human disease, vol 36. Elsevier, San Diego, pp 37–55
107. Frolov AA, Woodford JK, Murphy EJ, Billheimer JT, Schroeder F (1996) Fibroblast membrane sterol kinetic domains: modulation by sterol carrier protein 2 and liver fatty acid binding protein. J Lipid Res 37:1862–1874
108. Schroeder F, Kinden DA (1983) Measurement of phagocytosis using fluorescent latex beads. J Biochem Biophys Methods 8:15–27
109. Stangl H, Cao G, Wyne KL, Hobbs HH (1998) Scavenger receptor, class B, type 1-dependent stimulation of cholesterol esterification by high density lipoproteins, and nonlipoprotein cholesterol. J Biol Chem 273:31008
110. Hauser H, Dyer JH, Nandy A, Vega MA, Werder M, Bieliauskaite E, Weber FE, Compassi S, Gemperli A, Boffelli D, Wehrli E, Schulthess G, Phillips MC (1998) Identification of a receptor mediating absorption of dietary cholesterol in the intestine. Biochemistry 37:17843–17850

Historical Perspective

In order to resolve the dynamics and factors governing cholesterol trafficking within cells, it is important to recognize that the cholesterol molecule has very few polar constituents (Fig. 1a). Consequently, cholesterol is poorly soluble in aqueous environments such as cytosol as evidenced by critical micellar concentrations of cholesterol and other sterols being very low, near 20–30 nM [1–5]. The physiological impact of cholesterol's low aqueous solubility is that spontaneous cholesterol desorption from the cytofacial leaflet of the plasma membrane or lysosomal membrane into the cytosol for transfer to intracellular sites for esterification, oxidation, or secretion is extremely slow ($t_{1/2}$ 3 h-days) [6–9]. Therefore, it is important to resolve factors that influence the solubility of cholesterol in the cytoplasm as well as to understand how the architecture and properties of cholesterol in the plasma membrane govern cholesterol movement from serum lipoproteins/albumin into the membrane exofacial leaflet, across the bilayer, and from the membrane cytofacial leaflet into the cytoplasm either as vesicles or to cholesterol binding proteins.

Multiple physical approaches in model or fixed cell systems have been used to resolve the properties of cholesterol in membranes and the influence of cholesterol on membrane structure. Membrane cholesterol organization has been examined using electron microscopy to visualize the membrane at magnifications up to 100,000× [10]. X-ray diffraction has been applied to membranes to determine cholesterol orientation and depth as well as determine lipidic crystal structures [11, 12]. By using deuterated molecules and cooled neutron beams, neutron scattering profiles of phospholipid/cholesterol bilayers have been measured and neutron scatter off of the deuterium atom has been used to accurately determine cholesterol's location within the membrane [11, 12]. Electron scattering has had limited use due to high vacuum requirements but has yielded some packing orientation of cholesterol-rich domains [11–13]. Calorimetry or thermal analysis resolves the effects of cholesterol level on lipid phase transitions in model membranes of various lipid compositions [14]. Unfortunately the complexity of lipid compositions in biological membranes broadens/abolishes lipid phase transitions—thereby limiting the usefulness of calorimetry. By placing the membranes in a strong magnetic field with exposure to electromagnetic radiation, nuclear magnetic resonance (NMR) measurements involving the interaction with the nonzero spin of certain nuclei such as ^{1}H and ^{13}C have provided not only detailed structural information (e.g. order parameter) on cholesterol but also its interaction strengths with phospholipid constituents of the membrane [12, 15, 16]. While ^{1}H and ^{13}C labeled cholesterols provide probes with structure most closely resembling that of cholesterol, it is difficult to incorporate large amounts of these labeled sterols into biological membranes and the time-scale of NMR measurements precludes resolution of cholesterol dynamics on the biological time scale [17]. Another technique, electron spin resonance (EPR) involves the exploitation of the paramagnetism of certain molecules with unpaired spins, usually ^{14}N [15]. Due to the nature of the low natural paramagnetism of lipids, EPR probes are synthesized with spin labels such as nitroxide free radicals (e.g. dimethyl nitroxide referred to as doxyl). The properties of doxyl labeled sterol analogs such as

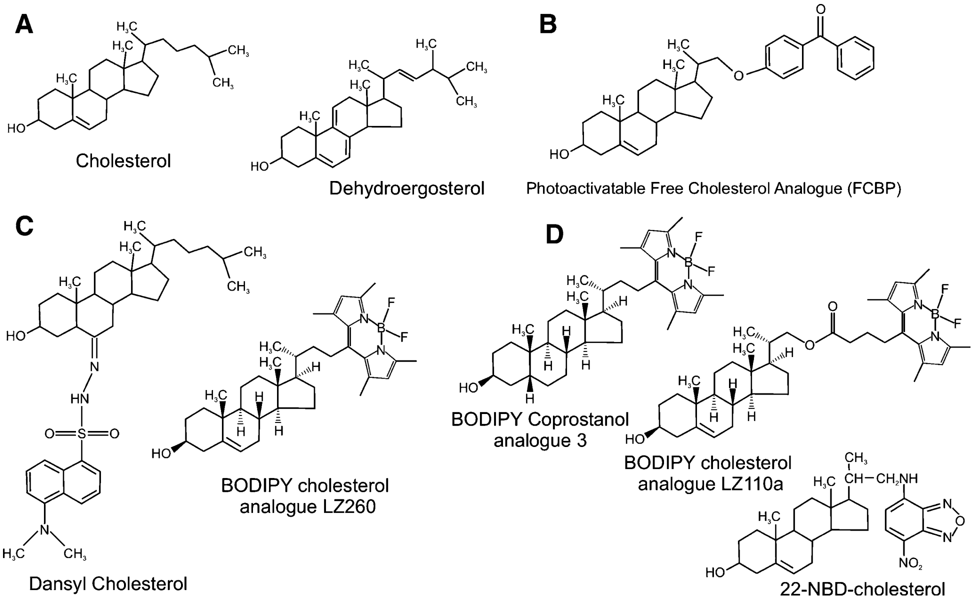
A
Cholesterol
Dehydroergosterol
B
Photoactivatable Free Cholesterol Analogue (FCBP)
C
Dansyl Cholesterol
BODIPY cholesterol analogue LZ260
D
BODIPY Coprostanol analogue 3
BODIPY cholesterol analogue LZ110a
22-NBD-cholesterol

Fig. 1 Structures of cholesterol and fluorescent cholesterol analogs. **a** Naturally occurring sterols: cholesterol and fluorescent sterol dehydroergosterol (DHE). **b** Photo-activatable cholesterol analog (FCBP). **c** Cholesterol-rich microdomain preferring cholesterol analogs: Dansyl-cholesterol (DChol); BODIPY-cholesterol analog (LZ260). **d** Cholesterol-poor microdomain preferring cholesterol analogs: BODIPY-coprostanol analog 3; BODIPY-cholesterol analog LZ110a; 22-NBD-cholesterol

SL-cholestane, SL-cholesterol, and SL-androstane have recently been examined in POPC large unilamellar vesicles (LUVs). Using EPR, it was found that the SL-cholestane was moved deeper within the membrane as a result of the bulky doxyl replacing the OH group but with correct membrane orientation similar to the SL-cholesterol which had the doxyl replacing two methyl groups in the cholesterol tail [16]. However, EPR showed that the SL-androstane molecule was upside down in membrane orientation. This was due to the hydroxyl at the terminal end of the lipid chain and the replacement of the OH by the doxyl group [16]. Other techniques to examine cholesterol architecture in membranes have included radiolabeled methods, Raman scattering, and absorption techniques including infrared and optical rotation dispersion/circular dichroism. While these approaches have been very useful for studies of model membrane systems, purified biological membrane fractions in vitro, or membranes of fixed cells, they have not provided much insight into cholesterol dynamics in living cells.

Obviously, a great deal of effort has been made to design both suitable cholesterol analogs and the respective experimental methods to gain insights into the lipid domain structure and dynamics of biological membranes. Nevertheless, there is concern whether the behavior of the cholesterol analogues truly reflects that of cholesterol. Most of the probes have been chosen for the respective studies based on their close structural and organizational resemblance to the cholesterol molecule in both natural and artificial membranes. Until recently it was almost universally accepted that cholesterol represents the unique and essential building block of the cell membrane which defines, to a great extent, the normal function of biological organisms including man and most animals. Under this paradigm even small alterations in the chemical structure of cholesterol would be predicted to be incompatible with animal life (rev. in [18]. But is cholesterol really essential for normal cell organization and function? How stringent are the stereo- and physico-chemical criteria for the membrane sterol molecule that creates a platform (environment) for membrane proteins? Several studies suggest that many aspects of the original paradigm—i.e. compatibility with life—may be met by sterols other than cholesterol. (i) Simple animal cells such as yeast (*Candida tropicalis*, *Saccharomyces cerevisiae*) and Red Sea sponge (*Biemna fortis*) synthesize dehydroergosterol (DHE, Fig. 1a) as a major membrane sterol component [19–21]. DHE differs from cholesterol by having an ergosterol side-chain (i.e. branched methyl and double bond), an ergosterol B ring (two double bonds), and a C ring with an additional double bond that maintains the extended cyclopentanophenanthrene ring structure (Fig. 1a). (ii) DHE completely replaces the requirement for cholesterol as the only sterol source in the diet of the worm *C. elegans* [19]. (iii) Mouse L-cell fibroblasts lack the enzyme 3β-hydroxysteroid-Δ^{24}-reductase (desmosterol reductase, Dhcr24) [22]. Desmosterol differs from cholesterol in having an extra double bound in the side chain. When cultured in chemically defined medium the L-cells synthesize desmosterol, replace membrane cholesterol with desmosterol, and grow normally despite the absence of cholesterol [22, 23]. (iv) Mouse L-cells cultured in chemically defined medium containing DHE accumulate DHE which replaces as much as 90% of endogenous membrane sterol without adverse effects on membrane phospholipid or fatty acid composition, sterol/phospholipid ratio, activity of cholesterol sensitive enzymes in the plasma membrane, or cell growth [24]. Similar observations have been made with cultured human fibroblasts and MDCK cells [25–27]. (v) Most of the cholesterol in the developing and early neonatal rat retina can be replaced by desmosterol without alteration in function [28]. (vi) Ablation of the enzyme 3β-hydroxysteroid-Δ^{24}-reductase (desmosterol reductase, Dhcr24) in mice is not lethal and such mice exhibit only a mildly altered phenotype evidenced by disturbances occurring in steroid homeostasis [18, 29]. The development of these viable "cholesterol-free mice", where almost all of the cholesterol is replaced by desmosterol, shows that there is not an absolute requirement for cholesterol to maintain life [18, 29]. It should be noted, however, that the same mutation in humans causes severe abnormalities, likely due to the inability of human embryos to access maternal cholesterol which is in contrast to mouse embryogenesis where maternal cholesterol is available [18]. Taken together, these data suggest that the membranes of mammalian and other animal cells can tolerate small changes in the structure of the cholesterol side (desmosterol, DHE) and ring structure (DHE) and remain viable. However, not all small changes in the cholesterol structure are equally well tolerated. For example, loss of the Dhcr7 gene in mice (Smith–Lemli–Opitz syndrome in humans) results in accumulation of 7-dehydrocholesterol and very short-lived mice (rev. in [29]. Much further work needs to be done to establish the exact substitutions/changes in cholesterol structure that can be accommodated to maintain viability.

Advent of Fluorescent Sterols

More recently fluorescence detection has been widely used to study cholesterol not only in vitro, but also in real-time imaging of fluorescent sterols (Fig. 1b–f) in living cultured cells or in vivo. Fluorescent sterols, like other fluorescent probes, provide ease of handling with very high level sensitivity of detection, relatively short detection times, and multiplexing of several probes [17]. These characteristics of fluorescence detection have made it very beneficial in utilizing small quantities of fluorescent sterols not only for use with traditional spectrofluorometers but also in newly developed systems. In particular, fluorescent sterols and other probes have brought about the widespread use of laser scanning confocal microscopy (LSCM) and multiphoton laser scanning microscopy (MPLSM) to simultaneously study the interaction of lipids like cholesterol and proteins/receptors in real-time within living cells.

With rare exception, the fluorophores present in most commercially available fluorescent sterols (Avanti Polar Lipids, Alabaster, AL; Invitrogen, Carlsbad, CA; Sigma, St. Louis, MO, USA) as well as those synthesized in individual laboratories are synthetic chemical tags that have been used to localize cholesterol in membranes. This includes the weakly fluorescent photoactivatable free cholesterol benzophenone FCBP that photocross-links to proteins or lipids (Fig. 1b), the cholesterol-rich microdomain preferring cholesterol analogs such as dansyl-cholesterol (6-dansyl-cholestanol) and BODIPY-cholesterol analog LZ260 (Fig. 1c), and the cholesterol-poor microdomain preferring BODIPY-coprostanol, BODIPY-cholesterol analog LZ110a, 22-NBD-cholesterol (Fig. 1d), 25-NBD-cholesterol (not shown), etc. [16, 30–38]. Although there is considerable discussion regarding the solubility and orientation of these synthetic fluorescent sterol probes in membrane bilayers, especially 22-NBD-cholesterol and 25-NBD-cholesterol, at low concentrations some are thought to mimic the distribution and orientation of cholesterol [16, 35–37]. However, relatively few have been examined with regards to their ability to be bound by intracellular cholesterol-binding proteins (e.g. SCP-2, ADRP) or their real-time uptake, distribution, and efflux dynamics in living cells. One exception is 22-NBD-cholesterol which has been shown to be not only bound with high affinity (nM K_ds) by SCP-2 and ADRP, but with orientation within the binding site similar to cholesterol—suggesting that this probe may be suitable for study of intracellular cholesterol trafficking [4, 39–44]. Indeed, 22-NBD-cholesterol has proven useful for real-time imaging of HDL-mediated cholesterol uptake, efflux, and intracellular trafficking in living cells such as L-cell fibroblasts as well as rat macrophages and lymphocytes [43, 45, 46]. Sterol carrier protein-2 (SCP-2) overexpression facilitated (i.e. decreased $t_{1/2}$ of efflux) of protein mediated NBD-cholesterol cytosolic efflux [43]. Concomitantly SCP-2 overexpression decreased the slower, vesicular cholesterol transfer—likely by binding and sequestering ligands (i.e. phosphatidylinositides, fatty acyl CoAs) that regulate vesicular trafficking [43, 47–53].

However, there is a small group of naturally fluorescent lipids that includes sterols such as DHE (Fig. 1a) as well as some fatty acids (parinaric acids), retinoids (retinol, retinoic acid), carotenes, and steroids (estriol). Because of the tremendous interest of biologists and membraneologists in cholesterol-rich microdomains (also called lipid rafts or caveolae) over the past 15 years (review in [54–63], DHE has emerged as a popular, potentially less perturbing fluorescent sterol probe since it does not contain additional bulky fluorescent groups added to the sterol structure. Although this ultraviolet (UV) light absorbing and fluorescent sterol (i.e. DHE) was first chemically synthesized over 50 years ago [64], it was its detection at high level in membranes of eukaryotes such as yeast *C. tropicalis* [19] and Red Sea sponge *B. fortis* [21] that suggested its potential usefulness as a probe for cholesterol. Consequently, the focus of the remainder of the current review is on the use of naturally fluorescent DHE as a probe of cholesterol behavior in sterol-protein interactions, lipoproteins, model membranes, biological membranes, and lipid rafts/caveolae. Since cholesterol itself has very few structural/chemical features suitable for UV/VIS or optical imaging, the advent of DHE with many properties mimicking or very similar to those of cholesterol, has proven to be a major asset for probing/elucidating real-time sterol dynamics by video and MPLSM imaging in living cells. For additional insights, the reader is referred to earlier reviews on DHE, synthetic fluorescent sterols, spin labeled sterols, photoreactive sterols, and chemical tags of cholesterol [65–68].

Effect of Sterol Structure and Purity on Sterol Architecture and Dynamics in Membranes

Despite the fact that DHE is a naturally occurring fluorescent sterol appearing in sponge and yeast, it is not generally obtained from these sources. Instead, DHE from commercial (Sigma, St. Louis, MO, USA) as well as laboratory sources is chemically synthesized by an adaptation of a 50-year-old method [64, 69–71]. However, synthetic DHE prepared by this established method, especially that obtained from commercial sources, may contain a significant sterol impurity, varying from batch to batch, and as high as 20–40% [43, 70, 71]. It is important to note that not only the quantity, but also the chemical structure of the sterol and the presence of cholesterol oxidation products are known to significantly affect the structure and/or function of model membranes (rev. in [54, 55, 70, 72, 73], biological membranes [13, 74–80], lipid raft/caveolae [58, 81–88], and cholesterol-requiring plasma membrane receptors [66, 89–91]. Because of this sensitivity it is essential that fluorescent sterols such as DHE not contain other sterols (e.g. ergosterol starting material or side products produced during DHE synthesis) or oxidation products. Such sterols/oxidation products may be non-fluorescent, potentially toxic (e.g. oxidized sterols), alter membrane structure, and/or not faithfully reflect the properties of cholesterol as accurately as pure DHE. This is even more important for real-time imaging of fluorescent DHE in living cells where such impurities may compete with DHE for uptake and/or may be toxic. Therefore, the following text deals with procedures for removing unreacted substrate (ergosterol), identifying side reaction or oxidation products, removing impurities, and modifying the synthesis procedure to prevent these artifacts. The DHE synthesis procedures described below tested ergosterol substrate obtained from several manufacturers (Steraloids, Wilmington, NH, USA; Aldrich Chemical Co., Milwaukee, WI, USA; Fluka Chemie, Steinheim, Switzerland; Sigma Chemical, St Louis, MO, USA), but all other reagents were in common from the same manufacturer: "Purified Plus" methanol, chloroform, and ethyl ether were from Burdick–Jackson (Muskegon, MI, USA); "Baker Analyzed" 99^+% pure glacial acetic acid was from Mallinckrodt Baker (Phillipsburg, NJ, USA), 99^+% pure acetic anhydride was from VWR (Atlanta, GA, USA), and anhydrous mercuric acetate was from Fisher Scientific (Pittsburgh, PA, USA).

Identification of Potential Impurities Obtained Through the Classical DHE Synthesis Procedure

DHE was synthesized from ergosterol by a classical procedure established over 50 years ago [64, 69]. Purity of DHE was determined by high performance liquid chromatography as described [69]. The HPLC elution profile was monitored as follows: absorbance at 205 nm (all constituents), absorbance at 325 nm (DHE), and fluorescence emission at 375 nm (DHE). When the elution profile of commercially available DHE was monitored at 205 nm absorbance, at least two major peaks were obtained with retention times of 11.75 and 15.3 min, respectively (Fig. 2a). The latter peak comprised at least 20% of total sterol. To determine which of these peaks represented DHE, the elution profile was monitored by absorbance at 325 nm (Fig. 2b) and fluorescence emission at 375 nm (Fig. 2c). Only the larger peak near 11.75 min absorbed at 325 nm (Fig. 2b) and fluoresced (Fig. 2c). The smaller peak at 15.3 min comprising about 20% of total sterol was not DHE since it did not absorb or fluoresce at wavelengths typical of DHE. HPLC chromatograms (not shown) of DHE prepared by our laboratory from only one lot of ergosterol (Steraloids), but not from subsequent lots from the same or other sources, yielded pure DHE (>99%). All other preparations yielded DHE which was highly (20–40%) impure. To further resolve the impurity, complete absorbance spectra were obtained. The absorption spectrum of >99% pure DHE showed maxima at 310, 325, and 342 nm (Fig. 3a). In contrast, absorbance spectra of impure synthetic DHE exhibited several additional peaks at 235, 242, and 251 nm (Fig. 3b), more clearly revealed by a difference spectrum (Fig. 3c). The latter absorbance maxima were not consistent with the starting material, ergosterol, which exhibited absorption maxima at much longer wavelengths 271, 281, and 293 nm (not shown). It is important to note that HPLC elution profiles, whether monitored at 205 or 242 nm (wavelength at which the impurity absorption was highest), were unable to clearly distinguish whether the impurity was unreacted ergosterol or an as yet unidentified compound with similar retention time (not shown). While mass spectra of the impure DHE detected DHE at $(M + 1)^+$ of 395.3 and $(M\text{-}OH)^+$ of 377.5 as expected (Fig. 4a), an additional component appeared with $(M + 1)^+$ of 397.3 and $(M\text{-}OH)^+$ of 379.3 (Fig. 4a).

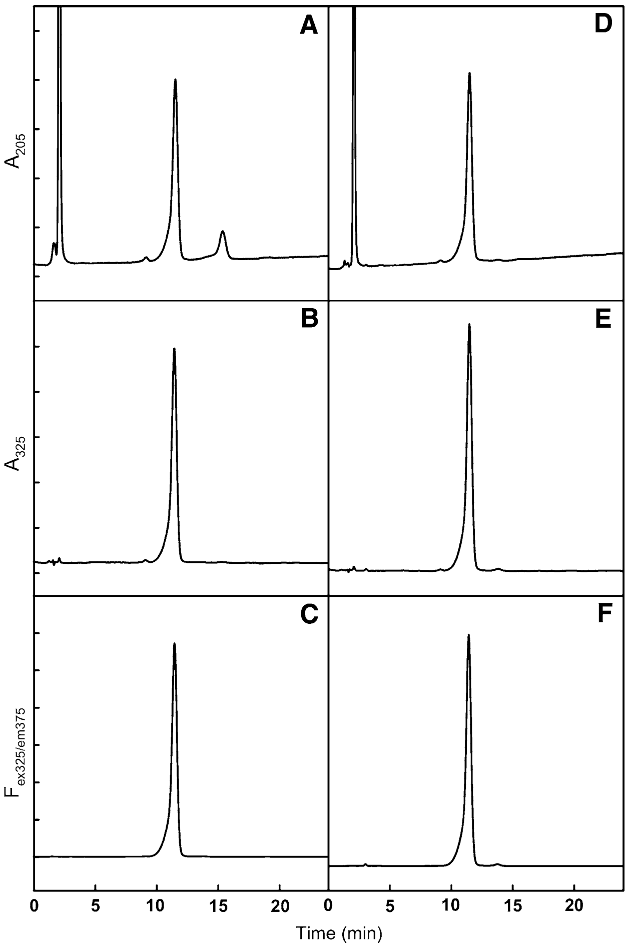

Fig. 2 HPLC analysis of DHE. **a**–**c** DHE synthesized by established method as described in Methods. **d**–**f** DHE synthesized by an improved method as described in Methods. Reversed phase HPLC was performed and elution of organic compounds was detected by absorbance at 205 nm (**a**, **d**). Elution of DHE was specifically detected by absorbance at 325 nm (**b**, **e**) and by fluorescence emission at 375 nm upon excitation at 325 nm (**c**, **f**). The peak with retention time at 11.75 min was due to DHE while that at 15.3 min was due to a non-fluorescent sterol

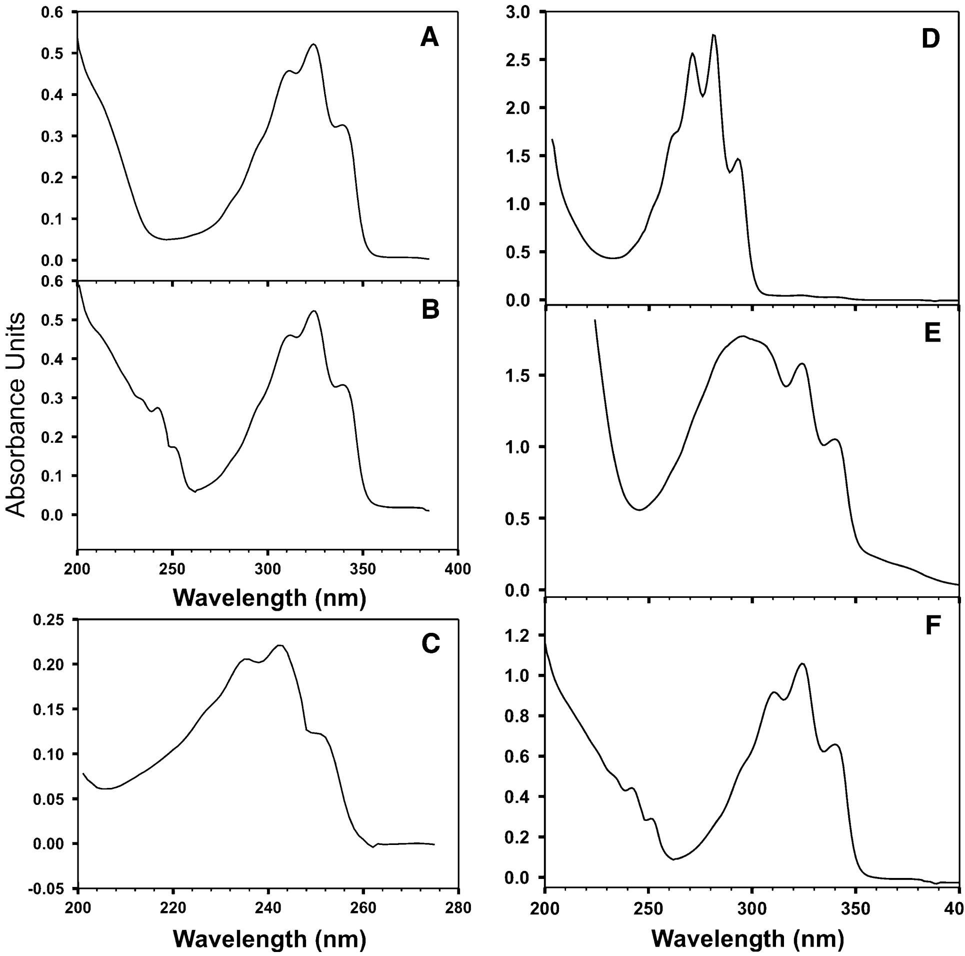

Fig. 3 Absorption spectra of DHE. **a** Pure (~99%) DHE synthesized by an improved method as described in Methods. **b** Commercially available DHE (Sigma). **c** Difference spectrum was calculated by subtraction of **a** from **b**. This spectrum shows the triene impurity alone. Note: it was necessary to use absorbance spectra to characterize the impurity, since the emission and excitation spectra determined the impurity was non-fluorescent (not shown). **d** UV absorbance spectrum of ergosterol acetate. **e** UV absorbance spectrum taken after 16 h dehydration of ergosterol acetate. **f** UV absorbance spectrum of the resultant DHE acetate with impurity from the dehydration step

Surprisingly the APCI mass spectrum of this additional component was identical to that of ergosterol (Fig. 4b)—suggesting that the impurity was possibly an isomer of ergosterol. Indeed it was reported nearly 60 years ago that small amounts of nitric acid or mercuric nitrate catalyze not only the formation of the tetraene DHE but also a side product, i.e., mercurated triene, of ergosterol due to double bond rearrangement [92, 93]. The spectral characteristics (i.e., maxima at 235, 242, and 251 nm) of the DHE impurity were the same as those of an isomer of ergosterol (5,7,22-cholestatrien-24β-methyl-3β-ol) known as ergosterol D [64, 94]. Ergosterol D is a triene [i.e. (7,9(11),22-cholestatrien-24β-methyl-3β-ol)] which differs from ergosterol (i.e. 5,7,22-cholestatrien-24β-methyl-3β-ol) in that the double bonds in the B ring are each displaced one carbon atom position.

Based on the above data, a general scheme of DHE synthesis and formation of the ergosterol D isomer was established (Fig. 5). This scheme suggests that the synthesis of pure DHE involved steps I, II (but *not* IIA), and III (Fig. 5). The presence of some as yet unknown factor ("impurity") in starting material ergosterol, however, resulted in rearrangement in the double bonds in the B ring of ergosterol (essentially a competing side reaction) as shown in step IIA (Fig. 5). This side reaction product was an isomer of ergosterol, ergosterol D [i.e. (7,9,22-cholestatrien-24β-methyl-3β-ol)] distinct from the original ergosterol (5,7,22-cholestatrien-24β-methyl-3β-ol) and DHE. In further support of this scheme, the absorbance spectrum of each product during DHE was monitored (Fig. 5). The UV absorbance spectrum of ergosterol acetate (step I, Fig. 5) exhibited three absorption maxima (Fig. 3d) essentially identical to pure ergosterol (not shown). Hence, ergosterol acetate formation did not alter UV absorbance spectrum of ergosterol. In Fig. 3e is shown the UV absorbance spectrum of the intermediate product taken 16 h into the 18 h dehydration step (step II, Fig. 5). This spectrum was broad with vibrational bands that were no longer distinct (cf. Fig. 3d). Figure 3f clearly showed that during formation of DHE acetate (step II in Fig. 5), the side reaction product ergosterol D acetate (step IIA in Fig. 5) was concomitantly formed. Finally, saponification (step III, Fig. 5) of the DHE acetate and the ergosterol D acetate and recrystallization resulted in a UV absorbance spectrum (Fig. 3f) consistent with presence of both DHE (longer wavelength peaks) and

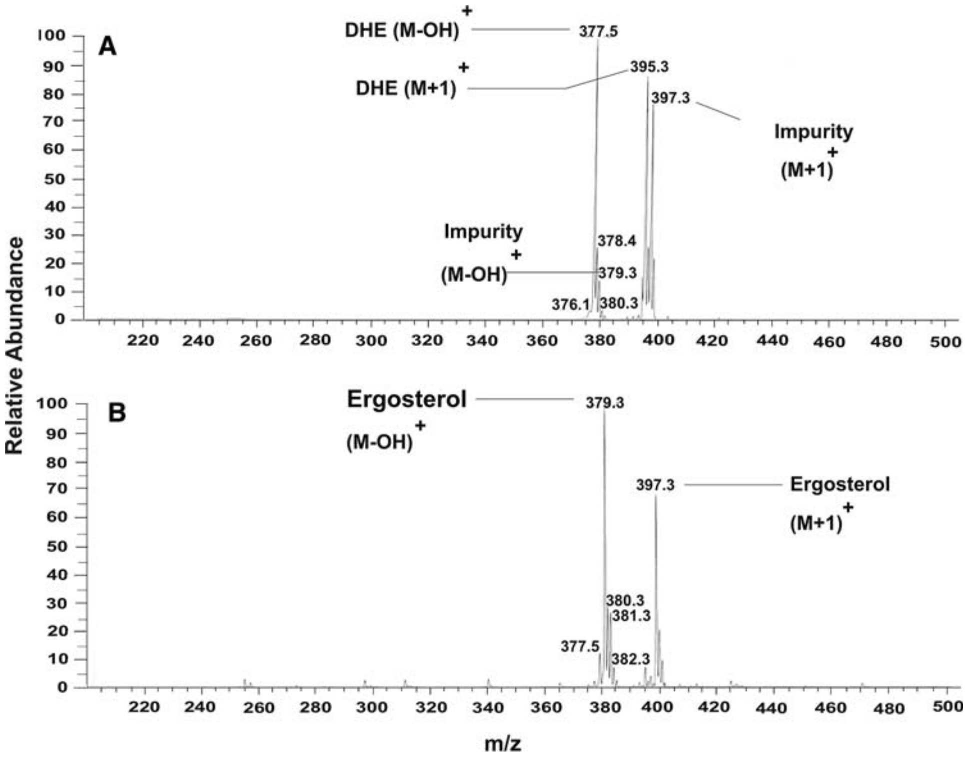

Fig. 4 Atmospheric pressure chemical ionization (APCI) mass spectra of the DHE and ergosterol. Mass spectral analysis was performed with a Thermo Finnigan LCQ Deca ion trap liquid chromatograph mass spectrometer (Thermo Finnigan, San Jose, CA, USA) in atmospheric pressure chemical ionization (APCI) ion mode with sample flow rates of 200 µl/min near the quadrupole ion trap mass analyzer involving ultra-high purity helium gas. Samples were brought up in 1 µM solutions of equal volumes of MeOH and H_2O where both the methanol and H_2O were HPLC grade Burdick and Jackson (Muskegon, MI, USA) purchased from VWR (Atlanta, GA, USA). **a** Mass spectrogram of impure DHE (Fig. 2a–c). The daughter ion resulting from the parent ion minus a hydroxyl group was indicated by $(\text{M-OH})^+$ while plus a proton was indicated by $(\text{M} + 1)^+$. The impurity was observed as a daughter ion resulting from the parent ion losing a hydroxyl group $(\text{M-OH})^+$ and gaining a proton $(\text{M} + 1)^+$. **b** Mass spectrogram of commercially available ergosterol (99% pure), with the observed $(\text{M} + 1)^+$ and $(\text{M-OH})^+$ daughter ions. Note that the ergosterol had the same mass as the triene impurity

ergosterol D (peaks between 230 and 260 nm) as indicated.

Removal of Impurities from DHE: Modified DHE Synthesis Procedure

The fact that HPLC, absorbance spectra, and mass spectral analysis did not detect any other organic contaminant in ergosterol starting material suggested that a water soluble inorganic contaminant might be a contributing factor to the formation of the non-fluorescent ergosterol D side reaction product. Therefore, in an effort to remove potential water-soluble contaminants, the ergosterol was dissolved in chloroform, washed at least three times with an equal amount of deionized water, dried under N_2, dissolved in hot methanol and recrystallized three times, and then dried under N_2. HPLC analysis to detect all constituents (absorbance at 205) revealed only a single peak was detectable, retention time 11.7 min (Fig. 2d). Likewise, when DHE was specifically monitored by absorbance at 325 nm (Fig. 2e) and fluorescence emission at 375 nm (Fig. 2f) in each case only a single peak was detectable, again with retention time of 11.7 min. HPLC chromatograms and absorbance spectra indicated that DHE synthesized by the modified method was $\geq$99% pure. Furthermore, APCI mass spectroscopy detected only a single peak with >99% (not shown).

Monomeric Versus Crystalline DHE

Many of the spectroscopic properties of DHE as a fluorescent sterol probe have been elucidated in organic solvents [64, 65, 95] and in aqueous buffers [69, 70, 96]. In organic solvents such as ethanol, DHE exhibits three UV excitation maxima (311, 324, and 340 nm) and three red-shifted emission maxima (354, 371, and 390 nm) characteristic of the DHE monomer. Interestingly, however, in aqueous buffers DHE exhibits a prominent spectral enhancement of the emission maxima near 404 and 426 nm

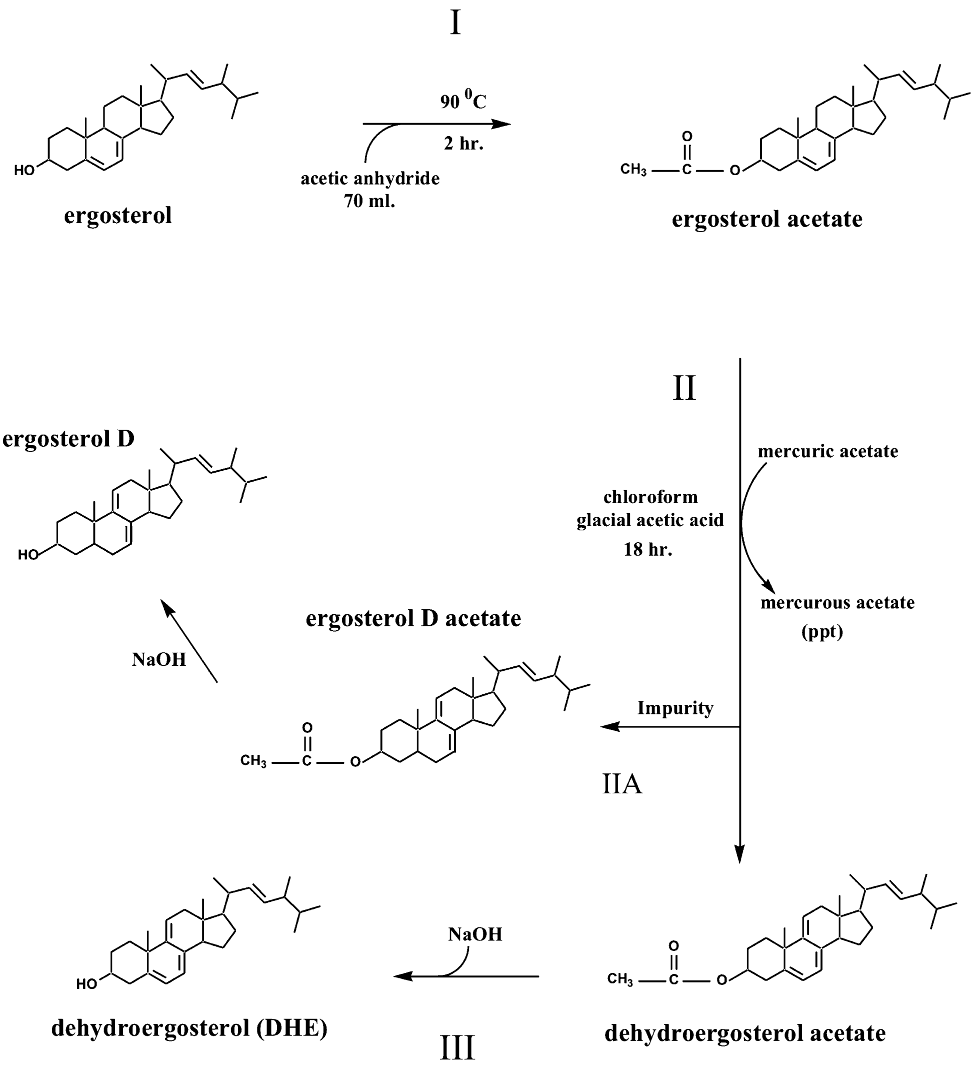

Fig. 5 General scheme of synthesis of DHE. Step I is the conversion of ergosterol to ergosterol acetate. Step II is the dehydration of the ergosterol acetate to form a new double bond in the C ring. Step IIA is the competing side reaction which causes formation of the triene impurity in DHE. Note that this triene impurity had the same molecular mass as ergosterol because it was an isomer of ergosterol, i.e. ergosterol D. Step III is the saponification of the DHE acetate to yield DHE product

as a possible result of excimeric emission—reflecting DHE in microcrystalline structures, but with only a slight (about 5 nm) red shift in both absorbance maxima and emission maxima [70]. For instance, the respective excitation and emission maxima at 324 and 370 nm in ethanol shifted to 329 and 375 nm in aqueous such that the difference in the similar vibronic levels was maintained at 46 nm. This was consistent with solvent polarity (i.e. dielectric constant) or pH having only a very minor effect on DHE and that charge separation does not occur. Many different organic solvents were used in a previous study to show that the Stokes shift varied between 3,867 and 4,000 cm^{-1} [95]. The DHE excitation and emission of the aqueous dispersion was similar to spectra of DHE polycrystalline powder; and both forms also exhibited similar lifetimes and corresponding fractions in a dual lifetime analysis [96].

Advantage has been taken of the distinction in the spectral characteristics to differentiate monomeric and microcrystalline (mostly in lysosomes) forms of DHE in living cells visualized by multiphoton imaging [70]. In order to determine quantitatively the amount of the crystalline component and monomeric, the DHE was examined by fluorescence spectroscopy wherein the ratio of fluorescence intensity measurements at the wavelengths 426 and 373 nm was computed. Under monomeric conditions, such as the case in an organic solvent (e.g. ethanol) or low concentrations of DHE in model membranes (e.g. large unilamellar vesicles or LUVs), the ratio was measured as $I_{426}/I_{373} \sim 0.3$ and would increase to approximately $I_{426}/I_{373} \sim 3.4$ for an aqueous dispersion of DHE in a buffered solution with pH. 7.4 [70]. Thus, the spectral properties of DHE give important insights on the cholesterol organization in membranes or organelles (e.g. lysosomes).

DHE Properties in Lipoproteins, Cholesterol-Binding Proteins, and Peptides

Dehydroergosterol has been directly incorporated into lipoproteins in vitro [97–99] or in vivo by feeding animals (rats, rabbits) dietary DHE followed by isolation of serum lipoproteins [100, 101]. These studies showed that DHE was localized in the surface monolayer surrounding the neutral lipid cores of triglyceride/cholesteryl ester rich lipoproteins similarly as cholesterol. In addition, DHE and a similar synthetic fluorescent cholesterol analog (cholestatrienol, CTE) have been used to examine the structure of the sterol binding site of cholesterol-binding proteins such as sterol carrier protein-2 (SCP-2) [2, 39, 102–105] and liver fatty acid binding protein (L-FABP) [2, 106, 107]. SCP-2 and L-FABP generally bound one mole of fluorescent sterol/mole protein. The fluorescent DHE or CTE were highly ordered in the binding pockets as indicated by markedly increased polarization as compared to aqueous buffer. The intermolecular distance between the DHE or CTE fluorophore and Trp or Tyr residues of these proteins measured by a fluorescence resonance energy transfer (FRET) in these studies was in the range of 16–19 Å, indicating close molecular interaction [108]. Finally, FRET between Trp of mellitin (peptide from bee venom) and DHE incorporated in model membranes indicated that mellitin bound to the membrane, bound mellitin Trp was in close proximity to DHE (i.e. a few angstroms), and DHE was non-randomly distributed within the model membrane [109]. Taken together these findings were consistent with DHE as a useful probe for examining the interactions and location of cholesterol in cholesterol-binding proteins and lipoproteins.

DHE Properties in Membranes

Model Membranes

The usefulness of DHE and cholestatrienol (CTE) as fluorescent cholesterol analogs in model membranes in a series of investigations spanning several decades demonstrated the usefulness of these probes to monitor cholesterol structural (polarization, limiting anisotropy, order) and dynamic (lifetime, rotational rate) properties in membranes [12, 65, 70, 95, 96, 108, 110–120]. The lifetime studies resolved for the first time at least two DHE domains in model membranes, one less sensitive to the aqueous than the other, and that these domains were dependent on the lipid composition, temperature, and other properties of the membrane [54, 119]. This possibility was further supported by model membrane studies of DHE exchange which provided kinetic evidence for the existence of multiple sterol containing domains in membranes [118, 121–124]. DHE was especially useful for these studies because the spontaneous exchange of DHE between model membranes was very similar to that of radiolabeled cholesterol [117]. Further, these dynamic and kinetic pools of DHE represent lateral sterol-rich and—poor domains rather than pools in the outer *vs.* inner leaflet because: (i) the transbilayer distribution of sterol across model membrane bilayers is uniform, unless membranes are very highly curved (rev. in [12]), (ii) the transbilayer migration rate of DHE is very rapid (much faster than kinetic exchange rates between membranes) and is very similar to that of cholesterol [108], (iii) Dynamic (lifetime) and DHE kinetic exchange studies determined that the presence of a large and a small DHE pool, (iv) DHE kinetic exchange studies determined that the large sterol pool corresponded to very-slowly (days) exchangeable sterol, while the small pool (generally <10%) was rapidly exchangeable. The pool size and half-times of exchange were dramatically affected by the presence of acidic phospholipids and, even more so by the presence of sphingolipids in the model membranes. The sterol carrier protein SCP-2 rapidly facilitated DHE transfer between model membranes by decreasing the half-time of exchange and increasing the size of the rapidly exchangeable domain. This action of SCP-2 was mechanistically due not only to the presence of a sterol binding site in this protein, but also the membrane interaction domain comprised on a positively charged face of an N-terminal amphipathic α-helix [125–127]. These studies demonstrated that the properties of DHE and/or CTE closely reflected those of cholesterol in model membranes.

Suitability of DHE as a Probe for Cholesterol in Biological Membranes

Dehydroergosterol is non-toxic to animal cells as shown by its presence in membranes of yeast (*C. tropicalis*, *S. cerevisiae*) and Red Sea sponge (*B. fortis*) as well as its ability to completely replace cholesterol as the only sterol source in the diet of animals such as *C. elegans* or cultured L-cells [19–21, 24, 128]. Unlike most synthetic fluorescent tagged sterols which can only be incorporated at very low amounts into cell membranes, DHE taken up by cultured cells can replace nearly 90% of total cholesterol without adverse effect on cell viability, plasma membrane structure, plasma membrane phospholipid composition or sterol/phospholipid ratio, or plasma membrane sterol sensitive enzymes [24]. Plasma membrane receptors such as the oxytocin receptor are exquisitely sensitive to the structure of the sterol with which it interacts. In cholesterol-depleted membranes, only cholesterol and DHE are effective in reconstituting activity of this highly sterol-sensitive plasma membrane protein [89–91]. In cultured cells DHE codistributes with cholesterol in plasma membranes, microsomes, mitochondria, and lysosomes [24, 129, 130].

Delivery of DHE into Cultured Cell Membranes

Dehydroergosterol may be delivered to living cells for uptake and incorporation into plasma membranes by several methods: (i) While relatively slow, the simplest is *delivery as micro-crystalline DHE* from a stock solution in ethanol over a 2-day period as described previously [24, 70]. DHE can enter the cells by exchange between the micro-crystals and the cell surface plasma membrane, a process that may be facilitated by albumin in the medium [131–134]. Concomitantly, the cultured cells also phagocytose DHE micro-crystals from the medium as shown by MPLSM colocalization with lysosomal markers [70]. Over time the endocytosed DHE micro-crystals may be digested/disrupted in the lysosome or outside the lysosome by intracellular cholesterol-binding proteins such as SCP-2. Consequently, most DHE delivered in this fashion is codistributed similarly as cholesterol in all subcellular membranes including plasma membranes, plasma membrane cholesterol-rich lipid rafts, plasma membrane cholesterol-poor non-rafts, lysosomes, endoplasmic reticulum, and mitochondria [6, 7, 24, 26, 27, 129, 135–137]. The presence of DHE micro-crystals in MPLSM images of cells cultured with DHE micro-crystals can be reduced by pulse labeling the cells with DHE micro-crystals for several hours followed by washing and incubation in DHE free medium for several days. (ii) An even slower, but more physiological method is to *deliver DHE complexed to serum lipoproteins* [100, 101]. In this method, the DHE is dissolved in organic solvent which is used to coat the inside of a tube or (to increase surface area) a tube containing celite (diatomaceous earth), the solvent is evaporated, serum lipoproteins are added in buffer with antimicrobial agent, incubated overnight with shaking at 37 °C, followed by sedimentation to remove particulates and filtration to assure sterility. (iii) A faster, but less efficient method to *deliver DHE as a component of large unilamellar vesicles (LUVs)* over a 1-day period as described previously [70]. The DHE present in the LUVs enters the cell either by exchange with the cell plasma membrane (potentially facilitated by albumin in the medium) or, depending on the charge of the LUV, by facilitated fusion with the cell plasma membrane. While the LUV method completely avoids the presence of micro-crystalline DHE, less total DHE is incorporated into the cells since incubation with larger amounts of LUVs concomitantly results in incorporation large amounts of carrier phospholipid which itself may alter cell membrane properties depending on the specific phospholipid polar head group (e.g. choline, ethanolamine, etc.) and esterified fatty acids (saturated, monounsaturated, polyunsaturated). (iv) The most rapid method for delivery of large amounts of DHE into cells is to *deliver DHE as dehydroergosterol-methyl-β-cyclodextrin (DHE-MβCD) complexes* prepared by adding DHE to an aqueous solution of MβCD (3 mM DHE and 30 mM MβCD). This mixture was overlaid with N_2, continuously vortexed under light protection for 24 h at room temperature, and filtered through a 0.2-μm filter to remove insoluble material and DHE crystals. Then, 20 μg of DHE was added to the cells in the form of DHE-MβCD complexes and allowed to incubate for 45 min at room temperature in PBS. Prior to imaging, cells were washed three times with PBS. With this technique DHE enters the cell by exchange between the DHE-MβCD complexes and the cell plasma membrane. The cyclodextrin-based method for DHE delivery to the cell may proceed, in addition to the clathrin mediated pathway, through the caveolae-dependent endocytosis due to non-selective cholesterol loading onto the plasma membrane by cyclodextrin. The major drawback of this method is that large excess of MβCD by itself can deplete cells of cholesterol while very high quantities of DHE-MβCD at high molar ratios can increase total sterol content. Therefore, care must be taken to optimize the DHE-MβCD molar ratio and concentration in the medium to maintain unaltered total sterol content in the cell and cell membranes.

In summary, the above methods of DHE delivery differ in rapidity, the amount of DHE that can be delivered, and potentially DHE distribution in the cell may differ from one loading method or another. The latter may be an advantage of a particular method if it is desirable to preferentially label a specific cellular compartment. Alternately, if uniform distribution of DHE is desired, this potential problem may be minimized if the cells are incubated over sufficient time for the DHE to equilibrate between all cellular compartments.

DHE Architecture in Purified Biological Membranes

Dehydroergosterol has been used to probe the structural (polarization, limiting anisotropy, order), dynamic (lifetime, rotational rate), and kinetic (exchange) environment of cholesterol in plasma membranes [6, 7, 54, 55, 135, 138–141], microsomes [6, 7], mitochondria [6, 7, 142, 143], and lysosomes [8, 129]. DHE has revealed several important structural and dynamic aspects of the cholesterol microenvironment in biological membranes.

First, in contrast to model membranes, DHE was found to be asymmetrically distributed across the plasma membrane bilayer (rev. in [12, 144, 145]. DHE revealed that the cytofacial leaflet of plasma membranes from L-cell fibroblasts [12, 24, 146, 147], erythrocytes [144], and brain synaptosomes [145, 148–151]. While other methods (filipin staining, exchange, cholesterol oxidase accessibility, neutron diffraction, etc.) have also been used to measure transbilayer cholesterol distribution, many have significant limitations including accessibility of membrane cholesterol (filipin, cholesterol oxidase), production of a potential perturbant (cholesterol oxidase produces cholesterone), and poor dynamic resolution (neutron diffraction) (rev. in [12].

While measurements of transbilayer sterol distribution by different methods may therefore not necessarily agree, multiple methods (DHE, NBD-cholesterol quenching, and exchange assays) indicate that the cytofacial leaflet of erythrocytes has more cholesterol than the exofacial leaflet [144, 152]. Likewise, several methods (DHE, cholesterol oxidase) indicate that the synaptosomal plasma membrane has more cholesterol in the cytofacial leaflet than the exofacial leaflet [12, 145, 148–150]. The transbilayer distribution of sterol is a major determinant of the transbilayer fluidity gradient present in these membranes, the cytofacial cholesterol-rich leaflet is more rigid (less fluid) than the relatively cholesterol-poor exofacial leaflet (rev. in [146, 147, 149, 153–159]. The transbilayer migration rate of DHE in model membranes and plasma membranes is relatively fast, $t_{1/2}$ of sec–min depending on the membrane examined (rev. in [12, 108, 144, 145]. Rapid transbilayer migration of DHE is also supported by the finding that uptake of DHE into and non-vesicular transport across cultured hepatocyte-derived cells (i.e. from basolateral to canalicular plasma membrane) is also very rapid, i.e. $t_{1/2}$ of 1–3 min [160]. The finding of rapid transbilayer sterol movement suggested that the asymmetric transbilayer distribution in the plasma membrane was not due to restricted movement of cholesterol from one leaflet to the other, but was instead a property of the lipid bilayer itself. DHE transbilayer distribution has broad applicability in studies of the action of anesthetics, cholesterol lowering drugs (statins), alcohol (chronic and acute), lupus erythematosus, aging, apoE, and sterol carrier proteins all of which can alter plasma membrane or synaptosomal plasma membrane transbilayer sterol distribution and/or transbilayer fluidity [26, 135, 136, 145, 149, 150, 154, 161–172].

Second, the DHE lateral distribution in both model and biological membranes was not uniform, but instead reflected sterol-rich and poor domains (rev. in [54, 55]. The exchange kinetics of DHE and radiolabeled cholesterol between model membranes was indistinguishable [117]. For a kinetic sterol exchange assay between biological membranes, cellular organellar membranes can be isolated from cells supplemented with DHE to act as donors and without supplementation of DHE to act as acceptors. Not only exchange kinetics but also lifetime analysis resolved multiple sterol domains; and cholesterol binding/transfer proteins such as SCP-2 (and less so L-FABP) rapidly facilitated DHE transfer from these purified membrane fractions to other intracellular membranes in vitro [54, 55]. With regards to cholesterol movement between purified intracellular organelle membrane fractions, the most rapid spontaneous DHE transfer occurred from mitochondrial membranes to microsomal membranes, mitochondrial to lysosomal and to plasma membranes, and plasma membranes to microsomal membranes [173]. Least rapid spontaneous DHE transfer occurred from lysosomal to plasma membranes. However, in the presence of the SCP-2, the DHE transfer was markedly enhanced in the approximate order of plasma membrane to microsomal membranes and plasma membranes to lysosomal membranes [173]. This order was followed by enhanced transfer from mitochondrial membranes to microsomal membrane, mitochondrial membranes to plasma membranes, and a nearly equal transfer between mitochondrial and plasma membranes. Other than the transfer between mitochondrial and plasma membranes, the reverse transfer was markedly slower in both spontaneous and SCP-2 mediated [173]. Thus, in vitro exchange dynamics of DHE revealed that: (i) spontaneous sterol transfer was very slow, but vectorial; (ii) spontaneous sterol transfer from lysosomes and lysosomal membranes was extremely slow, despite the fact that this is the route of LDL-receptor mediated cholesterol uptake; (iii) cholesterol-binding proteins such as SCP-2 rapidly enhanced the extent and directional transfer of sterol transfer from lysosomes and lysosomal membranes to the plasma membrane.

Physiological Significance of in Vitro Studies with DHE and Other Fluorescent Sterols: Cultured Cells and Animals

The significance of the above findings in living cells was confirmed with DHE and other fluorescent sterols in a variety of cultured cells including L-cells, CHO cells, macrophages, and hepatocyte derived cell lines [39, 43, 45, 160, 174–176]. Studies with transfected L-cells showed that uptake and efflux of fluorescent sterols was highly dependent on the expression of cholesterol binding proteins (e.g. such as SCP-2) in the cytosol. Furthermore, transhepatocyte transfer of DHE was very rapid and not vesicular. Since hepatocytes have very high levels of intracellular cholesterol binding proteins (e.g. SCP-2, L-FABP) taken together such data suggested that rapid transhepatocyte cholesterol trafficking from the basolateral to canalicular membrane for efflux was facilitated by these proteins in the cytosol. The physiological impact of cholesterol binding proteins such as SCP-2 and L-FABP on cholesterol uptake, esterification, and excretion into bile was confirmed by studies with SCP-2 transgenic (i.e. overexpressing or antisense cDNA treated) mice and rats [177–179] and gene-targeted mice wherein SCP-2/SCP-x [180–182], SCP-x [183], or L-FABP [184–189] were ablated.

Studies with radiolabeled cholesterol were consistent with many of the findings shown with the fluorescent DHE and other sterols in cultured cells [43, 45, 172, 190–197]. In one study, it was shown that overexpression of L-FABP in L-cell fibroblasts enhanced the transfer or radiolabeled cholesterol from the plasma membrane to the endoplasmic reticulum for esterification [194]. Transfer was inhibited by drugs that bound/competed with cholesterol for the L-FABP binding site. In another study, L-cells were transfected with the cDNA that encodes for the 13.2 and 15 kDa SCP-2 proteins respectively. In nearly all tissues and cells examined the 15 kDa SCP-2 undergoes complete *N*-terminal post-translational cleavage to yield the mature 13.2 kDa SCP-2 (rev. in [173]. Despite the fact that only the 13.2 kDa protein was found in both cases, different effects on the intracellular trafficking of cholesterol were observed [191]. In early experiments using radiolabeled cholesterol, 15 kDa SCP-2 transfected L-cells showed an enhanced uptake of [^{3}H]cholesterol after 4 hours including a resultant increase in esterification of the exogenous radiolabeled cholesterol as shown by the 30% increase in [^{3}H]cholesteryl ester levels with no enhancement in the 13.2 kDa SCP-2 transfected L-cells as compared to the control cells. Both the 15-kDa- and the 13.2-kDa SCP-2 transfected L-cells showed a significant increase (15- and 11-fold, respectively) in the initial [^{3}H]cholesteryl ester synthesis rate compared to control cells after treatment with sphingomyelinase. This experiment was important in order to examine the effect of SCP-2 expression on the intracellular movement of cholesterol from the plasma membrane to the endoplasmic reticulum for esterification [192]. The resulting data corresponded with the aforementioned fluorescent in vitro assays where greater enhancement occurred in the direction of exchange of DHE from plasma membrane to microsomal vesicle [6, 173]. The increased rate in ester synthesis resulted in a 1.5 increase in the [^{3}H]cholesteryl ester levels, while at saturation (1 hr treatment), the radiolabeled cholesteryl ester levels were increased 1.6- and 1.3-fold for 15- and 13.2-kDa SCP-2 overexpression [192]. Inhibition of microsomal cholesteryl ester synthesis by drug treatment in the sphingomyelinase treated cells showed no differences. The overexpression of 13.2-kDa SCP-2 did not elevate cholesterol homeostasis of free cholesterol while elevating esterified cholesterol levels [192]. Treatment with [^{3}H]oleic acid revealed that the 15-kDa SCP-2 overexpression resulted in a specific increase of cholesterol esterification as opposed to the 13.2-kDa SCP-2 overexpression which resulted in esterification into triacylglycerols[192]. Using [^{3}H]cholesterol and the fluorescent 22-NBD-cholesterol in conjunction with high density lipoproteins (HDL), L-cells overexpressing SCP-2 were shown to inhibit the HDL mediated efflux of cholesterol of 61 and 157%, respectively [43]. However, most of the inhibition occurred in the slower component while the faster component of the efflux pool (protein-mediated) was somewhat less affected. Clearly, both the radiolabeled cholesterol uptake and HDL-mediated 22-NBD-cholesterol efflux studies in living cells reveal that the effects of SCP-2 expression on cellular cholesterol transport become increasingly significant over longer time periods.

Overexpression of SCP-2 also had an inhibitory effect on the in vitro enhancement of SCP-2 on the exchange of DHE and cholesterol between purified lysosomal membranes as seen by the initial rates [8]. Lipid analysis of lysosomal membranes revealed a significant decrease in the cholesterol to phospholipid ratio as a result of a small decrease in the cholesterol mass with a corresponding increase in phosphatidylserine; however, lyso-bis-phosphatidic acid (LBPA), which is involved in lysosomal cholesterol trafficking, was dramatically decreased by nearly threefold. Furthermore, sterol exchanges involving lysosomal membranes isolated from normal CWN human fibroblasts and NPC1 human fibroblasts revealed an apparent similar effect [25]. The exchange of sterol from the fast kinetic pool was increased dramatically (twofold increase in initial rate) upon addition of SCP-2 in vitro for the NPC1 lysosomal membranes when compared to the control CWN lysosomal membranes as determined by DHE polarization exchange assays. The decreased expression of SCP-2 in NPC1 fibroblasts, as seen in murine models of Niemann-Pick type C disease [198], allowed for a higher exchange rate of the fast kinetic pool as compared to CWN fibroblasts with larger normal expression of SCP-2. In fact, the lysosomal membranes from CWN human fibroblasts showed much slower spontaneous initial rate of sterol exchange as well. However, the trend was reversed in the slower but larger kinetic pool, where higher levels of SCP-2 caused a higher rate of sterol transfer in vitro. Both cell types exhibited similar sterol kinetic pool fractions for the isolated lysosomal membranes [25] despite differences in sterol transfer rates. With the exception of the pool fraction sizes, sterol transfer characteristics examined as a function of expression of SCP-2 in lysosomal membranes isolated from control and transfected murine fibroblasts appeared consistent with those seen in CWN and NPC1 human fibroblasts [8] possibly through membrane lipid domain alteration and/or involvement with LBPA [199]. Exchanges between lysosomal donors to mitochondrial acceptors revealed similar results whereas SCP-2 overexpression removed the fast kinetic pool but enhanced the slower kinetic pool both in rate and in pool size [173]. In the reverse exchange (mitochondrial donor to lysosomal acceptors), no fast kinetic pool was detected in the control. However, SCP-2 overexpression still reduced the early exchange of sterol as seen by the 6-fold reduction in initial rate by shifting most of the sterol into the non-exchangeable pool [173]. In part, this might explain the large pool of non-exchangeable sterol observed in exchange assays using mitochondrial membrane vesicles isolated from steroidogenic MA-10 Leydig cells [143].

Thus, modulation of directional cholesterol transport and cholesterol esterification as well as membrane lipid composition has been demonstrated to occur as a function of expression levels of L-FABP or SCP-2, possibly through the interaction of proteins/receptors involved with cholesterol trafficking and lipid sensing/signaling. The resulting evidence has been obtained with assays using different labeled sterols including the fluorescent cholesterol analog DHE.

Plasma Membrane Sterol-Rich Microdomains: In Vitro Studies

Based on findings with delivery of dansyl-cholesterol, the method and duration of fluorescent sterol delivery (e.g. micro-crystals, lipoproteins, LUV, or cyclodextrin complexes) may affect the distribution of fluorescent sterol to lipid rafts/caveolae or non-rafts (see Sect. 6.3 and [32]. When transformed cells (L-cells, MDCK cells) or primary mouse hepatocytes were cultured with DHE (micro-crystals or LUV) under conditions to maximize DHE incorporation and equilibration, biochemical fractionation by affinity chromatography of purified plasma membrane vesicles yielded sterol-rich lipid rafts/caveolae, caveolae, and lipid rafts, respectively [26, 27, 70, 136]. DHE was codistributed similarly as cholesterol into sterol-rich and—poor domains [26, 27, 70, 82, 102, 135, 136, 172, 182, 196]. Lipid raft/caveolae associated receptors such as the oxytocin receptor are sensitive to the structure of the sterol with which it interacts and both cholesterol and DHE, but not other sterols, are effective in reconstituting activity of this highly sterol-sensitive plasma membrane protein in cholesterol-depleted lipid rafts/caveolae [89–91]. DHE mobility (fluorescence polarization) differed significantly in lipid rafts/caveolae from non-rafts. While spontaneous DHE transfer from lipid rafts/caveolae was relatively slow, that from non-rafts was essentially non-detectable. SCP-2 dramatically enhanced DHE transfer from lipid rafts/caveolae, but not from non-raft domains. Further examination of the plasma membrane cholesterol partitioning revealed that sterol transfer, as resolved using DHE in fluorescence polarization kinetic assays, from caveolae/raft domains with introduction of SCP-2 was enhanced as compared to plasma membrane vesicles [136]. Principally, the initial rate of the caveolae/raft fractions was increased by a factor of 5 with a larger portion of the sterol arranged in an exchangeable kinetic pool as compared to the overall plasma membrane fraction [136]. A possible mechanism for this enhancement may involve: (i) SCP-2 directly binding cholesterol as shown by fluorescent sterol binding assays and cross-linking by photoactivatable cholesterol (Fig. 1b) [39–41, 44]; (ii) SCP-2 directly interacting with caveolin-1 within the plasma membrane as observed from in vitro (coIP, CD) and in vivo (two hybrid, double immunofluorescence FRET, double immunogold EM) assays that revealed an average molecular interaction distance of ∼48Å was measured [200]. Specifically, SCP-2 has been shown to directly interact with the *N*-terminal sequence of amino acids of caveolin-1 [201]. Finally, DHE transfer from lipid rafts/caveolae to serum lipoproteins was remarkably specific for the type of lipoprotein/apoprotein, while that to non-rafts was very slow and not specific [27]. The importance of resolving cholesterol structure and dynamics in these cholesterol-rich plasma membrane microdomains is underscored by the fact that lipid rafts/caveolae function not only in reverse cholesterol transport, but also in cell recognition, signaling, immune function, and potocytosis (rev. in [58, 60, 82, 84, 85, 87]. Furthermore, lipid rafts/caveolae were shown to mediate the action of potential bioterror toxins and serve as entry portals for a host of bioterror pathogens (rev. in [82, 202].

Plasma Membrane Sterol-rich Microdomains: Real-time Imaging of DHE in Plasma Membranes of Living Cells

Recent improvements in imaging microscopy allowed the direct, real-time visualization of DHE in living cells by conventional (DHE delivered as micro-crystals) or video (DHE delivered as cyclodextrin complexes) UV fluorescence microscopy [39, 160, 174–176] and by MPLSM (DHE delivered as LUV or micro-crystals) multiphoton laser scanning microscopy [71, 82, 203, 204]. Analysis of intracellular localization and distribution of DHE at the plasma membrane can be accomplished after segmentation of specific regions of interest such as cellular organelles and performed on a cell by cell basis [70, 203]. Previously, two techniques involving image segmentation of the plasma membrane of cells labeled with DHE and multiple fluorescent probes (i.e. Nile Red, ECFP-Mem, and DiO) were validated and compared [203]: (i) subtraction and sliding window and (ii) rank statistic-based methodology. The subtraction technique was performed with the DHE and Nile Red colocalization experimental results by subtracting the DHE channel from the Nile Red channel. This procedure worked very well with Nile Red as it only very weakly stained the PM as compared to the significantly brighter labeling by the DHE. Noise was reduced by using a sliding window analysis technique where window size, intensity thresholding, and the signal to noise ratio was optimized. In the rank statistic-based technique, two small windows are created in the image and the pixel intensities in each window ranked from the lowest to highest; then a comparison is made by using Miller's rank statistic. The solution is optimized based upon intensity thresholding. The segmented plasma membrane regions were smoothed using geometric moments functions based on the intensity distribution within the segmented PM. Subsequently, geometric reference and spatial intensity measurements were calculated. Spatial statistical analysis was performed using pixels with DHE intensities higher than the median intensity to test for complete spatial randomness (CSR). Monte Carlo simulations were run using the narrowed data set (peak intensities—relative higher concentrations) as well as the complete data set [203].

Multiphoton Imaging of DHE Incorporated into L-Cells from Ethanolic Stock Diluted in Aqueous Medium

L-Cell fibroblasts grown on chambered coverglass were incubated with the fluorescent sterol analog, DHE, from ethanolic stock solution as described above and imaged by multi-photon microscopy. Despite multiple washings of the cells, images from a single channel covering the range 350–450 nm revealed very bright patches of fluorescence

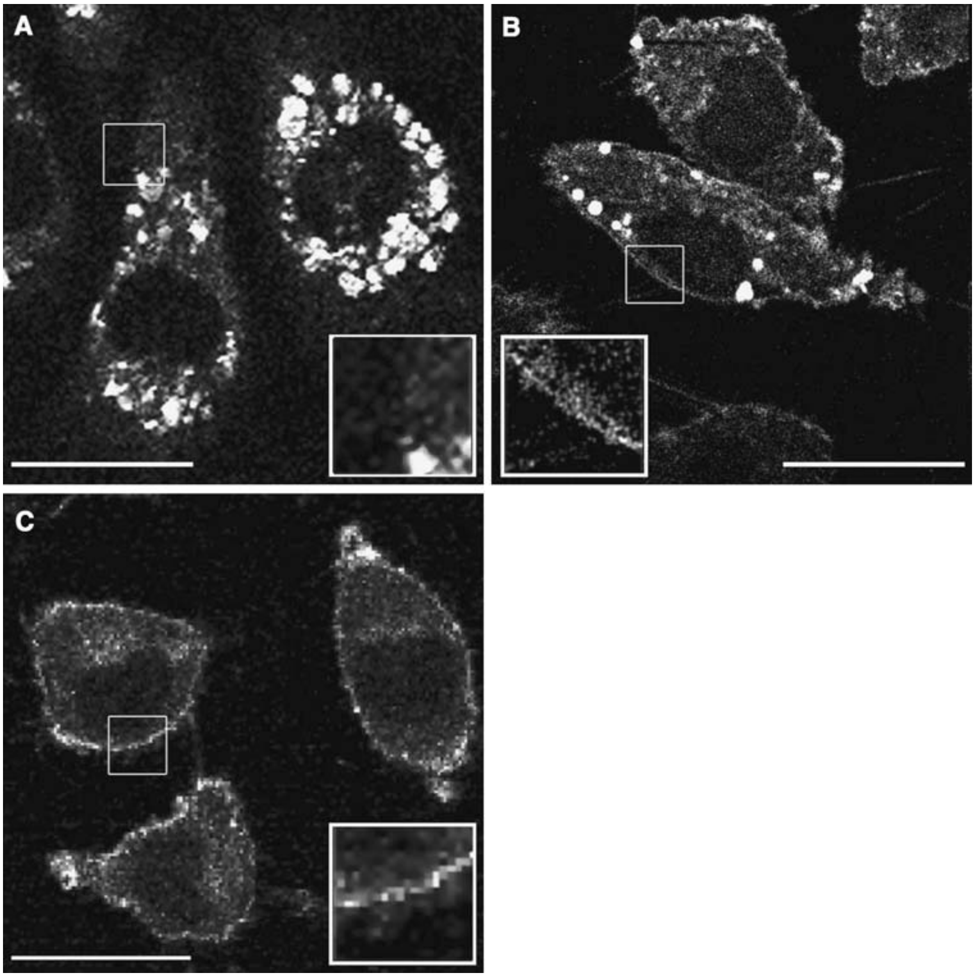

Fig. 6 Real-time multiphoton imaging of DHE in living L-cell fibroblasts. L-cells were plated onto chambered coverglass incubated with DHE by three different techniques and imaged by multi-photon laser scanning microscopy using a MRC-1024MP system with external non-descanned detection. Excitation occurred at a wavelength of 900 nm using a femto-second modelocked titanium:sapphire laser and the emission was detected through a D400/100 and UV 440LP dichroic filter. **a** Image of L-cells that were incubated for two days with 20 μg DHE from ethanolic stock solution added to 1 ml media (ethanol < 0.5%) wherein large accumulation of crystalline DHE occurred. The high intensities (crystalline DHE) was kept under saturation levels and within the instrumental dynamic range; thus lowering the sensitivity of detection of monomeric DHE within the plasma membrane. **b** Image of L-cells that were incubated for one day with 20 μg DHE in the form of large unilamellar vesicles (65:35 mol % POPC:DHE). **c** Image of L-cells that were incubated for 45 min with 20 μg dehydroergosterol methyl-β-cyclodextrin complexes. *Insets* Regions that included a section of the plasma membrane and outlined in a white rectangle were magnified ×2.5. *Bars* 20 μm

emission (Fig. 6a). By monitoring the ratio of the 455 to 375 nm region, the areas that were either mostly micro-crystalline or mostly monomeric were distinguished [70]. The micro-crystalline DHE phagocytosed by the cells was largely found to be in lysosomes [70] but breakdown of the microcrystals occurred over time (~2–3 days) such that monomeric DHE was distributed throughout the cell into the plasma membrane, lipid storage droplets, endoplasmic reticulum, and other organellar membranes. This was also observed in organelles isolated from cells incubated for several days on DHE from ethanolic stock solution [6, 8, 70, 102, 129]. As a result of the increased localized concentration of micro-crystalline DHE and its enhanced excimeric fluorescence, difficulties arise in detecting low to moderate amounts of monomeric DHE (Fig. 6a, inset). This is due to the intense emission arising from crystalline DHE which can cause saturation of the PMTs [70, 204]. Plasma membrane sterol can be detected by imaging cells that do not have residual large amounts of crystalline DHE.

Multiphoton Imaging of DHE Incorporated into L-Cells from LUV Diluted in Medium

Dehydroergosterol in the form of LUVs was taken up by living cells (Fig. 6b) in largely monomeric form as indicated by the emission peak ratios [70]. There was almost no appearance of DHE micro-crystals [70]. As a result, sensitivity of detection can be increased by using an emission dichroic/filter combination with broader bandwidth and higher photomultiplier gain. Thus, DHE with its low quantum yield can easily be detected at the plasma membrane (Fig. 6b, inset) and in intracellular compartments as had been observed from previous spectroscopic studies [8, 70, 102, 135, 172]. Signal saturation may occur as a result of accumulation of unesterified or esterified monomeric DHE in lipid storage vesicles (Fig. 6b), distinct and much less intense than micro-crystalline DHE observed in lysosomes upon culturing cells with DHE micro-crystals. MPLSM images of cells supplement with DHE as LUV revealed that DHE was non-randomly distributed into sterol-rich and poor-domains within the plasma membrane of living L-cells [70, 203, 204].

Multiphoton Imaging of DHE Incorporated into L-Cells from DHE-MβCD Complexes Diluted in Aqueous Medium

L-Cell incubation with DHE-MβCD complexes also yielded the monomeric DHE form as visualized by real-time multi-photon imaging in a confocal slice through the cell (Fig. 6). Within 45 min, heterogeneous regions of the plasma membrane were strongly labeled with DHE (Fig. 6c, inset), evidenced by the strong patchy outline at the cellular periphery. Other intracellular membranes were weakly labeled throughout the cell (Fig. 6c). In many of the cells, morphological structures such as microvilli and filopodia were also visible as a result of the strong signal from the fluorescent DHE. The non-random distribution of DHE in to sterol-rich and poor-domains at the plasma membrane was consistent with other studies wherein DHE was supplemented as LUV to the cells [70, 203, 204]. This would suggest that supplementation of cells with DHE-MβCD complexes also non-selectively loaded the different domains in the plasma membrane.

Image Analysis of DHE Distribution After Multiphoton Imaging

While MPLSM and visual inspection of DHE at the plasma membrane of cells supplemented with DHE as micro-crystals, LUV, or DHE-MβCD complexes revealed that DHE was non-randomly distributed into sterol-rich and poor domains, a mathematical framework substantiating this observation requires additional analysis [70, 203, 204].

Image analysis originally consisted of intensity measurements using region of interests and the use of colocalization, ratiometric, and fluorogram techniques. Further structured segmentation of the plasma membrane has permitted examination of the distribution of DHE through the use of inferential statistics, utilizing hypothesis testing and correlation determination, and has opened up an opportunity to do distributional modeling [71, 203]. Segmentation analysis of the MPLSM images of cells supplement with DHE as LUV confirmed that DHE was indeed non-randomly distributed into sterol-rich and poor-domains within the plasma membrane of living L-cells [203, 204].

Summary and Discussion

The naturally occurring fluorescent sterol DHE [19, 21] has proven a powerful probe for use in investigating membrane structure and cholesterol domain dynamics in vitro [8, 54, 55, 65, 70, 102, 172], for examining cholesterol-protein interactions in vitro [2, 39, 96, 101, 102, 108, 205], and for first time visualization in real-time of the distribution of cholesterol in the plasma membranes in living cells [70, 203, 204]. Successful application of the fluorescent DHE to investigation of the function and organization of sterols in membranes, especially lipid raft/caveolae microdomains of living cells, requires the use of highly purified DHE. This is due to the fact that lipid rafts/caveolae are highly sensitive not only to cholesterol content [58, 60, 82, 84, 85, 87, 88], but also to sterol structure [89], and sterol oxidation. The present review yielded new insights into this problem and potential applications of DHE imaging in living cells.

The presence of a non-fluorescent sterol impurity was observed not only in commercially available DHE, but also in DHE synthesized in the present laboratory from ergosterol obtained from multiple commercial sources. The appearance of the non-fluorescent sterol impurity was somewhat variable (20–40%) depending on the commercial source and batch of the ergosterol substrate but without dependence on any other reagent used for the synthesis. While both HPLC and APCI mass spectroscopy suggested that the impurity was either ergosterol or an ergosterol isomer, the unique UV spectral absorption characteristics of this impurity provided evidence that the non-fluorescent sterol impurity was an isomer of the initial ergosterol (5,7,22-cholestatrien-24β-methyl-3β-ol). This isomer, known as ergosterol D [i.e. 7,9(11),22-cholestatrien-24β-methyl-3β-ol], was not present in the ergosterol starting material but potentially arose from the rearrangement of double bonds in the B ring of the ergosterol during the dehydration step (Step IIA, Fig. 5). Purifying the ergosterol created a non-detectable yield of the ergosterol D impurity during DHE synthesis. While the nature of the water soluble component facilitating formation of the side reaction ergosterol D isomer was not identified, it has been reported that small amounts of nitric acid or mercuric nitrate catalyze the formation of the tetraene DHE as well as a side product, i.e., mercurated triene, and so such impurities may be possible contaminants in the original ergosterol [64].

Recently, real-time multiphoton imaging of the naturally occurring fluorescent sterol DHE in the plasma membrane of living cells [70, 82, 203, 204] was used to examine sterol distribution directly with high optical sectioning capability [206–209]. While subcellular distribution (plasma membrane, lysosome, lipid droplet, etc.) of DHE was highly dependent on the method of delivery (microcrystals, LUV, MβCD), DHE at the plasma membrane was found to be distributed non-randomly into sterol-rich and sterol-poor regions in plasma membranes of living cells with the size range of sterol-rich clustering domains estimated to be from 200 (limit of optical microscopy) to 565 nm [70, 71, 82, 203]. Due to the diffraction limit of resolution, there is uncertainty about whether these regions, as visible under laser scanning microscopy, are contiguous lateral domains [70, 71, 203] or represent artificial enhancement of the intensity as a result of microvillar/filopodial extensions and/or folding [210, 211] of the plasma membrane.

Video imaging studies involving HepG2 cells had resolved regions in the size range of 2,000–3,000 nm and had shown evidence of sterol-rich and sterol-poor distribution in the plasma membrane as well as canalicular microvilli of the polarized cells [210]. It was concluded, however, that these were not regions of enrichment but represented microvilli [210]. This same conclusion was reached following subsequent video imaging studies involving methyl-β-cyclodextrin complexes using a pulse chase method and the cell lines Hep G2, J774, and TRVb1 [211] where artifactual enhancement of the fluorescent emission was the result of rough surface topology and cell protrusions [211]. However, other studies using filipin, which labels all cholesterol in the plasma membrane without differentiating between sterol-rich or sterol-poor, did not reveal any enhancement in intensity as a result of plasma membrane ruffling or tubule sizing issues [212, 213].

Differences in results obtained by video imaging may be due to several factors: strong photobleaching of the fluorescent sterol as a result of video imaging techniques, saturation of all the plasma membrane with fluorescent sterol for video imaging, and video imaging's weak resolution in the *Z*-axis facilitating the need for deconvolution. In contrast, the MPLSM imaging studies used a loading methodology wherein only small amounts (non-saturable) of DHE were introduced into the plasma membrane over longer period of time to minimize the initial perturbations within the membrane [70, 71, 203]. With multi-photon excitation used in MPLSM, less extraneous photobleaching of the fluorescent sterol occurred with fluorescence emission from only the excitation volume at a radial resolution on the order of 300 nm while shorter dwell times minimized photodamage. The combination of probing sterol organization and distribution with low amounts of fluorescent sterol together with the resolution enhancement resulting from low yield in the 3-photon excitation volume element, cross-interference from the rough surface topology was reduced.

Available data from many experimental studies of the plasma membrane in general suggest cholesterol is the driving force for microdomain formation and cholesterol is not uniformly or homogeneously distributed but that the plasma membrane of living cells consists of areas of cholesterol segregation (regions that are cholesterol-rich and cholesterol-poor) [56, 214]. Biochemical studies also support this concept and demonstrate that purified cholesterol-rich microdomains isolated from cultured cell (L-cell, MDCK, primary hepatocytes) represent nearly one-third of the plasma membrane, are rich in cholesterol as well as saturated/monounsaturated fatty acylated phospholipids, and are comprised of physically distinct, liquid-ordered membrane phases intermediate between fluid liquid-crystalline and rigid gel phases [26, 82, 102, 136, 172, 182, 215–217]. Studies with purified microdomains from L-cell and MDCK plasma membranes showed that both exogenous (e.g. HDL) and endogenous (e.g. SCP-2) cholesterol binding proteins preferentially donate or extract cholesterol from cholesterol-rich, but not cholesterol-poor, microdomains [26, 27, 136, 137, 172]. The microdomain/lipid raft concept, despite controversy in details, provides a framework for biologists studying localization and function of membrane protein receptors, transporters, and downstream signaling molecules that regulate uptake of cholesterol [86, 87, 218–239], fatty acids [240–242], glucose [243–254], and other activities [216, 255–260].

Acknowledgments This work was supported in part by the by the USPHS, NIH GM31651 (FS, ABK), GM72041 (Project 2, ABK,FS), and Mentored Quantitative Research Career Development Award (K25) DK062812 (AMG).

References

1. Haberland ME, Reynolds JA (1973) Self-association of cholesterol in aqueous solution. Proc Natl Acad Sci 70:2313–2318
2. Fischer RT, Cowlen MS, Dempsey ME, Schroeder F (1985) Fluorescence of delta 5, 7, 9(11), 22-ergostatetraen-3 beta-ol in micelles, sterol carrier protein complexes, and plasma membranes. Biochemistry 24:3322–3331
3. Fischer RT, Stephenson FA, Shafiee A, Schroeder F (1984) delta 5, 7, 9(11)-Cholestatrien-3 beta-ol: a fluorescent cholesterol analogue. Chem Phys Lipids 36:1–14
4. Avdulov NA, Chochina SV, Igbavboa U, Warden CH, Schroeder F, Wood WG (1999) Lipid binding to sterol carrier protein-2 is inhibited by ethanol. Biochim Biophys Acta 1437:37–45
5. Castanho MA, Brown W, Prieto M (1992) Rod-like cholesterol micelles in aqueous solution studied using polarized and depolarized dynamic light scattering. Biophys J 63:1455–1461
6. Frolov A, Woodford JK, Murphy EJ, Billheimer JT, Schroeder F (1996) Spontaneous and protein-mediated sterol transfer between intracellular membranes. J Biol Chem 271:16075–16083
7. Frolov AA, Woodford JK, Murphy EJ, Billheimer JT, Schroeder F (1996) Fibroblast membrane sterol kinetic domains: modulation by sterol carrier protein 2 and liver fatty acid binding protein. J Lipid Res 37:1862–1874
8. Gallegos AM, Atshaves BP, Storey SM, Schoer J, Kier AB, Schroeder F (2002) Molecular and fluorescent sterol approaches to probing lysosomal membrane lipid dynamics. Chem Phys Lipids 116:19–38
9. Holthuis JCM, Levine TP (2005) Lipid traffic: floppy drives and superhighway. Nature Rev Mol Cell Biol 6:209–220
10. Warren RC (1987) Membrane microscopy. In: Warren RC (ed) Physics and the architecture of cell membranes. Adam Hilger, Bristol, pp 48–69
11. Warren RC (1987) Membrane crystallography. In: Warren RC (ed) Physics and the architecture of cell membranes. Adam Hilger, Bristol, pp 70–108
12. Schroeder F, Nemecz G (1990) Transmembrane cholesterol distribution. In: Esfahami M, Swaney J (eds) Advances in cholesterol research. Telford, Caldwell, pp 47–87
13. Small DM (1986) The physical chemistry of lipids. Plenum, New York, p 276
14. Warren RC (1987) Thermal analysis. In: Warren RC (ed) Physics and the architecture of cell membranes. Adam Hilger, Bristol, pp 109–121
15. Warren RC (1987) Membrane magnetic resonance. In: Warren RC (ed) Physics and the architecture of membranes. Adam Hilger, Bristol, pp 122–162
16. Scheidt HA, Muller P, Herrmann A, Huster D (2003) The potential of fluorescent and spin-labeled steroid analogues to mimic natural cholesterol. J Biol Chem 278:45563–45569
17. Badley RA (1976) Fluorescent probing of dynamic and molecular organization of biological membranes. In: Wehry EL (ed) Modern fluorescence spectroscopy, vol 2. Plenum, New York, pp 91–168
18. Wechsler A, Brafman A, Shafir M, Heverin M, Gottlieb H, Damari G, Gozlan-Kelner S, Spivak I, Moshkin O, Fridman E, Becker Y, Skaliter R, Einat P, Faerman A, Bjorkhem I, Feinstein E (2003) Generation of viable cholesterol-free mice. Science 302:2087
19. Sica D, Boniforti L, DiGiacomo G (1982) Sterols of *Candida tropicalis* grown on n-alkanes. Phytochemistry 21:234–236
20. Bocking T, Barrow KD, Netting AG, Chilcott TC, Coster HGL, Hofer M (2000) Effects of singlet oxygen on membrane sterols in the yeast *Saccharomyces cerevisiae*. FEBS Lett 267:1607–1618
21. Delseth C, Kashman Y, Djerassi C (1979) Ergosta-5, 7, 9(11), 22-tetraen-3beta-ol and its 24epsilon-ethyl homolog, two new marine sterols from the red sea sponge *Biemna fortis*. Helv Chim Acta 62:2037–2045
22. Rothblat GH, Burns CH, Conner RL, Landrey JR (1970) Desmosterol as the major sterol in L-cell mouse fibroblasts grown in sterol free culture medium. Science 169:880–882
23. Schroeder F, Perlmutter JF, Glaser M, Vagelos PR (1976) Isolation and characterization of mammalian membranes with altered phospholipid composition from cultured fibroblasts. J Biol Chem 251:6739–6746
24. Hale JE, Schroeder F (1982) Asymmetric transbilayer distribution of sterol across plasma membranes determined by fluorescence quenching of dehydroergosterol. Eur J Biochem 122:649–661
25. Schroeder F, Gallegos AM, Atshaves BP, Storey SM, McIntosh A, Petrescu AD, Huang H, Starodub O, Chao H, Yang H, Frolov A, Kier AB (2001) Recent advances in membrane cholesterol microdomains: rafts, caveolae, and intracellular cholesterol trafficking. Exp Biol Med 226:873–890
26. Gallegos AM, Storey SM, Kier AB, Schroeder F, Ball JM (2006) Structure and cholesterol dynamics of caveolae/raft and nonraft plasma membrane domains. Biochemistry 45:12100–12116
27. Storey SM, Gallegos AM, Atshaves BP, McIntosh AL, Martin GG, Landrock K, Kier AB, Ball JA, Schroeder F (2007) Selective cholesterol dynamics between lipoproteins and caveolae/lipid rafts. Biochemistry 46:13891–13906
28. Fliesler SJ, Richards MJ, Miller CY, Cenedella RJ (2000) Cholesterol synthesis in the vertebrate retina: effects of U1866A on rat retinal structure, photoreceptor membrane assembly, and sterol metabolism and composition. Lipids 35:289–296
29. Heverin M, Meaney S, Brafman A, Shafir M, Olin M, Shafaati M, von Bahr S, Larsson L, Lovgren-Sandblom A, Diczfalusy U, Parini P, Feinstein E, Bjorkhem I (2007) Studies on the cholesterol-free mouse: strong activation of LXR-regulated hepatic genes when replacing cholesterol with desmosterol. Arterioscler Thromb Vasc Biol 27:2191–2197
30. Wang P, Spencer TA (2005) Preparation of isotopically labelled benzophenone-containing lipid analogues. J Labelled Compd Radiopharm 48:781–788
31. Wiegand V, Chang T-Y, Strauss JFIII, Fahrenholz F, Gimpl G (2003) Transport of plasma membrane derived cholesterol and the function of Niemann–Pick C1 protein. FASEB J 17:782–784
32. Huang H, McIntosh AL, Atshaves BP, Kier AB, Schroeder F (2008) Polarity sensitive dansyl-cholesterol as a probe for sterol-rich and -poor domains in plasma membranes of living cells. Biochemistry (submitted)

33. Li Z, Mintzer E, Bittman R (2005) First synthesis of free cholesterol-BODIPY conjugates. J Org Chem 71:1718–1721
34. Li Z, Bittman R (2007) Synthesis and spectral properties of cholesterol- and FTY720-containing boron dipyrromethene dyes. J Org Chem 72:8367–8382
35. Chattopadhyay A, London E (1987) Parallax method for direct measurement of membrane penetration depth utilizing fluorescence quenching by spin-labeled phospholipids. Biochemistry 26:39–45
36. Mukherjee S, Chattopadhyay A (1996) Membrane organization at low cholesterol concentrations: a study using NBD-labeled cholesterol. Biochemistry 35:1311–1322
37. Mukherjee S, Chattopadhyay A (2005) Monitoring cholesterol organization in membranes at low concentrations utilizing the wavelength-selective fluorescence approach. Chem Phys Lipids 134:79–84
38. Shaw JE, Epand RF, Epand RM, Li Z, Bittman R, Yip CM (2006) Correlated fluorescence-atomic force microscopy of membrane domains: structure of fluorescence probes determines lipid localization. Biophys J 90:2170–2178
39. Schroeder F, Frolov A, Schoer J, Gallegos A, Atshaves BP, Stolowich NJ, Scott AI, Kier AB (1998) Intracellular sterol binding proteins, cholesterol transport and membrane domains. In: Chang TY, Freeman DA (eds) Intracellular cholesterol trafficking. Kluwer Academic, Boston, pp 213–234
40. Stolowich NJ, Frolov A, Petrescu AD, Scott AI, Billheimer JT, Schroeder F (1999) Holo-sterol carrier protein-2: ^{13}C-NMR investigation of cholesterol and fatty acid binding sites. J Biol Chem 274:35425–35433
41. Schroeder F, Frolov A, Starodub O, Russell W, Atshaves BP, Petrescu AD, Huang H, Gallegos A, McIntosh A, Tahotna D, Russell D, Billheimer JT, Baum CL, Kier AB (2000) Pro-sterol carrier protein-2: role of the *N*-terminal presequence in structure, function, and peroxisomal targeting. J Biol Chem 275:25547–25555
42. Serrero G, Frolov A, Schroeder F, Tanaka K, Gelhaar L (2000) Adipose differentiation related protein: expression, purification of recombinant protein in E. coli and characterization of its fatty acid binding properties. Biochim Biophys Acta 1488:245–254
43. Atshaves BP, Starodub O, McIntosh AL, Roths JB, Kier AB, Schroeder F (2000) Sterol carrier protein-2 alters HDL-mediated cholesterol efflux. J Biol Chem 275:36852–36861
44. Martin GG, Hostetler HA, Tichy SE, Russell DH, Berg JM, Woldegiorgis G, Spencer TA, Ball JA, Kier AB, Schroeder F (2008) Structure and function of the sterol carrier protein-2 (SCP-2) N-terminal pre-sequence. Biochemistry 47:5915–5934
45. Frolov A, Petrescu A, Atshaves BP, So PTC, Gratton E, Serrero G, Schroeder F (2000) High density lipoprotein mediated cholesterol uptake and targeting to lipid droplets in intact L-cell fibroblasts. J Biol Chem 275:12769–12780
46. Portioli Silva EP, Peres CM, Mendonca JR, Curi R (2004) NBD-cholesterol incorporation by rat macrophages and lymphocytes: a process dependent on the activation state of the cells. Cell Biochem Funct 22:23–28
47. Schroeder F, Zhou M, Swaggerty CL, Atshaves BP, Petrescu AD, Storey S, Martin GG, Huang H, Helmkamp GM, Ball JM (2003) Sterol carrier protein-2 functions in phosphatidylinositol transfer and signaling. Biochemistry 42:3189–3202
48. Gadella TW, Wirtz KW (1994) Phospholipid binding and transfer by non-specific lipid transfer protein (SCP-2): a kinetic model. Eur J Biochem 220:1019–1028
49. Frolov A, Cho TH, Billheimer JT, Schroeder F (1996) Sterol carrier protein-2, a new fatty acyl coenzyme A-binding protein. J Biol Chem 271:31878–31884
50. Dansen TB, Westerman J, Wouters F, Wanders RJ, van Hoek A, Gadella TW, Wirtz KW (1999) High affinity binding of very long chain fatty acyl CoA esters to the peroxisomal non-specific lipid transfer protein (sterol carrier protein-2). Biochem J 339:193–199
51. Pfanner N, Glick BS, Arden SR, Rothman JE (1990) Fatty acylation promotes fusion of transport vesicles with Golgi cisternae. J Cell Biol 110:955–961
52. Pfanner N, Orci L, Glick BS, Amherdt M, Arden SR, Malhotra V, Rothman JE (1989) Fatty acyl CoA is required for budding of transport vesicles from Golgi cisternae. Cell 59:95–102
53. Schroeder F, Atshaves BP, McIntosh AL, Gallegos AM, Storey SM, Parr RD, Jefferson JR, Ball JM, Kier AB (2007) Sterol carrier protein-2: new roles in regulating lipid rafts and signaling. Biochim Biophys Acta 1771:700–718
54. Schroeder F, Jefferson JR, Kier AB, Knittell J, Scallen TJ, Wood WG, Hapala I (1991) Membrane cholesterol dynamics: cholesterol domains and kinetic pools. Proc Soc Exp Biol Med 196:235–252
55. Schroeder F, Frolov AA, Murphy EJ, Atshaves BP, Jefferson JR, Pu L, Wood WG, Foxworth WB, Kier AB (1996) Recent advances in membrane cholesterol domain dynamics and intracellular cholesterol trafficking. Proc Soc Exp Biol Med 213:150–177
56. Bretscher MS, Munro S (1993) Cholesterol and the Golgi apparatus. Science 261:1280–1281
57. Smart EJ, Ying Y, Mineo C, Anderson RGW (1995) A detergent-free method for purifying caveolae membrane from tissue culture cells. Proc Natl Acad Sci 92:10404–10408
58. Brown DA, London E (2000) Structure and function of sphingolipid- and cholesterol-rich membrane rafts. J Biol Chem 275:17221–17224
59. Brown DA, London E (1998) Structure and origin of ordered lipid domains in biological membranes. J Membr Biol 164:103–114
60. Anderson RGW, Jacobson K (2002) A role for lipid shells in targeting proteins to caveolae, rafts, and other lipid domains. Science 296:1821–1825
61. Jacobson K, Vaz WL (1992) Domains in biological membranes. Comments Mol Cell Biophys 8:1–15
62. Pike LJ (2004) Lipid rafts: heterogeneity on the high seas. Biochem J 378:281–292
63. Pike LJ (2006) Rafts defined: a report on the Keystone symposium on lipid rafts and cell function. J Lipid Res 47:1597–1598
64. Ruyle WV, Jacob TA, Chemerda JM, Chamberlin EM, Rosenburg DW, Sita GE, Erickson RL, Aliminosa LM, Tishler M (1953) The preparation of delta7, 9(11)-allo-steroids by the action of mercuric acetate on delta7-allo steroids. J Am Chem Soc 75:2604–2609
65. Schroeder F (1984) Fluorescent sterols: probe molecules of membrane structure and function (review). Prog Lipid Res 23:97–113
66. Gimpl G, Gehrig-Burger K (2007) Cholesterol reporter molecules. Biosci Rep. doi:10.1007/s10540-007-9060-1
67. Wustner D (2007) Fluorescent sterols as tools in membrane biophysics and cell biology. Chem Phys Lipids 146:125
68. McIntosh AL, Huang H, Atshaves BP, Kier AB, Schroeder F (2007) Fluorescent sterols to study cholesterol trafficking in living cells. In: Miller L (ed) Selective probes and tags to study biomolecular function in vivo. Wiley VCH, Weinheim
69. Fischer RT, Stephenson FA, Shafiee A, Schroeder F (1985) Structure and dynamic properties of dehydroergosterol, delta 5, 7, 9(11), 22-ergostatetraen-3 beta-ol. J Biol Phys 13:13–24
70. McIntosh A, Gallegos A, Atshaves BP, Storey S, Kannoju D, Schroeder F (2003) Fluorescence and multiphoton imaging resolve unique structural forms of sterol in membranes of living cells. J Biol Chem 278:6384–6403

71. McIntosh AL, Atshaves BP, Huang H, Gallegos AM, Kier AB, Schroeder F, Xu H, Zhang W, Liu S (2007) Multiphoton laser scanning microscopy and spatial analysis of dehydroergosterol distributions on plasma membrane of living cells. In: McIntosh TJ (ed) Lipid rafts, vol 398. Humana, Totowa
72. Bittman R (1993) A review of the kinetics of cholesterol movement between donor and acceptor bilayer membranes. In: Finegold L (ed) Cholesterol in membrane models. CRC, Baton Raton, pp 45–66
73. Kan CC, Yan J, Bittman R (1992) Rates of spontaneous exchange of synthetic radiolabeled sterols between lipid vesicles. Biochemistry 31:1866–1874
74. Bittman R, Clejan S, Hui SW (1990) Increased rates of lipid exchange between *Mycoplasma capricolum* membranes and vesicles in relation to the propensity of forming nonbilayer lipid structures. J Biol Chem 265:15110–15117
75. Clejan S, Bittman R (1984) Distribution and movement of sterols with different side chain structures between the two leaflets of the membrane bilayer of mycoplasma cells. J Biol Chem 259:449–455
76. Abbott AJ, Nelsestuen GL (1987) Association of a protein with membrane vesicles at the collisional limit: studies with blood coagulation factor Va light chain also suggest major differences between small and large unilamellar vesicles. Biochemistry 26:7994–8003
77. McLean LR, Phillips M (1984) Cholesterol transfer from small and large unilamellar vesicles. Biochim Biophys Acta 776: 21–26
78. Small DM (1988) Progression and regression of atherosclerotic lesions: insights from lipid physical chemistry. Arteriosclerosis 8:103–129
79. Small DM, Shipley GG (1974) Physical-chemical basis of lipid deposition in atherosclerosis. Science 185:222–229
80. Tangirala RK, Jerome WG, Jones NL, Small DM, Johnson WJ, Glick JM, Mahlberg FH, Rothblat GH (1994) Formation of cholesterol monohydrate crystals in macrophage-derived foam cells. J Lipid Res 35:93–104
81. Smart EJ, Ying Y, Conrad PA, Anderson RGW (1994) Caveolin moves from caveolae to the Golgi apparatus in response to cholesterol oxidation. J Cell Biol 127:1185–1197
82. Schroeder F, Atshaves BP, Gallegos AM, McIntosh AL, Liu JC, Kier AB, Huang H, Ball JM (2005) Lipid rafts and caveolae organization. In: Frank PG, Lisanti MP (eds) Advances in molecular and cell biology, vol 36. Elsevier, Amsterdam, pp 3–36
83. Anderson R (1998) The caveolae membrane system. Ann Rev Biochem 67:199–225
84. Lavie Y, Liscovitch M (2000) Changes in lipid and protein constituents of rafts and caveolae in multidrug resistant cancer cells and their functional consequences. Glycoconj J 17:253–259
85. Everson WV, Smart EJ (2001) Influence of caveolin, cholesterol, and lipoproteins on nitric oxide synthase. TCM 11: 246–250
86. Everson WV, Smart EJ (2005) Caveolae and the regulation of cellular cholesterol homeostasis. In: Lisanti MP, Frank PG (eds) Caveolae and lipid rafts: roles in signal transduction and the pathogenesis of human disease, vol 36. Elsevier, San Diego, pp 37–55
87. Smart EJ, van der Westhuyzen DR (1998) Scavenger receptors, caveolae, caveolin, and cholesterol trafficking. In: Chang TY, Freeman DA (eds) Intracellular cholesterol trafficking. Kluwer Academic, Boston, pp 253–272
88. Kirsch C, Eckert GP, Mueller WE (2002) Statins affect cholesterol micro-domains in brain plasma membranes. Biochem Pharmacol 65:843–856
89. Burger K, Gimpl G, Fahrenholz F (2000) Regulation of receptor function by cholesterol. Cell Mol Life Sci 57:1577–1592
90. Gimpl G, Burger K, Fahrenholz F (1997) Cholesterol as modulator of receptor function. Biochemistry 36:10959–10974
91. Gimpl G, Fahrenholz F (2000) Human oxytocin receptors in cholesterol-rich vs. cholesterol-poor microdomains of the plasma membrane. Eur J Biochem 267:2483–2497
92. Bergmann W, Klacsmann JA (1947) Ergosterol F. J Org Chem 13:21–25
93. Bergmann W, Stevens PG (1947) Studies on the conversion of ergosterol to adrenal cortical hormones. J Org Chem 13:10–25
94. Budziarek R, Newbold GT, Stevenson R, Spring FS (1952) Steroids. Part I: 11-oxygenated steroids from ergosteryl-D acetate. Part 1. J Chem Soc July:2892–2900
95. Smutzer G, Crawford BF, Yeagle PL (1986) Physical properties of the fluorescent sterol probe dehydroergosterol. Biochim Biophys Acta 862:361–371
96. Loura LMS, Prieto M (1997) Dehydroergosterol structural organization in aqueous medium and in a model system of membranes. Biophys J 72:2226–2236
97. Yeagle PL, Bensen J, Greco M, Arena C (1982) Cholesterol behavior in human serum lipoproteins. Biochemistry 21:1249–1254
98. Schroeder F, Goh EH (1979) Regulation of very low density lipoprotein interior core lipid physicochemical properties. J Biol Chem 254:2464–2470
99. Schroeder F, Goh EH, Heimberg M (1979) Investigation of the surface structure of the very low density lipoprotein using fluorescence probes. FEBS Lett 97:233–236
100. Bergeron RJ, Scott J (1982) Fluorescent lipoprotein probe. Anal Chem 119:128–134
101. Bergeron RJ, Scott J (1982) Cholestatriene and ergostatetraene as in vivo and in vitro membrane and lipoprotein probes. J Lipid Res 23:391–404
102. Schroeder F, Gallegos AM, Atshaves BP, McIntosh A, Petrescu AD, Huang H, Chao H, Yang H, Frolov A, Kier AB (2001) Recent advances in membrane microdomains: rafts, caveolae and intracellular cholesterol trafficking. Exp Biol Med 226: 873–890
103. Stolowich NJ, Petrescu AD, Huang H, Martin G, Scott AI, Schroeder F (2002) Sterol carrier protein-2: structure reveals function. Cell Mol Life Sci 59:193–212
104. Colles SM, Woodford JK, Moncecchi D, Myers-Payne SC, McLean LR, Billheimer JT, Schroeder F (1995) Cholesterol interactions with recombinant human sterol carrier protein-2. Lipids 30:795–804
105. Nemecz G, Schroeder F (1991) Selective binding of cholesterol by recombinant fatty acid-binding proteins. J Biol Chem 266:17180–17186
106. Schroeder F, Dempsey ME, Fischer RT (1985) Sterol and squalene carrier protein interactions with fluorescent delta 5, 7, 9(11)-cholestatrien-3 beta-ol. J Biol Chem 260:2904–2911
107. Schroeder F, Butko P, Nemecz G, Jefferson JR, Powell D, Rymaszewski Z, Dempsey ME, Kukowska-Latallo J, Lowe JB (1989) Sterol carrier protein: a ubiquitous protein in search of a function. In: Verna R, Blumenthal R, Frati L (eds) Bioengineered molecules: basic and clinical aspects. Raven, New York, pp 29–45
108. Kubelt JK, Muller P, Wustner D, Hermann A (2002) Rapid transbilayer movement of the fluorescent sterol dehydroergosterol in lipid membranes. Biophys J 83:1525–1534
109. Raghuraman H, Chattopadhyay A (2004) Interaction of mellitin with membrane cholesterol: a fluorescence approach. Biophys J 87:2419–2432
110. Schroeder F, Nemecz G, Gratton E, Barenholz Y, Thompson TE (1988) Fluorescence properties of cholestatrienol in phosphatidylcholine bilayer vesicles. Biophys Chem 32:57–72

111. Schroeder F, Barenholz Y, Gratton E, Thompson TE (1987) A fluorescence study of dehydroergosterol in phosphatidylcholine bilayer vesicles. Biochemistry 26:2441–2448
112. Schroeder F, Nemecz G, Barenholz Y, Gratton E, Thompson TE (1988) Cholestatrienol time resolved fluorescence in phosphatidylcholine bilayers. In: Lakowicz JR, Eftink M, Wampler J (eds) Time resolved laser spectroscopy in biochemistry, vol 909. SPIE, Washington, pp 457–465
113. Bar LK, Chong PLG, Barenholz Y, Thompson TE (1989) Spontaneous transfer between phospholipid bilayers of dehydroergosterol: a fluorescent sterol analog. Biochim Biophys Acta 983:109–112
114. Chong PL, Liu F, Wang MM, Truong K, Sugar IP, Brown RE (1996) Fluorescence evidence for cholesterol regular distribution in phosphatidylcholine and in sphingomyelin lipid bilayers. J Fluoresc 6:221–224
115. Chong PLG (1994) Evidence for regular distribution of sterols in liquid crystalline phosphatidylcholine bilayers. Proc Natl Acad Sci 91:10069–10073
116. Liu F, Sugar IP, Chong PL (1997) Cholesterol and ergosterol superlattices in three-component liquid crystalline lipid bilayers as revealed by dehydroergosterol fluorescence. Biophys J 72:2243–2254
117. Nemecz G, Fontaine RN, Schroeder F (1988) A fluorescence and radiolabel study of sterol exchange between membranes. Biochim Biophys Acta 943:511–521
118. Butko P, Hapala I, Nemecz G, Schroeder F (1992) Sterol domains in phospholipid membranes: dehydroergosterol polarization measures molecular sterol transfer. J Biochem Biophys Methods 24:15–37
119. Nemecz G, Schroeder F (1988) Time-resolved fluorescence investigation of membrane cholesterol heterogeneity and exchange. Biochemistry 27:7740–7749
120. Schroeder F, Nemecz G (1989) Interaction of sphingomyelins and phosphatidylcholines with fluorescent dehydroergosterol. Biochemistry 28:5992–6000
121. Butko P, Hapala I, Scallen TJ, Schroeder F (1990) Acidic phospholipids strikingly potentiate sterol carrier protein 2 mediated intermembrane sterol transfer. Biochemistry 29:4070–4077
122. Hapala I, Kavecansky J, Butko P, Scallen TJ, Joiner C, Schroeder F (1994) Regulation of membrane cholesterol domains by sterol carrier protein-2. Biochemistry 33:7682–7690
123. Hapala I, Butko P, Schroeder F (1990) Role of acidic phospholipids in intermembrane sterol transfer. Chem Phys Lipids 56:37–47
124. Schroeder F, Butko P, Hapala I, Scallen TJ (1990) Intermembrane cholesterol transfer: role of sterol carrier proteins and phosphatidylserine. Lipids 25:669–674
125. Huang H, Ball JA, Billheimer JT, Schroeder F (1999) The sterol carrier protein-2 amino terminus: a membrane interaction domain. Biochemistry 38:13231–13243
126. Huang H, Ball JA, Billheimer JT, Schroeder F (1999) Interaction of the *N*-terminus of sterol carrier protein-2 with membranes: role of membrane curvature. Biochem J 344:593–603
127. Huang H, Gallegos A, Zhou M, Ball JM, Schroeder F (2002) Role of sterol carrier protein-2 N-terminal membrane binding domain in sterol transfer. Biochemistry 41:12149–12162
128. Matyash V, Geier C, Henske A, Mukherjee S, Hirsh D, Thiele C, Grant B, Maxfield FR, Kurzchalia TV (2001) Distribution and transport of cholesterol in *Caenorhabditis elegans*. Mol Biol Cell 12:1725–1736
129. Schoer J, Gallegos A, Starodub O, Petrescu A, Roths JB, Kier AB, Schroeder F (2000) Lysosomal membrane cholesterol dynamics: role of sterol carrier protein-2 gene products. Biochemistry 39:7662–7677
130. Chao H, Billheimer JT, Kier AB, Schroeder F (1999) Microsomal long chain fatty acyl-CoA transacylation: differential effect of sterol carrier protein-2. Biochim Biophys Acta 1439:371–383
131. Deliconstantinos G (1987) Effect of rat serum albumin-cholesterol on the physical properties of biomembranes. Biochem Int 45:467–474
132. Deliconstantinos G (1986) Evidence for the existence of non-esterified cholesterol carried by albumin in rat serum. Atherosclerosis 61:67–75
133. Fielding CJ, Moser K (1982) Evidence for the separation of albumin- and apo A-/-dependent mechanisms of cholesterol efflux from cultured fibroblasts into human plasma. J Biol Chem 257:10955–10960
134. Zhao Y, Marcel YL (1996) Serum albumin is a significant intermediate in cholesterol transfer between cells and lipoproteins. Biochemistry 35:7174–7180
135. Gallegos AM, Atshaves BP, Storey S, McIntosh A, Petrescu AD, Schroeder F (2001) Sterol carrier protein-2 expression alters plasma membrane lipid distribution and cholesterol dynamics. Biochemistry 40:6493–6506
136. Gallegos AM, McIntosh AL, Atshaves BP, Schroeder F (2004) Structure and cholesterol domain dynamics of an enriched caveolae/raft isolate. Biochem J 382:451–461
137. Gallegos AM, McIntosh AL, Kier AB, Schroeder F (2008) Membrane domain distributions: analysis of fluorescent sterol exchange kinetics. Curr Anal Chem 4:1–7
138. Woodford JK, Colles SM, Myers-Payne S, Billheimer JT, Schroeder F (1995) Sterol carrier protein-2 stimulates intermembrane sterol transfer by direct membrane interaction. Chem Phys Lipids 76:73–84
139. Woodford JK, Jefferson JR, Wood WG, Hubbell T, Schroeder F (1993) Expression of liver fatty acid binding protein alters membrane lipid composition and structure in transfected L-cell fibroblasts. Biochim Biophys Acta 1145:257–265
140. Woodford JK, Hapala I, Jefferson JR, Knittel JJ, Kavecansky J, Powell D, Scallen TJ, Schroeder F (1994) Mechanistic studies of sterol carrier protein-2 effects on L-cell fibroblast plasma membrane sterol domains. Biochim Biophys Acta 1189:52–60
141. Woodford JK, Behnke WD, Schroeder F (1995) Liver fatty acid binding protein enhances sterol transfer by membrane interaction. Mol Cell Biochem 152:51–62
142. Gallegos AM, Schoer J, Starodub O, Kier AB, Billheimer JT, Schroeder F (2000) A potential role for sterol carrier protein-2 in cholesterol transfer to mitochondria. Chem Phys Lipids 105:9–29
143. Petrescu AD, Gallegos AM, Okamura Y, Strauss IJF, Schroeder F (2001) Steroidogenic acute regulatory protein binds cholesterol and modulates mitochondrial membrane sterol domain dynamics. J Biol Chem 276:36970–36982
144. Schroeder F, Nemecz G, Wood WG, Joiner C, Morrot G, Ayraut-Jarrier M, Devaux PF (1991) Transmembrane distribution of sterol in the human erythrocyte. Biochim Biophys Acta 1066:183–192
145. Wood WG, Schroeder F, Hogy L, Rao AM, Nemecz G (1990) Asymmetric distribution of a fluorescent sterol in synaptic plasma membranes: effects of chronic ethanol consumption. Biochim Biophys Acta 1025:243–246
146. Schroeder F, Kier AB, Sweet WD (1990) Role of polyunsaturated fatty acids and lipid peroxidation in LM fibroblast plasma membrane structure. Arch Biochem Biophys 276:55–64
147. Sweet WD, Schroeder F (1988) Polyunsaturated fatty acids alter sterol transbilayer domains in LM fibroblast plasma membrane. FEBS Lett 229:188–192
148. Hayashi H, Igbavboa U, Hamanaka H, Kobayashi M, Fujita SC, Wood WG, Yanagisawa K (2002) Cholesterol is increased in the exofacial leaflet of plasma membranes of human apoE4 knock-in mice. Neuroreport 13:383–386

149. Igbavboa U, Avdulov NA, Schroeder F, Wood WG (1996) Increasing age alters transbilayer fluidity and cholesterol asymmetry in synaptic plasma membranes of mice. J Neurochem 66:1717–1725
150. Igbavboa U, Avdulov NA, Chochina SV, Wood WG (1997) Transbilayer distribution of cholesterol is modified in brain synaptic plasma membranes of knockout mice deficient in the LDL receptor, apoE, or both proteins. J Neurochem 69:1661–1667
151. Wood WG, Eckert GP, Igbavboa U, Mueller WE (2003) Amyloid beta-protein interactions with membranes and cholesterol: causes or casualties of Alzheimer's disease. Biochim Biophys Acta 1610:281–290
152. Brasaemle DL, Robertson RD, Attie AD (1988) Transbilayer movement of cholesterol in the human erythrocyte membrane. J Lipid Res 29:481–489
153. Schroeder F, Sweet WD (1988) The role of membrane lipid and structure asymmetry on transport systems. In: Jorgensen PL, Verna R (eds) Advances in biotechnology of membrane ion transport, vol 51. Serono Symposia, New York, pp 183–195
154. Sweet WD, Wood WG, Schroeder F (1987) Charged anesthetics selectively alter plasma membrane order. Biochemistry 26: 2828–2835
155. Sweet WD, Schroeder F (1986) Plasma membrane lipid composition modulates action of anesthetics. Biochim Biophys Acta 861:53–61
156. Sweet WD, Schroeder F (1988) Lipid domains and enzyme activity. In: Aloia RC, Cirtain CC, Gordon LM (eds) Advances in membrane fluidity: lipid domains and the relationship to membrane function. Alan R. Liss, New York, pp 17–42
157. Wood WG, Gorka C, Schroeder F (1989) Acute and chronic effects of ethanol on transbilayer membrane domains. J Neurochem 52:1925–1930
158. Wood WG, Rao AM, Schroeder F, Igbavboa U (1993) Membrane cholesterol and ethanol: domains, kinetics, and protein function. In: Alling C, Diamond I, Leslie SW, Sun GY, Wood WG (eds) Alcohol, cell membranes, and signal transduction in brain. Plenum, New York, pp 13–32
159. Wood WG, Schroeder F, Rao AM, Igbavboa U, Avdulov NA (1996) Membranes and ethanol: lipid domains and lipid protein interactions. In: Dietrich R, Erwin VG (eds) Pharmacological effects of ethanol on the nervous system. CRC, Boca Raton, pp 13–27
160. Wustner D, Herrmann A, Hao M, Maxfield FR (2002) Rapid nonvesicular transport of sterol between the plasma membrane domains of polarized hepatic cells. J Biol Chem 277:30325–30336
161. Colles SM, Wood WG, Myers-Payne SC, Igbavboa U, Avdulov NA, Joseph J, Schroeder F (1995) Structure and polarity of mouse brain synaptic plasma membrane: effects of ethanol in vitro and in vivo. Biochemistry 34:5945–5959
162. Schroeder F, Morrison WJ, Gorka C, Wood WG (1988) Transbilayer effects of ethanol on fluidity of brain membrane leaflets. Biochim Biophys Acta 946:85–94
163. Schroeder F, Gorka C, Williamson LS, Wood WG (1987) The influence of dolichols on fluidity of mouse synaptic plasma membranes. Biochim Biophys Acta 902:385–393
164. Wood WG, Lahiri S, Gorka C, Armbrecht HJ, Strong R (1987) In vitro effects of ethanol on erythrocyte membrane fluidity of alcoholic patients: an electron spin resonance study. Alcohol Clin Exp Res 11:332–335
165. Wood WG, Chochina SV, Igbavboa U, O'Hare EO, Schroeder F, Cleary JP, Avdulov NA (1997) Amyloid B alters brain synaptic plasma membrane lipid structure and lipid-protein interaction. J Neurochem 68:2086–2091
166. Wood WG, Schroeder F, Avdulov NA, Chochina SV, Igbavboa U (1999) Recent advances in brain cholesterol dynamics: transport, domains, and Alzheimer's disease. Lipids 34:225–234
167. Harris RA, Schroeder F (1982) Effects of barbiturates and ethanol on the physical properties of brain membranes. J Pharm Exp Ther 223:424–431
168. Harris RA, Schroeder F (1981) Ethanol and the physical properties of brain membranes: fluorescence studies. Mol Pharmacol 20:128–137
169. Schroeder F, Goetz I, Roberts E (1984) Age-related alterations in cultured human fibroblast membrane structure and function. Mech Ageing Dev 25:365–389
170. Schroeder F, Goetz IE, Roberts E (1984) Membrane anomalies in Huntington's disease fibroblasts. J Neurochem 43:526–539
171. Schroeder F (1984) Role of membrane lipid asymmetry in aging (review). Neurobiol Aging 5:323–333
172. Atshaves BP, Gallegos A, McIntosh AL, Kier AB, Schroeder F (2003) Sterol carrier protein-2 selectively alters lipid composition and cholesterol dynamics of caveolae/lipid raft vs. non-raft domains in L-cell fibroblast plasma membranes. Biochemistry 42:14583–14598
173. Gallegos AM, Atshaves BP, Storey SM, Starodub O, Petrescu AD, Huang H, McIntosh A, Martin G, Chao H, Kier AB, Schroeder F (2001) Gene structure, intracellular localization, and functional roles of sterol carrier protein-2. Prog Lipid Res 40:498–563
174. Mukherjee S, Zha X, Tabas I, Maxfield FR (1998) Cholesterol distribution in living cells: fluorescence imaging using dehydroergosterol as a fluorescent cholesterol analog. Biophys J 75:1915–1925
175. Wustner D, Mondal M, Tabas I, Maxfield FR (2005) Direct observation of rapid internalization and intracellular transport of sterol by macrophage foam cells. Traffic 6:396–412
176. Wustner D, Mondal M, Huang A, Maxfield FR (2004) Different routes of transport for high density lipoprotein and its associated free sterol in polarized hepatic cells. J Lipid Res 45:427–437
177. Puglielli L, Rigotti A, Amigo L, Nunez L, Greco AV, Santos MJ, Nervi F (1996) Modulation on intrahepatic cholesterol trafficking: Evidence by in vivo antisense treatment for the involvement of sterol carrier protein-2 in newly synthesized cholesterol transfer into bile. Biochem J 317:681–687
178. Amigo L, Zanlungo S, Miquel JF, Glick JM, Hyogo H, Cohen DE, Rigotti A, Nervi F (2003) Hepatic overexpression of sterol carrier protein-2 inhibits VLDL production and reciprocally enhances biliary lipid secretion. J Lipid Res 44:399–407
179. Zanlungo S, Amigo L, Mendoza H, Glick J, Rodriguez A, Kozarsky K, Miquel JF, Rigotti A, Nervi F (2000) Overexpression of sterol carrier protein-2 in mice leads to increased hepatic cholesterol content and enterohepatic circulation of bile acids. Gastroenterology 118:135 A1165
180. Fuchs M, Hafer A, Muench C, Kannenberg F, Teichmann S, Scheibner J, Stange EF, Seedorf U (2001) Disruption of the sterol carrier protein 2 gene in mice impairs biliary lipid and hepatic cholesterol metabolism. J Biol Chem 276:48058–48065
181. Muench C, Hafer A, Katzberg N, Scheibner J, Stange EF, Seedorf U, Fuchs M (2000) Relevance of the sterol carrier protein-2 gene for bile acid synthesis and gallstone formation in genetically susceptible mice (abstract). Part 1. Gastroenterology 118(4, Suppl 2):1167
182. Atshaves BP, McIntosh AL, Payne HR, Gallegos AM, Landrock K, Maeda N, Kier AB, Schroeder F (2007) Sterol carrier protein-2/sterol carrier protein-x gene ablation alters lipid raft domains in primary cultured mouse hepatocytes. J Lipid Res 48:2193–2211
183. Atshaves BP, McIntosh AL, Landrock D, Payne HR, Mackie J, Maeda N, Ball JM, Schroeder F, Kier AB (2007) Effect of

SCP-x gene ablation on branched-chain fatty acid metabolism. Am J Physiol 292:939–951

184. Martin GG, Danneberg H, Kumar LS, Atshaves BP, Erol E, Bader M, Schroeder F, Binas B (2003) Decreased liver fatty acid binding capacity and altered liver lipid distribution in mice lacking the liver fatty acid binding protein (L-FABP) gene. J Biol Chem 278:21429–21438
185. Martin GG, Huang H, Atshaves BP, Binas B, Schroeder F (2003) Ablation of the liver fatty acid binding protein gene decreases fatty acyl CoA binding capacity and alters fatty acyl CoA pool distribution in mouse liver. Biochemistry 42:11520–11532
186. Martin GG, Atshaves BP, McIntosh AL, Mackie JT, Kier AB, Schroeder F (2005) Liver fatty acid binding protein (L-FABP) gene ablation alters liver bile acid metabolism in male mice. Biochem J 391:549–560
187. Martin GG, Atshaves BP, McIntosh AL, Mackie JT, Kier AB, Schroeder F (2006) Liver fatty acid binding protein (L-FABP) gene ablation potentiates hepatic cholesterol accumulation in cholesterol-fed female mice. Am J Physiol 290:G36–G48
188. Martin GG, Atshaves BP, McIntosh AL, Mackie JT, Kier AB, Schroeder F (2008) Increased age-dependent obesity in liver fatty acid binding protein gene-ablated mice. J Nutr (submitted)
189. Martinn GG, Atshaves BP, McIntosh AL, Payne HR, Mackie JT, Kier AB, Schroeder F (2008) Liver fatty acid binding protein gene ablation enhances age-dependent obesity in male mice. Mol Cell Biochem (submitted)
190. Puglielli L, Rigotti A, Greco AV, Santos MJ, Nervi F (1995) Sterol carrier protein-2 is involved in cholesterol transfer from the endoplasmic reticulum to the plasma membrane in human fibroblasts. J Biol Chem 270:18723–18726
191. Moncecchi DM, Murphy EJ, Prows DR, Schroeder F (1996) Sterol carrier protein-2 expression in mouse L-cell fibroblasts alters cholesterol uptake. Biochim Biophys Acta 1302:110–116
192. Murphy EJ, Schroeder F (1997) Sterol carrier protein-2 mediated cholesterol esterification in transfected L-cell fibroblasts. Biochim Biophys Acta 1345:283–292
193. Jefferson JR, Powell DM, Rymaszewski Z, Kukowska-Latallo J, Schroeder F (1990) Altered membrane structure in transfected mouse L-cell fibroblasts expressing rat liver fatty acid-binding protein. J Biol Chem 265:11062–11068
194. Jefferson JR, Slotte JP, Nemecz G, Pastuszyn A, Scallen TJ, Schroeder F (1991) Intracellular sterol distribution in transfected mouse L-cell fibroblasts expressing rat liver fatty acid binding protein. J Biol Chem 266:5486–5496
195. Baum CL, Reschly EJ, Gayen AK, Groh ME, Schadick K (1997) Sterol carrier protein-2 overexpression enhances sterol cycling and inhibits cholesterol ester synthesis and high density lipoprotein cholesterol secretion. J Biol Chem 272:6490–6498
196. Atshaves BP, Jefferson JR, McIntosh AL, McCann BM, Landrock K, Kier AB, Schroeder F (2007) Effect of sterol carrier protein-2 expression on sphingolipid distribution in plasma membrane lipid rafts/caveolae. Lipids 42:871–884
197. Kriska T, Levchenko VV, Korytowski W, Atshaves BP, Schroeder F, Girotti AW (2006) Hypersensitivity of sterol carrier protein-2 overexpressing hepatoma cells to lethal peroxidative damage induced by an exogenous cholesterol hydroperoxide. J Biol Chem 281:23643–23651
198. Roff CF, Pastuszyn A, Strauss JFI, Billheimer JT, Vanier MT, Brady RO, Scallen TJ, Pentchev PG (1992) Deficiencies in sex-regulated expression and levels of two hepatic sterol carrier proteins in a murine model of Niemann-Pick type C disease. J Biol Chem 267:15902–15908
199. Kobayashi T, Beuchat M-H, Lindsay M, Frias S, Palmiter RD, Sakuraba H, Parton RG, Gruenberg J (1999) Late endosomal membranes rich in lysobisphosphatidic acid regulate cholesterol transport. Nat Cell Biol 1:113–118
200. Zhou M, Parr RD, Petrescu AD, Payne HR, Atshaves BP, Kier AB, Ball JA, Schroeder F (2004) Sterol carrier protein-2 directly interacts with caveolin-1 in vitro and in vivo. Biochemistry 43:7288–7306
201. Parr RD, Martin GG, Hostetler HA, Schroeder ME, Mir KD, Kier AB, Ball JM, Schroeder F (2007) A new N-terminal recognition domain in caveolin-1 interacts with sterol carrier protein-2 (SCP-2). Biochemistry 46:8301–8314
202. Duncan MJ, Abraham SN (2005) Lipid raft mediated entry of bacteria into host cells. In: Lisanti MP, Frank PG (eds) Caveolae and lipid rafts: roles in signal transduction and the pathogenesis of human disease, vol 36. Elsevier, San Diego, pp 79–88
203. Zhang W, McIntosh A, Xu H, Wu D, Gruninger T, Atshaves BP, Liu JCS, Schroeder F (2005) Structural analysis of sterol distribution in the plasma membrane of living cells. Biochemistry 44:2864–2984
204. McIntosh A, Atshaves BP, Huang H, Gallegos AM, Kier AB, Schroeder F, Xu H, Zhang W, Liu S (2007) Multiphoton laser scanning microscopy and spatial analysis of dehydroergosterol distributions on plasma membranes of living cells. In: McIntosh T (ed) Lipid rafts. Humana, Totowa, pp 85–105
205. Schroeder F, Butko P, Nemecz G, Scallen TJ (1990) Interaction of fluorescent delta 5, 7, 9(11), 22-ergostatetraen-3β-ol with sterol carrier protein-2. J Biol Chem 265:151–157
206. Denk W, Strickler JH, Webb WW (1990) Two-photon laser scanning fluorescence microscopy. Science 2:73–76
207. Williams RM, Zipfel WR, Webb WW (2001) Multiphoton microscopy in biological research. Curr Opin Chem Biol 5:603–608
208. Maiti S, Shear JB, Williams RM, Zipfel WR, Webb WW (1997) Measuring serotonin distribution in live cells with three-photon excitation. Science 275:530–532
209. Williams RM, Shear JB, Zipfel WRMS, Webb WW (1999) Mucosal mast cell secretion processes imaged using three-photon microscopy of 5-hydroxytryptamine autofluorescence. Biophys J 76:1835–1846
210. Wustner D (2005) Improved visualization and quantitative analysis of fluorescent membrane sterol in polarized hepatic cells. J Microscopy 220:47–64
211. Wustner D (2007) Plasma membrane sterol distribution resembles the surface topography of living cells. Mol Biol Cell 18:211–228
212. Mobius W, Ohno-Iwashita Y, van Donselaar E, Oorschot VMJ, Shimada Y, Fujimoto T, Heijnen HFG, Geuze HJ, Slot JW (2002) Immunoelectron microscopic localization of cholesterol using biotinylated and non-cytolytic perfringolysin O. J Histochem Cytochem 50:43–55
213. Waheed AA, Shimada Y, Heijnen HFG, Nakamura M, Inomata M, Hayashi M, Iwashita S, Slot JW, Ohno-Iwashita Y (2001) Selective binding of perfringolysin *O* derivative to cholesterol-rich membrane microdomains (rafts). Proc Natl Acad Sci USA 98:4926–4931
214. Sankaram MB, Thompson TE (1991) Cholesterol-induced fluid-phase immiscibility in membranes. Proc Natl Acad Sci 88:8689–8690
215. Schroeder R, London E, Brown D (1994) Interactions between saturated acyl chains confer detergent resistance on lipids and glycosylphosphatidylinositol (GPI)-anchored proteins: GPI-anchored proteins in liposomes and cells show similar behavior. Proc Natl Acad Sci 91:12130–12134
216. Anderson RG (1993) Caveolae: where incoming and outgoing messengers meet (review, 68 refs). Proc Natl Acad Sci USA 90:10909–10913

217. Mukherjee S, Maxfield FR (2004) Membrane domains. Annu Rev Cell Biol 20:839–866
218. Babitt J, Trigatti B, Rigotti A, Smart EJ, Anderson RGW, Xu S, Krieger M (1997) Murine SR-BI, a high density lipoprotein receptor that mediates selective lipid uptake, is *N*-Glycosylated and fatty acylated and colocalizes with plasma membrane caveolae. J Biol Chem 272:13242–13249
219. Barlage S, Boettcher D, Boettcher A, Dada A, Schmitz G (2006) High density lipoprotein modulates platelet function. Cytometry: Part A. J Int Soc Anal Cytol 69A:196–199
220. Chao WT, Tsai S-H, Lin Y-C, Lin W-W, Yang VC (2005) Cellular localization and interaction of ABCA1 and caveolin-1 in aortic endothelial cells after HDL incubation. Biochem Biophys Res Commun 332:743–749
221. Connelly MA, Williams DL (2004) Scavenger receptor B1: a scavenger receptor with a mission to transport high density lipoprotein lipids. Cur Opin Lipidol 15:287–295
222. Demeule M, Jodoin J, Gingras D, Beliveau R (2000) P-glycoprotein is localized in caveolae in resistant cells and in brain capillaries. FEBS Lett 466:219–224
223. Drobnik W, Borsukova H, Bottcher A, Pfeiffer A, Liebisch G, Schutz GJ, Schindler H, Schmitz G (2002) Apo AI/ABCA1-dependent and HDL3-mediated lipid efflux from compositionally distinct cholesterol-based microdomains. Traffic 3:268–278
224. Duong M, Collins HL, Jin W, Zanotti I, Favari E, Rothblat G (2006) Relative contributions of ABCA1 and SR-BI to cholesterol efflux to serum from fibroblasts and macrophages. Arterioscler Thromb Vasc Biol 26:541–547
225. Graf GA, Connell PM, van der Westhuyzen DR, Smart EJ (1999) The class B, type 1 scavenger receptor promotes the selective uptake of high density lipoprotein cholesterol into caveolae. J Biol Chem 274:12034–12048
226. Hinrichs JWJ, Klappe K, Hummel I, Kok JW (2004) ATP-binding cassette transporters are enriched in non-caveolar detergent insoluble glycosphingolipid-enriched membrane domains (DIGs) in human multidrug resistant cancer cells. J Biol Chem 279:5734–5738
227. Jessup W, Gelissen I, Gaus K, Kritharides L (2006) Roles of ATP binding cassette transporters A1 and G1, scavenger receptor BI and membrane lipid domains in cholesterol export from macrophages. Curr Opin Lipidol 17:247–267
228. Kamau SW, Kramer SD, Gunthert M, Wunderlich-Allenspach H (2005) Effect of the modulation of the membrane lipid composition on the localization and function of P-glycoprotein in MDR1-MDCK cells. In Vitro Cell Dev Biol 41:207–216
229. Lavie Y, Fiucci G, Liscovitch M (1998) Up-regulation of caveolae and caveolar constituents in multidrug resistant cancer cells. J Biol Chem 273:32380–32383
230. Luker GD, Pica CM, Kumar AS, Covey DF, Piwnica-Worms D (2000) Effect of cholesterol and enantiomeric cholesterol on *P*-glycoprotein localization and function in low density membrane domains. Biochemistry 39:7651–7661
231. Mendez AJ, Lin G, Wade DP, Lawn RM, Oram JF (2001) Membrane lipid domains distinct from cholesterol/sphingomyelin-rich rafts are involved in the ABCA1-mediated lipid secretory pathway. J Biol Chem 276:3158–3166
232. Nieland TJF, Chroni A, FitzGerald LM, Maliga Z, Zannis VI, Kirchhausen T, Krieger M (2004) Cross-inhibition of SR-BI- and ABCA1-mediated cholesterol transport by the small molecules BLT-4 and glyburide. J Lipid Res 45:1256–1265
233. Orso E, Broccardo C, Kaminski WE, Bottcher A, Liebisch G, Drobnik W, Gotz A, Chambenoit O, Diederich W, Langmann T, Spruss T, Luciani M-F, Rothe G, Lackner KJ, Chimini G, Schmitz G (2000) Transport of lipids from Golgi to plasma membrane is defective in Tangier disease patients and Abc1-deficient mice. Nat Genet 24:192–196
234. Parathath S, Connelly MA, Rieger RA, Klein SM, Abumrad NA, de la Llera-Moya M, Iden CR, Rothblat GH, Williams DL (2004) Changes in plasma membrane properties and phosphatidylcholine subspecies of insect Sf9 cells due to expression of scavenger receptor class B, type 1, and CD36. J Biol Chem 279:41310–41318
235. Peng Y, Akmentin W, Conneely MA, Lund-Katz S, Phillips MC, Williams DL (2003) Scavenger receptor B1 (SR-B1) clustered on microvillar extensions suggests that this plasma membrane domain is a way station for cholesterol trafficking between cells and high density lipoprotein. Mol Biol Cell 15:384–396
236. Rigotti A, Miettinen H, Kreiger M (2003) The role of the high-density lipoprotein receptor SR-B1 in the lipid metabolism of endocrine and other tissues. Endocrine Rev 23:357–383
237. Schmitz G, Kaminski WE, Orso E (2000) ABC transporters in cellular lipid trafficking. Curr Opin Lipidol 11:493–501
238. Smart EJ (2005) Caveolae and the regulation of cellular cholesterol homeostasis. In: Lisanti MP, Frank PG (eds) Advances in molecular and cell biology, vol 36. Elsevier, Amsterdam, p 35
239. Yancey PG, Bortnick AE, Kellner-Weibel G, de la Llera-Moya M, Phillips MC, Rothblat GH (2003) Importance of different pathways of cellular cholesterol efflux. Arterioscler Thromb Vasc Biol 23:712–719
240. Ehehalt R, Fullekrug J, Pohl J, Ring A, Herrmann T, Stremmel W (2006) Translocation of long chain fatty acids across the plasma membrane–lipid rafts and fatty acid transport proteins. Mol Cell Biochem 284:135–140
241. Koonen DPY, Glatz JFC, Bonen A, Luiken JJFP (2006) Long-chain fatty acid uptake and FAT/CD36 translocation in heart and skeletal muscle. Biochim Biophys Acta 1736:163–180
242. Ortegren U, Karlsson M, Blazic N, Blomqvist M, Nysrom FH, Gustavsson J, Fredman P, Stralfors P (2007) Lipids and glycosphingolipids in caveolae and surrounding plasma membrane of primary rat adipocytes. Eur J Biochem 271:2028–2036
243. Balbis ABG, Mounier C, Posner BI (2004) Effect of insulin on caveolin-enriched membrane domains in rat liver. J Biol Chem 279:39348–39357
244. Cohen AW, Combs TP, Scherer PE, Lisanti MP (2003) Role of caveolin and caveolae in insulin signaling and diabetes. Am J Physiol Endocrinol Metab 285:E1151–E1160
245. Elmendorf JS (2004) Fluidity of insulin action. Mol Biotech 27:127–138
246. Ikonen E, Vainio S (2005) Lipid microdomains and insulin resistance: is there a connection? Sci STKE pe3:1–3
247. Ishikawa Y, Otsu K, Oshikawa J (2005) Caveolin; different roles for insulin signal? Cell Signal 17:1175–1182
248. Kumar AS, Xiao Y-P, Laipis PJ, Fletcher BS, Frost SC (2004) Glucose deprivation enhances targeting of GLUT1 to lipid rafts in 3T3–L1 adipocytes. Am J Physiol Endocrinol Metab 286:E568–E576
249. Matthews LC, Taggart MJ, Westwood M (2005) Effect of cholesterol depletion on mitogenesis and survival: the role of caveolar and noncaveolar domains in insulin-like growth factor-mediated cellular function. Endocrinology 146:5463–5473
250. Ortegren U, Yin L, Ost A, Karlsson H, Nystrom FH, Stralfors P (2006) Separation and characterization of caveolae subclasses in the plasma membrane of primary adipocytes; segregation of specific proteins and functions. FEBS J 273:3381–3392
251. Rauch MC, Ocampo ME, Bohle J, Amthauer R, Yanez AJ, Rodriguez-Gil JE, Slebe JC, Reyes JG, Concha II (2006) Hexose transporters GLUT1 and GLUT3 are colocalized with hexokinase I in caveolae microdomains of rat spermatogenic cells. J Cell Physiol 207:397–406
252. Saltiel AR, Pessin JE (2003) Insulin signaling in microdomains of the plasma membrane. Traffic 4:711–716

253. Syme CA, Zhang L, Bisello A (2006) Caveolin-1 regulates cellular trafficking and function of the glucagon-like peptide 1 receptor. Mol Endocrinol 20:3400–3411
254. Vainio S, Bykov I, Hermansson M, Jokitalo E, Somerharju P, Ikonen E (2005) Defective insulin receptor activation and altered lipid rafts in Niemann–Pick type C disease hepatocytes. Biochem J 391:465–472
255. Yamamoto M, Toya f Y, Schwencke C, Lisanti MP, Myers MG, Iskikawa Y (1998) Caveolin is an activator of insulin receptor signaling. J Biol Chem 273:26962–26968
256. Smart EJ, Graf GA, McNiven MA, Sessa WC, Engelman JA, Scherer PE, Okamoto T, Lisanti MP (1999) Caveolins, liquid-ordered domains, and signal transduction. Mol Cell Biol 19:7289–7304
257. Liu P, Rudick M, Anderson RGW (2002) Multiple functions of caveolin-1. J Biol Chem 277:41295–41298
258. Stralfors P (2005) Insulin signaling and caveolae. In: Lisanti MP, Frank PG (eds) Caveolae and lipid rafts: roles in signal transduction and human disease, vol 36. Elsevier, San Diego, pp 141–169
259. Igarashi J (2005) eNOS regulation by sphingosine 1 phosphate and caveolin. In: Lisanti MP, Frank PG (eds) Caveolae and lipid rafts: roles in signal transduction and the pathogenesis of human disease. Elsevier, New York, pp 125–140
260. Morris R, Cox H, Mombelli E, Quinn P (2004) Rafts, Little caves and large potholes: how lipid structure interacts with membrane proteins to create functionally diverse membrane environments. In: Quinn P (ed) Subcellular biochemistry: membrane dynamics and domains, vol 37. Kluwer Academic, New York, pp 35–118